XENOBIOTICA , 2000, VOL. 30, NO. 1, 1–25

Molecular modelling of human CYP2E1 by homology with the CYP102 haemoprotein domain: investigation of the interactions of substrates and inhibitors within the putative active site of the human CYP2E1 isoform

D. F. V. LEWIS†*, M. G. BIRD‡, M. DICKINS§, B. G. LAKE¶, P. J. EDDERSHAW§, M. H. TARBIT§ and P. S. GOLDFARB†

† Molecular Toxicology Group, School of Biological Sciences, University of Surrey, Guildford, GU2 5XH, UK
‡ Toxicology Division, Exxon Biomedical Sciences, Inc., Mettlers Road, CN 2350, East Millstone, NJ, 08875–2350, USA
§ GlaxoWellcome Research and Development Ltd., Park Road, Ware SG12 0DP, UK
¶ BIBRA International, Woodmansterne Road, Carshalton SM5 4DS, UK

Received 23 May 1999

1. The construction of a three-dimensional model of human CYP2E1 is reported. It is based on homology with the haemoprotein domain of the unusual bacterial P450, CYP102, which is of known crystal structure.

2. Interactive docking of a number of human CYP2E1 substrates is consistent with their known positions of CYP2E1-mediated metabolism, where specific interactions with key active site amino acid side-chains appear to rationalize the binding and orientation of substrate molecules.

3. Amino acid residues within the putative active site of human CYP2E1, including those associated with the binding of substrates and inhibitors, are shown to correspond with those identified by site-directed mutagenesis experiments conducted on CYP2 family isoforms, and they are known to affect substrate metabolism regioselectivity.

4. Consequently, it was found that the CYP2E1 active site exhibits complementarity with the structural characteristics of known substrates and inhibitors of this enzyme, including their relatively low molecular weights and disposition of hydrogen bond-forming groups.

Introduction

The cytochromes P450 (CYP) constitute a superfamily of haem-thiolate enzymes present in most species, where they possess important roles primarily in the oxidation of many endogenous and exogenous chemicals (Nelson *et al*. 1996). The CYP2 family appears to have arisen ~ 470 million years ago and has subsequently undergone further divergence into at least five major subfamilies (CYP2A–E), of which CYP2E is thought to have emerged via bifurcation with CYP2C ~ 230 million years ago (reviewed in Lewis *et al*. 1998a). Although CYP2E may possess an endogenous role in gluconeogenesis from acetone (Johansson *et al*. 1986) it is clear that a substantial number of xenobiotics is metabolized by this isoform (Ingelman-Sundberg *et al*. 1993, Ronis *et al*. 1996), including nitrosamines (Yang *et al*. 1990), paracetamol (Raucy *et al*. 1989), acetone (Koop and Casazza 1985), 4-nitrophenol (Tassaneeyakul *et al*. 1993), ethanol (Elkstrom *et al*. 1986), halogenated hydrocarbons (Raucy *et al*. 1993, Loizou *et al*. 1994, Urban *et al*. 1994) and other low

* Author for correspondence; e-mail: d.lewis@surrey.ac.uk

Xenobiotica ISSN 0049–8254 print/ISSN 1366–5928 online © 2000 Taylor & Francis Ltd
http://www.tandf.co.uk/journals/tf/00498254.html

molecular weight organic chemicals (Guengerich *et al*. 1991). In addition, it is generally accepted that CYP2E plays a role in the carcinogenicity of a number of compounds such as benzene, dialkylnitrosamines, butadiene, chloroform, vinyl chloride, acrylonitrile and carbon tetrachloride (Gonzalez and Gelboin 1994, Guengerich 1995). It is known that unlike most other P450, CYP2E contains a proportion of the haemoprotein that is present naturally in the high-spin state even in the absence of substrate (Koop *et al*. 1982, Guengerich and Johnson 1997), and this may contribute to this enzyme's ability to generate hydroxyl radicals together with other reactive oxygen species (ROS) following its induction (Elkstrom *et al*. 1986, Cederbaum 1987, Kukielka and Cederbaum 1994). ROS can cause DNA damage (Halliwell and Gutteridge 1990, Wiseman and Halliwell 1996) and can, therefore, represent factors in the overall carcinogenicity of some CYP2E substrates and inducers (Parke 1987, 1994, Terelius *et al*. 1993, Ioannides *et al*. 1995) although genetic predisposition may also play a role (Raunio and Pelkonen 1995). Furthermore, the involvement of CYP2E (and possibly its association with ROS generation) has been implicated in a number of disease states, including diabetes (Barnett *et al*. 1994, Bellward *et al*. 1988), and it appears that both fasting (Liu *et al*. 1993) and vigorous exercise (Ardies *et al*. 1994) may potentiate the levels of CYP2E, especially when combined with moderate inducers of this enzyme.

It is possible that the ability of certain CYP2E substrates and inducers to generate oxygen radicals and other ROS may explain the greater tumorigenic susceptibility of small rodents towards dimethylnitrosamine (DMN) and other small molecular weight nitrosamines (Lewis *et al*. 1997a) together with that of other typical CYP2E substrates, including butadiene (Lewis *et al*. 1997b). The induction time of tumours in various animal species treated with DMN is related to their body weight (Lijinsky 1993) and there are also clear species differences in the carcinogenicity of butadiene (Csanady *et al*. 1992) and low molecular weight chloroalkanes (Parke and Ioannides 1990), all of which represent CYP2E substrates (Yang *et al*. 1990, Nakajima *et al*. 1993, Duescher and Elfarra 1994, Lewis *et al*. 1997a, b, Tan *et al*. 1997). Circumstantial evidence suggests that the increased carcinogenic susceptibility of small rodents towards these chemicals could be linked with their relatively low tolerance to oxygen radical/ROS production, due to rapid depletion of cellular glutathione (Lorenz *et al*. 1984). Nevertheless, it is clear that a substantial number of recognized CYP2E substrates and/or inducers are suspected to be human carcinogens, including butadiene (Melnick and Kohn 1995) together with other small molecular weight hydrocarbons, such as benzene and styrene (Guengerich 1995) and also certain chloroalkanes and chloroalkenes, like chloroform, tetrachloromethane, trichloroethene and vinyl chloride (Guengerich *et al*. 1991, Gonzalez and Gelboin 1994). However, it can be argued that the normal exposure levels to such chemicals are likely to lie below the probable thresholds for carcinogenic effects to occur (Bond *et al*. 1995, Lewis *et al*. 1997a), whereas dietary supplements of ROS scavengers/antioxidants such as ascorbic acid, together with the consumption of garlic, which contains diallyl sulphide, a known CYP2E inhibitor (Brady *et al*. 1991), may ameliorate the potentially deleterious effects of exposure to CYP2E substrates and inducers in the environment and diet.

In addition to its role in the metabolism, both oxidative and reductive (Koop 1992), of volatile environmental chemicals and halogenated solvents, CYP2E can metabolize a number of drug substrates (Parkinson 1996, Smith *et al*. 1997), and it has been reported that $\sim 4\%$ of drug oxidations in *Homo sapiens* is CYP2E-

mediated (Rendic and Di Carlo 1997). Furthermore, the active site of human CYP2E1 has been investigated using probe substrates (Wang *et al*. 1995) and haem-binding inhibitors (Mackman *et al*. 1996), whereas the CYP2E inhibitory potencies of small molecular aromatic and heterocyclic compounds have been studied in rat (Hargreaves *et al*. 1994), thus suggesting that CYP2E isoforms exhibit relatively constrained haem environments compared with other microsomal mammalian P450s. However, it is apparent, that medium chain-length carboxylic acids such as lauric acid (Wang *et al*. 1995, Amet *et al*. 1998) and arachidonic acid (Laetham *et al*. 1993) can occupy the CYP2E active site, indicating that an elongated substrate access channel may be present close to the haem pocket. Quantitative structure–activity relationship (QSAR) studies on series of structurally related CYP2E substrates and inhibitors (reviewed in Lewis *et al*. 1997b) clearly show that molecular size is a factor in the CYP2E-mediated activity of alcohols (Lewis 1987) and nitriles (Lewis *et al*. 1994), whereas frontier orbital energy levels play a role in the relative potency of dialkyl nitrosamines (Lewis *et al*. 1997a) and in the CYP2E-catalyzed rates of halothane metabolism (Lewis *et al*. 1998b), although hydrogen abstraction energies are also important in the latter (Yin *et al*. 1995).

In a previous study the homology modelling of rat, mouse and human CYP2E1 isoforms was reported (Lewis *et al*. 1997b), based on the substrate-free CYP102 crystal structure (Ravichandran *et al*. 1993), showing that relatively few changes within the protein sequences appear to govern species differences in the oxidative metabolism of chemicals attributable to CYP2E involvement. In the current work, the present authors focus on the human form of the enzyme to explore site interactions with substrates and inhibitors, employing the recently reported crystal structure of substrate-bound CYP102 (Li and Poulos 1997) as a template for homology modelling of CYP2E1. The new crystal structure exhibits certain differences from that of the substrate-free enzyme in that the former shows a more 'open' conformation for the active site region, whereas the substrate-bound enzyme structure represents a relatively 'closed' conformation. The presence of a bound substrate in the template structure aids the modelling of enzyme–substrate interactions because one has a starting point for investigating these in the model.

Materials and methods

The three-dimensional structural model of human CYP2E1 was generated from the atomic coordinates of the palmitoleate-bound CYP102 haemoprotein domain (Brookhaven Protein Databank code: 1fag), as described by Li and Poulos (1997), based on a sequence alignment between CYP102 and several CYP2E subfamily proteins (Lewis 1996, Lewis *et al*. 1997b) (figure 1). Although the CYP2E primary sequences are $\sim 25\%$ homologous with that of the CYP102 haemoprotein domain, alignment was facilitated by comparison with other CYP2 family proteins where there is more comprehensive mutagenesis information (reviewed in Lewis 1998). Initial alignment between the amino acid sequences of CYP102 and selected CYP2E subfamily proteins was carried out using the GCG package (Genetics Computer Group, Madison, WI, USA) and some degree of manual editing was undertaken to achieve a self-consistency with site-directed mutagenesis data from the CYP2 family in general, and with the substrate recognition sites (SRS) identified by Gotoh (1992) within various CYP2 family proteins. Some site-specific mutagenesis experiments have been carried out in CYP2E subfamily isoforms, but these are of highly conserved residues, namely, the distal threonine (Thr303) and a proximal phenylalanine (Phe429) which are thought to be involved in oxygen binding and activation of substrates (Fukuda *et al*. 1993), and redox interactions (Porter 1994) respectively. Shimizu (1997) has suggested that conserved aromatic residues, including Phe429 in CYP2E1, play an important role in electron transfer to the nearby haem moiety from an interacting redox partner, although an assistance in binding the haem group is a second possibility.

The methodology for homology modelling of P450 from the CYP102 template has been described previously (Lewis 1995, 1996, 1998) and involves residue replacement as required by the alignment,

```
                                                          10         20
   cyp102  .......... .......... ........TI KEMPQPKTFG ELKNLPLLNT
cyp2e1hum  MSALGVTVAL LVWAAFLLLV SMWRQVHSSW NLPPGPFPLP IIGNLFQLEL
cyp2e1rab  MAVLGITVAL LGWMVILLFI SVWKQIHSSW NLPPGPFPLP IIGNLLQLDL
cyp2e1rat  MAVLGITIAL LVWVATLLVI SIWKKIYNSW NLPPGPFPLP ILGNIFQLDL
cyp2e1mou  MAVLGITVAL LVWIATLLLV SIWKQIYRSW NLPPGPFPIP FFGNIFQLDL

                30         40         50         60         70
   cyp102  DKPVQALMKI ADELGEIFKF EAPGRVTRYL SSQRLIKEAC DESRFDKNLS
cyp2e1hum  KNIPKSFTRL AQRFGPVFTL YVGSQRMVVM HGYKAVKEAL LDYKDEFSGR
cyp2e1rab  KDIPKSFGRL AERFGPVFTV YLGSRRVVVL HGYKAVREML LNHKNEFSGR
cyp2e1rat  KDIPKSFTKL AKRFGPVFTL HLGSRRIVVL HGYKAVKEVL LNHKNEFSGR
cyp2e1mou  KDIPKSLTKL AKRFGPVFTL HLGQRRIVVL HGYKAVKEVL LNHKNEFSGR

                80         90         100        110        120
   cyp102  QALKFVRDFA GDGLFTSWTH EKNWKKAHNI LLPSFSQQAM .K.GYHAMMV
cyp2e1hum  GDLPAFHAHR DRGIIFN..N GPTWKDIRRF SLTTLRNYGM GKQGNESRIQ
cyp2e1rab  GEIPAFREFK DKGIIFN..N GPTWKDTRRF SLTTLRDYGM GKQGNEDRIQ
cyp2e1rat  GDIPVFQEYK NKGIIFN..N GPTWKDVRRF SLSILRDWGM GKQGNEARIQ
cyp2e1mou  GDIPVFQEYK NKGIIFN..N GPTWKDVRRF SLSILRDWGM GKQGNEARIQ

               130        140        150        160        170
   cyp102  DIAVQLVQKW ERLNADEHIE VPEDMTRLTL DTIGLCGFNY RFNSFYRDQP
cyp2e1hum  REAHFLLEAL RKTQG.QPFD PTFLIGCAPC NVIADILFRK HFDYNDEKF.
cyp2e1rab  KEAHFLLEEL RKTQG.QPFD PTFVIGCTPF NVIAKILFND RFDYKDKQA.
cyp2e1rat  REAQFLVEEL KKTKG.QPFD PTFLIGCAPC NVIADILFNK RFDYNDKKC.
cyp2e1mou  REAHFLVEEL KKTKG.QPFD PTFLIGCAPC NVIADILFNK RFDYDDKKC.

               180        190            200        210
   cyp102  HPFITSMVRA LDEAMNKLQR A..NPDDP.. AYDENKRQFQ EDIKVMNDLV
cyp2e1hum  LRLMYLFNEN FHLLSTPWLQ LYNNFPSFLH YLPGSHRKVI KNVAEVKEYV
cyp2e1rab  LRLMSLFNEN FYLLSTPWLQ VYNNFSNYLQ YMPGSHRKVI KNVSEIKEYT
cyp2e1rat  LRLMSLFNEN FYLLSTPWIQ LYNNFADYLR YLPGSHRKIM KNVSEIKQYT
cyp2e1mou  LELMSLFNEN FYLLSTPWIQ AYNYFSDYLQ YLPGSHRKVM KNVSEIRQYT

              220        230          240            250        260
   cyp102  DKIIADRKAS GEQS..DDLL THMLNGKDPE ...TGEPLDD ENIRYQIITF
cyp2e1hum  SERVKEHHQS LDPNCPRDLT DCLLVEMEKE KHSAERLYTM DGITVTVADL
cyp2e1rab  LARVKEHHKS LDPSCPRDFI DSLLIEMEKD KHSTEPLYTL ENIAVTVADM
cyp2e1rat  LEKAKEHLQS LDINCARDVT DCLLIEMEKE KHSQEPMYTM ENVSVTLADL
cyp2e1mou  LGKAKEHLKS LDINCPRDVT DCLLIEMEKE KHSQEPMYTM ENISVTLADL

               270        280        290            300        310
   cyp102  LIAGHETTS GLLSFALYFL VKNPHVLQKA AEEAARVLV. DPVPSYKQVKQ
cyp2e1hum  FFAGTETTS TTLRYGLLIL MKYPEIEEKL HEEIDRVIGP SRIPAIKDRQE
cyp2e1rab  FFAGTETTS TTLRYGLLIL LKHPEIEEKL HEEIDRVIGP SRMPSVRDRVQ
cyp2e1rat  FFAGTETTS TTLRYGLLIL MKYPEIEEKL HEEIDRVIGP SRVPAVRDRLD
cyp2e1mou  FFAGTETTS TTLRYGLLIL MKYPEIEEKL HEEIDRVIGP SRAPAVRDRMN

                320        330          340        350
   cyp102  LKYVGMVLN EALRLWPTAP A.FSLYAKED TVLGGEYPLE KGDELMVLIPQ
cyp2e1hum  MPYMDAVVH EIQRFITLVP SNLPHEATRD TIFRG.YLIP KGTVVVPTLDS
cyp2e1rab  MPYMDAVVH EIQRFIDLVP SNLPHEATRD TTFQG.YVIP KGTVVIPTLDS
cyp2e1rat  MPYMDAVVH EIQRFINLVP SNLPHEATRD TVFQG.YVIP KGTVVIPTLDS
cyp2e1mou  MPYMDAVVH EIQRFINLVP SNLPHEATRD TVFRG.YVIP KGTVVIPTLDS

              360        370        380          390        400
   cyp102  LHRDKTIWG DDVEEFRPER FENPSAI..P QHAFKPFGNG QRACIGQQFAL
cyp2e1hum  VLYDNQEFP .DPEKFKPEH FLNENGKFKY SDYFKPFSTG KRVCAGEGLAR
cyp2e1rab  LLYDKQEFP .DPEKFKPEH FLNEEGKFKY SDYFKPFSAG KRVCVGEGLAR
cyp2e1rat  LLYDSHEFP .DPEKFKPEH FLNENGKFKY SDYFKAFSAG KRVCVGEGLAR
cyp2e1mou  LLFDNYEFP .DPETFKPEH FLNENGKFKY SDYFKAFSAG KRVCVGEGLAR

              410        420        430        440        450
   cyp102  HEATLVLGM MLKHFDFE.D HTNYELDIKE TLTLKPEGFV VKAKSKKIPLGG
cyp2e1hum  MELFLLLCA ILQHFNLKPL VDPKDIDLSP IHIGFGC.IP PRYKLCVIPRS
cyp2e1rab  MELFLLLSA ILQHFNLKPL VDPEDIDLRN ITVGFGR.VP PRYKLCVIPRS
cyp2e1rat  MELFLLLSA ILQHFNLKSL VDPKDIDLSP VTVGFGS.IP PQFKLCVIPRS
cyp2e1mou  MELFLLLSA ILQHFNLKSL VDPKDIDLSP VTIGFGS.IP REFKLCVIPRS
```

Figure 1. An alignment between CYP2E subfamily protein sequences and that of the CYP102 haemoprotein domain, based on accession numbers from Nelson *et al.* (1996). The designations hum, rab, rat and mou refer to CYP2E proteins from human, rabbit, rat and mouse respectively.

Table 1. Substrates and inhibitors of CYP2E1.

Substrates	Catalyzed reaction	Reference
A		
Chlorzoxazone	6-hydroxylation	Dresibach *et al*. (1996)
4-Nitrophenol	2-hydroxylation	Tassaneeyakul *et al*. (1993)
Paracetamol	N-hydroxylation	Koop (1992), Nelson (1990)
Aniline	4-hydroxylation	Parkinson (1996)
Ethanol	C_{α}-hydroxylation	Koop (1992)
Diethylnitrosamine	N-deethylation	Tan *et al*. (1997)
Inhibitors	Mechanism of inhibition	
B		
4-Methyl pyrazole	haem ligation?	Parkinson (1996)
3-Amino-1,2,4-triazole	haem ligation?	Smith (1994)
Diallyl sulphide	haem ligation?	Ono *et al*. (1996)
Disulphiram (Diethyl-dithiocarbamate)*	haem interaction?	Parkinson (1996)
Phenethylisothiocyanate	haem interaction?	Parkinson (1996)
Propofol	competitive?	Chen *et al*. (1995)

Rendic and Di Carlo (1997), Ronis *et al*. (1996), Parkinson (1996).
* DEDTC can also act as an inhibitor of CYP2A6.

followed by residue deletions and insertions. The raw structure is then energy minimized using molecular mechanics to yield a low energy, stable geometry for the P450 enzyme which, in most instances, have total energies < –1000 kcal.mole^{-1}. In the case of human CYP2E1, the geometry-optimized conformation has an energy of –1466 kcal.mole^{-1}, thus indicating a stable structure for the haemoprotein.

The final three-dimensional structural model of CYP2E1 was investigated using known substrates and inhibitors (table 1). Each small molecular structure was produced from preminimized fragments and then geometry-optimized using the same procedures described above. Interactive docking of substrates and inhibitors within the putative active site of human CYP2E1 was carried out using the position of the original substrate, palmitoleic acid, as a guide, and it is important to recognize that relatively long-chain fatty acids can act as substrates for CYP2E1 as well as for CYP102 (Nahri and Fulco 1986, Wang *et al*. 1995), thus facilitating the process. Moreover, it has also been reported that arachidonic acid is epoxidized by both CYP102 (Graham-Lorence *et al*. 1997) and CYP2E1 (Laetham *et al*. 1993). All molecular modelling procedures were conducted using the Sybyl 6.5 package (Tripos Associates, St Louis, MO, USA).

Results and discussion

CYP2E1 active site

The overall disposition of the human CYP2E1 model is shown in figure 2. There are several favourable contacts between amino acid residues that may be involved in maintaining the overall tertiary structure of the haemoprotein, and some are listed in table 2. In particular, ion-paired interactions between oppositely charged side-chains appear to bridge sequentially distant regions of the structure, including some which are conserved both in CYP102 and broadly across the CYP2 family in general (reviewed in Lewis 1998). In the case of CYP2E, it would appear that certain ion-pairs and π–π stacked aromatic residues give rise to a relatively constrained active site that precludes the entry of fairly large molecules, thus explaining to some extent the substrate preferences of this isoform. As far as monocyclic aromatic substrates are concerned, it is possible that a pair of π-stacked phenylalanines (Phe78 and Phe88) close to the active site are involved in the recognition and access of benzenoid compounds, such as 4-nitrophenol, aniline, chlorzoxazone and paracetamol, for example. Furthermore, the salt bridge between Arg72 and Asp74, possibly also involving an extended hydrogen-bonded framework comprising His437 and Ser185,

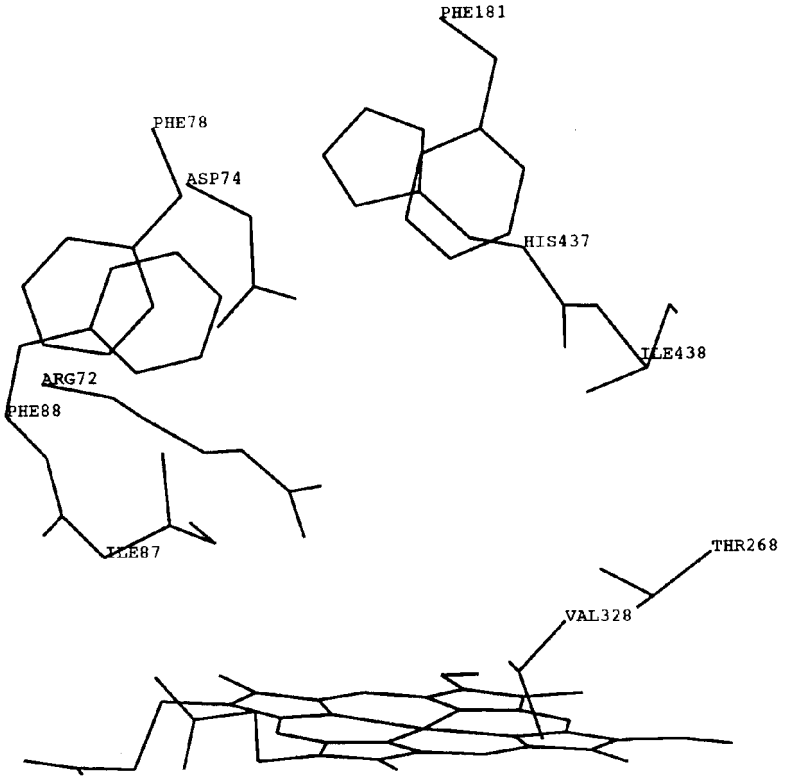


Figure 2. A view of the putative active site of human CYP2E1 showing the disposition of potential substrate-binding contacts.

Table 2. Favourable contacts within the human CYP2E1 structure.

Ion-pairs	π-π Stacking	Hydrogen bonds
D74-H437	F36-F40	Q19-N16
R82-D260	F88-F78	H437-S185
D83-K213	F262-F158	R72-substrate
R84-D252	Y362-F324	N151-N165
H223-D232	Y386-Y389	T268-substrate
D235-R231	F181-substrate	H437-substrate
E240-R231		
H333-haem propionate		
D358-K27		
E382-K385		
E366-K56		
R407-E403		
R72-D74		

The substrate in this case was 4-nitrophenol, as shown in figure 4.

ensures a constricted haem environment which can, nevertheless, become more open following substrate binding; a second ion-pair comprising Arg82 and Asp260 may also cooperate in restraining the size and flexibility of the active site area. It appears that the main contacts with substrates include Phe181, Arg72, His437, Asp74 and Thr268, together with some hydrophobic side-chains, such as Ile87, Ile438, Ala264 and Val328.

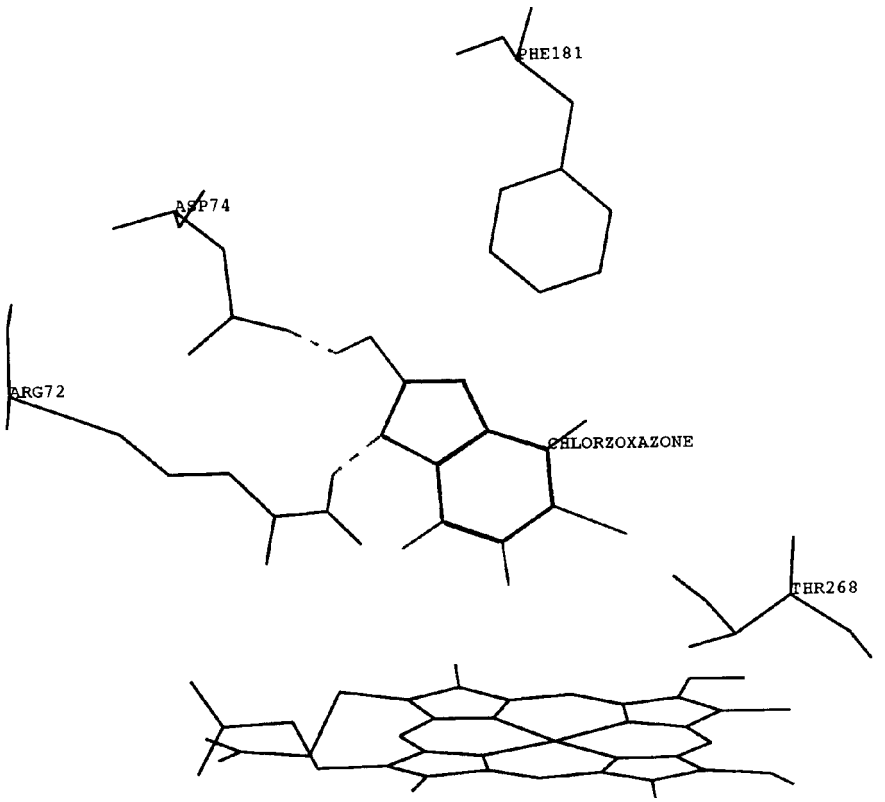


Figure 3. Chlorzoxazone fitted into the CYP2E1 active site where there are complementary contacts with key amino acid residues.

All of these residues have counterparts in other CYP2 family isoforms, which also contact substrates, and most have been the subject of site-directed mutagenesis in these proteins (reviewed in Lewis 1998). However, only Thr268 (Thr303 in CYP2E1) has been mutated in this subfamily (Fukuda *et al*. 1993) where it appears to play a role in substrate binding and metabolism. The haem environment of the CYP2E1 model shows agreement with the experimental studies of Mackman *et al*. (1996) on haem adduct formation, in that sterically hindered pyrrole rings of the haem moiety (i.e. rings B and C) prevent full access by the phenyldiazene inhibitor. In the model, active site residues Thr266 and Ala264 cover these, whereas pyrrole ring D is open for the binding of substrates in accordance with the covalent adduct data (Mackman *et al*. 1996).

Substrates in the CYP2E1 site

Chlorzoxazone. Figure 3 shows a possible orientation of the substrate, chlorzoxazone, within the putative active site of human CYP2E1. A number of interactions with amino acid residues appear to be involved in binding the chlorzoxazone structure such that hydroxylation at the 6-position occurs. For example, the aromatic ring of the substrate forms a π–π stacking interaction with the side-chain of Phe181, whereas hydrogen bonding is possible between chlorzoxazone and complementary groupings on His437, Arg72 and Asp74. There is also a likelihood

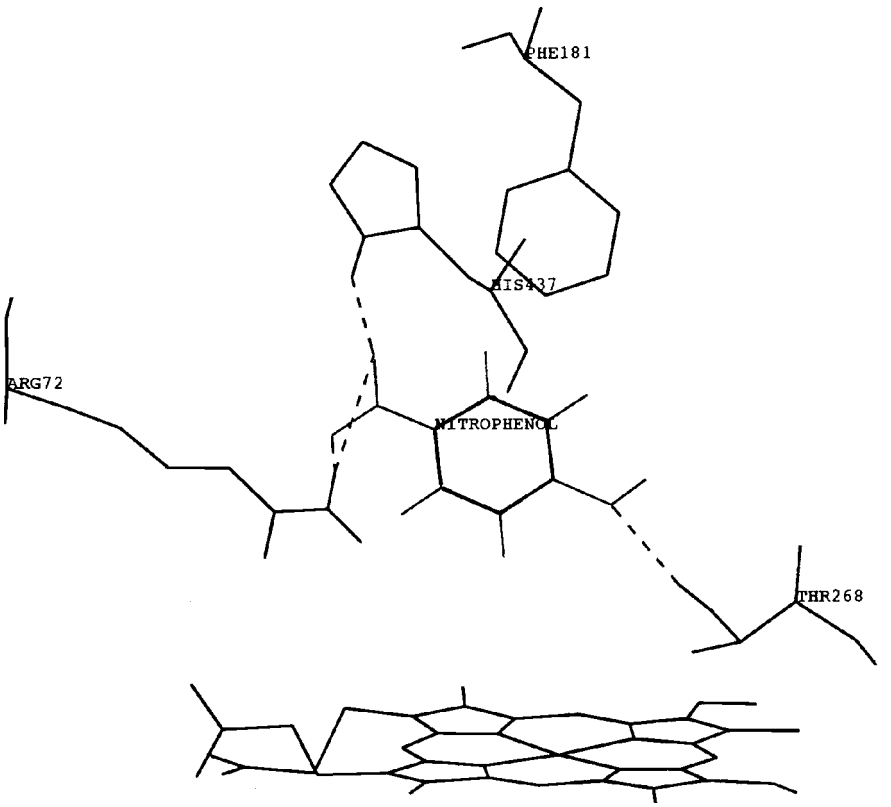


Figure 4. The substrate 4-nitrophenol presented binding within the CYP2E1 active site, with certain amino acid side-chains contributing to its orientation relative to the haem.

that the side-chain of Thr268 can form a weak hydrogen bond with the chloro substituent of the substrate, and it is known that chlorine can enter into weak hydrogen bond formation (Stenlake 1979). The orientation of chlorzoxazone in the human CYP2E1 active site is, therefore, consistent with its known position of metabolism (Dresibach *et al.* 1996) because the aforementioned complementary interactions with amino acid residues (presented in figure 3) ensure that the 6-hydrogen of the substrate is closest to the haem iron at 4.4 Å.

4-Nitrophenol. A fairly specific CYP2E1 substrate, 4-nitrophenol, is oxygenated at the 2-position (Tassaneeyakul *et al.* 1993) and a likely orientation of this substrate in the putative active site is shown in figure 4. There are some similarities in the interactions exhibited for 4-nitrophenol in CYP2E1 with that of the previous substrate, chlorzoxazone, because almost all of the same amino acid residues are involved in binding the molecule for oxygenation at the experimentally observed position. In particular, the 4-nitro group is held by hydrogen bonds from Arg72 and His437, whereas the hydroxyl group forms another hydrogen bond with Thr268, and the aromatic ring of the substrate π-stacks with Phe181. In addition, the close proximity of a pair of phenylalanine residues (Phe78 and Phe88) suggests a possible entry point for this, and other, monoaromatic substrates. In the orientation shown in figure 4, the 2-hydrogen is positioned relatively close to the haem iron, at 4.65 Å,

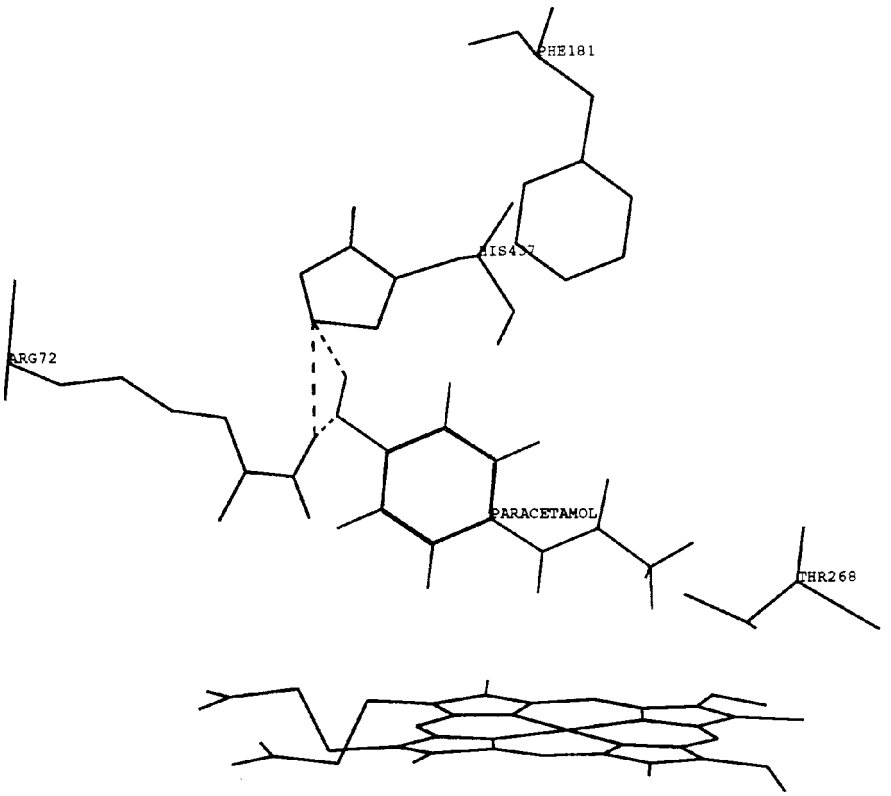


Figure 5. Paracetamol (acetaminophen) indicated in a possible mode of interaction with the putative active site of CYP2E1.

thus demonstrating that the proposed mode of interaction depicted in figure 4 is consistent with the formation of the observed hydroxylated product, 4-nitrocatechol.

Paracetamol (*acetaminophen*). Figure 5 indicates a possible orientation of paracetamol within the putative active site of CYP2E1, where there are complementary interactions with amino acid side-chains which tend to favour N-hydroxylation of the substrate, as is observed experimentally (Nelson 1990, Koop 1992). As shown in figure 5 the aromatic ring of the substrate forms a π–π stacking interaction with the side-chain of Phe181, whereas the amide and hydroxyl groups are positioned by hydrogen bonds with Thr268 and His437 respectively. These contacts, possibly augmented by a further hydrogen bond from Arg72, tend to orientate the paracetamol molecule such that the amide hydrogen atom is positioned directly above the haem iron at 3.67 Å, which is in good agreement with the 3.8 Å determined by NMR spectroscopic measurements (S. D. Nelson, University of Washington, personal communication).

Aniline. This substrate undergoes 4-hydroxylation by CYP2E1 (reviewed in Rendic and Di Carlo 1997, Parkinson 1996) and figure 6 shows how the molecule may become orientated with the putative active site such that oxygenation at the *para*-position will be preferred. In this manner, the amino group of aniline forms

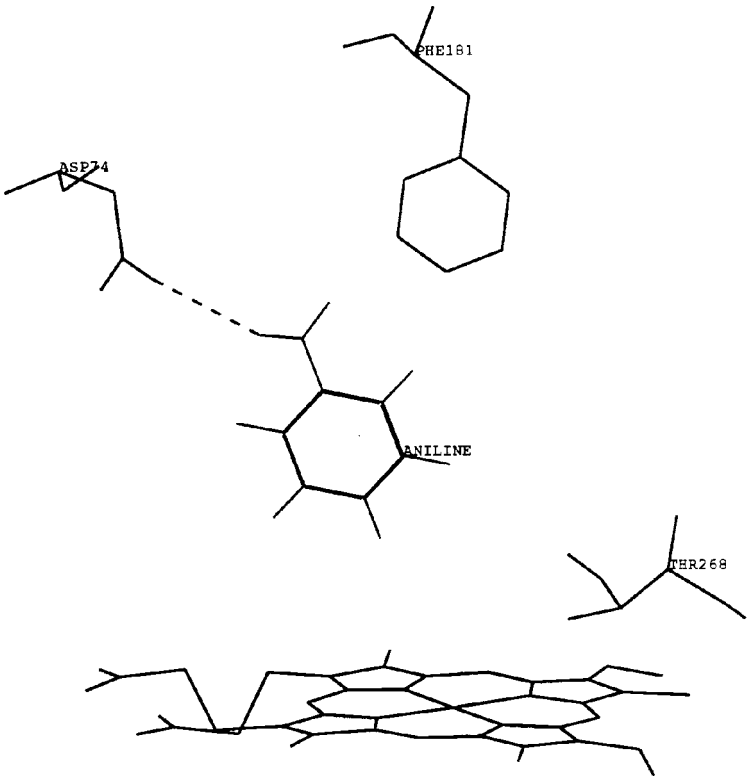


Figure 6. Aniline docked within the CYP2E1 active site for 4-hydroxylation via contacts with complementary amino acids.

hydrogen bonds with Asp74 and His437, with the aromatic ring of the substrate π-stacking with Phe181, as is found with all of the benzenoid compounds investigated in this study. Figure 6 indicates that the hydrogen atom in the 4-position lies directly over the haem iron at 4.62 Å, although it is possible that the substrate molecule could move closer to the haem by entering into a second type of interaction which includes a hydrogen bond with Asp74, as before, together with a somewhat unusual weak intermolecular association between one of the amine hydrogens of aniline and the centre of the Phe181 aromatic ring. Levitt and Perutz (1988) have shown that such interactions can occur when donor and acceptor species are at short-range distances, where the partial positive charge on the hydrogen is attracted to the electron-rich aromatic ring. It is possible, therefore, that a similar interaction occurs in the aniline-CYP2E1 complex.

Ethanol. Figure 7 shows the possible disposition of ethanol within the putative active site of CYP2E1, which is in agreement with experimental findings (Elkstrom *et al.* 1986) showing that acetaldehyde is the major metabolite (reviewed in Koop 1992). It appears that the main interaction involves a hydrogen bond between the hydroxyl group of the substrate and the side-chain of Thr268. There is also a hydrophobic interaction between the substrate's methyl group and the Phe181 side-chain, whereas the close proximity of Val328 could represent a second point of hydrophobic contact with the substrate. In the orientation presented in figure 7, one

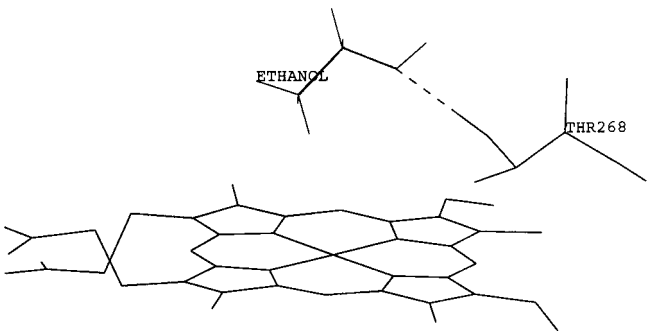


Figure 7. Ethanol presented within the active site of CYP2E1 such that a combination of amino acid residues directs the preferred position of metabolism to the α-methylene group.

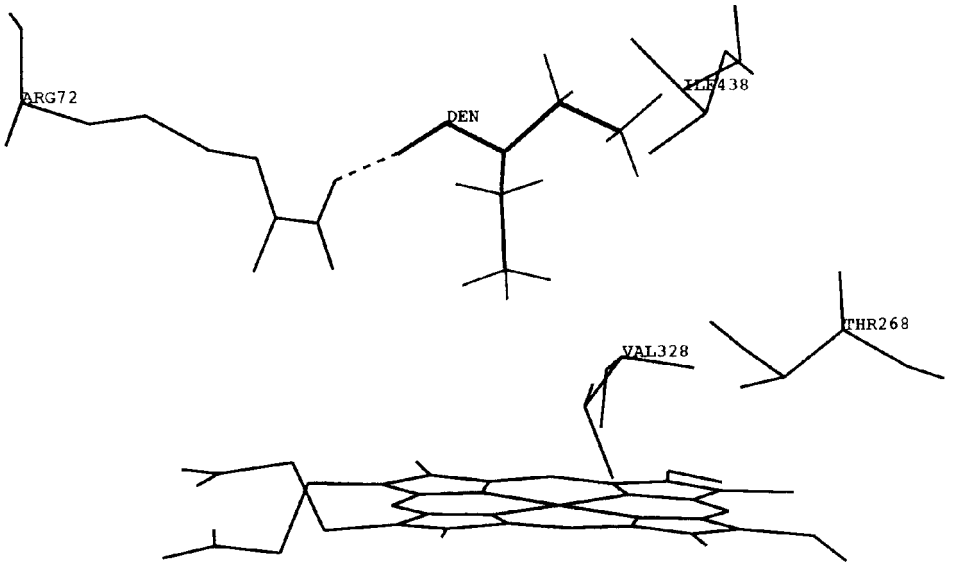


Figure 8. Diethylnitrosamine in the CYP2E1 active site where dealkylation is indicated by contacts with certain amino acid side-chains.

of the α-hydrogens of ethanol lies directly over the haem iron at 4.32 Å, which is consistent with the experimentally observed oxygenation catalyzed by CYP2E1 (Elkstrom *et al*. 1986, Koop 1992).

Diethylnitrosamine (*DEN*). Small chain dialkylnitrosamines such as DEN undergo mono N-dealkylation mediated by CYP2E1 (Tan *et al*. 1997), and figure 8 indicates how this substrate may become orientated for this reaction via complementary contacts with nearby amino acid residues in the CYP2E1 active site. In particular, there are hydrogen bonds between Arg72 and His437 side-chains and the nitroso group, whereas hydrophobic contacts may occur between Ile438 and one of the ethyl groups on the substrate. The side-chain of Thr268 lies close to this interaction and, consequently, the methyl group of this residue may also form a hydrophobic contact with one of the DEN ethyl groups. These interactions orientate the DEN molecule such that its other ethyl group is positioned above the

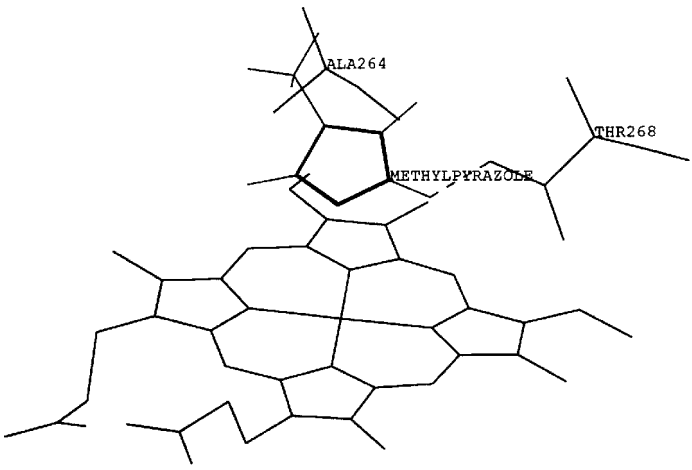


Figure 9. The inhibitor 4-methylpyrazole docking into the CYP2E1 site for haem ligation via contacts with key amino acid residues.

haem iron, where one of the hydrogen atoms lies at 4.86 Å from the iron. However, due to its relatively small molecular size it is possible that the substrate could rotate within the putative active site whereby the nitroso oxygen may form a hydrogen bond with Arg72. This would bring the one of the α-hydrogens of DEN nearer to the haem iron, and it is likely that oxygenation at this position will be preferred, in agreement with the results of electronic structure calculations (Lewis *et al*. 1997a). Consequently, it is apparent that the six known substrates of human CYP2E1 (listed in table 1) all fit the putative active site of the enzyme in a manner which is consistent with available experimental findings.

Inhibitors in the CYP2E1 site

Some of the known inhibitors of CYP2E1 (table 1) display structural similarity with certain substrates mentioned previously and, consequently, there are analogous interactions with active site residues. Some examples are discussed here, and it should be recalled that some of these inhibitors are not exclusively specific for this P450 isoform. In fact, as with certain substrates (e.g. paracetamol and DEN), diethyl dithiocarbamate (DEDTC) can also interact with CYP2A6. Propofol, however, can act as an inhibitor of human CYP1B1 as well as for CYP2E1 (Rendic and Di Carlo 1997).

4-Methyl pyrazole and 3-amino-1,2,4-triazole. Figure 9 shows a possible mode of interaction between 4-methyl pyrazole and the active site of CYP2E1, where the sp^2 nitrogen of the inhibitor ligates the haem iron. In such an orientation, the adjacent ring nitrogen can form a hydrogen bond with the side-chain of Thr268 and there is also the possibility of a hydrophobic contact between the 4-methyl group on the inhibitor and the complementary methyl of the Ala264 residue which, like Thr268, forms part of the distal I-helix. Although small molecular weight heterocyclics, such as imidazole and pyridine, can also act as inhibitors of CYP2E1 their selectivity is not as well defined as 4-methyl pyrazole and 3-amino-1,2,4-triazole, presumably due to the specific active site interactions described herein. The latter compound, for

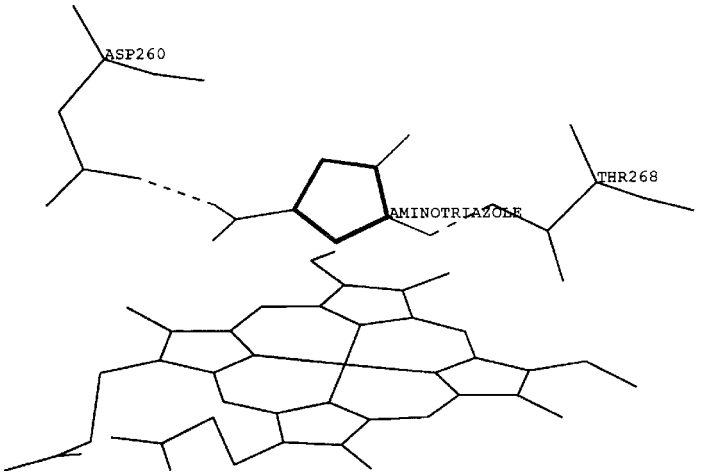


Figure 10. The inhibitor 3-amino-1,2,4-triazole docked within the CYP2E1 site where haem ligation is possible due to certain key residue interactions.

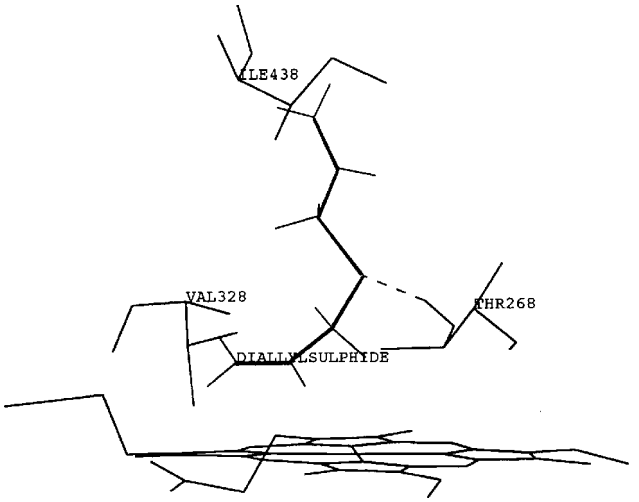


Figure 11. Diallyl sulphide within the CYP2E1 active site where key contacts with complementary amino acid residues position the molecule for interaction with the haem moiety.

example, appears to form the same haem ligation and hydrogen bonding as 4-methyl pyrazole but, instead of the hydrophobic interaction with Ala264, 3-aminotriazole hydrogen bonds with the side-chain of Asp260 via its amino group. There is also the possibility of a third hydrogen bond being formed via the triazole ring nitrogen atom (4-position) of the inhibitor and the Arg72 residue (figure 10).

Diallyl sulphide. The mechanism of CYP2E1 inhibition by diallyl sulphide is not known but, presumably, involves some form of haem interaction either via the sulphur atom (which could act as a haem ligand) or through one of the reactive allyl groups. By structural analogy with other CYP2E1 inhibitors, such as pyridine and thiophene, it is proposed that diallyl sulphide may interact by sulphur coordination to the haem iron (figure 11). Furthermore, the allyl groups can form π–π stacking

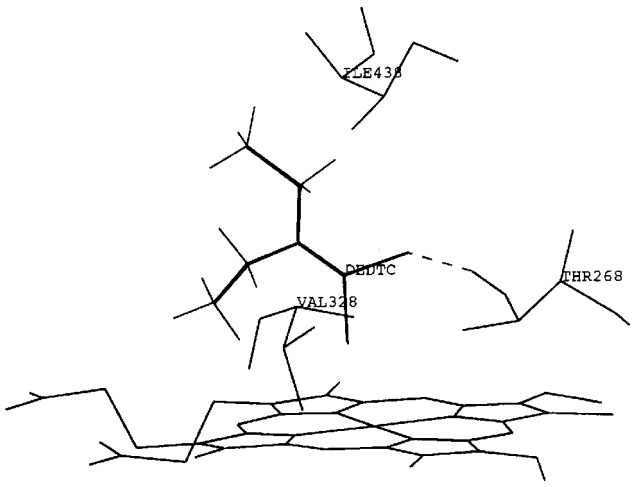


Figure 12. Diethyldithiocarbamate, a breakdown product of the inhibitor disulphiram, is presented as binding with CYP2E1 in the region of the haem such that an interaction with the iron is possible.

interactions with the aromatic side-chain of Phe181 in this orientation; presumably, a similar position would be adopted by heteroaromatic ligands like pyridine, although one cannot rule out the possibility of covalent adduct formation between an allyl group of the inhibitor and the porphyrin ring system of the haem moiety.

Disulphiram. Figure 12 shows one particular mode of interaction between disulphiram and the CYP2E1 active site, where the inhibitor molecule has cleaved symmetrically to form diethyldithiocarbamate (DEDTC). There is some structural analogy between DEDTC and diethylnitrosamine and it is possible, therefore, that the active site binding interactions are similar. However, one of the sulphur atoms on DEDTC could act as a haem ligand via coordination to the central iron atom, by comparison with the diallyl sulphide interaction described previously. Consequently, figure 12 indicates that the thiolate group of DEDTC ligates the haem moiety of CYP2E1 and, in this orientation, the two ethyl groups on the inhibitor can form hydrophobic interactions with the side-chains of Ile438 and Val328, although there is also the possibility of contact between DEDTC and the side-chain of Thr268.

Phenethylisothiocyanate. A likely mode of interaction between phenethylisothiocyanate and the putative active site of CYP2E1 is shown in figure 13. In this case, the aromatic ring of the inhibitor forms a π–π stacking contact with the side-chain of Phe181, whereas hydrogen bonding with Thr268 serves to hold the molecule close to the haem such that the reactive isothiocyanate moiety could covalently bind to the porphyrin ring. In addition, the ethyl group of the inhibitor can form a hydrophobic interaction with the complementary Ile438 residue, thus reinforcing the aforementioned contacts, which would also impart some degree of selectivity for this compound.

Propofol. Figure 14 shows a possible orientation for propofol within the putative active site of human CYP2E1, where there are certain complementary interactions with nearby amino acid residues. Although this compound can act as CYP1B1

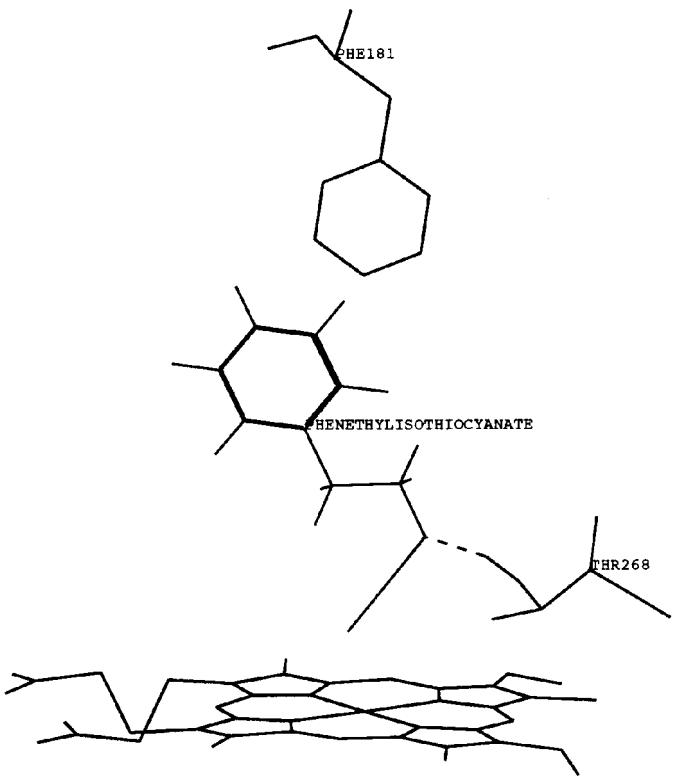


Figure 13. The inhibitor phenethylisothiocyanate docked within the active site of CYP2E1 for haem interaction via contacts with amino acid residues in the vicinity of the haem.

inhibitor (Rendic and Di Carlo 1997), it is likely to be more selective towards CYP2E1 due to the similarity between propofol and certain substrates of the enzyme, particularly those containing the phenolic group.

In addition to the hydrogen bond with Thr268 and the π–π stacking interaction with Phe181, the propofol molecule can form a hydrophobic contact with Ile438 via one of its isopropyl groups. In such an orientation (figure 14) the other isopropyl is positioned above the haem moiety, thus either blocking the binding of oxygen to the iron or being able to act as a competitive inhibitor.

QSARs in CYP2E1 specific compounds

Lewis (1987) showed that the relative ability for aliphatic alcohols to inhibit CYP2E1 activity, as measured by aniline 4-hydroxylation, is determined by two separate structural factors. These are the overall length of the molecule and the lowest unoccupied molecular orbital (LUMO) population on the α-carbon, and table 3 shows that the former gives a satisfactory correlation ($r = 0.74$) for 22 compounds, whereas the latter produces a significantly better correlation ($r = 0.92$) for 20 compounds (Lewis 1987). It is possible that molecular length of the alcohols is more important than suggested by the relatively poor correlation, and Wang *et al.* (1995) also indicated that chain length correlates with CYP2E1 inhibition.

Wang *et al.* (1995) investigated a homologous series of primary and secondary alcohols, together later with a series of long-chain carboxylic acids, and found that

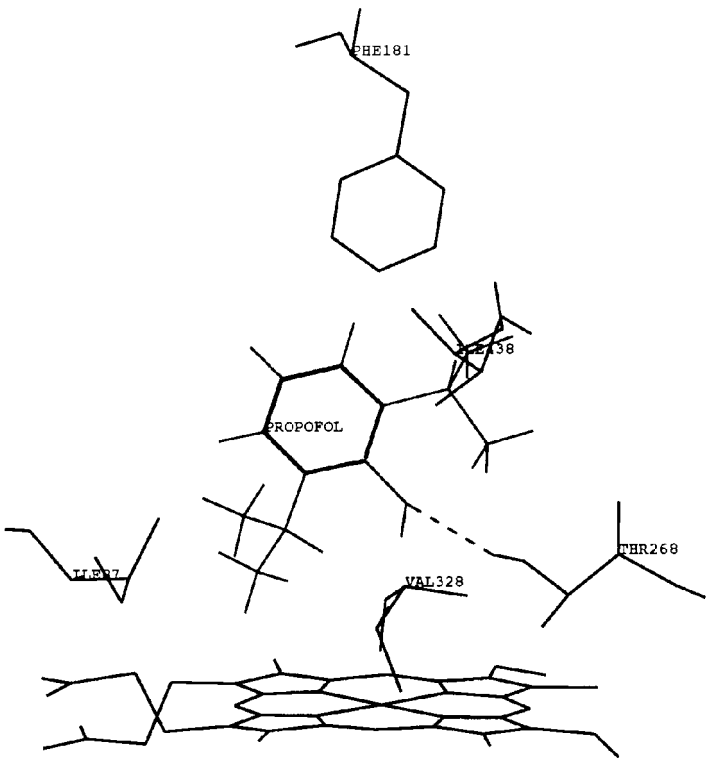


Figure 14. Propofol in a possible mode of interaction with CYP2E1 active site residues, which could explain its inhibitory effect.

inhibition of CYP2E1 increased linearly with carbon chain length up to a maximum for seven carbons in the chain for both primary and secondary alcohols, whereupon the inhibitory activity diminished with increasing chain length. A similar effect was observed for carboxylic acids although, in this case, maximum inhibition occurred for dodecanoic (lauric) acid. The inference drawn from these findings would be that the substrate binding site of CYP2E1 includes a hydrophobic channel of length sufficient to accommodate a seven-carbon chain for alcoholic compounds, but where carboxylic acids can optimally fit up to the extent of 11 carbons in the chain.

Table 4 presents the CYP2E1 inhibitory data (pK_i) for the aforementioned series together with their lipophilicities in the form of log P, where P is the octanol/water partition coefficient. It is clear from these data that parabolic relationships exist between log P and CYP2E1 inhibition (figure 15). The graph indicates that the optimal log P for maximum inhibition of CYP2E1 in each series is ~ 2.50 irrespective of the structural class of compound. However, this does not explain the fact that longer chain fatty acids fit the CYP2E1 binding site than do alcohols, and it may be that a complementary basic amino acid residue is situated at a certain distance from the haem for the binding of the carboxylate group of fatty acid substrates.

As both lauric acid (C_{12}) and arachidonic acid (C_{20}) can act as substrates for CYP2E1 (Amet *et al.* 1998, Laetham *et al.* 1993, Wang *et al.* 1995) it is possible that long-chain carboxylic acids require some degree of chain-folding to fit the active site, and it has been reported (Sharma *et al.* 1989) that both lauric and arachidonic

Table 3. Quantitative structure–activity relationships in CYP2E substrates and inhibitors.

Expression	*n*	*s*	*R*	*F*
1. Alcohols (Lewis 1987)				
$pIC_{50} = 0.45$ length $- 4.04$	22	0.64	0.74	23.6
$pIC_{50} = 6.42 - 13.3\ Q_C$LUMO	20	0.34	0.92	93.0
2. Nitriles (Lewis *et al*. 1994)				
log EtOH/Glucose $= 0.277 - 0.006\ \alpha_{mol}$	20	0.05	0.79	30.5
$pLD_{50} = 0.43 - 0.03\ \alpha_{mol}$	16	0.20	0.87	42.1
$(\alpha_{mol})^{1/3} = 0.53$ diameter	20	0.08	0.98	361.6
3. Nitrosamines (Lewis *et al*. 1998)				
$pTD_{50} = 4.79\Delta E - 67.47$	6	0.33	0.95	35.7
$pTD_{50} = 3.57 - 67.92\ Q_C$HOMO	25	0.33	0.84	51.5
4. Halothanes (Yin *et al*. 1995, Lewis and Pratt, 1998, Lewis *et al*. 1998)				
log Rate $= 26.90 - 2.58$ IP	6	0.13	0.99	145.2

n, Number of points; *s*, standard error; *R*, correlation coefficient; *F*, variance ratio.

log Rate = logarithm of the rate of metabolism attributable to CYP2E (Yin *et al*. 1995).

pIC_{50} = negative logarithm of the concentation required for 50% inhibition of aniline *para*-hydroxylation.

log EtOH/glucose = logarithm of the fold increase in ethanol metabolism relative to that of glucose.

pLD_{50} = negative logarithm of the lethal dose in 50% of the treated animals.

pTD_{50} = negative logarithm of the dose required to produce tumours in 50% of rats exposed to the chemical.

length = molecular length (Å).

Q_CHOMO = HOMO electron population of the α-carbon.

Q_CLUMO = LUMO population density on the α-carbon.

α_{MOL} = Molecular polarizability (Å^3) calculated via the CNDO/2 MO method.

$\Delta E = E_{LUMO} - E_{HOMO}$ (eV), where $E_{LUMO/HOMO}$ is the lowest unoccupied/occupied molecular orbital energies respectively.

IP = ionization potential (eV) calculated using the AM1 MO procedure (Yin *et al*. 1995).

acids can adopt a hairpin' conformation whereby the two structures are readily superimposable. In fact, even a molecule of the size of arachidonic acid can fit the CYP2E1 active site, and in an orientation which is consistent with its position of metabolism, where ion-pairing with Arg47 at the mouth of the access channel can occur (figure 16). Presumably, this basic residue represents the most likely contact point for salt-bridge formation with the carboxylate moiety of long-chain carboxylic acids.

In addition to carboxylic acids and alcohols, other series of CYP2E-specific compounds have been studied via QSAR analysis and the results of some of these investigations are summarized in table 3. For example, in a series of 20 nitriles it was reported (Lewis *et al*. 1994) that both CYP2E1-mediated activity (as determined by the increase in ethanol metabolism relative to glucose) and toxicity are proportional to molar polarizability, which is itself closely related ($r = 0.98$) to molecular diameter (table 2). These findings suggest that the lower molecular weight congeners are the more preferred substrates and inducers of CYP2E1, and it has also been reported that a molecular diameter of up to ~ 6.5 Å is discriminatory for CYP2E1 substrates (Lewis *et al*. 1997b). Furthermore, with symmetric dialkyl-nitrosamines it is found that the lower molecular compounds are more potent carcinogens, and it

Table 4. Lipophilicity and CYP2E1 inhibition data for alcohols and acids.

	log *P*	pK_i†
Primary alcohols		
1. Methanol	−0.74	−2.785
2. Ethanol	−0.30	−2.009
3. Propanol	0.25	−1.301
4. Butanol	0.84	−1.114
5. Pentanol	1.51	−0.954
6. Hexanol	2.03	−0.778
7. Heptanol	2.62	−0.477
8. Octanol	3.07	−0.778
9. Nonanol	4.02	−0.778
10. Decanol	4.57	−1.724
Secondary alcohols		
1. Propan-2-ol	0.05	−1.518
2. Butan-2-ol	0.65	−1.491
3. Pentan-2-ol	1.25	−1.230
4. Hexan-2-ol	1.76	−1.041
5. Heptan-2-ol	2.31	−0.903
6. Octan-2-ol	2.90	−0.477
7. Nonan-2-ol	3.49	−0.954
Carboxylic acids*		
1. Hexanoic	−0.61	−3.417
2. Heptanoic	−0.02	−2.516
3. Octanoic	0.54	−2.209
4. Nonanoic	0.95	−2.053
5. Decanoic	1.59	−1.819
6. Undecanoic	1.95	−1.362
7. Dodecanoic	2.50	−1.342
8. Tridecanoic	2.95	−1.653
9. Tetradecanoic	3.46	−2.079
10. Pentadecanoic	3.97	−2.471
11. Hexadecanoic	4.27	−2.531

* Log *P* (Sangster 1989) has been ionization-corrected using the relevant pK_a data.

† Data from Wang *et al*. (1995).

Regression equations	*n*	*s*	*R*	*F*
1. pK_i[a] = 0.98 log *P* − 0.20 log P^2 − 1.79 (±0.11) (±0.03)	10	0.22	0.96	89.4
2. pK_i[b] = 0.48 log *P* − 0.06 log P^2 − 1.66 (±0.25) (±0.01)	7	0.21	0.88	13.9
3. pK_i[c] = 1.05 log *P* − 0.24 log P^2 − 2.66 (±0.10) (±0.02)	11	0.17	0.97	119.0

n, No. of observations; *s*, standard error; *R*, correlation coefficient; *F*, variance ratio.

[a] Data for primary alcohols.

[b] Data for secondary alcohols.

[c] Data for carboxylic acids.

is thought that CYP2E1 is primarily responsible for the metabolic activation of small molecular weight nitrosamines (Lewis *et al*. 1997a). Table 3 shows, however, that relative carcinogenic potency of nitrosamines is related to electronic structural parameters, namely, the difference in frontier orbital energies (ΔE) and the highest occupied molecular orbital (HOMO) electron population on the α-carbon (Lewis *et al*. 1997a). Clearly, therefore, it is apparent that both molecular structure in the form of overall size, and electronic structure as determined by either overall reactivity, or

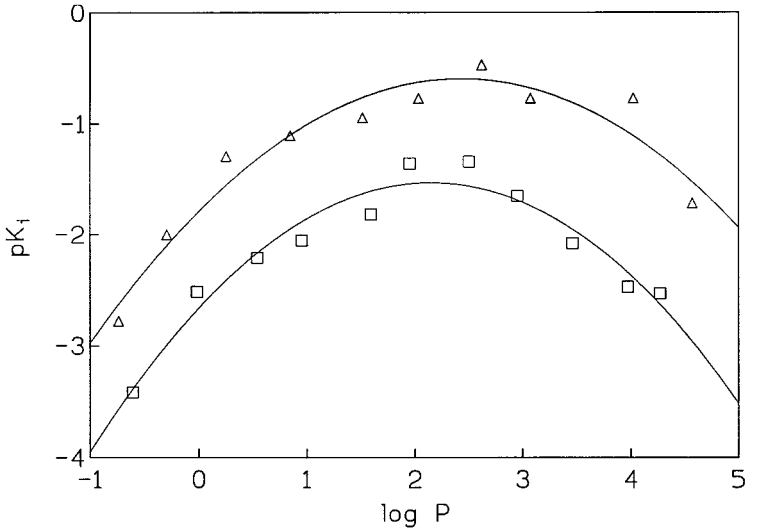


Figure 15. Parabolic relationships between pK_i and log P for primary aliphatic alcohols (triangles) and carboxylic acids (squares) based on data presented in table 3.

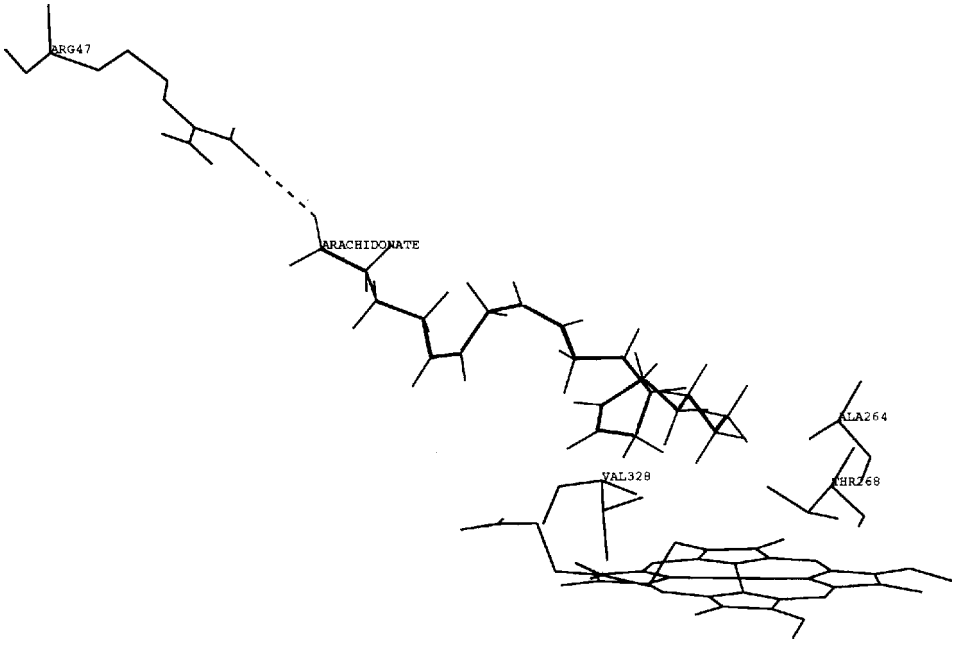


Figure 16. Possible mode of interaction between arachidonic acid and the active site of CYP2E1.

that of specific atoms involved in the enzyme–substrate interaction, are relevant to CYP2E1-mediated activity. Indeed, for a series of structurally related halothanes (Yin *et al*. 1995), the rate of metabolism via human CYP2E1 can be equated ($r = 0.99$) with ionization energy (Lewis and Pratt 1998, Lewis *et al*. 1998b) which is a reactivity parameter equivalent to E_{HOMO}. Both frontier orbital energies (E_{HOMO}, E_{LUMO}) have been shown to be of relevance to P450-mediated metabolism of volatile

Table 5. Physicochemical and structural data for 22 CYP2E substrates.[a]

	Compound	log P[b]	ΔE (eV)	μ (D)	Area/ depth[a]	Length/ width	Diameter (Å)
1.	Halothane	2.30	10.94	1.730	1.707	1.130	5.6
2.	Azoxymethane	−0.94[c]	10.09	5.085	2.272	1.355	5.1
3.	4-Nitrophenol	1.91	9.01	5.262	6.047	1.357	6.0
4.	Tetrachloromethane	2.83	11.26	0.005	1.322	1.000	5.5
5.	Isoniazid	−1.14	9.76	1.563	3.440	1.426	6.1
6.	Paracetamol	0.25	8.77	4.513	3.561	1.668	6.4
7.	Dimethlynitrosamine	−0.57	10.87	3.371	2.290	1.001	5.1
8.	Nitrosopyrrolidine	−0.19	10.85	3.818	2.451	1.232	5.6
9.	Dimethylsulphoxide	−1.35	9.60	4.488	2.379	1.195	5.2
10.	Aniline	0.90	9.16	1.541	5.371	1.206	5.6
11.	Xylene	3.15	9.55	0.070	3.394	1.334	6.0
12.	Pyridine	0.65	10.07	1.975	4.354	1.018	5.2
13.	Pyrazole	0.13	10.66	2.105	3.616	1.137	4.9
14.	Imidazole	−0.08	10.14	3.601	3.721	1.160	4.9
15.	Acetone	−0.24	11.51	2.896	2.017	1.098	4.9
16.	Benzene	2.13	10.20	0.001	4.850	1.100	5.4
17.	Butan-2-ol	0.76	14.51	1.624	2.135	1.405	5.4
18.	Pentane	3.11	14.89	0.007	2.719	1.762	5.6
19.	Ether	0.83	13.38	1.247	2.351	1.933	5.4
20.	Propan-2-ol	0.05	14.39	1.617	1.780	1.160	5.0
21.	Acetonitrile	−0.34	14.13	2.893	1.348	1.346	4.4
22.	Ethanol	−0.32	14.44	1.550	1.565	1.491	4.5

[a], Data compiled from Lewis *et al*. 1997b.
[b], experimental log P octanol value
$\Delta E = E_{LUMO} - E_{HOMO}$.
[c], calculated value
μ, dipole moment.
Diameter = molecular collision diameter calculated via the COSMIC package (Vinter *et al*. 1987).

organochlorines (Waller *et al*. 1996), whereas for a series of alkenes it has been demonstrated that the rate of epoxidation correlates with ionization energy (Traylor and Xu 1988). It is possible that the dependence of metabolic rate on ionization energy of the substrate is due to interaction with an electrophilic species as the active oxygenating agent in P450 catalysis (Lewis and Pratt 1998), and the reported finding that the rate of reaction with hydroxyl radicals for many diverse chemicals correlates closely with ionization potential (Sabljic and Gusten 1990) indicates that $OH^{\cdot}$ could represent the active oxygen species in P450-mediated reactions.

Although CYP2E1 substrates and inducers can be discriminated from those of other P450s on the grounds of molecular diameter and ΔE (where $\Delta E = E_{LUMO} - E_{HOMO}$), these parameters do not entirely differentiate between carcinogens and non-carcinogens (Lewis *et al*. 1997b). However, it has been reported previously that the molecular dipole moment is an important factor in this form of discriminate analysis (Lewis *et al*. 1997b) as carcinogenic CYP2E1 substrates/inducers tend to possess relatively low dipole moments and low ΔE, coupled with molecular diameters of between 5.0 and 6.0 Å, although some exceptions exist. Table 5 shows the relevant molecular and electronic structural parameters for 22 CYP2E substrates, together with their log P. In fact, one finds that a combination of rectangularity (length/width ratio) and ΔE provides a fairly satisfactory differentiation between the more carcinogenic/hepatotoxic CYP2E-specific compounds from those of relatively low toxicity (figure 17), and it should also be noted that dipole moment provides further discrimination of weak carcinogens/hepatotoxins from potent carcinogens, although molecular diameter (or size) is another factor in the overall analysis.

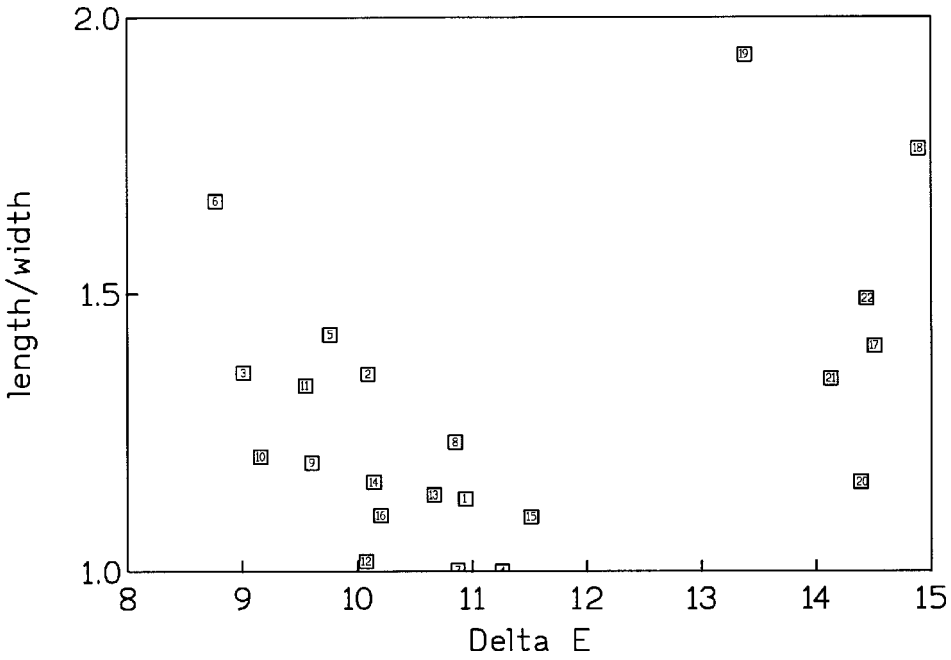


Figure 17. Plot of length/width versus ΔE for 22 CYP2E1 substrates and inducers as described in the text and using the data shown in table 4.

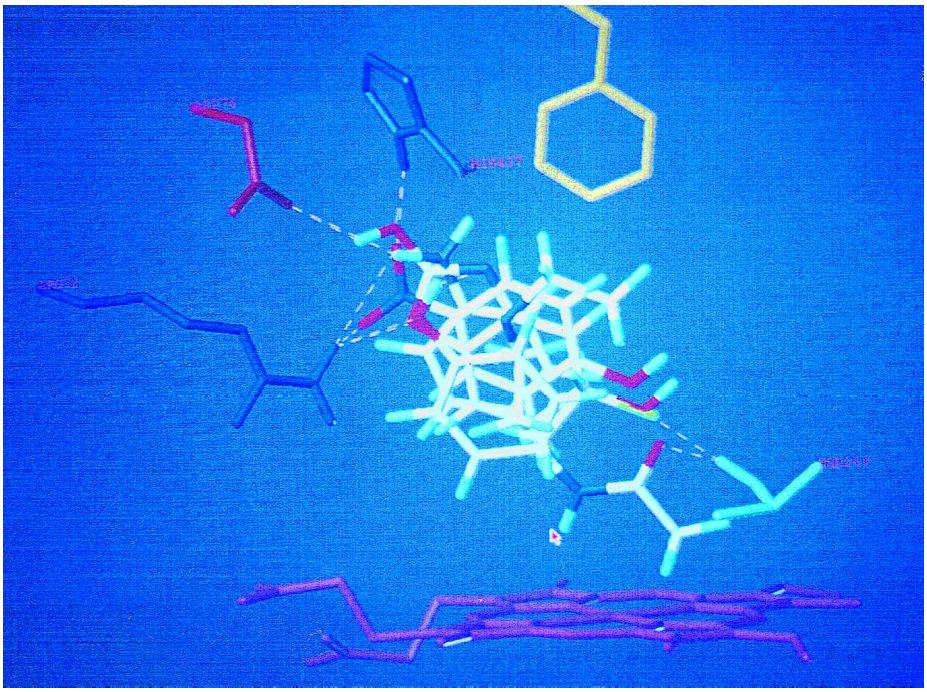


Figure 18. Molecular template of six CYP2E1 substrates docked within the putative active site of the enzyme where there is a reinforcement of several interactions with key amino acid residues.

Figure 18 shows that it is possible to superimpose all of the human CYP2E1 substrates, studied in this work, within the putative active site of the enzyme, where certain amino acid residues are involved in complementary interactions with key groups on the substrate molecules. In fact, this substrate template indicates that active site interactions consistently explain the observed CYP2E-mediated metabolism products for the compounds concerned. It is hoped, therefore, that a combination of homology modelling and molecular parametric analysis will prove fruitful in formulating rules governing P450 selectivity and potential toxicity.

Acknowledgements

The financial support of GlaxoWellcome Research and Development Ltd, Merck, Sharp and Dohme Ltd, the European Union Biomed 2 programme and the University of Surrey Foundation Fund is gratefully acknowledged by D.F.V.L.

References

Amet, Y., Lucas, D., Zhang-Gouillon, Z.-Q. and French, S. W., 1998, P450-dependent metabolism of lauric acid in alcoholic liver disease: comparison between rat and kidney microsomes. *Alcoholism: Clinical and Experimental Research*, **22**, 455–462.

Ardies, C. M., Zachman, E. K. and Koehn, B. J., 1994, Effect of swimming exercise and ethanol on rat liver P450-dependent monooxygenases. *Medicine and Science in Sports and Exercise*, **26**, 1453–1458.

Barnett, C. R., Flatt, P. R. and Ioannides, C., 1994, Modulation of the rat hepatic cytochrome P450 composition by long-term streptozotocin-induced insulin-dependent diabetes. *Journal of Biochemical Toxicology*, **9**, 63–69.

Bellward, G. D., Chang, T., Rodrigues, B., McNeill, J. H., Maines, S., Levin, W. and Thomas, P. E., 1988, Hepatic cytochrome P450j induction in the spontaneously diabetic BB rat. *Molecular Pharmacology*, **33**, 140–143.

Bond, J. A., Recio, L. and Andjelkovich, D., 1995, Epidemiological and mechanistic data suggest that 1,3-butadiene will not be carcinogenic to humans at exposures likely to be encountered in the environment or workplace. *Carcinogenesis*, **16**, 165–171.

Brady, J. F., Ishizaki, H., Fukuto, J. M., Lin, M. C., Fadel, A., Gapac, J. M. and Yang, C. S., 1991, Inhibition of cytochrome P450 2E1 by diallyl sulphide and its metabolites. *Chemical Research in Toxicology*, **4**, 642–647.

Cederbaum, A. I., 1987, Microsomal generation of hydroxyl radicals: its role in microsomal ethanol oxidizing system (MEOS) activity and requirement for iron. *Annals of the New York Academy of Sciences*, **492**, 35–49.

Chen, T. L., Ueng, T. H., Chen, S. H., Lee, P. H., Dan, S. Z. and Liu, C. C., 1995, Human cytochrome P450 mono-oxygenase system is suppressed by propofol. *British Journal of Anaesthesia*, **74**, 558–562.

Csanady, G. A., Guengerich, F. P. and Bond, J. A., 1992, Comparison of the biotransformation of 1,3-butadiene and its metabolite butadiene monoepoxide by hepatic and pulmonary tissues from humans, rats and mice. *Carcinogenesis*, **13**, 1143–1153.

Dresibach, A. W., Fertencz, N., Hopkins, N. E., Fuentes, M. G., Rege, A. B., George, W. J. and Lertora, J. J. L., 1996, Urinary excretion of 6-hydroxychlorozoxazone (CXZ-OH, as an index of cytochrome P450 2E1 activity. *Clinical Pharmacology and Therapeutics*, **58**, 498–505.

Duescher, R. J. and Elfarra, A. A., 1994, Human liver microsomes are efficient catalysts of 1,3-butadiene oxidation: evidence for major roles by cytochromes P450 2A6 and 2E1. *Archives of Biochemistry and Biophysics*, **311**, 342–349.

Elkstrom, G., Cronholm, T. and Ingelman-Sundberg, M., 1986, Hydroxyl radical production and ethanol oxidation by liver microsomes from ethanol-treated rats. *Biochemical Journal*, **233**, 755–761.

Fukuda, T., Imai, Y., Komori, M., Nakamura, M., Kusunose, E., Satouchi, K. and Kusunose, M., 1993, Replacement of Thr-303 of P450 2E1 with serine modifies the regioselectivity of its fatty acid hydroxylase activity. *Journal of Biochemistry*, **113**, 7–12.

Gonzalez, F. J. and Gelboin, H. V., 1994, Role of human cytochromes P450 in the metabolic activation of chemical carcinogens and toxins. *Drug Metabolism Reviews*, **26**, 165–183.

Gotoh, O., 1992, Substrate recognition sites in cytochrome P450 family 2 (CYP2, inferred from comparative analyses of amino acid and coding nucleotide sequences. *Journal of Biological Chemistry*, **267**, 83–90.

Graham-Lorence, S., Truan, G., Peterson, J. A., Falck, J. R., Wei, S., Helvig, C. and Capdevila, J. H., 1997, An active site substitution, F87V, converts cytochrome P450BM3 into a regio- and stereoselective (14*S*,15*R*)-arachidonic acid epoxygenase. *Journal of Biological Chemistry*, **272**, 1127–1135.

Guengerich, F. P., 1995, Human cytochrome P450 enzymes. In P. R. Ortiz de Montellano (ed.), *Cytochrome P*450 (New York: Plenum), pp. 473–535.

Guengerich, F. P. and Johnson, W. W., 1997, Kinetics of ferric cytochrome P450 reduction by NADPH-cytochrome P450 reductase: rapid reduction in the absence of substrate and variations among cytochrome P450 systems. *Biochemistry*, **36**, 14741–14750.

Guengerich, F. P., Kim, D.-H. and Iwasaki, M., 1991, Role of human cytochrome P450 IIE1 in the oxidation of many low molecular weight cancer suspects. *Chemical Research in Toxicology*, **4**, 168–179.

Halliwell, B. and Gutteridge, J. M. C., 1990, Role of free radicals and catalytic metal ions in human disease: an overview. *Methods in Enzymology*, **186**, 1–85.

Hargreaves, M. B., Jones, B. C., Smith, D. A. and Gescher, A., 1994, Inhibition of *p*-nitrophenol hydroxylase in rat liver microsomes by small aromatic and heterocyclic molecules. *Drug Metabolism and Disposition*, **22**, 806–810.

Ingelman-Sundberg, M., Johansson, I., Terelius, Y., Eliasson, E., Ekstrom, G., Buhler, R. and Lindros, K. O., 1993, Ethanol-inducible CYP2E1: toxicological importance and regulation by nutrients. In D. V. Parke, C. Ioannides and R. Walker (eds), *Food, Nutrition and Chemical Toxicity* (London: Smith-Gordon), pp. 147–160.

Ioannides, C., Lewis, D. F. V. and Parke, D. V., 1995, Mechanisms of chemical carcinogenesis and molecular parametric analysis in the safety evaluation of chemicals. In C. Ioannides and D. F. V. Lewis (eds), *Drugs, Diet and Disease*, vol. 1: *Mechanistic Approaches to Cancer* (Chichester: Ellis Horwood), pp. 1–46.

Johansson, I., Eliasson, E., Norsten, C. and Ingelman-Sundberg, M., 1986, Hydroxylation of acetone by ethanol- and acetone-inducible cytochrome P450 in liver microsomes and reconstituted membranes. *FEBS Letters*, **196**, 59–64.

Koop, D. R., 1992, Oxidative and reductive metabolism by cytochrome P450 2E1. *FASEB Journal*, **6**, 726–730.

Koop, D. R. and Casazza, J. P., 1985, Identification of ethanol-inducible P450 isozyme 3a as the acetone and acetol monooxygenase of rabbit microsomes. *Journal of Biological Chemistry*, **260**, 13607–13612.

Koop, D. R., Morgan, E. T., Torr, G. E. and Coon, M. J., 1982, Purification and characterization of a unique isozyme of cytochrome P450 from liver microsomes of ethanol-treated rabbits. *Journal of Biological Chemistry*, **257**, 8472–8480.

Kukielka, E. and Cederbaum, A. I., 1994, DNA strand cleavage as a sensitive assay for the production of hydroxyl radicals by microsomes: role of cytochrome P4502E1 in the increased activity after ethanol treatment. *Biochemical Journal*, **302**, 773–779.

Laetham, R. M., Balazy, M., Falck, J. R., Laetham, C. L. and Koop, D. R., 1993, Formation of 19(*S*)-, 19(*R*)-, and 18(*R*)-hydroxyeicosatetraenoic acids by alcohol-inducible cytochrome P450 2E1. *Journal of Biological Chemistry*, **268**, 12912–12918.

Levitt, M. and Perutz, M. F., 1988, Aromatic rings act as hydrogen bond acceptors. *Journal of Molecular Biology*, **201**, 751–754.

Lewis, D. F. V., 1987, Quantitative structure–activity relationships in a series of alcohols exhibiting inhibition of cytochrome P450-mediated aniline hydroxylation. *Chemico-Biological Interactions*, **62**, 271–280.

Lewis, D. F. V., 1995, Three-dimensional models of human and other mammalian microsomal P450 constructed from an alignment with P450102 ($P450_{bm3}$). *Xenobiotica*, **25**, 333–366.

Lewis, D. F. V., 1996, *Cytochromes P*450: *Structure, Function and Mechanism* (London: Taylor & Francis).

Lewis, D. F. V., 1998, The CYP2 family: models, mutants and interactions. *Xenobiotica*, **28**, 617–661.

Lewis, D. F. V., Bird, M. G. and Parke, D. V., 1997b, Molecular modelling of CYP2E1 enzymes for rat, mouse and man: an explanation for species differences in butadiene metabolism and potential carcinogenicity, and rationalization of CYP2E substrate specificity. *Toxicology*, **118**, 93–113.

Lewis, D. F. V., Brantom, P. G., Ioannides, C., Walker, R. and Parke, D. V., 1997a, Nitrosamine carcinogenesis: rodent assays, quantitative structure–activity relationships and human risk assessment. *Drug Metabolism Reviews*, **29**, 1055–1078.

Lewis, D. F. V., Eddershaw, P. J., Tarbit, M. H. and Goldfarb, P. S., 1998b, Structural determinants of cytochrome P450 substrate specificity, binding affinity and catalytic rate. *Chemico-Biological Interactions*, **115**, 175–199.

Lewis, D. F. V., Ioannides, C. and Parke, D. V., 1994, Interaction of a series of nitriles with the alcohol-inducible isoform of P450: computer analysis of structure–activity relationships. *Xenobiotica*, **24**, 401–408.

Lewis, D. F. V. and Pratt, J. M., 1998, The cytochrome P450 catalytic cycle and mechanism of oxygenation. *Drug Metabolism Reviews*, **30**, 739–786.
Lewis, D. F. V., Watson, E. and Lake, B. G., 1998a, Evolution of the cytochrome P450 superfamily: sequence alignments and pharmacogenetics. *Mutation Research*, **410**, 245–270.
Li, H. and Poulos, T. L., 1997, The structure of the cytochrome $P450_{BM_3}$ haem domain complexed with the fatty acid substrate, palmitoleic acid. *Nature Structural Biology*, **4**, 140–146.
Lijinsky, W., 1993, Life-span and cancer: the induction time of tumors in diverse animal species treated with nitrosodiethylamine. *Carcinogenesis*, **14**, 2373–2375.
Liu, P. T., Ioannides, C., Shavila, J., Symons, A. M. and Parke, D. V., 1993, Effects of ether anaesthesia and fasting on various cytochromes P450 of rat liver and kidney. *Biochemical Pharmacology*, **45**, 871–877.
Loizou, G. D., Urban, G., Dekant, W. and Anders, M. W., 1994, Gas-uptake pharmacokinetics of 2,2-dichloro-1,1,1-trifluoroethane (HCFC-123). *Drug Metabolism and Disposition*, **22**, 511–517.
Lorenz, J., Glatt, H. R., Fleischmann, R., Ferlinz, R. and Oesch, F., 1984, Drug metabolism in man and its relationship to that in three rodent species: monooxygenase, epoxide hydrolase and glutathione *S*-transferase activities in subcellular fractions of lung and liver. *Biochemical Medicine*, **32**, 43–56.
Mackman, R., Guo, Z., Guengerich, F. P. and Ortiz de Montellano, P. R., 1996, Active site topology of human cytochrome P450 2E1. *Chemical Research in Toxicology*, **9**, 223–226.
Melnick, R. L. and Kohn, M. C., 1995, Mechanistic data indicate that 1,3-butadiene is a human carcinogen. *Carcinogenesis*, **16**, 157–163.
Nakajima, T., Wang, R.-S., Elovaara, E., Park, S. S., Gelboin, H. V. and Vainio, H., 1993, Cytochrome P450-related differences between rats and mice in the metabolism of benzene, toluene and trichloroethylene in liver microsomes. *Biochemical Pharmacology*, **45**, 1079–1085.
Nahri, L. O. and Fulco, A. J., 1986, Characterization of a catalytically self-sufficient 119,000-dalton cytochrome P450 monooxygenase induced by barbiturates in *Bacillus megaterium*. *Journal of Biological Chemistry*, **261**, 7160–7169.
Nelson, D. R., Koymans, L., Kamataki, T., Stegeman, J. J., Feyereisen, R., Waxman, D. J., Waterman, M. R., Gotoh, O., Coon, M. J., Estabrook, R. W., Gunsalus, I. C. and Nebert, D. W., 1996, P450 superfamily: update on new sequences, gene mapping, accession numbers and nomenclature. *Pharmacogenetics*, **6**, 1–42.
Nelson, S. D., 1990, Molecular mechanisms of the hepatotoxicity caused by acetaminophen. *Seminars in Liver Disease*, **10**, 267–278.
Ono, S., Hatanaka, T., Hotta, H., Satoh, T., Gonzalez, F. J. and Tsutsu, M., 1996, Specificity of substrate and inhibitor probes for cytochrome P450: evaluation of in vitro metabolism using cDNA-expressed human P450 and human liver microsomes. *Xenobiotica*, **26**, 681–693.
Parke, D. V., 1987, Activation mechanisms to chemical toxicity. *Archives of Toxicology*, **60**, 5–15.
Parke, D. V., 1994, The cytochromes P450 and mechanisms of chemical carcinogenesis. *Environmental Health Perspectives*, **102**, 852–853.
Parke, D. V. and Ioannides, C., 1990, Roles of cytochromes P450 in mouse liver tumor production. In D. E. Stevenson, R. M. McClain, J. A. Popp, T. G. Slaga, J. M. Ward and H. C. Pitot (eds), *Mouse Liver Carcinogenesis*: *Mechanisms and Species Comparisons* (New York: Alan Liss), pp. 215–230.
Parkinson, A., 1996, An overview of current cytochrome P450 technology for assessing the safety and efficacy of new materials. *Toxicologic Pathology*, **24**, 45–57.
Porter, T. D., 1994, Mutagenesis at a highly conserved phenylalanine in cytochrome P450 2E1 affects heme incorporation and catalytic activity. *Biochemistry*, **33**, 5942–5946.
Raucy, J. L., Kraner, J. C. and Lasker, J. M., 1993, Bioactivation of halogenated hydrocarbons by cytochrome P4502E1. *Critical Reviews in Toxicology*, **23**, 1–20.
Raucy, J. L., Lasker, J. M., Lieber, C. S. and Black, M., 1989, Acetaminophen activation by human liver cytochromes P450IIE1 and P450IA2. *Archives of Biochemistry and Biophysics*, **271**, 270–283.
Raunio, H. and Pelkonen, O., 1995, Cancer genetics: genetic factors in the activation and inactivation of chemical carcinogens. In C. Ioannides and D. F. V. Lewis (eds), *Drugs, Diet and Disease*, vol. 1: *Mechanistic Approaches to Cancer* (Chichester: Ellis Horwood), pp. 229–258.
Ravichandran, K. G., Boddupalli, S. S., Hasemann, C. A., Peterson, J. A. and Deisenhofer, J., 1993, Crystal structure of hemoprotein domain of $P450_{BM_3}$, a prototype for microsomal P450. *Science*, **261**, 731–736.
Rendic, S. and Di Carlo, F. J., 1997, Human cytochrome P450 enzymes: a status report summarizing their reactions, substrates, inducers and inhibitors. *Drug Metabolism Reviews*, **29**, 413–580.
Ronis, M. J. J., Lindros, K. O. and Ingelman -Sundberg, M., 1996, The CYP2E Subfamily. In C. Ioannides (ed.), *Cytochromes P*450 - *Metabolic and Toxicological Aspects* (Boca Raton: CRC Press), pp. 211–239.
Sabljic, A. and Gusten, H., 1990, Predicting the night-time NO_3 radical reactivity in the troposphere. *Atmospheric Environment*, **24A**, 73–78.

Sangster, J., 1989, Octanol–water partition coefficients of simple organic compounds. *Journal of Physical and Chemical Reference Data*, **18**, 1111–1229.

Sharma, R. K., Doig, M. V., Lewis, D. F. V. and Gibson, G. G., 1989, Role of hepatic and renal cytochrome P450 IVA1 in the metabolism of lipid substrates. *Biochemical Pharmacology*, **38**, 3621–3629.

Shimizu, T., 1997, Diverse role of conserved aromatic amino acids in the electron transfer of cytochrome P450 catalytic functions: site-directed mutagenesis studies. *Recent Research Developments in Pure and Applied Chemistry*, **1**, 169–175.

Smith, D. A., 1994, Chemistry and enzymology: their use in the prediction of human drug metabolism. *European Journal of Pharmaceutical Sciences*, **2**, 69–71.

Smith, D. A., Ackland, M. J. and Jones, B. C., 1997, Properties of cytochrome P450 isoenzymes and their substrates. Part 2: Properties of cytochrome P450 substrates. *Drug Discovery Today*, **2**, 479–486.

Stenlake, J. B., 1979, *Foundations of Molecular Pharmacology*, vol. 2: *The Chemical Basis of Drug Action* (London: Athlone).

Tan, Y., White, S. P., Paranawithana, S. R. and Yang, C. S., 1997, A hypothetical model for the active site of human cytochrome P4502E1. *Xenobiotica*, **27**, 287–299.

Tassaneeyakul, W., Veronese, M. E., Birkett, D. J., Gonzalez, F. J. and Miners, J. O., 1993, Validation of 4-nitrophenol as an *in vitro* substrate probe for human liver CYP2E1 using cDNA expression and microsomal kinetic techniques. *Biochemical Pharmacology*, **46**, 1975–1981.

Terelius, Y., Lindros, K. O., Albano, E. and Ingelman -Sundberg, M., 1993, Isoenzyme specificity of cytochrome P450 mediated hepatotoxicity. *Frontiers in Biotransformation*, **8**, 186–232.

Traylor, T. G. and Xu, F., 1988, Model reactions related to cytochrome P450. Effects of alkene structure on the rates of epoxide formation. *Journal of the American Chemical Society*, **110**, 1953–1958.

Urban, G., Speerschnaider, P. and Dekant, W., 1994, Metabolism of the chlorofluorocarbon substitute 1,1-dichloro-2,2,2-trifluoroethane by rat and human liver microsomes. *Chemical Research in Toxicology*, **7**, 170–176.

Vinter, J. G., Davis, A. and Saunders, M. R., 1987, Strategic approaches to drug design. I. An integrated software framework for molecular modelling. *Journal of Computer-Aided Molecular Design*, **1**, 31–51.

Waller, C. L., Evans, M. V. and McKinney, J. D., 1996, Modeling the cytochrome P450-mediated metabolism of chlorinated volatile organic compounds. *Drug Metabolism and Disposition*, **24**, 203–210.

Wang, M.-H., Wade, D., Chen, L., White, S. and Yang, C. S., 1995, Probing the active sites of rat and human cytochrome P450 2E1 with alcohols and carboxylic acids. *Archives of Biochemistry and Biophysics*, **317**, 299–304.

Wiseman, H. and Halliwell, B., 1996, Damage to DNA by reactive oxygen and nitrogen species: role in inflammatory disease and progression to cancer. *Biochemical Journal*, **313**, 17–29.

Yang, C. S., Yoo, J.-S. H., Ishizaki, H. and Hong, J., 1990, Cytochrome P450IIE1: role in nitrosamine metabolism and mechanisms of regulation. *Drug Metabolism Reviews*, **22**, 147–159.

Yin, H., Anders, M. W., Korzekwa, K. R., Higgins, L., Thummel, K. E., Kharasch, E. D. and Jones, J. P., 1995, Designing safer chemicals: predicting the rates of metabolism of halogenated alkanes. *Proceedings of the National Academy of Sciences, USA*, **92**, 11076–11080.

XENOBIOTICA , 2000, VOL. 30, NO. 1, 27–46

Cytochrome P450 enzyme activity and protein expression in primary porcine enterocyte and hepatocyte cultures

T. HANSEN†, J. BORLAK†* and A. BADER‡

† Fraunhofer Institute of Toxicology and Aerosol Research, Department of Molecular Toxicology and Pharmacokinetics, Nikolai-Fuchs-Str. 1, D-30659 Hannover, Germany
‡ Leibniz Research Laboratories for Biotechnology and Artificial Organs, Medizinische Hochschule, Hannover, Germany

Received 23 May 1999

1. A method for the isolation and cultivation of porcine hepatocytes and porcine duodenal enterocytes for the investigation of drug oxidation reactions has been established.

2. Hepatocytes as well as enterocytes metabolized ethoxyresorufin (EROD) and ethoxycoumarin (ECOD) effectively, the rate being 31 ± 17 pmol/h·dish (EROD) and 9530 ± 4062 pmol/h·dish (ECOD) in the case of hepatocytes, and 9 ± 4 pmol/h·dish (EROD) and 510 ± 467 pmol/h·dish (ECOD) in the case of enterocytes. Diazepam, another CYP monooxygenase substrate, was also metabolized by porcine hepatocytes but not with porcine enterocytes, thus indicating differences in the metabolic competence of the liver and the gut.

3. The ability to induce enzymes responsible for the metabolism of ethoxyresorufin and ethoxycoumarin was investigated *in vitro* on treatment of the cell cultures with either 50 μM 3-methylcholanthrene (3-MC) or 50 μM β-naphthoflavone (β-NF). With enterocyte cultures, ECOD activity was inducible up to 20-fold, whereas EROD remained unchanged following treatment with either 3-MC or β-NF.

4. Western blotting provided additional evidence for the expression of CYP1A1 and CYP3A4 at the protein level and treatment of cultured enterocytes with 30 μM Aroclor 1254 or 50 μM β-NF resulted in enhanced expression of the CYP1A protein, and CYP3A4 protein expression was induced following treatment with 50 μM DEX, 2 mM PB, 30 μM Aroclor 1254 or 50 μM β-NF.

5. The metabolism of diazepam was also investigated with baculovirus-expressed human CYP enzymes (2C8, 2C9-ARG, 2C9-CYS, 2C19, 3A4, 3A4 + cytochrome b_5 and 3A5) and evidence was obtained to suggest the formation of temazepam and oxazepam by enzymes of the CYP3A subfamily. Small amounts (32 ± 12 ng/ml) of desmethyldiazepam were additionally recovered in microsomal preparations of all CYP-transfected cell lines.

6. In conclusion, porcine duodenal enterocytes can successfully be cultured for a short period and may be used as a tool for studying intestinal metabolism, whereas porcine hepatocytes can be cultured for prolonged periods (>10 days) reliably to investigate hepatic drug oxidation reactions.

Introduction

Studies with dog, rat and mouse are common when assessing the biotransformation of new drug candidates at early stages of drug development (Humphrey and Smith 1992) but due to large interspecies variations in the expression of drug-metabolizing enzymes (Caldwell 1992) extrapolation of animal data to humans is often problematical. The biotransformation pathways of new chemical entities (NCE) can, however, be predicted *in vitro*, which enables rational species selections

* Author for correspondence; e-mail: Borlak@ita.fhg.de

Xenobiotica ISSN 0049–8254 print/ISSN 1366–5928 online © 2000 Taylor & Francis Ltd
http://www.tandf.co.uk/journals/tf/00498254.html

for toxicity studies (most human-like tox species) and a better planning of clinical trials at the preclinical stage of drug development. *In vitro* systems also enable the identification of major metabolites when used as 'bioreactors' and permit an assessment of the enzymes responsible for the metabolic clearance of drugs (Rodrigues 1994, Parkinson 1996). This information enables, in a cost-effective manner, an intelligent planning of clinical studies with reduced risk for adverse drug reactions due to idiosyncratic metabolic pathways or the formation of toxic metabolites (Tucker 1992, Wrighton *et al*. 1995).

The potential for drug–drug interactions can reliably be studied *in vitro* and this information is of paramount importance for drug safety as shown by the recent and voluntary withdrawal of the cardiovascular drug posicor due to unexpected drug–drug interactions (SoRelle 1998).

Pig exhibits many similarities with man in cardiovascular anatomy and physiology and in digestive physiology. Because of these similarities pigs become increasingly attractive as toxicological models and offer several advantages compared with other non-rodent species, the non-human primate and dog. There are now efforts to replace companion animals such as the dog in toxicity testing. Therefore, the pig appears to be a suitable substitute particularly with respect to drug metabolism and hepatic toxicity of new chemical entities (Olsen *et al*. 1997, Skaanild and Friis 1998, Witkamp and Monshouwer 1998).

As the biotransformation of drugs is not restricted to the liver other tissues may significantly contribute to the overall metabolism of foreign chemicals (Kolars *et al*. 1991, Krishna and Klotz 1994). Indeed, to be absorbed, drugs and xenobiotics have to cross the mucus gel layer, the intestinal epithelial cells, the lamina propria and the endothelium of the blood or lymphatic capillaries respectively. The epithelial cells are the main component of this barrier. While passing the epithelial barrier, xenobiotics are subjected to intestinal metabolism including the cytochrome P450 (CYP) monooxygenase system (Gan *et al*. 1996). CYPs are expressed in the intestinal epithelium with highest concentrations in the duodenum but less so towards the distal end of the gut (Kaminsky and Fasco 1991).

The most abundant CYP isoenzyme in the human intestinal tract is CYP3A4 (Kolars *et al*. 1994). The expression of the CYP3A gene family in human intestinal tissue has also been investigated using *in situ* hybridization techniques (McKinnon *et al*. 1995) and RT-PCR (Kivistö *et al*. 1996). Drugs that are substrates for the intestinal CYP3A4 have a low and often interindividual variable bioavailability because of first-pass metabolism in the intestinal mucosa. Examples for intestinal first-pass include the immunosuppressive drugs cyclosporin (Wu *et al*. 1995) and tacrolimus (Lampen *et al*. 1996), the CNS-drug midazolam (Thummel *et al*. 1996) and the HIV protease inhibitor saquinavir (Fitzsimmons and Collins 1997).

Although needed, primary cell cultures for the study of intestinal biotransformation are difficult to obtain presumably due to the complex control of intestinal cell proliferation and differentiation (Adams and Watt 1993) and the short life span *in vivo* of enterocytes. Intestinal epithelial cells are renewed every 2–3 days in rodents (Cairne *et al*. 1965, Gordon 1989) and about every 5–6 days in humans (Lipkin 1973). The overall production of enterocytes in humans is very impressive indeed and may be as much as 8 tons over an entire life span. Therefore, the short life span of intestinal epithelial cells may be a prohibitive factor for long-term culture of enterocytes. Interestingly, Perreault and Beaulieu (1998) isolated epithelial cells from foetal small intestine using a non-enzymatic dissociation

method and the cultures were confluent monolayers and retained expression of brush border enzymes as well as morphologic characteristics of differentiated enterocytes, such as tight junctions, zonula adherens and desmosomal components.

On the other hand, when adult human enterocytes are isolated, a rapid loss of viability and differentiation can be observed, as reported by Gibson *et al.* (1989), who isolated human colonic crypts from resected mucosa or biopsy specimens. Cells maintained structural and functional integrity only for 16 h, as assessed by electron microscopy and ^{3}H-thymidine uptake. Moreover, Sträter *et al.* (1996) investigated the effect of collagenase tissue digest on human colonic crypt cells and found a rapid disintegration shortly after isolation, e.g. 4 h. The rapid loss of cellular integrity and the formation of amorphous cell clusters 4 h following isolation was caused by epithelial cells undergoing apoptosis, as judged by DNA-fragment labelling. According to Sträter *et al.* (1996), survival of epithelial cells depends on β_1-integrin-collagen type I interaction, which is destroyed by detachment of cells during the isolation procedure. This finding suggests that the extracellular matrix might play a crucial role in the regulation of enterocyte differentiation.

Using rodent intestinal tissue, differentiated enterocytes can successfully be isolated and cultured from foetal (Hahn *et al.* 1990) or suckling (Hahn *et al.* 1987, Evans *et al.* 1992) animals, but the isolation and culture of primary porcine epithelial cells has not been investigated as yet.

Since the expression of drug-metabolizing enzymes is differentially regulated during ontogenesis, a culture model for adult primary enterocytes could be of value to investigate intestinal drug biotransformation. Therefore, the objective of the present study was to develop a system for porcine enterocyte cultures to study intestinal biotransformation of drugs and to compare the metabolic competence of enterocytes to that of cultured hepatocytes and to that of individual human CYP isoforms, which are studied in a heterologous expression system. Since cell cultures of primary small intestinal enterocytes are not routinely available, a new method for the isolation and cultivation of enterocytes had to be developed.

Ethoxyresorufin, ethoxycoumarin and diazepam were used as marker substrates of CYP monooxygenases and the effects of treatment with 3-MC, β-NF, dexamethasone, phenobarbital or Aroclor 1254 (a mixture of PCBs) were also investigated to obtain a more comprehensive view for the potential of monooxygenase enzyme induction in culture.

Material and methods

Isolation and culture of porcine enterocytes

Small intestinal tissue was from healthy young female German landrace pigs weighing 150± 20 kg. A-30 cm segment of duodenum was swiftly removed and transported to the laboratory within 20 min in ice-cold PBS. The intestinal tube was rinsed gently with ice-cold phosphate-buffered saline (PBS) to remove any remnants of excreta. The intestinal segment was filled with prewarmed (37 °C) PBS containing 0.05% (w/v) 1,4-dithiothreitol (DTT), closed with clips and submerged in PBS 37 °C for 10 min. During the incubation the intestinal segment was manually kneaded several times. The incubation solution was discharged and the intestinal tube was flushed with PBS (37 °C). Subsequently the intestinal segment was filled with incubation buffer containing 0.05% (w/v) pronase and 0.075% collagenase H (w/v) (both Boehringer Mannheim) in the same manner. Incubation buffer consisted of 0.07 g/l $NaH_2PO_4 \times 2\ H_2O$, 0.18 g/l $Na_2HPO_4 \times 2\ H_2O$, 4.09 g/l NaCl, 0.37 g/l KCl, 1.7 g/l $NaHCO_3$, 11.9 g/l Hepes, 2.9 g/l $CaCl_2 \times 2\ H_2O$, 6.1 g/l $MgCl_2 \times 6\ H_2O$ and 2 g/l glucose. The incubation solution was collected in a precooled beaker and the intestinal tube was rinsed gently with ice-cold incubation buffer containing 0.2% (w/v) bovine serum albumin (Sigma Chemie GmbH, Deisenhofen, Germany). The resulting cell suspension was centrifuged at 170 *g* and 4 °C for 5 min. After removal of the supernatant the pellet was resuspended in buffer III. The washing procedure was repeated three times. The resulting

cell pellet was resuspended in William's E medium without phenol red (Cytogen, Berlin, Germany). The total yield of cells ranged from 4 to 8×10^7. Viability of freshly isolated cells ranged between 90 and 98% as assessed by the trypan blue exclusion test.

Immunohistochemistry

The efficiency of each of the cell isolations was assessed by histologic examination of the duodenum. Cryosections of the duodenum were stained with haematoxylin and eosin (H&E) and examined by light microscopy. For immunohistochemistry, cytospots were prepared from enterocyte cultures and immediately frozen at -80 °C. Immunoperoxydase staining was done using the avidin–biotin–peroxydase method. Monoclonal anti human cytokeratin peptide 18 (CY-90) was from Sigma. Cytospots of human intestinal epithelial Caco-2 cells were used as positive controls.

Marker enzyme assay for enterocytes

Alkaline phosphatase (AP) activity was measured from cell homogenates using a colorimetric kit (Sigma) with *p*-nitrophenyl phosphate as a substrate. Protein concentrations of the cell homogenates were determined according to the method of Smith *et al*. (1985). Levamisole (100 μM) was added to the incubation mixture to confirm that the detected AP activities were of intestinal origin. There are three distinct forms of alkaline phosphatases in mammalian tissues: placental, intestinal and liver/bone/kidney, which are distinguished by differences in molecular weight, heat stability and sensitivity to inhibitors (Suzuki *et al*. 1994). Suzuki *et al*. reported that the AP activity from placenta and kidney was inhibited by levamisole with a $K_{i0.5} = 10$–12 μM whereas the activity of the intestinal AP was not affected by levamisole until the concentration was increased to 240 μM levamisole.

Isolation of porcine hepatocytes

For isolation of porcine hepatocytes, female German landrace pigs weighing 20–30 kg were used. Following *in situ* perfusion with Kreb's–Ringer buffer (KRB) (4 °C) via the portal vein, the liver was removed and immediately dissected into pieces. Single liver lobes were then transported to the laboratory in ice-cold KRB. Blood vessels visible on the cut surface were cannulated and the liver specimen was perfused with 200 ml buffer I containing 8.3 g/l NaCl, 0.5 g/l KCl, 2.4 g/l HEPES and 0.19 g/l EGTA at pH 7.4 and 37 °C. This was followed by perfusion with 200 ml buffer II at pH 7.4 and 37 °C. Buffer II consisted of 8.3 g/l NaCl, 0.5 g/l KCl and 2.4 g/l HEPES. Thereafter collagenase perfusion was done with 200 ml buffer III containing 100 μg collagenase type IV, 3.9 g/l NaCl, 0.5 g/l KCl, 2.4 g/l HEPES and 0.7 g/l $CaCl_2 \cdot 2\ H_2O$ at 37 °C. The collagenase perfusate was recirculated. Flow rates ranged between 20 and 50 ml according to the size of the specimen. Following perfusion, the liver capsule was carefully removed and the dissolved cells were liberated by gentle shaking of the liver specimen in ice-cold buffer IV. Buffer IV contained 9.91 g/l Hanks' buffered salt solution without calcium and magnesium, 2.4 g/l HEPES and 2.0 g/l bovine serum albumin. The resulting cell suspension was filtered through a nylon mesh with 100 μm pore size and washed three times with buffer IV at 4 °C. Viability of the hepatocytes ranged between 90 and 99% as assessed by trypan blue exclusion. About 3×10^9 cells were isolated from liver resection material.

Cell culture

Primary porcine enterocytes and hepatocytes were cultivated in William's E medium without phenol red supplemented with 5% (v/v) foetal bovine serum, prednisolone 9.6 μg/ml, glucagon 0.014 μg/ml (Novo, Mainz, Germany) insulin 0.16 U/ml (Hoechst, Frankfurt, Germany), penicillin 200 U/ml and streptomycin 200 μg/ml (Biochrom, Berlin, Germany). Enterocytes were seeded at 2×10^6 cells per 60-mm dish. In suspension culture enterocytes spontaneously formed spheroidal aggregates.

Porcine hepatocytes were enclosed within two layers of collagen. Rat tail collagen type I was prepared according to the method of Elsdale and Bard (1972). Of collagen solution containing 1.1 mg/ml collagen, 1 ml was used for coating a 60-mm Petri dish. The pH of the collagen was adjusted to 7.4 using a $10\times$ DMEM (Dulbecco's modified eagle medium) concentrate (Biochrom). Thirty minutes after coating the dishes, 2×10^6 hepatocytes per dish were seeded. At four h following seeding and attachment of the cells, culture medium was removed along with non-adherent cells. After 48 h in culture, the medium was aspirated and a second layer of collagen was pipetted on top of the cells. After gelation of this second layer, culture medium was added. Culture medium (2 ml) was changed daily.

Albumin assay

ELISA as described (Dunn et al. 1992) determined albumin production by porcine hepatocytes. The 96-well plates were coated with 5 μg pig albumin overnight at 4 °C and pH 9.6. The wells were washed three times with PBS-Tween (PBS containing 0.5% v/v, Tween 20). Of the sample (cell culture supernatant), 50 μl was mixed with equal volume of antibody and incubated overnight at 4 °C. The wells

were washed three times with PBS-Tween and were then developed with 3,3′,5,5′-tetramethylbenzidine (TMB) for 7 min. The presence of bound antibodies was detected by the conversion of TMB by the conjugated horseradish peroxidase. The reaction was stopped with 8 N sulphuric acid and the absorbance was subsequently measured at 490 nm with a Dynatech MR600 microplate reader. A standard curve was generated for each ELISA plate using purified pig albumin as standard.

Treatment of cultures

The experiments started 4 h following seeding. The inducibility of CYP activities in enterocyte cultures was studied by addition of 50 μM 3-MC, 50 μM β-NF, 50 μM dexamethasone, 2 mM phenobarbital or 30 μM Aroclor 1254 to the cell cultures 4 h following seeding. With porcine hepatocyte cultures, experiments were started at day 4 in culture, since matrix overlaid hepatocytes are known to maintain expression of CYP enzymes for up to 14 days (Kern *et al*. 1997). EROD and ECOD activities were determined after 24- or 48-h treatment.

All substrates and inducing agents were dissolved in dimethyl sulphoxide (DMSO) and diluted to the working concentration with culture medium. The final concentration of DMSO never exceeded 0.5%.

Enzyme assays

Unless otherwise stated, all enzyme reactions were measured within the linear range of the assay.

7-Ethoxyresorufin O-deethylation (EROD) assay

7-Ethoxyresorufin (Sigma) was added to the cell cultures at a concentration of 2.4 μM. Dicumarol (10 μM) was added to the culture medium to prevent biotransformation of resorufin by cytosolic diaphorase (Nims *et al*. 1984). The kinetics of 7-ethoxyresorufin *O*-deethylation over 24 h was studied by adding 7-ethoxyresorufin to cell cultures for 0, 1, 2, 4, 8 and 24 h. The incubations were stopped by removal and immediate freezing of the cell culture supernatant at –20 °C. Formation of resorufin was measured using a Perkin–Elmer fluorimeter with an excitation wavelength of 530 nm and an emission wavelength of 585 nm. Fluorescences were converted to pmol with a calibration curve of resorufin fluorescence.

7-Ethoxycoumarin O-deethylation (ECOD) assay

To study the time dependence of 7-ethoxycoumarin *O*-deethylation over 24 h, 7-ethoxycoumarin (Sigma) was added to the cells for 0, 1, 2, 4, 8 and 24 h using a substrate concentration of 130 μM. At each time point cell culture supernatants were frozen at –20 °C. Formation of 7-hydroxycoumarin was quantitated based on the published procedures using a fluorimeter with an excitation wavelength of 380 nm and an emission wavelength of 460 nm. The fluorimeter was calibrated using 7-hydroxycoumarin (Sigma) standards.

Metabolism of diazepam

Diazepam was added to the cell culture medium for 0, 1, 2, 4, 8 and 24 h. A stock solution of diazepam was prepared in DMSO. The final concentration of diazepam used in the experiments was 35 μM. Samples were stored at – 20 °C and analysed by HPLC.

Midazolam was used as an internal standard for the quantification of diazepam and metabolites in the HPLC assay. Midazolam (1 μg) was added to 1 ml cell culture supernatant and the sample was subsequently alkalized using 20 μl 4 M NaOH. Following addition of 100 μl isopropanol the samples were extracted with 5 ml ethylacetate by gentle shaking for 30 min. The recovery was 99.4$\pm$0.2% (n = 3). Extracts were evaporated to dryness and the residues were dissolved in 120 μl mobile phase (acetonitril/methanol/triethylamine, 40/10/50 v/v/v) and 80 μl of the samples were injected in the HPLC system (Merck–Hitachi). The mobile phase was delivered at 0.8 ml/min with a HPLC pump (type L-7100). The 80-μl sample aliquots were applied to a C18-HD column (Nucleosil, 250 × 4 mm, particle size 5 μm, Macherey–Nagel) using an autosampler type L7200. Metabolites were detected by UV-absorption at 236 nm with L-7450 UV-detector.

Diazepam biotransformation studies with human supersomes

Recombinantly expressed human cytochrome P450 proteins were from Gentest corporation (Woburn, MA, USA). CYP proteins were expressed in an insect cell line using the baculovirus vector BTI-TN-5B1–4. Microsomal preparations from insect cells expressing human CYP2C8, CYP2C9-CYS144 mutant, 2C9-ARG144 mutant, CYP2C19, CYP3A4, CYP3A4 with cytochrome b_5 and CYP3A5 were used in this study. All preparations contained NADPH-cytochrome P450 reductase. Microsome preparations from wild-type cells were used as controls (Gentest). Microsomes were incubated with 100 μM diazepam and 1 mM NADPH for 30 min at 37 °C according to the manufacturer's recommendation. P450 protein (50 pmol) was used for each individual assay.

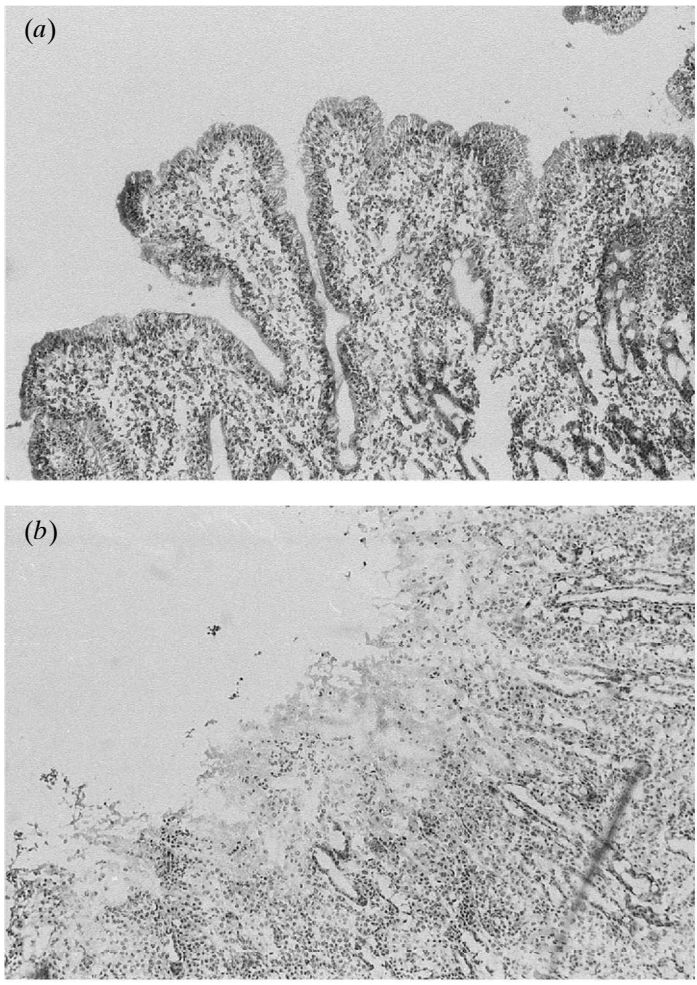


Figure 1. Cryosections of the duodenum stained with H&E before (a) and after (b) enterocyte isolation where intestinal epithelial cells are completely removed following collagenase digestion.

Western blot experiments

Western blotting techniques studied induction of individual CYP isozymes in control and treated cell cultures. For detailed description see Borlak *et al*. (1996). Before the preparation of microsomes the culture medium was removed and the cell cultures washed with PBS. Enterocytes in suspension culture were separated from the culture medium by centrifugation at 170 *g*. Microsomes were isolated by differential centrifugation according to Guengerich (1982). Protein concentrations of the microsomal suspension were determined by the method of Smith *et al*. (1985) with bicinchoninic acid using bovine serum albumin as standard. The protein loading for each gel was adjusted to 10 or 5 μg total protein respectively.

Results

Enterocyte isolation and culture

Light microscopic examination of the duodenum following collagenase-digestion provided evidence for villus-enterocytes to be completely removed from the intestine (figure 1). Viability of freshly isolated enterocytes ranged between 90 and 98% as estimated by trypan blue exclusion. The viability of cultured porcine

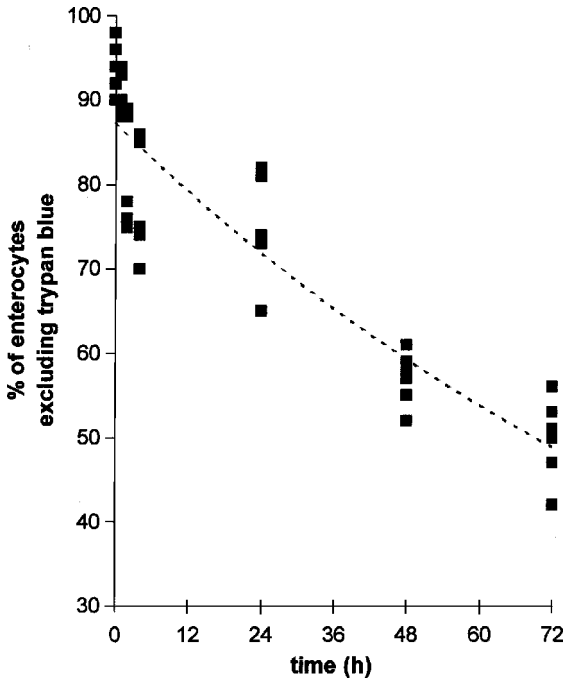


Figure 2. Viability of cultured porcine enterocytes. Viability was assessed by trypan blue exclusion ($n = 6$). An exponential regression function ($86e^{-0,01x}$) was fitted (determined with Microsoft Excel 5.0).

Table 1. Alkaline phosphatase activities in cultured porcine enterocytes.

Days in culture	nmol/min · mg protein
0	394 ± 97
1	488 ± 212
2	506 ± 241
3	373 ± 60
4	408 ± 90
5	423 ± 91
6	435 ± 83
8	489 ± 179

AP activity was measured from cell homogenates using *p*-nitrophenyl phosphate as a substrate. Protein concentrations of the cell homogenates were determined according to Smith *et al.* (1985). Levamisole (100 μM) was added to the incubation mixture. Data are the mean ± SD of six determinations.

enterocytes declined rapidly as shown in figure 2. During the first 4 h in culture, the percentage of viable enterocytes decreased from 94 ± 3 to 77 ± 6%. Following 24 h in culture, 75 ± 6% remained viable. In 48-h cultures of porcine enterocytes, 57 ± 3% excluded trypan blue and a further decline to 50 ± 3% was observed after 72 h in culture.

Alkaline phosphatase activity is a marker of differentiated villus tip cells. Immediately after enterocyte isolation, alkaline phosphatase activities of cell homogenates were 349.2 ± 97.1 nmol/mg protein min and the activity remained almost unchanged during 8 days in culture (table 1). Addition of 100 μM levamisole,

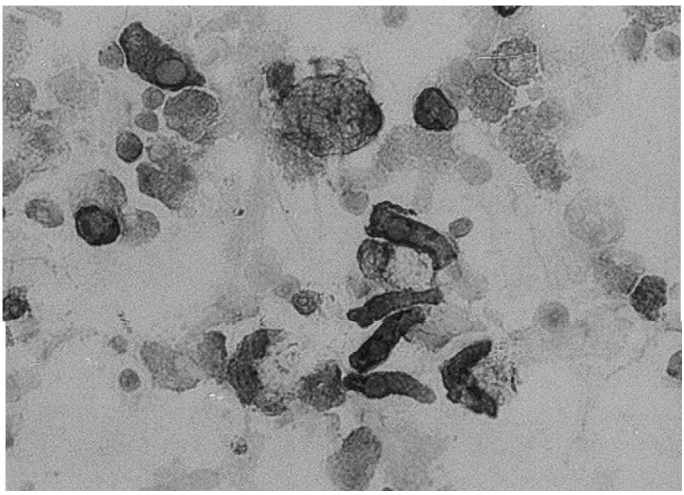


Figure 3. Cytospin preparation of enterocytes following 24 h in culture. Immunohistochemical staining used a avidin–biotin–peroxidase method with the anti human cytokeratin peptide 18 antibody.

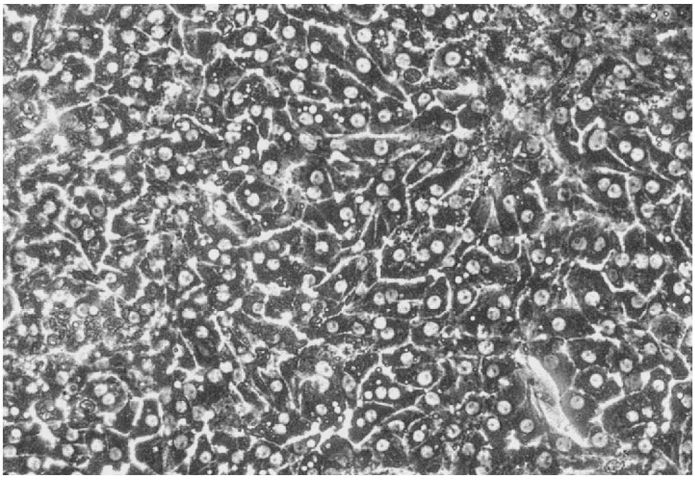


Figure 4. Phase contrast micrograph of porcine hepatocytes at 96 h in culture.

an inhibitor of placental and bone/liver/kidney AP activities, to the incubation mixture confirmed that the AP activities measured in enterocyte homogenates were not caused by contamination with other cell types expressing non-specific alkaline phosphatase.

Immunohistochemical staining of the cytospots showed, that the majority of cells contained cytokeratin 18, confirming the epithelial origin of the isolated cells (figure 3). The specificity of the cytokeratin 18 antibody used in the present study has been demonstrated previously (Levy *et al*. 1988). Cytokeratin 18 is found in a wide variety of simple and glandular epithelia, but is it not expressed in stratified squamous epithelia and in non-epithelial cells.

Enterocytes did not adhere to the surface of the cell culture dish and therefore only suspension cultures could be prepared where the cells formed three-dimensional aggregates. The size of cell aggregates increased with culture time.

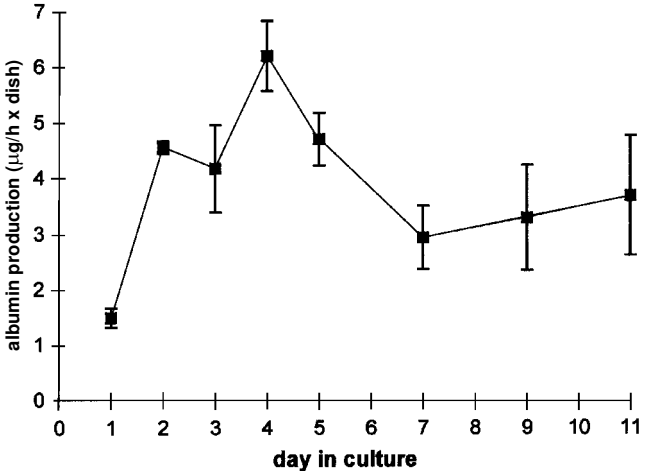


Figure 5. Albumin secretion by porcine hepatocytes in a collagen sandwich culture. Albumin was determined in the culture medium by ELISA. Results are mean ± SD of six dishes.

Table 2. Monooxygenase activities in cultured porcine hepatocytes and enterocytes.

	Pig hepatocytes	Pig enterocytes
EROD (free resorufin)	31 ± 17	9 ± 4
ECOD (free hydroxycoumarin)	9530 ± 4062	510 ± 467

Enzyme activities are expressed as pmol metabolite/h × culture dish (2×10^6 cells). Metabolites were detected fluorimetrically in the cell culture medium. Data are the mean ± SD of three determinations.

Staining of cell cultures with trypan blue and subsequent light microscopic examination confirmed that enterocyte aggregates were viable (excluding trypan blue), whereas single cells took up the dye, indicating an increased membrane permeability and thus cell damage (data not shown).

Hepatocyte culture

Immediately after seeding, pig hepatocytes were of rounded shape. Following 24 h in culture, the majority of the cells regained the normal polygonal cell shape and formed confluent monolayers, which could be maintained for 14 days (figure 4).

The secretion of albumin (figure 5) by cultured porcine hepatocytes increased during the first days in culture reaching a maximum value at day 4 of culture. The albumin secretion declined thereafter by ~ 50% but remained stable from day 7 onwards, e.g. to day 11.

Monooxygenase activities with marker substrates

Porcine cultured hepatocytes and enterocytes were able to metabolize ethoxyresorufin as well as ethoxycoumarin albeit at different levels and overall ECOD activities were considerably higher than those estimated for EROD (table 2). Furthermore, cultured hepatocytes had higher monooxygenase activities for both substrates, when compared with cultured enterocytes.

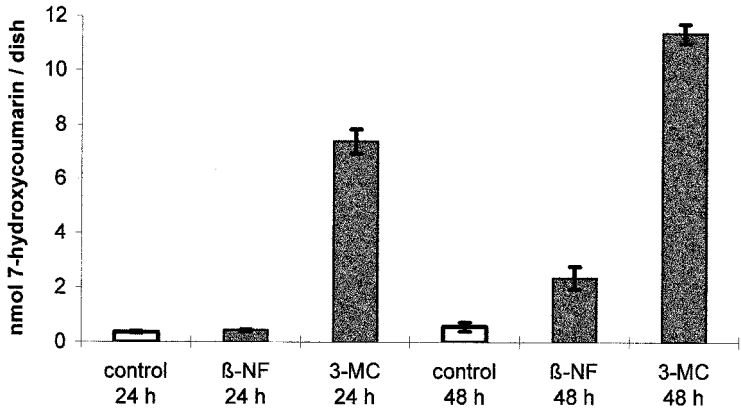


Figure 6. Induction of ECOD activity in cultured duodenal enterocyte cultures following treatment with 50 μM β-naphtoflavone or 50 μM 3-methylcholanthrene. Data are mean $\pm$ SD of four experiments.

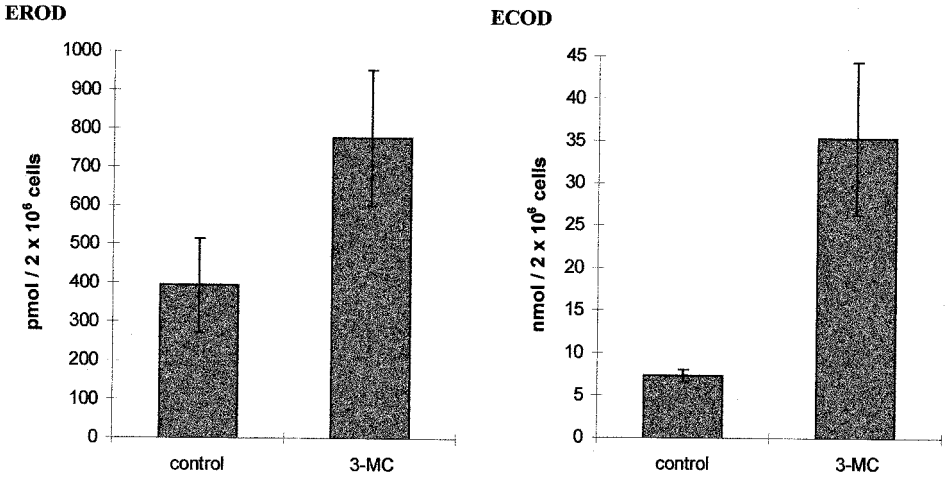


Figure 7. Induction of EROD activity and ECOD activity in porcine hepatocyte cultures following treatment with 50 μM 3-methylcholanthrene for 48 h. Data are mean $\pm$ SD of four experiments.

Pretreatment of enterocyte cultures with β-NF or 3-MC

The effects of 3-MC and β-NF treatment on ECOD activities in porcine enterocyte cultures are shown in figure 6. Treatment of enterocyte cultures with 50 μM 3-MC for 24 h led to an 8–16-fold increase in the ECOD activity (figure 6). Treatment of enterocyte cultures with 50 μM β-NF for 24 h did not alter the ECOD activity. Following 48 h of treatment with 3-MC or β-NF the ECOD activity increased 12–20- and 3–6-fold respectively (figure 6). EROD activity was not altered in enterocyte cultures by treatment with either 3-MC or β-NF for 24 or 48 h.

Pretreatment of hepatocyte cultures with β-NF or 3-MC

The metabolism of ethoxyresorufin and ethoxycoumarin was inducible by 3-MC in hepatocyte cultures (figure 7) and treatment of hepatocyte cultures with 50 μM for 48 h produced a 1.5–2-fold (EROD) and 4–6-fold (ECOD) increase in activities. This compares with a 12–20-fold induction seen with cultured enterocytes following treatment with 3-MC for 48 h.

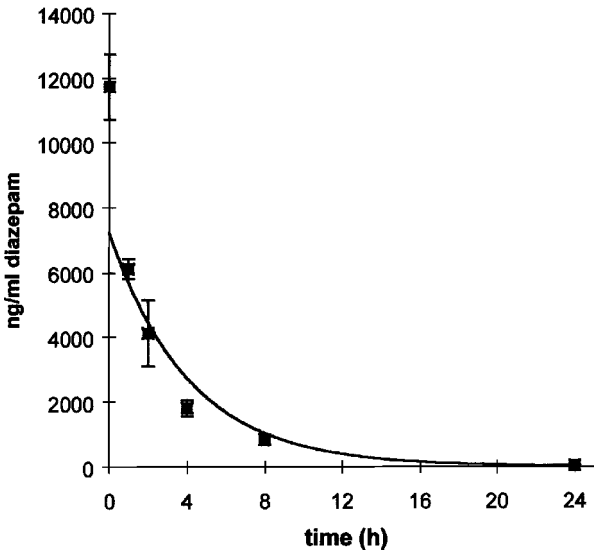


Figure 8. Time-dependent elimination of diazepam in hepatocyte cultures. Diazepam (35 μM) was added to the cell culture medium. Determination of diazepam and metabolites was by HPLC. Data are the mean $\pm$ SD from three experiments.

Metabolism of diazepam by enterocytes and hepatocytes

Cultured porcine enterocytes were unable to metabolize diazepam during a 24-h experiment and its metabolism could not be induced in enterocyte cultures by either phenobarbital or dexamethasone treatment (data not shown). In contrast, porcine hepatocyte cultures metabolized diazepam extensively to temazepam, desmethyldiazepam and oxazepam, which are well known and clinically important metabolites of diazepam. The time-course of diazepam metabolism by porcine hepatocyte cultures is shown in figure 8. Following 24 h of incubation the total amount of diazepam was completely metabolized.

Temazepam was by far the most rapidly generated metabolite. As shown in figure 9, the concentration of temazepam reached a maximum after 2 h of incubation and declined thereafter. The decrease in the temazepam concentration might be the result of additional metabolism, perhaps the formation of glucuronic acid conjugates. Phase II metabolites, however, could not be detected with the HPLC method used and validated in this study. Desmethyldiazepam formation by porcine hepatocytes was slower than temazepam formation and the desmethyldiazepam concentration was highest following 8 h of incubation (figure 9).

Typical HPLC-chromatograms showing baseline separation of the major metabolites of diazepam is given in figure 10a and b.

Diazepam metabolism by insect cell microsomes expressing human CYP enzymes

Insect cell microsomes expressing human CYP monooxygenases were used to establish the relative contribution of individual isozymes toward the metabolism of diazepam. These findings are then compared with those from porcine hepatocytes and enterocytes and with the findings reported by other investigators.

At a substrate concentration of 100 μM, hydroxylation of diazepam was the preferred metabolic pathway. Members of the CYP3A family exclusively generated

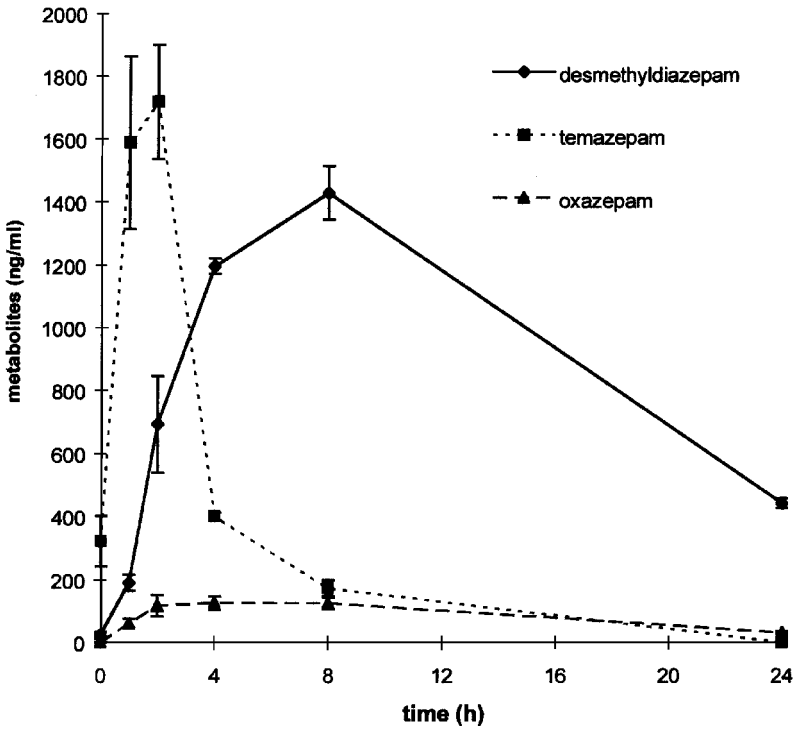


Figure 9. Metabolism of diazepam in hepatocyte cultures with respect to time. Diazepam (35 μM) was added to the cell culture medium. Determination of diazepam and metabolites was by HPLC. Data are the mean $\pm$ SD from three experiments.

Temazepam with highest activities in the preparations containing additionally cytochrome b_5 to CYP3A4 (table 3). Small amounts of desmethyldiazepam were detected in all microsomal preparations. Considerable amounts of desmethyldiazepam were produced by CYP3A4 only with the addition of cytochrome b_5. Oxazepam was exclusively generated by CYP3A4 containing cytochrome b_5.

Protein expression of cytochrome P450

Porcine enterocytes—CYP1A protein expression. The expression of the CYP1A and the CYP3A protein was studied by Western blotting as detailed in the Material and methods. Considering the CYP1A protein expression (figure 11, A), high levels were expressed in enterocytes immediately after isolation but only small amounts of the immunoreactive protein were seen in controls 24 h post-isolation. Thereafter the expression of this protein was below the limit of detection. When the cultures were treated with 30 μM Aroclor 1254, 50 μM β-NF, 2 mM phenobarbital or 50 μM dexamethasone, the following results were obtained. With Aroclor 1254, a substantial induction of the CYP1A protein was seen 48 h post-treatment and this induction declined thereafter (see 72 h value). No induction of this protein was seen in the 24 h treatment group. The pattern of induction of the CYP1A protein following treatment of enterocytes with β-NF was similar to that seen with Aroclor 1254 with maximum expression of the protein 48 h post-treatment. The enhanced expression declined thereafter and was highly significantly reduced following 72 h of

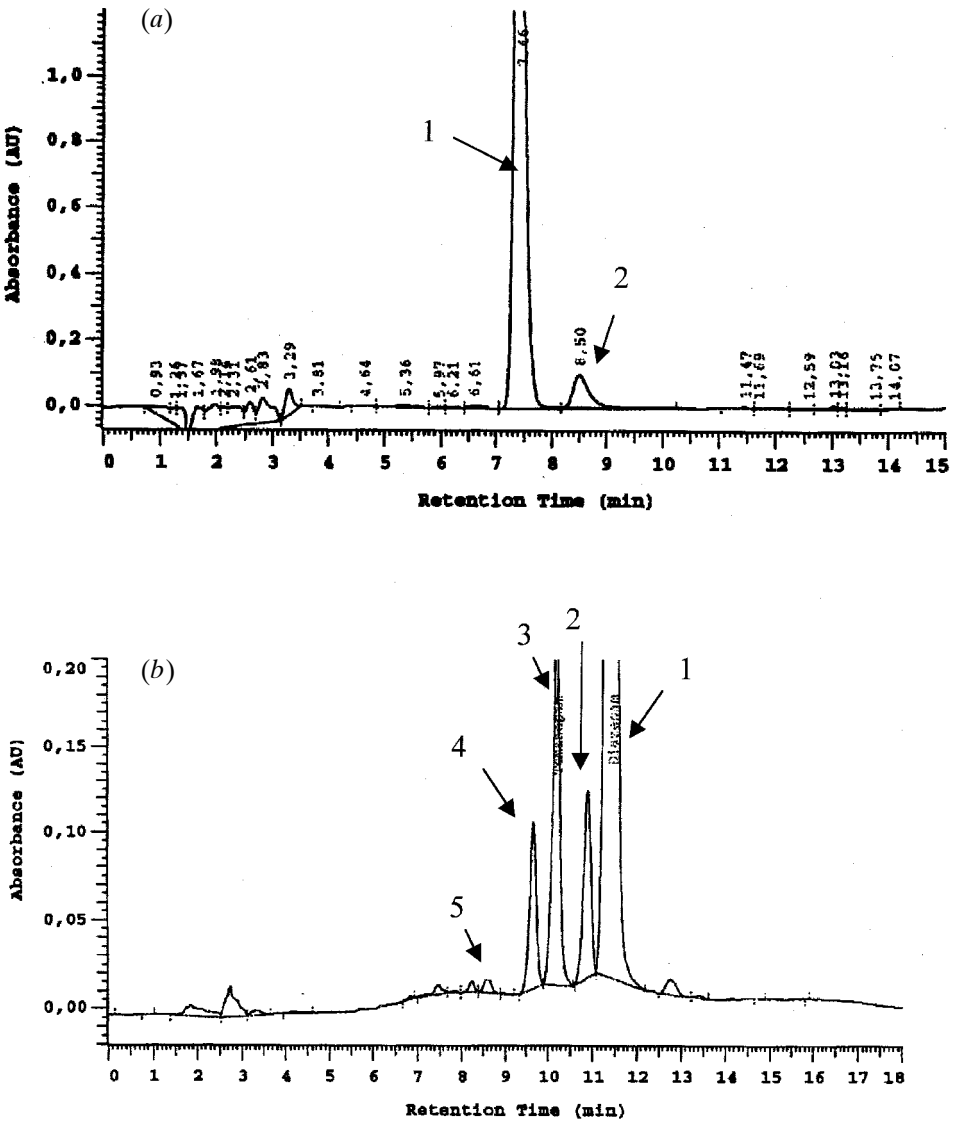


Figure 10. Metabolism of diazepam by porcine enterocyte cultures (a) and porcine hepatocyte cultures (b). Diazepam and its metabolites were quantified by HPLC after incubation of cell cultures with 35 μM diazepam for 2 h. 1, Diazepam; 2, midazolam (internal standard); 3, temazepam; 4, desmethyldiazepam; 5, oxazepam.

treatment. In contrast to Aroclor 1254, dosing of enterocyte cultures with β-NF resulted in increased expression of the CYP1A protein 24 h post-treatment. It is noteworthy that treatment of enterocyte cultures with dexamethasone and phenobarbital also resulted in small increases in the expression of the CYP1A protein but the effect was not seen in the 72-h phenobarbital treatment group.

Porcine enterocytes—CYP3A protein expression. The expression of the CYP3A protein was studied in enterocyte cultures in controls and in the presence of 50 μM dexamethasone, 2 mM phenobarbital, 30 μM Aroclor 1254 and 50 μM β-NF. Results

Table 3. Diazepam metabolism with insect cell microsomes expressing human CYP enzymes.

Human CYP isoform	Temazepam	Desmethyldiazepam	Oxazepam
2C8	n.d.	36.3± 10.3	n.d.
2C9 ARG	n.d.	31.7± 10.9	n.d.
2C9 CYS	n.d.	36.0± 2.8	n.d.
2C19	10.3± 1.3	48.3± 13.6	n.d.
3A4	275.7± 24.7	30.0± 0.8	n.d.
$3A4_{b5}$	4376.3± 1156.8	431.0± 105.0	106.3± 38.4
3A5	432.3± 58.4	9.0± 0.8	n.d.
Control	n.d.	n.d.	n.d.

Microsomes were incubated with 100 μM diazepam, as detailed in the Materials and methods. Diazepam and metabolites were analysed by HPLC. The amounts of metabolites (temazepam, desmethyldiazepam, oxazepam) are ng/ml. Data are the mean± SD of three experiments.

n.d., Not detected.

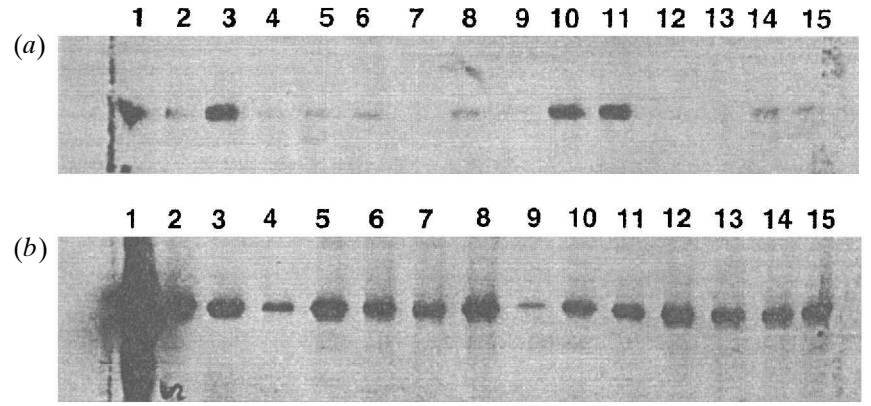


Figure 11. Western blotting of porcine enterocyte microsomes. Microsomes (10 μg total protein) were prepared from porcine enterocyte cultures (as detailed in the Material and methods) and subjected to Western blot analysis. Blots were probed with polyclonal antibodies raised against CYP1A1 (A) and recombinant CYP3A4 (B) and then developed by ECL. Lanes 1, RB marker; 2, standard; 3, control (0 h); 4, control (24 h); 5, 50 μM dexamethasone treated (24 h); 6, 2 mM phenobarbital treated (24 h); 7, 30 μM Aroclor 1254 treated (24 h); 8, 50 μM β-naphthoflavone treated (24 h); 9, control (48 h); 10, 30 μM Aroclor 1254 treated (48 h); 11, 50 μM β-naphthoflavone treated (48 h); 12, control (72 h); 13, 2 mM phenobarbital treated (72 h); 14, 30 μM Aroclor 1254 treated (72 h); 15, 50 μM β-naphthoflavone treated (72 h).

are shown in figure 11 (B). In the controls, the CYP3A4 protein expression was similar between freshly isolated enterocytes and those cultured for 72 h. The expression appeared to decline during the 24- and the 48-h culture possibly as a result of the cell isolation procedure, which most certainly traumatized the cells, although cell recovery occurred thereafter. When compared with the appropriate control (24-h culture), treatment of enterocytes with dexamethasone, phenobarbital, Aroclor 1254 and β-NF resulted in enhanced expression of the CYP3A protein. β-NF treatment resulted in the largest induction of CYP3A, a somewhat surprising result. A similar effect was seen when 48-h old enterocyte cultures were compared with Aroclor and β-NF treatment groups as these chemicals produced a highly significant induction of this protein. This effect was not seen when enterocyte cultures were compared within the 72 h treatment, where the expression of CYP3A was almost identical among all experimental groups.

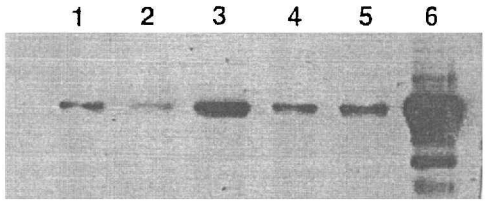


Figure 12. Western blotting of porcine hepatocyte microsomes. Microsomes (5 μg total protein) were prepared from porcine hepatocyte cultures (as detailed in the Material and methods) and subjected to Western blot analysis. Hepatocyte cultures were treated with either 30 μM Aroclor 1254, 2 mM phenobarbital or 50 μM 3-methylcholanthrene for 24 h. Blots were probed with a polyclonal antibody raised against recombinant CYP3A4 and then developed by ECL. Lanes 1, control (0 h); 2, control (24 h); 3, Aroclor 1254 treated; 4, phenobarbital treated; 5, 3-methylcholanthrene treated; 6, standard.

Porcine hepatocytes—CYP3A protein expression. For comparison, the expression of the CYP3A protein was also studied in control cultures and in hepatocyte cultures treated with 30 μM Aroclor 1254, 2 mM phenobarbital and 50 μM 3-MC (figure 12). In the controls, expression of the CYP3A protein was strongest in freshly isolated cells but declined thereafter continuously being below the limit of detection in 72- and 96-h cultures respectively. Treatment of sandwiched porcine hepatocytes with Aroclor 1254, phenobarbital and 3-MC resulted in a highly significant induction of the CYP3A4 protein with Aroclor 1254 producing the greatest induction and phenobarbital and 3-MC being of similar extent. The induction of the CYP3A protein was not seen in hepatocyte cultures following 72 and 96 h of treatment with Aroclor 1254 and phenobarbital and the expression of this protein was close to the limit of detection upon treatment of porcine hepatocytes with 3-MC for 72 and 96 h. It is noteworthy to point out that 3-MC treatment produced a highly significant induction of the CYP3A protein, which points to a complex regulation of the CYP3A gene that appears to be different from its regulation *in vivo*.

Discussion

The aim of the present study was to develop a cell isolation and cultivation protocol for porcine hepatocytes and porcine small intestinal enterocytes for the study of hepatic and intestinal xenobiotransformation. It has been shown that hepatocytes can be maintained in culture for 14 days while retaining their morphological integrity. In contrast, a rapid loss of cellular differentiation and cell viability was observed when enterocytes were cultured for prolonged periods (>24 h).

Small intestinal epithelial cells have *in vivo* a normal life span of ~ 2–6 days. During their life, intestinal epithelial cells migrate from the crypt to the villus tip and undergo differentiation. It is clear that mature primary enterocytes can not be maintained in culture for a prolonged period of time (>4 days). Nevertheless, the results of the present study show that porcine duodenal enterocytes can successfully be used for drug metabolism studies and for enzyme-induction studies during a short-term cultivation. Indeed, the AP activities measured in homogenates of the cultured small intestinal cells and the lack of inhibition by levamisole confirm that cultured cells were in fact mature enterocytes. The identification of immunoreactive cytokeratin 18 protein provided further evidence for cultured cells to be of epithelial

origin, since cytokeratins 8, 18 and 19 are good markers for intestinal epithelial cells (Franke *et al.* 1979). Porcine enterocytes also deethylated the CYP marker substrates ethoxyresorufin and ethoxycoumarin and in the Western blotting experiments the expression of CYP1A and CYP3A protein was confirmed. Therefore, enterocytes express CYP enzymes at the protein and catalytic level following isolation and cultivation in a extracellular matrix-free environment.

In contrast, hepatocytes could be maintained in culture without any sign of deterioration for up to 14 days. The time-course of albumin synthesis (figure 5) agrees well with the recovery of hepatocytes following isolation. Whether the decline in albumin synthesis after 4 days in culture correlates with a decline in CYP activities remains the subject of further investigations.

EROD and ECOD activities measured in hepatocyte cultures were ~ 3.4-fold (EROD) or 20-fold (ECOD) higher respectively than those obtained with enterocyte cultures when compared on the basis of cell number. This difference in enzyme activity most certainly corresponds to the total P450 amount available in the dish, which is considerably higher in the liver than the gut on a weight basis.

Induction and/or inhibition of intestinal CYP enzymes can be of significant pharmacological and toxicological importance in drug therapy and can occur for instance via digestion of dietary constituents that are inducers/inhibitors of CYP enzymes (Bailey *et al.* 1994, Kupferschmidt *et al.* 1998). In the case of enzyme induction–enhanced expression of CYP proteins can occur in the mucosa and as the intestine is the first metabolic site where orally ingested xenobiotics are metabolized an increase in enzyme expression would enhance the intestinal 'first-pass' effect. Similarly, ingestion of inhibitors of intestinal drug-metabolizing enzymes is of significant importance in drug therapy, as reported for some components of grapefruit juice that effectively inhibit CYP3A (Kupferschmidt *et al.* 1998).

In the present study, the potential of 3-MC, β-NF, dexamethasone, Aroclor 1254 and phenobarbital to induce CYP was investigated in enterocyte and in hepatocyte cultures. ECOD activity was increased 12–20- and 3–6-fold following treatment of enterocyte cultures with 3-MC and β-NF respectively, whereas EROD activity remained unchanged. It remains to be determined whether EROD activity was not induced in enterocyte cultures due to the release of some inhibitory factor as CYP1A protein expression was extensively induced in enterocytes. Also the binding of the inducing agent to CYP enzymes can lead to a suppression of catalytic activities. Similar results were obtained with porcine hepatocytes upon treatment with 3-MC as EROD activities were merely increased by 1.5–2-fold.

It was somewhat unexpected, that treatment of enterocyte cultures with phenobarbital and dexamethasone caused an increased expression of the CYP1A protein, as determined by Western blotting experiments. Interestingly, Zaher *et al.* (1998) investigated the induction of CYP1A proteins *in vivo* upon phenobarbital treatment using the Ah-receptor –/– knockout mouse. These authors also report that phenobarbital caused marked CYP1A2 induction in the null mouse at the protein and mRNA level, but CYP1A1 was not affected. The present findings with porcine enterocytes and the results of Zaher *et al.* (1998) provide strong evidence for CYP1A2 to be regulated by a mechanism, which is independent of the Ah-receptor, whereas CYP1A1 appears highly dependent on the nuclear Ah-transcription factor.

Moreover, phenobarbital-induction of P450 enzymes in cell cultures that are specifically induced *in vivo* by 3MC-type inducers has been previously reported. For instance, Althaus *et al.* (1979) provided data that PB induced AHH activity

~ 10-fold in primary cultures of chick embryo hepatocytes and Forster *et al.* (1986) reported that treatment of primary rat hepatocytes with PB caused an 8-fold increase in EROD activity. It is unknown whether the molecular mechanism leading to transcriptional activation of CYP genes differs in isolated and cultured cells as compared with the *in vivo* regulation, although the studies by Zaher *et al.* and the results shown in this study are in good agreement and provide evidence for a complex regulation. Further studies are needed to understand in detail the molecular mechanisms of CYP enzyme induction. The substantial induction of the CYP3A protein in β-NF treated enterocyte cultures and the induction of the CYP3A protein observed in treated hepatocyte cultures are further examples of such events, in view of the fact that β-NF and 3-MC are known ligands of the Ah-receptor (Okey 1990, Whitlock *et al.* 1996) and therefore are expected to primarily induce CYP1A proteins.

Differences at the molecular level in the regulation of enzyme induction in cultured cells and in intact animals have to be investigated further, particularly if cell culture experiments are to be used for the prediction of adverse drug effects *in vivo*.

Diazepam was chosen as an additional marker substrate for CYP enzymes. The major proportion of a given dose (60%) is demethylated, yielding desmethyldiazepam (nordazepam). C_3-hydroxylation of diazepam gives rise to temazepam. Oxazepam can also be formed by either C_3-hydroxylation of desmethyldiazepam or demethylation of temazepam. In a recent study, Ono *et al.* (1996) investigated the metabolism of diazepam using various P450 isoenzymes, which were recombinantly expressed in HepG2 cells with a vaccinia vector system. Ono *et al.* reported that CYP3A4 is responsible for diazepam N-demethylation as well as 3-hydroxylation in the human liver, even though at a high K_m (low substrate specificity). According to Ono *et al.* diazepam N-demethylation in the human liver is also mediated by CYP2C19, which is polymorphically expressed in humans (Goldstein *et al.* 1997). In the study of Jung *et al.* (1997) it was reported that CYP2C19 and CYP3A4 contribute to microsomal diazepam N-demethylation in human liver at low substrate concentrations, whereas CYP3A4 is the major enzyme responsible for 3-hydroxylation. The results of Ono *et al.* (1996) and Jung *et al.* (1997) are comparable in so far as CYP3A4 was identified as the major enzyme responsible for diazepam metabolism in human liver. The results of the present study obtained with the 'supersomes' are also in good agreement with these findings.

Porcine enterocytes did not metabolize diazepam in culture and this result is in good agreement with the good oral bioavailability of diazepam reported for humans ($100 \pm 14\%$). Significant metabolism of diazepam by intestinal cells is therefore unlikely. As shown in this study, porcine hepatocytes effectively metabolized diazepam to the principal metabolites desmethyldiazepam, temazepam and oxazepam and, therefore, porcine hepatocytes will reasonably well predict the metabolism of diazepam as was shown with the supersomes, which contain individual human P450 isozymes.

It is now established, that hepatic metabolism of drugs can be reasonably well predicted from *in vitro* data (Houston 1994) but pharmacokinetic models, which have been developed for the evaluation of hepatic extraction, are not suitable for the prediction of intestinal metabolism. For instance, Hebert *et al.* (1992) investigated the influence of the macrolid antibiotic rifampicin on the bioavailability of cyclosporine and compared the experimentally generated results with the change in bioavailability, which would have been predicted by computation with a pharmaco-

kinetic model. The decrease in cyclosporine bioavailability was greatly underestimated using the measured plasma cyclosporine clearance and an estimated hepatic blood flow. Hebert *et al*. proposed that induction of intestinal CYP enzymes by rifampicin was more pronounced than hepatic enzyme induction and thus the model was insufficient to predict the correct pharmacokinetics observed *in vivo*.

The effects of intestinal enzyme induction on the bioavailability of orally ingested compounds can be marked. This is often referred to as 'intestinal extraction' (as opposed to hepatic extraction) and changes in pharmaceutical formulations such as slow release preparations and drug targeting to specific sites in the gut may alleviate the negative effects of drug oxidation, which often leads to pharmacological inactivation. An improved pharmacokinetic behaviour of drugs is the key to a better pharmacotherapy and patient compliance.

Acknowledgements

The authors are grateful to Professor C. R. Wolf, University of Dundee, Ninewells Hospital and Medical School, Biomedical Research Centre, for carrying out the Western blot experiments.

References

Adams, J. C. and Watt, F. M., 1993, Regulation of development and differentiation by the extracellular matrix. *Development*, **117**, 1183–1198.

Althaus, F. R., Sinclair, J. F., Sinclair, P. and Meyers, U. A., 1979, Drug-mediated induction of cytochromes P-450 and drug metabolism in cultured hepatocytes maintained in chemically defined medium. *Journal of Biological Chemistry*, **254**, 2148–2153.

Bailey, D. G., Arnold, J. M. and Spence, J. D., 1994, Grapefruit juice and drugs. How significant is the interaction? *Clinical Pharmacokinetics*, **26**, 91–98.

Borlak, J. T., Scott, A., Henderson, C. J., Jenke, H. J. and Wolf, C. R., 1996, Transfer of PCB's via lactation simultaneously induces the expression of P450 isoenzymes and the protooncogenes c-Ha-ras and c-raf in neonates. *Biochemical Pharmacology*, **51**, 517–529.

Cairne, A. B., Lamerton, L. F. and Steel, G. G., 1965, Cell proliferation studies in the intestinal epithelium of the rat. I: Determination of the kinetic parameters. *Experimental Cell Research*, **39**, 528–538.

Caldwell, J., 1992, Problems and opportunities in toxicity testing arising from species differences in xenobiotic metabolism. *Toxicology Letters*, **64/65**, 651–659.

Dunn, J. C., Tompkins, R. G. and Yarmush, M. L., 1992, Hepatocytes in collagen sandwich: evidence for transcriptional and translational regulation. *Journal of Cell Biology*, **116**, 1043–1053.

Elsdale, T. and Bard, J., 1972, Collagen substrata for studies on cell behavior. *Journal of Cell Biology*, **54**, 626–637.

Evans, G. S., Flint, N., Somers, A. S., Eyden, B. and Potten, C. S., 1992, The development of a method for the preparation of rat intestinal epithelial cell primary cultures. *Journal of Cell Science*, **101**, 219–231.

Fitzsimmons, M. E. and Collins, J. M. 1997, Selective biotransformation of the human immunodeficiency virus protease inhibitor saquinavir by human small-intestinal cytochrome P4503A4: potential contribution to high first-pass metabolism. *Drug Metabolism and Disposition*, **25**, 256–266.

Forster, U., Luippold, G. and Schwarz, L. R., 1986, Induction of monooxygenase and UDP-glucuronosyltransferase activities in primary cultures of rat hepatocytes. *Drug Metabolism and Disposition*, **14**, 353–360.

Franke, W. W., Appelhans, B., Schmid, E., Freudenstein, C., Osborn, M. and Weber, K., 1979, The organization of cytokeratin filaments in the intestinal epithelium. *European Journal of Cell Biology*, **19**, 255–268.

Gan, L. S., Moseley, M. A., Khosla, B., Augustijns, P. F., Bradshaw, T. P., Hendren, R. W. and Thakker, D. R., 1996, CYP3A-like cytochrome P450-mediated metabolism and polarized efflux of cyclosporin A in Caco-2 cells. *Drug Metabolism and Disposition*, **24**, 344–349.

Gibson, P. R., van de Pol, E., Maxwell, L. E., Gabriel, A. and Doe, W. F., 1989, Isolation of colonic crypts that maintain structural and metabolic viability *in vitro*. *Gastroenterology*, **96**, 283–291.

Goldstein , J. A., Ishizaki , T., Chiba , K., de Morais , S. M., Bell , D., Krahn , P. M. and Evans , D. A., 1997, Frequencies of the defective CYP2C19 alleles responsible for the mephenytoin poor metabolizer phenotype in various Oriental, Caucasian, Saudi Arabian and American black populations. *Pharmacogenetics*, **7**, 59–64.

Gordon , J. I., 1989, Intestinal epithelial differentiation: new insights from chimeric and transgenic mice. *Journal of Cell Biology*, **108**, 1187–1194.

Guengerich , F., 1982, Microsomal enzymes involved in toxicology—analysis and separation. In A. Hayes (ed.), *Principles and Methods of Toxicology* (New York: Raven), pp. 609–637.

Hahn , U., Stallmach , A. and Riecken , E. O., 1990, Basement membrane components are potent promotors of rat intestinal epithelial cell differentiation *in vitro*. *Gastroenterology*, **98**, 322–335.

Hahn , U., Cho , A., Schuppan , D., Hahn , E. G., Merker , H. J. and Riecken , E. O., 1987, Intestinal epithelial cells preferentially attach to a biomatrix derived from human intestinal mucosa. *Gut*, **28 (S1)**, 153–158.

Hebert , M. F., Roberts , J. P., Prueksaritanont , T. and Benet , L. Z., 1992, Bioavailability of cyclosporine with concomitant rifampin administration is markedly less than predicted by hepatic enzyme induction. *Clinical Pharmacology and Therapeutics*, **52**, 453–437.

Houston , J. B., 1994, Utility of *in vitro* drug metabolism data in predicting *in vivo* metabolic clearance. *Biochemical Pharmacology*, **47**, 1469–1479.

Humphrey , M. J. and Smith , D. A., 1992, Role of metabolism and pharmacokinetic studies in the discovery of new drugs—present and future perspectives. *Xenobiotica*, **22**, 743–755.

Jung , F., Richardson , T. H., Raucy , J. L. and Johnson , E. F., 1997, Diazepam metabolism by cDNA-expressed human 2C P450: identification of P4502C18 and P4502C19 as low K_m diazepam N-demethylases. *Drug Metabolism and Disposition*, **25**, 133–139.

Kaminsky , L. S. and Fasco, M. J., 1991, Small intestinal cytochromes P450. *Critical Reviews in Toxicology*, **21**, 407–422.

Kern , A., Bader, A., Pichlmayr , R. and Sewing , K. F., 1997, Drug metabolism in hepatocyte sandwich cultures of rats and humans. *Biochemical Pharmacology*, **54**, 761–772.

Kivist Ö, K. T., Bookjans , G., Fromm , M. F., Griese , E. U., Munzel , P. and Kroemer , H. K., 1996, Expression of CYP3A4, CYP3A5 and CYP3A7 in human duodenal tissue. *British Journal of Clinical Pharmacology*, **42**, 387–389.

Kolars, J. C., Awni , W. M., Merion , R. M. and Watkins , P. B., 1991, First pass metabolism of cyclosporine by the gut. *Lancet*, **338**, 1488–1490.

Kolars, J. C., Lown , K. S., Schmiedlin -Ren , P., Ghosh , M., Fang , C., Wrighton , S. A., Merion , R. M. and Watkins , P. B., 1994, CYP3A gene expression in human gut epithelium. *Pharmacogenetics*, **4**, 247–259.

Krishna , D. R. and Klotz , U., 1994, Extrahepatic metabolism of drugs in humans. *Clinical Pharmacokineticsics*, **26**, 144–160.

Kupferschmidt , H. H., Fattinger , K. E., Ha, H. R., Follath , F. and Krahenbuhl , S., 1998, Grapefruit juice enhances the bioavailability of the HIV protease inhibitor saquinavir in man. *British Journal of Clinical Pharmacology*, **45**, 355–359.

Lampen , A., Christians , U., Gonschior , A. K., Bader, A., Hackbarth , I., von Engelhardt , W. and Sewing , K. F., 1996, Metabolism of the macrolide immunosuppressant, tacrolimus, by the pig gut mucosa in the Ussing chamber. *British Journal of Pharmacology*, **117**, 1730–1734.

Levy , R., Czernobilsky , B. and Geiger , B., 1988, Subtyping of epithelial cells of normal and metaplastic human uterine cervix, using polypeptide-specific cytokeratin antibodies. *Differentiation*, **39**, 185–196.

Lipkin , M., 1973, Proliferation and differentiation of gastrointestinal cells. *Physiology Reviews*, **53**, 891–915.

McKinnon , R. A., Burgess , W. M., Hall , P. M., Roberts -Thomson , S. J., Gonzalez , F. J. and McManus , M. E., 1995, Characterisation of CYP3A gene subfamily expression in human gastrointestinal tissues. *Gut*, **36**, 259–267.

Nims , R. W., Prough ,R. A. and Lubet , R. A., 1984, Cytosol-mediated reduction of resorufin : a method for measuring quinone oxidoreductase. *Archives in Biochemistry and Biophysics*, **229**, 459–465.

Okey , A. B., 1990, Enzyme induction in the cytochrome P450 system. *Pharmacology and Therapeutics*, **45**, 241–298.

Olsen , A. K., Hansen , K. T. and Friis , C., 1997, Pig hepatocytes as an *in vitro* model to study the regulation of human CYP3A4—prediction of drug–drug interactions with 17-alpha-ethynyl-estradiol. *Chemico-Biological Interactions*, **107**, 93–108.

Ono, S., Hatanaka , T., Miyazawa , S., Tsutsui , M., Aoyama , T., Gonzalez , F. J. and Satoh , T., 1996, Human liver microsomal diazepam metabolism using cDNA-expressed cytochrome P450: role of CYP2B6, 2C19 and the 3A subfamily. *Xenobiotica*, **26**, 1155–1166.

Parkinson , A., 1996, An overview of current cytochrome P450 technology for assessing the safety and efficacy of new materials. *Toxicology and Pathology*, **24**, 45–57.

Perreault , N. and Beaulieu , J. F., 1998, Primary cultures of fully differentiated and pure human intestinal epithelial cells. *Experimental Cell Research*, **25**, 34–42.

Rodrigues, A. D., 1994, Use of *in vitro* human metabolism studies in drug development. *Biochemical Pharmacology*, **48**, 2147–2156.

Skaanild, M. T. and Friis, C., 1998, Characterisation of the P450 system in Göttingen minipigs. *Scandinavian Journal of Laboratory Animal Science, Suppl*. 1., **25**, 171.

Smith, P. K., Krohn, R. I., Hermanson, G. T., Mallia, A. K., Gartner, F. H., Provenzano, M. D., Fujimoto, E. K., Goeke, N. M., Olson, B. J. and Klenk, D. C., 1985, Measurement of protein using bicinchoninic acid. *Annals in Biochemistry*, **150**, 76–85.

SoRelle, R, 1998, Withdrawal of Posicor from market. *Circulation*, **1**, 831–832.

StrÄter, J., Wedding, U., Barth, T. F., Koretz, K., Elsing, C. and Moller, P., 1996, Rapid onset of apoptosis *in vitro* follows disruption of beta 1-integrin/matrix interactions in human colonic crypt cells. *Gastroenterology*, **110**, 1776–1784.

Suzuki, K., Yoshimura, Y., Hisada, Y. and Matsumoto, A., 1994, Sensitivity of intestinal alkaline phosphatase to L-homoarginine and its regulation by subunit–subunit interaction. *Japanese Journal of Pharmacology*, **64**, 97–102.

Thummel, K. E., Paine, M. F., Shen, D. D., Kunze, K. L., Perkins, J. D. and Wilkinson, G. R., 1996, Oral first-pass elimination of midazolam involves both gastrointestinal and hepatic CYP3A-mediated metabolism. *Clinical Pharmacology and Therapeutics*, **59**, 491–502.

Tucker, G. T., 1992, The rational selection of drug interaction studies: Implication of recent advances in drug metabolism. *International Journal of Clinical Pharmacology and Therapeutic Toxicology*, **30**, 550–553.

Whitlock, J. P., Jr., OKINO, S. T., Dong, L., Ko, H. P., Clarke-Katzenberg, R., Ma, Q. and Li, H., 1996, Cytochromes P450 5: Induction of cytochrome P450 1A1: a model for analyzing mammalian gene transcription. *FASEB Journal*, **10**, 809–818.

Witkamp, R. and Monshouwer, M., 1998, Pharmakokinetics *in vivo* and *in vitro* in swine. *Scandinavian Journal of Laboratory Animal Science Suppl*. 1, **25**, 45–56.

Wrighton, S. A., Ring, B. J. and Vanden Branden, M., 1995, The use of *in vitro* metabolism techniques in the planning and interpretation of drug safety studies. *Toxicology and Pathology*, **23**, 199–208.

Wu, C. Y., Benet, L. Z., Hebert, M. F., Gupta, S. K., Rowland, M., Gomez, D. Y. and Wacher, V. J., 1995, Differentiation of absorption and first-pass gut and hepatic metabolism in humans: studies with cyclosporine. *Clinical Pharmacology and Therapeutics*, **58**, 492–497.

Zaher, H., Yang, T. J., Gelboin, H. V., Fernandez-Salguero, P. and Gonzalez, F. J., 1998, Effect of phenobarbital on hepatic CYP1A1 and CYP1A2 in the Ahr-null mouse. *Biochemical Pharmacology*, **55**, 235–238.

XENOBIOTICA , 2000, VOL. 30, NO. 1, 47–59

Interspecies comparison and role of human cytochrome P450 and flavin-containing monooxygenase in hepatic metabolism of L-775,606, a potent 5-HT_{1D} receptor agonist

T. PRUEKSARITANONT†*, P. LU†, L. GORHAM†, F. STERNFELD‡ and K. P. VYAS†

† Department of Drug Metabolism, Merck Research Laboratories, West Point, PA 19486, USA

‡ Neuroscience Research Center, Merck Research Laboratories, Terlings Park, Essex, UK

Received 28 April 1999

1. Quantitative species differences and human liver enzymes involved in the metabolism of L-775,606, a potent and selective 5-HT_{1D} receptor agonist developed for the acute treatment of migraine headache, have been investigated *in vitro*.

2. In human, monkey, dog and rat liver microsomes, formation of the hydroxylated M1 and the *N*-dealkylated M2 was mediated by enzyme(s) of high-affinity (apparent $K_m \sim 1$–6 μM), and that of the two *N*-oxide isomers (M3) was catalysed by those of low affinity (apparent $K_m \sim 50$–110 μM). In dog, M3 constituted a major pathway ($\sim 40\%$), whereas in all other species it was a minor metabolite ($< 5\%$).

3. In human liver microsomes, a marked inhibition ($\geqslant 80\%$) of M1 and M2 formation was observed by SKF525-A, troleandomycin, ketoconazole and anti-CYP3A antibodies, whereas the inhibition was modest (~ 20–40%) with quercetin. Of seven cDNA-expressed human P450 tested, only CYP3A4 and CYP2C8 were capable of oxidizing L-775,606, resulting primarily in M1 and M2. However, CYP3A4 possessed much higher affinity ($\geqslant$ 20-fold) and much higher intrinsic activity ($>$100-fold) than CYP2C8.

4. In contrast, *N*-oxidation was not inhibited by any inhibitors of P450 tested, but rather was reduced significantly by heat treatment and methimazole, and was increased substantially with an incubation pH >7.4. Human flavin-containing monooxygenase form 3 (FMO3) catalysed exclusively the *N*-oxidation to M3, with apparent K_m and optimum pH comparable with those observed in human liver microsomes.

5. These results demonstrated quantitative interspecies differences in the metabolism of L-775,606. In human, metabolism of L-775,606 to the principal metabolites, M1 and M2, was mediated primarily by CYP3A4 with minimal contribution from CYP2C8, whereas the minor *N*-oxidative pathway was catalysed mainly by FMO3.

Introduction

The serotonin 5-$HT_{1D/1B}$ receptor agonists, collectively referred as triptans, have been used or tested in clinical trials for the acute treatment of migraine headache (Plosker and McTavish 1994, Hamel 1996). Potential coronary vasoconstrictive side-effects common to these compounds are believed to mediate through the 5-HT_{1B} receptor, precluding their use in patients with known coronary heart diseases. In an attempt to overcome this undesirable effect, several selective 5-HT_{1D} agonists have been developed (MacLeod *et al.* 1997). Among them, L-775,606, 3-(3-{4-[2-(3-fluorophenyl)ethyl]piperazin-1-yl}propyl)-5-[1,2,4]triazol-4-yl-1H-indole

* Author for correspondence; e-mail: thomayant-prueksaritanont@merck.com

Xenobiotica ISSN 0049–8254 print/ISSN 1366–5928 online © 2000 Taylor & Francis Ltd
http://www.tandf.co.uk/journals/tf/00498254.html

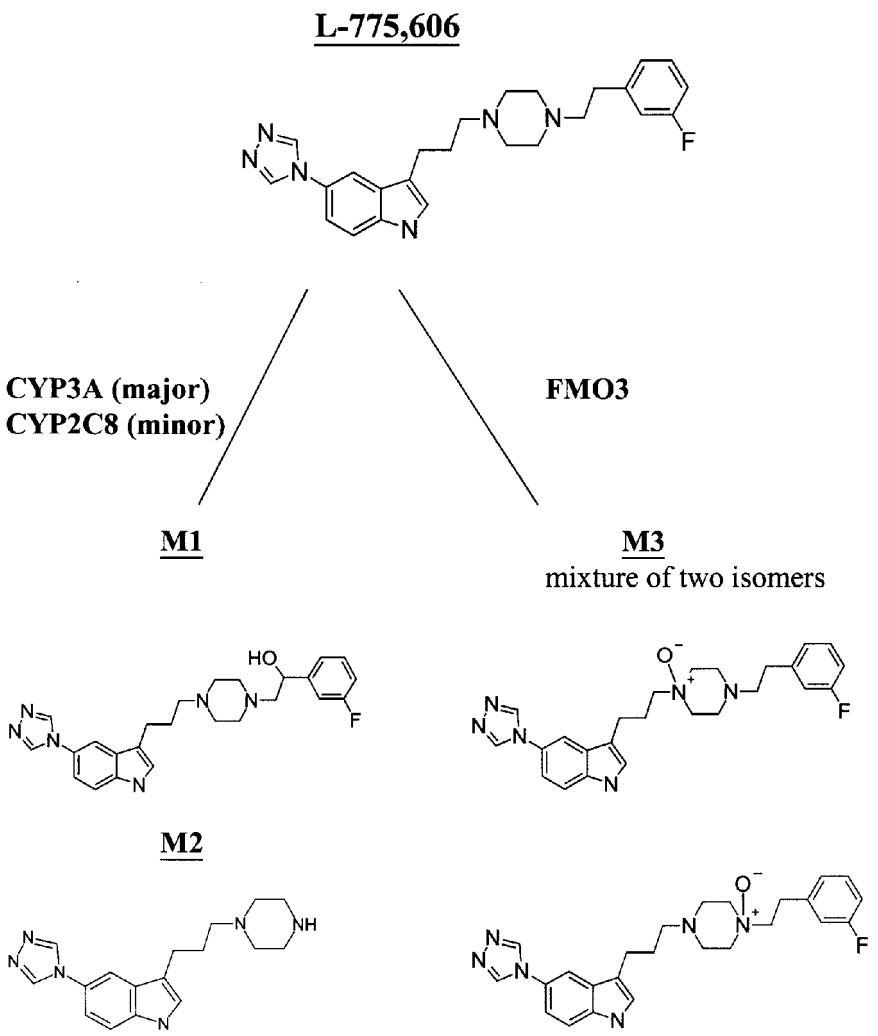


Figure 1. Structures of L-775,606 and its metabolites.

(figure 1), exhibited reasonable oral bioavailability in animal species and thus was selected for further development (MacLeod *et al*. 1997). Early studies (Neuroscience Research Centre, Merck Research Laboratories, Terlings Park, UK) suggested that L-775,606 underwent extensive metabolism and several oxidative metabolites have been identified (figure 1) from *in vitro* incubations with animal and human liver preparations (A. Watt, manuscript in preparation). Qualitatively, the metabolites of L-775,606 were similar across the species studied. To understand better species differences and similarities in the disposition of L-775,606, quantitative metabolism studies were later undertaken in rat, dog monkey and human liver microsomes. Additionally, since knowledge of drug-metabolizing enzymes is crucial in the prediction of drug–drug interactions, specific human liver monooxygenases involved in these biotransformations were also identified. In the current study, the potential involvement of cytochrome P450 (P450) and flavin-containing monooxygenase (FMO), the two major enzyme systems known for oxidative metabolism of

xenobiotics, have been investigated using combination of several different strategies, namely (1) metabolism by cDNA-expressed P450 and FMO isoforms, (2) chemical inhibition, (3) immuno-inhibition, (4) correlation analysis and (5) pH-dependent metabolism.

Materials and methods

Materials

L-775,606, M1, M2 and a mixture of M3 (figure 1) were synthesized at Merck Research Laboratories, Neuroscience Research Centre, Terlings Park (UK). Their identity was confirmed by NMR, and the purity, judged by thin-layer chromatography and HPLC was >98.5%. Markers and chemical inhibitors of the cytochrome P450 family of enzymes were from Sigma Chemical Co. (St Louis, MO, USA) (coumarin, 7′-hydroxycoumarin, phenacetin, testosterone, tolbutamide, troleandomycin (TAO), quercetin, quinidine, 8-methoxsalen, tranylcypromine and methimazole), Steraloids (Wilton, NH, USA) (6β-hydroxytestosterone), Research Biochemical International (Natick, MA, USA) (SKF-525A), Ultrafine (UK) (*S*-mephenytoin, 4′-hydroxymephenytoin, 3-methylhydroxytolbutamide, 1′-hydroxybufuralol and sulphaphenazole), and Hoffman–La Roche, Inc. (Nutley, NJ, USA) ((+)-bufuralol). Furafylline (>98% purity) was synthesized at Merck Research Laboratories (Rahway, NJ, USA).

Polyclonal antibodies raised against rat CYP3A1 known to cross react with human CYP3A were from Xenotech (Kansas City, KS, USA). The antibodies are specific to CYP3A and do not cross-react with CYP2D6 and CYP2C or 1A subfamilies. Microsomal preparations of cDNA expressed human FMO3 and P450 isoforms with (CYP3A4, CYP2C8, CYP2C9 and CYP2C19 supersomes™) or without co-expressed oxidoreductase (CYP1A2, CYP2A6 and CYP2D6 microsomes) were from Gentest (Woburn, MA, USA). All other reagents were of analytical or HPLC grade. Human liver microsomes were prepared from 11 individual subjects (Keystone Skin Bank, Exton, PA and University of New Mexico, Albuquerque, NM, USA), while those from the male Sprague–Dawley rat (~260–310 g), beagle dog (9–11 kg) and rhesus monkey (4–6 kg) were pooled from three to five animals.

In vitro *metabolism of L-775,606*

A typical incubation mixture, in a final volume of 0.1 ml, contained 0.1 mg (human, dog and monkey) or 0.05 mg (rat) liver microsomal protein, 10 μmol sodium phosphate buffer (pH 7.4), 1 μmol $MgCl_2$ and 0.1 μmol NADPH. Unless otherwise specified, the reaction was started by the addition of L-775,606 following a 3-min pre-incubation at 37 °C, and the reaction was terminated after 10-min incubation by the addition of 0.15 ml methanol. The resulting mixture was centrifuged and the supernatant was injected directly onto HPLC (see below). A preliminary experiment showed that the rates of formation of all metabolites were linear during the 10-min incubation.

Kinetic studies were conducted using 0.2–200 μM L-775,606 in liver microsomal preparations from human, rat, dog and monkey. All other experiments described below were performed using human liver microsomes. Experiments with known chemical inhibitors of P450 and FMO were performed at a substrate concentration of 20 μM and inhibitor concentrations of 10 μM quinidine or 8-methoxsalen, 25 μM sulphaphenazole, 50 μM furafylline, TAO or tranylcypromine, 200 μM methimazole, or 500 μM SKF-525A. At these concentrations, quinidine, furafylline, sulphaphenazole and TAO have been demonstrated specifically to abolish activities for CYP2D6, CYP1A2, CYP2C9 and CYP3A respectively (Chang *et al*. 1994, Newton *et al*. 1995). 8-Methoxsalen is a potent inhibitor of 2A6 (Draper *et al*. 1997), and tranylcypromine has been shown to strongly inhibit both CYP2A6 and CYP2C19 (Wienkers *et al*. 1996, Draper *et al*. 1997). Quercetin, at the concentration used, greatly inhibited CYP2C8, and slightly inhibited CYP3A activities (Minisalco *et al*. 1992, Rahman *et al*. 1994). In experiments with furafylline and TAO, the inhibitors were pre-incubated with liver microsomes and NADPH for 30 min at 37 °C before adding the substrate. All other inhibitors were co-incubated with the substrate. In the heat inactivation experiment, the microsomal mixture minus NADPH was incubated at 45 °C for 10 min before adding NADPH to start the reaction. For immuno-inhibition studies, microsomes were first incubated at room temperature for 20 min with the antibodies or control sera, and the reaction then was carried out as described above.

Incubations with human recombinant P450/FMO3 were performed using the same conditions as described herein for human liver microsomes, except that the mixture contained 20 pmol P450 (CYP3A4, CYP2C8, CYP2C9 and CYP2C19) or 50–100 pmol P450 (CYP2A6, CYP2D6, and CYP1A2), or 50 μg FMO3 and was incubated for up to 40 min. Control incubations using microsomes isolated from the same cell line, containing the vector but without a cDNA insert, also were included. Kinetic studies of L-775,606 metabolism by CYP3A4, CYP2C8 and FMO3 also were conducted using 10 pmol CYP3A4, 20 pmol CYP2C8 or 0.05 mg FMO3/incubation, 0.2–200 μM L-775,606 and 5-min (CYP3A4) or 10-min (CYP2C8 and FMO3) incubation.

Assays for enzyme activities

Assays described previously for CYP3A (testosterone 6β-hydroxylation), CYP2D6 (bufuralol 1′-hydroxylation), CYP2C9 (tolbutamide 3-methylhydroxylation), CYP2C19 (mephenytoin 4′-hydroxylation) and CYP1A2 (phenacetin *O*-deethylation) activities (Newton *et al.* 1995, Prueksaritanont *et al.* 1997) were used for the present studies.

Analytical procedures for L-775,606 and its metabolites

An HPLC method was used for the simultaneous determination of L-775,606 and its metabolites. The HPLC system consisted of a Waters 600E multisolvent delivery system, a Waters 717 plus autosampler and a Hewlett Packard 1046A fluorescence detector. The samples were chromatographed on a C8-Zorbax Rx column (250 4.6 mm, 5 μm), preceded by a C8 guard column, with a linear gradient of acetonitrile and 0.02 M phosphate buffer, pH 2.5 (10% acetonitrile to 22% acetonitrile in 3 min and increased to 28% at 14 min and held at 28% for 4 min). The effluent was monitored at λ_{ex} and λ_{em} of 240 and 380 nm respectively. For all metabolites, the limits of assay detection were 1 ng (on column).

Data analysis

Apparent K_m and V_{max} were estimated using a non-linear regression program (Enfit, Biosoft, Ferguson, MO, USA). The intrinsic clearance (Cl_{int}) was estimated by dividing V_{max} by K_m.

Results

Metabolism of L-775,606 in liver microsomes from human and animals

Figure 2A and B illustrates L-775,606 metabolite profiles in human and dog liver microsomal incubates respectively. Similar profiles were also obtained in rat and monkey liver microsomes (data not shown). In all species, the hydroxylated M1, the *N*-dealkylated product M2 and the *N*-oxide isomers (M3) were detected and confirmed by liquid chromatography-tandem mass spectrometry (LC-MS) analysis of the incubation mixtures, in comparison with metabolite standards (data not shown). All metabolites of L-775,606 were observed only in the presence of both NADPH and microsomal proteins, suggesting possible involvement of either P450 or FMO or both enzyme systems in the oxidative metabolism of this drug. In human, large interindividual variations were observed in the formation of these metabolites (figure 3). However, the metabolic pattern was qualitatively similar in all 11 subjects, with M3 being a minor product (figure 3).

Formation of the NADPH-dependent metabolites of L-775,606 in human, dog, monkey and rat liver microsomes was best described by single-enzyme Michaelis–Menten kinetics over the substrate range studied. In all species, the formation of M1 and M2 was mediated by enzyme(s) with much lower apparent K_m or higher affinity (4–60-fold) than those catalysing the formation of M3 (both isomers). Species differences were observed in the relative contribution of each individual metabolite to overall metabolism (table 1). In human and monkey, the intrinsic clearance, Cl_{int} (V_{max}/K_m), for the formation of M1 accounted for $\sim$ 60% of the total Cl_{int}, followed by that of M2 ($\sim$ 40%) and M3 ($<$ 5%), suggesting that M1 and M2 were major metabolites, and M3 was a minor product in these species. In rat, M1 predominated, accounting for $\sim$ 85%, with M2 ($\sim$ 14%) and M3 ($<$ 5%) constituting minor pathways. In contrast, in dog, M3 contributed primarily ($\sim$ 55%) to the total Cl_{int} of L-775,606, followed by M1 ($\sim$ 30%) and M2 ($\sim$ 15%). Species differences also were observed in the overall metabolism rate of L-775,606; the total Cl_{int} were $\sim$ 6–10-fold higher in rat and monkey than in dog and human (table 1).

Metabolism of L-775,606 by recombinant P450 isoforms and FMO3

Studies on L-775,606 metabolism by human recombinant P450 isoforms indicated that CYP3A4 oxidized L-775,606 efficiently to the primary metabolites

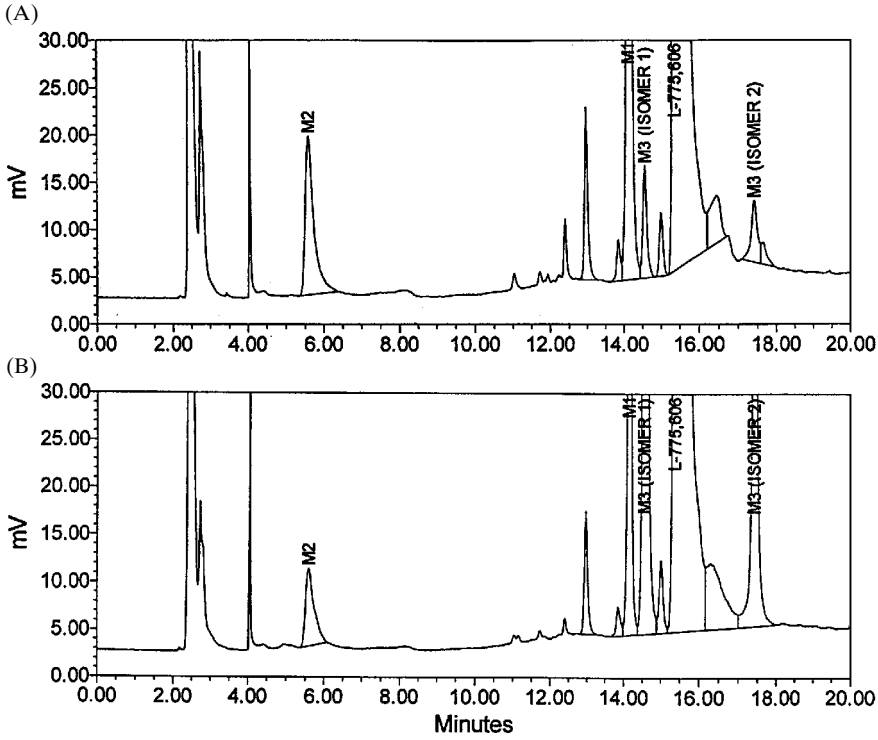


Figure 2. Representative HPLC profiles of L-775,606 metabolites in human (A) and dog (B) liver microsomal incubates. Incubations were carried out at 37 °C for 10 min using liver microsomes (1 mg/ml) and L-775,606 (20 μM) with NADPH (1 mM).

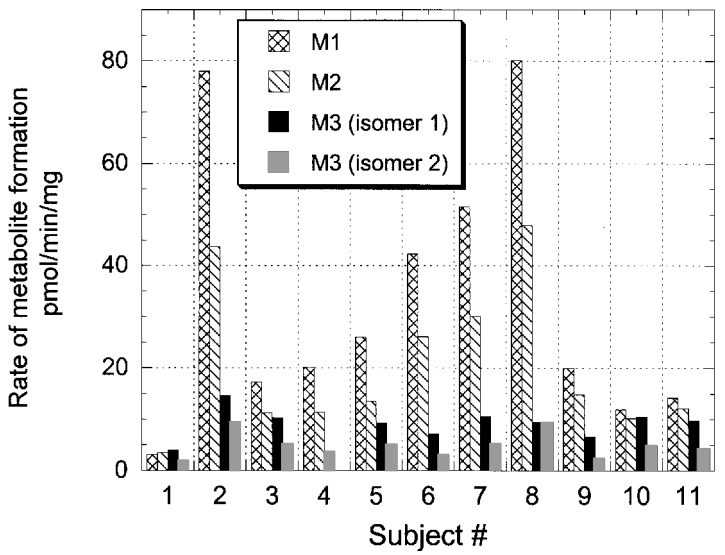


Figure 3. Interindividual variations in the metabolism of L-775,606 by human liver microsomes. Incubations were carried out at 37 °C for 10 min using human liver microsomes (1 mg/ml) and L-775,606 (20 μM) with NADPH (1 mM). Data are the mean of duplicate determinations.

Table 1. Kinetics of L-775,606 metabolism in liver microsomes from human, dog, monkey and rat.

		M1			M2			M3 (isomer 1)			M3 (isomer 2)			Total
Species	*n*	K_m (μM)	V_{max} (pmol/min/mg)	Cl_{int} (ml/min/g)	K_m (μM)	V_{max} (pmol/min/mg)	Cl_{int} (ml/min/g)	K_m (μM)	V_{max} (pmol/min/mg)	Cl_{int} (ml/min/g)	K_m (μM)	V_{max} (pmol/min/mg)	Cl_{int} (ml/min/g)	Cl_{int} (ml/min/g)
Human	11	2.2 ± 0.8	40.2 ± 28	18.2 ± 10.4	2.4 ± 0.8	25.3 ± 16	13.7 ± 12	86 ± 40	70 ± 51	0.64 ± 0.2	60 ± 23	22.9 ± 13	0.33 ± 0.1	32.7 ± 22
Dog	3 (pooled)	5.6	33.8	6.04	13.5	43.6	3.23	55.0	478.6	8.70	52.0	153.5	2.95	20.9
Monkey	3 (pooled)	1.3	167.80	129.1	1.4	104.7	74.8	46.0	55.0	1.20	75.0	68.0	0.91	206.0
Rat	5 (pooled)	4.0	796.2	199.1	6.1	207.3	34.0	114.0	291.0	2.55	n.a.	n.a.	n.a.	235.6

n.a., Not applicable due to low levels.

Table 2. Formation kinetics of L-775,606 metabolites by CYP3A4, CYP2C8 and FMO3.

	M1			M2			M3 (isomer 1)			M3 (isomer 2)		
	K_m (μM)	V_{max} (nmol/min/nmol P450 or mg FMO)	Cl_{int} (ml/min/nmol P450 or mg FMO)	K_m (μM)	V_{max} (nmol/min/nmol P450 or mg FMO)	Cl_{int} (ml/min/nmol P450 or mg FMO)	K_m (μM)	V_{max} (nmol/min/nmol P450 or mg FMO)	Cl_{int} (ml/min/nmol P450 or mg FMO)	K_m (μM)	V_{max} (nmol/min/nmol P450 or mg FMO)	Cl_{int} (ml/min/nmol P450 or mg FMO)
CYP3A4 + reductase + b5	2.3	2.60	1.13	2.4	1.70	0.71		n.a.			n.a.	
CYP3A4 + reductase	2.2	0.48	0.22	2.0	0.35	0.18		n.a.			n.a.	
CYP2C8 + reductase + b5	42	0.62	0.015	64	0.03	0.0005		n.a.			n.a.	
FMO3		n.d.			n.d.		115	729	6.34	118	340	2.88

n.a., Not applicable due to low levels.
n.d., Not detected.
Data are mean of duplicate determinations.

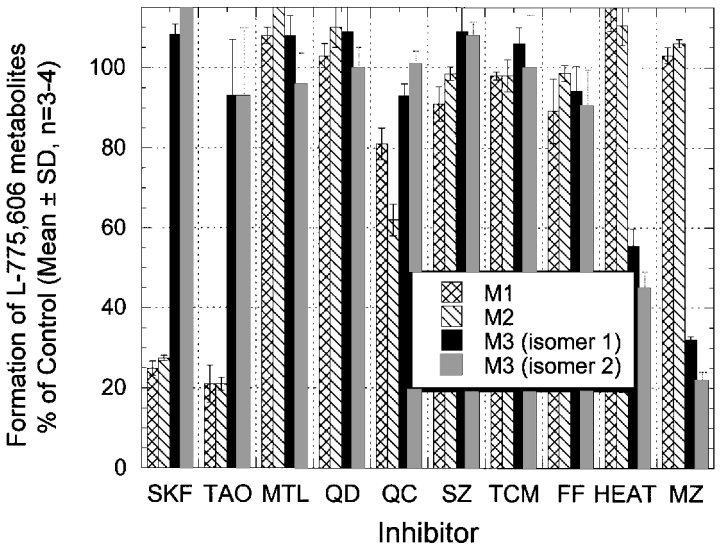


Figure 4. Effects of chemical inhibitors of P450 and FMO on the metabolism of L-775,606 by human liver microsomes. Results (mean ± SD) were based on triplicate or quadruplicate determinations. All incubations were carried out in the absence or presence of inhibitors, as described in the Materials and methods, at 37 °C for 10 min using human liver microsomes (1 mg/ml) and L-775,606 (20 μM) with NADPH (1 mM). Control activities (in the absence of inhibitors) = 50, 24, 8 and 3 pmol/min/mg protein for the formation of M1, M2, M3 (isomer 1) and M3 (isomer 2) respectively. SKF, SKF525-A; TAO, troleandomycin; MTL, 8-methoxsalen; QD, quinidine; QC, quercetin; SZ, sulphaphenazole; TCM, tranylcypromine; FF, furafylline; MZ, methinazole.

M1 and M2, and to a trace amount of the *N*-oxide isomers (M3). Kinetic studies suggested that CYP3A4, either with or without cytochrome b_5, catalysed the formation of M1 and M2 with high-affinity; the apparent K_m were comparable with those observed with human liver microsomes (table 2). In the presence of cytochrome b_5, the capacity (V_{max}) for metabolism of L-775,606 by CYP3A4 was markedly increased. Also, as was observed with human liver microsomes, the Cl_{int} of M1 (~60% of total) was higher than that of M2 (~40% of total) in the incubation with CYP3A4, with or without cytochrome b5 (table 2). CYP2C8 also was capable of oxidizing L-775,606 by all three metabolic pathways, with M1 constituting the primary metabolite (>90% of total). However, CYP2C8 exhibited much lower affinity and capacity, resulting in much lower intrinsic activity (Cl_{int}) than CYP3A4 (table 2). The apparent K_m for the formation of M1 and M2 obtained with CYP2C8 was ~ 18–30-fold higher, while Cl_{int} for CYP2C8 was < 1/100 of that with CYP3A4. All other P450 tested (CYP2D6, CYP2A6, CYP2C9, CYP2C19, CYP1A2) and the control microsomes failed to metabolize L-775,606 to any appreciable extent (data not shown).

Unlike CYP3A4 and CYP2C8, human FMO3, a major FMO isoform in adult human livers (Overby *et al*. 1997), catalysed metabolism of L-775,606 exclusively to M3, with no evidence for the formation of M1 or M2 (data not shown). Kinetic studies showed that FMO3 mediated the *N*-oxidation reaction with K_m = ~120 μM (table 2), being comparable with those observed in human liver microsomal incubations (table 1).

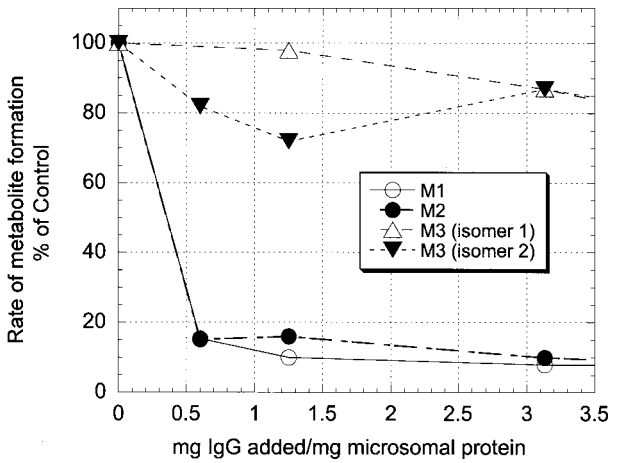


Figure 5. Effects of anti-CYP3A antibodies on the human liver microsomal metabolism of L-775,606. Results were based on duplicate determinations. Human liver microsomes (1 mg/ml), pre-incubated in the absence or presence of IgG, were incubated with L-775,606 (20 μM) and NADPH (1 mM) at 37 °C for 10 min. Control activities (in the absence of IgG) = 50, 30, 8 and 3 pmol/min/mg protein for the formation of M1, M2, M3 (isomer 1) and M3 (isomer 2) respectively.

Table 3. Correlation of L-775,606 metabolite formation and P450 activities in human liver microsomes ($n = 11$).

	Correlation (R^2)			
	M1	M2	M3 (isomer 1)	M3 (isomer 2)
M1	1.00*	0.99*	0.31	0.61
M2		1.00*	0.32	0.62
M3 (isomer 1)			1.00*	0.72*
M3 (isomer 2)				1.00*
Testosterone 6β-hydroxylation (CYP3A)	0.86*	0.87*	0.30	0.62
Tolbutamide 3-methyl hydroxylation (CYP2C9)	0.64	0.59	0.20	0.45
Bufuralol 1′-hydroxylation (CYP2D6)	0.28	0.25	0.51	0.43
S-mephenytoin 4-hydroxylation (CYP2C19)	0.04	0.04	0.15	0.03
Phenacetin *O*-deethylation (CYP1A2)	0.01	0.01	0.31	0.06

* $p < 0.0001$.

Chemical inhibition studies

The role of the above isozymes in the metabolism of L-775,606 in human liver microsomes was further investigated using known chemical inhibitors of P450 and FMO. None of the P450 inhibitors tested, including the non-specific P450 inhibitor SKF-525A, significantly inhibited the hepatic formation of M3 (figure 4), suggesting minimal involvement of P450 in the *N*-oxidative pathway in human livers. Among the P450 inhibitors tested, SKF-525A and the specific CYP3A inhibitor TAO inhibited the hepatic formation of M1 and M2 by ~ 80%, whereas quercetin, a relatively potent inhibitor of CYP2C8, inhibited the formation of M1 and M2 by 20 and 40% respectively (figure 4). The marked inhibition by SKF-525A and TAO indicated the important role of P450 in general and CYP3A in particular, whereas the modest inhibition by quercetin suggested a possibly partial contribution of

CYP2C8 in the formation of the two principal metabolites M1 and M2. Quinidine, sulphaphenazole, tranylcypromine, 8-methoxsalen and furafylline did not affect the oxidative metabolism of L-775,606 (figure 4), indicating that CYP2D6, CYP2C9, CYP2C19, CYP2A6 and CYP1A2 respectively did not play a significant role.

In contrast, pre-incubation of the reaction mixture at 45 °C without NADPH or incubation of L-775,606 in the presence of methimazole, a known FMO substrate (Overby *et al*. 1997, Ripp *et al*. 1999), substantially suppressed (45–80%) the formation of *N*-oxide metabolites, with minimal effect on the production of M1 and M2 (figure 4). These results suggested that FMO was a primary enzyme system responsible for the formation of M3 by human liver microsomes.

Immunoinhibition studies

Immuno-inhibition studies were subsequently conducted to confirm the involvement of CYP3A in the microsomal metabolism of L-775,606. Anti-CYP3A antibodies selectively inhibited the formation of L-775,606 metabolites; M1 and M2 formation was almost completely abolished, whereas M3 is slightly reduced (figure 5). These results supported the above chemical inhibition study that CYP3A is the primary contributor to the human hepatic microsomal formation of M1 and M2, but not M3.

Correlation studies

Table 3 summarizes results from correlation studies between L-775,606 metabolite formation and several CYP activities obtained in human liver microsomes from a panel of 11 subjects. Good correlation was observed between the rates of formation of M1 and M2 and between those of the two isomers of M3 (table 3). Formation of the two major metabolites did not correlate with that of the *N*-oxide isomers (table 3). The results were consistent with the findings that both M1 and M2 were catalysed by the same enzyme, and that this enzyme was different from the one that catalysed M3. Of the P450 marker activities examined, only testosterone 6β-hydroxylase activity (CYP3A) showed a strong correlation ($r^2 > 0.8, p < 0.001$) with the formation of M1 and M2, but not M3, further supporting the primary role of CYP3A in mediating the two principal metabolic pathways in human.

pH-dependent metabolism

The involvement of FMO3 in the *N*-oxidation reaction of L-775,606 in human liver microsomes also was confirmed by studying its metabolism as a function of pH since FMO, unlike P450, are known to exhibit high catalytic activity at pH > 7.4. In human liver microsomes, the formation of the major metabolites M1 and M2 was highest at pH 7.4, whereas that of M3 (both isomers) was optimal at pH > 8 (figure 6A). Control experiments with CYP3A4 (figure 6B) and FMO3 (figure 6C) agreed well with the observations in human liver microsomes, further supporting the aforementioned findings of the different regioselectivities between CYP3A4 and FMO3 in the oxidative metabolism of L-775,606.

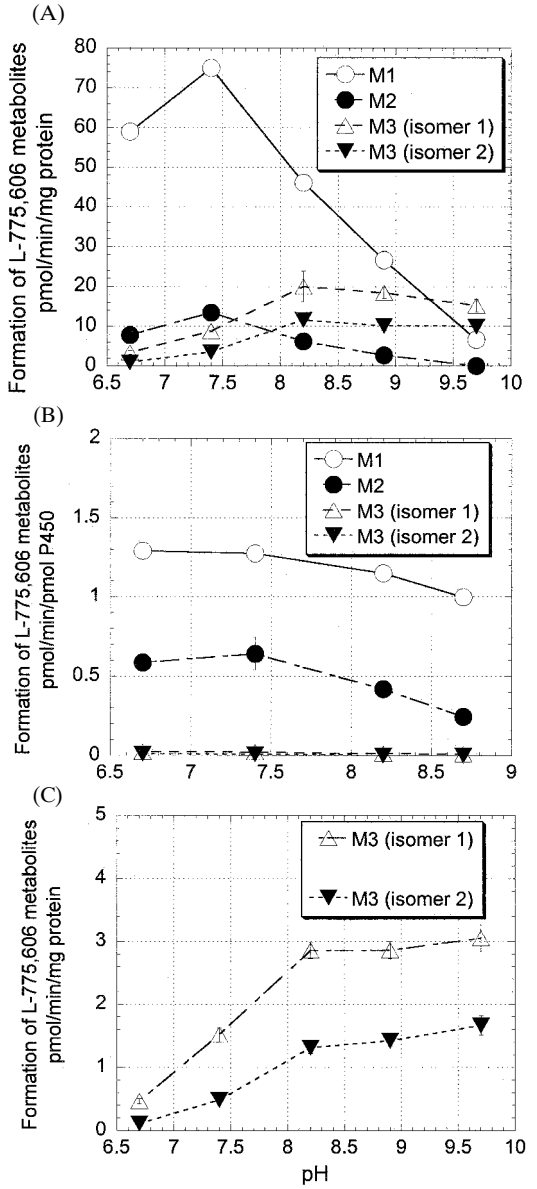


Figure 6. pH-dependent metabolism of L-775,606 by human liver microsomes (A), recombinant CYP3A4 (B) and FMO3 (C). Results (mean± SD) were based on triplicate determinations. Incubations (0.1 ml) were carried out at 37 °C for 10 min using human liver microsomes (0.1 mg), CYP3A4 (10 pmol P450) or FMO3 (0.05 mg) and L-775,606 (20 μM) with NADPH (1 mM).

Discussion

The data presented here have demonstrated marked quantitative differences in the *in vitro* hepatic metabolism of L-775,606 in animals and human. Considering that liver contains high levels of drug-metabolizing enzymes, the present hepatic metabolism results likely reflect the metabolism of L-775,606 *in vivo*. In a previous study, L-775,606 was shown to be metabolized extensively *in vivo* in dog; < 10% of the intact drug was recovered in urine and bile following i.v. administration (data

not shown). Since the total intrinsic clearance obtained *in vitro* was much faster in rat and monkey than in dog and human, the *in vivo* metabolism of L-775,606 in all other species examined could also be as extensive as was in dog. The *in vitro* findings of species differences observed in the formation pattern of L-775,606 metabolites suggested that similar differences would likely exist *in vivo*. Based on values for the Cl_{int} for each individual metabolite relative to the total Cl_{int}, the *in vivo* formation of M3 is expected to be minimal in all species except in dog. Of the three animal species examined, monkey exhibited L-775,606 metabolite profile, with the relative contribution from M1 and M2 closest to human. Potentially, monkey may be a better model than dog for the assessment of potential toxicological risks of L-775,606 metabolites.

The present study clearly indicated that both P450 and FMO systems are involved in oxidative metabolism of L-775,606 in human, with different affinities and regioselectivities. P450 preferentially catalysed the formation of M1 and M2 with high-affinity, whereas FMO exclusively catalysed M3 formation with relatively low affinity. Based on chemical inhibition, immuno-inhibition, kinetics of metabolism and correlation analysis, CYP3A was identified as the major P450 enzyme subfamily involved in L-775,606 metabolism in human. Although CYP2C8 might also be involved, its contribution is expected to be minimal. This conclusion is based mainly on the kinetic studies with human liver microsomes that showed apparently monophasic characteristics, with K_m comparable with those obtained with CYP3A4. These monophasic kinetics also were consistent with the findings that CYP2C8 possessed much lower (>100-fold) intrinsic activity (V_{max}/K_m), as compared with CYP3A4, and that in human livers, CYP3A subfamily is more abundant than CYP2C subfamily (Shimada *et al*. 1994). Moreover, the finding that the extent of inhibition of L-775,606 metabolism by the potent but non-specific CYP2C8 inhibitor quercetin was much less than that by the specific CYP3A inhibitor TAO also substantiated the above conclusion, considering that both inhibitors, at the concentrations used in the present study, are known to inhibit the respective CYP2C8 and CYP3A activities almost completely (Rahman *et al*. 1994, Newton *et al*. 1995). Similarly, the results from experiments with recombinant P450 enzymes and chemical inhibition and correlation studies with known P450 marker activities suggested that CYP2D6, CYP2C9, CYP1A2, CYP2C19 and CYP2A6 did not play a significant role in the metabolism of L-775,606.

The involvement of human FMO3 in the *N*-oxidative reaction of L-775,606 was elucidated on the basis of known characteristics of FMO (heat lability and high optimum pH), chemical inhibition with methimazole, and comparative studies of L-775,606 metabolism kinetics by FMO3 and human liver microsomes. It should be pointed out that based on the present data, involvement of FMO other than FMO3 in this reaction could not be ruled out. FMO are known to oxidize hetero-atom-containing compounds in human and animals (Cashman *et al*. 1995, Tugnait *et al*. 1997, Lang *et al*. 1998). In the case of L-775,606, a FMO(s) also was likely involved in the formation of M3 in rat, dog and monkey liver microsomes, based on heat inactivation experiments (data not shown). The finding that the formation of M3 was much higher in dog than in human suggested species differences in the abundance of FMO and/or in the catalytic activity of specific isoforms. Species differences have been shown earlier for the FMO-catalysed reaction of several compounds (Cashman *et al*. 1995, Hadley *et al*. 1996, Huan *et al*. 1998, Ripp *et al*. 1999).

The human CYP3A subfamily is known to exhibit a wide range of interindividual variability (Shimada *et al*. 1994). It has also been reported to be involved in the metabolism of structurally diverse xenobiotics, as well as to be inducible and inhibited by several xenobiotics (Thummel and Wilkinson 1998). Considering that L-775,606 would likely undergo extensive metabolism *in vivo* in human and that CYP3A is the primary enzyme responsible for the major metabolic pathways of L-775,606, the *in vivo* disposition kinetics of L-775,606 in human would likely be subjected to large interindividual variations and potentially could be affected by CYP3A4 substrates, inducers or inhibitors. Although several xenobiotics have been identified as FMO substrates and polymorphic metabolism of trimethylamine by FMO has been reported (Al-Waiz *et al*. 1987, Cashman *et al*. 1997), the clinical implications of FMO involvement in the metabolism of L-775,606 are limited since M3 is a minor component in human. Obviously, all the above *in vivo* implications remain to be verified in clinical studies.

To conclude, the present *in vitro* results demonstrated marked quantitative species differences in the metabolism of L-775,606 in human, dog, rat and monkey livers. Both P450 and FMO are involved in the human hepatic metabolism of L-775,606. CYP3A4 is identified as the major metabolizing enzyme subfamily, leading primarily to the major metabolites M1 and M2. CYP2C8 contributes minimally to, and CYP2D6, CYP2C8, CYP2C9, CYP1A2, CYP2E1 and CYP2A6 are not involved in oxidative metabolism of L-775,606. FMO3 is the major contributor to the formation of the minor *N*-oxide metabolites in human. Potentially, the *in vivo* metabolism of L-775,606 could be affected considerably by substrates, inhibitors or inducers of CYP3A4, but minimally by those of CYP2C8 or FMO3.

Acknowledgements

The authors thank Dr J. H. Lin for critical review of the manuscript, Drs Margaret Davis and Donald E. Slaughter and Mr S. Yu for LC/MS studies, Mr A. Watt, Neuroscience Research Centre, Merck Research Laboratories, Terlings Park, for information on L-776,606 metabolites, and Ms D. Walsh for preparation of human liver microsomes.

References

Al-Waiz, M., Ayesh, R., Mitchell, S. C., Idle, J. R. and Smith, R. L., 1987, Trimethylaminuria (fish-odour syndrome)—an inborn error of oxidative metabolism. *Lancet*, **1**, 634–635.

Cashman, J. R., Park, S. B., Berkman, C. E. and Cashman, L. E., 1995, Role of hepatic flavin-containing monooxygenase 3 in drug and chemical metabolism in adult human. *Chemico-Biological Interactions*, **96**, 33–46.

Cashman, J. R., Bi, Y.-A, Youil, R., Knight, M., Forrest, S. and Treacy, E., 1997, Human flavin-containing monooxygenase form 3: cDNA expression of the enzymes containing amino acid substitutions observed in individuals with trimethylaminuria. *Chemical Research in Toxicology*, **10**, 837–841.

Chang, T. K. H., Gonzalez, F. J. and Waxman, D. J., 1994, Evaluation of triacetyloleandromycin, α-naphthoflavone and diethyldithiocarbamate as selective chemical probes for inhibition of human cytochromes P450. *Archives of Biochemistry and Biophysics*, **311**, 437–442.

Draper, A. J., Madan, A. and Parkinson, A., 1997, Inhibition of coumarin 7-hydroxylase activity in human liver microsomes. *Archives of Biochemistry and Biophysics*, **341**, 47–61.

Hadley, M. R., Oldham, H. G., Camilleri, P., Damani, L. A. and Hutt, A. J., 1996, Species differences in the stereoselectivity of *N*-oxygenation of *N*-ethyl-*N*-methylaniline *in vitro*. *Chirality*, **8**, 430–440.

Hamel E., 1996, 5-HT_{1D} receptors: pharmacology and therapeutic potential. *Serotonin*, **1**, 19–29.

Huan, J.-Y., Miranda, C. L., Buhler, D. R. and Cheeke, P. R., 1998, Species differences in the hepatic microsomal enzyme metabolism of the pyrrolizidine alkaloids. *Toxicology Letters*, **99**, 127–137.

Lang, D. H., Yeung, C. K., Peter, R. M., Ibarra, C., Gasser, R., Itagaki, K., Philpot, R. M. and Retti, A. E., 1998, Isoform specificity of triethylamine *N*-oxygenation by human flavin-containing monooxygenase (FMO) and P450 enzymes. *Biochemical Pharmacology*, **56**, 1005–1012.

MacLeod, A. M., Street, L. J., Reeve, A. J., Jelley, R. A., Sternfeld, F., Beer, M. S., Stanton, J. A., Watt, A. P., Rathbone, D. and Matassa, V. G., 1997, Selective, orally active 5-HT_{1D} receptor agonists as potential antimigraine agents. *Journal Medicinal Chemistry*, **40**, 3501–3503.

Minisalco, A., Lundahl, J., Regardh, C. G., Edgar, B. and Eriksson, U. G., 1992, Inhibition of dihydropyridine metabolism in rat and human liver microsomes by flavonoids found in grapefruit juice. *Journal Pharmacology Experimental Therapeutics*, **261**, 1195–1199.

Newton, D. J., Wang, R. W. and Lu, A. H. Y., 1995, Cytochrome P450 inhibitors: Evaluation of specificities in the *in vitro* metabolism of therapeutic agents by human liver microsomes. *Drug Metabolism Disposition*, **23**, 154–158.

Overby, L. H., Carver, G. C. and Philpot, R. M., 1997, Quantitation and kinetics properties of hepatic microsomal and recombinant flavin-containing monooxygenases 3 and 5 from human. *Chemico-Biological Interactions*, **106**, 29–45.

Plosker, G. L. and McTavish, D., 1994, A reappraisal of its pharmacology and therapeutic efficacy in the acute treatment of migraine and cluster headache. *Drugs*, **47**, 622–651.

Prueksaritanont, T., Gorham, L. M., Ma, B., Liu, L., Yu, X., Zhao, J. J., Slaughter, D. E., Arison, B. H. and Vyas, K. P., 1997, *In vitro* metabolism of simvastatin in human: identification of metabolizing enzymes and effect of the drug on hepatic P450. *Drug Metabolism Disposition*, **25**, 1191–1199.

Rahman, A., Korzekwa, K. R., Grogan, J., Gonzalez, F. J. and Harris, J. W., 1994, Selective biotransformation of taxol to 6α-hydroxytaxol by human cytochrome P450 2C8. *Cancer Research*, **54**, 5543–5546.

Ripp, S. L., Itagaki, K., Philpot, R. M. and Elfarra, A. A., 1999, Species and sex differences in the expression of flavin-containing monooxygenase form 3 in liver and kidney microsomes. *Drug Metabolism Disposition*, **27**, 46–52.

Shimada, T., Yamazaki, H., Mimura, M., Inui, Y. and Guengerich, F. P., 1994, Interindividual variations in human liver cytochrome P-450 enzymes involved in the oxidation of drugs, carcinogens and toxic chemicals: Studies with liver microsomes of 30 Japanese and 30 Caucasians. *Journal of Pharmacology and Experimental Therapeutics*, **270**, 414–423.

Thummel, K. E. and Wilkinson, G. R., 1998, *In vitro* and *in vivo* drug interactions involving human CYP3A. *Annual Review Pharmacology and Toxicology*, **38**, 389–430.

Tugnait, M., Hawes, E. M., McKay, G., Rettie, A. E., Haining, R. L. and Midha, K. K., 1997, *N*-oxygenation of clozapine by flavin-containing monooxygenase. *Drug Metabolism Disposition*, **25**, 524–527.

Wienkers, L. C., Wurden, C. J., Storch, E., Kunze, K. L., Rettie, A. E. and Trager, W. F., 1996, Formation of *R*-8-hydroxywarfarin in human liver microsomes—a new metabolic marker for the (*S*)-mephenytoin hydroxylase, P4502C19. *Drug Metabolism Disposition*, **24**, 610–615.

XENOBIOTICA , 2000, VOL. 30, NO. 1, 61–70

In vitro inhibitory effects of troglitazone and its metabolites on drug oxidation activities of human cytochrome P450 enzymes: comparison with pioglitazone and rosiglitazone

H. YAMAZAKI†*, M. SUZUKI†, K. TANE†, N. SHIMADA‡, M. NAKAJIMA† and T. YOKOI†

† Division of Drug Metabolism, Faculty of Pharmaceutical Sciences, Kanazawa University, 13–1 Takara-machi, Kanazawa 920–0934, Japan
‡ Daiichi Pure Chemicals, Ibaraki 319–1182, Japan

Received 21 June 1999

1. Investigated were the effects of a new oral antidiabetic drug, troglitazone, and its three metabolites and antidiabetic drug candidates pioglitazone and rosiglitazone on xenobiotic oxidations catalyzed by nine recombinant human cytochrome P450 (P450 or CYP) enzymes and by human liver microsomes.

2. Troglitazone (5 μM) significantly inhibited CYP2C8-dependent paclitaxel 6α-hydroxylation and CYP2C9-dependent *S*-warfarin 7-hydroxylation. On the other hand, pioglitazone and rosiglitazone (50 μM) only slightly inhibited these xenobiotic oxidation activities catalyzed by CYP2C enzymes.

3. The inhibitory potential of troglitazone (50% inhibition concentration, IC_{50}) was $\sim$ 5 μM for drug oxidations catalyzed by CYP2C9 and CYP2C8 and $\sim$ 20 μM for activities catalyzed by CYP2C19 and CYP3A4 respectively. For the three metabolites of troglitazone tested, a quinone-type metabolite (M3) was the most potent inhibitor for CYP2C enzymes, followed by a sulphate conjugate (M1); effects of a glucuronide (M2) were very weak. The inhibitory effects of the parent drug were more potent than those of metabolites. Troglitazone and M3 inhibited P450 activities mainly through a competitive manner with K_i = 0.2–1.7 μM and 1.4–8.8 μM respectively.

4. In three human liver microsomes, troglitazone and its metabolites also inhibited paclitaxel 6α-hydroxylation, *S*-warfarin 7-hydroxylation, *S*-mephenytoin 4′-hydroxylation, and testosterone 6β-hydroxylation with similar IC_{50}, as observed for the recombinant P450 enzyme systems.

5. These results suggest that xenobiotic oxidations by P450 enzymes are more substantially affected by troglitazone and its metabolites than pioglitazone or rosiglitazone, and that drug interactions may be of much importance to understand the basis for the pharmacological and toxicological actions of this new oral antidiabetic drug.

Introduction

Cytochrome P450 (P450 or CYP) comprises a superfamily of enzymes that catalyze oxidation of many xenobiotic chemicals such as drugs, toxic chemicals and carcinogens as well as endobiotic chemicals including steroids, fatty acids and lipid soluble vitamins (Guengerich and Shimada 1991, Guengerich 1995, Nelson *et al*. 1996). Xenobiotic oxidations have been shown to be catalyzed mainly by P450 enzymes belonging to the CYP1, CYP2 and CYP3 subfamilies in mammals (Nelson *et al*. 1996) and these P450 enzymes have also been reported to have roles in the metabolism of endobiotic chemicals (Guengerich and Shimada 1991).

Troglitazone (Noscal® or Rezulin®, Sankyo, Tokyo, Japan or Parke-Davis, Morris Plains, NJ, USA) is a new oral antidiabetic drug approved in Japan and the

* Author for correspondence; e-mail: yanazak@kenroku.kamazawa-u.ac.jp

Xenobiotica ISSN 0049–8254 print/ISSN 1366–5928 online © 2000 Taylor & Francis Ltd
http://www.tandf.co.uk/journals/tf/00498254.html

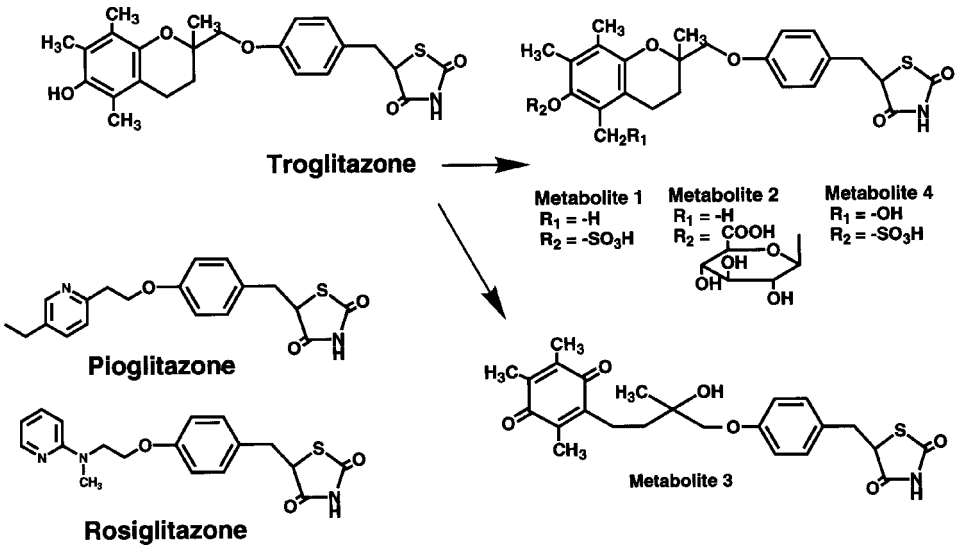


Figure 1. Chemical structures of troglitazone, its sulphate and glucuronide conjugates, oxidized metabolites and pioglitazone and rosiglitazone.

USA for use in the treatment of non-insulin-dependent diabetes mellitus (Sparano and Seaton 1998). Rosiglitazone (SmithKline Beecham, Epsom, UK) is now marketed in the USA, and pioglitazone (Takeda, Osaka, Japan) is recently approved in the USA; these are also novel antidiabetic thiazolidinedione derivatives that offer promise as oral insulin-sensitizing agents. The chemical structure of troglitazone contains a vitamin E moiety; however, in contrast, pioglitazone and rosiglitazone do not (figure 1). Troglitazone metabolism has been investigated in rat, mouse, dog, monkey and humans, and it has been reported to be mainly metabolized to sulphate (M1) and glucuronide (M2) conjugates (Izumi *et al.* 1997a, b, Kawai *et al.* 1998). The oxidized metabolite, a quinone-type metabolite (M3), has been found in human and monkey (PDR 1999). Rat CYP2C12, a female-specific form, has been reported to catalyze the hydroxylation of M1 to M4 (Odaka *et al.* 1995), the latter being found in the bile in the female rat (Kawai *et al.* 1997, Odaka *et al.* 1995). Troglitazone has been reported to be an inducer of CYP3A4 (PDR 1999) and significantly to decrease cyclosporine (Kaplan *et al.* 1998), terfenadine, and ethinyl estradiol (Koup *et al.* 1998, PDR 1999) concentrations in humans.

Recently it was reported that troglitazone is oxidized to a quinone-type metabolite catalyzed by CYP2C8 and CYP3A4 in human liver microsomes (Yamazaki *et al.* 1999a). To characterize further the inhibitory effects of troglitazone and its metabolite, the present study was undertaken to determine if troglitazone and its oxidative metabolite and conjugates and the new antidiabetic drugs pioglitazone and rosiglitazone inhibit P450-dependent xenobiotic oxidations in humans. Nine recombinant human P450 isoforms were used including CYP1A2, CYP2A6, CYP2B6, CYP2C8, CYP2C9, CYP2C19, CYP2D6, CYP2E1, CYP3A4 and also human liver microsomes. Substrates used for the determination of catalytic activities by P450 included 7-ethoxycoumarin, coumarin, paclitaxel, diclofenac, *S*-warfarin, *S*-mephenytoin, bufuralol and testosterone.

Materials and methods

Chemicals

Troglitazone (purity >99%), its sulphate (purity >98%) and glucuronide (purity >98%) conjugates, its quinone-type metabolite ((±)-5-[4-[2-hydroxy-2-methyl-4-(3,5,6-trimethyl-1,4-benzoquinon-2-yl)butoxy]benzyl]-2,4-thiazolidine-dione, purity >98%), pioglitazone (purity >99%) and rosiglitazone (purity >99%) were provided by Sankyo (Tokyo, Japan). 7-Ethoxycoumarin, coumarin, paclitaxel, *S*-warfarin, diclofenac, *S*-mephenytoin, bufuralol, testosterone, and their metabolites and reagents used in the study were from sources described previously or were of highest qualities commercially available (Yamazaki and Shimada 1999).

Enzyme preparations

Recombinant P450 enzymes expressed in microsomes of insect cells infected with baculovirus containing human P450 and human NADPH-P450 reductase cDNA inserts were from Gentest (Woburn, MA, USA); the P450 contents in these systems were used as described in the data sheets provided by the manufacturer. Human liver microsomes were prepared in 10 mM Tris-HCl buffer (pH 7.4) containing 0.10 mM EDTA and 20% glycerol (v/v) as described (Guengerich 1994). Concentrations of P450 (Omura and Sato 1964) and protein (Lowry *et al.* 1951) were measured as previously described. Total P450 contents in liver microsomes of human samples HL-3, HL-4 and HL-10 were 0.53, 0.32 and 0.45 nmol P450/mg protein respectively.

Enzyme assays

Standard incubation mixtures (final volume of 0.20 ml) contained recombinant P450 (0.010 μM) in 50 mM potassium phosphate buffer (pH 7.4) containing an NADPH-generating system (0.5 mM $NADP^+$, 5 mM glucose 6-phosphate, 0.5 unit glucose 6-phosphate dehydrogenase/ml) and substrates (1–100 μM). For determination of CYP1A2, CYP2B6, CYP2E1 and CYP3A4 activities, 100 mM potassium phosphate buffer (pH 7.4) was used. When human liver microsomes were used as the enzyme source, 500, 25, 100 and 25 pmol total P450 per ml were used for paclitaxel 6α-hydroxylation, *S*-warfarin 7-hydroxylation, *S*-mephenytoin 4′-hydroxylation and testosterone 6β-hydroxylation respectively. Product formation was determined by HPLC with a C_{18} 5-μm analytical column (Mightysil, Kanto Chemicals, Tokyo, Japan, 4.6×150 mm).

7-Ethoxycoumarin *O*-deethylation by CYP1A2, CYP2B6 and CYP2E1, coumarin 7-hydroxylation by CYP2A6, paclitaxel 6α-hydroxylation by CYP2C8, *S*-warfarin 7-hydroxylation and diclofenac 4′-hydroxylation by CYP2C9, *S*-mephenytoin 4′-hydroxylation by CYP2C19, bufuralol 1′-hydroxylation by CYP2D6, and testosterone 6β-hydroxylation by CYP3A4 were determined as described (Yamazaki *et al.* 1998a, b, 1999a, b, Yamazaki and Shimada 1999).

Inhibition experiments

The antidiabetic drugs and troglitazone metabolites (dissolved in methanol) were added simultaneously with marker substrates to the P450 enzymes and incubation was carried out at 37 °C for 10 min for the determination of substrate oxidation. The final concentration of solvent in the incubation mixture was < 1%. In some cases, troglitazone (0.5–2.0 μM) was first metabolized by recombinant CYP2C9 (0.010 μM) in the presence of an NADPH-generating system at 37 °C for 5–20 min (preincubation). Preincubation mixtures were then mixed with *S*-warfarin (10 μM) and incubated at 37 °C for 10 min and the 7-hydroxylated products of warfarin were determined. Control (100%) values were obtained in incubations without antidiabetic drugs or metabolites.

Kinetic analysis for substrate oxidations by P450 enzymes were calculated from the fitted curves using a computer program (KaleidaGraph, Synergy Software, Reading, PA, USA) designed for non-linear regression analysis. Kinetic constants and inhibition types for substrate oxidations by P450 enzymes were also estimated using a computer program (K·cat, BioMetallics, Princeton, NJ, USA) designed for non-linear regression analysis. All data were analysed using the mean of duplicate determinations.

Results

Effects of troglitazone, pioglitazone, rosiglitazone and troglitazone metabolites on drug oxidation activities catalyzed by recombinant human P450 enzymes

Effects of 5 and 50 μM concentration of each of troglitazone, pioglitazone, rosiglitazone and troglitazone metabolites on xenobiotic oxidation at 100 μM substrate concentrations (except for 10 μM S-warfarin) catalyzed by nine forms of

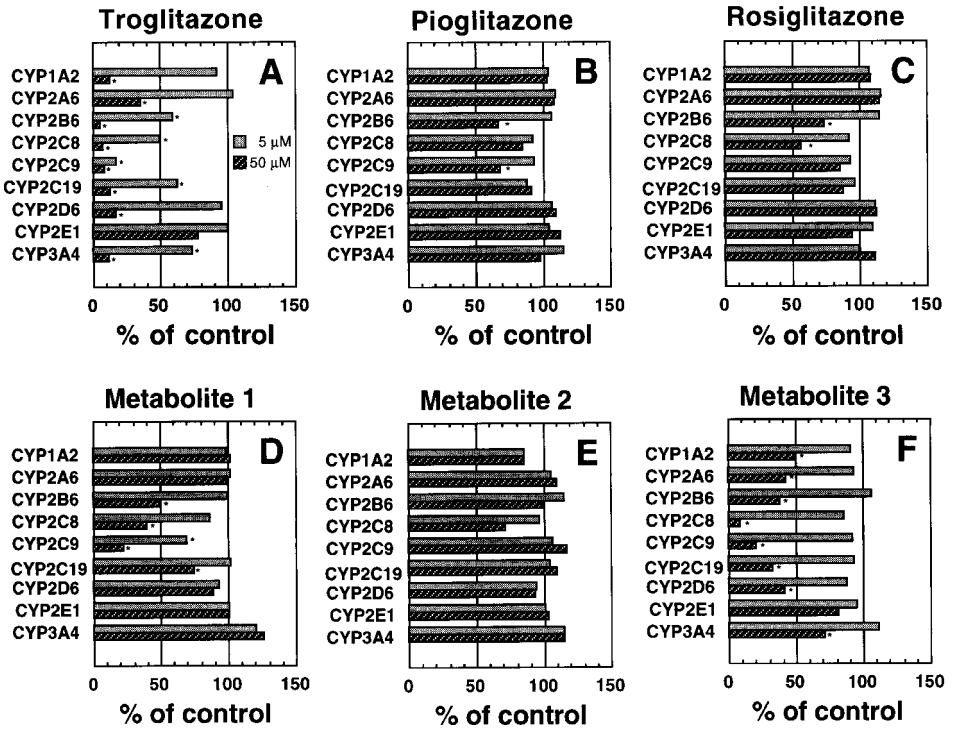


Figure 2. Effects of troglitazone (A), pioglitazone (B), rosiglitazone (C) and troglitazone metabolites (D–F) on drug oxidations catalyzed by recombinant human P450 enzymes. Marker substrate concentrations for P450 enzymes used were 100 μM, except for *S*-warfarin (10 μM), and chemicals were added at 5 μM (upper, shaded bar) and 50 μM (lower, striped bar). Control activities without inhibitors were 1.9 nmol/min/nmol P450 7-ethoxycoumarin *O*-deethylation catalyzed by CYP1A2, 5.1 nmol/min/nmol P450 coumarin 7-hydroxylation by CYP2A6, 0.9 nmol/min/nmol P450 7-ethoxycoumarin *O*-deethylation by CYP2B6, 2.1 nmol/min/nmol P450 paclitaxel 6α-hydroxylation by CYP2C8, 0.04 nmol/min/nmol P450 *S*-warfarin 7-hydroxylation by CYP2C9, 3.4 nmol/min/nmol P450 *S*-mephenytoin 4′-hydroxylation by CYP2C19, 8.4 nmol/min/nmol P450 bufuralol 1′-hydroxylation by CYP2D6, 1.8 nmol/min/nmol P450 7-ethoxycoumarin *O*-deethylation by CYP2E1, and 47 nmol/min/nmol P450 testosterone 6β-hydroxylation respectively, in microsomes of insect cells expressing human P450 enzymes and reductase. Data are the mean of duplicate determinations. *Significantly different from controls ($p < 0.01$).

cDNA-expressed human P450 enzymes were investigated (figure 2). Troglitazone (5 μM) significantly inhibited the CYP2C8-dependent paclitaxel 6α-hydroxylation and CYP2C9-dependent *S*-warfarin 7-hydroxylation. This chemical (50 μM) also extensively suppressed CYP2C19-dependent *S*-mephenytoin 4′-hydroxylation and CYP3A4-dependent testosterone 6β-hydroxylation and moderately influenced the CYP1A2- and CYP2B6-dependent 7-ethoxycoumarin *O*-deethylation, CYP2A6-dependent coumarin 7-hydroxylation and CYP2D6-dependent bufuralol 1′-hydroxylation. CYP2E1-dependent 7-ethoxycoumarin *O*-deethylation was not inhibited.

Pioglitazone and rosiglitazone (figure 2B, C) did not inhibit the xenobiotic oxidations catalyzed by recombinant P450 enzymes examined here, except that they affected slightly the activities of CYP2C enzymes; >50% inhibition was not observed under these conditions.

M3 of troglitazone (50 μM) inhibited on the xenobiotic oxidations catalyzed by CYP2C8, CYP2C9 and CYP2C19 (figure 2F). M1 was also found to be a inhibitor

Table 1. IC_{50} of troglitazone and its metabolites for drug oxidation activities catalyzed by recombinant P450 enzymes.

P450	Marker reaction	Substrate (μM)	IC_{50} (μM)‡		
			Troglitazone	M1	M3
1A2	7-ethoxycoumarin *O*-deethylation	20	27	>50	50
		100	30	>50	50
2A6	coumarin 7-hydroxylation	1	42	>50	43
		100	41	>50	43
2B6	7-ethoxycoumarin *O*-deethylation	20	28	>50	48
		100	35	>50	50
2C8	paclitaxel 6α-hydroxylation	10	1	9	6
		100	5	41	26
2C9	*S*-warfarin 7-hydroxylation	10	3	24	32
2C19	*S*-mephenytoin 4′-hydroxylation	100	17	>50	37
2D6	bufuralol 1′-hydroxylation	1	27	>50	41
		100	33	>50	42
2E1	7-ethoxycoumarin *O*-deethylation	100	>50	>50	>50
3A4	testosterone 6β-hydroxylation	100	23	>50	>50

Control activities at higher substrate concentrations without inhibitors were the same as the legends of figure 2. Control activities at lower substrate concentrations were 1.0 nmol/min/nmol CYP1A2 7-ethoxycoumarin *O*-deethylation, 2.4 nmol/min/nmol CYP2A6 coumarin 7-hydroxylation, 0.3 nmol/min/nmol CYP2B6 7-ethoxycoumarin *O*-deethylation, 1.1 nmol/min/nmol CYP2C8 paclitaxel 6α-hydroxylation and 4.0 nmol/min/nmol CYP2D6 bufuralol 1′-hydroxylation respectively.

‡ Data are the mean of duplicate determinations.

for CYP2C8- and CYP2C9-dependent xenobiotic oxidations (figure 2D). M2 did not extensively inhibit the xenobiotic oxidations catalyzed by recombinant P450 enzymes in the present study (figure 2E).

The IC_{50} (the concentration of an inhibitor that gives 50% inhibition at a specified substrate concentration) for anti-diabetic drugs are summarized in table 1. IC_{50} for troglitazone with CYP2C8 and CYP2C9 were very low (1–5 μM). IC_{50} for troglitazone inhibition of CYP1A2, CYP2A6, CYP2B6 and CYP2D6 were almost similar at both substrate concentrations tested, suggesting that troglitazone mainly inhibited these catalytic activities through a non-competitive mechanism. Among the troglitazone metabolites tested, M3 had the most potent inhibitory effects and the IC_{50} for M1 for CYP2C9-dependent *S*-warfarin 7-hydroxylation seemed to be smaller than that of M3. However, the parent drug troglitazone itself was a more potent inhibitor of all of human P450 enzymes tested.

Kinetic constants for inhibitory effects of troglitazone and its metabolites on drug oxidation activities in recombinant human P450 enzymes

Kinetic constants for inhibitory effects of troglitazone, M1 and M3 on drug oxidation activities in recombinant human P450 enzymes are summarized in table 2. Troglitazone exhibited mainly competitive inhibition with $K_i = 0.3 \pm 0.1$ μM for paclitaxel 6α-hydroxylation, 0.3 ± 0.1 μM for *S*-warfarin 7-hydroxylation (figure 3), 0.2 ± 0.1 μM for diclofenac 4′-hydroxylation, 1.2 ± 0.8 μM for *S*-mephenytoin 4′-hydroxylation, 1.7 ± 0.2 μM for testosterone 6β-hydroxylation. M3 also exhibited competitive inhibitory effects (except for CYP2C19) having higher K_i than those of troglitazone. M1 exhibited a lower K_i than that of M3 for both *S*-warfarin 7-hydroxylation and diclofenac 4′-hydroxylation catalyzed by CYP2C9.

Since troglitazone markedly inhibited CYP2C9-dependent drug oxidation

Table 2. Kinetic constants for the inhibitory effects of troglitazone and its metabolites on drug oxidation activities in recombinant human P450 enzymes.[a]

Enzyme	Marker reaction[b]	Inhibitor[c]	Inhibition type[d]	K_m (μM)	K_{is} (μM)	K_{ii} (μM)[e]	V_{max} (min^{-1})
CYP2C8	paclitaxel	troglitazone	competitive	6.8±2.2	0.3±0.1		3.0±0.2
	6α-hydroxylation	M3	competitive		3.0±0.2		
CYP2C9	*S*-warfarin	troglitazone	competitive	5.8±0.7	0.3±0.1		0.040±0.001
	7-hydroxylation	M1	competitive		2.6±0.5		
		M3	competitive		8.8±1.0		
	diclofenac	troglitazone	competitive	0.9±0.1	0.2±0.1		27±1
	4′-hydroxylation	M1	mixed		1.3±1.2	8.0±1.4	
		M3	mixed		2.9±0.1	4.0±0.2	
CYP2C19	*S*-mephenytoin	troglitazone	mixed	69±34	1.2±0.8	4.0±2.6	4.7±0.7
	4′-hydroxylation	M3	non-competitive			1.4±0.1	
CYP3A4	testosterone	troglitazone	competitive	60±21	1.7±0.2		126±9
	6β-hydroxylation	M3	competitive		5.1±0.8		

[a] Kinetic constants (means± SE for duplicate determinations) and inhibition type were determined from the fitted curves using the program K·cat.
[b] Substate concentrations of 10–200 μM paclitaxel and testosterone, 5–50 μM *S*-warfarin and diclofenac and 50–500 μM *S*-mephenytoin were used.
[c] Inhibitor concentrations of 0.2–2.0 μM troglitazone (for CYP2C8 and CYP2C9), 1–10 μM troglitazone (for CYP2C19 and CYP3A4), 5–50 μM of M1 and M3 were used.
[d] Inhibition type was determined by the best fit to competitive and non-competitive models.
[e] K_{is}, inhibition constant of slope (competitive); K_{ii}, inhibition constant on the intercept (non-competitive).

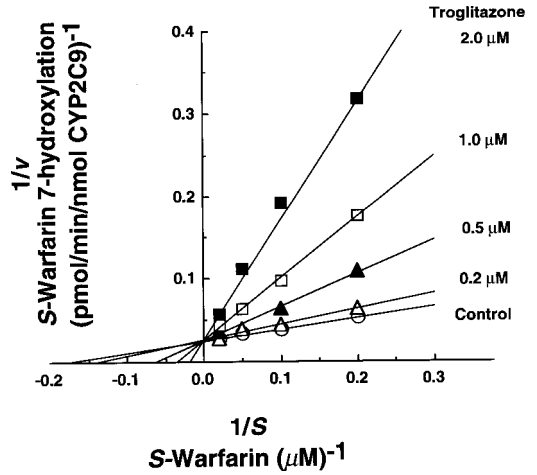


Figure 3. Inhibitory effect of troglitazone on *S*-warfarin 7-hydroxylation catalyzed by recombinant human CYP2C9. Troglitazone (0–2.0 μM) was incubated with *S*-warfarin (5–50 μM) and microsomes of insect cells expressing CYP2C9 and reductase. Data are the mean of duplicate determinations.

Table 3. IC_{50} for troglitazone and its metabolites for drug oxidation activities in three human liver microsomal samples.

Marker reaction	Substrate (μM)	Human liver sample	Catalytic activity[a]	IC_{50} (μM)‡		
				Troglitazone	M1	M3
Paclitaxel 6α-hydroxylation	100	HL-3	0.15	15	nd	>50
		HL-4	0.11	20	nd	43
		HL-10	0.11	20	nd	39
S-Warfarin 7-hydroxylation	10	HL-3	0.004	4	5	28
		HL-4	0.008	3	19	30
		HL-10	0.012	3	8	30
S-Mephenytoin 4′-hydroxylation	100	HL-3	0.04	21	nd	37
		HL-4	0.31	21	nd	32
		HL-10	0.14	22	nd	37
Testosterone 6β-hydroxylation	100	HL-3	18	25	nd	>50
		HL-4	4.0	5	nd	37
		HL-10	12	27	nd	34

[a] nmol products/min/nmol P450.
nd, Not determined.
‡ Data are the mean of duplicate determinations.

activities, effects of pre-incubation on the inhibitory effects of troglitazone were examined. Mechanism based inhibition by troglitazone on CYP2C9-dependent *S*-warfarin 7-hydroxylation was not detected (data not shown).

Effects of troglitazone and its metabolites on drug oxidations catalyzed by human liver microsomes

Four reactions—paclitaxel 6α-hydroxylation, *S*-warfarin 7-hydroxylation, *S*-mephenytoin 4′-hydroxylation and testosterone 6β-hydroxylation—were chosen for the determination of activities of CYP2C8, CYP2C9, CYP2C19 and CYP3A4

respectively in three human liver microsomes (table 3). Troglitazone and M3 significantly inhibited paclitaxel 6α-hydroxylation, *S*-warfarin 7-hydroxylation, *S*-mephenytoin 4′-hydroxylation and testosterone 6β-hydroxylation by each of the three human liver microsomes investigated. The IC_{50} for these reactions in human liver microsomes were almost the same as those observed in the recombinant human P450 systems (tables 1 and 3). The effect of troglitazone on paclitaxel 6α-hydroxylation by human liver microsomes was less than that by recombinant CYP2C8. More potent inhibitory effects of M1 than M3 on CYP2C9-catalyzed *S*-warfarin 7-hydroxylation were also observed in human liver microsomes.

Discussion

It has been recently reported the inhibitory effects of arachidonic acid, retinol, retinoic acid and cholecarciferol on xenobiotic oxidations catalyzed by human cytochrome P450 enzymes (Yamazaki and Shimada 1999). Xenobiotic oxidation by P450 enzymes are affected by endobiotic chemicals and that endobiotic–xenobiotic interactions as well as drug–drug interactions may be of great importance to understand the basis for various actions of a number of xenobiotic chemicals. In the previous study, marker substrate concentrations in *in vitro* experiments were 100 μM to observe nearly maximal catalytic activities of recombinant human P450 enzymes. In the present study, first investigated were the effects of new hypoglycemic agents on drug oxidation activities at marker substrate concentrations of 100 μM and $\sim K_m$ for each drug oxidation according to a previous study (Nakajima *et al.* 1999) (table 1). Inhibitor concentrations first were chosen at clinically relevant concentration of troglitazone (5 μM) and an order of magnitude higher. The potent inhibitory effects of troglitazone and its metabolites were further investigated in more detail by kinetic analysis (table 2).

Troglitazone is a new oral hypoglycemic agent approved for use in type II diabetes mellitus. Pioglitazone and rosiglitazone are also thiazolidinedione derivatives and have recently been approved for use in human. The chemical structure of troglitazone contains a vitamin E moiety, in contrast to pioglitazone and rosiglitazone (figure 1). Although troglitazone is not supposed to be metabolized by CYP1A1, CYP1A2, CYP2A6, CYP2B6, CYP2D6, CYP2E1 and CYP3A4 (PDR 1999), it is a inducer of CYP3A4 (Kaplan *et al.* 1998, Koup *et al.* 1998). Troglitazone has been suggested to be non-enzymatically converted to a quinone-type metabolite by lipid peroxides and active oxygen (Fu *et al.* 1996). In contrast, it has been recently reported that both CYP2C8 and CYP3A4 are major P450 enzymes involved in the oxidation of troglitazone to a quinone-type metabolite in human liver microsomes and that the roles of these two P450s vary depending on the contents of CYP2C8 and CYP3A4 in human livers (Yamazaki *et al.* 1999a). In the current study, potent inhibitory effects of troglitazone were clearly observed and it is likely that the hydroxychroman moiety is metabolized by human CYP2C8 and CYP2C9 and/or human liver microsomes and resulted in the observed extensive competitive inhibition.

Recently rare cases of severe idiosyncratic hepatocellular injury has been reported during marketed the use of troglitazone (Watkins and Whitcomb 1998, PDR 1999). Hepatic injury occurred after both short- and long-term troglitazone treatment in the USA (PDR 1999) and after troglitazone treatment for a period not shorter than 4 weeks in Japan (Kuramoto *et al.* 1998). It has been reported that

maximum plasma concentrations of troglitazone increase proportionally with increasing doses over range of 200–600 mg/day (PDR 1999). Following daily drug administration, steady-state plasma concentrations of troglitazone are reached within 3–5 days; the maximum plasma concentrations are 0.9–2.8 μg/ml (2.0–6.4 μM) at steady-state in normal volunteers (PDR 1999). Because of the high protein binding of troglitazone (>99%) (PDR 1999), plasma concentration of troglitazone in humans should be very low (< 0.020–0.064 μM). Based on these free plasma concentration of troglitazone *in vivo* and the 0.1 μM order of K_i *in vitro*, drug interactions via competitive inhibition of CYP2C9 activities would be rare. To date, troglitazone is reported to have no clinical significant effect on prothrombin time when administered to patients receiving chronic warfarin therapy (PDR 1999). However, it has been reported that plasma concentrations of troglitazone, M1, and M3 in patients with chronic liver disease were increased by ~30, 400 and 100% respectively, compared with those in healthy subjects without hepatic dysfunction (PDR 1999). In these latter cases, drug interactions caused by competitive inhibition of human P450 enzymes should be viewed with caution.

More extensive competitive inhibition by M1 of troglitazone than M3 on the catalytic activities of both recombinant CYP2C9 and human liver microsomes would suggest that human CYP2C9 might also take part in the hydroxylation of M1 to M4 in humans, as has been reported with rat CYP2C12 (Odaka *et al*. 1995). It should be mentioned that determination of unknown metabolites such as M4 in human is important to understand the basis for the pharmacokinetics of troglitazone.

It has been previously reported that troglitazone does not inhibit any of major P450 enzymes at clinically relevant concentrations but that the inhibitory characteristics of M3 of troglitazone have not been investigated yet (PDR 1999). However, the present results clearly show that troglitazone and its M3 inhibited human P450 activities mainly through a competitive mechanism with K_i = 0.2–1.7 μM and 1.4–8.8 μM respectively. M1 also showed extensive inhibitory effects on CYP2C9-dependent drug oxidation mainly through a competitive mechanism with K_i = 1.3–2.6 μM.

In conclusion, xenobiotics or endobiotics oxidations catalyzed by human P450 enzymes may be affected by troglitazone and its metabolites, but not by pioglitazone or rosiglitazone. *In vitro* studies of drug interactions may be of substantial importance in understanding the basis for the pharmacological and toxicological actions of this new oral antidiabetic drug.

Acknowledgements

This work was supported in part by Grants from the Ministry of Education, Science, Sports, and Culture of Japan, and the Ministry of Health and Welfare of Japan. Dr F. Peter Guengerich is thanked for providing the human liver samples; also Sankyo is thanked for providing troglitazone and its metabolites, pioglitazone and rosiglitazone.

References

Fu, Y., She, C., Fujita, T. and Foote, C. S., 1996, Photooxidation of troglitazone, a new antidiabetic drug. *Photochemistry and Photobiology*, **63**, 615–620.

Guengerich, F. P., 1994, Analysis and characterization of enzymes. In A. W. Hayes (ed.), *Principles and Methods of Toxicology* (New York: Raven), pp. 1259–1313.

Guengerich , F. P., 1995, Human cytochrome P450 enzymes. In P. R. Oritiz de Montellano (ed.), *Cytochrome P450* (New York: Plenum), pp. 473–535.

Guengerich , F. P. and Shimada , T., 1991, Oxidation of toxic and carcinogenic chemicals by human cytochrome P-450 enzymes. *Chemical Research in Toxicology*, **4**, 391–407.

Izumi , T., Enomoto , S., Hoshiyama , K., Sasahara, K. and Sugiyama , Y., 1997a, Pharmacokinetic stereoselectivity of troglitazone, an antidiabetic agent, in the KK mouse. *Biopharmaceutical and Drug Disposition*, **18**, 305–324.

Izumi , T., Hoshiyama , K., Enomoto , S., Sasahara, K. and Sugiyama , Y., 1997b, Pharmacokinetics of troglitazone, an antidiabetic agent: prediction of *in vivo* stereoselective sulphation and glucuronidation from *in vitro* data. *Journal of Pharmacology and Experimental Therapeutics*, **280**, 1392–1400.

Kaplan , B., Friedman , G., Jacobs , M., Viscuso , R., Lyman , N., DeFranco , P., Bonomini , L. and Mulgaonkar , S. P., 1998, Potential interaction of troglitazone and cyclosporine. *Transplantation*, **65**, 1399–1400.

Kawai , K., Kawasaki-Tokui , Y., Odaka, T., Tsuruta , F., Kazui , M., Iwabuchi , H., Nakamura , T., Kinoshita , T., Ikeda , T., Yoshioka , T., Komai , T. and Nakamura , K., 1997, Disposition and metabolism of the new oral antidiabetic drug troglitazone in rats, mice and dogs. *Arzneimittel Forschung*, **47**, 356–368.

Kawai , K., Odaka, T., Tsuruta , F., Tokui , T., Ikeda , T. and Nakamura , K., 1998, Stereoselective metabolism of new oral anti-diabetic agent troglitazone stereoisomers in liver. *Xenobiotic Metabolism and Disposition*, **13**, 362–368.

Koup , J. R., Anderson , G. D. and Loi , C. M., 1998, Effect of troglitazone on urinary excretion of 6β-hydroxycortisol. *Journal of Clinical Pharmacology*, **38**, 815–818.

Kuramoto , K., Shimizu , N. and Toda , G., 1998, Liver dysfunction associated with troglitazone (Noscal®). *Rinsho-Iyaku*, **14**, 461–466.

Lowry , O. H., Rosebrough , N. J., Farr , A. L. and Randall , R. J., 1951, Protein measurement with the Folin phenol reagent. *Journal of Biological Chemistry*, **193**, 265–275.

Nakajima , M., Ohyama , K., Nakamura , S., Shimada , N., Yamazaki , H. and Yokoi , T., 1999, Inhibitory effects of azelastine and its metabolites on drug oxidation catalyzed by human cytochrome P-450 enzymes. *Drug Metabolism and Disposition*, **27**, 792–797.

Nelson , D. R., Koymans , L., Kamataki , T., Stegeman , J. J., Feyereisen , R., Waxman , D. J., Waterman , M. R., Gotoh , O., Coon , M. J., Estabrook , R. W., Gunsalus , I. C. and Nebert , D. W., 1996, P450 superfamily: update on new sequences, gene mapping, accession numbers and nomenclature. *Pharmacogenetics*, **6**, 1–42.

Odaka, T., Kawai , K., Tsuruta , F., Ikeda , T., Kinoshita , T., Nakamura , K., Shimada , M. and Yamazoe , Y., 1995, Pharmacokinetics of troglitazone (CS-045), a new oral antidiabetic drug: phase I and phase II metabolism in female rats. *Xenobiotic Metabolism and Disposition*, **10** (suppl.), S-386.

Omura , T. and Sato , R., 1964, The carbon monoxide-binding pigment of liver microsomes. I. Evidence for its hemoprotein nature. *Journal of Biological Chemistry*, **239**, 2370–2378.

PDR, 1999, Rezulin ™. In *Physicians' Desk Reference* (Montvale: Medical Economics Co.), pp. 2310–2314.

Sparano , N. and Seaton , T. L., 1998, Troglitazone in type II diabetes mellitus. *Pharmacotherapy*, **18**, 539–548.

Watkins , P. B. and Whitcomb , R. W., 1998, Hepatic dysfunction associated with troglitazone. *New England Journal of Medicine*, **338**, 916–917.

Yamazaki , H., Inoue , K., Chiba , K., Ozawa, N., Kawai , T., Suzuki , Y., Goldstein , J. A., Guengerich , F. P. and Shimada , T., 1998a, Comparative studies on the catalytic roles of cytochrome P450 2C9 and its Cys- and Leu- variants in the oxidation of warfarin, flurbiprofen, and diclofenac by human liver microsomes. *Biochemical Pharmacology*, **56**, 243–251.

Yamazaki , H., Inoue , K. and Shimada , T., 1998b, Roles of two allelic variants (Arg144Cys and Ile359Leu) of cytochrome P450 2C9 in the oxidation of tolbutamide and warfarin by human liver microsome. *Xenobiotica*, **28**, 103–115.

Yamazaki , H., Nakajima , M., Shibata , A., Suzuki , M., Shimada , N., Guengerich , F. P. and Yokoi , T., 1999a, Oxidation of troglitazone to a quinone-type metabolite catalyzed by cytochrome P450 2C8 and P450 3A4 in human liver microsomes. *Drug Metabolism and Disposition* **27**.

Yamazaki , H. and Shimada , T., 1999, Effects of arachidonic acid, prostaglandins, retinol, retinoic acid, and cholecalciferol on xenobiotic oxidations catalysed by human cytochrome P450 enzymes. *Xenobiotica*, **29**, 231–241.

Yamazaki , H., Tanaka , M. and Shimada , T., 1999b, Highly sensitive HPLC assay for coumarin 7-hydroxylation and 7-ethoxycoumarin *O*-deethylation by human liver cytochrome P450 enzymes. *Journal of Chromatography B: Biomedical Applications*, **721**, 13–19.

XENOBIOTICA , 2000, VOL. 30, NO. 1, 71–80

Identification of CYP3A4 as the predominant isoform responsible for the metabolism of ambroxol in human liver microsomes

N. ISHIGURO†, C. SENDA†, W. KISHIMOTO†, K. SAKAI†, Y. FUNAE‡ and T. IGARASHI†*

† Department of Drug Metabolism and Pharmacokinetics, Kawanishi Pharma Research Institute, Nippon Boehringer Ingelheim Co., Ltd, 3–10–1, Yato, Kawanishi, Hyogo 666–0193, Japan
‡ Department of Chemical Biology, Osaka City University Medical School, 1–4-3, Asahimachi, Abeno-ku, Osaka 545–8585, Japan

Received 4 June 1999

1. In humans, ambroxol is metabolized to dibromoanthranilic acid (DBAA) and 6,8-dibromo-3-(*trans*-4-hydroxycyclohexyl)-1,2,3,4-tetrahydroquinazoline (DHTQ). The formation of DHTQ proceeds non-enzymatically, whereas that of DBAA requires NADPH. Studies have been performed to identify the CYP isozyme(s) involved in the formation of DBAA using human liver microsomes and microsomes expressing recombinant human CYP isozymes (1A1, 1A2, 2A6, 2B6, 2C8, 2C9, 2C19, 2D6, 2E1, 3A4 and 4A11).

2. The apparent V_{max} and K_m for the formation of DBAA were 472 ± 192 pmol/min/mg protein and 248 ± 40.6 μM respectively (mean ± S.D., $n = 3$).

3. Of the recombinant CYP examined, only CYP3A4 metabolized ambroxol to DBAA. The apparent V_{max} and K_m were 1.42 pmol/min/pmol P450 and 287 μM respectively.

4. Among the CYP inhibitors examined (furafylline, sulphaphenazole, quinidine, diethyldithiocarbamic acid, ketoconazole), only ketoconazole inhibited the production of DBAA (>80%) at 1 μM and anti-CYP3A antiserum almost completely inhibited the formation of DBAA.

5. These results suggest that CYP3A4 is predominantly involved in the metabolism of ambroxol to DBAA in humans.

Introduction

Ambroxol (*trans*-4-((2-amino-3,5-dibromobenzyl)amino)cyclohexanol hydrochloride) is a mucolubricant that promotes secretion of surfactant and airway fluid, enhances ciliary movement and normalizes airway mucosa (Curti 1972, Nagaoka and Kase 1981). It is used in the treatment of acute bronchitis, chronic bronchitis, asthma bronchiale, bronchiectasia, lung tuberculosis and coniosis, for which it may be co-administered with many other types of drugs, such as bronchodilators, steroids, antibiotics, antitussive, expectorant and anti-allergic agents (Hinobara and Abe 1997). After oral administration of ^{14}C-ambroxol in humans, the radioactivity was excreted mainly in urine within 72 h (~70% of administered oral dose). Ambroxol is well absorbed, and excreted into urine as ~50% glucuronides of the unchanged drug, ~10% as glucuronides of the oxidized metabolites, dibromoanthranilic acid (DBAA), ~10% as unchanged drug and a minor formylated cyclization product, 6,8-dibromo-3-(*trans*-4-hydroxycyclohexyl)-1,2,3,4-tetrahydroquinazoline (DHTQ) (Seki *et al*. 1977).

* Author for correspondence; e-mail: igarashi@boehringer-ingelheim.co.jp

Xenobiotica ISSN 0049–8254 print/ISSN 1366–5928 online © 2000 Taylor & Francis Ltd
http://www.tandf.co.uk/journals/tf/00498254.html

Cytochrome P450 (CYP) is the major catalytic component of the liver microsomal mixed-function oxidase system that catalyzes the biotransformation of endogenous substrates, including steroids and lipids, and exogenous substrates, such as drugs and chemical carcinogens (Gonzalez *et al*. 1991, Guengerich and Shimada 1991, Gonzalez and Gelboin 1994). It is generally accepted that the broad substrate specificity of the system is due to the existence of numerous isoforms of CYP, exhibiting distinct but overlapping specificities (Horai and Ishizaki 1988, Gonzalez 1992, Guengerich 1994). Recently, there has been much interest in drug interactions occurring during drug metabolism due to simultaneous co-medication. For example, an interaction between the bronchodilator theophylline and quinolone antibacterial agents *in vivo*, causing adverse side-effects, is attributed to the involvement of the same CYP isozyme in the metabolism of both drugs (Davies *et al*. 1984, Wijnands *et al*. 1984). Thus, for the prediction of potential drug–drug interactions through the inhibition of CYP-mediated drug metabolism, it is very important to identify the CYP isozymes responsible for the metabolism of drugs.

In the present study, the CYP isozyme predominantly responsible for ambroxol metabolism is identified by using human liver microsomes and microsomes expressing recombinant CYP isoforms. The potential for drug–drug interactions of ambroxol *in vivo* is also discussed.

Materials and methods

Chemicals

Ambroxol, ß-nicotineamide adenine dinucleotide phosphate reduced (tetrasodium salt) (NADPH), D-glucose 6-phosphate (monosodium salt) (G6P), glucose 6-phosphate dehydrogenase (type VII from yeast) (G6PDH), sulphaphenazole, diethyldithiocarbamic acid (DDC) and quinidine were from Sigma Chemical Co. (St Louis, MO, USA). Ketoconazole and furafylline were from Funakoshi Co., Ltd (Tokyo, Japan) and Daiichi Pure Chemicals Co., Ltd (Tokyo, Japan) respectively. 6,8-Dibromo-3-(*trans*-4-hydroxycyclohexyl)-1,2,3,4-tetrahydroquinazoline (DHTQ) and 3,5-dibromoanthranilic acid (DBAA) were synthesized by Boehringer Ingelheim Co. (Germany). The purities of DBAA and DHTQ determined by high-performance liquid chromatography (HPLC) were >99 and >80 % respectively. Microsomes from human B-lymphoblastoid cell line AHH-1 $TK^{+/-}$, expressing human CYP1A1, 1A2, 2A6, 2B6, 2C8, 2C9-Arg, 2C19, 2D6-Val, 2E1, 3A4 or 4A11, were from GENTEST Co. (Woburn, MA, USA). Human liver microsomes (HHM-195, HHM-224 and HHM-232) were from the International Institute for the Advancement of Medicine (Exton, PA, USA) via K. A. C. (Kyoto, Japan). All other chemicals and reagents were of analytical grade.

Microsomal incubations with ambroxol

Human liver microsomes. HHM-195, HHM-224 and HHM-232 were from a 42-year-old male Caucasian, a 64-year-old female Caucasian and a 29-year-old black female respectively.

Reactions. Human liver microsomes were diluted with 100 mM phosphate buffer (pH 7.4) to give a final protein concentration of 0.3–1.0 mg/ml. Microsomes expressing recombinant CYP isozymes (1A1, 1A2, 2B6, 2C8, 2C19, 2D6-Val, 2E1, 3A4, 4A11) were diluted with 100 mM phosphate buffer (pH 7.4) to give a final protein concentration of 0.6 or 1.0 mg/ml. For CYP2A6 or 2C9-Arg, 100 mM phosphate buffer was replaced with 50 mM Tris-HCl buffer (pH 7.4) because the activity of these isozymes is inhibited by phosphate. All microsomal suspensions were pre-incubated with ambroxol (1–1000 μM) or DHTQ (100 μM) for 5 min at 37 °C. After pre-incubation, the reaction was initiated by the addition of an NADPH-generating system (10 mM G6P, 1 mM NADPH, 1 unit/ml G6PDH and 4 mM $MgCl_2$) and the mixture was incubated for 45 min. The reaction was terminated by the addition of 0.5 vol. cold methanol with vortex mixing and the tubes placed on ice. After centrifugation at 15000*g* for 10 min, the supernatant was injected into the HPLC column for analysis.

Effect of specific CYP inhibitors on ambroxol metabolism in human liver microsomes. The CYP inhibitors sulphaphenazole (CYP2C9, 1–10 μM), quinidine (CYP2D6, 1–20 μM), DDC (CYP2E1, 20–100 μM) and

ketoconazole (CYP3A4, 0.05–20 μM) were added to microsomal suspensions as described above just before incubation. The incubation mixture containing the CYP inhibitor furafylline (CYP1A, final concentration 1–5 μM) was pre-incubated in the presence of NADPH-generating system at 37 °C for 15 min, and the reaction was initiated by addition of ambroxol. At appropriate times, the reaction was stopped by addition of 0.5 vol. cold methanol.

Immuno-inhibition study

For immuno-inhibition studies, rabbit anti-rat CYP3A2 antiserum (provided by Professor Funae, Osaka City University, Japan) was used. The antibody cross-reacted with all human CYP3A, but not with other CYP (Imaoka *et al*. 1990). The immuno-inhibition of ambroxol metabolism was examined by pre-incubation of 60 μg human liver microsomes with various concentrations of antiserum at room temperature for 15 min. Ambroxol (100 μM) and 100 mM phosphate buffer were added to the mixture on ice. The reaction was initiated by addition of an NADPH-generating system at 37 °C and incubation was continued for 60 min. The incubations were terminated by addition of 0.33 vol. 30% perchloric acid (PCA) with vortex mixing and the tubes were placed on ice. After centrifugation at 15000*g* for 2 min, the supernatant was injected into the HPLC column for analysis.

HPLC analysis

Ambroxol and its metabolites (DHTQ and DBAA) were determined by an HPLC method. Aliquots (50 μl), as described above, were injected (model 507, Beckman) into a reverse-phase column (Inertsil ODS-2, 4.6×150 mm, 5 μm, GL Science Inc., Tokyo, Japan). The mobile phase, consisting of (A): acetonitrile/15 mM triethylamine, pH 3.9 (20/80 v/v) and (B): acetonitrile/15 mM triethylamine, pH 3.9 (50/50 v/v) was delivered at a 1.0 ml/min by a pump (model 126, Beckman). Samples were eluted as follows: the initial eluent profile was isocratic 80% A/20% B for 1 min, followed by a linear gradient to 100% B by 10 min and isocratic 100% B for a further 2 min. A column temperature of 35 °C was maintained by using an oven (model 507, Beckman). The absorbance of the column effluent was measured at 220 nm with a UV-detector (model 156, Beckman); under these conditions, the retentions of DHTQ and DBAA were ~4.5 and 12.3 min respectively. DBAA was quantitated from linear calibration plots based on the peak heights of authentic DBAA (0.1–10 μM). Intra- and interassay coefficients of variation (CV) were < 5 and 10% respectively.

Kinetic analysis

Apparent K_m (Michaelis–Menten constant) and V_{max} (maximum rate of metabolite formation) were estimated by fitting data to the Michaelis–Menten equation using the enzyme kinetic program 'Leonora' with a least-squares non-linear regression method (Cornish-Bowden 1995).

Results

Metabolism of ambroxol by human liver microsomes

In human liver microsomes (1.0 mg/ml protein concentration), ambroxol (100 μM concentration) was metabolized to two main metabolites (DHTQ and DBAA; figure 1) and some minor peaks, which were separated and determined by HPLC (figure 2). DBAA did not form in the absence of NADPH, or with heat-inactivated microsomes or on incubation in the presence of SKF-525A a typical CYP inhibitor. However, under the same conditions, DHTQ was formed (data not shown). Furthermore, incubation of 100 μM DHTQ with human liver microsomes did not produce DBAA (data not shown). The formation of DBAA proceeded linearly with respect to incubation time up to 30 min and protein concentration up to 0.6 mg/ml (figure 3).

Typical velocity versus concentration curve (S-v plots) and Eadie–Hofstee plots for the formation of DBAA by human liver microsomes (HHM-195) are shown in figure 4. The S-v plots seemed to fit to simple Michaelis–Menten kinetics well and Eadie–Hofstee plots seemed to be linear, indicating the involvement of a single CYP

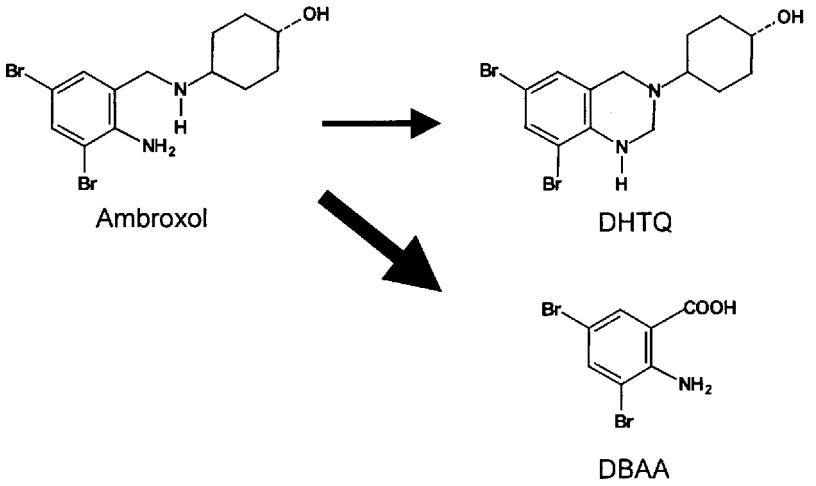


Figure 1. Ambroxol and its two major metabolites, DHTQ and DBAA.

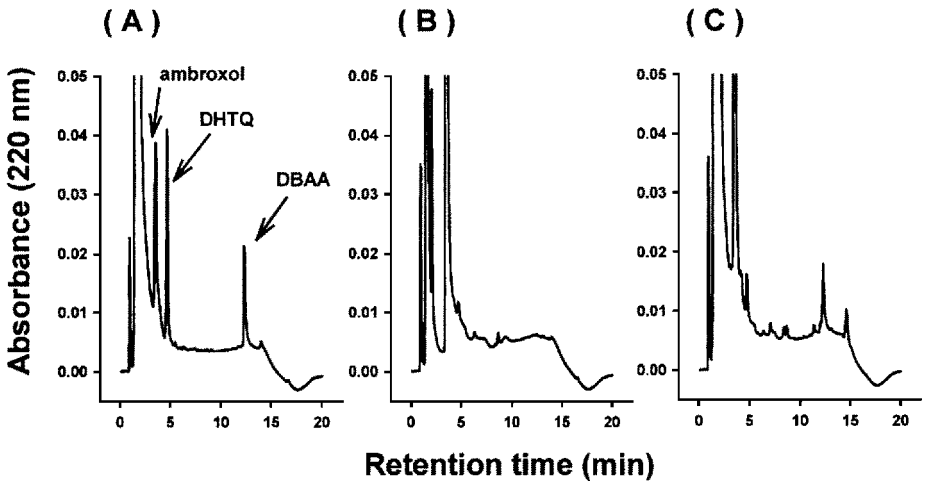


Figure 2. Representative HPLC chromatograms of ambroxol and its metabolites produced by human liver microsomes. (A) Elution pattern of ambroxol (4 μM), DHTQ (4 μM) and DBAA (4 μM) spiked into an ice-cold reaction mixture containing human liver microsomes and an NADPH-generating system. (B, C), Elution patterns of the reaction mixture incubated without and with an NADPH-generating system for 60 min respectively. Liver microsome preparation HHM-224 was used. Retentions (min): ambroxol, 3.5; DHTQ, 4.5; DBAA, 12.3.

isoform in the reaction. The mean K_m and V_{max} obtained from the Michaelis–Menten equation for one enzyme kinetics with these three human liver microsomes were 248 μM and 472 pmol/min/mg protein respectively (table 1).

Metabolism of ambroxol by recombinant CYP

Metabolism of ambroxol by microsomes expressing recombinant human CYP (1A1, 1A2, 2A6, 2B6, 2C8, 2C9-Arg, 2C19, 2D6-Val, 2E1, 3A4, 4A11) was investigated. CYP3A4 metabolized ambroxol, whereas other CYP examined did not

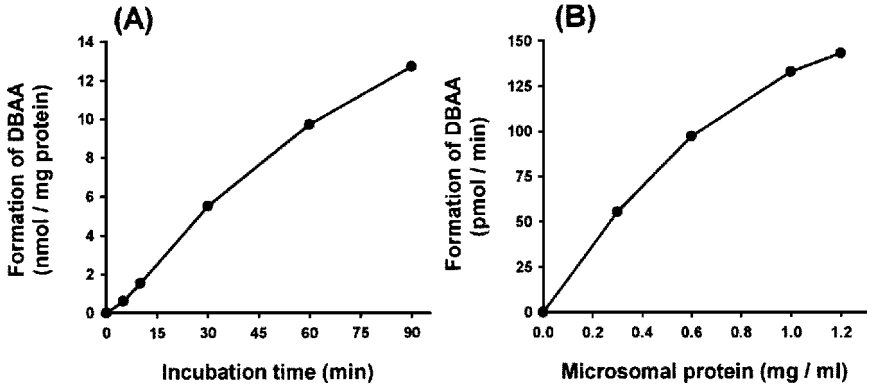


Figure 3. Formation of DBAA by human liver microsomes (HHM-195) as a function of incubation time or the amount of microsomal protein. Incubations were carried out for various periods (A) or with various amounts of human liver microsomes (B). The substrate concentration was 100 μM; data are the mean of duplicate determinations.

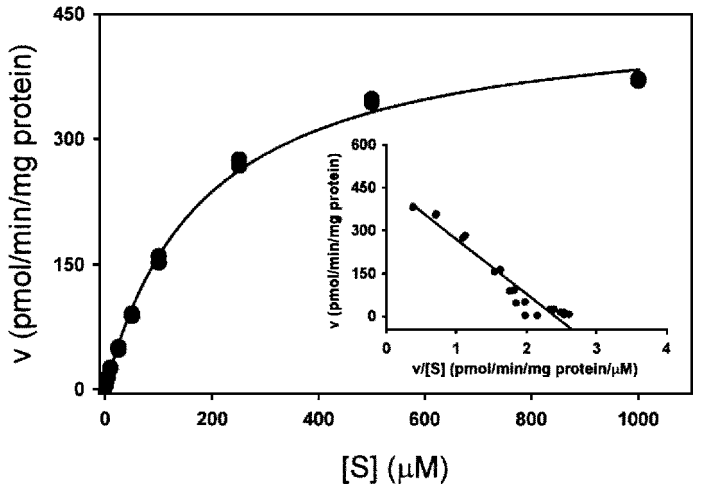


Figure 4. Representative Michaelis–Menten plots of DBAA formation by human liver microsomes (HHM-195). (inset) Eadie–Hofstee plots. Lines were estimated by least-squares linear regression. The substrate and protein concentrations were 1–1000 μM and 0.6 mg/ml respectively.

Table 1. Michaelis-Menten parameters for ambroxol metabolism in human liver microsomes.

Human liver microsomes	V_{max} (pmol/min/mg protein)	K_m (μM)	V_{max}/K_m
HHM-195	470	201	2.34
HHM-224	665	274	2.43
HHM-232	280	269	1.04
Mean	472	248	1.94
SD	192	40.6	0.77

Each point was measured in duplicate.

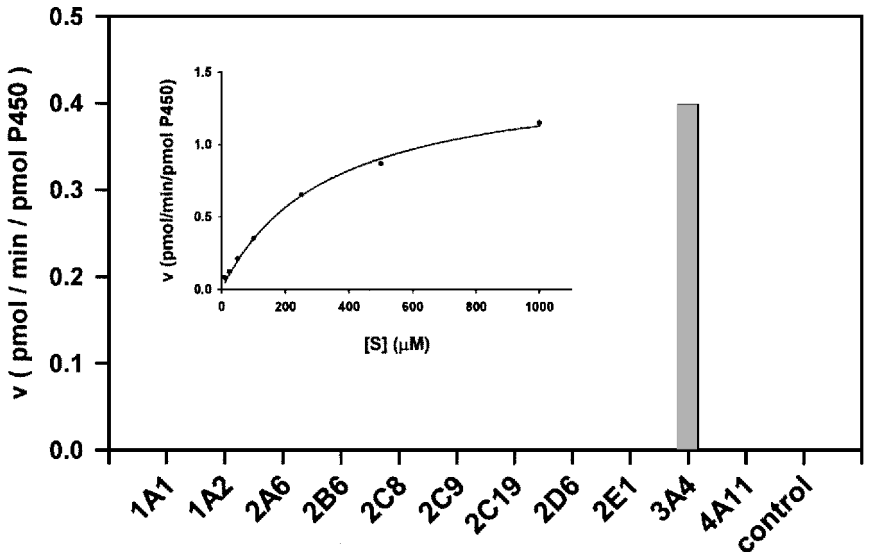


Figure 5. Metabolism of ambroxol by specific human CYP expressed in microsomes of B-lymphoblastoid cells. Ambroxol and microsomal protein concentrations used were at 100 μM and 1.0 mg/ml. (inset) Typical Michaelis–Menten plots for CYP3A4. Lines indicate the best fit of the Michaelis–Menten equation to the data. The substrate and microsomal protein concentrations were 10–1000 μM and 0.6 mg/ml respectively. Each point represents the mean of duplicate determinations.

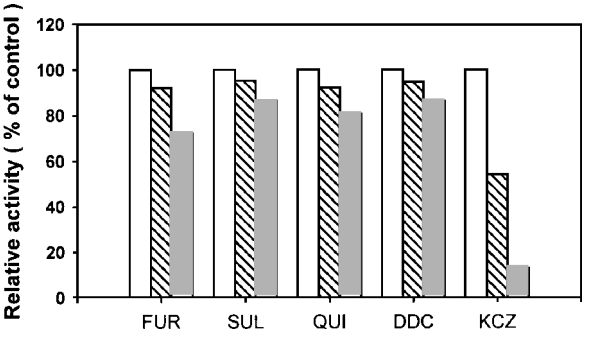


Figure 6. Effect of CYP isozyme inhibitors on the formation of DBAA in human liver microsomes (HHM-195). Ambroxol and microsomal protein concentrations used were at 15 μM and 0.6 mg/ml respectively. Data are the mean of duplicate determinations. Open, hatched and closed columns indicate control (no inhibitor), and low concentration and high concentration of inhibitors respectively. FUR, furafylline (CYP1A2 LOW, 1 μM; HIGH, 5 μM); SUL, sulphaphenazole (CYP2C9 LOW, 1 μM; HIGH, 10 μM); QUI, quinidine (CYP2D6 LOW, 1 μM; HIGH, 20 μM); DDC, diethyldithiocarbamic acid (CYP2E1 LOW, 20 μM; HIGH, 100 μM); KCZ, ketoconazole (CYP3A4 LOW, 0.1 μM; HIGH, 1 μM).

(figure 5). The apparent K_m and V_{max} for the formation of DBAA by recombinant CYP3A4 were 287 μM and 1.42 pmol/min/pmol P450 (figure 5, inset).

Chemical inhibition studies

The effects of furafylline (Clarke *et al.* 1994, Newton *et al.* 1995), sulphaphenazole (Baldwin *et al.* 1995, Newton *et al.* 1995), quinidine (Newton *et al.* 1995, Bourrie *et al.* 1996), diethyldithiocarbamic acid (Newton *et al.* 1995), ketoconazole

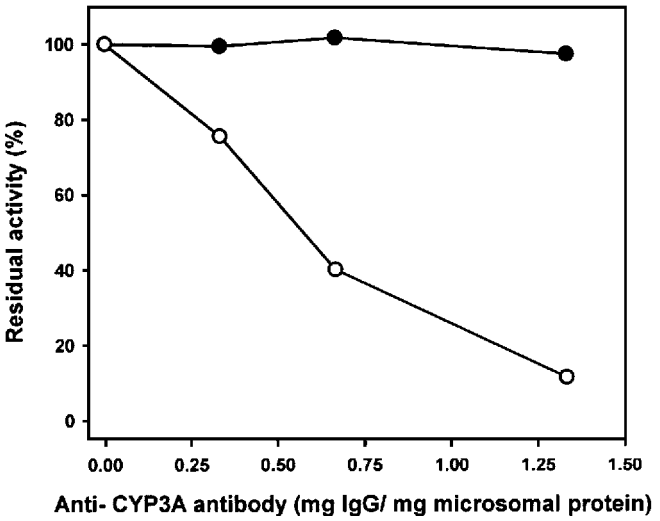


Figure 7. Immuno-inhibition by anti-human CYP3A antiserum of the formation of DBAA by human liver microsomes. Ambroxol was used at 100 μM. Microsomes (HHM-195) were pre-incubated in the presence of indicated amounts of rabbit anti-human CYP3A antibodies (open circles) and rabbit control rabbit IgG (closed circles) at room temperature for 15 min. Each point represents the mean of duplicate determinations.

(Baldwin *et al*. 1995, Bourrie *et al*. 1996), known specific inhibitors of CYP1A2, 2C9, 2D6, 2E1, 3A4 respectively on the formation of DBAA in human liver microsomes were investigated at an ambroxol concentration of 15 μM (figure 6) and 100 μM (data not shown). Furthermore, at 15 and 100 μM ambroxol concentration, only ketoconazole (0.05–1.0 and 0.5–20 μM respectively) markedly inhibited the formation of DBAA in a concentration-dependent manner.

Immuno-inhibition study

To confirm the involvement of CYP3A4 in the metabolism of ambroxol, an immuno-inhibition study was performed (figure 7). During incubation for 60 min, rabbit anti-human CYP3A antibodies almost completely inhibited the formation of DBAA.

Discussion

This is the first detailed study on the *in vitro* metabolism of ambroxol by human liver microsomes and microsomes expressing recombinant CYP isoforms. In human liver microsomes, DHTQ, DBAA and some unidentified minor peaks were produced from ambroxol. The formation of DHTQ from ambroxol was occurred with the incubation of heat-inactivated microsomes, suggesting that the formation was proceeded non-enzymatically. A slight increase in DHTQ formation in the presence of NADPH compared with in the absence of NADPH (figure 2) seems to indicate that an enzyme partly catalyzes the reaction. The source of supply of carbon to DHTQ may relate to the tetrahydrofolic acid (THF) pool (Jauch *et al*. 1978). Furthermore, DBAA was not generated from DHTQ. The formation of DBAA from ambroxol was completely inhibited by SKF-525A and did not occur in the

absence of NADPH. These results suggest that DBAA formation is catalyzed by one or more cytochrome P450s. Further studies were therefore performed to identify the CYP isozyme(s) involved. Using three different preparations of human liver microsomes (HHM-195, HHM-224 and HHM-232), Eadie–Hofstee plots suggested that DBAA was formed in a monophasic manner.

Among various specific CYP inhibitors examined, ketoconazole (1 μM) extensively inhibited the formation of DBAA ($>80\%$) from 15 μM ambroxol (figure 6). Another inhibition study was performed with 100 μM ambroxol, because the 15-μM concentration was different from the mean K_m estimated from three different human liver microsomes. The inhibitory effects of each inhibitor to 100 μM ambroxol were the same as that obtained from 15 μM, and only ketoconazole inhibited the formation of DBAA. In this study, the inhibition by DDC was performed without pre-incubation with NADPH, although several reports (Hickman *et al*. 1998, Zeng *et al*. 1998) use DDC after pre-incubation.

In the experiment using microsomes expressing recombinant human CYP (1A1, 1A2, 2A6, 2B6, 2C8, 2C9, 2C19, 2D6, 2E1, 3A4, 4A11) were used. Although CYP1A1 is scarcely detected in the liver, it is expressed in extrahepatic tissues including lung (Antilla *et al*. 1992). Since ambroxol is a drug for the respiratory system, CYP1A1 seemed to be of significance in ambroxol metabolism and was used in this study. Among these isoforms examined only CYP3A4 exhibited significant activity for the formation of DBAA and the estimated K_m corresponded well with the mean K_m from the three different preparations of human microsomes.

In the immuno-inhibition study, antibodies against human CYP3A almost completely inhibited the formation of DBAA. These data show that CYP3A4 is the isozyme that predominantly catalyzes the formation of DBAA from ambroxol.

CYP3A4 plays an important role in the metabolism of many drugs. Side-effects due to drug–drug interaction have been reported in patients concomitantly taking several drugs that are metabolized by CYP3A4, such as the H_1 receptor antagonist terfenadine and the antifungal agent itraconazole (Honig *et al*. 1993). Kishimoto *et al*. (1997) reported that terfenadine is extensively metabolized to terfenadine acid with an apparent K_m of 1.19 and 3.19 μM and V_{max}/K_m (metabolic clearance) of 130 and 85 μl/min/mg protein by two of the human microsomal preparations used in this study (HHM-195, HHM-224). These are 84- and 169-fold smaller (K_m) and 56- and 82-fold higher (V_{max}/K_m) than those of ambroxol respectively. These differences in K_m and metabolic clearance estimated using the same microsomal preparations indicate that ambroxol is poorly metabolized compared with terfenadine. In fact, ambroxol is mainly excreted in urine in the form of glucuronic acid conjugates of the unchanged drug (Seki *et al*. 1977). These data suggest that the main metabolic pathway of ambroxol is glucuronidation *in vivo*. Thus, the pharmacokinetic features (e.g. plasma concentration and ambroxol clearance) of ambroxol may not be greatly altered even if CYP3A4 inhibitor or substrate would suppress the metabolism of ambroxol. However, it is of interest to investigate the inhibitory effects of ambroxol on the metabolism of CYP3A4 substrates because many such drugs may be co-administered with ambroxol. It was found that CYP3A4-mediated testosterone 6ß-hydroxylation activity was inhibited weakly ($\sim 20\%$ inhibition) by ambroxol at 15 μM concentration, that is 150-fold more than its maximum plasma concentration after a single 15-mg oral medication (Seki *et al*. 1977). This finding suggests that the potential for drug–drug interaction through competition for CYP3A4 is low in the case of ambroxol. However, it should be

considered that ambroxol may inhibit other CYP isoforms because it is well known that quinidine, a substrate for CYP3A4, is a potent inhibitor of CYP2D6 (Guengerich *et al*. 1986) and cimetidine, a poor substrate for CYP, is a non-selective inhibitor for this enzyme (Murray 1987).

In conclusion, it has been demonstrated that formation of DBAA from ambroxol in human liver microsomes is predominantly catalyzed by CYP3A4.

References

Antilla , S., Vainio , H., Hietanen , E., Camus , A. M., Malaveille , C., Brun, G., Husgafvel-Pursiainen , K., Heikkila¨, L., Karjalainen , A. and Bartsch , H., 1992, Immunohistochemical detection of pulmonary cytochrome P4501A and metabolic activities associated with P4501A1 and P4501A2 isozymes in lung cancer patients. *Environmental Health Perspectives*, **98**, 179–182.

Baldwin , S. J., Bloomer , J. C., Smith , G. J., Ayrton , A. D., Clarke, S. E. and Chenery , R. J., 1995, Ketoconazole and sulphaphenazole as the respective selective inhibitors of P4503A and 2C9. *Xenobiotica*, **25**, 261–270.

Bourrie , M., Meunier , V., Berger , Y. and Fabre , G., 1996, Cytochrome P450 isoform inhibitors as a tool for the investigation of metabolic reactions catalyzed by human liver microsomes. *Journal of Pharmacology and Experimental Therapeutics*, **277**, 321–332.

Clarke , S. E., Ayrton , A. D. and Chenery , R. J., 1994, Characterization of the inhibition of P4501A2 by furafylline. *Xenobiotica*, **24,** 517–526.

Cornish -Bowden , A., 1995, Fitting the Michaelis–Menten equation by least squares. In A. Cornish-Bowden (ed.), *Analysis of Enzyme Kinetic Data* (Oxford: Oxford University Press), pp. 27–36.

Curti , P. C., 1972, Steigerung der produktion der oberflächenaktiven substanz der alveolen durch NA872. *Pneumonologic*, **147**, 62–74.

Davies , B. I., Maesen , F. P. V. and Teengs , J. P., 1984, Serum and sputum concentrations of enoxacin after single oral dosing in a clinical and bacteriological study. *Journal of Antimicrobial Chemotherapy*, **14 (suppl. C)**, 83–89.

Gonzalez , F. J., 1992, Human cytochrome P450: problems and prospects. *Trends in Pharmacological Science*, **13**, 346–352.

Gonzalez , F. J., Crespi , C. L. and Gelboin , H. V., 1991, cDNA-expressed human cytochrome P450s: a new age of molecular toxicology and human risk assessment. *Mutation Research*, **247**, 113–127.

Gonzalez , F. J. and Gelboin , H. V., 1994, Role of human cytochrome P450 in the metabolic activation of chemical carcinogens and toxins. *Drug Metabolism Reviews*, **26**, 165–183.

Guengerich , F. P., 1994, Catalytic selectivity of human cytochrome P450 enzymes: relevance to drug metabolism and toxicity. *Toxicology Letters*, **70**, 133–138.

Guengerich , F. P., Müller-Enoch , D. and Blair , I. A., 1986, Oxidation of quinidine by human liver cytochrome P-450. *Molecular Pharmacology*, **30**, 287–295.

Guengerich , F. P. and Shimada , T., 1991, Oxidation of toxic and carcinogenic chemicals by human cytochrome P-450 enzymes. *Chemical Research in Toxicology*, **4**, 391–407.

Hickman , D., Wang, J., Wang, Y. and Unadkat , J. D., 1998, Evaluation of the selectivity of in vitro probes and suitability of organic solvents for the measurement of human cytochrome P450 monooxygenase activities. *Drug Metabolism and Disposition*, **26**, 207–215.

Hinobara , S. and Abe , M., 1997, Respiratory disease. In S. Hinobara and M. Abe (eds), *Today's Therapy* 1997 (Tokyo: Igakushoin), pp. 283–317.

Honig , P. K., Wortham , D. C., Hull , R., Zamani , K., Smith , J. E. and Cantilena , L. R., 1993, Itraconazole affects single-dose terfenadine pharmacokinetics and cardiac repolarization pharmacodynamics. *Journal of Clinical Pharmacology*, **33**, 1201–1206.

Horai , Y. and Ishizaki , T., 1988, Pharmacogenetics and its clinical implications. Part II. Oxidation polymorphism. *Rational Drug Therapy*, **22**, 1–8.

Imaoka , S., Enomoto , K., Oda, Y., Asada, A., Fujimori , M., Shimada , T., Fujita , S., Guengerich , F. P. and Funae , Y., 1990, Lidocaine metabolism by human cytochrome P-450s purified from hepatic microsomes: comparison of those with rat hepatic cytochrome P-450s. *Journal of Pharmacology and Experimental Therapeutics*, **255**, 1385–1391.

Jauch, R., Bozler, G., Hammer , R. and Koss, F. W., 1978, Ambroxol, studies of metabolism in man and quantitative determination in biological samples. *Arzneimittel forschung*, **28**, 904–911.

Kishimoto , W., Hiroi , T., Sakai, K., Funae , Y. and Igarashi , T., 1997, Metabolism of epinastine, a histamine H_1 receptor antagonist, in human liver microsomes in comparison with that of terfenadine. *Research Communications in Molecular Pathology and Pharmacology*, **98**, 273–292.

Murray , M., 1987, Mechanisms of the inhibition of cytochrome P-450-mediated drug oxidation by therapeutic agents. *Drug Metabolism Reviews*, **18**, 55–81.

Nagaoka, S. and Kase, Y., 1981, Pharmacological study of ambroxol (NA872). *Japanese Pharmacology and Therapeutics*, **9**, 127–136.

NEWTON, D. J., WANG, R. W. and LU, A. Y. H., 1995, Cytochrome P450 inhibitors evaluation of specificities in the *in vitro* metabolism of therapeutic agents by human liver microsomes. *Drug Metabolism and Disposition*, **23**, 154–158.

SEKI, T., MATSUMURA, R. and KOHEI, H., 1977, A clinico-pharmacological study on *trans*-4-(2-amino-3,5-dibromobenzylamino) cyclohexanol hydrochloride. *Japanese Journal of Clinical Pharmacology and Therapeutics*, **8**, 25–31.

WIJNANDS, W. J. A., VAN HERWAARDEN, C. L. A. and VREE, T. B., 1984, Enoxacin raises plasma theophylline concentrations. *Lancet*, **ii**, 108–109.

ZENG, Z., ANDREW, N. W., ARISON, B. H., LUFFER-ATLAS, D. and WANG, R. W., 1998, Identification of cytochrome P4503A4 as the major enzyme responsible for the metabolism of ivermectin by human liver microsomes. *Xenobiotica*, **28**, 313–321.

XENOBIOTICA , 2000, VOL. 30, NO. 1, 81–92

Pronounced differences in inhibition potency of lactone and non-lactone compounds for mouse and human coumarin 7-hydroxylases (CYP2A5 and CYP2A6)

R. O. JUVONEN†*, J. GYNTHER‡, M. PASANEN¶, E. ALHAVA§ and A. POSO‡

† Departments of Pharmacology and Toxicology, ‡ Pharmaceutical Chemistry and § Surgery, University of Kuopio, PO Box 1627, 70211 Kuopio, Finland
¶ Department of Pharmacology, University of Oulu, Kajaanintie 52 A, 90220 Oulu, and National Agency for Medicines, Helsinki, Finland

Received 5 July 1999

1. The structural requirements for a compound to be a potent inhibitor for mouse CYP2A5 and human CYP2A6 enzymes catalysing coumarin 7-hydroxylase activity have been studied.

2. The IC_{50} of 28 compounds for the pyrazole-treated male DBA/2 mouse and human liver microsomal coumarin 7-hydroxylation were determined at 10 μM coumarin concentration 15 times over K_m of coumarin.

3. The three most potent inhibitors for CYP2A5 were γ-nonanoic lactone, γ-decanolactone and γ-phenyl-γ-butyrolactone with an $IC_{50} = 1.9 \pm 0.4$, 2.1 ± 0.2 and 2.4 ± 0.3 μM and for CYP2A6 7-methylcoumarin, butylcyclohexane and indan with an $IC_{50} = 30 \pm 3.2$, 43 ± 9 and 50 ± 11 μM.

4. Among the 28 compounds studied, only 2-benzoxazolinone, 2-indanone and γ-valerolactone showed similar inhibitory activity in both species. Indan had a lower IC_{50} for human than for mouse coumarin 7-hydroxylation, whereas the IC_{50} of 24 other compounds was higher for human than for mouse coumarin 7-hydroxylation.

5. The largest difference in IC_{50} between mouse and human activity was observed with 5-substituted phenyl, pentyl, hexyl, heptyl or octyl γ-lactones or 6-substituted δ-lactones. IC_{50} of γ-undecanolactone and γ-decanolactone was 500 times lower for mouse than human coumarin 7-hydroxylation.

6. The difference in the IC_{50} between human and mouse coumarin 7-hydroxylation decreased substantially with the corresponding compounds without the lactone ring.

7. It is concluded that certain 5- or 6-position substituted γ- and δ-lactones are potent inhibitors for mouse CYP2A5 but not for the orthologous human CYP2A6 and that the active site of CYP2A6 could be smaller than the active site of CYP2A5.

Introduction

Mouse CYP2A5 and its human counterpart, CYP2A6, are key enzymes in the elimination of coumarin and in the bioactivation of some promutagens and procarcinogens (Chang and Waxman 1996, Honkakoski and Negishi 1997, Pelkonen *et al*. 1997). CYP2A6 plays a major role in nicotine C-oxidation in human (Messina *et al*. 1997). CYP2A5 and CYP2A6 are in liver, share 82% amino acid similarity and are the principal enzymes of liver microsomes catalysing the hydroxylation of coumarin in the 7-position (Miles *et al*. 1990, Yamano *et al*. 1990, Chang and Waxman 1996). Coumarin 7-hydroxylation is a highly specific and widely used probe reaction for mouse liver CYP2A5 and human liver CYP2A6 (Chang and

* Author for correspondence; e-mail. risto.juvonen@uku.fi

Xenobiotica ISSN 0049–8254 print/ISSN 1366–5928 online © 2000 Taylor & Francis Ltd
http://www.tandf.co.uk/journals/tf/00498254.html

Waxman 1996, Draper *et al.* 1997, Pelkonen *et al.* 1997). In liver microsomes of the pyrazole-treated DBA/2N mouse, no other CYP enzymes catalyse this activity (Juvonen *et al.* 1985, Negishi *et al.* 1989). The polyclonal antibody against purified CYP2A5 inhibits 100% of coumarin 7-hydroxylase activity and the other mouse CYP2A members, CYP2A4 and CYP2A12, do not have any coumarin 7-hydroxylase activity (Lang *et al.* 1989, Lindberg and Negishi 1989, Raunio *et al.* 1998). In human, only CYP2A6 catalyses coumarin 7-hydroxylation (Raunio *et al.* 1990, Yamano *et al.* 1990, Yun *et al.* 1991, Ding *et al.* 1995). Therefore, *in vitro* inhibition of coumarin 7-hydroxylation in mouse and human liver microsomes by the compounds tested herein reflects only the inhibition of CYP2A5 or CYP2A6.

In vitro inhibition studies have shown that only pilocarpine inhibits coumarin 7-hydroxylation with almost equal potency in mouse and human liver microsomes (Mäenpää *et al.* 1993, Kinonen *et al.* 1995), whereas the linear furanocoumarins of psoralen, bergapten, imperatorin and isopimpinellin, and the angular furanocoumarin, pimpinellin and metyrapone more potently inhibit mouse coumarin 7-hydroxylation than human coumarin 7-hydroxylation (Mäenpää *et al.* 1993, Draper *et al.* 1997). Moreover, 7-ethoxycoumarin *O*-deethylation exhibits a much higher turnover number by CYP2A5 than by CYP2A6 (Juvonen *et al.* 1988, Yun *et al.* 1991) and only menadione and angelicin have been shown to be more potent at inhibiting human than mouse coumarin 7-hydroxylation. The above data indicate that CYP2A5 and 2A6 have much in common in their substrate/inhibitor specificity, but there are some fundamental differences in the nature of the compounds causing inhibition as well as in turnover of substrates. The reasons for those differences remain unknown.

In the current study, systematic inhibition experiments of mouse and human liver microsomal coumarin 7-hydroxylation activities were performed to determine the chemical characteristics that influence the inhibition potency of compound for CYP2A5 and CYP2A6 and to identify potent inhibitors for these enzymes. Twenty-eight commercially available compounds, most of which contained a lactone structure, were tested to determine their IC_{50} for both mouse and human coumarin 7-hydroxylation. Surprisingly, remarkable differences in inhibition potency of mouse and human coumarin 7-hydroxylation were observed with γ- and δ-lactone derivatives.

Materials and methods

Chemicals

γ-Butyrolactone, δ-valerolactone, 5,6-dihydro-2H-pyrano-2-one, 2H-pyran-2-one, ε-caprolactone, γ-valerolactone, γ-caprolactone, γ-heptalactone, γ-octanoic lactone, γ-nonanoic lactone, γ-decanolactone, γ-undecanolactone, γ-dodecanolactone, δ-hexalactone, δ-decanolactone, δ-undecanoic lactone, 2-coumarone, 2-indanone, 2,3-dihydrobenzofuran, indan, 2-benzoxazolinone, 7-methylcoumarin, butylcyclohexane, butylbenzene, biphenyl, γ-phenyl-γ-butyrolactone, 4-methoxy-2(5H)-furanone and 4,6-dimethyl-α-pyrone were the highest purity available, usually 99% pure as indicated by the manufacturer (Aldrich-Chemie GmbH & Co. KG, Heidenheim, Germany) (figure 1).

Biological material

Male (7–12 weeks old, 15–25 g body weight) DBA/2N//Kuo mice were given pyrazole in saline (150 mg kg^{-1}, i.p.) on three consecutive mornings and killed 24 h after the last injection. Livers were removed into ice cold saline and pooled microsomes prepared as described by Lang and Nebert (1981). The Ethics Committee for Animal Experiments, University of Kuopio approved these experiments. Human liver samples were from patients undergoing surgery in connection with laparoscopy with the approval of the Ethics Committee of the University of Kuopio. Liver samples were frozen in liquid

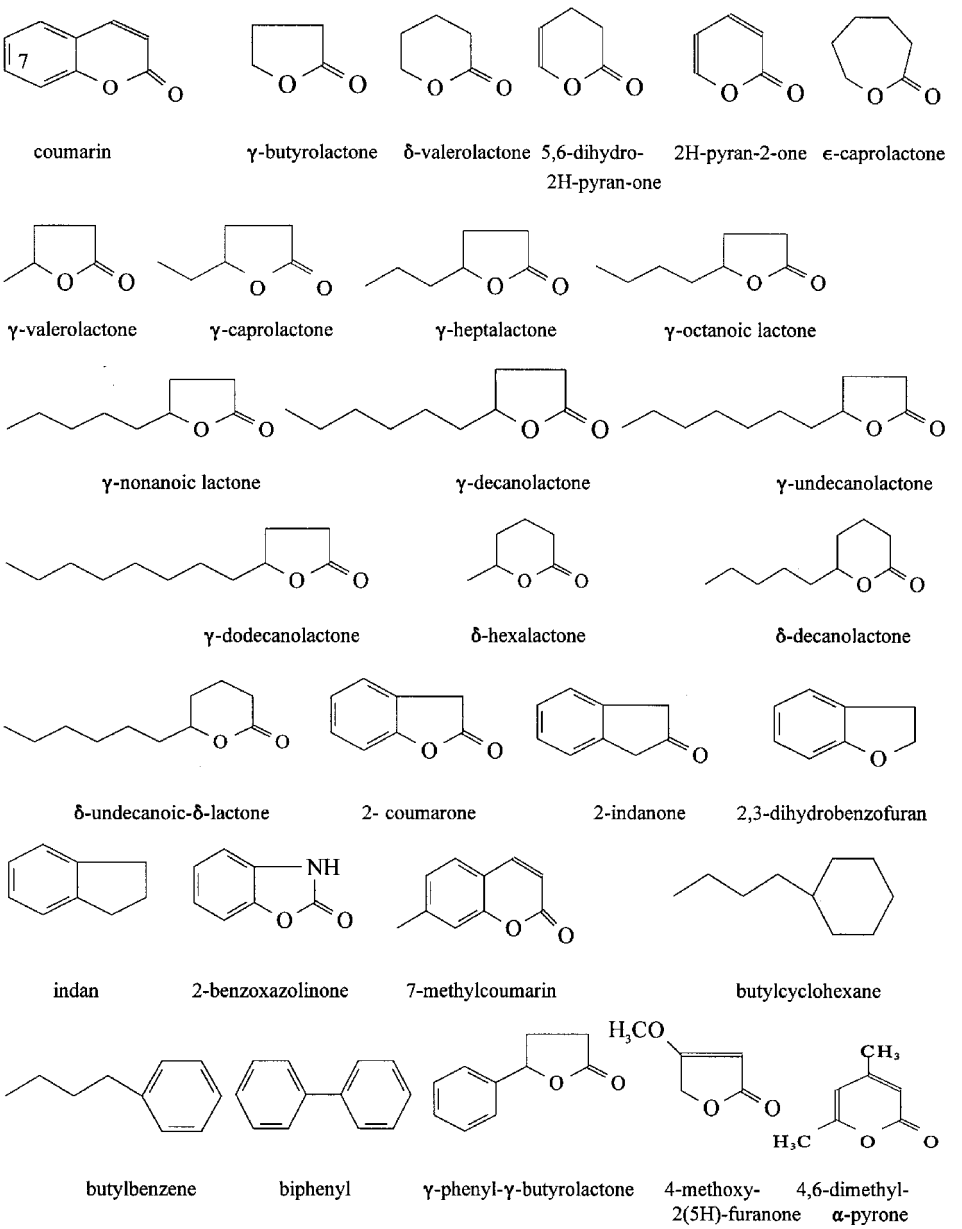


Figure 1. Chemical structures of coumarin and 28 compounds whose inhibition potency against mouse and human liver microsomal coumarin 7-hydroxylase were tested.

nitrogen and stored at − 80 °C. Only tissue free of tumour was used. The preparation of microsomes was made within 1 week of biopsy according to Lang and Nebert (1981). Female patients HL16, HL212 and HL237 have been described previously by Kimonen *et al.* (1995).

Biochemical assays

Microsomal protein was determined by the method of Smith *et al.* (1985). The 7-hydroxycoumarin formed was measured as described by Aitio (1978). The incubation mixture contained 50–200 μg microsomal protein, 10 μM coumarin, 0–0.4 M inhibitor, 2% ethanol (as a solvent for coumarin and inhibitors), 5 mM $MgCl_2$, 0.5 mM NADPH in 0.5 ml 50 mM Tris-HCl buffer, pH 7.4, in a total volume

of 0.5 ml. The mixture was incubated for 10 min, stopped by adding 0.5 ml 6% trichloroacetic acid, centrifuged for 10 min at 3000*g*, 0.5 ml supernatant mixed with 2 ml 1.6 M glycine buffer, pH 10.4, just before the transfer into a cuvette and the fluoresence was measured immediately using 440 nm emission and 390 nm excitation. Two blank reactions were used in the incubation mixture, one with inhibitor but no coumarin, the other being the mixture in which the reaction was stopped before addition of NADPH. This 7-hydroxycoumarin assay can detect 10 pmol 7-hydroxycoumarin and its reproducibility in different working days is < 15%. In the case of 4-methoxy-2(5H)-furanone and 4,6-dimethyl-α-pyrone, these fluoresences differed and hence both blank fluoresences were subtracted from the total fluoresence of the reaction.

Analysis of inhibition data

The analysis of IC_{50} was carried out from three measurements of different pooled mouse or individual human microsomes with the non-linear analysis for one binding site in the Prism 2.0 NW program.

Results

Inhibition of mouse and human liver coumarin 7-hydroxylation

The IC_{50} of 28 compounds for mouse and human liver coumarin 7-hydroxylase activity was determined in dose–response experiments (figures 2 and 3, table 1.). The three lowest IC_{50} (~ 2 μM) were obtained with γ-nonanoiclacotne, γ-decanolactone and γ-phenyl-γ-butyrolactone, and values as high as 19 mM were obtained with γ-butyrolactone for mouse coumarin 7-hydroxylation. IC_{50} for human coumarin 7-hydroxylation was distributed between the lowest value of 30 μM 7-methylcoumarin and the highest value of 350 mM γ-butyrolactone. Most of the compounds more potently inhibited mouse rather than human coumarin 7-hydroxylase.

The simple lactone rings were weak inhibitors of both mouse and human coumarin 7-hydroxylase (table 1, and A and B panels in figures 2 and 3). As the size of the lactone ring increased, IC_{50} for both hydroxylase activities decreased. There was a slight tendency to a more potent inhibition of both mouse and human coumarin 7-hydroxylases by increasing the content of double bonds of six atom lactone ring. According to these results, the size of the lactone ring determines its potency to inhibit mouse and human coumarin 7-hydroxylation.

When the size of inhibitor was increased with any substituent in either the five or six atom lactone ring, IC_{50} decreased as compared with the unsubstituted lactones (table 1, and figures 2 and 3). Five-substituted γ-lactones and 6-substituted δ-lactones exhibited progressively lower IC_{50} when the side-chain length increased from methyl to pentyl group such that the IC_{50} decreased almost 40 times for human coumarin 7-hydroxylase but > 3000 times for mouse (figures 2–4). The longest side-chains of six or seven carbons did not improve or even decrease the inhibition potency of lactones for both mouse and human coumarin 7-hydroxylase. γ-Phenyl-γ-butyrolactone was one of the most potent inhibitors for both enzymes. Interestingly, 2-coumarone, a smaller analogue of coumarin has a five and 30 times higher IC_{50} for mouse and human coumarin 7-hydroxylase than the 10 μM substrate concentration in the incubation mixture. In contrast, the compound with one methyl group more than coumarin, 7-methylcoumarin, had an IC_{50} lower than 10 μM coumarin concentration for the mouse but higher for the human coumarin 7-hydroxylase. In summary, it can be concluded that substituents at 5- and 6-positions of γ- and δ-lactones decrease the IC_{50} of a compound for coumarin 7-hydroxylation, such that the optimum size of inhibitor is the size of γ-octanoiclactone, γ-nonanoiclactone, γ-decanolactone, γ-phenyl-γ-butyrolactone or δ-decanolactone.

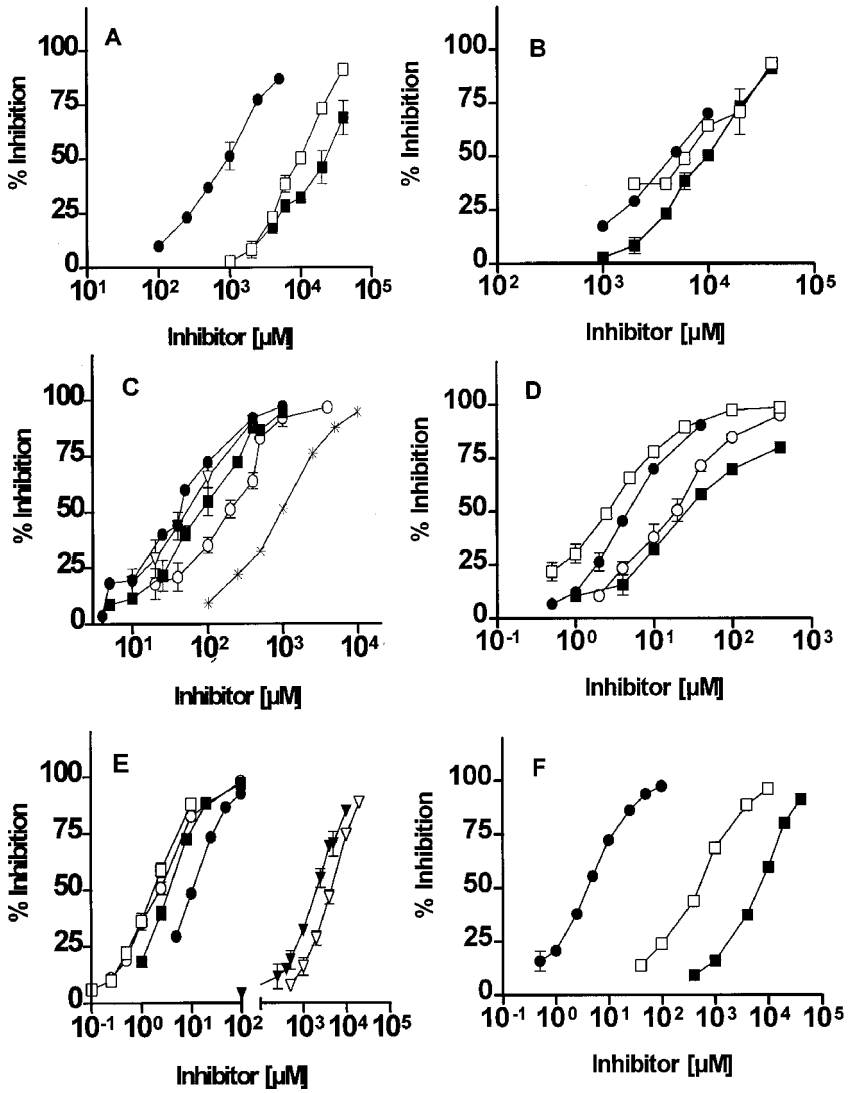


Figure 2. Inhibition of mouse coumarin 7-hydroxylase. DBA/2N mouse liver microsomal coumarin 7-hydroxylase activity using 10 μM coumarin concentration was inhibited by increasing concentrations of various compounds. (A) ε-Caprolactone (●), δ-valerolactone (□); γ-butyrolactone (■). (B) δ-Valerolactone (■), 5,6-dihydro-2H-pyran-2-one (□); 2H-pyran-2-one (●). (C) 2-Coumaranone (●), 2-indanone (▽), 2,3-dihydrobenzofuran (■), indan (○); benzoxazolinone (*). (D) γ-Phenyl-γ-butyrolactone (□), butylcyclohexane (●), butylbenzene (○); biphenyl (■). (E) γ-Valerolactone (▽), δ-hexalactone (▽), γ-nonanoiclactone (□), δ-decanoiclactone (■), γ-decanoiclactone (○); δ-undecanoiclactone (●). (F) 7-Methylcoumarin (●), 4,6-dimethyl-α-pyrone (□) and 4-methoxy-2(5H)-furanone (■) were used as inhibitors. Results are the average of three different samples.

Although the lactone structure of a compound is important for inhibiting mouse and human coumarin 7-hydroxylations (Juvonen *et al.* 1991), compounds also lacking a lactone ring can inhibit this enzyme. Surprisingly, butylcyclohexane was a potent inhibitor for both coumarin 7-hydroxylases such that its IC_{50} was equal for the mouse activity and five-to-six times lower for the human activity compared with the IC_{50} of corresponding γ-octanoic lactone (figures 1 and 2, D, and table 1). If the

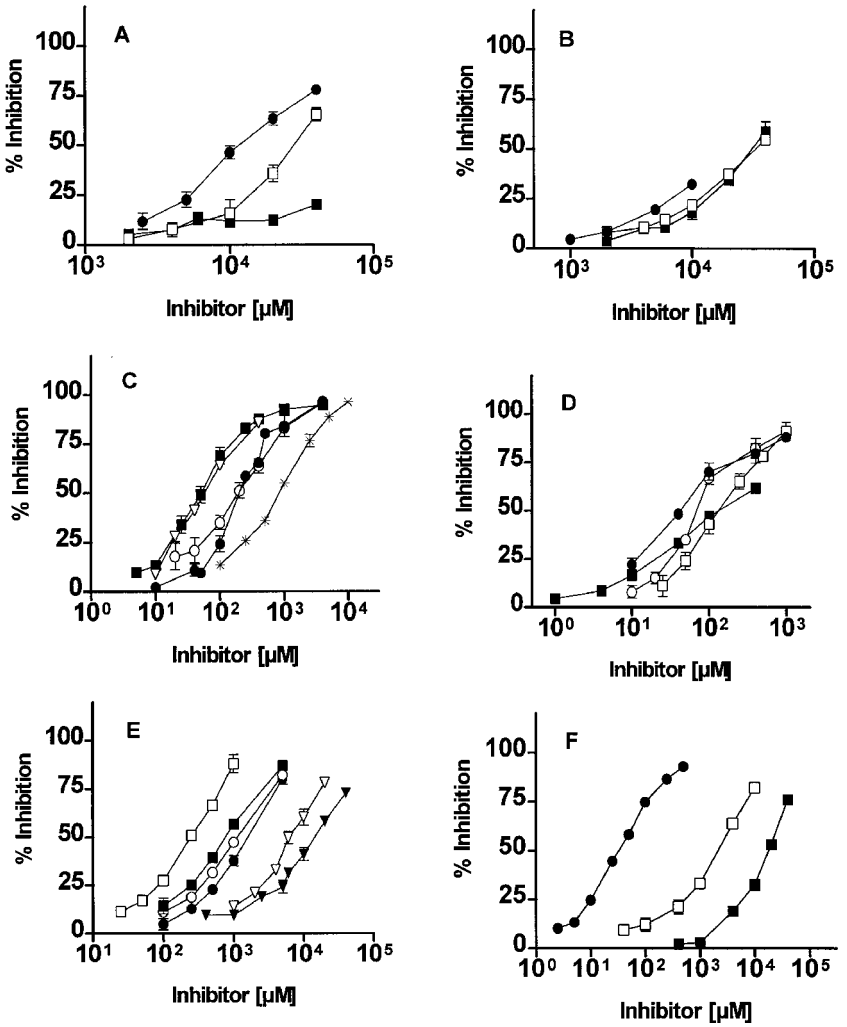


Figure 3. Inhibition of human coumarin 7-hydroxylase. Human liver microsomal coumarin 7-hydroxylase activity using 10 μM coumarin concentration was inhibited by increasing concentrations of various compounds. (A) ε-Caprolactone (●), δ-valerolactone (□); γ-butyrolactone (■). (B) δ-Valerolactone (■), 5,6-dihydro-2H-pyran-2-one (□); 2H-pyran-2-one (●). (C) 2-Coumaranone (●), 2-indanone (▽), 2,3-dihydrobenzofuran (■), indan (○); benzoxazolinone (*). (D) γ-Phenyl-γ-butyrolactone (□), butylcyclohexane (●), butylbenzene (○); biphenyl (■). (E) γ-Valerolactone (▽), δ-hexalactone (▽), γ-nonanoiclactone (□), δ-decanoiclactone (■), γ-decanoiclactone (○); δ-undecanoiclactone (●). (F) 7-Methylcoumarin (●), 4,6-dimethyl-α-pyrone (□) and 4-methoxy-2(5H)-furanone (■) were used as inhibitors. Results are the average of three different human samples.

cyclohexane ring was replaced by phenyl, the IC_{50} of butylbenzene increased 1.7–2.8 times. Furthermore, the IC_{50} of biphenyl was somewhat higher but still < 100 μM. Indan and 2,3-dihydrobenzofuran (lacking the carbonyl group) exhibited almost a twice higher IC_{50} for mouse coumarin 7-hydroxylase than 2-coumarone and 2-indanone. However, indan and 2-indanone were equally potent inhibitors for human coumarin 7-hydroxylase and 2-coumarone was the least potent in this series of compounds. When a nitrogen atom replaced the carbon atom 3 of 2-coumarone, the IC_{50} of benzoxazolinone was increased considerably compared with 2-

Table 1. IC_{50} of 28 compounds tested toward mouse and human coumarin 7-hydroxylation. Mouse and human coumarin 7-hydroxylation (using 10 μM coumarin concentration) was inhibited with increasing concentrations of inhibitors. IC_{50} and its 95 % confidence intervals in parenthesis were determined from dose–response curves of three separate experiments.

Compound	Mouse IC_{50} (μM)		Human IC_{50} (μM)	
γ-Butyrolactone	19000	(7900–30000)	350000	(100000–500000)
δ-Valerolactone	9800	(5000–15000)	29000	(10000–50000)
5,6-Dihydro-2H-pyran-2-one	6100	(4600–7600)	33000	(21000–49000)
2H-Pyran -2-one	5300	(4600–7600)	22000	(16000–25000)
ε-Caprolactone	890	(530–1200)	16000	(10000–22000)
γ-Valerolactone	5900	(4900–5700)	8300	(6100–11000)
γ-Caprolactone	720	(570–860)	3800	(3100–4600)
γ-Heptalactone	29	(21–36)	560	(470–650)
γ-Octanoic lactone	5.7	(5.1–6.3)	250	(190–310)
γ-Nonanoic lactone	1.9	(1.6–2.3)	240	(170–310)
γ-Decanolactone	2.1	(1.9–2.3)	1100	(940–1200)
γ-Undecanolactone	3.9	(3.5–4.3)	2100	(1600–2700)
γ-Dodecanolactone	3.9	(3.0–4.8)	1100	(600–1600)
δ-Hexalactone	2200	(1700–2600)	12000	(9000–16000)
δ-Decanolactone	3.8	(3.2–4.4)	740	(620–850)
Undecanoic-δ-lactone	12	(9.6–14)	2200	(1500–2900)
2-Coumarone	47	(40–54)	300	(180–430)
2-Indanone	51	(31–71)	57	(45–68)
2,3-Dihydrobenzofuran	80	(66–93)	180	(130–220)
Indan	84	(65–103)	50	(42–58)
2-Benzoxazolinone	1100	(910–1200)	870	(750–990)
7-Methylcoumarin	4.0	(3.5–4.4)	30	(27–34)
Butylcyclohexane	5.7	(4.5–6.9)	43	(25–61)
Butylbenzene	16	(13–20)	75	(53–97)
Biphenyl	29	(23–36)	82	(59–105)
γ-Phenyl-γ-butyrolactone	2.4	(2.1–2.7)	160	(110–210)
4-Methoxy-2(5H)-furanone	7200	(6100–8400)	18000	(10000–27000)
4,6-Dimethyl-α-pyrone	420	(340–490)	1600	(1000–2100)

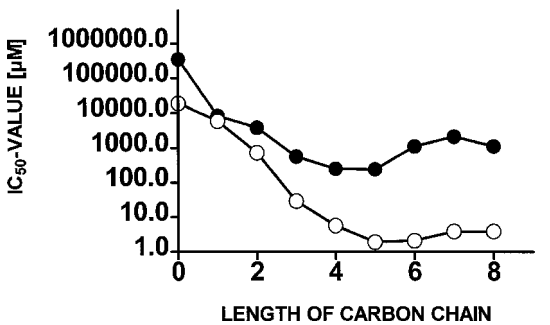


Figure 4. Effect of the size of γ-lactones on the inhibition of coumarin 7-hydroxylations. Mouse (○) and human (●) liver microsomal coumarin 7-hydroxylation were inhibited at 10 μM coumarin concentration by nine different γ-lactones (γ-butyrolactone, γ-valerolactone, γ-caprolactone, γ-heptalactone, γ-octanoiclactone, γ-nonanoiclactone, γ-decanoiclactone, γ-undecanoiclactone, γ-dodecanoiclactone) and then their was IC_{50} determined. Number on the x-axis is the length of alkyl side-chain in position 5 of γ-lactones. Each point is the average of three different experiments.

coumarone. These results indicate that nitrogen as an electron pair donating atom in the lactone ring of a compound substantially increases the IC_{50} for coumarin 7-hydroxylation and that compounds of optimum size but without the lactone ring also have a low IC_{50} .

Table 2. Comparison of IC_{50} between human and mouse coumarin 7-hydroxylation. A human/mouse IC_{50} ratio for each inhibitor was calculated by dividing the IC_{50} for human coumarin 7-hydroxylation by the IC_{50} for mouse coumarin 7-hydroxylation. IC_{50} are indicated in table 1.

Inhibitor	Human/mouse IC_{50} ratio
Indan	0.59
2-Benzoxazolinone	0.79
2-Indanone	1.1
γ-Valerolactone	1.4
2,3-Dihydrobenzofuran	2.3
4-Methoxy-2(5H)-furanone	2.5
Biphenyl	2.8
δ-Valerolacatone	3.0
4,6-Dimethyl-α-pyrone	3.8
2H-Pyran-2-one	4.2
Butylbenzene	4.7
γ-Caprolactone	5.3
5,6-Dihydro-2H-pyrano-2-one	5.4
δ-Hexalactone	5.7
2-Coumaranone	6.4
Butylcyclohexane	7.5
7-Methylcoumarin	7.5
ε-Caprolactone	18.0
γ-Butyrolactone	18.4
γ-Heptalactone	19.3
γ-Octanoiclactone	43.9
γ-Phenyl-γ-butyrolactone	66.7
γ-Nonanoiclactone	126
Undecanoic-δ-lactone	183
δ-Decanolactone	195
γ-Dodecanolactone	282
γ-Decanolactone	523
γ-Undecanolactone	538

Comparison of inhibition between mouse and human coumarin 7-hydroxylation

The tested compounds could be divided to three groups according to the difference in their IC_{50} between mouse and human coumarin 7-hydroxylation. For this purpose, a human to mouse IC_{50} ratio for each inhibitor was calculated by dividing the human by the mouse IC_{50} for coumarin 7-hydroxylation (table 2). Compounds in the first group were clearly more potent for human coumarin 7-hydroxylase than for mouse coumarin 7-hydroxylase and, therefore, their human to mouse IC_{50} ratio was < 0.67. Only indan belonged to this group. Compounds in the second group inhibited coumarin 7-hydroxylation equally potently in both species and their human mouse IC_{50} ratio was between 0.67 and 1.49. 2-Benzoxazolinone, 2-indanone and γ-valerolactone were classified in this group as should also the probe substrate, coumarin, because the K_m of coumarin for both mouse and human coumarin 7-hydroxylase reactions is equal, ~ 1 μM (Juvonen *et al*. 1991, Kinonen *et al*. 1995, Draper *et al*. 1997). All of the other compounds belonged to the third group whose human mouse IC_{50} ratio was > 1.49.

However, in the third group, it was possible to separate a further three subgroups: The human mouse IC_{50} ratio of 2,3-dihydrobenzofuran, 4-methoxy-2(5H)-furanone, biphenyl, δ-valerolactone, 4,6-dimethyl-α-pyrone, 2H-pyran-2-one, butylbenzene, γ-caprolactone, 5,6-dihydro-2H-pyran-2-one, δ-hexalactone, 2-coumaranone, butylcyclohexane and 7-methylcoumarin varied between 1.5 and 10

indicating that they more potently inhibit mouse rather than human coumarin 7-hydroxylation. Caprolactone, γ-butyrolactone, γ-heptalactone, γ-octanoic lactone and γ-phenyl-γ-butyrolactone inhibited much more potently mouse than human coumarin 7-hydroxylation, such that the human to mouse IC_{50} ratios were between 10 and 70. The human-to-mouse IC_{50} ratios for the compounds of the third subgroup were >70 and indicated that they were even more potent inhibitors for mouse than for human coumarin 7-hydroxylation. γ-Nonanoic lactone, undecanoic-δ-lactone, δ-decanolactone, γ-dodecanolactone, γ-decanolactone and γ-undecanolactone belonged to this latter group.

Discussion

Species-dependent differences in the inhibition of mouse CYP2A5 and human CYP2A6 have been studied and eight new lactone compounds and one non-lactone compound were potent inhibitors (IC_{50} < 10 μM) for mouse liver microsomal coumarin 7-hydroxylase (i.e. CYP2A5) *in vitro*. The lactone compounds were γ-octanoic lactone, γ-nonanoic lactone, γ-decanolactone, γ-dodecanolactone, γ-dodecanolactone, δ-decanolactone, γ-phenyl-γ-butyrolactone and 7-methylcoumarin, and non-lactone compound was butylcyclohexane. However, they all were much less potent inhibitors of human liver microsomal coumarin 7-hydroxylase (i.e. CYP2A6). Interestingly, the difference in inhibition potency between CYP2A5 and CYP2A6 with γ-decanolactone and γ-undecanolactone were as high as 500 times. Second, some lactone-containing compounds were more potent inhibitors than the corresponding compounds without the lactone structure in the case of CYP2A5 but vice versa in the case of CYP2A6. Third, according to the results of this study the active site of CYP2A5 could be smaller than the active site of CYP2A6.

The three most potent inhibitors of CYP2A5 in this study were γ-nonanoiclactone, γ-decanolactone and γ-phenyl-γ-butyrolactone whose IC_{50} were ~ 2 μM and five times smaller than the substrate concentration used in the assay. That means that their K_i are also smaller than the 0.74 μM K_m of coumarin for CYP2A5 (Kinonen *et al.* 1995) and their K_i would be 0.1–0.2 μM. Methoxsalen is an even more potent CYP2A5 inhibitor and it is also equally potent inhibitor for CYP2A6 (Mäenpää *et al.* 1993, Draper *et al.* 1997). Other known potent inhibitors of CYP2A5 are pilocarpine, metyrapone, miconatzole, psoralen and some other furanocoumarins (Mäenpää *et al.* 1993, Kimonen *et al.* 1995, Kinonen *et al.* 1995). Metyrapone, psoralen and furanocoumarins are much less potent inhibitors of CYP2A6 than CYP2A5, as were many inhibitors examined in this study (Mäenpää *et al.* 1993, Draper *et al.* 1997). Therefore, these orthologous mouse and human CYP enzymes show inhibitor specificity differences with certain chemical structures although they catalyse similarly coumarin 7-hydroxylation and are inhibited similarly by pilocarpine.

The difference in substrate/inhibitor specificity between CYP2A5 and CYP2A6 is understandable since the substrate specificity of CYP enzymes can be determined by the types of amino acid residues at only a few key positions (Lindberg and Negishi 1989, Matsunaga *et al.* 1990, Halpert and He 1993, Sraub *et al.* 1994) and since the amino acid similarity between CYP2A5 and CYP2A6 is only 82% (Miles *et al.* 1990, Yamano *et al.* 1990). According to the alignment study of Gotoh (1992) there are six substrate recognition sites in the amino acid sequences of CYP2

enzymes. Although these sites are highly homologous there are some differences between CYP2A5 and CYP2A6. At the moment it is too speculative to indicate which amino acid residues are responsible for the differences in inhibition specificity. However, this study gives excellent tools to study this question, e.g. by site-directed mutagenesis or computer modelling.

In the current study, larger compounds were poorer inhibitors for CYP2A6 than for CYP2A5 catalysed coumarin 7-hydroxylation, which could be interpreted that the active site of CYP2A6 is smaller than the active site of CYPA5. In contrast, it should be noted that methoxsalen, a relatively large compound, is almost an equally potent inhibitor of both enzymes (Mäenpää *et al.* 1993, Draper *et al.* 1997). However, several experimental results support the idea that the size of the active sites of these CYPs differ. First, the optimum length of the 5-alkyl side-chain in γ-butyrolactones was longer for CYP2A5 than for CYP2A6 such that butyl and pentyl side-chains were optimal for CYP2A6 and pentyl and hexyl for CYP2A5 activities. Second, the K_m for coumarin was similar for CYP2A5 and CYP2A6; however, the IC_{50} of 7-methylcoumarin differed seven times between these enzymes. The IC_{50} of 7-methylcoumarin was half of the coumarin concentration in the assay indicating that this larger compound interacts better than coumarin with the active site of CYP2A5. However, the IC_{50} of 7-methylcoumarin increased three times compared with the coumarin concentration in the incubation mixture indicating a possible reduction of its interaction in the active site of CYP2A6. Linear furanocoumarins (e.g. bergapten, imperatorin and isopimpinellin being larger compounds than coumarin) were also weaker inhibitors for CYP2A6 than CYP2A5 (Mäenpää *et al.* 1993). Therefore, the size of the active site of CYP2A6 appears to be smaller than that of CYP2A5.

Parkinson's and Pelkonen's groups have produced much useful information of the structure–activity relationship of CYP2A5 and CYP2A6 enzymes by examining inhibitory effects of many common drugs and model compounds used in biotransformation studies (Mäenpää *et al.* 1993, Draper *et al.* 1997). Their studies were valuable to evaluate if CYP2A5 and CYP2A6 could be involved in the metabolism of tested compounds and if CYP2A6 is involved in drug interactions. This study demonstrates that occupational chemicals tested in experimental animals may possess substantial differences in their effects on human biochemical parameters compared with animal models. According to previous studies, 2-coumarone and undecanoic-δ-lactone are competitive type inhibitors of recombinant CYP2A5 and mouse liver microsomal coumarin 7-hydroxylation *in vitro* (Juvonen *et al.* 1991, Asikainen *et al.* 1996). The inhibitory effect of other tested compounds for mouse coumarin 7-hydroxylation was reduced when the concentration of coumarin was increased (unpublished data) and they could, therefore, also be competitive inhibitors. However, to confirm the type of inhibition, further studies are needed.

In summary, the inhibition potency of 28 compounds for mouse and human liver microsomal coumarin 7-hydroxylase catalysed by CYP2A5 and CYP2A6 enzymes were tested. Interestingly, the most potent inhibitory compounds like γ-octanoic lactone, γ-nonanoic lactone, γ-decanolactone, γ-undecanolactone, γ-dodecanolactone, δ-decanolactone, undecanoic-δ-lactone and γ-phenyl-γ-butyrolactone were potent inhibitors for CYP2A5 but more than two orders of magnitude less potent for CYP2A6. The IC_{50} makes it possible to compare inhibition potencies between the compounds or to undertake structure–activity relationship studies with computer modelling.

Acknowledgements

The authors thank Pirjo Hänninen and Jaana Leskinen for excellent technical help, and Ewen MacDonald, Paavo Honkakoski and Olavi Pelkonen for critical and constructive comments. The help of Tapio Nevalainen is also appreciated.

References

Aitio, A., 1978, A simple and sensitive assay of 7-ethoxycoumarin deethylation. *Analytical Biochemistry*, **85**, 488–491.

Asikainen, J., Pasanen, M. and Juvonen, R. O., 1996, Inhibition of mice coumarin 7-hydroxylase bu undecanoic σ-lacton, benzoxazole and 2H-pyran-2-one. *Experimental and Toxicologic Pathology*, **48 (suppl. II)**, 13–17.

Chang, T. K. H. and Waxman, D. J., 1996, The CYP2A subfamily. In C. Ioannides (ed.), *Cytochromes P450: Metabolic and Toxicological Aspects* (Boca Raton: CRC Press), pp. 99–134.

Ding, S., Lake, B. G., Friedberg, T. and Wolf, C. R., 1995, Expression and alternative splicing of the cytochrome P-450 CYP2A7. *Biochemical Journal*, **306**, 161–166.

Draper, A. J., Madan, A. and Parkinson, A., 1997, Inhibition of coumarin 7-hydroxylase activity in human liver microsomes. *Archives of Biochemistry and Biophysics*, **341**, 47–61.

Gotoh, O., 1992, Substrate recognition sites in cytochrome P450 family 2 (CYP2) proteins inferred from comparative analyses of amino acid and coding nucleotide sequences. *Journal of Biological Chemistry*, **267**, 83–90.

Halpert, J. R. and He, Y., 1993, Engineering of cytochrome P4502B1 specificity: conversion of an androgen 16β-hydroxylase to a 15α-hydroxylase. *Journal of Biological Chemistry*, **268**, 4453–4457.

Honkakoski, P. and Negishi, M., 1997, The structure, function and regulation of cytochrome P4502A enzymes. *Drug metabolism reviews*, **29**, 977–996.

Juvonen, R. O., Iwasaki, M. and Negishi, M., 1991, Structural function of residue-209 in coumarin 7-hydroxylase (P450coh). Enzyme-kinetic studies and site-directed mutagenesis. *Journal of Biological Chemistry*, **266**, 16431–16435.

Juvonen, R. O., Kaipainen, P. K. and Lang, M. A., 1985, Selective induction of coumarin 7-hydroxylase by pyrazole in D2 mice. *European Journal of Biochemistry*, **152**, 3–8.

Juvonen, R. O., Shkumatov, V. M. and Lang, M. A., 1988, Purification and characterization of a liver microsomal cytochrome P-450 isoenzyme with a high affinity and metabolic capacity for coumarin from pyrazole-treated D2 mice. *European Journal of Biochemistry*, **171**, 205–211.

Kimonen, T., Juvonen, R. O., Alhava, E. and Pasanen, M., 1995, The inhibition of CYP enzymes in mouse and human liver by pilocarpine. *British Journal of Pharmacology*, **114**, 832–836.

Kinonen, T., Pasanen, M., Gynther, J., Poso, A., Järvinen, T., Alhava, E. and Juvonen, R. O., 1995, Competitive inhibition of coumarin 7-hydroxylation by pilocrpine and its interaction with mouse CYP 2A5 and human CYP 2A6. *British Journal of Pharmacology*, **116**, 2625–2630.

Lang, M. A., Juvonen, R. O., Järvinen, P., Honkakoski, P. and Raunio, H., 1989, Mouse liver P450coh: genetic regulation of the pyrazole-inducible enzyme and comparison with other P450 isoenzymes. *Archives of Biochemistry and Biophysics*, **271**, 139–148.

Lang, M. A. and Nebert, D. W., 1981, Structural gene products of the Ah locus. Evidence for many unique P-450-mediated monooxygenase activities reconstituted from 3-methylcholantrene-treated C57BL/6N mouse liver microsomes. *Journal of Biological Chemistry*, **256**, 12058–12067.

Lindberg, R. L. P. and Negishi, M., 1989, Alteration of mouse cytochrome P450coh substrate specificity by mutation of a single amino-acid residue. *Nature*, **339**, 632–634.

Mäenpää, J., Sigusch, H., Raunio, H., Syngelmä, T., Vuorela, P., Vuorela, H. and Pelkonen, O., 1993, Differential inhibition of coumarin hydroxylase activity in mouse and human liver microsomes. *Biochemical Pharmacology*, **45**, 1035–1042.

Matsunaga, E., Zeugin, T., Zanger, U. M., Aoyama, T., Meyer, U. A. and Gonzalez, F. J., 1990, Sequence requirements for cytochrome P-450IID1 catalytic activity: a single amino acid change (ILE380Phe specifically decreases V_{max} of the enzyme for bufuralol but not debrisoquine hydroxylation. *Journal of Biological Chemistry*, **265**, 17197–17201.

Messina, E. S., Tyndale, R. F. and Sellers, E. M., 1997, A major role for CYP2A6 in nicotine C-oxidation by human liver microsomes. *Journal of Pharmacology and Experimental Therapeutics*, **282**, 1608–1614.

Miles, J. S., McLare, A. W., Forrester, L. M., Glancey, M. J., Lang, M. A. and Wolf, C. R., 1990, Identification of the human liver cytochrome P-450 responsible for coumarin 7-hydroxylase activity. *Biochemical Journal*, **267**, 365–371.

Negishi, M., Lindberg, R., Burkhart, B., Ichikawa, T., Honkakoski, P. and Lang, M., 1989, Mouse steroid 15alpha-hydroxylase gene family: identification of type II P-450(15)alpha as coumarin 7-hydroxylase. *Biochemistry*, **28**, 4169–4172.

Pelkonen , O., Raunio , H., Rautio , A., Pasanen , M. and Lang , M. A., 1997, The metabolism of coumarin. In *Coumarins*: *Biology*, *Applications and Mode of Action* (Chichester: John Wiley), pp. 67–92.

Raunio , H., Juvonen , R., Pasanen , M., Pelkonen , O., Pääkkö, P. and Soini , Y., 1998, Cytochrome P4502A6 (CYP2A6) expression in human hepatocellular carcinoma. *Hepatology*, **27**, 427–432.

Raunio , H., Valtonen , J., Honkakoski , P., Lang , M. A., Stahlberg , M., Kairaluoma , M. A., Rautio , A., Pasanen , M. and Pelkonen , O., 1990, Immunochemical detection of human liver cytochrome P450 forms related to phenobarbital-inducible forms in the mouse. *Biochemical Pharmacology*, **40**, 2503–2509.

Smith , P. K., Krohn , R. I., Hermanson , G. T., Mallia , A. K., Gartner , F. H., Provenzano , M. D., Fujimoto , E. K., Goeke , N. M., Olson , B. J. and Klenk , D. C., 1985, Measurement of protein using bicinchonic acid. *Analytical Biochemistry*, **150**, 76–85.

Sraub, P., Lloyd , M., Johnson , E. F. and Kemper , B., 1994, Differential effects of mutation in substrate recognition site 1 of cytochrome P450 2C2 on lauric acid and progesterone hydroxylation. *Biochemistry*, **33**, 8029–8034.

Yamano , S., Tatsuno , J. and Gonzalez, F. J., 1990, The CYP2A3 gene product catalyzes coumarin 7-hydroxylation in human liver microsomes. *Biochemistry*, **29**, 1322–1329.

Yun, C. H., Shimada , T. and Guengerich , F. P., 1991, Purification and characterization of human liver microsomal cytochrome P450 of the IIA subfamily from human liver microsomes. *Molecular Pharmacology*, **40**, 679.

XENOBIOTICA , 2000, VOL. 30, NO. 1, 93–102

Comparison of the pharmacokinetics of verapamil in the pregnant and non-pregnant rabbit: study of maternal and foetal tissue levels

C. SOLANS†, M. A. BREGANTE†*, J. J. ARAMAYONA†, L. J. FRAILE† and M. A. GARCIA‡

† Departments of Pharmacology and Physiology and ‡ Analytical Chemistry, Faculty of Veterinary Science, University of Zaragoza, Miguel Servet 177, E-50013 Zaragoza, Spain

Received 16 February 1999

1. The comparison of the pharmacokinetics of verapamil (VER) has been studied between the non-pregnant and pregnant rabbit following VER intravenous (i.v.) bolus administration. Also studied has been VER tissue distribution in the non-pregnant and pregnant rabbit and its foetuses following an i.v. infusion of VER.

2. When the pharmacokinetic variables were compared between the pregnant and non-pregnant rabbit, it was observed that $t_{1/2}\lambda_z$, V_1 and V_D were significantly higher in the non-pregnant than in the pregnant rabbit. Moreover, λ_z was significantly lower in the non-pregnant than in the pregnant rabbit. However, AUC and CL showed no significant differences between the pregnant and non-pregnant rabbit.

3. When tissue concentrations were examined, it was found that in most of the tissues studied high concentrations of VER were found both in the pregnant and non-pregnant rabbit. Furthermore, VER concentrations in the uterus, heart, spleen and kidney were significantly higher in the non-pregnant than in the pregnant rabbit.

4. The results suggest that VER diffuses poorly through the placenta, given that VER blood concentrations were lower in blood foetuses than in maternal blood. Moreover, the concentrations of VER in the selected foetal tissues were either similar (brain and liver) or lower than those observed in maternal tissues.

Introduction

During pregnancy the body develops into a complex physiological unit consisting of the mother, the placenta and the foetus. Furthermore, several physiological changes occur during this time (Jeffries *et al*. 1988, Loebstein *et al*. 1997), which may lead to significant variations in pharmacokinetic processes.

It is a common practice to administer drugs to pregnant animals, with this being a potential risk for the foetus or neonates. Neonatal risks could result from the effect of trans-placentally acquired drugs on immature neonatal systems. Thus, the need for information on the disposition and pharmacokinetics of several drugs during pregnancy is a very important factor for therapeutic uses.

To this end, verapamil (VER), a synthetic papaverine derivative, has been used. It is a well-known calcium channel blocker with anti-anginal, anti-hypertensive and anti-arrhythmic properties (McTavish *et al*. 1989). The pharmacokinetics of VER have been described in dog (Bai *et al*. 1993), rat (Manitpisitkul *et al*. 1993), rabbit (Giacomini *et al*. 1985) and humans (Fort *et al*. 1992). Moreover, it is known that the drug is extensively metabolized by N-demethylation, N-dealkylation and O-

* Author for correspondence; e-mail: bregante@posta.unizar.es

Xenobiotica ISSN 0049–8254 print/ISSN 1366–5928 online © 2000 Taylor & Francis Ltd
http://www.tandf.co.uk/journals/tf/00498254.html

demethylation (Hamann *et al.* 1984, McTavish *et al.* 1989). The N-demetylated metabolite of VER (norverapamil; NOR) is pharmacologically active and may contribute to the overall pharmacological action of the drug (McTavish *et al.* 1989).

The use of VER for the treatment of hypertension during pregnancy has been postulated by different authors (Orlandi *et al.* 1986, Byerly *et al.* 1991, Szymanski *et al.* 1992, Ito *et al.* 1994), but to the present authors' knowledge no information is yet available on VER pharmacokinetics in the pregnant animal.

The aim of the present study has been to investigate the effect of pregnancy on VER pharmacokinetics in rabbit following intravenous (i.v.) administration and to compare it with that observed in the non-pregnant rabbit. VER tissue distribution in the non-pregnant rabbit and in the pregnant rabbit and its foetus has also been examined.

Materials and methods

Animals

Twenty-three New Zealand White rabbits (body weights 4.5–5.0 kg, age 1.5–2.0 years) were acclimatized in the laboratory for 7 days before their enrolment in the experiment. During this period, the does were housed in rooms with a controlled temperature (20 °C) and light cycle (12/12 h), and maintained on water and standard diet *ad libitum*. Each animal was judged to be clinically normal by way of physical examination before beginning the experiment. During this procedure, the heart and respiratory rate, and rectal temperature were evaluated.

Reagents

Verapamil (VER) and norverapamil (NOR) were from Knoll AG. Imipramine was from Sigma Chemical Co. All other chemicals were of reagent or HPLC grade.

Intravenous bolus administration

The effect of pregnancy on VER pharmacokinetics was studied in eight rabbits in a crossover design (washout period, 6 weeks). The female rabbits were co-habited with male breeders and pregnancy was determined 11 days later by abdominal palpation. When necessary, the mating protocol was repeated. When pregnancy was confirmed, the weight of the animals was recorded every 4 days to verify the normal course of gestation. In pregnant rabbits, the experiment was conducted on day 28 of gestation. The does whelped from days 30 to 32 of gestation. The litter sizes, perinatal mortality and offsprings' growth were recorded. Rabbits were administered VER i.v. as a bolus dose of 1 mg/kg body weight in the marginal ear vein. Serial blood samples (1 ml) were drawn from a catheter inserted in the contra-lateral central ear artery at 0, 5, 15, 30, 60, 90, 120, 180, 240, 360 and 480 min. Blood samples were immediately haemolysed by the addition of an equal volume of water. Thereafter, samples were placed in 10 ml of a cold extraction medium (hexane:isobutanol, 98:2 v/v, − 20 °C) and assayed for VER and NOR concentration.

Maternal and foetal tissue distribution of VER and its metabolite

Nine female rabbits, four on day 28 of gestation, were used. To obtain the steady-state concentration of VER, an infusion programme was set up using the mean of the estimated pharmacokinetics parameters obtained from an earlier experiment. The infusion rate (Q) was calculated as $Q = C_{ss} * \mathrm{CL}$, where C_{ss} is the desired maternal blood concentration at steady-state (160 ng/ml) and CL is the body clearance (30 $ml.min^{-1}.kg^{-1}$). VER solutions were prepared by dilution to an appropriate concentration that permitted infusion rates in every animal of $\leqslant 0.2$ ml/min. The time at which the equilibrium between maternal and foetal VER concentration was achieved was determined in an earlier experiment. Briefly, a pregnant rabbit was maintained under i.v. pentobarbital anaesthesia for 3 h after VER infusion had commenced. The uterus was exposed to allow for foetal blood sampling. Maternal and foetal blood samples were simultaneously drawn at 30, 120 and 180 min and assayed for VER and NOR concentration.

In the main experiment ($n = 3$), maternal blood samples were drawn through a catheter inserted in the ear artery at 0, 5, 15, 30, 45, 60, 90, 120 and 180 min after the start of VER infusion to observe if the steady-state had been reached. After reaching the steady-state plateau (180 min after the start of the infusion), the does were anaesthetized by an i.v. administration of sodium pentobarbital (30 mg/kg) and

a midline incision was carried out in the ventral abdominal wall passing through the skin and linea alba. In the pregnant animal, the horns of the uterus were exteriorized and an incision was made in the dorsal surface of the uterine body in such a way that the placental sacs were intact ($n = 4$ in each dam). Amniotic fluid (0.5 ml) was drawn by a syringe from each implantation site. The foetuses were then freed from the membranes and placenta. Blood samples (0.5 ml) were obtained from the foetuses by way of cardiac puncture under light ether anaesthesia. Maternal and foetal tissue were quickly excised in the following order: perirenal fat, spleen, kidney, uterus, liver, heart, lung, brain and muscle. Thereafter, the tissues were rinsed with cold saline, blotted and weighed. All specimens were rapidly frozen at –20 °C until assayed for VER and NOR concentrations. The same protocol was followed in the non-pregnant rabbit ($n = 6$) but, obviously, without foetal sampling.

The tissue samples (~ 2 g) were homogenized at 4000 *g* for 2 min in 10 ml cold 0.01 M phosphate buffer (pH 7.4) using a tissue homogenizer (Ultra-Turrax T25, Janke and Kunkel, GmbH and Co.). Thereafter, the homogenates were centrifuged for 5 min at 1000 *g* (Beckman Model J2–21, Palo Alto, CA, USA) and the supernatant fraction was collected. An aliquot of 5 ml homogenate was separated for analysis.

Hplc assay of VER and its metabolite

VER and its metabolite were assayed in blood and tissue homogenates, following hexane:isobutanol (98:2 v/v) extraction, according to a previously publicized HPLC method (Garcia *et al.* 1997). The HPLC system consisted of an isocratic pump (Model 145) a 5-μm reversed-phase column (Novapack C18, 150 × 3.9 mm i.d.) and an UV-VIS detector fixed at 210 nm (Model 484; all Water Associates, Mildford, MA, USA). The method was shown to be linear for concentrations ranging from 1 to 1000 ng/ml VER and NOR respectively. The detection limit was 5 ng/ml for VER and NOR. Recovery was determined as > 80% for each drug. Inter- and intra-assay precision, determined by injection of control standards, were 3 and 2% for VER, and 4 and 3% for NOR respectively.

Data analysis

To describe the time-course of VER in the non-pregnant or pregnant rabbit, and after using the Akaike criterion (Yamaoka *et al.* 1978), the following equation (1) was used:

$$C = A_i * e^{-\lambda_i t} + A_n * e^{-\lambda n t},$$

where A_i and λ_i are the compartmental kinetic variables obtained by non-linear least squares regression analysis using a weighting factor of $1/c^2$. The half-life in the distributive and post-distributive phases was calculated as:

$$t_{1/2\lambda i} = \ln 2/\lambda_i,$$

where λ_i is the slope of the distributive and post-distributive phases.

Total body clearance was calculated as:

$$\mathrm{CL} = \mathrm{dose}/\mathrm{AUC}_{\mathrm{VER}},$$

where $\mathrm{AUC}_{\mathrm{VER}}$ is the area under the VER blood concentration versus time curve, calculated by the trapezoidal rule to the last datum point and extrapolated to infinity by dividing C_{last} for the slope of the elimination phase. Finally, the volume of distribution under the area was calculated as:

$$V_{\mathrm{Darea}} = \mathrm{dose}/(\mathrm{AUC}_{\mathrm{VER}} . \lambda_n).$$

Statistics

The pharmacokinetic values obtained in the non-pregnant and pregnant rabbit are presented as mean ± SD, except for half-life where the harmonic mean was calculated. Comparisons between i.v. pharmacokinetic parameters from the non-pregnant and pregnant rabbit were carried out using Student's paired *t*-test. The differences between the VER or NOR tissue concentrations observed in the non-pregnant and pregnant rabbit, as well as in the foetus, were determined by one-way analysis of variance (ANOVA). In all instances, $p < 0.05$ was considered as statistically significant.

Results

Intravenous bolus administration

The time-course of VER concentrations in blood after i.v. administration of a dose of 1 mg/kg body weight to both the pregnant and non-pregnant rabbit were described by a bi-exponential decrease (figure 1), determined by using the Akaike

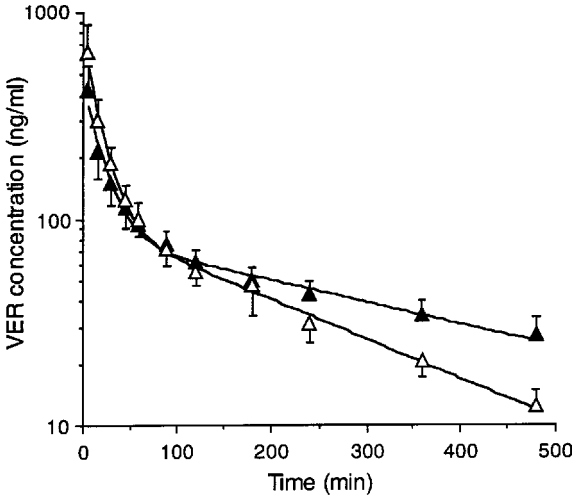


Figure 1. Mean± SD blood concentrations of VER following an endovenous bolus dose of 1 mg/kg VER. Non-pregnant, △; pregnant, ▲. Data are derived from eight determinations at each time point.

Table 1. Mean pharmacokinetic variables of VER determined following i.v. administration of 1 mg VER/kg body weight to the non-pregnant and pregnant rabbit (concentration data fit to equation 1).

Parameters		Non-pregnant	Pregnant
A_1	(ng ml^{-1})	824± 483	363± 114
λ_1	(min^{-1})	0.0790± 0.0478	0.0556± 0.0242
A_z	(ng ml^{-1})	101± 31	79± 15
λ_z	(min^{-1})	0.0044± 0.0007	0.0024± 0.0006†
$t_{1/2}\lambda_1$	(min)	9*	12*
$t_{1/2}\lambda_z$	(min)	155*	294*†
AUC_{VER}	(ng.min.ml^{-1})	34051± 5555	42017± 6824
V_1	(ml.kg^{-1})	1463± 899	2398± 745†
V_{Darea}	(ml.kg^{-1})	7737± 2079	10663± 1928†
CL	(ml.min^{-1}.kg^{-1})	30± 5	23± 4

A_1 and A_z are the coefficients and λ_1 and λz are the exponents derived by non-linear least squares regression of concentration data to equation (1). These terms are related to rate constants for the specific two-compartment pharmacokinetic model and were used to derive the following pharmacokinetic values: $t_{1/2}\lambda_1$ = distribution half life; $t_{1/2}\lambda_z$ = elimination half life; V_1 = volume of the central compartment; V_{Darea} = apparent volume of distribution calculated by the area method; AUC = area under the blood concentration–time curve; CL = body clearance.

*Harmonic mean

#Significantly different from the non-pregnant rabbit.

Data are the mean± SEM for eight animals.

criterion (Yamaoka *et al.* 1978). Table 1 shows the values obtained for the pharmacokinetic variables established from the model. After i.v. administration, VER had a distributive phase in both the pregnant and non-pregnant rabbit, which extended for ~ 80 min. Thereafter, linear elimination decrease began and extended until the last time point examined. When the pharmacokinetic variables of both the pregnant and non-pregnant rabbit were compared, significant differences were observed in λ_z, $t_{1/2}\lambda_z$, V_1 and V_D($p < 0.05$). The parameters that determine drug disposition (AUC and CL) showed no significant differences.

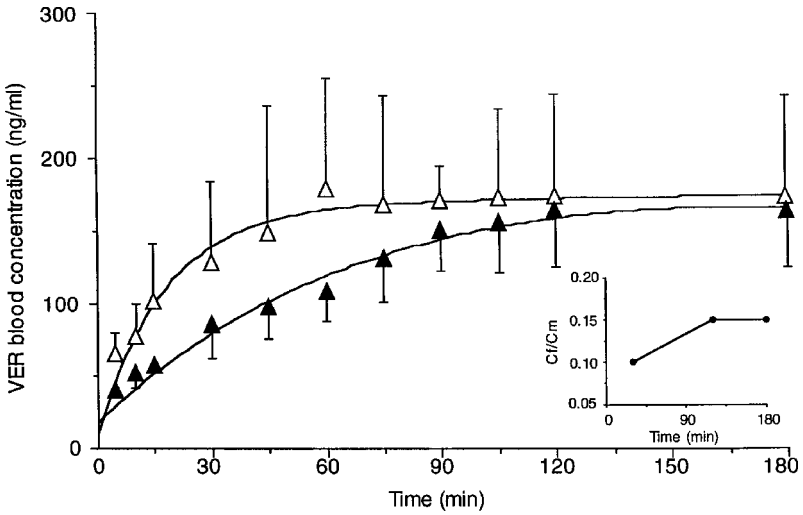


Figure 2. Mean ± SD concentrations of VER during the VER infusion programme in the non-pregnant (△; $n = 6$) and pregnant (▲) rabbit ($n = 3$). The insert in the bottom panel is the foetal-to-maternal blood concentration ratio (C_f/C_m) of VER determined in an additional pregnant rabbit (●).

After i.v. administration of the parent compounds, the presence of the NOR metabolite could not be detected in the blood of either the pregnant or non-pregnant rabbit (data not shown).

Tissue distribution

Figure 2 shows the mean blood levels of VER during the i.v. infusion of VER in both the pregnant and non-pregnant rabbit. After the i.v. infusion of VER, the steady-state blood levels of this drug were maintained in the range of 160 ng/ml for both the pregnant and non-pregnant rabbit. This result shows that there were no statistical differences between the two groups with respect to body clearance. However, statistical differences in V_D were not found between the pregnant (10305 ± 274 ml. kg^{-1}) and non-pregnant (4043 ± 1525 ml. kg^{-1}) rabbit. The steady-state was reached ~ 100 min after the beginning of infusion. The presence of the NOR metabolite could not be observed at any time throughout the infusion period (data not shown). The VER foetal-to-maternal ratio was constant 180 min after the start of VER infusion, indicating that the steady-state had been obtained.

When the VER concentrations in the tissues and the blood were examined, it was found that, in general, in all the tissues examined from both the pregnant and non-pregnant rabbit the VER concentration was higher than that measured in the blood, However, the accumulation observed in the different tissues was not homogeneous; thus, it was observed that some tissues, such as lung homogenates, showed very high concentrations, which were 80 and 66 times higher than those observed in the blood for both the non-pregnant and pregnant rabbit respectively. However, other tissues, such as the liver, showed a tissue-to-blood ratio of ~ 1.9 and 2.4 respectively.

When the tissue levels of VER were compared in the pregnant and non-pregnant rabbit, statistical differences were observed in the uterus, kidney, heart and spleen.

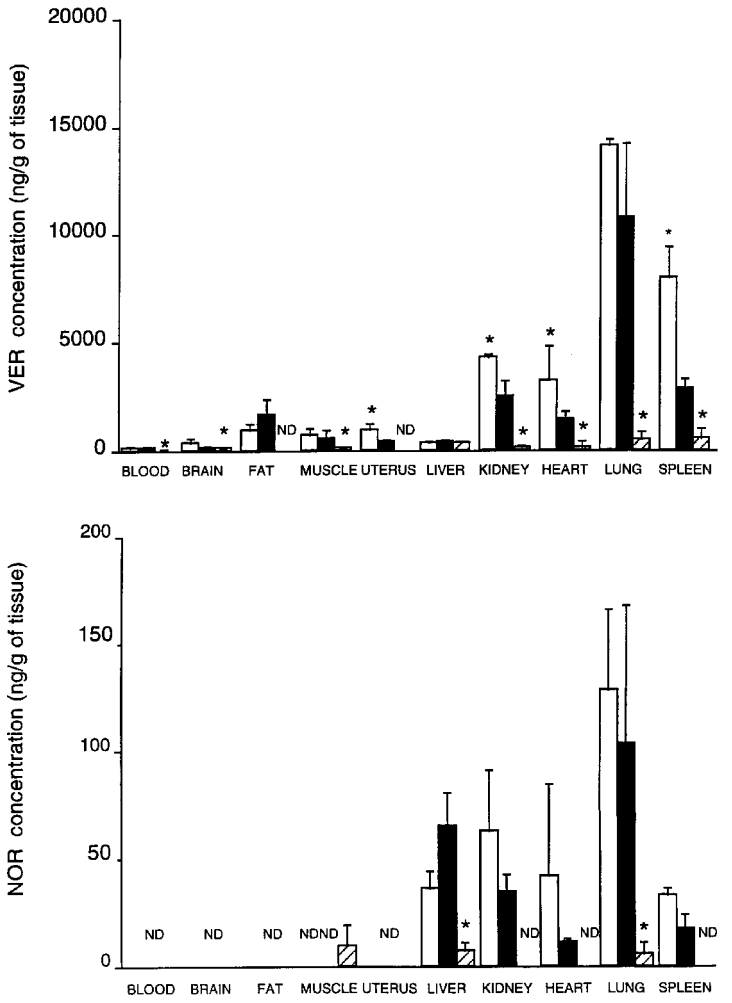


Figure 3. Mean ± SD concentrations of VER (top) and NOR (bottom) in several tissues and in whole blood determined in the non-pregnant rabbit ($n = 6$), pregnant rabbit ($n = 3$) and its foetuses ($n = 12$) after reaching steady-state following a VER infusion programme. Non-pregnant, □; pregnant, ■; foetuses, ▨. ND, not determined. *Significantly different from the pregnant rabbit, $p < 0.05$.

VER concentrations in these tissues were always higher in the non-pregnant than in the pregnant rabbit. On the other hand, NOR concentrations could only be observed in the liver, kidney, heart, lung and spleen. Moreover, NOR concentrations were smaller than VER concentrations in the same tissues. No statistical differences were found in any of the tissues examined when comparing the tissue levels of NOR in both the pregnant and non-pregnant rabbit (figure 3).

On the basis of placental transfer, it seems that VER crosses the placenta poorly, given that the concentrations of VER observed in the foetal blood were smaller and showed statistical differences with the levels of this compound found in the does blood. It was also found that neither VER nor NOR could be detected in the amniotic fluid. Finally, the foetal-to-maternal ratios of VER and NOR in the foetal and maternal tissues shown in table 2 indicate that for VER this ratio was very small

Table 2. Foetal-to-maternal ratios of VER and NOR the blood and in selected tissues determined following an i.v. infusion programme of VER.

Organ	VER	NOR
Blood	0.15± 0.05	–
Brain	1.16± 0.36	–
Muscle	0.47± 0.21	–
Heart	0.12± 0.03	–
Spleen	0.21± 0.16	–
Kidney	0.07± 0.01	–
Liver	0.81± 0.36	0.12± 0.09
Lung	0.05± 0.02	0.04± 0.03

Data are the mean± SEM for three pregnant rabbits and 12 foetuses (four for each dam).

Table 3. Tissue-to-blood ratios of VER determined following an i.v. infusion programme of VER.

Organ	Non-pregnant	Pregnant	Foetus
Brain	2.1	0.8	6.7
Muscle	4.2	3.7	7.1
Heart	20.0	9.0	7.1
Spleen	50.0	20.0	25.0
Kidney	25.0	16.7	6.7
Lung	81.1	65.7	20.0
Liver	1.9	2.4	14.3
Fat	5.3	10.0	–
Uterus	5.6	2.7	–

Data are the mean of six non-pregnant rabbits, three pregnant rabbits and 12 foetus.

in the blood, with only the brain and the liver showing ratios close to 1. This indicates a lower accumulation in the foetal tissues than that observed in the pregnant animal. On the other hand, the values shown in table 3 indicate that the foetal tissue-to-blood ratios showed higher VER concentrations in tissues than in foetal blood. This suggests that the foetuses would undergo greater exposure than that predicted from the blood foetal-to-blood maternal ratio values alone.

Finally, in foetal tissues NOR could only be observed in the liver, lung and muscle.

Discussion

It is well known that an optimal dosage regime has to be established on the basis of a knowledge of the pharmacokinetic variables. Many drugs have to be administered during pregnancy and, for this reason, the pharmacokinetic variables have to be known in order for an optimal treatment to be administered during this period.

The pharmacokinetics of VER have been described in dog (Bai *et al*. 1993), rat (Manitpisitkul *et al*. 1993), rabbit (Giacomini *et al*. 1985) and humans (Fort *et al*. 1992), but to our knowledge no information is yet available about VER pharmacokinetics in either pregnant animals or maternal and foetal tissue levels. Thus, the main aim of this study has been to determine whether pregnancy modifies the disposition of VER in rabbit. It was found that some pharmacokinetic variables were

modified by pregnancy; thus, $t_{1/2}\lambda_z$ was lower in the non-pregnant than in the pregnant rabbit, while V_D and V_1 were higher in the pregnant than in the non-pregnant rabbit. On the other hand, other parameters, such as AUC and CL, did not show significant differences between both groups of animals.

It is known that VER has a high hepatic extraction ratio and, as a result, its hepatic clearance is largely dependent on blood flow to the liver. No significant changes in body clearance between the pregnant and non-pregnant state may simply reflect the absence of any significant alteration in hepatic blood flow in pregnancy. Confirming this approach, Witter (1993) pointed out that high-extracted drugs do not usually show an altered disposition as a consequence of pregnancy. Furthermore, others have observed that propranolol (O'Hare *et al*. 1984), fenoterol (Hildebrandt *et al*. 1993) and diltiazem (Fraile 1996), disposition drugs which are mainly dependent on metabolism for elimination, showed hardly any modifications during pregnancy.

On the other hand, the present authors found that V_1 and V_D were higher in the pregnant than in the non-pregnant rabbit. Important modifications in body composition have been observed (Mitani *et al*. 1987) during pregnancy. Thus, in humans body water is increased by between 7 and 8 litres (Loebstein *et al*. 1997), the blood and plasma volume are increased to 30 and 20% respectively, during the second part of pregnancy, and at the end of pregnancy the plasma volume may be increased by 50% (Krauer *et al*. 1983, Ward 1992, Murray *et al*. 1994). In addition, fat may also be increased in human (3 or 4 kg) or animal. Therefore, in general during pregnancy the volume of distribution is modified both in water- and fat-soluble drugs (Jeffries *et al*. 1988) and, for this reason, the volume of distribution for VER in the pregnant rabbit is increased with respect to the non-pregnant rabbit. With regard to the half-life of VER in the pregnant rabbit, the present authors observed that this value increased. As the body clearance did not change, the present authors think that this modification has to be due to changes in the volume of distribution.

Finally, it should be pointed out that NOR could not be detect in either the pregnant or non-pregnant rabbit and, for this reason, the pharmacokinetic variations of this metabolite during pregnancy could not be studied.

All of the tissues examined in both the non-pregnant and pregnant rabbit and foetus showed higher levels of VER than those present in the blood, indicating that VER extensively accumulated in the tissues. It has been reported that basic amines, such as VER, are accumulated in specific tissues (Wilson 1979). Moreover, it has also been reported that tissues such as the lung have a high affinity for VER (Hamann *et al*. 1983, Gillespie *et al*. 1984). These results may be important from the pharmacodynamic point of view because some of these tissue are considered the target organs for VER. In the present study statistical differences have been detected when the VER tissue levels were compared in the pregnant and non-pregnant animal, with statistical differences being found in the uterus, heart, spleen and kidney in both the pregnant and non-pregnant rabbit. The VER concentrations in these tissues were higher in the non-pregnant than in the pregnant rabbit. The increased cardiac output to different organs during pregnancy results in changes in the protein binding and in the volume of distribution, as observed, and, finally, a different tissue affinity of VER could explain the differences in its tissue distribution. On the other hand, NOR could only be detected in the liver, kidney, heart, lung and spleen and no statistical differences in any of the tissues examined could be found

when comparing the tissue levels of NOR in the pregnant and non-pregnant rabbit. It is concluded that pregnancy affects the tissue distribution of VER, which may be important from a clinical point of view.

The results presented here indicate that VER crosses the placenta poorly, in that the VER concentrations observed in the foetal blood were significantly lower than those detected in the maternal blood. These results are similar to those reported by others (Wolff *et al*. 1980, Orlandi *et al*. 1986). Moreover, the concentration of VER and NOR in foetal tissues was either similar (brain and liver) or lower than that observed in maternal tissues, indicating a different tissue affinity in the foetuses as compared with their mothers. On the other hand, our results indicate that VER accumulated in the foetal tissues and, as a result, the foetuses would experience greater exposure than that predicted from blood foetal-to-blood maternal ratio values alone.

In conclusion, the differences observed in VER disposition in the pregnant as compared with the non-pregnant rabbit following VER i.v. administration could have some practical significance. Important modifications in the volume of distribution and half-life have been observed. The different tissue levels of VER and its metabolite in foetuses, the pregnant and non-pregnant rabbit could be explained by significant modifications in the blood disposition of VER. Finally, although the results indicate that VER crosses the placenta poorly, the foetuses would experience a greater exposure because of the accumulation observed in the different foetal tissues.

References

Bai, S. A., Lankford, S. M. and Johnson, L. M., 1993, Pharmacokinetics of the enantiomers of verapamil in the dog. *Chirality*, **5**, 436–442.

Byerly, W. G., Hartmann, A., Faster, D. E. and Tannenbaun, A. K., 1991, Verapamil in the treatment of maternal paroxysmal supraventricular tachycardia. *Annals of Emergency Medicine*, **20**, 552–554.

Fort, D. J. S., Lewis, M. J. and Luscombe, D. K., 1992, Pharmacokinetics and pharmacodynamics of verapamil following sublingual and oral administration to healthy volunteers. *British Journal of Clinical Pharmacokinetics*, **33**, 623–627.

Fraile, L. J., 1996, Paso transplacentario y modificaciones en la cinética del diltiazem durante la gestación y la ontogénesis en el conejo. Tesis doctoral, University of Zaragoza.

Garcia, M. A., Aramayona, J. J., Bregante, M. A., Fraile, L. and Solans, C., 1997, Simultaneous determination of verapamil and norverapamil in biological samples by high performance liquid chromatography using UV detection. *Journal of Chromatography B*, **693**, 377–382.

Giacomini, J. C., Nelson, W. L., Theodore, L., Wong, F. M., Rood, D. and Giacomini, K. M., 1985, The pharmacokinetics and pharmacodynamics of D- and D-L,verapamil in rabbits. *Journal of Cardiovascular Pharmacology*, **7**, 469–475.

Gillespie, M. N., Felder, T. B., Blanford, S. L., Reinsel, C. N. and Kostenbauer, H. B., 1984, Pulmonary disposition and pharmacodynamics of verapamil. *Journal of Cardiovascular Pharmacology*, **6**, 802–807.

Hamann, S. R., Blouin, R. A. and McAllister, R. G., 1984, Clinical pharmacokinetics of verapamil. *Clinical Pharmacokinetics*, **9**, 26–41.

Hamann, S. R., Todd, G. D. and McAllister, R. G., 1983, The pharmacology of verapamil. V. Tissue distribution of verapamil and norverapamil in rat and dog. *Pharmacology*, **27**, 1–8.

Hildebrandt, R., Weitzel, H., Warnke, K. and Gundert-Remy, U., 1993, Pharmacokinetics of fenoterol in pregnant and nonpregnant women. *European Journal of Clinical Pharmacology*, **45**, 275–277.

Ito, S., Magee, L. and Smallhorn, J., 1994, Drug therapy for fetal arrhythmias. *Clinica Perinatologica*, **21**, 543–572.

Jeffries, W. S. and Bochner, F., 1988, The effect of pregnancy on drug pharmacokinetics. *Medical Journal of Australia*, **149**, 675–677.

Krauer, B. and Krauer, F., 1983, Drug kinetics in pregnancy. In M. Gibaldi and L. Prescott (eds), *Handbook of Clinical Pharmacokinetics* (Balgowlah: ADIS Health Science Press), pp. 1–17.

Loebstein , R., Lalkin , A. and Koren , G., 1997, Pharmacokinetic changes during pregnancy and their clinical relevance. *Clinical Pharmacokinetics*, **33**, 328–343.

Manitpisitkul , P. and Chiou , W. L., 1993, Intravenous verapamil kinetic in rats: marked arteriovenous concentration difference and comparison with humans. *Biopharmaceutics and Drug Disposition*, **14**, 555–566.

McTavish , D. and Sorkin , E. M., 1989, Verapamil. An updated review of its pharmacodynamic and pharmacokinetic properties, and therapeutic use in hypertension. *Drugs*, **38**, 19–76.

Mitani , G. M., Steinberg , I., Lien , E., Harrison , C. and Elkayan , U., 1987, The pharmacokinetics of antiarrythmic agents in pregnancy and lactation. *Clinical Pharmacokinetics*, **12**, 253–291.

Murray, L. and Seger, D., 1994, Drug therapy during pregnancy and lactation. *Emergency Medical Clinical North America*, **12**, 129–149.

O'Hare, M. F., Kinney , C. D., Murnaghan , G. A. and McDevitt , D. G., 1984, Pharmacokinetics of propranolol during pregnancy. *European Journal of Clinical Pharmacology*, **27**, 583–587.

Orlandi , C., Marlettini , M. G., Cassani , A., Trabatti , M., Agostini , D., Salomone , T. and Testoni , N., 1986, Treatment of hypertension during pregnancy with the calcium antagonist verapamil. *Current Therapeutics Research Clinical and Experimental*, **39**, 884–893.

Szymanski , W., Skublicki , S., Jankowski , A. and Kotzbach , R., 1992, Pharmacokinetic investigations of verapamil used an a concomitant drug in treatment of premature labor. *Ginecologica. Polska*, **63**, 166–171.

Ward, R. M., 1992, Maternal drug therapy for fetal disorders. *Seminary Perinatology*, **16**, 12–20.

Wilson , A. G. E., Pickett , R. D., Eling , T. E. and Anderson , M. W., 1979, Studies on the persistence of basic amines in the rabbit lung. *Drug Metabolism and Disposition*, **76**, 420–424.

Witter , F. R., 1993, Clinical pharmacokinetics in the treatment of rheumatoid arthritis in pregnancy. *Clinical Pharmacokinetics*, **25**, 444–449.

Wolff , F., Breuker , K. H., Schlensker , K. H. and Bolte , A., 1980, Prenatal diagnosis and therapy of fetal heart rate anomalies: with a contribution on the placental transfer of verapamil. *Journal of Perinatal Medicine*, **8**, 203–208.

Yamaoka, K., Nakagawa, T. and Uno, T., 1978, Application of the Akaike's information criterion (AIC) in the evaluation of linear pharmacokinetics. *Journal of Pharmacokinetics and Biopharmaceutics*, **6**, 165–175.

XENOBIOTICA , 2000, VOL. 30, NO. 1, 103–109

Biotransformation of the xanthine oxidase inhibitor BOF-4272 and its metabolites in the liver and by the intestinal flora in rat

S. NAITO* and M. NISHIMURA

Laboratory of Drug Metabolism Research, Naruto Research Institute, Otsuka Pharmaceutical Factory, Inc., Naruto, Tokushima 772-8601, Japan

Received 21 June 1999

1. BOF-4272, (±)-8-(3-methoxy-4-phenylsulfinylphenyl) pyrazolo[1,5-a]-1,3,5-triazine-4(1H)-one), is a new drug intended for the treatment of hyperuricaemia.

2. This paper describes the detailed biotransformation of BOF-4272 and its metabolites in the liver and by the intestinal flora in rat.

3. Only the sulphoxide metabolite (M6) was detected in plasma in small amounts after the intravenous administration of M4 (hydroxy-BOF-4272) and in culture medium after the addition of M4.

4. Only M3 (the sulphide metabolite of M4) was detected in faeces, and its amount was ~ 50% of the administered dose within 1 day after the intravenous administration of M4.

5. These findings suggest that M4, which is excreted in the bile, is metabolized mainly to M3 (the corresponding sulphide of M4) by the intestinal flora in rat, whereas little M4 is metabolized to the sulphoxide (M6) in the rat liver.

6. M2, which is the demethylated form of BOF-4269, was detected in faeces after the oral administration of BOF-4272 to rat in which the common bile duct was cannulated, suggesting that BOF-4272 is metabolized to BOF-4269 and then to M2 by the intestinal flora.

7. These findings suggest that in rat the sulphoxide of BOF-4272 and its metabolites are demethylated and reduced by the intestinal flora, with other types of biotransformation occurring in the liver.

Introduction

BOF-4272, a derivative of pyrazolotriazine, inhibits the *de novo* biosynthesis of uric acid by blocking the xanthine oxidase/xanthine dehydrogenase system (Sato *et al*. 1991, Uematsu and Nakashima 1994). The mechanism of the inhibitory action of BOF-4272 was elucidated by an *in vitro* study using milk xanthine oxidase/xanthine dehydrogenase (Okamoto and Nishino 1995). BOF-4272 significantly decreases the concentration of the free radicals generated by xanthine oxidase and consequently reduces cellular necrosis (Suzuki *et al*. 1994). The pharmacological activity of BOF-4276 (the sulphoxide of BOF-4272) is weaker than that of BOF-4272, whereas BOF-4269 (the sulphide of BOF-4272) has no activity (Okamoto *et al*. 1993). It has also been demonstrated that the linear range of absorption and/or elimination of BOF-4272 is very wide in the mouse and in rat (Naito *et al*. 1999). Recent studies have demonstrated that the hepatic elimination of BOF-4272 is quite substantial (Nishimura *et al*. 1994–96). The present paper describes the detailed biotransformation of BOF-4272 and its metabolites in the liver and by the intestinal flora in rat.

* Author for correspondence.

Xenobiotica ISSN 0049–8254 print/ISSN 1366–5928 online © 2000 Taylor & Francis Ltd
http://www.tandf.co.uk/journals/tf/00498254.html

Materials and methods

Materials

^{14}C-labelled BOF-4272 (3.89 MBq/mg) and ^{14}C-labelled BOF-4269 (5.78 MBq/mg) were from Amersham International (Amersham, UK). Radiochemical purity was >97.0%. ^{14}C-labelled M4 (1.52 MBq/mg) was synthesized at Otsuka Pharmaceutical Factory, Inc. (Tokushima, Japan) and radiochemical purity was >98.8%. BOF-4272 and its metabolites used were synthesized at Otsuka Pharmaceutical Factory, Inc. (Tokushima, Japan) and chemical purities were >99.0%. Carboxymethyl cellulose sodium salt (CMC), diethyl ether, acetonitrile, ethyl acetate, dexamethasone and collagenase were from Wako Pure Chemical Industries Ltd (Osaka, Japan). Polyethylene glycol 400 (PEG 400) was from Nacalai Tesque, Inc. (Kyoto, Japan). Trypsin inhibitor, insulin, β-glucuronidase from *Escherichia coli* type IX, and sulphatase from Helix pomatia type H-1 were from Sigma Chemical Co. (St Louis, MO, USA). Trypan blue was from Flow Laboratories Ltd (Irvine, UK). Williams' medium E and calf bovine serum were from Dainippon Pharmaceutical Co. Ltd (Osaka, Japan). All other chemicals and reagents used were of analytical reagent grade.

Animals

Male Wistar rats, 7 weeks of age and weighing between 170 and 208 g ($n = 51$), were from Charles River Japan (Kanagawa, Japan). During the experiments, the rats were housed individually in metabolic cages at 23±2 °C and a relative humidity of 55%±10% with a 12-h night/day cycle. Animals were allowed free access to food (CRF-1-R, Oriental Yeast Co. Ltd, Tokyo, Japan), except during periods of fasting, and to drinking water.

Chromatography

The concentrations of BOF-4272 and its metabolites were measured using high-performance liquid chromatography (HPLC) systems (CCP & 8010 Series, Tosoh Co., Tokyo, Japan) with a stationary phase of TSKgel ODS-120T (250 4.6 mm i.d.; Tosoh). The HPLC systems consisted of a system controller (PX-8010), pump (CCPM), autosampler (AS-48), UV detector (UV-8010) and integrated data analyser (C-R4AX Chromatopac, Shimadzu Co., Kyoto, Japan). Detector wavelength and the flow rate were 323 nm and 1.0 ml/min respectively. Column temperature was ambient. The mobile phase was a mixture of solution A (10 mm $NH_4H_2PO_4$, pH 3.0) and solution B (acetonitrile and solution A, 80:20 v/v), with a linear gradient from 70/30 to 0/100% over 31 min.

Animal studies

Rats were fasted from 20 h before to 4 h after the intravenous (i.v) or oral administration of the test drugs. BOF-4269 and M4 were dissolved in 50% PEG 400 for i.v. administration and were administered to rats i.v. at 5 mg/kg (0.74 MBq/kg). BOF-4272 was dissolved in 0.5% CMC solution for oral administration and was administered to rats orally at 5 mg/kg (1.85 MBq/kg).

Rats were decapitated and blood samples were obtained. Blood samples were drawn into heparinized test tubes at eight time points (0 [predose], 0.083, 0.25, 0.5, 1, 2, 3 and 4 h) after bolus i.v. injection. All blood samples were immediately centrifuged to obtain plasma.

Rats from which bile samples were obtained were anaesthetized with diethyl ether, and the common bile duct was cannulated with a polyethylene tube (0.61 mm o.d., PE-10, Becton Dickinson & Co., Parsippany, NJ, USA). Bile, urine and faeces samples were collected at 4 °C up to 48 h after oral administration to rats in which the common bile duct was cannulated.

Urine and faeces samples were collected daily for 4 days after i.v. administration.

Isolation and monolayer culture of hepatocytes

Liver perfusion was performed as described by Moldeus *et al*. (1978). Briefly, rat liver was perfused at 37 °C for 4 min with Ca^{2+}- and Mg^{2+}-free Hanks' solution (pH 7.4) containing 0.5 mm EGTA and for 6 min with Hanks' solution (pH 7.4) containing 0.1% collagenase and 0.05% trypsin inhibitor. Hepatocytes were liberated from the perfused liver by blunt dissection and dispersed by gentle shaking in Ca^{+}- and Mg^{2+}-free Hanks' solution (pH 7.4). After filtration through gauze, the hepatocytes were separated from non-parenchymal cells by centrifugation three times, with the cells washed and resuspended in Ca^{+}- and Mg^{2+}-free Hanks' solution (pH 7.4) each time. Finally, the cells were resuspended in Williams' medium E (pH 7.4) containing 10% calf bovine serum, 1 nm insulin and 10 nm dexamethasone. Cell suspensions with a viability >90% as assessed by trypan blue exclusion were used for the experiments. The number of cells was counted using a Coulter Counter. The cell suspensions were diluted to a final concentration of 106 viable cells/ml, and inocula of 4106 viable cells/ml were introduced into 60-mm diameter dishes that had been coated with collagen. The cells were cultured for 6 h after inoculation under 5% CO2 and 95% air at 37 °C. The medium was then replaced with fresh medium, and the cells were used for experiments at 24 h after inoculation.

Experiments using monolayer cultures of hepatocytes

The medium was replaced with the same medium containing M4 at 2 μg/ml. The concentrations of each substrate and its metabolites were determined at 24 h after the addition of substrate.

Sample analysis

Total ^{14}C concentrations were measured. Aliquots of plasma (0.5 ml), bile (0.2 ml) and urine (0.5 ml) samples were each mixed with 0.5 ml water and 16 ml ACS II® (Amersham). The total ^{14}C concentration in each mixture was determined using a liquid scintillation analyser (TRI-CARB Model 4530, Packard Instruments Co., Meriden, CT, USA). Each faeces sample was added to 5 vols water at room temperature and homogenized with a Polytron® homogenizer (Kinematica, Switzerland). Aliquots ($\sim$ 0.5 g) of homogenized faeces samples were dried in Combusto Cones with Combusto Pads at 50 °C and oxidized with a Tri-Carb sample oxidizer (Model 307). The combustion products were mixed with 9 ml CarbosorbTM and 12 ml Permafluor VTM. Total ^{14}C in the mixture was determined using a liquid scintillation analyser (TRI-CARB Model 4530; all Packard).

Enzyme treatment

Each plasma, bile, urine, homogenized faeces and culture medium sample was prepared by the successive addition of an equal volume of enzyme solution (1000 units sulphatase or β-glucuronidase) at 37 °C, and then incubated for 24 h after the addition of the enzyme solution.

Preparation of HPLC samples from plasma and culture medium

Each plasma, culture medium, enzyme-treated plasma and enzyme-treated culture medium sample was prepared by the successive addition of 2 vols acetonitrile at 4 °C with shaking. After centrifugation, the supernatant was transferred to another tube, 2 vols 10 mm $NH_4H_2PO_4$ (pH 3.0) were added, and the mixture was shaken again. The mixture was then filtered through a membrane filter (pore size, 0.2 μm). An aliquot (500 μl) of the filtrate was injected into the HPLC system.

Preparation of HPLC samples from bile and urine

Each bile sample (0.2 ml) was mixed with 1 N HCl (0.1 ml) and ethyl acetate (4 ml) and shaken. After centrifugation, 1 ml the ethyl acetate layer was transferred to another tube and dried under reduced pressure. The dried sample was redissolved in 3 ml 10 mm $NH_4H_2PO_4$ (pH 3.0) containing 20% acetonitrile. The sample was then filtered through a membrane filter (pore size, 0.2 μm). An aliquot (500 μl) of the filtrate was injected into the HPLC system.

Enzyme-treated bile samples (0.4 ml), urine samples (0.5 ml) and enzyme-treated urine samples (1.0 ml) were prepared using the same method.

Preparation of HPLC samples from faeces

Each faeces and enzyme-treated faeces sample was prepared by the successive addition of 10 vols acetonitrile at 4 °C with shaking. After centrifugation, the supernatant was transferred to another tube, 10 vols 10 mm $NH_4H_2PO_4$ (pH 3.0) were added, and the mixture was shaken again. The mixture was then filtered through a membrane filter (pore size, 0.2 μm). An aliquot (500 μl) of the filtrate was injected into the HPLC system.

Data analysis

The concentration at time 0 (C_0) for i.v. administration was estimated by the residual method. The maximum plasma concentration (C_{max}) and the time to reach the maximum plasma concentration (t_{max}) were read directly from the mean plasma concentration data. The elimination half-life ($t_{1/2}$) was calculated using $t_{1/2} = \ln 2/K$, where K is the slope of the terminal portion of the natural logarithm of the plasma concentration–time curve obtained by linear regression. The area under the plasma concentration–time curve from time 0 to the last detectable concentration (AUC_{0-t}), the area under the plasma concentration–time curve from time 0 to infinity ($AUC_{0-\infty}$), and the mean residence time (MRT) were calculated according to the trapezoidal rule (Yamaoka *et al.* 1978). The total systemic clearance (Cl) and the volume of distribution (Vd_{ss}) were calculated using:

$$Cl = D/\mathrm{AUC}$$

$$Vd_{ss} = D \cdot \mathrm{MRT}/\mathrm{AUC}_{0-\infty},$$

where D is the administered dose.

Results and discussion

Previously, the metabolic pathways of BOF-4272 in the rat were clarified (Naito and Nishimura 1999). However, the biotransformation of M4, which is a metabolite of BOF-4272, has not yet been clarified. M4 was detected in plasma after the oral

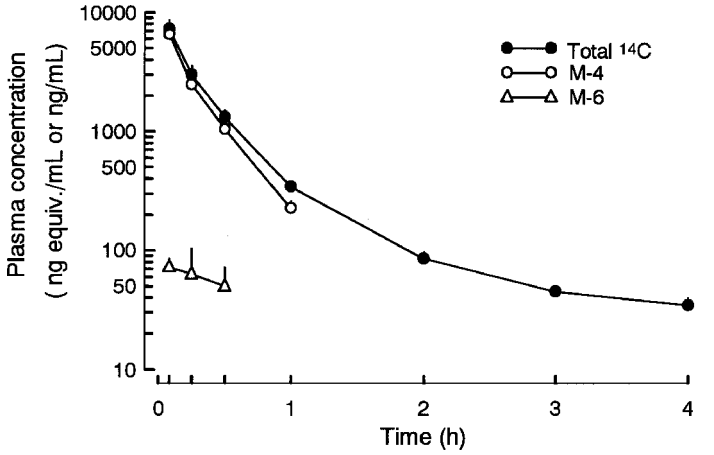


Figure 1. Plasma concentration profiles for total ^{14}C, M4 and its metabolites after the i.v. administration of M4 at 5 mg/kg (0.74 MBq/kg) to rat. Each point represents the mean ± SD of four rats.

Table 1. Pharmacokinetic parameters for total ^{14}C, M4, and its metabolites in plasma after the i.v. administration of ^{14}C-labelled M4 to rat.

Parameter	Total ^{14}C	M4	M6
5 mg/kg			
C_0 (ng/ml)	9320	8424	
C_{max} (ng/ml)			72
t_{max} (h)			0.083
$t_{1/2}$ (h)	1.53	0.22	0.78
AUC_{0-t} (ng·h/ml)	2800	2114	28
$AUC_{0-\infty}$ (ng·h/ml)	2872	2184	85
MRT (h)	0.54	0.25	
Cl (ml/h/kg)	1786	2365	
Cl* (ml/h/kg)	1741	2289	
Vd_{ss} (ml/kg)	940	572	

C_0, plasma concentration at time 0; C_{max}, maximum plasma concentration; t_{max}, time to maximum plasma concentration; $t_{1/2}$, elimination half-life; AUC_{0-t}, area under the plasma concentration–time curve from time 0 to the last measurement point; $AUC_{0-\infty}$, area under the plasma concentration–time curve from time 0 to infinity; MRT, mean residence time; *Cl*, clearance = dose/AUC_{0-t}; *Cl**, dose/$AUC_{0-\infty}$; Vd_{ss}, volume of distribution. Data are calculated from the means obtained from four rats.

administration of BOF-4272 to healthy human volunteers, and the AUC of M4 was about four times higher than that of the parent compound (BOF-4272) (Uematsu and Nakashima 1994). Investigated, therefore, was the detailed biotransformation of M4 in the liver and by the intestinal flora in rat. Only M6 was detected in small amounts in plasma after the i.v. administration of M4 to rats (figure 1). AUC_{0-t} of M4 and M6 after the i.v. administration of M4 to rat was 2114 and 28 ng·h/ml respectively (table 1). Only M6 was detected in small amounts in the culture medium after the addition of M4 (table 2). About 25% of the parent compound (M4) was recovered in urine within 1 day after the i.v. administration of M4 to rat (table 3). Only M3 (the sulphide metabolite of M4) was detected in faeces, and its amount was ~50% of the administered dose within 1 day after the i.v. administration of M4 to rats (table 3). In a previous study, it was demonstrated that

Table 2. Concentrations of M4 and its metabolite in culture medium at 24 h after the addition of M4 at 2 μg/ml.

	Concentration (ng/ml)
M4	1402
M6	36

Experiments were performed in duplicate.
Values are means ($n = 2$).

Table 3. Cumulative urinary and faecal excretion of total ^{14}C, M4, and its metabolites after the i.v. administration of ^{14}C-labelled M4 to rat.

	Time (days)	Total ^{14}C	M4	M3
5 mg/kg ($n = 6$)				
Urine	1	34.5± 3.1	26.5± 12.4	nd
	4	34.7± 3.1	26.5± 12.4	nd
Faeces	1	56.5± 5.0	nd	47.6± 3.1
	4	62.1± 4.0	nd	51.0± 2.0

Values are mean± SD (% of dose).
nd, Not detected.

Table 4. Cumulative biliary, urinary, and faecal excretion of total ^{14}C, BOF-4272 and its metabolites after the oral administration of ^{14}C-labelled BOF-4272 to rat in which the common bile duct was cannulated.

Time (h)	Total ^{14}C	BOF-4272	BOF-4269	M1 sulphate	M2	M2 glucuronide
5 mg/kg ($n = 5$)						
Bile						
4	1.9± 0.8	0.5± 0.2	nd	0.6± 0.3	nd	nd
8	5.0± 1.6	0.9± 0.3	nd	0.8± 0.4	nd	nd
12	10.9± 4.8	1.1± 0.4	nd	2.3± 1.8	nd	0.4± 0.5
24	26.2± 10.4	1.1± 0.4	nd	6.1± 3.5	nd	3.6± 2.3
48	30.7± 8.2	1.1± 0.4	nd	6.2± 3.4	nd	5.3± 1.9
Urine						
24	4.4± 2.1	1.7± 0.6	nd	0.9± 0.8	nd	nd
48	5.2± 2.0	1.9± 0.5	nd	1.0± 0.8	nd	nd
Faeces						
24	46.7± 11.4	3.4± 1.6	11.3± 5.9	nd	9.4± 3.7	nd
48	58.5± 7.1	3.9± 2.0	12.5± 6.5	nd	12.8± 2.1	nd

Values are mean± SD (% of dose).
nd, Not detected.

M4, which is a metabolite of BOF-4272 in rat liver, is excreted in rat bile (Naito and Nishimura 1999). It has been demonstrated previously that sulphoxide drugs are metabolized to sulphides by the intestinal flora (Renwick *et al*. 1982, Strong *et al*. 1985, 1987). It was, therefore, suggested that BOF-4272 is also metabolized to BOF-4269 (the sulphide metabolite of BOF-4272) by the intestinal flora in rat (Naito and Nishimura 1999). These findings suggest that M4, which is excreted in the bile, may be mainly metabolized to M3 by the intestinal flora in rat, whereas little M4 is metabolized to M6 in the rat liver.

M2, which is a metabolite of BOF-4269, and M2 glucuronide generated from M2 were not detected in the culture medium after the addition of BOF-4269 to rat

Table 5. Cumulative urinary and faecal excretion of total ^{14}C, BOF-4269 and its metabolites after the i.v. administration of ^{14}C-labelled BOF-4269 to rat.

Time (days)	Total ^{14}C	BOF-4269	BOF-4272	M1	M1 sulphate	M2	M3
5 mg/kg (n = 6)							
Urine 1	6.1±1.6	nd	2.2±0.8	0.3±0.3	2.3±0.6	nd	nd
4	6.2±1.6	nd	2.2±0.8	0.3±0.3	2.3±0.6	nd	nd
Faeces 1	86.0±1.8	5.2±1.9	nd	58.1±7.4	nd	0.4±0.6	2.3±0.3
4	91.7±2.7	5.2±1.9	nd	58.9±7.8	nd	0.5±0.9	2.3±0.3

Values are mean± SD (% of dose).
nd, Not detected.

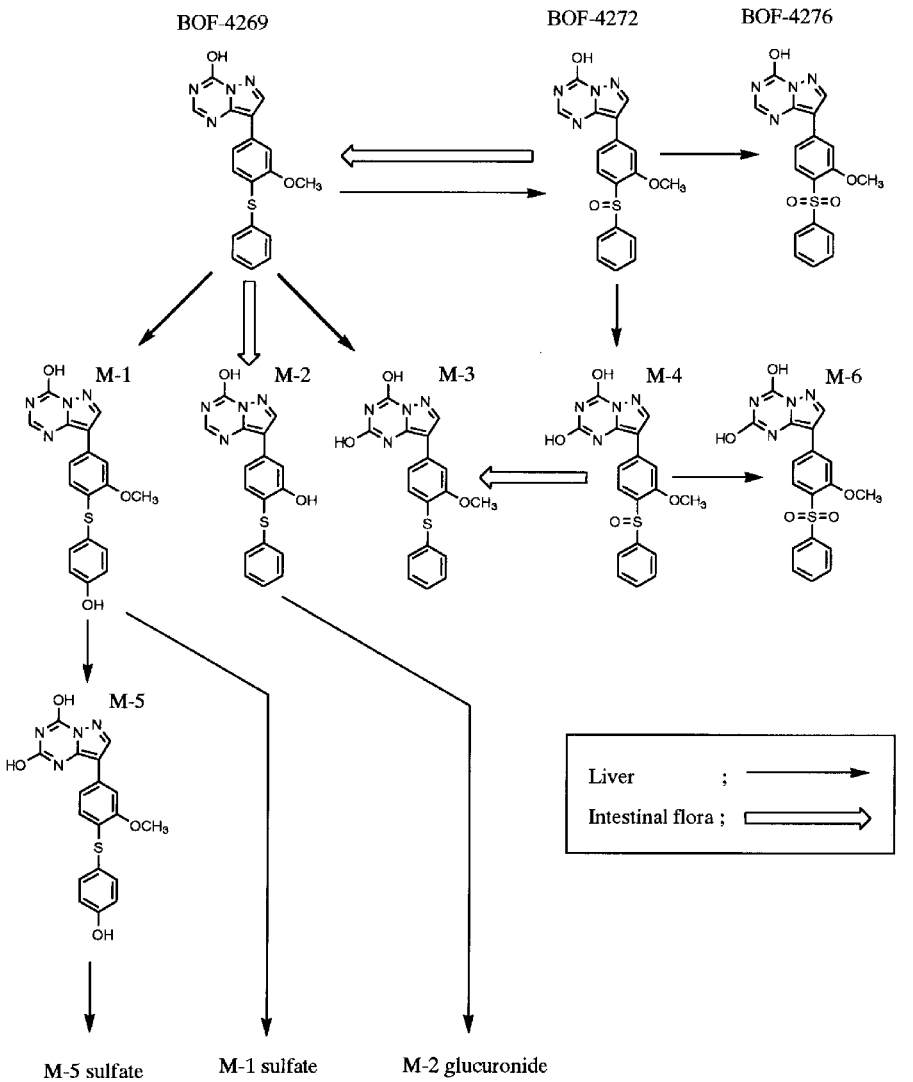


Figure 2. Proposed metabolic pathways of BOF-4272 in rat.

hepatocytes in primary culture (Naito and Nishimura 1999). However, M2 glucuronide was detected in bile after the oral administration of BOF-4272 to rat (Naito and Nishimura 1999). BOF-4269 and M2 were detected in faeces after the oral administration of BOF-4272 to rat in which the common bile duct was cannulated (table 4). M2 was detected in small amounts in faeces after the i.v. administration of BOF-4269 to rat (table 5). Thus, it was concluded that M2 was not excreted into the intestines by way of the intestinal tract. It has been suggested that compounds are demethylated by the intestinal flora (Axelson and Sjövall 1983). These findings suggest that BOF-4269, which is metabolized from BOF-4272 by the intestinal flora (Naito and Nishimura 1999), is further metabolized to M2 by the intestinal flora, and the M2 is then absorbed from the intestinal tract.

In conclusion, the findings of the present study suggest that in rat the intestinal flora is responsible for the biotransformation of BOF-4272 to BOF-4269, BOF-4269 to M2, and M4 to M3, with other types of biotransformation occurring in the liver (figure 2).

References

Axelson, M. and Sjövall, J., 1983, Formation of catechol estrogens by intestinal bacterial demethylation of 2-methoxyestrone. *Biochimica et Biophysica Acta*, **751**, 162–165.

Moldeus, P., Hogberg, J. and Orrenius, S., 1978, Isolation and use of liver cells. *Methods in Enzymology*, **52**, 60–71.

Naito, S. and Nishimura, M., 1999, Pharmacokinetics and proposed metabolic pathways of BOF-4272, a sulfoxide-containing drug, based on in-vivo and in-vitro studies in rats. *Pharmacy and Pharmacology Communications*, **5**, 123–131.

Naito, S., Nishimura, M. and Nogawa, H., 1999, Pharmacokinetics of BOF-4272, a xanthine oxidase inhibitor, after single intravenous or oral administration to male mice and rats. *Journal of Pharmacy and Pharmacology*, **51**, 347–351.

Nishimura, M., Yamaoka, K., Naito, S. and Nakagawa, T., 1996, Hepatic local disposition of a drug with high protein binding and high hepatic clearance using BOF-4272 as a model drug. *Biological and Pharmaceutical Bulletin*, **19**, 1197–1202.

Nishimura, M., Yamaoka, K., Yasui, H., Naito, S. and Nakagawa, T., 1994, Local disposition of new xanthine oxidase/xanthine dehydrogenase inhibitor, BOF-4272, in rat liver. *Biological and Pharmaceutical Bulletin*, **17**, 1301–1304.

Nishimura, M., Yamaoka, K., Yasui, H., Naito, S. and Nakagawa, T., 1995, Effect of temperature in perfusate on local hepatic disposition of BOF-4272, a new xanthine oxidase inhibitor. *Biological and Pharmaceutical Bulletin*, **18**, 980–983.

Okamoto, K., Iwamoto, T. and Nishino, T., 1993, New tight binding inhibitors of xanthine oxidase. In *Flavins and Flavoproteins* (Berlin: Walter de Gruyter), pp. 731–734.

Okamoto, K. and Nishino, T., 1995, Mechanism of inhibition of xanthine oxidase with a new tight binding inhibitor. *Journal of Biological Chemistry*, **270**, 7816–7821.

Renwick, A. G., Evans, S. P., Sweatman, T. W., Cumberland, J. and George, C. F., 1982, The role of the gut flora in the reduction of sulphinpyrazone in the rat. *Biochemical Pharmacology*, **31**, 2649–2656.

Sato, S., Tatsumi, K. and Nishino, T., 1991, A novel xanthine dehydrogenase inhibitor, BOF-4272. *Advances in Experimental Medicine and Biology*, **309A**, 135–138.

Strong, H. A., Renwick, A. G., George, C. F., Liu, Y. F. and Hill, M. J., 1987, The reduction of sulphinpyrazone and sulindac by intestinal bacteria. *Xenobiotica*, **17**, 685–696.

Strong, H. A., Warner, N. J., Renwick, A. G. and George, C. F., 1985, Sulindac metabolism: The importance of an intact colon. *Clinical Pharmacology and Therapeutics*, **38**, 387–393.

Suzuki, H., Suematsu, M., Ishii, H., Kato, S., Miki, H., Mori, M., Ishimura, Y., Nishino, T. and Tsuchiya, M., 1994, Prostaglandin E1 abrogates early reductive stress and zone-specific paradoxical oxidative injury in hypoperfused rat liver. *Journal of Clinical Investigation*, **93,** 155–164.

Uematsu, T. and Nakashima, M., 1994, Pharmacokinetic and pharmacodynamic properties of a novel xanthine oxidase inhibitor, BOF-4272, in healthy volunteers. *Journal of Pharmacology and Experimental Therapeutics*, **270**, 453–459.

Yamaoka, K., Nakagawa, T. and Uno, T., 1978, Statistical moments in pharmacokinetics. *Journal of Pharmacokinetics and Biopharmaceutics*, **6**, 547–558.

XENOBIOTICA , 2000, VOL. 30, NO. 2, 111–116

Fenamates and the potent inhibition of human liver phenol sulphotransferase

M. VIETRI†, C. DE SANTI†, A. PIETRABISSA‡, F. MOSCA‡ and G. M. PACIFICI†*

† Department of Neurosciences, Section of Pharmacology, Medical School, Via Roma 55, I-56126 Pisa, Italy
‡ Department of Oncology, Section of Surgery, Cisanello Hospital at University of Pisa, I-56124 Cisanello, Pisa, Italy

Received 4 June 1999

1. The inhibition of the human liver phenol sulphotransferase (HL-PST) and catechol sulphotransferase (HL-CST) by five fenamates has been studied and the activities of HL-PST and HL-CST were measured with 4-nitrophenol and dopamine as substrates, respectively.

2. The IC_{50} for inhibition of HL-PST were 0.02 μM (mefenamic acid); 0.12 μM (tolfenamic acid); 0.28 μM (niflumic acid); 0.87 μM (meclofenamic acid) and 1.50 μM (flufenamic acid).

3. HL-CST was less susceptible than HL-PST to the inhibition by fenamates and the IC_{50} for HL-CST were 36 μM (tolfenamic acid); 70 μM (flufenamic acid); 76 μM (mefenamic acid); 180 μM (niflumic acid) and 185 μM (meclofenamic acid).

4. The ratios of the IC_{50} for HL-CST:HL-PST were drug-dependent and ranged from 47 (flufenamic acid) to 3800 (mefenamic acid). Mefenamic acid is a relatively potent and selective inhibitor of HL-PST.

5. The IC_{50} for HL-PST obtained with mefenamic acid was three orders of magnitude lower than the peak plasma concentration of this drug after an oral dose of 0.5 g. Accordingly, mefenamic acid should impair sulphation *in vivo*.

Introduction

Sulphotransferase (EC 2.8.2) is an important enzyme in the metabolism of drugs, chemicals, hormones and neurotransmitters as sulphated compounds are more readily eliminated and sulphation is believed to be an important detoxification pathway (Mulder and Jakoby 1990, Weinshilboum and Otterness 1994, Pacifici and De Santi 1995). Inhibition of sulphotransferase results in the reduction of the sulphation rate with consequent decreased detoxification capacity. There are several forms of phenol sulphotransferase (EC 2.8.2.1) and two differ in substrate specificity, inhibitor sensitivity, thermal stability and regulation. One form is sensitive to the inhibition of 2,6-dichloro-4-phenol (Campbell et al., 1987), is relatively thermostabile and is named TS-PST (Weinshilboum 1986) or P form (Bonham Carter *et al.* 1983) or simply phenol sulphotransferase (Cappiello *et al.* 1990, Pacifici and De Santi 1995). This form is named hTSPST1 according to a classification based on the primary amino acid sequence (Raftogianis *et al.* 1996). The other form is thermolabile and it is named TL-PST (Weinshilboum 1986) or M form (Bonham Carter *et al.* 1983) or catechol sulphotransferase as its functional moiety is the catecholic group of dopamine (Cappiello *et al.* 1990, Pacifici and De Santi 1995). According to a classification based on the primary amino acid sequence it is named hTLPST (Raftogianis *et al.* 1996).

Fenamates are non-steroidal anti-inflammatory drugs that inhibit cyclo-

* Author for correspondence; e-mail: pacifici@biomed.unipi.it

Xenobiotica ISSN 0049–8254 print/ISSN 1366–5928 online © 2000 Taylor & Francis Ltd
http://www.tandf.co.uk/journals/tf/00498254.html

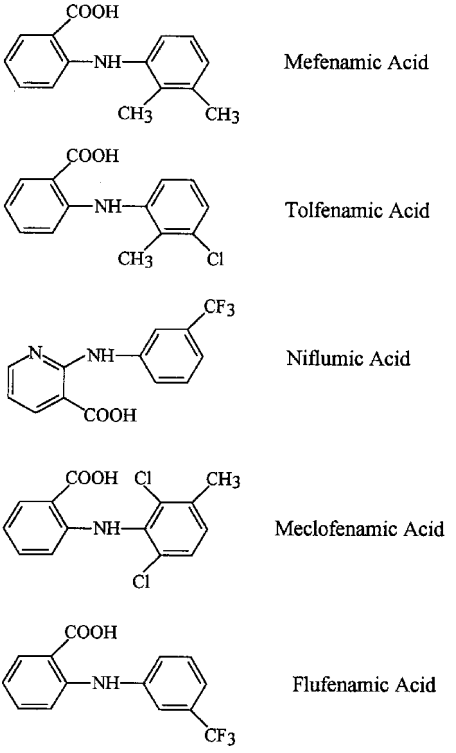


Figure 1. Structure of fenamates.

oxygenase, and mefenamic acid is used to treat pain from rheumatic disease, soft tissue injury (Insel 1996) and dysmenorrhea (Bonnar and Sheppard, 1996; Insel 1996; Zhang and Li Wan Po, 1998). Meclofenamic acid is effective in providing temporary relief of the symptoms of arthritis (Insel 1996), menorrhagia and it is also used to treat dysmenorrhea (Conroy *et al.* 1991). The other fenamates are tolfenamic acid, niflumic acid and flufenamic acid, which are mainly used as analgesics and antipyretics and are on the market in many countries.

In preliminary experiments, it was observed that mefenamic acid is a potent inhibitor of the human liver phenol sulphotransferase (HL-PST). Fenamates are a class of drugs with similar molecular structures (figure 1) and the aim of this study was to see whether the various fenamates share the inhibiting capacity of mefenamic acid.

Materials and methods

Chemicals

3′-Phosphoadenosine-5′-phosphosulphate[^{35}S] (specific activity 1.52 Ci/mmol) was from NEN Life Science Products, Inc. (Brussels, Belgium). 4-Nitrophenol, dopamine, tolfenamic acid, niflumic acid, meclofenamic acid, flufenamic acid, pargyline, dithiothreitol and bovine serum albumin were from Sigma Chemical Co. (Milan, Italy). Monobasic and dibasic potassium phosphate, barium hydroxide, barium acetate and zinc sulphate were from Carlo Erba (Milan, Italy). Mefenamic acid was a generous gift of SIMS (Florence, Italy).

Biological material

Specimens of human liver were obtained after clinically indicated partial hepatotectomy; the Ethical Committee of the Medical School approved the work. Liver samples were from three patients (one man, two women) aged between 47 and 71 years. Of liver, 1 g was homogenized in 5 vols 0.25 M sucrose

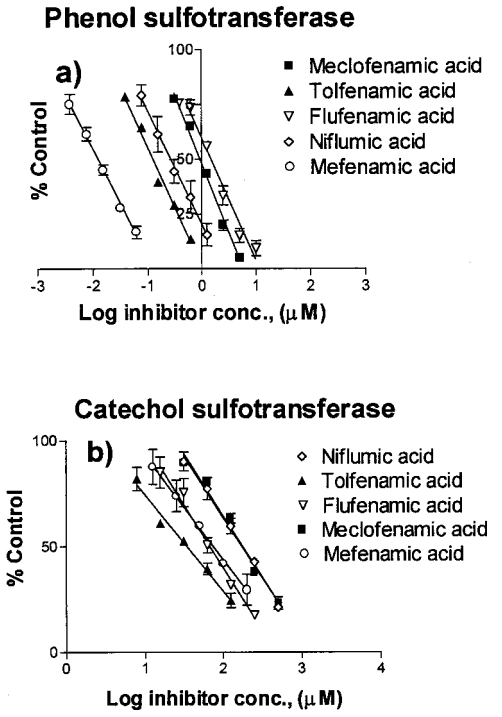


Figure 2. Inhibition curves of the human liver phenol (a) and catechol (b) sulphotransferases by various fenamates. Points are the mean of three livers; vertical bars are 2 × SD. IC_{50} estimates are summarized in tables 1 and 2. The activities (mean ± SD) of phenol- and catechol-sulphotransferases in the control samples were 967 ± 72 and 25 ± 3 pmol/min/mg respectively.

dissolved in 5 mM potassium orthophosphate buffer (pH 7.4) using a glass–Teflon homogenizer. The homogenates were centrifuged at 12000 *g* for 15 min and the resulting supernatants were centrifuged again at 105000 *g* for 1 h. The high-speed cytosolic fraction was divided in aliquots, stored at − 80 °C and designated as the cytosolic fraction. The protein concentration was measured as described by Lowry *et al.* (1951) using bovine serum albumin as a standard.

Phenol and catechol sulphotransferase assays

The activity of HL-PST was measured with 4 μM 4-nitrophenol and 0.4 μM PAPS as substrates and that of HL-CST was measured with 60 μM dopamine and 0.4 μM PAPS as substrates as described by Foldes and Meek (1973), modified by Anderson and Weinshilboum (1980) and adapted by Cappiello *et al.* (1990) to the human liver. The various fenamates were dissolved in acetone and added in 2 μl to the incubation mixture (final volume 150 μl). This volume of acetone did not affect the activities of HL-PST and HL-CST. Each sample was assayed in duplicate and had two blank samples that had the same composition of the active samples with the exception that the sulphate acceptor substrate was omitted. The enzyme activity was measured based on the specific radioactivity of PAPS after correction for blanks and the inhibition curves were constructed using five concentrations of the inhibitor.

Calculations

The IC_{50} estimates were calculated using the software package Dose–Effect Analysis with Microcomputer (Biosoft, Cambridge, UK).

Results and discussion

The inhibition of HL-PST by mefenamic acid was first examined and the IC_{50} for this drug was 0.02 μM and was the lowest IC_{50} observed in this study. The IC_{50} estimates obtained with the other fenamates ranged from 0.12 μM (tolfenamic acid)

Table 1. Inhibition of the human liver phenol sulphotransferase by fenamates.

Drug	$IC_{50} \pm SD$ (μM)	Peak plasma concentration (μM)*	Reference
Mefenamic acid	0.02 ± 0.003	28 (1)	Neuvonen and Kivisto (1988)
Tolfenamic acid	0.12 ± 0.004	21 (2)	Neuvonen and Kivisto (1988)
Niflumic acid	0.28 ± 0.10	68 (3)	Houin *et al.* (1983)
Meclofenamic acid	0.87 ± 0.02	16 (4)	Conroy *et al.* (1991)
Flufenamic acid	1.50 ± 0.20	40 (5)	Lentjes and van Ginneken (1987)

IC_{50} estimates are the mean $\pm$ SD of three livers.

* Average peak plasma concentration after oral administration of (1) 500 mg of mefenamic acid; (2) 400 mg of tolfenamic acid; (3) 250 mg of niflumic acid; (4) 100 mg of meclofenamic acid and (5) 200 mg of flufenamic acid.

Table 2. Inhibition of the human liver catechol sulphotransferase by fenamates.

Drug	$IC_{50} \pm SD$ (μM)	$\frac{IC_{50}\ CST}{IC_{50}\ PST}$	Peak plasma concentration (μM)†	Reference
Tolfenamic acid	36 ± 1	300	21 (1)	Neuvonen and Kivisto (1988)
Flufenamic acid	70 ± 14	47	40 (2)	Lentjes and van Ginneken (1987)
Mefenamic acid	76 ± 6	3800	28 (3)	Neuvonen and Kivisto (1988)
Niflumic acid	180 ± 14	643	68 (4)	Houin *et al.* (1983)
Meclofenamic acid	185 ± 4	213	16 (5)	Conroy et al. (1991)

IC_{50} estimates are the mean $\pm$ SD of three livers.

* Ratio of IC_{50} for catechol sulphotransferase/IC_{50} for phenol sulphotransferase.

† Average peak plasma concentrations after oral administration of (1) 400 mg of tolfenamic acid; (2) 200 mg of flufenamic acid; (3) 500 mg of mefenamic acid; (4) 250 mg of niflumic acid and (5) 100 mg of meclofenamic acid.

and 1.5 μM (flufenamic acid; table 1). The inhibition curves are shown in figure 1(a). The comparison of the IC_{50} estimates with the peak plasma concentrations for the various fenamates obtained from the literature revealed that the IC_{50} estimates were lower than the peak plasma concentrations (table 1). In particular, the peak plasma concentration of mefenamic acid after an oral dose of 0.5 g was three orders of magnitude greater than the IC_{50} for this drug.

Mefenamic acid inhibits the sulphation of (−)-salbutamol and minoxidil in the human liver and the IC_{50} were 72 nM and 1.5 μM respectively (data not shown). These data should suggest that mefenamic acid might inhibit the sulphation of drugs *in vivo*.

Table 2 summarizes the IC_{50} of HL-CST and the figures ranged from 36 μM (tolfenamic acid) and 185 μM (meclofenamic acid) and were greater than those of HL-PST. HL-CST is less susceptible than HL-PST to the inhibition by fenamates and the inhibition curves for the various drugs are shown in the figure 1(b). The peak plasma concentrations of the various fenamates were smaller than the respective IC_{50} for these drugs (table 2). The ratios of the IC_{50} for HL-CST to the IC_{50} for HL-PST were drug-dependent and ranged from 47 (flufenamic acid) to 3800 (mefenamic acid; table 2). Mefenamic acid is, therefore, a potent and selective inhibitor of HL-PST.

The present results show that fenamates inhibit HL-PST and their IC_{50} estimates are smaller than the peak plasma concentrations of these drugs. Mefenamic acid is the most powerful inhibitor of HL-PST and its IC_{50} is three orders of

magnitude lower than the peak plasma concentration of this drug obtained after an oral dose of 0.5 g. The molecular structures of mefenamic acid and tolfenamic acid differ for the substitution of a methyl group by a chlorine atom and the latter drug is a less potent inhibitor than the former one of HL-PST. The other three fenamates (niflumic acid, meclofenamic acid, flufenamic acid) have two or three atoms of chlorine or fluorine in their molecules and their IC_{50} are greater than those of mefenamic acid and tolfenamic acid.

A comparison of the peak plasma concentrations with the IC_{50} is complicated by the fact that the pharmacokinetic data were obtained with different doses of the various drugs. The literature on the fenamates is limited and had not been possible to identify kinetic studies of fenamates performed with similar doses.

Acidic drugs are extensively bound in plasma (Pacifici and Viani, 1992) and only the unbound fraction distributes to the tissues. The unbound fraction of flufenamic acid and tolfenamic acid is 1% (Anon. 1998). When the peak plasma concentration was corrected for the unbound fraction, which was hypothetically estimated at 1% for all fenamates, the unbound concentration of mefenamic acid was an order of magnitude greater than its IC_{50} estimate, whereas the unbound concentrations of the other fenamates were lower than their respective IC_{50} estimates. These *in vitro* results suggest that mefenamic acid should inhibit PST *in vivo* with consequent impairment of sulphation and this possibility should be investigated. Likely, the other fenamates should not inhibit HL-PST *in vivo*.

HL-CST is less susceptible than HL-PST to the inhibition by fenamates and the IC_{50} for HL-CST are greater than the respective peak plasma concentrations of these drugs. The ratio of the IC_{50} for HL-CST to that of HL-PST ranges from 47 (flufenamic acid) to 3800 (mefenamic acid) with the latter drug being a relatively selective inhibitor of HL-PST. The compound 2,6-dichloro-4-phenol (DCNP) has been used as a selective inhibitor of phenol sulphotransferase and the IC_{50} measured with isolated HL-PST is 2.3 μM (Campbell et al., 1987), i.e. two orders of magnitude greater than that of mefenamic acid. This latter drug is, therefore, relatively more potent than DCNP as an inhibitor of HL-PST. As sulphotransferase and UDPGA-glucuronosyl transferase often share the same substrates, further work has to be done to ascertain whether fenamates also inhibit UDPGA-glucuronosyl transferase.

Acknowledgements

This work was supported by the European Commission, Brussels, by the contract BMH1-CT94–1622 and by the Italian Ministry of the University, Rome.

References

ANDERSON, R. J. and WEINSHILBOUM, R. M., 1980, Phenolsulphotransferase in human tissue: radiochemical enzymatic assay and biochemical properties. *Clinica et Chimica Acta*, **103**, 79–90.

ANON., 1998, *Drug Data Handbook*, 3rd edn (Auckland: ADIS), pp. 6–48.

BONHAM CARTER, S. M., REIN, G., GLOVER, V. and SANDLER, M., 1983, Human platelet phenol-sulphotransferase M and P: substrate specificities and correlation with *in vivo* sulphoconjugation of paracetamol and salicylamide. *British Journal of Clinical Pharmacology*, **15**, 323–330.

BONNAR, J. and SHEPPARD, B. L., 1996, Treatment of menorrhagia during menstruation: randomised controlled trial of ethamsylate, mefenamic acid, and tranexamic acid. *British Medical Journal*, **313**, 579–582.

CAMPBELL, N. R. C., VAN LOON, J. A. and WEINSHILBOUM, R. M., 1987, Human liver phenol sulphotransferase: assay conditions, biochemical properties and partial purification of isoenzymes of the thermostable form. *Biochemical Pharmacology*, **36**, 1435–1446.

CAPPIELLO, M., GIULIANI, L. and PACIFICI, G. M., 1990, Differential distribution of phenol and catechol sulphotransferase in human liver and intestinal mucosa. *Pharmacology*, **40**, 69–76.

CONROY, M. C., RANDINITIS, E. J. and TURNER, J. L., 1991, Pharmacology, pharmacokinetics, and therapeutic use of meclofenamate sodium. *Clinical Journal of Pain*, **7 (suppl. 1)**, S44–48.

FOLDES, A. and MEEK, J., 1973, Rat brain phenolsulphotransferase-partial purification and some properties. *Biochimica et Biophysica Acta*, **327**, 365–374.

HOUIN, G., TREMBLAY, D., BREE, F., DUFOUR, A., LEDUDAL, P. and TILLEMENT, J. P., 1983, The pharmacokinetics and availability of niflumic acid in humans. *International Journal of Clinical Pharmacology, Therapy and Toxicology*, **21**, 130–134.

INSEL, P. A., 1996, Analgesic–antipyretic and antiinflammatory agents and drug employed in the treatment of gout. In J. G. Hardman, L. E. Limbird, P. B. Molinoff, R. W. Ruddon and A. Goodman Gilman (eds), *The Pharmacological Basis of Therapeutics*, 9th edn (New York: McGraw-Hill), pp. 617–659.

LENTJES, E. G. and VAN GINNEKEN, C. A., 1987, Pharmacokinetics of flufenamic acid in man. *International Journal of Pharmacology, Therapy and Toxicology*, **25**, 185–187.

LOWRY, O. H., ROSEBROUGH, N. J., FARR, A. and RANDALL, R. J., 1951, Protein measurement with Folin phenol reagent. *Journal Biological Chemistry*, **193**, 265–275.

MULDER, G. J. and JAKOBY, W. B., 1990, Sulfation. In G. J. Mulder (ed.), *Conjugation Reactions in Drug Metabolism* (New York: Taylor & Francis), pp. 107–161.

NEUVONEN, P. J. and KIVISTO, K. T., 1988, Effect of magnesium hydroxide on the absorption of tolfenamic and mefenamic acids. *European Journal of Clinical Pharmacology*, **35**, 495–501.

PACIFICI, G. M. and DE SANTI, C., 1995, Human sulphotransferase. Classification and metabolic profile of the major isoforms. The point of view of the clinical pharmacologist. In G. M. Pacifici and G. N. Fracchia (eds), *Advances in Drug Metabolism in Man* (Luxembourg: European Commission), pp. 311–349.

PACIFICI, G. M. and VIANI, A., 1992, Methods of determining plasma and tissue binding of drugs. Pharmacokinetic consequences. *Clinical Pharmacokinetics*, **23**, 449–468.

RAFTOGIANIS, R. B., HER, C. and WEINSHILBOUM, R. M., 1996, Human phenol sulphotransferase pharmacogenetics: STP1* gene cloning and structural characterisation. *Pharmacogenetics*, **6**, 473–487.

WEINSHILBOUM, R. M., 1986, Phenol sulphotransferase in humans: properties, regulation, and function. *Federation Proceedings*, **45**, 2223–2228.

WEINSHILBOUM, R. M. and OTTERNESS, D. M., 1994, Sulfotransferase enzymes. In: F. C. Kauffman (ed.), *Conjugation–Deconjugation Reactions in Drug Metabolism and Toxicity*. Handbook of Experimental Pharmacology Series, Volume 112 (Berlin: Springer), pp. 45–78.

ZHANG, W. Y. and LI WAN PO, A., 1998, Efficacy of minor analgesics in primary dysmenorrhoea: a systematic review. *British Journal of Obstetrics and Gynaecology*, **105**, 780–789.

XENOBIOTICA , 2000, VOL. 30, NO. 2, 117–129

Comparative *in vitro* metabolism of indinavir in primates – a unique stereoselective hydroxylation in monkey

M. CHIBA*, J. A. NISHIME, W. NEWAY, Y. LIN and J. H. LIN

Department of Drug Metabolism, Merck Research Laboratories, West Point, PA 19486, USA

Received 21 June 1999

1. The *in vitro* metabolism of indinavir (CRIXIVAN, MK-0639, L-735,524), an HIV protease inhibitor, was evaluated using liver microsomes from cynomolgus monkey, rhesus monkey, chimpanzee and human. Indinavir exhibited marked species differences in metabolism. The overall rate of indinavir metabolism varied > 4-fold among primates (84 pmol/min/mg protein in cynomolgus monkey versus 20.4 pmol/min/mg protein in human) and followed the rank order: cynomolgus monkey > rhesus monkey > chimpanzee > human.

2. The *cis*-(indan)hydroxylated metabolite of indinavir was formed only in cynomolgus and rhesus monkey livers, whereas *trans*-(indan)hydroxylation and *N*-dealkylation were observed as the major metabolites in all primates tested. Inhibition studies with P450-selective inhibitors (ketoconazole, quinine, quinidine) and monoclonal antibodies (against CYP2D6 or CYP3A4) indicated that a cytochrome P450 isoform of the CYP2D subfamily is involved in the formation of the unique *cis*-(indan) hydroxylated metabolite in monkey, whereas all other oxidative metabolites, including the *trans*-(indan)hydroxylated metabolite, are formed by CYP3A isoform(s).

3. The present study has demonstrated that monkeys were unique in their abilities to form the stereoselective metabolite and were not appropriate surrogates for the qualitative prediction of indinavir metabolism in human.

Introduction

For human risk assessment, regulatory agencies require that systemic exposures of an unchanged drug and its major metabolites in animal toxicity studies are demonstrated and that they exceed the results expected in human to ensure a safety margin. Therefore, it is important to select animal species that have a metabolite profile similar to human. However, it is well known that the metabolism of drugs may differ significantly between species, both in qualitative and quantitative terms (Smith 1991, Lin 1995, Chauret *et al.* 1997, Zhao and Ishizaki 1997). Because very high doses are normally administered in toxicity studies and a much smaller dose is used clinically, the systemic exposure of a drug and its metabolites are sufficient in toxicity animals to cover the safety margin in patients. Therefore, the 'qualitative' species difference in metabolism is of greater concern than the 'quantitative' species difference.

Non-human primates have been long considered the most appropriate animal models for the prediction of drug metabolism in human, and there are many publications that suggest that the monkey may provide more reliable predictions for human drug metabolism than the rodent and dog (Yasumori *et al.* 1992, Wu *et al.* 1993, Ring *et al.* 1994, Sharer *et al.* 1995, Igarashi *et al.* 1997). This general belief

* Author for correspondence; e-mail: Masato_Chiba@merck.com

Xenobiotica ISSN 0049–8254 print/ISSN 1366–5928 online © 2000 Taylor & Francis Ltd
http://www.tandf.co.uk/journals/tf/00498254.html

is derived from the basis of homology of drug-metabolizing enzymes. It has been shown that the nucleotide and the deduced amino acid sequences of P450 isoforms (CYP2D and 3A) in cynomolgus monkey (*Macaca fasicularis*) and marmoset (*Callithrix jacchus*) had $>90\%$ identities to the human P450s (Laddison *et al.* 1995, Igarashi *et al.* 1997). However, it must be noted that even a few amino acid changes can substantially influence the substrate specificity and enzyme activity (Smith *et al.* 1998) and there are several evidence suggesting that drug metabolism is quantitatively dissimilar between monkey and human (Stevens *et al.* 1993, Lin 1995, Sharer *et al.* 1995, Shimada *et al.* 1997).

Indinavir (CRIXIVAN, MK-0639, L-735,524) is a potent and highly selective inhibitor for HIV protease (Vacca *et al.* 1994). The pharmacokinetics of the drug have been studied in rat, dog and monkey, and the *in vitro* kinetic parameters reasonably well predicted the *in vivo* pharmacokinetics of indinavir in the animal species tested (Lin *et al.* 1996). In addition, it was demonstrated that P450 isoform(s) in the CYP3A subfamily played an important role in the oxidative metabolism of indinavir in both rat (Chiba *et al.* 1997) and human (Chiba *et al.* 1996).

The aim of the current paper was to compare the metabolism of indinavir in liver microsomes from rhesus monkey (*Macaca mulatta*), cynomolgus monkey, chimpanzee (*Pan troglodytes*) and human. Whereas the metabolic pathways of indinavir were similar in these three species, only monkey (both rhesus and cynomolgus monkey) formed a novel metabolite, 2′,3′-*cis*-dihydroxyindan (M7). Additionally, the possible involvement of a P450 isoform(s) in CYP2D subfamily in this unique metabolism in monkey has been investigated.

Materials and methods

Chemicals

Indinavir and its ^{14}C form (CRIXIVAN, MK-0639, L-735,524, *N*-[2(*R*)-hydroxy-1(*S*)-indanyl]-5-[[2(S)-tertiary-butylaminocarbonyl]-4-(3-pyridylmethyl)piperazino]-4(*S*)-hydroxy-2(*R*)-phenylmethyl-pentanamide) were synthesized at Merck Research Laboratories (West Point, PA, USA). The labelled indinavir was prepared with ^{14}C in the 1-position of the pentanamide moiety, with a specific activity of 33.08 μCi/mg (figure 1). The drug occasionally was purified according to the HPLC method described below and the purity was $>99\%$. Authentic metabolites used to assign the chromatogram were: 2′,3′-*trans*-dihydroxyindan (M3), pyridine *N*-oxide (M4a), *p*-hydroxyphenylmethyl (M4b) and *N*-depyridomethylated (M6) analogues of indinavir. The synthesized *cis*-isomer of M3 (M7) was also used. Quinine, quinidine and ketoconazole were from Sigma Chemical Co. (St Louis, MO, USA). Debrisoquin and its 4-hydroxylated metabolite were from Gentest Corp. (Woburn, MA, USA). All other reagents were of analytical grade.

Liver microsomes

Animal liver microsomes were prepared from male adult cynomolgus monkey (*M. fasicularis*; 3–6 kg body weight), male adult rhesus monkey (*M. mulatta*; 3–6 kg body weight) and male adult chimpanzees (*P. troglodytes*; 50 kg body weight) (Charles River, Key Lois, FL, USA). Microsomes were prepared by differential ultracentrifugation (Omura and Sato 1964). Microsomal final pellets were resuspended in 0.15 M Tris-HCl buffer (pH 7.4). Microsomal protein was measured by the method of Lowry *et al.* (1951) with bovine serum albumin as the standard. Human liver microsomes were from Keystone Skin Bank (Exton, PA, USA).

Antibodies and recombinant P450s

Monoclonal anti-CYP3A4 antibody and recombinant CYP3A4 (batch no. 103097) were prepared at Merck Research Laboratories (West Point, PA, USA). The antibody showed a high inhibitory potency for testosterone 6β-hydroxylase activity in recombinant CYP3A4, 3A5 and 3A7 without cross-inhibition for recombinant CYP1A1, 1A2, 2A6, 2B6, 2C8, 2C9, 2C19, 2D6 or 2E1-catalyzed marker metabolism (Dr Magang Shou, MRL, personal communication). Monoclonal anti-CYP2D6 antibody (cat. no. A366), recombinants CYP2D1 (cat. no. P517) and CYP2D6 (cat. no. P217) were from Gentest.

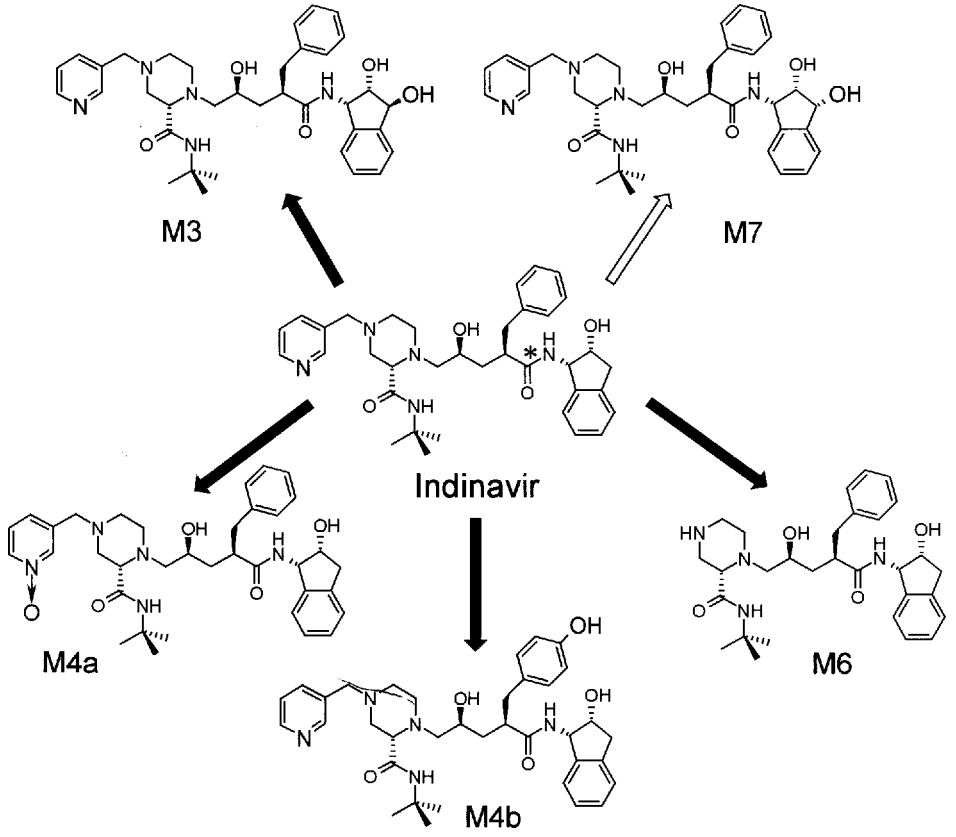


Figure 1. Primary metabolites of indinavir in animals and human. Metabolic structures have been identified in human urine and faeces samples (Balani *et al.* 1995). Primary metabolites formed by P450 are shown. *Position of ^{14}C label.

Indinavir metabolism studies

Indinavir metabolism was measured in a reaction mixture consisting of NADPH-fortified liver microsomes from cynomolgus monkey, rhesus monkey, chimpanzee and human (or NADPH-fortified recombinant P450s) according to the methods outlined herein.

Metabolite profiling studies. The incubation mixture (total volume = 120 μl in 0.15 M Tris-HCl buffer, pH 7.4) consisted of an NADPH-generating system (10 mM G6P, 2 IU/ml G6P dehydrogenase, 10 mM $MgCl_2$), 1 mM EDTA, 4 mg/ml microsomal protein and 10 μM [^{14}C]indinavir. Time-course studies indicated that the formation of primary metabolites was linear up to 10 (monkey) or 20 (chimpanzee and human) min at 4 mg/ml protein (data not shown). After a 5-min pre-incubation at 37 °C, the reaction was initiated by the addition of 5 μl 50 mM NADPH. The incubation was conducted at 37 °C for 10, 20 and 20 min in monkey, chimpanzee and human liver microsomes respectively, and the reaction terminated by adding 375 μl ice-cold acetonitrile. The resulting suspension was mixed vigorously and centrifuged at 16000 *g* for 4 min to precipitate protein, and the supernatant transferred to a clean test tube. The sample was evaporated to dryness under nitrogen and reconstituted with 125 μl 10% acetonitrile in water for injection onto the HPLC system described as follows.

Chemical inhibition studies. For the competitive inhibition studies with chemical inhibitors (ketoconazole, quinine, quinidine), the incubation mixture (total volume = 120 μl in 0.15 M Tris-HCl buffer, pH 7.4) consisted of an NADPH-generating system (same composition as described above), 1 mM EDTA, 2 μM [^{14}C]indinavir, various concentrations of inhibitors (0, 0.5, 1, 5, 10 μM for ketoconazole; 0, 2, 5, 20, 50, 100 μM for quinine and quinidine) and 4 mg/ml rhesus monkey liver microsomes. The reaction was initiated by the addition of 5 μl 50 mM NADPH, and the incubation was conducted at 37 °C for 10 min. The reaction was terminated by adding 375 μl ice-cold acetonitrile and the sample for HPLC injection was prepared as described above.

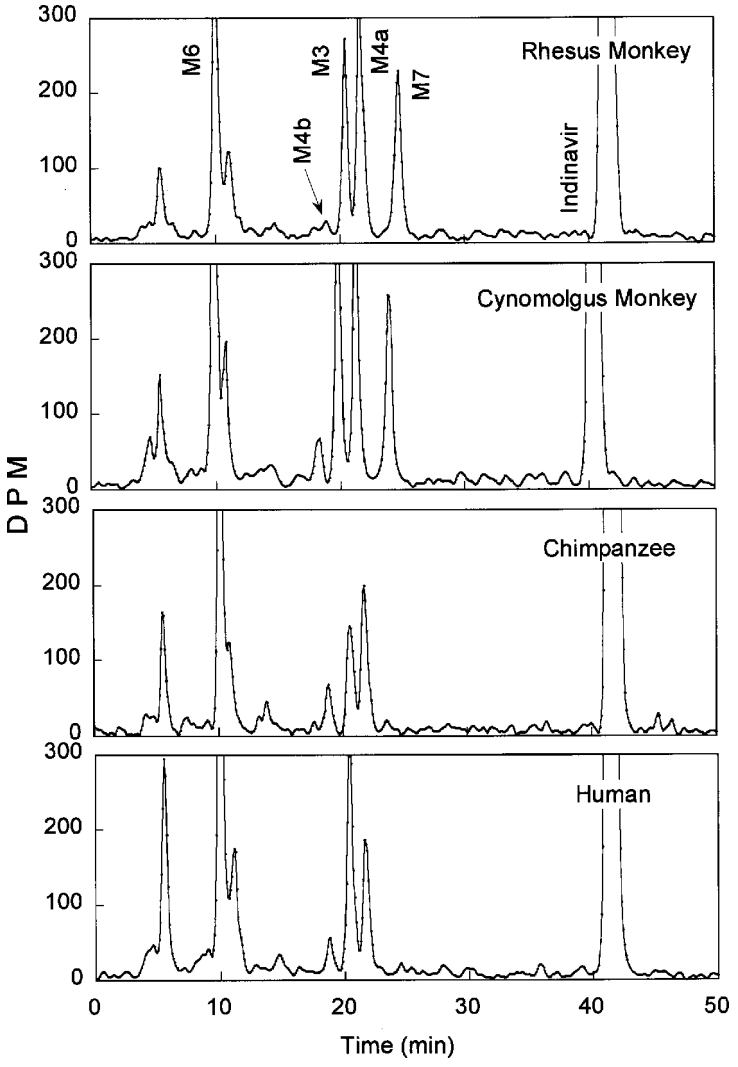


Figure 2. Indinavir metabolism by rhesus monkey, cynomolgus monkey, chimpanzee and human liver microsomes. Microsomes (4 mg/ml) were incubated with 10 μM [^{14}C]indinavir in the presence of an NADPH-generating system at 37 °C for 10 (monkey) or 20 (chimpanzee and human) min. Chromatograms were obtained by HPLC system with a flow scintillation analyzer.

Immunochemical inhibition studies. Immunochemical inhibition studies were performed with monoclonal anti-CYP2D6 antibody (for indinavir and debrisoquin metabolism) and anti-CYP3A4 antibody (for indinavir metabolism). The liver microsomal suspension from rhesus monkey or human (0.5 mg) was pre-incubated with 0, 5, 10, 20, 50 and 100 μl ascites/mg microsomal protein (anti-CYP2D6 antibody) or 0, 0.5, 1, 2, 5, 10 and 20 μl ascites/mg microsomal protein (anti-CYP3A4 antibody) for 30 min at room temperature. After pre-incubation the reaction mixture (same composition described above) and 10 μM [^{14}C]indinavir (or 50 μM debrisoquin) were added to the microsomal suspension and incubated for 5 min at 37 °C. The reaction was initiated by the addition of 5 μl 50 mM NADPH, and the incubation conducted at 37 °C for 10 min for indinavir and 30 min for debrisoquin. The reaction was terminated by adding 375 μl ice-cold acetonitrile for the indinavir assay and 10 μl 70% perchloric acid for the debrisoquine assay. The metabolites were determined according to the HPLC methods described below.

Recombinant P450 studies. Recombinant P450 isoforms (25 pmol P450/incubation) were incubated with an NADPH-generating system (same composition as noted above), 1 mM EDTA and 10 μM

Table 1. Hepatic microsomal metabolism of indinavir in primates[a].

Species[b]		Metabolite formation rate (pmol/min/mg)						
		M2 + M5[c]	M3	M4a	M4b	M6	M7	Total
Rhesus monkey[d]	mean	5.26	15.8	12.3	3.90	19.6	17.6	74.5
	SD	1.71	2.9	1.7	0.79	3.6	1.0	11.0
Cynomolgus monkey	mean	9.19	12.7	13.6	3.25	29.2	16.0	84.0
	SD	1.99	2.7	3.6	0.59	6.8	3.6	17.5
Chimpanzee	mean	5.62	2.94	4.83	0.80	12.5	nd[e]	26.7
	SD	1.53	0.89	0.92	0.10	2.5		2.6
Human	HL-1	7.82	7.09	5.94	2.5	16.0	nd	39.4
	HL-2	1.28	1.13	1.19	0.727	2.11	nd	6.44
	HL-3	1.06	0.763	0.744	0.202	1.61	nd	4.38
	HL-4	3.98	2.89	3.67	2.27	5.69	nd	18.5
	HL-5	2.56	0.959	1.46	0.478	3.65	nd	9.11
	HL-6	8.58	7.60	7.27	4.82	16.1	nd	44.4
	mean	4.21	3.41	3.38	1.83	7.53		20.4
	SD	3.27	3.15	2.73	1.75	6.75		17.4

[a] Metabolite formation rates were measured at 10 (monkey) or 20 (chimpanzee and human) min after the onset of incubation in the presence of NADPH and 4 mg/ml microsomal protein. Indinavir concentration was 10 μM. Data are the mean of results from three individual microsomal preparations except human ($n = 6$).

[b] All experimental animals were male.

[c] Formation rates for secondary metabolites (M2 and M5) were summed.

[d] Data were taken from Lin *et al.* (1996) for the comparison.

[e] ND, Not detectable.

[^{14}C]indinavir at 37 °C for 10 (CYP3A4) and 60 (CYP2D1 or CYP2D6) min following the addition of 5 μl 50 mM NADPH. The reaction was terminated by adding 375 μl ice-cold acetonitrile. The sample for HPLC injection was prepared as described previously.

HPLC assay for indinavir and metabolites

Indinavir and its metabolites were measured by an HPLC system as described in Chiba *et al.* (1996). Briefly, an HPLC system consisted of a pump/auto-injector (Thermo Separation Products P4000/AS3000, Fremont, CA, USA), an UV detector (Thermo Separation Products UV2000) and a flowscintilation analyzer (Packard 515TR, Downers Grove, IL, USA). The assay was performed on a reversed-phase column (Supercosil LC-18, 15 cm × 4.6 mm, 5 μm). Mobile phase A consisted of 10 mM phosphate buffer (pH 5.2) and 0.005 M hexyltriethylammonium phosphate. Mobile phase B consisted of acetonitrile. The following gradient system was used: 25% B to 30% B linearly over the first 40 min; isocratic 30% B for 10 min; and then 30% to 25% B for 5 min. Flow rate was 1 ml/min. Each biological sample was treated with a mixture of synthetic indinavir metabolites, elution of which from the column was monitored at 210 nm. The recovery after HPLC analysis was calculated as > 90%, as determined by comparing the injected counts with the integrated counts in the eluted samples.

Debrisoquin–quinidine and debrisoquin–indinavir interaction studies

Debrisoquin 4-hydroxylase activity (at 50 μM) was measured in rhesus monkey liver microsomes (1 mg/ml) incubated with different concentrations of indinavir (or quinidine), or in human liver microsomes (1 mg/ml) with different concentrations of quinidine, in the presence of an NADPH-generating system (same composition as noted previously) for 30 min at 37 °C. The reaction was terminated by the addition of 10 μl 70% perchloric acid, and the resulting mixture was vortex-mixed. The supernatant was separated by centrifugation (16 000*g* for 4 min) and injected directly onto the HPLC. An HPLC assay was performed on a Vydac protein-peptide C_{18} column (5 μm, 4.6 mm × 25 cm) using an HPLC system (Thermo Separation Products P4000/AS3000) and a spectrofluorometer (FL2000). The HPLC method involved the isocratic elution for 10 min with 5% acetonitrile in 0.1 M NaH_2PO_4 at 1.0 ml/min. At 10 min a gradient was initiated and the acetonitrile was increased to 10% at 15 min. The acetonitrile was then decreased to 5% at 20 min and remained at 5% for an additional 10 min. The metabolite was monitored at 210 and 290 nm for excitation and emission respectively. The inhibition of M7 formation from [^{14}C]indinavir (10 μM) by debrisoquin was measured in rhesus monkey liver microsomes (4 mg/ml) incubated with the designated concentrations of debrisoquin in the

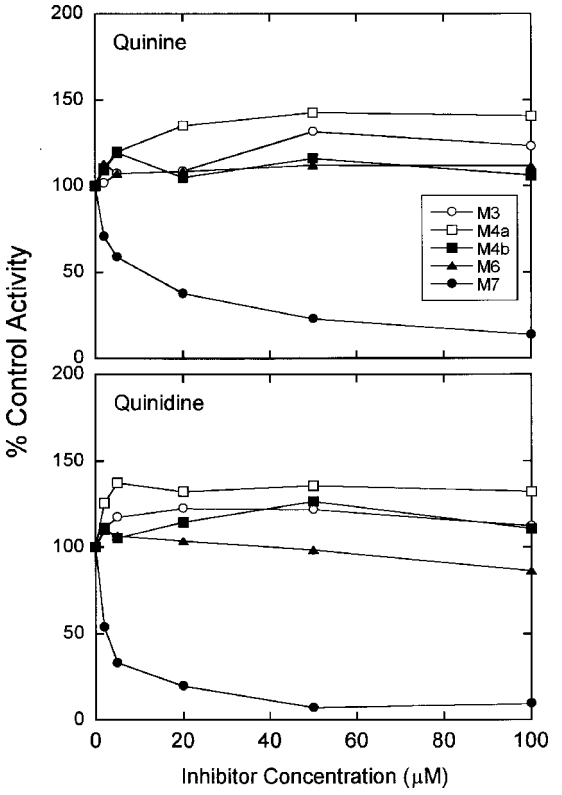


Figure 3. Inhibition of indinavir metabolism by quinine and quinidine in rhesus monkey liver microsomes. Rhesus monkey liver microsomes (4 mg/ml) were incubated with 2 μM [^{14}C]indinavir and various concentrations of inhibitor (0, 2, 5, 20, 50, 100 μM) in the presence of an NADPH-generating system for 10 min at 37 °C. Data are the average of duplicate samples. Controls for indinavir metabolism were: 13.7 pmol/min/mg protein for M3 formation; 9.13 pmol/min/mg protein for M4a formation; 3.16 pmol/min/mg protein for M4b formation; 18.3 pmol/min/mg protein for M6 formation; and 7.72 pmol/min/mg protein for M7 formation.

presence of an NADPH-generating system (same composition as described previously) for 10 min at 37 °C. The reaction was terminated by the addition of 375 μl ice-cold acetonitrile. The sample for HPLC injection was prepared as described above.

Results

Biotransformation of indinavir in monkey, chimpanzee and human

In previous studies (Balani *et al.* 1995) the major metabolic pathways were identified in human as (1) pyridine *N*-oxidation (M4a), (2) *para*-hydroxylation of the phenylmethyl group (M4b), (3) *trans* 3′-hydroxylation of the indan moiety (M3) and (4) *N*-depyridomethylation (M6) (figure 1). Two additional secondary metabolites (M2, a product of pyridine *N*-oxidation and *trans* 3′-hydroxylation; M5, a product of *N*-depyridomethylation and *trans* 3′-hydroxylation) were also found in the human samples. Six major metabolites (M2, M3, M4a, b, M5 and M6) were formed in all primates studied when indinavir was incubated with NADPH-fortified liver microsomes. An additional metabolite, *cis*-2′,3′-dihydroxylated indan (M7), was observed only in rhesus and cynomolgus monkey (figure 2 and table 1). The total metabolic activity measured by the formation of all metabolites in the

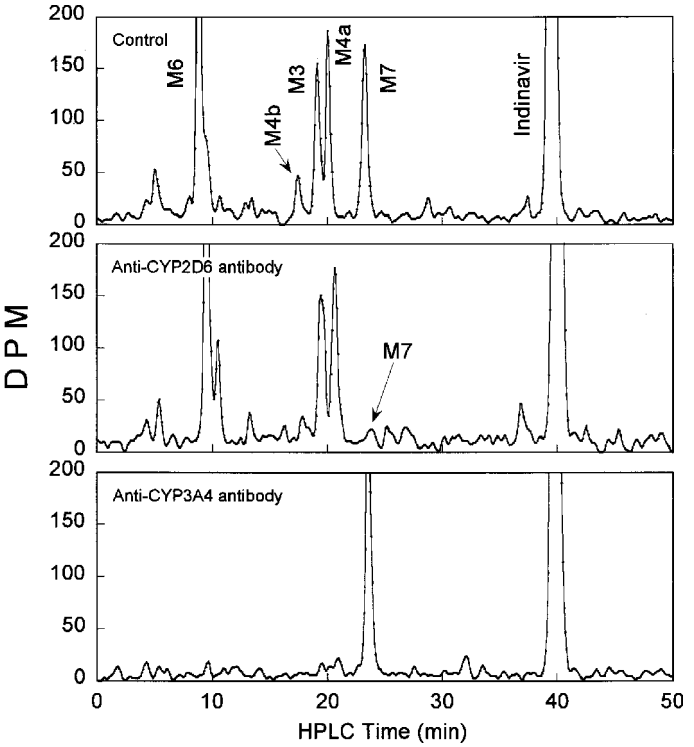


Figure 4. Immuno-inhibition by monoclonal anti-CYP2D6 antibody and anti-CYP3A4 antibody on indinavir metabolism in rhesus monkey liver microsomes. Rhesus monkey liver microsomes were pre-incubated with 0 (control), 100 (anti-CYP2D6 antibody) or 20 (anti-CYP3A4 antibody) μl ascites/mg microsomal protein for 30 min at room temperature. The reaction was then initiated by the addition of NADPH after a 5-min pre-incubation in the presence of an NADPH-generating system and 10 μM [^{14}C]indinavir at 37 °C. The incubation was conducted for 10 min.

monkey was the largest among species (table 1). It should be noted that the metabolic activity varied >10-fold in human liver microsomes from six independent subjects.

P450 isoform(s) involved in M7 formation in monkey

Ketoconazole (0.5–10 μM), a potent CYP3A inhibitor, completely inhibited all oxidative metabolites in a concentration-dependent manner without affecting M7 formation in monkey liver microsomes (data not shown). In contrast, both quinine and quinidine (CYP2D-selective inhibitors) extensively inhibited M7 formation with little effect on the other oxidative metabolism pathways (figure 3). Quinidine appeared to be more potent inhibiting M7 formation than quinine. IC_{50} for M7 inhibition by quinidine and quinine was 2.5 and 10 μM respectively. These results suggest that the involvement of CYP2D-like isoform in the formation of M7.

The inhibition studies with monoclonal antibodies for CYP2D6 and 3A4 further supported the involvement of CYP2D-like isoform in M7 formation. Monoclonal anti-CYP2D6 antibody showed a specific inhibitory potency for M7 formation in monkey liver microsomes, whereas anti-CYP3A4 antibody clearly inhibited the formation of all metabolites, but not M7 formation (figure 4).

The metabolism of indinavir was also examined using recombinant CYP3A4,

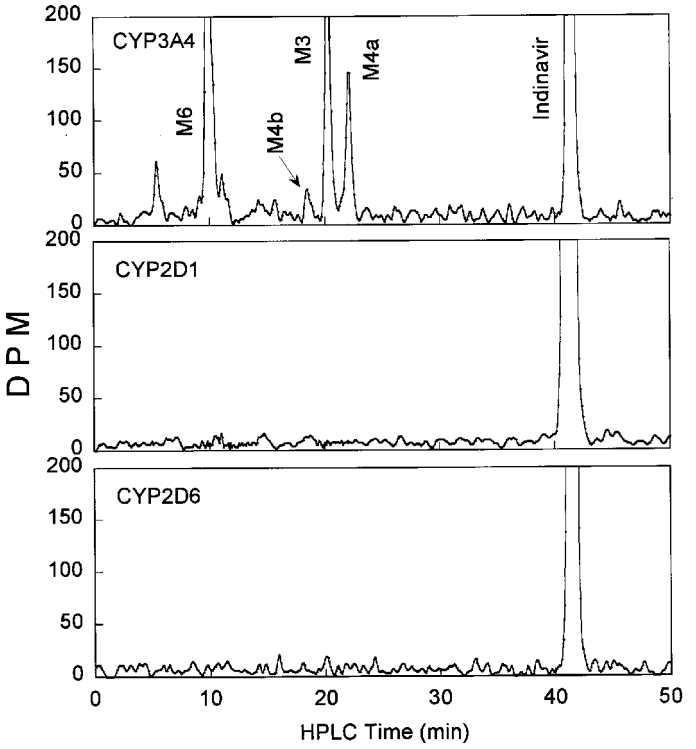


Figure 5. Indinavir metabolism by recombinant P450s. Recombinant CYP3A4, CYP2D1 and CYP2D6 (25 pmol each) were incubated with 10 μM [^{14}C]indinavir at 37 °C for 10 (CYP3A4) or 60 (CYP2D1 and 2D6) min in the presence of an NADPH-generating system.

Table 2. Kinetics of indinavir metabolism in rhesus monkey liver microsomes[a].

Metabolite	K_m (μM)	V_{max} (pmol/min/mg protein)	V_{max}/K_m (μl/min/mg protein)
M3	5.39± 1.16	14.8± 4.5	2.79± 0.9
M4a	5.45± 1.44	21.0± 3.3	3.97± 0.69
M4b	3.75± 2.23	3.52± 0.66	1.44± 1.20
M6	2.64± 0.39	29.2± 4.6	11.3± 2.5
M7	10.8± 2.4	23.3± 8.0	2.21± 0.69

[a] Kinetic studies were conducted using indinavir concentrations between 0.5 and 20 μM. Incubation was carried out for 2 min to minimize the secondary metabolite formation (< 15% of total metabolism). Numbers are the mean± SD of three individual monkey liver microsomal preparations.

2D1 or 2D6 (figure 5). CYP3A4 formed all oxidative metabolites found in monkey liver microsomes, with the exception of M7. Neither CYP2D1 nor 2D6 showed any capability to metabolize indinavir during a 60-min incubation.

Kinetic studies on M7 formation in rhesus monkey

To characterize the unique formation of M7, kinetic studies were conducted to evaluate K_m and V_{max} for each metabolic pathway of indinavir using rhesus monkey liver microsomes (table 2). K_m for M7 was 2–3-fold larger than that for the other

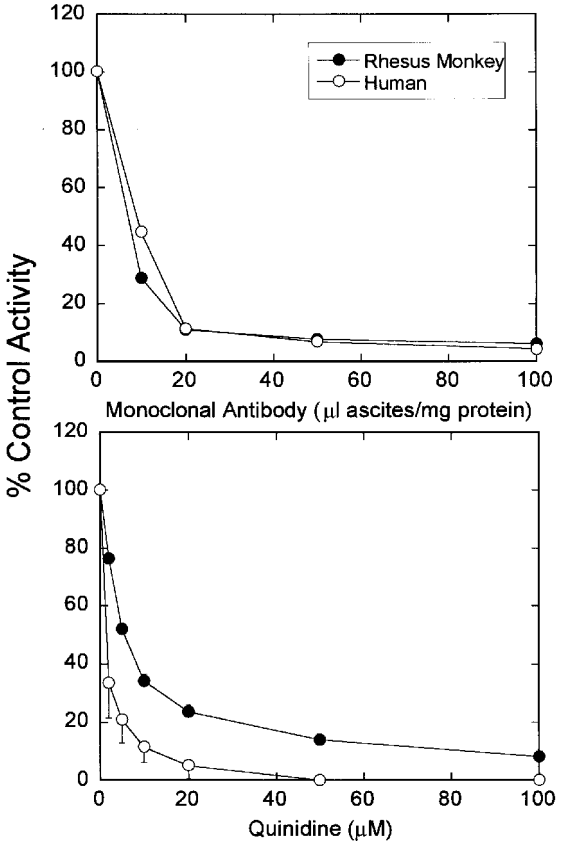


Figure 6. Inhibition of debrisoquin 4-hydroxylation by monoclonal anti-CYP2D6 antibody and quinidine in monkey and human. Rhesus monkey and human liver microsomes were pre-incubated with different concentrations of monoclonal anti-CYP2D6 antibody for 30 min before the incubation at 37 °C for 30 min in the presence of an NADPH and 50 μM debrisoquin. For the inhibition studies with quinidine, microsomes were incubated with different concentrations of quinidine in the presence of an NADPH and 50 μM debrisoquin at 37 °C for 30 min. IC_{50} were 1.16± 0.56 μM (n = 3, mean± SD) for human; 5.80± 0.4 μM (n = 3, mean± SD) for monkey.

metabolic pathways. V_{max} for M7 formation was comparable with that for M4a or M6 formation. Metabolic clearance calculated from V_{max}/K_m predicted that the formation of M6 is the major metabolic pathway in the lower concentration range. K_m for the CYP3A-catalyzed metabolism (M3, M4a, M4b, M6 formations) were relatively similar, and that for the M7 formation was somewhat larger than those for CYP3A-mediated metabolism.

Indinavir and debrisoquin interaction in rhesus monkey

Debrisoquin 4-hydroxylation, a CYP2D-mediated activity, was inhibited > 95% by monoclonal anti-CYP2D6 antibody and quinidine in a concentration-dependent manner in rhesus monkey liver microsomes, as well as in human (figure 6). Since both debrisoquin 4-hydroxylase activity and indinavir M7 formation were almost completely inhibited by quinidine and the same monoclonal anti-CYP2D6 antibody, it is expected that there is an interaction between debrisoquin 4-hydroxylation and indinavir M7 formation. Surprisingly, debrisoquin showed

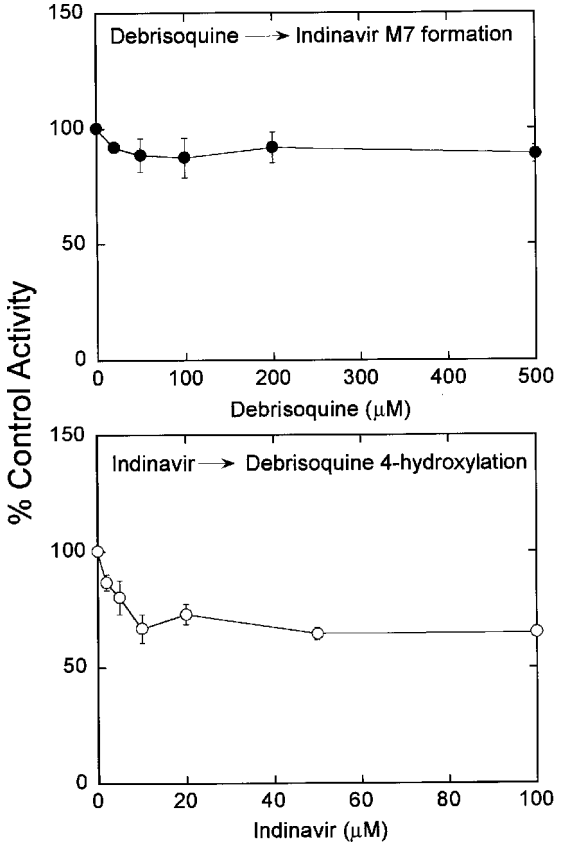


Figure 7. Indinavir and debrisoquin interaction in rhesus monkey liver microsomes. M7 formation from [^{14}C]indinavir (10 μM) was measured in the rhesus monkey liver microsomes incubated with different concentrations of debrisoquin in the presence of an NADPH-generating system for 10 min at 37 °C (upper). Control M7 formation rate was 15.5± 2.5 pmol/min/mg protein (n = 3, mean± SD). Debrisoquin 4-hydroxylase activity (at 50 μM) was measured in the rhesus monkey liver microsomes incubated with different concentrations of indinavir in the presence of an NADPH-generating system for 30 min at 37 °C (lower). Control debrisoquin 4-hydroxylase activity was 2.2± 0.3 pmol/min/mg protein (n = 3, mean± SD).

little effect (< 10%) on M7 formation rate up to 500 μM (figure 7, upper). Indinavir moderately inhibited debrisoquin 4-hydroxylase activity; ~ 35% of control activity was inhibited by indinavir at 100 μM (figure 7, lower).

Discussion

In vitro studies on indinavir metabolism have been conducted with liver microsomes from monkey (rhesus and cynomolgus), chimpanzee and human. Only monkey formed the *cis*-hydroxylated indan metabolite of indinavir (M7 in figure 1). Inhibition studies with P450-selective inhibitors and monoclonal antibodies suggested that a P450 isoform(s) in CYP2D subfamily is involved in the unique formation of the *cis*-hydroxylated metabolite (M7), whereas the CYP3A isoform catalyzed the *trans*-hydroxylation (M3 formation) as well as all other oxidative metabolism in monkey.

The species differences in regio- and stereo-selective metabolism catalyzed by P450s have been studied for many compounds including digitoxin (Eberhart *et al.*

1991), mephenytoin (Yasumori *et al.* 1992), phenanthrene (Shou *et al.* 1994), progesterone (Duignan *et al.* 1988), testosterone (Niwa *et al.* 1995), tolbutamide (Sharer *et al.* 1995, Smith 1991) and warfarin (Kaminsky 1989). It has been suggested that primates are better surrogates for human than rodent or dog in qualitatively predicting human drug metabolism (Eberhart *et al.* 1991, Yasumori *et al.* 1992, Ring *et al.* 1994). However, the present data strongly indicate that the metabolism of indinavir in monkey is qualitatively different from that in human, whereas the indinavir metabolism in chimpanzee is similar to that in human.

Both immunochemical and chemical inhibition studies indicated that M7 formation in monkey liver microsomes was catalyzed by CYP2D isoform(s). Similarly, debrisoquin 4-hydroxylation was also metabolized by CYP2D isoform in monkey. However, debrisoquin had little inhibitory effect ($< 10\%$) on the M7 formation of indinavir, whereas indinavir significantly ($\sim 30\%$) inhibited debrisoquin 4-hydroxylation (figure 7). These results suggest that there may be (at least) two distinct CYP2D isoforms in monkey liver microsomes. In a study by Jacqz-Aigrain *et al.* (1991), two distinct proteins of 49 and 47 kDa were electrophoretically cross-reacted with anti-LKM(CYP2D6) antibody in monkey liver microsomes. These results appear to support the present hypothesis that monkey may have multiple CYP2D isoforms.

Although the homology of the nucleotide and the deduced amino acid sequences of a CYP2D isoform in cynomolgus monkey (CYP2D17) were reported to be 96 and 94% respectively to human CYP2D6 (Laddison *et al.* 1995), there is little known about the substrate specificity of monkey CYP2D isoforms. It has been demonstrated that cloned CYP2D isoforms (CYP2D1, 2D2, 2D3, 2D4), all belonging to the rat CYP2D subfamily, had distinct substrate specificities toward bufuralol, debrisoquin and lidocaine (Wan *et al.* 1997). Furthermore, Smith *et al.* (1998) demonstrated that a single amino acid substitution (F483I) had conferred on CYP2D6 the ability to metabolize testosterone to the novel product, 15α-hydroxytestosterone without losing its catalytic activity for bufuralol metabolism. Therefore, it is not surprising that a minor difference in the critical structure of monkey CYP2D isoform(s) could result in the acquisition of a metabolic capability to form a stereoselective metabolite distinct from the other primates.

The present results suggest that chimpanzee might be a good animal model in predicting drug metabolism in human. However, it was reported that the stereoselectivity of ABT-418 metabolism catalyzed by flavin-containing monooxygenase (FMO) in chimpanzee was different from rat, rabbit, dog and human (Rodrigues *et al.* 1995). Therefore, the species differences and similarity in drug metabolism appears to depend on the enzyme system(s) involved in the metabolism of interest.

In summary, the present authors have observed that monkey liver microsomes uniquely converted indinavir to a novel *cis*-hydroxylated metabolite. The formation appeared to be mediated by P450 isoform(s) in the CYP2D subfamily, yet is distinct from the isoform(s) responsible for catalyzing the widely used CYP2D marker, debrisoquin 4-hydroxylation. Monkey has been demonstrated to be a useful surrogate for human in predicting P450(CYP2D)-catalyzed drug metabolism (Jacqz-Aigrain *et al.* 1991, Otton *et al.* 1992, Wu *et al.* 1993). The present study, however, re-emphasizes the fact that qualitative differences in metabolic profiles can still exist among primates. Thus, caution must be taken when extrapolating drug metabolism and pharmacokinetic data from monkey to human.

Acknowledgements

The authors gratefully acknowledge the support and thoughtful discussion of Dr Thomas A. Baillie during the course of this study. They are indebted to Ms Michelle L. Ok for technical support and to Dr M. Shou for the monoclonal anti-CYP3A4 antibody and recombinant CYP3A4. Also thank is Ms A. Gibson for preparation of the manuscript.

References

Balani, S. K., Arison, B. H., Mathai, L., Kauffman, L., Miller, R. R., Sterns, R. A., Chen, I.-W. and Lin, J. H., 1995, Metabolites of L-735,524, a potent HIV-1 protease inhibitor, in human urine. *Drug Metabolism and Disposition*, **23**, 266–270.

Chauret, N., Gauthier, A., Martin, J. and Nicoll-Griffith, D. A., 1997, *In vitro* comparison of cytochrome P450-mediated metabolic activities in human, dog, cat, and horse. *Drug Metabolism and Disposition*, **25**, 1130–1136.

Chiba, M., Hensleigh, M. and Lin, J. H., 1997, Hepatic and intestinal metabolism of indinavir, an HIV protease inhibitor, in rat and human microsomes. *Biochemical Pharmacology*, **53**, 1187–1195.

Chiba, M., Hensleigh, M., Nishime, J. A., Balani, S. and Lin, J. H., 1996, Role of cytochrome P450 3A4 in human metabolism of MK-639, a potent human immunodeficiency virus protease inhibitor. *Drug Metabolism and Disposition*, **24**, 307–314.

Duignan, D. B., Sipes, I. G., Ciaccio, P. J. and Halpert, J. R., 1988, The metabolism of xenobiotics and endogenous compounds by the constitutive dog liver cytochrome P450 PBD-2. *Archives of Biochemistry and Biophysics*, **267**, 294–304.

Eberhart, D. C., Gemzik, B., Halvorson, M. R. and Parkinson, A., 1991, Species differences in the toxicity and cytochrome P450 IIIA-dependent metabolism of digitoxin. *Molecular Pharmacology*, **40**, 859–867.

Igarashi, T., Sakuma, T., Isogai, M., Nagata, R. and Kamataki, T., 1997, Marmoset liver cytochrome P450s: Study for expression and molecular cloning of their cDNAs. *Archives of Biochemistry and Biophysics*, **339**, 85–91.

Jacqz-Aigrain, E., Gueguen, M., Zanger, U. M., Robieux, I. and Alvarez, F., 1991, Cytochrome P450IID subfamily in non-human primates. Catalytical and immunological characterization. *Biochemical Pharmacology*, **41**, 1657–1663.

Kaminsky, L. S., 1989, Warfarin as a probe of cytochrome P450 function. *Drug Metabolism Reviews*, **20**, 479–487.

Laddison, K. J., Speirs, A., Mankowski, D. C., Tweedie, D. and Lawton, M. P., 1995, Cloning, sequencing, and expression of the cynomolgus monkey liver cytochrome P450 that is orthologous to human CYP2D6. *ISSX Proceedings*, **8**, 367.

Lin, J. H., 1995, Species similarities and differences in pharmacokinetics. *Drug Metabolism and Disposition*, **23**, 1008–1021.

Lin, J. H., Chiba, M., Balani, S. K., Chen, I.-W., Kwei, G. Y.-S., Vastag, K. J. and Nishime, J. A., 1996, Species differences in the pharmacokinetics and metabolism of indinavir, a potent HIV protease inhibitor. *Drug Metabolism and Disposition*, **24**, 1111–1120.

Lowry, O. H., Rosenbrough, N. J., Farr, A. L. and Randal, R. J., 1951, Protein measurement with Folin phenol reagent. *Journal of Biological Chemistry*, **193**, 265–275.

Niwa, T., Kaneko, H., Naritomi, Y., Togawa, A., Shiraga, T., Iwasaki, K., Tozuka, Z. and Hata, T., 1995, Species and sex differences of testosterone and nifedipine oxidation in liver microsomes of rat, dog and monkey. *Xenobiotica*, **25**, 1041–1049.

Omura, T. and Sato, R., 1964, The carbon monoxide binding pigment of liver microsomes. *Journal of Biological Chemistry*, **239**, 2370–2378.

Otton, S. V., Tyndale, R. F., Wu, D., Inaba, T., Kalow, W. and Sellers, E. M., 1992, Catalytic and immunologic similarities between monkey and human liver cytochrome P-450db1 (human cytochrome P-450 2D6). *Drug Metabolism and Disposition*, **20**, 1–5.

Ring, B. J., Parli, C. J., George, M. C. and Wrighton, S. A., 1994, *In vitro* metabolism of zatosetron. Interspecies comparison and role of CYP3A. *Drug Metabolism and Disposition*, **22**, 352–357.

Rodrigues, A. D., Kukulka, M. J., Ferrero, J. L. and Cashman, J. R., 1995, *In vitro* hepatic metabolism of ABT-418 in chimpanzee (*Pan troglodytes*). A unique pattern of microsomal flavin-containing monooxygenase-dependent stereoselective N′-oxidation. *Drug Metabolism and Disposition*, **23**, 1143–1152.

Sharer, J. E., Shipley, L. A., Vandenbranden, M. R., Binkley, S. N. and Wrighton, S. A., 1995, Comparisons of phase I and phase II *in vitro* hepatic enzyme activities of human, dog, rhesus monkey, and cynomolgus monkey. *Drug Metabolism and Disposition*, **23**, 1231–1241.

Shimada, T., Mimura, M., Inoue, K., Nakamura, S., Oda, H., Ohmori, S. and Yamazaki, H., 1997,

Cytochrome P450-dependent drug oxidation activities in liver microsomes of various animal species including rats, guinea pigs, dogs, monkey, and human. *Archives of Toxicology*, **71**, 401–408.

SHOU, M., KORZEKWA, K. R., KRAUSZ, K. W., CRESPI, C. L., GONZALEZ, F. J. and GELBOIN, H. V., 1994, Regio- and stereo-selective metabolism of phenanthrene by twelve cDNA-expressed human, rodent and rabbit cytochromes P-450. *Cancer Letters*, **83**, 305–313.

SMITH, D. A., 1991, Species differences in metabolism and pharmacokinetics: are we close to an understanding? *Drug Metabolism Reviews*, **23**, 355–373.

SMITH, G., MODI, S., PILLAI, I., LIAN, L.-Y., SUTCLIFFE, M. J., PRITCHARD, M. P., FRIEDBERG, T., ROBERTS, G. C. K. and WOLF, C. R., 1998, Determinants of the substrate specificity of human cytochrome P-450 CYP2D6: design and construction of a mutant with testosterone hydroxyase activity. *Biochemical Journal*, **331**, 783–792.

STEVENS, J. C., SHIPLEY, L. A., CASHMAN, J. R., VANDERBRANDEN, M. and WRIGHTON, S. A., 1993, Comparison of human and rhesus monkey *in vitro* phase I and phase II hepatic drug metabolism activities. *Drug Metabolism and Disposition*, **21**, 753–760.

VACCA, J. P., DORSEY, B. D., SCHLEIF, W. A., LEVIN, R. B., MCDANIEL, S. L., DARKE, P. L., ZUGAY, J., QUINTERO, J. C., BLAHY, O. M., ROTH, E., SARDANA, V., SCHLABACH, A. J., GRAHAM, P. I., CONDRA, J. H., GOTLIB, L., HOLLOWAY, M. K., LIN, J. H., CHEN, I.-W., VASTAG, K., OSTOVIC, D., ANDERSON, P. S., EMINI, E. A. and HUFF, J. R., 1994, L-735,524: An orally bioavailable human immunodeficiency virus type 1 protease inhibitor. *Proceedings of the National Academy of Sciences, USA*, **91**, 4096–4100.

WAN, J., IMAOKA, S., CHOW, T., HIROI, T., YABUSAKI, Y. and FUNAE, Y., 1997, Expression of four rat CYP2D isoforms in *Saccharomyces cerevisiae* and their catalytic specificity. *Archives of Biochemistry and Biophysics*, **348**, 383–390.

WU, D., OTTON, V., MORROW, P., INABA, T., KALOW, W. and SELLERS, E. M., 1993, Human hepatic cytochrome P450 2D6-like activity in nonhuman primates: catalytic characterization *in vitro*. *Journal of Pharmacology and Experimental Therapeutics*, **266**, 715–719.

YASUMORI, T., CHEN, L., NAGATA, K., YAMAZOE, Y. and KATO, R., 1992, Species differences in stereoselective metabolism of mephenytoin by cytochrome P450 (CYP2C and CYP3A). *Journal of Pharmacology and Experimental Therapeutics*, **264**, 89–94.

ZHAO, X. J. and ISHIZAKI, T., 1997, The *in vitro* hepatic metabolism of quinidine in mice, rats and dogs: comparison with human liver microsomes. *Journal of Pharmacology and Experimental Therapeutics*, **283**, 1168–1176.

XENOBIOTICA , 2000, VOL. 30, NO. 2, 131–140

Metabolite-intermediate complexation and inhibition of microsomal CYP3A in rat liver by diltiazem

L. TRIEU† and M. MURRAY‡*

† Storr Liver Unit, University of Sydney, Westmead Hospital, Westmead, NSW 2145 and Department of Pharmacology, University of Sydney, NSW 2006
‡ School of Physiology and Pharmacology, University of New South Wales, Sydney, NSW 2052, Australia

Received 15 July 1999

1. The formation of metabolite intermediate (MI)-complexes between cytochrome P450 (CYP) and the alkylamine-substituted drugs diltiazem (DTZ) and desipramine (DES) and their effect on CYP activities was investigated in rat liver.

2. Dexamethasone and phenobarbitone pretreatment enhanced MI-complexation by DTZ (36% and 11% of total CYP complexed, respectively), whereas β-naphthoflavone induction was without effect. All three treatments decreased MI-complexation produced by DES.

3. After a preincubation step in NADPH-supplemented microsomes DTZ and DES were effective inhibitors of the activities of CYPs 3A and 2C11 (testosterone 6β- and 16α-hydroxylations, respectively).

4. Although MI-complexation by DTZ was more extensive in microsomes from dexamethasone-induced rats, the apparent inhibition potency of the drug toward CYP activity was unchanged. By comparison, inhibition of CYP activity by DES was less pronounced than in control liver.

5. These findings indicate that drug-mediated MI-complexation of CYPs does not necessarily potentiate the inhibitory effect on monooxygenase activity, although the duration of inhibition is longer. The extent of inhibition produced by stable drug metabolites may be similar to that from MI-complexation, but their duration of action is limited by diffusion from the active site of the enzyme.

Introduction

The alkylamine-substituent is a structural feature common to many drug classes, including macrolide antibiotics, the calcium channel blocker diltiazem (DTZ) and tricyclic antidepressants, including desipramine (DES) and nortriptyline. Therapy with agents such as DTZ and DES is likely to be long term and to involve the coadministration of other drugs. Pharmacokinetic drug interactions arising from the inhibition of cytochrome P450 (CYP) drug oxidases have been reported during therapy with DTZ and DES (Piepho *et al.* 1987, Sirmans *et al.* 1988, Dayer *et al.* 1992).

The inhibitory effects of some alkylamine-substituted drugs on CYP monooxygenases may operate by several mechanisms, including metabolite intermediate (MI)-complexation. Troleandomycin and DES are oxidised by CYPs to reactive metabolites that remain within the active site of the CYP and generate MI-complexes (Delaforge *et al.* 1983, Murray and Field 1992). Because these complexes are quite stable *in vivo* it is generally considered that they may elicit potent,

* Author for correspondence: Dr Michael Murray, email: M.Murray@unsw.edu.au

Xenobiotica ISSN 0049–8254 print/ISSN 1366–5928 online © 2000 Taylor & Francis Ltd
http://www.tandf.co.uk/journals/tf/00498254.html

irreversible impairment of drug oxidation. However, not all alkylamine-substituted drugs generate MI-complexes with CYPs and are converted to stable (isolable) metabolites. Such metabolites may also elicit significant inhibition of monooxygenase activity, as is the case with some of the major isolable metabolites of DTZ and DES (Murray and Butler 1996, McNeil and Murray 1996). As these metabolites can dissociate from the CYP active site, the mode of inhibition is reversible.

Reports from other laboratories have demonstrated that induction of CYP by dexamethasone increases the extent of MI-complexation (Bensoussan *et al.* 1995). Thus, CYPs 3A are a major target for MI-complexation by reactive DTZ metabolites, although it is unclear whether this involves potentiation of inhibition potency over that produced by isolable DTZ metabolites. The present study evaluated the effect of induction on MI-complexation and inhibition of the major hepatic monooxygenases CYPs 3A and 2C11; testosterone 6β- and 16α-hydroxylations, respectively, were used as catalytic markers of these enzymes (Waxman *et al.* 1985). The major finding was that, although MI-complexation of CYP3A by DTZ was enhanced by dexamethasone, inhibition of monooxygenation was not significantly enhanced over that produced by stable metabolites in control liver, in which an MI-complex was not formed. In comparison, induction decreased the extent of MI-complexation and CYP inhibition by DES. Thus, it emerges from these studies that MI-complexation does not necessarily enhance the potency of CYP inhibition processes, although more protracted effects are likely.

Materials and methods

Chemicals

[^{14}C] Testosterone (sp. act. 59 mCi/mmol) was purchased from Amersham Australia (North Ryde, NSW, Australia). Hydroxysteroid standards were from the Sigma Chemical Co. (St. Louis, MO, USA), Steraloids (Wilton, NH, USA) and the MRC Steroid Reference Collection (Queen Mary's College, London, UK). DTZ HCl (*d-cis* isomer), DES HCl, dexamethasone, β-naphthoflavone and biochemicals were purchased from Sigma. Analytical grade solvents and miscellaneous chemicals were from Ajax Chemicals (Sydney, Australia).

Animals and preparation of microsomal fractions

Experimental protocols were approved by Institutional Animal Ethics Committees. Male Wistar rats ($\sim$ 250 g) were held (four per cage) under conditions of constant temperature and lighting (12 h light/dark cycle) and allowed free access to standard rat chow (Young Stock Feeds, Young, NSW) and water. Induction regimen consisted of either dexamethasone (100 mg/kg in corn oil by i.p. injection, once daily for 3 days), phenobarbitone (100 mg/kg in saline by i.p. injection, once daily for 3 days) or β-naphthoflavone (40 mg/kg in corn oil by i.p. injection, once daily for 3 days); controls received no pretreatment. Animals were killed by exsanguination under anaesthesia 48 h after the final treatment and livers were collected and perfused with cold saline. Livers were minced and homogenised and hepatic microsomes were prepared by differential ultracentrifugation (Murray *et al.* 1983). Washed microsomal pellets were resuspended in potassium phosphate buffer (50 mM, pH 7.4, containing 20% glycerol and 1 mM EDTA), frozen in liquid nitrogen and stored at -70 °C until required. Microsomal protein was estimated by the procedure of Lowry *et al.* (1951).

Microsomal testosterone hydroxylation assay

[^{14}C] Testosterone (50 μM; 0.18 μCi/0.4 ml incubation) hydroxylation reactions (0.15 mg protein) were conducted at 37 °C in potassium phosphate buffer (0.1 M, pH 7.4 containing 1 mM EDTA) (Butler and Murray 1993). DTZ or DES were added in 50 μl of distilled water and incubations were initiated with NADPH (1 mM). After 2.5 min, reactions were terminated by addition of 5 ml of chloroform, placed in an ice bath and shaken for 5 min. The organic phase was collected after centrifugation (2000 g for 2 min) and evaporated to dryness under N_2. The residue was dissolved in a small volume of chloroform and applied to TLC plates (Merck silica gel 60 F_{254} type; Darmstadt, Germany). Plates were developed in dichloromethane/acetone (4:1), air dried, and then developed in chloroform/ethyl acetate/ethanol

(4:1:0.7) (Waxman *et al.* 1983). Zones containing radioactive metabolites were detected on plates by autoradiography (Hyperfilm-MP; Amersham) over ~ 60 h and subjected to scintillation counting (ACS II; Amersham).

For the determination of IC_{50}s, incubations were conducted in duplicate using at least 4 concentrations of DTZ or DES. IC_{50}s were calculated from plots of *percentage activity remaining* versus log_{10} (*inhibitor concentration*).

The effect of DTZ or DES biotransformation on the extent of CYP inhibition was also assessed. In these experiments drugs were incubated with NADPH-supplemented microsomes, aliquots were withdrawn at intervals and transferred to tubes containing [^{14}C] testosterone. Incubations were continued for a further 2.5 min for the determination of steroid hydroxylation activities as described above. Control incubations (no drug) were conducted in parallel.

Interactions of DTZ with NADPH-supplemented CYP in rat hepatic microsomes

The interaction of DTZ (5–40 μM) with CYP in NADPH-supplemented rat hepatic microsomes was monitored by difference spectroscopy essentially as described previously (Murray 1992). DTZ was added to the sample cuvette (2 mg microsomal protein/ml) and NADPH (1 mM final) was added to both cuvettes. MI-complexation was indicated by the time-dependent formation of a 452 nm absorbance maximum in the optical difference spectrum; the reaction was conducted for a period of at least 10 min. After 30 min, CYP content was calculated according to the method of Omura and Sato (1964). In one experiment, potassium ferricyanide (50 μM final) was used to restore the CYP that had been sequestered as an MI-complex (Murray 1988). Testosterone hydroxylation activities were also estimated after addition of potassium ferricyanide to microsomes. In this experiment the microsomes were reisolated by differential centrifugation after ferricyanide treatment and testosterone hydroxylation was conducted as described above. This confirmed that MI-complexation and not autocatalytic destruction was the mode of mechanism-based inhibition of CYP by DTZ.

Immunoblotting for CYP3A protein in rat hepatic microsomes

Microsomal fractions (5 μg per lane) were incubated at 100 °C for 5 min with 2% sodium dodecyl sulphate and 5% 2-mercaptoethanol and subjected to electrophoresis on 7.5% polyacrylamide gels (Laemmli 1971) with minor modifications (Murray *et al.* 1986). Proteins were then transferred to nitrocellulose sheets (Towbin *et al.* 1979) and incubated with anti-CYP3A IgG (3.7 μg/ml); these conditions fell within the linear response range. Immunoreactive proteins were detected by enhanced chemiluminescence and autoradiography on Hyperfilm-MP and the resultant signals were analysed by densitometry (Bio-Rad, Richmond, CA, USA).

Statistics

Differences between means from two or more than two treatment groups were detected using, respectively, the Student's *t*-test or one-way analysis of variance in conjunction with the Student-Newman-Keuls *q*-test.

Results

Spectrophotometric studies of MI-complexation of rat liver microsomal CYP by DTZ

Incubation of DTZ with NADPH-supplemented microsomes from dexamethasone-induced rats for 30 min resulted in a CYP loss of 0.41 nmol/mg protein to 64% of initial levels (0.73 ± 0.17 *versus* 1.14 ± 0.18 nmol/mg protein; $p < 0.01$; Figure 1A). By comparison, DTZ produced a smaller, but still significant, loss of 0.31 nmol CYP/mg protein in microsomes from phenobarbitone-treated rats (2.45 ± 0.10 *versus* 2.76 ± 0.06 nmol/mg protein; $p < 0.01$; Figure 1A). However, a decrease in spectrally apparent CYP was not observed when DTZ was incubated with microsomes from untreated or β-naphthoflavone-induced rats

In addition to the effect of DTZ on apparent CYP content, MI-complexation was also monitored directly (Figure 1B). Thus, the characteristics of MI-complex formation after NADPH addition (as determined by the time-dependent appearance of a 452 nm wavelength absorbance in the optical difference spectrum) were

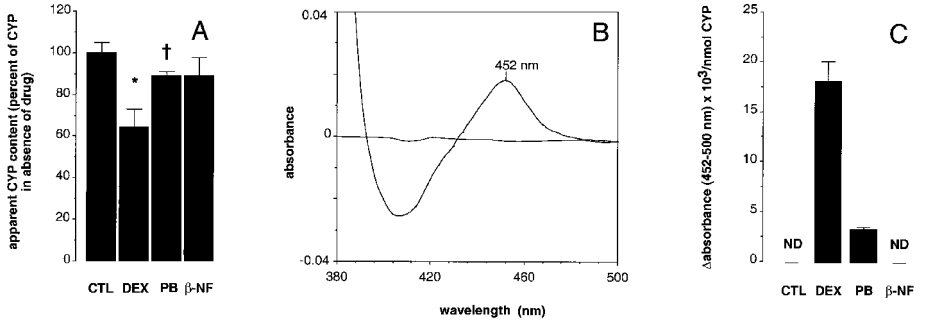


Figure 1. MI-complexation of CYP in rat liver microsomes by DTZ. (A) Apparent CYP content after incubation of DTZ (40 μM) with NADPH (1 mM) and hepatic microsomes from untreated (CTL), dexamethasone-(DEX), phenobarbitone(PB)- and β-naphthoflavone (β-NF)-pretreated rats. CYP contents (nmol/mg protein) in these fractions were 0.62 ± 0.04, 1.14 ± 0.18, 2.76 ± 0.06 and 1.00 ± 0.13, respectively ($n = 4$ animals per group). Different from CYP content in absence of DTZ: $*p < 0.01$, $\dagger p < 0.05$. (B) Appearance of 452 nm absorbance in the optical difference spectrum of hepatic microsomes from dexamethasone-induced rats after addition of DTZ (40 μM) and NADPH (1 mM). The spectrum was recorded 10 min after NADPH addition. (C) Apparent optimal magnitude of MI-complex ($\Delta_{452-500\ nm}$/nmol CYP) in microsomes from untreated (CTL), dexamethasone-(DEX), phenobarbitone(PB)- and β-naphthoflavone (β-NF)-pretreated rats. ND, not detected.

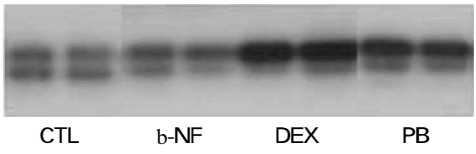


Figure 2. Western immunoblots of CYP3A proteins in hepatic microsomes from untreated (CTL), dexamethasone-(DEX), phenobarbitone (PB)- and β-naphthoflavone (β-NF)-pretreated rats (signals were obtained with 1 μg microsomal protein; two individual livers per treatment are shown). The appearance of at least two proteins immunoreactive with the anti-CYP3A IgG is typical of our Wistar rat strain.

examined (DTZ 5–40 μM). Formation of this absorbing species was noted in hepatic microsomes from dexamethasone- and, to a lesser extent, phenobarbitone-induced rats ($\Delta A_{452-500\ nm}$ of $18 \pm 2 \times 10^3$/nmol CYP and 3.3 ± 0.2 nmol $\times 10^3$/nmol CYP, respectively; Figure 1C). An MI-complex was not detected in microsomes from either control or β-naphthoflavone-treated rat liver.

Consistent with observations from other laboratories, dexamethasone and phenobarbitone were effective inducers of total CYP3A at the protein level (Waxman *et al.* 1985). Thus, in our Wistar strain, dexamethasone and phenobarbitone treatment increased CYP3A immunoreactive protein to 3.0- and 2.2-fold of levels in untreated rat liver (Figure 2). Accordingly, the extent of MI-complexation by DTZ in liver parallelled the apparent hepatic content of CYP3A.

Inhibition of microsomal CYP steroid hydroxylation activities by DTZ

The inhibition of CYP activities in microsomal fractions from untreated and dexamethasone-induced male rats was assessed. DTZ inhibited CYP3A-mediated steroid 6β-hydroxylation in control liver in a concentration-related fashion (figure 3), from which an IC_{50} value of 67 μM was determined. The corresponding value in micorosomes from dexamethasone-induced rat liver was 41 μM, representing an

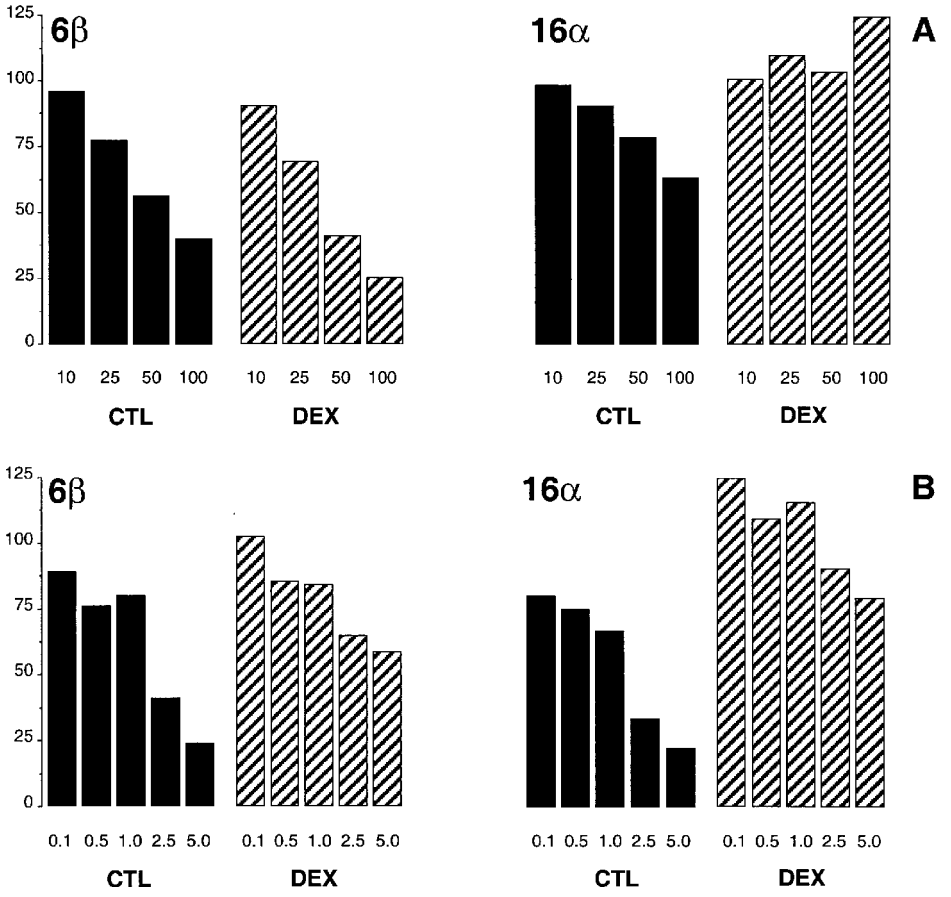


Figure 3. Concentration-related effects of DTZ on testosterone 6β- and 16α-hydroxylation activities in microsomes from untreated (CTL) and dexamethasone (DEX)-pretreated rats. (A) No preincubation step, (B) after a 20 min preincubation step between DTZ, NADPH (1 mM) and microsomal fractions. DTZ concentrations (μM) are indicated below each bar; data are averages of at least duplicate determinations that varied by $< 8\%$ from the stated values. Uninhibited activities: (CTL) 6β- and 16α-hydroxylation: 2.26 ± 0.16 and 4.28 ± 0.38 nmol/mg protein/min and (DEX) 6β- and 16α-hydroxylation 8.69 ± 0.43 and 1.91 ± 0.02 nmol/mg protein/min.

approximate 60 % increase in the apparent potency of direct inhibition of CYPs 3A after induction (figure 3). Preincubation of DTZ with NADPH and microsomes from untreated and dexamethasone-pretreated liver enhanced the extent of inhibition observed (Figure 3; apparent IC_{50}s of 1.8 and 12 μM, respectively). Thus, there was an approximate 37-fold enhancement of the potency of inhibition of CYP3A activity in microsomes from untreated rat liver, but only a 3.4-fold increase in dexamethasone-treated liver, under conditions that favoured MI-complexation. Treatment of microsomes with potassium ferricyanide restored CYP3A-mediated testosterone 6β-hydroxylation to the activity detected in dexamethasone-induced rat liver (data not shown). In contrast, in microsomal fractions from control and dexamethasone-induced rat liver, CYP2C11 activity was inhibited only slightly by DTZ (figure 3). Preincubation of DTZ with these microsomes enhanced the observed inhibition, especially in control liver, but not to the extent seen with steroid 6β-hydroxylation.

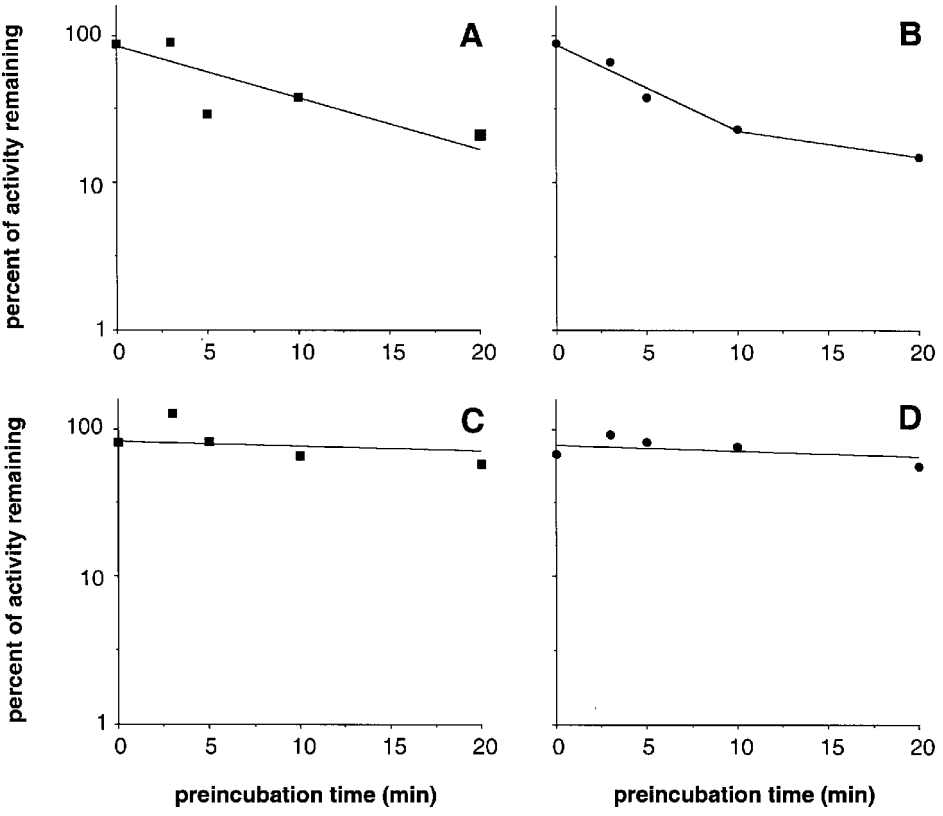


Figure 4. Time-dependent decrease in testosterone hydroxylation activities during the biotransformation of DTZ (5 μM): testosterone 6β-hydroxylation in hepatic microsomes from (A) untreated and (B) dexamethasone-induced rats, and testosterone 16α-hydroxylation in hepatic microsomes from (C) untreated and (D) dexamethasone-induced rats. Data are averages of experiments conducted in duplicate and that varied by $< 8\%$ from the stated values.

Figures 4A and 4B indicate the relationship between time of preincubation of DTZ (5 μM) with NADPH-supplemented microsomal fractions from untreated and dexamethasone-pretreated rat liver and the inhibition of steroid 6β-hydroxylation activity. Times that were required for decreases in apparent enzyme activity to 50% of the initial levels were determined. In the case of steroid 6β-hydroxylation in control and dexamethasone-induced rat liver these times were 8.1 min and 4.9 min, respectively. Loss of CYP3A activity in dexamethasone-induced liver exhibited a biphasic decline under these conditions: a rapid initial phase followed by a slower secondary phase. In contrast, the half-times for loss of CYP2C11-dependent testosterone 16α-hydroxylation were not determined because of the much slower rate of loss of this activity during the preincubation phase (> 20 min; figures 4C and 4D indicate the effect in control and dexamethasone-induced rat liver, respectively).

MI-Complexation and CYP inhibition in rat liver microsomes by DES

Analogous studies were undertaken with DES, because this alkylamine-substituted drug generates a prominent MI-complex in untreated rat hepatic microsomes. As indicated in figure 5A, $\sim 35\%$ of the CYP in hepatic microsomes

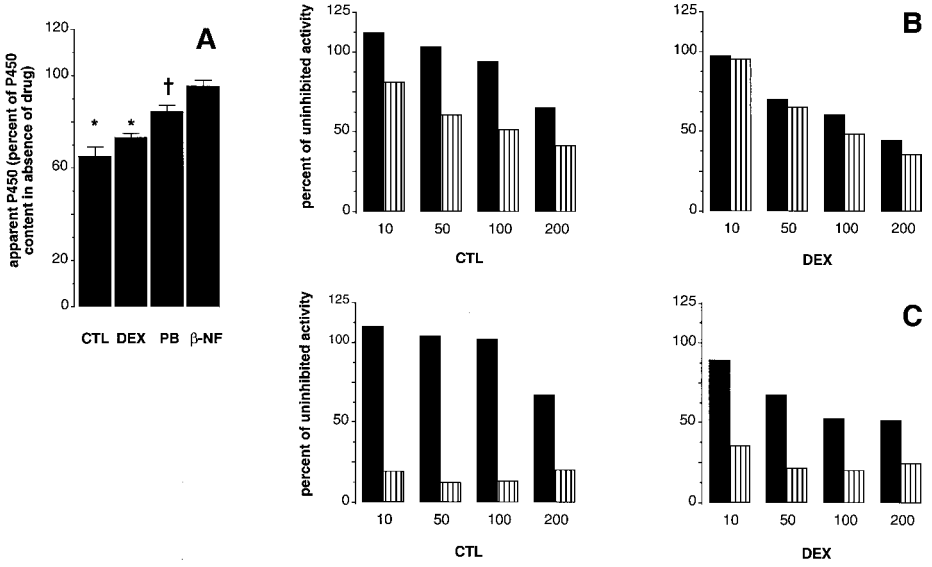


Figure 5. MI-complexation and inhibition of CYP-mediated testosterone hydroxylation by DES. (A) Apparent CYP content after incubation of DES (50 μM) with NADPH (1 mM) and hepatic microsomes from untreated (CTL), dexamethasone-(DEX), phenobarbitone(PB)- and β-naphthoflavone (β-NF)-pretreated rats ($n = 4$ per group). Different from CYP content in absence of DES: *$p < 0.01$, †$P < 0.05$. (B) Testosterone 6β-hydroxylation, and (C) testosterone 16α-hydroxylation in hepatic microsomes from untreated (CTL) and dexamethasone (DEX)-induced rats. Solid bars indicate activities in the absence of preincubation and vertical hatching indicates activities after a 20 min preincubation step between DES, NADPH (1 mM) and microsomal fractions. DES concentrations (μM) are indicated below each bar; data are averages of at least duplicate determinations that varied by $< 8\%$ from the stated values.

from untreated rats was unavailable for detection as a CO-complex after a 30 min incubation with DES (50 μM) and NADPH (1 mM). All three induction protocols decreased the apparent extent of MI-complexation elicited by DES (from 35% of total CYP to 27%, 16% and 5% of total CYP, respectively, after dexamethasone, phenobarbitone and β-naphthoflavone; figure 5A).

Inhibition by DES of microsomal CYP activities was evaluated in fractions from control and dexamethasone-induced male rats. In contrast to DTZ, DES preferentially inhibited CYP2C11-mediated steroid 16α-hydroxylation in control liver in a concentration-related fashion (Figure 5B). In the absence of a preincubation step inhibition was weak and an IC_{50} value could not be determined over the range of test concentrations (10–200 μM), but a 20 min preincubation step markedly enhanced the observed inhibition at all concentrations ($< 20\%$ activity remaining). The situation in microsomes from dexamethasone-induced rats was similar, although direct inhibition was noted in this case (to $\sim 55\%$ of the uninhibited reaction was produced by 100–200 μM DES). Preincubation of DES with NADPH and microsomes from dexamethasone-pretreated liver for 20 min enhanced the observed extent of inhibition of 16α-hydroxylation activity. In contrast with these findings, CYP3A activity in microsomal fractions was essentially refractory to direct inhibition, although again DES (200 μM) produced $\sim 50\%$ inhibition of CYP3A activity in hepatic microsomes from dexamethasone-treated rats. Preincubation enhanced the observed inhibition of steroid 6β-hydroxylation activity in microsomes from untreated, but not dexamethasone-induced, rat liver. However, this en-

hancement was much less pronounced than the effect on testosterone 16α-hydroxylation activity.

Discussion

The initial report that microsomal drug oxidation is susceptible to inhibition by DTZ (Renton 1985) has been complemented by later findings that DTZ metabolites participate in the process (Abernethy and Montamat 1987, Hoglund and Nilsson 1989, Murray and Butler 1996). The inhibition of CYP function by MI-complexation follows the biotransformation of an *N*-alkylamine substituent to a reactive metabolite, probably a nitroso species, that forms a quasi-covalent ligand with the CYP haem iron atom (Mansuy *et al.* 1978, Lindeke *et al.* 1979). Thus, complexes are formed between CYP and metabolites of macrolide antibiotics, such as erythromycin and troleandomycin (Delaforge *et al.* 1983), and the anti-parkinsonian agent orphenadrine (Reidy *et al.* 1989). MI-Complexation may contribute to the documented drug interactions between erythromycin and warfarin, carbamazepine and alfentanil (Wong *et al.* 1982, Hassel and Utt 1985, Bartowski *et al.* 1989).

Apart from MI-complexation, it has been established that inhibition of CYP activity also occurs when chemicals bind to ferric CYP (Rein and Ristau 1978, Rein *et al.* 1979). This process impairs the first step of the CYP cycle, in which substrate binds to the enzyme, and the subsequent reduction of substrate-coordinated CYP by an electron from NADPH. Thus, drugs and drug metabolites may inhibit CYP reactions. For example, the 4′-hydroxy- and sulphoxide metabolites of fenbendazole (Murray *et al.* 1992), *N*,*N*-didesmethyldesipramine (McNeil and Murray 1996) and *N*-demethylated metabolites of DTZ (Murray and Butler 1996) are all potent, reversible CYP inhibitors; MI-complexation is not part of the inhibition mechanism. However, because the metabolite can diffuse away from the CYP active site, such processes are probably of shorter duration than those produced by MI-complexation (which leads to CYP modification).

From these considerations it emerges that inhibition of CYP activity by alkylamine drugs can occur by either reversible binding or complexation of CYPs, by stable and reactive metabolites, respectively (Murray and Reidy 1990, Bensoussan *et al.* 1995). Both DTZ and DES generate MI-complexes with CYPs under certain conditions and undergo enzymic oxidation to stable metabolites that also inhibit CYPs. Altering the profile of CYP expression in liver by treatment of animals *in vivo* with inducers like dexamethasone has been shown to influence the amount of MI-complex generated by some drugs, including DTZ (Bensoussan *et al.* 1995). The present study characterised the effect of induction on the extent of MI-complexation produced by DTZ and DES. MI-Complex formation by reactive DTZ metabolites was greatest with dexamethasone and phenobarbitone and was not observed in microsomes from untreated or β-naphthoflavone-pretreated liver. In the case of DES, MI-complexation declines with all three regimens. These findings are consistent with earlier reports that DTZ generates an MI-complex with CYPs 3A (Bensoussan *et al.* 1995) and that DES interacts preferentially with CYP2C11 (Murray and Field 1992). The present study evaluated the effect of enhanced MI-complexation on the extent of inhibition produced by DTZ. It emerged from this work that complexation did not markedly alter the percentage of CYP3A activity that was inhibited by DTZ but, since induction greatly increased CYP3A activity,

the residual activity after inhibition was also greater than in control liver. In addition, the duration of the inhibitory effect produced by MI-complex-forming DTZ metabolites would be longer than that produced by stable DTZ metabolites.

It is already clear that multiple CYPs 3A are differentially regulated by xenobiotic inducers. Using a sensitive reverse transcriptase-polymerase chain reaction (RT-PCR) method Mahnke *et al.* (1996) found that CYP3A23 in male rat liver was extensively upregulated by dexamethasone and phenobarbitone (to ~ 10–12-fold of control). CYP3A18 was also highly inducible by dexamethasone (to ~ 12-fold of control), but its expression relative to β-actin was much lower than CYP3A23. In the present study induction by dexamethasone and phenobarbitone increased the MI-complexation of these CYPs 3A by DTZ.

CYPs within subfamilies are closely related but are often functionally different. Human CYPs 3A4 and 3A5 are 84% related at the protein level but exhibit different catalytic capabilities toward several substrates, including erythromycin (Gillam *et al.* 1995), a drug that forms an MI-complex. Expression of CYPs 3A4 and 3A5 is variable in human liver; CYP3A5 constituted all of the CYP3A expressed in one sample (Wrighton *et al.* 1990). In light of the present findings it will be important to consider whether individuals whose livers contain relatively large quantities of particular CYPs, such as CYP3A5, are at greater risk from adverse pharmacokinetic interactions due to MI-complex-forming drugs.

Acknowledgements

This work was supported by a grant from the Australian National Health and Medical Research Council and in the form of a John Wait scholarship from the Faculty of Medicine, University of Sydney (to L. T.).

References

ABERNETHY, D. R. and MONTAMAT, S. C., 1987, Acute and chronic studies of diltiazem in elderly versus young hypertensive patients. *American Journal of Cardiology*, **60**, 116I–120I.

BARTOWSKI, R. R., GOLDBERG, M. E., LARIJANI, G. E. and BOERNER, T., 1989, Inhibition of alfentanil metabolism by erythromycin. *Clinical Pharmacology and Therapeutics*, **46**, 99–102.

BENSOUSSAN, C,. DELAFORGE, M. and MANSUY, D., 1995, Particular ability of cytochromes P450 3A to form inhibitory CYP-iron-metabolite complexes upon metabolic oxidation of aminodrugs. *Biochemical Pharmacology*, **49**, 591–602.

BUTLER, A. M. and MURRAY, M., 1993, Inhibition and inactivation of constitutive cytochromes P450 in rat liver by parathion. *Molecular Pharmacology*, **43**, 902–908.

DAYER, P., DESMEULES, J. and STRIBERNI, R., 1992, *In vitro* forecasting of drugs that may interfere with codeine bioactivation. *European Journal of Drug Metabolism and Pharmacokinetics*, **17**, 115–120.

DELAFORGE, M., JAOUEN, M. and MANSUY, D., 1983 Dual effects of macrolide antibiotics on rat liver cytochrome P-450. Induction and formation of metabolite-complexes: A structure-activity relationship. *Biochemical Pharmacology*, **32**, 2309-2318.

GILLAM, E. M. J., GUO, Z., UENG, Y.-F., YAMAZAKI, H., COCK, I., REILLY, P. E. B., HOOPER, W. D. and GUENGERICH, F. P., 1995, Expression of cytochrome P450 3A5 in *Escherichia coli*: Effects of 5′ modification, purification, spectral characterization, reconstitution conditions, and catalytic activities. *Archives of Biochemistry and Biophysics*, **317**, 374–384.

HASSEL, D. and UTT, J. K., 1985, Suspected interaction: warfarin and erythromycin. *Southern Medical Journal*, **78**, 1015–1016.

HOGLUND, P. and NILSSON, L. G., 1989, Pharmacokinetics of diltiazem and its metabolite after single and multiple dosing in healthy volunteers. *Therapeutic Drug Monitoring*, **11**, 558–566.

LAEMMLI, U. K., 1971, Cleavage of structural proteins during assembly of the head of bacteriophage T4. *Nature*, **227**, 680–685.

LINDEKE, B., PAULSEN, U. and ANDERSON, E., 1979, Cytochrome P-455 complex formation in the metabolism of phenylalkylamines-IV. Spectral evidences for metabolic conversion of methamphetamine to *N*-hydroxyamphetamine. *Biochemical Pharmacology*, **28**, 3629–3635.

LOWRY, O. H., ROSEBROUGH, N. J., FARR, A. L. and RANDALL, R. J., 1951, Protein measurement with the Folin phenol reagent. *Journal of Biological Chemistry*, **193**, 265–275.

MAHNKE, A., STROTKAMP, D., ROOS, P. H., HANSTEIN, W. G., CHABOT, G. G. and NEF, P., 1997, Expression and inducibility of cytochrome P450 3A9 (CYP3A9) and other members of the CYP3A subfamily in rat liver. *Archives of Biochemistry and Biophysics*, **337**, 62–68.

MANSUY, D., ROUER, E., BACOT, C., GANS, P., CHOTTARD, J. C. and LEROUX, J. P., 1978, Interaction of aliphatic *N*-hydroxylamines with microsomal cytochrome P450: nature of the different derived complexes and inhibitory effects on monoxygenases activities. *Biochemical Pharmacology*, **27**, 1229–1237.

MCNEIL, C. M. and MURRAY, M., 1996, Inhibition of microsomal cytochromes P450 in rat liver by the tricyclic antidepressant drug desipramine and its primary oxidized metabolites. *Biochemical Pharmacology*, **51**, 15–20.

MURRAY, M., 1988, Complexation of cytochrome P450 isozymes in hepatic microsomes from SKF-525-A-induced rats. *Archives of Biochemistry and Biophysics*, **262**, 381–388.

MURRAY, M., 1992, Metabolite intermediate complexation of microsomal cytochrome P450 2C11 in male rat liver by nortriptyline. *Molecular Pharmacology*, **42**, 931–938.

MURRAY, M. and BUTLER, A. M., 1996, Enhanced inhibition of microsomal cytochrome P450 3A2 in rat liver during diltiazem biotransformation. *Journal of Pharmacology and Experimental Therapeutics*, **279**, 1447–1452.

MURRAY, M. and FIELD, S. L., 1992, Inhibition and metabolite complexation of rat hepatic microsomal cytochrome P450 by tricyclic antidepressants. *Biochemical Pharmacology*, **43**, 2065–2071.

MURRAY, M., ZALUZNY, L. and FARRELL, G. C., 1986, Drug metabolism in cirrhosis: Selective changes in cytochrome P-450 isozymes in the choline-deficient rat model. *Biochemical Pharmacology*, **35**, 1817–1824.

MURRAY, M. and REIDY, G. F., 1990, Selectivity in the inhibition of mammalian cytochromes P-450 by chemical agents. *Pharmacological Reviews*, **42**, 85–101.

MURRAY, M., HUDSON, A. M. and YASSA, V., 1992, Hepatic microsomal metabolism of the anthelmintic benzimidazole fenbendazole: Enhanced inhibition of cytochrome P450 reactions by oxidized metabolites of the drug. *Chemical Research in Toxicology*, **5**, 60–66.

MURRAY, M., WILKINSON, C. F. and DUBE, C. E., 1983, Effects of dihydrosafrole on cytochromes P-450 and drug oxidation in hepatic microsomes from control and induced rats. *Toxicology and Applied Pharmacology*, **68**, 66–76.

OMURA, T. and SATO, R., 1964, The carbon monoxide binding pigment of liver microsomes. I. Evidence for its hemoprotein nature. *Journal of Biological Chemistry*, **239**, 2370-2378.

PIEPHO, R. W., CULBERTSON, V. L. and RHODES, R. S., 1987, Drug interactions with the calcium-entry blockers. *Circulation*, **75**, V-181–194.

REIDY, G. F., MEHTA, I. and MURRAY, M., 1989, Inhibition of oxidative drug metabolism by orphenadrine: *In vitro* and *in vivo* evidence for isozyme-specific complexation of cytochrome P-450 and inhibition kinetics. *Molecular Pharmacology*, **35**, 736–743.

REIN, H. and RISTAU, O., 1978, The importance of the high spin/low spin equilibrium existing in cytochrome P-450 for the enzymatic mechanism. *Pharmazie*, **33**, 325–328.

REIN, H., RISTAU, O., MISSELWITZ, R., BUDER, E. and RUCKPAUL, K., 1979, The importance of the spin equilibrium in cytochrome P-450 for the reduction rate of the heme iron. *Acta Biologica et Medica Germanica*, **38**, 187–199.

RENTON, K. W., 1985, Inhibition of hepatic microsomal drug metabolism by the calcium channel blockers diltiazem and verapamil. *Biochemical Pharmacology*, **34**, 2549-2553.

SIRMANS, S. M., PIEPER, J. A., LALONDE, R. L., SMITH, D. G. and SELF, T. H., 1988, Effect of calcium channel blockers on theophylline disposition. *Clinical Pharmacology and Therapeutics*, **44**, 29–34, 1988.

TOWBIN, H., STAEHELIN, T. and GORDON, J., 1979, Electrophoretic transfer of proteins from polyacrylamide gels to nitrocellulose sheets: Procedure and some applications. *Proceedings of the National Academy of Sciences, USA*, **76**, 4350–4354.

WAXMAN, D. J., DANNAN, G. A. and GUENGERICH, F. P., 1985, Regulation of rat hepatic cytochrome P-450: Age-dependent expression, hormonal imprinting, and xenobiotic inducibility of sex-specific isoenzymes. *Biochemistry*, **24**, 4409–4417.

WAXMAN, D. J., KO, A. and WALSH, C., 1983, Regioselectivity and stereoselectivity of androgen hydroxylations catalysed by cytochrome P-450 isozymes purified from phenobarbital-induced rat liver. *Journal of Biological Chemistry*, **258**, 11937–11947.

WONG, Y. Y., LUDDEN, T. M. and BELL, R. D., 1982, Effect of erythromycin on carbamazepine kinetics. *Clinical Pharmacology and Therapeutics*, **33**, 460–464, 1982.

WRIGHTON, S. A., BRIAN, W. R., SARI, M.-A., IWASAKI, M., GUENGERICH, F. P., RAUCY, J. L., MOLOWA, D. T. and VANDENBRANDEN, M., 1990, Studies on the expression and metabolic capabilities of human liver cytochrome P450IIIA5 (HLp3). *Molecular Pharmacology*, **38**, 207–213.

XENOBIOTICA , 2000, VOL. 30, NO. 2, 141–154

Automated high throughput human CYP isoform activity assay using SPE-LC/MS method: application in CYP inhibition evaluation

H. YIN†, J. RACHA, S.-Y. LI†, N. OLEJNIK, H. SATOH and D. MOORE*

Drug Metabolism and Pharmacokinetics, Hoffmann-La Roche Inc., 340 Kingsland Street, Nutley, NJ 07110,USA

Received 23 May 1999

1. A high throughput screening (HTS) method for the evaluation of the seven major human hepatic CYP isoform activities was developed on a 96-well format, with automation. The method utilized pooled human liver microsomes and seven probe substrates, generic conditions for incubation, reaction termination and metabolite extraction with solid phase extraction (SPE) plates. Metabolites from the seven reactions were pooled and quantified using a generic liquid chromatography and tandem mass spectrometry (LCMS/MS) method.

2. The HTS method was validated based on K_m values obtained, which were in agreement with literature data.

3. The isoform inhibition profiles of ketoconazole, quinidine, sulfaphenazole, tranylcypromine, α-naphthoflavone, and 4-methylpyrazole against CYPs 3A4, 2D6, 2C9, 2A6 (and 2C19), 1A2 and 2E1, respectively, were obtained by this HTS method. Graphically obtained IC_{50}values are in agreement with literature reported values.

4. The HTS method represents a significant efficiency and selectivity improvement over traditional methods, and can be used for CYP inhibition assay and can be extended for liver activity profiling.

Introduction

Drug–drug interaction is an important issue in pharmaceutical research and development (Bertz and Granneman 1997, Guengerich 1997). Many factors, such as induction of drug-metabolizing enzymes, inhibition of drug-metabolizing enzymes (Bertz and Granneman 1997, Guengerich 1997), inhibition and induction of p-glycoproteins (Lown *et al.* 1997, Shuetz *et al.* 1996), competition of plasma protein binding (Bertz and Granneman 1997), contribute to the interaction by co-administered drugs, which could compromise a drug's efficacy and safety profile. Cytochromes P450 (CYP) are the most important class of phase-I enzymes in the biotransformation and bioactivation of drugs, pesticides, and environmental chemicals (Yin *et al.* 1995a). There are at least twelve human hepatic CYP isoforms identified to date, seven of which, namely CYPs 3A4, 2D6, 2C9, 2C19, 1A2, 2E1 and 2A6, play significant roles in drug metabolism (Nelson *et al.* 1996). The most predominant CYP isoform in the human intestinal lumen is CYP3A4, which has the same amino acid sequence as the hepatic counterpart (Lown *et al.* 1998). Inhibition of CYP in the liver and intestine by co-administered drugs or dietary agents affects bioavailability and/or half-lives of many drugs (Kupferschmidt *et al.* 1998, Warwick and Corrall 1998).

* Author for correspondence; e-mail: David.Moore@Roche.com

† Current address: Department of Drug Metabolism Pharmacokinetics, Novartis Pharmaceuticals Corporation, 59 Route 10, East Hanover, NJ 07936, USA.

Xenobiotica ISSN 0049–8254 print/ISSN 1366–5928 online © 2000 Taylor & Francis Ltd
http://www.tandf.co.uk/journals/tf/00498254.html

Prior to clinical trials of new chemical entities in humans, *in vitro* CYP isoform inhibition studies are typically carried out to evaluate their inhibition potential. Although each CYP isoform has broad and overlapping substrate selectivity, there are isoform-selective substrates identified as probes, for example, midazolam 1′-hydroxylation and testosterone 6-β hydroxylation for CYP3A4; ethoxyresorufin O-deethylation and caffeine *N*-demethylation for CYP1A1/2; coumarin 7-hydroxylation for CYP2A6; bufuralol 1′-hydroxylation for CYP2D6; tolbutamide methylhydroxylation for CYP2C9; *S*-mephenytoin 4′-hydroxylation for CYP2C19; and chlorzoxazone 6-hydroxylation for CYP2E1 (Kivisto and Kroemer 1997, Hickman *et al* 1998). The determinations of enzymatic activity for each of the seven CYP isoforms have been traditionally carried out under quite different conditions (Hickman et al 1998, Wynalda and Wienkers 1997) and are laborious and time consuming. Crespi and Penman (1997) recently reported a high throughput method for CYP inhibition screening using cDNA-expressed human hepatic CYPs and fluorescent substrates in 96-well format. Although superior to traditional assays, the method suffers from sensitivity for certain CYP isoforms, and occasional interference by test compounds which may be fluorescent or fluorescence modifying. In addition, a high throughput assay for inhibition of binding to CYP 3A4 using solid scintillants has recently been reported (Hopkins *et al.* 1998). Solid phase extraction (SPE)-radioassays using probe substrates with ^{14}C-methyl group have been also reported for catalytic evaluation of CYP enzymes (Rodrigues *et al.* 1994, Bloomer *et al.* 1995, Riley and Howbrook 1997). During the preparation of this manuscript, the fully automated analytical methods for the major human liver CYPs that utilize the SPE-radioassays and fluorometry has been published (Moody *et al.* 1999). Here, a high throughput screening (HTS) method for CYP isoform activity determinations is reported, which can be used for the evaluation of inhibition potential of drug candidates. The method utilizes human liver microsomes and generic conditions for incubation, metabolite extraction on a 96-well platform, and liquid chromatography and tandem mass spectrometry (LCMS/MS) quantification. The method is rapid, highly selective, with high throughput capacity, and therefore the procedure may also be extended for liver bank phenotyping and P450 induction evaluations.

Materials and methods

Chemicals

Resorufin, 7-ethoxyresorufin, coumarin, 7-hydroxycoumarin, tolbutamide, chlorzoxazone, phenacetin, α-naphthoflavone, tranylcypromine, 4-methylpyrazole, quinidine and NADPH were purchased from Sigma (St. Louis, MO). *S*-Mephenytoin, 4-hydroxy-*S*-mephenytoin, sulfaphenazole and ketoconazole were from Ultrafine Chemicals (Manchester, UK). Bufuralol, 1-hydroxybufuralol, hydroxytolbutamide, midazolam, 1′-hydroxymidazolam, 6-hydroxychlorzoxazone were synthesized by the Chemical Synthesis group of Hoffmann-La Roche (Nutley, NJ).

A pool of human liver microsomes from 8 male and 8 female donors were prepared in-house according to published method (Ghosal *et al.* 1996). Protein concentration was measured by the method of Lowry (Lowry *et al.* 1951). All other reagents were of the highest grade commercially available.

Microsomal incubations

Incubation mixtures contained a final concentration of 0.1 M potassium phosphate buffer (pH 7.4), 5 mM $MgCl_2$, 1 mM EDTA, 0.2 mg/ml microsomal protein, substrate (concentrations as below), and 1 mM NADPH in a total volume of 0.5 ml. The probe substrates for human CYP isoforms used were: CYP1A2 (1.7 μM ethoxyresorufin), CYP2A6 (3.6 μM coumarin), CYP2C9 (166 μM tolbutamide), CYP2C19 (40 μM *S*-mephenytoin), CYP2D6 (30 μM bufuralol), CYP2E1 (40 μM chlorzoxazone), and

Table 1. Scan function parameters for the MS/MS detection of metabolites generated by seven human hepatic CYP isoforms.

Scan function No.	CYP isoform	Analyte	Transition	Scan time (min)	Polarity	Cone voltage (V)	Collision energy (eV)	Dwell time (s)	Inter channel delay (s)
1	2D6	1′-Hydroxybufuralol	278.1 > 186	0.8–2.7	ESP +	28	20	0.5	0.03
2	2C19	4′Hydroxymephenytoin	235.1 > 150	2.0–3.8	ESP +	27	20	0.3	0.20
3	2E1	6-Hydroxychlorzoxazone	184 > 120	2.0–3.7	ESP−	25	20	0.3	0.30
4	2A6	7-Hydroxycoumarin	163 > 107	2.6–4.3	ESP +	30	25	0.2	0.30
5	2C9	Hydroxytolbutamide	287.1 > 171	4.0–6.5	ESP +	25	18	0.3	0.03
6	Int.Std.	Phenacetin	180 > 110	4.6–7.0	ESP +	28	24	0.3	0.03
7	3A4	1′-Hydroxymidazolam	342.1 > 203	7.4–9.4	ESP +	35	28	0.1	0.03
8	1A2	Resorufin	214 > 186	7.4–9.3	ESP +	50	25	0.9	0.03

Selected reaction monitoring (SRM) ion chromatograms of CYP isoform oxygenated products of probe substrates and internal standard (phenacetin). 1′-Hydroxybufuralol, 4′-hydroxymephyenytoin, 7-hydroxycoumarin, hydroxytolbutamide, phenacetin, 1′-hydroxymidaxolam and resorufin were monitored in electrospray positive ion mode and 6-hydroxychlorzoxazone were monitored in electrospray negative ion mode.

CYP3A4 (10 μM midazolam). The reactions were carried out in 96 well plates and initiated by the addition of NADPH after a 5-min preincubation at 37 °C. After 10-min incubation at 37 °C, an aliquot of reaction mixture (0.45 ml) was transferred into a preconditioned SPE plate to immediately stop the reactions by removing the NADPH cofactor from the incubation mixture. All procedures were carried out on a Tomtec Quadra 96™ multiwell plate processor. For the determination of intra- and inter-assay variations, experiments were carried out in triplicates and repeated for three consecutive days. For the determination of the linear range of each reaction, a series of incubations were carried out under the same conditions except at a protein concentration of 0.5 mg/ml and stopped at 0, 5, 10, 20 and 30 min.

Positive control inhibition experiments included the following inhibitors: α-naphthaflavone for CYP1A2, quinidine for CYP2D6, 4-methyl pyrazole for CYP2E1, ketoconazole for CYP3A4, tranylcypromine for CYP2A6 and CYP2C19, and sulfaphenazole for CYP2C9 (Bourrie *et al.* 1996, Yamazaki *et al.* 1992, Newton *et al.* 1995).

Solid phase extraction (SPE)

For reaction termination and metabolite extraction, 96-well HLB plates that contain 30 mg macroporous copolymer, [poly(divinylbenzene-co-N-vinylpyrrolidone)] /well from Waters Oasis (Milford, MA) were used on a Tomtec Quadra 96™ multiwell plate processor (Wallac Inc., Gaithersburg, MD). The plates were preconditioned with 0.8 ml methanol followed by 1.0 ml distilled water. Microsomal incubations (0.45 ml) were transferred to the plates, and metabolites were washed with 1 ml distilled water and then eluted with 0.7 ml methanol into 96-well receiving plates†. Vacuum from 2 to 10 psi was applied during extraction. An aliquot (0.15 ml) of each of the seven eluents were pooled and evaporated in a TurboVap (Zymark, Hopkinton, MA) set at 25 °C and then reconstituted in 150 μl of 50/50 (v/v) methanol/H_2O containing 0.1% acetic acid. Internal standard (0.2 nmol phenacetin) was added prior to evaporation. The samples were then analysed by LCMS/MS in MRM (multiple reaction monitoring) mode.

LCMS/MS analysis

The quantitation of metabolites was carried out on a HP 1100 HPLC instrument coupled to a Micromass (Manchester, UK) Quattro II triple quadrupole mass detector with an electrospray ionization source. A YMC (Wilmington, NC) C_{18} column (ODS-AQ, 2 × 50 mm, 5μ) was utilized for separation. The column temperature was set at 30 °C. Mobile phase consisted of 0.1% acetic acid in water (A) and 0.1% acetic acid in methanol (B). The initial condition was set at 35% B, remained at initial condition for 4.2 min, then increased to 100% B over 2 min, remained at 100% B for 3 min, finally brought back to initial condition in 1 min. The total run time was 15 min at a flow rate of 0.2 ml/min. A 25 μl aliquot was injected onto the column and the initial 0.8 min was diverted to waste in order to protect the mass spectrometer. The operating parameters of the MS detector were set as follows: capillary voltage 3.32 KV, HV lens 0.68 KV, RF lens 0.5 V, and ion energy 1 V, skimmer lens offset 5 V, skimmer 1.5 V, resolution 15 for both LM and HM, drying gas flow rate ~ 350 L/hr, and source temperature 130 °C. The scan function parameters, including cone voltages and collision energies were optimized to accommodate all analytes and are listed in table 1.

Determination of K_m *values*

In the experiment for K_m determination, incubations were carried out with five substrate concentrations: 0.5-, 0.7-, 1.0-, 1.7- and 5.0-fold of literature K_m concentration (table 3) for each CYP isoform. K_m values were obtained from the basic Michaelis-Menten enzyme kinetics equation using GraFit, Version 4 (Erithacus Software). Experiments were carried out in duplicate in parallel.

Statistics

Standard deviation (SD) and per cent coefficient of variation (CV%) were used to describe variability.

Results

Analytical characteristics

Enzyme activity was expressed as the rate of formation of the seven characteristic metabolites (table 1 and figure 1) in the form of area ratio of metabolite over internal standard. The reaction time courses (figure 4) of the seven CYP isoforms were

† Separate experiments determined 0.7 ml as the minimal volume to elute all analytes of interest.

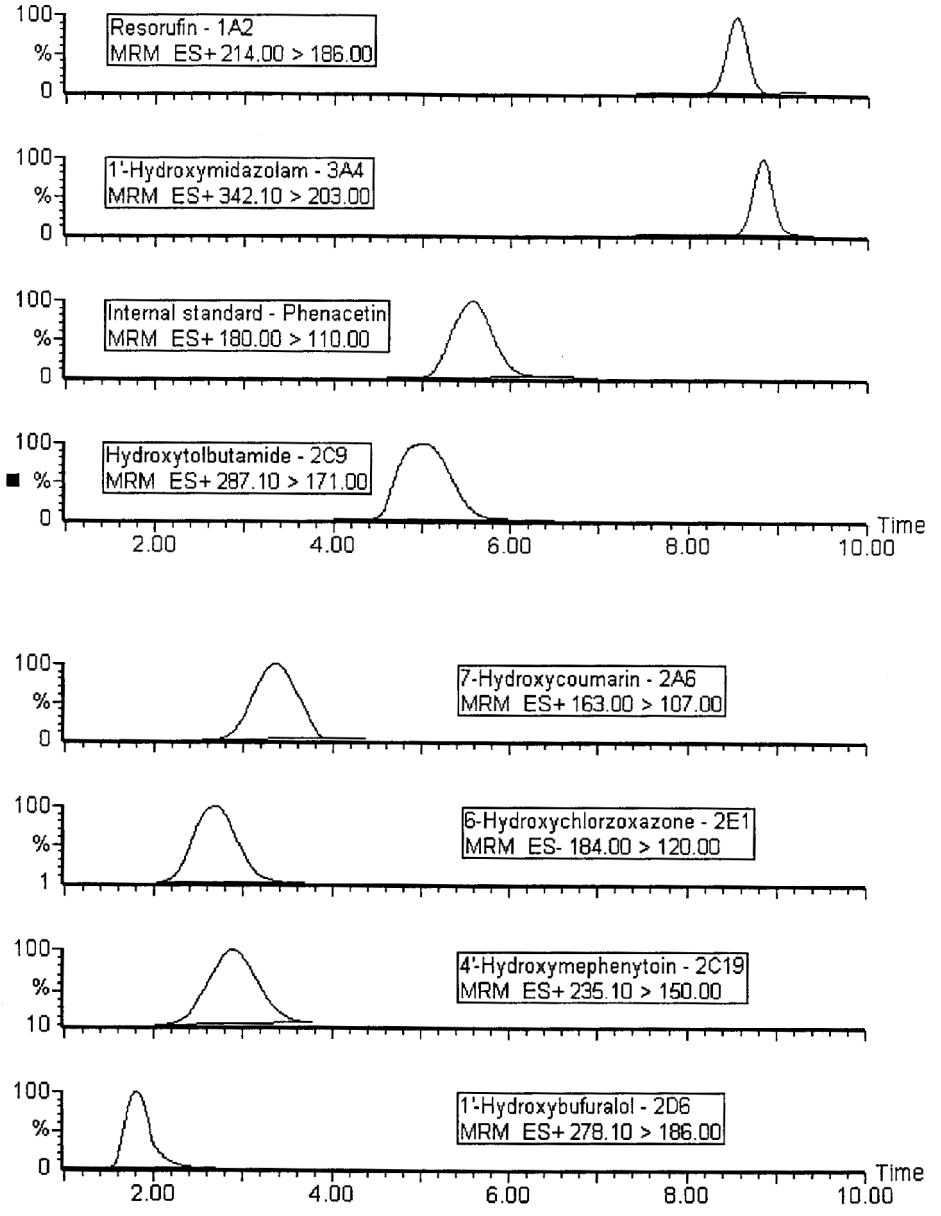


Figure 1. Multiple reaction monitoring (MRM) ion chromatograms of CYP isoform oxygenated products of probe substrates and internal standard (phenacetin). 1′-Hydroxybufuralol, 4′-hydroxymephenytoin, 7-hydroxycoumarin, hydroxytolbutamide, phenacetin, 1′-hydroxymidazolam, resorufin were monitored in electrospray positive ion mode and 6-hydroxychlorzoxazone were monitored in electrospray negative ion mode.

determined under the conditions specified in Materials and methods. Lower and higher detection limits of each probe metabolite in the incubation tube are presented in table 2. A linear relationship of each probe metabolite was detected by LCMS/MS in MRM mode in a range of 5–5000 nM for 1′-hydroxymidazolam and hydroxytolbutamide, 5–1000 nM for resorufin, 10–5000 nM for 7-hydroxycoumarin, 1′-

Table 2. Sensitivity and lower limit of detections of CYP probe metabolites by LCMS/MS assay. The experiment was carried out by adding probe metabolites in the blank incubation mixture with boiled microsomes.

CYP isoform:	3A4	1A2	2C9	2A6	2C19	2E1	2D6
Marker metabolites:	1′Hydroxy-midazolam	Resorufin	Hydroxy-tolbutamide	7-Hydroxy-coumarin	4′-Hydroxy-mephenytoin	6-hydroxy-chlorzoxazone	1′-hydroxy-bufuralol
LDL (nM)	5	5	5	10	10	25	10
HDL (nM)	5000	1000	5000	5000	5000	5000	5000
R2	0.9969	0.9985	0.9921	0.9949	0.9981	0.9988	0.9988

LDL, Lower detection limit.
HDL, Higher detection limit.
nM, nM concentration of probe metabolite in the reaction mixture.
R2, correlation coefficient.

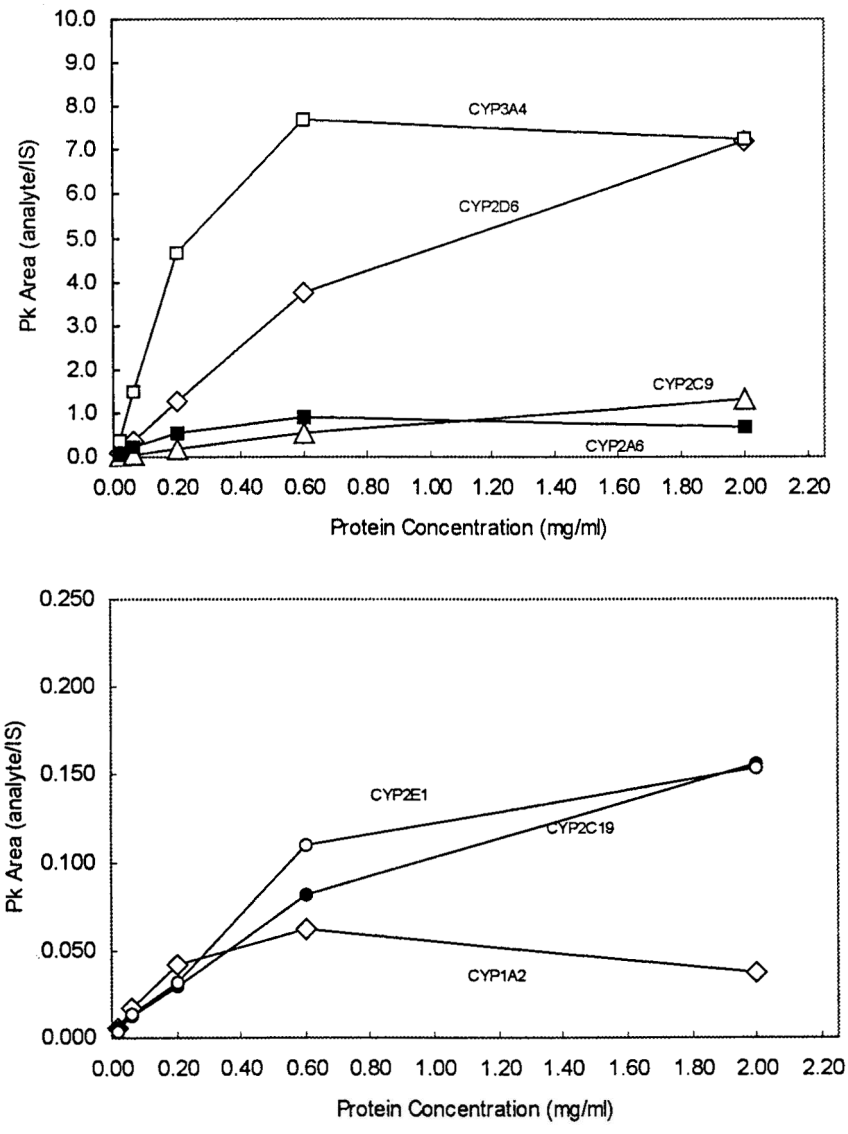


Figure 2. Microsomal protein concentration versus CYP marker metabolite formation; Top: CYP3A4 (1′-hydroxymidazolam), CYP2D6 (1′-hydroxybufuralol), CYP2C9 (hydroxytolbutamide) and CYP2A6 (7-hydroxycoumarin). Bottom: CYP1A2 (resorufin), CYP2C19 4′-hydroxymephenytoin) and CYP2E1 (6-hydroxychlorzoxazone). Y axis represents relative peak area (paek area of probe metabolite over internal standard). Probe substrates used were: CYP1A2 (1.7 μM ethoxyresorufin), CYP2A6 (3.6 μM coumarin), CYP2C9 (166 μM tolbutamide), CYP2C19 (40 μM *S*-mephenytoin, CYP2D6 (30 μM bufuralol), CYP2E1 (40 μM chlorzoxazone), and CYP3A4 (10 μM midazolam). Incubation was carried out in duplicate for 10 min and each sample was analysed twice by LCMS/MS, therefore each datum point represents average of four numbers.

hydroxybufuralol and 4′-hydroxymephenytoin, 25–5000 nM for 6-hydroxychlorzoxazone. The relationship of each probe metabolite production versus microsome concentration is demonstrated by this method (figure 2). As linear ranges are different depending upon CYP activity, 0.2 mg/ml microsome concentration was used as the generic microsome concentration for the current CYP inhibition

Table 3. Comparison of K_m values determined by HTS method to those from literature reports. Cited literature values are all human derived.

CYP isoform	Probe substrate	K_m in literature (μM)	Measured K_m (μM)[a]	SD[a]	Reference
1A2	Ethoxyresorufin	0.5	0.5	0.05	Draper *et al.* 1997
2A6	Coumarin	0.9± 0.14	1.7	0.4	Hickman *et al.* 1998
2C9	Tolbutamide	206± 123			Hickman *et al.* 1998
		151± 70	93.1	8.3	Sharer *et al.* 1995
2C19	S-Mephenytoin	35± 18	29.1	2.4	Sharer *et al.* 1995
2D6	Bufuralol	13± 10			Sharer *et al.* 1995
		9.4	14.8	5.1	Ring *et al.* 1996
		50, 100 250			Yamazaki *et al.* 1994
2E1	Chlorzoxazone	56.8± 6.8			Hickman *et al.* 1998
		148± 18	157.1	6.9	Peter *et al.* 1990
		39± 9			
3A4	Midazolam	2.6± 1.1			Sharer *et al.* 1995
		9.6	2.4	0.7	Ring *et al.* 1996
		2.5–5.6			Ghosal *et al.* 1996

[a] Experiments were carried out in duplicates and the results are expressed as mean and SD. K_m values were obtained by Michaelis-Menten enzyme kinetics equation (Grafit, version 4, Erithacus Software).

Table 4. Intra- and inter-assay variation of the 7 major human hepatic CYP isoforms with the HTS method.

CYP isoform	1A2	2A6	2C9	2C19	2D6	2E1	3A4
Intra assay CV% [a]	0.9	7.4	14.0	5.4	5.3	12.0	1.8
Inter assay CV% [b]	7.1	3.8	9.5	7.6	6.0	2.2	2.0

[a] %SD of triplicate determinations of area ratio of probe metabolites over internal standard from the incubations (without inhibitor) a day.
[b] %SD of determinations from assays of three independent days.

assay. At substrate concentrations between approximately K_m and saturation points, and a protein concentration at 0.5 mg/ml, the reaction was linear up to 30 min for isoforms CYP 2C9, 2C19, 2E1 and 2D6; and up to nearly 10 min for isoforms CYP1A2, 2A6 and 3A4 (figure 4). Therefore, subsequent analyses used a universal reaction time of 10 min, at 0.2 mg/ml protein concentration.

Determination of K_m

As part of the HTS assay validation, the K_m value of each reaction was measured (table 3). All numbers are in close agreement with literature values (Draper *et al.* 1997, Bourrie *et al.* 1996, Hickman *et al.* 1998, Sharer *et al.* 1995, Yamazaki *et al.* 1994, Ghosal *et al.* 1996, Ring *et al.* 1996).

Assay variations

Triplicates of control reactions were carried out on each day for three consecutive days to evaluate assay variability. Area ratio of metabolites over internal standard (I. S.) had CV% of 0.9–14.0% and 2.0–9.5% for intra- and inter-assay, respectively (table 4).

Inhibition study with known isoform inhibitors

Inhibition profiles of known isoform inhibitors were determined at various concentration levels with this HTS assay (figure 3). Ketoconazole (0.003–1 μM), 4-methylprazole (0.01–10 μM), quinidine (0.03–3 μM), sulfaphenazole (0.1–3 μM), α-naphthoflavone (0.003–0.3 μM) and tranylcypromine (0.9–90 μM) showed inhibition against CYP3A4, 2E1, 2D6, 2C9, 1A2 and 2A6, respectively, in a concentration-dependent manner. Graphically obtained IC_{50} values of CYP inhibitors from the figure are: CYP 1A2 (0.082 μM of α-naphthoflavone to resorufin deethylase), CYP2A6 (0.96 μM of tranylcypromine to coumarin 7-hydroxylase), CYP2C9 (1.3 μM of sulfaphenazole to tolbutamide hydroxylase), CYP2D6 (0.18 μM of quinidine to bufuralol 1′-hydroxylase), CYP2E1 (1μM of 4-methylpyrazole to chlorzoxazone 6-hydroxylase) and CYP3A4 (0.09 μM of ketoconazole to midazolam 1′hydroxylase). This is in agreement with previous reports (Testa and Jenner 1981, Netter 1980, Eagling *et al.* 1998). Selectivity of inhibition was dependent on inhibitor concentration, especially for ketoconazole and tranylcypromine: ketoconazole at high concentration (10 μM) also significantly inhibited CYP 1A2, 2C9, 2C19 and 2D6 (data not shown); and tranycypromine at high concentration (above 10 μM) also inhibited CYP 1A2, 2C9, and 2E1 significantly (data not shown).

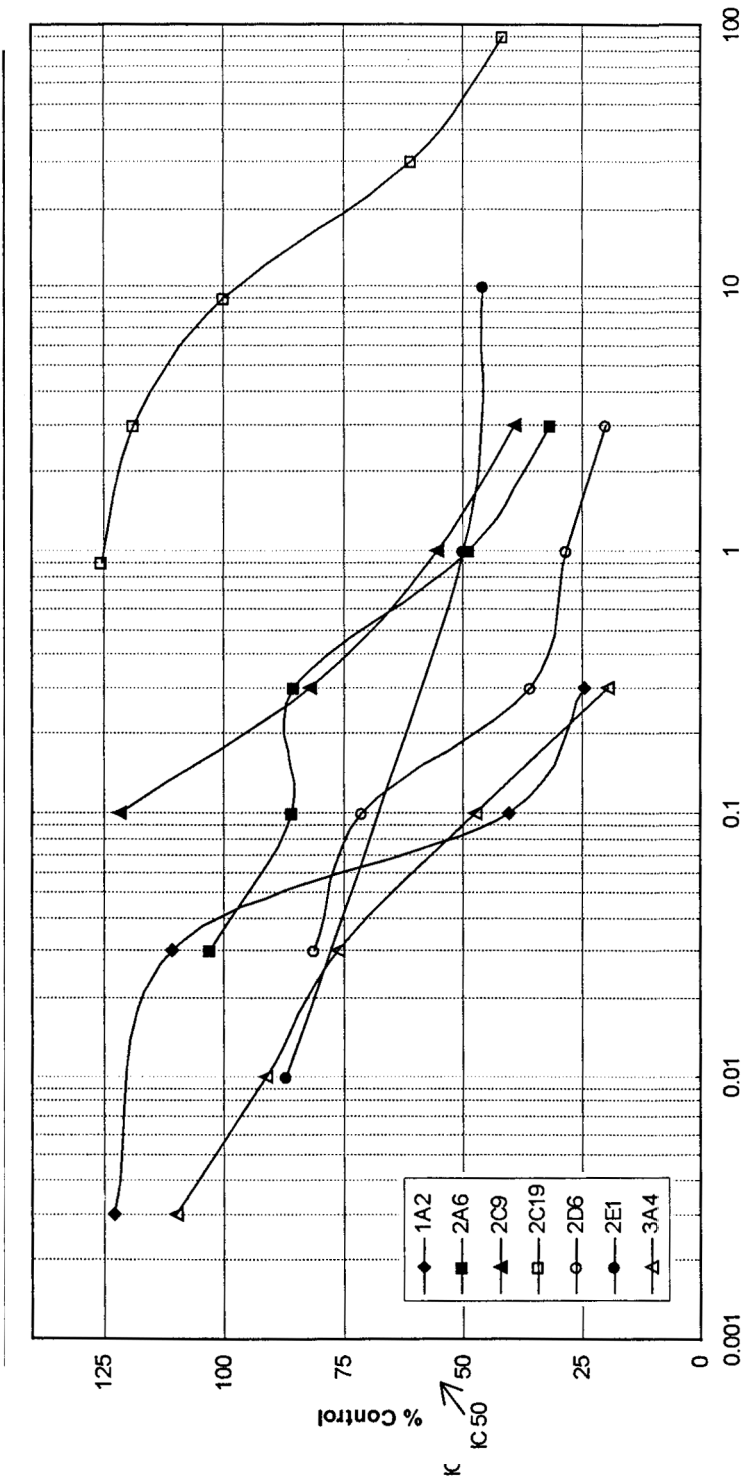


Figure 3. Inhibition of CYP activities in human liver microsomes by known inhibitors. Incubation was carried out in duplicate and each sample was analysed twice by LCMS/MS, therefore each datum point represents average of four numbers. Microsome concentration: 0.2 mg/ml, incubation time: 10 min, CYP isoform probe substrate concentrations are the same as described for Figure 2. CYP inhibitors used were; α-naphthoflavone against CYP1A2, tranylcypromine against CYP2A6, sulfaphenazole against CYP2C9, quinidine against CYD2D6, 4-methylpyrazole against CYP2E1 and ketoconazole against CYP3A4. Graphically obtained IC_{50} values are reported under Inhibition study of the Results section. Y axis indicates per cent of vehicle control (relative peak area of probe metabolites over internal standard).

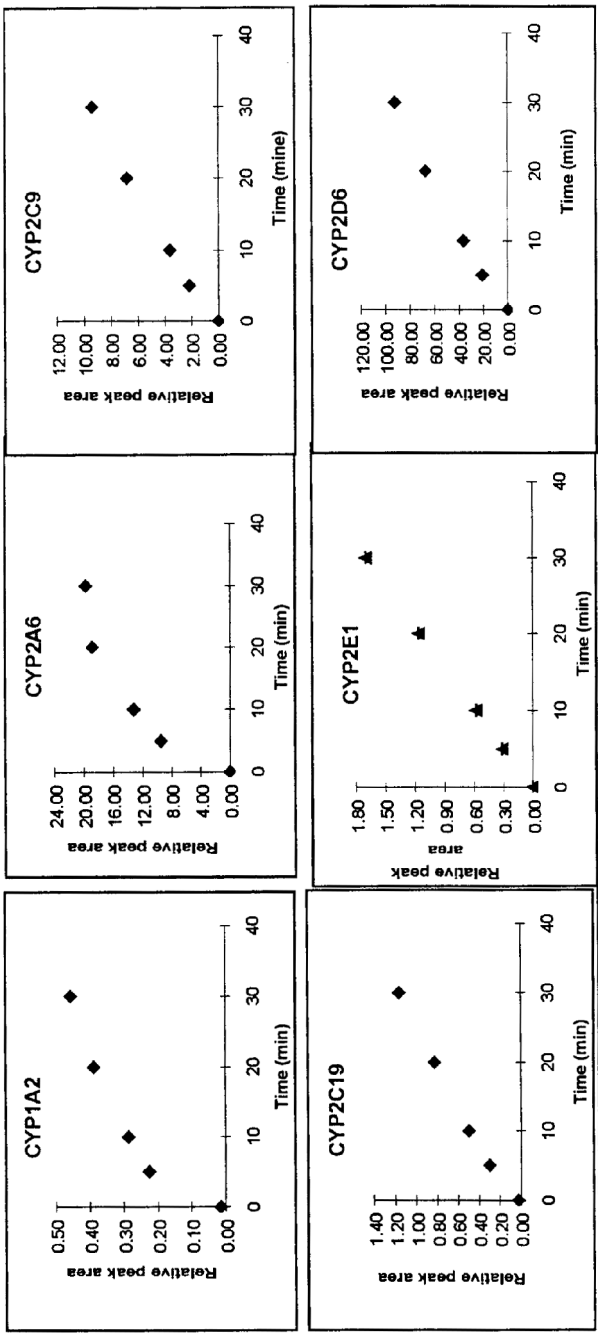


Figure 4. Reaction time course of the seven CYP isoforms. Incubation was carried out in duplicate and each sample was analysed twice by LCMS/MS, therefore each datum point represents average of four numbers, microsome concentration used was 0.5 mg/ml. CYP probe substrates and their concentrations are described under Figure 2. Probe metabolite formation is expressed on Y axis as relative peak height (area ratio of metabolite over internal standard).

Tranylcypromine, which was previously proposed as a selective inhibitor against CYP2C19 and 2A6 (Draper *et al.* 1997), showed 50% inhibition against CYP2C19 at 51 μM and was not isoform-selective at that concentration.

Discussion

A high throughput CYP isoform activity assay was developed on a 96-well platform utilizing liver microsomes and a generic condition for incubation, reaction termination, metabolite extraction, and LCMS/MS quantification. The assay used pooled human liver microsomes, and seven probe substrates for the major human hepatic CYP isoforms 1A2, 2A6, 2C9, 2C19, 2D6, 2E1, and 3A4 at around K_m concentrations, and with automation. Metabolites from the seven reactions were pooled and quantified during a single LC injection by a generic LCMS/MS method with a short LC run time of 15 min. This HTS method represents a major improvement in assay efficiency and selectivity for CYP isoform activity assay, and can be used for the screening of CYP inhibition potentials of drug candidates, and for the profiling of liver activities.

A YMC ODS-AQ C_{18} column, which has good retention property for ionic analytes, helped achieve an elution profile that is satisfactory for all seven metabolites ranging from ionic (e.g., 6-hydroxychlorzoxazone) to highly lipophilic (e.g., 1′-hydroxymidazolam). Under the gradient conditions, a total LC run time of 15 min was sufficient for the elution of all remaining substrates off the column (data not shown), such that variation of possible ion suppression could be minimized between injections. The formation of the seven characteristic metabolites was simultaneously quantified by mass spectrometry in MRM mode during a single LC run. Mass analysis of the seven characteristic metabolites was highly selective and signal intensities were within MS detection linear range (data not shown).

Solid phase cartridges were used to stop the metabolic reactions through the removal of NADPH, and also to extract metabolites. The solid phase plates were capable of retaining all the seven metabolites, some of them ionic. Maximal recovery of all seven metabolites was reached when 0.7 ml of methanol was used for elution. Such a combination of reaction termination and metabolites extraction is superior to traditional methods such as acid precipitation, liquid–liquid extraction, heat-inactivation or CO saturation, in light of its compatibility with 96-well format and to the diverse range of metabolite polarity.

Two parameters were used to validate this HTS assay: (1) K_m value and (2) inhibition profile with known isoform inhibitors. The measured K_m values of each isoform were in close agreement with those obtained by traditional incubation, liquid–liquid extraction and HPLC procedures (table 3). The inhibition profiles of known selective inhibitors determined by this HTS (figure 3) method were also in good agreement with literature reports (Testa and Jenner 1981, Netter 1980, Eagling *et al.* 1998, Moody *et al.* 1999). The selectivity of inhibition appears to be dependent on inhibitor concentration, and conceivably also on probe substrate concentrations.

Compared to traditional CYP assays, which use liquid chromatograph with UV, fluorescence detection or SPE-radioassays, the HTS method using MS detection is advantageous in uniformity of assay conditions, speed of throughput and high selectivity. Although the current procedure was primarily developed to evaluate competitive CYP inhibition, it could be modified to evaluate mechanism-based CYP

inhibition as well. In the early drug discovery phase, compounds could be screened at a single concentration (i.e. 10 μM), whereas the HTS method takes an average of 15 min to obtain a full spectrum of CYP inhibition profile. When significant levels of inhibition (i.e. 50% or greater) are identified at the initial screening, further experiments with different concentrations could be carried out to define K_i values. Such CYP inhibition information could help the selection of better drug candidates at the discovery phase, and guide the design of interaction studies in clinical trials.

In summary, a HTS method was developed for the determination of human CYP isoform activities. This method can be used to evaluate the *in vitro* drug interaction potentials using known probe substrates for the individual CYP isoforms. The method also can be applied to profile microsomal activities from different species and different individuals, and may likewise be used for other assays such as P450 induction evaluations.

Acknowledgments

The authors wish to thank our colleagues at Hoffmann-La-Roche, Nutley: Dr Zhenmin Liang for technical help in instrumentation; Dr Roger Blain and Natalya Khelemskaya for help with Tomtec workstation and solid phase extraction cartridges; and Drs Ernest Bush and Daniel Liberato for critical review of the paper and helpful discussions.

References

Bertz, R. J. and Granneman , G. R., 1997, Use of *in vitro* and *in vivo* data to estimate the likelihood of metabolic pharmacokinetic interactions. *Clinical Pharmacokinetics*, **32**, 210–258.

Bloomer , J. C., Clarks, S. E. and Chenery , R. J., 1995, Determination of P4501A2 activity in human liver microsomes using [3-^{14}C-methyl]caffein. *Xenobiotica*, **25**, 917–927.

Bourrie , M., Meunier , V., Berger, Y. and Fabre, G., 1996, Cytochrome P450 isoform inhibitors as a tool for the investigation of metabolic reactions catalyzed by human liver microsomes. *Journal of Pharmacology and Experimental Therapeutics*, **277**, 321–332.

Crespi , C. L. and Penman , B. W., 1997, Use of cDNA-expressed human cytochrome P450 enzymes to study potential drug–drug interactions. *Advances in Pharmacology*, **43**, 171–188.

Draper, A. J., Madan, A. and Parkinson , A., 1997, Inhibition of Coumarin 7-hydroxylase activity in human liver microsomes. *Archives of Biochemistry and Biophysics*, **341**, 47–61.

Eagling , V. A., Tjia, J. F. and Back, D. J., 1998, Differential selectivity of cytochrome P450 inhibitors against probe substrates in human and rat liver microsomes. *British Journal of Clinical Pharmacology*, **45**, 107–114.

Ghosal , A., Satoh , H., Thomas , P. E., Bush, E. and Moore, D., 1996, Inhibition and kinetics of cytochrome P4503A activity in microsomes from rat, human and CDNA-expressed human cytochrome P450. *Drug Metabolism and Disposition*, **24**, 940–947.

Guengerich , F. P., 1997, Role of cytochrome P450 enzymes in drug–drug interactions. *Advances in Pharmacology*, **43**, 7–35.

Hickman , D., Wang, J. P., Wang, Y. and Unadkat, J. D., 1998, Evaluation of the selectivity of *in vitro* probes and suitability of organic solvents for the measurement of human cytochrome P450 monooxygenase activities. *Drug Metabolism and Disposition*, **26**, 207–215.

Hopkins, A., Price-Jones, M. J., Hughes, K. T., Eddershaw, P. J., Hood, S. R., Woodrooffe, A. J. and Tarbit , M. H., 1998, A high throughput screening assay for the inhibition of binding to CYP3A4 using SpA. *12th International conference on microsomes and drug oxidation*, Montpellier, France.

Kivisto , K. T. and Kroemer , H. K., 1997, Use of probe drugs as predictors of drug metabolism in humans. *Journal of Clinical Pharmacology*, **37(1 Suppl)**, 40S–48S.

Kupferschmidt , H. H., Fattinger , K. E., Ha, H. R., Follath , F. and Krahenbuhl , S., 1998, Grapefruit juice enhances the bioavailability of the HIV protease inhibitor saquinavir in man *British Journal of Clinical Pharmacology*, **45**, 355–359.

Lown, K. S., Mayo, R. R., Leichtman , A. B., Hsiao, H. L., Turgeon, K., Schmiedlin -Ren, P., Brown, M. B., Guo, W., Rossi , S. J., Benet , L. Z. and Watkins , P. B., 1997, Pharmacokinetics and drug disposition: Role of intestinal P-glycoprotein (*mdr*1) in interpatient variation in the oral bioavailability of cyclosporine. *Clinical Pharmacology & Therapeutics*, **62**, 248–260.

LOWN, K. S., GHOSH, M. and WATKINS, P. B., 1998, Sequences of intestinal and hepatic cytochrome P450 3A4 cDNAs are identical. *Drug Metabolism Disposition*, **26**, 185–187.

LOWRY, O., ROSEBROUGH, A., FARR, A. and RANDALL, R., 1951, Protein measurement with the folin phenol reagent. *Journal of Biological Chemistry*, **193**, 265–275.

MOODY, G. C., GRIFFIN, S. J., MATHER, A. N., MCGINNITY, D. F. and RILEY, R. J., 1999, Fully automated analysis of activities catalysed by the major human liver cytochrome P450 (CYP) enzymes: assessment of human CYP inhibition potential. *Xenobiotica*, **29**, 53–75.

NELSON, D. R., KOYMANS, L., KAMATAKI, T., STEGEMAN, J. J., FEYEREISEN, R., WAXMAN, D. J., WATERMAN, M. R., GOTOH, O., COON, M. J., ESTABROOK, R. W., GUNSALUS, I. C. and NEBERT, D. W., 1996, P450 superfamily: update on new sequences, gene mapping, accession numbers and nomenclature. *Pharmacogenetics*, **6**, 1–42.

NETTER, K. J., 1980, Inhibition of oxidative drug metabolism in microsomes. *Pharmacology and Therapeutics*, **10**, 515–535.

NEWTON, D. J., WANG, R. W. and LU, Y. H. A., 1995, CYTOCHROME P450 INHIBITORS EVALUATION OF SPECIFICITIES IN THE *in vitro* metabolism of therapeutic agents by human liver microsomes. *Drug Metabolism and Dispos*, **23**, 154–158.

PATTEN, C. J., ISHIZAKI, H., AOYAMA, T., LEE, M., NING, S. M., HUANG, W., GONZALEZ, F. J. and YANG, C. S., 1992, Catalytic properties of the human cytochrome P450 2E1 produced by cDNA expression in mammalian cells. *Archives of Biochemistry and Biophysics* **229**, 163–171.

PETER, R., BOCHER, R., BEAUNE, P. H., IWASAKI, M., GUENGERICH, P. and YANG, C. S., 1990, Hydroxylation of chlorzoxazone P-450IIE1. *Chemical Research in Toxicology*, **3**, 566–573.

RILEY, R. J. and HOWBROOK, D., 1997, *In vitro* analysis of the activity of the major human hepatic CYP enzyme (CYP3A4) using [n-methyl-^{14}C]-erythromycin. *Journal of Pharmacological and Toxicological Methods*, **38**, 189–193.

RING, B. J., BINKLEY, S. N., VANDENBRANDEN, M. and WRIGHTON, S..A., 1996, *In vitro* interaction of the antipsychotic agent olanzapine with human cytochromes P450 CYP2C9, CYP2C19, CYP2D6 and CYP3A. *British Journal of Clinical Pharmacology*, **41**, 181–186.

RODRIGUES, A. D., KUKULKA, M. J., SURBER, B. W., THOMAS, S. B., UCHIC, J. T., ROTERT, G. A., MICHEL, G., THOME -KROMER, B. and MACHINIST, J. M., 1994, Measurement of liver microsomal cytochrome P450 (CYP2D6) activity using [O-methyl-^{14}C] dextromethorphan. *Analytical Biochemistry*, **219**, 309–320.

SCHUETZ, E. G., BECK, W. T. and SCHUETZ, J. D., 1996, Modulators and substrates of P-glycoprotein and cytochrome P4503A coordinately up-regulate these proteins in human colon carcinoma cells. *Molecular Pharmacology*, **49**, 311–318.

SHARER, J. E., SHIPLEY, L. A., VANDENBRANDEN, M. R., BRINKLEY, S. N. and WRIGHTON, S. A., 1995, Comparisons of phase I and phase II *in vitro* hepatic enzyme activities of human, dog, rhesus monkey and cynomolgus monkey. *Drug Metabolism and Disposition*, **23**, 1231–1241.

TESTA, B. and JENNER, P., 1981, Inhibitors of cytochrome P-450s and their mechanism of action. *Drug Metabolism Reviews*, **12**, 1–117.

WARWICK, J. A. and CORRALL, R. J., 1998, Serious interaction between warfarin and oral terbinafine. *British Medical Journal*, **316**, 440–447.

WYNALDA, M. A. and WIENKERS, L. C., 1997, Assessment of potential interactions between dopamine receptor agonists and various human cytochrome P450 enzymes using a simple *in vitro* inhibition screen. *Drug Metabolism and Disposition*, **25**, 1211–1214.

YAMAZAKI, H., INUI, Y., YUN, C. H., MIMURA, M., GUENGERICH, F. P. and SHIMADA, T., 1992, Cytochrome P450 2E1 and 2A6 enzymes as major catalysts for metabolic activation of *N*-nitrosodialylamines and tobacco-related nitrosamines in human liver microsomes. *Carcinogenesis*, **13**, 1789–1794.

YAMAZAKI, H., GUO, Z., PERSMARK, M., MIMURA, M., INOUE, K., GUENGERICH, F. P. and SHIMADA, T., 1994, Bufuralol hydroxylation by cytochrome P450 2D6 and 1A2 enzymes in human liver microsomes. *Molecular Pharmacology*, **46**, 568–577.

YIN, H., ANDERS, M. W., HIGGINS, L., KOWZEKWA, K. R. and JONES, J. P., 1995a, Designing safer chemicals: Predicting the rates of halogenated alkane metabolism. *Proceedings of the National Academy of Sciences USA*, **92**, 11076–11080.

YIN, H., JONES, J. P., and ANDERS, M. W., 1995b, Metabolism studies of 1,1,1-trifluoro-2-chloroethane, 1,2,-dichloro-1,1-difluoroethane and 1-fluoro-1,1,2-trichloroethane. *Chemical Research in Toxicology*, **8**, 262–268.

XENOBIOTICA , 2000, VOL. 30, NO. 2, 155–177

DNA arrays: technology, options and toxicological applications

JOHN C. ROCKETT* and DAVID J. DIX

Reproductive Toxicology Division, National Health and Environmental Effects Research Laboratory, US Environmental Protection Agency, Research Triangle Park, NC 27711, USA

The human genome contains an estimated 3 billion bases of DNA making up some 100000 genes, and the variation within this genome accounts for human diversity and, in many cases, disease. Defining and understanding the expression profile of given genotypes is essential to understanding adverse effects from acute or chronic exposure to environmental toxicants or other stimuli. DNA array technology could help researchers understand how organisms function in response to exposure by elucidating the molecular mechanisms that underlie them. DNA arrays have been developed and refined over the past 5 years and matured into a relatively accessible and affordable technology. They vary in design from membrane-based filters with a few hundred cDNAs, to glass-based 'chips' with tens of thousands of genetic elements. Mammalian DNA arrays will soon allow expression analysis on a genome-wide scale, similar to that already accomplished in some lower organisms (e.g. *S. cerevisiae*, *E. coli*). These whole-genome arrays will be powerful tools for identifying and characterizing toxicants in environmental and pharmaceutical science. This review discusses the technology behind the production of DNA arrays, the options available to those interested in applying them to their own research, and the possible toxicological applications of this exciting new technology.

Introduction

The rapid emergence of and advances in molecular biology over the past 30 years have led to the development of many new techniques for analysing the function of the genome. Indeed, it is now possible to determine the entire DNA sequence of any genome, the first step in understanding how it works. Since the first sequencing of a whole genome from a free-living organism (*H. influenza*; Fleischmann *et al.* 1995), over 20 more genomes have been sequenced and >60 more are currently underway (http://www-fp.mcs.anl.gov/~gaasterland/genomes.html). Although most of these are microbial species, there are high-profile projects sequencing and mapping more complex genomes. The foremost effort is, of course, the Human Genome Mapping Project (http://www.hgmp.mrc.ac.uk, http://www.er.doe.gov/production/ober/hugtop.html, http://www.nhgri.nih.gov/HGP/). However, the genomes of a number of commonly used laboratory and agricultural species are also under intensive investigation, including *Arabidopsis*, barley, chicken, cow, dog, *Drosophila*, rice, maize, mouse, pig, rat and zebrafish (table 1).

The phenotype and/or functional state of an organism is determined not only by the genotype *per se*, but also by spatial and temporal fluctuations in expression of the genes that it encodes. These in turn can be differentially regulated by environmental factors such as physical injury, lack of an essential nutrient(s) or insult by a toxicant. Thus, for sequence data to be of practical value, genotyping of organisms must be supported by large-scale gene or protein expression mapping. The premier experimental technique capable of analysing gene expression in a high-throughput format is the DNA array. Also called gene arrays, gene chips or micro-arrays, DNA

* Author for correspondence: e-mail: rockett.john@epa.gov

Xenobiotica ISSN 0049–8254 print/ISSN 1366–5928 on line © 2000 Taylor & Francis Ltd
http://www.tandf.co.uk/journals/tf/00498254.html

Table 1. Web addresses of major genome mapping projects.

Species	Sequencing project web address
Arabidopsis	http://www.nsf.gov/bio/pubs/arabid
Barley	http://www.css.orst.edu/barley/nabgmp/nabgmp.htm
Chicken	http://www.ri.bbsrc.ac.uk/chickmap/ChickMapHomePage.html
Cow	http://locus.jouy.inra.fr/cgi-bin/bovmap/intro.pl
Dog	http://mendel.berkeley.edu/dog.html
Drosophila	http://www.fruitfly.org
Human	http://www.hgmp.mrc.ac.uk http://www.er.doe.gov/production/ober/hugtop.html http://www.nhgri.nih.gov/HGP/
Maize	http://www.math.iastate.edu/danwell/maize/homepage.html
Mouse	http://www.informatics.jax.org
Pig	http://www.ri.bbsrc.ac.uk/pigmap/pigmap.html
Rat	http://ratmap.gen.gu.se
Rice	http://www.staff.or.jp
Zebrafish	http://zfish.uoregon.edu/zfinfo/zfmap.html

arrays have recently emerged (Schena *et al*. 1995) as one of the most promising new techniques in molecular biology since the polymerase chain reaction (PCR). This potential has been highlighted in a number of ways, including the publication of an entire *Nature Genetics* supplement (1999) dedicated to the technology, the high ratio of review to data papers, the protracted and bitter disputes in the courts over patent rights, the initiation of multiple start-up companies focusing almost exclusively on array-related products, and the plethora of zealous articles in the lay press.

It is anticipated that the knowledge attained through genome and expression mapping projects will provide new and detailed insight into how organisms function, both normally and in response to environmental stimuli. DNA arrays can be applied to current issues in toxicology such as screening therapeutic compounds for relative toxicity to prioritize for further development, developing more thorough comparisons of toxicity endpoints across multiple species and the screening of compounds for common toxicological properties. Indeed, the advent of genome-scale sequence and expression analysis is producing a paradigm shift that may address the longstanding imbalance between experimental models and real-world exposure scenarios. After many years of elucidating the function of single genes and their individual responses to single compounds, toxicologists can now study the effects of single and mixed chemicals on entire gene expression networks. The new scientific subdiscipline of toxicogenomics has thus been born. Toxicogenomics combines the emerging technologies of genomics and bioinformatics to identify and characterize mechanisms of action of known and suspected toxicants (see Chemical Industry Institute of Toxicology website, http://www.ciit.org/TOXICOGENOMICS/homepage.html) and is poised to create new approaches to experimental and regulatory issues.

Technology

What is a DNA array?

Almost 25 years ago, Ed Southern showed that immobilized single-stranded DNA molecules can hybridize with their complementary sequences (Southern 1975). The method he described, later termed the 'Southern blot', has become a core technique for molecular biologists. In the typical Southern blot, a size-separated target DNA population is immobilized on a membrane and a labelled

probe, normally composed of a single gene species, is hybridized to it. The dot-blot was later developed as a means to probe a target population for multiple genes. Dot-blots are effectively reverse Southerns, in that gene-specific probes are immobilized on the membrane and then hybridized against the labelled target population of multigenic genomic or cDNA. DNA arrays are essentially second-generation dot-blots. However, unlike dot-blots, which are typically prepared on membranes and rarely contain more than 100 individual gene spots, DNA arrays can also be prepared on glass or silicon substrates and have a much higher number and density of spots.

The DNA spots that constitute a DNA array can be composed of short oligonucleotides (20–25 bp), partial gene sequences (500–2000 bp) or full-length cDNAs. The source of the DNA components varies accordingly. For example, companies such as Incyte (Palo Alto, CA, USA) and AlphaGene (Woburn, MA, USA) utilize clones from their extensive collections of proprietary full-length cDNAs. However, the most commonly used approach is to utilize the cDNA clone libraries that have been assembled by the Integrated Molecular Analysis of Genomes and their Expression (IMAGE) consortium (http://www-bio.llnl.gov/bbrp/image/image.html; Lennon *et al.* 1996). This program offers the most accessible and affordable means to procure large numbers of genes for use in arrays, although the selection of species is currently limited to human, mouse and zebrafish. IMAGE clones are available free of royalties and may be used by anyone agreeing with the distribution guidelines (http://www.atcc.org/hilights/imagemta.html). Not surprisingly, the main condition for use is that all sequencing, mapping and expression data derived from using the IMAGE clones will be made publicly available at little or no fee. The clones themselves, which are largely partial cDNA sequences, may be obtained from a number of distributors in the USA (American Type Culture Collection, Genome Systems and Research Genetics) and Europe (UK Human Genome Mapping Project, Hinxton, UK; Resource Center of the German Human Genome Project, Berlin, Germany). The total number of clones available from IMAGE is vast, wand the National Center for Biotechnology Information (http://www.ncbi.nlm.nih.gov) has aided the selection of non-redundant clones through its Unigene project (http://www.ncbi.nlm.nih.gov/UniGene/index.html). UniGene is a system for partitioning GenBank sequences into a non-redundant set of gene-oriented clusters. Each cluster contains sequences representing a unique gene, as well as related information such as the tissue types in which the gene is known to be expressed.

Prefabricated arrays derived from IMAGE clones are currently available through either Research Genetics, Inc. (Huntsville, AL, USA) or Genome Systems, Inc. (St Louis, MO, USA). These companies utilize PCR products and lysed colonies respectively to prepare membrane-based arrays. While it seems likely that commercial suppliers will continue to concentrate largely on human DNA arrays and those of the small core of commonly used laboratory species, completion of other genome mapping projects will hopefully encourage a divergence in the species for which arrays are available.

Whether buying prefabricated arrays or arraying a library of one's own (see below), two caveats exist for those utilizing IMAGE clones. First, there have been problems with T1-phage contamination of some of the storage plates. Although badly contaminated clones have been withdrawn, IMAGE will ship lightly contaminated clones if the customer is willing to receive them. In addition, it is

known that the clones have about a 20% error rate in sequence matches (Research Genetics, Inc., suppliers of IMAGE clones, personal communication), i.e. in ~ 20% of cases, the sequence given in the IMAGE database will not match the sequence of the clone in the corresponding storage plate and well. Thus, in most cases it is prudent to purchase sequence-verified clones or verify them in-house before using them.

Array substrates

The printing of DNA arrays on nylon or nitrocellulose does not require special preparation of the membrane as the technology and commercial supply of products for immobilizing nucleic acids onto this medium is already well established. Glass-based arrays can be divided into two types. Affymetrix prepare their arrays on glass wafers called 'chips', while the majority of other users utilize glass (microscope) slides. One of the most important factors in generating consistently reproducible micro-array expression data from glass-based arrays is the quality and preparation of the glass substrate. Although standard microscope slides may be used to make DNA arrays, they require prespotting preparation to facilitate binding of the DNA targets. Several different coatings have been used successfully to accomplish this, including silyl (reactive aldehyde) and silane (reactive amine) groups, lysine and polylysine. In a unique approach, Grace Biolabs (Bend, OR, USA) have combined the binding ability of nitrocellulose with the glass slide format to produce their 'Oncyte' nitrocellulose-coated slides. Coating can easily be carried out in the laboratory, although many prefer the convenience of precoated slides available from a number of suppliers, e.g. Sigma (St Louis, MO, USA) or TeleChem International (Sunnyvale, CA, USA). Furthermore, though less expensive the use of self-coated slides may not necessarily be the best option because standard microscope slides often have a high and non-uniform autofluoresence and are not always ground flat enough to accommodate the narrow focal range of confocal scanners. The result is that the fluorescence of spots in some parts of a slide may appear less intense than others. Companies such as Corning (Corning, NY, USA) and Surmodics (Eden Prairie, MI, USA) now supply precoated slides designed specifically for DNA arrays, and it may be worth the extra cost of these quality controlled slides to minimize background fluorescence and to facilitate more consistent scanning results.

Third-generation slides tailored even more finely to the needs of micro-arrays will soon be available from companies such as Genometrix (The Woodlands, TX, USA). The latter company has developed methods to apply active surface films that can be 'tuned' to enhance hybridization. These films, made from short synthetic peptides, hold a weak positive charge during hybridization, and a high negative charge during washing, resulting in a reported 20-fold increase in hybridization rate relative to standard hybridization protocols (http://www.genometrix.com/PRODSERV.HTM).

Printing arrays

Two distinct methods exist for depositing DNA elements onto the support medium. In their unique approach to producing DNA arrays, Affymetrix (Santa Clara, CA, USA) utilize short oligonucleotide probes (25 bp) which are synthesized directly *in situ*, one base at a time, to make their GeneChip® probe arrays. This is carried out using a light-directed chemical synthesis process, which combines solid-phase chemical synthesis with fabrication techniques employed in the semi-

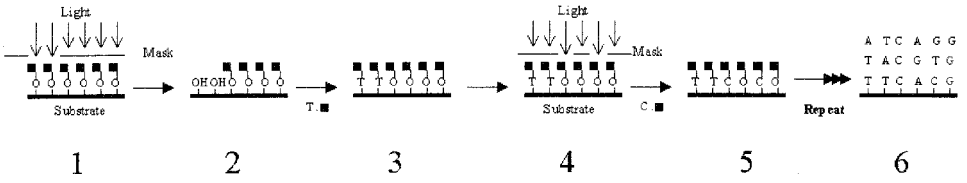


Figure 1. Process used to produce Affymetrix GeneChip probe arrays. A photo-protected glass substrate is selectively illuminated by light passing through a photolithographic mask. Deprotected areas are activated. With nucleoside incubation, chemical coupling occurs at activated positions. A new mask pattern is then applied and the coupling step repeated. The process is repeated until the desired set of probes is obtained. (Image courtesy of Affymetrix, Inc., Santa Clara, CA, USA. Affymetrix® and GeneChip® are US registered trademarks used by Affymetrix, Inc.)

conductor industry to make silicon microchips. In this process (figure 1), the glass chip is selectively illuminated through a photolithographic mask using a high-intensity mercury lamp. As a result, the illuminated areas are deprotected. Incubation of the chip with a nucleoside solution permits chemical coupling to the resident terminal nucleotides at the activated positions. A new mask is then applied and the process repeated until the oligonucleotide of desired length (typically 20–25 bp) is produced. Being small, >400000 such probes can be placed on a single chip measuring 1.28×1.28 cm.

However, most laboratories utilize the approach developed by Pat Brown and colleagues at Stanford, CA (http://cmgm.stanford.edu/pbrown/array.html). Rather than synthesizing the DNA elements *in situ*, prepared clones are simply spotted onto the support medium using high-speed robotic technology. Typically, a library of cDNA clones is first amplified in 96-well plates using PCR. The PCR products (usually between ~ 500 and 2000 bp) are then precipitated, washed and resuspended in printing buffer. Different printers are available that can be used to transfer sample from plate to substrate. In common to all are the print-heads, which are attached to and controlled by robotic arms capable of high-speed yet precise 3-D movement. High-density arrays (up to 6400 spots cm^{-2}) can thus be produced on multiple slides (up to 100 at a time) in one run by incremental changes in the addressing coordinates between subsequent samples. The printing process can be categorized as either contact or non-contact printing depending on the type of printing mechanism used.

Contact printers. Contact printers utilize finely machined metal pins that are dipped in the sample and then touched briefly to the surface of the support medium to deposit a small aliquot. Current print-heads can accommodate between 1 and 48 pins. Some pins are solid, with a tip that tapers to a small flat surface perpendicular to the shaft. These pins utilize surface tension forces to pick up and deposit small (a few hundred picolitres), fixed volumes of liquid. Other pins have a fine groove cut vertically up from the tip. In this way, they pick up and deposit sample through capillar action, much as a fountain pen picks up and deposits ink. The deposit volume is typically between 100 and 500 pl, and is dependent on several factors. These include the fluidity of the sample, the diameter of the pin-tip or groove, the length of time the pin is in contact with the surface, the age of the pin (wearing of the pin tip occurs) and the substrate being printed on.

An alternative to investing large sums of money in robotic printing technology or contract printing is to obtain hand-held arraying devices from a company such as

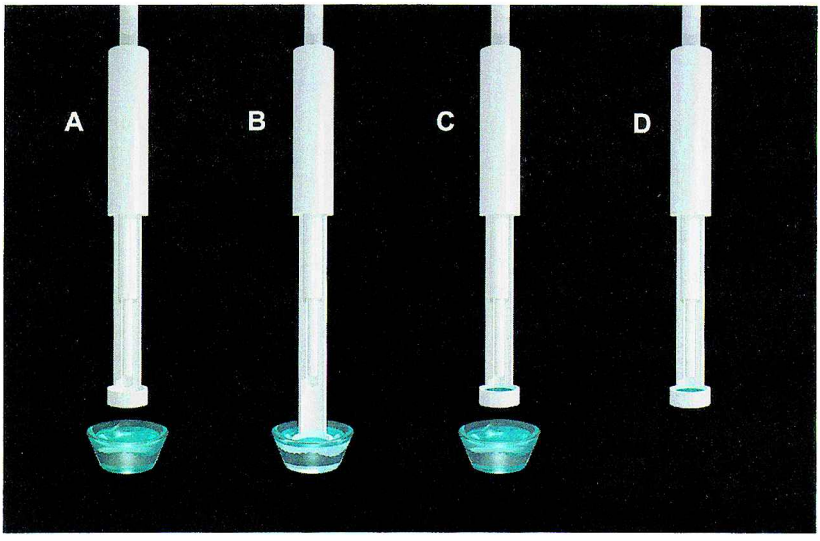
V&P Scientific, Inc. (San Diego, CA, USA). The printing pins of these devices are 96, 384 or 1536 stainless steel solid or split-pins designed to deposit micro- to nanolitre volumes. These can be used to construct large high-density membrane-based arrays. For example, up to 9216 spots can be addressed to a single 30×30 cm membrane. The large size of such membranes means that a relatively large amount of labelled cDNA sample is required for hybridization. However, those with an adequate supply of RNA may find this inexpensive alternative an attractive proposition.

Non-contact printing. A different approach to automated printing is employed by Genetic MicroSystems (Woburn, MA, USA). In this non-contact system (figure 2A and B), the split-pin is replaced by the 'ring-pin', and the printing mechanism relies on fluid transport and transfer based on surface tension forces. One advantage of the pin-ring over the split-pin is that the printing tip cannot be blocked. It can thus be used with a broader range of samples, including cell suspensions and particulates.

Other types of non-contact printer utilize thermal, solenoid or piezoelectric technology to spray aliquots of solution onto the support matrix. In this way they may be used to produce arrays on any substrate with equal ease. Cartesian Technologies (Irvine, CA, USA) supplies a printing station that can utilize either split-pins or its proprietary nQUAD (nanoliter Quantitative Aspirate and Dispense) technology. The latter couples a syringe pump with a micro-solenoid valve, a combination that provides rapid, quantitative dispensing of nanoliter volumes over a wide volume range (20 nl to 250 μl).

Irrespective of their design, all array printers should be sent through a preprint sequence before producing the actual experimental arrays. For reasons which are not very clear, the first ~ 100 spots of a new run tend to be somewhat variable in their size and quality. Factors affecting spot reproducibility include slide treatment and coating homogeneity, sample differences and instrumental errors. Other factors that come into play include clean ejection of the drop and clogging (nQUAD printing), and mechanical variations and long-term alteration in print-head surface (pin-heads). The most frequent problem encountered in printing glass-based arrays is the so-called 'donut' effect, whereby the probe spot dries unevenly due to dirty slides or atmospheric influence, e.g. dry room or exposure to air currents. In this case, following hybridization of the labelled population the signal appears uneven, with a dark area in the centre of the spot. Although such spots are aesthetically displeasing, the latest image analysis software can compensate for their variability and return reliable signal intensity data. Even so, printing should be carried out in a controlled environment and humidified chambers are available in which to place printers. These help to prevent dust contamination and produce a uniform drying rate, which is important in determining the spot size, quality and reproducibility. Uneven signals may also be generated due to the kinetics of hybridization, particularly if short hybridization times are used. Typically, a long (overnight) hybridization is enough to overcome this problem. Overall, with careful preparation and protocol, it is possible to get the coefficient of variation for spot reproducibility down $< 10\%$.

Another important consideration for printing is the potential problem of sample carryover. Repeated washing, blotting and drying (vacuum) of print-pins between samples is normally effective at reducing sample carryover to negligible amounts.



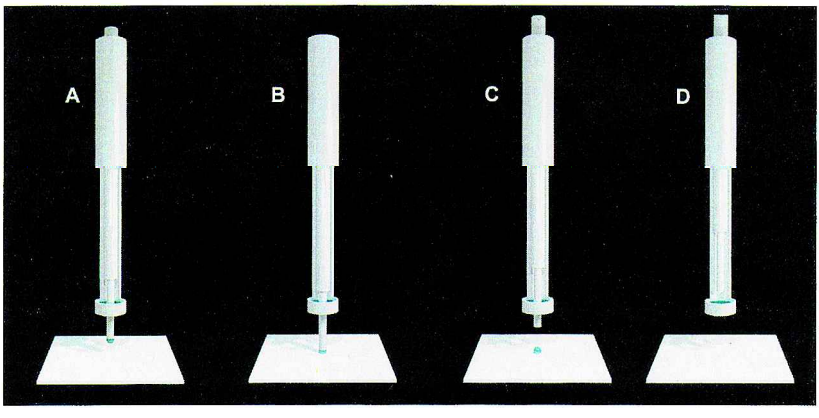


Figure 2A. Loading of GMS pin-ring array printer. (Panel A) A single ring and pin are centred over the source well poised to acquire the sample. (Panel B) The pin is kept stationary while the ring independently lowers into the sample source. When the ring is immersed it fills with fluid, and this fluid, held in place by surface tension and the surface activity of the inner portion of the ring, forms a meniscus after the ring is raised (C). The inner surface of the ring is threaded to add surface area and increase the 'holding power' of the contained liquid. (D) The filled ring is moved to the sites of deposition with enough sample to create between 600 and 1000 spots. (Used with permission from Genetic Microsystems Inc, Woburn, MA, USA.)

Figure 2B. Spotting process of GMS pin-ring array printer. (Panel A) The pin-ring assembly is positioned over the target, the ring maintains its Z-height and the pin is lowered through the meniscus, collecting pendant drop of the sample liquid at the end of the pin. When the pendant drop makes initial contact with the substrate, the combination of surface tension and gravity transfer the droplet onto the substrate (B). The droplet is released when the pin is lifted (C), and the process is ready to be repeated after the pin is lifted through and above the meniscus (D). The cycle may be repeated at the same spot for deposition of additional material, shifted slightly for creation of duplicate sites, or moved to another slide. (Used with permission from Genetic Microsystems Inc, Woburn, MA, USA.)

Table 2. Amount and type of RNA required, suggested or reported for hybridization to various types of DNA arrays.

DNA array	Amount of polyA RNA required per slide or membrane	Amount of total RNA required per slide or membrane
Prefabricated membrane arrays		
Clontech Atlas Array	1 μg	2–5 μg
Genome Systems, Inc. Gene Discovery Array	2.5 μg	–
Research Genetics, Inc. GeneFilter	20 ng	125–250 ng
Prefabricated glass chip arrays		
Affymetrix GeneChip	1 μg	–
Incyte Gene Expression Micro-array (contract service only)	600 ng	100 μg*
NEN MICROMAX	mRNA not required	2 μg‡
DIY glass slide arrays		
Albert Einstein College of Medicine†	2.5 μg	100 μg
Stanford (De Risi *et al.* 1997)	1.25 μg	–
(Lashkari *et al.* 1997)	2 μg	–
(Schena *et al.* 1996)	3 μg	–
NHGRI (Khan *et al.* 1998)	–	100–200 μg

* Incyte workers extract mRNA for use in screening GEM
† http://sequence.aecom.yu.edu/bioinf/micro-array/protocol2.html
‡ NEN utilizes Tyramide Signal Amplification (TSA)

The final word that must accompany any account on the current status of array printing is that although several different printing technologies are available, none has yet been established as particularly outstanding. It is certain that printing technology will improve over the next few years to provide faster machines capable of printing higher density arrays of more reproducible spots.

Probe preparation and hybridization

Strictly speaking, where arrays are concerned it is not the probe that is labelled, but the test population of RNA/cDNA. The hybridization protocol used depends upon the type of array. The amount of starting material, which can be either total RNA or mRNA depending on the type and nature of the array, also varies. Table 2 indicates the amounts required by a number of systems and demonstrates one of the perceived problems of DNA arrays; namely, that they require relatively large amounts of RNA, amounts which are sometimes difficult to extract from small samples such as biopsies or the organs of embryonic laboratory animals.

With membrane-based arrays, the control and treated mRNA populations are reverse-transcribed to cDNA, and in the process labelled with isotope. ^{33}P is the isotope of choice for higher density arrays, e.g. those marketed by Research Genetics and Genome Systems, since it is a lower energy emitter and, therefore, creates fewer problems with bleed-over than ^{32}P. The latter, which is less expensive and more sensitive than ^{33}P, may be used with lower density arrays such as those marketed by Clontech Laboratories (Palo Alto, CA, USA). The probes prepared from the control and treated samples are hybridized independently on parallel (different) arrays or in series to the same array. In theory it is preferable to carry out serial hybridizations of control and treated samples on the same membrane to remove the effects of intermembrane variability. However, this requires either a decay period (6 months in a freezer) or stripping (boiling the membrane briefly with SDS) to remove the first

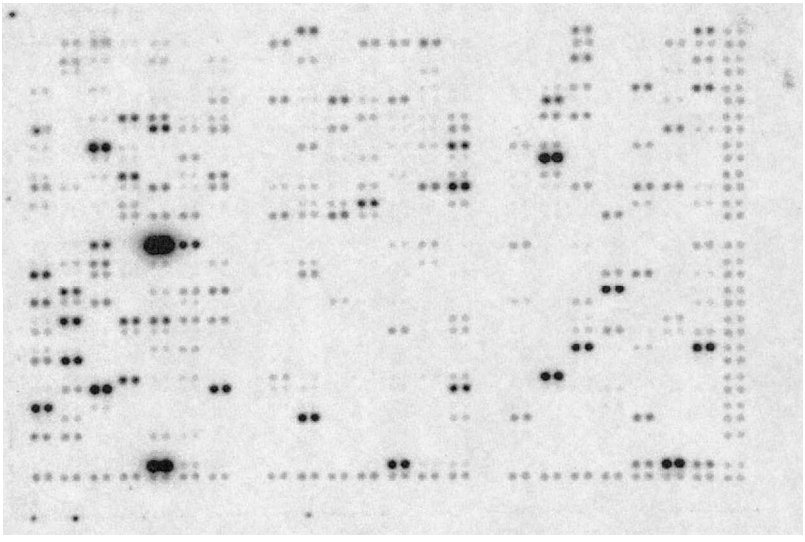


Figure 3. Membrane-based DNA array. A human cDNA expression array (Clontech) following hybridization to human testicular RNA is shown. Total RNA (2 μg) was reverse-transcribed in the presence of ^{32}P-labelled dATP, and unincorporated nucleotides removed via column chromatography. The labelled cDNA was hybridized against the membrane overnight, and the image captured using a phosphorimager. The nylon membrane, which measures 12 × 8 cm, contains 588 different genes spotted in duplicate, plus a number of positive and negative controls and 'landing-lights' (bottom row, right two columns) for orientation.

hybridized population. The former option is normally impractical, and while manufacturers claim that membrane-based arrays can be stripped and reused several times, it has been commonly reported that this process is not efficient and that more reliable results are obtained when control and test samples are applied to different membranes. Parallel blotting is also useful where tissue or RNA is limiting in that a control blot does not have to be prepared in every experiment. For instance, in a concentration or time response experiment, only one blot needs to be used as the control against which numerous points may be compared. An example of a hybridized, membrane-based array is shown in figure 3.

An alternative to radioactive labelling is enzymatic detection. In this case the probe may be biotinylated, haptenylated or have alkaline phosphatase or horse radish peroxidase attached. Hybridization is detected by an enzymatic reaction yielding a colour reaction (Chen *et al.* 1998). Whether an isotopic or enzymatic approach to labelling is used, differences in hybridization signals can usually be detected by eye. However, it is more accurate to capture the signal with a phosphor or other imaging device and quantify the signals using one of the various software packages available from the companies that market membrane-based arrays.

Hybridization of samples to glass-based DNA arrays can proceed in a similar manner to that of membranes, in that control and test samples may be labelled with the same fluor and hybridized to duplicate arrays. However, it is more common that control and treated mRNA populations are labelled with different coloured fluors, and then hybridized simultaneously to the *same* slide/chip. The advantage of this is that relative signal intensity is independent of variations in slides or hybridization conditions that may arise if independent slides are used. The method for preparation and labelling of the mRNA populations being tested depends on the array format.

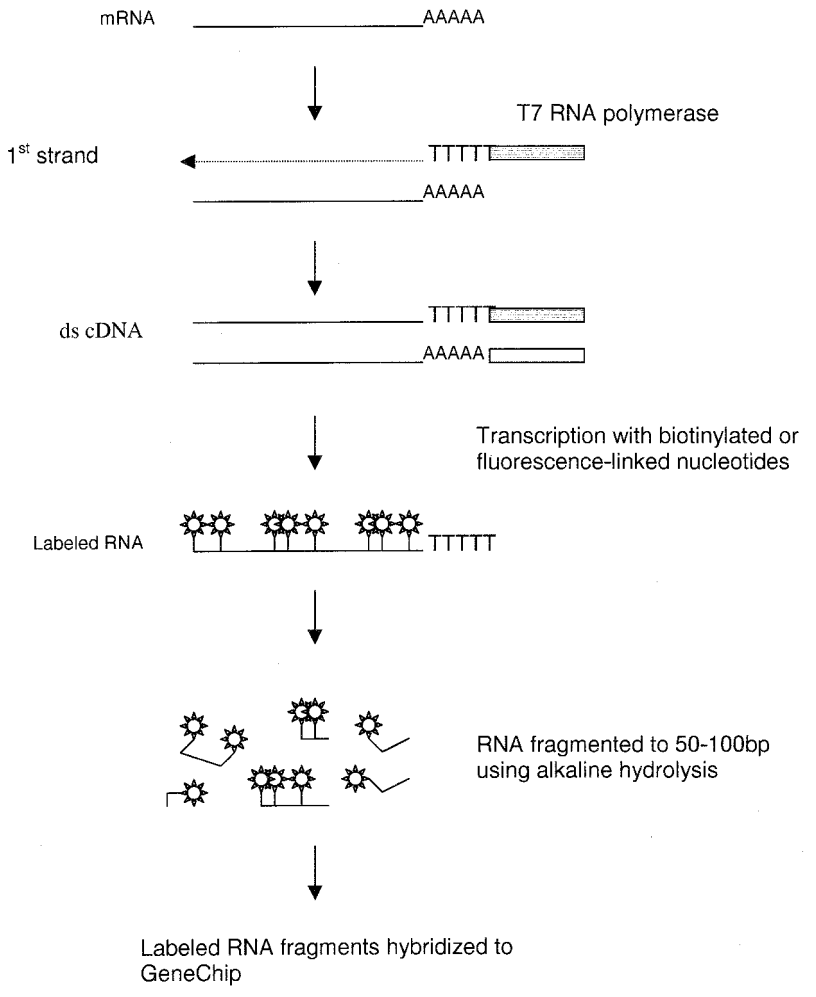


Figure 4. Preparation of probe for use with Affymetrix GeneChips. The arrays contain many thousands of small (20–25 bp) nucleotides. Hybridization is, therefore, carried out with small labelled fragments of cRNA prepared from RNA of the control and test populations. The RNA is first converted to cDNA using an oligodT primer, which has a T7 RNA polymerase promoter attached to the 5′ end. This enables RNA probes to be produced from the cDNA representations of the original populations. Incorporation of fluorescence-linked or biotinylated nucleotides into the transcription reaction produced labelled cRNA. Hybridization is carried out following fragmentation of the labelled RNA probes in an alkaline buffer. Method described by Zhu *et al.* (1998).

Affymetrix chips are probed with labelled antisense RNA, which is fragmented before hybridization so as to be compatible with the small (25 bp) probes (figure 4). Arrays that have been spotted with full- or partial-length cDNA clones are normally hybridized with single-stranded partial/full length cDNA (figure 5).

There are several approaches to labelling the populations that will be hybridized to the arrays. Most commonly, fluor-labelled nucleotides are directly incorporated into the cDNA in the process of converting RNA to cDNA. End-labelled primers may also be used for cDNA synthesis. A fluor is linked to the 5′ end of the cDNA primer to permit direct visualization of the hybridized array. Alternatively, biotin (De Saizieu *et al.* 1998) or a hapten may be attached to the primer, in which case a

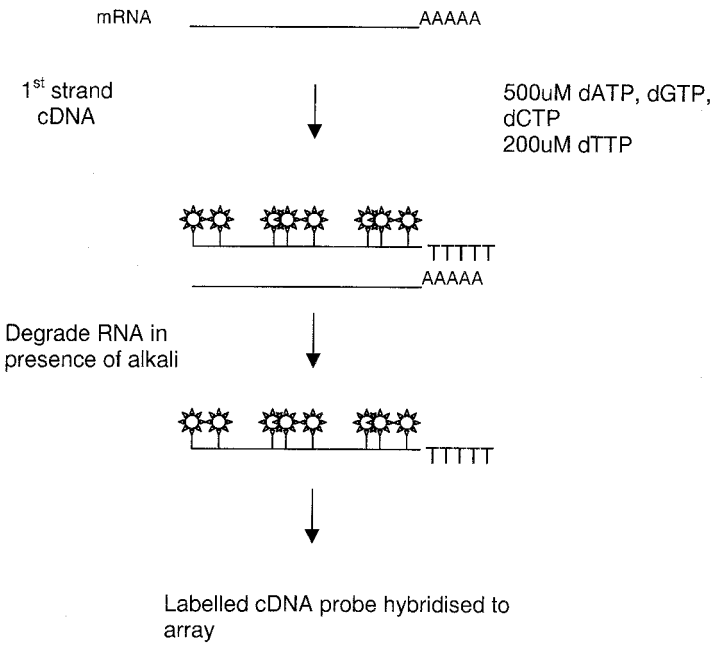


Figure 5. Preparation of probe for use with glass-based arrays. cDNA is prepared from total or mRNA extracted from the control and target cell populations using a poly dT primer. Cy-3- and Cy-5-labelled nucleotides are included in the reverse transcription mix to label the first strand cDNA. Following first strand cDNA synthesis the RNA strand is degraded with alkali and the remaining single-stranded cDNA is then used to hybridize against the array. Method described by Khan *et al.* (1998).

fluor-labelled streptavidin or antibody must be applied before a signal can be generated. The most commonly used fluors at present are Cyanine3 (Cy-3) and Cyanine5 (Cy-5) (Amersham Pharmacia Biotech, Uppsala, Sweden). However, the relative expense of these conjugates has driven a search for cheaper alternatives. Fluorescein, rhodamine and TX, USA red have all been used, and companies such as Molecular Probes, Inc. (Eugene, OR, USA) have developed a number of alternative fluors, e.g. the Alexa dyes, which cover a wide range of excitation and emission spectra and may prove to function as well as the 'Cy-dyes'. The development of second generation scanners housing multiple lasers and detectors (up to five are currently available in the latest scanner from GSI Lumonics, Watertown, MA, USA) will increase the versatility and throughput of samples. For example, one control and three treated RNA populations (perhaps representing different doses of a chemical or different time points) can be hybridized to the same slide if they are labelled with different fluors (table 3).

Although the Affymetrix system, with its multiple probe pairings, can distinguish very closely related sequences (single-point mutations), the issue of probe specificity has not yet been answered satisfactorily for cDNA arrays, which use much larger gene segments. This is important for discriminating closely related genes (e.g. the cytochrome P450 family), and different gene splice variants could be vital in elucidating the molecular mechanism of a given phenotype or response. Although the stringency of hybridization can be controlled to increase the specificity, it still may be difficult accurately and reproducibly to differentiate between sequences with $>70\%$ homology. The choice of sequence spotted onto the

Table 3. Excitation and emission wavelengths of four fluorescent dyes. Four fluorescent dyes currently available for use in hybridizations using glass-based arrays. The excitation and emission spectra are sufficiently distinct to allow use of all four dyes on a single DNA array. Adapted from Pickering (1999).

Fluorophore	Excitation (nm)	Emission (nm)	Excitation laser (nm)
Alexa 488	490	520	Blue Argon, 488
Cy-3	550	570	Green HeNe, 543
Alexa 594	590	615	Yellow HeNe, 594
Cy-5	649	670	Red HeNe, 633

membrane or slide is, therefore, highly important, and it is a good idea to incorporate at least a portion of the 3′ untranslated region of a gene (normally the most unique part of a gene) into the probe sequence if possible.

Analysis of DNA micro-arrays

Analysis of hybridized DNA arrays is composed of two steps – image capture and signal quantitation. The first step is relatively straightforward. For example, the hybridization signal from membrane-based arrays can easily be captured on film or with a phosphorimager. However, the scanners used to stimulate and capture the fluorescence signal from chip-based hybridizations are somewhat more specialized and relatively expensive. They are available from a number of companies, including Applied Precision (Issaquah, WA, USA), Axon Instruments (Foster City, CA, USA), Genetic MicroSystems, GSI Lumonics, Molecular Dynamics (Sunnyvale, CA, USA) and others. The scanners can be divided into three main types according to how they capture the array image: charge-coupled device (CCD) camera systems and non-confocal and confocal laser scanners. Each has particular advantages and disadvantages. For example, confocal laser scanners have a very high resolution (down to 5 μm/pixel) that increases the number of pixels per spot and helps to increase accuracy of quantitation. They also have a small depth of field, which serves to reduce the effects of artefacts such as dust on the bottom of the slide. However, they are about twice as slow as the other scanners and their small depth of focus requires very flat slides and scanning precision. CCD-based scanners are the current main alternative to confocal scanners. They are faster and focus over a large depth of field, but currently have a lower resolution ($\sim$ 30 μm per pixel) and are more prone to optical scatter, which can make them less appropriate for dim samples. Still, with most machines, signal can be detected down to levels of < 1 fluor molecule μm^{-2}, which translates to detecting a message at about one copy per cell or less. This high sensitivity is important for detecting rarely expressed genes, as well as small changes in the relative expression of those which are more abundant.

Given that a typical spot on a micro-array can contain $> 10^8$ molecules, it is clear that, depending on the abundance of a particular message being studied, a large variation in signal strength may occur. Most scanners cannot work across this many orders of magnitude. However, the scanning parameters may be adjustable to collect more or less signal, such that two or three scans of the same array should permit the detection of the whole gene expression spectrum.

When a micro-array is scanned, the fluorescent images generated by the fluors are captured by software normally included with the scanner. Image processing (quantitation of the signals) and data mining (trying to understand what the

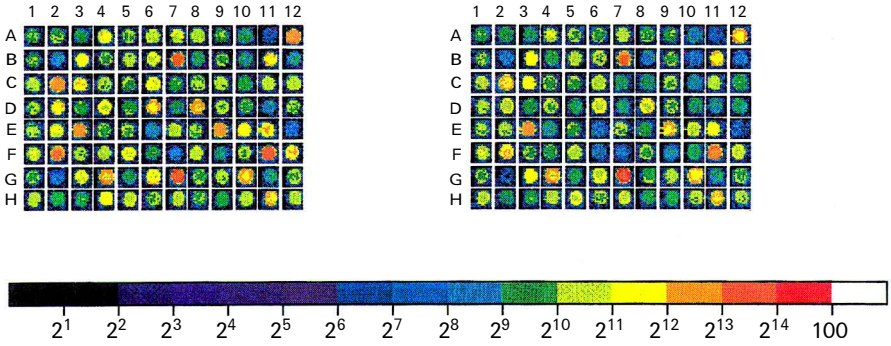


Figure 6. Two mouse testicular cDNA samples, one labelled with Cy-3 (control, left image), the other with Cy-5 (test, right image), were hybridized simultaneously to an Incyte mouse GEM I micro-array. The signal intensities are represented as false-colour images, with the scale indicating the relative fluorescence intensity. Relative changes in the fluorescence intensity of each spot (gene) can subsequently be calculated after adjusting for efficiency of fluor-labelling. The mouse GEM 1 micro-array, which is about the size of a microscope slide, contains 8734 sequence-verified IMAGE clones representing both known genes and EST, which are mapped to the National Center for Biotechnology Information's UniGene database.

expression patterns could mean) is carried out using more complex software. For example, programs such as ArrayVision (Imaging Research, Inc., Ontario, Canada), ImaGene (BioDiscovery, Los Angeles, CA, USA) and IP Lab MicroArray Suite (Scanalytics, Inc., Faifax, VA, USA) are used for fast and accurate quantitation of hybridization signals. In this process, the fluorescence intensity for each fluor is measured for every spot as a monochromatic signal. The images are then combined and false-colour added to represent which of the fluors was most abundant, and to what degree. An example of a two-colour image is shown in figure 6. Keeping track of the many thousands of data points generated by even a few experiments is a formidable task. The National Human Genome Research Institute (NHGRI; Ermolaeva *et al.* 1998) and others are developing relational databases designed to facilitate data input and report generation. Other software programs such as GeneSpring (Silicon Genetics, San Carlos, CA, USA), Spotfire Pro (Spotfire, Cambridge, MA, USA) and Expressionist (GeneData, Basel, Switzerland) are geared towards the identification of trends, clusters, patterns and outliers in large data sets.

The software tools for quantitation of DNA array images and data mining are constantly evolving as an increasing number of companies face up to the bioinformatics challenge that has arisen with this type of very high throughput technology. This is encouraging as the processing of the data into meaningful conclusions is currently the bottleneck for those using the method. Molecular Dynamics and Affymetrix has formed the Genetic Analysis Technology Consortium (GATC) to standardize the rapidly growing field of array-based genetic analysis. The consortium was created to provide a unified technology platform to design, process, read and analyse DNA arrays. According to the GATC consortium, researchers will benefit from chips, readers, reagents and database architectures that are GATC compliant and compatible, thus allowing direct comparison with data from other GATC compliant systems.

Summary

Being a new technology, the majority of hardware and software is in a relatively rapid state of development. Indeed, suppliers of such products are almost continuously upgrading their products to meet the new requirements which researchers are demanding. It should, therefore, come as no surprise to the reader if, by the time this paper is published, new developments have already taken place in the field. Nevertheless, current technology is generally considered robust enough to provide meaningful, reproducible data. The bottleneck for utilizing DNA arrays does not appear to be in the technology, but rather in the analysis and interpretation of the data. Faced with a mountain of expression data, many scientists still do not how to analyse it in the most useful and/or appropriate manner. This situation will improve as researchers and software engineers develop ideas and algorithms for analysing the large, complex sets of data generated by DNA arrays. The introduction of specialized bioinformatics courses at an increasing number of academic institutions should facilitate this process, as will the large number of workshops and seminars dedicated to DNA arrays which generate cross-fertilization and peer-review of ideas generated by the array community.

Options

Although DNA arrays are a relatively new development, there are already many options available for the investigator wishing to incorporate this technology into their research. They range from little or no hands-on work through intimate technology partnerships with large companies using the latest technology, to the use of hand-held devices to spot PCR products on membranes. It is the aim of this part of the review to describe these options.

Contract-screening

Those who are interested in fast results with a minimum investment of hands-on time may choose to pay for a contract screening service. Several companies offer such a service, although most utilize either the Incyte Gene Expression Microarrays (GEM) or Affymetrix GeneChip probe arrays. In this approach the investigator submits total RNA or mRNA samples that have been extracted from the samples to be compared, e.g. control and treated. Hybridization is carried out on a specified array and the data analysed to identify (1) the genes that are expressed in each sample and (2) those genes which show altered expression.

Incyte offers contract services for screening its GEM arrays, several of which are available with human, mouse, rat, *C. albicans*, *S. aureus* or *S. cerevisiae* clones. However, only the human UniGEM V and mouse GEM I arrays are currently available to all researchers. Other arrays require subscription to a related Incyte sequence database. Alternatively, Incyte will build custom arrays containing genes which are specified by the researcher (as long as clones of those genes are available). The company specifications appear impressive: sensitivity is reported to be high enough to detect genes which are expressed once per cell, while statistically significant changes of 2-fold can be reliably detected. Besides the high cost, probably the main drawback with the Incyte system is that clones that are $>70\%$ homologous may be difficult to differentiate.

Research Genetics, Inc. offers a gene expression analysis service using the Affymetrix GeneChip array platform, which currently includes human, rat, mouse

and yeast chips. In contrast to the spotting approach, in which a single clone is used to analyse each mRNA, every gene on a GeneChip array is represented by ~ 20 pairs of different, specific oligonucleotides biased toward the 3′ end of the gene. Each pair of oligonucleotides consists of a perfect match and a mismatch oligonucleotide, which differs only by a single base at the centre base position. This pairing strategy helps identify and minimize the effects of non-specific hybridization and background signal. GeneChip arrays are thus able specifically to detect individual gene transcripts and splice variants, and differentiate among closely related members of gene families. Although the range of species available for analysis is currently limited, one of the main advantages of this system in that the same technology may be used for expression monitoring, sequence analysis, genotyping and single nucleotide polymorphism (SNP) mapping. A gene expression analysis service is offered by Research Genetics and several not-for profit research institutions. Those trying to identify currently available services or local contractors should consider subscribing to the (free) Gene-Arrays Listserv (http://www.people.cornell.edu/pages/alm13/listserv.html), an internet forum for discussing anything to do with arrays. Although they do not carry out expression analysis, Gene Logic (Gaithersburg, MD, USA) and Lab Corp (Research Triangle Park, NC, USA) offer p53 and HIV SNP screening respectively using the Affymetrix GeneChip system.

Complete systems

At the next level of laboratory interaction, and still at very high cost, one can purchase entire systems so that the hands-on hybridizing and analysis can be carried out in-house. Affymetrix offers this complete approach to array technology through the integrated GeneChip system, which includes arrays, protocols, instrumentation, software and service – all the researcher needs is the labelled probes. Affymetrix has also gone on to form the aforementioned GATC in collaboration with Molecular Dynamics and a number of other corporate partners. The goal of GATC is to provide a unified technology platform to design, process, read and analyse DNA arrays through developing standards and certifying compliance of various hardware and software applications.

Genomic Solutions (Ann Arbor, MI, USA) also offers a complete system approach that includes everything except the DNA arrays themselves. Genomic Solutions also offers a contract printing service and is preparing to market prefabricated arrays of human, rat and mouse clones.

Off-the-shelf arrays

Contract screening of arrays or the purchase of integrated systems is very costly. One alternative is to purchase prefabricated arrays and the hardware to scan them in-house. Membrane-based arrays probably offer the best value at present, since they are less expensive than chips to purchase and do not require expensive consumables or the use of a specialized scanner. Instead, they can be read using a phosphorimager or by simply capturing the image on film. Although the manufacturers claim that membrane arrays can be stripped and reused, a large proportion of users has reported difficulty in carrying this out efficiently.

Prefabricated membrane-based DNA-arrays are currently or imminently available for human (Clontech, Genome Systems and Research Genetics), mouse

(Clontech and Genome Systems), rat (Clontech and Research Genetics) and *E. coli* (Genosys, The Woodlands, TX, USA). Clontech prints PCR products, corresponding to relatively small regions (a few hundred base pairs) of the target genes onto nylon membranes. Included with each pair of Clontech filter arrays is a set of primers that only transcribe and amplify the mRNA of genes which are present on that specific array. In this way the specificity of the probes is increased and false-positives due to non-specific cross-hybridization are reduced. The Clontech approach to arrays is also unique in that they have chosen to use a relatively small set of sequences (~ 1200 on their largest arrays), all derived from known genes. Thus, Clontech arrays are suitable for generating small expression profiles, or perhaps monitoring the expression of genes of known function which are involved in regulating a model system. Clontech also produce smaller arrays of just a few hundred clones which are aimed at specific research areas (e.g. stress/toxicology and cell cycle) and are preparing to offer a custom printing service.

Genome Systems and Research Genetics each produce arrays containing several thousand different genes or 'clusters' as delineated through UniGene. Both companies utilize partial- and full-length clones obtained from the IMAGE consortium and/or the Cancer Genome Anatomy Project (CGAP, http://www.ncbi.nlm.nih.gov/ncicgap). Genome Systems prepare their arrays by growing dense grids of bacterial clones (containing plasmids with the gene of interest) on a nylon membrane. After a specified growth time, the colonies are lysed and processed to allow the plasmid cDNAs to remain fixed to the membrane. Research Genetics uses a similar technique to Clontech in that it PCR-amplifies the cDNAs and spots the products on a filter. The genes available on each array depends upon the species. According to the UniGene database (http://www.ncbi.nlm.nih.gov/UniGene/index.html), the most genes (clusters) are available for human, with rat and mouse being the next best represented. Many clusters are represented only by Expressed Sequence Tags (EST; Adams *et al.* 1991). While these cloned DNA sequences have no formal identification, they may be usefully incorporated into DNA-arrays since identification and/or characterization of the gene they represent can be carried out later if the EST is seen to be regulated in some way in the chosen model. Genome Systems' and Research Genetics' arrays can thus be used to generate large expression profiles and to hunt for genes (in the form of EST) which are potentially important in the model system, but which are unidentified or uncharacterized.

Incyte and Affymetrix currently dominate the market for DNA arrays prepared on glass. Unfortunately, their marketing strategy excludes routine use of their products by all but the most highly funded laboratories. The only other commercial supplier of such off-the-shelf arrays is NEN® Life Science Products (Boston, MA, USA), which recently introduced the MICROMAX™ Human cDNA Micro-array System. This kit includes two identical glass slides prespotted with 2400 human genes, all key reagents for cDNA labelling and hybridization, and NEN's proprietary TSA™ (Tyramide Signal Amplification) reagents. TSA reduces the amount of starting sample required by as much as 50-fold (table 2), and because of its high sensitivity, permits the detection of mRNA expression at levels below those detectable by other methods. It could thus prove to be a valuable system for those working with small samples such as tissue biopsies. Arrays currently require at least several hundred nanograms mRNA per sample (or the equivalent in total RNA), which is another reason why they are not yet broadly used.

Do-it-yourself arrays

Contract screening and prefabricated arrays suffer from several drawbacks. For instance, the researcher is limited to screening the species and gene sequences that the suppliers have placed on their arrays. Unfortunately, many researchers study animals, plants or microbes that are outside the small core of laboratory species currently covered by such off-the-shelf arrays. In addition, many who wish to utilize DNA-array technology may be dissuaded by the relatively high cost of the hardware, software and even consumables. However, since the preparation and use of DNA-arrays is a multi-step procedure (preparation of the array, probe preparation, hybridization, scanning of the hybridized array, analysis of the hybridization signals and interpretation of data), options are available to reduce capital or recurring costs.

Clone library

To produce arrays, one must first obtain the library of clones which are to be arrayed. Whether such a library is composed of known or unknown genes or a mixture of the two is ultimately determined by the aims of the investigator. Although some individuals may carry extensive libraries of clones, in most cases it is probable that they will wish to incorporate even larger numbers into the array, in which case purchase from an appropriate supplier is required. Clones (including sequence-verified clones) are available for human, rat and mouse through IMAGE distributors.

Printing arrays

The small number of species for whom large numbers of clones is available at a reasonable price can be a block or a hindrance to those working on unusual genes or species, in which case the only real option is to print one's own array. The pioneers of this approach were the laboratories of Pat Brown (http://cmgm.Stanford.edu/pbrown) and Ron Davis (http://cmgm.stanford.edu/biochem/davis.html) at Stanford. A detailed plan for building the printer they used can be found on Brown's web site. Although these and other academic groups have done much to promote and advance array technology, they have recently been joined by companies focusing their efforts on producing various off-the-shelf components and systems for those wishing to enter the world of arrays.

Contract-printing

Several companies have emerged recently who offer a printing service, e.g. Radius Biosciences (Medfield, MA, USA), Genometrix and Genomic Solutions. The researcher provides PCR products (or chooses from the library held by the printing company), and the company prints arrays in the specified format. There are several advantages to contract-printing. Foremost is that it eliminates the purchase of a costly printing device. In addition, the technology of printing is still developing and is likely to improve rapidly over the next few years. Finally, the problems invariably encountered in the use of new, high throughput technology are not the researcher's to solve. The use of contract printing is a good option for those who are considering using small numbers of arrays. However, laboratories or core facilities who project using hundreds of arrays over months or years will probably find it more cost-effective to purchase a printing robot and carry out the process in-house.

In summary, the use of DNA arrays is not necessarily the prerogative of the rich. There are ways in which anyone wishing to utilize them can achieve this aim. From the contract screening of high-density glass chips with numerous researcher-provided samples, to the in-house hand-printing of small libraries of genes on membranes, products and services are now available to fit the budget of most laboratories.

Applications of DNA arrays

Although analysis by arrays is still an emerging technology which is certain to undergo improvement and alteration, it has already been applied usefully to a number of different applications. Arrays are at their most powerful when they contain clones for the entire genome of the species they are being used to study. For this reason, they have found strong support with, among others, researchers studying yeast (http://cmgm.Stanford.EDU/pbrown) and *C. elegans*. (http://www.mcb.arizona.edu/wardlab/micro-array.html, http://cmgm.Stanford.EDU/~kimlab). The genomes of both these species have been sequenced, and manuscripts published describing the deposition of the entire yeast genome onto a chip and subsequent use of that chip in the examination of altered gene expression following mutation or environmental challenge of cells (DeRisi *et al.* 1997, Lashkari et al. 1997). With both these species it is a relatively easy matter to perturb individual gene expression. Thus, by a process of systematic gene disruption, it is possible to examine the cause and effect relationships between different genes in these simple organisms. This kind of approach should help facilitate the elucidation of biochemical pathways and genetic control processes, unravel polygenic interactions, and define the architecture of cellular and genetic networks. Polygenic interactions will become increasingly important as researchers start to move away from single gene analysis when examining the nature of responses to external stimuli. This is especially important in toxicology since the phenotype produced by a given environmental insult is likely never the result of the action of a single gene, but a complex interaction of one or multiple cellular pathways which together produce the manifested phenotype. Phenomena such as quantitative trait (the continuous variation of phenotype), epistatsis (the effect of alleles of one or more genes on the expression of other genes) and penetrance (proportion of individuals of a given genotype that display a particular phenotype) will become increasingly evident and important as toxicologists push towards matching the responses of an individual genome to different environmental stimuli.

At present, DNA arrays are primarily a tool for examining the differential gene expression in a given model. In this context they are referred to as 'closed' systems, since they lack the ability of other differential expression technologies, e.g. differential display (Liang and Pardee 1992) and subtractive hybridization (Sargent and Dawid 1983), to detect previously unknown genes which are not present on the array. This would appear to limit the power of DNA arrays to the imaginations and preconceptions of the researcher in selecting an array of genes which have been previously characterized and been shown or thought to be involved in the model system. However, the various gene sequencing projects have thrown up a new way of identifying expressed genes (as EST) which has partially mollified this deficiency. EST represent genes which have been identified as being expressed in a particular model or tissue, many of which show little or no homology to previously

Table 4. Toxicity fingerprints as a means to assess the toxic potential of chemical compounds at an early stage of development. In this simple representation of the utility of toxicity signatures/fingerprints for screening new compounds, each group of known toxic chemicals is plotted against the relative change in expression of a series of genes or gene families at a predetermined exposure level (e.g. NOAEL, LOAEL). Each gene or gene family represents predetermined biomarkers of one or more groups of toxic chemicals, and their expression may be upregulated (+), downregulated (−) or unchanged (=). Degrees of change could also be introduced if deemed necessary. Thus, each row represents the toxicity signature/fingerprint of that particular group of toxic chemicals. The fingerprints of new or untested chemicals can be compared against the established toxicity signature/fingerprints to check for indications of toxicity. In this case, test compound 1 would be eliminated from further development as its toxicity fingerprint appears to match that of known neurotoxins 1, while the test compound 2 would be retained for further development as its toxicity fingerprint does not match any of the known toxicant groups.

Test compound 1	+	+	+	−	−	−	=	=	=
Test compound 2	=	=	=	−	+	−	+	=	=
Peroxisome proliferators	=	=	=	−	−	−	+	+	+
Non-genotoxic carcinogens	−	=	=	−	−	−	+	+	+
Genotoxic carcinogens	−	−	−	+	−	+	=	−	−
Endocrine disruptors	−	+	+	+	+	+	−	=	=
Neurotoxins 1	+	+	+	−	−	−	=	=	=
Neurotoxins 2	+	+	+	+	+	−	=	=	=
Heavy metals	+	+	+	−	=	−	−	+	+
Teratogens	+	+	−	+	−	+	−	+	−
	A	B	C	D	E	F	G	H	etc.
				Gene or gene family					

=, Unchanged; +, upregulated; −, downregulated.

characterized genes. In this way, their expression, function and biological significance is unknown. By incorporating EST clones into an array, it is possible to monitor the expression of these unknown genes. Thus, DNA arrays can potentially be used as a springboard for the identification and investigation of previously uncharacterized genes that may have biological significance in the model system.

The use of the 'transcriptome' (the expression level of all the genes in a given cell population) in toxicological research will depend on the successful development and application of DNA arrays. Once a transcriptome has been assembled, it can then be transferred onto arrays and used to screen gene expression in any chosen system. For example, the EPA MicroArray Consortium (EPAMAC; Rockett and Dix 1999) is looking to assemble testes transcriptomes for human, rat and mouse. Other groups have assembled what is effectively a 'toxicological transcriptome' – a library of human and mouse genes which have previously been shown or implicated to be involved in responses to toxicological insults (Nuwaysir *et al.* 1999). Thus, rather than being tissue or cell-specific, they can be used across a variety of model systems to look for alterations in toxicologically important genes. The potential to identify toxicant 'families' based on tissue or cell-specific gene expression could revolutionize toxicology and drug testing. These so called molecular 'signatures' or 'fingerprints' could point to the possible toxicity/carcinogenicity of compounds (table 4) and aid in elucidating their mechanism of action through identification of gene expression networks. By extension, such signatures might identify biomarkers to assess the degree, time and nature of exposure. Furthermore, it may be that these gene expression signatures are more highly conserved between species than individual biomarkers. An example of the gene expression signature for etoposide-induced apoptosis in human cells was recently published by Wang *et al.* (1999) using a 6591 element micro-array. Several p53-regulatory genes and novel p53 target

genes, as well as p53-independent signalling pathways, were identified by the array and confirmed by Northern blot.

A further use of micro-arrays is the identification of SNP. These genomic variations are very abundant – occurring about every 1 kb - and are the basis of RFLP-analysis used in forensic analysis. Affymetrix has designed GeneChip probe arrays that contain multiple repeats of the same gene sequence. Each position is present with all four possible bases. Following hybridization of the sample, the degree of hybridization to the different sequences can be measured and the exact sequence of the target gene deduced. SNP are thought as being of vital importance in drug metabolism and might explain, for example, why some people can metabolize certain xenobiotics better than others (e.g. Hengstler *et al.* 1998, Longuemaux *et al.* 1999). Thus, arrays provide a further tool for the toxicologist investigating the nature of toxicological responses and susceptible subpopulations.

Sequencing by hybridization (SBH) chips being developed by HySeq (Sunnyvale, CA, USA) and Perkin Elmer (Norwalk, CT, USA) contain universal oligonucleotides with all possible combinations of sequences in a given length. The DNA to be sequenced is cleaved, fluorescently labelled and hybridized to the SBH chip. The target DNA sequence is then resolved from the pattern of fluorescence emitted from the SBH chip. If SBH development is successful, it will result in a universal chip able rapidly and inexpensively to analyse any DNA sequence without prior knowledge of the gene sequence.

Other technologies are available that may complement or supplant DNA array applications to toxicology in certain areas, including serial analysis of gene expression (SAGE; Velculescu *et al.* 1995), proteomics and cell-based arrays for combinatorial analysis. SAGE applications in toxicology are being developed and marketed by Genzyme Molecular Oncology (Framingham, MA, USA). SAGE is a proprietary sequence-based technology for gene identification and quantitation, and is touted as being more efficient and less biased (it is an open system, unaffected by the prejudices or constraints of the investigator in retrieving differentially expressed genes) than DNA arrays.

Cutting-edge proteomics systems include high-throughput two-dimensional electrophoresis coupled with automated mass spectrometry rapidly to identify and characterize expressed proteins (i.e. the proteome) of a given model system. The use of high-density arrays is not limited to DNA sequences. Analysis of protein–protein and protein–ligand interactions can be conducted on peptide arrays available from academic (http://www.hi.helsinki.fi/hi/cf/peptide/SPOT.html) and commercial sources (Genosys Biotechnologies, Inc., The Woodlands, TX, USA; Jerini BioTools GmbH, Berlin, Germany). Other protein arrays are being developed to enable the detection of trace amounts of specific proteins directly from biological fluids (Ciphergen BioSystems, Inc.), enabling comparison of protein expression in diseased or exposed states versus normal. Cellomics, Inc. (Pittsburgh, PA, USA) have gone one step further and developed ArrayScan™, a system for subcellular resolution of fluorescence signals in multiple cells in a field within a well of a microtiter plate. Such cell-based information can be used to understand the temporal and spatial expression of and interaction between, the ions, metabolites, macromolecules and organelles that are responsible for life functions. A further new technology under development utilizes multicoloured microbeads to identify individual binding (protein) or hybridization (nucleic acid) reactions, the extent of which can be quantitated using fibreoptic (Illumina, San Diego, CA, USA; Michael

et al. 1998) or flow sorting (Luminex, Austin, TX, USA; Fulton *et al.* 1997) technology. In this approach, antibodies (if protein is the intended target) or cDNA probes (for RNAs/cDNAs) are attached to the surface of the microbead. Each microbead and, therefore, its probe can be identified by its unique identifying colour, while the amount of target attached to its surface is quantitated through direct (nucleic acids) or indirect (protein) labelling with fluorescent dyes. Although this approach to gene/protein expression analysis appears to offer some benefits, e.g. decreased costs and increased speed and sensitivity (http://www.devicelink.com/mddi/archive/97/04/020.html), it will probably be some time before the true value and potential of this technology is fully realised.

The high-density high throughput approach of arrays has also been applied to tissues. Tsao-Wu *et al.* (1998) described a method to array thousands of thin tissue sections from fish larvae in agarose. They performed histological- and PCR-based genotypic analysis from section of individual larvae. This type of approach could be applied to tissue sections from laboratory animals, and possibly even extended to include the treatment of live tissue slices, e.g. liver, with different xenobiotics before fixation and analysis.

Of course, the potential of these and other methodologies does not diminish the utility of DNA arrays to toxicological studies with multiple time- and dose-points, particularly as new fluors and scanners allow four or five labelled populations to be hybridized simultaneously to a single slide or chip. Indeed, such tissue-, cell- and protein-based systems will serve to complement DNA arrays through providing a means to simultaneously analyse multiple characteristics of a toxicant or drug.

Summary

Fortune magazine readers were recently treated to the following attention-grabbing leader: 'Microprocessors have reshaped our economy, spawned vast fortunes and changed the way we live. Gene chips could be even bigger' (Stipp 1997). Although the world may not face meltdown on 1 January 2000 as a result of badly designed DNA arrays, the sci-fi implications are indeed grand. It is possible that one day it could be possible to place the entire genome of an individual on small glass 'chips' and use it to diagnose the exact nature of a disease or xenobiotic exposure. Indeed, it may even be possible to predict the onset of a genetically inherited disease or to warn against exposure to specific environmental antigens or chemicals. However, such grandiose ideas are still a long way off as DNA array technology is at a relatively early stage of development. This means that the hardware is still improving and there is no current consensus for standard procedures, quantitation and interpretation. In addition, one of the dark regions of array technology – strife in the courts over who owns what bits of the technology – has erected a further barrier towards the development of consensus procedures. However, perhaps the greatest hurdle is the actual interpretation of data. Cross-referencing results from multiple experiments (time, dose, repeats, different animals, different species) to identify commonly expressed genes is a very great challenge.

For the toxicologist there is a need to carry out multiple experiments – dose-responses, time curves, multiple animals, repeats. Glass-based DNA-arrays are most attractive in this context because they can be prepared in large batches from the same DNA source and accommodate control and treated samples in the same

hybridization. However, one problem with prefabricated arrays at this time is that they often do not contain the particular genes a group is interested in. An alternative is to obtain and/or produce a set of custom clones and have contract printing carried out. Contracting out the work can be cheaper than laying out capital for ones own equipment, but if array technology is to be established, there will come a point where buying some clones, a printer, a scanner and the appropriate software must be seriously considered.

Finally, DNA arrays are currently a team game. They are a technology that utilizes a range of fields, including engineering, statistics, biochemistry, molecular biology and bioinformatics. Since most individuals are skilled in only one or perhaps two of these areas, it appears that success with arrays may be best expected by teams or collaborations consisting of individuals whose combined skills encompass all of these fields. The large amounts of data obtained from even a single chip could also lead to a new approach to collaboration if a single chip could provide useful information to several different groups interested in different gene networks.

There are still many months, if not years, from the time when DNA arrays will become used as routinely as, for example, current blotting techniques, DNA sequencing or perhaps even PCR. However, the fact that DNA arrays report the expression of so many genes in a single experiment is a powerful incentive to develop the technology into an accessible platform routinely used by life-science laboratories. Toxicologists should be among those who benefit most from this new technology – one that could just turn out to be a key that opens up whole new avenues for delineating toxicological responses and developing new prognostic and diagnostic tests for safeguarding public health and enhancing our quality of life.

Acknowledgements

This paper was reviewed in accordance with the US Environmental Protection Agency policy and was approved for publication. Companies, trade names or products cited herein do not signify endorsement of such by the EPA.

References

Adams, M. D., Kelley, J. M., Gocayne, J. D., Dubnick, M., Polymeropoulos, M. H., Xiao, H., Merril, C. R., Wu, A., Olde, B., Moreno, R. F., Kerlavage, A. R., McCombie, W. R. and Ventor, J. C., 1991, Complementary DNA sequencing: expressed sequence tags and human genome project. *Science*, **252**, 1651–1656.

Chen, J. J., Wu R., Yang, P. C., Huang, J. Y., Sher, Y. P., Han, M. H., Kao, W. C., Lee, P. J., Chiu, T. F., Chang, F., Chu, Y. W., Wu, C. W. and Peck, K., 1998, Profiling expression patterns and isolating differentially expressed genes by cDNA micro-array system with colorimetry detection. *Genomics*, **51**, 313–324.

DeRisi, J. L., Iyer, V. R. and Brown, P. O., 1997, Exploring the metabolic and genetic control of gene expression on a genomic scale. *Science*, **278**, 680–686.

Ermolaeva, O., Rastogi, M., Pruitt, K. D., Schuler, G. D., Bittner, M. L., Chen, Y., Simon, R., Meltzer, P., Trent, J. M. and Boguski, M. S., 1998, Data management and analysis for gene expression arrays. *National Genetics*, **20**, 19–23.

Fleischmann, R. D., Adams, M. D., White, O., Clayton, R. A., Kirkness, E. F., Kerlavage, A. R., Bult, C. J., Tomb, J. F., Dougherty, B. A., Merrick, J. M., McKenney, K., Sutton, G., Fitzhugh, W., Fields, C., Gocayne, J. D., Scott, J., Shirley, R., Liu, L.-I., Glodek, A., Kelley, J. M., Weidman, J. F., Philips, C. A., Spriggs, T., Hedblom, E., Cotton, M. D., Utterback, T. R., Hanna, M. C., Nguyen, D. T., Saudek, D. M., Brandon, R. C., Fine, L. D., Fritchman, J. L., Fuhrmann, J. L., Geoghagen, N. S. M., Gnehm, C. L., McDonald, L. A., Small, K. V., Fraser, C. M., Smith, H. O. and Venter, J. C., 1995, Whole-genome random sequencing and assembly of *Haemophilus influenzae* Rd. *Science*, **269**, 496–512.

FULTON, R. J., MCDADE, R. L., SMITH, P. L., KIENKER, L. J. and KETTMAN, J. R., 1997, Advanced multiplexed analysis with the FlowMetrix system. *Clinical Chemistry*, **43**, 1749–1756.

HENGSTLER, J. G., ARAND, M., HERRERO, M. E. and OESCH, F., 1998, Polymorphisms of N-acetyltransferases, glutathione *S*-transferases, microsomal epoxide hydrolase and sulfotransferases: influence on cancer susceptibility. *Recent Results in Cancer Research*, **154**, 47–85.

KHAN, J., SIMON, R., BITTNER, M., CHEN, Y., LEIGHTON, S. B., POHIDA, T., SMITH, P. D., JIANG, Y., GOODEN, G. C., TRENT, J. M. and MELTZER, P. S., 1998, Gene expression profiling of alveolar rhabdomyosarcoma with cDNA micro-arrays. *Cancer Research*, **58**, 5009–5013.

LASHKARI, D. A., DERISI, J. L., MCCUSKER, J. H., NAMATH, A. F., GENTILE, C., HWANG, S. Y., BROWN, P. O. and DAVIS, R. W., 1997, Yeast micro-arrays for genome wide parallel genetic and gene expression analysis. *Proceedings of the National Academy of Sciences, USA*, **94**, 13057–13062.

LENNON, G., AUFFRAY, C., POLYMEROPOULOS, M. and SOARES, M. B., 1996, The I.M.A.G.E. Consortium: an integrated molecular analysis of genomes and their expression. *Genomics*, **33**, 151–152.

LIANG, P. and PARDEE, A. B., 1992, Differential display of eukaryotic messenger RNA by means of the polymerase chain reaction. *Science*, **257**, 967–971.

LONGUEMAUX, S., DELOMENIE, C., GALLOU, C., MEJEAN, A., VINCENT-VIRY, M., BOUVIER, R., DROZ, D., KRISHNAMOORTHY, R., GALTEAU, M. M., JUNIEN, C., BEROUD, C. and DUPRET, J. M., 1999, Candidate genetic modifiers of individual susceptibility to renal cell carcinoma: a study of polymorphic human xenobiotic-metabolizing enzymes. *Cancer Research*, **59**, 2903–2908.

MICHAEL, L. L., TAYLOR, L. C., SCHULTZ, S. L. and WALT, D. R., 1998, Randomly ordered addressable high-density optical sensor arrays. *Annals in Chemistry*, **70**, 1242–1248.

Nature Genetics, 1999, The chipping forecast. *Nature Genetics*, **(suppl. 1, January).**

NUWAYSIR, E. F., BITTNER, M., TRENT, J., BARRETT, J. C. and AFSHARI, C. A., 1999, Micro-arrays and toxicology: the advent of toxicogenomics. *Molecular Carcinogenesis*, **24**, 153–159.

PICKERING, L., 1999, Micro-array technologies: using range of techniques to sped the drug discovery process. *Genetic Engineering News*, **19**, 21.

ROCKETT, J. C. and DIX, D. J., 1999, U.S. EPA workshop: Application of DNA arrays to toxicology. *Environmental Health Perspectives*, **107**, 681–686.

DE SAIZIEU, A., CERTA, U., WARRINGTON, J., GRAY, C., KECK, W. and MOUS, J., 1998, Bacterial transcript imaging by hybridization of total RNA to oligonucleotide arrays. *Nature Biotechnology*, **16**, 45–47.

SARGENT, T. D. and DAWID, I. B., 1983, Differential gene expression in the gastrula of *Xenopus laevis*. *Science*, **222**, 135–139.

SCHENA, M., SHALON, D., DAVIS, R. W. and BROWN, P. O., 1995, Quantitative monitoring of gene expression patterns with a complementary DNA micro-array. *Science*, **270**, 467–470.

SOUTHERN, E. M., 1975, Detection of specific sequences among DNA fragments separated by gel electrophoresis. *Journal of Molecular Biology*, **98**, 503–517.

STIPP, D., 1997, Gene chip breakthrough. *Fortune*, **31 March**, 56–73.

TSAO-WU, G. S., WEBER, C. H., BUDGEON, L. R. and CHENG, K. C., 1998, Agarose-embedded tissue arrays for histologic and genetic analysis. *Biotechniques*, **25**, 614–618.

VELCULESCU, V. E., ZHANG, L., VOGELSTEIN, B. and KINZLER, K. W., 1995, Serial analysis of gene expression. *Science*, **270**, 484–487.

WANG, Y., REA, T., BIAN, J., GRAY, S. and SUN, Y., 1999, Identification of the genes responsive to etoposide-induced apoptosis: application of DNA chip technology. *FEBS Letters*, **445**, 269–273.

ZHU, H., CONG, J.-P., MAMTORI, G., GINERAS, T. and SHENK, T., 1998, Cellular gene expression altered by human cytomagalovirus: global monitoring with oligonucleotide arrays. *Proceedings of the National Academy of Sciences, USA*, **95**, 14470–14475.

XENOBIOTICA , 2000, VOL. 30, NO. 2, 179–192

Metabolic fate of delmopinol in man after mouth rinsing and after oral administration

B. ERIKSSON*, G. HALLSTRÖM†, A.-K. OTTERSGÅRD BRORSSON, L. SVENSSON and P. O. GUNNARSSON

Pharmacokinetics and Metabolism, Active Biotech Research AB, PO Box 724, SE-220 07 Lund, Sweden

Received 4 March 1999

1. The metabolism of delmopinol, an inhibitor of plaque formation and gingivitis, has been studied after mouth rinsing or an oral dose of ^{14}C-delmopinol to healthy male volunteers. The metabolite pattern was studied in urine and plasma samples (unhydrolysed or hydrolysed with conjugate cleaving enzymes) by liquid chromatography (LC) with radio detection. Metabolite identifications were carried out by gas chromatography–electron-impact mass spectrometry (GC-MS) and by liquid chromatography–thermospray mass spectrometry (LC-MS).

2. The metabolic clearance of delmopinol was high, and $< 0.2\%$ of the dose was excreted as intact delmopinol in the urine. The main metabolites were, for both administration routes, glucuronide conjugates of delmopinol and of (ω-1-hydroxy) delmopinol. These metabolites were predominant and accounted for nearly the entire urinary radioactivity and most of the plasma radioactivity. After mouth rinsing, parent delmopinol was also one of the main compounds in plasma.

3. Several other products of oxidation of the aliphatic side-chain were present in minor amounts in urine. These metabolites also appeared to be excreted as glucuronic acid conjugates.

4. Glucuronidated (ω-1-hydroxy) delmopinol separated into three peaks by the LC system used. This could be due to different chromatographic properties of conjugate isomers, positional or optical.

Introduction

Delmopinol (Decapinol®, *rac*-4-(2-hydroxyethyl)-3-(4-propylheptyl)-morpholine) is a surface active agent with low antimicrobial properties intended to act locally by preventing bacteria from adhering to and colonizing the tooth surface. The agent has been shown to be effective against dental plaque formation and gingivitis *in vivo* (Collaert *et al.* 1992a, b, Moran *et al.* 1992) and is well tolerated by patients in long-term studies (Claydon *et al.* 1996).

The pharmacokinetics of ^{14}C-delmopinol (figure 1), 20 mg, in humans have been reported previously (Eriksson *et al.* 1998). After mouth rinsing with an aqueous solution of ^{14}C-delmopinol HCl, $\sim 72\%$ of the dose was expectorated and 25% was excreted in the urine. Renal excretion was also predominant after oral administration with 92% of the dose excreted in the urine. Very little material was found in the faeces. The excretion was rapid, and at 24 h after administration, 96 ± 2 and $93 \pm 2\%$ of the dose had been recovered following mouth rinsing and oral administration, respectively. A high clearance was indicated, and after oral administration the plasma concentration of parent delmopinol was much lower than after mouth rinsing, probably due to a high first-pass metabolism.

* Author for correspondence: e-mail; birgitta.eriksson@activebiotech.com
† Present address: AstraZeneca, R&D Lund, SE-221 87 Lund, Sweden.

Xenobiotica ISSN 0049–8254 print/ISSN 1366–5928 online © 2000 Taylor & Francis Ltd
http://www.tandf.co.uk/journals/tf/0049825.html

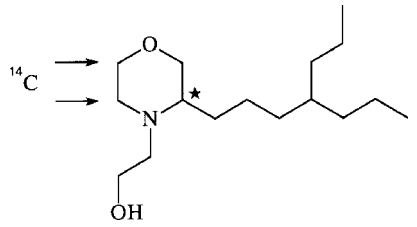


Figure 1. Structural formula of delmopinol. Arrows show the position of the ^{14}C-labelling, the asterisk the chiral centre.

A detailed investigation of the delmopinol metabolites in urine and plasma samples collected in the above study was performed. The present paper reports the identification and quantifications of delmopinol metabolites in urine and plasma from healthy male volunteers administered ^{14}C-delmopinol HCl by mouth rinsing or orally.

Materials and methods

Chemicals

Delmopinol HCl (*rac*-4-(2-hydroxyethyl)-3-(4-propylheptyl) morpholine HCl; chemical purity 99%) and delmopinol glucuronide (2-[3-(4-propylheptyl)morpholino]ethyl β-D-glucopyranosiduronic acid; chemical purity 98%) were synthesized at the request of Biosurface Pharma AB (Malmoe, Sweden). ^{14}C-delmopinol (*rac*-4-(2-hydroxyethyl)-3-(4-propylheptyl)-[5,6-^{14}C]-morpholine HCl; radiochemical purity 98%) was synthesized by Amersham (Amersham, Buckinghamshire, UK). The position of the ^{14}C-labelling is shown in figure 1. β-Glucuronidase/arylsulphatase (from *Helix pomatia*, ~ 5.5 U/ml glucuronidase activity at 38 °C = ~ 100000 Fishman units/ml; ~ 2.6 U/ml arylsulphatase activity at 38 °C = ~ 800000 Roy units/ml) and sulphatase-free β-glucuronidase (from *E. coli* K12, ~ 200 U/ml at 37 °C) were from Boehringer Mannheim GmbH (Mannheim, Germany). D-Saccharic acid 1,4-lactone was from Sigma Chemical Co. (St Louis, MO, USA). BSTFA (N,O-bis(trimethylsilyl)trifluoroacetamide) with 1% trimethylchlorosilane was from Pierce Chemical Co. (Rockford, IL, USA). Water was purified in a MilliQ system (Millipore Corp., Milford, MA, USA). Other chemicals were standard products of analytical or HPLC grade.

Investigation of metabolite pattern

Metabolites in urine and plasma were separated and quantified by LC with radioactivity detection. The samples were from healthy male volunteers after mouth rinsing with ($n = 6$) or oral administration ($n = 6$) of 10-ml aqueous solution of ^{14}C-delmopinol HCl, 2 mg/ml. Metabolites were quantified in urine collected 0–36 h (24% of dose; 86% of not expectorated) or 0–24 h (91% of dose) after mouth rinsing or oral administration respectively. Metabolites in plasma were quantified in samples obtained 0–6 h after mouth rinsing and 0–4 h after oral administration. The LC system (Waters Corp., Milford, MA, USA) consisted of 600E liquid chromatography delivery system with U6K injector, a NovaPak C18 precolumn, a Radial Pak NovaPak C18 column (8 mm × 10 cm cartridge), and a 441 UV detector set at 214 nm. On-line detection of radioactivity was achieved with a Flo-One β-radioactive flow detector, model CR (Radiomatic Instruments & Chemicals Co., Meriden, CT, USA) equipped with a 2.5 ml liquid cell, and using Monophase-S as scintillation cocktail at 3.5 ml/min. For collection of fractions, a Gilson Model 202 Fraction collector (Gilson Medical Electronics, Middleton, WI, USA) was used. Metabolites were separated with a gradient of methanol and 0.01 mol/l ammonium/triethylammonium acetate (0.1% TEA), pH 5.6 (0–35 min, 33% methanol; 35–37 min, 33–55% methanol; 37–56 min, 55% methanol; 56–58 min, 55–95% methanol; 58–75 min, 95% methanol). The flow rate was 1 ml/min.

Untreated urine samples were mixed with 33% methanol and filtered (Accords 4184; 0.45 μm, 25 mm, polysulphone membrane, Gelman Sciences, Ann Arbor, MI, USA) before injection onto the LC system. All other samples were extracted on solid-phase (see below) before LC analysis.

Representative individual and pooled urine and plasma samples were treated with β-glucuronidase/arylsulphatase. Major LC peaks in urine were fractionated and hydrolysed after evaporation of the methanol content. In addition, pooled urine was hydrolysed with β-glucuronidase and also treated with D-saccharic acid 1,4-lactone, a specific inhibitor of β-glucuronidase, in combination with β-glucuronidase/arylsulphatase. The samples were diluted with an equal volume of 0.2 mol/l sodium acetate, pH 5, and incubated at 37 °C with β-glucuronidase/arylsulphatase (β-glucuronidase activity 0.8 U/ml sample, 15000 Fishman units/ml sample), β-glucuronidase (12 U/ml sample) or β-glucuronidase/arylsulphatase combined with D-saccharo-lactone (5 mmol/l) for ~ 24 h.

Unhydrolysed plasma and hydrolysed samples of plasma, urine and LC fractions of urine were solid-phase extracted on Bond Elut C8 columns (Analytichem, Harbor City, CA, USA) before analysis by LC. The samples were diluted 1:1 with 0.01 mol/l ammonium acetate, pH 5.1, and vortex-mixed. A diluted sample was passed through a column that had been pre-activated with methanol and 0.01 mol/l ammonium acetate, pH 5.1. The sorbent was washed with 1 vol. 0.01 mol/l ammonium acetate, pH 5.1. Retained ^{14}C-components were eluted with 2 vols 200 μl (100 mg column) or 2 vols 600 μl (500 mg columns) acetonitrile–0.01 mol/l ammonium acetate, pH 5.1 (80:20 v/v) and 2 vols 200 μl or 2 vols 600 μl 0.5% 1 mol/l ammonium acetate in methanol. If necessary, the eluate was filtered through Acrodisc or LC13 PVDF (0.45 μm, 13 mm polyvinylidene difluoride membrane; Gelman Science, USA) before or after evaporation under a gentle stream of nitrogen and redissolution in 200–400 μl mobile phase (33% methanol, 67% 0.01 mol/l ammonium/triethylammonium acetate, pH 5.6). The recoveries of radioactivity following solid-phase extraction and filtration were essentially quantitative.

Mass spectrometric identifications of metabolites

The metabolites in urine and plasma were identified by gas chromatography–mass spectrometry (GC-MS) after hydrolysis by conjugate cleaving enzymes and solid-phase extraction. Samples with the highest radioactivity were used; urine collected 0–8 h after dosing and plasma samples at t_{max} (1.5 h after mouth rinse, 0.5 h after oral administration). Selected samples were also fractionated by LC prior to GC-MS analysis. Solid phase eluates and pooled LC-fractions were evaporated and dissolved in acetone, transferred to autosampler vials and again evaporated. The residue was either dissolved in 25 μl acetone and subjected to GC-MS directly, or derivatized by heating with 25 μl BSTFA for 30 min at $\sim$ 50 °C.

GC-MS was run on a HP 5890-TSQ70 system (Hewlett-Packard Co., Palo Alto, CA, and FinniganMAT, St. Jose, CA, USA). The autosampler (HP7673A) performed split/splitless injections (ratio $\sim$ 1/50, split valve closed for 1 min) of 2 μl sample on a 25 m $\times$ 0.2 mm fused silica column with a 0.33 μm film of HP-5 (95% methyl, 5% phenyl silicone). The column temperature was programmed as follows for all silylated samples: 150 °C for 2 min; 25 °/min for 2 min; 10 °/min for 8.5 min; 285 °C for 6 min. Underivatized delmopinol was run at 55 °C for 2 min; 25 °/min for 6 min; 10 °/min for 8 min; 285 °C for 3 min.

The heated interface to the mass spectrometer was held at 280 °C and the ion source at 150 °C. Electron-impact (70 eV, 200 μA) mass spectra were produced by scanning quadrupole 1 of the triple quadrupole set-up from m/z 40 to 600 with a scan cycle of 1 s. From the repeated scanning, spectra of relevant GC peaks were selected and background-subtracted, using FinniganMAT ICIS-I software. Reconstructed ion chromatograms (mass chromatograms) were scrutinized to ensure chromatographic peak integrity.

Metabolites were also identified, without prior treatment with hydrolysing enzymes, by liquid chromatography–mass spectrometry (LC-MS). The samples (urine collected after oral administration) had been solid-phase extracted and fractionated by LC before analysis. The pooled fractions were evaporated and dissolved in the mobile phase below (80/20). Aliquots of 20 μl were injected.

LC-MS was run on the same FinniganMAT TSQ70 mass spectrometer interfaced with a FinniganMAT thermospray (TSP-1) unit. The samples (20 μl) were injected onto a C18 column (8 mm $\times$ 10 cm cartridge Radial Pak NovaPak, Waters). The mobile phases, delivered by a Pharmacia LKB 2248 pump (Pharmacia LKB, Uppsala, Sweden), were 50% methanol and 50% 0.05 mol/l ammonium acetate for more polar samples and 80% methanol and 20% 0.05 M ammonium acetate for the less polar samples as well as for the delmopinol glucuronide reference. The flow rate was 1 ml/min.

The operating conditions of the interface were: vaporizer temperature 90 °C, source temperature 260 °C, repeller voltage 80 V. Mass spectra were recorded from m/z 250 to 700, scan cycle 1 s.

Pharmacokinetic calculations

The methods used for calculation of the pharmacokinetic parameters were as described previously (Eriksson *et al.* 1998). The elimination half-lives were estimated in the intervals 2–6 h after buccal administration and 1.5–4 h after oral administration.

Results

Metabolite pattern in urine and plasma

Urine. The metabolite patterns in urine were very similar after the two administration routes (figure 2). Four peaks were present and dominated the chromatograms of all analysed samples of unhydrolysed urine. These metabolites, denoted M1–4, collectively represented 20% of the dose administered by mouth rinsing (71% of that not expectorated) and 69% of the oral dose (table 1). Highest concentration of

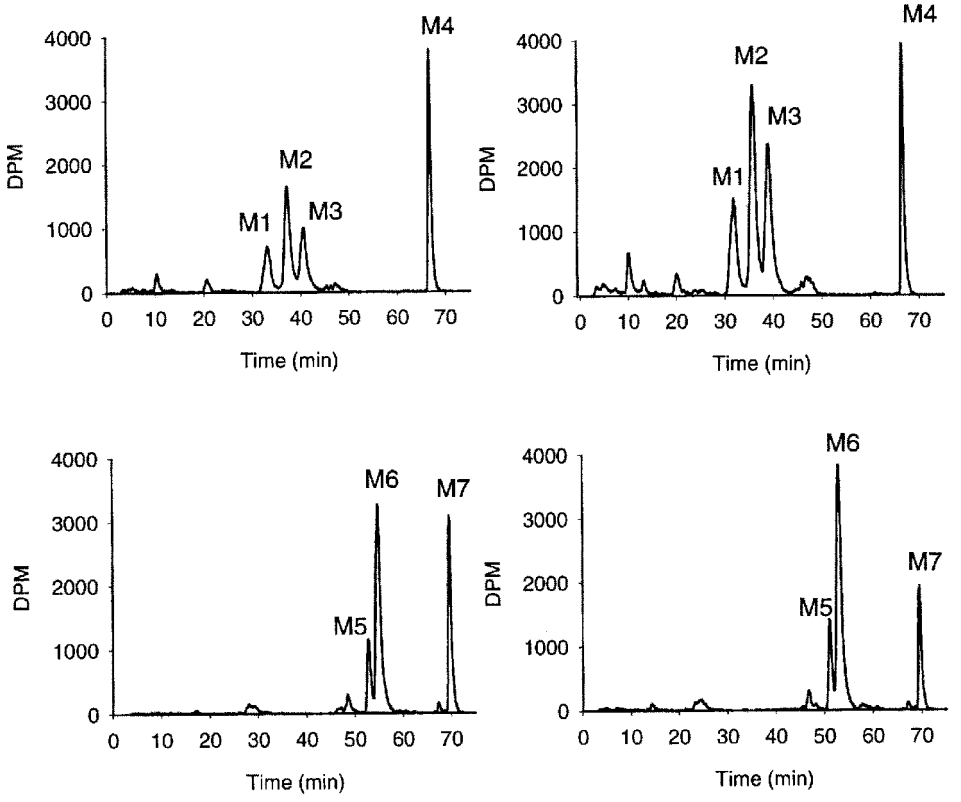


Figure 2. Liquid radio chromatograms of urine collected after administration of ^{14}C-delmopinol by mouth rinsing (left) and oral administration (right). Chromatograms of the corresponding enzymatically hydrolysed samples are shown below.

Table 1. Delmopinol and its main ^{14}C-metabolites in urine (percentage of dose) after administration of 20 mg delmopinol HCl.

	Unhydrolysed urine[a]		Hydrolysed urine[c]	
Route	Rinse	Oral	Rinse	Oral
Sampling interval (h):	0–36	0–24	0–8	0–8
Whole sample	24[a,b]	91	20	86
Metabolites[d]				
M1	3	12	nd	nd
M2	6	22	nd	< 0.1
M3	5	19	nd	nd
M4	6	16	nd	< 0.4
M5	< 0.1	< 0.3	3	11
M6	nd	< 0.1	11	43
M7	< 0.2	< 0.1	5	16

[a] Data are the sum of means from single determinations in six volunteers (intervals 0–4 and 8–12 h) and from pooled samples from six volunteers (intervals 4–8, 12–24 and 24–36 h).

[b] Corresponds to 86% of non expectorated dose.

[c] Data are the sum of determinations in pooled samples from six volunteers (intervals 0–4, 4–8 h).

[d] Retentions of M4 and M7 correspond to those of delmopinol glucuronide and delmopinol respectively.

nd, Not detected.

Table 2. Delmopinol and its main ^{14}C-metabolites in plasma after administration of 20mg, delmopinol HCl.

	Unhydrolysed plasma[a]				Hydrolysed plasma[b]			
	% in sample		Concentration[c] (nmol/l)		% in sample		Concentration[c] (nmol/l)	
Route:	Rinse	Oral	Rinse	Oral	Rinse	Oral	Rinse	Oral
Sampling time (h):	1.5	0.5	1.5	0.5	1.5	0.5	1.5	0.5
Whole sample	100	100	192	3020	100	100	192	3020
Metabolites[d]								
M1	8	10	15	290	nd	nd	nd	nd
M2	23	20	45	610	nd	< 0.1	nd	< 1
M3	16	16	30	470	nd	nd	nd	nd
M4	26	47	50	1400	nd	2	nd	46
M5	nd	< 0.1	nd	2	8	10	16	310
M6	nd	0.3	nd	9	45	38	87	1200
M7	23	< 1	45	5	42	39	81	1200

[a] Data are the means of single determinations in six volunteers.
[b] Data are the sum of determination in pooled samples from six volunteers.
[c] Concentrations were calculated from the specific activity of ^{14}C-delmopinol HCl.
[d] Retentions of M4 and M7 correspond to those of delmopinol glucuronide and delmopinol respectively.
nd, Not detected.

all the metabolites were in the urine collected 0–4 h after administration. All four metabolites eluted earlier than the delmopinol reference in the LC system used. The retention of the last main peak (M4) corresponded to that of authentic delmopinol glucuronide. The remaining metabolites each represented < 5% of the administered dose. Only traces of parent delmopinol were found. The total amount of each metabolite excreted in the urine was three-to-four times higher after oral administration than after mouth rinsing.

After hydrolysis with β-glucuronidase/arylsulphatase, the urinary metabolite pattern was almost completely changed. Hydrolysed samples yielded mainly three compounds (M5–7), all with longer retentions than that of the corresponding unhydrolysed metabolite. The three compounds collectively represented 19% of the dose administered by mouth rinsing (67% of the non-expectorated dose) and 70% of the oral dose. The chromatographic behaviour of the compound with the longest retention (M7) corresponded to that of intact delmopinol. Two of the main metabolites from the unhydrolysed sample, M2 and M3, both eluted as M6 after hydrolysis (figure 2). Several of the minor peaks were also shifted after enzyme hydrolysis. Hydrolysis with β-glucuronidase alone resulted in the same metabolite pattern as did hydrolysis with β-glucuronidase/arylsulphatase. When urine was incubated with β-glucuronidase/arylsulphatase in combination with D-saccharic acid 1,4-lactone the hydrolysis was inhibited and the initial metabolite pattern was maintained.

Plasma. Chromatograms of plasma showed a pattern similar to that obtained for urine, with the same four main metabolites appearing in samples from both treatment groups (table 2 and figure 3). After oral administration, these four compounds constituted 93% of the total metabolite concentration in plasma at 0.5 h (t_{max}, time of peak concentration) and only a trace (< 1%) of parent delmopinol was

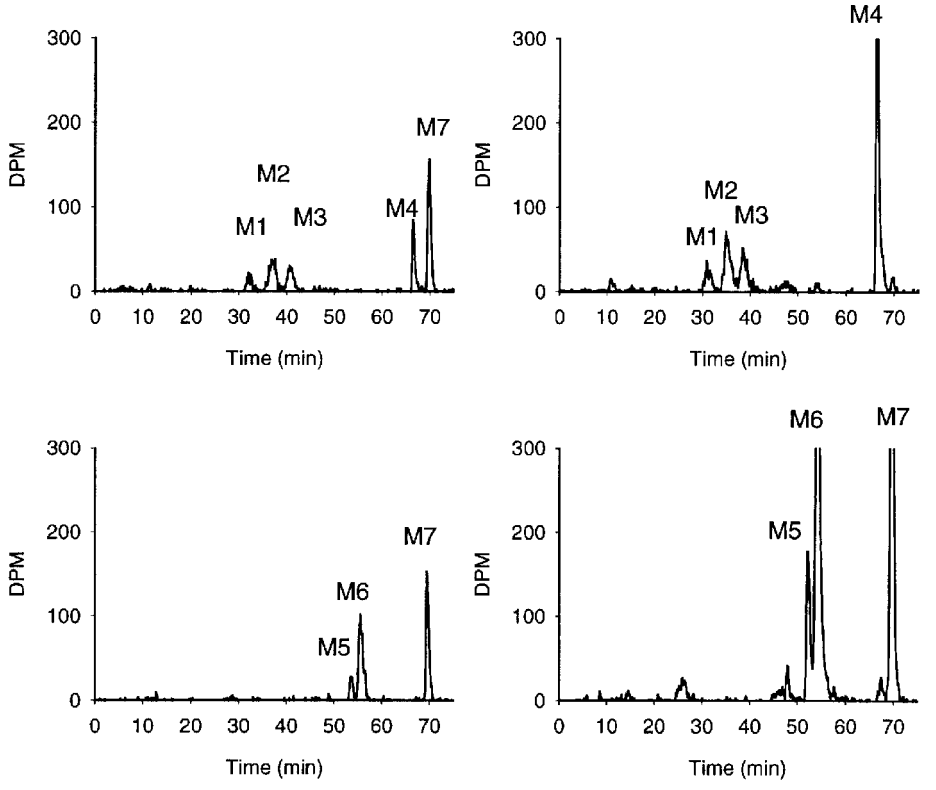


Figure 3. Liquid radio chromatograms of plasma sampled after administration of ^{14}C-delmolpinol by mouth rinsing (left) and oral administration (right). Chromatograms of the corresponding enzymatically hydrolysed samples are shown below.

detected. In contrast, in the plasma samples collected at 1.5 h (t_{max}) after mouth rinsing intact delmopinol represented 23% of the total concentration and the four main metabolites represented 73% of the total concentration. Plasma concentration–time curves for the major metabolites after mouth rinsing or oral administration of delmopinol are shown in figure 4. After oral administration, the peak plasma concentration was found at 0.5 h for all major metabolites. After mouth rinsing, however, peak concentrations were reached later, namely between 1 and 2 h after administration. No other metabolite had, at t_{max}, a concentration $>1\%$ of the total concentration after mouth rinsing or 3% after oral administration. Approximate AUC and half-lives were estimated for the metabolites (table 3). AUC of M1–3 after an oral dose were about three-to-four times higher than those after rinsing. AUC of M4 was ~ 6 times larger after swallowing than after rinsing. After mouth rinsing the metabolite profiles seemed approximately parallel to that of delmopinol, and the elimination half-life was estimated as ~ 2 h. For the oral route the estimated elimination half-lives of the metabolites seemed to be shorter than that after rinsing, namely ~ 1 h.

Hydrolysed plasma (figure 3) yielded delmopinol and the two main metabolites also found in hydrolysed urine; together representing 96% (mouth rinsing) and 87% (oral) of the sample.

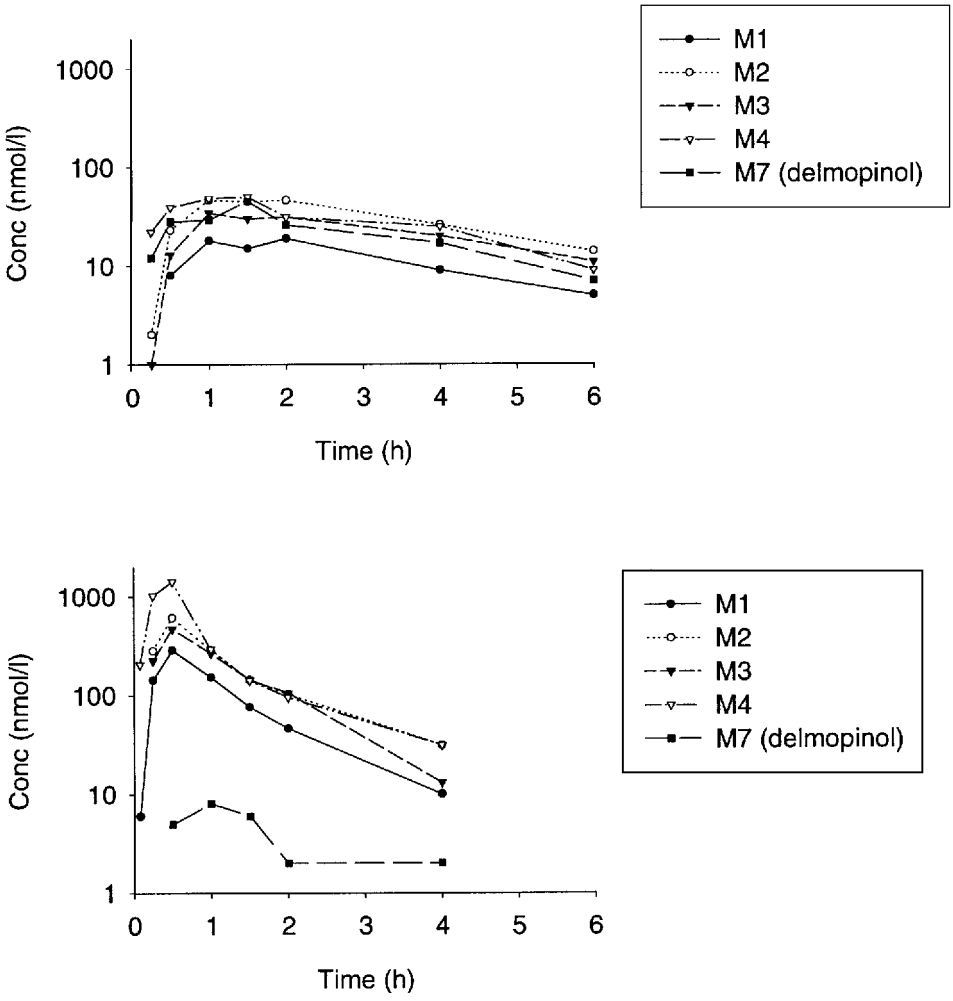


Figure 4. Plasma levels of the main delmopinol metabolites after mouth rinsing (upper) or an oral dose (lower) of ^{14}C-delmopinol.

Table 3. Estimated pharmacokinetic parameters of delmopinol and its main metabolites in man after administration of 20 mg, delmopinol HCl.

Route:	Rinse					Oral				
Metabolites[a]	C_{max} (nmol/l)	t_{max} (h)	$t_{1/2}$ (h)	AUC_{0-4} (nmol·h/l)	$AUC_{0-\infty}$ (nmol·h/l)	C_{max} (nmol/l)	t_{max} (h)	$t_{1/2}$ (h)	AUC_{0-4} (nmol·h/l)	$AUC_{0-\infty}$ (nmol·h/l)
M1	19	2.0	2.1	65	80	290	0.5	0.9	320	330
M2	46	1.0	2.3	180	230	610	0.5	1.1	640	690
M3	34	1.0	2.7	130	170	470	0.5	0.7	550	570
M4	50	1.5	2.2	160	200	1400	0.5	1.2	1100	1200
M7	45	1.5	2.1	120	150	8	1.0	2.2	13	18

[a] Retentions of M4 and M7 correspond to those of delmopinol glucuronide and delmopinol respectively.

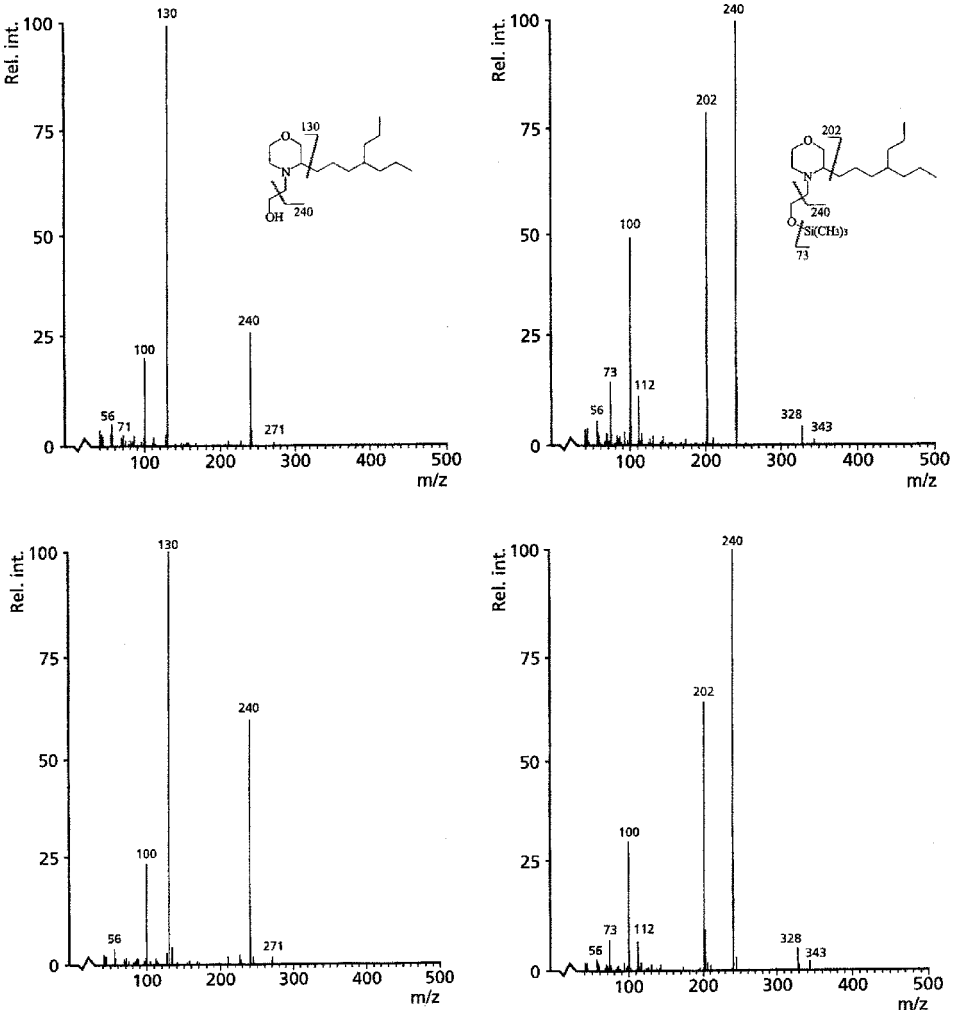


Figure 5. Electron-impact mass spectrum by GC-MS of authentic delmopinol (upper left), the corresponding trimethylsilyl derivative (upper right), compound in M7 identified as delmopinol (lower left), and the corresponding trimethylsilyl derivative (lower right).

Mass spectrometric identifications by GC-MS

The identity of metabolites in LC fractions corresponding to M5–7 was determined from an extract of hydrolysed urine collected after oral administration. Metabolites were subjected to trimethylsilylation with BSTFA before GC-MS analysis. M7 was also identified without prior silylation. The structures of M5–7 were verified in urine collected after mouth rinsing, but the amounts of ^{14}C-labelled compounds were generally ~ 10% of those found in urine after oral administration.

LC-fractions of hydrolysed plasma pools, corresponding to M5–7, were analysed by GC-MS after silylation. The identity of the main component of each fraction corresponded to that identified in the urine samples.

The electron-impact mass spectrum of authentic delmopinol (figure 5) is characterized by a small molecular ion peak (m/z 271) and the spectrum is dominated by α-cleavage relative to the nitrogen, forming m/z 240 or 130 (base

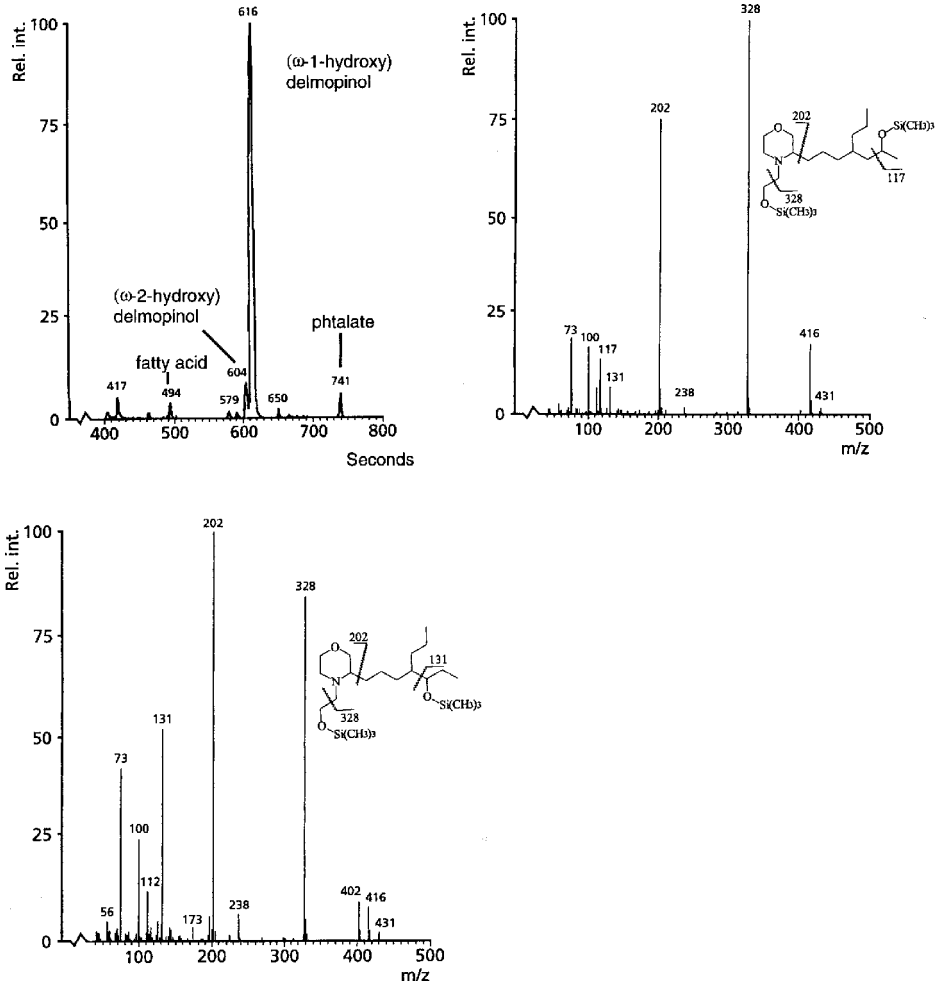


Figure 6. Reconstructed ion current profile (total ions) from GC-MS of trimethylsilyl derivatized M6 (upper left), electron-impact mass spectrum of the major compound in trimethylsilyl derivatized M6, identified as (ω-1-hydroxy) delmopinol (upper right) and electron-impact mass spectrum of the minor compound in trimethylsilyl derivatized M6, identified as (ω-2-hydroxy) delmopinol (lower).

peak). The m/z 100 ion retains the backbone of the morpholine ring and the adjacent carbon of the hydroxyethyl substituent. After trimethylsilylation, the spectrum (figure 5) of the authentic compound showed the expected mass shifts. The low intensity molecular ion (m/z 343) readily loses $\cdot CH_3$from the TMS moiety, but also in this case the spectrum is dominated by m/z 240, 202 (in analogy with m/z 130) and 100. The TMS component is also apparent in a distinct m/z 73 peak.

M7, with the expected LC retention of delmopinol, gave a mass spectrum of the main component (figure 5) identical to that of authentic delmopinol. Silylation of this sample afforded a compound with the same mass spectrum as that of the derivatized delmopinol reference. The GC retentions of underivatized and derivatized sample agreed with those of authentic delmopinol before and after silylation.

M6, the fraction corresponding to the major LC peak was found to contain at least two metabolites, when subjected to silylation and GC-MS analysis (figure 6).

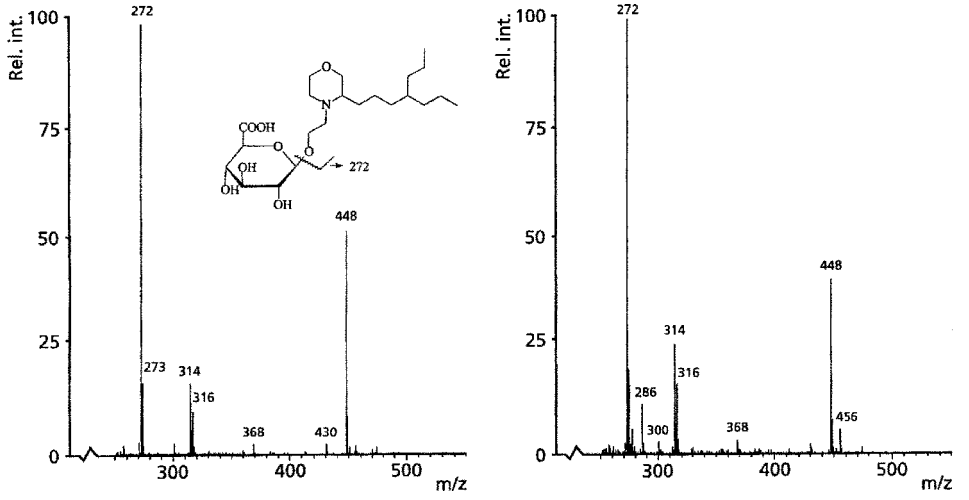


Figure 7. Thermospray mass spectrum of authentic delmopinol glucuronide (left) and of M4, identified as delmopinol glucuronide (right).

The major component was identified as (ω-1-hydroxy) delmopinol (figure 6). The mass increase of 88 in the molecular ion (m/z 343 → 431) and the base peak (m/z 240 → 328), with m/z 100 and 202 intact indicate a hydroxylation in the hydrocarbon substituent. The increased tendency of losing $\cdot CH_3$, and the presence of m/z 117 rather than higher homologues defines the position as ω-1.

A minor component was (ω-2-hydroxy) delmopinol. Its spectrum (figure 6) is similar to that of the ω-1 isomer ($[M\cdot^+]$, base peak, etc.). However, the peaks at m/z 402 (loss of ethyl) and m/z 131 both indicate the ω-2 position of the TMSO group. Assuming identical response it amounted to $< 10\%$ of the dominating compound, (ω-1-hydroxy) delmopinol, in this sample.

M5, the smaller LC peak fused to the largest peak consisted of the same main metabolite, (ω-1-hydroxy) delmopinol (spectrum not shown). Apparently, isomers have been separated into different LC peaks, but appear with identical GC retentions and mass spectra.

Some of the quantitatively less important LC peaks were also investigated and tentatively identified (data not shown). Among the metabolites found in small amounts were (ω-1-oxo) delmopinol, (ω-1-hydroxy, ω'-1-oxo) delmopinol and isomers of dihydroxy delmopinol and certain carboxylic acid analogues.

Mass spectrometric identifications by LC-MS

The major metabolites M1–4 were identified in LC fractions of urine collected after oral administration.

The thermospray mass spectrum of authentic delmopinol glucuronide (figure 7) shows two dominant peaks, namely m/z 448 and 272 (base peak). The former corresponds to the protonated molecule (MH^+), and the latter to the delmopinol moiety.

M4 was identified as delmopinol glucuronide. The LC retentions were the same and the mass spectrum (figure 7) showed the same dominant peaks as did authentic delmopinol glucuronide.

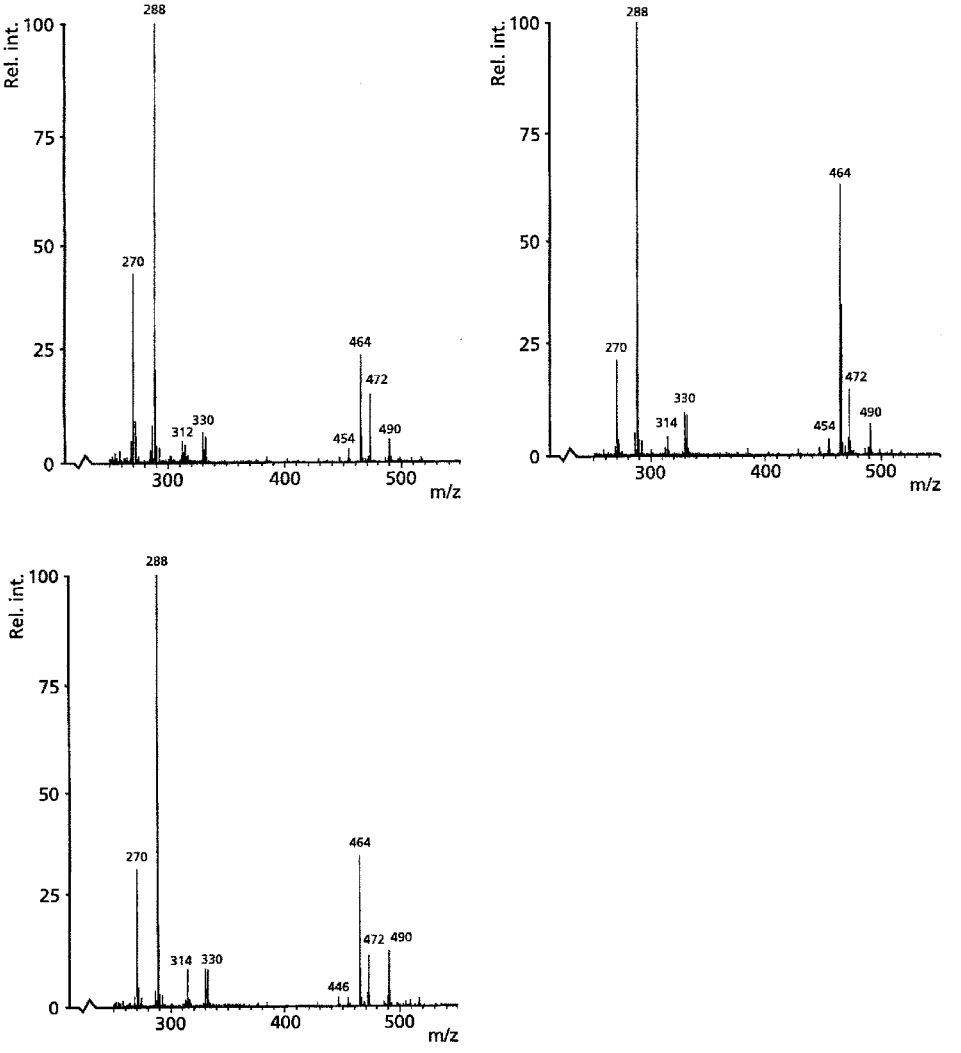


Figure 8. Thermospray mass spectrum of M1 (upper left), M2 (upper right) and M3 (lower) identified as glucuronides of (ω-1-hydroxy) delmopinol.

M1–3, although having different retentions, all gave practically identical thermospray mass spectra (figure 8). Characteristic peaks were m/z 464 (MH^+) and 288 (aglycone) showing the mass increase of 16 units expected for glucuronides of monohydroxylated delmopinol. The minor peaks at m/z 472 and 490 cannot at present be explained. They are, however, likely to originate from some non-covalent adducts formed in the LC-MS interface, as corresponding ions can be seen as minor peaks in the spectrum of authentic delmopinol glucuronide (m/z 456, 474 in figure 7). By recording spectra up to m/z 700, the possibility of di-glucuronide formation was excluded (data not shown). Based on the identifications of the ω-1-hydroxy delmopinol as the main component in hydrolysis products of these metabolites, they are proposed to be isomeric glucuronides of this compound.

Discussion

A rapid elimination of delmopinol in humans has previously been reported (Eriksson *et al.* 1998). Furthermore, a high clearance and an extensive first-pass metabolism were indicated. In the present investigation the metabolism of delmopinol has been examined and the results confirm that delmopinol is extensively metabolized after oral administration as well as after mouth rinsing, the latter being the intended route of therapy.

For both routes of administration, the LC radioactivity pattern indicated the formation of four main metabolites that accounted for nearly all of the radioactivity excreted, and only trace amounts of parent delmopinol were found in the urine. Thus, the high clearance of delmopinol is due to a high metabolic clearance, and the renal clearance is low.

The same four metabolites also accounted for nearly all of the radioactivity in plasma after oral administration and most of the radioactivity after mouth rinsing. However, after mouth rinsing parent delmopinol was also a main compound. This is in agreement with the higher bioavailability of delmopinol after mouth rinsing than after oral treatment as previously reported (Eriksson *et al.* 1998).

Hydrolysis and inhibition experiments suggested all four metabolites being glucuronides, and the one with the longest retention being glucuronidated delmopinol. GC-MS analysis of hydrolysed samples showed that the phase I metabolites were products of oxidation in the aliphatic side chain of the parent compound. Mainly ω-1-hydroxylation, a common metabolic pathway, was encountered. No products of N-dealkylation or N-oxidation, which are also common routes of metabolism for amine compounds, were found in this study. LC-MS analysis of unhydrolysed urine showed that the main metabolites were indeed mono glucuronides of delmopinol and of (ω-1-hydroxy) delmopinol. The major pathways found in this study are depicted in figure 9.

Glucuronidated monohydroxylated delmopinol separated into three LC peaks, with reproducible retentions. Analysis of aglycones after hydrolysis showed only the ω-1-hydroxy isomer in amounts that could explain LC peaks of this intensity (some minor contribution from other isomers is possible) and the present conclusion is that all three peaks represent glucuronides of ω-1-hydroxy delmopinol. The separation may be explained by the presence of conjugate isomers, positional or optical, as glucuronides of chiral compounds appear as diastereomers which can often be separated (e.g. Ruelius *et al.* 1979, Thompson *et al.* 1981, El Moeuelhi *et al.* 1987). The position of the glucuronic acid moiety at the hydroxyethyl substituent, as for delmopinol glucuronide, or at the ω-1-hydroxy group remains unknown, although it is likely that both positions are involved. Delmopinol glucuronide, however, did not separate into its diastereomers with the present LC system. After hydrolysis, the (ω-1-hydroxy) delmopinol isomers separated into two peaks. The prochiral character of the aliphatic side chain branching results in eight possible stereoisomers of the hydroxylated compound. Some diastereomers could be expected to have different chromatographic properties, whereas other isomers might be difficult to separate.

The relative amounts of the different metabolites excreted were similar for the two routes. Similar ratios between the metabolites for the different routes of absorption indicate that the metabolites were mainly formed in the liver rather than in the gastrointestinal tract after oral administration. After rinsing, the plasma elimination profiles of the main metabolites seemed to parallel that of delmopinol

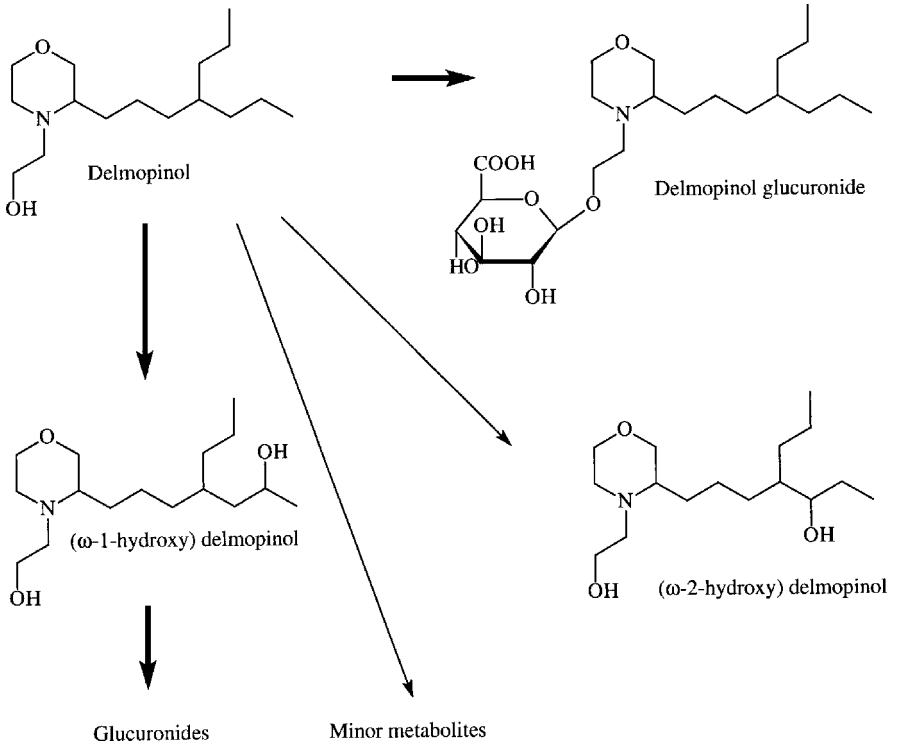


Figure 9. Metabolic pathways of delmopinol in man.

indicating formation rate limitation of the metabolites. After oral administration, the metabolites were mainly formed during first-pass, and the elimination was independent of that of delmopinol. Shorter half-lives (~ 1 h) were indicated for the metabolites.

In conclusion, the metabolic clearance of delmopinol is high and only trace amounts are excreted unchanged. The metabolism is well characterized both qualitatively and quantitatively. The main route of elimination for delmopinol as well as for its oxidized metabolites is glucuronidation.

References

CLAYDON, N., HUNTER, L., MORAN, J., WADE, W., KELTY, E., MOVERT, R. and ADDY, M., 1996, A 6-month home-usage trial of 0.1% and 0.2% delmopinol mouthwashes (I). Effects on plaque, gingivitis, supragingival calculus and tooth staining. *Journal of Clinical Periodontology*, **23**, 200–228.

COLLAERT, B., ATTSTRÖM, R., DE BRUYN, H. and MOVERT, R., 1992a, The effect of delmopinol rinsing on dental plaque formation and gingivitis healing. *Journal of Clinical Periodontology*, **19**, 274–280.

COLLAERT, B., EDWARDSSON, S., ATTSTRÖM, R., HASE, J. C., ASTRÖM, M. and MOVERT, R., 1992b, Rinsing with delmopinol 0.2% and chlorhexidine 0.2% : short-term effect on salivary microbiology, plaque, and gingivitis. *Journal of Periodontology*, **63**, 618–625.

EL MOUELHI, M., RUELIUS, H. W., FENSELAU, C. and DULIK, D. M., 1987, Species-dependent enantioselective glucuronidation of three 2-arylpropionic acids. Naproxen, ibubrofen, and benoxaprofen. *Drug Metabolism and Disposition*, **15**, 767–772.

ERIKSSON, B., OTTERSGÅRD BRORSSON, A.-K., HALLSTRÖM, G., SJÖDIN, T. and GUNNARSSON, P. O., 1998. Pharmacokinetics of ^{14}C-delmopinol in the healthy male volunteer. *Xenobiotica*, **28**, 1075–1081.

MORAN, J., ADDY, M., WADE, W. G.., MAYNARD, J. H., ROBERTS, S. E. ASTRÖM, M. and MOVERT, R., 1992, A comparison of delmopinol and chlorhexidine on plaque regrowth over a 4-day period and salivary bacterial counts. *Journal of Clinical Periodontology*, **19**, 749–753.

RUELIUS, H. W., TIO, C. D., KNOWLES, J. A., MCHUGH, S. L., SCHILLINGS, R. T. and SISENWINE, S. F., 1979, Diastereoisomeric glucuronides of oxazepam. Isolation and stereoselective enzymic hydrolysis. *Drug Metabolism and Disposition*, **7**, 40–43.

THOMPSON, J. A., HULL, J. E. and NORRIS, K. J., 1981, Glucuronidation of propranolol and 4′-hydroxypropranolol. Substrate specificity and stereoselectivity of rat liver microsomal glucuronyltransferases. *Drug Metabolism and Disposition*, **9**, 466–471.

XENOBIOTICA , 2000, VOL. 30, NO. 2, 193–199

Pharmacodynamic analysis between plasma level and inhibition of acid output after administration of a new histamine H_2-receptor antagonist (Z-300) in dog

S. FURUTA*, T. SUGIMOTO, M. SUZUKI, T. YONETA, Y. HORI, H. MORITA, H. AITA and H. SANO

Central Research Laboratories, Zeria Pharmaceutical Co., Ltd, Kohnan-machi, Ohsato-gun, Saitama 360-0111, Japan

Received 8 June 1999

1. The relationship between plasma levels of a new H_2-receptor antagonist, Z-300, and an active sulphoxide metabolite, and inhibitory effects on gastric acid secretion after intravenous or oral administration to dog have been examined. After both routes of administration, Z-300 in plasma eliminated with two phases, and the terminal half-lives were ~2 h. The level of sulphoxide in plasma reached a maximum at 0.6–0.7 h after administration, then subsequently eliminated with a half-life of ~6 h.

2. The maximal pharmacological effect of inhibition of gastric acid secretion (90–91%) was observed at 2 h (i.v.) and 6 h (p.o.), and the action persisted until 7 h after administration.

3. Since there was no correlation between plasma levels of Z-300 and pharmacological effects, the pharmacological effects were calculated by pharmacodynamic model including the effect compartment. The inhibition of acid output could be calculated by the amounts of Z-300 and sulphoxide corrected by pharmacological efficacy in the effect compartment.

4. These findings suggest that Z-300 contributes to the rapid appearance of the pharmacological effects in dog, whereas the sulphoxide, which eliminates slowly in plasma, contributes to duration.

Introduction

N-[3-[3-(piperidinomethyl)phenoxy]-propyl]-2-(2-hydroxyethyl-1-thio) acetamido·2-(4-hydroxy benzoyl)benzoate (Z-300) is a selective and competitive histamine H_2-receptor antagonist (Okabe *et al.* 1992) presently developed by Zeria Pharmaceutical Co. (Tokyo, Japan). This agent inhibited gastric acid secretion in rat in response to histamine stimuli after oral, intraduodenal or intravenous administration, protected the gastric mucosa in water immersion stress-related ulcers, indomethacin-, aspirin- or ethanol hydrochloride-induced ulcers, and protected the duodenal mucosa in mepirizole- or cystamine-induced ulcers. Furthermore, Z-300 promoted the spontaneous healing of acetic acid-induced ulcers and inhibited delayed healing of indomethacin-induced ulcers. Therefore, Z-300 may be useful for the treatment of peptic ulcer, not only by inhibiting gastric acid secretion, but also by protecting the gastric mucosa (Okabe *et al.* 1992, Ichikawa *et al.* 1994, Umemura *et al.* 1994).

In the current study, the plasma concentrations of Z-300 and its metabolites, and the acid output after administration of Z-300 to dog were measured. Z-300 is eliminated mainly by metabolism to a sulphoxide metabolite, which has similar

* Author for correspondence.

Xenobiotica ISSN 0049–8254 print/ISSN 1366–5928 online © 2000 Taylor & Francis Ltd
http://www.tandf.co.uk/journals/tf/00498254.html

potency to Z-300, as H_2-receptor antagonists. Therefore, investigated was the relationship between the plasma levels of Z-300 and sulphoxide, and the pharmacological effect.

Materials and methods

Compounds

Z-300 and its metabolites, N-[3-[3-(piperidinomethyl) phenoxy]-propyl]-2-(2-hydroxyethyl-1-sulphinyl) acetamido (sulphoxide), N-[3-[3-(piperidinomethyl) phenoxy]-propyl]-2-(2-hydroxyethyl-sulphonyl) acetamide (sulphone) (figure 1) and an internal standard, N-[3-[3-(piperidinomethyl) phenoxy]-propyl]-2-(2-hydroxypropyl-1-thio) acetamido were synthesized by our laboratory, and their chemical purities were >99%. Other materials and solvents were of analytical grade.

Animals

To measure the plasma concentration, five 6-month-old male Beagles (Japan Clea, Tokyo, Japan) weighing ~10 kg were used. To measure gastric acid secretion, four beagles, weighing 12–15 kg, with Heidenhain pouches (Okabe *et al*. 1992), were used.

Drug administration

Z-300 was dissolved in physiological saline for intravenous administration and 0.5% sodium carboxymethylcellulose for oral administration at a dose of 3 mg/2 ml/kg to dog. Dogs had been fasted for 16 h before administration (water was given *ad libitum*), and solid Canine Diet #4360 (Purina Taiyo Pet Food Co., Ltd, Tokyo, Japan) was given 8 h after administration.

In a study examining gastric acid secretion in dogs, 160 μg/h/kg histamine was continuously injected intravenously to the Heidenhain pouched dog for stimulation of gastric acid secretion. Z-300 was administered to dog after 1 h following the initiation of the constant rate of infusion of histamine.

Measurement of plasma levels

Blood was serially collected through a forelimb cephalic vein and samples were centrifuged to separate plasma, which were stored at −80 °C until measurement. Plasma levels of Z-300, sulphoxide and sulphone were measured by a high-performance liquid chromatography (HPLC) method (Hoshino *et al*. 1993).

Measurement of inhibition of gastric acid secretion

Gastric acid was collected at 30-min intervals. The gastric acid secretion was calculated from hydrogen ion levels (mEq). Simultaneously, gastric acid secretion was measured in the untreated control group. The rate of inhibition of gastric acid secretion (I) was calculated from acid output in the treated ($I_{Z\text{-}300}$) and control ($I_{control}$) group using equation (1):

$$I\ (\%) = (I_{control}\ (\mathrm{mEq/h}) - I_{Z\text{-}300}\ (\mathrm{mEq/h}))/I_{control}\ (\mathrm{mEq/h}) \times 100. \quad (1)$$

Pharmacokinetic and pharmacodynamic analysis

Model-independent pharmacokinetic parameters were calculated based on plasma levels of Z-300 and sulphoxide. These parameters were the time required until the maximal concentration (T_{max}), the maximal concentration (C_{max}), the area under the plasma concentration–time curve (AUC) and the plasma clearance (Cl). AUC was calculated by extrapolation from the slope during the terminal phase to the infinite value using the trapezoidal method. Cl was calculated from dividing the dose by the AUC.

Pharmacokinetic and pharmacodynamic parameters were calculated from plasma Z-300 (C_1) and sulphoxide (C_3) levels using nonlinear least square method software, MULTI(RUNGE) (Yamaoka and Nakagawa 1983) according to simultaneous differential equations based on a two-compartment open model considering the metabolic process from Z-300 to sulphoxide (figure 2).

$$dC_1/dt = k_{12} \times C_2 - (k_{12} + k_{13}) \times C_1 \quad (2)$$

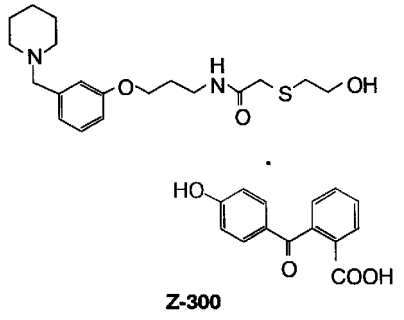
$$dC_1/dt = k_a \times F \times X_D/V_1 + k_{12} \times C_2 - (k_{12} + k_{13}) \times C_1 \quad (3)$$

$$dC_2/dt = k_{21} \times C_1 - k_{21} \times C_2 \quad (4)$$

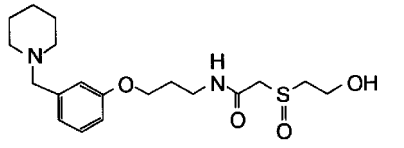
$$dC_3/dt = k_{13} \times C_1 \times V_1/V_3 - k_{30} \times C_3 \quad (5)$$

$$dX_D/dt = -k_a \times F \times X_D, \quad (6)$$

where C is the drug concentration in each compartment, k is the rate constant between the indicated



Z-300



sulphoxide

Figure 1. Chemical structures of Z-300 and its metabolites.

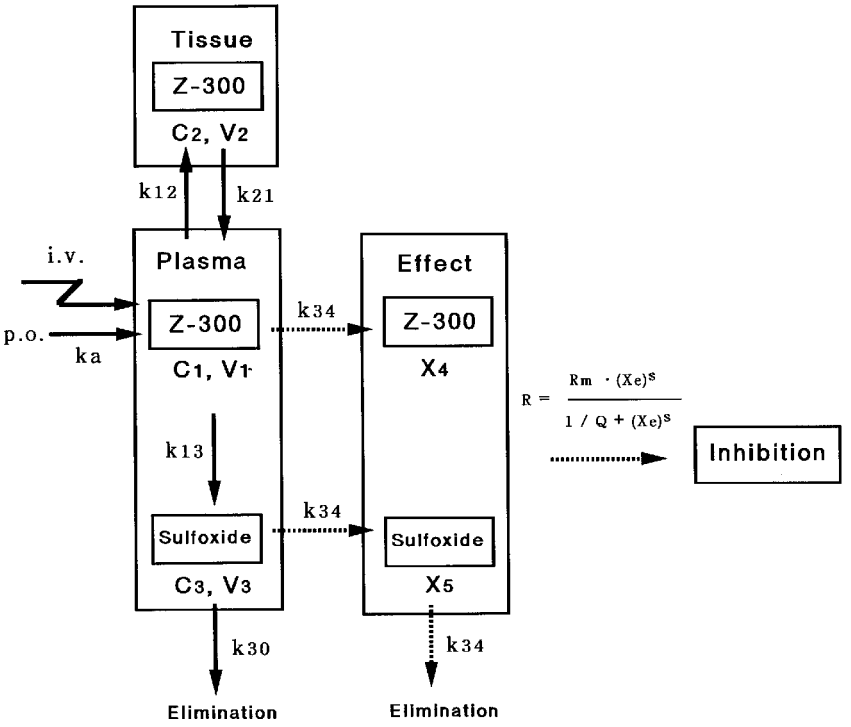


Figure 2. Pharmacokinetic and pharmacodynamic model after administration of Z-300 to the male dog.

compartments, V is the distribution volume of each compartment, X_D is the amount of a given drug in the absorption site and F is the bioavailability of Z-300. The plasma concentration of Z-300 was fitted to equation (2) for intravenous administration and equation (3) for oral administration. Where the initial values are: $C_1 = X_D/V_1$ for intravenous administration, and $C_1 = 0$ for oral administration, $C_2 = 0$, $C_3 = 0$, X_D = dose.

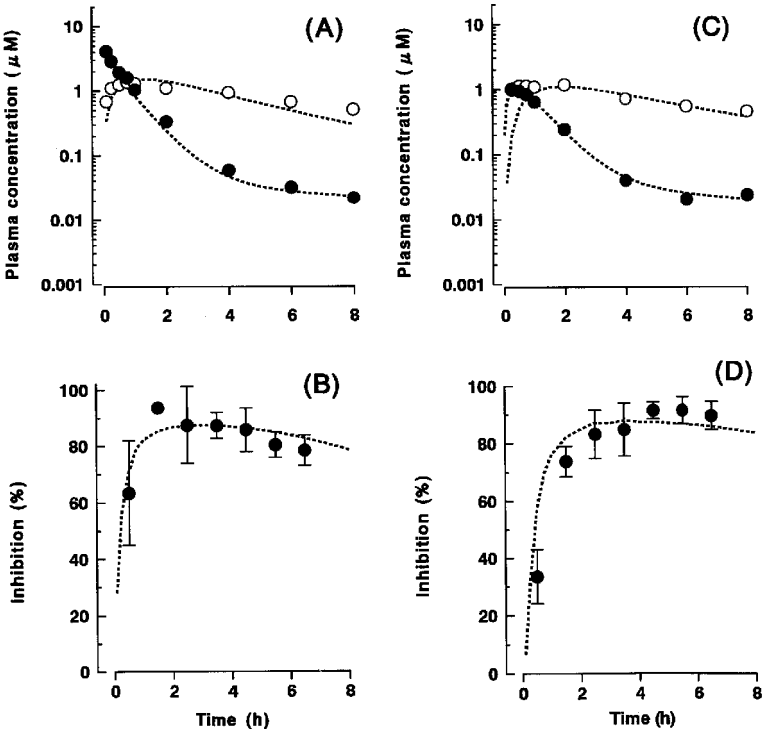


Figure 3. Plasma levels of Z-300 and sulphoxide, and inhibition rates of acid output after intravenous (A, B) or oral (C, D) administration of Z-300 to the male dog (dose 3 mg/kg). ●, Z-300; ○, sulphoxide. Data are the mean± SE ($n = 4$ or 5). Dotted lines were calculated by the pharmacodynamic model shown in figure 2.

The amount of Z-300 (X_4) and sulphoxide (X_5) in the effect compartment were calculated based on equations (7) and (8).

$$dX_4/dt = k_{34} \times (C_1 \times V_1 - X_4) \quad (7)$$

$$dX_5/dt = k_{34} \times (C_3 \times V_3 - X_5), \quad (8)$$

where k_{34} is the rate constant from plasma to the effect compartment of both Z-300 and the sulphoxide.

From a binding study to the H_2-receptor by using the isolated right atrium of guinea pig, pA_2 of Z-300 and its active metabolite, sulphoxide, was 6.80 and 6.59 respectively (unpublished data). It suggested that sulphoxide shows 62% efficacy compared with Z-300, total amount of effect compartment (X_e) was calculated from Z-300 (X_4) and sulphoxide (X_5) corrected by the efficacy ratio according to equation (9):

$$X_e = X_4 + 0.62 \times X_5. \quad (9)$$

The pharmacological effect was defined as Hill equation (10) (Holford and Sheiner 1981) based on the mean inhibition rate (R) of gastric acid secretion per h after Z-300 administration and the amount of Z-300 and sulphoxide in the effect compartment:

$$R = R_m \cdot (X_e)^S / (1/Q + (X_e)^S), \quad (10)$$

where R_m is the maximum efficacy, Q is a parameter describing drug affinity for receptors and S is the Hill coefficient.

Results

Plasma concentrations

Changes in plasma Z-300 and sulphoxide levels after intravenous or oral administration of 3 mg/kg of Z-300 to dog are shown in figure 3A and C. Pharmacokinetic parameters are shown in table 1.

Table 1. Pharmacokinetic and pharmacodynamic parameters for Z-300 and its sulphoxide metabolite after administration of Z-300 to dog.[a]

Parameter	3 mg/kg i.v.	3 mg/kg p.o.
Model-independent pharmacokinetic parameters		
Z-300		
C_{max} (μM)	—	1.16± 0.24
T_{max} (h)	—	0.4± 0.1
AUC (μM·h)	3.81± 0.90	1.93± 0.40
Cl/F (l/h/kg)	1.35± 0.30	2.65± 0.60
$t_{1/2}.\beta$ (h)	2.4± 0.2	1.8± 0.2
F	—	0.52± 0.12
Sulphoxide		
C_{max} (μM)	1.51± 0.35	1.26± 0.34
T_{max} (h)	0.7± 0.2	0.6± 0.4
AUC (μM·h)	12.07± 4.02	10.21± 3.28
$t_{1/2}.\beta$ (h)	6.0± 1.4	6.2± 2.5
Model-dependent pharmacokinetic parameters[b]		
Z-300		
ka (1/h)	—	5.52± 0.92
k_{12} (1/h)	0.26± 0.03	0.28± 0.04
k_{21} (1/h)	0.21± 0.13	0.12± 0.03
k_{13} (1/h)	1.16± 0.10	0.94± 0.06
k_{30} (1/h)	0.34± 0.05	0.29± 0.04
V_1 (l/kg)	1.23± 0.14	1.51± 0.16
V_2 (l/kg)	3.79± 1.24	4.45± 1.12
V_3 (l/kg)	1.68± 0.24	1.20± 0.14
Pharmacodynamic parameters[b]		
k_{34} (1/h)	0.25± 0.00	0.25± 0.01
S	1.34± 0.02	1.13± 0.06
$1/Q$ (nmol/kg)	0.10± 0.00	0.07± 0.02

[a] Data are the mean± SE of five animals.
[b] Data are calculated by the pharmacokinetic and pharmacodynamic model shown in figure 2.

The plasma level of Z-300 showed a biphasic disposition profile with a half-life of 2.4 h between 2 and 8 h after intravenous administration. The plasma level was almost at the detection limit at 24 h after administration, and AUC was 3.81 μM/h. The plasma level of sulphoxide reached a maximum of 1.51 μM at 0.7 h after administration, and decreased with a half-life of 6.0 h. AUC was 12.07 μM/h.

The plasma level of Z-300 reached a maximum concentration of 1.16 μM at 0.4 h after oral administration, and decreased with half-life of 1.8 h. AUC was 1.93 μM/h; and bioavailability was 52%. The plasma level of the sulphoxide reached a maximum of 1.26 μM at 0.6 h after administration, and decreased with a half-life of 6.2 h. AUC was 10.21 μM/h. The level of sulphone was much lower than the level of Z-300 or sulphoxide after intravenous and oral administration (Sugimoto *et al.* 1999a).

Plasma levels of Z-300 and the sulphoxide were analyzed by a two-compartment model analysis including the metabolic process, and observed values were in good agreement with calculated values (figure 3A and C, table 1). The distribution volumes of Z-300 and sulphoxide in plasma compartment were almost equal.

Rate of inhibition of gastric acid secretion

The rate of inhibition of gastric acid secretion of each 1-h period until 7 h after Z-300 administration is shown in figure 3B and D. The rate of inhibition reached a maximum of 89.6% at 2 h after intravenous administration, and gradually decreased

thereafter. However, inhibition was still 75.0% at 7 h after administration. The rate of inhibition after oral administration gradually increased until it reached a maximum of 91.1% at 6 h, and was still 89.5% at 7 h after administration.

Based on the pharmacodynamic model, the amount of Z-300 and sulphoxide in the effect compartment and the pharmacological response were calculated. The rate of inhibition of gastric acid secretion was analyzed using the Hill equation from the total amount of Z-300 and sulphoxide in the effect compartment corrected by pA_2. The observed values were in good agreement with theoretical ones (figure 3B and D) and it was determined that S was 1.34 and 1.13, whereas $1/Q$ was 0.10 and 0.07 after intravenous or oral administration respectively (table 1).

Discussion

After intravenous or oral administration of Z-300 to dog, Z-300 in plasma disappeared rapidly. However, the rates of inhibition of gastric acid secretion as a pharmacological effect were 75 and 89% at 7 h after intravenous and oral administration respectively. The plasma level of sulphoxide (a metabolite of Z-300) reached a maximum at 0.7 and 0.6 h after intravenous and oral administration, and remained high (0.68 and 0.55 μM) at 6 h after administration. Comparing the $t_{1/2}$ between 2 and 8 h, those values for the sulphoxide were longer than those of Z-300. Sulphoxide and sulphone metabolites also show inhibition of gastric acid secretion, and pA_2 obtained using the right atrium of guinea pig were 6.80, 6.59 and 6.67 for Z-300, sulphoxide and sulphone respectively (unpublished data). The plasma levels of Z-300 were higher than sulphoxide levels up to 1 h after intravenous administration, but after this time sulphoxide levels were higher than Z-300 levels. Plasma sulphoxide levels were higher than Z-300 levels at 0.5 h after oral administration; however, Z-300 levels were higher than the levels of sulphoxide corrected by the efficacy ratio up to 1 h. Therefore, Z-300 may contribute to the rapid appearance of the pharmacological effect and the duration may be closely related to sulphoxide level. In addition, the effect of the sulphone was negligible due to its low plasma level.

It is known that blood levels of H_2-receptor antagonists such as cimetidine (Cohen *et al.* 1980), ranitidine (Peden *et al.* 1979) and nizatidine (Callaghan *et al.* 1985) correlate with their pharmacological effects. The plasma Z-300 levels, sulphoxide levels or total Z-300 and sulphoxide levels corrected by the pA_2 values were plotted on the transverse axis, and the rate of inhibition of gastric acid secretion was plotted on the longitudinal axis. There were no correlation between plasma levels and pharmacological effects, and the plots showed an anti-clockwise hysteresis (not shown). In clinical studies, gastric pH after administration of Z-300 was almost consistent with plasma Z-300 and metabolite (Umemura *et al.* 1994). However, pharmacological effects appeared slightly later than the plasma levels during the initial phase after administration. These findings suggested that there was a time lag in the appearance of the inhibitory effects on gastric acid secretion, and the effect compartment associated with sites of action was considered (Zhu and Koizumi 1987). H_2-receptor antagonists inhibit histamine stimuli and acid secretion by binding to receptors in gastric mucosal parietal cells (Burland *et al.* 1975) and a specific period may be required until this agent is distributed in gastric parietal cells via plasma and inhibits gastric acid secretion.

Therefore, a pharmacokinetic and pharmacodynamic model with an effect

compartment was established (figure 2) and plasma levels, the amounts of effect compartment and pharmacological effects were calculated using the Hill equation. The elimination of Z-300 from the plasma compartment without metabolism to sulphoxide was neglected because the excretion of Z-300 in urine was negligible and $>90\%$ of Z-300 was metabolized to sulphoxide in an *in vitro* dog liver microsome study (Sugimoto *et al.* 1999b). The bioavailability of Z-300 was 52% in dog. It is suggested that the first-pass effect of Z-300 is not negligible; therefore, the dose of oral administration was corrected by F in this model. As the calculated curves were in good agreement with the observed values, the model might be appropriate. The parameters were similar between intravenous and oral administration, $k_a = 5.52/h$ and the absorption of Z-300 from the gut was rapid in dog. Furthermore, S was almost 1, indicating that these agents bind reversively to the H_2-receptor.

In conclusion, Z-300 contributes to the rapid appearance of the pharmacological effects in dog, whereas its sulphoxide metabolite, which eliminates from the plasma slowly, may contribute to the duration of the pharmacological effect.

References

Burland, W. L., Duncan, W. A. M., Hesselbo, T., Mills, J. C., Sharpe, P. C., Haggie, S. J. and Wyllie, J. H., 1975, Pharmacological evaluation of cimetidine, a new histamine H_2-receptor antagonist, in healthy man. *British Journal of Clinical Pharmacology*, **2**, 481–486.

Callaghan, J. T., Bergstom, R. F., Obermeyer, B. D., King, E. P. and Offen, W. W., 1985, Intravenous nizatidine kinetics and acid suppression. *Clinical Pharmacology and Therapeutics*, **37**, 162–165.

Cohen, I. A., Siepler, J. K., Nation, R., Bombeck, C. T. and Nyhus, L. M., 1980, Relationship between cimetidine plasma levels and gastric acidity in acutely III patients. *American Journal of Hospital Pharmacology*, **37**, 375–379.

Holford, N. H. G. and Sheiner, L. B., 1981, Understanding the dose–effect relationship: Clinical application of pharmacokinetic–pharmacodynamic models. *Clinical Pharmacokinetics*, **6**, 429–453.

Hoshino, M., Watanabe, Y., Hamasaki, Y., Masubuchi, M. and Okahira, A., 1993, Determination of new H_2-receptor antagonist Z-300 in plasma by high-performance liquid chromatography with fluorescence detection. *Yakugaku Zasshi*, **113**, 586–590.

Ichikawa, T., Ishihara, K., Ogata, Y., Ohara, S., Saigenji, K. and Hotta, K., 1994, Effects of Z-300, a new histamine H_2-receptor antagonist, on mucin biosynthesis in rat gastric mucosa. *Japanese Journal of Pharmacology*, **65**, 63–66.

Okabe, S., Takagi, K., Igata, H., Kato, S., Shimosako, K., Yamaji, Y. and Seiki, M., 1992, Effects of a new histamine H_2-receptor antagonist, Z-300, on gastric secretion and gastro-duodenal lesions in rats: Comparison with roxatidine. *Japanese Journal of Pharmacology*, **59**, 275–289.

Peden, N. R., Richards, D. A., Saunders, J. H. B. and Wormsley, K. G., 1979, Pharmacologically effective plasma concentrations of ranitidine. *Lanset*, **July 28**, 199–200.

Sugimoto, T., Furuta, S., Kawamata, H., Suzuki, M., Sano, H., Ito, T., Hirabayashi, N., Imamura, F. and Matsuki, Y., 1999a, Pharmacokinetics of a new histamine H_2-receptor antagonist, Z-300, in rat and dog. *Xenobiotica*, **29**, 425–433.

Sugimoto, T., Furuta, S., Suzuki, M. and Sano, H., 1999b, The metabolic fate of a new histamine H_2-receptor antagonist, Z-300 in rat. *Xenobiotica*, **29**, 803–814.

Umemura, K., Uematsu, T., Kosuge, K., Nakano, M., Mizuno, A., Wada, K. and Nakajima, M., 1994, Metabolic fate and the effect of the gastric pH of new H_2-receptor antagonist Z-300. *Japanese Journal of Clinical Pharmacology Therapeutics*, **25**, 239–240.

Yamaoka, K. and Nakagawa, T., 1983, A nonlinear least squares program based on differential equations, MULTI(RUNGE) for microcomputers. *Journal of Pharmacobio-Dynamics*, **6**, 595–606.

Zhu, J. and Koizumi, T., 1987, The diuretic effect of furosemide in relation to its disposition in man. *Journal of Pharmacobio-Dynamics*, **10**, 377–383.

XENOBIOTICA , 2000, VOL. 30, NO. 2, 201–217

Metabolism of levormeloxifene, a selective oestrogen receptor modulator, in the Sprague–Dawley rat, Cynomolgus monkey and postmenopausal woman

R. J. MOUNTFIELD†*, A. M. PANDURO‡, O. WASSMANN‡, M. THOMPSON§, B. JOHN¶ and N. VAN DER MERBEL‖

† F. Hoffman-La Roche Ltd, Pharmaceutical Division, CH-4070 Basel, Switzerland
‡ Departments of Drug Metabolism and §Clinical Pharmacology, Novo Nordisk A/S, Novo Nordisk Park, 2760 Maaloev, Denmark
¶ Department of Drug Metabolism, HLS Ltd, PO Box 2, Huntingdon PE18 6ES, UK
‖ Pharma Bio-Research International BV, PO Box 200, 9470 AE Zuidlaren, The Netherlands

Received 21 June 1999

1. The metabolic fate of levormeloxifene in the Sprague–Dawley rat, Cynomolgus monkey and postmenopausal volunteer has been investigated.

2. Two doses of [^{14}C]levormeloxifene, 0.7 and 50 mg/kg, were given to the male and female rat and monkey, and a single 20-mg dose to the postmenopausal volunteer.

3. The primary route of excretion in all three species was the faeces. Metabolism was similar in all three species, with demethylation forming the major metabolite in the rat and postmenopausal volunteer. One of the major metabolites in the monkey involved an oxidative ring opening of a pyrrole ring.

4. The main site of metabolism of levormeloxifene is the liver and the majority of the drug and its metabolites is excreted via the faecal route. Metabolic pathways appear to be similar in the three species studied.

Introduction

Symptoms of the menopause can have a profound effect on the quality of life of the menopausal woman and the administration of oestrogen has been associated with beneficial effects on vasomotor symptoms, the cardiovascular system and bone (Witt and Lousberg 1997). Oestrogen is, however, generally accepted to have adverse effects on the endometrium (Antunes *et al.* 1979). Co-administration of progestins can provide endometrial protection, but there have been reports of loss of some of the cardiovascular effects of oestrogen alone (Lobo *et al.* 1994) and, in a recent study, oestrogen and progestin therapy did not reduce the overall rate of coronary heart disease events in women with established coronary disease (Hulley *et al.* 1998). Therefore, selective oestrogen receptor agonists and antagonists may prove an attractive alternative to hormone replacement therapy, potentially protecting the cardiovascular system and bone but without affecting endometrial or breast tissue. Raloxifene (Black *et al.* 1994) was the first selective oestrogen receptor agonist to be approved for the treatment of osteoporosis in the postmenopausal woman and others, such as levormeloxifene (Bain *et al.* 1997) and droloxifene (Ke *et al.* 1995) were under investigation for this indication.

Levormeloxifene (figure 1) is a partial oestrogen agonist selected as an alternative to current oestrogen replacement therapy (ERT) as a development candidate for the treatment and prevention of postmenopausal bone loss. Preclinical experiments

* Author for correspondence: e-mail; richard.mountfield@roche.com

Xenobiotica ISSN 0049–8254 print/ISSN 1366–5928 online © 2000 Taylor & Francis Ltd
http://www.tandf.co.uk/journals/tf/00498254.html

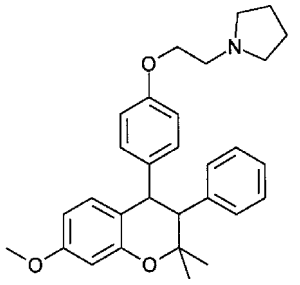


Figure 1. Structure of levormeloxifene.

have shown that levormeloxifene prevents bone loss in the ovariectomized rat and stimulates the uterus without increasing endometrial proliferation (Bain *et al.* 1996). Further, levormeloxifene lowers serum cholesterol and has a direct anti-atherogenic effect on the arterial wall of the cholesterol-fed rabbit (Holm *et al.* 1997a), an action thought to be mediated through its effect on endothelial nitric oxide (Holm *et al.* 1997b). This is achieved without any appreciable effect on the uterine tissue in the female rabbit or testicular tissue in the male.

Therefore, this paper describes the excretion pattern and metabolic fate of levormeloxifene in the rat, monkey and postmenopausal volunteer following oral administration of a single dose of [^{14}C]levormeloxifene.

Materials and methods

Chemicals

[^{14}C]levormeloxifene((−)-3,4-*trans*-7-methoxy-2,2-dimethyl-3-phenyl-4-(4-(2-pyrrolidin-1-yl)-ethoxy)phenyl)chromane) hydrogen fumarate was synthesized at Amersham, (Amersham, UK) and purified at Novo Nordisk A/S (2760 Maaloev, Denmark). Radiochemical purity was >99% based on high-performance liquid chromatography (HPLC) analysis. Non-radiolabelled levormeloxifene (99.7% chemical purity; figure 1) and chromatographic reference compounds were synthesized at Novo Nordisk A/S. All animal studies were performed in accordance with the relevant UK (1996) or Danish (1993) animal acts. Ethics committee approval and written informed consent were obtained before starting the human study, which was carried out in accordance with the Helsinki Declaration and with GCP (Good Clinical Practice).

Animal dosing and sample collection

Rat. Albino Sprague–Dawley rats, CD strain (200–230 g bodyweight), were housed in groups of six or fewer in stainless steel cages or singly in glass metabolism cages (Jencons Ltd, Leighton Buzzard, UK). [^{14}C]Levormeloxifene was dissolved in 0.1 M H_2SO_4, 10% (v/v) Tween 80 and injection grade water, and the pH of the solution was adjusted to 4 with sodium hydroxide. Three male and three female rat received single oral doses (0.7 or 50 mg/kg bodyweight, based on the free base) of levormeloxifene by gavage, and were then housed in glass metabolism cages (Jencons) to allow the collection of urine and faeces samples. Urine was collected from 0–6, 6–24, and at 24-h intervals during the study, and faeces over 24-h intervals, up to 168 h post-dose. Rats were killed at 168 h post-dose by cervical dislocation. Blood samples were obtained from rats killed at 4 and 24 h after dosing. These rats were anaesthetized using isofluorane, blood was collected by exsanguination (cardiac puncture) and stored in heparinized tubes and the rats killed by cervical dislocation.

To identify metabolites present in the bile, a further four male and five female rat were anaesthetized using Mebumal (phenobarbital; DAK, Copenhagen, Denmark), then operated on to produce permanent bile fistulas (Remie *et al.* 1991). Between 5 and 10 days after recovery from surgery, animals were administered levormeloxifene (0.7 or 50 mg/kg bodyweight) by oral gavage and bile collected every 2 h, for 24 h post-dose. Animals used for investigation of enterohepatic circulation were dosed by infusion of bile into the stomach. Animals were dosed as follows: two males and two females received 0.7 mg/kg bodyweight levormeloxifene; two males and two females received 50 mg/kg bodyweight levormeloxifene and one female received a fixed volume of bile from one female dosed with 50 mg/kg bodyweight levormeloxifene. All samples were stored at $< -15\,^{\circ}$C until analysis.

Monkey. Three male and three female Cynomolgus monkeys (*Macaca fascicularis*, bodyweights from 2.3 to 2.9 kg) were housed in purpose-built metabolism cages designed to facilitate the separate collection of urine and faeces. A single dose of levormeloxifene (0.7 or 50 mg) in ethanol, distilled water, glycerine and 10% hydroxypropylmethylcellulose was administered intragastrically by oral gavage. After each single oral dose, urine was collected from 0–6, 6–24 and during 24-h periods thereafter, up to 168 h post-dose. Faeces were collected during 24-h intervals, until 168 h post-dose. Blood samples were taken by venepuncture from a femoral vein at 6, 24, 48, 72, 96, 120, 144 and 168 h after drug dosing and processed for plasma, then stored at < -15 °C until analysis. The same animals were used at both dose levels after a suitable 'wash out' period.

Postmenopausal volunteer. Six healthy, postmenopausal volunteers (age range 49–62 years, bodyweight from 66.3 to 80.4 kg) received 20 mg levormeloxifene in a 20 ml drinking solution that contained [^{14}C]levormeloxifene (25 μCi) and levormeloxifene hydrogen fumarate. Volunteers had not received any other medication for 2 weeks before dose administration. After dosing, urine was collected into containers from 0–12 and 12–24 h and during 24 h periods thereafter, up to 36 days or until the level of radioactivity was < 50 dpm/ml. Faeces samples were collected into suitable vessels, allowing for quantitation, from 0–24 h post dosing and at 24-h intervals through to, in some instances, 71 days, although generally the last sampling day for most volunteer was day 42 following dosing. Blood samples were collected 1, 2, 3, 4, 9, 12 and 24 h after dosing and once only on days 2, 3, 4, 5, 7, 8, 10, 13, 17, 21, 25 and 36. Faeces samples from days 4, 5, 7, 9, 13–15 (combined) and 20–22 (combined) were pooled, after determination of radioactivity, for metabolite profiling purposes, as were plasma samples for 2 and 4 h (combined), 9 and 24 h. Sample pools were prepared by mixing equal weights of faeces or plasma samples from all six volunteers. For metabolite profiling of urine, samples taken during 0–12, 12–24 and 24–48 h from one volunteer only were used. Samples were stored at -20 °C until analysis.

Quantitation of radioactivity

Rat and monkey. Radioactivity in liquid samples was quantified by mixing aliquots with scintillation cocktail MI-31 (Packard Instruments Ltd, Pangbourne, UK) and conventional liquid scintillation counting (LSC). Faeces were homogenized to a paste in distilled water and burned in oxygen in a Packard automatic sample oxidizer (Model 307, Packard). The products of combustion were absorbed in Optisorb I and mixed with Optisorb S scintillator (Fisons plc, Loughborough, UK). Radioactivity was measured using a Wallac 1409 or 1410 (Pharmacia-Wallac Oy, Turku, Finland) automatic liquid scintillation analyser with appropriate quench correction.

Postmenopausal volunteer. Aliquots of faeces samples, previously homogenized to a paste in methanol:water (1:1), were mixed with Pico 30^{TM} and aqueous samples were mixed with Pico Aqua^{TM} and analysed in a Model 1900TR liquid scintillation analyser (Canberra Packard, Downers Grove, IL, USA). To ensure satisfactory recovery of radioactivity, control experiments were conducted and involved either spiking blank faeces samples with a known amount of ^{14}C-levormeloxifene and determining recovery using the above extraction procedures or alternatively certain faeces were homogenized to a paste and burned in oxygen in a Zinsser OX 500 automatic sample oxidizer. The products of combustion were absorbed in Pico Solve C-300 scintillator (Canberra Packard) and the recovery of radioactivity compared with the liquid extraction method.

Chromatography

Rat and monkey. Samples (0.3–1 ml) were injected onto the HPLC column along with the reference sample mix (25–100 μl) for initial identification based on co-chromatographic behaviour. Samples were analysed using a LiChrospher 100 C_{18} column (particle size 5 μm, 25 cm $\times$ 4 mm internal diameter (i.d.); E. Merck, Darmstadt, Germany) with a μBondaPak C_{18} Guard-Pak precolumn (Millipore®; Waters Ltd, Watford, UK). A UV 2000 variable wavelength UV detector (Thermo Separation Products, Stone, UK) and a Ramona-5 or β-RAM on-line radioactivity detector (LabLogic Systems Ltd, Sheffield, UK) fitted with a solid scintillator flow cell were used. UV emission was detected at 279 nm. Mobile phase was prepared by mixing acetonitrile and 0.1 M ammonium formate, pH 3.3. The following mobile phase gradients were used: 0–55 min a 3:7 ratio of 0.1 M ammonium formate, pH 3.3:acetonitrile; 55.1–57.0 min a 1:1 ratio; 57.1–59.0 min a 7:3 ratio. A flow rate of 1.0 ml/min was used except during 27.6–55.1 min when it was increased to 1.3 ml/min. Data were captured using LabChrom chromatography software (LabLogic Systems Ltd, Sheffield, UK). A similar chromatographic gradient was utilized for the analysis of bile samples.

Postmenopausal volunteer. Samples were analysed using a LiChrospher 100 C_{18} column (particle size 5 μm, 25 cm $\times$ 4 mm i.d.; E. Merck), with an LC 75 spectrophotometric detector (Perkin Elmer Ltd, UK). The UV emission was detected at 240 nm. The mobile phase consisted of ammonium acetate (pH 3.3):acetonitrile (60:40 v/v) (eluant A) and acetonitrile (B) and the flow rate was 1 ml/min. The gradient

was 100% A for the first 15 min, decreasing to 50% A and 50% B in a linear fashion over the next 25 min. From 40 to 45 min, 30% A was used, and was increased to 100% A at 45 min and maintained until 55 min.

Metabolic profiling

Rat and monkey. Tentative identification of metabolites in faecal extracts, urine, plasma and bile was achieved by HPLC co-chromatography with authentic standards where possible. Rat and monkey faeces extracts were made by homogenization of samples in diethylether, evaporation of solvent and suspension in the HPLC mobile phase. Plasma samples (native or enzyme-treated) were applied to Isolute-Confirm HCX mixed-mode solid-phase extraction (SPE) columns (3 ml/300 mg size; Jones Chromatography, Hengoed, UK) which were preconditioned with methanol and phosphate buffer (0.1 M; pH 2). After sample loading, the column was rinsed with acetic acid (1 M) and phosphate buffer (0.1 M; pH 2.0) and the analytes eluted with methanol:triethylamine (98:2 v/v). Certain rat and monkey bile, urine and plasma samples were mixed in equal proportions with β-glucoronidase (type H-1, EC3.2.1.31, also containing sulphatase activity; Sigma-Aldrich Chemical Co., Poole, UK) and incubated overnight at 37 °C in acetate buffer (pH 5) to effect the relevant deconjugations.

Postmenopausal volunteer. Faeces, urine and plasma samples from the postmenopausal woman were pretreated by solid-phase extraction (SPE) using Isolute-Multimode cartridges (1 g) which were preconditioned with methanol (5 ml) and sodium phosphate buffer (5 ml, pH 2). Plasma was diluted with buffer, urine was acidified to < pH 2 and faeces centrifuged, the supernatant acidified to < pH 2 and the pellet extracted with methanol (6 × 1 ml) before SPE. Eluate fractions were subsequently concentrated in propyleneglycol, then reconstituted in methanol containing 2% diethylamine before HPLC.

Each human urine sample and one representative faeces sample homogenate (day 7) was acidified to pH 5, treated with a highly concentrated solution of β-glucuronidase (type H-1, Sigma-Aldrich Chemical Co. containing 10^5 units/ml, giving a final enzyme concentration of 1000 units/ml, and incubated at 37 °C overnight. Aliquots of enzyme-treated sample were then processed as described above.

Identification of metabolites

Rat and monkey. Metabolites present in faeces, urine and plasma samples were analysed using a TSQ7000 mass spectrometer (Finnigan MAT, San Jose, CA, USA) following HPLC purification. All samples and reference standards were analysed by atmospheric pressure chemical ionization (APCI) or electrospray mass spectrometry (MS) in both positive and negative-ionization modes, where appropriate. A portion of the sample ($\sim$ 100 μl) was infused through the ESI interface at 5 μl/min, using a syringe pump. Ionization conditions were optimized by infusing the reference standard and varying the octapole offset (range -2.9 to -3.3 V in positive-ion mode, $+3.0$ V in negative-ion mode), capillary (range 20–91.8 V in positive-ion mode, -20 to -96.8 V in negative-ion mode) and tube lens voltages (range 72–181.5 V in positive-ion mode, -72 to -187.1 V in negative-ion mode) using the data system. One or more blank runs of infusion solvent (acetonitrile:water, 1:1 v/v) and/or methanol were analysed between each infusion to ensure there was no carry over. Mass spectra of the compound(s) of interest were recorded by averaging Q1 scans over an appropriate mass range for 1 min at a scan rate of 3 s/scan. To obtain further structural information, ions of interest were subjected to tandem mass spectrometry (MS/MS) analysis in product ion mode. The Q1 mass analyser was set to pass only ions of mass corresponding to the candidate molecular ion species identified from the mass spectrum. This ion was fragmented by collision with argon in the Q2 region at a collision energy, which was empirically optimized to provide maximum structural information. A mass spectrum of the fragments produced was recorded by scanning Q3 across a mass range from m/z 10 to a point several mass units above the selected Q1 mass, at a scan rate of 3 s/scan. Ion scans were averaged over a 1 min to produce the product ion mass spectra of the compound(s) of interest. Metabolites present in bile samples were analysed by LC-MS and LC-MS/MS using an API 300 triple quadruple mass spectrometer (Perkin Elmer Sciex Instruments, UK). The HPLC system consisted of a Perkin Elmer 200LC HPLC pump.

Postmenopausal volunteer. Based on initial HPLC profiling, metabolites from the ether extracts were further separated using semipreparative HPLC (gradient as described above, column: Li-Chrospher 100 C_{18}, semipreparative). Aliquots of each collected fraction were counted by LSC to determine the amount of radioactivity in each fraction, thus allowing for selected metabolites to be identified for isolation. Fractions containing appreciable amounts of radioactivity were pooled from subsequent runs. Excess solvent was removed under reduced pressure and the residue dissolved in HPLC mobile phase. Individual fractions, after assessment of total radioactivity, were analysed by LC-MS/MS.

Samples and reference compounds were analysed using an API 300 triple quadruple LC-MS/MS mass spectrometer (Perkin Elmer Sciex Instruments). The HPLC system consisted of a Perkin Elmer 200LC HPLC pump (Norwark, CT, USA), a Rheodyne 8125 injection valve (Cotati, CA, USA), a Waters Symmetry C_{18} (3.5 mm) column and a Perkin Elmer APB 785 UV detector operating at 254 nm.

After UV detection the mobile phase was split ~ 25:1 and the minor portion was sent to a Sciex API300 mass spectrometer equipped with an Ionspray® interface (Thornhill, Canada). The mobile phase consisted of acetonitrile:ammonium formate (linear gradient 95% acetonitrile:70% acetonitrile over 30 min).

In the MS mode (full scan) the mass spectrometer scanned in the range m/z 100–700 with a dwell time of 0.5 ms and a step size of 0.1 amu. The electrospray and orifice voltages were set to 5000 and 30 V respectively. In the MS/MS mode (product ion scan) the mass spectrometer scanned in the range m/z 50–500 (or higher, dependent upon the mass of the precursor ion) with a dwell time of 0.5 ms and a step size of 0.1 amu. The electrospray and orifice voltages were set to 5000 and 30 V respectively; and the fragmentation energy was 35 V.

Results

Excretion studies

Levormeloxifene and its metabolites were primarily excreted in the faeces in the Sprague–Dawley rat, Cynomolgus monkey and postmenopausal woman (table 1). Although recovery of radioactivity was essentially complete in the rat and Cynomolgus monkey, traces of radioactivity were identified in rat urine (0.02%) and faeces (1.45%) samples collected during the final collection period (144–168 h).

Radioactivity was excreted more rapidly by the male than the female rat, with 51.1 and 84.3% of total dose excreted by the male during the first 24 and 48 h compared with 23.5 and 52.8% excreted by the female rat during the same period. Excretion was relatively rapid in the monkey, with 90% of the total urinary and faecal radioactivity being excreted over 48 and 72 h respectively. There were no significant differences in the excretion pattern in the male and female monkey. Elimination of levormeloxifene was slow in the postmenopausal volunteer, with the last collection of faeces from three volunteers on day 42 following dosing, on day 48 in one volunteer, on day 56 for one volunteer and on day 71 for the final volunteer. The recovery was relatively poor (mean total recovery 82.7%) and the majority of the radiolabel was excreted in the faeces (79%) over 22 days, with 3.7% being excreted in the urine (figure 2).

Metabolism of levormeloxifene

Rat. Proportions of radioactive components in the faeces and plasma of the rat following a single, oral dose of levormeloxifene (0.7 mg/kg) are shown in tables 2 and 3 respectively. HPLC traces of faeces, plasma and urine samples from the female rat are shown in figure 3.

The greatest proportion of faecal radioactivity was associated with metabolite A and accounted for 32.2% of the total dose in the male rat during 0–48 h and 28.3% in the female rat during 0–72 h. Unchanged drug accounted for a further 7.8% of the total dose in the male rat during 0–48 h and 10.4% in the female rat during 0–72 h. Several other components were excreted in the faeces, each accounting for 0.2–9.1% of the total dose. The metabolic profile after administration of the higher dose (50 mg/kg) was similar to that obtained following the lower dose and differences between the male and the female rat were minimal.

At 4 and 24 h post-dose, unchanged drug was the major radioactive component in male and female plasma. This accounted for 71.9 and 61.5% respectively of plasma extract radioactivity in the male and female rat at 4 h and 28.6 and 48.8% respectively in the male and female at 24 h. At 4 h, metabolites B and C were detected in plasma. These components accounted for 7.3 and 7.1% respectively of radioactivity in the male rat and 11.5 and 5.4% respectively in the female rat. No other components accounted for $>5\%$ of total radioactivity. At 24 h, the proportion

Table 1. Excretion of total radioactivity following a single oral dose of [^{14}C]levormeloxifene in the rat, monkey and postmenopausal woman.

	Sex	Dose (mg/kg)	Time (days)	Dose excreted (%) Urine	Faeces	Total
Rat	male	0.7	7	0.58	99.95	100.53
	($n = 3$)	50	7	0.84	97.72	98.56
	female	0.7	7	1.32	93.58	94.90
	($n = 3$)	50	7	1.30	94.52	95.82
Monkey	male	0.7	7	0.76	89.45	90.21
	($n = 3$)	50	7	1.16	95.48	96.64
	female	0.7	7	0.68	90.86	91.54
	($n = 3$)	50	7	0.83	93.83	94.66
Woman	20 mg single dose					
	($n = 6$)		42–71*	3.74	79.00	82.74

*Variability in period due to incomplete recovery during days 1–40.

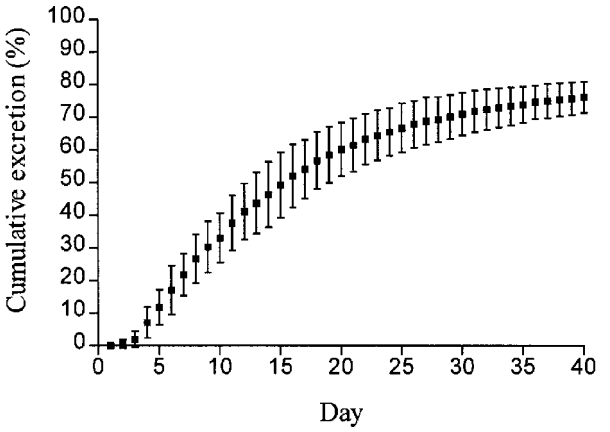


Figure 2. Cumulative excretion profile of radioactivity following oral administration of 20 mg levormeloxifene (containing 25 μCi [^{14}C]-levormeloxifene) to the postmenopausal volunteer ($n = 6$, data shown represent mean$\pm$ SD).

of metabolite B increased to 16.8% in the male and decreased to 1.3% in the female. The proportion of radioactivity associated with several polar components was greater at 24 than at 4 h; metabolite D accounted for 13.5 and 15.9% of plasma extract radioactivity in the male and female rat respectively at 24 h. The metabolic profile following administration of the higher dose was similar, in that unchanged drug was the main component in the plasma. At 4 h post-dose, however, unchanged drug accounted for a lower proportion of the total plasma radioactivity, indicating more extensive metabolism at the higher dose. Deconjugation of plasma samples following both doses resulted in a metabolite profile similar to that of the deconjugated sample, suggesting that there was little phase II metabolism in rat plasma.

Following administration of both doses to the male and female rat, a large proportion of the radioactivity excreted in the urine (91%) was associated with a number of polar components. Deconjugation with β-glucoronidase and sulphatase led to a decrease of 30–50% in the radioactivity associated with polar metabolites, whereas the proportion of radioactivity associated with metabolites A and E

Table 2. Excretion of levormeloxifene and metabolites (% of sample extract radioactivity) in rat and monkey faeces following a single oral dose (0.7 mg/kg).

	Rat				Monkey			
	Male		Female		Male		Female	
Metabolite	0–24 h	24–48 h	0–24 h	24–48 h	0–24 h	24–48 h	0–24 h	24–48 h
A	36.5 (18.7)	40.7 (13.5)	38.5 (9.1)	39.7 (11.6)	10.2 (2.6)	13.2 (5.2)	8.1 (2.1)	14.0 (6.2)
B	9.7 (5.0)	10.1 (3.3)	0.1 (0.02)	3.8 (1.1)	22.2 (5.6)	18.1 (7.2)	15.8 (4.0)	19.6 (8.7)
C	1.8 (0.9)	2.7 (0.9)	0.4 (0.1)	3.5 (1.0)	16.3 (4.1)	13.6 (5.4)	23.7 (6.1)	21.3 (9.4)
D	ND	ND	ND	ND	ND	ND	ND	ND
E	10.6 (5.4)	11.7 (3.9)	4.5 (1.1)	11.1 (3.3)	17.8 (4.5)	21.0 (8.3)	14.7 (3.8)	18.0 (8.0)
F	ND	ND	ND	ND	ND	ND	ND	ND
G	3.8 (1.9)	4.2 (1.4)	5.9 (1.4)	5.7 (1.7)	ND	ND	ND	ND
H	1.8 (0.9)	2.7 (0.9)	0.4 (0.1)	3.5 (1.0)	ND	ND	ND	ND
Levormeloxifene	14.2 (7.3)	1.6 (0.5)	33.0 (7.8)	6.1 (1.8)	7.1 (1.8)	5.2 (2.1)	15.9 (4.1)	9.5 (4.2)

Figures in parenthesis are % dose.
ND, Not detected.
Data are the average of three animals.

Table 3. Excretion of levormeloxifene and metabolites (% of sample extract radioactivity) in rat and monkey plasma following a single oral dose (0.7 mg/kg).*

	Rat 0–24 h post-dose				Monkey 0–6 h post-dose			
	Male		Female		Male		Female	
Metabolite	U	E	U	E	U	E	U	E
A	6.0 (0.9)	8.7 (1.4)	1.9 (0.5)	17.7 (4.4)	4.8 (2.4)	9.2 (4.6)	4.8 (2.6)	11.0 (6.1)
B	16.8 (2.7)	8.7 (1.4)	1.3 (0.3)	ND	ND	ND	ND	ND
C	5.9 (0.9)	5.6 (0.9)	5.0 (1.3)	6.2 (1.6)	8.2 (4.1)	7.4 (3.7)	6.2 (3.4)	9.5 (5.2)
D	13.5 (2.2)	13.8 (2.2)	15.9 (4.0)	5.9 (1.5)	5.9 (2.9)	ND	3.1 (1.7)	2.6 (1.4)
E	ND	1.8 (0.3)	3.0 (0.8)	ND	ND	2.0 (1.0)	3.5 (1.9)	ND
F	ND	ND	ND	ND	ND	ND	ND	ND
G	ND	ND	ND	ND	ND	ND	ND	ND
H	ND	ND	ND	ND	ND	ND	ND	ND
Levormeloxifene	28.6 (4.6)	16.8 (2.7)	48.8 (11.0)	38.7 (9.7)	19.6 (9.8)	25.1 (12.5)	25.5 (14.1)	14.3 (7.9)

Figures in parenthesis are ng equivalents/ml.

*Rat samples taken 24 h post-dose, monkey samples taken 6 h post-dose since data are not available for male monkeys at 24 h post-dose. Data are the average of three animals.

U, untreated plasma sample; E, plasma sample treated with β-glucuronidase.

ND, Not detected.

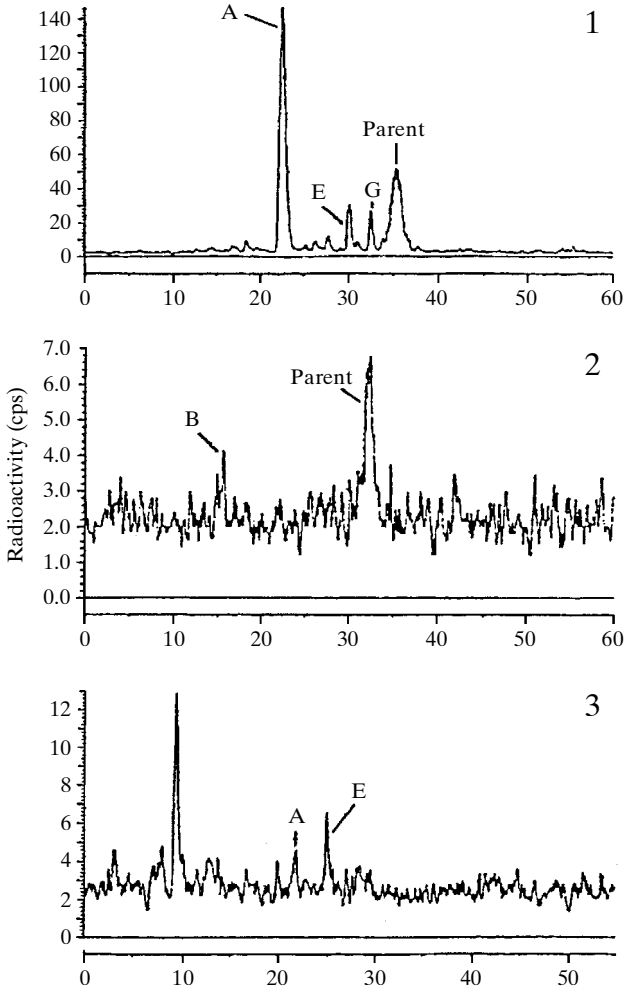


Figure 3. HPLC chromatograms of levormeloxifene and metabolites in faeces (1), plasma (2) and urine (3) samples taken 24, 4 and 24–48 h respectively following oral administration of levormeloxifene (0.7 mg/kg) to the female Sprague–Dawley rat. Letters indicate metabolite assignment.

increased from 1.7 and 1.2% respectively in male rat urine, to 1.8 and 10.5% respectively. The proportion of radioactivity associated with metabolites A and E increased from 10.4 and 11.9% respectively in female rat urine, to 35.4 and 12.1% respectively. Similar increases were seen following deconjugation of samples obtained after administration of the higher dose. Unchanged drug was seen in the enzyme-treated urine of rat dosed at 0.7 mg/kg and accounted for 19.7 and 8.3% of radioactivity in the male and the female rat respectively, but was not detected in rat treated with the higher dose.

After oral administration of 0.7 mg/kg [^{14}C]levormeloxifene, a significant proportion (16–35%) of the total dose of radioactivity was excreted into the bile in the male and female rat. The major radioactive component seen in the bile during 0–24 h was metabolite D, which accounted for 14.3 and 8.8% of the administered dose in the male and the female rat respectively. No other component accounted for $>5\%$ of the administered dose in the male rat. In the female rat no other component

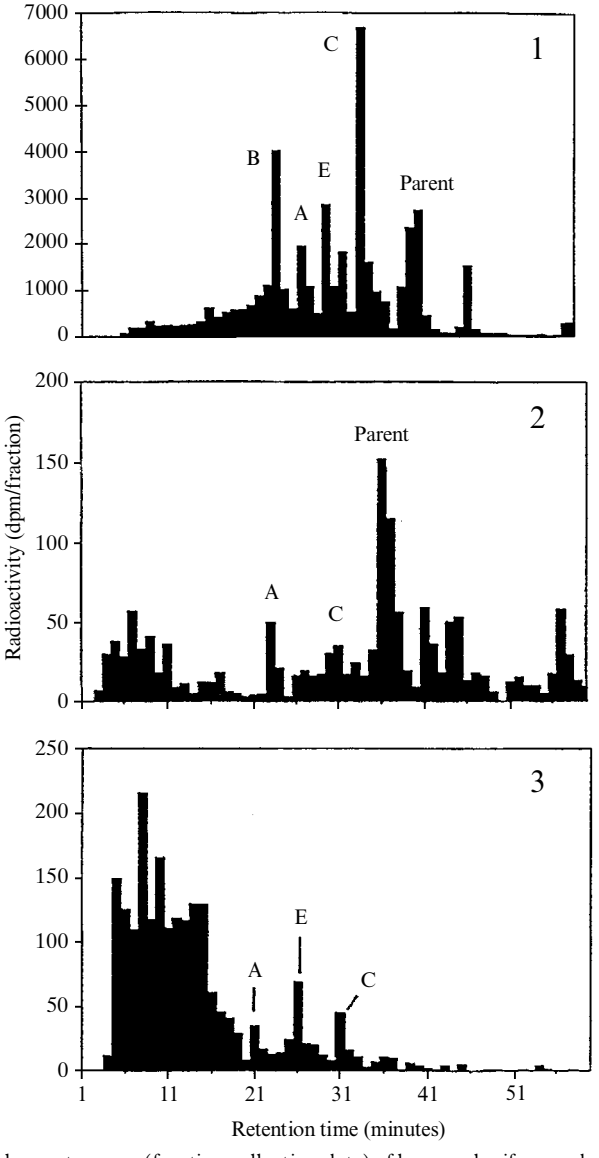


Figure 4. HPLC chromatograms (fraction collection data) of levormeloxifene and metabolites in faeces (1), plasma (2) and urine (3) samples taken 24, 6 and 6–24 h respectively following oral administration of levormeloxifene (0.7 mg/kg) to the female Cynomolgus monkey. Letters indicate metabolite assignment

accounted for $>1\%$ of the administered dose. Similar results were seen following administration of the higher dose of levormeloxifene. The major component in the deconjugated sample was metabolite A.

After intraduodenal infusion of bile from rat treated with 50 mg/kg levormeloxifene, the major component present was again metabolite D, which accounted for 19.7% of the administered dose 0–24 h after administration.

Monkey. HPLC traces for female monkey faeces, plasma and urine samples are shown in figure 4. Proportions of radioactive components excreted in monkey

Table 4. Excretion of levormeloxifene and metabolites, expressed as % of sample extract radioactivity in faeces and urine following a single oral dose (20 mg) to the postmenopausal volunteer.

Metabolite	Faeces Day 4*	Urine 12–24 h
A	20.6 (1.1)	10.7 (0.02)
B	11.4 (0.6)	ND
C	ND	ND
D	ND	ND
E	6.5 (0.3)	ND
F	11.3 (0.6)	ND
G	NQ	ND
H	ND	ND
Levormeloxifene	4.7 (0.3)	ND

Figures in parenthesis show % dose.

* Day 4 represented the highest excretion of radioactivity into faeces.

ND, Not detected; NQ, Not quantifiable.

Data for faeces samples are the average of six volunteers.

Data for the urine sample obtained from one volunteer only.

plasma and faeces following a single oral dose (0.7 mg/kg) of levormeloxifene, during 0–24 and 24–48 h (faeces) are shown in tables 2 and 3.

The greatest proportion of faecal radioactivity (13.6–23.7% of sample radioactivity) was generally associated with metabolite C, while metabolites A, B and E accounted for 8.1–14.0, 15.8–22.2 and 14.7–21.0% of the faecal radioactivity respectively. Unchanged levormeloxifene was also noted, in particular in the female, where it accounted for 15.9% of radioactivity at 0–24 h and 9.5% of radioactivity at 24–48 h (table 2). At the higher dose, unchanged levormeloxifene accounted for a greater proportion of faecal radioactivity, up to 55% in the male and up to 74% in the female. Other radioactivity was associated with metabolites A–C and E, which accounted for up to 10.7, 10.6, 13.1 and 9.6% of total radioactivity respectively.

At 6 and 24 h after oral administration of both doses of levormeloxifene, unchanged drug was the largest component in the systemic circulation of both the male and female (table 3). Other components accounting for $>5\%$ of total plasma radioactivity at 6 h included metabolites C and A. These components were also detected in female plasma at 24 h. Several polar compounds were also detected. After incubation with β-glucuronidase/sulphatase, the proportions of radioactivity associated with these components decreased markedly, indicating that these were products of phase II metabolism. An increase was seen in metabolite A, but due to the low levels of radioactivity in the plasma, no other significant increases were identified.

As seen in the rat, urine from monkey dosed with a single dose (0.7 or 50 mg/kg) of levormeloxifene contained a number of polar components. Several non-polar metabolites were identified, but of these only metabolites A and E accounted for $>3\%$ of the total urine radioactivity. After treatment with β-glucuronidase/sulphatase, radioactivity associated with the polar metabolites decreased, and the proportion of radioactivity associated with metabolite A increased. This amounted to $\sim 11.5\%$ in animals dosed at 0.7 mg/kg and 33% of total urinary radioactivity in animals dosed at 50 mg/kg. Conjugates of unchanged levormeloxifene were seen only in the female monkey and only after administration of the 50 mg/kg dose.

Postmenopausal volunteer. Owing to the large numbers of samples collected following administration of levormeloxifene to women, levels of radioactivity were low and a large number of metabolites could not be identified. Proportions of radioactive components in the faeces and plasma following a single oral dose of levormeloxifene (20 mg) are shown in table 4, and figure 5 shows the HPLC traces of faeces, plasma and urine samples from the postmenopausal woman.

The major single metabolite in the faeces was metabolite A (20–25%), with the highest level being at day 5, with minor components including unchanged drug (accounting for $< 0.3\%$ of the dose) and metabolites B and E–G ($< 10\%$ of the extracted radioactivity). Samples taken after day 15 were below the limit of quantitation. Urinary radioactivity was predominately associated with polar material (consisting of three separate peaks, including conjugated metabolite A) in addition to metabolite A which accounted for 5, 10 and 5% of the extracted radioactivity for the 0–12-, 12–24- and the 24–48 h samples respectively. No compound accounted for $> 0.2\%$ of the administered dose. Meaningful analysis was limited due to the samples selected containing only 1% of the administered dose (excreted in three periods; 0–12, 12–24 and 24–48 h). The main component in the plasma in the first 24 h was unchanged drug (45–60% of plasma extract radioactivity), with a second component which accounted for $< 5\%$ of the total plasma radioactivity at 2 and 4 h, but which was not detectable thereafter. There was no evidence of polar conjugated material in the systemic circulation in the samples analysed. Further radioactive peaks were below the limit of quantitation.

Identification of metabolites

Initially, identification of the major metabolites seen in faeces, plasma and urine of the rat, monkey and postmenopausal woman (metabolites A–H) was attempted by comparison of their HPLC retentions with those of known standards. In this manner, metabolite A was identified as 7-desmethyl-levormeloxifene (figure 6). Reference compounds corresponding to other components were not available and consequently metabolite identification was made on the basis of mass spectra of material purified by HPLC. No attempt was made to isolate sufficient quantities of these compounds in order to obtain conclusive NMR spectra. Table 5 shows the fragmentation pattern of levormeloxifene and potential metabolites. The proposed metabolic pathway for levormeloxifene is shown in figure 6.

APCI MS and MS/MS confirmed that the structure of metabolite A was most likely 7-desmethyl-levormeloxifene since the spectra of the authentic compound were spectrometrically identical to those of metabolite A.

Based on the appearance in the MS of metabolite B of a major ion at m/z 474, 16 mass units higher than the mass of levormeloxifene, it was proposed that metabolite B was a ring-hydroxylated analogue of levormeloxifene. MS/MS of the major protonated metabolite at 474 amu had fragment ions at m/z 71 and 98, indicating the presence of an intact pyrrole ring. The fragment ion at m/z 283, corresponding to the ion at m/z 267 in levormeloxifene, indicated that the hydroxyl group had been added to the lower half of the parent molecule. The fragment at m/z 271, corresponding to the loss of 71 and 132 amu, provided further evidence that hydroxylation had taken place on the phenyl ring, as shown in figure 6, and not on either of the methyl groups or the 2-phenyl group.

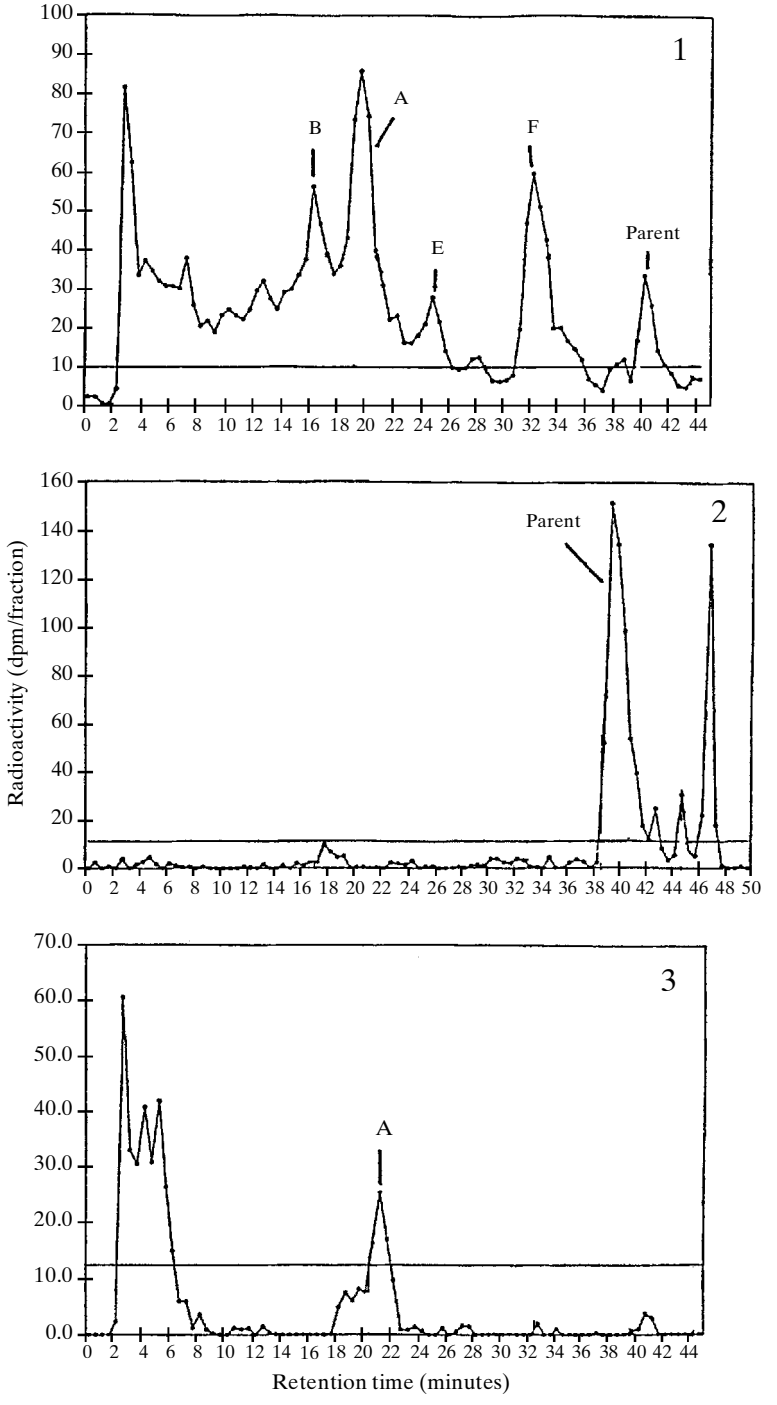


Figure 5. HPLC chromatograms (fraction collection data) of levormeloxifene and metabolites in faeces (1), plasma (2) and urine (3) samples taken 4 days, 2–4 h and 12–24 h respectively following oral administration of levormeloxifene (20 mg containing 25 μCi radioactivity) to the postmenopausal volunteer. Letters indicate metabolite assignment. Horizontal lines represent the limit of quantitation

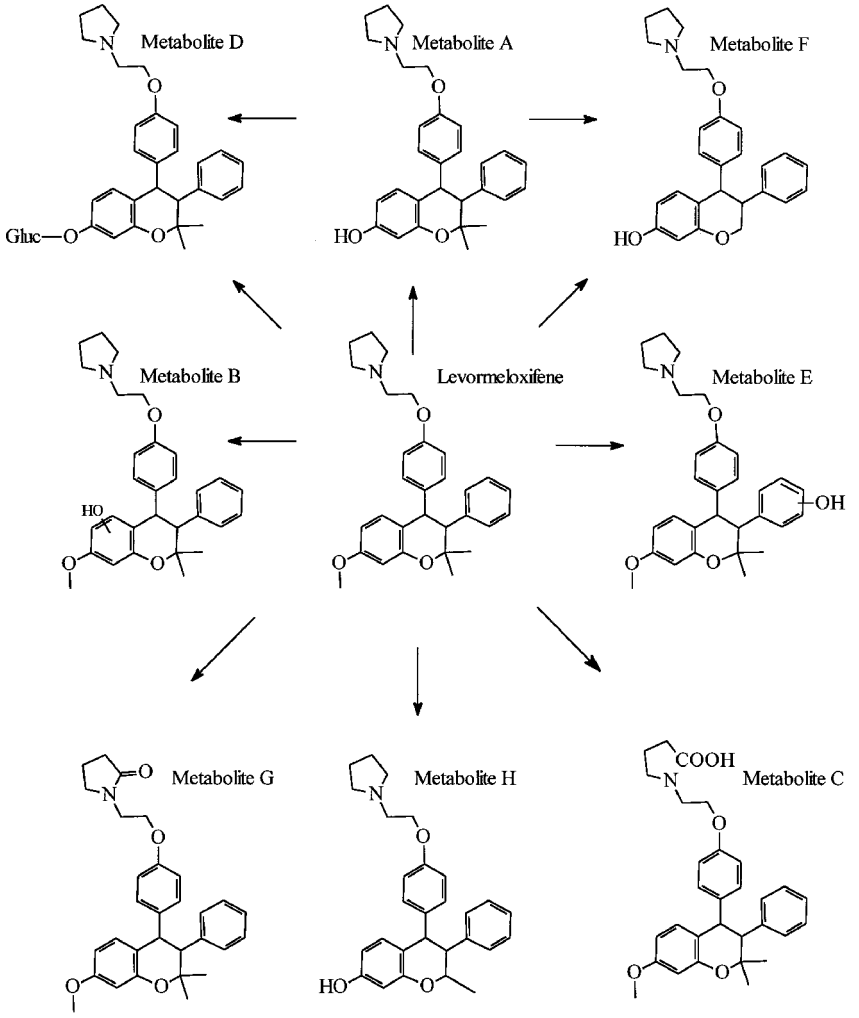


Figure 6. Proposed major metabolic pathways of levormeloxifene following oral administration of a single dose of [^{14}C]levormeloxifene to rat, monkey and the postmenopausal woman. Metabolites F, G and H are tentatively identified.

Table 5. Mass spectra profiles of levormeloxifene metabolites isolated from rat, monkey and the postmenopausal volunteer.

Metabolite	Metabolite source	*m/z*	Productions
A	faeces extract	444	241, 192, 119, 98, 91, 71,
B	faeces extract	474	283, 271, 192, 181, 143, 119, 98, 71
C	faeces extract	490	472, 326, 267, 229, 223, 165, 130, 112, 91, 87, 84, 69, 44
D	bile	620	444, 294, 151, 98
E	faeces extract	474	283, 255, 215, 165, 135, 107, 98, 71
F	faeces extract	ND	
G	faeces extract	472	414, 267, 165, 119, 112, 91
H	faeces extract	430	239, 211, 159, 98, 91, 71
Levormeloxifene	faeces extract	458	267, 189, 175, 165, 119, 98, 91, 71,

ND, Not detected.

Analysis of the rat HPLC fraction thought to contain metabolite C showed that there were two components present, at m/z 430 (metabolite H) and 490 (C). H had a mass corresponding to that of C-didemethylated levormeloxifene, but did not co-chromatograph with authentic didemethylated levormeloxifene and, as a result, was tentatively identified as monodemethylated 7-desmethyl-levormeloxifene. The product ion analysis of the second component, C, contained fragment ions at m/z 165 and 267, as seen in the spectrum of levormeloxifene. Oxidative ring-opening of the pyrrole ring could be expected to give rise to metabolite C, as shown in figure 6, and ions at m/z 130, 112, 84, 87 and 44, suggesting that the pyrrole ring had undergone some modification. The presence of m/z 472 would indicate a condensation reaction of the ring opened pyrrole moiety.

The major ions found in the electrospray mass spectrum of metabolite D, found in rat bile, were at m/z 444 and 620. The ion at 620 is 176 amu higher than that at 444, suggesting that metabolite D was a glucuronide conjugate. Fragments at m/z 444 and 98 in the product ion spectrum obtained following MS/MS analysis of the ion at 620 are consistent with the fragmentation pattern of 7-desmethyl-levormeloxifene. Following incubation of metabolite D with β-glucuronidase/sulphatase, electron impact ionization LC/MS of the product gave rise to a fragmentation pattern identical to that of authentic 7-desmethyl-levormeloxifene. Co-chromatography of deconjugated metabolite D with 7-desmethyl-levormeloxifene resulted in identical retentions.

Analysis of the fraction containing metabolite E suggested that this too was a ring-hydroxylated analogue of levormeloxifene, as the major ion was at m/z 474. The presence of fragment ion at m/z 107, corresponding to an hydroxybenzyl fragment, suggested that hydroxylation had taken place on the 2-phenyl ring, as shown in figure 6.

Sufficient quantities of metabolite F could not be isolated to allow MS identification; therefore, the tentative characterization of F as 2,2-didesmethyl-7-desmethyl-levormeloxifene was made based on co-chromatography with the authentic material. The APCI mass spectrum obtained following analysis of metabolite G, contained major ions at m/z 472.2, 438.4, 357.3, 316.2 and 281.2 (thought not to be related to levormeloxifene and/or its metabolites). The ion at 472 is 14 mass units higher than levormeloxifene (m/z 458), consistent with the addition of a single atom of oxygen and the loss of two H atoms, most likely as a ketone group. The fragment ion at m/z 112 indicates that the pyrrolidine side chain of levormeloxifene has been modified, and the remaining fragments are consistent with the fragmentation pattern of levormeloxifene, further substantiating the proposal that the incorporated oxygen was located in a pyrrolidinone side chain.

Discussion

Administration of ^{14}C-levormeloxifene to rat and monkey was followed by almost complete recovery of parent compound and metabolites, with $>92\%$ being recovered within 7 days in the rat and 90% in the monkey in 3 days. Excretion was much slower in the postmenopausal woman, with total urinary and faecal radioactivity being excreted in 16–23 and 41–71 days respectively. The major route of excretion in all three species was the faeces, with $<1\%$ of the administered radioactivity being excreted in the urine in rat and monkey, and $<5\%$ in human urine. There were only minor sex differences in excretion patterns in the rat and monkey. The proposed metabolism of levormeloxifene is shown in figure 6.

Major metabolic pathways in the rat involved 7-demethylation and ring hydroxylation and the major components in rat faeces included 7-desmethyl-levormeloxifene, hydroxylevormeloxifene and unchanged drug. Unchanged drug was the major component in rat plasma, whereas conjugates of 7-desmethyl-levormeloxifene and hydroxylevormeloxifene were seen in rat urine. Results from an experiment in which a female rat was infused with bile from another rat that had received a single dose of levormeloxifene suggest that there was some uptake of bile from the intestine, and hence enterohepatic recirculation, although the main metabolite in this animal was a glucuronide conjugate of desmethyl-levormeloxifene.

A ring-opened pyrrolidine derivative, metabolite C, was seen in the monkey, presumably arising from oxidative ring-opening of levormeloxifene. Demethylation and ring hydroxylation were also seen in the monkey, giving rise to metabolites A, B and E. Unchanged drug was also present, particularly following administration of the 50 mg/kg dose, presumably due to saturation of metabolizing enzymes. As seen in rat, unchanged drug was the main component in monkey plasma, while monkey urine contained conjugates of 7-desmethyl-levormeloxifene and unchanged drug. Differences in the metabolic profiles of the male and female monkey were minimal. These results are consistent with those obtained in rat, although there are differences in the relative quantities of observed metabolites, possibly reflecting lack of absorption of the higher level dose or saturation of drug-metabolizing enzymes.

Levormeloxifene has a half-life of 219 h in the healthy postmenopausal volunteer studied (B. Kiehr, personal communication). This meant that samples were collected over an extended period, with some women remaining on the study for up to 45 days. Consequently, amounts of radioactivity were low in samples obtained, leading to difficulties in detection and identification of metabolites. Metabolism was extensive in these women. Levormeloxifene was the major radioactive component in the systemic circulation, accounting for $\sim 60\%$ of radioactivity. Some unchanged drug ($< 5\%$) was seen in the faeces, along with 7-desmethyl-levormeloxifene, 7-desmethyl-2,2-didesmethyl-levormeloxifene and several unidentified metabolites. The small proportion of unchanged drug in the faeces may be due in part to the lower doses used in women, relative to rat and monkey, as saturation of metabolizing enzymes and non-absorbed drug may be considerable in these animals. The choice of the rat as a preclinical model for the clinical situation was fortuitous given the similarity of the metabolic profiles seen in the rat and the postmenopausal woman.

The proportions of unchanged drug in the plasma were high in all three species studied. This is consistent with the bioavailability of levormeloxifene in animal species which is 50 and 65% in rat and monkey respectively. Other species detected in the plasma included desmethyl-levormeloxifene, hydroxylevormeloxifene and glucuronides of these compounds. The detection of levormeloxifene in the systemic circulation over extended periods would seem to indicate that the mode of action of this particular drug may be attributable to the parent structure rather than by the formation of an active metabolite. This was confirmed in pharmacology receptor binding assays where the major metabolite, desmethyl-levormeloxifene, was demonstrated to be less active with respect to the indication being studied. Further, plasma profiles at later times (not shown) also resulted in the detection of levormeloxifene as the major component.

In summary, the major metabolic pathways for levormeloxifene in rat, monkey and the postmenopausal woman involve oxidation to a variety of metabolites and

further conjugation of these products. Formation of the major metabolite is proposed to proceed via oxidation in the liver to desmethyl-levormeloxifene, formation of the glucuronide and entry into the bile. Excretion of the glucuronide into the digestive system would be followed by hydrolysis of the conjugate and excretion of the demethylated metabolite in the faeces. Although the relative proportions of the metabolites vary slightly between species and sexes, all three species appear to be exposed to the same chemical entities after administration of levormeloxifene. However, there can be little doubt that the major pathway of levormeloxifene involves O-demethylation. What has not been established during these preclinical studies is the effect of systemic exposure on the adverse reactions reported in the clinic. What may be appropriate is an evaluation of dosing regimens that maintain efficacious plasma concentrations while keeping overall exposures at steady-state within limits not associated with adverse events, although designing such a regimen would be difficult due to the half-life of this compound. Interestingly, a similar compound under development for osteoporosis, idoxifene, also has a long half-life and clinical development was recently stopped due to adverse events in the clinic (SCRIP, 1999, 2431, p. 21).

Acknowledgements

Bile duct cannulation procedures were by Ms T. Pederson. Mass spectra were obtained by Mr O. Wassmann and Dr D. Watson. The authors thank Ms D. Carman for assistance in the preparation of the manuscript.

References

ANTUNES, C. M. F., STROLLEY, P. D., ROSENSHEIN, N. B., DAVIES, J. L., TONASCIA, J. A., BROWN, C., BURNETT, L., RUTLEDGE, A., POKEMPNER, M. and GARCIA, R., 1979, Endometrial cancer and estrogen use: report of a large case-control study. *New England Journal of Medicine*, **300**, 9–13.

BAIN, S., SHALMI, M. and KORSGAARD, N., 1997, Levormeloxifene, a non-steroidal estrogen receptor therapeutic, prevents bone loss, reduces serum cholesterol and has differentiated uterine effects in the ovariectomised rat. *Maturita*, **27 (suppl. 1)**, 144.

BLACK, L. J., SATO, M., ROWLEY, E. R., MAGEE, D. E., BEKELE, A., WILLIAMS, D. C., CULLINAN, G. J., BENDELE, R., KAUFMANN, R. F., BENSCH, W. R., FROLIK, C. A., TERMINE, J. D. and BRYANT, H. U., 1994, Raloxifene prevents bone loss and reduces serum cholesterol without causing uterine hypertrophy in ovariectomised rats. *Journal of Clinical Investigation*, **93**, 63–69.

HOLM, P., KORSGAARD, N., SHALMI, M., ANDERSEN, H. L., HOUGAARD, P., SKOUBY, S. O. and STENDER, S., 1997b, Significant reduction of the antiatherogenic effect of estrogen by long-term inhibition of nitric oxide synthesis in cholesterol-clamped rabbits. *Journal of Clinical Investigation*, **100**, 821–828.

HOLM, P., SHALMI, M., KORSGAARD, N., GULDHAMMER, B., SKOUBY, S. O. and STENDER, S., 1997a, A partial estrogen receptor agonist with strong antiatherogenic properties without noticeable effect on reproductive tissue in cholesterol-fed female and male rabbits. *Arteriosclerosis, Thrombosis, and Vascular Biology*, **17**, 2264–2272.

HULLEY, S., GRADY, D., BUSH, T., FURBERG, C., HERRINGTON, D., RIGGS, B., VITTINGHOFF, E. for the HEART AND ESTROGEN/PROGESTIN REPLACEMENT STUDY (HERS) RESEARCH GROUP, 1998, Randomized trial of estrogen plus progestin for secondary prevention of coronary heart disease in the postmenopausal woman. *Journal of the American Medical Association*, **280**, 605–613.

KE, H. Z., SIMMONS, H. A., PIRIE, C. M., CRAWFORD, D. T. and THOMPSON, D. D., 1995, Droloxifene, a new estrogen antagonist/agonist, prevents bone loss in ovariectomized rats. *Endocrinology*, **136**, 2435–2441.

LOBO, R. A., PICKAR, J. H., WILD, R. A., WALSH, B. and HIRVONEN, E., 1994, Metabolic impact of adding medroxyprogesterone acetate to conjugated estrogen therapy in the postmenopausal woman. *Obstetrics and Gynecology*, **84**, 987–995.

REMIE, R., RENSEMA, J. W., HAVINGA, R. and KUIPERS, F., 1991, The permanent bile fistula rat model. In *Progress in Pharmacology and Clinical Pharmacology*, 8/4 (Stuttgart: Gustav Fischer), pp. 127–145.

WITT, D. M. and LOUSBERG, T. R., 1997, Controversies surrounding estrogen use in the postmenopausal woman. *Annals of Pharmacotherapy*, **31**, 745–755.

XENOBIOTICA , 2000, VOL. 30, NO. 3, 219–233

Regioselective hydroxylation of debrisoquine by cytochrome P4502D6: implications for active site modelling

T. LIGHTFOOT†, S. W. ELLIS†*, J. MAHLING‡, M. J. ACKLAND§, F. E. BLANEY¶, G. J. BIJLOO‖, M. J. DE GROOT§, N. P. E. VERMEULEN‖, G. M. BLACKBURN‡, M. S. LENNARD† and G. T. TUCKER†

† University of Sheffield, Section of Molecular Pharmacology and Pharmacogenetics, Division of Clinical Sciences, Royal Hallamshire Hospital, Sheffield S10 2JF, UK
‡ University of Sheffield, Department of Chemistry, Dainton Building, Sheffield S3 7HF, UK
§ Department of Drug Metabolism, Pfizer Central Research, Sandwich, UK
¶ SmithKline Beecham Pharmaceuticals, New Frontier Science Park North, Third Avenue, Harlow CM19 5AW, UK
‖ Division of Molecular Toxicology, Department of Pharmacochemistry, Vrije Universiteit, De Boelelaan 1083, 1081HV Amsterdam, The Netherlands

Received 5 August 1999

1. Debrisoquine, a prototypic probe substrate for human cytochrome P4502D6 (CYP2D6), is hydroxylated at the alicyclic C4-position by this enzyme. Phenolic metabolites of debrisoquine (5-, 6-, 7- and 8-hydroxydebrisoquine) have also been reported as *in vivo* metabolites, but the role of CYP2D6 in their formation is unclear.

2. As part of studies to develop a predictive model of the active site of CYP2D6 using pharmacophore and homology modelling techniques, it became important to determine the precise regioselective hydroxylation of debrisoquine by CYP2D6.

3. Data from studies with human liver microsomes and yeast microsomes containing cDNA-derived CYP2D6 demonstrated unequivocally that debrisoquine was hydroxylated by CYP2D6 at each aromatic site in the molecule, as well as at the alicyclic 4-position. The four phenolic metabolites amounted to $>60\%$ of the total identified products and the pattern of regioselective hydroxylation (4-HD > 7-HD > 6-HD > 8-HD > 5-HD) was similar in both *in vitro* systems.

4. A pharmacophore model for CYP2D6 indicated that while the hydroxylation of debrisoquine at alternative positions could arise from the substrate adopting multiple binding orientations, the energy constraints for the aromatic hydroxylations were unfavourable. An alternative proposal involving essentially a single binding orientation and a mechanism of hydroxylation based on benzylic radical spin delocalization could satisfactorily rationalize all the hydroxylations of debrisoquine.

5. This latter proposal demonstrates the need to consider the mechanism of oxidation as well as the spatial orientation of the substrate in the development of a predictive model of the active site of CYP2D6.

Introduction

Debrisoquine is a prototypic probe substrate with respect to the polymorphic oxidation of drugs and other xenobiotics by cytochrome P4502D6 (CYP2D6) (Mahgoub *et al.* 1977, Tucker *et al.* 1977). Thus, the urinary ratio of parent drug to 4-hydroxydebrisoquine, considered to be formed principally by CYP2D6, is commonly used to phenotype individuals as extensive (EM) or poor metabolizers (PM). However, *in vivo*, only up to 30% of the dose of debrisoquine is recovered in the urine of EM as the 4-hydroxy metabolite, along with varying amounts of

* Author for correspondence: e-mail: S.Ellis@Sheffield.ac.uk

Xenobiotica ISSN 0049–8254 print/ISSN 1366–5928 online © 2000 Taylor & Francis Ltd
http://www.tandf.co.uk/journals/tf/00498254.html

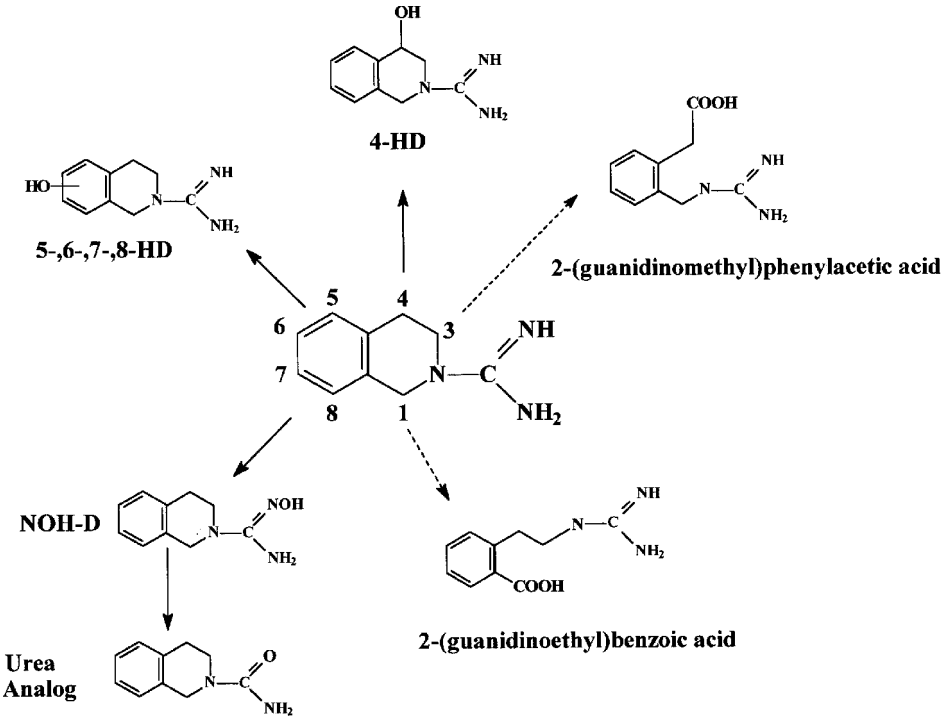


Figure 1. Pathways of debrisoquine metabolism.

phenolic 5-, 6-, 7- and 8-hydroxy products as well as traces of diphenolic and ring-opened compounds (Allen *et al.* 1975, Angelo *et al.* 1978, Silas *et al.* 1978, Idle *et al.* 1979, Ritchie *et al.* 1986, Clement *et al.* 1993) (figure 1). Some *in vivo* studies indicate that the aromatic hydroxylations, particularly the formation of the most abundant 7-hydroxy product, are also mediated by CYP2D6 (Woolhouse *et al.* 1979, Bertilsson *et al.* 1993) but others are more equivocal (Ritchie *et al.* 1986). In general, *in vitro* studies with heterologously expressed CYP2D6 have only reported formation of the 4-hydroxy metabolite (Penman *et al.* 1993, Crespi *et al.* 1995, Ellis *et al.* 1995, Krynetski *et al.* 1995), although Kronbach *et al.* (1987) also detected 6-hydroxydebrisoquine and an unidentified metabolite (shown not to be the 8-hydroxy compound) using a reconstituted purified CYP2D6 preparation.

As part of studies to define the topography of the active site of CYP2D6 based on protein homology modelling (Koymans *et al.* 1993, Ellis *et al.* 1996, de Groot *et al.* 1996, 1999, Lewis *et al.* 1997) and site-directed mutagenesis (Ellis *et al.* 1995), the present authors have used debrisoquine as a relatively rigid, planar model substrate. In this context, it became important to define precisely the regioselectivity of its oxidation to understand further the binding and orientation of this substrate in the active site. Accordingly, a simple HPLC assay has been developed for the alicyclic and aromatic hydroxy metabolites of debrisoquine and the formation of these products by human liver microsomes and microsomes from yeast cells expressing cDNA-derived CYP2D6 was compared (Ellis *et al.* 1992). The results are discussed in light of whether the regioselectivity in hydroxylation of debrisoquine is primarily a consequence of the substrate adopting multiple binding orientations or whether it is a consequence of a mechanism of oxidation involving benzylic radical spin

delocalization in which the substrate adopts essentially a single binding orientation in the active site.

Materials and methods

Chemicals

Debrisoquine hemisulphate and its 4-hydroxydebrisoquine (4-HD) metabolite were gifts from Roche Products Ltd (Welwyn Garden City, UK). Authentic standards of metabolites 5-, 6-, 7- and 8-hydroxydebrisoquine (5-HD, 6-HD, 7-HD, 8-HD) were generously provided by Professor R. L. Smith, Department of Pharmacology and Toxicology, Imperial College School of Medicine at St Mary's, London, UK. Further quantities of the phenolic metabolites (purity, 92–95%) were synthesized in the Department of Chemistry, University of Sheffield. All other chemicals were obtained commercially and were of the highest grade of purity.

Yeast microsomes

Microsomes from yeast cells expressing human wild-type CYP2D6 (CYP2D61) and control microsomes from yeast cells transformed with plasmid lacking *CYP2D6* cDNA were prepared as described by Ellis *et al.* (1996). The cytochrome P450 holoprotein content of microsomes was quantified by reduced carbon monoxide difference spectroscopy using an absorbance coefficient of 91 mM^{-1} cm^{-1} between 450 and 490 nm, essentially according to the method of Omura and Sato (1964).

Human liver microsomes

Samples of human livers (HL), coded HL1, 3, 4, 6, 7 and 9–12, were obtained from renal transplant donors and from patients undergoing partial hepatectomy, with the approval of the local Ethics Committee and the Coroner. Clinical details of the donors have been published by Williams *et al.* (1994). HL1 and 3 were phenotyped and genotyped as being from PMs with respect to the CYP2D6 polymorphism; the remaining livers were characterized as being from EM subjects. Each liver studied had been evaluated with respect to CYP2D6 activity by measuring the rate of microsomal formation of α-hydroxymetoprolol from racemic metoprolol (40 μM), a CYP2D6 specific reaction (Otton *et al.* 1988). Microsomes from the human livers were prepared as described by Otton *et al.* (1988). Microsomal protein was quantified by the method of Lowry *et al.* (1951) using bovine serum albumin as standard.

Incubation conditions

Incubation mixtures comprised 40 pmol (equivalent to 0.5 mg microsomal protein) yeast-derived CYP2D6 or 0.25–0.5 mg human liver microsomal protein, 20 or 250 μM debrisoquine dissolved in water, and a NADP(H)-generating system dissolved in 0.2 M potassium phosphate buffer (pH 7.4). The NADP(H)-generating system comprised 0.8 μmol glucose 6-phosphate, 0.08 μmol NADP, 0.08 U glucose 6-phosphate dehydrogenase and 0.4 μmol $MgCl_2$. The total incubation volume was 0.2 ml. All reactions were initiated by the addition of microsomes and were carried out at 37 °C for 5 min (yeast-derived CYP2D6) or 60 min (human liver) in a shaking water bath (100 oscillations/min). The metabolic reactions were terminated by the addition of 15 μl 60% (v/v) perchloric acid. Preliminary experiments indicated that the formation velocities of metabolites were linear up to 10 min with yeast-derived CYP2D6 and over 60 min with human liver microsomes. Kinetic analyses of the hydroxylation of debrisoquine by yeast-derived CYP2D6 were conducted over a substrate concentration range of 10–1000 μM. Incubations at each substrate concentration were performed in duplicate, and each experiment was conducted in triplicate. As controls, boiled human liver microsomes and microsomes prepared from yeast cells transformed with plasmid lacking *CYP2D6* cDNA were included in each set of incubations.

Assay of debrisoquine metabolites

Following inactivation of incubates with perchloric acid, the samples were vortex-mixed (15 s) and centrifuged at 12000 *g* for 15 min to precipitate protein, and the aqueous supernatant was assayed immediately by HPLC. Chromatographic analysis was performed using an APEX Symmetry Base Deactivated cartridge containing 5 μM silica-based C18 reverse-phase packing material (Jones Chromatography, Hengoed, UK), a NovaPak C18 guard column, a model 510 pump, a model 712 auto-injector (WISP, all Waters Ltd, UK), and a Model 970S Schoeffel fluorometric detector (Kratos,

Manchester, UK) operated at an excitation wavelength of 193 nm and with an emission filter at 300 nm. The mobile phase consisted of 4 mM potassium dihydrogen orthophosphate (adjusted to pH 2.5 with orthophosphoric acid)/acetonitrile in the proportions 99:1 (v/v). Chromatography was performed at ambient temperature and isocratically at a flow rate of 0.7 ml/min.

Calibration graphs, prepared by the addition of known amounts of metabolite standards to heat inactivated microsomes, were linear ($r^2 > 0.99$) and passed through the origin. The respective intra-assay coefficients of variation for 4-, 5-, 6-, 7- and 8-hydroxydebrisoquine were 2.3, 2.0, 1.7, 1.2 and 5.4% at 500 ng/ml and 2.4, 2.0, 1.6, 1.7 and 6.0% at 50 ng/ml. The limits of determination based on a signal-to-noise ratio of 3:1 were 0.072, 0.029, 0.096, 0.032 and 0.185 pmol product/min/pmol P450 for 4-, 5-, 6-, 7- and 8-hydroxydebrisoquine respectively.

The identity of the peaks assigned to specific metabolites was confirmed by on-line liquid chromatography-mass spectrometry (LCMS) using a TSQ 700 mass spectrometer (Finnigan MAT) in electrospray mode (data not shown). Samples of the incubate plus authentic standards were analysed on a C18 column (Hichrom) using a gradient mobile phase ramped from 5% acetonitrile/0.1% trifluoroacetic acid (TFA) up to 45% acetonitrile/0.1% TFA over 20 min. Chromatographic peaks were identified by retention time, mass and fragmentation pattern.

Data analysis

Data from kinetic experiments were analysed by NONLIN, an iterative least-squares fitting program, using initial estimates of K_m and V_{max} obtained from Eadie–Hofstee plots. The kinetic parameters were compared by analysis of variance. When significant differences were noted between groups, the data were compared using the Mann–Whitney test.

Substrate modelling

The hydroxylation of debrisoquine at alternative positions could arise as a consequence of the substrate adopting multiple binding orientations in the active site of the enzyme. This proposal was assessed using a recently refined substrate model for CYP2D6 (de Groot *et al.* 1997) that incorporated steric constraints imposed by the haem moiety and the I-helix of the active site. The initial conformation of debrisoquine was taken from the published debrisoquine-template complex (de Groot *et al.* 1997), and subsequent rigid and flexible fitting procedures were carried out with the ChemX molecular modelling program (Chemical Design Ltd, Oxford, UK). In the rigid fitting procedure, only global rotations and translations are allowed. The flexible fitting minimizer uses the ChemX non-bonded energy forcefield and minimizes the internal non-bonded energy of the fitted molecule with respect to user-defined exocyclic dihedral angles and enforced penalty functions.

An aspartic acid residue representing Asp^{301}, shown previously to be a critical substrate-binding residue of the active site of CYP2D6 (Ellis *et al.* 1995), was attached to the guanidinium nitrogen atom(s) of debrisoquine as described de Groot *et al.* (1997). This procedure allows greater flexibility in the possible positions of the basic nitrogen atom in the substrate model. In contrast to the original refined substrate model (de Groot *et al.* 1997), however, the direction of ANTI lone pair electrons (figure 2a) of the carboxylate moiety was also considered, in addition to the direction of the SYN lone pair electrons (figure 2a), in the ionic interaction with the basic nitrogen of the substrate. This procedure allows even greater flexibility in the possible positions of the basic nitrogen. In the interactions shown in figure 2 (with debrisoquine binding in a SYN-orientation), the strength of the hydrogen bonding between the protonated debrisoquine and the aspartic acid residue decreases in the order: double SYN-SYN > SYN-SYN > ANTI-SYN (figure 2b–d respectively) (ter Laak 1995).

The different sites of hydroxylation of debrisoquine were matched (rigidly) with the position of the haem-bound oxygen, located distally between pyrrole rings A and B of the haem moiety, this position representing the '7 A' site of oxidation as defined in the refined substrate model (de Groot *et al.* 1997). The flat hydrophobic region of the substrate was then superimposed onto a grid used for matching substrate planar regions (de Groot *et al.* 1997). Subsequently, using a flexible fitting procedure (de Groot *et al.* 1997), the C_α- and C_β-atoms of the aspartic acid residue attached to debrisoquine were superimposed onto the corresponding atoms of Asp^{301} located in the I-helix of CYP2D6. The position of the I-helix relative to the haem moiety was determined from a recently improved homology model of the active site of the enzyme (de Groot *et al.* 1996), thereby incorporating steric restrictions and orientation preferences into the substrate model. In general, conformations with distances > 0.5 A between the superimposed C_α- and C_β-atoms of Asp^{301} were rejected. Close contacts between debrisoquine and the protein components of the model (I-helix and haem moiety) were checked and, when necessary, the orientation of the substrate was slightly adjusted manually. The subsequent conformation was accepted as a good fit when the difference in density functional energy (ΔE) between minimal energy conformation and fitted conformation (unprotonated, without the attached aspartic acid residue) of the debrisoquine-template complex did not exceed 25 kcal/mol (preferably < 10 kcal/mol) (de Groot *et al.* 1997).

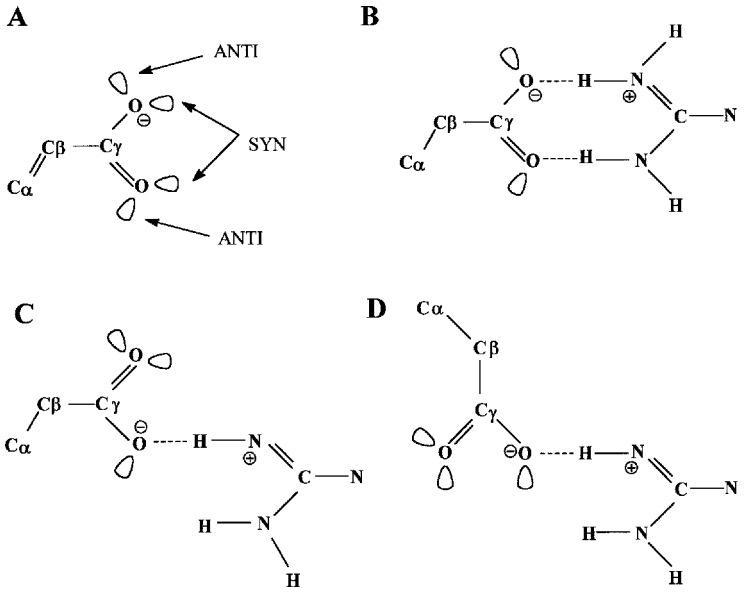


Figure 2. Possible hydrogen bonding directions for a carboxylate moiety (ter Laak 1995). (A) Nomenclature and directionality; (B–D) interactions with debrisoquine in decreasing order: (B) double SYN-SYN, (C) SYN-SYN, (D) ANTI-SYN.

Molecular orbital calculations

In principle, the observed regioselective hydroxylation of debrisoquine could arise as a consequence of a mechanism of oxidation involving hydrogen abstraction, spin delocalization and hydroxyl radical recombination (Korzekwa *et al.* 1985, Koymans *et al.* 1989, Riley and Hanzlik 1994, de Groot *et al.* 1995, Che *et al.* 1997). To test this hypothesis, a quantum mechanical analysis was carried out on the potential radical intermediates involved in such a mechanism. Hydrogen abstraction is presumed to occur through attack by a [porphyrin-Fe(IV)-O$^{\bullet}$] species to produce a [porphyrin-Fe(IV)-OH] intermediate and a substrate radical. The substrate radical cation (protonated on the guanidine group), formed by hydrogen atom abstraction at each of the seven possible oxidation sites of debrisoquine, was optimized by two different methods. In method 1, the semi-empirical program, VAMP 6.0 (Oxford Molecular Ltd, Oxford, UK), was used with the AM1 Hamiltonian (UHF; spin = 2; charge = 1). In method 2, optimization was performed at the *ab initio* level, using the SPARTAN suite of programs (Wavefunction, Inc., Irvine, CA, USA), with a gaussian 3–21G* basis set (again using UHF; spin = 2; charge = 1). In both methods the guanidine moiety was fixed in an idealized geometry, taken from X-ray data with optimization of the NH bonds. This was necessary to prevent the usual distortion of the nitrogens from planarity, which is commonly found during optimization with lower level methods. The resulting geometries from both methods were essentially identical. Hydrogen abstraction at the benzylic positions (C1 and C4) produce planar radical intermediates, whereas abstraction at the C3 alicyclic position maintained some sp^3 character. *Ab initio* single-point calculations were then carried out on these optimized structures at the UHF/6-31G* level. Particular attention was paid to the development of the spin density in the radicals. The spin density at a particular atom can be thought of as the degree of radical character associated with that centre, and thus is the main indicator of the site of oxidation (de Groot *et al.* 1995).

Results

Debrisoquine metabolism

Metabolites, identified as 4-, 5-, 6-, 7- and 8-hydroxydebrisoquine by co-chromatography with authentic standards and mass spectroscopy, were detected in

incubations with recombinant CYP2D6 (figure 3). A further two metabolites with mass ions corresponding to unidentified monohydroxylated debrisoquine products were also detectable by mass spectroscopy, but were minor products relative to the other metabolites (data not shown). Co-incubation of debrisoquine with quinidine (10 μM), a potent selective inhibitor of CYP2D6 (Otton *et al.* 1988), abolished hydroxylation at all sites, and no metabolite formation was detectable in incubates containing yeast control microsomes (data not shown).

Estimates of apparent Michaelis–Menten constants for the formation of the identified hydroxylated metabolites of debrisoquine by recombinant CYP2D6 are shown in table 1. The K_m for each hydroxylation reaction was not significantly different and was in the low micromolar range (15–19 μM). V_{max} showed that hydroxylation at the alicyclic 4-position was the major route of oxidation (2.11 pmol product/min/pmol P450), with 7-hydroxydebrisoquine being the major phenolic metabolite (1.51 pmol product/min/pmol P450). The relative rates of formation of the hydroxylated products were in the order 4-HD > 7-HD > 6-HD > 8-HD > 5-HD (table 1); the extent of each hydroxylation expressed as a percentage of total hydroxylation was 36, 26, 19, 12 and 7% respectively.

The debrisoquine metabolites detected in incubations with human liver microsomes were identical to those found in incubates containing recombinant CYP2D6. At a substrate concentration equivalent to the apparent K_m of the enzyme (20 μM), the relative rates of formation of the five hydroxylated metabolites with microsomes from each human EM liver were identical to those determined with recombinant CYP2D6 (4-HD > 7-HD > 6-HD > 8-HD > 5-HD; figure 4). However, at a saturating substrate concentration of 250 μM, some variation in the relative proportions of the metabolites was observed across the livers, principally with respect to the relative amounts of the 4- and 7-hydroxy products (figure 5). Nevertheless, in all EM livers studied there were highly significant correlations between metoprolol α-hydroxylase activity (a measure of specific CYP2D6 activity) and the rate of formation of each hydroxylated metabolite of debrisoquine (4-HD $r_s = 0.92$; 5-HD $r_s = 0.95$; 6-HD $r_s = 0.95$; 7-HD $r_s = 0.95$; 8-HD $r_s = 0.95$).

At a substrate concentration of 250 μM, the formation of the debrisoquine metabolites by microsomes from the two PM livers, HL1 and HL3, was greatly decreased relative to that by microsomes from EM livers (figure 5). Nevertheless, with the exception of 8-hydroxydebrisoquine, each metabolite was detectable in HL1 but only 4-hydroxydebrisoquine was detectable in HL3 (figure 5). At a lower substrate concentration of 20 μM, only trace amounts of 4-HD were detectable in incubates from PM livers (figure 4).

Substrate modelling

All the sites of oxidation of debrisoquine could be accommodated in the refined substrate model of CYP2D6 (table 2). However, some of the fits are clearly better than others. Only the 4- and 8-hydroxylation sites could be fitted using the most stable double SYN-SYN hydrogen bond orientation between the aspartic acid residue and debrisoquine (figure 2b). The other three sites of oxidation in the aromatic ring could only be modelled by employing a single hydrogen bond (ANTI-SYN; figure 2d). For each site of oxidation, the superposition of the C_β-atoms of Asp^{301} was generally poorer than the superposition of the C_α-atoms. Of major

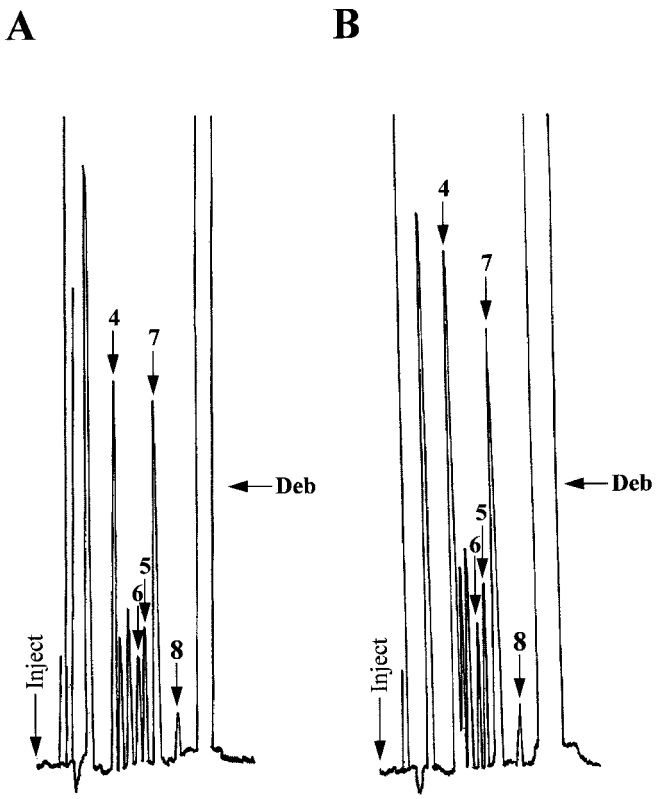


Figure 3. Representative chromatograms depicting formation of hydroxy metabolites of debrisoquine (20 μM) by (A) cDNA-derived CYP2D6 and (B) HL10 microsomes. 4, 4-hydroxydebrisoquine; 5, 5-hydroxydebrisoquine; 6, 6-hydroxydebrisoquine; 7, 7-hydroxydebrisoquine; 8, 8-hydroxydebrisoquine; Deb, debrisoquine.

Table 1. Estimates of the apparent Michaelis–Menten constants for the hydroxylation of debrisoquine by cDNA-derived CYP2D6

Debrisoquine oxidation site	K_m (μM)	V_{max} (pmol/min/pmol CYP2D6)
4-Hydroxylation	14.9 ± 0.9	2.11 ± 0.08[a]
5-Hydroxylation	17.1 ± 2.2	0.44 ± 0.02[b]
6-Hydroxylation	15.2 ± 2.2	1.11 ± 0.06[c]
7-Hydroxylation	14.0 ± 0.3	1.51 ± 0.04[d]
8-Hydroxylation	18.5 ± 7.9	0.72 ± 0.07

Values are means ± SD of three experiments, each data point being replicated three times.

[a] Significantly different ($p < 0.005$) from all other metabolites; [b] $p < 0.003$ from 8-hydroxy; [c] $p < 0.002$ from 7- and 8-hydroxy; [d] $p < 0.0001$ from 8-hydroxy.

significance is the observation that the conformation of each debrisoquine-active site complex leading to aromatic hydroxylation was > 20 kcal/mol above the energy of the molecule in its minimum energy conformation (table 2).

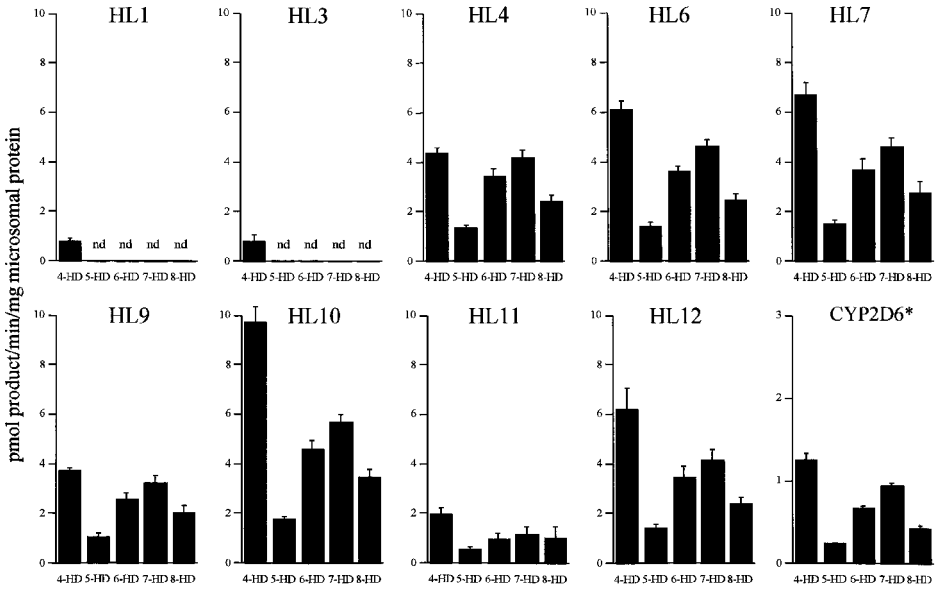


Figure 4. Rates of formation of hydroxy metabolites of debrisoquine (20 μM) by microsomes from nine human livers and cDNA-derived CYP2D6. HL1 and HL3 are from PM with respect to CYP2D6. CYP2D6*, rate expressed as pmol product/min/pmol P450. Data are mean± SD derived from three determinations.

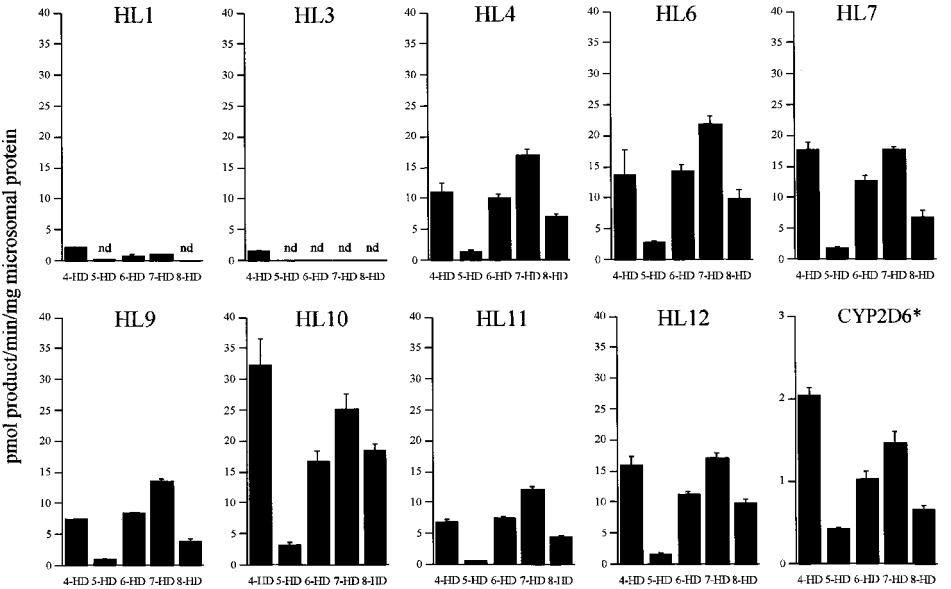


Figure 5. Rates of formation of hydroxy metabolites of debrisoquine (250 μM) by microsomes from nine human livers and cDNA-derived CYP2D6. HL1 and HL3 are from PM with respect to CYP2D6. CYP2D6*, rate expressed as pmol product/min/pmol P450. Data are mean± SD derived from three determinations.

Table 2. Type of hydrogen bond, results of rigid and flexible fits, and energy differences between fitted conformation and minimal energy conformation.

Debrisoquine oxidation site[a]	Type of hydrogen bonding interaction[b]	Rigid fit	Flexible fit		
		$\Delta r_{(ox\text{-}ox)}$[c] ($10^{-3}$ Å)	$\Delta C\alpha$[d] (Å)	$\Delta C\beta^{5\text{-}e}$ (Å)	ΔE(opt-fit)[f] (kcal/mol)
4-Hydroxylation	double SYN-SYN	10.0	0.01	1.00	0.0
5-Hydroxylation	ANTI-SYN	3.0	0.05	0.89	27.6
6-Hydroxylation	ANTI-SYN	8.4	0.12	1.03	22.2
7-Hydroxylation	ANTI-SYN	4.9	0.06	0.80	21.2
8-Hydroxylation	double SYN-SYN	3.9	0.56	0.63	23.3

[a] For each metabolite the distance between the site of oxidation and the basic nitrogen atom is 7Å except for the 4-hydroxylation metabolite (5Å).

[b] See figure 2 for an explanation.

[c] $\Delta r_{(ox\text{-}ox)}$, distance between the site of oxidation above the haem moiety (between pyrrole rings A and B) and the site of oxidation in the substrate after the rigid fitting procedure.

[d] $\Delta C\alpha/\Delta C\beta$, distance between $C\alpha/C\beta$ atoms of aspartic acid residue attached to the substrate and the corresponding atoms in Asp^{301} of the I-helix after the flexible fitting procedure.

[e] For each hydroxylation, the Cα-atoms and the site of oxidation could be superimposed without difficulty, whereas the Cβ-atoms could not be superimposed without sacrificing the match of the flat hydrophobic region with the grid and/or the hydrogen bond interaction(s) between the basic nitrogen atom(s) and the carboxylate moiety of Asp^{301}. The same difficulty was observed with the fitting of other 5Å substrates as described previously (de Groot *et al.* 1997).

[f] ΔE(opt-fit), density functional energy difference between minimal energy conformation and fitted conformation.

Molecular orbital calculations

The relative energies of the potential radicals formed by hydrogen abstraction at each of the seven oxidation sites of debrisoquine can be compared either as heats of formation from the AM1 calculations or as energies above the minimum (the C1 radical) from the *ab initio* 6–31G* calculations (table 3). With both methods, the trends in the data are almost identical. The radicals formed by hydrogen abstraction at the C1 and C4 benzylic positions are relatively low in energy, indicating that these radicals would be expected to form readily. The higher values associated with the aromatic radicals (C5–C8) indicate that direct hydrogen atom abstraction from the phenyl ring would be extremely unfavourable, as demonstrated by previous calculations (de Groot *et al.* 1995). The radical formed by hydrogen abstraction at C3 is intermediate in energy and would be expected to form a minor component of the overall reaction.

Hydrogen abstraction at the favoured C1 and C4 benzylic positions is also accompanied by extensive spin delocalization into the aromatic ring (table 3), hence the relative stability of these intermediates. The C4 radical has significant spin density at C5 and C7, whereas the C1 radical delocalizes into C6 and C8 (table 3; figure 6). Only a small amount of spin density (0.063) develops on the guanidinium carbon. In contrast to C1 and C4, hydrogen abstraction at C3, C5, C6, C7 or C8 sites, which are not favoured sites for hydrogen abstraction, gives rise to debrisoquine radicals with more localized spin densities (table 3).

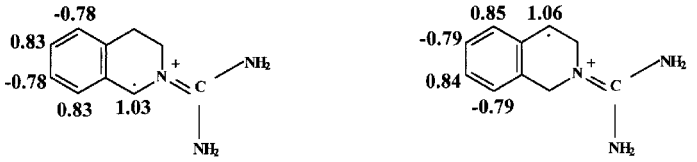
Discussion

In vitro data generated with recombinant CYP2D6 demonstrated unequivocally the capacity of the enzyme to hydroxylate debrisoquine at the 5-, 6-, 7- and 8-

Table 3. Relative energies and spin density of radical intermediates of debrisoquine.

	Relative energy[a]		Mulliken spin density at each carbon position						
Radical	AM1	(6–31G*)	C1	C3	C4	C5	C6	C7	C8
C1	208.440	0.0	1.0333	0.0171	−0.0996	−0.7842	0.8295	−0.7805	0.8345
C3	228.604	19.810	0.0318	1.1980	−0.1679	−0.0853	0.0838	−0.0791	0.0805
C4	213.056	2.773	−0.0987	0.1367	1.0590	0.8465	−0.7868	0.8365	−0.7888
C5	243.877	28.665	−0.0802	−0.0092	0.1043	1.7428	−0.8083	0.7685	−0.7527
C6	244.153	29.708	0.0862	0.0095	−0.0807	−0.8270	1.7320	−0.8075	0.7841
C7	244.149	29.728	−0.0808	−0.0086	0.0859	0.7854	−0.8136	1.7347	−0.8326
C8	243.183	28.283	0.1035	0.0084	−0.0804	−0.7496	0.7708	−0.8049	1.7399

[a] AM1 energies refer to the calculated heats of formation in kcal/mol. The *ab initio* energies (6–31G*) are in kcal/mol above that of the minimum species which is the C1 radical.



C1 Radical **C4 Radical**

Figure 6. Mulliken spin distribution of the radicals formed by hydrogen abstraction at the C1 and C4 benzylic positions of debrisoquine.

aromatic positions, as well as at the alicyclic 4-position. Furthermore, when incubations were conducted with human liver microsomes at a debrisoquine concentration equivalent to the apparent K_m of the enzyme (20 μM), the relative rates of formation of the hydroxylated metabolites by each EM liver were identical to those observed with recombinant CYP2D6 (4-HD > 7-HD > 6-HD > 8-HD > 5-HD). This observation, together with a lack of significant metabolite formation by PM liver microsomes at 20 μM debrisoquine, and the highly significant correlation between debrisoquine metabolite formation and metoprolol α-hydroxylase activity indicate a major contribution of CYP2D6 to both alicyclic and aromatic hydroxylation of debrisoquine in human liver. However, the observed variation in the regioselective hydroxylation of debrisoquine by EM liver microsomes at a saturating substrate concentration (250 μM), and the residual metabolite formation in the PM livers, especially HL1, at this high substrate concentration, suggest the involvement of additional enzyme(s) in the hydroxylation of debrisoquine in human liver, albeit to a minimal extent.

The predominance of phenolic metabolite formation (64% of total hydroxylated products) with both recombinant CYP2D6 and human liver microsomes contrasts markedly with all other *in vitro* data (Kronbach *et al.* 1987, Penman *et al.* 1993, Crespi *et al.* 1995, Ellis *et al.* 1995, Krynetski *et al.* 1995) and the majority of *in vivo* data (Allen *et al.* 1975, Angelo *et al.* 1978, Silas *et al.* 1978, Idle *et al.* 1979, Ritchie *et al.* 1986, Bertilsson *et al.* 1993, Clement *et al.* 1993). Only in two patients with carbimazole-induced agranulocytosis has the extent of aromatic hydroxylation of debrisoquine been reported to approach 50% of total hydroxylation, consistent with

our *in vitro* studies (Woolhouse *et al.* 1979). The urinary recovery of phenolic metabolites was ~5% of the dose in most other *in vivo* studies. The disparity between our *in vitro* data and the majority of *in vivo* findings might be explained by conjugation of the phenolic metabolites *in vivo* to glucuronide/sulphate conjugates, although earlier *in vivo* studies failed to detect such products (Allen *et al.* 1975, Idle *et al.* 1979).

The capacity of CYP2D6 to hydroxylate debrisoquine at alternative sites in the molecule raises the issue as to whether this is achieved through multiple binding orientations. In the present study, a recently refined CYP2D6 substrate model (de Groot *et al.* 1997) was utilized to address this notion. This pharmacophore model incorporated features to improve its predictive capability including steric constraints imposed by the haem and I-helix, and the directionality of Asp^{301}, the residue located in the I helix presumed to bind via an ion-pair interaction with the basic nitrogen of CYP2D6 substrates (Ellis *et al.* 1995). However, although the formation of each hydroxylated product of debrisoquine could be rationalized by the substrate adopting multiple orientations, some of the fits in the substrate model were clearly better than others. Indeed, some of the orientations of debrisoquine could only be achieved after further refinement of the model by incorporating an ANTI direction of the carboxylate lone pair electrons of Asp^{301}, thus allowing greater flexibility in the direction of the hydrogen bonds formed between the carboxylate moiety and the basic nitrogen of debrisoquine. However, even after these adjustments, the difference in the density functional energy between the minimal energy conformation representing 4-hydroxylation and the fitted conformation for each aromatic hydroxylation was >20 kcal/mol, exceeding the preferred limit of 10 kcal/mol (de Groot *et al.* 1997). Such large energy differences could reflect limitations in the current substrate model, although it is also possible that debrisoquine binds in the active site in one orientation only, as represented by the conformation for the 4-hydroxylation reaction. The concept of multiple binding orientations may therefore be inappropriate to rationalize the aromatic hydroxylations of debrisoquine.

Whether debrisoquine binds in the active site of CYP2D6 in one or multiple orientations, the question still arises about the mechanism(s) of the benzylic and aromatic hydroxylation reactions. It is generally acknowledged that P450-catalysed benzylic hydroxylation is best represented by hydrogen abstraction to generate a substrate radical species, which collapses via oxygen rebound (recombination reaction) to generate the enzyme-hydroxylated product complex (Mueller *et al.* 1996). The substrate model (table 2) and molecular orbital calculations (table 3) confirm that the 4-hydroxylation of debrisoquine can proceed via such a mechanism. The introduction of a hydroxyl group into an aromatic ring by P450, on the other hand, is generally considered to proceed via direct electrophilic attack by the iron-bound oxygen species leading to the formation of epoxide intermediates (Akhtar and Wright 1991). However, the formation of epoxide intermediates as a primary reaction step in the pathway leading to the formation of phenolic metabolites has been challenged (Rizk and Hanzlik 1995), and, furthermore, cannot satisfactorily account for all the phenolic metabolites of debrisoquine. Other mechanisms including one electron abstraction (Ortiz de Montellano 1996), direct attack at carbon atoms (Zakhariva *et al.* 1998), and benzylic radical spin delocalization into the aromatic ring (Korzekwa *et al.* 1985, Koymans *et al.* 1989, Riley and Hanzlik 1994, de Groot *et al.* 1995, Che *et al.* 1997) have also been proposed to account for

aromatic hydroxylation reactions. In relation to the latter mechanism, the molecular orbital calculations shown in table 3 and figure 6 suggest that primary hydrogen abstraction at the benzylic C1 and C4 positions of debrisoquine (the favoured sites of hydrogen abstraction), and the subsequent delocalization of spin of these two radicals into the aromatic ring, could rationalize all the sites of hydroxylation of debrisoquine. Thus, since the distribution of spin is considered to be an indicator of the site of oxidation (de Groot *et al.* 1995), hydrogen abstraction at C1 could give rise to 1-, 6- and 8-hydroxydebrisoquine, while abstraction at the alternative C4 benzylic site could account for the formation of 4-, 5- and 7-hydroxydebrisoquine. For such a proposal to be feasible, the C1 and C4 sites of debrisoquine require to be close to the iron-oxygen species. In this respect, docking of the two twist-boat conformations of debrisoquine into the CYP2D6 homology model of Modi *et al.* (1996) does allow the C1 and C4 (and C3) sites to come within a similar distance to the [porphyrin-Fe(IV)-O$^{\bullet}$] complex. These two twist-boat conformations represent essentially identical binding orientations since the flat aromatic ring of the molecule is flipped 180° through the plane of the ring.

According to the above proposal, hydrogen abstraction at the C1 and C3 centres should also allow the respective formation of 1- and 3-hydroxydebrisoquine. However, these metabolites were not identified as products in the present study, although two unknown monohydroxylated debrisoquine metabolites were detected in trace quantities during LC/MS analysis. Because of the lack of standards, the identities of these metabolites were not confirmed as 1- and 3-hydroxydebrisoquine. However, a recent report has confirmed the *in vivo* formation of 1- and 3-hydroxydebrisoquine by CYP2D6 (Eireman *et al.* 1998) and, as such, further supports the concept of benzylic radical spin delocalization as a mechanism for the aromatic hydroxylation of debrisoquine. If, indeed, the aromatic hydroxylation of debrisoquine is a consequence of benzylic radical rearrangement, hydrogen atom substitution with methyl or fluorine at the C4 (or C1) positions should prevent this process and abolish formation of the appropriate hydroxylated products. This hypothesis will be the subject of further investigation.

Although hydrogen abstraction at the benzylic carbon atoms and subsequent radical spin delocalization into the aromatic ring can rationalize all the observed sites of hydroxylation of debrisoquine, the rank order of hydroxylations will undoubtedly be dependent on a number of additional interrelated factors. While orientation will obviously define the distance between the iron-oxygen species and the sites of hydrogen abstraction and/or hydroxylation, steric constraints imposed by both the substrate and active site residues will also influence the energetic favourability of hydrogen abstraction and/or oxygen rebound to different sites on the substrate. Such factors will apply whether the substrate binds in one or multiple orientations. Only from more refined active site models of CYP2D6, and ultimately a crystal structure of a substrate-bound CYP2D6 protein, will the precise nature of these interactions be elucidated.

In conclusion, the data presented here clearly demonstrate the ability of CYP2D6 to hydroxylate debrisoquine at a number of aromatic sites in the molecule, as well as the alicyclic C4-position. Although binding in multiple orientations is generally accepted as a concept to account for alternative sites of oxidation, the computational data presented in this study suggest that product selectivity may also be determined by the mechanism(s) of oxidation. As such, in addition to the spatial orientation of the substrate in the active site relative to the FeO$^{\bullet}$ species, the potential mechanism(s)

of oxidation, reflecting in part the electronic properties of the substrate, should also be considered in the development of predictive models of the active sites of cytochromes P450.

Acknowledgements

The authors gratefully acknowledge the technical support of J. R. Harlow and J. Chowdry, University of Sheffield. This work was supported in part by Wellcome Trust Grant 038735.

References

Akhtar, M. and Wright, J. N., 1991, A unified mechanistic view of oxidative reactions by P-450 and related Fe-containing enzymes. *Natural Product Reports*, **8**, 527–551.

Allen, J. G., East, P. B., Francis, R. J. and Haigh, J. L., 1975, Metabolism of debrisoquine sulphate. Identification of some urinary metabolites in rat and man. *Drug Metabolism and Disposition*, **3**, 332–337.

Angelo, M., Dring, L. G., Idle, J. R., Lancaster, R., Mahgoub, A. and Smith, R. L., 1978, Defective alicyclic hydroxylation of debrisoquine in man. *British Journal of Clinical Pharmacology*, **4**, 725P.

Bertilsson, L., Meese, C. O., Yue, Q. Y., Dahl, M. L., Ingelman-Sundberg, M., Johansson, I., Säwe, J. and Eichelbaum, M., 1993, Quinidine inhibition of debrisoquine S(+)-4- and 7-hydroxylations in Chinese of different CYP2D6 genotypes. *Pharmacogenetics*, **3**, 94–100.

Che, H., de Groot, M. J., Vermeulen, N. P. E. and Hanslik, R. P., 1997, Oxidative N-dealkylation of *p*-cyclopropyl-*N*, *N*-dimethylanaline. A substituent effect on a radical clock reaction rationalized by *ab initio* calculations on radical cation intermediates. *Journal of Organic Chemistry*, **62**, 8227–8230.

Clement, B., Shultze-Mosgau, M.-H. and Wohlers, H., 1993, Cytochrome P450 dependent N-hydroxylation of a guanidine (debrisoquine), microsomal catalysed reduction and further oxidation of the N-hydroxy-guanidine metabolite to the urea derivative. *Biochemical Pharmacology*, **46**, 2249–2267.

Crespi, C. L., Steimel, D. T., Penman, B. W., Korzekwa, K. R., Fernandez-Salguero, P., Buters, J. T. M., Gelboin, H. V., Gonzalez, F. J., Idle, J. R. and Daly, A. K., 1995, Comparison of substrate metabolism by wild-type CYP2D6 protein and a variant containing methionine, not valine, at position 374. *Pharmacogenetics*, **5**, 234–243.

De Groot, M. J., Ackland, M. J., Horne, V. A., Alex, A. A. and Jones, B. C., 1999, Novel approach to predicting P450-mediated drug metabolism: development of a combined protein and pharmacophore model for CYP2D6. *Journal of Medicinal Chemistry*, **42**, 1515–1524.

De Groot, M. J., Bijloo, G. J., Martens, B. J., van Acker, F. A. A. and Vermeulen, N. P. E., 1997, A refined substrate model for human cytochrome P450 2D6. *Chemical Research in Toxicology*, **10**, 41–48.

De Groot, M. J., Donne-Op den Kelder, G. M., Commandeur, J. N. M., van Lenthe, J. H. and Vermeulen, N. P. E., 1995, Metabolite predictions for *para*-substituted anisoles based on *ab initio* complete active space self consistent field calculations. *Chemical Research in Toxicology*, **8**, 437–443.

De Groot, M. J., Vermeulen, N. P. E., Kramer, J. D., van Acker, F. A. A. and Donne-Op den Kelder, G. M., 1996, Three-dimensional protein model for human cytochrome P450 2D6 based on the crystal structures of P450 101, P450 102, and P450 108. *Chemical Research in Toxicolology*, **9**, 1079–1091.

Eireman, B., Edlund, P. O., Tjernberg, A., Dalen, P., Dahl M.-L. and Bertilsson, L., 1998, 1- and 3-hydroxylations, in addition to 4-hydroxylation, of debrisoquine are catalyzed by cytochrome P450 2D6 in humans. *Drug Metabolism and Disposition*, **26**, 1096–1101.

Ellis, S. W., Ching, M. S., Watson, P. F., Henderson, C. J., Simula, A. P., Lennard, M. S., Tucker, G. T. and Woods, H. F., 1992, Catalytic activities of human debrisoquine 4-hydroxylase cytochrome P450 (CYP2D6) expressed in yeast. *Biochemical Pharmacology*, **44**, 617–620.

Ellis, S. W., Hayhurst, G. P., Smith, G., Lightfoot, T., Wong, M. M. S., Simula, A. P., Ackland, M. J., Sternberg, M. J. E., Lennard, M. S., Tucker, G. T. and Wolf, C. R., 1995, Evidence that aspartic acid 301 is a critical substrate-contact residue in the active site of cytochrome P450 2D6. *Journal of Biological Chemistry*, **270**, 29055–29058.

ELLIS, S. W., ROWLAND, K., ACKLAND, M. J., REKKA, E., SIMULA, A. T., LENNARD, M. S., WOLF, C. R. and TUCKER, G. T., 1996, Influence of amino acid residue 374 of cytochrome P450 2D6 (CYP2D6) on the regio- and enantio-selective metabolism of metoprolol. *Biochemical Journal*, **361**, 647–654.

IDLE, J. R., MAHGOUB, A., ANGELO, M. M., DRING, L. G., LANCASTER, R. and SMITH, R. L., 1979, The metabolism of [^{14}C]-debrisoquine in man. *British Journal of Clinical Pharmacology*, **7**, 257–266.

KORZEKWA, K. R., TRAGER, W. F., GOUTERMAN, M., SPRANGLER, D. and LOWE, G. H., 1985, Cytochrome P450 mediated aromatic oxidations: a theoretical study. *Journal of American Chemical Society*, **107**, 4273–4279.

KRONBACH, T., MATHYS, D., GUT, J., CALIN, T. and MEYER, U. A., 1987, High-performance liquid chromatographic assays for bufuralol 1′-hydroxylase, debrisoquine 4-hydroxylase and dextromethorphan *O*-demethylase in microsomes and purified cytochrome P450 isozymes of human liver. *Analytical Biochem*istry, **164**, 24–32.

KOYMANS, L. M. H., VAN LENTHE, J. H., VAN DE STRAAT, R., DONNE-OP DEN KELDER, G. M. and VERMEULEN, N. P. E., 1989, A theoretical study on the metabolic activation of paracetamol by cytochrome P-450: indications for a uniform oxidation mechanism. *Chemical Research in Toxicology*, **2**, 60–66.

KOYMANS, L. M. H., VERMEULEN, N. P. E., BRAARSLAG, A. and DONNE-OP DEN KELDER, G. M., 1993, A preliminary 3D model for cytochrome P450 2D6 constructed by homology model building. *Journal of Computer-Aided Molecular Design*, **7**, 281–289.

KRYNETSKI, E. Y., DRUTSA, V. L., KOVALERA, I. E. and LUZIKOV, V. N., 1995, High yield expression of functionally active human liver CYP2D6 in yeast cells. *Pharmacogenetics*, **5**, 103–109.

LEWIS, D. F. V., EDDERSHAW, P. J., GOLDFARB, P. S. and TARBIT, M. H., 1997, Molecular modelling of cytochrome P4502d6 (CYP2D6) based on an alignment with CYP102: structural studies on specific CYP2D6 substrate metabolism. *Xenobiotica*, **27**, 319–340.

LOWRY, O. H., ROSEBROUGH, N. J., FARR, A. L. and RANDALL, R. J., 1951, Protein measurement with the Folin phenol reagent. *Journal of Biological Chemistry*, **193**, 265–275.

MAHGOUB, A., IDLE, J. R., DRING, L. G., LANCASTER, R. and SMITH, R. L., 1977, Polymorphic hydroxylation of debrisoquine in man. *Lancet*, **i**, 584–586.

MODI, S., PAINE, M. J., SUTCLIFFE, M. J., LIAN, L.-Y., PRIMROSE, W. U., WOLF, C. R. and ROBERTS, G. C. K., 1996, A model for human cytochrome P450 2D6 based on homology modeling and NMR studies of substrate binding. *Biochemistry*, **35**, 4540–4550.

MUELLER, E. J., LOIDA, P. J. and SLIGAR, G. S., 1996, Twenty-five years of P450cam research: mechanistic insights into catalysis. In P. R. Ortiz de Montellano (ed.), *Cytochrome P450 – Structure, Mechanism, and Biochemistry*, 2nd edn (New York: Plenum), pp. 83–124.

OMURA, T. and SATO, R., 1964, Carbon monoxide-binding pigment of liver microsomes. I. Evidence for its hemoprotein nature. *Journal of Biological Chemistry*, **239**, 2370–2378.

ORTIZ DE MONTELLANO, P. R., 1996, Oxygen activation and reactivity. In P. R. Ortiz de Montellano (ed.), *Cytochrome P450 – Structure, Mechanism, and Biochemistry*, 2nd edn (New York: Plenum), pp. 245–304.

OTTON, S. V., CREWE, H. K., LENNARD, M. S., TUCKER, G. T. and WOODS, H. F., 1998, Use of quinidine inhibition to define the role of sparteine/debrisoquine cytochrome P450 in metoprolol oxidation by human liver microsomes. *Journal of Pharmacology and Experimental Therapeutics*, **247**, 242–247.

PENMAN, B. W., REECE, J., SMITH, T., YANG, C. S., GELBOIN, H. V., GONZALEZ, F. J. and CRESPI, C. L., 1993, Characterization of a human cell line expressing high levels of cDNA-derived CYP2D6. *Pharmacogenetics*, **3**, 28–39.

RILEY, P. and HANZLIK, R. P., 1994, Electron transfer in P450 mechanisms. Microsomal metabolism of cyclopropylbenzene and *p*-cyclopropylanisole. *Xenobiotica*, **24**, 1–16.

RITCHIE, J. C., CROTHERS, M. J., SHAH, R. R., IDLE, J. R. and SMITH, R. L., 1986, The metabolism of debrisoquine in man: (1) regioselectivity of hydroxylation and (2) aberrant oxidative metabolism in two sibling patients with carbimazole-induced agranulocytosis. *Xenobiotica*, **16**, 503–509.

RIZK, P. N. and HANZLIK, R. P., 1995, Oxidative and non-oxidative metabolism of 4-iodoanisole by rat liver microsomes. *Xenobiotica*, **25**, 143–150.

SILAS, J. H., LENNARD, M. S., TUCKER, G. T., SMITH, A. J., MALCOLM, S. L. and MARTEN, T. R., 1978, The disposition of debrisoquine in hypertensive patients. *British Journal of Clinical Pharmacology*, **5**, 27–34.

TER LAAK, A. M., 1995, Histamine H_1-receptor agonists and antagonists. Molecular modeling and drug design. PhD thesis, Vrije Universiteit Amsterdam.

TUCKER, G. T., SILAS, J. H., LYUN, A. O., LENNARD, M. S. and SMITH, A. J., 1977, Polymorphic hydroxylation of debrisoquine. *Lancet*, **ii**, 718.

WILLIAMS, M. L., LENNARD, M. S., MARTIN, I. J. and TUCKER, G. T., 1994, Interindividual variation in the isomerization of 4-hydroxytamoxifen by human liver microsomes: involvement of cytochromes P450. *Carcinogenesis*, **15**, 2733–2738.

WOOLHOUSE, N. M., ANDOH, B., MAHGOUB, A., SLOAN, T. P., IDLE, J. R. and SMITH, R. L., 1997, Debrisoquine hydroxylation polymorphism among Ghanaians and Caucasians. *Clinical Pharmacology and Therapeutics*, 26, 584–591.

ZAKHARIVA, O., GRODZICKI, M., TRAUTWEIN, A. X., VEEGER, C. and RIETJENS, I. M. C. M., 1998, Molecular orbital study of porphyrin–substrate interactions in cytochrome P450 catalysed aromatic hydroxylation of substituted anilines. *Biophysical Chemistry*, **73**, 9–203.

XENOBIOTICA , 2000, VOL. 30, NO. 3, 235–251

In vitro inhibition of human P450 enzymes by prenylated flavonoids from hops, *Humulus lupulus*

M. C. HENDERSON†, C. L. MIRANDA†, J. F. STEVENS‡, M. L. DEINZER‡ and D. R. BUHLER†*

† Departments of Environmental and Molecular Toxicology and
‡ Chemistry, Oregon State University, Corvallis, OR 97331, USA

Received 5 July 1999

1. Several unique flavonoid compounds have recently been isolated from hops, *Humulus lupulus*, and their presence has been detected in beer. Their chemical structures are similar to other plant-derived compounds, many present in the human diet, that have been shown to have cancer chemopreventive properties due, in part, to inhibition of cytochrome P450 enzymes that activate carcinogens. Additionally, preliminary studies have shown these flavonoids (at 100 μM) to be inhibitory of P450-mediated activation reactions in a variety of *in vitro* systems. Thus, the *in vitro* effects of these phytochemicals on cDNA-expressed human CYP1A1, CYP1B1, CYP1A2, CYP3A4 and CYP2E1 were currently examined by the use of diagnostic substrates and the carcinogen AFB_1.

2. At 10 μM, the prenylated chalcone, xanthohumol (XN), almost completely inhibited the 7-ethoxyresorufin *O*-deethylase (EROD) activity of CYP1A1. At the same concentration, other hop flavonoids decreased the EROD activity by 90.8–27.0%.

3. At 10 μM, XN completely eliminated CYP1B1 EROD activity, whereas the other hop flavonoids showed varying degrees of inhibitory action ranging from 99.3 to 1.8%.

4. In contrast, the most effective inhibitors of CYP1A2 acetanilide 4-hydroxylase activity were the two prenylated flavonoids, 8-prenylnaringenin (8PN) and isoxanthohumol (IX), which produced $>90\%$ inhibition when added at concentrations of 10 μM.

5. CYP1A2 metabolism of the carcinogen AFB_1 was also inhibited by IX and 8PN as shown by decreased appearance of dihydrodiols and AFM_1 as analysed by hplc. IX and 8PN also decreased covalent binding of radiolabelled AFB_1 to microsomal protein in a concomitant manner.

6. XN, IX and 8PN, however, were poor inhibitors of CYP2E1 and CYP3A4 as measured by their effect on chorzoxazone hydroxylase and nifedipine oxidase activities respectively.

7. These results suggest that the hop flavonoids are potent and selective inhibitors of human cytochrome P450 and warrant further *in vivo* investigations.

Introduction

Many chemicals in the environment act as carcinogens following activation by cytochrome P450 (Gonzalez and Gelboin 1994). Accordingly, one approach to cancer prevention is to inhibit the carcinogen activation process with inhibitors of these phase I enzymes (Wattenburg 1983, Pezzuto 1997). Metabolic activation of chemical carcinogens is mediated by a limited number of human P450 species, namely CYP1A1, CYP1A2, CYP1B1, CYP2A6, CYP2E1 and CYP3A4 (Guengerich *et al.* 1992, 1994, Gonzalez and Gelboin 1994, Guengerich 1995, Shimada *et al.* 1996); CYP2A3 and CYP3A3 (Aoyama *et al.* 1990); CYP2B6 (Shou *et al.* 1996a, Code *et al.* 1997), CYP2C8 (Shou *et al.* 1994) and CYP2C9 (Shou *et al.* 1996a, b). Since CYP1A1 is not significantly expressed in human liver, CYP1A2, CYP2B6 and CYP2C9 probably are the major contributors to the metabolic

* Author for correspondence; email: Donald.Buhler@orst.edu

Xenobiotica ISSN 0049–8254 print/ISSN 1366–5928 online © 2000 Taylor & Francis Ltd
http://www.tandf.co.uk/journals/tf/00498254.html

activation of polycyclic aromatic hydrocarbons in this organ (Shou *et al.* 1996c). CYP1A1 and CYP1B1 are mainly expressed in extrahepatic tissues (Guengerich 1995) and may contribute to metabolic activation and carcinogenicity of polycyclic aromatic hydrocarbons (PAH) at these sites. CYP1A2 and CYP3A4 have been shown to be responsible for the oxidation of the liver carcinogen aflatoxin B_1 (Gallagher *et al.* 1996). Additionally, CYP1A2 in human liver microsomes is responsible for the activation of heterocyclic aromatic amines to genotoxic species, in particular, the *N*-hydroxylation of 2-amino-1-methyl 6-phenylimidazo(4,5-*b*)pyridine (PhIP) (Zhao *et al.* 1994). Inhibition of the activity of these enzymes could result in the inhibition of the carcinogenic effects of the chemicals activated by these enzymes.

Synthetic and naturally occurring flavonoids belonging to different chemical classes [flavones (chrysin, tangeretin, flavone, 5,6-benzoflavone, 7,8-benzoflavone), flavonols (quercetin), and flavanones (pinocembrin, eriodictyol, flavanone) have been examined for their ability to inhibit ethoxyresorufin *O*-deethylase (EROD) and benzyloxyresorufin *O*-debenzylase (BROD) activities of human liver microsomes (Siess *et al.* 1995). Flavonoids without hydroxyl groups were more effective than those with hydroxyl groups in inhibiting EROD activity. Furthermore, flavanones were more inhibitory than the flavones toward EROD activity of human liver microsomes. In contrast, non-hydroxylated flavones were activators of BROD activity. In another study, quercetin inhibited aryl hydrocarbon hydroxylase activity while activating 7-methoxyresorufin *O*-dealkylase activity of cDNA-expressed human CYP1A2 (Tsyrlov *et al.* 1994). Differential effects of 7,8-benzoflavone on enzyme activities were observed in that the chemical is an inhibitor of human CYP1A1 and CYP1A2 (Tassaneeyakul *et al.* 1993) but an activator of CYP3A4 (Guengerich *et al.* 1994). The flavonoid present in grapefruit, naringenin, is an inhibitor of CYP3A4 and inhibits the activation of aflatoxin B_1 (AFB_1) to the carcinogenic metabolite, AFB_1-*exo*-8,9-epoxide (Guengerich and Kim 1990, Guengerich *et al.* 1994). Additionally, tangeretin from citrus fruits, and green tea flavonoids inhibit EROD (CYP1A2) and nifedipine oxidase (CYP3A4) activity in human liver microsomes (Obermeier *et al.* 1995). Thus, flavonoids can be either inhibitors or activators of human cytochrome P450 depending upon their chemical structures. Those flavonoids that inhibit P450-mediated reactions for pro-carcinogens could be useful as cancer chemopreventive agents at the initiation stage of carcinogenesis by blocking carcinogen activation.

Recently, several flavonoids (figure 1) have been isolated from hops (Stevens *et al.* 1997), and several of these chemicals have been detected in beer (Stevens *et al.* 1998, 1999a, b). These flavonoids are unique in that they contain one or two prenyl groups or a geranyl group. The prenylated flavonoids have the basic structure of either a flavanone like that of naringenin, or a chalcone (figure 1). Prenylation occurs at the 6 and/or 8 position yielding 6-prenylnaringenin, 8-prenylnaringenin and 6,8-diprenylnaringenin. Unlike the flavanones, chalcones lack the heterocyclic C ring (Bohm 1993). The unsubstituted chalcone has been shown to inhibit 7-ethoxyresorufin and 7-methoxyresorufin *O*-dealkylase activities of liver microsomes from the Aroclor 1254-treated rat (Edenharder *et al.* 1997).

Miranda *et al.* (1999) reported anti-proliferative and cytotoxic effects of several of the prenylated hop flavonoids on human cancer cell lines. Additionally, preliminary studies (Henderson *et al.* 1998) with the hop flavonoids at relatively high concentration (100 μM) showed inhibition of certain P450-mediated activities

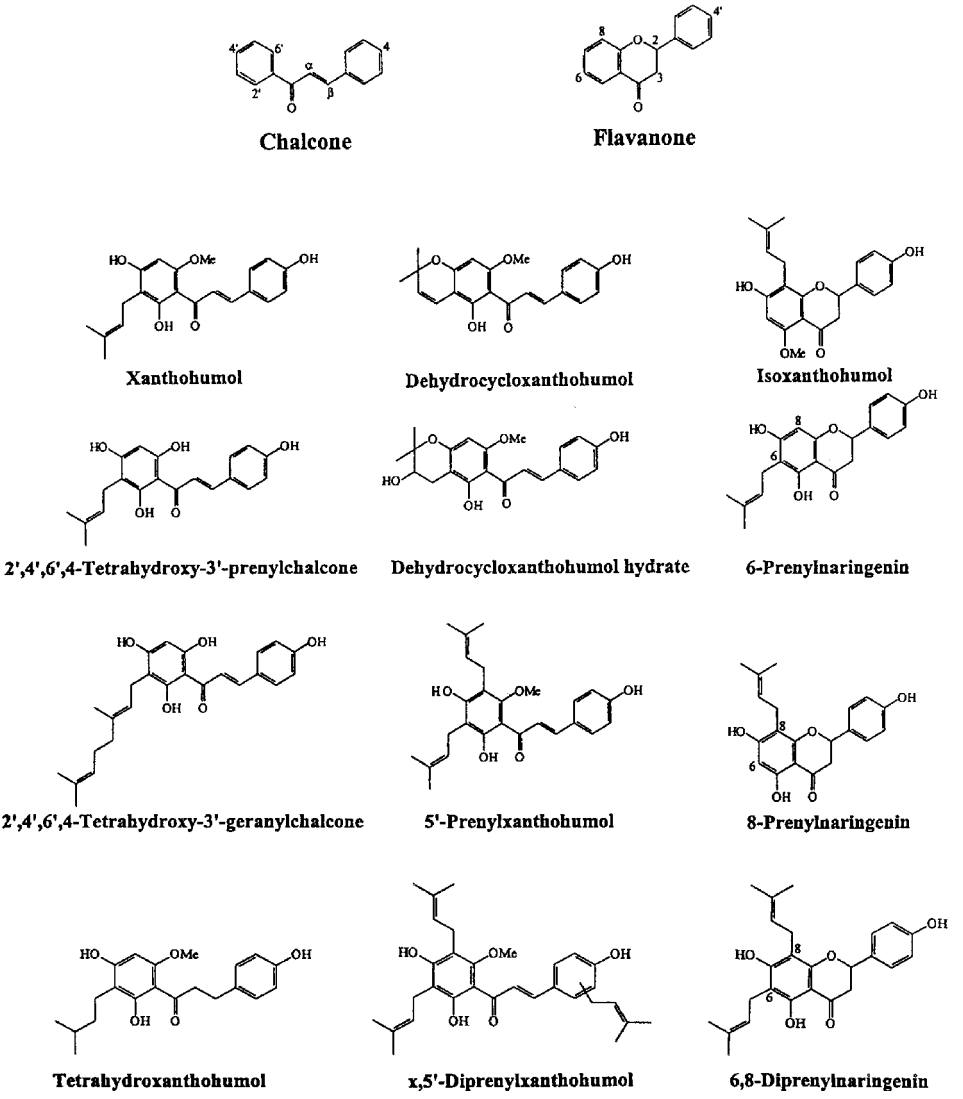


Figure 1. Chemical structures of hop flavonoids.

in a variety of *in vitro* systems including the metabolism of DMBA by liver microsomes from the male rat treated with β-naphthoflavone, the CYP3A-mediated activation of pyrrolizidine alkaloid senecionine to toxic pyrroles in cattle liver microsomes and the metabolic activation of AFB_1 by trout liver microsomes.

The biological activities of prenylated flavanones and prenylated chalcones in terms of their ability to inhibit human P450, particularly at lower concentrations, have not been examined. Thus, the aim of the present study was to determine if these hop flavonoids are inhibitors of human P450s involved in carcinogen activation. Other phytochemicals were examined for comparative purposes. As limited quantities of the hop flavonoids are available, studies with cDNA-expressed human cytochrome P450 were undertaken as a first step in determining which flavonoids might warrant further *in vivo* investigations which require large amounts of test

compound. Evidence is presented that two of the prenylated flavanones, 8-prenylnaringenin and isoxanthohumol, are the most effective inhibitors of CYP1A2, whereas the prenylated chalcone, xanthohumol is the best inhibitor of CYP1A1 and CYP1B1.

Materials and methods

Materials

Acetanilide, 4-hydroxyacetanilide, chlorzoxazone, nifedipine, genistein (GS), naringenin (NG), resveratrol (RV) and unlabeled aflatoxin B_1 were from Sigma Chemical Co. (St Louis, MO, USA). [^{3}H(G)]-aflatoxin B_1 (15.8 mCi/mmol) with a radiochemical purity of 97.5% was from Moravek Biochemicals, Inc. (Brea, CA, USA). 6-Hydroxychlorzoxazone was from Research Biochemicals Intl. (Natick, MA, USA). Oxidized nifedipine was obtained from Ultrafine Chemicals. Chalcones [xanthohumol (XN); 2′,4′,6′,4-tetrahydroxy 3′-prenylchalcone (TP); 2′,4′,6′,4-tetrahydroxy 3′-geranylchalcone (TG); dehydrocycloxanthohumol (DX); dehydrocycloxanthohumol hydrate (DH); 5′-prenylxanthohumol (PX); tetrahydroxyxanthohumol (TX); and x,5′-diprenylxanthohumol (DPX)] and flavanones [isoxanthohumol (IX); 6-prenylnaringenin (6PN); 8-prenylnaringenin (8PN); and diprenylnaringenin (DPN)] (figure 1) were isolated and purified from hops or synthesized as described by Stevens *et al.* (1997, 1999a, b) The purity of the materials was estimated at $>98\%$ by hplc-UV, atmospheric pressure chemical ionization-mass spectrometry and ^{1}NMR spectroscopy.

Microsomes

Insect cell (BTI-TN-5B1–4) microsomes (Supersomes) containing cDNA-expressed human cytochromes P450 CYP1A1, CYP1A2, CYP1B1, CYP2E1 or CYP3A4 were from GENTEST Corp. The Supersomes with the cDNA-expressed P450 also contained cDNA-expressed NADPH cytochrome P450 reductase, and in some cases, cytochrome b_5 (for CYP3A4 and CYP2E1).

7-Ethoxyresorufin O-*deethylase* (*EROD*) *assay*

EROD activity of cDNA-expressed human CYP1A1 and CYP1B1 was determined as described by Pohl and Fouts (1980) with some modifications. Briefly, each incubation tube (16×100 mm) contained 0.1 M Tris-HCl (pH 7.4), P450 (5 pmole for CYP1A1, 10 pmole for CYP1B1), 2 mM magnesium chloride, 0.1 mM EDTA, 1 mM NADPH and 2 μM 7-ethoxyresorufin, in a final volume of 1 ml. After a 5-min incubation at 37 °C, the reaction was stopped by the addition of 1 ml methanol. The tubes were centrifuged and the fluorescence of product (resorufin) in the supernatant was measured at 585 nm in a Perkin–Elmer fluorescence spectrophotometer using an excitation wavelength of 530 nm. Under the described incubation conditions, the reaction was linear for 5 min as confirmed in a dynamic assay where the reaction in a 1 ml incubation mixture was monitored fluorometrically.

In the inhibition studies comparing the effects of the various flavonoids, 1 μl flavonoid in ethanol (ethanol alone for controls, 0.1% final concentration) was added to the incubation mixture to give a final concentration of 10 μM before starting the reaction with NADPH. Similar incubations with NG, GS or RV (each at 10 μM) were run for comparative purposes. To generate kinetic data, xanthohumol was added to the incubation mixture at concentrations of 0.5, 0.75 or 1.0 μM for CYP1A1 and at 0.5, 1.0 or 2.0 for CYP1B1. 7-Ethoxyresorufin was added at final concentrations of 0.0625, 0.125, 0.25, 0.5 or 1 μM.

Acetanilide 4-hydroxylase (AC-4-OH) assay

The metabolism of acetanilide to 4-hydroxyacetanilide was determined according to the procedure of Liu *et al.* (1991) with some modifications. The incubation mixture contained 50 mM potassium phosphate buffer (pH 7.4), 20 pmole cDNA-expressed human CYP1A2, 5 mM magnesium chloride, 1 mM EDTA, 10 mM glucose 6-phosphate, 1 unit/ml glucose 6-phosphate dehydrogenase and 1 mM NADPH in a final volume of 0.25 ml. The flavonoids were added to the incubation mixture in 0.5 μl ethanol at a final concentration of 10 μM. Similar incubations with other phytochemicals (NG, GS, RV) were run for comparative purposes (each at 10 μM). Controls contained ethanol alone (0.2% final concentration). For the determination of IC_{50}, the concentration of flavonoid in the incubation mixture ranged from 1 to 100 μM. For kinetic data, incubations contained 8PN at concentrations of 2, 3 or 4 μM with varying substrate concentrations of 50, 100, 250 or 500 μM. The reaction was started by adding NADPH and terminated after 1-h incubation at 37 °C by the addition of 25 μl H_3PO_4. The samples were vortexed and centrifuged at 16000 *g* for 20 min before analysis of the supernatant by hplc.

Concentrations of 4-hydroxyacetanilide were determined using a Waters (Milford, MA, USA) 3 μm Novapak C_{18} reverse-phase column (3.9×150 mm) at a flow rate of 0.8 ml/min and detection at 240 nm. Instrumentation included a Waters 2690 hplc with a 996 photo-diode array detector. The solvent system was 15% methanol and 85% 0.001 M H_3PO_4 for 3.5 min, then a linear gradient to 40% methanol in 1 min with a return to initial conditions at 8 min. The column was equilibrated for 5 min before the next injection.

AFB_1 metabolism

Inhibition of AFB_1 metabolism was examined by hplc analysis of the reactive metabolites produced and trapped as Tris-dihydrodiols (DHD), and aflatoxin M_1 (AFM_1) (Manson *et al.* 1997). Incubation mixtures contained 100 mM Tris-HCl (pH 7.5), 2 mM magnesium chloride, 10 mM KCl, 0.2 mM EDTA, 40 pmole cDNA-expressed human CYP1A2, 100 μM AFB_1 and 1 mM NADPH in a final volume of 0.5 ml. Flavonoids were added in 0.5 μl ethanol at concentrations of 5, 25 or 100 μM. Controls contained ethanol only (0.1% final concentration). Incubations were for 30 min at 37 °C. Reactions were stopped by the addition of 100 μl 2 M acetic acid. Samples were frozen for 2 h at − 20 °C, thawed, centrifuged 20 min at 16000*g* in a microfuge, then analysed by hplc using the instrumentation described above and a Pirkle-concept column essentially as described by Stresser *et al.* (1994). The mobile phase was 40% methanol and 60% 20 mM potassium phosphate buffer (pH 4.0) at 1 ml/min with detection at 360 nm. After 25 min, methanol concentration was increased to 80% over 2 min and kept at this concentration for 18 min before being returned to initial conditions.

AFB_1–protein covalent binding

Incubations were completed as described above but with [^{3}H]-AFB_1. IX and 8PN concentrations were 25 μM. After protein precipitation and centrifugation, the supernatants were removed and the pellets exhaustively extracted with methanol. The protein was then redissolved in 1 N NaOH and an aliquot counted by scintillation spectrometry.

Chlorzoxazone 6-hydroxylase assay

Chlorzoxazone 6-hydroxylase activities of cDNA-expressed CYP2E1 were determined by the method of Peter *et al.* (1990). The typical incubation mixture consisted of 50 mM Tris-HCl (pH 7.4), insect cell microsomes (equivalent to 20 pmols CYP2E1), 1 mM magnesium chloride, 5 mM potassium chloride, 1.0 mM NADPH, substrate and flavonoid (dissolved in 0.5 μl ethanol) in a final volume of 250 μl. As ethanol is highly inhibitory of CYP2E1, the flavonoid was added first to the tubes, then the ethanol evaporated under N_2. Based on the solubility of the flavonoids, they would readily redissolve when buffer and water were added to the tubes. Substrate concentration was 100 μM chlorzoxazone (CZX). The final concentration of flavonoid in the incubation mixture was 10 μM. Incubations were carried out at 37 °C for 60 min following the addition of NADPH. The reactions were terminated by the addition of 50 μl H_3PO_4. After centrifugation, the supernatant was analysed by hplc for 6-hydroxy CZX formed during incubation. The instrumentation and column used were the same as for the acetanilide assay. Detection was by UV at 287 nm. Solvent flow was an isocratic system of 25% acetonitrile and 85% 0.001 M H_3PO_4 at a flow rate of 0.8 ml/min.

Nifedipine oxidase assay

Nifedipine oxidase activity of cDNA-expressed CYP3A4 was determined by the method of Guengerich (1989) with modification. Incubation mixtures contained 0.1 M potassium phosphate buffer (pH 7.85), insect cell microsomes (equivalent to 20 pmols CYP3A4), 200 μM nifedipine and 10 μM flavonoid (added in 0.5 μl ethanol), in a final volume of 0.25 ml. Reactions were initiated by the addition of 1 mM NADPH and stopped after 15-min incubation at 37 °C by the addition of 0.25 ml methanol. After centrifugation to remove protein, supernatants were analysed by hplc for oxidized nifedipine. Hplc analysis used the same column and instrumentation as above. Detection was at 254 nm. Solvent flow was 0.8 ml/min of 64% methanol and 36% water run isocratically.

Statistical analysis

Statistical significance of treatment versus ethanol control for some experiments was determined by Student's *t*-test at $p \leqslant 0.05$, as indicated in legends. In others, differences between treatment groups were analysed by one-way analysis of variance (ANOVA) followed by the LSD test using the SAS program. Values were considered statistically significant at $p \leqslant 0.05$. Lineweaver–Burke plots were generated by graphing the reciprocal of the substrate concentration versus the reciprocal of the rate of metabolite formation and using the linear regression function of the SigmaPlot 4.0 program.

Results

Effects of flavonoids on EROD activity of cDNA-expressed human CYP1A1 and CYP1B1

As an initial step to reveal the inhibitory activity of hop flavonoids on the activation of chemical carcinogens by human CYP1A1 and CYP1B1, their effects on the EROD activity of these carcinogen-activating enzymes were evaluated. These

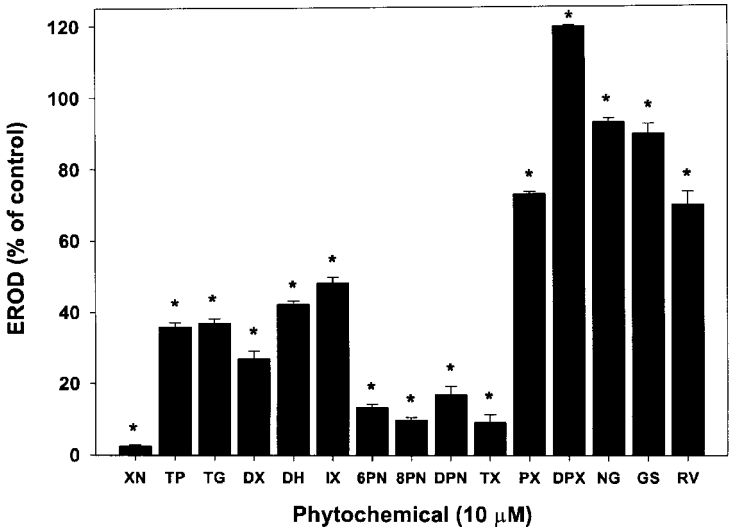


Figure 2. Inhibition of 7-ethoxyresorufin *O*-deethylase (EROD) activity of human P450 CYP1A1 by phytochemicals. Chemicals tested are: xanthohumol (XN); 2′,4′,6′,4-OH-3′-prenylchalcone (TP); 2′,4′,6′,4-OH-3′-geranylchalcone (TG); dehydrocycloxanthohumol (DX); dehydrocycloxanthohumol hydrate (DH); isoxanthohumol (IX); 6-prenylnaringenin (6PN); 8-prenylnaringenin (8PN); 6,8-diprenylnaringenin (DPN); tetrahydroxanthohumol (TX); 5′-prenylxanthohumol (PX); x,5′-diprenylxanthohumol (DPX); naringenin (NG); genistein (GS) and resveratrol(RV). Values are the means ± SE of three determinations. *Significantly different from ethanol control at $p \leq 0.05$ as determined by ANOVA followed by LSD test. Absolute value of ethanol controls = 15.8 ± 0.58 nmol/min/nmol P450.

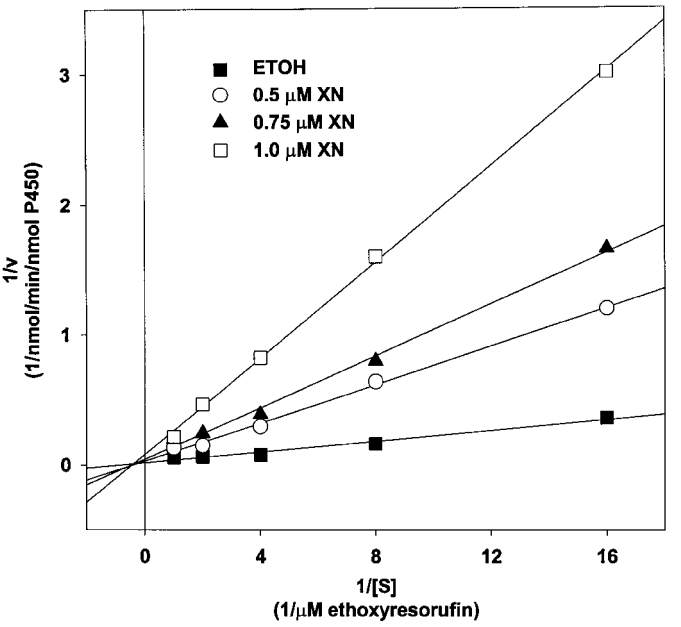


Figure 3. Lineweaver–Burke plot of inhibition of 7-ethoxyresorufin *O*-deethylase (EROD) activity of cDNA-expressed human P450 CYP1A1 by xanthohumol (XN) at 0 [ETOH (ethanol), ■], 0.5 μM (○), 0.75 μM (△) and 1.0 μM (□) concentrations. Values are means of at least four determinations.

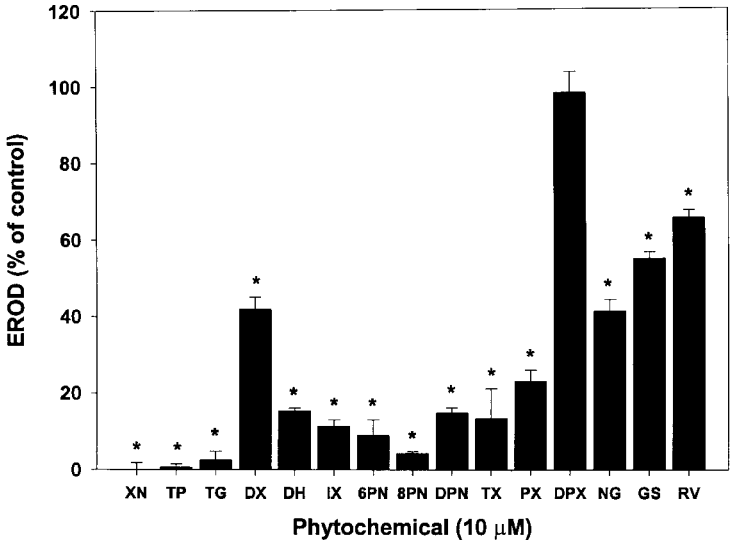


Figure 4. Inhibition of 7-ethoxyresorufin *O*-deethylase (EROD) activity of human P450 CYP1B1 by phytochemicals. Chemicals tested are xanthohumol (XN); 2′,4′,6′,4-OH-3′-prenylchalcone (TP); 2′,4′,6′,4-OH-3′-geranylchalcone (TG); dehydrocycloxanthohumol (DX); dehydrocycloxanthohumol hydrate (DH); isoxanthohumol (IX); 6-prenylnaringenin (6PN); 8-prenylnaringenin (8PN); 6,8-diprenylnaringenin (DPN); tetrahydroxanthohumol (TX); 5′-prenylxanthohumol (PX); x,5′-diprenylxanthohumol (DPX); naringenin (NG); genistein (GS) and resveratrol (RV). Values are the means ± SE of three determinations. *Significantly different from ethanol control as determined by ANOVA followed by LSD at $p \leqslant 0.05$. Absolute value of ethanol controls = 1.40 ± 0.01 nmol/min/nmol P450.

two human P450 expressed in the insect cell microsomes exhibit EROD activity as disclosed by the supplier (GENTEST Corp.) and by our own enzyme assay. EROD activity of CYP1A1 and CYP1B1 was measured in the presence of the hop chalcones (XN, TP, TG, DX, DH, TX, PX, DPX), hop flavanones (6PN, 8PN, DPN, IX), and other phytochemicals (NG, GS, RV) without pre-incubation.

Figure 2 shows that, at 10 μM concentration, XN almost completely inhibited EROD activity of CYP1A1 (2.5% of control). The next most inhibitory flavonoid at 10 μM concentration was TX, followed by 8PN, 6PN and DPN (9.2, 9.8, 13.3 and 16.8% of control respectively). The other hop flavonoids (TP, TG, DX, DH, IX) were less inhibitory, causing < 75% inhibition of EROD activity of CYP1A1. NG, a non-prenylated flavanone present in grapefruit, and GS, an isoflavone in soybeans, were the least inhibitory (10% inhibition or less) toward EROD activity of CYP1A1. Inhibition by RV, a stilbene compound from grapes, was also significantly less (30%) than all the hop flavonoids except PX. Additionally, DPX showed a slight, but significant, increase in EROD activity (119.6% of control). All of the hop flavonoids, except PX and DPX, were significantly more effective inhibitors (as analysed by ANOVA and the LSD test) than the phytochemicals from other sources (RV, NG, GS). Although the suppression by XN was not significantly greater than that of TX or 8PN, it was selected for further analysis because it is the most prevalent in hops and the most readily available for study. Inhibition of CYP1A1-mediated EROD activity by XN appeared to be non-competitive as shown by the kinetic plots in figure 3 with a calculated $K_i = 50$ nM.

The effects of the hop flavonoids and other phytochemicals (all at 10 μM) on EROD activity of CYP1B1 were also investigated (figure 4). The EROD activity of

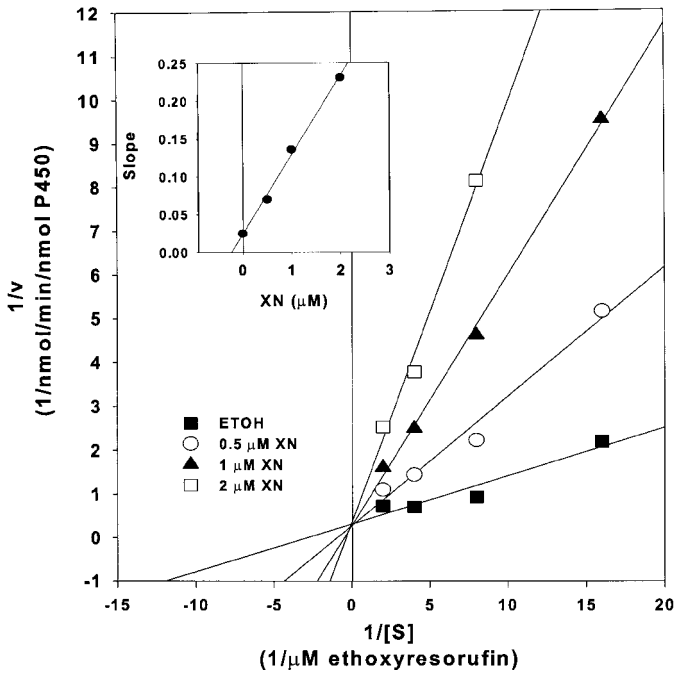


Figure 5. Lineweaver–Burke plot of inhibition of 7-ethoxyresorufin *O*-deethylase (EROD) activity of cDNA-expressed human P450 CYP1B1 by xanthohumol (XN) at 0 [ETOH (ethanol), ■], 0.5 μM (○), 1.0 μM (△) and 2.0 μM (□) concentrations. Values are means of at least four determinations. The inset graph shows a replot of the slope of the lines (apparent K_m) versus XN concentration. The linear regression equation and correlation coefficient for the line are $y = -0.2249 + 9.5229x$; $r^2 = 0.9958$.

CYP1B1 was completely eliminated by XN. TP, TG, 8PN and 6PN were the next most potent inhibitors (>90% inhibition). DH, IX, TX, DPN and PX were also effective in inhibiting CYP1B1-mediated EROD activity (75–90% inhibition). The least inhibitory flavonoids (40–60% inhibition) toward EROD activity of CYP1B1 were DX, NG and GS. RV was even less inhibitory. DPX had no effect on activity. Similarly to the data from CYP1A1, all the hop flavonoids except for DX and DPX were significantly (as analysed by ANOVA and LSD test) better inhibitors of CYP1B1 EROD activity than the phytochemicals from other sources (NG, GS, RV). Although XN was not significantly more inhibitory than TP, TG, 8PN or 6PN, it was chosen for further kinetic analysis because of its availability, occurrence in hops, and because its presence in incubations resulted in virtually no CYP1B1 activity toward EROD. As illustrated by Lineweaver–Burke plots of kinetic data shown in figure 5, inhibition of CYP1B1-mediated EROD activity by XN appeared competitive in nature with lines for all concentrations examined converging on the y axis. When the data were replotted as the slope of the lines (apparent K_m) versus XN concentration, a straight line with a $r^2 = 0.9958$ was obtained which confirmed XN as a competitive inhibitor.

Collectively, these findings indicate that XN is the most effective inhibitor of both CYP1A1 and CYP1B1 and that, in general, prenylated flavanones are more active than non-prenylated flavanones (NG) or isoflavones (GS) in inhibiting these two human P450 enzymes expressed in insect cells. Additionally, the kinetic data suggests that the flavonoids act by more than one mechanism.

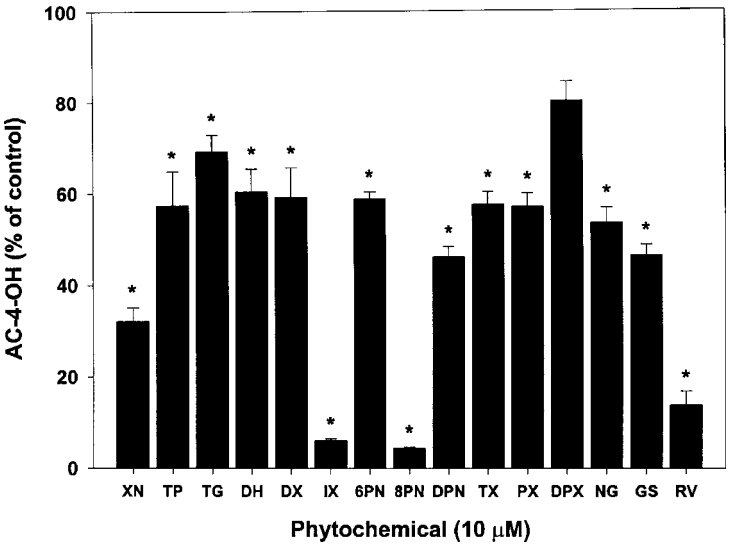


Figure 6. Inhibition of acetanilide 4-hydroxylase (AC-4-OH) activity of cDNA-expressed human P450 CYP1A2 by phytochemicals. Chemicals tested are xanthohumol (XN); 2′,4′,6′,4-OH-3′-prenylchalcone (TP); 2′,4′,6′,4-OH-3′-geranylchalcone (TG); dehydrocycloxanthohumol (DX); dehydrocycloxanthohumol hydrate (DH); isoxanthohumol (IX); 6-prenylnaringenin (6PN); 8-prenylnaringenin (8PN); 6,8-diprenylnaringenin (DPN); tetahydroxanthohumol (TX); 5′-prenylxanthohumol (PX); x,5′-diprenylxanthohumol (DPX); naringenin (NG); genistein (GS) and resveratrol (RV). Values are the means ± SE of three determinations. *Significantly different from ethanol control at $p \leqslant 0.05$ as determined by ANOVA followed by LSD test. Absolute value of ethanol controls = 32.9 ± 3.55 nmol/min/nmol P450.

Effects of flavonoids on AC-4-OH activity of cDNA-expressed human CYP1A2

The 4-hydroxylation of acetanilide is exclusively catalysed by CYP1A2 in human liver (Liu *et al.* 1991) and is one of the typical reactions mediated by cDNA-expressed human CYP1A2 (Liu *et al.* 1991, Penman *et al.* 1994). The inhibition of AC-4-OH activity of human CYP1A2 heterologously expressed in insect cells by various hop flavonoids and phytochemicals (all at a final concentration of 10 μM) was examined. All the flavonoids tested, except DPX, significantly inhibited AC-4-OH activity of CYP1A2 as compared with ethanol controls (figure 6), but the most effective inhibitors were the two prenylated flavanones, 8PN and IX (4.4 and 6.0% of control respectively) followed by XN (32.2% of control). 6PN, however, was 10 times less inhibitory than 8PN. DPX, with two prenyl groups, was the least inhibitory (80.3% of control). The stilbene RV was also a strong inhibitor of AC-4-OH (13.8% of control). None of the other flavonoids, including NG and GS, inhibited > 54% of the activity. By ANOVA and LSD test, 8PN, IX and RV were significantly most inhibitory, followed by XN. Analysis of Lineweaver–Burke plots of kinetic data generated using 8PN (figure 7) suggests that the inhibition of CYP1A2 by 8PN is of the mixed type as the lines generated by the reciprocal plots neither converge nor are they parallel.

When the inhibitory activity of a chalcone (XN) and a flavanone (IX) toward AC-4OH activity of CYP1A2 were compared in a dose–response study (figure 8), IX and XN gave IC_{50} = 4.5 and 31.4 μM respectively.

Together, these results indicate that prenylated flavanones are more inhibitory than prenylated chalcones of human CYP1A2. Furthermore, the number and

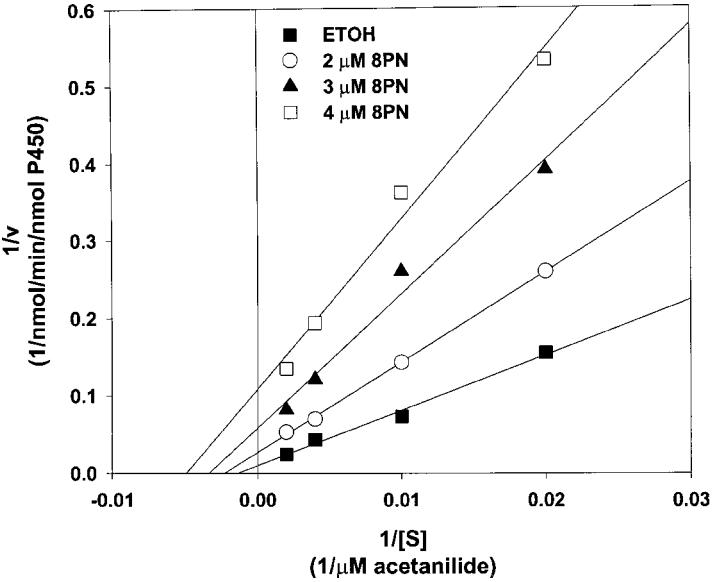


Figure 7. Lineweaver–Burke plot of inhibition of acetanilide 4-hydroxylase (AC-4-OH) activity of cDNA-expressed human P450 CYP1A2 by 8-prenylnaringenin (8PN) at 0 [ETOH (ethanol), ■], 2 μM (○), 3 μM (△) and 4 μM (△) concentrations. Values are means of at least four determinations.

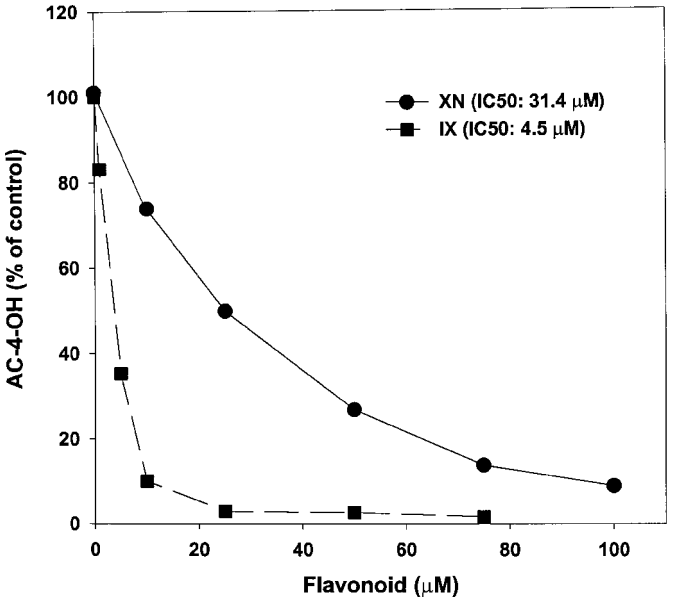


Figure 8. Dose–response study of inhibition of cDNA-expressed human P450 CYP1A2-mediated acetanilide 4-hydroxylase (AC-4-OH) activity by xanthohumol (XN) and isoxanthohumol (IX). Data points are means of three determinations.

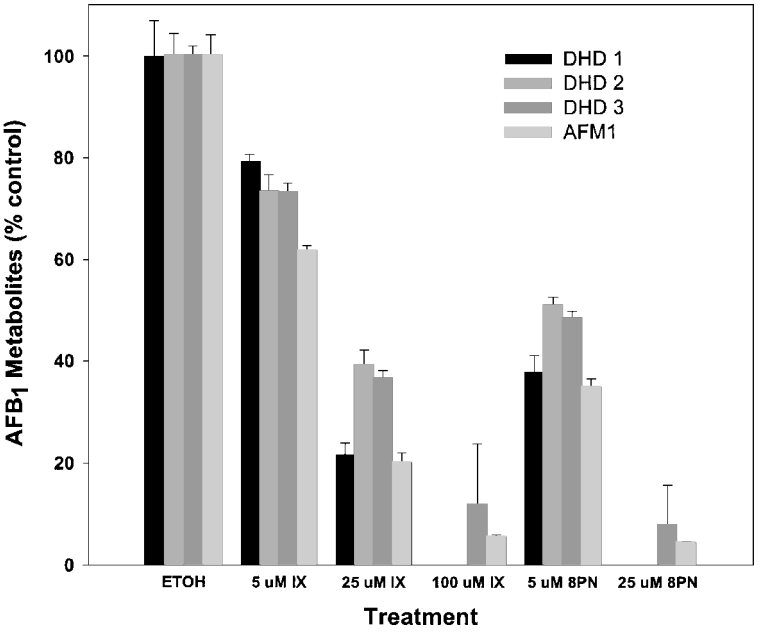


Figure 9. Effects of two flavanones [isoxanthohumol (IX) and 8-prenylnaringenin (8PN)] on the cDNA-expressed human P450 CYP1A2-mediated metabolism of AFB_1. DHD1, 2 and 3 are representative of three different Tris-dihydrodiol peaks. Data are means of three determinations ± SE

position of the prenyl group in the flavanone structure was important in the inhibitory action.

Effects of flavonoids on AFB_1 metabolism mediated by cDNA-expressed human CYP1A2

The inhibitory activity of XN, IX and 8PN toward the metabolism of the carcinogen AFB_1 was examined since it has been shown by Gallagher *et al.* (1996) to be mediated, in part, by CYP1A2. As shown in figure 9, both flavanones inhibited the oxidation of AFB_1 to dihydrodiols and AFM_1 mediated by cDNA-expressed human CYP1A2. Metabolism was almost completely eliminated by 25 μM 8PN and 100 μM IX. Binding of ^{3}H-AFB_1 to microsomal protein (figure 10) was inhibited in a concomitant manner with 25 μM 8PN virtually eliminating binding while 25 μM IX showed a lesser degree of inhibitory activity.

Effects of flavonoids on chlorzoxazone activity of cDNA-expressed human CYP2E1 and on nifedipine oxidase activity of cDNA-expressed human CYP3A4

Chlorzoxazone and nifedipine are known to be diagnostic substrates for human CYP2E1 (Peter *et al.* 1990) and CYP3A4 (Guengerich *et al.* 1986) respectively. Inhibition of the activity of cDNA-expressed human CYP2E1 and CYP3A4 by flavonoids was determined with these substrates. The catalytic activities of CYP2E1 and CYP3A4 toward chlorzoxazone and nifedipine respectively were poorly or not inhibited at all by flavonoids (data not shown) that were demonstrated to be strong inhibitors of CYP1A1-, CYP1A2- and CYP1B1-mediated activities. At 10 μM, none

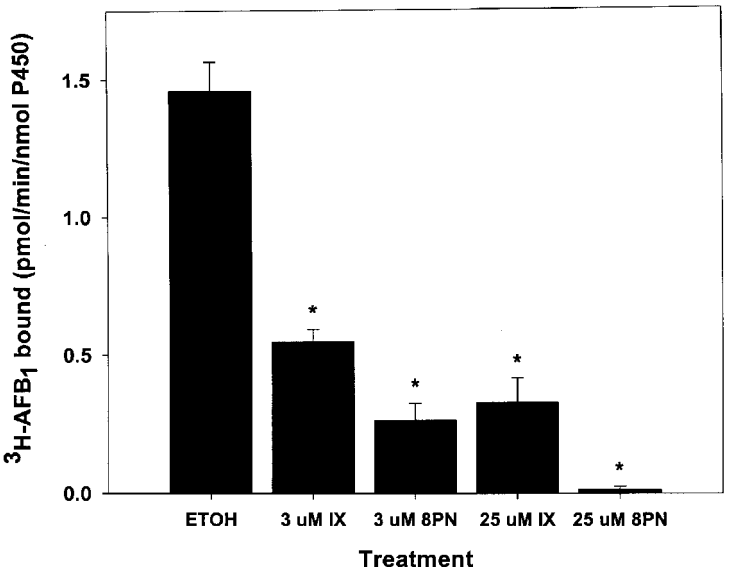


Figure 10. Binding of ^{3}H-AFB$_1$ to cDNA-expressed human P450 CYP1A2 microsomal protein in the presence of ETOH (vehicle control at 0.1%), isoxanthohumol (IX) or 8-prenylnaringenin (8PN) (3 or 25 μM). Data are means of three determinations± SE. *Significantly different from ethanol control at $p \leqslant 0.05$ by Student's t-test.

of the 12 hop flavonoids or NG inhibited either activity at $>35\%$. For example, XN, which inhibited EROD activity of CYP1A1 and CYP1B1, did not inhibit chlorzoxazone 6-hydroxylase activity of CYP2E1 whereas IX, a potent inhibitor of CYP1A2-mediated AC-4-OH activity caused only a 17% reduction of CYP2E1 activity. IX, though the most effective flavonoid inhibitor of nifedipine oxidase activity of CYP3A4, inhibited this activity only by 35% as compared with the 94% inhibition of AC-4-OH activity of CYP1A2.

Discussion

Flavonoids are phytochemicals that are either flavones, isoflavones, flavanones or chalcones that have certain biological activities that may be of benefit to the protection of human health. Some of these compounds, in edible and non-edible plants, have anti-allergenic, anti-bacterial, antioxidant, anti-inflammatory, anti-proliferative and anti-carcinogenic activities (for reviews, see Middleton and Kandaswami 1994). Flavonoids may act as anti-carcinogens by inhibiting the initiation stage of carcinogenesis through inhibition of cytochromes P450 involved in carcinogen activation. Human CYP1A1 and CYP1B1 catalyse the metabolic activation of carcinogenic PAH (Guengerich 1995) whereas CYP1A2 activates AFB$_1$ (Gallagher *et al.* 1996) and heterocyclic amines (Guengerich 1995). Therefore, it is expected that inhibition of the activities of these P450 enzymes could lead to a suppression of chemical carcinogenesis at the initiation stage by preventing the formation of reactive electrophiles that bind to DNA. The flavonoid quercetin has been reported to inhibit AHH activity of cDNA-expressed human CYP1A2. Similarly, in the present study, the present authors identified flavonoids from hops, IX and 8PN, that were highly effective in inhibiting cDNA-expressed human

CYP1A2. Furthermore, another hop flavonoid, the chalcone XN, was shown to be a potent inhibitor of cDNA-expressed human CYP1A1 and CYP1B1. By interfering with the activities of the CYP1A1 and CYP1B1 enzymes, the hop flavonoids may be potentially useful in inhibiting the bioactivation of procarcinogens which are substrates of these P450 enzymes.

If the hop flavonoids or other compounds are to be considered as potential anti-tumour initiating agents, they should have selectivity in the inhibition of human P450. Ideally, the flavonoid should be a specific inhibitor of P450 involved in carcinogen activation and not of P450 which are necessary catalysts of the metabolism of endogenous compounds and pharmaceutical drugs. Although the hop flavonoids have not been examined for their inhibitory activity toward all human P450, the present study showed that XN, IX and 8PN were poor inhibitors of CYP2E1 and CYP3A4 at concentrations (10 μM) that completely or almost completely abolished the activities of CYP1A2 (figure 6), CYP1A1 and CYP1B1 (figures 2 and 4). Additional studies are needed to demonstrate that the hop flavonoids are not inhibitors of other human P450. Earlier reports showed that the synthetic flavonoid, α-naphthoflavone, was a selective inhibitor of CYP1A1 and CYP1A2 (Guengerich and Shimada 1991) but subsequent studies revealed that this compound also inhibited other human P450 such as CYP2A6, CYP2B6, CYP2C8 and CYP2C9 (Chang *et al.* 1994).

Structure–activity studies on flavonoids as inhibitors of P450 have been conducted predominantly with rodent enzymes and with liver microsomal enzyme systems. Little information has been available on their effects on cDNA-expressed human P450. In the present study, a single human P450 enzyme was chosen instead of human liver microsomes to avoid the confounding effects of competing or other P450-mediated metabolic pathways for the substrate. Using cDNA-expressed human CYP1A2-mediated AC-4-OH activity as the endpoint, the present authors analysed the importance of the following factors in determining inhibitory activity of the hop flavonoids: presence, position and number of prenyl groups; substitution of a prenyl group with a geranyl group in a chalcone; cyclization of the prenyl substituent in a chalcone (XN versus DX); replacement of a hydroxyl group with a methoxy group in chalcone; presence (in IX) or absence (XN) of the C ring; flavanone (NG) versus isoflavone (GS); and hydrogenation of the double bond in the prenyl substituent (TX versus XN). From the data presented in figure 6, the following conditions increased inhibitory activity of the hop flavonoids toward CYP1A2: (1) addition of a prenyl group to a flavanone (8PN) was more inhibitory than NG); (2) presence of a prenyl substituent in the 8 position (8PN) instead of the 6 position (6PN) in the A ring of the flavanone nucleus; (3) presence of a methoxy group (XN) instead of a hydroxyl group at the 6′ position (TG) of the A ring of a chalcone; (4) presence (IX) rather than absence (XN) of the C ring; and (5) presence of a double bond in a prenyl substituent at the 3′ position in the A ring of a chalcone (XN versus TX). The substitution of a prenyl group (in TP) with a geranyl group (in TG) did not appreciably influence inhibitory activity of the chalcones toward CYP1A2. Cyclization of the prenyl substituent in a chalcone (XN versus DX or DH) reduced inhibitory activity by half. The use of an isoflavone (GS) instead of a flavanone (NG) also did not significantly increase the inhibitory action of the flavonoids. RV, a phytochemical from grapes with a stilbene structure, showed considerable inhibitory activity but not as much as 8PN or IX (though this difference was not statistically significant).

It was of interest to determine if the structure–activity relationships noted for the high inhibitory activity of the flavonoids toward CYP1A2 also apply to CYP1A1 or CYP1B1. As in the case of CYP1A2, the presence of a prenyl substituent increased the inhibitory activity of the flavanones toward CYP1A1 and CYP1B1. The presence of a methoxy group (in XN) instead of a hydroxyl group at the 6′ position (in TP) of the A ring was important for enhancing inhibitory activity of the chalcone for CYP1A1 but not for CYP1B1. In contrast to the case of CYP1A2, XN (a prenylated chalcone) was significantly more inhibitory than IX (a prenylated flavanone) toward CYP1A1 and CYP1B1 (figures 1 and 3). These findings suggest that there is no consistent structure–activity relationships in the inhibitory activity of the prenylated flavonoids toward different forms of human P450.

XN was a potent inhibitor of both human CYP1A1 and CYP1B1 but the type of inhibition produced by XN differed with the two P450. XN was a competitive inhibitor of CYP1B1 (figure 5) but inhibited CYP1A1 in a non-competitive manner (figure 3). In contrast, 8PN appeared to be a mixed-type inhibitor of CYP1A2 (figure 7), as were IX and XN (data not shown). These differences in inhibitory patterns indicate the complexity of the inhibitory mechanisms for the hop flavonoids toward human P450 and suggest possible exploitation of that property in developing the flavonoids as chemopreventive agents. Studies determining possible synergistic effects would also be useful.

The studies with the carcinogen AFB_1 indicate that IX and 8PN, the two most effective suppressors of CYP1A2 activity toward acetanilide, were also very successful in preventing formation of Tris dihydrodiols and AFM_1. Although the conversion to AFM_1 is often considered a detoxifying step, the conversion to dihydrodiols results in protein binding (Manson *et al.* 1997), probably associated with a toxic effect. The elimination of diols by 25 μM 8PN correlates with the reduction of AFB_1 protein binding by the same concentration of flavonoid. Even 3 μM IX (near the calculated IC_{50}) reduced protein binding by more than half.

Though IX and 8PN showed similar potencies in the inhibition of CYP1A2 activity using acetanilide as a diagnostic substrate, they were different with AFB_1 as the marker. This discrepancy could be explained by different rates and modes of metabolism by the two substrates. Although we were examining the inhibition of only one P450 enzyme, the mechanism of catalysis may vary with the nature of the substrate. The metabolism of one substrate by a given P450 could be inhibited more strongly than the metabolism of another substrate (Newton *et al.* 1995).

Of the flavonoids studied, XN is the most prevalent in hops, but IX is present in the highest concentration in a variety of beers (Stevens *et al.* 1999a) since XN is converted to its isomeric counterpart IX, in the brewing process. A recent study by Arimoto-Kobayashi *et al.* (1999) reports inhibitory effects of beer on mutagenesis and DNA adduct formation induced by carcinogens, such as heterocyclic amines. The effects were not seen from treatment with ethanol alone and the authors concluded that the results were due to some yet unidentified components of the beer. It is possible that the hop flavonoids could be involved in these effects. Recent work by Miranda *et al.* (1999) showed that XN, IX and 8PN at 2 μM concentration, are capable of inhibiting the mutagenic activity of the heterocyclic amine, IQ, in the Ames/Salmonella TA98 assay. XN also inhibited the binding of IQ to calf-thymus DNA catalyzed by cDNA-expressed human CYP1A2. These results support the possibility these flavonoids, which are found in beer (Stevens *et al.* 1999a, b) may contribute to the inhibitory activity reported by Arimoto-Kobayashi *et al.* (1999).

An additional advantage to the hop flavonoids as chemopreventive agents for some types of carcinogens may be their ability to induce the phase II detoxifying enzymes, quinone reductase (Aponso *et al.* 1998) and glutathione *S*-transferase. As the ultimate outcome of carcinogenicity is dependent on a balance of bioactivation and detoxification enzymes, compounds which inhibit bioactivation while inducing detoxification could be particularly useful.

Preliminary results from our laboratory showed that control, phenobarbital-induced, β-naphthoflavone-induced and isosafrole-induced liver microsomes can metabolize XN (Yilmazer *et al.* 1999). These findings indicate that several P450 enzymes may be involved in the metabolism of XN, the major prenylchalcone in hops and beer. This suggests the possible decrease in the levels of parent compound available, thus the effective concentration required for inhibition may be higher than that shown by incubations with a single P450 enzyme.

While these results are promising, it is possible that the hop flavonoids shown to inhibit carcinogen-activating enzymes *in vitro* may become inducers *in vivo*. However, recent evidence (Miranda *et al.*, unpublished data) suggests that the hop flavonoids XN and IX and other chalcones do not induce CYP1A1/CYP1A2 but rather suppress the expression of these enzymes in mouse hepatoma Hepa 1c1c7 cells. Preliminary studies conducted in our laboratory showed that oral or i.p. administration of XN or IX does not induce EROD activities in mouse liver microsomes (Miranda *et al.*, unpublished data).

Additional *in vivo* studies are necessary before flavonoids could be considered for any type of clinical or prophylactic application. Information concerning absorption and excretion, bioavailability, as well as gastrointestinal and hepatic metabolism of the hop flavonoids would be pertinent.

A recent discussion article by Mukhtar and Ahmad (1999), suggests 'a ''cocktail approach'' that relies on a combination of agents, which individually are effective against distinct targets'. It is felt that the hop favonoids may have a place in such an approach in the chemoprevention of cancer.

In summary, several unique flavonoids from hops, particularly XN, IX and 8PN, were shown to be potent and selective inhibitors of certain human P450 known to bioactivate carcinogens. This inhibitory ability could be exploited in developing cancer prevention strategies and warrants further *in vitro* and *in vivo* studies including those examining effects on other carcinogen-activating enzymes in humans (CYP2A6, CYP2B6, CYP2C8, CYP2C9), possible synergistic activity and effects on DNA binding and tumour formation.

Acknowledgements

This work was supported by the Hop Research Council and NIEHS grant 00210. The manuscript was issued by the Oregon State University Agricultural Experiment Station as Technical Paper No. 11416.

References

Aoyama, T., Yamano, S., Guzelian, P. S., Gelboin, H. V. and Gonzalez, F. J., 1990, Five of 12 forms of vaccinia virus-expressed human hepatic cytochrome P450 metabolically activate aflatoxin B_1. *Proceedings of the National Academy of Sciences, USA*, **87**, 4790–4793.

Aponso, L., Miranda, C. L., Stevens, J. F., Deinzer, M. L. and Buhler, D. R., 1998, Induction of quinone reductase by flavonoids from hops (*Humulus lupulus*) in cultured mouse hepatoma (Hepa 1c1c7) cells. *Toxicological Sciences*, **42**, 185.

ARIMOTO -KOBAYASHI , S., SUGIYAMA , C., HARADA, N., TAKEUCHI , M., TAKEMURA , M. and HAYATSU, H., 1999, Inhibitory effects of beer and other alcoholic beverages on mutagenesis and DNA adduct formation induced by several carcinogens. *Journal of Agricultural and Food Chemistry*, **47**, 221–230.

BOHM , B. A., 1993, The minor flavonoids. In J. B. Harborne (ed.), *The Flavonoids* (New York: Chapman & Hall), pp. 387–440.

CHANG , T. K. H., GONZALEZ, F. J. and WAXMAN , D. J., 1994, Evaluation of triacetyloleandomycin, α-naphthoflavone and diethyldithiocarbamate as selective chemical probes for inhibition of human P450. *Archives of Biochemistry and Biophysics*, **311**, 437–442.

CODE, E. L., CRESPI , C. L., PENMAN , B. W., GONZALEZ, F. J., CHANG , T. K. and WAXMAN , D. J., 1997, Human cytochrome P4502B6: interindividual hepatic expression, substrate specificity, and role in procarcinogen activation. *Drug Metabolism and Disposition*, **25**, 985–993.

EDENHARDER , R., RAUSCHER , R. and PLATT , K. L., 1997, The inhibition by flavonoids of 2-amino-3-methylimidazo[4,5-*f*]quinoline metabolic activation to a mutagen: a structure–activity relationship study. *Mutation Research*, **379**, 21–32.

GALLAGHER , E. P., KUNZE, K. L., STAPLETON , P. L. and EATON , D. L., 1996, The kinetics of aflatoxin B_1 oxidation by human cDNA-expressed and human liver microsomal cytochromes P450 1A2 and 3A4. *Toxicology and Applied Pharmacology*, **141**, 595–606.

GONZALEZ, F. J. and GELBOIN , H. V., 1994, Role of human cytochromes P450 in the metabolic activation of chemical carcinogens and toxins. *Drug Metabolism Reviews*, **26**, 165–183.

GUENGERICH , F. P., 1989, Analysis and characterization of enzymes. In A. Wallace Hayes (ed.), *Principles and Methods of Toxicology*, 2nd edn, pp. 777–813.

GUENGERICH , F. P., 1995, Human cytochrome P450 enzymes. In P. R. Ortiz de Montellano (ed.), *Cytochrome P450: Structure, Mechanism, and Biochemistry*, 2nd edn (New York: Plenum), pp. 473–535.

GUENGERICH , F. P. and KIM , D. H., 1990, *In vitro* inhibition of dihydropyridine oxidation and aflatoxin B1 activation in human liver microsomes by naringenin and other flavonoids. *Carcinogenesis*, **11**, 2275–2279.

GUENGERICH , F. P., MARTIN , M. V., BEAUNE , P. H., KREMERS , P., WOLFF , T. and WAXMAN , D. J., 1986, Characterization of rat and human liver microsomal cytochrome P-450 forms involved in nifedipine oxidation, a prototype for genetic polymorphism in oxidative drug metabolism. *Journal of Biological Chemistry*, **261**, 5051–5060.

GUENGERICH , F. P. and SHIMADA , T., 1991, Oxidation of toxic and carcinogenic chemicals by human cytochrome P-450 enzymes. *Chemical Research in Toxicology*, **4**, 391–407.

GUENGERICH , F. P., SHIMADA , T., RANEY , K. D., YUN, C. H., MEYER , D. J., KETTERER , B., HARRIS, T. M., GROOPMAN , J. D. and KADLUBAR , F. F., 1992, Elucidation of the catalytic specificities of human cytochromes P450 and glutathione *S*-transferase enzymes and relevance to molecular epidemiology. *Environmental Health Perspectives*, **98**, 75–80.

GUENGERICH , F. P., SHIMADA , T., YUN, C. H., YAMAZAKI , H., RANEY , K. D., THIER , R., COLES , B. and HARRIS, T. M., 1994, Interactions of ingested food, beverage, and tobacco components involving human cytochrome P4501A2, 2A6, 2E1, and 3A4 enzymes. *Environmental Health Perspectives*, **102 (suppl. 9)**, 49–53.

HENDERSON , M. C., MIRANDA , C. L., STEVENS , J. F., DEINZER , M. L. and BUHLER , D. R., 1998, *In vitro* inhibition of carcinogen metabolism by flavonoids from hops (*Humulus lupulus*) in various species. *Toxicological Science*, **42**, 185.

LIU , G., GELBOIN , H. V. and MYERS , M. J., 1991, Role of cytochrome P450 1A2 in acetanilide 4-hydroxylation as determined with cDNA expression and monoclonal antibodies. *Archives of Biochemistry and Biophysics*, **284**, 400–406.

MANSON , M. M., BALL , H. W. L., BARRETT , M. C., CLARK, H. L., JUDAH , D. J., WILLIAMSON , G. and NEAL , G. E. 1997, Mechanism of action of dietary chemoprotective agents in rat liver: induction of phase I and II drug metabolizing enzymes and aflatoxin B_1 metabolism. *Carcinogenesis*, **18**, 1729–1738.

MIDDLETON , E. JR and KANDASWAMI , C., 1994, The impact of plant flavonoids on mammalian biology: implications for immunity, inflammation and cancer. In J. B. Harborne (ed.), *The Flavonoids* (New York: Chapman & Hall), pp. 619–652.

MIRANDA , C. L. STEVENS , J. F., HELMRICH , A., HENDERSON , M. C., RODRIGUEZ , R. J., YANG , Y.-H., DEINZER , M. L., BARNES , D. W. and BUHLER , D. R., 1999, Anti-proliferative and cytotoxic effects of prenylated flavonoids from hops (*Humulus lupulus*) in human cancer cell lines. *Food and Chemical Toxicology*, **37**, 271–285.

MUKHTAR , H. and AHMAD , N., 1999, Cancer chemoprevention: future holds in multiple agents. *Toxicology and Applied Pharmacology*, **158**, 207–210.

NEWTON , D. J., WANG , R. W. and LU, A. Y. H., 1995, Cytochrome P450 inhibitors. Evaluation of specificities in the *in vitro* metabolism of therapeutic agents by human liver microsomes. *Drug Metabolism and Disposition*, **23**, 154–158.

OBERMEIER , M. T., WHITE , R. E. and YANG, C. S., 1995, Effects of bioflavonoids on hepatic P450 activities. *Xenobiotica*, **25**, 575–584.

PENMAN , B. W., CHEN , L., GELBOIN , H. V., GONZALEZ, F. J. and CRESPI , C. L., 1994, Development of a human lymphoblastoid cell line constitutively expressing human CYP1A1 cDNA: substrate specificity with model substrates and promutagens. *Carcinogenesis*, **15**, 1931–1937.

PETER , R., BOCKER , R. G., BEAUNE , P. H., IWASAKI , M., GUENGERICH , F. P. and YANG, C. S., 1990, Hydroxylation of chlorzoxazone as a specific probe for human liver cytochrome P-450 IIE1. *Chemical Research in Toxicology*, **3**, 566–573.

PEZZUTO, J. M., 1997, Plant-derived anticancer agents. *Biochemical Pharmacology*, **53**, 121–133.

POHL , R. J. and FOUTS , J. R., 1980, A rapid method for assaying the metabolism of 7-ethoxyresorufin by microsomal subcellular fractions. *Annals of Biochemistry*, **107**, 150–155.

SHIMADA , T., HAYES, C. L., YAMAZAKI , H., AMIN , S., HECHT , S. S., GUENGERICH , F. P. and SUTTER , T. R., 1996, Activation of chemically diverse procarcinogens by human cytochrome P-450 1B1. *Cancer Research*, **56**, 2979–2984.

SHOU , M., KORZEKWA, K. R., CRESPI , C. L., GONZALEZ, F. J. and GELBOIN , H. V., 1994, The role of 12 cDNA-expressed human, rodent, and rabbit cytochromes P450 in the metabolism of the benzo[*a*]pyrene and benzo[*a*]pyrene trans-7,8-dihydrodiol. *Molecular Carcinogenesis*, **10**, 159–168.

SHOU , M., KORZEKWA, K. R., KRAUSZ, K. W., BUTERS , J. T., GROGAN , J., GOLDFARB , I., HARDWICK , J. P., GONZALEZ, F. J. and GELBOIN , H. V., 1996b, Specificity of cDNA-expressed human and rodent cytochrome P450 in the oxidative metabolism of the potent carcinogen 7,12-dimethybenz[*a*]anthracene. *Molecular Carcinogenesis*, **17**, 241–249.

SHOU , M., KRAUSZ, K. W., GONZALEZ, F. J. and GELBOIN , H. V., 1996a, Metabolic activation of the potent carcinogen dibenzo[a,l]pyrene by human recombinant cytochromes P450, lung and liver microsomes. *Carcinogenesis*, **17**, 2429–2433.

SHOU , M., KRAUSZ, K. W., GONZALEZ, F. J. and GELBOIN , H. V., 1996c, Metabolic activation of the potent carcinogen dibenzo[a,h]anthracene by cDNA-expressed human cytochromes P450. *Archives of Biochemistry and Biophysics*, **328**, 201–207.

SIESS , M.-H., LECLERC , J., CANIVENC -LAVIER , M.-C., RAT, P. and SUSCHETET , M., 1995, Heterogenous effects of natural flavonoids on monooxygenase activities in human and rat liver microsomes. *Toxicology and Applied Pharmacology*, **130**, 73–78.

STEVENS , J. F., IVANCIC , M., HSU, V. L. and DEINZER , M. L., 1997, Prenylflavonoids from *Humulus lupulus*. *Phytochemistry*, **44**, 1575–1585.

STEVENS , J. F., MIRANDA , C. L., BUHLER , D. R. and DEINZER , M. L, 1998, Chemistry and biology of hop flavonoids. *Journal of the American Society of Brewing Chemistry*, **56**, 136–145.

STEVENS , J. F., TAYLOR , A. W. and DEINZER , M. L., 1999a, Quantitative analysis of xanthohumol and related flavonoids in hops and beer by liquid chromatography tandem mass spectrometry. *Journal of Chromatography*, **A832**, 97–107.

STEVENS , J. F. TAYLOR , A. W., CLAWSON , J. E. and DEINZER , M. L., 1999b, Fate of xanthohumol and related prenylflavonoids from hops to beer. *Journal of Agricultural and Food Chemistry*, **47**, 2421–2428.

STRESSER , D. M., WILLIAMS , D. E., MCLELLAN , L. I., HARRIS , T. M. and BAILEY , G. S., 1994, Indole 3-carbinol induces a rat liver glutathione transferase subunit (yc2) with high activity toward aflatoxin B_1-*exo*-epoxide. *Drug Metabolism and Disposition*, **22**, 392–399.

TASSANEEYAKUL , W., BIRKETT , D. J., VERONESE , M. E., MCMANUS , M. E., TUKEY , R. H., QUATTROCHI , L. C., GELBOIN , H. V. and MINERS , J. O., 1993, Specificity of substrate and inhibitor probes for human cytochromes P450 1A1 and 1A2. *Journal of Pharmacology and Experimental Therapeutics*, **265**, 401–407.

TSYRLOV , I. B., MIKHAILENKO , V. M. and GELBOIN , H. V., 1994, Isozyme- and species-specific susceptibility of cDNA-expressed CYP1A P-450s to different flavonoids. *Biochimica et Biophysica Acta*, **1205**, 325–335.

WATTENBURG , L. W., 1983, Inhibition of neoplasia by minor dietary constituents. *Cancer Research*, 26, 1520–1526.

YILMAZER , M., STEVENS , J. F., DEINZER , M. L. and BUHLER , D. R., 1999, *In vitro* biotransformation of xanthohumol by rat liver microsomes. *Toxicological Sciences*, **48**, 223.

ZHAO, K., SURRAY, S., DAVIES, D. S., BOOBIS , A. R. and GOODERSHAM , N. J., 1994, Metabolism of the food derived mutagen and carcinogen 2-amino-1-methyl 6-phenylimidazo(4,5-*b*)pyridine (PhIP) by human liver microsomes. *Carcinogenesis*, **15**, 1285–1288.

XENOBIOTICA , 2000, VOL. 30, NO. 3, 253–261

Sulphonation of N-hydroxy-2-acetylaminofluorene by human dehydroepiandrosterone sulphotransferase

A. J. LEWIS, Y. OTAKE, U. K. WALLE and T. WALLE*

Department of Cell and Molecular Pharmacology and Experimental Therapeutics, Medical University of South Carolina, 173 Ashley Avenue, PO Box 250505, Charleston, SC 29425, USA

Received 28 April 1999

1. The aim was to determine which human recombinant sulphotransferase (ST) isoform(s) were responsible for the sulphonation and, thus, potential further bioactivation of the classical hepatic procarcinogen N-hydroxy-2-acetylaminofluorene (N-OH-2AAF).

2. N-OH-2AAF was incubated together with the cosubstrate 3′-phosphoadenosine-5′-phosphosulphate (PAPS) and either human liver cytosol or recombinant P-form phenol-sulphotransferase (P-PST), M-form PST, dehydroepiandrosterone-ST (DHEA-ST) or oestrogen ST (EST). Formation of 3′-phosphoadenosine-5′-phosphate (PAP) from PAPS, measured by HPLC, was used as the assay for determination of sulphoconjugation rates.

3. The liver cytosol produced a 100% increase in PAP formation in the presence of 200 μM N-OH-2AAF as compared with baseline levels ($p < 0.01$), corresponding to a rate of 19 pmol/min/mg protein. Recombinant P-PST, however, was without effect. This is in contrast to previous suggestions using crude enzyme preparations. Like P-PST, recombinant M-PST and EST did not sulphonate N-OH-2AAF. On the other hand, recombinant DHEA-ST produced a 161% increase in PAP formation in the presence of 200 μM N-OH-2AAF as compared with baseline values ($p < 0.001$).

4. Kinetic studies of N-OH-2AAF sulphonation by DHEA-ST and human liver cytosol gave similar apparent K_ms. Interestingly, the V_{max} for N-OH-2AAF sulphonation by DHEA-ST was very similar to that of DHEA, the natural substrate for DHEA-ST.

5. This is the first paper to demonstrate the involvement of the human DHEA-ST in the sulphonation of an N-hydroxylated aromatic amide carcinogen.

Introduction

Bioactivation of the classical carcinogenic aromatic amide 2-acetylaminofluorene (2AAF) in animals and human initially involves cytochrome P450 oxidation to the corresponding N-hydroxylated aromatic amide N-OH-2AAF (Heflich and Neft 1994). However, subsequent esterification by sulphonation and/or acetylation further increases the ability of this hepatic procarcinogen to react with DNA, preferentially forming N-(deoxyguanosin-8-yl) adducts (for reviews, see Miller and Surh 1994, Michejda and Kroeger Koepke 1994). The occurrence of sulphonation as a bioactivation step for N-OH-2AAF in human was established with the liver cytosol as the sulphotransferase (ST) enzyme source, using either a DNA binding assay (Abu-Zeid *et al.* 1992, Chou *et al.* 1995) or an assay based on the formation of PAP from the co-substrate PAPS (Gilissen *et al.* 1994). These studies suggested that the phenol (P) form phenolsulphotransferase (PST) is the ST isoform responsible for the sulphonation of N-OH-2AAF.

Preliminary observations in our laboratory prompted a more thorough analysis of the STs involved in the sulphonation of N-OH-2AAF, using recombinant human

* Author for correspondence; e-mail: wallet@musc.edu

Xenobiotica ISSN 0049–8254 print/ISSN 1366–5928 online © 2000 Taylor & Francis Ltd
http://www.tandf.co.uk/journals/tf/00498254.html

isoforms. Because sulphuric acid esters of the aromatic N-hydroxylated amides are highly unstable in aqueous medium, direct assays of these metabolites are not possible. As it has been suggested that bioactivated N-OH-2AAF preferentially binds to protein rather than DNA (DeBaun *et al.* 1970, Heflich and Neft 1994), the PAPS to PAP conversion assay was selected (Duffel *et al.* 1989, Gilissen *et al.* 1992, 1994) as a measure of sulphonation rates.

Materials and methods

Chemicals

N-Hydroxy-2-acetylaminofluorene (N-OH-2AAF) was from the National Cancer Institute Chemical Carcinogen Reference Standard Repository at the Midwest Research Institute, Kansas City, MO, USA. Its purity, determined by HPLC, was ~95%. Ultrapure 3′-phosphoadenosine-5′-phosphosulphate (PAPS) was from S. S. Singer, University of Dayton, Dayton, OH. [^{35}S]-Labelled PAPS (specific activity 1.0–1.5 Ci mmol^{-1}), [^{3}H]-labelled dehydroepiandrosterone (DHEA) (89 Ci mmol^{-1}) and [^{3}H]-labelled 17β-oestradiol (50 Ci mmol^{-1}) were from DuPont NEN (Wilmington, DE, USA). *p*-Nitrophenol, DHEA, DHEA sulphate, dopamine hydrochloride, 17β-oestradiol and adenosine 3′,5′-diphosphate (PAP) were from Sigma Chemical Co. (St Louis, MO, USA). Other chemicals were obtained from standard sources of the highest available purity.

Liver cytosol

Human liver tissue was from the Liver Tissue Procurement and Distribution System (LTPADS, University of Minnesota) and the 100000*g* cytosol was prepared from a 25% homogenate in 250 mM sucrose/3 mM 2-mercaptoethanol in pH 6.5, 5 mM potassium phosphate buffer (Campbell *et al.* 1987, Walle *et al.* 1993) and was stored at −80 °C.

Recombinant sulphotransferases

Recombinant human dehydroepiandrosterone sulphotransferase (DHEA-ST), human M-form phenolsulphotransferase (M-PST) and human oestrogen sulphotransferase (EST) were purified from DHEA-ST/pKK233-2, M-PST/pKK233-2 and EST/pKK233-2 constructs respectively expressed in *E. coli*, as described (Falany *et al.* 1994, 1995b, Ganguly *et al.* 1995). Recombinant human histidine-labelled P-form phenolsulphotransferase (P-PST) was purified from a P-PST/pET-15b construct expressed in *E. coli*, as described (Lewis *et al.* 1996). Because of the efficient affinity column cleanup, P-PST was >99% pure; however, the other ST isoforms contained multiple non-ST proteins, even after ion-exchange chromatography, as evident by SDS-PAGE. Because of limited stability, further purification of these isoforms was unsuccessful.

N-OH-2AAF sulphonation assay

N-OH-2AAF sulphonation activity was determined by measuring the formation of PAP from PAPS, as described (Duffel *et al.* 1989, Gilissen *et al.* 1994), with minor modifications. Briefly, the reaction mixture (30 μl) consisted of 25 μM ultrapure PAPS, 200 μM N-OH-2AAF, 8.3 mM dithiothreitol and 6 μl either liver cytosol (120–150 μg protein), P-PST (0.4 μg protein), DHEA-ST (7 μg protein), M-PST (9 μg) or EST (6 μg) in 250 mM potassium phosphate buffer (pH 7.0). As the specific activities of the ST in these preparations were very different, the amounts of the enzyme preparations used in the incubations were selected to produce similar rates of PAP formation in the presence of the respective model substrates, i.e. *p*-nitrophenol for P-PST, DHEA for DHEA-ST, dopamine for M-PST and 17β-oestradiol for EST. After a 30-min incubation at 37 °C, the reaction was terminated by addition of 30 μl ice-cold methanol and 20 μl supernatant (after centrifugation) was analyzed by HPLC. Control incubations represent both enzymatic and nonenzymatic hydrolysis of PAPS to PAP in the absence of substrate. In the kinetic experiments a range of N-OH-2AAF concentrations (25–400 μM) was used. In some experiments 500 μM DHEA sulphate was added to the recombinant DHEA-ST and liver cytosol incubates in an attempt to inhibit N-OH-2AAF-mediated PAP formation.

The validity of the PAPS to PAP conversion assay was originally tested with 1-naphthalenemethanol as the substrate and rat arylsulphotransferase IV as the enzyme (Duffel *et al.* 1989). In the present study DHEA as substrate and human DHEA-ST as the enzyme were used. In both cases HPLC measured the sulphonated substrates. For both substrates, PAP formation was stoichiometric with the amount of sulphate conjugates formed.

HPLC analysis of PAP formation

The supernatant from N-OH-2AAF incubations was analyzed by a modification of a previous HPLC method (Duffel *et al.* 1989). An Econosphere C18 column (Alltech Associates, Deerfield, IL, USA) was used with a mobile phase of ammonium chloride (100 mM), octylamine (2 mM), in potassium phosphate buffer (75 mM, pH 5.45) with 18% methanol (v/v) at a flow rate of 1.2 ml/min and UV detection at 254 nm. PAP standard curves were generated by injecting known amounts of PAP (0–200 pmole).

Determination of ST activities in human liver cytosols

P-PST and M-PST activities in the liver cytosols were measured with 1 μM *p*-nitrophenol and 40 μM dopamine as the substrates with 0.4 μM [^{35}S]-labelled PAPS as the co-substrate, as described (Anderson and Weinshilboum 1980, Walle and Walle 1990). After $Ba(OH)_2/ZnSO_4$ precipitation (Foldes and Meek 1973), the radioactivity content in the supernatants was measured by liquid scintillation spectrometry. The DHEA-ST activity in the liver cytosols was measured with 3 μM [^{3}H]DHEA as the substrate and 20 μM unlabelled PAPS as the co-substrate (Falany *et al.* 1989). The formation of [^{3}H]DHEA sulphate was measured by counting the supernatant after chloroform extraction. EST activity measurements used 10 nM [^{3}H]17β-oestradiol as the substrate (Falany *et al.* 1995b).

Immuno-inhibition and immunoprecipitation of DHEA-ST in human liver cytosol

Immuno-inhibition experiments were carried out by pre-incubating human liver cytosol and PAPS for 5 min with increasing amounts (0.01–10 μg) of either rabbit anti-rat DHEA-ST IgG (Sharp *et al.* 1993), previously shown to cross-react with human DHEA-ST, or rabbit anti-human DHEA-ST IgG (Comer and Falany 1992) before adding 3 μM [^{3}H]DHEA. The formation of DHEA sulphate after 30 min at 37 °C was measured as above (Falany *et al.* 1989). In immunoprecipitation experiments, human liver cytosol was incubated with 0.01–10 μg of the rat or human DHEA-ST antibodies in 1 ml immunoprecipitation buffer (50 mM HEPES, pH 7.4, 0.15 M NaCl, 1 mM EDTA) (Oemar *et al.* 1991) for 24 h at 4 °C. After incubation, the immune complexes were precipitated by the addition of 40 μl protein A agarose beads (Boehringer Mannheim Corp., Indianapolis, IN, USA). The complexes were then washed for 3 × 20 min with immunoprecipitation buffer at 4 °C. The final pellets were boiled in SDS sample buffer and the precipitated proteins were resolved in a 12% SDS-polyacrylamide gel (Laemmli 1970). The degree of immunoprecipitation, or DHEA-ST clearance, was visualized by immunoblot analysis (Lewis *et al.* 1996) of both the precipitated antibody/antigen complex and the remaining liver cytosol, using the same antibodies as for the precipitation. In addition, antibody removal of DHEA-ST was measured as the activity remaining in the liver cytosol after immunoprecipitation, using 3 μM DHEA as the substrate (Falany *et al.* 1989).

Results

Sulphonation of N-OH-2AAF by human liver cytosol

The sulphonation reaction carried out according to the Materials and methods was linear for 45 min (data not shown) and subsequent experiments used a 30-min incubation. When the reaction was studied with respect to volume of liver cytosol, it showed evidence of saturation with volumes > 6 μl. This volume, corresponding to 120–150 μg protein, was used in further experiments. In addition, the reaction was saturable with respect to PAPS concentration. A concentration of 25 μM was used.

Figure 1A depicts the formation of PAP from PAPS in the presence of human liver cytosol. The basal rate (Control) of 2.3 ± 0.3 pmol/min (mean $\pm$ SE; $n = 6$ from two human livers) appears to be due mainly to enzymatic hydrolysis of PAPS. Thus, the PAP content in the PAPS used was very low ($< 1\%$) and incubation of PAPS in the absence of liver cytosol gave rise to only low levels of hydrolysis ($\leqslant 0.5$ pmol/min). In the presence of 200 μM N-OH-2AAF, the PAP formation increased 2-fold in the same liver cytosols to 4.6 ± 0.7 pmol/min (figure 1A) ($p < 0.01$), corresponding to an increase of 19 pmol/min/mg protein.

Apparent enzyme kinetic determinations for the sulphonation of this procarcinogen, not previously reported, using N-OH-2AAF concentrations of 25–400 μM, showed saturation kinetics, as demonstrated for one of the human liver

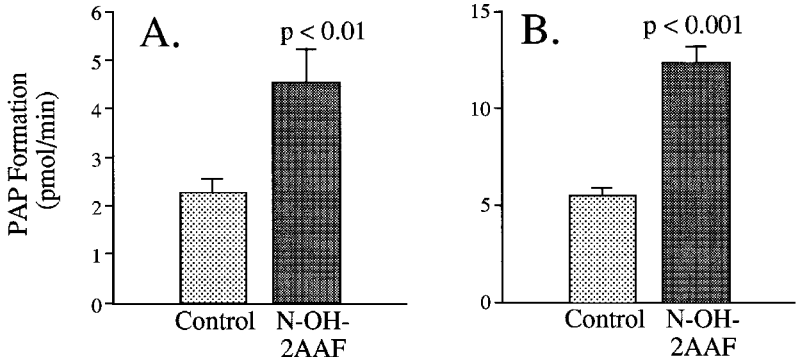


Figure 1. Sulphonation activity in the absence (Control) and presence of N-OH-2AAF (200 μM) using the PAPS to PAP conversion assay. (A) Human liver cytosol, (B) recombinant DHEA-ST. Each bar is the mean $\pm$ SE of five-to-six experiments. For experimental conditions, see the Materials and methods.

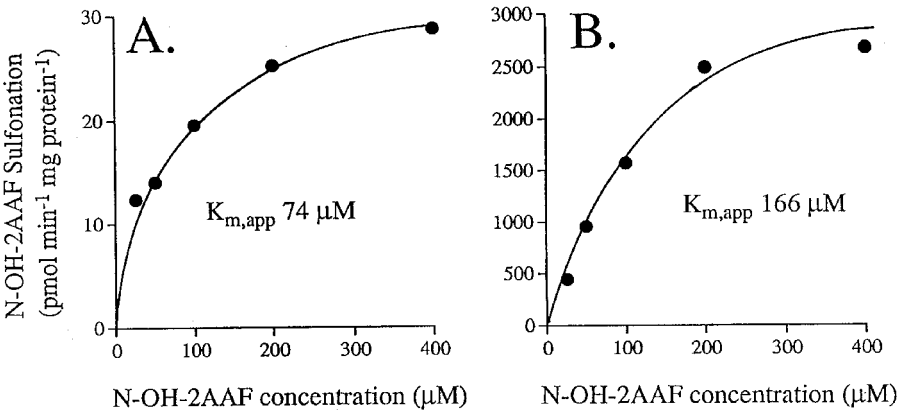


Figure 2. Effect of increasing substrate concentrations on N-OH-2AAF sulfonation by liver cytosol (A) and recombinant DHEA-ST (B). Results from representative experiments are shown. See table 1 for all observations.

Table 1. Apparent enzyme kinetic parameters for the sulphonation of N-OH-2AAF by human liver cytosol and DHEA-ST.

Human liver cytosol	K_m (μM)	V_{max} (pmol min^{-1} mg protein^{-1})	V_{max}/K_m (μl min^{-1} mg protein^{-1})
UM528	51	110	2.1
UM256	74	35	0.47
UM592	290	81	0.28
UM208	100	39	0.39
DHEA-ST	170	4130	24.9

Data for individual human livers and DHEA-ST are the mean of two determinations.

cytosols (UM256) (figure 2A). This gave an apparent $K_m = 74$ μM and a $V_{max} =$ 35 pmol/min/mg protein. Apparent enzyme kinetic parameters derived from four livers are summarized in table 1. One liver, UM528, appeared to be about four times more efficient (V_{max}/K_m) in sulphonating N-OH-2AAF than the others.

Sulphonation of N-OH-2AAF by recombinant DHEA-ST

The rate of hydrolysis of PAPS to PAP in the presence of DHEA-ST, but absence of substrate, was 5.6± 0.5 pmol/min, i.e. twice that of the liver cytosol, indicating DHEA-ST-mediated PAPS hydrolysis. In the presence of 200 μM N-OH-2AAF, PAP formation increased > 2-fold to 12.4± 1.0 pmol/min ($n = 5$; $p < 0.001$) (figure 1B), corresponding to 970 pmol/min/mg protein after subtraction of background, clearly demonstrating DHEA-ST-mediated sulphonation of N-OH-2AAF. Under the same conditions, 3 μM of the prototype substrate for DHEA-ST, i.e. DHEA, hydrolyzed PAPS at ~ 440 pmol/min/mg protein after subtraction of background, i.e. similar to N-OH-2AAF.

Apparent enzyme kinetic determinations, using N-OH-2AAF concentrations of 25–400 μM with recombinant DHEA-ST as the enzyme source, showed saturable kinetics (figure 2B) producing an apparent $K_m = 166$ μM (table 1).

Sulphonation of N-OH-2AAF by P-PST and other recombinant STs

The hydrolysis of PAPS to PAP in the presence of recombinant P-PST but in the absence of substrate was 3.0± 0.8 pmol/min ($n = 5$), i.e. similar to that for the liver cytosol (cf. figure 1A), but only one-half that for recombinant DHEA-ST. In the presence of 200 μM N-OH-2AAF the PAP production of 2.9± 0.8 pmol/min ($n = 5$) did not change from the control value. These studies were repeated at N-OH-2AAF concentrations ranging from 25 to 400 μM. There was no statistically significant increase in the PAPS to PAP hydrolysis ($n = 6$) over this concentration range. In parallel experiments sulphonation of 4 μM *p*-nitrophenol (positive control) produced an increase in PAP formation of 1.6± 0.2 pmol/min ($n = 3$).

The ability of recombinant M-PST and EST to sulphonate N-OH-2AAF was investigated over the same 25–400 μM concentration range. There was no evidence of sulphonation. The background PAP formation for M-PST was very low (~ 0.5 pmol/min), whereas for EST it was similar to that of DHEA-ST. As positive controls the sulphonation of dopamine (M-PST) and 17β-oestradiol (EST) was used.

ST isoforms in human liver cytosol

As a basis for evaluation of the contribution of various ST isoforms to the sulphonation of N-OH-2AAF *in vivo*, it was important to assess these levels in the cytosol of normal human livers. It was known from previous studies that the human liver expresses DHEA-ST (Comer and Falany 1992) as well as P-PST and M-PST (Campbell *et al.* 1987) enzyme protein. Table 2 summarizes the activity levels for these isoforms in the cytosols from five human livers. Each isoform was measured at the optimal concentration for its respective model substrate, i.e. 3 μM DHEA for DHEA-ST, 1 μM *p*-nitrophenol for P-PST and 40 μM dopamine for M-PST. As expected, DHEA-ST and P-PST demonstrated high activity whereas M-PST had very low activity. Whereas there was as much as an 8-fold variability in M-PST activity, the activities for DHEA-ST and P-PST were more uniform in these livers.

Although EST is expressed at low levels in the human liver (Falany *et al.* 1995b, Song *et al.* 1998), measurements of its activity with 17β-oestradiol as the substrate were low and erratic, potentially due to the fact that P-PST may also contribute to its sulphonation (Hernández *et al.* 1992).

Table 2. DHEA-ST, P-PST and M-PST activities in human liver cytosol. DHEA-ST activity was measured with 3 μM DHEA as the substrate, P-PST activity with 1 μM *p*-nitrophenol and M-PST with 40 μM dopamine. PAPS concentrations were 20, 0.4 and 0.4 μM respectively.

	DHEA-ST		P-PST		M-PST	
Liver cytosol	(nmol h^{-1} g $liver^{-1}$)	(pmol min^{-1} mg $protein^{-1}$)	(nmol h^{-1} g $liver^{-1}$)	(pmol min^{-1} mg $protein^{-1}$)	(nmol h^{-1} g $liver^{-1}$)	(pmol min^{-1} mg $protein^{-1}$)
UM528	2320	180	750	120	53	8.4
UM256	2020	160	640	100	120	19.0
UM592	1770	140	570	93	15	2.4
UM208	1540	140	540	96	29	5.1
UM350	1150	74	650	84	20	2.5

Data are the average of two determinations.

Inhibition of DHEA-ST in human liver cytosol

To assess further the importance of DHEA-ST in liver cytosol for the sulphonation of N-OH-2AAF, inhibition experiments were attempted. The only known inhibitor of DHEA-ST, aside from the substrate DHEA, i.e. DHEA sulphate (Watabe *et al.* 1987), produced a 70% inhibition of the sulphonation of N-OH-2AAF by recombinant DHEA-ST at very high concentration (500 μM). However, with liver cytosol there was no inhibition, presumably due to the very high protein binding of DHEA sulphate (Plager 1965).

Another approach used antibodies raised against DHEA-ST (Comer and Falany 1992, Sharp *et al.* 1993). In immuno-inhibition experiments the direct effect of DHEA-ST antibodies on the sulphonation of 3 μM DHEA was examined. Even at the highest amounts of antibody (10 μg) only 50% inhibition was observed. In attempts to use the antibodies for immunoprecipitation, only small amounts of DHEA-ST were precipitated. Greater than 90% of the enzyme still remained in the cytosol, as determined by Western blot analysis.

Discussion

The primary observation in this study was that sulphonation of the classical hepatic procarcinogen N-OH-2AAF by the human liver appeared to be catalyzed by DHEA-ST. This was established by the sulphonation activity observed with recombinant DHEA-ST and the absence of activity with other recombinant STs known to be expressed in the human liver.

Previous studies with the liver cytosol, using either the PAPS to PAP conversion or the DNA binding assay, have demonstrated high levels of sulphonation-induced bioactivation of N-OH-2AAF in rat (Gilissen *et al.* 1992, Abu-Zeid *et al.* 1992). In contrast, the first studies with human liver cytosol and the DNA-binding assay indicated that sulphonation-induced activation of N-OH-2AAF was low in comparison with rat (Falany 1991, Abu-Zeid *et al.* 1992, Chou *et al.* 1995). Using the PAPS to PAP conversion assay, Gilissen *et al.* (1994) detected an activity of 3.5 pmol/min/mg cytosolic protein. In the present study with four human livers, using identical experimental conditions, an even higher activity, 19 pmol/min/mg cytosolic protein, was observed.

The observations with the recombinant ST enzymes clearly demonstrated that sulphonation of N-OH-2AAF can be catalyzed by DHEA-ST. The apparent K_m observed with the cytosol from human livers (51–291 μM) and recombinant DHEA-

ST (166 μM) were similar. Although the binding affinity of N-OH-2AAF for DHEA-ST was considerably lower than for the primary substrate of this enzyme, i.e. DHEA (5–10 μM), its V_{max} = 35–106 pmol/min/mg protein was very similar to that for DHEA (43–211 pmol/min/mg protein) (Bamforth *et al.* 1992), measured under identical conditions.

As further shown in table 2, the activity of DHEA-ST in the human liver was high compared with P-PST and, in particular, M-PST. These activities compare well with previous reports for DHEA-ST (Falany *et al.* 1989, Wood *et al.* 1996), P-PST and M-PST (Campbell *et al.* 1987, Pacifici *et al.* 1994, Ozawa *et al.* 1998). Although a correlation analysis between V_{max}/K_m for N-OH-2AAF sulphonation and DHEA-sulphonation would not be meaningful with the small number of livers investigated, it is of interest that the highest V_{max}/K_m (table 1) was seen in the liver with the highest DHEA-ST activity (table 2). It is also noteworthy that N-OH-2AAF in preliminary experiments appears to be mutagenic in *Salmonella typhimurium* TA1538, genetically engineered to express the human DHEA-ST (Falany *et al.* 1995a).

The role of P-PST, which based on previous studies (Abu-Zeid *et al.* 1992, Gilissen *et al.* 1994, Chou *et al.* 1995) was proposed as the main ST involved, appears from the present study to be minor. When the enzyme responsible for N-OH-2AAF sulphonation was isolated from human liver in a previous study (Gilissen *et al.* 1994), it appeared that P-PST was the only enzyme involved. However, as has been shown previously (Otterness *et al.* 1992), even when using multiple chromatography techniques the P-PST protein cannot be physically separated from the DHEA-ST protein, the isoform now shown to have high catalytic activity for the sulphonation of N-OH-2AAF. Recombinant EST, shown to have very similar substrate specificity as P-PST (Falany *et al.* 1995b), also did not sulphonate N-OH-2AAF. In contrast, P-PST as well as EST have very high catalytic activities for the sulphonation/bioactivation of the colon and mammary procarcinogen N-OH-PhIP (Ozawa *et al.* 1994, Lewis *et al.* 1998).

Although attempts were made to identify an inhibitor of DHEA-ST that was not itself sulphonated, no chemicals or currently available antibodies are efficient in a heterogeneous mixture such as the human liver cytosol. This would certainly be a worthwhile area of future investigation.

In spite of the findings in this study that recombinant P-PST did not sulphonate N-OH-2AAF, several previous studies using human liver cytosol as the enzyme source indicate an important role of P-PST, primarily based on high correlations between sulphonation of *p*-nitrophenol, a prototype substrate of P-PST, and the liver cytosol-induced DNA binding of N-OH-2AAF among a number of human livers (Abu-Zeid *et al.* 1992, Chou *et al.* 1995). This discrepancy has no clear explanation. The conditions of the experiments, including an N-OH-2AAF concentration of 200 μM, were the same as in the present study. Part of this discrepancy may be due to the indirect methodologies used to assess the sulphonation of this procarcinogen. Whereas the PAPS to PAP conversion assay used by us and Gilissen *et al.* (1994) specifically measures sulphonation rates, the DNA binding assay used by Abu-Zeid *et al.* (1992) and Chou *et al.* (1995), although functionally very important, only measures a fraction of the sulphonation rate. This is due to the fact that bioactivated N-OH-2AAF shows a much greater propensity for binding to protein than to DNA (DeBaun *et al.* 1970, Heflich and Neft 1994).

In summary, this study represents the first report demonstrating that for certain

N-hydroxylated aromatic amides, and maybe also amines, sulphonation in humans can occur by DHEA-ST. This finding may be rationalized based on similar spatial configuration of N-OH-2AAF and DHEA, as previously observed for the hydroxymethylated polyaromatic hydrocarbons, including 1-hydroxymethylpyrene (Glatt *et al.* 1995). These findings do, however, not rule out minor contributions of other ST isoforms.

Acknowledgements

This study was supported by a grant from the National Cancer Institute (CA69138). The work was presented in part at the 8th North American Meeting of the International Society for the Study of Xenobiotics, Hilton Head, SC, 26–30 October 1997. The authors gratefully acknowledge the gift of the DHEA-ST, EST and M-PST cDNAs expressed in *E. coli* XL1-Blue as well as rabbit anti-human DHEA-ST antiserum from Dr Charles N. Falany, University of Alabama, Birmingham, AL. They also thank Dr Michael W. H. Coughtrie for providing rabbit anti-rat DHEA-ST IgG.

References

Abu-Zeid, M., Yamazoe, Y., and Kato, R., 1992, Sulfotransferase-mediated DNA binding of *N*-hydroxyarylamines(amide) in liver cytosols from human and experimental animals. *Carcinogenesis*, **13**, 1307–1314.

Anderson, R. J., and Weinshilboum, R. M., 1980, Phenolsulphotransferase in human tissue: radiochemical enzymatic assay and biochemical properties. *Clinica et Chimica Acta*, **103**, 79–90.

Bamforth, K. J., Dagliesh, K. and Coughtrie, M. W. H., 1992, Inhibition of human liver steroid sulfotransferase activities by drugs: a novel mechanism of drug toxicity? *European Journal of Pharmacology—Environmental Toxicology and Pharmacology Section*, **228**, 15–21.

Campbell, N. R. C., van Loon, J. A. and Weinshilboum, R. M., 1987, Human liver phenol sulfotransferase: assay conditions, biochemical properties and partial purification of isozymes of the thermostable form. *Biochemical Pharmacology*, **36**, 1435–1446.

Chou, H.-C., Lang, N. P. and Kadlubar, F. F., 1995, Metabolic activation of *N*-hydroxy arylamines and *N*-hydroxy heterocyclic amines by human sulfotransferase(s). *Cancer Research*, **55**, 525–529.

Comer, K. A. and Falany, C. N., 1992, Immunological characterization of dehydroepiandrosterone sulfotransferase from human liver and adrenal. *Molecular Pharmacology*, **41**, 645–651.

DeBaun, J. R., Smith, J. Y. R., Miller, E. C. and Miller, J. A., 1970, Reactivity *in vivo* of the carcinogen N-hydroxy-2-acetylaminofluorene: increase by sulfate ion. *Science*, **167**, 184–186.

Duffel, M. W., Binder, T. P. and Rao, S. I., 1989, Assay of purified aryl sulfotransferase suitable for reactions yielding unstable sulfuric acid esters. *Analytical Biochemistry*, **183**, 320–324.

Falany, C. N., 1991, Molecular enzymology of human liver cytosolic sulfotransferases. *Trends in Pharmacological Sciences*, **12**, 255–259.

Falany, C. N., Comer, K. A., Dooley, T. P. and Glatt, H., 1995a, Human dehydroepiandrosterone sulfotransferase—purification, molecular cloning, and characterization. *Annals of the New York Academy of Sciences*, **774**, 59–72.

Falany, C. N., Krasnykh, V. and Falany, J. L., 1995b, Bacterial expression and characterization of a cDNA for human liver estrogen sulfotransferase. *Journal of Steroid Biochemistry and Molecular Biology*, **52**, 529–539.

Falany, C. N., Vazquez, M. E. and Kalb, J. M., 1989, Purification and characterization of human liver dehydroepiandrosterone sulfotransferase. *Biochemical Journal*, **260**, 641–646.

Falany, C. N., Wheeler, J., Oh, T. S. and Falany, J. L., 1994, Steroid sulfation by expressed human cytosolic sulfotransferases. *Journal of Steroid Biochemistry and Molecular Biology*, **48**, 369–375.

Foldes, A. and Meek, J. L., 1973, Rat brain phenolsulfotransferase—partial purification and some properties. *Biochimica et Biophysica Acta*, **327**, 365–374.

Ganguly, T. C., Krasnykh, V. and Falany, C. N., 1995, Bacterial expression and kinetic characterization of the human monoamine-sulfating form of phenol sulfotransferase. *Drug Metabolism and Disposition*, **23**, 945–950.

Gilissen, R. A. H. J., Bamforth, K. J., Stavenuiter, J. F. C., Coughtrie, M. W. H. and Meerman, J. H. N., 1994, Sulfation of aromatic hydroxamic acids and hydroxylamines by multiple forms of human liver sulfotransferases. *Carcinogenesis*, **15**, 39–45.

GILISSEN, R. A. H. J., RINGER, D. P., STAVENUITER, H. J. F. C., MULDER, G. J. and MEERMAN, J. H. N., 1992, Sulfation of hydroxylamines and hydroxamic acids in liver cytosol from male and female rats and purified aryl sulfotransferase IV. *Carcinogenesis*, **13**, 1699–1703.

GLATT, H., PAULY, K., CZICH, A., FALANY, J. L. and FALANY, C. N., 1995, Activation of benzylic alcohols to mutagens by rat and human sulfotransferases expressed in *Escherichia coli*. *European Journal of Pharmacology*, **293**, 173–181.

HEFLICH, R. H. and NEFT, R. E., 1994, Genetic toxicity of 2-acetylaminofluorene, 2-aminofluorene and some of their metabolites and model metabolites. *Mutation Research*, **318**, 73–174.

HERNÁNDEZ, J. S., WATSON, R. W. G., WOOD, T. C. and WEINSHILBOUM, R. M., 1992, Sulfation of estrone and 17β-estradiol in human liver: catalysis by thermostable phenol sulfotransferase and by dehydroepiandrosterone sulfotransferase. *Drug Metabolism and Disposition*, **20**, 413–422.

LAEMMLI, U. K., 1970, Cleavage of structural proteins during the assembly of the head of bacteriophage T4. *Nature*, **227**, 680–685.

LEWIS, A. J., KELLY, M. M., WALLE, U. K., EATON, E. A., FALANY, C. N. and WALLE, T., 1996, Improved bacterial expression of the human P form phenolsulfotransferase: applications to drug metabolism. *Drug Metabolism and Disposition*, **24**, 1180–1185.

LEWIS, A. J., WALLE, U. K., KING, R. S., KADLUBAR, F. F., FALANY, C. N. and WALLE, T., 1998, Bioactivation of the cooked food mutagen *N*-hydroxy-2-amino-1-methyl-6-phenylimidazo[4,5-*b*]pyridine by estrogen sulfotransferase in cultured human mammary epithelial cells. *Carcinogenesis*, **19**, 2049–2053.

MICHEJDA, C. J. and KROEGER KOEPKE, M. B., 1994, Carcinogen activation by sulfate conjugate formation. *Advances in Pharmacology*, **27**, 331–363.

MILLER, J. A. and SURH, Y.-J., 1994, Sulfonation in chemical carcinogenesis. In F. C. Kauffman (ed.), *Conjugation–Deconjugation Reactions in Drug Metabolism and Toxicity* (Berlin: Springer), **112**, pp. 429–457.

OEMAR, B. S., FOELLMER, H. G., HODGDON-ANANDANT, L. and ROSENZWEIG, S. A., 1991, Regulation of insulin-like growth factor I receptors in diabetic mesangial cells. *Journal of Biological Chemistry*, **266**, 2369–2373.

OTTERNESS, D. M., WIEBEN, E. D., WOOD, T. C., WATSON, R. W. G., MADDEN, B. J., MCCORMICK, D. J. and WEINSHILBOUM, R. M., 1992, Human liver dehydroepiandrosterone sulfotransferase: molecular cloning and expression of cDNA. *Molecular Pharmacology*, **41**, 865–872.

OZAWA, S., CHOU, H.-C., KADLUBAR, F. F., NAGATA, K., YAMAZOE, Y. and KATO, R., 1994, Activation of 2-hydroxyamino-1-methyl-6-phenylimidazo[4,5-*b*]pyridine by cDNA-expressed human and rat arylsulfotransferases. *Japanese Journal of Cancer Research*, **85**, 1220–1228.

OZAWA, S., TANG, Y.-M., YAMAZOE, Y., KATO, R., LANG, N. P. and KADLUBAR, F. F., 1998, Genetic polymorphisms in human liver phenol sulfotransferases involved in the bioactivation of *N*-hydroxy derivatives of carcinogenic arylamines and heterocyclic amines. *Chemico-Biological Interactions*, **109**, 237–248.

PACIFICI, G. M., TEMELLINI, A., CASTIGLIONI, M., D'ALESSANDRO, C., DUCCI, A. and GIULIANI, L., 1994, Interindividual variability of the human hepatic sulphotransferases. *Chemico-Biological Interactions*, **92**, 219–231.

PLAGER, J. E., 1965, The binding of androsterone sulfate, etiocholanolone sulfate, and dehydroisoandrosterone sulfate by human plasma protein. *Journal of Clinical Investigation*, **44**, 1234–1239.

SHARP, S., BARKER, E. V., COUGHTRIE, M. W. H., LOWENSTEIN, P. R. and HUME, R., 1993, Immunochemical characterisation of a dehydroepiandrosterone sulfotransferase in rats and humans. *European Journal of Biochemistry*, **211**, 539–548.

SONG, W.-C., QIAN, Y. and LI, A. P., 1998, Estrogen sulfotransferase expression in the human liver: marked interindividual variation and lack of gender specificity. *Journal of Pharmacology and Experimental Therapeutics*, **284**, 1197–1202.

WALLE, T. and WALLE, U. K., 1990, Stereoselective sulphate conjugation of racemic terbutaline by human liver cytosol. *British Journal of Clinical Pharmacology*, **30**, 127–133.

WALLE, U. K., PESOLA, G. R. and WALLE, T., 1993, Stereoselective sulphate conjugation of salbutamol in humans: comparison of hepatic, intestinal and platelet activity. *British Journal of Clinical Pharmacology*, **35**, 413–418.

WATABE, T., HIRATSUKA, A. and OGURA, K., 1987, Sulphotransferase-mediated covalent binding of the carcinogen 7,12-dihydroxymethylbenz[*a*]anthracene to calf thymus DNA and its inhibition by glutathione transferase. *Carcinogenesis*, **8**, 445–453.

WOOD, T. C., HER, C., AKSOY, I., OTTERNESS, D. M. and WEINSHILBOUM, R. M., 1996, Human dehydroepiandrosterone sulfotransferase pharmacogenetics: quantitative Western analysis and gene sequence polymorphisms. *Journal of Steroid Biochemistry and Molecular Biology*, **59**, 467–478.

XENOBIOTICA , 2000, VOL. 30, NO. 3, 263–272

Metabolism and disposition of luminol in the rat

J. M. SANDERS*, L.-J. CHEN, L. T. BURKA
and H. B. MATTHEWS

Laboratory of Pharmacology and Chemistry, National Toxicology Program, National Institute of Environmental Health Sciences, Research Triangle Park, NC 27709, USA

Received 4 June 1999

1. The metabolism and disposition of Luminol (LMN, 3-aminophthalhydrazide), a widely used forensic and laboratory reagent that chemiluminesses upon oxidation, was determined as part of its overall toxicological characterization.

2. Radiolabelled LMN was well absorbed, metabolized and excreted following p.o. administration of a range of doses. About 90% of the total dose was recovered within 24 h of administration in urine in the form of two metabolites identified as LMN N^8-glucuronide and LMN N^8-sulphamic acid. 3-Aminophthalic acid, the oxidative product of LMN in the light-emitting reaction, was apparently not formed *in vivo*.

3. Metabolism and disposition of an i.v. administered dose was similar to that following gavage. Little or no LMN-derived radioactivity was present in tissue within 12 h post-dosing. Excretion of radioactivity in bile following i.v. injection was minimal (~ 8% of the total dose in 6 h) and consisted of the same urinary-excreted glucuronide and sulphate conjugates.

4. LMN was not absorbed dermally in rat, potentially a major route of exposure to human. If the fate of LMN is similar between species, this compound should have little potential for either dermal absorption, bioaccumulation in tissues following other routes of exposure or chronic toxicity in humans.

Introduction

Luminol (LMN, 3-aminophthalhydrazide) is widely used in forensic toxicology and as a laboratory reagent because it chemiluminesses upon oxidation. For example, LMN is used as an enhancer of weak cellular chemiluminescence and can be used to monitor the generation of reactive oxygen species produced by the respiratory burst in leukocytes following tissue insult or pathogen exposure (Kricka 1995). Specifically, LMN-enhanced chemiluminescence probes have been used to characterize the role of granulocyte-derived reactive oxygen species in post-ischaemic myocardial damage (Becker *et al.* 1993), to investigate the effect of respiratory syncytial virus particles on cytokine release and respiratory burst in granulocytes (Arnold *et al.* 1994), and to determine neutrophil phagocytic capacity in patients with diabetes mellitus (Marhoffer *et al.* 1994). LMN-derived chemiluminescence detection methods have been used in protein blotting (Shewry and Fido 1998), for monitoring total antioxidant activity and capacity in biological fluids such as serum, saliva and semen (Hirayama *et al.* 1997, Saez *et al.* 1998), and with capillary electrophoresis instrumentation to investigate the production and consumption of hydrogen peroxide by enzyme systems (Regehr and Regnier 1996). Therapeutic uses for LMN, including treatment for baldness, fluid accumulation and promotion of blood clotting, were briefly investigated in the early 1960s (Irie

* Author for correspondence: e-mail: sandersm@niehs.nih.gov

Xenobiotica ISSN 0049–8254 print/ISSN 1366–5928 online 2000 US Government work
http://www.tandf.co.uk/journals/tf/00498254.html

1960a–c); but there is no evidence that LMN is currently used for clinical purposes. Possibly the most well-known use for LMN is as a forensic tool for the detection of blood at crime scenes (Yeshion 1991). Light is emitted upon oxidation of LMN by sodium perborate using the peroxidase activity of haeme as the catalyst for the reaction.

LMN-induced toxicity has not been well characterized, although its widespread use poses considerable potential for exposure to individuals working in certain laboratory and forensic occupations. The oral LD_{50} of LMN in rat has been reported to be >500 mg/kg (RTECS 1999). Little or no LMN-induced toxicity was observed following 10 weeks of administration of LMN in an investigation of the role of poly(ADP-ribose) synthetase in liver tumour promotion (Tsujiuchi *et al.* 1990). In this latter study, tumour promotion activity of phenobarbital was reduced in a dose-dependent manner when LMN, an inhibitor of poly(ADP-ribose) synthetase, was added to the diet. Inhibition of the enzyme by LMN has been shown to induce sister-chromatid exchanges (SCE) in mammalian cells, a characteristic of many mutagenic carcinogens. However, LMN-derived SCE lesions are short-lived, unlike those caused by other potent poly(ADP-ribose) synthetase inhibitors such as mitomycin C (Ikushima 1990). Further, LMN did not exhibit mutagenic activity in *Salmonella typhimurium* with or without S9 metabolic activation (Zeiger *et al.* 1992). In humans, no adverse effects associated with LMN exposure were observed in clinical trials as reported by Irie (1960a–c).

Although the previous work indicates that the toxic potential of LMN may be low, the compound has arylamine and hydrazide functionality, both structural alerts for carcinogenicity (Ashby and Tennant 1991). Few carcinogenicity studies of hydrazides exist to test this structural feature adequately, but the carcinogenic potential of aromatic amines is well known. Carcinogenic activity of aromatic amines can differ considerably, probably due to variations in their metabolic fates (Lilienblum and Bock 1984). Since there is potential for human exposure to this compound and no data are available describing the fate of LMN in intact animals, the present study has determined the metabolism and disposition of LMN in rat when administered either dermally, orally or by i.v. injection.

Materials and methods

Animals and dose preparation

About 60 Male F344 rats obtained from Charles River Laboratories (Raleigh, NC, USA), with an age range of 2–3 months and weight range of 203–304 g, were used in the experiments. All procedures involving animals were carried out in accordance with institutional guidelines. Each rat received single doses of either 0.5, 5 or 50 mg/kg by gavage, 0.5 mg/kg by i.v. injection into a tail vein or a dermally applied dose as described below. Dosing solutions administered either orally or intravenously (dose volumes of 5 and 1 ml/kg respectively) were prepared by suspending the desired concentration of unlabeled LMN (Aldrich Chemical Co., Inc., Milwaukee, WI, USA) and/or 50–90 μCi/kg (ring ^{14}C) LMN (NEN, Boston, MA, USA) in water and adding Na_2CO_3 until LMN went into solution at a pH range of 9.6–10.1. Radiolabelled LMN was added as a suspension in ethanol; therefore, dosing solutions contained up to 5% ethanol by volume. The purity of LMN (radiolabelled and unlabelled) was 97% or greater.

Disposition

The rates and routes of elimination of LMN-derived radioactivity were determined following either p.o. or i.v. administration to four rats/treatment group. Animals were individually housed in metabolism cages for the collection of urine and faeces at time-points ranging from 4 to 72 h following dosing. Food (NIH rodent diet #31) and water were provided for *ad libitum* consumption. All urine excreted up to 12 h post-dosing was collected in receptacles jacketed by containers of dry ice. Urine was briefly thawed and

aliquots were taken for analysis of radioactivity content. A drop of chloroform was added to suppress biotic degradation of LMN-derived metabolites, and the samples were immediately frozen and stored at − 20 °C for later HPLC analysis. The percentage of the total dose excreted in urine was determined by counting ^{14}C contained in triplicate 20-μl aliquots of each sample, as well as triplicate 50-μl aliquots of a water rinse of the cage at each collected time-point, directly in Ecolume® (ICN, Research Products Division, Costa Mesa, CA, USA), in either a model LS 5801 or model 9800 scintillation counter (Beckman Instruments, Inc., Fullerton, CA, USA). The percentage of the total dose excreted in faeces was determined after combusting and trapping ^{14}C contained in triplicate 100-mg samples using a model 306 biological sample oxidizer (Packard Instruments Co., Meriden, CT, USA). Before oxidation, faecal samples were air-dried, weighed and ground to a fine-powder using a mortar and pestle. Oxidized samples were analysed for radioactivity content in the scintillation counter. All animals used in these and subsequently described experiments were euthanized by CO_2 asphyxiation. At time of death, blood was collected by cardiac puncture, then triplicate 50-μl aliquots were taken, oxidized and counted in the scintillation counter. Selected animals were necropsied and triplicate aliquots (up to 100 mg) of tissues were taken for determination of radioactivity content following oxidation and scintillation counting.

Analysis for LMN-derived radioactivity in expired air

Each rat receiving 5 mg/kg by gavage was placed into an individual glass metabolism cage (Wyse Glass Specialties, Inc., Freeland MI, USA), attached to a vacuum system that pulled air through the cage at a flow rate of 0.4–0.6 l/min. Air exiting the cage passed through a trap containing 200–400 ml 95% ethanol for collection of organic volatile ^{14}C, then through a trap containing 200–400 ml 7:3 (v/v) mixture of ethylene glycol monomethyl ether and ethanolamine for collection of expired $^{14}CO_2$. Moisture and CO_2 content were reduced in the ambient cage air by filtering the intake air through a cylinder containing calcium sulphate and soda lime. This increased the efficiency of the trapping solutions that were changed and sampled at 4, 8, 12 and 24 h post-dosing. Sampling for radioactivity excreted in expired air was discontinued at the 24-h time-point. Total exhaled radioactivity was determined by counting triplicate 1-ml aliquots of each trapping solution in Ecolume in the scintillation counter.

Dermal administration of LMN to rat

Twenty-four hours before dermal administration of LMN, each rat ($n = 4$) was lightly anaesthetized with metafane and hair was shaved from the interscapular region of the back with animal clippers. At time of application, rats were again lightly anaesthetized with metafane, and ^{14}C LMN, dissolved in a dose volume of 50 μl ethanol, was applied directly to the skin in a marked circular area of 1 cm^2. Each rat received an approximate dose concentration of 0.1 mg/kg. The dosing site was covered with a small perforated metal cap glued to the skin with cyanoacrylate glue (to prevent ingestion of the dose by grooming). Animals were placed in metabolism cages for 48 h for collection of urine and faeces as described above. Following sacrifice, the skin dosing site was washed repeatedly with 10 ml ethanol until all unabsorbed LMN was recovered.

Bile duct cannulations of LMN-treated rat

Each F344 rat ($n = 3$) was anaesthetized with 50 mg/kg pentobarbital i.p. at a dose volume of 1 ml/kg. A midline incision was made and the bile duct was isolated, distally ligated and punctured with a 25-gauge needle. A bevelled PE10 cannula was inserted through the puncture site into the bile duct for ~ 1 cm and secured with a suture. Flow of bile was confirmed and the incision was closed with wound clips. Following i.v. administration of 0.5 mg/ml/kg into a tail vein, bile was collected on ice for 6 h at time-points of 0.25, 0.5, 0.75, 1, 1.5, 2, 2.5, 3, 4, 5 and 6 h. Rats were placed on heated pads (40 °C), changed hourly to maintain a constant body temperature throughout surgery and bile collection. A 75 W incandescent light placed above the supine animals provided additional heat. The body temperature of the rats, monitored hourly, ranged from 35 to 38 °C. Each rat remained anaesthetized throughout the entire procedure as a result of hourly i.p. injections of 0.1 ml pentobarbital. Concurrent i.p. injections of 300–500 μl 0.85% saline containing 2.5 mM taurocholic acid were made to maintain hydration.

Metabolism

The relative amounts of LMN and radiolabelled metabolites in urine and bile were determined by HPLC analysis. Waters Corp. (Milford, MA, USA) Millennium® software controlled dual Waters model 510 pumps, a Radiomatic model 280 radiochemical detector (Packard Instrument Co., Meriden, CT, USA), and a Waters model 481 spectrophotometer ($\lambda = 254$ nm). The system utilized a 10 μm Waters μBondapak® C_{18} steel column with a linear gradient from 100% 0.01 M sodium phosphate buffer (pH 6) to 50% acetonitrile in 15 min at a flow rate of 1.5 ml/min. Urine and bile were centrifuged for 5 min at maximum speed in an Eppendorf® model 5412 microcentrifuge (Brinkmann Instruments, Westbury, NY, USA) before injection ($\leqslant 50$ μl aliquots) into the HPLC system.

Metabolite identification

Isolation and collection using UV detection at 254 nm characterized the two major radiolabelled peaks of interest in urine. Initial isolation was performed using the previously described HPLC system with a linear gradient of 0–25% acetonitrile in 15 min, starting from 100% water:trifluoroacetic acid (TFA) (99.9:0.1). Peak A was successfully purified using one additional isolation in the TFA–acetonitrile HPLC system. Peak B proved to be labile in the acidic TFA HPLC system; therefore, initial isolation was performed using the initially described sodium phosphate–acetonitrile HPLC system. Phosphate was removed with a second isolation utilizing a linear gradient from 100% 20 mM ammonium acetate to 50% acetonitrile in 15 min. Purified peaks A and B were identified using NMR and mass spectral analysis. ^{1}H-NMR spectra were acquired on a Nicolet NT-360 NB (Fremont, CA, USA) spectrometer. The chemical shifts are reported in ppm relative to solvent peaks. The fast atom bombardment (FAB) mass spectrum was run on a Fisons ZAB-E instrument using thioglycerol as the FAB matrix. The electrospray (ESI) mass spectrum was obtained on a Micromass Platform II (Altrincham, UK) single-quadruple mass spectrometer equipped with an electrospray ionization interface.

Urinary metabolite A

This metabolite was identified as LMN N^8-glucuronide. Negative-ion FAB-MS contained ions at 352 (M-H^+), 176 (M-glucuronide-H^+). ^{1}H-NMR (D_2O, 360 MHz): δ 7.80 (t, $\mathcal{J}$ = 8.0 Hz, 1H, C_5-H), 7.76 (d, $\mathcal{J}$ = 7.0 Hz, 1H, C_6-H), 7.46 (d, $\mathcal{J}$ = 7.3 Hz, 1H, C_4-H), 5.80 (d, $\mathcal{J}$ = 8.0 Hz, 1H, C_1'-H of glucuronic acid), 4.18 (dd, $\mathcal{J}$ = 7.3, 2.6 Hz, 1H, C_5'-H of glucuronic acid), 3.73 (td, $\mathcal{J}$ = 7.3, 2.2 Hz, 1H, C_4'-H of glucuronic acid), 3.67–3.61 (m, 2H, C_2'-H and C_3'-H of glucuronic acid); ^{1}H-NMR (DMSO-d_6, 360 MHz): δ 11.58 (s, 1H, CONH), 7.51 (t, $\mathcal{J}$ = 7.9 Hz, 1H, C_5-H), 7.36 (br. s, 2H, C_3-NH_2), 7.01 (d, $\mathcal{J}$ = 7.3 Hz, 1H, C_6-H), 6.93 (d, $\mathcal{J}$ = 8.4 Hz, 1H, C_4-H), 6.55 (s, 1H, -OH), 5.53 (d, $\mathcal{J}$ = 7.3 Hz, 1H, C_1'-H of glucuronic acid), 5.48 (d, $\mathcal{J}$ = 4.8 Hz, 1H, -OH), 5.30 (d, $\mathcal{J}$ = 4.0 Hz, 1H, -OH), 3.73 (d, $\mathcal{J}$ = 9.2 Hz, 1H, C_5'-H of glucuronic acid), 3.5–3.3 (C_2'-, C_3'- and C_4'-H's of glucuronic acid, overlapping with the water peak). The signals at δ 11.58, 7.36, 6.55, 5.48 and 5.30 disappeared after exchange with D_2O.

Urinary metabolite B

This metabolite was identified as LMN N^8-sulphamic acid. Negative-ion ESI-MS contained ions at 256 (M-H^+), 176 (M-SO_3-H^+). ^{1}H-NMR (DMSO-d_6, 360 MHz) of the ammonium salt of LMN N^8-sulphamic acid: δ 11.65 (s, 1H, CONH), 7.46 (t, $\mathcal{J}$ = 7.7 Hz, 1H, C_5-H), 7.26 (br. s, 2H, C_3-NH_2), 7.11 (br. s, NH_4^+), 6.99 (d, $\mathcal{J}$ = 7.7 Hz, 1H, C_6-H), 6.86 (d, $\mathcal{J}$ = 8.1 Hz, 1H, C_4-H).

Statistical analysis

Statistical analyses were performed using Student's *t*-test (JMP Statistical Software, SAS Institute Inc., Cary, NC, USA).

Results

Disposition

LMN-derived radioactivity was rapidly eliminated in urine following administration of either 0.5, 5 or 50 mg by gavage to the male F344 rat (table 1). At 4 h post-dosing, 50% or more of the radiolabel had been excreted in urine following p.o. administration of the low and median doses. Excretion of the highest dose lagged behind the two lower doses somewhat at earlier time-points but by 12 h post-dosing there were no significant differences between treatment groups in the cumulative amount of LMN-derived radioactivity excreted in urine. Cumulative 24-h urine contained ~ 90% of the dose with the remainder excreted in faeces. No radiolabel was excreted in expired air within 24 h of dose administration and major tissues contained little or no LMN-derived radioactivity at the assayed time-points of either 48 or 72 h post-dosing (data not shown).

The rate of elimination of LMN-derived radioactivity in urine following i.v. administration of 0.5 mg/kg was more rapid than that observed following gavage (table 1). Up to 90% of the total dose was excreted in urine within 4 h post-dosing. In contrast to the gavaged rat, no more than a trace of radioactivity was detected in faeces of the i.v. injected rat.

Table 1. Cumulative excretion of LMN-derived radioactivity (% total dose) in urine and faeces over time following either p.o. or i.v. administration to rat.

		Dose (mg/kg) and route			
Excreta	Time (h)	0.5 p.o.	5 p.o.	50 p.o.	0.5 i.v.
Urine	4	50.1± 11.1[a]	54.6± 10.3	29.2± 13.8	94.7± 3.8
	8	71.1± 7.1	77.6± 5.1	63.6± 7.8	100.2± 3.5
	12	81.8± 4.1	85.4± 2.6	81.1± 9.4	104.5± 3.1
	24	87.2± 3.1	90.1± 2.5	86.7± 10.2	106.4± 3.0
	48	88.3± 3.0	91.0± 2.6	88.9± 10.5	nd[b]
Faeces	24	9.1± 3.8	8.3± 3.4	2.5± 0.3	0.3± 0.1
	48	9.7± 3.8	8.5± 3.4	3.3± 0.5	nd

[a] Each value represents the mean± SD of four rats.
[b] Not determined.

Table 2. Concentration[a] of LMN-derived radioactivity in tissues over time following i.v. administration of 0.5 mg/kg to rats

	Time (hr)						
Tissue	0.25	0.75	2	4	8	12	24
Blood	268.8± 22.0[b]	89.9± 95.0	9.3± 1.2	5.3± 0.7	3.0± 0.5	2.1± 0.5	3.2± 0.9
Liver	194.8± 19.1	28.0± 5.1	8.9± 1.4	4.0± 0.4	3.5± 1.0	1.1± 0.2	1.1± 0.1
Kidney	2443.5± 629.8	239.4± 68.5	57.5± 15.2	42.6± 18.8	19.8± 6.7	3.9± 0.8	3.2± 0.2
Muscle	80.7± 21.8	13.7± 11.3	2.2± 0.2	1.5± 0.6	0.8± 0.2	0.4± 0.6	0.3± 0.1
Skin	273.2± 42.7	45.4± 7.2	8.2± 2.2	3.9± 0.3	6.8± 2.3	3.0± 0.8	2.7± 0.9
Adipose	74.2± 41.4	40.1± 14.6	8.9± 4.9	2.8± 3.1	5.0± 2.4	2.0± 0.3	0.9± 0.2
Brain	41.0± 30.6	2.9± 1.1	2.9± 4.1	0.3± 0.1	0.2± 0.1	< 0.1	0.2± 0.1

[a] ng LMN equivalents/g tissue.
[b] Each value represents the mean± SD for three-to-four rats.

The concentration of LMN-derived radioactivity in tissues over time was investigated in the i.v. injected rat (table 2). Of assayed tissues, only kidney consistently contained higher concentrations of radioactivity over time than those found in blood. Tissue contained little LMN-derived radioactivity by 12 h post-dosing.

Transdermal absorption of LMN was investigated in rat, with results indicating < 1% of the total dose present in cumulative 48 h urine and faeces. About 100% of the LMN-derived radioactivity was recovered from the dose site following extensive washing of the skin with ethanol (data not shown).

Biliary excretion of LMN-derived radioactivity was investigated in rat following i.v. injection. Only 7.6± 1.8% total dose was excreted within 6 h of LMN administration, with the greatest amount (3.5± 0.6% total dose) excreted within the first 15 min following administration.

Metabolism

Two radiolabelled LMN-derived metabolites were detected by HPLC analysis of urine of rats receiving either p.o. or i.v. doses (figure 1). Both peaks were isolated from urine and identified by NMR and mass spectral analysis as direct conjugates of parent LMN (details of the NMR and mass spectra are included in Materials and

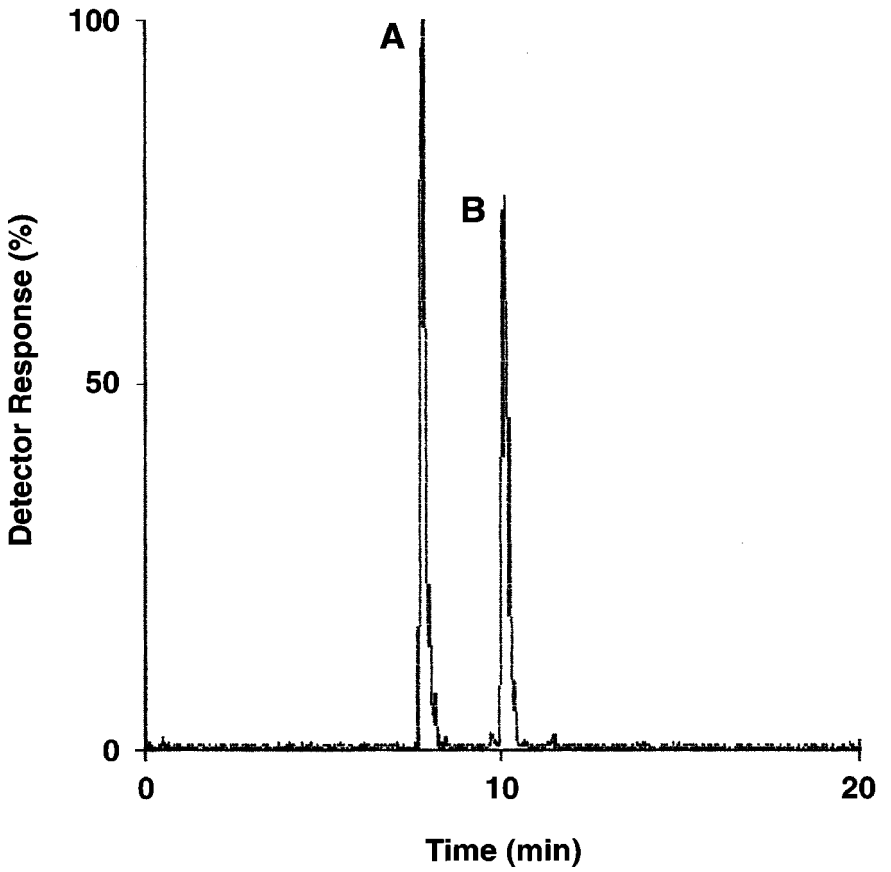


Figure 1. Representative HPLC chromatogram of LMN-derived radioactivity excreted in cumulative 4-h urine of a rat receiving 5 mg/kg by gavage. (A) LMN N^8-glucuronide; (B) LMN N^8-sulphamic acid. (3-Aminophthalic acid, the product formed in the chemiluminescence reaction, elutes near the void volume and parent LMN elutes at 11.2 min in this system.)

methods). The proposed structure for peak A eluting at 7.6 min is LMN N^8-glucuronide, and for peak B eluting at 10 min is LMN N^8-sulphamic acid (figure 2). Metabolic profiles of radioactivity in urine were qualitatively similar among all treatment groups (table 3). However, the ratio of the glucuronide to the sulphamic acid varied from 1:1 to 3:1 depending on treatment group and assayed time-point, with the ratio favouring the glucuronide conjugate over time. In preliminary experiments (data not shown), HPLC analysis indicated that up to 50% of the ^{14}C present in urine samples collected at room temperature and without chloroform added to retard bacterial growth, consisted of parent LMN, with a glucuronide:sulphamic acid ratio of 1:4. In contrast, amounts of parent LMN in urine samples collected on dry ice ranged from a mean of < 0.1–5% of the total sample radioactivity (table 3). The half-life of the glucuronide conjugate in urine at room temperature was 9.2 h, as determined by serial injections on the HPLC. Concurrently, the peak corresponding to parent LMN increased at the expense of the glucuronide, but not the sulphamic acid. The latter conjugate, stable for up to 24 h in urine at room temperature, proved extremely labile at lower pH in the HPLC system utilizing TFA in the mobile phase (data not shown).

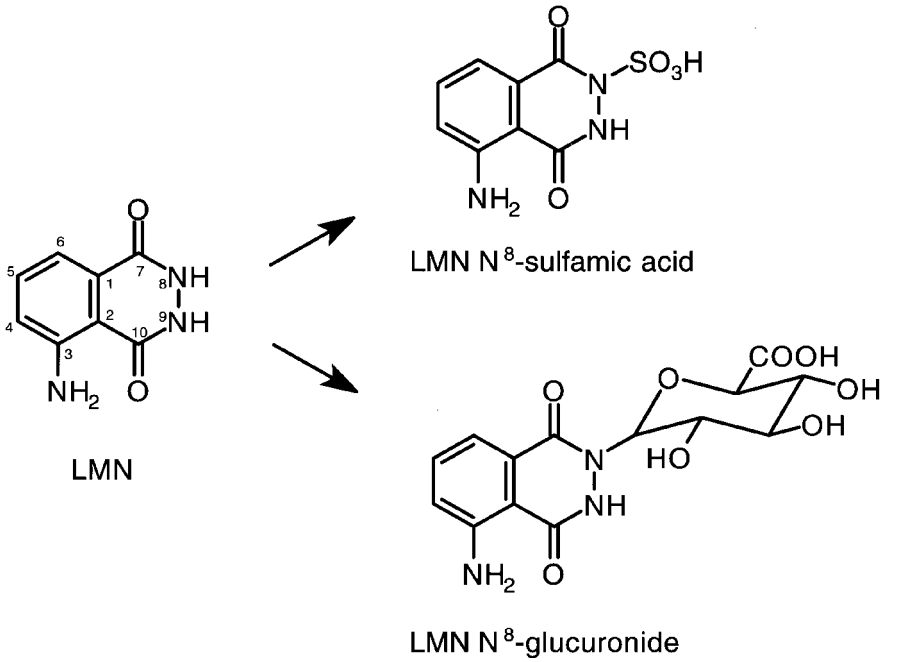


Figure 2. Proposed metabolic scheme for LMN in rat.

Table 3. Amount (% total radioactivity) of LMN N^8-glucuronide (A), LMN N^8-sulphamic acid (B) and parent LMN (C) in urine.

Dose (mg/kg)/route	Time (h)	Radiolabelled peak		
		A	B	C
5 p.o.	0–4	65.5± 5.5[a]	32.1± 3.7	2.5± 3.6
	4–8	74.0± 5.2	23.2± 2.5	2.9± 3.4
	8–12	73.2± 6.3	22.2± 3.0	4.7± 4.6
50 p.o.	0–4	50.4± 4.9	49.1± 4.8	0.6± 0.4
	4–8	67.1± 2.6	32.0± 3.2	1.0± 0.7
	8–12	71.6± 3.0	28.2± 3.1	0.2± 0.5
0.5 i.v.	0–4	47.9± 2.0	52.1± 2.0	< 0.1
	4–8	62.0± 1.6	36.5± 2.7	1.6± 1.1
	8–12	60.7± 5.4	36.2± 4.6	3.0± 0.9

[a] Mean± SD of four rats.

HPLC analysis of radioactivity in the 0.25, 0.5, 0.75 and 1 h bile samples indicated the presence of two radiolabelled peaks co-eluting with the two LMN-derived conjugates detected in urine. The glucuronide:sulphamic acid ratio was variable among the rats, ranging from 1:2 to 2:1. Parent LMN was present at trace levels in only two of 12 assayed samples (data not shown).

Discussion

LMN was rapidly and nearly completely absorbed from the GI tract of rat as demonstrated by the rapid rate and amount of elimination of LMN-derived radioactivity in urine following gavage. A measurable portion of radiolabel was

present in faeces, especially at the two lower p.o. administered doses, possibly due to cross-contamination of ^{14}C from urine as well as binding of a small portion of the lower doses to unabsorbed fibre in the diet. This might explain the lower amount of ^{14}C excreted in faeces of rat receiving the high dose. LMN disposition appeared to be dose-dependent over time at the two lower doses as indicated by comparable rates and routes of dose elimination. In contrast, some initial saturation of absorption and/or elimination pathways apparently occurred following administration of the highest dose. However, this effect was short-lived, with rates of elimination of radiolabel in urine becoming comparable with those of the lower doses within 8 h post-dosing. In the i.v. injected rat the rate of elimination of ^{14}C in urine was more rapid and the amount of ^{14}C excreted in faeces was less, compared with gavaged animals at the same dose. The effect of dosing route on overall disposition is probably insignificant given the extensive elimination of radiolabel in the urine of gavaged animals.

Oxidation of LMN to 3-aminophthalate produces chemiluminescence, rendering LMN useful as a detection agent in many different *in vitro* biochemical assays. However, in the present *in vivo* work, no phase I metabolism of the compound, including oxidation, was detected. Metabolism of LMN in the F344 rat, although complete (see below), proved relatively uncomplicated. Only two radiolabelled metabolites were detected in either urine or bile, both direct conjugates of the parent compound. The assigned structures of the metabolites are LMN N^8-glucuronide and LMN N^8-sulphamic acid, based on MS and NMR analysis. Negative-ion MS of the metabolites gave ions at m/z 352 and 256, consistent with conjugation of LMN with either a glucuronic acid or a sulphate ion respectively. The fragmentation of both molecular ions gave an ion at m/z 176 (the LMN anion), an indication that both metabolites are direct LMN conjugates. The sites of N-conjugations are likely to be at the N^8 positions for both metabolites based on their NMR data. Only one amide proton signal was observed and the two amino protons remained intact in the ^1H-NMR spectra of both metabolites, indicating that the conjugations are at one of the amide nitrogens (N^8 or N^9). The signal for C_6-H of LMN N^8-sulphamic acid is shifted 0.05 ppm downfield relative to that of LMN, whereas the chemical shifts for C_4- and C_5-H's remain similar. Because sulphate conjugation should generate a deshielding effect on nearby protons, this observation favours assignment as N^8- over N^9-substitutions; however, the assignment is not unambiguous. The chemical shift for the anomeric proton (C_1'-H) of LMN N^8-glucuronide is unusually downfield (δ 5.80 in D_2O; δ 5.53 in DMSO-d_6) compared with that of nirvanol N-glucuronide (δ 4.66 in DMSO-d_6), a hydantoin (Maguire *et al.* 1982). This is probably due to the presence of the additional nitrogen in the hydrazide structure of LMN. The magnitude of the coupling constant of the anomeric proton (a doublet, $\mathcal{J} = 8$ Hz) indicates that C_1'-H and C_2'-H are *trans*-diaxially oriented, and LMN N^8-glucuronide has a β-anomer configuration.

Several aromatic amines such as 2-naphthylamine and benzidine are known bladder carcinogens, with a mechanism of action that involves N-oxidation followed by glucuronidation of the hydroxyl group (Orzechowski *et al.* 1992). Conjugation serves as a transport mechanism to the bladder where acid hydrolysis of the conjugate can release the hydroxylamine that may then be activated by protonation or acetylation. Direct glucuronide conjugates also form with both 2-naphthylamine and benzidine, without prior N-oxidation (Orzechowski *et al.* 1992, Zenser *et al.* 1998). Zenser *et al.* (1998) implicated the N-glucuronide in the transport mechanism

scheme of benzidine-initiated bladder cancer. They postulated that parent benzidine, released upon hydrolysis of the conjugate in urine, can be metabolically activated by prostaglandin H synthase in bladder epithelium.

LMN has arylamine functionality and is primarily eliminated in urine of rat indicating a structure–activity alert for toxic insult to bladder tissue. However, in contrast to the previously mentioned arylamines, there is no metabolism at the primary amine group of LMN in rats. Instead, conjugation to the hydrazide moiety of LMN was extensive and both the glucuronide and sulphamic acid that were formed were observed to be labile under certain conditions. Reactivity of the LMN sulphamic acid does not appear to be an issue, since it was resistant to either biotic-mediated degradation or acidic hydrolysis at urine pH and was excreted intact in urine. On the other hand, parent LMN was detected in some urine samples following hydrolysis of the glucuronide conjugate by either urine acidity and/or microflora. Rats urinate frequently and appear to excrete the glucuronide relatively intact; the present observations indicated that most if not all of the hydrolysis of the conjugate was biotically mediated after elimination from the body. The stability of the glucuronide conjugate (if formed) is uncertain in the bladder of higher species such as dog and human that urinate less frequently. However, the potential reactivity of the secondary amide site of the aglycone in the bladder would be minimal, at best. Therefore, hydrolysis of LMN conjugates *in situ* should be of little consequence for LMN-induced toxicity.

In conclusion, the results presented here indicated that LMN, administered orally to rat, was rapidly absorbed and completely conjugated to form products that were readily excreted in urine. Excretion of the dose proceeds at such a rapid rate that there is little probability of accumulation of LMN-derived species in tissues. Further, there is no evidence for potential reactive species involved in the proposed metabolic scheme for this compound. LMN was not absorbed transdermally in rat and metabolism of the compound following i.v. administration was similar to that observed following gavage. It is probable that metabolism following inhalation exposure would also be similar. In humans, major exposure to this compound appears to be by the dermal route and possible inhalation of aerosolized particles from spray applications of LMN used in forensic work. If LMN disposition and metabolism are similar in rat and human, then anticipated levels of exposure by either route should not result in appreciable toxicity to humans.

Acknowledgements

The authors thank Ms T. M. Lewter for expert technical assistance.

References

ARNOLD, R., WERNER, F., HUMBERT, B., WERCHAU, H. and KONIG, W., 1994, Effect of respiratory syncytial virus-antibody complexes on cytokine (IL-8, IL-6, TNF-α) release and respiratory burst in human granulocytes. *Immunology*, **82**, 184–191.

ASHBY, J. and TENNANT, R. W., 1991, Definitive relationships among chemical structure, carcinogenicity and mutagenicity for 301 chemicals tested by the U. S. NTP. *Mutation Research*, **257**, 229–306.

BECKER, B. F., RASCHKE, P., BARDENHEUER, H. and GERLACH, E., 1993, Granulocytes, reactive oxygen species and uric acid. *Pharmaceutical and Pharmacological Letters*, **3**, 93–96.

HIRAYAMA, O., TAGAGI, M., HUKUMOTO, K. and KATOH, S., 1997, Evaluation of antioxidant activity by chemiuminescence. *Analytical Biochemistry*, **247**, 237–241.

IKUSHIMA, T., 1990, Bimodal induction of sister-chromatid exchanges by luminol, an inhibitor of poly(ADP-ribose) synthetase, during the S-phase of the cell cycle. *Chromosoma*, **99**, 360–364.

IRIE, S., 1960a, The treatment of alopecia areata with 3-aminophthalhydrazide. *Current Therapeutic Research*, **2**, 107–110.

IRIE, S., 1960b, Observations on the diuretic effects of 3-aminophthalhydrazide. *Current Therapeutic Research*, **2**, 132–136.

IRIE, S., 1960c, Influence of 3-aminophthalhydrazide on the prothrombin time. *Current Therapeutic Research*, **2**, 153–157.

KRICKA, L. J., 1995, Chemiluninescence and bioluminescence. *Analytical Chemistry*, **67**, 499R–502R.

LILIENBLUM, W. and BOCK, K. W., 1984, N-glucuronide formation of carcinogenic aromatic amines in rat and human liver microsomes. *Biochemical Pharmacology*, **33**, 2041–2046.

MAGUIRE, J. H., BUTLER, T. C. and DUDLEY, K. H., 1982, 5-Ethyl-5-phenylhydantoin N-glucuronide, the major urinary metabolite of 5-ethyl-5-phenylhydantoin (Nirvanol) in the dog. *Drug Metabolism and Disposition*, **10**, 595–598.

MARHOFFER, W., STEIN, M., SCHLEINKOFER, L. and FEDERLIN, K., 1994, Monitoring of polymorphonuclear leukocyte functions in diabetes mellitus-A comparative study of conventional radiometric function tests and low-light imaging systems. *Journal of Bioluminescence and Chemiluminescence*, **9**, 165–170.

ORZECHOWSKI, A., SCHRENK, D. and BOCK, K. W., 1992, Metabolism of 1- and 2-naphthylamine in isolated rat hepatocytes. *Carcinogenesis*, **13**, 2227–2232.

REGEHR, M. F. and REGNIER, F. E., 1996, Chemiluminescent detection for capillary electrophoresis and EMMA enzyme assays. *Journal of Capillary Electrophoresis*, **3**, 117–124.

RTECS, 1999, ONLINE. BIBLIOGRAPHIC DATABASE.

SAEZ, F., MOTTA, C., BOUCHER, D. and GRIZARD, G., 1998, Antioxidant capacity of prostasomes in human semen. *Molecular Human Reproduction*, **4**, 667–672.

SHEWRY, P. R. and FIDO, R. J., 1998, Protein blotting. In R. Rapley and J. M. Walker (eds), *Molecular Biomethods Handbook* (Totawa: Humana), pp. 435–444.

TSUJIUCHI, T., TSUTSUMI, M., DENDA, A., KONDOH, S., NAKAE, D., MARUYAMA, H. and KONISHI, Y., 1990, Possible involvement of poly ADP-ribosylation in phenobarbital promotion of rat hepatocarcinogenesis. *Carcinogenesis*, **11**, 1783–1787.

YESHION, T. E., 1991, The forensic application of luminol as a presumptive blood test. In P. E. Stanley, P. E and L. J. Krika (eds), *Chemiluminescence and Bioluminescence*: *Current Status* (Chichester: Wiley), pp. 379–384.

ZEIGER, E., ANDERSON, B., HAWORTH, S., LAWLOR, T. and MORTELMANS, K., 1992, Salmonella mutagenicity tests: V. Results from the testing of 311 chemicals. *Environmental Molecular Mutagenesis*, **19**, 2–141.

ZENSER, T. V., LAKSHMI, V. M. and DAVIS, B. B., 1998, 1996 ASPET N-glucuronidation of xenobiotics symposium. N-glucuronidation of benzidine and its metabolites. Role in bladder cancer. *Drug Metabolism and Disposition*, **26**, 856–859.

XENOBIOTICA , 2000, VOL. 30, NO. 3, 273–284

Effect of troglitazone on cytochrome P450 enzymes in primary cultures of human and rat hepatocytes

J. SAHI†, G. HAMILTON‡, M. SINZ†, S. BARROS‡, S.-M. HUANG§, L. J. LESKO§ and E. L. LECLUYSE‡*

† Parke-Davis Pharmaceutical Research, Ann Arbor, MI, USA
‡ UNC School of Pharmacy, Chapel Hill, NC, USA
§ Office of Clinical Pharmacology and Biopharmaceutics, CDER, FDA, Rockville, MD, USA

Received 5 August 1999

1. Troglitazone was the first thiazolidinedione approved for clinical use in the treatment of non-insulin-dependent diabetes mellitus. During clinical investigations of drug–drug interactions with therapeutics (terfenadine and cyclosporine) known to be metabolized by CYP3A4, pharmacokinetic interactions were noted upon troglitazone multiple-dose treatments. The nature of the interactions suggested induction of CYP3A enzymes.

2. Primary cultures of human hepatocytes were used to investigate the induction potential of troglitazone with respect to CYP3A4, CYP2B6 and CYP1A1/2. In human hepatocytes, troglitazone induced both immunoreactive CYP3A4 protein and testosterone 6β-hydroxylase activity in a dose-dependent fashion (EC_{50} = 5–10 μM), accompanied by an increase in CYP3A4 mRNA. The capacity of troglitazone to induce CYP3A4 was between that of rifampin (EC_{50} = ~ 0.8 μM) and dexamethasone (40–50 μM). Troglitazone increased CYP2B6 immunoreactive protein but did not significantly effect CYP1A1/2 activity, immunoreactive protein or mRNA.

3. Troglitazone produced significant increases in CYP3A message, protein and activity in primary rat hepatocytes, a slight increase in CYP2B1/2 activity and no change in CYP1A1/2 message or activity.

4. These results provide evidence that troglitazone can induce CYP3A and CYP2B enzymes while apparently not altering CYP1A. This provides a rationale for the clinically observed interactions of troglitazone with selected CYP3A4 substrates.

Introduction

Troglitazone (± -5-[4-[3′4-dihydro 6-hydroxy-2,5,7,8-tetramethyl-2H-1-benzopyran-2-yl)-methoxy]phenyl]methyl]-2,4 thiazolidinedione, Rezulin®, TRZ) is a thiazolidinedione derivative proven to lower plasma glucose levels in patients with type II diabetes mellitus (Spencer and Markham 1997). In addition to reducing hyperglycaemia, TRZ decreases plasma insulin and triglyceride concentrations (Kumar *et al.* 1996, Cavaghan *et al.* 1997). TRZ is also useful in the non-diabetic patient with impaired glucose tolerance as it causes a significant reversal of hyperinsulinaemia, increased sensitivity to insulin and increased glucose tolerance. An enhanced glucose response has been observed in pancreatic β-cells (Antonucci *et al.* 1997, Cavaghan *et al.* 1997), although TRZ does not have a direct effect on insulin release from these cells (Fujiwara *et al.* 1998). TRZ acts by increasing skeletal muscle, liver and adipose tissue sensitivity to insulin and by decreasing hepatic glucose production. The mode of action is believed to be through binding to

* Author for correspondence at: University of North Carolina at Chapel Hill, School of Pharmacy, Division of Pharmaceutics, CB #7360, Beard Hall, Chapel Hill, NC 27599–7360, USA; e-mail: edlecluyse@unc.edu

Xenobiotica ISSN 0049–8254 print/ISSN 1366–5928 online © 2000 Taylor & Francis Ltd
http://www.tandf.co.uk/journals/tf/00498254.html

and activation of the peroxisome proliferator-activated receptor γ (PPAR-γ), which results in induction of DNA transcription and stimulation of the glucose kinase promoter (Lehmann *et al.* 1995, Vidal-Puig *et al.* 1996).

Troglitazone is predominantly metabolized via formation of sulphate and glucuronide conjugates and a quinone metabolite (Loi *et al.* 1999a). Drug interaction studies have shown that TRZ does not effect the steady state pharmacokinetics of digoxin (Loi *et al.* 1998a), acetaminophen, glyburide or warfarin (Loi *et al.* 1999a). TRZ does, however, decrease the trough concentration of cyclosporine in the renal transplant patient (Burgess *et al.* 1998, Kaplan *et al.* 1998) and decreases plasma concentrations of terfenadine, ethinyl oestradiol, norethindrone (Parke Davis 1997, package insert) and atorvastatin (Lipitor®; Loi *et al.* 1999b). These drugs are extensively metabolized by CYP3A4, thereby implying that TRZ may be an inducer of this enzyme—most likely in the liver. Supporting the induction of CYP3A4 in humans were results from a TRZ multiple dose study where a marked increase in levels of 6β-hydroxycortisol, a metabolite of endogenous cortisol formed by CYP3A4, were measured (Koup *et al.* 1998).

Several preclinical *in vitro* and *in vivo* models have been used to investigate different aspects of drug–drug interactions, including induction and inhibition potentials. It has been established that under appropriate culture conditions mammalian hepatocytes remain differentiated and retain the ability to respond to inducers for several days (LeCluyse *et al.* 1996a, Strom *et al.* 1996). For the present studies, primary cultures of rat and human hepatocytes were used to examine the induction of P450 enzymes by troglitazone. The specific CYP enzymes investigated were CYP1A, CYP2B and CYP3A, based on their importance in xenobiotic metabolism (Parkinson 1996). Inasmuch as enzyme induction can occur through either an increase in mRNA or through stabilization of the protein, the levels of P450 enzyme mRNA, protein and activities have been examined to see how they differentiate the mechanism(s) of P450 enzyme induction by TRZ. The results presented here provide supporting evidence for involvement of CYP3A4 induction in troglitazone drug–drug interactions observed in the clinic.

Materials and methods

Male Wistar rats (150–200 g) were from Charles River (Portage, MI, USA). ITS+ (insulin, transferrin, selenium, linoleic acid, BSA supplement), Hepatostim culture media and Matrigel® were from Collaborative Biomedical Research (Bedford, MA, USA). Collagenase type IV was from Sigma Chemical Co. (St Louis, MO, USA) and collagen, type I (Vitrogen) was from CelTrix (Santa Clara, CA, USA). Petri dishes (60 mm, LUX, Permanox) were from NUNC (Naperville, IL, USA). All other media and culture reagents were from Gibco BRL (Grand Island, NY, USA). Western blotting kits for rat CYP1A1, CYP2B1 and CYP3A1 were from Amersham Life Science (Amersham, UK). BCIP/NBT phosphatase substrate was from Kirkegaard & Perry Laboratories (Gaithersburg, MD, USA). RNA STAT-60 was from Tel Test, Inc. (Friendswood, TX, USA) and the Titan one tube RT-PCR system from Boehringer Mannheim (Indianapolis, IN, USA). Glucose 6-phosphate, glucose 6-phosphate dehydrogenase, 11β-hydroxy-testosterone, $NADP^+$, testosterone, β-naphthoflavone and dexamethasone were from Sigma. Resorufin and 7-ethoxyresorufin were from Molecular Probes (Junction City, OR, USA) and 6β-hydroxytestosterone from Steraloids, Inc. (Wilton, NH, USA). All solvents and other chemicals used were of HPLC grade or the highest purity available.

Isolation of human hepatocytes

All tissues were obtained through qualified medical staff, with donor consent and the approval of the UNC Hospitals Ethics Committee. Hepatocytes were isolated from human liver specimens from patients undergoing hepatic resections for hepatic cancer (three males, two females) or from a rejected donor organ (one female) by a modification of the two-step collagenase digestion method of Strom *et al.* (1996),

with minor modifications as described by LeCluyse *et al.* (1996a). In most cases encapsulated liver tissue (25–100 g) was perfused with calcium-free buffer containing 5.5 mM glucose and 0.5 mM EGTA for 10–15 min at a flow rate of 30–50 ml/min followed by perfusion with buffer containing 1.5 mM calcium and collagenase (0.3–0.4 mg/ml) for 20–25 min. Hepatocytes were dispersed from the digested liver in Dulbecco's modified Eagle's medium (DMEM) containing 5% foetal calf serum, insulin and dexamethasone and washed by low-speed centrifugation (70 *g*, 4 min). Cell pellets were resuspended in supplemented DMEM and 90% isotonic Percoll (3:1 v/v) and centrifuged at 100 *g* for 5 min. The resulting pellets were washed with fresh medium by low-speed centrifugation and resuspended in supplemented DMEM. Viability was determined by trypan blue exclusion and was typically between 80 and 90%.

Primary cultures of human hepatocytes

Hepatocytes were cultured according to the method of LeCluyse *et al.* (1996a). Briefly, 4.0–4.5 million hepatocytes were added to 60-mm NUNC Permanox® culture dishes coated with a simple collagen substratum in 3 ml serum-free modified Chee's medium (MCM) containing 0.1 μM dexamethasone, 6.25 μg/ml insulin, 6.25 μg/ml transferrin and 6.25 ng/ml selenium (ITS+) and allowed to attach for 2–4 h at 37 °C in a humidified chamber with 95% /5% air/CO_2. Culture dishes were gently swirled and medium containing unattached cells was then aspirated. Fresh ice-cold medium containing 0.25 mg/ml Matrigel® was added to each dish and cultures were returned to the humidified chamber (Sidhu *et al.* 1993). Medium was changed on a daily basis thereafter. Unless otherwise specified, primary cultures of human hepatocytes were maintained for 36–48 h before initiating treatment with test compounds.

P450 enzyme induction

Hepatocytes were plated onto Permanox® culture dishes and overlaid with Matrigel® as described above. The cells were maintained in MCM supplemented with ITS+ and 0.1 μM dexamethasone before initiating treatment with TRZ and other prototypical inducers (rifampin or dexamethasone). Groups of hepatocyte cultures ($n = 2–3$ dishes per treatment group) were then treated for 3 consecutive days with drug at concentrations as outlined in the Results. Control cultures were treated with vehicle alone (0.1% DMSO). At the end of each study period cells were harvested for the preparation of microsomes.

Cell harvest and microsome preparation

At appropriate time points, cultures of human hepatocytes from each treatment group were rinsed twice with ice-cold PBS. Homogenization buffer (50 mM Tris-HCl, pH 7.0, 150 mM KCl, 2 mM EDTA) was added to each dish (0.5 ml/dish) and cells were scraped with a rubber policeman. Harvested cells from each treatment were then pooled and sonicated with a Vibra-Cell probe sonicator (Sonics & Materials, Danbury, CT, USA) at 40 watts for 15–20 s (Wortelboer 1990). Cell lysates were centrifuged at 9000 *g* for 20 min at 4 °C. Supernatants were collected and centrifuged at 100 000 *g* for 60 min at 4 °C. The final microsomal pellets were resuspended in 0.2–0.4 ml 0.25 M sucrose with the aid of a Dounce homogenizer fitted with a Teflon pestle. A small aliquot was taken for protein determination and all samples were subsequently stored at − 80 °C.

Isolation and culture of rat hepatocytes

Animals. Male Wistar rats (150–200 g) were housed in accordance to the guidelines set by the National Institute of Health and the Institutional Animal Care Committee. Rats were fed water and Prolab RMH 3000 rodent chow (PMI Nutrition International, Inc., Brentwood, MO, USA) *ad libitum*.

Hepatocytes were isolated from rat livers using the two-step collagenase perfusion method described above (LeCluyse *et al.* 1996a). Animals were anaesthetized with ether and a U-shaped incision exposed the liver. The hepatic artery was cannulated and the superior vena cava incised before starting perfusion. Cells were used for experiments if viability was >85%, as determined by trypan blue exclusion. Six million hepatocytes were seeded on each 100-mm tissue culture dish precoated with a thick Matrigel matrix (3 mg/100 mm dish) and cultured in 8 ml Hepatostim culture media. Media was changed after a 4-h attachment.

P450 enzyme induction

Twenty-four hours after seeding, the media was removed and fresh medium containing the vehicle (control), TRZ (25 or 50 μM), dexamethasone (50 μM, positive control for CYP3A induction), β-naphthoflavone (50 μM, positive control for CYP1A1/2 induction) or phenobarbital (50–100 μM, positive control for CYP2B1/B2 induction) was added. Cells were harvested 48 h post-treatment using cold phosphate-buffered saline (PBS, pH 7.4) containing 5 mM EDTA, and microsomes were prepared as described above.

Enzyme assays

CYP1A (rat and human), CYP3A (rat and human) and CYP2B1/2 (rat) activities were determined by measuring 7-ethoxyresorufin *O*-dealkylation, testosterone 6β-hydroxylation and 7-pentoxyresorufin *O*-dealkylation activities respectively in microsomal samples from hepatocyte cultures (Pearce *et al.* 1996). To determine resorufin *O*-dealkylation, liver microsomes (0.1–0.2 mg) were incubated at 37$\pm$1 °C in 0.5-ml (final volume) incubation mixtures containing potassium phosphate buffer (100 mM, pH 7.4), $MgCl_2$ (3 mM), EDTA (1 mM), NADP (1 mM), glucose 6-phosphate (5 mM), glucose 6-phosphate dehydrogenase (1 Unit/ml) and 7-ethoxyresorufin (10 μM), at the final concentrations indicated. 7-Ethoxyresorufin (2.5 mM) was added to each incubation mixture in 4 μl dimethylsulphoxide. Reactions were started by addition of the NADPH-generating system and stopped after 2–16 min by addition of 1 ml ice-cold acetone. Precipitated protein was removed by centrifugation (2000 *g* for 5 min). The amount of resorufin in the clear supernatant fraction was determined fluorometrically (λ_{ex} = 535 nm, λ_{em} = 585 nm) with a Shimadzu RF 540 Spectrofluorometer. Zero-time incubations served as blanks, and blanks spiked with up to 1000 pmol resorufin served as standards.

To measure testosterone 6β-hydroxylation, reaction mixtures were essentially as described above except for the addition of testosterone as substrate at a final concentration of 250 μM. Testosterone (12.5 mM) was added to each 0.5-ml incubation in 20 μl methanol; reactions were started by addition of the NADPH-generating system and were stopped after 8–16 min by addition of 1.5 ml dichloromethane. Zero-time incubations served as blanks. Testosterone and its metabolites were extracted from incubation samples and resolved by binary gradient HPLC on a Supelcosil LC-18 reverse-phase octyldecylsilane column (5 μm particle size, 15 cm$\times$4.6 mm i.d.) (Supelco, Bellefonte, PA, USA) preceded by a Supelcosil LC-18 guard column (40 μm particle size, 2 cm$\times$4.6 mm, i.d.) (Pearce *et al.* 1996).

Western blot analysis

The protein content of CYP1A1, 1A2, 2B1/2 and 3A1/2 in the rat hepatic microsomes and 1A2, 2B6, and 3A4 in the human microsomes was visualized using Western immunoblotting (Parkinson and Gemzik 1991). Microsomal protein samples (10 μg) were resolved by SDS-PAGE and electrophoretically transferred to nitrocellulose membranes. Membranes were probed with specific polyclonal antibodies raised in rabbit to rat CYP1A1, CYP1A2, CYP2B1/2 or CYP3A1/2 or human CYP1A2, CYP2B6, CYP3A4, followed by an anti-rabbit Ig-biotinylated secondary antibody and streptavidin-horseradish peroxidase or alkaline phosphatase conjugate. For rat CYP enzymes, the protein was visualized on autoradiography film after ECL detection. For human CYP enzymes the protein was visualized using BCIP/NBT (5-bromo-4-chloroindolyl-phosphatase/nitrobenzotetrazolium) phosphatase substrate.

RT-PCR

RT-PCR examined the induction of RNA transcript after treatment with TRZ. Briefly, the cells were lysed directly on the culture dish by adding RNA STAT-60. RNA was extracted using chloroform, precipitated with isopropanol, washed with ethanol and reconstituted in DEPC-treated water. RT-PCR was conducted using the Titan one tube RT-PCR kit and primers specific for each enzyme (Muntane-Relat *et al.* 1990, Omiesinski *et al.* 1990, Morris and Davila 1996). cDNA content was visualized under UV light after running the cDNA on agarose gels containing ethidium bromide.

Statistical analysis

Data were analyzed for statistically significant differences between control and treated rat and human hepatocyte cultures by Dunnett's two-way analysis of variance at the 5% level of significance (Dunnett 1964). Results are expressed as mean$\pm$SD of hepatocyte preparations from three-to-five separate livers. Within each experiment, assays were performed in triplicate.

Results

Effect of troglitazone on cytochrome P450 enzymes in human hepatocytes

Figure 1 shows the mean CYP1A1/2 activity in three separate preparations of human hepatocytes after treatment with 25 μM TRZ. Basal CYP1A1/2 activity (7.12 pmol ethoxyresorufin dealkylated/min/mg protein) increased by $<$ 2-fold as compared with nearly 9-fold after treatment with the known CYP1A1/2 inducer βNF. Microsomes prepared from the primary hepatocyte cultures were subjected to Western blot analysis using anti-CYP1A1/2 antibodies. A marked increase in protein levels was observed with βNF, whereas no change in levels was found after TRZ treatment (figure 1).

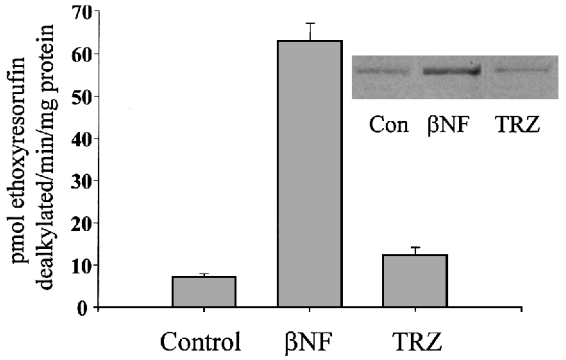


Figure 1. Effect of βNF and TRZ on CYP1A protein levels and activity in primary cultures of human hepatocytes. Freshly isolated hepatocytes were prepared from human liver and placed in primary culture for 24 h before treatment with DMSO (vehicle, control group), βNF (50 μM, positive control) and TRZ (50 μM). Twenty-four hours post-treatment, cells were harvested, microsomal membranes made and activity assays run, as per procedures in the Materials and methods. The data reflect the mean of triplicate determinations of three different preparations of human hepatocytes. The insert shows the effect of βNF (50 μM, positive control) and TRZ (50 μM) on the expression of CYP1A2 immunoreactive protein in the primary cultures of human hepatocytes. Microsomes were isolated and analysed (10 μg/lane) by Western blot hybridization for CYP1A2, as described in the Materials and methods.

Testosterone 6β-hydroxylase activity assessed the effects of TRZ on CYP3A4 activity. Rifampin (figure 2a) and dexamethasone (figure 2b) were used as positive controls. TRZ increased CYP3A4 activity in a concentration-dependent manner (figure 2c). The maximum extent of induction observed was between 5- and 6-fold. CYP3A4 activity was also increased in a dose-dependent manner with rifampin (figure 2a) and dexamethasone (figure 2b). The maximum extent of induction for rifampin and dexamethasone was $\sim$7-fold for both compounds. EC_{50} for RIF, DEX, and TRZ were 0.5–1.0, 40–50 and 5–10 μM respectively. These results were supported by Western blot analysis using anti-CYP3A4 antibody and microsomes prepared from troglitazone-treated primary hepatocytes over a concentration range of 0.5–50 μM (figure 3a). Microsomes from rifampin (10 μM) -treated primary hepatocytes also showed a marked increase in CYP3A4 protein (figure 3a).

CYP2B6 induction also was observed in the TRZ-treated primary cultures of human hepatocytes. An initial increase in CYP2B6 immunoreactive protein was observed with TRZ concentrations as low as 5 μM, with further increases in protein levels observed in a concentration-dependent manner with increasing concentrations of TRZ (figure 3b). Treatment of the hepatocytes with rifampin (10 μM) resulted in a marked increase in the levels of immunoreactive CYP2B6 (figure 3b).

The mRNA extracted from primary hepatocytes was reverse-transcribed to cDNA and subjected to the polymerase chain reaction using primers specific for human CYP1A1/2 and CYP3A4. No change was observed in CYP1A1/2 cDNA after treatment with TRZ (figure 4a). This was consistent with activity assays and Western blot analysis (figure 1), where no increase was observed in protein activity and content in cells treated with TRZ. RT-PCR analysis showed a marked increase in mRNA for CYP3A4 (figure 4a) in hepatocytes consistent with the increase in enzyme activity and protein content observed with TRZ treatment (figures 2 and 3).

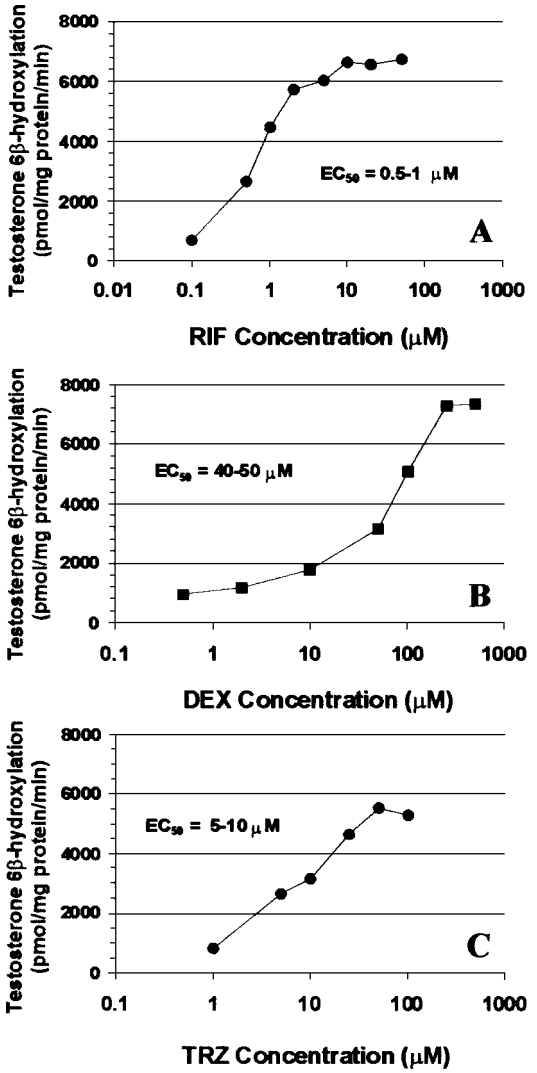


Figure 2. Concentration-dependant induction of CYP3A4 activity by RIF, DEX and TRZ. Freshly isolated hepatocytes prepared from human liver were placed in primary culture for 36–48 h before initializing treatment with (A) rifampin (0.1–50 μM), (B) dexamethasone (0.5–500 μM) and (C) TRZ (1–100 μM). Seventy-two hours post-treatment, cells were harvested, microsomal membranes made and testosterone 6β-hydroxylation activity assay run, as per the procedures in the Materials and methods. The data are representative results taken from a single preparation of human hepatocytes.

Effect of troglitazone on cytochrome P450 enzymes in rat hepatocytes

CYP1A1/2 activity was evaluated in the primary rat hepatocytes after 48 h of treatment in culture. As shown in table 1, TRZ did not change basal activity of this enzyme, while βNF treated rat hepatocytes, used as a positive control, increased CYP1A1/2 activity by 40-fold. Microsomal membranes derived from rat hepatocytes were probed with anti CYP1A1 and CYP1A2 antibodies (figure 5). CYP1A1 was not detected in untreated cultures consistent with the known expression of this enzyme in rat. This enzyme was expressed after 48 h of exposure to βNF. CYP1A1 protein was not detectable after a 48-h treatment with TRZ. CYP1A2 was visualized

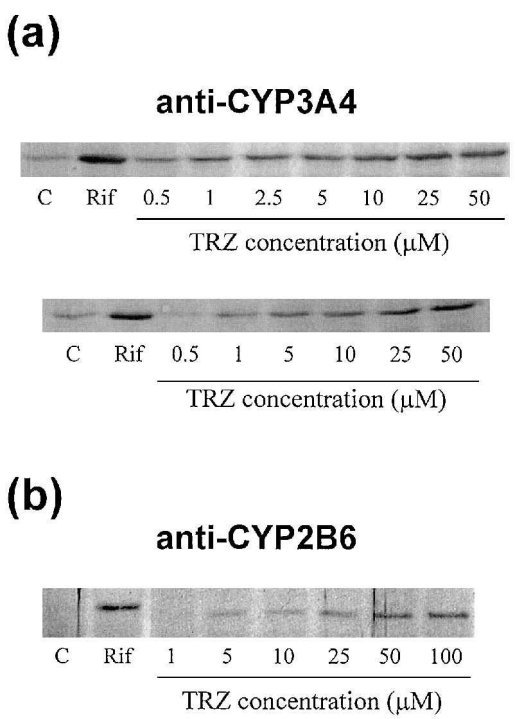


Figure 3. Induction of CYP3A4 and CYP2B6 immunoreactive protein in primary cultures of human hepatocytes. (a) Freshly isolated hepatocytes prepared from two separate human livers were placed in primary culture for 36–48 h before treating with rifampin (10 μM) or TRZ (0.5–50 μM) for 72 h. Microsomes were isolated and analysed (10 μg/lane) by Western blot hybridization for CYP3A4 immunoreactive protein as described in the Materials and methods. (b) Freshly isolated hepatocytes prepared from a single donor were treated with rifampin (10 μM) or TRZ (0.5–50 μM) as in (a). Microsomes were isolated and analysed (10 μg/lane) by Western blot hybridization for CYP2B6 immunoreactive protein.

in the control microsomes and the protein content remained unchanged after TRZ treatment. Following βNF treatment, a significant increase was observed in CYP1A2. Taken together, these results confirm that the CYP1A1 and CYP1A2 protein are not induced by TRZ in primary cultures of rat hepatocytes, consistent with the results observed in the human hepatocytes.

The dealkylation of 7-pentoxyresorufin by rat liver microsomes was measured as an indicator of CYP2B1/2 activity (table 1). Phenobarbital (100 μM) was used as a positive control and induced a significant (62-fold) increase in the basal levels of CYP2B1/2 while only a slight increase (2.3-fold) was observed with TRZ (25 μM). Phenobarbital (25 μM) induced a 5-fold increase (data not shown). Western blot analysis of microsomes prepared from TRZ- and PB-treated hepatocytes was probed with anti-CYP2B1/2 antibody. CYP2B1/2 protein was detected in the preparations from control hepatocytes and a marked increase in protein content was observed after phenobarbital treatment. A slight increase in CYP2B1/2 content was detected with 25 μM TRZ (figure 5).

CYP3A activity was measured by examining the metabolism of testosterone to 6β-hydroxy testosterone in rat microsomes prepared from primary rat hepatocytes treated with dexamethasone (50 μM) and TRZ (25 μM). A significant 3.5-fold increase was observed with TRZ compared with control and a 5-fold increase was

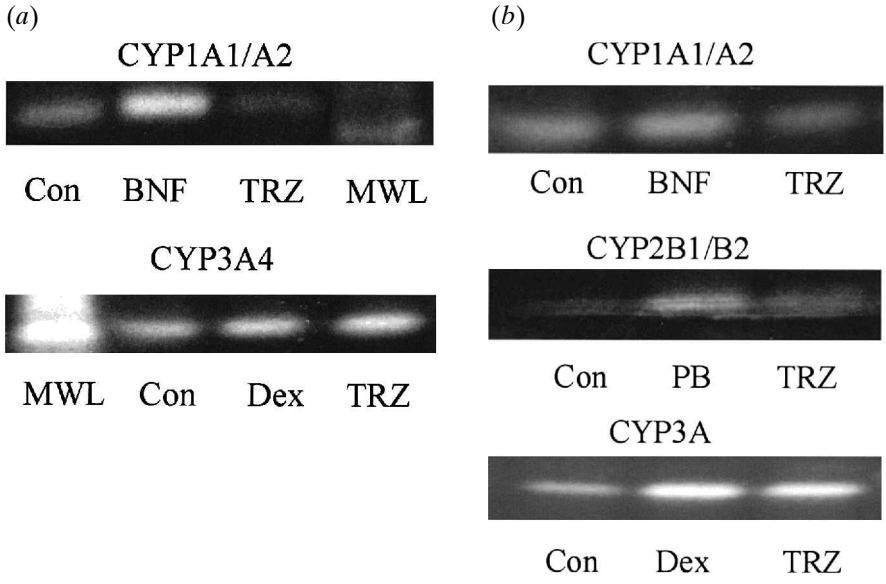


Figure 4. Effect of TRZ on CYP1A, CYP2B and CYP3A message in primary cultures of human and rat hepatocytes. (*a*) Freshly isolated hepatocytes prepared from human liver were placed in primary culture for 24 h before treating with βNF (50 μM), DEX (50 μM) or TRZ (25 μM). (*b*) Freshly isolated hepatocytes prepared from rat liver were placed in primary culture for 24 h before treating with βNF (50 μM), DEX (50 μM), PB (50 μM) or TRZ (25 μM). Twenty-four hours post-treatment, total cellular RNA was extracted and RT-PCR conducted as described in the Materials and methods. All samples (10 μg /lane) were run in triplicate. MWL is the molecular weight ladder.

Table 1. Effects of troglitazone and prototypical P450 inducers on the activities of the major inducible drug-metabolizing P450 enzymes in primary cultures of rat hepatocytes[a].

	CYP1A	CYP2B	CYP3A
Control (DMSO)	14± 5	6± 1	833± 146
Dexamethasone (50 μM)	nd	nd	4140± 306***
β-naphthoflavone (50 μM)	560± 30***	nd	nd
Phenobarbital (100 μM)	nd	396± 67***	nd
Troglitazone (25 μM)	15± 4	15± 3**	2900± 800***

[a] Freshly isolated rat hepatocytes were placed in primary culture for 24 h before treatment with DMSO (control), phenobarbital (50 μM), rifampin (50 μM), βNF (50 μM) and TRZ (25 μM). Forty-eight hours post-treatment, cells were harvested, microsomal membranes made and 7-ethoxyresorufin, 7-pentoxyresorufin and testosterone 6β-hydroxylation activity assays run, for the CYP1A, CYP2B and CYP3A activities respectively as described in the Materials and methods. Data reflect the mean± SE of triplicate determinations from four different preparations of rat hepatocytes. Activities are pmol/min/mg protein. *$p < 0.05$, **$p < 0.01$ and ***$p < 0.001$, p is the level of statistical significance of differences between treated and control values.

found in microsomes from the dexamethasone-treated hepatocytes (table 1). Immunoblots for CYP3A content in rat microsomes reveal a significant increase in CYP3A protein after treatment with both dexamethasone and TRZ (figure 5).

The mRNA isolated from primary rat hepatocytes was reverse transcribed to cDNA and subjected to the polymerase chain reaction using primers specific for

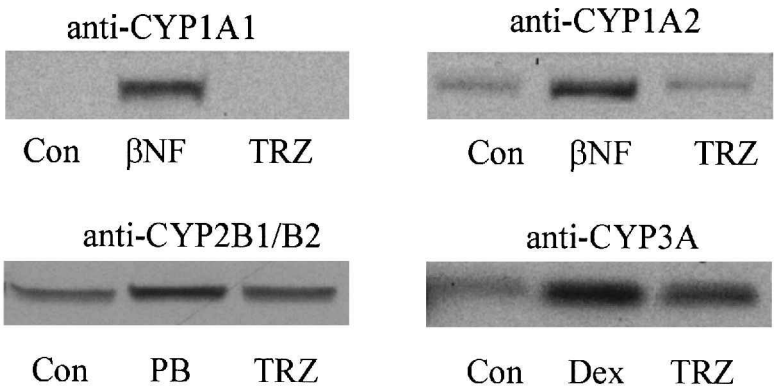


Figure 5. Effect of βNF, PB, DEX and TRZ on the immunoreactive proteins of CYP1A1, CYP1A2, CYP2B1/B2 and CYP3A respectively in primary cultures of rat hepatocytes. Freshly isolated hepatocytes prepared from rat liver were placed in primary culture for 24 h before treating with βNF (50 μM), dexamethasone (50 μM), phenobarbital (50 μM) or TRZ (25 μM). Forty-eight hours post-treatment, cells were harvested. Microsomes were isolated and analysed (5 μg/lane) by Western blot hybridization for CYP1A1, CYP1A2, CYP2B1/2 and CYP3A4, as described in the Materials and methods.

CYP1A1/2, CYP2B1/2 and CYP3A. The results show that the increase in CYP3A activity in the rat hepatocytes is at the level of the mRNA, as a corresponding increase was seen in the cDNA (figure 4b). No change was observed in CYP1A1/2 cDNA after TRZ treatment, consistent with activity assays and Western blot analysis. CYP2B1/2 expression in rat hepatocytes increased slightly after treatment with TRZ, consistent with the activity and protein expression results.

Discussion

Induction of drug-metabolizing enzymes, especially CYP enzymes, is a relatively common phenomenon characteristic of many drugs. Whether induction results in clinically significant drug–drug interactions depend on the enzyme(s) induced, magnitude of the induction and pharmacokinetic profile of co-administered drugs. TRZ is currently available for prescription use in the USA to treat patients with type II diabetes mellitus, although its use in the UK is still under consideration. Pharmacokinetic drug–drug interactions have been noted following multiple dose administration of TRZ with such drugs as ethinyl oestradiol, norethindrone (Loi *et al.* 1999d), fexofenadine (Loi *et al.* 1999c) and cholestyramine (Young *et al.* 1998) through either metabolism- or transport-related mechanisms. Other compounds, whose clearance have been increased in conjunction with TRZ, are atorvastatin (Lipitor®) (Loi, personal communication), cyclosporine (Burgess *et al.* 1998, Kaplan *et al.* 1998), terfenadine (Cowie *et al.* 1996, Loi *et al.* 1998b) and midazolam (unpublished data). The metabolism of these four drugs is known to be mediated by CYP3A4, suggesting that TRZ may be an inducer of CYP3A4 activity. CYP3A4 is known to be inducible by a wide variety of structurally diverse compounds, including rifampin, carbamazepine, phenytoin and dexamethasone (Parkinson 1996).

Initial studies to assess the effect of TRZ on the levels of hepatic drug-metabolizing enzymes have been employed *in vivo* in rat and monkey models. The rat studies showed small changes in the enzymes studied—a 9–14% increase in

activity of aminopyrine N-demethylase and a 13–24% increase in 7-ethoxycoumarin *O*-deethylase activity. In the monkey, small increases were found in the total P450 content and activities of hepatic 7-methoxycoumarin *O*-demethylase and ethoxycoumarin *O*-deethylase (unpublished data). The induction observed in both these species was minor and, although the probes used in the *in vivo* studies were not specific for CYP3A, no significant drug-interactions were anticipated in the human. Whereas the rat and monkey *in vivo* models for TRZ induction were not predictive of the human situation, the present authors explored using primary cultures of human hepatocytes. This model system was chosen because primary hepatocyte cultures are the most appropriate *in vitro* method to examine the effect of chemicals on hepatic CYP expression and activity in the relevant species. Thus, the advantage of using this *in vitro* model is that the direct effect on cellular processes such as enzyme regulation can be examined selectively in the species of choice.

Human hepatic tissue has limited availability and is highly variable in its quality – both as a result of donor history and lag time between harvesting of tissue and procurement at the laboratory. As a result, parallel studies were also conducted using rat primary hepatocytes to validate them as an alternative model system for studying human hepatic induction by glitazones. Whereas heterogeneity exists between species, it is possible to extrapolate results from one species to the other, with the appropriate supporting data, as described in these studies. However, this is often drug specific. For example, RIF is a potent inducer of human CYP3A4, but a poor inducer of rodent CYP3A1/2 (Kocarek *et al.* 1995, Parkinson 1996). On the other hand, PCN is a potent inducer of rodent CYP3A1/2, but a poor inducer of human CYP3A4.

The effect of TRZ on CYP3A expression confirmed what has been implied by the clinical studies - that TRZ is an inducer of this enzyme subfamily in the human liver. The present results showed an increase in CYP3A mRNA levels accompanied by an increase in CYP3A immunoreactive protein and enzyme activity in both the human and rat hepatocytes treated with TRZ. This occurs, most likely, via pregnane X receptor (PXR)-mediated CYP3A4 gene activation (Lehmann *et al.* 1998). Notably, TRZ binds to and activates human PXR at a similar EC_{50} as described here (S. Kliewer, personal communication). However, these studies do not exclude the added possibility that TRZ may also cause stabilization of the CYP3A message.

The concentration–response curves and the derived EC_{50} with human hepatocytes, suggest that TRZ is a moderate inducer of CYP3A4 activity, that it is less potent than rifampin and more potent than dexamethasone or phenobarbital. Although the EC_{50} for CYP3A4 induction by TRZ *in vitro* is slightly above the steady-state plasma concentrations observed *in vivo* (2 μM), tissue distribution studies in rat have shown that TRZ concentrations within liver tissue are much higher (10–12-fold), indicating that levels sufficient to activate PXR can be easily achieved *in vivo* (R. Boyd, Parke-Davis, personal communication).

CYP1A activity was also examined in both rat and human hepatocytes. No significant induction in activity was observed at the level of CYP1A transcript, protein content or enzyme activity. These results imply that administering drugs that are metabolized predominantly by the CYP1A enzymes will not result in clinically significant drug–drug interactions.

The results from the present studies also show that TRZ could potentially be an inducer of human CYP2B6 *in vivo*, as a marked increase in immunoreactive CYP2B6 protein was observed. This suggests that TRZ may cause interactions with

drugs that are metabolized by CYP2B6, including cyclophosphamide, ifosfamide, tamoxifen, nevirapine, bupropion and nicotine (Parkinson 1996). In rat hepatocytes, TRZ treatment results in a minor increase in the level of the CYP2B1/2 immunoreactive protein and activity. Since rat and human hepatocytes show a similar induction profile for CYP1A and CYP3A, it is possible that this trend will also hold true for CYP2B. Additional studies, including activity assays, are currently being conducted to corroborate these findings.

In conclusion, these studies show that in human hepatocytes, TRZ is a moderate inducer of CYP3A4 activity compared with the prototypical inducers, rifampin and dexamethasone. The mechanism of induction appears to be through gene activation, as TRZ caused a marked increase in CYP3A4 mRNA, accompanied by an increase in immunoreactive protein and enzyme activity. No significant induction in CYP1A was observed at the level of the mRNA, protein content or enzyme activity. Western blot analysis indicates that TRZ is an inducer of CYP2B6 in primary cultures of human hepatocytes. The interactions resulting from the induction of P450 enzymes by TRZ could have clinical implications, particularly because CYP3A4 metabolizes such a large number of drugs. The data also suggest that the rat appears to be a reasonable model for future studies with TRZ, as results obtained were comparable with those with human hepatocytes. Further, these studies illustrate the utility of primary cultures of hepatocytes in the assessment of the induction potential of new chemical entities.

Acknowledgements

This work was supported in part by a grant from the FDA (Centre for Drug Evaluation and Research) (#223–97–3004). The authors thank Dr Rebecca Boyd for valuable comments during the preparation of the manuscript.

References

ANTONUCCI, T., MCLAIN, R., WHITCOMB, R. *et al.*, 1997, Impaired glucose tolerance is normalized by treatment with the thiazoldinedione, troglitazone. *Diabetes Care*, **20**, 188–193.

BURGESS, S. J., SINGER, G. G. and BRENNAN, D. C., 1998, Effect of troglitazone on cyclosporine whole blood levels. *Transplantation*, **66**, 1399–1400.

CAVAGHAN, M. K., EHRMANN, D. A., BYRNE, M. M. *et al.*, 1997, Treatment with oral antidiabetic agent troglitazone improves β cell responses to glucose in subjects with impaired glucose tolerance. *Journal of Clinical Investigation*, **100**, 530–537.

COWIE, C. C. and EBERHARDT, M. S. (eds), 1996, *Diabetes 1996 Vital Statistics* (Alexandria: American Diabetes Association).

DUNNETT, G. W., 1964, New tables for multiple comparisons with a control. *Biometrics* **20**, 482–491.

FUJIWARA, T., YOSHIOKA, U. *et al.*, 1998, Characterization of new oral antidiabetic agent CS-045. Studies in KK and ob/ob mice and Zucker fatty rats. *Diabetes*, **37**, 1549–1558.

KAPLAN, B., FRIEDMAN, G., JACOBS, M. *et al.*, 1998, Potential interaction of troglitazone and cyclosporine. *Transplantation*, **65**, 1399–1400.

KUMAR, S., BOULTON, A. J. M., BECK-NIELSEN, H. *et al.*, 1996, Troglitazone, an insulin action enhancer, improves metabolic control in type II diabetes patients. *Diabetelogia*, **39**, 701–709.

LECLUYSE, E. L., BULLOCK, P. and PARKINSON, A., 1996b, Strategies for restoration and maintenance of normal hepatic structure and function in long-term cultures of rat hepatocytes. *Advanced Drug Delivery Reviews*, **22**, 133–186.

LECLUYSE, E. L., BULLOCK, P., PARKINSON, A. and HOCHMAN, J. H., 1996a, Cultured rat hepatocytes. In R. T. Borchardt, G. Wilson and P. Smith (eds), *Model Systems for Biopharmaceutical Assessment of Drug Absorption and Metabolism* (New York: Plenum), pp. 121–159.

LEHMANN, J. M., MCKEE, D. D., WATSON, M. A., WILLSON, T. M., MOORE, J. T. and KLIEWER, S. A., 1998, The human orphan nuclear receptor PXR is activated by compounds that regulate *CYP3A4* gene expression and cause drug interactions. *Journal of Clinical Investigation*, **102**, 1016–1023.

LEHMANN, J. M., MOORE, L. B., SMITH-OLIVER, T. A. *et al.*, 1995, An antidiabetic thiazolidinedione is a high affinity ligand for peroxisome proliferator-activated receptor γ (PPAR γ). *Journal of Biological Chemistry*, **270**, 12953–12956.

KOCAREK, T. A., SCHUETZ, E. G., STROM, S. C., FISHER, R. A. and GUZELIAN, P. S., 1995, Comparative analysis of cytochrome P4503A induction in primary cultures of rat, rabbit, and human hepatocytes. *Drug Metabolism and Disposition*, **23**, 415–421.

KOUP, J. R., ANDERSON, G. and LOI, C. M., 1998, Effect of troglitazone on urinary excretion of cortisol and 6β-hydroxycortisol. *Journal of Clinical Pharmacology*, **38**, 815–818.

LOI, C. M., KNOWLTON, P. W., STERN, R. *et al.*, 1998a, Effect of troglitazone on steady-state pharmacokinetics of digoxin. *Journal of Clinical Pharmacology*, **38**, 178–183.

LOI, C. M., MALCOLM, Y. RANDINITIS, E. *et al.*, 1999a, Clinical pharmacokinetics of Troglitazone. *Clinical Pharmacokinetics*, **37**, 91–104.

LOI, C. M., STERN, R., ABEL, R. *et al.*, 1999b, Effect of troglitazone on pharmacokinetics and pharmacodynamics of atorvastatin. *Clinical Pharmacology and Therapeutics*, **65**, PIII39.

LOI, C. M., STERN, R., VASSOS, A. B. *et al.*, 1998b, Effect of troglitazone on terfenadine pharmacokinetics. *Clinical Pharmacology and Therapeutics*, **63**, 228.

LOI, C. M., KOUP, J. R., VASSOS, A. B. and SEDMAN, A. J., 1999c, Effect of TRZ on fexofenadine pharmacokonetics. *Clinical Pharmacology and Therapeutics*, **65**, PIII40.

LOI, C. M., STERN, R., KOUP, J. R. *et al.*, 1999d, Effect of troglitazone on the pharmacokinetics of an oral contraceptive agent. *Journal of Clinical Pharmacology*, **39**, 410–414.

MORRIS, D. L. and DAVILA, J. C., 1996, Analysis of rat cytochrome P450 isoenzyme expression using semi-quantitative reverse transcriptase-polymerase chain reaction (RT-PCR). *Biochemical Pharmacology*, **52**, 781–792.

MUNTANE-RELAT, J., OURLIN, J. C., DOMERGUE, J. and MAUREL, P., 1995, Differential effects of cytokines on the inducible expression of CYP1A1, CYP 1A2 and CYP3A4 in human hepatocytes in primary culture. *Hepatology*, **22**, 1143–1153.

OMIESINSKI, C. J., HASSETT, C. and COSTA, P., 1990, Developmental expression and *in situ* localization of the phenobarbital-inducible rat hepatic mRNAs for cytochromes CYP2B1, CYP2B2, CYP2C6 and CYP3A1. *Molecular Pharmacology*, **38**, 462–470.

PARKINSON, A., 1996, Biotransformation of xenobiotics. In C. D. Klaassen (ed.), *Casarett and Doull's Toxicology. The Basic Science of Poisons*, 5th edn (New York: McGraw-Hill), pp. 113–186.

PARKINSON, A. and GEMZIK, B., 1991, Production and purification of antibodies against rat liver P450 enzymes. *Methods in Enzymology*, **206**, 233–245.

PEARCE, R. E., MCINTYRE, C. J., MADAN, A., SANZGIRI, U., DRAPER, A. J., BULLOCK, P. L., COOK, D. C., BURTON, L. A., LATHAM, J., NEVINS, C. and PARKINSON, A., 1996, Effects of freezing, thawing, and storing human liver microsomes on cytochrome P450 activity. *Archives of Biochemistry and Biophysics*, **331**, 145–169.

REZULIN® PRODUCT LABELLING (package insert), 1998, Warner–Lambert Co. (Morris Plains, NJ, USA).

SIDHU, J. S., FARIN, F. M. and OMIECINSKI, C. J., 1993, Influence of extracellular matrix overlay on phenobarbital-mediated induction of CYP2B1, 2B2, and 3A1 genes in primary adult rat hepatocyte culture. *Archives of Biochemistry and Biophysics*, **30**, 103–113.

STROM S. C., PISAROV, L. A., DORKO, K., THOMPSON, M. T., SCHUETZ, J. D. and SCHUETZ, E. G., 1996, Use of human hepatocytes to study P450 gene induction. *Methods in Enzymology*, **272**, 388–401.

VIDAL-PUIG, A., JIMINEZ-LINAN, M., LOWELL, B. B. *et al.*, 1996, Regulation of PPARγ gene expression by nutrition and obesity in rodents. *Journal of Clinical Investigation*, **97**, 2553–2561.

WORTELBOER, H. M., DE KRUIF, C. A,. VAN IERSEL, A. A. J., FALKE, H. E., NOORDHOEK, J. and BLAAUBOER, B. J., 1990, The isoenzyme pattern of cytochrome P450 in rat hepatocytes in primary culture, comparing different enzyme activities in microsomal incubations and in intact monolayers. *Biochemical Pharmacology*, **40**, 2525–2534.

YOUNG, M. A., LETTIS, S. and EASTMOND, R., 1998, Concomitant administration of cholestyramine influences the absorption of troglitazone. *British Journal of Clinical Pharmacology*, **45**, 37–40.

XENOBIOTICA , 2000, VOL. 30, NO. 3, 285–295

Ethnic-related differences in the frequency distribution of genetic polymorphisms in the *CYP1A1* and *CYP1B1* genes in Japanese and Caucasian populations

K. INOUE, T. ASAO and T. SHIMADA*

Osaka Prefectural Institute of Public Health, 3–69 Nakamichi 1-chome, Higashinari-ku, Osaka 537–0025, Japan

Received 23 July 1999

1. Race-related differences in the frequency distribution of genetic polymorphisms in the *CYP1A1* and *CYP1B1* genes were studied in 39 Japanese and 45 Caucasians.

2. Four types of *CYP1A1* polymorphism, namely m1 (a nucleotide change at T6235C in the 3′-flanking region), m2 (A4889G at exon 7), m3 (T5639C in the 3′-flanking region) and m4 (C4887A at exon 7), and three types of *CYP1B1* genetic polymorphism, namely m1 (C488G and G701T leading to Arg48Gly and Ala119Ser exchanges respectively), m2 (C1294G leading to a Leu432Val exchange) and m3 (A1358G leading to an Asn453Ser exchange) were studied.

3. The distribution of the m1-, m2-, m3-, and m4-types of *CYP1A1* polymorphism in the Japanese population was 30.8, 17.9, 0 and 0% respectively; those in Caucasians were 3.3, 6.7, 0 and 2.2% respectively. Two types (m1, and m2) of *CYP1B1* polymorphism were expressed at 14.1 and 21.8% respectively in the Japanese, and by 28.9 and 37.5% respectively in the Caucasian. Ethnic differences were also noted in the m3-type *CYP1B1* polymorphism in which the incidence in Caucasians was 23.9%, whereas no cases in the 39 Japanese subjects were observed.

4. No apparent association was found in the incidence in each of the genetic polymorphisms of *CYP1A1* and *CYP1B1* genes, nor in methylenetetrahydrofolate reductase gene, except that the occurrence of the m2-type of *CYP1A1* genetic polymorphism was related to that of the m1-type *CYP1A1* polymorphism in the Japanese population.

5. These results suggest that there are race-related differences in the occurrence of genetic polymorphisms in both *CYP1A1* and *CYP1B1* genes in Japanese and Caucasian populations and that these differences in P450 genetic polymorphisms may, in part, cause differences in the occurrence of lung and breast cancers in these ethnic groups.

Introduction

Cytochrome P450 (P450, CYP) comprises a superfamily of enzymes that catalyze oxidation of diverse xenobiotic chemicals including drugs, toxic chemicals and carcinogens, as well as endobiotic chemicals such as steroids, fatty acids, fat soluble vitamins and prostaglandins (Nelson *et al.* 1993). Major P450 enzymes involved in the detoxication and activation of a number of environmental procarcinogens include CYP1A1, 1A2, 1B1, 2B6, 2A6, 2E1, 3A4, 3A5 and 4B1 in humans (Gonzalez and Gelboin 1994, Guengerich *et al.* 1998). Of these P450 enzymes, CYP1A1 and CYP1B1 have been shown to be expressed predominantly in the extrahepatic organs and they catalyze activation of a number of carcinogenic polycyclic aromatic hydrocarbons to reactive metabolites that cause initiation of DNA damage in cells (Guengerich and Shimada 1991, Shimada *et al.* 1996, Larsen *et al.* 1998).

Relationships between *Msp*I polymorphism in the *CYP1A1* gene and lung

* Author for correspondence; e-mail, shimada@iph.pref.osaka.jp

Xenobiotica ISSN 0049–8254 print/ISSN 1366–5928 online © 2000 Taylor & Francis Ltd
http://www.tandf.co.uk/journals/tf/00498254.html

cancer susceptibilities were first reported by Kawajiri *et al.* (1990; Hayashi *et al.* 1992) in the Japanese population. However, some contrasting results have been demonstrated in several laboratories in which there is no direct evidence supporting the fact that *Msp*I polymorphism in the *CYP1A1* gene is actually linked to lung cancer susceptibilities (Hayashi *et al.* 1992, Hirvonen *et al.* 1992, Cosma *et al.* 1993, Drakoulis *et al.* 1994, Kelsey *et al.* 1994). Such contradictory results in these different laboratories may, in part, be accounted by differences in the distribution of genetic polymorphisms in the *CYP1A1* gene in different ethnic groups. In fact, recent studies have shown that there are at least four types of genetic polymorphisms in the *CYP1A1* gene, namely m1 (nucleotide change T6235C in the 3′-flanking region), m2 (A4889G at exon 7), m3 (T5639C in the 3′-flanking region) and m4 (C4887A at exon 7), and that there are race-related differences in the distribution of the m1- and m2-type polymorphisms in the *CYP1A1* gene (Hayashi *et al.* 1992, Kelsey *et al.* 1994, Taioli *et al.* 1995). Recently, it has also been reported that there are at least three types of genetic polymorphisms in the *CYP1B1* gene in humans (Bailey *et al.* 1998, Bejjani *et al.* 1998, Watanabe *et al.* 1999).

In the current study, the occurrence of genetic polymorphisms in the *CYP1A1* and *CYP1B1* genes was determined in 39 Japanese and 45 Caucasians and the incidence of these genetic polymorphisms was compared in these ethnic groups. Four types of *CYP1A1* polymorphisms have been investigated in these populations, namely m1-, m2-, m3-, and m4-types which correspond to nucleotide changes at T6235C, A4889G, T5639C and C4887A respectively, and three types of *CYP1B1* polymorphisms, m1-, m2-, and m3-types, which correspond to nucleotide changes at C488G and G701T, C1294G, and A1358G respectively. (Recently, recommended nomenclatures for the genetic polymorphisms in human P450 genes and proteins have appeared at http://www.imm.ki.se/CYPalleles) We also determined and compared these latter polymorphisms with a polymorphism in the methylenetetrahydrofolate reductase (MTHFR) gene whose polymorphism associated with a m4-type of *CYP1A1* polymorphism has been suggested to influence susceptibility to endometrial cancer in Caucasians (Esteller *et al.* 1997).

Materials and methods

Isolation of genomic DNA from human livers

Human liver samples were from organ donors or patients undergoing liver resection as described (Shimada *et al.* 1994, Inoue *et al.* 1997, Yamazaki *et al.* 1997). About 2 g liver was suspended in 10 mM Tris-HCl buffer (pH 7.5) containing 10 mM EDTA and 100 mM NaCl and homogenized with a Teflon-pestle homogenizer. Nuclear fractions, collected by centrifugation at 3500 *g* for 5 min at 4 °C, were washed twice with the same buffer by centrifugation at 9000 *g* for 15 min. Genomic DNA was isolated from the nuclear fraction by a commercial Nucleic Acid Purification System (Perkin-Elmer ABI 341, Norwalk, CT, USA).

Analysis of genetic polymorphisms in the CYP1A1 *and* 1B1 *genes*

Four types of genetic polymorphisms in the *CYP1A1* gene, namely m1–m4 of *CYP1A1* (table 1), were examined using RFLP analysis of PCR products as described (Kawajiri *et al.* 1990, 1996, Hayashi *et al.* 1991, Crofts *et al.* 1993, Cascorbi *et al.* 1996, Watanabe *et al.* 1999). Briefly, polymorphisms in m1- and m3-types were determined after digestion of a PCR product using primers M3F and P80 (Cascorbi *et al.* 1996) with the restriction enzyme *Msp*I and the fragments thus obtained were analyzed on an ethidium bromide-stained agarose gel. Amplification for the analysis of the m2-type of *CYP1A1* polymorphism was done using PCR primers M2F and M2R (Cascorbi *et al.* 1996) and the 204-bp fragments thus obtained were digested with *Bsr*DI. The 204-bp PCR products were also used for the analysis of the m4-type of *CYP1A1* polymorphism after digestion with *Bsa*I.

All PCR reactions were performed with a Perkin-Elmer GeneAmp PCR System 2400 thermocycler with an AmpliTaq Gold® DNA polymerase (Perkin-Elmer ABI 341).

PCR primers used for the analysis of the *CYP1B1* genetic polymorphisms are shown in table 2. A

Table 1. Characteristics of polymorphisms in the *CYP1A1* and *CYP1B1* genes determined in the study.

Characteristics	CYP1A1	CYP1B1
Type	m1	m1
Allele*	*CYP1A1*2A*	*CYP1B1*2*
Mutation site	3′-flanking region	exon 2
Restriction enzyme	*Msp*I	
Nucleotide change	T6235C	C488G, G701T
Amino acid change	—	Arg48Gly, Ala119Ser
Type	m2	m2
Allele*	*CYP1A1*2C*	*CYP1B1*3*
Mutation site	exon 7	exon 3
Restriction enzyme	*Bsr*DI	*Eco*57I
Nucleotide change	A4889G	C1294G
Amino acid change	Ile462Val	Leu432Val
Type	m3	m3
Allele*	*CYP1A1*3*	*CYP1B1*4*
Mutation site	3′-flanking region	exon 3
Restriction enzyme	*Msp*I	*Cac*8I
Nucleotide change	T5639C	A1358G
Amino acid change	—	Asn453Ser
Type	m4	
Allele*	*CYP1A1*4*	
Mutation site	exon 7	
Restriction enzyme	*Bsa*I	
Nucleotide change	C4887A	
Amino acid change	Thr461Asn	

*Allele nomenclatures recommended recently; http:www.imm.ki.se/CYPalleles

Table 2. Primers used for genotyping of the *CYP1B1* gene.

Primers	Sequence	References
1B1-E1F	5′-TACGGCGACGTTTTCCAGAT-3′	Watanabe *et al.* (2000)
1B1-E1R	5′-CGTGAAGAAGTTGCGCATCA-3′	Watanabe *et al.* (2000)
1B1-3F	5′-TCCCAGAAATATTAATTTAGTCACTG-3′	Stoilov *et al.* (1998)
1B1-3R	5′-TATGGAGCACACCTCACCTG-3′	Stoilov *et al.* (1998)
1B1-JF	5′-ATGCGCTTCTCCAGCTTTGT-3′	Watanabe *et al.* (2000)
1B1-1294C	5′-TCCGGGTTAGGCCACTTCAG-3′	present study
1B1-1294G	5′-TCCGGGTTAGGCCACTTCAC-3′	present study
1B1-JF	5′-ATGCGCTTCTCCAGCTTTGT-3′	Watanabe *et al.* (2000)
1B1-1358A	5′-TCTGCTGGTCAGGTCCTTGT-3′	present study
1B1-1358G	5′-TCTGCTGGTCAGGTCCTTGC-3′	present study

231-bp fragment using primers 1B1-E1F and 1B1-E1R (Kurabo Biomedical Dept, Osaka, Japan) was used for the PCR-SSCP (single-strand conformation polymorphism) analysis of m1-type genetic polymorphism in the *CYP1B1* gene (Watanabe *et al.* 1999). Briefly, the reaction mixture contained 200 ng genomic DNA, 0.25 μM of each primer, 200 μM dNTP, 10 mM Tris-HCl (pH 8.3), 50 mM KCl, 1.5 mM $MgCl_2$, 0.001% gelatin and 1 U DNA polymerase in a final volume of 50μl. PCR products were resolved by electrophoresis on a 3% AmpliSize agarose (Bio-Rad)-ethidium bromide gels and visualized using an UV trans-illuminator. The amplified products were analyzed by non-radioactive SSCP by the method of Kumeda and Asao (1996) with slight modifications. The products were denatured in an equal volume of gel-loading buffer consisted of 40% sucrose, 5×TBE buffer (90 mM Tris-boric acid containing 2 mM EDTA, pH 8.3), and 0.25% bromophenol blue at 95 °C for 5 min and the denatured mixtures were applied to polyacrylamide gel electrophoresis in systems containing 10% gel, 0.6×TBE buffer (pH 8.3) and 5% glycerol. Electrophoresis was conducted at 15 °C (figure 1).

For the analysis of the m2- and m3-types of *CYP1B1* polymorphisms, two-step PCR procedures were designed, and the primers were obtained from Amersham Pharmacia Biotech (Tokyo, Japan). An 885-bp DNA fragment was first amplified using 0.5 unit DNA polymerase, 0.25 μM primers 1B1-3F and

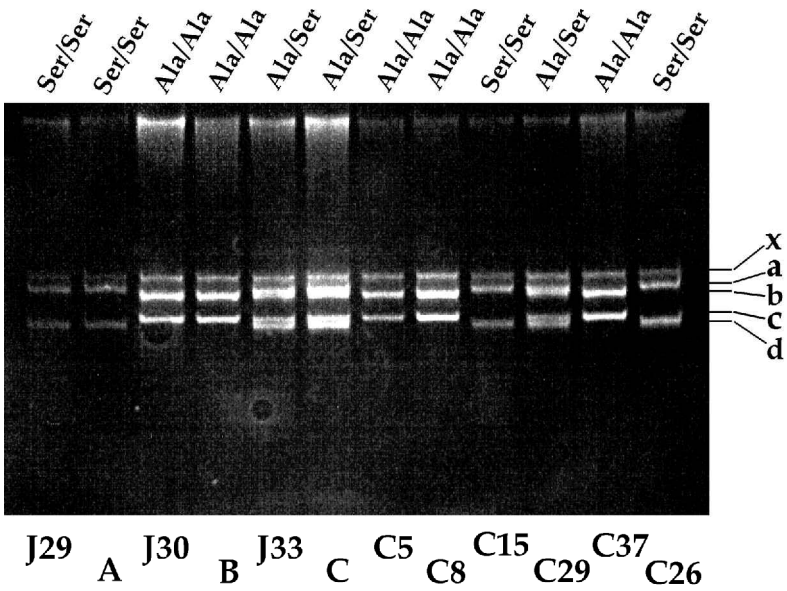


Figure 1. Single-strand conformation polymorphism of Ala119Ser (m1) genetic polymorphism in the *CYP1B1* gene in Japanese and Caucasian populations. Experimental details are described in the Materials and methods. J, Japanese; C, Caucasian; A, B, and C, Japanese samples of blood DNA whose genotypes have already been identified as Ser/Ser, Ala/Ala and Ala/Ser respectively. The genotypes identified in this study are shown at top. 'a', 'b', 'c' and 'd' denote fragments related to *CYP1B1* gene; 'x' denotes a non-specific fragment not related to *CYP1B1* gene.

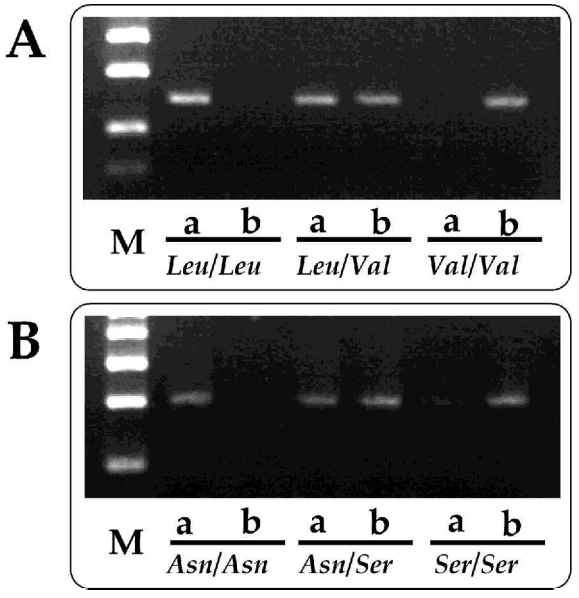


Figure 2. Detection of Leu432Val (m2)-type (A) and Asn453Ser (m3)-type (B) of genetic polymorphisms in the *CYP1B1* gene in humans. Experimental details are described in the Materials and methods.

1B1-3R, 200 μM dNTP, 1.5 mM $MgCl_2$, 50 mM KCl, 10 mM Tris-HCl (pH 8.3), 0.001% gelatin and 200 ng genomic DNA in a final volume of 25 μl. A pre-PCR heat step at 95 °C for 10 min was performed, followed by 35 cycles of amplification. The PCR cycle comprised denaturation at 94 °C for 30 s, annealing at 56 °C for 30 s, extension at 72 °C for 1 min for 35 cycles, and the final extension for 10 min at 72 °C. The mixture for the mutation-specific reaction contained 0.05–1 μl PCR I product, 0.5 unit DNA polymerase, 0.25 μM primers 1B1-JF and either 1B1-1294C or 1B1-1294G for the analysis at codon Leu432Val and either 1B1-1358A or 1B1-1358G for the analysis at codon Asn453Ser, 200 μM dNTP, 1.5 mM $MgCl_2$, 50 mM KCl, 10 mM Tris-HCl (pH 8.3), and 0.001% gelatin in a final volume of 25 μl. A pre-PCR heat step at 95 °C for 10 min was performed, followed by 15 cycles of amplification. The PCR cycle comprised denaturation at 94 °C for 30 s, annealing at 60 °C for 30 s, extension at 72 °C for 30 s for 15 cycles, and the final extension for 10 min at 72 °C. PCR products were resolved by electrophoresis as described above (figure 2).

Genetic polymorphism in the *MTHFR* gene was determined as described (Esteller *et al.* 1997).

Results

Genetic polymorphisms in the *CYP1A1*, *CYP1B1* and *MTHFR* genes were determined in liver DNA of 39 Japanese (table 3) and 45 Caucasians (table 4) as described in Materials and methods. In the tables, each of the genetic polymorphisms in the *CYP1A1, CYP1B1*, and *MTHFR* genes was classified as wild-type (○), heterozygous mutant (▲) or homozygous mutant (■) (table 1).

There were no cases of m3- and m4-types of *CYP1A1* genetic polymorphisms and m3-type of *CYP1B1* genetic polymorphism in the Japanese population (table 3). Of the 39 Japanese examined, four were homozygous and 16 were heterozygous mutants of the m1-type of *CYP1A1* polymorphism (incidence 30.8%), and one was homozygous and 12 were heterozygous mutant of the m2-type of *CYP1A1* polymorphism (incidence 17.9%). Interestingly, 13 Japanese who had heterozygous or homozygous mutants of the m2-type of *CYP1A1* polymorphism also had a m1-type of *CYP1A1* mutation. However, seven Japanese, having the m1-type of *CYP1A1* mutation, did not have the m2-mutation in the *CYP1A1* gene.

Of the 39 Japanese studied, nine were heterozygous and one was homozygous mutants of the m1-type of *CYP1B1* polymorphism, and five were heterozygous and six were homozygous mutant of the m2-type of *CYP1B1* polymorphism, and as a result the incidence of m1- and m2-types of these polymorphisms was 14.1 and 21.8% respectively. Note too that there was no apparent linkage in the incidence of genetic polymorphisms of the *CYP1A1* and *CYP1B1* genes. There were no apparent relationships between the incidence in polymorphisms of the *MTHFR* gene, and the *CYP1A1* and *CYP1B1* genes in the Japanese population.

In the Caucasian population, there were very few occurrences of the m1- and m2-types of *CYP1A1* genetic polymorphisms, the incidence being 3.3 and 6.7% respectively (table 4). It was also found that two of 45 Caucasians had the heterozygous mutant of the m4-type of *CYP1A1* polymorphism; there were no cases in this polymorphism in the Japanese population (table 3). No linkage was observed between incidence in the m1- and m2-types of *CYP1A1* mutation in the Caucasian population. The incidence of the m1- and m2-types of *CYP1B1* polymorphisms in Caucasians was 28.9 and 37.5% respectively. In contrast to the Japanese group, a high incidence in the genetic polymorphisms of the *CYP1B1* gene was noted in the Caucasian population in that 19 had heterozygous and one had homozygous mutants of the m3-type of *CYP1B1* polymorphism; there were no cases of this polymorphism in the Japanese group. There was no clear relationship in incidence between several types of genetic polymorphisms in the *CYP1A1*, *CYP1B1* and *MTHFR* genes in the Caucasian population.

Genotypic distribution in the *CYP1A1* gene in the Japanese and Caucasian

Table 3. Distribution of genetic polymorphisms in the *CYP1A1*, *CYP1B1* and *MTHFR* genes in the Japanese population.

Human liver sample	*CYP1A1*				*CYP1B1*			*MTHFR*
	m1	m2	m3	m4	m1	m2	m3	
J1	▲	▲	○	○	▲	○	○	○
J2	▲	○	○	○	○	○	○	▲
J3	○	○	○	○	○	○	○	○
J4	○	○	○	○	▲	▲	○	▲
J5	▲	○	○	○	▲	○	○	○
J6	■	■	○	○	○	○	○	▲
J7	○	○	○	○	○	■	○	▲
J8	▲	▲	○	○	○	▲	○	▲
J9	▲	○	○	○	○	■	○	■
J10	▲	▲	○	○	○	○	○	○
J11	○	○	○	○	○	○	○	▲
J12	▲	▲	○	○	○	○	○	○
J13	○	○	○	○	○	○	○	▲
J14	■	▲	○	○	○	○	○	▲
J15	○	○	○	○	○	○	○	○
J16	▲	▲	○	○	▲	○	○	▲
J17	■	▲	○	○	▲	○	○	▲
J18	○	○	○	○	○	○	○	▲
J19	○	○	○	○	▲	■	○	■
J20	○	○	○	○	○	○	○	■
J21	▲	▲	○	○	○	○	○	○
J22	○	○	○	○	▲	▲	○	○
J23	○	○	○	○	○	○	○	○
J24	▲	○	○	○	○	○	○	○
J25	■	○	○	○	○	■	○	○
J26	○	○	○	○	○	○	○	○
J27	○	○	○	○	○	■	○	▲
J28	○	○	○	○	○	▲	○	▲
J29	▲	▲	○	○	■	○	○	▲
J30	○	○	○	○	○	■	○	▲
J31	▲	▲	○	○	○	▲	○	▲
J32	○	○	○	○	○	○	○	▲
J33	▲	▲	○	○	▲	○	○	■
J34	▲	○	○	○	○	○	○	■
J35	○	○	○	○	○	○	○	○
J36	○	○	○	○	○	○	○	■
J37	○	○	○	○	▲	○	○	■
J38	▲	▲	○	○	○	○	○	▲
J39	▲	○	○	○	○	○	○	○

○, Wild-type; ▲, heterozygous mutant; ■, homozygous mutant.

populations was determined based on the above results (table 5). At least nine genotypes of the *CYP1A1* gene in humans were detected; in the Japanese population there were no cases in the occurrence of genotypes T6235/A4889/T5639/C4887A, T6235/A4889G/T5639/C4887 or T6235/A4889G/T5639/C4887A, and in Caucasians there were no cases in genotypes T6235C/A4889G/T5639/C4887, C6235/A4889/T5639/C4887 and C6235/G4889/T5639/C4887.

There were at least 14 genotypes in the *CYP1B1* gene in humans (table 6). Since the m3-type of genetic polymorphism in the *CYP1B1* gene in the Japanese population was not detected, only seven genotypes in *CYP1B1* gene were found. In Caucasians no cases were observed for the G701T/G1294/A1358 genotypes; however, 13 other genotypes were detected. These 13 genotypes of the *CYP1B1* gene were randomly distributed in the Caucasian population.

Table 4. Distribution of genetic polymorphisms in the *CYP1A1*, *CYP1B1* and *MTHFR* genes in the Caucasian population.

Human liver sample	*CYP1A1*				*CYP1B1*			
	m1	m2	m3	m4	m1	m2	m3	*MTHFR*
C1	○	○	○	○	○	■	○	■
C2	○	○	○	○	○	▲	▲	○
C3	○	○	○	○	▲	○	▲	○
C4	○	○	○	○	▲	○	○	▲
C5	○	○	○	○	○	■	▲	○
C6	○	○	○	▲	▲	▲	○	○
C7	○	○	○	○	■	○	○	○
C8	○	○	○	○	○	■	○	○
C9	○	▲	○	○	○	○	▲	■
C10	○	▲	○	○	▲	○	▲	▲
C11	○	○	○	○	▲	○	▲	▲
C12	○	○	○	○	▲	○	▲	○
C13	○	○	○	○	○	○	○	▲
C14	○	○	○	○	▲	○	▲	▲
C15	○	○	○	○	■	○	○	▲
C16	○	○	○	○	○	▲	○	○
C17	○	○	○	○	○			▲
C18	○	○	○	○	○	○	▲	▲
C19	○	○	○	○	○	▲	▲	○
C20	○	○	○	○	○	■	○	▲
C21	○	○	○	○	○	■	○	▲
C22	▲	○	○	○	▲	▲	○	○
C23	○	○	○	○	▲	▲	○	○
C24	○	○	○	○	○	■	○	■
C25	○	○	○	○	▲	▲	○	▲
C26	○	○	○	○	■	○	○	▲
C27	○	○	○	○	○	■	○	▲
C28	○	▲	○	○	○	○	■	○
C29	○	○	○	○	▲	▲	○	■
C30	○	○	○	○	■	○	○	■
C31	○	○	○	○	▲	○	○	▲
C32	○	▲	○	▲	○	■	○	▲
C33	○	○	○	○	○	○	▲	▲
C34	○	○	○	○	■	○	▲	○
C35	○	○	○	○	○	▲	▲	○
C36	○	○	○	○	▲	○	▲	■
C37	○	○	○	○	○	■	○	▲
C38	○	○	○	○	▲	○	▲	○
C39	○	▲	○	○	○	▲	▲	▲
C40	○	○	○	○	○	▲	▲	▲
C41	■	▲	○	○	▲	○	○	○
C42	○	○	○	○	▲	▲	▲	▲
C43	○	○	○	○	○	▲	▲	○
C44	○	○	○	○	○	○	○	▲
C45	○	○	○	○	○	■	○	○

○, Wild-type; ▲, heterozygous mutant; ■, homozygous mutant.

A 885-bp PCR fragment in sample C17 could not be obtained probably due to the condition of liver sample storage before analysis.

Discussion

The human *CYP1B1* gene is localized on chromosome 2, whereas *CYP1A1* and *1A2* genes are on chromosome 15 in humans (Sutter *et al.* 1994, Nelson *et al.* 1996). Different substrate specificities towards procarcinogen metabolism are known in these three P450 enzymes in that CYP1A1 and CYP1B1 metabolize a variety of carcinogenic polycyclic aromatic hydrocarbons, whereas CYP1A2 participates in

Table 5. Distribution of genotypes of the *CYP1A1* gene in 39 Japanese and 45 Caucasians.

Genotype of the *CYP1A1* gene				Japanese ($n = 39$)		Caucasian ($n = 45$)	
Nucleotide at position:							
6235 (m1)	4889 (m2)	5639 (m3)	4887 (m4)	*n*	%	*n*	%
T	A	T	C	19	48.7	37	82.2
T	A	T	C/A	0	0.0	1	2.2
T	A/G	T	C	0	0.0	4	8.9
T	A/G	T	C/A	0	0.0	1	2.2
T/C	A	T	C	6	15.4	1	2.2
T/C	A/G	T	C	10	25.6	0	0.0
C	A	T	C	1	2.6	0	0.0
C	A/G	T	C	2	5.1	1	2.2
C	G	T	C	1	2.6	0	0.0

Table 6. Distribution of genotypes of the *CYP1B1* gene in Japanese and Caucasian populations.

Genotype of the *CYP1B1* gene			Japanese ($n = 39$)		Caucasian ($n = 44$)	
Nucleotide at position:						
701 (m1)	1294 (m2)	1358 (m3)	*n*	%	*n*	%
G	C	A	21	53.8	2	4.5
G	C	A/G	0	0	3	6.8
G	C	G	0	0	1	2.3
G	C/G	A	3	7.7	1	2.3
G	C/G	A/G	0	0	6	13.6
G	G	A	5	12.8	9	20.5
G	G	A/G	0	0	1	2.3
G/T	C	A	6	15.4	3	6.8
G/T	C	A/G	0	0	7	15.9
G/T	C/G	A	2	5.1	5	11.4
G/T	C/G	A/G	0	0	1	2.3
G/T	G	A	1	2.6	0	0
T	C	A	1	2.6	4	9.1
T	C	A/G	0	0	1	2.3

the activation of structurally diverse arylamines and heterocyclic amines (Shimada *et al.* 1996, 1998). Since the former two P450 enzymes are predominantly expressed in extrahepatic organs, such as the mammary gland, lung, uterus, prostate, testis, adrenals, kidney, etc., the levels of expression of these P450 forms in humans are thought to be one of the important factors that determine the susceptibilities of individuals to lung and breast cancers (Shimada *et al.* 1996).

The race-related differences in the several types of polymorphisms in the *CYP1A1* gene, previously reported in several laboratories (Hayashi *et al.* 1992, Kelsey *et al.* 1994, Taioli *et al.* 1995, d'Errico *et al.* 1996), were confirmed in this study using 39 Japanese and 45 Caucasians. The present results have shown that distributions in the m1- and m2-types of *CYP1A1* genetic polymorphisms were more frequent in the Japanese population than the Caucasians. These results are of interest since several investigators have shown that the *Msp*I (m1-) and Ile-Val (m2-) polymorphisms in the *CYP1A1* gene are associated with a high susceptibility to squamous cell carcinoma of the lung in the Japanese population (Kawajiri *et al.* 1990, Nakachi *et al.* 1991). It should be noted, however, that there were no cases in the m4-type of *CYP1A1* genetic polymorphisms in the Japanese population,

whereas two out of 45 Caucasians were classified as the heterozygous m4-mutant. The present results also showed that the m3-type of *CYP1A1* polymorphism, a known type specific for the African black (Crofts *et al.* 1993), was not detected in both the Japanese and Caucasian populations studied here (Cascorbi *et al.* 1996, Aynacioglu *et al.* 1998).

In the current study, it has been shown that the m2-mutation in the *CYP1A1* gene is exclusively linked to the m1-mutation in the Japanese population, but not in the Caucasian population, although seven Japanese subjects who were identified to be of the m1-type of *CYP1A1* polymorphism did not have the m2-mutation in the *CYP1A1* gene. The linkage between the m2-type mutation with the m1-mutation in the *CYP1A1* gene has already been reported in a Turkish population (Aynacioglu *et al.* 1998). It is not known, however, why there is no apparent linkage of the m1- and m2-types of *CYP1A1* mutation in the Caucasians.

In contrast to the genetic polymorphisms in the *CYP1A1* gene, the incidence of the genetic polymorphisms in the *CYP1B1* gene was more frequent in Caucasians than the Japanese population studied. The incidence of the m1- and m2-types of *CYP1B1* polymorphisms in the Caucasians was 28.9 and 37.5% respectively, whereas that in the Japanese was 14.1 and 21.8% respectively. The clear differences in the occurrence of the *CYP1B1* genetic polymorphism in these ethnic groups was that there were no cases of the m3-type in the Japanese population, whereas in the Caucasians the incidence of this type of *CYP1B1* mutation was 23.9%.

Recently, the present authors have reported that both CYP1B1 and CYP1A1 are very active in catalyzing the activation of lung carcinogens such as (+)- and (−)-benzo[*a*]pyrene-7,8-diol, dibenzo[*a,l*]pyrene-11,12-diol, 7,12-dimethylbenz[*a*]-anthracene-3,4-diol, 5-methylchrysene-1,2-diol and 5,6-dimethylchrysene-1,2-diol (Shimada *et al.* 1996). Some of these chemicals are also known to be mammary carcinogens in experimental animals and recent studies have established that CYP1B1 is expressed at substantial levels in human mammary epithelial cells (Huang *et al.* 1996, Eltom *et al.* 1998, Larsen *et al.* 1998). CYP1B1 has also been reported to catalyze the oxidation of 17β-oestradiol at a higher rate at the 4-position than at the 2-position; the former metabolite has been suggested to be involved in the development of breast cancer in humans (Spink *et al.* 1992, 1997, Liehr and Rocci 1996). It is of great interest to study the roles of CYP1B1 and its variants in the metabolism of these chemicals to understand the basis of interindividual differences in the formation of lung and breast cancers in humans. In fact, our recent studies involving recombinant (*Escherichia coli*) CYP1B1 and its variants have shown that the polymorphism in the human *CYP1B1* gene causes some alterations in catalytic function towards procarcinogens and gonadal steroid hormones, and thus may have some contribution to susceptibilities of individuals towards mammary and lung cancers in humans (Shimada *et al.* 1999).

In conclusion, the present study has shown that there were ethnic-related differences in the frequently distribution in genetic polymorphisms of the *CYP1A1* and *CYP1B1* genes in Japanese and Caucasian populations. The incidence of the *CYP1A1* genetic polymorphism was more frequent in Japanese than that in the Caucasian population, whereas the reverse is the case for genetic polymorphisms in the *CYP1B1* gene. There was no clear linkage in the frequencies of several types of genetic polymorphisms in these P450 genes, except that the incidence in the m2-type of *CYP1A1* polymorphisms was linked to that of the m1-type in the Japanese population. Ethnic-related differences in the occurrence of genetic polymorphisms

in *CYP1A1* and *CYP1B1* genes may determine the different susceptibilities in individuals towards environmental procarcinogens that result in lung and breast cancers.

Acknowledgements

This work was supported in part by Grants from the Ministry of Education, Science, and Culture of Japan, and the Ministry of Health and Welfare of Japan. The authors thank Drs J. Watanabe and K. Kawajiri for advice in the analysis of CYP1B1 polymorphism, H. Yamazaki for help in handling the DNA samples, and F. Peter Guengerich for human samples used.

References

Aynacioglu, A. S., Cascorbi, I., Mrozikiewicz, P. M. and Ropp, J. D., 1998, High frequency of *CYP1A1* mutations in a Turkish population. *Archives of Toxicology*, **72**, 215–218.

Bailey, L. R., Roodi, N., Dupont, W. D. and Parl, F. F., 1998, Association of cytochrome P450 1B1 (CYP1B1) polymorphism with steroid receptor status in breast cancer. *Cancer Research*, **58**, 5038–5041.

Bejjani, B. A., Lewis, R. A., Tomey, K. F., Anderson, K. L., Dueker, D. K., Jabak, M., Astle, W. F., Otterud, B., Leppert, M. and Lupski, J. R., 1998, Mutations in *CYP1B1*, the gene for cytochrome P4501B1, are the predominant cause of primary congenital glaucoma in Saudi Arabia. *American Journal of Human Genetics*, **62**, 325–333.

Cascorbi, I., Brockmoller, J. and Roots, I., 1996, A C4887A polymorphism in exon 7 of human *CYP1A1*: population frequency, mutation linkages, and impact on lung cancer susceptibility. *Cancer Research*, **56**, 4965–4969.

Cosma, G., Crofts, F., Taioli, E., Toniolo, P. and Garte, S., 1993, Relationship between genotype and function of the human *CYP1A1* gene. *Journal of Toxicology and Environmental Health*, **40**, 309–316.

Crofts, F., Cosma, G. N., Currie, D., Taioli, E., Toniolo, P. and Garte, S. J., 1993, A novel *CYP1A1* gene polymorphism in African-Americans. *Carcinogenesis*, **14**, 1729–1731.

D'Errico, A., Taioli, E., Chen, X. and Vineis, P., 1996, Genetic metabolic polymorphisms and the risk of cancer: a review of the literature. *Biomarkers*, **1**, 149–173.

Drakoulis, N., Cascorbi, I., Brockmoller, J., Gross, C. R. and Roots, I., 1994, Polymorphisms in the human *CYP1A1* gene as susceptibility factors for lung cancer: exon-7 mutation (4889 A to G), and a T to C mutation in the 3′-flanking region. *Clinical Investigations*, **72**, 240–248.

Eltom, S. E., Larsen, M. C. and Jefcoate, C. R., 1998, Expression of CYP1B1 but not CYP1A1 by primary cultured human mammary stromal fibroblasts constitutively and in response to dioxin exposure: role of the Ah receptor. *Carcinogenesis*, **19**, 1437–1444.

Esteller, M., Garcia, A., Martinez-Palones, J. M., Xercavins, J. and Reventos, J., 1997, Germ line polymorphisms in cytochrome P450 1A1 (C4887 CYP1A1) and methylenetetrahydrofolate reductase (MTHFR) genes and endometrial cancer susceptibility. *Carcinogenesis*, **18**, 2307–2311.

Gonzalez, F. J. and Gelboin, H. V., 1994, Role of human cytochromes P450 in the metabolic activation of chemical carcinogens and toxins. *Drug Metabolism Reviews*, **26**, 165–183.

Guengerich, F. P., Hosea, N. A., Parikh, A., Bell-Parikh, L. C., Johnson, W. W., Gillam, E. M. J. and Shimada, T., 1998, Twenty years of biochemistry of human P450s. *Drug Metabolism and Disposition*, **26**, 1175–1178.

Guengerich, F. P. and Shimada, T., 1991, Oxidation of toxic and carcinogenic chemicals by human cytochrome P-450 enzymes. *Chemical Research in Toxicology*, **4**, 391–407.

Hayashi, S., Watanabe, J. and Kawajiri, K., 1992, High susceptibility to lung cancer analyzed in terms of combined genotypes of P4501A1 and Mu-class glutathione S-transferase genes. *Japanese Journal of Cancer Research*, **83**, 866–870.

Hayashi, S. I., Watanabe, J., Nakachi, K. and Kawajiri, K., 1991, Genetic linkage of lung cancer-associated *Msp*I polymorphisms with amino acid replace'ment in the heme binding region of the human cytochrome P4501A1 gene. *Journal of Biochemistry*, **110**, 407–411.

Hirvonen, A., Husgafvel-Pursiainen, K., Karjalainen, A., Anttila, S. and Vainio, H., 1992, Point-mutational *Msp*I and *Ile-Val* polymorphisms closely linked in the *CYP1A1* gene: lack of association with susceptibility to lung cancer in a Finnish study population. *Cancer Epidemiology, Biomarkers and Prevention*, **1**, 485–489.

Huang, Z., Fasco, M. J., Figge, H. L., Keyomars, F. K. and Kaminsky, L. S., 1996, Expression of cytochromes P450 in human breast tissue and tumors. *Drug Metabolism and Disposition*, **24**, 899–905.

Inoue, K., Yamazaki, H., Imiya, K., Akasaka, S., Guengerich, F. P. and Shimada, T., 1997,

Relationship between *CYP2C9* and *2C19* genotypes and tolbutamide methyl hydroxylation and *S*-mephenytoin 4′-hydroxylation activities in livers of Japanese and Caucasian populations. *Pharmacogenetics*, **7**, 103–113.

KAWAJIRI, K., NAKACHI, K., IMAI, K., YOSHII, A., SHINODA, N. and WATANABE, J., 1990, Identification of genetically high risk individuals to lung cancer by DNA polymorphisms of the cytochrome P4501A1 gene. *FEBS Letters*, **263**, 131–133.

KAWAJIRI, K., WATANABE, J. and HAYASHI, S., 1996, Identification of allelic variants of the human *CYP1A1* gene. *Methods in Enzymology*, **272**, 226–232.

KELSEY, K. T., WIENCKE, J. K. and SPITZ, M. R., 1994, A race-specific genetic polymorphism in the CYP1A1 gene is not associated with lung cancer in African Americans. *Carcinogenesis*, **15**, 1121–1124.

KUMEDA, Y. and ASAO, T., 1996, Single-strand conformation polymorphism analysis of PCR-amplified ribosomal DNA internal transcribed spacers to differentiate species of *Aspergillus* section *Flavi*. *Applied and Environmental Microbiology*, **62**, 2947–2952.

LARSEN, M. C., ANGUS, W. G. R., BRAKE, P. B., ELTOM, S. E., SUKOW, K. A. and JEFCOATE, C. R., 1998, Characterization of CYP1B1 and CYP1A1 expression in human mammary epithelial cells: role of the aryl hydrocarbon receptor in polycyclic aromatic hydrocarbon metabolism. *Cancer Research*, **58**, 2366–2374.

LIEHR, J. G. and ROCCI, M. J., 1996, 4–Hydroxylation of estrogens as marker of human mammary tumors. *Proceedings of the National Academy of Sciences, USA*, **93**, 3294–3296.

NAKACHI, K., IMAI, K., HAYASHI, S. and KAWAJIRI, K., 1991, Genetic susceptibility to squamous cell carcinoma of the lung in relation to cigarette smoking dose. *Cancer Research*, **51**, 5177–5180.

NELSON, D. R., KAMATAKI, T., WAXMAN, D. J., GUENGERICH, F. P., ESTABROOK, R. W., FEYEREISEN, R., GONZALEZ, F. J., COON, M. J., GUNSALUS, I. C., GOTOH, O., OKUDA, K. and NEBERT, D. W., 1993, The P450 superfamily: update on new sequences, gene mapping, accession numbers, early trivial names of enzymes, and nomenclature. *DNA and Cell Biology*, **12**, 1–51.

NELSON, D. R., KOYMANS, L., KAMATAKI, T., STEGEMAN, J. J., FEYEREISEN, R., WAXMAN, D. J., WATERMAN, M. R., GOTOH, O., COON, M. J., ESTABROOK, R. W., GUNSALUS, I. C. and NEBERT, D. W., 1996, P450 superfamily: update on new sequences, gene mapping, accession numbers and nomenclature. *Pharmacogenetics*, **6**, 1–42.

SHIMADA, T., HAYES, C. L., YAMAZAKI, H., AMIN, S., HECHT, S. S., GUENGERICH, F. P. and SUTTER, T. R., 1996, Activation of chemically diverse procarcinogens by human cytochrome P450 1B1. *Cancer Research*, **56**, 2979–2984.

SHIMADA, T., WATANABE, J., KAWAJIRI, K., SUTTER, T. R., GUENGERICH, F. P., GILLAM, E. M. J. and INOUE, K., 1999, Catalytic properties of polymorphic human cytochrome P450 1B1 variants. *Carcinogenesis*, **20**, 1607–1613.

SHIMADA, T., WUNSCH, R. M., HANNA, I. H., SUTTER, T. R., GUENGERICH, F. P. and GILLAM, E. M. J., 1998, Recombinant human cytochrome P450 1B1 expression in *Escherichia coli*. *Archives of Biochemistry and Biophysics*, **357**, 111–120.

SHIMADA, T., YAMAZAKI, H., MIMURA, M., INUI, Y. and GUENGERICH, F. P., 1994, Interindividual variations in human liver cytochrome P-450 enzymes involved in the oxidation of drugs, carcinogens and toxic chemicals: studies with liver microsomes of 30 Japanese and 30 Caucasians. *Journal of Pharmacology and Experimental Therapeutics*, **270**, 414–423.

SPINK, D. C., EUGSTER, H. P., LINCOLN II, D. W., SCHUETZ, J. D., SCHUETZ, E. G., JOHNSON, J. A., KAMINSKY, L. S. and GIERTHY, J. F., 1992, 17β-Estradiol hydroxylation catalyzed by human cytochrome P450 1A1: a comparison of the activities induced by 2,3,7,8–tetrachlorodibenzo-*p*-dioxin in MCF-7 cells with those from heterologous expression of the cDNA. *Archives of Biochemistry and Biophysics*, **293**, 342–348.

SPINK, D. C., SPINK, B. C., CAO, J. Q., GIERTHY, J. F., HAYES, C. L., LI, Y. and SUTTER, T. R., 1997, Induction of cytochrome P450 1B1 and catechol estrogen metabolism in ACHN human renal adenocarcinoma cells. *Journal of Steroid and Biochemical Molecular Biology*, **62**, 223–232.

SUTTER, T. R., TANG, Y. M., HAYES, C. L., WO, Y.-Y. P., JABS, W., LI, X., YIN, H., CODY, C. W. and GREENLEE, W. F., 1994, Complete cDNA sequence of a human dioxin-inducible mRNA identifies a new gene subfamily of cytochrome P450 that maps to chromosome 2. *Journal of Biological Chemistry*, **269**, 13092–13099.

TAIOLI, E., CROFTS, F., TRACHMAN, J., BAYO, S., TONIOLO, P. and GARTE, S. J., 1995, Racial differences in CYP1A1 genotype and function. *Toxicology Letters*, **77**, 357–362.

WATANABE, J., SHIMADA, T., GILLAM, E. M. J., IKUTA, T., SUEMATSU, K., HIGASHI, Y., GOTOH, O. and KAWAJIRI, K., 1999, Association of *CYP1B1* genetic polymorphism with incidence to breast and lung cancer. *Pharmacogenetics* (in press).

YAMAZAKI, H., INOUE, K., TURVY, C. G., GUENGERICH, F. P. and SHIMADA, T., 1997, Effects of freezing, thawing, and storage of human liver samples on the microsomal contents and activities of cytochrome P450 enzymes. *Drug Metabolism and Disposition*, **25**, 168–174.

XENOBIOTICA , 2000, VOL. 30, NO. 3, 297–306

Metabolism of N,N-dialkylated amphetamines, including deprenyl, by CYP2D6 expressed in a human cell line

M. V. BACH†, R. T. COUTTS†* and G. B. BAKER‡

Neurochemical Research Unit, †Faculty of Pharmacy and Pharmaceutical Sciences, and ‡Department of Psychiatry, University of Alberta, Edmonton, Alberta T6G 2N8, Canada

Received 21 June 1999

1. Five N,N-dialkylated amphetamines, N-methyl-N-propargylamphetamine (deprenyl; DEP), N-benzyl-N-methylamphetamine (benzphetamine; BPA), N-allyl-N-methylamphetamine (AMA), N,N-diallylamphetamine (DAA) and N-methyl-N-propylamphetamine (MPA), were metabolized *in vitro* with a microsomal preparation from cells expressing human CYP2D6 to determine what influence the N,N-dialkyl substituents had on the extent of N-dealkylation and/or aromatic ring oxidation.

2. The results obtained from experiments with the first two substrates, DEP and BPA, were surprisingly different. Whereas DEP was N-demethylated and N-depropargylated by the CYP2D6 enzyme system, no metabolites were formed from BPA. Subsequently, it was determined that AMA, DAA and MPA also underwent CYP2D6-catalysed N-dealkylation. Both N-methyl- and N-allylamphetamine were identified as products of AMA metabolism; similarly, metabolism of MPA produced both N-methyl- and N-propargylamphetamine, and N-allylamphetamine was the sole metabolite of DAA.

3. No N,N-didealkylated product (i.e. amphetamine) was isolated from incubates of any of the five substrates, and none of the N,N-dialkylated substrates was metabolized to a ring-hydroxylated product.

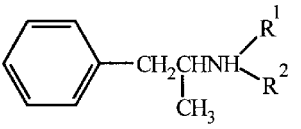
4. Rates of these CYP2D6-catalysed reactions were dependent on the nature and degree of unsaturation of the N-substituents.

Introduction

Our interest in the involvement of CYP2D6 in the N-dealkylation of amphetamine derivatives (Bach *et al.* 1999) has been extended to include N,N-dialkylated derivatives. In a preliminary study, benzphetamine [(+)-N-benzyl-N-methylamphetamine; BPA] and (−)-deprenyl [(−)-N-methyl-N-propargylamphetamine; DEP] were metabolized with a fortified expressed CYP2D6 enzyme preparation using experimental conditions that had previously been employed successfully to metabolize other amphetamine derivatives and some tricyclic antidepressants (Coutts *et al.* 1994a, Bach *et al.* 1999). Surprisingly, whereas DEP was extensively metabolized to two major products in this system, no metabolites were produced from BPA. Others (Grace *et al.* 1994, Wacher *et al.* 1996) have since identified DEP's two CYP2D6-catalyzed metabolites as N-methylamphetamine (MA) and N-propargylamphetamine (PgA), but there was an appreciable difference in the relative amounts of both metabolites produced by recombinant CYP2D6 and CYP2D6-containing liver microsomes. PgA formation was favoured 13-fold over MA formation in the studies by Grace *et al.* (1994), but both metabolites were isolated by Wacher *et al.* (1996) in approximately equal quantities. Grace *et al.*

* Author for correspondence; e-mail: ronald.coutts@ualberta.ca

Xenobiotica ISSN 0049–8254 print/ISSN 1366–5928 online © 2000 Taylor & Francis Ltd
http://www.tandf.co.uk/journals/tf/00498254.html



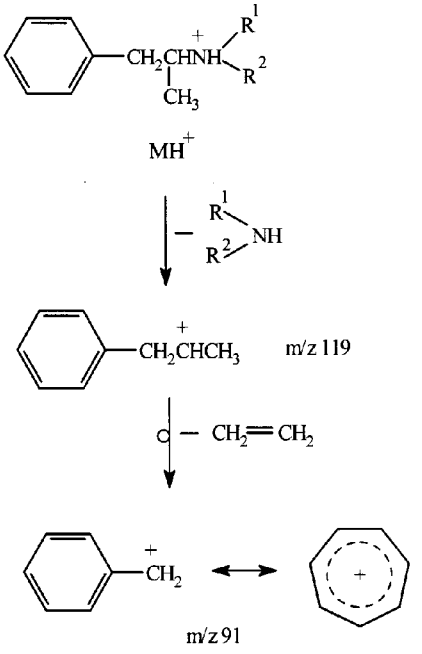
Compound	R^1	R^2
AA	H	CH_2-CH=CH_2
AMA	CH_3	CH_2-CH=CH_2
MPA	CH_3	$(CH_2)_2CH_3$
DEP	CH_3	CH_2-C≡CH
PgA	H	CH_2-C≡CH
DAA	CH_2-CH=CH_2	CH_2-CH=CH_2
DPgA	CH_2-C≡CH	CH_2-C≡CH
MA	H	CH_3
PA	H	$(CH_2)_2CH_3$
BPA	CH_3	$PhCH_2$

Figure 1. Structures of N,N-dialkylamphetamine analogues and N-dealkylated metabolites. Abbreviations are identified in the text.

(1994) described this metabolism of DEP as being an 'atypical' dealkylation, presumably because very few examples of CYP2D6-catalyzed N-dealkylation of basic drugs were known at that time. It is now recognized that many drugs, including amiflamine, amitriptyline, desmethylcitalopram, haloperidol, imipramine, 1-methyl-4-phenyl-1,2,3,6-tetrahydropyridine (MPTP), mianserin, tomoxetine, trazodone and venlafaxine, do undergo CYP2D6-catalyzed N-dealkylation (Coutts *et al.* 1994a, Coutts and Urichuk 1999), although in most instances CYP2D6's role in this important metabolic reaction is relatively minor.

Our observation that the N-demethylation and N-depropargylation of DEP were catalysed to some extent by CYP2D6, whereas no N-demethylation or N-debenzylation of BPA was catalysed by this enzyme, prompted the determination whether other N-methyl-N-alkylamphetamines could be N-demethylated and/or N-dealkylated by the catalytic action of CYP2D6. Three additional N,N-dialkylated amphetamines, N-allyl-N-methylamphetamine (AMA), N,N-diallylamphetamine (DAA) and N-methyl-N-propylamphetamine (MPA) were selected for this study. They were readily synthesized and their structures (figure 1) were confirmed by nuclear magnetic resonance (NMR) and electrospray mass spectrometry (ESMS; figure 2). N-allylamphetamine (AA), a potential metabolite of AMA and DAA, and DEP's metabolite, PgA, were also synthesized and similarly characterized. (−)-N,N-dipropargylamphetamine (DPgA) was isolated in low yield as a by-product in the synthesis of PgA, but its CYP2D6-catalyzed metabolism was not investigated at this time. Its mass spectrum was recorded for comparison with those of the other amphetamine derivatives (figure 2).

To determine whether the N-allyl and N-propyl analogues of DEP were suitable substrates for CYP2D6-catalyzed N-dealkylation, the *in vitro* metabolism of AMA, DAA, MPA, and also DEP and BPA, under identical conditions, was studied using CYP2D6 expressed in a human cell line. Since all of the compounds investigated,



	R^1	R^2
AA	$CH_2CH{=}CH_2$	H
AMA	$CH_2CH{=}CH_2$	CH_3
MPA	$CH_2CH_2CH_3$	CH_3
DEP	$CH_2C{\equiv}CH$	CH_3
PgA	$CH_2C{\equiv}CH$	H
DAA	$CH_2CH{=}CH_2$	$CH_2CH{=}CH_2$
DPgA	$CH_2C{\equiv}CH$	$CH_2C{\equiv}CH$

Compound	m/z	% Relative Abundance		
		MH^+	m/z 119	m/z 91
AA	176	100.0	36.1	63.0
AMA	190	100.0	19.9	29.8
MPA	192	100.0	13.5	18.0
DEP	188	100.0	35.2	53.1
PgA	174	79.1	43.8	100.0
DAA	216	100.0	20.9	32.2
DPgA	212	87.3	68.7	100.0

Figure 2. Characteristic fragment ions in the electrospray mass spectra of N-mono- and N,N-dialkylated amphetamines.

except DAA, are N-methylated and also N-alkylated with another moiety, to avoid confusion 'demethylation' has been used to indicate the loss of the methyl group, and 'dealkylation' to indicate the loss of the other moiety.

Materials and methods

Instrumentation

GC analyses were conducted using a DB-5 fused capillary column, 13 m × 0.25 mm i.d. × 0.25 μm film thickness (J&W Scientific, Folsom, CA, USA) on a HP 5890 GC (Hewlett Packard, PA, USA) equipped with a nitrogen-phosphorus detector and a HP-3396A integrator. The carrier gas was ultrapure helium (Union Carbide, Edmonton, Canada) and its flow rate was adjusted to maintain a column head pressure of 10 psi. The make-up gas at the detector was a mixture of hydrogen (3 ml min^{-1}) and air (80 ml min^{-1}). The injector and detector temperatures were 260 and 310 °C respectively. Chromatographic peak areas were measured with a HP 3396A. GC conditions were: an initial column temperature of 110 °C held for 2 min and then raised by automatic temperature programming at 8 °C min^{-1} to 240 °C.

Electrospray mass spectrometric analyses were performed on Fisons Trio 2000. Samples were sprayed at 75 °C at a probe voltage of 3.5 KV.

NMR spectra were recorded on a Bruker 300 MHz instrument using $CDCl_3$ as a solvent and TMS as an internal standard

Chemicals

Amphetamine sulphate and 4-methoxy-N-methylamphetamine (MMA).HCl were gifts from the former Smith, Kline and French Laboratories (Philadelphia), and benzphetamine HCl was kindly supplied by Professor A. H. Beckett and Dr D. A. Cowan, King's College, London. N-(*n*-propyl) amphetamine.HCl and N-methylamphetamine.HCl were prepared by a reported method (Coutts *et al.* 1976, 1978). Other chemicals were purchased from various commercial sources: allyl bromide, 1-bromopropane, analytical grade trifluoroacetic acid (Aldrich Chemical Co., Milwaukee, WI, USA);

R-(−)-deprenyl.HCl (Research Biochemicals International, Natick, MA, USA); $NADP^+$ sodium salt from yeast, D-glucose 6-phosphate monosodium salt (G6P) and glucose 6-phosphate dehydrogenase (G6PD) type XII from *Tortula* yeast (Sigma Chemical Co., St Louis, MO, USA); potassium carbonate (K_2CO_3), methanol (CH_3OH), *n*-hexane, HPLC-grade acetonitrile (CH_3CN), isopropanol, dichloromethane (CH_2Cl_2), diethyl ether, toluene (BDH, Toronto, Canada). All solvents were distilled before use. The K_2CO_3 solution used was a 25% w/v aqueous solution. The buffer solution used in all experiments was 100 mM, pH 7.4.

Synthesis of potential substrates of CYP2D6 and their metabolites

(±)-*N-allylamphetamine* (*AA*) *and* (±)-*N,N-diallylamphetamine* (*DAA*). (±)-Amphetamine sulphate (500 mg; 2.71 mmol) was suspended in CH_3CN (3 ml) and basified with K_2CO_3 solution (25% w/v; 1.5 ml; 2.71 mmol). The CH_3CN solution was decanted into another flask. The residue of K_2SO_4 was washed with CH_3CN (2.5 ml × 2). To the combined organic solution, allyl bromide (117.45 μl; 1.36 mmol) was added, followed by K_2CO_3 solution (1.5 ml). The reaction mixture was left to stir at room temperature for 1 h during which time samples of the reaction mixture were examined by tlc using 10% CH_3OH in CH_2Cl_2 as the developing solvent. When the absence of allyl bromide was indicated, the reaction mixture was evaporated (rotatory evaporator) and the residue obtained was dissolved in water (40 ml). This solution was basified with K_2CO_3 solution (1.5 ml) and extracted with CH_2Cl_2 (5 ml × 3). The combined extract was evaporated to dryness and the product was purified by silica gel column chromatography, using 2% CH_3OH in CH_2Cl_2 as eluting solvent. Two products were obtained: (±)-N,N-diallylamphetamine (DAA; 24.80 mg) eluted first, followed by (±)-N-allylamphetamine (AA; 112.20 mg). Both were liquids. Total yield was 67.4%. AA was converted to a salt by treating a solution of it in diethyl ether with dry HCl gas, with cooling (solid CO_2 in acetone). The melting point of AA.HCl (recrystallized from ethyl acetate) was 168.5–169.5 °C. ^{1}H-NMR ($CDCl_3$) for AA, δ: 7.22–7.17 (m, 5H, **Ph**); 5.91–5.78 (m, 1H, allyl C**H**); 5.15–5.03 (m, 2H, terminal allyl C$\mathbf{H}_2$); 3.36–3.29 (m, 1H) and 3.24–3.16 (m, 1H) (allyl N-C$\mathbf{H}_2$); 3.00–2.90 (m, 1H, N-C**H**); 2.80–2.73 and 2.64–2.57 (two dd, 2H, $\mathcal{J}_{gem}$ = 10 H_z, $\mathcal{J}_{vic}$ = 5 Hz; C$\mathbf{H}_2$Ph); 1.07–1.05 (d, 3H, $\mathcal{J}$ = 5 Hz, CH-C$\mathbf{H}_3$).

The electrospray mass spectrum of AA was consistent with the proposed structure (figure 2).

When this reaction was repeated using excess allyl bromide (four equivalents relative to the quantity of amphetamine), a single product, DAA, was detected by tlc. The crude DAA was subjected to silica gel column chromatography using a mixture of ethyl acetate and *n*-hexane (1:4 v/v ratio) as developing solvent. The chromatographed product was converted to its HCl salt as described above in the synthesis of AA.HCl. (±)-DAA.HCl was obtained in 85% yield as a colourless solid, m.p. 162.0–163.0 °C when recrystallized from ethyl acetate. ^{1}H-NMR ($CDCl_3$) for DAA, δ: 7.25–7.14 (m, 5H, **Ph**); 5.88–5.75 (m, 2H, two allyl C**H**); 5.22–5.08 (m, 4H, two terminal allyl C$\mathbf{H}_2$); 3.22–3.06 (m, 5H, two allyl N-C$\mathbf{H}_2$ overlapping N-C**H**); 2.96–2.90 (dd, 1H, $\mathcal{J}$ = 8 Hz and $\mathcal{J}$ = 6 Hz; C$\mathbf{H}_2$Ph); 2.44–2.36 (dd, 1H, $\mathcal{J}$ = 8 and 3 Hz, C$\mathbf{H}_2$Ph); 0.95–0.93 (d, 3H, $\mathcal{J}$ = 5 Hz, CH-C$\mathbf{H}_3$).

The electrospray mass spectrum of DAA was consistent with the proposed structure (figure 2).

(±)-*N-allyl-N-methylamphetamine* (*AMA*). (±)-N-methylamphetamine.HCl (200.0 mg; 1.08 mmol) was suspended in CH_3CN (10 ml) and converted to its free base by the addition of K_2CO_3 solution (1 ml). To the base (isolated by the method used in the preparation of AA and DAA), an excess of allyl bromide (2.69 mmol; 233 μl) was added, followed by K_2CO_3 solution (1 ml). The resulting mixture was stirred at room temperature for 45 min at which time tlc monitoring of the reaction mixture indicated that > 90% of MA had been consumed. The residue obtained after solvent evaporation was dissolved in H_2O (10 ml) and basified with K_2CO_3 solution, then extracted into CH_2Cl_2. Chromatographic purification of the crude product on silica gel using 2.5% CH_3OH in CH_2Cl_2 as eluting solvent yielded (±)-AMA base (224.0 mg; liquid) in 92.1% yield. The base was converted to its HCl salt and recrystallized from ethyl acetate as a colourless solid, m.p. 130.5–132 °C. ^{1}H-NMR ($CDCl_3$), δ: 7.30–7.16 (m, 5H, **Ph**); 5.95–5.82 (m, 1H, allyl C**H**); 5.30–5.12 (m, 2H, terminal allyl C$\mathbf{H}_2$); 3.17–3.15 (d, 2H, allyl N-C$\mathbf{H}_2$); 3.02–2.95 (m, 2H, one H of C$\mathbf{H}_2$Ph overlapping N-CH); 2.45–2.37 (dd, one H of C$\mathbf{H}_2$Ph); 2.30 (s, 3H, N-C$\mathbf{H}_3$); 0.96–0.94 (d, 3H, $\mathcal{J}$ = 5 Hz, CH-C$\mathbf{H}_3$).

The electrospray mass spectrum of AMA was consistent with the proposed structure (figure 2).

(±)-*N-methyl-N-propylamphetamine* (*MPA*). This N-dialkylamphetamine was synthesized by a procedure similar to that used for the preparation of AMA. The amine and halide reagent used was (±)-N-methylamphetamine.HCl (1.38 mmol; 257.0 mg) and 1-bromopropane (2.76 mmol; 251.66 μl) respectively. After 1 day of stirring at room temperature, a tlc of the reaction mixture was developed with 7% CH_3OH in CH_2Cl_2. This showed that almost no reaction had occurred, so more 1-bromopropane (121 μl) and K_2CO_3 solution (1.02 ml) were added and the reaction continued for another day. The crude product (isolated as described in the preparation of AA and DAA) was chromatographed on a silica gel column, initially with 2%, and subsequently with 5% CH_3OH in CH_2Cl_2. Fractions were collected and examined by tlc. Those containing the desired product were eluted by 5% CH_3OH in CH_2Cl_2. Evaporation of the combined eluates gave MPA as a liquid in modest yield (40%). MPA.HCl salt,

prepared as described for AMA.HCl, was a colourless solid, m.p. 113.0–114.0 °C. ^{1}H-NMR ($CDCl_3$), δ: 7.32–7.27 (m, 2H of Ph) and 7.22–7.17 (m, 3H of Ph); 3.10–2.86 (m, 2H, one H of C**H**$_2$Ph overlapping N-C**H**); 2.46–2.37 (m, 3H, one H of C**H**$_2$Ph and 2H of N-C**H**$_2$CH$_2$CH$_3$); 2.32 (s, 3H, N-C**H**$_3$); 1.58–1.44 (m, 2H, C**H**$_2$CH$_3$); 0.95–0.89 (overlapping d and t, 6H, CHC**H**$_3$ and CH$_2$C**H**$_3$).

The electrospray mass spectrum of MPA was consistent with the proposed structure (figure 2).

(−)-*N-propargylamphetamine* (*PgA*). PgA was synthesized according to the method of MacGregor *et al.* (1988). The crude product obtained from a reaction of (−)-amphetamine sulphate (250 mg; 1.36 mmol) with propargyl bromide (75 μl; 0.86 mmol) was purified on a silica column (0.75 × 8 inches) using 2% CH_3OH in CH_2Cl_2 as eluting solvent. A small amount of DPgA as side product eluted first, followed by PgA as a liquid in 75% yield. NMR data of the PgA coincided with reported literature values. PgA.HCl and DPgA.HCl salts were prepared as described for AMA.HCl. Both products were colourless solids when recrystallized from ethyl acetate. PgA.HCl had a m.p. = 162.5–163.5 °C (m.p. reported by MacGregor *et al.* 158–160 °C). The melting point of DPgA.HCl was 166–167 °C. Their electrospray mass spectra were consistent with the proposed structures (figure 2).

Microsomal protein

Human CYP2D6 microsomal preparation used in this study was purchased from Gentest Corporation (Woburn, MA, USA). It was derived from a human AHH-1 TK+/− cell line transfected with complementary DNA that encoded human CYP2D6. Total protein content was 10 mg/ml in 100 mM potassium phosphate (pH 7.4) and CYP2D6 content was 260 pmol/mg protein. Control microsomes obtained from the same human cell line that had not been transfected with specific cDNA, were purchased from the same source.

NADPH-generating system

An NADPH-generating system was prepared by mixing freshly prepared stock solutions of $NADP^+$ (1.3 mM; 1 mg/ml), G6P (3.3 mM; 1 mg/ml), $MgCl_2.6H_2O$ (3.3 mM; 0.67 mg/ml) and G6PD (50 U/ml buffer) in a 5:5:10:2 volume ratio.

In vitro *microsomal incubation, extraction and derivatization*

Metabolism of N-allyl-N-methylamphetamine (*AMA*). An incubation mixture containing AMA (6.9 nmol), CYP2D6 (12.5 μl; 0.125 mg) and phosphate buffer to a volume of 97.5 μl was preheated at 37 °C for 5 min before the enzymatic reaction was started by an addition of NADPH-generating system (27.5 μl). The resulting mixture (125 μl) was incubated at 37 °C for 2 h. The reaction was terminated by cooling in an ice bath, followed by the addition of K_2CO_3 solution (100 μl). Internal standard (MMA; 0.7 nmol) was added and the mixture was extracted with a mixed organic solvent (2% v/v isopropanol in *n*-hexane; 2 × 3.5 ml) by vortexing vigorously for 1 min, shaking mechanically for 5 min and then centrifuging for 5 min at 2300 rpm in a Du Pont Sorvall GLC-2B General Laboratory Centrifuge (Mississauga, ON, Canada). The organic layer was transferred to a clean tube and evaporated to dryness under a stream of nitrogen at room temperature. The residue was trifluoroacetylated under anhydrous conditions as described below, and the derivatized sample was analyzed by GC as described above.

An identical incubation with control microsomes instead of CYP2D6 microsomes was also performed for comparison.

Derivatization procedure

The dried residue obtained at the end of each metabolic reaction was mixed with trifluoroacetic anhydride (50 μl) and acetonitrile (25 μl) in a test tube which was capped tightly with a screw cap before its insertion in a metal heating module at 60 °C for 30 min. The reaction mixture was allowed to cool to room temperature before the tube was opened and its contents evaporated to dryness at room temperature under a stream of dry nitrogen. The residue was dissolved in toluene (30 μl) and aliquots (2 μl) were analyzed by GC.

Quantitative analysis of metabolites

Known but varying amounts of authentic standards of all substrates (1.58–22.15 nmol) and metabolites (0.09–1.05 nmol) and a fixed quantity of internal standard (0.7 nmol MMA) was added to a series of tubes containing the same amount of NADPH-generating system, control microsomes and substrate as indicated in incubation samples. Extraction and derivatization procedures were then applied to these tubes, and their trifluoroacetylated products were analyzed by GC. Peak area ratios of metabolite to internal standard were plotted against concentrations of metabolite to produce calibration curves. The concentration of each metabolite in incubation mixtures was determined from the equation of the straight line derived from its calibration curve.

Metabolism of N-methyl-N-propylamphetamine (MPA), N,N-diallylamphetamine (DAA), deprenyl (DEP) and benzphetamine (BPA). The incubation procedure described above was repeated, except that substrate AMA was individually replaced with MPA, DAA, DEP or BPA (6.9 nmol).

The metabolism of DEP was also conducted in the presence of quinidine (0.638 nmol), an inhibitor of CYP2D6.

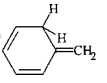
Results

The envisaged study required the synthesis of the substrates N-allyl-N-methylamphetamine, N,N-diallylamphetamine (a by-product of the synthesis of N-allylamphetamine) and N-methyl-N-propylamphetamine, and metabolites N-allylamphetamine and N-propargylamphetamine. The structures of these five compounds were confirmed by NMR and electrospray MS. Diagnostic ions (MH^+, m/z 119 and 91) were present in the mass spectra of all N-mono- and N,N-di-substituted compounds (figure 2). Most spectra also contained additional fragments of low abundance that were consistent with the structures from which they were derived. These fragment ions are identified in table 1.

When five N,N-dialkylated amphetamines (AMA, MPA, DAA, DEP, BPA) were individually incubated with the CYP2D6 isozyme fortified with appropriate

Table 1. Identities of minor fragment ions in the electrospray mass spectra of the synthesized N-mono- and N,N-dialkylated amphetamines.

Compound†	Fragment‡ (m/z; % rel. ab.)	Probable identity	
AA	84 (5.8%)	$CH_3CH{=}N^+HCH_2CH{=}CH_2$	(MH^+–C_7H_8)§
MPA	74 (7.8%)	$CH_3CH_2CH_2N^+H_2CH_3$	(MH^+–$C_6H_5CH{=}CHCH_3$)
DAA	174 (4.7%)	$C_6H_5CH_2C(CH_3){=}N^+HCH_2CH{=}CH_2$	(MH^+–$CH_3CH{=}CH_2$)
DAA	98 (7.2%)	$CH_2{=}CHCH_2N^+H_2CH_2CH{=}CH_2$	(MH^+–$C_6H_5CH{=}CHCH_3$)
DPgA	94 (17.9%)	$CH{\equiv}CHCH_2N^+H_2CH_2C{\equiv}CH$	(MH^+–$C_6H_5CH{=}CHCH_3$)

† Structures identified in Fig. 1; ‡ rel. ab., relative abundance; § C_7H_8= 

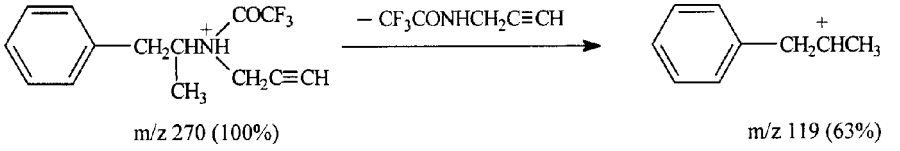


Figure 3. Diagnostic ions in the electrospray mass spectrum of the trifluoracetylated metabolite of deprenyl (PgA). Figures in brackets are % relative abundances.

Table 2. Yields of metabolites formed when various amphetamines were incubated with CYP2D6 and cofactors. Data are averages that differed by < 5% in duplicated experiments.

Substrate (6.9 nmol/incubation)	MA (pmol/incubation)	Nor metabolite (pmol/incubation)
AMA	98	279
MPA	44	73
DAA	(a)	594
DEP	624	1160
BPA	0	0

[a] Metabolism of DAA to MA is not possible.

cofactors, no ring hydroxylation of any of these substrates was observed. N-dealkylated metabolites, however, were detected in the incubation mixtures that contained AMA, MPA, DAA and DEP. AMA underwent two N-dealkylations to form the N-demethylation and N-deallylation products, AA and MA respectively. Similarly, CYP2D6-catalyzed metabolism of MPA produced MA and PA, and CYP2D6 promoted the production of MA and PgA from DEP.

In agreement with literature data (Grace *et al.* 1994, Wacher *et al.* 1996), DEP was metabolized by N-demethylation to nordeprenyl and by N-depropargylation to MA. As expected, these two metabolites were not observed when quinidine was included in the metabolism reaction. DAA was metabolized to AA, but no dideallylated product (amphetamine) was observed. The structures of these metabolites were confirmed by comparing their retention times with those of authentic reference samples of MA, PA and AA, and by interpretation of the mass spectrum of the N-demethylated metabolite of DEP after its trifluoroacetylation. This spectrum had two prominent ions of m/z 270 and 119, which are readily identified (figure 3). The quantities of metabolites formed are listed in table 2. No N-demethylated or N-dealkylated metabolites were detected in incubations of these substrates with control microsomes. This confirmed that CYP2D6 catalyzed these N-demethylations and N-dealkylations. Typical GC traces of derivatized incubation mixtures of DEP, AMA, MPA and DAA are shown in figure 4a and b.

Discussion

The anticipated result of this study on amphetamine derivatives was that the N,N-dialkylated amphetamines bearing an N-methyl substituent (AMA, MPA, DEP, BPA) would at least be N-demethylated since this pathway is known to be catalyzed partially by CYP2D6 (Coutts and Urichuk 1999). Ring hydroxylation was also expected because CYP2D6 can mediate the ring oxidation of other amphetamines such as N-*n*-butylamphetamine, N-ethylamphetamine and amphetamine (Bach *et al.* 1999). Three of the compounds investigated (AMA, MPA, DEP) were N-demethylated to varying extents (table 2) but, surprisingly, no CYP2D6-catalyzed N-demethylation or N-dealkylation occurred when BPA was incubated with CYP2D6 and none of the substrates was ring-hydroxylated. Aromatic ring-hydroxylated metabolites of the five dialkylated amphetamines (AMA, BPA, DEP, DAA, MPA) were not available to provide GC retention times of their O-acetylated derivatives and their mass spectra. However, it has been our experience that the GC retention times of the O-acetylated derivatives of many ring-hydroxylated drugs, including imipramine (Coutts *et al.* 1976, Su *et al.* 1993), trimipramine (Bolaji *et al.* 1993), methoxyphenamine, an amphetamine derivative (Coutts *et al.* 1994b), and N-alkylated amphetamines (Bach *et al.* 1999) are always in close proximity to those of the parent drug. If aromatic ring-hydroxylated metabolites had been formed in the present study, it probable that they would have been observed after acetylation in the GC traces and would have been readily identified by MS. No GC or MS evidence in favour of their presence was found.

The major structural difference in the four N-methylated substrates (AMA, MPA, DEP, BPA) is the nature of the N-alkyl groups (figure 1). These N-substituents appeared to influence the catalytic activity of CYP2D6 in the N-dealkylation pathway. Of the four alkyl groups, allyl ($CH_2CH{=}CH_2$), benzyl ($PhCH_2$), propargyl ($CH_2C{\equiv}CH$: and *n*-propyl ($CH_2CH_2CH_3$), the presence of

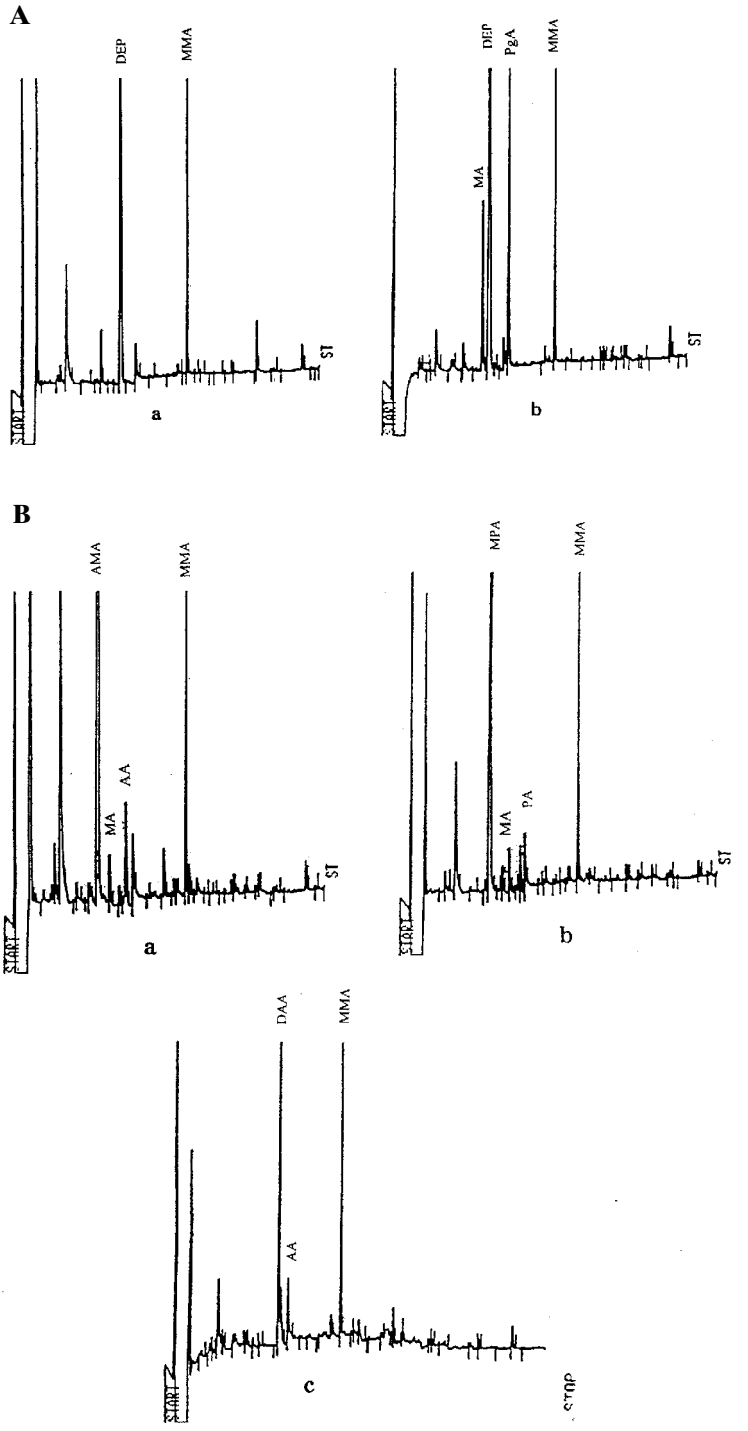


Figure 4. A. GC traces of trifluoracetylated dried extracts of DEP incubation with: (a) control microsomal protein; and (b) CYP2D6 enzyme preparation. MMA is the internal standard. B. (a) GC trace of trifluoroacetylated dried extract of AMA incubation with CYP2D6; (b) GC trace of trifluoroacetylated dried extract of MPA incubation with CYP2D6; (c) GC trace of trifluoroacetylated dried extract of DAA incubation with CYP2D6. Incubations were carried out under identical conditions. MMA is the internal standard.

the propargyl group had the greatest effect on CYP2D6 activity. Indeed, DEP was a very good *in vitro* substrate of CYP2D6 (table 2 and figure 4a). The two N-dealkylated metabolites of DEP (MA, nordeprenyl) were formed at different rates, indicating that CYP2D6 selectively mediated the cleavage of N-C bonds. When the propargyl group of DEP was replaced with an allyl group in AMA, the extent of N-dealkylation was much reduced, and when the propargyl group was replaced with an *n*-propyl group in MPA, a further reduction in the extent of N-dealkylation was observed. Finally, replacing the propargyl group with a benzyl moiety in benzphetamine resulted in a complete absence of CYP2D6-catalyzed metabolic N-demethylation or N-dealkylation. It appears that when the N atom of amphetamine contains both a 3-carbon substituent and a methyl group, the degree of unsaturation of the 3-carbon unit has an important influence on the extent of CYP2D6-catalyzed N-dealkylation. In addition, when the N-methyl group of AMA was replaced by an allyl substituent in DAA (which is N,N-diallylated), the extent of N-dealkylation was again increased (table 2). These findings suggest that the affinities of N-methyl, N-propyl, N-allyl and N-propargyl groups for CYP2D6 vary considerably.

In summary, this study has shown that human expressed CYP2D6 enzyme can catalyze the N-demethylation and N-dealkylation of four N,N-dialkylated amphetamines, namely AMA, MPA, DAA and DEP, but that it does not mediate the N-dealkylation of benzphetamine. Rates of these N-dealkylation reactions were clearly dependent upon the nature and extent of unsaturation of the N-substituents. Another noteworthy observation from this study was that none of the N,N-dialkylated substrates was ring-hydroxylated, in contrast to what was observed with N-monoalkylated amphetamines (Bach *et al.* 1999).

Results from the present study complemented those of previous investigators (Guengerich *et al.* 1986, Shet *et al.* 1993) who concluded that the N-demethylation of benzphetamine was catalyzed *in vitro* in humans by CYP3A4 and not by CYP2D6. Also, four of the five N,N-dialkylated amphetamines investigated were racemates. Only DEP was a single enantiomer. It would be of interest to extend the study to the enantiomers of all five N,N-dialkylated amphetamines to determine whether stereoselective metabolism is observed.

Acknowledgements

The authors are grateful to the Alberta Mental Health Fund and the Medical Research Council of Canada for funding.

References

Bach, M. V., Coutts R. T. and Baker G. B., 1999, Involvement of CYP2D6 in the metabolism of amphetamine, two N-alkylamphetamines and their 4-methoxylated derivatives. *Xenobiotica*, **29**, 719–732.

Bolaji, O. O., Coutts, R. T. and Baker, G. B., 1993, Metabolism of trimipramine *in vitro* by human CYP2D6 isozyme, *Research Communications in Chemical Pathology and Pharmacology*, **82**, 111–120.

Coutts, R. T., Bolaji, O. O., Su, P. and Baker, G. B., 1994b, Metabolism of methoxyphenamine *in vitro* by a CYP2D6 microsomal preparation, *Drug Metabolism and Disposition*, **22**, 756–760.

Coutts, R. T., Dawson, G. W. and Jones, G. R., 1978, *In vivo* metabolism of N-alkylamphetamines in the rat – the effect of N-alkyl chain length on oxidation of the aromatic ring. *Research Communications in Chemical Pathology and Pharmacology*, **22**, 589–592.

Coutts, R. T., Dawson, G. W., Kazakoff, C. W. and Wong, J. Y., 1976, *In vivo* phenolic metabolites of N-alkylamphetamines in the rat. Evidence in favor of catechol formation. *Drug Metabolism and Disposition*, **4**, 256–261.

COUTTS, R. T., SU, P. and BAKER, G. B., 1994a, Involvement of CYP2D6, CYP3A4, and other cytochrome P450 isozymes in N-dealkylation reactions. *Journal of Pharmacological and Toxicological Methods*, **31**, 177–186.

COUTTS, R. T., SU, P., BAKER, G. B. and DANESHTALAB, M., 1993, Metabolism of imipramine *in vitro* by isozyme CYP2D6 expressed in a human cell line, and observations on metabolite stability, *Journal of Chromatography, Biomedical Applications*, **615**, 265–272.

COUTTS, R. T. and URICHUK L. J., 1999, Polymorphic cytochromes P450 and drugs used in psychiatry. *Cellular and Molecular Neurobiology*, **17**, 325–354.

GRACE, J. M., KINTER M. T. and MACDONALD, T. L., 1994, Atypical metabolism of deprenyl and its enantiomer, (S)-(+)-N,α-dimethyl-N-propynylphenethylamine, by cytochrome P4502D6. *Chemical Research in Toxicology*, **7**, 286–290.

GUENGERICH, F. P., MARTIN, M. V., BEAUNE, P. H., KREMERS, P., WOLFF, T. and WAXMAN, D. J., 1986, Characterization of rat and human liver microsomal cytochrome P-450 forms involved in nifedipine oxidation, a prototype for genetic polymorphism in oxidative drug metabolism. *Journal of Biological Chemistry*, **261**, 5051–5061.

MACGREGOR, K. R., FOWLER, J. S. and WOLF, A. F., 1988, Synthesis of suicide inhibitors of monoamine oxidase: carbon-11 labeled clorgyline, L-deprenyl and D-deprenyl. *Journal of Labelled Compounds and Radiopharmaceuticals*, **25**, 1–9.

SHET, M. S., FISHER, C. W., HOLMANS, P. L. and ESTABROOK, R. W., 1993, Human cytochrome P450 3A4: enzymatic properties of a purified recombinant fusion protein containing NADPH-P450 reductase. *Proceedings of the National Academy of Sciences, USA*, **90**, 11748–11752.

SU, P., COUTTS, R. T., BAKER, G. B. and DANESHTALAB, M., 1993, Analysis of imipramine and three metabolites produced by isozyme CYP2D6 expressed in a human cell line. *Xenobiotica*, **23**, 1289–1298.

WACHER, V. J., WONG, S., WONG, H. T. and BENET, L. Z., 1996, Contribution of CYP3A to selegiline metabolism in rat and human microsomes. In *Proceedings of the 7th North American International Society for the Study of Xenobiotics Meeting*, San Diego, 10, 351.

XENOBIOTICA , 2000, VOL. 30, NO. 3, 307–315

Absorption, distribution, metabolism and excretion of *p*-bromophenylacetylurea in the female rat

J. XU†*, W. M. PURCELL† and D. E. RAY‡

†Faculty of Applied Sciences, University of the West of England, Frenchay Campus, Coldharbour Lane, Bristol BS16 1QY, UK
‡Medical Research Council Toxicology Unit, University of Leicester, Leicester, U.K.

Received 15 July 1999

1. This study has investigated absorption, distribution, metabolism and excretion of *p*-bromophenylacetylurea (BPAU) in the F344 female rat. BPAU and its metabolites were determined by HPLC.

2. Following a single p.o. dose of 150 mg/kg BPAU, the absorbed fraction of dosed BPAU was 65.9% and its half-life in the blood was 9.4 h. The relative distribution of BPAU (tissue/serum ratio) at 6 h (peak time point) after a single i.p. dose of 150 mg/kg BPAU was spinal cord (4.6 ± 0.2) > liver (3.7 ± 0.1) > brain (2.9 ± 0.1) (mean ± SD, $n = 5$), and they were significantly different from each other ($p < 0.05$). BPAU in spinal cord reached the highest level.

3. Absorbed BPAU was metabolized *in vivo* into three major metabolites. N′-hydroxy-*p*-bromophenylacetylurea (M1) was a dominant metabolite in tissues, whereas 4-(4-bromophenyl)-3-oxapyrrolidine-2,5-dione (M2) reached a high concentration in blood. N′-methyl-*p*-bromophenylacetylurea (M3) was mainly found in the urine. All three metabolites were excreted via the urine and together accounted for 87% of absorbed BPAU.

4. This study provides a basic understanding of BPAU absorption, distribution, metabolism and elimination in rat.

Introduction

p-Bromophenylacetylurea (BPAU) was originally synthesized as one of a series of halogenated congeners of phenylacetylurea (Phenurone, Abbott), an anti-epileptic agent, in a search for a more effective anticonvulsive drug, but it produced serious delayed neuropathy in rats (Diezel and Quadbeck 1960). BPAU can induce pathological damages in the spinal cord and peripheral nerves in rat (Cavanagh and Chen 1968, Jakobsen *et al.* 1982, Troncoso *et al.* 1982, Nagata and Brimijoin 1986, Nagata *et al.* 1987, Oka and Brimijoin 1990, Jortner *et al.* 1997). Either a single high dose (100–400 mg/kg) or lower repeated daily doses (10–40 mg/kg for 2–8 months) produced similar clinical ataxia and histopathological damage in the spinal cord and peripheral nerves (Cavanagh and Chen 1968, Troncoso *et al.* 1982). This delayed neurotoxicity was clinically and histopathologically similar to organophosphorous ester-induced delayed neuropathy in hen (Cavanagh and Chen 1968). Rat is more susceptible to BPAU-induced neurotoxicity than other species (Cavanagh and Chen 1968) and BPAU has been widely used as a model compound for mechanistic studies of delayed neuropathy in rat. BPAU is metabolized *in vivo* into three metabolites (Xu *et al.* 1999a). Phenylmethanesulphonyl fluoride (PMSF) interferes with BPAU metabolism and potentiates BPAU-induced neurotoxicity (Xu *et al.* 1999b). This

* Author for correspondence; e-mail: Jinsheng.Xu@uwe.ac.uk

Xenobiotica ISSN 0049–8254 print/ISSN 1366–5928 online © 2000 Taylor & Francis Ltd
http://www.tandf.co.uk/journals/tf/00498254.html

suggests that metabolic and pharmacokinetic factors play a role in BPAU-induced neurotoxicity. The present study has investigated the absorption, distribution, metabolism and excretion of BPAU in rat to explore the relevance of pharmacokinetic factors in BPAU-induced neurotoxicity.

Materials and methods

Chemicals

p-Bromophenylacetylurea (BPAU, 99%) was synthesized by Dr R. Mattocks (MRC Toxicology Unit); acetonitrile (HPLC grade) was from Sigma; dimethyl sulphoxide (DMSO) was from BDH Laboratory Supplies; ammonium acetate was from Fisons.

Three metabolites of BPAU, N′-hydroxy-*p*-bromophenylacetylurea [3-hydroxy-5-(4-bromophenyl)-1,3-diazapentane-2,4-dione, M1], 4-(4-bromophenyl)-3-oxapyrrolidine-2,5-dione (M2), and N′-methyl-*p*-bromophenylacetylurea [3-methyl-5-(4-bromophenyl)-1,3-diazapentane-2,4-dione, M3] were purified from the liver, serum and urine of the BPAU-dosed rat using a HPLC method in our laboratory (Xu *et al.* 1999a). Their purities were $>98\%$.

Animals and procedures

BPAU absorption, metabolism and excretion after an oral dose. A group of five female F344 rats, body weight 250–280 g, were given a single oral dose of 150 mg/kg BPAU in DMSO (BPAU was dissolved in DMSO, 150 mg/ml, 0.1 ml/100 g body weight). Each rat was housed in a metabolic cage, with free access to food and water at 22 ± 1 °C with a 12 h light/dark cycle. Faeces and urine were collected daily for 5 days. Blood samples of 30–50 μl were taken by pricking the tail of rats at 1, 2, 4, 6, 12, 24, 48, 72, 96 and 122 h after BPAU dosing and anti-clotting with heparin. Control faeces, urine and blood samples were collected 1 day before dosing.

BPAU disposition in individual tissues. Groups of four female F344 rats, body weight 170–210 g, were given a single i.p. dose of 150 mg/kg BPAU in DMSO (BPAU was dissolved in DMSO, 150 mg/ml, 0.1 ml/100 g body weight). All animals were housed in plastic cages with stainless steel grill tops and had free access to food and water. The animals were sacrificed at 1, 2, 4, 6, 12, 18, 24, 48 or 72 h after dosing. One rat was used as solvent control and given the same volume of DMSO alone, and was sacrificed at 18 h after administration.

Sample preparation

Whole blood. Each blood sample was mixed with methanol/DMSO (95:5 v/v) in the ratio 1:5 (v/v) and was sedimented in a microcentrifuge at 9000 *g* for 5 min. The supernatant was retained for HPLC analysis.

Faeces and urine. Faeces samples were extracted with methanol/DMSO at 1 g/ml and urine samples were mixed with methanol/DMSO at 1:1 and then centrifuged at 6000 *g* for 20 min. The supernatants were stored at 4 °C and sedimented again in a microcentrifuge at 9000 *g* before HPLC injection.

Serum and tissues. Animals for the pharmacokinetic studies of BPAU in tissues were sacrificed by carbon dioxide at each time point. Blood samples were collected by cardiac puncture after death and allowed to clot. Brain, spinal cord, liver and muscle tissues were removed, weighed and stored at −20 °C. Before analysis, tissues were thawed and homogenized in the methanol/DMSO solution at 100 mg tissue per ml solution. Blood was centrifuged at 3000 *g* for 10 min. Serum was removed and mixed with methanol/DMSO solution at the ratio 1:4 (v/v). All samples were centrifuged at 9000 *g* for 5 min and the supernatant analysed for BPAU and its metabolites with HPLC.

HPLC analytical conditions

The HPLC method for the determination of BPAU and its metabolites has been previously described (Xu *et al.* 1999a). In brief, a Waters HPLC system with a Controller 600, a tunable absorbance detector 486 and an autosampler plus 717 was employed. Column: S5 ODS2 250 4.6 mm (Spherisorb); detection: UV at 240 nm; mobile phase: A = 0.1 M ammonium acetate, pH 6.5; B = acetonitrile; flow rate: 1 ml/min. Gradient programme: 75:25 (v/v) A:B linear to 50:50 (v/v) A:B within 10 min and then hold at 50:50 (v/v) A:B for 10 min. The injected volume of each sample was 25–50 μl for quantitative assays.

Table 1. Pharmacokinetic parameters of BPAU in whole blood of rat after a single oral dose of 150 mg/kg BPAU.

C_0[a] (μg/ml)	F[b] (%)	r^2[c]	k[d] (h^{-1})	V[e] (ml)	AUC[f] ($\mu g.ml^{-1}.h^{-1}$)	$T_{1/2}$[g] (h)
14.8	65.9	0.761[h]	0.074	1230± 160	103.7	9.4± 1.3

[a] The concentration estimated from the extrapolated line of $-k/2.303$ when time $t = 0$.
[b] Absorbed fraction.
[c] The square of regression coefficient between logarithmic concentrations and time of elimination phase.
[d] Apparent first-order elimination rat constant.
[e] Apparent distribution volume.
[f] The area under concentration-time curve.
[g] Half-life of elimination.
[h] $p < 0.001$, $n = 5$ (regression test).

Statistics and pharmacokinetics

ANOVA was used for the comparisons of the concentration of BPAU or its metabolites in different tissues and the blood/tissue ratios. Student's *t*-test was employed for two sample comparisons. The standard errors of elimination rate constants were calculated according to the method given by Mead and Curnow (1987). The *Z*-test was used for half-life comparisons.

Pharmacokinetic data were analysed according to the methods and equations given by Gibaldi and Perrier (1982). The area under the concentration–time curve (AUC) was estimated using the trapezoidal rule (Martin 1986).

Results

Pharmacokinetics of BPAU after a single oral dose

Absorption. Following a single oral dose of 150 mg/kg BPAU, ~ 30% of the dosed BPAU was found in faeces within the first 24 h, and 4% was detected in faeces between 24 and 48 h after dosing. Less than 1% of the BPAU was excreted via the urine. Thus, the absorption fraction was 65.9% of dosed BPAU. The fraction of absorbed BPAU is shown in table 1. M1 was just detectable, but M2 and M3 were undetectable in faeces.

Pharmacokinetic parameters. Figure 1 shows the curve of logarithmic concentration data versus time of BPAU in blood after a single oral dose. BPAU given orally followed apparent first-order absorption and elimination kinetics in the blood of rat. The kinetic data for BPAU in whole blood was best fitted with a one-compartment model and the pharmacokinetic parameters were determined according to the method of Gibaldi and Perrier (1982). The AUC in whole blood was estimated using the trapezoidal rule (Martin 1986). The pharmacokinetic parameters of BPAU in whole blood are shown in table 1.

M1 and M2 kinetics in blood. M1 and M2 were major metabolites of BPAU detected in blood. M1 reached a peak value at 18 h after dosing, which was 12 h later compared with the parent compound (BPAU), whereas M2 reached a peak value at 48 h after dosing. M2 was much higher than M1 in blood (figure 2). M3 in blood was just detectable but had a high concentration in urine.

Excretion of metabolites. All three metabolites were excreted in the urine. The total metabolites recovered in urine is shown in table 2. The three metabolites excreted from urine accounted for 86.6% of the absorbed BPAU, with M2 predominating.

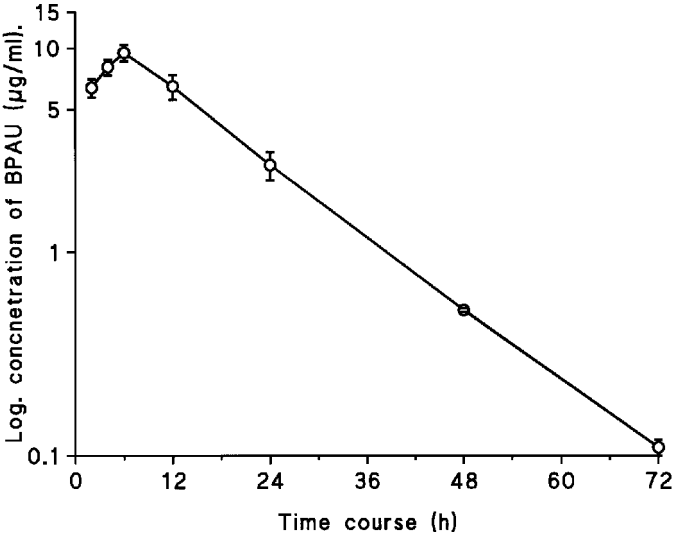


Figure 1. Logarithmic concentration–time curve of BPAU in the whole blood of rat following a single oral dose of 150 mg/kg BPAU. Data are mean± SME, $n = 5$.

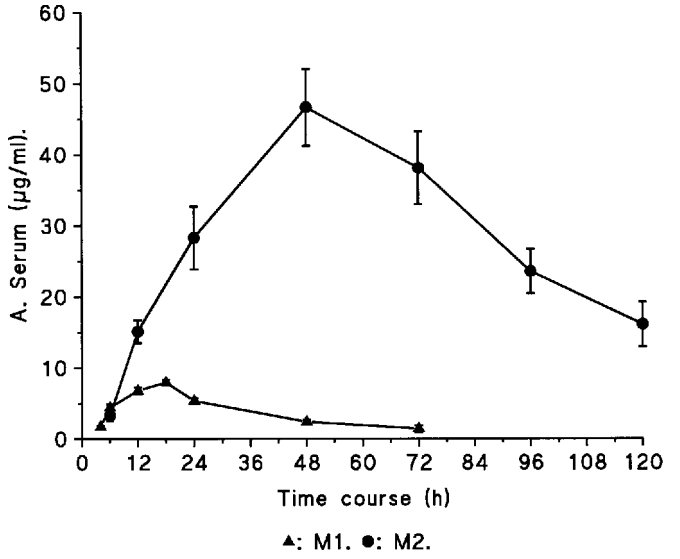


Figure 2. Concentration–time curves of BPAU metabolites M1 and M2 in the whole blood of rat following a single oral dose of 150 mg/kg BPAU. Data are mean± SEM, $n = 5$.

Table 2. Excretion of M1, M2 and M3 from urine after a single oral dose of 150 mg/kg BPAU.

	Absorbed BPAU	M1	M2	M3	M1 + M2 + M3
Amount (μmol./rat[a])	71.76± 2.74[b]	8.7± 1.3	35.8± 5.3	17.7± 4.5	62.2
% of dosage	65.9	8.0	32.9	16.3	57.1

[a] Rat body weight 186± 5 g.
[b] Values in the table are expressed as mean or mean± SD, $n = 5$.

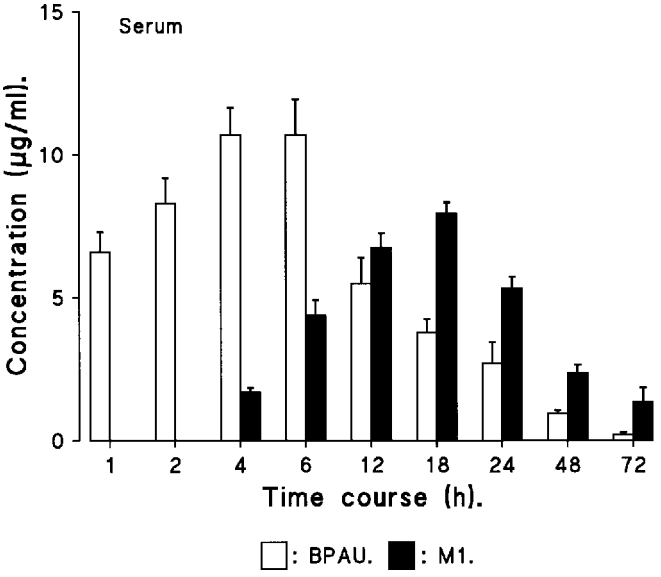


Figure 3. Time-courses of BPAU and M1 in rat serum following a single i.v. dose of 150 mg/kg BPAU. Data are mean± SEM, $n = 5$.

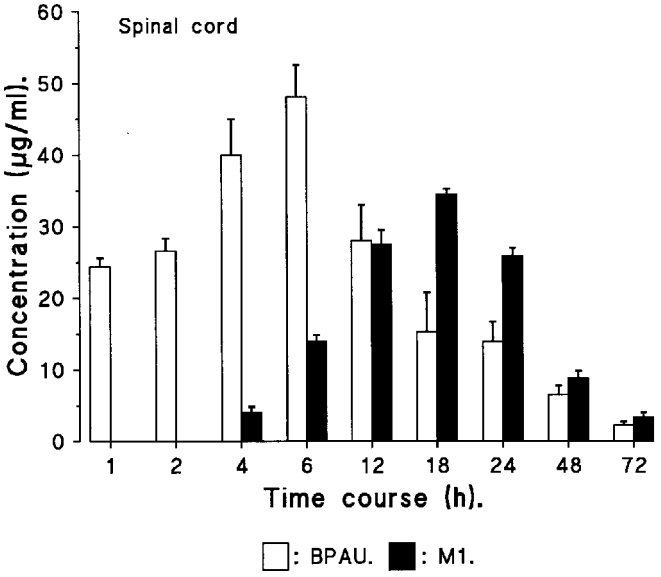


Figure 4. Time-courses of BPAU and M1 in rat spinal cord following a single i.v. dose of 150 mg/kg BPAU. Data are mean± SEM, $n = 5$.

BPAU disposition in individual tissues after a single intraperitoneal dose

*BPAU and M*1 *kinetics in serum*. BPAU and M1 kinetics in serum after a single i.p. dose are shown in figure 3. Although the dosing route was different from the whole blood data, their kinetic processes were similar.

BPAU reached peak values in tissues 6 h after a single i.p. dose (figures 4–6). Its relative concentration in different tissues was expressed as tissue/serum ratios. The

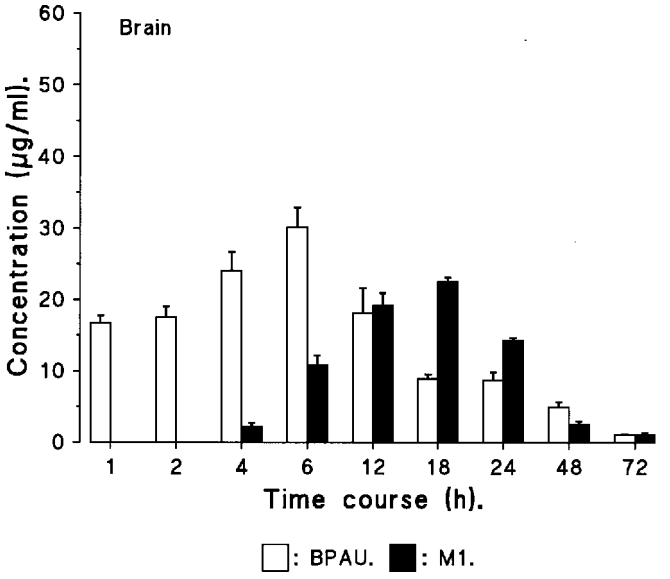


Figure 5. Time-courses of BPAU and M1 in rat brain following a single i.v. dose of 150 mg/kg BPAU. Data are mean± SEM, $n = 5$.

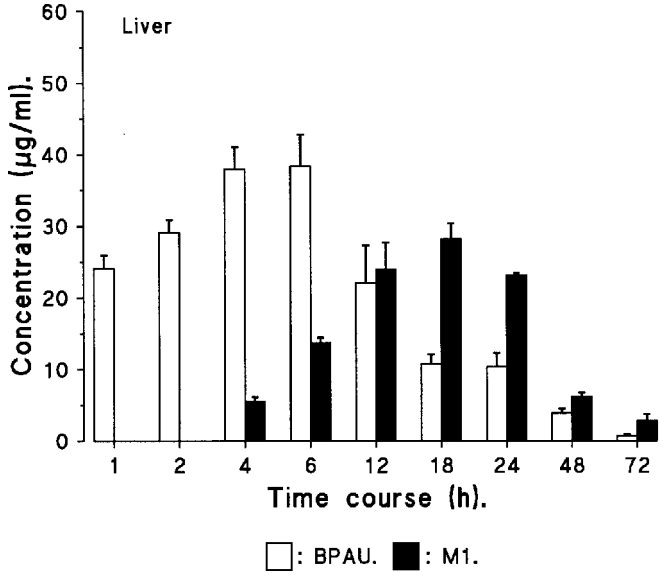
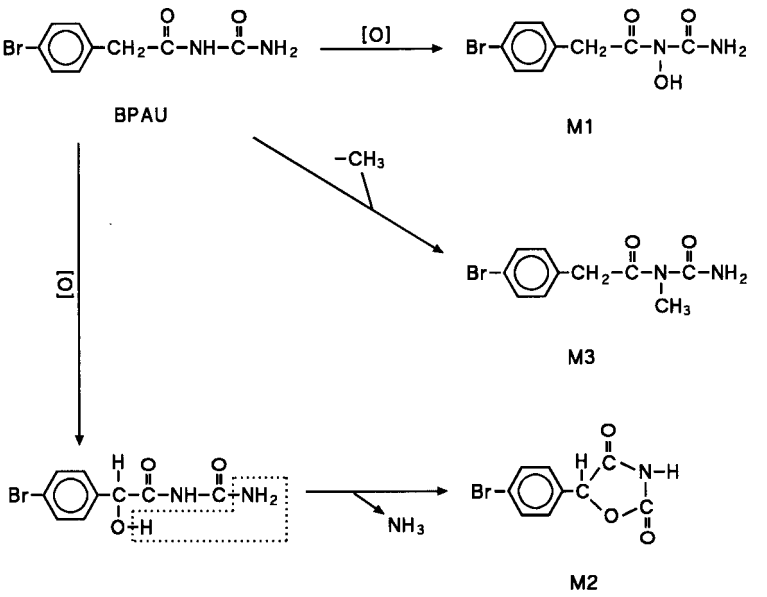


Figure 6. Time-courses of BPAU and M1 in rat liver following a single i.v. dose of 150 mg/kg BPAU. Data are mean± SEM, $n = 5$.

order of the tissue/serum ratios at 6 h (peak time point) was spinal cord (4.6± 0.2) > liver (3.7± 0.1) > brain (2.9± 0.1) (mean± SD, $n = 5$). These latter values were significantly different from each other ($p < 0.05$ or 0.01). M1 was a dominant metabolite of BPAU in tissues and reached peak values in tissues 18 h after dosing (figures 4–6) and its distribution paralleled that of BPAU. The level of M1 in spinal cord was significantly higher than that in other tissues ($p < 0.01$). The levels of M2



BPAU: p-bromophenylacetylurea

M1: N'-hydroxy-p-bromophenylurea

M2: 4-(bromophenyl)-3-oxapyrrolidine-2,5-dione

M3: N'-methyl-p-bromophenylacetylurea

Figure 7. Proposed metabolic pathways of BPAU.

in tissues were low (data are not shown) and blood contamination may also contribute to tissue M2 levels because the concentration of M2 in blood was very high.

The proposed metabolic pathways of BPAU is shown in figure 7.

Discussion

It has previously been reported that spinal cord and peripheral nerves are the target sites of BPAU-induced neurotoxicity (Cavanagh and Chen 1968, Troncoso *et al.* 1982). The current study has shown that BPAU was widely distributed over a range of tissues, but reached the highest level in the spinal cord and the distribution characteristics of BPAU may be responsible for the vulnerability of the spinal cord.

The current study has shown that the absorption of BPAU was not complete. The absorption fraction was 65.9%, which might be greater than bioavailability due to the first-pass effect of liver. Only a small fraction ($< 1\%$) of absorbed BPAU was excreted in the urine in its original form. Most BPAU was eliminated via biotransformation and all the three identified metabolites were excreted through urine. M2 had a high concentration in blood and was a dominant metabolite in the urine. Hence, M2 is likely to be a detoxified metabolite. M3 was detected principally in the urine and, therefore, has no direct neurotoxic potential. However, M1 was formed by hydroxylation at the secondary nitrogen on BPAU. The formation of the = N-OH group often increases toxic potential (Parkinson 1996). Therefore, M1 is likely to be an activated metabolite and may play a role in BPAU-induced

neuropathy. This proposal would require further confirmation by *in vitro* studies. M1 remained in the tissues much longer than BPAU itself because its peak values in tissues appeared at 18 h after dosing and, hence, when repeated daily doses are given, it is more likely to maintain or increase a certain level in target tissues after each dose. Troncoso *et al.* (1982) reported that rat given daily doses of either 40 or 10 mg/kg BPAU for 2–6 months developed clinical ataxia and histological damage in the spinal cord and peripheral nerves, which were similar to that induced by a higher single dose. The pharmacokinetic characteristics of BPAU and its metabolites in tissues may be responsible for the toxic effect of repeated low doses.

The liver was thought to be the major site for BPAU metabolism since the observation that partially removing the liver by surgical operation or chemically damaging the tissue before BPAU dosing significantly increased BPAU-induced neurotoxicity (Chen and Cavanagh 1971). However, the present study shows that the peak value of M1 in the liver and CNS were similarly proportional to that of the parent compound, BPAU. This might have been due to either *in situ* metabolism of BPAU in the central nervous system, or redistribution from the liver, but the former was likely the case because BPAU is a lipophilic compound and, therefore, is difficult to redistribute away from lipid-rich tissues to other tissues (Caldwell *et al.* 1995).

The present study provides a basic understanding of BPAU absorption, distribution, metabolism and excretion in rat, and implies a pharmacokinetic reason for the vulnerability of spinal cord as the main target of BPAU-induced neurotoxicity.

Acknowledgements

This study was supported by Medical Research Council Toxicology Unit, Leicester, UK.

References

Caldwell, J., Gardner, I. and Swales, N., 1995, An introduction to drug disposition: the basic principles of absorption, distribution, metabolism, and excretion, *Toxicology and Pathology*, **23**, 102–114.

Cavanagh, B. and Chen, F. C.-K., 1968, The experimental neuropathy in rats caused by *p*-bromophenylacetylurea. *Journal of Neurosurgery and Psychiatry*, **31**, 471–478.

Chen, F. C.-K. and Cavanagh, L. B., 1971, Factors affecting neurotoxicity by *p*-bromophenylacetylurea in rats. *British Journal of Experimental Pathology*, **52**, 315–321.

Diezel, B. and Quadbeck, G., 1960, Nervenschadigung durch *p*-bromphenylacetylharnstoff, *Naunyn. Schmiedeberg's Archives and Experimental Pharmakologie and Pathology*, **238**, 534–541.

Gibaldi, M. and Perrier, D. 1982, *Pharmacokinetics*, 2nd edn (New York: Marcel Dekker).

Jakobsen, J., Lambert, E. H., Carlson, G. and Brimijoin, S, 1982, Clinical and electrophysiological characteristics of the experimental neuropathy caused by *p*-bromophenylacetylurea. *Experimental Neurology*, **75**, 158–172.

Jortner, S., Dyer, K., Walton, A. and Ehrich, M., 1997, Synaptophysin immunoreactive axonal swelling in *p*-bromophenylacetylurea-induced neuropathy. *Neurotoxicology*, **18**, 161–168.

Martin, B. K., 1986, Pharmacokinetics. In H. Glenny and P. Nelmes (eds), *Handbook of Clinical Drug Research* (London: Blackwell), pp. 59–93.

Mead, R. and Curnow, R. N., 1987, *Statistical Methods in Agriculture and Experimental Biology* (London: Chapman & Hall).

Nagata, H. and Brimijoin, S., 1986, Neurotoxicity of halogenated phenylacetylureas is linked to abnormal onset of rapid axonal transport. *Brain Research*, **385**, 136–142.

Nagata, H., Brimijoin, S., Low, P. and Schmelzer, J. D., 1987, Slow axonal transport in experimental hypoxia and in neuropathy induced by *p*-bromophenylacetylurea. *Brain Research*, **422**, 319–326.

Oka, N. and Brimijoin, S., 1990, Premature onset of fast axonal transport in bromophenylacetylurea neuropathy: an electrophoretic analysis of proteins exported into motor nerve. *Brain Research*, **509**, 107–110.

PARKINSON , A., 1996, Biotransformation of xenobiotics. In C. D. Klaassen (ed.), *Casarett & Doull's Toxicology*: *The Basic Science of Poisons* (New York: McGraw-Hill, Inc.), pp. 113–186.

TRONCOSO , J. C., GRIFFIN , J. W., PRICE, D. L. and HESS-KOZLOW, K. M., 1982, Pathology of the peripheral neuropathy induced by *p*-bromophenylacetylurea. *Laboratory Investigation*, **46**, 215–223.

XU, J., LAMB , J., DUKES, R., PURCELL , W. M. and RAY, D. E., 1999a, Application of the high-performance liquid chromatographic method for separation, purification and characterisation of *p*-bromophenylacetylurea and its metabolites. *Journal of Chromatography B*, **732**, 349–356.

XU, J., LISTER , T., PURCELL , W. M. and RAY, D. E., 1999b, Neurotoxic potentiation is related to a metabolic interaction between *p*-bromophenylacetylurea and phenylmethanesulfonyl fluoride. *Toxicology and Applied Pharmacology*, **157**, 222–226.

XENOBIOTICA , 2000, VOL. 30, NO. 3, 317–326

Hippuric acid as a major excretion product associated with black tea consumption

M. N. CLIFFORD†*, E. L. COPELAND†, J. P. BLOXSIDGE‡ and L. A. MITCHELL†

† Food Safety Research Group, School of Biological Sciences and ‡Department of Chemistry, University of Surrey, Guildford GU2 5XH, UK

Received 10 August 1999

1. Nine habitual tea-drinking volunteers were recruited and asked to follow a low-polyphenol and low-caffeine diet for 6 days and to provide daily 24-h urine samples. On day 4 of the experiment strong black tea brewed under standardized conditions was re-introduced to the volunteers' diet.

2. ^{1}H-NMR and HPLC profiling of the urine samples indicated that consumption of black tea (6–10 mugs per day) was associated with a significant ($p = 0.00017$) increase in hippuric acid excretion relative to control, increasing from 153–512 to 742–1374 mg day^{-1}. The excretion of substantial amounts of hippuric acid has not previously been associated with black tea consumption.

3. For some volunteers, the quantity of benzoic acid processed exceeded the acceptable daily intake (ADI), but this is not considered to constitute any hazard.

4. A mass-balance analysis indicated that the necessary quantity of benzoic acid could not be obtained from the contents of gallic acid, flavanols, flavonol glycosides and theaflavins in black tea even if 100% transformation was obtained, suggesting that the thearubigins (the major and chemically ill-defined polyphenols of black tea) may be an important source.

Introduction

It has been claimed that tea is the most popular beverage, consumed by over two-thirds of the world's population. Freshly harvested tea leaf is processed differently in different parts of the world to give oolong tea (2%), green tea (20%) or black tea (78%) (Kuroda and Hara 1999), of which black tea is the most important form in the UK and Europe.

Fresh tea leaf is rich in water-soluble polyphenols, particularly flavanols, flavanol gallates and flavonol glycosides (Graham 1992, Willson and Clifford 1992, Clifford 1997). Black tea ('black' used in this context relates solely to the method of leaf processing and not to the optional addition of milk to the beverage before consumption) is produced from fresh green leaf by 'fermentation'—enzymic (polyphenol oxidase-driven) and coupled chemical oxidation of the flavanols and flavanol gallates and, to a lesser extent, the flavonol (especially myricetin) glycosides and the non-flavonoid theogallin. These transformations produce a unique range of pigments including the brownish thearubigins and the red-orange theaflavins, theaflavic acids and theaflagallins, as reviewed by Harbowy and Balentine (1997). More recently, the structures of the red-orange theaflavates (Wan *et al.* 1997) and the yellow theacitrins (Davis *et al.* 1997) have been reported and the theafulvins, a thearubigin subfraction, have been partially characterized (Clifford and Powell 1996).

The thearubigins are difficult to analyse, but they are the major polyphenols of black tea leaf and beverage. Their content has been variously estimated as ~ 3–6%

* Author for correspondence; e-mail: M.Clifford@surrey.ac.uk

Xenobiotica ISSN 0049–8254 print/ISSN 1366–5928 online © 2000 Taylor & Francis Ltd
http://www.tandf.co.uk/journals/tf/00498254.html

of the black leaf or ~ 20% of the total solutes extracted during brewing. The theaflavins form ~ 1–2% of the black leaf or ~ 3–5% of brew solids, making black tea brew one of the major sources of dietary phenols (Clifford 1997, Harbowy and Balentine 1997). The lack of commercial sources of theaflavins and thearubigins, compounded by the complexity and ill-defined chemistry of the latter, has impeded investigation of their biological properties in both animals and man. It has been reported that consumption of black tea leads to an increased content of total phenols in human plasma (He and Kies 1994). The nature of these plasma metabolites was not defined and it is not known whether the theaflavins and thearubigins contributed. The objectives of this study using healthy volunteers were:

- to estimate by ^{1}H-NMR and HPLC-profiling of urine the quantity of phenolic and/or aromatic compounds excreted after consuming a low-phenol diet;
- to investigate whether the amount excreted increased significantly when the volunteers introduced black tea to their diet; and
- to identify the major metabolite(s) excreted after consuming black tea.

Materials and methods

Volunteer study

Volunteers were recruited by word-of-mouth within the University of Surrey. Nine volunteers (two males, seven females, 25–28 years of age, body weight 57–83 kg) were selected on the basis that they were habitual drinkers of black tea. Volunteers were advised about the objectives of the study, provided with tea bags and milk, and trained in a standardized tea brewing procedure (see below). For 6 days, volunteers were asked to exclude polyphenol-rich components (fruits, fruit juices, vegetables, herbs, spices, soy products, green tea, black tea, coffee) from their diet. Diet records were kept throughout the 6 days so that the foods and drinks consumed on day 1 could be replicated for day 4 (likewise, diets were matched on days 2 and 5, and days 3 and 6). During days 4–6 of this period, black tea was re-introduced to the diet at a level that each volunteer selected. One female volunteer repeated the experiment on two further occasions to compare the effect of drinking caffeine-containing black tea with milk, caffeine-containing black tea without milk, and decaffeinated black tea.

Standard tea brewing procedure

Volunteers were trained to use the following procedure and provided with the tea bags and skimmed milk as required. Boiling water (250 ml) was poured from a domestic kettle into a mug containing a readily available tea bag, and the bag squeezed with a spoon against the mug for 2 min. Skimmed milk (60 ml) was added and the volunteers were asked to consume the total volume as rapidly as possible. The same supermarket's decaffeinated tea bag was substituted as necessary, and when tea was consumed without milk, cold tap water (60 ml) was added instead.

Twenty-four-hour urine collection

Collection was made into a plastic container (G and N, Billingshurst, UK) containing 1 M HCl (10 ml) to retard bacterial growth. The 24-h urine volume was recorded, the contents of the bottle mixed thoroughly by inversion, 4 × 20 ml aliquots kept for analysis (− 20 °C) and the remainder of the sample discarded.

HPLC analysis

Urine (as collected) was centrifuged (1360 *g*, 3 min) to remove solids. Direct, duplicate injections (50 µl) were made onto a Phenomenex Luna HPLC column (25 cm × 4.6 mm). Detection was at 240, 280 and 360 nm using a Spectra Physics forward optical scanning detector. Mobile phase: A: 0.5% formic acid in water; B: 50% acetonitrile in 0.5% aqueous formic acid. Gradient: isocratic elution with 100% solvent A (10 min), falling linearly to 45% solvent A at 65 min, and linearly to 0% solvent A at 70 min. Total flow rate: 1 ml min^{-1}. Preparative HPLC was performed similarly, but using repeated 250-µl injections and automated fraction collection. The bulked fraction was evaporated at reduced pressure to remove organic solvents and the aqueous residue freeze-dried.

Tea brews were analysed as previously described (Powell *et al.* 1995). The peaks corresponding to caffeine, gallic acid, (+)-catechin, (−)-epicatechin, (−)-epigallocatechin, (−)-epicatechin gallate and (−)-epigallocatechin gallate were identified by spiking and spectral matching, and quantified against standard calibration curves (five concentrations). Regression analysis determined the relationship between concentration and peak area (duplicate injections). The main peaks having maximum absorption

near 360 nm but lacking absorption > 400 nm were assigned as flavonol glycosides and quantified as rutin equivalents. The late eluting peaks with strong absorption at 360 and 460–470 nm were assigned as theaflavin, theaflavin-3-gallate, theaflavin-3′-gallate and theaflavin-3,3′-digallate as previously determined (Opie 1992). These four components were quantified as theaflavin equivalents using theaflavin provided by Dr A. L. Davis (Unilever, Sharnbrook, UK). These chemically defined components of black tea brews elute from reversed-phase HPLC columns as distinct peaks superimposed on the thearubigins that appear on the chromatogram as an approximately gaussian 'hump' (McDowell *et al.* 1991, 1995a, b, Powell *et al.* 1992, Shao *et al.* 1995, Temple and Clifford 1997, Bruschi *et al.* 1999). As described, the peak areas for the chemically defined components are calculated electronically to the upper surface of the 'hump' rather than to the horizontal baseline (Clifford *et al.* 1996, Ozawa *et al.* 1996). The area associated with the thearubigins is calculated as the difference between the total chromatogram area and the sum of all resolved peaks that are superimposed thereon (Powell *et al.* 1992, Shao *et al.* 1995). This calculated area is interpreted against a calibration curve prepared from isolated theafulvin, a thearubigin fraction previously shown to be free from caffeine, gallic acid, flavanols, flavonol glycosides and theaflavins, and thought to consist of phenolic compounds having masses up to ~ 2500 daltons (Powell *et al.* 1992, Powell 1995, Shao *et al.* 1995, Clifford and Powell 1996).

^{1}H-NMR analysis

Urine (as collected) was centrifuged (1360 *g*, 3 min) to remove solids, and aliquots (2 ml) were transferred to plastic Sterilin tubes, frozen and lyophilized. The residue was redissolved in 2 ml sodium formate (1 mg ml^{-1} in D_2O) and stored at − 20 °C to await ^{1}H-NMR analysis. The signal at 8.22 ppm from the sodium formate was used as an internal standard to facilitate quantification of the area under the curve as described elsewhere (Copeland 1996). The area calculated was corrected for the total volume of urine excreted per 24 h.

GC–MS analysis

The material collected by HPLC, after freeze-drying, was reconstituted in distilled water (5 ml). An aliquot (1 ml) was adjusted to pH 1 with HCl, applied to an SPE column and eluted with ethyl accetate. The eluate was evaporated under nitrogen and derivatized with bis-silyl trifluoroacetamide (BSTFA).

GC was performed with a Hewlett Packard HP5890 GC–MS using a CP-Sil-5 capillary column and a temperature gradient from 80 to 155 °C at 15 °C min^{-1}, from 155 to 185 °C at 6 °C min^{-1} and 185 to 290 °C at 15 °C min^{-1}. Injection port temperature was 250 °C. Hippuric acid eluted at 14.9 min. Peak detection and characterization was performed using EI ionization. Target ions were 105, 206 and 308 with the ratio 105/206 = 0.57 and the ratio 105/308 = 0.18.

Results

The volunteers selected were habitual drinkers of black tea. Two volunteers regularly consumed seven mugs per day, the others between two and four, giving a mean habitual consumption of about four mugs per day. This level is considered to be slightly higher than the UK national average. The 2-min brewing period used here is considerably longer than current common practice. Three of the volunteers reported that before the study they also consumed between one and three mugs of coffee per day. This would add to their total intake of phenolic compounds, providing a significant intake of cinnamates (Clifford 1999), but not of those polyphenols associated with black tea beverage.

The composition of black tea beverage brewed by the method in which the volunteers were trained was estimated by analysing eight brews prepared by two people. Theogallin was not detected. Gallic acid contents averaged 22.6± 0.7 mg l^{-1}. The flavonol glycoside content (as rutin) was 33.0± 1.4 mg l^{-1} (or 16.3± 0.7 mg l^{-1} as the aglycone quercetin), the flavanol content 55.2± 1.6 mg l^{-1}, thearubigins 1.2± 0.1 g l^{-1}, and total theaflavins (as theaflavin) 85.7± 12.9 mg l^{-1}. The caffeine content was 136.2± 1.0 mg l^{-1}. These data are in keeping with literature values and indicate that the composition of a mug of tea (310 ml) brewed in this standardized manner varied comparatively little.

The volunteers were asked to not leave tea brew in the mug in order to maximize and better standardize the quantity of polyphenols consumed. They were asked to consume the beverage as quickly as possible to minimize loss from the beverage of polyphenols by precipitation as the tea cooled. This precipitation, known as

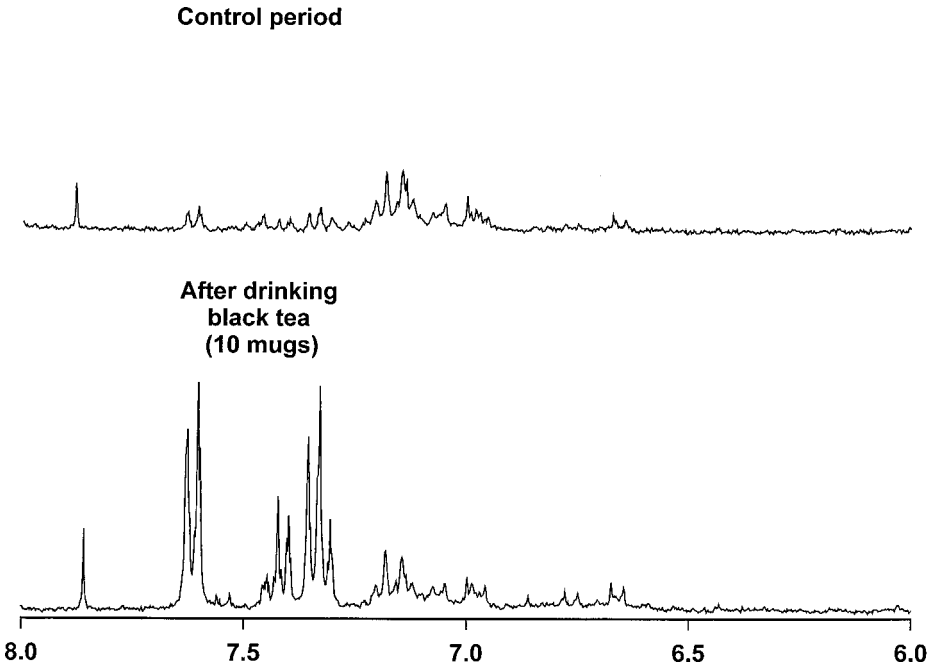


Figure 1. ^{1}H-NMR (6.0–8.0 ppm) of 24-h urine samples from the control period (low-phenol diet) and from the test period for the same volunteer (after consuming 10 mugs of tea).

creaming, involves the formation in caffeine-containing (but not decaffeinated) tea brews of caffeine complexes that are insoluble at $< 60\ ^{\circ}C$ (Powell *et al.* 1992), and which tend to adsorb to the mug.

Clearly it was not possible to control brewing and consumption absolutely, and therefore it was not possible to calculate precisely the intake of polyphenols for each volunteer. However, on average, it may be concluded that such a mug of tea would supply some 415 mg polyphenols comprising thearubigins ($\sim$ 360 mg), theaflavins ($\sim$ 26 mg), flavonol glycosides ($\sim$ 5 mg as aglycones), flavanols ($\sim$ 17 mg) and gallic acid ($\sim$ 7 mg). In addition, each mug contained some 40 mg caffeine when the caffeine-containing tea bags were used.

Although diet diaries were kept, no attempt was made to estimate the intake or identity of polyphenols arising from the low-phenol diet because there is no database available for such a purpose. One could infer that the additional intake would be relatively small compared with that derived from tea. All volunteers completed the study without reporting any untoward effects. During the tea-drinking part of the study, three volunteers selected 10 mugs per day, three selected seven mugs per day, and two selected six mugs per day. HPLC chromatograms and ^{1}H-NMR spectra were obtained for all control and test urine samples, i.e. those collected following the consumption of tea.

For a given volunteer, the area under the curve (expressed as arbitrary units relative to the internal standard) for the aromatic region (6.0–8.0 ppm) of the NMR spectrum was considerably larger for the urine from the tea drinking period (2.44–3.89) compared with that for the control period (1.77–2.19). A Mann–Whitney two-tailed test returned $p = 0.001$. A major contributor to the aromatic portion of each spectrum, and always larger in the test urine samples, was a distinctive series of peaks that were consistent with the presence of hippuric acid (figure 1).

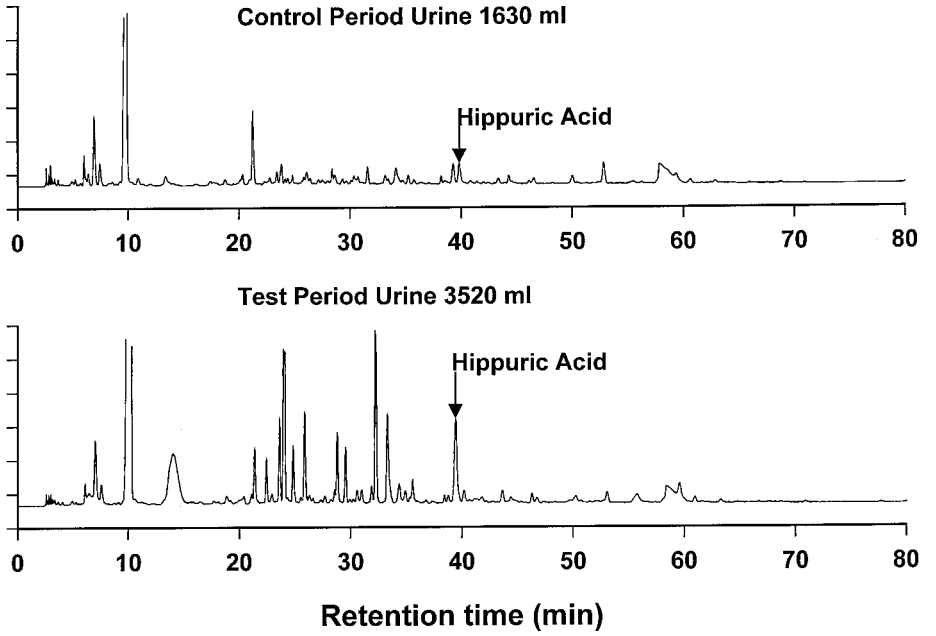


Figure 2. Reversed-phase chromatograms of 24-h urine from the control period (low-phenol diet) and from the test period for the same volunteer (after consuming 10 mugs of tea).

Table 1. Excretion of hippuric acid and the equivalent amount of benzoic acid processed (mg 24 h^{-1}) by volunteers during the control period (low phenol diet) and the experimental (black tea-drinking) period.

	Volunteer		Hippuric acid excreted (mg 24 h^{-1})			
	Body weight (kg)	Black tea (mugs day^{-1})	Control period	Test period	Test control	Equivalent benzoic acid
1	57.0	7	208.8	254.9	46.1	31.4
2	63.5	7	109.9	288.8	178.8	122.0
3	80.0	7	62.4	239.1	176.7	120.5
4	62.0	10	59.6	515.7	456.0	311.0
5	76.2	10	99.5	480.3	380.8	259.7
6	65.0	6	110.7	342.9	232.2	158.4
7	83.0	10	163.2	544.6	381.4	260.1
8	63.5	6	195.9	410.6	214.7	146.4
9	75.0	10	55.7	401.8	346.1	236.0
9	75.0	10[a]	55.7	458.4	402.7	274.6
9	75.0	10[b]	55.7	440.4	384.7	262.3

[a] Without milk.
[b] Decaffeinated black tea.

HPLC analysis revealed in all urine samples a well-resolved peak eluting close to 40 min (figure 2), which by spiking was indistinguishable from authentic hippuric acid, and which was quantified as such. The results are presented in table 1. This HPLC peak was collected and subjected to GC–MS. The only component observed had a GC retention time (14.9 min), target ions (105, 205, 206, 308) and target ion ratios identical with authentic hippuric acid similarly processed, thus confirming the NMR and HPLC data.

The quantity of hippuric acid excreted by nine volunteers during the control period (153–512 mg day^{-1}) was significantly lower (Mann–Whitney, two-tailed, $p =$

0.00017) than the corresponding excretion (742–1374 mg day^{-1}) following consumption of 6–10 mugs of black tea. The increase in excretion relative to control ranged from 334 to 1141 mg day^{-1} or 47–114 mg per mug of tea consumed. As far as the present authors are aware, the excretion of such quantities of hippuric acid has not previously been associated with black tea consumption. Initially, it seemed surprising that previous investigators should have overlooked the excretion of such substantial amounts of hippuric acid. However, hippuric acid has generally been investigated in relation to the metabolism of (poly)phenols and it should be noted that the methods used to detect and quantify phenols (absorbance at 280 nm, colour-producing reactions involving a phenolic hydroxyl, or native fluorescence) are not appropriate for the detection and quantification of hippuric acid.

In successive study periods, one volunteer consumed 10 mugs of decaffeinated black tea without added milk, 10 mugs of caffeine-containing black tea without milk and 10 mugs of caffeine-containing black tea with added skimmed milk. The 24-h excretion of hippuric acid following 10 mugs of caffeine-containing black tea with skimmed milk was 1140 mg. For caffeine-containing black tea and decaffeinated black tea without added skim milk, the corresponding values were 1257 mg ($\sim$ 110%) and 1303 mg ($\sim$ 115%) respectively. These modest increases may well have been a reflection of the tendency of certain black tea polyphenols to associate and precipitate, or to adsorb to the mug, following interaction with caffeine or milk proteins. The tedium and inconvenience associated with the diets precluded replication of this study. Accordingly, it is not possible to judge whether the presence of milk or caffeine has a statistically significant effect on the excretion of hippuric acid, but if so, it would appear to be modest.

Discussion

Hippuric acid (benzoyl glycine) is produced in mammals from the metabolism of benzoic acid and it has been reported in urine samples from volunteers consuming benzoic acid-rich fruits (Cathcart-Rake *et al.* 1975). Free benzoic acid was not found in the urine samples during the current study. The increased excretion of hippuric acid associated with black tea consumption in this study correspond to requirements for between 227 and 778 mg benzoic acid, but its exact origin is uncertain. Since the volunteers maintained their diets as constant as possible on control and test days, it would appear to be associated with the consumption of black tea. Since benzoic acid has not been reported to occur naturally in tea and is not a permitted additive in tea products (Anon. 1981), it seems unlikely that pre-existing benzoic acid can be the origin.

Other origins for hippuric acid include formation endogenously or by the gut microflora, or by both in concert. It has been demonstrated that several species (particularly guinea pig) (Svardal and Scheline 1985a–c) can convert quinic acid to benzoic acid in the liver. Early work reviewed by Scheline (1978) indicates that humans given quinic acid per os excrete a substantial amount of hippuric acid relative to the dose of quinic acid, but whether the aromatization is entirely endogenous or whether the gut microflora are involved is not clear. Quinic acid is not a known constituent of tea, but theogallin (5-galloylquinic acid) may be present (Shao *et al.* 1995, Kiehne and Engelhardt 1996, Harbowy and Balentine 1997). However, theogallin was not detected in the brews consumed during this study and, therefore, cannot be the source of benzoic acid. Hippuric acid and glycine conjugates of hydroxybenzoic and methylbenzoic acids have been reported in the urine of man

(Hackett *et al.* 1983, Pietta *et al.* 1997) or animals (Griffiths 1964, Das and Griffiths 1969, 1966) and have been associated with the gut flora metabolism of flavonoids (Winter *et al.* 1989, Meselhy *et al.* 1977, Kim *et al.* 1998) and drugs (Kershaw *et al.* 1987, Cupid *et al.* 1996) but always as minor products relative to the doses.

Since the volunteers in this study were not taking medication, it seems likely, therefore, that the benzoic acid arises from the gut flora metabolism of some constituent(s) in black tea brew. While some might be formed from non-aromatic precursors, it seems more plausible that the majority is derived from black tea polyphenols by the action of the gut microflora followed by absorption and endogenous conjugation.

It has been established that the gut microflora in humans and animals can produce 3-(3′-hydroxyphenyl)propionic and 3-(4′-hydroxyphenyl)propionic acids from a range of dietary phenols (including flavonoids, cinnamates and tyrosine) (Hackett *et al.* 1983, Skjevrak *et al.* 1986, Goodwin *et al.* 1994, Cremin *et al.* 1995, Pietta *et al.* 1995, Merfort *et al.* 1996, Phipps *et al.* 1998). It has been reported that rat gut microflora can produce 3-phenylpropionic acid from 5-caffeoylquinic acid (Phipps *et al.* 1998) and a flavonoid dimer (procyanidin B3) (Groenewoud and Hundt 1986). Similarly, human gut microflora can convert 3-(4′-hydroxyphenyl)propionic acid to 3-phenylpropionic acid *in vitro* but faecal extracts from different individuals vary markedly in their ability to carry out this dehydroxylation probably reflecting variations in the gut flora (Curtius *et al.* 1976, Bennett *et al.* 1992, Chesson *et al.* 1999). It has been reported that infants do not acquire the necessary gut microflora until $\sim$ 4 months of age (Bennett *et al.* 1992).

Humans absorb 3-phenylpropionic acid and normally convert it to benzoic acid by β-oxidation, followed by excretion as hippuric acid (Curtius *et al.* 1976, Bennett *et al.* 1992, Pietta *et al.* 1997). However, in cases of medium-chain acyl-CoA dehydrogenase (MCAD) deficiency, an autosomal recessively transmitted inborn error of C6–C12-carboxylic acid metabolism, 3-phenylpropionic acid cannot be efficiently chain-shortened and is excreted as 3-phenylpropionylglycine (Bennett *et al.* 1992, Glasgow *et al.* 1992, Lehnert 1993). The safety of benzoic acid taken per os has been associated with regard to the use of benzoates as preservatives permitted for use in foods (Anon. 1996), and it has been noted that its conversion to hippuric acid is a saturable process in which the availability of glycine is the rate-limiting factor. Even with saturation, clearance is relatively rapid, although at sufficiently high doses there is evidence of interference with intermediary metabolism, including the urea cycle, gluconeo-genesis, fatty acid metabolism and the tricarboxylic acid cycle, probably by sequestering coenzyme A before its conjugation with glycine (Anon. 1996). Although volunteers given occasional substantial doses of benzoic acid have suffered no ill-effects, the Joint WHO/FAO Expert Committee on Food Additives nevertheless applied an acceptable daily intake (ADI) of up to 5 mg kg^{-1} b.wt (Anon. 1996). The total amount of benzoic acid processed by the volunteers during the control period ranged from 0.7 to 3.1 mg kg^{-1} b.wt day^{-1}, well within this ADI. However, during the tea drinking period, the equivalent values ranged from 3.0 to 8.3 mg kg^{-1} b.wt day^{-1}, with the 'extra' benzoic acid attributed to tea drinking ranging from 0.6 to 5.0 mg kg^{-1} b.wt day^{-1}. In assessing the significance of these observations, it should be noted that these levels were only achieved at rates of tea consumption well above the UK average, and for beverage prepared by a brewing time (2 min) and method intended to maximize extraction of polyphenols, and considerably harsher than is common current practice. Moreover, bearing in mind

the relatively conservative nature of the calculations used in defining an ADI, coupled with the fact that to exceed the ADI modestly on a regular basis or even more substantially on an occasional basis, is not automatically indicative of any toxicological hazard, these observations do not seem to be a cause for alarm. However, they do highlight a source of benzoic acid that has not previously been taken into consideration and deserving of greater attention in the future.

As discussed above, the yield of hippuric acid per mug of black tea consumed ranged from 47 to 114 mg, which corresponds to between 32 and 76 mg benzoic acid per mug. In view of the composition of the tea brew, it is clear that even the lowest yield of benzoic acid (32 mg per mug) could not be accounted for by the contents of gallic acid, flavanols and flavonol glycosides since these would total only 29 mg, and one would not expect 100% conversion.

Similarly, it is clear that the highest yield of benzoic acid (76 mg per mug) could not be supplied solely by these classes of polyphenols even in combination with the theaflavins (total 55 mg). It seems reasonable, therefore, to suggest that a significant part of the benzoic acid is derived from the thearubigins, the major and least well-characterized polyphenols of the black tea brew.

Based on the estimated consumption of tea polyphenols, the yield of benzoic acid excreted (after conjugation) varied between 1 and 8% and was not obviously related to the amount of tea consumed during the study, body weight, or habitual level of tea or coffee consumption before the study. It is suspected that a major factor responsible for this substantial person-to-person variation might be significant differences in the competence of their gut microflora to metabolize these black tea constituents. However, any imprecision in our estimates of the volunteers' consumption of tea polyphenols would be another consideration.

Whether benzoic acid or 3-phenylpropionic acid are associated in any way with the suspected health benefits ascribed to the consumption of black tea, or whether they are of any physiological significance whatsoever is not clear at present. Claims made for the putative benefits of dietary phenols often cite their antioxidant activity in rationalization. Benzoic acid and 3-phenylpropionic acid, however, are not antioxidants (although they could be radical scavengers). It follows, therefore, that the greater the flux of dietary phenols along this pathway, the lower the potential for phenolic metabolites to enter the tissues for a given polyphenol burden. In addition, any biological effects that might accrue from this production of benzoic acid must, therefore, be mediated by some non-antioxidative mechanism(s).

Conclusions

It has been demonstrated conclusively that the consumption of black tea by habitual tea drinkers leads to an increased excretion of hippuric acid. The increase relative to the control period on a low-phenol diet ranged from 334 to 1141 mg day^{-1} and was not obviously related in a simple manner to the volunteer's body weight or the quantity of tea consumed during the study. The origin of the hippuric acid is thought to be gut flora metabolism of black tea polyphenols (including the ill-defined thearubigins) to 3-phenylpropionic acid, followed by endogenous β-oxidation and conjugation to glycine. For some volunteers the amount of benzoic acid processed exceeded the ADI.

Acknowledgements

This study was part of the EU Shared Cost Project CT95–0653 'CPT and Health'. Dr Peter C. H. Hollman, State Institute for Quality Control of Agricultural

Products (RIKILT-DLO), 6708 PD Wageningen, The Netherlands, is thanked for assistance with the GC–MS analysis described here.

References

ANON., 1981, *Butterworth's Law of Food and Drugs* (London: Butterworths).

ANON., 1996, Miscellaneous substances: benzyl acetate, benzyl alcohol, benzaldehyde and benzoic acid and its salts. In *Toxicological Evaluation of Certain Food Additives* (Geneva: WHO), pp. 29–80.

BENNETT, M. J., BHALA, A., POIRIER, S. F., RAGNI, M. C., WILLI, S. M. and HALE, D. E., 1992, When do gut flora in the newborn produce 3-phenylpropionic acid? Implications for early diagnosis of medium-chain acyl-CoA dehydrogenase deficiency. *Clinical Chemistry*, **38**, 278–281.

BRUSCHI, L., COPELAND, E. L. and CLIFFORD, M. N., 1999, Unexpected hyperchromic interactions during the chromatography of theafulvins and simple flavonoids. *Food Chemistry*, **67**, 143–146.

CATHCART-RAKE, W., PORTER, R., WHITTIER, F., STEIN, P., CAREY, M. and GRANTHAM, J., 1975, Effect of diet on serum accumulation and renal excretion of aryl acids and secretory activity in normal and uremic man. *American Journal of Clinical Nutrition*, **28**, 1110–1115.

CHESSON, A., PROVENZA, F., RUSSELL, W. R., SCOLLARD, D. J., RICHART, C. and STEWART, C., 1999, Hydroxycinnamic acids in the digestive tract of livestock and humans. *Journal of the Science of Food and Agriculture*, **79**, 373–378.

CLIFFORD, M. N., 1997, Tea. In M. D. Ranken, R. C. Kill and C. J. G. Baker (eds), *Food Industries Manual*, 24 edn (London: Blackie), pp. 379–395.

CLIFFORD, M. N., 1999, Chlorogenic acids and other cinnamates—nature, occurrence and dietary burden. *Journal of the Science of Food and Agriculture*, **79**, 362–372.

CLIFFORD, M. N. and POWELL, C., 1996, A partial resolution of 'black tea tannins' by HPLC. In J. Vercauteren, C. Chèze, M. C. Dumon and J. F. Weber (eds), *Polyphenols 96: XVIII^e Journées Internationales Groupe Polyphénols* (Paris: INRA), pp. 217–218.

CLIFFORD, M. N., HARDEN, G., DAVIS, A. L., OPIE, S. C., POWELL, C. and TEMPLE, C., 1996, Black tea thearubigins. In J. Velisek and J. Davidek (eds), *Chemical Reactions in Foods III* (Prague: Czech Chemical Society), pp. 13–16.

COPELAND, E. L., 1996, Biomarkers of flavonoid consumption for the evaluation of dietary burden. PhD thesis, University of Surrey.

CREMIN, J. D., MCLEOD, K. R., HARMON, D. L., GOETSCH, A. L., BOURQUIN, L. D. and FAHEY, G. C., 1995, Portal and hepatic fluxes in sheep and concentrations in cattle ruminal fluid of 3-(4-hydroxyphenyl)propionic, benzoic, 3-phenylpropionic, and *trans*-cinnamic acids. *Journal of Animal Science*, **73**, 1766–1775.

CUPID, B. C., BEDDELL, C. R., LINDON, J. C., WILSON, I. D. and NICHOLSON, J. K., 1996, Quantitative structure–metabolism relationships for substituted benzoic acids in the rabbit: prediction of urinary excretion of glycine and glucuronide conjugates. *Xenobiotica*, **26**, 157–176.

CURTIUS, H. C., METTLER, M. and ETTLINGER, L., 1976, Study of the intestinal tyrosine metabolism using stable isotopes and gas chromatography–mass spectrometry. *Journal of Chromatography*, **126**, 569–580.

DAS, N. P. and GRIFFITHS, L. A., 1966, Studies on flavonoid metabolism. Metabolism of (+)-catechin in the guinea pig. *Biochemical Journal*, **100**, 449–456.

DAS, N. P. and GRIFFITHS, L. A., 1969, Studies on flavonoid metabolism. Metabolism of (+)-[^{14}C]catechin in the rat and guinea pig. *Biochemical Journal*, **115**, 831–836.

DAVIS, A. L., LEWIS, J. R., CAI, Y., POWELL, C., DAVIES, A. P., WILKINS, J. P. G., PUDNEY, P. and CLIFFORD, M. N., 1997, A polyphenolic pigment from black tea. *Phytochemistry*, **46**, 1397–1402.

GLASGOW, J. F., MOORE, R., ROBINSON, P. H. and MCKIERNAN, P. J., 1992, The phenylpropionic acid load test: experience with 72 children at-risk for beta-oxidation disorders. *Irish Journal of Medical Science*, **161**, 586–588.

GOODWIN, B. L., RUTHVEN, C. R. J. and SANDLER, M., 1994, Gut flora and the origin of some urinary aromatic phenolic compounds. *Biochemical Pharmacology*, **47**, 2294–2297.

GRAHAM, H. N., 1992, Green tea composition, consumption and polyphenol chemistry. *Preventive Medicine*, **21**, 334–350.

GRIFFITHS, L. A., 1964, Studies on flavonoid metabolism. Identification of the metabolites of (+)-catechin in rat urine. *Biochemical Journal*, **92**, 173–179.

GROENEWOUD, G. and HUNDT, H. K. L., 1986, The microbial metabolism of condensed (+)-catechins by rat caecal microflora. *Xenobiotica*, **16**, 99–107.

HACKETT, A. M., GRIFFITHS, L. A., BROILLET, A. and WERMEILLE, M., 1983, The metabolism and excretion of (+)-[^{14}C]cyanidanol-3 in man following oral administration. *Xenobiotica*, **13**, 279–286.

HARBOWY, M. E. and BALENTINE, D. A., 1997, Tea chemistry. *CRC Critical Reviews in Plant Sciences*, **16**, 415–480.

HE, Y. H. and KIES, C., 1994, Green and black tea consumption by humans: impact on polyphenol concentrations in feces, blood and urine. *Plant Foods and Human Nutrition*, **46**, 221–229.

KERSHAW, R. A., MAYS, D. C., BIANCHINE, J. R. and GERBER, N., 1987, Disposition of aspirin and its metabolites in the semen of man. *Journal of Clinical Pharmacology*, **27**, 304–309.

KIEHNE, A. and ENGELHARDT, U. H., 1996, Thermospray-LC-MS analysis of various groups of polyphenols in tea. I. Catechins, flavonol-*O*-glycosides and flavone-*C*-glycosides. *Zeitschrift für Lebensmittel-Untersuchung und -Forschung*, **202**, 48–54.

KIM, D.-H., JUNG, E.-H., SOHNG, I.-S., HAN, J.-H., KIM, T.-H. and HAN, M. J., 1998, Intestinal bacterial metabolism of flavonoids and its relation to some biological activities. *Archives of Pharmacology Research*, **21**, 17–23.

KURODA, Y. and HARA, Y., 1999, Antimutagenic and anticarcinogenic activity of tea polyphenols. *Mutation Research*, **436**, 69–97.

LEHNERT, W., 1993, Experience with the 3-phenylpropionic acid loading test for diagnosis of medium-chain acyl-CoA dehydrogenase deficiency (MCADD). *Padiatrie und Padologie*, **28**, 9–12.

MCDOWELL, I., FEAKES, J. and GAY, C., 1991, Phenolic composition of black tea liquors as a means of predicting price and country of origin. *Journal of the Science of Food and Agriculture*, **55**, 627–641.

MCDOWELL, I., TAYLOR, S. and GAY, C., 1995a, The phenolic composition of black tea liquors—Part I. Predicting quality. *Journal of the Science of Food and Agriculture*, **69**, 467–474.

MCDOWELL, I., TAYLOR, S. and GAY, C., 1995b, The phenolic pigment composition of black tea liquors—Part II. Discriminating origin. *Journal of the Science of Food and Agriculture*, **69**, 475–480.

MERFORT, I., HEILMANN, J., WEISS, M., PIETTA, P. and GARDANA, C., 1996, Radical scavenger activity of three flavonoid metabolites studied by inhibition of chemiluminescence in human PMNs. *Planta Medica*, **62**, 289–292.

MESELHY, M. R., NAKAMURA, N. and HATTORI, M., 1997, Biotransformation of (−)-epicatechin 3-*O*-gallate by human intestinal bacteria. *Chemical and Pharmaceutical Bulletin*, **45**, 888–893.

OPIE, S. C., 1992, Black tea thearubigins. PhD thesis, University of Surrey.

OZAWA, T., KATAOKA, K. and NEGISHI, O., 1996, Elucidation of the partial structure of polymeric thearubigins from black tea by chemical degradation. *Bioscience, Biotechnology and Biochemistry*, **60**, 2023–2027.

PHIPPS, A. N., STEWART, J., WRIGHT, B. and WILSON, I. D., 1998, Effect of diet on the urinary excretion of hippuric acid and other dietary-derived aromatics in rat. A complex interaction between diet, gut microflora and substrate specificity. *Xenobiotica*, **28**, 527–537.

PIETTA, P. G., GARDANA, C. and MAURI, P. L., 1997, Identification of *Gingko biloba* flavanol metabolites after oral administration to humans. *Journal of Chromatography B: Biomedical Applications*, **693**, 249–255.

PIETTA, P. G., GARDANA, C., MAURI, P. L., MAFFEI FACINO, R. and CARINI, M., 1995, Identification of flavonoid metabolites after oral administration to rats of a *Gingko biloba* extract. *Journal of Chromatography B: Biomedical Applications*, **673**, 75–80.

POWELL, C., 1995, The polyphenolic pigments of black tea. PhD thesis, University of Surrey.

POWELL, C., CLIFFORD, M. N., OPIE, S. C., FORD, M. A., ROBERTSON, A. and GIBSON, C. L., 1992, Tea cream formation: the contribution of black tea phenolic pigments determined by HPLC. *Journal of the Science of Food and Agriculture*, **63**, 77–86.

POWELL, C., CLIFFORD, M. N., OPIE, S. C. and GIBSON, C. L., 1995, Use of Porter's reagents for the characterisation of thearubigins and other non-proanthocyanidins. *Journal of the Science of Food and Agriculture*, **68**, 33–38.

SCHELINE, R. R., 1978, *Mammalian Metabolism of Plant Xenobiotics* (London: Academic Press).

SHAO, W., POWELL, C. and CLIFFORD, M. N., 1995, The analysis by HPLC of green, black and Pu'er teas produced in Yunnan. *Journal of the Science of Food and Agriculture*, **69**, 535–540.

SKJEVRAK, I., SOLHEIM, E. and SCHELINE, R. R., 1986, Dihydrochalcone metabolism in the rat: trihydroxylated derivatives related to phloretin. *Xenobiotica*, **16**, 35–45.

SVARDAL, A. M. and SCHELINE, R. R., 1985a, Intracellular localization and some properties of the system in guinea pig liver responsible for the aromatization of cyclohexanecarboxylic acid to hippuric acid. *Molecular and Cellular Biochemistry*, **65**, 107–115.

SVARDAL, A. M. and SCHELINE, R. R., 1985b, The aromatization of cyclohexanecarboxylic acid to hippuric acid: substrate specificity and species differences. *Molecular and Cellular Biochemistry*, **67**, 171–179.

SVARDAL, A. M. and SCHELINE, R. R., 1985c, The aromatization of cyclohexanecarboxyl-CoA to hippuric acid by guinea pig liver mitochondria: submitochondrial localization. *Molecular and Cellular Biochemistry*, **67**, 181–188.

TEMPLE, C. M. and CLIFFORD, M. N., 1997, The stability of theaflavins during HPLC analysis of a decaffeinated aqueous tea extract. *Journal of the Science of Food and Agriculture*, **74**, 536–540.

WAN, X. C., NURSTEN, H. E., CAI, Y., DAVIS, A. L., WILKINS, J. P. G. and DAVIES, A. P., 1997, A new type of tea pigment from the chemical oxidation of epicatechin gallate and isolated from tea. *Journal of the Science of Food and Agriculture*, **74**, 401–408.

WILLSON, K. C. and CLIFFORD, M. N., 1992, *Tea: Cultivation to Consumption* (London: Chapman & Hall).

WINTER, J., MOORE, L. H., DOWELL, V. R. and BOKKENHEUSER, V. D., 1989, C-ring cleavage of flavonoids by human intestinal bacteria. *Applied and Environmental Microbiology*, **55**, 1203–1208.

XENOBIOTICA , 2000, VOL. 30, NO. 4, 327–343

Assessment of specificity of eight chemical inhibitors using cDNA-expressed cytochromes P450

Y. SAI†, R. DAI†, T. J. YANG†, K. W. KRAUSZ†,
F. J. GONZALEZ‡, H. V. GELBOIN† and M. SHOU§*

† Laboratories of Molecular Carcinogenesis and ‡ Metabolism, National Cancer Institute, National Institutes of Health, Bethesda, MD 20892, USA
§ Department of Drug Metabolism, WP75A-203, Merck Research Laboratories, West Point, PA 19486, USA

Received 21 June 1999

1. The selectivity of eight chemical inhibitors has been extensively evaluated with 10 cDNA-expressed human cytochrome P450 isoforms (CYP). The results indicate that sulphaphenazole, quinidine and α-naphthoflavone are selective inhibitors of CYP2C9 (IC_{50} = 0.5–0.7 μM), CYP2D6 (0.3–0.4 μM) and CYP1A (0.05–5 μM) respectively on the basis of the IC_{50}, which are much lower than those of other P450 isoforms (> 10-fold).

2. Ketoconazole exhibited potent inhibition of both CYP3A4-catalysed metabolism of phenanthrene, testosterone, diazepam (IC_{50} = 0.03–0.5 μM) and CYP1A1-catalysed de-ethylation of 7-ethoxycoumarin (0.33 μM). The selectivity of ketoconazole for other P450s was highly related to the concentration used.

3. Diethyldithiocarbamate, orphenadrine and furafylline were shown separately to be less selective inhibitors of CYP2E1, CYP2B6 and CYP1A isoforms by a broad range of IC_{50} that overlap those observed with other P450 isoforms.

4. Furafylline, quinidine and α-naphthoflavone activated CYP3A4-catalysed phenanthrene metabolism by 1.7-, 2- and 15-fold respectively.

5. The selectivity of orphenadrine and ketoconazole was further examined by using inhibitory monoclonal antibodies (MAb). Inhibitory MAb specific for the individual P450 isoforms may be of greater value than chemical inhibitors.

Introduction

The correct assignment of individual cytochrome P450 (P450 or CYP) isoforms to particular metabolic routes is an area of considerable importance, especially for prediction of drug–drug interactions and *in vitro–in vivo* correlation for pharmacokinetics. Many different strategies are currently used for the identification of P450 isoforms responsible for the biotransformation of therapeutic agents. These approaches include the use of specific chemical inhibitors and inhibitory monoclonal antibodies (MAb) to individual P450 isoforms (Gelboin *et al.* 1993, Halpert *et al.* 1994), studies with individual cDNA-expressed P450 enzymes (Gonzalez and Korzekwa 1995), and metabolic correlation of a given candidate with a diagnostic substrate as well as an association between the metabolic rate and quantitative level of specific P450 isoforms (Shimada *et al.* 1994). Owing to the commercial availability and the simplicity in use of chemical inhibitors, characterization of the catalytic specificity of individual P450 isoforms involved in drug metabolism has been facilitated greatly and proven valuable. Several chemical inhibitors have previously been demonstrated selectively to inhibit P450-mediated reactions and, thus, have been used extensively as tools for the identification of individual P450 isoforms (Johnson *et al.* 1979, Tyndale *et al.* 1991, Smith and Jones 1992, Yun *et al.* 1992, Chang *et al.* 1993, 1994, Kharasch and Thummel 1993, Kunze and Trager 1993,

* Author for correspondence; e-mail: magang_shou@merck.com

Xenobiotica ISSN 0049-8254 print/ISSN 1366-5928 online © 2000 Taylor & Francis Ltd
http://www.tandf.co.uk/journals

Hasegawa *et al.* 1994, Baldwin *et al.* 1995, Newton *et al.* 1995, Bonnabry *et al.* 1996, Bourrie *et al.* 1996, Spracklin *et al.* 1996, Lakshmi *et al.* 1997, Lang *et al.* 1997, Sanderink *et al.* 1997, Stevens *et al.* 1997). However, many available chemical inhibitors used to target individual P450 isoforms are poorly or incompletely characterized, or exhibit considerable overlapping inhibition of P450 isoforms.

Hence, the selectivity of chemical inhibitors can be fully characterized using cDNA-expressed individual human P450s. This may lead to a better understanding of how inhibitor probes can be correctly used for predicting individual P450 isoforms that are involved in the metabolism of a particular drug in human tissue. In the present study, the selectivity of eight of the most commonly used chemical inhibitors—troleandomycine (TAO), ketoconazole (KET), diethyldithiocarbamate (DDC), orphenadrine (ORP), furafylline (FUR), α-naphthoflavone (ANF), quinidine (QUI), sulphaphenazole (SUL)—has been examined by determining the IC_{50} for the metabolic reactions of designated substrates that were metabolized by individual cDNA-expressed P450 isoforms.

Materials and methods

Chemicals

Chemicals were from the following commercial sources: ANF from Fluka Chemie AG (Ronkonkoma, NY, USA), TAO, KET and DDC from ICN Biomedicals, Inc. (Aurora, OH, USA); ORP, QUI and 7-ethoxycoumarin from Aldrich Chemical Co. (Milwaukee, WI, USA); DZ, TMZ, NDZ, SUL, IMI, PHE and β-NADPH from Sigma Chemical Co. (St Louis, MO, USA); FUR and BUF from Ultrafine Chemicals (UK); testosterone from ICN Nutritional Biochemicals (Cleveland, OH, USA); benzo(*a*)pyrene-*trans*-9,10-dihydrodiol, benzo(*a*)pyrene-*trans*-4,5-dihydrodiol and phenanthrene-*trans*-9,10-dihydrodiol from the National Cancer Institute Chemical Carcinogen Repository (Kansas, MO, USA); testosterone (TES) and 6β-hydroxytestosterone from Steraloids (Wilton, NH, USA).

Preparation of baculovirus- and vaccinia virus-expressed P450s

cDNAs encoding for individual cytochrome P450 isoforms were constructed into vaccinia (Battula *et al.* 1987, Gonzalez *et al.* 1991a) and baculovirus vectors (Gonzalez *et al.* 1991b). TK^- embryoblasts or Hep G_2 cells infected with recombinant vaccinia viruses were used to express human CYP1A2, CYP2B6, CYP2C8, CYP2C9, CYP2E1 and CYP3A4. Hep G_2 cells were used as hosts for expression since they have ample endoplasmic reticulum, oxidoreductase (OR) and cytochrome b_5 (Gonzalez *et al.* 1995). Owing to the lack of recombinant vaccinia vectors, CYP2A6 and CYP2D6 with OR were expressed separately in Sf9 insect cells infected with respective recombinant baculoviruses. The microsomes from Sf9 cells were prepared as described below. For the metabolism studies, previously harvested frozen Hep G_2 cells were thawed, lysed by sonication and centrifuged at 100000 *g* for 15 min. The resulting pellet was re-suspended in 50 mM potassium phosphate buffer (KPi) by homogenization. P450 content and protein concentration were measured according to reported procedures (Lowry *et al.* 1951, Miller 1959, Omura and Sato 1964). The microsomes containing human baculovirus-expressed CYP1A1, and CYP2C19 were from Gentest Corp. (Woburn, MA, USA).

Microsomal preparation from human livers

Normal liver specimens from six subjects of 20–55 years of age (two female, four male Caucasians) were from the National Cancer Institute Cooperative Human Tissue Network (Philadelphia, PA, USA). Clinical information on the donors was provided and indicated that the causes of death were automobile accidents (three cases), coronary artery disease (one) and respiratory failure (two). Donors were non-smokers and non-alcoholics, and their renal and hepatic function tests were normal. Microsomes were prepared as described by Wang *et al.* (1983) and were reconstituted in a buffer (pH 7.4) containing 0.25 M sucrose, 1 mM EDTA, 0.5 mM DTT, 1.15% KCl and 0.1 M KPi. Six individual human liver microsomal preparations were pooled at an equivalent amount of P450 and stored at -80 °C until used.

Chemical inhibition of P450-catalysed metabolism

A typical 1.0-ml incubation contained 25 pmol expressed P450, 1.0 μmol NADPH, 100 μM of each substrate in the absence and presence of various concentrations of a chemical inhibitor (0.01–500 μM) as needed, 50 mM KPi or Tris buffer (pH 7.4). The mixture was pre-incubated for 5 min at 37 °C in a shaking waterbath and reactions were initiated by the addition of substrate and incubated for 15 min except for TAO, DDC and FUR, which were pre-incubated for 10 min. All incubations were in triplicate

Table 1. Selected substrates and their P450-mediated reactions

Substrates	P450	Reaction
Phenanthrene	1A1, 1A2, 2A6, 2B6, 2C8, 2C9, 2E1, 3A4	hydroxylation
7-Ethoxycoumarin	1A1, 1A2, 2A6, 2B6, 2E1	*O*-deethylation
Diazepam	2B6, 2C8, 2C9, 2C19	*N*-demethylation
	3A4	hydroxylation
Imipramine	1A2, 2C19, 2D6	*N*-demethylation
	2D6, 2C19, 1A2	hydroxylation
Bufuralol	2D6	hydroxylation
Testosterone	3A4	hydroxylation

and were terminated by adding 9 ml dichloromethane. Internal standards added separately to the incubation mixture were benzo(*a*)pyrene-*trans*-9,10-dihydrodiol for phenanthrene (PHE) metabolism, benzo(*a*)pyrene-*trans*-4,5-dihydrodiol for the metabolism of bufuralol, 7-ethoxycoumarin and testosterone, 2-oxo-quazepam for diazepam metabolism, and temazepam for imipramine metabolism. Samples were vortexed for 20 s, centrifuged for 10 min at 3000 rpm (Sorvall RT600 centrifuge, Du Pont) and the organic phases were dried under a stream of nitrogen gas. Finally, the residues were dissolved in 100 μl of 50% methanol in water and analysed by HPLC.

High-performance liquid chromatography

HPLC was performed on a Hewlett-Packard Model HP1050 liquid chromatography equipped with a HP model 1050 autosampler, a ternary solvent delivery system and a multiple-wavelength detector controlled by Hewlett-Packard HPLC^{2D} ChemStation software installed in a Compaq DeskPro 5133 personal computer.

The metabolites of phenanthrene, 7-ethoxycoumarin and diazepam were analysed as described (Shou *et al.* 1994b, Sai *et al.* 1999, Yang *et al.* 1998). The analysis for bufuralol metabolism was performed by reverse-phase HPLC (ODS, 200×4.6 mm, TLC, Springfield, VA, USA) using a 25-min linear gradient elution from 20 to 70% acetonitrile in a phosphate buffer (0.05 M, pH 3.0) containing 0.2% triethylamine at a flow rate of 1 ml/min. The metabolite, 1′-hydroxybufuralol were detected at 245 nm. Testosterone and its metabolite (6β-hydroxytestosterone) were separated on a reverse-phase column as described above, which was eluted with a 20-min linear gradient from the elution of 10:5:85 to 95:5:0 (methanol:THF: H_2O) at a flow rate of 1 ml/min and detection of the metabolite was 242 nm. Imipramine and its N-demethylated metabolite were separated on a Phenomnex C8 luna column (250×4.6 mm, 5 μm) eluted with a 25-min linear gradient from elution of 30:10:70 to 50:10:40 (acetonitrile:methanol: 0.05 M phosphate buffer, pH 6.0) containing 0.05% triethylamine. The flow rate was 1 ml/min and UV detection was 250 nm. Quantitation of the metabolite was achieved by comparison between the chromatographic peaks under the areas of metabolite formed and internal standard.

Data analysis

The values of all kinetic parameters, e.g. s and IC_{50}, were adjusted with an iteration that best fits the data by using a program of the nonlinear least squares algorithm. Plots of equations were prepared and fits of kinetic parameter statistics were determined by a regression analysis using Grafit version 3.09 (Data analysis and Graphics Program, Erithancus Software Ltd, Staines, UK). The inhibitory constant (IC_{50}) was calculated from the equation as follows:

$$v = \frac{V_o}{1 + \left(\frac{I}{IC_{50}}\right)^S}$$

where V_o is the uninhibited velocity, v is the observed velocity, s is the slope factor and I is the inhibitor concentration. Alternatively, the inhibition of enzyme activities was expressed as % control activities. Inhibition results were expressed as the mean$\pm$ SD, where SD was obtained by seven measurements.

Results

Selectivity of chemical inhibitors for 10 individual cDNA-expressed P450 isoforms

To determine IC_{50} for the eight chemical inhibitors for individual P450 isoforms, six substrates were selected for metabolism, four of which were shown to be metabolized by multiple P450 isoforms, e.g. phenanthrene, 7-ethoxycoumarin,

Table 2. Inhibitory effects of eight chemical inhibitors on P450-mediated metabolism *in vitro*.

CYP450	Substrate	IC_{50} (μM)*							
		TAO (3A4)	KET (3A4)	DDC (2E1)	ORP (2B6)	FUR (1A2)	ANF (1A1/2)	SUL (2C9)	QUI (2D6)
1A1	phenanthrene	N	7.4± 0.5	N	N	404.7± 207.1	5.3± 3.7	N	N
	7-ethoxycoumarin	517.6± 55.2	0.33± 0.03	54.9± 6.5	N	153.5± 12.0	0.6± 0.1	N	36.2± 2.8
1A2	phenanthrene	N	N	N	N	361.6± 43.1	3.8± 0.6	N	N
	7-ethoxycoumarin	N	432.9± 174.4	432.9± 82.0	N	208.3± 36.0	0.4± 0.2	N	240.2± 48.6
	imipramine	N	509.5± 36.9	N	263.9± 10.9	20.0± 1.4	0.05± 0.01	N	395.0± 95.7
2A6	phenanthrene	N	50.4± 5.4	93.5± 12.5	N	N	467.9± 53.1	N	158.9± 29.8
	7-ethoxycoumarin	N	47.5± 9.4	45.6± 7.9	N	N	N	N	476.3± 111.3
2B6	phenanthrene	N	80.6± 41.8	268.3± 34.5	275.0± 11.9	867.1± 39.5	N	N	770.1± 54.5
	diazepam	N	35.5± 13.4	600.2± 60.8	234.4± 23.6	N	N	443.2± 139.5	236.8± 22.3
	7-ethoxycoumarin	N	8.8± 1.3	144.8± 37.0	227.6± 64.7	519± 69.7	N	144.6± 28.7	191.7± 35.6
2C8	phenanthrene	953.0± 128.7	8.9± 4.2	464.1± 49.2	249.1± 10.6	N	A	N	135.4± 16.8
	diazepam	N	4.0± 0.3	129.5± 8.9	278.8± 23.9	N	A	172.0± 17.7	98.5± 18.3
2C9	phenanthrene	N	28.2± 6.5	539.2± 201.7	600.3± 86.6	N	468.1± 187.1	0.7± 0.1	597.3± 52.3
	diazepam	N	10.7± 1.9	75.0± 17.5	620.4± 172.3	N	353.1± 87.4	0.5± 0.1	234.5± 33.7
2C19	diazepam	N	4.2± 0.4	20.8± 1.8	277.8± 66.2	261.9± 27.3	57.2± 49.5	378.8± 32.9	321.2± 36.1
	imipramine	N	21.9± 1.8	193.4± 21.0	N	983.4± 274.9	494.0± 33.6	N	449.1± 45.9
2D6	bufuralol	N	N	673.9± 85.7	54.0± 5.9	N	N	N	0.4± 0.1
	imipramine	N	70.7± 14.4	N	455.5± 136.6	N	N	N	0.3± 0.1
2E1	phenanthrene	N	720.3± 94.0	46.0± 13.0	996.8± 86.1	N	N	N	N
	7-ethoxycoumarin	N	171.0± 67.0	40.1± 7.0	N	N	N	398.5± 45.4	N
3A4	phenanthrene	324.1± 22.4	0.03± 0.01	N	312.1± 37.3	A	A	N	A
	testosterone	152.3± 10.7	0.04± 0.01	806.4± 116.1	273.8± 17.3	137.6± 39.4	N	N	161.7± 5.3
	diazepam	135.5± 22.6	0.49± 0.03	521.7± 74.4	520.9± 77.4	N	N	213.3± 24.3	89.6± 25.9

*Calculation by Grafit Version 3.09, Data Analysis and Graphics Program.

N, negligible inhibition ($IC_{50} > 1000$ μM, inhibition $< 30\%$ in 500 μM of inhibitor concentration); A, no inhibition, but activation.

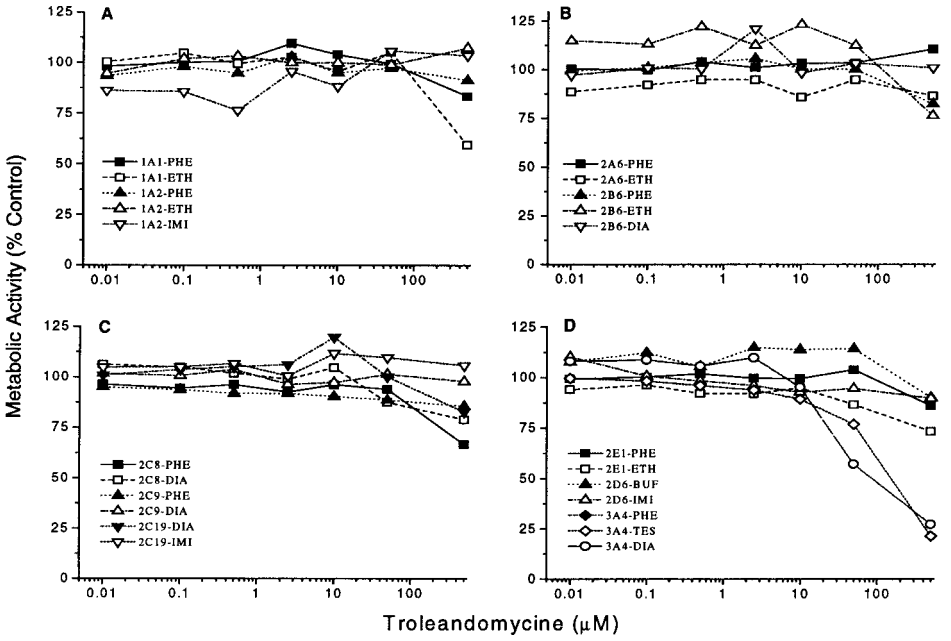


Figure 1. Inhibitory effects of troleandomycine (TAO) on (**A**) cDNA-expressed CYP1A1 and CYP1A2 activity; (**B**) CYP2A6 and CYP2B6 activity; (**C**) CYP2C8/9/19 activity; and (**D**) CYP2E1, CYP2D6 and CYP3A4 activity. Substrates used are phenanthrene (PHE), 7-ethoxycoumarin (ETH), imipramine (IMI), diazepam (DIA), bufuralol (BUF) and testosterone (TES). Data are the average in triplicate.

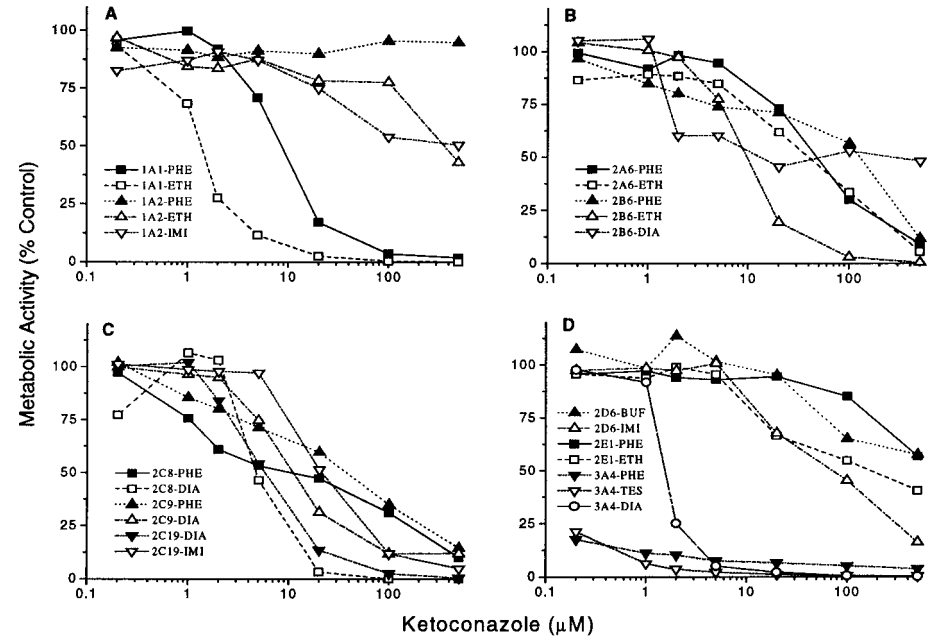


Figure 2. Inhibitory effects of ketoconazole (KET) on (**A**) CYP1A1 and CYP1A2 activity; (**B**) CYP2A6 and CYP2B6 activity; (**C**) CYP2C8/9/19 activity; and (**D**) CYP2E1, CYP2D6 and CYP3A4 activity. Substrates used are PHE, ETH, IMI, DIA, BUF and TES.

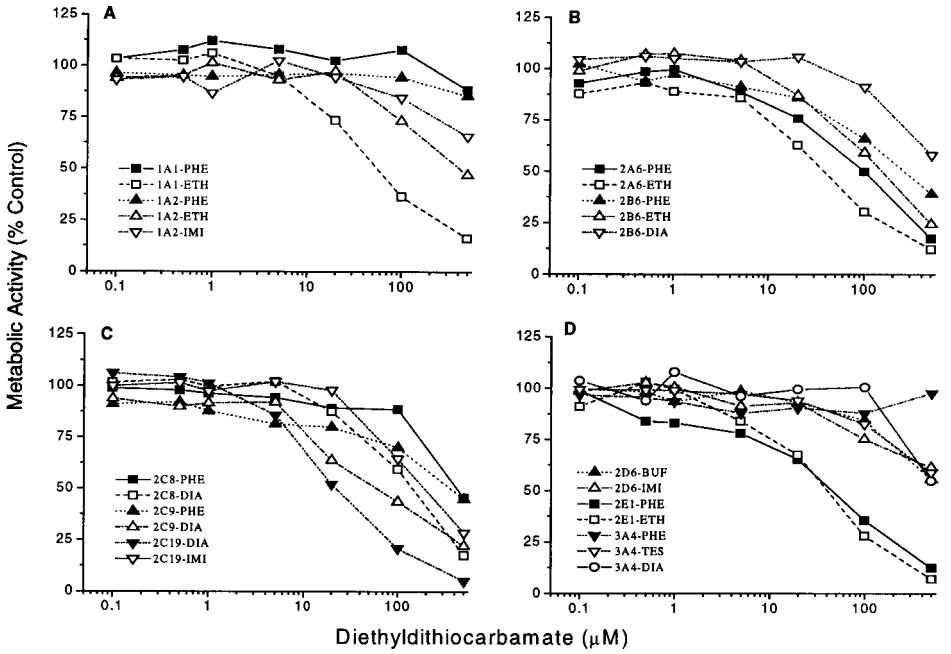


Figure 3. Inhibitory effects of diethyldithiocarbamate (DDC) on (**A**) CYP1A1 and CYP1A2 activity; (**B**) CYP2A6 and CYP2B6 activity; (**C**) CYP2C8/9/19 activity; and (**D**) CYP2E1, CYP2D6 and CYP3A4 activity. Substrates used are PHE, ETH, IMI, DIA, BUF and TES.

diazepam and impramine (table 1). The selectivity and potency of the inhibitors for individual cDNA-expressed P450-mediated reactions of the respective substrates were evaluated by their IC_{50} (table 2).

TAO, a selective inhibitor for CYP3A4, inhibited $>70\%$ of the oxidation of testosterone and diazepam catalysed by CYP3A4, and slightly inhibited the CYP3A4-catalysed hydroxylation of phenanthrene when used at 500 μM (figure 1). The IC_{50} of TAO was determined as 152, 135 and 324 μM for the metabolism of testosterone, diazepam and phenanthrene respectively. TAO had no significant effect on the activities of other P450 isoforms at the inhibitor concentration used ($< 50\%$ inhibition).

KET, the most commonly used inhibitor of CYP3A4, exhibited the most potent inhibition of CYP3A4-catalysed metabolism of phenanthrene ($IC_{50} = 0.03$ μM), and testosterone (0.04 μM) by $\sim 80\%$ at 0.2 μM respectively (figure 2A). However, KET also inhibited metabolism of other P450 isoforms when the concentration used was slightly increased (figure 2 and table 2). More than 90% of the inhibition of CYP3A4-catalysed diazepam oxidation and CYP1A1-catalysed *O*-deethylation of 7-ethoxycoumarin at 5 μM KET was observed with $IC_{50} = 0.49$ and 0.33 μM respectively (figure 2A and D). KET at 500 μM inhibited the activities of CYP2B6, CYP2C8, CYP2C9, CYP2C19, CYP2A6 and CYP2D6 by $>90\%$ (IC_{50} range = 4.0–80.6 μM; figure 2B and C). KET was less inhibitory to CYP2E1- and CYP1A2-catalysed reactions ($IC_{50} = 171$–510 μM), and inhibited CYP2D6-catalysed bufuralol metabolism by $< 50\%$ when used at 500 μM (Figure 2D).

DDC is widely used as an inhibitor to probe CYP2E1 activity in tissue preparations. The inhibition potency of DDC for 10 individual cDNA-expressed human P450 isoforms was determined. Results showed that DDC extensively

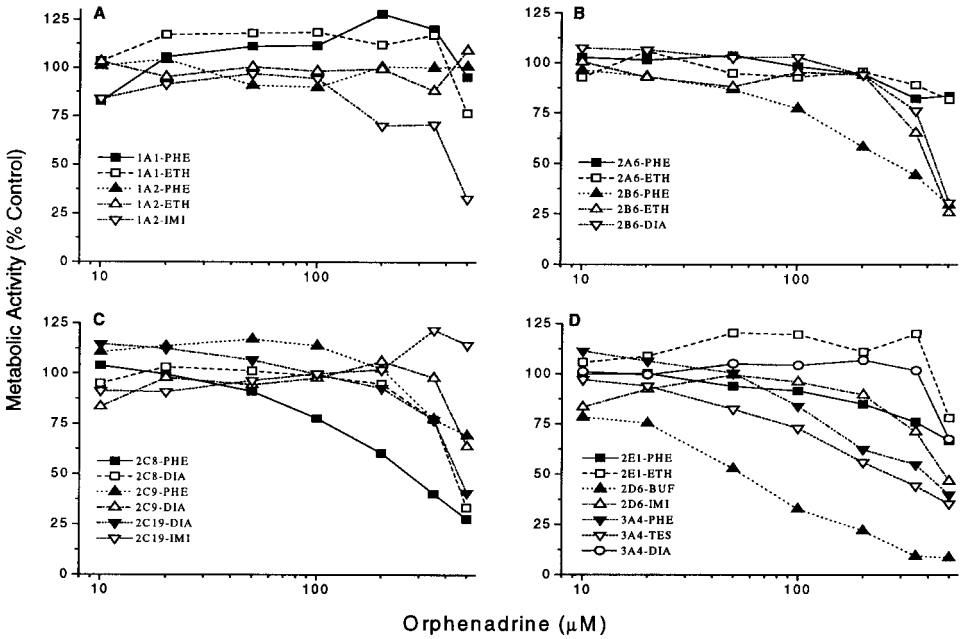


Figure 4. Inhibitory effects of orphenadrine (ORP) on (**A**) CYP1A1 and CYP1A2 activity; (**B**) CYP2A6 and CYP2B6 activity; (**C**) CYP2C8/9/19 activity; and (**D**) CYP2E1, CYP2D6 and CYP3A4 activity. Substrates used are PHE, ETH, IMI, DIA, BUF and TES.

inhibited CYP2E1, CYP1A1 and CYP2A6 activities towards 7-ethoxycoumarin *O*-deethylation with $IC_{50} = 40.1$, 54.9 and 45.6 μM respectively. DDC only slightly inhibited CYP1A2 and CYP2B6 activities in the same reaction (table 2 and figure 3). For the metabolism of phenanthrene, DDC inhibited CYP2A6 and CYP2E1 activities with $IC_{50} = 93.5$ and 46.0 μM, and had little effect on the activities of CYP2B6, CYP2C8 and CYP2C9. When diazepam was used as a substrate, DDC exhibited extensive inhibition of CYP2C9- and CYP2C19-catalysed *N*-demethylation, resulting in $IC_{50} = 75.0$ and 20.8 μM respectively, but exhibited no specific inhibition of CYP2C8, CYP1A1, CYP1A2 or CYP3A4.

ORP has been reported as a selective inhibitor for CYP2B6 (Chang *et al.* 1993, Heyn *et al.* 1996). However, when comparing the IC_{50} for different isozyme-specific reactions, ORP (300 μM) extensively inhibited CYP2D6-catalysed bufuralol metabolism ($IC_{50} = 54$ μM) by $> 90\%$. The IC_{50} for CYP2B6-catalysed reactions of phenanthrene, diazepam and 7-ethoxycoumarin were $\sim$ 200–300 μM (table 2 and figure 4D), in which only $< 85\%$ inhibition was observed with 500 μM of ORP (figure 4B). In addition, the IC_{50} of ORP for CYP1A2-, CYP2C8-, CYP2C19- and CYP3A4-catalysed reactions were similar to that of CYP2B6 (table 2 and figure 4). ORP inhibition of the metabolism of other substrates that were catalysed by specific P450 isoforms did not appear to be significant ($IC_{50} = 300$–1000 μM) (table 2).

FUR has been widely used as a probe to determine the role of CYP1A2 in liver microsomal metabolism of drugs. The data in figure 5 and table 2 have shown that FUR selectively inhibited CYP1A2-catalysed imipramine hydroxylation ($IC_{50} =$ 20 μM) and yielded $> 90\%$ inhibition at a concentration of 200 μM. The IC_{50} of FUR for CYP1A1- and CYP1A2-catalysed metabolism of phenanthrene and 7-ethoxycoumarin, and CYP3A4-catalysed testosterone 6β-hydroxylation ranged

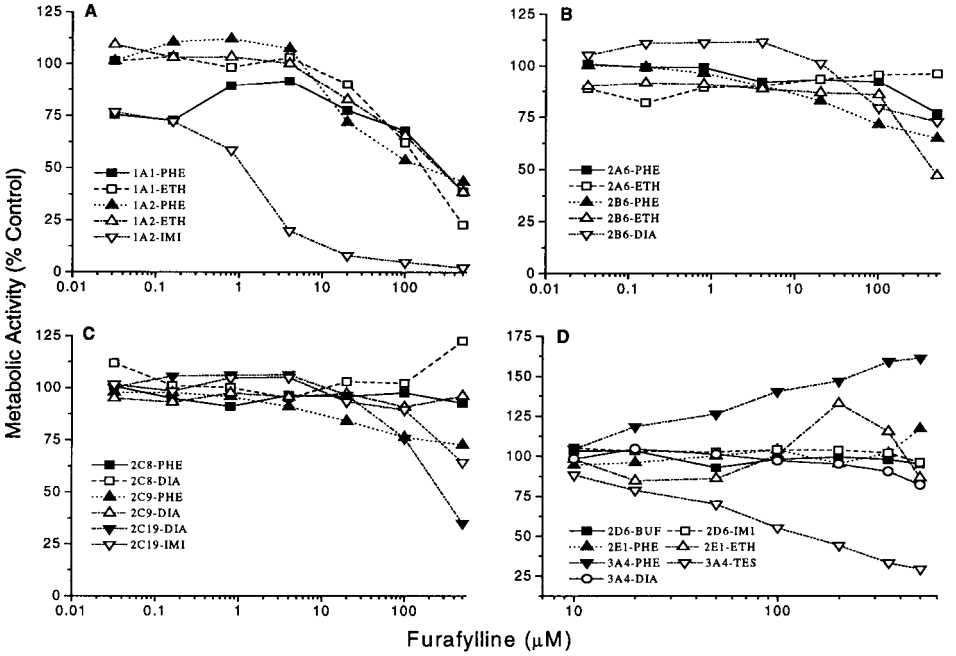


Figure 5. Inhibitory effects of furafylline (FUR) on (**A**) CYP1A1 and CYP1A2 activity; (**B**) CYP2A6 and CYP2B6 activity; (**C**) CYP2C8/9/19 activity; and (**D**) CYP2E1, CYP2D6 and CYP3A4 activity. Substrates used are PHE, ETH, IMI, DIA, BUF and TES.

from 100 to 405 μM (table 2 and figure 5). Interestingly, FUR increased CYP3A4 activity in the hydroxylation of phenanthrene up to 1.7-fold in the concentrations between 50 and 500 μM (figure 5D).

ANF is a complicated modulator of P450 isoforms, as it can act as an activator, inducer or inhibitor for different P450 isoforms (Middleton and Kandaswanmi 1993). ANF extensively inhibited both CYP1A1- and CYP1A2-catalysed reactions with IC_{50} ranging from 0.4 to 5.3 μM (table 2 and figure 6A) except for imipramine metabolism in which a very low IC_{50} (0.05 μM) was found. ANF had no influence on the reactions that were catalysed by P450 isoforms other than CYP1A. However, ANF extensively stimulated CYP2C8 and CYP3A4 activities towards the metabolism of phenanthrene and diazepam by 3- and 15-fold respectively (figure 6C and D).

SUL is a probe for CYP2C9 (Baldwin *et al.* 1995) and was very sensitive towards the metabolism of phenanthrene and diazepam by CYP2C9 (IC_{50} = 0.7 and 0.5 μM respectively) and 100 μM resulted in metabolism inhibition by > 90% (table 2 and figure 7C). Relative to CYP2C9, SUL was less selective towards CYP2C8 (IC_{50} = 172 μM) and CYP2C19 (IC_{50} = 379 μM) for the metabolism of diazepam. SUL also slightly inhibited CYP2B6 and CYP2E1 activities (7-ethoxycoumarin *O*-deethylation). The IC_{50} for CYP2B6, CYP2C19 and CYP3A4 in diazepam metabolism ranged from 100 to 450 μM.

QUI, an inhibitor of CYP2D6, displayed an extensive inhibition of the CYP2D6-catalysed metabolism of bufuralol and imipramine (figure 8 and table 2), with IC_{50} = 0.4 and 0.3 μM respectively. When 5 μM QUI was used in the metabolism of the two individual substrates, CYP2D6 activity was inhibited by > 90% (figure 8D). QUI also suppressed CYP1A1 activity towards 7-ethoxycoumarin *O*-deethylation

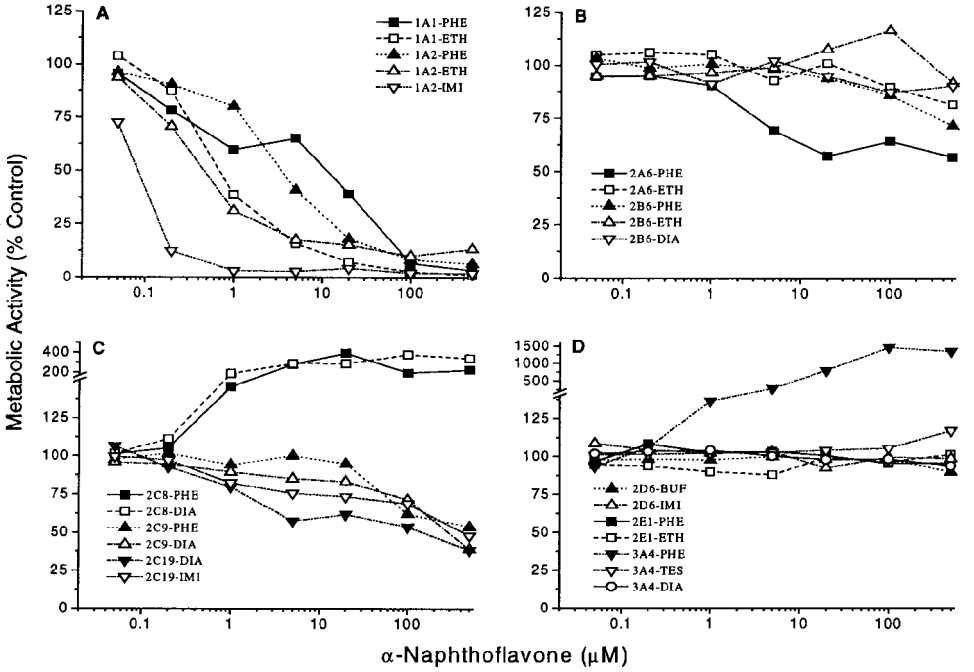


Figure 6. Inhibitory effects of α-naphthoflavone (ANF) on (**A**) CYP1A1 and CYP1A2 activity; (**B**) CYP2A6 and CYP2B6 activity; (**C**) CYP2C8/9/19 activity; and (**D**) CYP2E1, CYP2D6 and CYP3A4 activity. Substrates used are PHE, ETH, IMI, DIA, BUF and TES.

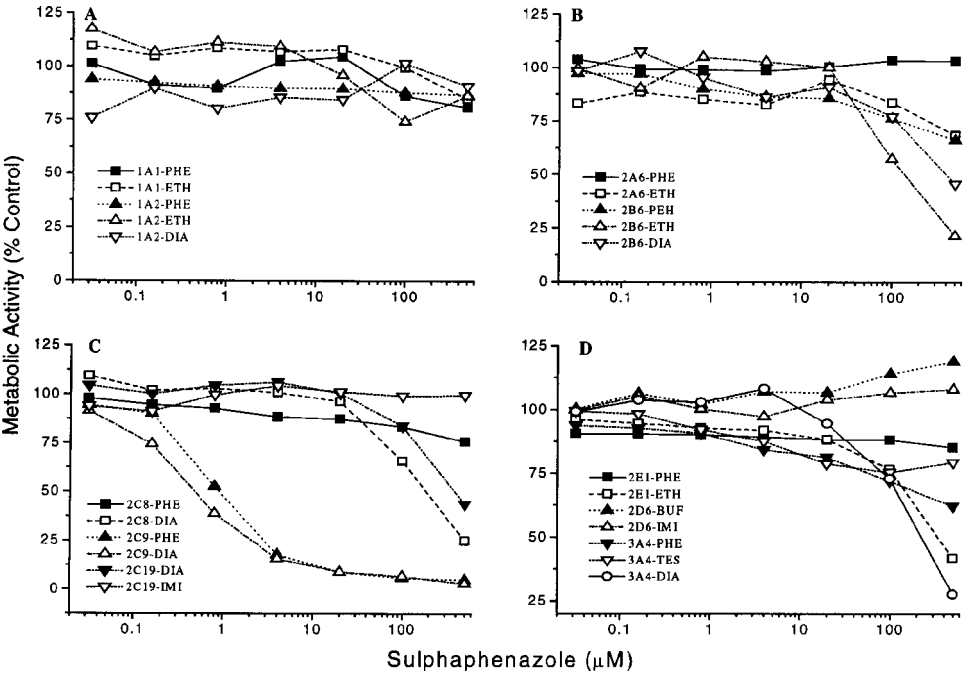


Figure 7. Inhibitory effects of sulphaphenazole (SUL) on (**A**) CYP1A1 and CYP1A2 activity; (**B**) CYP2A6 and CYP2B6 activity; (**C**) CYP2C8/9/19 activity; and (**D**) CYP2E1, CYP2D6 and CYP3A4 activity. Substrates used are PHE, ETH, IMI, DIA, BUF and TES.

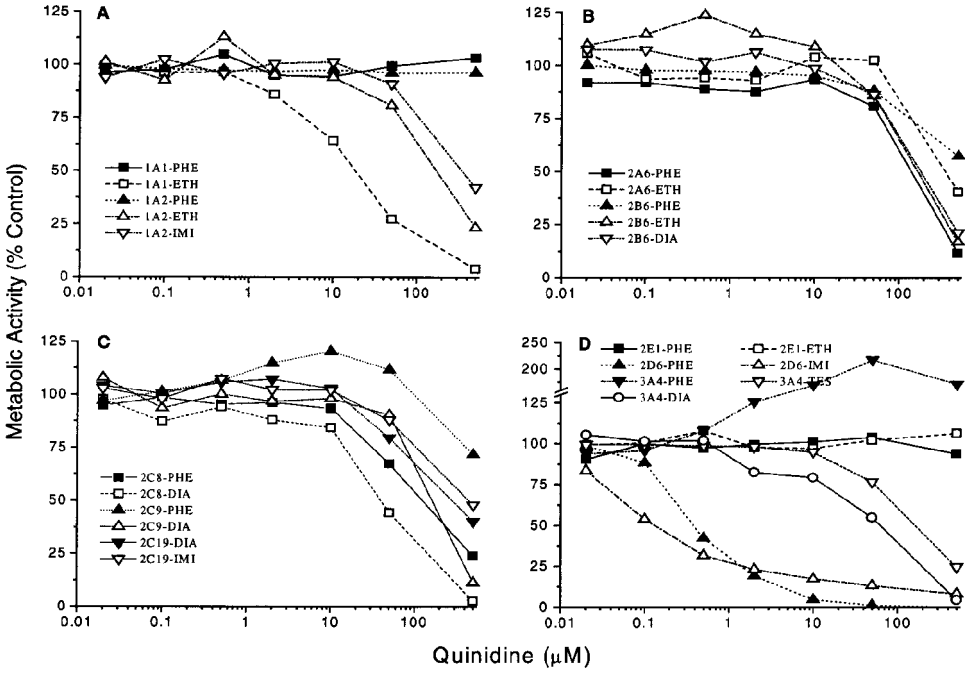


Figure 8. Inhibitory effects of quinidine (QUI) on (**A**) CYP1A1 and CYP1A2 activity; (**B**) CYP2A6 and CYP2B6 activity; (**C**) CYP2C8/9/19 activity; and (**D**) CYP2E1, CYP2D6 and CYP3A4 activity. Substrates used are PHE, ETH, IMI, DIA, BUF and TES.

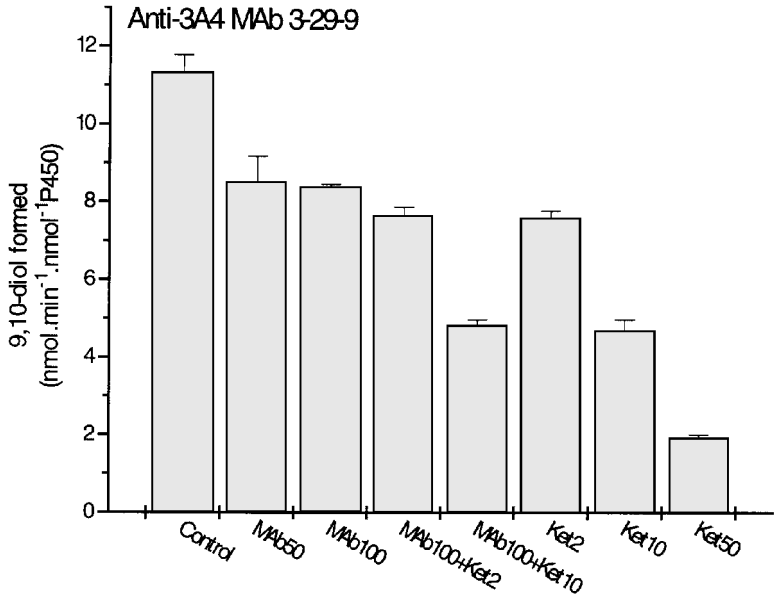


Figure 9. Inhibitory effects of MAb 3-29-9 and ketoconazole (KET) on phenanthrene hydroxylation in human liver microsomes. MAb50 (50 nM MAb 3-29-9); MAb100 (100 nM MAb 3-29-9); MAb100 + KET2 (100 nM MAb 3-29-9 and 2 μM KET); MAb100 + KET10 (100 nM MAb 3-29-9 and 10 μM KET); KET2 (2 μM KET); KET10 (10 μM KET), KET50 (50 μM KET) and control (IgG against hen egg white lysozyme).

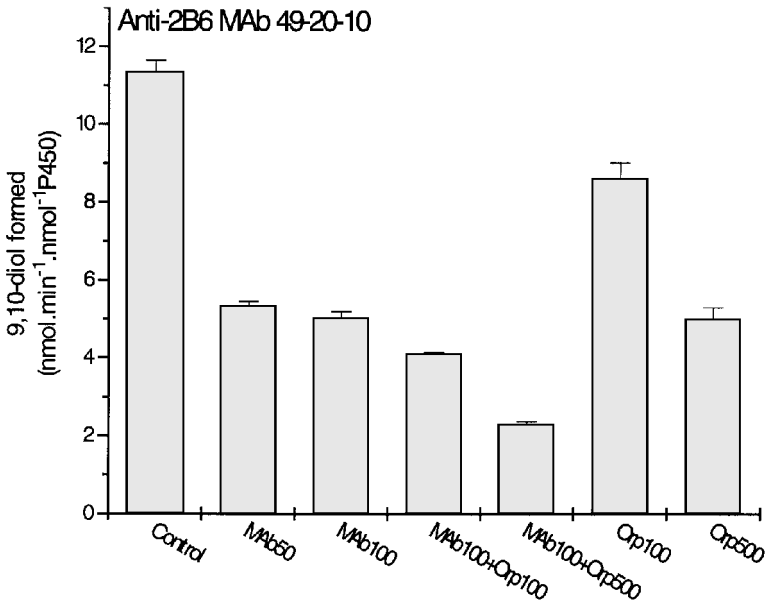


Figure 10. Inhibitory effects of MAb 49-10-20 (anti-CYP3A4) and orphenadrine (ORP) on the phenanthrene hydroxylation by human liver microsomes. MAb50 (50 nM MAb 49-10-20); MAb100 (100 nM MAb 49-10-20); MAb100 + Orp100 (100 nM MAb 49-10-20 and 100 μM ORP); MAb100 + Orp500 (100 nM MAb 49-10-20 and 500 μM ORP); Orp100 (100 μM ORP); Orp500 (500 μM ORP), control (IgG against hen egg white lysozyme).

(IC_{50} = 36.2 μM), and inhibited the metabolism of diazepam by CYP2C8 and CYP3A4 (IC_{50} = 90–100 μM).

Use of inhibitory MAbs to determine the selectivity of chemical inhibitors

To determine the contribution of a specific P450 to the metabolism of a given drug in human liver microsomes containing multiple P450 isoforms, both immuno-inhibition and chemical inhibition have been commonly employed. MAb 3-29-9 (anti-CYP3A4) and 49-10-20 (anti-CYP2B6) have been characterized to be highly specific (Gelboin *et al.* 1995, Yang *et al.* 1998), and they inhibit CYP3A4 and CYP2B6 activity by >90% using phenanthrene, a substrate metabolized by multiple P450 isoforms, as a probe (Shou *et al.* 1994b, Gelboin *et al.* 1995, Yang *et al.* 1998). Thus, two MAbs, which assess the contribution of CYP3A4 and CYP2B6 isoforms in human liver microsomes, were combined separately with KET and ORP to determine the selectivity of the inhibitors in the phenanthrene metabolism. Thus, the question regarding the accuracy and selectivity of the chemical inhibitors can be addressed.

As shown in figure 9, when MAb 3-29-9 determined the contribution of CYP3A4 to phenanthrene metabolism in human liver microsomes, the maximum inhibition (25%) was achieved at an optimal MAb concentration (usually >50 nM), suggesting that the MAb bound to the CYP3A4 and completely blocked the CYP3A4-catalysed reaction. However, whenever the MAb 3-29-9 at the optimal concentration was absent or present, KET (2 μM) inhibited the phenanthrene metabolism in liver microsomes by ~ 33%, which is greater than that observed by

MAb 3-29-9 (25%). When the KET concentration was increased to 10 and 50 μM, the inhibition achieved was 59 and 88% respectively. These results suggest that 25% immuno-inhibition is due to the sole inhibition of CYP3A4 and the additional inhibition caused by KET is due to other P450(s) for phenanthrene metabolism, e.g. CYP2A6, CYP2C9 and CYP2B6 according to their relatively low IC_{50} in table 2.

Similarly, MAb 49–10–20, an inhibitory MAb for CYP2B6, inhibited human liver microsomal metabolism of phenanthrene by 50% at a concentration of 100 nM and no further significant inhibition was observed by up to 500 nM, indicating that CYP2B6 contained in liver microsomes contributes ~ 50% to the phenanthrene hydroxylation (figure 10). When ORP at 100 and 500 μM was used alone, the phenanthrene metabolism in human liver microsomes was inhibited to 23 and 55% of the control value respectively. Furthermore, addition of MAb 49-20-10 enhanced the inhibition caused by ORP at 100 and 500μM by 63 and 79% respectively (figure 10). Since the IC_{50} of ORP (275 μM) for CYP2B6 is comparable with those for CYP2C8 (249 μM) and CYP3A4 (312 μM), the inhibition percentage by ORP may be attributed to the combined inhibition of CYP2B6, CYP2C8 and CYP3A4. The inhibition of phenanthrene metabolism (63 and 78%) by combining MAb 49-20-10 (100 nM) with ORP (100 and 500 μM) is clearly due to the contribution of CYP2B6 (50%) and other P450 isoforms (13 and 29%).

Discussion

Two approaches frequently used for identification of specific P450 isoforms in a crude tissue preparation containing multiple P450 isoforms responsible for the metabolism of a drug include selective chemical inhibition and immuno-inhibition. Chemical inhibitors have proven to be extremely valuable and in some cases are used specifically for individual P450 isoforms. These compounds have inherent advantages in that they are readily available either from chemical synthesis or from chemical or pharmaceutical companies. In addition, chemical inhibitors can be used with intact cells and *in vivo*, even with human subjects, thus making it possible to link a particular P450 with a specific toxicological or pharmacological response. The fractional inhibition of a reaction in microsomes reflects the extent to which a particular P450 (or class of P450 isoforms) is responsible for a reaction. Although chemical inhibitors can be very useful in the elucidation of catalytic specificity of human P450 isoforms, full information regarding selectivity of many previously used inhibitors is less clear. For instance, DDC was initially described as a selective inhibitor of CYP2E1 (Guengerich *et al.* 1991), but was later found to inhibit CYP2A6, CYP2C8, CYP2B6 and CYP3A4 (Yamazaki *et al.* 1992, Chang *et al.* 1994). Thus, the specificity of an inhibitor should be characterized by kinetic parameters (IC_{50} or K_i) with diagnostic substrates for as many P450 isoforms as possible.

The inhibition potency of chemical inhibitor can be influenced by the kinetic natures of inhibitor, enzyme and substrate. A competitive inhibitor can act only to increase the apparent K_m for the substrate but has no effect on V_{max}. The degree of inhibition exhibited by a competitive inhibitor depends on [*S*], [*I*], K_m, and K_i:

$$\left\{ \% \text{ inhibition} = \frac{[I]}{[I] + K_i\left(1 + \frac{[S]}{K_m}\right)} \right\}.100$$

When [*S*] is comparable with K_m, inhibition can be treated as a non-competitive inhibition, which is only related to [*I*] and K_i:

$$\left(\% \text{ inhibition} = \frac{[I]}{K_i + [I]}\right).100$$

The inhibition by an inhibitor is always a constant fraction, regardless of the substrate concentration or K_m, as long as the enzyme is saturated by [*I*] (Rodrigues 1999).

In the present study, the selectivity of eight chemical inhibitors for 10 individual cDNA-expressed P450 isoforms has been evaluated by their IC_{50}. The results indicate that SUL and QUI are relatively selective for CYP2C9- and CYP2D6-catalysed oxidations respectively. Differences in the IC_{50} of these inhibitors for their specific P450 isoforms as compared with other P450 isoforms varied markedly by >150-fold (table 2). ANF is a relatively selective inhibitor for CYP1A subfamily and its IC_{50} differed by >10-fold from that observed for other P450 isoforms.

KET has been widely used as a specific inhibitor for CYP3A4 (Baldwin *et al.* 1995). Similarly, the present study has confirmed that KET exhibits very low IC_{50} for inhibition of the metabolism of phenanthrene, testosterone and diazepam respectively (0.03, 0.04 and 0.49 μM). However, KET also inhibited CYP1A1-catalysed deethylation of 7-ethoxycoumarin ($IC_{50} = 0.33$ μM; table 2) at a potency equivalent to CYP3A4. A lower concentration of KET (0.2 μM) inhibited the CYP3A4-catalysed metabolism of testosterone and phenanthrene by $\sim 80\%$, but had no effect on diazepam metabolism. Other P450 reactions, e.g. CYP1A1 and CYP2C8/9/19, were also inhibited when the KET concentration was increased (figure 2), results which are consistent with previous reports (Otton *et al.* 1984, Back *et al.* 1988, Ward and Back 1993). Therefore, KET is implicated in the inhibition of the CYP2C-mediated reaction and is thought to be a good inhibitor of a broad spectrum of P450 isoforms depending on the concentration used. Thus, when KET is used to define a role of CYP3A4 in the metabolism of a given drug, it must be used carefully and other approaches may be helpful to support the conclusion made when using KET.

The IC_{50} of DDC for CYP2E1, CYP2C9, CYP2C19 and CYP2A6 were determined and exhibited almost equivalent values (table 2). Activities of CYP2C8 and CYP2B6 were also moderately decreased when the DDC concentration was increased. As compared with Chang's report, DDC at 125 μM ($IC_{50} = 125$ μM) inhibits not only CYP2E1-mediated *N*-nitrosodimethylamine *N*-demethylation and chlorzoxazone 6-hydroxylation, but also it substantially reduced CYP2A6, CYP2B6 and CYP2C8 activities ($>75\%$ inhibition) among which the CYP2A6 activity is almost completely blocked (Yamazaki *et al.* 1992, Chang *et al.* 1994). Thus, DDC must be used with caution in light of these observations for probing P450 isoforms responsible for a metabolic reaction. The IC_{50} of ORP for CYP2B6 (227–275 μM) overlapped with those for CYP2D6, CYP2C8, CYP2C19 and CYP3A4. FUR, used as a mechanism-based inhibitor for CYP1A2, displays variable IC_{50} for CYP1A2-catalysed reactions of phenanthrene, 7-ethoxycoumarin and impramine (361, 208 and 20 μM) respectively, and also exhibited overlapping inhibition of CYP1A1-, CYP2C19- and CYP3A4-mediated metabolism. Hence, IC_{50} assessment of an inhibitor on the same or the different P450 isoforms responsible for the metabolism of substrate molecules could largely differ depending

on the enzyme and the substrate of test, i.e. kinetic characteristics (K_m and V_{max}) and physicochemical properties (hydrophobic, steric, electronic). These suggest that the IC_{50} of the inhibitor for a known substrate may not be confidently used for other uncharacterized substrates for the identification of P450 isoforms.

If a drug is metabolized by multiple P450 isoforms, the specificity and concentration of an inhibitor are important for defining a role for an individual P450 in the metabolism of a drug. With rapid development of inhibitory MAbs that specifically target a single or subfamily of P450, MAbs can support the identification of the P450 isoforms with chemical inhibitors or can be a replacement of chemical inhibitor that is poor in P450 selectivity. MAb 3-29-9 specific for CYP3A and 49-20-10 specific for CYP2B6 do not cross-react with other human P450 isoforms and are known to inhibit $>90\%$ of the metabolism of phenanthrene and other substrates by cDNA-expressed CYP3A4 and CYP2B6 (Gelboin *et al.* 1995, Yang *et al.* 1998). The present authors used the MAb to aid in the evaluation of the selectivity of chemical inhibitors. Phenanthrene is a common substrate metabolized by most P450 isoforms in families 1–3 (Shou *et al.* 1994b). Activities of cDNA-expressed P450 isoforms for phenanthrene metabolism are ranked in the order of CYP2B6 > CYP1A > CYP2C > CYP3A. Two selective chemical inhibitors, KET for CYP3A4 and ORP for CYP2B6, defined the quantitative role of CYP3A4 and CYP2B6 in the metabolism of phenanthrene in human liver microsomes. When KET was added to human liver microsomes, 2, 10 and 50 μM KET ($IC_{50} = 0.03$ μM for CYP3A4) inhibited phenanthrene metabolism by 33, 59 and 88% respectively, which exhibited greater inhibitions than that observed with MAb 3-29-9 alone (25%). When the MAb (100 nM) and KET (2 or 10 μM) were combined together, no additional inhibition obtained (figure 9) as compared with KET alone, suggesting that $\sim 25\%$ of the metabolism in human liver is due to CYP3A4, whereas metabolism (8 or 34%) can be attributed to other P450 isoforms, e.g. CYP2C8/9/19, CYP2B6 and CYP2A6 according to the IC_{50} reported in this study ($IC_{50} =$ 8.9–80.6 μM).

ORP was not shown to be selective in this study, which was confirmed by the immuno-inhibition data. MAb 49–10–20, at an optimal concentration, caused 50% inhibition of phenanthrene metabolism, suggesting that CYP2B6 plays a role. When ORP at concentrations of 100 and 500 μM was used to assess CYP2B6 involvement, phenanthrene metabolism was inhibited by 23 and 55% respectively. Since the IC_{50} of ORP (275 μM) for CYP2B6 is comparable with those for CYP2C8 (249 μM) and CYP3A4 (312 μM), the inhibition percentage from ORP in human liver may not accurately represent the contribution of CYP2B6. When the MAb was added together with ORP (100 and 500 μM), the inhibition by ORP was increased to 63 and 79% respectively relative to that obtained with ORP only (figure 10). Thus, the 63 or 79% contribution to phenanthrene metabolism can be attributed to a combination of 50% of CYP2B6 and 13 or 29% of other P450 isoforms. These studies suggest that assessing the quantitative roles for individual P450 isoforms in the metabolism of a substrate catalysed by multiple P450 isoforms can be misleading when using poorly defined and non-selective inhibitors or inappropriate concentrations.

If an inhibitor is a modulator, inhibiting one P450 and activating other P450(s), P450 assessment can be complicated by a given compound that is a substrate for both P450 isoforms. FUR and ANF, inhibitors of CYP1A, activated CYP3A4-mediated phenanthrene hydroxylation by ~ 1.7- and 15-fold respectively (figures 5 and 6), the latter of which is consistent with previous report (Shou *et al.* 1994a). QUI

and ANF were also capable of increasing CYP3A4-catalysed metabolism of phenanthrene by 2-fold and enhanced CYP2C8 activities for phenanthrene hydroxylation and diazepam *N*-demethylation by >3-fold (figures 6 and 8). Thus, care should be exerted when FUR, ANF and QUI are considered as diagnostic probes for such substrates. Hence, it is necessary that the inhibitors should be tested with a panel of individual cDNA-expressed P450 isoforms for an untested substrate unless full information of the inhibitor in P450 modulation is obtained.

In summary, the selectivity of eight chemical inhibitors has been extensively evaluated with 10 cDNA-expressed P450 isoforms by using six substrates. SUL and QUI are highly selective inhibitors of CYP2C9 and CYP2D6 for the substrates tested. ANF is selective for CYP1A1 and CYP1A2 although it may regulate the activity of some other P450 isoforms for a specific substrate. KET is selective but its selectivity is concentration-dependent and may interact a variety of P450 isoforms. DDC, ORP and FUR are less selective when they are used to probe CYP2E1, CYP2A6 and CYP1A respectively. Thus, the present study provides valuable information that leads to an understanding of P450 identification in *in vitro* drug metabolism by using selective chemical inhibitors.

References

Back, D. J., Tjia, J. F., Karbwang, J. and Colbert, J., 1988, *In vitro* inhibition studies of tolbutamide hydroxylase activity of human liver microsomes by azoles, sulphonamides and quinolines. *British Journal Clinical Pharmacology*, **26**, 23–29.

Baldwin, S. J., Bloomer, J. C., Smith, G. J., Ayrton, A. D., Clarke, S. E., Chener, Y. and Henery, R. J., 1995, Ketoconazole and sulphaphenazole as the respective selective inhibitors of P4503A and 2C9. *Xenobiotica*, **25**, 261–270.

Battula, N., Sagara, J. and Gelboin, H. V., 1987, Expression of P1-450 and P3-450 DNA coding sequences as enzymatically active cytochromes P-450 in mammalian cells. *Proceedings of the National Academy of Sciences, USA*, **84**, 4073–4077.

Bonnabry, P., Leemann, T. and Dayer, P., 1996, Role of human liver microsomal CYP2C9 in the biotransformation of lornoxicam. *European Journal of Clinical Pharmacology*, **49**, 305–308.

Bourrie, M., Meunier, V., Berger, Y. and Fabre, G., 1996, Cytochrome P450 isoform inhibitors as a tool for the investigation of metabolic reactions catalyzed by human liver microsomes. *Journal of Pharmacology and Experimental Therapeutics*, **277**, 321–332.

Chang, T. K., Gonzalez, F. J. and Waxman, D. J., 1994, Evaluation of triacetyloleandomycin, alpha-naphthoflavone and diethyldithiocarbamate as selective chemical probes for inhibition of human cytochromes P450. *Archives of Biochemistry and Biophysics*, **311**, 437–442.

Chang, T. K., Weber, G. F., Crespi, C. L. and Waxman, D. J., 1993, Differential activation of cyclophosphamide and ifosphamide by cytochromes P-450 2B and 3A in human liver microsomes. *Cancer Research*, **53**, 5629–5637.

Gelboin, H. V. 1993, Cytochrome P450 and monoclonal antibodies. *Pharmacological Review*, **45**, 413–453

Gelboin, H. V., Krausz, K. W., Goldfarb, I., Buters, J. T., Yang, S. K., Gonzalez, F. J., Korzekwa, K. R. and Shou, M., 1995. Inhibitory and non-inhibitory monoclonal antibodies to human cytochrome P450 3A3/4. *Biochemical Pharmacology*, **50**, 1841–1850.

Gonzalez, F. J., Aoyama, T. and Gelboin, H. V., 1991a, Expression of mammalian cytochrome P450 using vaccinia virus. *Methods Enzymology*, **206**, 85–92.

Gonzalez, F. J., Kimura, S., Tamura, S. and Gelboin, H. V., 1991b, Expression of mammalian cytochrome P450 using baculovirus. *Methods Enzymology*, **206**, 93–99.

Gonzalez, F. J. and Korzekwa, K. R., 1995, Cytochromes P450 expression systems. *Annual Review of Pharmacology and Toxicology*, **35**, 369–390.

Guengerich, F. P., Kim, D. H. and Iwasaki, M., 1991, Role of human cytochrome P-450 IIE1 in the oxidation of many low molecular weight cancer suspects. *Chemical Research in Toxicology*, **4**, 168–179.

Halpert, J. R., Guengerich, F. P., Bend, J. R. and Correia, M. A. 1994, Selective inhibitors of cytochromes P450. *Toxicology and Applied Pharmacology*, **125**, 163–175.

Hasegawa, T., Hara, K., Kenmochi, T. and Hata, S., 1994, *In vitro* metabolism of dorzolamide, a novel potent carbonic anhydrase inhibitor, in rat liver microsomes. *Drug Metabolism and Disposition*, **22**, 916–921.

HEYN, H., WHITE, R. B. and STEVENS, J. C., 1996, Catalytic role of cytochrome P4502B6 in the N-demethylation of *S*-mephenytoin. *Drug Metabolism and Disposition*, **24**, 948–954.

JOHNSON, E. F., SCHWAB, G. E. and MULLER-EBERHARD, U., 1979, Multiple forms of cytochrome P-450: catalytic differences exhibited by two homogeneous forms of rabbit cytochrome P-450. *Molecular Pharmacology*, **15**, 708–718.

KHARASCH, E. D. and THUMMEL, K. E., 1993, Identification of cytochrome P450 2E1 as the predominant enzyme catalyzing human liver microsomal defluorination of sevoflurane, isoflurane, and methoxyflurane. *Anesthesiology*, **79**, 795–807.

KUNZE, K. L. and TRAGER, W. F., 1993, Isoform-selective mechanism-based inhibition of human cytochrome P450 1A2 by furafylline. *Chemical Research in Toxicology*, **6**, 649–656.

LAKSHMI, V. M., ZENSER, T. V. and DAVIS, B. B., 1997, Rat liver cytochrome P450 metabolism of N-acetylbenzidine and N,N′-diacetylbenzidine. *Drug Metabolism and Disposition*, **25**, 481–488.

LANG, D. H., RETTIE, A. E. and BOCKER, R. H., 1997, Identification of enzymes involved in the metabolism of atrazine, terbuthylazine, ametryne, and terbutryne in human liver microsomes. *Chemical Research in Toxicology*, **10**, 1037–1044.

LOWRY, O. H., ROSEBROUGH, N. J., RARR, A. L. and RANDALL, R. J., 1951, Protein measurement with the Folin reagent. *Journal of Biological Chemistry*, **193**, 265–275.

MIDDLETON, JR, E. and KANDASWANMI, C., 1993, The flavonoids. In J. B. Harborne (ed.), *Advances in Research since* 1986 (London: Chapman & Hall), pp. 619–652.

MILLER, G. L., 1959, Protein determination for a large number of samples. *Analytical Chemistry*, **31**, 964–969.

NEWTON, D. J., WANG, R. and LU, A. Y., 1995, Cytochrome P450 inhibitors. Evaluation of specificities in the *in vitro* metabolism of therapeutic agents by human liver microsomes. *Drug Metabolism and Disposition*, **23**, 154–158.

OMURA, T. and SATO, K. R., 1964, The carbon monoxide-binding pigment of lover microsomes. Evidence for its hemoprotein nature. *Journal of Biological Chemistry*, **239**, 2370–2378.

OTTON, S. V., INABA, T. and KALOW, W., 1984, Competitive inhibition of sparteine oxidation in human liver by beta-adrenoceptor antagonists and other cardiovascular drugs. *Life Science*, **34**, 73–80.

RODRIGUES, A. D., 1999, Integrated cytochrome P450 reaction phenotyping: attempting to bridge the gap between cDNA-expressed cytochromes P450 and native human liver microsomes. *Biochemical Pharmacology*, **57**, 465–480.

SAI, Y., YANG, T. J., KRAUSZ, K. W., GONZALEZ, F. J. and GELBOIN, H. V., 1999, An inhibitory monoclonal antibody to human cytochrome P450 2A6 defines its role in the metabolism of coumarin, 7-ethoxycoumarin and 4-nitroanisole in human liver. *Pharmacogentics*, **9**, 229–237.

SANDERINK, G. J., BOURNIQUE, B., STEVENS, J., PETRY, M. and MARTINET, M., 1997, Involvement of human CYP1A isoenzymes in the metabolism and drug interactions of riluzole *in vitro*. *Journal of Pharmacology and Experimental Therapeutics*, **282**, 1465–1472.

SHIMADA, T., YAMAZAKI, H., MIMURA, M., INUI, Y. and GUENGERICH, F. P., 1994, Interindividual variations in human liver cytochrome P-450 enzymes involved in the oxidation of drug, carcinogens and toxic chemicals; studies with liver microsomes of 30 Japanese and 30 Caucasians. *Journal of Pharmacology and Experimental Therapeutics*, **270**, 414–423.

SHOU, M., GROGAN, J., MANCEWICZ, J. A., KRAUSZ, K. W., GONZALEZ, F. J., GELBOIN, H. V. and KORZEKWA, K. R., 1994a, Activation of CYP3A4: evidence for the simultaneous binding of two substrates in a cytochrome P450 active site. *Biochemistry*, **33**, 6450–6455.

SHOU, M., KORZEKWA, K. R., KRAUSZ, K. W., CRESPI, C. L., GONZALEZ, F. J. and GELBOIN, H. V., 1994b, Regio- and stereo-selective metabolism of phenanthrene by twelve cDNA-expressed human, rodent, and rabbit cytochromes P-450. *Cancer Letters*, **83**, 305–313.

SMITH, D. A. and JONES, B. C., 1992, Speculations on the substrate structure–activity relationship (SSAR) of cytochrome P450 enzymes. *Biochemical Pharmacology*, **44**, 2089–2098.

SPRACKLIN, D. K., THUMMEL, K. E. and KHARASCH, E. D., 1996, Human reductive halothane metabolism *in vitro* is catalyzed by cytochrome P450 2A6 and 3A4. *Drug Metabolism and Disposition*, **24**, 976–983.

STEVENS, J. C., WHITE, R. B., HSU, S. H. and MARTINET, M., 1997, Human liver CYP2B6-catalyzed hydroxylation of RP 73401. *Journal of Pharmacology and Experimental Therapeutics*, **282**, 1389–1395.

TYNDALE, R. F., KALOW, W. and INABA, T., 1991, Oxidation of reduced haloperidol to haloperidol: involvement of human P450IID6 (sparteine/debrisoquine monooxygenase). *British Journal of Clinical Pharmacology*, **31**, 655–660.

WARD, S. and BACK, D. J., 1993, Metabolism of gestodene in human liver cytosol and microsomes *in vitro*. *Journal of Steroid Biochemistry and Molecular Biology*, **46**, 235–243.

YAMAZAKI, H., INUI, Y., YUN, C. H., GUENGERICH, F. P. and SHIMADA, T., 1992, Cytochrome P450 2E1 and 2A6 enzymes as major catalysts for metabolic activation of N-nitrosodialkylamines and tobacco-related nitrosamines in human liver microsomes. *Carcinogenesis*, **13**, 1789–1794.

YANG, T. J., KRAUSZ, K. W., SHOU, M., YANG, S. K., BUTERS, J. Y., GONZALEZ, F. J. and GELBOIN,

H. V., 1998, Inhibitory monoclonal antibody to human cytochrome P450 2B6. *Biochemical Pharmacology*, **55**, 1633–1640.

YUN, C. H., SHIMADA , T. and GUENGERICH , F. P., 1992, Roles of human liver cytochrome P4502C and 3A enzymes in the 3-hydroxylation of benzo(a)pyrene. *Cancer Research*, **52**, 1868–1874.

WANG, P. P., BEAUNE, P., KAMINSKY , L. S., DANNAN, G. A., KADLUBAR, F. F., LARREY, D. and GUENGERICH , F. P., 1983, Purification and characterization of six cytochrome P-450 isozymes from human liver microsomes. *Biochemistry*, **22**, 5375–5383.

XENOBIOTICA , 2000, VOL. 30, NO. 4, 345–357

Thyroid hormone modulation of rat sulphotransferase mRNA expression

R. T. DUNN, II and C. D. KLAASSEN*

Department of Pharmacology, Toxicology and Therapeutics, University of Kansas Medical Center, 3901 Rainbow Blvd, Kansas City, KS 66160–7417, USA

Received 15 July 1999

1. Thyroid hormones modulate sulphotransferase (SULT) enzyme expression. Specific substrates are not available for the study of the SULT isoforms, so the regulation of hepatic SULT mRNA expression by thyroid hormones was examined by Northern blot analysis with oligonucleotide probes specific for each SULT mRNA, including male-dominant phenol SULT (1A1, 1C1, 1E2), female-dominant hydroxysteroid SULT (20/21, 40/41, 60), and a non-sex-dependent SULT, 1B1. The male and female rat were either untreated, thyroidectomized (TX), or TX and given thyroid hormones (thyroxine [T_4, 20 μg kg^{-1} day^{-1}] and 3,5,3′-triiodothyronine [T_3, 5 μg kg^{-1} day^{-1}]).

2. With regard to phenol SULTs, expression of SULT1A1 or SULT1B1 mRNA was not altered in either sex by TX. TX increased SULT1E2 mRNA expression 3-fold in the male and 2.5-fold in the female rat. The increase in SULT1E2 mRNA was partially reversed by infusion of T_3/T_4 in the male, and was not reversed in the female.

3. With regard to hydroxysteroid SULTs, TX decreased expression of SULT20/21 mRNA in the male rat by 70 and 60% in the female, and these decreases were reversed by T_3/T_4 infusion. SULT40/41 mRNA expression increased in the male rat 3-fold and decreased in the female TX rat by 25%. SULT60 mRNA expression increased 3-fold by TX in the female rats. The effects of TX on SULT40/41 and SULT60 mRNA expression were reversed by infusion of T_3/T_4.

5. Thus, phenol sulphotransferases were not markedly affected by thyroid hormones except for SULT1E2, but each hydroxysteroid sulphotransferase isoform was affected by thyroidectomy. Therefore, thyroid hormones regulate SULT gene expression in an isoform-specific manner.

Introduction

The sulphotransferase (SULT) family of enzymes catalyses the transfer of a sulphonate moiety to a variety of substrates, which results in enhanced excretion of these substrates. The substrates for the SULT enzymes include a variety of hormones (e.g. oestrogens, corticosteroids, dehydroepiandrosterone, thyroid hormones) and neurotransmitters, including dopamine (Mulder *et al.* 1990, Visser 1994). In addition to the numerous endogenous molecules, xenobiotics are also substrates of SULT (e.g. 4-nitrophenol and 1-naphthol). Minoxidil, an antihypertensive drug (Thomas and Harpootlian 1975), has been exploited for its ability to stimulate hair growth. The biological activity of minoxidil is dependent on its conversion to minoxidil sulphate, by a phenol-preferring sulphotransferase (Clissold and Heel 1987). The analgesic drug acetaminophen is a substrate of the SULT enzymes, and is often used as a model compound to study the kinetics of the sulphation reaction (Goon and Klaassen 1990), as well as species differences in sulphation activity (Liu and Klaassen 1996a, Gregus *et al.* 1988). Thus, SULT enzymes metabolize a wide range of both endogenous and xenobiotic compounds.

While the SULT enzymes have been studied extensively in terms of substrates

* Author for correspondence; e-mail: cklaasse@kumc.edu

Xenobiotica ISSN 0049-8254 print/ISSN 1366-5928 online © 2000 Taylor & Francis Ltd
http://www.tandf.co.uk/journals

and conversion of substrates to reactive species, less is known about how the expression of SULTs are is regulated physiologically. Sex-specific expression of certain SULT isoforms has been observed in rat and linked to the susceptibility of the male rat to cancer induced by *N*-hydroxyacetylaminofluorine (DeBaun *et al.* 1970). This susceptibility is likely due to the male-predominant sulphation activity of the SULT 1C1 isoform. Alternatively, the female rat is more sensitive to the carcinogenic effects of hydroxymethyl polyaromatic hydrocarbons (PAH), because the female rat expresses hydroxysteroid SULT, which preferentially catalyses the sulphation of certain hydroxymethyl-PAH, at higher levels than the male rat (Watabe *et al.* 1994).

Recent studies have identified hormones that regulate the expression of SULT isoforms. Our previous studies have demonstrated that growth hormone secretion patterns are important for SULT gene expression (Liu and Klaassen 1996b, c). The expression of mRNA for the male-specific isoform, SULT1C1, was abolished upon hypophysectomy (HX). Expression of SULT1C1 mRNA was restored in the HX male rat by daily injection of growth hormone (male pattern). Alternatively, infusion of growth hormone (female pattern) failed to restore SULT1C1 expression to pre-HX levels. By contrast, hypophysectomy of the female rat resulted in a decrease of hydroxysteroid SULT mRNA expression. mRNA expression of the hydroxysteroid SULT was only partially restored in the HX female rat by infusion of growth hormone (i.e. female pattern). The hormonal regulation of two female-predominant hydroxysteroid SULT (20/21 and 40/41) has been further substantiated by Ueda *et al.* (1997). Thus, growth hormone as well as growth hormone secretion patterns are important in the regulation of SULT gene expression (Yamazoe *et al.* 1997). Regulation of SULT gene expression by steroidal chemicals, including dexamethasone and the anti-glucocorticoid pregnenolone-16α-carbonitrile (PCN), has been demonstrated (Runge-Morris and Wilusz 1994).

The influence of thyroid hormones on drug-metabolizing enzymes, such as cytochrome P450, has been examined at the enzyme level (Skett and Weir 1983, Kato and Yamazoe 1992). Thyroid hormone negatively regulated expression of CYP 3A2 and CYP 2A2 (Ram and Waxman 1991). In addition, T_3 was shown to modulate constitutive expression of CYP 4A2 (Webb *et al.* 1996). Expression of certain SULT enzyme activities also appears to be regulated, at least in part, by thyroid hormones. Gong *et al.* (1992) demonstrated that sulphation of 3,5,3′-triiodothyronine was decreased by administration of T_3 in the hypophysectomized rat. Borthwick *et al.* (1995) showed that thyroxine administration to the hypophysectomized male rat dramatically decreased ($>75\%$) oestrogen sulphation and oestrogen SULT immunoreactive protein. Thus, it is important to examine the effects of thyroid hormones on SULT mRNA expression.

Two methods used to study SULT enzymes: (1) substrate-based enzyme assays and (2) anti-SULT antibodies can lead to inappropriate conclusions regarding specificity, due to the overlap in substrate specificity and possible antibody cross reactivity, respectively. Therefore, our approach to the study of SULT gene regulation utilizes specific oligonucleotides that can distinguish between mRNA for each SULT isoform. The objective of the present study was systematically to analyse the effect of thyroidectomy on the expression of the seven major SULT isoforms in the male and female rat to define the thyroid hormonal regulation of SULT mRNA expression.

Table 1. Oligonucleotide sequences and GENBANK accession numbers.

SULT isoform	Oligonucleotide sequence	GENBANK accession number
Phenol SULT		
SULT1A1	5′-CTT CAC ATG CAC TAG CGG TG-3′	X52883
SULT1B1	5′-TGT TCC AGA CAA TTT CTT CTT-3′	U38419
SULT1C1	5′-CAC CTA GTG TGG AAG GTC TC-3′	L22339
SULT1E2	5′-GCA CTC CAG GTC AGG TAT TC-3′	M86758
Hydroxysteroid SULT		
SULT20/21	5′-CCT TTC CTC ATG AGG CCA GT-3′	M31363
SULT40/41	5′-TGT CTA ATT CTC GCA TAG AC-3′	M33329
SULT60	5′-TTT CTT CTC CAG GGC GAT CT-3′	D14989

Materials and methods

Animals

Male and female Sprague–Dawley rats (8 weeks of age, 150–250 g, 18/sex) were used in the study. They were divided into three groups of six rats per group: (1) intact control rats (CONT), (2) thyroidectomized (TX) rats given saline via Alzet osmotic minipumps (Model 2002, Alza Corp., Palo Alto, CA, USA), and (3) thyroidectomized rats given T_3 and T_4 via osmotic minipumps (TX + T_3/T_4). Rats were surgically thyroidectomized by the supplier (Charles River, Madison, WI, USA) and allowed to acclimatize for a minimum of 10 days before implantation of the osmotic minipumps. The animals were allowed free access to food (Harlan-Teklad 4%, Mouse/Rat Diet, #7001) and tap water throughout the duration of the experiment. TX animals were given 0.1% calcium chloride in the drinking water to prevent excess loss of calcium from bone, which occurs with the removal of the parathyroid glands.

After an acclimatization period of 10 days, rats were anaesthetized with diethyl ether. Osmotic minipumps were implanted subcutaneously, delivering 20 μg T_4 kg^{-1} body weight day^{-1} and 5 μg T_3 kg^{-1} body weight day^{-1} dissolved in 0.1 N NaOH in 0.9% saline. This experimental protocol has been utilized previously in our laboratory, and restored thyroid hormones to levels observed in intact animals (Barter and Klaassen 1992).

After the 14-day period of hormone replacement, animals were euthanized with CO_2, and livers immediately removed and frozen in liquid N_2. Tissues were stored at − 80 °C until further use.

Analysis of thyroid hormones

On day 0, before implantation of osmotic minipumps, and on days 3, 7, 10 and 14 following implantation of osmotic minipumps, rats were lightly anaesthetized with diethyl ether, and blood (1.0–1.5 ml) was drawn from the orbital sinus with a heparinized capillary tube. The blood was allowed to clot and subsequently centrifuged at 12 000 *g* to obtain serum. Serum samples were stored at − 80 °C before determination of total and free T_3 and T_4. Hormone levels (total and free T_3 and T_4) were determined by radio-immunoassay (RIA) using kits supplied by Diagnostic Products Corp. (Los Angeles, CA, USA).

RNA isolation and separation

Total RNA was isolated using RNAzol B reagent (Tel-Test Inc., Friendswood, TX, USA) utilizing instructions provided by the manufacturer. Briefly, 0.2 g liver was added to 2.0 ml RNAzol B in sterile polypropylene vials and subjected to homogenization with a Polytron (PTA 10S generator, Brinkman, Westbury, NY, USA). Chloroform (0.25 ml) was added to each homogenate, and the vials were vigorously shaken for 45 s, followed by incubation at 4 °C for 7–8 min. The vials were then subjected to centrifugation at 12000*g* for 15 min. The aqueous (upper) phase containing RNA was removed, transferred to a clean vial and total RNA precipitated for a minimum of 30 min at − 20 °C in 2–3 ml isopropanol. After precipitation, the vials were centrifuged at 12000*g* for 15 min. The supernatant was removed and each pellet was washed with 3.0 ml 75% ethanol and centrifuged again at 7500 *g* for 10 min. After centrifugation, the supernatant was discarded and the residual ethanol evaporated. Each pellet was redissolved in 0.2 ml 0.1% SDS in 10 mM Tris (pH 7.5). RNA concentration was assessed by UV absorbance at 260 nm using a Beckman DU 650 spectrophotometer (Beckman, Palo Alto, CA, USA).

Oligonucleotide probes

Oligonucleotides were designed to be complementary to certain sequences of the respective SULT cDNA and sequences and GenBank accession numbers are given in table 1. SULT1A1, SULT1B1, SULT1C1 and SULT1E2 are complementary to nucleotides 82–101 of the cDNA sequence reported by

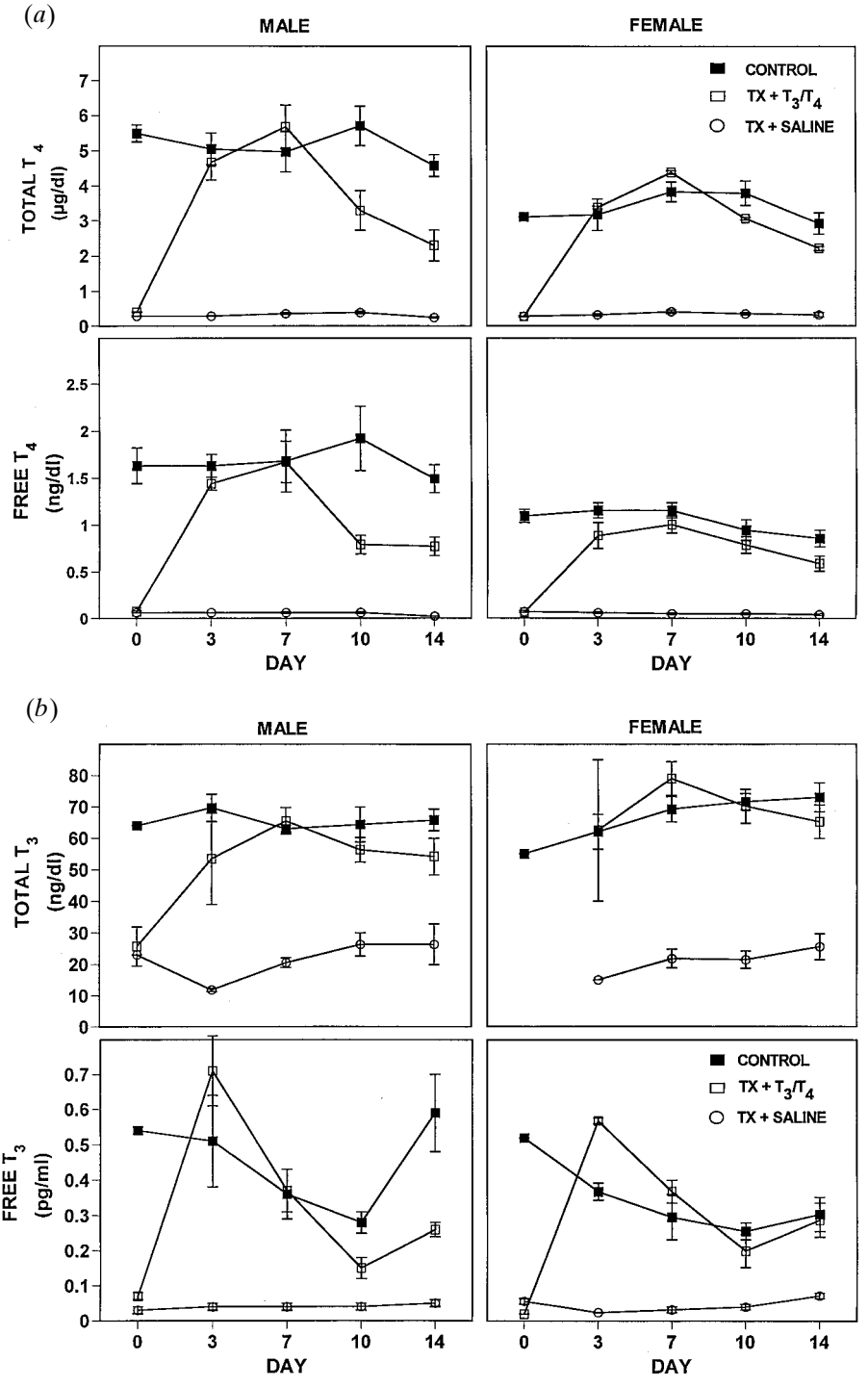


Figure 1. For legend see opposite.

Ozawa *et al.* (1990), nucleotides 814–834 of the cDNA sequence reported by Sakakibara *et al.* (1995) and nucleotides 882–903 of the sequence reported by Fujita *et al.* (1997), nucleotides 1050–1069 of the cDNA sequence reported by Nagata *et al.* (1993), and nucleotides 364–383 of the cDNA sequence reported by Demyan *et al.* (1992) respectively. SULT-20, SULT-40 and SULT-60 are complementary to nucleotides 761–780 of the cDNA sequence reported by Ogura *et al.* (1989), nucleotides 547–566 of the cDNA sequence reported by Ogura *et al.* (1990) and nucleotides 436–455 of the cDNA sequence reported by Watabe *et al.* (1994) respectively. The oligonucleotides used in this study were designed to distinguish only between the major SULT isoforms indicated above.

Each oligonucleotide was labeled with [α-^{32}P]dATP (6000 Ci/mmole) (Amersham, Arlington Heights, IL, USA) by tailing with terminal deoxynucleotidyl transferase (Boehringer-Mannheim, Indianapolis, IN, USA). The blots were stripped and reprobed with an oligonucleotide specific for 28S rRNA utilized as a control for loading.

Northern blot analysis

Following separation of total RNA, RNA was blotted onto nylon membranes (Zeta Probe-GT, BioRad, Hercules, CA, USA) by capillary action in 10× standard sodium citrate (SSC). Once transfer of RNA was complete, each membrane was dried for 2 h at 70 °C, then cross-linked under UV light for 30 s. Before hybridization each membrane was prehybridized for 4 h in 0.5× prehybridization solution (Sigma, St Louis, MO, USA) (5× SSC, 5× Denhardt's, DNA 100 μg ml^{-1}) prepared in 7% SDS, 20% formamide, 0.25 mg ml^{-1} tRNA in 0.02 M sodium phosphate buffer, pH 7.5. Following prehybridization, each membrane was hybridized overnight (18 h) in hybridization solution (Sigma) (5×SSC, 2× Denhardt's, DNA 100 μg ml^{-1}) prepared in 7% SDS, 20% formamide, 0.25 mg ml^{-1} tRNA in 0.02 M sodium phosphate buffer, pH 7.5. To each 1.0 ml hybridization solution was added 2.0×10^{6} cpm [^{32}P]dATP-labelled oligonucleotide specific for each SULT mRNA. After hybridization, each blot was washed twice in 2×SSC, 2% SDS for 15 min per wash at 45 °C. Blots were washed subsequently in 1×SSC, 2% SDS for 20 min at 45 °C, then for 30 min at 50 °C. Blots were exposed to phosphor screens (Molecular Dynamics, Sunnyvale, CA, USA) for 24–48 h. Quantification was performed using a PhosphorImager and Imagequant software (Molecular Dynamics). RNA from each animal ($n = 5$–6 animals per group) in the study was analysed in quadruplicate. Results are presented as mean± SEM ratio of SULT hybridization signal relative to 28S rRNA hybridization signal. Analysis of variance was performed to determine significance ($p \leqslant 0.05$) followed by Duncan's *post-hoc* test.

Results

Analysis of serum T_3 and T_4 levels

Serum was analysed for total and free T_3 and T_4 by RIA. Blood samples were collected the day before implantation of the osmotic minipumps (day 0), and then on each experimental day indicated (3, 7, 10, 14). In the thyroidectomized rat, the levels of thyroid hormones were consistently near or below the limit of detection for the RIA analysis. Infusion of thyroid hormones restored the levels of both T_3 (figure 1a) and T_4 (figure 1b) to approximately the same levels observed in control animals. There was no statistical difference between the levels of thyroid hormones in the control versus the TX + T_3/T_4 infused rat ($p \leqslant 0.05$).

Further evidence for the completeness of thyroidectomy and the effectiveness of T_3/T_4 infusion is provided in Figure 2. The weight of each rat was recorded on the indicated experimental day. The TX rat infused with saline did not increase in weight over the course of the study. By contrast, the TX rat treated with thyroid hormones gained weight at rates parallel with the intact controls.

Figure 1. Effect of thyroid hormone infusion on serum levels of 3,5,3′-triiodothyronine (T_3, (a)), and thyroxine (T_4, (b)) in male and female rat serum by radio-immunoassay (RIA). Blood was drawn from the orbital sinus on day 0, 3, 7, 10 and 14. Serum was separated and analysed by RIA for thyroid hormones (total and free T_4 and total and free T_3). Values are mean ± SEM of five to six animals per group. Symbols are: (■) control, (□) TX + T_3/T_4, (○) TX + saline. The approximate sensitivity of each assay according to the manufacturer is: total $T_4 = 0.25$ μg dl^{-1}; free $T_4 = 0.01$ ng dl^{-1}; total $T_3 = 7$ ng dl^{-1}; free $T_3 = 0.2$ pg ml^{-1}.

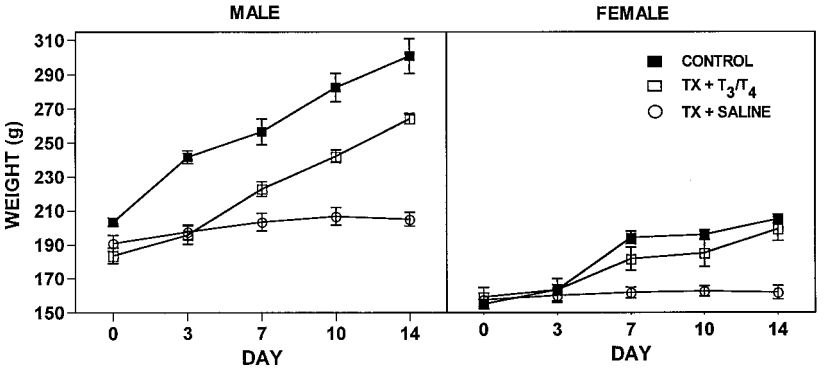


Figure 2. Effect of thyroidectomy and thyroidectomy + T_3 and T_4 on male and female rat weights during the course of the 14-day study. Rat weights (g) were measured on the days indicated and are the mean ± SEM from five to six animals per group.

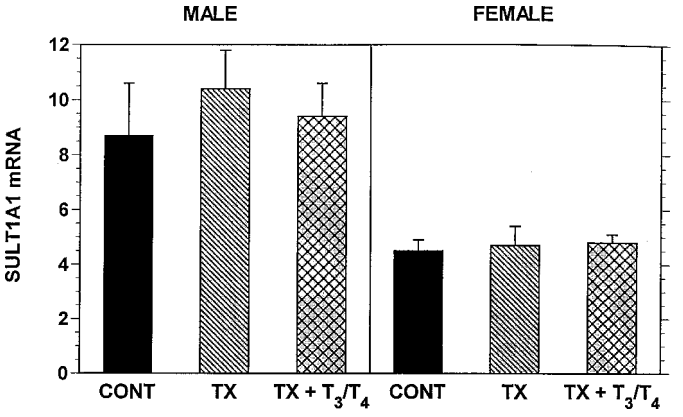


Figure 3. Effect of thyroidectomy on the expression of hepatic SULT1A1 mRNA in male and female rat. Rats were either intact (CONT), thyroidectomized (TX) given saline by osmotic minipump or thyroidectomized and given thyroid hormones T_3 (5 μg kg^{-1} day^{-1}) + T_4 (20 μg kg^{-1} day^{-1}) (TX + T_3/T_4) via osmotic minipump for 14 days. Values are the ratio of SULT hybridization to 28S rRNA hybridization ($\times$1000). Results are the mean ± SEM for five to six rats.

Total RNA was collected from the liver of control (CONT), thyroidectomized (TX) and thyroidectomized rat given thyroid hormones (TX + T_3/T_4), and analysed for expression of mRNA for the seven major sulphotransferase isoforms, including male-predominant isoforms SULT1A1, SULT1C1 and SULT1E2, and female-predominant isoforms SULT 20/21, SULT 40/41 and SULT 60, in both male and female rat. The expression of SULT1B1 mRNA that exhibits comparable expression between male and female rat (Sakakibara *et al.* 1995, Fujita *et al.* 1997) was also examined.

Expression of the male-predominant isoform SULT1A1 was not appreciably altered by thyroidectomy in either male or female rat (figure 3). Thyroid hormone replacement also did not alter SULT1A1 mRNA expression relative to the control or TX male or female rat. Expression of SULT1B1 mRNA was also relatively resistant to the effect of thyroidectomy in both male and female rat

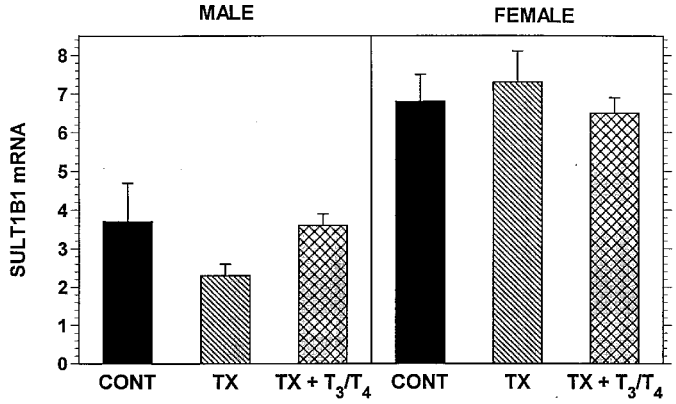


Figure 4. Effect of thyroidectomy on the expression of hepatic SULT1B1 mRNA in the male and female rat. Rats were either intact (CONT), thyroidectomized (TX) given saline by osmotic minipump or thyroidectomized and given thyroid hormones T_3 (5 μg kg^{-1} day^{-1}) + T_4 (20 μg kg^{-1} day^{-1}) (TX + T_3/T_4) via osmotic minipump for 14 days. Values are the ratio of SULT hybridization to 28S rRNA hybridization ($\times$1000). Results are the mean$\pm$ SEM for five to six rats.

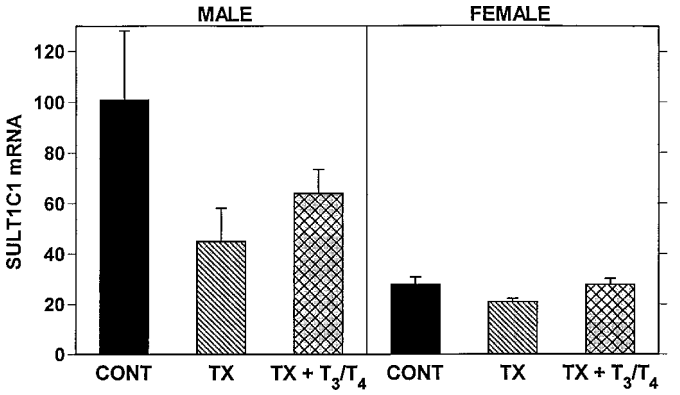


Figure 5. Effect of thyroidectomy on the expression of hepatic SULT1C1 mRNA in the male and female rat. Rats were either intact (CONT), thyroidectomized (TX) given saline by osmotic minipump or thyroidectomized and given thyroid hormones T_3 (5 μg kg^{-1} day^{-1}) + T_4 (20 μg kg^{-1} day^{-1}) (TX + T_3/T_4) via osmotic minipump for 14 days. Values are the ratio of SULT hybridization to 28S rRNA hybridization ($\times$1000). Results are the mean$\pm$ SEM for five to six rats.

(figure 4). Expression of the male-specific isoform SULT1C1 tended to be decreased in TX male rat, although the decrease was not statistically significant (figure 5). TX had no effect on SULT1C1 in female rat. In contrast, expression of the male-specific SULT isoform SULT1E2 was increased $\sim$ 2.5-fold by thyroidectomy in male rat (figure 6). This effect was only partially reversed by replacement of thyroid hormones. While SULT1E2 mRNA is very low in female rat, thyroidectomy also induced expression of SULT1E2 mRNA in the female, and the induction was not reversed by infusion of thyroid hormones. Despite the induction of SULT1E2 mRNA in female rat, expression was still near the limit of detection by Northern blot analysis.

The expression of hydroxysteroid-SULT isoforms was also examined in both the male and female rat. These isoforms (i.e. SULT20/21, SULT40/41, SULT60) are

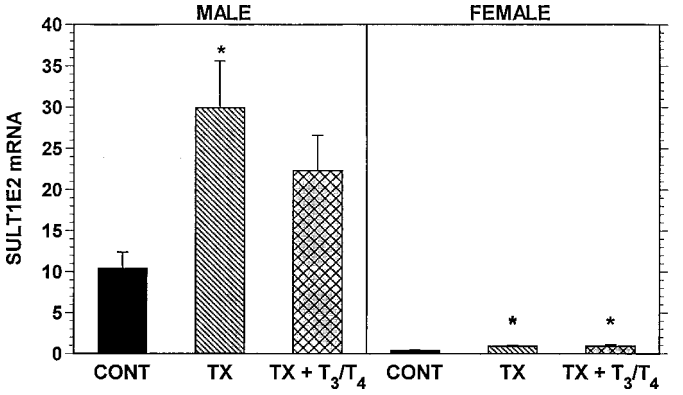


Figure 6. Effect of thyroidectomy on the expression of hepatic SULT1E2 mRNA in the male and female rat. Rats were either intact (CONT), thyroidectomized (TX) given saline by osmotic minipump or thyroidectomized and given thyroid hormones T_3 (5 μg kg^{-1} day^{-1}) + T_4 (20 μg kg^{-1} day^{-1}) (TX + T_3/T_4) via osmotic minipump for 14 days. Values are the ratio of SULT hybridization to 28S rRNA hybridization ($\times$1000). Results are the mean $\pm$ SEM for five to six rats. *Significant difference from control at $p \leqslant 0.05$.

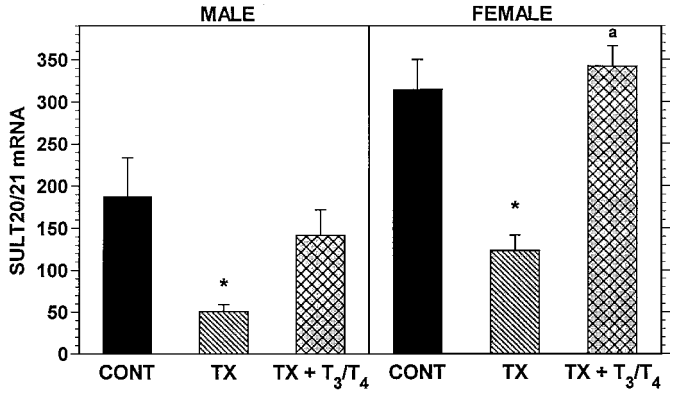


Figure 7. Effect of thyroidectomy on the expression of hepatic SULT20/21 mRNA in the male and female rat. Rats were either intact (CONT), thyroidectomized (TX) given saline by osmotic minipump or thyroidectomized and given thyroid hormones T_3 (5 μg kg^{-1} day^{-1}) + T_4 (20 μg kg^{-1} day^{-1}) (TX + T_3/T_4) via osmotic minipump for 14 days. Values are the ratio of SULT hybridization to 28S rRNA hybridization ($\times$1000). Results are the mean $\pm$ SEM for five to six rats. *Significant difference from control; 'a', significant difference from TX group at $p \leqslant 0.05$.

considered to be female-predominant. Expression of hydroxysteroid SULT20/21 was similarly affected in both the male and female rat (figure 7). In the male rat, SULT20/21 mRNA expression was decreased to $\sim$75% of control by thyroidectomy. Infusion of thyroid hormones restored SULT20/21 mRNA expression in the TX male rat to a similar level observed in controls although the expression level in the thyroid hormone treated rat was not statistically different from the TX male rat. TX decreased expression of SULT20/21 in the female rat by 50%, and this decrease was completely reversed by infusion of thyroid hormones. SULT40/41 mRNA was increased 3-fold in the TX male rat from nearly undetectable levels in the control male rat (figure 8). The induction of SULT40/41 in the TX male rat

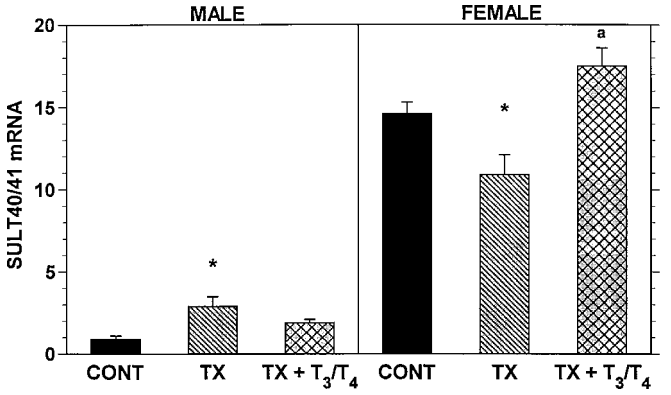


Figure 8. Effect of thyroidectomy on the expression of hepatic SULT40/41 mRNA in the male and female rat. Rats were either intact (CONT), thyroidectomized (TX) given saline by osmotic minipump or thyroidectomized and given thyroid hormones T_3 (5 μg kg^{-1} day^{-1}) + T_4 (20 μg kg^{-1} day^{-1}) (TX + T_3/T_4) via osmotic minipump for 14 days. Values are the ratio of SULT hybridization to 28S rRNA hybridization ($\times$1000). Results are the mean $\pm$ SEM for five to six rats. *Significant difference from control at $p \leqslant 0.05$.

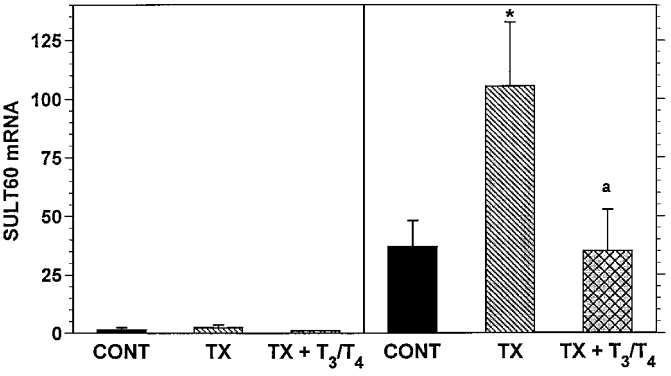


Figure 9. Effect of thyroidectomy on the expression of hepatic SULT60 mRNA in the male and female rat. Rats were either intact (CONT), thyroidectomized (TX) given saline by osmotic minipump or thyroidectomized and given thyroid hormones T_3 (5 μg kg^{-1} day^{-1}) + T_4 (20 μg kg^{-1} day^{-1}) (TX + T_3/T_4) via osmotic minipump for 14 days. Values are the ratio of SULT hybridization to 28S rRNA hybridization ($\times$1000). Results are the mean $\pm$ SEM for five to six rats. *Significant difference from control; 'a', significant difference from TX group at $p \leqslant 0.05$.

was reversed by thyroid hormone infusion although SULT40/41 mRNA expression in the thyroid hormone-treated rat was not statistically different from the TX male rat. In the female rat, thyroidectomy reduced expression of SULT40/41 mRNA in contrast to the induction of SULT40/41 seen in the TX male rat. Infusion of thyroid hormones restored the SULT40/41 mRNA to that observed in the intact control female rat. In contrast to the SULT20/21 and SULT40/41, SULT60 mRNA expression was not changed in the TX male rat (figure 9). However, SULT60 mRNA was induced in the TX female rat to twice the expression observed in the intact control female rat. Infusion of thyroid hormones effectively reversed the induction of SULT60 mRNA seen in the TX female rat.

Discussion

The regulation of sulphotransferase gene expression has recently become an area of active investigation. Numerous hormones have been implicated in the modulation of SULT gene expression; among these are growth hormone, glucocorticoids and certain sex steroids, including oestrogen and testosterone (Liu and Klaassen 1996b–d, Runge-Morris *et al.* 1996, Ueda *et al.* 1997). SULT gene expression is modified by xenobiotics, including 3-methylcholanthrene (Runge-Morris and Wilusz 1994) and PCN (Liu and Klaassen 1996d). However, the mechanism(s) by which the above-mentioned hormones and xenobiotics act on SULT genes is unknown.

To investigate the hormonal regulation of SULT gene expression *in vivo*, studies have been conducted that involve endocrine manipulation, including removal of hormone secretory organs (e.g. pituitary, gonads, adrenal glands), followed by hormone replacement, or alternatively, studies with hormone inhibitors (e.g. tamoxifen) (Hellriegel *et al.* 1996, Nuwaysir *et al.* 1996). The objective of the present study was to analyse the effect of thyroidectomy and thyroid hormone replacement with physiological levels of T_3 and T_4 on hepatic expression of the seven major SULT mRNAs in the male and female rat. The present approach to analyse SULT gene expression relies on oligonucleotides specific for each SULT isoform, which is advantageous over analyses involving less specific antibodies and enzyme assays.

SULT mRNA expression is affected by thyroidectomy. In certain cases TX resulted in the induction of SULT mRNA (e.g. SULT1E2 in the male and female rat, SULT40/41 in the male rat, SULT60 in the female rat). TX also elicited reductions in specific SULT mRNAs (e.g. SULT1C1 in male rat, SULT20/21 in the male and female rat, SULT40/41 in the female rat). Thus, thyroidal control of SULT gene expression is dependent on SULT isoforms and can be either negative as in the cases of SULT1E2, SULT40/41 (male), and SULT60 (female) or positive in the cases of SULT1C1 (male), SULT20/21 (male and female) and SULT40/41 (female).

Another aspect of thyroid hormone regulation of SULT gene expression that emerged from these experiments was that the effects of thyroidectomy were both similar to and different from the effects caused by hypophysectomy (Liu and Klaassen 1996b, c). Induction of SULT1E2 mRNA in the male rat by TX is in contrast to the lack of effect that HX has upon SULT1E2 mRNA expression; however, TX induces SULT1E2 in the female rat, albeit to a lesser degree than HX (Liu and Klaassen 1996b, c). SULT20/21 mRNA expression was decreased similarly by HX and TX in both the male and female rat. The effects of TX and HX are similar for SULT40/41 in the male and female rat. Finally, SULT60 mRNA expression is differentially altered by TX, which increases SULT60 mRNA expression and HX, which decreases SULT60 mRNA expression (Liu and Klaassen 1996b, c). Thus, the regulation of SULT1E2 and SULT60 appears independent of a pituitary factor. These observations of differential responsiveness to pituitary and thyroid hormones are similar to those observed previously for two cytochrome P450 isoenzymes, CYP2B1 and CYP2B2. Each cytochrome P450 isoform is expressed at low levels in the normal adult rat but can be induced up to 100-fold in the GH-depleted rat (Yamazoe *et al.* 1987, 1989). CYP2B1 is more responsive to induction by HX than to induction by TX, but the induction of CYP2B2 by HX is effectively reversed by T_3 (Murayama *et al.* 1991).

The present studies have led to more precise conclusions about the regulation of SULT expression. Our previous studies that analysed the effect of HX and HX + hormonal replacement could not delineate responses due solely to thyroid hormone. Hypophysectomy, in addition to causing deficiencies in GH, also induces a hypothyroid state (Jones *et al.* 1990, Levy *et al.* 1992). The results of the present study, coupled with previous studies (Liu and Klaassen 1996b, c) with the HX rat, indicate that SULT1E2 and SULT60 mRNA expression is influenced by thyroid hormone independent of a pituitary factor(s). SULT1E2 enzyme levels and activity were induced in the HX rat and the induction was completely reversed by administration of T_4 (Borthwick *et al.* 1995). These previous results are similar to our present studies that indicate SULT1E2 mRNA is negatively regulated by thyroid hormones. Although not directly investigated in these studies, there are at least two possibilities for thyroid hormone regulation of SULT expression. One is positive regulation via thyroid hormone receptor interacting with regulatory elements of the SULT gene(s) and increasing transcription directly. Alternatively, thyroid hormone (T_3) has been observed negatively to regulate DHEA-induced expression of rat CYP3A23 and CYP4A by an as yet undefined mechanism (Singleton *et al.* 1999).

These findings further support the role of the pituitary-thyroid axis in the control of SULT gene expression and are similar to those observed previously for certain cytochromes P450. Taken together, the influence of thyroid hormones in drug-metabolizing enzyme regulation is broad and affects both phase I and phase II drug-metabolizing enzyme systems.

Acknowledgements

Work supported by grant ES-03192. R. T. D. was supported in part by Training Grant ES-07079.

References

BARTER, R. A. and KLAASSEN, C. D., 1992, UDP-glucuronosyltransferase inducers reduce thyroid hormone levels in rats by an extrathyroidal mechanism. *Toxicology and Applied Pharmacology*, **113**, 36–42.

BORTHWICK, E. B., VOICE, M. W., BURCHELL, A. and COUGHTRIE, M. W., 1995, Effects of hypophysectomy and thyroxine on the expression of hepatic oestrogen, hydroxysteroid and phenol sulphotransferases. *Biochemical Pharmacology*, **49**, 1381–1386.

CLISSOLD, S. P. and HEEL, R. C., 1987, Topical minoxidil. A preliminary review of its pharmacodynamic properties and therapeutic efficacy in alopecia areata and alopecia androgenetica. *Drugs*, **33**, 107–122.

DEBAUN, J. R., MILLER, E. C. and MILLER, J. A., 1970, *N*-hydroxy-2-acetylaminofluorene sulphotransferase: its probable role in carcinogenesis and in protein-(methion-*S*-yl) binding in rat liver. *Cancer Research*, **30**, 577–595.

DEMYAN, W. F., SONG, C. S., KIM, D. S., HER, S., GALLWITZ, W., RAO, T. R., SLOMCZYNSKA, M., CHATTERJEE, B. and ROY, A. K., 1992, Estrogen sulphotransferase of the rat liver: complementary DNA cloning and age- and sex-specific regulation of messenger RNA. *Molecular Endocrinology*, **6**, 589–597.

FUJITA, K., NAGATA, K., OZAWA, S., SASANO, H. and YAMAZOE, Y., 1997, Molecular cloning and characterization of rat ST1B1 and human ST1B2 cDNAs, encoding thyroid hormone sulfotransferases. *Journal of Biochemistry (Tokyo)*, **122**, 1052–1061.

GONG, D. W., MURAYAMA, N., YAMAZOE, Y. and KATO, R., 1992, Hepatic triiodothyronine sulphation and its regulation by growth hormone and triiodothyronine in rats. *Journal of Biochemistry Tokyo*, **112**, 112–116.

GOON, D. and KLAASSEN, C. D., 1990, Dose-dependent intestinal glucuronidation and sulphation of acetaminophen in the rat *in situ*. *Journal of Pharmacology and Experimental Therapeutics*, **252**, 201–207.

Gregus, Z., Madhu, C. and Klaassen, C. D., 1988, Species variation in toxication and detoxication of acetaminophen *in vivo*: a comparative study of biliary and urinary excretion of acetaminophen metabolites. *Journal of Pharmacology and Experimental Therapeutics*, **244**, 91–99.

Hellriegel, E. T., Matwyshyn, G. A., Fei, P., Dragnev, K. H., Nims, R. W., Lubet, R. A. and Kong, A. N., 1996, Regulation of gene expression of various phase I and phase II drug-metabolizing enzymes by tamoxifen in rat liver. *Biochemical Pharmacology*, **52**, 1561–1568.

Jones, P. M., Burrin, J. M., Ghatei, M. A., O'Halloran, D. J., Legon, S., and Bloom, S. R., 1990, The influence of thyroid hormone status on the hypothalamo-hypophyseal growth hormone axis. *Endocrinology*, **126**, 1374–1379.

Kato, R. and Yamazoe, Y., 1992, Sex-specific cytochrome P450 as a cause of sex- and species-related differences in drug toxicity. *Toxicology Letters*, **64–65**, 661–667.

Levy, A., Matovelle, M. C., Lightman, S. L. and Young, W. S., 1992, The effects of pituitary stalk transection, hypophysectomy and thyroid hormone status on insulin-like growth factor 2-, growth hormone releasing hormone, and somatostatin mRNA prevalence in rat brain. *Brain Research*, **579**, 1–7.

Liu, L. and Klaassen, C. D., 1996a, Different mechanism of saturation of acetaminophen sulphate conjugation in mice and rats. *Toxicology and Applied Pharmacology*, **139**, 128–134.

Liu, L. and Klaassen, C. D., 1996b, Ontogeny and hormonal basis of male-dominant rat hepatic sulphotransferases. *Molecular Pharmacology*, **50**, 565–572.

Liu, L. and Klaassen, C. D., 1996c, Ontogeny and hormonal basis of female-dominant rat hepatic sulphotransferases. *Journal of Pharmacology and Experimental Therapeutics*, **279**, 386–391.

Liu, L. and Klaassen, C. D., 1996d, Regulation of hepatic sulphotransferases by steroidal chemicals in rats. *Drug Metabolism and Disposition*, **24**, 854–858.

Meerman, J. H. N. and Vandepoll, M. L. M., 1994, Metabolic activation routes of arylamines and their genotoxic effects. *Environmental Health Perspectives*, **102**, 153–159.

Mulder, G. J., Jakoby, W. B. and Mulder, G. J. (eds), 1990, Sulphation. In *Conjugation Reactions in Drug Metabolism* (London: Taylor & Francis), pp. 107–161.

Murayama, N., Shimada, M., Yamazoe, Y. and Kato, R., 1991, Difference in the susceptibility of two phenobarbital-inducible forms, P450IIB1 and P450IIB2, to thyroid hormone- and growth hormone-induced suppression in rat liver: phenobarbital-inducible P450IIB2 suppression by thyroid hormone acting directly, but not through the pituitary system. *Molecular Pharmacology*, **39**, 811–817.

Nagata, K., Ozawa, S., Miyata, M., Shimada, M., Gong, D. W., Yamazoe, Y. and Kato, R., 1993, Isolation and expression of a cDNA encoding a male-specific rat sulphotransferase that catalyzes activation of *N*-hydroxy-2-acetylaminofluorene. *Journal of Biological Chemistry*, **268**, 24720–24725.

Nuwaysir, E. F., Daggett, D. A., Jordan, V. C. and Pitot, H. C., 1996, Phase II enzyme expression in rat liver in response to the antiestrogen tamoxifen. *Cancer Research*, **56**, 3704–3710.

Ogura, K., Kajita, J., Narihata, H., Watabe, T., Ozawa, S., Nagata, K., Yamazoe, Y. and Kato, R., 1989, Cloning and sequence analysis of a rat liver cDNA encoding hydroxysteroid sulphotransferase. *Biochemical and Biophysical Research Communication*, **165**, 168–174.

Ogura, K., Kajita, J., Narihata, H., Watabe, T., Ozawa, S., Nagata, K., Yamazoe, Y. and Kato, R., 1990, cDNA cloning of the hydroxysteroid sulphotransferase STa sharing a strong homology in amino acid sequence with the senescence marker protein SMP-2 in rat livers. *Biochemical Biophysical Research Communications*, **166**, 1494–1500.

Ozawa, S., Nagata, K., Gong, D., Yamazoe, Y. and Kato, R., 1990, Nucleotide sequence of a full-length cDNA (PST-1) for aryl sulphotransferase from rat liver. *Nucleic Acids Research*, **18**, 4001.

Ram, P. A. and Waxman, D. J., 1991, Hepatic P450 expression in hypothyroid rats: differential responsiveness of male-specific P450 forms 2a (IIIA2), 2c (IIC11), and RLM2 (IIA2) to thyroid hormone. *Molecular Endocrinology*, **5**, 13–20.

Runge-Morris, M., Rose, K. and Kocarek, T. A., 1996, Regulation of rat hepatic sulphotransferase gene expression by glucocorticoid hormones. *Drug Metabolism and Disposition*, **24**, 1095–1101.

Runge-Morris, M. and Wilusz, J., 1994, Suppression of hydroxysteroid sulphotransferase-a gene expression by 3-methylcholanthrene. *Toxicology and Applied Pharmacology*, **125**, 133–141.

Sakakibara, Y., Takami, Y., Zwieb, C., Nakayama, T., Suiko, M., Nakajima, H. and Liu, M. C., 1995, Purification, characterization, and molecular cloning of a novel rat liver Dopa/tyrosine sulphotransferase. *Journal of Biological Chemistry*, **270**, 30470–30478.

Singleton, D. W., Lei, X. D., Webb, S. J., Prough, R. A. and Geoghegan, T. E., 1999, Cytochrome P-450 mRNAs are modulated by dehydroepiandrosterone, nafenopin, and triiodothyronine. *Drug Metabolism and Disposition*, **27**, 193–200.

Skett, P. and Weir, A., 1983, Sex- and substrate-dependent effects of the thyroid gland on drug metabolism in the rat. *Biochemical Pharmacology*, **32**, 3115–3117.

Surh, Y. J., Lai, C. C., Miller, J. A. and Miller, E. C., 1987, Hepatic DNA and RNA adduct formation from the carcinogen 7-hydroxymethyl-12-methylbenz[a]anthracene and its electro-

philic sulphuric acid ester metabolite in preweanling rats and mice. *Biochemical and Biophysical Research Communications*, **144**, 576–582.

THOMAS, R. C. and HARPOOTLIAN, H., 1975, Metabolism of minoxidil, a new hypotensive agent II: biotransformation following oral administration to rats, dogs, and monkeys. *Journal of Pharmacological Science*, **64**, 1366–1371.

UEDA, R., SHIMADA, M., HASHIMOTO, H., ISHIKAWA, H. and YAMAZOE, Y., 1997, Distinct regulation of two hydroxysteroid sulphotransferases, ST2A1 and ST2A2, by growth hormone: a unique type of growth hormone regulation in rats. *Journal of Pharmacology and Experimental Therapeutics*, **282**, 1117–1121.

VISSER, T. J., 1994, Role of sulphation in thyroid hormone metabolism. *Chemico and Biological Interactions*, **92**, 293–303.

WATABE, T., OGURA, K., SATSUKAWA, M., OKUDA, H. and HIRATSUKA, A., 1994, Molecular cloning and functions of rat liver hydroxysteroid sulfotransferases catalysing covalent binding of carcinogenic polycyclic arylmethanols to DNA. *Chemico and Biological Interactions*, **92**, 87–105.

WEBB, S. J., XIAO, G. H., GEOGHEGAN, T. E. and PROUGH, R. A., 1996, Regulation of CYP4A expression in rat by dehydroepiandrosterone and thyroid hormone. *Molecular Pharmacology*, **49**, 276–287.

YAMAZOE, Y., MANABE, S., MURAYAMA, N. and KATO, R., 1987, Regulation of hepatic sulfotransferase catalyzing the activation of N-hydroxyarylamide and N-hydroxyarylamine by growth hormone. *Molecular Pharmacology*, **32**, 536–541.

YAMAZOE, Y., GONG, D., MURAYAMA, N., ABU-ZEID, M. and KATO, R., 1989, Regulation of hepatic cortisol sulfotransferase in rats by pituitary growth hormone. *Molecular Pharmacology*, **35**, 707–712.

YAMAZOE, Y., MANABE, S., MURAYAMA, N. and KATO, R., 1997, Regulation of hepatic sulphotransferase catalyzing the activation of *N*-hydroxylamide and *N*-hydroxylarylamine by growth hormone. *Molecular Pharmacology*, **32**, 536–541.

XENOBIOTICA , 2000, VOL. 30, NO. 4, 359–369

Reduction of stilbene oxide and styrene oxide to the corresponding alkenes by intestinal bacteria

S. KITAMURA*, M. MITA, K. MATSUDA, S. OHTA and K. TATSUMI

Institute of Pharmaceutical Science, Hiroshima University School of Medicine, Kasumi 1–2-3, Minami-ku, Hiroshima 734–8551, Japan

Received 23 July 1999

1. This study provides the first evidence that stilbene oxide and styrene oxide are reductively metabolized to the corresponding alkenes by intestinal bacteria in animals.

2. When *trans*- or *cis*-stilbene oxide were incubated with the caecal contents of rat under anaerobic conditions, both *trans*- and *cis*-stilbene were isolated from the incubation mixture. Styrene oxide was also reduced to styrene by rat caecal contents.

3. Caecal contents of mouse, hamster and guinea pig also exhibited alkene oxide reductase activities toward *cis*- and *trans*-stilbene oxides, and styrene oxide. In contrast, liver microsomes or cytosol exhibited no epoxide reductase activities toward these substrates.

4. Seven pure strains of intestinal bacteria exhibited alkene oxide reductase activities of varying degrees under anaerobic conditions, with the highest activity being observed in *Clostridium sporogenes*.

5. Cell-free extracts of either the intestinal bacteria in rat caecal contents or *C. sporogenes* exhibited reductase activity when supplemented with both NAD(P)H and FMN under anaerobic conditions. Reductase activity was also observed on addition of the photochemically reduced form of FMN instead of both NAD(P)H and FMN.

Introduction

Aromatic hydrocarbons or alkene compounds undergo metabolic oxidation to their epoxides, and some epoxides are known to be active intermediates in carcinogenesis and mutagenesis (Marquardt *et al.* 1972, Jerina and Daly 1974, Hemminki *et al.* 1994). The epoxides formed are further metabolized to the corresponding dihydrodiols and to glutathione conjugates (Watabe and Akamatsu 1972, Jakoby and Habig 1980, Oesch 1980, Luo and Guenthner 1994). Of the epoxide compounds, the arene oxides formed from arenes are also known to be reduced to regenerate the parent compounds (Booth *et al.* 1975, Kato *et al.* 1976, Yamazoe *et al.* 1978, Sugiura *et al.* 1980, Wrighton *et al.* 1982), and this interconversion between arenes and arene oxides occurs in the animal body. Booth *et al.* (1975) reported that several arene oxides were reduced by rat liver microsomes in the presence of NADPH. The participation of cytochrome P450 in microsomal arene oxide reduction was demonstrated mainly by using benz[a]pyrene 4,5-oxide as a substrate (Kato *et al.* 1976, Yamazoe *et al.* 1978, Sugiura *et al.* 1980, Wrighton *et al.* 1982). Wrighton *et al.* (1982) reported that a cytosolic factor is essential in the microsomal reduction of benzo[a]pyrene 4,5-oxide. Recently, Hirao *et al.* (1994) reported that naphthalene 1,2-oxide and benzo[a]pyrene 4,5-oxide are also reduced in rat liver cytosol and are catalysed by aldehyde oxidase.

However, a few studies concerning the reduction of alkene oxides to the parent

* Author for correspondence; e-mail: kitamura@pharm.hiroshima-u.ac.jp

Xenobiotica ISSN 0049-8254 print/ISSN 1366-5928 online © 2000 Taylor & Francis Ltd
http://www.tandf.co.uk/journals

alkenes have been conducted to date. Sugiura *et al.* (1980) reported that benzo[a]pyrene 7,8-dihydrodiol 9,10-oxide was not reduced by the cytochrome P450 system of rat liver microsomes in the presence of NADPH. Hirao *et al.* (1994) also reported that the reduction of alkene oxides such as styrene oxide and *trans*-stilbene oxide did not occur in the cytosolic fraction of rat liver even in the presence of an electron donor for aldehyde oxidase, even though arene oxides were reduced in the cytosol under the same conditions. In contrast, Ivie (1976) demonstrated that dieldrin, an alkene oxide of aldrin, was reduced to aldrin in sheep rumen. However, a detailed examination concerning the nature of alkene oxide reduction in intestinal bacteria has not been conducted. In the present study, the reductive metabolism of *trans*-stilbene oxide, *cis*-stilbene oxide and styrene oxide to the alkene products by intestinal bacteria have been examined to examine the nature of alkene oxide reduction in significantly more detail.

Materials and methods

Chemicals

Trans-stilbene oxide (98% pure), *trans*-stilbene (96%) and styrene oxide (97%) were from Tokyo Chemical Industry Co. Ltd (Tokyo, Japan), *cis*-stilbene (96%) and styrene (99%) from Nacalai Tesque, Inc. (Kyoto, Japan), and *cis*-stilbene oxide (97%) from Aldrich Chemical Co. (Milwaukee, WI, USA). Reduced FMN was prepared photochemically from FMN by the method of Yubisui *et al.* (1980).

Animals and treatment with antibiotics

Male Wistar rats (185–240 g), ddY mice (27–38 g), Syrian golden hamsters (85–98 g) and Hartley guinea pigs (235–260 g) were used. Treatment of rat with antibiotics was performed according to the method of Kinouchi *et al.* (1993). A mixture of neomycin sulphate, streptomycin sulphate and bacitracin (200 mg kg^{-1} each) was given orally to rat twice daily for 6 days.

Cecal contents and bacterial strains

Caecal contents quickly prepared from the exanguinated animals, suspended in 4 vols deoxygenated GAM broth (Gifu anaerobic medium broth for general culture and susceptibility test; Nissui Pharmaceutical Co., Ltd, Tokyo, Japan) and centrifuged at 500*g* for 5 min to exclude food materials. The supernatant was used as the suspension of caecal contents. Pure strains of intestinal bacteria, *Clostridium sporogenes*, *Bifidobacterium bifidum*, *Escherichia coli*, *Salmonella typhimurium*, *Pseudomonas fluorescens*, *Lactobacillus rhamnosus* and *Streptococcus faecalis*, were from the Institute for Fermentation (Osaka, Japan). Facultative anaerobic bacteria were grown in *l*-broth at 37 °C and harvested by centrifugation at 10 000*g* for 10 min. Cells were washed twice with sterilized 0.1 M K,Na-phosphate buffer (pH 7.4), and resuspended in the latter phosphate buffer. Anaerobic bacteria were grown in GAM broth using a BBL Gas Pack anaerobic jar (Becton-Dickinson, Cockeysville, MD, USA). Cells harvested by centrifugation were suspended in sterilized GAM broth. The concentration of the cell suspensions was adjusted on the basis of the absorbance at 600 nm, namely when the absorbance was 0.1, the cell concentration was estimated to be 2×10^8 ml^{-1}.

Preparation of cell-free extracts

Caecal contents ($\sim$ 6 g) or *C. sporogenes* cells ($\sim$ 4 g) were suspended in 15 ml sterilized 0.1 M K,Na-phosphate buffer (pH 7.4), and sonicated using a Tomy Ultrasonic Disruptor (UR-200P, Tomy Seiko Co. Ltd, Tokyo, Japan). Any undisrupted cells in the suspension were removed by centrifugation at 10000*g* for 20 min, and the supernatant was used as cell-free extracts. Protein contents in the cell-free extracts from *C. sporogenes* and caecal contents were determined as 4.6–5.5 and 14.8–16.6 mg protein ml^{-1} respectively by the method of Lowry *et al.* (1951).

High-performance liquid chromatography (HPLC)

HPLC was performed in a Hitachi L-6000 chromatograph (Tokyo, Japan) fitted with a 250 × 4.6 mm Capcell Pak C_{18} UG 120 Å (5 μm) column (Shiseido, Tokyo, Japan). The mobile phase was acetonitrile-H_2O (7 : 3 v/v). The chromatograph was operated at a flow rate of 1.0 or 0.5 $mlmin^{-1}$ in the case of stilbene oxide or styrene oxide respectively at a wavelength of 254 nm. The elution times of *cis*-stilbene oxide,

trans-stilbene oxide, *trans*-stilbene, *cis*-stilbene, diphenyl (an internal standard in the case of stilbene oxide), styrene oxide, styrene and diphenyl (an internal standard in the case of styrene oxide) were 6.0, 7.5, 10.2, 10.8, 9.0, 7.8, 12.6 and 17.8 min respectively.

Isolation of alkene oxide metabolites from the incubation mixture of caecal contents

An incubation mixture consisted of 10 μmol of an alkene oxide and a bacterial suspension from rat caecal contents in a final volume of 20 ml 0.1 M phosphate buffer (pH 7.4). The following experiments were carried out in the dark. The incubation was performed at 37 °C for 6 h under nitrogen. The mixture was adjusted to pH 10 with 1 N NaOH and extracted twice with 2 vols benzene in the case of *cis*- and *trans*-stilbene oxides, or with diethyl ether in the case of styrene oxide. The combined extract was dried over anhydrous Na_2SO_4 and evaporated to dryness *in vacuo*. In the case of *cis*- and *trans*-stilbene oxides, HPLC analysis showed that either extract contains two metabolites corresponding to *cis*- and *trans*-stilbene. In the case of styrene oxide, HPLC analysis showed that the extract contains the metabolite corresponding to styrene. The metabolites were purified by HPLC from the extract.

Assays of alkene oxide reductase activities

A typical incubation mixture consisted of 0.5 μmol of an alkene oxide, 1 μmol of an electron donor, 0.2 μmol FMN or methyl viologen, and an enzyme source in a final volume of 2 ml 0.1 M K,Na-phosphate buffer (pH 7.4). When caecal contents or bacteria were used, an electron donor and FMN were omitted, and 1 ml (equivalent to 20 mg) of caecal contents or 1 ml ($8–13\times10^{10}$ cells) of intestinal bacterial suspension was added. The following experiments were carried out in the dark. The incubation was performed at 37 °C for 6 h under anaerobic conditions using a Thunberg tube. The side arm contained the substrate and the body contained all other components. The tube was gassed for 5 min with nitrogen, evacuated with an aspirator for 5 min, and again gassed with nitrogen. Mixing the components of the side arm and the body started the reaction. After incubation, 100 μg biphenyl was added as an internal standard, and the mixture was extracted with 5 ml benzene. The extract was evaporated to dryness, the residue dissolved in 0.1 ml methanol and an aliquot was analyzed by HPLC. The limit of detection for *cis*-stilbene, *trans*-stilbene and styrene in the incubation mixture was 0.03, 0.05 and 0.12 nmol respectively.

Results

Metabolites of trans-stilbene oxide by rat caecum contents

When *trans*-stilbene oxide was incubated with caecal contents of rat, two metabolites were detected in organic extracts of the incubation mixtures on HPLC analysis. The retentions of these metabolites (10.2, 10.8 min) were identical to those of *trans*- and *cis*-stilbene respectively. These metabolites were then designated stilbene product M1 and stilbene product M2. These peaks were not detected in the chromatogram of the extract of control incubation mixtures (figure 1). These metabolites were isolated from the mixture as described in the Materials and methods. The mass spectra of the two metabolites gave the same molecular ion at m/z 180, suggesting that these metabolites are the corresponding alkene compound. Furthermore, the spectra showed the same fragment ions at m/z 165, 102, 89 and 77 (figure 2A). However, the UV spectra of these metabolites in ethanol revealed an absorption maximum at 296 nm with shoulders at 320, 309 and 242 nm for stilbene product M1 and at 274 nm with shoulders at 332 and 242 for stilbene product M2. The mass and UV spectra, and the HPLC behaviour of these metabolites were identical to those of authentic samples of *trans*- and *cis*-stilbene. The two metabolites were also isolated from the incubation mixture with *cis*-stilbene oxide, and identified as *cis*- and *trans*-stilbene.

The time-course of the reduction of *trans*-stilbene oxide by rat caecum contents was essentially linear up to 12 h, whereupon the amounts of the alkenes formed from the alkene oxide decreased with time. Accordingly, incubations were carried out for 6 h under anaerobic conditions. When the caecal contents were sonicated or boiled, the reductase activity toward *trans*-stilbene oxide was abolished, and low activity

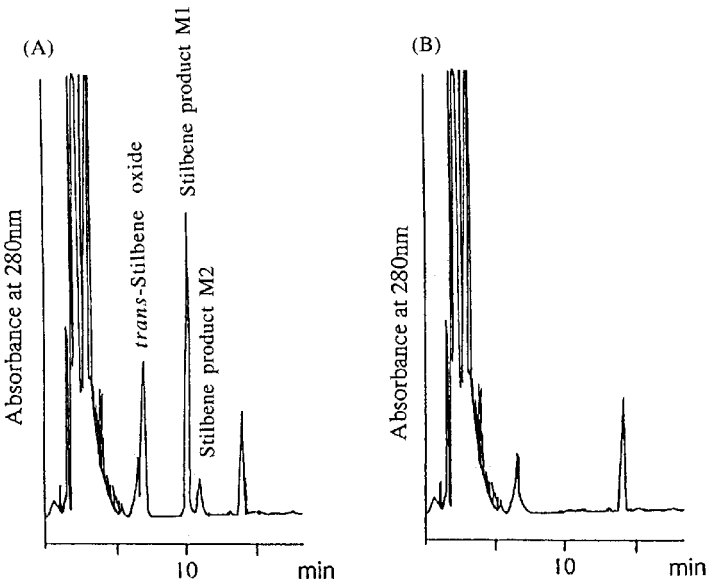


Figure 1. HPLC of the metabolites of *trans*-stilbene oxide produced by the intestinal bacteria of rat. (A) Extract of the incubation mixture of *trans*-stilbene oxide with rat caecum contents. (B) Extract of the incubation mixture without substrate.

was observed under aerobic conditions. When *trans*-stilbene oxide was incubated with the caecal contents of the antibiotic-treated rat under anaerobic conditions, low reductase activity was observed (figure 3).

When styrene oxide was incubated with rat caecum contents in a similar manner, one metabolite designated styrene product M1 was isolated from the mixture. The mass spectrum of the metabolite showed a molecular ion at m/z 104, suggesting that the metabolite is styrene (figure 2B). The UV spectrum of the metabolite in ethanol revealed an absorption maximum at 247 nm with shoulders at 220 and 269 nm. The mass and UV spectra, and the HPLC behaviour of the metabolite were identical with those of an authentic sample of styrene.

Reduction of alkene oxides by caecal contents of animals

The caecal contents of rat, mouse, hamster and guinea pig had the ability to catalyze the reduction of *trans*-stilbene oxide, *cis*-stilbene oxide and styrene oxide to the alkenes under anaerobic conditions. In the case of stilbene oxide, *cis*- and *trans*-stilbenes were formed simultaneously from *cis*- and *trans*-stilbene oxides. Among the mammalian species examined, the highest activity toward *trans*-stilbene oxide was observed with hamster (table 1). The liver microsomes of these animals exhibited no reductase activity toward the alkene oxides even in the presence of NADPH and liver cytosols of the animals also had no ability to reduce the alkene oxides in the presence of an electron donor for aldehyde oxidase (data not shown).

The ability of the sonicated cell-free extracts of intestinal bacteria from the caecal contents of rat to reduce alkene oxides to alkenes was examined. When NADH, NADPH or FMN was added to the incubation mixture, limited reductase activity was observed. However, the activity was enhanced by addition of both NADH and FMN, or NADPH and FMN under anaerobic conditions (table 2). The activity was inhibited by oxygen (data not shown).

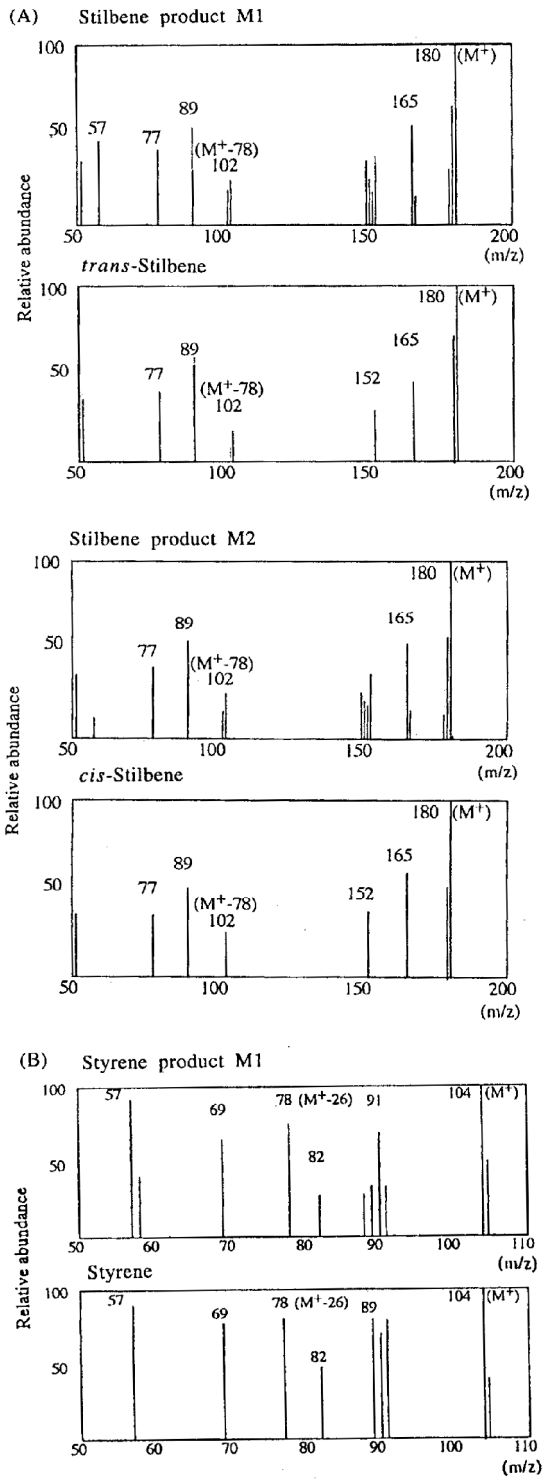


Figure 2. Mass spectra of the metabolites of *trans*-stilbene oxide (A) and styrene oxide (B) by rat caecum contents, and authentic samples.

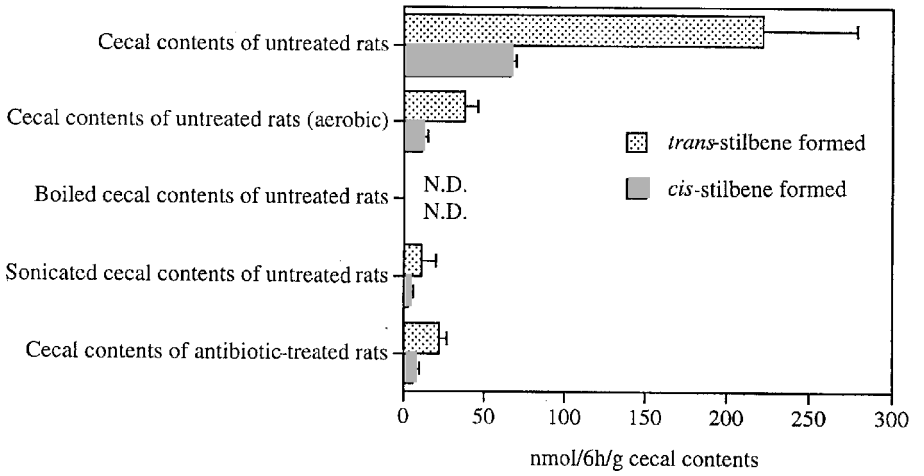


Figure 3. Reduction of *trans*-stilbene oxide to *cis*- and *trans*-stilbene by rat caecum contents. Each value represents the mean± SD of three experiments. Reactions were conducted with rat caecum contents under anaerobic conditions and other experimental details are described in the Materials and methods. ND, not detected.

Table 1. Reduction of *cis*- and *trans*-stilbene oxides and styrene oxide by caecum contents of several mammalian species.

	trans-Stilbene oxide		*cis*-Stilbene oxide		Styrene oxide
Species	*trans*-Stilbene formed	*cis*-Stilbene formed	*trans*-Stilbene formed	*cis*-Stilbene formed	Styrene formed
Rat	222± 57	66± 4	30± 8	68± 10	53± 5
Mouse	101± 70	17± 9	18± 8	88± 62	64± 5
Hamster	595± 263	114± 43	11± 1	44± 12	75± 8
Guinea pig	48± 18	2± 3	2± 3	58± 31	48± 5

Each value represents the mean± S.D. of three animals and is expressed as nmol/6 h/g caecum content.

A mixture containing an alkene oxide (5×10^{-4} M) and caecum contents in 0.1 M phosphate buffer (pH 7.4) was incubated at 37°C for 6 h under anaerobic conditions.

The alkene formed was determined using HPLC, and other experimental details are described in the Materials and methods.

Reduction of alkene oxides by colonies of single intestinal bacteria

The caecal contents contain a variety of bacteria and the ability of seven types of intestinal bacteria to reduce alkene oxides was therefore examined. These bacteria exhibited reductase activity toward the alkene oxides to varying degrees. Among the strains tested, the highest activity was observed in *C. sporogenes*, and the lowest in *S. faecalis* under anaerobic conditions (figure 4).

Reduction of alkene oxides by a cell-free extract of C. sporogenes

The ability of a cell-free extract from *C. sporogenes* to reduce alkene oxides was also examined. The reductase activity of the cell-free extract was enhanced by addition of NAD(P)H and FMN, or NAD(P)H and methyl viologen under anaerobic conditions. Significant reductase activity of the cell-free extract was

Table 2. Reduction of *cis*- and *trans*-stilbene oxides and styrene oxide by cell-free extracts of rat caecum contents.

Addition	*trans*-Stilbene oxide Stilbene formed*	*cis*-Stilbene oxide	Styrene oxide Styrene formed
None	5±2	nd	nd
NADH	120±23	18±5	10±3
NADPH	50±12	8±3	nd
NADH + FMN	308±48	38±12	27±12
NADPH + FMN	248±43	20±8	22±10
FMN	8±2	2±2	nd

Each value represents the mean± SD of three experiments and is expressed as pmol h^{-1} mg $protein^{-1}$.
nd, Not detected.
* Sum of *cis*- and *trans*-stilbenes formed.
A mixture containing an alkene oxide (5×10^{-4} M), NADH or NADPH (5×10^{-4} M), FMN (10^{-4} M) and the cell-free extract from sonicated caecum contents of rat (~8 mg protein) in 0.1 M phosphate buffer was incubated at 37°C for 6 h under anaerobic conditions. The alkene formed was determined using HPLC and other experimental details are described in the Materials and methods.

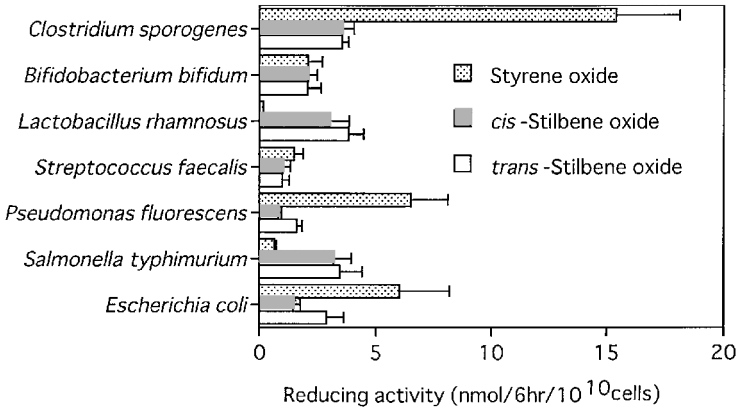


Figure 4. Reduction of alkene oxides by various intestinal bacteria. Each value represents the mean± SD of three experiments. Reactions were conducted at 37 °C for 6 h with bacterial strains under anaerobic conditions and alkenes formed were determined by HPLC. In the case of stilbene oxides, the sum of *cis*- and *trans*-stilbenes formed is shown. Other experimental details are described in the Materials and methods.

observed when photochemically reduced FMN was added instead of FMN and NAD(P)H (table 3). In this case, reduced FMN could not reduce these substrates without the cell-free extracts. When the cell-free extract was boiled, reduction did not occur in the presence of cofactors and the reductase activity of the cell-free extracts was not observed under aerobic conditions (data not shown).

Discussion

Previous workers have suggested that alkene oxides can not be reduced in the animal body on the basis of the findings that the alkene oxides are not reduced by liver microsomes or cytosol *in vitro* (Sugiura *et al.* 1980, Hirao *et al.* 1994). The present study provides the first evidence that *cis*- and *trans*-stilbene oxides, and styrene oxide are reduced to the parent alkene compounds by intestinal bacteria.

Table 3. Reduction of *cis*- and *trans*-stilbene oxides and styrene oxide by cell-free extracts from *Clostridium sporogenes*.

	trans-Stilbene oxide	*cis*-Stilbene oxide	Styrene oxide
Addition	Stilbene formed*		Styrene formed
None	112± 95	52± 43	32± 27
NADH	237± 102	140± 20	57± 32
NADPH	145± 127	75± 35	42± 37
NADH + FMN	517± 132	262± 60	67± 37
NADPH + FMN	415± 48	185± 38	50± 43
FMN	173± 77	95± 82	35± 20
NADH + methyl viologen	358± 67	170± 35	38± 33
NADPH + methyl viologen	210± 82	113± 22	35± 30
Methyl viologen	145± 125	62± 52	18± 17
$FMNH_2$	753± 125	542± 77	178± 7

Each value represents the mean± S.D. of three experiments and is expressed as pmol h^{-1} mg $protein^{-1}$.

* Sum of *cis*- and *trans*-stilbenes formed.

A mixture containing an alkene oxide (5×10^{-4} M), NADH or NADPH (5×10^{-4} M), FMN or methyl viologen (10^{-4} M) and the cell-free extract from *Clostridium sporogenes* (~ 3 mg protein) in 0.1 M phosphate buffer (pH 7.4) was incubated at 37°C for 6 h under anaerobic conditions. The alkene formed was determined using HPLC and other experimental details are described in the Materials and methods.

The importance of intestinal bacteria in the metabolism of xenobiotics has been increasingly recognized and Scheline (1973) has reviewed the reduction of certain xenobiotics by intestinal bacteria. Involvement of intestinal bacteria in the reduction of nitro, azo, sulphoxide, hydroxamic acid and double bond compounds, and in the reductive cleavage of the benzisoxazole ring has been reported (Williams *et al.* 1970, Gingell *et al.* 1971, Levin and Dent 1982, Renwick *et al.* 1982, Ishida *et al.* 1996, Kitamura *et al.* 1997). However, little is known about the reduction of alkene oxides by intestinal bacteria. Fukushima *et al.* (1990) reported that an epoxysuccinic acid derivative was reduced by rat caecal contents; the corresponding alkene derivative was tentatively identified as an intermediate, but the reduction mechanism of intestinal bacteria was not examined using cell-free extracts of intestinal bacteria. Ivie (1976) reported that a juvenile hormone mimic, 1-(4′-ethylphenoxy)-3,7-dimethyl-6,7-epoxy-*trans*-2-octene, and an insecticide, dieldrin, were reduced to the corresponding alkene compounds by sheep rumen, and suggested that the reaction was microbial. In contrast, Hoffman *et al.* (1973) reported that the alkene derivative of the former compound was not formed and they suggested that the alkene compound was due to contamination of the parent compound.

The present authors have demonstrated that *trans*- and *cis*-stilbenes were formed from *trans*- or *cis*-stilbene oxide by intestinal bacteria and the pathway of formation of both isomers has been examined in caecal contents of rat. When *cis*- or *trans*-stilbene oxide were incubated with intestinal bacteria, *cis*- and *trans*-stilbene were formed simultaneously (figure 1, table 1). In other preliminary experiments, when *cis*- or *trans*-stilbene (5×10^{-4} M) was incubated with rat caecal contents for 6 h under anaerobic conditions, the *cis*- and *trans*-isomers were again formed from each isomer. The rates of isomerization from *cis*- to *trans*-isomer was 115 nmol h^{-1} g^{-1} caecum contents and that from *trans*- to *cis*-isomer was 35 nmol h^{-1} g^{-1} caecum contents and the activity was not influenced by oxygen. It is likely that isomerization proceeded enzymatically because activity was not observed in boiled caecum

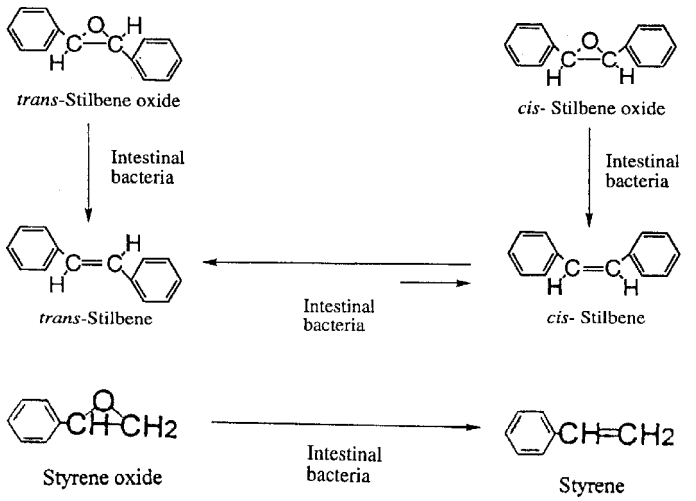


Figure 5. Proposed pathway of alkene formation from alkene oxides by intestinal bacteria.

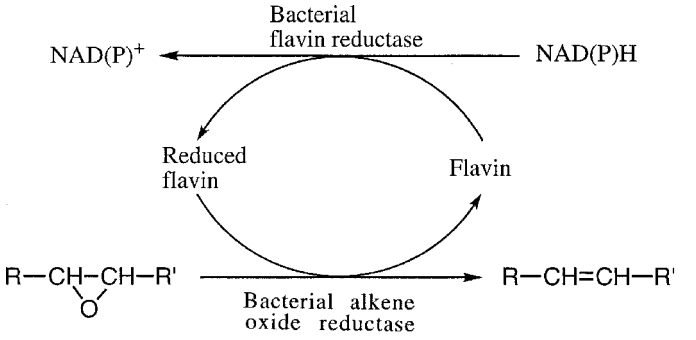


Figure 6. Proposed mechanism of the reduction of alkene oxides by intestinal bacteria.

contents. These results suggest that the *cis*- and *trans*-stilbene oxides were reduced to the corresponding alkenes, and intestinal bacteria isomerized cis- and trans-stilbene to each other (figure 5).

A cell-free extract from *C. sporogenes* or intestinal bacteria in rat caecal contents exhibited NAD(P)H and FMN-dependent reductase activity toward alkene oxides. Photochemically reduced FMN was more effective for the reduction by the cell-free extracts. However, reduced FMN could not reduce alkene oxides without the cell-free extracts. The reduction of alkene oxides by intestinal bacteria presented in this study appears to proceed in two steps. The first step is reduction of FMN by a bacterial flavin reductase in the presence of a reduced pyridine nucleotide as described by Fieschi *et al.* (1995) or non-enzymatic reduction by NADPH or NADH as reported by Singer and Kearney (1950). The second step is reduction of alkene oxide to the corresponding alkene by a flavin-dependent bacterial reductase with the reduced flavin as an electron donor (figure 6). Recently, the present authors reported that a similar flavin-dependent enzyme system in cell-free extracts of intestinal bacteria functions in the reduction of 1-nitropyrene, zonisamide and α-(bromoisovaleryl)urea (Narai *et al.* 1984, Kitamura *et al.* 1997, 1998). A detailed

investigation of the reduction mechanism of xenobiotics by intestinal bacteria is underway.

References

Booth, J., Hewer, A., Keysell, G. R. and Sims, P., 1975, Enzymic reduction of aromatic hydrocarbon epoxides by the microsomal fraction of rat liver. *Xenobiotica*, **5**, 197–203.

Fieschi, F., Nivie'Re, V., Frier, C., De'Cout, J.-L. and Fontecave, M., 1995, The mechanism and substrate specificity of the NADPH:flavin oxidoreductase from *Escherichia coli*. *Journal of Biological Chemistry*, **270**, 30392–30400.

Fukushima, K., Arai, M., Suwa, T. and Satoh, T., 1990, Enzymatic reduction of an epoxysuccinic acid derivative by rat caecal microflora. *Drug Metabolism and Disposition*, **18**, 264–266.

Gingell, R., Bridges, J. W. and Williams, R. T., 1971, The role of the gut flora in the metabolism of prontosil and neoprontosil in the rat. *Xenobiotica*, **1**, 143–156.

Hemminki, A., Väyrynen, T. and Hemminki, K., 1994, Reaction kinetics of alkyl epoxides with DNA and other nucleophiles. *Chemico-Biological Interactions*, **93**, 51–58.

Hirao, Y., Kitamura, S. and Tatsumi, K., 1994, Epoxide reductase activity of mammalian liver cytosols and aldehyde oxidase. *Carcinogenesis*, **15**, 739–743.

Hoffman, L. J., Ross, J. H. and Menn, J. J., 1973, Metabolism of 1-(4′-ethylphenoxy)-6,7-epoxy-3,7-dimethyl-2-octene (R 20458) in the rat. *Journal of Agricultural and Food Chemistry*, **21**, 156–163.

Ishida, M., Kitamura, S. and Tatsumi, K., 1996, Purification of an α,βketoalkene double bond reductase from *Salmonella typhimurium*. *Biochemistry and Molecular Biology International*, **39**, 1157–1165.

Ivie, G. W., 1976, Epoxide to olefin: a novel biotransformation in the rumen. *Science*, **191**, 959–961.

Jakoby, W. B. and Habig, W. H., 1980, Glutathione transferases. In W. B. Jakoby (ed.), *Enzymatic Basis of Detoxication*, vol. II (New York: Academic Press), pp. 63–94.

Jerina, D. M. and Daly, J. W., 1974, Arene oxides: a new aspect of drug metabolism. *Science*, 185, 573–582.

Kato, R., Iwasaki, K., Shiraga, T. and Noguchi, H., 1976, Evidence for the involvement of cytochrome P-450 in reduction of benzo(a)pyrene 4,5-oxide by rat liver microsomes. *Biochemical and Biophysical Research Communications*, 70, 681–687.

Kinouchi, T., Kataoka, K., Miyanishi, K., Akimoto, S. and Ohnishi, Y., 1993, Biological activities of the intestinal microflora in mice treated with antibiotics or untreated and the effects of the microflora on absorption and metabolic activation of orally administered glutathione conjugates of K-region epoxides of 1-nitropyrene. *Carcinogenesis*, **14**, 869–874.

Kitamura, S., Kuwasako, M., Ohta, S. and Tatsumi, K., 1998, Reductive debromination of α-(bromoisovaleryl)urea by intestinal bacteria. *Journal of Pharmacy and Pharmacology*, **51**, 79–84.

Kitamura, S., Sugihara, K., Kuwasako, M. and Tatsumi, K., 1997, The role of mammalian intestinal bacteria in the reductive metabolism of zonisamide. *Journal of Pharmacy and Pharmacology*, **49**, 253–256.

Levin, A. A. and Dent, J. G., 1982, Comparison of the metabolism of nitrobenzene by hepatic microsomes and caecal microflora from Fischer-344 rats *in vitro* and the relative importance of each *in vivo*. *Drug Metabolism and Disposition*, **10**, 450–454.

Lowry, O. H., Rosebrough, N. J., Farr, A. L. and Randall, R. J., 1951, Protein measurement with the Folin phenol reagent. *Journal of Biological Chemistry*, **193**, 265–275.

Luo, G. and Guenthner, T. M., 1994, Detoxication of the 2′,3′-epoxide metabolites of allylbenzene and estragole: conjugation with glutathione. *Drug Metabolism and Disposition*, **22**, 731–737.

Marquardt, H., Kuroki, T., Huberman, E., Selkirk, J. K., Heidelberg, C., Grover, P. L. and Sims, P., 1972, Malignant transformation of cells derived from mouse prostate by epoxides and other derivatives of polycyclic hydrocarbons. *Cancer Research*, **32**, 716–720.

Narai, N., Kitamura, S. and Tatsumi, K., 1984, A comparative study on 1-nitropyrene and nitrofurazone reductases in *Escherichia coli*. *Journal of Pharmacobio-Dynamics*, **7**, 407–413.

Oesch, F., 1980, Microsomal epoxide hydrolase. In W. B. Jakoby (ed.), *Enzymatic Basis of Detoxication*, vol. II (New York: Academic Press), pp. 277–290.

Renwick, A. G., Evans, S. P., Sweatman, T. W., Cumberland, J. and George, C. F., 1982, The role of the gut flora in the reduction of sulphinpyrazone in the rat. *Biochemical Pharmacology*, **31**, 2649–2656.

Scheline, R. R., 1973, Metabolism of foreign compounds by gastrointestinal microorganisms. *Pharmacological Reviews*, **25**, 451–523.

Singer, T. P. and Kearney, F. B., 1950, The non-enzymatic reduction of cytochrome *c* by pyridine nucleotides and its catalysis by various flavins. *Journal of Biological Chemistry*, **183**, 409–429.

Sugiura, M., Yamazoe, Y., Kamataki, T. and Kato, R., 1980, Reduction of epoxy derivatives of benzo(a)pyrene by microsomal cytochrome P-450. *Cancer Research*, **40**, 2910–2914.

WATABE, T. and AKAMATSU, K., 1972, Stereoselective hydrolysis of acyclic olefin oxides to glycols by hepatic microsomal epoxide hydrolase. *Biochimica et Biophysica Acta*, **279**, 297–305.

WILLIAMS, J. R., GRANTHAM, P. H., MARSH, H. H. and WEISBURGER, J. H., 1970, Participation of liver fractions and of intestinal bacteria in the metabolism of intestinal bacteria in the metabolism of *N*-hydroxy-*N*-2-fluorenylacetamide in the rat. *Biochemical Pharmacology*, **19**, 173–188.

WRIGHTON, S. A., FAHL, W. E., SHINNICK, F. L. JR and JEFCOATE, C. R., 1982, Characteristics of microsomal reduction of benzo[a]pyrene 4,5-oxide. *Chemico-Biological Interactions*, **40**, 345–356.

YAMAZOE, Y., SIGIURA, M., KAMATAKI, T. and KATO, R., 1978, Reconstitution of benzo[a]pyrene 4,5-oxide reductase activity by purified cytochrome P-450. *FEBS Letters*, **88**, 337–340.

YUBISUI, T., MATSUKAWA, S. and YONEYAMA, Y., 1980, Stopped flow studies on the non-enzymatic reduction of methemoglobin by reduced flavin mononucleotide. *Journal of Biological Chemistry*, **255**, 11694–11697.

XENOBIOTICA , 2000, VOL. 30, NO. 4, 371–380

Metabolism of roquinimex in mouse and rat: an *in vitro/in vivo* comparison

H. TUVESSON†‡*, K. STRANDGÅRDEN†, Ö. NORDLE†, P. O. GUNNARSSON†, J. SEIDEGÅRD‡ and R. PERSSON†

† Pharmacokinetics and Metabolism, Active Biotech Research AB, Box 724, SE-220 07 Lund, Sweden
‡ Department of Cell and Molecular Biology, Lund University, SE-223 62 Lund, Sweden

Received 18 August 1999

1.1. *In vitro* studies with roquinimex, an immuno-modulator, in liver microsomes from mouse and rat were conducted to evaluate the primary metabolism and compare the metabolite pattern as well as the rate of metabolism with the *in vivo* pharmacokinetics of the compound in these two species.

2. In the presence of NADPH, roquinimex was metabolized to six primary metabolites (R1–6) by liver microsomes from mouse and rat. The formation of these metabolites was qualitatively similar in both species, and was greatly enhanced by pretreatment with PCN, an inducer of cytochrome P4503A.

3. The identification of the R1–6 demonstrated that roquinimex had been hydroxylated and demethylated. Hydroxylation at different sites of the quinoline moiety was the dominating reaction in both species.

4. Comparison of the resulting microsomal intrinsic clearance of 0.3 μmol mg^{-1} protein min^{-1} in mouse liver microsomes, versus 0.03 μmol mg^{-1} protein min^{-1} in rat liver microsomes demonstrated that the mouse possesses about a 10-fold greater metabolic capacity for roquinimex than the rat.

5. The *in vivo* pharmacokinetics of roquinimex demonstrated a 7-fold higher clearance in mouse than in the rat (82 ml h^{-1} kg^{-1} in mouse, 10.6 ml h^{-1} kg^{-1} in rat), which is in concordance with the *in vitro* findings.

Introduction

Roquinimex (Linomide, N-methyl-N-phenyl-1,2-dihydro-4-hydroxy-1-methyl-2-oxoquinoline-3-carboxamide) is a compound in a series of quinoline 3-carboxamide derivatives with an immuno-modulating capacity. Inhibitory effects on disease progression have been demonstrated in various animal models for systemic lupus erythematosus, insulin-dependent diabetes mellitus and experimental auto-immmune encephalomyelitis (Tarkowski *et al.* 1986a, b, Karussis *et al.* 1993, 1995, Slavin *et al.* 1993). The mouse has been used as the major pharmacological species, and studies for the toxicological and safety evaluation of the compound were conducted primarily in rat. Pharmacokinetic studies have demonstrated that roquinimex has a low clearance and is highly metabolized: $< 10\%$ of the parent compound is excreted unchanged in the mouse and rat (K. Strandgården, unpublished data). The involvement of cytochrome P450 enzymes (CYP), the major enzyme system involved in the metabolism of drugs (Nelson *et al.* 1996), has not been demonstrated. CYP can be selectively induced by various xenobiotics such as β-naphthoflavone (β-NF), phenobarbital (PB) and cyanopregnenolone (PCN) (Masaki *et al.* 1984, Bock *et al.* 1990, Boobis *et al.* 1990). In mouse and rat liver, β-

* Author for correspondence.

NF is known preferentially to induce members of the CYP1A family, whereas PB and PCN preferentially induce members of the CYP2B and CYP3A families respectively.

In the present investigation, studies *in vitro* were conducted with mouse and rat liver microsomes from untreated and induced animals to evaluate and compare the primary metabolism of roquinimex in these two species. In addition, the *in vitro* metabolism was compared with the *in vivo* pharmacokinetics in these two species.

Materials and methods

Chemicals

^{3}H-roquinimex (PNU-212616, N-methyl-N-[^{3}H]-phenyl-1,2-dihydro-4-hydroxy-1-methyl-2-oxo-quinoline-3-carboxamide, specific activity 10.4 Ci/mmol 950314 32 μg ml^{-1}) was synthesized at Amersham (Amersham, UK), and ^{14}C-PNU-212616 (N-methyl-N-phenyl-1,2-dihydro-4-hydroxy-1-methyl-2-[^{14}C]-oxoquinoline-3-carboxamide, specific activity 12.2 mCi/mmol) was synthesized at Pharmacia & Upjohn AB (Helsingborg, Sweden) with a radiochemical purity >95%. The non-radioactive reference substances, PNU-212616, PNU-212684 (R1), PNU-213708 (R2), PNU-214608 (R3), PNU-213831 (R4), PNU-212679 (R5) and PNU-211944 (R6), were all synthesized at Pharmacia & Upjohn with a chemical purity >97%. NADPH and troleandomycin (TAO) were from the Sigma Chemical Co. (St Louis, MO, USA). All other chemicals were commercially available and of analytical grade.

Animals and preparations

Pooled microsomes from the male CD1 mouse and male Sprague–Dawley rat control animals and animals pretreated with PCN were from XENOTECH$_{LLC}$ (Kansas City, KS, USA).

Female Sprague–Dawley rats, ~ 200 g, were from Charles River (Sweden). For enzyme induction, rats were treated with daily intraperitoneal doses of β-NF (80 mg kg^{-1}, suspension in corn oil) for 4 days, PB (80 mg kg^{-1}, in saline) for 3 days or PCN (25 mg kg^{-1}, suspension in corn oil) for 3 days. Twenty-four hours after the last dose the animals were euthanized, and livers were dissected, frozen in dry ice and stored at − 70 °C. Hepatic microsomes were prepared by differential centrifugation of liver homogenates based on standard methods (Ernster *et al*. 1962, Lu and Lewin 1972).

In the *in vivo* experiment, 20 male C57Bl/6J mice (~ 18 g; Bomholtgaard, Denmark) and 20 male Sprague–Dawley rats (~ 200 g; Möllegaard Breeding Center, Denmark) were given a single intravenous dose of roquinimex (80 mg kg^{-1} in mouse, 50 mg kg^{-1} in rat). Blood samples were taken from the vena cava or aorta and collected in heparinized tubes at 5, 15, 30 min, 1, 2, 4, 6, 8, 12 and 24 h after the administration of roquinimex in mouse, and after 5, 15, 30 min, 1, 2, 4, 8, 24, 48 and 72 h in rat. At each sampling time, blood was withdrawn from two animals. Plasma was separated by centrifugation at 1300 *g*, 4 °C for 15 min and stored at − 20 °C.

Biotransformation of roquinimex

Metabolism of ^{3}H-roquinimex (5–3010 μM, final concentration) was determined with 1–3.5 mg ml^{-1} microsomal protein in 50 mM sodium phosphate buffer, pH 7.4 at 37 °C for 60 min, in a final incubation volume of 200 μl. All incubations were made in duplicate. Preliminary experiments established conditions for reasonable substrate consumption and time and protein linearity of metabolite formation in control and PCN treated mouse and rat microsomes (data not shown). The incubation mixture was allowed to pre-incubate for 5 min at 37 °C before the addition of NADPH (5 mM, final concentration). The reaction was terminated after 60 min by addition of an equal volume of ice-cold acetone. After centrifugation at 10000*g* for 10 min, the supernatant was mixed with roquinimex standards and transferred to HPLC auto-injector vials. Experiments with TAO (100 μM) were performed with ^{14}C-roquinimex and 1 mg (PCN mouse), 3.5 mg (PCN rat) microsomal protein for 60 min. A pre-incubation (equilibrium and inactivation period) was performed for 10 min at 37 °C, and the metabolic reaction was initiated by the addition of roquinimex.

HPLC analyses

Quantification of roquinimex and metabolites in the incubated samples were obtained with an HPLC-system. The samples were injected (10–100 μl) into the chromatographic system and separated on a Nova-Pak C18 column, 4 μm, (3.9 × 150 mm) with guard column Nova-Pak C18 (Waters Associates)

and with a linear gradient system from 15:65:20 to 80:0:20 (methanol with 20% tetrahydrofuran:deionized water:25% formic acid). The analyses were performed at room temperature at a flow of 1.0 ml min^{-1}. Radioactivity was detected by a flow detector (Flo-One β, Radiomatic Instruments), with a 0.5 ml flow cell. The mobile phase was mixed post-column with Ultima Flo AP (Packard Instrument Co.) at a flow of 3 ml min^{-1}. The retentions of formed metabolites were compared with the retentions of synthesized reference compounds and their identity was further confirmed by electrospray ionization mass spectrometry.

The concentrations of roquinimex in the plasma samples were determined by HPLC. A chlorinated analogue (N-methyl-N-chlorophenyl-1,2-dihydro-4-hydroxy-1-methyl-2-oxoquinoline-3-carboxamide) of roquinimex used as internal standard was added to the sample. The sample was then applied on a solid-phase extraction column (Sep-Pak C18 cartridge, Waters Associates). After a clean-up step, roquinimex and the internal standard were eluted from the cartridge with methanol, the eluate was evaporated, redissolved and injected into the chromatographic system. The separation was achieved on a reversed-phase column (μ-Bondapak C18 or Nova-Pak C18, Waters Associates) using a mixture of acetonitrile–water–1 M phosphoric acid (325:525:150 v/v) as the mobile phase. Roquinimex and internal standard were detected by UV-monitoring. The peak-height ratio between roquinimex and internal standard was used for evaluation.

Data analyses

The nature of roquinimex microsomal metabolism was characterized graphically by Eadie–Hoffstee plots for the different metabolites and the kinetic parameters K_m , V_{max} and intrinsic microsomal clearance (Cl_{Int}) (Lineweaver and Burke 1934) were estimated by the non-linear procedure PROC NLIN in the SAS statistical software (SAS/STAT 1989). The model

$$\log(V) = \log(V_{max} * S^n/(K_m{}^n + S^n)) = \log(K_m * Cl_{Int} * S^n/(K_m{}^n + S^n))$$

was fitted to data. The weight after log-transformation was 1, which corresponds to a multiplicative error on untransformed data. Cl_{Int} was calculated from the V_{max}/K_m ratio.

The pharmacokinetic parameters clearance (Cl), volume of distribution (V) and terminal elimination half-life ($t_{\frac{1}{2}}$) were calculated according to standard non-compartmental methods (Gibaldi and Perrier 1982). The area under the curve of plasma concentration versus time (AUC) was calculated using the logarithmic trapezoidal method and adding the residual area. Data were analysed using the program WinNonlin Professional (v.2.1) (WinNonlin 1997). The standard error (SE) of AUC (and Cl) was estimated as a linear combination of SE of the concentrations at each time-point and SE of λ (and $t_{\frac{1}{2}\lambda}$) was estimated from the linear regression equation (Tiveron *et al*. 1993).

Results

Metabolism of roquinimex

Roquinimex was metabolized by liver microsomes from both mouse and rat. No metabolites were formed in the absence of NADPH, which indicated a likely involvement of CYP enzymes in the metabolism of roquinimex. Six primary metabolites were detected and their identity was confirmed by comparison with the retentions and mass spectra of synthesized reference standards (data not shown). The metabolites were identified as the hydroxylated R1 (p-OH), R2 (6-OH), R3 (7-OH), R4 (8-OH) and the demethylated metabolites of roquinimex R5 and R6 (figure 1).

The metabolism of roquinimex was greatly increased in liver microsomes from both mouse and rat pretreated with PCN, $\sim$ 9- and 37-fold in mouse and rat respectively, based upon a comparison of sum of Cl_{Int} in microsomes from induced/non-induced animals. The metabolism was also slightly increased ($\sim$ 2-fold) in microsomes from the PB-treated rat, whereas no increase was observed with microsomes from the β-NF-treated rat. For evaluation of the role of CYP enzymes in the metabolism of roquinimex, experiments with liver microsomes from animals pretreated with PCN were performed. Chromatographic profiles of ^{3}H-roquinimex

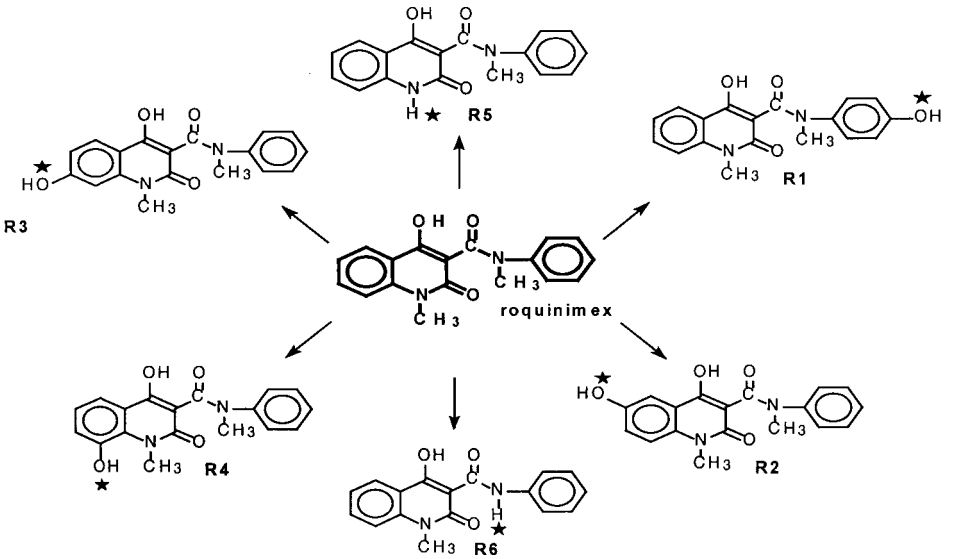


Figure 1. Primary metabolic pathways of roquinimex. The metabolite structurs of R1 to R6 have been identified in microsomal incubates by LC/MS. *Site of metabolism.

and its metabolites generated by liver microsomes from the untreated and PCN-treated mouse and rat are shown in figure 2.

Metabolite formation was very low in untreated animals, especially in rat. Thus, after 60 min of incubation with rat liver microsomes $< 1\%$ (of the initial substrate concentration) of metabolites was formed, while after 60 min with liver microsomes from the PCN-treated rat $\sim 10\%$ of metabolites was formed. Examination of the profiles showed formation of the same metabolites in both species and also with microsomes from PCN treated animals. Incubations with PCN-induced liver microsomes, pre-incubated with TAO (100 μM), a mechanism-based inhibitor of CYP3A enzymes (Larrey *et al.* 1983) demonstrated an almost complete inhibition of the formation of all metabolites in both species (data not shown).

Enzyme kinetics of roquinimex metabolism

Cl_{Int} for roquinimex metabolism in non-induced mouse and rat liver microsomes was estimated using the sum of formed metabolites and demonstrated a low rate of metabolism in both species, with a 10-fold higher rate in the mouse: 0.3 μmol mg^{-1} protein min^{-1} as compared with 0.03 μmol mg^{-1} protein min^{-1} in liver microsomes from the rat. Owing to the low rate of metabolism in microsomes from untreated animals, further kinetic characterization and estimation of the Michaelis–Menten parameters for the primary metabolites was performed using liver microsomes from PCN-treated animals. Metabolite formation was linear with time up to at least 60 min and to 1.0 (mouse) and 3.5 (rat) mg ml^{-1} of microsomal protein in these microsomes (data not shown). Saturation curves were obtained for the formation of primary metabolites and in figure 2 typical curves for the major metabolites are shown. Eadie–Hoffstee plots of the metabolite formation (R1–6) were visually inspected and demonstrated linear enzyme kinetics. The kinetic parameters were calculated from statistical analysis, which was done on the logarithm of replicated V as this method gave the best residual plots and lowest coefficient of variation. Determination of kinetic constants (table 1) for the formation of the roquinimex

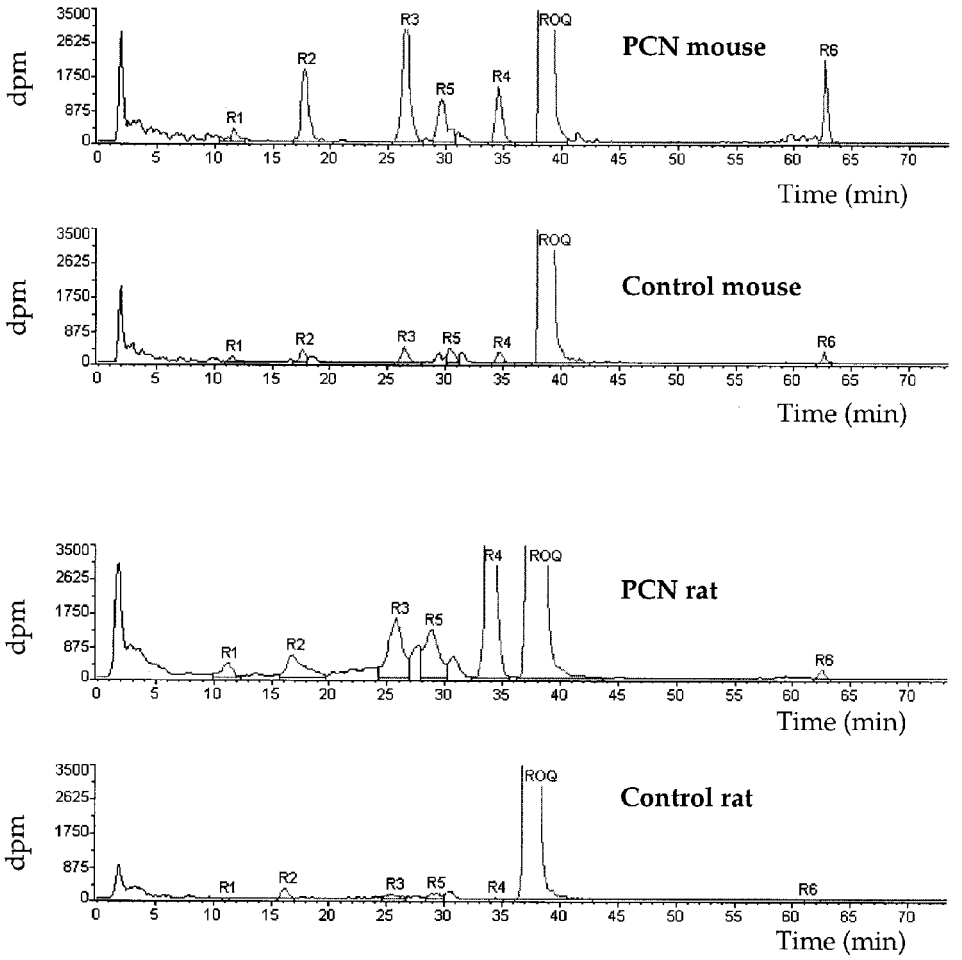


Figure 2. HPLC radiochromatograms of metabolites formed in incubations of roquinimex (100 μM) for 60 min with liver microsomes from control and PCN-treated mouse and rat. From each incubation 50μl (about 400000 dpm) was analysed.

metabolites R1 to R6 described apparent K_m in PCN-treated mouse liver microsomes in the range of 0.19–1.36 mM and V_{max} of 27–794 pmol mg^{-1} protein min^{-1}. In PCN-treated rat liver microsomes the apparent K_m ranged from 0.72 to 2.55 mM and V_{max} from 15 to 636 pmol mg^{-1} protein min^{-1}.

In the PCN-treated mouse, Cl_{Int} ranged from 100 to 700 nl mg^{-1} protein min^{-1} and the highest Cl_{Int} was for the formation of R3 followed by R2, R6, R5, R4 and R1. In the PCN-treated rat, Cl_{Int} ranged from 21 to 616 nl mg^{-1} protein min^{-1}, and the highest Cl_{Int} was for the formation of R4 followed by R5, R6, R3, R2, and R1 (table 1).

Pharmacokinetics of roquinimex

The plasma concentrations of roquinimex were in the range of 0.2–778 μM after a single intravenous dose of the compound to the mouse (80 mg kg^{-1}) and rat (50 mg kg^{-1}) (figure 4). The volume of distribution of roquinimex was small in

Table 1. Kinetic parameters for the formation of roquinimex metabolites in liver microsomes from the PCN-treated mouse and rat. Incubations of ^{3}H-roquinimex (5–3010 μM) were conducted for 60 min at 37°C with microsomes from mouse (1 mg protein ml^{-1}) and rat (3.5 mg protein ml^{-1}). Results are obtained values (SE) from non-linear regression analysis.

		R1	R2	R3	R4	R5	R6
Mouse	V_{max} (pmol mg protein^{-1} min^{-1})	7 (4)	794 (228)	131 (35)	143 (20)	501 (166)	298 (155)
	K_m (mM)	0.28 (0.05)	1.36 (0.43)	0.19 (0.07)	0.41 (0.07)	1.31 (0.48)	0.67 (0.41)
	Cl_{Int} (nl mg protein $^{-1}$ min^{-1})	100 (10)	580 (30)	700 (110)	350 (20)	380 (20)	450 (70)
Rat	V_{max}	15 (3)	54 (6)	128 (21)	636 (61)	563 (50)	193 (19)
	K_m	0.72 (0.18)	0.99 (0.25)	1.82 (0.38)	1.03 (0.14)	2.55 (0.27)	1.46 (0.18)
	Cl_{Int}	21 (2)	54 6)	70 (5)	616 (32)	220 (6)	132 (6)

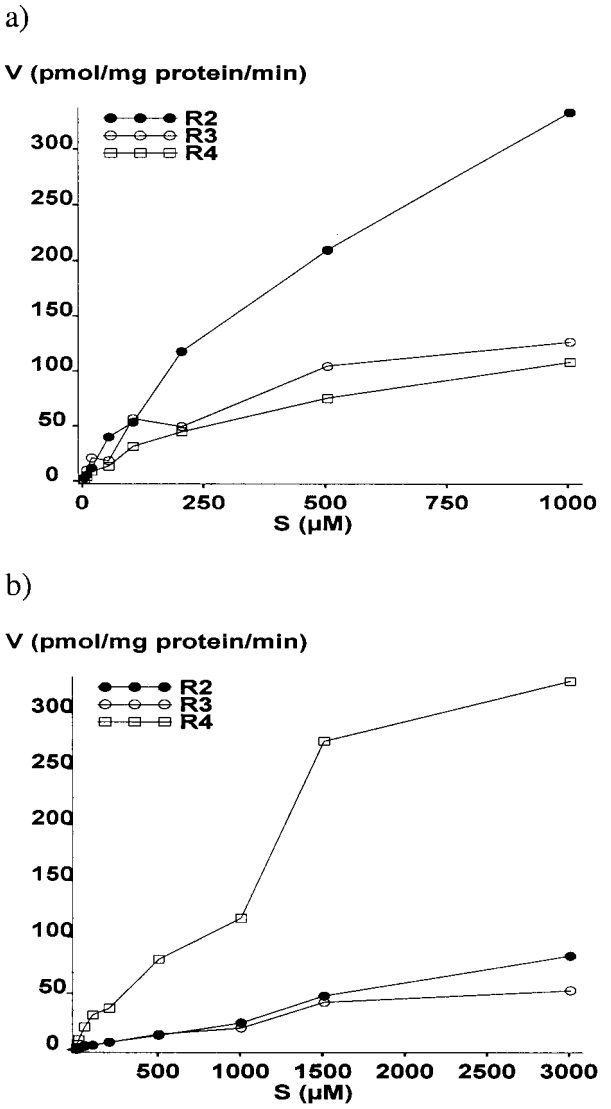


Figure 3. Saturation curves for the formation of the quinoline hydroxylated metabolites (R2-R4) in liver microsomes from PCN pre-treated mouse (a) and rat (b).

mouse and rat: 0.22 and 0.37 litres kg^{-1} respectively. *Cl* was low in both species: 82 ml h^{-1} kg^{-1} in mouse, 10.6 ml h^{-1} kg^{-1} in rat. These primary pharmacokinetic parameters resulted in a terminal elimination half-life of ~ 2 h in mouse and ~ 24 h in rat (table 2).

Discussion

Mouse and rat are two species that have been used for the pharmacological and toxicological evaluation of roquinimex. In the present investigation, roquinimex was metabolized by liver microsomes from both species and the same metabolites were formed, to relatively the same extent. Metabolism was greatly increased, with

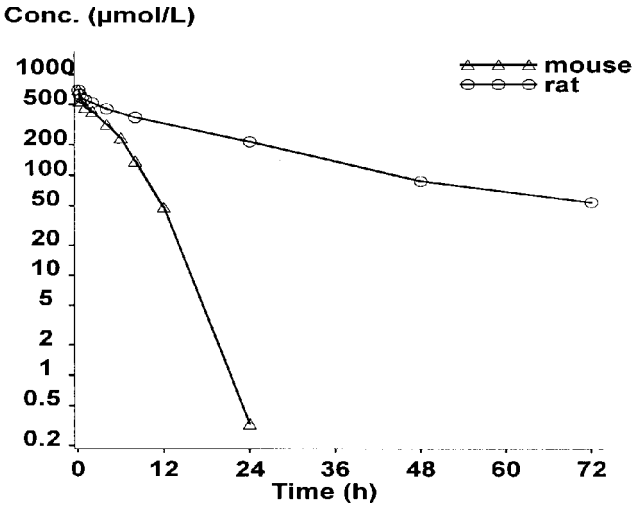


Figure 4. Plasma concentrations of roquinimex after a single intravenous dose of roquinimex to mouse and rat. Twenty C57Bl/6J mice and twenty Sprague-Dawley rats were given a single intravenous dose of roquinimex (mouse, 80 mg/kg, rat 50 mg/kg). Blood samples were taken from two animals at each indicated time and analysed with respect to the parent compound.

Table 2. Pharmacokinetic parameters of roquinimex after a single intravenous dose of roquinimex to mouse and rat. Male C57B1/6J mice and male Sprague–Dawley rats were used, and blood samples were taken at 10 time points (two animals per time point) over a period of 5 min to 72 h. Results are estimated values (SE).

Parameter	Mouse	Rat
Dose (mg kg^{-1})	80	50
Cl (ml h^{-1} kg^{-1})	82 (7)	10.6 (0.2)
V(l kg^{-1})	0.22	0.37
$t_{1/2}$ (h)	1.8 (0.2)	24 (2)

a similar metabolite pattern, in microsomes from animals pretreated with PCN. Furthermore, a slight increase in roquinimex metabolism was demonstrated in microsomes from the PB-treated rat. In both mouse and rat, treatment with PCN increased the content and activity of CYP3A in the liver (Simmons *et al.* 1985, Mannering *et al.* 1992, Gonzalez *et al.* 1986). The induction response after PB treatment involves not only enzymes of the CYP2B family (Nebert and Gonzalez 1987, Nebert *et al.* 1989) but also an increase in the content of CYP3A, which has been reported in rat (Gonzalez 1989, Soucek and Gut 1992) and which could explain the observed induction of roquinimex metabolism with PB in this study. Roquinimex metabolism was almost completely inhibited by co-incubation with TAO, an inhibitor of CYP3A enzymes in both mouse and rat (Larrey *et al.* 1983, Xue-Jun and Takashi 1997). Taken together, the presented results demonstrated a role for enzymes of the CYP3A subfamily in the metabolism of roquinimex in both mouse and rat.

The uninduced mouse showed ~10-fold higher metabolic capacity for roquinimex compared with that of the uninduced rat. To compare further the rate of metabolism, as well as the magnitude of the different metabolite pathways in mouse and rat, enzyme kinetics for roquinimex metabolites were obtained in microsomes from PCN-treated animals. The overall metabolism of roquinimex,

estimated as the sum of the individual Cl_{Int} for each pathway, resulted in a 2.5 times higher Cl_{Int} in mouse than in rat (2.6 versus 1.1 μl mg^{-1} protein min^{-1}), after PCN treatment. The formation of roquinimex metabolites demonstrated high K_m and low V_{max} in both species. However, apparent K_m was generally lower and the corresponding V_{max} higher in the mouse than in rat.

The pharmacokinetics of roquinimex in mouse and rat *in vivo* demonstrated a low *Cl* of the compound in both species, although there were apparent differences. The plasma *Cl* of roquinimex was considerably higher (about seven times) in the uninduced mouse than in the uninduced rat, which is in reasonably good agreement with data obtained *in vitro*. For low *Cl* drugs such as roquinimex, the hepatic *Cl* is a function of both the unbound fraction in plasma and the intrinsic ability of the liver to eliminate the drug. Plasma protein binding was not an objective of the present investigation, but preliminary data (not shown) in mouse and rat indicate no differences in protein binding between the two species at doses used in the present study. Thus, the clearance will mainly be affected by the metabolism.

In both species, hydroxylation of the quinoline moiety (R2–4) was the major pathway and constituted $\sim$64 and 67% of the sum of Cl_{Int} for the individual pathways in mouse and rat respectively. In mouse the hydroxylated products R2 (6-OH) and R3 (7-OH) were the major metabolites, while R4 (8-OH) was dominant in the rat. No obvious difference in the rates of formation of the N-demethylated metabolites (R5, R6) was obtained.

Preliminary data from studies with human liver microsomes indicated that a metabolite pattern similar to that detected with mouse and rat liver microsomes was formed. Furthermore, a role for CYP3A4, the human orthologue of the rat CYP3A2 (Soucek and Gut 1992) was indicated. Whether any of the hydroxylated and/or demethylated metabolites of roquinimex possess pharmacological and/or toxicological activity remains to be clarified.

Acknowledgements

The authors thank Lillemor Halvarsson and Bengt Olofsson for excellent technical assistance.

References

Bock, K. W., Lipp, H-P. and Bock-Hennig, B. S., 1990, Review: Induction of drug-metabolising enzymes by xenobiotics. *Xenobiotica*, **20**, 1101–1111.

Boobis, A. R., Sesardic, D., Murray, B. P., Edwards, R. J., Singelton, A. M., Rich, K. J., Murray, S., De La Torre, R., Segura, J., Pelkonen, O., Pasanen, M., Kobayashi, S., Zhi-Guang, T. and Davies, D. S., 1990, Species variation in the response of the cytochrome P-450-dependent monooxygenase system to inducers and inhibitors. *Xenobiotica*, **20**, 1139–1161.

Ernster, L., Siekevitz, P. and Palade G. E., 1962, Enzyme–structure relationships in the endoplasmic reticulum of rat liver. *Journal of Cell Biology*, **15**, 541–562.

Gibaldi, M. and Perrier, D., 1982, *Pharmacokinetics*, 2nd edn (New York. Marcel Dekker).

Gonzalez, F. J., 1989, The molecular biology of cytochrome P450s. *Pharmacology Reviews*, **41**, 91–92.

Gonzalez, F. J., Song, B.-J. and Hardwick, J. P., 1986, Pregnenolone 16 α-carbonitrile-inducible P450 gene family: gene conversion and differential regulation. *Molecular Cell Biology*, **6**, 2969–2976.

Karussis, D. M., Lehmann, D., Slavin, S., Kalland, T., Vourka-Karussis, U., Mizrachi-Koll, R., Ovadia, H. and Abramsky, O., 1995, Immunomodulation of autoimmunity by Linomide. *Israel Journal of Medical Science*, **31**, 38–41.

Karussis, D. M., Lehmann, D., Slavin, S., Vourka-Karussis, U., Mizrachi-Koll, R., Ovadia, H., Kalland, T. and Abramsky, O., 1993, Treatment of chronic-relapsing experimental autoimmune encephalomyelitis with the synthetic immunomodulator Linomide (quinoline-3-carboxamide). *Proceedings of the National Academy of Sciences, USA*, **90**, 6400–6404.

LARREY, D., TINEL, M. and PESSAYRE, D., 1983, Formation of inactive cytochrome P450 Fe(II)-metabolite complexes with several erythromycin derivatives but not with josamycin and midecamycin in rats. *Biochemical Pharmacology*, **32**, 1487–1492.

LINEWEAVER, H. and BURKE, D., 1934, The determination of enzyme dissociation constants. *Journal of the American Chemical Society*, **56**, 658–666.

LU, A. H. and LEWIN, W., 1972, Partial purification of cytochromes P450 and P448 from rat liver microsomes. *Biochemical and Biophysical Research Communications*, **46**, 1334–1339.

MANNERING, G. J., SHOEMAN, J. A. and DELORIA, L. B., 1992, Identification of the antibiotic hops component, colupulone as an inducer of hepatic cytochrome P4503A in the mouse. *Drug Metabolism and Disposition*, **20**, 142–147.

MASAKI, R., MATSUURA, S. and TASHIRO, Y., 1984, A biochemical and electron microscopic study of changes in the content of cytochrome P450 in rat livers after cessations of treatment with phenobarbital, β-naphtoflavone or 3-methylcholantrene. *Cell Structure and Functions*, **9**, 53–66.

NEBERT, D. W. and GONZALEZ, F. J., 1987, P450 genes: structure, evolution and regulation. *Annual Reviews in Biology*, **56**, 945–993.

NEBERT, D. W., NELSON, D. R. and FEYEREISEN, R., 1989, Evolution of the cytochrome P450 genes. *Xenobiotica*, **19**, 1149–1160.

NELSON, D. R., KOYMANS, L., KAMATAKI, T., STEGEMAN, J. J., FEYEREISEN, R., WAXMAN, D. J., WATERMAN, M. R., GOTOH, O., COON, M. J., ESTABROOK, R. W., GUNSALUS, I. C. and NEBERT, D. W., 1996, P450 superfamily: update on new sequences, gene mapping, accession numbers and nomenclature. *Pharmacogenetics*, **6**, 1–42.

SAS/STAT, 1989, *User's Guide, Version* 6, 4th edn, vol. 1 (Cary: SAS Institute).

SIMMONS, D. L., LALLEY, P. A. and KASPER, C. B., 1985, Chromosomal assignment of genes coding for component of the mixed-function oxidase system in mouse. *Journal of Biological Chemistry*, **260**, 515–521.

SLAVIN, S., SIDI, H., WEISS, L., ROSENMAN, E., KALLAND, T. and GROSS, D., 1993, Linomide, a new treatment for autoimmune diseases: The potential in type I diabetes. *Diabetes Metabolism Reviews*, **9**, 311–315.

SOUCEK, P. and GUT, I., 1992, Review. Cytochromes P-450 in rats: structures, functions, properties and relevant human forms. *Xenobiotica*, **22**, 83–103.

TARKOWSKI, A., GUNNARSSON, K. and STÅLHANSKE, T., 1986a, Effects of LS 2616 administration upon the autoimmune disease of (NZB × NZW) F1 hybrid mice. *Immunology*, **59**, 589–594.

TARKOWSKI, A., GUNNARSSON, K., NILSSON, L. Å., LINDHOLM, L. and STÅLHANSKE, T., 1986b, Successful treatment of autoimmunity in MRL/1 mice with LS 2616, a new immunomodulator. *Arthritis and Rheumatism*, **29**, 1405–1409.

TIVERON, C., HARTLEY-ASP, B., JOHANSSON, C. J. and PACCHIEROTTI, F., 1993, Noscapine does not show aneugenic activity in mouse oocytes. *Mutagenesis*, **8**, 311–315.

WIN NONLIN, 1997, *Professional User's Guide, vers* 1.5 (Lexington: Scientific Consulting, Inc.).

XUE-JUN, Z. and TAKASHI, I., 1997, The *in vitro* hepatic metabolism of quinine in mice, rats and dogs: comparison with human liver microsomes. *Journal of Pharmacology and Experimental Therapeutics*, **283**, 1168–1176.

XENOBIOTICA , 2000, VOL. 30, NO. 4, 395–406

Metabolism of Cyanox in rat. II. Sex-related differences in oxidative dearylation and desulphuration

Y. TOMIGAHARA*, M. ONOGI, K. SAITO, N. ISOBE, H. KANEKO and I. NAKATSUKA

Environmental Health Science Laboratory, Sumitomo Chemical Co., Ltd, 1-98, 3-Chome, Kasugade-Naka, Konohana-Ku, Osaka 554-8558, Japan

Received 28 April 1999

1. To examine the metabolites of Cyanox (*O*-4-cyanophenyl *O*,*O*-dimethyl phosphorothioate, cyanophos, CYAP) in brain, liver, blood cells and plasma during the early toxic period, the male and female rat was administered a single oral dose of [phenyl-^{14}C]Cyanox at dose levels of 50 mg/kg and killed 5, 10 and 20 min thereafter.

2. Sex-related differences in the concentrations of metabolites were observed. Cyanoxon, produced by oxidative desulphuration, was observed in the brains of both sexes at all time points, but the concentrations were 2–6 times higher in the male. The same metabolite was detected in the liver, blood cells and plasma of the male but not the female. The total concentrations of oxidative dearylation metabolites (4-cyanophenol + 4-cyanophenylsulphate + glucuronide of 4-cyanophenol) in plasma, blood cell, brain and liver were larger in the male at all time points than those in the female, whereas the reverse was the case for demethylated metabolites (desmethylcyanox + desmethylcyanoxon) in all tissues except for the brain.

3. Studies of the *in vitro* metabolism of Cyanox revealed no sex-related difference for hepatic cytosolic fractions in terms of the major *in vitro* metabolic reaction, demethylation. On the other hand, the major reactions in microsomal fractions, oxidative desulphuration and oxidative dearylation, were significantly (2–3 times) greater in the male than in the female.

4. Oxidative desulphuration and oxidative dearylation, involving cytochrome P450 enzymes, were inhibited by male-specific rat CYP2C11 antiserum. The degree of inhibition was more pronounced in the male case. Thus, the results strongly suggest that the 2C family of cytochrome P450 (male, CYP2C11 and CYP2C13; female, CYP2C12) contributes to oxidative desulphuration and dearylation of cyanox in the rat and that the activity of male-specific CYP2C11 (and CYP2C13) is greater than that of female-specific CYP2C12. The consequent greater formation of cyanoxon in the male is consistent with the higher toxicity in this sex.

Introduction

The organophosphorous insecticide, Cyanox (*O*-4-cyanophenyl *O*,*O*-dimethyl phosphorothioate, cyanophos, CYAP) is widely used and, therefore, may be present in agricultural environments. The metabolism of phosphorothionate triesters has been well established from studies of various organophosphorus insecticides incorporating this structure, including Cyanox itself (Wakimura and Miyamoto 1971), fenitrothion (Miyamoto *et al.* 1976, 1978), salithoin (Mihara and Miyamoto 1974), and tolchlofos-methyl (Mihara *et al.* 1981). The major metabolic reactions are common, namely demethylation of the P-O-methyl group, conversion of P = S to P = O (oxidative desulphuration) and cleavage of the P-O-aryl bond (oxidative dearylation).

* Author for correspondence; e-mail: tomigahara@sc.sumitmo-chem.co.jp

Xenobiotica ISSN 0049-8254 print/ISSN 1366-5928 online © 2000 Taylor & Francis Ltd
http://www.tandf.co.uk/journals

It is well established that the parent phosphorothionates of phosphorothionate triesters are poor acetylcholinesterase (AChE) inhibitors, requiring metabolical bioactivation by the cytochrome P450 monooxygenase system to the corresponding oxon analogues for potent effects to be exhibited (Kulkarni and Hodgson 1980, Testa and Jenner 1976).

Acute toxicity studies on Cyanox have demonstrated a marked sex difference: the male rat shows more severe symptoms than the female (Hiromori *et al.* 1989, unpublished data). In a previous study (Tomigahara *et al.* 1995), the metabolic fate of Cyanox in the rat was investigated and sex differences in metabolic reactions were observed. Oxidative dearylation and oxidative desulphuration were greater in the male. On the other hand, demethylation was more pronounced in the female. The first two have been reported to be catalyzed by cytochrome P450 (CYP) (Nakatsugawa and Dahm 1967, Neal 1967, Eto 1974), whereas glutathione *S*-transferase is considered responsible for demethylation (Matsumura 1975). Therefore, the severe toxic effects in the male is presumably related to the higher production of cyanoxon by oxidative desulphuration. In contrast, detoxification by demethylation predominates in the female.

With regard to sex differences in CYP in rat, CYP2A2, CYP2C11, CYP2C13, CYP3A2 and CYP4A2 are well-known to be male-specific forms and CYP2C12 is a female-specific form (Kamataki *et al.* 1983, Imaoka *et al.* 1991, Funae and Imaoka 1993). Glutathione *S*-transferases in rat have been separated into four classes: alpha, mu, pi and theta, based on differences in their structural, immunological and enzymatic properties (Mannervik *et al.* 1985, Hiratsuka *et al.* 1990, Meyer *et al.* 1991). However, reports of sex-dependent expression have not appeared to date. Consequently, it is considered that the more severe toxicity in the male is due to the sex-specific CYP.

The objectives of this study were (1) to investigate sex differences in metabolites in brain, liver, blood cell and plasma and (2) to clarify the main CYP participating in oxidative dearylation and desulphuration reactions.

Materials and methods

Chemicals and reagents

[Phenyl-^{14}C]Cyanox (4.50 GBq/mmol) was synthesized in our laboratory, purified by preparative TLC developed in chloroform prior to use. Its radiochemical purity was $>99\%$ based on TLC analysis.

Unlabelled Cyanox (99.4% purity) and cyanoxon (*O*-4-cyanophenyl *O*,*O*-dimethyl phosphate, 98.2% purity) were also synthesized in our laboratory. The unlabelled authentic standard, 4-cyanophenol (95% purity), was from Aldrich (USA).

The ^{14}C-labelled authentic standards, 4-cyanophenylsulphate, desmethylcyanox (*O*-4-cyanophenyl *O*-hydrogen *O*-methyl phosphorothioate), desmethylcyanoxon (*O*-4-cyanophenyl *O*-hydrogen *O*-methyl phosphate) and the glucuronide of 4-cyanophenol, were purified from urine and faeces of rat administered [phenyl-^{14}C]Cyanox and identified (Tomigahara *et al.*, unpublished data).

NADPH was from Oriental Yeast Co. (Japan) and anti-rat CYP2C11 goat serum and non-immunized goat serum were commercially obtained from Daiichi Pure Chemicals Co., Ltd (Japan). In the specification of the CYP2C11 antiserum, it is reported that it inhibits CYP2B1 and CYP2B2 activities slightly, although it does not inhibit CYP2E1, CYP3A2 or CYP4A1 activities.

Chromatographic procedures

Thin-layer chromatography (TLC) analyses were conducted essentially as described by Kaneko *et al.* (1988) and Saito *et al.* (1991). Precoated silica gel 60 F_{254} chromatoplates (Art. 5715, 20×20 cm, 0.25 mm layer thickness; E. Merck, Darmstadt, Germany) were used for analyses of metabolites. The following solvent systems were used: (A) benzene/ethyl acetate (4/1, v/v), and (B) ethyl acetate/methanol/acetic acid (10/3/1, v/v/v).

Table 1. TLC R_f for Cyanox and authentic standards.

Compounds	R_f A	R_f B
Cyanox	0.53	*
Cyanoxon	0.14	0.86
Desmethylcyanox	**	0.76
Desmethylcyanoxon	**	0.48
4-Cyanophenol	0.27	0.92
4-Cyanophenylsulphate	**	0.80
Glucuronide of 4-cyanophenol	**	0.32

Solvent systems: (A) benzene/ethyl acetate = 4/1 (v/v); (B) ethyl acetate/methanol/acetic acid = 10/3/1 (v/v/v).
* Solvent front.
** Origin.

Unlabelled standards on TLC plates were detected by viewing under ultraviolet (UV) light (254 nm). The radioactive metabolites on TLC plates were detected by exposure of imaging plates (Type BAS-III, Fuji Photo Film Co. Ltd., Japan) for a few days at room temperature, followed by visualization with a Bio-Image Analyzer (BAS2000, Fuji Photo Film). R_f of authentic standards are shown in table 1.

Treatments of animals

Charles River-derived CD (Sprague–Dawley) male and female rats at 6 weeks of age were purchased from Charles River Japan, Inc. (Japan) and maintained in an air-conditioned room at 22–24 °C with an alternating 12 h light and 12 h dark cycle for 1 week before use. The animals were given free access to pelleted diet (CRF-1, Oriental Yeast, Inc.) and water *ad libitum* during all treatments.

Distribution study

[phenyl-^{14}C]Cyanox was dissolved in corn oil at 50 mg/5 ml, and orally administered to nine males and nine females at 5 ml/kg. This dose level was chosen because male and female rats showed toxic signs until 30 min after administration and these indicators of toxicity were more severe in the male than the female in a previous study (Tomigahara *et al.* 1995). The dosed ^{14}C was adjusted to 18.5 MBq/kg. Groups of three rats per sex were killed by decapitation at 5, 10 and 20 min after administration, and the corpses immediately immersed in crushed ice. These times were selected as the early toxic period. The brain and liver from each animal were dissected out as quickly as possible, washed with ice cold saline and stored frozen at −80 °C until analysis (radioanalysis and TLC). Heparinized blood was divided into blood cell and plasma by centrifugation at 1000*g* for 10 min. These tissues were selected as main target tissues of toxicity.

Microsomes and cytosol preparation

Microsomal and cytosolic fractions were prepared according to Lake (1987). Three male and three female rats were decapitated, the livers quickly dissected out, weighed and immediately placed in saline on ice. The livers were individually rinsed with saline, chopped into pieces and homogenized (20% w/v) individually in ice cold 50 mM phosphate buffer (pH 7.4) containing 1.15% KCl using a glass Potter–Elvehjem homogenizer and a Teflon pestle at 4 °C. The homogenates were centrifuged at 10000*g* for 10 min at 4 °C. The resultant supernatant fractions were removed, centrifuged at 105000*g* for 60 min at 4 °C, and decanted (designated as the cytosolic fraction). The resulting pellets were rehomogenized with the buffer and centrifuged at 105000*g* for 60 min at 4 °C. The microsomal pellets were resuspended in the buffer to a concentration of 0.20 g fresh liver equivalent/ml (20%, w/v) before assays (the microsomal fraction). Protein content was measured by the method of Bradford (1976) using a protein assay kit (Bio-Rad Laboratory, CA, USA) and bovine serum albumin as the standard. The CYP content was determined by the method of Omura and Sato (1964).

Determination of demethylation, oxidative dearylation and oxidative desulphuration activities

To assess potential for (1) demethylation of the P-O-methyl group, (2) conversion of P = S to P = O (oxidative desulphuration) and (3) cleavage of the P-O-aryl bond (oxidative dearylation), the following *in vitro* study was conducted. About 20 nmol [phenyl-^{14}C]Cyanox in 10 μl acetone, NADPH (final

concentration 3 mM) and 0.5 ml 50 mM phosphate buffer (pH 7.4) were mixed with 0.5 ml aliquots of the 20% microsomal or cytosolic preparations and incubated for 10, 20, 40 and 60 min at 37 °C. Reactions were terminated by adding 2 ml ice-cold ethanol. Denatured proteins were removed by centrifugation at 1500*g* for 10 min and the supernatant fractions were stored at −20 °C until TLC analysis. Biotransformation activities were calculated from the amounts of identified metabolites.

Incubation of microsomes with CYP antiserum

An *in vitro* inhibition study with CYP antiserum was conducted using the methods of Neville *et al.* (1993) with some modifications. Microsomal suspensions (60–70 μl) containing ~300 pmol CYP (~0.3–0.4 mg protein) were pre-incubated for 30 min at room temperature with 0, 5, 15 or 25 μl CYP2C11 antiserum. The reaction was initiated by adding NADPH (final concentration 3 mM), 10 μl acetone solution of [phenyl-^{14}C]Cyanox (2 nmol) and 50 mM phosphate buffer to give a final volume of 1 ml and incubation was conducted at 37 °C for 20 min. Reactions were terminated by adding 2 ml ice-cold ethanol. Denatured proteins were removed by centrifugation at 1500*g* for 10 min and the supernatant fractions were stored at −20 °C until TLC analysis. Inhibition rates were calculated by subtracting the percentages of extents of each metabolic reaction by hepatic microsomes pre-incubated with antiserum from control values set at 100%.

Radioanalysis

Radioanalysis was conducted in the same manner as reported previously (Tomigahara *et al.* 1994). Radioactivity in organosoluble fractions and silica gel was quantified by conventional liquid scintillation counting (LSC). Radioactivity in brain, liver, blood cell, plasma and tissue residues was assessed using a Tri-Carb® 307 Sample Oxidizer (Packard, USA) where ^{14}C was determined as $^{14}CO_2$ trapped in a scintillation solution of 8 ml CARBO-SORB$_2$® and 12 ml PERMAFLUOR®E+ (Packard) prior to LSC after being air-dried. Brain, liver, blood cell and plasma samples from rats were extracted three times with a 3-fold quantity of methanol/water, 9/1 (v/v), and the extracts and residues were radioassayed.

The ^{14}C-residue levels were expressed as μg equivalents of Cyanox/g wet tissue (ppm).

Radioactivity on TLC plates was measured by scraping the appropriate silica gel regions and counting in scintillation vials (scraping method). The quantitative limit of each metabolite was < 0.03 ppm.

Analysis of metabolites in tissues for the in vivo *study, and in samples for the* in vitro *study*

The tissue extracts for the *in vivo* study, and the samples for the *in vitro* study were tentatively identified by TLC co-chromatography with authentic standards using solvent systems A and B. Quantification of each metabolite was performed by the TLC scraping method using solvent systems A and B.

Statistical analysis

Student's *t*-test was used for statistical analysis of the data.

Results

^{14}C- and metabolites concentrations in tissues

^{14}C-concentrations in plasma, blood cell, brain and liver are given in tables 2 and 3. Figure 1 shows the major metabolic reactions of Cyanox *in vivo* in rat (Tomigahara *et al.* 1995). Figure 2 illustrates a representative TLC autoradiogram of metabolites in brain extracts. Peak ^{14}C-concentrations in plasma, blood cells, brain and liver in both sexes occurred 10 min after administration. The maximum concentrations in these tissues were 38.5, 11.7, 10.2 and 65.9 ppm respectively in the male, and 26.4, 7.1, 7.1 and 56.3 ppm respectively in the female.

In liver, the main metabolites, 4-cyanophenylsulphate and desmethylcyanox, were found with the parent compound. The concentrations of the parent compounds in the male and the female at 10 min after administration were 32.2 and 13.1 ppm respectively. The concentrations of 4-cyanophenylsulphate at 10 min after administration were 4.6 and 2.2 ppm respectively with the same sex difference. In contrast, the concentrations of desmethylcyanox in the male and female liver at 10 min after

Table 2. Amounts of metabolites in plasma, blood cell, brain and liver samples of the male rat, 5, 10 and 20 min after a single oral administration of [phenyl-^{14}C]Cyanox at 50 mg/kg.

	Male (ppm)		
Metabolite	5 min	10 min	20 min
Plasma			
Cyanox	n.d.	4.6± 0.77	2.9± 0.61
4-Cyanophenol	1.4± 0.17	3.8± 0.82	1.6± 0.24
Cyanoxon	n.d.	n.d.	0.1± 0.05
4-Cyanophenylsulphate	6.2± 0.80	12.3± 2.48	8.0± 1.25
Desmethylcyanox	1.8± 0.25	11.4± 2.10	11.2± 1.98
Desmethylcyanoxon	1.4± 0.23	3.4± 0.60	1.9± 0.32
Glucuronide of 4-cyanophenol	0.2± 0.05	0.3± 0.09	0.3± 0.18
Others	0.7± 0.12	0.8± 0.30	0.6± 0.13
Unextractable	0.5± 0.12	1.9± 0.15	1.5± 0.18
Total	12.0± 1.35	38.5± 6.95	28.0± 4.17
Blood cell			
Cyanox	0.2± 0.06	1.8± 0.34	1.0± 0.09
4-Cyanophenol	0.7± 0.09	2.4± 0.58	0.9± 0.09
Cyanoxon	n.d.	0.1± 0.01	n.d.
4-Cyanophenylsulphate	1.0± 0.15	2.4± 0.58	1.3± 0.17
Desmethylcyanox	0.6± 0.13	2.9± 0.66	1.9± 0.17
Desmethylcyanoxon	0.2± 0.05	0.8± 0.15	0.2± 0.02
Glucuronide of 4-cyanophenol	0.0± 0.00	0.1± 0.03	0.0± 0.01
Others	0.3± 0.10	0.2± 0.12	0.3± 0.03
Unextractable	0.2± 0.03	1.0± 0.08	0.6± 0.10
Total	3.3± 0.57	11.7± 2.22	6.3± 0.51
Brain			
Cyanox	n.d.	5.6± 1.00	3.7± 0.84
4-Cyanophenol	0.3± 0.05	0.9± 0.23	0.5± 0.26
Cyanoxon	0.6± 0.07	1.2± 0.37	0.4± 0.18
4-Cyanophenylsulphate	0.2± 0.04	0.3± 0.08	0.4± 0.09
Desmethylcyanox	n.d.	0.5± 0.11	0.3± 0.05
Desmethylcyanoxon	0.3± 0.08	0.7± 0.13	0.4± 0.14
Glucuronide of 4-cyanophenol	0.0± 0.01	0.2± 0.04	0.2± 0.04
Others	0.0± 0.03	0.4± 0.10	0.6± 0.13
Unextractable	0.1± 0.01	0.4± 0.06	0.3± 0.05
Total	1.5± 0.23	10.2± 1.90	6.9± 1.76
Liver			
Cyanox	11.2± 1.70	32.2± 5.62	5.2± 2.17
4-Cyanophenol	3.0± 0.45	2.1± 0.60	1.6± 0.83
Cyanoxon	0.3± 0.15	0.4± 0.14	0.0± 0.01
4-Cyanophenylsulphate	6.6± 1.58	4.6± 0.50	2.1± 0.87
Desmethylcyanox	17.2± 2.87	18.8± 2.13	17.5± 4.32
Desmethylcyanoxon	6.5± 1.48	4.1± 0.35	2.6± 0.85
Glucuronide of 4-cyanophenol	0.4± 0.07	0.4± 0.15	0.3± 0.15
Others	0.9± 0.67	0.3± 0.09	0.5± 0.34
Unextractable	2.3± 0.30	3.1± 0.32	1.5± 0.22
Total	48.4± 8.37	65.9± 9.28	31.2± 9.74

Figures are mean± SD for three rats.
n.d., Not detected.

administrations were 18.8 and 32.9 ppm respectively, with a higher concentration in the female. Cyanoxon (a potent AchE inhibitor) was detected in the male but not in the female liver.

In brain, cyanoxon were detected in both sexes at all time points, with the male and female values after 10 min being 1.2 and 0.2 ppm respectively. The other main metabolites in the male brain at the 10 min time-point were the parent compound, 4-cyanophenol and desmethylcyanoxon, at 5.6, 0.9 and 0.7 ppm

Table 3. Amounts of metabolites in blood cell, plasma, brain and liver samples of the female rat, 5, 10 and 20 min after a single oral administration of [phenyl-^{14}C]Cyanox at 50 mg/kg.

	Female (ppm)		
Metabolite	5 min	10 min	20 min
Plasma			
Cyanox	0.9± 0.20	3.1± 0.23	1.9± 0.51
4-Cyanophenol	1.0± 0.17	1.2± 0.18	1.2± 0.42
Cyanoxon	n.d.	n.d.	n.d.
4-Cyanophenylsulphate	3.3± 0.52	3.8± 0.33	4.0± 1.35
Desmethylcyanox	4.4± 0.92	13.7± 1.47	9.6± 2.33
Desmethylcyanoxon	1.7± 0.29	2.4± 0.19	1.8± 0.76
Glucuronide of 4-cyanophenol	0.2± 0.04	0.3± 0.03	0.2± 0.02
Others	0.6± 0.16	0.7± 0.12	0.6± 0.31
Unextractable	0.6± 0.06	1.4± 0.06	1.3± 0.08
Total	12.7± 2.27	26.4± 2.33	20.7± 5.69
Blood cell			
Cyanox	0.5± 0.03	1.4± 0.19	1.3± 0.16
4-Cyanophenol	0.6± 0.08	0.8± 0.18	0.7± 0.15
Cyanoxon	n.d.	n.d.	n.d.
4-Cyanophenylsulphate	0.5± 0.05	0.9± 0.15	0.6± 0.14
Desmethylcyanox	0.7± 0.06	2.5± 0.27	2.0± 0.27
Desmethylcyanoxon	0.4± 0.08	0.5± 0.15	0.3± 0.06
Glucuronide of 4-cyanophenol	0.0± 0.00	0.0± 0.02	0.0± 0.02
Others	0.4± 0.06	0.5± 0.11	0.4± 0.16
Unextractable	0.1± 0.02	0.6± 0.23	0.4± 0.17
Total	3.2± 0.23	7.1± 0.93	5.7± 0.86
Brain			
Cyanox	1.0± 0.23	4.9± 0.75	2.5± 0.92
4-Cyanophenol	0.1± 0.02	0.4± 0.02	0.4± 0.11
Cyanoxon	0.1± 0.03	0.2± 0.00	0.2± 0.11
4-Cyanophenylsulphate	n.d.	0.1± 0.03	0.2± 0.06
Desmethylcyanox	n.d.	0.5± 0.11	0.3± 0.08
Desmethylcyanoxon	0.2± 0.03	0.4± 0.10	0.2± 0.08
Glucuronide of 4-cyanophenol	n.d.	0.1± 0.06	0.1± 0.01
Others	0.3± 0.03	0.1± 0.00	0.4± 0.10
Unextractable	0.1± 0.02	0.4± 0.04	0.2± 0.04
Total	1.8± 0.33	7.1± 1.06	4.4± 1.37
Liver			
Cyanox	3.8± 0.23	13.1± 0.54	2.8± 0.58
4-Cyanophenol	1.1± 0.52	1.3± 0.20	0.8± 0.12
Cyanoxon	n.d.	n.d.	n.d.
4-Cyanophenylsulphate	2.2± 0.03	2.2± 0.37	2.3± 0.38
Desmethylcyanox	24.9± 3.32	32.9± 2.73	19.6± 2.85
Desmethylcyanoxon	3.5± 1.32	3.5± 0.14	2.3± 0.34
Glucoronide of 4-cyanophenol	0.4± 0.13	0.4± 0.16	0.1± 0.07
Others	0.6± 0.44	0.6± 0.15	0.1± 0.05
Unextractable	1.8± 0.17	2.4± 0.29	1.4± 0.23
Total	38.2± 5.78	56.3± 3.99	29.3± 4.20

Figures are mean± SD for three rats.
n.d., Not detected.

respectively. The main metabolites in the female were the parent compound and desmethylcyanox, accounting for 4.9 and 0.5 ppm respectively. At 5 min after administration, the main metabolites were cyanoxon (0.6 ppm) in the male and Cyanox (1.0 ppm) in the female.

In plasma, the main metabolites in both sexes at 10 min after the administration were the parent compound, 4-cyanophenylsulphate and desmethylcyanox, accounting for 4.6, 12.3 and 11.4 ppm respectively in the male, and 3.1, 3.8 and

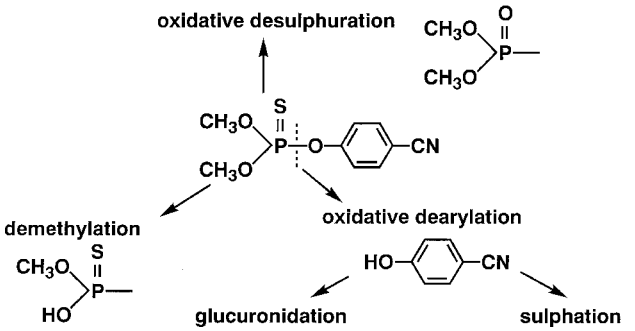


Figure 1. Chemical structure of Cyanox and sites of metabolic reactions in rat.

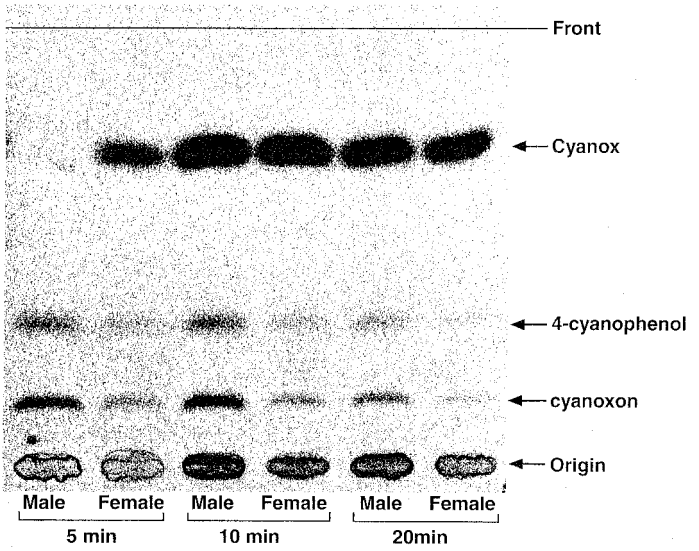


Figure 2. Representative TLC autoradiogram of metabolites in brain extracts. Solvent system: benzene/ethyl acetate = 4/1 (v/v).

13.7 ppm respectively in the females. A similar tendency was also observed in blood cells with cyanoxon being detected in male plasma and blood cells but not in the female.

Demethylation, oxidative dearylation and oxidative desulphuration activities in liver

Figure 3 shows representative TLC autoradiograms of metabolites in hepatic cytosolic and microsomal fractions from the male and female rat in the *in vitro* metabolism study. Liver weight, cytosolic protein content, microsomal protein content and total CYP content were 11.4± 1.02 g, 55.5± 5.81 mg/g liver, 31.3± 1.50 mg/g liver and 0.87± 0.09 nmol/mg protein respectively in three males, and 8.7± 0.57 g, 60.7± 7.17 mg/g liver, 30.2± 1.60 mg/g liver and 0.74± 0.14 nmol/mg protein respectively in three females. Figure 4 shows plots of time versus amounts of Cyanox metabolites formed in hepatic microsomal and cytosolic fractions. As shown in figure 3, desmethylcyanox was the only product observed in the cytosolic

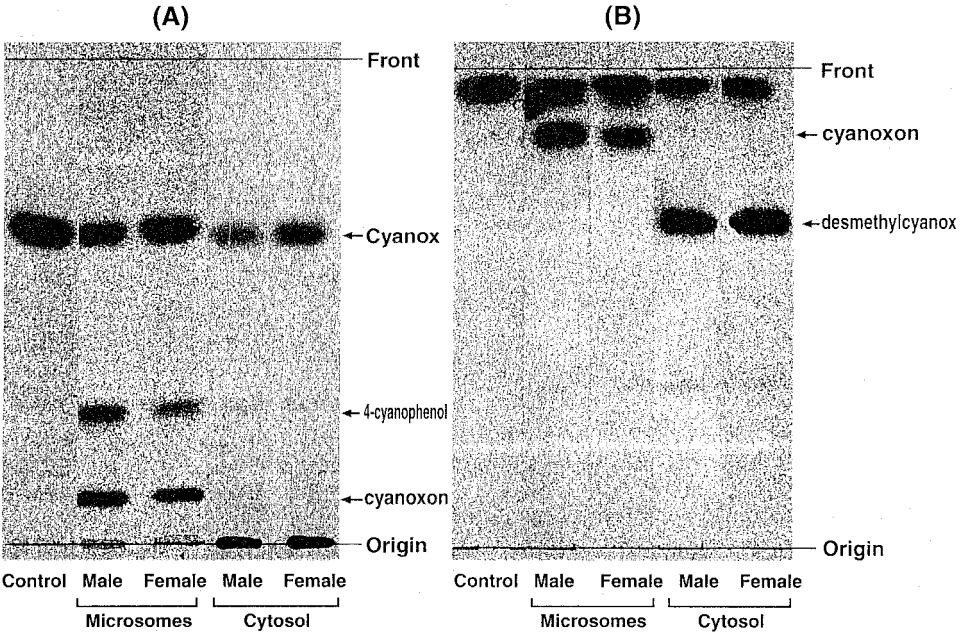


Figure 3. Representative TLC autoradiogram of metabolites in hepatic cytosolic and microsomal fractions from the male and female rat. [Phenyl-^{14}C]cyanox was applied to microsomes or cytosol and incubated for 20 min at 37 °C. Solvent systems: (A) benzene/ethyl acetate = 4/1 (v/v); (B) ethyl acetate/methanol/acetic acid = 10/3/1 (v/v/v).

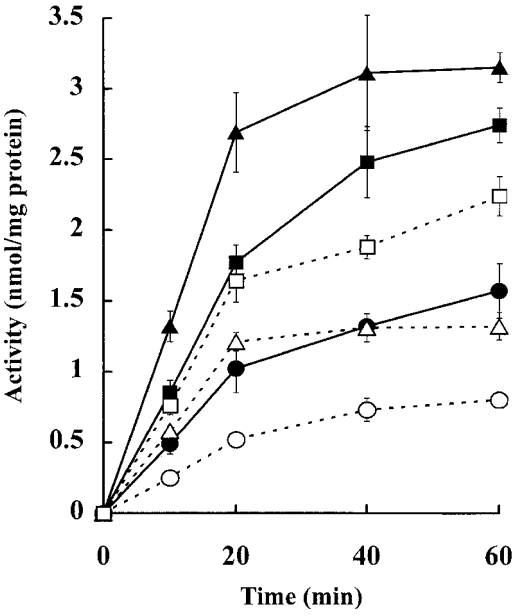


Figure 4. Rates of Cyanox metabolites formation in the male and female rat liver. ●, Male, 4-cyanophenol (microsomes); ▲, male, cyanoxon (microsomes); ○, female, 4-cyanophenol (microsomes); △, female, cyanoxon (microsomes); ■, male, desmethylcyanox (cytosol); □, female, desmethylcyanox (cytosol).

Table 4. Metabolic activity in the hepatic microsomal and cytosolic fractions of the male and female rat.

		pmol/min/mg protein		nmol/min/g liver	
Metabolic transformation	Product	Male	Female	Male	Female
Microsomal fraction					
Oxidative dearylation	4-Cyanophenol	51.0± 8.58*	26.1± 1.59	18.1± 3.29*	6.9± 0.99
Oxidative desulphulation	Cyanoxon	134.5± 14.11**	60.4± 3.26	47.7± 5.48**	15.9± 2.31
Cytosolic fraction					
Demethylation	Desmethylcyanox	88.7± 6.14	82.0± 7.61	55.6± 9.19	42.9± 1.22

Metabolic activity was calculated using amounts formed during 20-min incubation.
Figures are mean± SD for three rats.
*$p < 0.05$, **$p < 0.01$, significantly different from the female value (t-test).

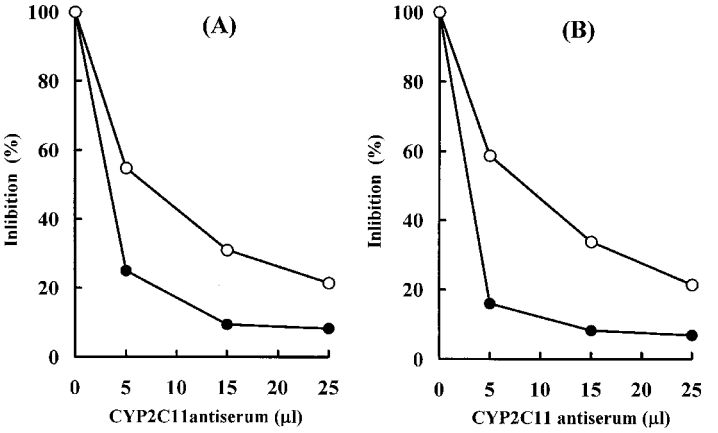


Figure 5. Influence of rat CYP2C11 antiserum on metabolic reactions of Cyanox. (A) Oxidative dearylation; (B) oxidative desulphuration; ●, male; ○, female.

fractions whereas 4-cyanophenol and cyanoxon were the main metabolites in the microsomes for both sexes. Values for activities (table 4) were calculated using data for the 20 min time-point because the plots between 0 and 20 min were linear, as demonstrated in figure 4. As shown in table 4, no marked sex difference was evident for the production of desmethylcyanox (demethylation activity) in the cytosol. On the other hand, significant sex-dependence was observed for 4-cyanophenol and cyanoxon production (oxidative dearylation and oxidative desulphuration activities) in the microsomes, these activities being 2–3-fold greater in the male than in the female.

Incubation of microsomes with CYP2C11 antiserum

Figure 5 shows the influence of rat CYP2C11 antiserum on the metabolism of Cyanox. For both sexes, oxidative dearylation (producing 4-cyanophenol) and oxidative desulphuration (producing cyanoxon) were inhibited by incubation of microsomes with CYP2C11 antiserum. The observed inhibition with 5 and 25 μl antiserum was more extensive in the male ($>$75 and 90% for oxidative dearylation; 75 and 93%, and oxidative desulphuration; 84 and 91%) as opposed to $\sim$45 and 70% in females for oxidative dearylation (45 and 78%), and oxidative desulphuration (41 and 72%).

Discussion

In a previous study (Tomigahara *et al.* 1995), the metabolic fate of Cyanox in the male and female rat was investigated and sex differences in metabolic reactions were demonstrated. Oxidative dearylation and oxidative desulphuration were more pronounced in the male than in the female. Examination of the metabolites in brain, liver, blood cell and plasma of male and female at early time-points after administration in the present study similarly demonstrated sex differences. In all male tissues examined, cyanoxon (a potent AChE inhibitor) was detected. On the other hand, in the female, cyanoxon was only found in brain and even in this tissue the concentration was 2–6-fold higher in the male at all time-points.

The findings indicate that the sex-dependence of toxic symptoms is directly related to amounts of cyanoxon at early time-points after administration of Cyanox. As for the reason for the greater formation of cyanoxon in the male, the following two points should be considered. First, oxidative desulphuration and dearylation activities in the male are greater than those in the female. Second, demethylation activity in the female is greater than that in the male. It has been reported that oxidative desulphuration and dearylation are catalyzed by CYP (Nakatsugawa and Dahm 1967, Neal 1967, Eto 1974), whereas demethylation is considered due to the action of glutathione *S*-transferase (Matsumura 1975). In our *in vitro* study, all of the phase I reactions shown in figure 1 occurred in microsomes and/or cytosol from both sexes. No sex difference was observed for the major cytosolic metabolic reaction, which is demethylation. On the other hand, oxidative desulphuration and oxidative dearylation were 2–3 times greater in the microsomes of the male. The existence of sex-specific CYP in rat liver microsomes is well established (Kamataki *et al.* 1983, Kato and Yamazoe 1990, Imaoka *et al.* 1991, Funae and Imaoka 1993) and it is currently accepted that sex- and age-related differences in metabolism arise due to changes in the relative composition of the various enzymes comprising the drug-metabolizing CYP family (Neville *et al.* 1993). Therefore, one can conclude that the greater formation of cyanoxon in the male is due to the influence of sex-specific CYP. The isozymes CYP2A2, CYP2C11, CYP2C13, CYP3A2 and CYP4A2 are reported to be male-specific forms, whereas CYP2C12 is female-specific form (Funae and Imaoka 1993, Ryan and Levin 1993). Since antiserum against CYP2A2, CYP2C12, CYP2C13, CYP3A2 and CYP4A2 were not available, only that against CYP2C11 was examined in the present study. Both oxidative desulphuration and dearylation were inhibited, the effect being, as expected, most pronounced in the male. The inhibition in the female might have been due to a cross-reaction with female-specific rat CYP2C12. A similar cross-reaction with CYP2C13 could also have occurred in the male. As for CYP3A2 and CYP4A2, the possibility of participation in oxidative dearylation and desulphuration is considered to be low, because it has been reported that CYP2C11 antiserum does not inhibit CYP3A2 or CYP4A1 activities. With respect to CYP2A2, although there is a possibility of participation in these reactions due to the fact that the antiserum inhibits CYP2B1 and CYP2B2 activities slightly, it seems not to be predominant because the CYP2A2 content in the male is so small (at 7 weeks of age, 10 pmol/mg protein) (Imaoka *et al.* 1991). Furthermore, the following results in our previous study using several human CYP expressed by yeast support the consideration mentioned above. Oxidative dearylation and oxidative desulphuration reactions mainly occurred in human CYP2C8, CYP2C9 and CYP2C18, occurred slightly in CYP1A2, CYP2B6, CYP2D6 and CYP2E1 and occurred hardly in CYP2A6 and CYP3A4 (data not

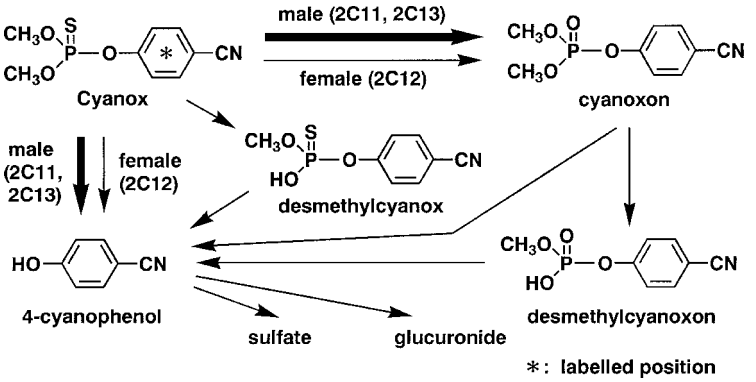


Figure 6. Proposed metabolic pathways of Cyanox in rat.

shown). In conclusion, the results strongly imply that the 2C family of CYP (CYP2C11 and CYP2C13 for the male, CYP2C12 for the female) is involved in oxidative desulphuration and oxidative dearylation of Cyanox in the rat. Imaoka *et al.* (1991) reported the CYP2C11 content in the male at 7 weeks of age was 250 pmol/mg protein, while the CYP2C12 content in the female at the same age was 200 pmol/mg protein, the proportions of each isozyme being ~ 50% of the total hepatic microsomal CYP (400–600 pmol/mg protein) in both cases. Furthermore, Imaoka *et al.* (1990) found 437 and 123 pmol/mg protein of CYP2C11 and CYP2C13 respectively in the male rat weighing 200–220 g. Therefore, the total amount of CYP2C11 and CYP2C13 in the male would appear to be only 1.3-fold that of CYP2C12 in the female. The fact that the two reactions were 2–3 more active in the male, however, indicates more efficient catalysis of male-specific CYP2C11 (and CYP2C13) in comparison with female-specific CYP2C12 (figure 6). Consequently, the greater formation of cyanoxon by the 2C family of CYP in males is consistent with the greater toxicity in this sex.

Acknowledgement

The authors thank Ms Michiko Murotani and Ms Kaeko Tanaka for expert technical assistance.

References

Bradford, M. M., 1976, A rapid and sensitive method for the quantitation of microgram quantities of protein utilizing the principle of protein-dye binding. *Analytical Biochemistry*, **72**, 248–254.

Eto, M., 1974, *Organophosphorus Pesticides: Organic and Biological Chemistry* (Ohio: CRC Press), pp. 158–175.

Funae, Y. and Imaoka, S., 1993, Cytochrome P-450 in Rodents. In J. B. Schenkman and H. Greim (eds), *Handbook of Experimental Pharmacology*, vol. 105: *Cytochrome P-450* (Berlin: Springer), pp. 221–238.

Hiratsuka, A., Sebata, N., Kawashima, K., Okuda, H., Ogura, K., Watabe, T., Satoh, K., Hatayama, I., Tsuchida, S., Ishikawa, T. and Sato, K., 1990, A new class of rat glutathione S-transferase Yrs-Yrs inactivating reactive sulfate esters as metabolites of carcinogenic arylmethanols. *Journal of Biological Chemistry*, **265**, 11973–11981.

Imaoka, S., Fujita, S. and Funae, Y., 1991, Age-dependent expression of cytochrome P-450s in rat liver. *Biochimica et Biophysica Acta*, **1097**, 187–192.

Imaoka, S., Terano, Y. and Funae, Y., 1990, Changes in the amount of cytochrome P450s in rat hepatic microsomes with starvation. *Archives of Biochemistry and Biophysics*, **278**, 168–178.

KAMATAKI, T., MAEDA, K., YAMAZOE, Y., NAGAI, T. and KATO, R., 1983, Sex difference of cytochrome P-450 in the rat: Purification, characterization, and quantitation of constitutive forms of cytochrome P-450 from liver microsomes of male and female rats. *Archives of Biochemistry and Biophysics*, **225**, 758–770.

KANEKO, H., TAKAMATSU, Y., OKUNO, Y., YOSHITAKE, A. and MIYAMOTO, J., 1988, Substrate Specificity for Formation of Cholesterol Ester Conjugates from Fenvalerate Analogues and for Granuloma Formation. *Xenobiotica*, **18**, 11–19.

KATO, R. and YAMAZOE, Y., 1990, Sex-dependent regulation of cytochrome P-450 expression. In K. Ruckpaul and H. Rein (eds), *Principle, Mechanisms and Biological Consequences of Induction* (London: Taylor & Francis), pp. 82–112.

KULKARNI, A. P. and HODGSON, E., 1980, Metabolism of insecticides by mixed function oxidase systems. *Pharmacology and Experimental Therapeutics*, **8**, 379–475.

LAKE, B. G., 1987, Preparation and characterisation of microsomal fractions for studies on xenobiotic metabolism. In K. Snell and B. Mullock (eds), *Biochemical Toxicology* (Washington, DC: IRL Press), pp. 183–215.

MANNERVIK, B., ALIN, P., GUTHENBERG, C., JENSON, H., TAHIR, M. K., WARHOLM, M. and JORNVALL, H., 1985, Identification of three classes of cytosolic glutathione transferase common to several mammalian species: correlation between structural data and enzymatic properties. *Proceedings of the National Academy of Sciences, USA*, **82**, 7202–7206.

MATSUMURA, F., 1975, *Toxicology of Insecticides* (New York: Plenum), pp. 174–176.

MEYER, D. J., COLES, B., PEMBLE, S. E., GILMORE, K. S., FRASER, G. M. and KETTERER, B., 1991, Theta, a new class of glutathione transferase purified from rat and man. *Biochemistry Journal*, **274**, 409–414.

MIHARA, K. and MIYAMOTO, J., 1974, Metabolism of salithion (2-methyoxy-4H-1,3,2-benzodioxaphosphorin-2-sulfide) in rats and plants. *Agriculture and Biological Chemistry*, **38**, 1913–1924.

MIHARA, K., OHKAWA, H. and MIYAMOTO, J., 1981, Metabolism of Tolclofos-methyl in rats and mice. *Journal of Pesticide Science*, **6**, 65–74.

MIYAMOTO, J., MIHARA, K. and HOSOKAWA, S., 1976, Comparative metabolism of *m*-methyl-^{14}C-sumithion in several species of mammals *in vivo*. *Journal of Pesticide Science*, **1**, 9–21.

MIYAMOTO, J., MIKAMI, N., MIHARA, K., TAKIMOTO, Y., KOHDA, H. and SUZUKI, H., 1978, Biological activity of fenitrothion and its degradation products. *Journal of Pesticide Science*, **3**, 35–41.

NAKATSUGAWA, T. and DAHM, P. A., 1967, Microsomal metabolism of parathion. *Biochemistry and Pharmacology*, **16**, 25–38.

NEAL, R. A., 1967, Studies on the metabolism of diethyl 4-nitrophenyl phosphorothionate (parathion) *in vitro*. *Biochemistry Journal*, **103**, 183–192.

NEVILLE, C. F., NONOMIYA, S., SHIMADA, N., KAMATAKI, T., IMAOKA, S. and FUNAE, T., 1993, Characterization of specific cytochrome P450 enzymes responsible for the metabolism of diazepam in hepatic microsomes of adult male rats. *Biochemistry and Pharmacology*, **45**, 59–65.

OMURA, T. and SATO, R., 1964, The carbon monooxide-binding pigment of liver microsomes. I. Evidence for its hemoprotein nature. *Journal of Biological Chemistry*, **239**, 2370–2378.

RYAN, D. E. and LEVIN, W., 1993, Age- and gender-related expression of rat liver cytochrome P450. In J. B. Schenkman and H. Greim (eds), *Handbook of Experimental Pharmacology*, vol. 105: *Cytochrome P-450* (Berlin: Springer), pp. 461–476.

SAITO, K., KANEKO, H., SATOH, K., YOSHITAKE, A. and YAMADA, H., 1991, Agerelated changes in metabolism of diethofencarb: Relationship between metabolism in rat and hepatic drug metabolizing enzyme activities. *Xenobiotica*, **21**, 575–582.

TESTA, B. and JENNER, P., 1976, *Drugs and the Pharmaceutical Sciences*, vol. 4: *Drug Metabolism: Chemical and Biochemical Aspects* (New York: Marcel Dekker), pp. 112–113.

TOMIGAHARA, Y., MORI, M., SHIBA, K., ISOBE, N., KANEKO, H., NAKATSUKA, I. and YAMADA, H., 1994, Metabolism of tetramethrin isomers in rat: II. Identification and quantitation of metabolites. *Xenobiotica*, **24**, 1205–1214.

TOMIGAHARA, Y., ONOGI, M., SAITO, K., SHIBA, K., KANEKO, H., NAKATSUKA, I. and YAMADA, H., 1995, Metabolism of Cyanox in the rat. I. Absorption, disposition, excretion and biotransformation. *Xenobiotica*, **25**, 1195–1206.

WAKIMURA, A. and MIYAMOTO, J., 1971, Metabolism of cyanox, *O,O*-dimethyl *O*-(4-cyanophenyl) phosphorothioate in the rats. *Agriculture and Biological Chemistry*, **35**, 410–416.

XENOBIOTICA , 2000, VOL. 30, NO. 4, 407–426

Urinary metabolites of a novel quinoxaline non-nucleoside reverse transcriptase inhibitor in rabbit, mouse and human: identification of fluorine NIH shift metabolites using NMR and tandem MS

G. J. DEAR, I. M. ISMAIL*, P. J. MUTCH, R. S. PLUMB, L. H. DAVIES and B. C. SWEATMAN

International Development, Bioanalysis and Drug Metabolism Division, Glaxo Wellcome Research and Development, Park Road, Ware SG12 0DP, UK

Received 10 August 1999

1. The urinary metabolites of (*S*)-2-ethyl-7-fluoro-3-oxo-3,4-dihydro-2H-quinoxaline-carboxylic acid isopropylester (GW420867X) have been investigated in samples obtained following oral administration to rabbit, mouse and human. GW420867X underwent extensive biotransformation to form hydroxylated metabolites and glucuronide conjugates on the aromatic ring, and on the ethyl and isopropyl side-chains in all species. In rabbit urine, a minor metabolite was detected and characterized as a cysteine adduct that was not observed in mouse or man.

2. The hydroxylated metabolites and corresponding glucuronide conjugates were isolated by semi-preparative HPLC and characterized using NMR, LC-NMR and LC-MS/MS. The relative proportions of fluorine-containing metabolites were determined in animal species by ^{19}F-NMR signal integration.

3. The fluorine atom of the aromatic ring underwent NIH shift rearrangement in the metabolites isolated and characterized in rabbit, mouse and human urine.

4. The characterization of the NIH shift metabolites in urine enabled the detection and confirmation of the presence of these metabolites in human plasma.

Introduction

(*S*)-2-ethyl-7-fluoro-3-oxo-3,4-dihydro-2H-quinoxaline-carboxylic acid isopropylester (GW420867X; figure 1) is a member of the quinoxaline class of non-nucleoside reverse transcriptase inhibitors and is currently under development for the treatment of HIV infection. The identification of metabolites is an important part of the development process of any potential drug candidate and as part of this process the metabolism of GW420867X following oral dosing to human and various animal species has been studied. The present authors have previously reported the urinary metabolites in dog, cynomolgus monkey and mini-pig using a combination of ^{19}F- and ^{1}H-NMR spectroscopy and mass spectrometry (MS) (Ismail *et al.* 1999).

HPLC coupled to tandem mass spectrometry (LC-MS/MS) has been the industry method of choice for quantitative and qualitative analysis of drugs and their metabolites in complex samples of biological origin, and many examples have been reported (Dear *et al.* 1995, 1998a). NMR spectroscopy is another valuable technique for elucidating the structures of organic compounds and recently it has found an ever-increasing role in drug metabolite identification particularly when coupled to HPLC (Nicholson and Wilson 1989, Spraul *et al.* 1994, Lindon *et al.* 1997). Owing

* Author for correspondence; e-mail: imi2682@glaxowellcome.co.uk

Xenobiotica ISSN 0049-8254 print/ISSN 1366-5928 online © 2000 Taylor & Francis Ltd
http://www.tandf.co.uk/journals

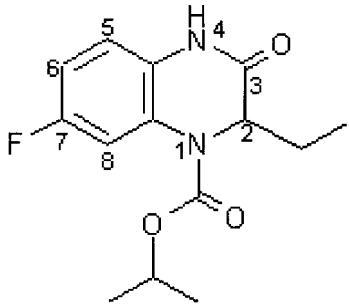


Figure 1. Structure of GW420867X.

to the low ^{19}F background noise in biological samples, ^{19}F-NMR provides a powerful and rapid means of gaining qualitative and quantitative information about metabolites of fluorinated drugs (Everett *et al.* 1985, Vialaneix *et al.* 1987, Wade *et al.* 1988).

The present authors have previously demonstrated the value of using semi-preparative HPLC to isolate drug metabolites in sufficient quantities such that they may be rapidly characterized by the effective use of NMR and MS (Plumb *et al.* 1999). The combination of this semi-preparative approach with ^{1}H-NMR as a non-selective detector for screening is a very efficient method for the isolation and characterization of xenobiotic-related material in biological matrices (Ismail *et al.* 1999). Analytical-scale LC-NMR and LC-NMR/MS analysis can be applied to these fractions if further chromatographic resolution is required to yield unequivocal structural elucidation of metabolite structures (Dear *et al.* 1998b). The combined power of NMR and MS has recently been highlighted (Pullen *et al.* 1995, Shockcor *et al.* 1996, Holt *et al.* 1997, Dear *et al.* 1998a).

This paper describes the identification of metabolites of GW420867X, including, for the first time, fluorine NIH shift metabolites in both human urine and plasma, by a combination of NMR, LC-NMR and LC-MS/MS, preceded by semi-preparative LC.

Aromatic hydroxylation of drug molecules is commonly observed both *in vitro* and *in vivo* and occasionally a substitutent present at the site of hydroxylation is seen to migrate to an adjacent carbon atom. It is now accepted that this rearrangement proceeds via arene oxide (epoxide) and/or keto intermediates and has been termed the NIH shift (Guroff *et al.* 1967, Daly *et al.* 1972, Jerina and Daly 1974, Korzekwa *et al.* 1985). This NIH rearrangement has been reported for deuterium and tritium aromatic labels, and also for larger bulkier moieties such as halide and alkyl substituents (Guroff *et al.* 1967, Daly *et al.* 1972, Jerina and Daly 1974). The propensity of a substituent to undergo migration is dependent on the nature of the substituent itself and also on the nature of other substituents that may be present in the molecule (Safe *et al.* 1976).

Generally, the importance of the NIH shift of halogen substituents in the course of aromatic hydroxylation is less well documented than the NIH shift of deuterium or tritium substituents. For cytochrome P450-catalysed hydroxylation of halogenated aromatic compounds, evidence of the NIH shift has been presented primarily for substrates containing chlorine and bromine substituents (Kohli *et al.* 1976, Chu *et al.* 1984, Schwartz *et al.* 1987, Den Besten *et al.* 1991, 1992). In contrast, reference to fluorine migration is particularly sparse in the literature, and

it has been reported that the NIH shift plays only a minor role in the *in vivo* metabolism of fluorobenzenes (Koerts *et al*. 1998). This has been attributed, in part, to the possible existence of alternative pathways for metabolism of the epoxide intermediate, such as glutathione conjugation, which is more efficient for fluorinated than chlorinated arene oxides. This latter conclusion is supported by *in vitro* data obtained using liver microsomes, which showed a significant amount of NIH-shifted metabolite for 1,4-difluorobenzene (Koerts *et al*. 1998).

Described here for the first time is the isolation and characterization of the NIH shift metabolites of GW420867X in human urine and the confirmation of the presence of these NIH shift metabolites circulating in human plasma. These same metabolites were also observed in the urine of mouse and rabbit but not in that of cynomolgus monkey, dog and mini-pig (Ismail *et al*. 1999).

Materials and methods

Chemicals

GW420867X was synthesized by Hoechst Marion Roussel (Frankfurt-am-Main, Germany) (purity 99.3%). HPLC grade acetonitrile was from Rathburn (Walkerburn, UK), and HPLC-grade water and formic acid (AR grade) were from Fisons Chemicals (Loughborough, UK). Deuterium oxide and acetonitrile (Reidel-de-Haën, 'Pestanal' grade) for NMR studies was supplied by Fluorochem Ltd (Old Glossop, UK). All other chemicals and reagents were of analytical grade or equivalent.

Urine collection

Mouse urine was collected over 0–24 h following the ninth daily oral dose of GW420867X to the male CD-1 mouse at a target dose level of 250 mg kg^{-1} day^{-1}. The dose was formulated as a suspension in a 0.5% (w/v) solution of hydroxypropylmethyl cellulose in sterile water for irrigation with 0.1% (w/v) Poloxamer 188. Samples from eight animals (age range 6–7 weeks at start of study) were pooled before analysis. Rabbit urine was collected over 0–24 h following the seventh daily oral dose of GW420867X to two female New Zealand White rabbits at a target dose level of 125 mg kg^{-1} day^{-1}. The dose was formulated as a suspension in a 0.5% (w/v) solution of hydroxypropylmethyl cellulose in sterile water for irrigation with 0.1% (w/v) Poloxamer 188. Samples from the two animals (age range 7–10 months at start of study) were pooled before analysis.

Human urine was collected over 0–24 h following a single oral dose of GW420867X at a dose level of 1200 mg/subject to four healthy male volunteers. Each dose of 1200 mg was administered as 6×200 mg tablets. The age range of the volunteers was 19–29 years, and the weight range 62.3–83.7 kg. Samples from individual subjects (2% of total volume) were pooled before analysis. For all human volunteer studies, the protocol had been approved by ethical review, and volunteers provided informed consent.

Plasma

Plasma was obtained from human volunteers at 1.5–6 h following a single oral administration of GW420867X of 900 mg/subject to four healthy male volunteers. Each dose of 900 mg was administered as 4×200 mg and 2×50 mg tablets. The following blood samples were taken from individual volunteers into lithium heparin blood tubes: subject 70, 3 and 4 h post-dose; subject 72, 1.5 and 2 h post-dose; subject 74, 1.5, 2 and 3 h post-dose; subject 75, 3, 4 and 6 h post-dose. Plasma was separated from whole blood by centrifugation (2000*g*, 10 min). From each sample 1 ml plasma was taken and pooled. The age range of the volunteers was 23–36 years, and the weight range 75.1–86.8 kg.

In addition, plasma was obtained at 2–4 h following the last of 14 daily oral administrations of 200 mg/subject day^{-1} to seven healthy male volunteers. Each dose of 200 mg was administered as 1×200 mg tablet. Blood samples were taken from individual volunteers into lithium heparin blood tubes at 2 and 4 h post-dose. Plasma was separated from whole blood by centrifugation (2000*g*, 10 min). From each sample, 150 μl plasma was taken and pooled. The age range of the volunteers was 20–30 years, and the weight range 57.2–94.9 kg. All samples were kept stored frozen at -20 °C before analysis.

Sample preparation

Urine. Pooled urine samples collected following oral administration of GW420867X to rabbit and human (50 and 110 ml respectively) were freeze-dried and reconstituted in 10 ml distilled water; mouse

urine (15 ml) was centrifuged and the supernatant used without any further treatment. The concentrated rabbit and human urine samples were centrifuged at 14500*g* for 5 min and the supernatants removed and stored at 0–8 °C before isolation by preparative HPLC as described below.

Preparative HPLC. Preparative chromatography was performed on a Magellen C18 60 × 21 mm 5 μm column (Phenomenex, UK) using a Gilson 233-XL autosampler and two Gilson 307 pumps (Gilson, France) controlled by Unipoint (v.1.6) software. The sample eluent was monitored by UV absorbance at 254 nm using a LDC Spectro-Monitor 3100 (Thermoseparations, USA). Injections of the prepared urine samples (9.5 ml) were made onto the preparative column. The column eluent was collected into 96-well microtitre plates, under the control of the Unipoint software, using 15 s fractions (corresponding to 1 ml column eluent). Separations were achieved at 4 ml min^{-1} using a mobile phase of 0.1% formic acid in an aqueous/acetonitrile gradient. The proportion of acetonitrile was held at 0% for an initial 3 min and then programmed to increase linearly from 0 to 95% over 35 min. Collected fractions were evaporated to dryness under a constant flow of nitrogen at 25 °C, re-dissolved in 600 μl Pestanal grade acetonitrile/deuterium oxide (50/50 v/v) and transferred individually to 5-mm NMR tubes for analysis.

Plasma. Pooled human plasma (2 ml) was prepared by simple protein precipitation using acetonitrile (1 : 3 v/v). Precipitated samples were centrifuged at 1300*g* for 15 min and the supernatant aspirated and taken to dryness under a stream of nitrogen. The dried sample was reconstituted in 0.1% aqueous formic acid and transferred to an HPLC vial ready for injection.

NMR. NMR experiments were performed on a Bruker DRX-600 spectrometer (Bruker, Rheinstetten, Germany) equipped with a dual ^{1}H-^{19}F 5-mm NMR probe or a ^{1}H-^{19}F flow probe (cell 4 mm i.d. with an active cell volume of ~ 120 μl) operating at 600.13 MHz for ^{1}H and 564.4 MHz for ^{19}F. Isolated fractions were analysed by ^{1}H- and ^{19}F-NMR spectroscopy for the presence of drug-related material. ^{19}F-NMR measurements were obtained using a single 90° pulse observed with broad-band proton decoupling using the Waltz-16 sequence. Typically 1024 transients were acquired into 128 K data points over a spectral width of 28 248 Hz (50 ppm) producing a total pulse repetition time of 5 s. The data were line broadened by 2 Hz before Fourier transformation and the chemical shifts referenced externally to $CFCl_3$ (δ 0.0).

The peak areas of fluorine-containing components in individual fractions were quantified by integrating the ^{19}F-NMR peaks (XWIN-NMR software, v.2.1, Bruker). Following assignment of peak identity the relative proportions of components containing a fluorine atom were calculated and thus major drug-related components quantified.

^{1}H- and LC-NMR spectra were acquired using a standard NOESYPRESAT pulse sequence for solvent suppression with time-shared double presaturation of the water and acetonitrile frequencies. In these experiments typically 256 transients were acquired into 32 K data points over a spectral width of 12019 Hz (20 ppm) giving a pulse repetition time of 3.2 s. Before Fourier transformation, an exponential line-broadening function of 0.3 Hz was applied to each spectrum to improve the signal-to-noise ratio. Chemical shifts are given in ppm referenced to CH_3CN at δ2.00.

Aliquots of fractions containing metabolites were analysed by LC-MS/MS as described below.

LC-MS/MS. LC-MS/MS experiments were conducted on a Hewlett-Packard Model 1100 liquid chromatograph (Walderbron, Germany) coupled in series to a Bruker Esquire ion-trap mass spectrometer (Bruker-Fransen, Bremen, Germany), fitted with an atmospheric pressure ionization source (API). The analytical chromatography was performed on a 250 × 4.6 mm i.d. Zorbax RxC8 column operated at 25 °C, using a mobile phase consisting of 0.1% formic acid in an aqueous/acetonitrile gradient. The proportion of acetonitrile was programmed to increase linearly from 0% to 95% over 30 min. A flow rate of 1 ml min^{-1} was used for all analyses.

The column eluent was split 1 in 10, directing ~ 100 μlmin^{-1} to a pneumatically assisted electrospray interface. Nitrogen was the nebulizer gas at 30–40 psi, and the drying gas at 6 l min^{-1} and 150 °C. The MS was operated in positive-ion mode with a scan rate of 13000 amu s^{-1} and a range of 50–600 m/z. Generated ions were monitored by the ion-trap using automatic MS/MS, in which the base peak intensity was constantly compared with a user-defined threshold (10^6 in this case). When this threshold was exceeded, the ion-trap mass spectrometer first isolated the base peak over a given mass window and then induced fragmentation using resonant excitation at 1.2 V. In essence, during LC-MS/MS sample acquisition, where base peak intensity exceeded the threshold, alternate single scans of MS and MS/MS were acquired. All MS/MS experiments were performed using the ion charge control (ICC) facility automatically to adjust the accumulation time as the ion abundance changed. Instrument control, data acquisition and data processing were performed on a DEC station 5000/33 using Bruker proprietary software.

Additional LC-MS/MS experiments on plasma extracts were carried out on a Hewlett-Packard Model 1090 liquid chromatograph coupled in series to a Finnigan MAT TSQ 700 mass spectrometer (Finnigan, Palo Alto, CA, USA), fitted with an API. Analytical chromatography was performed as described above. The column eluent was split 1 in 10, directing ~ 100 μl min^{-1} to a pneumatically

assisted electrospray interface. The API-heated capillary was maintained at 220 °C and nitrogen was the nebulizer gas at 60 psi. MS/MS experiments were based on collision-induced dissociations (CID) occurring in the RF-only collision cell of the triple quadrupole, using a collision energy of 25 eV and argon as the collision gas at 2.0 mTorr. Selected reaction monitoring (SRM) experiments were performed using a dwell time of 200 ms per transition. Instrument control, data acquisition and data processing were performed on a DEC station 5000/33 using Finnigan proprietary software.

LC-NMR. The LC-NMR probe head contained a flow cell with an active volume of 120 μl. The chromatographic separation for LC-NMR was performed under the control of Bruker HyStar (v.1.0) software operating in loop storage mode. Analytical chromatography was performed on a 250 × 3.2 mm i.d. Phenomenex Magellen C18 column at 0.6 ml min^{-1}. The mobile phase consisted of 0.1% formic acid in deuterium oxide/acetonitrile. The proportion of acetonitrile was increased linearly from 0 to 80% over 35 min. The column eluent was monitored at a wavelength of 254 nm using a Knauer VWM (Bruker) detector and eluting peaks of interest were stored in the loops of the Bruker BPSU-36/BSFU-0 peak sampling unit before transfer to the NMR probe for analysis.

When a sufficient number of scans had been acquired to produce a good-quality ^{1}H-NMR spectrum, the sample was recovered from the NMR probe for subsequent analysis by MS.

Results

Analysis of urinary metabolites

NMR. The majority of the urinary metabolites characterized in this study were isolated as semi-pure fractions by preparative HPLC and identified as being drug-related by ^{19}F- and ^{1}H-NMR spectroscopy. Inspection of the NMR and MS data of the metabolites following isolation by preparative HPLC without further treatment enabled their characterization. In cases where semi-preparative chromatography provided insufficient separation or the metabolite was not present in sufficient quantity to enable the characterization, further analytical separation and longer data acquisition times were used utilizing LC-NMR. In the case of one particular metabolite, M17, LC-NMR-MS was necessary to elucidate the structure of the metabolite and this has been reported elsewhere (Dear *et al.* 1998b). This process was also facilitated by the comparison of NMR and mass spectra obtained here with the spectra of M1–6, previously isolated and characterized from the urine of dog, cynomolgus monkey and mini-pig (Ismail *et al.* 1999).

A ^{1}H-NMR stack plot from rabbit urine fractions (figure 2) shows that metabolites have been isolated as semi-pure fractions in some cases enabling characterization of the metabolite without further treatment. This is illustrated by the relative purity of the ^{1}H-NMR spectrum obtained for the fraction containing M12 (figure 3). Additionally, the isolation of sufficient quantities of material using this semi-preparative approach allows the performance of relatively insensitive information-rich NMR experiments such as nuclear Overhauser enhancement (nOe) that have enabled the unambiguous characterization of novel metabolites such as M12.

The isolated fractions containing M8 (in all species) and M14 (in rabbit urine) gave rise to no ^{19}F signals and, thus, gave no immediate indication of containing xenobiotic-related material. However, inspection of the ^{1}H-NMR spectra showed that these fractions contained the ethyl as well as the isopropyl side-chain of GW420867X and thus contained drug-related material. The ^{1}H-NMR spectrum of M14 indicated the loss of the 6-H aromatic proton and the absence of fluorine or proton coupling to the remaining aromatic protons at δ7.06 and 7.23. Additionally, the appearance of protons at δ3.7, 3.11 and 3.43 suggested that the structure of M14 was the 7-desfluoro-6-cysteine adduct. Further evidence to support the position of the cysteine adduct on the aromatic ring as being at the 6-position was obtained by

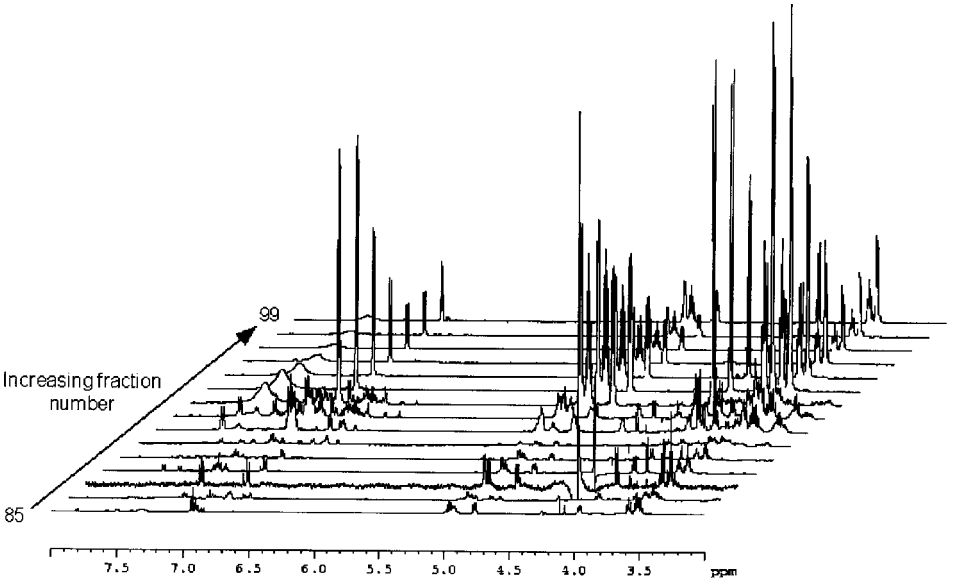
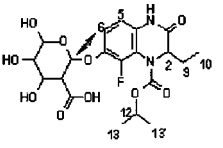


Figure 2. [1]H-NMR stack plot of individual rabbit urine fractions acquired following preparative HPLC.



Metabolite M12

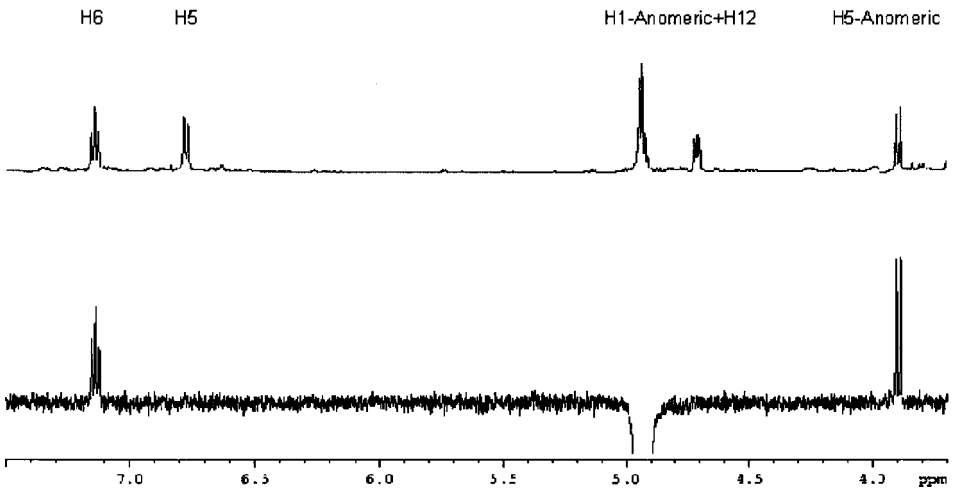


Figure 3. [1]H-NMR spectrum of M12 and selective nOe (nuclear Overhauser effect) enhancement of multiplet at 4.95 ppm.

means of a positive nOe from the 5-H proton at δ7.06 to the methylene protons of the cysteine moiety at δ3.11 and 3.43.

The structures of M8 and M15 were established by means of further analytical chromatographic separation performed on the isolated rabbit urine fractions in which M8 and M15 were in adjacent fractions and poorly resolved. Analytical LC-NMR was performed, using the semi-purified fractions from the semi-preparative chromatography separation, to resolve these metabolites and obtain NMR spectra of these metabolites. Analysis of the chemical shifts and coupling constants from the LC-NMR together with mass spectral data enabled the confirmation of the structure of the 7-desfluoro-7-hydroxyglucuronide conjugate, M8. Once having been identified in the rabbit, the presence of M8 in mouse and human urine was readily confirmed by comparison of the ^{1}H-NMR data.

The ^{1}H-NMR spectrum of M15 clearly indicated a glucuronide conjugate that is substituted in the aromatic region. The ^{19}F-NMR data (not shown) that produced a signal in the -135 to -136 ppm region for M15 is consistent with a ^{19}F signal *ortho* to oxygen. In the ^{1}H-NMR spectrum of M15, the size of the coupling constant on the observed aromatic proton at δ 6.88 ppm is 11.0 Hz, which is consistent with an *ortho* ^{19}F-^{1}H coupling. On warming of the sample, the aromatic proton signal for 8-H at δ7.44, which is normally broad through restricted rotation of the isopropyl group, was sharpened sufficiently to observe coupling, and a coupling constant of 6.14 Hz was recorded, which is consistent with a *meta* ^{19}F-^{1}H coupling. Further confirmation of the structure of M15 was provided by a positive nOe from the anomeric β-H1 glucuronide proton at δ4.95 to the 8-H aromatic proton at δ7.44 (figure 4). This result strongly suggests that the fluorine and the hydroxyl group (and thus the glucuronide) are at the 6- and 7-positions respectively and thereby confirms that the M15 metabolite is a 6-fluoro-7-hydroxyglucuronide.

The ^{19}F-NMR chemical shift of M12 was similar to that of M15 and consistent with substitution *ortho* to the fluorine atom. Unlike M15 and the other metabolites, there is a noticeable absence of the broad signal corresponding to the aromatic proton at the 8-position. Only two aromatic signals were observed at δ7.12 and 6.77, each showing a fine coupling. A positive nOe was obtained from the anomeric H1 proton at δ4.95 of the glucuronic acid moiety and confirmed its proximity to the aromatic proton seen as a triplet at δ7.12 (figure 3). From these data it can be deduced that the fluorine and the hydroxyl groups are at the 8- and 7-position respectively. This metabolite, therefore, represents an 8-fluoro-7-hydroxy-glucuronide conjugate.

The migration of the fluorine atom from the 7- to the 6-position (M15) and from the 7- to the 8-position (M12) of the aromatic ring is consistent with the occurrence of an NIH shift.

M13 was readily characterized in that aromatic hydroxylation and glucuronide conjugation had occurred in a similar manner to M3, but in this case the carboxylic acid isopropyl ester side-chain was not present, indicating that it had undergone a biotransformation to give M13.

The absence of any changes to the aromatic protons or to the protons of the carboxylic acid isopropyl ester side-chain of the metabolites observed in mouse, M9 and M11, indicated that no substitution had occurred in these positions for these metabolites. The loss of the methyl protons observed for the ethyl side-chains together with the appearance of signals at δ3.5 for the newly formed CH_2OH group leads to the deduction of the structure of M9.

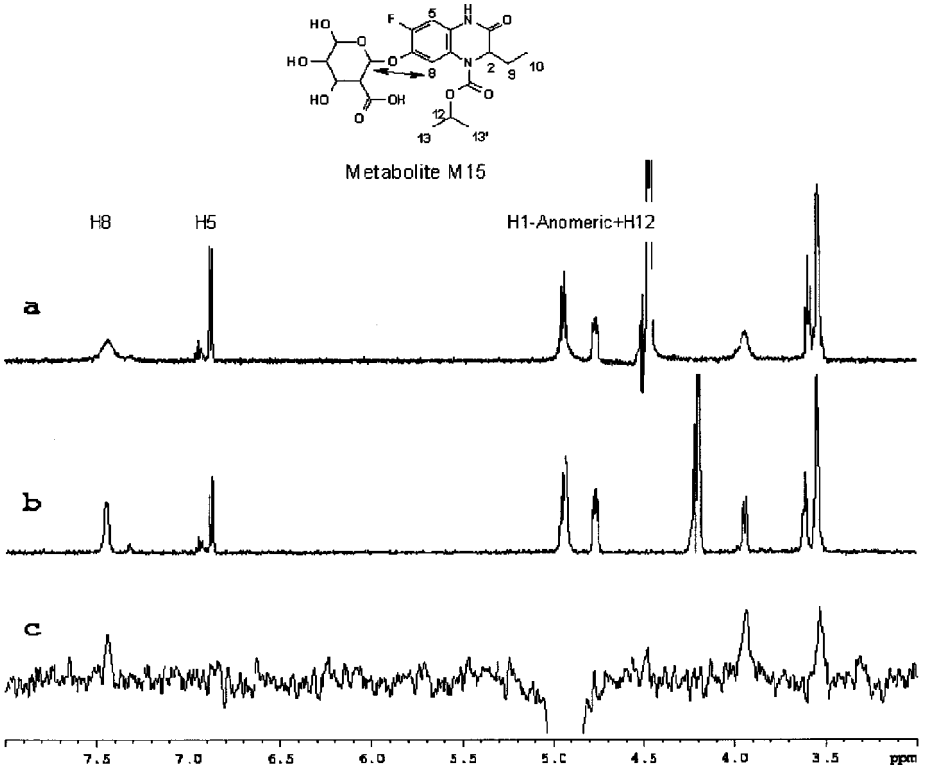


Figure 4. ^{1}H-NMR spectrum of M15 measured at (a) 293 and (b) 323 K; and (c) selective nOe enhancement of multiplet at 4.95 ppm.

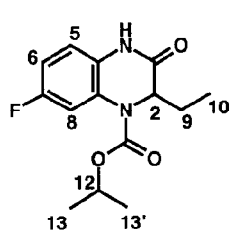
Similarly, for M11, the chemical shifts of the CH_2 group adjacent to the newly formed COOH group appeared at δ2.54 and 2.42 in comparison with δ1.60 and 1.35 for GW420867X, and the disappearance of the methyl protons of the ethyl side-chain indicated metabolism occurred in this position. This, together with the mass spectral evidence, led to the confirmation of the structure of M11.

The structure of M17 from human urine was characterized by means of LC-NMR/MS and has already been published (Dear *et al.* 1998b). M10 was not present in sufficient quantities for analysis by NMR and its structure was deduced solely on the evidence of the mass spectral data given below.

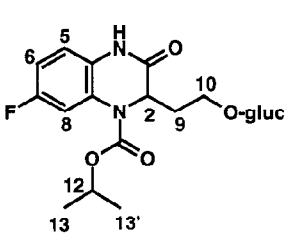
Chemical shifts for parent GW420867X and metabolites assigned by NMR are given in tables 1–3. The relative proportions of fluorine-containing components in rabbit and mouse urine are given in table 4.

LC-MS/MS. The structure of urinary metabolites isolated by preparative HPLC and identified as drug-related by ^{19}F- and ^{1}H-NMR spectroscopy were characterized, in part, by LC-MS/MS using the ion-trap mass spectrometer, as described above. Interpretation of the MS/MS spectra of metabolites was based on comparisons with the product ions formed from authentic parent drug. The MS/MS product ion spectrum of GW420867X was formed using the MH^+ ion, m/z 281, as the precursor ion. The spectrum, which is relatively simple, is dominated by a collision-induced loss of the isopropyl group, following cleavage of the ester link,

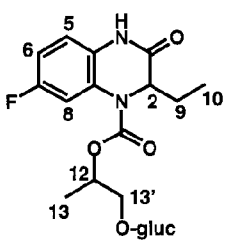
Table 1. ^{1}H-NMR chemical shifts and coupling constants of GW420867X and M1–4.



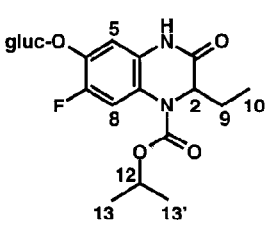
GW420867



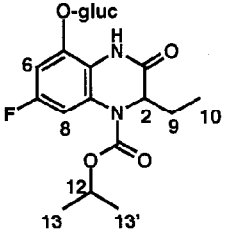
M1



M2



M3

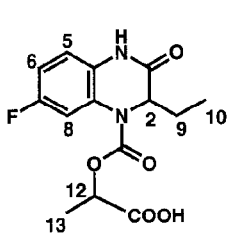


M4

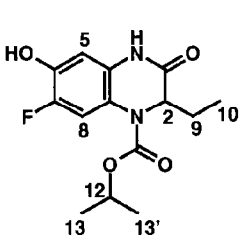
	2-H	5-H	6-H	8-H	9-H	10-H	12-H	13-H/13′-H	H1-Glu	H5-Glu	H2-H4-Glu
GW420867X	4.78	6.98 (dd,5.1, 8.8 Hz)	6.94 (dt, 8.8; 8.8, 2.2 Hz)	7.38 (broad)	1.60 and 1.35	0.85 (t, 7.3)	4.96	1.29 and 1.22			
M1	5.03	6.96 (dd, $\mathcal{J}$ = 8.8, 5.1 Hz)	6.99 (broad)	1.80 and 1.66	3.83 and 3.55 (m)	4.96	1.30 and 1.23	4.31	3.8	3.48–3.22	
M2	4.8	6.9	7.01	n/o	1.61 and 1.38	0.85	5.05	1.21 (broad)	n/o	3.85	3.6–3.4
M3	4.76	6.88 (d, 8.1 Hz)	—	7.43 (broad)	1.6 and 1.35	0.85	4.98	1.29 and 1.22	5.06	3.99	3.6–3.5
M4	4.79	–	6.82 (dd,10.3, 2.9 Hz)	7.14 (broad)	1.60 and 1.36	0.85	4.95	1.29 and 1.22	5.02	4.06	3.65–3.5

Chemical shift measurements are quoted in ppm and $\mathcal{J}$ values in Hz, d, doublet; dd, doublet of doublets; t, triplet; dt, doublet of triplets.

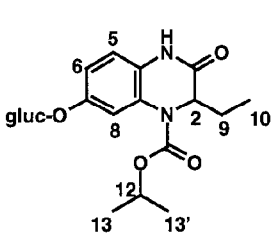
Table 2. ^{1}NMR chemical shifts and coupling constants of M5, M6, M8, M9 and M11



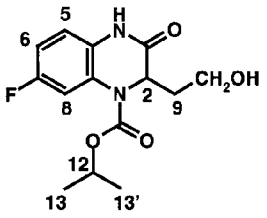
M5



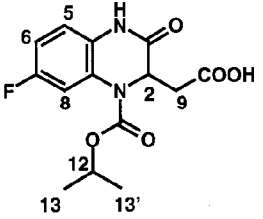
M6



M8



M9

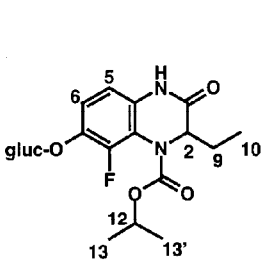


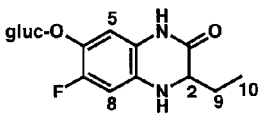
M11

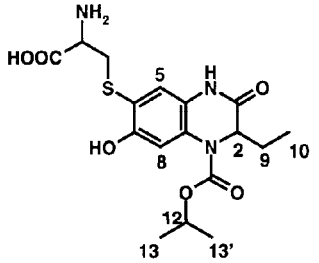
	2-H	5-H	6-H	8-H	9-H	10-H	12-H	13-H/13′-H	H1-Glu	H5-Glu	H2-H4-Glu
M5	4.78 (broad)	7.00 (dd, 5.9, 8.8 Hz)	6.94 (dt, 8.8, 8.8, 2.9 Hz)	n/o	n/o	n/o	5.11 (m, 7.3 Hz)	n/o			
M6	4.74	6.59 (d, 8.8 Hz)	—	n/o	1.59 and 1.36	0.85	4.95	1.29 and 1.22			
M8	4.78	6.96 (d, 8.8Hz)	6.93 (dd, $\mathcal{J}$ = 8.8, 2.2 Hz)	7.33 (broad)	1.60 and 1.36	0.85	4.46	1.29 and 1.22	4.96	3.96	3.6–3.5
M9	5.0–4.9 (overlapped)	6.9	7.03	7.34	3.5	—	5.0–4.9 (overlapped)	1.27 and 1.19			
M11	5.28	6.9	7.03	7.38	2.54 (14.7 and 5.1Hz) and 2.42 (14.7 & 9.5Hz)	—	4.95	1.29 and 1.23			

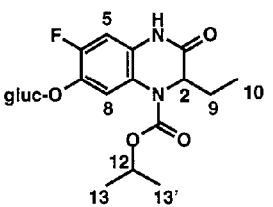
Chemical shift measurements are quoted in ppm and $\mathcal{J}$ values in Hz, d, doublet; dd, doublet of doublets; t, triplet; dt, doublet of triplets.

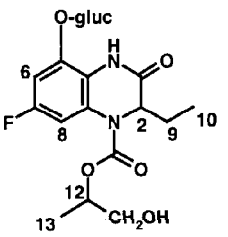
Table 3. ^{1}H NMR chemical shifts and coupling constants of M12, M13, M14, M15 and M17.











	2-H	5-H	6-H	8-H	9-H	10-H	12-H	13–H/13′-H	H1-Glu	H5-Glu	H2-H4-Glu
M12	4.70	6.77 (dd, 8.8, 1.2 Hz)	7.2 (t, 8.8, 8.8Hz)	—	1.61 and 1.29	0.89	4.92	1.23 and 1.16	4.95	3.94	3.6–3.4
M13	3.73	6.81 (d, 8.0 Hz)	—	6.6 (d, 11.7 Hz)	1.68 and 1.55	0.90 (t, 7.3 Hz)	—	—	4.76 (7.3Hz)	3.65 (9.5 Hz)	3.6–3.4
M14	4.75	7.06	—	7.23 (broad)	1.6 and 1.38	0.86	4.96	1.29 and 1.24	α-cysteine 3.7 (3.7, 9.5 Hz) β-cysteine 3.43 and 3.11 (3.7, 9.5, 14.7 Hz)		
M15	4.77	6.88 (d, 11.0 Hz)	—	7.44 (d, 6.1 Hz)	1.59 and 1.36	0.85	4.95	1.28 and 1.21	4.95	3.84	3.6–3.5
M17	4.82	-	6.84 (dd, 10.6, 1.5 Hz)	7.15 (broad)	1.61 and 1.39	0.85	4.90	1.26	5.04 (7.3 Hz)	4.06	3.6–3.5

Chemical shift measurements are quoted in ppm and J values in Hz, d, doublet; dd, doublet of doublets; t, triplet; dt, doublet of triplets.

Table 4. Comparative proportions of fluorine-containing drug-related material in urine after repeat oral dosing of GW420867X to rabbit (seven daily doses of 125 mg kg^{-1} day^{-1}) and mouse (nine daily doses of 250 mg kg^{-1} day^{-1}).

	Percentage of quantified fluorine-containing drug-related material											
Species	GW420867X	M1	M2	M3	M4	M5	M6	M9	M11	M12	M13	M15
Rabbit	nd	3	3	38	35	4	nd	nd	nd	9	3	5
Mouse	2	25	nd	29	2	9	4	7	19	2	nd	nd

nd, Component not detected in urine.

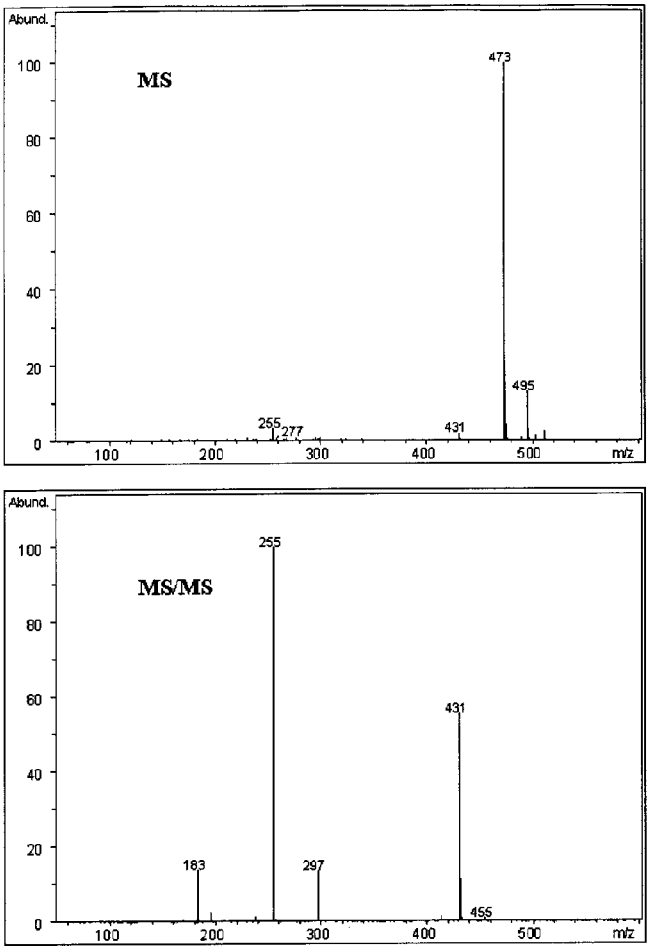


Figure 5. MS and MS/MS spectra of a representative hydroxyglucuronide (m/z 473) isolated from rabbit urine.

generating the base peak at m/z 239. A concerted loss of the carboxyl group and the ethyl side-chain subsequently generates the product ion at m/z 167.

Using LC-MS/MS, four fluorinated aromatic hydroxyglucuronides were detected in rabbit urine fractions. The MS and MS/MS spectra of one of these hydroxylated conjugates are given in figure 5. The MS spectrum is dominated by the MH^+ ion at m/z 473, with a smaller Na^+ adduct ion discernible at m/z 495. The peak in the product ion spectrum at m/z 297 (figure 5) corresponds to the hydroxylated species formed by loss of the glucuronyl moiety. Such a loss (− 176 amu) is characteristic of such conjugates (Baille 1994). Subsequent loss of the isopropyl group to form m/z 255, equivalent to m/z 239 generated from parent drug, indicates that the likely site of hydroxylation (and thus glucuronidation) is either the aromatic ring or the ethyl side-chain. Further loss of the carboxyl group and the ethyl side-chain, confirms the aromatic ring as the site of biotransformation. These product ions have previously been rationalized (Dear *et al.* 1998b). This spectrum is representative of the aromatic hydroxyglucuronides found in isolated rabbit urine

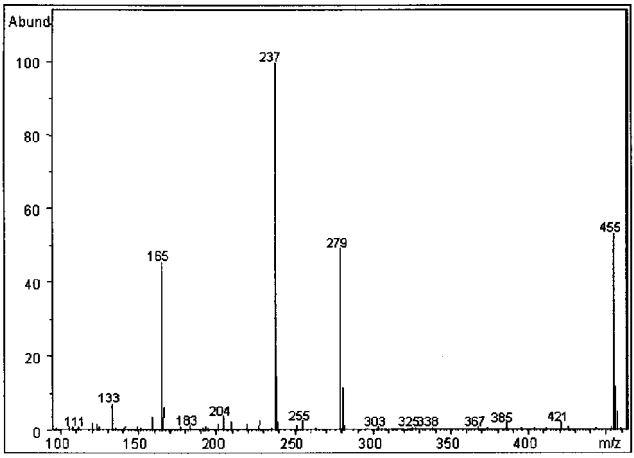


Figure 6. MS/MS spectrum of the dehalogenated hydroxyglucuronide (m/z 455) M8.

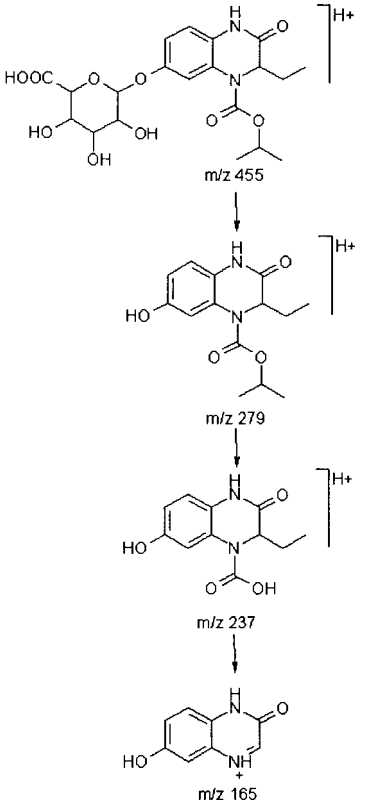


Figure 7. Rationalization of the major product ions formed following MS/MS of m/z 455 of M8.

fractions. In total, four aromatic hydroxyglucuronides were detected in rabbit, three in mouse and four in human urine.

An additional metabolite, rationalized as the dehalogenated aromatic hydroxyglucuronide (M8), was detected in rabbit, mouse and human urine fractions. It gave

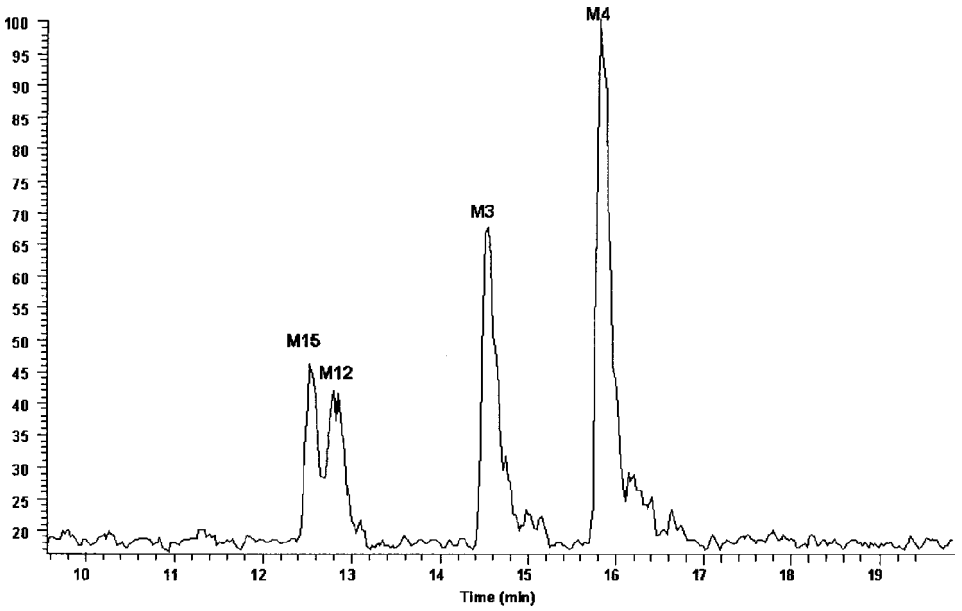


Figure 8. Ion chromatogram (m/z 473⇒183) formed following SRM analysis of extracted human plasma.

rise to an MH^+ ion at m/z 455 and the proposed structural assignment was supported by subsequent MS/MS data (figure 6). The resulting product ions are rationalized in figure 7. The fragmentation pattern was compared with parent drug to confirm the structure of M8. M9–11, 13 and 14 were characterized in an identical manner. Assignment of M17 has been described (Dear *et al.* 1998b).

Analysis of plasma metabolites

LC-MS/MS. Following successful characterization of the aromatic hydroxyglucuronides (M3, 4, 15, 12) in urine, extracted human plasma was selectively screened. Screening was performed using selected reaction monitoring (SRM)-based experiments, using a triple quadrupole mass spectrometer, as described above.

Aromatic hydroxyglucuronides were detected in human plasma through the transitions m/z 473⇒255 and 473⇒183. In total, four aromatic hydroxyglucuronides were detected, eluting at 12.5, 12.8, 14.6 and 15.8 min. The SRM chromatogram corresponding to m/z 473⇒183 is given in figure 8. These peaks were confirmed as M3, 4, 15 and 12 respectively by co-chromatography with the purified and characterized metabolites obtained previously from rabbit and cynomolgus monkey urine. The 7-desfluoro-7-hydroxyglucuronide was also detected in human plasma by the transitions m/z 455⇒237 and 455⇒165.

Therefore, all the aromatic hydroxyglucuronides characterized in human urine, including the two NIH shift metabolites, were present as circulating metabolites in the plasma.

In addition, the hydroxylated metabolite of the ethyl side-chain (M9) was characterized by LC-MS/MS in plasma from human volunteers after both single

and repeated administration of GW420867X. M9 was shown by SRM to give rise to characteristic product ions at m/z 165 and 237.

The glucuronide conjugate of M9 (M1) was detected in human plasma following repeated administration of GW420867X. M1 had previously been characterized by LC-MS/MS of rat and cynomolgus plasma with a retention of 14.2 min (unpublished data). In human repeat dose plasma a component with a retention similar to this, but with a molecular weight 176 less than M1, was detected. It is therefore presumed that the glucuronide conjugate M1, although present in human plasma, broke down thermally in the source of the MS so that the aglycone and not the molecular ion was detected at this retention time. The hydroxylated component, M9, had a retention of 16.1 min in this system.

Discussion

It has been shown that GW420867X, a fluorinated xenobiotic, undergoes extensive metabolism, and the combined metabolic scheme of GW420867X based on metabolites identified in human and laboratory animal urine and human plasma is given in figure 9. A range of biotransformation products was detected in rabbit, mouse and human urine, resulting from aromatic and aliphatic hydroxylation and conjugation with glucuronic acid. In addition, defluorinated components were identified, including a cysteinyl conjugate in rabbit urine.

This work has also shown that GW420867X undergoes fluorine NIH shift rearrangement to form the 8-fluoro-7-hydroxyglucuronide (M12) in human, rabbit and mouse, and 6-fluoro-7-hydroxyglucuronide (M15) in rabbit and human in addition to the expected 5- and 6-hydroxyglucuronides (M3 and 4), which are observed in all species studied. Additionally, the 7-defluoro-7-hydroxyglucuronide species M8 was also observed. Therefore, NIH shift rearrangement of GW420867X, presumably via arene oxide formation, and subsequent conjugation with glucuronic acid is an observed route of metabolism in these species. Similar NIH shift rearrangements for fluorinated aromatics have been reported in dog for the spirohydantoin aldose inhibitor, imirestat (Gilbert *et al.* 1992), and in rat and dog for the novel anti-psychotic, sertindole (Sakamoto *et al.* 1995). A proposed NIH shift metabolic scheme for GW420867X is presented in figure 10.

Metabolism of arene oxide intermediates by glutathione (GSH) conjugation was not observed to any significance. This is in contrast to work reported by Koerts *et al.* (1998) on the occurrence of the NIH shift *in vivo* and *in vitro* using a series of fluorobenzenes. This latter work, using microsomal incubations (in the presence and absence of GSH and cytosol) and the GSH-depleted rat, showed that the formation of NIH-shifted phenolic metabolites was reduced in the presence of an active GSH pathway.

NIH shift rearrangement does not appear to be a major route of metabolism in dog, cynomolgus monkey and mini-pig (Ismail *et al.* 1999). The observation of 6- and 5-hydroxy metabolites could also be attributed to the formation of an arene oxide intermediate, although these may also form via an alternative mechanism. The absence of an 8-hydroxy metabolite is possibly due to steric hindrance.

This first report of fluorine migration in humans confirms that the NIH shift rearrangement can have a significant role in the metabolism of fluorinated xenobiotics confirming earlier work done in animal and *in vitro* systems (Gilbert *et*

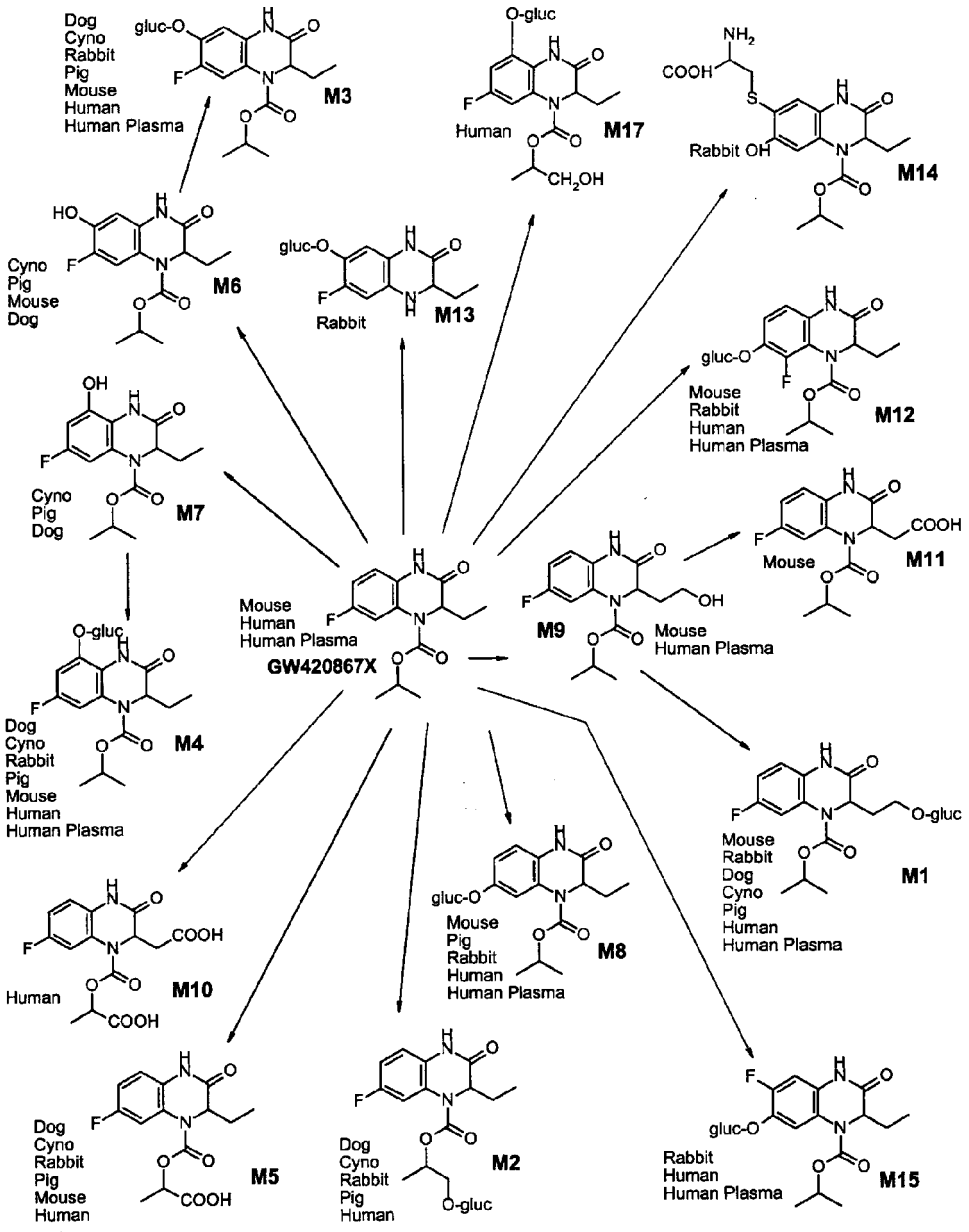


Figure 9. Metabolites of GW420867X in urine of human and animal species and in human plasma.

al. 1992, Sakamoto *et al.* 1995, Koerts *et al.* 1998). The unambiguous characterization of these metabolites by NMR and LC-MS/MS in urine enabled the detection of these NIH shifted metabolites in human plasma.

This work highlights the complementary role of MS and NMR within a structural elucidation laboratory. These techniques employed in conjunction with each other and with a systematic semi-preparative approach to sample isolation enable the rapid structure elucidation of novel metabolites in complex mixtures of biological origin. The presence of fluorine in a molecule offers an extremely useful

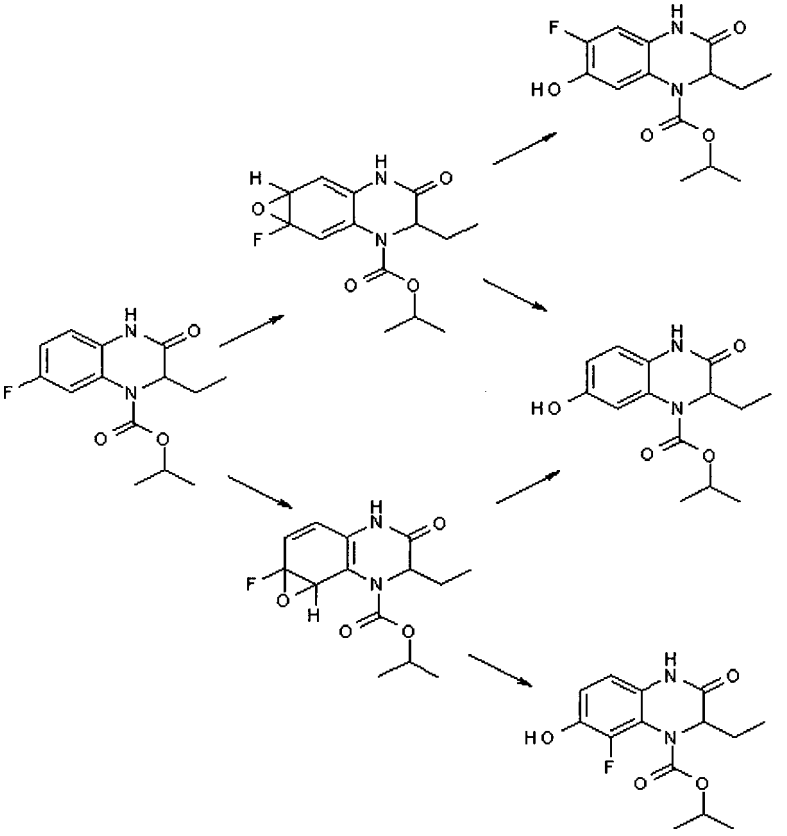


Figure 10. Proposed NIH shift metabolic scheme for GW420867X.

tool that can be used readily to detect the presence of drug-related material and to quantify the relative amount of the respective metabolites. However, as this work demonstrates, care must be taken to take account of any possible defluorinated metabolites, which would otherwise not be detected by ^{19}F-NMR and places a limitation on the use of ^{19}F-NMR in the quantification of xenobiotic-related material. In this work the formation of the 7-desfluoro-7-hydroxyglucuronide was characterized by a combination of LC-MS/MS and ^{1}H-NMR techniques, which are obviously not reliant on the presence of a fluorine atom.

Having established the main routes of metabolism, MS alone can analyse samples in cases where there is insufficient material for NMR analysis, such as in circulating plasma metabolites. In this instance, initial metabolite identification was performed using NMR and an ion-trap spectrometer, in contrast to the plasma screening experiments, which were carried out using a quadrupole instrument. The use of a quadrupole mass spectrometer for the screening of plasma samples was chosen in preference to the ion-trap spectrometer due to the enhanced sensitivity gained through selected target analysis. Direct comparison of the ion-trap spectrometer scanning in full-scan mode versus the triple quadrupole instrument scanning in SRM showed a difference in sensitivity of $\sim$ 25-fold, in favour of the triple quadrupole (Dear *et al.* 1999). However, the ion-trap spectrometer remains the instrument of choice for qualitative metabolite identification work, which is

heavily reliant on full-scan analysis. The faster scan rates of the ion-trap spectrometer relative to a quadrupole spectrometer can greatly improve detection limits because the ion current increases and the resulting shorter scan functions allow for improved signal averaging (de Hoffmann 1996).

References

BAILLE T., 1994, The role of LC-ionspray MS/MS in studies of drug metabolism and toxicology. In *Proceedings of the 42nd ASMS Conference on MS and Allied Topics*, Chicago 29 May–3 June 1994, p. 862.

CHU, I., VILLENEUVE , D. C., VIAU, A., BARNES, C. R., BENOIT , F. M. and QIN , Y. H., 1984, Metabolism of 1,2,3,4–1,2,3,5-, and 1,2,4,5-tetrachlorobenzene in the rat. *Journal of Toxicology and Environmental Health*, **13**, 777–786.

DALY, J. W., JERINA , D. M. and WITKOP , B., 1972, Arene oxides and the NIH shift: the metabolism, toxicity and carcinogenicity of aromatic compounds. *Experientia*, **28**, 1129–1264.

DE HOFFMAN , E., 1996, Tandem mass spectrometry: a primer. *Journal of Mass Spectrometry*, **31**, 129–137.

DEAR, G. J., HARRELSON , J. C., JONES, A. E., JOHNSON , T. E. and PLEASANCE , S., 1995, Identification of urinary and biliary conjugated metabolites of the neuromuscular blocker 51W89 by liquid chromatography/mass spectrometry. *Rapid Communications in Mass Spectrometry*, **9**, 1457–1464.

DEAR, G. J., FRASER, I. J., PATEL, D. K., LONG, J. and PLEASANCE , S., 1998a, Use of liquid chromatography-tandem mass spectrometry for the quantitative and qualitative analysis of an anti-psychotic agent and its metabolites in human plasma and urine. *Journal of Chromatography A*, **794**, 27–36.

DEAR, G. J., AYRTON , J., PLUMB , R., SWEATMAN , B. C., ISMAIL , I. M., FRASER, I. J. and MUTCH , P. J., 1998b, A rapid and efficient approach to metabolite identification using NMR, LC/MS and LC/NMR/Sequential MS. *Rapid Communications in Mass Spectrometry*, **12**, 2023–2030.

DEAR, G. J., AYRTON , J., PLUMB , R. and FRASER, I. J., 1999, The rapid identification of drug metabolites using capillary liquid chromatography coupled to an ion-trap mass spectrometer. *Rapid Communications in Mass Spectrometry*, **13**, 456–463.

DEN BESTEN , C., ELLENBROEK , M., VAN DER REE, M. A. E., RIETJENS , I. M. C. M. and VAN BLADEREN , P. J., 1992, The involvement of primary and secondary metabolism in the covalent binding of 1,2- and 1,4-dichlorobenzens. *Chemico-Biological Interactions*, **84**, 223–233.

DEN BESTEN , C., SMINK , M. C. C., DE VRIES , E. J. and VAN BLADEREN , P. J., 1991, Metabolic activation of 1,2,4-trichlorobenzene by rat liver microsomes: a major role for quinone metabolites. *Toxicology and Applied Pharmacology*, **108**, 223–233.

EVERETT , J. R., JENNINGS , K. and WOODNUT , G., 1985, ^{19}F-NMR spectroscopy study of the metabolism of flucloxacillin in rat urine. *Journal of Pharmacy and Pharmacology*, **37**, 869–873.

GILBERT , P. J., HARTLEY , T. E., TROKE , J. A., TURCAN, R. G., VOSE , C. W. and WATSON , K. V., 1992. Applications of ^{19}F-NMR spectroscopy to the identification of dog urinary metabolites of imirestat, a spirohydantoin aldose reductase inhibitor. *Xenobiotica*, **22**, 775–787.

GUROFF , G., DALY , J. W., JERINA , D. M., RENSON , J., WITKOP , B. and UDENFRIEND , S., 1967, Hydroxylation-induced migration: the NIH shift. *Science*, **157**, 1524–1530.

HOLT , R. M., NEWMAN , M. J., PULLEN , F. S., RICHARDS , D. S. and SWANSON , A. G., 1997, High-performance liquid chromatography NMR spectrometry mass spectrometry - further advances in hyphenated technology. *Journal of Mass Spectrometry*, **32**, 64–70.

ISMAIL , I, DEAR, G. J., MUTCH , P. J., DAVIES , L. H., PLUMB , R. and SWEATMAN , B. C., 1999 The urinary metabolism of the novel non-nucleoside reverse transcriptase inhibitor GW420867X in dog, cynomolgus monkey and mini-pig. *Xenobiotica*, **29**, 957–967.

JERINA , D. M. and DALY , J. W., 1974, Arene oxides: a new aspect of drug metabolism. *Science*, **185**, 573–582.

KOERTS , J., SOFFERS , A. E. M. F., VERVOOT , J., DE JAGER, A. and RIETJENS , I. M. C. M., 1998, Occurrence of the NIH shift upon the cytochrome P450-catalyzed *in vivo* and *in vitro* aromatic ring hydroxylation of fluorobenzenes. *Chemical Research in Toxicology*, **11**, 503–512.

KOHLI , J., JONES , D. and SAFE , S., 1976, The metabolism of higher chlorinated benzene isomers. *Canadian Journal of Biochemistry*, **54**, 203–208.

KORZEKWA, K., TRAGER, W., GOUTERMAN , M., SPANGLER , D. and LOEW , G. H., 1985, Cytochrome P450 mediated aromatic oxidation: a theoretical study. *Journal of the American Chemical Society*, **107**, 4273–4279.

LINDON , J. C., NICHOLSON , J. K., SIDELMANN , U. G. and WILSON , I. D., 1997, Directly coupled HPLC-NMR and its application to drug metabolism. *Drug Metabolism Reviews*, **29**, 705–746.

NICHOLSON , J. K. and WILSON , I. D., 1989, High resolution proton magnetic resonance spectroscopy of biological fluids. *Progress in NMR Spectroscopy*, **21**, 449–501.

PLUMB, R. S., AYRTON, J., DEAR, G. J., SWEATMAN, B. C. and ISMAIL, I. M., 1999, The use of preparative high performance liquid chromatography with tandem mass spectrometric directed fraction collection for the isolation and characterisation of drug metabolites in urine by nuclear magnetic resonance spectroscopy/sequential mass spectrometry. *Rapid Communications in Mass Spectrometry*, **13**, 845–854.

PULLEN, F. S., SWANSON, A. G., NEWMAN, M. J. and RICHARDS, D. S., 1995, On-line liquid chromatography nuclear magnetic resonance mass spectrometry - a powerful spectroscopic tool for the analysis of mixtures of pharmaceutical interest. *Rapid Communications in Mass Spectrometry*, **9**, 1003–1006.

SAFE, S., JONES, D. and HUTZINGER, O., 1976, Metabolism of 4,4′-dihalogenobiphenyls. *Journal of the Chemical Society, Perkin Transactions*, **1**, 357–359.

SAKAMOTO, K., NAKAMURA, Y., AIKOH, S., BABA, T., PERREGAARD, J., PEDERSEN, H., MOLTZEN, K., MULFORD, D. J. and YAMAGUCHI, T., 1995, Metabolism of sertindole: identification of the metabolites in rat and dog, and species comparison of liver microsomal metabolism. *Xenobiotica*, **25**, 1327–1343.

SCHWARTZ, H., CHU, I., VILLENEUVE, D. C. and BENOIT, F. M., 1987, Metabolism of 1,2,3,4-, 1,2,3,5-, and 1,2,4,5-tetrachlorobenzene in the squirrel monkey. *Journal of Toxicology and Environmental Health*, **22**, 341–350.

SHOCKCOR, J. P., UNGER, S. E., WILSON, I. D., FOXALL, P. J. D., NICHOLSON, J. K. and LINDON, J. C., 1996, Combined HPLC, NMR spectroscopy, and ion-trap mass spectrometry with application to the detection and characterisation of xenobiotic and endogenous metabolites in human urine. *Analytical Chemistry*, **68**, 4431–4435.

SPRAUL, M., HOFFMAN, M., LINDON, J. C., FARRANT, R. D., SEDDON, M., NICHOLSON, J. K. and WILSON, I. D., 1994, Evaluation of liquid chromatography coupled with high field ^{1}H-NMR spectroscopy for drug metabolism detection and characterisation; the identification of paracetamol metabolites in urine and bile. *NMR BioMedicine*, **7**, 295–303.

VIALANEIX, J. P., MALET-MARTINO, M. C., HOFFMAN, J. S., PRIS, J. and MARTINO, R., 1987, Direct detection of new flucytosine metabolites in human biofluids by ^{19}F nuclear magnetic resonance. *Drug Metabolism and Disposition*, **5**, 718–724.

WADE, K. E., TROKE, J., MACDONALD, C. M., WILSON, I. D. and NICHOLSON, J. K., 1988, ^{19}F studies of the metabolism of trifluoro-methylaniline. In E. Reid, J. D. Robinson and I. D. Wilson (eds), *Bioanalysis of Drug Metabolites* (London: Plenum).

XENOBIOTICA , 2000, VOL. 30, NO. 4, 427–440

Identification of turkey biliary metabolites of ractopamine hydrochloride and the metabolism and distribution of synthetic [^{14}C]ractopamine glucuronides in the turkey

D. J. SMITH*, V. J. FEIL and G. D. PAULSON

US Department of Agriculture, Agricultural Research Service, Biosciences Research Laboratory, PO Box 5674 University Station, Fargo, ND 58105-5674, USA

1. The bile duct cannulated turkey poult (n = 3) dosed orally with [^{14}C]ractopamine HCl {(1*R**,3*R**),(1*R**,3*S**)-4-hydroxy-α-[[[3-(4-hydroxy[^{14}C]phenyl)-1-methylpropyl]-amino]methyl]-benzenemethanol hydrochloride; 19.9 mg; 9.28 μCi] excreted 37.4± 12.1% (mean± SD) of the administered radioactivity in bile by 24 h post-dosing.

2. A mono-glucuronide, conjugated at C-10 (the methylpropylamino phenol) of ractopamine, accounted for 76.6% of biliary radioactivity.

3. Urine collected from the colostomized turkey poult (n = 3) orally dosed with synthetic [^{14}C]ractopamine-glucuronides (10.1 mg; 3.6 μCi) contained 11.9± 1.0% (mean± SD) of the administered radioactivity 24 h after dosing, indicating that some absorption of radioactivity occurred. Faeces contained 60.6% of the administered radioactivity and carcasses (with gastrointestinal tracts) contained 23.3% of the starting radioactivity.

4. Five colostomized poults were fitted with bile duct cannulas and were dosed intraduodenally with 10.2 mg (3.6 μCi) synthetic [^{14}C]ractopamine-glucuronides. Urine and bile contained 15.5± 2.2 and 16.8± 2.1% respectively of the administered radiocarbon by 24 h post-dosing. Faeces contained 54.3% of the administered radioactivity. Total absorption of the dosed radioactivity averaged 33.4%.

5. Bile and urine collected from the colostomized, bile-duct cannulated bird contained mainly ractopamine glucuronides. Indirect evidence suggests that the dosed ractopamine glucuronides were not absorbed intact.

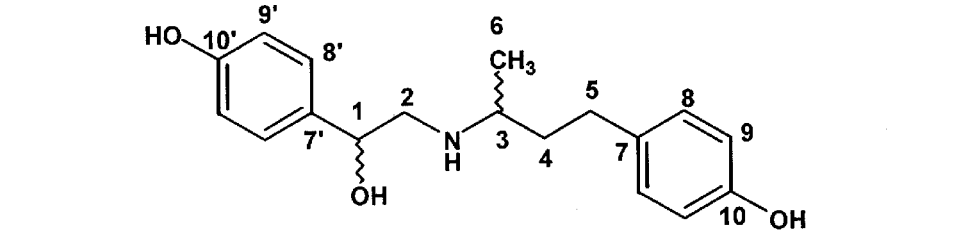
Introduction

Ractopamine HCl (figure 1) is a phenethanolamine β-adrenergic agonist that increases growth rates and carcass leanness in ruminant and non-ruminant mammals (Anderson *et al.* 1990), turkey (Wellenreiter and Tonkinson 1990a, b) and fish (Mustin and Lovell 1993) when used as a feed additive. In addition to causing improvements in carcass composition, ractopamine also increases the efficiency of feed utilization in some test species.

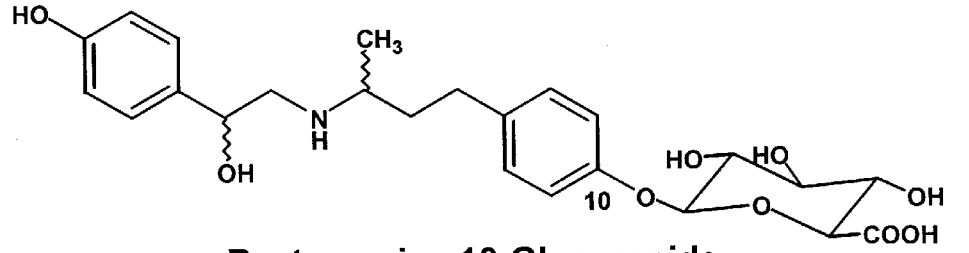
The metabolism and disposition of β-adrenergic agonists in livestock species is not well understood (Smith 1998) even though several livestock species have been targets for illegal β-adrenergic agonists use (Kuiper *et al.* 1998, Mitchell and Dunnavan 1998). Smith (1998) has reasoned that the development of safe and effective β-adrenergic agonists for use as livestock feed additives is possible. Such a viewpoint is defensible when one considers the pharmacokinetics, metabolism and disposition of individual compounds. For example, although ritodrine and clenbuterol are both phenethanolamine β-adrenergic agents, their oral potencies and pharmacokinetic properties in humans are not similar.

* Author for correspondence; e-mail: smithd@fargo.ars.usda.gov

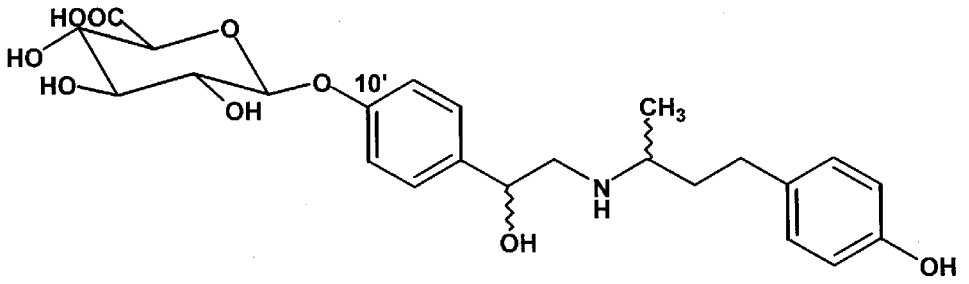
Xenobiotica ISSN 0049-8254 print/ISSN 1366-5928 online 2000 US Government work
http://www.tandf.co.uk/journals



Ractopamine Hydrochloride



Ractopamine 10-Glucuronide



Ractopamine 10'-Glucuronide

Figure 1. Ractopamine HCl and ractopamine glucuronide conjugates. Carbons 1 and 3 are chiral. Diastereo-isomers of ractopamine 10-glucuronides were separable by the HPLC conditions used in the study; the earliest ractopamine 10-glucuronide was composed of the *RS*, *SR* ractopamine stereo-isomers and the later eluting ractopamine 10-glucuronide was composed of the *RR*, *SS* ractopamine stereo-isomers.

Urinary biotransformation products of ractopamine have been studied in rat, dog, swine and turkey (Dalidowicz *et al.* 1992, Smith *et al.* 1993). In each species, mono-glucuronides were the major urinary product of ractopamine metabolism. Rat bile, however, contained a ractopamine mono-sulphate conjugate and a ractopamine mono-sulphate/mono-glucuronic acid diconjugate (Smith *et al.* 1995) that were not present in rat urine. These metabolites had not been previously identified as urinary excretion products of ractopamine in any species.

The general objective of the current study was to gain a better understanding of the absorption and distribution of the β-adrenergic agonist ractopamine HCl in a species sensitive to the leanness enhancing effects of the compound. Specific objectives of this study were (1) to determine the extent of excretion of metabolites in turkey bile after oral administration of [^{14}C]ractopamine; (2) to identify the major metabolites of ractopamine excreted in bile; (3) to determine the extent of absorption of radioactivity from the gastrointestinal tracts of turkey after oral administration of synthetic [^{14}C]ractopamine mono-glucuronides; and (4) to determine the metabolic

disposition of radioactivity in the urine and bile of turkey that was intraduodenally administered synthetic [^{14}C]ractopamine-glucuronides.

Materials and methods

The use of trade, firm or corporation names in this publication is for the information and convenience of the reader. Such use does not constitute an official endorsement or approval by the US Department of Agriculture or the Agricultural Research Service of any product or service to the exclusion of others that may be suitable.

Trial 1 : Biliary excretion of radioactivity after oral administration of [^{14}*C*]*ractopamine*

Three male turkey poults (4–5 kg; Nicholas strain) were bile-duct cannulated and given duodenal re-entry cannulas according to the method of Paulson and Struble (1981). Racemic [^{14}C]ractopamine HCl {(1*R**,3*R**),(1*R**,3*S**)-4-hydroxy-α-[[[3-(4-hydroxy[^{14}C]phenyl)-1-methylpropyl]amino]methyl]-benzenemethanol hydrochloride; provided by Elanco Animal Health, Greenfield, IN, USA] was purified to a radiochemical purity of 97% as described by Smith *et al.* (1993), dissolved in water (20 mg.ml^{-1}, 9.3 μCi.ml^{-1}), and 1 ml was added to each of three gelatin capsules containing 4–5 g feed. [^{14}C]ractopamine was administered to the turkeys by placing the gelatin capsules, lubricated with vegetable oil, into the oral cavity of each poult. Each capsule was gently manoeuvred through the oesophagus until it could be felt at the junction of the thoracic cavity and neck in the region of the crop. Animal dosing was completed in $<$ 1 min per bird without notable incident.

Bile was collected from each bird over a 24-h period in three 8-h increments. During the collection period each bird was re-perfused with blank bile at 1–3 ml.h^{-1} depending on the rate of bile excretion during the previous 8-h period. Urine and faeces were collected together. At the end of the 24-h collection, each bird was euthanized.

Biliary radioactivity was quantified by diluting quadruplicate 0.1 g aliquots in 15 ml scintillation fluid (ICN Biochemicals, Costa Mesa, CA, USA), and by counting each sample with a liquid scintillation counter (LSC, Beckman, Fullerton, CA, USA). Quench was corrected using the external standard channels method (Chapman and Ayrey 1981).

Identification of biliary ractopamine metabolites

Portions of period 1 (0–8 h) bile from each bird, containing equal amounts of radioactivity, were pooled so that the bile pool contained $\sim$ 2000 μg ractopamine HCl equivalents. Pooled bile was diluted with an equal mass of purified water and placed onto a 30 $\times$ 2 cm glass column packed with 80 g XAD-2 resin (Sigma, St Louis, MO, USA), which had previously been washed with 750 ml methanol followed by 1000 ml purified water. The sample was loaded and allowed to elute from the column by gravity (fraction 1); the XAD-2 was then washed sequentially with 500 ml each of purified water, water/acetonitrile (1 : 1), 0.05 M ammonium acetate (pH 4.5)/acetonitrile (1 : 1) and 100% acetonitrile (fractions 2–5 respectively). Quadruplicate aliquots (2–4 g) of each fraction were diluted with 15 ml scintillation fluid, and radioactivity was quantified by LSC as described above.

Volumes of XAD-2 fractions 2 and 3 were reduced on a rotary evaporator and aliquots of each fraction were analyzed by HPLC. The HPLC system consisted of a Waters 600E controller and pump (Waters Associates, Millford, MA, USA) equipped with tandem 250 $\times$ 4.6 mm Apex I-ODS (Jones Chromatography, Lakewood, CO, USA) columns. Initial solvent composition was 95% 0.05 M ammonium acetate (pH 4.5) and 5% acetonitrile (flow rate of 1.25 ml.min^{-1}); a linear gradient of 5–25% acetonitrile over 40 min was used to elute metabolites from the column. Detection was with a Waters Model 441 absorbance detector set at 254 nm. As UV absorbing compounds eluted, they were collected into scintillation vials, diluted in 15-ml scintillation fluid, and the radioactivity in each fraction was determined by LSC. Radioactive peaks were located, and crude metabolite preparations were collected from XAD-2 fraction 3 using the same chromatographic conditions as above except that tandem 250 $\times$ 8 mm Apex-I ODS semi-preparative columns (Jones Chromatography) were used at 3.78 ml.min^{-1}. Metabolites isolated from the crude preparations were further purified using the same semi-preparative HPLC columns but with an isocratic solvent system consisting of 8% acetonitrile and 92% 0.05 M ammonium acetate, pH 4.5. Before analysis by ^{1}H-NMR and negative-ion FAB-mass spectroscopy, each metabolite fraction was desalted on 6-ml C-18 solid-phase extraction cartridges (J. T. Baker, Phillipsburg, NJ, USA). Purified metabolite fractions were applied, the cartridges washed with 10 ml purified water, and the radioactive metabolites were eluted from the cartridges with acetonitrile/water (1 : 1). At each step of the purification process, recovery of radioactivity was monitored and recorded.

Solvent was evaporated from purified metabolites under a steady stream of nitrogen. Metabolites were exchanged, and then re-dissolved in deuterated methanol ($>$ 99.8 atom% ; Cambridge Isotope

Labs, Woburn, MA, USA). ^{1}H-NMR spectra, referenced against TMS, were generated on a Bruker AM 400 spectrometer. Negative-ion FAB mass spectra were obtained on a VG-Autospec mass spectrometer; ionization was induced with a Cs ion source.

Chiral composition of individual metabolites was determined by chiral derivatization of metabolite fractions after hydrolysis with û-glucuronidase (type VII-A from *E. coli*, Sigma; unknown sulphatase activity). Purified metabolites (~ 50 μg each) were dissolved in 0.01 M phosphate buffer, pH 6.8, and were hydrolyzed at 37 °C over 2 h with 50 units β-glucuronidase. The free base of unconjugated ractopamine was extracted into ethyl acetate after adjusting the pH of the incubation supernatant to 10 with 0.1 M ammonium bicarbonate. Ethyl acetate was evaporated and the residue was derivatized at 60 °C for 1 h with 3 mg (4*S cis*)-2,2-dimethyl-5-isothiocyanato-4-phenyl-1,3-dioxane (PHEDIT), which was synthesized according to Desai and Gal (1992). The PHEDIT was dissolved in 100 μl acetonitrile and 5 μl triethylamine and was added to the residue remaining after evaporating ethyl acetate from the β-glucuronidase incubation extract. After 1 h at 60 °C the reaction mixture was diluted with 200 μl acetonitrile, vortexed, and 25 μl of the diluted mixture was injected on an analytical reverse-phase HPLC system consisting of a single 4.6 × 250 mm Apex I ODS column (Jones Chromatography). Ractopamine-PHEDIT derivatives were eluted isocratically with 0.05 M ammonium acetate and acetonitrile (1:1) at 1.25 ml.min^{-1}. The elution order of the ractopamine-PHEDIT derivatives was determined by derivatizing individually synthesized ractopamine stereo-isomers (Ricke *et al.* 1999) with PHEDIT and chromatographing them under identical conditions as described for the derivatized metabolite fractions.

Synthesis and purification of [^{14}C]ractopamine-glucuronides

Rabbit liver microsomes were prepared, solubilized and immobilized on Sepharose® 4B-200 (Sigma) as described by Pallante *et al.* (1986). Racemic [^{14}C]ractopamine HCl {(1*R**,3*R**),(1*R**,3*S**)-4-hydroxy-α-[[[3-(4-hydroxyphenyl)-1-methylpropyl]amino]methyl]-[^{14}C]benzenemethanol hydrochloride; 117.4 mg; 0.5045 μCi/mg] was added to a round-bottom flask containing 60 ml 0.1 M KH_2PO_4 buffer (pH 7.4), 140 ml (packed volume) of previously washed (0.1 M KH_2PO_4 buffer) Sepharose beads containing immobilized microsomal proteins (590 mg protein), 140 mg $MgCl_2$, and 406.2 mg uridine diphosphoglucuronic acid (UDPGA; Sigma) in a round-bottom flask. The round-bottom flask was placed on a rotary evaporator, rotated slowly at 37 °C with no vacuum, and the reaction mixture was allowed to incubate. After 19 h the slurry was filtered on a coarse 0.5 litres sintered glass funnel and the beads were rinsed four times with 50 ml 0.1 M KH_2PO_4 buffer (pH 7.4). Filtrates from each rinse were collected into tared flasks and assayed for total radioactivity. The filtered Sepharose beads were re-diluted in ~ 100 ml buffer, removed from the filter and placed into a round-bottom flask. A second incubation was initiated by adding 140 mg $MgCl_2$, 407 mg UDPGA and 117.4 mg [^{14}C]ractopamine. The slurry was again placed on the rotary evaporator, without vacuum, and allowed to incubate overnight at 37 °C. After 24 h the incubation was stopped by filtration, the beads rinsed thoroughly with phosphate buffer and the total filtrate collected and pooled.

Ractopamine glucuronides were purified by eluting the filtrates through a 1 litre sintered glass funnel packed with ~ 220 g C-18 packing (Separations Technology, Wakefield, RI, USA) by applying a light vacuum. The C-18 packing was then rinsed consecutively with 500 ml each of acetonitrile in water (1:24 v/v), acetonitrile in water (1:1 v/v), acetonitrile in 0.05 M ammonium acetate buffer, pH 4.5 (1:1 v/v), and 100% acetonitrile. Water/acetonitrile (1:1) fractions from separate runs were pooled, the acetonitrile was removed under vacuum, and the remaining aqueous solution was re-applied to the reversed-phase packing to remove residual parent ractopamine. Ractopamine glucuronides were eluted from the packing with 50% acetonitrile in water (v/v). Radiochemical purity of the synthetic glucuronides was 99.0% as assessed using analytical reversed-phase HPLC and LSC of fractions taken during triplicate HPLC runs. Ractopamine C-10 glucuronides (figure 1), which eluted on the reverse-phase HPLC system as two distinct diastereo-isomer peaks made up 30.8% of the total radiocarbon (19.5% *RS*/*SR* and 11.4% *RR*/*SS* diastereo-isomers); ractopamine C-10′ glucuronides (figure 1) which eluted as a single peak represented 68.2% of the total ractopamine glucuronides.

Trial 2: Disposition of radioactivity administered orally as [^{14}C]ractopamine-glucuronides

Three turkeys (8.1 ± 0.6 kg) were colostomized according to Paulson (1969) except that anaesthesia was induced with 4–5% halothane in oxygen. The poults were placed in restraining cages and allowed to recover for 24 h. Only birds that were observed to eat, drink, urinate and defecate were used in the study. The mixture of synthetic [^{14}C]ractopamine glucuronides (10.1 ± 0.04 mg; 3.60 ± 0.02 μCi), dissolved in water, was added to gelatin capsules containing 3–4 g feed. Poults were orally dosed as described above. Urine and faeces were collected for the next 24 h in three 8-h periods. Radioactivity in excreta was quantified as described by Smith *et al.* (1993).

Trial 3: Disposition of radioactivity administered intraduodenally as [^{14}C]ractopamine-glucuronides

Five male turkey poults (2.9 ± .4 kg) were anesthetized with sodium pentobarbital (Fort Dodge, Fort Dodge, IA, USA) and their bile ducts were cannulated as described above; re-entry cannulas were placed directly into the duodenum, 4–5 cm distal to the gastric sphincter. The same poults were also

colostomized as described by Paulson (1969) except that adapters were not placed around the colostomy. Instead, faeces dropped directly onto a stainless steel tray below the restraining cage. Urine was kept separate from faeces by suturing a plastic adapter, constructed from the mouth of a 250 ml narrow-mouth Nalgene® bottle (Nalge, Rochester, NY, USA) to the cloaca. A hole (18 mm) was bored through the screw-on lid of each narrow mouth bottle and a 1 × 18 inches (width × length) piece of penrose tubing was secured to the outer circumference of the lid. The lids, with penrose tubing attached, were screwed onto the mouths of the plastic adapters sutured to the cloacal orifices of the turkeys. This arrangement allowed for the sequential passage of urine through the cloaca, adapter, lid and penrose conduit directly into a container placed below the restraining cage.

Bile was collected from the poults for the duration of the 24–48-h recovery. About 4 h before dosing, reperfusion of blank bile into the duodenum was initiated. The mixture of synthetic [^{14}C]ractopamine-glucuronides (3.62 ± 0.09 μCi; 10.20 ± 0.27 mg), dissolved in water, was diluted in ~ 9 ml bile per bird and dosed to each turkey by reperfusing into the duodenum during the first 4 h of the study period. Blank bile was then perfused into each bird throughout the remainder of the study.

Urine, faeces and bile were collected during the 24-h study in three 8-h periods. At the end of the study each poult was euthanized with CO_2 and dissected to ensure the patency of the bile-duct and re-entry cannulas. Gastrointestinal tracts were separated from the carcasses and were separately ground with a Hobart grinder. Radioactivity in urine was measured in quadruplicate by LSC; faecal, carcass and gastrointestinal tract radioactivity was measured in quintuplicate as described by Smith *et al.* (1993).

Metabolism of [^{14}C]ractopamine-glucuronides by the turkey poult

Within a study period aliquots of urine from each bird were combined forming a urine pool that contained 113 μg ractopamine HCl equivalents. In a similar fashion, bile from each bird was combined, by period, forming a pool which contained 113 μg ractopamine HCl. Radioactivity in urine and bile was fractionated on XAD-2 resin into five fractions as described above. Aliquots of bile and urine XAD-2 fractions 3 were injected onto the analytical HPLC system as described above, except that the HPLC columns were tandem 100 × 8 mm Novapak C-18 radial compression columns (Waters Associates). Fractions were collected for each HPLC run and radioactivity was quantified by LSC. Ractopamine mono-glucuronides were trapped from the crude XAD-2 fraction and purified metabolites were identified by co-chromatography with synthetic mono-glucuronide standards. Radioactive metabolites other than ractopamine mono-glucuronides were not isolated from urine or bile XAD-2 fractions from the [^{14}C]ractopamine glucuronide-dosed bird.

Results

Trial 1: Biliary excretion of radioactivity after oral administration of [^{14}C]ractopamine HCl

Figure 2 shows the cumulative excretion of radioactivity into bile after oral administration of [^{14}C]ractopamine HCl. By 24 h after dosing, 37.4 ± 12.1% of the administered radiocarbon had been excreted in the bile. As the figure indicates, total biliary excretion of radioactivity, as well as excretion of activity within a given period, were variable among the three birds. Nevertheless, it was evident that biliary excretion of ractopamine or ractopamine metabolites was a significant route of elimination in turkeys and further studies were pursued.

Identification of biliary ractopamine HCl metabolites

Bile XAD-2 fractions 1–5 contained 0, 6.5, 93.2, 1.2 and 0% of the applied radioactivity respectively (figure 3). Analysis of XAD-2 fractions 2–4 by analytical reverse-phase HPLC and LSC of fractions from each HPLC run indicated that the radioactivity in XAD-2 fractions 2 and 3 eluted into three regions A–C; analysis of XAD-2 fraction 4 indicated that the radioactivity eluted in four regions, A–D (figure 3). Radioactive regions A–C corresponded among the respective XAD-2 fractions indicating that the metabolites were incompletely resolved by the XAD-2 fractionation. Radioactive region 3C from XAD-2 fraction 3 was collected and re-chromatographed on an isocratic HPLC system where it was resolved into two

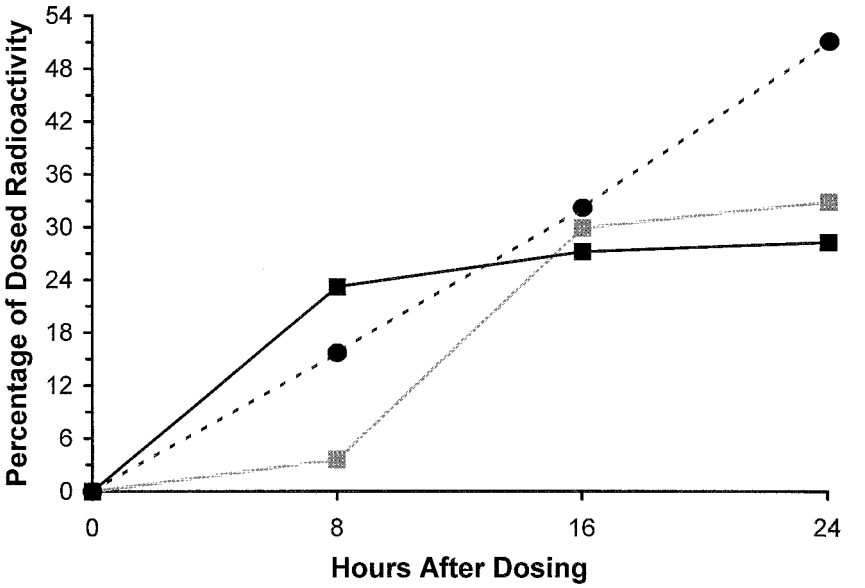


Figure 2. Elimination of radiocarbon in bile of the colostomized turkey poult orally administered 20 mg (9.3 μCi) [^{14}C]ractopamine HCl. The solid black, hatched black and solid grey lines represent poults 11, 13 and 14 respectively.

peaks, 3C1 and 3C2 representing 36.8 and 36.7% of the biliary radioactivity respectively. Radioactive region 3B, representing ~5.8% of the biliary radioactivity, was not identified. Metabolites from fractions 2 and 4 were not purified further.

3C1 and 3C2 were identified as ractopamine mono-glucuronides conjugated at the C-10 hydroxyl group (figure 1) based on negative-ion FAB-MS, ^{1}H-NMR and co-chromatography (data not shown) with well-characterized synthetic mono-glucuronide standards (Smith *et al.* 1993). In addition, 3C1 and 3C2 were readily hydrolyzed by β-glucuronidase. No glucuronides conjugated to C-10′ of ractopamine were isolated from the turkey bile.

Chiral derivatization and chromatography of the β-glucuronidase hydrolysis products of 3C1 and 3C2 revealed that glucuronide conjugate 3C1 was composed of the *SR* and *RS* stereo-isomers of ractopamine (retentions of ~16.6 and 20.4 min respectively), and glucuronide 3C2 was composed of the *SS* and *RR* stereo-isomers of ractopamine (retentions of ~19.1 and 14.9 min respectively). The ratio of *SR*:*RS* in 3C1 was ~0.7 and the ratio of *SS*:*RR* in 3C2 was ~2.7. Chiral analysis indicated that the *SR*, *RS*, *SS* and *RR* stereo-isomers represented 20.7, 29.4, 36.5 and 13.5% of the C-10 glucuronide conjugates respectively. Stereoselective hydrolysis of glucuronides 3C1 and 3C2 did not occur because >96% of the starting radioactivity was extracted into the ethyl acetate after each β-glucuronidase incubation (data not shown).

Synthesis and purification of [^{14}C]*ractopamine-glucuronides*

[^{14}C]ractopamine mono-glucuronides were synthesized to determine the disposition of ractopamine-glucuronides in turkey. Analysis of the crude incubation supernatant taken from an aliquot of the first incubation (19 h) by HPLC indicated

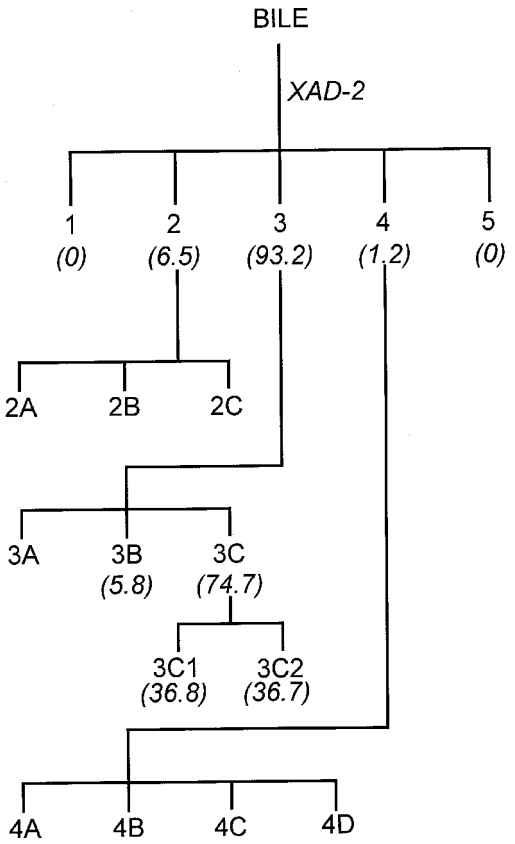


Figure 3. Fractionation of biliary radioactivity collected from the [^{14}C]ractopamine HCl-dosed poult by XAD-2 column chromatography and HPLC. Parenthetical numerals are the percentage of biliary radioactivity present in each fraction.

that 66% of the injected radioactivity was present as ractopamine-glucuronides. Conversion of [^{14}C]ractopamine to [^{14}C]ractopamine-glucuronides in the second incubation (24 h) was 79%. Final radiochemical purity of the ractopamine mono-glucuronides was 99.0%. The synthetic ractopamine-glucuronide mixture was composed of C-10 glucuronides (30.8% of the total conjugates) and C-10′ glucuronides (68.2% of the total radioactivity). A total of 216.2 mg [^{14}C]ractop-amine-glucuronides was recovered, representing an overall yield of 69.6%.

Trial 2 : Disposition of radioactivity administered orally as [^{14}C]ractopamine-glucuronides

Table 1 shows the disposition of radioactivity in urine, faeces and carcasses when the bile-duct cannulated turkey was dosed orally with a mixture of synthetic [^{14}C]ractopamine mono-glucuronides. Poults excreted 72.5% of the administered radioactivity within 24 h in urine and faeces. Most of the radioactivity was excreted in faeces (60.6%) with the majority of the faecal radioactivity being excreted during the second 8-h period after dosing. About 12% of the administered radioactivity was excreted in urine indicating that significant absorption of radioactivity occurred. Most of the radioactivity that was excreted in the urine was excreted during the

Table 1. Disposition of radioactivity in the colostomized turkey poult ($n = 3$) dosed orally with 10.10± 0.04 mg (3.60± 0.16 μCi) synthetic [^{14}C]ractopamine glucuronides.

		Percentage of administered radioactivity excreted				
		Poult number			Mean (± SD)	
Item	Period[a]	21	23	24	By period	Cumulative
Urine	1	1.38	0.90	5.34	2.54± 2.44	2.54± 2.44
	2	6.32	8.98	4.49	6.60± 2.26	9.14± 1.24
	3	3.06	2.91	2.37	2.78± 0.36	11.92± 0.36
Faeces	1	6.75	3.67	42.97	17.80± 21.86	17.80± 21.86
	2	25.90	52.52	28.32	35.58± 14.72	53.38± 19.47
	3	11.76	6.17	3.78	7.24± 4.10	60.61± 15.40
Carcass[b]		33.75	24.04	11.97	na[c]	23.25± 10.91
Cage Wash		0.60	0.01	0.13	na	0.24± 0.32
Total		89.52	99.20	99.37	na	96.03± 5.64

[a] Periods 1, 2, and 3 represent consecutive 8-h intervals.
[b] Gastrointestinal tracts were not separated from carcasses.
[c] na, Not applicable.

Table 2. Disposition of radioactivity administered intraduodenally to the bile-duct cannulated, colostomized turkey ($n = 5$) as [^{14}C]ractopamine glucuronides (10.15± 0.27 mg; 3.61± 0.96 μCi) dissolved in turkey bile. Data are expressed as a percentage of the administered dose.

		Percentage of administered radioactivity					
		Poult					
Item	Period[a]	27	31	32	33	34	Mean (± SD)
Urine	1	8.61	5.35	3.55	6.90	6.01	6.08± 1.87
	2	6.66	7.14	5.30	5.93	8.19	6.64± 1.11
	3	2.31	1.65	3.60	3.30	3.17	2.81± 0.80
Cumulative:		17.58	14.14	12.45	16.13	17.37	15.53± 2.20
Bile	1	8.31	8.06	3.83	7.08	4.51	6.36± 2.06
	2	9.12	5.63	6.88	6.54	8.32	7.30± 1.41
	3	2.48	2.06	3.77	4.13	3.15	3.12± 0.86
Cumulative:		19.91	15.75	14.48	17.75	15.98	16.77± 2.11
Faeces	1	54.19	54.75	41.46	40.68	41.09	46.45± 7.33
	2	0.82	2.26	4.91	1.06	1.29	2.07± 1.68
	3	0.15	0.24	0.47	6.64	21.33	5.77± 9.13
Cumulative:		55.16	57.25	46.84	48.38	63.71	54.27± 6.87
Carcass		5.36[b]	1.70	1.60	1.47	0.62	1.35± 0.49[c]
GI tract		–[b]	7.37	13.91	9.19	0.74	7.80± 5.46[c]
Cage wash		0.44	0.33	2.55	0.84	0.19	0.87± 0.97
Apparent absorption[d]		37.49	31.59	28.53	35.35	33.97	33.39± 3.46
Total Recovery:[e]		98.45	96.54	91.83	93.76	98.61	95.84± 2.97

[a] Periods 1, 2, and 3 each represent 8-h intervals.
[b] Gastrointestinal tract was not separated from the carcass for poult 27.
[c] Value does not include poult 27.
[d] Apparent absorption represents the summation of urinary, biliary and carcass radioactivities.
[e] Total recovery represents the summation of urinary, biliary, fecal, carcass, gastrointestinal tract and cage wash radioactivities.

Table 3. XAD-2 fractionation of radioactivity present in turkey urine and bile pools from the bile duct-cannulated and colostomized poult dosed intraduodenally with [^{14}C]ractopamine glucuronides.

		Percentage of administered radioactivity					
		Fraction[a]					
Excreta	Period	1	2	3	4	5	Total
Urine	1	0.74	1.88	95.32	0.39	0.15	98.48
	2	0.57	1.33	95.00	0.50	0.08	97.48
	3	1.51	1.57	93.99	0.47	0.10	97.64
Bile	1	0.75	6.46	92.59	0.52	0.10	100.42
	2	0.55	5.36	93.80	0.42	0.07	100.20
	3	1.12	7.33	89.94	0.26	0.05	98.70

[a] XAD-2 column loaded and eluted as described in the Materials and methods; fraction 1, load; fraction 2, water wash; fraction 3, water/acetonitrile (1:1); fraction 4, buffer/acetonitrile (1:1); fraction 5, acetonitrile.

second 8-h period. Carcasses retained ~ 23% of the administered radioactivity; however, gastrointestinal contents were not separated from carcasses in this trial so the contribution of the gastrointestinal contents to the total carcass radioactivity was unknown. Because radioactivity dosed as [^{14}C]ractopamine-glucuronide was absorbed, a study was executed designed to assess the degree of total absorption of radioactivity after administration of [^{14}C]ractopamine glucuronides.

Trial 3: Disposition of radioactivity administered intraduodenally as [^{14}C]ractopamine-glucuronides in the colostomized turkey with bile duct cannulas

Table 2 shows the disposition of radioactivity dosed intraduodenally as a mixture of [^{14}C]ractopamine mono-glucuronides in urine, faeces, carcasses and gastrointestinal tracts of turkey poults. Urine contained 15.5% of the administered radioactivity and bile contained 16.8% of the administered radiocarbon. Periods 1 and 2 contained roughly equal quantities of radioactivity in both urine and bile, with lesser amounts being excreted in the third period. Almost half (46.5%) of the administered radioactivity was eliminated in faeces during period 1. Smaller amounts (2–6%) of faecal radiocarbon were excreted in periods 2 and 3. Carcasses (minus the gastrointestinal tracts) contained ~ 1% of the total administered radioactivity 24 h after dosing. Gastrointestinal tracts contained ~ 8% of the total administered radioactivity at slaughter. Apparent absorption of radioactivity (summation of urinary, biliary and carcass radioactivity) represented ~ 33% of the total dose administered.

Table 3 shows the fractionation of urinary and biliary radioactivity on XAD-2 resin. Bile XAD-2 fraction 3 contained > 90% of the biliary radioactivity, regardless of the period; urine XAD-2 fractions 3 contained 94%, or greater, of the urinary radioactivity excreted within a given period. Bile and urine XAD-2 fractions 2 contained ~ 6.4 and 1.6% of the radioactivity respectively suggesting the presence of more polar metabolites in bile.

Table 4 summarizes the composition of the [^{14}C]ractopamine metabolites present in bile and urine XAD-2 fractions 3. The major portion of the urinary and biliary radioactivity was identified as ractopamine mono-glucuronides, with 67–84% of the radioactivity in fraction 3 associated with ractopamine mono-glucuronides. Bile

Table 4. Metabolite composition of XAD-2 fractions 3 from urine and bile of turkey dosed intraduodenally with [^{14}C]ractopamine mono-glucuronides.

Excreta	Metabolite fraction	Percent of injected radioactivity[a]		
		Period 1[b]	Period 2[b]	Period 3[b]
Bile	pre-glucuronide	7.6	7.7	6.5
	glucuronides	82.3	82.4	84.01
	post-glucuronide	2.5	2.5	1.0
Urine	pre-glucuronide	2.9	3.6	3.3
	glucuronides	79.3	67.7	67.0
	post-glucuronide	11.0	32.9	25.1

[a] Percent of radioactivity eluting in fractions representing $>1\%$ of injected radioactivity.
[b] Periods 1, 2, and 3 represent consecutive 8-h intervals.

contained more glucuronides, on a percentage basis than urine. Urine XAD-2 fraction 3 contained substantial radioactivity (11–33% of injected radioactivity) that eluted after the ractopamine glucuronides. Most of this radioactivity eluted in the vicinity of parent ractopamine, but smaller amounts of uncharacterized radiocarbon (1%) eluted before parent.

Discussion

The extent of ractopamine HCl absorption has not been widely studied in target species. Dalidowicz *et al.* (1992) demonstrated that swine excrete ~ 85% of an oral [^{14}C]ractopamine dose in urine within 24 h of dosing. The rapid and extensive absorption correlates well with ractopamine's biological activity in swine (Anderson *et al.* 1990). Previous data from our lab demonstrated that the urinary excretion of radioactivity in turkey was lower than in swine with only 50% of the administered activity being excreted in the urine by 24 h after dosing. About 39% of the dosed activity was excreted in faeces during the same period (Smith *et al.* 1993). Because ractopamine has excellent biological activity in turkey (Wellenreiter and Tonkinson 1990a, b), and because rat excretes nearly 60% of orally dosed ractopamine in bile (Smith and Paulson 1994), it is expected that biliary excretion may have contributed significantly to the faecal excretion of radiocarbon in turkey. This supposition was confirmed in trial 1 of this study because nearly 40% of the radioactivity in an orally administered [^{14}C]ractopamine dose was eliminated in the bile of turkeys within a 24-h period. However, the identity of these biliary metabolites was unknown.

The only data on the identity of biliary ractopamine metabolites available in the literature was collected from rat. Ractopamine metabolites excreted in rat bile differed somewhat from those excreted in rat urine. Ractopamine mono-glucuronides are the major metabolites excreted in the urine of swine, dog, rat and turkey (Dalidowicz *et al.* 1992, Smith *et al.* 1993, 1995). Metabolites excreted in rat bile were identified as ractopamine-sulphate esters, a ractopamine-sulphate/glucuronate diconjugate, and ractopamine mono-glucuronides (Smith *et al.* 1995). Metabolites present in bile of other species have not been reported although Dalidowicz *et al.* (1992) mentioned the possible presence of a glucuronide diconjugate in cattle bile.

The present authors have demonstrated that turkeys excrete ractopamine primarily as mono-glucuronides in the urine (Smith *et al.* 1993) and in bile (present study). Mono-glucuronides present in turkey bile were conjugated to the C-10

phenol of ractopamine (figure 1) with no evidence for the presence of ractopamine C-10′ glucuronide. Metabolites in this study were identified on the basis of FAB-MS, ^{1}H-NMR and co-chromatography with synthetic standards. Exhaustive proof of structure for these metabolites is discussed by Smith *et al.* (1993). Previous work in this lab demonstrated the presence of both C-10- and C-10′-ractopamine glucuronides in turkey urine (Smith *et al.* 1993). The exclusive biliary excretion of glucuronides conjugated to C-10 in bile of turkey is interesting and unexplained. It is possible that liver glucuronosyl transferases are regio-specific for the C-10 phenol of ractopamine, but seems unlikely given the fact that immobilized liver microsomal UDP-glucuronosyl transferases from rabbit (Smith *et al.* 1993, present study) and swine (Smith, unpublished data) efficiently glucuronidated both phenolic groups of ractopamine. In addition, results of Smith *et al.* (1995) indicated that rat bile contained ractopamine mono-glucuronides conjugated to the C-10 and C-10′ phenols, although the major conjugation site was the C-10 phenol. For the sulphate/glucuronide diconjugate present in rat bile, sulphation occurred exclusively at C-10′ and glucuronidation occurred exclusively at C-10. This study, along with others (Smith *et al.* 1993, 1995) provides consistent evidence that the glucuronidation of ractopamine is regio-selective and not regio-specific. For example, in turkey urine the major metabolite of ractopamine was the C-10 conjugate (59.8% of urinary radioactivity) with lesser amounts of the C-10′ glucuronide being excreted (12.7% of urinary radioactivity).

The C-10′ glucuronide previously isolated from turkey urine by Smith *et al.* (1993) was conjugated exclusively to the *RS* and *RR* stereo-isomers of ractopamine whereas the C-10 glucuronides were conjugated to the *RS*, *SR*, *SS* and *RR* stereo-isomers. In turkey urine, the *RS*-, *SR*-ractopamine C-10 glucuronides represented 34% of the urinary radioactivity and the *RR*-, *SS*-ractopamine C-10 glucuronides represented 25% of the radioactivity (Smith *et al.* 1993). In the present study, *RR*-, *SS*-C-10 glucuronides and the *RS*-, *SR*-C-10 glucuronides each represented ~ 36% of the biliary radioactivity (73.5% of biliary activity). However, the individual ractopamine stereo-isomers were not present in equal proportions. Chiral HPLC analysis of the C-10 conjugates, after hydrolysis with β-glucuronidase, indicated that the *SR*, *RS*, *SS* and *RR* stereo-isomers represented 20.7, 29.4, 36.5 and 13.5% of the C-10 glucuronide conjugates respectively. Thus, the *SS* stereo-isomer was conjugated and excreted at a rate nearly three times that of the *RR* stereo-isomer.

Because glucuronidation at the C-10 phenol is a major route of metabolism, and because biliary excretion of this metabolite in the bile is significant in turkeys, the impact of these processes on the biological action of ractopamine could be significant. For example, Ricke *et al.* (1999) have shown that the leanness-enhancing effects of ractopamine reside primarily with the *RR* stereo-isomer. Ricke *et al.*'s results are consistent with the theory that, for direct-acting phenethanolamine β-adrenergic agonists, levorotatory stereo-isomers are biologically active (Ruffalo 1991, Smith 1998). Biological activity of ractopamine in turkey could be due to the fact that the *RR* stereo-isomer is retained at target tissues and receptors for longer periods relative to the other inactive stereo-isomers. Chiral analysis of ractopamine tissue residues would resolve this issue.

Synthetic ractopamine glucuronides were prepared to evaluate the role of enterohepatic circulation on ractopamine distribution in turkeys. Preliminary experiments (trial 2) with the colostomized turkey poult (table 1) indicated that at

least some of the radioactivity in an oral dose of [^{14}C]ractopamine glucuronides was absorbed and subsequently excreted in urine. Total absorption could not be calculated because bile was not collected, and gastrointestinal tracts were not separated from the turkey carcasses at the termination of the experiment. Nevertheless, this preliminary trial clearly indicated a capacity of turkeys to absorb radioactivity administered as [^{14}C]ractopamine glucuronides.

Trial 3 was therefore conducted with the bile-duct cannulated, colostomized turkey. [^{14}C]ractopamine glucuronides were formulated in blank bile that was infused into the duodenum to mimic biliary excretion. Apparent absorption of radioactivity was calculated by summing the percentage of radioactivity present in excreted urine and bile, and in the carcass (excluding the gastrointestinal tract) at the termination of the study (table 2). Results from the study clearly indicate that 28–37% of the radioactivity administered as biliary [^{14}C]ractopamine glucuronides was absorbed. It is currently unknown whether the radioactivity was absorbed intact as ractopamine glucuronides or whether the glucuronide conjugates were hydrolyzed to parent ractopamine before absorption. Available evidence suggests that intact glucuronides are very poorly absorbed and that enzymatic hydrolysis of glucuronides to parent compound precedes absorption of parent drug for a variety of compounds (Huckle *et al.* 1981, Pohland *et al.* 1982, Ruelius *et al.* 1985, Sim and Back 1985). Because ractopamine glucuronides are readily hydrolyzed by β-glucuronidase (Smith *et al.* 1993, 1995) the likelihood of intact absorption of ractopamine glucuronide is remote.

Additional data from this study provide circumstantial evidence supporting the supposition that ractopamine glucuronides were not absorbed intact. For example, most of the radioactivity in urine or bile of the [^{14}C]ractopamine glucuronide-treated bird was excreted during the first 16 h after dosing, with the distribution of radioactivity nearly equal between the first and second 8-h periods after dosing. In contrast, colostomized birds dosed with parent ractopamine excreted 75% of the total urinary radiocarbon during the first 8 h after dosing (Smith *et al.* 1993). The temporal distribution of urinary and biliary radioactivity observed in this study suggests that there was a delay in the absorption of radioactivity relative to the time it takes for parent ractopamine to be absorbed and excreted. One could note that the combination of bile-duct cannulation, duodenal re-entry cannulation and colostomization of birds significantly altered the absorptive and(or) digestive processes so that delayed and partial absorption occurred. This observation is countered by the fact that only birds that resumed eating, drinking, urination and defecation were used for the study. In most instances, birds had resumed feed consumption within 4 h of the completion of the surgery. A more likely explanation for the prolonged elimination of [^{14}C]ractopamine-glucuronide derived radioactivity in urine and bile is that the dose was infused over a 4-h period, and the fact that the ractopamine glucuronides would likely be hydrolyzed to parent ractopamine before re-absorption. Delays in absorption of xenobiotic-glucuronides, relative to parent compound, have been observed for oestradiol 17β-glucuronide (Coppoc *et al.* 1982, Pohland *et al.* 1982, Sim and Back 1985) and 3-phenoxybenzoic acid glucuronide (Huckle *et al.* 1981). Hydrolysis of the ractopamine glucuronides had to occur at some point because urine collected from trial 3 birds contained substantial quantities of non-glucuronide radioactivity.

Certainly it is known that phenolic phenethanolamine β-adrenergic agonists are cleared very rapidly after absorption (Smith 1998) so it would not be surprising that

a large fraction of the absorbed radioactivity from [^{14}C]ractopamine-glucuronide dosed poults would be excreted as metabolites. Such was the case for swine dosed with [^{3}H]-oestradiol 17β-glucuronide. None of the radioactivity present in urine or plasma was present as free drug, but the presence of conjugated oxidized metabolites of oestradiol indicated that hydrolysis of parent had occurred before absorption (Coppoc *et al.* 1982, Pohland *et al.* 1982). Circumstantial evidence provided by Smith and Paulson (1994) also suggests that ractopamine glucuronide would likely be hydrolyzed prior to absorption and then re-conjugated by intestinal or hepatic tissues. They provided evidence that rapid and extensive biotransformation of ractopamine HCl by the intestinal tract removes parent drug from circulation.

References

Anderson, D. B., Veenhuizen V. L., Jones, D. J., Schroeder, A. L. and Hancock, D. L., 1990, The use of phenethanolamines to reduce fat and increase carcass leanness in meat animals. In G. Bray (ed.), *Fat and Cholesterol Reduced Foods: Technologies and Strategies* (Wood: Portfolio), pp. 43–73.

Chapman, J. M. and Ayrey, G., 1981. *The Use of Radioactive Isotopes in the Life Sciences* (London: George Allen & Unwin), pp. 41–76.

Coppoc, G. L., Bottoms, G. L., Moore, A. B. and Roesel, O. F., 1982, Metabolism of estrogens in the gastrointestinal tract of swine. II. Orally administered oestradiol-17β-D-glucruonide. *Journal of Animal Science*, **55**, 135–144.

Dalidowicz, J. E., Thomson, T. D. and Babbitt, G. E., 1992, Ractopamine hydrochloride, a phenethanolamine repartitioning agent: metabolism and residues. In D. H. Hutson, D. R. Hawkins, G. D. Paulson and C. B. Struble (eds), *Xenobiotics and Food-producing Animals*. Symposium Series 503 (Washington, DC: American Chemical Society), pp. 234–243.

Desai, D. M. and Gal, J., 1992, Reversed-phase high-performance liquid chromatographic separation of the stereo-isomers of labetalol via derivatization with chiral and non-chiral isothiocyanate reagents. *Journal of Chromatography*, **579**, 165–171.

Huckle, K. R., Chipman, J. K., Hutson, D. H. and Millburn, P., 1981, Metabolism of 3-phenoxybenzoic acid and the enterohepatorenal disposition of its metabolites in rats. *Drug Metabolism and Disposition*, **9**, 360–368.

Kuiper, H. A., Noordam, M. Y., van Dooren-Flipsen, M. M. H., Schilt, R. and Roos, A. H., 1998, Illegal use of β-adrenergic agonists: European Community. *Journal of Animal Science*, **76**, 195–207.

Mitchell, G. A. and Dunnavan, G., 1998, Illegal use of β-adrenergic agonists in the United States. *Journal of Animal Science*, **76**, 208–211.

Mustin, W. T. and Lovell, R. T., 1993, Feeding the repartitioning agent, ractopamine, to channel catfish (*Ictalurus punctatus*) increases weight gain and reduces fat deposition. *Aquaculture*, **109**, 145–152.

Pallante, S. L., Lisek, C. A., Dulik, D. M. and Fenselau, C. M., 1986, Glutathione conjugates: Immobilized enzyme synthesis and characterization by fast atom bombardment mass spectrometry. *Drug Metabolism and Disposition*, **14**, 313–318.

Paulson, G. D., 1969, An improved method for separate collection of urine, faeces, and expiratory gases from the mature chicken. *Poultry Science*, **48**, 1331–1336.

Paulson, G. D. and Struble, C., 1981, Bile collection and intestinal perfusion in the restrained chicken. *Poultry Science*, **60**, 867–870.

Pohland, R. C, Coppoc, G. L., Bottoms, G. D. and Moore, A. B., 1982, Metabolism of estrogens in the gastrointestinal tract of swine. III. Oestradiol-17β-D-glucuronide instilled into sections of the intestine. *Journal of Animal Science*, **55**, 145–152.

Ricke, E. A., Smith, D. J., Feil, V. J., Larsen, G. L. and Caton, J. S., 1999, Effects of ractopamine HCl stereo-isomers on growth, nitrogen retention, and carcass composition in rats. *Journal of Animal Science*, **77**, 701–707.

Ruelius, H. W., Young, E. M., Kirkman, S. K., Schillings, R. T., Sisenwine, S. F. and Janssen, F. W., 1985, Biological fate of acyl glucoronides in the rat. The role of rearrangement, intestinal enzymes, and reabsorption. *Biochemical Pharmacology*, **34**, 451–452.

Ruffalo, R. R., 1991, Chirality in α- and β-adrenoceptor agonists and antagonists. *Tetrahedron*, **47**, 9953–9980.

Sim, S. M. and Back, D. J. 1985. Intestinal absorption of oestrone, oestrone glucuronide and oestrone sulphate in the rat *in situ* - I. Importance of hydrolytic enzymes on conjugate absorption. *Journal of Steroid Biochemistry*, **22**, 781–785.

SMITH , D. J., 1998, The pharmacokinetics, metabolism, and tissue residues of β-adrenergic agonists in livestock. *Journal of Animal Science*, **76**, 173–194.

SMITH , D. J., FEIL V. J., HUWE J. K. and PAULSON , G. D., 1993, Metabolism and disposition of ractopamine hydrochloride by turkey poults. *Drug Metabolism and Disposition*, **21**, 624–633.

SMITH , D. J., GIDDINGS , J. M., FEIL , V. J. and PAULSON , G. D., 1995, Identification of ractopamine hydrochloride metabolites excreted into rat bile. *Xenobiotica*, **25**, 511–520.

SMITH , D. J. and PAULSON , G. D., 1994, Growth characteristics of rats receiving ractopamine hydrochloride and the metabolic disposition of ractopamine hydrochloride after oral or intraperitoneal administration. *Journal of Animal Science*, **72**, 404–414.

WELLENREITER , R. H. and TONKINSON , L. V., 1990a, Effect of ractopamine hydrochloride on growth performance of turkeys. *Poultry Science*, **69(suppl. 1)**, 142.

WELLENREITER , R. H. and TONKINSON , L. V., 1990b, Effect of ractopamine hydrochloride on carcass parameters of turkeys. *Poultry Science*, **69(suppl. 1)**, 143.

XENOBIOTICA , 2000, VOL. 30, NO. 5, 441–456

Rapid determination of rat hepatocyte mRNA induction potential using oligonucleotide probes for CYP1A1, 1A2, 3A and 4A1

D. D. SURRY†*, G. MENESES-LORENTE†, R. HEAVENS‡, A. JACK§ and D. C. EVANS†

Departments of †Drug Metabolism and Pharmacokinetics, ‡Pharmacology and §Biostatistics, Neuroscience Research Centre, Merck Research Laboratories, Harlow, UK

Received 14 October 1999

1. A new assay to quantify mRNA levels in small numbers of rat hepatocytes has been developed for cytochrome P450 (CYP) isoforms 1A1, 1A2, 3A and 4A1. The assay uses sets of oligonucleotide probes end-labelled with [^{35}S]-dATP to hybridize to mRNA in control- or drug-treated rat hepatocytes cultured on Cytostar-T™ 96-well scintillating microplates.

2. The rat hepatocyte induction potential (RHIP) assays for CYP3A, 1A1, 1A2 and 4A1 are sensitive and selective and have an excellent qualitative relationship with CYP induction data *ex vivo*. The robustness of the CYP3A assay was determined following a run of >40 plates. The variation of the dexamethasone (DEX) response on each plate, calculated as %coefficient of variation, showed that there was no significant difference between the variability of the response to DEX.

3. Assay specificity for each CYP isoform was achieved by designing probes (four per isoform) antisense to coding regions of each CYP gene sequence. In the CYP3A RHIP assay, pregnenalone 16α-carbonitrile (PCN), DEX, clotrimazole (CLOT) and miconazole (MIC) were all good inducers of CYP3A mRNA; β-napthoflavone (BNF) and methyl-clofenapate (MCP), however, did not induce CYP3A mRNA, further defining the specificity of this methodology. Specificity was similarly confirmed for the other CYP isoforms.

4. Ind_{50}, the concentration of inducer required to elicit a 50% induction of CYP-specific mRNA, was derived for prototypical CYP inducers: BNF 0.54 and 0.17 μM (CYP1A1 and 1A2 respectively), 3-methylcholanthrene (3MC) 0.11 and 0.04 μM (CYP1A1 and 1A2 respectively), PCN 0.03 μM, DEX 0.17 μM, CLOT 0.48 μM, MIC 3 μM, TAO 3 μM (CYP3A), MCP 1.8 μM, clofibrate (CLOF) 65 μM and ciprofibrate (CIP) 1.9 μM (CYP4A1). Ind_{50} for BNF and 3MC at CYP1A2 was 3-fold lower than that at CYP1A1 indicating a subfamily difference in inducer potency.

5. Reducing the numbers of animals and the amount of compound required to study CYP induction is an important advantage of the RHIP assays over conventional evaluations *in vivo*. Typically four rats are dosed for 4 days using oral doses in the range 50–500 mg kg^{-1} day^{-1}. In comparison, the amount of hepatocytes required to carry out all the studies reported herein may be obtained from a single animal ($< 2\times10^8$ viable cells) and CYP induction investigated using μg rather than g quantities of drug substance.

6. With appropriately designed oligonucleotide probes, the RHIP technology can assess CYP induction in human hepatocytes, which together with preclinical data can contribute to improving the quality of compounds progressing into the expensive process of drug development.

Introduction

The cytochromes P450 (CYP) are a superfamily of enzymes responsible for the metabolism of a range of endogenous molecules, e.g. steroids, retinoids and eicosinoids (Meyer *et al.* 1995). CYPs are also responsible for a majority of xenobiotic

* Author for correspondence; e-mail: Dominic_Surry@Merck.com

Xenobiotica ISSN 0049-8254 print/ISSN 1366-5928 online © 2000 Taylor & Francis Ltd
http://www.tandf.co.uk/journals

metabolism (Wrighton and Stevens 1992, Spatzenegger and Jaeger 1995). The families are subdivided into individual subfamilies (isoforms) based on their genetic and amino acid sequence homology (Nelson 1998). The genes in this superfamily are under transcriptional controls and can be modulated by xenobiotics via cellular receptors. The best studied are the CYP1A genes under the control of the aryl hydrocarbon (*Ah*) receptor (Safe and Krishnan 1995) and the CYP4A genes under the control of the peroxisome proliferator-activated receptor (PPAR, Meyer *et al.* 1995). Recent advances in the study of CYP3A transcription have implicated the orphan nuclear receptor PXR (pregnane X receptor) in some studies including activation of promoter-reporter constructs by a range of known CYP3A inducers (Kliewer *et al.* 1998, Lehmann *et al.* 1998).

Increases in CYP transcription, translation or stabilization of the resultant protein are known as induction. Repeated doses of xenobiotic can result in induction of hepatic CYP at the transcriptional level, e.g. CYP1A, 4A, 3A (Dogra *et al.* 1998) and post-translationally, e.g. the induction of CYP2E by isoniazid (Park *et al.* 1993). The consequences of CYP induction can lead to significant effects in laboratory animals and in the clinic.

CYP1A1 has been shown to activate environmental procarcinogens such as polycyclic aromatic hydrocarbons (PAH) while CYP1A2 is responsible for the N-oxidation of many carcinogenic aromatic and heterocyclic amines (Kadlubar and Guengerich 1992). Induction of these latter two CYP is therefore undesirable since a greater activation of such compounds would result and increase the risk of tumour formation (Schrenk 1998). CYP3A has been shown to be responsible for the metabolism of a large number of drugs in the clinic (Michalets 1998). Clinically significant loss of efficacy due to CYP3A induction has been reported for the contraceptive steroids (Breckenridge *et al.* 1980, Guengerich 1988) and increased metabolism of the non-benzodiazepine anxiolytic, buspirone (Lambeg *et al.* 1998). Preclinically, CYP4A inducers cause the proliferation of peroxisomes in rat (Lake 1995). Such compounds can cause an increase in the size and number of peroxisomes in a number of tissues. Long-term dosing of peroxisome proliferators (PP) can cause liver cancer in these animals and belong to a class of compounds known as non-genotoxic carcinogens, i.e. they cause cancer through mechanisms that do not involve direct DNA damage (Gonzalez *et al.* 1998).

The study of CYP induction before costly clinical trials is therefore desirable. Studies normally involve repeat dosing of compound to rat over a number of days, followed by analysis of hepatic CYP content for changes in CYP expression and activity. Such studies are labour-, animal- and compound-intensive. Hence, the ability to study CYP induction using simple *in vitro* methodologies has resulted in significant research efforts.

Hepatocytes are the most widely used *in vitro* model for induction studies and have a number of advantages (Wortelboer *et al.* 1988, Nishibe and Hirata 1993, Kostrubsky *et al.* 1995, Li *et al.* 1997a, b). They are relatively simple to isolate and culture large numbers of viable cells in a number of different environments, and the amounts of compound required for *in vitro* studies is small (μm versus g). The disadvantages with such systems can be the scarcity of material for studying effects on human cells and the numbers of cells required to obtain sufficient protein or mRNA for analysis of CYP expression. Methods used to study CYP expression include metabolism of probe substrates (Sharer *et al.* 1995), Western blotting and ELISA (Bars *et al.* 1989, Wright *et al.* 1994), Northern blotting (Ryu *et al.* 1996),

ribonuclease protection assays (Schuetz *et al.* 1988, Kostrubsky *et al.* 1995) and reverse transcriptase polymerase chain reaction (rtPCR; Willey *et al.* 1997) methods.

Described here is a method that allows the CYP-inductive capacity of xenobiotics to be assessed in rat hepatocytes cultured on Cytostar-T™ scintillating 96-well plates. Following treatment with xenobiotics, hepatocytes are fixed and then hybridized *in situ* with a set of four specific [^{35}S]-dATP-labelled oligonucleotide probes antisense to discreet regions of CYP mRNA. Prototypical inducers of CYP3A, 1A and 4A have been used to validate this methodology.

Materials and methods

Animals

Male and Female Sprague–Dawley International Standard rats (170–180g) supplied by Charles River, UK were allowed food (Bantin and Kingman rat and mouse expanded diet) and water *ad libitum*.

Chemicals

Collagenase H from *Clostridium histolyticum* was from Boehringer (Lewes, UK). Earle's balanced salt solution (EBSS), Williams' E medium without L-glutamine, penicillin/streptomycin, L-glutamine, non-essential amino acids, formamide, saline sodium citrate buffer (SSC), Dulbecco's phosphate-buffered saline (DPBS) and dithiothreiotol (DTT) were from Life Technologies (Paisley, UK). Sodium bicarbonate, gentamycin, dextran sulphate, EDTA, diethyl pyrocarbonate (DEPC), dexamethasone (DEX), pregnenalone 16α-carbonitrile (PCN), β-napthoflavone (BNF), clotrimazole (CLOT), troleadomycin (TAO), miconazole (MIC), 3-methylcholanthrene (3MC), isoniazid (ISN), clofibrate (CLOF), ciprofibrate (CIP), dimethyl sulphoxide (DMSO) and sulphorhodamine-based (TOX-6) kits were from Sigma Chemical Co. (Poole, UK). Cytostar-T scintillating microplates were from Amersham Life Sciences (Amersham, UK). Matrigel was from Stratech Scientific (Surrey, UK). Heparin was from CP Pharmaceuticals (Wrexham, UK). MCP was a kind gift from Dr B Lake (BIBRA, Carshalton, UK). [^{35}S]-dATP was from New England Nuclear (Brussels, Belgium).

Hepatocyte preparation and culture

One rat was injected with 500 units heparin 5 min before decapitation. The liver was carefully removed to ice-cold DPBS and taken for a three-stage perfusion of the largest lobes based on cut surface perfusion models (Reese and Byard 1981, Strom *et al.* 1982). Following digestion with collagenase, cells were filtered through nylon bolting cloth and cleaned by three sterile washes by centrifugation and resuspension in DPBS. Hepatocytes were finally resuspended at 0.15×10^6 viable cells ml^{-1}, determined by trypan blue exclusion, in Williams' E medium containing L-glutamine (2 mM), penicillin and streptomycin (100 U ml^{-1} and 0.1 mg ml^{-1}), gentamycin (50 mg ml^{-1}) DEX (100 nM) and insulin (1 μM). Typical yields of hepatocytes were 150×10^6 viable ($>80\%$) cells.

Cells were dispensed onto the Cytostar-T plates at 30 000 viable hepatocytes/well previously coated with 25 μl Matrigel (1:25 dilution in DPBS) and dried overnight at 37 °C. After allowing cells to settle for 24 h at 37 °C in a CO_2 incubator with 95% humidity, non-viable cells and debris was aspirated and the media replaced. Following a further 24 h the cells were then available for challenge with prototypical CYP inducers.

Treatment of cells

Stock solutions of prototypical inducers were prepared in sterile DMSO at a concentration of 10 mM. Treatments (n = eight wells/treatment) were directly added to cells so that the DMSO concentration was constant at 1% v/v. DMSO was added as one treatment to act as a dose vehicle control. The final concentrations of the compounds (unless a range was used; see figures) were DEX (10 μM), PCN (2 μM), CLOT (5 μM), MIC (10 μM), BNF (10 μM), 3MC (10 μM), PB (100 μM), ISN (10 μM), MCP (10 μM), CLOF (500 μM) and CIP (100 μM). At the end of induction (24 h) media were replaced with formaldehyde fixative (3.8% v/v in sterile DPBS, 100 μl/well) for 10 min. Fixative was aspirated and replaced with sterile DPBS (100 μl/well) for storage at 4 °C before analysis for CYP mRNA levels.

Production, labelling and purification of oligonucleotide probes

Isoform-specific oligonucleotides of either 44, 45, 46 or 48 bases were designed using published CYP gene sequences (table 1). The CYP3A oligonucleotides were designed to encompass a number of isoforms from this family known to be inducible by xenobiotics. The oligonucleotides antisense to the mRNAs

Table 1. Oligonucleotide sequences used in the RHIP assays showing isoform specificity and the published sequences used to design and align antisense probes.

CYP isoform	Oligo number	Oligonucleotide sequences	Number of bases	Reference
1A1	1	ATGCCTTCTGTGTATGGATTCCCAGCCTTCACATCAGCCACAGAGC	46	Sogawa *et al.* (1984)
1A1	2	GTCACTGACAAAGCTGAGTCAGCAGTATGGGGACGTGCTGCAGA	44	Sogawa *et al.* (1984)
1A1	3	GGCCACATCCGGGACATCACAGACAGCCTCATTGAGCATTGTCAGG	46	Sogawa *et al.* (1984)
1A1	4	GGATACAGAGAAAGATCCAGGAGGAGTTAGGTAGGTGGTGGCTCC	45	Sogawa *et al.* (1984)
1A2	1	ATGGCGTTCTCCCAGTATATCTCCTTAGCCACCGAGCTGCTACTGGCC	48	Sogawa *et al.* (1985)
1A2	2	CGTCATCGGAGCCATGTGCTTTGGGAAGAACTTCCCCAGGAAGAG	45	Sogawa *et al.* (1985)
1A2	3	GTATCCAGGACATCACAGGCGCCCTGTTCAAGCACAGTGAGAACT	45	Sogawa *et al.* (1985)
1A2	4	TGATTGGCAGAGATCGGCAGCCACGGCTTTCTGACAGACCCCAGC	45	Sogawa *et al.* (1985)
3A1/23	1	GCAGCACACTTTCCTTTGTCCTGCATTCCCTGGCCACTCACCCAG	45	van den Broek *et al.* (1996), Kirita and Matsubara (1993)
3A1/23	2	GATCGACAGGGCTCTGCCCAATAAGGCACCTCCCACCTATGATAC	45	van den Broek *et al.* (1996), Kirita and Matsubara (1993)
3A1/23/18	3	CGCCCAGAAAGGTTCAGCAAGGAGAACAAGGGCAGCATTGATCC	45	van den Broek *et al.* (1996), Kirita and Matsubara (1993), Strotkamp *et al.* (1995)
3A1/2/23	4	CCCAGGAACTGCATTGGCATGAGGTTTGCTCTCATGAATATG	45	van den Broek *et al.* (1996), Miyata *et al.* 1991, Strotkamp *et al.* (1995)
4A1	1	ATGAGCGTCTCTGCACTGAGCTCCACCCGCTTCACGGGCAGCATCTCT	48	Kimura *et al.* (1989)
4A1	2	TTCCCAAGTGCCTTTCCTCGATGGTTCTGGGGAAGCAAAGCCTAC	45	Kimura *et al.* (1989)
4A1	3	GATAGGTAGCAACCAAGGGAGAGAGCTGTTTGAACTTTCAGCTCC	45	Kimura *et al.* (1989)
4A1	4	TCCGGTAAGGACAAGGACAGACTCTATGAACATGTGGCCTGGCAC	45	Kimura *et al.* (1989)

were synthesized (Applied Biosystems 394 synthesizer) and purified on 8% polyacrylamide/8 M urea preparative sequencing gels.

The oligonucleotides were 3′-end labelled with [^{35}S]-dATP in a 30:1 molar ratio of radioisotope to oligonucleotide using terminal deoxynucleotidyl transferase (Boehringer Mannheim).

The reaction was stopped after 15 min by the addition of 40 μl DEPC-treated water and purified using Sephadex G50 spin columns. The spin columns were prepared by packing a small amount of silanized glass wool into the barrel of a 1 ml sterile plastic syringe. The barrel was filled with a 5% w/v Sephadex G50 suspension (5 M NaCl, 1 M Tris, 0.5 M EDTA, 10% w/v SDS in DEPC-treated water). The syringe was placed into a 15-ml tapered tube and centrifuged at 500 *g* for 2 min. The excess buffer was removed from the tapered tube and an Eppendorf tube put in place to collect the labelled oligonucleotide following addition of the reaction mix to the top of the column and a further 2-min spin at 500 *g*. The total volume of recovered probe was measured and 4 μl taken for scintillation counting to assess the yield of each reaction. DTT (2 μl, 1 M) was added to the oligonucleotides to stabilize the products before use.

The volumes of labelled oligonucleotide required to give a final concentration of 0.5 million counts ml^{-1}/oligonucleotide were mixed in hybridization buffer (50% v/v formamide, 10% w/v dextran sulphate, 0.1 M DTT and 4×SSC in DEPC-treated water).

Hybridization conditions

DPBS was removed and cells permeabilized with Triton X100 in DPBS (0.25% w/v) for 10 min. After removing the detergent, hybridization buffer containing the four labelled oligonucleotides was added (100 μl) to each well and incubated overnight at 42 °C. Unbound oligonucleotide was then removed by a series of washes in 1×SSC; two 30-min washes at 55 °C followed by two 30-min washes at room temperature. Washed plates were aspirated and counted in a Wallac MicroBeta 96-well plate scintillation counter for 1 min/well using a program normalized for 35S and Cytostar-T plates to give CPM data.

Total cellular protein assay

To account for differences in the number of cells in each well a sulphorhodamine dye-based total cellular protein assay (Sigma TOX-6 kit) was carried out on plates following scintillation counting according to the manufacturers instructions. Basically, sulphorhodamine dye (50 μl) was incubated for 30 min at room temperature. After washing excess dye away using acetic acid (1% v/v, 100 μl×3) the bound dye was released from the cells using Tris (0.1 M, 200 μl) and repeat pipetting. The absorbance at 500 nm (equivalent to the total cellular protein and directly proportional to the number of cells in each well) was read using a 96-well plate UV spectrophotometer (Molecular Devices SpectraMax 250). The absorbance at 500 nm was corrected for background absorbance at 690 nm.

In vivo *studies*

Microsomes from a previous study (Lake *et al.* 1998) where hepatic homogenates and microsomes were prepared from the female Sprague–Dawley rat repeatedly dosed with a range of cytochrome P450 inducers were used to determine testosterone 6β-hydroxylase activity and cyanide-insensitive palmitoyl CoA oxidation as markers for CYP3A and 4A activity respectively.

Data analysis and statistics

CPM data obtained from the Wallac MicroBeta 96-well plate scintillation counter was normalized for the number of cells that were in the well using the absorbance data (Abs) from the sulphorhodamine-based assay (CPM/Abs).

Results (CPM/Abs) were converted to %DMSO control and the SEM was inflated by 5% of the treatment mean to take into account intrinsic variation on the plates.

Where concentration range experiments were carried out, results (%DMSO control) were expressed as a percentage of the maximal induction observed for that compound. This was sometimes limited by the cytotoxicity of the compounds used and therefore it does not appear to have reached a plateau. The concentration at which 50% of maximal induction was observed (Ind_{50}) was calculated using the GraphPad Prism® curve-fitting package.

For comparisons of different treatments, values are expressed as %mRNA in DMSO-treated cells. All data are the mean of eight observations with inflated standard errors indicated. Differences from control observations were determined using one-way ANOVA with Dunnett's post-test.

To demonstrate the robustness of the CYP3A assay the %coefficient of variation (%CV) was determined for DEX treatment on 42 different plates. The data were then compared with 3 or 2 SD of the mean CV.

Results

CYP3A induction

A direct comparison of induction of CYP3A mRNA *in vitro* using the RHIP assay with induction of testosterone 6β-hydroxylase activities in hepatic microsomes from *in vivo* studies previously published (Lake *et al.* 1998) has been carried out (figure 1). Animals treated with the prototypical CYP3A inducers DEX and PCN showed a marked increase in CYP3A activity, while other CYP3A inducers, TAO and MIC, showed only a modest elevation in activity. (TAO was, however, not statistically significant different from control under these conditions). Testosterone 6β-hydroxylase activities in liver microsomes prepared from vehicle-treated (corn oil or gum tragacanth) animals are also presented. The RHIP assay (figure 1B) shows a remarkable similarity in response to the same inducers. Under these conditions DEX, PCN, TAO, MIC and CLOT were statistically significantly different from the vehicle (DMSO)-treated control. The levels of induction seen for DEX, PCN and CLOT were of the same magnitude. Both the *in vivo* and *in vitro* assays showed that the inducers of other CYP isoforms, namely BNF (CYP1A) and MCP (CYP4A), had no effect on the CYP3A activity *in vivo* or on mRNA expression *in vitro*.

Using the RHIP assay the effect of inducer concentration on CYP3A mRNA expression was investigated (figure 2). It could be seen that the concentration needed to obtain maximal induction, i.e. their effective potencies as CYP3A inducers, was quite different. The most potent of the inducers was PCN with an $Ind_{50} = 0.03$ μM followed by DEX (0.17 μM), CLOT (0.48 μM), MIC (3 μM) and TAO (3 μM).

The robustness of the CYP3A assay was determined by comparing the %CV of individual results against 2 and 3 SD of the overall mean CV of 42 separate plates. The data show that none of the results fall outside the 3 SD level (figure 3).

CYP1A1 and CYP1A2 induction

The RHIP assay confirmed that BNF is a potent inducer of both CYP1A1 and 1A2 mRNA expression as is the prototypical CYP1A inducer, 3MC (figure 4). Neither DEX, MCP nor PB induced CYP1A1 or 1A2 mRNA levels. The effect of BNF and 3MC concentration on both CYP1A1 and 1A2 induction was investigated (figure 5) and the Ind_{50} derived (table 2).

CYP4A1 induction

The effect of prototypical inducers on palmitoyl-CoA oxidase activity, an enzyme activity co-induced with that of CYP4A, has been demonstrated previously (Lake *et al.* 1998). Of the compounds dosed to the animals, the prototypical CYP4A inducer MCP had a very significant effect, and BNF (a prototypical CYP1A inducer) a small but significant effect on palmitoyl-CoA oxidation. Using the RHIP assay, MCP induced CYP4A mRNA expression to a significant level (figure 6A). Other prototypical inducers of CYP4A (CLOF and CIP, not studied *in vivo*) increased mRNA expression to the same extent as MCP. Inducers of other CYP isoforms—DEX for CYP3A, BNF for CYP1A, PB for CYP2B and ISN for CYP2E—had no effect on the expression of CYP4A1 mRNA.

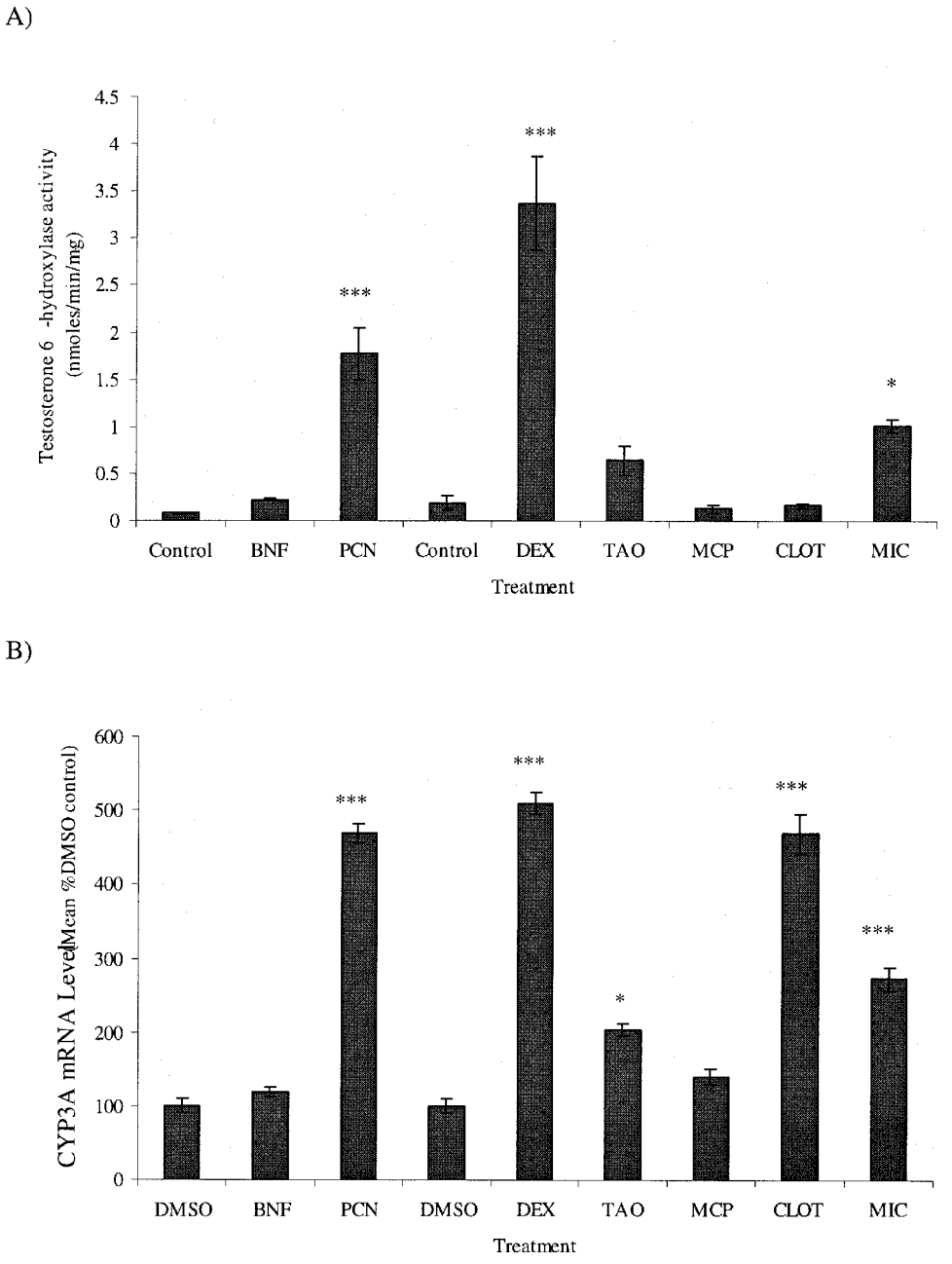


Figure 1. Induction of CYP3A. (A) testosterone 6β-hydroxylase activity in hepatic microsomes from the female Sprague–Dawley rat following repeat dosing with the same compounds (adapted from Lake *et al.* 1998); (B) mRNA levels in female rat hepatocytes following 24-h exposure to prototypical CYP inducers (BNF, 10 μM, PCN, 2 μM, DEX, 10 μM, TAO, 10 μM, MCP, 10 μM, CLOT, 5 μM, MIC, 10 μM). Data are presented as mean ($\pm$ SEM) of 6 and 8 determinations per treatment for A and B respectively. Statistically significant difference from DMSO or appropriate *in vivo* control determined using One-way ANOVA with Dunnett's post-test. *** $p < 0.001$, * $p < 0.005$.

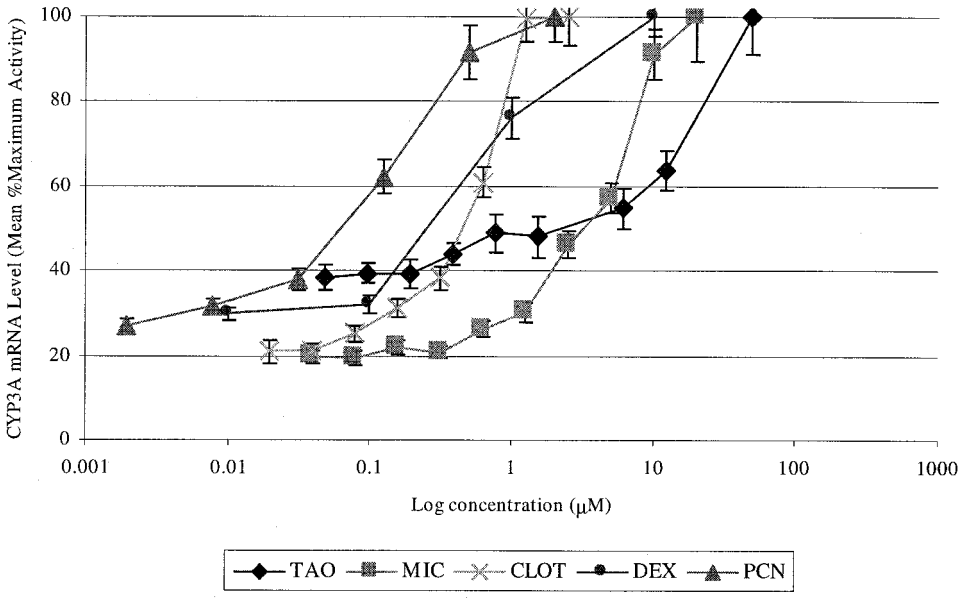


Figure 2. Effect of prototypical CYP3A inducer concentration on CYP3A mRNA expression in female rat hepatocytes following 24-h exposure. Data shown are the mean (± SEM) of 8 determinations of each point.

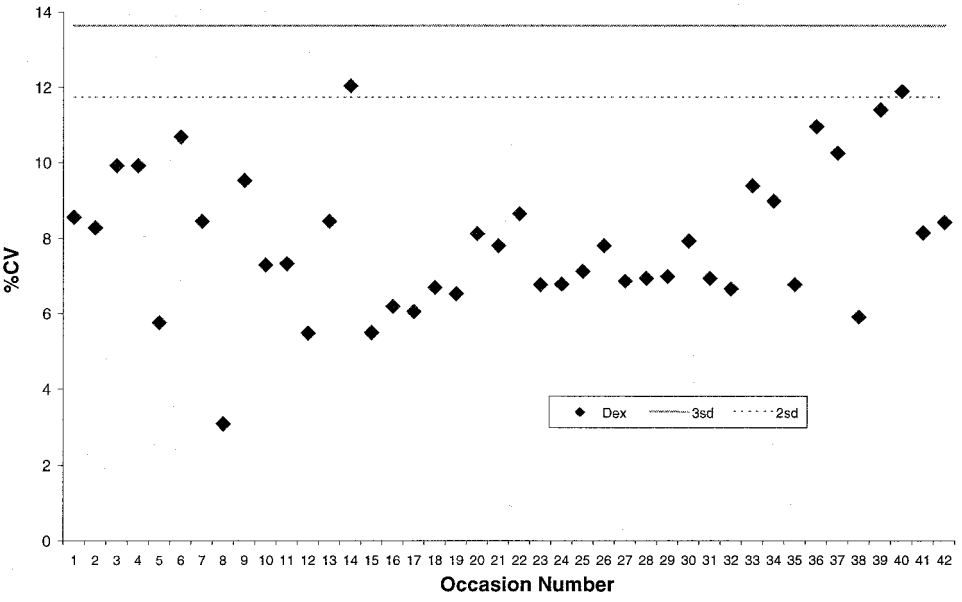


Figure 3. Variation of %CV associated with DEX treatment on different occasions in the CYP3A RHIP assay (limits define 3 or 2 SD away from mean). The %CV is a measurement of the variability of the DEX within each plate. None of the CV's fall outside 3 SD's of the mean CV, which indicates that there is no significant difference between the variability of DEX on the plates. Individual data points (%CV) were calculated from data derived from 8 determinations of DEX induction.

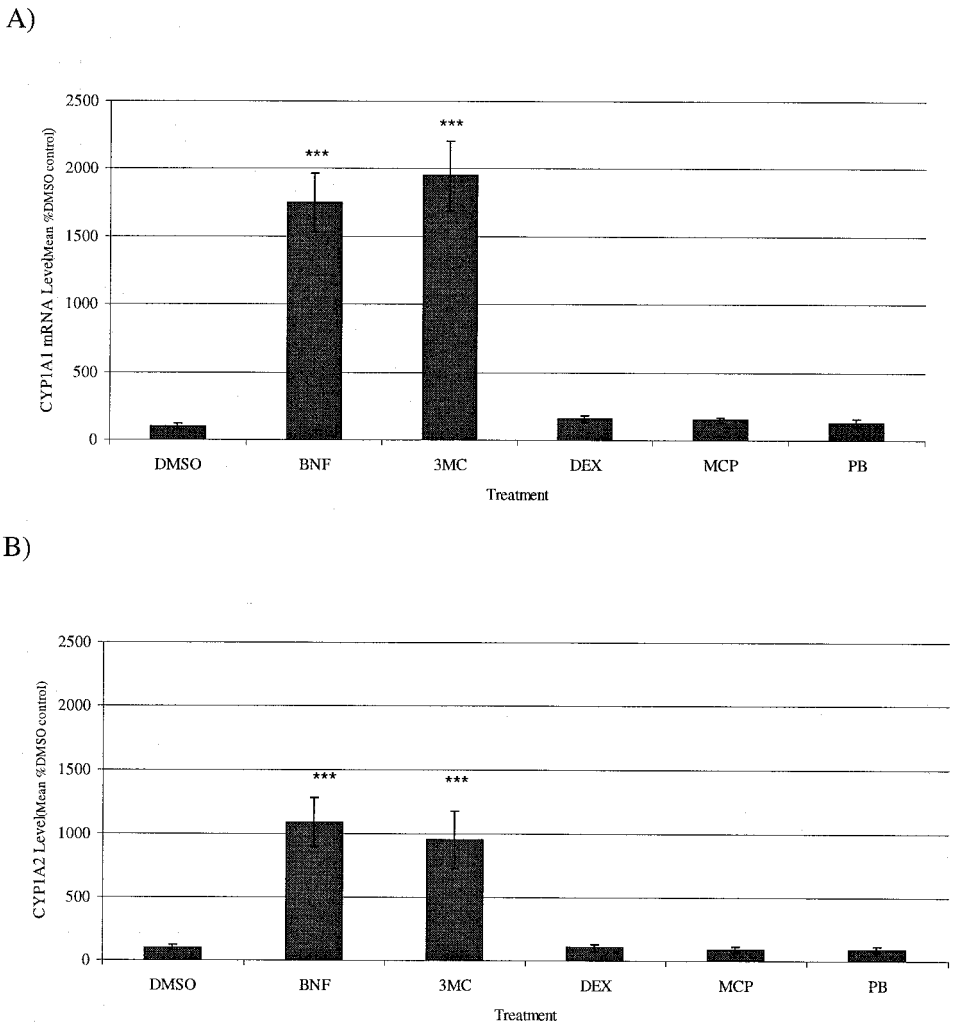


Figure 4. Induction of (A) CYP1A1 mRNA and (B) CYP1A2 mRNA in female rat hepatocytes following 24-h exposure to various prototypical CYP inducers (BNF, 10 μM, 3MC, 10 μM, DEX, 10 μM, MCP, 10 μM, PB, 100 μM). Data are presented as mean ($\pm$ SEM) of 8 determinations per treatment. Statistically significant difference from DMSO or appropriate *in vivo* control determined using One-way ANOVA with Dunnett's post-test. ***$p < 0.001$, *$p < 0.005$.

As for CYP3A, 1A1 and 1A2, the effect of inducer concentration on CYP4A1 mRNA induction was demonstrated for MCP, CIP and CLOF (figure 6B, table 2).

Discussion

Chronic administration of CYP1A (BNF) and CYP2B1 (PB, PCN) inducers to rat can, as a consequence of hepatocellular hyperplasia/hypertrophy, produce liver tumours (Lake *et al.* 1998). Also, administration of MCP to rat (a CYP4A1 inducer) can induce peroxisome proliferation in rodents (Parkinson 1996). These inducers all result in a significant increase in relative liver weight and CYP-specific probe substrate activity (microsomal EROD and 16β-hydroxytestosterone activities for

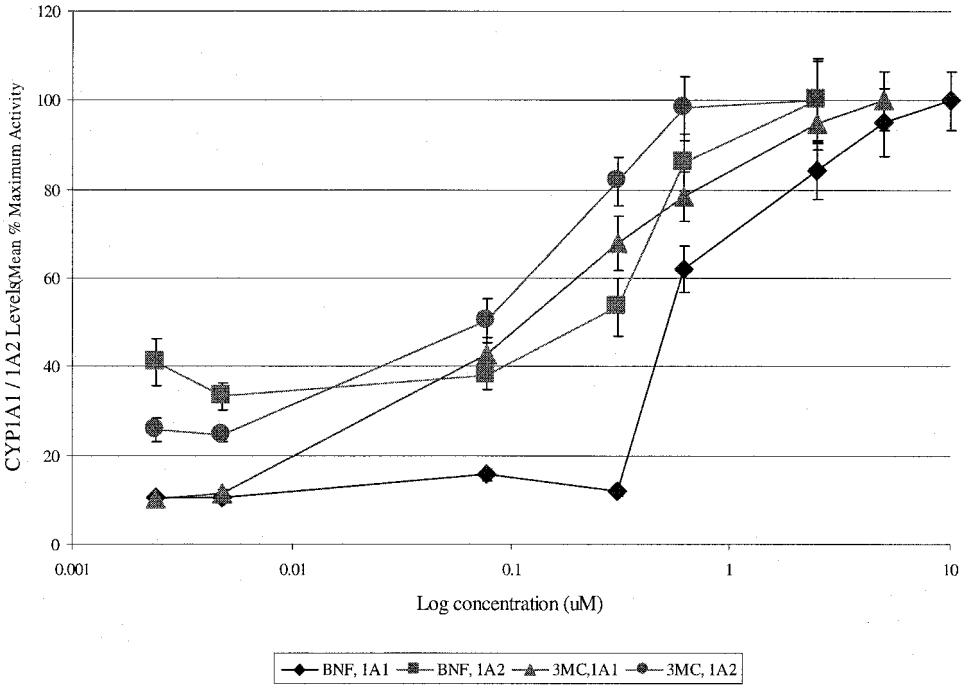


Figure 5. Effect of prototypical CYP1A inducer concentration on CYP1A1 and CYP1A2 mRNA expression in female rat hepatocytes following 24-h exposure. Data are presented as mean (± SEM) of 8 determinations of each point.

Table 2. Ind_{50} for prototypical CYP450 inducers in female rat hepatocytes.

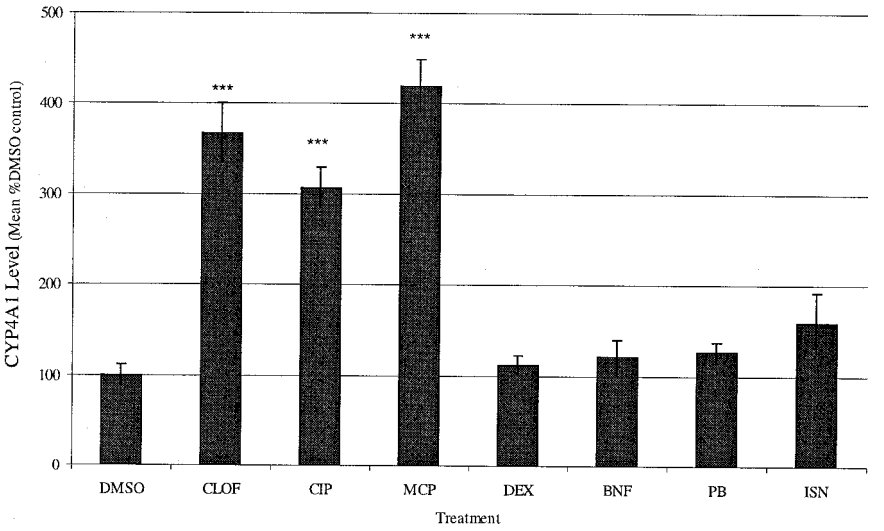
	Inducer	Ind_{50} (μM)
CYP3A	PCN	0.03
	DEX	0.17
	CLOT	0.48
	MIC	2.96
	TAO	3.00
CYP1A1	BNF	0.54
	3MC	0.11
CYP1A2	BNF	0.17
	3MC	0.04
CYP4A1	CLOF	65.2
	MCP	1.82
	CIP	1.92

Data are derived from single curves with a minimum of six concentrations and eight determinations per concentration.

1A2 and 2B1 respectively), and hepatic whole homogenate cyanide-insensitive palmitoyl-CoA oxidation activity and CYP4A1 (Weaver *et al.* 1994, Lake *et al.* 1998).

Inducers of CYP3A are of most concern clinically since this isoform is the major drug-metabolizing CYP (Michalets 1998). The antituberculosis drug, rifampicin, is the best studied example of CYP3A4 induction in human where its co-administration with medications used to treat potentially life-threatening conditions

A)



B)

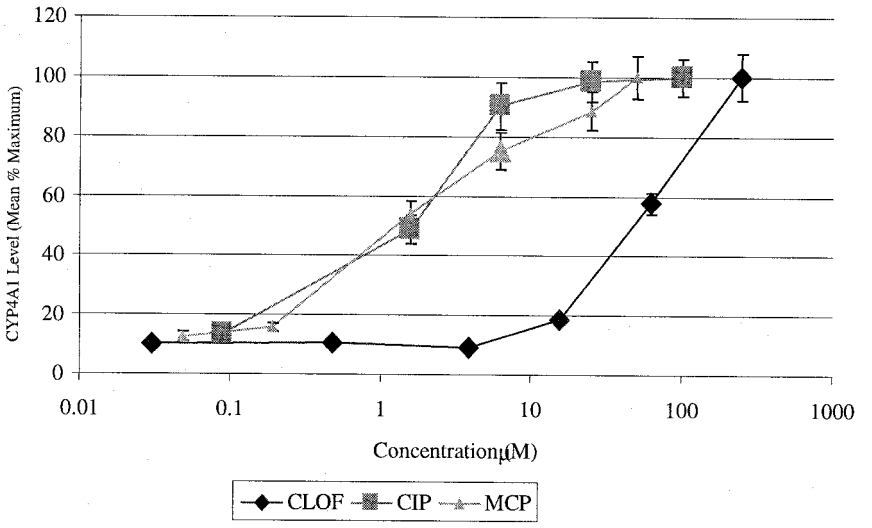


Figure 6. Induction of (A) CYP4A1 mRNA in female rat hepatocytes following 24-h exposure to various CYP450 inducers (CLOF, 500 μM, CIP, 100 μM, MCP, 10 μM, DEX, 10 μM, BNF, 10 μM, PB, 100 μM) and (B) effect of inducer concentration on CYP4A1 mRNA expression in female rat hepatocytes. Data presented are the mean ($\pm$ SEM) of 8 determinations. Statistically significant difference from DMSO control determined using One-way ANOVA with Dunnett's post-test. ***$p < 0.001$.

can lead to adverse events. Loss of efficacy following interaction of rifampicin with CYP3A-metabolized drugs used to treat blood pressure—calcium channel blockers, e.g. nifedipine (Ndanusa *et al.* 1997), HIV (protease inhibitors, e.g. nelfinavir (Jarvis and Faulds 1998), and breast cancer anti-estrogens, e.g. tamoxifen (Kivisto *et al.* 1998)—are just three of many examples in the literature.

Clear advantages are to be gained in preventing inducers of rodent and human CYP inducers from coming to market. In rodents, the aberrant histology associated with CYP inducers may mask underlying toxicology. Also, where the induced CYP isoform is primarily responsible for the metabolic clearance of the dose, the actual level of systemic exposure might well be below that expected based on a single-dose study. In such cases, the level of drug systemic exposure at the toxicological no effect level can be alarmingly close to that required for clinical efficacy.

Obtaining CYP induction information on a drug candidate early in the development process therefore can prevent toxicological and clinical hurdles having to be addressed at critical times in the drug life cycle. The context of this paper is to bring choice to early chemical series or final stage compound selection during the research stage of drug discovery. Compounds essentially not CYP inducers in rodents or humans but which have optimum pharmaceutical properties in all other respects will ultimately benefit from expedient drug development and optimum clinical usage—a benefit that has clear clinical and economic advantages. Here is described a method that addresses the preclinical phase of this drug optimization process, a method which uses rat hepatocytes cultured on Cytostar-T™ 96-well scintillating plates to assess the ability of xenobiotics to induce CYP1A1, 1A2, 3A and 4A1.

Assay specificity for each isoform was achieved by designing oligonucleotide probes (four per isoform) antisense to coding regions of each CYP gene sequence. Greatest specificity was achieved for CYP1A and CYP4A where subfamily definition for 1A1, 1A2 and 4A1 was confirmed by sequence alignment (Genbank). A utilitarian set of CYP3A probes, which does not discriminate between CYP3A1, 3A2, 3A18 or 3A23, was generated to provide a measure of total CYP3A transcription. The greatest emphasis here has been on CYP3A since this is the main drug-metabolizing isoform.

In the CYP3A RHIP assay, the prototypical CYP3A inducers PCN, DEX, CLOT and MIC (Kocarek *et al.* 1995, Lake *et al.* 1998) were all good inducers of CYP3A mRNA. BNF and MCP, which are well-known inducers of CYP1A (Bars and Elcombe 1991, Lefevre *et al.* 1994) respectively, did not induce CYP3A mRNA (figure 1), further defining the specificity of this methodology. Testosterone-6β-hydroxylase activity of hepatic microsomes prepared *ex vivo* from rats that had received four daily oral doses of various CYP inducers (Lake *et al.* 1998) indicated a good qualitative *in vivo* to *in vitro* CYP3A induction relationship. This relationship was qualitative and best for PCN and DEX; that for TAO, CLOT and MIC was less well defined due, it is proposed here, to the compound being carried through in the microsomal preparation procedure and inhibiting testosterone-6β-hydroxylase activity. This finding has previously been reported for CLOT, TAO and MIC by Parkinson (1996).

The RHIP methodology can generate Ind_{50} (the concentration of inducer required to elicit 50% of the maximum induction of CYP-specific mRNA, figures 2, 5 and 6, and table 1), and therefore provides information on inducer potency normalized for inducer concentration. Since exposure of hepatocytes to inducers *in*

vivo is dependent on both the extent of dose absorbed and subsequently upon its distribution within the liver, it is not surprising that the apparent relationship between induction *in vivo* (enzyme activity) and that *in vitro* (mRNA) is not quantitative (figure 1). This is exemplified by DEX and PCN induction of CYP3A activity by 17- and 8-fold *in vivo* respectively, and induction of mRNA 5-fold for both compounds *in vitro* (figure 1). In addition to exposure considerations, differences between the extents of induction by DEX *in vivo* and *in vitro* (17- and 5-fold respectively) could also be due to a single mRNA transcript *in vivo* being translated into protein a number of times.

The robustness of the CYP3A RHIP assay has also been investigated. The interplate variation of %CV associated with DEX treatment on different occasions in the CYP3A RHIP assay is presented in figure 3. %CV is a measurement of the variability of the DEX on each plate. None of the CVs fell outside 3 SD of the mean CV, which indicates that there was no significant difference between the variability of DEX on the plates.

In the CYP1A1 and 1A2 RHIP assays, the prototypical CYP1A inducers BNF and 3MC (Lake *et al.* 1998) were good inducers of both CYP1A1 and 1A2 mRNA (figure 4). DEX, PB and MCP, inducers of CYP3A, 2B and 4A respectively, did not induce CYP1A1 or 1A2, showing that these oligonucleotide probes were specific. Subfamily specificity of CYP1A1 over 1A2 was defined by the oligonucleotide probe base sequences (table 1). BNF and 3MC appear as more potent inducers of CYP1A2 than of 1A1 (figure 5). Ind_{50} for BNF and 3MC at CYP1A2 was 0.17 and 0.04 μM respectively, while Ind_{50} for these inducers at CYP1A1 was 3-fold higher (0.54 and 0.11 μM respectively).

In the CYP4A1 RHIP assay, the prototypical CYP4A1 inducers, CLOF, CIP and MCP were selective (over DEX, BNF, PB and ISN) inducers of CYP4A1 mRNA (figure 6). Ind_{50} of these three inducers was 65.2, 1.92 and 1.82 μM respectively (figure 6B and table 2).

Some of the latest 96-well plate mRNA technologies require cellular extracts of mRNA to be transferred to a capture plate, e.g. in bDNA and TaqMan methodologies (Burris *et al.* 1999, Wang and Brown 1999). This may inherently introduce error into an already variable system. The RHIP assay has the advantage of all procedures taking place within a single 96-well plate—from culture to hybridization to final result. There is also no need for labour-intensive cloning studies to generate antisense probes as in the ribonuclease protection assay methodology reported by Surry *et al.* (1999) since the oligonucleotide probes can be custom-synthesized automatically. This methodology does not detect, however, compounds that result in induction via post-translational stabilization of proteins where no increase in mRNA would be observed, e.g. isoniazid and CYP2E1 induction (Park *et al.* 1993).

Reducing the amounts of animals and compound required to study CYP induction are important advantages of the RHIP assays over conventional evaluations *in vivo*. Typically four rats are dosed for 4 days using oral doses in the range 50–500 mg kg^{-1} day^{-1} (Lake *et al.* 1998). In comparison, the amount of hepatocytes required to carry out all the studies reported herein could be obtained from a single animal ($< 200 \times 10^6$ viable cells) and CYP induction investigated using μg rather than g quantities of drug substance. With such small compound requirements, there is now scope to investigate the effect of chemical structure on CYP induction as part of the lead selection phase of the drug discovery process.

The RHIP assays for CYP3A, 1A1, 1A2 and 4A are sensitive and selective, and they have an excellent qualitative relationship with CYP induction data *ex vivo*. Ind_{50} allows quantitative comparisons to be made about the potency of an inducer. With appropriately designed oligonucleotide probes, this technology can assess CYP induction in human hepatocytes, which together with preclinical data can contribute to improving the quality of compounds progressing into the expensive process of drug development.

Acknowledgements

The authors thank Brian Lake for the data reproduced from his original publication.

References

Bars, R. G. and Elcombe , C. R., 1991, Dose-dependent acinar induction of cytochromes P450 in rat liver. Evidence for a differential mechanism of induction of P450IA1 by β-naphthoflavone and dioxin. *Biochemical Journal*, **277**, 577–580.

Bars, R. G., Mitchell , A. M., Wolf , C. R. and Elcombe , C. R., 1989, Induction of cytochrome P-450 in cultured rat hepatocytes. The heterogeneous localisation of specific isoenzymes using immunocytochemistry. *Biochemical Journal*, **262**, 151–158.

Breckenridge , A. M., Back, D. J., Crawford, F. E., MaCiver , M., Orme , N. and Rowe, P. H., 1980, Drug interactions with oral contraceptives: clinical and experimental studies. *International Congress Symposium Series—Royal Society of Medicine*, **31**, 1–11.

Burris, T. P., Pelton , P. D., Zhou , L., Osborne , M. C., Cryan, E. and Demarest , K. T., 1999, A novel method for analysis of nuclear receptor function at natural promoters: peroxisome proliferator-activated receptor γ agonist actions on aP2 gene expression detected using branched DNA messenger RNA quantitation. *Molecular Endocrinology*, **13**, 410–417.

Dogra, S. C., Whitelaw , M. L. and May, B. K., 1998, Transcriptional activation of cytochrome P450 genes by different classes of chemical inducers. *Clinical and Experimental Pharmacology and Physiology*, **25**, 1–9.

Gonzalez, F. J., Peters , J. M. and Cattley , R. C., 1998, Mechanism of action of the nongenotoxic peroxisome proliferators: role of the peroxisome proliferator-activated receptor alpha. *Journal of the National Cancer Institute*, **90**, 1702–1709.

Guengerich , F. P., 1988, Oxidation of 17 α-ethynylestradiol by human liver cytochrome P-450. *Molecular Pharmacology*, **33**, 500–508.

Jarvis, B. and Faulds, D., 1998, Nelfinavir: a review of its therapeutic efficacy in HIV infection. *Drugs*, **56**, 147–167.

Kadlubar , F. F. and Guengerich , F. P., 1992, Inducibility of human cytochromes P-450 primarily involved in the activation of chemical carcinogens. *Chemosphere*, **25**, 201–204.

Kimura , S., Hanioka , N., Matsunaga , E. and Gonzalez, F. J., 1989, The rat clofibrate-inducible CYP4A gene subfamily. I. Complete intron and exon sequence of the CYP4A1 and CYP4A2 genes, unique exon organisation, and identification of a conserved 19-bp upstream element. *DNA*, **8**, 503–516.

Kirita , S. and Matsubara , T., 1993, cDNA cloning and characterisation of a novel member of steroid-induced cytochrome P450 3A in rats. *Archives of Biochemistry and Biophysics*, **307**, 253–258.

Kivisto , K. T., Villikka , K., Nyman , L., Anttila , M. and Neuvonen , P. J., 1998, Tamoxifen and toremifene concentrations in plasma are greatly decreased by rifampin. *Clinical and Pharmacological Therapeutics* (*St Louis*), **64**, 648–654.

Kliewer , S. A., Moore , J. T., Wade , L., Staudinger , J. L., Watson , M. A., Jones , S. A., McKee , D. D., Oliver , B. B., Willson , T. M., Zetterstrom , R. H., Perlmann , T. and Lehmann , J. M., 1998, An orphan nuclear receptor activated by pregnanes defines a novel steroid signaling pathway. *Cell* (*Cambridge, Mass.*), **92**, 73–82.

Kocarek , T. A., Schuetz , E. G., Strom , S. C., Fisher , R. A. and Guzelian , P. S., 1995, Comparative analysis of cytochrome P4503A induction in primary cultures of rat, rabbit, and human hepatocytes. *Drug Metabolism and Disposition*, **23**, 415–421.

Kostrubsky , V. E., Strom , S. C., Wood , S. G., Wrighton , S. A., Sinclair , P. R. and Sinclair , J. F., 1995, Ethanol and isopentanol increase CYP3A and CYP2E in primary cultures of human hepatocytes. *Archives of Biochemistry and Biophysics*, 3**22**, 516–520.

Lake, B. G., 1995, Mechanisms of hepatocarcinogenicity of peroxisome-proliferating drugs and chemicals. *Annual Reviews in Pharmacology and Toxicology*, **35**, 483–507.

LAKE, B. G., RENWICK , A. B., CUNNINGHAME , M. E., PRICE, R. J., SURRY, D. and EVANS, D. C., 1998, Comparison of the effects of some CYP3A and other enzyme inducers on replicative DNA synthesis and cytochrome P450 isoforms in rat liver. *Toxicology*, **131**, 9–20.

LAMBEG , T. S., KIVISTO , K. T. and NEUVONEN , P. J., 1998, Concentrations and effects of buspirone are considerably reduced by rifampicin. *British Journal of Clinical Pharmacology*, **45**, 381–385.

LEFEVRE , P. A., TINWELL , H., GALLOWAY , S. M., HILL , R., MACKAY, J. M., ELCOMBE , C. R., FOSTER , J., RANDALL , V., CALLANDER , R. D. and ASHBY , J., 1994, Evaluation of the genetic toxicity of the peroxisome proliferator and carcinogen methyl clofenapate, including assays using Muta mouse and Big Blue transgenic mice. *Human Experimental Toxicology*, **13**, 764–775.

LEHMANN , J. M., MCKEE, D. D., WATSON , M. A., WILLSON , T. M., MOORE, J. T. and KLIEWER , S. A., 1998, The human orphan nuclear receptor PXR is activated by compounds that regulate CYP3A4 gene expression and cause drug interactions. *Journal of Clinical Investigation*, **102**, 1016–1023.

LI, A. P., MAUREL, P., GOMEZ -LECHON , M. J., CHENG , L. C. and JURIMA -ROMET , M., 1997a, Preclinical evaluation of drug–drug interaction potential: Present status of the application of primary human hepatocytes in the evaluation of cytochrome P450 induction. *Chemico-Biological Interactions*, **107**, 5–16.

LI, A. P., REITH , M. K., RASMUSSEN , A., GORSKI , J. C., HALL , S. D., XU, L., KAMINSKI , D. L. and CHENG , L. K., 1997b, Primary human hepatocytes as a tool for the evaluation of structure–activity relationship in cytochrome P450 induction potential of xenobiotics: evaluation of rifampin, rifapentine and rifabutin. *Chemico-Biological Interactions*, **107**, 17–30.

MEYER , U. A., GONZALEZ, F. J., GUENGERICH , F. P., MCMANUS, M. E. and OKUDA, K.-I., 1995, Human cytochromes P450: regulation and functional variability. In A. Cuello (ed.), *Conference Proceeding, 1994* (Basle: Birkhaeuser), pp. 153–159.

MICHALETS , E. L., 1998, Update: clinically significant cytochrome P-450 drug interactions. *Pharmacotherapy*, **18**, 84–112.

MIYATA , M., NAGATA, K., YAMAZOE, Y. and KATO, R., 1991, A gene structure of testosterone 6β-hydroxylase (P450IIIA). *Biochemical and Biophysical Research Communications*, **177**, 68–73.

NDANUSA , B. U., MUSTAPHA , A. and ABDU -AGUYE , I., 1997, The effect of single dose of rifampicin on the pharmacokinetics of oral nifedipine. *Journal of Pharmacology and Biomedical Annals*, **15**, 1571–1575.

NELSON , D. R., 1998, Cytochrome P450 nomenclature. *Methods in Molecular Biology* (*Totowa, NJ*), **107**, 15–24.

NISHIBE , Y. and HIRATA , M., 1993, Effect of phenobarbital and other model inducers on cytochrome P450 isoenzymes in primary culture of dog hepatocytes. *Xenobiotica*, **23**, 681–692.

PARK, K. S., SOHN , D. H., VEECH , R. L. and SONG , B. J., 1993, Translational activation of ethanol-inducible cytochrome P450 (CYP2E1) by isoniazid. *European Journal of Pharmacology, Environmental Toxicology and Pharmacology Section*, **248**, 7–14.

PARKINSON , A., 1996, An overview of current cytochrome P 450 technology for assessing the safety and efficacy of new materials. *Toxicology and Pathology*, **24**, 45–57.

REESE , J. A. and BYARD, J. L., 1981, Isolation and culture of adult hepatocytes from liver biopsies. *In Vitro*, **17**, 935–940.

RYU, D.-Y., LEVI , P. E., FERNANDEZ -SALGUERO , P., GONZALEZ, F. J. and HODGSON , E., 1996, Piperonyl butoxide and acenaphthylene induce cytochrome P450 1A2 and 1B1 mRNA in aromatic hydrocarbon response receptor knock-out mouse liver. *Molecular Pharmacology*, **50**, 443–446.

SAFE, S. and KRISHNAN , V., 1995, Cellular and molecular biology of aryl hydrocarbon (Ah) receptor-mediated gene expression. *Archives of Toxicology*, **17 (suppl.)**, 99–115.

SCHRENK , D., 1998, Impact of dioxin-type induction of drug-metabolising enzymes on the metabolism of endo- and xenobiotics. *Biochemical Pharmacology*, **55**, 1155–1162.

SCHUETZ, E. G., LI, D., OMIECINSKI , C. J., MULLER -EBERHARD , U., KLEINMAN , H. K., ELSWICK , B. and GUZELIAN , P. S., 1988, Regulation of gene expression in adult rat hepatocytes cultured on a basement membrane matrix. *Journal of Cellular Physiology*, **134**, 309–323.

SHARER , J. E., SHIPLEY , L. A., VANDENBRANDEN , M. R., BINKLEY , S. N. and WRIGHTON , S. A., 1995, Comparisons of phase I and phase II *in vitro* hepatic enzyme activities of human, dog, rhesus monkey, and cynomolgus monkey. *Drug Metabolism and Disposition*, **23**, 1231–1241.

SOGAWA, K., GOTOH , O., KAWAJIRI , K. and FUJII -KURIYAMA , Y., 1984, Distinct organisation of methylcholanthrene- and phenobarbital-inducible cytochrome P-450 genes in the rat. *Proceedings of the National Academy of Sciences, USA*, **81**, 5066–5070.

SOGAWA, K., GOTOH , O., KAWAJIRI , K., HARADA, T. and FUJII -KURIYAMA , Y., 1985, Complete nucleotide sequence of a methylcholanthrene-inducible cytochrome P-450 (P-450d) gene in the rat. *Journal of Biological Chemistry*, **260**, 5026–5032.

SPATZENEGGER , M. and JAEGER , W., 1995, Clinical importance of hepatic cytochrome P450 in drug metabolism. *Drug Metabolism Reviews*, **27**, 397–417.

STROM , S. C., JIRTLE , R. L., JONES , R. S., NOVICKI , D. L., ROSENBERG , M. R., NOVOTNY , A., IRONS , G., MCLAIN , J. R. and MICHALOPOULOS , G., 1982, Isolation, culture, and transplantation of human hepatocytes. *Journal of the National Cancer Institute*, **68**, 771–778.

STROTKAMP, D., ROOS, P. H. and HANSTEIN, W. G., 1995, A novel CYP3 gene from female rats. *Biochimica et Biophysica Acta*, **1260**, 341–344.

SURRY, D., MCALLISTER, G., MENESES-LORENTE, G. and EVANS, D. C., 1999, High throughput ribonuclease protection assay for the determination of CYP3A mRNA induction in cultured rat hepatocytes. *Xenobiotica*, **29**, 827–838.

VAN DEN BROEK, P. J. A., BARROSO, M. and LECHNER, M. C., 1996, Critical amino-terminal segments in insertion of rat liver cytochrome P450 3A1 into the endoplasmic reticulum membrane. *Experientia*, **52**, 851–855.

WANG, T. and BROWN, M. J., 1999, mRNA Quantification by real time TaqMan polymerase chain reaction: validation and comparison with RNase protection. *Analytical Biochemistry*, **269**, 198–201.

WEAVER, R. J., THOMPSON, S., SMITH, G., DICHINS, M., ELCOMBE, C. R., MAYER, R. T. and BURKE, M. D., 1994, A comparative study of constitutive and induced alkoxyresorufin O-dealkylation and individual cytochrome P450 forms in cynomolgus monkey (*Macaca fascicularis*), human, mouse, rat and hamster liver microsomes. *Biochemical Pharmacology*, **47**, 763–773.

WILLEY, J. C., COY, E. L., FRAMPTON, M. W., TORRES, A., APOSTOLAKOS, M. J., HOEHN, G., SCHUERMANN, W. H., THILLY, W. G., OLSON, D. E., HAMMERSLEY, J. R., CRESPI, C. L. and UTELL, M. J., 1997, Quantitative RT-PCR measurement of cytochromes P450 1A1, 1B1, and 2B7, microsomal epoxide hydrolase, and NADPH oxidoreductase expression in lung cells of smokers and nonsmokers. *American Journal of Respiratory Cell and Molecular Biology*, **17**, 114–124.

WORTELBOER, H. M., DE KRUIF, C. A., DE BOER, W. I., VAN IERSEL, A. A. J., FALKE, H. E. and BLAAUBOER, B. J., 1988, Induction and activity of several isoenzymes of cytochrome P-450 in primary cultures of rat hepatocytes, in comparison with *in vivo* data. *Molecular Toxicology*, **1**, 373–381.

WRIGHT, M. C., PAINE, A. J., SKETT, P. and AULD, R., 1994, Induction of rat hepatic glucocorticoid-inducible cytochrome P450 3A by metyrapone. *Journal of Steroid Biochemistry and Molecular Biology*, **48**, 271–276.

WRIGHTON, S. A. and STEVENS, J. C., 1992, The human hepatic cytochromes P450 involved in drug metabolism. *Critical Reviews in Toxicology*, **22**, 1–21.

XENOBIOTICA , 2000, VOL. 30, NO. 5, 457–467

Reduction of hydroxamic acids to the corresponding amides catalyzed by rabbit blood

K. SUGIHARA, S. KITAMURA*, S. OHTA and K. TATSUMI

Institute of Pharmaceutical Science, Hiroshima University School of Medicine, Kasumi 1-2-3, Minami-ku, Hiroshima, 734-8551 Japan

Received 17 September 1999

1. The hydroxamic acids *N*-hydroxyphenacetin and *N*-hydroxy-2-acetylaminofluorene were reduced to the corresponding amides, phenacetin and 2-acetylaminofluorene respectively by rabbit blood supplemented with both NAD(P)H and FAD. These reducing activities were found in erythrocytes but not in plasma, and were sensitive to inhibition by carbon monoxide and oxygen. When blood or erythrocytes were boiled, these activities were not abolished.

2. Haemoproteins such as haemoglobin and catalase exhibited the reductase activity in the presence of both NAD(P)H and FAD under anaerobic conditions. The activity was not abolished when the haemoproteins were boiled.

3. Haematin showed a significant reducing activity in the presence of these cofactors. The activity of haematin was also observed with the photochemically reduced form of FAD.

4. The reduction system in blood was composed of NAD(P)H, FAD and haemoglobin. Reduction appears to proceed in two steps, i.e. the reduction of FAD by NADH or NADPH, followed by the non-enzymatic reduction of the hydroxamic acids to the amides by reduced FAD, catalyzed by the haem group of haemoglobin in rabbit erythrocytes.

Introduction

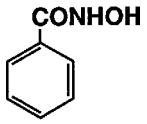
Hydroxamic acids possess a variety of important biological activities (Munson 1982) and can be divided into three groups in terms of chemical structure, i.e. (1) aromatic hydroxamic acids such as benzohydroxamic acid and salicylhydroxamic acid, (2) heterocyclic hydroxamic acids such as nicotinohydroxamic acid, and (3) aliphatic hydroxamic acids such as *N*-hydroxyphenacetin and *N*-hydroxy-2-acetylaminofluorene (*N*-OH-AAF) (figure 1). Acetohydroxamic acid, salicylhydroxamic acid and *N*-acylglycinohydroxamic acid have been used clinically as therapeutic agents (Griffith *et al.* 1978, Munson 1982). Some aliphatic hydroxamic acids are known to be toxic metabolites of arylamides such as 2-acetylaminofluorene (AAF) and 2-formylaminofluorene (Miller *et al.* 1960, Weeks *et al.* 1980, Allaben *et al.* 1982).

Several workers have demonstrated that hydroxamic acids undergo enzymatic reduction to the corresponding amides (Lowenthal 1954, Hirsch and Kaplan 1961, Irving 1964, Bernheim 1965, Grantham *et al.* 1965, Lotlikar *et al.* 1965, Gutmann and Erickson 1969, Bernheim 1972, Putcha *et al.* 1984). However, these reports did not identify the enzymes responsible for the reduction. Our previous study reported that aldehyde oxidase (EC 1.2.3.1) in the presence of its electron donor has an ability to reduce various types of hydroxamic acids such as salicylhydroxamic acid, benzohydroxamic acid, anthranilhydroxamic acid, nicotinohydroxamic acid and *N*-OH-AAF (Sugihara *et al.* 1983, Sugihara and Tatsumi 1986, Kitamura *et al.* 1994). Furthermore, other hydroxamic acid reductases, *N*-hydroxy-2-acetylaminofluorene reductase and salicylhydroxamic acid reductase, have been purified from rabbit and

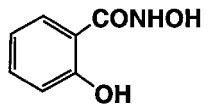
* Author for correspondence: e-mail: kitamura@pharm.hiroshima-u.ac.jp

Xenobiotica ISSN 0049-8254 print/ISSN 1366-5928 online © 2000 Taylor & Francis Ltd
http://www.tandf.co.uk/journals

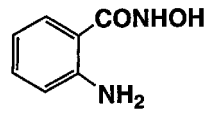
Aromatic hydroxamic acids



Benzohydroxamic acid

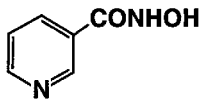


Salicylhydroxamic acid



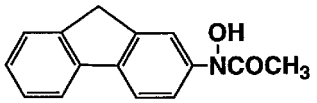
Anthranilhydroxamic acid

Heterocyclic hydroxamic acid

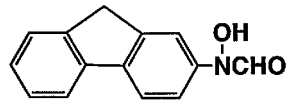


Nicotinohydroxamic acid

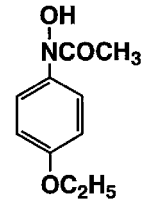
Aliphatic hydroxamic acids



N-Hydroxy-2-acetylaminofluorene



N-Hydroxy-2-formylaminofluorene



N-Hydroxyphenacetin

Figure 1. Structures of hydroxamic acids.

rat liver cytosols respectively (Kitamura and Tatsumi 1985, Katsura *et al.* 1993). The former enzyme catalyzes the reduction of *N*-OH-AAF, *N*-hydroxy-4-acetylaminobiphenyl and *N*-hydroxyphenacetin, but not aromatic or heterocyclic hydroxamic acids. The latter enzyme is highly specific for salicylhydroxamic acid and dependent on NADH or NADPH, and it is sensitive to allopurinol.

In the present study, a novel system in blood for the reduction of aliphatic hydroxamic acids, composed of haemoglobin, NAD(P)H and a flavin, was investigated using *N*-hydroxyphenacetin and *N*-OH-AAF as substrates.

Materials and methods

Materials

Phenacetin (98%) and AAF (97%) were from Tokyo Chemical Industry Co. Ltd (Tokyo, Japan). NADPH and NADH were from Oriental Yeast Co. (Tokyo, Japan); and FAD, bovine blood haemoglobin, horse skeletal muscle myoglobin, bovine liver catalase, horseradish peroxidase, horse heart cytochrome *c* and bovine blood haematin (Fe^{3+}) from Sigma Chemical Co. (St Louis, MO, USA). *N*-hydroxyphenacetin (98%) and *N*-OH-AAF (96%) were synthesized according to the methods of Hinson and Mitchell (1976) and Cramer *et al.* (1960) respectively. Reduced FAD was prepared photochemically from FAD by the method of Yubisui *et al.* (1980).

Preparation of blood and erythrocytes

Male Japanese albino rabbits (2.8–3.2 kg) were used in this study and blood samples collected from the jugular vein. Blood was put into polystyrene tubes containing heparin as an anticoagulant and was centrifuged for 5 min at 4 °C at 1000 *g*. Plasma was removed and the pellet (erythrocyte fraction) was

washed with 2 vols cold isotonic saline. Erythrocytes were suspended and haemolyzed in 1 vol. 0.01 M K, Na phosphate buffer (pH 7.4).

Assay of reductase activity

In the case of reduction of *N*-hydroxyphenacetin, the incubation mixture consisted of 0.2 μmol *N*-hydroxyphenacetin, 1 μmol NADPH or NADH, 0.2 μmol FAD, and haemoprotein or blood or a related compound in a final volume of 2 ml 0.01 M K, Na phosphate buffer (pH 7.4). Blood (10 μl), erythrocytes equivalent to 10 μl blood, 5 nmol haemoglobin or 5 nmol haematin was used. In some experiments, the incubation mixture excluding substrate and cofactors was heated in a boiling water bath for 5 min. Incubation was performed using a Thunberg tube under anaerobic conditions. The side arm contained NADPH or NADH, and the body contained all other components. The tube was gassed for 3 min with nitrogen, evacuated with an aspirator for 5 min and again gassed with nitrogen. The reaction was started by mixing the components of the side arm and the body, continued for 10 min at 37 °C, and stopped by adding 0.2 ml 1 N HCl. The mixture, after addition of 20 μg acetanilide as an internal standard, was extracted once with 5 ml ether and the extract was evaporated to dryness *in vacuo*. The residue was dissolved in 0.2 ml methanol and then subjected to high-performance liquid chromatography (HPLC). HPLC was performed in a Hitachi L-6000 high-performance liquid chromatograph (Tokyo, Japan) equipped with an UV absorption detector. The instrument was fitted with a 4×125 mm LiChrospher 100 RP-18(e) (5 μm) column (Merck, Darmstadt, Germany). The mobile phase was acetonitrile–H_2O (4:6 v/v). The chromatograph was operated at 0.8 ml min^{-1} at ambient temperature and at a wavelength of 254 nm. Elution times of *N*-hydroxyphenacetin, acetanilide and phenacetin were 2.5, 5.7 and 8.0 min respectively. The peak ratio of phenacetin formed and an internal standard was determined from their peak areas.

In the case of *N*-OH-AAF, the hydroxamic acid was incubated as described above. AAF formed was assayed according to Kitamura and Tatsumi (1985). Nicotinohydroxamic acid, salicylhydroxamic acid and anthranilhydroxamic acid were also incubated with blood or a related compound, and amides formed were measured by HPLC according to Sugihara and Tatsumi (1986).

Measurement of protein contents

Protein contents were determined by the method of Lowry *et al.* (1951) with bovine serum albumin as standard.

Results

When *N*-hydroxyphenacetin or *N*-OH-AAF was incubated with rabbit blood, phenacetin or AAF respectively was formed in the presence of NADH or NADPH under both aerobic and anaerobic conditions (table 1). These hydroxamic acid-reducing activities were stimulated by addition of FAD under anaerobic conditions. The activities were sensitive to inhibition by carbon monoxide. When the blood was boiled, these activities were not abolished but were enhanced. The activities of boiled blood were markedly inhibited by carbon monoxide (table 1). When FAD was replaced with FMN or riboflavin in the presence of NADH or NADPH, similar activities were observed (data not shown).

Rabbit erythrocytes, which were haemolyzed by adding 0.01 M phosphate buffer, also exhibited a significant reducing activity toward *N*-hydroxyphenacetin in the presence of both NAD(P)H and FAD under anaerobic conditions (figure 2). When the erythrocytes were boiled, the activity was not abolished, as had been found with blood. The activity was inhibited by carbon monoxide. In contrast, plasma exhibited no reducing activity even in the presence of the cofactors (figure 2). These results suggested that haemoglobin is involved in the reduction of hydroxamic acids in rat erythrocytes.

When haemoglobin was used instead of blood, reducing activities towards *N*-hydroxyphenacetin and *N*-OH-AAF, which were sensitive to carbon monoxide, were observed in the presence of NADH or NADPH and FAD (figure 3). Boiled haemoglobin with both NAD(P)H and FAD also exhibited reducing activities and were 2–5-fold higher than those seen with native haemoglobin (figure 3). When

Table 1. Reduction of *N*-hydroxyphenacetin and *N*-hydroxy-2-acetylaminofluorene by rabbit blood.

	Reduced product formed[a] (nmol/10 min/ml blood)					
	N-hydroxyphenacetin			*N*-hydroxy-2-acetylaminofluorene		
	Blood		Boiled blood[b]	Blood		Boiled blood
Addition	Aerobic	Anaerobic	Anaerobic	Aerobic	Anaerobic	Anaerobic
None	34± 17	35± 14	69± 12	202± 24	242± 20	1464± 188
NADH	42± 11	37± 8	64± 11	186± 22	197± 26	3041± 462
NADPH	53± 18	49± 17	73± 21	223± 28	193± 27	3262± 389
FAD	109± 20	130± 19	137± 18	242± 24	244± 29	1880± 204
NADH, FAD	164± 22	502± 57	2828± 167	441± 47	8232± 1020	18730± 2140
NADPH, FAD	166± 24	493± 52	2774± 187	389± 38	8555± 1100	13160± 1820
NADH, FAD, CO	–	130± 20	290± 44	–	874± 90	1788± 194

Each value represents the mean± SD of four experiments.

[a] Hydroxamic acids were incubated with 10 μl rabbit blood in the presence of cofactors for 10 min. Phenacetin or 2-acetylaminofluorene was determined by HPLC. Other details are as described in the Materials and methods.

[b] Blood was heated for 10 min in a boiling water bath.

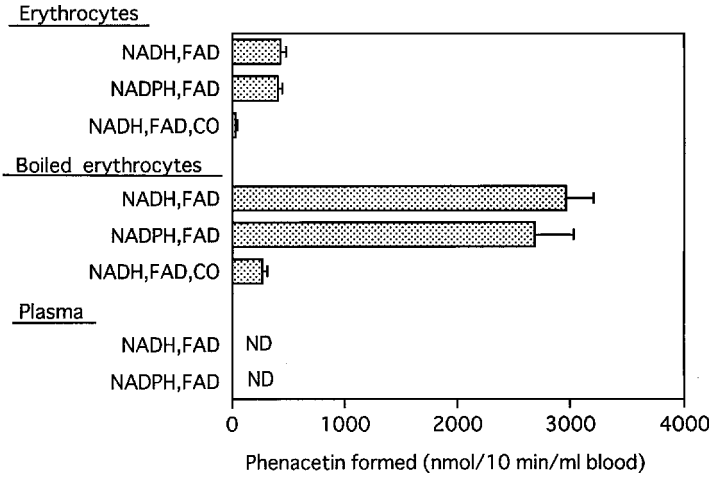


Figure 2. Reduction of *N*-hydroxyphenacetin to phenacetin by erythrocytes and plasma of rabbit in the presence of NAD(P)H and FAD. Each bar represents the mean ±SD of four experiments. Reactions were conducted at 37 °C with 10 μl erythrocytes or 50 μl plasma of rat in the presence of both NAD(P)H and FAD under anaerobic conditions. Phenacetin formed was determined by HPLC. Other details are described in the Materials and methods. ND, Not detected.

myoglobin, catalase, peroxidase and cytochrome *c* were used instead of haemoglobin as a haemoprotein, reducing activity toward *N*-hydroxyphenacetin was also observed to varying degrees (table 2). When the haemoproteins were boiled, the activities were not abolished but were enhanced except in the case of cytochrome *c* (table 2).

Furthermore, haematin showed significant reducing activities towards *N*-hydroxyphenacetin and *N*-OH-AAF in the presence of both NADH and FAD (table 3). The non-enzymatic reduction by haemoglobin or haematin was also observed in the presence of the photochemically reduced form of FAD (table 4). However, protoporphyrin, ferric chloride or ferrous chloride had no effect on the reduction of these hydroxamic acids (data not shown).

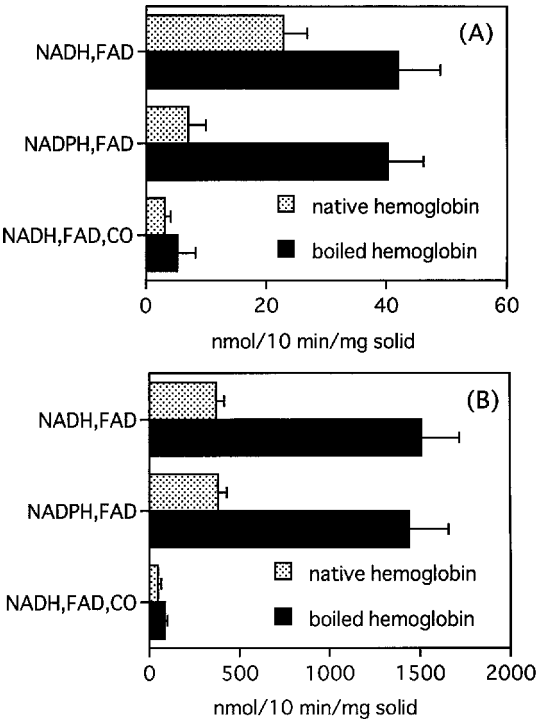


Figure 3. Reduction of *N*-hydroxyphenacetin (A) and *N*-hydroxy-2-acetylaminofluorene (B) by haemoglobin. Each bar represents the mean± SD of four experiments. Reactions were conducted at 37 °C with 0.32 mg haemoglobin in the presence of both NAD(P)H and FAD for 10 min under anaerobic conditions. Phenacetin or 2-acetylaminofluorene formed was determined by HPLC. Other details are described in the Materials and methods.

Table 2. Reduction of *N*-hydroxyphenacetin by haemoproteins.

	Phenacetin formed[a] (nmol/10 min/μmol heme)	
Addition	Haemoprotein	Boiled haemoprotein
Haemoglobin	368± 22	677± 56
Myoglobin	99± 13	461± 33
Cytochrome *c*	34± 6	21± 3
Peroxidase	64± 6	220± 31
Catalase	150± 24	222± 37

Each value represents the mean± SD of four experiments.

[a] *N*-hydroxyphenacetin was incubated with 0.3–1 mg hemoproteins in the presence of NADH and FAD for 10 min under anaerobic conditions. Phenacetin formed was determined by HPLC. Other details are described as in the Materials and methods.

These results led us to the conclusion that *N*-hydroxyphenacetin and *N*-OH-AAF can be reduced to the corresponding amides non-enzymatically by the catalytic action of the haem group of haemoglobin in the presence of a flavin and a reduced pyridine nucleotide, both of which can be replaced with a reduced flavin.

N-hydroxyphenacetin was also reduced by haemoglobin in the presence of 1,4-dihydroxynaphthalene, dithionite, 2-mercaptoethanol or dithiothreitol instead of a

Table 3. Reduction of *N*-hydroxyphenacetin and *N*-hydroxy-2-acetylaminofluorene by haematin.

	Reduction product formed[a] (nmol/min/μmol heme)	
Addition	*N*-hydroxyphenacetin	*N*-hydroxy-2-acetylaminofluorene
None	nd	nd
NADH	0.2±0.1	1.1±0.6
NADH, FAD	215±34	711±68

Each value represents the mean± SD of four experiments.

[a] Hydroxamic acids were incubated with 5 nmol haematin in the presence of cofactors for 10 min under anaerobic conditions. Phenacetin or 2-acetylaminofluorene formed was determined by HPLC. Other details are described as in the Materials and methods.

nd, Not detected.

Table 4. Reduction of *N*-hydroxyphenacetin and *N*-hydroxy-2-acetylaminofluorene by haemoglobin and haematin in the presence of reduced FAD.

	Reduction product formed[a] (nmol/min/μmol heme)	
Addition	*N*-hydroxyphenacetin	*N*-hydroxy-2-acetylaminofluorene
None	nd	nd
Haemoglobin	194±27	766±63
Haematin	308±31	1009±114

Each value represents the mean± SD of four experiments.

[a] Hydroxamic acids were incubated with 0.32 mg haemaglobin or haematin in the presence of reduced FAD for 10 min under anaerobic conditions. Phenacetin or 2-acetylaminofluorene formed was determined by HPLC. Other details are described as in the Materials and methods.

nd, Not detected.

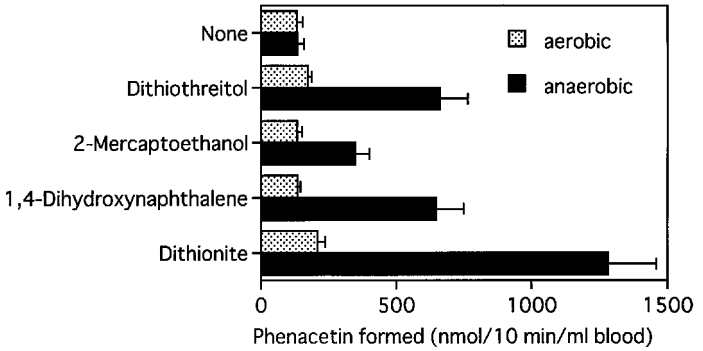


Figure 4. Reduction of *N*-hydroxyphenacetin by haemoglobin in the presence of various reducing agents. Each bar represents the mean ± SD of four experiments. Reactions were conducted at 37 °C with 0.32 mg haemoglobin in the presence of reducing agents for 10 min under aerobic or anaerobic conditions. Phenacetin formed was determined by HPLC. Other details are described in the Materials and methods.

reduced flavin under anaerobic conditions (figure 4). These chemicals could not reduce *N*-hydroxyphenacetin without haemoglobin. Thus, mild reducing agents such as dithionite, dihydroquinones and SH reagents were also effective in the reduction of hydroxamic acids by haem instead of reduced flavins.

When the reducing activity towards aromatic hydroxamic acids and heterocyclic hydroxamic acids was examined using nicotinohydroxamic acid, salicylhydroxamic acid and anthranilhydroxamic acid as substrates, these hydroxamic acids were not reduced by rabbit blood or haemoglobin even in the presence of both NAD(P)H and FAD (data not shown).

Discussion

Arylacetamides such as phenacetin and AAF are oxidized to the corresponding hydroxamic acids in biological systems (Irving 1964, Miller 1970, Nery 1971). *N*-hydroxylation of AAF is an essential first step in the metabolic activation of this carcinogen (Cramer *et al.* 1960, Miller *et al.* 1960, Irving 1962). The *N*-hydroxylated product of the carcinogen is also reduced to the parent arylacetamide (Irving 1964, Grantham *et al.* 1965, 1970, Lotlikar *et al.* 1965, Gutmann and Erickson 1969, Williams *et al.* 1970, Weisburger *et al.* 1970, Lenk and Scharmer 1980, Yamazoe *et al.* 1980). The reduction of *N*-OH-AAF to the parent compound AAF is a detoxification step of the hydroxamic acid. Therefore, the reductase activity toward *N*-OH-AAF in tissues is of importance in the determination of the carcinogenicity. *N*-hydroxyphenacetin is also formed from phenacetin in animals, and is toxic, like the parent compound (Nery 1971, Hinson and Mitchell 1976). The hydroxamic acid is known to be a liver carcinogen and is mutagenic in the presence of an S-9 mix (Calder *et al.* 1976, Dybing *et al.* 1981, Johansson 1981, Wirth *et al.* 1982, Corbett *et al.* 1983). The interconversion between phenacetin and *N*-hydroxyphenacetin is also important in relation to the toxicity of phenacetin. However, the reductive metabolism of *N*-hydroxyphenacetin has not been reported except for a brief communication that the hydroxamic acid was reduced by aldehyde oxidase as for *N*-OH-AAF (Kitamura *et al.* 1994).

Gutmann and Erickson (1969) reported that *N*-OH-AAF was reduced to AAF by mammalian liver cytosol. The present authors investigated the liver cytosolic enzymes responsible for the reduction of *N*-OH-AAF, and purified a new enzyme, *N*-hydroxy-2-acetylaminofluorene reductase, capable of reducing *N*-OH-AAF from rabbit liver cytosol (Kitamura and Tatsumi 1985). The enzyme required cysteine, glutathione, NADH or NADPH as an electron donor. Furthermore, the present authors demonstrated that aldehyde oxidase is another liver cytosolic enzyme responsible for the reduction of *N*-OH-AAF (Kitamura *et al.* 1994). Yamazoe *et al.* (1980) reported that *N*-OH-AAF was also reduced by mammalian liver microsomes, with participation of cytochrome P450. The present authors demonstrated that the microsomal reduction of *N*-OH-AAF by cytochrome P450 proceeded non-enzymatically (Kitamura *et al.* 1999c). On the other hand, Weisburger *et al.* (Grantham *et al.* 1970, Weisburger *et al.* 1970, Williams *et al.* 1970) demonstrated the role of intestinal bacteria in the reduction of *N*-OH-AAF. In the current study, it is reported that blood is another important site for the reduction of hydroxamic acids, in addition to liver and intestinal bacteria.

Clement *et al.* reported that amidines, amidinohydrazones and guanidines are oxidized to their *N*-hydroxy metabolites, and retroreduction to the parent compounds occurs in liver microsomes (Clement *et al.* 1993, 1994, Clement and Jung 1994, Clement and Demesmaeker 1997). The reducing activity was much higher than the oxidative activity in liver microsomes. Thus, the equilibrium of interconversion may favour the reduced state *in vivo*. When the present authors

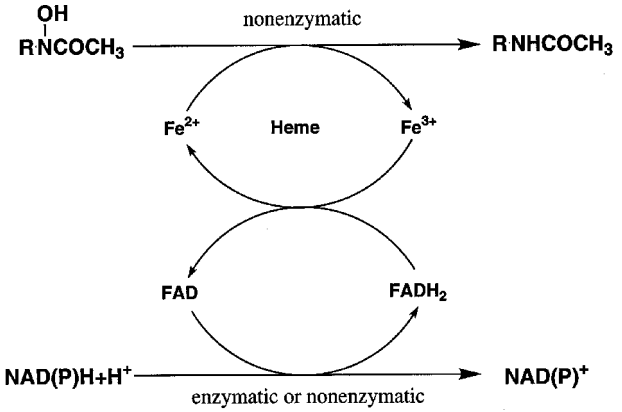


Figure 5. Proposed mechanism of the reduction of hydroxamic acids by blood.

compared the reducing activity of *N*-OH-AAF in blood to the oxidizing activity of AAF by rabbit liver as reported in the literature, the reducing activity is higher. However, interconversion between hydroxamic acids and amides may not occur in blood because oxidizing activity towards the hydroxamic acid in blood has not been reported. These facts suggest that the equilibrium of interconversion between hydroxamic acids and amides is heavily weighted towards the reduced state, and that the reducing system composing haemoglobin and cofactors in blood plays an important role in the detoxification of hydroxamic acids.

Recently, it was reported that *p,p′*-DDT (1,1,1-trichloro-2,2-bis(*p*-chlorophenyl)ethane) and *α*-(bromoisovaleryl)urea, a hypnotic, were dehalogenated to *p,p′*-DDD (1,1-dichloro-2,2-bis(*p*-chlorophenyl)ethane) and to isovalerylurea respectively by rat blood, and the reaction involved reduced pyridine nucleotides and flavins (Sugihara *et al.* 1998, Kitamura *et al.* 1999a). The activity of dehalogenation by blood was of the same order as the reducing activity towards hydroxamic acids reported in the current study. The reduction of xenobiotics by blood or related compounds has also been reported in the reduction of tertiary amine *N*-oxides to the tertiary amines (Vaisey 1956, Terayama 1963, Bickel *et al.* 1968, Kiese *et al.* 1971, Powis and DeGraw 1980). However, the reduction mechanism has not been established. Recently, it has been demonstrated that the reduction of imipramine *N*-oxide to imipramine was catalyzed by haem in the presence of dihydroquinones as a reducing agent (Kitamura *et al.* 1998, 1999b).

The reduction of hydroxamic acids by haemoproteins with both NAD(P)H and FAD presented in this study appears to proceed in two steps (figure 5). The first is reduction of flavin by a reduced pyridine nucleotide; in native blood, flavin is reduced by NADPH-flavin reductase with NADPH (Yubisui *et al.* 1977), whereas in boiled blood the flavin appears to be reduced non-enzymatically by NADPH or NADH (Singer and Kearney 1950). The second step is non-enzymatic reduction of the hydroxamic acids to the corresponding amides catalyzed by the haem moiety of rabbit haemoglobin in the presence of reduced flavin. This step is replaceable by a mild reducing agent such as dithionite and 1,4-dihydroxynaphthalene. In the spectral experiments, it was found that when haemoglobin was incubated with dithionite under anaerobic condition, the UV maximum at 406 nm due to the oxidized form of haemoglobin was changed to 432 nm due to the reduced form, and,

upon addition of *N*-OH-AAF, it returned to 406 nm. This suggested that interconversion between oxidized and reduced forms of haemoglobin were involved in the catalytic action. In boiled blood or erythrocytes, the reducing activity was markedly increased compared with native preparations, possibly because the substrate and reduced flavin have easy access to the haem moiety of denatured haemoglobin.

Presented here is evidence for the reduction of *N*-hydroxyphenacetin and *N*-OH-AAF in rabbit blood. However, salicylhydroxamic and nicotinohydroxamic acids were not reduced by the system. *N*-hydroxy-2-acetylaminofluorene reductase and salicylhydroxamic acid reductase also showed high substrate specificity in the reduction of hydroxamic acids, i.e. the former enzyme reduced *N*-OH-AAF but not *N*-hydroxyphenacetin, and the activity of the latter was specific to salicylhydroxamic acid (Kitamura and Tatsumi 1985, Katsura *et al.* 1993). Aldehyde oxidase showed reductase activity towards various types of hydroxamic acids (Sugihara *et al.* 1986, Kitamura *et al.* 1994). Thus, the reducing system in blood is very different from the cytosolic enzymes in terms of substrate specificity. However, this system is widely distributed in the animal body, and is likely to be of significance in the *in vivo* metabolism of hydroxamic acids.

References

Allaben, W. T., Weeka, C. E., Weis, C. C., Burger, G. T. and King, C. M., 1982, Rat mammary gland carcinogenesis after local injection of *N*-hydroxy-*N*-acyl-2-aminofluorene: relationship to metabolic activation. *Carcinogenesis*, **3**, 233–240.

Bernheim, M. L., 1965, Metabolism of anthranilic hydroxamic acid by rat liver. *Archives of Biochemistry Biophysics*, **112**, 191–195.

Bernheim, M. L., 1972, The reduction of hydroxylamine and some arylhydroxamates by liver mitochondria from mammals and birds. *Enzymologia*, **43**, 167–176.

Bickel, M. H., Weder, H. J. and Aebi, H., 1968, Metabolic interconversions between imipramine, its *N*-oxide, and its desmethyl derivative in rat tissues *in vitro*. *Biochemical and Biophysical Research Communications*, **33**, 1012–1018.

Calder, I. C., Goss, D. E., Williams, P. J., Funder, C. C., Green, C. R., Ham, K. N. and Tange, J. D.,1976, Neoplasia in the rat induced by *N*-hydroxyphenacetin, a metabolite of phenacetin. *Pathology*, **8**, 1–6.

Clement, B. and Demesmaeker, M., 1997, Formation of guanoxabenz from guanabenz in human liver. A new metabolic marker for CYP1A2. *Drug Metabolism and Disposition*, **25**, 1266–1271.

Clement, B. and Jung, F., 1994, *N*-Hydroxylation of the antiprotozoal drug pentamidine catalyzed by rabbit liver cytochrome P-450 2C3 or human liver microsomes, microsomal retroreduction, and further oxidative transformation of the formed amidoximes. *Drug Metabolism and Disposition*, **22**, 486–497.

Clement, B., Schultze-Mosgau, M. H., Richter, P. H. and Besch, A., 1994, Cytochrome P450-dependent *N*-hydroxylation of an aminoguanidine (amidinohydrazone) and microsomal retroreduction of the *N*-hydroxylated product. *Xenobiotica*, **24**, 671–688.

Clement, B., Schultze-Mosgau, M. H. and Wohlers, H., 1993, Cytochrome P450 dependent *N*-hydroxylation of a guanidine (debrisoquine), microsomal catalysed reduction and further oxidation of the *N*-hydroxy-guanidine metabolite to the urea derivative. *Biochemical Pharmacology*, **46**, 2249–2267.

Corbett, M. D., Wei, C. L., Fernando, S. Y., Doergo, D. R. and Corbett, B. R., 1983, The synthesis and mutagenicity of *N*-formyl analog of *N*-hydroxyphenacetin. *Carcinogenesis*, **4**, 1615–1618.

Cramer, J. W., Miller, J. A. and Miller, E. C., 1960, *N*-Hydroxylation: a new metabolic reaction observed in the rat with the carcinogen 2-acetylaminofluorene. *Journal of Biological Chemistry*, **235**, 885–888.

Dybing, E., Saxholm, H. J., Aune, T., Wirth, P. J. and Thorgeirsson, S. S., 1981, Studies on mutagenic and carcinogenic *N*-substituted aryl compounds: cosmetics and drugs. *National Cancer Institute Monographs*, **58**, 21–26.

Grantham, P. H., Horton, R. E., Weisburger, E. K. and Weisburger, J. H., 1970, Metabolism of the carcinogen *N*-hydroxy-*N*-2-fluorenylacetamide in germ-free and conventional rats. *Biochemical Pharmacology*, **19**, 163–171.

GRANTHAM, P. H., WEISBURGER, E. K. and WEISBURGER, J. H., 1965, Dehydroxylation and deacetylation of *N*-hydroxy-*N*-2-fluorenylacetamide by rat liver and brain homogenates. *Biochimica et Biophysica Acta*, **107**, 414–424.

GRIFFITH, D. P., GIBSON, J. R., CLINTON, C. W. and MUSHER, D. M., 1978, Acetohydroxamic acid: clinical studies of a urease inhibitor in patients with staghorn renal calculi. *Journal Urology*. **119**, 9–15.

GUTMANN, H. R. and ERICKSON, R. R., 1969, The conversion of the carcinogen *N*-hydroxy-2-fluorenylacetamide to *o*-amindophenols by rat liver *in vitro*. *Journal of Biological Chemistry*, **244**, 1729–1740.

HINSON, J. A. and MITCHELL, J. A., 1976, *N*-Hydroxylation of phenacetin by hamster liver microsomes. *Drug Metabolism and Disposition*, **4**, 430–435.

HIRSCH, P. F. and KAPLAN, N. O., 1961, The conversion of pyridine hydroxamic acids to amides by mouse liver mitochondria. *Journal of Biological Chemistry*, **236**, 926–930.

IRVING, C. C., 1962, *N*-Hydroxylation of 2-acetylaminofluorene in the rabbit. *Cancer Research*, **22**, 867–873.

IRVING, C. C., 1964, Enzymatic *N*-hydroxylation of the carcinogen 2-acetylaminofluorene and the metabolism of *N*-hydroxy-2-acetylaminofluorene-9-^{14}C *in vitro*. *Journal of Biological Chemistry*, **239**, 1589–1596.

JOHANSSON, S. L., 1981, Carcinogenicity of analgesics: long-term treatment of Sprague–Dawley rats with phenacetin, phenazone, caffeine and paracetamol (acetamidophen). *International Journal of Cancer*. **27**, 521–529.

KATSURA, H., KITAMURA, S. and TATSUMI, K., 1993, Purification and characterization of salicylhydroxamic acid reductase from rat liver. *Archives of Biochemistry and Biophysics*, **302**, 356–361.

KIESE, M., RENNER, G. and SCHLAEGER, R., 1971, Mechanism of the autocatalytic formation of ferrihemoglobin by *N*, *N*-dimethylaniline *N*-oxide. *Naunyn–Schmiedebergs Archives of Pharmacology*, **268**, 247–263.

KITAMURA, S., KUWASAKO, M., SUGIHARA, K. and TATSUMI, K., 1999a, Debromination of α-(bromo-iso-valeryl)urea catalyzed by rat blood. *Journal of Pharmacy and Pharmacology*, **51**, 73–78.

KITAMURA, S., SUGIHARA, K. and TATSUMI, K., 1994, Reductase activity of aldehyde oxidase toward the carcinogen *N*-hydroxy-2-acetylaminofluorene and the related hydroxamic acids. *Biochemistry and Molecular Biology International*, **34**, 1197–1203.

KITAMURA, S., SUGIHARA, K. and TATSUMI, K., 1999b, A unique tertiary amine *N*-oxides reduction system composed of quinone reductase and heme in rat liver preparations. *Drug Metabolism and Disposition*, **27**, 92–97.

KITAMURA, S., TAKEKAWA., K., SUGIHARA, K., TATSUMI, K. and OHTA, S., 1999c, Pseudoenzymatic reduction of *N*-hydroxy-2-acetylaminofluorene to 2-acetylaminofluorene mediated by cytochrome P450. *Carcinogenesis*, **20**, 347–350.

KITAMURA, S. and TATSUMI, K., 1985, Purification of *N*-hydroxy-2-acetylaminofluorene reductase from rabbit liver cytosol. *Biochemical and Biophysical Research Communications*, **133**, 67–74.

KITAMURA, S., TERADA, A., INOUE, N., KAMIO, H., OHTA, S. and TATSUMI, K., 1998, Quinone-dependent tertiary amine *N*-oxide reduction in rat blood. *Biological and Pharmaceutical Bulletin*, **21**, 1344–1347.

LENK, W. and SCHARMER, U., 1980, Reaction of microsomal and cytosolic enzymes with *N*-arylacetohydroxamic acids. *Xenobiotica*, **10**, 573–591.

LOTLIKAR, P. D., MILLER, E. C., MILLER, J. A. and MARGRETH, A., 1965, The enzymatic reduction of the *N*-hydroxy derivatives of 2-acetylaminofluorene and related carcinogens by tissue preparations. *Cancer Research*, **25**, 1743–1752.

LOWENTHAL, J., 1954, Enzymatic conversion of salicylhydroxamic acid to salicylamide. *Nature (London)*, **174**, 36–37.

LOWRY, O. H., ROSEBROUGH, N. J., FARR, A. L. and RANDALL, R. J., 1951, Protein measurement with the Folin phenol reagent. *Journal of Biological Chemistry*, **193**, 265–275.

MILLER, J. A., 1970, Carcinogenesis by chemicals: an overview. G. H. A. Clowes Memorial Lecture. *Cancer Research*, **30**, 559–576.

MILLER, J. A., CRAMER, J. W. and MILLER, E. C., 1960, The *N*- and ring-hydroxylation of 2-acetylaminofluorene during carcinogenesis in the rat. *Cancer Research*, **20**, 950–962.

MUNSON, J. W., 1982, Chemistry and biology of hydroxamic acids—an overview. In H. Kehl (ed.), *Chemistry and Biology of Hydroxamic Acids* (New York: Karger), pp. 1–13.

NERY, R., 1971, The possible role of *N*-hydroxylation in the biological effects of phenacetin. *Xenobiotica*, **1**, 339–343.

POWIS, G. and DE GRAW, C. L., 1980, *N*-Oxide reduction by hemoglobin, cytochrome *c* and ferrous ions. *Research Communications Chemical Pathology and Pharmacology*, **30**, 143–150.

PUTCHA, L., GRIFFITH, D. P. and FELDMAN, S., 1984, Disposition of ^{14}C-acetohydroxamic acid and ^{14}C-acetamide in the rat. *Drug Metabolism and Disposition*, **12**, 438–443.

SINGER, T. P. and KEARNEY, F. B., 1950, The non-enzymatic reduction of cytochrome *c* by pyridine nucleotides and its catalysis by various flavins. *Journal of Biological Chemistry*, **183**, 409–429.

SUGIHARA, K., KITAMURA, S. and OHTA, S., 1998, Reductive dechlorination of DDT to DDD by rat blood. *Biochemistry and Molecular Biology International*, **45**, 85–91.

SUGIHARA, K., KITAMURA, S. and TATSUMI, K., 1983, Evidence for reduction of hydroxamic acids to the corresponding amides by liver aldehyde oxidase. *Chemical and Pharmaceutical Bulletin*, **31**, 3366–3369.

SUGIHARA, K. and TATSUMI, K., 1986, Participation of liver aldehyde oxidase in reductive metabolism of hydroxamic acids to amides. *Archives of Biochemistry and Biophysics*, **247**, 289–293.

TERAYAMA, H., 1963 Aminoazo dye amine-*N*-oxide as a possible intermediate metabolite preceding *N*-demethylation and *ortho*-hydroxylation, as well as azo dye–protein binding. *Gann*, **55**, 195–204.

VAISEY, E. B., 1956, The non-enzymic reduction of trimethylamine oxide to trimethylamine, dimethylamine, and formaldehyde. *Canadian Journal of Biochemistry and Physiology*, **34**, 1085–1090.

WEEKS, C. E., ALLABEN, W. T., TRESP, N. M., LOUIE, S. C., LAZEAR, E. J. and KING, C. M., 1980, Effect of structure of *N*-acyl-*N*-2-fluorenylhydroxylamines on arylhydroxamic acid acyltransferase, sulfotransferase, and deacylase activities, and on mutations in *Salmonella typhimurium* TA 1538. *Cancer Research*, **40**, 1204–1211.

WEISBURGER, J. H., GRANTHAM, P. H., HORTON, R. E. and WEISBURGER, E. K., 1970, Metabolism of the carcinogen *N*-hydroxy-*N*-2-fluorenylacetamide in germ-free rats. *Biochemical Pharmacology*, **19**, 151–162.

WILLIAMS, J. R., GRANTHAM, P. H., MARSH, H. H., WEISBURGER, J. H. and WEISBURGER, E. K., 1970, Participation of liver fractions and of intestinal bacteria in the metabolism of *N*-hydroxy-*N*-2-fluorenylacetamide in the rat. *Biochemical Pharmacology* **19**, 173–188.

WIRTH, P. J., ALEWOOD, P., CALDER, I. and THORGEIRSSON, S. S., 1982, Mutagenicity of *N*-hydroxy-2-acetylaminofluorene and *N*-hydroxyphenacetin and their respective deacetylated metabolites in nitroreductase deficient *Salmonella* TA98FR and TA100FR. *Carcinogenesis*, **3**, 167–170.

YAMAZOE, Y., ISHII, K., YAMAGUCHI, N., KAMATAKI, T. and KATO, R., 1980, Reduction of *N*-hydroxy-2-acetylaminofluorene by liver microsomes. *Biochemical Pharmacology*, **29**, 2183–2188.

YUBISUI, T., MATSUKI, T., TANISHIMA, K., TAKESHITA, M. and YONEYAMA, Y., 1977, NADPH-flavin reductase in human erythrocytes and the reduction of methemoglobin through flavin by the enzyme. *Biochemical and Biophysical Research Communications*, **76**, 174–182.

YUBISUI, T., MATSUKAWA, S. and YONEYAMA, Y., 1980, Stopped flow studies on the nonenzymatic reduction of methemoglobin by reduced flavin mononucleotide. *Journal of Biological Chemistry*, **255**, 11694–11697.

XENOBIOTICA , 2000, VOL. 30, NO. 5, 469–483

Dermal penetration and metabolism of five glycidyl ethers in human, rat and mouse skin

P. J. BOOGAARD*, M. A. DENNEMAN
and N. J. VAN SITTERT

Department of Molecular Toxicology, Shell Research and Technology Center, Amsterdam, Shell International Chemicals BV, PO Box 38000, 1030 BN Amsterdam, The Netherlands

Received 23 July 1999

1. Glycidyl ethers (GE), an important class of industrial chemicals, are considered to be potentially mutagenic *in vivo* because some GE have been shown to be direct mutagens in short-term *in vitro* tests.

2. The percutaneous penetration and metabolism of representatives of different classes of GE was studied in the fresh, full-thickness C3H mouse, and dermatomed human and Fisher 344 rat skin to determine the apparent permeability constants, lag times and metabolic profiles.

3. Five different GE, the diglycidyl ethers of bisphenol A (BADGE), 4,4′-dihydroxy-3,3′,5,5′-tetramethylbiphenyl (Epikote YX4000) and 1,6-hexanediol (HDDGE) and the GE of 1-dodecanol (C_{12}GE) and *o*-cresol (*o*-CGE), were synthesized by reaction of their alcohols with epichlorohydrin. Their radiolabelled analogues were synthesized with a ^{14}C-label using [U-^{14}C]-epichlorohydrin.

4. There was a large variation (four orders of magnitude) in percutaneous penetration between the five GE. In general, penetration through full-thickness mouse skin was higher than through dermatomed rat skin, whereas dermatomed human skin was the least permeable. The permeability increased in the order YX4000 < BADGE < C_{12}GE < *o*-CGE < HDDGE.

5. The relative skin permeability of the five GE could be explained for a significant part by the lipophilicity, expressed as log $P_{o/w}$, in combination with the molecular weight of the compounds.

6. During skin penetration, all GE were extensively metabolized to their corresponding (*bis*-)diols. Virtually no YX4000, and only very small amounts of C_{12}GE and BADGE, penetrated the skin unchanged, but significant amounts of HDDGE and *o*-CGE penetrated the skin unchanged. For *o*-CGE, but none of the other GE, the percentage of the applied dose that penetrated the skin unchanged increased over time.

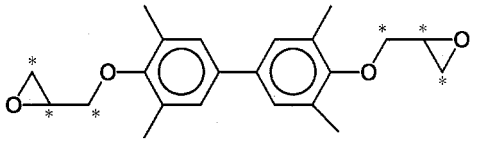
7. The large variation in response observed with the five selected GE indicates that GE should not be considered as a single class of compounds but rather on the basis of their individual properties.

Introduction

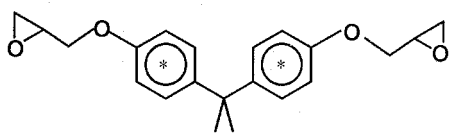
Glycidyl ethers (GE) form an important and highly diverse group of industrial chemicals used for manufacturing epoxy resin systems applied in adhesives, coatings, plastics, electronics and structural composites. Phenyl glycidyl ether (PGE) and resorcinol diglycidyl ether have been reported as causing tumours in animal studies and consequently have been classified by the IARC as group 2B carcinogens (possibly carcinogenic to humans) (IARC 1985, 1989, 1999a). Some other glycidyl ethers, such as BADGE and triethylene glycol diglycidyl ether, were considered not classifiable as to their carcinogenicity to humans (group 3) since only limited or inadequate evidence in experimental animals and no epidemiological data in humans relevant to their carcinogenicity were available (IARC 1989, 1999c, d).

* Author for correspondence; e-mail: Peter.J.Boogaard@opc.shell.com

Xenobiotica ISSN 0049-8254 print/ISSN 1366-5928 online © 2000 Taylor & Francis Ltd
http://www.tandf.co.uk/journals



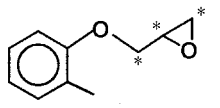
Epikote YX4000 (**YX4000**); MW = 354.4, log $P_{o/w}$ = 5.2



Bisphenol A diglycidyl ether (**BADGE**); MW = 340.8, log $P_{o/w}$ = 3.8



1-Dodecyl glycidyl ether (**C_{12}GE**); MW = 242.2, log $P_{o/w}$ = 5.0



o-Cresyl glycidyl ether (***oCGE***); MW = 164.2, log $P_{o/w}$ = 2.2



1,6-Hexanediol diglycidyl ether (**HDDGE**); MW = 230.2, log $P_{o/w}$ = 0.84

Figure 1. Structures of synthesized chemicals with their molecular weights (MW) and logarithm of the octanol/water partition coefficient (log $P_{o/w}$). *Position of radiolabels.

Nevertheless, glycidyl ethers as a group are under scrutiny, because several epoxy compounds have been associated with mutagenicity and cancer. It is indeed likely that the epoxy group is responsible for the direct mutagenic effects observed in bacteria exposed to glycidyl ethers (Gardiner *et al.* 1992) and for the DNA adducts observed in *in vitro* systems (Plná *et al.* 1996, Deforce *et al.* 1998). GE are often used as reactive diluents and as components of paints and glues. Most of the GE have a low volatility, and as a consequence one of the primary portals of entry for GE is the skin through direct contact with the compounds. Any systemic but also any topical effects of GE will be highly dependent on the extent of percutaneous penetration and metabolism. Both penetration and metabolism of a particular compound are largely determined by its structure and physical chemical properties that vary widely among the GE.

The main objective of the current study was to compare the percutaneous absorption and metabolism of a series of selected GE (figure 1) in viable skin explants of dorsal skin of rat and mouse and human breast skin. Based on previous experience with subcellular fractions from skin and viable skin, it was decided to study dermal metabolism in viable skin only since it appeared that viable skin gave

a much better reflection of the *in vivo* situation than subcellular fractions from the same individual (Boogaard *et al.* 1999).

Materials and methods

Chemicals

[U-^{14}C]-epichlorohydrin, radiochemical purity > 98%, specific activity 38 mCi/mmol, was custom-synthesized by ChemSyn Laboratories (Lenexa, KS, USA). [Ring-U-^{14}C]-*bis*-phenol A diglycidyl ether (radiochemical purity > 98% ; specific activity 11 mCi/mmol) was a gift from Dr John Waechter (Dow Chemical Co., Midland, MI, USA). Recrystallized BADGE (chemical purity > 99%) and its *bis*-diol (*bis*-phenol A diglycerol ether) (chemical purity > 96%) were from the Department of Basic & Exploratory Research (Shell Research & Technology Centre, Amsterdam). Gentamicin solution, Hanks' buffered salts and bovine serum albumin (fraction V) (BSA) were from Sigma Chemical Co. (St Louis, MO, USA). 4-Phenylchalcone oxide (4-PCO) was from ICN Biomedicals BV (Zoetermeer, The Netherlands); its chemical purity was 99%. Tetraethylammonium hydroxide (20% aqueous solution) was from E. Merck (Darmstadt, Germany). All other chemicals used were from Aldrich and were at least reagent grade with a purity > 95%. Solvents used for HPLC were HPLC grade.

Synthesis of reference materials (figure 1)

The glycidyl and glycerol ethers of *o*-cresol and 1-dodecanol as well as the diglycidyl and diglycerol ethers of 1,6-hexanediol, 4,4′-dihydroxy-3,3′,5,5′-tetramethylbiphenyl and diphenylol propane were synthesized from the corresponding alcohols and epichlorohydrin (ECH). The ^{14}C-labelled analogues were synthesized from the same alcohols and [U-^{14}C]-epichlorohydrin, diluted with non-labelled ECH to a specific activity of 0.2 mCi/mmol. The chemical and radiochemical purities for the (di)glycidyl ethers were: YX4000 > 97% and > 98% ; HDDGE > 92% and > 98% ; C_{12}GE > 95% and > 98% ; *o*-CGE > 94% and > 92% respectively. The chemical purities for the (di)glycerol ethers were: YX4000 > 97% ; HDDGE > 93% ; C_{12}GE > 90% ; *o*-CGE > 85%. Details of synthesis and analysis are given in Van Elburg *et al.* (1999).

Liquid scintillation counting (LSC)

Radioactivity in solutions was measured using TriCarb 2200CA liquid scintillation counters (Canberra Packard, Groningen, The Netherlands) in antistatic scintillation vials after mixing with 5–10 vols Ultima Gold Scintillation cocktail (Canberra Packard). The machine was calibrated using commercial ^{3}H and ^{14}C internal standard kits for organic solvents (Wallac, Turku, Finland). Calibration was checked daily by counting a set of quenched standards commercially prepared in sealed glass vials. Counting efficiency was determined using the spectral index of the internal standard (SIE) and cpm was automatically transformed to dpm. Samples were corrected for background and counted for periods sufficiently long to reach a relative standard deviation of < 0.02.

High-performance liquid chromatography (HPLC)

HPLC analyses were carried out using various systems. For analysis of radiolabelled compounds, a Ramona D or 2000 on-line radioactivity detector (Raytest, Straubenhardt, Germany), both equipped with solid scintillant cells, were used. In addition, because the total radioactivity in individual peaks was in most cases below the limit of quantitation of the on-line detectors, fractions were collected using LKB fraction collectors. The radioactivity in the collected fractions was determined by LSC. HPLC analyses were carried out using the following equipment and conditions:

System A. Apparatus: HP1050 liquid chromatograph with UV detection ($\lambda = 230$ nm) (Hewlett Packard, Amstelveen, The Netherlands); column: Phenomenex Jupiter 300 Å, 5 μm ODS, 250 × 4.6 mm (Phenomenex, Torrance, CA, USA) with HiChrom security guard column NC120-5C18-10C (HiChrom, Reading, UK); eluent: purified water (A) and methanol (B); flow: 1.0 ml/min; gradient: 0–18 min, linear increase from 25 to 92.5% B; 18–20 min, 92.5% B; 20–22 min: linear increase from 92.5 to 100% B, 30–35 min linear decrease from 100 to 25% B.

System B. Apparatus: HP1100 liquid chromatograph with UV detection ($\lambda = 230$ nm) (Hewlett Packard); column: Phenomenex Jupiter 300 Å, 5 μm ODS, 250 × 4.6 mm, with Phenomenex Security Guard (widepore 4 × 3.0 mm ODS cartridge); eluent: purified water (A) and acetonitrile (B); flow: 1.0 ml/min; gradient: 0–31 min, linear increase from 25 to 48.5 % B; 31–35 min, linear increase from 48.5% to 100% B; 35–40 min, linear decrease from 100 to 25% B; 40–45 min 25 % B.

System C. As for system B, but with a different gradient: 0–15 min, linear increase from 0 to 30% B; 15–25 min, linear increase from 30% to 45% B; 25–30 min, linear increase from 45 to 100% B; 30–33 min, 100% B; 33–35 min linear decrease from 100 to 0% B.

Liquid chromatography-mass spectrometry (LC-MS)

LC-MS analyses were performed using system A on a HP 1050 liquid chromatograph coupled to a Micromass Quattro quadrupole mass spectrometer. Electrospray was used as the LC-MS interfacing and ionization technique (positive ions). The scan range was 100–1500 Dalton with 0.5 scan/s.

Human skin

Fresh full-thickness healthy human breast skin was from five female Caucasian patients, aged 17–41 years, undergoing mammoplastic reduction surgery in a regional hospital (MCA, Alkmaar, The Netherlands). The skin was placed on ice in a Petri dish and transported to the laboratory where it was used within 3 h from the time it was surgically removed. The use of human tissue in the present studies was according to the guidelines of the 1984 Declaration of Helsinki. Patients gave written, informed consent and the hospital's medical–ethical committee approved the use of viable human tissue for this study.

Rodent skin

Male Fisher 344 rats ($\sim$ 250 g) and male C3H mice ($\sim$ 25 g) were from the Central Laboratories for the Blood Banks (CLB) (Amsterdam, The Netherlands). Animals were kept on a 12 h light/dark cycle in humidity- ($60\pm 15\%$ relative humidity) and temperature- (22 ± 2 °C) controlled mass-air-displacement rooms. A standard rodent diet (VRF-I, Broekman Instituut [Charles River Laboratories], Someren, The Netherlands) and de-ionized water were supplied *ad libitum*. Following an acclimation of 1 week, the animals were used as the source for viable rodent skin. Animals were killed with a lethal dose of sodium pentobarbital, and the dorsal region shaved. The skin was removed and placed in a Petri dish on ice until used (within 2 h from removal).

Skin preparation

Skin penetration and metabolism was studied using viable skin. Three different skin donors (both for human and animal skin) were used for each of the five GE under study. Human skin was dissected from the tissue removed during mammoplastic reduction surgery using a scalpel and cleaned with physiological saline. The shaved area from the rodent skin was cut out with dissecting scissors. Excess subcutaneous tissue was removed from the skin samples with a scalpel. The skin was placed on a Teflon dissecting board and full-thickness skin circles were cut out using a circular sharpened steel cutter. Mouse skin was always used at full thickness since it is so thin that it can not be dermatomed. Human and rat skin was only used following dermatomization. The skin, epidermis up, was stretched over a small band of Teflon and a sheet of skin was cut off using a hand-held keratotome (Storz Instrument Co., US). Skin circles were cut out of this sheet using small dissection scissors. The gross integrity of the skin was assessed visually. Skin membranes were rejected if very high quantities of the applied dose appeared in the receptor fluid immediately after application. Previous studies have shown that the enzymes essential for inactivation of glycidyl compounds are present and active in skin membranes prepared with this procedure (Boogaard *et al.* 1999).

Diffusion system

The skin was mounted, epidermis uppermost, in a flow-through diffusion cell system that has been described (Boogaard *et al.* 1999) and which is based on the system developed by Bronaugh and Stewart (1984) and Hotchkiss *et al.* (1990). The system consisted of (1) 12 stainless steel diffusion cells, which were stirred continuously with magnetic stirrer bars (Variomag HP 15 Multipoint, HP Labortechnik, Munich, Germany) to prevent irregular penetration due to air bubbles underneath the skin membrane, (2) a fraction collector holding 20 ml glass scintillation vials, (3) a thermostatically controlled water circulator (PolyScience, USA) to heat the jackets holding the cells in such a way that the skin surface temperature was kept at 32 ± 1 °C, and (4) a cassette peristaltic pump (Watson Marlow, Falmouth, UK). The exposed skin surface was 0.636 cm^2. The underside of the skin was exposed to continuously flowing (flow rate $\sim$ 1.5 ml/h) receptor fluid consisting of Hanks' balanced salt solution, without phenol red and sodium bicarbonate, buffered with 25 mM HEPES (pH 7.40) and containing 2.5% w/v BSA and 50 μg gentamicin per ml. The receptor fluid was transported to the cells and from the cells, through the pump, to the fraction collector through PVC tubing (Accurated tubing, Elkay). In some experiments the cells were occluded by placing a polycarbonate lid over the cells.

Dosing and determination of penetration

In each experiment, which was carried out in triplicate, three-to-four cells with skin from the same donor (human or animal) were used to study the penetration of each of the GE under study.

Aliquots of 5.0 μl GE dissolved in acetone at a concentration of 636 mM were applied to the exposed skin surface using a micropipette (final concentration 5.0 μmol/cm^2). The receptor fluid was collected in

3-hourly fractions for 24 h following application of the GE. The fractions were weighed for determination of the actual flow rates and the radioactivity in an aliquot of the fractions was determined by LSC. The remaining portions of the collected fractions were extracted twice with a double volume of ethyl acetate. An aliquot of DMSO was added to the combined fractions and a gentle stream of nitrogen evaporated the ethyl acetate. The DMSO residues were mixed with an equal volume of methanol and subsequently analysed by HPLC with radiodetection. For studies with *o*-CGE and C_{12}GE system A was used, for BADGE and YX4000 system B was used, for HDDGE system C was used. The (radioactive) products formed were identified by co-elution with reference standards and by LC-MS.

At the end of the experiment the skin was removed from the cell and soaked twice for 12 h in 2 ml ethyl acetate to dissolve GE remaining on the skin. The combined ethyl acetate fractions were dissolved in Ultima Gold scintillation cocktail and the radioactivity determined by LSC. The skin itself was dissolved over 48 h in 1.0 ml tetraethylammonium hydroxide and the total radioactivity in the resulting solution was determined by LSC. The receptor fluid remaining in the cell and the tubing was collected; the tubing was subsequently flushed with receptor fluid and water. The combined fluids were counted by LSC. Finally, to obtain a mass balance, the complete cells (including supportive grids and stirrer bars) were individually sonicated in 100 ml ethyl acetate for 30 min to dissolve any traces of the GE, and an aliquot of the ethyl acetate was counted by LSC.

Estimation of the octanol/water partition coefficient ($P_{o/w}$)

Compounds with a log $P_{o/w} > 2$ may accumulate in the fatty compartment of the dermis. To study the skin permeation of such compounds and avoid the dermis acting as a reservoir, the skin of rat and humans, which have a relatively thick dermis, should be dermatomed. For BADGE, a log $P_{o/w} = 4.0$ was determined by HPLC (Eadsforth 1983). For the other GE, however, no log $P_{o/w}$ has been determined. For these GE log $P_{o/w}$ was estimated using the KOWWIN software package, v.1.57 (Syracuse Research Software, Whitstable, UK). The following were determined: YX4000 log $P_{o/w} = 5.2$, C_{12}GE log $P_{o/w} = 5.0$, BADGE log $P_{o/w} = 3.8$, *o*-CGE log $P_{o/w} = 2.2$ and HDDGE log $P_{o/w} = 0.84$.

Calculations and statistics

Multiple linear regression analyses were performed using the LINEST function of the Excel for Windows 95 software package (v.7.0a; Microsoft Co., Redmond, WA, USA).

Results

Percutaneous penetration

Percutaneous penetration varies considerably between the various GE and also between the three species. In figure 2A–E the actual dermal penetration, as percentage of the applied dose, for the five GE through the skin is depicted. The mass balances show that the recovery of YX4000 and BADGE is complete, but that there is a small loss of C_{12}GE and HDDGE and a significant loss of *o*-CGE (table 1). The incomplete mass balance is due to the volatility of the GE: whereas YX4000 and BADGE have virtually no vapour pressure and C_{12}GE and HDDGE have a low vapour pressure, *o*-CGE is relatively volatile. The skin permeation of YX4000, BADGE and C_{12}GE is linear with time over the entire 24 h for human, rat and mouse skin. For *o*-CGE and HDDGE a substantial deviation from linearity was observed after ~ 6 h in rat and mouse skin. In human skin the absorption of *o*-GCE also deviated from linearity, but the absorption of HDDGE through the human skin was linear with time over the entire 24 h. With *o*-CGE, the dermal penetration reached a plateau at absorption of ~ 10, 18 and 23% of the applied dose with human, rat and mouse skin respectively. In all three cases, the curves started levelling off after ~ 12 h. Based on the mass balance and the relatively high volatility of *o*-CGE, it is assumed that at this point nearly all *o*-CGE had evaporated from the skin. For HDDGE, the curves for rat and mouse skin also seemed to reach a plateau, but at a later point in time and at significantly higher absorption levels (65–80% of applied dose). Occlusion of the skin significantly enhanced the dermal penetration of *o*-CGE through human, rat as well as mouse skin: the percentage of the applied dose

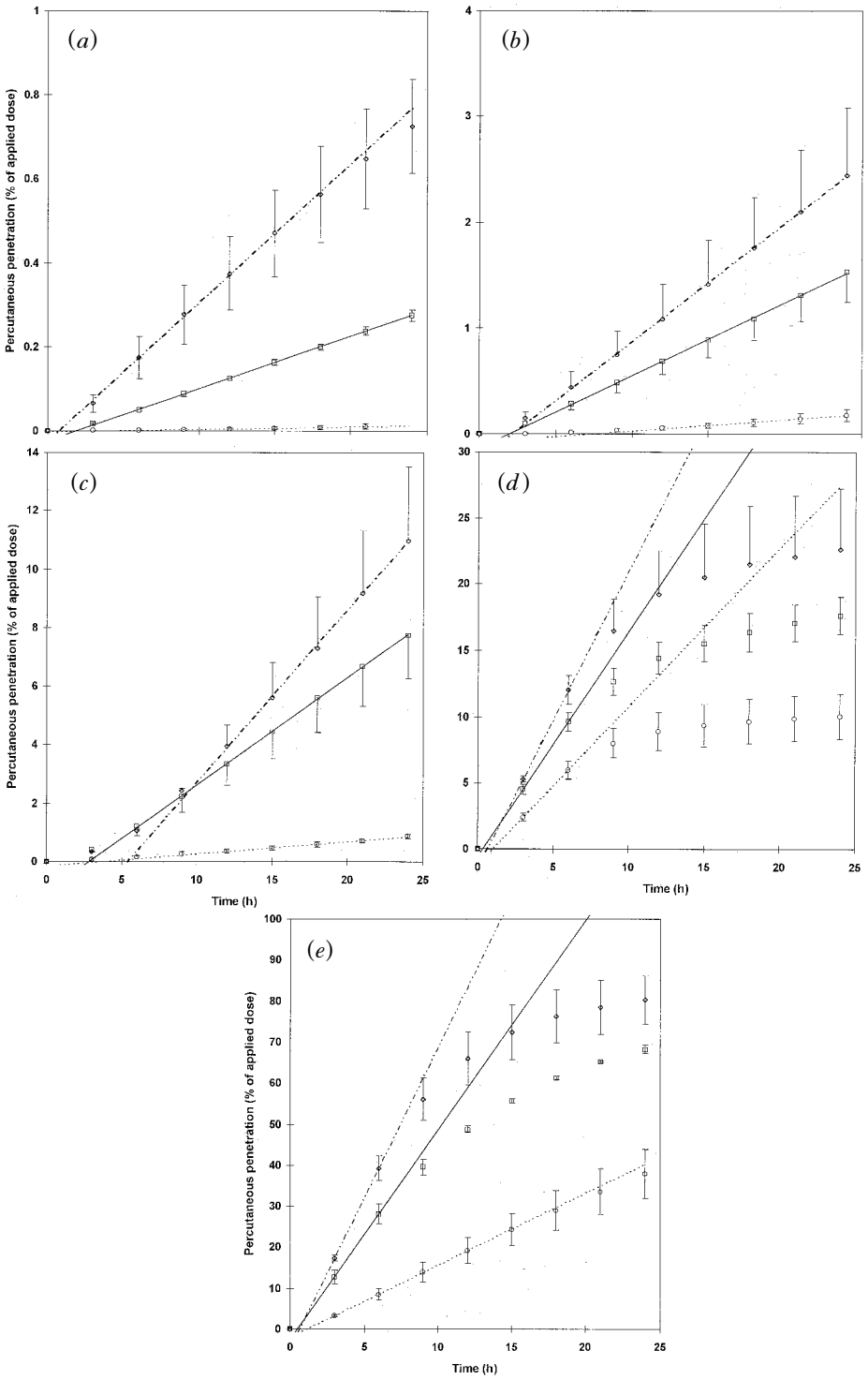


Figure 2. Penetration of glycidyl ethers through viable skin. Human and rat skin were used dermatomed, whereas mouse skin was used at full-thickness (undermatomed). Data are averages of three separate experiments with skin from different human or animal donors (each experiment

Table 1. Mass balance of skin permeation experiments percentage of applied dose of GE recovered from the surface of the skin, from the skin itself, in the receptor fluid and from the percutaneous penetration equipment.

Species	YX4000	BADGE	C_{12}GE	*o*-CGE	HDDGE
Human	99.6± 0.6	102± 10	70.9± 0.6	13± 3	83± 13
Rat	105± 5	98± 11	88± 6	22± 3	90± 6
Mouse	104± 8	98± 8	70± 3	26± 5	89± 10

Data are means± SD of triplicate determinations.

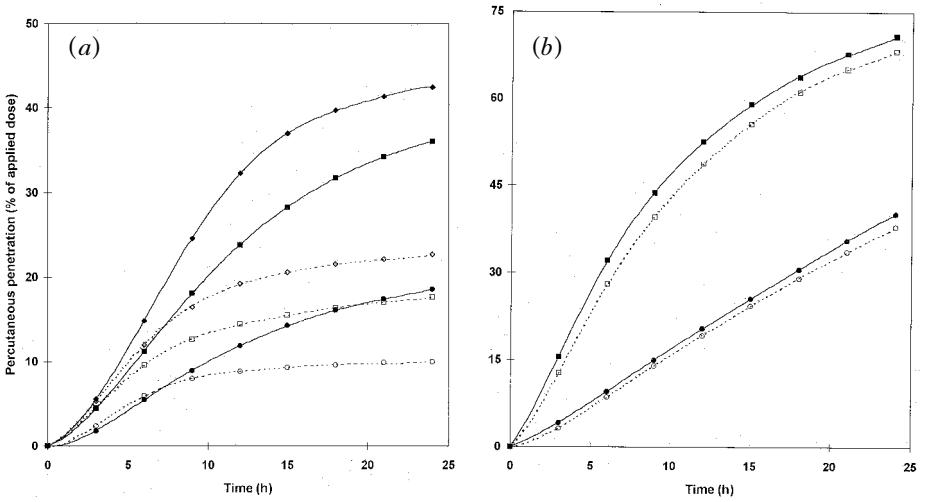


Figure 3. Penetration of glycidyl ethers through occluded and non-occluded viable skin. Human and rat skin were used dermatomed, whereas mouse skin was used at full-thickness (undermatomed). Data for non-occluded skin are identical to those in figure 2, but without error bars for clarity. Mouse skin ◆, ◇; rat skin ■, □; human skin, ●, ○. Filled symbols indicate occluded; open symbols indicate non-occluded skin. (a) *o*-CGE (*o*-cresyl glycidyl ether). (b) HDDGE (1,6-hexanediol diglycidyl ether).

that had penetrated through the skin was roughly doubled by occlusion (figure 3A). In contrast, the dermal penetration of HDDGE was not significantly influenced by occlusion of the skin (figure 3B). The data on the occlusion of *o*-CGE and HDDGE indicate that the increased dermal penetration is mainly due to diminished volatilization of the GE and not to alterations of the skin, such as increased hydratation, caused by the occlusion.

with three-to-four separate cells). Values are means± SE ($n = 3$). Mouse skin, ◇; rat skin, □; ○; human skin. (a) YX4000 (4,4′-dihydroxy-3,3′,5,5′-tetramethylbiphenyl diglycidyl ether). Lines are obtained by linear regression analysis on all data points; $R^2 = 0.9977$, 0.9999 and 0.9992 for human, rat and mouse skin respectively. (b) BADGE (*bis*phenol A diglycidyl ether). Lines are obtained by linear regression analysis on all data points; $R^2 = 0.9916$, 0.9996 and 0.9997 for human, rat and mouse skin respectively. (c) C_{12}GE (1-dodecyl glycidyl ether). Lines are obtained by linear regression analysis on all data points; $R^2 = 0.9958$, 0.9996 and 0.9993 for human, rat and mouse skin respectively. (d) *o*-CGE (*o*-cresyl glycidyl ether). Lines are obtained by extrapolation of the linear part of the permeation curves. (e) HDDGE (1,6-hexanediol diglycidyl ether). The line representing the penetration through human skin is obtained by linear regression analysis on all data points; $R^2 = 0.9999$. Lines representing the penetration through rodent skin are obtained by extrapolation of the initial, linear part of the penetration curve.

Table 2. Apparent permeability constant[a] (in 10^{-6} cm/h) in dermatomed human and rat skin and full-thickness mouse skin of five glycidyl ethers.

Species	YX4000	BADGE	C_{12}GE	*o*-CGE	HDDGE
Human	0.047± 0.02	0.48± 0.22	3.31± 0.19	93± 11	136± 28
Rat	0.98± 0.02	5.5± 1.5	29.0± 7.3	134± 15	402± 22
Mouse	2.63± 0.55	8.6± 1.6	46.1± 17.2	176± 32	577± 86

Data are means± SE of triplicate determinations.
[a] A *finite* amount of the glycidyl ethers, 5 μmol/cm^2, was applied to the skin surface, therefore, P is the *apparent* permeability constant.

Table 3. Percutaneous penetration (as percentage of the applied dose) through dermatomed human and rat skin and full-thickness mouse skin of five glycidyl ethers over 24 h

Species	YX4000	BADGE	C_{12}GE	*o*-CGE	HDDGE
Human	0.011± 0.003	0.137± 0.055	0.870± 0.065	10.2± 1.6	37.8± 8.5
Rat	0.275± 0.010	1.57± 0.41	7.73± 2.09	17.4± 1.8	67.2± 0.5
Mouse	0.726± 0.113	2.98± 0.80	10.97± 3.63	22.7± 4.6	80.3± 8.3

Data are means± SE of triplicate determinations.
Data represent total radioactivity, i.e. parent compounds plus metabolites.

Table 4. Lag time (h) in dermal penetration of five glycidyl ethers through dermatomed human and rat skin and full-thickness mouse skin.

Species	YX4000	BADGE	C_{12}GE	*o*-CGE	HDDGE
HumanHuman	2.4± 1.5	6.1± 1.7	3.8± 1.6	0.96± 0.23	0.92± 0.18
Rat	1.87± 0.09	1.8± 0.5	3.0± 0.6	0.36± 0.26	0.40± 0.18
Mouse	0.92± 0.50	2.3± 1.0	5.3± 0.7	0.51± 0.47	0.62± 0.23

Data are means± SE of triplicate determinations.

Table 5. Correlation between the logarithm of the apparent permeability coefficient (log P) of five glycidyl ethers (YX4000, BADGE, C_{12}GE, *o*-CGE and HDDGE) and their intrinsic physical parameters molecular weight (MW) and logarithm of the octanol/water partition coefficient (log $P_{o/w}$).

	Regression coefficient (± SE) for		Regression constant	
Species	MW	log $P_{o/w}$	(± SE)	R
Human	−0.386± 0.114	−0.0113± 0.0026	4.91± 0.58	0.987
Rat	−0.283± 0.145	−0.0073± 0.0034	4.30± 0.74	0.957
Mouse	−0.261± 0.134	−0.0065± 0.0031	4.22± 0.69	0.955
All	−0.310± 0.118	−0.0084± 0.0027	4.48± 0.61	0.880

The apparent permeability constant, in non-occluded skin, varies over >4 orders of magnitude, from 4.7 (SE 0.2)$\times 10^{-8}$ cm/h, for YX4000 in human skin, to 5.8 (SE 0.9)$\times 10^{-4}$ cm/h, for HDDGE in mouse skin (table 2). Regardless of species, the permeability increased in the order: YX4000< BADGE< C_{12}GE< *o*-CGE< HDDGE. For all GE, full-thickness mouse skin had the highest permeability and human dermatomed skin was the least permeable (tables 2 and 3). The lag time is longest in human skin for all GE, with the exception of C_{12}GE, where the lag time in mouse skin is longer (table 4). Rather poor linear correlations were

Table 6. Correlation between the logarithm of the apparent permeability coefficient (log P) of five glycidyl ethers (YX4000, BADGE, C_{12}GE, *o*-CGE and HDDGE) and their intrinsic physical parameters square root of molecular weight ($\sqrt{}$MW) and logarithm of the octanol/water partition coefficient (log $P_{o/w}$).

Species	Regression coefficient (± SE) for MW	Regression coefficient (± SE) for log $P_{o/w}$	Regression constant (± SE)	R
Human	−0.396± 0.136	−0.351± 0.102	7.62± 1.42	0.981
Rat	−0.293± 0.159	−0.223± 0.120	5.99± 1.67	0.948
Mouse	−0.271± 0.147	−0.197± 0.111	5.71± 1.54	0.946
All	−0.320± 0.122	−0.257± 0.092	6.44± 1.28	0.872

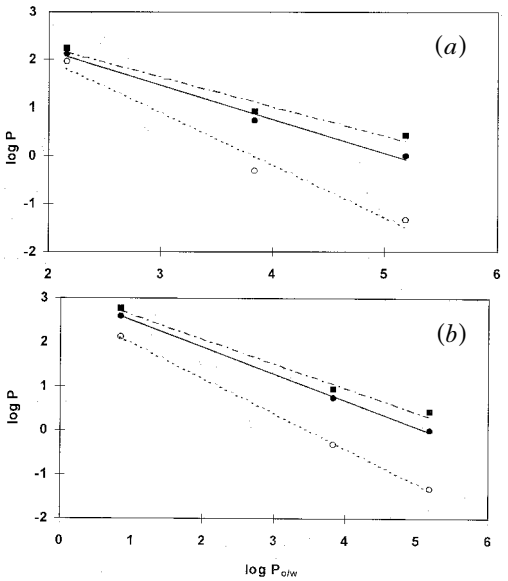


Figure 4. Correlation between the logarithm of the apparent permeability constant (log P) and the logarithm of the octanol/water partition coefficient (log $P_{o/w}$) for the aromatic glycidyl ethers (A) and the bifunctional glycidyl ethers (B). Log P was determined experimentally (table 2) and log $P_{o/w}$ was estimated (the Materials and methods) Symbols are the log P determined in viable dermatomed human skin (rat skin (●) or undermatomed mouse skin (■). (A) Aromatic glycidyl ethers: *o*-CGE, YX4000 and BADGE. Lines are obtained by linear regression analysis; $R^2 = 0.975, 0.988$ and 0.967 for human, rat and mouse skin respectively. (B) Bifunctional glycidyl ethers: YX4000, BADGE and HDDGE. Lines are obtained by linear regression analysis; $R^2 = 0.946, 0.922$ and 0.958 for human, rat and mouse skin respectively.

obtained by plotting the logarithm of the apparent permeability constant (log P) for the 5 GE against their log $P_{o/w}$ ($R^2 = 0.75, 0.72$ and 0.73 for human, rat and mouse respectively) or their molecular weight (MW) ($R^2 = 0.83, 0.75$ and 0.76 for human, rat and mouse respectively). MW gave slightly better correlations than the square root of MW ($\sqrt{}$MW) (tables 5 and 6). In contrast, highly significant linear correlations were found between the log P and log $P_{o/w}$ if only the bifunctional GE or only the aromatic GE were considered (figure 4). Multiple regression analysis with the log P obtained for all five GE under study as dependent variables and their intrinsic physical properties log $P_{o/w}$ and either MW (table 5) or $\sqrt{}$MW (table 6) as independent variables showed statistically highly significant correlations for each of the species separately as well as for all data grouped together.

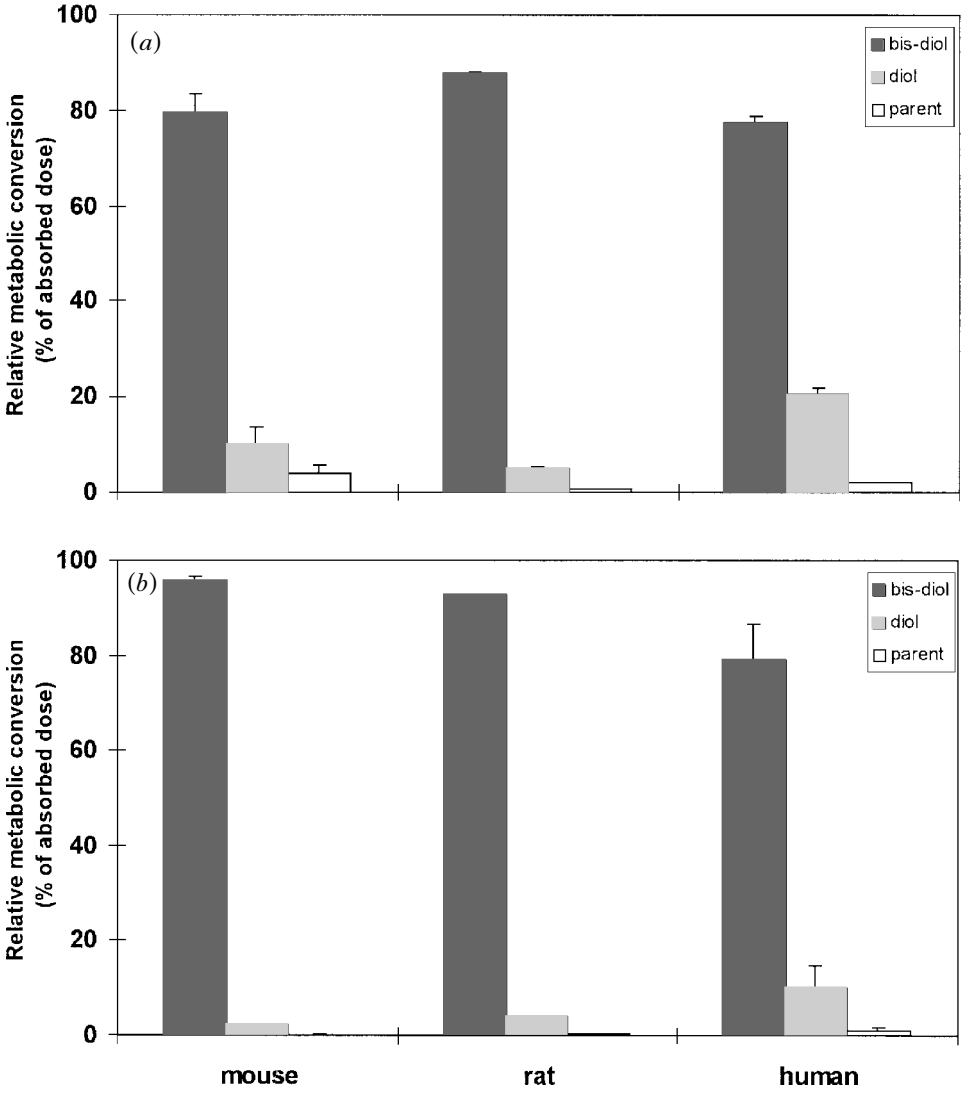


Figure 5. For legend see facing page.

Percutaneous metabolism

Extensive metabolism of all five GE was observed in the skin. As can be seen in figure 5A and B, YX4000 and BADGE are almost completely converted to their *bis*-diol during absorption. Note that the relative metabolic conversion in figure 5 is given as a percentage of the dose penetrated, which is more than an order of magnitude lower in humans than in rodents. Therefore, the absolute amount of YX4000, BADGE or C_{12}GE that penetrates the skin unchanged is much lower for human skin than either rat or mouse skin. The major part of the limited amount of YX4000 that penetrates the skin is metabolized to the *bis*-diol (77 ± 2, 87.9 ± 0.2 and 80 ± 4% of the penetrated dose for human, rat and mouse skin respectively) and only a minor portion of the penetrated material is present as the mono-diol (20 ± 1, 5.1 ± 0.3 and 10 ± 4% of the penetrated dose for human, rat and mouse skin respectively). The percentage of the penetrated dose that permeated the skin as

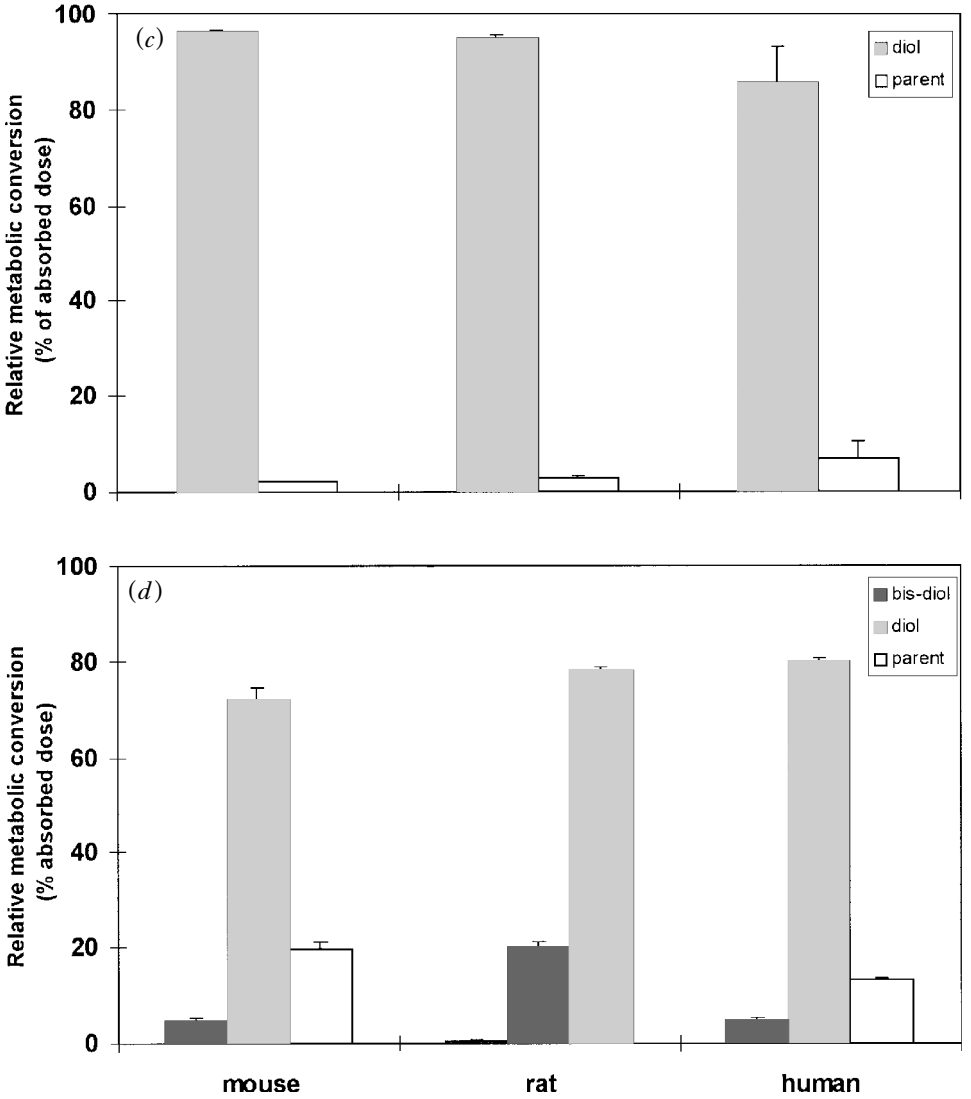


Figure 5. Hydrolysis of glycidyl ethers in viable skin. Human and rat skin were used dermatomed, whereas mouse skin was used at full-thickness (undermatomed). Bars are means ± SE ($n = 3$) of the metabolic conversion of each glycidyl ether to its corresponding diol, and for bifunctional glycidyl ethers also their *bis*-diols, as a percentage of the total penetrated dose in 24 h. (a) YX4000 (4,4′-dihydroxy-3,3′,5,5′-tetramethylbiphenyl diglycidyl ether). (b) BADGE (*bis*phenol A diglycidyl ether). (c) C_{12}GE (1-dodecyl glycidyl ether). (d) HDDGE (1,6-hexanediol diglycidyl ether).

YX4000 was only 2.1 ± 0.1, 0.67 ± 0.03 and 3.9 ± 1.7% in human, rat and mouse respectively. For BADGE very similar results were found: 79 ± 8, 92.9 ± 0.1 and 96 ± 1% of the penetrated dose was converted to the *bis*-diol in human, rat and mouse skin respectively, 10 ± 5, 3.8 ± 0.1 and 2.0 ± 0.2% of the penetrated dose was hydrolysed to the mono-diol in human, rat and mouse skin respectively, and 1.1 ± 0.7, 0.29 ± 0.02 and 0.15 ± 0.07% of the penetrated dose was recovered as BADGE itself in human, rat and mouse skin. For the third bifunctional GE under study, HDDGE, a very different picture was observed. First, HDDGE penetrates

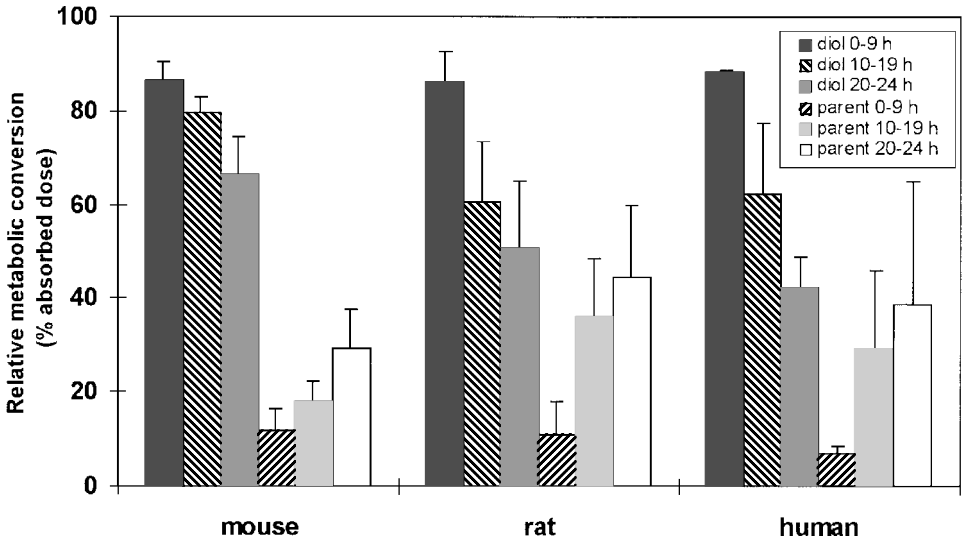


Figure 6. Hydrolysis of *o*-cresyl glycidyl ether in viable skin over time. Human and rat skin were used dermatomed, whereas mouse skin was used at full-thickness (undermatomed). Bars are means± SE ($n = 3$) of the metabolic conversion of *o*-cresyl glycidyl ether to mephenesin (the diol) as a percentage of the total amount permeated during the 24 h of the experiment.

the skin rapidly and efficiently and, second, only a minor portion of the penetrated amount is fully hydrolysed to the *bis*-diol. Especially in rat only very little metabolism takes place and 78± 1% of the absorbed dose penetrates through the skin unaltered. Virtually no *bis*-diol (0.41± 0.25% of the absorbed dose) was formed in rat skin during penetration. Mouse and human are very similar with 13.4± 0.3 and 20± 1% of the absorbed dose penetrating unchanged respectively, and 79.8± 0.7 and 72± 3% as the mono-diol and 4.8± 0.4 and 4.5± 1.0% as the *bis*-diol respectively. C_{12}GE was almost completely hydrolysed with 86± 7, 95.1± 0.7 and 96.5± 0.3% of the absorbed dose being recovered as the diol and only 7± 4, 2.8± 0.4 and 2.1± 0.2% of the absorbed dose as unchanged C_{12}GE in human, rat and mouse skin respectively. For YX4000, BADGE, C_{12}GE and HDDGE the relative amount of various hydrolysis products in the receptor fluid did not change during the 24 h of the study. For *o*-CGE, however, the picture was very dissimilar (figure 6): a considerable amount of the penetrated dose (86–88%), was hydrolysed to mephenesin (the glycerol ether of *o*-cresol) during the first hours of penetration in human, rat as well as mouse skin, but as the study progressed less *o*-CGE was hydrolysed and more unchanged compound was recovered from the receptor fluid (39± 26, 45± 15 and 29± 8% of the penetrated dose from 20 to 24 h of the exposure in human, rat and mouse skin respectively). This effect was more pronounced in human skin than rodent skin, but the absolute amounts of *o*-CGE penetrating the skin were lower in human skin than in either rat or mouse skin.

Discussion

In the present study, the percutaneous penetration and metabolism of selected GE, representatives of different classes of GE were investigated. Since considerable exposure to GE may also occur through inhalation, either as aerosol or as vapour for

the more volatile GE, or through ingestion of inhaled GE or food stuffs containing GE, the metabolism of GE in subcellular fractions of liver and lung were investigated in a separate study (Boogaard *et al.* 2000).

The dermal penetration studies demonstrate substantial differences in percutaneous penetration of the various GE. In general, the penetration through full-thickness mouse skin is higher than through dermatomed rat skin, whereas dermatomed human skin is the least permeable of all. The percutaneous penetration of the various GE increases in the following order: YX4000 < BADGE < C_{12}GE < *o*-CGE < HDDGE. The corresponding apparent skin permeability constants vary over > 4 orders of magnitude, from 0.047×10^{-6} cm/h for YX4000 through human skin and HDDGE to 577×10^{-6} cm/h through mouse skin respectively. In general, the skin permeation of a compound correlates with its octanol/water partition coefficient ($P_{o/w}$) and/or with its molecular weight (MW) (Wilschut *et al.* 1995). In the current study, percutaneous penetration was indeed correlated with the log $P_{o/w}$ as well as with the MW of the GE. These correlations were most clear if only the aromatic or only the bifunctional GE were taken into account (figure 6). A number of mathematical models have been constructed to describe this correlation. Compared with several other models, the relatively simple model by Guy and Potts (1993) gave one of the best predictions for the skin permeation of a large set of chemicals (Wilschut *et al.* 1995). Using this model (which described the permeability constant as a linear function of log $P_{o/w}$ and the square root of MW) a highly significant correlation for the 5 GE was found. Using MW directly, instead of its square root, gave a slightly better correlation, which is probably due to the fact that a relatively small and homogeneous group of compounds is being modelled here. The correlations were very strong within one species ($R > 0.95$) but still highly significant if data for human and rodent skin were pooled ($R = 0.88$). These results indicate that the skin penetration of other GE will probably be highly predictable as well.

Most of the GE were effectively metabolized during absorption through the skin. Virtually no YX4000 penetrated human skin unchanged: only 0.00024% of the applied dose permeated unchanged. Although still low, these percentages were significantly higher in rat and mouse skin: 0.0018 and 0.029% of the applied dose of YX4000 respectively. For BADGE the amounts were very similar for rat and mouse skin (0.0046 and 0.0045% of the applied dose) and substantially higher than for human skin, through which only 0.0015% of the applied dose permeated unchanged. Most of the absorbed YX4000 and BADGE was completely hydrolysed to the corresponding *bis*-diol in human as well as rodent skin. To the best of our knowledge the only *in vivo* studies on the metabolism of GE following dermal application were carried out with BADGE (Climie *et al.* 1981a, b, Steiner *et al.* 1992a, b). Only the study by Climie *et al.* presents data on the disposition of BADGE following dermal occluded application in CF1 mouse. It was reported that the total urinary and faecal excretion of radioactivity over the first 24 h following occluded application of radiolabelled BADGE amounted to ~ 4%, of which 99% was metabolized to more polar metabolites. This matches well with the present *in vitro* results, where 3.0 ± 0.8% of BADGE penetrated the skin after 24 h unoccluded application, of which 96 ± 1 and 2.0 ± 0.2% was converted to the *bis*-diol and the mono-diol respectively.

The picture seen with HDDGE, the third bifunctional glycidyl ether studied, was very different from that of YX4000 and BADGE. Quite a significant amount of

the applied dose penetrated the skin unchanged: 5.07, 52.4 and 15.9% of the applied dose for human, rat and mouse skin respectively. The high percentage of HDDGE that penetrated the rat skin unchanged was particularly striking and suggests that there is relatively little metabolism of HDDGE in rat skin. This is, however, in agreement with the observations in subcellular fractions of rat liver and lung where significantly less hydrolysis also occurred than in human or mouse fractions (Boogaard *et al.* 2000). Most of the HDDGE was hydrolysed during penetration to the mono-diol and only a small percentage to the *bis*-diol. For C_{12}GE, as for BADGE, there was only a marginal difference in the percentage of the applied dose that penetrated unchanged (0.23 and 0.21% for mouse and rat skin respectively) but this amount was much larger than for human skin (only 0.057% of the applied dose penetrated unchanged). Virtually all C_{12}GE was being hydrolysed to its diol during its penetration of the skin.

Like HDDGE, *o*-CGE was extensively absorbed and, compared with the other GE, was not very extensively hydrolysed. In addition, the hydrolysis of *o*-CGE diminished over time. For instance, in the first 9 h of the experiment only 0.69% of the applied dose had permeated human skin unchanged, but in the following period of 9 h this rose to 2.9% and in the last 5 h to 3.9%. In rodents the same phenomenon was observed; in rat the percentage rose from 1.9% to 6.3 and 7.8% and in mouse from 2.6 to 4.1 and 6.7%. In addition, *o*-CGE evaporated from the skin, thus reducing the amount of *o*-CGE on the skin. Occlusion of the skin increased the dermal uptake of *o*-CGE about twice but had no significant influence on the extent of metabolism: the same percentage of *o*-CGE passed the skin unchanged. This suggests that *o*-CGE influences its own metabolism over time. This phenomenon is probably not due to an increased permeability of the skin, thus reducing the time for metabolism but rather to an inhibitory effect. The mass balance data (table 1) and the shape of the permeation curve (figure 2D) indicate that after $\sim$ 12 h virtually all *o*-CGE has evaporated from the surface of the skin. This means that most of the *o*-CGE entering the receptor fluid in the last two periods over which metabolism was studied (10–19 and 20–24 h; figure 6) was already absorbed into the skin and released unchanged to the receptor fluid. This effect might be due to *o*-CGE itself, inhibiting its own metabolism for instance through alkylation of the active site of the epoxide hydrolase (EH), or by mephenesin, for instance through allosteric inhibition or competition for the binding site which would increase when the concentration of mephenesin in the skin increases. Elucidation of the exact mechanism by which *o*-CGE influences its own dermal metabolism requires additional research.

From the present study it can be concluded that there is a substantial variation in the extent of dermal penetration of the GE studied. The permeability increases in the order: YX4000 < BADGE < C_{12}GE < *o*-CGE < HDDGE. For all GE, full-thickness mouse skin is more permeable than dermatomed rat skin and that human skin is the least permeable of all. During skin penetration, all GE are extensively metabolized to their corresponding (*bis*-)diols. The large variation in response observed with the five selected GE indicates that GE should not be considered as a single class of compounds but rather on the basis of their individual properties.

Acknowledgements

The authors are grateful to Drs Klaassens and Stevens, plastic surgeons at the Medical Centre Alkmaar, for their kind and efficient cooperation in the supplying of fresh human skin samples.

References

BOOGAARD, P. J., VAN ELBURG, P. A., DE KLOE, K. P., WATSON, W. P. and VAN SITTERT, N. J., 1999, Metabolic inactivation of 2-oxiranomethyl 2-ethyl-2,5-dimethyl hexanoate (C_{10}GE) in skin, lungs, and liver of humans, rats and mice. *Xenobiotica*, **29**, 987–1006.

BOOGAARD, P. J., DE KLOE, K. P., DENNEMAN, M. A., BIERAU, J., KUIKEN, G., BORKULO, P. E. D. and VAN SITTERT, N. J., 2000, Metabolic inactivation of five glycidyl ethers in lungs and liver of humans, rats and mice. *Xenobiotica*, **30**, 485–502.

BRONAUGH, R. L. and STEWART, R. F., 1984. Methods for *in vitro* percutaneous absorption studies. IV: the flow through diffusion cell. *Journal of Pharmaceutical Science*, **74**, 64–67.

CLIMIE, I. J. G., HUTSON, D. H. and STOYDIN, G., 1981a, Metabolism of the epoxy resin component 2,3-bis[4-(2,3-epoxypropoxy)phenyl]propane, the diglycidyl ether of bisphenol A (DGEBPA) in the mouse. I. A comparison of the fate of a single dermal application and of a single oral dose of ^{14}C-DGEBPA. *Xenobiotica*, **11**, 391–399.

CLIMIE, I. J. G, HUTSON, D. H. and STOYDIN, G., 1981b, Metabolism of the epoxy resin component 2,3-bis[4-(2,3-epoxypropoxy)phenyl]propane, the diglycidyl ether of bisphenol A (DGEBPA) in the mouse. II. Identification of metabolites in urine and faeces following of a single oral dose of ^{14}C-DGEBPA. *Xenobiotica*, **11**, 401–424.

DEFORCE, D. L. D., LEMIÊRE, F., HOES, I., MILLECAMPS, R. E. M., ESMANS, E. L., DE LEENHEER, A. and VAN DEN EECKHOUT, E. G., 1988, Analysis of the DNA adducts of phenyl glycidyl ether in a calf thymus DNA hydrolysate by capillary zone electrophoresis - electrospray mass spectrometry: evidence for phosphate alkylation. *Carcinogenesis*, **19**, 1077–1086.

EADSFORTH, C. V., 1983, *EPIKOTE 828: Determination of the N-octanol/Water Partition Coefficient using a Reverse-phase HPLC Method.* Report no. SBGR 83.385 (Sittingbourne: Shell Research Centre).

GARDINER, T. H., WAECHTER, J. M., WIEDOW, M. A. and SOLOMON, W. T., 1992, Glycidyloxy compounds used in epoxy resin systems: a toxicology review. *Reviews in Toxicology and Pharmacology*, **15**, S1–77.

GUY, R. H. and POTTS, R. O., 1993, Penetration of industrial chemicals across the skin: a predictive model. *American Journal of Industrial Medicine*, **23**, 711–719.

HOTCHKISS, S. A., CHIDGEY, M. A. J., ROSE, S. and CALDWELL, J., 1990, Percutaneous absorption of benzyl acetate through rat skin *in vitro*. 1. Validation of an *in vitro* model against *in vivo* data. *Food and Chemical Toxicology*, **28**, 443–447.

IARC, 1985, *Allyl Compounds, Aldehydes, Epoxides and Peroxides. Diglycidyl Resorcinol Ether* (Lyons: IARC), **36**, 181–188.

IARC, 1989, *Some Organic Solvents, Resin Monomers and Related Compounds, Pigments and Occupational Exposures in Paint Manufacture and Painting. Some Glycidyl Ethers* (Lyon: IARC), **47**, 237–261.

IARC, 1999a, *Re-evaluation of Some Organic Chemicals, Hydrazine and Hydrogen Peroxide. Phenyl Glycidyl Ether* (Lyon: IARC), **71**, 1525.

IARC, 1999b, *Re-evaluation of Some Organic Chemicals, Hydrazine and Hydrogen Peroxide. Diglycidyl Resorcinol Ether* (Lyon: IARC), **71**, 1417.

IARC, 1999c, *Re-evaluation of Some Organic Chemicals, Hydrazine and Hydrogen Peroxide. Bisphenol A Diglycidyl Ether* (Lyon: IARC), **71**, 1265.

IARC, 1999d, *Re-evaluation of Some Organic Chemicals, Hydrazine and Hydrogen Peroxide. Triethylene Glycol Diglycidyl Etheri* (Lyon: IARC), **71**, 1285.

PLNÁ, K., SEGERBÄCK, D. and SCHWEDA, E. K. H., 1996, DNA adduct formation by allyl glycidyl ether. *Carcinogenesis*, **17**, 1465–1471.

STEINER, S., CRANE, A. E. and WATSON, W. P., 1992a, Molecular dosimetry of DNA adducts in C3H mice treated with glycidaldehyde. *Carcinogenesis*, **13**, 119–124.

STEINER, S., HÖNGER, G. and SAGELSDORFF, P., 1992b, Molecular dosimetry of DNA adducts in C3H mice treated with bisphenol A diglycidyl ether. *Carcinogenesis*, **13**, 969–972.

VAN ELBURG, P. A., ORMSKERK, O. A., DE KLOE, K. P. and BOOGAARD, P. J., 2000, Synthesis of [^{14}C]-labelled glycidyl and glycerol ethers of aliphatic and aromatic alcohols. *Journal of Labelled Compound Radiopharmacology*, **43**, 147–167.

WILSCHUT, A., TEN BERGE, W. F., ROBINSON, P. J. and MCKONE, T. E., 1995, Estimating skin permeation, the validation of five mathematical skin permeation models. *Chemosphere*, **30**, 1275–1296.

XENOBIOTICA , 2000, VOL. 30, NO. 5, 485–502

Metabolic inactivation of five glycidyl ethers in lung and liver of humans, rats and mice *in vitro*

P. J. BOOGAARD*, K. P. DE KLOE, J. BIERAU, G. KUIKEN, P. E. D. BORKULO and N. J. VAN SITTERT

Department of Molecular Toxicology, Shell Research and Technology Center, Amsterdam, Shell International Chemicals BV, PO Box 38000, 1030 BN Amsterdam, The Netherlands

Received 23 July 1999

1. Some glycidyl ethers (GE) have been shown to be direct mutagens in short-term *in vitro* tests and consequently GE are considered to be potentially mutagenic *in vivo*. However, GE may be metabolically inactivated in the body by two different enzymatic routes: conjugation of the epoxide moiety with the endogenous tripeptide glutathione (GSH) catalysed by glutathione *S*-transferase (GST) or hydrolysis of the epoxide moiety catalysed by epoxide hydrolase (EH).

2. The metabolic inactivation of five different GE, the diglycidyl ethers of *bis*phenol A (BADGE), 4,4′-dihydroxy-3,3′,5,5′-tetramethylbiphenyl (Epikote YX4000) and 1,6-hexanediol (HDDGE) and the GE of 1-dodecanol (C_{12}GE) and *o*-cresol (*o*-CGE), has been studied in subcellular fractions of human, C3H mouse and F344 rat liver and lung.

3. All GE were chemically very stable and resistant to aqueous hydrolysis, but were rapidly hydrolysed by EH in cytosolic and microsomal fractions of liver and lung. The aromatic GE were very good substrates for EH. In general, microsomal EH is more efficient than cytosolic EH in hydrolysis of GE, and human microsomes are more efficient than rodent microsomes.

4. The more water-soluble GE, *o*-CGE and HDDGE, were good substrates for GST whereas the more lipophilic GE, YX4000 and C_{12}GE, were poor substrates for GST. In general, rodents are more efficient in GSH conjugation of GE than humans.

5. In general, the epoxide groups of YX4000 are the most and those of HDDGE the least efficiently inactivated of the five GE under study. For the other three GE no general trend was observed: the relative efficiency of inactivation varied with organ and species.

6. The large variation in metabolism observed with five representative GE indicate that GE have variable individual properties and should not be considered as a single, homogenous class of compounds.

Introduction

Glycidyl ethers (GE) form an important group of chemicals used widely and in a large variety in the manufacture of epoxy resin systems employed in adhesives, coatings, plastics, electronics and structural composites. Some glycidyl compounds have been reported to show direct mutagenic properties in bacteria and in a small number of examples to cause tumours in animal studies (Gardiner *et al.* 1992). For example, phenyl glycidyl ether (PGE) and resorcinol diglycidyl ether have been classified by IARC as Class 2B carcinogens ('possibly carcinogenic to humans') (IARC 1985, 1989, 1999a, b). Other glycidyl ethers are under scrutiny because of their structural relationship to this glycidyl ether.

On the basis of previous metabolic studies *in vivo* on glycidyl compounds (Climie *et al.* 1981a, b, Boogaard *et al.* 1999) it is expected, however, that most GE would be rapidly and effectively detoxified by epoxide hydrolysis or by conjugation with

* Author for correspondence; e-mail: Peter.J.Boogaard@opc.shell.com

Xenobiotica ISSN 0049-8254 print/ISSN 1366-5928 online © 2000 Taylor & Francis Ltd
http://www.tandf.co.uk/journals

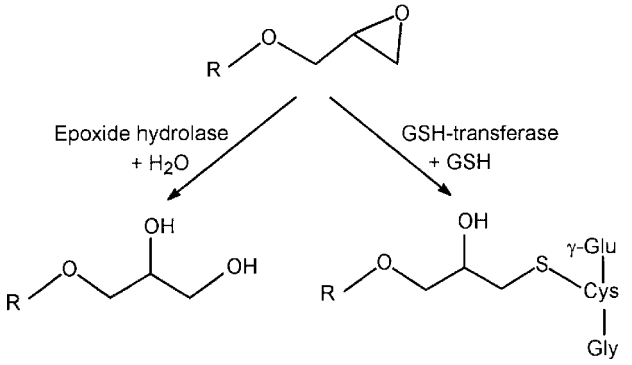


Figure 1. Metabolic detoxification pathways for glycidyl ethers.

glutathione (GSH) (figure 1). Therefore, comparative metabolism studies on GE of different classes were carried out to identify the role of these detoxification reactions in the overall toxicology, such that glycidyl ethers which are readily susceptible to hydrolytic or conjugative detoxification reactions can be clearly differentiated. Moreover, it is essential to generate data to substantiate the view that glycidyl compounds should not be considered as a single class of compounds but that susceptibility to metabolic hydrolysis and intrinsic and enzyme catalysed conjugation with glutathione should be taken into account.

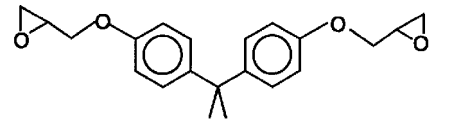
One of the primary portals of entry for GE is the lungs through inhalation of aerosols or vapours. Nevertheless, hepatic metabolism was also considered relevant for two reasons. First, residues of GE may be present in foodstuffs and ingestion of GE might occur, either directly or from swallowing material deposited in the airways after inhalation. In these cases hepatic metabolism may play a significant role. Second, the metabolic capacity of the liver is considerable and will probably be the single most important factor in the overall metabolism of GE that became systemically available, regardless of the way it entered the body. The skin may also be an important route of exposure for GE through direct dermal contact. Percutaneous penetration and metabolism of the five selected GE has also been studied and will be reported in Boogaard *et al.* (2000).

The overall objective of this study was generation of mechanistic data on the detoxifying metabolism of a series of GE to assist its appropriate classification and labelling. Representatives of four classes of GE (mono- and difunctional aromatic GE and mono- and difunctional aliphatic GE) were selected and synthesized and their rates of epoxide hydrolase (EH) catalysed hydrolysis and glutathione *S*-transferase- (GST) catalysed conjugation with GSH were studied in subcellular fractions of liver and lung of human, Fisher 344 rat and C3H mouse.

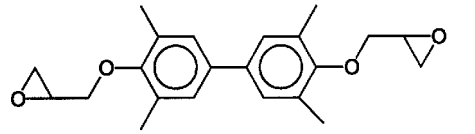
Materials and methods

Chemicals

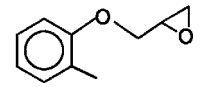
[U-^{14}C]-epichlorohydrin, radiopurity $\geqslant$ 97%, specific activity 30 mCi/mmol, was from ChemSyn Laboratories (Lenexa, KS, USA), and [glycine-2-^{3}H]-glutathione, radiopurity $\geqslant$ 97%, specific activity 44.8 mCi/mmol, from NEN Life Science Products (Boston, MA, USA). [Ring-U-^{14}C]-*bis*-phenol A diglycidyl ether, radiopurity $\geqslant$ 98%, specific activity 11 mCi/mmol, was a gift from Dr John Waechter (Dow Chemical Co., Midland, MI, USA). Re-crystallized BADGE (chemical purity $>$99%) and its *bis*-diol (*bis*-phenol A diglycerol ether; chemical purity $>$98%) were from the department of Basic & Exploratory Research (Shell Research & Technology Centre, Amsterdam). 1,2-Epoxy-3,3,3-trichloro-



Bisphenol A diglycidyl ether (BADGE)



Epikote YX4000 (YX4000)



o-Cresyl glycidyl ether (*o*CGE)



1,6-Hexanediol diglycidyl ether (HDDGE)



1-Dodecyl glycidyl ether (C_{12}GE)

Figure 2. Structures of synthesized chemicals.

Table 1. Characteristics of human liver donors.

No.	Sex	Race	Age (years)	COD[a]	Medication/ illnesses[b]	Alcohol	Smoker	Protein (mg/ml) Microsomes	Protein (mg/ml) Cytosol
1	F	Caucasian	49	ICH	premarin, ditropan, desyrel/HTN	no	no	20	18.8
2	F	Caucasian	42	ICH	clonidine/HTN	no	no	20	20
3	F	Caucasian	53	ICH	oestrogen/ CNS tumor	no	no	20	20
4	M	Caucasian	32	CHI	none	yes	no	20	20
5	M	Caucasian	39	ICH	none	yes	no	20	19.8
6	M	Caucasian	51	CHI	HTN	no	no	20	20

[a] Cause of death (COD): ICH, intracranial haemorrhage; CHI: closed-head injury.
[b] HTN, hypertension; CNS, central nervous system.

propane (TCPO), reduced glutathione (GSH), oxidized glutathione (GSSG) and micro-protein determination kits were from Sigma Chemical Co. (St Louis, MO, USA). 4-Phenylchalcone oxide (4-PCO) was from ICN Biomedicals BV (Zoetermeer, The Netherlands). Solvents were of the highest grades available. All other chemicals used were from Aldrich and were at least reagent grade with a purity $> 95\%$.

Reference materials

The glycidyl and glycerol ethers of *o*-cresol and 1-dodecanol as well as the diglycidyl and diglycerol ethers of 1,6-hexanediol, 4,4′-dihydroxy-3,3′,5,5′-tetramethylbiphenyl and diphenylol propane were synthesized from the alcohols and epichlorohydrin (ECH) (figure 2). The corresponding ^{14}C-labelled

compounds were synthesized from the alcohols and [U-^{14}C]-ECH, diluted with non-labelled ECH to a specific activity of 0.2 mCi/mmol. The aromatic alcohols were converted to the corresponding glycidyl ethers using sodium hydroxide and aliphatic alcohols using tin(IV) chloride as catalyst. All compounds were identified by ^{1}H- and ^{13}C-NMR and mass spectrometry. Chemical purities (from $>$92 to 99%) were determined using GC-MS or LC-MS. Radiopurities (from $>$95 to $>$98%) were determined by GC and LC with on-line radiodetection. Details of synthesis and analysis are in van Elburg *et al.* (2000).

Biological materials

Human organs. Human liver and lung microsomes, prepared by standard differential centrifugation methods (Boogaard *et al.* 1996), were from the Human Cell Culture Center (Laurel, MD, USA). Liver and lung donor characteristics are listed in tables 1 and 2 respectively.

Animals. Male Fisher 344 rats ($\sim$250 g) and male C3H mice ($\sim$25 g) were from the Central Laboratories for the Blood Banks (CLB) (Amsterdam, The Netherlands). Animals were kept on a 12 h light/dark cycle in humidity- (60$\pm$15% relative humidity) and temperature- (22$\pm$2 °C) controlled mass-air-displacement rooms and following an acclimation of 1 week were used as the source for skin, liver and lung tissue. A standard rodent diet (VRF-I, Broekman Instituut (Charles River Laboratories), Someren, The Netherlands) and de-ionized water were supplied *ad libitum*.

Subcellular tissue fractions

Rodents were anaesthetized with sodium pentobarbital, the abdomen was opened and the abdominal aorta cut. The animals were subsequently perfused *in situ* with ice-cold isotonic 0.05 M TRIS-buffered (pH 7.40) 0.15 M potassium chloride solution. Livers and lungs were excized, weighed and placed on ice. The lungs were minced with scissors and pulverized in liquid nitrogen using a hammer mill (6700 Freezer/Mill, Glen Creston, Inc., Stanmore, UK). Livers were only minced with scissors. Lung powder and minced livers were homogenized in TRIS-buffered (pH 7.40) isotonic KCl solution with six passes (1100 rpm) of a Teflon–glass homogenizer (Braun). Homogenates were centrifuged at 10 000*g* at 4 °C for 20 min, the lipid layer was removed and the supernatant was centrifuged at 105000*g* at 4 °C for 60 min. The supernatant (cytosolic fraction) was stored frozen at $-$80 °C. The pellet was dispersed with four passes of a Teflon–glass homogenizer in 0.05 M TRIS buffer (pH 7.40) containing 0.25 M sucrose and 1 mM EDTA and centrifuged again at 105000*g* at 4 °C for 60 min. The supernatant was discarded and the pellet resuspended with four passes of a Teflon–glass homogenizer in 0.1 M potassium phosphate buffer (pH 7.40) containing 0.25 M sucrose (microsomal fraction). The microsomes were stored at $-$80 °C. Subcellular fractions were used within 6 months of preparation. No apparent loss of activity was observed during this period as determined by assaying epoxide hydrolysis and GSH conjugation of standard substrates (Boogaard and Bond 1996, Boogaard *et al.* 1996).

Protein concentrations of all lung and liver subcellular preparations of rodents were assayed using the modified micro-Lowry assay for total micro-protein. Human liver and lung subcellular preparations were assayed for total micro-protein using the Coomassie blue method (all Sigma).

Analyses

Liquid scintillation counting (LSC). Radioactivity in solutions was measured using TriCarb 2200CA liquid scintillation counters (Canberra Packard, Groningen, The Netherlands) in antistatic scintillation vials after mixing with 5–10 vols Ultima Gold Scintillation cocktail (Canberra Packard). The machine was calibrated using commercial ^{3}H and ^{14}C internal standard kits for organic solvents (Wallac, Turku, Finland). The calibration was checked daily by counting a set of quenched standards commercially prepared in sealed glass vials. Counting efficiency was determined using the spectral index of the internal standard (SIE) and cpm were automatically transformed to dpm. Samples were corrected for background and counted for periods sufficiently long to reach a relative SD $<$ 0.02.

Capillary zone electrophoresis (CZE). CZE was carried out on a Beckman P/ACE 2100 system equipped with a UV absorbance detector, set at $\lambda = 214$ nm. The temperature of the capillary was controlled by liquid cooling and was maintained at 23$\pm$1 °C. Data were recorded with Beckman System Gold software. Beckman pretreated fused-silica capillary cartridges, 50 cm $\times$ 75 μm (internal diameter) were used for separation using a 12.5 mM Borax-HCl buffer, pH 8.35, as separation buffer. The capillaries were subsequently rinsed with 0.1 M NaOH for 30 s, with purified water for 30 s, and with separation buffer for 1 min, samples were injected by application of high pressure for 1–2 s, all separations were carried out at 19 kV in 16.5 min. The GSH conjugates of BADGE, *o*-CGE and HDDGE had retentions of 12.7, 13.0 and 13.2 min respectively, while GSH and GSSG had retentions of 13.7 and 14.2 min respectively. Initially, aspartame (retention 12.7 min) was chosen as internal standard based on the structural similarity to the GSH conjugate of *o*-CGE. However, it appeared unstable in aqueous solution as it demethylated over time. L-Asp-L-Phe, in contrast, was stable and appeared as a suitable internal standard (retention 15.8 min) for the determination of the GSH conjugates

Table 2. Characteristics of human lung donors.

No.	Sex	Race	Age (years)	COD[a]	Medication/ illnesses[b]	Alcohol	Smoker	Protein (mg/ml) Microsomes	Protein (mg/ml) Cytosol
1	F	Caucasian	35	anoxia	none	yes	yes	17.5	17.7
2	F	Caucasian	66	ICH	HTN medication/ HTN, KS	no	no	10	8.4
3	F	Caucasian	17	CHI	cannabis, Prozac/ anorexia	yes	yes	20	7.7
4	M	Caucasian	43	ICH	none	social	no[c]	15	18.9
5	M	Caucasian	56	ICH	coumadin, aterol, K-du, prenivil/HD	social	no	20	14.5
6	M	Caucasian	59	SDH	dilantin/HTN	social	no	10	3.4

[a] Cause of death (COD): ICH, intracranial haemorrhage; SDH, subdural hematoma.
[b] HTN, hypertension; KS, kidney stones; HD, heart disease.
[c] Stopped smoking 9 years ago.

of other GE as well. Several *N*-benzoylated amino acids, such as *N*-benzoyl-L-methionine (retention 13.9 min) and *N*-benzoyl-histidine (retention 13.7 min) were tested as external standards to correct for differences in injection volume. Based on a retention of 13.8 min and the large molecular extinction coefficient, *N*-benzoyl-L-Phe was selected as external standard.

Typical injection volumes for CZE were 9 nl, which is far too small to calibrate the analyses with radiolabelled reference material used for calibration of the EH-catalysed metabolism. As it was desirable to calibrate all analytical methods with the same reference material, all radiolabelled GE were incubated with mouse hepatic cytosol and GSH. The reaction was stopped by addition of methanol and following precipitation of the protein, the supernatant was serially diluted to obtain a series of solutions with different concentrations of GE. These solutions were subsequently analysed for the parent compound and its GSH conjugate both by HPLC with LSC and by CZE to enable calibration of the latter method of analysis.

High-performance liquid chromatography (*HPLC*). HPLC analyses were carried out using various liquid chromatographs. For analysis of radiolabelled compounds, a Ramona D or 2000 on-line radioactivity detector (Raytest, Straubenhardt, Germany), both equipped with 500 μl solid scintillant cells, were used. In addition, since the total radioactivity in individual peaks was in most cases below the detection limit of the on-line detectors, fractions were collected using fraction collectors. The radioactivity in the collected fractions was determined by LSC. HPLC analyses were carried using the following equipment and conditions.

System A. Apparatus: HP1050 liquid chromatograph with UV detection ($\lambda = 230$ nm) (Hewlett Packard, Amstelveen, The Netherlands); column: Phenomenex Jupiter 300 Å, 5 μm ODS, 250 × 4.6 mm (Phenomenex, Torrance, CA, USA) with HiChrom security guard column NC120–5C18–10C (HiChrom, Reading, UK); eluent: purified water (A) and methanol (B); flow: 1.0 ml/min; gradient: 0–18 min, linear increase from 25 to 92.5% B; 18–20 min, 92.5% B; 20–22 min: linear increase from 92.5 to 100% B, 30–35 min linear decrease from 100 to 25% B.

System B. Apparatus: HP1090 liquid chromatograph with UV detection ($\lambda = 230$ nm); column: Waters Novapak C18, 3 μm ODS, 15 × 3.9 mm (Waters, Etten-Leur, The Netherlands), with Phenomenex Security Guard (widepore 4 × 3.0 mm ODS cartridge); eluent: purified water (A) and acetonitrile (B); flow: 1 ml/min; gradient: 0–31 min, linear increase from 25 to 48.5% B; 31–35 min, linear increase from 48.5 to 100% B; 35–40 min: linear decrease from 100 to 25% B; 40–45 min: 25% B.

System C. Apparatus: HP1100 liquid chromatograph with UV detection ($\lambda = 230$ nm) (Hewlett Packard); column: Phenomenex Jupiter 300 Å, 5 μm ODS, 250 × 4.6 mm, with Phenomenex Security Guard (widepore 4 × 3.0 mm ODS cartridge); eluent: purified water (A) and acetonitrile (B); flow: 1.0 ml/min; gradient: 0–31 min, linear increase from 25 to 48.5 % B; 31–35 min, linear increase from 48.5 to 100% B; 35–40 min, linear decrease from 100 to 25% B; 40–45 min 25% B.

System D. Apparatus: HP1100 liquid chromatograph with UV detection ($\lambda = 230$ nm) (Hewlett Packard); column: Phenomenex Jupiter 300 Å, 5 μm ODS, 250 × 4.6 mm, with Phenomenex Security Guard (widepore 4 × 3.0 mm ODS cartridge); eluent: purified water (A) and acetonitrile (B); flow:

1.0 ml/min; gradient: 0–15 min, linear increase from 0 to 30% B; 15–25 min, linear increase from 30 to 45% B; 25–30 min, linear increase from 45 to 100% B; 30–33 min, 100% B; 33–35 min linear decrease from 100 to 0% B.

System E. Apparatus: HP1100 liquid chromatograph with UV detection ($\lambda = 230$ nm) (Hewlett Packard); column: Phenomenex Jupiter 300 Å, 5 μm ODS, 250×4.6 mm, with Phenomenex Security Guard (widepore 4×3.0 mm ODS cartridge); eluent: purified water (A) and acetonitrile (B); flow: 1.0 ml/min; gradient: 0–20 min, linear increase from 25 to 40% B; 20–21 min, linear increase from 40 to 100% B, 21–25.5 min 100% B; 25.5–26.5 min, linear decrease from 100 to 25% B; 26.5–30 min 25% B.

System F. Apparatus: Knauer HPLC Pumps 64, controlled by a Programmer 50 and equipped with a Dynamic Mixing Chamber and a Variable UV Detector (set at $\lambda = 230$ nm) (Herbert Knauer, Berlin, Germany); column: Phenomenex Jupiter 300 Å, 5 μm ODS, 250×4.6 mm, with HiChrom security guard column NC120–5C18–10C; eluent: Purified water (A) and acetonitrile (B); flow: 1.0 ml/min; gradient: 0–25 min, linear increase from 25 to 100% B; 25–32 min, 100% B; 32–37 min: linear decrease from 100 to 25% B.

Gas chromatography-mass spectrometry (*GC-MS*). GC-MS analyses were carried out using a HP 6890 GC equipped with auto-injector and a HP 5973 mass selective detector on a HP-5 MS, fused silica column of 30 m×0.25 mm (internal diameter) with a film thickness of 0.25 μm and a phase ratio of 250. The mobile phase was He at a constant flow of 1.0 ml/min (pressure ~ 7.7 psi). The injector was kept at 275 °C and 1 μl split/splitless injections were made. The following temperature programme was used: 50 °C for 1 min, then at 10 °C/min to 200 °C, maintained at 200 °C for 10 min; then second ramp (10 °C/min) to 250 °C, maintained at 250 °C for 10 min. Temperature transfer line was kept at 250 °C. The mass detector was used at electron impact mode; the quadrupole was kept at 106 °C and the source at 230 °C. The ionization potential was 70 eV and the multiplier voltage was set at the autotune voltage plus 400 eV. The data collection was either in scan mode from m/e 20 to 500 or, for quantitation, by single ion monitoring (100 ms dwell time) of the following fragments: m/e 111 and 197 (fragments of C_{12}GE), m/e 199 and 219 (fragments of the diol of C_{12}GE).

Liquid chromatography-mass spectrometry (*LC-MS*). LC-MS analyses were performed using system A on a HP 1050 liquid chromatograph coupled to a Micromass Quattro quadrupole mass spectrometer. Electrospray was used as the LC-MS interfacing and ionization technique (positive ions). The scan range was 100–1500 Dalton with 0.5 scan/s.

GSH conjugation

Uncatalysed chemical reaction. The chemical reaction of the GE with GSH was studied with both labelled and non-labelled GE. Each individual, unlabelled GE was dissolved in DMSO at a concentration of 20 mM. After dissolution an equal volume of a 20 mM solution of ^{3}H-GSH, freshly prepared in deoxygenated 100 mM phosphate buffer, pH 7.4, was added to a final volume of 5 ml. The mixture was kept at room temperature in an amber vial for 18 h and aliquots were analysed by HPLC (system A, see above) and CZE. ^{14}C-labelled GE were allowed to react with non-labelled GSH similarly and analysed by HPLC and CZE.

Enzymatic reaction for GSH conjugation. Individual GE under study were dissolved in acetone, aliquots were transferred into 1.5 ml vials and the acetone was carefully evaporated with a gentle stream of nitrogen. Phosphate buffer (0.1 M, pH 7.40), containing L-Asp-L-Phe as internal standard, was deoxygenated with He for 10 min. GSH was dissolved in the deoxygenated phosphate buffer. For cytosolic incubations, an aliquot of 4-PCO, an inhibitor of cytosolic EH (Mullin and Hammock 1982) was dissolved in acetone and transferred into a 2.0 ml vial and the acetone was evaporated under a gentle stream of nitrogen. Cytosol was diluted with the deoxygenated phosphate buffer and transferred into the vial with 4-PCO. For microsomal incubations, microsomes were diluted with the deoxygenated phosphate buffer and transferred into 2.0 ml vials. TCPO, an inhibitor of microsomal EH (Guest and Dent 1980), dissolved in DMSO was added in a small volume (concentration of DMSO was < 5% v/v). The mixtures of subcellular protein and inhibitors were incubated at 37 °C for ~ 2 min and aliquots of the GSH solution were added. The final concentrations of inhibitors, L-Asp-L-Phe and GSH during the incubation were 50 μM, 1.5 mM and 10 mM respectively. After pre-incubation for another 2 min, aliquots of the subcellular protein mixtures were transferred to the vials with the GE. The final concentrations of the GE were 0, 0.041, 0.12, 0.37, 1.11, 3.33 and 10.0 mM. Incubation was stopped by the addition of an equal volume of ice-cold methanol (kept on dry ice), containing 127 μM *N*-benzoyl-L-Phe, and the precipitated protein pelleted by centrifugation (10 min, 2500*g*, 4 °C). The supernatants were analysed by CZE. Linearity of the GSH conjugation with protein concentration was tested by incubation during 10 min with varying amounts of liver cytosol protein ranging from 0.2 to 5.0 mg protein/ml. Linearity

with time was investigated by incubation during 0.5, 1, 2, 5, 10, 15, 20 and 30 min with a liver cytosol protein concentration of 1 mg/ml. Spontaneous reaction of GSH with GE or inhibitors was measured from incubations without addition of cytosolic protein. All values for enzymatic reactions were corrected for the measured uncatalysed chemical reaction.

Hydrolysis

Incubations were carried out with both microsomal and cytosolic fractions. Following pre-incubation of the subcellular fractions, the reaction was started by addition of the GE dissolved in DMSO. The final concentrations of the GE ranged from 0.013 to 20.0 mM. The maximum concentration of DMSO in the final incubation mixture was 5% v/v.

For HPLC analysis, the incubation was stopped by addition of an equal volume of cold methanol (kept on dry ice), mixing and precipitation of the denaturated protein by centrifugation (2400*g*, 15 min). Various HPLC systems analysed the hydrolysis products of the different GE: BADGE was analysed using system B, YX4000 was analysed using system C, HDDGE was analysed using system D, *o*-CGE was analysed using system E, and C_{12}GE was analysed using system F. Since the UV absorptions of HDDGE and C_{12}GE are not suitable for UV detection, hydrolysis of these compounds was studied using radiolabelled material and HPLC with fraction collection followed by LSC. Linearity of the hydrolytic reactions with protein concentration was tested by incubation during 10 min with varying amounts of liver microsomal protein. Linearity with time was investigated by incubation during 0.5, 1, 2, 5, 10, 15, 20 and 30 min with a liver microsome concentration of 1 mg protein/ml.

Estimation of the octanol/water partition coefficient ($P_{o/w}$)

Log $P_{o/w}$ is in many cases an important determinant of enzyme affinity. For BADGE log $P_{o/w} = 4.0$ was determined by HPLC (Eadsforth 1983). For the other GE, however, no log $P_{o/w}$ has been determined. For these GE, log $P_{o/w}$ was estimated using the KOWWIN software package, v.1.57 (Syracuse Research Software, Whitstable, UK). The following were calculated: YX4000 log $P_{o/w} = 5.2$, C_{12}GE log $P_{o/w} = 5.0$, BADGE log $P_{o/w} = 3.8$, *o*-CGE log $P_{o/w} = 2.2$ and HDDGE log $P_{o/w} = 0.84$.

Calculations and statistics

The formation of GSH conjugates or hydrolysis products in the incubation mixtures, after correction for non-enzymatic GSH conjugation, was fitted to the Michaelis–Menten equation with parameter value optimization by the Levenberg–Marquardt approximation, using the DeltaGraph software package (v.4.0.5d; SPSS, Inc., Chicago, IL, USA). Experiments for the construction of Michaelis–Menten plots were done at least in duplicate for mouse and rat subcellular fractions, but if the results of duplicate determinations differed $> 20\%$, which sometimes happened with subcellular fractions with low activity, additional series of incubations were performed to reduce the relative error associated with the fitted parameters. Since V_{max} and K_m are interdependent variables, their ratio, V_{max}/K_m, which may be interpreted as a measure of enzyme efficiency, was chosen as the best value for comparison of the efficiency of the reactions between organs and species. In some cases no Michaelis–Menten kinetics were observed. In these instances the rate of the reaction was determined by linear regression analysis using the least squares approximation. These reaction rates were expressed as μl/min/mg protein, units identical to those in which V_{max}/K_m is expressed, to allow easier comparison.

In vivo V_{max} was scaled from *in vitro* V_{max} and K_m and by adjustment for the interspecies differences in microsomal and cytosolic protein concentrations and liver volumes (Boogaard and Bond 1996). *In vivo* hepatic clearances were estimated by division of the calculated *in vivo* V_{max} by the corresponding *in vitro* K_m for the enzymatic reaction. Average liver volumes for humans, mouse and rat were taken as 3.1, 5.4 and 3.7% of lean body weight respectively, and average lung volumes for humans, mice and rats were 0.65, 1.09 and 0.57% of lean body weight respectively (ILSI 1994). In this study, the cytosolic protein content was assayed as 41.7, 72.6 and 50.1 mg/g liver and 16.7, 45.1 and 10.4 mg/g lung for human, rat and mouse respectively, and the microsomal protein content was 16.7, 18.4 and 5.8 mg/g liver and 2.7, 2.4 and 4.4 mg/g lung for human, rat and mouse respectively.

Results

GSH conjugation

No detectable chemical or enzyme catalysed reaction of YX4000 and C_{12}GE with GSH could be observed with either rat liver cytosol or microsomes (data not shown). Both a small degree of chemical reaction and some inconsistent enzyme-catalysed GSH conjugation of BADGE was observed under the given experimental

Table 3. Kinetic constants for enzymatic conjugation of *o*-cresyl glycidyl ether

Organ	Species	V_{max} (nmol/mg/min)	K_m (mM)	V_{max}/K_m µl/min/mg	*n*	*R*
Liver	human	84.5	14.5	5.84	6	0.999
	rat	61.3	2.72	22.5	3	0.998
	mouse	150	6.63	22.7	2	0.998
Lung	human	50.1	20.9	2.40	6	0.997
	rat	29.0	5.79	5.01	2	0.993
	mouse	29.5	3.95	7.45	2	0.998

n, Number of individuals /animals.
R, Correlation coefficient of the fitted curve.

Table 4. Kinetic constants for enzymatic conjugation of 1,6-hexanediol diglycidyl ether with glutathione by liver and lung cytosol.

Organ	Species	V_{max} (nmol/mg/min)	K_m (mM)	V_{max}/K_m µl/min/mg	*n*	*R*
Liver	human	nd[a]	nd[a]	4.95[a]	6	0.998[a]
	rat	257	5.69	45.2	3	0.937
	mouse	523	13.4	38.9	3	0.998
Lung	human	nd[a]	nd[a]	1.44[a]	6	0.996[a]
	rat	98.6	6.0	16.4	3	0.954
	mouse	129	11.6	11.0	3	0.970

n, Number of individuals /animals.
R, Correlation coefficient of the fitted curve.
[a] No apparent Michaelis–Menten kinetics, but enzymatic formation of glutathione conjugate appeared proportional to the concentration of substrate under the incubation conditions. V_{max}/K_m and *R* were obtained by linear regression analysis.

conditions. In contrast, *o*-CGE and HDDGE showed only a small but significant chemical reactivity towards GSH under the experimental conditions, but a rapid enzyme catalysed reaction. The radiolabelled products formed during incubation of *o*-CGE and HDDGE with ^{3}H-GSH were identified by LC-MS as GSSG and as the GSH conjugates of *o*-CGE and HDDGE respectively. The GST-catalysed reactions, for both *o*-CGE and HDDGE, were linear with time for at least up to 15 min and linear with protein concentrations up to 3 mg/ml. All data are based on 10 min incubations with protein concentrations varying from 0.4 to 3.0 mg/ml. The parameters describing the above kinetic behaviour are tabulated in tables 3 and 4. The enzyme-catalysed GSH conjugation of *o*-CGE, corrected for intrinsic chemical reaction, was well described by Michaelis–Menten kinetics for both liver and lung cytosol of rodents as well as humans. The hepatic GSH conjugation, expressed as V_{max}/K_m, was about equal in rodents but higher than in humans. Typical Michaelis–Menten plots for the GSH conjugation of *o*-CGE and HDDGE in the presence of lung cytosol are represented in figure 3. GSH conjugation in lung cytosol was lower than in liver and decreased by: mouse > rat > human. The GSH conjugation of HDDGE was less well described by Michaelis–Menten kinetics. In human liver and lung cytosol, no Michaelis–Menten kinetics were observed, but the increase in conjugation (corrected for the chemical reaction of HDDGE with GSH) was proportional to the concentration of HDDGE (figure 3B), and a straight line fitted better to the data obtained for the GSH conjugation of HDDGE in human liver and lung cytosol than the rectangular hyperbola which would result from

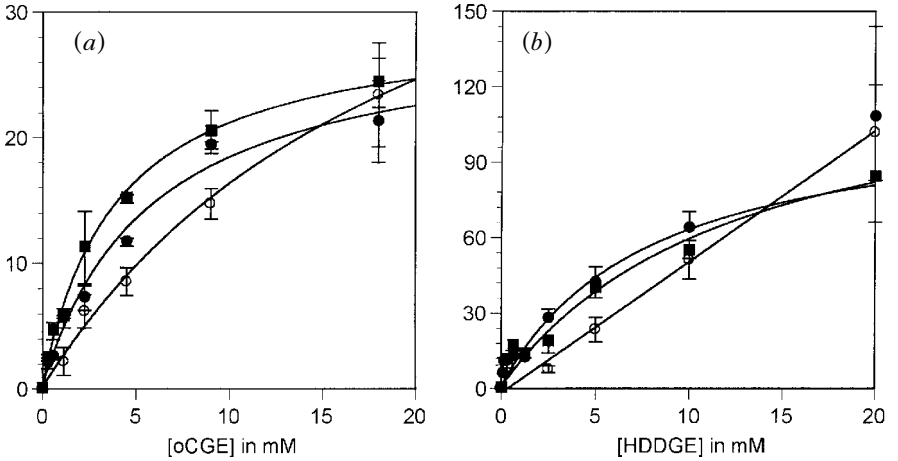


Figure 3. Enzymatic formation of the GSH conjugate of *o*-cresyl glycidyl ether (*o*-CGE) and 1,6-hexanediol diglycidyl ether (HDDGE) by human (○), Fisher 344 rat (●) and C3H mouse (■) lung cytosolic fractions. Data points represent means ± SE of six separate experiments with lung cytosol from six individuals (three males, three females) or two (*o*-CGE) or three (HDDGE) separate experiments with lung cytosol from rodents. (a) *o*-CGE. The lines are model simulations for the Michaelis–Menten equation fitted to the data points ($R^2 = 0.994$, 0.986 and 0.996 for human, rat and mouse lung respectively). (b) HDDGE. The lines for rat and mouse are model simulations for the Michaelis–Menten equation fitted to the data points ($R^2 = 0.910$ and 0.941 for rat and mouse lung respectively). The data obtained for the GSH conjugation of HDDGE by human lung cytosol did not fit to the Michaelis–Menten equation, but a linear increase of GSH conjugates with the concentration HDDGE was found ($R^2 = 0.992$).

Michaelis–Menten kinetics. This might be caused by a low affinity (high K_m) of HDDGE for GST resulting in an apparently straight curve. Alternatively, the formation of the mono-conjugate and *bis*-conjugate, for which the peaks were not well resolved at low concentration, might obscure the observation of Michaelis–Menten kinetics. Again, the conjugation rates were higher in liver than in lung fractions, and higher in rodents than in human. The GSH conjugation of HDDGE was, in contrast to *o*-CGE, slightly higher in rat than in mouse.

Hydrolysis

All five GE studied were rapidly hydrolysed to the corresponding (di)glycerol ethers upon incubation with either cytosolic or microsomal fractions (figure 4). The only exception was *o*-CGE for which no EH-catalysed hydrolysis was observed with rat lung cytosol (tables 5–9). The identity of the hydrolysis products formed was confirmed by co-elution on HPLC with the synthesized reference compounds and by comparison of the mass spectra obtained LC-MS, with exception of C_{12}GE for which the mass spectrum was obtained by GC-MS. The EH-catalysed hydrolysis was linear with time for at least 10 min and linear with protein concentrations up to 1.5 mg/ml for liver and 3.0 mg/ml for lung subcellular fractions. All data are based on 10 min incubations and protein concentrations of 1.0 mg/ml for liver and 0.4–2.0 mg/ml for lung preparations. In general, the V_{max}/K_m ratio for microsomal EH was higher than for cytosolic EH. The only exception to this general observation was seen with YX4000 and C_{12}GE in mouse liver. In these two cases, cytosolic hydrolysis was more effective, as determined by the V_{max}/K_m ratio, than microsomal

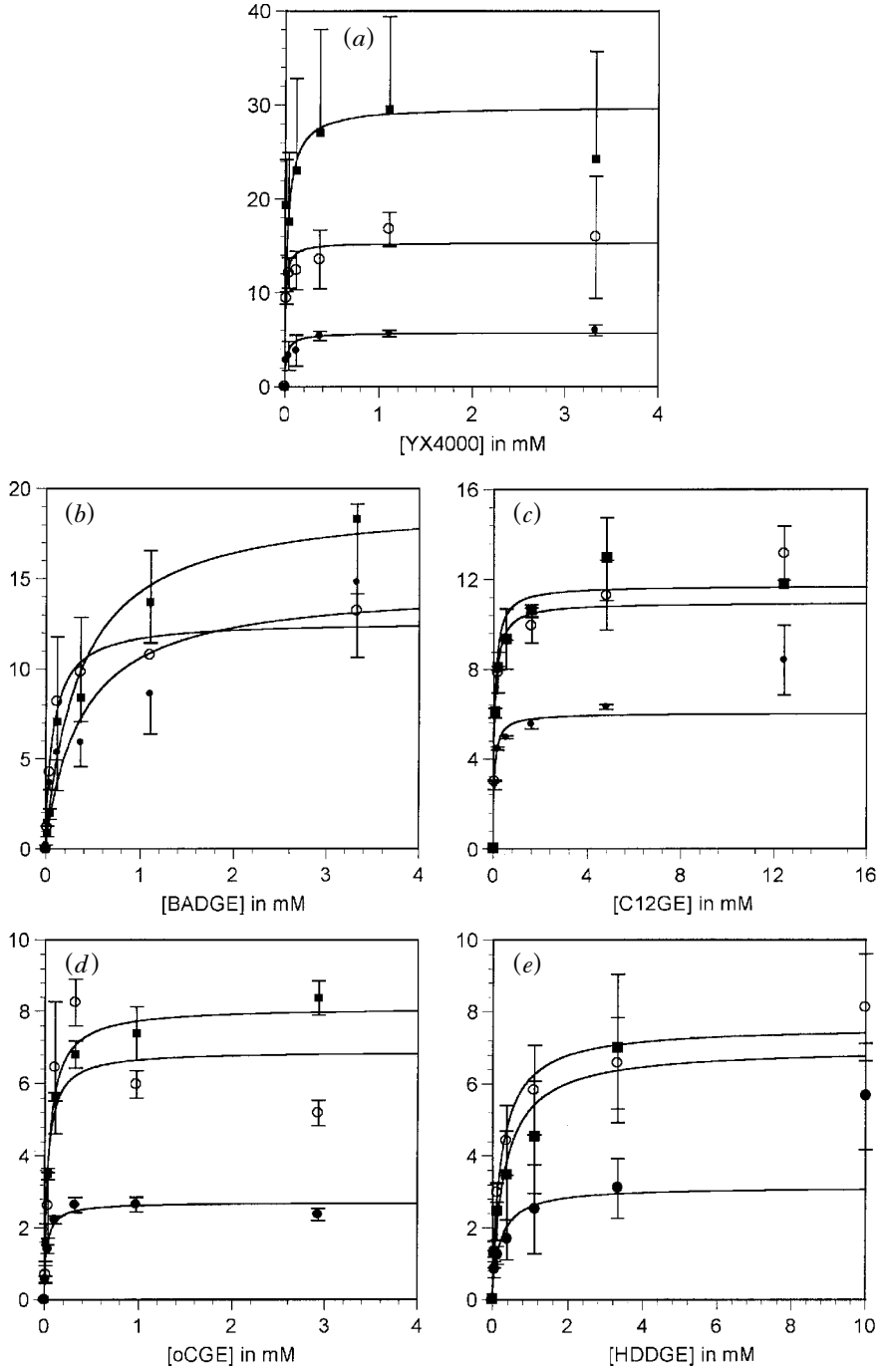


Figure 4. Enzymatic hydrolysis of various glycidyl ethers by human (○), Fisher 344 rat (●) and C3H mouse (■) lung microsomal fractions. Data points represent means ± SE of six separate experiments with lung microsomes from six individuals (three males, three females) or two-to-four separate experiments with lung microsomes from rodents. (a) YX4000 (4,4′-dihydroxy-3,3′,5,5′-tetramethylbiphenyl diglycidyl ether). The lines represent model simulations for the Michaelis–Menten equation fitted to the data points ($R^2 = 0.957$, 0.943 and 0.998 for hydrolysis by human, rat and mouse lung microsomes respectively). (b) BADGE (*bis*phenol A diglycidyl ether). The lines represent model simulations for the Michaelis–Menten equation fitted to the data

Table 5. Apparent kinetic constants for enzymatic hydrolysis of YX4000 (4,4′-dihydroxy-3,3′,5,5′-tetramethylbiphenyl diglycidyl ether) by liver and lung cytosol and microsomes.

Organ	Fraction	Species	V_{max} (nmol/mg/min)	K_m (mM)	V_{max}/K_m μl/min/mg	*n*	*R*
Liver	cytosol	human	24.5	0.067	365	6	0.996
		rat	3.91	0.024	162	3	0.967
		mouse	16.8	0.027	619	3	0.988
	microsomes	human	133	0.18	731	6	0.984
		rat	30.6	0.064	475	3	0.987
		mouse	12.0	0.12	102	3	0.972
Lung	cytosol	human	1.01	0.022	47	6	0.848
		rat	1.04	0.020	52	2	0.999
		mouse	1.61	0.011	141	2	0.984
	microsomes	human	15.2	0.010	1524	6	0.978
		rat	5.59	0.023	241	3	0.970
		mouse	29.7	0.030	978	4	0.999

n, number of individuals /animals.
R, correlation coefficient of the fitted curve.

Table 6. Apparent kinetic constants for enzymatic hydrolysis of BADGE by liver and lung cytosol and microsomes.

Organ	Fraction	Species	V_{max} (nmol/mg/min)	K_m (mM)	V_{max}/K_m μl/min/mg	*n*	*R*
Liver	cytosol	human	26.1	0.22	117	4	0.999
		rat	12.2	0.37	32.6	6	0.948
		mouse	52.1	0.27	198	3	0.987
	microsomes	human	150	0.63	239	6	0.998
		rat	63.0	0.34	188	3	0.993
		mouse	46.6	0.23	203	3	0.991
Lung	cytosol	human	2.90	0.16	18.7	6	0.942
		rat	2.02	0.26	7.80	3	0.994
		mouse	3.45	0.25	13.6	5	0.940
	microsomes	human	12.5	0.08	157	6	0.993
		rat	14.5	0.38	38.1	3	0.950
		mouse	19.3	0.36	53.4	2	0.985

n, number of individuals /animals.
R, correlation coefficient of the fitted curve.

hydrolysis. In general, for the five GE under study, V_{max}/K_m was highest for YX4000 hydrolysis and least for HDDGE hydrolysis. For the other three GE, no general trend was observed: the V_{max}/K_m ratio for hydrolysis varied with organ and species. Comparing species, it appears that human microsomes, both of liver and

points ($R^2 = 0.982$, 0.971 and 0.898 for hydrolysis by human, rat and mouse lung microsomes respectively). (c) C_{12}GE (1-dodecyl glycidyl ether). The lines represent model simulations for the Michaelis–Menten equation fitted to the data points ($R^2 = 0.992$, 0.987 and 0.961 for hydrolysis by human, rat and mouse lung microsomes respectively). (d) *o*-CGE (*o*-cresyl glycidyl ether). The lines represent model simulations for the Michaelis–Menten equation fitted to the data points ($R^2 = 0.821$, 0.975 and 0.994 for hydrolysis by human, rat and mouse lung microsomes respectively). (e) HDDGE (1,6-hexanediol diglycidyl ether). The lines represent model simulations for the Michaelis–Menten equation fitted to the data points ($R^2 = 0.978$, 0.964 and 0.946 for hydrolysis by human, rat and mouse lung microsomes respectively).

Table 7. Apparent kinetic constants for enzymatic hydrolysis of 1-dodecanol glycidyl ether by liver and lung cytosol and microsomes.

Organ	Fraction	Species	V_{max} (nmol/mg/min)	K_m (mM)	V_{max}/K_m µl/min/mg	*n*	*R*
Liver	cytosol	human	21.1	0.17	124	6	0.9995
		rat	1.05	0.023	45.4	2	0.999
		mouse	12.7	0.10	129	2	0.969
	microsomes	human	137	0.71	192	6	0.984
		rat	48.2	0.31	156	2	0.997
		mouse	40.3	0.36	111	2	0.983
Lung	cytosol	human	0.77	0.20	3.88	6	0.950
		rat	0.21	0.78	0.26	2	0.953
		mouse	0.22	0.076	2.89	2	0.997
	microsomes	human	10.9	0.076	143	6	0.996
		rat	6.0	0.069	87.3	2	0.993
		mouse	11.7	0.072	163	2	0.983

n, number of individuals/animals.
R, correlation coefficient of the fitted curve.

Table 8. Apparent kinetic constants for enzymatic hydrolysis of *o*-cresyl glycidyl ether by liver and lung cytosol and microsomes.

Organ	Fraction	Species	V_{max} (nmol/mg/min)	K_m (mM)	V_{max}/K_m µl/min/mg	*n*	*R*
Liver	cytosol	human	12.7	0.062	204	6	0.981
		rat	1.16	0.019	60.2	2	0.995
		mouse	45.8	1.60	28.6	2	0.9999
	microsomes	human	106	0.43	244	6	0.966
		rat	61.4	0.26	232	2	0.984
		mouse	23.2	0.086	268	2	0.989
Lung	cytosol	human	0.40	0.013	30.7	6	0.985
		rat	no reaction	–	–	4	–
		mouse	0.91	3.04	0.30	3	0.998
	microsomes	human	6.86	0.036	189	6	0.906
		rat	2.68	0.032	84.5	2	0.987
		mouse	8.08	0.049	165	2	0.997

n, number of individuals/animals.
R, correlation coefficient of the fitted curve.

lung, have in general, a higher hydrolytic activity, as expressed by V_{max}/K_m, towards the GE than rat or mouse microsomes (tables 5–9). The only exceptions being the V_{max}/K_m ratio for HDDGE in rat liver microsomes, for *o*-CGE in mouse liver microsomes and for C_{12}GE in mouse lung microsomes. In these latter three cases, the V_{max}/K_m ratio of the human microsomes roughly equalled those of the rodent microsomes and had the lowest hydrolytic capacity towards the GE, the only exception being the activity of liver microsomes towards HDDGE where rat and human are equal. The V_{max}/K_m ratio for hydrolysis was highest in human lung cytosol for all GE except for YX4000 for which V_{max}/K_m was higher in mouse lung cytosol. V_{max}/K_m was higher in human liver cytosol than in mouse liver cytosol for *o*-CGE and HDDGE, and the opposite was found for YX4000 and BADGE, whereas about equal values were observed for C_{12}GE.

Table 9. Apparent kinetic constants for enzymatic hydrolysis of 1,6-hexanediol diglycidyl ether by liver and lung cytosol and microsomes.

Organ	Fraction	Species	V_{max} (nmol/mg/min)	K_m (mM)	V_{max}/K_m µl/min/mg	*n*	*R*
Liver	cytosol	human	36.6	1.05	34.7	6	0.992
		rat	3.48	1.01	3.45	2	0.989
		mouse	96.9	3.07	31.5	3	0.9999
	microsomes	human	93.7	0.77	122	6	0.999
		rat	23.0	0.18	129	2	0.984
		mouse	18.9	0.26	74.0	2	0.977
Lung	cytosol	human	0.52	0.11	4.78	6	0.982
		rat	1.42	2.42	0.59	2	0.9991
		mouse	3.31	6.69	0.49	2	0.9995
	microsomes	human	7.57	0.24	31.6	6	0.989
		rat	3.11	0.22	14.3	2	0.983
		mouse	6.98	0.33	21.1	2	0.972

n, number of individuals /animals.
R, correlation coefficient of the fitted curve.

Discussion

The epoxy moiety makes glycidyl ethers chemically reactive compounds, a characteristic which on the one hand is an essential prerequisite for their commercial use, but on the other hand makes them toxicologically active since some epoxy compounds have been associated with cancer. In a small number of cases, glycidyl ethers have been reported to cause tumours in animal studies. For example, in an inhalation study of phenyl glycidyl ether (PGE) in rat, nasal carcinomas, squamous cell metaplasia, hyperplasia and dysplasia and chronic rhinitis were observed (Lee *et al.* 1983). Based on this latter study, the IARC classified PGE as a group 2B carcinogen (possibly carcinogenic to humans) (IARC 1989, 1999a). Other glycidyl ethers such as BADGE and triethylene glycol diglycidyl ether, were considered not classifiable as to their carcinogenicity to humans (group 3) since only limited or inadequate evidence in experimental animals and no epidemiological data in humans relevant to their carcinogenicity was available (IARC 1989, 1999c, d). The epoxy group is also responsible for the direct mutagenic effects observed in bacteria exposed to glycidyl ethers (Gardiner *et al.* 1992) and for the DNA adducts observed in *in vitro* systems (Plná *et al.* 1996, Deforce *et al.* 1998). However, these observations might be less relevant for the *in vivo* situation since GE may be detoxified by hydrolysis of the epoxide group or by GSH conjugation. In the present study, these two detoxification reactions were quantified for representatives of four classes of GE.

Glutathione conjugation

All GE were chemically stable in an aqueous environment as no measurable rate of hydrolysis was observed at maximum solubility. A small, but measurable, chemical reaction of GSH with the two most water-soluble GE, *o*-CGE and HDDGE, with estimated log $P_{o/w} = 2.2$ and 0.84 respectively, was observed under the given experimental conditions. Upon incubation with both liver and lung cytosol, rapid GSH conjugation was observed for both *o*-CGE and HDDGE (figure 3). The observed conjugation rates were considerably lower in human cytosol than

Table 10. Estimated rate constants for *in vivo* hepatic clearance ($l \times h^{-1} \times kg^{-1}$) of various glycidyl ethers in human and rodents[a].

Glycidyl ether	Species	Cytosolic glutathione *S*-transferase	Epoxide hydrolase
YX4000	human	nd[b]	51
	rat	nd	45
	mouse	< LOQ	103
BADGE	human	nd	17
	rat	< LOQ	13
	mouse	< LOQ	35
C_{12}GE	human	nd	16
	rat	nd	14
	mouse	< LOQ	23
o-CGE	human	0.45	24
	rat	3.6	19
	mouse	3.7	10
HDDGE	human	0.38	6.5
	rat	7.2	5.7
	mouse	6.4	6.5

[a] See the Materials and methods for calculations.
[b] nd, Not determined; < LOQ: below limit of quantitation.

in rodent cytosol, which is in agreement with the relative rates of GSH conjugation observed for other epoxides such as 1,2-epoxy-3-butene and 1,2:3,4-diepoxybutane (Csánady *et al.* 1992, Boogaard *et al.* 1996, 1999).

In contrast to *o*-CGE and HDDGE, only a very limited chemical reaction with GSH was observed with BADGE (estimated log $P_{o/w} = 3.8$) and no chemical reaction with the most lipophilic GE C_{12}GE and YX4000 (estimated log $P_{o/w} = 5.0$ and 5.1 respectively), which is probably explained by their poor solubility in water. Low, inconsistent GSH conjugation with BADGE and no measurable GSH conjugation with YX4000 and C_{12}GE were observed upon incubation with liver cytosol. Climie *et al.* (1981b) reported that incubation of 6 μM ^{14}C-BADGE with CF1 mouse liver cytosol (2 mg protein/ml) for 30 min in the presence of 5 mM GSH, gave a polar compound which did not migrate in a TLC system (ethyl acetate–formic acid–water [70:4:4] on silicagel) and which was assumed to be the GSH conjugate since the compound was not found in the absence of GSH. Although this non-migrating compound was not identified, 80% of the radioactivity applied to the TLC plate migrated and was recovered as the *bis*-diol of BADGE. In our system, EH activity was inhibited by pre-incubation with 4-PCO and only traces of the diol and *bis*-diol could be identified (data not shown). In the current study, the formation of a GSH conjugate of BADGE was confirmed in two ways. First, small radio-peaks with identical retentions appeared in both conjugation experiments with ^{3}H-GSH and unlabelled BADGE and with unlabelled GSH and ^{14}C-BADGE. Second, the identity of the peak was confirmed by LC-MS.

In general, it seems that the more hydrophilic the GE is, the faster its enzyme-catalysed GSH conjugation proceeds. This is in agreement with the relative GSH conjugation rates for substituted phenyl glycidyl ethers in Sprague–Dawley rat liver cytosol: 17.7, 25.3 and 77.74 nmol/mg protein/min for *p*-methoxyphenyl-, phenyl- and *p*-nitrophenyl-glycidyl ether (Sinsheimer *et al.* 1987), which are closely related to *o*-CGE for which a $V_{max} = 61.3$ nmol/mg protein/min was measured in rat liver cytosol in our study. Although little, if any, GSH conjugation was measured for

Table 11. Estimated rate constants for *in vivo* pulmonary clearance ($l \times h^{-1} \times kg^{-1}$) of various glycidyl ethers in human and rodents[a].

Glycidyl ether	Species	Cytosolic glutathione *S*-transferase	Epoxide hydrolase
YX4000	human	nd[b]	1.9
	rat	nd	0.87
	mouse	nd	2.6
BADGE	human	nd	0.28
	rat	nd	0.13
	mouse	nd	0.17
C_{12}GE	human	nd	0.17
	rat	nd	0.066
	mouse	nd	0.33
o-CGE	human	0.02	0.40
	rat	0.07	0.060
	mouse	0.03	0.32
HDDGE	human	0.01	0.064
	rat	0.22	0.018
	mouse	0.05	0.043

[a] See the Materials and Methods and Materials for calculations.
[b] nd, Not determined.

YX4000, BADGE and C_{12}GE, it is clear from the estimated values in tables 10 and 11 that GSH conjugation is an important route of detoxification for *o*-CGE and HDDGE, especially in rodents. The estimated hepatic clearances were 0.45, 3.6 and 3.7 l/h/kg for *o*-CGE in human, rat and mouse respectively, and 0.38, 7.2 and 6.4 for HDDGE in human, rat and mouse respectively. In a identical way, *in vivo* clearances were estimated based on *in vitro* data for a limited number of simple aliphatic epoxides. Compared with these epoxides, the estimated clearances by GSH conjugation are strikingly similar: 0.47, 5.66 and 4.36 l/h/kg for hepatic clearance of 1,2-epoxy-3-butene by human, rat and mouse respectively (Csánady *et al.* 1993) and 0.26, 2.51 and 7.82 l/h/kg for hepatic clearance of 1,2:3,4-diepoxybutane by human, rat and mouse respectively (Boogaard *et al.* 1996, Boogaard and Bond 1996). This indicates that, with regard to enzyme-catalysed GSH conjugation, *o*-CGE and HDDGE behave like simple aliphatic epoxides.

Epoxide hydrolysis

Epoxide hydrolysis is the most important route of detoxification for most GE. All GE were rapidly hydrolysed to the corresponding (*bis*-)diols. The two glycidyl groups in the bifunctional GE, YX4000, BADGE and HDDGE, behave independently. This is in agreement with the results for BADGE reported by Climie *et al.* (1981a). Apparently, the affinity of the EH for the unchanged GE and the corresponding mono-diol is equal or only negligibly different, which allows the use of the total of the mono-diol and *bis*-diol to calculate the Michaelis–Menten parameters. There is a considerable difference between the various GE in efficiency of hydrolysis, expressed as V_{max}/K_m. In general, the microsomal EH is more efficient than the cytosolic EH, and human microsomal fractions are more efficient in hydrolysis of the GE than rodent microsomal fractions at low substrate concentrations, which are more relevant for human exposure. Although no simple relationship was found, the reaction catalysed by the microsomal EH seems to be

related with the aromaticity and lipophilicity of the compounds. GE with an aromatic ring have higher V_{max}/K_m than aliphatic GE, and V_{max}/K_m is higher for GE with a higher log $P_{o/w}$. For human liver microsomes, for instance, the V_{max}/K_m decrease in the following order YX4000 > BADGE > *o*-CGE > C_{12}GE > HDDGE. The estimated *in vivo* clearance for the five GE (tables 10 and 11) indicate that rat has the poorest clearance, both in liver and lung, with exception of the hepatic clearance of *o*-CGE, which is least in mouse. Generally, there is not much difference in hepatic clearance: it differs no more than 1 order of magnitude from one GE to the other and from one species to the other. The differences in pulmonary clearance are larger: although there is < 1 order of magnitude of difference between species for the same GE, much larger differences are found between the various GE. Despite this variation, on the whole the *in vivo* clearances for both liver and lung are much larger (about 2 orders of magnitude) than for simple aliphatic epoxides such as 1,2-epoxy-3-butene and 1,2:3,4-diepoxybutane (Csánady *et al.* 1993, Boogaard and Bond 1996). In experimental animals, the relative importance of epoxide hydrolysis compared with GSH conjugation was demonstrated *in vivo* for PGE and *o*-CGE. Upon administration of PGE to rat and rabbit, either by oral gavage or by subcutaneous injection, the major urinary metabolite was 2-hydroxy-3-phenoxyproprionic acid, formed by hydrolysis of the epoxy group of PGE and subsequent oxidation. In addition, *N*-acetyl-*S*-(2-hydroxy-3-phenoxypropyl)-L-cysteine, the mercapturic acid of PGE formed following GSH conjugation of PGE, was excreted as a minor metabolite in urine (James *et al.* 1978). More recently, the urinary metabolite profile of PGE and *o*-CGE was studied in rat following intraperitoneal administration (De Rooij *et al.* 1998). In this latter study a novel metabolite of PGE was found: *N*-acetyl-*O*-phenylserine, which is believed to result from oxidation of 2-hydroxy-3-phenoxyproprionic acid followed by transamination and *N*-acetylation, and thus a metabolite from the epoxide hydrolysis pathway. A similar metabolite was also found for *o*-CGE. At low doses of PGE the GSH pathway accounted for > 25% of the metabolites excreted in urine, and with increasing dose, this percentage declined to ~ 10%. In contrast, the epoxide hydrolysis pathway accounted for ~ 40% of the urinary metabolites, irrespective the dose. For *o*-CGE a similar pattern was observed (De Rooij *et al.* 1998).

Oxidative dealkylation

Theoretically, metabolism of GE might also lead to more toxic compounds since oxidative de-alkylation of the GE might lead to the formation of glyceraldehyde and glycidaldehyde. The latter is classified by IARC as a group 2B carcinogen (possibly carcinogenic to humans) (IARC 1976, 1999e). Although it has been argued that glyceraldehyde, and not glycidaldehyde, is formed *in vivo* (Climie *et al.* 1981a, b), there is still concern about the formation of glycidaldehyde as its formation from PGE and allyl glycidyl ether has been demonstrated *in vitro* (Plná *et al.* 1996. Deforce *et al.* 1998). Evidence for the *in vivo* formation of glycidaldehyde from BADGE and allyl glycidyl ether has also been reported following topical administration (Bentley *et al.* 1989, Steiner *et al.* 1992a, b, Plná and Segerbäck 1997). It has previously been shown that oxidative de-alkylation of BADGE only occurred at high doses, leading to saturation of the EH pathway, or when EH was inhibited (Bentley *et al.* 1989). Like BADGE, glycidaldehyde is a good substrate for EH and glycidaldehyde is a particularly good substrate for GST. GSH conjugation rates in

rat, after incubation of 3.0 mM glycidaldehyde with 3.0 mM GSH, were 4.1 ± 0.4 and 1.9 ± 0.1 μmol/mg protein/min for liver (1 mg/ml) and lung (1.5 mg/ml) cytosol respectively, and hydrolysis rates, after incubation of 0.1 mM glycidaldehyde with liver (3.3 mg/ml) or lung (5 mg/ml) microsomes, were 26 and 20 nmol/mg/min respectively (Patel *et al.* 1980). Accordingly, it is unlikely that the formation of glycidaldehyde from BADGE or other GE will pose an important genotoxic risk as the small amounts of glycidaldehyde will be rapidly detoxified.

In conclusion, the selected GE, which represent different classes of GE, show a very large variation with regard to the rate of inactivation of the epoxide moiety indicating that GE have highly variable properties and should not be considered as a single class of compounds. In addition, the rates for hydrolysis of the epoxide moiety, the most important inactivation pathway for most of the GE, are ~ 2 orders of magnitude higher than for some simple aliphatic epoxides.

References

Bentley, P., Bieri, F., Kuster, H., Muakkassah-Kelly, S., Sagelsdorff, P., Stäubli, W. and Waechter, F., 1989, Hydrolysis of bisphenol A diglycidylether by epoxide hydrolases in cytosolic and microsomal fractions of mouse liver and skin: inhibition by bis epoxycyclopentylether and the effects upon the covalent binding to mouse skin DNA. *Carcinogenesis*, **10**, 321–327.

Boogaard, P. J. and Bond, J. A., 1996, The role of hydrolysis in the detoxification of 1,2:3,4-diepoxybutane by human, rat, and mouse liver and lung *in vitro*. *Toxicology and Applied Pharmacology*, **141**, 617–627.

Boogaard, P. J., Denneman, M. A. and van Sittert, N. J., 2000, Dermal penetration and metabolism of five glycidyl ethers in human, rat and mouse skin. *Xenobiotica*, **30**, 469–483.

Boogaard, P. J., Sumner, S. C. J. and Bond, J. A., 1996, Glutathione conjugation of 1,2:3,4-diepoxybutane in human liver and rat and mouse liver and lung *in vitro*. *Toxicology and Applied Pharmacology*, **136**, 307–316.

Boogaard, P. J., van Elburg, P. A., de Kloe, K. P., Watson, W. P. and van Sittert, N. J., 1999, Metabolic inactivation of 2-oxiranomethyl 2-ethyl-2,5-dimethyl hexanoate (C_{10}GE) in skin, lungs, and liver of humans, rats and mice. *Xenobiotica*, **29**, 987–1006.

Climie, I. J. G., Hutson, D. H. and Stoydin, G., 1981a, Metabolism of the epoxy resin component 2,3-bis[4-(2,3-epoxypropoxy)phenyl]propane, the diglycidyl ether of bisphenol A (DGEBPA) in the mouse. I. A comparison of the fate of a single dermal application and of a single oral dose of ^{14}C-DGEBPA. *Xenobiotica*, **11**, 391–399.

Climie, I. J. G., Hutson, D. H. and Stoydin, G., 1981b, Metabolism of the epoxy resin component 2,3-bis[4-(2,3-epoxypropoxy)phenyl]propane, the diglycidyl ether of bisphenol A (DGEBPA) in the mouse. II. Identification of metabolites in urine and faeces following of a single oral dose of ^{14}C-DGEBPA. *Xenobiotica*, **11**, 401–424.

Csanády, G. A., Guengerich, F. P. and Bond, J. A., 1992a, Comparison of the biotransformation of 1,3-butadiene and its metabolite, butadiene monoepoxide, by hepatic and pulmonary tissues from humans, rats and mice. *Carcinogenesis*, **13**, 1143–1153. [Erratum *Carcinogenesis*, **14**, 784.]

De Rooij, B. M., Commandeur, J. N. M., Hommes, J. W., Aalbers, T., Groot, E. J. and Vermeulen, N. P. E., 1998, Urinary metabolite profile of phenyl and *o*-cresyl glycidyl ethers in rats: identification of a novel pathway leading to *N*-acetylserine O-conjugates. *Chemical Research in Toxicology*, **11**, 111–118.

Deforce, D. L. D., Lemière, F., Hoes, I., Millecamps, R. E. M., Esmans, E. L., de Leenheer, A. and van den Eeckhout, E. G., 1998, Analysis of the DNA adducts of phenyl glycidyl ether in a calf thymus DNA hydrolysate by capillary zone electrophoresis–electrospray mass spectrometry: evidence for phosphate alkylation. *Carcinogenesis*, **19**, 1077–1086.

Eadsforth, C. V., 1983, *EPIKOTE* 828: *Determination of the* N-*Octanol/water Partition Coefficient Using a Reverse-phase HPLC Method*. Report no. SBGR 83. 385 (Sittingbourne: Shell Research Centre).

Gardiner, T. H., Waechter, J. M., Wiedow, M. A. and Solomon, W. T., 1992, Glycidyloxy compounds used in epoxy resin systems: a toxicology review. *Reviews in Toxicology and Pharmacology*, **15**, S1–77.

Guest, D. and Dent, J. G., 1980, Effects of epoxide hydratase inhibitors in forward and reversion bacterial mutagenesis assay systems. *Environmental Mutagenesis*, **2**, 27–34.

IARC, 1976, *Cadmium, Nickel, some Epoxides, Miscellaneous Industrial Chemicals and General Considerations on Volatile Anaesthetics. Glycidaldehyde* (Lyon: IARC), **11**, 175–181.

IARC, 1985, *Allyl Compounds, Aldehydes, Epoxides and Peroxides. Diglycidyl Resorcinol Ether* (Lyon: IARC), **36**, 181–188.

IARC, 1989, *Some Organic Solvents, Resin Monomers and Related Compounds, Pigments and Occupational Exposures in Paint Manufacture and Painting. Some Glycidyl Ethers* (Lyon: IARC), **47**, 237–261.

IARC, 1999a, *Re-evaluation of Some Organic Chemicals, Hydrazine and Hydrogen Peroxide. Phenyl Glycidyl Ether* (Lyon: IARC), **71**, 1525.

IARC, 1999b, *Re-evaluation of Some Organic Chemicals, Hydrazine and Hydrogen Peroxide. Diglycidyl Resorcinol Ether* (Lyon: IARC), **71**, 1417.

IARC, 1999c, *Re-evaluation of Some Organic Chemicals, Hydrazine and Hydrogen Peroxide. Bisphenol A Diglycidyl Ether* (Lyon: IARC), **71**, 1265.

IARC, 1999d, *Re-evaluation of Some Organic Chemicals, Hydrazine and Hydrogen Peroxide. Triethylene Glycol Diglycidyl Ether* (Lyon: IARC), **71**, 1285.

IARC, 1999e, *Re-evaluation of Some Organic Chemicals, Hydrazine and Hydrogen Peroxide. Glycidaldehyde* (Lyon: IARC), **71**, 1459.

ILSI, 1994, *Physiological Parameter Values for PBPK Models*. Report prepared by the ILSI Risk Science Institute Working Group on Physiological Parameters (Washington, DC: International Life Science Institute).

James, S. P., Pheasant, A. E. and Solheim, E., 1978, Metabolites of 1,2-epoxy-3-phenoxy- and 1,2-epoxy-3-(*p*-nitrophenoxy)propane. *Xenobiotica*, **8**, 219–228.

Lee, K. P., Schneider, P. W. and Trochimowicz, H. J., 1983, Morphological expression of glandular differentiation in the epidermoid nasal carcinomas induced by phenyl glycidyl ether inhalation. *American Journal of Pathology*, **3**, 140–148.

Mullin, C. A. and Hammock, B. D., 1982, Chalcone oxides – potent selective inhibitors of cytosolic epoxide hydrolase. *Archives of Biochemistry and Biophysics*, **216**, 423–439.

Patel, J. M., Wood, J. C. and Leibman, K. C., 1980, The biotransformation of allyl alcohol and acrolein in rat liver and lung preparations. *Drug Metabolism and Disposition*, **8**, 305–308.

Plná, K. and Segerbäck, D., 1997, ^{32}P-postlabelling of DNA adducts formed by allyl glycidyl ether *in vitro* and *in vivo*. *Carcinogenesis*, **18**, 1457–1462.

Plná, K., Segerbäck, D. and Schweda, E. K. H., 1996, DNA adduct formation by allyl glycidyl ether. *Carcinogenesis*, **17**, 1465–1471.

Sinsheimer, J. E., van den Eeckhout, E., Hooberman, H. B. and Beylin, V. G., 1987, Detoxification of aliphatic epoxides by diol formation and glutathione conjugation. *Chemico-Biological Interactions*, **63**, 75–90.

Steiner, S., Crane, A. E. and Watson, W. P., 1992a, Molecular dosimetry of DNA adducts in C3H mice treated with glycidaldehyde. *Carcinogenesis*, **13**, 119–124.

Steiner, S., Hönger, G. and Sagelsdorff, P., 1992b, Molecular dosimetry of DNA adducts in C3H mice treated with bisphenol A diglycidyl ether. *Carcinogenesis*, **13**, 969–972.

Van Elburg, P. A., Ormskerk, O. A., de Kloe, K. P. and Boogaard, P. J., 2000, Synthesis of [^{14}C]-labelled glycidyl and glycerol ethers of aliphatic and aromatic alcohols. *Journal of Labelled Compound Radiopharmacology*, **43**, 147–167.

XENOBIOTICA , 2000, VOL. 30, NO. 5, 503–513

Identification of cytochrome P450 isoform involved in the metabolism of YM992, a novel selective serotonin re-uptake inhibitor, in human liver microsomes

K. NOGUCHI†*, A. MERA†, T. WATANABE†, S. HIGUCHI†, and K. CHIBA‡

† Drug Metabolism Laboratories, Yamanouchi Pharmaceutical Co., Ltd, 1–8, Azusawa 1-chome, Itabashi-ku, Tokyo 174–8511, Japan
‡ Laboratory of Biochemical Pharmacology and Toxicology, Faculty of Pharmaceutical Sciences, Chiba University, 1-33 Yayoi-cho, Inage-ku, Chiba 263–8522, Japan

Received 24 September 1999

1. *In vitro* studies were conducted to identify the hepatic cytochrome P450 isoform involved in the metabolism of YM992, ((*S*)-2-[[(fluoro-4-indanyl)oxy]methyl]morpholine monohydrochloride), a novel serotonin re-uptake inhibitor, in human liver microsomes.

2. Microsomes prepared from yeast expressing CYP1A1, CYP1A2 and CYP2D6 effectively metabolized YM992. A significant correlation was observed between the rate of YM992 metabolism and 7-ethoxyresorufin *O*-deethylation, CYP1A1/2 specific activity, in liver microsomes from 16 individual donors ($r^2 = 0.628$, $p < 0.001$). α-Naphtoflavone and isosafrole, CYP1A1/2 inhibitors, suppressed the metabolism of YM992 in human liver microsomes in a concentration-dependent manner.

3. The metabolism of YM992 in human liver microsomes was inhibited by ~ 95% by antibodies which recognize both CYP1A1 and CYP1A2 whereas antibodies specific for CYP1A1 did not show inhibitory effects.

4. The same major metabolites, M6 and M7, were generated from YM992 after incubation with human liver microsomes and recombinant human CYP1A2.

5. These results suggest that the metabolism of YM992 in human liver microsomes is mainly catalysed by CYP1A2, and that YM992 might increase plasma concentration of concomitant drugs metabolized by CYP1A2 due to competitive inhibition.

Introduction

Recently selective serotonin re-uptake inhibitors (SSRI) have been widely used for the treatment of depression because of their safety profile over tricyclic antidepressants. YM992, ((*S*)-2-[[(fluoro-4-indanyl)oxy]methyl]morpholine monohydrochloride), is a newly synthesized SSRI (figure 1) and exhibits a dual mode of action, namely selective serotonin re-uptake inhibition and 5-HT_{2A} antagonistic activity (Hatanaka *et al.* 1996, Takeuchi *et al.* 1997). Therefore, YM992 is expected to show faster onset of pharmacological action in comparison with conventional SSRI.

After oral administration of ^{14}C-YM992 to humans, almost 100% of radioactivity was excreted into urine. Urinary unchanged YM992 accounted for < 10% of radioactivity, and the rest of radioactivity was recovered as oxidative metabolites and their conjugates (unpublished data). These findings suggest that YM992 is

* Author for correspondence; e-mail: noguchik@yamanouchi.co.jp

Xenobiotica ISSN 0049-8254 print/ISSN 1366-5928 online © 2000 Taylor & Francis Ltd
http://www.tandf.co.uk/journals

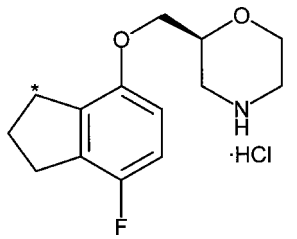


Figure 1. Chemical structure of YM992. * Labelled position.

almost completely absorbed from the gastrointestinal tract and that its elimination mainly depends on metabolism. It is well known that cytochrome P450 catalyses the biotransformation of a variety of drugs and carcinogens (Gonzalez 1992, Guengerich 1994). The characterization of the isoform(s) responsible for the *in vitro* metabolism of YM992 provides information to predict the potential drug–drug interactions between YM992 and other medications and genetic polymorphism on the metabolic disposition of YM992.

In the present study, the principal P450 isoform involved in the metabolism of YM992 have been identified by using human liver microsomes and cDNA-expressed human P450 isoforms. YM992 is transformed to various metabolites in human liver microsomes and their metabolic rates are very low. It is therefore difficult to estimate the rate of metabolism for each metabolite at physiologically relevant YM992 concentration. Consequently, the principal P450 isoform was identified from the disappearance rate of YM992 from the incubation mixture, instead of the formation rate of each metabolite.

Materials and methods

Chemicals

YM992 (chemical purity 99%) and 2-[[4-fluoro-5,6,7,8-tetrahydro-1-naphtyl)oxy]methyl]morpholine hemifumarate (YM-35005, 99%) used as the internal standard for HPLC were synthesized in Chemical Technology Laboratories and Neuroscience and Gastrointestinal Research Laboratories of Yamanouchi Pharmaceutical Co., Ltd respectively. ^{14}C-YM992, labelled at the C-3 position of the indan ring (98% radiochemical purity, 1.74 MBq/mg), was synthesized at Amersham Pharmacia Biotech (Cardiff, UK). Glucose 6-phosphate, glucose 6-phosphate dehydrogenase and $NADP^+$ were from Boehringer Mannheim GmbH (Mannheim, Germany), α-naphthoflavone and quinidine from Nacalai Tesque, Inc. (Kyoto, Japan), isosafrole, quercetin and 4-fluoro-7-nitrobenzofurazan from Wako Pure Chemical Industries, Ltd (Osaka, Japan), orphenadrine and troleandomycin from Sigma Chemical Co. (St Louis, MO, USA), *S*-mephenytoin from Sumika Chemical Analysis Service Ltd (Osaka, Japan), ketoconazole from Research Biochemical, Inc. (Natik, MA, USA). Sulphaphenazole was a gift of Meiji Yakuhin Co. (Tokyo, Japan). Goat anti-rat CYP1A1 serum, which exclusively inhibits human CYP1A1, and rabbit anti-rat CYP1A2 serum, which inhibits human both CYP1A1 and CYP1A2, were from Daiichi Pure Chemicals (Tokyo, Japan). All other chemicals and solvents used were of the highest commercially available quality.

Microsomal preparation

Human liver microsomes were from XENOTCH LLC (Kansas City, KS, USA) as the Reaction Phenotyping Kit®. The test kit contained microsomes from 16 individual donors. Microsomes were also supplied as pool of individual samples from 15 donors. Microsomal protein, total P450 concentrations and P450 isoform selective activities were provided by XENOTECH LLC. Microsomes from yeast expressing human CYP1A1, CYP1A2, CYP2A6, CYP2B6, CYP2C8, CYP2C9, CYP2C18, CYP2C19, CYP2D6, CYP2E1 and CYP3A4 were from Sumika Chemical Analysis Service Ltd (Osaka, Japan).

Analytical procedure

A typical incubation mixture contained 0.2 mg/ml human liver microsomes, 0.33 mM $NADP^+$, 8 mM glucose 6-phosphate, 0.1 U/ml glucose 6-phosphate dehydrogenase, 6 mM $MgCl_2$, 0.1 mM EDTA, 100 mM sodium-potassium phosphate buffer (pH 7.4) and YM992, in a final volume of 0.5 ml. In kinetic analysis, 5–50 ng/ml YM992 was used, and 10 ng/ml YM992 was used in other studies. The mixture was incubated at 37 °C. The reaction times were set to decrease the substrate concentrations by ~ 80% of the initial values: namely, 20 min for 5 ng/ml samples, 30 min for 10– 20 ng/ml samples, 40 min for 25 and 30 ng/ml samples, 50 min for 40 ng/ml samples, and 60 min for 50 ng/ml samples. Following the incubation, the reaction was stopped by the addition of 6 ml *n*-hexane. To the reaction mixtures, 0.1 ml 500 ng/ml YM-35005 (the internal standard) and 1 ml 0.2 M sodium bicarbonate solution were added. After shaking (10 min) and centrifugation (550*g*, 10 min), the organic phase was transferred to brown glass centrifuge tubes. To the organic phase, 1 ml 0.1 M HCl was added. After shaking (10 min) and centrifugation (550 *g*, 10 min), the organic phase was aspirated off. To the aqueous phase, 1 ml 0.2 M sodium hydroxide and 6 ml *n*-hexane were added. After shaking (10 min) and centrifugation (550 *g*, 10 min), the organic phase was transferred to another brown glass centrifuge tube. The organic solvent was evaporated to dryness under reduced pressure. To the residue, 0.15 ml 0.1 M borate buffer (pH 7.5) and 0.1 ml 1 mM 4-fluoro-7-nitrobenzofurazan ethanol solution were added to convert YM992 and the internal standard to fluorescent derivatives. After standing at room temperature for 20 min, 0.02 ml 1 M HCl was added to stop the reaction, and a portion of 100 µl of the resultant solution was injected onto an HPLC system. The HPLC system consisted of a model LC 10AS pump, a model CRO-10A column oven, a model SCL-10A system controller, a model SIL-10A autosampler, a model RF-10A$_{XL}$ fluorescence detector, a model C-R4AX integrator (all Shimadzu Corp., Kyoto, Japan) and a TSK gel ODS-80 Ts (4.6×150 mm; Tosoh Corp., Tokyo, Japan). A mixture of 50 mM phosphoric acid:acetonitrile (38:62 v/v) was delivered at 1 ml/min. The column eçuent was monitored at 547 nm with 487 nm excitation. The column temperature was kept at 35 °C.

Kinetic analysis

Initially, the data were examined on Eadie–Hofstee plots to assess the potential for multiplicity of enzymes. Then, the data were analysed by non-linear least-squares regression analysis fitting the data to the equation $v = (V_{max} \times S)/(K_m + S)$, where v is the reaction velocity corresponding to S, the substrate concentration, V_{max} is the maximal velocity, and K_m is the substrate concentration at which the reaction velocity equals 50% of V_{max}. K_m was corrected by non-specific binding of YM992 to microsomal fraction.

Determination of non-specific binding of YM992 to microsomes

Non-specific binding of YM992 to microsomal fraction was determined by an ultrafiltration method. The mixtures containing 10, 20 and 50 ng/ml YM992 without the NADPH-generating system in a total volume of 2 ml were prepared. A portion of 0.2 ml was sampled for the determination of total YM992 concentration. The remainder of the sample (1.8 ml) was applied to an ultrafiltration tube (ULTRACENT30, Tosoh) and centrifuged at 37 °C, at 550 *g* for 30 min. The filtrate (0.2 ml) was used for the determination of unbound YM992 concentration. The unbound fraction ratio was defined as (unbound concentration)/(total concentration).

Correlation study

The activities of YM992 metabolism in human liver microsomes were compared with 7-ethoxyresorufin *O*-deethylation (CYP1A1/2), coumarin 7-hydroxylation (CYP2A6), tolbutamide methyl-hydroxylation (CYP2C9), *S*-mephenytoin 4′-hydroxylation (CYP2C19) and testosterone 6β-hydroxylation (CYP3A4). These P450 isoform selective activities were specified by the supplier. For details of the P450 isoform selective activity assays, see Pearce *et al.* (1996), *passim*.

Chemical inhibition study

The effects of P450 inhibitors on the metabolism of YM992 in human liver microsomes were studied. The inhibitors used were α-naphthoflavone (CYP1A1/2) (Chang *et al.* 1994), isosafrole (CYP1A1/2) (Pastrakuljic *et al.* 1997), orphenadrine (CYP2B6) (Stevens *et al.* 1997), quercetin (CYP2C8) (Rahman *et al.* 1994), sulphaphenazole (CYP2C9) (Bourrié *et al.* 1996), *S*-mephenytoin (CYP2C19) (Küpfer *et al.* 1984), quinidine (CYP2D6) (Guengerich *et al.* 1986), ketoconazole (CYP3A4) (Back *et al.* 1992) and troleandomycin (CYP3A4) (Newton *et al.* 1995). All inhibitors were dissolved in methanol and added to the incubation mixture and control experiments without inhibitors confirmed that methanol (0.1% in the incubation mixture) did not affect the metabolic activity of YM992 in human liver microsomes. When

troleandomycin was used, microsomes were firstly incubated with the inhibitor and the NADPH-generating system at 37 °C for 10 min before the addition of the substrate.

Immunoinhibition

Immuno-inhibition of the metabolism of YM992 was examined by pre-incubation of 0.05 mg human liver microsomes with various concentrations of anti-human CYP1A1 serum or anti-human CYP1A1/2 serum at room temperature for 30 min. Then, other components of the incubation medium were added to give a final volume of 0.25 ml, and the reactions were carried out as described above.

Metabolism of YM992 by cDNA-expressed human P450 isoform

Incubation mixtures consisted of 100 pmole/ml recombinant human P450 isoform, 0.33 mM $NADP^+$, 8 mM glucose 6-phosphate, 0.1 U/ml glucose 6-phosphate dehydrogenase, 6 mM $MgCl_2$, 0.1 mM EDTA, 100 mM sodium-potassium phosphate buffer (pH 7.4) and 10 ng/ml YM992 in a final volume of 0.25 ml. The incubations were carried out at 37 °C for 60 min. Other methods were the same as described in the analytical procedure.

Chromatographic monitoring of metabolites

Incubation mixtures consisted of 1 mg/ml human liver microsomes or 100 pmole/ml recombinant human CYP1A2, 0.33 mM $NADP^+$, 8 mM glucose 6-phosphate, 0.1 U/ml glucose 6-phosphate dehydrogenase, 6 mM $MgCl_2$, 0.1 mM EDTA, 100 mM sodium-potassium phosphate buffer (pH 7.4) and 10 μg/ml ^{14}C-YM992, in a final volume of 0.25 ml. The mixtures were incubated at 37 °C for 180 min. After the reaction was stopped by addition of 50 μl 25% trichloroacetic acid, the mixture was centrifuged at 6500 *g* for 10 min. A portion of 200 μl supernatant was injected onto an HPLC system consisting of a model CCPM-II pump, a model CO-8020 column oven a model AS-8020 autosampler, a model SC-8020 controller and a model RS-8020 radio detector (all Tosoh). YM992 and metabolites were separated by reversed-phase HPLC with a gradient elution. The mobile phase A was a mixture of 50 mM ammonium acetate buffer (pH 4.5) and acetonitrile (95:5 v/v), and the mobile phase B was a mixture of 50 mM ammonium acetate buffer (pH 4.5) and acetonitrile (30:70 v/v). The mobile phase was delivered at 1 ml/min to TSK gel ODS-80Ts (4.6×250 mm; Tosoh) maintained at 40 °C and a gradient of decreasing polarity [time (min)/% of mobile phase B: 0/0, 60/25, 85/70]. Radioactivity in the eçuent was monitored for metabolites of YM992.

Results

Kinetic profile of YM992 metabolism in human liver microsomes

Eadie–Hofstee plots for the metabolism of YM992 in human liver microsomes showed that a single component was responsible for the YM992 metabolism (figure 2a). The nominal concentrations of the substrate and the metabolic activities were analysed by non-linear least-squares regression analysis to the Michaelis–Menten plots (figure 2b). K_m and V_{max} for YM992 metabolism were 15.5 ng/ml (= 0.054 μM) and 1.26 ng/mg protein/min (= 4.38 pmole/mg protein/min) respectively. The unbound fraction ratio was almost constant at every YM992 concentration tested, namely 0.572, 0.603 and 0.655 at 10, 20 and 50 ng/ml respectively with a mean of unbound fraction of YM992 of 0.61. Thus, the corrected K_m based on unbound concentration of YM992 was calculated as 9.5 ng/ml (= 0.033 μM).

Metabolism of YM992 by cDNA-expressed human P450 isoforms

The ability of cDNA-expressed P450 isoforms (CYP1A1, 1A2, 2A6, 2B6, 2C8, 2C9, 2C18, 2C19, 2D6, 2E1 and 3A4) to metabolize YM992 was investigated. Of the P450 isoforms tested, CYP1A1, 1A2 and 2D6 exhibited high rates of YM992

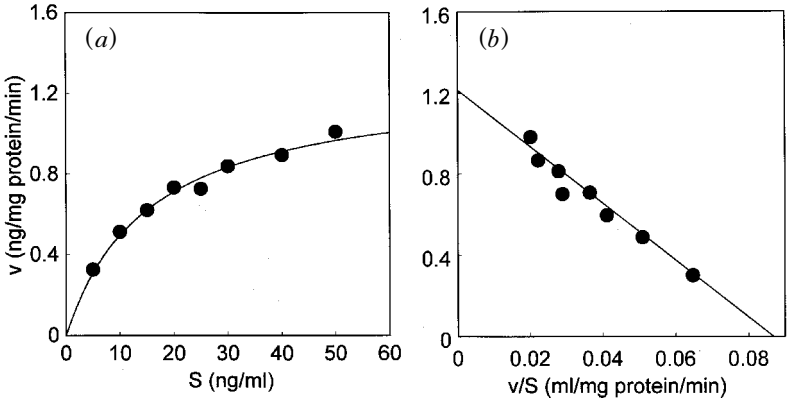


Figure 2. YM992 metabolism at various substrate concentrations in human liver microsomes. Solid limes were determined by least-squares regression analysis. Values are averages of duplicate determinations. (a) Michaelis–Menten plot; (b) Eadie–Hofstee plot.

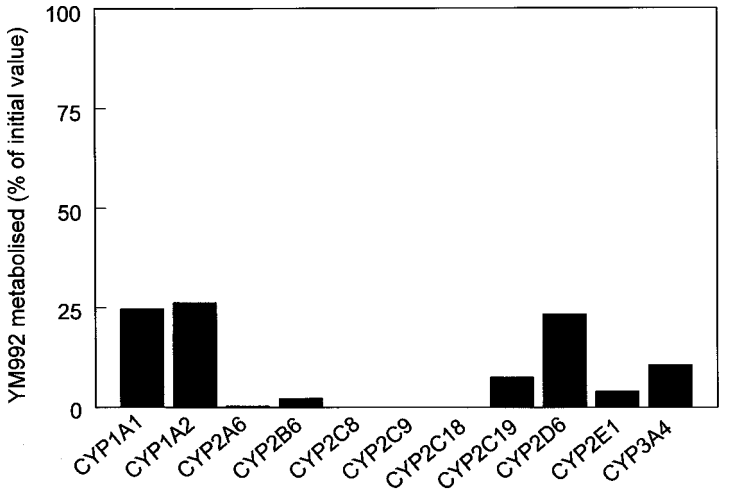


Figure 3. Metabolism of YM992 by microsomes of genetically engineered yeast cells expressing specific human P450 isoforms. Each datum point represents the average of duplicate determinations.

metabolic activity (figure 3). Relatively high metabolic activity was observed with CYP3A4 and CYP2C19. Other isoforms (CYP2A6, 2B6, 2C8, 2C9, 2C19 and 2E1) showed low or negligible activity for the metabolism of YM992, suggesting low contribution of these isoforms to the overall metabolism of YM992 in the human liver microsomes.

Correlation study

The correlations between activities for the metabolism of YM992 with P450 isoform specific enzyme activities in human liver microsomes from 16 individual donors are shown in table 1. A significant correlation was observed between the metabolic activities of YM992 with 7-ethoxyresorufin *O*-deethylation (CYP1A1/2, $r^2 = 0.628$, $p < 0.001$). No significant correlation was observed between the

Table 1. Correlation of YM992 metabolism with specific P450 isozyme activities in human liver microsomes.

P450 isozyme	Selective activity	Correlation coefficient (r^2)
CYP1A/12	7-ethoxyresorufin *O*-deethylation	0.628*
CYP2A6	coumarin 7-hydroxylation	0.021
CYP2C9	tolbutamide methyl-hydroxylation	0.044
CYP2C19	*S*-mephenytoin 4′-hydroxylation	0.202
CYP2D6	dextromethorphan *O*-demethylation	0.105
CYP2E1	chlorzoxazone 6-hydroxylation	0.121
CYP3A4	testosterone 6β-hydroxylation	0.085

Correlation coefficients were determined with liver microsomes from 16 individual donors.

* $p < 0.001$.

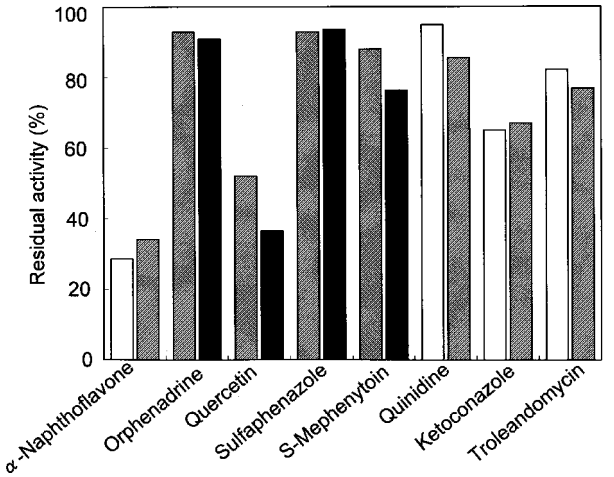


Figure 4. Effects of P450 inhibitors on the metabolism of YM992 in human liver microsomes. Inhibitor was added to the incubation mixture at a concentration of 1 μM (open column), 10 μM (hatched column) and 100 μM (closed column). Values are averages of duplicate determinations.

metabolic activities of YM992 with metabolic activities of other P450 isoforms (CYP2A6, CYP2C9, CYP2C19, CYP2D6, CYP2E1, CYP3A4). These results suggest that the metabolism of YM992 is mainly catalysed by CYP1A1/2.

Chemical inhibition study

The effects of inhibitors on the activities of YM992 metabolism in human liver microsomes were examined. As shown in figure 4, α-naphthoflavone, an inhibitor of CYP1A1/2, inhibited the activities of YM992 metabolism by 71 and 66% at 1 and 10 μM respectively. Quercetin (CYP2C8, 100 μM) showed 64% inhibition of the activities of YM992 metabolism. Ketoconazole (CYP3A4, 10 μM), troleandomycin (CYP3A4, 10 μM) and *S*-mephenytoin (CYP2C19, 100 μM) inhibited the activities of YM992 metabolism by 33, 23 and 24% respectively. Inhibitory effects of orphenadrine (CYP2B6), sulphaphenazole (CYP2C9) and quinidine (CYP2D6) were $< 20\%$. These results are consist with the results of the correlation study and support the possibility that CYP1A1/2 is mainly involved in the metabolism of

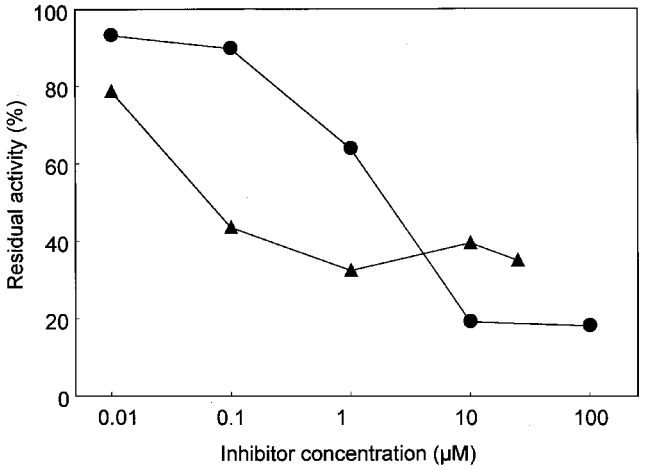


Figure 5. Inhibition of the metabolism of YM992 in human liver microsomes in relation to concentration of α-naphthoflavone and isosafrole, CYP1A1/2 inhibitors. Incubations were performed in duplicate.

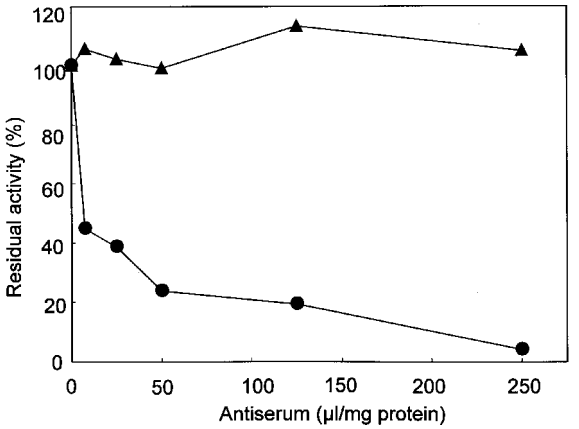


Figure 6. Immuno-inhibition of the metabolism of YM992 by antiserum for CYP1A1 and antiserum for CYP1A1/2. Each datum point represents the average of duplicate determinations. ●, Antiserum for CYP1A1/2; ▲, antiserum for CYP1A1.

YM992. To confirm further the involvement of CYP1A1/2 in the metabolism of YM992, the effects of α-naphthoflavone and isosafrole, inhibitors of CYP1A1/2, were examined at various concentrations on the metabolism of YM992 in human liver microsomes. The metabolism of YM992 was inhibited by both α-naphthoflavone and isosafrole in a concentration-dependent manner (figure 5).

Immunoinhibition study

As shown in figure 6, antibodies that recognize both CYP1A1 and 1A2 inhibited the metabolism of YM992 in human liver microsomes. At the highest concentration of antibody examined (250 μl/mg protein), the metabolism of YM992 was inhibited by $\sim$ 95%. On the contrary, antibodies specific for CYP1A1 did not show inhibitory effects on the metabolism of YM992.

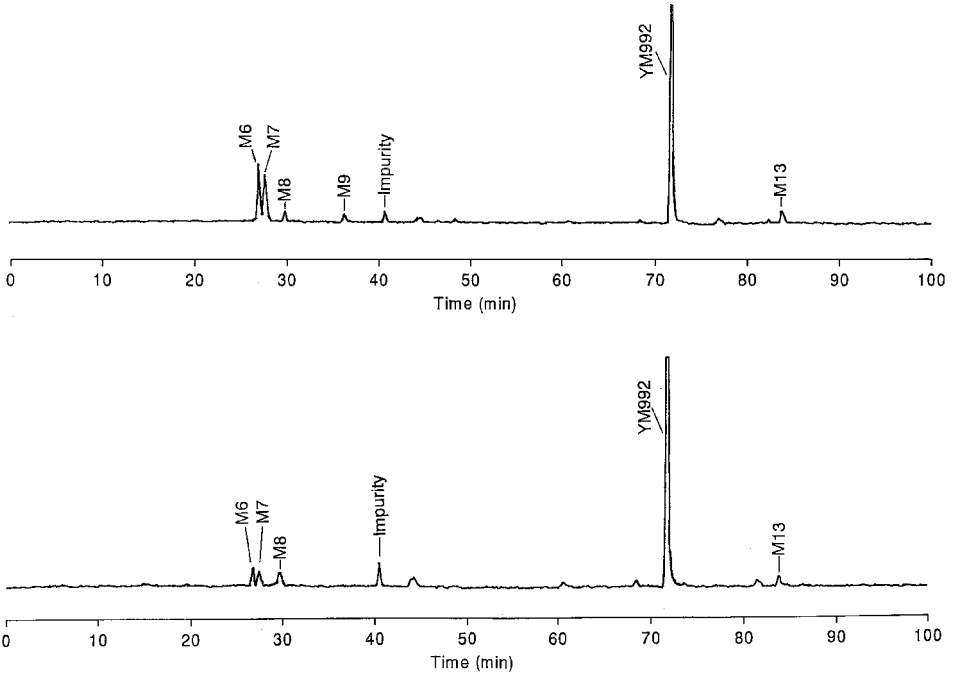


Figure 7. Representative chromatograms of an extract from (a) human liver microsomal incubation with ^{14}C-YM992 with on-line radioactivity detection, and (b) cDNA-expressed human CYP1A2 incubation with ^{14}C-YM992 with on-line radioactivity detection.

Metabolite fingerprinting

Figure 7 illustrates a typical chromatogram of an extracted incubation mixture of ^{14}C-YM992 with human liver microsomes. The radioactivity trace demonstrated that YM992 was metabolized to the five known metabolites and some unidentified metabolites in human liver microsomes. The predominant ones were M6 and M7 followed by M8 and M9 and M13. After incubation of ^{14}C-YM992 with microsomes prepared from yeast expressing CYP1A2, M6 and M7 were observed as the predominant metabolites. Small amounts of M8 and M13 were also detected.

Discussion

It is very important to know the enzyme or isozyme responsible for the metabolism of a particular drug for predictions of drug–drug interactions, which may influence the pharmacokinetics, therapeutic response and potency of side effects. This knowledge is also helpful to predict the influence of genetic polymorphism on the metabolic disposition of drugs under development. Usually, identification of P450 isoform is performed by using combinations of *in vitro* studies (Guengerich 1996). It is important that a metabolism reaction used *in vitro* studies reflects the main metabolism pathway *in vivo*. Therefore, if a drug is transformed into various metabolites, the sum of the metabolites may be used for the estimation of overall metabolic activities (Iwatsubo *et al.* 1997, Bourrié *et al.* 1999). Preliminary studies showed that human liver microsomes transform YM992 into various metabolites. Therefore, overall metabolic activities of YM992 were used to

identify the P450 isoform(s) responsible for the metabolism of YM992. However, the determination of each metabolite is very difficult because of low metabolic activities of YM992 in human liver microsomes. Consequently, the decrease in the substrate concentration was determined to estimate the overall metabolism of YM992.

K_m and V_{max} for YM992 metabolism in human liver microsomes were calculated as 15.5 ng/ml (= 0.054 μM) and 1.26 ng/mg protein/min (= 4.38 pmole/mg protein/min) respectively. However, it has been reported that several drugs show non-specific and non-covalent binding to microsomal protein (Obach 1996, 1997). In this case, correcting for binding of a substrate to microsomal protein is necessary to prevent overestimation of K_m. The unbound fraction ratio of YM992 was 0.61; thus, corrected K_m based on the unbound substrate concentration was calculated as 9.5 ng/ml (= 0.033 μM). After the oral administration of 100 mg YM992 to humans, C_{max} is $\sim$ 200 ng/ml. C_{max}, expressed as unbound concentration, is calculated as $\sim$ 10 ng/ml by using the 0.06 unbound fraction ratio of YM992 in human plasma. Therefore, the concentration of YM992 used in this study can be considered as clinically relevant.

After incubation of YM992 with cDNA-expressed P450 isoforms, several P450 isoforms metabolized YM992. Of them, CYP1A1, 1A2 and 2D6 showed high activities for YM992 metabolism. This finding suggests that these isoforms play a significant role in the metabolism of YM992. However, it is difficult to estimate relative contribution of each P450 isoform to the metabolism of YM992 in the human liver based on only the metabolism study using cDNA-expressed P450s, because the relative expression level of P450 isoform protein is quite different (Shimada *et al.* 1994). Therefore, correlation, inhibition and immuno-inhibition studies were also performed in human liver microsomes.

The metabolism rate of YM992 in human liver microsomes showed a significant correlation only with 7-ethoxyresorufin *O*-deethylation, which is relatively specific for CYP1A1/2 (Forrester *et al.* 1992). In addition, α-naphthoflavone and isosafrole, inhibitors of CYP1A1/2, inhibited substantially the YM992 metabolism. These results suggest that CYP1A1/2 is the major enzyme that catalyses the metabolism of YM992 in human liver. Quercetin, an inhibitor of CYP2C8, also inhibited the YM992 metabolism by $\sim$ 60%. However, this result supports the fact that YM992 is mainly catalysed by CYP1A1/2 rather than CYP2C8, because quercetin inhibits also CYP1A1/2 (Tsyrlov *et al.* 1994) and cDNA-expressed CYP2C8 did not metabolize YM992 (figure 3). The metabolism of YM992 in human liver microsomes was inhibited by antibodies that recognize both CYP1A1 and 1A2 by $\sim$ 95%, whereas antibodies specific for CYP1A1 did not show any inhibitory effect. These results are consistent with the results of the correlation and chemical inhibition studies. Furthermore, these results clearly indicate that the contribution of CYP1A1 to the metabolism of YM992 in human liver microsomes is negligible, in agreement with the low level of expression of CYP1A1 in human liver (Murray *et al.* 1993).

To characterize the metabolites formed from YM992 *in vitro*, ^{14}C-YM992 was incubated with human liver microsomes in the presence of NADPH. As shown in figure 7, the predominant metabolites were M6 and M7 and a small amount of M8, M9 and M13 was detected. The same metabolites, except M9, were generated in the incubation of CYP1A2 and ^{14}C-YM992. These findings suggest that CYP1A2 contributes to the majority of metabolic pathways of YM992 in human liver

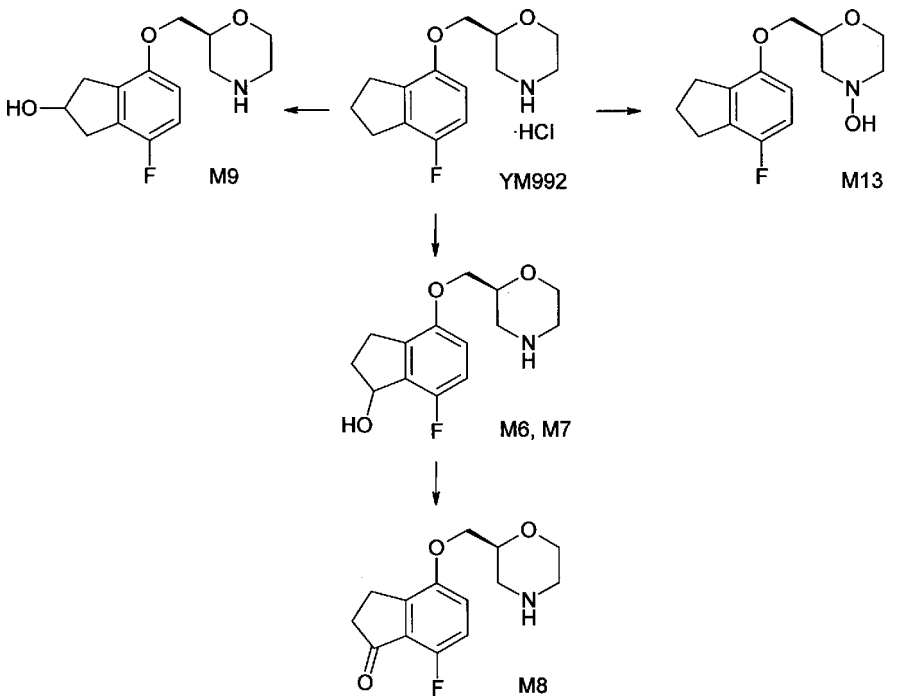


Figure 8. Proposed *in vitro* metabolic pathway of YM992 in human liver microsomes.

microsomes. The formation of the minor metabolite M9 might be catalysed CYP isoform(s) other than CYP1A2 (figure 8 illustrates *in vitro* metabolic pathway of YM992).

In conclusion, a combination of *in vitro* procedures using human liver microsomes and recombinant human P450 isoforms has strongly suggested that the metabolism of YM992 is catalysed mainly by CYP1A2. K_m for the metabolism of YM992 in human liver microsomes is low at 9.5 ng/ml (= 0.033 μM, as unbound concentration). In addition, unbound plasma concentrations after oral administration to humans can reach this level. Therefore, YM992 might act as a competitive inhibitor of CYP1A2 *in vivo*. In consequence, YM992 might increase plasma concentration of co-administered drugs, which are also metabolized by CYP1A2, such as theophylline (Tjia *et al.* 1996) and tacrine (Spaldin *et al.* 1995).

References

Back, D. J. and Tjia, J. F., 1992, Comparative effects of the antimycotic drugs ketoconazole, fluconazole, itraconazole and terbinafine on the metabolism of cyclosporin by human liver microsomes. *British Journal of Clinical Pharmacology*, **32**, 624–626.

Bourrié, M., Meunier, V., Berger, Y. and Fabre, G., 1996, Cytochrome P450 isoform inhibitors as a tool for the investigation of metabolic reactions catalyzed by human liver microsomes. *Journal of Pharmacology and Experimental Therapeutics*, **227**, 321–332.

Bourrié, M., Meunier, V., Berger, Y. and Fabre, G., 1999, Role of cytochrome P-4502C9 in irbesartan oxidation by human liver microsomes. *Drug Metabolism and Disposition*, **27**, 288–296.

Chang, T. K. H., Gonzales, F. J. and Waxman, D. J., 1994, Evaluation of triacetyloleandomycin, α-naphthoflavone and diethyldithiocarbamate as selective chemical probes for inhibition of human cytochromes P450. *Archives of Biochemistry and Biophysics*, **311**, 437–442.

Gonzales, F. J., 1992, Human cytochrome P450: problems and prospects. Trends in Pharmacological Science, **13**, 346–356.

FORRESTER, L. M., HENDERSON C. J., GLANCEY, M. J., BACK, D. J., PARK, B. K., BALL, S. E., KITTERRINGHAM, N. R., MCLAREN, A. W., MILES, J. S., SKETT, P. and WOLF, C. R., 1992, Relative expression of cytochrome P450 isoenzymes in human liver and association with the metabolism of drugs and xenobiotics. *Biochemical Journal*, **280**, 359–368.

GUENEGERICH, F. P., 1994, Catalytic selectivity of human cytochrome P450: relevance to drug metabolism and toxicity. *Toxicology Letters*, **70**, 133–138.

GUENGERICH, F. P., 1996, *In vitro* techniques for studying drug metabolism. *Journal of Pharmacokinetics and Biopharmaceutics*, **24**, 521–533.

GUENGERICH, F. P., MÜLLER-ENOCH, D. and BLAIR, I. A., 1986, Oxidation of quinidine by human liver cytochrome P-450. *Molecular Pharmacology*, **30**, 287–295.

HATANAKA, K., NOMURA, T., HIDAKA, K., TAKEUCHI, H., YATUSGI, S., FUJII, M. and YAMAGUCHI, T., 1996, Biochemical profile of YM992, a novel selective serotonin reuptake inhibitor with 5-HT_{2A} receptor antagonistic activity. *Neuropharmacology*, **35**, 1621–1626.

IWATSUBO, T., SUZUKI, H., SHIMADA, N., CHIBA, K., ISHIZAKI, T., GREEN, C., TYSON, C., YOKOI, T., KAMATAKI, T. and SUGIYAMA, Y., 1997, Prediction of *in vivo* hepatic metabolic clearance of YM796 from *in vitro* data by use of human liver microsomes and recombinant P-450 isozymes. *Journal of Pharmacology and Experimental Therapeutics*, **282**, 909–919.

KÜPFER, A. and PREISIG, R., 1984, Pharmacogenetics of mephenytoin: a new drug hydroxylation polymorphism in man. *European Journal of Clinical Pharmacology*, **26**, 753–759.

MURRAY, B. P., EDWARDS, R. J., MURRAY, S., SINGLETON, A. M., DAVIES, D. S. and BOOBIS, A., 1993, Human hepatic CYP1A1 and CYP1A2 content, determined with specific anti-peptide antibodies, correlates with the mutagenic activation of PhIP. *Carcinogenesis*, **14**, 585–595.

NEWTON, D. J., WANG, R. W. and LU, A. Y. H., 1995, Evaluation of specificities in the *in vitro* metabolism of therapeutic agents by human liver microsomes. *Drug Metabolism and Disposition*, **23**, 154–158.

OBACH, R. S., 1996, The importance of nonspecific binding in *in vitro* matrices, its impact on enzyme kinetic studies of drug metabolism reactions, and implications for *in vitro–in vivo* correlations. *Drug Metabolism and Disposition*, **24**, 1047–1049.

OBACH, R. S., 1997, Non-specific binding to microsomes: impact on scale-up of *in vitro* intrinsic clearance to hepatic clearance as assessed through examination of warfarin, imipramine, and propranolol. *Drug Metabolism and Disposition*, **25**, 1359–1369.

PASTRAKULJIC, A., TANG, B. K., ROBERTS, E. A. and KALOW, W., 1997, Distinction of CYP1A1 and CYP1A2 activity by selective inhibition using fluvoxamine and isosafrole. *Biochemical Pharmacology*, **53**, 531–538.

PEARCE, R. E., MCINTYRE, C. J., MADAN, A., SANZGIRI, U., DRAPER, A. J., BULLOCK, P. L., COOK, D. C., BURTON, L. A., LATHAM, J., NEVINS, C. and PARKINSON, A., 1996, Effects of freezing, thawing, and storing human liver microsomes on cytochrome P450 activity. *Archives of Biochemistry and Biophysics*, **331**, 145–169.

RAHMAN, A., KORZEKWA, K. R., GROGAN, J., GONZALES, F. J. and HARRIS, J. W., 1994, Selective biotransformation of taxol to 6α-hydroxytaxol by human cytochrome P450 2C8. *Cancer Research*, **54**, 5543–5546.

SHIMADA, T., YAMAZAKI, M., MIMURA, M., INUI, Y. and GUENGERICH, F. P., 1994, Interindividual variations in human liver cytochrome P-450 enzymes involved in the oxidation of drugs, carcinogens and toxic chemicals: studies with liver microsomes of 30 Japanese and 30 Caucasians. *Journal of Pharmacology and Experimental Therapeutics*, **270**, 414–423.

SPALDIN, V., MADDEN, S., ADAMS, D. A., EDWARDS, R. J., DAVIES, D. S. and PARK, B. K., 1995, Determination of human hepatic cytochrome P4501A2 activity *in vitro* use of tacrine as an isoenzyme-specific probe. *Drug Metabolism and Disposition*, **23**, 929–935.

STEVENS, J. C., WHITE, R. B., HSU, S. H. and MARTINET, M., 1997, Human liver CYP2B6-catalyzed hydroxylation of RP-73401. *Journal of Pharmacology and Experimental Therapeutics*, **282**, 1389–1395.

TAKEUCHI, H., YATSUGI, S., HATANAKA, K., NAKATO, K., HATTORI, H., SONODA, R., KOSHIYA, K. and YAMAGUCHI, T., 1997, Pharmacological studies on YM992, a novel antidepressant with selective serotonin re-uptake inhibitory and 5-HT_{2A} receptor antagonistic activity. *European Journal of Pharmacology*, **329**, 27–35.

TJIA, J. F., COLBERT, J. and BACK, D. J., 1996, Theophylline metabolism in human liver microsomes: inhibition studies. *Journal of Pharmacology and Experimental Therapeutics*, **276**, 912–917.

TSYRLOV, I. B., MIHAILENKO, V. M. and GELBOIN, H. V., 1994, Isozyme- and species-specific susceptibility of cDNA expressed CYP1A P-450s to different flavonoids. *Biochimica et Biophysica Acta*, **1205**, 325–335.

XENOBIOTICA , 2000, VOL. 30, NO. 5, 515–521

Pharmacokinetics of the anticoagulant ^{14}C-DX-9065a in the healthy male volunteer after a single intravenous dose

N. MURAYAMA†*, H. McMAHON‡, C. G. YOUNG‡, N. W. McCRACKEN‡, Y. OKAMURA§, H. HAKUSUI† and M. TANAKA†

† Drug Metabolism and Analytical Chemistry Research Laboratory, Daiichi Pharmaceutical Co., Ltd, 16-13, Kitakasai 1-chome, Edogawa-ku, Tokyo 134-8630, Japan
‡ Pharmaceutical Metabolism, Inveresk Research, Tranent EH33 2NE, UK
§ Metabolism Research Group, Tokai Research Laboratories, Daiichi Pure Chemicals Co., Ltd, Ibaraki 319-1182, Japan

Received 6 September 1999

1. The plasma pharmacokinetics, excretion and metabolism of DX-9065a were studied in the healthy male Caucasian volunteer after a single intravenous dose of 10 mg ^{14}C-labelled DX-9065a.

2. At the end of a 1 h infusion, the mean plasma concentration of total radioactivity was 380 ng ml^{-1} (equivalent to unchanged DX-9065). Thereafter, it decreased in a bi-exponential manner and was below the detection limit by 48 h after dosing. The half-life for the distribution phase was 6.93 h.

3. The total radioactivity recovered in urine and faeces by 336 h post-dose was 83.8% of the administered dose, with excretion ongoing at the end of the 14-day collection. The major route of excretion was via urine, accounting for a mean of 77.6% of the administered radioactivity. The urinary excretion profile was biphasic, consisting of rapid (0–24 h) and slow (24–336 h) phases. A large renal clearance suggested that renal tubular secretion might contribute to the excretion of DX-9065 via urine.

4. No metabolite peaks in the radio-HPLC chromatograms of urine samples were detected, indicating that biotransformation of DX-9065 does not play a significant role in the elimination of DX-9065 in man.

Introduction

DX-9065a, (2S)-2-[4-[[(3S)-1-acetimidoyl-3-pyrrolidinyl]oxy]phenyl]-3-[7-amidino-2-naphthyl]propanoic acid hydrochloride pentahydrate, a novel low-molecular weight anticoagulant, is currently under development by Daiichi Pharmaceutical Co. Ltd. It has a specific anti-Xa activity (Hara *et al.* 1994, 1995a, Lin and Johnson 1995, Stubbs *et al.* 1995, Brandstetter *et al.* 1996), and its anticoagulation effect is independent of antithrombin III (Morishima *et al.* 1997), thereby minimizing the risk of bleeding (Hara *et al.* 1995b, Morishima *et al.* 1997). This compound is therefore expected to be useful in the treatment of a number of thrombotic disorders, such as unstable angina, deep vein thrombosis and disseminated intravascular coagulation.

The good tolerability and good agreement of pharmacokinetics/pharmacodynamics of the drug were already confirmed in an intravenous dosing study with healthy male volunteers (Ikeda *et al.* 1998, Murayama *et al.* 1999). It is therefore expected that the anticoagulant effect of DX-9065a in clinical usage will be

* Author for correspondence; e-mail: muraycjs@daiichipharm.co.jp

Xenobiotica ISSN 0049-8254 print/ISSN 1366-5928 online © 2000 Taylor & Francis Ltd
http://www.tandf.co.uk/journals

easily predicted from its pharmacokinetic parameters. Furthermore, the complicated optimization and individualization of the dosage may not be essential for the anticoagulant therapy with the drug in fixed dose due to its tolerated profile.

The aim of the present study was to investigate the plasma kinetics, distribution, excretion and metabolic fate of the drug after a single intravenous administration of ^{14}C-DX-9065a to the healthy male volunteer.

Materials and methods

Chemicals

^{14}C-DX-9065a, with a specific activity of 1.95 MBq mg^{-1}, was synthesized by Daiichi Pure Chemicals Co., Ltd (Ibaraki, Japan). The chemical structure of ^{14}C-DX-9065a is shown in figure 1. For the dose formulation, ^{14}C-DX-9065a was diluted with unlabelled compound (chemical purity 99.0%) to achieve a specific activity of 190 kBq mg^{-1} (5.2 μCi mg^{-1}). The radiochemical purity in the dose formulation was assessed by HPLC before administration and was 99.1%. The dose and all concentration data in this report are expressed as equivalents of DX-9065, the anhydrous free-base of DX-9065a.

Study design

The study was performed at Inveresk Research (Tranent, UK) in accordance with the Declaration of Helsinki and the ICH guidelines on Good Clinical Practice (CPMC/ICH/135/95). The study protocol was approved by an independent Ethics Review Committee and the administration of the radioactive dose was approved by the UK Department of Health Administration of Radioactive Substances Advisory Committee (ARSAC).

Six healthy male Caucasian volunteers (33–55 years, 171–185 cm, 60.9–85.5 kg), who had given their informed consent, participated in the study. They were selected from a panel of volunteers held at Inveresk Research on the basis of a satisfactory medical history, clinical examination and laboratory investigations. For all volunteers included in the study, the following haematological screening examinations were also performed: Xa clotting time, activated partial thromboplastin time (APTT), prothrombin time (PT) and bleeding time. Alcohol- and caffeine-containing beverages were prohibited during the study.

Drug administration

^{14}C-DX-9065a and DX-9065a were dissolved in 1% lactose/saline, and the solution was diluted to a concentration of 0.2 mg ml^{-1}. After adjusting the pH to $\sim$4.3, the solution was drawn into sterile syringes through a sterile filter unit (0.22 μm). Each volunteer received an intravenous administration of $\sim$ 50 ml the dose formulation via an antecubital vein at 0.83 ml min^{-1} over a duration of 1 h. This dose was equivalent to 10 mg DX-9065 and a radioactive dose of 1.9 MBq (52 μCi).

The volunteers remained seated or recumbent until $\sim$ 4 h post-dose, and remained within the ward area under continuous supervision until 24 h post-dose.

Sample collection

Venous blood samples ($\sim$ 12 ml) were collected from *in situ* venous cannula inserted in the anticubital vein contralateral to the infusion site or by venipuncture, into lithium heparin tubes at the following times: predose, 0.5, 1, 1.5, 2, 3, 4, 6, 8, 12, 24, 48, 72, 96, 120, 144, 168; and 336 h post-dose. Plasma was separated by centrifugation (1800 g for 10 min). A small portion ($\sim$ 1 ml) of whole blood sample was reserved and duplicate $\sim$ 0.3-ml aliquots were used for the determination of total radioactivity.

Urine samples were collected at the following intervals: predose, 0–2, 2–4, 4–6, 6–8, 8–12, 12–24 h and subsequently at 24-h intervals up to 336 h after dosing. Faeces were collected daily up to 14 days after dosing.

Samples not analysed immediately were stored frozen at -20 °C until analysis.

Preparation of samples

Duplicate aliquots of urine (1 ml), and plasma (100, 250, 500 μl or 1 ml) were taken for the analysis of total radioactivity by liquid scintillation counting. Each aliquot was mixed with 10 ml Quickszint I scintillation fluid (Zinsser Analytic, Maidenhead, UK) before analysis. Duplicate aliquots of each whole blood sample were combusted using a Tri-Carb 306 Automatic Sample Oxidizer (Packard, USA). The resultant $^{14}CO_2$ was collected by absorption in 8 ml Carbo-sorb® CO_2 absorbing fluid (Canberra Packard, UK) and 10 ml Permafluor E$^+$ scintillation fluid (Canberra Packard). Combustion of standards during sample combustion showed that recovery efficiencies were $>$97% throughout.

Faeces samples were homogenized in water. Duplicate aliquots of the homogenate ($\sim$ 0.3 g) were weighed and combusted as for whole blood samples above.

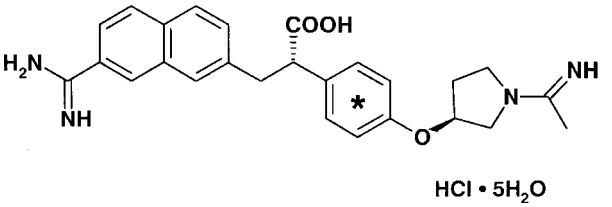


Figure 1. Chemical structure of ^{14}C-DX-9065a. * Position of ^{14}C-label.

Quantification of total radioactivity

Radioactivity was quantified using a liquid scintillation counter with automatic quench correction using an external standard method. Samples were allowed to heat and light stabilize before analysis and each sample was analysed for 5 min.

HPLC analysis of urine sample

HPLC analysis with radiometric detection was performed to evaluate the metabolism of DX-9065a, with 0–2 and 12–24 h urine samples obtained from all the volunteers. Urine samples obtained from one of the volunteers at 0–2, 2–4, 4–6, 6–8, 8–12 and 12–24 h after administration were also analysed. After extraction with 1% trifluoroacetic acid/methanol from the lyophilized urine sample solvents were evaporated *in vacuo*. The residue was dissolved in HPLC mobile phase and analysed by radio-HPLC chromatography. The HPLC conditions were: column: L-column ODS (4.6 i.d. × 150 mm; Chemicals Inspection & Testing Institute, Japan; mobile phase: potassium phosphate buffer (pH 6.8) containing 5 mM *n*-octylamine-acetonitrile (90:10) (detection UV 242 nm). The eluent from the analytical column was collected at 30-s intervals, and the radioactivity in each sample was determined by liquid scintillation counting. Mean recoveries of radioactivity for the sample processing, and from the HPLC column were 100.0 and 99.4% respectively.

Pharmacokinetic analysis

The pharmacokinetic parameters were calculated by non-compartmental analysis using WinNonlin (ver. 1.1, Scientific Consulting, USA) from the individual plots of the concentration of radioactivity in plasma against time. The following parameters were calculated: maximum radioactivity concentrations (C_{max}), time to reach C_{max} (T_{max}), half-life of plasma concentrations up to 24 h of distribution phase ($t_{1/2}$), area under the concentration-time curve (AUC_{0-24h}, up to 24 h; and $AUC_{0-\infty}$, 0–infinity), total clearance (Cl_t), renal clearance (Cl_r), and steady-state of volume of distribution (Vd_{ss}). C_{max} and T_{max} were observed values. Cl_t was calculated by using the equation $Cl_t = \text{dose}/AUC_{0-\infty}$. Vd_{ss} was calculated using $Vd_{ss} = Cl_t/\lambda_z$, where λ_z is the elimination constant of distribution phase. Cl_r was obtained from the equation $Cl_r = Ux/AUC_{0-24h}$, where Ux is the cumulative urinary excretion of radioactivity from 0 to 24 h.

Results

Clinical aspects

The drug was well tolerated in each volunteer. No clinically significant changes were recorded from any volunteers throughout the study.

Plasma and whole blood pharmacokinetics of radioactivity

The time-courses of radioactivity in plasma and whole blood after a single intravenous administration of ^{14}C-DX-9065a are shown in figure 2. C_{max}, 380 and 195 ng ml^{-1} equivalents of DX-9065 in plasma and whole blood respectively, was observed at the end of the 1-h infusion. Thereafter, the concentration decreased in a bi-exponential manner and was below the detection limit at 48 h after dosing. The time-course of the concentrations of total radioactivity in plasma paralleled that in whole blood. The mean concentration of total radioactivity in whole blood was below the limit of detection by 6 h after dosing. The whole blood/plasma ratio of

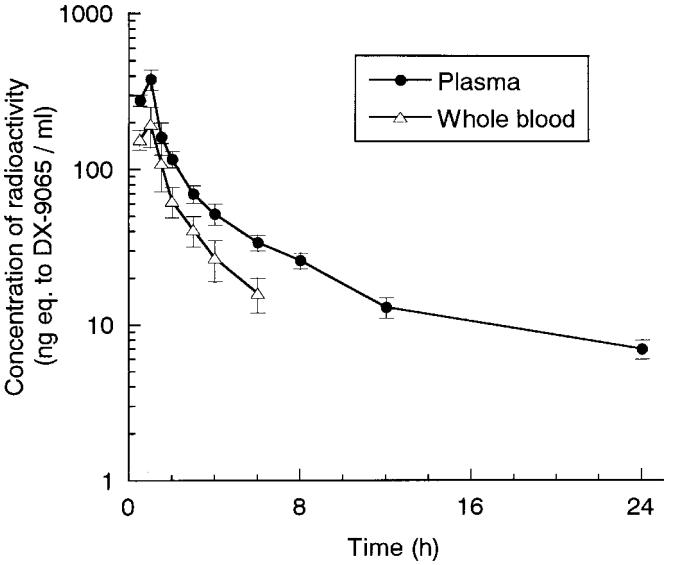


Figure 2. Time-course of concentration of total radioactivity in plasma and whole blood following a single intravenous dosing of ^{14}C-DX-9065a to the male Caucasian volunteer. Values are mean± SD ($n = 6$).

Table 1. Pharmacokinetic parameters for concentration of ^{14}C-radioactivity in plasma with single intravenous dosing of ^{14}C-DX-9065a to the healthy male Caucasian volunteer.

Parameters	Mean± SD ($n = 6$)
C_{max} (ng/ml)	380± 47
$t_{1/2}$* (h)	6.93± 0.82
AUC_{0-24} (ng × h/ml)	933± 171
Cl_t (ml/min)	171± 30
Cl_r (ml/min)	152± 34
Vd_{ss} (litres)	101± 12

* t-24 h.

mean total radioactivity was ~0.55, suggesting that the association of the radioactivity with red blood cells was minimal and radioactivity was essentially confined to plasma.

The pharmacokinetic parameters in the Caucasian volunteers after dosing of ^{14}C-DX-9065a are summarized (table 1). $t_{1/2}$ for the distribution phase was 6.93 h. Mean Cl_t and Cl_r were 171 and 152 ml min^{-1} respectively. Cl_r exceeded the glomerular filtration rate in humans (125 ml min^{-1}; Davies and Morris 1993) and this suggests net renal tubular secretion plays a role in the excretion of this compound via urine. The large Vd_{ss} (101 litres) indicated the possibility that radioactivity was highly distributed in organs at steady-state.

Excretion of radioactivity

The cumulative excretion of radioactivity over 336 h following intravenous administration of ^{14}C-DX-9065a is shown in table 2. The total recovery of radioactivity in urine and faeces was in the range 78.2–88.5% (mean 83.7%). The

Table 2. Cumulative excretion of radioactivity in urine and faeces.

Interval (h)	Excretion of radioactivity (% of dose)		
	Urine	Faeces	Total
0–4	30.8 ± 5.2	–	30.8 ± 5.2
0–8	40.1 ± 4.1	–	40.1 ± 4.3
0–12	42.7 ± 3.4	–	42.7 ± 3.4
0–24	47.2 ± 4.5	0.2 ± 0.3	47.4 ± 4.6
0–48	51.7 ± 4.9	1.5 ± 0.5	53.2 ± 4.8
0–96	58.6 ± 4.7	3.3 ± 0.8	61.9 ± 4.0
0–144	64.2 ± 4.6	4.3 ± 1.2	68.5 ± 3.7
0–192	68.5 ± 4.6	5.0 ± 1.3	73.5 ± 3.8
0–240	72.3 ± 4.6	5.4 ± 1.5	77.7 ± 3.7
0–288	75.1 ± 4.7	5.8 ± 1.7	80.9 ± 3.8
0–312	76.5 ± 4.7	6.0 ± 1.7	82.5 ± 3.9
0–336	77.6 ± 4.7	6.1 ± 1.7	83.7 ± 4.0

Values are mean ± SD ($n = 6$).

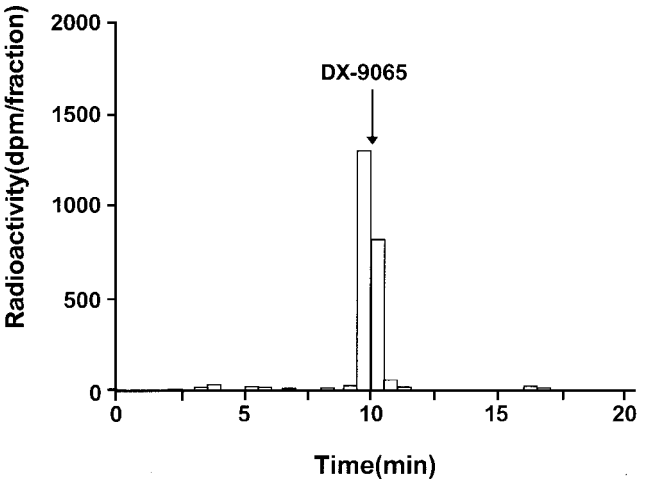


Figure 3. Representative metabolic profile radio-HPLC of urine collected 8–12 h after dosing. Radioactivity was determined by liquid scintillation counting following collection of eluent fractions (30-s intervals).

major route of excretion was via the urine, accounting for a mean of 77.6% (range 69.8–83.4%) of the administered dose by 336 h. The excretion profile in urine was biphasic with an initial rapid phase in which a mean of 47.2% was recovered at 24 h after dosing, followed by a slow phase with a total of 83.7% recovered by the end of the 14-day collection (336 h). Radioactivity recovered in the faeces accounted for a mean of 6.1% of the administered radioactivity at 336 h post-dose. Excretion of the radioactivity in urine and faeces was ongoing at the end of the 14-day collection, with daily totals of recovery of 1.2%. Therefore, the cumulative excretion of total radioactivity would have been greater if urine and faeces samples had been collected for >14 days.

Metabolic profile of ^{14}C-DX-9065a in human urine

A typical chromatogram of radioactivity extracted from urine samples is shown in figure 3. The only radioactive peak observed was that of unchanged DX-9065. Taking into account the high recovery ($>99\%$) of radioactivity throughout the entire process for the sample analysis, this result suggests that DX-9065 was not metabolized to any significant extent in man.

Discussion

After administration of ^{14}C-DX-9065a to rat and monkey, no metabolites were observed in plasma, urine, faeces or liver (unpublished data). In the present human study with ^{14}C-DX-9065a, no metabolites were observed in urine, the major pathway for excretion of radioactivity. This result suggests that biotransformation of DX-9065 was a negligible process in its elimination in man, and that the pharmacokinetic parameters obtained from the total radioactivity concentration were equivalent to those for the unchanged DX-9065.

After administration of ^{14}C-DX-9065a to the male Caucasian volunteer, the majority of the radioactivity was excreted via urine in a biphasic manner. This was consistent with the plasma concentration profile that exhibited a bi-exponential decrease. Up to 24 h after dosing, the excretion of total radioactivity was rapid. Moreover, the large Cl_r, which exceeded the glomerular filtration rate without correction for the plasma protein binding ratio (~ 0.7; Murayama *et al.* 1999), suggested that renal tubular secretion might contribute to the excretion of DX-9065 in urine. However, after 48 h the rate of excretion became very slow, with excretion apparently ongoing after the end of the 336-h collection. The large Vd_{ss} suggests that DX-9065 was well distributed to organs at later times. These results indicate that the slow excretion of radioactivity observed at later time points after dosing was due to a slow redistribution of DX-9065 from organs to plasma.

The half-life (6.93 h) for the total radioactivity in plasma was shorter than that for unchanged drug (26.1 h; Murayama *et al.* 1999), which was obtained after dosing of 10 mg unlabelled DX-9065a to the Japanese volunteer. This difference was due to the difference in the detection limits of the analytical methods used for the different studies. Since the radio-immunoassay method (Murayama *et al.* 1996) used for the determination of unchanged drug in plasma is 10 times more sensitive than radiometric detection, this accounts for the observed terminal elimination phase with the longer half-life in the Japanese volunteer. The relatively short half-life may result in an underestimation of the AUC and an overestimation of Cl_t. However, the Cl_r/Cl_t ratio (0.889), which represents the contribution of urinary excretion to the total elimination, was in good agreement with the extrapolated excretion ratio in urine at infinity (87.3%). This indicates that the effect of the short half-life on other pharmacokinetic parameters was practically negligible in this study.

In conclusion, after a single intravenous administration of ^{14}C-DX-9065a to the male Caucasian volunteer, 83.7% of the administered radioactivity was excreted after 14 days. The main route of elimination was via the urine. Therefore, impairment of renal function may have an effect on clearance of DX-9065. However the small amount of DX-9065 excreted in the faeces and the fact that no metabolites were found in urine makes it unlikely that hepatic dysfunction will significantly change the clearance of DX-9065.

References

BRANDSTETTER , H., KÜHENE , A., BODE, W., HUBER,. R., VON DER SAAL, W., WIRTHENSOHN , K. and ENGH , R. A., 1996, X-ray structure of active site-inhibited clotting factor Xa. *Journal of Biological Chemistry*, **271**, 29988–29992.

DAVIES, B. and MORRIS, T., 1993, Physiological parameters in laboratory animals and humans. *Pharmaceutical Research*, **10**, 1093–1095.

HARA, T., MORISHIMA , Y., ISHIHARA , H., MURAYAMA , N., TANAKA, S., SUDO, K. and KUNITADA , S., 1995a, Inhibition of thrombin generation effectively prevents thrombus formation without aggravation of bleeding. *Thrombosis and Haemostasis*, **73**, 1308.

HARA, T., YOKOYAMA , A., ISHIHARA , H., YOKOYAMA , Y., NAGAHARA, T. and IWAMOTO , M., 1994, DX-9065a, a new synthetic, potent anticoagulant and selective inhibitor for factor Xa. *Thrombosis and Haemostasis*, **71**, 314–319.

HARA, T., YOKOYAMA , A., TANABE , K., ISHIHARA , H. and IWAMOTO , M., 1995b, DX-9065a, an orally active, specific inhibitor of factor Xa, inhibits thrombosis without affecting bleeding time in rats. *Thrombosis and Haemostasis*, 74, 635–639.

IKEDA, Y., FUJITA , M., MURAYAMA , N., YAMADA, H., INOUE , T., SASANO , H. and KUNITADA , S., 1998, Human pharmacokinetics, pharmacodynamics, and tolerability of activated factor Xa inhibitor DX-9065a. *Circulation*, **98(suppl.)**, 1454.

LIN , Z. and JOHNSON , M. E., 1995, Proposed cation-π mediated binding by factor Xa: a novel enzymatic mechanism for molecular recognition. *FEBS Letters*, **370**, 1–5.

MORISHIMA , Y., TANABE , K., TERADA, Y., HARA, T. and KUNITADA , S., 1997, Antithrombotic and hemorrhagic effects of DX-9065a, a direct and selective factor Xa inhibitor : comparison with a direct thrombin inhibitor and antithrombin III-dependent anticoagulants. *Thrombosis and Haemostasis*, **78**, 1366–1371.

MURAYAMA , N., TANAKA, S., KIKUCHI , T., NAKAOKA, M. and SUDO, K. 1996, Radioimmunoassay method for DX-9065a, an anticoagulant agent. Development, evaluation and application to human plasma. *Journal of Pharmaceutical and Biomedical Analysis*, **14**, 1435–1445.

MURAYAMA , N., TANAKA, M., KUNITADA , S., YAMADA, H., INOUE , T., TERADA, Y., FUJITA , M. and IKEDA, Y., 1999, Tolerability, pharmacokinetics and pharmacodynamics of DX-9065a, a new synthetic, potent and specific factor Xa inhibitor, in healthy male volunteers. *Clinical Pharmacology and Therapeutics*, **66**, 258–264.

STUBBS , M. T., HUBER , R. and BODE, W., 1995, Crystal structures of factor Xa specific inhibitors in complex with trypsin: structural grounds for inhibition of factor Xa and selectivity against thrombin. *FEBS Letters*, **375**, 103–107.

XENOBIOTICA , 2000, VOL. 30, NO. 5, 523–533

Effect of diet and gavage on the dose- and dose-mode-dependent absorption and metabolism of bidisomide in rat

C. S. COOK*, M. LONIEN and J. HRIBAR

Metabolism and Safety Evaluation, G. D. Searle & Co., 4901 Searle Parkway, Skokie, IL 60077, USA

Received 17 September 1999

1. The metabolism of bidisomide was investigated to examine how dose and mode of drug administration (i.e. diet admixture versus oral solution) affect the absorption and metabolism of bidisomide in the toxicity studies.

2. After dietary admixture, bidisomide was more absorbed and less metabolized at the higher doses. Reduced metabolism at the high doses resulted from saturation of stereo-specific formation of the N-desisopropyl-arylhydroxy bidisomide (NDABD) metabolite.

3. The rat-specific NDABD metabolite was formed only from (−)-bidisomide on incubation with rat liver microsomes.

4. After oral solution dosing, absorption was increased and metabolism reduced compared with the dietary admixture.

5. After 24-h infusion, plasma concentrations of radioactivity were approximately dose-proportional. However, the concentrations in the liver were similar at the 200 and 400 mg/kg doses due to saturation of liver uptake of the NDABD metabolite.

Introduction

Bidisomide, SC-40230 (± α-[acetyl(1-methylethyl)amino] ethyl]-α-(2-chloro-phenyl)-1-piperidinebutamide) is a potential anti-arrhythmic agent. The average effective doses in the Harris dog arrhythmia model were 9 and 15 mg bidisomide/kg body weight after intravenous (IV) and oral administration respectively (Hatley *et al.* 1987, Frederick *et al.* 1989, Garthwaite *et al.* 1995). Absorption of bidisomide in rat and human was relatively low (Cook *et al.* 1993a, b, Lee *et al.* 1997). Furthermore, bidisomide exhibited remarkable food effects with a reduction in the systemic availability of ~50% (Cook *et al.* 1998, Pao *et al.* 1998). In dog and human, N-dealkylation and/or piperidine ring hydroxylation were the major metabolic pathways (figure 1). However, in rat, N-desisopropylarylhydroxy bidisomide (NDABD), an additional metabolite of bidisomide, was found.

Bidisomide exhibited atypical dose- and dose-mode-dependent toxicity in rat. During a 1-year toxicity study with dietary admixture, activities of alanine and aspartate transaminase (ALT and AST) were elevated in some animals at a daily dose of 300 mg/kg, whereas at the 90 and 900 mg/kg doses, no notable elevations of the enzyme activities were observed (Vandenberghe *et al.* 1995). Similar phenomena were observed in the 13-week dietary admixture study. In contrast, during a 13-week rat toxicity study using gavage administration, no changes were observed in ALT and AST levels at daily doses of 80, 250 and 800 mg/kg, even though the systemic availability was much greater after administration of the drug as gavage

* Author for correspondence; e-mail: chyung.s.cook@monsanto.com

Xenobiotica ISSN 0049-8254 print/ISSN 1366-5928 online © 2000 Taylor & Francis Ltd
http://www.tandf.co.uk/journals

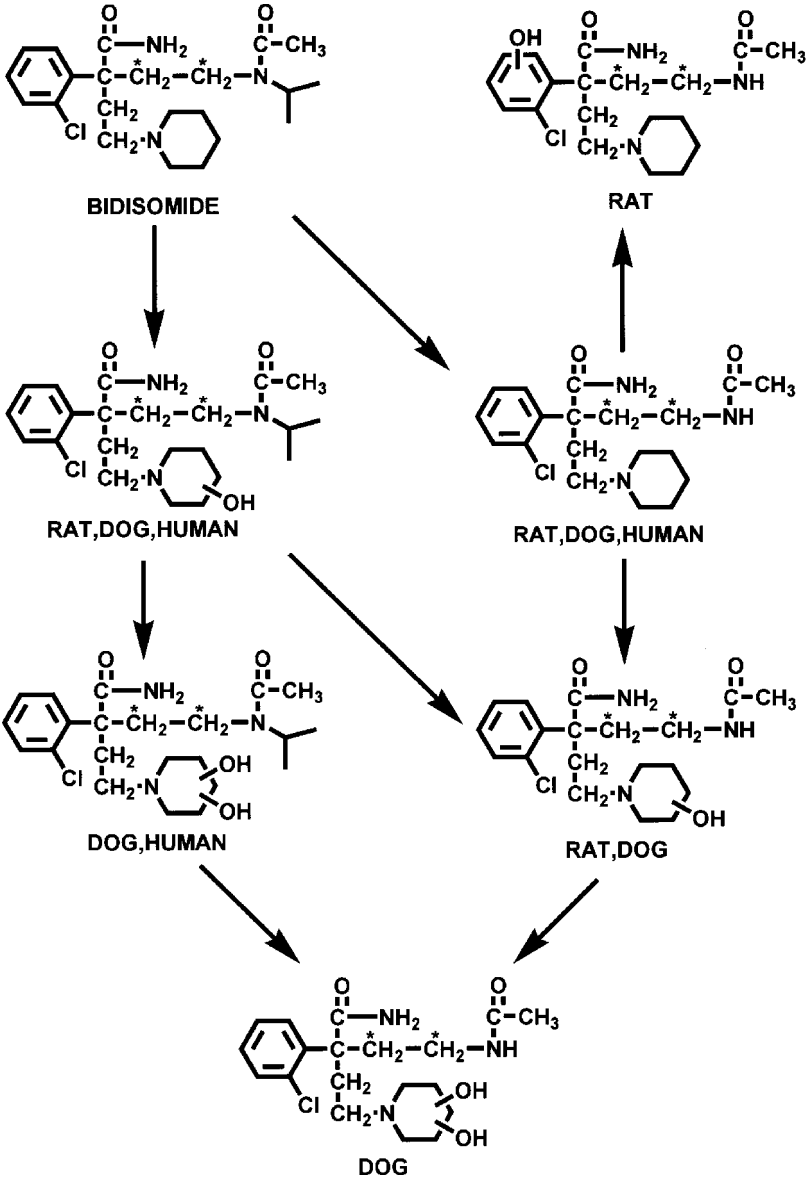


Figure 1. Chemical structure of bidisomide and its metabolic pathways. *Position of labelled carbons.

than dietary admixture at comparable doses. Furthermore, in a 13-week dog toxicity study at daily doses of 15, 20 and 30 mg/kg, and a 1-year dog toxicity study at daily doses 20, 30 and 45 mg/kg, there was no evidence of notable changes in transaminase activities. Higher plasma concentrations of bidisomide were achieved at the 45 mg/kg dose in dog than at the 300 mg/kg dose in rat.

Effect of diet and gavage on drug absorption has been reported in rat for a cephalosporin antibiotic (Vanharken and Hottendorf *et al.* 1978) and other compounds (Smyth *et al.* 1979). The differences in toxicity of a drug administered with diet admixture and by gavage have also been demonstrated. Fluperlapine, a

potential agent for treatment of psychoses, exhibited liver toxicity when administered with diet to rat at doses of 40 and 80 mg/kg but not by gavage at 80 mg/kg (Dain and Jaffe *et al.* 1988). This was explained by the quantitative differences of the possible toxic metabolite (an arylhydroxy metabolite) produced after administration of dietary admixture and gavage solution.

The present study examined how dose and mode of bidisomide administration (i.e. diet admixture versus oral solution) affect absorption and metabolism and it investigated whether the dose- and dose-mode-dependent toxicity could be explained by differences in the exposure to the rat-specific metabolite NDABD in the toxicity studies.

Materials and methods

Materials

The following materials were supplied by G. D. Searle & Co. (Skokie, IL, USA): bidisomide (chemical purity > 95%), [^{14}C]bidisomide (lot no. MRC-GDS1539 6–1, specific activity 33.2 μCi/mg, radiochemical purity > 97%). (+)- and (−)-[^{14}C]bidisomide, and (+)- and (−)-bidisomide were prepared using a chiral HPLC procedure. Optical and chemical purity of the enantiomers was > 95%. Pseudo-(±)-[^{14}C]bidisomide was prepared by mixing an equal amount of either (+)-[^{14}C]bidisomide and (−)-bidisomide or (−)-[^{14}C]bidisomide and (+)-bidisomide. All other chemicals were commercially available unless otherwise stated.

Animal studies

One-year dietary admixture. Twelve male and 12 female Crl:CD (SD) rats (Charles River, Wilmington, MA, USA) weighing 150–200 g were selected from the pharmacokinetic group of animals in the 1-year dietary admixture study where daily doses of 90, 300 and 900 mg/kg were administered to each group of animals. On week 52 after initiation of the study, radioactive [^{14}C]bidisomide was administered orally for 2 consecutive days as a dietary admixture to the same three-dose groups of rats (four rats/sex/group). Doses administered were determined by multiplying the amount diet consumed (g) for 24 h by the amount of the drug per g of diet. Blood, urine and faecal samples were collected at the time intervals specified after administration of [^{14}C]bidisomide.

Dietary admixture versus oral solution. To compare metabolic profiles in the liver between dietary admixture and aqueous solution, bidisomide was also administered to male Crl:CD (SD) rats (150–200 g, three rats/group) as dietary admixture for 1 week at doses of 90, 300 and 900 mg/kg. On day 8, [^{14}C]bidisomide was given as dietary admixture at the same doses for 24 h. On day 9, immediately after completion of the dark cycle (at 07:00 hours), food was withdrawn, the rats killed and liver samples collected. In addition, [^{14}C]bidisomide was administered as an aqueous solution to three male Crl:CD (SD) rats (150–200 g) at 300 mg/kg. The rats were killed 3 h after drug administration and liver samples collected. All liver samples were cut into small pieces and homogenized in methanol immediately. Urine samples were collected for 24 h from a separate group of animals ($n = 4$).

Intravenous infusion. [^{14}C]bidisomide was administered by IV infusion to male Crl:CD (SD) rats (150–200 g, $n = 4$/dose group) for 24 h at total doses of 100, 200 and 400 mg/kg. These doses were selected such that the steady-state plasma concentrations of total radioactivity at these doses are similar to those after administration of bidisomide diet admixture at the doses of 90, 300 and 900 mg/kg respectively. The steady-state plasma concentrations and liver concentrations of total radioactivity were determined. In addition, metabolic profiles were obtained from plasma and the liver.

In vitro *study*

Pseudoracemic [^{14}C]bidisomide defined as a mixture of (−)-[^{14}C]bidisomide and (+)-unlabelled bidisomide or vice versa, and a racemic [^{14}C]bidisomide were incubated at 37 °C for 30 min with rat liver microsomes in phosphate buffer with NADPH-generating cofactors as described (Cook *et al.* 1993a, b). A cofactor mixture was prepared in phosphate buffer at pH 7.4 (0.1 M), glucose 6-phosphate (15 mM), $MgCl_2$ (10 mM), NADP (3 mM) and glucose 6-phosphate dehydrogenase (1.5 units). The cofactor mixture (3 ml) was added to 1 ml rat hepatic microsomes (1 mg protein/ml) and the substrate added to achieve a final concentration of 1 μg/ml incubation mixture. Formation of metabolites was linear up to 30-min incubation. Bond Elut extracts of the incubation mixtures were analyzed by HPLC.

Sample analysis

Plasma. Aliquots (100 μl) of each sample were mixed with 10 ml Aquassure (DuPont Co., Boston, MA, USA) after which ^{14}C concentrations were determined by liquid scintillation counting (LSC).

For determination of the representative distribution of plasma radioactivity, 0.2 ml 1 M NaOH per ml plasma was added to an aliquot (2–4 ml) of plasma at selected time intervals, and the sample was mixed for ~ 0.2 min using a Vortex Genie mixer (Scientific Products, Evanston, IL, USA). The sample was transferred to a C-18 Bond Elut column (3 ml, C18, Analytichem International, Inc., Harbor City, CA, USA), which was preconditioned with 6 ml methanol and rinsed with 6 ml water. The column containing the sample was then washed with 3 ml water. The radioactive compounds retained on the column were eluted with 6 ml methanol. Total Bond Elut and HPLC recovery were determined from the HPLC counting data. The remaining eluent was dried under a stream of nitrogen. The residue was reconstituted with 0.25 ml 5% methanol in 0.01 M dibutylamine phosphate and analyzed by non-chiral HPLC for metabolic profiles.

Urine. Duplicate aliquots (0.05 ml) of each urine sample were mixed with 10 ml Aquassure and the concentrations of total radioactivity were determined by LSC. The percentages of the dose excreted in urine were calculated by dividing total dpm recovered in urine by total dpm administered.

For metabolic profiles, urine samples were dried under a stream of nitrogen. The residue was reconstituted with 0.25 ml 5% methanol in 0.01 M dibutylamine phosphate and analyzed using the non-chiral HPLC system. The percentages of the parent drug and metabolites were calculated using: % parent drug or metabolite = % dose recovered in urine × fraction of radioactivity associated with parent drug or metabolite.

For determination of enantiomeric ratios and concentrations of each enantiomer in urine, the HPLC eluents containing bidisomide or the N-desisopropyl bidisomide (NDBD) metabolite were collected using a Foxy fraction collector (Foxy ISCO, Lincoln, NE, USA). The collected eluents were dried under a stream of nitrogen. The residue was reconstituted and extracted using the Bond Elut column procedure as described above for plasma samples. The Bond Elut extracts were subjected to chiral HPLC analysis. Concentrations of (−)- and (+)-bidisomide were calculated by multiplying the fraction of each enantiomer from the chiral HPLC metabolic profile analysis by the respective concentration of (±)-bidisomide determined by the non-chiral HPLC.

Faeces. Each faecal sample was homogenized in a Stomacher (Lab-Blender 400, A. J. Seward, London, UK). Triplicate aliquots of each homogenized sample were dried at room temperature for at least 15 h and oxidized with a Packard Model 306 Tri-Carb Sample Oxidizer (Packard Instrument Co., Downers Grove, IL, USA). The combustion products were mixed with ~ 9 ml Carbosorb and 12 ml Permafluor, and the total radioactivity in the mixture was determined by LSC.

Tissues. Tissues were homogenized after adding water to the tissues using a Brinkman Polytron (System Technik AG/Ruschlikon, Switzerland). Duplicate aliquots (200 μl) of the homogenates were mixed with 10 ml Aquassure and the ^{14}C concentrations were determined by LSC.

To determine the metabolic profiles of faecal samples, an aliquot from each of the faecal samples of the same dose and sex group (four rats/sex/dose) was pooled proportional to its total weight. Aliquots (20–30 g) of the pooled faecal samples were extracted with methanol (80 ml) and the methanol layer was dried under a stream of nitrogen. The methanol extractability was > 90%. The dried residue was reconstituted in HPLC mobile phase A (5% methanol in 0.01 M dibutylamine phosphate) and analyzed using the non-chiral HPLC system. Since methanol extractability was > 90%, the percentages of bidisomide excreted in faeces were calculated using a similar equation described for the urine samples without correcting for the extractability.

For determination of enantiomeric ratios and concentrations of each enantiomer in faeces, the samples were prepared and analyzed using the same procedure as for urine samples.

HPLC system

Non-chiral HPLC was performed on a Hewlett-Packard HPLC (Germany) equipped with HP series 1050 pumps, 1050 auto-injector and a C-18 Radial-Pak liquid chromatography cartridge (8 mm i.d., 10 μm particle size). For metabolic profiles of plasma, urine and faecal samples, a linear gradient system was employed from 5% methanol in 0.01 M dibutylamine phosphate to 90% methanol in 0.01 M dibutylamine phosphate over 60 min. The flow rate of the mobile phase was 1.5 ml/min.

For the plasma extracts, the eluents from the HPLC column were collected every 0.5 min in liquid scintillation vials using a Foxy fraction collector (Foxy ISCO, Lincoln, NE, USA). Aquassure (10 ml) was added to each vial and radioactivity was determined by LSC.

For the urine and faecal samples the eluents from the HPLC column were mixed with Flo Scint IIIR (Radiomatic Instruments and Chemical Co., Inc., Tampa, FL, USA) at a ratio of 1.5:6.0 (by vol.). A Flo-One radioactive detector (Flo-One/Beta Model IC or A250) detected radioactivity.

LSC system

Radioactivity was measured with liquid scintillation spectrometers (Mark III, Tracor Analytic, Elk Grove, IL, USA). Chemical quenching was corrected by the automatic external standard channels ratio method. In all radioactivity measurements, values of radioactivity disintegrations per min (dpm) less than two times background values were considered insignificant.

Results

One-year dietary admixture

After dietary admixture administration of [^{14}C]bidisomide to the male and female rat at ~ 90, 300 and 900 mg/kg for 48 h, the mean percentages of total radioactivity excreted in 0–48-h urine increased as dose increased (table 1). Total recovery of the administered dose decreased as dose increased. This appeared to be due to premature termination of sample collection since at the higher doses slower elimination of total radioactivity is expected. Urinary excretion of the parent drug was increased to a greater extent as dose increased. Faecal excretion of total radioactivity and the parent drug was also dose-dependent with lower percentages of the dose being excreted at the higher doses. The majority of the urinary radioactivity (> 60%) was associated with the parent drug at all doses of [^{14}C]bidisomide given as dietary admixture (figure 2). However, the percentages of the parent drug peak increased as dose increased. The percentages of total radioactivity associated with NDBD metabolite (peak 2 with an HPLC retention of 9 min) and the rat-specific NDABD metabolite (peak 1 with a retention of ~ 5 min) decreased as dose increased. The NDABD metabolite in urine counted for 0.21 ± 0.07, 0.19 ± 0.05 and 0.13 ± 0.05% of the dose at the 90, 300 and 900 mg/kg doses respectively.

In faeces, > 90% of faecal radioactivity was due to the parent drug regardless of the dose and the percentages of each metabolite were < 2%. This was due to unabsorbed bidisomide in addition to biliary excretion of the drug. There were no notable sex differences in urinary and faecal excretion of total radioactivity and the parent drug.

The mean percentages of total radioactive dose recovered in the liver at 07:00 hours were 0.41 ± 0.02, 0.55 ± 0.02 and 0.28 ± 0.04% at 90, 300 and 900 mg/kg respectively.

After [^{14}C]bidisomide administration as a dietary admixture, the percentages of (−)- and (+)-bidisomide were similar in both urine (figure 3) and faeces with an overall (−)/(+)-isomer ratio of ~ 1 regardless of dose. However, the percentages of (−)- and (+)-NDBD metabolite in urine were dose-dependent and the mean ratios of (−)/(+)-isomer were 0.05, 0.34 and 0.72 at doses of 90, 300 and 900 mg/kg respectively (figure 4). As observed in urine, the percentages of (−)- and (+)-NDBD metabolite in faeces were also dose-dependent. The ratios of (−)/(+)-isomer were 0.38, 0.45 and 0.74 at doses of 90, 300 and 900 mg/kg respectively.

Dietary admixture versus oral solution

In an 8-day dietary admixture study to compare metabolic profiles in the liver between dietary admixture and aqueous solution at the 300 mg/kg dose, the mean percentage of total radioactive dose in the liver was 0.61%. About 14% of the liver radioactivity was due to the parent drug and the rest of the liver radioactivity (0.5% of the dose) was due to the rat-specific metabolite, NDABD (figure 5).

Table 1. Percentages of the dose excreted as total radioactivity and bidisomide in urine (0–48 h) and faeces (0–96 h) after initiation of 48-h dietary admixture of [^{14}C]bidisomide to the male and female rat.

		Male		Female	
Dose (mg/kg)	matrix	^{14}C	Bidisomide	^{14}C	Bidisomide
90	urine	3.44± 0.35	2.27± 0.26	3.27± 0.48	2.03± 0.36
	faeces	75.4± 1.7	73.4[a]	73.1± 1.0	70.4[a]
300	urine	8.15± 0.78	6.96± 0.78	6.80± 0.49	5.65± 0.47
	faeces	67.3± 0.7	62.8[a]	64.9± 1.6	61.8[a]
900	urine	14.4± 0.9	13.5± 0.92	13.1± 1.2	12.2± 1.2
	faeces	55.6± 2.6	50.7[a]	51.3± 6.4	48.7[a]

Data are the mean (± SEM) from four animals.
[a] Obtained from the pooled faeces of the four rats in each group.

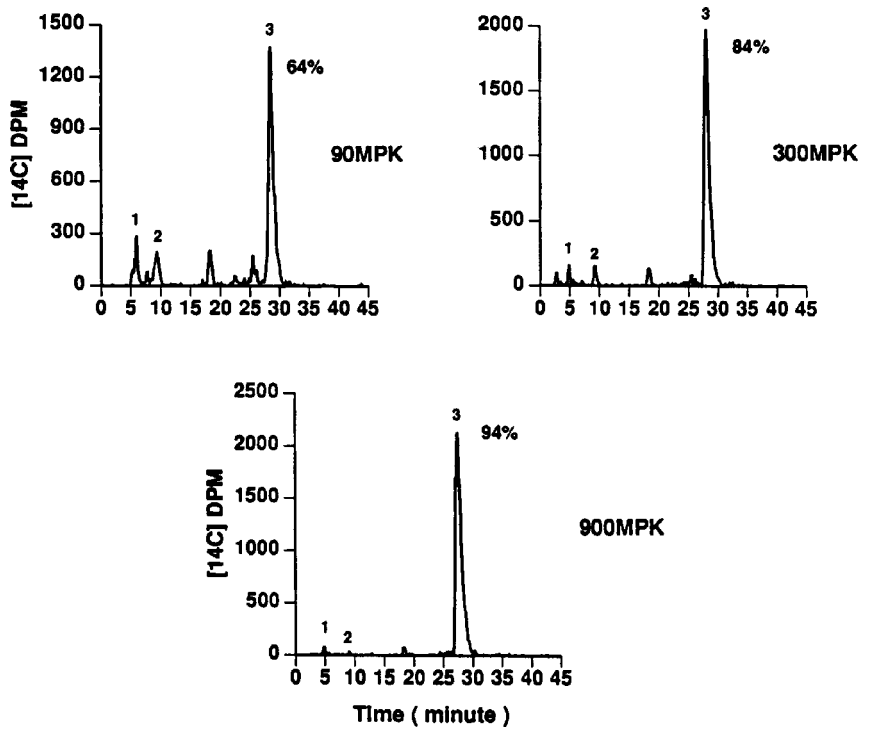


Figure 2. Representative non-chiral HPLC of male urine samples after [^{14}C]bidisomide was given as a dietary admixture to rat at doses of 90 (top left), 300 (top right) and 900 mg/kg (bottom). Peaks 1–3, NDABD, NDBD and bidisomide respectively.

After oral administration of [^{14}C]bidisomide at a dose of 300 mg/kg as a solution, the mean percentage of the radioactive dose remaining in the liver at 3 h post-dose (the time point to reach maximum plasma concentration) was 1.73± 0.37%. Of this, 28% was due to NDABD metabolite, which corresponded to 0.5% of the dose. The remaining radioactivity was due to the parent drug (figure 5).

The mean percentage of the dose excreted in urine following drug administration as a solution was 16.4± 0.9% and ~ 2-fold higher than that after administration of

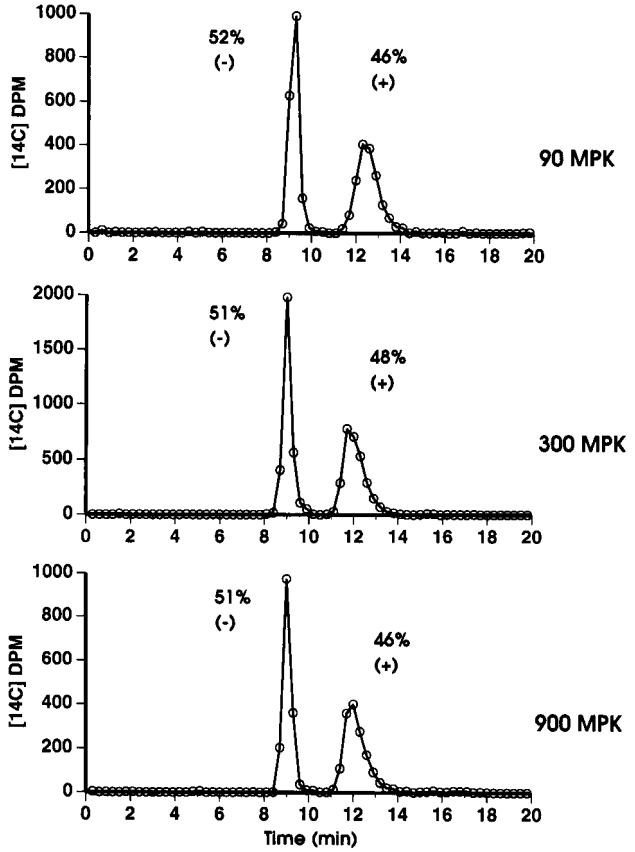


Figure 3. Representative chiral HPLC of [^{14}C]bidisomide isolated from urine after [^{14}C]bidisomide dietary admixture was given to rat at doses of 90 (top left), 300 (top right) and 900 mg/kg (bottom). Peaks at retentions of ~ 9 and 12 min are (−)- and (+)-[^{14}C]bidisomide respectively.

the dietary admixture. However, the NDABD excreted in urine with the solution dose was 0.23± 0.05% and approximately the same as that following dietary administration. As observed in the dietary admixture study, excretion of bidisomide in urine was not stereoselective when administered as a solution. The excretion of NDBD in urine was less stereoselective after administration of the drug as a solution than as a dietary admixture at the 300 mg/kg dose. This was due to more saturation in metabolism of (−)-NDBD to NDABD metabolite after drug administration as an oral solution.

Intravenous infusion

During IV infusion of [^{14}C]bidisomide at total doses of 100, 200 and 400 mg/kg over 24 h, the mean plasma concentrations of total radioactivity at the steady-state were 0.93–2.1, 3.5–4.1 and 8.9–10 μg/ml respectively. These concentrations were similar to the plasma concentrations at 07:00 hours after dietary admixture administration of bidisomide at doses of 90, 300 and 900 mg/kg respectively. The increase in plasma concentrations of total radioactivity was approximately pro-

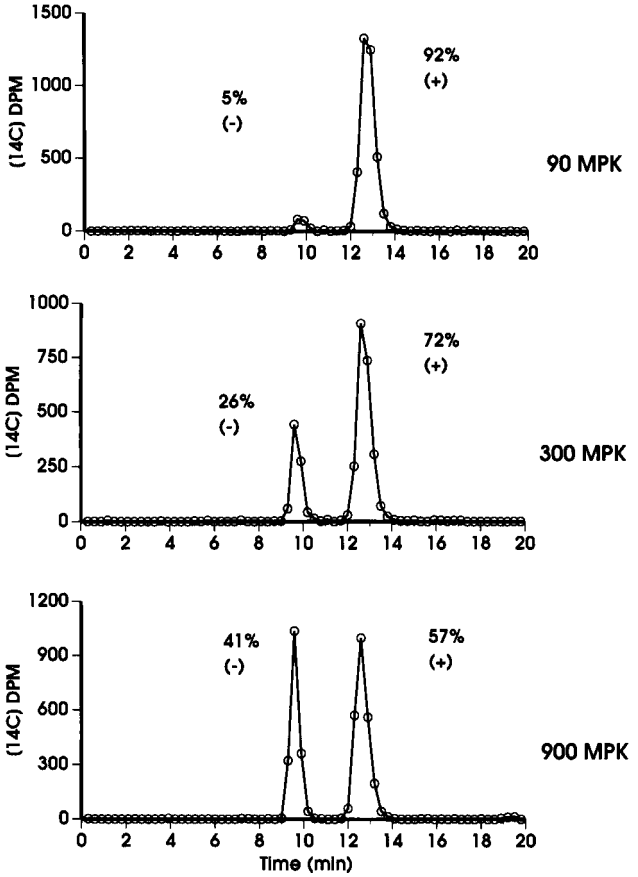


Figure 4. Representative chiral HPLC of [^{14}C]N-desisopropyl bidisomide metabolite was isolated from urine samples after [^{14}C]bidisomide dietary admixture was given to rat at doses of 90 (top), 300 (middle) and 900 mg/kg (bottom).

portional to the increase in dose. However, the concentrations of radioactivity in the liver did not increase substantially as dose increased, particularly at the 400 mg/kg dose. The mean concentrations of total radioactivity were 84.8± 10.2, 124± 6 and 145± 9 μg eq./g liver at doses of 100, 200 and 400 mg/kg respectively. These correspond to 3.91± 0.11, 2.55± 0.12, and 1.62± 0.07% of the dose respectively. The liver concentrations of the parent drug at these doses were 5.1, 16 and 30 μg/g respectively; the concentrations of NDABD metabolites were 80, 107 and 115 μg eq./g respectively. The concentrations of total radioactivity in tissues other than liver (heart, stomach, small intestine, colon) increased at the higher doses more than expected from dose-proportionality.

In vitro *metabolism*

Pseudoracemic [^{14}C]bidisomide and racemic [^{14}C]bidisomide were incubated with rat liver microsomes to examine the stereoselectivity of bidisomide metabolism. The NDBD metabolite was formed from both (−)- and (+)-enantiomers. However, the NDABD metabolite was formed only from (−)-bidisomide (figure 6).

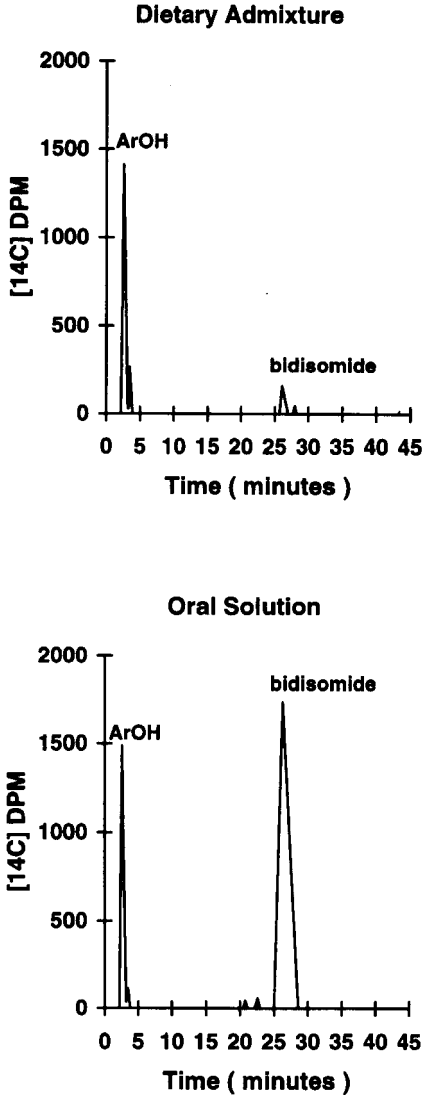


Figure 5. Representative non-chiral HPLC of Bond Elut-extractable radioactivity in the liver after [^{14}C]bidisomide administration at 300 mg/kg as a dietary mixture or an oral solution. ArOH is the NDABD metabolite.

Discussion

The present study has demonstrated that the pharmacokinetics of bidisomide in rat were not only dose-dependent over the dose range 90–900 mg/kg when administered as a dietary admixture, but also dose-mode-dependent when dietary admixture was compared with the oral solution at a comparable dose. The remarkable dose-dependent pharmacokinetics after dietary admixture administration were due to greater absorption as well as reduction of metabolism of bidisomide at the higher doses. This atypical dose-dependent absorption is thought to be due to both reduced interaction of the drug with food as the ratios of the diet to drug reduced at the high doses and also reduced secretion (e.g. biliary excretion, intestinal secretion) into the gastrointestinal tract. Small but consistent dose-

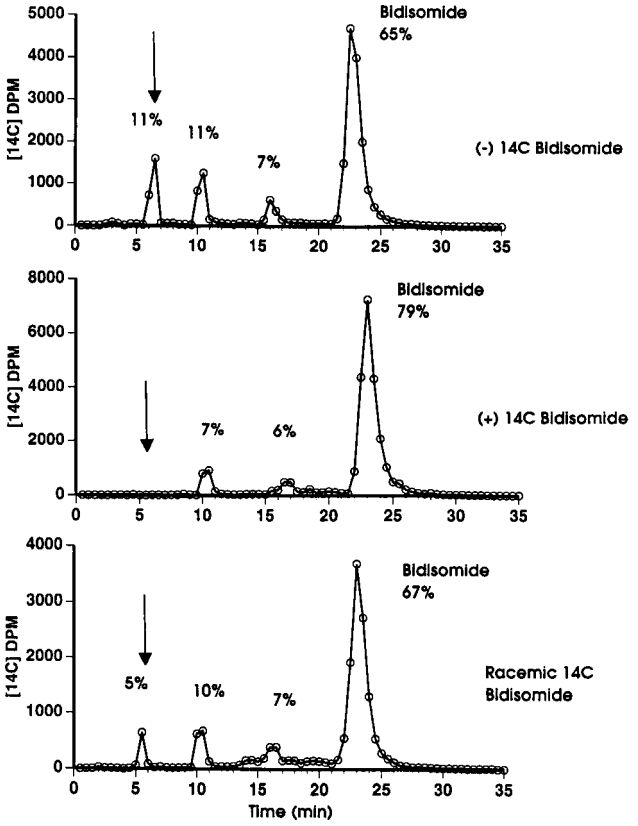


Figure 6. *In vitro* metabolic profiles of pseudoracemic (top and middle) mixtures of [^{14}C]bidisomide using rat liver microsomes. Peaks at 6 and 10 min are NDABD and NDBD respectively.

dependent systemic availability was observed even with a solution dosage form in the rat (unpublished data).

Metabolism of bidisomide was saturated at the higher doses and the proportion of the NDBD and NDABD in urine decreased as dose increased. With dietary admixture, the percentages of the dose excreted in urine as the rat-specific metabolite NDABD, was the same at the 90 and 300 mg/kg doses, whereas at the 900 mg/kg dose the percentage of the dose was lower. This was due to saturation of stereospecific arylhydroxylation of (−)-NDBD at the high dose. Liver uptake of total radioactivity was also dose-dependent, which is consistent with urinary excretion data. The percentages in the liver were the same at the 90 and 300 mg/kg doses but lower at the 900 mg/kg dose. The dose-dependent disposition of the metabolite in the liver was also evident in the IV infusion study even though apparent dose-proportionality was achieved in plasma concentrations over a dose range of 100–400 mg/kg. This IV infusion study mimicked the dietary admixture study in that constant blood levels maintained over an extended period.

Although the percentage of NDABD formed was less at the 900 mg/kg dose than at the 90 and 300 mg/kg doses, the total amount of the metabolite increased as dose increased. Therefore, the dose-dependent toxicity of bidisomide could not be explained by the dose-dependent metabolism alone. Transaminase levels were elevated at the 300 mg/kg dose but not at the 90 and 900 mg/kg doses.

After bidisomide administration as a solution, metabolism was reduced as compared with that after dietary admixture administration. The majority of liver radioactivity was due to the parent drug for the solution, whereas the majority of the liver radioactivity was due to NDABD metabolite for the dietary admixture. This was due to the fact that formation of the stereo-specific metabolite was more saturated after oral solution administration. However, reduction of metabolism was compensated by increased absorption and the total amount of the NDABD metabolite excreted in urine was similar whether bidisomide was administered as an oral solution or a dietary admixture. Therefore, the dose-mode-dependent toxicity of bidisomide after administration of the dietary admixture or oral solution could not be explained by the differences in the NDABD metabolite formation.

A dose-proportionality of drug disposition is generally assumed when an apparent dose-proportionality was achieved in plasma concentrations. However, in the IV infusion study, uptake of NDABD by the liver was saturated at the high doses even though plasma and liver concentrations of the parent drug were approximately dose-proportional. Concentrations of total radioactivity in the other organs were greater than expected from the dose-proportionality. These findings are of significance and caution must be exercized when plasma concentration data are correlated to the exposure to the drug-related materials in toxicity studies.

References

COOK, C. S., AMES, G. B., SMITH, M. E., KOWALSKI, K. G. and KARIM, A., 1993a, Absorption and disposition of a new antiarrhythmic agent bidisomide in man. *Pharmaceutical Research*, **10**, 1675–1681.

COOK, C. S., HAUSWALD, C., OPPERMANN, J. A. and SCHOENHARD, G. L., 1993b, Involvement of cytochrome P-450 IIIA in mechanism of inhibition of the epoxide formation by spironolactone and its sulfur-containing metabolite. *Journal of Pharmacology Experimental and Therapeutics*, **266**, 1–7.

COOK, C. S., ZHANG, L., OSIS, J., SCHOENHARD, G. L. and KARIM, A., 1998, Mechanism of compound- and species-specific food effects of structurally related antiarrhythmic drugs, disopyramide and bidisomide. *Pharmaceutical Research*, **15**, 429–433.

DAIN, J. D. and JAFFE, J. M., 1988, Effect of diet and gavage on the absorption and metabolism of fluperlapine in the rat. *Drug Metabolism Disposition*, **16**, 238–242.

FREDERICK, L. G., MCDONALD, S. J. and GARTHWAITE, S. M., 1989, Cardiovascular profile of a new antiarrhythmic agent, SC-40230. *Cardiovascular Research*, **23**, 897–903.

GARTHWAITE, S., HASHIMOTO K., KARIM, A., COOK, C. S., DESAI, D., TOOL, J., ANDRESS, J. and FERRO, L., 1995, Bidisomide: an investigational antiarrhythmic agent. *Cardiovascular Drug Review*, **13**, 19–32.

HATLEY, F., GARTHWAITE, S., FREDERICK, L., RUBY, J., OTTINGER, J., COOK, C. and MAHONEY, R., 1987, Antiarrhythmic profile of SC-40230. *Federation Proceedings*, **46**, 871.

LEE, K. H., XU, G. X., SCHOENHARD, G. L. and COOK, C. S., 1997, Mechanisms of food effects of structurally related antiarrhythmic drugs, disopyramide and bidisomide in the rat. *Pharmaceutical Research*, **14**, 1032–1040.

PAO, L. H., ZHOU, S. Y., COOK, C. S., KARARLI, T., KIRCHHOFF, C., TRUELOVE, J., KARIM, A. and FLEISHER, D., 1998, Reduced systemic availability of antiarrhythmic drugs, bidisomide, with meal co-administration: relationship with region-dependent intestinal absorption. *Pharmaceutical Research*, **15**, 221–227.

SMYTH, R. D., GAVER, R. C., DANDEKAR, K. A. VAN HARKEN, D. R. and HOTTENDORF, G. H., 1979, Evaluation of the availability of drugs incorporated in rat laboratory diet. *Toxicology and Applied Pharmacology*, **50**, 493–499.

VANDENBERGHE, Y., MASSON, M., PALATE, B. and ROBA. J., 1995, Effect of folate supplementation on clinical chemistry and hematologic changes related to bidisomide administration in the rat. *Drug Chemical Toxicology*, **18**, 235–270.

VANHARKEN, D. R. and HOTTENDORF, G. H., 1978, Comparative absorption following the administration of a drug to rats by oral gavage and incorporation in the diet. *Toxicology Applied Pharmacology*, **43**, 407–410.

XENOBIOTICA , 2000, VOL. 30, NO. 5, 535–545

Effects of phenethylisothiocyanate on the expression of glutathione *S*-transferases and hepatotoxicity induced by acetaminophen

K. W. SEO*, J. G. KIM, M. PARK, T. W. KIM and H. J. KIM

Department of Toxicology, National Institute of Toxicological Research, Korea Food and Drug Administration, 5 Nokbundong, Eunpyunggu, Seoul 122–020, Korea

1. The effect of PEITC on the expression of hepatic glutathione *S*-transferases (GST) and the glutathione (GSH) conjugation has been investigated in the Sprague–Dawley rat, and it has been determined whether hepatotoxicity of acetaminophen (AA) could be inhibited through the induction of GST expression in mouse.

2. The hepatic GST activity and protein levels of α class (Ya, Yc) and μ class (Yb1, Yb2) of GST were elevated in a dose-dependent manner after treatment with PEITC (0, 3.16, 10, 31.6, 100 and 200 mg/kg, p.o., 3 days). The mRNA levels of GST Ya and GST Yb1 were also markedly increased 1 day after treatment with PEITC at dosages ranging from 31.6 to 200 mg/kg. The hepatic GSH content was significantly increased to 200% of control at dose of 200 mg/kg PEITC.

3. Pretreatment with 100 mg/kg PEITC significantly enhanced the biliary excretion of glutathione conjugate of AA 2-fold, whereas treatment with 200 mg/kg did not affect it.

4. In mouse, PEITC (100 and 200 mg/kg, 3 days) decreased the lethality and hepatotoxicity caused by AA.

5. These results indicate that (1) the induction of GST by PEITC is presumably under transcriptional regulation, and (2) PEITC may have a protective function against AA-induced hepatotoxicity by induction effect on GST, in combination of enhancement of hepatic GSH.

Introduction

Consumption of vegetables and fruit can significantly decrease the risk of human cancer (Trock *et al.* 1990, Steinmetz and Potter 1991). The human diet contains a variety of compounds that inhibit mutagenesis and/or carcinogenesis in laboratory models (Ames 1983, Carr 1985, Hayatsu *et al.* 1988). These compounds consist of structurally diverse compounds, of which the protective mechanisms are generally unknown. Phenethylisothiocyanate (PEITC) (figure 1), occurring in certain cruciferous vegetables (Tookey *et al.* 1980), has been shown to inhibit carcinogenesis induced by several nitrosamines and polycyclic aromatic hydrocarbons (Morse *et al.* 1989a, b). The anticarcinogenic action of PEITC has been ascribed to its ability to inhibit activation of carcinogens, and also to enhanced detoxification systems, such as glutathione *S*-transferase (Morse *et al.* 1989b, Guo *et al.* 1991, 1992, Doerr *et al.* 1991, Smith *et al.* 1993). Guo *et al.* reported that PEITC dramatically decreased the activities of cytochrome P4502E1, cytochrome P4501A2 and P4503A in liver microsomes. In contrast, hepatic NADPH quinone oxidoreductase activity and glutathione *S*-transferase (GST) activity were increased in the PEITC-treated rat (Guo *et al.* 1992).

* Author for correspondence; e-mail: kwseo@kfda.go.kr

Xenobiotica ISSN 0049-8254 print/ISSN 1366-5928 online © 2000 Taylor & Francis Ltd
http://www.tandf.co.uk/journals

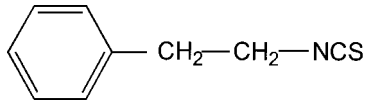


Figure 1. Structure of PEITC.

GST is a family of multifunctional enzymes that detoxify a number of mutagenic electrophiles by catalysing their conjugation with reduced glutathione. Multiple forms of GST provide diversity in ligand binding and catalytic specificities. A widely accepted, species-independent scheme for classifying major mammalian cytosolic GST into α, μ and π categories is based on sequence homologies, subunit assembly patterns, immunological and other common properties (Mannervik and Danielson 1988). The human μ class (GSTM) has attracted considerable attention because of notable genetic polymorphisms. GSTM1 is one of five μ class enzymes (M1–5; Hussey and Hayes 1993, Heagerty *et al.* 1994, Hayes and Pulford 1995), and detoxifies the mutagenic metabolites produced by cytochrome P4501A1-catalyzed oxidation of polycyclic aromatic hydrocarbon such as benzo(α)pyrene (Mannervik and Danielson 1988). A number of studies have reported that GSTM1 gene deletion is associated with an increased incidence of tumours, particularly adenocarcinoma of stomach and caecum and multiple skin cancers in human (Strange *et al.* 1991, Heagerty *et al.* 1994).

The current study was designed to investigate whether the expression of GST is responsible for the chemopreventive effect of PEITC. For this purpose the expressions of GST α (Ya, Yc) and GST μ (Yb1, Yb2), as well as the activities of GST, were measured in rat liver after administration of PEITC. In addition, to examine if formation of glutathione conjugate can be increased through induction of GST, glutathione conjugate of acetaminophen (AA-GS) in bile was also quantified in rat pretreated with PEITC. The second aim of this work was to determine whether acetaminophen (AA)-induced hepatotoxicity could be inhibited through the induction of GST expression. AA is a widely used analgesic that undergoes biotransformation reactions that may toxify or detoxify the drug (Boyd and Bereczky 1966, Davidson and Eastham 1966). Toxification presumably involves formation of an electrophile, *N*-acetyl-*p*-benzoquinoneimine, that may arylate cellular macromolecules and produce liver necrosis (Corcoran *et al.* 1980, Hinson 1982, Jollow *et al.* 1982). However, when sufficient glutathione is available, the electrophile can be detoxified by conjugation with glutathione (GSH). Because GST plays an important role in glutathione conjugation, it was also of interest to know whether the toxication/detoxication pathways for AA are altered by induction of GST. For this purpose, the effect of PEITC pretreatment on AA-induced hepatotoxicity was examined in the mouse.

Materials and methods

Chemicals

PEITC were from Aldrich Chemical Co. (Milwaukee, WI, USA). Monoclonal antibodies against rat GST α (Ya, Yc) and GST μ (Yb1, Yb2) were from Biotrin International (Dublin, Ireland). Biotinylated goat anti-rabbit IgG was from Life Technologies, Inc. (Gaithersburg, MD, USA). Vectastatin Elite ABC kit and DAB-Ni kit for Western blotting were from Vector Laboratories, Inc. (Burlingame, CA, USA). All other chemicals were from Sigma Chemical Co. (St Louis, MO, USA).

Animal treatment

Male Sprague–Dawley rats (180–220 g) and male ICR mice (20–25 g) were from Korea Food and Drug Administration (Seoul, Korea) and fed with rodent chow (Shinchon Diet Co., Seoul, Korea) and tap water *ad libitum*. The rats were orally treated with PEITC for consecutive 3 days using the following dosages: 3.16, 10, 31.6, 100 and 200 mg/kg for the investigations of GST activity, GSH content and Western blot analysis, 100 and 200 mg/kg for analysis of AA-GS in bile. Northern blot hybridization was performed 1 day after administration of PEITC (3.16, 10, 31.6, 100, 200 mg/kg). To estimate the effects of PEITC on toxification of AA, mice were pretreated with PEITC (100 and 200 mg/kg, p.o.) for 3 days, and then were injected i.p. with AA (500 mg/kg) in saline.

Preparation of cytosol

The livers were quickly excized and rinsed in cold KCl-Tris buffer (150–50 mM Tris-HCl, pH 7.4). A portion of the liver was homogenized in 2 vols KCl-Tris using a motor-driven Teflon and glass tissue grinder. Homogenates were diluted to 250 mg liver/ml with KCl-Tris and centrifuged at 105000 *g* for 90 min in a Kontron ultracentrifuge. The supernatant was carefully collected and diluted to the desired protein concentration. Cytosolic suspensions were stored in aliquots at -75 °C until assayed. Cytosolic protein was determined by the method of Lowry *et al.* (1951).

Analysis of GSH

Hepatic GSH concentration was determined according to the procedure of Tietze (1969) with a minor modification. Liver tissues were homogenized with 4 vols 3% sulphosalicylic acid as rapidly as possible upon death. The homogenate was centrifuged at 10000 *g* for 10 min, and then supernatant was diluted 100-fold with phosphate buffer. Reaction mixtures consisted of 0.1 M sodium phosphate buffer (containing 5 mM EDTA, pH 7.5), 0.5 mM 5,5-dithiobis (2-nitrobenzoic acid), 0.5 unit/ml glutathione reductase and 100 μl tissue sample. After mixing, the increase in absorbance at 412 nm/min was determined. Glutathione was used for a standard.

GST assays

GST activity in cytosol was determined according to Habig *et al.* (1974) using 1-chloro-2,4-dinitrobenzene as a substrate. The reaction mixtures consisted of 1 mM GSH and 1 mM 1-chloro-2,4-dinitrobenzene (CDNB) in 0.1 M potassium phosphate buffer, pH 6.5. The reaction was initiated by the addition of 10 μg cytosolic protein (final reaction volume = 2.0 ml) and the increase in absorbance at 340 nm due to the formation of CDNB-GS conjugates was recorded for 4 min. The activity was calculated using the extinction coefficient of 9.6 mM^{-1} cm^{-1}.

Western blot analysis

Western blot analysis was accomplished according to previously published procedures (Davis *et al.* 1989). The cytosolic proteins were separated by 12% SDS-PAGE (Laemmili 1970) using a BioRad Mini-Protein II system and electrophoretically transferred to nitrocellulose paper. Immunoblots were incubated with rabbit anti-rat GST Ya, Yc, Yb1 and Yb2 antibodies. The specific binding of the monoclonal antibodies to the isozymes was detected with 4-chloro-1-naphthol after incubation with peroxidase-conjugated goat anti-rabbit IgG as a second antibody.

Isolation of total RNA and poly(A)$^+$ RNA

Total RNA was isolated using the improved single-step method of thiocyanate–phenol–chloroform RNA extraction according to the methods of Cathala *et al* (1983) and Chomczynski and Sacchi (1987), as modified by Puissant and Houdebine (1990). Poly(A)$^+$ RNA was isolated from the total RNA using an oligo(dT)-cellulose column according to the method of Jacobson (1987). cDNA probes (Ya 287–684, Yb1 643–963) were derived from hepatic poly(A)$^+$ RNA from rat treated with pyrazine. cDNA was amplified using a PCR technique, and the amplified DNA was cloned in pGEM + T Vector (Promega, Madison, WI, USA).

Northern blot hybridization

The poly(A)$^+$ RNA isolated from rat livers was resolved by electrophoresis in a 1% agarose gel containing 2.2 M formaldehyde and then transferred to supported nitrocellulose paper by capillary transfer. The nitrocellulose paper was baked in a vacuum oven at 80 °C for 2 h. The blot was incubated with hybridization buffer containing 50% de-ionized formamide, 5 × Denhardt's solution (0.1% Ficoll, 0.1% polyvinylpyrrolidine and 0.1% bovine serum albunim (Pentex Fraction V)), 0.1% SDS, 200 μg/ml sonicated salmon sperm DNA and 5 × SSPE (1 × SSPE: 0.15 M NaCl, 10 mM NaH_2PO_4 and

1 mM Na_2EDTA, pH 7.4) without probe for 1 h at 42 °C. Hybridization was performed at 42 °C for 18 h with a heat-denatured cDNA probe, which was random prime-labelled with [α-^{32}P]dATP. Filters were washed twice in 2 × standard saline citrate (SSC) and 0.1% SDS for 10 min at room temperature. Filters were finally washed in the solution containing 0.1 × SSC and 0.1% SDS for 60 min at 60 °C, followed by autoradiography with Kodak X-Omat AR film at − 80 °C using intensifying screens.

Quantification of AA-GS in bile

After treatment with PEITC (100 and 200 mg/kg) for 3 days, rats were anaesthetized with pentobarbital (50 mg/kg, i.p.) and the common bile duct cannulated using polyethylene tubing (PE-50). AA (150 mg/kg in saline) was injected into the saphenous vein and then bile was collected for 2 h. AA-GS in bile was determined by isocratic reverse-phase HPLC with UV absorbance detection as described by Howie *et al* (1977). The concentration of AA-GS was calculated from AA standard curve as its molar extinction coefficient is the same that of AA. Bile was diluted 100-fold with methanol and centrifuged before analysis.

Hepatotoxicity of AA in mouse

Mice were orally pretreated with PEITC (100 or 200 mg/kg) for 3 consecutive days and the control animals were given the vehicle. After 3 days, a single dose of AA (500 mg/kg) was injected i.p. Liver samples for histopathology were fixed in 10% buffered formalin, processed by standard histopathological techniques and stained with haematoxylin and eosin. Two observers examined it by light microscopy by the method of Chalkley (1943). The quantitation of hepatic necrosis was: 0, absent; 1, necrosis of < 6% of the parenchymal hepatocytes; 2, necrosis of 6–25% of hepatocytes; 3, necrosis of 26–50% of hepatocyte; and 4, necrosis of > 50% of hepatocytes.

Statistics

One-way analysis of variance assessed the statistical significance of changes in all indices, followed by Duncan's multiple range test with $p < 0.05$ set at the minimum level of significance.

Results

Effect of PEITC on the activities and expressions of GST

The specific activity of GST after administration of PEITC is given in table 1. Treatment with 100 and 200 mg/kg PEITC elevated GST activity 1.6- and 1.8-fold respectively. Also at dosages ranging from 3.16 to 31.6 mg/kg, PEITC tended to increase GST activity, but these changes were not statistically significant.

GST induction was monitored by measuring GST (Ya, Yc, Yb1 and Yb2) protein levels immunochemically as shown in figure 2. These blots showed the dose-dependent increases in GST Ya, Yb1 and Yb2 proteins following PEITC treatment. PEITC produced the largest increase in the Ya subunit, with somewhat lesser increases in Yb1 and Yb2. The protein level of Yc was not affected by PEITC treatment.

To determine whether GST induction was accompanied by increases in mRNA, Northern blot hybridization was performed using poly(A)$^+$ RNA isolated from rat treated with PEITC (figure 3). GST Ya and GST Yb1 were selected because they represented marked increases in protein level. Northern blot analysis revealed that GST Ya and GST Yb1 mRNA levels in rats treated with PEITC were dramatically elevated after dosage of 31.6 mg/kg PEITC.

Effect of PEITC on the hepatic GSH content

Since GSH content is important factor in glutathione conjugation, the hepatic GSH content after pretreatment with PEITC was measured. Table 1 demonstrates the hepatic GSH content in rat treated with PEITC. The hepatic GSH concen-

Table 1. Effect of PEITC on the GST activity and GSH content in liver, and biliary excretion of AA-GS.[a,b]

Dose of PEITC (mg/kg)	GST activity (nmol/min/mg protein)	GSH content (μmol/g liver)	AA-GS (mmoles/kg B.W.)
0	346.1± 9.77	4.8± 0.07	17.9± 3.81
3.16	369.2± 20.00	4.0± 0.21*	
31.6	409.6± 43.53	4.0± 0.15*	
10	427.2± 30.07	4.2± 0.18	
100	550.2± 46.66*	4.5± 0.23	37.8± 3.63*
200	606.1± 41.92*	7.9± 0.39*	21.6± 3.56

[a] For the investigations of GST activity and GSH content, rats were orally treated with PEITC (0, 3.16, 10, 31.6, 100 and 200 mg/kg) for 3 consecutive days. Values are mean± SE of 10 rats.

[b] After pretreatment with PEITC (0, 100 and 200 mg/kg, p.o., 3 days) rats were injected with AA (150 mg/kg, i.v.), and then AA-GS in bile was measured. Values are mean± SE of six rats.

* Significantly different from the control rat ($p < 0.05$).

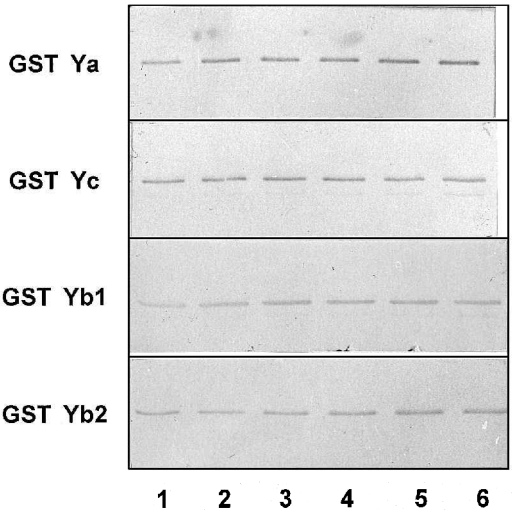


Figure 2. Immunoblot analysis of rat hepatic cytosol with rabbit anti-rat GST Ya, Yc, Yb1 and Yb2 antibodies. This blot exhibited GST levels in hepatic cytosols isolated from the untreated (lanes 1), 3.16 mg/kg PEITC- (2), 10 mg/kg PEITC- (3), 31.6 mg/kg PEITC- (4), 100 mg/kg PEITC- (5) or 200 mg/kg PEITC- (6) treated rat (p.o., 3 days). Each lane was loaded with 20 μg rat liver cytosol.

tration was slightly, but significantly, decreased at dosages of 3.16 and 10 mg/kg PEITC, whereas it gradually increased to a control level at larger dosages of PEITC (31.6 and 100 mg/kg), and was substantially elevated to 165% of control at the highest dosage (200 mg/kg).

Effect of PEITC on the glutathione conjugation of AA

To examine whether PEITC increases the formation of glutathione conjugate through induction of GST, AA-GS in bile was analyzed. The effect of pretreatment with PEITC on the biliary excretion of AA-GS is demonstrated in the table 1. The

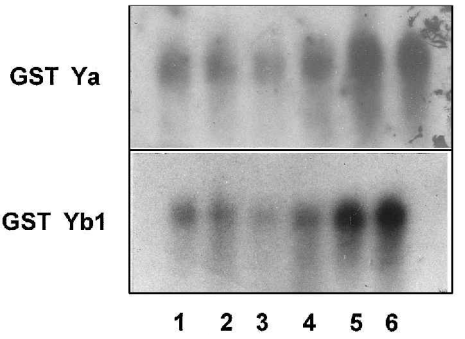


Figure 3. Northern blot hybridization of poly(A)$^+$ mRNA with cDNA probes of GST Ya and Yb1. This blot exhibited GST mRNA levels in hepatic cytosols isolated from the untreated (lanes 1), 3.16 mg/kg PEITC- (2), 10 mg/kg PEITC- (3), 31.6 mg/kg PEITC- (4), 100 mg/kg PEITC- (5) or 200 mg/kg PEITC- (6) treated rat (p.o., 3 days). Each lane was loaded with 20 μg hepatic total RNA.

Table 2. Effect of PEITC on AA-induced mortality rate and hepatic necrosis[a].

Treatment (mg/kg)	Mortality rate (%)	Incidence of necrosis (%)			
		Severity of necrosis[b]			
		0	1	2	3<
AA alone	83	—	—	—	100
PEITC alone (200)	0	100	—	—	—
PEITC (100)+AA	43	14	—	29	57
PEITC (200)+AA	29	—	—	29	71

[a] Mice ($n = 7$) were injected i.p. with AA (500 mg/kg) after pretreatment with PEITC (100 or 200 mg/kg) for 3 consecutive days.
[b] Hepatic necrosis 24 h after administration of AA was scored by the criteria given under the Materials and methods.

treatment with 100 mg/kg PEITC markedly increased the biliary excretion of AA-GS to 211% of control, but treatment with 200 mg/kg had no effect.

Effect of PEITC on AA-induced mortality and hepatotoxicity

Mice were pretreated for 3 days with PEITC and on the fourth day 500 mg/kg AA was injected i.p. As demonstrated in table 2, PEITC pretreatment (100 and 200 mg/kg) had a significant effect on the mortality rate induced by AA. In the control mouse administered 500 mg/kg AA, the lethality was 83% ; however, the mortality rate was markedly decreased to 43 and 20% in mouse pretreated with 100 and 200 mg/kg PEITC respectively.

Figure 4 shows photomicrographs of livers from mouse; and table 2 illustrates quantitative effect of PEITC pretreatment on AA-induced liver necrosis. As shown in figure 4, administration of AA elicited parenchymal degeneration and severe necrosis, and liver necrosis was scored from levels 1 to 3 according to severity. Up to 200 mg/kg PEITC by itself did not produce any histophathological evidence of liver. In the control mouse injected with 500 mg/kg AA, all the livers exhibited

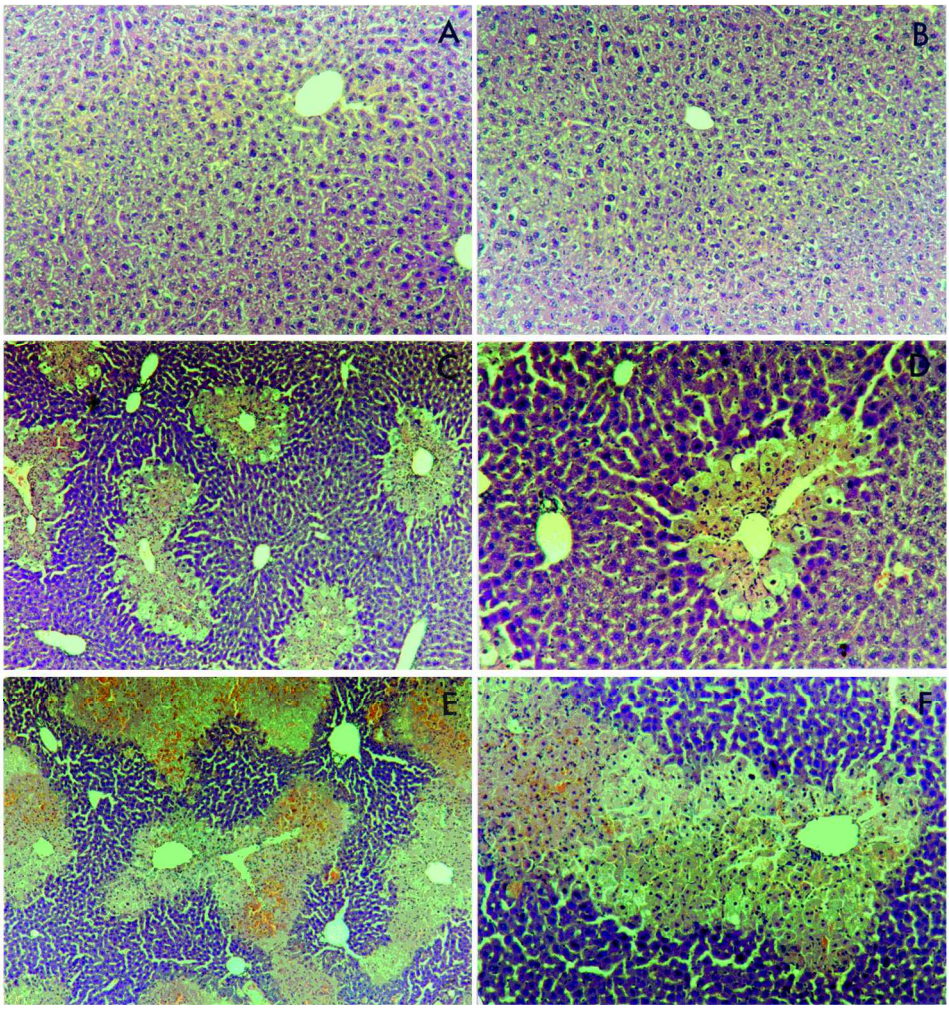


Figure 4. (A) Liver lobule from the control mouse. (B) Liver lobule from the 200 mg/kg PEITC-treated mouse. Note the normal appearance of the hepatic parenchyma and sinusoids surrounding the central vein. (C, D) Level 2; (E, F) level 3 <. Liver lobule from a mouse sacrificed 24 h after administration of AA (500 mg/kg, i.p.). Severe necrosis and congestion of sinusoids are more prominent in the centrilobular area. H&E ×40 and ×100.

severe necrosis of at least level 3. However, the administration of 500 mg/kg AA to mouse pretreated with PEITC (100 and 200 mg/kg) resulted in 57 and 71% of the livers showing necrosis (level 3 <) respectively.

Discussion

In the present study, significant induction of GST activity by PEITC (100 and 200 mg/kg) was demonstrated in accordance with the results of Guo *et al.* (1993) who reported that treatment with PEITC (0.25 and 1.0 mmol/kg) resulted in a slight increase in liver GST activity. On the other hand, studies by Lieshout *et al.* (1996) and Smith *et al.* (1993) reported that dietary intake of PEITC (1 and 3 μmol/g diet) did not significantly enhance hepatic GST activity in the Wistar rat. These

differences might be due to a species-specific effect, and concentration- and/or duration-dependent effects, which make it virtually impossible to extrapolate from one study to another.

In addition to the measurement of total GST activity it is important to study changes in levels of specific isoenzymes. The increase in GST activity by PEITC was paralleled by rises in protein levels of GST α and GST μ in the same order of magnitude, and treatment with 100 and 200 mg/kg PEITC resulted in marked increases of GST α and GST μ protein levels. Although GST activity was not significantly increased by PEITC treatment at doses ranging from 3.16 to 31.6 mg/kg, the hepatic GST α and GST μ protein levels were elevated at these dosages. This induction of hepatic GST protein levels correlate with the increases of GST mRNA levels, resulting in marked enhancement of GST mRNA in the PEITC-treated rat (31.6 mg/kg). These results provide evidence that PEITC induces GST and that GST induction involves large increases in GST mRNA, probably due to transcriptional activation.

The correlation between the induction in GST activities and increases in glutathione conjugates has previously been investigated. Wallin *et al.* (1978) reported that phenobarbital (PB) treatment caused an increase in GST activity in rat liver, resulting in a significant increase of glutathione conjugate of ethacrynic acid in bile. A similar argument has been made for sulphobromophthalein clearance and PB induction of ligandin (Reyes *et al.* 1971). Ligandin has been demonstrated to be a GST (Habig *et al.* 1974). These results indicate that hepatic GST induction is responsible for the increased biliary excretion of glutathione conjugate and clearance of parent compound. In the present study it was observed that biliary excretion of AA-GS was increased (2-fold) in the PEITC-pretreated rat (100 mg/kg). Because glutathione conjugates are known to be excreted predominantly in bile (Smith 1973), the biliary excretion of AA-GS was used to estimate the formation of AA-GS. Thus, our observation that treatment of rat with 100 mg/kg PEITC enhanced the biliary excretion of AA-GS reflects the increased formation of the AA-GS. In this study the increased biliary excretion of AA-GS as a result of PEITC treatment (100 mg/kg) without a change in hepatic GSH levels favours the view that the increase is enzymatically mediated. Therefore, it is concluded that PEITC induces GST and that the induction of this enzyme results in increased formation of AA-GS.

In contrast to finding at dosage of 100 mg/kg (0.6 mmol/kg), treatment of rat with 200 mg/kg (1.2 mmol/kg) PEITC did not significantly increase the formation of AA-GS. Because AA-GS was produced from conjugation of *N*-acetyl-*p*-benzoquinoneimine (reactive metabolite of AA) with GSH, formation of AA-GS may not only be dependent on the rate of glutathione conjugate formation by GST, but also on the amount of *N*-acetyl-*p*-benzoquinoneimine produced by P450 enzymes. Cytochrome P450s is a family of enzymes and it appears that the ethanol-inducible form, P4502E1, and the β-naphthofalvone-inducible form, P4501A2, are most effective in producing this reactive metabolite (Harvison *et al.* 1988). It has been reported that a single dose of PEITC (1 mmol/kg) to rat decreased the activities of liver P4502E1 and P4501A2 (Guo *et al.* 1992). Thus, unchanged excretion of AA-GS in the 200 mg/kg PEITC-pretreated rat may be due to inhibition of the P450-mediated formation of *N*-acetyl-*p*-benzoquinoneimine.

AA-induced hepatotoxicity varies considerably among species (Davis *et al.* 1974, Siegers *et al.* 1978). Hamster and mouse are the laboratory animals most sensitive to

the hepatotoxic properties of AA, whereas rat and guinea pig are relatively resistant to AA-induced liver injury. The species variation in hepatotoxicity is thought to be largely due to differences in the activation of AA to its reactive metabolite by the P450 (Davis *et al.* 1974, Jollow *et al.* 1974, Coldwell *et al.* 1976, Gregus *et al.* 1988). Therefore, to investigate the effect of PEITC on the AA-induced hepatotoxicity, the mouse was chosen as the target species.

Pretreatment of mouse with PEITC (100 and 200 mg/kg) markedly decreased the hepatotoxicity produced by AA as evidenced by decreased mortality and the marked decrease in necrosis produced by AA. Therefore, these data clearly indicate that PEITC pretreatment protects against AA-induced hepatotoxicity. It is known that the hepatotoxic effects of AA are caused by *N*-acetyl-*p*-benzoquinoneimine (Mitchell and Jollow 1975, Dahlin *et al.* 1984), which is normally detoxified by conjugation with GSH. However, if the reactive metabolite is formed at a faster rate than it can be detoxified by GSH, the reactive metabolite will bind to cellular macromolecules and produce cell death (Mitchell *et al.* 1973a, b, Potter *et al.* 1974). Therefore, the availability of GSH is critical in mitigating AA hepatotoxicity. For example, pretreatment of animals with GSH precursors decreased AA hepatotoxicity (Potter *et al.* 1974, Hazelton *et al.* 1986) and GSH depletors, such as diethyl maleate, increased AA hepatotoxicity (Mitchell *et al.* 1973a). Very little information on the effects on GSH levels of PEITC has previously been reported. Recently, PEITC administration was reported to induce GSH content in the colon, and elevation of GSH levels occurred in parallel with induction of GST (Lieshout *et al.* 1996). In the present study, treatment with 200 mg/kg PEITC caused a substantial increase in hepatic GSH concentration. Although the specific mechanism of this increase remains unclear, this increase in GSH produced by PEITC probably contributes to its ability to decrease AA hepatotoxicity.

The GST plays an important role in glutathione conjugation, detoxified metabolic reaction of AA. In the present study it was demonstrated that PEITC increases GST activity, resulting in enhancement of glutathione conjugation. Therefore, the increase of hepatic GST activity by PEITC may be of significance in the protection against hepatotoxicity of AA. Hepatoprotective effects of PEITC may be mediated by enzyme systems other than GST. PEITC is known to inhibit the activities of P4502E1 and P4501A2 (Guo *et al.* 1992), which are active in the formation of a highly reactive metabolite of AA, namely *N*-acetyl-*p*-benzoquinoneimine. Thus it appears that PEITC decreases the hepatotoxicity of AA in mouse both by a decrease in activation of AA as well as by an increase in detoxication.

In conclusion, the results of the present study demonstrate that PEITC treatment significantly increases hepatic GST activities, and that the induction of GST is likely under transcriptional regulation. This study also suggests that PEITC may have protective function against AA-induced hepatotoxicity by inducing GST, in combination of enhancement of hepatic GSH content.

References

AMES, B. N., 1983, Dietary carcinogens and anticarcinogens. *Science*, **221**, 1256–1264.

BOYD, E. M. and BERECZKY, G. M., 1966, Liver necrosis from paracetamol. *British Journal of Pharmacology and Chemotherapy*, **26**, 606–614.

CARR, B. I., 1985, Chemical carcinogens and inhibitors of carcinogenesis in the human diet. *Cancer*, **55**, 218–224.

CATHALA, G., SAVOURET, J.-F., MENDEZ, B., WEST, B. L., KARIN, M., MARTIAL, J. A. and BAXTER, J. D., 1983, Laboratory methods; A method for isolation of intact, translationally active ribonucleic acids. *DNA*, **2**, 329–335.

CHALKLEY, H. W., 1943, Methods for the quantitative morphologic analysis of tissues. *Journal of National Cancer Institute*, **4**, 47–53.

CHOMCZYNSKI, P. and SACCHI, N., 1987, Single-step method of RNA isolation by acid guanidinium thiocyanate–phenol–chloroform extraction. *Analytical Biochemistry*, **162**, 156–159.

COLDWELL, B. B., THOMAS, B. H., WHITEHOUSE, L. W., WONG, L. T. and HYNIE, I., 1976, Metabolism of ^{14}C-acetaminophen in humans and laboratory animals. *Proceedings of the Society of Environmental Toxicology*, **17**, 269–276.

CORCORAN, G. B., MITCHELL, J. R., VAISHNAV, Y. N. and HORNING, E. C., 1980, Evidence that acetaminophen and *N*-hydroxyacetaminophen form a common arylating intermediate, *N*-acetyl-*p*-benzoquinoneimine. *Molecular Pharmacology*, **18**, 536–542.

DAHLIN, D. C., MIWA, G. T., LU, A. Y. H. and NELSON, S. D., 1984, *N*-acetyl-*p*-benzoquinoneimine; A cytochrome P450-mediated oxidation product of acetaminophen. *Proceedings of the National Academy of Sciences, USA*, **81**, 1327–1331.

DAVIDSON, D. G. and EASTHAM, W. N., 1966, Acute liver necrosis following overdose of paracetamol. *British Medical Journal*, **2**, 497–499.

DAVIS, D. C., POTTER, W. Z., JOLLOW, D. J. and MITCHELL, J. R., 1974, Species differences in hepatic glutathione depletion, covalent binding and hepatic necrosis after acetaminophen. *Life Science*, **14**, 2099–2109.

DAVIS, I. G., DIBNER, M. D. and BATTERY, J. F., 1989, Western blot analysis. In *Basic Methods in Molecular Biology* (New York: Elsevier), pp. 311–314.

DOERR-O'ROURKE, K., TRUSHIN, N., HECHT, S. S. and STONER, G. D., 1991, Effect of phenethyl isothiocyanate on the metabolism of the tobacco-specific nitrosamine 4-(methylnitroamino)-1-(3-pyridyl)-1-butanone by cultured rat lung tissue. *Carcinogenesis*, **12**, 1029–1034.

GREGUS, Z., MADHU, C. and KLAASSEN, C. D., 1988, Species variation in toxication and detoxication of acetaminophen *in vivo*; a comparative study of biliary and urinary excretion of acetaminophen metabolites. *Journal of Pharmacology and Experimental Therapeutics*, **244**, 91–99.

GUO, Z., SMITH, T. J., THOMAS, P. E. and YANG, C. S., 1991, Metabolic activation of 4-(methylnitrosamine)-1-(3-pyridyl)-1-butanone as measured by DNA alkylation *in vitro* and its inhibition by isothiocyanates. *Cancer Research*, **51**, 4798–4803.

GUO, Z., SMITH, T. J., WANG, E., EKLIND, K. I., CHUNG, F.-L. and YANG, F. S., 1993, Structure–activity relationships of arylalkyl isothiocyanates for the inhibition of 4-(methylnitrosamino)-1-(3-pyridyl)-1-butanone metabolism and the modulation of xenobiotic-metabolizing enzymes in rats and mice. *Carcinogenesis*, **14**, 1167–1173.

GUO, Z., SMITH, T. J., WANG, E., SADRICH, N., MA, Q., THOMAS, P. E. and YANG, C. S., 1992, Effects of phenylhexyl isothiocyanate, a carcinogenesis inhibitor, on xenobiotic-metabolizing enzymes and nitrosamine metabolism in rats. *Carcinogenesis*. **13**, 2205–2210.

HABIG, W. H., PABST, M. J. and JAKOBY, W. B., 1974, Glutathione *S*-transferase; the first enzymatic step in mercapturic acid formation. *Journal of Biological Chemistry*, **249**, 7130–7139.

HARVISON, P. J., GUENGERICH, F. P., RASHED, M. S. and NELAON, S. D., 1988, Cytochrome P450 isozymes selectivity in the oxidation of acetaminophen. *Chemical Research in Toxicology*, **1**, 47–52.

HAYATSU, H., ARIMOTO, S. and NEGISHI, T., 1988, Dietary inhibitors of mutagenesis and carcinogenesis. *Mutation Research*, **202**, 429–446.

HAYES, J. D. and PULFORD, D. J., 1995, The glutathione *S*-transferase supergene family. Regulation of GST and the contribution of the isoenzymes to cancer chemoprotection and drug resistance. *Critical Reviews in Biochemistry and Molecular Biology*, **30**, 445–600.

HAZELTON, G. A., HJELLE, J. J. and KLAASSEN, C. D., 1986, Effect of cysteine pro-drugs on acetaminophen-induced hepatotoxicity. *Journal of Pharmacology and Experimental Therapeutics*, **237**, 341–349.

HEAGERTY, A. H. M., FITZGERALD, D., SMITH, A., BOWERS, B., JONES, P., FRYER, A., ZHAO, L., ALLDERSEA, J. and STRANGE, R. C., 1994, Glutathione *S*-transferase GSTM1 phenotypes and protection against cutaneous malignancy. *Lancet*, **343**, 266–268.

HINSON, J. A., 1982, Biochemical toxicology of acetaminophen. In E. Hodgson, J. R. Bend and R. M. Philpot (eds), *Reviews in Biochemical Toxicology* (New York: Elsevier/North Holland), pp. 103–109.

HOWIE, D., ADRIAENSSENS, P. and PRESCOTT, L. F., 1977, Paracetamol metabolism following overdosage; application of high performance liquid chromatography. *Journal of Pharmacy and Pharmacology*, **29**, 235–237.

HUSSEY, A. J. and HAYES, J. D. H., 1993, Human μ-class glutathione *S*-transferases present in liver, skeletal muscle and testicular tissue. *Biochimica et Biophysica Acta*, **1203**, 131–141.

JACOBSON, A., 1987, Purification and fractionation of poly(A)$^+$ RNA. *Methods in Enzymology*, **152**, 254–261.

JOLLOW, D. J., ROBERTS, S., PRICE, V. and SMOTH, C., 1982, Biochemical basis for dose response

relationships in reactive intermediate toxicity. In R. Snyder, D. V. Parke, J. J. Kocois, G. Gibson and D. J. Jollow (eds), *Biological Reactive Intermediates. II: Chemical Mechanisms and Biological Effects* (New York: Plenum), pp. 99–113.

JOLLOW, D. J., THORGEIRSSON, S. S., POTTER, W. Z., HASHIMOTO, M. and MITCHELL, J. R., 1974, Acetaminophen-induced hepatic necrosis. VI. Metabolic disposition of toxic and nontoxic doses of acetaminophen. *Pharmacology (Basel)*, **12**, 251–271.

LAEMMILI, U. K., 1970, Cleavage of structural proteins during assembly of the head bacteriophage T4. *Nature*, **227**, 680–685.

LIESHOUT, E. M. M., PETERS, W. H. M. and JANSEN, J. B. M. J., 1996, Effect of oltipraz, α-tocopherol, β-carotene and phenethylisothiocyanate on rat oesophageal, gastric, colonic and hepatic glutathione, glutathione *S*-transferase and peroxidase. *Carcinogenesis*, **17**, 1439–1445.

LOWRY, O. H., ROSEBROUGH, N. J., FARR, A. L. and RANDALL, R. T., 1951, Protein measurement with the Folin phenol reagent. *Journal of Biological Chemistry*, **193**, 265–275.

MANNERVIK, B. and DANIELSON, U. H., 1988, Glutathione transferases; structure and catalytic activity. *Critical Reviews in Biochemistry and Molecular Biology*, **23**, 281–337.

MITCHELL, J. R. and JOLLOW, D. J., 1975, Metabolic activation of drugs to toxic substances. *Gastroenterology*, **68**, 392.

MITCHELL, J. R., JOLLOW, D. J., POTTER, W. Z., DAVIS, D. C., GILETTE, J. R. and BRODIE, B. B., 1973b, Acetaminophen-induced hepatic necrosis. I. Role of drug metabolism. *Journal of Pharmacology and Experimental Therapeutics*, **187**, 185–194.

MITCHELL, J. R., JOLLOW, D. J., POTTER, W. Z., DAVIS, D. C., GILETTE, J. R. and BRODIE, B. B., 1973a, Acetaminophen-induced hepatic necrosis. IV. Protective role of glutathione. *Journal of Pharmacology and Experimental Therapeutics*, **187**, 211–217.

MORSE, M. A., AMIN, S. G., HECHT, S. S. and CHUNG, F.-L., 1989b, Effects of aromatic isothiocyanates on tumorigenicity, O^6-methylguanine formation, and metabolism of the tobacco-specific nitrosamine 4-(methylnitrosamino)-1-(3-pyidyl)-1-butanone in A/J mouse lung. *Cancer Research*, **49**, 2894–2897.

MORSE, M. A., WANG, C.-X., STONER, G. D., MANDAL, S., CONRAN, P. B., AMIN, S. G., HECHT, S. S. and CHUNG, F.-L., 1989a, Inhibition of 4-(methylnitrosamino)-1-(3-pyridyl)-1-butanone-induced DNA adduct formation and tumorigenicity in the lung of F344 rats by dietary phenethyl isothiocyanate. *Cancer Research*, **49**, 549–553.

POTTER, W. Z., THORGEIRSSON, S. S., JOLLOW, D. J. and MITCHELL, J. R., 1974, Acetaminophen-induced hepatic necrosis, V. Correlation of hepatic necrosis, covalent binding and glutathione depletion in hamsters. *Pharmacology (Basel)*, **12**, 129–143.

PUISSANT, C. and HOUDEBINE, L. M., 1990, An improvement of the single-step method of RNA isolation by acid guanidinium thiocyanate–phenol–chloroform extraction. *Biotechniques*, **8**, 148–149.

REYES, H., LEVI, A. J., GATMAITAN, Z. and ARIAS, I. M., 1971, Studies of Y and Z, two hepatic cytoplasmic organic anion-binding proteins; Effect of drugs, chemicals, hormones, and cholestasis. *Journal of Clinical Investigation*, **50**, 2242–2252.

SIEGERS, C.-P., STRUBLET, O. and SCHUTT, A, 1978, Relations between hepatotoxicity and pharmacokinetics of paracetamol in rats and mice. *Pharmacology (Basel)*, **16**, 273–278.

SMITH, R. L., 1973, The excretory function of bile. In *The Elimination of Drugs and Toxic Substances in Bile* (London: Chapman & Hall).

SMITH, T. J., GUO, Z., LI, C., NING, S. M., THOMAS, P. E. and YANG, C. S., 1993, Mechanisms of inhibition of 4-(methylnitrosamino)-1-(3-pyridyl)-1-butanone bioactivation in mouse by dietary phenethyl isothiocyanate. *Cancer Research*, **53**, 3276–3282.

STEINMETZ, K. A. and POTTER, J. D., 1991, Vegetables, fruit and cancer. I. Epidemiology. *Cancer Causes and Control*, **2**, 325–357.

STRANGE, R. C., MATHAROO, B., FAULDER, G. C., JONES, P., COTTON, W., ELDER, J. B. and DEAKIN, M., 1991, The human glutathione *S*-transferases; a case control study of the incidence of the GST1 0 phenotype in patients with adenocarcinoma. *Carcinogenesis*, **2**, 25–28.

TIETZE, F., 1969, Enzymatic method for quantitative determination of nanogram amounts of total and oxidized glutathione; Application to mammalian blood and other tissues. *Analytical Biochemistry*, **27**, 502–522.

TOOKEY, H. L., VANETTEN, C. H. and DAXENBICHLER, M. E., 1980, Glucosinolates. In I. E. Liener (ed.), *Toxic Constituents of Plant Foodstuffs* (New York: Academic Press), pp. 103–142.

TROCK, B., LANZA, E. and GREENWALD, P., 1990, Dietary fiber, vegetables and colon cancer; a critical review and meta-analysis of the epidemiologic evidence. *Journal of the National Cancer Institute*, **82**, 650–661.

WALLIN, J. D., CLIFTON, G. and KAPLOWITZ, N., 1978, The effect of phenobarbital, probenecid and diethyl maleate on the pharmacokinetics and biliary excretion of ethacrynic acid in the rat. *Journal of Pharmacology and Experimental Therapeutics*, **205**, 471–479.

XENOBIOTICA, 2000, VOL. 30, NO. 6, 547–564

Regional and cellular distribution of CYP2D subfamily members in rat brain

S. MIKSYS, Y. RAO, E. M. SELLERS, M. KWAN, D. MENDIS and R. F. TYNDALE*

Centre for Addictions and Mental Health, and Department of Pharmacology, Medical Sciences Building, Room 4336, University of Toronto, Toronto, Ontario, Canada M5S 1A8

Received 10 August 1999; accepted 10 November 1999

1. Human CYP2D6 is present in brain, metabolizes many drugs and has been implicated in Parkinson's and Alzheimer's diseases and some cancers. It is still unclear which of the six known rat CYP2D subfamily members is/are homologous to human CYP2D6.

2. In this study, RT-PCR, Southern and Western blotting and immunohistochemical techniques were used to study the distribution of CYP2D subfamily member mRNA and proteins across 10 rat brain regions. CYP2D subfamily mRNA and protein levels were correlated with brain dextromethorphan *O*-demethylation (DOD), a measure of human CYP2D6 and rat CYP2D1 activities.

3. The data showed a strong relationship between CYP2D1 and CYP2D1–18 with brain DOD activity. In addition, it was shown that CYP2D proteins are present in brain mitochondrial as well as microsomal membranes. CYP2D subfamily member mRNA and proteins varied across brain regions and were highly concentrated in specific cell types.

4. These data strongly suggest that CYP2D1 and not CYP2D5 mediates DOD activity in rat brain, and may be the rat homologue of human CYP2D6. The highly localized nature of CYP2D indicates that in specific neurones enzyme levels may approach hepatic levels and, hence, contribute to local alterations in brain drug metabolism.

Introduction

Cytochromes P450 (CYP) are a superfamily of haem-containing mono-oxygenases that metabolize a variety of endogenous (e.g. fatty acids, steroids) and exogenous (e.g. drugs, carcinogens) compounds (reviewed by Parkinson 1996). The liver is the major site of CYP-mediated xenobiotic metabolism, but these enzymes are also expressed in extrahepatic tissues such as the gastrointestinal tract, colon, lung, kidney, skin (reviewed by Krishna and Klotz 1994), nasal epithelium (Hadley and Dahl 1982), placenta (Pasanen and Pelkonen 1994), breast (Warner *et al*. 1997) and the brain (Tyndale *et al*. 1991, Warner *et al*. 1997, Riedl *et al*. 1999).

Although the amount of CYP in the brain is a small fraction of that in liver, the presence and activity of many different isozymes have been demonstrated in rat (Jolivalt *et al*. 1995), dog (Niznik *et al*. 1990), monkey (Iscan *et al*. 1990) and human (Ghersi-Egea *et al*. 1993) brain tissue. The overall metabolic capacities of these enzymes are low in the whole brain, but recent immunocytochemical investigations show that CYP are unevenly distributed across brain regions, and that different isozymes are localized in discrete neurones and/or glial elements (Ghersi-Egea *et al*. 1993, Norris *et al*. 1996, Riedl *et al*. 1999), as well as in the endothelium of the blood

* Author for correspondence: e-mail: r.tyndale@utoronto.ca

Xenobiotica ISwSN 0049–8254 print/ISSN 1366–5928 online © 2000 Taylor & Francis Ltd
http://www.tandf.co.uk/journals

brain barrier (Ghersi-Egea *et al*. 1994). The activity of a specific CYP isozyme may therefore be relatively high in one region, or even one cell type, while absent in another. For a full understanding of the significance of brain CYP in xenobiotic metabolism, it is necessary to establish the regional and cellular localization of each isozyme, and its relative metabolic activity in each region.

CYP2D6, the only known functional member of the CYP2D subfamily in humans, metabolizes a wide variety of substances including therapeutically used drugs and drugs of abuse. This enzyme is genetically polymorphic (Meyer 1990) leading to impaired metabolism in 5–10% of Caucasians of many centrally acting drugs and toxins such as tricyclic antidepressants, SSRI, monoamine oxidase inhibitors, amphetamines, codeine, neuroleptics and MPTP (1-methyl-4-phenyl-1,2,3,6-tetrahydropyridine) (reviewed by Parkinson 1996). Polymorphic expression of CYP2D6 in the brain may contribute to the interindividual differences observed in pharmacological actions of drugs and susceptibility to neuronal damage by neurotoxins. In addition, there is some evidence of a link between defects in the CYP2D6 gene and Parkinson's disease (Riedl *et al*. 1998a), Alzheimer's disease (Tanaka *et al*. 1998), certain types of cancer (Wundrack *et al*. 1994, Elexpuru-Camiruaga *et al*. 1995), and neuroleptic-induced disorders (Ohmori *et al*. 1998), although not all studies agree.

The CYP2D family has evolved differently in the rat, where six genes have been described for the enzymes CYP2D1–5 and 18 (Gonzalez 1987, Matsunaga *et al*. 1990, Nelson *et al*. 1993, Kawashima *et al*. 1996). Human CYP2D6 and the rat homologue CYP2D1 are both expressed in the liver. CYP2D6 is also present in human brain (Tyndale *et al*. 1991, Bhamre *et al*. 1993, Gilham 1997), and CYP2D6 has been characterized in canine and human brain using binding studies (Niznik *et al*. 1990, Allard *et al*. 1994). CYP2D1 catalytic activity (Jolivalt *et al*. 1995, Laurenzana and Owens 1997, Tyndale *et al*. 1999) and CYP2D immunoreactivity have been shown in rat brain (Norris *et al*. 1996, Riedl *et al*. 1999). The mRNA for CYP2D4 and for CYP2D1 and/or 5 have been isolated from rat brain, with that for CYP2D4 being the most abundant (Komori 1993, Wyss *et al*. 1995). Although present in the liver, neither rat CYP2D2 nor CYP2D3 have yet been demonstrated in brain, possibly because they are present in very low quantities, and/or their presence is masked by much higher levels of CYP2D4.

In the current study, a variety of techniques, including RT-PCR, immunocytochemistry and Western blotting, demonstrated the variation in mRNA levels for individual CYP2D subfamily members, and the concomitant variation in expression of CYP2D protein among 10 brain regions. In addition, this variation in subfamily member mRNA and protein has been related to catalytic activity in the same brain regions (Tyndale *et al*. 1999) to determine the CYP2D isozyme most likely to be responsible for this activity in brain.

Materials and methods

Animals

Adult, male Wistar rats (250–300 g) (Charles River, PQ, Canada) were either killed by decapitation for RNA extraction ($n = 5$) and membrane preparation for Western blotting ($n = 4$), or anaesthetized with a lethal dose of sodium pentobarbital, then perfused transcardially with 30 ml 0.1% heparin in saline followed by 300 ml 4% paraformaldehyde in 0.1 M phosphate buffer, pH 7.4, for immunocytochemistry ($n = 4$). Brain regions were identified and dissected according to Paxinos and Watson's (1986) stereotaxic atlas of the rat brain. These were the same dissections used for catalytic activity studies

(Tyndale *et al*. 1999). All the experimental procedures described here were carried out in accordance with the guidelines for the care and use of laboratory animals, and approved by the Animal Care Committee of the University of Toronto.

RT-PCR

Random hexamer primers (pd(N)6), deoxynucleotide triphosphates (dNTP), and RNA guard were obtained from Pharmacia (PQ, Canada), and first strand buffer, dithiothreitol (DTT), M-MLV reverse transcriptase, and *T. aquaticus* polymerase were from Canadian Life Technologies (ON, Canada). Ten brain regions and liver were dissected from each animal, immediately frozen in liquid nitrogen and stored at –80 °C. RNA was extracted by a guanidinium thiocyanate single-step method (Xie and Rothblum 1991) followed by cDNA synthesis. For each sample, 20 μg RNA was added to first strand buffer, 50 mM Tris-HCl, pH 8.3, 74 mM KCl, 3 mM $MgCl_2$, 100 mM DDT, 2.5 U pd(N)6, 25 mM of each dNTP, 1.6 U M-MLV reverse transcriptase, and 140 mU RNA guard. cDNA synthesis was carried out in a total volume of 400 μl at 37 °C for 2 h, followed by cDNA precipitation with 40 μl 3 M sodium acetate, pH 5.2, 800 μl 100% ethanol, and cooling to −80 °C for at least 30 min. PCR amplification was carried out with 1–5 μl cDNA template in 20 mM Tris-HCl, pH 8.4, 50 mM KCl, 5% DMSO, 0.5 mM dNTP, 2–2.5 mM MgCl2, 1 U *T. aquaticus* polymerase and 1 mM PCR primers (table 1), in a total volume of 20 μl. PCR was performed in a PTC 200 thermal cycler (M. J. Research, Fisher Scientific, ON, Canada) with cycle conditions of 84 °C for 4 min, followed by 25–35 cycles of 94 °C for 1 min, 55 °C for 1 min, and 72 °C for 1 min.

Southern blotting

PCR products were either untreated or digested with restriction enzymes (Hinf I and Bsa H1), separated electrophoretically in 3% agarose, and transferred to Zeta-Probe membranes (BioRad, CA, USA). Membranes were prehybridized in 50% formamide, 120 mM Na_2HPO_4, pH 7.2, 250 mM NaCl, 7% w/v SDS for 0.5–1 h at 43 °C, then hybridized in the same buffer overnight at 43 °C with a ^{32}P-end-labelled oligonucleotide probe specific for CYP2D1 (table 1), for CYP2D1 primers, or ^{32}P-random-primed full-length CYP2D6 cDNA probe (generously provided by F. J. Gonzalez, NIH, USA), for CYP2D1+5 and CYP2D1–18 primers. Membranes were washed with 2×, followed by 0.5×, then by 0.1×standard sodium citrate (SSC) with 0.1% SDS for 15 min each at room temperature. Exposure times varied from several minutes to days.

Controls

RNA blanks were used in every RT-PCR reaction for every set of primers to control for contaminant cDNA/RNA/DNA. Primers for ubiquitous mRNA (non-neuronal enolase, NNE) ensured that RNA isolation, cDNA synthesis and precipitation were successful and equivalent among samples. Following titration experiments to determine the amount of cDNA which resulted in equal production of NNE over three different cycles, experiments were carried out at several cycles using CYP2D primers to ensure that all samples were amplified, and that their product density fell within the linear range of the standard curve of serial dilutions of liver cDNA template which were included in every experiment. Primer pairs were designed to cross over introns to identify any genomic DNA contamination (resulting in larger size products). Genomic DNA contamination was not observed in any experiments.

Western blotting

Brains from each animal (n = 4) were dissected into 10 regions: cerebellum, hippocampus, frontal cortex, parietal cortex, temporal cortex, striatum, olfactory bulbs, medulla oblongata, pons and spinal cord. These regions were chosen because they are easily identifiable for microdissection and provide a survey of almost all of the brain. This is the maximum number of regions that can be separated and still yield enough tissue for each assay. Brain regions were homogenized manually in glass on glass homogenizers in 100 mM Tris (pH 7.4) with 0.1 mM EDTA and 0.32 M sucrose (homogenizing solution) on ice. Mitochondrial and microsomal membranes were prepared according to Ghersi-Egea *et al*. (1993) whose methodology resulted in no cross-contamination. Homogenates were centrifuged at 3000 *g* for 5–10 min to remove cellular and nuclear debris, then the supernatant (1) was either centrifuged at 110000 *g* for 90 min at 4 °C for a whole membrane pellet, or separated into mitochondrial and microsomal pellets, as follows. Mitochondrial and microsomal membranes were prepared by centrifuging supernatant (1) at 12500 *g* for 30 min at 4 °C, saving supernatant (2). The pellet was resuspended in homogenizing solution and recentrifuged at 11000 *g* for 30 min at 4 °C, for a mitochondrial pellet. Supernatant (2) was centrifuged at 110000 *g* for 90 min at 4 °C for a microsomal pellet. Pellets were resuspended in a storage solution, consisting of 100 mM Tris (pH 7.4), 0.1 mM EDTA, 0.1 mM DTT, 1.15% w/v KCl and 20% v/v glycerol, aliquoted and stored at −80 °C. Microsomes were prepared from rat liver for use as positive controls and for standard curves.

Table 1A. Primer sequence for PCR.

Isozyme	Direction	Primer sequence	Starting at base	Size (bp)
2D1	forward	5′-GTGATGCCTTCACTGCCCAGGC-3′	490	269
	reverse	5′-GGAAGGCCATGAAGGTCTTCTGACCTT-3′		
2D1+5	forward	5′-TGCCTGGGTGTGAAGCCCAG-3′	334	426
	reverse	5′-GGAAGGCCATGAAGGTCTTCT-3′		
2D1−18	forward	5′-CCTGAGAGCAGCTTCAATGATGA-3′	865	520
	reverse	5′-AGGTGAAGAAGAGGAAGAGCTCCA-3′		
2D1 Hybridization Probe (HP)		5′-TGGGATTGATGGACT-3′	518	

Table 1B. Homology of primers to CYP2D family members (%)

Primer	2D1	2D2	2D3	2D4	2D5	2D18
	M16654					
	JO2867	M16655			J02869	
Accession	M16654	M22330	J02868	M22331	M22329	U48220
no.:	M22328	AB008523	AB008424	AB008425	M25143	U48219
2D1 F	100	63.7**	81.8	68.0*	90.9**	72.7***
2D1 R	96.3+	59.3***	59.3***	66.7**	100	66.7**
2D1 HP	100	73.3	60.0	60.0	93.3	60–66.7
2D1+5 F	100	55–60***	65.0	55–60***	100	60.0***
2D1+5 R	95.2+	66.7***	66.7***	76.2	100	76.2
2D1−18F	95.7+	100	86.7+	100	95.7+	100
2D1−18R	100	100	100	100	100	100

1 (*), 2 (**), or ⩾ 3(***) nucleotide mismatches at 3′ end of primer.
+, Nucleotide mismatch in middle of primer.

Table 1C. Restriction enzyme cutting sites and fragment sizes from the CYP2D1−18 amplification.

	Hinf I		Bsa HI	
CYP2D isozyme	Cutting site (underlined)	Fragment size (b)	Cutting site (underlined)	Fragment size(b)
CYP2D1	865-974-999-1137-1385	109, 25, 138, 248	none	
CYP2D2	865-999-1385	134, 386	none	
CYP2D3	865-1252-1385	113, 387	none	
CYP2D4/18	865-1385	520	865-1039-1385	174, 346
CYP2D5	865-974-999-1385	134, 25, 386	none	

The protein content of each sample was assayed by the method of Bradford (1976). Proteins (60 μg/brain sample) were separated by SDS polyacrylamide gel electrophoresis (4% stacking, 10% separating gels), then transferred onto nitrocellulose membranes. Membranes were blocked with 3% skim milk powder and 1% BSA in TBST (50 mM Tris pH 7.4, 150 mM NaCl, 0.1% v/v Triton X-100), immunoblotted with primary antibody, anti-CYP2D6 peptide antiserum (1:5000), biotinylated goat anti-rabbit IgG (1:500, Vector Laboratories Canada, ON, Canada), horse-radish peroxidase-conjugated streptavidin (1:2500), then detected with enhanced chemiluminescence reagents (both Amersham, ON, Canada). The primary antiserum (a gift from A. Cribb and Merck & Co., NJ, USA) contained antibodies raised in rabbits against a peptide corresponding to amino acids 254–273 of human CYP2D6 (Cribb *et al.* 1995). This peptide is 65% (CYP2D2), 75% (CYP2D1,3,5) and 85% (CYP2D4, CYP2D18) homologous to the corresponding epitopes of rat CYP2D subfamily members, and therefore the antiserum cross-reacts with the whole subfamily. All antibodies were diluted in TBST with 1% BSA. No signal was detected on control blots incubated with pre-immune serum instead of primary antibody. Standard curves for liver microsomal and cerebellar whole membrane CYP2D protein dilutions were

constructed, and a liver standard (1 μg protein) included in all experiments. This allowed the analysis of only those blots that fell within the linear region of detection on the standard curve. Blots were analysed with an imaging system (Imaging Research, Inc., ON, Canada), and means of all animals (n = 4) were calculated.

Immunocytochemistry

Brains were dissected and post-fixed in fresh perfusate overnight at 4 °C, transferred to 20% sucrose in 0.1 M phosphate buffer at 4 °C for cryoprotection, rinsed and rapidly frozen in 2-methyl butane at −80 °C. Frozen sections (16 μm) were collected on silane-coated slides and stored at −20 °C. Sections were washed twice in phosphate-buffered saline (PBS, 10 mM sodium phosphate buffer, 0.9% sodium chloride, pH 7.4), then incubated for 1 h in blocking buffer (PBS with 1% skim milk powder, 2% BSA, 4% Triton X-100 and 10% normal goat serum, NGS). Sections were incubated in anti-CYP2D6 antiserum (1:500 dilution in PBS with 2% BSA, 0.4% Triton X-100 and 2% NGS) for 48 h at 4 °C. Sections were washed three times in PBS, 10 min each, incubated with biotinylated goat anti-rabbit IgG (Vector Laboratories) for 1 h at room temperature, washed again with PBS, and then the antigen–antibody complex was visualized using the avidin-biotin complex technique (ABC Elite kit, Vector Laboratories) followed by reaction with 3,3′-diaminobenzidine and hydrogen peroxide (DAB Kit, Vector Laboratories). Sections were dehydrated and mounted via xylene in Permount (Fisher Scientific). Control sections were incubated either with pre-immune serum in place of antiserum, or with antiserum which had been pre-absorbed overnight with a lysate of 1.8×10^7 CYP2D6-expressing cells, line h2D6-Val (Gentest Corporation, MA, USA).

Statistical analysis

Protein and RNA values were tested for differences between brain regions by ANOVA, followed by the *a posteriori* Duncan's new multiple range test. Pearson correlation coefficients were calculated for all data sets and their significance calculated by a t-test. Significance level was set at 5%.

Results

RT-PCR analysis of brain CYP2D mRNA

To investigate the regional distribution of the CYP2D family mRNA in male Wistar rat brain, pairs of primers were designed specifically to amplify CYP2D1, CYP2D1 and CYP2D5 (CYP2D1+5), and all rat CYP2D family members CYP2D1–5 and CYP2D18 (referred to as CYP2D1–18) (table 1A). The sequence homology of these primers with the members of the CYP2D family is shown in table 1B. Digestion of CYP2D1 primer product with Hph I (digests CYP2D1 to 145 and 124 bp fragments) and Sfa NI (digests CYP2D5 to 122 and 147 bp fragments) confirmed that only CYP2D1 (not CYP2D5) was being amplified by the CYP2D1 primers. Restriction digestion of CYP2D1–18 primer product with Hinf I and Bsa HI (table 1C) and Southern blotting confirmed that all six members were identified in the product.

mRNA was detected in all 10 brain regions with all three sets of primers (see figure 1 for data from one animal for CYP2D1 primers). cDNA from each brain region was amplified at least three separate times from each animal to ensure reproducibility of the assays, and the means for each brain region from five individual animals are shown in figure 2. CYP2D1 and CYP2D1+5 mRNA showed no significant variation in distribution among regions (ANOVA, p = 0.70 and 0.30 respectively). However, CYP2D1+5 mRNA showed a different distribution from CYP2D1 alone (Pearson correlation, r = 0.37, p = 0.31), and also much more variability among brain regions (figure 2). Whole family CYP2D mRNA showed significant variation between brain regions (ANOVA, p = 0.03). Both cerebellum (CB) and medulla oblongata (MO) were significantly higher than frontal cortex (FC), striatum (ST), pons (PO) and spinal cord (SC) ($p < 0.05$; figure 2).

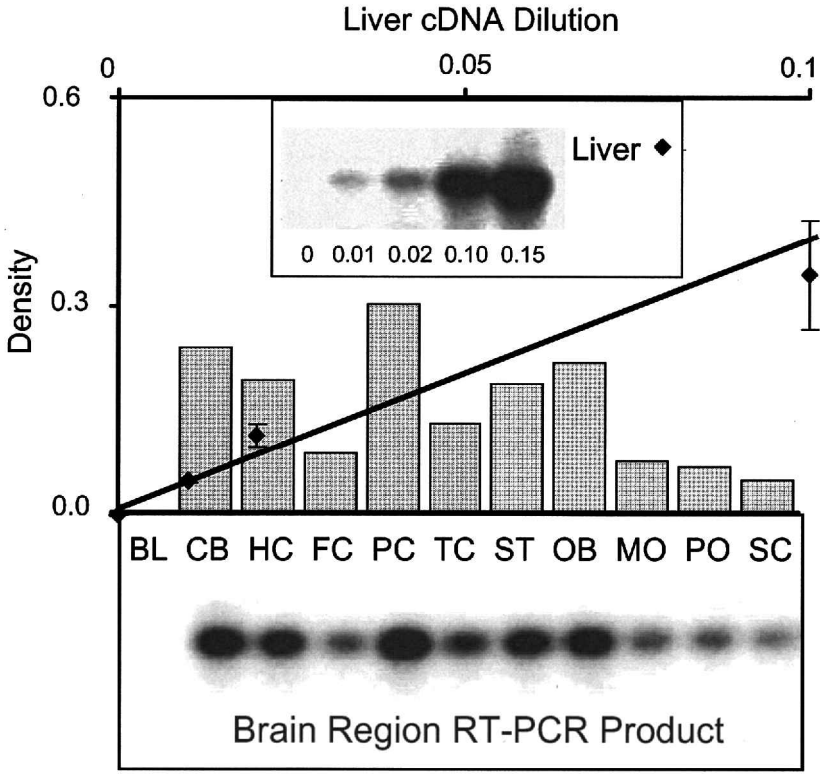


Figure 1. Brain regional distribution of CYP2D1 mRNA determined by RT-PCR amplification. The line graph represents densitometer readings of RT-PCR Southern blots of standard curves of rat liver cDNA (boxed inset). This is superimposed on a histogram of densitometer readings of a representative Southern blot of RT-PCR product from a single animal (lower) demonstrating that brain regions fall within a linear range of detection. Distilled water was used in place of cDNA template for the blank lane (BL). CB, cerebellum; HC, hippocampus; FC, frontal cortex; PC, parietal cortex; TC, temporal cortex; ST, striatum; OB, olfactory bulbs; MO, medulla oblongata; PO, pons; SC, spinal cord.

Table 2. Pearson coefficients of correlation (r) between CYP2D protein, enzyme activity and mRNA.

	Protein						mRNA		
	Mitochondrial		Microsomal		Whole member				
	Upper	Lower	Upper	Lower	Upper	Lower	CYP2D1	CYP2D1+5	CYP2D1−18
Activity	0.23	0.70*	0.36	0.61*	0.60	0.80**	0.65*	−0.14	0.68*
Mit. upper		−0.29	0.53	0.07	0.01	−0.05	−0.16	0.24	0.07
Mit. lower			0.09	0.56	0.66*	0.83*	0.39	−0.52	0.26
Mic. upper				0.49	0.31	0.50	0.29	0.24	0.84**
Mic. lower					0.65*	0.85**	0.11	−0.30	0.53
Whole upper						0.75*	0.03	−0.58	0.44
Whole lower							0.30	−0.50	0.67*
CYP2D1								0.37	0.30
CYP2D1+5									0.09

* $p < 0.05$, ** $p < 0.01$.

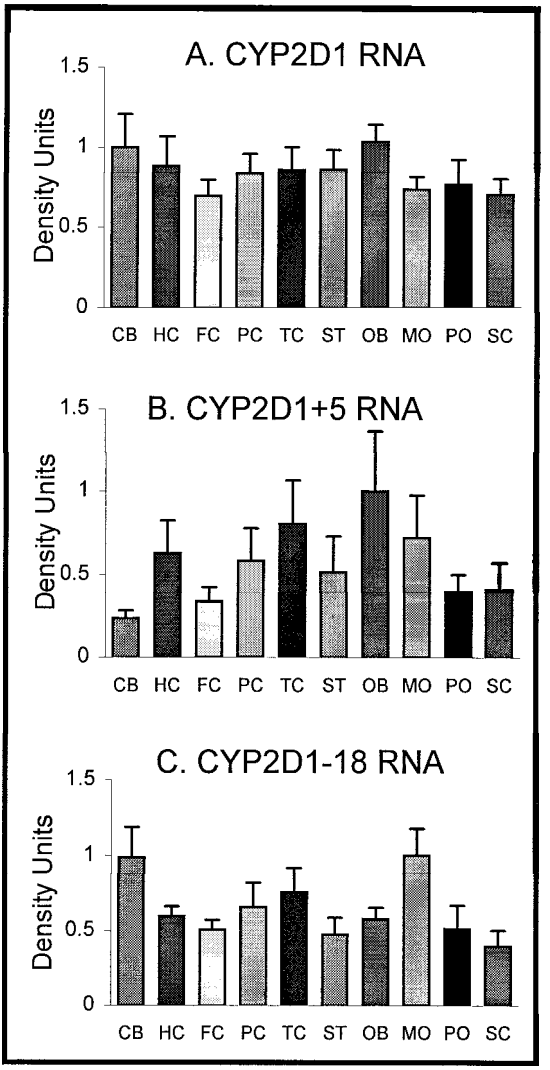


Figure 2. Brain regional distribution of RT-PCR products (mean ± SEM, $n = 5$ animals assayed separately) using primers for CYP2D1, CYP2D1+5 and CYP2D1−18. In each case the region with the highest value was set as 1.0 density unit, a direct comparison of amount of PCR product for different isozymes would be inappropriate due to different amplification efficiency of primary pairs. CYP2D1 mRNA shows the least variation, while CYP2D1+5 and whole family CYP2D1−18 mRNA show variation among brain regions. For abbreviations, see figure 1.

Western blotting

All brain regions expressed CYP2D protein in varying amounts and two bands were always visible (figure 3). There was significantly more CYP2D protein in the lower bands of all membrane preparations. Liver microsomal membranes also separated into two discrete but very close bands of even density. Based on the deduced molecular weights and on the mobilities of CYP2D isozymes reported in Wan *et al.* (1997), and assuming no post-translational modification, the upper (lower mobility) CYP2D protein band is likely to be CYP2D3 and CYP2D5 (m.w. 57 kDa; Matsunaga *et al.* 1989). The lower (higher mobility) band probably consists of

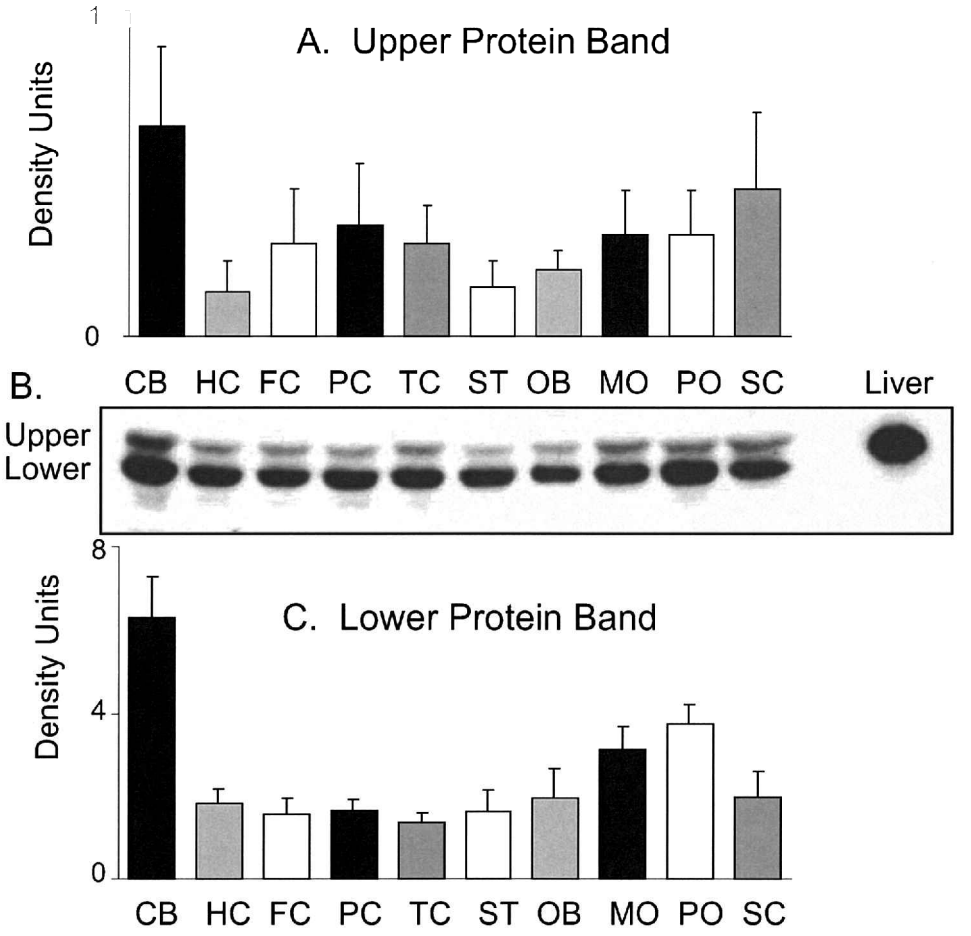


Figure 3. Brain regional distribution of CYP2D protein by Western blotting (mean±SEM, $n = 4$ animals assayed separately, 60 μg brain protein and 2 μg liver protein loaded per lane) for upper band (A) and lower band (C). A representative blot from one animal is shown (B). For each region the upper band is significantly ($p < 0.05$) less dense than the lower band. For abbreviations, see figure 1.

CYP2D1, CYP2D2 (m.w. 52 kDa; Gonzalez *et al.* 1987), and CYP2D4 and CYP2D18 (m.w. 50 kDa; Wyss *et al.* 1995, Kawashima *et al.* 1996). The present authors have confirmed that CYP2D1 migrates with the lower band, and that CYP2D5 migrates with the upper band using highly specific anti-peptide antisera against these isozymes, a gift from R. J. Edwards (data not shown).

As it has been reported that most brain CYP are present in mitochondrial membranes (Ghersi-Egea *et al.* 1993), the distribution of CYP2D proteins has been investigated between mitochondrial and microsomal membranes as well as whole membrane preparations. CYP2D protein was found in both microsomal and mitochondrial fractions, but in different relative amounts (figure 4). The ratios of microsomal to mitochondrial protein (sum of upper and lower bands) for the various brain regions were: cerebellum (1.7), hippocampus (2.2), frontal cortex (1.3), parietal cortex (1.8), temporal cortex (3.1), striatum (2.8), olfactory bulbs (1.7) and medulla oblongata (3.7), pons (2.0), spinal chord (2.7). The distribution patterns for

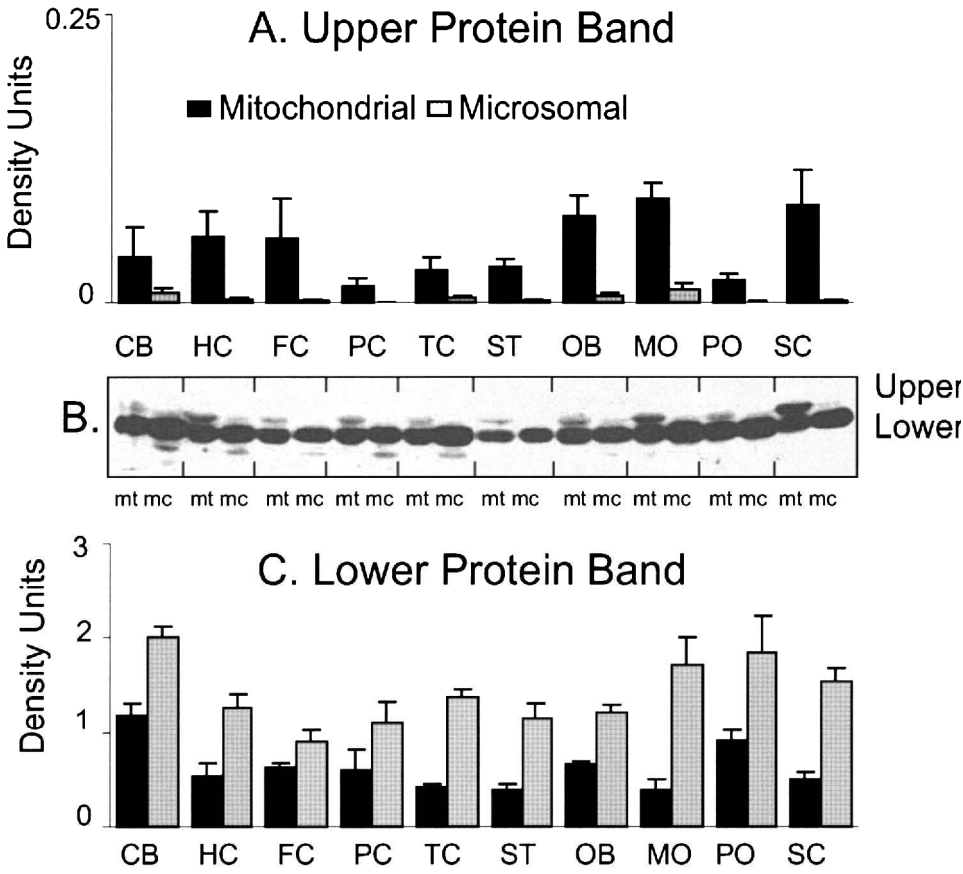


Figure 4. Subcellular brain region distribution of CYP2D protein by Western blotting (mean±SEM, $n = 4$ animals assayed separately, 60 μg brain protein loaded per lane). (A) Mitochondrial and microsomal protein in the upper protein band. This band is predominantly in the mitochondrial membranes and is barely detectable in microsomal membranes. (B) A representative blot from one animal showing mitochondrial and microsomal membrane CYP2D protein levels side by side for each brain region. (C) Brain region distribution of mitochondrial and microsomal CYP2D protein in the lower band. There is significantly more CYP2D protein in microsomal membranes for all regions. For abbreviations, see figure 1.

each membrane preparation were quite different, indicating little or no cross-contamination consistent with the established methodology (Ghersi-Egea *et al.* 1993). The upper protein band was much stronger in the mitochondrial membranes and barely discernible in microsomal membranes of some regions (figure 4). For whole, mitochondrial and microsomal membrane preparations, there was significant variation among brain regions in the lower CYP2D band density (figures 3 and 4).

Immunocytochemistry

Immunoreactivity was observed in almost all brain regions examined, but the intensity and cellular distribution of staining varied regionally (summarized in table 3). Omission of the primary antiserum and its pre-incubation with a lysate of h2D6-Val cells eliminated all immunostaining (figure 5).

Table 3. Summary of cellular location and intensity of CYP2D immunoreactivity in rat brain.

Brain region	Immunoreactivity
Cerebellum, white matter	−
granular cell layer	+
Purkinje cells	+++
molecular cell layer	+++
Hippocampus, dentate gyrus granule cells	−
dentate gyrus polymorphic cells	++
CA1,2 pyramidal cells	−
CA1,2 molecular and polymorphic cell layer	++
Frontal cortex, parietal cortex	
medial and ventral orbital cortex	++
olfactory tubercle	+++
piriform cortex, layer I	+++
nucleus accumbens	++
occipital cortex	+++
Temporal cortex	+
Striatum, caudate/putamen	++
globus pallidus	++
corpus callosum	−
Olfactory bulbs, aci	−
lateral olfactory tract	−
internal granular layer	+++
anterior olfactory nucleus	+
Anterior commissure	−
Choroid plexus	++++
Amygdaloid complex	+++
Lateral septal nucleus	++
Thalamus	++
Hypothalamus	+
Arcuate hypothalamic nucleus	++
Medial habenular nucleus	+
Mammillary nuclei	+++
Pons, substantia nigra	++
red nucleus	+
interpeduncular nucleus	+
Medulla oblongata, subcommissural organ	+
central (periaquaductal) grey	++
facial nucleus, large neurons	++
supragenual nucleus	++
vestibulo cochlear ganglion	+++
ventral cochlear nucleus	+++
Spinal cord, glial cells in lateral and ventral funiculus	++
motor neurons	+++/++
neuropile of ventral and dorsal horns	++

Staining intensity was scored as: −, none; +, weak; ++, moderate; +++, strong; ++++, very strong.

The cerebellum, the most intensely immunoreactive region on Western blots, showed the strongest staining in neurones of the molecular (stellate and basket cells) and Purkinje cell layers. There was some staining of the Bergmann glial cells in the molecular layer, but very little immunoreactivity in the granular cell layer, confined to the granule cells and absent in the glomeruli (figure 5 and table 3). Very strong staining was observed in the endothelial cells of the choroid plexus (figure 6B). The neocortex showed moderate glial and neuropilar staining in all layers, with strong staining of pyramidal neurones in some layers, e.g. layers II–V in the frontal cortex, and II, III in the olfactory tubercle (figure 6C and table 3). The hippocampus showed moderate staining confined to the neuronal and glial elements of the

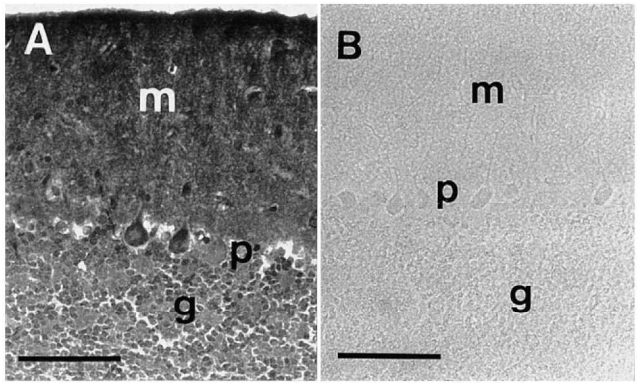


Figure 5. Immunocytochemical staining of coronal sections of rat cerebellum (A) with anti-CYP2D6 peptide antiserum (B) with control antiserum pre-absorbed with a lysate of CYP2D6-expressing cells (h2D6-Val, Gentest Corp.). m, Molecular layer; p, Purkinje cells; g, granule cell layer. Bar = 100 μm.

molecular and polymorphic layers of the hippocampus and dentate gyrus, and notably absent in the granule and pyramidal cell layers (figure 6D). The striatum showed moderate glial and some neuronal staining in the caudate-putamen and globus pallidus, but none in the corpus callosum (table 3). There was strong staining of neurones in the internal granular layer of the olfactory bulbs, with some light glial and neuropilar staining in the outer layers, and cell bodies of the anterior olfactory nucleus (table 3).

The overall immunoreactivity of the medulla oblongata was moderately high on Western blots, and immunocytochemistry showed that this was confined to certain areas such as the central peri-aquaductal grey and subcommissural organ (figure 6B). Strongly immunoreactive neurones were observed in the facial nuclei, in the anterior ventral cochlear nuclei and the vestibulo cochlear ganglia (figure 6A). In the pons, the second highest immunoreactive region on Western blots, there was light-to-moderate glial and neuropilar staining, with strong staining of neurones of the substantia nigra pars compacta and pars reticulata, and light-to-moderate staining of cell bodies of the red nucleus and interpeduncular nucleus. In the cervical spinal cord there was some glial staining in the ventral and lateral funiculus (white matter), moderate neuropilar staining and strong staining of motor neurones in the dorsal and ventral horns (figure 6E and table 3).

Correlation with enzyme activity

Dextromethorphan *O*-demethylation (DOD) to dextrorphan is a measure of human CYP2D6 and rat CYP2D1 liver activities (Wu *et al*. 1993). To investigate whether DOD activity in rat brain is attributable to rat CYP2D1, the human CYP2D6 homologue, the degree of correlation between protein and mRNA levels was determined with DOD activities from Tyndale *et al*. (1999) in various brain regions. Dissections of brain regions by Tyndale *et al*. were performed identically to those in the present study. Whole membrane preparations were incubated with 10 μM dextromethorphan and 1 mM NADPH and the production of dextrorphan quantified by HPLC. For further details see Tyndale *et al*. (1999). Some correlations are displayed in figure 7, and Pearson coefficients of correlation (r) are shown in table

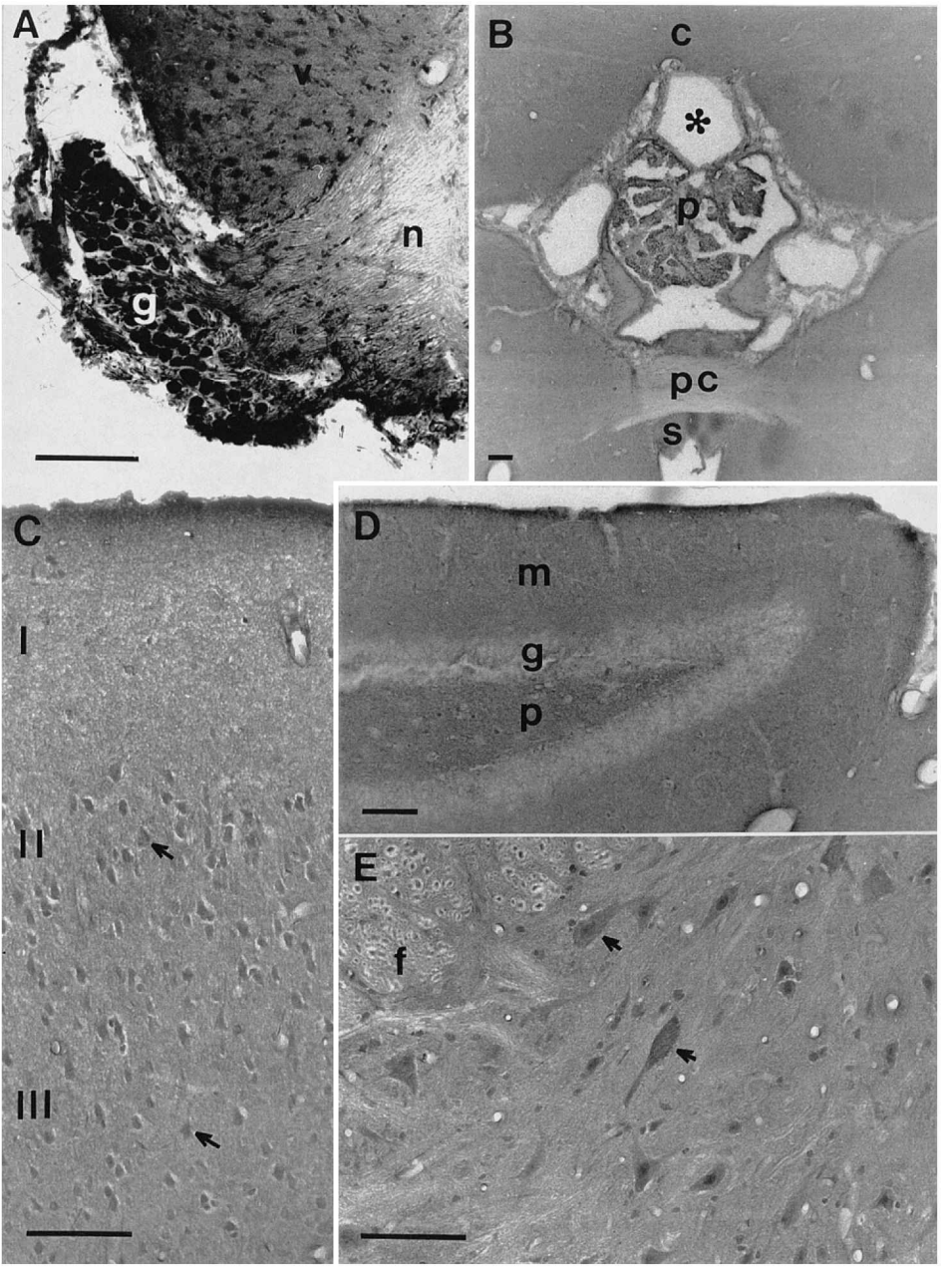


Figure 6. Immunocytochemical staining of coronal sections of rat brain regions using anti-CYP2D6 peptide antiserum (A) intense staining of neurons in the vestibulocochlear ganglion (g) adjacent to the anterior ventral cochlear nucleus (v) and the cochlear root vestibulocochlear nerve (n). (B) Strong staining of endothelial cells of the choroid plexus (p) in the third ventricle pineal recess (*). c, Corpus callosum; pc, posterior commissure; s, subcommissural organ. (C) Pyramidal neurons (arrows) in layers two and three of the frontal cerebral cortex stain strongly. (D) In the dentate gyrus of the hippocampus there is light-to-moderate staining of the molecular and polymorphic layers, but no staining in the granule cell layer. (E) Motor neurons (arrows) in layer 9 of the ventral horn stain intensely. f, Lateral funiculus of spinal cord. Bar = 100 μm.

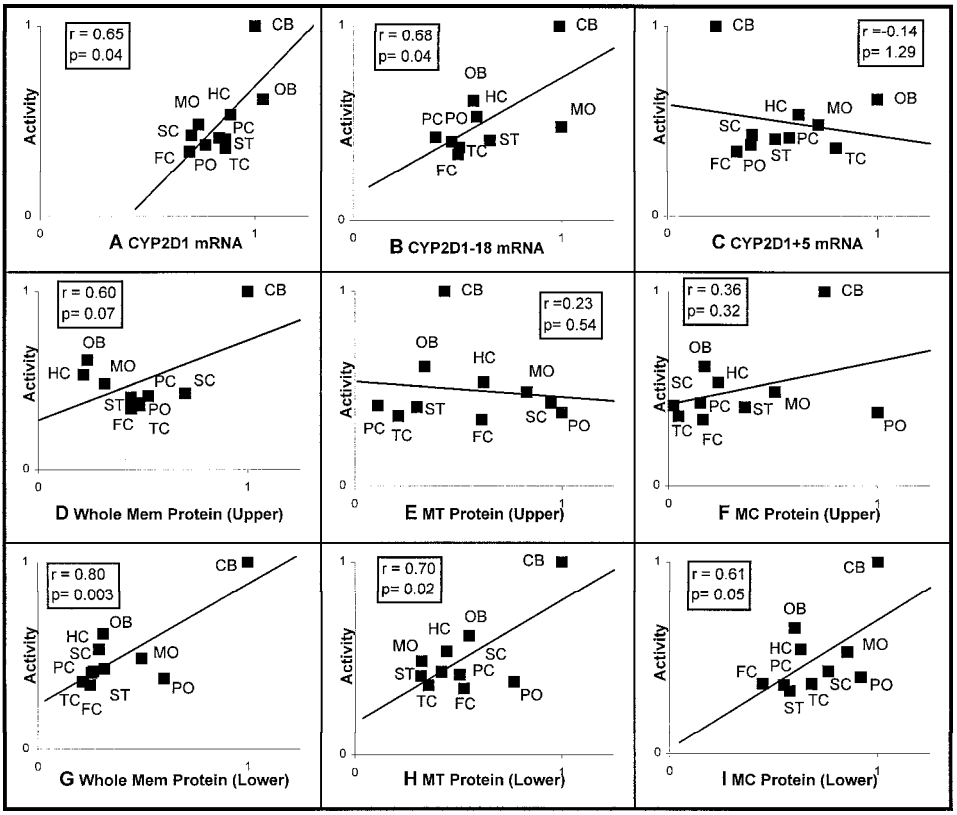


Figure 7. Relationship between dextromethorphan *O*-demethylase (DOD) activity ($n = 4$) and mRNA ($n = 5$) of CYP2D family members (A–C) and DOD activity and CYP2D protein ($n = 4$) in different membrane preparations (D–I). All parameters were normalized with the brain region of highest value set to a 1.0 density unit. DOD activity correlates best with CYP2D1 mRNA (Pearson coefficient of correlation $r = 0.65$, $p = 0.04$). There is no significant correlation between DOD activity and upper protein bands (CYP2D3,5) of whole (D), mitochondrial (E) or microsomal (F) membrane preparations. DOD activity correlates well with lower protein bands (CYP2D1,2,4,18) of whole (G), mitochondrial (H) and microsomal (I) membrane preparations.

2. DOD activity correlated significantly with CYP2D1 ($r = 0.65, p = 0.04$) and with CYP2D1–18 mRNA ($r = 0.68$, $p = 0.04$) (figure 7). These relationships held when each brain region was omitted in turn and r recalculated, showing that a single brain region did not drive the relationship. The lower bands of all membrane preparations correlated significantly with DOD activity in contrast to the upper bands (figure 7 and table 2). These data and correlations suggest that the DOD activity correlated best with a faster migrating isozyme(s) in the lower band (CYP2D1, 2, 4 or 18). In addition, the lower bands of whole membrane preparations correlated significantly with whole family CYP2D mRNA ($r = 0.67$, $p = 0.03$, table 2), which is to be expected as the antiserum recognizes all members of the CYP2D family.

Discussion

Presence of CYP2D isozymes in brain

The polymorphic enzyme CYP2D6 is involved in metabolism of therapeutic drugs, drugs of abuse and neurotoxins, such as the Parkinsonism-related compounds

MPTP and TIQ (1,2,3,4-tetrahydroisoquinoline). As such there is an interest in studying this enzyme's homologue in the rat (CYP2D1), particularly to establish an animal model for the study of this enzyme in the brain.

There have been very few studies on the presence and distribution of specific CYP2D subfamily member proteins and mRNA in rat brain regions, and these are confounded by the use of animals of both genders as it appears that CYP2D brain levels are influenced by sex steroid hormones (Bergh and Strobel 1996). Immunodetection studies for specific isozymes are difficult because the CYP2D subfamily members in the rat all have highly homologous mRNA and amino acid sequences. This study, using the untreated male Wistar rat, is the first detailed description of the distribution of mRNA of CYP2D1 and other subfamily members in rat brain regions. Like Komori (1993), Wyss *et al.* (1995) and Hiroi *et al.* (1998), the present authors observed that the most abundant species of mRNA was CYP2D4/18; other subfamily members were also expressed at lower levels in the brain. Although others have been unable to detect mRNA of individual CYP2D isozymes in whole brain, the present authors showed that mRNA of different CYP2D family members are present in brain, with region-specific patterns of distribution. CYP2D protein also varied between brain regions with the upper and lower bands showing very different distribution patterns (figures 3 and 4). These data strongly suggest that CYP2D isozymes are present and are distributed differently among brain regions.

Relationship of CYP2D isozymes to enzyme activity

Although dextromethorphan *O*-demethylase activity has been demonstrated in rat brain membranes (Jolivalt *et al.* 1995, Tyndale *et al.* 1999), it was not clear which CYP2D isozyme(s) was responsible for the metabolism. This activity measured in Tyndale *et al.* (1999) had a K_m (2–5 μM) identical to that found in rat liver, and was inhibited by quinine and by anti-CYP2D6 antibody (Tyndale *et al.* 1999), suggesting that CYP2D1 is involved, but this does not eliminate the possibility of contribution from other CYP2D subfamily members within the brain. Both CYP2D2 (Yamamoto *et al.* 1996, 1998, Wan *et al.* 1997) and CYP2D5 (Riedl 1998b) have been suggested as the human CYP2D6 homologue. Recently Yamamoto *et al.* (1998) suggested that lower levels of both CYP2D1 and CYP2D2 confer impaired debrisoquine metabolism in the Dark Agouti rat. In other cell expression systems CYP2D1 has been shown to have CYP2D6-like enzymatic properties, and can catalyse bufuralol oxidation (Matsunaga *et al.* 1989), debrisoquine 4-hydroxylation (Matsunaga 1990), and lidocaine 3-hydroxylation (Ohishi 1993). We took advantage of the different isozyme distributions to investigate which CYP2D family members showed a similar distribution to dextromethophan *O*-demethylase activity (from Tyndale *et al.* 1999). Our data indicate that CYP2D5 is not involved in dextromethorphan metabolism and is not homologous to CYP2D6 because (1) it was found that DOD activity correlated well with CYP2D1 mRNA ($r = 0.65$, $p = 0.04$) but poorly with CYP2D1+5 ($r = -0.14$, $p = 1.29$; figure 7 and table 2), and (2) lower protein bands (CYP2D1, 2, 4 and 18) correlated strongly with DOD activity, whereas upper protein bands (CYP2D 3 and 5) correlated poorly. Although one cannot exclude CYP2D2 as a possible candidate, the present data strongly suggest that CYP2D1 is the isozyme that metabolizes dextromethorphan, and is the human CYP2D6 homologue.

Almost all of the metabolism studies reported to date focus on hepatic CYP2D isozymes, yet it is clear that at least the antidepressant desmethylimipramine is

metabolized differently in rat brain and liver (Hansson *et al*. 1992). It has been shown that there is a brain-specific CYP2D subfamily member, CYP2D18, which differs from CYP2D4 by only five amino acids in the C-terminal region (Kawashima *et al*. 1996). This isozyme N-demethylates imipramine (Kawashima *et al*. 1996), in contrast to human CYP2D6 which metabolizes imipramine by 2-hydroxylation (Brosen *et al*. 1991). The differences in overall metabolism between brain and liver may be due in part to different proportions of CYP2D isozymes in these tissues. This emphasizes the need for further investigations into the properties of rat brain CYP2D subfamily members.

Cellular distribution of CYP2D

The present immunocytochemical and CYP2D1–18 mRNA data are in close agreement with that of Norris *et al*. (1996), who described the cellular distribution of CYP2D1-like immunoreactivity and mRNA throughout rat brain, although their antibody and *in situ* probes were likely to have detected all subfamily members. Recently Riedl *et al*. (1999) used peptide-specific antibodies to show differential expression of individual CYP2D subfamily members in rat basal ganglia. The present study shows the importance of using a combination of the techniques of Western blotting and immunocytochemistry to localize enzyme levels in brain regions to specific structures and/or cell types. For example, the medulla oblongata showed a much lower overall CYP2D level than the cerebellum on immunoblots (figure 3), yet there were some areas, such as neurones in the vestibulo cochlear ganglion, which stained very intensely (figure 6A and table 3). In the cerebellum, immunoreactivity was confined to the Purkinje and molecular cell layers, with very little staining in the cells of the granular layer (figure 5 and table 3). Although the overall levels of CYP are lower in brain than in liver, their high degree of regional and cellular localization in the brain may result in sufficiently high enzyme levels to influence local drug metabolism and concentration, thereby altering CNS response to a drug. This could occur with no detectable changes in the plasma drug and metabolite concentrations. Differences in local CNS drug metabolism could account, at least in part, for the large interindividual variability in CNS response to some drugs (Britto and Wedlund 1992).

Subcellular distribution of CYP2D

It is evident that CYP are present in many subcellular membrane compartments including mitochondria in rat (Bhagwat *et al*. 1995), monkey (Iscan *et al*. 1990) and human brain (Ghersi-Egea *et al*. 1993) and the plasma membrane (Loeper *et al*. 1993). Mitochondrial CYP can metabolize xenobiotics and are inducible (Ghersi-Egea *et al*. 1993, Bhagwat *et al*. 1995). The present authors observed that CYP2D mitochondrial and microsomal proteins were distributed differently among brain regions (figure 4A and B). The upper protein bands were much stronger in the mitochondrial membranes, indicating that the CYP2D isozymes are present in different relative amounts in these two cellular membranes. The lower protein band of both subcellular membrane fractions correlated significantly with DOD activity (figure 7 and table 2), suggesting that the human CYP2D6 homologue is present in both membrane types in brain, but with slightly different regional distributions.

The brain is a heterogeneous organ, relying on the perfect synchrony of its constituents to function normally. Pathological change in any region, caused by

genetic deficiency, disease, toxins, drugs, etc. will result in a disturbance in normal brain function. The data presented here suggest that indeed CYP2D1 is homologous to human CYP2D6 at least with respect to dextromethorphan metabolism. These data contribute to the knowledge of the anatomical distribution and functioning of the CYP2D family of proteins in rat brain, and represent one type of study necessary for the development of animal models for the investigation of the role of central CYP in drug response, toxicity and brain function.

Acknowledgements

The authors thank Dr P. Wu and Ms Yvette Grabowski for technical assistance. Work was funded by an MRC grant MT14173, NIDA grant DA06889 and the Centre for Addictions and Mental Health.

References

Allard, P., Marcusson, J. O. and Ross, S. B., 1994, [3]GBR-12935 binding to cytochrome P450 in the human brain. *Journal of Neurochemistry*, **62**, 342–348.

Bergh, A. F. and Strobel, W., 1996, Anatomical distribution of NADPH-cytochrome P450 reductase and cytochrome P4502D forms in rat brain: effects of xenobiotics and sex steroids. *Molecular and Cellular Biochemistry*, **162**, 31–41.

Bhagwat, S. V., Boyd, M. R. and Ravindranath, V., 1995, Brain mitochondrial cytochromes P450: Xenobiotic metabolism, presence of multiple forms and their selective inducibility. *Archives in Biochemistry and Biophysics*, **320**, 73–83.

Bhamre, S., Anandatheerthavarada, H. K., Shankar, S. K., Boyd, M. R. and Ravindranarth, V., 1993, Purification of multiple forms of cytochrome P450 from a human brain and reconstitution of catalytic activities. *Archives in Biochemistry and Biophysics*, **301**, 251–255.

Bradford, M. M., 1976, A rapid and sensitive method for the quantification of microgram quantities of protein utilizing the principle of protein–dye binding. *Annals of Biochemistry*, **72**, 248–254.

Britto, M. R. and Wedlund, P. J., 1992, Cytochrome P0450 in the brain. Potential evolutionary and therapeutic relevance of localization of drug-metabolizing enzymes. *Drug Metabolism and Disposition*, **20**, 446–450.

Brosen, K., Zeugin, T. and Meyer, U. A., 1991, Role of P450IID6, the target of the sparteine-debrisoquin oxidation polymorphism, in the metabolism of imipramine. *Clinical Pharmacology and Therapeutics*, **49**, 609–617.

Cribb, A., Nuss, C. and Wang, R., 1995, Antipeptide antibodies against overlapping sequences differentially inhibit human CYP2D6. *Drug Metabolism and Disposition*, **23**, 671–675.

Elexpuru-Camiruaga, J., Buxton, N., Kandula, V., Dias, P. S., Campbell, D., McIntosh, J., Broome, J., Jones, P., Inskip, A., Alldersea, J. *et al.*, 1995, susceptibility of astrocytoma and meningioma: influence of allelism at glutathione *S*-transferase (GSTT1 and GSTM1) and cytochrome P-450 (CYP2D6) loci. *Cancer Research*, **55**, 4237–4239.

Ghersi-Egea, J.-F., Leninger-Muller, B., Suleman, G., Siest, G. and Minn, A., 1994, Localization of drug-metabolizing enzyme activities to blood–brain interfaces and circumventricular organs. *Journal of Neurochemistry*, **62**, 1089–1096.

Ghersi-Egea, J.-F., Perrin, R., Leninger-Muller, B., Grassiot, M.-C., Jeandel, C., Floquet, J., Cuny, G., Siest, G. and Minn, A., 1993, Subcellular localization of cytochrome P450 and activities of several enzymes responsible for drug metabolism in the human brain. *Biochemical Pharmacology*, **45**, 647–658.

Gilham, D. E., Cairns, W., Paine, M. J., Modi, S., Poulsom, R., Roberts, G. C. and Wolf, C. R., 1997, Metabolism of MPTP by cytochrome P4502D6 and the demonstration of 2D6 mRNA in human foetal and adult brain by in situ hybridization. *Xenobiotica*, **27**, 111–125.

Gonzalez, F. J., Matsunaga, T., Nagata, K., Meyer, U. A., Nebert, D. W., Pastewka, J., Kozak, C. A., Gillette, J. Gelboin, H. V. and Hardwick, J. P., 1987, Debrisoquine 4-hydroxylase: characterization of a new P450 gene subfamily, regulation, chromosomal mapping, and molecular analysis of the DA rat polymorphism. *DNA*, **6**, 149–161.

Hadley, W. M. and Dahl, A. R., 1982, Cytochrome P-450 dependent monooxygenase activity in rat nasal epithelial membranes. *Toxicology Letters*, **10**, 417–422.

Hansson, T., von Bahr, C., Marklund, M., Svensson, J.-O., Ingelman-Sundberg, M. and Lundstrom, J., 1992, Different regiospecificity in the hydroxylation of the antidepressant desmethylimipramine between rat brain and liver. *Pharmacology and Toxicology*, **71**, 416–419.

Iscan, M., Reuhl, K., Weiss, R. and Maines, M. D., 1990, Regional and subcellular distribution of cytochrome P-450-dependent drug metabolism in monkey brain: the olfactory bulb and the mitochondrial fraction have high levels of activity. *Biochemical and Biophysical Research Communications*, **169**, 858–863.

Jolivalt, C., Minn, A., Vincent-Viry, M., Galteau, M.-M. and Siest, G., 1995, Dextromethorphan *O*-demethylase activity in rat brain microsomes. *Neuroscience Letters*, **187**, 65–68.

Kawashima, H., Sequeira, D. J., Nelson, D. R. and Strobel, H. W., 1996, Genomic cloning and protein expression of a novel rat brain cytochrome P-450 CYP2D18* catalyzing imipramine N-demethylation. *Journal of Biological Chemistry*, **271**, 28176–28180.

Komori, M., 1993, A novel P450 expressed at high level in rat brain. *Biochemical and Biophysical Research Communications*, **196**, 721–728.

Krishna, D. R. and Klotz, U., 1994, Extrahepatic metabolism of drugs in humans. *Clinical Pharmacokinetics*, **26**, 144–160.

Laurenzana, E. M. and Owens, S. M., 1997, Brain microsomal metabolism of phencyclidine in male and female rats. *Brain Research*, **756**, 256–265.

Loeper, J., Descatoire, V., Maurice, M., Beaune, P., Belghiti, J., Houssin, D., Ballet, F., Feldmann, G., Guengerich, F. P. and Pessayre, D., 1993, Cytochromes P-450 in human hepatocyte plasma membrane: recognition by several autoantibodies. *Gastroenterology*, **104**, 203–216.

Matsunaga, E., Umeno, M. and Gonzalez, F. J., 1990, The rat P450IID subfamily: complete sequences of four closely linked genes and evidence that gene conversions maintained sequence homogeneity at the heme-binding region of the cytochrome P450 active site. *Journal of Molecular Evolution*, **30**, 155–169.

Matsunaga, E., Zanger, U. M., Hardwick, J. P., Gelboin, H. V., Meyer, U. A. and Gonzalez, F. J., 1989, The CYP2D gene subfamily: analysis of the molecular basis of the debrisoquine 4-hydroxylase deficiency in DA rats. *Biochemistry*, **28**, 7349–7355.

Meyer, U. A., Skoda, R. C. and Zanger, U. M., 1990, The genetic polymorphism of debrisoquine/sparteine metabolism - molecular mechanisms. *Pharmacology and Therapeutics*, **46**, 297–308.

Nelson, D. R., Kamataki, T., Waxman, D. J., Guengerich, F. P., Estabrook, R. W., Feyereisen, R., Gonzalez, F. J., Coon, M. J., Gunsalus, I. C., Gotoh, O., Okuda, K. and Nebert, D. W., 1993, The P450 superfamily - update on new sequences, gene mapping, accession numbers, early trivial names of enzymes, and nomenclatures. *DNA Cell Biology*, **12**, 1–51.

Niznik, H. B., Tyndale, R. F., Sallee, F. R., Gonzalez, F. J., Hardwick, J. P., Inaba, T. and Kalow, W., 1990, The dopamine transporter and cytochrome P450IID1 (debrisoquine 4-hydroxylase) in brain: resolution and identification of two distinct [3H]GBR-12935 binding proteins. *Archives in Biochemistry and Biophysics*, **276**, 424–432.

Norris, P. J., Hardwick, J. P. and Emson, P. C., 1996, Regional distribution of cytochrome P450 2D1 in the rat central nervous system. *Journal of Comp. Neurology*, **366**, 244–258.

Ohishi, N., Imaoka, S., Suzuki, T. and Funae, Y., 1993, Characterization of two P-450 isozymes placed in the rat CYP2D subfamily. *Biochimica et Biophysica Acta*, **1158**, 227–236.

Ohmori, O., Suzuki, T., Kojima, H., Shinkai, T., Terao, T., Mita, T. and Abe, K., 1998, Tardive dyskinesia and debrisoquine 4-hydroxylase (CYP2D6) genotype in Japanese schizophrenics. *Schizophrenia Research*, **32**, 107–113.

Parkinson, A., 1996, Biotransformation of xenobiotics. In C. D. Klasson (ed.), *Casarett and Doull's Toxicology: The Basic Science of Poisons*, 5th edn (New York: McGraw-Hill), pp. 113–185.

Pasanen, M. and Pelkonen, O., 1994, The expression and environmental regulation of P450 enzymes in human placenta. *Critical Reviews in Toxicology*, **24**, 211–229.

Paxinos, G. and Watson, C., 1986, *The Rat Brain in Stereotaxic Coordinates*, 2nd edn (San Diego: Academic Press).

Riedl, A. G., Brown, C. T., Rose, S., Schulz-Utermoehl, T., Edwards, R. J., Boobis, A. R. and Jenner, P., 1998b, Localisation of CYP2D enzymes in naive rat basal ganglia. Proceedings of the BPS, December 1997. British Journal of Pharmacology, **123 (suppl.)**.

Riedl, A. G., Watts, P. M., Edwards, R. J., Schulz-Utermoehl, T., Boobis, A. R., Jenner, P. and Marsden, C. D., 1999, Expression and localisation of CYP2D enzymes in rat basal ganglia. *Brain Research*, **822**, 175–191.

Riedl, A. G., Watts, P. M., Jenner, P. and Marsden, C. D., 1998a, P450 enzymes and Parkinson's disease: the story so far. *Mov Disorder*, **13**, 212–220.

Tanaka, S., Chen, X., Xia, Y., Kang, D. E., Matoh, N., Sundsmo, M., Thomas, R. G., Katzman, R., Thal, L. J., Trojanowski, J. Q. Saitoh, T. Ueda, K. and Masliah, El, 1998, Association of CYP2D microsatellite polymorphism with Lewy body variant of Alzheimer's disease. *Neurology*, **50**, 1556–1562.

Tyndale, R. F., Li, Y., Li, N.-Y., Messina, E., Miksys, S. and Sellers, E. M., 1999, Characterization of CYP2D1 activity in rat brain: high affinity kinetics for dextromethorphan. *Drug Metabolism and Disposition*, **27**, 924–930.

Tyndale, R. F., Sunahara, R., Inaba, T., Kalow, W., Gonzalez, F. J. and Niznik, H. B., 1991,

Neuronal cytochrome CYP2D1 (debrisoquine/sparteine-type): potent inhibition of activity by (–)-cocaine and nucleotide sequence identity with human hepatic P450 gene CYP2D6. *Molecular Pharmacology*, **40**, 63–68.

Wan, J., Imaoka, S., Chow, T., Hiroi, T., Yabusaki, Y. and Funae, Y., 1997, Expression of four rat CYP2D isoforms in *Saccharomyces cerevisiae* and their catalytic specificity. *Archives in Biochemistry and Biophysics*, **348**, 383–390.

Warner, M., Hillmold, H., Yoshida, S., Liao, D., Hedlund, E. and Gustafsson, J.-A., 1997, Cytochrome P450 in the breast and brain: role in tissue-specific activation of xenobiotics. *Mutation Research*, **376**, 79–85.

Wu, D., Otton, V. S., Morrow, P., Inaba, T., Kalow, W. and Sellers, E. M., 1993, Human hepatic cytochrome P450 2D6-like activity in nonhuman primates: catalytic characterization *in vitro*. *Journal of Pharmacology and Experimental Therapeutics*, **266**, 715–719.

Wundrack, I., Meese, E., Mullenbach, R. and Blin, N., 1994, Debrisoquine hydroxylase gene polymorphism in meningioma. *Acta Neuropathologica* (*Berlin*), **88**, 472–474.

Wyss, A., Gustafsson, J.-A. and Warner, M., 1995, Cytochromes P450 of the 2D subfamily in the rat brain. *Molecular Pharmacology*, **47**, 1148–1155.

Xie, W. and Rothblum, L. I., 1991, Rapid, small-scale RNA isolation from tissue culture cells. *Biotechniques*, **11**, 325–327.

Yamamoto, Y., Nakamura, A., Tasaki, T., Umeda, S., Sugimoto, C., Iaoka, S., Funae, Y., Masuda, M., Kazusaka, A. and Fujita, S., 1996, Impaired expression in DA rats of catalytically active p450btl immunochemically distinguishable from p4502d1: immunological evidence with specific antipeptide antibodies. *Biomedical Research*, **17**, 331–337.

Yamamoto, Y., Talaki, T., Nakamura, A., Iwata, H., Kazusaka, A., Gonzaliz, F. J. and Fujita, S., 1998, Molecular basis of the dark agouti rat drug oxidation polymorphism: importance of CYP2D1 and CYP2D2. *Pharmacogenetics*, **8**, 73–82.

XENOBIOTICA, 2000, VOL. 30, NO. 6, 565–574

Identification of enzymes responsible for rifalazil metabolism in human liver microsomes

T. MAE†*, T. INABA‡, E. KONISHI†, K. HOSOE† and T. HIDAKA†

† Takasago Research Laboratories, Kaneka Corporation, 1–8, Miyamae-machi, Takasago-cho, Takasago-shi, Hyogo, 676–8688, Japan
‡ Department of Pharmacology, Faculty of Medicine, University of Toronto, Toronto M5S1A8, Canada

Received 21 June 1999

1. The major metabolites of rifalazil in human are 25-deacetyl-rifalazil and 32-hydroxy-rifalazil. Biotransformation to these metabolites in pooled human liver microsomes, cytosol and supernatant 9000*g* (S9) fractions was studied, and the enzymes responsible for rifalazil metabolism were identified using inhibitors of esterases and cytochromes P450 (CYP).

2. The 25-deacetylation and 32-hydroxylation of rifalazil occurred in incubations with microsomes or S9 but not with cytosol, indicating that both the enzymes responsible for rifalazil metabolism were microsomal. K_m and V_{max} of the rifalazil-25-deacetylation in microsomes were 6.5 μM and 11.9 pmol/min/mg with NADPH, and 2.6 μM and 6.0 pmol/min/mg without NADPH, indicating that, although rifalazil-25-deacetylation did not require NADPH, NADPH activated it. Rifalazil-32-hydroxylation was NADPH dependent, and its K_m and V_{max} were 3.3 μM and 11.0 pmol/min/mg respectively.

3. Rifalazil-25-deacetylation in microsomes was completely inhibited by diisopropyl fluorophosphate, diethyl *p*-nitrophenyl phosphate and eserine, but not by *p*-chloromercuribenzoate or 5,5′-dithio-bis(2-nitrobenzoic acid), indicating that the enzyme responsible for the rifalazil-25-deacetylation is a B-esterase.

4. Rifalazil-32-hydroxylation in microsomes was completely inhibited by CYP3A4-specific inhibitors (fluconazole, ketoconazole, miconazole, troleandomycin) and drugs metabolized by CYP3A4 such as cyclosporin A and clarithromycin, indicating that the enzyme responsible for the rifalazil-32-hydroxylation is CYP3A4.

Introduction

Rifalazil (KRM-1648) is a new rifamycin derivative (Yamane *et al*. 1993) and this antibiotic exhibits potent activity against Gram-positive bacteria (Fujii *et al*. 1994) and mycobacteria including *Mycobacterium avium* complex and *M. tuberculosis* (Saito *et al*. 1991, Tomioka *et al*. 1992, 1993, Bermudez *et al*. 1994, Inderlied *et al*. 1994, Luna-Herrera *et al*. 1995). The antibacterial activity of rifalazil is higher than that of other rifamycin derivatives such as rifampicin, rifabutin and rifapentine both *in vitro* and *in vivo* (Klemens *et al*. 1994, Hirata *et al*. 1995, Kelly *et al*. 1996, Moghazeh *et al*. 1996, Mor *et al*. 1996, Reddy *et al*. 1996, Yang *et al*. 1998).

The pharmacokinetics of rifalazil have been studied in animals. After a single oral administration in mouse, rifalazil is distributed at higher levels in tissues than in plasma, and eliminated more slowly than either rifampicin or rifabutin (Yamane *et al*. 1993). In rat and dog these same pharmacokinetic properties are observed and the elimination half-life is 12.3–15.6 and 15.2–24.0 h respectively (Hosoe *et al*. 1996a). Rifalazil is biotransformed to 25-deacetyl-rifalazil (M1) in rat, to M1, 30-hydroxy-rifalazil (M2) and 25-deacetyl-30-hydroxy-rifalazil (M3) in dog (Hosoe *et*

* Author for correspondence.

Xenobiotica ISSN 0049–8254 print/ISSN 1366–5928 online © 2000 Taylor & Francis Ltd
http://www.tandf.co.uk/journals

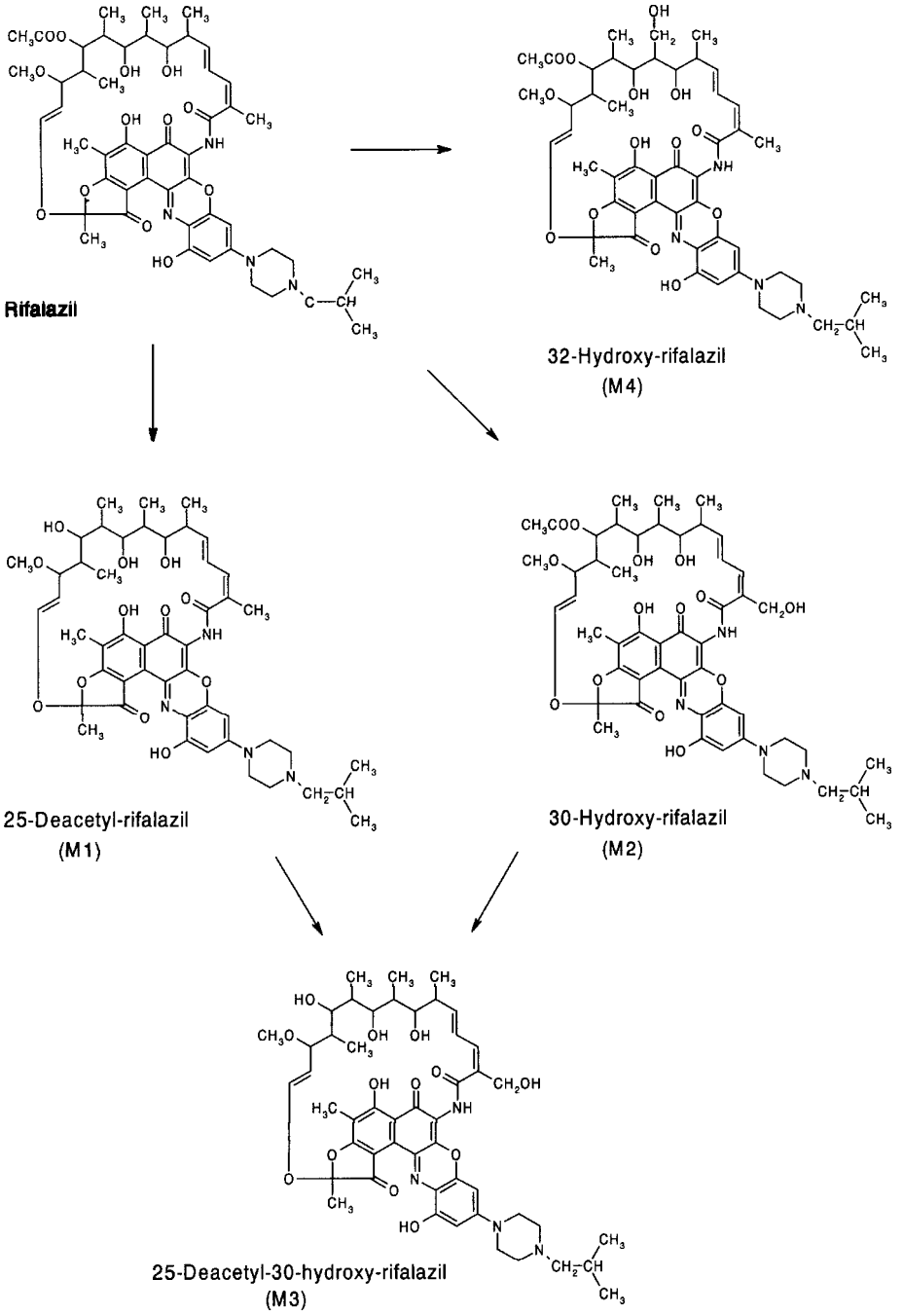


Figure 1. Metabolic pathways of rifalazil.

al. 1996b), and to M1 and 32-hydroxy-rifalazil (M4) in mouse (Mae *et al*. 1999). The major metabolic pathways of rifalazil are deacetylation to form M1 and hydroxylation to form M2 and M4 (figure 1). Rifalazil is not an inducer of microsomal drug-metabolizing enzymes in rat or dog liver (Mae *et al*. 1998).

In human, rifalazil is biotransformed to M1 and M4 (Mae *et al*. 1999). Conjugated metabolites of rifalazil are undetectable after incubations of rifalazil with human liver S9, an NADPH-generating system, or uridine 5′-diphosphoglucuronic acid and 3′-phosphoadenosine 5′-phosphosulphate (unpublished data). Our preliminary study using expressed human cytochrome P450 (CYP) isoforms reported that rifalazil is hydroxylated by cell lysates containing CYP3A3 and 3A4 (Mae *et al*. 1996). However, the enzyme responsible for the deacetylation of rifalazil has not been identified.

The identity of a number of rifabutin metabolites in human is known (Vigevani *et al*. 1985, Cocchiara *et al*. 1989, Battaglia *et al*. 1990, Utkin *et al*. 1997) and contributing metabolic pathways are deacetylation, hydroxylation and demethylation. Rifabutin is metabolized by CYP3A4 (Iatsimirskaia *et al*. 1997, Trapnell *et al*. 1997) and the deacetylation of rifabutin is catalyzed by a microsomal B-esterase (Iatsimirskaia *et al*. 1997, Jamis-Dow *et al*. 1997). B-Esterases are inhibited by organophosphates (Aldridge 1953), and include cholinesterases and carboxylesterases (Williams 1985). Rifalazil has unique properties foremost of which is a much longer elimination half-life than rifampicin or rifabutin.

In this paper, the kinetic parameters for rifalazil metabolism in human liver microsomes have been determined and the enzymes involved using inhibitors of esterases and CYP have been identified. The *in vitro* drug interactions of rifalazil with compounds likely to be co-administered in multidrug treatment have also been investigated.

Materials and methods

Drug and chemicals

Rifalazil, 3′-hydroxy-5′-(4-isobutyl-1-piperazinyl)benzoxazinorifamycin (KRM-1648, purity 99.9%) and 3′-hydroxy-5′-(4-isopentyl-1-piperazinyl)benzoxazinorifamycin (99.7%, an internal standard for hplc analysis) were synthesized at the Takasago Research Laboratories of Kaneka Corporation. ^{14}C-rifalazil (15.1 mCi/mmol) was synthesized at Wizard Laboratories (West Sacramento, CA, USA).

Esterase inhibitors: *p*-chloromercuribenzoate (PCMB), 5,5′-dithio-bis(2-nitrobenzoic acid) (DTNB), eserine, neostigmine bromide and diethyl *p*-nitrophenyl phosphate (DNPP) were from Sigma (St Louis, MO, USA); bis(*p*-nitrophenyl) phosphate (BPNP) from Aldrich (Milwaukee, WI, USA); and diisopropyl fluorophosphate (DFP) from Wako Pure Chemical Industries (Osaka, Japan). CYP inhibitors: phenacetin, sulphaphenazole, mephenytoin, quinidine, chlorzoxazone, troleandomycin, miconazole, ketoconazole and fluconazole were from Sigma. These inhibitors of esterases and CYP were dissolved in dimethyl sulphoxide (DMSO).

Metabolism of rifalazil in human liver microsomes, cytosol and S9

Pooled human liver microsomes (lot H0610, from 15 donors), cytosol (lot H1000.C, 10 donors) and S9 (lot H0610.S9, 15 donors) were from XenoTech LLC (Kansas City, KS, USA).

The reaction mixture of 1 ml contained 100 mM phosphate buffer (pH 7.4), 1 mM EDTA, 1 mM NADPH, 1 mg protein/ml human liver microsomes, cytosol or S9, and 10 μg/ml (= 10.6 μM) rifalazil was incubated at 37 °C for 15, 30, 60, 90 and 120 min. For determination of the kinetic parameters (K_m and V_{max}), 2–50 μg/ml (= 2.13–53.1 μM) rifalazil was added and incubated at 37 °C for 15 min. The reaction was initiated by adding rifalazil, 10 μl 1 mg/ml solution in ethanol, and terminated by adding 5 ml acetone, mixing and cooling on ice. An internal standard, 20 μl 50 μg/ml solution in methanol, was added and mixed. After centrifugation at 2000 *g* for 10 min, the supernatant was evaporated to dryness under reduced pressure. The residue was reconstituted in 200 μl methanol, and an aliquot of 50 μl was analyzed by hplc.

Inhibition of rifalazil-25-deacetylation in human liver microsomes

The reaction mixture of 0.99 ml contained 100 mM phosphate buffer (pH 7.4), 1 mM EDTA, 1 mg protein/ml human liver microsomes (lot H0610), and 10 μM esterase inhibitors, added as 10 μl 1 mM solution in DMSO, was pre-incubated at 37 °C for 10 min. Rifalazil, 10 μl 1 mg/ml solution in ethanol, was then added to final concentration of 10 μg/ml (= 10.6 μM) and incubation at 37 °C for 60 min.

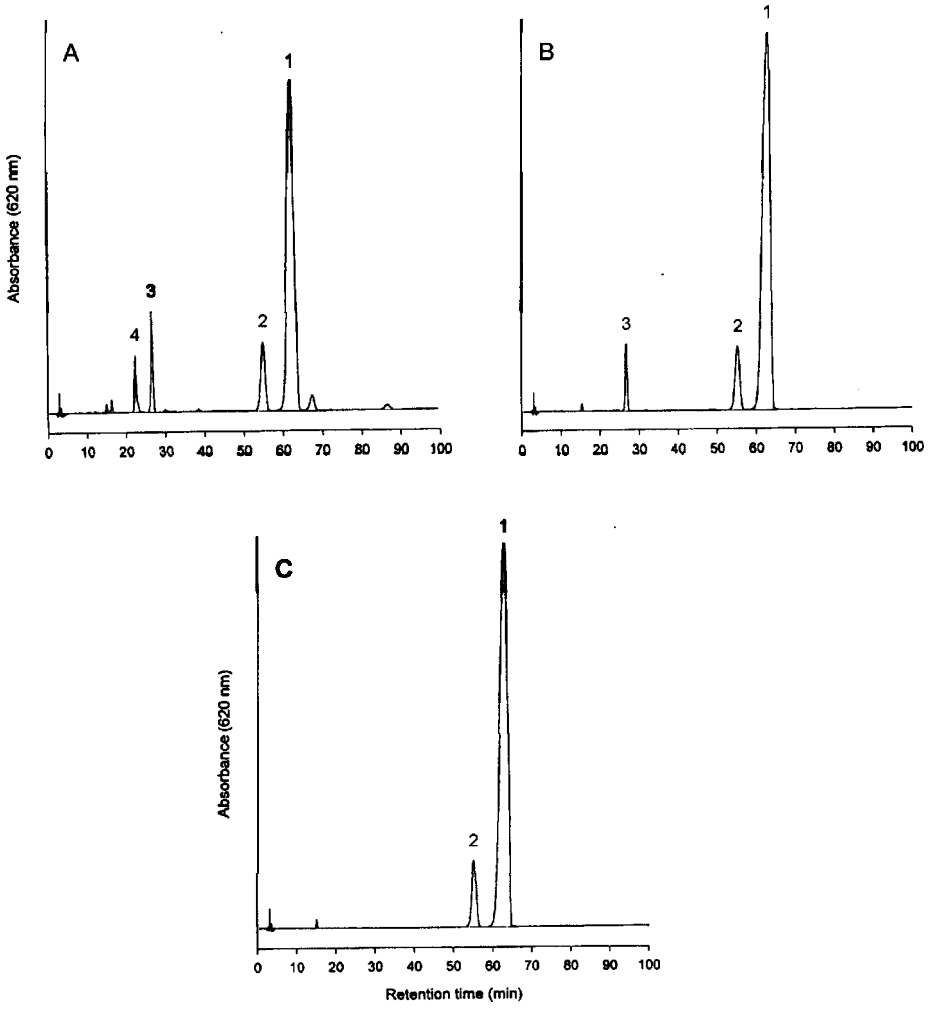


Figure 2. Typical hplc chromatograms of rifalazil metabolites in human liver microsomes. Rifalazil (10 μg/ml = 10.6 μM) was incubated with human liver microsomes (1 mg protein/ml) in the presence or absence of NADPH at 37 °C for 120 min, and analyzed by hplc as described in the Materials and methods. Chromatograms: A, incubation in the presence of NADPH; B, incubation in the absence of NADPH; C, no incubation. Peaks: 1, rifalazil; 2, internal standard; 3, 25-deacetyl-rifalazil; 4, 32-hydroxy-rifalazil.

Inhibition of rifalazil-32-hydroxylation in human liver microsomes

Human liver samples (from kidney donors, K20 and K27; Sumida *et al.* 1999) in the University of Toronto Liver Bank, stored at −70 °C, were partially thawed, homogenized 1:1 in 1.15% KCl and centrifuged at 9000*g* for 20 min, and the supernatant was obtained after sedimentation (Tyndale *et al.* 1990). The microsomal pellet was washed and resuspended in 100 mM phosphate buffer (pH 7.4) and stored at −70 °C until used. Protein concentrations were determined by the bicinchoninic acid method (Pierce Chemical Co., Rockford, IL, USA) with bovine serum albumin as the standard.

The reaction mixture of 0.5 ml contained 100 mM phosphate buffer (pH 7.4), 5 mM $MgCl_2$, 1 mM NADPH, 2 mg protein/ml human liver microsomes, 10 or 100 μM inhibitors and 15 μM rifalazil (including 0.1 μCi [^{14}C]-labelled) were incubated at 37 °C for 20 min. The reaction was terminated by adding 2 ml ethyl acetate, the samples vortexed for 30 s and then centrifuged at 2000*g* for 5 min. The ethyl acetate layers were removed, placed in a heating block set at 45 °C and evaporated to dryness under a stream of nitrogen. The residues were reconstituted in 30 μl chloroform, and 10 μl aliquots were analyzed by tlc.

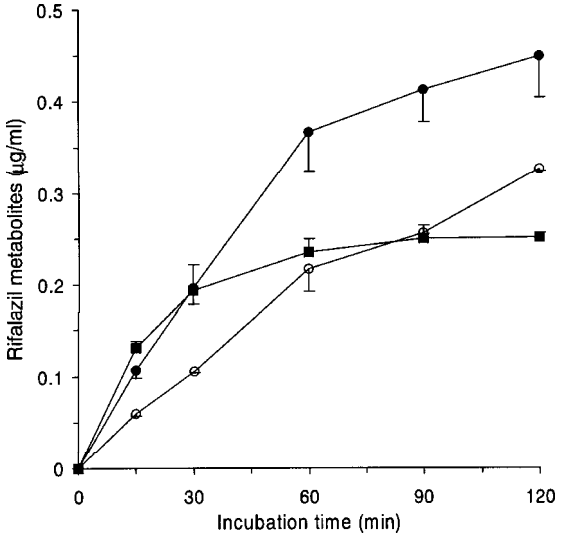


Figure 3. Time-course of rifalazil metabolism in human liver microsomes. Rifalazil (10 μg/ml = 10.6 μM) was incubated with human liver microsomes (1 mg protein/ml) in the presence or absence of NADPH at 37 °C for 0–120 min, and analyzed by hplc as described in the Materials and methods. Each point is presented as the mean ± SD of two-to-five experiments. ●, 25-Deacetyl-rifalazil produced in the presence of NADPH; ■, 32-hydroxy-rifalazil produced in the presence of NADPH; ○, 25-deacetyl-rifalazil produced in the absence of NADPH.

Hplc and tlc analysis for measurement of rifalazil metabolites

Hplc methods were described in Mae *et al*. (1999) and tlc methods as in Inaba *et al*. (1997).

Results

When rifalazil was incubated with human liver microsomes in the presence of NADPH, it was converted to two major metabolites, 25-deacetyl-rifalazil and 32-hydroxy-rifalazil, and some minor metabolites (figure 2, A). When incubated in the absence of NADPH, only 25-deacetyl-rifalazil was produced (figure 2, B). The 25-deacetylation of rifalazil was linear for up to 60 min under both conditions, but the amount of this metabolite produced with NADPH was ~2-fold greater than without NADPH (figure 3).

The Michaelis–Menten constants, K_m and $V_{max,}$ for the 25-deacetylation and the 32-hydroxylation of rifalazil are shown in table 1. In the presence of NADPH, V_{max} was comparable for 25-deacetylation and 32-hydroxylation, but K_m for the 25-deacetylation was ~2-fold higher than that of 32-hydroxylation. Both K_m and V_{max} for the 25-deacetylation of rifalazil with NADPH were ~2-fold higher than those without NADPH.

When rifalazil was incubated with human liver S9 fractions, the same metabolites detected in the microsomal incubations were produced, but the conversion was about one-fifth of that in the microsomal incubations (data not shown). In contrast, no metabolites of rifalazil were detected in the incubations with human liver cytosol (data not shown), indicating that enzymes responsible for rifalazil metabolism were microsomal enzymes in human liver.

Effects of esterase inhibitors on the 25-deacetylation of rifalazil in human liver microsomes without NADPH were examined, and the results shown in figure 4.

Table 1. Kinetic parameters for rifalazil metabolism in human liver microsomes.

	In the presence of NADPH		In the absence of NADPH	
	K_m (μM)	V_{max} (pmol/min/mg protein)	K_m (μM)	V_{max} (pmol/min/mg protein)
Rifalazil-25-deacetylation	6.54±0.69	11.89±0.39	2.57±0.52	5.97±0.27
Rifalazil-32-hydroxylation	3.32±0.41	11.00±0.33	—	—

K_m, Michaelis–Menten constant; V_{max}, maximal velocity.

Kinetic parameters (±SE) were determined by computerized curve-fitting to the Michaelis–Menten equation. Data are the mean±SEM of triplicate determinations.

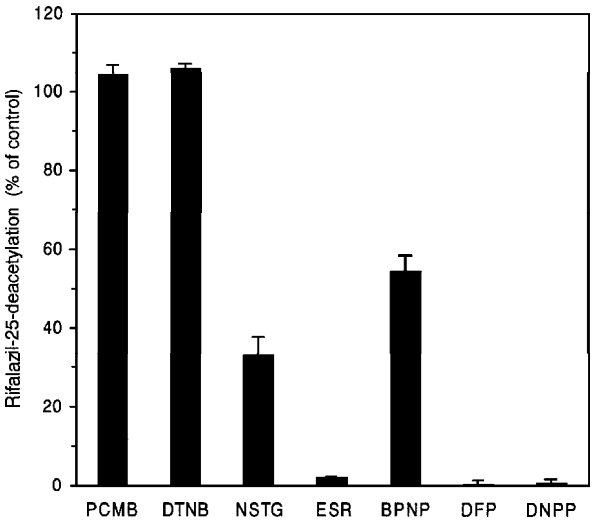


Figure 4. Effect of esterase inhibitors on rifalazil-25-deacetylation in human liver microsomes in the absence of NADPH. After pre-incubation with human liver microsomes (1 mg protein/ml) and esterase inhibitors (10 μM) at 37 °C for 5–10 min, rifalazil (10 μg/ml = 10.6 μM) was added and incubated at 37 °C for 60 min. Control activity for rifalazil-25-deacetylation was 0.210±0.006 μg/mg protein/h. Data are the mean±SD of three experiments. PCMB, *p*-chloromercuribenzoate; DTNB, 5,5′-dithio-bis(2-nitrobenzoic acid); NSTG, neostigmine bromide; ESR, eserine; BPNP, bis(*p*-nitrophenyl) phosphate; DFP, diisopropyl fluorophosphate; DNPP, diethyl *p*-nitrophenyl phosphate.

The organophosphates diisopropyl fluorophosphate (DFP) and diethyl *p*-nitrophenyl phosphate (DNPP) inhibited completely the 25-deacetylation of rifalazil, and bis(*p*-nitrophenyl) phosphate (BPNP) inhibited moderately. Eserine and neostigmine, inhibitors of cholinesterases, also inhibited the 25-deacetylation of rifalazil. However, *p*-chloromercuribenzoate (PCMB) and 5,5′-dithio-bis(2-nitrobenzoic acid) (DTNB), inhibitors of arylesterases, had no effect. In the presence of NADPH, the same results were observed, i.e. the 25-deacetylation of rifalazil was inhibited completely by DFP, DNPP and eserine, and moderately by BPNP and neostigmine, but not by PCMB or DTNB. These esterase inhibitors did not affect the NADPH-dependent formation of rifalazil metabolites except one minor metabolite that had a retention of 68 min.

Effects of specific CYP inhibitors on the 32-hydroxylation of rifalazil in human liver microsomes with NADPH were examined, and the results are shown in table

Table 2. Inhibition of rifalazil-32-hydroxylation in human liver microsomes by CYP inhibitors.

	Rifalazil-32-hydroxylation (% of control)	
	[I] = 10 μM	[I] = 100 μM
Phenacetin	84	92
Sulphaphenazole	107	71
Mephenytoin	71	86
Quinidine	85	98
Chlorzoxazone	91	93
Troleandomycin	56	8
Fluconazole	33	2
Ketoconazole	14	2
Miconazole	2	4

Rifalazil (10 μM + ^{14}C-labelled 5 μM) was incubated at 37 °C for 20 min with human liver microsomes (2 mg protein/ml), NADPH (1 mM) and CYP inhibitors (10 and 100 μM), extracted with ethyl acetate, and radiometrically analyzed by tlc. Data are the mean of duplicate determinations. Control rate was 2·34 pmol/min/mg protein.

2. The 32-hydroxylation of rifalazil was completely inhibited by fluconazole, ketoconazole, miconazole and troleandomycin (inhibitors of CYP3A4), but not by phenacetin (CYP1A2), sulphaphenazole (CYP2C8/9), mephenytoin (CYP2C19), quinidine (CYP2D6) or chlorzoxazone (CYP2E1) even at a concentration of 100 μM.

Table 3 shows the effects of clinically used drugs on the 32-hydroxylation of rifalazil in human liver microsomes with NADPH. Cyclosporin A exhibited the largest inhibition of the 32-hydroxylation of rifalazil among all drugs studied. Clarithromycin, terfenadine, loratadine and astemizole were potent inhibitors, and azithromycin, nifedipine, midazolam and clofazimine were moderate inhibitors of the 32-hydroxylation of rifalazil. However, AZT, ddC, ddI, ethambutol, pyrazinamide, streptomycin, cimetidine, ranitidine, dextromethorphan, cocaine, acetaminophen, naringenin, ofloxacin, sparfloxacin, pipemidic acid and enoxacin showed no inhibition.

Discussion

In this study, the enzymes responsible for the 25-deacetylation and the 32-hydroxylation of rifalazil were identified. Rifalazil was biotransformed to two major metabolites, namely 25-deacetyl-rifalazil and 32-hydroxy-rifalazil, in human liver microsomes and S9 but not in cytosol. Organophosphates and inhibitors of cholinesterases inhibited the deacetylation of rifalazil, and CYP3A4-specific inhibitors inhibited the hydroxylation of rifalazil. This indicates that the enzymes responsible for rifalazil metabolism are a microsomal B-esterase and CYP3A4.

Iatsimirskaia *et al*. (1997) reported that the K_m and V_{max} of rifabutin metabolism in human liver microsomes were 16.4 μM and 78.5 pmol/min/mg for the deacetylation, and 10.9 μM and 104.6 pmol/min/mg for the CYP-mediated metabolism. As shown in table 1, the V_{max} of rifalazil metabolism was seven-to-ten times lower than that of rifabutin, indicating that rifalazil is metabolized much more slowly than rifabutin. The long elimination half-life of rifalazil can be explained by this slow phase I metabolism, which may be attributable to the benzoxazine moiety.

The addition of NADPH to the microsomal incubations of rifalazil increased the amount of 25-deacetyl-rifalazil produced and the K_m and V_{max} for deacetylation by

Table 3. Effects of clinically-used drugs on rifalazil-32-hydroxylation in human liver microsomes.

	Rifalazil-32-hydroxylation (% of control)	
	[I] = 10 μM	[I] = 100 μM
Anti-AIDS drugs:		
AZT	120	112
ddC	119	101
ddI	91	104
Anti-MAC/TB drugs:		
Azithromycin	85	60
Clarithromycin	68	21
Ethambutol	130	87
Isoniazid	98	96
Pyrazinamide	93	91
Streptomycin	105	99
Antihistamines:		
Terfenadine	43	6
Loratadine	79	10
Astemizole	67	22
Cimetidine	105	101
Ranitidine	96	126
CYP3A4 substrates:		
Dextromethorphan	96	101
Cocaine	101	88
Acetaminophen	128	118
Cyclosporin A	2	1
Naringenin	113	102
Nifedipine	115	51
Midazolam	71	51
Antibiotics:		
Ofloxacin	95	97
Sparfloxacin	119	92
Clofazimine	113	53
Pipemidic acid	nd	90
Enoxacin	nd	113

nd, Not determined.

The control rate was 2·96 pmol/min/mg protein. Data are derived from duplicate determinations.

~ 2-fold. Deacetylation catalyzed by a B-esterase is a metabolic pathway common to the rifamycin derivatives, rifabutin, rifampicin and rifapentine (Iatsimirskaia *et al*. 1997, Jamis-Dow *et al*. 1997, Reith *et al*. 1998). Jamis-Dow *et al*. showed that the addition of NADPH to microsomal incubations of rifabutin and rifampicin produces small but opposite changes in the amount of the deacetylated metabolites, namely a decrease of 25-deacetyl-rifabutin and an increase of 25-deacetyl-rifampicin. Although cytochrome P450 can cleave ester bonds (Parkinson 1996), the complete inhibition of the deacetylation of rifalazil by DFP, DNPP and eserine in the presence of NADPH was observed. This suggests the activation of a B-esterase by NADPH.

Since multidrug treatment is very common and efficacious for chemotherapy of *M. avium* complex and *M. tuberculosis*, it was appropriate to investigate drug interactions between rifalazil and other clinically used drugs, especially those metabolized by CYP3A4, which is responsible for the metabolism of a large number of compounds (Shimada *et al*. 1994). In contrast to other rifamycin derivatives, rifalazil is not an inducer of drug-metabolizing enzymes (Mae *et al*. 1998). The present authors have shown that the hydroxylation of rifalazil catalyzed by CYP3A4

was inhibited by drugs such as cyclosporin A and clarithromycin, which are metabolized by CYP3A4. Inaba *et al*. (1997) reported that the HIV protease inhibitors ritonavir, indinavir and saquinavir also inhibit the hydroxylation of rifalazil. However, the inhibitory impact on rifalazil metabolism may be insignificant since the rate of rifalazil metabolism is extremely slow.

In conclusion, the enzymes responsible for the 25-deacetylation and 32-hydroxylation of rifalazil in human liver are a microsomal B-esterase and CYP3A4 respectively. It appears that these enzymes contribute significantly to the metabolism of all rifamycin derivatives, but rifalazil is the most slowly metabolized of the compounds reported to date.

Acknowledgement

Ms Nancy Fischer is thanked for critically reading the manuscript.

References

Aldridge, W. N., 1953, Serum esterases: two types of esterase (A and B) hydrolysing *p*-nitrophenyl acetate, propionate and butyrate, and a method for their determination. *Biochemical Journal*, **53**, 110–117.

Battaglia, R., Pianezzola, E., Salgarollo, G., Zini, G. and Strolin-Benedetti, M., 1990, Absorption, disposition and preliminary metabolic pathway of ^{14}C-rifabutin in animals and man. *Journal of Antimicrobial Chemotherapy*, **26**, 813–822.

Bermudez, L. E., Kolonoski, P., Young, L. S. and Inderlied, C. B., 1994, Activity of KRM-1648 alone or in combination with ethambutol or clarithromycin against *Mycobacterium avium* in beige mouse model of disseminated infection. *Antimicrobial Agents and Chemotherapy*, **38**, 1844–1848.

Cocchiara, G., Strolin Benedetti, M., Vicario, G. P., Ballabio, M., Gioia, B., Vioglio, S. and Vigevani, A., 1989, Urinary metabolites of rifabutin, a new antimycobacterial agent, in human volunteers. *Xenobiotica*, **19**, 769–780.

Fujii, K., Tsuji, A., Miyazaki, S., Yamaguchi, K. and Goto, S., 1994, *In vitro* and *in vivo* antibacterial activities of KRM-1648 and KRM-1657, new rifamycin derivatives. *Antimicrobial Agents and Chemotherapy*, **38**, 1118–1122.

Hirata, T., Saito, H., Tomioka, H., Sato, K., Jidoi, J., Hosoe, K. and Hidata, T., 1995, *In vitro* and *in vivo* activities of the benzoxazinorifamycin KRM-1648 against *Mycobacterium tuberculosis*. *Antimicrobial Agents and Chemotherapy*, **39**, 2295–2303.

Hosoe, K., Mae, T., Konishi, E., Fujii, K., Yamashita, K., Yamane, T., Hidaka, T. and Ohasi, T., 1996a, Pharmacokinetics of KRM-1648, a new benzoxazinorifamycin, in rats and dogs. *Antimicrobial Agents and Chemotherapy*, **40**, 2749–2755.

Hosoe, K., Mae, T., Yamashita, K., Fujii, K., Yamane, T., Hidaka, T. and Ohasi, T., 1996b, Identification and antimicrobial activity of urinary metabolites of a rifamycin derivative in dog. *Xenobiotica*, **26**, 321–332.

Iatsimirskaia, E., Tulebaev, S., Storozhuk, E., Utkin, I., Smith, D., Gerber, N. and Koudriakova, T., 1997, Metabolism of rifabutin in human enterocyte and liver microsomes: kinetic parameters, identification of enzyme systems, and drug interactions with macrolides and antifungal agents. *Clinical Pharmacology and Therapeutics*, **61**, 554–562.

Inaba, T., Fischer, N. E., Riddick, D. S., Stewart, D. J. and Hidaka, T., 1997, HIV protease inhibitors, saquinavir, indinavir and ritonavir: inhibition of CYP3A4-mediated metabolism of testosterone and benzoxazinorifamycin, KRM-1648, in human liver microsomes. *Toxicology Letters*, **93**, 215–219.

Inderlied, C. B., Barbara-Burnham, L., Wu, M., Young, L. and Bermudez, L. E., 1994, Activity of the benzoxazinorifamycin KRM-1648 against the *Mycobacterium avium* complex *in vitro* and in macrophages. *Antimicrobial Agents and Chemotherapy*, **38**, 1838–1843.

Jamis-Dow, C. A., Katki, A. G., Collins, J. M. and Klecker, R. W., 1997, Rifampicin and rifabutin and their metabolism by human liver esterases. *Xenobiotica*, **27**, 1015–1024.

Kelly, B. P., Furney, S. K., Jessen, M. T. and Orme, I. M., 1996, Low-dose aerosol infection model for testing drugs for efficacy against *Mycobacterium tuberculosis*. *Antimicrobial Agents and Chemotherapy*, **40**, 2809–2812.

Klemens, S. P., Grossi, M. A. and Cynamon, M. H., 1994, Activity of KRM-1648, a new benzoxazinorifamycin, against *Mycobacterium tuberculosis* in a murine model. *Antimicrobial Agents and Chemotherapy*, **38**, 2245–2248.

Luna-Herrera, J., Reddy, M. V. and Gangadharam, P. R. J., 1995, *In vitro* activity of the benzoxazinorifamycin KRM-1648 against drug-susceptible and multidrug-resistant tubercle bacilli. *Antimicrobial Agents and Chemotherapy*, **39**, 440–444.

Mae, T., Hosoe, K., Fujii, K., Yamashita, K., Yamane, T., Hidaka, T. and Ohashi, T., 1996, *In vitro* metabolism of a rifamycin derivative by animal and human liver microsomes, whole blood and expressed human CYP3A isoform. *Xenobiotica*, **26**, 793–802.

Mae, T., Hosoe, K., Yamamoto, T., Hidaka, T., Ohashi, T., Kleeman, J. M. and Adams, P. E., 1998, Effect of a new rifamycin derivative, rifalazil, on liver microsomal enzyme induction in rat and dog. *Xenobiotica*, **28**, 759–766.

Mae, T., Konishi, E., Hosoe, K. and Hidaka, T., 1999, Isolation and identification of major metabolites of rifalazil in mouse and human. *Xenobiotica*, **29**, 1073–1087.

Moghazeh, S. L., Pan, X., Arain, T., Stover, C. K., Musser, J. M. and Kreiswirth, B. N., 1996, Comparative antimycobacterial activities of rifampin, rifapentine, and KRM-1648 against a collection of rifampin-resistant *Mycobacterium tuberculosis* isolates with known rpoB mutations. *Antimicrobial Agents and Chemotherapy*, **40**, 2655–2657.

Mor, N., Simon, B. and Heifets, L., 1996, Bacteriostatic and bactericidal activities of benzoxazinorifamycin KRM-1648 against *Mycobacterium tuberculosis* and *Mycobacterium avium* in human macrophages. *Antimicrobial Agents and Chemotherapy*, **40**, 1482–1485.

Parkinson, A., 1996, Biotransformation of xenobiotics. In C. D. Klaassen (eds), *Casaret & Doull's Toxicology*: *The Basic Science of Poisons*, 5th edn (New York: McGraw-Hill), pp. 113–186.

Reddy, M. V., Luna-Herrera, J., Daneluzzi, D. and Gangadharam, P. R., 1996, Chemotherapeutic activity of benzoxazinorifamycin, KRM-1648, against *Mycobacterium tuberculosis* in C57BL/6 mice. *Tubercle and Lung Disease*, **77**, 154–159.

Reith, K., Keung, A., Toren, P. C., Cheng, L., Eller, M. G. and Weir, S. J., 1998, Disposition and metabolism of ^{14}C-rifapentine in healthy volunteers. *Drug Metabolism and Disposition*, **26**, 732–738.

Saito, H., Tomioka, H., Sato, K., Emori, M., Yamane, T., Yamashita, K., Hosoe, K. and Hidaka, T., 1991, *In vitro* antimycobacterial activities of newly synthesized benzoxazinorifamycins. *Antimicrobial Agents and Chemotherapy*, **35**, 542–547.

Shimada, T., Yamazaki, H., Mimura, M., Inui, Y. and Guengerich, F. P., 1994, Interindividual variations in human liver cytochrome P-450 enzymes involved in the oxidation of drugs, carcinogens and toxic chemicals: studies with liver microsomes of 30 Japanese and 30 Caucasians. *Journal of Pharmacology and Experimental Therapeutics*, **270**, 414–423.

Sumida, A., Kinoshita, K., Fukuda, T., Matsuda, H., Yamamoto, I., Inaba, T. and Azuma, J., 1999, Relationship between mRNA levels quantified by reverse transcription-competitive PCR and metabolic activity of CYP3A4 and CYP2E1 in human liver. *Biochemical and Biophysical Research Communications*, **262**, 499–503.

Tomioka, H., Saito, H., Fujii, K., Sato, K. and Hidaka, T., 1993, *In vitro* antimicrobial activity of benzoxazinorifamycin, KRM-1648, against *Mycobacterium avium* complex determined by the radiometric method. *Antimicrobial Agents and Chemotherapy*, **37**, 67–70.

Tomioka, H., Saito, H., Sato, K., Yamane, T., Yamashita, K., Hosoe, K., Fujii, K. and Hidaka, T., 1992, Chemotherapeutic efficacy of a newly synthesized benzoxazinorifamycin, KRM-1648, against *Mycobacterium avium* complex infection induced in mice. *Antimicrobial Agents and Chemotherapy*, **36**, 387–393.

Trapnell, C. B., Jamis-Dow, C., Klecker, R. W. and Collins, J. M., 1997, Metabolism rifabutin and its 25-desacetyl metabolite, LM565, by human liver microsomes and recombinant human cytochrome P-450 3A4: relevance to clinical interaction with fluconazole. *Antimicrobial Agents and Chemotherapy*, **41**, 924–926.

Utkin, I., Koudriakova, T., Thompson, T., Cottrell, C., Iatsimirskaia, E., Barry, J., Vouros, P. and Gerber, N., 1997, Isolation and identification of major urinary metabolites of rifabutin in rats and humans. *Drug Metabolism and Disposition*, **25**, 963–969.

Vigevani, A., Ballabio, M., Gioia, B., Marsili, L., Vioglio, S. and Franceschi, G., 1985, Identification of urinary metabolites of rifamycin LM 427 in man. *Journal of Antibiotics*, **38**, 1799–1802.

Williams, F. M., 1985, Clinical significance of esterases in man. *Clinical Pharmacokinetics*, **10**, 392–403.

Yamane, T., Hashizume, T., Yamashita, K., Konishi, E., Hosoe, K., Hidata, T., Watanabe, K., Kawaharada, H., Yamamoto, T. and Kuze, F., 1993, Synthesis and biological activity of 3′-hydroxy-5′-aminobenzoxazinorifamycin derivatives. *Chemical and Pharmaceutical Bulletin*, **41**, 148–155.

Yang, B., Koga, H., Ohno, H., Ogawa, K., Fukuda, M., Hirakata, Y., Maesaki, S., Tomono, K., Tashiro, T. and Kohno, S., 1998, Relationship between antimycobacterial activities of rifampicin, rifabutin and KRM-1648 and rpoB mutations of *Mycobacterium tuberculosis*. *Journal of Antimicrobial Chemotherapy*, **42**, 621–628.

XENOBIOTICA, 2000, VOL. 30, NO. 6, 575–588

Evidence for propofol hydroxylation by cytochrome P4502B11 in canine liver microsomes: breed and gender differences

B. L. HAY KRAUS†, D. J. GREENBLATT‡,
K. VENKATAKRISHNAN‡ and M. H. COURT†‡*

†Department of Clinical Sciences and ‡Department of Pharmacology and Experimental Therapeutics, Tufts University School of Veterinary Medicine, North Grafton, Massachusetts, USA

Received 19 November 1999

1. The study aimed to ascertain the enzyme kinetic basis for breed differences in the biotransformation of propofol in dog and to identify the responsible canine cytochrome P450 (CYP) isoenzymes.

2. The NADPH-dependent formation of 4-hydroxypropofol (the rate-limiting biotransformation in dog) was assayed using hepatic microsomes from the male greyhound and beagle, and from both sexes in mixed-breed dogs (five of each).

3. Enzyme kinetic analysis revealed that whereas there were no significant differences in K_m, V_{max} averaged > 3-fold lower in greyhound compared with beagle ($p = 0.032$). Although average V_{max} was > 3-fold higher in the male compared with female mixed-breed dogs, this difference did not achieve statistical significance ($p = 0.095$), probably because of the high variability of data from mixed-breed dogs.

4. Chloramphenicol (a specific CYP2B11 inhibitor) and diethyldithiocarbamate (a non-specific CYP2 inhibitor) inhibited propofol hydroxylation in all microsomes. Quinine (a CYP2D15 inhibitor) was also inhibitory, but only in one-half of the microsomes examined. Immuno-inhibition by anti-CYP2B1 sera resulted in > 50% reduction in metabolite formation in all dogs except mixed-breed females, which showed a 30% reduction. Differences in propofol hydroxylase activity between microsomal preparations were primarily attributed to a component that was sensitive to inhibition by chloramphenicol and anti-CYP2B1 sera.

5. The results indicate that propofol hydroxylation in dog is primarily mediated by CYP2B11 and that breed (and possibly gender) differences in propofol metabolism may result from differences in the liver content of this CYP.

Introduction

Propofol (2,6-diisopropylphenol) is becoming popular for anaesthesia and sedation in dog (Robertson *et al*. 1992, Zoran *et al*. 1993, Mandsager *et al*. 1995, Court 1999). Perhaps the major advantage of propofol over similar agents is that anaesthetic recovery is rapid and complete even after relatively prolonged intravenous infusions (Mandsager *et al*. 1995). Termination of the drug's effect is largely attributed to rapid and extensive biotransformation by the liver to inactive metabolites, which are excreted in the urine. In dog the two major urinary metabolites of propofol are the glucuronide and sulphate conjugates of 4-hydroxypropofol (2,6-diisopropyl-1,4-quinol) (Simons *et al*. 1991). The formation of this latter intermediate derivative by aromatic hydroxylation of propofol appears to be a critical initial step in the biotransformation and elimination of propofol in dog (Court *et al*. 1999).

* Author for correspondence at: Department of Pharmacology and Experimental Therapeutics, Tufts University, 136 Harrison Avenue, Boston, MA 02111, USA; e-mail: mcourt01@emerald.tufts.edu

Xenobiotica ISSN 0049–8254 print/ISSN 1366–5928 online © 2000 Taylor & Francis Ltd
http://www.tandf.co.uk/journals

Pharmacokinetic studies indicate that there may be breed differences in the clearance of propofol by metabolism. Greyhounds have significantly slower drug clearance and longer recoveries compared with other breeds (Robertson *et al*. 1992, Zoran *et al*. 1993). In a previous study an *in vitro* propofol hydroxylase assay was developed and used to compare enzyme activities in liver microsomes from male greyhound, beagle and mixed-breed dogs (Court *et al*. 1999). Propofol hydroxylation was NADPH-dependent and therefore likely to be mediated by one or more hepatic cytochrome P450 (CYP) isoforms. Furthermore, enzyme activities were almost 3-fold lower in greyhound compared with beagle microsomes, which is in good agreement with *in vivo* pharmacokinetic clearance differences. Activities in mixed-breed dog microsomes tended to span the range of activities in greyhound and beagle microsomes.

Based on these findings it was speculated that dog breed differences in propofol metabolism might result from differences in hydroxylation of propofol by a specific canine CYP isoform. Although the identity of this CYP has yet to be determined, the results of a recent pharmacokinetic study indicate that it could be CYP2B11, a major constitutive CYP isoenzyme in canine liver (Mandsager *et al*. 1995). In the latter study, administration of chloramphenicol to greyhounds anaesthetized with propofol decreased propofol clearance by 50% and increased anaesthetic recovery from 60 min to >9 h. Although chloramphenicol inhibits multiple CYP isoforms in human and rat, the drug appears a specific inhibitor of CYP2B11 in dog (Ciaccio *et al*. 1987). Unfortunately, chloramphenicol can also inhibit drug glucuronidation (LeGuellec *et al*. 1995). Consequently, *in vitro* studies are needed to ascertain whether the drug interaction is mediated via oxidative or conjugative pathways.

The objectives of the current study were to utilize the hepatic microsomal assay system to identify the major CYP isoforms responsible for propofol hydroxylation in dog and to ascertain the enzyme kinetic basis for breed-related differences in this activity. In addition to hepatic microsomes from male greyhound, beagle and mixed-breed dogs, microsomes from female mixed-breed dogs were studied to investigate possible gender-related differences in propofol hydroxylation independent of the effect of dog breed.

Materials and methods

Chemicals and reagents

Pure propofol was from Zeneca Pharmaceuticals (Wilmington, DE, USA) and kept in a Teflon-sealed glass vial with nitrogen overlay at -80 °C. A small quantity (4 mg) of pure 4-hydroxypropofol was a gift from Dr J. Guitton (Université Claude Bernard, Lyon, France). Thymol (5-methyl 2-isopropylphenol), resorufin, benzyloxyresorufin, $NADP^+$, isocitrate dehydrogenase, DL-isocitrate and dimethylsulphoxide (DMSO) were from Sigma Chemical Company (St Louis, MO, USA). Chemical inhibitors, including coumarin, sulphaphenazole, quinine, chloramphenicol, diethyldithiocarbamate, troleandomycin and furafylline, were also from Sigma. Acetonitrile and methanol were chromatographic grade and were from Fisher Scientific (Fairlawn, NJ, USA). Control pre-immune and anti-rat CYP2B1 sera were from Daiichi Pure Chemicals Co. (Tokyo, Japan). CYP2B1 antiserum was produced in goat and is inhibitory to both CYP2B1 and 2B2, but not CYP1A1, 1A2, 2C11, 2E1, 3A2 or 4A1. Stock solutions of propofol in DMSO (8.9 mg propofol/ml DMSO) and thymol in methanol (10 μg/ml methanol) were kept in screw-capped polypropylene tubes with neoprene O-rings at -80 °C.

Liver microsomes

Liver tissue was from male beagle, greyhound and mixed-breed dogs, and from female mixed-breed dogs (five in each group) with approximate ages ranging from 1 to 3 years and bodyweights from 15 to

31 kg. All dogs were untreated controls from studies in which tissue other than the liver was collected. The Institutional Animal Care and Use Committee at Tufts University approved the procedures. Immediately after euthanasia by overdose of pentobarbital, liver tissue was collected and placed in plastic freezer bags on dry ice and transported for final storage at −80 °C.

Liver microsomes were prepared by differential centrifugation as described (von Moltke *et al*. 1993, Court *et al*. 1997). The resultant pellet was reconstituted in 100 mM phosphate buffer (pH 7.5), divided into aliquots and stored at −80 °C. Microsomes prepared in this fashion in this laboratory are stable (no significant loss of marker activities) for at least 12 months. Frozen microsomes were thawed on ice (once only), immediately before use. Microsomal protein concentrations were determined using the bicinchoninic acid assay (Pierce, Rockford, IL, USA).

Propofol hydroxylation assay

Microsomal propofol hydroxylation activities were determined as described (Court *et al*. 1999). Briefly, glass gas chromatography vials were prepared on ice containing 50 μl liver microsomes (100 μg/ml protein, final concentration) and 100 μl of an NADPH regeneration system (0.5 mM $NADP^+$; 3.75 mM racemic isocitrate; 1 unit/ml isocitrate dehydrogenase; 6 mM $MgCl_2$, final concentrations). Reactions were started by addition of 100 μl propofol working solution (0–100 μM propofol for kinetic studies, 20 μM propofol for inhibition studies, with 0.2% DMSO, final concentrations). All working solutions were made up in 50 mM phosphate buffer (pH 7.5) and the total incubation volume was 250 μl. The tubes were immediately vortexed and placed in a 37 °C agitating water bath. After 10 min the reaction was stopped by addition of 250 μl acetonitrile containing the internal standard (25–50 ng thymol) to each tube, and immediately vortexed and placed on ice. This mixture was transferred to polypropylene tubes and spun at 20000 *g* in a microcentrifuge for 5 min at 4 °C. The supernatant was then transferred to vials for immediate analysis or for storage at 4 °C until assay within 2 weeks. 4-Hydroxypropofol concentrations were determined by high-performance liquid chromatography (HPLC) with fluorescence detection (Model 474, Waters, Milford, MA, USA) as described (Court *et al*. 1999). The excitation wavelength was 276 nm, emission wavelength was 310 nm, and slit widths were 15 nm. The column was a C_{18} μBondapack (300×3.9 mm i.d., Waters, Milford, MA, USA) and the mobile phase consisted of 50% acetonitrile, 40% water and 10% methanol with a flow rate of 2 ml/min. A standard curve was generated by assay of samples containing varying amounts of pure 4-hydroxypropofol standard and a fixed amount of internal standard. Metabolite concentrations were then calculated by linear regression of calibration curve data using measured metabolite–internal standard peak height ratios. Enzyme activity was calculated by dividing the amount of product formed by incubation time and microsomal protein content, and expressed as nmol/min/mg. Incubation time (10 min) and microsomal protein concentration (100 μg/ml) were minimized to ensure linearity of product formation with respect to these variables. This was substantiated in each assay by demonstrating proportionally greater product formation when reaction mixtures contained 50% more microsomal protein or were incubated for 50% longer than usual at the lowest substrate concentration (data not shown).

Enzyme kinetic analysis

For each microsomal preparation, propofol hydroxylation activities were determined at propofol concentrations from 1 to 100 μM. Non-linear regression analysis then derived the Michaelis-Menten kinetic parameters apparent V_{max} and apparent K_m according to:

$$V = \frac{V_{max} \times S}{K_m + S} \quad (1)$$

where S is propofol concentration and V is enzyme activity. For some sets of data, Eadie–Hofstee plots (V versus V/S) were non-linear and indicated the possible contribution of high- and low-affinity components to the observed activity. Consequently, data were additionally analyzed by non-linear regression using:

$$V = \frac{V_{max1} \times S}{K_{m1} + S} + \frac{V_{max2} \times S}{K_{m2} + S} \quad (2)$$

where subscripts 1 and 2 represent V_{max} and K_m for apparent high- and low-affinity activities. The equation that best described the set of data (equation 1 or 2) was determined by comparison of the sum of the squared residual errors. Estimates of intrinsic clearance were calculated by dividing V_{max} by K_m. In instances where a multicomponent model was used, total intrinsic clearance was calculated by summing high- and low-affinity V_{max}/K_m. The relative contribution of each component was then determined by expressing individual V_{max}/K_m as a percent of total intrinsic clearance.

Chemical inhibition

Seven chemical inhibitors were assessed for their ability to inhibit formation of 4-hydroxypropofol by hepatic microsomes. These were chosen either because they inhibit particular canine CYP isoforms, as reported for chloramphenicol (Ciaccio *et al*. 1987), quinine (Roussel *et al*. 1998) and troleandomycin (Ciaccio and Halpert 1989), or because they are used in human to implicate the involvement of a specific major drug-metabolizing CYP subfamily (Newton *et al*. 1995). The inhibitors used and CYP subfamily inhibited included furafylline (CYP1A), coumarin (CYP2A), chloramphenicol (CYP2B), sulphaphenazole (CYP2C), quinine (CYP2D), diethyldithiocarbamate (CYP2E) and troleandomycin (CYP3A). Inhibitor concentrations examined were between 0.1 and 1000 μM except for furafylline, which was limited to 100 μM because of low solubility. Stock solutions of these chemicals were dissolved in pure methanol and stored at −20 °C. For assays, aliquots were added to gas chromatography vials and then dried down in a vacuum oven without heat. The vials were then placed on ice and 100 μl liver microsomes (100 μg/ml final protein concentration) and 100 μl of the NADPH regeneration system added. Vials containing furafylline, chloramphenicol, diethyldithiocarbamate and troleandomycin were pre-incubated with the microsomes and NADPH regeneration system for 15 min in an agitated water bath at 37 °C. For all inhibitors, the reactions were started with 50 μl propofol (final concentration 20 μM in 50 mM phosphate buffer and 0.2% DMSO) and incubated for 10 min in an agitated water bath at 37 °C. The reactions were stopped by addition of 250 μl acetonitrile containing internal standard (25–50 ng thymol), vortexed and placed on ice. The mixture was then processed and assayed by HPLC as described above.

The percent inhibition of activity at each inhibitor concentration was calculated as the percent of control (i.e. no inhibitor added) activity. IC_{50} (inhibitor concentration resulting in 50% inhibition of 4-hydroxypropofol production) was used as an index of inhibitor potency and was derived by linear regression of plots of inhibitor concentration (log transformed) versus percent inhibition.

To evaluate dog breed and gender differences further in the effects of chloramphenicol, propofol hydroxylase activities insensitive (residual activity) and sensitive (by subtracting residual activity from control activity) to inhibition by 100 μM chloramphenicol were calculated for each set of microsomes.

Immunoinhibition

An immuno-inhibition study was performed using goat anti-rat CYP2B1 and pre-immune sera. Equal amounts of microsomal protein from each liver were pooled into four groups of microsomes according to dog breed and gender, including male beagle, greyhound, and mixed-breed dogs, and female mixed-breed dogs. These microsomes (20 μg protein) were pre-incubated with a mixture of inhibitory and control sera (total 400 μg serum protein) for 30 min at room temperature in a volume of 100 μl. For each set of pooled microsomes, the mixture of inhibitory and control serum was adjusted such that the ratio of inhibitory serum to microsomal protein was 0:1, 5:1, 10:1, 15:1 and 20:1. The reaction was started by adding 50 μl propofol (final concentration 20 μM in 50 mM phosphate buffer and 0.2% DMSO) and 100 μl of the NADPH cofactor solution. This mixture was vortexed and incubated for 10 min at 37 °C. The reaction was stopped by adding 250 μl acetonitrile/thymol solution, vortexed and placed on ice. The samples were then processed as before and analyzed by HPLC. The percent inhibition of activity at each ratio of inhibitory serum to microsomal protein was calculated as the percent decrease from control (i.e. no inhibitory sera added) activity. To evaluate further dog breed and gender differences in the effects of anti-CYP2B1, propofol hydroxylase activities insensitive (residual activity) and sensitive (by subtracting residual activity from control activity) to inhibition by a 20:1 ratio of anti-CYP2B1 were calculated for each set of pooled microsomes.

Benzyloxyresorufin O-debenzylase activity

Benzyloxyresorufin *O*-debenzylase (BROD) activity was determined for each set of microsomes based on methods previously described with minor modifications (Klekotka and Halpert 1995). Instrumentation consisted of a fluorescence spectrophotometer (Model LS50B, Perkin-Elmer, Beaconsfield, UK) with a stirred and thermostatted (37 °C) cuvette holder. Briefly, reactions were performed in a quartz cuvette containing NADPH cofactor mix and 300 μg microsomal protein to a final volume of 2 ml. Benzyloxyresorufin (1 μM final concentration) was added in 10 μl DMSO. Resorufin formation was continuously monitored with excitation and emission wavelengths set at 530 and 585 nm respectively. At the end of each incubation (1–20 min depending on microsomal activity), 100 pmoles resorufin in 10 μl DMSO was added to calibrate the fluorescence output. Activities were calculated from the slope of the initial linear portion of the fluorescence intensity–time curve and expressed relative to microsomal protein content and incubation time (pmoles/mg/min). Linearity of activities with respect to microsomal protein concentration was established in preliminary studies (data not shown).

Statistical analyses

Statistical analyses were performed using the Sigmastat software package (Jandel Scientific, San Rafael, CA, USA). The influence of dog breed and gender on V_{max}, K_m, and chloramphenicol inhibitable

and residual activities was evaluated by multiple comparisons analyses. Initial analysis showed that data sets failed tests of equal variance (V_{max}, K_m, and chloramphenicol inhibitable and residual activities). Consequently, a non-parametric approach utilizing the Mann–Whitney rank sum test was employed. Differences were considered significant when $p < 0.05$.

The relationship between BROD and propofol hydroxylation activities (measured at 20 μM propofol concentration) was determined by linear regression analysis and calculation of the Pearson product–moment correlation coefficient (r). A similar approach was also used to explore possible relationships between IC_{50} for chemical inhibitors.

Results

Enzyme kinetic analysis (figure 1) showed that data from 16 of 20 dogs, including all beagle and male mixed-breed dogs were well described by the Michaelis-Menten model (equation 1). Estimates ranged between 3.5 and 16 μM and between 0.88 and 13 nmoles/mg/min for K_m and V_{max} respectively. However, Eadie-Hofstee plots of data from three of five female mixed-breed and one of five greyhound dogs were non-linear (figure 1). Subsequent non-linear regression analysis confirmed that the two-component enzyme kinetic model (equation 2) best described these data. Estimates ranged between 1.8 and 3.2 μM and between 0.52 and 1.2 nmoles/mg/min for high-affinity K_{m1} and V_{max1} respectively. For low-affinity K_{m2} and V_{max2}, estimates ranged from 120 to 230 μM and from 0.88 to 6.5 nmoles/mg/min respectively. Calculation of the relative contribution of high- and low-affinity components to total intrinsic clearance ($\Sigma V_{max}/K_m$) in these dogs showed that the high-affinity component provided between 91 and 97% of total intrinsic clearance. Consequently, for comparison purposes, the mean ($\pm$SEM) K_m and V_{max} shown in figure 2 were calculated using the high-affinity component for these dogs. Statistical analysis of the effect of dog breed on these data showed that V_{max} were significantly lower ($p = 0.032$) in microsomes from greyhounds (2.0 ± 0.50 nmoles/mg/min; mean$\pm$SEM) compared with beagle (7.0 ± 1.8 nmoles/mg/min), but were not different ($p = 0.26$) from male mixed-breed dogs (3.8 ± 1.3 nmoles/mg/min). There were also no differences ($p = 0.18$) between microsomes from beagles and male mixed-breed dogs. While V_{max} averaged >3-fold lower for microsomes from female mixed-breed dogs (1.1 ± 0.20 nmoles/mg/min) compared with male mixed-breed dogs, this difference did not achieve statistical significance ($p = 0.095$). There was no significant effect of breed or gender on K_m.

Chemical inhibition studies (table 1) showed inhibition by both chloramphenicol and diethyldithiocarbamate in virtually all of the microsomal samples assayed. IC_{50} were < 100 μM in 19 of 20 microsomes treated with chloramphenicol and in all 20 microsomes treated with diethyldithiocarbamate. Of the other chemicals evaluated, only quinine was inhibitory; however, this effect was inconsistent, being observed in only 50% of the microsomal samples. IC_{50} for quinine were < 100 μM in microsomes from two of five greyhounds, two of five beagles, three of five male mixed-breed and three of five female mixed-breed dogs. Correlation analysis showed that there was a relatively weak, although statistically significant, correlation ($r = 0.47$, $p = 0.038$) between IC_{50} for chloramphenicol and diethyldithiocarbamate. r was < 0.01 for all other combinations of inhibitors examined.

An immuno-inhibition study using pooled microsomes and anti-rat CYP2B1 showed an effect on propofol hydroxylase activity, which was dependent on the amount of specific antisera added (figure 3). At an antisera-microsomal protein ratio of 20:1 there was $>50\%$ inhibition of propofol hydroxylase activity in all

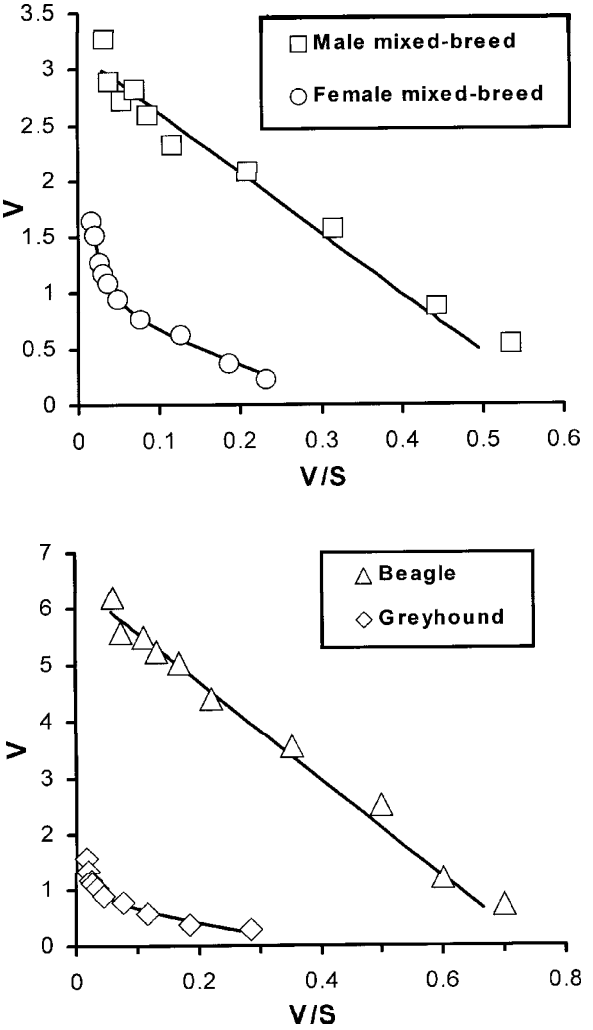


Figure 1. Representative examples of raw activity data used to derive enzyme kinetic parameters for propofol hydroxylation. Shown are Eadie–Hofstee plots (V versus V/S, where V is enzyme activity in nmoles/mg/min and S is substrate concentration in μM) of microsomal propofol hydroxylation activities measured at substrate concentrations between 1 and 100 μM. Microsomes were from a male mixed-breed dog (#19), a female mixed-breed dog (#6), a beagle (#1) and a greyhound (#4). Also shown are the curves of best fit derived by non-linear regression of data to either the Michaelis-Menten model (equation 1; male mixed-breed and beagle dogs) or a two-component kinetic model (equation 2; female mixed-breed and greyhound dogs). Data points represent the average of duplicate determinations.

microsomes except those from female mixed-breed dogs, which showed ~ 30% inhibition.

Dissection of propofol hydroxylase activities into components that were sensitive and insensitive to inhibition by 100 μM chloramphenicol (figure 4) showed that differences in total activity resulted almost exclusively from the chloramphenicol-inhibitable component. A similar, although less apparent, trend was also observed with the CYP2B1 antisera (figure 4). Statistical analysis of chloramphenicol-

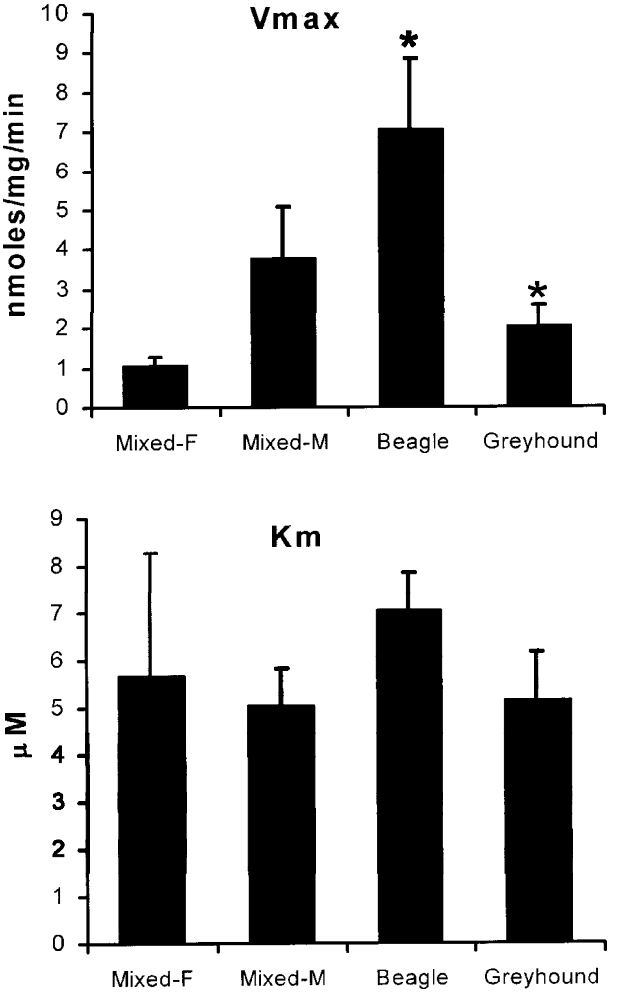


Figure 2. Dog breed and gender differences in the enzyme kinetics of propofol hydroxylation. Propofol hydroxylase activities were determined in hepatic microsomes from male mixed-breed, beagle and greyhound, and from female mixed-breed dogs (five livers per group) with substrate concentrations varied between 1 and 100 μM. Enzyme kinetic (V_{max}, K_m) were determined by non-linear regression of data to the Michaelis-Menten model (equation 1). For three of the female mixed-breed dog livers and one of the greyhound dog livers, a two-component kinetic model (equation 2) best described the data. Since the high-affinity component contributed $> 90\%$ of the calculated total intrinsic clearance, high-affinity from these dogs were used for comparison purposes. Individual determinations were made for each liver and averaged. Error bars indicate the SEM. V_{max} was significantly lower in greyhound compared with beagle microsomes (*$p = 0.032$). No significant differences were found between K_m.

inhibitable activities was similar to analysis of V_{max} data in that values for greyhound microsomes were significantly less than for beagle microsomes ($p = 0.032$), whereas gender differences were less pronounced and did not achieve statistical significance ($p = 0.056$). There were no significant breed or gender differences in activities that were residual to chloramphenicol inhibition.

Propofol hydroxylation activity was strongly correlated ($r = 0.97, p < 0.01$) with BROD activity in the 20 sets of microsomes (figure 5).

Table 1. IC_{50} (μM) for chemical inhibitors of propofol hydroxylation by dog liver microsomes*.

Dog breed and liver ID#	IC_{50} (μM)						
	Furafylline	Coumarin	Chloramphenicol	Sulphaphenazole	Quinine	Diethyldithiocarbamate	Troleandomycin
Male mixed-breed							
12	>100	670	3.4	990	360	5.5	>1000
13	>100	530	4.1	>1000	200	10	>1000
17	>100	>1000	0.40	>1000	5.4	12	>1000
18	>100	>1000	0.10	>1000	12	7.4	>1000
19	>100	>1000	1.2	800	34	8.8	>1000
Female mixed-breed							
5	52	570	7.3	880	160	23	>1000
6	>100	660	130	>1000	430	21	>1000
7	>100	>1000	33	>1000	64	9.1	>1000
11	>100	380	8.5	580	0.1	16	>1000
14	97	>1000	23	>1000	48	12	>1000
Beagle							
1	>100	860	2.5	360	700	17	>1000
2	>100	690	3.9	860	910	8.4	>1000
15	>100	300	6.7	950	810	3.7	>1000
16	>100	>1000	0.50	>1000	11	18	>1000
20	>100	>1000	7.3	>1000	18	21	>1000
Greyhound							
3	>100	>1000	54	>1000	120	19	>1000
4	>100	330	56	>1000	120	28	>1000
8	>100	240	3.6	>1000	1.6	13	>1000
9	>100	380	4.8	600	1.3	17	>1000
10	>100	280	6.5	590	150	6.4	>1000

* Hepatic microsomes from male mixed-breed, beagle and greyhound, and female mixed-breed dogs (five livers per group) were assayed for propofol hydroxylase activity (20 μM substrate concentration) in the absence and presence of chemical inhibitors. For mechanism-based inhibitors (furafylline, chloramphenicol, diethyldithiocarbamate, troleandomycin) the substrate was added after 15 min of pre-incubation. Inhibitor concentrations ranged from 0.1–1000 μM, except for furafylline, which was 0.1–100 μM. IC_{50} was determined by linear regression analysis of log-transformed inhibition data for each set of liver microsomes.

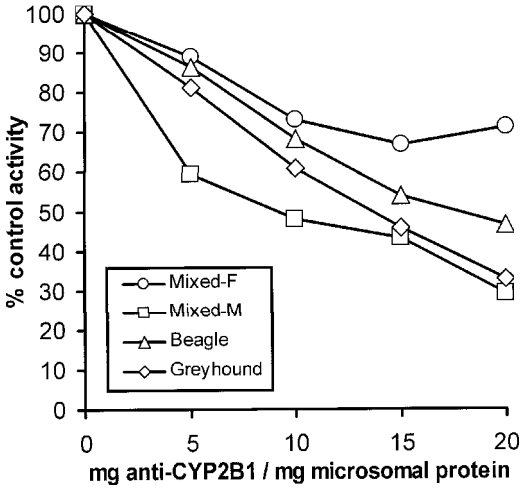


Figure 3. Immuno-inhibition of microsomal propofol hydroxylation. Pooled hepatic microsomes (five livers each) from male mixed-breed, beagle and greyhound, and female mixed-breed dogs were pre-incubated with increasing amounts of anti-CYP2B1 sera (relative to microsomal protein) and then assayed for propofol hydroxylase activity. Pre-immune serum was also included in each incubation such that the total protein content of specific inhibitory and pre-immune sera was constant. Results are the average of duplicate determinations and expressed as percentage of activity of incubations that contained only pre-immune serum.

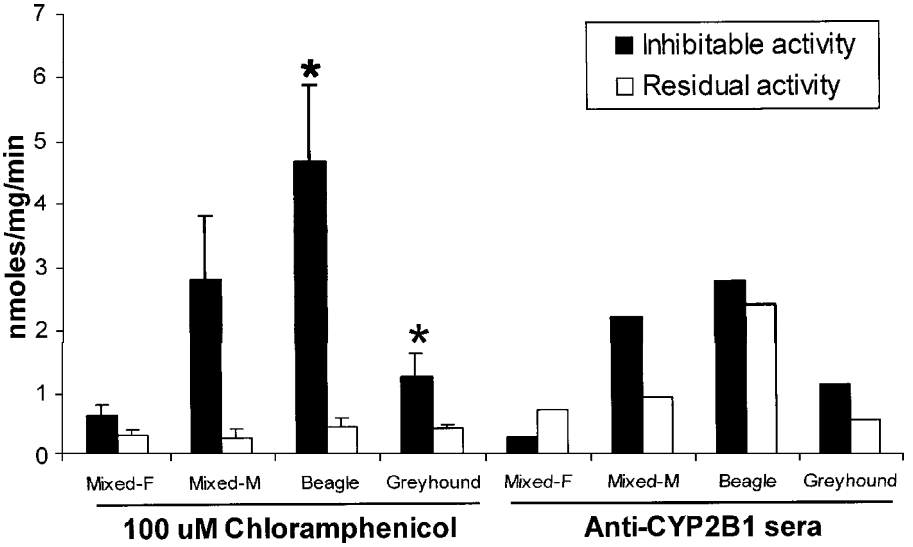


Figure 4. Dog breed and gender differences in microsomal propofol hydroxylation activity sensitive (inhibitable) and insensitive (residual) to inhibition by 100 μM chloramphenicol or anti-CYP2B1 antibody (20:1 antibody to microsomal protein). For chloramphenicol inhibition, data were determined using microsomes from male mixed-breed, beagle and greyhound, and female mixed-breed dogs (five livers per group) and averaged. Error bars indicate the SEM. For antibody inhibition, data are the average of duplicate determinations using pooled microsomes from five livers. Values for chloramphenicol-inhibitable activity were significantly lower ($*p = 0.032$) in greyhound compared with beagle microsomes.

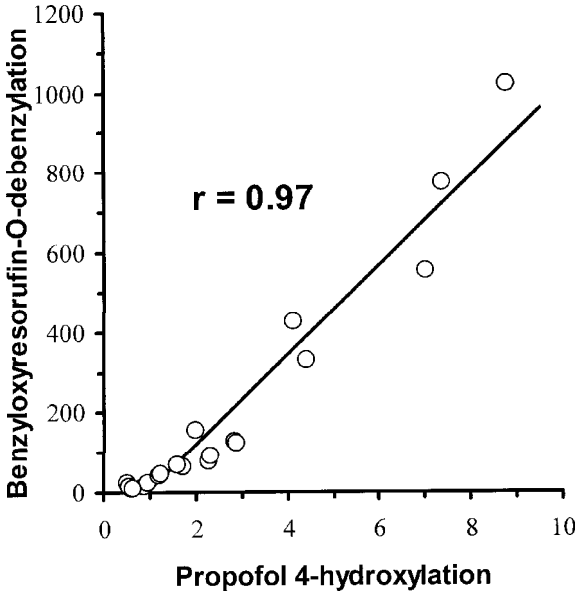


Figure 5. Correlation between propofol hydroxylation activity (nmoles/mg/min) and benzyloxyresorufin-*O*-debenzylation activity (pmoles/mg/min) in dog liver microsomes. Substrate concentrations were 20 and 1 μM respectively. Activities were measured using liver microsomes from male mixed breed, beagle and greyhound dogs and from female mixed breed dogs (five livers each, one data point per liver). Also shown is the regression line ($y = 112^{*} \times -104$), and the correlation coefficient ($r = 0.97$; $p < 0.01$).

Discussion

Chemical inhibition, immuno-inhibition and marker activity correlation studies indicate that CYP2B11 is a major CYP isoform mediating hydroxylation of propofol in dog liver microsomes. Only chloramphenicol and diethyldithiocarbamate consistently inhibited propofol hydroxylase activity in all microsomes examined. Previous inhibition kinetic studies and protein labelling by ^{14}C-chloramphenicol have shown that this drug is a specific mechanism-based inactivator of CYP2B11 in dog liver microsomes with a $K_i \sim 5$ μM (Ciaccio *et al.* 1987). This contrasts with other species in which chloramphenicol is much less specific and can inhibit other CYP2 family as well as CYP3 family isoforms (Halpert *et al.* 1985).

Involvement of CYP2B11 in propofol hydroxylation was also supported by demonstrating immuno-inhibition of microsomal activities by an antiserum to a rat CYP2B isoform, and by showing an excellent correlation between propofol hydroxylase and BROD activities measured in the same set of microsomes. There is good evidence that BROD is a marker activity for CYP2B11 in dog (Klekotka and Halpert 1995). Additional contributions from other CYP isoforms, however, cannot be excluded since immuno-inhibition was not complete, and, with the exception of chloramphenicol, the efficacy and specificity of the chemical inhibitors used have not been established for dog CYP isoforms.

Inhibition by diethyldithiocarbamate probably also represents an effect on CYP2B11 since diethyldithiocarbamate can inhibit CYP2 subfamilies other than CYP2E1 (Chang *et al.* 1994, Eagling *et al.* 1998). In support of this, there was a

significant although weak correlation between IC_{50} for diethyldithiocarbamate and chloramphenicol, which was not found for any other inhibitor combination. To date, no chemical inhibitor has been identified that specifically inhibits CYP2E1. Consequently diethyldithiocarbamate is used to implicate a possible role for CYP2E1 in a biotransformation reaction, which can then confirmed by other techniques, such as immuno-inhibition by a CYP2E1-specific antibody.

Inhibition by quinine was variable but in almost half of the microsomal samples (with a distribution independent of dog breed and gender) resulted in IC_{50} consistent with a role for canine CYP2D15 in addition to CYP2B11. A recent study has shown that K_i for quinine is ~ 3.1 μM in cDNA-expressed canine CYP2D15 and 0.22 μM in canine liver microsomes (Roussel *et al*. 1998). Interestingly, these latter researchers also identified CYP2D15 variants with functional differences compared with the wild-type enzyme. Such differences could explain the inconsistency in quinine inhibition that we observed between individual dogs in this study. Unfortunately, the specificity of quinine as a CYP2D15 inhibitor has yet to be established, and so involvement of CYP2D15 in propofol hydroxylation would need to be supported by immuno-inhibition studies.

All of the remaining chemical inhibitors, including furafylline, coumarin, sulphaphenazole and troleandomycin, essentially had no effect. Although these compounds were chosen because they are used as specific inhibitors of CYP subfamilies 1A, 2A, 2C and 3A (respectively) in humans, only troleandomycin has been shown to inhibit a canine CYP isoform (CYP3A12), and the specificity of this inhibition has not been determined (Ciaccio and Halpert 1989).

A recent study using liver microsomes and cDNA-expressed enzymes indicates that multiple CYP isoforms can mediate propofol hydroxylation in humans (Guitton *et al*. 1998). The rank order of activity was CYP2C9 > 2A6 > 1A1 > 2C8 > 2C18 > 2C19 > 1A2. Minimal or no activity was observed with CYP2D6, 2E1, 3A4 or 3A5. CYP2C9 was proposed as the predominant hepatic propofol hydroxylase based on expressed enzyme activity, relative abundance, correlation of microsomal metabolism to CYP2C9 immunoreactivity, and inhibition by sulphaphenazole. Unfortunately, metabolism by expressed CYP2B6, a possible human orthologue of canine CYP2B11 was not examined. Significant involvement of CYP2B6 was excluded based on a lack of microsomal inhibition by orphenadrine and low abundance of this isoform in human liver (< 1% of microsomal CYP content). However, the concentration of orphenadrine used (50 μM) was > 10-fold lower than what has been used to inhibit CYP2B6-mediated activities in other studies (Granvil *et al*. 1999). Also, more recent work indicates that CYP2B6 may be more abundant in liver than first realised, representing as much as 6% of total microsomal CYP (Stresser and Kupfer 1999). In view of these findings and the results of this study, the role of CYP2B6 in propofol hydroxylation should be re-evaluated.

As reported (Court *et al*. 1999) there were breed differences in microsomal propofol hydroxylation. Enzyme kinetic analysis showed that these differences result from lower V_{max} in greyhound compared with beagle microsomes rather than from differences in K_m. Furthermore, differences in propofol hydroxylation were also attributed to lower amounts of activity sensitive to inhibition by chloramphenicol and CYP2B1 antisera in greyhound compared with beagle microsomes. Data from male mixed-breed dog microsomes tended to span the range of data from beagle and greyhound microsomes ($\sim$ 14-fold difference in V_{max}). Together, these

findings suggest that the amount of hepatic CYP2B11 varies considerably between dogs, and that greyhound livers contain significantly less functional CYP2B11 than do beagle livers. There are possible explanations for this difference, including the presence of a deleterious mutation within the greyhound CYP2B11 gene, or perhaps there are breed-dependent differences in the extrinsic regulation of CYP2B11 expression. Further studies of CYP2B11 in beagles compared with greyhounds hopefully will establish the molecular basis for this phenomenon.

Mixed-breed dog microsomes were studied to determine whether there were gender-associated differences in propofol metabolism independent of dog breed. The investigation of the effect of gender on propofol hydroxylation was inconclusive probably because of the relatively high variability of data from these animals. Despite this, there was an apparent trend in the data (higher V_{max}, $p = 0.095$; and chloramphenicol-inhibitable activity, $p = 0.056$) that suggested microsomal content of CYP2B11 is greater in the male compared with female dogs. Until recently, relatively few studies have examined drug metabolism in both male and female dogs. More rapid *in vivo* clearance and *in vitro* biotransformation of indinavir, a viral protease inhibitor, has been reported for female compared with male beagles, which was attributed to relatively higher levels of CYP3A immunoreactive protein (by Western blot) in female dog (Lin *et al*. 1996). Evidence against this conclusion, however, comes from a study of the specific content of CYP1A1/2, 2B11, 2C21 and 3A12 measured by enzyme-linked immunosorbent assay in hepatic microsomes (Eguchi *et al*. 1996). The latter authors failed to detect any significant differences in enzyme content between the male and female beagle dog, although the number of dogs examined was relatively small. On the other hand, these same investigators in a later study reported that there was greater induction of CYP3A12 by rifampicin in the female as compared with the male dog (Nishibe *et al*. 1998).

Sexual dimorphism of a hepatic CYP2B isoform (CYP2B1) has been described in rat (Larsen *et al*. 1994). While constitutive levels of this enzyme are similar between genders, there is greater induction of CYP2B1 in the male compared with the female rat (Chang *et al*. 1997). This difference appears to be caused by a differential suppressive effect of growth hormone (GH) in the male (intermittent and pulsatile GH secretion) as compared with the female rat (continuous GH secretion) on phenobarbital induction mechanisms. This effect is not seen with CYP2B2 (equal induction) and is also dependent on the strain of rat studied (Larsen *et al*. 1994). GH does not appear to affect constitutive expression of CYP2B1 probably because constitutive levels of this enzyme are very low in rat. As mentioned previously, constitutive expression of CYP2B11 in dog is much greater (Eguchi *et al*. 1996). Consequently, a gender-dependent effect of GH secretion (or other effector) on CYP2B11 expression is more likely to be discernible in the uninduced dog than in the uninduced rat. However, as was found with different rat strains, such gender differences may depend on the dog breed evaluated. Gender-related differences in CYP2B6 expression in human livers have not been found, but expression of CYP2B6 is less than half that of CYP2B11, and like the present data, is highly variable.

In conclusion, the results of this study indicate that propofol hydroxylation is primarily mediated by CYP2B11 in dog liver microsomes. Other CYP (such as 2D15) may also contribute, but to a lesser and more variable extent. Furthermore, dog breed (and possibly gender) differences in propofol biotransformation may reflect differences in the hepatic content of functional CYP2B11.

Acknowledgements

The authors gratefully acknowledge the assistance of Dr Wendy Norman at the University of Florida, College of Veterinary Medicine, Gainesville, for obtaining the greyhound livers used in the study. We also thank Dr Ray Connelly, Surgical Research, New England Medical Center, Boston, Massachusetts, for help in procuring beagle and mixed-breed dog livers. This study was funded in part by the Hill's Pet Product College Feeding Program, Hill's Pet Products, PO Box 148, Topeka, KS, and by National Institutes of Health grants MH-34223, MH-01237 and MH-19924. M.H.C. was supported by a Special Emphasis Research Career Award (SERCA) from the National Center for Research Resources, National Institutes of Health (RR-K01-00104).

References

Chang, T. K., Anderson, M. D., Bandiera, S. M. and Bellward, G. D., 1997, Effect of ovariectomy and androgen on phenobarbital induction of hepatic CYP2B1 and CYP2B2 in Sprague-Dawley rats. *Drug Metabolism and Disposition*, **25**, 994–1000.

Chang, T. K. H., Gonzalez, F. J. and Waxman, D. J., 1994, Evaluation of triacetyloleandomycin, alpha-naphthoflavone and diethyldithiocarbamate as selective chemical probes for inhibition of human cytochromes P450. *Archives of Biochemistry and Biophysics*, **311**, 437–442.

Ciaccio, P. J., Duignan, D. B. and Halpert, J. R., 1987, Selective inactivation of the major phenobarbital inducible isozyme of dog liver cytochrome P-450. *Drug Metabolism and Disposition*, **15**, 852–856.

Ciaccio, P. J. and Halpert, J. R., 1989, Characterization of a phenobarbital-inducible dog liver cytochrome P450 structurally related to rat and human enzymes of the P450IIIA (steroid-inducible) gene subfamily. *Archives of Biochemistry and Biophysics*, **271**, 284–299.

Court, M. H., 1999, Anaesthesia of the sighthound. *Clinical Techniques in Small Animal Practice*, **14**, 38–43.

Court, M. H., Hay-Kraus, B. L., Hill, D. W., Kind, A. J. and Greenblatt, D. J., 1999, Propofol hydroxylation by dog liver microsomes: assay development and dog breed differences. *Drug Metabolism and Disposition*, **27**, 1293–1299.

Court, M. H., von Moltke, L. L., Shader, R. I. and Greenblatt, D. J., 1997, Biotransformation of chlorzoxazone by hepatic microsomes from humans and ten other mammalian species. *Biopharmaceutics and Drug Disposition*, **18**, 213–226.

Eagling, V. A., Tjia, J. F. and Back, D. J., 1998, Differential selectivity of cytochrome P450 inhibitors against probe substrates in human and rat liver microsomes. *British Journal of Clinical Pharmacology*, **45**, 107–114.

Eguchi, K., Nishibe, Y., Baba, T. and Ohno, K., 1996, Quantitation of cytochrome P450 enzymes (CYP1A1/2, 2B11, 2C21 and 3A12) in dog liver microsomes by enzyme-linked immunosorbent assay. *Xenobiotica*, **26**, 755–763.

Granvil, C. P., Madan, A., Sharkawi, M., Parkinson, A. and Wainer, I. W., 1999, Role of CYP2B6 and CYP3A4 in the *in vitro* N-dechloroethylation of (*R*)- and (*S*)-ifosfamide in human liver microsomes. *Drug Metabolism and Disposition*, **27**, 533–541.

Guitton, J., Buronfosse, T., Desage, M., Flinois, J.-P., Perdrix, J.-P., Brazier, J.-L. and Beaune, P., 1998, Possible involvement of multiple cytochrome P450 isoforms in the liver metabolism of propofol. *British Journal of Anaesthesia*, **80**, 788–795.

Halpert, J., Balfour, C., Miller, N. E., Morgan, E. T., Dunbar, D. and Kaminsky, L. S., 1985, Isozyme selectivity of the inhibition of rat liver cytochromes P-450 by chloramphenicol *in vivo*. *Molecular Pharmacology*, **28**, 290–296.

Klekotka, P. A. and Halpert, J. R., 1995, Benzyloxyresorufin as a specific substrate for the major phenobarbital-inducible dog liver cytochrome P450 (P4502B11). *Drug Metabolism and Disposition*, **23**, 1434–1435.

Larsen, M. C., Brake, P. B., Parmar, D. and Jefcoate, C. R., 1994, The induction of 5 rat hepatic P450 cytochromes by phenobarbital and similarly acting compounds is regulated by a sexually dimorphic, dietary-dependent endocrine factor that is highly strain specific. *Archives of Biochemistry and Biophysics*, **315**, 24–34.

LeGuellec, C., Lacarelle, B., Villard, P.-H., Point, H., Catalin, J. and Durand, A., 1995, Glucuronidation of propofol in microsomal fractions from various tissues and species including humans: effect of different drugs. *Anaesthesia and Analgesia*, **81**, 855–861.

Lin, J. H., Chiba, M., Chen, I. W., Nishime, J. A. and Vastag, K. J., 1996, Sex-dependent pharmacokinetics of indinavir : *in vivo* and *in vitro* evidence. *Drug Metabolism and Disposition*, **24**, 1298–1306.

Mandsager, R. E., Clarke, C. R., Shawley, R. V. and Hague, C. M., 1995, Effects of chloramphenicol on infusion pharmacokinetics of propofol in greyhounds. *American Journal of Veterinary Research*, **56**, 95–99.

Newton, D. J., Wang, R. W. and Lu, A. Y., 1995, Cytochrome P450 inhibitors. Evaluation of specificities in the *in vitro* metabolism of therapeutic agents by human liver microsomes. *Drug Metabolism and Disposition*, **23**, 154–158.

Nishibe, Y., Wakabayashi, M., Harauchi, T. and Ohno, K., 1998, Characterization of cytochrome P450 (CYP3A12) induction by rifampicin in dog. *Xenobiotica*, **28**, 549–557.

Robertson, S. A., Johnston, S. and Beemsterboer, J., 1992, Cardiopulmonary, anaesthetic and postanesthetic effects of intravenous infusions of propofol in greyhounds and non-greyhounds. *American Journal of Veterinary Research*, **53**, 1027–1032.

Roussel, F., Duignan, D. B., Lawton, M. P., Obach, R. S., Strick, C. A. and Tweedie, D. J., 1998, Expression and characterization of canine cytochrome P450 2D15. *Archives of Biochemistry and Biophysics*, **357**, 27–36.

Simons, P. J., Cockshott, I. D., Douglas, E. L., Gordon, E. A., Knott, S. and Ruane, R. J., 1991, Species differences in blood profiles, metabolism and excretion of ^{14}C-propofol after intravenous dosing to rat, dog and rabbit. *Xenobiotica*, **21**, 1243–1256.

Stresser, D. M. and Kupfer, D., 1999, Monospecific antipeptide antibody to cytochrome P-450 2B6. *Drug Metabolism and Disposition*, **27**, 517–525.

Von Moltke, L. L., Greenblatt, D. J., Harmatz, J. S. and Shader, R. I., 1993, Alprazolam metabolism *in vitro*: Studies of human, monkey, mouse and rat liver microsomes. *Pharmacology*, **47**, 268–276.

Zoran, D. L., Riedesel, D. H. and Dyer, D. C., 1993, Pharmacokinetics of propofol in mixed-breed dogs and greyhounds. *American Journal of Veterinary Research*, **54**, 755–760.

XENOBIOTICA, 2000, VOL. 30, NO. 6, 589–607

Expression and induction of CYP1A1/1A2, CYP2A6 and CYP3A4 in primary cultures of human hepatocytes: a 10-year follow-up

V. MEUNIER, M. BOURRIÉ, B. JULIAN, E. MARTI, F. GUILLOU, Y. BERGER and G. FABRE*

Sanofi Recherche, Department of Preclinical Metabolism and Pharmacokinetics, 371 Rue du Professeur Joseph Blayac, F-34184 Montpellier, Cédex 4, France

Received 24 November 1999

1. The aims were to refine experimental conditions (using 76 human hepatocyte preparations) in terms of the selection of enzyme inducers and their optimal concentration, the treatment duration with inducers and the choice of specific cytochrome P450 isoform(s) probes to optimize the use of primary hepatocytes for predicting the potential induction by new chemical entities of cytochrome P450 isoforms *in vivo* in man.

2. In the absence of any inducer, basal cytochrome P450 isoform(s)-mediated activities decreased to 20% of their initial activity (end of the seeding period) by 72–96 h. In contrast, UGT-dependent enzyme activities remained at a constant level (±20%) up to the fifth day of culture.

3. β-Naphthoflavone, at an optimal concentration of 50 μM and after a 3-day treatment, specifically and potently induced 7-ethoxyresorufin (10.4±10.4-fold, $n = 74$) and phenacetin (6.6±6.4-fold, $n = 60$) *O*-deethylation processes, markers for CYP1A1 and CYP1A2 isoforms respectively. Only a 2-fold increase was noted following treatment with 2 mM phenobarbitone, whereas dexamethasone and rifampicin had no effect at all.

4. A 3-day treatment of human hepatocytes with 50 μM dexamethasone was associated with a major induction of both coumarin 7-hydroxylation (9.4±11.4-fold, $n = 49$) and nifedipine dehydrogenation (4.7±3.8-fold, $n = 61$), markers for CYP2A6 and CYP3A4 respectively. Phenobarbitone, however, exhibited a broad but moderate inducing effect on 7-ethoxyresorufin (2.2±1.5-fold, $n = 55$) and phenacetin (1.7±0.9-fold, $n = 54$) *O*-deethylation, coumarin 7-hydroxylation (3.9±9.2-fold, $n = 50$) and nifedipine dehydrogenation (2.1±2.0-fold, $n = 47$).

5. K_m obtained for the different cytochrome P450 isoform substrates in untreated hepatocytes were in the same range of magnitude that those determined on human hepatic microsomal fractions. Enzyme induction processes were characterized by a large increase in apparent V_{max} whereas apparent K_m were not affected.

6. These studies demonstrate that human hepatocytes in primary culture can respond specifically and quantitatively to model inducers. This *in vitro* system offers a useful approach to study the regulation of human hepatic biotransformation activities and should facilitate the demand for a reproducible method for addressing cytochrome P450 induction.

Introduction

It is now well accepted by both regulatory authorities and the pharmaceutical industry that *in vitro* models provide valuable information to investigate which enzyme/isoform systems are involved in the production of a single metabolite, and what is the impact (inhibition, induction or repression) of the development candidate on various cytochrome P450-dependent reactions (Wrighton and Stevens 1992). Whereas *in vitro* tools and models for the characterization of cytochrome P450 isoforms (Nelson *et al*. 1993) involved in the formation of a specific metabolite are now available and currently used (Tucker 1992, Birkett *et al*. 1993, Miners *et al*.

* Author for correspondence; e-mail: gerard.fabre@sanofi.com

Xenobiotica ISSN 0049–8254 print/ISSN 1366–5928 online © 2000 Taylor & Francis Ltd
http://www.tandf.co.uk/journals

1994, Rodrigues 1994), such as specific isoforms inhibitors (including their specificity and range of selectivity), cytochrome P450 isoform-mediated reactions or cytochrome P450 isoform engineered systems, models for investigating enzyme induction still require further development. Although induction of monooxygenase activities may be of clinical relevance (Wadhwa *et al.* 1987, Pichard *et al.* 1990), the effects of xenobiotics on the expression and induction of cytochrome P450 isoforms have been difficult to explore for obvious ethical reasons. In the past few years, different laboratories reported that human hepatocytes in primary culture retain not only drug-metabolizing activities (Fabre *et al.* 1988a, Ekins *et al.* 1996, Guillouzo 1997, Iwatsubo *et al.* 1997), but also the ability to increase specific cytochrome P450 activities upon incubation with inducers (Combalbert *et al.* 1989, Daujat *et al.* 1990, Fabre *et al.* 1990, Daujat *et al.* 1991, Maurice *et al.* 1992, Donato *et al.* 1995, Kocarek *et al.* 1995, Li *et al.* 1995, Li 1997, Silva *et al.* 1998). Although most of these latter studies have amply demonstrated the utility of primary cultures of human hepatocytes as an *in vitro* model for investigating cytochrome P450 isoform(s) inducibility, much less information is available concerning the choice of enzyme inducers, their optimal concentration and the shortest time for achieving a maximal induction response.

To characterize this model better, the behaviour of basal activities of CYP1A1/A2, 2A6 and 3A4 was examined as a function of culture time, as well as response to model cytochrome P450 inducers, inducer concentration and treatment duration. These latter activities were monitored using specific cytochrome P450 isoform-mediated reactions (Bourrié *et al.* 1996), and were generated between 1987 and 1998 from 76 different human hepatocyte preparations.

Materials and methods

Chemicals

The drug substrates, specific metabolites and inducers used in this study were obtained from different sources as follows: nifedipine and its oxidized metabolite (i.e. BAY b-4759) were a kind gift of Bayer. Coumarin, dexamethasone, 7-hydroxycoumarin, 3-methylcholanthrene, α-naphthol, β-naphthoflavone, β-nicotinamide adenine dinucleotide, reduced form (β-NADPH), phenacetin, phenobarbitone, resorufin, rifampicin, testosterone, troleandomycin, uridine 5′-diphosphoglucuronic acid (UDPGA), 4-acetamidophenol and α-naphthol-β-D-glucuronide were obtained from Sigma-Aldrich-Fluka (St-Quentin Falavier, France), and 7-ethoxyresorufin from Pierce (Bezons, France).

[^{14}C]-lauric acid (57 mCi/mmol) and [^{14}C]-testosterone (46 mCi/mmol) were from Amersham (Les Ulis, France). [^{3}H]-digitoxigenine monodigitoxoside (dt1) was generated following a 2-h hydrolysis of [^{3}H]-digitoxine (from New England Nuclear, Le Blanc-Mesnil, France; 18.8 Ci/mmol) at 37 °C in the presence of 0.2 N HCl (v/v). After neutralization with NaOH (0.2 N), the mixture of digitoxine, digitoxigenine, mono- and di-digitoxoside was fractionated by HPLC on a μBondapak C18 column using a linear elution gradient of 25/75 to 40/60 bidistilled water/acetonitrile (v/v) at a 2.2 ml/min flow rate. Dt1 was collected, purified and used as a radioactive tracer for enzymatic reactions. All other chemicals and reagents used were of the highest commercially available quality.

Human hepatocyte isolation and culture

Fresh human liver tissues (n = 76) were obtained from donors undergoing partial hepatectomies (termed 'HTL-x', n = 70) and from unused liver portions from patients undergoing liver transplants (termed 'FH-x', n = 6) (table 1). Olinga *et al.* (1998) reported that in terms of metabolic capacity, hepatocytes obtained following perfusions of liver lobes from partial hepatectomy or from transplantation could be used in the same study without consideration of the procurement of the tissue.

Tissue samples were transported from the operating room in ice-cold University of Wisconsin solution at 4 °C. Hepatocytes were obtained according to the two-step collagenase perfusion technique described by Fabre *et al.* (1988a). This perfusion technique allows several billions of cells to be obtained, up to 4×10^9 hepatocytes according to the size of the hepatic sample, with a viability $> 85\%$ (as measured by trypan blue exclusion).

Table 1. Characteristics of patients from whom samples of livers were obtained and hepatocytes prepared.

Patients	Sex	Age (years)	Pathology	Patients	Sex	Age (years)	Pathology
FH−1	M	25	none	HTL−71	F	70	hepatocarcinoma
FH−3	F	19	none	HTL−73	F	59	rectum adenocarcinoma
FH−4	F	47	none	HTL−74	F	55	hepatic adenoma
FH−6	F	55	none	HTL−75	F	55	pancreatic carcinoma
FH−7	M	30	none	HTL−76	F	65	colon adenocarcinoma
FH−68	M	36	amyeloid neuropathie	HTL−77	F	62	colon adenocarcinoma
HTL−8	M	63	rectum adenocarcinoma	HTL−78	F	50	bile duct carcinoma
HTL−9	M	45	rectum adenocarcinoma	HTL−79	F	24	hepatic adenoma
HTL−11	F	43	sigmoid adenoma	HTL−84	F	70	colon adenocarcinoma
HTL−14	M	67	rectum adenocarcinoma	HTL−87	F	66	colon adenocarcinoma
HTL−21	M	na	na	HTL−88	M	68	colon adenocarcinoma
HTL−23	F	77	colon adenocarcinoma	HTL−89	F	42	hepatocarcinoma
HTL−26	F	47	colon adenocarcinoma	HTL−90	F	42	hepatic adenoma
HTL−33	F	77	hepatocarcinoma	HTL−91	F	60	hepatic adenoma
HTL−36	M	46	colon adenocarcinoma	HTL−92	F	68	colon adenocarcinoma
HTL−38	M	32	liver adenoma	HTL−93	F	43	colon adenocarcinoma
HTL−39	F	32	angioma	HTL−94	F	68	colon adenocarcinoma
HTL−40	F	64	colon adenocarcinoma	HTL−100	F	30	hepatic adenoma
HTL−42	F	70	colon adenocarcinoma	HTL−101	M	58	colon adenocarcinoma
HTL−46	F	55	colon adenocarcinoma	HTL−102	F	60	colon adenocarcinoma
HTL−47	F	69	hepatocarcinoma	HTL−103	F	63	colon adenocarcinoma
HTL−48	M	49	rectum adenocarcinoma	HTL−106	na	na	na
HTL−49	M	51	colon adenocarcinoma	HTL−107	M	73	colon adenocarcinoma
HTL−51	F	31	hepatoma	HTL−108	F	70	hepatic adenoma
HTL−52	F	51	colon adenocarcinoma	HTL−109	M	50	colon adenocarcinoma
HTL−53	na	na	bile duct carcinoma	HTL−110	M	58	colon adenocarcinoma
HTL−54	F	65	colon adenocarcinoma	HTL−111	F	61	hepatic adenoma
HTL−55	F	53	bile duct carcinoma	HTL−112	F	49	hepatocarcinoma
HTL−56	F	73	bile duct carcinoma	HTL−114	F	46	hepatic adenoma
HTL−58	F	33	angioma	HTL−115	M	71	colon adenocarcinoma
HTL−59	F	53	rectum adenocarcinoma	HTL−120	M	71	colon adenocarcinoma
HTL−60	F	50	hepatocarcinoma	HTL−121	F	47	breast adenocarcinoma
HTL−64	F	32	melanoma	HTL−122	M	61	colon adenocarcinoma
HTL−65	M	64	colon adenocarcinoma	HTL−124	na	na	na
HTL−67	F	41	colon adenocarcinoma	HTL−128	F	52	colon adenocarcinoma
HTL−68	F	41	colon adenocarcinoma	HTL−139	M	71	colon adenocarcinoma
HTL−69	M	65	rectum adenocarcinoma	HTL−140	F	61	colon adenocarcinoma
HTL−70	F	22	na	HTL−141	M	66	rectum adenocarcinoma

na: Not available.

Following different washing steps (filtration through 150 and 250 μm nylon mesh, and low-speed centrifugation at 50 *g* for 5 min, 3-fold), freshly isolated hepatocytes were plated on collagen-coated plastic dishes in a chemically defined medium described by Isom and Georgoff (1984), consisting of a 50/50 (v/v) mixture of Ham F12/Williams' E medium supplemented with 10% decomplemented foetal calf serum, 10 mg/l insulin, 0.8 mg/l glucagon and antibiotics (100 IU penicillin, 100 μg/ml streptomycin). After 4–6 h of incubation at 37 °C in a 5% CO_2 and 100% humidified atmosphere, a period during which hepatocytes attached to the collagen–matrix, the plating medium was removed and replaced by the same serum-free culture medium supplemented with HEPES (3.6 g/l), ethanolamine (4 mg/l), transferrin (10 mg/l), linoleic acid–albumin (1.4 mg/l), glucose (252 mg/l), sodium pyruvate (44 mg/l), ascorbic acid (50 mg/l), arginine (104 mg/l) and L-glutamine (0.7 g/l).

Human hepatocyte treatment

The enzyme inducers were directly added to the incubation medium. Regardless of the final concentration investigated, the final solvent (DMSO) concentration never exceeded 0.1% (v/v). DMSO was used for the solubilization of different enzyme inducers, except for phenobarbitone that was dissolved in bidistilled water. Since preliminary studies did not demonstrate any improvement in either residual enzyme activity or enzyme induction, in comparison with DMSO, control hepatocytes were

treated with DMSO (0.1%). Culture medium supplemented with enzyme inducers was renewed daily over the entire period of experimentation. For determining the initial turnover rate of the different cytochrome P450 isoforms (i.e. time '0' corresponding to the end of the plating period), hepatocytes were immediately scraped into phosphate buffered saline at 4 °C and stored at −80 °C until further analysis.

Preparation of hepatocyte microsomal fractions

After treatment of human hepatocytes with the various enzyme inducers, hepatocytes from eight to 12 100-mm diameter plastic dishes ($80–120 \times 10^6$ hepatocytes were theoretically plated) were scraped into phosphate buffered saline at 4 °C. Following centrifugation at 200*g* for 10 min, and removal of the supernatant, hepatocyte pellets were immediately frozen in dry ice and stored at −80 °C until further use. After thawing at 4 °C and homogenization in Tris acetate buffer (0.1 M, pH 7.4), hepatocyte homogenates were ultracentrifuged for 90 min at 105 000*g* and 4 °C. The protein pellet was suspended in 0.1 M KH_2PO_4 buffer (pH 7.4) containing 0.1 mM EDTA and 20% glycerol (v/v), and frozen at −80 °C until use (Fabre *et al*. 1988b).

Protein concentration and enzyme assays

Protein concentration was determined using the method of Bradford (Pollard *et al*. 1978). For each investigated substrate (Bourrié *et al*. 1996), preliminary enzyme experiments were performed to determine incubation conditions under which metabolite formation was maximal, i.e. V_{max}. The enzymatic rate was determined by the quantity of metabolite formed per unit time and per mg protein. For determination of K_m and $V_{max,}$ hepatocyte microsomal fractions were incubated with increasing substrate concentrations and metabolic rates were analysed by non-linear regression analysis of data using the EnzPack-3 software (BioSoft). K_m and V_{max} were obtained from either specific microsomal fractions obtained from a single hepatocyte preparation, or from a pool of microsomal fractions obtained from different hepatocytes preparations ($n = 30$).

Incubation of CYP isoform substrates with hepatocyte microsomal fractions was carried out at 37 °C in 0.1 M KH_2PO_4 buffer (pH 7.4), under continuous stirring. 7-Ethoxyresorufin *O*-deethylation, an enzyme reaction catalysed by CYP1A1/1A2 isoforms, was evaluated over 2–10 min following incubation of human hepatocyte microsomes (0.1 mg/ml) in the presence of 1 mM NADPH, with 5 μM 7-ethoxyresorufin. The appearance of the resorufin derivative was evaluated with respect to time, by a spectrofluorimetric method (Burke *et al*. 1985).

Phenacetin *O*-deethylation (Sesardic *et al*. 1988), an enzyme reaction specifically catalysed by CYP1A2 (Butler *et al*. 1989) was determined following a 30-min incubation of human hepatocyte microsomes (final protein concentration = 1 mg/ml) with 200 μM phenacetin and 1 mM NADPH. At the end of the incubation, 2-min heat-inactivated proteins were removed by centrifugation (2500*g* for 10 min) and supernatant fluid was directly analysed by HPLC (C_{18} μBondapak column; flow rate = 1 ml/min; UV absorbance = 245 nm; 0.02 M KH_2PO_4 buffer at pH 4/acetonitrile; 10–25% acetonitrile over a 10-min linear gradient, followed by a 1-min linear gradient from 25 to 70% acetonitrile).

Coumarin 7-hydroxylation, an enzyme reaction specifically catalysed by CYP2A6 (Pelkonen *et al*. 1989) was assayed using the method previously described by Creaven *et al*. (1965). Human hepatocyte microsomes (final concentration = 0.1 mg/ml) were incubated for 10 min in 1 mg/ml bovine serum albumin-supplemented phosphate buffer, with 10 μM coumarin in the presence of 1 mM NADPH. The enzymatic reaction was stopped by addition of a one-fifth volume of trichloroacetic acid (solution at 10% in bidistilled water). The precipitated proteins were removed by centrifugation and 9 vols of 0.4 M glycine buffer (adjusted at pH 10.4 with 10 N NaOH) were added to the supernatant fluid. 7-Hydroxycoumarin formed was determined fluorometrically (λ_{ex} = 390 nm; λ_{em} = 450 nm) relative to a standard curve of authentic 7-hydroxycoumarin.

Nifedipine dehydrogenation was measured as previously described by Guengerich *et al*. (1986). Human hepatocyte microsomes (final protein concentration = 1 mg/ml) were incubated for 30 min with 200 μM nifedipine and 1 mM NADPH. The proteins that precipitated with one-half volume of a acetonitrile/20% trichloroacetic acid mixture (50/50), were removed by centrifugation (2500*g* for 10 min) and the clear supernatant was analysed by HPLC (ODS-2 column, 5 μm particle size; flow rate = 1.5 ml/min; UV absorbance = 254 nm; 0.1% diethylamine buffer adjusted at pH 6.0 with acetic acid/acetonitrile, 65/35 v/v).

Lauric acid 12-hydroxylation was evaluated following incubation of hepatocyte microsomal fractions (final protein concentration = 0.5 mg/ml) for 30 min with 200 μM [^{14}C]-lauric acid and 1 mM NADPH. The proteins that precipitated with one-half volume of acetonitrile, were removed by centrifugation (2500*g* for 10 min) and the clear supernatant was analysed by HPLC (C_{18} μBondapak column, 10 μm particle size; flow rate = 1 ml/min; on-line radioactive detection; 0.1% acetic acid/acetonitrile; 30% acetonitrile isocratically over 10 min followed by a 20-min linear gradient up to 90% acetonitrile).

Incubation of UGT isoform-substrates with hepatocyte microsomal fractions, was carried out at 37 °C in 0.1 M Tris HCl buffer supplemented with 5 mM $MgCl_2$ buffer (pH 7.4), under continuous stirring.

[^{3}H]-Dt1 (10 μM final concentration) was incubated for 30 min with 2 mg/ml hepatocyte microsomal

fractions and 3 mM UDPGA. Enzyme reactions were stopped by addition of 1 vol. ethyl alcohol. Following extraction of unmetabolized dt1 by 2 vols chloroform (twice), dt1-glucuronide was quantified by liquid scintillation counting in the aqueous phase.

α-Naphthol (500 μM final concentration) was incubated for 30 min with 0.1 mg/ml hepatocyte microsomal fractions and 3 mM UDPGA, in a total volume of 0.5 ml. Enzyme reactions were stopped with the addition of 170 μl 0.4 M trichloroacetic acid/0.6 M glycine (v/v). Unmetabolized α-naphthol was removed following extraction with 5 ml dichloromethane and centrifugation at 3000*g* for 10 min. Following addition of 1.6 ml 0.35 M Na_2HPO_4 to 0.4 ml aqueous phase, α-naphthol-β-D-glucuronide was determined fluorometrically (λ_{ex} = 290 nm; λ_{em} = 330 nm) relative to a standard curve of authentic α-naphthol-β-D-glucuronide.

[^{14}C]-testosterone (500 μM final concentration) was incubated for 30 min with 2 mg/ml hepatocyte microsomal fractions and 3 mM UDPGA, in a total volume of 0.5 ml. Enzyme reactions were optimized with lubrol (0.1 mg/mg of protein). At the end of the incubation period, unmetabolized testosterone was removed following extraction with 8 ml dichloromethane and centrifugation at 3000*g* for 10 min, and testosterone-glucuronide was quantified by liquid scintillation counting of the aqueous phase.

Immunoblot analysis

Cytochrome P450 isoforms CYP1A2 and CYP3A4 were quantified by immunoblot analysis of electrophoretically separated microsomal proteins. Usually 5–10 μg proteins were submitted to electrophoresis and the immunoblots were developed in the presence of 0.1 mg/ml specific IgG (anti-CYP1A2 and anti-CYP3A6 respectively) as described (Daujat *et al*. 1990). The methods for preparation of both the polyclonal antibody directed against CYP3A6 and of the monoclonal antibody directed against CYP1A2, as well as the purification of CYP1A2 and CYP3A4 (also termed HLp or cytochrome P450 cyclosporin A oxidase) standards, have been described (Daujat *et al*. 1987, 1990). Results are reported in terms of staining intensity

Results

Effect of increasing enzyme inducer concentrations on CYP-mediated enzyme activities

CYP1A1/A2 isoform(s). Human hepatocytes were cultured over 3 days with increasing enzyme inducers concentrations and specific enzyme activities towards different cytochrome P450 isoforms were monitored. In figure 1, the effects of increasing β-naphthoflavone (ranging from 5 to 100 μM) and phenobarbitone (ranging from 250 μM to 4 mM) concentrations, on CYP1A activity, using phenacetin *O*-deethylation as a specific enzyme reaction are illustrated. In FH-4 human hepatocyte preparations, the turnover rate for phenacetin *O*-deethylation was ~ 0.2 nmol/min/mg. This activity was increased in a concentration-dependent manner from 5 to 50 μM β-naphthoflavone, the highest increase, i.e. 16-fold increase, being observed at 50 μM. A 8-fold increase in enzyme activity was already apparent at 5 μM. At the highest β-naphthoflavone concentration tested (100 μM), a large decrease in induction was observed, which is probably associated with β-naphthoflavone cytotoxicity. Similar results were obtained, using 7-ethoxyresorufin *O*-deethylation as specific enzyme activity (data not shown). Of particular interest was the observation that even at 4 mM phenobarbitone concentration, phenacetin *O*-deethylation was only slightly increased, i.e. 2-fold, suggesting that this enzyme reaction was a good marker for CYP1A-catalytic activity.

In addition to CYP1A-substrates (phenacetin and 7-ethoxyresorufin), lauric acid 12-hydroxylation was also evaluated. Whichever the inducer and its final concentration, lauric acid 12-hydroxylation was only slightly, either increased (0.88 nmol/min/mg in 4 mM phenobarbitone-treated cells versus 0.55 nmol/min/mg in controls) or decreased (0.37 nmol/min/mg in 50 μM β-naphthoflavone-treated cells). Lauric acid 12-hydroxylation was also not induced following a 3-day incubation of human hepatocytes with either clofibrate (50 to 500 μM) or di(2-ethylhexyl)phthalate (50 μM).

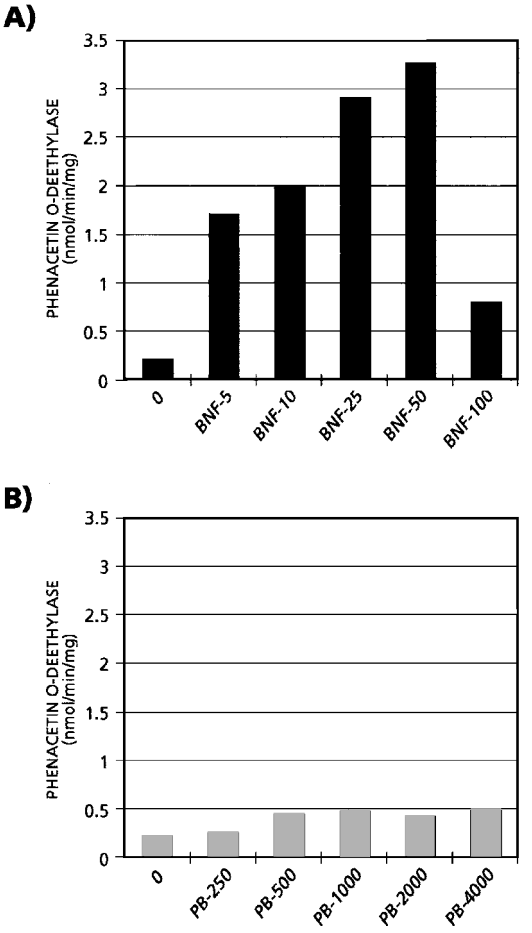


Figure 1. Representative effect of a 3-day treatment of human hepatocytes with increasing either β-naphthoflavone (A) or phenobarbitone (B) concentrations, on phenacetin *O*-deethylation process. Human hepatocytes in primary culture (preparation FH-4) were incubated for 3 days with either β-naphthoflavone (5–100 μM) or phenobarbitone (0.5–4 mM). Cells were then scraped, microsomal fractions prepared and the phenacetin *O*-deethylation rate determined.

The Michaelis–Menten characteristics of 7-ethoxyresorufin *O*-deethylation were determined on microsomal fractions (preparation HTL-90) prepared from either control hepatocytes or hepatocytes treated for 3 days with 50 μM b-naphthoflavone. Similar K_m were obtained (0.35 μM in control versus 0.50 μM in β-naphthoflavone-treated hepatocytes), whereas V_{max} were 2.3 nmol/min/mg and 25 nmol/min/mg in control and β-naphthoflavone-treated hepatocytes respectively.

CYP2A6 isoform. The Michaelis–Menten characteristics of coumarin 7-hydroxylation were determined on microsomal fractions prepared from either untreated or inducer-treated hepatocytes. In preparation HTL-56, hepatocytes were treated over 3 days in the absence or the presence of 50 μM dexamethasone. Similar K_m were obtained (1.22 μM in control versus 1.10 μM in dexamethasone-treated hepatocytes), whereas V_{max} were 0.28 nmol/min/mg and 1.14 nmol/min/mg in control and dexamethasone-treated hepatocytes respectively. In preparation HTL-69, similar

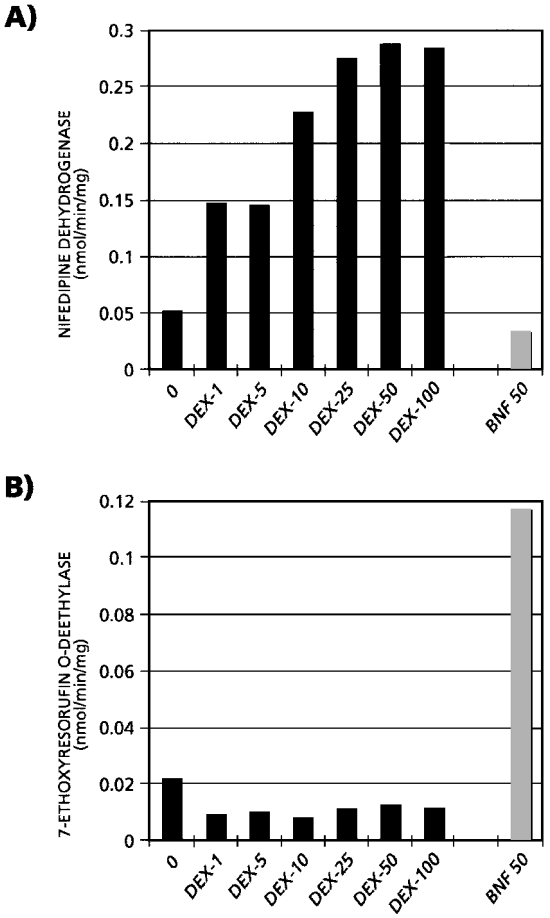


Figure 2. Representative effect of a 3-day treatment of human hepatocytes with either increasing dexamethasone concentrations, or 50 μM β-naphthoflavone, and nifedipine oxidation (A) and 7-ethoxyresorufin *O*-deethylation (B) processes were monitored. Human hepatocytes in primary culture (preparation HTL-48) were incubated for 3 days with either increasing dexamethasone concentrations (1–100 μM range) or 50 μM β-naphthoflavone. Cells were then scraped, microsomal fractions prepared, and nifedipine dehydrogenation and 7-ethoxyresorufin *O*-deethylation rates determined.

K_m were also obtained in control (0.37 μM) and phenobarbitone-treated hepatocytes (0.46 μM), whereas V_{max} were 0.017 nmol/min/mg and 0.038 nmol/min/mg in control and phenobarbitone-treated hepatocytes respectively.

Following β-naphthoflavone-treatment, no changes in either K_m or V_{max} were observed.

CYP3A4 isoform. Human hepatocytes (preparation HTL-48) were cultured over 3 days in the absence, or the presence of either increasing dexamethasone concentrations (ranging from 1 to 100 μM) or 50 μM β-naphthoflavone. Both nifedipine dehydrogenation and 7-ethoxyresorufin *O*-deethylation activities were monitored (figure 2). In this preparation, the turnover rate for nifedipine dehydrogenation was about 0.05 nmol/min/mg. This activity was increased in a concentration-dependent manner from 1 to 25 μM dexamethasone. The highest increase (6-fold), was observed for concentrations ranging between 25 and 100 μM.

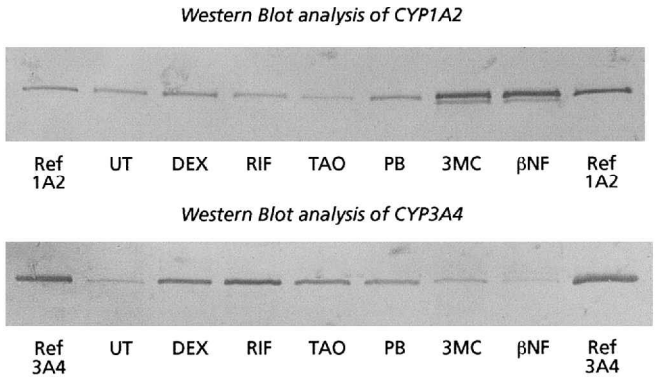


Figure 3. Western blot analysis of CYP1A2 (A) and CYP3A6 (B) orthologous isoforms following a 5-day treatment of human hepatocytes with various enzyme inducers. Human hepatocytes in primary culture (preparation FH-1) were incubated for 5 days in the absence (UT) or the presence of either 50 μM dexamethasone (DEX), rifampicin (RIF), troleandomycin (TAO), 3-methylcholanthrene (3MC), β-naphthoflavone (βNF) or 2 mM phenobarbitone (2 mM). Cells were then scraped, microsomal fractions prepared and proteins (40 μg) were immunoblotted using anti-CYP1A2 monoclonal (A) and anti-CYP3A6 polyclonal (B) antibodies.

At the lowest concentration used (1 μM), a 3-fold increase in nifedipine dehydrogenation was already apparent. Even following a 3-day treatment with 50 μM β-naphthoflavone, no increase at all in this enzyme activity was demonstrated, whereas 7-ethoxyresorufin and phenacetin *O*-deethylase activities were increased by 5.3-(figure 2) and 2.8-fold (data not shown) respectively.

Effect of increasing enzyme inducer concentrations on CYP isoform expression

Human hepatocytes in primary culture (preparation FH-1) were incubated for 5 days after cell seeding with different well-known enzyme inducers of the CYP1A gene subfamily such as 3-methylcholanthrene (50 μM) and β-naphthoflavone (50 μM), and of CYP3A gene subfamily such as dexamethasone (50 μM), rifampicin (50 μM), phenobarbitone (2 mM) and troleandomycin (50 μM). After the fifth day of treatment, hepatocytes were scraped, hepatocyte microsomal fractions prepared, and analyzed by immunoblotting with anti-CYP1A and anti-CYP3A6 antibodies (figure 3). All hepatocyte samples, either untreated or treated with potent enzyme inducers, reacted with both antibodies.

When immunoblots were developed with a monoclonal antibody directed against CYP1A2, a single immunoreactive band was detected in untreated hepatocytes co-migrating with a CYP1A2 standard on SDS-PAGE, consistent with previous studies that reported that CYP1A2 was constitutively present in human liver (Daujat *et al.* 1990, McKinnon *et al.* 1991). This immunoreactive isoform remained unchanged following treatment of hepatocytes with rifampicin and troleandomycin, and was only slightly increased following treatment with dexamethasone and phenobarbitone. However, following treatment of hepatocytes with aromatic polycyclic hydrocarbons, not only was a large increase in constitutive CYP1A2 observed, but also the appearance of an additional band was demonstrated, exhibiting characteristics of CYP1A1 (Daujat *et al.* 1990).

When the same immunoblots were developed with a polyclonal antibody directed against CYP3A6 (orthologous to CYP3A4; figure 3, bottom), a well-known

glucocorticoid and macrolide antibiotic-inducible isoform, a single band was visualized co-migrating with authentic CYP3A4. Quantitative analyses of the blot indicated that hepatocytes pretreated with rifampicin and dexamethasone had the highest amount of CYP3A4, whereas phenobarbitone and troleandomycin were moderate inducers.

Effect of treatment duration on the induction of CYP-mediated enzyme activity

The effect of enzyme inducers on the behaviour of CYP isoform(s)-mediated activities was investigated. As illustrated in figures 4 and 5, a decrease in basal enzyme activity was noted for all hepatocyte preparations and specific enzyme activities monitored. In general a 30–60% decrease in enzyme activity was observed between time '0' corresponding to the end of the plating period, i.e. 4–6 h following obtention of hepatocytes at the end of the dissociation period, and time '24 h'. Basal enzyme activities continued to decrease down to 10–20% of initial enzyme activity by the third or fourth day of culture.

Following treatment of hepatocytes with the different enzyme inducers, a decrease in all basal activities was also observed over the first 24 h of culture, followed by a large increase in the enzyme activity specifically regulated by the inducer used (figure 4). Hence, in both hepatocytes preparations, a decrease in 7-ethoxyresorufin and phenacetin *O*-deethylase activities was observed following treatment of hepatocytes with dexamethasone and phenobarbitone, whereas a large increase in these enzyme activities was observed following treatment with β-naphthoflavone. For coumarin 7-hydroxylation and nifedipine dehydrogenation, an increase in enzyme activities was only observed following treatment of hepatocytes with 50 μM dexamethasone. After a 3-day treatment with the respective specific enzyme inducer, all enzyme activities were much higher than those determined in untreated hepatocytes either at time '0' of the culture or at time '72 or 96 h'.

In addition to the standard enzyme inducers used, the effects of 3-methylcholanthrene and rifampicin were also investigated (figure 5). 3-Methylcholanthrene and rifampicin specifically and selectively induced 7-ethoxyresorufin *O*-deethylation and nifedipine dehydrogenation respectively.

Inter-individual variability in CYP-mediated enzyme activity inducibility

In figure 6, the effects of different enzyme inducers on specific CYP-mediated enzyme activities are summarized. 7-Ethoxyresorufin *O*-deethylation was largely induced following treatment with β-naphthoflavone with increases relative to control ranging between 2- and 37.3-fold with a mean at 10.4 ± 10.4-fold ($n = 74$). No increase at all was observed following treatment with either rifampicin or dexamethasone, whereas a 2.2 ± 1.5-fold increase was observed following treatment with phenobarbitone. In a similar manner, both rifampicin and dexamethasone have no effect on phenacetin *O*-deethylation, whereas a 1.7 ± 0.9-fold increase was observed following treatment with phenobarbitone. Following treatment with β-naphthoflavone, increases in phenacetin *O*-deethylation relative to control ranged between 1.8- and 24.4-fold with a mean at 6.6 ± 6.4-fold ($n = 60$).

Similar induction was obtained using either 7-ethoxyresorufin or phenacetin as specific substrates. These data clearly demonstrated that both substrates were specific markers for both CYP1A1 and CYP1A2 isoforms.

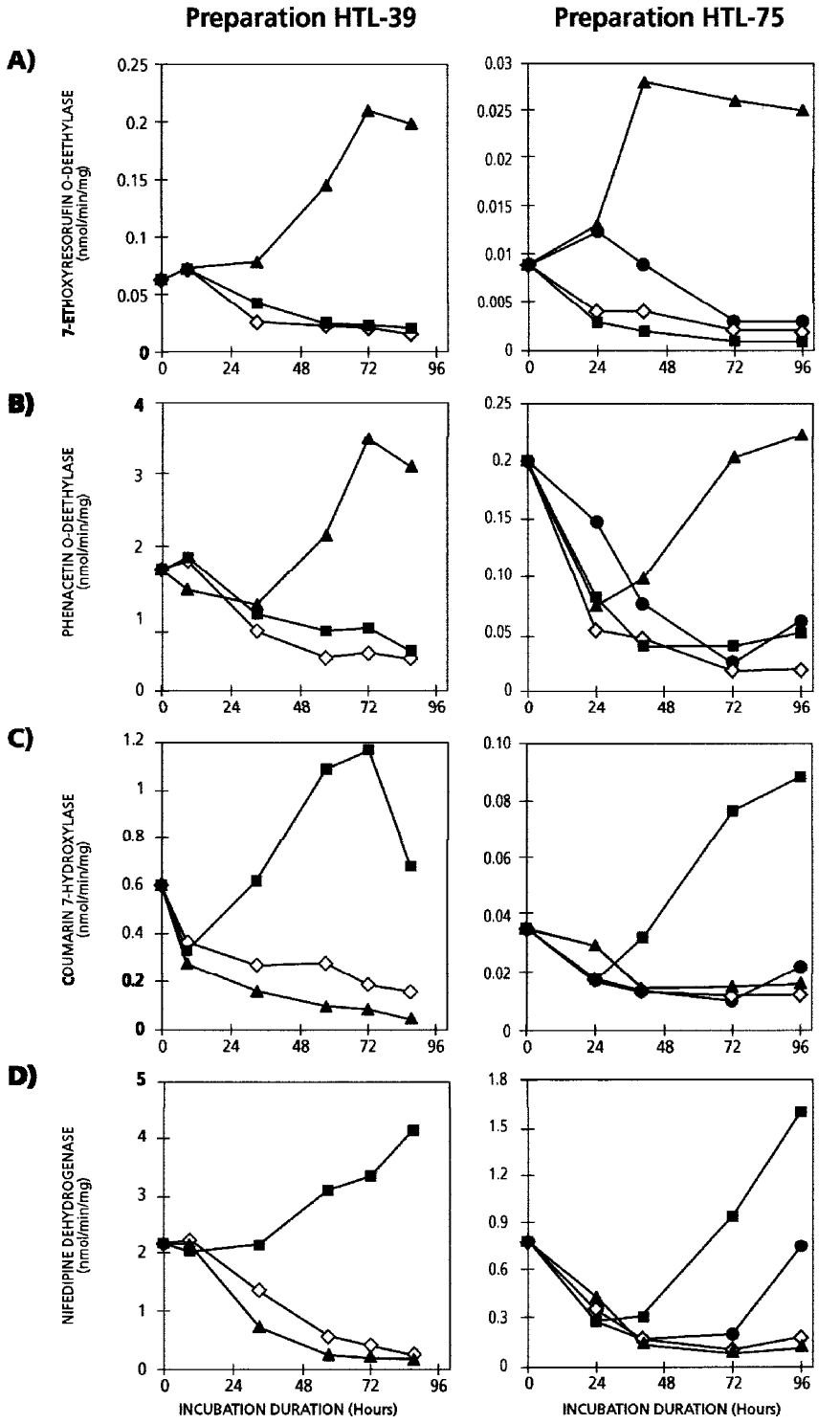


Figure 4. Time-dependent effect of enzyme inducers on 7-ethoxyresorufin (A) and phenacetin (B) *O*-deethylation, coumarin 7-hydroxylation (C) and nifedipine oxidation (D) processes using primary cultures of human hepatocytes. Human hepatocytes in primary culture (preparations HTL-39

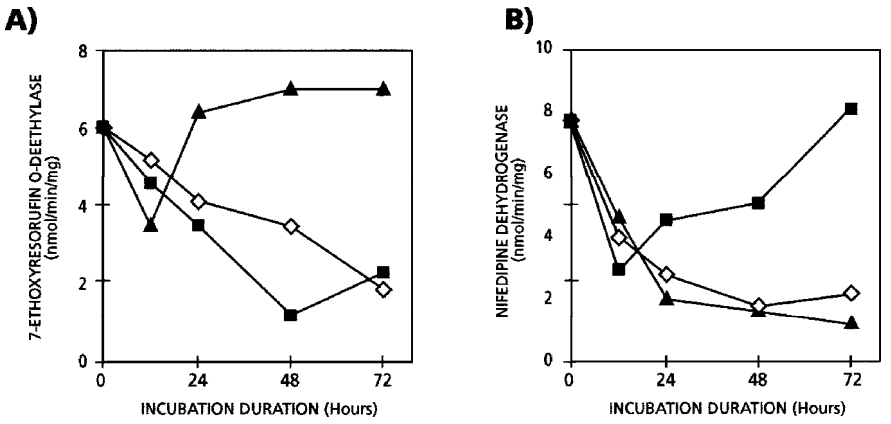


Figure 5. Time-dependent effect of enzyme inducers (rifampicin and 3-methylcholanthrene) on 7-ethoxyresorufin *O*-deethylation (A) and nifedipine oxidation (B) processes using primary cultures of human hepatocytes. Human hepatocytes in primary culture (preparation HTL-14) were incubated over 3 days with DMSO alone (◇), 50 μM rifampicin (■) or 50 μM 3-methylcholanthrene (▲). Cells were then scraped, microsomal fractions prepared, and 7-ethoxyresorufin *O*-deethylation and nifedipine dehydrogenation rates determined.

Coumarin 7-hydroxylation was not increased but rather decreased following treatment of hepatocytes with rifampicin and β-naphthoflavone. However, large increases in enzyme activity were observed following treatment of hepatocytes with dexamethasone and phenobarbitone, with induction factors of 9.4 ± 11.4-fold (n = 49) and 3.9 ± 9.2-fold (n = 50) respectively. Although mean demonstrated that both dexamethasone and phenobarbitone induced CYP2A6-mediated activity, large interindividual differences were observed. Hence, coumarin 7-hydroxylation was induced by dexamethasone in the 49 human hepatocytes preparations investigated with individual increases ranging between 1.5- and 53.7-fold relative to control. By contrast, coumarin 7-hydroxylation was only increased in 22 of 50 human hepatocytes preparations by phenobarbitone, the highest increase being 57.5-fold compared with control. Of particular interest were the differences in CYP2A6 induction from one preparation to another. In human hepatocyte preparation HTL-114, coumarin 7-hydroxylation was 53.7-fold increased following dexamethasone-treatment, whereas no increase (1.2-fold) was observed following phenobarbitone-treatment. By contrast, in preparation HTL-103, a 57.5- and a 10.3-fold increase in coumarin 7-hydroxylation was observed following phenobarbitone- and dexamethasone-treatment respectively.

Nifedipine dehydrogenation induction was also evaluated following treatment of hepatocytes with the different enzyme inducers. No increase in this enzyme activity was observed following treatment with either β-naphthoflavone or 3-methylcholanthrene. By contrast, a large increase in nifedipine dehydrogenation was

---

and HTL-75) were incubated up to 96 h with DMSO alone (◇), 50 μM dexamethasone (■), 2 mM phenobarbitone (●) or 50 μM β-naphthoflavone (▲). At specified times after cell seeding (time 0 of the kinetic), hepatocyte monolayers were scraped, microsomal fractions prepared, and 7-ethoxyresorufin and phenacetin *O*-deethylation, coumarin 7-hydroxylation and nifedipine dehydrogenation rates determined.

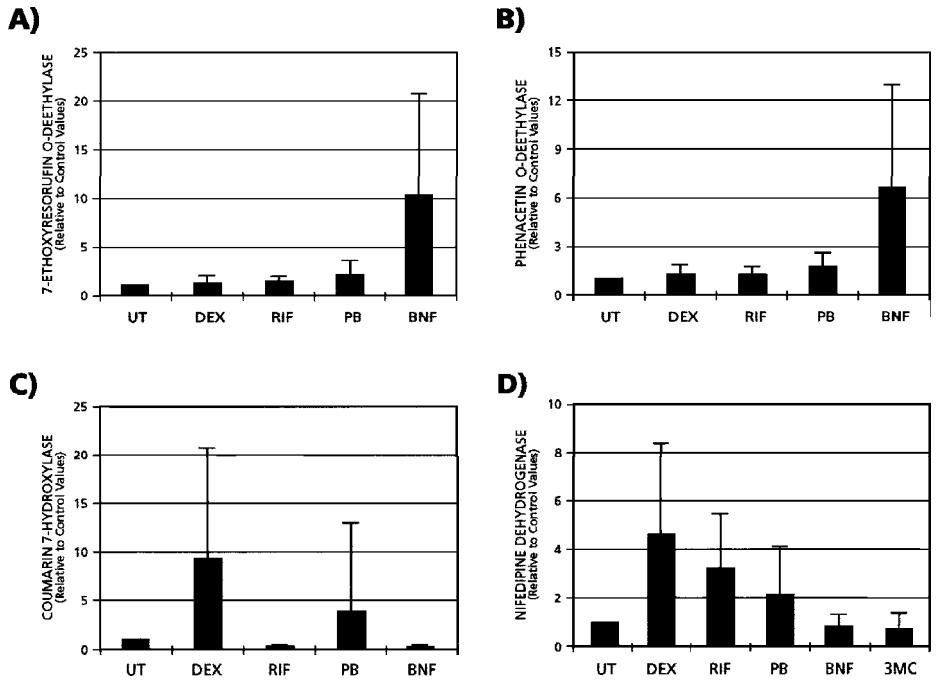


Figure 6. Inducing effects of various enzyme inducers on 7-ethoxyresorufin and phenacetin *O*-deethylation, coumarin 7-hydroxylation and nifedipine oxidation processes using primary cultures of human hepatocytes. Human hepatocytes in primary culture were incubated for 3 days with DMSO alone (control), 50 μM dexamethasone, 50 μM rifampicin, 2 mM phenobarbitone or 50 μM b-naphthoflavone. Cells were then scraped, microsomal fractions prepared and 7-ethoxyresorufin *O*-deethylation (A), phenacetin (B) *O*-deethylation, coumarin 7-hydroxylation (C) and nifedipine dehydrogenation (D) rates determined.

observed following treatment of hepatocytes with dexamethasone (4.7$\pm$3.8-fold, n = 61), rifampicin (3.2$\pm$2.3-fold, n = 7) or phenobarbitone (2.1$\pm$2.0-fold, n = 47). Owing to the low number of human hepatocyte preparations treated with rifampicin in comparison with dexamethasone, one could not differentiate between the potency of these two inducers. Whereas CYP3A4-mediated activity was demonstrated in most of hepatocyte preparations treated with dexamethasone (53 from 61) and rifampicin (five from seven), only 50% of hepatocytes preparations (25 from 47) could be induced with phenobarbitone.

Since the degree of induction could be linked to the basal enzyme activity in the hepatocyte preparation, this parameter being potentially itself linked to the quality of the hepatocytes preparation, also investigated was the potential link between these parameters.

Hepatocyte viability was evaluated at the end of liver perfusion, using the Trypan blue dye exclusion test. Only hepatocytes exhibiting a percentage of viability $>$85% were seeded on collagen-coated plastic dishes. After a 2–4 h incubation, during which hepatocytes attached to the matrix, the quality of the cell attachment was checked by optical micrography. Only preparations for which hepatocytes overlapped at least 70% of the cell dish area were used for investigating enzyme induction processes. In addition to morphological and viability criteria, additional parameters were investigated; (1) the recovery in microsomal proteins from hepatocyte cultures was also determined, and each hepatocyte preparation

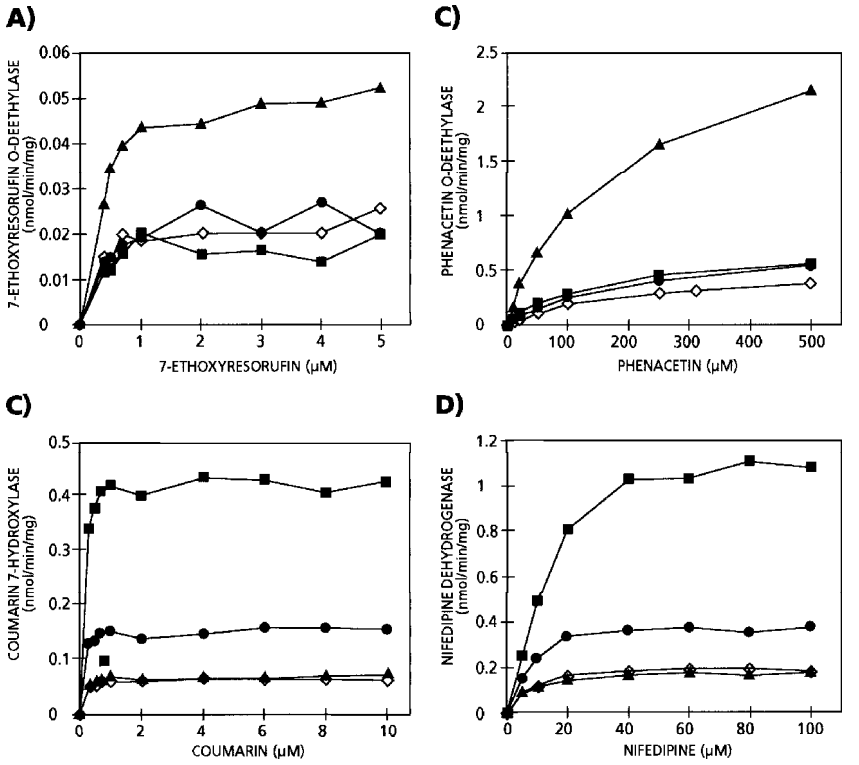


Figure 7. Effect of enzyme inducers on Michaelis–Menten characteristics of specific enzyme reactions, using pooled hepatocytes microsomal fractions. Pooled microsomal fractions (n = 30 preparations) obtained from either untreated hepatocytes (◇) or cells treated for 3 days with 50 μM dexamethasone (■), 2 mM phenobarbitone (●) or 50 μM β-naphthoflavone (▲), were incubated with increasing concentrations of 7-ethoxyresorufin (A), phenacetin (B), coumarin (C) and nifedipine (D), and metabolic rates were determined and illustrated according to Lineweaver–Burk representations.

with a recovery in microsomal proteins < 5 μg/10^6 hepatocytes was discarded, (2) each single human hepatocyte preparation for which one did not observe an at least 4-fold increase in at least one enzyme activity following a 3-day treatment with at least one enzyme inducer (either dexamethasone, β-naphthoflavone or phenobarbitone), was discarded, (3) all human hepatocytes preparations for which low enzyme activity towards all the different cytochrome P450 isoforms was observed, were also discarded. Finally, not observed was any relationship between the basal enzyme activity and the degree of enzyme induction.

Effect of enzyme inducers on Michaelis–Menten characteristics of CYP isoforms

Microsomal fractions (n = 30) obtained from either untreated human hepatocytes (3 days of culture) or hepatocytes treated for 3 days with either 50 μM dexamethasone, 50 μM β-naphthoflavone or 2 mM phenobarbitone, were pooled to constitute a large pool of control and induced material. These hepatocyte microsomal fractions were enzymatically characterized for their ability to metabolize the different CYP isoform-substrates. The Michaelis–Menten characteristics are illustrated in figure 7, and both K_m and V_{max} determinations are summarized in

Table 2. Michaelis–Menten characteristics of specific enzyme reactions, obtained on a pool of hepatocytes microsomal fractions prepared from either untreated hepatocytes or cells treated for 3 days with 50 μM dexamethasone, 2 mM phenobarbitone or 50 μM β-naphthoflavone.

	7-ethoxyresorufin *O*-deethylase		Phenacetin *O*-deethylase		Coumarin 7-hydroxylase		Nifedipine dehydrogenase	
Hepatocyte treatment	K_m	V_{max}	K_m	V_{max}	K_m	V_{max}	K_m	V_{max}
Control	0.23	0.024	174	0.51	0.09	0.06	6.2	0.21
β-naphthoflavone	0.31	**0.054**	172	**2.87**	0.11	0.07	5.2	0.19
Phenobarbitone	0.32	0.026	205	0.76	0.06	**0.15**	6.5	0.40
Dexamethasone	0.17	0.018	137	0.71	0.08	**0.43**	**15.0**	**1.30**

K_m are expressed as μM.
V_{max} are expressed as nmol metabolite formed/min/mg hepatocyte microsomal protein.
Bold indicates values that are at least 2-fold higher than controls.

table 2. When the specific CYP isoform-mediated reactions were investigated, Michaelis–Menten plots of the data showed a large increase in V_{max} and a less significant change in K_m, following treatment of hepatocytes with the corresponding enzyme inducer.

Hence, V_{max} for 7-ethoxyresorufin and phenacetin *O*-deethylation processes were increased 2.3- and 5.6-fold increased respectively, following a 3-day treatment with β-naphthoflavone, whereas dexamethasone and phenobarbitone had no significant effect on either V_{max} or K_m.

Following treatment of hepatocytes with dexamethasone, the V_{max} for nifedipine dehydrogenation and coumarin 7-hydroxylation were 6.3- and 7.2-fold increased respectively. These increases were much lower following phenobarbitone-treatment, namely 2.0- and 2.5-fold respectively. β-naphthoflavone-treatment did not affect CYP2A6- and CYP3A4-mediated reactions.

K_m obtained from control hepatocyte microsomal fractions were similar to those obtained in human hepatic microsomal fractions, using the same experimental conditions, i.e. incubation duration, protein concentration, range of substrate concentration, analytical techniques for metabolite quantification (Bourrié *et al.* 1996).

Effect of treatment duration on the induction of UGT-mediated enzyme activity

The data clearly demonstrate a decrease in basal cytochrome P450 isoform-mediated activities as a function of culture duration. This decrease in enzyme activity could be associated with either a loss of viability of hepatocytes or a dedifferentiation process. In order to evaluate the metabolic capacity of hepatocytes, different UGT-mediated activities were monitored as a function of time and over 72–120 h, on different human hepatocytes preparations.

Different UGT isoform(s)-mediated reactions were investigated using 1-naphthol, testosterone and digitoxigenine monodigitoxoside (dt1) as substrates. Turnover numbers were determined after the plating period, i.e. t = '0', and after 72–120 h of culture.

1-Naphthol glucuronidation rates at t = '0' and = '72–120 h' were 31.6 ± 13.7 nmol/min/mg ($n = 6$) and 27.4 ± 9.4 nmol/min/mg ($n = 6$) respectively. Dt1 glucuronidation rates at t = '0' and = '72 h' were 7.1 ± 0.4 nmol/

min/mg ($n = 2$) and 5.0 ± 1.5 nmol/min/mg ($n = 2$) respectively. In one single human hepatocyte preparation, testosterone glucuronidation rate increased from 9 to 19 pmol/min/mg over 120 h.

Analysis of these different UGT-dependent reactions catalysed by several isoforms, clearly showed no significant decreases in activity and further confirmed the viability of hepatocytes maintained in primary culture up to 5 days, at least with respect to this parameter.

Discussion

The effects of xenobiotics on the expression and induction of cytochrome P450 isoforms(s) has been largely investigated in animals, mostly rodents, although some attempts have been performed in dog and monkey. However, these effects in humans have been difficult to explore. The majority of results in humans were obtained either from unexpected drug–drug interactions or from the erythromycin breath test. Hence, CYP3A4, the major CYP3A gene expressed in adult human livers (Shimada *et al*. 1994), was increased (or induced) when patients were treated with a variety of compounds including the commonly used antibiotic rifampicin (Ged *et al*. 1989, Watkins *et al*. 1989). There is now a good evidence that, when isolated and cultured properly, intact hepatocyte preparations recapitulate the *in vivo* response of the liver to modulators of drug metabolizing enzymes to a great extent. The fact that, to date, most of the known human cytochrome P450 inducers studied (Ged *et al*. 1989, Daujat *et al*. 1990, Diaz *et al*. 1990, Fabre *et al*. 1990) also lead to enzyme induction in primary cultures of human hepatocyte, coupled with the demonstrated ability to reproduce the well-known species differences, e.g. rat versus human (Silva *et al*. 1998), is particularly impressive. Hence, the effect of rifampicin on CYP3A4 expression was reproduced in hepatocytes in primary culture (Pichard *et al*. 1990) which have been demonstrated to retain the expression of several liver functions including drug-metabolizing activities. More recently, this model was used to predict potential drug adverse effects with drugs such as cyclosporin A (Pichard *et al*. 1990) or lidocaine (Li *et al*. 1995).

Although the widespread availability of high-quality human hepatocyte preparations will increase our understanding of enzyme induction in humans, the main pitfall appears to be the lack of standardized culture conditions. In addition to different basal media, with their own special supplementation needs, and various cellular substrata, many different induction protocols have been reported in the literature in terms of treatment duration, choice of inducers, metabolic reactions selected and optimal concentration of inducers.

In some studies, the culture medium used was already supplemented with 1 μM dexamethasone to maintain cytochrome P450 differentiation, a concentration for which we demonstrated a 3-fold increase in nifedipine dehydrogenation, whereas a 5.6-fold maximal increase was achieved with 25–100 μM dexamethasone. In other studies, enzyme inducers were added to the culture medium for 1–3 days, either directly after cell attachment (Fabre *et al*. 1990) or following 1 (Gomez-Lechon *et al*. 1990, Donato *et al*. 1995, Kocarek *et al*. 1995), 2 (Daujat *et al*. 1990, Silva *et al*. 1998) or 3 days (Li *et al*. 1995) after cell attachment. If for well-known model enzyme inducers, this experimental protocol allowed for characterization of the induction process, false-negative results could be encountered. Indeed, after a 2–3-day lag, the ability of hepatocytes to metabolize active cytochrome P450 inducers to inactive products or to convert inactive precursor molecules to substantial

cytochrome P450 inducers, could be highly reduced. It is now well recognized that during culture, human hepatocytes tend to lose expression of specific liver functions, including cytochrome P450-dependent activities, as they adapt to culture conditions over time. Hence, a 80–90% decrease in basal cytochrome P450-dependent activities has been observed over 3 days (Fabre *et al*. 1990, Li *et al*. 1995, Guillouzo 1997).

The potency of aryl hydrocarbons, such as 3-methylcholanthrene and β-naphthoflavone, or omeprazole to induce CYP1A1 and 1A2 isoforms has been widely described. Using 7-ethoxyresorufin as specific CYP1A-mediated reaction, a maximal increase was observed following treatment of hepatocytes with 10 μM omeprazole (investigated range = 2–10 μM) (Li 1997). For other inducers, usual concentrations ranged between 2 μM (Donato *et al*. 1995) and 25 μM (Fabre *et al*. 1990) for 3-methylcholanthrene, and ~ 50 μM for β-naphthoflavone. However, little is known about the concentration dependency of these various inducers. Under our culture conditions, 3-methylcholanthrene concentrations > 25 μM were associated with cytotoxicity, the latter not being observed for β-naphthoflavone up to 50 μM. Using either phenacetin or 7-ethoxyresorufin as specific substrates for CYP1A1/A2 isoforms, it has been demonstrated that a significant increase in enzyme activity was already observed at 2 μM β-naphthoflavone, but the maximal effect was observed at 50 μM. At this higher concentration and even following a 3-day treatment, the response to β-naphthoflavone was very specific. Hence, neither coumarin 7-hydroxylation nor nifedipine dehydrogenation were induced (table 2).

Although induction of metabolic enzymes by phenobarbitone is a well-established phenomenon in rodents, only few reports have evidenced the effect of clinical phenobarbitone-treatment on human drug metabolizing enzymes (Bock and Bock-Hennig 1987, Bachmann *et al*. 1991). Using human hepatocytes in primary culture, the effect of phenobarbitone has been demonstrated. Hence, Daujat *et al*. (1991) reported a 4.0–33-fold increased accumulation of the CYP3A-haemoprotein following a 3-day treatment with 2 mM phenobarbitone. Phenobarbitone (1.5 mM final concentration; 2-day treatment) was also reported (Donato *et al*. 1995) to increase moderately 7-ethoxyresorufin *O*-deethylation (1.2–1.9-fold), 7-pentoxyresorufin *O*-dealkylation (1.5–2.0-fold) and testosterone 16α- (1.5–4.5-fold) and 2β-hydroxylations (1.3–2.0-fold), but to have no effect on *p*-nitrophenol hydroxylation.

In our study, it was clearly demonstrated that phenobarbitone was a broad but moderate inducer of different cytochrome P450 isoforms in man. CYP1A1/A2- and CYP3A4-mediated reactions were induced by 2.2±1.5-fold (7-ethoxyresorufin *O*-deethylation, $n = 54$; maximal increase = 6.5-fold, whereas in the same preparation a 69.5-fold increase was observed following β-naphthoflavone-treatment), 1.7±0.9-fold (phenacetin *O*-deethylation, $n = 53$; maximal increase = 4.5-fold), and 2.1±2.0-fold (nifedipine dehydrogenation, $n = 47$; maximal increase = 13-fold). The more predominant effect was observed for coumarin 7-hydroxylation where a 3.8±9.2-fold ($n = 50$; maximal increase = 57.5-fold) increase was observed. This study revealed both a very large interindividual variability among (1) the basal activities obtained from different liver donors, (2) the degree of CYP2A6 induction from one human hepatocyte preparation to another, and (3) the regulation of the induction process, e.g. some preparations being more sensitive to dexamethasone-treatment and others being more sensitive to phenobarbitone-treatment.

There is abundant evidence that hepatic CYP3A4 is inducible in man (Watkins *et al*. 1985). Clinical observations indicate that high levels of CYP3A isozymes were

observed after treatment of patients with either dexamethasone (Molowa *et al*. 1986, Watkins *et al*. 1989) or rifampicin (Watkins *et al*. 1989), by measuring either the rate of production of breath $^{14}CO_2$ after injection of a test dose of [^{14}C]-*N*-methyl erythromycin (Watkins *et al*. 1989) or the cumulative urinary excretion of 6β-hydroxycortisol after a standard period (Ged et *al*. 1989). The major *in vitro* model inducers for CYP3A4 induction are dexamethasone and rifampicin. However, protocols vary both in terms of concentration and treatment duration. For rifampicin, concentrations ranged from 2 μM (Silva *et al*. 1998) to 50 μM, i.e. the most often used (Daujat *et al*. 1990, Fabre *et al*. 1990, Li *et al*. 1995). The effect of increasing rifampicin concentrations (0.1–50 μM range) on CYP3A4 expression and related lidocaine metabolism was reported by Li *et al*. (1995). Although a significant 3-fold increase in lidocaine metabolism was already achieved following a 2-day treatment with 1 μM rifampicin, an optimal 7-fold-increase was observed following incubation with 50 μM rifampicin. In a recent review and using testosterone 6β-hydroxylation as a CYP3A4 probe, Li (1997) reported that optimal inducer concentrations were 3.3 mM for phenobarbitone (range 0.1–10 mM), 100 μM for dexamethasone (range 1–100 μM) and 10 μM for rifampicin (range 1–100 μM). For this latter inducer, a decrease in testosterone 6β-hydroxylation was observed when hepatocytes were treated with higher rifampicin concentrations, i.e. 33.3 and 100 μM. Large differences were also observed in dexamethasone concentrations used from one laboratory to another, ranging from 1 μM (Donato *et al*. 1995) to 50 μM, i.e. the most often used (Daujat *et al*. 1990, Fabre *et al*. 1990, Silva *et al*. 1998). Using a large range of dexamethasone concentrations (1–100 μM), one could demonstrate that in agreement with Donato *et al*. (1995), a significant increase in CYP3A4-related activities was observed at 1 μM dexamethasone, but an optimal increase was achieved for dexamethasone concentrations >25 μM. It has to be noted that some standard culture media (Li *et al*. 1995) are already supplemented with 1 μM dexamethasone, to maintain cell differentiation.

This study, performed on a large number of human hepatocyte preparations, confirms the validity of this model to evaluate cytochrome P450 isoforms induction. This was supported by the optimization of experimental conditions, in terms of the choice of maximal specific inducer concentration and treatment duration.

Acknowledgements

The authors thank Dr Patrick Maurel, INSERM U-128, Montpellier, for a critical reading of the manuscript. Grateful thanks are also due to Josiane Villard for invaluable help in the preparation of the manuscript.

References

Briquette, D. J., MacKenzie, P. I., Veroneze, M. E. and Miners, J. O., 1993, In vitro approaches can predict human drug metabolism. *Trends in Pharmacological Sciences*, **14**, 292–294.

Bourrié, M., Meunier, V., Berger, Y. and Fabre, G., 1996, Cytochrome P450 isoform inhibitors as a tool for the investigation of metabolic reactions catalysed by human liver microsomes. *Journal of Pharmacology and Experimental Therapeutics*, **277**, 321–332.

Burke, M. D., Thompson, S., Elcombe, C. R., Halpert, J., Haaparanta, T. and Mayer, R. T., 1985, Ethoxy-, pentoxy-, and benzoyloxy-phenoxazones and homologues: a series of substrates to distinguish between different induced cytochromes P-450. *Biochemical Pharmacology*, **34**, 3337–3345.

Butler, M. A., Iwasaki, M., Guengerich, F. P. and Kadlubar F. F., 1989, Human cytochrome P-450PA (P-450IA2), the phenacetin *O*-deethylase, is primarily responsible for the hepatic 3-

demethylation of caffeine and N-oxidation of carcinogenic arylamines. *Proceedings of the National Academy of Sciences, USA*, **86**, 7696–7700.

Combalbert, J., Fabre, I., Fabre, G., Dalet, C., Derancourt, J., Cano, J. P. and Maurel, P., 1989, Metabolism of cyclosporin A: IV. Purification and identification of the rifampicin-inducible human liver cytochrome (cyclosporin A oxidase) as a product of P-450IIIA gene subfamily. *Drug Metabolism and Disposition*, **17**, 197–207.

Creaven, P. J., Parke, D. V. and Williams, R. T., 1965, A spectrofluorimetric study of the 7-hydroxylation of coumarin by liver microsomes. *Biochemical Journal*, **96**, 390–398.

Daujat, M., Fabre, I., Diaz, D., Pichard, L., Fabre, G,. Fabre, J. M., Saint-Aubert, B. and Maurel, P., 1990, Inducibility and expression of class IA and IIIA cytochromes P450 in primary cultures of adult human hepatocytes. *Biochemical Pharmacology* (*Life Sciences Advances*), **9**, 315–326.

Daujat, M., Pichard, L., Dalet, C., Larroque, C., Bonfils, C., Pompon, D., Li, D., Guzelian, P. S. and Maurel, P., 1987, Expression of five forms of microsomal cytochrome P-450 in primary cultures of rabbit hepatocytes treated with various classes of inducers. *Biochemical Pharmacology*, 36, 3597–3607.

Daujat, M., Pichard, L., Fabre, I., Pineau, T., Fabre, G., Bonfils, C. and Maurel, P., 1991, Induction protocols for cytochrome P450IIIA *in vivo* and in primary cultures of animal and human hepatocytes. *Methods in Enzymology*, 206, 345–353.

Diaz, D., Fabre, I., Daujat, M., Saint Aubert, P., Bories, P., Michel, H. and Maurel, P., 1990, Omeprazole is an aryl hydrocarbon-like inducer of human cytochrome P450. *Gastroenterology*, **99**, 737–747.

Donato, M. T., Castell, J. V. and Gomez-Lechon, M. J., 1995, Effect of model inducers on cytochrome P450 activities of human hepatocytes in primary culture. *Drug Metabolism and Disposition*, **23**, 553–558.

Ekins, S., Williams, J. A., Murray, G. I., Burke, M. D., Marchant, N. C., Engeset, J. and Hawksworth, G. M., 1996, Xenobiotic metabolism in rat, dog and human precision-cut liver slices, freshly isolated hepatocytes and vitrified precision-cut liver slices. *Drug Metabolism and Disposition*, **24**, 990–995.

Fabre, G., Bourrié, M., Marti, E., Fabre, I., Roque, C., Saint-Aubert, B., Joyeux, H., Maurel, P., Berger, Y. and Cano, J. P., 1990, Inducibility of both cytochrome P-450 and UDP-glucuronosyl transferase isozymes in primary cultures of human hepatocytes. *Biochemical Pharmacology* (*Life Sciences Advances*), **9**, 79–91.

Fabre, G., Crevat-Pizano, P., Dragna, S., Covo, J., Barra, Y. and Cano, J. P., 1988b, Involvement of the macrolide antibiotic cytochrome P450-LM3c in the metabolism of midazolam by microsomal fractions prepared from rabbit liver. *Biochemical Pharmacology*, **37**, 1947–1953.

Fabre, G., Rahmani, R., Placidi, M., Combalbert, J., Covo, J., Cano, J. P., Coulange, C., Ducros, M. and Rampal, M., 1988a, Characterization of midazolam metabolism using human hepatic microsomal fractions and hepatocytes in suspension obtained by perfusing whole human livers. *Biochemical Pharmacology*, **37**, 4389–4397.

Ged, C., Rouillon, J. M., Pichard, L., Combalbert, J., Bressot, N., Bories, P., Michel, H., Beaune, P. and Maurel, P., 1989, The increase in urinary excretion of 6β-hydroxycortisol as a marker of human hepatic cytochrome P450IIIA induction. *British Journal of Clinical Pharmacology*, **28**, 373–387.

Gomez-Lechon, M. J., Lopez, P., Donato, T., Montoya, A., Larrauri, P., Gimenez, P., Trullenque, R., Fabra, R. and Castell, J. V., 1990, Culture of human hepatocytes from small surgical liver biopsies: biochemical characterization and comparison with *in vivo*. *In Vitro Cell Development in Biology*, 26, 67–74.

Guengerich, F. P., Martin, M. V., Beaune, P. H., Kremers, P., Wolff, T. and Waxman, D. J., 1986, Characterization of rat and human liver microsomal cytochrome P-450 forms involved in nifedipine oxidation, a prototype of genetic polymorphism in oxidative drug metabolism. *Journal of Biological Chemistry*, 261, 5051–5060.

Guillouzo, A., 1997, Biotransformation of drugs by hepatocytes. In *In Vitro Methods in Pharmaceutical Research* (Orlando: Academic Press), pp. 411–429.

Isom, H. C. and Georgoff, I., 1984, Quantitative assay for albumin-producing liver cells after simian virus 40 transformation of rat hepatocytes maintained in a chemically-defined medium. *Proceedings of the National Academy of Sciences, USA*, **81**, 6378–6382.

Iwatsubo, T., Hirota, N., Ooie, T., Suzuki, H., Shimada, N., Chiba, K., Ishizaki, T., Green, C. E., Tyson, C. A. and Sugiyama, Y., 1997, Prediction of *in vivo* drug metabolism in the human liver from *in vitro* metabolism data. *Pharmacology and Therapeutics*, **73**, 147–171.

Kocarek, T. A., Schuetz, E. G., Strom, S. C., Fisher, R. A. and Guzelian, P. S., 1995, Comparative analysis of cytochrome P4503A induction in primary cultures of rat, rabbit, and human hepatocytes. *Drug Metabolism and Disposition*, **23**, 415–421.

Li, A. P., 1997, Primary hepatocyte cultures as an *in vitro* experimental model for the evaluation of pharmacokinetic drug–drug interactions. In *Advances in Pharmacology*, vol. 43 (Orlando: Academic Press), pp. 103–130.

Li, A. P., Rasmussen, A., Xu, L. and Kaminski, D. L., 1995, Rifampicin induction of lidocaine metabolism in cultured human hepatocytes. *Journal of Pharmacology and Experimental Therapeutics*, **274**, 673–677.

Maurice, M., Pichard, L., Daujat, M., Fabre, I., Joyeux, H., Domergue, J. and Maurel, P., 1992, Effects of imidazole derivatives on cytochromes P450 from human hepatocytes in primary culture. *FASEB Journal*, 6,752–758.

McKinnon, R. A., Hall, P. M., Quattrochi, L., Tukey, R. H. and McManus, M. E., 1991, Localization of CYP1A1 and CYP1A2 messenger RNA in normal human liver and in hepatocellular carcinoma by *in situ* hybridization. Hepatology, **14**, 848–852.

Miners, M. O. Veronese, M. E. and Birkett, D. J., 1994, *In vitro* approaches for the prediction of human drug metabolism. In J. A. Bristol (ed.), *Annual Reports in Medicinal Chemistry*, vol. 29 (Orlando: Academic Press), pp. 306–316.

Nelson, D. R., Kamataki, T., Waxman, D. J., Guengerich, F. P., Estabrook, R. W., Feyereizen, R., Gonzalez, F. J., Coon, M. J., Gunsalus, I. C., Gotoh, O., Okuda, K. and Nebert, D. W., 1993, The P450 superfamily: update on new sequences, gene mapping, accession numbers, early trivial names of enzymes, and nomenclature. *DNA Cell Biology*, **12**, 1–51.

Olinga, P., Merema, M., Hof, I. H., De Jong, K. P., Slooff, M. J. H., Meijer, D. K. F. and Groothuis, G. M. M., 1998, Effect of human liver source on the functionality of isolated hepatocytes and liver slices. *Drug Metabolism and Disposition*, **26**, 5–11.

Pelkonen, O., Sotaniemi, E. A. and Ahokas, J. T., 1985, Coumarin 7-hydroxylase activity in human liver microsomes. Properties of the enzyme and inter-species comparison. *British Journal of Clinical Pharmacology*, **19**, 59–66.

Pichard, P., Fabre, I., Fabre, G., Domergue, J., Saint Aubert, B., Mourad, G. and Maurel P., 1990, Cyclosporin A drug interactions: screening for inducers and inhibitors of cytochrome P450 (cyclosporin A oxidase) in primary cultures of human hepatocytes. *Drug Metabolism and Disposition*, **18**, 595–606.

Pollard, H. B., Menard, R., Brandt, H. A., Pazoles, C. J., Creutz, C. E. and Ramu, A., 1978, Application of Bradford's protein assay to adrenal gland subcellular fractions. *Analytical Biochemistry*, 86, 761–763.

Rodrigues, A. D., 1994, Use of *in vitro* human metabolism studies in drug development. An industrial perspective. *Biochemical Pharmacology*, **48**, 2147–2156.

Sesardic, D., Boobis, A. R., Edwards, R. J. and Davies, D. S., 1988, A form of cytochrome P450 in man, orthologous to form d in the rat, catalyses the *O*-deethylation of phenacetin and is inducible by cigarette smoking. *British Journal of Clinical Pharmacology*, **26**, 363–372.

Silva, J. M., Morin, P. E., Day, S. H., Kennedy, P. P., Rushmore, T., Yergey, J. A. and Nicoll-Griffith, D. A., 1998, Refinement of an *in vitro* cell model for cytochrome P450 induction. *Drug Metabolism and Disposition*, 26, 490–496.

Shimada, T., Yamazaki, H., Minura, M., Inui, Y. and Guengerich F. P., 1994, Inter-individual variations in human liver cytochrome P450 enzymes involved in the oxidation of drugs, carcinogens and toxic chemicals; studies with liver microsomes of 30 Japanese and 30 Caucasians. *Journal of Pharmacology and Experimental Therapeutics*, **270**, 414–423.

Tucker, G. T., 1992, The rational selection of drug interaction studies; Implications of recent advances in drug metabolism. *International Journal of Clinical Pharmacology, Therapeutics and Toxicology*, **30**, 550–553.

Wadhwa, N. K., Schroeder, T. J., Pesce, A. J., Myre, S. A., Clardy, C. W. and First, M. R., 1987, Cyclosporin drug interactions: a review. *Therapeutics and Drug Monitoring*, **9**, 399–406.

Watkins, P. B., Murray, S. A., Winkelman, L. G., Heuman, D. M., Wrighton, S. A. and Guzelian, P. S., 1989, Erythromycin breath test as an assay of glucocorticoid-inducible liver cytochromes P-450. *Journal of Clinical Investigation*, **83**, 688–697.

Watkins, P. B., Wrighton, S. A., Maurel, P., Schuetz, E. G., Mendez-Picon, G., Parker, G. A. and Guzelian, P. S., 1985, Identification of an inducible form of cytochrome P-450 in human liver. *Proceedings of the National Academy of Sciences, USA*, **82**, 6310–6314.

Wrighton, S. A. and Stevens, J. C., 1992, The human hepatic cytochromes P450 involved in drug metabolism. *Critical Review in Toxicology*, 22, 1–21.

XENOBIOTICA, 2000, VOL. 30, NO. 6, 619–625

An inhibitory monoclonal antibody to human cytochrome P450 that specifically binds and inhibits P4502C9II, an allelic variant of P4502C9 having a single amino acid change Arg144 Cys

K. W. KRAUSZ†, I. GOLDFARB†, T. J. YANG†,
F. J. GONZALEZ‡ and H. V. GELBOIN†*

Laboratories of †Molecular Carcinogenesis and ‡Metabolism, National Cancer Institute, National Institutes of Health, 37 Convent Drive, Bldg 37, Rm 3E24 Bethesda, MD 20892 USA

A monoclonal antibody (MAb 292-2-3) has been isolated that binds specifically to a single allele of three expressed human cytochrome P4502C9 alleles. The MAb binds to $2C9_{Cys144}$ (II), and does not bind to the wild-type $2C9_{Arg144}$ (I), or the third allele $2C9_{Ile \rightarrow Leu359}$ (III) and thus the MAb detects an allele with $>99\%$ homology and differing from the wild-type $2C9_{Arg144}$ (I) by a single amino acid. The MAb 292-2-3 does not bind to the other 2C isoforms (2C8, 2C18, 2C19) or the other human cytochrome P450s, 1A1, 1A2, 2A6, 2B6, 2C8, 2D6, 2E1 or 3A4/5. MAb 292-2-3 inhibits the metabolism of tolbutamide, diclofenac and phenanthrene by the target $2C9_{Cys144}$ (II) allele by $>90\%$ and does not inhibit the catalytic activity of the wild-type $2C9_{Arg144}$ (I), or $2C9_{Ile \rightarrow Leu359}$ (III) the other 2C isoforms 2C8, 2C18, 2C19, or the other non-2C human P450s listed above. The MAb 292-2-3 is thus a prototype of an ideal and extraordinarily specific reagent for the detection and measurement of the metabolic role of highly related isoforms and polymorphic alleles of human cytochrome P450s. MAbs of high specificity can also determine the amount of phenotypic expression of polymorphic alleles and their metabolic role in drug and non-drug xenobiotic metabolism in heterozygote individuals. The inhibitory MAb might also identify allele-specific substrates of polymorphic human cytochrome P450s.

Introduction

Cytochromes P450 are a superfamily of haemoproteins that metabolically activate and detoxify a vast variety of drugs and non-drug xenobiotics, and their collective metabolic role in humans is catalyzed by ~12 major isoforms of cytochromes P450 found in human liver (Montellano 1995, Ioannides 1996, Rendic and Di Carlo 1997). Monoclonal antibodies (MAb) are reagents 'par excellence' (Kohler and Milstein 1975) for determining the amount of individual cytochrome P450 protein and their metabolic contribution to the metabolism of a drug or non-drug xenobiotic in human liver microsomes (Gelboin 1993, Gelboin *et al*. 1999, Yang *et al*. 1999). The present authors have previously isolated and characterized 14 MAbs to individual forms of cytochrome P450 in human liver which specifically immunoblot and/or inhibit the catalytic activity of human cytochrome P4501A1 (Fujino *et al*. 1982, Tassaneeyakul *et al*. 1993), 1A2 (Yang *et al*. 1998b), 2A6 (Sai *et al*. 1999), 2B6 (Yang *et al*. 1998a), 2C8 (Gelboin *et al*. 1999), 2D6 (Gelboin *et al*. 1997), 2E1 (Gelboin *et al*. 1996) and 3A3/4 (Gelboin *et al*. 1995). In addition, one MAb that inhibits four of the P450s of the 2C family, 2C8, 2C9, 2C18, 2C19 (Gelboin *et al*. 1997) has been isolated. The inhibitory MAb quantitate the role

* Author for correspondence; e-mail: gelboinh@intra.nci.nih.gov

Xenobiotica ISSN 0049–8254 print/ISSN 1366–5928 online © 2000 Taylor & Francis Ltd
http://www.tandf.co.uk/journals

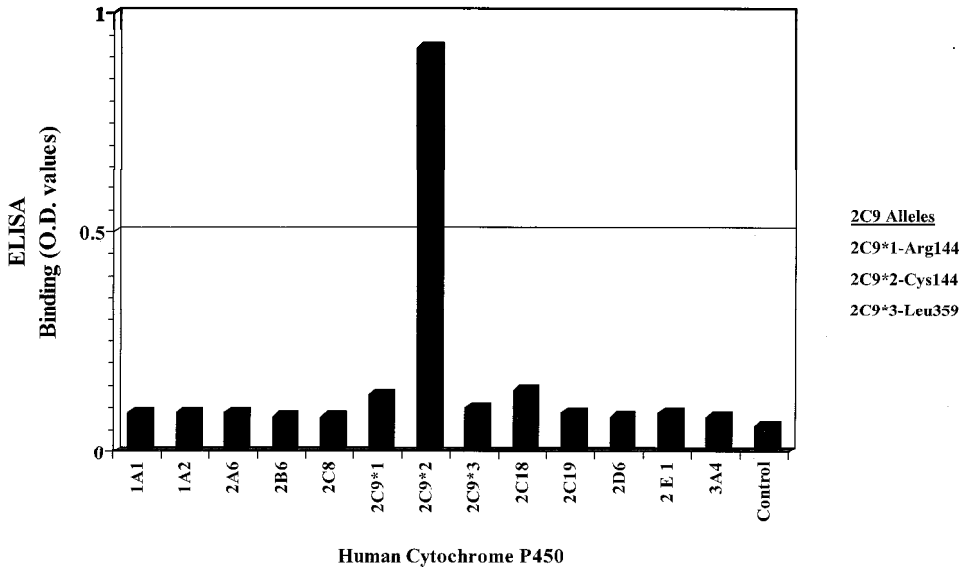


Figure 1. Specificity of binding of monoclonal antibody 292–2-3 to expressed human cytochrome P450s. ELISA plates were coated with 1.5 pmole of the indicated cytochrome P450. MAb 292-2-3 (10 μg/ml) was incubated on the plate as described in the Material and methods. The amount of binding to each enzyme was measure by absorbance (OD) at 405 nm. Controls are without expressed cytochrome P450. Data are the mean of duplicate incubations.

of a target P450 by their inhibition of substrate metabolism in human liver microsomes (HLM).

The major importance of human P4502C9 and its properties have been extensively reviewed (Miners and Birkett 1998). The P4502C9 cDNAs encode proteins comprised of 490 amino acids. P4502C9 has three allelic forms, the wild-type (WT) $2C9_{Arg144}$ (I), $2C9_{Cys144}$ (II) and $2C9_{Ile \rightarrow Leu359}$ (III). Cytochrome P4502C9 is a major form of the 2C family (2C8, 9, 18, 19) and is responsible for the metabolism of a variety of important drugs among which are tolbutamide, *S*-warfarin, phenytoin, tienillic acid and losartan, as well as non-steroidal anti-inflammatory drugs such as diclofenac and ibuprofen (Miners and Birkett 1998).

This paper reports the isolation of a hybridoma that produces a monoclonal antibody (MAb 292-2-3) which specifically binds and inhibits the metabolism catalyzed by one of the three human 2C9 allele products, $P4502C9_{Cys144}$ (II), and does not bind or inhibit the wild-type $2C9_{Arg144}$ (I), or the third allele $2C9_{Ile \rightarrow Leu359}$ (III). Thus, MAb 292-2-3 specificity targets the single $2C9_{Cys144}$ (II) allele that differs from the wild-type by substituting Cyst for Arg at position 144 and does not bind or inhibit the other two 2C9 alleles, the other isoforms of the 2C family (8, 18, 19) or eight other human P450 isoforms (1A1, 1A2, 2B6, 2C8, 2D6, 2E1 or 3A4/5). The $2C9_{Cys144}$ (II) has $> 99\%$ homology with the wild-type $2C9_{Arg144}$ (I) and differs by a single amino acid.

The extraordinary and super specificity of the MAb 292-2-3 is a paradigm illustrating the potential of the MAb system for the highly specific targeting of the metabolic function of closely related P450s and their polymorphic allelic forms. The MAb system can be usefully applied to other xenobiotic metabolizing isoformic systems such as those of the phase two enzymes or other non-cytochrome P450 enzyme systems composed of multiple isoforms.

Materials and methods

Hybridoma production

Cytochrome P4502C9$_{Cys144}$ (II) was expressed using a vaccinia vector in Hep G2 cells (Battula *et al.* 1987) or from a baculovirus vector in insect cells (Gonzalez *et al.* 1991) and extracted according to Gelboin *et al.* (1998). The extracted cytochrome P450 baculovirus-expressed 2C9$_{Cys144}$ (II) was used as the immunogen. The vaccinia-expressed P450s were used for some of the enzyme analysis. The Balb/c mouse was immunized with 50 μg baculo-expressed cytochrome P4502C9 (II) for 3 weeks, the spleen cells isolated and fused with myeloma cells (NS-1). The resulting hybridomas were screened for antibody production and binding specificity to single expressed human cytochrome P450s by ELISA as described (Gelboin *et al.* 1998). Of 1086 hybridomas screened for antibody production and binding specificity, one bound specifically to P4502C9$_{Cys144}$ (II). All the other hybridomas yielded MAb that were either non-binding or non-specific to the target P450. The hybridoma producing the desired MAb 292-2-3 was cloned three times, and the MAb was produced in cell culture or by ascites production in mouse as described (Gelboin *et al.* 1998).

Immuno-assay assays

ELISA was performed on 96-well plates coated with 1.5 pmole of a single cytochrome P450. MAb derived from culture fluids or by diluted ascites fluid were applied and incubated at room temperature for 2 h. After washing, labelled antibody (alkaline phosphatase goat anti-mouse IgG$_{Fc}$) was applied for 1 h. After washing, the wells were developed with the appropriate substrate (*p*-nitrophenyl phosphate) and the absorbance was measured at 405 nm. SDS-PAGE gels and immunoblots (IB) were performed as described (Gelboin *et al.* 1998).

Immunoinhibition studies were performed using cDNA vaccinia-expressed cytochrome P450 enzymes from Hep G2 cells, Supersomes (Gentest Corp.) and/or Baculosomes (Panvera Corp.). Generally the incubations contained 30–60 μg ascites protein containing the MAb which was pre-incubated with 30–50 pmole cytochrome P450 enzyme in 0.5 ml in buffer (100 mM Tris pH 7.5) and incubated at 37 °C for 5 min. The substrate in 10 μl methanol, NADPH (1.0 mM, final concentration) and additional buffer were added to a final volume of 1.0 ml. The incubation was for 30 min (60 min for tolbutamide) and the metabolites were extracted with 8 ml dichloromethane. Phenanthrene (200 μM) was used for examining the specificity of inhibition of the target P450s by the MAb (Shou *et al.* 1994). Phenanthrene conversion to the 9,10 diol was catalyzed by 1A1, 1A2, 2B6, 2C8, 2C9 (I), 2C9 (II), 2C9 (III), 2C18, 2C19, 2E1, 3A4, and 3A5; Burfuralol (50 μM) conversion to 1-OH bufuralol was used for measuring 2D6 metabolism (Gelboin *et al.* 1997). Diclofenac (50 μM) conversion to 4′OH (Crespi and Penman 1997) and tolbutamide (200 μM) (Relling *et al.* 1990) were used for testing the specificity of the MAb 292-2-3 inhibition of metabolism catalyzed by each of the three 2C9 allelic variants: 2C9$_{Arg144}$ (I), 2C9$_{Cys144}$ (II) and 2C9$_{Ile\rightarrow Leu359}$ (III). Metabolites formed were separated by HPLC performed using A Hewlett Packard Model 1050 Series system equipped with an autosampler, a quaternary pump, and a dio-array detector controlled by the Hewlett Packard Chemstations software. Metabolite retentions were compared with authentic standards and metabolite peaks were quantitated based on their ratios to internal standards. Control incubations contained a MAb against hen egg white lysozyme (MAb HyHel-9) (Gelboin *et al.* 1998). Percent of control metabolism was calculated from that observed in the absence and presence of the MAb 292-2-3.

Results

Figure 1 shows the specificity of binding of the MAb 292-2-3 to the expressed cytochrome P450s determined by ELISA. The MAb 292-2-3 binds only to the single expressed 2C9$_{Cys144}$ (II) and does not bind the wild-type (WT) 2C9$_{Arg144}$ (I) or the 2C9$_{Ile\rightarrow Leu359}$ (III) Further the MAb 292-2-3 does not bind to other members of the 2C family, 2C8, 2C18, 2C19 and none of the non-2C isoforms of human liver cytochrome P450s, i.e. 1A1, 1A2, 2A6, 2B6, 2D6, 2E1 or 3A4/5. The MAb 292-2-3 does not immunoblot any of the above three 2C9 alleles.

Figure 2 shows the specificity of inhibition of MAb 292-2-3 for the metabolism of phenanthrene catalyzed by the 2C9$_{Arg144}$ (I) and 2C9$_{Cys144}$ (II) allelic cytochrome P450s and other isoforms in human liver except for 2D6 measured by bufuralol metabolism and 2C9$_{Ile\rightarrow Leu359}$ (III) measured by diclofenac metabolism. The metabolism by 2C9$_{Cys144}$ (II) was completely inhibited by MAb 292-2-3, which exhibits no inhibition of the two other 2C9 alleles, 2C isoforms (8, 18, 19) or the non-2C P450 isoforms, 1A1, 1A2, 2A6, 2B6, 2C8, 2D6, 2E1 or 3A4/5. All of the

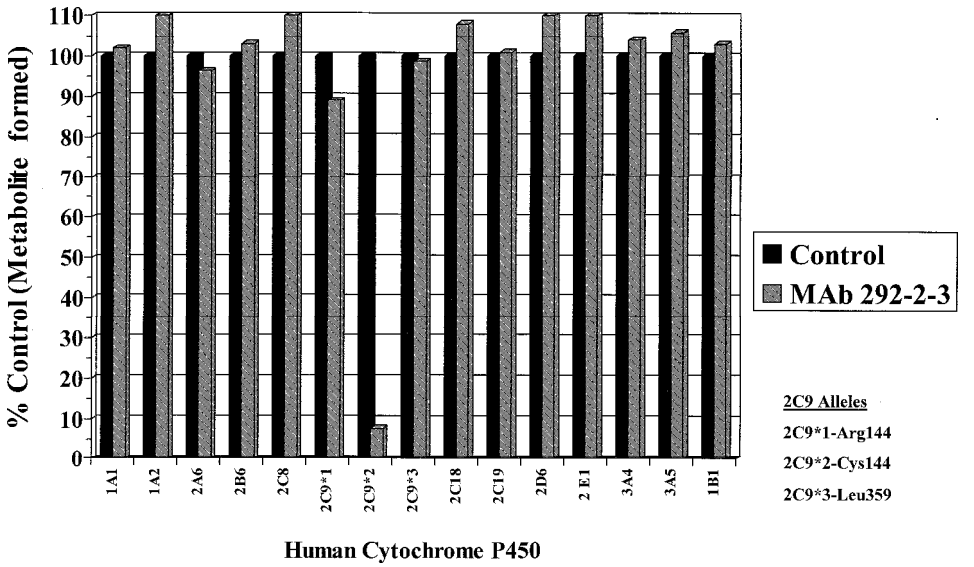


Figure 2. Specificity of MAb 292-2-3: inhibition of metabolism by P4502C9 alleles and other cytochrome P450s. Each enzyme was incubated in the presence of a control antibody (MAb Hy-Hel) or MAb 292–2-3 along with phenanthrene for all cytochrome P450s except bufuralol for 2D6 and diclofenac for $2C9_{Ile \rightarrow Leu359}$ (III) (see Materials and methods).

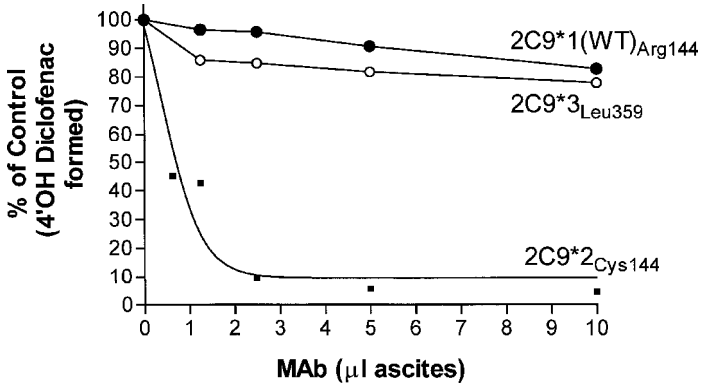


Figure 3. MAb 292-2-3 inhibition of P4502C9 allele diclofenac metabolism. Diclofenac was incubated with the expressed cytochrome P450s from the 2C9 alleles with MAb 292-2-3 or control antibody. Data are the mean of duplicate incubations.

Table 1. Tolbutamide and diclofenac metabolism by 2C9: specific inhibition of the $2C9_{Cys144}$ Allele by MAb 292-2-3.

	2C9 Allele[a]								
	*1-WT Arg144			*2-Arg144Cys			*3-Ile359Leu		
Substrate	Control	+MAb	% Inh	Control	+MAb	% Inh	Control	+MAb	% Inh
Tolbutamide	1.0	0.98	1.3	0.85	0.03	96.4	0.22	0.02	9.3
Diclofenac	0.3	0.3	0.1	0.42	0.02	95.1	0.35	0.30	14.4

[a] P450 activity is (nmolproduct/min/nmolP450).

measurements of enzyme activity and inhibition by the MAb were performed with P450s expressed from either vaccinia or baculovirus vectors.

Figure 3 shows the concentration dependence of inhibition of diclofenca metabolism by the MAb 292-2-3.

Table 1 shows the specificity of MAb 292-2-3 toward each of the three 2C9 cytochrome P450 alleles catalyzed metabolism of two major 2C9 substrates, tolbutamide and diclofenac. The MAb 292-2-3 inhibited $2C9_{Cys144}$ (II) by $>95\%$ and did not exhibit significant inhibition of the wild-type $2C9_{Arg144}$ (I) or $2C9_{Ile\rightarrow Leu359}$ (III).

Discussion

Human cytochrome P4502C9 is of major importance being responsible for the metabolism of numerous drugs and non-drug xenobiotics including tolbutamide, *S*-warfarin, phenytoin, diclofenac, ibuprofen and losarten. The three major alleles of cytochrome P4502C9 are the wild-type $2C9_{Arg144}$ (I), $2C9_{Cys144}$ (II) and $2C9_{Ile\rightarrow Leu359}$ (III) (Haining *et al*. 1996, Miners and Birkett 1998). A genetic study of the 2C9 polymorphism indicated that the frequency of the $2C9_{Arg144}$ (II) and $2C9_{Ile\rightarrow Leu359}$ (III) alleles in a Caucasian American Population were 0.08 and 0.06% respectively and 0.005 and 0.01 for 2C9III and 2C9II respectively in African-Americans (Sullivan-Klose *et al*. 1996). In a Japanese population the $2C9_{Cys144}$ (II) allele was absent and the frequency of $2C9_{Ile\rightarrow Leu359}$ (III) was 0.021 (Nasu *et al*. 1997). In another study of 100 Caucasians the allelic frequency for the 2C9 wild-type, $2C9_{Arg144}$ (I), $2C9_{Cys144}$ (II) and $2C9_{Ile\rightarrow Leu359}$ (III) were 0.79, 0.12 and 0.085 respectively (Stubbins *et al*. 1996). These results are consistent with a more recent study of 450 Swedish volunteers that found a distribution of 0.819, 0.107 and 0.074 respectively for the 2C9I, 2C9II and 2C9III alleles (Yasar *et al*. 1999).

The catalytic roles of the (WT) $2C9_{Arg144}$ (I), $2C9_{Cys144}$ (II) and $2C9_{Ile\rightarrow Leu359}$ (III) for the metabolism of warfarin, flurbuprofen and diclofenac were studied in liver microsomes from 30 humans genotyped for the three 2C9 alleles. Nineteen of the humans were wild-type, eight were heterozygous $2C9_{Cys144}$ (II) and three were heterozygous for $2C9_{Ile\rightarrow Leu359}$ (III). All individuals with the $2C9_{Cys144}$ (II) allele had similar but slightly lower activities for the metabolism of the three substrates. One of the three samples from heterozygotes for $2C9_{Ile\rightarrow Leu359}$ (III) had low V_{max} and high K_m whereas the other two samples were comparable with that of the $2C9_{Arg144}$ (I) wild-type and the $2C9_{Cys144}$ (II). The conclusion of this latter study was that the $2C9_{Cys144}$ (II) allele exhibited comparable but slightly lower metabolic activity than the wild-type and the $2C9_{Ile\rightarrow Leu359}$ (III) had lower rates of oxidation compared with the wild-type (Yamazaki *et al*. 1998). In another study, Veronese *et al*. (1991) reported that the V_{max} for the $2C9_{Cys144}$ (II) allele for tolbutamide and phenytoin metabolism were 2–3 times lower than the wild-type 2C9. In another study, the V_{max} of (*S*)-7-hydroxy warfarin formation was 20-fold greater in the wild-type than the $2C9_{Cys144}$ (II). V_{max} for methylhydroxy tolbutamide formation however was similar in the wild-type and the $2C9_{Cys144}$ (II) allele (Rettie *et al*. 1994).

Previous studies from our laboratory have reported the production of monoclonal antibodies highly specific and highly inhibitory to the major isoforms of cytochromes P450 in human liver. This highly allele specific MAb can be of unique value for determining the amount of expression of the P4502C9II allele in HLM from a heterozygote with a genotype 2C9WTI/II. Using the MAb 292-2-3, differences were found in the relative expression of each allele in different HLM samples from

heterozygote individuals (unpublished data). The MAb-based analytic system can identify drugs metabolized by a single or multiple P450s and partner drugs metabolized by a common P450, which may thereby result in toxicity. The MAb can also determine cytochrome P450 substrate and product specificity, interindividual variation in cytochrome P450-based drug metabolism in liver and other tissues, and the effects of cytochrome P450 inducers, inhibitors, genetic factors, ethnic differences, age, gender, developmental and nutritional states and environmental factors (Gelboin *et al*. 1999).

Polymorphic genetically defective cytochrome P450 genes can be identified by genomic methods (Ingelman-Sundberg *et al*. 1999) and MAb-based proteomic methods can quantitatively measure cytochrome P450 gene expression at the functional protein level. The MAb system can identify drugs metabolized by polymorphic cytochrome P450s that may be defective in certain populations. The clinical use of those drugs in the defective population would depend on the relative amount of the drug metabolized by other non-polymorphic cytochrome P450s and the presence and activity of allelic forms. A major application of the MAb system is the identification of drugs that can be used *in vivo* for phenotyping an individual P450 profile. *In vivo* determination of the P450 isoform phenotype requires that the metabolic pathway of a probe drug be entirely catalyzed by a single cytochrome P450.

The MAb 292-2-3 is specific to a single allele of 2C9 and may be a prototype for MAb specific to single alleles which may be used to determine in a heterozygote individual the amount of expression of a target allele into functional cytochrome P450 enzyme. It is quite possible that some drugs can be identified that are metabolized by only a single allelic form and thus be used as an *in vivo* marker for the specific allele. Characterization of drugs P450-based metabolism coupled with knowledge of the phenotype of the individual will be clinically useful for the goal of toxicity reduction.

References

Battula, N., Sagara, J. and Gelboin, H. V., 1987, Expression of P1–450 and P3–450 DNA coding sequences as enzymatically active cytochromes P-450 in mammalian cells. *Proceedings of the National Academy of Sciences, USA*, **12**, 4073–4077.

Crespi, C. L. AND Penman, B. W., 1997, Use of cDNA-expressed human cytochrome P450 enzymes to study potential drug-drug interactions. *Advances in Pharmacology*, **43**, 171–188.

Fujino, T., Park, S. S., West, D. and Gelboin, H. V., 1982, Phenotyping of cytochromes P-450 in human tissues with monoclonal antibodies. *Proceedings of the National Academy of Sciences, USA*, **79**, 3682–3686.

Gelboin, H. V., 1993, Monoclonal antibodies and cytochrome P450. *Pharmacological Reviews*, 45, 413–453.

Gelboin, H. V., Goldfarb, I., Krausz, K. W., Grogan, J., Korzekwa, K. R., Gonzalez, F. J. and Shou, M., 1996, Inhibitory and non-inhibitory monoclonal antibodies to human cytochrome P450 2E1. *Chemical Research Toxicology*, **9**, 1023–1030.

Gelboin, H. V., Krausz, K. W., Goldfarb, I., Buters, J. T. M., Yang, S. K., Gonzalez, F. J., Korzekwa, K. R. and Shou, M., 1995, Inhibitory and non inhibitory monoclonal antibodies to human cytochrome P450 3A3/4. *Biochemical Pharmacology*, **50**, 1841–1850.

Gelboin, H. V., Krausz, K. W., Gonzalez, F. J. and Yang, T. J., 1999, Monoclonal antibodies and human cytochromes P450: a new avenue for drug discovery. *Trends in Pharmacological Science*, **20**, 432–438.

Gelboin, H. V., Krausz, K. W., Shou, M., Gonzalez, F. J. and Yang, T. J., 1997, A monoclonal antibody inhibitory to human P450 2D6: a paradigm for use in combinatorial determination of individual P450 role in specific drug tissue metabolism. *Pharmacogenetics*, **7**, 469–477.

Gelboin, H. V., Shou, M., Goldfarb, I., Yang, T. J. and Krausz, K. W., 1998, Monoclonal antibodies to cytochrome P450. In I. R. Phillips and E. A. Shephard (eds), *Methods in Molecular Biology*: *Cytochrome P450 Protocols* (New Jersey: Humana), pp. 227–237.

Gonzalez, F. J., Kimura, S., Tamura, S. and Gelboin, H. V., 1991, Expression of mammalian cytochrome P 450 using baculovirus. *Methods in Enzymology*, **206**, 93–99.

Haining, R. L., Hunter, A. P., Veronese, M. E., Trager, W. F. and Rettie, A. E., 1996, Allelic variants of human cytochrome P450 2C9: baculovirus-mediated expression, purification, structural characterization, substrate stereoselectivity, and prochiral selectivity of the wild-type and I359L mutant forms. *Archives of Biochemistry and Biophysics*, **333**, 447–458.

Ingelman-Sundberg, M., Oscarson, M. and McLellan, R. A., 1999, Polymorphic human cytochrome P450 enzymes: an opportunity for individualized drug treatment. *Trends in Pharmacological Sciences*, **20**, 342–349.

Ioannides, C. (ed.), 1996, *Cytochrome P*450: *Metabolic and Toxicology Aspects* (Boca Raton: CRC Press), pp. 1–411.

Kohler, G. and Milstein, C., 1975, Continuous cultures of fused cells secreting antibody of predefined specificity. *Nature*, **7**, 495–497.

Miners, J. O. and Birkett, D. J. 1998, Cytochrome P 450 2C9: an enzyme of major importance in human drug metabolism. *British Journal of Clinical Pharmacology*, **45**, 525–538.

Montellano, O. (ed.), 1995, *Cytochrome P* 450: *Structure, Mechanism and Biochemistry* (London: Plenum), pp. 473–535.

Nasu, K., Kubota, T. and Ishizaki, T., 1997, Genetic analysis of CYP2C9 polymorphism in a Japanese population. *Pharmacogenetics*, **7**, 405–409.

Relling, M. V., Aoyama, T., Gonzalez, F. J. and Meyer, U. A., 1990, Tolbutamide and mephenytoin hydroxylation by human cytochrome P450s in the CYP2C subfamily. *American Society for Pharmacology and Experimental Therapeutics*, **252**, 442–447.

Rendic, S. and Di Carlo, F. J., 1997, Human cytochrome P450 enzymes: status report summarizing their reactions, substrates, inducers, and inhibitors. *Drug Metabolism Reviews*, **29**, 413–580.

Rettie, A. E., Wienkers, L. C., Gonzalez, F. J., Trager, W. F. and Korzekwa, K. R., 1994, Impaired (*S*)-warfarin metabolism catalysed by the R144C allelic variant of CYP2C9. *Pharmacogenetics*, **4**, 39–42.

Sai, Y., Yang, T. J., Krausz, K. W., Gonzalez, F. J. and Gelboin, H. V., 1999, An inhibitory monoclonal antibody to human cytochrome P450 2A6 defines its role in the metabolism of coumarin, 7-ethoxycoumarin and 4-nitroanisole in human liver. *Pharmacogenetics*, **9**, 229–237.

Shou, M., Korzekwa, K. R., Krausz, K. W., Crespi, C. L., Gonzalez, F. J. and Gelboin, H. V., 1994, Regio- and stereo-selective metabolism of phenanthrene by twelve cDNA expressed human, rodent, and rabbit cytochromes P-450. *Cancer Letters*, **83**, 305–313.

Stubbins, M. J., Harries, L. W., Smith, G., Tarbit, M. H. and Wolf, C. R., 1996, Genetic analysis of the human cytochrome P450 CYP2C9 locus. *Pharmacogenetics*, **6**, 429–439.

Sullivan-Klose, T. H., Ghanayem, B. I., Bell, D. A., Zhang, Z. Y., Kaminsky, L. S., Shenfield, G. M., Miners, J. O., Birkett, D. J. and Goldstein, J. A., 1996, The role of the CYP2C9-Leu359 allelic variant in the tolbutamide polymorphism. *Pharmacogenetics*, **6**, 341–349.

Tassaneeyakul, W., Birkett, D. J., Veronese, M. E., McManus, M. E., Tukey, R. H., Quattrochi, L. C., Gelboin, H. V. and Miners, J. O., 1993, Specificity of substrate and inhibitor probes for human cytochromes P 450 1A1 and 1A2. *Journal of Pharmacology Experimental Therapy*, **1**, 401–407.

Veronese, M. E., Mackenzie, P. I., Doecke, D. J., McManus, M. E., Minors, J. O. and Birkett, D. J., 1991, Tolbutamide and phenytoin hydroxylations by cDNA-expressed human liver cytochrome P450 2C9. *Biochemical Biophysical Research Communications*, **175**, 1112–1118.

Yamazaki, H., Inoue, K., Chiba, K., Ozawa, N., Kawai, T., Suzuki, Y., Goldstein, J. A., Guengerich, F. P. and Shimada, T., 1998, Comparative studies on the catalytic roles of cytochrome P450 2C9 and its Cys- and Leu- variants in the oxidation of warfarin, flurbiprofen, and diclofenac by human liver microsomes. *Biochemical Pharmacology*, **56**, 243–251.

Yang, T. J., Krausz, K. W., Shou, M., Yang, S. K., Buters, J. T. M., Gonzalez, F. J. and Gelboin, H. V., 1998a, Inhibitory monoclonal antibody to human cytochrome P450 2B6. *Biochemical Pharmacology*, **55**, 1633–1640.

Yang, T. J., Krausz, K. W., Sai, Y., Gonzalez, F. J. and Gelboin, H. V., 1999, Eight inhibitory monoclonal antibodies define the role of individual P450s in human liver microsomal diazepam, 7-ethoxycoumarin and imipramine metabolism. *Drug Metabolism and Disposition*, **27**, 102–109.

Yang, T. J., Sai, Y., Krausz, K. W., Gonzalez, F. J. and Gelboin, H. V., 1998b, Inhibitory Monoclonal Antibodies to Human cytochrome P450 1A2: analysis of phenacetin *o*-deethylation in human liver. *Pharmacogenetics*, **8**, 375–382.

Yasar, U., Eliasson, E., Dahl, M. L., Johansson, I., Ingelman-Sundberg, M. and Sjoqvist, F., 1999, Validation of methods for CYP2C9 genotyping: frequencies of mutant alleles in a Swedish population. *Biochemical and Biophysical Research Communications*, **254**, 628–631.

XENOBIOTICA, 2000, VOL. 30, NO. 6, 627–642

Pharmacokinetics and metabolism of a sulphamide NK_2 antagonist in rat, dog and human

K. BEAUMONT†*, A. HARPER†, D. A. SMITH† and S. ABEL‡

† Department of Drug Metabolism and ‡ Early Clinical Research Group, Pfizer Central Research, Sandwich CT13 9NJ, UK

Received 19 November 1999

1. UK-224,671 is a sulphamide-containing NK_2 antagonist with moderate lipophilicity and basicity.

2. The physicochemical properties of UK-224,671 are reflected in its pharmacokinetics following intravenous (i.v.) administration. The compound partitioned extensively into red blood cells in all species examined and the blood clearance was moderate to low with respect to liver blood flow and distribution into tissues was extensive.

3. UK-224,671 exhibited species differences in oral bioavailability. In dog, the compound exhibited moderate bioavailability (55%), whereas in rat and man oral bioavailability was $< 10\%$.

4. In rat and dog, the major excreted form after i.v. administration was unchanged UK-224,671 in both urine and faeces. In addition, of three metabolites observed, the most abundant was the N-descyclopropylmethyl (UK-280,045).

5. The profile of radioactivity in rat following oral administration of [^{14}C]-UK-224,671 was not consistent with a 10% absorbed compound with 40% of the dose present as metabolites. This suggests that the low bioavailability of UK-224,671 in rat is due to a combination of moderate intestinal permeability and extensive first-pass metabolism by the gut and does not result from poor gastrointestinal absorption *per se*.

Introduction

UK-224,671 [(*S*)-(+)-4-(1-{2-[1-(cyclopropylmethyl)-3-(3,4-dichlorophenyl)-6-oxo-3-piperidyl]ethyl}azetidin-3-yl)-1-piperazine sulphamide] (figure 1) is a new chemical entity shown in-house to be a potent and selective NK_2 receptor antagonist *in vitro* and *in vivo* (unpublished data). NK_2 receptor antagonists have the potential to relax smooth muscle and as such could have applications in the treatment of diseases such as asthma.

In the current study, the pharmacokinetics of UK-224,671 have been determined in rat, dog and human following intravenous (i.v.) and oral administration, using a specific hplc-mass spectrometry method for the analysis of drug in biological fluids. In addition, the excretion and metabolic fate of the compound has been determined in rat and dog following i.v. and oral administration of [^{14}C]-labelled UK-224,671. The pharmacokinetic parameters obtained have been rationalized in terms of the physicochemical and structural properties of UK-224,671.

Materials and methods

Chemicals

UK-224,671 (regulatory quality material always $> 95\%$ chemically pure) and internal standard UK-339,501 (UK-224,671 labelled with eight deuterium atoms) were obtained from Medicinal Chemistry or Process Research Departments (Pfizer Central Research, Sandwich). [^{14}C]-UK-224,671 was prepared by

* Author for correspondence; e-mail: kevin_beaumont@sandwich.pfizer.com

Xenobiotica ISSN 0049–8254 print/ISSN 1366–5928 online © 2000 Taylor & Francis Ltd
http://www.tandf.co.uk/journals

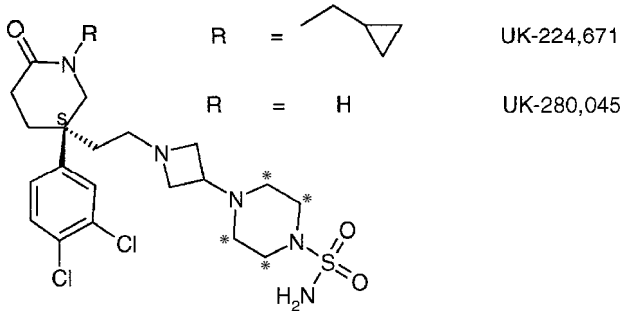


Figure 1. Structure of UK-224,671 and UK-280,045. *Positions of [^{14}C]-labels.

Amersham International (Cardiff, UK). The nominal specific activity was 33.2 μCi/mg (1.23 MBq/mg) and the radiochemical purity was $>98.5\%$ by thin layer chromatography (tlc) in two solvent systems and by hplc. The identity of the [^{14}C]-UK-224,671 was checked by mass spectrometry.

Administration to animals

Wherever possible the dose levels and formulations of UK-224,671 were chosen to reflect those used in toxicology evaluation. All vehicles used were deemed to be acceptable for use in the animal species.

Pharmacokinetic studies. For i.v. administration to rat and dog, UK-224,671 (monosulphate trihydrate salt) was dissolved in a vehicle containing propylene glycol/saline (20/80 v/v) and the pH was adjusted to 3.5 with 1 M sodium hydroxide. For oral administration to rat and dog, UK-224,671 was prepared as a suspension in 0.5% methylcellulose/0.1% Tween 80 in water (w/v). The suspensions were prepared to reflect toxicology studies aiming at particle sizes of <40 μm with stability appropriate for the duration of the study.

Male and female Sprague–Dawley rats (Charles River, mean weight 271 ± 25 g) were housed in Techniplast cages in facilities maintained at 19–21 °C and $50\pm20\%$ humidity with a 12-h dark/light cycle. They had free access to food (Rat and mouse maintenance diet no. 1, Special Diet Services) and water.

Rats received either i.v. doses of UK-224,671 (0.2 ml, $\sim$0.8 ml/kg) via the tail vein (n = 2 male, n = 2 female) or oral doses (0.5 ml, $\sim$2 ml/kg) by gavage tube (n = 2 male, n = 2 female). Dose levels were 3 mg/kg (i.v.) or 20 mg/kg (oral). Blood (0.2 ml) was sampled from previously implanted jugular vein cannulae and made up to a final volume of 1 ml with control blood for analysis.

Two male and two female beagle dogs (weight range 12–15 kg, age 2.5–6.5 years) from the colony at Pfizer Central Research were used in the studies. The dogs had previously been used for other studies but an appropriate wash out period (at least 1 month) was allowed before completing these studies. The dogs were housed in pens of 4.5 m^2 area on a solid floor with graded sawdust bedding. The temperature was maintained at 18.5 ± 2 °C with $55\pm10\%$ humidity and a 12-h dark/light cycle. They received $\sim$400 g Teklad dog maintenance diet (Harlan) and water *ad libitum*.

Intravenous doses of UK-224,671 (3 mg/kg) were administered into the saphenous vein as an infusion of 12–15 min duration. Infusion administration was used as standard practice within the Department of Drug Metabolism as in the unlikely event of an adverse reaction, administration of the compound could be terminated. Oral doses (20 mg/kg) were administered by gavage 2 weeks later. To obtain samples up to 48 h, one male and one female dog were dosed at 09:00 hours on the first day of the study. Following dosing they were kept in slings for the first 6 h and blood was sampled from the saphenous vein by means of indwelling catheters. After this period, samples were obtained from the cephalic vein by venepuncture. Another male and female dog were dosed at 21:00 hours on day 1 and blood samples taken from 09:00 hours the next day (i.e. 12–24 h) via indwelling saphenous vein catheters. Again subsequent samples were taken by venepuncture. The overall blood sample volume taken per animal for each leg of the study was $\sim$80 ml. All blood samples were collected into heparinized tubes and stored at ~-20 °C before analysis.

Metabolism studies

For i.v. administration to rat and dog, unlabelled UK-224,671 and [^{14}C]-UK-224,671 were dissolved in the same vehicle as outlined for the pharmacokinetic studies. For oral administration unlabelled and [^{14}C]-UK-224,671 were dissolved in PEG 200/distilled water (25/75 v/v). A solution formulation was used for these studies as opposed to the suspension to ensure homogeneity of the labelled and unlabelled UK-224,671.

Four male and four female Sprague–Dawley rats (mean weight 246±12 g) received i.v. doses of [^{14}C]-UK-224,671 (3 mg/kg, 21 μCi, 0.8 ml/kg) via the tail vein. A further four male and four female Sprague–Dawley rats (mean weight 247±14 g) received oral doses (20 mg/kg, 21 μCi, 2 ml/kg) by gavage tube. For each administration route following dosing, two male and two female rats were housed singly in metabolism cages designed for separate collection of urine and faeces, and two male and two female rats were housed in stock boxes for blood collection at different time points.

For the excretion study the total output of urine and faeces was collected and weighed daily for 5 days after administration. Daily faecal output was macerated with an equal weight of water and stored frozen (−20 °C) until analysed. For the blood study, rats were anaesthetized (halothane) and exsanguinated via the vena cava. The blood was stored frozen until analysed.

One male and one female beagle dog from the Pfizer colony were used for metabolism studies. For i.v. administration (3 mg/kg, 40 μCi, 0.5 ml/kg), individual doses were infused into the saphenous vein for 12–15 min. For oral administration (20 mg/kg, 38 μCi, 2 ml/kg), individual doses were administered by gavage. There were 28 days between the successive doses. Following dosing the dogs were housed individually in metabolism cages. The total output of urine and faeces was weighed daily for 6 days (i.v.) and 5 days (oral) after dosing. Urine was stored frozen (−20 °C) before analysis. Daily faecal output was macerated with water in a ratio of 4:1 and stored frozen before analysis. Blood samples (5 ml per sample up to a total of ~ 80 ml) were taken into heparinized tubes at specific times after dosing and stored frozen before analysis. For analysis of radioactive content, samples (0.25 ml) were dried in Combusto cones (Packard).

Administration to human volunteers

To determine the pharmacokinetics of UK-224,671 in human, eight male volunteers (age 18–45 years; weight 60–100 kg) participated in a randomized four-way crossover study conducted at the Pfizer Clinical Research Unit and Canterbury Hospital. The volunteers provided written informed consent and the protocol was approved by the local ethics committee. The study was conducted to the requirements of GCP. Each volunteer was screened within 3 weeks of the study start, and then followed-up within 7–10 days of the final dose. The following safety assessments were made at each study period, on admission and discharge (48 h post-dose): physical examination, 12-lead ECG and laboratory safety tests (blood and urine). In addition, a neurological examination was conducted predose and at 45 min post-dose, and blood pressure was measured at regular intervals from predose to 48 h post-dose.

The four treatment groups consisted of placebo, 0.1 mg/kg UK-224,671 by i.v. infusion of 15 min and oral solution administration of 150 mg UK-224,671 to fed and fasted individuals. UK-224,671 exhibited appropriate stability in the solutions used and the i.v. dose was prepared under sterile conditions. On each dosing day, each subject received a single dose of UK-224,671 and whole blood samples were taken up to 72 h. The overall volume of blood taken from each volunteer was ~ 600 ml.

Analysis of whole-blood samples for UK-224,671

The concentrations of UK-224,671 in rat and dog whole blood were determined by a specific hplc-mass spectrometry method. UK-224,671 and the internal standard UK-339,501 (deuterium-labelled UK-224,671) were extracted from blood (1 ml) after addition of buffer (1 M Tris, pH 11.2, 1 ml) and water (1 ml), using Chem-elut tubes (1 ml capacity, Varian). Compounds were eluted from the Chem-elut tubes with 2×6 ml ethyl acetate/isopropanol (9/1 v/v) and evaporated to dryness under nitrogen at 50 °C.

The residues were reconstituted in 2 ml isopropanol/water (50/50 v/v) and then extracted by ion pair solid-phase extraction. Samples were loaded onto Propylsulphonic acid (PRS) solid-phase extraction cartridges (100 mg, 1 ml, Varian) pretreated with 1 ml methanol, followed by 2 ml 5% HCl in methanol and followed by another 1 ml methanol. The contents of the cartridges were washed with 1 ml water and 2 ml methanol/ethyl acetate (50/50 v/v). Compounds were eluted with 1.5 ml 5% ammonia in methanol and evaporated to dryness under nitrogen at 30 °C. The residues were dissolved in 200 μl methanol/water (40/60 v/v) containing 20 mM ammonium acetate for analysis by LC-MS-MS. The assay was validated for a lower calibration range of 0.5–25 ng/ml and for a higher calibration range of 25–250 ng/ml. For the lower range 150 μl of sample was injected onto the mass spectrometer and for the higher range 15 μl of sample was injected to prevent saturation of ionization. The mobile phase was methanol/water (70/30 v/v) containing 20 mM ammonium acetate and the column was a Kromasil KR100-5C18 (15 cm×4.6 mm i.d.) with a 1 cm KR100-5C18 guard column. Detection used a Sciex API III+mass spectrometer (Perkin Elmer, Sciex, Ontario, Canada) in positive atmospheric pressure chemical ionization mode (heated nebulizer probe at 500 °C). The mass spectrometer was tuned to detect the precursor to product transitions of 544 to 465 for UK-224,671 and 552 to 473 for UK-339,501. Imprecision and inaccuracy determinations for the analysis of UK-224,671 in animal blood are shown in table 1.

The concentrations of UK-224,671 in human blood were determined by a similar specific hplc mass spectrometry method, modified to facilitate more rapid sample throughput and a wider calibration range of 1–100 ng/ml. UK-224,671 and internal standard (UK-339,501) were extracted from blood (100 μl)

Table 1. Imprecision and inaccuracy of the UK-224,671 bioanalytical method in blood from rat and dog.

Concentration (ng/ml)	Imprecision (%)	
0.5–25 ng/ml range	Rat	Dog
0.5	11.3	12.4
6	1.2	2.7
25	1.2	1.7
Mean % QC error (inaccuracy)	9.1	7.5
25–250 ng/ml range		
25	4.8	7.9
75	1.5	2.9
250	0.7	3.4
Mean % QC error (inaccuracy)	8.2	10.6

Imprecision was determined by the analysis of blood containing UK-224,671 at the concentrations stated (n = 5 determinations per concentration) and was calculated by dividing the standard deviation by the mean concentration found. Inaccuracy was determined from quality control (QC) samples (n = 6) containing concentrations of UK-224,671 unknown to the analyst. Error was determined as the concentration found relative to the actual concentration.

Table 2. Imprecision and inaccuracy for the UK-224,671 bioanalytical methods in human blood and urine.

QC concentration (ng/ml)	Mean concentration found (ng/ml)	Standard deviation	Imprecision (%)	Inaccuracy (%)
Human blood				
2	1.9	0.17	8.8	−4.0
25	23.6	1.4	6.0	−5.7
75	70.9	5.5	7.8	−5.5
Human urine				
200	224	5.8	2.6	11.8
1000	976	59.4	6.1	−2.4
2500	2310	108	4.7	−7.6
25000	23100	2220	9.6	−7.7

Imprecision was calculated by dividing the standard deviation by the mean concentration found. Inaccuracy was determined from the mean concentration found relative to the actual concentration. Results are derived from 36 determinations for human blood and eight determinations for human urine.

after addition of 0.2 M sodium borate buffer, pH 10 (300 μl) using Chem-elut tubes (0.3 ml capacity, Varian). Compounds were eluted from the Chem-elut tubes with 2×2 ml aliquots of ethyl acetate/propan-2-ol (9/1 v/v) and evaporated to dryness under nitrogen at 50 °C. The residues were dissolved in 150 μl methanol/water (40/60 v/v) containing 20 mM ammonium acetate, and 75 μl was injected onto the hplc-mass spectrometer. The same mass spectrometry conditions were used for analysis except that the eluent from the hplc column was diverted to waste for the first 3 min following injection, by use of a six-port switching valve. The eluent was then diverted to the mass spectrometer after 3 min to detect UK-224,671 and internal standard (UK-339,501). Imprecision and inaccuracy determinations for the analysis of UK-224,671 in human blood and urine are shown in table 2. Assay validation was completed to the standards described by Shah *et al*. (1992). Quality control samples were included in each analytical run.

Urinary excretion of unchanged UK-224,671 in rat and dog was determined from the excretion studies. Urinary concentrations of UK-224,671 in human were determined by an adaptation of the above blood assay. Urine was diluted with methanol/water (40/60 v/v) containing 20 mM ammonium acetate and internal standard. Aliquots of this were injected into the hplc-mass spectrometer under the conditions outlined above. The lower limit of quantification was 100 ng/ml. Validation of the human urinary assay is shown in table 2.

Pharmacokinetic analysis of data

The terminal phase rate constant (k_{el}) was determined by linear regression of the log blood concentration–time profile. The terminal elimination half-life ($t_{1/2}$) was calculated from $0.693/k_{el}$. Area under the blood concentration versus time curve $AUC_{(0-t)}$ was calculated to the last time point (24 or 48 h) by the linear trapezoidal rule. $AUC_{(0-\infty)}$ was calculated from $AUC_{(0-t)}$ by extrapolation to infinity using k_{el}. Clearance (Cl) was calculated from the i.v. data by the relationship dose/$AUC_{(0-\infty)}$ and the volume of distribution at steady-state was calculated from moment analysis. Oral bioavailability (F) was calculated from the ratio of AUC after oral and i.v. doses after normalizing for dose.

Analysis of radioactivity

Radioactivity in weighed samples of rat and dog urine was determined by liquid scintillation counting in Starscint (Packard). Radioactivity in rat and dog faecal homogenate and whole blood was measured by combustion of triplicate weighed samples in an Oximate Sample Oxidizer (Packard Instruments). The evolved $^{14}CO_2$ was trapped using Carbosorb (Packard) and the amount of radioactivity determined by liquid scintillation counting in 10 ml Permafluor E+ (Packard).

Analysis of faecal metabolite profiles

Excretion of drug and metabolites was measured by radio hplc of extracts of faeces. Pooled faecal samples were prepared for each species by mixing proportionate amounts of faecal homogenates to represent 1% (rat) or 0.1% (dog) of the excreted radioactivity over 0–48 h. Pooled samples were basified by addition of 5 mg sodium carbonate and extracted using 10 ml methanol (rat) or 25 ml methanol (dog) with thorough mixing for 1 h. Following centrifugation, the methanol layer was removed and evaporated to dryness under nitrogen. The solid particles were re-extracted with fresh methanol twice more and the residues combined. The combined residues from rat and dog faeces were dissolved in 10 ml methanol and an aliquot taken for liquid scintillation counting. The recoveries of radioactivity from rat and dog faecal homogenates were 74 and 92% respectively. When calculating the percentage of the dose excreted as one particular metabolite (table 6), the assumption was made that the relative proportions of radioactivity in the faecal extracts represented those present in the faeces.

Following recovery determination, the methanol was evaporated to dryness and the residues redissolved in 0.1 M ammonium acetate pH 7.4, for injection onto the gradient hplc. The hplc consisted of a semi-preparative Spherisorb-5-ODS-2 column (25×0.8 cm i.d. Hichrom) over which two linear gradients were developed; 25–70% methanol in 0.1 M ammonium acetate, pH 7.4 during 10 min, continuing to 100% during a further 10 min, then at 100% for 15 min. Detection was by a radioflow detector (β-ram, INUS systems) with data analysis on LAURA software (Lablogic, Sheffield, UK). Blood samples were analysed for UK-224,671 using the same procedure as before.

Analysis of urinary metabolite profiles

Excretion of drug and metabolites was measured by radio hplc of urine produced in the 0–24-h period post-dose. Following centrifugation to remove particulate matter, aliquots of the urine samples were injected directly onto the same gradient hplc as described for the faecal extract analysis above.

Determination of metabolite identities

Confirmation of the chemical identity of the radioactive components collected as fractions of the hplc eluate was inferred from molecular weight values obtained by mass spectral analysis. Fractions were introduced onto the mass spectrometer following chromatography on a Phenomenex Magellen C18 column (3 μm, 5 cm×4.6 mm diameter) at a flow rate of 1 ml/min in a mobile phase of methanol/water (55/45 v/v) containing 2 mM ammonium acetate. The mass spectrometer was a Sciex API III triple quadrupole mass spectrometer in positive-ion mode (using ion spray probe or heated nebulizer). Q1 analysis of parent ions and MS/MS analysis of daughter ions was compared with that of known standards, as were retention times on hplc.

Blood distribution studies

Preliminary information on the extent of blood cell distribution of UK-224,671 was obtained using a bioanalytical method which was not formally validated. Whole blood from rat, dog and human was prepared containing 200 ng/ml UK-224,671 and incubated at 37 °C in a shaking water bath. At 0-, 0.5-, 1-, 1.5- and 2-h incubations, 3 ml blood was withdrawn and plasma prepared by centrifugation. Following addition of an internal standard (UK-202,413, an analogue of UK-224,671) plasma (1 ml) was extracted using solid-phase extraction. The extraction cartridges (CN Bond Eluts, 1 ml capacity, Analytichem International) were activated with 1 ml methanol and washed with 1 ml 0.1 M potassium dihydrogen orthophosphate buffer, pH 7.4. Following application of the plasma, the columns were washed with 1 ml 0.1 M potassium dihydrogen orthophosphate buffer, pH 7.4 followed by 1 ml methanol/water (20/80 v/v). The compounds were eluted with 1 ml methanol, which was evaporated to dryness under nitrogen. The residues were resuspended in 100 μl of the hplc mobile phase and 80 μl was injected onto the hplc. The hplc consisted of an HiRPB column(25 cm × 0.5 cm i.d., Hichrom) with a mobile phase of acetonitrile/10 mM octane sulphonic acid, 10 mM potassium dihydrogen orthophosphate pH 3 (39/61 v/v). Detection was by UV absorbance at 210 nm. On this system UK-224,671 and UK-202,413 exhibited retentions of 8 and 11 min respectively. The analytical method performance was monitored by assessing linearity of the calibration curve and analysing concentrations of UK-224,671 unknown to the analyst. Distribution into the blood cell fraction was generally complete within 1 h and the data quoted in the results are from the 2-h time point.

Plasma protein binding

Samples of rat, dog and human plasma (1 ml) containing UK-224,671 (500 ng/ml) were dialysed (Spectrapor 1 dialysis membrane 6000–8000 molecular weight cut off; Spectrum Medical Industries) against isotonic Krebs–Ringer Bicarbonate buffer, pH 7.4 (1 ml) for 4 h at 37 °C in a rotating dialyser (Dianorm M.S.E.). Following dialysis, samples of buffer and plasma were analysed for UK-224,671 using the hplc UV method described above for the blood distribution experiments.

Blood binding studies

The extent of binding of UK-224,671 in whole blood from rat, dog and human was determined using the radiolabelled compound. Blood (1 ml) containing [^{14}C]-UK-224,671 (500 ng/ml) was dialysed under the same conditions reported for the plasma protein binding determination. Following dialysis, the radioactivity in buffer was determined by liquid scintillation counting in Starscint (Packard). Blood samples were combusted and analysed as previously described.

Results

Red blood cell partitioning and equilibrium dialysis in whole blood and plasma

UK-224,671 is a sulphamide-containing compound and structurally similar compounds have been previously reported to distribute unevenly between plasma and the red cell fraction (Lettieri and Portelli 1983). Thus, partitioning studies were carried out in rat, dog and human blood. In addition, the free fractions of UK-224,671 in both plasma and whole blood were determined in the same species. The results from these studies are shown in table 3.

As expected, UK-224,671 distributed preferentially into the red cell fraction in blood with most extensive distribution into human red cells. However, the free fraction of UK-224,671 in whole blood varied < 2-fold across the species tested. Thus, to understand fully the pharmacokinetics of UK-224,671 a whole blood assay was developed.

UK-224,671 Pharmacokinetics

The blood concentration versus time profiles of UK-224,671 following single i.v. and oral administration to rat, dog and human are shown in figure 2 and the pharmacokinetic parameters are shown in table 4. In rat, dog and human, following

Table 3. Red blood cell partitioning and free fractions of UK-224,671 in the plasma and blood from rat, dog and man.

Species	% Unbound in plasma	% Unbound in blood	% in Red cells
Rat	34±2.8	16±0.65	89
Dog	28±2.9	11±0.79	79
Man	42±2.7	8±0.51	96

Results are from five determinations per species from binding studies and a single determination per species at 2 h from the blood distribution studies (see Materials and methods). Plasma protein binding and blood distribution studies are estimates only since the bioanalytical method used was not fully validated.

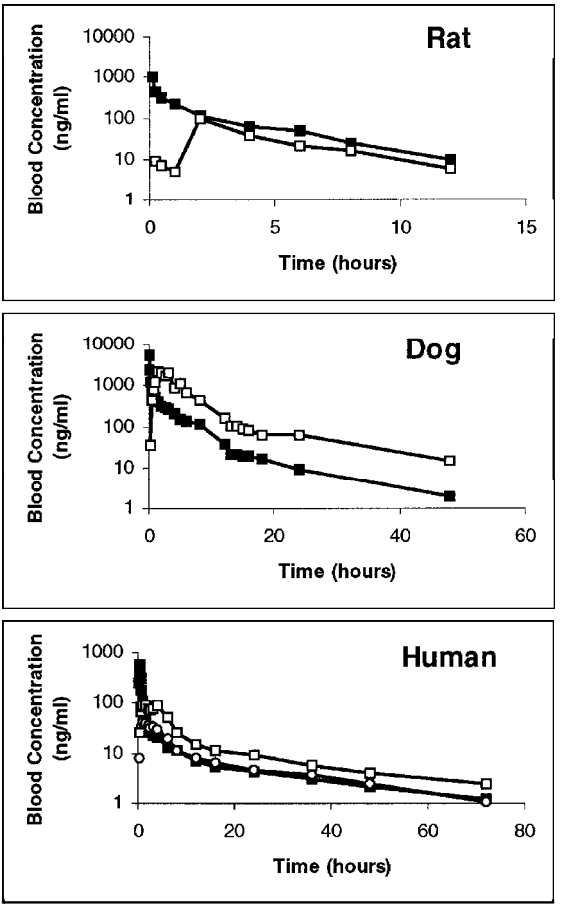


Figure 2. Mean blood concentrations of UK-224,671 following single i.v. and oral administration to rat, dog and man. Data are i.v. (closed squares) and oral (open squares). Dose levels were 3 mg/kg i.v. and 20 mg/kg oral in dog (n = 4) and rat (n = 4) and 100 μg/kg i.v. and 150 mg oral (fasted, n = 8, open squares and fed, n = 8, open circles) in human.

i.v. administration, UK-224,671 exhibited moderate to long terminal phase half-lives of 3.3, 10 and 28 h respectively. These were due to moderate to low blood clearance (rat 47, dog 15 and man 2.3 ml/min/kg) combined with volumes of distribution greater than body water (rat 10, dog 7 and man 2.4 l/kg).

Table 4. Mean pharmacokinetic parameters for UK-224,671 in rat, dog and man following i.v. and oral administration.

Parameter	Rat (n = 4)	Dog (n = 2)	Man (n = 8)	
Intravenous				
Dose (mg/kg)	3.0	3.0	0.1	
Terminal phase half-life (h)	3.3±1.0	10	28±5.2	
Blood clearance (ml/min/kg)	47±13	15	2.3±0.38	
Volume of distribution at steady state (l/kg)	10±0.6	7	2.4±0.74	
AUC_t (ng.h/ml)	970±134	3287	685±103	
AUC_{inf} (ng.h/ml)	1117±264	3321	741±112	
Oral			Fasted	Fed
Dose (mg/kg)	20	20	1.92[a]	1.92[a]
C_{max} (ng/ml)	100±127	2216	124±68	46±16
Terminal phase half-life (h)	3.1[b]	13	26±3.2	32±12
T_{max} (h)	2.7±1.15	1.5	3.2±1.9	1.5±0.7
Bioavailability (%)	7	55	7.5	3.6

[a] Mean weight of volunteers = 78 kg.
[b] Owing to variability, a terminal phase half-life could only be calculated for two rats.

Table 5. Excretion of radioactivity in rat and dog following single i.v. and oral doses of [^{14}C]-UK-224,671.

Species	Route	Dose (mg/kg)	Urine	Faeces	Total excretion 0–48 h	Total excretion 0–120 h[a]
Rat (n = 4)	i.v.	3.0	18	74	91	93
Dog (n = 2)	i.v.	3.0	14	78	82	92
Rat (n = 4)	Oral	20	2	99	100	101
Dog (n = 2)	Oral	20	10	86	89	96

[a] In the i.v. dog, excretion study collections were made up to 144 h post-dose. Results expressed as percentage of administered dose.

Following oral administration of UK-224,671 to rat, blood concentrations were low and variable such that for one rat no pharmacokinetic parameters could be calculated. Comparison of the area under the blood concentration versus time curves for the three other rats versus that for the i.v. dosed rat (normalized for dose) showed that the oral bioavailability in rat was 7%. However, following oral administration of UK-224,671 to dog, bioavailability was 55%. Oral bioavailability in human was similar to rat with an oral bioavailability of 7.5% following administration in the fasted state and 3.6% following administration in the fed state.

Excretion studies

The excretion of radioactivity in the urine and faeces of rat and dog following i.v. and oral administration of [^{14}C]-UK-224,671 are shown in table 5. Following i.v. and oral administration, radioactivity was extensively excreted in the faeces in both species. In rat, following i.v. administration 74% of the dose was excreted in the faeces with 18% in the urine. Following oral administration 99% of the dose was excreted in the faeces.

Table 6. Excretion of radioactive metabolites in urine and faeces of rat and dog after i.v. and oral administration of [^{14}C]-UK-224,671*.

	Intravenous		Oral	
	Faeces	Urine	Faeces	Urine
Rat				
MP (UK-224,671)	50	14	60	0.7
P1 (UK-280,045)	8	0.4	23	0.1
P2	13	0.2	13	nd
P3	nd	1.1	4	0.6
Dog				
MP (UK-224,671)	59	6	54	8
P1 (UK-280,045)	20	1	13	1
P3	nd	2	nd	1

* Data are expressed as a percentage of the administered dose and are derived from two determinations per species.

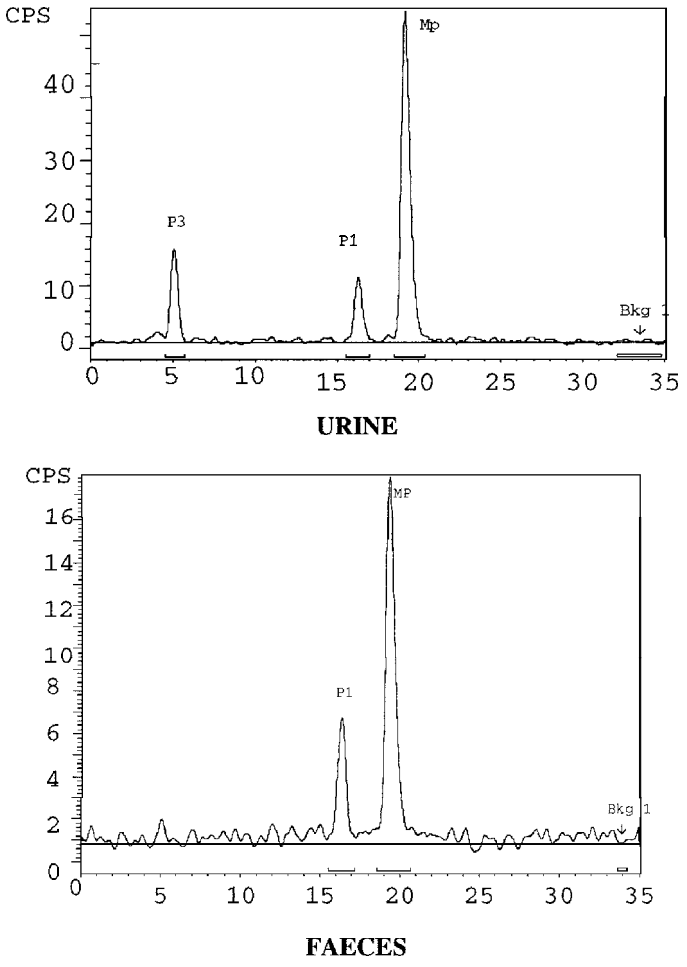


Figure 3. Profiles of urinary and faecal radioactivity after oral administration of [^{14}C]-UK-224,671 to dog. MP is unchanged UK-224,671; P1 is UK-280,045.

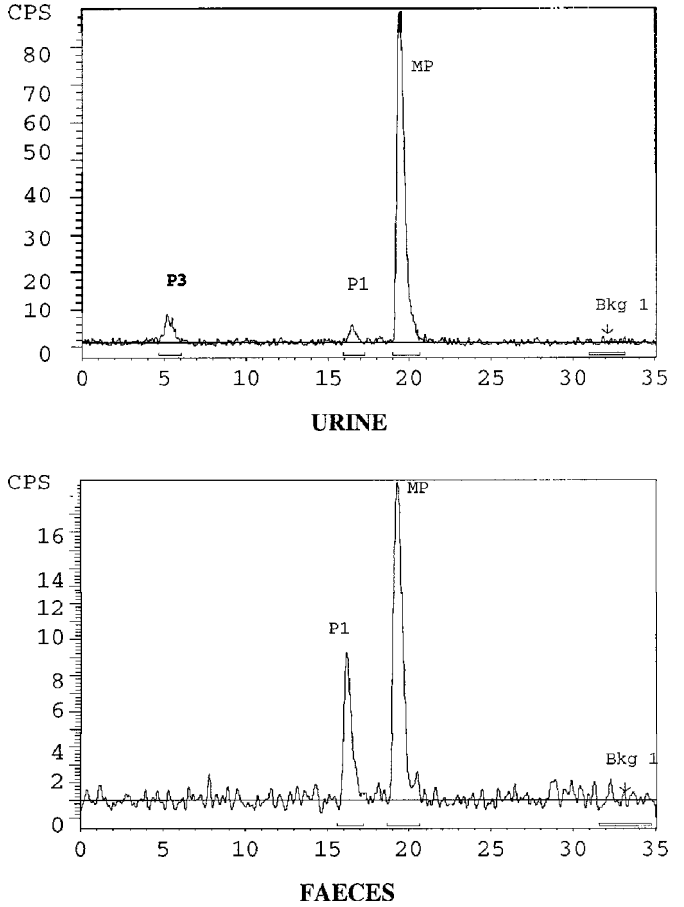


Figure 4. Profiles of urinary and faecal radioactivity after i.v. administration of [^{14}C]-UK-224,671 to dog. MP is unchanged UK-224,671; P1 is UK-280,045.

In dog, 78 and 86% of the dose was excreted in the faeces following i.v. and oral administration respectively. Urinary recovery of radioactivity was 14 and 10% of the dose respectively. Excretion was rapid in both rat and dog with the majority of the dose (at least 82% in both species) being recovered within 48 h post-dose. Overall excretion of radioactivity was essentially complete by 120 h post-dose.

Metabolite profiles

The proportions of the dosed radioactivity excreted as unchanged drug and metabolites, in faeces and urine for both rat and dog are shown in table 6.

The profiles of urinary and faecal metabolites are shown in figures 3 and 4 (dog) and figures 5 and 6 (rat). Metabolite characterization was carried out by comparison of the retention time of the authentic material (where available) and by analysis of the API mass spectrum.

In rat, after dosing by either route about one-half of the dose was excreted as unchanged UK-224,671. The remainder of the excreted radioactivity was accounted for by three metabolites. P1, a dealkylation product (identified as UK-280,045;

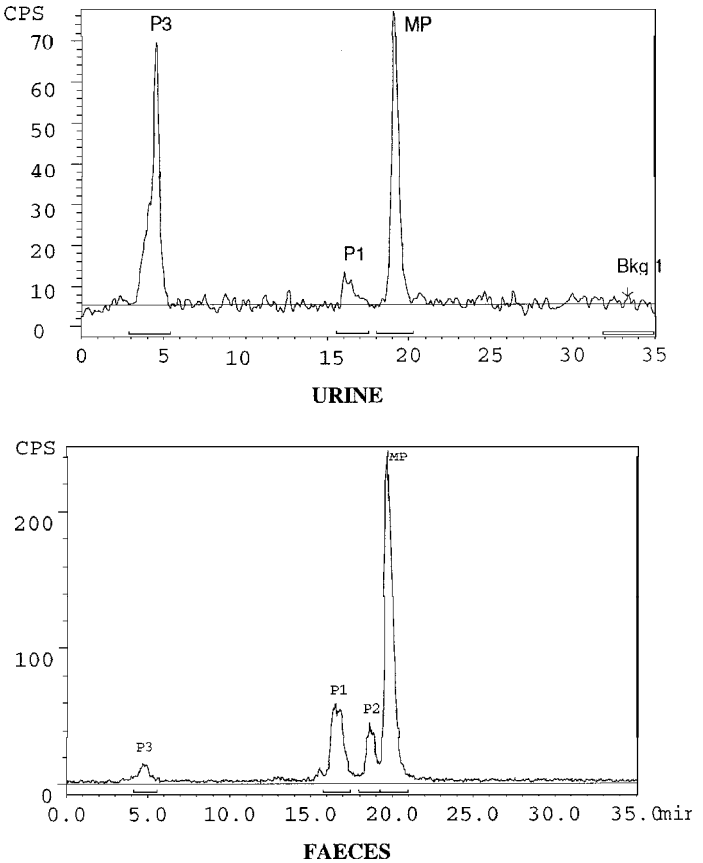


Figure 5. Profiles of urinary and faecal radioactivity after oral administration of [^{14}C]-UK-224,671 to rat. MP is unchanged UK-224,671; P1 is UK-280,045.

figure 1), accounted for 8% of the i.v. dose, compared with 23% after oral dose. P2, identified as a mono-oxidation product (but not further characterized), was excreted equally in the faeces (13%) after both dose routes. Traces of an uncharacterized third metabolite (P3) were present, mainly in faeces (4% of dose) after the oral dose.

In dog, the majority of the excreted radioactivity was identified as unchanged UK-224,671 in both urine and faeces, accounting for a mean of 65 and 62% after i.v. and oral doses respectively. A smaller proportion of excreted radioactivity was identified as metabolites, the most abundant of which (P1, 20 and 13% i.v. and oral respectively) was identified as the N-dealkylation product UK-280,045 (figure 1).

Blood concentrations of radioactivity and of unchanged UK-224,671 measured by specific assay at 1 and 4 h after i.v. and oral dose for both rat and dog are shown in table 7.

In rat, after an i.v. dose $\sim$ 50% of the circulating radioactivity was UK-224,671, whereas after an oral dose, $<$ 5% was UK-224,671 which indicates the presence of circulating metabolites and of first-pass metabolism.

In dog, the close correlation of the values for either dose route and gender indicate that up to 12 h after dose the circulating radioactivity comprised largely of UK-224,671.

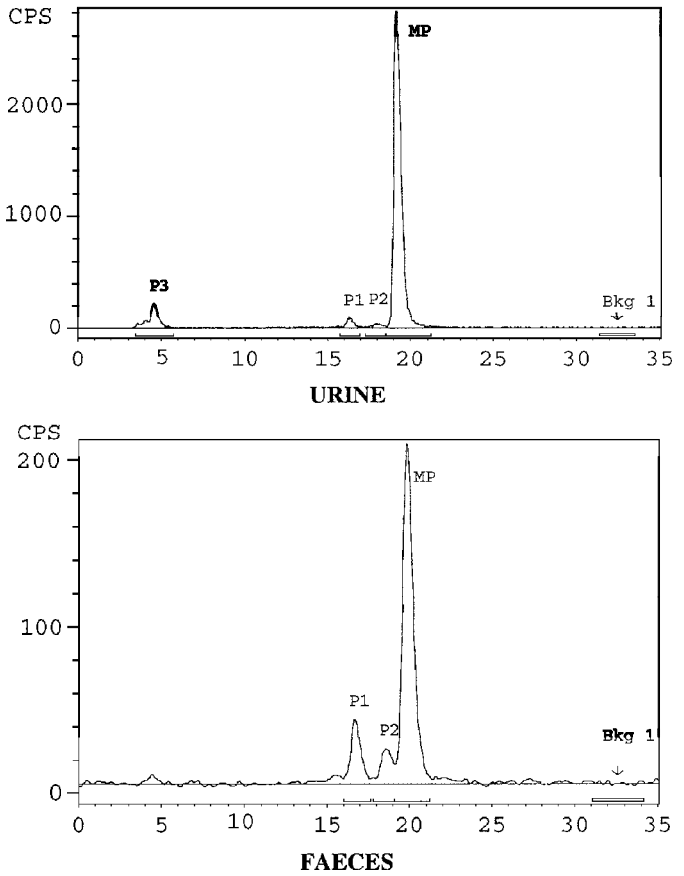


Figure 6. Profiles of urinary and faecal radioactivity after i.v. administration of [^{14}C]-UK-224,671 to rat. MP is unchanged UK-224,671; P1 is UK-280,045.

Table 7. Concentrations of total radioactivity and of UK-224,671 in blood of the male and female rat and dog following single i.v. and oral doses of [^{14}C]-UK-224,671.

			Male		Female	
Species	Route	Time (h)	Radioactivity	UK-224,671	Radioactivity	UK-224,671
Rat	i.v.	1	0.39±0.05	0.19	0.27±0.01	0.14
	i.v.	4	0.16±0.05	0.06	0.10±0.01	0.05
	oral	1	0.29±0.04	0.01	0.36±0.11	0.01
	oral	4	0.43±0.12	0.03	0.41±0.05	0.03
Dog	i.v.	1	0.38±0.01	0.36	0.61±0.05	0.56
	i.v.	4	0.16±0.01	0.15	0.27±0.01	0.23
	oral	1	3.55±0.04	3.52	4.71±0.32	4.80
	oral	4	1.67±0.14	1.57	1.85±0.04	1.40

Concentrations expressed as μg equiv./ml and are derived from three determinations for radioactivity and one determination for unchanged UK-224,671.

Discussion

UK-224,671 has been shown to partition unevenly into the red cell fraction of blood. Such partitioning is a precedented phenomenon particularly for sulphonamide containing drugs such as indapamide (Lettieri and Portelli 1983) and also

Table 8. Total renal clearance and calculated relative clearances for filtration and tubular secretion of UK-224,671.

Species	% Dose unchanged in urine	Renal clearance (ml/min/kg)	GFR (ml/min/kg)	Clearance by GFR (ml/min/kg)	Clearance by tubular secretion (ml/min/kg)
Rat	14	6.6	11	1.8	4.8
Dog	6	0.9	4	0.44	0.46
Man	18	0.4	2	0.16	0.34

Percentage of the dose excreted unchanged in the urine of animals was determined from the excretion and metabolism experiments (table 6) and were derived from two determinations. Human urinary excretion was determined by specific assay and was derived from eight determinations. Clearance by GFR was calculated by the product of the fraction of UK-224,671 unbound in blood and the glomerular filtration rate. The difference between this and the renal clearance represents clearance by tubular secretion.

occurs with the antimalarial chloroquine (Bergqvist and Domeij-Nyberg 1983). For such drugs, a knowledge of the extent of partitioning is important as it determines the most appropriate biological fluid to measure to put pharmacokinetic parameters into context with organ blood flows (Hinderling 1997). For UK-224,671, whole blood was the most appropriate biological fluid to measure and a blood assay was developed.

UK-224,671 is a moderately lipophilic (log $D_{(7.4)}$ 1.8) and weakly basic molecule (pK_a 7.6) and this is reflected in its pharmacokinetics. The compound exhibits volumes of distribution greater than body water in all species (10, 7 and 2.4 l/kg in rat, dog and human respectively) indicating extensive distribution into tissues. The volume of distribution of the unbound drug (calculated by correcting for the free fraction in blood) is similar across the species (63, 44 and 27 l/kg in rat, dog and human respectively), again underlining the use of the whole blood assay. Blood clearances are low to moderate with respect to liver blood flow in all species (47, 15 and 2.3 ml/min/kg in rat, dog and human respectively) indicating that hepatic extraction is not extensive. A proportion of the clearance of UK-224,671 occurs via the kidney with 14, 6 and 18% of the dose recovered unchanged in rat, dog and human respectively (table 8). Thus, renal clearance represents 6.6, 0.9 and 0.4 ml/min/kg respectively. Since these are greater than the maximum clearance by GFR, it appears that there is an active secretion component to the renal clearance of UK-224,671.

UK-224,671 exhibits species differences in pharmacokinetics following oral administration. In the rat, the oral bioavailability was estimated at 7% although there was variability between the individual rats. This low oral bioavailability was not expected from the blood clearance of UK-224,671 in the rat with respect to liver blood flow and suggests that in this species, UK-224,671 is poorly absorbed from the GI tract. In the dog, oral bioavailability was 55% suggesting that UK-224,671 was ~ 75% absorbed (assuming liver blood flow in the dog is 50 ml/min/kg). Oral bioavailability in man was similar to that in rat (7.5%) suggesting that UK-224,671 is ~ 9% absorbed from the GI tract (liver blood flow in human assumed as 25 ml/min/kg). Moreover, the oral absorption (and hence oral bioavailability) of UK-224,671 in man was reduced in the presence of food (3.6%).

This species difference in absorption of UK-224,671 is indicative of absorption by the paracellular (aqueous pore) route. Oral absorption is higher in the dog than

the rat due to a larger pore size and frequency of pores in the paracellular pathway of dog compared with rat (He *et al*. 1998). Furthermore, rat appears to be a better predictor than dog of absorption of such compounds in human (He *et al*. 1998). Paracellular absorption of compounds such as UK-224,671 in human is always likely to be low due to the requirement for low molecular size to move through the aqueous pore (He *et al*. 1998). The molecular weight of UK-224,671 is 544.

It is perhaps surprising that, given the lipophilicity of UK-224,671 (log $D_{(7.4)}$ 1.8), the compound is not well absorbed by the transcellular route. However, lipophilicity is not the only determinant of absorption for a molecule. Lipinski *et al*. (1997) showed that absorption is also dependent upon molecular size and the degree of hydrogen bonding potential of the molecule. Molecular size is regarded as important since to be transcellularly absorbed a compound must overcome steric interactions with the lipid chains in the membrane. Thus, larger molecules will move more slowly through a membrane than smaller ones. Hydrogen bonding is important since it determines the extent to which a molecule is surrounded by water solvation shells. The extent of solvation of a molecule will determine the rate at which it can cross a membrane. This is because the solvation shell must be removed before the compound can cross the lipophilic environment of the membrane. A good example of this comes from Chan and Stewart (1996) who showed the effect of increasing molecular weight and hydrogen bond capacity on the permeability of a series of renin inhibitor molecules across a cell monolayer. With its high molecular weight and moderate to high degree of hydrogen bonding potential, it is likely that UK-224,671 will show low membrane flux.

The excretion and metabolism experiment with [^{14}C]-UK-224,671 in dog and rat also provided information on the absorption of the compound. In the dog, the recovery of radioactivity in the urine represented 14 and 9.7% of the dose following i.v. and oral administration respectively. This is indicative of 69% oral absorption which is consistent with that assumed from the blood clearance and the oral bioavailability (75%, see above). The majority of the dose of [^{14}C]-UK-224,671 was excreted in the faeces (78 and 86% following i.v. and oral administration respectively). Analysis of the faecal metabolite profiles showed two major components, one of which was unchanged UK-224,671. This suggests that there is significant excretion of UK-224,671 following i.v. administration, probably via the bile. The second major faecal component was identified as loss of the cyclopropylmethyl moiety (UK-280,045; figure 1).

In rat, urinary excretion of radioactivity (18 and 1.8% following i.v. and oral administration respectively) indicates that oral absorption is low (10%) which is consistent with the pharmacokinetic data. The major component of radioactivity in the urine of rat following i.v. administration was unchanged UK-224,671 (14% of the dose), suggesting a renal component to the clearance of UK-224,671. However, the faecal metabolite profiles were not consistent with a 10% absorbed compound. Following i.v. administration, the major component of radioactivity in the faeces was unchanged UK-224,671 representing 50% of the dose. Again, this suggests that biliary secretion of UK-224,671 is a major clearance mechanism in the rat. Following oral administration, faecal excretion of unchanged UK-224,671 represented only 60% of the dose. For a compound which is 10% absorbed following oral administration, this should approach 90%. The remainder of the radioactivity comprised metabolites including UK-280,045 (23% of the dose) and two unidentified metabolites (13 and 3.5% of the dose respectively).

There are two potential explanations for these observations. First, there may be degradation of UK-224,671 by the bacteria present in the faeces. However, the presence of UK-280,045 as a metabolite may suggest that this is not the case since an oxidative process forms this metabolite. Scheline (1973) showed that the majority of metabolic reactions carried out by gut bacteria are hydrolytic or reductive although they are capable of the type of N-dealkylation which would yield UK-280,045. The second explanation is that UK-224,671 is metabolized on first-pass through the gut wall. Thus, the relatively slow paracellular absorption of UK-224,671 allows it to pass into the gut wall cell where it is metabolized to UK-280,045 and other products. These metabolites could then be removed from the cell into the lumen of the gut. Under these circumstances, drug-related material is not absorbed into the animal and the overall appearance is that of a drug which is poorly absorbed.

There is growing evidence that first-pass metabolism by the gut wall can contribute to the disposition of many drugs following oral administration, particularly if the compound is a substrate for both CYP3A and P-glycoprotein. Many authors have suggested that gut wall CYP3A and P-glycoprotein act in a concerted manner to control the absorption of their substrates (Hebert 1997, Lown *et al*. 1997, Lampen *et al*. 1998, van Asperen *et al*. 1998, Wacher *et al*. 1998, Hall *et al*. 1999). This is based on the large overlap of substrates between the two (Wacher *et al*. 1996) and the proximity of their expression within the gut wall. Thus, it is proposed (Hebert 1997) that P-glycoprotein effectively recycles its substrates allowing CYP3A several opportunities to metabolize compounds in the gut. In this way, a small amount of CYP3A in the gut wall (relative to the liver content) can exert a profound extraction of the compound. This certainly appears to be the case for cyclosporin which is a substrate for both CYP3A4 and P-glycoprotein, and intestinal metabolism accounts for up to 50% of oral cyclosporin metabolism (Wacher *et al*. 1996). Our unpublished data have indicated that UK-224,671 may be a substrate for P-glycoprotein. Indeed, UK-224,671 contains all the structural features that are known to be requirements for this transporter (basic centre and hydrogen bonding; Seelig 1998). The enzymology of the formation of UK-280,045 from UK-224,671 has not been determined but there is the potential for this to be carried out by CYP3A. Thus, it may be that the observed poor absorption of UK-224,671 could be due to extensive first-pass extraction in the gut wall driven by P-glycoprotein and CYP3A. Extensive investigations are underway to examine this latter hypothesis.

In summary, UK-224,671 exhibits species differences in its disposition following oral administration. In dog, the compound is well absorbed but in rat and human, oral absorption is poor. The majority of a radioactive dose in rat and dog is excreted as unchanged UK-224,671 following i.v. administration. In addition, a few metabolites are observed. The faecal profile of radioactivity in rat is not consistent with a 10% absorption value since a significant amount of metabolites are present. This suggests that UK-224,671 may well be metabolized on first-pass through the gut wall and that this is responsible for the observed low absorption of the compound.

Acknowledgements

The authors gratefully acknowledge the assistance of Dr Donald Middleton and colleagues in the Medicinal Chemistry Department, Pfizer Central Research, for supplying UK-224,671 and UK-280,045. Also, acknowledgements to Ms Jenny

Gedge and Mr Richard Hucker of the Drug Metabolism Department for technical assistance in the metabolism studies and analysis of human blood samples respectively. The clinical phase was conducted at the Pfizer Clinical Research Unit and at Canterbury Hospital, Kent, and principal investigator was Dr M. D. Eve.

References

Bergqvist, Y. and Domeij-Nyberg, B., 1983, Distribution of chloroquine and its metabolite desethylchloroquine in human blood cells and its implication for the quantitative determination of these compounds in serum and plasma. *Journal of Chromatography*, **272**, 137–148.

Chan, O. H. and Stewart, B. H., 1996, Physicochemical and drug-delivery considerations for oral drug bioavailability. *Drug Discovery Today*, **1**, 461–473.

Hall, S. D., Thummel, K. E., Watkins, P. B., Lown, K. S., Benet, L. Z., Paine, M. F., Mayo, R. R., Turgeon, D. K., Bailey, D. G., Fontana, R. J. and Wrighton, S. A., 1999, Molecular and physical mechanisms of first-pass extraction. *Drug Metabolism and Disposition*, **27**, 161–166.

He, Y., Murby, S., Warhurst, G., Gifford, L, Walker, D., Ayrton, J., Eastmond, R. and Rowland, M., 1998, Species differences in size discrimination in the paracellular pathway reflected by oral bioavailability of polyethylene glycol and D-peptides. *Journal of Pharmaceutical Sciences*, **87**, 626–633.

Hebert, M. F., 1997, Contributions of hepatic and intestinal metabolism and P-glycoprotein to cyclosporine and tacrolimus oral drug delivery. *Advanced Drug Delivery Reviews*, **27**, 201–214.

Hinderling, P. H., 1997, Red blood cells: a neglected compartment in pharmacokinetics and pharmacodynamics. *Pharmacology Reviews*, **49**, 279–295.

Lampen, A., Zhang, Y., Hackbarth, I., Benet, L. Z., Sewing K.-F. and Christians, U., 1998, Metabolism and transport of the macrolide immunosuppressant sirolimus in the small intestine. *Journal of Pharmacology and Experimental Therapeutics*, **285**, 1104–1112.

Lettieri, J. T., and Portelli, S. T., 1983, Effects of competitive red blood cell binding and reduced haematocrit on the blood and plasma levels of [^{14}C]-indapamide in the rat. *Journal of Pharmacology and Experimental Therapeutics*, **224**, 266–272.

Lipinski, C. A., Lombardo, F., Dominy, B. W. and Feeney, P. J., 1997, Experimental and computational approaches to estimate solubility and permeability in drug discovery and development settings. *Advanced Drug Delivery Reviews*, **23**, 3–25.

Lown, K. S, Bailey, D. G., Fontana, R. J., Janarden,S. K., Adair, C. H., Fortlage, L. A., Brown, M. B., Guo, W. and Watkins P. B., 1997, Grapefruit juice increase felodipine oral availability in humans by decreasing intestinal CYP3A protein expression. *Journal of Clinical Investigation*, **99**, 2545–2553.

Scheline, R. R., 1973, Metabolism of foreign compounds by gastrointestinal microorganisms. *Pharmacological Reviews*, **25**, 451–523.

Seelig, A., 1998, A general pattern for substrate recognition by P-glycoprotein. *European Journal of Biochemistry*, **251**, 252–261.

Shah, V. P., Midha, K. K., Dighe, S., McGilveray, I. J., Skelley, J. P., Yacobi, A., Layloff, T., Viswanathan, C. T., Cook, C. E., McDowall, R. D., Pittman, K. A. and Spector, S., 1997, Analytical methods validation: Bioavailability, bioequivalence and pharmacokinetic studies. *Journal of Pharmaceutical Sciences*, **81**, 309–312.

Van Asperen, J., Van Tellingen, O. and Beijnen, J. H., 1998, The pharmacological role of P-glycoprotein in the intestinal epithelium. *Pharmacology Research*, **37**, 429–435.

Wacher, V. J., Salphati, L. and Benet, L. Z., 1996, Active secretion and enterocytic drug metabolism barriers to drug absorption. *Advanced Drug Delivery Reviews*, **20**, 99–112.

Wacher, V. J., Silverman, J. A., Zhang, Y. and Benet, L. Z., 1998, Role of P-glycoprotein and cytochrome P450 3A in limiting oral absorption of peptides and peptidomimetics. *Journal of Pharmaceutical Sciences*, **87**, 1322–1330.

XENOBIOTICA, 2000, VOL. 30, NO. 6, 643–653

Metabolism of a novel hypnotic, N^3-phenacyluridine, and hypnotic and sedative activities of its enantiomer metabolites in mouse

T. KIMURA†, M. MIKI†, K. WATANABE†, S. KONDO‡, I. K. HO§ and I. YAMAMOTO†*

† Department of Hygienic Chemistry, Faculty of Pharmaceutical Sciences, Hokuriku University, 3-Ho, Kanagawa-machi, Kanazawa 920–1181, Japan
‡ Nissui Pharmaceutical Co., Ltd, Yuuki Ibaraki 307-0036, Japan
§ Department of Pharmacology and Toxicology, University of Mississippi Medical Center, 2500 North State Street, Jackson, MS 39216–4505, USA

Received 19 November 1999

1. The metabolism of N^3-phenacyluridine (3-phenacyl-1-β-D-ribofuranosyluracil), a potent hypnotic nucleoside derivative, was studied in mouse.

2. Of the radioactivity, 65% was excreted in urine within 48 h after intraperitoneal (i.p.) administration of [^{3}H]N^3-phenacyluridine. The urinary metabolites N^3-phenacyluracil and N^3-α-hydroxy-β-phenethyluridine were extracted, isolated and analyzed by mass spectrometry.

3. Racemates of N^3-α-hydroxy-β-phenethyluridine were synthesized and both isomers were separated as N^3-(*S*)-(+)-α-hydroxy-β-phenethyluridine and N^3-(*R*)-(−)-α-hydroxy-β-phenethyluridine by hplc (CHIRALCEL-OJ column) with retentions of 13.8 and 17.9 min respectively. The reduction process took place with high stereo-selectivity, which gave an alcohol product in the urine with the same retention (17.9 min) as one of the synthetic isomers separated by hplc.

4. One of urinary metabolites was identified as N^3-(*S*)-(+)-α-hydroxy-β-phenethyluridine. N^3-phenacyluridine was predominantly converted to an alcoholic metabolite of (*S*)-(+)-configuration.

5. N^3-phenacyluracil and uridine were also identified as minor metabolites.

6. The pharmacological effects of the metabolites and related compounds were also evaluated in mouse. N^3-(*S*)-(+)-α-hydroxy-β-phenethyluridine, but not N^3-(*R*)-(−)-α-hydroxy-β-phenethyluridine, possessed hypnotic activity and potentiated pentobarbital-induced sleeping time with a similar potency to the parent compound, N^3-phenacyluridine. N^3-α-hydroxy-β-phenethyluridine (racemate) had almost two thirds of the hypnotic activity of N^3-(*S*)-(+)-α-hydroxy-β-phenethyluridine. No other metabolites exhibited hypnotic activities.

7. The present study indicates that N^3-(*S*)-(+)-α-hydroxy-β-phenethyluridine, a major metabolite of N^3-phenacyluridine, is an active metabolite and contributes a significant CNS depressant effect.

Introduction

Uridine possesses central nervous system (CNS) depressant effects such as decreasing spontaneous activity in the mouse (Krooth *et al*. 1978) and protection of metrazol- and penicillin-induced seizures in frog (Roberts 1973). In addition, uridine was isolated as a sleep-promoting substance from 24 h sleep-deprived brainstems and promoted natural sleep by intracerebroventricular (i.c.v.) infusion in rat (Komoda *et al*. 1983, Honda *et al*. 1984, Inoue *et al*. 1984). However, unlike barbiturates and benzodiazepines, uridine does not possess any hypnotic action. Reported for the first time was that the N^3-benzyl substituted uridine possessed

* Author for correspondence; e-mail: i-yamamoto@hokuriku-u.ac.jp

Xenobiotica ISSN 0049–8254 print/ISSN 1366–5928 online © 2000 Taylor & Francis Ltd
http://www.tandf.co.uk/journals

hypnotic activity when the compound is administered by i.c.v. injection to mouse at 2.0 μmol/mouse (Yamamoto *et al*. 1985). N^3-benzyluridine, but not its metabolites, possessed hypnotic activity (Kimura *et al*. 1991). In addition, it was found that N^3-phenacyluridine is the most potent hypnotic agent in mouse (i.c.v. injection) among all the oxopyrimidine nucleoside derivatives synthesized to date (Yamamoto *et al*. 1986, 1987a,b, 1990, 1994, Koshigami *et al*. 1991, Kimura *et al*. 1993, 1996). However, the metabolite of N^3-phenacyluridine is different from that of N^3-benzyluridine because it has a ketone moiety in the N^3-substituent group. It is known that certain drugs having a ketone moiety are reduced to the corresponding hydroxy group by reductases in the cytosol to produce the active metabolite. Therefore, it is anticipated that N^3-phenacyluridine is also metabolized by reduction to form an alcohol product. Acetohexamide is widely used as an orally antidiabetic drug and has a ketone group in the structure. In man, acetohexamide was reported to be mainly biotransformed to (−)-hydroxyhexamide, which is a pharmacologically active metabolite (Imamura *et al*. 1985). Furthermore, McMahon *et al*. (1965) reported that (−)-hydroxyhexamide is 2.4 times as potent as acetohexamide with respect to its pharmacological effect. Therefore, in the present study, the metabolites of N^3-phenacyluridine were identified and their pharmacological effects on the CNS evaluated in mouse.

Materials and methods

Materials

[^{3}H]uridine (42.7 Ci/mmol, 97.8% purity) was from Daiichi Pure Chemical Co. Ltd/NEN (Tokyo, Japan) and other synthetic reagents were from Wako Pure Chemical Co. Ltd (Osaka, Japan). Male ddY mice (body weight 23–28 g) were from the Sankyo Laboratory Co. Ltd (Toyama, Japan).

Preparation of N^3*-phenacyluridine and* [^3H]N^3*-phenacyluridine*

N^3-phenacyluridine and [^{3}H]N^3-phenacyluridine were prepared according to Yamamoto *et al*. (1994) from uridine and [^{3}H]uridine respectively. [^{3}H]N^3-phenacyluridine was developed on thin layer chromatography (tlc) (solvent chloroform/methanol, 9/1 v/v), and the radioactivity of the spot was measured by a Radiochromanizer (Aloka, Japan). The purity of [^{3}H]N^3-phenacyluridine was > 98%.

Preparation of N^3*-phenacyluracil*

N^3-phenacyluracil was prepared by the method of Kimura *et al*. (1991) with slight modifications. Sodium hydride (60% purity), 1.07 g (120 mmol), was washed with petroleum ether and dissolved in 133 ml *N*,*N*-dimethylformamide (DMF). Uracil 7.5 g (67 mmol) was added to the mixture and stirred at room temperature for 30 min. Chloromethylether, 7.5 g (94 mmol), was added drop-wise to the mixture and stirred at room temperature for 90 min. After the reaction was completed, the solvent was evaporated to dryness and the residue applied to a silica gel column and eluted with chloroform/isopropanol (9/1 v/v) as the solvent. N^1-methoxymethyluracil was isolated and purified from the reaction mixture. The N^1-methoxymethyluracil obtained was recrystallized from chloroform and ligroin to yield 2.79 g (27.2%) of the compound with a m.p. = 153–156 °C, ^{1}H-nmr ($CDCl_3$) δ: 3.20 (3H, s, OCH_3), 5.13 (2H, s, NCH_2), 5.79 (1H, d, J = 8 Hz, 5-H), 7.32 (1H, d, J = 8 Hz, 6-H), 8.91 (1H, broad s, NH), MS, m/z = 156 [M^+]. N^1-methoxymethyl-N^3-phenacyluracil was prepared by N^3-phenacylation of N^1-methoxymethyluracil according to Kimura *et al*. (1991). The compound yielded 30% as an oil with ^{1}H-nmr ($CDCl_3$) δ: 3.30 (3H, s, OCH_3), 5.15 (2H, s, NCH_2), 5.34 (2H, s, NCH_2-CO), 5.75 (1H, d, J = 8 Hz, 5-H), 7.30–8.08 (6H, m, 6-H, C_6H_5), MS, m/z = 274 [M^+]. N^3-phenacyluracil was then from N^1-methoxymethyl-N^3-phenacyluracil by deprotection at N^1 position. N^1-methoxymethyl-N^3-phenacyluracil 210 mg (0.77 mmol) was refluxed in a mixture of 7 ml methanol, 8 ml HCl, 8 ml H_2SO_4 and 3 ml water at 100 °C for 24 h. The reaction mixture was neutralized with 0.1 N sodium hydroxide, extracted with chloroform, and the solvent evaporated followed by purification by a silica gel column chromatography with chloroform/isopropanol (9/1 v/v) as solvent. Finally, N^3-phenacyluracil was recrystallized from water to yield 110 mg (62.1%) of the compound with a m.p. = 195–199 °C, ^{1}H-nmr ($CDCl_3$) δ: 5.20 (2H, s, NCH_2), 5.69 (1H, d, J = 8 Hz, 5-H), 7.25–8.10 (6H, m, 6-H, C_6H_5). MS, m/z = 230 [M^+].

Synthesis of N^3*-α-hydroxy-β-phenethyluridine (racemate)*

N^3-phenacyluridine, 362 mg (1 mmol), was dissolved in anhydrous methanol and sodium borohydride, 47 mg (1 mmol), was added. The reaction mixture was stirred at room temperature for 30 min, followed by evaporation. The residue was applied to Amberlite XAD-2 and eluted with 250 ml ethanol after washing with 100 ml water. N^3-α-hydroxy-β-phenethyluridine was separated by silica gel column chromatography with chloroform/methanol (9/1 v/v). N^3-α-hydroxy-β-phenethyluridine was recrystallized from acetone and *n*-hexane, yielding 60.4 % of the compound. M.p. = 143–147 °C, ^{1}H-nmr (DMSO-d_6) δ: 3.22–3.63 (2H, m, 5′-H_2), 3.66–3.80 (1H, m, 4′-H), 3.90–4.12 (3H, m, 2′-H, 3′-H, -CH-), 5.07–5.81 (3H, m, NCH_2, 1′-H), 7.24–7.41 (5H, m, C_6H_5), 8.14–8.16 (1H, d, $\mathcal{J}$ = 8 Hz, 6-H). FAB-MS (magic bullet) m/z = 365 $[M+H]^+$.

Hplc separation of the racemic metabolites, N^3*-(R)-(−)-α-hydroxy-β-phenethyluridine and* N^3*-(S)-(+)-α-hydroxy-β-phenethyluridine*

Racemic mixtures of N^3-α-hydroxy-β-phenethyluridine (racemate) were separated by hplc (Hitachi 655–21, Japan) using a CHIRALCEL-OJ column (0.46 mm × 25 cm, Daisel Chemical Co. Ltd, Japan), eluent: *n*-hexane/isopropanol (7/3 v/v), flow rate = 1.0 ml/min, and detection at 254 nm.

Administration of N^3*-phenacyluridine and* [^3H]N^3*-phenacyluridine to mouse*

Unlabelled N^3-phenacyluridine (1.0 mmol/kg) or [^{3}H]N^3-phenacyluridine (1.0 mmol/kg, 1.7 MBq/kg) was suspended in 1% Tween-80 saline solution and administered by intraperitoneal (i.p.) injection to the male ddY mouse (weight 23–28 g). Each group consisted of three mice.

Excretion of [^3H]N^3*-phenacyluridine to urine and faeces*

Urine and faeces were collected 1, 3, 6, 12, 24, 48 h after the i.p. administration of [^{3}H]N^3-phenacyluridine to mouse. An aliquot of urine was added to Clear-sol I (Nacalai-tesque, Japan) and radioactivity was counted by a liquid scintillation counter (Aloka LSC-3000, Japan). An aliquot of faeces was subjected to Automatic Sample Combustion System (Aloka, Japan). The recovered radioactivity from the faeces was counted by a liquid scintillation counter.

Determination of metabolites

A 24-h urine sample from mouse was collected after the administration of [^{3}H]N^3-phenacyluridine. Of urine, 40 ml was pretreated with Bond Elut (Si) (Varian, CA, USA) with methanol as eluant, and was subsequently stirred with 40 ml Amberlite XAD-2 for 2 h. The residue was applied to a column, eluted with 250 ml methanol after washing with 100 ml water, and each fraction was evaporated and dissolved in ethanol. The fraction was developed on tlc (SIL-G25, Macherey-Nagel, Germany) (solvent chloroform/methanol/acetic acid/water, 80/20/6/4 v/v/v/v). The scraped band was added to Clear-sol I, and radioactivity was counted by a liquid scintillation counter. After administration of noneradioactive N^3-phenacyluridine, each tlc extract was analyzed by mass spectrometry for the determination of the metabolites. Twenty-four-hour urine samples from mouse were collected after the administration and were handled in a similar manner as mentioned above. The metabolite fraction was analyzed by hplc, optical rotation and FAB-MS. Hplc was carried out using a Hitachi hplc apparatus equipped with a CHIRALCEL-OJ column and a Hitachi UV monitor (254 nm). *n*-Hexane/isopropanol (7/3 v/v) was employed as a mobile phase at 1.0 ml/min. The optical rotation and FAB-MS were performed by using Nippon-bunko DIP-370 (Tokyo, Japan) and JEOL JMX-DX-300 instruments (Tokyo, Japan) respectively.

Hypnotic activity

Compounds tested (2.0 μmol/mouse) were injected i.c.v. to the male ddY mouse (body weight 23–28 g) according to Haley and McCormick (1957). Hypnotic activity was expressed as sleeping time (min) and was considered as the time between the loss of righting reflex of animals and the time they righted themselves. Each group had eight mice.

Pentobarbital-induced sleep prolongation

Compounds tested (0.5 μmol/mouse) were injected (i.c.v.) in the animals and pentobarbital (40 mg/kg) was injected (i.p.) 15 min after the i.c.v. administration of the tested compound. Sleeping time was measured as the time between the loss and recovery of righting reflex in the mouse, and the data were expressed as percentage of that of the controls. Each group had eight mice. Statistical significance of difference was calculated using Bonferroni test.

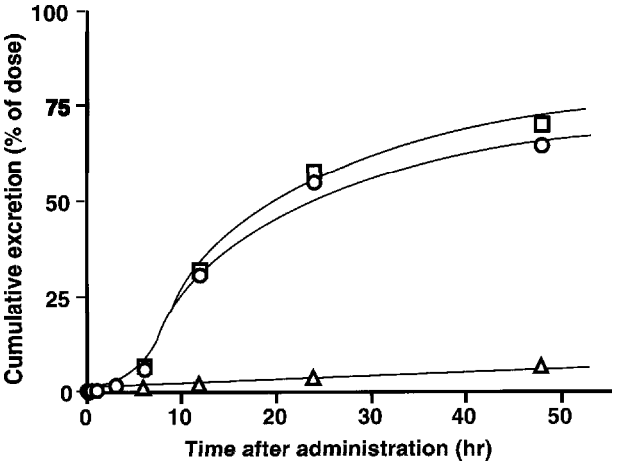


Figure 1. Excretion of radioactivity after the i.p. administration of [^{3}H]N^3-phenacyluridine to mouse. [^{3}H]N^3-phenacyluridine, 1.0 mmol/kg, was administered by i.p. injection. Total, □, urine, ○, faeces, △. Data are the average of three mice.

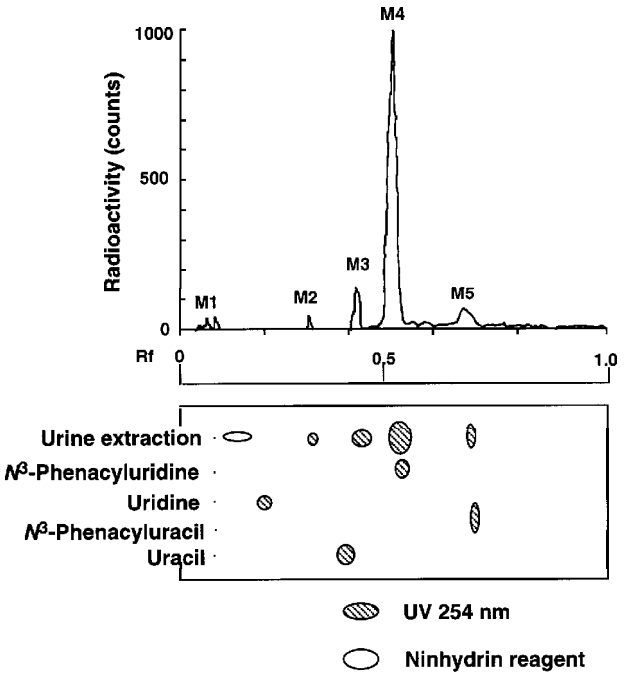


Figure 2. Analysis of [^{3}H]N^3-phenacyluridine and its urinary metabolites by radiochromanyzer analysis. Urinary extracts were developed on tlc (solvent chloroform/methanol/acetic acid/water, 80/20/6/4 v/v/v/v), and the radioactivity of the fractions were counted by liquid scintillation spectrometry.

Results

N^3-phenacyluridine and its metabolites were mainly excreted in the urine and by 48 h after [^{3}H]N^3-phenacyluridine administration (1.0 mmol/kg, i.p.), 65 and 7% of the radioactivity administered to mouse was found in the urine and faeces respectively (figure 1).

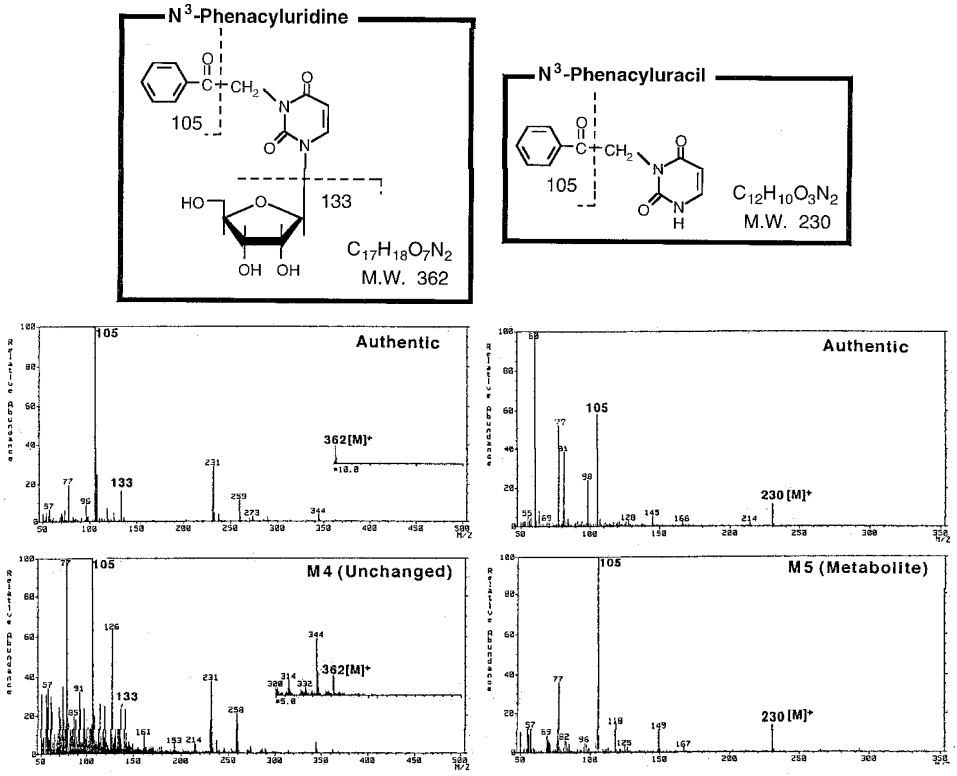


Figure 3. Mass spectra of M4 and M5 fractions after the i.p. administration of N^3-phenacyluridine to mouse.

The extracted sample from urine was developed on tlc and the radioactivity was analyzed. The amount of radioactivity in fractions of M1–5 were 13.0, 8.3, 11.6, 51.5 and 15.6% of that excreted in the urine respectively (figure 2). Each fraction was also extracted and the metabolite structures identified by mass spectrometry and compared with that of authentic samples.

Figure 3 shows mass spectra of M4 and M5 and the corresponding authentic samples. Since the mass spectra of M4 and M5 indicated molecular weights of 362 (m/z = 362 $[M]^+$) and 230 (m/z = 230$[M]^+$) respectively, the fractions were identified as N^3-phenacyluridine and the corresponding deribosylated compound, N^3-phenacyluracil respectively. The mass spectrum (FAB mass, magic bullet: Na) of M3 showed ions at 387 $[M+Na]^+$ and 365 (m/z = 364 $[M+H]^+$). The mass fragment of m/z = 107 was confirmed, whereas m/z = 105, derived from the phenacyl moiety disappeared, suggesting metabolic alteration of the phenacyl moiety (figure 4).

Additional data were also from authentic samples. The mass spectrum of M3 was compared with that of an authentic sample, indicating the reduction of the ketone moiety to an alcohol in the phenacyl group of N^3-phenacyluridine.

Figure 5 shows the urinary excretion of N^3-phenacyluridine, N^3-α-hydroxy-β-phenethyluridine and N^3-phenacyluracil. By 48 h after administration, 40% of N^3-phenacyluridine remained unchanged, whereas N^3-α-hydroxy-β-phenethyluridine and N^3-phenacyluracil accounted for 9 and 11% of the total amount of urinary excretion respectively.

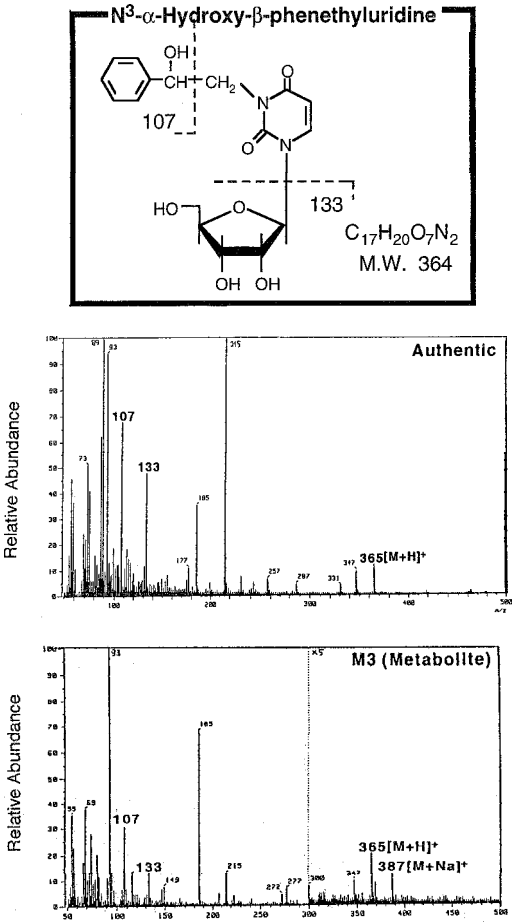


Figure 4. Mass spectra of the M3 fraction after the i.p. administration of N^3-phenacyluridine to mouse.

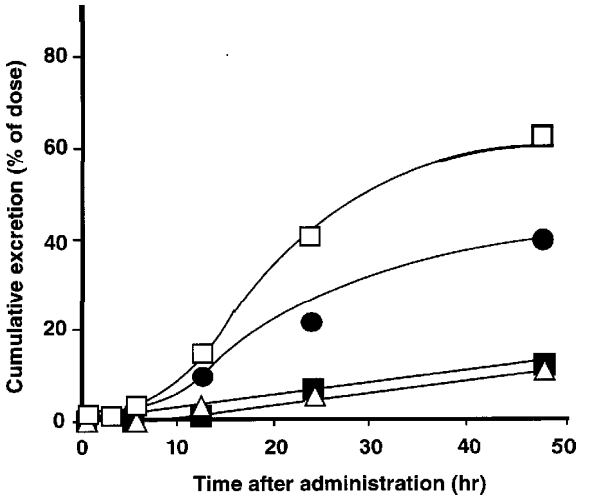


Figure 5. Urinary excretion of metabolites after the i.p. administration of [^{3}H]N^3-phenacyluridine. [^{3}H]N^3-phenacyluridine, 1.0 mmol/kg, was administered by i.p. injection. Total, □; N^3-phenacyluridine, ●; N^3-(*S*)-(+)-α-hydroxy-*β*-phenethyluridine, △; N^3-phenacyluracil, ■.

Table 1. Analytical data for the (*R*)- and (*S*)-enantiomers of N^3-α-hydroxy-β-phenethyluridine.

Compound	Hplc (min	Optical rotation $[\alpha]_D$	m.p. (°C)	FAB-MS (*m/z*)
N^3-α-hydroxy-β-phenethyluridine (racemate)	13·8, 17·9	+2·9	143–147	107 ($C_6H_5CH(OH)$) 365 ($[M+H]^+$) 387 ($[M+Na]^+$)
N^3-(*R*)-(−)-α-hydroxy-β-phenethyluridine	13·8	−82·5	145–147	107 ($C_6H_5CH(OH)$) 365 ($[M+H]^+$)
N^3-(*S*)-(+)-α-hydroxy-β-phenethyluridine	17·9	+81·3	145–148	107 ($C_6H_5CH(OH)$) 365 ($[M+H]^+$) 387 ($[M+Na]^+$)
Metabolite	17·9	+83·9	144–146	107 ($C_6H_5CH(OH)$) 365 ($[M+H]^+$) 387 ($[M+Na]^+$)

Compounds were injected onto an hplc (Hitachi 655-21, Japan) using a CHIRALCEL-OJ column (0·46 mm × 25 cm; Daisel Chemical Co. Ltd, Japan). Eluent: *n*-hexane/isopropanol (7/3 v/v). Flow rate = 1·0 ml/min. Detection = UV 254 nm.

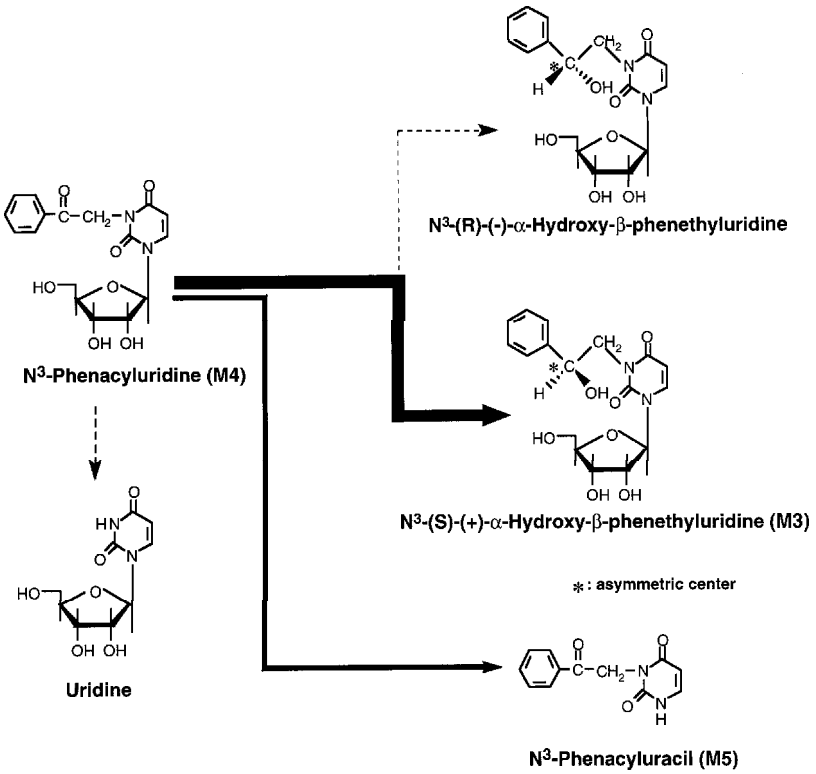


Figure 6. Proposed metabolic pathways of N^3-phenacyluridine in mouse.

N^3-α-hydroxy-β-phenethyluridine theoretically has either the (*R*)- or (*S*)-enantiomer configuration, derived from the asymmetric carbon of the phenacyl moiety. These isomers were successfully separated from the synthetic racemates by hplc using a CHIRACEL-OJ column, with retentions of 13.8 (PI) and 17.9 min (PII) for the (*R*)- and (*S*)-enantiomers respectively (table 1).

Table 2. Hypnotic activities of N^3-phenacyluridine, N^3-(*R*)-(−)- and N^3-(*S*)-(+)-α-hydroxy-β-phenethyluridine, and related compounds in mouse.

Compound	Hypnotic activity (min)	Pentobarbital-induced sleep (% of control)
N^3-phenacyluridine	487±47	423±31*
N^3-α-hydroxy-β-phenethyluridine (racemate)	279±24	447±26*
N^3-(*R*)-(−)-α-hydroxy-β-phenylethyluridine	27±7	259±54*
N^3-(*S*)-(+)-α-hydroxy-β-phenethyluridine	409±21	690±47*
N^3-phenacyluracil	none	105±12
Uridine	none	128±26
Uracil	none	136±21
D-Ribose	none	94±9

Compounds were administered i.c.v to the male ddY mouse (body weight 23–28 g) at 2.0 μmol/mouse. Hypnotic activity was evaluated as the time between loss and recovery of the mouse righting reflex. 'none' indicates that the compound did not show hypnotic activity. Pentobarbital (40 mg/kg, i.p.) was injected 15 min after the i.c.v. injection of the compound tested at 0.5 μmol/mouse. Data are the mean % of control sleeping time (53±9 min)±SEM, where $n = 8$.

* Significantly different from control ($P < 0.01$).

The analytical data for both enantiomers were compared with that of (*R*)- or (*S*)-*sec*-phenethylalcohol. The optical rotations of (*R*)- and (*S*)-*sec*-phenethylalcohol are +73.9 and −78.7 respectively. The (*R*)- and (*S*)-*sec*-phenethylalcohol were injected to hplc using the CHIRALCEL-OJ column, showing retentions of 35.1 and 31.8 min respectively. According to the Baumann and Prelog rule (1958), (*R*)- and (*S*)-*sec*-phenethylalcohol correspond to N^3-(*S*)-(+)- and N^3-(*R*)-(−)-α-hydroxy-β-phenethyluridine respectively. For N^3-α-hydroxy-β-phenethyluridine, the optical rotation of the racemate is +2.9, whereas compounds separated hplc (PI and PII) show −82.5 and +81.3 for the optical rotations respectively. One of the urinary metabolites showed a retention of 17.9 min on hplc and the optical rotation of +83.9. Furthermore, the data from measurement of m.p., FAB-MS and ^{1}H-nmr (data not shown) support the view that this metabolite is N^3-(*S*)-(+)-α-hydroxy-β-phenethyluridine (figure 6).

M1 and M2 have not been identified to date because of their trace amounts in urine. Since M1 showed a positive reaction with the ninhydrin reagent (data not shown), ring opening to an amino acid derivative may be possible.

The pharmacological properties of N^3-phenacyluridine, N^3-α-hydroxy-β-phenethyluridine (racemate) and the enantiomers were evaluated by their hypnotic activity and synergistic effects with pentobarbital in mouse.

As shown table 2, in mouse receiving an i.c.v. injection of 2.0 μmol/mouse N^3-phenacyluridine, the sleeping time was 487 min. The same dose of N^3-α-hydroxy-β-phenethyluridine (racemate) induced a sleeping time of 279 min, suggesting that there is an active metabolite of N^3-phenacyluridine. In the case of N^3-(*R*)-(−)-α-hydroxy-β-phenethyluridine and N^3-(*S*)-(+)-α-hydroxy-β-phenethyluridine, N^3-(*S*)-(+)-α-hydroxy-β-phenethyluridine induced a sleeping time of 409 min, whereas N^3-(*R*)-(−)-α-hydroxy-β-phenethyluridine only resulted in a sleeping time of 27 min at the same dose. With respect to the effects on the pentobarbital-induced sleeping time, N^3-phenacyluridine, N^3-α-hydroxy-β-phenethyluridine (racemate), N^3-(*R*)-(−)- and N^3-(*S*)-(+)-enantiomers significantly prolonged to 423, 447, 259 and 690% of the vehicle controlled group (53±9 min) respectively. N^3-phenacyluracil, uridine, uracil, and D-ribose did not show any significant changes in the pentobarbital-induced sleeping time.

Discussion

In a previous study, N^3-benzyluridine was biotransformed to N^3-benzyluracil and trace amounts of uridine in mouse (Kimura *et al*. 1991). Since these metabolites do not show any CNS depressant effects in mouse, the parent compound, N^3-benzyluridine, but not the metabolites possessed a hypnotic activity. In contrast, the structure of N^3-phenacyluridine differs from that of N^3-benzyluridine in that there is a carbonyl group in the phenacyl moiety. In the current study, urinary metabolites were analyzed by mass spectrometry and compared with authentic samples. M4 was identified as unchanged compound, N^3-phenacyluridine. Since M5 showed a molecular weight of 230 (m/z = 230 $[M]^+$), it was identified as N^3-phenacyluracil, a deribosylated product of N^3-phenacyluridine similar to that previously reported for N^3-benzyluridine (Kimura *et al*. 1991). R_f of M3 was smaller than that of N^3-phenacyluridine, suggesting a polar metabolite. The mass spectrum (FAB-MS, magic bullet: Na) of M3 showed ions at 387 $[M+Na]^+$ and 365 (m/z = 364 $[M+H]^+$). Mass fragmentation of m/z = 105 was derived from phenacyl moiety. Therefore, a fragment ion of m/z = 107 instead of 105 indicated an addition of two hydrogens to the phenacyl moiety. Since the mass spectrum of an authentic sample of N^3-α-hydroxy-β-phenethyluridine showed the same mass fragmentation of M3, N^3-α-hydroxy-β-phenethyluridine is one of metabolites of N^3-phenacyluridine.

In man, acetohexamide has been reported to be mainly biotransformed to (−)-hydroxyhexamide, a pharmacologically active metabolite (Imamura *et al*. 1985). In addition, McMahon *et al*. (1965) reported that (−)-hydroxyhexamide is 2.4 times as potent as acetohexamide. In addition, the carbonyl moiety of the anti-inflammatory agent, sodium 2-[4-(2-oxocyclopentylmethyl)-phenyl]propionate dihydrate (loxoprofen sodium), has been shown to be metabolized to the correspond hydroxy group (Tanaka *et al*. 1983). The *trans*-OH form was a pharmacologically active compound and has an anti-inflammatory effect. In the present study, the metabolite theoretically has (*R*)- and (*S*)-isomers derived from the asymmetric carbon of the phenacyl moiety. These isomers were separated by hplc and compared the synthetic racemates. In general, carbonyl groups are metabolized according to the Baumann–Prelog rule. In the cases of acetophenone (McMahon *et al*. 1965), warfaline (Moreland and Hewick 1975), nabilone (Billings *et al*. 1980) and 2-octanone (Gal *et al*. 1981), essentially one enantiomer, (*S*)-alcohols, is mainly formed in mammals. Optical rotation of the isomers indicated that one of the urinary metabolites is N^3-(*S*)-(+)-α-hydroxy-β-phenethyluridine. The metabolic pathways of N^3-phenacyluridine are proposed in figure 6 and the reactions are stereo-specific in that only the (*S*)-(+)-enantiomer is produced.

The CNS depressant effects of N^3-phenacyluridine, its metabolites and related compounds were also evaluated for hypnotic activity and synergistic effects with pentobarbital in mouse by i.c.v. injection. Since N^3-α-hydroxy-β-phenethyluridine (racemate) exhibited a sleeping time of 279 min in mouse at 2.0 μmol/mouse by i.c.v. injection, it is suggested that the metabolite retained depressant activity. For the pharmacological effects of both enantiomers, N^3-(*S*)-(+)-α-hydroxy-β-phenethyluridine exhibited a sleeping time of 409 min, whereas N^3-(*R*)-(−)-α-hydroxy-β-phenethyluridine had only ~ 6% of the effect as compared with the (*S*)-isomer at the same dose, indicating that the enantiomers possess stereo-selective pharmacological activity. N^3-phenacyluracil, uridine, uracil, and D-ribose did not exhibit any hypnotic action. N^3-phenacyluridine, N^3-α-hydroxy-β-phenethyluridine (racemate), (*R*)- and (*S*)-enantiomers significantly prolonged the

pentobarbital-induced sleeping time to 423, 447, 259 and 690% of the control. N^3-(*S*)-(+)-α-hydroxy-β-phenethyluridine possesses a strong synergistic effect but N^3-phenacyluracil, uridine, uracil and D-ribose did not show significant changes in the pentobarbital-induced sleeping time.

Acknowledgements

This work was supported by a Grant-in-Aid for Scientific Research from the Ministry of Education, Science, Sports, and Culture of Japan, and by the Special Fund of Hokuriku University.

References

Baumann, P. and Prelog, V., 1958, Reaktionen mit mikroorganismen. Die stereospezifische reduktion von stereoisomeren dekalindonen-(1,4). *Helvetica Chimica Acta*, **41**, 2362–2379.

Billings, R. E., Whitaker, G. W. and McMahon, R. E., 1980, The streoselective enzymic reduction of the synthetic 9-ketocannabinoid, nabilone, *in vivo*, in isolated liver cells and in liver homogenate. *Xenobiotica*, **10**, 33–36.

Gal, J., DeVito, D. and Harper, T. W., 1981, GAS-chromatographic resolution of enantiomeric secondary alcohols. Stereoselective reductive metabolism of ketone in rabbit-liver cytosol. *Drug Metabolism and Disposition*, **9**, 557–560.

Haley, T. J. and McCormick, W. G., 1957, Pharmacological effects produced by intracerebral injection of drugs in the conscious mouse. *British Journal of Pharmacology*, **12**, 12–15.

Honda K., Komoda, Y., Nishida, S., Nagasaki, H., Higashi, A., Uchizono, K. and Inoue, S., 1984, Uridine as an active component of sleep-promoting substance: its effects on nocturnal sleep in rats. *Neuroscience Research*, **1**, 243–252.

Imamura Y., Kojima, Y. and Ichibagase, H., 1985, Effect of simultaneous administration of drugs on absorption and excretion. XIX. Binding of acetohexamide and its major metabolite, (−)-hydroxyhexamide, to human serum albumin. *Chemical and Pharmaceutical Bulletin*, **33**, 1281–1284.

Inoue S., Honda, K., Komoda, Y., Uchizono, K., Ueno, R. and Hayaishi, O., 1984, Differential sleep-promoting effects of five sleep substances nocturnally infused in unrestrained rats. *Proceeding of the National Academy of Sciences, USA*, **81**, 6240–6244.

Kimura, T., Kuze, J., Watanabe, K., Kondo, S., Ho, I. K. and Yamamoto, I., 1996, N^3-Phenacyluridine, a novel hypnotic compound, interacts with the benzodiazepine receptor. *European Journal of Pharmacology*, **311**, 265–269.

Kimura T., Watanabe, K., Tateoka, Y., Kondo, S., Ho, I. K. and Yamamoto, I., 1993, Preparation and pharmacological evaluation of N^3-substituted thymidine derivatives as central depressants. *Chemical and Pharmaceutical Bulletin*, **41**, 1180–1182.

Kimura T., Yamamoto, I., Watanabe, K., Tateoka, Y. and Ho, I. K., 1991, *In vivo* and *in vitro* metabolic studies of N^3-benzyluridine which exhibits hypnotic activity in mice. *Research Communications in Chemical Pathology and Pharmacology*, **71**, 27–48.

Komoda Y., Ishikawa, M., Nagasaki, H., Iriki, M., Honda, K., Inoue, S., Higashi, A. and Uchizono K, 1983, Uridine, a sleep-promoting substance from brainstems of sleep-deprived rats. *Biomedical Research*, **4**, 223–228.

Koshigami, M., Watanabe, K., Kimura, T. and Yamamoto, I., 1991, Central depressant effects of N^3-substituted 6-azauridines in mice. *Chemical and Pharmaceutical Bulletin*, **39**, 2597–2599.

Krooth, R. S., Hsiao, W. L. and Lam, G. F. M., 1978, Effects of natural pyrimidines and of certain related compounds on the spontaneous activity of the mouse. *Journal of Pharmacology and Experimental Therapeutics*, **207**, 504–514.

McMahon, R. E., Marshall, F. J. and Culp, H. W., 1965, The nature of the metabolites of acetohexamide in the rat and in the human. *Journal of Pharmacology and Experimental Therapeutics*, **149**, 272–279.

Roberts, C. A., 1973, Anticonvulsant effects of uridine: comparative analysis of Metrazol and penicillin induced foci. *Brain Research*, **55**, 291–308.

Moreland, T. A. and Hewick, D. S., 1975, Studies on a ketone reductase in human and rat liver and kidney soluble faction using warfarin as a substrate. *Biochemical Pharmacology*, **24**, 1953–1957.

Tanaka, Y., Nishikawa, Y. and Hayashi, R., 1983, Species differences in metabolism of sodium 2-[4-(2-oxocyclopentylmethyl)-phenyl]propionate dihydrate (loxoprofen sodium), a new anti-inflammatory agent. *Chemical and Pharmaceutical Bulletin*, **31**, 3656–3664.

Yamamoto, I., Kimura, T., Tateoka, Y., Watanabe, K. and Ho, I. K., 1985, N^3-Benzyluridine exerts hypnotic activity in mice. *Chemical and Pharmaceutical Bulletin*, **33**, 4088–4090.

Yamamoto, I., Kimura, T., Tateoka, Y., Watanabe, K. and Ho, I. K., 1986, Central depressant activities of N^3-allyluridine and N^3-allylthymidine. *Research Communications in Chemical Pathology and Pharmacology*, **52**, 321–332.

Yamamoto I., Kimura, T., Tateoka, Y., Watanabe, K. and Ho, I. K., 1987a, *N*-Substituted oxopyrimidines and nucleosides: structure–activity relationship for hypnotic activity as central nervous system depressant. *Journal of Medicinal Chemistry*, **30**, 2227–2231.

Yamamoto, I., Kimura, T., Tateoka, Y., Watanabe, K. and Ho, I. K., 1987b, Hypnotic activity of N^3-benzylthymidine on mice. *Life Sciences*, **41**, 2791–2797.

Yamamoto, I., Kimura, T., Watanabe, K., Tateoka, Y. and Ho, I. K., 1990, Action mechanism for hypnotic activity of N^3-benzyluridine and related compounds. In S. Inoue and J. M. Krueger (eds), *Endogenous Sleep Factors* (The Netherlands: SPB Academic Publishing bv), pp. 133–142.

Yamamoto, I., Kuze, J., Kimura, T., Watanabe, K., Kondo, S. and Ho, I. K., 1994, The potent depressant effects of N^3-phenacyluridine in mice. *Biological and Pharmaceutical Bulletin*, **17**, 514–516.

XENOBIOTICA, 2000, VOL. 30, NO. 7, 655–664

In vitro metabolism of human and salmon calcitonins in rat liver and kidney evaluated by liquid chromatography-tandem mass spectrometry

N. KOBAYASHI*, N. YAMAMURA, M. KAMAGATA, A. KURIHARA and T. IKEDA

Drug Metabolism and Pharmacokinetics Research Laboratories, Sankyo Co., Ltd, 2–58, Hiromachi 1-chome, Shinagawa-ku, Tokyo 140, Japan

Received 17 September 1999

1. Using LC-MS and LC-MS/MS, an *in vitro* study was conducted on the metabolism of human calcitonin (*h*CT) and salmon calcitonin (*s*CT) in rat liver and kidney to determine the rates of metabolism and the positions of hydrolytic cleavage in both peptides.

2. In lysosomal fractions of rat liver and kidney, *h*CT was degraded 9–12 times faster than *s*CT. Many metabolites of *h*CT were produced in the lysosomal fractions, whereas the metabolites of *s*CT were scarcely found.

3. In the case of the cytosolic fractions, three positions of initial endoproteolytic cleavage were found in *h*CT, leading to the production of many peptide fragments via subsequent exoproteolytic metabolism. The initial cleavage position of *s*CT could not be identified precisely, but it was postulated that the rate-determining step in the metabolism of *s*CT is the endoproteolytic hydrolysis.

4. The studies using pure proteases and protease inhibitors indicated that the metabolism of calcitonins proceeds by initial endoproteolytic cleavage and subsequent exoproteolytic digestion, catalysed by an aspartate-protease in lysosomes and by a metalloprotease and cysteine-protease in combination in the cytosol.

5. The result suggested that the higher *in vivo* pharmacological activity of *s*CT compared with that of *h*CT may be due to a slower metabolism of the former.

Introduction

Calcitonin, a polypeptide hormone of 32 amino acids (figure 4), lowers the blood calcium level both by inhibiting bone resorption and by enhancing the urinary excretion of calcium (Austin *et al*. 1981). Salmon calcitonin (*s*CT) has been used clinically for the treatment of osteoporosis (Gennari *et al*. 1994, Scheiber *et al*. 1998), but human calcitonin (*h*CT) has not been successfully introduced into the therapeutic field because of its somewhat lower pharmacological activity (Galante *et al*. 1971). This difference in pharmacological activities has been confirmed in humans as well as in rat (Gaggi *et al*. 1985), and is believed to be caused mostly by the dissimilar affinities of *s*CT and *h*CT for the calcitonin receptor (Houssami *et al*. 1994). In addition to receptor affinity, metabolic resistance after binding to the receptor is expected to be another important factor in determining the *in vivo* potencies of these peptide hormones (Pontiroli 1990). The kidney and liver, the main organs for metabolism of calcitonins (Scarpace *et al*. 1977), are believed to be the sites of internalization of the receptor-calcitonin complex from the cell surface into the intracellular matrix (Findlay *et al*. 1982, 1989) and subsequent hydrolytic decomposition in the lysosome (Hicke 1997). Since the presence of the disulphide bond at the amino terminus and the amide bond at the carboxyl terminus in the

* Author for correspondence; e-mail: nobuhi@shina.sankyo.co.jp

Xenobiotica ISSN 0049-8254 print/ISSN 1366-5928 online © 2000 Taylor & Francis Ltd
http://www.tandf.co.uk/journals

molecule makes calcitonins resistant to exoproteolytic hydrolysis, endoproteolysis is very likely the initial process of the metabolism of calcitonin. To date, however, information about the *in vitro* metabolism of *h*CT and *s*CT in the liver and kidney and the chemical structures of their primary metabolites is sparse at best.

In the present study, the rate of metabolism of both calcitonins *in vitro* was investigated and the chemical structures of the primary metabolites were determined by liquid chromatography-mass spectrometry (LC-MS) and liquid chromatography-tandem mass spectrometry (LC-MS/MS), using subcellular fractions of rat liver and kidney.

Materials and methods

Materials

Rat calcitonin (*r*CT, peptide content 86%), the internal standard substance used in mass spectrometric measurements, was obtained together with *h*CT (peptide content ~ 80%) from Peninsula Laboratory Co. (CA, USA). Diisopropyl fluorophosphate (DFP), phenylmethylsulfonyl fluoride (PMFS), *N*-ethylmaleimide (NEM), pepstatin, ethylenediamine tetra-acetic acid (EDTA), and *s*CT (peptide content 78%) were from Sigma Chemical Co. (St Louis, MO, USA). Other reagents and solvents were of analytical grade and were used without further purification.

Preparation of subcellular fractions of rat liver and kidney

Three male Sprague–Dawley rats (body weight 300 g) were killed by exsanguination from the abdominal aorta under diethyl ether anaesthesia. The liver and kidneys were quickly removed, and each was homogenized in a 4-fold volume of 10 mM Tris-HCl buffer containing 0.25 M sucrose (pH 7.4). The homogenates from individual animals were centrifuged at 1000 *g* for 10 min at 4 °C to remove cell debris, and the supernatant fractions were centrifuged at 3300 *g* for 20 min at 4 °C. The supernatant fractions were centrifuged again at 12000 *g* for 20 min at 4 °C to sediment the lysosomal fractions, and were subsequently ultracentrifuged at 105000 *g* for 60 min to sediment the microsomal fractions. The supernatant fraction obtained by ultracentrifugation was used as the cytosolic fraction. The lysosomal fractions were washed with 10 mM Tris-HCl buffer containing 0.25 M sucrose (pH 7.4) by centrifugation, and the final lysosomal fractions were obtained by re-suspending the pellet in 10 mM potassium phosphate buffer containing 1.14% KCl. The lysosomal and cytosolic fractions were stored frozen at −80 °C until used. The protein concentration in each fraction was determined by Lowry's method (Lowry *et al*. 1951) using bovine serum albumin as standard.

Determination of rates of metabolism of h*CT and* s*CT in hepatic and renal subcellular fractions*

Rates of metabolism of *h*CT and *s*CT were measured as the rate of decrease of the parent compound in the presence of hepatic and renal subcellular fractions. The lysosomal fraction was diluted with 0.5 M glycine-HCl buffer (pH 3.0) (final protein concentration 2.5 mg.protein/ml). The cytosolic fraction was supplemented with 0.5 M potassium phosphate buffer (pH 7.0) (final protein concentration 0.5 mg/ml). A 0.5-ml aliquot of each fraction was pre-incubated for 2 min at 37 °C, and the reaction started by adding 0.5 ml *h*CT or *s*CT at a final concentration of 10 μg/ml. The reaction was stopped at 0, 10, 20, 30, 60 and 120 min by the addition of a 4-fold volume of methanol containing 2 μg/ml *r*CT as the internal standard (IS). The reaction mixture was centrifuged at 10 000*g* in an Eppendorf centrifuge, and the supernatant fraction analyzed by LC/MS.

For the LC analysis a Model HP1050 LC System (Hewlett-Packard, Silicon Valley, CA, USA) was used consisting of a low-pressure pump, an autosampler and a semi-micro column (Capcell Pak UG-120, C18, 50×2 mm i.d., Shiseido, Yokohama, Japan). A mixture of trifluoroacetic acid (TFA), water and acetonitrile (0.01:66:34 v/v/v) was used as the mobile phase at 0.2 ml/min. Of the sample, 5 μl was injected into the LC-electrospray ionization (ESI)-MS system. A triple-stage quadruple mass spectrometer (TSQ-700, Thermoquest, San Jose, CA, USA) equipped with an atmospheric ionization (API) source (Thermoquest) was used for the LC-MS/MS. The API source was fitted with an ESI inlet, and the positive-ion selected ion monitoring (SIM) mode was chosen for the quantification. The ESI voltage was set at −4.5 kV, and the capillary temperature was maintained at 200 °C. The sheath and auxiliary gas pressures were 60 and 15 psi respectively. The scan range was switched over at 0.8-s intervals. A triply charged positive ion was selected for the determination of the unchanged *h*CT or *s*CT (Kobayashi *et al*. 1995). The peak integration was calculated by peak-area ratios from the SIM mode of *h*CT/IS or *s*CT/IS.

Detection of metabolites of h*CT and* s*CT produced by hepatic and renal subcellular fractions or by purified lysosomal enzymes*

The lysosomal and cytosolic fractions of rat liver and kidney were incubated with *h*CT or *s*CT for 2 min in the same manner as described above, and the reaction was stopped by adding a 4-fold volume of methanol without containing *r*CT. In separate experiments, cathepsin B1 (0.5 units/ml final concentration) and cathepsin D (0.25 units/ml final concentration) were incubated with *h*CT and *s*CT. The supernatant fraction, obtained by centrifugation of the reaction mixture after addition of methanol, was evaporated to dryness under a nitrogen gas stream. The residue was re-dissolved in a small volume of the HPLC mobile phase and analyzed by LC-MS to detect the metabolites (scanning range m/z 500–1700). The same LC-MS operating conditions described above were used, but with the following modification of the elution method: a mixture of TFA, water and acetonitrile (0.05:95:5 v/v/v, mobile phase A) was run through the column, and the elution was conducted over 20 min by replacing mobile phase A in a linear gradient manner (0–100%) with mobile phase B consisting of TFA, water and acetonitrile (0.05:50:50 v/v/v).

Inhibition of h*CT and* s*CT metabolism*

DFP, PFMFS, NEM, pepstatin and EDTA were used as the protease inhibitors at increasing final concentrations of 0.1, 1 and 10 mM. Either the lysosomal fraction (2 mg protein/ml) or cytosolic fraction (1 mg protein/ml) was incubated with *h*CT or *s*CT at a final concentration of 100 μg/ml for 2 min at 37 °C in the presence or absence of the above protease inhibitors, and the reaction was stopped by adding a 4-fold volume of methanol containing *r*CT (2 μg/ml). Of the supernatant fraction, 20 μl was injected to an LC system equipped with a UV detector set at 225 nm. The LC system was used to assay only unchanged compound, and was an LC-10A System (Shimadzu, Kyoto, Japan) consisting of two high-pressure pumps, an autosampler and a reversed phase column (ASAHIPAK ODP-50 6D, C18, 150×6 mm i.d., Shodex, Tokyo, Japan). A mixture of TFA, water and acetonitrile (0.05:72.5:27.5 v/v/v) was used as the mobile phase at 1 ml/min.

Data processing for primary structures of h*CT and* s*CT metabolites*

The metabolites of *h*CT and *s*CT were structurally analyzed according to the following procedure using LC-MS and LC-MS/MS. The peaks of the metabolites were identified by comparing the LC/MS chromatogram of the sample with that of a control sample obtained after incubation without *h*CT or *s*CT. A protein analysis application, Bio Spec (Sciex, Toronto, Canada), searched for the peptide fragments in the ions of each peak. When necessary, the peak was collected and the amino acid structure was determined by LC-MS/MS.

Results and discussion

Rates of metabolism of h*CT and* s*CT in hepatic and renal lysosomal fractions*

Time-courses of the residual amounts of *h*CT and *s*CT after incubation with hepatic and renal lysosomal fractions of rats are shown in figure 1. The data collected at 10 min after starting the incubation are presented as the initial rate of metabolism in table 1. The disposition rates of *h*CT were nine times faster in the hepatic lysosomal fraction and 12 times faster in the renal lysosomal fraction compared with those of *s*CT. The rates of the *h*CT and *s*CT metabolism in the hepatic lysosomal fraction were similar to those in the renal lysosomal fraction.

It has been reported that after intravenous administration, calcitonin is taken up rapidly by the liver and kidney, organs rich in calcitonin receptors (Blower *et al*. 1998). It is believed that after binding to the receptor, calcitonin is internalized and metabolized to the amino acid components or the peptide fragments by hydrolysis mainly in the lysosomes in these organs (Schneider *et al*. 1988). Lysosomal inhibitor is known to suppress the internalization of *h*CT (Findlay *et al*. 1982), and such the metabolic process may be a determinant of the duration of the pharmacodynamic action of calcitonin.

In comparing *h*CT and *s*CT, the more rapid metabolism of the former observed in both hepatic and renal lysosomal fractions is consistent with its shorter plasma half-life, and may prove to be one of the reasons for the higher pharmacological activity of the latter *in vivo*.

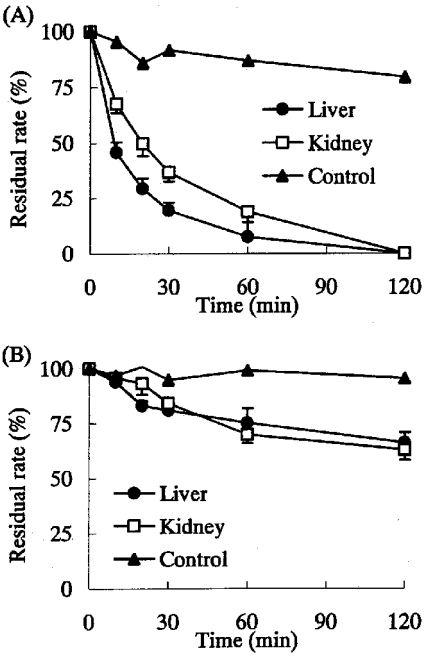


Figure 1. Disappearance of *h*CT (A) and *s*CT (B) in lysosomal fractions from rat liver and kidney. Data are mean±SD (n = 3), except for control (n = 1). Final protein concentration of lysosomal fraction: 2.5 mg protein/ml, final calcitonin concentration: 10 μg/ml, pH 3. Residual rates of *h*CT and *s*CT at 0 min were 100%, and *h*CT and *s*CT solutions without subcellular fractions were used for the control.

Table 1. Initial rates of proteolytic metabolism of *h*CT and *s*CT in subcellular fractions. Values were calculated by the decay in the initial 10 min and derived from three specimens.

	Fraction	Tissue	Initial rate (μg/ml/mg.protein/min)	SD
*h*CT	lysosomal	kidney	0.34	0.05
		liver	0.59	0.07
	cytosolic	kidney	>2.73	—
		liver	>3.21	—
*s*CT	lysosomal	kidney	0.04	0.02
		liver	0.05	0.02
	cytosolic	kidney	0.56	0.34
		liver	0.95	0.22

Rates of metabolism of h*CT and* s*CT in cytosolic fractions*

Time-courses of the residual amounts of *h*CT and *s*CT after incubation with hepatic and renal cytosolic fractions of rats are represented in figure 2. The data collected at 10 min after starting the incubation are presented as the initial rate of metabolism in table 1. The disposition rates of *h*CT were more than three times faster than those of *s*CT in both the hepatic and renal cytosolic fractions. The rates of *h*CT and *s*CT metabolism in the hepatic cytosolic fraction were similar to those in the renal cytosolic fraction. Under the given pH condition for the *in vitro* metabolism using cytosolic fractions (pH 7.0), a slow disappearance of *h*CT was observed without addition of the cytosolic fraction, but no such decrease of *s*CT was observed. This decrease of *h*CT was not associated with the production of any

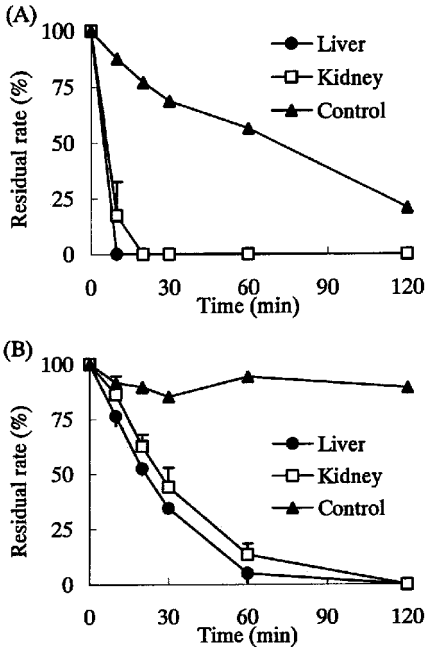


Figure 2. Disappearance metabolic rates of *h*CT (A) and *s*CT (B) in cytosolic fractions from rat liver and kidney. Data are mean ± SD (n = 3), except for control (n = 1). Final protein concentration of cytosolic fraction: 0.5 mg.protein/ml, final calcitonin concentration: 10 μg/ml, pH 7.

metabolites (data not shown). It has been reported that *h*CT aggregates in a neutral solution, and that aggregation is minimized in an acidic solution or when high *h*CT concentrations are avoided (Arvinte *et al.* 1993, Cudd *et al.* 1995). This aggregation phenomenon of *h*CT at neutral pH is quite likely to be the reason for the decrease of the parent compound without formation of the metabolites in the cytosolic fractions. In concordance with this reported finding, a decrease of *h*CT without formation of metabolites was not observed at pH 3 in a previously conducted control experiment for the metabolism by the lysosomal fraction.

The proteases in the cytosol are believed to have a physiological function to turn over the endogenous proteins produced inside the cells. Although calcitonins given exogenously are not considered to be metabolized by the cytosolic proteases, the peptide fragments of calcitonins produced *in vitro* by the cytosol were appropriate for demonstrating the suitability of LC-MS and LC-MS/MS for analyzing substances with relatively large molecular weights.

Metabolism of h*CT and* s*CT by purified lysosomal enzymes*

To examine the applicability of LC-MS/MS to the structural determination of peptide metabolites, the metabolites of calcitonins produced in a relatively simple system were investigated using purified lysosomal enzymes. As one of the main metabolites of *h*CT derived by hydrolysis by cathepsin D, a metabolite showing an $[M+H]^+$ ion with m/z 1261 was indicated as a peptide fragment of *h*CT from 1Cys to 12Tyr. As shown in figure 3, sequential elimination of Tyr, Thr, Gly, Leu and Met from this metabolite was consistent with the peptide fragment structure. In this manner, other metabolites of calcitonins were confirmed, and their amino acid

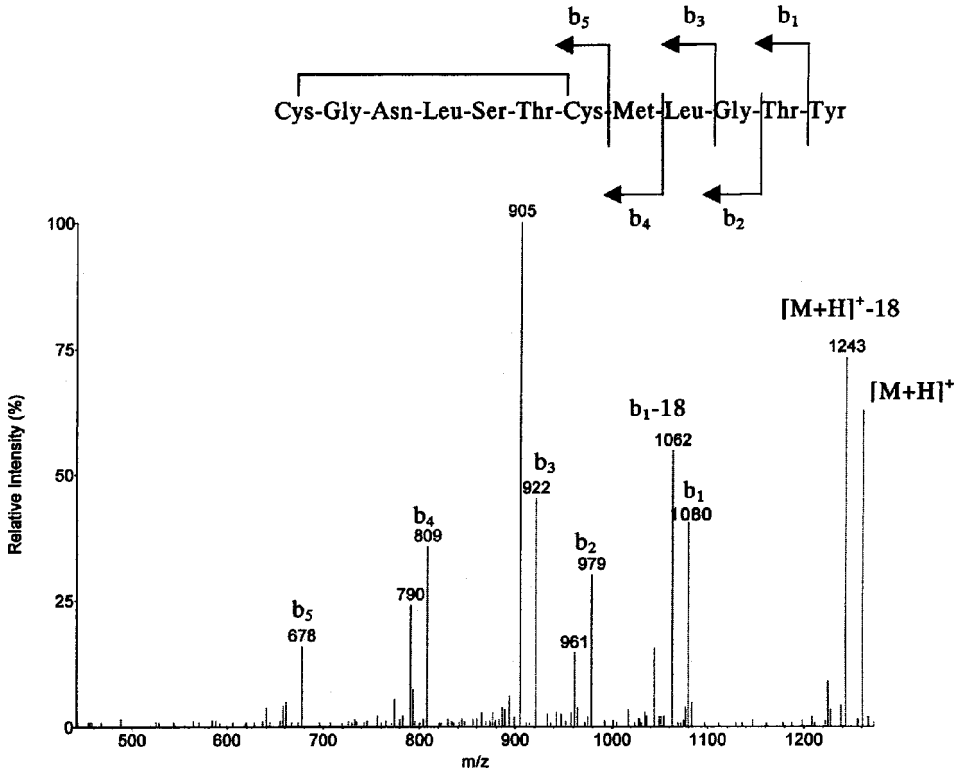


Figure 3. MS/MS spectrum of a main metabolite of *h*CT. Since one of the metabolites hydrolyzed by cathepsin D was detected as an ion at *m/z* 1261, it was presumed to be derived from a peptide fragment 1 Cys-12 Tyr. The product ions observed in this spectrum correspond to the amino sequence of the postulated peptide fragment.

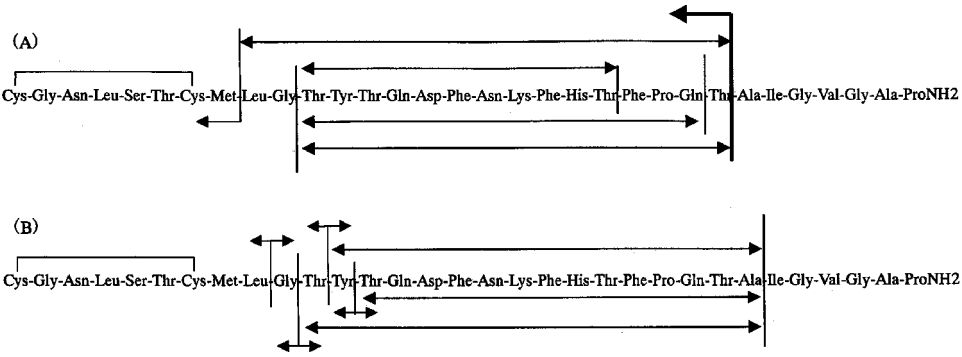


Figure 4. Proteolytic cleavage of *h*CT by cathepsin B1 (A) and cathepsin D (B). Vertical lines show the cleavage positions, and horizontal arrows the identified peptide fragment.

sequences were successfully determined by LC-MS/MS. The metabolites of *h*CT and *s*CT produced after incubation with the lysosomal enzymes, cathepsin B1 and cathepsin D (Sakai *et al*. 1978, Braulke *et al*. 1999), are shown in figures 4 and 5. As similarly observed after incubation with the hepatic lysosomal fraction, *h*CT was hydrolyzed at many positions by cathepsin B1 and cathepsin D. The metabolites primarily produced by the hydrolysis at the positions between 9Leu and 13Thr and between 24Gln an d27Ile were the main metabolites (figure 4). Hydrolysis of *s*CT by

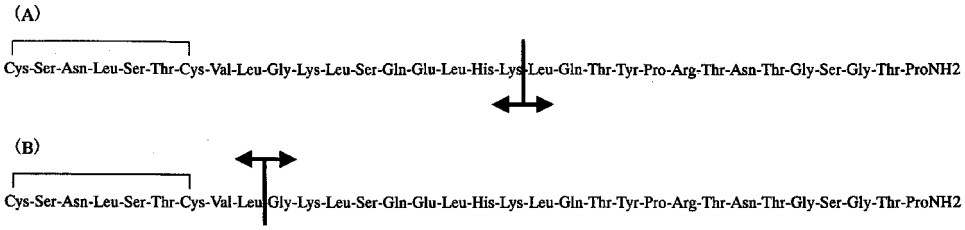


Figure 5. Proteolytic cleavage of *s*CT by cathepsin B1 (A) and cathepsin D (B).

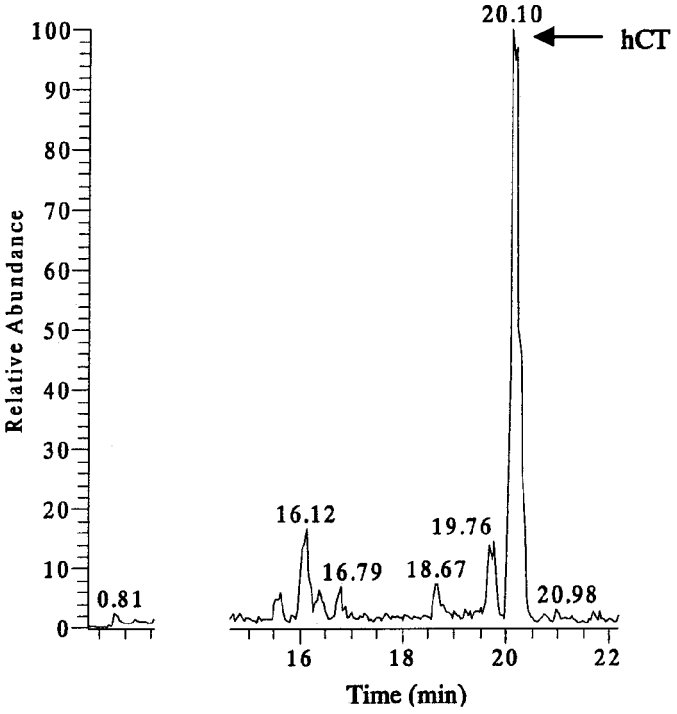


Figure 6. Typical LC-MS chromatogram of *h*CT metabolites produced by hepatic lysosomal fractions.

cathepsin B1 was observed only at the position between 18Lys and 19Leu (figure 5), and prolonged incubation up to 120 min failed to produce other metabolites. Cathepsin D cleaved *s*CT only at the position between 9Leu and 10Gly.

Identification of metabolites of h*CT and* s*CT produced in lysosomal fractions by LC-MS and LC-MS/MS*

Figure 6 shows a typical LC-MS chromatogram of *h*CT metabolites produced by hepatic lysosomal fraction. Many peaks of *h*CT metabolites were observed, demonstrating an extensive metabolism of *h*CT in the lysosomal fraction of the liver. The metabolites of *h*CT identified by mass spectrometric analysis are shown in figure 7. These metabolites were formed primarily by hydrolysis at positions between 9 Leu and 17 Asn and between 24 Gln and 27 Ile. A number of the metabolites produced by this endoproteolytic hydrolysis were associated with subsequent exoproteolytic digestion. Since both the N- and C-termini of *h*CT and

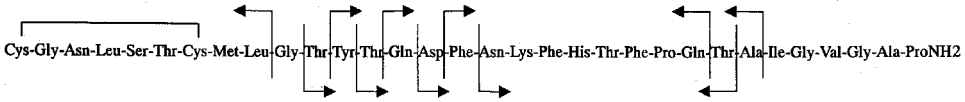


Figure 7. Proteolytic cleavages of *h*CT by the lysosomal fraction of the liver.

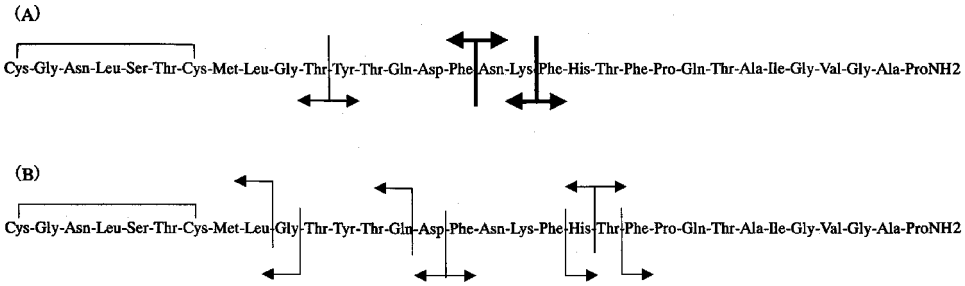


Figure 8. Proteolytic cleavages of *h*CT in the cytosolic fraction of the liver at 5 min (A) and 30 min (B). Metabolites shown in A were also confirmed in the fraction at 30 min, but are abbreviated in B.

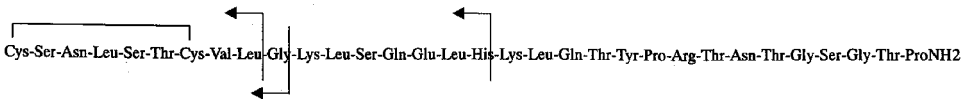


Figure 9. Proteolytic cleavage of *s*CT in kidney cytosolic fractions.

*s*CT are blocked, calcitonin is considered to be resistant to the exoproteolytic hydrolysis. Production of the metabolites primarily by the endoproteolytic hydrolysis supports this view. In the case of the renal lysosomal fraction (data not shown), only metabolites of *h*CT were produced by hydrolysis between 9 Leu and 11 Thr, and no metabolite was found to be produced by the hydrolysis between 24 Gln and 27 Ile. Metabolites of *s*CT were found only at a low level after incubation with the hepatic and renal lysosomal fractions extending over 120 min.

Identification of metabolites of h*CT and* s*CT produced in cytosolic fractions by LC/MS and LC/MS/MS*

The identified metabolites of *h*CT in the hepatic cytosolic fraction are shown in figure 8. Judging from the structures of the metabolites produced at 5 min after starting the incubation (figure 8A), it was assumed that *h*CT was initially cleaved at the positions between 11 Thr and 12 Tyr, between 16 Phe and 17 Asn, and between 18 Lys and 19 Phe since the peptide fragments at the both sides of these peptide bonds were detected. Prolonged incubation (30 min) led to the production of metabolites firstly by primary hydrolysis between 15 Asp and 16 Phe and between 20 His and 21 Thr, and second, by exoproteolytic digestion of the above peptides (figure 8B). The metabolites of *h*CT produced after incubation with the renal cytosolic fraction were almost the same as those produced in the hepatic cytosolic fraction (data not shown).

The metabolites of *s*CT produced after incubation with the renal cytosolic fraction are shown in figure 9. Since only three metabolites with short peptide sequences at the N-terminus were observed, the initial cleavage position of *s*CT

Table 2. Inhibition of metabolic activity of *h*CT and *s*CT by protease inhibitors. Proteolytic metabolism was completely inhibited when the percentage is 100%. Data are derived from three specimens. Final protein concentration of lysosomal fraction, 2 mg-protein/ml; final protein concentration of cytosolic fraction, 1 mg.protein/ml; final calcitonin concentration, 100 μg/ml.

	Inhibition (%)							
	Human calcitonin					Salmon calcitonin		
		Liver		Kidney			Liver	Kidney
Inhibitor	Final conc. (mM)	Lysosome	Cytosol	Lysosome	Cytosol	Final conc. (mM)	Cytosol	Cytosol
EDTA	0·1	—	—	—	9·4	0·1	9·6	—
	1	—	5·2	—	5·6	1	36·5	19·2
	10	—	104·9	—	66·2	10	99·6	53·6
DFP	0·1	—	—	—	2·6	0·1	—	15·6
	1	—	—	—	—	1	—	—
	10	—	—	—	—	10	—	4·7
NEM	0·1	—	12·8	—	0·8	0·1	—	24·6
	1	—	110·8	—	64·5	1	68·1	62·7
	10	7·5	91·7	—	72·2	10	99·9	65·3
Pepstatin	0·005	39·2	2·1	27·7	—	0·1	—	—
	0·05	51·8	7·1	44·7	5·2	1	—	9·2
	0·5	60·0	—	50·9	—	10	2·9	18·4
Leupeptin	0·005	—	—	5·4	—	—	—	—
	0·05	—	—	—	—	—	—	—
	0·5	—	—	11·0	—	—	—	—

—, Minus quantity.

could not be precisely identified. The absence of the primary metabolites and the slow metabolism of *s*CT indicated that the rate-determining step in the metabolism of *s*CT is endoproteolytic hydrolysis, and that the subsequent exoproteolytic digestion of the primary metabolites is very rapid.

Inhibition of h*CT and* s*CT metabolism by protease inhibitors*

According to the key amino acid residue in the active centre within the enzyme, proteases are divided into serine-proteases (specific inhibitors DFP and PMSF), cysteine-proteases (NEM and leupeptin), aspartate-proteases (pepstatin) and metalloproteases (EDTA).

Table 2 shows the inhibition of the metabolism of calcitonins in hepatic and renal subcellular fractions by these protease inhibitors. NEM and EDTA inhibited the metabolism of both *h*CT and *s*CT in the hepatic and renal cytosolic fractions. Pepstatin inhibited the metabolism of *h*CT in the lysosomal fractions. These results suggested the involvement of the metalloprotease and the cysteine-protease in the proteolytic metabolism of *h*CT and *s*CT in the cytosolic fraction, and the involvement of the aspartate-protease in the metabolism of *h*CT in the lysosomal fraction.

Conclusions

The metabolites of the peptide hormones, *s*CT and *h*CT, produced by subcellular fractions of rat liver and kidney were successfully separated by reversed-phase LC using linear gradient elution, and then investigated by LC-MS and LC-

MS/MS to determine their chemical structures. The results indicated that the metabolism of calcitonins proceeds by initial endoproteolytic cleavage and subsequent exoproteolytic digestion, catalysed by an aspartate-protease in lysosomes and by a metalloprotease and cysteine-protease in combination in the cytosol.

References

Arvinte, T., Cudd, A. and Drake, A. F., 1993, The structure and mechanism of formation of human calcitonin fibrils. *Journal of Biological Chemistry*, **268**, 6415–6422.

Austin, L. A. and Heath, H., 1981, Physiology and pathophysiology. *New England Journal of Medicine*, **304**, 269–278.

Blower, P. J., Puncher, M. R. B., Kettle, A. G., George, S., Dorsch, S., Leak, A., Naylor, L. H. and O'Doherty, M. J., 1998, Iodine-123 salmon calcitonin, an imaging agent for calcitonin receptors: synthesis, biodistribution, metabolism and dosimetry in humans. *European Journal of Nuclear Medicine*, **25**, 101–108.

Braulke, T., Dittmer, F., Gotz, W. and Von Figura, K., 1999, Alteration in pancreatic immunoreactivity of insulin-like growth factor (IGF)-binding protein (IGFBP) -6 and in intracellular degradation of IGFBP-3 in fibroblasts of IGF-II receptor/IGF-II-deficient mice. *Hormone and Metabolism Research*, **31**, 235–241.

Cudd, A., Arvinte, T., Gaines Das, R. E., Chinni, C. and MacIntyre, I., 1995, Enhanced potency of human calcitonin when fibrillation is avoided. *Journal of Pharmaceutical Science*, **84**, 717–719.

Findlay, D. M., Michelangeli, V. P. and Robinson, P. J., 1989, Protein kinase-C-induced down-regulation of calcitonin receptors and calcitonin-activated adenylate cyclase in T47D and BEN cells. *Endocrinology*, **125**, 2656–2663.

Findlay, D. M., Ng, K. W., Niall, M. and Martin, T. J., 1982, Processing of calcitonin and epidermal growth factor after binding to receptors in human breast cancer cells (T47D). *Biochemical Journal*, **206**, 343–350.

Gaggi, R., Beltrandi, E., Dall'Olio, R. and Ferri, S., 1985, Relationships between hypocalcaemic and anorectic effect of calcitonin in the rat. *Pharmacology Research Communications*, **17**, 209–215.

Galante, L., Horton, R., Joplin, G. F., Woodhouse, N. J. and MacIntyre, I., 1971, Comparison of human, porcine and salmon synthetic calcitonins in man and in the rat. *Clinical Science*, **40**, 9–10.

Gennari, C. and Agnusdei, D., 1994, Calcitonins and osteoporosis. *British Journal of Clinical Practice*, **48**, 196–200.

Hicke, L., 1997, Ubiquitin-dependent internalization and down-regulation of plasma membrane proteins. *FASEB Journal*, **11**, 1215–1226.

Houssami, S., Findlay, D. M., Brady, C. L., Martin, T. J., Epand, R. M., Moore, E. E., Murayama, E., Tamura, T., Orliwski, R. C. and Sexton, P. M., 1994, Divergent structural requirements exist for calcitonin receptor binding specificity and adenylate cyclase activation. *Molecular Pharmacology*, **47**, 798–809.

Kobayashi, N., Kanai, M., Seta, K. and Nakamura, K., 1995, Quantitative analysis of synthetic human calcitonin by liquid chromatography-mass spectrometry. *Journal of Chromatography B*, **672**, 17–23.

Lowry, O. H., Rosebrough, H. J., Farr, A. L. and Randall, R. J., 1951, Protein measurement with Folin phenol reagent. *Journal of Biological Chemistry*, **193**, 265–275.

Pontiroli, A. E., 1990, Intranasal administration of calcitonin and of other peptides: studies with different promoters. *Journal of Controlled Release*, **13**, 247–251.

Sakai, T., Makino, H. and Tanaka, R., 1978, Increased activity of cyclic AMP phosphodiesterase from frozen–thawed rat liver. A role of lysosomal protease in enzyme activation. *Biochimica et Biophysica Acta.*, **522**, 477–490.

Scarpace, P. J., Neuman, W. F. and Raisz, L. G., 1977, Metabolism of radioiodinated salmon calcitonin in rats. *Endocrinology*, **100**, 1260–1267.

Scheiber, L. B. N. and Torregrosa, L., 1998, Evaluation and treatment of postmenopausal osteoporosis. *Seminars in Arthritis and Rheumatism*, **27**, 245–261.

Schneider, H. G., Raue, F., Zink, A., Koppold, A. and Ziegler, R., 1988, Down-regulation of calcitonin receptors in T47D cells by internalization of calcitonin-receptor complexes. *Molecular and Cellular Endocrinology*, **58**, 9–15.

XENOBIOTICA, 2000, VOL. 30, NO. 7, 665–681

Metabolic activity of fresh and cryopreserved cynomolgus monkey (*Macaca fascicularis*) hepatocytes

N. J. HEWITT†, T. FISCHER†, U. ZUEHLKE‡, F. OESCH§ and D. UTESCH†

† Institute of Toxicology, Merck KGaA, Frankfurterstraße 250, D-64271 Darmstadt, Germany
‡ Covance Laboratories GmbH, Kesselfeld 29, D-48163 Münster, Germany
§ Institute of Toxicology, University of Mainz, Obere Zahlbacher Straße 67, D-55131, Mainz, Germany

Received 19 November 1999

1. The effect of cryopreservation on the metabolic capacity of monkey hepatocytes over 4 h in suspension and 24 h in culture was determined. Hepatocytes were diluted in a buffer containing 10% DMSO and frozen in a computer-controlled chamber.

2. Initial ethoxyresorufin and ethoxycoumarin *O*-deethylase (ECOD) activities were the same in fresh and cryopreserved (CP) hepatocytes. ECOD activity in suspensions declined over 4 h but was the same in fresh and CP hepatocytes.

3. The formation of testosterone hydroxy (OHT) metabolites (namely 6β-OHT, 2β-OHT, 16β-OHT, 16α-OHT, 15β-OHT, 2α-OHT and 6β-OHT) was unaffected by cryopreservation. The loss of OHT activities over 4 h in CP and fresh whole cell suspensions was attributed to a loss of cofactor. CP hepatocyte cultures had equivalent OHT activities to freshly isolated hepatocytes.

4. Initial UDP-glucuronyltransferase (UGT) activities, using the substrates 4-methylumbelliferone, ethoxycoumarin and hydroxycoumarin, were equivalent in fresh and CP whole hepatocytes. At later times, UGT activity was lower in CP than fresh hepatocytes but this was due to a loss of UDPGA. Initial sulphotransferase (SULT) activities, using the substrates 2-naphthol, ethoxycoumarin and hydroxycoumarin, were equivalent in fresh and CP hepatocytes. SULT activities were less stable than UGT activities but were the same in fresh and CP hepatocytes throughout the 4-h incubation.

5. Initial glutathione *S*-transferase activities (using 1-chloro-2,4-dinitrobenzene) were the same in fresh and CP hepatocytes and both did not decrease over 4 h.

6. CP monkey hepatocytes are a useful model for metabolic and cytotoxicity studies. These cells can be can be used either in suspension or in culture.

Introduction

During drug development, early toxicological and metabolic studies of xenobiotics are becoming more focused on species more relevant to man. Consequently, the cynomolgus monkey (*Macaca fascicularis*) is the most common primate species used for such studies (Blaauboer *et al*. 1990). In addition to *in vivo* studies, *in vitro* studies using monkey hepatocytes would provide important information for the selection and development of a prospective drug candidate. A major problem facing researchers using hepatocytes from the livers of larger species (including, and especially, monkeys and humans) is the scarcity of tissue availability. In addition, whenever liver sections are available, the amount of cells isolated may be much greater than is needed in a day. It is well known that hepatocytes are normally

* Author for correspondence; e-mail: nicola.hewitt@merck.de

Xenobiotica ISSN 0049-8254 print/ISSN 1366-5928 online © 2000 Taylor & Francis Ltd
http://www.tandf.co.uk/journals

quiescent and lose their differentiated functions rapidly (especially their drug-metabolizing enzyme activities), thus fresh hepatocytes have a limited life span. Effective techniques have been developed to improve and maintain metabolizing functions in long-term cultures of hepatocytes, which include collagen gel sandwich cultures (Dunn *et al*. 1989, 1991) and hepatocyte aggregate 'spheroids' (Landry *et al*. 1985, Tong *et al*. 1992). However, the only method developed so far for the indefinite storage of hepatocytes is cryopreservation, i.e. the step-wise freezing of cells in a protective agent and their subsequent storage in liquid nitrogen. Several freezing protocols for hepatocytes of different species have been published to date, all involving step-wise freezing in a cryoprotectant-containing buffer (the recovery of hepatocytes were determined using simple viability parameters) (Sun *et al*. 1990, Chesné *et al*. 1993, de Sousa *et al*. 1996). There are good *in vitro–in vivo* correlations of metabolism using fresh animal and human hepatocytes (Bayliss *et al*. 1999 and references therein), thus, for the acceptance of cryopreserved (CP) hepatocytes as a suitable test system, it is necessary that the metabolism of a compound in fresh hepatocytes is reflected in CP hepatocytes. Furthermore, interspecies differences in the metabolism of xenobiotics should be detectable. For metabolism studies, hepatocytes can either be used in short-term incubations in suspension for up to several hours or in long-term metabolism or enzyme induction studies in primary culture. Therefore, the drug-metabolizing capacity as well as the attachment efficiency of the CP cells have to be maintained after the thawing procedure.

There have been detailed reports of cytochrome P450 (CYP) activities in liver microsomes from different animal species, including the cynomolgus monkey, and the effects of enzyme inducers (Weaver *et al*. 1994, Bullock *et al*. 1995, Sharer *et al*. 1995, Shimada *et al*. 1997); however, only a few studies have investigated both phase I and phase II enzyme activities of CP monkey hepatocytes (Chesné *et al*. 1993, de Sousa *et al*. 1996).

The aim of this study was to analyse the drug-metabolizing enzyme activities of freshly isolated and CP monkey hepatocytes maintained in suspension for up to 4 h and to evaluate the quality of the CP cells obtained by using the methods already established in our laboratory for other species (Utesch *et al*. 1992, Swales and Utesch 1998). The rates of ethoxyresorufin-*O*-deethylation (EROD), ethoxycoumarin-*O*-deethylation (ECOD) and testosterone hydroxylation were compared as indicators of the activities of several CYP isoforms (Waxman *et al*. 1988, Weaver *et al*. 1994). UDP-glucuronyltransferase (UGT), glutathione *S*-transferase (GST) and sulphotransferase (SULT) activities were chosen as the most relevant enzyme activities to reflect phase II metabolism (Pickett and Lu 1989, Bock 1994, Falany and Wilborn 1994). To investigate whether any losses of enzyme activities were due to the loss of the respective cofactors or the protein itself, the activities in homogenates were measured with the required cofactors added and in intact cells without any additions. Also compared were the plating efficiencies of fresh and CP hepatocytes measuring lactate dehydrogenase (LDH) contents of monolayers after 24 h in culture.

Materials and methods

Animals

Liver sections of male cynomolgus monkeys (3–7 kg) were kindly provided by Covance Laboratories (Münster, Germany). They were from untreated animals of separate toxicity studies and were humanely killed by an overdose of pentobarbitone.

Chemicals and materials

Collagenase A (0.18 U/mg protein) was from Boehringer Mannheim (Germany). Hank's balanced salt solution without Ca^{2+} or Mg^{2+} (HBSS) was from GibcoBRL (Eggenstein, Germany). Percoll was from Biochrom (Berlin, Germany) and Brij®58 was from Fluka (Germany). The hydroxytestosterone (OHT) standards, 6β-OHT, 16α-OHT, 2α-OHT, 15β-OHT, 2β-OHT and 16β-OHT, 7-ethoxycoumarin (EC), 7-ethoxyresorufin (ER), 7-hydroxycoumarin (HC), 1-chloro-2,4 dinitrobenzene (CDNB), 4-methylumbelliferone (MUF), MUF-glucuronide, 2-naphthyl sulphate, uridine 5′-diphosphoglucuronic acid (UDPGA) and 3′-phosphoadenosine 5′-phosphosulphate (PAPS) were from Sigma (Deidenhofen, Germany). Ethyleneglycol-bis(β-aminoethyl ether) *N*,*N*,*N*′,*N*′-tetra-acetic acid (EGTA), bovine serum albumin, fraction V (BSA), 2-naphthol, dihydronicotinamide adenine dinucleotide phosphate (NADPH) and all other chemicals were from Merck (Darmstadt, Germany) and were of the highest grade available. Collagen (Type IV)-coated, Primaria and fibrinectin culture plates were from Beckton Dickinson GmbH (Heidelberg, Germany).

Cell isolation

Liver pieces (each with one cut surface) of 50–100 g were pre-perfused with HBSS to remove the blood and were transferred to our laboratory in ice-cold Krebs–Henseleit buffer, pH 7.6. Perfusion started about 4 h after liver resection. The hepatocytes were isolated by a two-step wedge perfusion technique as described by Moldéus *et al*. (1978). Briefly, two veins were cannulated and perfused with 0.5 mM EGTA-containing buffer for 10 min and then with a 0.15% (w/v) collagenase-containing buffer for 3–5 min at 37 °C. When the liver became soft, the liver section was immersed into ice-cold HBSS (pH 7.6) containing 2.5% BSA and cells were released by gently combing with sharp-pointed forceps. The cells were filtered through 150 μm nylon gauze and then centrifuged at 50 *g* for 5 min at 4 °C. Cells were washed twice in suspension buffer (50 *g* for 5 min at 4 °C) and once in Percoll-containing buffer (160 *g* for 20 min at 4 °C). The suspension buffer was a modified Krebs–Henseleit buffer containing 25 mM HEPES, 0.5% glucose, 0.2% BSA, 1 mM $CaCl_2$, 0.4 mM $MgSO_4$, 1 μg/ml insulin, 70 μg/ml glutamine and the amino acid mixture recommended by Seglen (1976). The Percoll solution consisted of 90% Percoll and 10% HBSS (10 concentrate containing Ca^{2+} and Mg^{2+}), pH 7.6. Cells (30 ml) were gently mixed with 20 ml Percoll buffer and then centrifuged at 160 *g* for 20 min at 4 °C. The hepatocytes were washed again in suspension buffer before viability and cell number were determined by Trypan blue exclusion.

Cryopreservation of hepatocytes

Hepatocytes were again pelleted by centrifugation at 50 *g* for 5 min at 4 °C and then resuspended in suspension buffer containing 4% DMSO at 24×10^6 viable cells/ml. Cells were left on ice for 5 min and an equal volume of a 16% DMSO-containing suspension buffer was added, resulting in a final density of 12×10^6 viable cells/ml. Cells were aliquoted into 2-ml cryotubes (Nunc, Wiesbaden, Germany) and frozen in a Cryoson TRA-14 programmable freezer (Cryoson, Schöllkrippen, Germany) using the freezing protocol described by Diener *et al*. (1993) and Swales and Utesch (1998). The freezing programme (of 51 min) comprised an initial slow-cooling rate (from 20 to 0 °C in 10 min), a shock-freeze at 17 min from −9.5 to −28 °C/min and, finally, a rapid freeze from −30 to −100 °C in the last 10 min. Cells were stored in liquid nitrogen until required.

Thawing of hepatocytes

Cells were rapidly thawed by immersing in a waterbath at 37 °C. The cryoprotectant was diluted in a stepwise fashion (Utesch *et al*. 1992). Briefly, the cells were transferred directly from the vials to a tube containing ice-cold suspension buffer (1 ml/vial thawed). After 5 min, a further 1 ml/vial was added to the cells. After a further 5 min, the volume was made up to 8 ml/vial by the addition of suspension buffer. Cells were pelleted by centrifugation at 50 *g* for 5 min at 4 °C. Cells were washed in suspension buffer (50 *g* for 5 min at 4 °C) and once in Percoll-containing buffer (160 *g* for 20 min at 4 °C). Percoll solution (18 ml) was added to 32-ml cell suspension and the tubes gently inverted to allow for even mixing. After Percoll differential centrifugation, the cells were again washed in suspension buffer (50 *g* for 5 min at 4 °C) before being counted for cell number and viability by Trypan blue exclusion.

Hepatocyte culture

Hepatocytes were diluted to 0.5×10^6 total cells/ml in Williams' medium E with Glutamax I, supplemented with 10 μg/ml insulin, 50 μg/ml gentamycin and 20% foetal calf serum (this medium was used throughout the culture incubation). Cultures (containing 2-ml cell suspension/plate) were allowed to attach for 4 h before the medium was replaced. After 24 h, the cells were harvested and lysed in 1% Triton X-100 in PBS. All media and lysates were retained for LDH measurement, using the method described by Jauregi *et al*. (1981).

Biochemical assays

Testosterone hydroxylase activities. Freshly isolated and thawed hepatocytes were diluted to 10^6 total cells/ml in suspension buffer and incubated for up to 4 h in a waterbath maintained at 37 °C. At 0, 2 and 4 h, 1 ml (in duplicate) cell suspension was removed and sonicated (Sonifier B12 cell disrupter, 2×5-s bursts) and NADPH (250 μM final concentration) was added. For whole cell incubations, 1 ml (in duplicate) was incubated without sonication or any cofactor addition. The reaction was started by the addition of testosterone (final concentration 250 μM) and terminated after 15 min by the addition of 6 ml dichloromethane, after which 2.5 μg 11α-hydroxyprogesterone was added as an internal standard. Aqueous and non-aqueous solutions were separated by passing the solution through an Extrelute column (Merck). The resulting organic phase eluent was blown down to dryness under a stream of nitrogen gas and reconstituted in 110 μl methanol:water (50:50). The metabolites were analysed by HPLC. Activities were expressed as pmol product formed/min/total (viable and dead) 10^6 cells.

A reversed-phase HPLC LiChrospher RP-18, 5 μm, 125×4 mm (LiChroCART) column was used with a corresponding C18 guard column. The gradient system was the same as that described by Arlotto *et al.* (1991). Testosterone and its metabolites were detected by UV absorbance at 254 nm. A standard curve of each metabolite was constructed for every HPLC run.

ECOD, UGT and SULT activities. Hepatocytes were diluted to 10^6 total cells/ml in incubation buffer. Cells were incubated as whole cells or homogenized by sonication and supplemented with 250 μM NADPH. Cells were allowed to warm to 37 °C before EC or HC (500 μM final concentration) were added. At various times up to 4 h an aliquot (0.2 ml) was removed from the incubation and the reaction was stopped by filtering this through a 0.2-μm Spartan 13/A filters directly into HPLC vials. HC-glucuronide, HC, HC-sulphate and EC were detected and quantified by HPLC as described previously (Ekins *et al.* 1995). A standard curve of 0–500 μM HC was constructed for each HPLC run. The absorbance coefficients of the HC-glucuronide and HC-sulphate were assumed to be identical to that of HC (according to Ekins *et al.* 1995). Activities for ECOD, UGT and SULT were expressed as pmol product formed/min/total 10^6 cells.

EROD activity. EROD activity was measured according to Lubet *et al.* (1985). Hepatocytes were diluted to 10^6 cells/ml in suspension buffer. Cells were homogenized by sonication and supplemented with 250 μM NADPH and 10 μm dicoumarol. Homogenates were warmed to 37 °C and then placed in an Hitachi spectrofluorometer with a cuvette water-jacket (heated to 37 °C). The reaction was started by the addition of ethoxyresorufin (5 μm final concentration) and the rate of resorufin production (pmol/min/total 10^6 cells) was measured over 3 min using an excitation wavelength of 535 nm and an emission wavelength of 582 nm. A standard curve of resorufin (0–500 pmol) was constructed for each assay.

GST activity. Homogenates were incubated in a 0.1 M potassium phosphate buffer (pH 6.5) and supplemented with 1 mM reduced glutathione (GSH). Samples were put into cuvettes and prewarmed in a spectrophotometer with a cuvette water jacket at 25 °C. Reaction was started by adding 1 mM CDNB and formation of the respective GSH-conjugate was observed at 340 nm for 3 min. Activity was calculated as μmol/min/10^6 total cells using the known extinction coefficient of CDNB at this wavelength (Habig *et al.* 1974).

SULT activity using 2-naphthol as the substrate. Freshly isolated and thawed hepatocytes were diluted to 10^6 total cells/ml in suspension buffer and incubated in a shaking waterbath for up to 4 h.

SULT activity in cell homogenates was determined according to Arand *et al.* (1987). This method measures maximal SULT activities under non-physiological conditions and, therefore, can not be measured in whole cells. At various time points, a 1 ml aliquot of cells was homogenized by sonication and pre-incubated at 37 °C in a 0.25 M sodium acetate buffer (pH 5.5) supplemented with 7.5 mM mercaptoethanol and 250 μM 2-naphthol. The reaction was started by adding 200 μM PAPS and terminated after 10 min by adding a 0.6 M glycine/0.4 M trichloroacetic acid buffer (pH 2.2) and centrifuged at 2000 *g* for 3 min. The supernatant was extracted with chloroform (2 ml) and the aqueous phase was diluted with 0.1 M NaOH. 2-Naphthyl sulphate formation was measured fluorometrically at an excitation wavelength of 285 nm and an emission wavelength of 335 nm. A standard curve using 2-naphthyl sulphate was run for each assay (Arand *et al.* 1987). Activities were expressed as pmol product formed/h/total 10^6 cells.

For whole cell SULT activity measurement, a 1-ml aliquot of cells was removed at various times and placed into a separate tube. The reaction was started by adding 100 μM 2-naphthol (250 μM was cytotoxic to whole hepatocytes). The reaction was stopped after 30 min by adding 2 ml chloroform. After the extraction of excess substrate, the aqueous phase was diluted with 0.1 M NaOH and activity was measured as described above.

UGT activity using MUF as the substrate. Freshly isolated and thawed hepatocytes were diluted to 10^6 total cells/ml in suspension buffer and incubated in a shaking waterbath for up to 4 h.

MUF-UGT activities were measured in cell homogenates according to Lilienblum *et al.* (1982).

Again, this method measures maximal activities of the enzyme in non-biological conditions and was, therefore, not used for whole cell measurements. Homogenates were incubated in a Tris buffer containing 5 mM $MgCl_2$ and 0.05% Brij®58 (pH 7.4). MUF was added to give a final concentration of 0.5 mM. Reactions were started with 3 mM UDPGA and terminated after 5 min by adding an equal volume of 0.5 M perchloric acid. After centrifugation at 2000 *g*, the supernatant was extracted with chloroform (2 ml). Aliquots of the aqueous phase were mixed with an equal volume of a glycine/NaOH solution (pH 10.3) and measured fluorometrically at an excitation wavelength of 315 nm and an emission wavelength of 365 nm, using an Hitachi spectrofluorometer. Activities (pmol product formed/h/total 10^6 cells) were calculated with respect to a standard curve of MUF-glucuronide, which was run for each assay (Lilienblum *et al*. 1982).

For whole cell incubations, hepatocytes were incubated (without any cofactor supplements) in suspension buffer for up to 4 h. The reaction was started by adding 0.1 mM MUF at the appropriate time points (0.5 mM MUF was cytotoxic to the cells). The reaction was stopped after 30 min by adding 2 ml chloroform. After the extraction of excess substrate, the aqueous phase was mixed with an equal amount of 1.6 M glycine/NaOH solution (pH 10.3) and UGT activity was measured as described above.

Statistics

Results were compared using the Student's unpaired *t*-test or the Dunnett's *t*-test. $p < 0.05$ was considered significant. '*n*' is the number of different hepatocyte preparations from different animals.

Results

Cell viability and attachment

The viabilities of freshly isolated and CP hepatocytes used for culture and metabolic studies are shown in table 1. The viable recovery was marginally increased (but not significantly) and the viability of CP hepatocytes was improved by including Percoll differential centrifugation in the thawing procedure. The viability of fresh and CP hepatocytes decreased when they were incubated in suspension, however, the loss of viability of CP hepatocytes was the same as that in fresh cells. The attachment efficiency of fresh and CP hepatocytes to collagen (type IV) after the initial plating period (4 h) was $\sim 60\%$. During the following 20 h, 17% of fresh cells detached, however, CP hepatocytes were more fragile and by 24 h, only $15 \pm 4\%$ of these cells remained attached. Attachment was markedly improved by the inclusion of Percoll differential centrifugation during the thawing of CP hepatocytes. The attachment of fresh and CP hepatocytes was not increased when cultured on human fibrinectin or Primaria plates (which have a positively charged surface, data not shown). CP hepatocytes appeared healthy under light microscopy, showing cytoplasmic spread, cell–cell contact and a non-blebbed appearance (figure 1).

Initial enzyme activities in hepatocyte homogenates

Table 2 shows enzyme activities in whole cells and homogenates of freshly isolated and CP hepatocytes immediately after thawing. ECOD activity was much higher in homogenates supplemented with NADPH than in whole cells and was not significantly different in fresh and CP hepatocytes. EROD and total testosterone hydroxylase activities (defined as the sum of the individual OHT activities given in Table 3) were also the same in fresh and CP hepatocytes (table 2). Table 3 shows the initial individual testosterone hydroxylase activities in fresh and CP hepatocytes. The rate of hydroxylase activities were not decreased by cryopreservation, moreover, CP whole hepatocytes (but not homogenates) had significantly higher rates of hydroxylation than the corresponding fresh values. The relative amount of each hydroxylase activity was not altered by cryopreservation, whereby 6β-OHT was the predominant metabolite in both fresh and CP hepatocytes (71–75% of the total OHT production). 2β-OHT and 16β-OHT represented 16 and 7% of the total

Table 1. Viability and attachment efficiencies of freshly isolated and cryopreserved (CP) monkey hepatocytes.

			CP	
		Fresh	Non-Percoll	Percoll-treated
Viability (%)[a]	0 h	91±7	67±14*	91±6
in suspension:	2 h	73±14	n.d.	82±5
	4 h	59±13	n.d.	74±7
% Viable recovery		–	26±11	36±17
Attachment (%)	4 h	59±9	53±7	63±7
in culture[b]	24 h	42±9	15±4*	45±7

Values are mean±SD, $n \geqslant 4$.

[a] Determined by Trypan blue exclusion after isolation and thawing.

[b] Determined by intracellular lactate dehydrogenase contents of attached cells

* Significantly different from the corresponding fresh value (Student's t-test, $p < 0.05$).

n.d., Not determined.

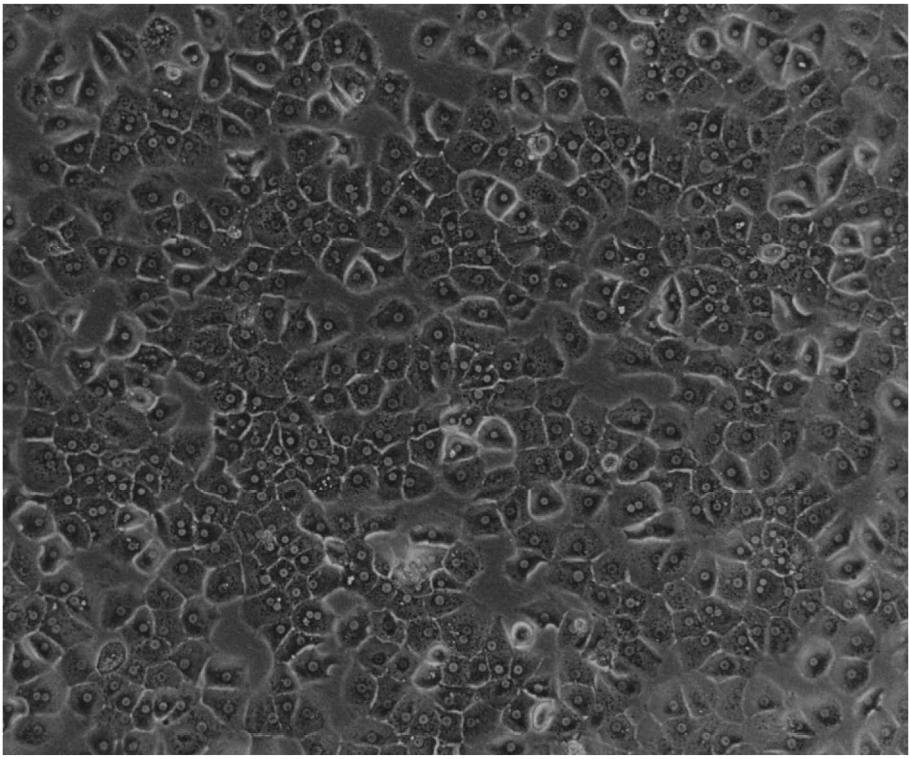


Figure 1. The appearance of cryopreserved monkey hepatocyte cultures (after 24 h) under light microscopy.

metabolites respectively, and 16α-OHT, 15β-OHT, 2α-OHT and 7α-OHT, were minor metabolites (each represented 1–2% of the total hydroxy-metabolite formation). The process of homogenization significantly increased the rate of all hydroxylases but not the relative ratio of each metabolite (i.e. 6β-OHT still represented 73–75% of the total OHT formation).

Table 2. Initial phase I and II enzyme activities of freshly isolated and cryopreserved (CP) monkey hepatocytes.

	Whole cells		Homogenates+cofactors	
	Fresh	CP	Fresh	CP
Phase I				
ECOD-activity[a]	108±14	170±85	1047±508	884±230
EROD-activity[a]	n.d.	n.d.	125±80	155±69
Total testosterone hydroxylation[a]	1039±209	1497±313	2959±607	3173±591
Phase II				
GST activity[b]	n.d.	n.d.	2.28±1.3	2.24±1.15
UGT activity				
MUF[c]	47.1±9.0	43.3±10.9	212±127	115±108
EC[a,d]	27.9±9.1	36.7±29.2	34.9±15.9	47.3±20.6
HC[a]	136±48	128±77	n.d.	n.d.
SULT activity				
2-naphthol[c]	40.0±23.2	32.2±24.3	33.6±25.5	19.5±11.6
EC[a,d]	23.4±7.5	31.7±19.2	15.1±5.0	18.2±12.4
HC[a]	29.4±15.3	40.6±17.7	n.d.	n.d.

Values are mean±SD, $n \geqslant 3$.

Enzyme activities of CP hepatocytes were not significantly different from fresh values.

Total hydroxylase activity is the sum of the individual hydroxylases (refer to table 3 for individual hydroxylase activities).

n.d., Not determined.

[a] Expressed as pmol/min/10^6 cells.

[b] Expressed as μmol/h/10^6 cells.

[c] Expressed as pmol/h/10^6 cells.

[d] Only NADPH was added to these homogenates.

Table 3. Initial testosterone hydroxylase activities in freshly isolated and cryopreserved (CP) monkey whole hepatocytes and homogenates supplemented with 250 μ_M NADPH.

	Whole cells		Homogenates+NADPH	
	Fresh	CP	Fresh	CP
6β-OHT[a]	751±167 (72%)	1069±232* (71%)	2209±490 (75%)	2324±481 (73%)
2β-OHT[a]	165±26 (16%)	241±54* (16%)	405±78 (14%)	433±85 (14%)
16β-OHT[a]	69±10 (7%)	102±26* (7%)	169±36 (6%)	178±40 (6%)
16α-OHT[a]	17±5 (2%)	35±23 (2%)	99±55 (3%)	153±83 (5%)
15β-OHT[a]	22±3 (2%)	33±8* (2%)	50±11 (2%)	50±13 (2%)
2α-OHT[a]	7±4 (1%)	9±3 (1%)	16±4 (0.5%)	22±5 (1%)
6α-OHT[a]	8±4 (1%)	8±2 (1%)	11±4 (0.4%)	13±5 (0.4%)

Values are mean±SD, $n = 6$.

[a] Expressed as pmol/min/10^6 cells.

Values in parentheses denote the percentage of total hydroxylase activity.

* Significantly different from the corresponding fresh value (Dunnett's test, $p < 0.05$).

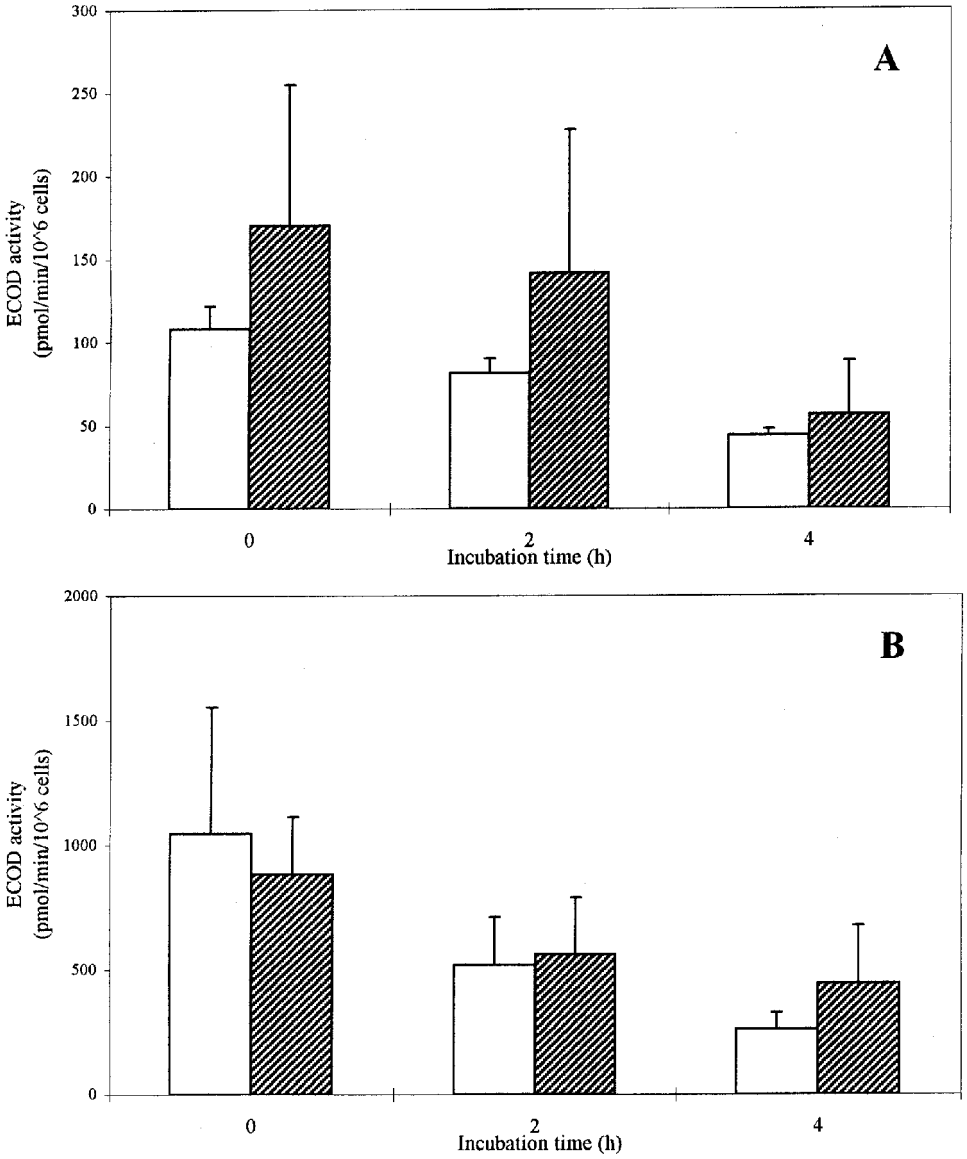


Figure 2. ECOD activities in fresh (□) and cryopreserved (▨) whole cells (A) and homogenates (B) over 4 h in suspension, (mean ±SD, n = 3).

Fresh and CP homogenates supplemented with GSH had the same initial GST activities (table 2). UGT activity was measured using three substrates, namely, MUF, EC and HC. EC was used as an indirect measurement of UGT activity since HC produced from *O*-deethylation of EC can be further metabolized by UGT (as well as SULT). UGT activities for all three substrates were equivalent in fresh and CP hepatocytes, whether incubated as whole cells or homogenates (table 2). SULT activities were also measured using three substrates, 2-naphthol, EC and HC (table 2). SULT activities for these substrates in CP hepatocytes did not differ from fresh cell activities.

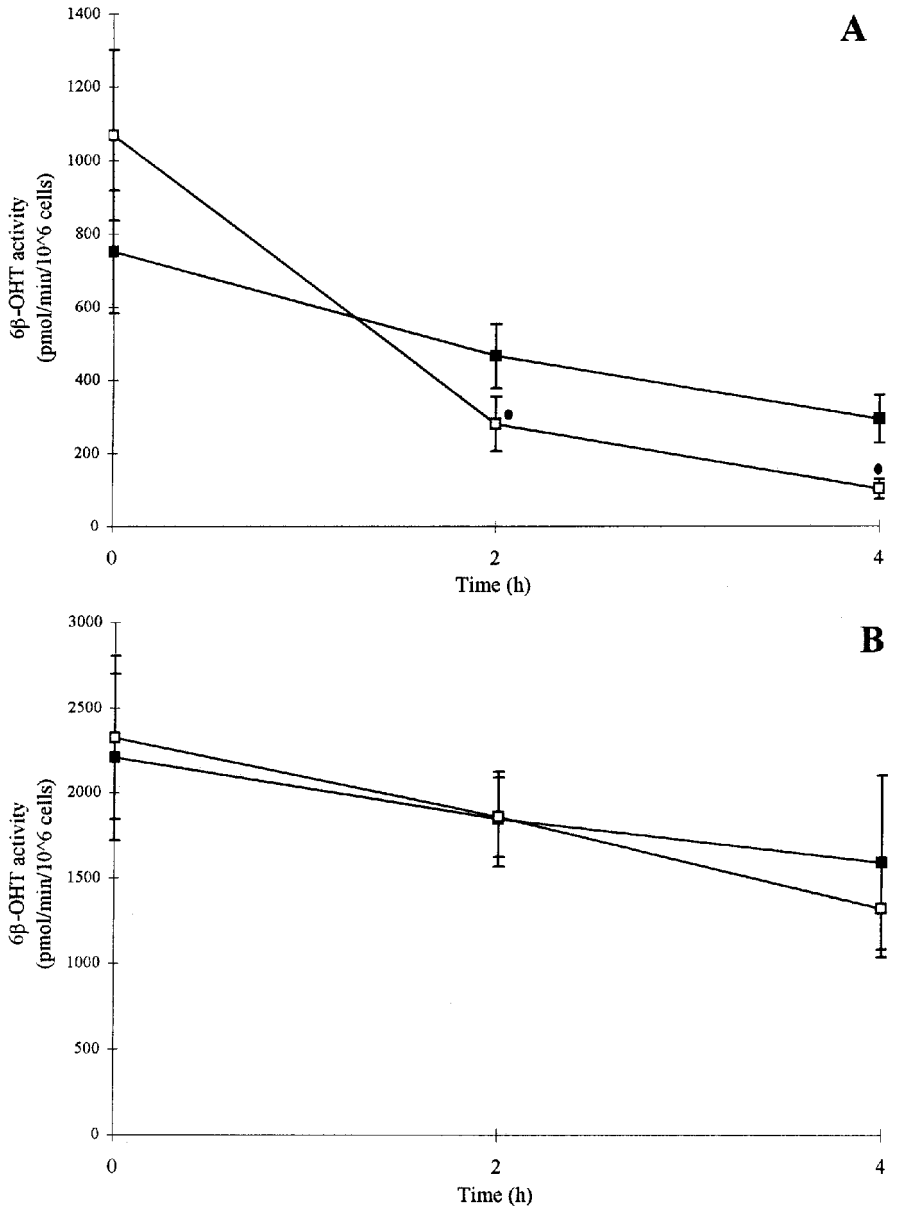


Figure 3. Testosterone 6β-Hydroxylase activities over 4 h in fresh (■) and cryopreserved (□) hepatocyte whole cell suspensions (A) and homogenates supplemented with 250 μM NADPH (B) (mean $\pm$SD, $n = 6$). ●Significantly different from the corresponding value of freshly isolated cells at the given time-point ($p < 0.05$, Dunnett's test).

Phase I enzyme activities over 4-h incubation

ECOD activity in CP hepatocytes was marginally higher over 4 h than in fresh whole cells (although this was not statistically significant; figure 2A) and equivalent in homogenates supplemented with NADPH (figure 2B). ECOD activity decreased during the 4-h incubation from 108$\pm$14 pmol/min/10^6 cells and 170$\pm$85 pmol/min/10^6 at 0 h to 44$\pm$4 pmol/min/10^6 and 57$\pm$32 pmol/min/10^6 at 4 h in fresh and

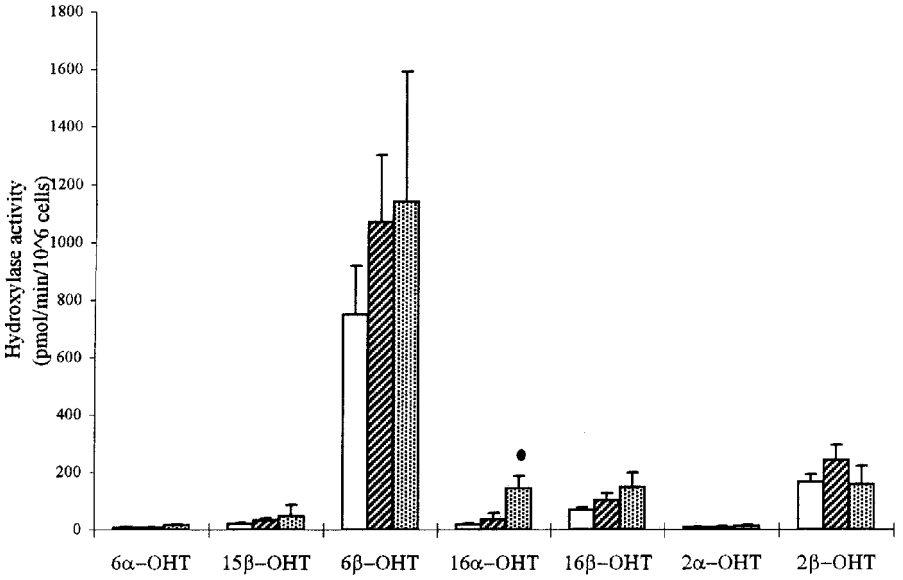


Figure 4. Testosterone hydroxylase activities in freshly isolated hepatocytes (n = 6, □), freshly thawed cryopreserved hepatocytes (n = 6, ▨) and cryopreserved hepatocyte cultures (24 h) (n = 4, ▨), (mean ±s.d.). ●Significantly different from fresh and cryopreserved cell activity at t = 0 ($p < 0.05$, Dunnett's test).

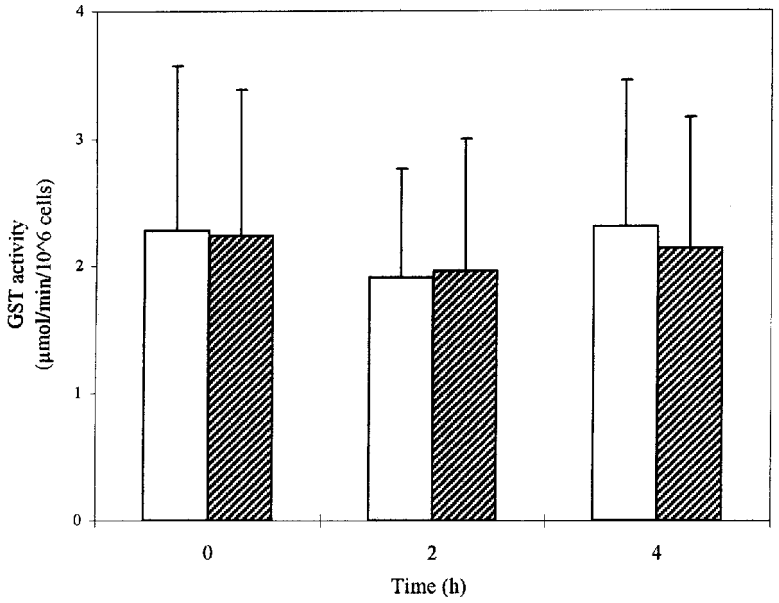


Figure 5. GST activities (using 1-chloro-2, 4 dinitrobenzene as a subtrate) in fresh (□) and cryopreserved (■) homogenates over 4 h in suspension, (mean ±SD, n = 3)

CP whole hepatocytes respectively. Likewise, ECOD activity decreased in hepatocyte homogenates from 1047±508 pmol/min/10^6 cells and 885±230 pmol/min/10^6 at 0 h to 263±66 pmol/min/10^6 and 446±233 pmol/min/10^6 at 4 h in fresh and CP homogenates respectively.

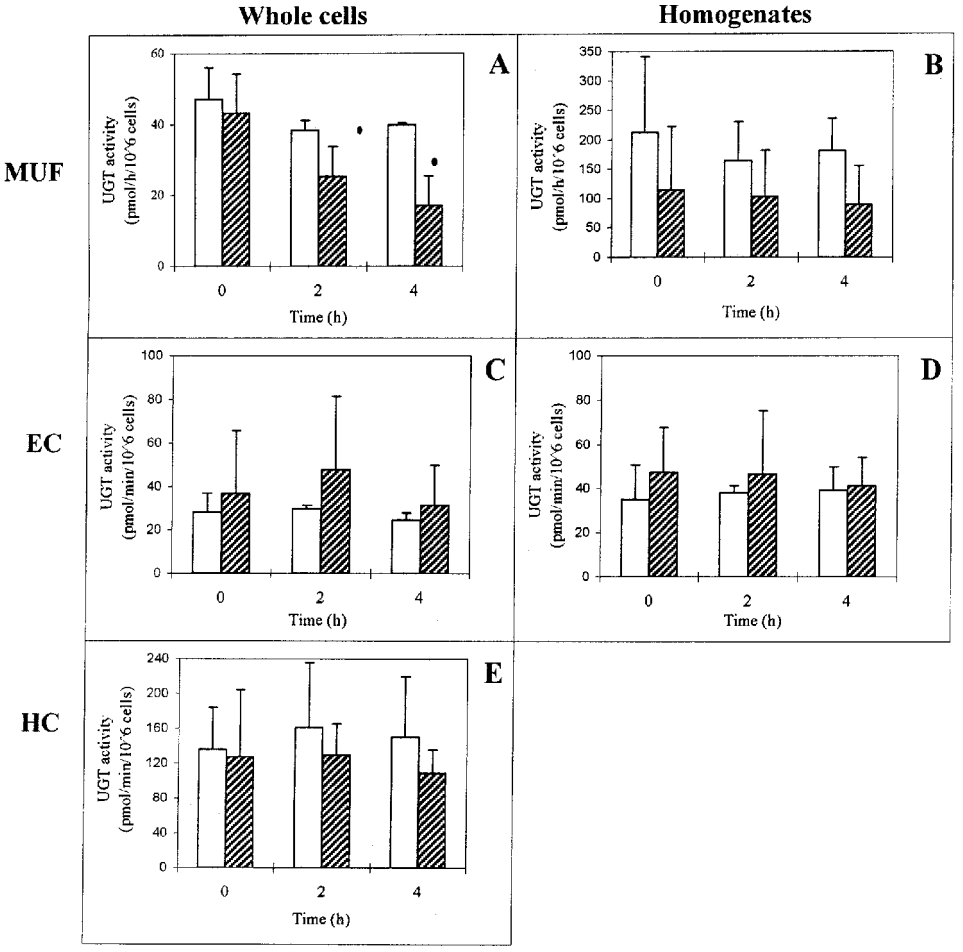


Figure 6. UGT activities in freshly isolated (□) and cryopreserved (▨) whole cells (A, C and E) and homogenates (B and D) over 4 h in suspension. Activities were measured using the substrates, MUF (A and B), EC (C and D) and HC (E) (mean ±SD., $n = 3$) ●Significantly different from the corresponding value of freshly isolated cells at the given time-point and from the corresponding $t = 0$ value ($p < 0.05$, Dunnett's test).

Figure 3 shows 6β-OHT activities in fresh and CP hepatocyte suspensions over a 4-h incubation. Whole hepatocytes (CP and fresh) lost more 6β-OHT activity than homogenates over 4 h. 6β-OHT activity was lower in CP whole hepatocytes than in fresh whole hepatocytes (60% (2 h) and 35% (4 h) of fresh values) but in homogenates supplemented with NADPH, the activities were very similar. The relative amounts of individual hydroxylase activities over 4 h incubation of whole cells and homogenates (supplemented with NADPH) were unchanged with time (data not shown). When placed into culture for 24 h, CP hepatocytes had testosterone hydroxylase activities equivalent to those in fresh and CP whole cells at 0 h (figure 4). 6β-OHT represented 69% of the total OHT formation, 2β-OHT and 16β-OHT each accounted for 9% of the total OHT formation and 6α-OHT and 15β-OHT were minor metabolites (1% of total OHT formation). 16α-OHT activity was marginally higher in 24 h cultures but this still represented only 9% of the total OHT metabolism.

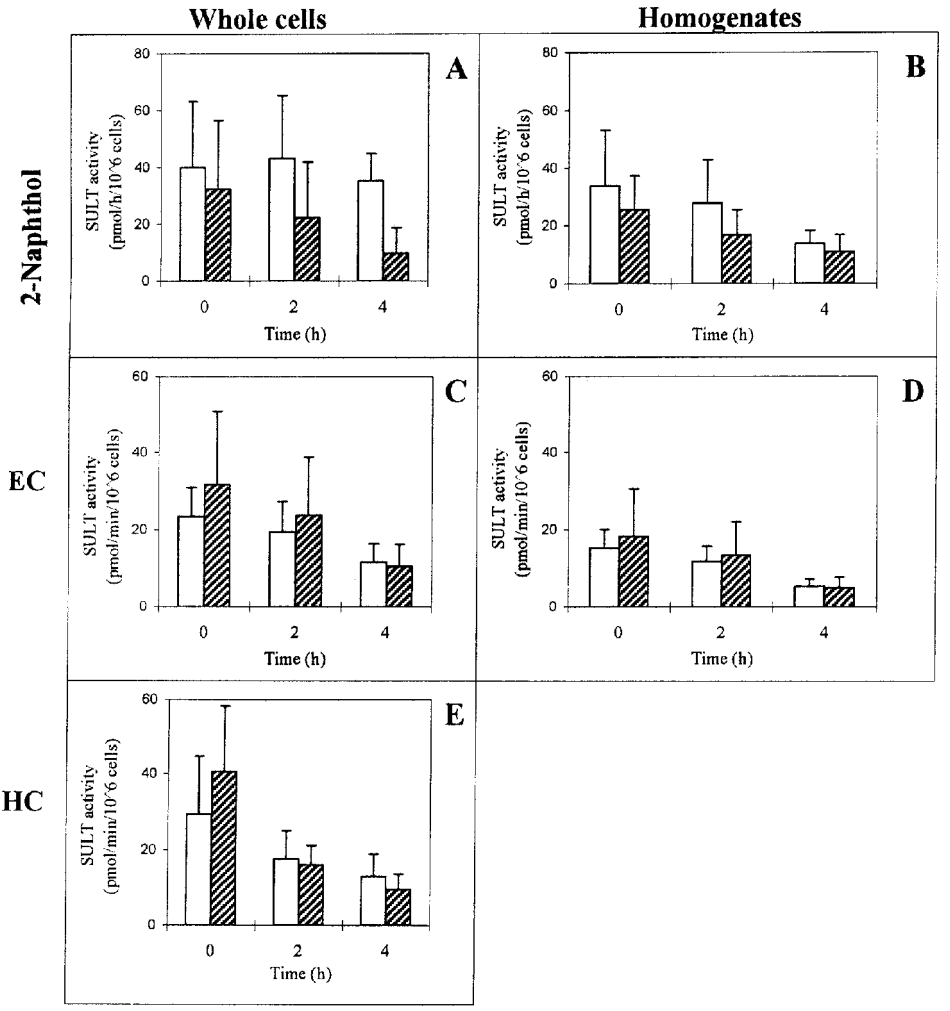


Figure 7. SULT activities in freshly isolated (□) and cryopreserved (▨) whole cells (A, C and E) and homogenates (B and D) over 4 h in suspension. Activities were measured using the substrates, 2-naphthol (A and B), EC (C and D) and HC (E) (mean ±SD., $n = 3$)

Phase II enzyme activities over 4-h incubation

GST activities could only be measured in homogenates, not in whole cells (possibly because whole cells are impermeable to CDNB). GST activities in both fresh and CP hepatocytes were well maintained over 4 h in suspension (figure 5). There was no difference in GST activities between fresh and CP hepatocytes at any time. Moreover, GST activities in fresh and CP hepatocytes at 4 h were the same as initial values.

Figure 6 shows UGT activities in freshly isolated and CP hepatocytes maintained in suspension for up to 4 h. UDPGA was added to homogenates incubated with MUF (but not EC), whereas intact hepatocytes were incubated without any cofactor supplements. UGT activities using MUF, EC and HC as substrates in fresh whole hepatocytes were 85, 88 and 111% of their initial values at 4 h respectively (figure 6A, C and E). UGT activities using EC and HC in CP hepatocytes were also well maintained, whereby 85% of the initial activity remained for both substrates (figure

6C and E). MUF-UGT activity was significantly lower in CP whole cells than in fresh whole cells and only 40% of the initial activity remained after 4 h (figure 6A). MUF-UGT activity was ~5-fold higher in homogenates supplemented with UDPGA than in whole cells (figure 6A and B). Although the average MUF-UGT activity was lower in CP homogenates than in fresh homogenates, the decline in this activity was less compared with the loss in whole cells (85 and 78% of the initial MUF activity in fresh and CP hepatocyte homogenates remained after 4 h respectively). EC-UGT activity in fresh and CP hepatocyte homogenates (in which no exogenous UDPGA was added) was still 113 and 88% of the initial value after 4 h incubation (figure 6D) and was not substantially different from values in whole cells.

SULT activities with all substrates were generally more unstable than UGT activities (in both CP and fresh hepatocytes), whereby only 20–40% of the initial SULT activities remained after 4 h of incubation, whether in whole cells or homogenates (figure 7A–E). The one exception to this was with fresh whole hepatocytes incubated with 2-naphthol, which lost only 15% of its initial activity over 4 h (figure 7A). CP whole cell SULT activity for 2-naphthol was, therefore, significantly lower than in fresh hepatocytes by 4 h incubation (figure 7A). Fresh homogenates supplemented with PAPS lost more 2-naphthol-SULT activity than fresh whole cells (figure 7B), therefore, this activity was equivalent in fresh and CP homogenates over 4 h. EC-SULT and HC-SULT activities in CP hepatocytes were equivalent in whole cell and homogenates throughout the incubation (figure 7C–E).

Discussion

There is a great demand in the chemical, pharmaceutical and cosmetics industries for *in vitro* model systems, particularly those using hepatocytes for either short-term incubations in suspension or for long-term studies in primary culture. The monkey is one of the most common non-rodent mammalian species used for metabolism and toxicity studies. Despite this, information about the cryopreservation of monkey hepatocytes is sparse (Sun *et al*. 1990, Chesné *et al*. 1993, de Sousa *et al*. 1996) and, to our knowledge, comprehensive studies on the metabolic capacity of these cells have yet to be published.

In the present study, the viability and phase I and II enzyme activities of freshly isolated monkey hepatocytes were compared with those cryopreserved using a method previously used in this laboratory. To distinguish whether any loss in enzyme activity was due to a loss of apoprotein or simply to the loss of the respective cofactor, enzyme activities were measured in intact cells and homogenates supplemented with cofactors.

The viability of CP hepatocytes was improved by Percoll purification and resulted in better attachment of these cells in culture, possibly due to the removal of leaky dead cells (the intracellular proteolytic contents released may prevent attachment of healthy cells). The advantage of the use of Percoll was that it effectively separated dead cells from viable cells (dead cells floated on top of the 50 ml buffer and viable cells pelleted firmly to the bottom of the tube) without decreasing the number of viable cells recovered (which was the same viable cell recovery (30–40%) as our previous thawing method which does not include this step; Swales and Utesch 1998). The viability and attachment of fresh and CP monkey hepatocytes described here compare well with that of others who also used Percoll in their thawing methods: Chesné *et al*. (1993) obtained viabilities of 86%

(fresh) and 61% (CP) and attachments of 60% (fresh) and 30% (CP); Sun *et al.* (1990) reported similar attachments of 54% (fresh) and 43% (CP). The attachment of hepatocytes, monolayer formation and the maintenance of CYP enzymes demonstrated herein is essential for the measurement of enzyme induction. Previous studies by de Sousa *et al.* (1996) showed that it is possible to measure CYP1A and GST induction at the mRNA level in cultures of CP monkey hepatocytes. Future work will be extended to CYP enzyme induction in CP monkey hepatocyte monolayers by measuring enzyme activities, rather than mRNA levels.

A fundamental requirement for many toxicity assays (e.g. those measuring genotoxicty and cytotoxicity) is the ability of cells to metabolize the test compound. It is, therefore, important to measure basic phase I and II metabolism of diagnostic substrates to establish whether or not monkey hepatocytes may be used in such assays. In human liver, ECOD activity is a measure of CYP1A2 and 2E1 (Yamazaki *et al.* 1996), these CYPs have amino acid sequences which are 92% identical with the corresponding CYPs in monkey liver (Komori *et al.* 1992). Thus, ECOD activity reflects CYP1A2 and 2E1 activities, rather than overall P450 activities. ECOD activities over 4 h and initial EROD activities (CYP1A in the cynomolgus monkey; Weaver *et al.* 1994, 1999) were the same in fresh and CP hepatoctyes, demonstrating that phase I metabolism in these cells is resistant to cryo-injury.

The rate of testosterone metabolism is a sensitive marker for the detection of cryo-injury, since decreases in total or selective testosterone hydroxylase activities are not always reflected by decreases in ECOD or EROD activities (as reported in previous studies using dog hepatocytes; Swales and Utesch 1998). Testosterone metabolism was, therefore, used as a parameter for assessing cell recovery. Testosterone hydroxylation is believed to be catalysed in the cynomolgus monkey liver by the CYP2B, 2C and 3A subfamilies (Weaver *et al.* 1994, 1999). Seven different hydroxylated metabolites were identified in both fresh and CP hepatocytes. The results concur with those of Wortelboer *et al.* (1992) in that both studies found 6β-OHT to be the major metabolite. Additionally, the relative activities of the individual hydroxylases were similar to those of fresh monkey hepatocyte cultures (Wortelboer *et al.* 1992) and liver microsomes of untreated monkeys (Bullock *et al.* 1995). Results presented here show that both the pattern and extent of testosterone metabolism by monkey hepatocytes is unaltered by cryopreservation. When incubated in suspension for longer times, the rate of testosterone metabolism decreased in fresh and CP whole hepatocytes, although the isoenzyme relative ratios of metabolites of both were unaffected. CP hepatocytes lost more hydroxylase activity than fresh cells but this was due to a greater loss of NADPH from the cells, rather than a loss of enzyme function, since the addition of NADPH returned the activities of CP cells back to fresh values and attenuated the loss of hydroxylases over 4 h. Hydroxylase activities in CP hepatocytes are much more stable when they are placed into culture, such that by 24-h culture, the hydroxylase activites are no different from freshly isolated hepatocytes.

Initial phase II enzyme activities (GST, UGT, SULT) were equivalent in fresh and CP whole hepatocytes and homogenates which were supplemented with cofactors. GST activities in fresh and CP hepatocytes were unaltered throughout the incubation. The maintained stability of GST by CP hepatocytes is important for their use in metabolic and toxicity studies since GST play a pivotal role in xenobiotic detoxification, and sometimes bioactivation (Meister 1988). In accordance with others (Wortelboer *et al.* 1992, Olinga *et al.* 1998), the predominant phase II

conjugation pathway in EC metabolism, in both fresh and CP hepatocytes, was glucuronidation. Importantly, UGT activities were stable throughout the 4-h incubation and any loss (which was only seen in with MUF metabolism in CP whole cells) was due to a loss of cofactor, since addition of UDPGA restored the UGT activity at 4 h to initial levels. Previous results with Beagle dog hepatocytes demonstrated that homogenization by sonication resulted in complete loss of phase II metabolism of EC (Swales and Utesch 1998); therefore, UDPGA was not included in the incubation of EC with homogenates in order to measure phase I metabolism only (hence, the addition of NADPH only). However, not only was the HC-glucuronide formed, but also the rate of glucuronidation was similar to that measured in whole cells. Likewise, homogenates which were not supplemented with exogenous PAPS could still form HC-sulphate, albeit at a lower rate than in whole cells. SULT activities were generally more labile than UGT activities but SULT activities in CP hepatocytes were always similar to those in fresh cells. The loss of SULT activities was due to a loss of enzyme function over time since addition of PAPS did not increase 2-naphthol-SULT activity. Others have reported SULT to be more unstable than UGT, for example, human liver slices lost most of their SULT but not UGT activity (using EC as the substrate) as a result of cryopreservation (de Kanter *et al*. 1998) and hypothermic storage (Olinga *et al*. 1998). The maintenance of phase II enzyme activities in CP monkey hepatocytes is in contrast to our previous data with Beagle dog hepatocytes (Swales and Utesch 1998), which showed significant losses of SULT and UGT activities in whole hepatocytes immediately after thawing (but which were restored to fresh values with the addition of PAPS and UDPGA). Thus, hepatocytes isolated from monkey livers are more resistant to cryo-injury than Beagle dog hepatocytes. This suggests that the recovery of the hepatoctyes using this cryopreservation method may depend largely on the general resilience of the cells. Indeed, preliminary results using a different breed of dog (Foxhound-Boxer cross-breed, FBI) have shown that FBI dog hepatocytes have much better viabilities and attachment efficiencies ($\sim 60\%$ after 24 h in culture) than Beagle hepatocytes.

The detection of species differences in metabolism is an important factor to address, especially with respect to testing of drug candidates. These data show a marked difference in EROD activities and OHT formation to that measured in rat hepatocytes. EROD activity was much higher in monkey hepatocytes than in rat hepatocytes (in which EROD activity was 8 ± 3 pmol/min/10^6 total cells in our studies; unpublished data). This observation was also made by Wortelboer *et al*. (1992). 6β-Hydroxylase activity in monkey hepatocytes is by far the major metabolite (71–75% of the total OHT formed) and was many-fold higher than that measured in rat hepatocytes (392 pmol/min/10^6 cells; Swales *et al*. 1996) or dog hepatocytes (390 pmol/min/10^6 cells; Swales and Utesch 1998). Such high 6β-OHT activity is also a feature of human hepatocytes (Waxman *et al*. 1988). 6β-OHT is not the major metabolite in rat hepatocytes and only contributes $\sim 20\%$ of the total OHT formation (Swales *et al*. 1996). Although 6β-OHT is the major OHT in dog hepatocytes, it accounts for only 48% of the total OHT formed. Moreover, other OHT strongly feature in the metabolites produced by these cells (namely 16α-OHT, 16β-OHT and 2β-OHT). Another minor species difference in testosterone metabolism was with respect to 7α-OHT formation. 7α-OHT was not detected in either fresh or CP monkey hepatocytes (which was also reported by Wortelboer *et al*. 1992) but is a minor metabolite in the rat (Swales *et al*. 1996).

In conclusion, data presented herein report that, phase I and II drug-metabolizing enzyme activities of monkey hepatocytes, measured immediately after thawing, were unaffected by cryopreservation. When placed into suspension or into culture, CP hepatocytes had similar metabolic characteristics to fresh cells. These results support the use of CP monkey hepatocytes for *in vitro* toxicological and metabolic studies: either for short-term assays, such as the comet assay (a genotoxicity test in which test compounds are incubated for a maximum of 2 h; Kuchenmeister *et al*. 1998) or long-term assays which require longer incubation times in culture (such as enzyme induction assays, proliferation assays and the unscheduled DNA assay). In whichever system these cells are used, they will undoubtedly provide important information for screening and evaluation of novel and existing compounds in drug development.

Acknowledgement

This work was supported by a grant from the Bundesministerium für Bildung, Wissenschaft, Forschung und Technologie (BMBF), Project no. 0311242.

References

Arand, M., Robertson, L. W. and Oesch, F., 1987, A fluorimetric assay for quantitating phenol sulphotransferase activities in homogenates of cells and tissues. *Analytical Biochemistry*, **163**, 546–551.

Arlotto, M. P., Trant J. M. and Estabrook R. W., 1991, Measurement of steroid hydroxylation reactions by high-performance liquid chromatography as an indicator of P450 identity and function. *Methods in Enzymology*, **206**, 454–462.

Bayliss, M. K., Bell, J. A., Jenner, W. N., Park, G. R. and Wilson, K., 1999, Utility of hepatocytes to model species differences in the metabolism of loxidine and to predict pharmakokinetic parameters in rat, dog and man. *Xenobiotica*, **29**, 253–268.

Blaauboer, B. J., Wortelboer, H. M. and Mennes, W. C., 1990, The use of liver cell cultures derived from different mammalian species in *in vitro* toxicological studies: implementation in extrapolation models? *ATLA*, **18**, 251–258.

Bock, K. W., 1994, UDP-glucuronosyltransferases and their role in metabolism and disposition of carcinogens. *Advances in Pharmacology*, **27**, 367–383.

Bullock, P., Pearce, R., Draper, A., Podval, J., Bracken, W., Veltman, J., Thomas, P. and Parkinson, A., 1995, Induction of liver microsomal cytochrome P450 in cynomolgus monkeys. *Drug Metabolism and Disposition*, **23**, 736–748.

Chesné, C., Guymard, C., Fautrel, A., Poullain, M.-G., Fremond, B., De Jong, H. and Guillouzo, A., 1993, Viability and function in primary culture of adult hepatocytes from various species and human beings after cryopreservation. *Hepatology*, **18**, 406–414.

De Kanter, R., Olinga, P., Hof, I., de Jager, M., Verwillegen, W. A., Slooff, M. J. H., Koster, H. J., Meijer, D. K. F. and Groothius, G. M. M., 1998, A rapid method for cryopreservation of human liver slices. *Xenobiotica*, **28**, 225–234.

De Sousa, G., Langou S0003Tët, S., Lorenzon, G., Placidi, M., Rahmani, R. and Guillouzo, A., 1996, Increase of CYP P-450 1A and glutathione transferase transcripts in cultured hepatocytes from dogs, monkeys, and humans after cryopreservation. *Cell Biology and Toxicology*, **12**, 351–358.

Diener, B., Utesch, D., Beer, N., Dürk, H. and Oesch, F., 1993, A method for the cryopreservation of liver parenchymal cells for studies of xenobiotics. *Cryobiology*, **30**, 116–127.

Dunn, J. C. Y., Tompkins, R. G. and Yarmush, M. L., 1991, Long-term *in vitro* function of adult rat hepatocytes in a collagen sandwich configuration. *Biotechnological Progress*, **7**, 237–245.

Dunn, J. C. Y., Yarmush, M. L., Koebe, H. G. and Tompkins, R. G., 1989, Hepatocyte function and extracellular matrix geometry: long-term culture in a sandwich configuration. *FASEB Journal*, **3**, 174–177.

Ekins, S., Murray, G. I., Burke, B. M., Williams, J. A., Marchant, N. C. and Hawkins, G. M., 1995, Quantitative differences in phase I and II metabolism between rat precision-cut liver slices and isolated hepatocytes. *Drug Metabolism and Disposition*, **23**, 1274–1279.

Falany, C. N. and Wilborn, T. W., 1994, Biochemistry of cytosolic sulfotransferases involved in bioactivation. *Advances in Pharmacology*, **27**, 302–330.

Habig, W. H., Pabst, M. J. and Jakoby, W. B., 1974, Glutathione-*S*-transferases. The first enzymatic step in mercapturic acid formation. *Journal of Biological Chemistry*, **249**, 7130–7139.

Jauregi, H., O., Hayner, N. T., Driscoll, J. L., Williams-Holland, R., Lipsky, M. H. and Galletti, P. M., 1981, Trypan blue uptake and lactate dehydrogenase in adult rat hepatocytes-freshly isolated cells, cell suspensions and primary monolayer cultures. *In Vitro*, **17**, 1100–1111.

Komori, M., Kikuchi, O., Sakuma, T., Funaki, J., Kitada, M. and Kamataki, T., 1992, Molecular cloning of monkey liver microsome P-450 cDNAs: similarity of the primary sequences to human cytochrome P-450. *Biochimica et Biophysica Acta*, **1171**, 141–146.

Kuchenmeister, F., Schmezer, P. and Engelhardt, G., 1998, Genotoxic bifunctional aldehydes produce specific images in the comet assay. *Mutation Research*, **419**, 69–78.

Landry, J., Bernier, D., Quillet, C., Goyette, R. and Maeceau, N., 1985, Spheroidal aggregate culture of rat liver cells: histotypic reorganization, biomatrix deposition, and maintenance of functional activities. *Journal of Cellular Biology*, **101**, 914–923.

Lilienblum, W., Walli, A. K. and Bock, K. W., 1982, Differential induction of rat liver microsomal UDP-glucuronosyltransferase activities by various inducing agents. *Biochemical Pharmacology*, **31**, 907–913.

Lubet, R. A., Nims, R. W., Mayer, R. T., Cameron, J. W. and Schechtman, L. M., 1985, Measurement of CYP P-450 dependent dealkylation of alkoxyphenoxazones in hepatic S9s and hepatocyte homogenates: effects of dicoumarol. *Mutation Research*, **142**, 127–131.

Meister, A., 1988, Glutathione. In I. M. Arias, W. B. Jakoby, H. Popper, D. Schachter and D. A. Shafritz (eds), *The Liver: Biology and Pathology*, 2nd edn (New York: Raven), pp. 401–417.

Moldéus, P., Högberg, J. and Orrhenius, S., 1978, Isolation and use of liver cells. *Methods in Enzymololgy*, **52**, 60–71.

Olinga, P., Merema, M. T., Hof, I. H., de Jager, M. H., de Jong, K. P., Sloof, M. J. H., Meijer, D. K. F. and Groothuis, M. M., 1998, Effect of cold ischaemia on drug metabolism in isolated hepatocytes and slices from human and monkey liver. *Xenobiotica*, **28**, 349–360.

Pickett, C. B. and Lu, A. Y. H., 1989, Glutathione *S*-transferases: gene structure, regulation and biological function. *Annual Reviews in Biochemistry*, **58**, 743–764.

Seglen, P. O., 1976, Preparation of isolated rat liver cells. In D. M. Prescott (ed.), *Methods in Cell Biology*, vol. 13 (New York: Academic Press), pp. 29–83.

Sharer, J. E., Shipley, L. A., Vandenbrande, M. R., Binkley, S. N. and Wrighton, S. A., 1995, Comparison of phase I and phase II *in vitro* hepatic enzyme activities of human, dog, rhesus monkey, and cynomolgus monkey. *Drug Metabolism and Disposition*, **23**, 1231–1241.

Shimada, T., Mimura, M., Inoue, K., Nakamura, S., Oda, H. and Ohmori, S., 1997, Cytochrome P450-dependent drug oxidation activities in liver microsomes of various animal species including rats, guinea pigs, dogs, monkeys, and humans. *Archives in Toxicology*, **71**, 401–408.

Sun, E. L., Aspar, D. G., Ulrich, R. G. and Melchior, G. W., 1990, Cryopreservation of cynomolgus monkey (*Macaca fascicularis*) hepatocytes for subsequent culture and protein synthesis studies. *In Vitro Cellular and Developmental Biology*, **25**, 147–150.

Swales, N. J., Johnson, T. and Caldwell, J., 1996, Cryopreservation of rat and mouse hepatocytes: II. Assessment of metabolic capacity using testosterone metabolism. *Drug Metabolism and Disposition*, **24**, 1224–1230.

Swales, N. J. and Utesch, D., 1998, Metabolic activity of fresh and cryopreserved dog hepatocyte suspensions. *Xenobiotica*, **28**, 937–948.

Tong, J. Z., Lagausie, P. D., Furlan, V., Cresteil, T., Bernard, O. and Alvarez, F., 1992, Long term culture of adult rat hepatocyte spheroids. *Experimental Cellular Research*, **200**, 326–332.

Utesch, D., Diener, B., Molitor, E., Oesch, F. and Platt, K. L.,1992, Characterization of cryopreserved rat liver parenchymal cells by metabolism of diagnostic substrates and activities of related enzymes. *Biochemical Pharmacology*, **44**, 309–315.

Waxman, D. J., Attizano, C., Guengerich, F. P. and Lapenson, D. P., 1988, Human liver microsomal steroid metabolism: identification of the major microsomal steroid hormone S0001T6b-hydroxylase cytochrome P-450 enzyme. *Archives of Biochemical Biophysics*, **263**, 424–436.

Weaver, R. J., Dickins, M. and Burke, M. D., 1999, A comparison of basal and induced hepatic microsomal cytochrome P450 monooxygenase activities in the cynomolgus monkey (*Macaca fascicularis*) and man. *Xenobiotica*, **29**, 467–482.

Weaver, R. J., Thompson, S., Smith, G., Dickins, M., Elcombe, C. R., Mayer, R. T. and Burke, D. M., 1994, A comparative study of constitutive and induced alkoxyresorufin *O*-dealkylation and individual cytochrome P450 forms in cynomolgus monkey (*Macaca fascicularis*), human, mouse, rat and hamster liver microsomes. *Biochemical Pharmacology*, **47**, 763–773.

Wortelboer, H. M., de Kruif, C. A, van Iersel, A. A. J., Falke, H. E., Noordhoek, J. and Blaauboer, B. J., 1992, Acid reaction products of indole-3-carbinol and their effects on cytochrome P450 and phase II enzymes in rat and monkey hepatocytes. *Biochemical Pharmacology*, **43**, 1439–1447.

Yamazaki, H., Inoue, K., Mimura, M., Oda, Y., Guengerich, F. P. and Shimada, T., 1996, 7-Ethoxycoumarin *O*-deethylation catalysed by cytochrome P450 1A2 and 2E1 in human liver microsomes. *Biochemical Pharmacology*, **51**, 313–319.

XENOBIOTICA, 2000, VOL. 30, NO. 7, 683–692

Concurrent induction of rat hepatic microsomal cytochrome P450 and haem oxygenase by 2,2′-dipyridyl ketone: comparison with the effect of 2,2′-dipyridyl amine

Y. KOBAYASHI†, N. OHSHIRO†, E. OKUI‡, T. SASAKI†, S. TOKUYAMA†, T. YOSHIDA‡ and T. YAMAMOTO†*

† Department of Clinical Pharmacy and ‡Department of Biochemical Toxicology, School of Pharmaceutical Sciences, Showa University, 1-5-8, Hatanodai, Shinagawa-ku, Tokyo 142-8555, Japan

Received 18 January 2000

1. The effect of 2,2′-dipyridyl ketone and 2,2′-dipyridyl amine on the induction of hepatic microsomal cytochrome P450 (P450) and heme oxygenase was compared, and their effects on five different P450 isoforms (P4501A1, 3A2, 2B1, 2E1 and 2C11) in rat were examined.

2. Treatment of rat with 2,2′-dipyridyl amine resulted in the marked induction of haem oxygenase to about seven-fold of the controls with a decrease in P450 content. 2,2′-Dipyridyl ketone produced concomitant induction of both P450 and haem oxygenase activity in a dose- and time-dependent manner without showing any sex differences.

3. Immunoblot analysis revealed that 2,2′-dipyridyl ketone slightly increased CYP2E1 and CYP3A2 at low doses, but not at high dose levels. There was no effect on P4502C11. P4502B1 was induced by the treatment with 2,2′-dipyridyl ketone in a dose-dependent manner.

4. These results indicate that dipyridyl compounds having different bridges between two aromatic moieties act as differential inducers of hepatic microsomal P450s and haem oxygenase.

Introduction

It has been shown that N-substituted azole antimycotic drugs and chemicals are potent inducers of hepatic microsomal cytochrome P450 (P450) (Ritter and Franklin 1987a, b, James 1988, Rodrigues *et al*. 1988, Laignelet *et al*. 1989, Franklin 1992, Franklin and Moody 1992). It has already been demonstrated that clotrimazole and its structurally related compounds also increased P450 content in the rat liver (Matsuura *et al*. 1991, Kobayashi *et al*. 1992, 1994). Of the compounds having a benzyl moiety bound to the imidazole- and pyridine-rings at the 1- or 4-position of the ring, 1-benzylimidazole and/or 4-benzylpyridine are the minimum structures for the induction of hepatic P450 (Matsuura *et al*. 1991, Kobayashi *et al*. 1992). In addition, 1-benzylimidazole induced hepatic P450 content and P4502B1/2 in a dose-dependent manner in the male rat, but it failed to induce P4502B1/2 in the female (Kobayashi *et al*. 1994), suggesting that induction of P4502B1/2 by 1-benzylimidazole may be mediated through the presence of sex steroids, such as testosterone. Moreover, both 4-phenylalkylpyridines and N-phenylalkylimidazoles increased hepatic and renal P450 in a chain-length-dependent manner (Kobayashi *et al*. 1995, 1996a).

* Author for correspondence; e-mail: yamagen@pharm.showa-u.ac.jp

Xenobiotica ISSN 0049-8254 print/ISSN 1366-5928 online © 2000 Taylor & Francis Ltd
http://www.tandf.co.uk/journals

With respect to the effect of simple diaryl pyridines on hepatic phase II drug-metabolizing enzymes, Franklin *et al.* reported that 2-substituted bipyridines dramatically increased phase II enzymes without affecting the total P450 content (Franklin 1991, 1992, Franklin and Moody 1992). With respect to the induction of microsomal epoxide hydrolase activity by imidazole compounds, Cho *et al.* (1995) reported that 1-benzylimidazole induces epoxide hydrolase protein and that the induction response of the enzyme is primarily associated with accumulation of microsomal epoxide hydrolase mRNA levels in the male rat. Additionally, others have shown that the induction of microsomal epoxide hydrolase activity by azole antimycotic drugs and chemicals is regulated by the transcriptional activation (Seidegard *et al.* 1981, Kim 1992, Kim *et al.* 1993, 1994, Kim and Kim 1993, Kim and Novak 1993). Thus, the induction responses of hepatic drug-metabolizing enzymes by these heterocyclic aromatic chemicals are of great interest for drug development from a toxicological viewpoint.

Hepatic microsomal haem oxygenase enzyme is well known as a rate-limiting enzyme of haem degradation (Maines 1992). Currently, it is reported here that 2,2′-dipyridyl and structurally related compounds are substantially decreased P450 content and result in the marked induction of haem oxygenase activity 24 h after its administration (Yoshida *et al.* 1995, Kobayashi *et al.* 1996b). Thus, imidazole- and pyridine-containing drugs and chemicals are good tools for examining the induction response of hepatic enzymes involved in drug and haem metabolism. However, information for the enzyme induction response by these compounds containing nitrogen heterocycles is less well established.

In this paper, the effect of 2,2′-dipyridyl amine and 2,2′-dipyridyl ketone on hepatic microsomal cytochrome P450 content and haem oxygenase activity was examined together with modulation of five different P450 species, including P4501A1, 3A2, 2B1, C11 and 2E1 in rat.

Materials and methods

Chemicals

2,2′-Dipyridyl amine and 2,2′-dipyridyl ketone were from Tokyo Kasei Co. Ltd (Tokyo, Japan). The chemical purities of 2,2′-dipyridyl amine and 2,2′-dipyridyl ketone used were >99 and $>98\%$ respectively. All anti-P450 antibodies were from Daiichi Pure Chemicals Co. Ltd (Tokyo, Japan). All other chemicals used and not listed were of the highest grade commercially available.

Animals and treatments

Male and female Wistar rats (7 weeks of age, 180–220 g) were fed a commercial solid diet (MF, Oriental Yeast, Tokyo) and water *ad libitum*. 2,2′-Dipyridyl amine and 2,2′-dipyridyl ketone were suspended in an appropriate volume of corn oil and injected intraperitoneally (i.p.) at doses of 0·10–0·80 mmol/kg. For the time-course study, rats were treated i.p. with 2,2′-dipyridyl amine and/or 2,2′-dipyridyl ketone at the fixed dose of 0·80 mmol/kg, and killed by decapitation at the times indicated. All animals were fasted for 24 h before being killed.

Tissue preparation

Livers were perfused *in situ* with ice-cold 0·9% NaCl solution and were homogenized with 5 vols 1·15% KCl using a Potter–Elvehjem homogenizer with a Teflon pestle. The microsomal fraction was obtained by differential centrifugation (Kobayashi *et al.* 1992) and the resulting pellet suspended in 0·1 M Na,K-phosphate buffer (pH 7·4), and was used for determination of haem oxygenase activity, P450 content, aminopyrine N-demethylase and aniline *p*-hydroxylase activities, in addition to immunoblot analysis.

Enzyme assays

P450 content was determined by CO-difference spectrum of dithionite-treated microsomes (about 2 mg protein/ml) as described by Omura and Sato (1964). Aminopyrine N-demethylase activity was measured by determining formaldehyde formation according to Nash (1953). Aniline *p*-hydroxylase activity was determined by the method of Imai *et al*. (1966). Microsomal haem oxygenase activity was assayed by the method of Tenhunen *et al*. (1970) using 105000*g* supernatant fractions obtained from untreated animals as the source of biliverdin reductase. Protein concentration was determined by the method of Lowry *et al*. (1951) using bovine serum albumin as a standard.

Electrophoresis and immunoblot analysis

Microsomes obtained from control and two dipyridyl compounds-treated rats were solubilized in sodium dodecyl sulphate and resolved by polyacrylamide gel electrophoresis (PAGE) according to Laemmli (1970). Antigenic components reactive with polyclonal antibodies raised against various P450 species were visualized with 4-chloro-1-naphthol in the presence of 0·006% hydrogen peroxide and peroxidase-labelled anti-gout IgG in 0·05 M Na,K-phosphate buffer (pH 7·4). All antibodies raised against P4501A1, 2B1, 2E1 and 3A2 predominantly cross-reacted with human 1A2, 2B6, 2E1 and 3A4, respectively. Anti-CYP2C11 antibody raised against P450 2C11 predominantly cross-reacted with human 2A6, 2C9 and 2E1.

Statistical analysis

Means were confirmed using a Student two-tailed *t*-test. Values were considered significantly different from the controls at $p < 0.05$.

Results and discussion

Effect of 2,2′-dipyridyl amine and 2,2′-dipyridyl ketone on cytochrome P450 content and haem oxygenase activity in rat

It is well accepted that there is an inverse relationship between the decrease in hepatic P450 content and the induction of haem oxygenase activity (Maines 1992). It is reported here that 2,2′-dipyridyl failed to induce P450, but that 2,4- and 4,4′-dipyridyls induced the haemoprotein (Yoshida *et al*. 1995). In addition, it was observed that 2,2′-dipyridyl is a powerful inducer of haem oxygenase (Yoshida *et al*. 1995). On the basis of previous findings, the effect of 2,2′-dipyridyl amine on the induction of hepatic microsomal cytochrome P450 and haem oxygenase activity in the male rat was examined and its effect with that of 2,2′-dipyridyl ketone was compared. Figure 1 shows the effect of 2,2′-dipyridyl amine on P450 and haem oxygenase in the male rat at doses ranging from 0·10 to 0·80 mmol/kg. No toxic manifestation was observed after the administration of these 2,2′-dipyridyls. As expected, 2,2′-dipyridyl amine slightly increased P450 at 0·10 mmol/kg, then decreased P450 content when increasing the dose to 0·80 mmol/kg (figure 1A). P450-dependent drug-metabolizing enzyme activities, such as aminopyrine N-demethylase and aniline *p*-hydroxylase activities, also decreased proportionally with decreasing P450 content (data not shown). Figure 1A also shows the result of the induction of hepatic microsomal haem oxygenase after treatment with 2,2′-dipyridyl amine in the male rat. As expected, 2,2′-dipyridyl amine increased haem oxygenase activity in a dose-dependent manner. At 0·80 mmol/kg, 2,2′-dipyridyl amine induced haem oxygenase activity to about seven-fold of the controls, suggesting that the amine bridge between the two pyridine rings produces induction of haem oxygenase and a decrease in P450 content as observed for 2,2′-dipyridyl treatment (Yoshida *et al*. 1995).

On the basis of these and previous results (Yoshida *et al*. 1995), the effect of 2,2′-dipyridyl ketone on haem oxygenase activity and P450 content in the male rat was

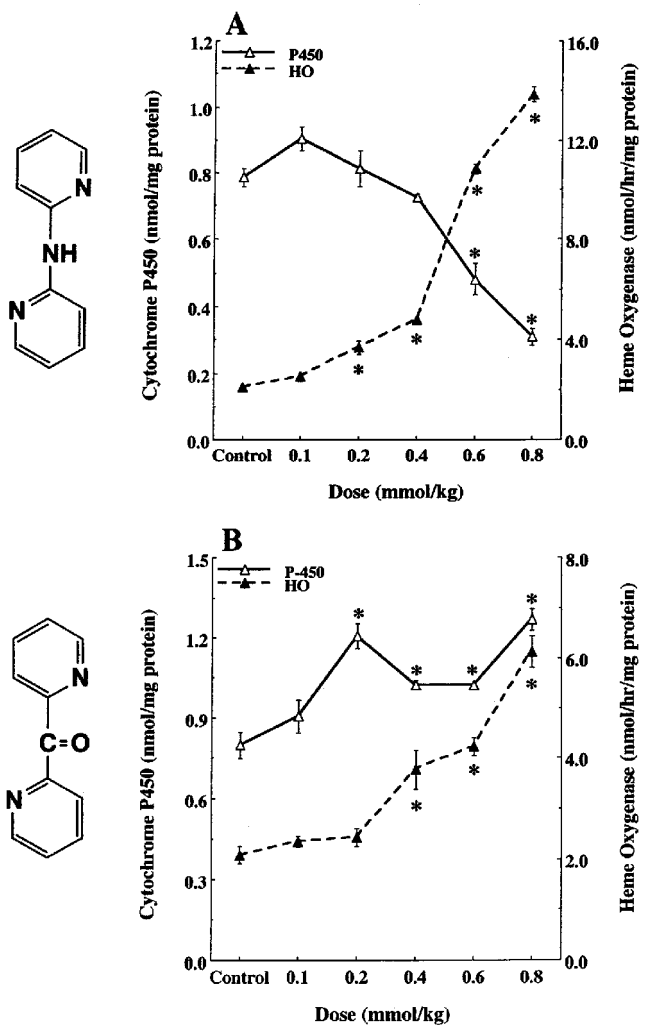


Figure 1. Dose–response effects of 2,2′-dipyridyl amine and 2,2′-dipyridyl ketone on the induction of hepatic microsomal cytochrome P450 and haem oxygenase activity in the male rat. Rats were treated i.p. with 2,2′-dipyridyl amine (A) and 2,2′-dipyridyl ketone (B) at doses ranging from 0·10 to 0·80 mmol/kg, and were killed 24 h after the treatment. Control rats were injected with an appropriate volume of the vehicle alone. All rats were fasted for 24 h before being killed. Each value is the mean ± SD of three-to-four different rats. HO, haem oxygenase. * Significantly different from controls; $p < 0.05$.

examined. The results are shown in figure 1B. Here, 2,2′-dipyridyl ketone induced both P450 content and haem oxygenase activity. However, a dose–response induction of P450 content after treatment with 2,2′-dipyridyl ketone was not observed. At 0·20 mmol/kg, 2,2′-dipyridyl ketone induced P450 content to about 1·7-fold of the controls without induction of haem oxygenase activity, then it slightly decreased with increasing doses of 0·40 and 0·60 mmol/kg, at which doses haem oxygenase activity was gradually increased. At the highest dose examined (0·80 mmol/kg), 2,2′-dipyridyl ketone markedly induced both P450 content and haem oxygenase activity to about two- and three-fold of the controls respectively. Parallel to the increase in P450 content, both aminopyrine N-demethylase and

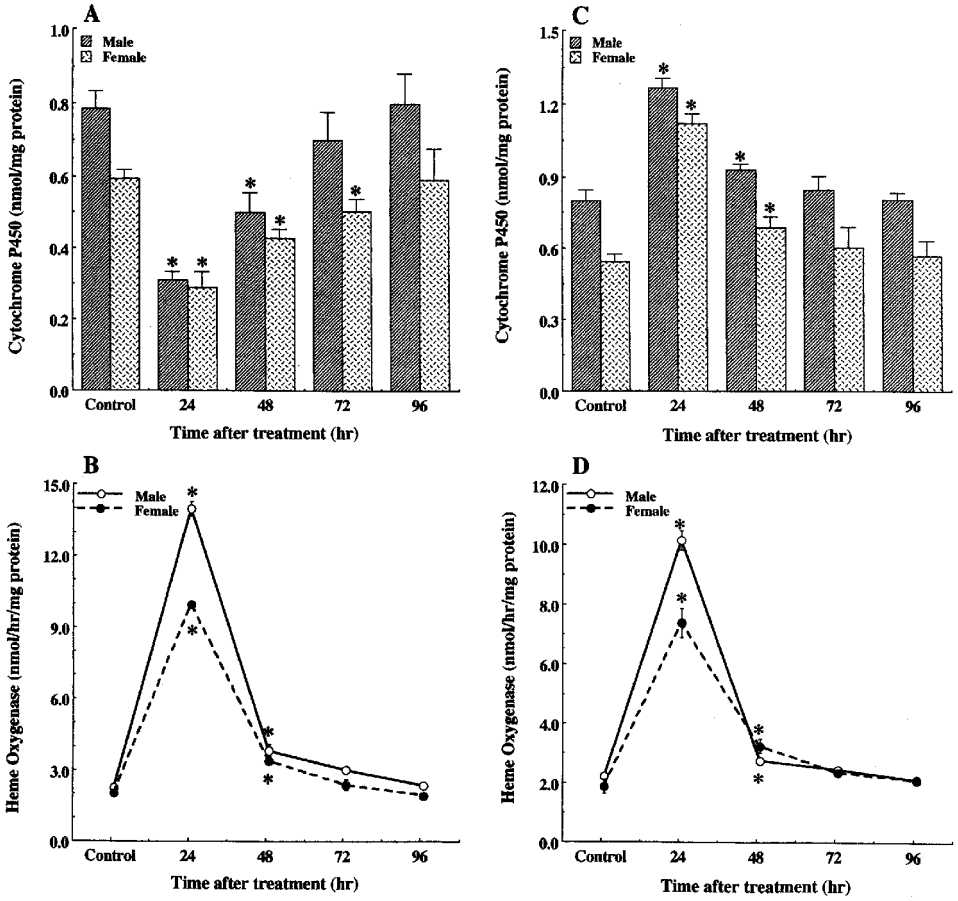


Figure 2. Time-course of the effects of 2,2′-dipyridyl ketone and 2,2′-dipyridyl amine on the induction of hepatic microsomal cytochrome P450 and haem oxygenase activity in the male and female rat. Rats were treated i.p. with 2,2′-dipyridyl ketone (A, B) and 2,2′-dipyridyl amine (C, D) at 0·80 mmol/kg, and were killed at the times indicated. Each value is the mean ± SD of three-to-four different rats. * Significantly different from controls; $p < 0.05$. Other experimental conditions were the same as described in figure 1.

aniline *p*-hydroxylase activities were also significantly increased (data not shown). The results indicate that 2,2′-dipyridyl ketone is an inducer of hepatic P450 and haem oxygenase.

Time-course effects of 2,2′-dipyridyl ketone and 2,2′-dipyridyl amine on hepatic microsomal P450 and haem oxygenase in rat

On the basis of the preceding data (figure 1), the effects of 2,2′-dipyridyl ketone and 2,2′-dipyridyl amine on hepatic microsomal P450 content and haem oxygenase activity in the male and female rat was investigated further to ascertain whether there exists sex-differences in the effect on hepatic enzymes. As shown in figure 2B, treatment of rat with 2,2′-dipyridyl amine at 0·80 mmol/kg resulted in a significant increase in haem oxygenase to about seven- and five-fold in the male and female rat respectively, then it returned to the controls levels by 72 h. The cytochrome P450

Table 1. Time-course effects of 2,2′-dipyridyl amine and 2,2′-dipyridyl ketone on hepatic microsomal aminopyrine N-demethylase and aniline *p*-hydroxylase activities in the male and female rat.

Time after treatment (h)	Aminopyrine N-demethylase (nmol/min/mg protein)	Aniline *p*-hydroxylase (nmol/min/mg protein)
2,2′-Dipyridyl amine		
Male control	6·19±0·17	2·09±0·09
24	3·68±0·31*	0·85±0·06*
48	4·22±0·17*	1·01±0·05*
72	5·28±0·13*	1·55±0·05*
96	5·96±0·12	1·82±0·06
Female control	3·99±0·05	1·43±0·11
24	2·18±0·02*	0·87±0·12*
48	2·46±0·02*	1·11±0·01*
72	3·05±0·06*	1·23±0·05*
96	3·88±0·06	1·39±0·04
2,2′-Dipyridyl ketone		
Male control	6·97±0·35	1·74±0·18
24	10·58±0·77*	2·56±0·25*
48	9·06±0·22*	2·45±0·11*
72	8·54±0·12*	1·83±0·09
96	7·21±0·02	1·77±0·03
Female control	3·38±016	1·21±0·02
24	4·87±0·60*	2·00±0·10*
48	4·33±0·22*	2·25±0·10*
72	3·85±0·01*	1·55±0·05*
96	3·21±0·04	1·33±0·07

Rats were treated i.p. with 2,2′-dipyridyl amine and 2,2′-dipyridyl ketone at 0·70 mmol/kg for a single treatment for each compounds, and were killed by decapitation 24 h after. Values are the mean±SD of three different animals. Other conditions are as described in the Materials and methods. * Significantly different from controls; $p < 0.05$.

content decreased to about < 50% of the controls at 24 h after the administration of 2,2′-dipyridyl amine in both sexes, at which time haem oxygenase activity was markedly increased (figure 2, A and B). The changed patterns of P450 content and haem oxygenase activity produced by this chemical in the male and female rat were very similar, suggesting that there are no significant sex differences in the effect of this chemical on the decrease of P450 content and the increase in haem oxygenase activity. As shown in table 1, hepatic enzymes involved in drug metabolism were also proportional to the decrease in P450 content at 24 h in both sexes. At present, a mechanism(s) of the induction of haem oxygenase and the decrease of P450 content produced by 2,2′-dipyridyl amine remains to be determined. However, the observed phenomena are very similar to 2,2′-dipyridyl treatment (Yoshida *et al.* 1995). In this respect, however, further detailed study will be needed.

The effects of 2,2′-dipyridyl ketone on P450 content and haem oxygenase activity are shown in figure 2 (C and D). Both enzymes were induced by the administration of 2,2′-dipyridyl ketone (0·80 mmol/kg) without showing any differences between sexes. Thus, as shown in figure 2C and D, 2,2′-dipyridyl ketone increased cytochrome P450 content to about twice that of the controls at 24 h after administration. The cytochrome contents gradually returned to the control levels by 72 h after 2,2′-dipyridyl ketone treatment in both sexes. Parallel to the increase in P450 content, 2,2′-dipyridyl ketone increased both aminopyrine demethylase and aniline hydroxylase activities to about 1·7- and 1·8-times of the controls, respectively, at 24 h after its administration (table 1), and it returned to control levels by

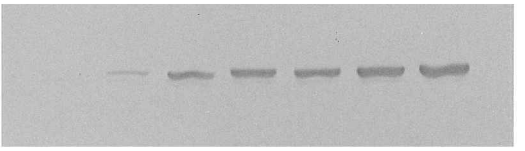


Figure 3. Immunoblot analysis for P4502B1 in hepatic microsomes from the male rat treated with with 2,2′-dipyridyl ketone. Microsomes were obtained from the male rat treated with 2,2′-dipyridyl ketone at 0·10–0·80 mmol/kg, and fasted for 24 h after the treatment. All rats were killed 24 h after the treatment. C, control; PB, phenobabital sodium (80 mg/kg for 2 consecutive days)-treated rat. Numbers indicate the dose of 2,2-dipyridyl ketone. Microsomal protein (10 μg) was loaded on SDS-PAGE.

Table 2. Levels of various P450 species in liver microsomes of rat treated with 2,2′-dipyridyl ketone.

Compounds	Dose (mmol/kg)	1A1	2B1	2E1	3A2	2C11
2,2′-Dipyridyl ketone	control	—	—	++	++	+
	0·1	—	±	++	++	+
	0·2	—	+	++	++	+
	0·4	—	+	+	+	+
	0·6	—	++	±	±	+
	0·8	—	++	±	±	+

—, Not detected; ±, weakly detected; +, clearly detected; ++, strongly detected.

96 h. Similar results obtained from the female rat with respect to drug-metabolizing enzymes are shown in table 1. Here, there is neither sex-related differential induction of hepatic P450 nor drug-metabolizing enzyme activities in the male and female rat.

Effects of 2,2′-dipyridyl amine and 2,2′,dipyridyl ketone on cytochrome P4502B1, 1A1, 2E1, 3A2 and 2C11 in the male rat

Previously reported has been that 2,2′-dipyridyl did not induce P4501A1/2 and P4502B1/2 subfamilies, but other positional isomers, such as 2,4′- and 4,4′-dipyridines, induced these P450 species in a dose-dependent manner (Yoshida *et al.* 1995). Taking these facts and the present data (figures 1 and 2) into consideration, the inducing effects of 2,2′-dipyridyl ketone and 2,2′-dipyridyl amine on various P450 species were examined further, including P4502B1, 1A1, 2E1, 3A2 and 2C11 in the male rat. Figure 3 shows the typical results of an immunoblot analysis carried out on microsomes from the 2,2′-dipyridyl ketone-treated male rat. Table 2 also illustrates the dose–response effects of 2,2′-dipyridyl ketone on the induction of P4502B1, 1A1, 2E1, 3A2 and 2C11 in the male rat. These two dipyridyl compounds produced dose-dependent induction of P450 species in the dose range 0·10–0·80 mmol/kg at 24 h after administration, by which time the bipyridines produced maximum induction of those P450s. Immunoblot analyses revealed that 2,2′-dipyridyl amine did not change appreciably those P450 species at various doses examined, suggesting that 2,2′-dipyridyl amine did not affect P450 levels,

irrespective of its slight inducing effect on P450 at the lowest dose employed (data not shown).

Treatment of rat with 2,2′-dipyridyl ketone resulted in a decrease of P4502E1 and 3A2 at higher doses (table 2). The ability of 2,2′-dipyridyl ketone to induce these isozymes weakened with increasing dose. 2,2′-Dipyridyl ketone did not induce P4502E1 and 3A2 at the highest dose examined (0·80 mmol/kg), despite the fact that the compound markedly increased total P450 content at this dose level. In contrast to these observations, P4502B1 was induced by the treatment with 2,2′-dipyridyl ketone in a dose-dependent manner with maximum induction of this isozyme at 0·80 mmol/kg dose (table 2), so indicating that this compound produced dose-related differential induction of P450 species in rat liver.

Seidegard and DePierre (1983) reported that *trans*-stilbene oxide and its derivatives having a carbon bridge between two phenyl rings play an important role in the induction of hepatic P450. Their results suggest that compounds having one or two carbonyl bridges may be necessary for extensive induction of some hepatic microsomal enzymes, such as P450, in rat. Additionally, the present authors have shown that both 4-benzoylpyridine and phenyl-4-pyridyl methanol induced P450 in a dose-dependent manner (Kobayashi *et al*. 1993). Both compounds preferentially induced P4502B1/2 at doses ranging from 0·10 to 0·80 mmol/kg, but did not induce P4501A1/2 even at the highest dose employed when compared with 4-benzyl-pyridine treatment (Kobayashi *et al*. 1992), so suggesting that the ketone bridge between the two pyridine rings plays an important role in the induction of P4502B1. As expected, 2,2′-dipyridyl ketone failed to induce P4501A1 at various doses examined (table 2). In addition, this chemical increased P4502B1 with an increase in P450 content. All of these findings suggest that a compound which does not have planar conformational structure nor a bulky moiety may induce P4502B1/2. It is not clear at present whether such dose-differentiated induction of P450 species by 2,2′-dipyridyl ketone is an isolated case, or whether it is a common phenomena after the treatment of rat with the inducers of both P450 and haem oxygenase remains to be determined. In this respect, Oguro *et al*. (1996) reported that *trans*-stilbene oxide is a potent inducer of P4502B1/2 at low doses, but it induced HO-1 with the increasing doses together with the decrease of P4502B1/2 and total content. Although they did not present details of the changes in other P450 species, it could be possible that drugs and chemicals that induce both P450 and HO-1 can affect the induction of P450 species. P4502C11 is known as one of the constitutively expressed forms of P450 in the male rat liver. Dipyridyl ketone slightly increased P4502C11 at the lowest dose examined, but it did not produce any changes at the higher doses examined.

In conclusion, the present study has revealed that 2,2′-dipyridyl ketone produces a concomitant induction of P450 and haem oxygenase. 2,2′-Dipyridyl amine decreased P450 in a dose- and time-dependent manner, and it caused a substantial induction of haem oxygenase activity in the male and female rat as observed with 2,2′-dipyridyl (Yoshida *et al*. 1995). There are various drugs and chemicals including toxic and essential heavy metals known to be either cytochrome P450 inducers or haem oxygenase inducers. However, as shown in figures 1 and 2, 2,2′-dipyridyl ketone produced induction of both P450 and haem oxygenase in a dose- and time-dependent manner. Thus, some 2,2′-substituted dipyridyls would be a good tool for understanding the mechanism(s) of the regulation of induction of P450 and haem oxygenase in rat liver.

Acknowledgements

The authors are grateful to Miss Hasegawa and Mr M. Suzuki for their skillful assistance in part of the study.

References

Cho, J. Y., Nam, S. Y. and Kim, S. G., 1995, 1-Benzylimidazole induces rat hepatic microsomal epoxide hydrolase with the elevation of its mRNA levels. *Xenobiotica*, **25**, 791–798.

Franklin, M. R., 1991, Drug metabolizing enzyme induction by simple diaryl pyridines; 2-Substituted isomers selectively increase only conjugation enzyme activities, 4-substituted isomers also induce cytochrome P450. *Toxicology and Applied Pharmacology*, **111**, 24–32.

Franklin, M. R., 1992, Whether cytochrome P450 induction accompanies glucuronosyl and glutathione transferase induction by isomers of dipyridyl appears unrelated to dose and iron chelation properties. *Journal of Biochemical Toxicology*, **7**, 81–85.

Franklin, M. R. and Moody, D. E., 1992, Concomitant induction of microsomal epoxide hydrolase and UDP-glucuronosyltransferase activities by dipyridine compounds. *Drug Metabolism and Disposition*, **20**, 726–729.

Imai, Y., Ito, A. and Sato, R., 1966, Evidence for biochemically different types of vesicles in the hepatic microsomal fraction. *Journal of Biochemistry (Tokyo)*, **60**, 417–428.

James, M. O., 1988, Acute and subacute effects of miconazole nitrate on hepatic styrene oxide hydrolase and cytochrome P-450-dependent monooxygenase activities in male and female AKR/J mice. *Toxicology*, **50**, 269–281.

Kim, S. G., 1992, Transcriptional regulation of rat microsomal epoxide hydrolase gene by imidazole antimycotic agents. *Molecular Pharmacology*, **42**, 273–279.

Kim, S. G., Jung, K. H., Yang, W. K. and Kim, N. D., 1994, Differential expression of microsomal epoxide hydrolase gene by azole heterocycles in rat. *Biochemical Pharmacology*, **48**, 111–120.

Kim, S. G., Kedderis, G. L., Batra, R. and Novak, R. F., 1993, Induction of rat liver microsomal epoxide hydrolase by thiazole and pyrazine: hydrolysis of 2-cyanoethylene oxide. *Carcinogenesis*, **14**, 1665–1670.

Kim, S. G. and Kim, Y. H., 1992, Gender-related expression of rat microsomal epoxide hydrolase during maturation: post-transcriptional reguration. *Molecular Pharmacology*, **42**, 75–81.

Kim, S. G. and Novak, R. F., 1993, The induction of cytochrome P4502E1 by nitrogen- and sulfur-containing heterocycles: expression and molecular reguration. *Toxicology and Applied Pharmacology*, **120**, 257–264.

Kobayashi, Y., Matuura, Y., Kotani, E., Iio, T., Fukuda, T., Aoyagi, T., Tobinaga, S., Yoshida, T. and Kuroiwa, Y., 1992, Induction of hepatic microsomal cytochrome P450 and drug-metabolizing enzymes by 4-benzylpyridine and its structurally related compounds in rats: dose- and sex-related differential induction of cytochrome P450 species. *Biochemical Pharmacology*, **43**, 2151–2159.

Kobayashi, Y., Matuura, Y., Kotani, E., Fukuda, T., Aoyagi, T., Tobinaga, S., Yoshida, T. and Kuroiwa, Y., 1993, Structural requirements for the induction of hepatic microsomal cytochrome P450 by imidazole- and pyridine-containing compounds in rats. *Journal of Biochemistry (Tokyo)*, **114**, 697–701.

Kobayashi, Y., Yamamoto, T., Okui, E., Kotani, E., Yoshida, T. and Kuroiwa, Y., 1996b, Regio-related differential induction of hepatic microsomal heme oxygenase and cytochrome P450 by substituted imidazole and pyridine compounds in rats. *Japanese Journal of Toxicology and Environmental Health*, **42**, 468–478.

Kobayashi, Y., Yoshida, T., Kotani, E., Aoyagi, T., Kuroiwa, Y. and Tobinaga, S., 1994, Involvement of testosterone in the induction of hepatic microsomal cytochrome P-450 2B1/2 (P-450 2B1/2) by 1-benzylimidazole in male and female rats: sex-differentiated induction of P-450 2B1/2 species. *Biochimica et Biophysica Acta*, **1200**, 11–18.

Kobayashi, Y., Yoshida, T., Kotani, E., Matsuura, Y., Egawa, H., Aoyagi, T., Imaoka, S., Funae, Y., Tobinaga, S. and Kuroiwa, Y., 1995, Induction of hepatic microsomal P450 by 4-phenylalkylpyridines in rat; chain length-dependent and sex-related differential induction of P450s. *Xenobiotica*, **25**, 779–789.

Kobayashi, Y., Yoshida, T., Yamamoto, T., Kotani, E., Imaoka, S., Funae, Y. and Kuroiwa, Y., 1996a, Differential induction of hepatic and renal microsomal cytochrome P450 by N-phenylalkylimidazoles in rats. *Japanese Journal of Toxicology and Environmental Health*, **42**, 127–135.

Laemmli, U. K., 1970, Cleavage of structural proteins during the assembly of the head of bacteriophage T4. *Nature*, **277**, 680–685.

Laignelet, L., Narbonne, J. F., Lhuguenot, J. C. and Riviere, J. L., 1989, Induction and inhibition of rat liver cytochrome(s) P-450 by an imidazole fungicide (prochloraz). *Toxicology*, **59**, 271–284.

LOWRY, O. H., ROSEBROGH, N. J., FARR, A. L. and RANDALL, R. J., 1951, Protein measurement with the Folin phenol reagent. *Journal of Biological Chemistry*, **193**, 265–275.

MAINES, M. D., 1992, *Heme Oxygenase: Clinical Applications and Functions* (Ann Arbor: CRC Press).

MATSUURA, Y., KOTANI, E., IIO, T., FUKUDA, T., TOBINAGA, S., YOSHIDA, T. and KUROIWA, Y., 1991, Structure–activity relationships in the induction of hepatic microsomal cytochrome P450 by clotrimazole and its structurally related compounds in rats. *Biochemical Pharmacology*, **41**, 1949–1956.

NASH, T., 1953, The colorimetric estimation of formaldehyde by means of the Hantzsch reaction. *Biochemical Journal*, **55**, 416–421.

OGURO, T., KANEKO, E., KANEKO, Y., NUMAZAWA, S., IMAOKA, S., FUNAE, Y., MIKAMI, T. and YOSHIDA, T., 1996, Suppressed expression of phenobarbital-inducible hepatic cytochrome P-450s in Eisai-hyperilirubinuria rats (EHBR/Eis). *Journal of Pharmacology and Experimental Therapeutics*, **277**, 1676–1684.

OGURO, T., YOSHIDA, T., NUMAZAWA, S. and KUROIWA, Y., 1990, Possible role of glutathione depletion in the induction of rate-limiting enzymes involved in heme degradation and polyamine biosynthesis in the liver of rats. *Journal of Pharmacobio-Dynamics* **13**, 628–636.

OMURA, T. and SATO, R., 1964, The carbon monoxide-binding pigment of liver microsomes. *Journal of Biological Chemistry*, **239**, 2370–2378.

RITTER, J. K. and FRANKLIN, M. R., 1987a, Induction and inhibition of rat hepatic drug metabolism by N-substituted imidazole drugs. *Drug Metabolism and Disposition*, **15**, 335–343.

RITTER, J. K. and FRANKLIN, M. R., 1987b, High magnitude hepatic cytochrome P-450 induction by an N-substituted imidazole antimycotic, clotrimazole. *Biochemical Pharmacology*, **36**, 2783–2787.

RODRIGUES, A. D., WADDELL, P. R., AH-SING, E., MORRIS, B. A., WOLF, C. R. and IOANNIDES, C., 1988, Induction of the rat hepatic microsomal mixed-function oxidases by 3 imidazole-containing antifungal agents: Selectively for the cytochrome P-450IIB and P-450III families of cytochrome P-450. *Toxicology*, **50**, 283–301.

SEIDEGARD, J. and DEPIERRE, J. W., 1983, Microsomal epoxide hydrolase properties, regulation and function. *Biochimica et Biophysica Acta*, **695**, 251–270.

SEIDEGARD, J., DEPIERRE, J. W., MORGENSTERN, R., PILOTTI, A. and ERNSTER, L., 1981, Induction of drug-metabolizing systems and related enzymes with metabolites and structural analogues of stilbene. *Biochimica et Biophysica Acta*, **672**, 65–78.

TENHUNEN, R., MARVER, H. S. and SCHMID, R., 1970, The enzymatic catabolism of hemoglobin: stimulation of microsomal heme oxygenase by hemin. *Journal of Laboratory Clinical Medicine*, **75**, 410–421.

YOSHIDA, T., KOBAYASHI, Y., MASUKO, T., HASHIMOTO, Y. and KUROIWA, Y., 1995, Differential effects of 3 dipyridyl isomers on hepatic microsomal cytochrome P450 and heme oxygenase in rats. *Toxicology Letters*, **76**, 145–153.

YOSHIDA, T., OGURO, T., NUMAZAWA, S. and KUROIWA, Y., 1987, Effects of phorone (diisopropyridene acetone), a glutathione (GSH) depletor, on hepatic enzymes involved in drug and heme metabolism in rats: evidence that phorone is a potent inducer of heme oxygenase. *Biochemical and Biophysical Research Communications*, **145**, 502–508.

XENOBIOTICA, 2000, VOL. 30, NO. 7, 693–705

Comparison of receptor-mediated endocytosis kinetics between wild-type t-PA and recombinant pamiteplase in isolated rat hepatocytes and liver cell plasma membranes

K. OIKAWA, T. WATANABE and S. HIGUCHI

Drug Metabolism Laboratories, Yamanouchi Pharmaceutical Co., Ltd, 1–8, Azusawa 1-Chome Itabashi-ku, Tokyo 174–8511, Japan

Received 6 January 2000

1. Differences in receptor-mediated endocytosis kinetics between pamiteplase, an engineered t-PA, and an unmodified rt-PA were examined using liver cell plasma membranes and isolated rat hepatocytes.

2. Whereas the binding site of pamiteplase on hepatocytes was the same as that of rt-PA, the K_d of pamiteplase was 5.1–7.7 times larger than that of rt-PA, indicating a lower affinity of pamiteplase for the t-PA receptor.

3. k_e for pamiteplase measured using parenchymal cells or non-parenchymal cells was slightly smaller than that for rt-PA, whereas k_{on} for pamiteplase were much lower than that of rt-PA, suggesting that the interaction between pamiteplase and the receptor is slower than that of rt-PA because of its structural modification.

4. Therefore, the difference in drug disposition between pamiteplase and rt-PA is mainly due to the difference in the hepatic clearance caused by a change in the interaction rate between the ligand and its cell-surface receptor.

Introduction

Tissue-type plasminogen activator (t-PA) is an endogenous glycoprotein that is widely used as a thrombolytic agent. The pharmacologic efficacy of recombinant t-PA (rt-PA) has been evaluated in many clinical studies and results of these studies have revealed lower patient mortality compared with the use of streptokinase or urokinase (Verstraete *et al*. 1985, Kanemoto *et al*. 1991). One major disadvantage of rt-PA is its short plasma half-life due to rapid hepatic uptake (Camani *et al*. 1994). Such rapid hepatic uptake is due to receptor-mediated endocytosis (RME) by specific receptors on the surface of parenchymal and endothelial cells in the liver (Camani *et al*. 1994).

To extend the short plasma half-life of wild-type t-PA, a novel t-PA pamiteplase was constructed. Pamiteplase bears a deletion in the Kringle-1 domain and a point mutation (Arg275 → Glu) in the Kringle-2 domain (Kawauchi *et al*. 1991). Pamiteplase administered at one-third the dose of rt-PA to rat and dog with induced thrombi has almost the same thrombolytic activity as a typical rt-PA (Kawasaki *et al*. 1993a–c), because pamiteplase has the same AUC at that dose as rt-PA (Oikawa *et al*. 1996a). Consequently, pamiteplase has the same biological effect as t-PA (Katoh *et al*. 1991) but with a much lower clearance (*Cl*) compared with wild-type t-PA (Oikawa *et al*. 1996a). In rat, unchanged pamiteplase and rt-PA are not excreted in

* Author for correspondence; e-mail: oikawa@yamanouchi.co.jp

Xenobiotica ISSN 0049-8254 print/ISSN 1366-5928 online © 2000 Taylor & Francis Ltd
http://www.tandf.co.uk/journals

urine, indicating their elimination is due to metabolic clearance (Iida *et al*. 1988, Oikawa *et al*. 1996b). Since the greatest tissue distribution of both compounds is in the liver where uptake and degradation occur, this tissue plays an important role in their metabolic clearance (Iida *et al*. 1988, Oikawa *et al*. 1996b).

The clearance of high molecular-weight compounds (HMWD) in the liver is due to RME via specific receptors (Sugiyama *et al*. 1989). A HMWD in the systemic circulation binds to a specific receptor on the surface of cell membranes, and this ligand–receptor complex is taken into the cell (Sugiyama *et al*. 1989). Subsequently, the ligand separates from receptors due to a change of pH, and is eliminated through either the lysosomal pathway or the shuttle pathway (Sugiyama *et al*. 1989). Since both pamiteplase and rt-PA are eliminated by hepatic clearance, the difference in drug disposition between two compounds is thought to be caused by interaction with the specific RME receptors. In this study, the cause for this difference between pamiteplase and rt-PA in rats was examined by comparing parameters related to RME, such as K_d, B_{max}, k_e, k_{on} and k_{off}, using liver cell plasma membranes and hepatocytes.

Materials and methods

All animal experiments complied with the regulations of Yamanouchi Pharmaceutical's Animal Experimentation Ethics Committee.

Materials

The pamiteplase molecule contains a finger domain, an EGF domain, a Kringle-2 domain, a serine protease domain, and a site mutation at the Kringle-2–serine protease linkage site (del 92–173, Arg275 → Glu) (Kawauchi *et al*. 1991). A lyophilized pharmaceutical preparation of pamiteplase was used in this study. rt-PA (Alteplase) was from Genentech, Inc. (CA, USA). Carrier-free $Na^{125}I$ was from DuPont NEN (MA, USA). Other reagents were commercially available and of analytical grade.

Preparation of ^{125}I-labelled pamiteplase (^{125}I-pamiteplase) and ^{125}I-labelled rt-PA (^{125}I-rt-PA)

Lyophilized formulations containing either 4 mg pamiteplase or 50 mg rt-PA were dissolved in physiologic saline to make stock solutions of both drugs (1 mg/ml). ^{125}I-pamiteplase or ^{125}I-rt-PA was synthesized by the chloramine T method using carrier-free $Na^{125}I$ (Oikawa *et al*. 1996b). The specific activity, concentration and radiochemical purity of ^{125}I-pamiteplase were 214.3 MBq/mg, 11.4 MBq/ml and $>95\%$ respectively; those of ^{125}I-rt-PA were 177.0 MBq/mg, 9.4 MBq/ml and $>95\%$ respectively.

Animals

Male Fischer rats (aged 6 weeks, 109–136 g), from Charles River Japan, were acclimated to an air-conditioned room (23 ± 2 °C, relative humidity $55\pm5\%$) on a light/dark cycle of 12/12 h for >1 week before the study. Animals had free access to pelleted food (MF, Oriental Yeast Co., Ltd, Japan) and water.

Preparation of liver cell plasma membranes

Rat liver cell plasma membranes were prepared by the method of Krause *et al*. (1990) and Stang *et al*. (1992) as follows. Freshly excized liver was finely chopped with scissors, suspended in cold homogenization buffer (0.25 M sucrose, 1 mM EGTA, 5 mM Tris at pH 7.4 (9 ml/g)), and homogenized at 0 °C in a 50-ml homogenizer. The homogenate was filtered through nylon gauze (40 threads per cm), and then was loaded on top of 4.8 ml buffered sucrose containing 1.45 M sucrose and 20 mM Tris, pH 7.4, in an ultracentrifuge tube. The homogenate was then centrifuged at 35000 *g* for 30 min at 4 °C. The pale interfacial layer was collected by upward displacement with buffered sucrose, diluted three-fold with

homogenization buffer, and centrifuged at 40000 *g* for 15 min at 4 °C. The pellets were diluted three-fold with homogenization buffer, and centrifuged at 40000 *g* for 20 min at 4 °C. The membranes were collected by adding 2 ml homogenization buffer to pellets and the isolated preparations were stored at −80 °C. The protein concentration was determined by the BCA protein assay (Pierce, IL, USA) with bovine serum albumin as the standard.

Preparation of hepatocytes

The preparation of isolated hepatocytes was performed by the method of Baur *et al.* (1975) with modification. Briefly, under pentobarbital anesthesia, the portal vein was cannulated and the liver perfused with 150 ml calcium-free Hanks' balanced salt solution (HBSS; Gibco BRL, MD, USA). Collagenase was added to 200 ml HBSS to make a 0.05% collagenase solution. The liver was perfused for 10 min with the collagenase solution and then washed with 100 ml calcium-free HBSS. The liver was then gently agitated in calcium-free HBSS. Parenchymal and non-parenchymal cells were purified by several filtration and centrifugation procedures. After washing, both hepatocyte preparations were resuspended in William's Medium E (WE; Sigma Chemical Co., St Louis, MO, USA).

Binding assay

^{125}I-labelled compound solution of ^{125}I-pamiteplase or ^{125}I-rt-PA was prepared by mixing the stock solution, ^{125}I-labelled compound solution and Krebs–Henseleit buffer containing 1.2 mM KH_2PO_4, 25 mM $NaHCO_3$, 118 mM NaCl, 5 mM KCl, 1.1 mM $MgSO_4$ and 2.5 mM $CaCl_2$ (KH buffer) to yield final concentrations ranging from 0.1 to 500 nM. In the case of liver cell plasma membranes, 100 μl KH buffer containing 2% BSA, 25 μl ^{125}I-labelled compound solution, 25 μl KH buffer and 50 μl membrane solution (2 mg/ml) prepared by diluting the liver cell plasma membrane suspension with KH buffer were added to a 96-well microplate (Costar, MA, USA). These reaction mixtures were incubated for 1 h at 37 °C. The mixtures were harvested onto glassfibre filters (UniFilterPlate GF/C 96, Packard, CT, USA), and the filters were dried and counted on TopCount (Packard, CT, USA) with a scintillation cocktail (MicroScint-O, Packard). Non-specific binding was determined by simultaneously measuring ^{125}I-radioactivity in the presence of 1 μM unlabelled compound. The specific binding was obtained by subtracting the non-specific binding from the total binding.

In the case of hepatocytes, 100 μl KH buffer containing 2% BSA and 0.1% D-glucose, 25 μl ^{125}I-labelled compound solution, 25 μl KH buffer and 100 μl cell suspension (10^6 cells/ml) prepared by diluting hepatocyte suspensions with KH buffer was added to a 96-well microplate. These reaction mixtures were incubated for 30 min at 37 °C. The specific binding was measured as described above.

The binding parameters (K_d, B_{max}) were calculated by simultaneous non-linear regression using WinNonlin software (v.1.5, Pharsight, Inc., CA, USA). The observed binding versus ligand (pamiteplase and rt-PA) concentration ([L]) data were fit to equation (1):

$$\text{Specific binding} = B_{max} \cdot [L]/(K_d + [L]). \quad (1)$$

Competition binding assay

In the case of liver cell plasma membranes, 25 μl KH buffer containing 2% BSA, 25 μl ^{125}I-labelled compound solution (10 nM), 25 μl competitor (unlabelled pamiteplase and rt-PA), 25 μl KH buffer and 50 μl membrane solution (2 mg/ml) were added to a 96-well microplate. The reaction mixtures were incubated for 1 h at 37 °C. In the case of hepatocytes, 100 μl KH buffer containing 2% BSA and 0.1% D-glucose, 25 μl ^{125}I-labelled compound solution, 25 μl competitor, 25 μl KH buffer and 100 μl cell suspension (10^6 cells/ml) were added to a 96-well microplate. These reaction mixtures were incubated for 1 h at 37 °C. The specific binding was measured as described above.

The inhibitory constant (IC_{50}) was calculated by simultaneous non-linear regression using WinNonlin software (v.1.5). The observed binding versus ligand concentration data were fit to equation 2 and are shown as a percentage of control binding in the absence of the inhibitor.

$$\text{Specific binding} = B_{max} \cdot [1 - [L]/([L] + IC_{50})]. \quad (2)$$

Analysis of pamiteplase and rt-PA binding using hepatocytes

KH buffer (50 μl) containing 2% BSA, 25 μl ^{125}I-labelled compound solution (10 nM), 25 μl KH buffer and 100 μl cell solution (10^6 cells/ml) was added to a 96-well microplate. In the case of measurement of total compound associated with cells, these reaction mixtures were incubated for 1 h at 37 °C. In the case of measurement of compound bound to the cell surface only, these reaction mixtures were incubated for 1 h at 4 °C. In the case of measurement of compound taken up by cells, these reaction mixtures were incubated for 1 h at 37 °C, washed with 100 μl 100 mM CH_3COOH and 130 mM NaCl for 5 min on ice to dissociate bound to the surface.

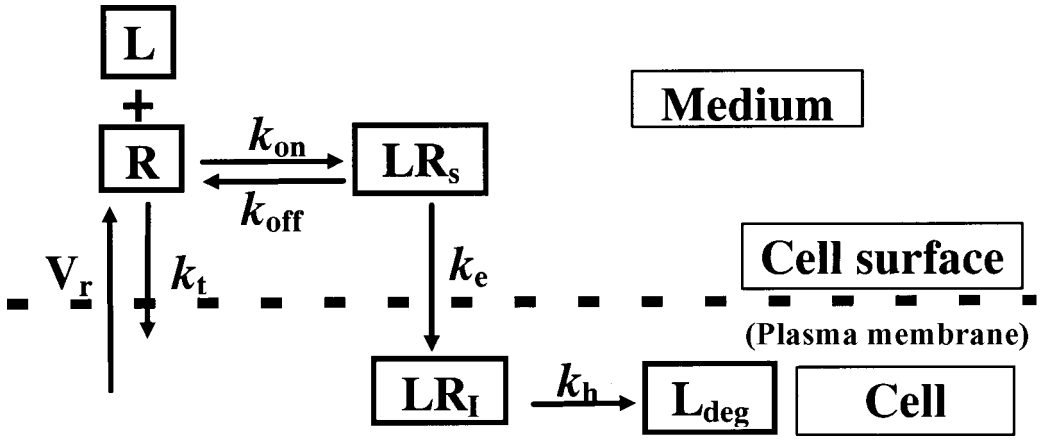


Figure 1. Mathematical model A for receptor-mediated handling of ligands.

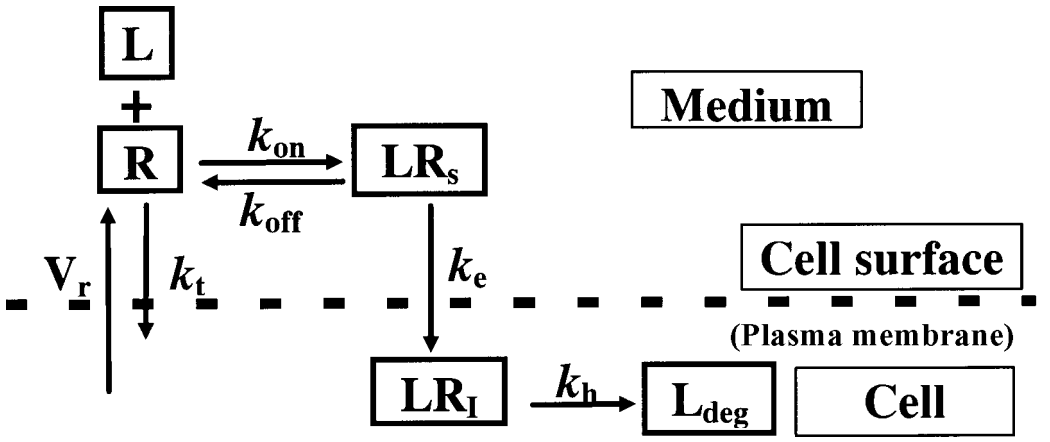


Figure 2. Mathematical model B for receptor-mediated handling of ligands.

These reaction mixtures were harvested onto glassfibre filters, and the filters dried and counted on TopCount with a scintillation cocktail (MicroScint-O). The specific binding was measured as described above.

Kinetic analysis of internalization

Differential equations were based on a simple model (model A) shown in figure 1 employing a single compartment for the ligand–receptor complex and operating at 37 °C. The binding of a compound to the membrane receptor (k_{on}, k_{off}), the internalization of the complex (k_e), the free receptors (k_t), the degradation of the ligand (k_h), and the receptor insertion into the surface membrane (V_r) are specified by linked differential equations:

$$d[L]/dt = k_{off} \cdot [LRs] - k_{on} \cdot [L][R] \quad (3)$$

$$d[R]/dt = V_r + k_{off} \cdot [LR_S] - k_{on} \cdot [L][R] - k_t \cdot [R] \quad (4)$$

$$d[LR_S]/dt = k_{on} \cdot [L][R] - k_{off} \cdot [LR_S] - k_e \cdot [LR_S] \quad (5)$$

$$d[LR_I]/dt = k_e \cdot [LR_S] - k_h \cdot [LR_I]. \quad (6)$$

When negligible k_h is assumed, equation (6) is simplified to:

$$d[LR_I]/dt = k_e \cdot [LR_S]. \quad (7)$$

Integration of equation (7) yields:

$$[LR_I]_{0-t} = k_e \cdot \int [LR_S] dt. \quad (8)$$

If the amount of internalized ligand at time t is plotted against the integrated amount of surface-bound ligand, as shown figure 8, the initial slope is the k_e.

Kinetic analysis of association and dissociation

The kinetic model (model B) shown in figure 2 for binding to the cell surface receptor (in the absence of sequestration and internalization of receptor) at 0 °C is specified by two linked differential equations:

$$d[L]/dt = k_{off} \cdot [LRs] - k_{on} \cdot [L][R] \quad (9)$$

$$d[LR_S]/dt = k_{on} \cdot [L][R] - k_{off} \cdot [LR_s] \quad (10)$$

The binding parameters (k_{on} and k_{off}) were calculated by simultaneous non-linear regression using WinNonlin software (v.1.5).

Results

Specific binding of pamiteplase and t-PA to liver cell plasma membranes

The specific binding of pamiteplase and t-PA to liver cell plasma membranes is shown in figure 3. The profile clearly shows both increased binding with increasing concentration of pamiteplase or rt-PA and the saturability of the binding. Binding is monophasic (Eadie–Hofstee plot, data not shown), suggesting the existence of one specific binding site for both proteins. K_d and B_{max} were obtained from simultaneous non-linear regression analysis by directly applying the Michaelis–Menten equation to data from the binding experiments were 33.1 nM and 4.41 pmole/mg for pamiteplase, and 13.1 nM and 5.00 pmole/mg for t-PA respectively (table 1).

The ratio of the specific binding to liver cell plasma membranes of pamiteplase or t-PA in the presence of a competitor compared with specific binding in the absence of a competitor is shown in figure 4. Unlabelled rt-PA was used as a competitor to examine the specific binding of ^{125}I-pamiteplase, while unlabelled pamiteplase was used to examine the specific binding of ^{125}I-t-PA. The specific binding of both compounds decreased as concentration of the competitor increased. The IC_{50} of pamiteplase obtained from a simultaneous non-linear regression analysis as a competitive inhibition against one specific site was 192 nM and the IC_{50} of t-PA was 43.6 nM.

Specific binding of pamiteplase and t-PA at hepatocytes

The specific binding of pamiteplase and t-PA to PC and NPC is shown in figure 5. The profile clearly shows both the increased binding with increasing concentration of the pamiteplase and t-PA and the saturability of the binding. Binding site were suggested to be one specific site for both proteins as determined by Eadie–Hofstee plots (data not shown). K_d and B_{max} of pamiteplase were obtained from simultaneous non-linear regression analysis by directly applying the Michaelis–Menten equation were 29.4 nM and 4.26 pmole/10^6 cells at PC, and were 36.4 nM and 5.50 pmole/10^6 cells at NPC, while those of t-PA were 18.8 nM and 5.04 pmole/10^6 cells at PC, and were 12.4 nM and 4.74 pmole/10^6 cells at NPC (table 2).

The ratio of the specific binding to PC and NPC of pamiteplase or t-PA in the presence of a competitor compared with specific binding in the absence of a competitor is shown in figure 6. The specific binding of both compounds decreased as concentration of the competitor increased. The IC_{50} at PC and NPC as a competitive inhibition against one specific site was 364.0 and 121.5 nM at pamiteplase, and 93.7 and 55.9 nM at t-PA respectively (table 3).

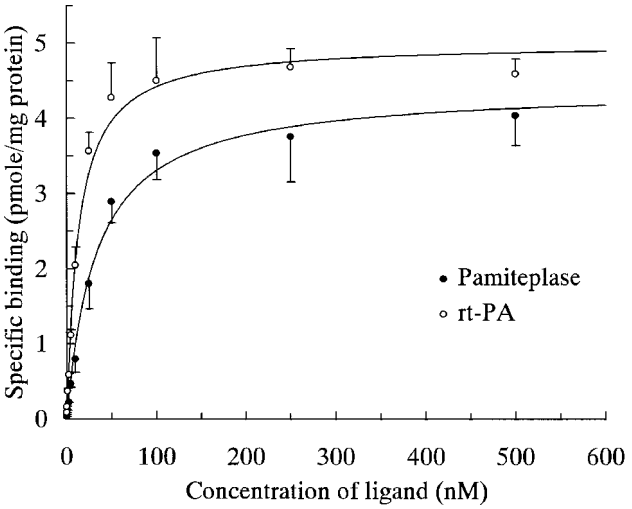


Figure 3. Specific binding of ^{125}I-pamiteplase and ^{125}I-rt-PA to liver cell plasma membranes. Data are the mean±SD from five determinations.

Table 1. Specific binding of ^{125}I-pamiteplase or ^{125}I-rt-PA to liver cell plasma membranes.

Drug	K_d (nM)	B_{max} (pmole/mg)
Pamiteplase	33.1±3.84	4.41±0.14
rt-PA	13.1±1.62	5.00±0.14

Data are the mean±SD from five determinations.

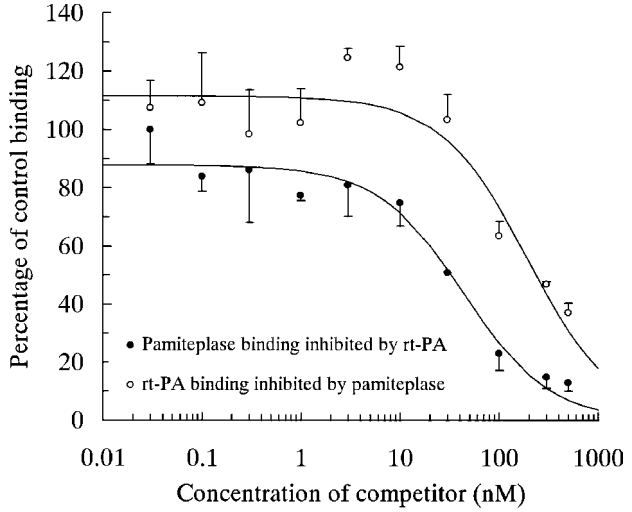


Figure 4. Competitive binding to liver cell plasma membranes of unlabelled rt-PA against ^{125}I-pamiteplase or of unlabelled pamiteplase against ^{125}I-rt-PA. Data are the mean±SD from five determinations.

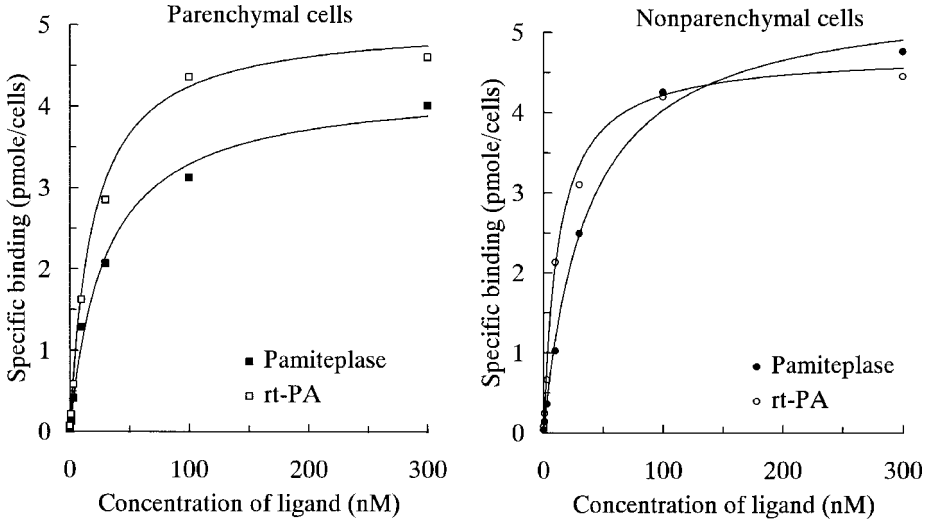


Figure 5. Specific binding of ^{125}I-pamiteplase and ^{125}I-rt-PA to rat hepatocytes (parenchymal and non-parenchymal cells). Data are the mean from five determinations.

Table 2. Specific binding of ^{125}I-pamiteplase or ^{125}I-rt-PA to hepatocytes.

	K_d (nM)		B_{max} (pmole/10^6 cells)	
Drug	Parenchymal cell	Non-parenchymal cell	Parenchymal cell	Non-parenchymal cell
Pamiteplase	29.4±3.97	36.4±4.18	4.26±0.16	5.50±0.19
rt-PA	18.8±1.93	12.4±1.69	5.04±0.14	4.74±0.16

Data are the mean±SD from five determinations.

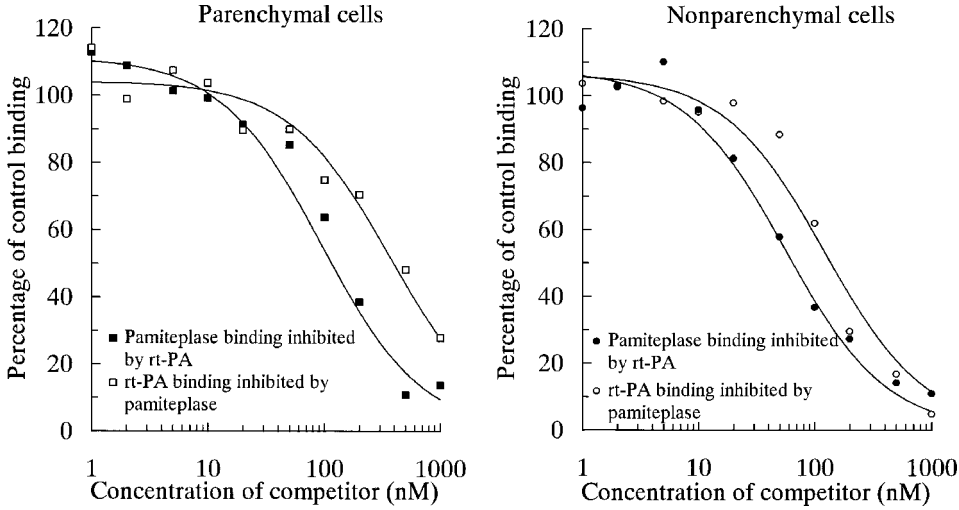


Figure 6. Competitive binding to rat hepatocytes (parenchymal and non-parenchymal cell) of unlabelled rt-PA against ^{125}I-pamiteplase or of unlabelled pamiteplase against ^{125}I-rt-PA. Data are the mean from five determinations.

Table 3. Inhibitory constant of ^{125}I-pamiteplase or ^{125}I-rt-PA to hepatocytes.

Inhibiting drug	IC_{50} (nM)	
	Parenchymal cell	Non-parenchymal cell
Pamiteplase	364.0±59.2	121.5±22.4
rt-PA	93.7±15.4	55.9±10.1

Data are the mean±SD from five determinations.

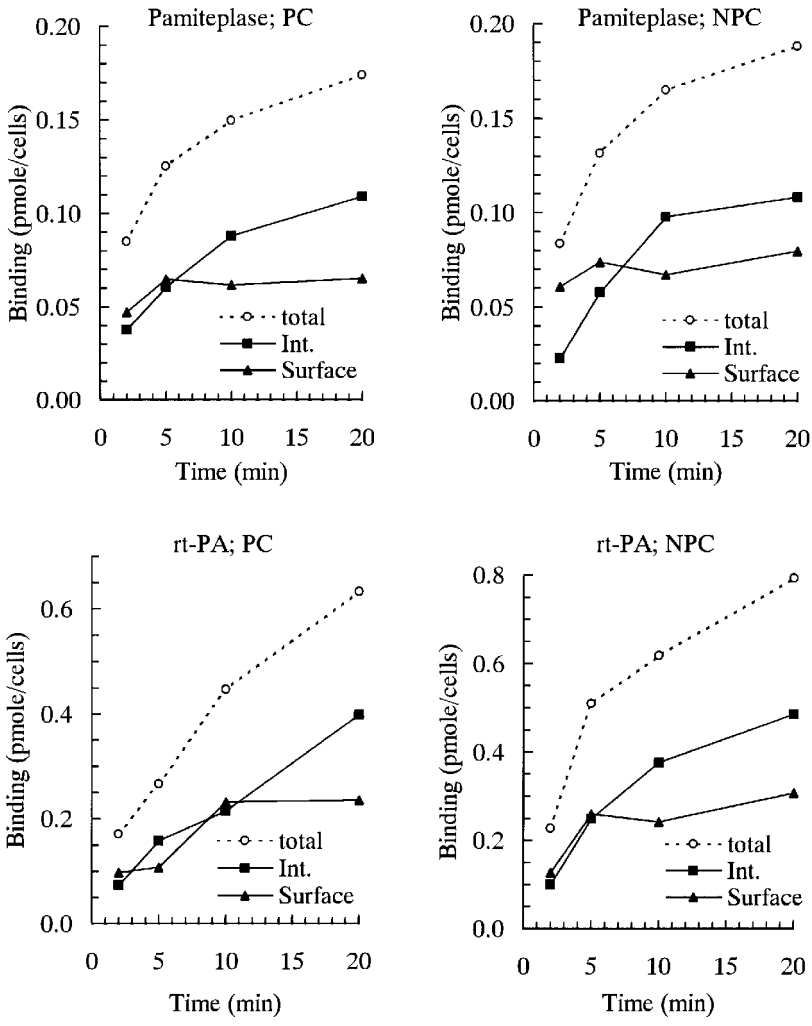


Figure 7. Time-course of cell surface-bound and internalized ^{125}I-pamiteplase or ^{125}I-rt-PA concentrations in rat hepatocytes (parenchymal and non-parenchymal cell). Data are the mean from five determinations.

Internalization rate constant for the ligand–receptor complex (k_e)

The amount of either ligand bound only to cell surface obtained by subtracting internalized ligand measured after an acid washing from the total bound ligand is shown figure 7. The internalization of the ligand–receptor complex for both

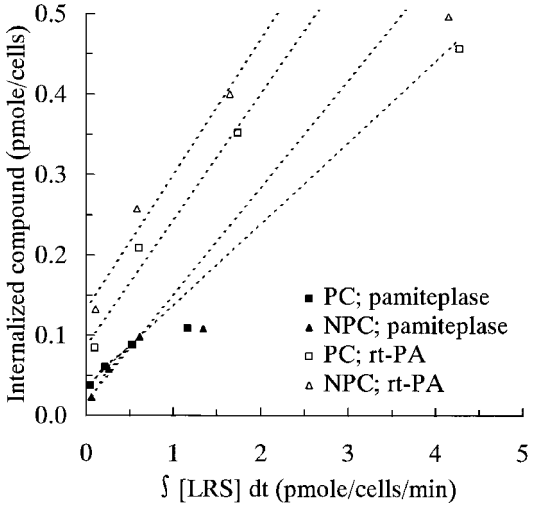


Figure 8. Plots for estimating apparent internalization rate constant of ^{125}I-pamiteplase or ^{125}I-rt-PA in rat hepatocytes (parenchymal and non-parenchymal cell). Data are the mean from five determinations.

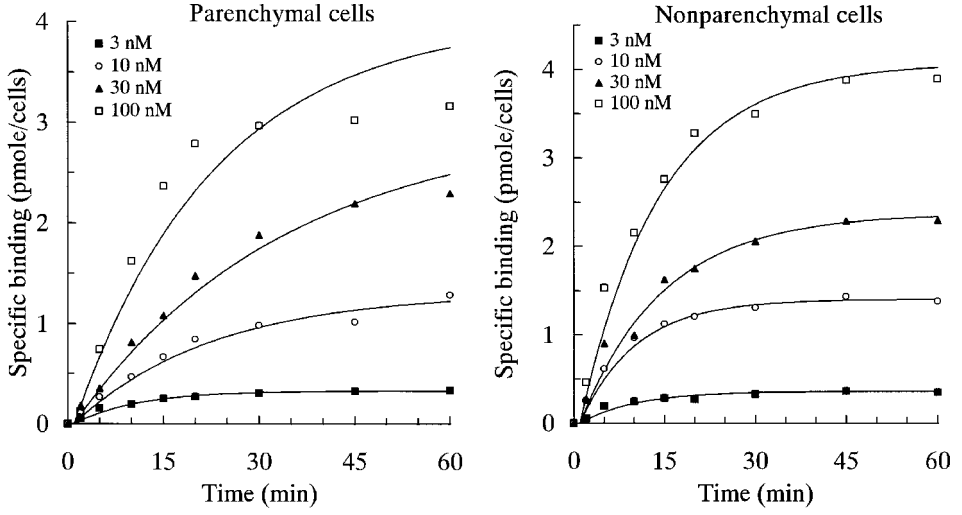


Figure 9. Time-dependent association of ^{125}I-pamiteplase with rat hepatocytes (parenchymal and non-parenchymal cell). Data are the mean from five determinations.

compounds increased with time. As shown in figure 8, $[LR_I]$ plotted against $\int[LR_S]dt$ (equation 8) yielded a linear relationship up to 10 min, where negligible degradation was assumed. The k_e of pamiteplase calculated from this slope was 0.156 min^{-1} for PC and 0.174 min^{-1} for NPC, and that of t-PA was 0.271 min^{-1} for PC and 0.247 min^{-1} for NPC.

Association and dissociation rate constant for ligand–receptor complex (k_{on} *and* k_{off})

The time-courses of specific binding of pamiteplase or t-PA to PC and NPC with unlabelled ligand at various concentrations (3–100 nM) at 0 °C are shown in figures 9 and 10. k_{on} and k_{off} of pamiteplase obtained from a simultaneous non-linear

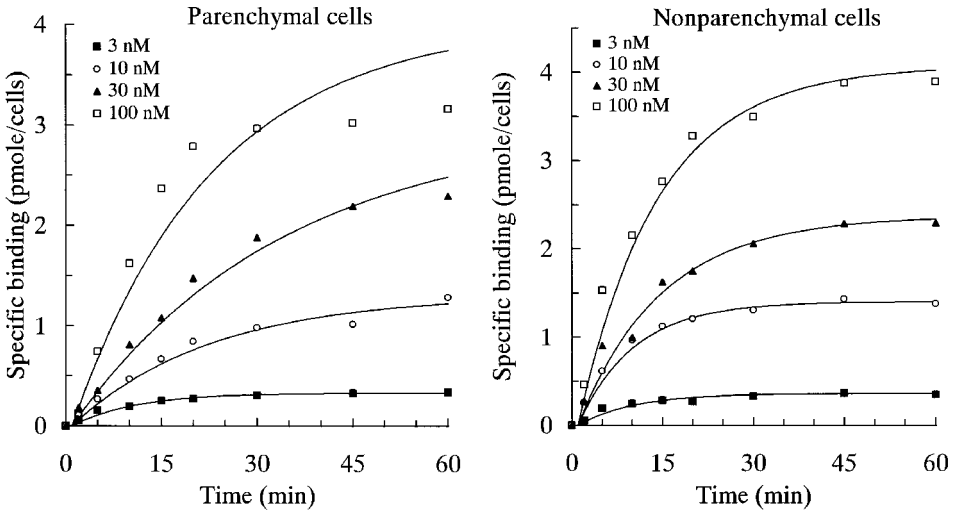


Figure 10. Time-dependent association of ^{125}I-rt-PA with rat hepatocytes (parenchymal and non-parenchymal cell). Data are the mean from five determinations.

Table 4. Association (k_{on}) and dissociation (k_{off}) constants of specific binding of ^{125}I-pamiteplase or ^{125}I-rt-PA to hepatocytes.

	Cell	k_{on} ($min^{-1} \cdot nM^{-1}$)	k_{on} (min^{-1})	K_d (nM)
Pamiteplase	PC	0·000490	0·0096	19·1
	NPC	0·000459	0·0153	33·3
rt-PA	PC	0·00162	0·0164	10·2
	NPC	0·00189	0·0158	8·4

Data are the mean from five determinations.

regression analysis of these results were 0.000490 $min^{-1}.nM^{-1}$ and 0.0096 min^{-1} for PC, and 0.000459 $min^{-1}.nM^{-1}$ and 0.0153 min^{-1} for NPC (table 4). k_{on} and k_{off} of t-PA were 0.00162 $min^{-1}.nM^{-1}$ and 0.0164 min^{-1} for PC, and 0.00189 $min^{-1}.nM^{-1}$ and 0.0158 min^{-1} for NPC (table 4).

Discussion

The kinetics for RME for the elimination of peptides such as asialoglycoproteins (Pardridge *et al.* 1983), GSF (Kuwabara *et al.* 1994), EGF (Yanai *et al.* 1991) and erythropoietin (Kato *et al.* 1997) have been reported for various types of cells. Protein uptake by hepatocytes through RME has been reported to contribute considerably to the elimination of wild-type t-PA (Krause *et al.* 1990, Tanswell *et al.* 1990). Pamiteplase is a novel t-PA analogue with a markedly lower Cl_{total} than that of rt-PA (Oikawa *et al.* 1996a). In this study, this difference in Cl_{total} was examined assuming RME as the primary mechanism, using liver cell plasma membranes and hepatocytes.

The specific binding of rt-PA in the liver has been examined in many studies. K_d has been reported to be 10 nM in isolated rat hepatocytes (Bakhit *et al.* 1987), 3.7 nM in the human hepatoma cell line Hep G_2 (Owensby *et al.* 1988), 1 nM in isolated rat

hepatocytes (Krause *et al*. 1990), 2 nM in purified hepatocyte plasma membranes (Krause *et al*. 1990), and 1.4 nM in rat Novikoff hepatoma cell (Nguyen *et al*. 1992) respectively. Furthermore, the IC_{50} of unlabelled rt-PA binding against ^{125}I-rt-PA was 19 nM in primary culture hepatocytes (Einarsson *et al*. 1988), $\sim$100 nM in isolated rat hepatocytes (Bakhit *et al*. 1987), $\sim$10 nM in isolated rat hepatocytes (Krause *et al*. 1990) and $\sim$10 nM in purified hepatocyte plasma membranes (Krause *et al*. 1990) respectively. Although slight differences in results were observed because of the difference in experimental conditions and matrices, there were no large differences in the results between this and other studies. Therefore, the results of rt-PA in this study were thought useful as a positive control when evaluating the kinetics of pamiteplase.

The specific binding of both compounds was examined using liver cell plasma membranes and hepatocytes. Concentration-dependent and saturated binding profiles were observed for both compounds, and linear analysis by Eadie–Hofstee plotting suggested the existence of only one specific binding site. Furthermore, there was no difference between receptor source (liver cell plasma membranes or hepatocytes), cell type (PC or NPC), or compounds (pamiteplase or rt-PA) in B_{max} calculated using the Michaelis–Menten equation. Furthermore, there was no difference between matrices and cell type in K_d. However, a difference in K_d was observed between the compounds, suggesting pamiteplase has a lower affinity for cell surface membranes in the liver. Furthermore, the specific binding of each ligand could be inhibited by the other, showing that both compounds share a common specific binding site. This was consistent with results showing that B_{max} was comparable between the compounds. The IC_{50}, however, was 121.5–364 nM for pamiteplase and 43.6–93.7 nM for t-PA, indicating that differences in K_d were responsible for the binding differences in IC_{50}.

The RME process can be separated main three steps (Sugiyama *et al*. 1989). In the first step (binding; association/dissociation), a polypeptide in systemic circulation easily transfers into the space of the Disse from the sinusoid and binds to a cell-surface receptor (Sugiyama *et al*. 1989). In the second step (internalization), a ligand–receptor complex is moved to a coated pit forming a coated vesicle and is pinocytosed (Sugiyama *et al*. 1989). In the third step, the ligand–receptor complex moving to the endosome dissociates due to low pH and the ligand is eliminated by lysosomal degradation or a shuttle pathway (Sugiyama *et al*. 1989). Model A (figure 1) kinetically describes the first and second step occurring at 37 °C under physiologic conditions. Compared with model A, model B (figure 2) could be kinetically described at 4 °C because of the lack of a second step. From these models, k_{on} and k_{off} are thought to play an important role in first step, whereas k_e mediates the second step.

On the basis of model A at 37 °C, the integration plot obtained from the amount of cell-surface binding and internalized ligand showed a linear relationship (slope; k_e) between $\int[LR_s]dt$ versus $[LR_I]_{0-t}$ (internalized ligand) up to 10 min of incubation, suggesting that degradation was negligible. There are no differences in the k_e of either compound between PC and NPC. Comparing results between the compounds, the value for pamiteplase was 1.4–1.7 times larger than that for rt-PA, indicating that the internalization of pamiteplase was slightly slower than that for rt-PA in both cells. Since the process of internalization can be separated mainly to transfer to coated pits and formation of coated vesicles, the cause of the difference in k_e was thought due to a structural or electrical interrelation between ligand and cell

surface component because of the difference in a ligand of ligand–receptor complex. However, the difference in $Cl_{hepatic}$ could not be explained only by this difference.

On the basis of model B at 4 °C, there was no difference in k_{on} and k_{off} for either compound between cells. In contrast, k_{on} of pamiteplase was 3.3–4.1 times larger than that of rt-PA, whereas the k_{off} of pamiteplase was 1.0–1.7 times larger. The rate constant of pamiteplase related to both the association (k_{on}) and dissociation (k_{off}) process was lower than that of rt-PA, with larger difference in k_{on} between the compounds. The k_{on} process was thought to be only an interaction between ligand and receptor. The RME of wild-type t-PA is mediated by two ligand structures (Camani *et al*. 1994). One is a mannose-rich carbohydrate chain at Asn117 in the rt-PA molecule that binds to the mannose receptor on the membrane of NPC (Camani *et al*. 1994). The other is amino acids near Try67 of the epidermal growth factor domain (EGF domain) in the rt-PA molecule that binds to the low-density lipoprotein receptor-related protein/α_2-macroglobulin receptor (LRP/α_2-M receptor) on the membrane of PC (Camani *et al*. 1994). The pamiteplase structure deletes the Kringle-1 domain and introduces a point mutation (Arg275 → Glu) in the Kringle-2 domain of wild-type t-PA (Kawauchi *et al*. 1991). Therefore, the k_{on} of pamiteplase for the mannose receptor on NPC was suggested to be lower in comparison with rt-PA because of such structural modifications. Additionally, the affinity of pamiteplase for the LRP/α_2-M receptor on PC might be affected because the three-dimensional structure of the EGF domain and finger domain next to Kringle-1 domain is changed by the deletion of the Kringle-1. Consequently, differences in K_d, $Cl_{hepatic}$ and *in vivo* pharmacokinetics between two compounds are suggested form k_e, k_{on} and k_{off}, which measure important steps in the RME process.

The previously described observations lead to the following conclusions. Whereas pamiteplase has a common binding site with rt-PA, the affinity of pamiteplase at this specific binding site is lower than that of rt-PA. Kinetic analysis shows the k_e, k_{on} and k_{off} of pamiteplase are relatively slower than that of rt-PA, with k_{on} showing a marked decrease. Accordingly, because less pamiteplase binds to hepatocytes at physiologic concentrations compared with t-PA, the $Cl_{hepatic}$ of pamiteplase is lower than that of t-PA, thus explaining how pamiteplase maintains its higher plasma concentration than t-PA for a large period of time.

References

Bakhit, C., Lewis, D., Billings, R. and Malfroy, B., 1987, Cellular catabolism of recombinant tissue-type plasminogen activator. *Journal of Biological Chemistry*, **262**, 8716–8720.

Baur, H. and Pond, S. M., 1975, Criteria of viability of isolated liver cells. *Hoppe-Seyler's Zeitschrift fur Physiologische Chemie*, **356**, 827–838.

Camani, C. and Kruithof, K. O., 1994, Clearance receptors for tissue-type plasminogen activator. *International Journal of Hematology*, **60**, 97–109.

Einarsson, M., Smedsrod, B. and Pertoft, H., 1988, Uptake and degradation of tissue plasminogen activator in rat liver. *Thrombosis and Haemostasis*, **59**, 474–479.

Iida, S., Iwamoto, M., Suzuki, M. and Komatsu, T., 1988, Metabolic fate of recombinant human tissue plasminogen activator (rt-PA) (1). *Xenobiotic Metabolism and Disposition*, **3**, 309–329.

Kanemoto, N., Goto, Y. and Hirosawa, K., 1991, Intravenous recombinant tissue-type plasminogen activator (rt-PA) and urokinase (UK) in patients with evolving myocardial infarction. A multicenter double-blind, randomised trial in Japan. *Japanese Circulation Journal*, **55**, 250–261.

Kato, M., Kamiyama, H., Okazaki, A., Kato, Y. and Sugiyama, Y., 1997, Mechanism for the non-linear pharmacokinetics of erythropoietin in rats. *Journal of Pharmacology and Experimental Therapeutics*, **283**, 520–527.

Katoh, M., Suzuki, Y., Miyamoto, I. and Watanabe, T., 1991, Biochemical and pharmacokinetics properties of pamiteplase, a novel fibrinolytic agent. *Thrombosis and Haemostasis*, **65**, 1193.

Kawasaki, T., Kawamura, S., Katoh, S. and Takenaka, T., 1993a, Experimental model of carotid artery thrombosis in rats and the thrombolytic activity of YM866, a novel modified tissue-type plasminogen activator. *Japanese Journal Pharmacology*, **63**, 135–142.

Kawasaki, T., Katoh, M., Kaku, S., Gushima, H., Takenaka, T, Yui, Y. and Kawai C., 1993b, Thrombolytic activity of a novel modified tissue-type plasminogen activator, YM866, in a canine model of coronary artery thrombosis. *Japanese Journal Pharmacology*, **63**, 9–16.

Kawasaki, T., Katoh, M., Kaku, S., Gushima, H., Takenaka, T., Yui, Y. and Kawai C., 1993c, Thrombolysis with intracoronary administration of YM866, a novel modified tissue-type plasminogen activator, in a canine model of coronary artery thrombosis. *Japanese Journal Pharmacology*, **63**, 319–325.

Kawauchi, Y., Morinaga, T., Yokota, M., Kinoshita, A., Kawamura, K., Suzuki, Y., Takayama, M., Furuichi, K. and Gushima, H., 1991, Gene construction and large scale production of a novel fibrinolytic agent(pamiteplase) in CHO cells. *Thrombosis and Haemostasis*, **65**, 1193.

Krause, J., Seydel, W., Heinzel, G. and Tansewell, P., 1990, Different receptors mediate the hepatic catabolism of tissue-type plasminogen activator and urokinase. *Biochemical Journal*, **267**, 647–652.

Kuwabara, T., Kato, Y., Kobayashi, S., Suzuki, H. and Sugiyama, Y., 1994, Non-linear pharmacokinetics of a recombinant human granulocyte colony-stimulation factor derivative (Nartograstim): species differences among rats, monkey and humans. *Journal of Pharmacology and Experimental Therapeutics*, **271**, 1535–1543.

Nguyen, G., Self, S. J. and Kruithof, E. K. O., 1992, Demonstration of a specific clearance for tissue-type plasminogen activator on rat Novikoff hepatoma cells. *Journal of Biological Chemistry*, **267**, 6249–6256.

Oikawa, K., Kamimura, H., Watanabe, T., Higuchi, S. and Miyamoto I., 1996a, Pharmacokinetics of YM866 and t-PA after intravenous administration to rats and dogs. *Clinical Pharmacology and Therapy*, **6**, 2391–2396.

Oikawa, K., Kamimura, H., Watanabe, T., Miyamoto, I. and Higuchi, S., 1996b, Metabolic fate of YM866, a novel fibrinolytic agent. *Xenobiotic Metabolism and Disposition*, **11**, 1–10.

Owensby, D. A., Sobel, B. E. and Schwartz, A. L., 1988, Receptor-mediated endocytosis of tissue-type plasminogen activator by the human hepatoma cell line Hep G2. *Journal of Biological Chemistry*, **263**, 10587–10594.

Pardridge, W. M., Herle, A. J. V., Naruse, R. T. and Costin, A., 1983, *In vivo* quantification of receptor-mediated uptake of asialoglycoproteins by rat liver. *Journal of Biological Chemistry*, **258**, 990–994.

Sugiyama, Y. and Hanano, M., 1989, Receptor-mediated transport of polypeptide hormones and its importance in the overall hormone disposition in the body. *Pharmaceutical Research*, **6**, 192–202.

Stang, E., Krause, J., Seydel, W., Berg, T. and Roos, N., 1992, Endocytosis and intracellular processing of tissue-type plasminogen activator by rat liver cells *in vivo*. *Biochemical Journal*, **282**, 841–851.

Tanswell, P., Heinzel, G., Greischel, A. and Krause, J., 1990, Non-linear pharmacokinetics of tissue-type plasminogen activator in three animal species and isolated perfused rat liver. *Journal of Pharmacology and Experimental Therapeutics*, **255**, 318–323.

Verstraete, M. and Collen, D., 1985, Randomized trial of intravenous recombinant tissue-type plasminogen activator versus intravenous streptokinase in acute myocardial infarction. *Lancet*, **i**, 842–847.

Yanai, S., Sugiyama, Y., Kim, D. C., Iga, T., Fuwa, T. and Hanano, M., 1991, Kinetic analysis of receptor-mediated endocytosis of epidermal growth factor by isolated rat hepatocyte. *American Journal of Physiology*, **260**, C457–467.

XENOBIOTICA, 2000, VOL. 30, NO. 7, 707–715

Intestinal absorption and excretion of troglitazone sulphate, a major biliary metabolite of troglitazone

K. KAWAI†*, T. HIROTA†, S. MURAMATSU†,
F. TSURUTA†, T. IKEDA†, K. KOBASHI‡
and K.-I. NAKAMURA§

† Drug Metabolism and Pharmacokinetics Research Laboratories, Sankyo Co. Ltd, 2–58, Hiromachi 1-chome, Shinagawa-ku, Tokyo 140–8710, Japan
‡ Faculty of Pharmaceutical Sciences, Toyama Medical and Pharmaceutical University, 2630 Sugitani, Toyama, 930–01, Japan
§ Sankyo USA Co., 780 Third Avenue, New York, NY 10017, USA

Received 17 September 1999

1. Deconjugation by sulphate transfer and intestinal absorption of troglitazone sulphate (M1), the major metabolite of a thiazolidinedione antidiabetic drug, troglitazone, were studied in the male F344 rat using ^{14}C-troglitazone, ^{14}C-M1 and ^{35}S-M1.

2. Some part of M1, produced in the liver and excreted mostly in the bile, was deconjugated in the intestine to the parent compound, troglitazone, by arylsulphate sulphotransferase originated from intestinal flora. However, deconjugation of M1 was not catalyzed by arylsulphatases. Caecal injection of M1 led to the appearance of troglitazone and M1 in plasma.

3. Biliary excretion mostly as M1, and, following absorption, as M1 and troglitazone after deconjugation, were indicated as the basis for the enterohepatic circulation of troglitazone.

4. Enterohepatic circulation may prolong the pharmacological effects of troglitazone.

Introduction

Troglitazone (CS-045), (±)-5-[4-(6-hydroxy-2,5,7,8-tetramethylchroman-2-ylmethoxy) benzyl] thiazolidine-2,4-dione, was developed as a novel oral antidiabetic drug (Fujiwara *et al*. 1988, Yoshioka *et al*. 1993, Barrie *et al*. 1994) for the treatment of non-insulin-dependent diabetes mellitus (NIDDM) (Iwamoto *et al*. 1991, Kathleen *et al*. 1996). The mechanism of action of thiazolidinediones is thought to be via the activation of peroxisome-proliferator-activated receptor γ (PPARγ) (Lehman *et al*. 1995, Burant *et al*. 1997), a member of the nuclear receptor superfamily shown to function in adipogenesis (Lambe and Tugwood 1996). In addition to this action (possibly a common one in thiazolidinedione hypoglycaemic agents), troglitazone has a characteristic anti-oxidative ability effective in suppressing the development of atherosclerosis by inhibiting the lipid peroxidation of low-density lipoprotein (Noguchi *et al*. 1996, Cominacini *et al*. 1998). It was reported that after initial metabolism of troglitazone in the liver mostly to the sulphate conjugate (M1) and the glucuronide (M2), M1 and M2 were excreted in the bile, whereas troglitazone was excreted in the bile only in very small amounts (Kawai *et al*. 1997). Also, the conjugation reactions of troglitazone proceeded in *in vitro* system of mouse, rat, monkey and human livers (Kawai *et al*. 1998). On the other

* Author for correspondence: e-mail: kawaik@shina.sankyo.co.jp

Xenobiotica ISSN 0049-8254 print/ISSN 1366-5928 online © 2000 Taylor & Francis Ltd
http://www.tandf.co.uk/journals

hand, the conjugated metabolites were excreted in the faeces in only negligible amounts, and only troglitazone was a main component in the faeces. Furthermore, administration of ^{14}C-labelled troglitazone revealed that the substances excreted in the bile were reabsorbed (Kawai *et al*. 1997).

Here, ^{14}C-troglitazone, ^{14}C-M1 and ^{35}S-M1 were administered to the bile duct-cannulated male rat, and the deconjugation and enterohepatic circulation of M1, the major and common metabolite of troglitazone in all animal species investigated to date, was investigated.

Materials and methods

Chemicals and enzymes

^{14}C-troglitazone was synthesized from [5-^{14}C]thiazolidine-2,4-dione in the Medicinal Chemistry Research Laboratories of Sankyo (Yoshioka *et al*. 1990) (specific activity, 562.4 kBq (15.2 μCi)/mg; radiochemical purity, >98%, TLC). ^{14}C-M1 (specific activity, 518.7 kBq (14.0 μCi)/mg; radiochemical purity, >98%, TLC) was synthesized by a condensation reaction using 1-ethyl-3-(3′-dimethylaminopropyl)carbodiimide (Chales *et al*. 1969) from ^{14}C-troglitazone and sulphonic acid (John *et al*. 1961). ^{35}S-M1 (specific activity, 845.7 kBq (22.9 μCi)/mg; radiochemical purity, >98%, TLC) was synthesized according to the same method from non-labelled troglitazone and ^{35}S-sulphonic acid.

Non-labelled troglitazone (purity, 99.6% by HPLC) and the standard compounds for the main metabolites, i.e. ROY-1357 (M1, (±)-5-[4-[2,5,7,8-tetramethyl-6-sulphoxychroman-2-ylmethoxy) benzyl] thiazolidine-2,4-dione, purity, 96.4%, HPLC), the sulphate of troglitazone (Yoshioka *et al*. 1987), and ROY-1515 (M2, 1-*O*-[2-[4-(2,4-dioxothiazolidin-5-ylmethyl)phenoxymethyl]-2,5,7,8-tetramethylchroman-6-yl]-β-D-glucopyranuronic acid, purity, 95.6%, HPLC), the glucuronide (Yoshioka *et al*. 1991) of troglitazone, were from the Process Development Laboratories and Medicinal Chemistry Research Laboratories of Sankyo. The structures of troglitazone and its related compounds are shown in figure 1.

Arylsulphate sulphotransferase (ASST) purified 150-fold from *Eubacterium* A-44 (Kim *et al*. 1986, Kobashi *et al*. 1986, Konishi-Imamura *et al*. 1991, 1992), one of the major intestinal bacteria, and was kindly provided by Fuji Chemical Industries. Several series of sulphatase, derived from *Aerobacter aerogenes*, *Abalone entrails* and *Helix pomatia*, were from Sigma. Glusulase® from *Helix pomatia* was from DuPont. β-Oestradiol, deoxycholic acid and taurolithocholic acid were from Sigma. Lithocholic acid and chenodeoxycholic acid were from Wako Pure Chemical. All other chemicals used were commercially available and either, guaranteed grade or HPLC-grade.

Animals

Male F344 rats (7 weeks of age, body weight 165–225 g) were from Charles River Japan and were used at 8–10 weeks of age. The animals were acclimatized in the animal room at 24±2 °C and a relative humidity of 55±10% with a 12-h light (7:00–19:00 hours) and dark cycle. Laboratory solid food (F-2, Funabashi Farm) and water were given *ad libitum*.

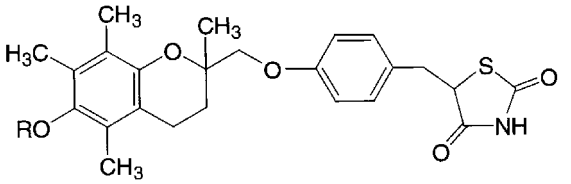
Dosing formulation, dosage, and dosing routes

Appropriate amounts of non-labelled M1 were added to ^{14}C-M1 and ^{35}S-M1, and each solution was dissolved in polyethylene glycol #400 (PEG, Wako Pure Chemicals), and the proportion of PEG in each solution was decreased to 60% by adding distilled water. Similarly, a solution of ^{14}C-troglitazone in 60% PEG was also prepared. A single dose of 5.9 mg/2 ml/kg ^{14}C-M1 or ^{35}S-M1 PEG solution was administered by in the intraduodenal route to the bile duct-cannulated rat (corresponding to 5 mg/kg troglitazone). For administration of M1 through the intracaecum route, a single dose of 1.23 mg/0.5 ml/rat (corresponding to ~1 mg troglitazone/animal) was employed.

^{14}C-troglitazone dosing solution, 1 mg/ml/kg troglitazone, was prepared for the intracaecum route using a mixture of PEG/bile/water (20:50:30 v/v/v). The bile used in this dosing formulation was collected from rats without drug administration.

Biliary, urinary and faecal excretion after intraduodenal administration of ^{14}C-M1 or ^{35}S-M1

Rats were subjected to laparotomy under diethyl ether anaesthesia, and a polyethylene tube was inserted into the common bile duct. Before suture of the wounds, intraduodenal administration of the labelled compound was conducted. The bile duct-cannulated rats (n = 4) were housed individually in



R: H Troglitazone

R: SO_3H M1 ^{14}C-M1 was in position 5 of the thiazolidine ring.

^{35}S-M1 was in sulphate group at position 6 of chroman ring.

R: M2

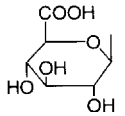


Figure 1. Structures of troglitazone and related compounds (^{14}C- and ^{35}C-M1 were the labelled position).

Bollman cages for collection of bile, urine and faeces. Bile samples were collected under constant cooling for 0–0.5, 0.5–1, 1–1.5, 1.5–2, 2–3, 3–4, 4–6, 6–8, 8–24, 24–30, 30–48 and 48–72 h post-dose. Urine and faecal samples were collected at 0–24, 24–48 and 48–72 h post-dose.

Absorption of M1 and ^{14}C-troglitazone from caecum

A solution of non-labelled M1 was injected into a ligated loop of caecum of the bile duct-cannulated rat (n = 4). After administration of M1, a fixed amount of blood was collected via the caecum vein at 10-min intervals over 1 h, and almost the same volume of blood was transfused via the jugular vein using an infusion pump (Harvard II).

A similar study with the bile duct-cannulated rat (n = 3) was conducted after administration of ^{14}C-troglitazone solution into the caecum loop at 1 mg/kg. Rats were housed individually in Bollman cages, bile samples were collected at 0–3, 3–24 and 24–48 h post-dose; faeces samples were collected at 0–24 and 24–48 h post-dose.

In vitro *deconjugation of ^{14}C-M1*

^{14}C-M1 was dissolved in dimethyl sulphoxide (1 mM DMSO) and 10 μl of this solution was added to either (1) 0.19 ml 0.5 M acetate buffer solution, pH 5.0, containing 100 units Glusulase® (DuPont, *Helix pomatia*) or (2) 0.19 ml 0.01 M Tris HCl buffer solutions, pH 7.0, containing 10 units of one of three types of sulphatase (Sigma) (types VI, *Aerobacter aerogenes*; VII, *Abalone entrails*; H-2, *Helix pomatia*) at a final concentration of 50 μM. These mixtures were then incubated at 37 °C for 2 and 24 h, the reactions being terminated by the addition of 2-fold vols ethanol, and the mixtures centrifuged at 4 °C and 1800 g for 3 min. A portion of each supernatant fraction was analyzed by TLC separation.

Radiometric TLC assay of unchanged troglitazone and its main metabolites in the bile and deconjugation reaction solution

The ethanolic supernatants obtained above and the bile samples collected after intraduodenal administration of ^{14}C-M1 or ^{35}S-M1 were spotted onto TLC plates (Kiesel gel 60 F_{254}, Art 5744, E. Merck) that had been previously spotted with ethanol solutions of unlabeled troglitazone, M1, and M2 as authentic standards. The TLC plates were developed with a solvent system of n-butanol/acetic acid/water (4:1:1 v/v/v). After development, the TLC plates were thoroughly air-dried. Radioactivity was monitored by a conventional direct counting method after scraping the spots from the plate or by a sensitive radioluminographic method (RLG). Radioactive metabolites separated by TLC were detected by exposure to X-ray film, and their positions were simultaneously confirmed with authentic standards on the plate by irradiation with a UV lamp. For quantification, silica gel on the TLC plate at the position of the unchanged drug or at the position of each metabolite was scraped into a vial, added to 0.5 ml methanol and mixed with 10 ml toluene/ethanol scintillant. In several studies, RLG was employed for the measurement of radioactivity on the TLC plate. The well-dried plates were covered with a protective film (4 μm, Dia Foil Hoechst) and placed into contact with an Imaging Plate (Fuji Photofilm) for 24 h.

The photoluminescence corresponding to the radioactivity was measured by a BAS-2000 Bioimaging Analyzer (Fuji Photofilm). The spots of authentic samples of the metabolites were visualized by UV irradiation.

Measurement of radioactivity

Biological samples were solubilized in 2 ml NCS-II® tissue solubilizer (DuPont NEN) and mixed with 10 ml toluene scintillant containing 6% Permafluor I® (Packard). For coloured specimens, a small amount of benzoyl peroxide was added for decolouration. Radioactivity was measured by a liquid scintillation counter (LSC-1000, Aloka), and was corrected for counting efficiency according to the calibration curve by an external standard method to calculate dpm.

HPLC assay for troglitazone and M1 in plasma

Plasma concentrations of troglitazone and M1 after intracaecum administration of non-labelled M1 were determined by HPLC. The plasma was deproteinized by the addition of a 2-fold volume of methanol. The supernatant was subjected to HPLC analysis under the following conditions: column, YMC-pack A312 (ODS, YMC); mobile phase, acetonitrile/water/H_3PO_4 (620:380:0·5 v/v/v); flow rate 1·0 ml/min (L-6250 pump, Hitachi); detection, UV at 230 nm (L-4200, Hitachi).

Preparation of suspension of intestinal contents and crude enzyme fraction

Three rats were killed to prepare the suspensions of intestinal contents. Whole intestine was removed from each rat under diethyl ether anaesthesia and divided into three parts, i.e. the small intestine, caecum and large intestine. The contents of each part of the digestive tract were washed out, diluted to 50 ml with 50 mM Tris-HCl buffer, pH 7·4, and homogenized by with a Polytron (Kinematica) to prepare the suspensions of intestinal contents. The crude enzyme solution from intestinal bacteria was prepared from caecum contents: Triton X-100 (2% final concentration) was added to suspensions of caecum contents and centrifuged at 3000*g* for 10 min. The pellet was resuspended in 50 mM Tris-HCl buffer, pH 7·4, and centrifuged again under the same conditions. This washing process was repeated six times and then the final suspension was used as the crude enzyme fraction.

Assay of activities of arylsulphate sulphotransferase (ASST) and deconjugation of M1

The activity of arylsulphate sulphotransferase (ASST) was determined according to Konishi-Imamura *et al.* (1991) with a minor modification. The reaction mixture (final volume 0·5 ml) contained 0·5 mM *p*-nitrophenyl sulphate as a donor substrate, 50 mM Tris-HCl buffer, pH 8·0, and 0·5 mM phenol as an acceptor substrate. The reaction was initiated by the addition of the enzyme solution; and absorbance at 405 nm was monitored. The molar extinction coefficient for *p*-nitrophenol at pH 8·0 ($1·42 \times 10^7$ l.mol^{-1}.cm^{-1}), determined by a separate measurement, was used for calculation of the enzyme activity. One unit of activity was defined as the amount of enzyme catalyzing the production of 1 μmole *p*-nitrophenol min^{-1}.

Deconjugation reaction of M1 was evaluated from the production rate of troglitazone as determined by HPLC. The reaction was carried out in a mixture of 0·1 mM M1, 50 mM Tris-HCl buffer, pH 8·0, and 0·1 mM of each acceptor in a final volume of 0·5 ml. The reaction was terminated by an addition of 2-fold ethanol, and the supernatant after centrifugation was subjected to the HPLC measurement.

Results and discussion

Excretion of radioactivity after administration of ^{14}C-M1 or ^{35}S-M1

Biliary excretion of the radioactivity after the intraduodenal administration of ^{14}C-M1 or ^{35}S-M1 in rat is given in figure 2. Urinary and faecal excretions of the radioactivity in percent of the dose administered are compared with the biliary excretion in table 1.

Radioactivity was excreted predominantly in the bile after administration of both ^{14}C-M1 and ^{35}S-M1, and the excretions of those conjugates were similar to each other 8 h post-dose. However, in the longer period extending over 72 h after administration, the biliary excretion of the radioactivity after ^{14}C-M1 administration was quite high (78·2%) and substantially greater than that after ^{35}S-M1 administration (51·9%). In contrast to the biliary excretion, the urinary excretion of

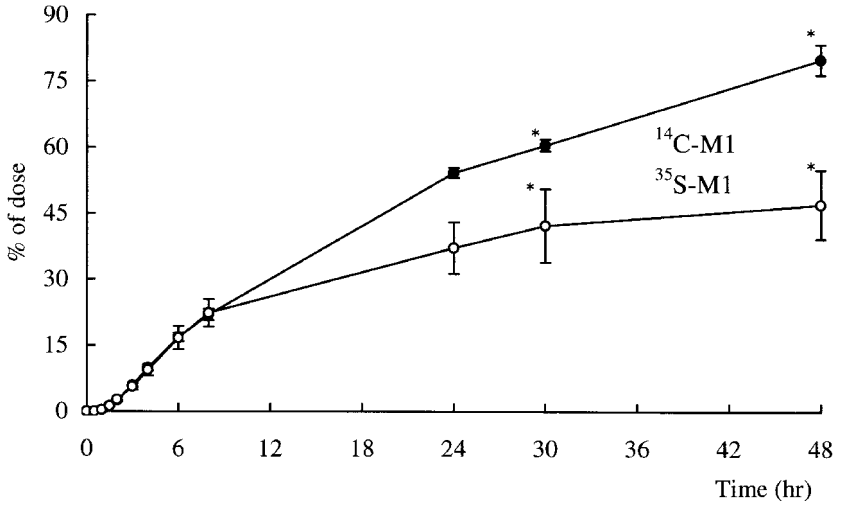


Figure 2. Cumulative biliary excretion of radioactivity after intraduodenal administration of ^{14}C-M1 and ^{35}S-M1 to rat (dose 5.9 mg/kg). Results are the mean ± SE of four animals. *$p < 0.05$.

Table 1. Excretion of radioactivity in bile, urine and faeces during 72 h after the intraduodenal administration of ^{14}C-M1 and ^{35}S-M1 to rat (dose 5.9 mg/kg).

	Excretion of radioactivity (% of administered dose)	
	^{14}C-M1	^{35}S-M1
Bile	78.17 ± 2.46*	51.9 ± 6.15*
Urine	0.30 ± 0.05**	24.58 ± 4.97**
Faeces†	18.87 ± 3.72	15.54 ± 2.97
Total	97.33 ± 4.09	92.03 ± 3.40

Data are the mean ± SE of four animals.
† Combined with the gastrointestinal contents.
* Significant ($p < 0.01$) difference between ^{14}C-M1 and ^{35}S-M1.
** Significant ($p < 0.05$) difference between ^{14}C-M1 and ^{35}S-M1.

the radioactivity after ^{35}S-M1 administration (24.6%) was much higher than that after ^{14}C-M1 administration (0.3%). The ^{35}S-radioactivity excreted in the urine is either inorganic sulphate or water-soluble endogenous acceptors, which have received radioactive sulphonate moiety from M1. On the other hand, the metabolites excreted in the bile were almost identical after administration of ^{14}C-M1 and ^{35}S-M1. The mean recovery of unchanged M1 in the bile within 0–6 h post-dose was 13.6% of the dose for both ^{14}C-M1 and ^{35}S-M1 administration. However, in the bile collected in the later period of 6–24 h post-dose, ^{14}C-M1 represented 24.0% of the dose, which was double the amount of ^{35}S-M1 (12.0%). Troglitazone was as low as 0.22% after administration of ^{14}C-M1. The biliary recovery of M1 after ^{14}C-M1 dosing indicates that about two-thirds of M1 excreted in the bile is reabsorbed as M1 itself, and the urinary recovery of ^{35}S-radioactivity after ^{35}S-M1 dosing indicates that one-quarter of M1 excreted in the bile is converted to troglitazone. The radioactivity excreted in the faeces within 72 h post-dose were

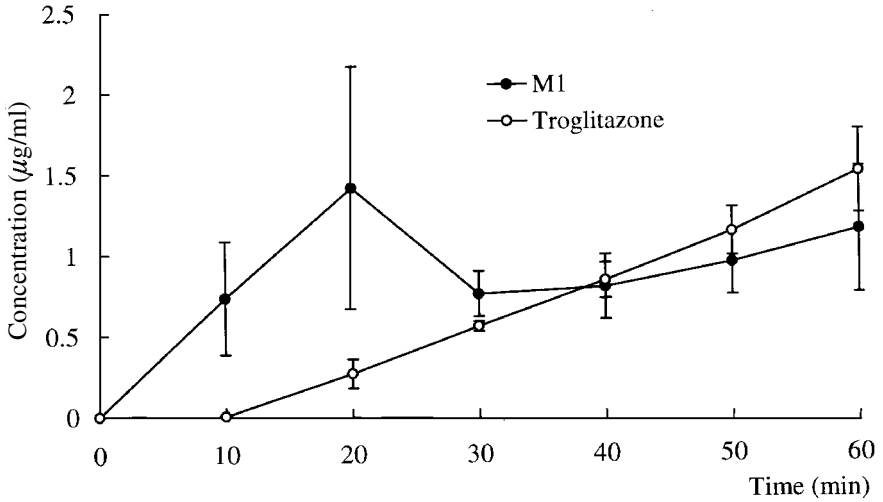


Figure. 3 Plasma concentrations of M1 and troglitazone in mesentery vein of caecum after intracaecal administration of M1 to rat (dose 1·23 mg/body). Results are the mean ± SE of four animals.

similar amounts of 18.9 and 15.5% after administration of ^{14}C-M1 and ^{35}S-M1 respectively. Assuming that the radioactivity excreted in the faeces accounts for the drug not absorbed from the digestive tract, ~ 80% of administered isotopes was considered to be equally absorbed after administration of both the labelled compounds.

Absorbed chemical form after caecum injection of M1

The time-course of plasma concentrations of M1 and troglitazone after injection of M1 in the caecum are given in figure 3. In the earlier period up to 20 min after injection, only M1 was observed. However, troglitazone was observed from 20 min after the injection, and its concentration increased linearly thereafter. This result strongly supports the view that M1 is absorbed predominantly as M1 and partially as troglitazone after deconjugation in the caecum of rat.

Biliary excretion of radioactivity after caecal injection of ^{14}C-troglitazone

The cumulative excretions of the radioactivity in the bile after caecal injection of ^{14}C-troglitazone to rat (n = 3, mean±SE) were 18·0±3·0, 55·2±7·9 and 66·9±8·9% of the dose administered during the periods of 0–3, 0–24 and 0–48 h respectively. These results also support the notion that troglitazone itself is absorbed slowly from lower parts of the intestine such as the caecum.

In vitro *deconjugation by sulphate transfer*

^{14}C-M1 was not hydrolyzed by Glusulase® or by three types of arylsulphatase originating from *Aerobacter aerogenes*, *Abalone entrails* and *Helix pomatia*, and it was concluded that the M1 conjugate is a sulphate conjugate resistant to direct hydrolysis by common arylsulphatases. On the other hand, troglitazone was generated from M1 after treatment with ASST, which catalyzes the sulphate transfer from the

Table 2. Acceptor specificity in sulphate transfer reaction using purified ASST and crude extract of rat intestinal flora as enzyme preparation and M1 as substrate.

		Enzyme rate			
		Human		Rat	
Acceptor	pK_a	(nmol/min/U)	(%)	(nmol/min/U)	(%)
2,4-Dinitrophenol	4·1	0·0	(0)	0·00	(0)
p-Nitrophenol	7·1	7·1	(13)	2·41	(33)
Phenol	9·9	55·5	(100)	7·15	(100)
Cresol	10·26	50·6	(91)	6·14	(86)
β-Oestradiol		21·5	(39)	4·71	(66)
Deoxycholic acid		26·1	(47)	0·05	(0·7)
Cholic acid		5·6	(10)	0·00	(0)
Taurolithotholic acid		0·4	(1)	0·00	(0)
Lithocholic acid		0·1	(0·2)	0·00	(0)
Chenodeoxycholic acid		6·1	(1)	0·00	(0)
Tyrosine	10·4	2·5	(5)	0·90	(13)
Tyramine	10·52	44·4	(80)	6·36	(89)

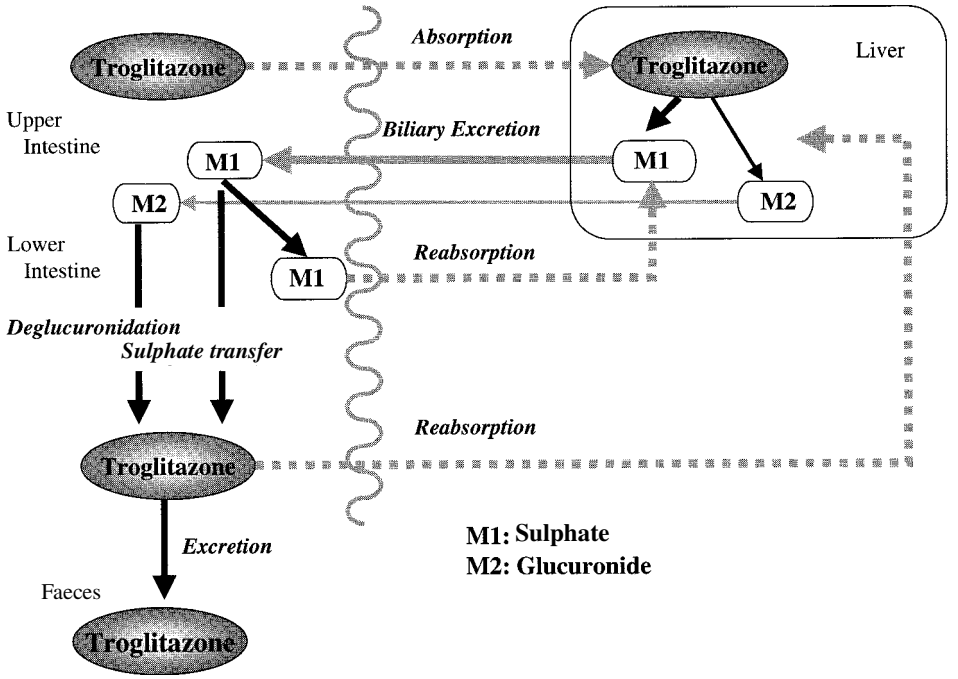


Figure 4. Proposed enterohepatic circulation of troglitazone and its conjugated metabolites in rat after oral administration of troglitazone.

sulphate conjugates to acceptor molecules originating from the human intestinal flora such as phenol. Troglitazone was also generated from M1 after treatment with a solubilized preparation of rat intestinal flora in the presence of phenol. The acceptor specificity of ASST purified from human intestinal bacteria was examined in the sulphate transfer reaction using M1 as donor (table 2). The rates of sulphate transfer from M1 per unit ASST activity in the presence of 12 acceptors (and their relative values to that of phenol, the best acceptor for the sulphate) are shown with

their pK_a in table 2 (Kortun *et al*. 1961). The sulphate transfer activity increased apparently with an increase of basicity up to $pK_a = 11$. Tyramine, a well-known standard acceptor of sulphonic acid in the ASST system, also showed a high activity in the sulphate transfer reaction of M1. Neither 2,4-dinitrophenol, acidic with a $pK_a = 4.11$, nor troglitazone served as an acceptor. β-Oestradiol exhibited a high activity but deoxycholic acid was the only bile acid to contribute to the conversion of M1 to troglitazone by sulphate transfer, and its activity as an acceptor was weak at best.

Therefore, M1, the sulphate conjugate of troglitazone found as the major metabolite both in the bile and systemic blood, was converted back to the parent compound, troglitazone, in the small intestine by arylsulphate sulphotransferase but not by sulphatase. This transferase is commonly found in the intestinal flora both in human and rat.

M2, the glucuronide of troglitazone, is another major conjugated metabolite of troglitazone, which is highly excreted in the bile. M2 was readily hydrolyzed to troglitazone by treatments either with Glusulase® or the caecum contents of rat (Kawai *et al*. 1997). In concordance with this observation, troglitazone was detected in the faeces of rat administered troglitazone, but its sulphate conjugate and glucuronide were not.

From these observations, a scheme is proposed for enterohepatic circulation of troglitazone and its major metabolites are given in figure 4. The enterohepatic circulation of M1, M2 and troglitazone may contribute to the prolonged pharmacological action of troglitazone, provided that the plasma levels are sufficiently high enough to produce a pharmacological effect.

References

Barrie, C. C. C., Michael, A. C. Graham, P. C., Peter, T. D., David, H., Ricard, M. H., Burant, C. F, Sreenan, S., Hirano, K., Tai, T., lohmiller, J., Lukens, J., Davidson, N. O., Ross, S. and Graves, R., 1997, Troglitazone action is independent of adipose tissue. *Journal of Clinical Investigation*, **100**, 2900–2908.

Carolyn, A. L., Stephen, A. S. and Peter, L. T., 1994, [[ω-(Heterocyclylamino)alkoxy]benzyl]-2,4-thiazolidinediones as potent antihyperglycemic agents. *Journal of Medicinal Chemistry*, **37**, 3977–3985.

Chales, P. H. and Ralph, O. M., 1969, Preparation of sulfate esters. Reactions of various alcohols, phenols, amines, mercaptans, and oximes with sulfuric acid and dicyclohexylcarbodiimide. *Journal of the American Chemical Society*, **91**, 4273–4278.

Cominacini, L., Grabin, U., Pasini, A. F., Campagnola, M., Davoli, A., Foot, E., Sighieri, G., Sironi, A. S., Cascio, V. L. and Ferrannini, E., 1998, Troglitazone reduces LDL oxidation and lower plasma E-selectin concentration in NIDDM patients. *Diabetes*, **47**, 130–133.

Fujiwara, T., Yoshioka, S., Yoshioka, T., Ushiyama, I. and Horikoshi, H., 1988, Characterisation of a new oral antidiabetic agent CS-045. *Diabetes*, **37**, 1549–1558.

Iwamoto, Y., Kuzuya, T., Matsuda, A., Awata, T., Kumakura, S., Inooka, G. and Shiraishi, I., 1991, Effect of new oral antidiabetic agent CS-045 on glucose tolerance and insulin secretion in patients with NIDDM. *Diabetes Care*, **14**, 1083–1086.

John, C. S., Philip, A. C. and Gregory, L. B., 1961, A convenient synthesis of water-soluble carbodiimides. *Journal of Organic Chemistry*, **26**, 2525–2528.

Kathleen, B., Ruth, P., Siri, L. K., Jose, G., Aura, M., Meleana, E. D., Anny, X., Stanley, A. and Thomas, A. B., 1996, Effect of troglitazone on insulin sensitivity and pancreatic β-cell function in women at high risk for NIDDM. *Diabetes*, **45**, 1572–1579.

Kawai, K., Kawasaki-Tokui, Y., Odaka, T., Tsuruta, F., Kazui, M., Iwabuchi, H., Nakamura, T., Kinoshita, T., Ikeda, T., Yoshioka, T., Komai, T. and Nakamura, K., 1997, Disposition and metabolism of the new oral antidiabetic drug troglitazone in rats, mice, and dogs. *Arzneim.-Forsh./Drug Research*, **47**, 356–368.

Kawai, K., Odaka, T., Tsuruta, F., Tokui, T., Ikeda, T. and Nakamura, K., 1998, Stereoselective metabolism of new oral anti-diabetic agent troglitazone stereoisomers in liver. *Xenobiotic Metabolism and Disposition*, **13**, 362–368. [in Japanese]

KIM, D.-H., KONISHI, L. and KOBASHI, K., 1986, Purification, characterisation and reaction mechanism of novel arylsulfotransferase obtained from an anaerobic bacterium of human intestine. *Biochimica et Biophysica Acta*, **872**, 33–41.

KOBASHI, K., FUKUYA, Y., KIM, D.-H., AKAO, T. and TAKEBE, S., 1986, A novel type of aryl sulfotransferase obtained from an anaerobic bacterium of human intestine. *Archives of Biochemistry and Biophysics*, **245**, 537–539.

KONISHI-IMAMURA, L., KIM, D.-H. and KOBASHI, K., 1991, Effect of enzymatic sulfation on biochemical and pharmacological properties of catecholamines and tyrosine-containing peptides. *Chemical and Pharmaceutical Bulletin*, **39**, 2994–2998.

KONISHI-IMAMURA, L., KIM, D.-H. and KOBASHI, K., 1992, Relationship between substrate activity and pKa value of phenols on sulfotransferase from *Eubacterium* A-44. *Biochemistry International*, **28**, 725–734.

KORTUN, G., VOGEL, W. and ANDRUSSOV, K., E. D. 1961, *Dissociation Constants of Organic Acids in Aqueous Solution* (London: Butterworths).

LAMBE, K. G. and TUGWOOD, J. D., 1996, A human peroxisome-proliferator-activated receptor-γ is activated by inducers of adipogenesis, including thiazolidinedione drugs. *European Journal of Biochemistry*, **239**, 1–7.

LEHMAN, J. M., MOORE, L. B., SMITH-OLIVER, T. A., WILKISON, W. O., WILLSON, T. M. and KLIEWER, S. A., 1995, An antidiabetic thiazolinedione is a high affinity ligand for peroxisome proliferator-activated receptor γ (PPARγ). *Journal of Biological Chemistry*, **270**, 12953–12956.

NOGUCHI, N., SASAKI, H., KATO, Y., TSUCHIYA, J., YAMAMOTO, Y., NIKI, E., HORIKOSHI, H. and KODAMA, T., 1996, Inhibition of oxidation of low density lipoprotein by troglitazone. *Atherosclerosis*, **123**, 227–234.

YOSHIOKA, T., AIZAWA, Y., KANAI, T., FUJITA, T. and KAWAI, K., 1990, Studies of hindered phenols. III. Synthesis of (±)-5-[4-(6-hydroxy-2,5,7,8-tetramethylchroman-2-yl-methoxy)benzyl]-5-^{14}C-thiazoline-2,4-dione (^{14}C-labelled CS-045). *Journal of Labelled Compounds and Radiopharmacology*, **28**, 911–920.

YOSHIOKA, T., AIZAWA, Y., FUJITA, T., NAKAMURA, K., SASAHARA, K., KUWANO, H., KINOSHITA, T. and HORIKOSHI, H., 1991, Studies on hindered phenols and analogues. V. Synthesis, identification, and antidiabetic activity of the glucuronide of CS-045. *Chemical and Pharmaceutical Bulletin*, **39**, 2124–2125.

YOSHIOKA, T., HORIKOSHI, H., AIZAWA, NAKAMURA, K., SASAHARA, K. and TAKEBAYASHI, T., 1987, *Japanese Kokai Tokkyo Koho*, JP 62–123186 [Chemical Abstract, 107, 176024c(1987)].

YOSHIOKA, S., NISHINO, H., SHIRAKI, T., IKEDA, K., KOIKE, H., OKUNO, A., WADA, M., FUJIWARA, T. and HORIKOSHI, H., 1993, Antihypertensive effects of CS-045 treatment in obese Zucker rats. *Metabolism*, **42**, 75–80.

XENOBIOTICA, 2000, VOL. 30, NO. 7, 717–729

Investigation of the metabolism of $^{14}C/^{13}C$-practolol in rat using directly coupled radio-HPLC-NMR-MS

G. B. SCARFE†, J. C. LINDON†, J. K. NICHOLSON†, P. MARTIN‡, B. WRIGHT‡, S. TAYLOR‡, E. LENZ‡ and I. D. WILSON‡*

† Biological Chemistry, Biomedical Sciences Division, Imperial College of Science, Technology and Medicine, Sir Alexander Fleming Building, South Kensington, London SW7 2AZ, UK
‡ Drug Metabolism and Pharmacokinetics Department, AstraZeneca Pharmaceuticals, Mereside, Alderley Park, Macclesfield SK10 4TG, UK

Received 28 January 2000

1. The metabolic fate of $^{14}C/^{13}C$-practolol was investigated using on-line HPLC-NMR-MS following oral administration to rat. The major route of elimination for the radiolabel was via the urine with the principal biotransformation products confirmed as the 2-hydroxy- and 2-hydroxyglucronide metabolites.

2. In addition, futile deacetylation, determined by the replacement of ^{13}C-labelled acetyl groups with endogenous ^{12}C-acetyls accounted for ~7–10% of the urinary metabolites, corresponding to ~5% of the dose undergoing N-deacetylation.

3. Evidence for chiral metabolism was sought via NMR of isolated metabolites using β-cyclodextrin as a chiral shift agent. Practolol was excreted as a racemate. However, some enantioselective metabolism/excretion had occurred as the hydroxy- and hydroxy-glucuronide were not excreted as racemic mixtures.

4. Directly coupled radio-HPLC-NMR-MS is extremely effective for the identification of the metabolites of radiolabelled xenobiotics in urine samples.

Introduction

Practolol (Eraldin™) was developed as a β-adrenoceptor antagonist for the treatment of angina pectoris, systemic hypertension and cardiac arrhythmias, but was subsequently withdrawn due to unwanted side-effects observed in a comparatively small proportion of patients receiving the drug. The metabolic fate of the compound has been extensively studied in a number of species. Thus, following administration of practolol to rat (20–500 mg kg^{-1}) and dog (16 mg kg^{-1}), urinary excretion was the major route of elimination (Scales and Cosgrove 1970) with >85% of the dose excreted as unchanged Practolol. The major metabolite (9% of total) was identified as the 2-hydroxy-4-(2-hydroxy-3-isopropylaminopropoxy)-acetanilide, which was excreted in the ratio 1:2 as the free and glucuronide conjugated metabolite. Practolol metabolism has also been studied in healthy human volunteers and patients (Reeves *et al*. 1978). Similar metabolism was seen in man and other species including mouse, guinea pig, hamster, rabbit and marmoset (Reeves *et al*. 1979). The only species difference that was noted was the extent of N-deacetylation (followed by re-acetylation). While this futile deacetylation was low in most species (< 5%), in the marmoset ~57% of the dose was N-deacetylated (Reeves *et al*. 1979). The extent of this deacetylation was monitored by measuring the evolution of $^{14}CO_2$ after the incorporation of a ^{14}C-acetyl group into the drug.

* Author for correspondence; e-mail: ian.wilson@astrazeneca.com

Xenobiotica ISSN 0049-8254 print/ISSN 1366-5928 online © 2000 Taylor & Francis Ltd
http://www.tandf.co.uk/journals

More recently, N-deacetylation/acetylation reactions have been monitored for a range of acetanilides using ^{13}C-labelled acetyl-labelled compound with ^{1}H-NMR to measure the acetyl methyl signals for the ^{12}C- and ^{13}C-labelled acetyls present in the samples (e.g. Nicholls *et al*. 1997a, 1999).

The opportunity has been taken here to compare this newer NMR spectroscopic approach with results previously obtained in the rat using the radiolabelled acetyl derivative. Also examined has been the use of more modern technology for drug metabolite identification such as combined HPLC-NMR and HPLC-NMR-MS techniques, which have proved particularly useful in this type of investigation, e.g. Nicholls *et al*. (1997a, 1999), Scarfe *et al*. (1999a–c). In addition, Practolol, in common with many other compounds of this class, was administered as a racemate, and the opportunity has been taken here to investigate the chiral metabolism of this compound.

Materials and methods

Sources and synthesis of test compounds

4-(2-Hydroxy-3-isopropylaminopropoxy)-acetanilide (practolol, Eraldin™, ICI 50172) with a ^{14}C-label in the isopropyl chain (radiochemical batch no. 35R) and a radiochemical purity $>95\%$ was from the Isotope Chemistry Unit, Department of Drug Metabolism and Pharmacokinetics, AstraZeneca Pharmaceuticals (Alderley Park, UK).

4-(2-Hydroxy-3-isopropylaminopropoxy)-[carbonyl-^{13}C]-acetanilide (^{13}C-practolol) was synthesized from 4-(2-hydroxy-3-isopropylaminopropoxy)-aniline (ICI 50138, 1.8 mmol; AstraZeneca Pharmaceuticals) by reaction with 2 mmol acetyl-1-[^{13}C]-chloride (Aldrich, Poole, UK). The solvent used was dimethylformamide, the majority of which was removed under vacuum after the reaction. The resulting product was impure, containing a number of unwanted acetylated derivatives and residual solvent, and was purified using semipreparative HPLC. The HPLC system consisted of a Perkin-Elmer Series 200 pump and UV detector at 254 nm. Chromatography was performed on a Partisil ODS-3 50 cm $\times$ 9.4 mm column (10 μm particles) with gradient elution. The mobile phases consisted of water containing 0.1% trifluoroacetic acid and acetonitrile (HPLC grade) with a linear gradient from 5 to 95% over 45 min. Flow rate was 2 ml min^{-1}. The reaction mixture was dissolved in 5 ml mobile phase and 0.5-ml portions of it were injected on to the column. Fractions corresponding to ^{13}C-practolol were collected into a flask and the mobile phase removed by rotary evaporation. The product was converted to the hydrochloride salt by dissolving in 0.1 m hydrochloric acid then freeze-drying, resulting in a product $>95\%$ pure by ^{1}H-NMR and carbon, hydrogen and nitrogen analysis.

Animal experiments

Three male Wistar rats (150–200 g) were acclimatized in metabolism cages for 24 h before dosing and predose urine was collected. Rats were permitted free access to food (R&M No. 1 Modified Irradiated Diet) and water throughout the study. ^{14}C-practolol (5.3 mg, specific activity 71.6 μCi mg^{-1}) was added to ^{13}C-practolol hydrochloride (162.7 mg, 143.2 mg free base) and dissolved in distilled water (6 ml) to give a dose solution with a nominal concentration of 25 mg ml^{-1} and a specific activity of 0.4 μCi mg^{-1}. Rats were dosed orally (p.o.) to give a nominal dose of 100 mg kg^{-1}, 40 μCi kg^{-1}. Urine was collected over solid CO_2 from 0 to 6, 6 to 24 and 24 to 48 h after dosing. Faeces and aqueous cage wash ($\sim$ 200 ml) were collected between 0–24 and 24–48 h after dosing. After the study, animals were killed by halothane inhalation; death was assured by cervical dislocation and the carcasses retained for analysis. All samples were weighed then stored at -20 °C until analysed.

Radiochemical methods

Liquid scintillation counting. A full excretion balance determination was obtained using liquid scintillation counting. Three aliquots per sample of urine (20–100 μl) and aqueous cage wash (1 ml) were weighed into 20-ml scintillation vials then diluted to 1 ml with distilled water where necessary. Packard Ultima Gold scintillant (10 ml) was added to each vial and radioactivity measured for 10 min or until 10^4 counts had accumulated using a Packard model 1600 liquid scintillation counter. Quench correction was calculated using the tSIE method (Packard). Faeces samples were homogenized in distilled water (1:2 w/v). Three weighed aliquots per sample were taken and allowed to dry in Packard CombustaCones before combustion on a Packard sample oxidizer model 307. $^{14}CO_2$ produced was trapped using Optisorb 1 (6 ml), and Optisorb S scintillant (12 ml) was added before measuring radioactivity by liquid

scintillation counting. Carcasses were solubilized by incubation with a caustic solution, each carcass being placed in a solution of 80 g sodium hydroxide, 600 ml distilled water, 300 ml methanol and 100 ml Triton X-100 (detergent). Carcasses were incubated overnight at 60 °C in a water bath. Three weighed aliquots of the solutions (200 μl) were neutralized with 4.4 m nitric acid (100 μl) then diluted to 1 ml with distilled water before addition of 10 ml Ultima Gold scintillant. Radioactivity was measured by liquid scintillation counting as described.

HPLC with radiochemical detection. Profiling and quantification of the urinary metabolites of $^{14}C/^{13}C$-practolol was achieved using HPLC with radiochemical detection. The HPLC system consisted of a Perkin-Elmer Series 200 pump and UV detector at 254 nm with a Berthold LB506C radioactivity detector using a solid scintillant cell. Urine samples (20–100 μl) were injected on to a Hypersil H5BDS C18 column (250×4.6 mm) with 5- μm particles and separation was effected at 25 °C using 0.01 M ammonium formate (adjusted to pH 7.0 with ammonia solution) and acetonitrile (HPLC grade) at a flow rate of 1 ml min^{-1}. Gradient elution was used starting with an isocratic period of 10 min at 0% acetonitrile then increasing to 30% acetonitrile after 35 min and to 50% after 45 min. Chromatography was controlled using Berthold HLABE v.1.65 software and the radioactive peaks were integrated relative to each other and correlation with the excretion balance data enabled the percentage of dose associated with each metabolite to be determined.

Radio-HPLC-NMR-MS

The HPLC system consisted of a Bruker (Coventry, UK) LC22 pump using a Bischoff Lambda 1000 variable wavelength UV detector, a Berthold LB506C radioactivity detector and a Bruker BPSU-12 collector with a Hypersil BDS C_{18} column (250×4.6 mm) with 5- μm particles (Hichrom, Reading, UK). Separation was effected at ambient temperature using D_2O (Fluorochem Ltd, Glossop, UK) containing 0.01 M ammonium formate (Fisons Ltd, Loughborough, UK) adjusted to pH 7.0 with ammonia solution and methanol-d_4 (Aldrich) at a flow rate of 1 ml min^{-1}. Gradient elution was used starting with an isocratic period of 10 min at 0% methanol-d_4 then increasing to 30% methanol-d_4 after 35 min and to 50% after 45 min. Chromatography was controlled by Bruker Chromstar™ software. The eluent from the column was monitored by a combination of UV detection at 254 nm, radioactivity detection, ^{1}H-NMR spectroscopy and positive-ion electrospray (ES) MS. Following UV and radioactivity detection of the chromatographic peaks, the eluent was split in the ratio of 95:5 to the NMR probe and MS inlet respectively. The major proportion was directed using a splitter, via the BPSU-12, to the flow-probe (cell volume 120 μl) of the NMR spectrometer. ^{1}H-NMR spectra were measured at 500.13 MHz using a Bruker DRX-500 spectrometer. For stop-flow HPLC-^{1}H-NMR experiments, typically 600–5000 free induction decays (FID) were collected over a spectral width of 8278 Hz into 16384 data points using an acquisition time of 0.99 s. The residual water and acetonitrile resonances were suppressed using a the NOESY presat pulse sequence (Bruker) with pre-irradiation during the relaxation delay of 2 s and the mixing time of 0.1 s. ^{1}H-NMR spectra were resolution enhanced using a Lorentzian-to-Gaussian transformation function before Fourier transformation (FT). ^{1}H chemical shifts were referenced to the acetonitrile signal at δ 2.0 relative to trimethylsilylpropionic acid at δ 0.0. The minor proportion of the eluent was directed using the splitter to the inlet of a Micromass (Altrincham, UK) Quattro LC mass spectrometer. Ionization was by positive-ion electrospray and mass spectra were acquired up to mass m/z 600 using alternating low and high cone voltages. The low cone voltage spectra provided essentially molecular ion information whereas the high cone voltage spectra gave, in favourable circumstances, meaningful fragment ion data.

Enzyme hydrolysis

Aliquots (600 μl) of urine from an appropriate period after dosing were adjusted to pH 7 or 5 using 1 M hydrochloric acid or sodium hydroxide solutions and 2500 units of β-glucuronidase (*Escherichia coli* type VII-A, sulphatase free) or 75–200 units aryl sulphatase (*Helix pomatia* type H-1) were added. In addition 50 μl 0.1 M solution of D-saccharic acid-1,4-lactone in distilled water was added to the sulphatase sample to inhibit β-glucuronidase activity. The samples were incubated at 37 °C overnight ($\sim$ 16 h) using a shaking water bath. Control samples of pH-adjusted urine were also incubated. All samples were analysed by HPLC with radiochemical detection as described.

Metabolite isolation

The HPLC system used for radio-HPLC-NMR-MS was adapted to isolate the various metabolites for subsequent chiral analysis. Metabolites were isolated from representative samples of the 0–6- and 6–24-h urines, which were freeze dried, reconstituted in 1 ml aqueous HPLC mobile phase, and injected as a series of 200- μl aliquots on to the HPLC column used for profiling. Individual radiolabelled peaks were collected, and the same peaks from individual runs were bulked together to provide purified 0–6- and 6–24-h Practolol, 0–6- and 6–24-h hydroxypractolol and 0–6- and 6–24-h hydroxypractolol-

glucuronide samples. Following removal of the mobile phase, the isolated metabolites were analysed by ^{1}H-NMR to determine their purity and, where necessary, were rechromatographed until pure by NMR spectroscopic criteria. Purity in methanol-d_4 was assessed using a Bruker DRX500 NMR spectrometer operating at 500.13 MHz ^{1}H-NMR resonance frequency. ^{1}H-NMR spectra were acquired with 64 scans collected into 16 K data points over a spectral width of 8278 Hz. Solvent suppression of residual water was achieved by gated irradiation at the water frequency during the relaxation delay of 3 s. No line-broadening function was applied before Fourier transformation. The ratio of diastereoisomers of the hydroxypractololglucuronide was determined directly from the ^{1}H-NMR spectrum by measuring the proportions of the peaks for the β-anomeric protons of the glucuronide moiety (δ 4.67 and 4.72 for each diastereoisomer). Once shown to be pure, the samples of practolol and its hydroxy-metabolite were taken to dryness and reconstituted in D_2O to which an excess ($\sim$ 20:1) of β-cyclodextrin was added before chiral NMR. The mixture was then gently heated (to $\sim$ 50 °C) to ensure dissolution and taken for ^{1}H-NMR. ^{1}H-NMR spectra were acquired with between 256 and 512 transients into 36 K data points over a spectral width of 6082 Hz, resulting in an acquisition time of 2.7 s. Pulses (90°) were employed together with a relaxation delay of 1 s. The residual water signal was suppressed via presaturation of the residual water signal for the duration of the relaxation delay. Resolution enhancement was achieved by the application of a Lorentzian–Gaussian window function before Fourier transformation.

Results and discussion

The percentage of the dose recovered in the various samples collected up to 48 h after dosing ^{14}C/^{13}C-practolol as determined by scintillation counting is shown in table 1. A total recovery of 92.7$\pm$2.6% of the dose was achieved with the major route of excretion via the urine. Thus, 61.9$\pm$2.0% of the administered radiolabel was recovered in urine with about a further 5% in the cage wash and 24.3$\pm$4.7% in the faeces. Excretion was rapid with 86.2$\pm$2.1% recovered in the first 24 h, and only $\sim$ 5% of the dose was excreted in the 24–48 h samples. A further 1.6$\pm$0.3% of the dose was in the carcasses of the rats analysed at the end of the study. These results are essentially the same as those determined by Reeves *et al*. (1979) in this species, who obtained a urinary recovery (up to 96 h after dosing) of 71.3% after oral administration (100 mg kg^{-1}), faecal recoveries were not reported.

Metabolite profiling and identification

Reversed-phase gradient HPLC, with radioactivity detection, showed the presence of three major components accounting for the majority of the radioactivity together with a number of minor peaks that accounted for $<$ 5% of the total. The major radioactive peak eluting at 33.2 min had the same retention time as unchanged parent compound, which is consistent with the reports from earlier studies (e.g. Reeves *et al*. 1979). HPLC radiochromatography also profiled the 0–6-h urine samples after treatment with enzymes to identify phase II conjugates. These studies showed that incubation with β-glucuronidase caused the peak with a retention of 27.7 min to disappear, implying the presence of a glucuronide conjugate.

To confirm the identity of the metabolites and to determine the extent of metabolism of the ^{13}C-acetyl group, HPLC-NMR-MS was performed. For this reason the HPLC-NMR-MS analyses used deuterated methanol as the organic modifier in the mobile phase rather than acetonitrile to enable the acetyl methyl resonance (at $\sim \delta_H$ 2.0) to be observed. The radioactivity detector was connected in-line (after the UV detector) and stop-flow NMR experiments were triggered using this. The UV 254 nm detected chromatogram for a 0–6-h sample is shown in figure 1a together with its corresponding radiochromatogram in and MS TIC (figure 1b, c).

The ^{1}H-NMR spectroscopic and MS data obtained for the peak with a retention

Table 1. Percentage of dose recovered in the various samples collected up to 48 h after dosing $^{14}C/^{13}C$-practolol (derived from radioassay).

Sample	0–6 h	6–24 h	24–48 h	Total
Urine	30·3±3·2	30·0±4·8	1·6±0·4	61·9±2·0
Faeces	21·5±4·7		2·9±0·2	24·3±4·7
Cage wash	4·3±3·6		0·5±0·6	4·8±3·2
Carcass				1·6±0·3
Total	86·2±2·1		4·9±0·9	92·7±2·6

Values are mean data (n = 3)±SD.

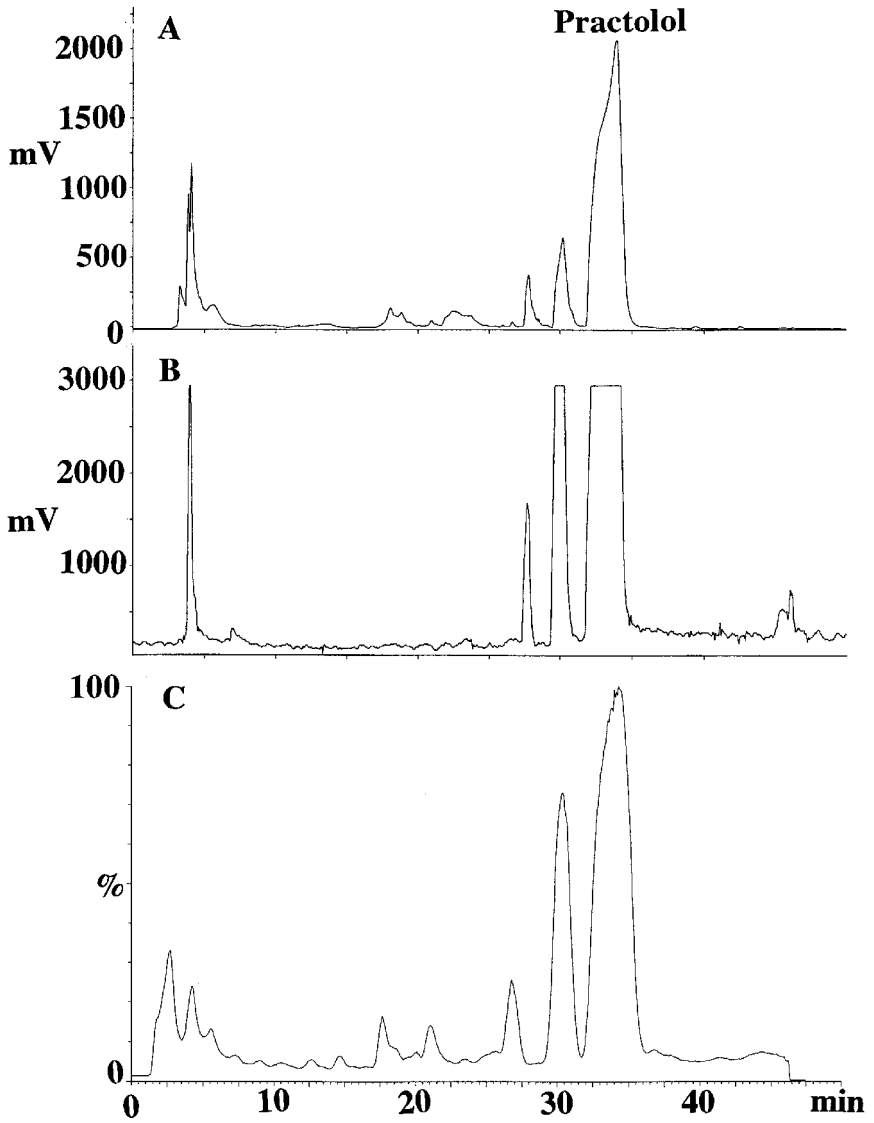


Figure 1. HPLC-UV (A), HPLC-[^{14}C] radioactivity (B) and HPLC-MS (C) total ion current traces for practolol metabolites in rat urine.

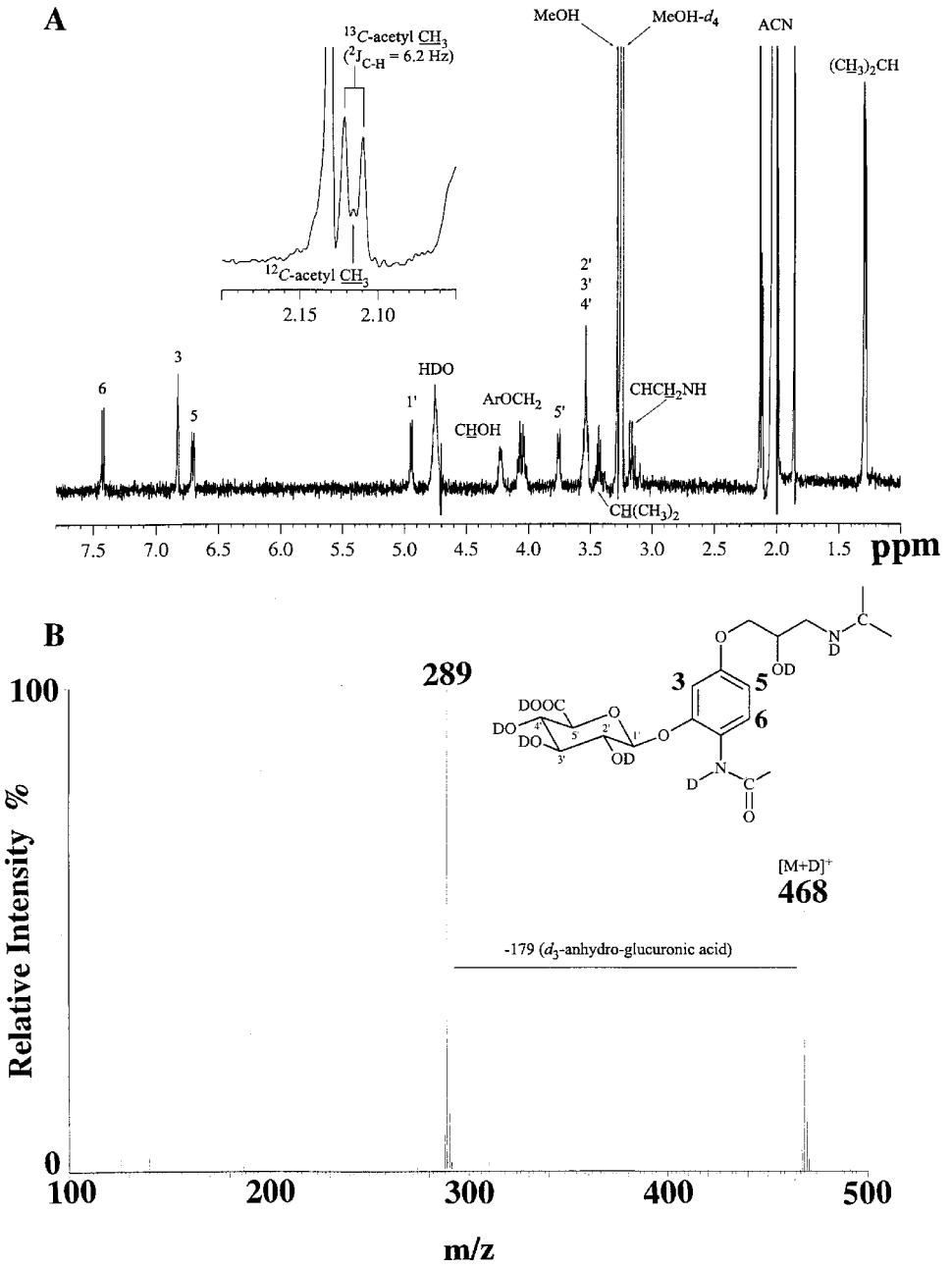


Figure 2. On-line NMR (a) and MS (b) spectra for the hydroxyglucuronide metabolite of practolol.

of 27.7 min are shown in figure 2a. In the aromatic region of the NMR spectrum signals from the metabolite could be seen that clearly showed that the *para*-disubstituted pattern of the aromatic protons of the parent compound had been lost. Three separate signals with doublets at δ_H 7.43 (H6) and δ_H 6.70 (H5) and a singlet at δ_H 6.83 were present showing that oxidation had occurred at the 2-position in the aromatic ring. In addition, diagnostic signals indicating that the metabolite was a glucuronide conjugate were present, with a distinctive β-anomeric proton doublet

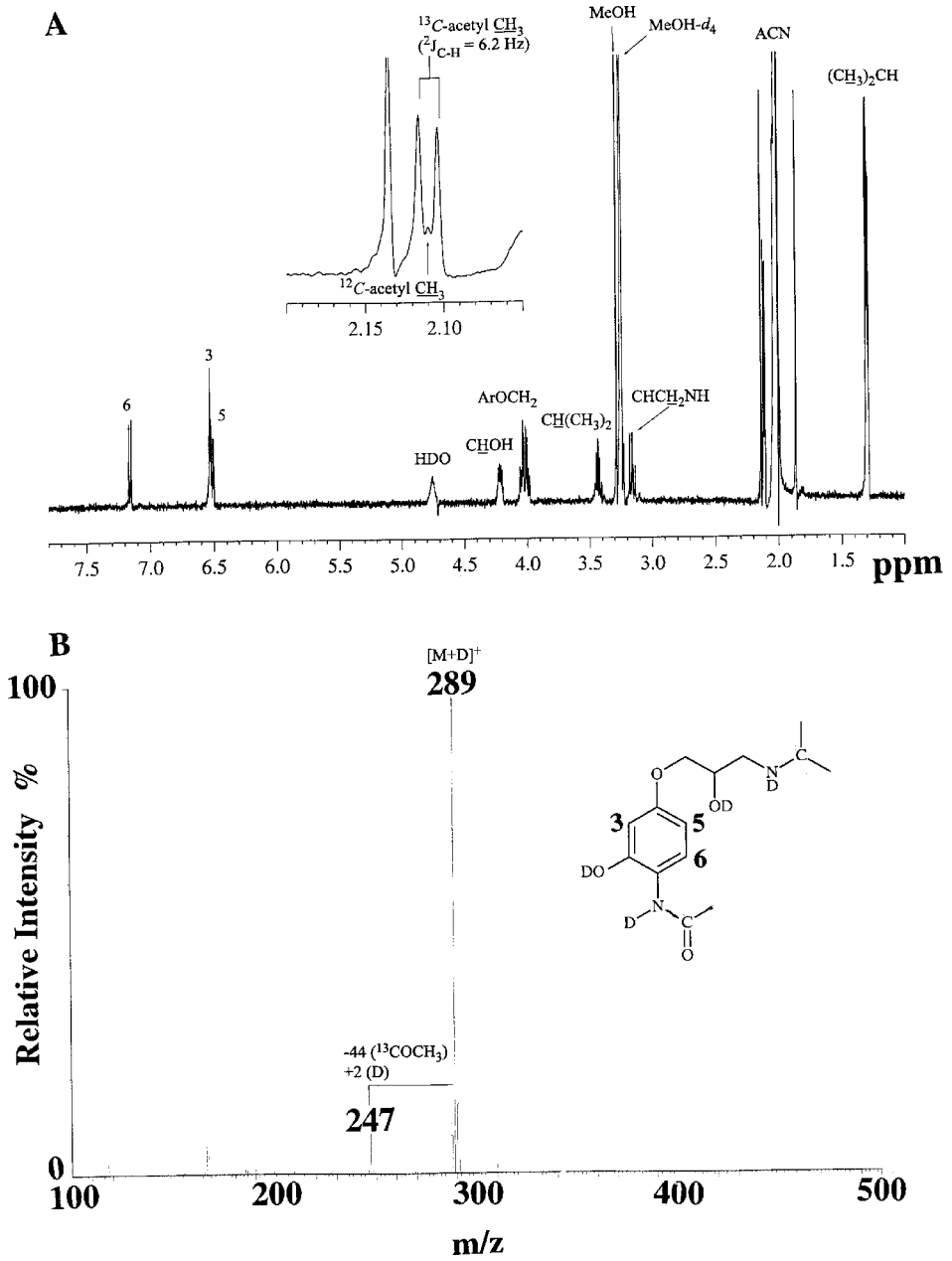


Figure 3. On-line NMR (a) and MS (b) spectra for the hydroxy- metabolite of practolol.

(H1′) at δH 4.95 and the remaining glucuronide protons H5′ at δ_H 3.76 and H2′, H3′, H4′ at δ_H 3.54 also visible. This result was in agreement with the results of enzyme hydrolysis studies which also indicated that the metabolite was a glucuronide conjugate. The other resonances in the aliphatic region of the spectrum at δ_H 4.23, 4.05, 3.43, 3.17 and 1.29 showed that the practolol side chain was still intact and no metabolism had occurred there. Although signals from acetonitrile were still present in the spectrum (due to contamination from previous runs), the resonances for the

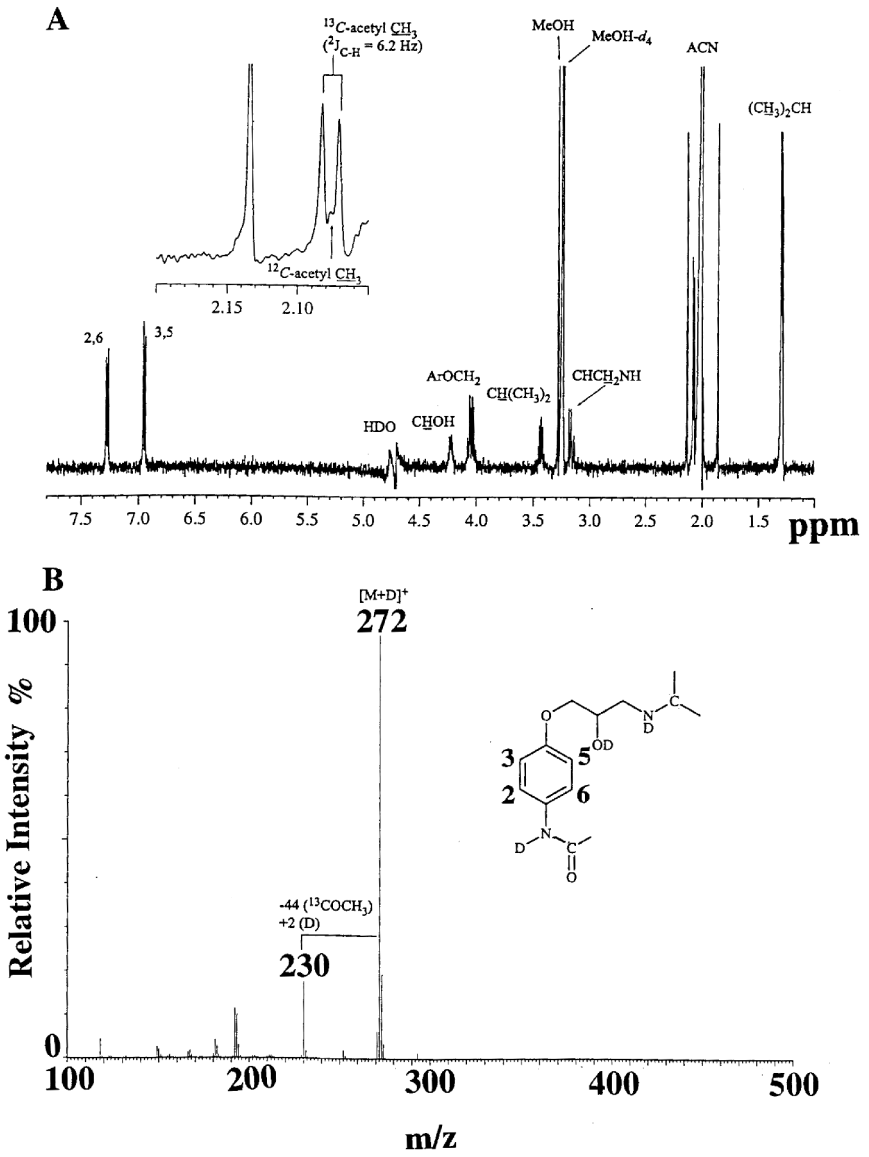


Figure 4. On-line NMR (a) and MS (b) spectra of practolol.

acetyl protons attached to the ^{12}C (singlet) and ^{13}C (doublet, $\mathcal{J}$ = ~ 14 Hz) acetyl methyl group for this metabolite could still clearly be observed. Thus, within the ^{13}C acetyl doublet a singlet was also present indicating that N-deacetylation and re-acetylation with endogenous ^{12}C-labelled material had occurred. Deconvolution and reconstruction of this portion of the spectrum enabled the peak areas and hence proportion of ^{12}C-labelled material to be estimated. It was found that 10% of the acetyl signal had undergone N-deacetylation and re-acetylation with ^{12}C-labelled material. The positive-ion electrospray mass spectrum of this metabolite gave a molecular ion $[M+D]^+$ at m/z 468 (figure 2b). This is consistent with the metabolite structure based on the ^{1}H-NMR data as 2-acetamido-5-(2-hydroxy-3-isopropyl-

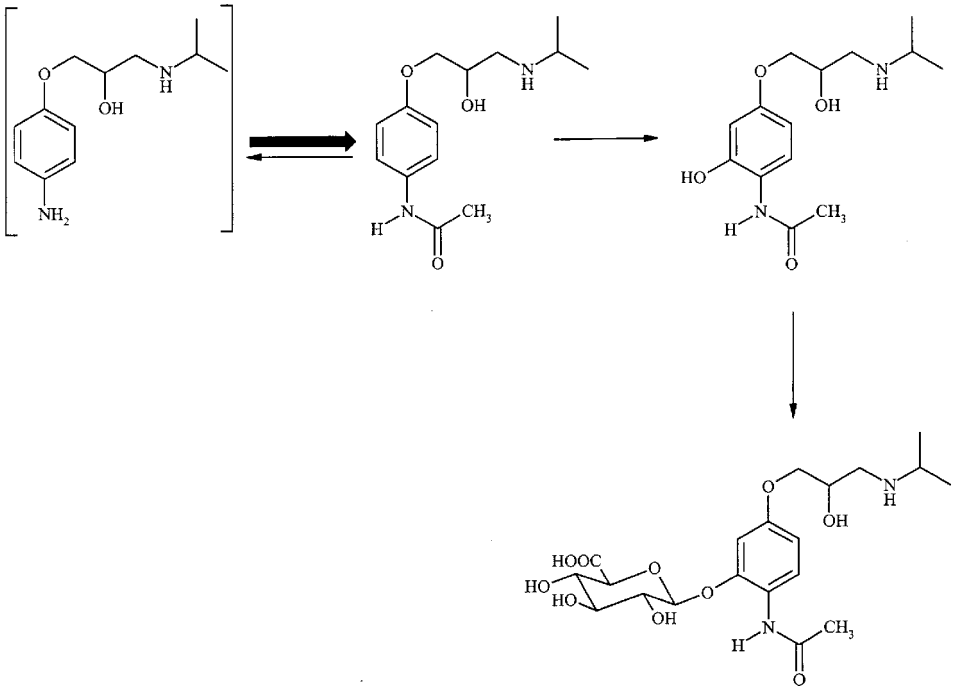


Figure 5. Metabolic pathway of practolol.

aminopropoxy)phenylglucuronide with an exchangeable deuterated molecular weight (d-MW) = 466. The fragmentation observed in this high cone voltage spectrum also confirms the assignment, showing the loss of 179 Da (d_3-dehydroglucuronic acid). Isotope patterns could be seen around the main molecular ion due to the ^{14}C-radiolabel (m/z 469) and the ^{12}C-acetyl labelled material (m/z 467) from which an estimate of the amount of futile deacetylation had occurred and ~ 7% ^{12}C-acetyl was present, a result consistent with that obtained by ^{1}H-NMR.

The NMR spectrum of the second eluting radiolabelled peak (retention = 30.0 min) showed three separate signals at δ_H 7.16 (H6, doublet), δ_H 6.53 (H3, singlet) and δ_H 6.51 (H5, doublet). This indicated that metabolism had occurred at the 2-position of the aromatic ring. The aliphatic region of the spectrum of this metabolite was unchanged compared with the parent compound. However, when the resonances for the acetyl methyl signal were examined, it appeared that ~ 10% of the ^{13}C label had been replaced with ^{12}C by futile acetylation. The positive-ion electrospray mass spectrum of this metabolite gave a molecular ion at m/z 289. This is consistent with the structure of the metabolite being 2-acetamido-5-(2-hydroxy-3-isopropylaminopropoxy)phenol (d-MW = 287). The isotope corresponding to the ^{12}C-acetyl labelled compound could be seen at m/z 288 and this accounted for ~ 7% of the total. Typical NMR and MS data for this metabolite are given in figure 3a and b.

The major radiolabelled peak, with a retention of 33.2, was confirmed as being practolol by NMR and MS. However, the compound was not entirely unmetabolized as the percentage of ^{12}C-acetyl labelled compound, calculated from the ^{1}H-NMR spectrum (figure 4a) and the isotope at m/z 271 (figure 4b) in the positive-ion electrospray mass spectrum, were again ~ 10 and 7% respectively.

Table 2. Percentage of dose recovered as the metabolites identified in urine up to 48 h after dosing $^{13}C/^{14}C$-practolol (derived from radio-HPLC and radioassay data; table 1).

Metabolite identified	HPLC t_r	Percentage dose in 0–6-h urine	Percentage dose in 6–24-h urine	Percentage dose in 24–48-h urine	Total % dose (0–48 h)
Practolol	23.4 min	20.8±2.8	16.2±2.3	n.d.	37.0±1.7
2-Acetamido-5-(2-hydroxy-3-isopropyl aminopropoxy)phenol	23.0 min	4.9±0.5	7.6±2.6	n.d.	12.5±3.0
2-Acetamido-5-(2-hydroxy-3-isopropyl aminopropoxy)phenyl glucuronide	20.4 min	1.7±0.4	4.4±0.5	n.d.	6.1±0.8
Minor metabolites†		2.9±0.5	1.8±0.1	n.d.	4.8±0.6
Total		30.3±3.2	30.0±4.8	1.6±0.4	61.9±2.0

Values are mean data (n = 3)±SD.
† Comprise three minor unidentified metabolites. n.d., not detected.

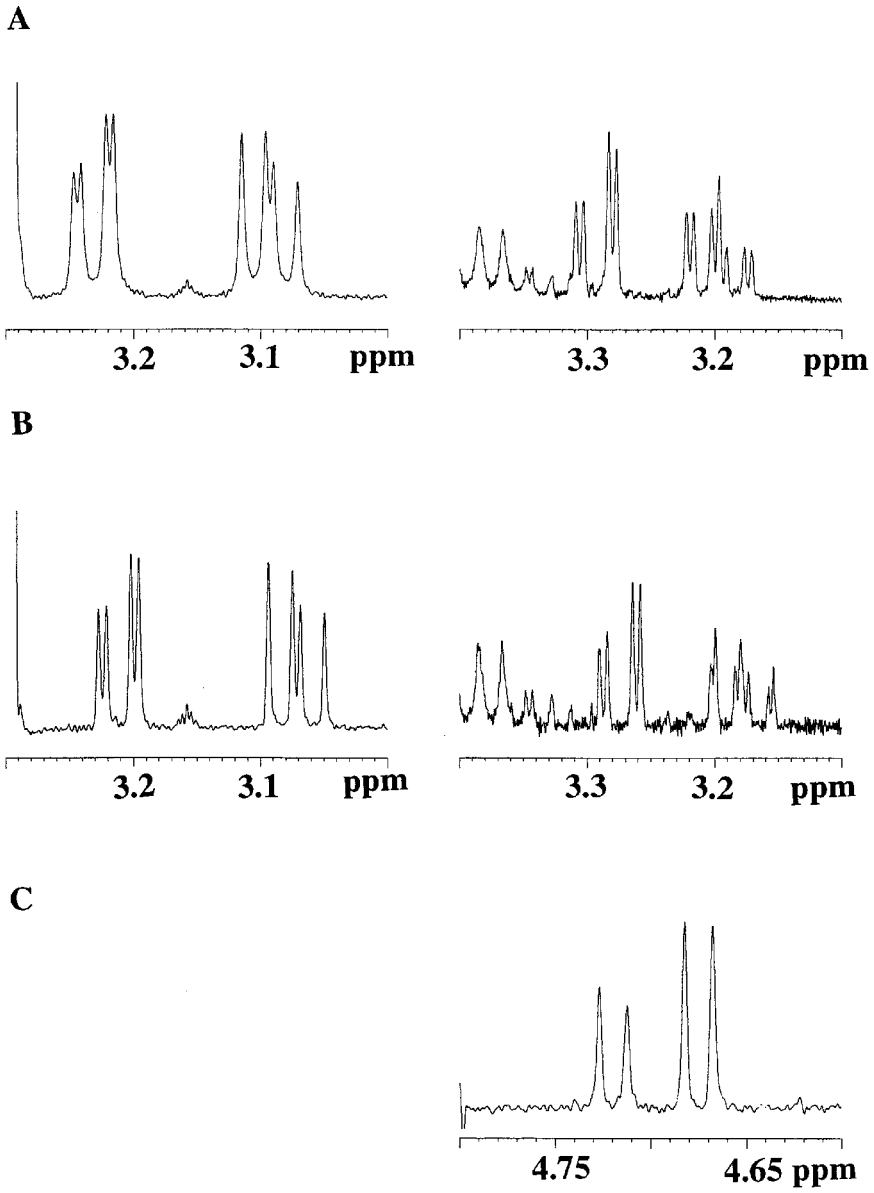


Figure 6. Chiral NMR studies on practolol and its urinary metabolites showing the aliphatic region of the NMR spectrum of (a) practolol and (b) hydroxypractolol. For these compounds, two traces are provided showing on the left spectra obtained in the absence of β-cyclodextrin while on the right the same region in the presence of this reagent. (c) NMR spectrum of the β-anomeric proton region of the glucuronic acid moiety of the diastereoisomeric hydroxyglucuronide metabolite of practolol.

Thus, both metabolites and 'unchanged parent compound' were shown by HPLC-NMR-MS to have undergone some N-deacetylation then re-acetylation (futile deacetylation) with endogenous material. The 7–10% futile acetylation seen here when related to the percentage of the dose excreted in the urine (66.7%) means that ~ 5% of the dose underwent N-deacetylation. This is comparable with the amount of N-deacetylation in rat reported by Reeves *et al.* (1979; 5.5% of the

dose) and Scales and Cosgove (1970; 4% of the dose) who determined the amount of $^{14}CO_2$ after administration of acetyl ^{14}C-labelled practolol. The amount of futile deacetylation of practolol (7–10%) was of the same order as that of paracetamol (10%; Nicholls *et al.* 1997a) but significantly lower than that for phenacetin (30%; Nicholls *et al.* 1997b). This is interesting from a structure–metabolism point of view as practolol and phenacetin are effectively both alkyl substituted analogues of paracetamol, but have quite different proportions of futile deacetylation. A metabolic pathway for practolol is given in figure 5. It was not possible to obtain interpretable mass or NMR spectra of the minor radiolabelled peaks.

Integration of the radioactive peaks from the radio-HPLC urine profiles enabled quantification of the urinary metabolites. Practolol accounted for $37.0 \pm 1.7\%$ of the total with the major metabolite, 2-acetamido-5-(2-hydroxy-3-isopropylamino-propoxy)phenol a further $12.5 \pm 3.0\%$ and its glucuronide conjugate (2-acetamido-5-(2-hydroxy-3-isopropylaminopropoxy)phenyl glucuronide) for $6.1 \pm 0.8\%$ of the dose. The three minor unidentified radiolabelled metabolites in total accounted for $\sim 5\%$ of the dose. These data are summarized in table 2.

Chiral metabolism of practolol

The practolol used in this study was dosed as a racemic mixture. Analysis of the parent compound following isolation from urine by chiral NMR using, β-cyclodextrin, showed that the drug was also excreted as a racemate. In contrast, similar analysis of the hydroxy-metabolite showed it to be excreted as a mixture of enantiomers in the ratio of $\sim 2:3$ (illustrative spectra are shown in figure 6a–e). A similar ratio was observed for the hydroxypractolol glucuronide metabolite, which by virtue of being excreted as a diastereosiomer could be observed directly by NMR, without the need for the addition of β-cyclodextrin. The fact that the spectra for the hydroxy-metabolite (in the presence B-cyclodextrin) and the hydroxyglucuronide show them to be no longer racemic clearly shows enantioselectivity at some stage. This might reflect either enatioselective formation, metabolism or excretion of these metabolites.

In the absence of authentic samples of resolved enantiomers of the metabolites, it was not possible to determine the absolute configuration of these metabolites to obtain the proportions of the R- and S-hydroxy- and hydroxypractolol glucuronide present in the samples.

Conclusions

These results show directly coupled radio-HPLC-NMR-MS to be extremely useful for the rapid identification of radiolabelled xenobiotics in complex biological fluids such as urine. The radiochromatogram showed unequivocally which peaks in the UV and MS chromatograms contained metabolites, and thereby enabled stop-flow NMR experiments to be triggered directly. In this way, practolol and its metabolites were identified rapidly, while the inclusion of the ^{13}C-acetyl group allowed the extent of futile acetylation to be determined efficiently and at the same time as the excretion balance study, thus avoiding the need for a second ^{14}C-study. The subsequent isolation of the individual metabolites and their analysis by chiral NMR showed that the contribution of chiral metabolism to the overall metabolic fate of the compound was minor.

References

Nicholls, A. W., Farrant, R. D., Shockcor, J. P., Unger, S. E., Wilson, I. D., Lindon, J. C. and Nicholson, J. K., 1997a, NMR and HPLC-NMR spectroscopic studies on the metabolism and futile deacetylation of paracetamol metabolites in rat and man. *Biochemical Pharmacology*, **49**, 1155–1164.

Nicholls, A. W., Lindon, J. C., Caddick, S., Farrant, R. D., Wilson, I. D. and Nicholson, J. K., 1997b, NMR spectroscopic studies on the metabolism and futile deacetylation of phenacetin in the rat. *Xenobiotica*, **27**, 1175–1186.

Nicholls, A. W., Lindon, J. C., Farrant, R. D., Shockor, J. P., Wilson, I. D. and Nicholson, J. K., 1999, Directly coupled HPLC-NMR spectroscopic studies of metabolism and futile deacetylation of phenacetin in the rat. *Journal of Pharmaceutics and Biomedical Annals*, **20**, 865–873.

Reeves, P. R., Case, D. E, Jepson, H. T., McCormick, D. J., Nicholls, J. T., Felix, R. H., Holt, P. J. L., Zacharias, F. J. and Fluke, R. W., 1978, Practolol metabolism. II. Metabolism in human subjects. *Journal of Pharmacology and Experimental Therapeutics*, **205**, 489–498.

Reeves, P. R., McCormick, D. J. and Jepson, H. T., 1979, Practolol metabolism in various small animal species. *Xenobiotica*, **9**, 453–458.

Scales, B. and Cosgrove, M. B., 1970, The metabolism and distribution of the selective adrenergic beta blocking agent, Practolol. *Journal of Pharmacology and Experimental Therapeutics*, **175**, 338–347.

Scarfe, G. B., Lindon, J. C., Nicholson. J. K., Wright, B., Clayton, E. and Wilson, I. D., 1999c, Investigation of the quantitative metabolic fate and urinary excretion of 3-methyl-4-trifluoro-aniline and 3-methyl-4-trifluroacetanilide in the rat. *Drug Metabolism and Disposition*, **27**, 1171–1178.

Scarfe G. B., Tugnait, M., Wilson, I. D. and Nicholson, J. K., 1999b, Studies on the metabolism of 4-fluoroaniline and 4-fluoroacetanilide in the rat: formation of 4-acetamidophenol (paracetamol) and its metabolites via defluorination and N-acetylation. *Xenobiotica*, **29**, 205–216.

Scarfe G. B., Wright, B., Clayton., Taylor, S., Wilson, I. D., Lindon, J. C. and Nicholson, J., 1999a, Quantitative studies on the urinary metabolic fate of 2-chloro-4-trifluormethylaniline in the rat using 19_F NMR spectroscopy and directly coupled HPLC-NMR-MS. *Xenobiotica*, **29**, 77–91.

XENOBIOTICA, 2000, VOL. 30, NO. 7, 731–744

Comparison of celecoxib metabolism and excretion in mouse, rabbit, dog, cynomolgus monkey and rhesus monkey

S. K. PAULSON†*, J. Y. ZHANG†, S. M. JESSEN‡, Y. LAWAL‡, N. W. K. LIU§, C. M. DUDKOWSKI†, Y.-F. WANG†, M. CHANG†, D. YANG†, J. W. A. FINDLAY†, M. A. BERGE¶, C. S. MARKOS†, A. P. BREAU†, J. D. HRIBAR§ and J. YUAN†

† Pharmacokinetics, Bioanalytical & Radiochemistry, ‡Regulatory Affairs and §Physical Methodology, G. D. Searle & Co., 4901 Searle Parkway, Skokie, IL, USA
¶ Metabolic Chemistry, Covance Laboratories, Inc., Madison, WI, USA

Received 2 February 2000

1. The metabolism and excretion of celecoxib, a specific cyclooxygenase 2 (COX-2) inhibitor, was investigated in mouse, rabbit, the EM (extensive) and PM (poor metabolizer) dog, and rhesus and cynomolgus monkey.

2. Some sex and species differences were evident in the disposition of celecoxib. After intravenous (i.v.) administration of [^{14}C]celecoxib, the major route of excretion of radioactivity in all species studied was via the faeces: EM dog (80.0%), PM dog (83.4%), cynomolgus monkey (63.5%), rhesus monkey (83.1%). After oral administration, faeces were the primary route of excretion in rabbit (72.2%) and the male mouse (71.1%), with the remainder of the dose excreted in the urine. After oral administration of [^{14}C]celecoxib to the female mouse, radioactivity was eliminated equally in urine (45.7%) and faeces (46.7%).

3. Biotransformation of celecoxib occurs primarily by oxidation of the aromatic methyl group to form a hydroxymethyl metabolite, which is further oxidized to the carboxylic acid analogue.

4. An additional phase I metabolite (phenyl ring hydroxylation) and a glucuronide conjugate of the carboxylic acid metabolite was produced by rabbit.

5. The major excretion product in urine and faeces of mouse, rabbit, dog and monkey was the carboxylic acid metabolite of celecoxib.

Introduction

Celecoxib, 4-[5-(4-methylphenyl)-3-(trifluoromethyl)-1H-pyrazol-1-yl] benzenesulphonamide, is a specific inhibitor of the inducible form of cyclooxygenase (COX-2) and does not inhibit COX-1 at plasma concentrations that are therapeutic in arthritis (Penning *et al*. 1997, Isakson *et al*. 1998, Simon *et al*. 1998). Constitutive COX-1 is widely expressed in most all tissues and appears responsible for most of the physiological prostaglandin production associated with gastric lining cytoprotection (O'Neill and Ford-Hutchinson 1993, Seibert *et al*. 1994). COX-2 expression is induced in inflammation (Crofford *et al*. 1994, Seibert *et al*. 1994). It has been hypothesized that COX-2 inhibitors will have the benefits of classical non-steroidal anti-inflammatory drugs (NSAID) without the risk of gastrointestinal toxicity (Isakson *et al*. 1998). Celecoxib was recently approved in the USA for the treatment of the signs of symptoms of rheumatoid arthritis and osteoarthritis.

* Author for correspondence: e-mail: Susan.K.Paulson@monsanto.com

Xenobiotica ISSN 0049-8254 print/ISSN 1366-5928 online © 2000 Taylor & Francis Ltd
http://www.tandf.co.uk/journals

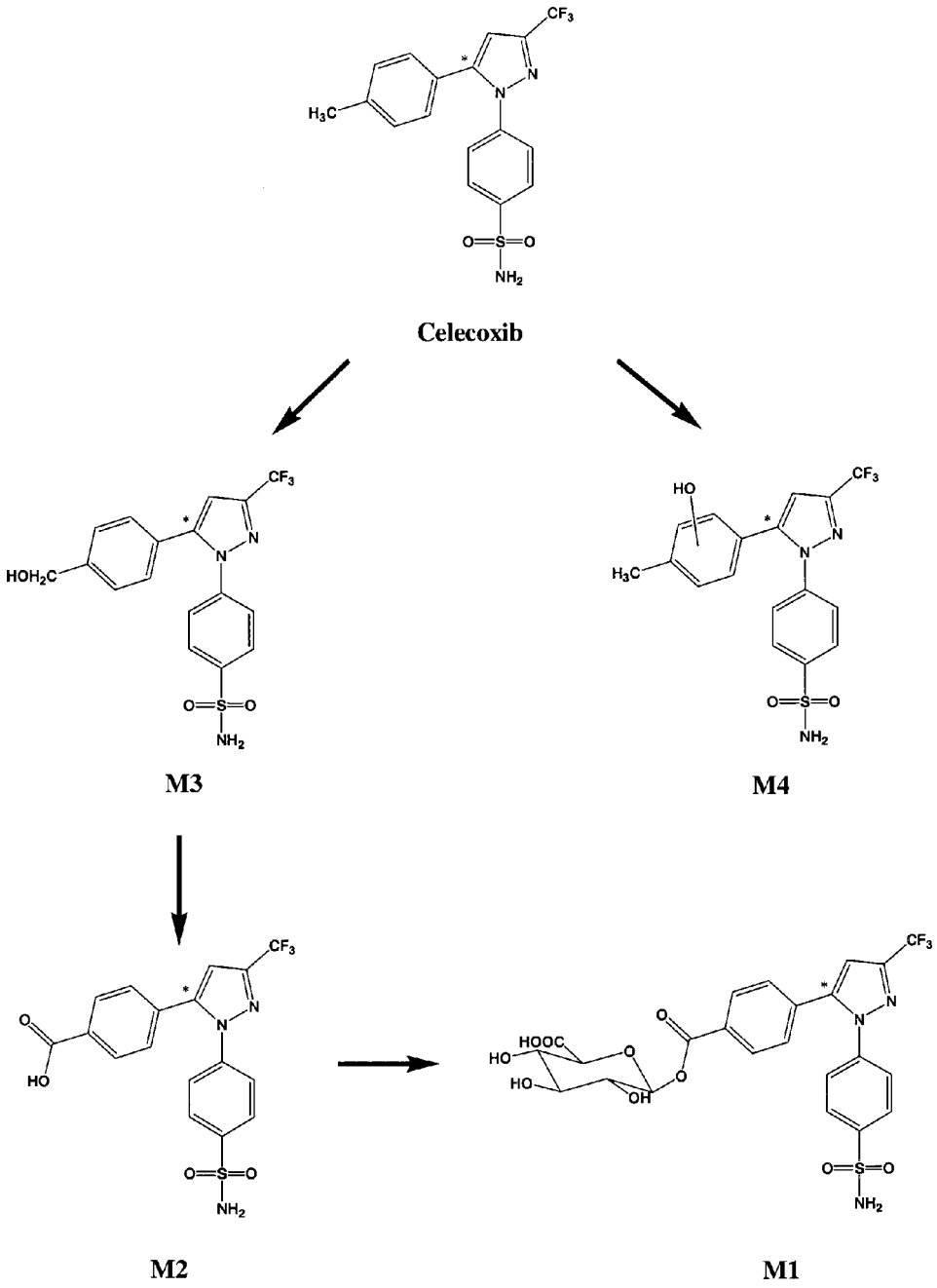


Figure 1. Proposed metabolic pathway for celecoxib.

The chemical structure of celecoxib is given in figure 1. Celecoxib is extensively metabolized in humans via a single metabolic pathway that involves hydroxylation of the aromatic methyl group of celecoxib followed by further oxidation of the hydroxymethyl metabolite to the carboxylic acid (Paulson *et al.* 2000a). The major excretion product of celecoxib in humans is the carboxylic acid metabolite.

Glucuronide conjugation of the carboxylic acid metabolite is a minor pathway of elimination of the carboxylic acid metabolite in humans.

In dog, celecoxib is metabolized *in vitro* to the hydroxymethyl metabolite with subsequent oxidation to the carboxylic acid analogue. There is a polymorphism in the canine metabolism of celecoxib associated with the formation of the hydroxymethyl metabolite (Paulson *et al*. 1999). At least two distinct populations of dog that have been described designated PM for 'poor metabolizers' and EM for 'extensive metabolizers' of celecoxib. An equal distribution of the two phenotypes, EM and PM, exists within a population of the beagle dog. The polymorphism appears due to a difference in the rate of metabolism of celecoxib by liver cytochrome P450. The specific cytochrome(s) responsible for the polymorphism is not understood.

The present study investigated the metabolism and excretion of celecoxib in several animal species : mouse, rabbit, dog, cynomolgus monkey and rhesus monkey. Routes of excretion were determined; metabolites were isolated from urine and faeces and their structures elucidated.

Materials and methods

Chemicals

Celecoxib and radiolabelled celecoxib, 4-[5-(4-methylphenyl)-3-(trifluoromethyl)-1H-pyrazol-1-yl-5-^{14}C], were synthesized at Searle (Skokie, IL, USA). The chemical purity of celecoxib was $>99\%$; chemical purity of the celecoxib metabolites was $>95\%$. Radiochemical purity of the radiolabelled celecoxib was $>96\%$ and the specific activity of the radiolabelled celecoxib was 56 mCi/mmol. The hydroxymethyl and carboxylic acid metabolites of celecoxib as well as the 1-*O*-glucuronide conjugate of the carboxylic acid metabolite of celecoxib were synthesized at Searle and MS and NMR (figure 1) confirmed the structures. The hydroxymethyl metabolite was synthesized from celecoxib by photocatalyzed bromination (NBS) of the methyl group followed by hydrolysis of the bromomethyl products. Sodium borohydride reduction of the hydrolysis mixture converted the mixture of hydroxymethyl and aldehyde products to the desired compound. Oxidation of the hydroxymethyl metabolite with Jones's chromic acid in acetone afforded the carboxylic acid metabolite. The carboxylic acid metabolite was condensed with the benzyl ester of TBDMS-protected glucal epoxide followed by protecting group removal to afford the glucuronide. All other chemicals and reagents were analytical grade and commercially available.

Animal studies

Mouse. CD-1 mice (n = 33/sex) with body weights 20–40 g (Charles River Breeding Laboratory, Portage, MI, USA) were administered [^{14}C]celecoxib in a solution of polyethylene glycol 400:water (2:1 w/v) by oral gavage at 35 mg/kg (175 μCi/kg). Mice were fasted overnight before dosing and for at least 4 h afterwards. They were housed in individual metabolism cages designed for the separation and collection of urine and faeces. Blood samples ($\sim$1 ml) were collected from the auricular artery or marginal ear vein (n = 30/sex) into chilled, heparinized vacutainers at 0.5, 2, 4, 8, 24, 48, 72, 96, 120 or 168 h after dosing. Three blood samples were collected for each time point and only one sample was collected from each mouse. All urine and faeces were collected from mice (n = 3/sex) at -18 to 0 h predose and at 24-h intervals for 7 consecutive days after dose administration. Urine was collected into containers surrounded by dry ice. Faeces were collected at ambient temperature into Stomacher bags and frozen immediately on dry ice at the end of each collection interval. Urine and faeces were stored at about -20 °C until analyses for radioactivity and metabolic profile.

Rabbit. Three female New Zealand White (Hra:SPF) rabbits with body weights of 2.8–3.2 kg (Hazelton Research Products, Denver, PA, USA) were administered [^{14}C]celecoxib in a solution of polyethylene glycol 400:water (2:1 w/v) by oral gavage at 10 mg/kg (60 μCi/kg). Rabbits were fasted overnight before dosing and for at least 4 h afterwards. They were housed in individual metabolism cages designed for the separation and collection of urine and faeces. Blood samples ($\sim$5 ml) were collected from the auricular artery or marginal ear into chilled, heparinized vacutainers at 0.5, 2, 8 and 24 h after dosing. All urine and faeces were collected at -18 to 0 h predose and at 24-h intervals for 7 consecutive days after dose administration. Urine was collected into containers surrounded by dry ice. Faeces were collected into at ambient temperature into Stomacher bags and frozen immediately on dry ice at the end

of each collection interval. Urine and faeces were stored at about −20 °C until analyses for radioactivity and metabolic profile.

Monkey. One female cynomolgus and one female rhesus monkey were administered i.v. [^{14}C]celecoxib in a solution of polyethylene glycol 400:water (2:1 w/v) at 1 mg/kg (20 μCi/kg) via the jugular vein. Monkeys were fasted overnight before dosing and for at least 4 h afterward. They were housed in individual metabolism cages designed for the separation and collection of urine and faeces. Blood samples (~5 ml) were collected from the femoral vein into chilled, heparinized vacutainers at 5, 15, 30 min, 2, 3, 4 and 6 h for the cynomolgus monkey, and at 3 and 4 h after dosing for the rhesus monkey. All urine and faeces were collected from the monkeys at −18 to 0 h predose and at 24-h intervals for 7 consecutive days after dose administration. Urine was collected into containers surrounded by dry ice. Faeces were collected at ambient temperature and frozen immediately on dry ice at the end of each collection interval. Urine and faeces were stored frozen at about −20 °C until analyses for radioactivity and metabolic profile.

Dog. Six pure-bred beagle dogs (n = 2 male, 4 female) (Hazelton Research Product, Inc., Cumberland, VA, USA) weighing 10–14 kg were characterized as PM or EM as described (Paulson *et al.* 1999). Briefly, dogs were administered a single 5 mg/kg i.v. bolus injection of celecoxib in a solution of polyethylene glycol 400:water (2:1 w/v). Venous blood samples were collected into chill tubes containing sodium heparin at ~6, 12 and 24 h post-dose. Plasma was analyzed for celecoxib concentrations. Dogs with a 24-h plasma celecoxib concentration below the limit of detection of the assay (0.010 μg celecoxib/ml plasma) were EM of celecoxib; dogs with a 24-h plasma celecoxib concentration above the limit of detection of the assay were PM of celecoxib. Dogs were allowed at least 1 week to recover from the pre-screen procedure. After recovery, dogs were administered i.v. [^{14}C]celecoxib in a solution of polyethylene glycol 400:water (2:1 w/v) at 5 mg/kg (20 μCi/kg) via the cephalic vein. The dogs (n = 3 EM, 3 PM) were fasted overnight before dosing and for at least 4 h afterward. They were housed in individual metabolism cages designed for the separation and collection of urine and faeces. Blood samples (~5 ml) were collected from the jugular vein into chilled, heparinized vacutainers predose and at 5, 15, 30 min, 1, 2, 4, 8, 24, 48, 72 and 96 h after dosing. All urine and faeces were collected from the dogs at −18 to 0 h predose and at 24-h intervals for the 7 consecutive days after dose administration. Urine was collected into containers surrounded by dry ice. Faeces were collected at ambient temperature and frozen immediately on dry ice at the end of each collection interval. Urine and faeces were stored at about −20 °C until analyses for radioactivity and metabolic profile.

Radioactivity analyses

Plasma. Blood samples were centrifuged at ~1000 *g* at 4 °C for 10 min. Aliquots of plasma (0.1–0.5 ml) were placed in 20-ml glass scintillation vials along with liquid scintillation cocktail (Ultima Gold XR, Radiomatic, Meriden, CT; or Aquassure™, Packard Instrument Co., Downers Grove, IL, USA) and radioactivity was determined in a Model 1500 or 1900 TF liquid scintillation counter (LSC) (Packard).

Urine. Total volumes of the urine samples were recorded. Aliquots of urine were placed in liquid scintillation vials along with Aquassure™ or Ultima Gold XR liquid scintillation cocktail and radioactivity was determined by LSC.

Faeces. Faecal samples were thawed at ambient temperature and weighed. About two-to-three times the sample weight of methanol:water (50:50 or 80:20 v/v) was added to the faecal samples and the samples were homogenized either using a probe-type homogenizers or in a Stomacher™ bag using a Stomacher™ Laboratory Blender 400 (A. J. Seward, London, UK). Duplicate or triplicate aliquots (0.3–0.6 g) of each faecal homogenate were placed in a Combustocone™ with pads (Packard) and allowed to dry overnight. Samples were combusted using a Packard Sample Oxidizer. The combustion products were trapped in 7 ml Carbosorb™ and mixed with 9 ml Permafluor™ (Packard) for determination of radioactivity by LSC.

The percentage of dose excreted in each urine and faecal sample was calculated as: (total radioactivity recovered in each urine and faecal sample divided by total radioactivity dosed)×100.

Quantitative metabolite profiling

Plasma. The mouse, rabbit and monkey plasma samples (1 ml) were acidified with ~0.2 vol. 1 N phosphoric acid and extracted by a 1-ml 100-mg C18 Bond Elut™ solid-phase extraction (SPE) column (Varian, Harbor City, CA, USA) preconditioned with 2-ml aliquots of acetonitrile, methanol and water. After loading the plasma sample, the column was washed with 2 ml water, then eluted with 2 ml acetonitrile. The eluate was dried under a stream of nitrogen and reconstituted into 0.2 ml solvent A of the mobile phase used in the HPLC analysis. The recoveries of radioactivity following extraction were 91.4, 87.4, 98.1 and 90.0% for mouse, rabbit, cynomolgus monkey and rhesus monkey respectively.

Dog plasma samples (~ 1 ml) were extracted with an equal volume of acetonitrile, mixed by vortexing and then centrifuged at 1000 *g* for 10 min. Supernatants were removed to a separate tube and 1 ml acetonitrile : water (50 : 50 v/v) was added to the pellet. The pellet and acetonitrile : water were vortexed and centrifuged as indicated above. Supernatants from the two extractions were combined. The recoveries of radioactivity following extractions were 108% for EM and 105% for PM dog.

Urine. The metabolic profile of [^{14}C]celecoxib in urine was determined by direct injection of urine samples (100 μl) onto the HPLC system. The percentage of the dose excreted as each metabolite in urine was calculated as: % dose recovered in the urine sample × the fraction of total HPLC radioactivity of each metabolite peak.

The urine samples from each dog (5% of the 0–72-h samples) were pooled. An aliquot (10 ml) of each pooled urine sample was concentrated under nitrogen to 1.5 ml. Acetonitrile (200 μl) was added to the concentrated urine. Samples were vortexed, sonicated for 10 min and then centrifuged at 1000 *g* for 15 min. The supernatant was removed and water : acetonitrile (80 : 20 v/v, 300 μl) was added to the pellet. The mixture was sonicated for 10 min and then centrifuged as above. The supernatants were removed and combined with the previous supernatant. The recoveries of radioactivity following extractions were 97.1% for EM and 95.3% for PM dog.

Faeces. To determine the distribution of radioactivity in faeces from mouse, rabbit and monkey, aliquots (~ 0.2 g) of faecal homogenates were pooled on a percentage weight basis and extracted with 15 ml methanol by end-over-end rotation for 1.5 h at room temperature. The faecal extracts were centrifuged at ~ 2000 *g* for 10 min at 5 °C using a Sorvall RT6000D centrifuge (Dupont Co., Wilmington, DE, USA). The supernatant volume was measured, aliquots taken and radioactivity determined by LSC. The pellet was resuspended in 15 ml methanol, vortexed briefly and extracted as described above. The extracts were combined and evaporated in a heated water bath under a stream of nitrogen. The residues were reconstituted in 3.0 ml methanol and centrifuged at ~ 2000 *g* for 10 min at 4 °C. Aliquots of the reconstituted residues were evaporated in a heated water bath, under a stream of nitrogen, and reconstituted in 15% acetonitrile containing 0.025 M sodium acetate, pH 4.5, and directly injected onto the HPLC system. The recovery of radioactivity from the extraction procedures were > 95, 80, ~ 100 and ~ 100% for mouse, rabbit, cynomolgus monkey and rhesus monkey respectively.

Dog faecal homogenate samples (~ 5 g) were acidified with 0.1 N HCl and extracted several times with acetonitrile or methanol at a ratio of 1 : 1. Samples were vortexed to mix, sonicated for 10 min and then centrifuged at 1000 *g* for 15 min at 5 °C. Supernatants from each extraction were combined. The recovery of radioactivity from the extraction procedure was 99.2% for EM and 99.3% for PM dog.

The percentage of the dose excreted as each metabolite in faeces was calculated as: % of dose recovered in the faecal sample × the fraction of total HPLC radioactivity of each metabolite peak.

HPLC

HPLC analyses of plasma, urine and faecal samples was performed using an HP1050 autosampler and HP1050 pump (Hewlett Packard, Wilmington, DE, USA) equipped with a Novapak C18 column (3.9 × 150 mm, 4 μm, Waters, Marlborough, MA, USA) and a Waters Novapak C18 guard column. A linear gradient was employed from 20% acetonitrile in 0.025 M sodium acetate buffer, pH 4.5 (mobile phase A) to 60% acetonitrile in 0.025 M sodium acetate buffer, pH 4.5 (mobile phase B) over 20 min and held at mobile phase B for 5 min before being re-equilibrated at mobile phase A for 20 min. The flow rate of mobile phase was 1 ml/min. Eluates from the HPLC column following injection of urine samples and faecal extracts were mixed with Ultima Flo™ (Packard) at 1 : 3 (v/v) and analysed for radioactivity using a Flo-One Beta A-500 radioactivity detector (Packard). Plasma extracts were injected on the HPLC and 0.5-min fractions were collected using a Foxy 200 (ISCO, Inc., Lincoln, NE, USA) fraction collector. Each fraction was mixed with 10 ml Ultima Gold scintillation cocktail (Radiomatic, Meriden, CT, USA) and ^{14}C content was determined by LSC.

LC-MS/MS

Liquid chromatography-mass spectrometry/mass spectrometry (LC-MS/MS) analyses were performed using a series 200 LC autosampler (Perkin-Elmer, Norwalk, CT, USA), and two LC-10A HPLC pumps (Shimadzu, Tokyo, Japan) coupled to a API-III Plus triple quadrupole mass spectrometer (PE Sciex, Concord, Ont., Canada). Separation was performed on a Waters NovaPak C18 HPLC column (3.9 × 150 mm, 4 μm, Marlborough, MA, USA) that was eluted isocratically at 1.0 ml/min, with mobile phase C (acetonitrile: 0.025 M ammonium acetate, 20 : 80, pH 4.5) for 5 min, then programmed with a linear gradient system to mobile phase D (acetonitrile: 0.025 M ammonium acetate, 60 : 40, pH 4.5) over 20 min and held at mobile phase D for another 5 min. About 20% of the flow was diverted to the mass spectrometer using a 1 : 4 T-splitter. The mass spectral analyses were performed in a negative-ion turbo-ionspray ionization mode set at 400 °C with the turbo-ionspray interface and orifice voltages maintained at −3700 and −65 V respectively. The nitrogen gas for nebulization was set at 50 psi, whereas the

nitrogen auxiliary and curtain gases were flow controlled at 2 and 1.8 l/min respectively. Collision-induced dissociation (CID) studies were performed using a collision energy of −30 eV and at a collision gas thickness of 250×1013 molecules/cm² argon.

Results

Radioactivity in urine and faeces

The excretion data after i.v. administration of [^{14}C]celecoxib to dog and monkey are given in tables 1 and 2 respectively. The total recovery of radioactivity in urine and faeces collected 0–168 h after dosing to EM dog, PM dog, cynomolgus monkey and rhesus monkey was 85.3±1.67, 87.3±0.87, 91.4 and >100% respectively. For dog, the majority of the radioactivity was excreted in the faeces (80.0±1.1% for EM; 83.4±0.7% for PM), with < 6% excreted in the urine (5.10±0.77% for EM; 3.47±0.41% for PM). A greater percentage of the radioactivity was excreted in urine of monkey (27.9% for cynomolgus; 24.9% for rhesus) with the remainder of the dose excreted in faeces (63.5% for cynomolgus; 83.1% for rhesus).

Data on the excretion of radioactivity after oral administration of [^{14}C]celecoxib to mouse and rabbit are given in tables 3 and 4 respectively. Total mean (±SEM) percentage of administered radioactivity recovered was 93.5±1.9% for the male mouse (22.4±5.4% in urine; 71.1±3.7% in faeces) and 92.4±1.3% for the female mouse (45.7±0.8% in urine; 46.7±0.7% in faeces). In rabbit, total mean (±SEM) percentage of administered radioactivity recovered was 97.2±0.4%, with 25.0±4.4% excreted in the urine and 72.2±4.6% excreted in the faeces.

Metabolites of celecoxib present in plasma, urine and faeces

Plasma. The plasma metabolite profiles for the rabbit revealed the presence of two metabolic pathways for celecoxib: oxidation of the methyl group or hydroxylation in the phenyl ring of celecoxib to form hydroxymethyl (M3) and hydroxylphenyl (M4) metabolites respectively (figure 1 and 2, and table 5). A carboxylic acid metabolite (M2), formed from further oxidation of M3, as well as its glucuronide (M1) were also in rabbit plasma. The plasma metabolic profiles of [^{14}C]celecoxib differed between the male and female mouse (table 5). In the male mouse, celecoxib was the major circulating radioactive component and only minor amounts of M3 (< 11%) and M2 (< 7%) metabolites were in plasma. In the female mouse, celecoxib represented 54.4% (0.5 h) and 26.6% (8 h) of the radioactive material in plasma. The female mouse had higher circulating levels of M2 and M3 than the male. Following i.v. administration of [^{14}C]celecoxib, M2 was the major circulating radioactive component for both the cynomolgus and rhesus monkey after 15 min (table 6). The plasma metabolic profiles were different between the EM and PM dog. The plasma of the PM dog contained primarily celecoxib with only minor amounts of M3, whereas the plasma of the EM dog contained M1–4 as well as celecoxib. Although, the plasma HPLC profile from the EM dog had radioactivity eluting at a position similar to M4 (hydroxyphenyl metabolite of rabbits), the structure was not confirmed by LC/MS. There was no evidence for phenyl ring hydroxylation in mouse, the PM dog or monkey.

Urine and faeces. Following i.v. administration of radiolabelled celecoxib to dog and monkey, M2 was the major excretion product accounting for 96.2, 71.4, 79.3

Table 1. Excretion of radioactivity in urine and faeces after a single i.v. dose of 5 mg/kg [^{14}C]celecoxib to the EM and PM dog.

	Radioactivity (% of administered dose)			
Collection interval (h)	EM (n = 3)		PM (n = 3)	
	Urine	Faeces	Urine	Faeces
0–24	4.52±0.56	50.0±8.96	2.63±0.33	55.6±5.73
24–48	0.44±0.23	24.6±8.28	0.57±0.15	23.1±4.00
48–72	0.07±0.02	4.31±3.90	0.13±0.01	3.30±1.42
72–96	0.03±0.01	0.97±0.87	0.05±0.00	1.04±0.65
96–120	0.01±0.00	0.08±0.04	0.05±0.01	0.25±0.14
120–144	0.02±0.01	0.07±0.05	0.03±0.01	0.08±0.03
144–168	0.02±0.00	0.02±0.01	0.01±0.00	0.03±0.00
0–168	5.10±0.77	80.0±1.10	3.47±0.41	83.4±0.70
Cage wash	0.21		0.42	
Total	85.3±1.67		87.3±0.87	

EM, extensive metabolizer of celecoxib ; PM, poor metabolizer of celecoxib.

Table 2. Excretion of radioactivity in urine and faeces after a single i.v. dose of 1 mg/kg [^{14}C]celecoxib to cynomologus and rhesus monkey.

	Radioactivity (% of administered dose)			
Collection interval (h)	Cynomolgus monkey (n = 1)		Rhesus monkey (n = 1)	
	Urine	Faeces	Urine	Faeces
0–24	18.9	0.02	21.6	18.5
24–48	8.1	6.4	0.5	56.8
48–72	0	34.2	2.6	7.2
72–96	0.6	13.0	0.1	0.5
96–120	0.1	7.9	0	0.1
120–144	0.1	1.8	0	0
144–168	0.1	0.2	0.1	0
0–168	27.9	63.5	24.9	83.1
Total	91.4		>100	

Table 3. Excretion of radioactivity in urine and faeces after a single oral dose of 35 mg/kg [^{14}C]celecoxib to mouse.

	Radioactivity (% of administered dose)			
Collection interval (h)	Male (n = 3)		Female (n = 3)	
	Urine	Faeces	Urine	Faeces
0–24	19.0±6.8	62.8±4.3	40.2±0.9	42.0±1.1
24–48	1.1±0.3	6.4±3.2	2.7±0.7	3.3±0.5
48–72	0.43±0.17	0.9±0.5	0.9±0.1	0.6±0.2
72–96	0.07±0.01	0.3±0.2	0.2±0.1	0.3±0.2
96–120	0.17±0.04	0.4±0.1	0.2±0.1	0.2±0.1
120–144	0.03±0.01	0.1±0.0	0.05±0.01	0.1±0.04
144–168	0.27±0.06	0.1±0.0	0.4±0.3	0.1±0.05
Cage wash	0.17±0.04		1.04±0.3	
0–168	22.4±5.4	71.1±3.7	45.7±0.8	46.7±0.7
Total	93.5±1.9		92.4±1.3	

Table 4. Excretion of radioactivity in urine and faeces after a single oral dose of 10 mg/kg [^{14}C]celecoxib to female rabbit (n = 3).

Time (h)	Radioactivity (% of administered dose)	
	Urine	Faeces
0–24	19.0±1.5	27.0±10.2
24–48	5.19±3.09	38.2±6.4
48–72	0.46±0.20	6.05±1.20
72–96	0.26±0.09	0.69±0.06
96–120	0.03±0.00	0.17±0.02
120–144	0.01±0.01	0.04±0.01
144–168	0.01±0.00	0.02±0.01
0–168	25.0±4.4	72.2±4.60
Total	97.2±0.4	

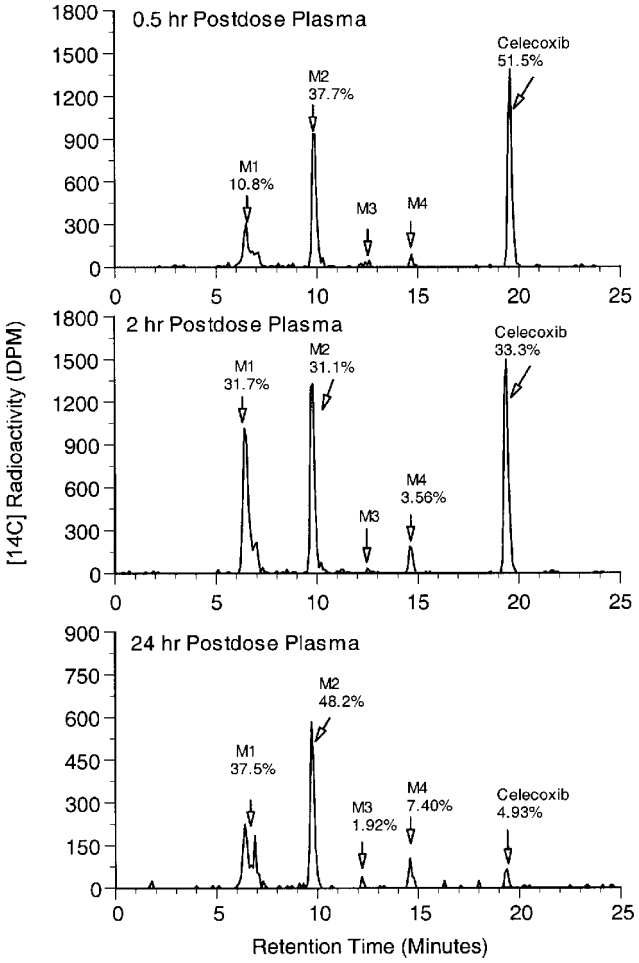


Figure 2. Representative radiochromatogram of an extract of plasma obtained from a female rabbit administered 10 mg/kg [^{14}C]celecoxib.

Table 5. Metabolite profiles in mouse and rabbit plasma after oral administration of [^{14}C]celecoxib.

		Metabolite (%)			
Sampling time (h)	Celecoxib	M1	M2	M3	M4
Female mouse[a]					
0.5	54.4	nd	13.9	30.0	nd
2	33.7	nd	22.0	39.2	nd
4	48.5	nd	17.9	30.4	nd
8	26.6	nd	39.6	26.6	nd
24	na	na	na	na	na
Male mouse[a]					
0.5	87.9	nd	2.32	7.3	nd
2	86.0	nd	1.66	10.4	nd
4	87.6	nd	1.74	8.93	nd
8	84.0	nd	6.48	2.77	nd
24	na	na	na	na	na
Female rabbit[b]					
0.5	51.5	10.8	37.7	nd	nd
2	37.8	33.1	25.4	0.71	2.85
4	na	na	na	na	na
8	28.9	7.40	33.0	nd	9.38
24	4.93	37.5	48.2	1.92	7.40

[a] Values are from pooled samples from $n = 3$ animals.

[b] Values for the 0.5-, 4-, 8- and 24-h samples are from pooled samples from $n = 3$ animals. The value for the 2-h sample represents mean of samples from $n = 3$ animals.

na, Sample was not analyzed due to low levels of radioactivity in mouse plasma at 24 h. A 4-h plasma sample was not collected for rabbit.

nd, no radioactivity detected in peak.

Table 6. Metabolite profiles in plasma after i.v. administration of 1 mg/kg [^{14}C]celecoxib to rhesus and cynomolgus monkey and i.v. administration of 5 mg/kg [^{14}C]celecoxib to EM and PM dog.

		Metabolite (%)			
Sampling time (h)	Celecoxib	M1	M2	M3	M4
Cynomolgus monkey					
0.083	72.6	nd	27.4	0	nd
0.25	34.4	nd	64.0	1.57	nd
0.5	28.6	nd	70.1	1.31	nd
2	34.2	nd	64.8	0.624	nd
3	20.5	nd	79.5	0	nd
4	24.7	nd	75.3	0	nd
6	9.2	nd	90.1	0	nd
Rhesus monkey					
3	36.7	nd	59.1	0	nd
4	30.2	nd	69.8	0	nd
EM dog					
0.5	78.4	2.24[a]	5.30	9.47	0.36[b]
4	50.3	2.36[a]	5.25	27.5	nd
PM dog					
0.5	94.0	nd	nd	1.77	nd
4	93.8	nd	nd	5.78	nd

[a] Metabolite elutes at a similar position to M1.

[b] Metabolite elutes at a similar position to M4.

nd, no radioactivity detected in peak.

Table 7. Percentage of the dose excreted as celecoxib or metabolites following a single i.v. dose given to dog, cynomolgus and rhesus monkey.

Species	Collection interval (h)	Metabolite (%)				
		Celecoxib	M1	M2	M3	M4
% of the Radioactive doses in urine						
Dog (EM)	0–72	nd	0.15[b]	4.6	nd	0.07[a]
Dog (PM)	0–72	nd	0.07[b]	3.0	0.03	0.07[a]
Cynomolgus monkey	0–24	nd	nd	18.7	nd	nd
Rhesus monkey	0–24	nd	nd	21.1	nd	nd
% of the Radioactive dose in faeces						
Dog (EM)	0–72	nd	nd	78.5	1.1	nd
Dog (PM)	0–72	nd	nd	76.3	2.0	nd
Cynomolgus monkey	0–96	nd	nd	52.7	nd	nd
Rhesus monkey	0–48	nd	nd	75.1	nd	nd

EM, extensive metabolizer of celecoxib; PM, poor metabolizer of celecoxib.
[a] Metabolite elutes at a similar position on the radiochromatogram as M4.
[b] Metabolite elutes at a similar position on the radiochroamtogram as M1.
nd, no radioactivity detected in peak.

Table 8. Percentage of the dose excreted as celecoxib or metabolites following oral administration of a single dose to mouse and rabbits.

Species	Collection interval (h)	Metabolite (%)				
		Celecoxib	M1	M2	M3	M4
% of the Radioactive dose in urine						
Mouse (M)	0–48	nd	nd	19.6	nd	nd
Mouse (F)	0–48	nd	nd	42.1	nd	nd
Rabbit	0–48	nd	1.6	21.9	nd	nd
% of the Radioactive dose in faeces						
Mouse (M)	0–48	8.3	nd	58.4	1.2	nd
Mouse (F)	0–48	0.4	nd	42.9	0.7	nd
Rabbit	0–48	0.5	0.1	63.9	nd	nd

nd, no radioactivity detected in peak.

and 83.1% of the dose in urine and faeces of rhesus and cynomolgus monkey, and PM and EM dog respectively (table 7). Minor amounts of M3 (< 2%) and the M1 (< 1%) were excreted in dog faeces. Dog, cynomolgus or rhesus monkey excreted no unchanged drug.

M2 was also a major excretion product of male and female mouse and rabbit, accounting for ~78.0, 85.0 and 85.8% of the dose excreted in the first 48 h respectively (table 8). Minor amounts (~1%) of M3 was excreted in faeces of both the male and female mouse. The female mouse differed from the male regarding the pathway of excretion of celecoxib and its metabolites. In the male, M2 represented 19.6% of the dose excreted in urine and 58.4% of the dose excreted in faeces, whereas in the female, 42.1% of the dose excreted in urine and 42.9% of the dose excreted in faeces was M2. Celecoxib (8.3% of the dose) was excreted unchanged in the faeces of the male, representing either unabsorbed dose or biliary excretion of the unchanged drug. Only 0.4% of the dose was excreted as celecoxib following oral administration to the female.

Structure elucidation of metabolites

The identity of celecoxib and its metabolites was elucidated by MS/MS. Because the rabbit produced all of the metabolites of celecoxib, details of the structure elucidation for only that species are presented. Representative radiochromatograms of plasma and urine samples from a rabbit administered [^{14}C]celecoxib are shown in figures 2 and 3. Ionspray ionization mass spectral data for celecoxib metabolites are shown in table 9.

Celecoxib. The HPLC retention time of the celecoxib peak was identical to that of an authentic celecoxib standard. The deprotonated molecular ion at 380 daltons in its negative-ion mass spectrum was consistent with that of the celecoxib standard. The CID spectrum of the negative-ion at m/z 380 generated a series of product ions identical to those in the CID spectrum of the celecoxib standard.

M1. The HPLC retention time of M1 was identical to that of an authentic standard of the 1-*O*-glucuronide conjugate of M1. The mass spectrum of M1 was identical to the mass spectrum of the synthetic standard of carboxylic acid celecoxib glucuronide (figure 1 and table 9). The HPLC and MS data indicate that M1 consisted of glucuronide conjugates of the carboxylic acid metabolite of celecoxib. The four peaks of glucuronide conjugates of M1 observed in the HPLC profiles of rabbit urine are likely to be positional isomers (Spahn-Langguth and Benet 1992, Sidelmann *et al*. 1996).

M2. M2 had the same HPLC retention time as the authentic standard of the carboxylic acid metabolite of celecoxib. The deprotonated molecular ion of M2 at m/z 410 in its negative-ion mass spectrum, 30 daltons higher than the parent compound celecoxib, suggested that M2 was a carboxylic acid metabolite. The CID spectrum of the negative-ion at m/z 410 generated a series of product ions similar to those in the CID spectrum of the synthetic carboxylic acid celecoxib (figure 1 and table 9). These data indicate that M2 was a carboxylic acid metabolite of celecoxib.

M3. M3 had the same HPLC retention time as the hydroxymethyl celecoxib standard. The deprotonated molecular ion of M3 at m/z 396 in its negative-ion mass spectrum was consistent with that of the synthetic hydroxymethyl metabolite of celecoxib. The CID spectrum of M3 (m/z 396) generated a series of product ions matching those in the CID spectrum of the synthetic hydroxymethyl celecoxib (figure 1 and table 9). These results confirmed that M3 was a monohydroxylated metabolite of celecoxib in which the hydroxylation occurred on the methyl moiety of the 5-(4-methyl)phenyl group.

M4. The HPLC retention time of the M4 peak was $\sim$ 2 min longer than that of M3. The deprotonated molecular ion of M4 at m/z 396 is 16 daltons higher than that of celecoxib, indicating that another monohydroxylated metabolite of celecoxib, different from M3, was formed. The CID spectrum of M4 (m/z 396) produced a series of product ions at m/z 332, 317, 312, 302, 297, 277, 178, 160 and 69, which was also different from the CID spectrum of M3. The sequential losses of 64 (SO_2), 15 (NH), 20 (HF) and 20 (HF) daltons from the m/z 396 produced the product ions at m/z 332, 317, 297 and 277 respectively. The base peak at m/z 302 was formed by a loss of 30 (CH_3) daltons from the m/z 317 ion, suggesting that the hydroxyl group

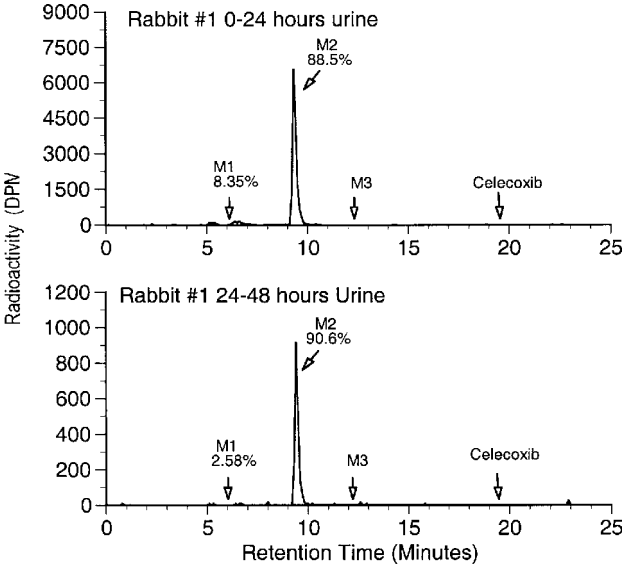


Figure 3. Representative radiochromatogram of urine from a female rabbit administered 10 mg/kg [^{14}C]celecoxib.

Table 9. Ionspray inonization mass spectral data for celecoxib metabolites.

Metabolite	$[M–H]^-$	CID mass spectral data, m/z (%)
M1	586	410 (28), M-H-$C_6H_8O_6$; 366 (60), M-H-$C_6H_80_6$-CO_2; 302 (28), M-H-$C_6H_8O_6$-CO_2-SO_2; 282 (7), M-H-$C_6H_8O_6CO_2$-SO_2-HF; 175 (5), $C_6H_7O_6$; 113 (100), $C_6H_7O_6$-CH_2OHCH_2OH.
M2	410	366 (32), M-H-CO_2; 302 (100), M-H-CO_2-SO_2; 282 (74), M-H-CO_2-SO_2-HF; 262 (98), M-H-CO_2-SO_2-2HF; 233 (52), M-H-CO_2-SO_2-CF_3; 179 (48), M-H-SO_2NH-$OCH_2C_6H_4C$-HF; 159 (26), M-H-SO_2NH-$OCH_2C_6H_4C$-2HF; 69 (82), CF_3.
M3	396	396 (12), M-H 366 (6), M-H-CH_2O; 302 (100), M-H-CH_2O-SO_2; 282 (48), M-H-CH_2O-SO_2-HF; 262 (45), M-H-CH_2O-SO_2-2HF; 233 (25), M-H-CH_2O-SO_2-CF_3; 179 (23), M-H-SO_2NH-$OCH_2C_6H_4C$-HF; 159 (10), M-H-SO_2NH-$OCH_2C_6H_4C$-2HF; 69 (35), CF_3.
M4	396	396 (9), M-H 332 (11), M-H-SO_2; 317 (35), M-H-SO_2-NH; 312 (11), M-H-SO_2-HF; 302 (100), M-H-SO_2-CHOH; 297 (24), M-H-SO_2-CH_3-HF; 277 (8), M-H-SO_2-CH_3-2HF; 178 (15), M-H-SO_2NH-$CH_3C_6H_3OHC$-HF; 160 (10), M-H-SO_2NH-$CH_3C_6H_3OHC$-2F; 69 (23), CF_3.

was at the phenyl moiety of the 5-(4-methyl)phenyl group. The product ion at m/z 69 was related to the CF_3 group. The MS results suggested that M4 was a monohydroxylated metabolite of celecoxib with the hydroxylation occurring on the phenyl moiety of the 5-(4-methyl)phenyl group (figure 1).

Discussion

The metabolism and excretion of celecoxib was investigated following i.v. administration to dog, cynomolgus and rhesus monkey, and after oral administration to mouse and rabbit. Celecoxib was extensively metabolized by all species studied. Only minor species differences in the metabolic pathway for celecoxib were observed. A gender difference in the disposition of celecoxib was observed in mouse. Two phase I oxidative pathways for the metabolism of celecoxib were demonstrated (figure 1). The major phase I pathway that occurred in mouse, rabbit, cynomolgus and rhesus monkey, and dog involved oxidation of the aromatic methyl group of celecoxib to form a hydroxymethyl metabolite (M3). M3 underwent further oxidation to the carboxylic acid metabolite (M2). M2 was produced by all the species studied. Oxidation of the aromatic methyl group of celecoxib was the metabolic pathway for elimination of celecoxib in humans and rat (Paulson *et al*. 2000a, b). A minor phase I pathway was the ring hydroxylation of the methylphenyl group of celecoxib to form M4, which was shown to occur only in rabbit and, possibly, EM dog.

In rabbit, the carboxylic acid metabolite of celecoxib (M2) was conjugated with glucuronic acid to form the *O*-glucuronide conjugate (M1). M1 was only a minor metabolite of celecoxib in the rabbit representing $< 2\%$ of the dose excreted. M1 was also only a minor metabolite in humans accounting for $< 2\%$ of the dose excreted (Paulson *et al*. 2000a). Conjugation of the hydroxy and the carboxylic acid metabolite of celecoxib also occurs in rat. Rat also produced a glucuronide conjugate of the hydroxymethyl metabolite (Paulson *et al*. 2000b).

There are two populations of dogs that have been reported as being PM or EM of celecoxib (Paulson *et al*. 1999). Qualitatively the metabolism of celecoxib was similar between the two populations with the primary metabolic pathway being hydroxylation of the aromatic methyl group. The polymorphism was associated primarily with the formation of M3 catalysed via liver microsomal CYP450. However, interestingly the EM dog contains a metabolite in plasma that elutes at a position similar to M4 (ring-hydroxylation) on a HPLC radiochromatogram that was not observed in plasma of the PM dog. Greater amounts of metabolites were found circulating in the EM dog than in the corresponding PM animal.

A gender difference in the disposition of celecoxib was observed in mouse. Although the metabolic pathway for celecoxib was the same for the male and female, metabolism was slightly more extensive in the female, with 0.4% of the dose excreted as unchanged celecoxib compared with 8.3% excreted as unchanged drug in the male. The male also had higher circulating levels of metabolites than the female.

Monkeys metabolize celecoxib via a single pathway with the formation of M3 and M2. The carboxylic acid metabolite (M2) appears to be the major circulating component of plasma and the major excretion product. However, since only a single cynomolgus monkey and rhesus monkey were studied, there can be no assessment of interanimal variability in this species.

After i.v. dosing to monkey and dog, excretion of the radioactivity was near complete in rhesus monkey and EM and PM dog by 48 h after dose administration. In the cynomolgus monkey, most of the dose was excreted by 5 days after dose administration. Most of the radioactivity was excreted in the faeces, suggesting that for dog and monkey the major route of elimination for celecoxib is metabolism followed by excretion of the metabolites in bile. Radiolabeled celecoxib was administered by oral gavage to mouse and rabbit. Excretion of radioactivity was near complete by 48 h in these species. Higher urinary excretion occurred in female (45.7%) compared with male (22.4%) mouse.

In conclusion, celecoxib was eliminated primarily by a single metabolic pathway, i.e. hydroxylation of the aromatic methyl group of celecoxib and further oxidation of the hydroxylated metabolite to a carboxylic acid metabolite. The major route of elimination of celecoxib was metabolism followed by excretion of the metabolites in the faeces, with the remainder of the metabolites excreted by the kidney.

Acknowledgements

Radiolabeled compounds were synthesized by Scott Harring at the Radiochemistry Department at G. D. Searle.

References

Crofford, L. J., Wilder, R. L., Ristimaki, A. P., Sano, H., Remmers, E. F., Epps, H. R. and Hla, T., 1994, Cyclooxygenase-1 and -2 expression in rheumatoid synovial tissues: effects of interleukin-1β, phorbol ester, and corticosteroids. *Journal Clinical Investigation*, **93**, 1095–1101.

Isakson, P., Zweifel, B., Masferrer, J., Koboldt, C., Seibert,. K, Hubbard, R., Geis, S. and Needleman, P. 1998, Specific COX-2 inhibitors: from bench to bedside. In J. Vane and J. Botting (eds), *Selective COX-2 Inhibitors: Pharmacology, Clinical Effects and Therapeutic Potential* (London: Kluwer and William Harvery), 127–133.

O'Neill, G. P. and Ford-Hutchinson, A. W., 1993, Expression of messenger mRNA for cyclooxygenase-1 and cyclooxygenase-2 in human tissues. *FEBS Letters*, **330**, 156–160.

Paulson, S. K., Engel, L., Reitz, B., Bolten, S., Burton, E. G., Maziasz, T. J., Yan, B. and Schoenhard, G. L., 1999, Evidence for polymorphism in the canine metabolism of the cyclooxygenase 2 inhibitor, celecoxib. *Drug Metabolism Disposition*, **27**, 1133–1142.

Paulson, S. K., Hribar, J. D., Liu, N. W. K., Hajdu, E., Bible, R. H., Piergies, A. and Karim, A., 2000a, Metabolism and excretion of [^{14}C] celecoxib in healthy male volunteers. *Drug Metabolism Disposition*, **28**, 308–314.

Paulson, S. K., Zhang, J., Breau, A. P., Hribar, J. D., Liu, N. W. K., Jessen, S. M., Lawal, Y. M., Cogburn, J. N., Gresk, C. J., Markos, C. S., Schoenhard, G. L. and Burton, E. G., 2000b, Pharmacokinetics, tissue distribution, metabolism and excretion of celecoxib in rats. *Drug Metabolism and Disposition*, **28**, 514–521.

Penning, T. D., Talley, J. J., Bertenshaw, S. R., Carter, J. D., Collins, P. W., Docter, S., Graneto, M. J., Lee, L. F., Malecha, J. W., Miyashiro, J. M., Rogers, R. S., Rogier, D. J., Yu, S. S., Anderson, G. D., Burton, E. G., Cogburn, J. N., Gregory, S. A., Koboldt, C. M., Perkins, W. E., Seibert, K., Veenhuizen, A. W., Zhang, Y. Y. and Isakson, P. C., 1997, Synthesis and biological evaluation of the 1,5-diarylpyrazole class of cyclooxygenase-2 inhibitors: identification of 4-[5-(4-methylphenyl)-3-(trifluoromethyl)-1H-pyrazol-1-yl]bezenesulfonamide (SC-58635, celecoxib). *Journal Medical Chemistry*, **40**, 1347–1365.

Seibert, K., Zhang, Y., Leahy, K., Hauser, S., Masferrer, J., Perkins, W., Lee, L. and Isakson, P. C., 1994, Pharmacological and biochemical demonstration of the role of cyclooxygenase 2 in inflammation and pain. *Proceedings of the National Academy of Sciences, USA*, **91**, 12013–12017.

Sidelmann, U. G., Lenz, E. M., Spraul, M., Hofmann, M., Troke, J., Sanderson, P. N., Lindon, J. C., Wilson, A. D. and Nicholson, J. K., 1996, 750 MHz HPLC-NMR spectroscopic studies on the separation and characterisation of the positional isomers of the glucuronides of 6,11-dihydro-11-oxodibenz[*b*,*e*]oxepin-2-acetic acid. *Analytical Chemistry*, **68**, 106–110.

Simon, L. S., Lanza, F. L., Lipsky, P. E., Hubbard, R. C., Talwalker, S., Schwartz, B. D., Isakson, P. C. and Geis, G. S., 1998, Preliminary study of the safety and efficacy of SC-58635, a novel cyclooxygenase 2 inhibitor, *Arthritis Rheumatology*, **41**, 1591–1602.

Spahn-Langguth, H. and Benet, L., 1992, Acyl glucuronides revisited: Is the glucuronidation process a toxification as well as a detoxification mechanism? *Drug Metabolism Reviews*, **241**, 5–48.

XENOBIOTICA, 2000, VOL. 30, NO. 8, 745–754

Characterization of transgenic mouse strains using six human hepatic cytochrome P450 probe substrates

D. C. MANKOWSKI†‡, M. P. LAWTON† and S. EKINS†*
† Central Research Division, Pfizer, Inc., Groton, CT 06340, USA

Received 2 February 2000

1. Transgenic mice were evaluated with six human cytochrome P450 (CYP) selective probe substrates, as little is known about their metabolism in the mouse. Mouse strains characterized include C57BL/SJL, FVB/N, mdr 1a/1b (−/−), ob/ob and ACCA.

2. Human CYP probe substrates used for characterization of mouse CYP activities included bufuralol, testosterone, dextromethorphan, phenacetin, diclofenac and *S*-mephenytoin. Activities were compared with those obtained in human liver microsomes and in human recombinant enzyme preparations. All transgenic mouse strains showed similar apparent K_m with bufuralol, testosterone and dextromethorphan which compared favourably with those observed in human liver microsomes.

3. K_m for phenacetin *O*-deethylase and *S*-mephenytoin 4′-hydroxylation were more variable across strains and in some cases demonstrated biphasic kinetics. Phenacetin *O*-deethylase activity was low in all mouse strains except FVB/N and mdr 1a/1b (−/−). Diclofenac 4-hydroxylation did not occur to any significant extent in the five strains of mouse evaluated here.

4. The findings suggest the validity of using five of the probes for transgenic mouse hepatic CYP characterization and gross comparison with data generated with human CYP.

Introduction

There are many techniques utilized in the discovery and development of new chemical entities in the pharmaceutical industry. While *in vitro* systems now play a major role in the determination of xenobiotic metabolism (Ekins *et al*. 1999), *in vivo* models, such as the transgenic mouse, are increasingly being evaluated with the hope of predicting human responses *in vivo*. The transgenic mouse is being widely used as surrogate models for disease states such as obesity (Karvonen *et al*. 1990, Roe *et al*. 1999, Watson *et al*. 1999), diabetes mellitus (Knodell *et al*. 1984) and fulminant hepatitis (Chemin *et al*. 1996). The transgenic mouse has also been widely used as a pharmacological tool for the study of growth hormone effects (Cheriathundam *et al*. 1998), drug transport (Schuetz *et al*. 1996, Perloff *et al*. 1999) or drug distribution (Schuetz *et al*. 1998), and the development of immortalized hepatocyte-like cells (Courjault-Gautier *et al*. 1997). Because the extrapolation of drug metabolism data from the transgenic mouse to human depends on a close agreement in the catalytic capabilities of the biotransformation enzymes, it is important to characterize the catalytic properties of drug-metabolizing enzymes in the transgenic mouse.

Unlike the extensive characterization of cytochrome P450 (CYP) activities in human, rat, monkey and dog hepatic tissues (Stevens *et al*. 1993, Sharer *et al*. 1995, Ekins 1996b), metabolism in hepatic subcellular fractions or other *in vitro* systems

* Author for correspondence at: Lilly Research Laboratories, Lilly Corporate Center, Drop Code 0730, Indianapolis, IN 46285, USA; email: ekins_sean@lilly.com
‡ Present address: University of Connecticut Health Center, Farmington, CT 06030, USA.

Xenobiotica ISSN 0049-8254 print/ISSN 1366-5928 online © 2000 Taylor & Francis Ltd
http://www.tandf.co.uk/journals

derived from the wild-type and transgenic mouse have not been extensively characterized (Ekins *et al*. 1999). Studies with mouse P450s have focused on their gender-dependent metabolism (Mugford and Kedderis 1998), which appears to result in larger intra- than interstrain differences, observed with classical CYP substrates (Mugford and Kedderis 1998, *passim*). Even though numerous mouse CYP have been identified (Nelson *et al*. 1996), few studies have evaluated multiple mouse strains for their ability to metabolize a single probe substrate. One of the few exceptions is the use of 12 inbred strains to study the *O*-demethylation and α-hydroxylation of metoprolol, a human CYP2D6 substrate (Adams *et al*. 1991). In contrast, Masubuchi *et al*. (1997) showed that four strains of mouse could not metabolize debrisoquine, another typical human CYP2D6 substrate.

Activities of hepatic CYP have been partially characterized in only a few strains of transgenic mouse. The ob/ob mouse is probably the most extensively studied transgenic mouse in this regard (Rouer and Leroux 1980, Stengard *et al*. 1987, Karvonen *et al*. 1990, Roe *et al*. 1999, Watson *et al*. 1999) as it has been characterized for CYP1A, CYP2B, CYP2E, CYP3A and CYP4A activities. The data obtained for this strain have been variable, especially with regard to CYP2E activity (Roe *et al*. 1999, Watson *et al*. 1999). Recent studies have used precision-cut mouse liver slices and the widely used human CYP probe substrate, testosterone, in an attempt to characterize multiple mouse CYP activities (Ekins 1996a, Ghokale *et al*. 1997). Testosterone 6β-, 7α- and 16α-hydroxylation were comparable for Swiss, nude, B6D2F1 and C57B6 mouse liver slices and it was ultimately representative of multiple CYP (Ekins 1996a).

With the current usage of the transgenic mouse and the previously conflicting metabolic studies for some strains, the objective of the present study was to characterize mouse hepatic CYP activities in several mouse strains. The C57BL/SJL and FVB/N mouse were used as control strains, and the ob/ob, ACCA and mdr 1a/1b (−/−) transgenic mouse was used for comparison. These strains were selected because of their use in projects related to diabetes, obesity, cardiovascular and psychotherapeutic areas of research. Microsomal CYP activities were evaluated using widely accepted human CYP-selective probe substrates for CYP1A2, CYP2C9, CYP2C19, CYP2D6 and CYP3A4/5 as the mouse is known to possess members of all of these major CYP families (Nelson *et al*. 1996). Additionally, intestinal microsomes were prepared from the mdr 1a/1b (−/−) and FVB/N mouse and CYP2D activity was assessed using bufuralol. The present study illustrates the overall differences between probes and strains compared with their kinetic characteristics in human liver microsomes and recombinant CYP.

Materials and methods

Materials

Diclofenac, dextromethorphan, dextrorphan, testosterone, 6β-hydroxytestosterone, 11β-hydroxytestosterone, phenacetin, 3-acetomidophenol and 4-acetomidophenol were from Sigma Chemical Co. (St Louis, MO, USA). Bufuralol, 1′-hydroxy bufuralol, 4′-hydroxy diclofenac, 4′-hydroxymephenytoin and *S*-mephenytoin were from Gentest (Woburn, MA, USA). The C57BL/SJL and ob/ob mouse were from Jackson Laboratories (Bar Harbor, ME, USA). The mdr 1a/1b (−/−) and FVB/N mouse were from Taconic Farms (Germantown, NY, USA). The ACCA mouse (triple transgenic containing human apolipoproteins A1 and C1 and cholesterol ester transfer protein) were bred at the Pfizer transgenic facility (Groton, CT, USA). The ACCA and ob/ob mouse were derived from the C57 strain; mdr 1a/1b (−/−) was derived from FVB/N. Recombinant human cytochrome P450 enzymes were prepared at Pfizer (Christopherson *et al*. 1995) or from Panvera (Madison, WI, USA).

Table 1. Protein and cytochrome P450 content of mouse microsomal preparations.

Mouse strain	Tissue	Total cytochrome P450 content (nmol/mg)†
C57BL/SJL	liver	0·47
ACCA	liver	0·24
ob/ob	liver	0·44
FVB/N	liver	0·36
FVB/N	intestine	n.d.‡
mdr 1a/1b (−/−)	liver	0·60
mdr 1a/1b (−/−)	intestine	n.d.

Protein concentrations and total cytochrome P450 were determined as described in the Materials and methods.

† n.d., Not determined.

‡ Date are an average of duplicate determinations from pooled livers or intestines (n = 3–10).

Human liver microsomal preparation

Human liver samples were from the International Institute for the Advancement of Medicine (Exton, PA, USA), and microsomes were generated according to Guengerich *et al*. (1977). Protein concentrations were determined using a BCA Protein Assay kit (Pierce Chemical Co. Rockford, IL, USA). Cytochrome P450 content was determined according to Omura and Sato (1964).

Mouse microsomal preparation

Microsomes were prepared from pooled livers or intestines (n = 3–10) using 100 mM potassium phosphate buffer, pH 7.4, with 0.25 M sucrose and 0.1 mM EDTA (Guengerich *et al*. 1977). In addition, heparin (3 U/ml) and trypsin inhibitor (5 mg/ml) were added to buffers for mouse intestinal microsome preparation (Rosenberg and Mankowski 1994). Protein concentrations and cytochrome P450 content were determined as described above. The following substrate probes were used to characterize mouse CYP under conditions linear for time and protein.

Phenacetin O-deethylation

Incubations containing mouse liver microsomes (0.2–0.8 mg/ml) were carried out with an NADPH-regenerating system (10 mM $MgCl_2$, 0.44 mM $NADP^+$, 5 mM DL-isocitric acid, 0.5 U/ml isocitric dehydrogenase) in 100 mM phosphate buffer, pH 7.4, after a 2-min pre-incubation at 37 °C in a final volume of 0.5 ml. Phenacetin (0.5–500 μM) was incubated for 30 min and terminated by addition of 5 ml ethylacetate and 20 μl internal standard (37 μg/ml 3-acetamidophenol in methanol). The vials were then vortexed for 2 min, then centrifuged at 3000 *g* for 3 min. The top layer was transferred to fresh tubes (3 ml) and allowed to dry under a gentle stream of nitrogen. The residues were reconstituted in 150 μl mobile phase A' (82/10/8 water/methanol/acetonitrile), and 25 μl was injected onto HPLC and analysed as follows. 4-Acetaminophenol (metabolite) was separated from phenacetin using a Beckman Ultrasphere ODS column (5 μm; 4.6 × 250 mm) with a mobile phase A consisting of water/methanol/acetonitrile (82/10/8 v/v) and mobile phase B consisting of methanol/acetonitrile/water (86/5/9 v/v) using a gradient of 100–50% A from 0 to 20 min (B 0–50% from 0 to 20 min), increasing to 100% A from 21 to 30 min at 1 ml/min. Metabolite formation was monitored by UV detection at 254 nm using a SpectroMonitor variable wavelength detector (LDC Analytical, Riviera Beach, FL, USA), and the Multichrom data acquisition system (Version 2.11, Fisons Instruments, Beverly, MA, USA) was used for data collection, analysis, and reporting.

Diclofenac 4′-hydroxylation

Incubations containing mouse liver microsomes (0.2–0.8 mg/ml) were carried out as described above using diclofenac (0.5–500 μM) for 30 min using a modification of the method of Leeman *et al*. (1993). Briefly, 0.5-ml incubations were quenched with 150 μl cold acetonitrile, centrifuged at 11 000 *g*, and 25 μl supernatant was injected onto HPLC. 4′-Hydroxydiclofenac was separated from diclofenac using a Waters Novapak C18 column (4 μm; 3.9 × 150 mm), using a mobile phase of 75/25 v/v 50 mM potassium

phosphate buffer/acetonitrile with 0.02% triethylamine. Flow rate was 2 ml/min; and the metabolite was detected with UV detection at 282 nm. 4′-Hydroxydiclofenac was quantitated by comparison with a standard curve with known concentrations of metabolite.

S-mephenytoin 4′-hydroxylation

Incubations containing mouse liver microsomes (0.2–0.8 mg/ml) were carried out as described using a modification of the method of Meier *et al*. (1985). *S*-mephenytoin (10–500 μM) was incubated for 60 min (0.5-ml reaction volume) and terminated by addition of 5 ml methylene chloride. Internal standard (100 μl 25 μM phenobarbital) was added, then tubes were vortexed and centrifuged at 3000 *g* for 3 min. The organic layer was dried under nitrogen, and residues were reconstituted in 150 μl mobile phase consisting of 20 mM sodium perchlorate (pH 2.5)/methanol/acetonitrile (69/25/6 v/v). The HPLC system consisted of a Supelcosil LC-18 column (15 × 4.6 mm) using a flow rate of 1.5 ml/min. 4′-Hydroxymephenytoin was quantitated using UV detection at 204 nm.

Bufuralol 1′-hydroxylation

Incubations containing mouse liver or intestinal microsomes were carried out as described above with bufuralol (0.2–50 μM) by using the method of Mankowski (1999).

Dextromethorphan O-demethylation

Incubations containing mouse liver microsomes were carried out as described above using dextromethorphan (0.5–50 μM) (Leeman *et al*. 1994). Briefly, 0.5-ml incubations were quenched with 50 μl 70% perchloric acid after a 20-min incubation. Dextromethorphan and its 3′-hydroxy metabolite (dextrorphan) were resolved on a Supelcosil LC 18 (3 μm; 4.6 × 5 cm) column with a mobile phase of 60% acetonitrile/40% 10 mM potassium phosphate, pH 3.0, with 0.02% triethylamine added, at 1 ml/min. Dextrorphan was monitored by fluorescence detection at an excitation wavelength of 280 nm and an emission wavelength of 310 nm. Metabolite levels were quantified by comparison with standard concentrations of authentic dextrorphan (1 μg/ml; n = 3).

Testosterone 6β hydroxylation

Testosterone (5–250 μM) was incubated with 0.2–0.8 mg/ml mouse liver or intestinal microsomes using the modification of Sonderfan *et al*. (1987). Briefly, 1-ml reactions were quenched with 5 ml methylene chloride and 100 μl 11β-hydroxytestosterone (internal standard) after a 20-min incubation. Reactions were processed as previously described, then organic residues were reconstituted in 150 μl mobile phase 10 mM potassium phosphate, pH 3.0/methanol (50/50 v/v). HPLC analysis consisted of a Supelcosil LC 18 column (5 × 4.6 mm; 3 μm) at 1 ml/min. UV detection was at 244 nm.

Human liver and recombinant microsomal incubation

Human liver microsomes and recombinant CYP were incubated with the substrate probes as described above (Mankowski *et al*. 1996).

Kinetic analysis

Substrate saturation data were plotted on Eadie–Hofstee plots to check for the linearity or non-linearity of the data. Data were then plotted on substrate saturation curves and fitted to the Michaelis–Menten equation using Deltagraph (Version 4.0, Monterey, CA, USA) to yield apparent K_m and V_{max} (Mankowski 1999).

Results

Characterization of mouse hepatic CYP

The total P450 contents of hepatic microsomes from the transgenic and wild-type mouse were comparable, ranging from 0.24 to 0.6 nmol/mg protein (table 1). When testosterone 6β-hydroxylation was used as a CYP probe for putative mouse

Table 2. Comparison of kinetic parameters for human CYP isoform-selective probe substrates in the transgenic male mouse liver microsomes.

Probe substrate	Mouse strain				
	C57BL/SJL	ACCA	ob/ob	mdr 1a/1b(−/−)	FVB/N
Testosterone					
$K_{m(apparent)}$ (μM)	137	154	115	183	159
V_{max}(nmol/min/nmol P450)	3.7	11	3.8	7.0	13.5
Bufuralol					
$K_{m(apparent)}$ (μM)	2.6	0.9	1.0	4.7	3.9
V_{max}(nmol/min/nmol P450)	2.2	5.4	1.4	2.1	2.0
Dextromethorphan					
$K_{m(apparent)}$ (μM)	6.2	2.6	3.3	4.0	4.4
V_{max}(nmol/min/nmol P450)	1.9	3.9	1.4	1.2	4.2
Phenacetin					
$K_{m(apparent)}$ (μM)	4.0	3.0	10, 40†	15	5
V_{max}(nmol/min/nmol P450)	0.6	0.7	0.6	2.3	2.2
Diclofenac					
$K_{m(apparent)}$ (μM)	n.d.‡	n.d.	n.d.	n.d.	n.d.
V_{max}(nmol/min/nmol P450)					
S-mephenytoin					
$K_{m(apparent)}$ (μM)	103	158	31, 159†	71	34, 195†
V_{max}(nmol/min/nmol P450)	0.09	0.72	0.06	0.15	0.23

Enzyme kinetic parameters were determined for metabolite formation by microsomes prepared from mouse livers as described in the Materials and methods. Data are an average of duplicate determinations.

† Two apparent K_m observed.

‡ nd, Not detectable.

CYP3A enzymes, $K_{m(apparent)}$ demonstrated little variability (range 115–183 μM) between the transgenic and wild-type mouse (table 2). V_{max} was more variable, ranging from 3.7 nmol/min/nmol P450 for C57BL/SJL to 13.5 nmol/min/nmol P450 for FVB/N. Bufuralol hydroxylation was the CYP2D probe with a $K_{m(apparent)}$ from 0.88 to 4.7 μM and V_{max} from 1.45 to 5.4 nmol/min/nmol P450. Dextromethorphan, a second probe used for CYP2D activities, produced a more consistent $K_{m(apparent)}$ and V_{max} for *O*-demethylation, from 2.6 to 6.2 μM and 1.16 to 4.2 nmol/min/nmol P450 respectively. Phenacetin was the probe for CYP1A activity and its *O*-deethylation illustrated variability between mouse strains with ob/ob and mdr 1a/1b (−/−) having a higher $K_{m(apparent)}$ than the respective controls. The ob/ob mouse hepatic microsomal phenacetin *O*-deethylase activity also appeared to have a high- and low-affinity component (table 2). Phenacetin *O*-deethylase activity was low in all mouse strains except in FVB/N and mdr 1a/1b (−/−). A substrate probe used for CYP2C activity, diclofenac, did not display detectable hydroxylation in any mouse strain. A second CYP2C probe, *S*-mephenytoin, displayed variable $K_{m(apparent)}$ across all strains. In addition, the ob/ob and FVB/N mouse generated biphasic kinetics for hydroxylation of this substrate (table 2).

Characterization of mouse intestinal CYP

Microsomes were prepared from the mdr 1a/1b(−/−) and FVB/N mouse intestines with much lower protein content than in the liver (table 1). Following characterization with bufuralol, the resulting kinetic parameters were similar across

Table 3. Comparison of kinetic parameters for human CYP isoform-selective probe substrates in human liver microsomes and recombinant CYPs.

Probe substrate	Human liver microsomes	Human recombinant CYP
Testosterone (CYP3A4)		
$K_{m(apparent)}$ (μM)	65	60
V_{max}(nmol/min/nmol P450)	66	59
Bufuralol (CYP2D6)		
$K_{m(apparent)}$ (μM)	5.4	3.4
V_{max}(nmol/min/nmol P450)	0.06	128
Dextromethorphan (CYP2D6)		
$K_{m(apparent)}$ (μM)	4.2	0.7
V_{max}(nmol/min/nmol P450)	1.1	36
Phenacetin (CYP1A2)		
$K_{m(apparent)}$ (μM)	30	47
V_{max}(nmol/min/nmol P450)	2.4	43
Diclofenac (CYP2C9)		
$K_{m(apparent)}$ (μM)	10	8
V_{max}(nmol/min/nmol P450)	17.5	55
S-mephenytoin (CYP2C19)		
$K_{m(apparent)}$ (μM)	40	32
V_{max}(nmol/min/nmol P450)	0.5	11

Enzyme kinetic parameters were determined for metabolite formation by microsomes prepared from human liver or baculovirus-expressed human recombinant CYPs as described in the Materials and methods. Data are an average of duplicate determinations.

† μM.

‡ nmol/min/nmol P450.

these two strains with $K_{m(apparent)}$ and V_{max} of 0.4 μM and 0.25 nmol/min/mg protein (mdr 1a/1b(−/−)) and 0.8 μM and 0.30 nmol/min/mg protein (FVB/N). Incubations with up to 250 μM testosterone with these microsomes produced no significant metabolism to any testosterone metabolite (data not shown).

Characterization of human microsomal and recombinant CYP

Human liver microsomes and recombinant CYP generated enzyme kinetic parameters with the widely used substrate probes previously used for characterization of different mouse strains. $K_{m(apparent)}$ for *S*-mephenytoin hydroxylation, diclofenac hydroxylation, phenacetin *O*-deethylation and bufuralol hydroxylation were comparable between human liver microsomes and recombinant CYP (table 3). $K_{m(apparent)}$ for dextromethorphan and testosterone was lower in recombinant CYP2D6 and CYP3A4 respectively (table 3) than in human liver microsomes.

Discussion

The use of *in vitro* techniques has increased in the past few decades as the pharmaceutical industry now uses more rapid metabolism screens to tackle compound failure earlier (Ekins *et al*. 1999). However, *in vivo* models still maintain a major role in drug metabolism and toxicology studies. The use of transgenic mouse

models has also increased to the point where many early pharmacology tests of efficacy occur in a mouse model of the disease under study. Perhaps the most widely studied transgenic mouse strains from the point of view of drug-metabolizing enzymes are ob/ob and db/db (Rouer and Leroux 1980, Stengard *et al*. 1987, Karvonen *et al*. 1990, Roe *et al*. 1999, Watson *et al*. 1999). More recently, the mdr 1a (−/−) mouse has become a useful tool in understanding drug transport mediated by P-glycoprotein (Schuetz *et al*. 1998) as well as in defining its relationship with CYP3A4 (Schuetz *et al*. 1996). Despite the increased use of the humanized' transgenic mouse, however, a thorough understanding of mouse CYP has lagged behind that of other species such as rat, dog, monkey and human (Stevens *et al*. 1993, Sharer *et al*. 1995).

Many of the early studies describing CYP in select transgenic and wild-type mouse strains used substrate probes that have since been identified as being metabolized by multiple CYP in other species. More recently, substrate probes known to be more selective for specific human CYP isoforms have characterized mouse strains. Examples include chlorzoxazone 6-hydroxylation (mediated by human CYP2E1; Watson *et al*. 1999), testosterone 6β-hydroxylation (CYP3A4; Watson *et al*. 1999), debrisoquine 4-hydroxylation (CYP2D6, Masubuchi *et al*. 1997), midazolam 1′- and 4′-hydroxylation, triazolam 1′- and 4′-hydroxylation and dexamethasone metabolism (CYP3A4; Perloff *et al*. 1999).

In the present study six CYP probe substrates were used (table 2 and 3) and they were previously identified as being useful for the determination of the catalytic activity of specific human CYP. As the mouse is known to contain members of CYP1A, CYP2C, CYP2D and CYP3A families (Nelson *et al*. 1996), we used testosterone 6β-hydroxylation mediated by CYP3A4 (Sonderfan *et al*. 1987), bufuralol 1′-hydroxylation (Kronbach *et al*. 1987) and dextromethorphan *O*-demethylation (Jacqz-Aigrain *et al*. 1993) mediated by CYP2D6, phenacetin *O*-deethylation mediated by CYP1A2 (Sesardic *et al*. 1988), diclofenac 4′-hydroxylation catalysed by CYP2C9 (Leeman *et al*. 1993) and *S*-mephenytoin 4′-hydroxylation catalysed by CYP2C19 in human (Wrighton *et al*. 1993). Overall, the mouse liver microsome $K_{m(apparent)}$ obtained using these human CYP probe substrates compared favourably with those obtained with human liver microsomes and recombinant CYP known to mediate the metabolism (tables 2 and 3). V_{max} showed some variability not only across mouse strains, but also when compared with human liver microsomes and recombinant CYP. In the case of recombinant CYP, the level of enzyme expression compared with human liver microsomes could explain this difference. In addition, human liver microsomal and human recombinant CYP kinetic parameters for the human CYP substrate probes corresponded with data generated by many other groups (reviewed in Pelkonen *et al*. 1998). Thus, it would appear that in general these human CYP selective probes can be used as gross markers of CYP activity related to human CYP in the five mouse strains assessed here.

One probe substrate for which there was a significant difference between human and mouse was diclofenac, which was not metabolized by liver microsomes from any of the five mouse strains. This finding is similar to that reported earlier with the CYP2D6 probe substrate debrisoquine, which was not metabolized by liver microsomes from four different mouse strains (Masubuchi *et al*. 1997) and would suggest catalytic differences for some CYP substrates between these species. Experiments are currently underway to screen several other human CYP2C9

substrates in these five mouse strains. Another difference between human and mouse liver was the biphasic kinetics observed with some CYP and mouse strains. Examples of this include phenacetin with ob/ob mouse and *S*-mephenytoin with ob/ob and FVB/N mouse (table 2), suggestive of multiple CYP involved in metabolism of these probes. In general, in these cases the high-affinity $K_{m(apparent)}$ is similar to that observed with human liver microsomes. Detailed enzymatic characterization of recombinant mouse CYP and a more complete understanding of isoform-specific expression in the mouse will be required unambiguously to explain the few differences among the catalytic properties of human and mouse liver microsomes.

Intestinal microsomes from the mdr 1a/1b (−/−) and FVB/N mouse were characterized because of the possible influence of a lack of mdr expression on CYP3A activity (Schuetz *et al*. 1996). Although previous studies have utilized human (Lown *et al*. 1994, Prueksaritanont *et al*. 1996, Zhang *et al*. 1999), rat (Stohs *et al*. 1976) or dog intestinal microsomes (Prueksaritanont *et al*. 1996), and characterized various CYP activities with standard human probes, there has been little study of mouse intestinal CYP using these same substrates. Intestinal microsomes from the mdr 1a/1b(−/−) and FVB/N mouse also showed that bufuralol 1′-hydroxylation illustrates a much power $K_{m(apparent)}$ than that observed in the mouse liver, human liver and recombinant CYP (table 2 and 3). This could be explained by a high-affinity bufuralol-metabolizing CYP expressed in the intestines of these two mouse strains but not in the liver. In fact, evidence for multiple bufuralol-metabolizing enzymes in the human has been shown (Mankowski 1999). Another unexpected finding was the lack of testosterone metabolism in these intestinal microsome preparations. This could be due to differing affinities of the mouse intestinal CYP towards testosterone compared with the liver. Additional experiments are needed completely to characterize mouse intestinal CYP activity with other human probe substrates.

The similarity in catalytic properties of CYP expressed in the transgenic or wild-type mouse liver microsomes and human liver microsomes suggests that the former species could be a good surrogate for the latter. This would also indicate an economic advantage to using wild-type mouse for pharmacokinetic and metabolism studies while using the expensive transgenic mouse for pharmacological testing. Of course, future studies will be required unequivocally to identify the mouse CYP involved in metabolism of each human CYP probe described here. This will necessitate use of numerous antibodies and inhibitor probes some of which continue to be used even though they present specificity issues across human CYP (Ekins *et al*. 1997) as well as across species. Experiments with the mouse strains used here are underway to test human CYP isoform-selective inhibitors with these CYP probe substrates. This information will be used to determine if the mouse may be a good surrogate for CYP inhibition studies usually performed with human liver microsomes or with recombinant CYP. The ultimate aim is that these characterization studies will provide confidence in the use of these mouse strains for ADME studies. Preliminary studies have shown that liver microsomes derived from the ACCA mouse are useful for generating clearance predictions for four proprietary compounds primarily metabolized by CYP3A4 and/or CYP2D6 (unpublished data). The future characterization of other metabolizing enzymes, particularly phase II systems, will be necessary to provide confidence in the use of the mouse as a potential surrogate for human metabolism studies *in vitro*.

Acknowledgements

The authors gratefully acknowledge Dr Shelby Anderson and Victor Soliman for communicating their data on proprietary compounds, and Drs R. Scott Obach and Robert Polzer for valuable discussions and a review of the manuscript.

References

Adams, M., Lennard, M. S., Otton, S. V., Tucker, G. T. and Woods, H. F., 1991, Assessment of the mouse as an experimental model for studying polymorphic oxidation of the sparteine/debrisoquine type. *Biochemical Pharmacology*, **42**, 947–949.

Chemin, I., Takahashi, S., Belloc, C., Lang, M. A., Ando, K., Guidotti, L. G., Chizari, F. V. and Wild, C. P., 1996, Differential induction of carcinogen metabolizing enzymes in a transgenic mouse model of fulminant hepatitis. *Hepatology*, **24**, 649–656.

Cheriathundam, E., Doi, S. Q., Knapp, J. R., Jasser, M. Z., Kopchick, J. J. and Alvares, A. P., 1998, Consequences of overexpression of growth hormone in transgenic mice on liver cytochrome P450 enzymes. *Biochemical Pharmacology*, **55**, 1481–1487.

Christopherson, P. A., Mankowski, D. C., Tweedie, D. J. and Lawton, M. P., 1995, Expression of human cytochromes P450 in insect cells. *ISSX* Proceedings, **8**, 358.

Courjault-Gautier, F., Antoine, B., Bens, M., Vallet, V., Cluzeaud, F., Pringault, E., Kahn, A., Toutain, H. and Vandewalle, A., 1997, Activity and inducibility of drug-metabolizing enzymes in immortalized hepatocyte-like cells (mhPKT) derived from a L-PK/Tag1 transgenic mouse. *Experimental Cell Research*, **234**, 362–372.

Ekins, S., 1996a, Maintenance and cryopreservation of xenobiotic metabolism in precision-cut liver slices. Evaluation of an alternative *in vitro* model to isolated hepatocytes. PhD thesis, University of Aberdeen.

Ekins, S., 1996b, Past, present, and future applications of precision-cut liver slices for *in vitro* xenobiotic metabolism. *Drug Metabolism Reviews*, **28**, 591–624.

Ekins, S., Mäenpää, J. and Wrighton, S. A., 1999, *In vitro* metabolism: subcellular fractions. In T. F. Wolff (ed.), *Handbook of Drug Metabolism* (New York: Marcel Dekker), pp. 363–399.

Ekins, S., VandenBranden, M., Ring, B. J. and Wrighton, S. A., 1997, Examination of purported probes of human CYP2B6. *Pharmacogenetics*, **7**, 165–179.

Ghokale, M. S., Bunton, T. E., Zurlo, J. and Yager, J. D., 1997, Cytochrome P450 isozyme activities in cultured rat and mouse liver slices. *Xenobiotica*, **27**, 341–355.

Guengerich, F. P., 1977, Separation and purification of multiple forms of cytochrome P450. *Journal of Biological Chemistry*, **252**, 3970–3979.

Jacqz-Aigrain, E., Funck-Brentano, C. and Cresteil, T., 1993, CYP2D6- and CYP3A-dependent metabolism of dextromethorphan in humans. *Pharmacogenetics*, **3**, 197–204.

Karvonen, I., Sormunen, R., Huupponen, R. and Sotaniemi, E. A., 1990, Reduced glucose-6-phosphorylase and NADPH generating enzyme activities associated with glibenclamide induced hypoglycemia and hypoinsulinemia in genetically obese mice. *Biomedicine and Pharmacotherapy*, **44**, 307–316.

Knodell, R. G., Handwerger, B. S., Morley, J. E., Levine, A. S. and Brown, D. M., 1984, Separate influences of insulin and hyperglycemia on hepatic drug metabolism in mice with genetic and chemically induced diabetes mellitus. *Journal of Pharmacology and Experimental Therapeutics*, **230**, 256–262.

Leeman, T., Bonnabry, P. and Dayer, P., 1994, Selective inhibition of major drug-metabolizing cytochrome P450 isoenzymes in human liver microsomes by carbon monoxide. *Life Sciences*, **54**, 951–956.

Leeman, T., Transon, C. and Dayer, P., 1993, Cytochrome P450TB (CYP2C): a major monoxygenase catalyzing diclofenac 4′-hydroxylation in human liver. *Life Sciences*, **52**, 29–34.

Lown, K. S., Kolars, J. C., Thummel, K. E., Barnett, J. L., Kunze, K. L., Wrighton, S. A. and Watkins, P. B., 1994, Interpatient heterogeneity in expression of CYP3A4 and CYP3A5 in small bowel. *Drug Metabolism and Disposition*, **22**, 947–955.

Mankowski, D. C., 1999, The role of CYP2C19 in the metabolism of (+/−) bufuralol, the prototypic substrate of CYP2D6. *Drug Metabolism and Disposition*, **27**, 1024–1028.

Mankowski, D. C., Elsenboss, L., Christopherson, P., Lawton, M. P. and Tweedie, D. J., 1996, Characterization of baculovirus-expressed human cytochromes P450. Paper presented at the 11th International Symposium on Microsomes and Drug Oxidations, 21–24 July, University of California, Los Angeles.

Masubuchi, Y., Iwasa, T., Hosokawa, S., Suzuki, T., Horie, T., Imaoka, S., Funae, Y. and Narimatsu, S., 1997, Selective deficiency of debrisoquine 4-hydroxylase activity in mouse liver microsomes. *Journal of Pharmacology and Experimental Therapeutics*, **282**, 1435–1441.

Meier, U. T., Kronbach, T. and Meyer, U. A., 1985, Assay of mephenytoin metabolism in human liver microsomes by high-performance liquid chromatography. *Annals of Biochemistry*, **151**, 286–291.

Mugford, C. A. and Kedderis, G. L., 1998, Sex-dependent metabolism of xenobiotics. *Drug Metabolism Reviews*, **30**, 441–498.

Nelson, D. R., Koymans, L., Kamataki, T., Stegeman, J. J., Feyereizen, R., Waxman, D. J., Waterman, M. R., Gotoh, O., Coon, M. J., Estabrook, R. W., Gunsalus, I. C. and Nebert, D. W., 1996, P450 superfamily: update on new sequences, gene mapping, accession numbers and nomenclature. *Pharmacogenetics*, **6**, 1–42.

Omura, T. and Sato, R., 1964, The carbon monoxide-binding pigment of human liver microsomes. I. Evidence for its hemoprotein nature. *Journal of Biological Chemistry*, **239**, 2370–2378.

Pelkonen, O., Mäenpää, J., Taavitsainen, P., Rautio, A. and Raunio, H., 1998, Inhibition and induction of human cytochrome P450 (CYP) enzymes. *Xenobiotica*, **28**, 1203–1253.

Perloff, M. D., von Moltke, L. L., Cotreau, M. M. and Greenblatt, D. J., 1999, Unchanged cytochrome P450 3A (CYP3A) expression and metabolism of midazolam, triazolam, and dexamethasone in mdr (−/−) mouse liver microsomes. *Biochemical Pharmacology*, **57**, 1227–1232.

Prueksaritanont, T., Gorham, L. M., Hochman, J. H., Tran, L. O. and Vyas, K. P., 1996, Comparative studies of drug-metabolizing enzymes in dog, monkey and human small intestines, and in Caco-2 cells. *Drug Metabolism and Disposition*, **24**, 634–642.

Roe, A. L., Howard, G., Blouin, R. and Snawder, J. E., 1999, Characterization of cytochrome P450 and glutathione *S*-transferase activity and expression in male and female ob/ob mice. *International Journal of Obesity*, **23**, 48–53.

Rosenberg, D. W. and Mankowski, D. C., 1994, Induction of cyp2e1 protein in mouse colon. *Carcinogenesis*, **15**, 73–78.

Schuetz, E. G., Schinkel, A. H., Relling, M. V., Schuetz, J. D., 1996, P-glycoprotein: a major determinant of rifampicin-inducible expression of cytochrome P4503A in mice and humans. *Proceedings of the National Academy of Sciences, USA*, **93**, 4001–4005.

Schuetz, E. G., Yasuda, K., Arimori, K. and Schuetz, J. D., 1998, Human MDR1 and mouse mdr1a P-glycoprotein alter the cellular retention and disposition of erythromycin, but not of retinoic acid or benzo(a)pyrene. *Archives of Biochemistry and Biophysics*, **350**, 340–347.

Sesardic, D., Boobis, A. R., Edwards, R. J. and Davies, D. S., 1988, A form of cytochrome P450 in man orthologous to form d in the rat, catalyses the *O*-deethylation of phenacetin and is inducible by cigarette smoking. *British Journal of Clinical Pharmacology*, **26**, 363–372.

Sharer, J. E., Shipley, L. A., VandenBranden, M., Binkley, S. N. and Wrighton, S. A., 1995, Comparisons of phase I and Phase II *in vitro* hepatic enzyme activities of human, dog rhesus monkey and cynomolgus monkey. *Drug Metabolism and Disposition*, **23**, 1231–1241.

Sonderfan, A. J., Arlotto, M. P., Dutton, D. R., McMillen, S. K. and Parkinson, A., 1987, Regulation of testosterone hydroxylation by rat liver microsomal cytochrome P450. *Archives of Biochemistry and Biophysics*, **255**, 27–41.

Stengard, J. H., Saarni, H. U., Karvonen, R. I., Lahtela, J. T., Karki, N. T., Stenback, F. and Sotaniemi, E. A., 1987, Hepatic drug metabolism and the activities of NADPH generating enzymes and glucose-6-phosphatase in phenobarbital treated genetically obese (ob/ob) mice. *Biomedical Pharmacotherapy*, **41**, 389–396.

Stevens, J. C., Shipley, L. A., Cashman J. R., VandenBranden, M. and Wrighton, S. A., 1993, Comparison of human and rhesus monkey *in vitro* phase I and II hepatic drug metabolism activities. *Drug Metabolism and Disposition*, **21**, 753–760.

Stohs, S. J., Grafson, R. C., Burke, M. D., Moldeus, P. W. and Orrenius, S. G., 1976, The isolation of rat intestinal microsomes with stable cytochrome P-450 and their metabolism of benzo(a)pyrene. *Archives of Biochemistry and Biophysics*, **177**, 105–116.

Watson, A. M., Poloyac, S. M., Howard, G. and Blouin, R. A., 1999, Effect of leptin on cytochrome P-450, conjugation, and antioxidant enzymes in the ob/ob mouse. *Drug Metabolism and Disposition*, **27**, 695–700.

Wrighton, S. A., Stevens, J. C., Becker, G. W. and VandenBranden, M., 1993, Isolation and characterization of human liver cytochrome P4502C19: Correlation between 2C19 and *S*-mephenytoin 4′-hydroxylation. *Archives of Biochemistry and Biophysics*, **306**, 240–245.

Zhang, Q.-Y., Dunbar, D., Ostrowska, A., Zeisloft, S., Yang, J. and Kaminsky, L. S., 1999, Characterization of human small intestinal cytochromes P450. *Drug Metabolism and Disposition*, **27**, 804–809.

XENOBIOTICA, 2000, VOL. 30, NO. 8, 755–769

Purification and characterization of oxidoreductases-catalyzing carbonyl reduction of the tobacco-specific nitrosamine 4-methylnitrosamino-1-(3-pyridyl)-1-butanone (NNK) in human liver cytosol

A. ATALLA†, U. BREYER-PFAFF‡ and E. MASER†*

†Department of Pharmacology and Toxicology, School of Medicine, Philipps-University of Marburg, D-35033 Marburg, Germany
‡Department of Toxicology, University of Tübingen, D-72074 Tübingen, Germany

Received 25 February 2000

1. Four enzymes were purified to homogeneity from human liver cytosol and were demonstrated to be responsible for carbonyl reduction of the tobacco-specific nitrosamine 4-methylnitrosamino-1-(3-pyridyl)-1-butanone (NNK).

2. Carbonyl reductase (EC 1.1.1.184), a member of the short-chain dehydrogenase/reductase (SDR) superfamily, was compared with three isoenzymes of the aldo-keto reductase (AKR) superfamily in terms of enzyme kinetics, co-substrate dependence and inhibition pattern.

3. AKR1C1, 1C2 and 1C4, previously designated as dihydrodiol dehydrogenases (DD1, DD2 and DD4), showed lower K_m (0.2, 0.3 and 0.8 mM respectively) than did carbonyl reductase (7 mM), whereas carbonyl reductase exhibited the highest enzyme efficiency (V_{max}/K_m) for NNK. Multiplication of enzyme efficiencies with the relative quantities of individual enzymes in cytosol resulted in a rough estimate of their contributions to total alcohol metabolite formation. These were ~ 60% for carbonyl reductase, 20% each for AKR1C1 and 1C2, and 1% for AKR1C4.

4. Except for AKR1C4, the enzymes had a strong preference for NADPH over NADH, and the highest activities were measured with an NADPH-regenerating system. Carbonyl reductase activity was extensively inhibited by menadione, rutin and quercitrin, whereas medroxyprogesterone acetate, phenolphthalein and flufenamic acid were potent inhibitors of AKR1C1, 1C2 and 1C4.

5. In conclusion, cytosolic members of the SDR and AKR superfamilies contribute to reductive NNK detoxification in human liver, the enzymes responsible being carbonyl reductase and aldoketo reductases of the AKR1C subfamily.

Introduction

The tobacco-specific nitrosamine 4-methylnitrosamino-1-(3-pyridyl)-1-butanone (NNK) is among the most abundant carcinogens in tobacco and tobacco smoke (Hecht and Hoffmann 1988, Fischer *et al*. 1990). Its carcinogenic potency in mouse, rat and hamster and its specificity for the lung has strongly implicated NNK as an important etiological factor in the causation of lung cancer in human smokers (Hecht and Hoffmann 1988, 1989).

NNK is a procarcinogen that requires metabolic activation by cytochrome P450 (CYP) enzymes to express its mutagenic and carcinogenic properties (Hecht and Hoffmann 1988, Crespi *et al*. 1991). This activation involves the α-hydroxylation of the two carbons bound to the *N*-nitroso group leading to the formation of reactive electrophilic species that methylate and pyridyloxobutylate purine bases of DNA (Murphy *et al*. 1990b). The pathway competing with NNK activation is

* Author for correspondence; e-mail: maser@mailer.uni-marburg.de

Xenobiotica ISSN 0049-8254 print/ISSN 1366-5928 online © 2000 Taylor & Francis Ltd
http://www.tandf.co.uk/journals

NNK carbonyl reduction. Like NNK, the resulting *N*-nitroso alcohol 4-(methylnitrosamino)-1-(3-pyridyl)-1-butanol (NNAL) has also been proposed to be carcinogenic in animals (Hecht 1994). Nevertheless, carbonyl reduction of NNK is important since it initiates the detoxification of NNK by providing the hydroxy butyl function necessary for glucuronosylation and final excretion (Hecht 1994). Pyridine *N*-oxidation of NNAL and NNK is also considered as a detoxification reaction, since NNK *N*-oxides are only one-tenth as carcinogenic as NNK, and metabolic studies in laboratory animals failed to demonstrate substantial amounts of metabolic activation products of these compounds (Castonguay *et al*. 1983a, Hecht 1994, 1996). However, NNAL *N*-oxide and NNK *N*-oxide are relatively minor NNK metabolites in the urine of smokers and smokeless tobacco users (Carmella *et al*. 1997), such that detoxification of NNK occurs mainly by carbonyl reduction and glucuronosylation in humans (Carmella *et al*. 1997, 1995, 1993, Hecht *et al*. 1993a).

The extent of the competing pathways α-hydroxylation versus carbonyl reduction of NNK that occur in different species and tissues may depend on the composition of enzymes present in the tissues and may be related to the organospecificity of and individual susceptibility to NNK-induced cancerogenesis. Therefore, to understand human susceptibility to NNK, it is important to identify the enzymes that catalyze the activation and detoxification reactions.

Several studies have addressed the question of which CYP enzymes mediate the activation of NNK. In human, strong evidence indicates involvement of CYP1A2, 2A6 and 3A4 in NNK activation (reviewed in Hecht 1994, 1998, Smith *et al*. 1997). However, it was estimated that 39–100% of the NNK dose was excreted as NNAL and NNAL-glucuronide in smoker's urine (Carmella *et al*. 1993). Although carbonyl reduction constitutes the major pathway of NNK metabolism *in vivo* and several tissues *in vitro* (reviewed in Maser 1998, 1997), research on the enzymes catalyzing this reaction has largely been neglected (Hecht *et al*. 1980).

Two major groups of enzymes can catalyze the reduction of xenobiotic ketones in mammals (Wermuth 1985, Flynn and Green 1993, Maser 1995). One constitutes the family of short-chain dehydrogenases/reductases (SDR), which comprises membrane-bound as well as soluble enzymes (Jörnvall *et al*. 1995). A member of this family, 11β-hydroxysteroid dehydrogenase 1 (11β-HSD 1; EC 1.1.1.146), was identified as a microsomal NNK reductase in mouse liver and lung (Maser 1998, Maser *et al*. 1996). A cytosolic SDR enzyme designated carbonyl reductase (CR; EC 1.1.1.184) occurs in all human tissues investigated (Wermuth 1985) and it can reduce a broad spectrum of ketones and quinones (Wermuth 1985, Wermuth 1981). On purification, it is separated into three forms (CR I–III) that differ in their *p*I, but which exhibit very similar enzymatic properties (Wermuth 1981, Inazu *et al*. 1992). Recently, NNK carbonyl reduction has been demonstrated in cytosol from mouse liver and lung (Atalla and Maser 1999) as well as human liver and lung (Maser *et al*. 2000). Experiments with various inhibitors pointed to the participation of CR in this reaction.

For the second superfamily of carbonyl-reducing enzymes, the aldoketo reductases (AKR), a systematic nomenclature has been proposed on the basis of amino acid sequence identities (Jez *et al*. 1997). The members of the various families and subfamilies bear no structural similarities to the SDR proteins in spite of overlapping substrate specificities (Flynn and Green 1993, Maser 1995). Human AKR capable of reducing xenobiotic ketones are primarily found in the AKR1C subfamily. They use NADPH as a co-substrate as does CR, but in contrast to the

latter they can catalyse efficiently the oxidation of aliphatic alcohols and diols in the presence of $NADP^+$. This reaction has led to their designation as dihydrodiol dehydrogenases (DD) (Vogel *et al*. 1980, Hara *et al*. 1990). Fractionation of human liver cytosol led to the purification of AKR1C1 (DD1 of Hara *et al*. 1990) with activity towards 20α-hydroxysteroids, AKR1C2 (DD2 of Hara *et al*. 1990), previously characterized as a bile-acid-binding protein (Stolz *et al*. 1993) and AKR1C4 (DD4 of Hara *et al*. 1990) that had been described as human liver chlordecone reductase (Molowa *et al*. 1986) and was later obtained in three molecular forms as 3α-hydroxysteroid dehydrogenase (Takikawa *et al*. 1990). The AKR have molecular masses of ~ 37 kDa (Hara *et al*. 1996a), whereas those of the SDR are ~ 30 kDa (Wermuth *et al*. 1988).

A procedure for the parallel purification of the three CR isoforms and of AKR1C1, 1C2 and 1C4 from human liver has been developed (Breyer-Pfaff and Nill 2000). In the present investigation, this procedure was used to obtain a complete survey of all cytosolic enzymes participating in NNAL formation in human liver by measuring the NNK reductase activity in each purification step. Human liver was selected for our studies, since, in contrast to other tissues, all possible cytosolic NNK carbonyl-reducing enzymes could be expected in this organ. Moreover, NNK is known to distribute throughout the entire body with the liver being the major site of NNK detoxification. According to our results, NNK was a substrate for CR as well as for aldoketo reductases, but the kinetic parameters varied widely among enzymes.

Some of the results have been presented in abstract form (Atalla *et al*. 1999).

Materials and methods

Materials

Human liver samples (female 25 years of age, female 54, male 70) were obtained from Professor Dr W. Lauchart, Department of Surgery, University of Tübingen, Germany. These were either samples from livers excluded from transplantation for medical reasons or excess normal tissue obtained on partial hepatectomy for tumour metastases. Pieces (5–10 g) were stored at −80 °C for up to 7 years, which did not affect specific enzyme activities towards standard substrates (4-benzoylpyridine and (*S*)-(+)-1-indanol).

Human recombinant CR was generously provided by Professor Dr B. Wermuth, Inselspital, Bern, Switzerland (Bohren *et al*. 1994).

Chemicals

NNK (⩾ 99% purity) was from Campro Scientific (Emmerich, Germany); NNAL was a gift from D. Hoffmann (American Health Foundation, Valhalla, NY, USA). Pyridine nucleotide co-substrates and glucose 6-phosphate dehydrogenase were from Boehringer (Mannheim, Germany), Sephadex G-100, Q Sepharose, CM Sepharose, DEAE Sepharose, Polybuffer Exchanger PBE 94, and the Polybuffers 74 and 96 from Pharmacia (Freiburg, Germany), hydroxyapatite Bio-Gel HTP from Bio-Rad (Munich, Germany), Reactive Red 120 Agarose, (*S*)-(+)- and (*R*)-(−)-1-indanol, medroxyprogesterone acetate, flufenamic acid, quercitrin, rutin, dexamethasone, phenolphthalein and the molecular weight standard Dalton Mark VII-L for protein electrophoresis from Sigma-Aldrich (Deisenhofen, Germany), 4-benzoylpyridine and menadione from Merck (Darmstadt, Germany), a 50-ml ultrafiltration chamber and filters YM10 from Amicon (Witten, Germany), the carrier ampholytes Servalyt 6–9 and 9–11 from Serva (Heidelberg, Germany), and Resolyte 3.5–10 and 6–9.5 from Merck.

Enzyme isolation

The preparation of liver cytosol and its fractionation by gel filtration, ion exchange, hydroxy apatite and affinity chromatography followed by chromatofocusing were largely carried out by a modification (Breyer-Pfaff and Nill 2000) of a procedure of Hara *et al*. (1990) (figures 1 and 2). Fractions were tested for AKR activity by measuring the NADPH production as reflected by an increase of absorbance at 339 nm on incubation with 0.5 mM (*S*)-(+)-1-indanol. CR activity was followed by the decrease of

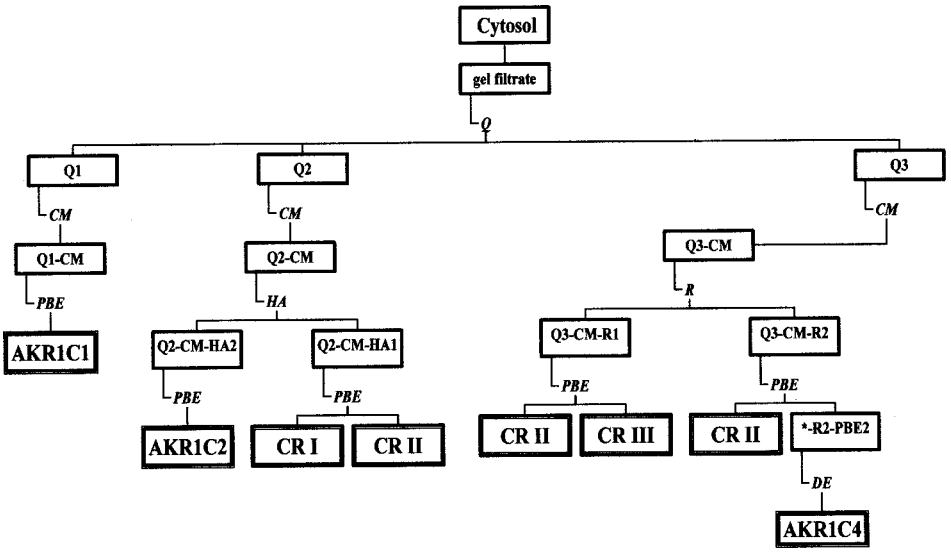


Figure 1. Purification scheme of the aldoketo reductases AKR1C1, 1C2 and 1C4, and the isoforms I–III of CR. For details, see the Materials and methods. Q, Q Sepharose; CM, CM Sepharose; HA, Bio-Gel HTP; R, Reactive Red 120 Agarose; PBE, polybuffer exchanger; DE, DEAE Sepharose; *, Q3-CM; AKR, aldoketo reductase; CR, carbonyl reductase.

NADPH absorbance at 339 nm with 1 mM 4-benzoylpyridine (Breyer-Pfaff and Nill 2000). Minor modifications were introduced in the present investigation (figure 1, table 1). Thus, the Q3 fraction resulting from Q Sepharose fractionation of the gel filtrate was applied to 10 ml CM Sepharose in 10 mM sodium phosphate pH 6.5 and the fraction not adsorbed (Q3-CM) was applied to 3 ml Reactive Red 120 Agarose. After 17 h at 4 °C, a first fraction with enzymatic activity (Q3-CM-R1) could be eluted with 10 mM Tris-HCl, pH 7.5, in 20% glycerol, whereas a second fraction (Q3-CM-R2) was obtained after adding 2.5 M NaCl to the eluent. On chromatofocusing on PBE 94 of these two fractions by the procedure of Breyer-Pfaff and Nill (2000), the first one was separated into CR II and III (eluted at pH 7.1 and 6.9 respectively), and the second one into CR II and several partially overlapping fractions displaying (*S*)-1-indanol oxidase activity. Of these, only the first one (Q3-CM-R2-PBE2, eluted at pH 6.3) served for purification by DEAE Sepharose chromatography to obtain pure AKR1C4 (Breyer-Pfaff and Nill 2000).

Enzyme identification

Except for CR III, the enzymes were homogeneous on SDS-gel electrophoresis (Laemmli 1970) with apparent molecular masses of 36 kDa for the aldoketo reductases and 32–33 kDa for the CR (figure 3). In isoelectric focussing, *p*I was 8.0 for AKR1C1, 7.25 for AKR1C2 and 6.3 for AKR1C4 in accordance with Hara *et al.* (1996b). Two more acidic isoforms of AKR1C4 were eluted from PBE 94 with decreasing pH of the polybuffer (Breyer-Pfaff and Nill 2000), but these were not obtained in pure form. CR I and II purified to homogeneity had *p*I = 7.8 and 7.3 in accordance with Wermuth (1981), while CR III with a *p*I = 6.7 showed an admixture on electrophoresis.

The identities of the enzymes were further confirmed by partial amino acid sequence analysis (4base lab, Reutlingen, Germany). Sequences of tryptic fragments were identical with published sequences for AKR1C2 (amino acids 305–318; Hara *et al.* 1996b), for CR I from a Q2 fraction and CR II from a Q3 fraction (amino acids 113–119; Wermuth *et al.* 1988). In addition, specific activities towards standard substrates and results of inhibition experiments were in accordance with published data (Breyer-Pfaff and Nill 2000).

Assay of NNK carbonyl reduction

The assay was performed by incubating 20 μl enzyme preparation (corresponding to 1–5 μg protein) and 100 μl of an NADPH-regenerating system (final concentrations: $NADP^+$, 0.2 mM; glucose 6-phosphate, 2 mM; glucose 6-phosphate dehydrogenase, 1 U/ml; $MgCl_2$, 8 mM) in 100 mM sodium phosphate buffer, pH 7.4, at 37 °C. The reaction was started by adding 10 μl NNK to final concentrations ranging from 0.5 to 8 mM (CR) or 0.05 to 4 mM (AKR) in a total volume of 400 μl. The reaction was stopped after 30 min by denaturating the protein for 3 min at 100 °C before cooling on ice. The samples were centrifuged in an Eppendorf centrifuge at 8000*g* for 5 min to sediment organic material, and 200 μl supernatant served for HPLC analysis.

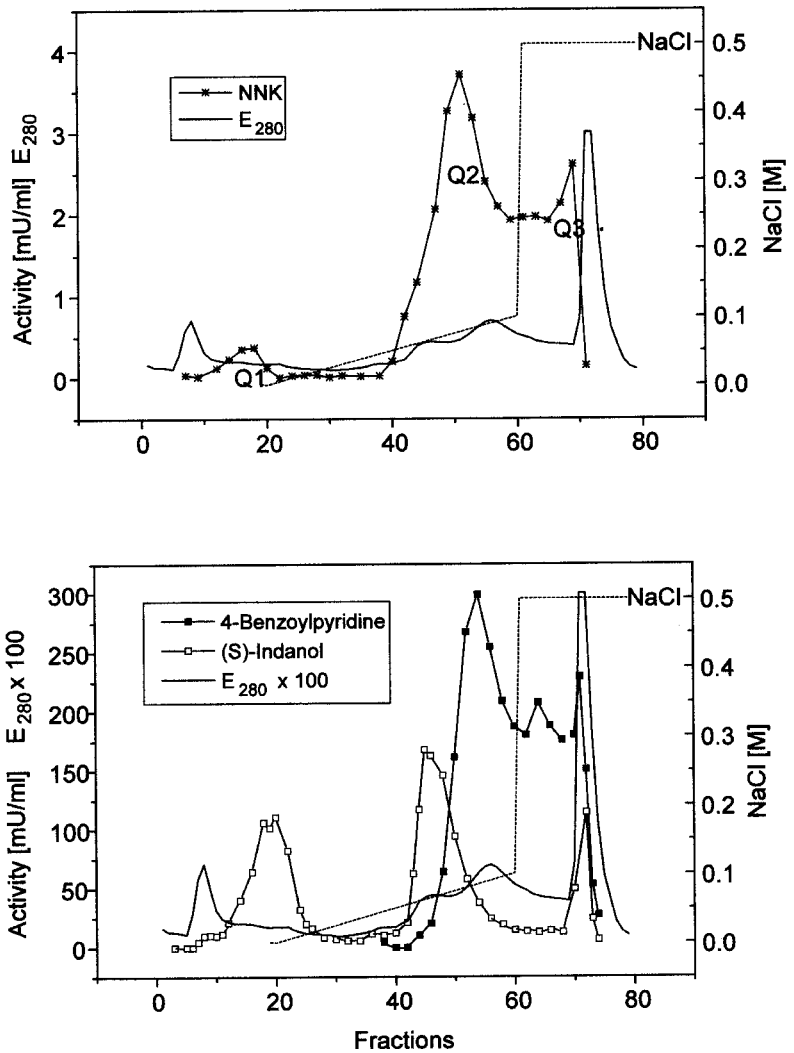


Figure 2. Elution patterns from Q Sepharose. (upper) Total proteins (UV, E_{280}) and reductase activity towards NNK (*); (lower) 4-benzoylpyridine reductase (■) and (*S*)-indanol oxidase (□) activities. Fractions combined were 12–26 (Q1), 43–62 (Q2) and 63–73 (Q3).

For determining the co-substrate dependency, 0.5 mM NADH or NADPH instead of the NADPH-regenerating system were employed. The pH dependence of NNK carbonyl reduction was tested between pH 4.5 and 11.5 by using a universal buffer containing acetic acid, MES, KH_2PO_4, Tris and glycine in a concentration of 30 mM each.

Control experiments with heat-inactivated enzyme fractions were performed to determine non-enzymatic substrate conversion.

Metabolite determination by HPLC

NNK and its reduced alcohol metabolite NNAL were detected on a reverse-phase HPLC system (Merck Hitachi L-6220 Intelligent Pump, Merck Hitachi AS-2000 A Autosampler, Merck Hitachi L-4000 A UV Detector), using a 4.6 mm x 25 cm LiChrosphere 100 RP18 column (Merck, Germany) and a Shimadzu C-R6A Chromatopac integrator. With an eluent of 25% acetonitrile (v/v) in 10 mM sodium phosphate buffer, pH 7.4, at a flow rate of 0.5 ml/min, NNK elutes at ~ 11.0 min and NNAL at 6.8 min. Substances were monitored at 230 nm. The identity of NNK and NNAL was determined by injecting authentic standards. Concentrations of NNK and NNAL were calculated from peak areas of samples and standards used for calibration curves.

Table 1. NNK carbonyl reductase activities and protein quantities of AKR1C1, AKR1C2, AKR1C4 and CR isoforms during the purification procedure.

Fraction or enzyme	Protein (mg)	Activity (mU)	Specific activity (mU NNAL/mg)
Cytosol	810	785	1.0
Gel filtrate	113	650	5.8
Q1	6.0	16	2.6
Q1-CM	2.6	8.8	3.4
AKR1C1	**0.6**	**6**	**10**
Q2	31	294	9.5
Q2-CM	9.2	124	14
Q2-CM-HA1	1.3	81	62
CR I	**0.16**	**29**	**180**
CR II	**0.15**	**23**	**160**
Q2-CM-HA2	3.7	28	7.8
AKR1C2	**1.7**	**19**	**11**
Q3	45	162	3.6
Q3-CM	26	124	4.7
Q3-CM-R1	14	53	3.8
CR II	**0.05**	**10**	**200**
CR III	**0.18**	**12**	**66**
Q3-CM-R2	3.5	72	20
CR II	**0.14**	**21**	**150**
Q3-CM-R2-PBE2	0.27	0.65	2.4
AKR1C4	**0.15**	**0.45**	**3.0**

Values of purified enzyme preparations are shown in **bold**.

Activities were determined using 0.5 mM NNK and an NADPH-regenerating system.

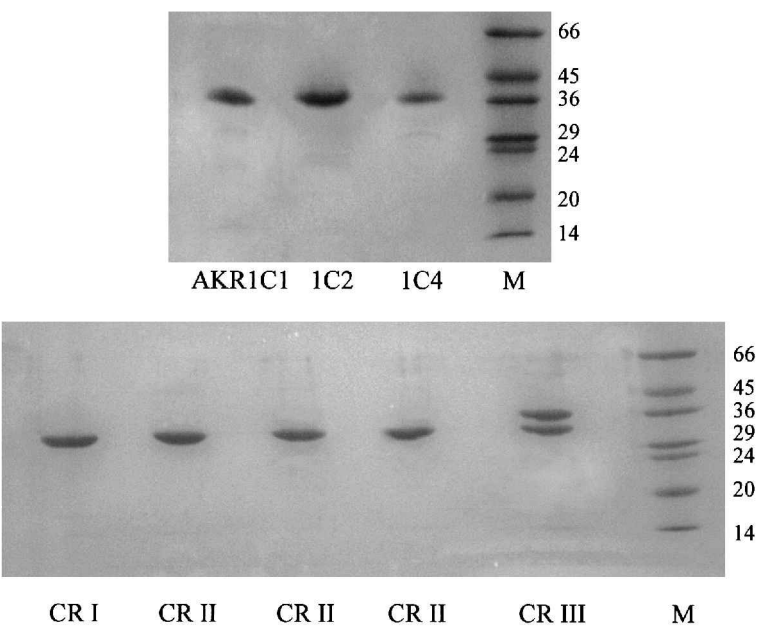


Figure 3. SDS-PAGE demonstrating the homogeneity of purified enzymes. (upper) Lanes 1, AKR1C1; 2, AKR1C2; 3, AKR1C4; M, molecular mass standard; (lower) lanes 1, CR I; 2, CR II from Q2; 3, CR II from Q3-CM-R1; 4, CR II from Q3-CM-R2; 5, CR III; M, molecular mass standard. Protein (3–6 μg) was applied per lane.

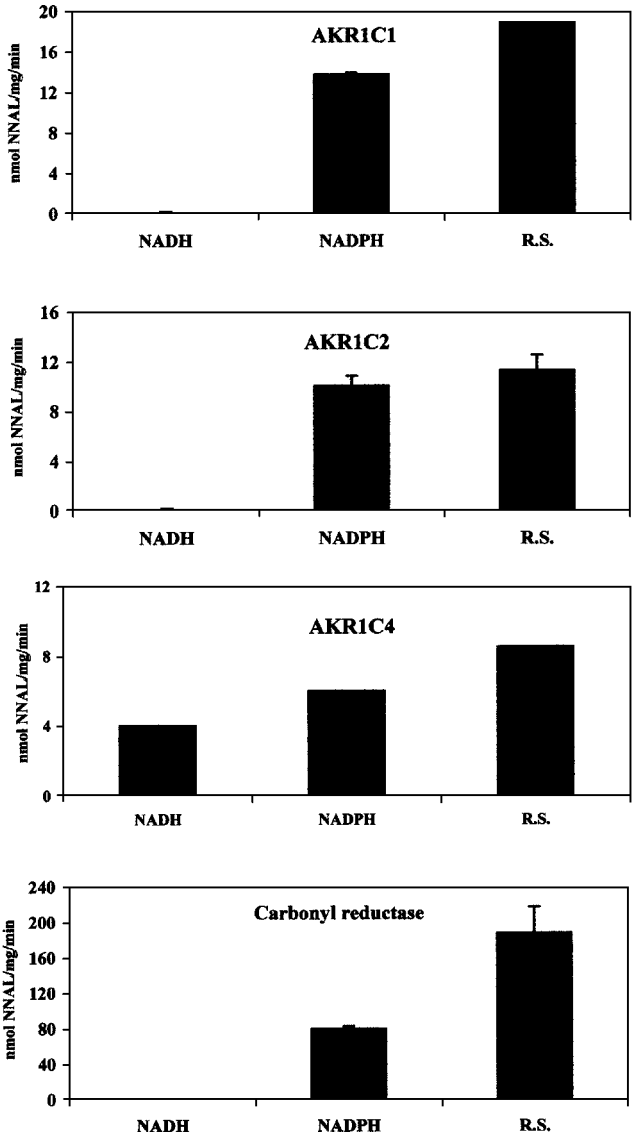


Figure 4. Co-substrate dependency of purified NNK carbonyl reducing enzymes. Enzyme activities were assayed in a reaction mixture containing 0.5 mM NNK and either 0.5 mM NADH, 0.5 mM NADPH or an NADPH-regenerating system (RS). Values represent the specific activity (nmol/mg/min) and are the means ± SD of three-to-four determinations (for AKR1C4: $n = 2$). Upper panel, AKR1C1; second panel, AKR1C2; third panel, AKR1C4; lower panel, CR I.

Inhibitor studies

Stock solutions of the inhibitors were added to the incubation mixtures. Inhibitors not sufficiently soluble in buffer were dissolved either in methanol or 0.03 M NaOH. Control velocities were determined in the presence of appropriate quantities of the solvents. After a pre-incubation of 5 min, the reaction was started by adding NNK.

Protein determination

Protein concentration was determined by the method of Bradford (1976) using bovine serum albumin as standard.

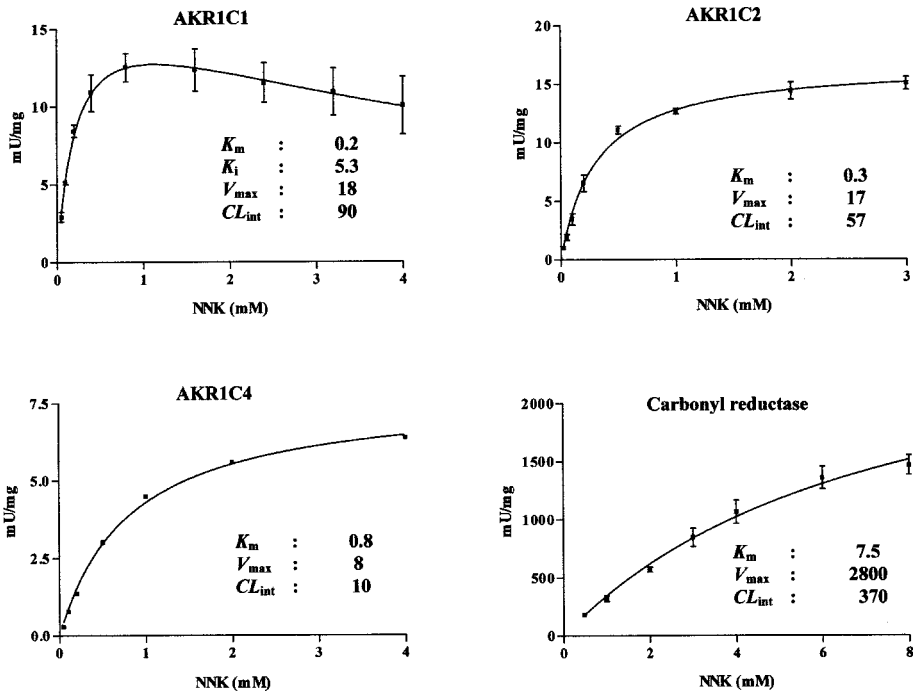


Figure 5. Kinetics of NNAL formation from NNK by purified enzymes. Values are means ± SD of three-to-four individual preparations. K_m (mM), V_{max} (mU/mg), Cl_{int} (μl/mg/min).

Kinetic parameter estimations

Time and enzyme protein concentrations were chosen so that reaction velocities were time linear, which was true at least for 1 h. Kinetic parameters were calculated according to the Michaelis–Menten equation by using GraphPad Inplot kinetic computer software. In cases of substrate inhibition, a formula for non-competitive inhibition was used. Enzyme efficiency (Cl_{int}) was calculated as V_{max}/K_m provided that maximal substrate concentrations exceeded K_m at least two-fold. Otherwise, Cl_{int} was derived from the ratios of reaction rate/substrate concentration at concentrations far below K_m. Specific activities are expressed as mU/mg (nmol NNAL/mg/min).

Results

Purification of NNK carbonyl reducing enzymes

The fractionation scheme is outlined in figure 1. The initial separation on Q Sepharose resulted in three enzymatically active fractions demonstrating that several soluble enzymes participate in NNK reduction to NNAL in human liver cytosol (figure 2). NNK carbonyl reducing activity was detected in all fractions exhibiting aldoketo reductase (AKR) and/or CR activities with standard substrates as shown, for example, in figure 2. During subsequent purification, specific activities increased (table 1) in parallel to those towards (*S*)-(+)-1-indanol on purification of AKR1C1, 1C2 and 1C4 and to those towards 4-benzoylpyridine on purification of the CR isoforms. The apparent homogeneity of the individual enzymes in gel electrophoresis is shown in figure 3. An exception is CR III which, in addition to the expected protein with a molecular mass of 32–33 kDa, obviously showed an admixture of an autocatalytically modified form of CR (Wermuth, personal communication). No NNK reduction was observed in fractions devoid of

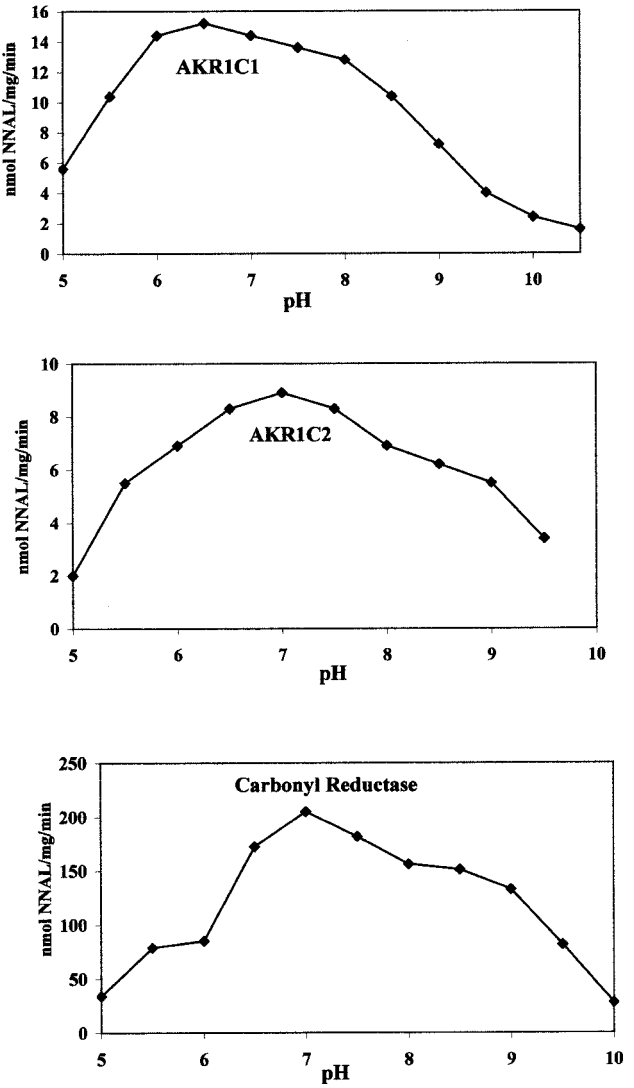


Figure 6. pH dependency of NNK carbonyl reductase activities of AKR1C1, AKR1C2 and carbonyl reductase (CR I). Activities were determined with 0.5 mM NNK as the substrate and an NADPH-regenerating system as co-substrate. Data points are the average of three determinations.

activity towards standard substrates. Determinations of kinetic parameters, pH dependence and inhibitor sensitivities were carried out with CR I.

Cosubstrate requirement of purified NNK reductases

Very little NNK reduction took place on incubating pure enzymes with NADH as the electron donor, except for AKR1C4, which produced considerable quantities of NNAL with NADH. Overall, NADPH was the preferred co-substrate, and highest reaction rates were obtained with an NADPH-regenerating system (figure 4), probably because $NADP^+$ produced during the incubation with NADPH alone can act as an inhibitor. All further experiments were carried out using the NADPH-regenerating system.

Table 2. Effect of inhibitors on carbonyl reduction mediated by AKR1C1, AKR1C2, AKR1C4 and CR I.

Enzyme	Inhibitor	Concentration (μM)	Inhibition (%)
AKR1C1	phenolphthalein	5	73
	medroxyprogesterone acetate	2	48
	flufenamic acid	10	51
	ethanol	5%	70
AKR1C2	phenolphthalein	1	26
	medroxyprogesterone acetate	2	60
	flufenamic acid	10	66
	ethanol	5%	42
AKR1C4	phenolphthalein	10	71
	medroxyprogesterone acetate	10	72
	dexamethasone	50	75
	ethanol	5%	27
Carbonyl reductase	menadione	100	81
	rutin	100	63
	quercitrin	100	43
	ethanol	5%	30

Activities were determined using 1 mM NNK and an NADPH-regenerating system. Values represent the mean of two or three determinations. Deviations were $< 9\%$.

Absolute (uninhibited) values were: AKR1C1 = 12, AKR1C2 = 9·6, AKR1C4 = 6·5 and carbonyl reductase = 285 nmol NNAL/mg/min.

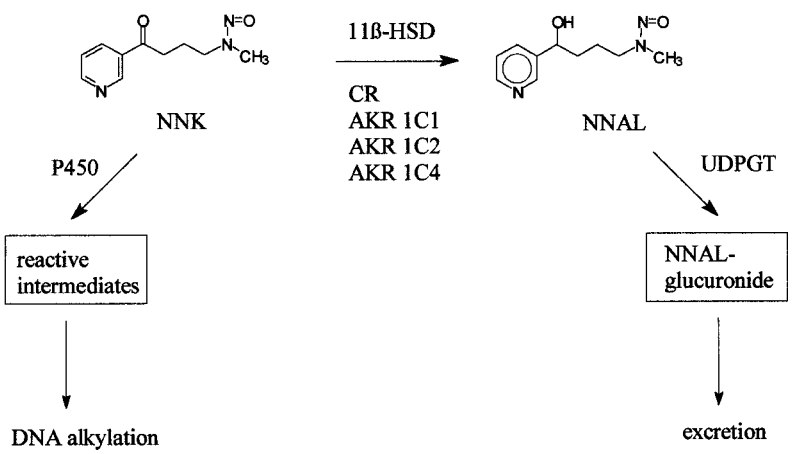


Figure 7. Metabolic pathways of NNK. UDPGT, uridine diphosphate glucuronosyl transferase.

Kinetics of purified NNK reductases

Substrate concentration dependencies of the enzymes with respect to NNAL production from NNK and kinetic parameters are given in figure 5. Low K_m and V_{max} were obtained with the AKR, whereas with CR saturation of NNAL formation was not apparent such that the kinetic parameters have to be regarded as estimates. Slight substrate inhibition occurred with AKR1C1 at NNK concentrations > 1 mM (figure 5). Carbonyl reduction efficiencies reflected by enzyme efficiencies (Cl_{int}) were highest with CR (370 μl/mg/min) compared with those of the AKR. When Cl_{int} for CR was calculated from the reaction rate/substrate concentration ratio at NNK concentrations of 0.5 or 1 mM, 450μl/mg/min was obtained. Interestingly, 400 μl/mg/min resulted from incubations of NNK with human recombinant CR by following a similar approach (data not shown).

pH-dependence of purified enzymes

AKR1C1 showed a broad optimum of NNK reduction rates at pH ~ 6–7 and AKR1C2 at pH ~ 6.5–7.5 (figure 6). Pure AKR1C4 was not available in quantities sufficient for studying pH dependence. CR exhibited an optimum at pH ~ 7.

Inhibition of purified enzymes

Selected substances were employed to inhibit the isolated NNK carbonyl reducing enzymes (table 2). NNK carbonyl reduction by AKR was potently inhibited by medroxyprogesterone acetate, phenolphthalein and flufenamic acid. In addition, dexamethasone potently inhibited AKR1C4. The formation of NNAL by CR was decreased most extensively by the competing substrate menadione, followed by the specific inhibitors rutin and quercitrin. Ethanol considerably affected all cytosolic NNK carbonyl reducing enzymes at a concentration of 5%, with AKR1C1 exhibiting a residual activity of 30%.

Discussion

Carbonyl-reducing enzymes are generally regarded as part of the metabolic systems protecting against toxic actions of endogenous and exogenous compounds. For instance, CR was the main quinone reductase in human liver cytosol. By transfer of two electrons the enzyme prevents one-electron reduction of quinones, which may give rise to oxidative stress and thus the enzyme protects against indirect toxic effects (Wermuth *et al*. 1986). Likewise, aldehydes and ketones are mostly more toxic than their corresponding alcohol metabolites (Wermuth 1985, Flynn and Green 1993). Even if an alcohol can exert similar toxic effects like the parent ketone, as is the case with NNAL and NNK, its toxic potential will mostly be less due to its easier elimination either in free form or following conjugation. Therefore, CR as well as aldoketo reductases can be considered as contributing to the detoxification of an important human carcinogen (figure 7).

In experiments with rat and monkey *in vivo*, NNK is rapidly reduced to NNAL, and in urine from human tobacco users NNAL and its glucuronide, but neither NNK nor NNK *N*-oxide can be detected (Hecht 1998). This is in accordance with the biochemical properties of the enzymes mediating NNK conversion to NNAL, because all of them, including microsomal 11β-HSD 1, prefer NADPH over NADH as co-substrate (Wermuth 1981, Hara *et al*. 1990, Maser and Bannenberg 1994, Maser *et al*. 1996, Maser 1998). In view of the high NADPH/$NADP^+$ ratio in cell cytosol (Veech *et al*. 1969), substrate reduction should predominate over the reverse reaction.

At NNK doses in the lower μg/kg range, rat excretes very low amounts of NNAL and/or NNAL-glucuronide, accounting for only 6–7% of the administered dose (Morse *et al*. 1990, Richter and Tricker 1994). In monkey urine, NNAL plus NNAL-glucuronides made up 21% (Hecht *et al*. 1993b) or 32% (Meger *et al*. 1999) of the NNK dose. Interestingly, in smokers' urine, the sum of NNAL and the two NNAL-glucuronides represent 40–100% of the estimated NNK uptake with cigarette mainstream smoke (Carmella *et al*. 1993), indicating large interindividual variations in the expression of NNK carbonyl reducing enzymes and/or NNAL-glucuronosyltransferases. Considering the fact that only 16% of habitual smokers develop lung cancer (Belinsky *et al*. 1997), these interindividual variations of NNK-detoxifying enzymes are of major interest since they may be linked to NNK-induced carcinogenesis. In view of the patterns of urinary metabolites, it may be hypothesized

that during evolution the capability to detoxify NNK *via* carbonyl reduction and glucuronosylation increased in the sequence rat–monkey–human.

Investigations on the *in vitro* metabolism of NNK have generally been performed with tissue homogenates, subcellular fractions, cultured cells, cultured tissues and isolated perfused tissues (Castonguay *et al*. 1983b, Murphy *et al*. 1990a, Richter *et al*. 1998, Schrader *et al*. 1998, Schulze *et al*. 1998, 1996) but to a lesser extent with purified enzymes. With respect to carbonyl reduction, 11β-hydroxysteroid dehydrogenase 1 (EC 1.1.1.146), an enzyme physiologically responsible for the interconversion of active 11-hydroxy-glucocorticoids to the inactive 11-oxo forms, has previously been identified as microsomal carbonyl reductase involved in the reduction of NNK to NNAL (Maser *et al*. 1996, Maser 1997). In the present study, four cytosolic enzymes have additionally been purified and characterized in terms of their NNK carbonyl-reducing activity. This multiplicity of NNK carbonyl reducing enzymes has to be taken into account when calculating kinetic values for NNAL formation in crude cellular fractions or whole tissues and assigning these values to individual enzymes. For example, in studies on NNK metabolism with isolated perfused liver, Schrader *et al*. (1998) observed a shift from α-hydroxylation towards NNAL formation at high compared with low NNK concentrations, reflecting the fact that several carbonyl reducing enzymes with different affinities to NNK are active in NNAL formation.

Estimates on the contribution of individual enzymes to total NNK reduction in human liver cytosol can be based on enzyme efficiencies and relative enzyme quantities. On the assumption that losses during purification of cytosolic enzymes are comparable for the aldoketo reductases and CR, ratios of enzyme quantities in liver cytosol in the present investigation and in a previous report (Breyer-Pfaff and Nill 2000) should be $\sim 3:3:1:1.5$ for AKR1C1, AKR1C2, AKR1C4 and CR I–III (table 1). Multiplication by the enzyme efficiencies (figure 5) results in relative contributions of ~ 20, 20, 1 and 60% to NNK reduction by the four enzymes. No indication was obtained of the occurrence of further cytosolic enzymes with NNK-reducing capacity in human liver.

The inhibitor sensitivities of aldoketo reductases have in previous investigations mainly been determined for dehydrogenase reactions. Nonetheless, the present data on the inhibition of NNK carbonyl reduction (table 2) are in accordance with reports on potent inhibition of AKR1C1, 1C2 and 1C4 by medroxyprogesterone acetate (Hara *et al*. 1990), of AKR1C4 by dexamethasone (Deyashiki *et al*. 1992) and of AKR1C1 and 1C2 by flufenamic acid (Matsuura *et al*. 1997). The extensive inhibitory effect of the flavonoids rutin and quercitrin on NNK reduction by CR corresponds to findings with 4-nitrobenzaldehyde as substrate (Wermuth 1981). A conspicuous finding was the efficient NNK reduction by AKR1C4 with NADH as a co-substrate (figure 4). Whereas chlordecone reduction by chlordecone reductase (later identified as AKR1C4) was not supported by NADH (Molowa *et al*. 1986), the dehydrogenation of (*S*)-1-indanol catalyzed by AKR1C4 proceeded at similar rates with 0.25 mM $NADP^+$ and 2 mM NAD^+ as co-substrates (Hara *et al*. 1990). In contrast, NAD^+ was a much poorer co-substrate in the same reaction mediated by AKR1C1 and 1C2 (Hara *et al*. 1990). Thus, in oxidative as well as in reductive reactions, the preference for triphospho- over diphosphopyridine nucleotides seems to be less distinct with AKR1C4 than with the other AKR.

No data are available on the product stereoselectivity of NNK carbonyl reduction by individual enzymes. NNAL is a chiral alcohol and separation of its diastereomeric

glucuronides excreted in urine indicated species-specific differences in the production and/or conjugation of the enantiomers (reviewed in Hecht 1998). Their absolute configurations were recently elucidated with the result that (*R*)-NNAL is mainly produced in rat liver microsomes, but (*S*)-NNAL-glucuronide predominates in rat urine. The patas monkey given NNK intravenously and human heavily using tobacco (snuffing) excreted more (*R*)- than (*S*)-NNAL-glucuronide in urine (Hecht *et al*. 1997). Interestingly, the higher tumorigenicity of (*R*)- compared with (*S*)-NNAL in the A/J mouse lung has been related to a preferential metabolic activation of (*R*)-NNAL and preferential glucuronidation of (*S*)-NNAL (Upadhyaya *et al*. 1999). Therefore, further investigations on the stereoselectivity of NNAL formation and disposition in man seem warranted.

In conclusion, four enzymes have been purified from human liver cytosol to homogeneity, AKR1C1, AKR1C2, AKR1C4 and CR, and it has been shown that these enzymes are responsible for carbonyl reduction of the tobacco-specific nitrosamine NNK. Considering that carbonyl reduction precedes glucuronosylation and excretion of NNK, it is conceivable that these cytosolic members of the AKR and SDR protein superfamilies contribute to the overall detoxification of this carcinogen.

Acknowledgements

This study was supported by grants (to E. Maser) from the Deutsche Forschungsgemeinschaft (MA 1704/3–1), the Stiftung Verhalten und Umwelt (Munich, Germany), and the European Commission (BIO4–97–2123).

References

Atalla, A., Breyer-Pfaff, U. and Maser, E., 1999, Carbonyl reductase and three aldo-keto reductases responsible for NNK carbonyl reduction in human liver cytosol. *Naunyn-Schmiedeberg's Archives of Pharmacology*, **Suppl. 359**, R154.

Atalla, A. and Maser, E., 1999, Carbonyl reduction of the tobacco-specific nitrosamine 4-(methylnitrosamino)-1-(3-pyridyl)-1-butanone (NNK) in cytosol of mouse liver and lung. *Toxicology*, **139**, 155–166.

Belinsky, S. A., Swafford, B. S., Finch, G. L., Mitchell, C. E., Kelly, G., Hahn, F. F., Anderson, M. W. and Nikula, K. J., 1997, Alterations in the K-ras and p53 genes in rat lung tumors. *Environmental Health Perspectives*, **105 (suppl. 4)**, 901–906.

Bohren, K. M., Wermuth, B., Harrison, D., Ring, D., Petsko, G. A. and Abby, K. H., 1994, Expression, crystallization and preliminary crystallographic analysis of human carbonyl reductase. *Journal of Molecular Biology*, **244**, 659–664.

Bradford, M. M., 1976, A rapid and sensitive method for the quantitation of microgram quantities of proteins using the principle of dye-binding. *Analytical Biochemistry*, **72**, 248–254.

Breyer-Pfaff, U. and Nill, K., 2000, High-affinity stereoselective reduction of the enantiomers of ketotifen and of ketonic nortriptyline metabolites by aldo-keto reductases from human liver. *Biochemical Pharmacology*, **59**, 249–260.

Carmella, S. G., Akerkar, S. and Hecht, S. S., 1993, Metabolites of the tobacco-specific nitrosamine 4-(methylnitrosamino)-1-(3-pyridyl)-1-butanone in smokers' urine. *Cancer Research*, **53**, 721–724.

Carmella, S. G., Akerkar, S. A., Richie, J. P. and Hecht, S. S., 1995, Intraindividual and interindividual differences in metabolites of the tobacco-specific lung carcinogen 4-(methylnitrosamino)-1-(3-pyridyl)-1-butanone (NNK) in smoker's urine. *Cancer Epidemiology Biomarkers and Prevention*, **4**, 635–652.

Carmella, S. G., Borukhova, A., Akerkar, S. A. and Hecht, S. S., 1997, Analysis of human urine for pyridine-N-oxide metabolites of 4-(methylnitrosamino)-1-(3-pyridyl)-1-butanone, a tobacco-specific lung carcinogen. *Cancer Epidemiology Biomarkers and Prevention*, **6**, 113–120.

Castonguay, A., Lin, D., Stoner, G. D., Radok, P., Furuya, K., Hecht, S. S., Schut, H. A. J. and Klaunig, J. E., 1983a, Comparative carcinogenicity in A/J mice and metabolism by cultured mouse peripheral lung of N′-nitrosonornicotine, 4-(methylnitrosamino)-1-(3-pyridyl)-1-butanone, and their analogues. *Cancer Research*, **43**, 1223–1229.

Castonguay, A., Stoner, G. D., Schut, H. A. and Hecht, S. S., 1983b, Metabolism of tobacco-specific N-nitrosamines by cultured human tissues. *Proceedings of the National Academy of Sciences, USA*, **80**, 6694–6697.

Crespi, C. L., Penman, B. W., Gelboin, H. V. and Gonzalez, F. J., 1991, A tobacco smoke-derived nitrosamine, 4-(methylnitrosamino)-1-(3-pyridyl)-1-butanone, is activated by multiple human cytochrome P450s including the polymorphic human cytochrome P4502D6. *Carcinogenesis*, **12**, 1197–1201.

Deyashiki, Y., Taniguchi, H., Amano, T., Nakayama, T., Hara, A. and Sawada, H., 1992, Structural and functional comparison of two human liver dihydrodiol dehydrogenases associated with 3 alpha-hydroxysteroid dehydrogenase activity. *Biochemical Journal*, **282**, 741–746.

Fischer, S., Spiegelhalder, B., Eisenbarth, J. and Preussmann, R., 1990, Investigations on the origin of tobacco-specific nitrosamines in mainstream smoke of cigarettes. *Carcinogenesis*, **11**, 723–730.

Flynn, T. G. and Green, N. C., 1993, The aldo-keto reductases: an overview. *Advances in Experimental Medicine and Biology*, **328**, 251–257.

Hara, A., Matsuura, K., Tamada, Y., Sato, K., Miyabe, Y., Deyashiki, Y. and Ishida, N., 1996a, Relationship of human liver dihydrodiol dehydrogenases to hepatic bile-acid-binding protein and an oxidoreductase of human colon cells. *Biochemical Journal*, **313**, 373–376.

Hara, A., Matsuura, K., Tamada, Y., Sato, K., Miyabe, Y., Deyashiki, Y. and Ishida, N., 1996b, Relationship of human liver dihydrodiol dehydrogenases to hepatic bile-acid-binding protein and an oxidoreductase of human colon cells. *Biochemical Journal*, **313**, 373–376.

Hara, A., Taniguchi, H., Nakayama, T. and Sawada, H., 1990, Purification and properties of multiple forms of dihydrodiol dehydrogenase from human liver. *Journal of Biochemistry, Tokyo*, **108**, 250–254.

Hecht, S. S., 1994, Metabolic activation and detoxification of tobacco-specific nitrosamines – a model for cancer prevention strategies. *Drug Metabolism Reviews*, **26**, 373–390.

Hecht, S. S., 1996, Recent studies on mechanisms of bioactivation and detoxification of 4-(methylnitrosamino)-1-(3-pyridyl)-1-butanone (NNK), a tobacco-specific lung carcinogen. *Critical Reviews in Toxicology*, **26**, 163–181.

Hecht, S. S., 1998, Biochemistry, biology, and carcinogenicity of tobacco-specific *N*-nitrosamines. *Chemical Research in Toxicology*, **11**, 559–603.

Hecht, S. S., Carmella, S. G., Murphy, S. E., Akerkar, S., Brunnemann, K. D. and Hoffmann, D., 1993a, A tobacco-specific lung carcinogen in the urine of men exposed to cigarette smoke. *New England Journal of Medicine*, **329**, 1543–1546.

Hecht, S. S. and Hoffmann, D., 1988, Tobacco-specific nitrosamines, an important group of carcinogens in tobacco and tobacco smoke. *Carcinogenesis*, **9**, 875–884.

Hecht, S. S. and Hoffmann, D., 1989, The relevance of tobacco-specific nitrosamines to human cancer. *Cancer Surveys*, **8**, 273–294.

Hecht, S. S., Spratt, T. E. and Trushin, N., 1997, Absolute configuration of 4-(methylnitrosamino)-1-(3-pyridyl)-1-butanol formed metabolically from 4-(methylnitrosamino)-1-(3-pyridyl)-1-butanone. *Carcinogenesis*, **18**, 1851–1854.

Hecht, S. S., Trushin, N., Reid Quinn, C. A., Burak, E. S., Jones, A. B., Southers, J. L., Gombar, C. T., Carmella, S. G., Anderson, L. M. and Rice, J. M., 1993b, Metabolism of the tobacco-specific nitrosamine 4-(methylnitrosamino)-1-(3-pyridyl)-1-butanone in the patas monkey: pharmacokinetics and characterization of glucuronide metabolites. *Carcinogenesis*, **14**, 229–236.

Hecht, S. S., Young, R. and Chen, C. B., 1980, Metabolism in the F344 rat of 4-(N-methyl-N-nitrosamino)-1-(3-pyridyl)-1-butanone, a tobacco-specific carcinogen. *Cancer Research*, **40**, 4144–4150.

Inazu, N., Ruepp, B., Wirth, H. and Wermuth, B., 1992, Carbonyl reductase from human testis: purification and comparison with carbonyl reductase from human brain and rat testis. *Biochimica et Biophysica Acta*, **1116**, 50–56.

Jez, J. M., Flynn, T. G. and Penning, T. M., 1997, A nomenclature system for the aldo-keto reductase superfamily. *Advances in Experimental Medicine and Biology*, **414**, 579–589.

Jörnvall, H., Persson, B., Krook, M., Atrian, S., Gonzalez-Duarte, R., Jeffery, J. and Ghosh, D., 1995, Short-chain dehydrogenases/reductases (SDR). *Biochemistry*, **34**, 6003–6013.

Laemmli, U. K., 1970, Cleavage of structural proteins during the assembly of the head of bacteriophage T4. *Nature*, **227**, 680–685.

Maser, E., 1995, Xenobiotic carbonyl reduction and physiological steroid oxidoreduction—the pluripotency of several hydroxysteroid dehydrogenases. *Biochemical Pharmacology*, **49**, 421–440.

Maser, E., 1997, Stress, hormonal changes, alcohol, food constituents and drugs: factors that advance the incidence of tobacco smoke-related cancer? *Trends in Pharmacological Sciences*, **18**, 270–275.

Maser, E., 1998, 11β-Hydroxysteroid dehydrogenase responsible for carbonyl reduction of the tobacco-specific nitrosamine 4-(methylnitrosamino)-1-(3-pyridyl)-1-butanone in mouse lung microsomes. *Cancer Research*, **58**, 2996–3003.

Maser, E. and Bannenberg, G., 1994, 11β-Hydroxysteroid dehydrogenase mediates reductive metabolism of xenobiotic carbonyl compounds. *Biochemical Pharmacology*, **47**, 1805–1812.

Maser, E., Richter, E. and Friebertshäuser, J., 1996, The identification of 11 beta-hydroxysteroid dehydrogenase as carbonyl reductase of the tobacco-specific nitrosamine 4-(methylnitrosamino)-1-(3-pyridyl)-1-butanone. *European Journal of Biochemistry*, **238**, 484–489.

Maser, E., Stinner, B. and Atalla, A., 2000, Carbonyl reduction of 4-(methylnitrosamino)-1-(3-pyridyl)-1-butanone (NNK) by cytosolic enzymes in human liver and lung. *Cancer Letters*, **148**, 135–144.

Matsuura, K., Deyashiki, Y., Sato, K., Ishida, N., Miwa, G. and Hara, A., 1997, Identification of amino acid residues responsible for differences in substrate specificity and inhibitor sensitivity between two human liver dihydrodiol dehydrogenase isoenzymes by site-directed mutagenesis. *Biochemical Journal*, **323**, 61–64.

Meger, M., Richter, E., Zwickenpflug, W., Oehlmann, C., Hargaden, M. B., A-Rahim, Y. I. and Vesell, E. S., 1999, Metabolism and disposition of 4-(methylnitrosamino)-1-(3-pyridyl)-1-butanone (NNK) in rhesus monkeys. *Drug Metabolism and Disposition*, **27**, 471–478.

Molowa, D. T., Shayne, A. G. and Guzelian, P. S., 1986, Purification and characterization of chlordecone reductase from human liver. *Journal of Biological Chemistry*, **261**, 12624–12627.

Morse, M. A., Eklind, K. I., Toussaint, M., Amin, S. G. and Chung, F. L., 1990, Characterization of a glucuronide metabolite of 4-(methyl-nitrosamino)-1-(3-pyridyl)-1-butanone (NNK) and its dose-dependent excretion in the urine of mice and rats. *Carcinogenesis*, **11**, 1819–1823.

Murphy, S. E., Heiblum, R. and Trushin, N., 1990a, Comparative metabolism of N′-nitrosonornicotine and 4-(methylnitrosamino)-1-(3-pyridyl)-1-butanone by cultured F344 rat oral tissue and esophagus. *Cancer Research*, **50**, 4685–4691.

Murphy, S. E., Palomino, A., Hecht, S. S. and Hoffmann, D., 1990b, Dose–response study of DNA and hemoglobin adduct formation by 4-(methylnitrosamino)-1-(3-pyridyl)-1-butanone in F344 rats. *Cancer Research*, **50**, 5446–5452.

Richter, E., Engl, J. and Tricker, A. R., 1998, Metabolism of 4-(methylnitrosamino)-1-(3-pyridyl)-1-butanone (NNK) and 4-(methylnitrosamino)-1-(3-pyridyl)-1-butanol (NNAL) in precision-cut human and rodent liver and lung tissue slices. *Toxicological Sciences*, **42 (suppl. 1)**, 183.

Richter, E. and Tricker, A. R., 1994, Nicotine inhibits the metabolic activation of the tobacco-specific nitrosamine 4-(methylnitrosamino)-1-(3-pyridyl)-1-butanone in rats. *Carcinogenesis*, **15**, 1061–1064.

Schrader, E., Hirsch-Ernst, K. I., Richter, E. and Foth, H., 1998, Metabolism of 4-(methylnitrosamino)-1-(3-pyridyl)-1-butanone (NNK) in isolated rat lung and liver. *Naunyn-Schmiedeberg's Archives of Pharmacology*, **357**, 336–343.

Schulze, J., Schrader, E., Foth, H., Kahl, G. F. and Richter, E., 1998, Effect of nicotine or cotinine on metabolism of 4-methylnitrosamino-1-(3-pyridyl)-1-butanone (NNK) in isolated rat lung and liver. *Naunyn-Schmiedeberg's Archives of Pharmacology*, **357**, 344–350.

Schulze, J., Schlager, W., Wunsch, R. and Richter, E., 1996, Metabolism of 4-(methylnitrosamino)-1-(3-pyridyl)-1-butanone (NNK) by hamster, mouse and rat intestine: relevance of species differences. *Carcinogenesis*, **17**, 1093–1099.

Smith, T. J., Liao, A. M., Liu, Y., Butler Jones, A., Anderson, L. M. and Yang, C. S., 1997, Enzymes involved in the bioactivation of 4-(methylnitrosamino)-1-(3-pyridyl)-1-butanone in patas monkey lung and liver microsomes. *Carcinogenesis*, **18**, 1577–1584.

Stolz, A., Hammond, L., Lou, H., Takikawa, H., Ronk, M. and Shively, J. E., 1993, cDNA cloning and expression of the human hepatic bile acid-binding protein. A member of the monomeric reductase gene family. *Journal of Biological Chemistry*, **268**, 10448–10457.

Takikawa, H., Stolz, A., Sugiyama, Y., Yoshida, H., Yamanaka, M. and Kaplowitz, N., 1990, Relationship between the newly identified bile acid binder and bile acid oxidoreductases in human liver. *Journal of Biological Chemistry*, **265**, 2132–2136.

Upadhyaya, P., Kenney, P. M., Hochalter, J. B., Wang, M. and Hecht, S. S., 1999, Tumorigenicity and metabolism of 4-(methylnitrosamino)-1-(3-pyridyl)-1-butanol enantiomers and metabolites in the A/J mouse. *Carcinogenesis*, **20**, 1577–1582.

Veech, R. L., Eggleston, L. V. and Krebs, H. A., 1969, The redox state of free nicotinamide-adenine dinucleotide phosphate in the cytoplasm of rat liver. *Biochemical Journal*, **115**, 609–619.

Vogel, K., Bentley, P., Platt, K. L. and Oesch, F., 1980, Rat liver cytoplasmic dihydrodiol dehydrogenase. Purification to apparent homogeneity and properties. *Journal of Biological Chemistry*, **255**, 9621–9635.

Wermuth, B., 1981, Purification and properties of an NADPH-dependent carbonyl reductase from human brain. *Journal of Biological Chemistry*, **256**, 1206–1213.

Wermuth, B., 1985, Aldo-keto reductases. In T. G. Flynn and H. Weiner (eds), *Enzymology of Carbonyl Metabolism: Aldehyde Dehydrogenase, Aldo/Keto Reductase, and Alcohol Dehydrogenase* (New York: Alan R. Liss), pp. 209–230.

Wermuth, B., Bohren, K. M., Heinemann, G., von Wartburg, J. P. and Gabbay, K. H., 1988, Human carbonyl reductase. Nucleotide sequence analysis of a cDNA and amino acid sequence of the encoded protein. *Journal of Biological Chemistry*, **263**, 16185–16188.

Wermuth, B., Platt, K. L., Seidel, A. and Oesch, F., 1986, Carbonyl reductase provides the enzymatic basis of quinone detoxication in man. *Biochemical Pharmacology*, **35**, 1277–1282.

XENOBIOTICA, 2000, VOL. 30, NO. 8, 771–779

Modulation of rat epididymal γ-glutamyl transpeptidase by nonylphenols

P. C. LEE†‡*, P. HO†, B. H. JELINEK† and M. STRUVE†

† Department of Pediatrics and ‡Department of Pharmacology and Toxicology, Medical College of Wisconsin, Milwaukee, WI 53226, USA

Received 18 January 2000

1. γ-Glutamyl-transpeptidase (γ-GTP), present at low levels in the testis, seminal vesicle, prostate gland and epididymis in rat at 4 days of age, showed rapid developmental increases at the time of weaning.

2. Administration of nonylphenols (NP) to the neonatal male rat pup (from days 1 to 15) impaired the subsequent development of γ-GTP in the epididymis but not in the testis, seminal vesicles or prostate gland.

3. Single injection of NP to weaned pups at ~ 22 days of age decreased γ-GTP in the epididymis but not in other male accessory sex organs. This effect was transient, dose-dependent and blocked by the oestrogen receptor-specific antagonist ICI 182,780.

4. Single injection of oestradiol to weaned rat at ~ 22 days of age also decreased γ-GTP in the epididymis but not in the testis, prostate gland or seminal vesicles.

5. In *in vitro* assays, NP did not inhibit epididymal γ-GTP activity even at 100 μM final concentration. Under similar conditions, acivicin, a specific inhibitor for γ-GTP, showed a dose-dependent inhibition of γ-GTP activity.

6. It is suggested that NP impair γ-GTP expression in the epididymis of developing male rat and act in part via the oestrogen receptor.

Introduction

Dysfunction of the human male reproductive system has been increasing in the past few decades (Sharpe and Skakkebaek 1993, Toppari *et al*. 1996) and abnormalities in the male reproductive organs in wild animals are also documented (Guillette *et al*. 1994, Facemire *et al*. 1995). Accumulating evidence suggests that these increases in male reproductive impairment are the result of increasing exposure to xeno-oestrogens (Purdom *et al*. 1994, Kavlock *et al*. 1996, Toppari *et al*. 1996, Foster 1998).

Alkylphenol ethoxylates have been used extensively in industrial processing and in household and institutional cleaning products (Metcalfe *et al*. 1996). The majority of alkylphenol ethoxylate surfactants are nonylphenol ethoxylates that yield the stable product, nonylphenols. Nonylphenols were first shown to have oestrogenic activity in their induction of proliferation and up-regulation of the progesterone receptor in human oestrogen-sensitive breast tumour cells and their ability to promote cell division in the endometrial epithelium of ovariectomized female rat (Soto *et al*. 1991). A commercial preparation of nonylphenols stimulates the production of vitellogenin in rainbow trout *in vivo* (Ren *et al*. 1996) and elicits the synthesis of another oestrogen-responsive protein, the zona radiata protein, in salmon (Arukwe *et al*. 1999). The present authors have shown that nonylphenols induce uterine growth in the immature female rat in a manner similar to that of oestrogen (Lee and Lee 1996). More importantly, alkylphenols affect the male reproductive system. When given to fish, nonylphenols caused testicular ab-

* Author for correspondence; e-mail: pclee@mcw.edu

Xenobiotica ISSN 0049-8254 print/ISSN 1366-5928 online © 2000 Taylor & Francis Ltd
http://www.tandf.co.uk/journals

normalities including spermatogenic cyst formation in seminiferous lobules with few spermatozoa and general degeneration of seminiferous lobules in male ellpout, *Zoarus viviparus* (Christiansen *et al*. 1998). In male Japanese Medaka, exposure to 4-tert-octylphenol resulted in inhibition of spermatogenesis and formation of oocytes in the testis (Gronen *et al*. 1999). In rat, Boockfor and Blake (1997) reported that long-term (up to 2 months) administration of octylphenols to young adult males led to reduction in sperm count and disruption of spermatogenesis. Sharpe *et al*. (1995) reported that feeding of octylphenol to the pregnant rat resulted in male progeny with smaller testes and reduced daily sperm production. Maternal exposure to nonylphenols results in abnormalities of the testis and epididymis of male progeny (DeJager *et al*. 1999). The present authors have shown that the male rat pup exposed to nonylphenols immediately after birth had a decreased size of testis and associated male reproductive organs and an increased incidence of cryptorchidism and infertility (Lee 1998) with accompanying testicular abnormalities including lack of differentiation of seminiferous tubules, lowering of epididymal sperm counts and reduction in sperm motility (Lee *et al*. 1999).

γ-GTP, a ubiquitous enzyme present in serum, urine (Dimov and Kulhanek 1967, Rosalki and Rau 1972) and many other tissues including the testis and seminal vesicle, has been used as a marker for testicular growth and development (Hodgen and Sherins 1973, Lu and Steinberger 1977). The content and specific activity of γ-GTP in the seminal vesicles responded to sex steroid hormones. This leads to speculation about the role of γ-GTP in seminal vesicle function (DeLap *et al*. 1975). Particularly relevant to the present study is that the mouse with genetic γ-GTP deficiency is infertile (Harding *et al*. 1997). Similarly, the γ-GTP knockout mouse is sexually immature and has hypoplastic testes, seminal vesicles and epididymis in the affected males (Lieberman *et al*. 1996). Both observations suggest the importance of γ-GTP in the development of male reproductive organs and their functions.

Here, the present authors have (1) documented the development of γ-GTP in the testis, seminal vesicles, epididymis and ventral prostate gland; (2) examined changes in γ-GTP activities in the testis and male accessory sex organs in the young rat exposed to nonylphenols for 15 days from birth, (3) defined the time-course and dose–response of γ-GTP changes after a single injection of nonylphenol to the weaned rat and (4) evaluated whether nonylphenols act as xeno-oestrogens in their action through the oestrogen receptor on the modulation of γ-GTP expression in the male reproductive tissues.

The National Institutes of Health Guidelines for the care and use of laboratory animals were followed and all the animal protocols were approved by the Animal Research Committee of the Medical College of Wisconsin.

Materials and methods

Chemicals

Unless otherwise stated, all chemicals were from Sigma Chemical Co. (St Louis, MO, USA). Technical grade nonylphenol was from American Cyanamid Co. (Wayne, NJ, USA). L-γ-Glutamyl-3,4-nitroanilide was from ICN Biochemicals (Aurora, OH, USA). ICI 182,780, a specific oestrogen receptor antagonist, was a gift from Dr A. Wakeling of Zeneca Pharmaceuticals (Cheshire, UK).

Animals

Pregnant Sprague–Dawley rats from an inbred colony maintained at the Medical College of Wisconsin were housed in individual cages and maintained on a 12-h alternate light–dark cycle. On the expected date of delivery, cages were inspected every 6 h for birth. The day of birth was designated as day 0. Pups were allowed to suckle freely until 21 days of age and were weaned. For the evaluation of enzyme

development, four to 24 animals (depending on age) were killed at various selected ages. Their testes, epididymis, ventral prostate glands and seminal vesicles were harvested, frozen immediately over dry ice and stored at −80 °C until analysed.

Neonatal exposure to nonylphenols. Newborn male pups (n = 16) were divided into two groups (eight in each). One group was given nonylphenols at 16 mg/kg body i.p. daily for 15 days. The other group was given vehicle only (dimethyl sulphoxide) for the same duration. Four animals from the control and NP-treated groups were killed at 25 and 30 days of age. Their testes, epididymis, ventral prostate glands and seminal vesicles were removed, and their weights were determined before being snap-frozen and stored separately at −80 °C until analysis.

Single injection experiments

Dose–response studies. Sixteen weaned males (21–22 days of age) were divided into four subgroups and given an injection of vehicle or nonylphenol at increasing doses of 0.6, 6.0 and 60 mg/kg body weight to each of the four subgroups. Animals were sacrificed 24 h latter. Their testes and male accessory sex organs were removed, frozen and stored at −80 °C for later analyses.

Time-course studies. Weaned male rat (21–22 days of age) were given an injection of vehicle (n = 16) or nonylphenols (60 mg/kg body weight) (n = 16). Four animals from each group were killed at 1, 2, 3 and 5 days later. Their testes and accessory sex organs were harvested and stored as described.

Effect of ER antagonist. To evaluate whether nonylphenols act through the oestrogen receptor, one group of male pups (n = 14) were given vehicle (n = 4) NP (60 mg/kg body weight) (n = 4) or NP (60 mg/kg) and ICI 182,780 (2.5 mg/kg body weight) (n = 6) simultaneously 24 h before sacrifice. Their testes and accessory sex organs were harvested and stored as described.

Effect of oestradiol. As an added control group, one group of male pups was given oestradiol (10 μg/animal) (n = 4) or vehicle (n = 4) also 24 h before sacrifice. Their testes and accessory sex organs were harvested and stored as described.

Methods

Thawed tissue samples were use for homogenization. Individual (~ 30 mg) tissue was homogenized in 0.5 ml Tris-HCl (100 mM, pH 8.25) containing aprotinin (10 μg/ml). An equal volume of the same buffer but with Triton X-100 (2%) was added to the homogenate, mixed and allowed to sit for 20 min with occasional stirring. The homogenate was centrifuged for 10 min at 4 °C and 20000 *g*. The supernatant fraction was collected for γ-GTP and protein determination. A preliminary study indicated that the recovery of γ-GTP activity in the supernatant fraction ranged from 98 to 100% of that found in the tissue. Activity was also shown to be proportional to the amount of homogenate added within the concentrations and time specified. Furthermore, γ-GTP activity did not change after 2 months of storage at −80 °C.

Protein concentration was determined by the Bradford (1976) method using the BioRad reagent (BioRad Laboratories) with BSA as standard.

The activity of γ-GTP was determined with a modification of the method of Tate and Meister (1974). The reaction mixture contained Tris-HCl buffer (100 mM, pH 8.25), L-γ-Glutamyl-3,4-nitroanilide (2.9 mM) and glycylglycine (100 mM). The amount of 3-carboxy-4-nitroaniline produced by the enzymatic reaction was measured at 405 nm over 2 h for tissue extracts from the testis and ventral prostate gland, and 30 min for tissue extracts from seminal vesicles and epididymis. Because of the substantial difference in γ-GTP activities among different tissues, the volume of tissue extract used for the assay was 50 μl (~ 160 μg protein) for the testis and prostate gland, 25 μl (~ 60 μg protein) for the seminal vesicle and 10 μl (~ 20 μg protein) for the epididymis. Enzyme activity was expressed as nmoles product formed per mg protein per min.

In *in vitro* inhibition studies, pooled epididymal extracts from the same age group (weaned animals) were used. Acivicin or nonylphenols at increasing doses (10, 25, 50 and 100 μM final concentrations in the assay mixture) were added individually to the assay buffer before the addition of tissue extract.

Statistics

Results are mean+SD. ANOVA evaluated the difference between multiple groups. If significance was observed between groups, then a *post-hoc* t-test compared the means of two specific groups, with $p < 0.05$ considered as statistically significant.

Results

Figure 1 shows the developmental profile of γ-GTP in rat from 4 days of age to adult. Rat pups at 4 days of age had low γ-GTP activity in their testis, epididymis,

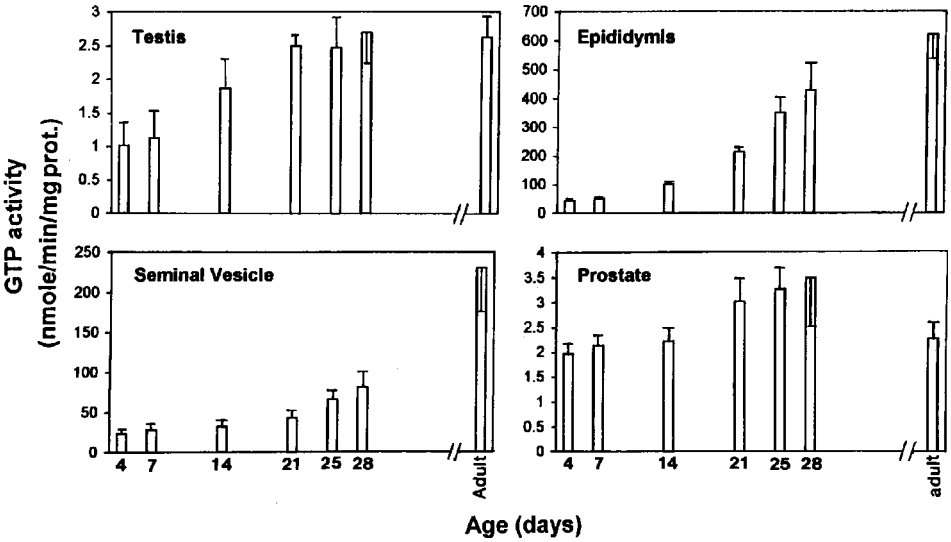


Figure 1. Developmental profile of γ-GTP in the testis, seminal vesicles, epididymis and prostate gland of the normal rat. Date of birth was designated as day 0. Values represent the mean ± SD from all animals killed at each time point. The number of animals varies from four to 24 depending on age. Adults were ~ 6 months of age. Vertical lines above the bars represent SD of the mean.

Table 1. Effects of neonatal NP treatment (days 1–15) on γ-GTP activity in testis and male accessory organs. γ-GTP activity (nmoles/min/mg protein).

Age (days)	Treatment	Testis	Epididymis	Seminal vesicle	Prostate
25	Control	2.5 ± 0.1	460.5 ± 6.1	68.8 ± 3.5	1.3 ± 0.1
	NP	2.4 ± 0.1	380.2 ± 46.5*	79.5 ± 14.4	1.4 ± 0.1
30	Control	2.3 ± 0.1	450.6 ± 23.8	102.0 ± 3.2	1.6 ± 0.4
	NP	2.3 ± 0.2	369.2 ± 50.6*	93.3 ± 10.1	1.5 ± 0.1

Newborn rats were given NP daily (16 mg/kg) from days 1–15 and killed on days 25 and 30. Values are means ± SD, with $n = 4$ in each group. *Significantly different from corresponding controls, $p \leq 0.05$.

seminal vesicles and prostate gland. The level of γ-GTP activity was highest in the epididymis followed by seminal vesicle but much less in the testis and prostate gland. As the rat developed, γ-GTP activity increased rapidly in both the epididymis and the seminal vesicle at ~ 14–25 days of age. The adult level of γ-GTP activity in the epididymis was ~ 14 times, and in the seminal vesicles, ~ 10 times of that found in the corresponding tissues from the 4-day-old rat. Increases in γ-GTP were also evident in the testis and prostate gland but to a much less extent, reaching ~ 1.5–2 times of the 4-day-old levels by the time the animal reached adulthood.

Nonylphenols administered to male rat pups starting from day 1 after birth for 15 days decreased γ-GTP activity in the epididymis at 25 and 30 days of age (table 1). In contrast, the γ-GTP activity in the testis, seminal vesicles and prostate gland was not affected.

To examine the kinetics of NP inhibition on γ-GTP in the epididymis, NP was given as a single injection to the weanling rat and the effects on the enzyme were followed in subsequent days. A decrease in epididymal γ-GTP activity was seen at

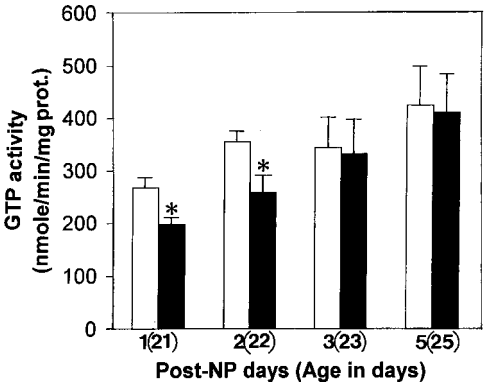


Figure 2. Time-course of epididymal γ-GTP response to a single dose of NP (60 mg/kg body weight) and killed at the times indicated. Values represent the mean ± SD from four animals. Numerals in brackets denote the age of animals at the time of sacrifice. Open bars represent values from the vehicle injected, control rat and solid bars from the NP-treated rat. Vertical lines above the bars represent the SD of the mean. *Significantly different from corresponding control values with $p < 0.05$.

1 and 2 days after NP administration (figure 2). γ-GTP activity then returned to the control level by the third day and was maintained at a level similar to the control level thereafter.

The effects of nonylphenols on the epididymal γ-GTP were dose-dependent. Treatment (0.6 mg/kg body weight) had no significant effect on the epididymal γ-GTP activity (table 2). Rat pups treated with 6 mg/kg body weight had decreased enzyme activity. Further reduction in epididymal γ-GTP activity was evident when the NP dose was increased to 60 mg/kg body weight. There was no change in γ-GTP activity in either the testis or prostate gland at any dose of NP used. The seminal vesicles showed inconsistent changes and only at the 60 mg/kg dose.

Nonylphenols have oestrogenic properties both *in vitro* and *in vivo* (Soto *et al.* 1991, Ren *et al.* 1996, Lee and Lee 1996, Lee 1998, Arukwe *et al.* 1999). Therefore, the present authors investigated whether the effects of NP on epididymal γ-GTP activity were mediated by the oestrogen receptor (ER). The weanling rat was given NP alone or together with ICI 182,780, a specific ER receptor antagonist. Age-matched control male pups were given the vehicle only. Table 3 shows that NP decreased epididymal γ-GTP activity. ICI 182,780 when given together with NP restored γ-GTP activity in the epididymis to a level intermediate between the control and NP-treated animals. Nonylphenol itself or in combination with ICI 182,780 did not affect γ-GTP activity in the testis, seminal vesicles and prostate gland.

As a comparison, the male rat pup was treated with oestradiol in a similar manner as with NP. A single injection of oestradiol given to the weanling rat also decreased epididymal γ-GTP activity (table 4). Like that of NP treatment, oestradiol did not affect the γ-GTP activity in the testis, seminal vesicles and the prostate gland.

Since NP are powerful surfactants, the present authors performed *in vitro* assays to evaluate whether NP affected γ-GTP enzyme activity *per se* rather than affecting its expression. The γ-GTP activity of a pooled epididymis extract was tested in the presence of increasing concentrations of NP. As a control, enzyme activity was also measured in the presence of acivicin, a known specific inhibitor for γ-GTP. As shown in figure 3, acivicin inhibited γ-GTP activity when present at 10 μM final

Table 2. Dose–response of γ-GTP activity in male reproductive tissues to NP administration. γ-GTP activity (nmoles/min/mg protein).

Treatments	Testis	Epididymis	Seminal vesicle	Prostate
Control	2.66±0.15	333.6±17.9	84.0±7.1	1.8±0.3
NP (0.6 mg/kg	2.80±0.07	297.0±20.6	85.1±3.5	1.7±0.2
NP (6.0 mg/kg	2.73±0.13	250.2±15.6*	97.0±17.1	1.6±0.3
NP (60 mg/kg)	2.83±0.11	190.3±20.0*	69.9±9.0	1.6±0.2

Weaned rats at 22 days of age were given NP at the doses specified and killed 24 h later. Values are means±SD, where $n = 4$ in each group. *Significantly different from corresponding controls.

Table 3. Effects of ER antagonist, ICI 182,780 on NP-induced changes in γ-GRP activity in testis and male accessory organs. γ-GTP activity (nmoles/min/mg protein).

Treatments	Testis	Epididymis	Seminal vesicle	Prostate
Control ($n = 4$)	2.11±0.10	269.8±29.8	66.7±2.5	1.95±0.3
NP ($n = 4$)	2.09±0.06	175.5±12.0*	63.7±8.1	1.98±0.6
NP+ICI ($n = 6$)	2.28±0.18	218.6±29.1*†	71.7±5.5	2.00±0.7

Weaned rats at 21 days were given NP (4 mg per animal) alone or together with ICI 182,780 (0.15 mg per animal) and killed at 22 days of age. Values are means±SD. *Significantly different from corresponding controls. †Significantly different from corresponding NP values with $p < 0.05$.

Table 4. Effect of oestradiol on γ-GTP activity in testis and other male accessory organs. γ-GTP activity (nmoles/min/mg protein).

Treatments	Testis	Epididymis	Seminal vesicle	Prostate
Control	2.39±0.4	286.5±30.7	69.0±2.1	2.42±0.6
Oestradiol	2.30±0.1	192.4±12.6*	70.1±4.9	2.72±0.5

Oestradiol was given at 10 μg per animal at 21 days of age and sacrificed after 24 h. Values are means±SD, where $n = 4$ in both groups. *Significantly different from corresponding controls with $p \leq 0.05$.

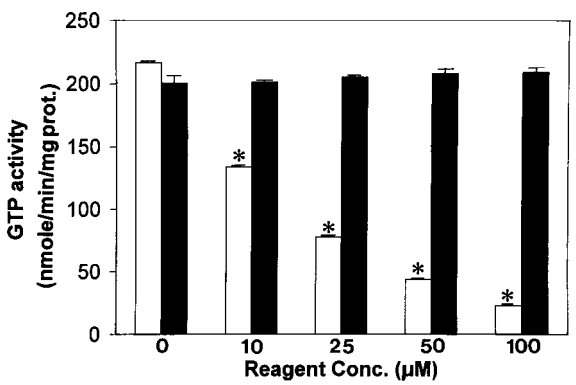


Figure 3. Effect of graded doses of acivicin (open bars) or NP (solid bars) on *in vitro* γ-GTP activity of pooled epididymal extract from the normal weaned rat. Values are the mean±SD of four separate assays. Vertical lines above bars represent the SD of the mean. *Significantly different from values obtained in the absence of acivicin or NP in the assay mixture with $p < 0.05$. Acivicin or NP were added to the reaction mixture before the addition of tissue extract.

concentration in the assay system. Inhibition was dose-dependent and at 100 μM concentration, the inhibition was > 90 %. In contrast, NP had no effect on the γ-GTP activity *in vitro* even at 100 μM concentration.

Discussion

γ-GTP is a ubiquitous enzyme present in serum, urine and other tissues including the testis and seminal vesicle (Dimov and Kulhanek 1967, Rosalki and Rau 1972, Hodgen and Sherins 1973, Lu and Steinberger 1977) and has been used as a marker for testicular growth and development (Hodgen and Sherins 1973, DeLap *et al*. 1975).

The present results show that γ-GTP activity is present not only in the testis and seminal vesicles, but also in the epididymis and ventral prostate gland. The epididymis, in particular, has very high γ-GTP activity in that the adult level of this enzyme in the epididymis is ~ 250 times of that found in the testis. Furthermore, γ-GTP activity exhibits developmental increases in the testis and male accessory sex organs ~ 14–25 day of age and reaches a near-adult level ~ 1–2 weeks after weanling (~ 5 weeks of age). Temporally, these increases occur before sexual maturation that happens ~ 7–8 weeks of age for the male rat and suggests that γ-GTP, particularly in the epididymis, may play a role in sexual maturity of these animals. The present results indicated that NP treatment of the male rat at neonatal ages (days 1–15) decreased the activity of γ-GTP in the epididymis but did not affect those in the seminal vesicle, testis and prostate gland. These results coupled with the observed lowering of epididymal sperm counts and decrease in sperm motility (Lee *et al*. 1999) and the reported requirement of γ-GTP for normal development of the testis and accessory sex organs and fertility (Lieberman *et al*. 1996, Harding *et al*. 1997) suggest a correlation between the decrease of epididymal γ-GTP levels and the overall dysfunction of the male reproductive system in the NP-treated male rat.

The lack of effect of NP on testicular γ-GTP is in contrast to that reported by Christiansen *et al*. (1998), who reported that NP treatment of the male eelpout decreased γ-GTP in its testis in a manner similar to that of treatment with oestradiol. This latter report did not examine other tissues of the male reproductive system and therefore could not be compared with the present results on the epididymis, seminal vesicles and prostate gland. The difference observed for the response of the fish testis to NP may be related to species differences.

The present results indicate that a single injection of NP to the weaned male rat leads to decreased epididymal γ-GTP activity but no change in the testis, seminal vesicles and prostate gland. Recovery of enzyme activity occurred in 3 days. The effect was dose-dependent and required a relatively high concentration of NP. Treatment with oestradiol also led to a decrease in epididymal γ-GTP activity, but activity in the testis, seminal vesicles and prostate gland were unaffected. More importantly, the decrease in epididymal γ-GTP activity by NP-treatment was blocked by the simultaneous administration of the oestrogen receptor (ER) specific antagonist, ICI 182,780. The blockage was not complete, since the γ-GTP activity of the ICI + NP treated animals was in between that of the control and NP-treated activity. The results suggested that, at least in part, NP acts through the ER in its modulation of the epididymal γ-GTP expression.

One possibility for NP to affect γ-GTP activity is that it may act as an inhibitor of the enzyme. However, in *in vitro* assays, NP even up to 100 μM final concentration

in the assay mixture, showed no detectable inhibition of γ-GTP activity. This concentration is about five times that would be present in the animal when given 6.0 mg/kg body weight (assuming NP distributes evenly throughout the entire body of the animal). In contrast, the same concentration of acivicin, a specific inhibitor for γ-GTP, inhibited > 90 % of the enzyme activity under similar assay conditions. Thus, the decrease in epididymal γ-GTP following NP-treatment cannot be due to direct inhibition of γ-GTP activity by NP but is more likely the result of down regulation of γ-GTP expression.

In conclusion, the present study has demonstrated that NP-treatment in neonates specifically decreases the level of γ-GTP in the epididymis but that it has no effect in the testis, seminal vesicles and the prostate gland. The reduced level of γ-GTP may contribute to the observed dysfunction of the male reproductive system following NP-treatment in the neonatal period and NP, in part, may act through the oestrogen receptor in their modulation of epididymal γ-GTP levels.

Acknowledgement

The authors thank Dr S. L. Werlin for his critical review of the manuscript.

References

Arukwe, A., Knudsen, S. R. and Goksoyr, A., 1997, Fish zona radiata (egg shell) protein. A sensitive bio-marker for environmental estrogen. *Environmental Health Perspectives*, **105**, 418–422.

Boockfor, R. R. and Blake, C. A., 1997, Chronic administration of 4-tert-octylphenol to adult male rats causes shrinkage of the testes and male accessory sex organs, disrupts spermatogenesis and increases the incidence of sperm deformities. *Biology of Reproduction*, **57**, 267–277.

Bradford, M. A., 1976, A rapid and sensitive method for quantitation of microgram quantities of protein utilising the principle of protein dye-binding. *Analytical Biochemistry*, **72**, 248–254.

Christiansen, T., Korsgaard, B. and Jespersen, A., 1998, Effects of nonylphenol and 17β-oestradiol on vitellogenin synthesis, testicular structure and cytology in male eelpout, *Zoarus viviparus*. *Journal of Experimental Biology*, **201**, 179–192.

DeJager, C., Bornman, M. S. and Oosthuizen, J. M., 1999, The effect of *p*-nonylphenol on the fertility potential of male rats after gestational, lactational and direct exposure. *Andrologia*, **31**, 107–113.

DeLap, L. W., Tate, S. S. and Meister, A., 1975, γ-Glutamyl transpeptidase of rat seminal vesicles: effect of orchidectomy and hormone administration on the transpeptidase in relation to its possible role in secretory activity. *Life Sciences*, **16**, 691–704.

Dimov, D. M. and Kulhanek, V., 1967, Comparison of four methods for the estimation of γ-glutamyl transpeptidase activity in biological fluids. *Clinica et Chimica Acta*, **16**, 271–277.

Facemire, C. F., Gross, T. S. and Guillette, L. J. Jr, 1995, Reproductive impairment in the Florida panther: nature or nurture? *Environmental Health Perspectives*, **103**, 79–86.

Foster, W. G., 1998, Endocrine disruptors and development of the reproductive systems in the fetus and children: is there cause for concern? *Canadian Public Health*, **suppl. 1**, S37–34, S52, S41–46.

Gronen, S., Denslow, N., Manning, S., Barnes, D. and Brouwer, M., 1999, Serum vitellogenin levels and reproductive impairment of male Japanese medaka (*Oryzius latipes*). *Environmental Health Perspectives*, **107**, 385–390.

Guillette, L. J. Jr, Gross, T. S., Masson, G. R., Matter, J. M., Percival, H. F. and Woodward, A. R., 1994, Developmental abnormalities of the gonad and abnormal sex hormone concentrations in juvenile alligators form contaminated and control lakes in Florida. *Environmental Health Perspectives*, **102**, 608–688.

Harding, C. O., Williams, P., Wagner, E., Chang, D. S., Wild, K., Colwell, R. E. and Wolff, J. A., 1997, Mice with genetic γ-glutamyl transpeptidase deficiency exhibit glutathionuria, severe growth failure, reduced life spans and infertility. *Journal of Biological Chemistry*, **272**, 12560–12567.

Hodgen, G. D. and Sherins, R. J., 1973, Enzymes as markers of testicular growth and development. *Endocrinology*, **93**, 985–989.

Kavlock, J. J., Daston, G. P., DeRosa, C., Fenner-Crisp, P., Gray, L. E., Kaattari, S., Lucier, G., Luster, M., Mac, M. J., Maczka, C., Miller, R., Moore, J., Rolland, R., Scott, G., Sheehan, D. M., Sinks, T. and Tilson, H. A., 1996, Research needs for the risk assessment of health and environmental effects of endocrine disruptors: a report of the U.S. EPA-sponsored workshop. *Environmental Health Perspectives*, **104 (suppl. 4)**, 715–740.

Lee, P. C., 1998, Disruption of male reproductive tract development by administration of the xenoestrogen, nonylphenol, to male newborn rats. *Endocrine*, **9**, 105–111.

Lee, P. C., Arndt, P. and Nickels, K. C., 1999, Testicular abnormalities in male rats after lactational exposure to nonylphenols. *Endocrine*, **11**, 61–68.

Lee, P. C. and Lee, W., 1996, *In vivo* estrogenic action of nonylphenol in immature female rats. *Bulletin of Environmental Contamination and Toxicology*, **51**, 341–348.

Lieberman, M. W., Wiseman, A. L., Shi, Z. Z., Carter, B. Z., Barrios, R., Ou, C. N., Chevez-Barrios, P., Wang, Y., Habib, G. M., Goodman, J. C., Huang, S. L., Lebovitz, R. M. and Matzuk, M. M., 1996, Growth retardation and cysteine deficiency in γ-glutamyl transpeptidase-deficient mice. *Proceedings of the National Academy of Sciences, USA*, **93**, 7923–7926.

Lu, C. and Steinberger, A., 1977, Gamma-glutamyl transpeptidase activity in the developing rat testis. Enzyme localisation in isolated cell types. *Biology of Reproduction*, **17**, 84–88.

Metcalfe, C., Hoover, L. and Sang, S., 1996, *Nonylphenol Ethoxylates and their Use in Canada*. Report (World Wild Life Fund Canada).

Purdom, C. E., Hardiman, P. A., Bye, V. J., Eno, N. C., Tyler, C. R. and Sumpter, J. R., 1994, Estrogenic effects of effluents from sewage treatment works. *Chemical Ecology*, **8**, 275–285.

Ren, L. F., Lattier, D. and Lech, J. J., 1996, Estrogenic activity of DDE and nonylphenol in rainbow trout determined with a new DNA probe for vitellogenesis pSG5Vg1. *Bulletin of Environmental Contamination and Toxicology*, **56**, 287–294.

Rosalki, S. and Rau, D., 1972, Serum γ-glutamyl transpeptidase activity in alcoholism. *Clinica Chimica Acta*, **39**, 41–47.

Sharpe, R. M., Fisher, J. S., Milla, M. M., Jobling, S. and Sumpter, J. P., 1995, Gestational and lactational exposure of rats to xenoestrogens results in reduced testicular size and sperm production. *Environmental Health Perspectives*, **103**, 1136–1143.

Sharpe, R. M. and Skakkebaek, N. E., 1993, Are estrogens involved in falling sperm counts and disorders of the male reproductive tract? *Lancet*, **341**, 1392.

Soto, A. M., Justica, H., Wray, J. and Sonnenschein, C., 1991, P-nonylphenol: an estrogenic xenobiotic released from modified' styrene. *Environmental Health Perspectives*, **92**, 167–173.

Tate, S. and Meister, A., 1974, Interaction of γ-glutamyl transpeptidase with amino acids, dipeptides and derivatives and analogs of glutathione. *Journal of Biological Chemistry*, **249**, 7593–7602.

Toppari, J., Chr. Larsen, J, Christiansen, P., Giwercman, A., Grandjean, P., Guillette, L. J., Jegou, B., Jensen, T. K., Jouannet, P., Keiding, N., Leffers, H., McLachlan, J. A., Meyer, O., Muller, J., Rajpert-De-Meyts, E., Scheike, T., Sharpe, S., Sumpter, J. and Skakkebaek, N. E., 1996, Male reproductive health and environmental xenoestrogen. *Environmental Health Perspectives*, **104**, 741–776.

XENOBIOTICA, 2000, VOL. 30, NO. 8, 781–795

CYP isoform induction screening in 96-well plates: use of 7-benzyloxy-4-trifluoromethylcoumarin as a substrate for studies with rat hepatocytes

R. J. PRICE†, D. SURRY‡, A. B. RENWICK†,
G. MENESES-LORENTE‡, B. G. LAKE†* and D. C. EVANS§

† TNO BIBRA International Ltd, Carshalton SM5 4DS, UK
‡ Merck Sharp and Dohme Ltd, Neuroscience Research Centre, Terlings Park, Harlow CM20 2QR, UK
§ Drug Metabolism, Merck and Co., 126 East Lincoln Avenue, Rahway, NJ 08535, USA

Received 8 March 2000

1. In this study, 7-benzyloxy-4-trifluoromethylcoumarin (BFC) was evaluated as a substrate to assess the induction of cytochrome P450 (CYP) isoform enzyme activities in rat hepatocytes using a 96-well plate format.

2. BFC was metabolized by both untreated and sodium phenobarbitone (NaPB)-treated rat hepatocytes in a time- and concentration-dependent manner to the highly fluorescent product 7-hydroxy-4-trifluoromethylcoumarin (HFC).

3. HFC was extensively conjugated with D-glucuronic acid and/or sulphate in both untreated and NaPB-treated rat hepatocytes, thus necessitating the inclusion of an enzymatic deconjugation step in the assay procedure.

4. The time-course of induction of 7-ethoxyresorufin metabolism by the CYP1A inducer β-naphthoflavone (BNF), 7-benzyloxyresorufin metabolism by the CYP2B inducer NaPB and BFC metabolism by both BNF and NaPB was studied in rat hepatocytes treated for 24–96 h. The optimal time for induction of metabolism of all three substrates was 72 h, with no medium changes being necessary during this period.

5. The effect of treatment with 0.5–20 μM BNF, 50–2000 μM NaPB, 2–20 μM dexamethasone (DEX), 20–100 μM methylclofenapate (MCP), and 50 and 200 μM isoniazid (ISN) for 72 h on BFC metabolism in cultured rat hepatocytes was studied. BFC metabolism was induced by treatment with BNF, NaPB and MCP, but not with either DEX or ISN.

6. The metabolism of BFC in liver microsomes from the control rat and rat treated with CYP isoform inducers was also studied. BFC metabolism was induced by treatment with NaPB, BNF and DEX.

7. The metabolism of BFC was also studied using microsomes from baculovirus-infected insect cells containing rat cDNA-expressed CYP1A, CYP2B, CYP2C and CYP3A isoforms. Whereas BFC was metabolized to some extent by all the rat cDNA-expressed CYP isoforms examined, at a substrate concentration of 2.5 μM the greatest rates of BFC metabolism were observed with the CYP1A1, CYP1A2 and CYP2B1 preparations.

8. In summary, the results demonstrate that BFC is a good substrate for assessing the induction of CYP1A and CYP2B isoforms in rat hepatocytes in a 96-well plate format.

Introduction

Mammalian cytochrome P450 (CYP) isoforms have a major role in the oxidative metabolism of both xenobiotics and certain endogenous compounds (Conney 1986, Nelson *et al*. 1996, Parkinson 1996). CYP isoform-dependent monooxygenase activities are either induced or inhibited by a wide range of chemicals including

* Author for correspondence; e-mail: blake@bibra.co.uk

Xenobiotica ISSN 0049-8254 print/ISSN 1366-5928 online © 2000 Taylor & Francis Ltd
http://www.tandf.co.uk/journals

many therapeutic agents (Conney 1986, Okey 1990, Parkinson 1996, Pelkonen *et al.* 1998). In the development of new therapeutic agents, it is important to ascertain whether the compound will be either an inducer or inhibitor of CYP isoform activities to minimize potential drug interactions. A knowledge of the properties of a new chemical entity is also important in preclinical studies as several non-genotoxic CYP2B, CYP3A and CYP4A isoform inducers (e.g. phenobarbitone, 2,2-bis(4-chlorophenyl)-1,1,1-trichloroethane, ciprofibrate, Wy-14,643) produce liver tumours in rodents (Nims *et al.* 1987, Grasso and Hinton 1991, Lake 1995, Whysner *et al.* 1996).

The effects of xenobiotics on hepatic CYP isoforms may be evaluated by both *in vivo* and *in vitro* techniques. Many studies have demonstrated that CYP isoforms in the CYP1A, CYP2B, CYP3A, CYP4A and other subfamilies can be induced in cultured rat hepatocytes (reviewed in Paine 1990, LeCluyse *et al.* 1996, Lake 1997). Induction of CYP isoforms in cultured rat hepatocytes can be assessed by a variety of procedures including measurement of CYP isoform mRNA levels, apoprotein levels and enzyme activities (Wortelboer *et al.* 1991, Sidhu *et al.* 1993, Herrero and Castell 1994, Sidhu and Omiecinski 1995, Silva *et al.* 1998, Surry *et al.* 1999). The induction of CYP isoform enzyme activities may be determined both in hepatocyte homogenates/subcellular fractions and in the intact monolayers by addition of the substrate to the culture medium. Indeed, by using substrates that can be metabolized to highly fluorescent products, it is possible to conduct CYP isoform induction studies in 96-well plates using only relatively small numbers of hepatocytes per well. For example, Castell *et al.* have investigated CYP isoform induction in rat and human hepatocytes cultured in 96-well plates using various substrates including 7-benzyloxyresorufin (7BR), 7-ethoxyresorufin (7ER), 7-methoxyresorufin and 7-pentoxyresorufin (Donato *et al.* 1992, 1993, Gómez-Lechón *et al.* 1997). Recently, species differences in coumarin metabolism to 7-hydroxycoumarin have been described in hepatocytes cultured in 96-well plates (Donato *et al.* 1998).

In addition to coumarin and the resorufin derivatives listed above, other fluorescent substrates have been described as sensitive markers for CYP isoform-dependent activities in tissue preparations and for use with cDNA-expressed CYP isoforms. These substrates include 7-alkoxyquinolines (Mayer *et al.* 1990) and coumarin derivatives such as 3-cyano-7-ethoxycoumarin (White 1988), 7-ethoxy-4-trifluoromethylcoumarin (DeLuca *et al.* 1988, Buters *et al.* 1993) and 7-benzyloxy-4-trifluoromethylcoumarin (BFC). BFC has been described as a useful substrate for cDNA-expressed human CYP3A4 in 96-well plate CYP isoform inhibition assays (Crespi *et al.* 1999).

The aim of the present study was to examine the use of BFC as a substrate for assessing the induction of xenobiotic metabolism in cultured rat hepatocytes employing a 96-well plate format. BFC is commercially available (Crespi *et al.* 1999) and is metabolized to 7-hydroxy-4-trifluoromethylcoumarin (HFC), which is highly fluorescent and may be readily quantified (DeLuca *et al.* 1988, Buters *et al.* 1993). The effect of some known inducers of CYP isoforms on BFC metabolism in rat hepatocytes has been compared with effects on 7ER and 7BR metabolism. 7ER and 7BR are often employed as substrates for the induction of CYP1A and CYP2B subfamily isoforms respectively in rat liver (Nerurkar *et al.* 1993, Burke *et al.* 1994). Finally, the sulphorhodamine B (SRB; Rubinstein *et al.* 1990, Skehan *et al.* 1990) and Lowry *et al.* (1951) methods for the assay of hepatocyte protein content in 96-well plates have also been compared.

Materials and methods

Materials

Tissue culture media and Nunclon™ MicroWell™ flat-bottomed 96-well polystyrene plates were from Life Technologies Ltd (Paisley, UK) and Matrigel® Basement Membrane Matrix from Stratech Scientific Ltd (Luton, UK). Other tissue culture materials were as described by Gray *et al*. (1983). 7BR, 7ER, resorufin, β-naphthoflavone, isoniazid, NADPH, SRB and Tris were from Sigma-Aldrich Co. Ltd (Poole, UK), BFC and HFC from UFC Ltd (Manchester, UK), sodium phenobarbitone from BDH Chemicals (Poole, UK) and methylclofenapate from Lancaster Synthesis (Morecambe, UK). A combined β-glucuronidase/arylsulphatase preparation (Catalogue no. 127 698, from *Helix pomatia*) was from Boehringer Mannheim UK Ltd (Lewes, UK). The β-glucuronidase and arylsulphatase activities in 1-ml of the preparation at 38 °C were stated to be 100000 Fishman units and 800000 Roy units respectively. Microsomes were from baculovirus-infected insect (BTI-TN-5B1–4) cells containing cDNA-expressed rat CYP isoforms (GENTEST Corp., Woburn, MA, USA) and stored at −80 °C. The samples of baculovirus-infected insect cell microsomes comprised control cell microsomes (i.e. no transfected CYP isoform, but containing rat NADPH-cytochrome P450 reductase (OR) cDNA) and cell microsomes containing CYP1A1+OR rat, CYP1A2+OR rat, CYP2B1+OR human OR+human cytochrome-b_5 (cyt-b_5) cDNA, CYP2C6+rat OR+human cyt-b_5, CYP2C12 + rat OR+human cyt-b_5, CYP2C13+rat OR+human cyt-b_5, CYP3A1+rat OR+human cyt-b_5 and CYP3A2+rat OR+human cyt-b_5.

Animals

Male Sprague-Dawley rats were from Harlan Olac (Bicester, UK) and allowed free access to R and M No. 1 laboratory animal diet (Special Diets Services, Witham, UK) and water. The animals were housed in polypropylene cages with stainless-steel grid tops and floors in rooms maintained at 22±3 °C with a relative humidity of 40–65% and were allowed to acclimatize to these conditions for at least 14 days before use.

Hepatocyte isolation and culture

Flat-bottomed 96-well plates were coated with Matrigel® before use. Stock Matrigel® was diluted 1:25 (v/v) with cold sterile Dulbecco's phosphate-buffered saline and 25 μl of this solution was added to each well. The plates were placed on a gyratory 96-well plate shaker for 30 s to spread the Matrigel® and then allowed to dry overnight in a 37 °C tissue culture incubator. The plates were washed with 200 μl per well of serum-free tissue culture medium (see below) before addition of hepatocytes. Hepatocytes were from rats (225–275 g body weight) by a collagenase perfusion procedure as described by Gray *et al*. (1983). Viability determined by trypan blue exclusion was 88.1±1.4% (mean±SEM, n = 10). Rat hepatocytes were cultured as described by Donato *et al*. (1992, 1993) and Gómez-Lechón *et al*. (1997). Isolated hepatocytes were seeded in Matrigel®-coated 96-well plates at 30000 viable cells per well in 200 μl per well of Ham F-12/Leibovitz L-15 medium (1:1 v/v) containing 2% (v/v) newborn calf serum, 10 mM D-glucose, 0.01 μM insulin, 50 μg/ml gentamicin and 0.2% (w/v) bovine serum albumin. Hepatocytes were cultured at 37 °C in a humidified incubator under an atmosphere of 95% air/5% CO_2. In the experiments on the comparison of the SRB and Lowry protein assays, hepatocytes were seeded at 10000–40000 viable cells per well. After a 1-h attachment, the medium was changed and the cells cultured for 24 h. Treatment was commenced after 24 h by replacing the medium with 200 μl per well of serum-free Ham F-12/Leibovitz L-15 medium (1:1 v/v) containing 10 mM D-glucose, 0.01 μM insulin, 0.01 μM dexamethasone, 50 μg/ml gentamicin, 0.2% (w/v) bovine serum albumin and the test compound dissolved in DMSO. The final DMSO concentration was 0.4% (v/v) in all cultures including the controls (no test compound) cultures. Hepatocytes were subsequently cultured for 24, 48, 72 and 96 h without any further medium changes.

Assay of 7ER and 7BR metabolism

At the end of the treatment periods the control medium or medium containing the test compounds was removed and the cells washed at 37 °C by the addition of 200 μl RPMI 1640 medium (phenol red free) to each well. The medium was removed and replaced with 100 μl per well of RPMI 1640 medium (phenol red free) containing either 8 μM 7ER and 10 μM dicumarol or 15 μM 7BR and 10 μM dicumarol. Stock solutions of 7ER, 7BR and dicumarol were prepared in DMSO and added to RPMI 1640 medium (phenol red free) at 37 °C so that the final DMSO concentration was 0.45% (v/v). A minimum of four replicate incubations was performed per condition per plate. The plates were quickly mixed on a gyratory shaker and returned to the incubator. At the end of the desired incubation (15–45 min) a 75-μl aliquot of medium was removed from each well into a 'V'-bottomed 96-well plate and the plate stored at −80 °C before analysis. The plates were thawed and 10 μl 0.5 M sodium acetate, pH 4.5, and 15 μl β-glucuronidase/arylsulphatase (freshly diluted 1:100 with distilled water) added to each well. The plates

were mixed on a gyratory shaker and incubated at 37 °C for 2 h. Enzymatic hydrolysis was terminated by the addition of 100 μl methanol to each well. The plates were mixed on a gyratory shaker and centrifuged at 260*g* for 5 min at 4 °C. From each well, a 100-μl aliquot was removed into a white Porvair 96-well plate (Perkin Elmer Ltd, Beaconsfield, UK) and 100 μl 0.5 M glycine-NaOH, pH 10.5, was added to each well. All fluorescence measurements were performed with a Perkin Elmer model LS-50B luminescence spectrophotometer equipped with a Perkin Elmer model LS50 plate reader. Fluorescence measurements were made with excitation and emission wavelengths of 535 and 582 nm respectively, employing 3-nm slits. Standard curves were constructed with 0–60 pmol resorufin per well, the standard being added to RPMI 1640 medium (phenol red free) and taken through the enzymatic hydrolysis procedure described above.

Assay of BFC metabolism

At the end of the treatment periods, the control medium or medium containing the test compounds was removed and the cells washed at 37 °C by the addition of 200 μl RPMI 1640 medium (phenol red free) to each well. The medium was removed and replaced with 100 μl per well of RPMI 1640 medium (phenol red free) containing 2–50 μM BFC. Stock solutions of BFC were prepared in DMSO and added to RPMI 1640 medium (phenol red free) at 37 °C so that the final DMSO concentration was 0.4% (v/v). A minimum of four replicative incubations was performed per condition per plate. The plates were quickly mixed on a gyratory shaker and returned to the incubator. At the end of the desired incubation (10–60 min) a 75-μl aliquot of medium was removed from each well into a 'V'-bottomed 96-well plate and the plate stored at −80 °C before analysis. The plates were thawed and 10 μl 0.5 M sodium acetate, pH 4.5, and 15 μl β-glucuronidase/arylsulphatase (freshly diluted 1:100 with distilled water) was added to each well. The plates were mixed on a gyratory shaker and incubated at 37 °C for 2 h. Enzymatic hydrolysis was terminated by the addition of 100 μl 0.25 M Tris base in 60% (v/v) acetonitrile and the plates were centrifuged as described above. A 100-μl aliquot from each well was removed into a white Porvair 96-well plate and the fluorescence was determined with excitation and emission wavelengths of 410 and 510 nm respectively, employing 3-nm slits. Standard curves were constructed with 0–167 pmol HFC per well, the standard being added to RPMI 1640 medium (phenol red free) and taken through the enzymatic hydrolysis procedure described above.

Determination of protein

At the end of the incubations with the CYP isoform substrates, the medium was removed from the plates and 100 μl 10% (w/v) trichloroacetic acid (TCA) added to each well. After leaving the plates for 30 min at 4 °C, the TCA solution was removed and the wells washed four times with distilled water. The wells were allowed to dry under air and the plates stored at 4 °C before protein determination with SRB (Rubinstein *et al*. 1990, Skehan *et al*. 1990). A 50-μl aliquot of 0.4% (w/v) SRB in 1% (v/v) glacial acetic acid was added to each well and the TCA-fixed cells stained for 30 min at room temperature. The unbound dye was discarded and the wells were quickly washed four times with 1% (v/v) glacial acetic acid. The plates were then dried under air and 200 μl 10 mM Tris base was added to each well and the plates mixed for 5 min on a gyratory shaker. The absorbance of each well was then determined at 490 nm, employing 630 nm as a reference wavelength. In some experiments hepatocyte protein content was also determined by the method of Lowry *et al*. (1951) as adapted for 96-well plates by Donato *et al*. (1998).

Metabolism of BFC in liver microsomes

Investigations were conducted with washed microsomal fractions (Lake 1987) from the livers of the female Sprague-Dawley CD rat (225–275 g body weight), prepared previously (Lake *et al*. 1998). Spectrofluorimeter cuvettes contained 20 μM BFC (added in 10 μl DMSO), 0.1 mg microsomal protein, 1 mM $NADP^+$, 7.5 mM DL-isocitric acid, 2 units isocitric dehydrogenase, 5 mM $MgSO_4$ and 100 mM phosphate buffer, pH 7.4, in a final volume of 2 ml. HFC formation at 37 °C was monitored with excitation and emission wavelengths of 410 and 510 nm respectively, employing 4-nm slits.

Metabolism of BFC by cDNA-expressed rat CYP isoforms

Incubations were performed in Nunc Micro Well™ (Life Technologies Ltd, Paisley, UK) polystyrene 96-well plates with conical wells. Incubation mixtures contained either 2.5 or 25 μM BFC (added in DMSO final concentration 0.2% v/v), 1 mM NADPH and 0.1 M phosphate buffer, pH 7.4, in a final volume of 100 μl. After a 5-min pre-incubation at 37 °C, the reaction was initiated with 4 pmol cDNA-expressed rat CYP isoform preparation (for the control baculovirus-infected insect cell preparation 20 μg microsomal protein was added). For each of the baculovirus-infected insect cell rat cDNA-expressed CYP isoform preparations and each incubation time, four wells were incubated with microsomes and one well without microsomes (blank; tissue added at the end of the incubation). Incubations were performed for 2.5–15 min at 37 °C and were terminated by the addition of 100 μl 0.25 M Tris base in 60% (v/v)

acetonitrile. The plates were centrifuged at 260 *g* for 10 min at 4 °C and a 150-μl aliquot removed from each well into a white Porvair 96-well plate. Fluorescence measurements were performed as described above.

Statistical analysis

Statistical evaluation of data was performed by one-way analysis of variance. Comparisons between means were made using the least significant difference test.

Results

Comparison of SRB and Lowry assays for hepatocyte protein

Rat hepatocytes were seeded in Matrigel® coated 96-well plates at densities of 10000–40000 viable cells per well and cultured for 24 h. At the end of this period, wells were assayed for protein content by either the SRB (Rubinstein *et al*. 1990, Skehan *et al*. 1990) or the Lowry (Lowry *et al*. 1951, Donato *et al*. 1998) procedures. In a series of three experiments, utilizing five different hepatocyte plating densities in each experiment, a good correlation (r^2 = 0.901) was observed between the SRB assay absorbance units and the Lowry protein assay (figure 1). From the data shown in figure 1, a factor of 102 was calculated to convert SRB assay absorbance units into μg hepatocyte protein as determined by the Lowry assay. Matrigel® was found not to affect the SRB assay (data not shown).

Induction of 7ER and 7BR metabolism in cultured rat hepatocytes

The time-course of induction of CYP1A and CYP2B isoforms in rat hepatocytes was studied in cells treated with either 0.05–50 μM β-naphthoflavone (BNF) or 5–2000 μM sodium phenobarbitone (NaPB) for 24, 48, 72 and 96 h. 7-Benzyloxyresorufin *O*-debenzylase activity was relatively constant in 24–96-h control cultures, ranging from 1.0 to 4.5 pmol/min/mg hepatocyte protein. In contrast, 7-ethoxyresorufin *O*-deethylase activity in control cultures increased with culture time, being 9 and 38 pmol/min/mg hepatocyte protein after 24 and 96 h culture respectively (figure 2). BNF treatment produced both a concentration- and time-dependent induction of 7-ethoxyresorufin *O*-deethylase activity (figure 2A). Compared with control cultures, maximum induction of enzyme activity to 1535–1570% of control was observed in cultures treated with either 0.5 or 2 μM BNF for either 48 or 72 h. NaPB treatment produced both a concentration- and time-dependent induction of 7-benzyloxyresorufin *O*-debenzylase activity (figure 2B). Compared with control cultures, maximum induction of enzyme activity to 790–800% of control was observed in cultures treated with either 200 or 500 μM NaPB for 72 h. With both the induction of 7-ethoxyresorufin *O*-deethylase and 7-benzyloxyresorufin *O*-debenzylase activities, compared with control cultures, enzyme induction was greater after 72-h treatment than after either 24- or 96-h treatment.

BFC metabolism in cultured rat hepatocytes

Initial studies were performed by adding HFC, the metabolite of BFC, to the culture medium. Good fluorescent intensities were observed when culture medium, following hydrolysis with β-glucuronidase/arylsulphatase (see below), was treated with 0.25 M Tris in 60% (v/v) acetonitrile and the fluorescence determined at

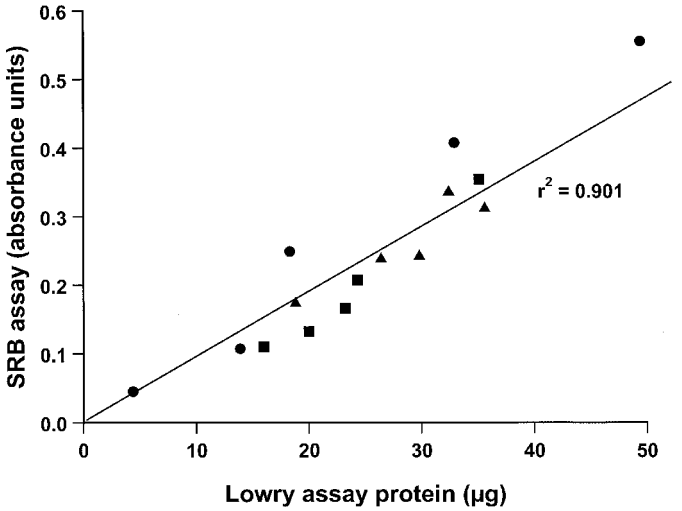


Figure 1. Relationship between SRB protein assay absorbance units and protein content determined by the Lowry assay. Cells were plated at densities of 10000–40000 viable cells per well and cultured for 24 h before determination of rat hepatocyte protein by the SRB and Lowry assays, as described in the Materials and methods. Three separate experiments (●, ■, ▲), utilizing five plating densities per experiment, were performed. A factor of 102 was calculated to convert SRB assay absorbance units into μg hepatocyte protein as determined by the Lowry assay.

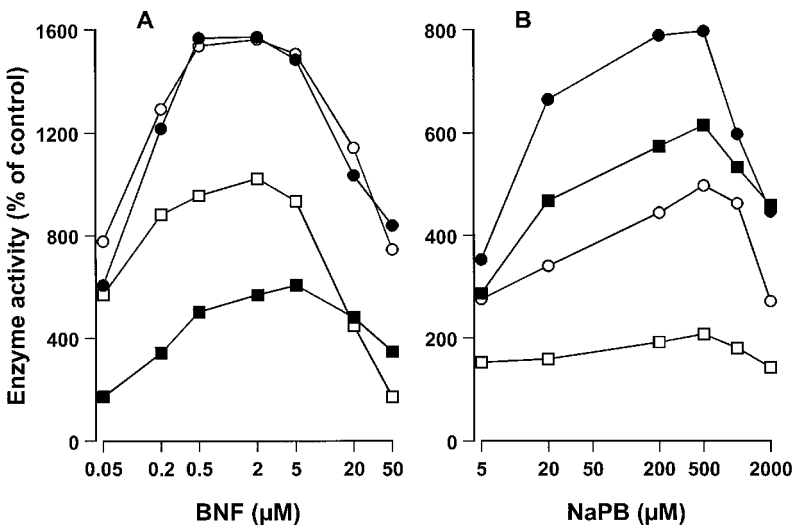


Figure 2. Time-course of induction of 7ER (A) and 7BR (B) metabolism in rat hepatocytes. Cells were cultured for 24 h in control medium and then for 24 (□), 48 (○), 72 (●) and 96 (■) h in either control medium (DMSO only treated) or medium containing 0.05–50 μM BNF (A) or 5–2000 μM NaPB (B). The medium was then changed to one containing either 8 μM 7ER (A) or 15 μM 7BR (B), and the hepatocytes cultured for 30 min before determination of total (i.e. free and conjugated) resorufin. Results are expressed as percentage of enzyme activities in control (DMSO only treated) cultures. Each point represents the mean of four separate experiments. Control rates of 7ER and 7BR metabolism in 24-, 48-, 72- and 96-h cultured hepatocytes were 9 ± 1 (mean$\pm$SEM of four experiments), 14 ± 3, 18 ± 6 and 38 ± 8 pmol/min/mg protein and 1.0 ± 0.4, 2.0 ± 0.4, 4.5 ± 3.2 and 3.4 ± 0.7 pmol/min/mg protein respectively.

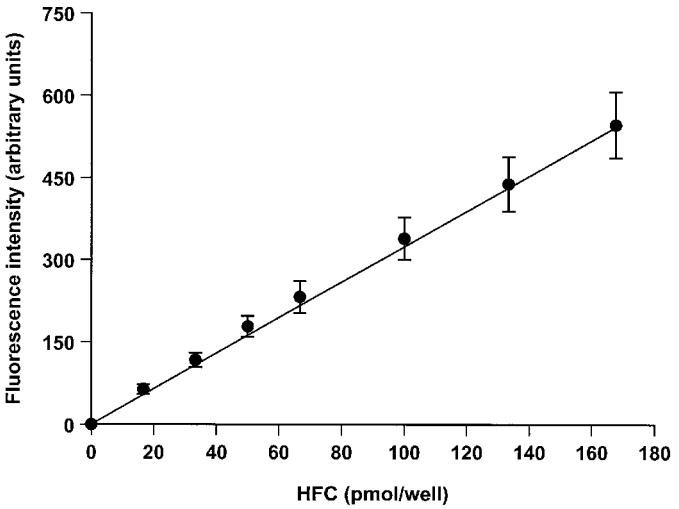


Figure 3. Plot of fluorescence intensity against HFC concentration (mean ± SEM of five experiments). HFC (0–167 pmol) was added to 75 μl phenol red free RPMI 1640 medium, hydrolysed with β-glucuronidase/arylsulphatase and treated with Tris/acetonitrile, as described in the Materials and methods. Fluorescence was determined with excitation and emission wavelengths of 410 and 510 nm respectively, employing 3-nm slits.

excitation and emission wavelengths of 410 and 510 nm respectively. Fluorescence intensity was linear with concentration up to at least 167 pmol HFC per well (figure 3). Under these conditions while HFC fluorescence was stable for short periods (e.g. up to 15 min), some decay of fluorescence intensity was observed if the samples were stored at room temperature (e.g. for $\geqslant$ 45 min) before measurement (data not shown).

Subsequent studies were conducted with rat hepatocytes cultured in either control medium (i.e. no test compound added) or in medium containing known CYP isoform inducers for various periods. Initial studies were conducted with a BFC concentration of 50 μM, this being essentially the limit of BFC solubility in RPMI 1640 medium. BFC metabolism was examined in rat hepatocytes cultured for 72 h in either control medium or medium containing 500 μM NaPB. HFC formation was linear for at least 60 min in control hepatocyte cultures (figure 4A) and for at least 30 min in NaPB-treated cultures (figure 4B). HFC was extensively conjugated with D-glucuronic acid and/or sulphate as rates of HFC formation were much lower in unhydrolysed medium samples from control and NaPB treated cultures (figure 4).

Figure 5 shows the effect of varying the BFC substrate concentration from 2 to 50 μM on HFC formation in rat hepatocytes cultured for 72 h in either control medium or medium containing 500 μM NaPB. With both control and NaPB-treated hepatocytes, HFC formation was maximal at BFC substrate concentrations $\geqslant$ 25 μM.

Induction of BFC metabolism in rat hepatocytes

Time-course studies were conducted with 200 μM NaPB and 20 μM BNF. Rat hepatocytes were cultured with the two inducers for 24, 48, 72 and 96 h. In control cultures, BFC metabolism ranged from 7 to 25 pmol/min/mg hepatocyte protein

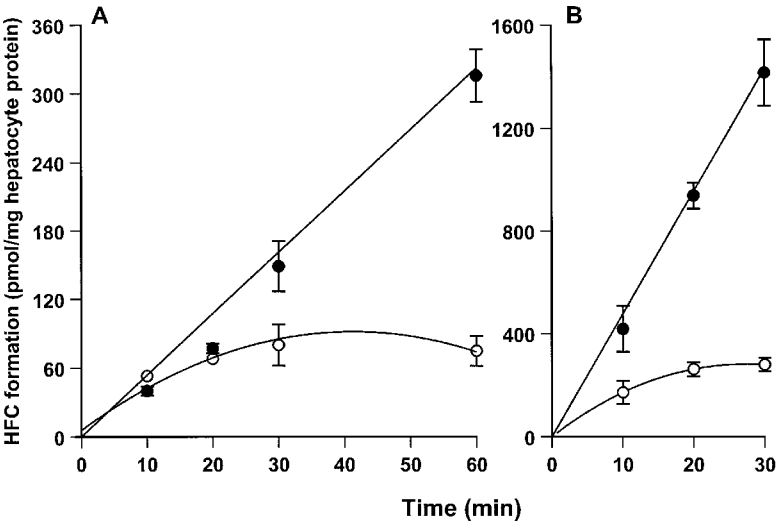


Figure 4. Time-course of BFC metabolism to free (○) and total (i.e. free and conjugated; ●) HFC in rat hepatocytes. Cells were cultured for 24 h in control medium and then for 72 h in either control medium (A) or medium containing 500 μM NaPB (B). The medium was then changed to one containing 50 μM BFC and the hepatocytes cultured for either 10–60 (control cells) or 10–30 (NaPB treated cells) min before determination of HFC. Each point represents the mean ± SEM of four wells. The results of a typical experiment are shown.

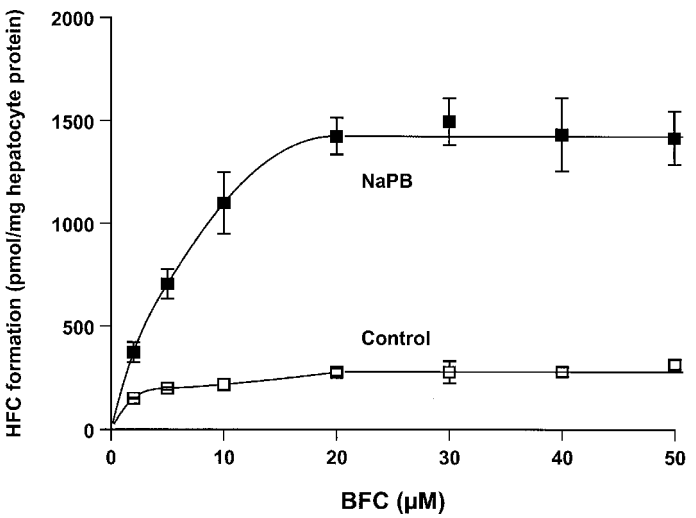


Figure 5. Effect of BFC substrate concentration on the rate of formation of total (i.e. free and conjugated) HFC. Rat hepatocytes were cultured for 72 h in control medium and then for a further 72 h in either control medium or in medium containing 500 μM NaPB. The medium was then changed to one containing 2–50 μM BFC and the hepatocytes cultured for either 30 (NaPB treated cells) or 60 (control cells) min before determination of HFC. Each point represents the mean ± SEM of four wells. The results of a typical experiment are shown.

(figure 6). While a small induction of BFC metabolism was observed after 24-h treatment, enzyme induction was more marked after 48-, 72- and 96-h culture. For both NaPB and BNF, the greatest induction of BFC metabolism was observed in 72-h cultured rat hepatocytes (figure 6).

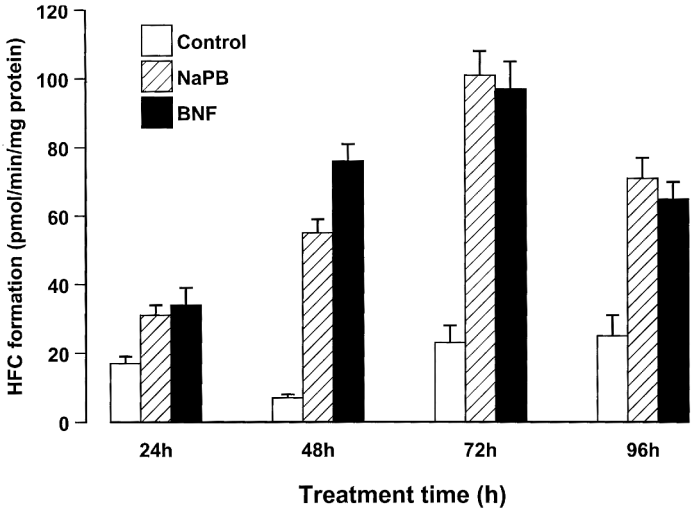


Figure 6. Time-course of induction of BFC metabolism to total (i.e. free and conjugated) HFC in rat hepatocytes. Cells were cultured for 24 h in control medium and then for 24, 48, 72 and 96 h in either control medium or medium containing either 200 μM NaPB or 20 μM BNF. The medium was then changed to one containing 50 μM BFC and the hepatocytes cultured for 20 min before determination of HFC. Each point represents the mean ± SEM of six wells. The results of a typical experiment are shown.

Further studies were conducted with NaPB, BNF and, for purposes of comparison, with dexamethasone (DEX), methylclofenapate (MCP) and isoniazid (ISN). DEX is a known inducer of CYP3A and also of CYP2B isoforms, MCP is a potent peroxisome proliferator and inducer of CYP4A subfamily isoforms, whereas ISN is known to induce CYP2E1 in rat liver (Lake 1995, Parkinson 1996, Lake *et al.* 1998). Hepatocytes were treated with 50–2000 μM NaPB, 0.2–20 μM BNF, 2–20 μM DEX, 20–100 μM MCP, and 50 and 200 μM ISN for 72 h. Treatment with NaPB and BNF for 72 h produced a marked induction of BFC metabolism in rat hepatocytes (figure 7). Maximal induction of BFC metabolism to 565 and 585% of control levels was observed after treatment with 200 μM NaPB and 20 μM BNF respectively. Treatment with MCP also resulted in an induction of BFC metabolism, with maximal induction to 495% of control being observed with 100 μM MCP. In contrast, neither 2–20 μM DEX nor 50 and 200 μM ISN had any marked effect on BFC metabolism in rat hepatocytes (figure 7). In other studies, 200 and 1000 μM NaPB and 2 and 20 μM BNF induced BFC metabolism in 72-h cultured female rat hepatocytes (data not shown).

BFC metabolism in rat hepatic microsomes

BFC metabolism was also examined in liver microsomes prepared previously (Lake *et al.* 1998) from the female Sprague-Dawley CD rat. Rats were treated with 100 mg/kg/day NaPB, 100 mg/kg/day BNF, 50 mg/kg/day DEX, 75 mg/kg/day MCP and 100 mg/kg/day ISN by daily oral gavage for 4 days. Figure 8 shows the effect of treatment with the five inducers on BFC metabolism and, for purposes of comparison, on 7-ethoxy-4-trifluoromethylcoumarin (EFC) *O*-deethylase. The metabolism of BFC and EFC was markedly induced by NaPB and BNF, whereas

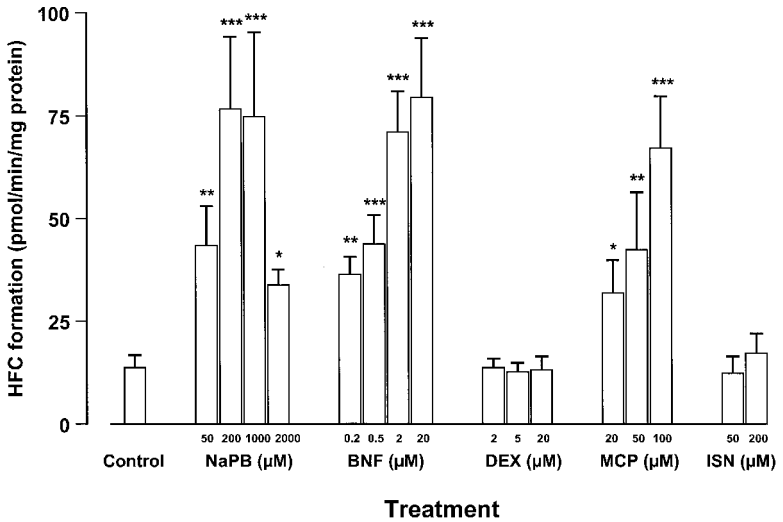


Figure 7. Induction of BFC metabolism to total (i.e. free and conjugated) HFC in rat hepatocytes. Cells were cultured for 24 h in control medium and then for 72 h in either control medium or medium containing 50–2000 μM NaPB, 0.2–20 μM BNF, 2–20 μM DEX, 20–100 μM MCP, and 50 and 200 μM ISN. The medium was then changed to one containing 50 μM BFC and the hepatocytes cultured for 20 min before determination of HFC. Results are the mean ± SEM of three-to-five experiments. Significantly different from control: $*p < 0.05$; $**p < 0.01$; $***p < 0.001$.

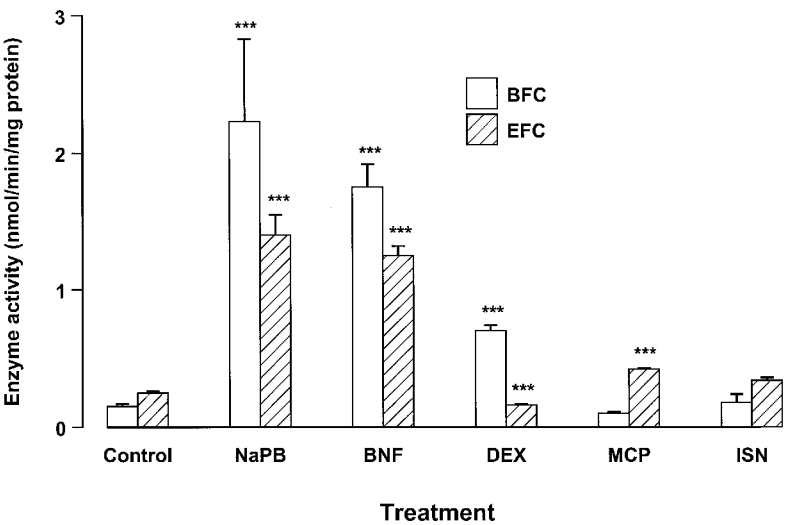


Figure 8. Effect of treatment of the female Sprague-Dawley rat with NaPB, BNF, DEX, MCP and ISN for 4 days on hepatic microsomal BFC and 7-ethoxy-4-trifluoromethylcoumarin (EFC) metabolism to HFC. Results are the mean ± SEM of four animals. EFC metabolism data are from Lake *et al.* (1998). Significantly different from control: $***p < 0.001$.

ISN had no significant effect (figure 8). DEX treatment produced some induction of BFC metabolism and an inhibition of EFC metabolism, whereas MCP treatment produced a small induction of EFC metabolism, but had no effect on BFC metabolism (figure 8).

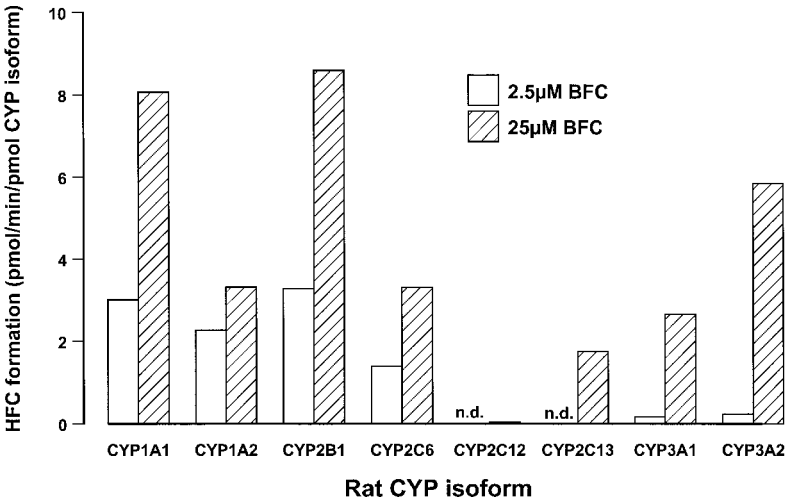


Figure 9. Metabolism of 2.5 and 25 μM BFC by baculovirus-infected insect cell microsomes containing cDNA-expressed rat CYP isoforms. The results of a single experiment are shown. Each value is the mean of four wells, except for incubations with CYP2C12 and CYP2C13 and 2.5 μM BFC substrate where enzyme activity was not determined (n.d.).

BFC metabolism by cDNA-expressed rat CYP isoforms

The metabolism of 2.5 and 25 μM BFC was examined in baculovirus-infected insect cell microsomes containing either no cDNA-expressed rat CYP isoform (control microsomes) or microsomes containing cDNA-expressed rat CYP1A1, CYP1A2, CYP2B1, CYP2C6, CYP2C12, CYP2C13, CYP3A1 and CYP3A2. The BFC substrate concentrations examined were $\sim$2.5 and 25 times respectively the K_m for the high-affinity component of BFC metabolism in liver microsomes from the untreated male Sprague-Dawley rat (Price, Renwick and Lake, unpublished data). With 25-μM substrate, BFC was metabolized by cDNA-expressed CYP1A1, CYP1A2, CYP2B1, CYP2C6, CYP2C13, CYP3A1 and CYP3A2 (figure 9). In contrast, only a very low rate of HFC formation was observed with the cDNA-expressed CYP2C12 preparation. With 2.5-μM substrate, the highest rates of BFC metabolism were observed with the cDNA-expressed CYP1A1, CYP1A2 and CYP2B1 microsome preparations (figure 9). No detectable HFC formation was observed when control (i.e. no transfected CYP isoform) baculovirus-insect cell microsomes were incubated with either 2.5 or 25 μM BFC (data not shown).

Discussion

The development of rapid *in vitro* systems for screening new chemical entities for CYP isoform induction would both reduce the cost of drug development and the usage of experimental animals. In this study, BFC was evaluated as a substrate for assessing the induction of CYP isoform enzyme activities in rat hepatocytes using a 96-well plate format.

Preliminary studies demonstrated that BFC was metabolized both by untreated and NaPB-treated rat hepatocytes in a time- and concentration-dependent manner

to the highly fluorescent product HFC. BFC metabolism to HFC was sufficiently sensitive to be easily quantified in untreated rat hepatocytes (seeded at 30000 viable cells per well) for up to 120 h after isolation (figure 6). Like resorufin formed from 7ER metabolism (Donato *et al.* 1993), HFC produced from BFC metabolism was extensively conjugated with either D-glucuronic acid and/or sulphate (figure 4), thus necessitating an enzymatic deconjugation step to be included in the assay procedure. Kinetic studies demonstrated that maximal rates of HFC formation in the untreated and NaPB-treated rat hepatocytes were observed with BFC medium concentrations of $\geqslant 25$ μM (figure 5).

In this study, two procedures were evaluated for the assay of hepatocyte protein content and the time-course for induction of CYP1A and CYP2B isoforms were investigated. A good relationship was observed between the SRB and Lowry protein assays (figure 1). The SRB assay requires fewer reagents than the Lowry assay and has the advantage that 96-well plates may be stored for extended periods at room temperature before assay of protein content. In agreement with the studies of Boyd *et al.* (Rubinstein *et al.* 1990, Skehan *et al.* 1990), a good concordance was observed between the SRB and Lowry protein assays, enabling a simple factor to be calculated to convert SRB absorbance units to μg protein as determined by the Lowry procedure. Using the SRB protein assay, the rates of 7ER metabolism in 48–96-h cultured rat hepatocytes were calculated as 9–18 pmol/min/mg hepatocyte protein. These rates are similar to the ~ 10 pmol/min/mg protein reported by Donato *et al.* (1992), where protein content was quantified by the Lowry assay.

Also investigated was the time-course for induction of CYP1A and CYP2B isoforms in cultured rat hepatocytes using 7ER and 7BR as substrates. Although 7ER is metabolized mainly by CYP2C6 in liver microsomes from the untreated rat and 7BR is metabolized by several CYP isoforms, 7ER and 7BR are considered good markers for induction of CYP1A and CYP2B isoforms respectively (Nerurkar *et al.* 1993, Burke *et al.* 1994). In a series of elegant studies, Castell *et al.* demonstrated that the resorufin derivatives 7ER, 7BR, 7-methoxyresorufin and 7-pentoxyresorufin might be utilized as substrates to determine the induction of CYP isoforms in cultured rat and human hepatocytes (Donato *et al.* 1992, 1993, Gómez-Lechón *et al.* 1997). The hepatocyte culture conditions described by Castell *et al.* were utilized in the present study. Following the end of an initial 24-h culture, treatment was commenced by changing the culture medium to one containing the test compounds. However, unlike the studies of Castell *et al.*, where the culture medium was changed daily, no further medium changes were performed. Even without daily medium changes, a concentration- and time-dependent induction of 7ER metabolism by BNF and 7BR metabolism by NaPB were observed (figure 2). A 72-h treatment appeared optimal for the induction of both CYP1A and CYP2B isoforms in cultured rat hepatocytes. The lower percentage induction of 7ER and 7BR metabolism after a 96-h culture may represent some degeneration of the cultures at this time point and for 7ER also to the increase in enzyme activity in the control cultures.

The effect of a number of CYP isoform inducers on BFC metabolism in cultured rat hepatocytes was investigated. Initial time-course studies with NaPB and BNF demonstrated that, like the induction of 7ER and 7BR metabolism, a 72-h treatment appeared optimal for assessing enzyme induction (figure 6). Whereas the induction of BFC metabolism was most marked following treatment with BNF and NaPB, induction was also observed with MCP, whereas both DEX and ISN had little effect on BFC metabolism. Whereas BNF is an inducer of CYP1A isoforms, NaPB can

induce CYP isoforms in several CYP subfamilies including CYP2A, CYP2B and CYP3A (Okey 1990, Parkinson 1996). MCP is a potent peroxisome proliferator and induces CYP4A1 mRNA and CYP4A-dependent lauric acid 12-hydroxylase activity in cultured rat hepatocytes (Bell and Elcombe 1991, Lake *et al*. 1993).

For purposes of comparison, the metabolism of BFC and a structurally related compound, EFC, was also studied in liver microsomes from rat treated with CYP isoform inducers. Although these studies were performed with female Sprague-Dawley rat liver microsomes, it was observed that BFC metabolism is inducible by both NaPB and BNF in hepatocytes from both the male and female rat (data not shown). BFC metabolism in liver microsomes was most markedly induced by NaPB and BNF, with DEX producing a small effect and MCP and ISN having no effect. EFC metabolism was similarly most induced by NaPB and BNF, with DEX and MCP producing respectively a small decrease and increase in enzyme activity. Other studies have also reported that EFC metabolism in rat liver microsomes can be stimulated by CYP1A and CYP2B isoform inducers (DeLuca *et al*. 1988).

Additional studies were conducted using cDNA-expressed rat CYP isoforms (figure 9). They demonstrate that BFC is a substrate for CYP1A, CYP2B, CYP2C and CYP3A subfamily isoforms in rat liver. However, at a low substrate concentration, BFC had a higher affinity for the CYP1A and CYP2B isoforms examined (namely CYP1A1, CYP1A2, CYP2B1), than for the CYP2C and CYP3A isoforms examined.

Overall, the present *in vitro* (hepatocytes and cDNA-expressed CYP isoforms) and *in vivo* (liver microsomes) studies suggest that BFC is primarily a probe substrate for induction of CYP1A and CYP2B isoforms in rat hepatocytes. The lack of effect of DEX on BFC metabolism in cultured rat hepatocytes suggests that BFC may not be a suitable probe substrate for CYP3A isoform induction. The induction of BFC metabolism by DEX in rat liver microsomes may be attributable to the observation that DEX induces both CYP2B and CYP3A isoforms in rat liver (Lake *et al*. 1998). Moreover, the difference in affinity of BFC for CYP1A/2B and CYP3A isoforms, together with the limited solubility of BFC in tissue culture medium, would appear to exclude BFC as a suitable probe substrate for induction of CYP3A isoforms in cultured rat hepatocytes. In contrast to DEX, MCP induced BFC metabolism in cultured rat hepatocytes, but not in liver microsomes. The induction of BFC metabolism by MCP in cultured rat hepatocytes is unlikely to be attributable to the induction of CYP4A isoforms. For example, clofibric acid, a structurally related peroxisome proliferator and CYP4A isoform inducer (Lake *et al*. 1993, Lake 1995), induces several CYP isoforms in cultured rat hepatocytes including CYP2B, CYP2C, CYP3A and CYP4A (Bars *et al*. 1989, Bell and Elcombe 1991). BFC does not appear to be a suitable probe for CYP2E isoform induction, as ISN did not stimulate BFC metabolism in either cultured rat hepatocytes or liver microsomes. Additional studies would be required to ascertain whether BFC is a suitable probe for induction of CYP isoforms other than CYP1A and CYP2B in cultured rat hepatocytes.

In summary, these results demonstrate that BFC is a useful substrate for CYP isoform induction studies in cultured rat hepatocytes employing a 96-well plate format. HFC formation could be readily quantified in untreated and CYP isoform inducer-treated rat hepatocyte cultures. From the present data, BFC appears to have the combined properties of 7ER and 7BR as a fluorescent probe substrate, in that BFC metabolism is inducible by both CYP1A and CYP2B isoform inducers.

Acknowledgements

The authors are grateful to MSD Research Laboratories (Harlow, UK) for provision of a research grant.

References

Bars, R. G., Mitchell, A. M., Wolf, C. R. and Elcombe, C. R., 1989, Induction of cytochrome *P*-450 in cultured rat hepatocytes. The heterogeneous localisation of specific isoenzymes by immunocytochemistry. *Biochemical Journal*, **262**, 151–158.

Bell, D. R. and Elcombe, C. R., 1991, Induction of acyl-CoA oxidase and cytochrome P450IVA1 RNA in rat primary hepatocyte culture by peroxisome proliferators. *Biochemical Journal*, **280**, 249–253.

Burke, M. D., Thompson, S., Weaver, R. J., Wolf, C. R. and Mayer, R. T., 1994, Cytochrome P450 specificities of alkoxyresorufin *O*-dealkylation in human and rat liver. *Biochemical Journal*, **48**, 923–936.

Buters, J. T. M., Schiller, C. D. and Chou, R. C., 1993, A highly sensitive tool for the assay of cytochrome P450 enzyme activity in rat, dog and man. Direct fluorescence monitoring of the deethylation of 7-ethoxy-4-trifluoromethylcoumarin. *Biochemical Pharmacology*, **46**, 1577–1584.

Conney, A. J., 1986, Induction of microsomal cytochrome P-450 enzymes: the first Bernard B Brodie Lecture at Pennsylvania State University. *Life Sciences*, **39**, 2493–2518.

Crespi, C. L., Miller, V. P., Ackermann, J. M., Stresser, D. M. and Busby, W. F., Jr., 1999, Novel high throughput fluorescent cytochrome P450 assays. *Toxicological Sciences*, **48(1-S)**, 69.

DeLuca, J. G., Dysart, G. R., Rasnick, D. and Bradley, M. O., 1988, A direct, highly sensitive assay for cytochrome P-450 catalysed *O*-deethylation using a novel coumarin analog. *Biochemical Pharmacology*, **37**, 1731–1739.

Donato, M. T., Castell, J. V. and Gómez-Lechón, M. J., 1992, A rapid and sensitive method for measuring monooxygenase activities in hepatocytes cultured in 96-well plates. *Journal of Tissue Culture Methods*, **14**, 153–157.

Donato, M. T., Castell, J. V. and Gómez-Lechón, M. J., 1998, The coumarin 7-hydroxylation microassay in living hepatic cells in culture. *ATLA*, **26**, 213–223.

Donato, M. T., Gómez-Lechón, M. J. and Castell, J. V., 1993, A microassay for measuring cytochrome P450IA1 and P450IIB1 activities in intact human and rat hepatocytes cultured on 96-well plates. *Analytical Biochemistry*, **213**, 29–33.

Gómez-Lechón, M. J., Donato, M. T., Ponsoda, X., Fabra, R., Trullenque, R. and Castell, J. V., 1997, Isolation, culture and use of human hepatocytes in drug research. In J. V. Castell and M. J. Gómez-Lechón (eds), *In Vitro Methods in Pharmaceutical Research* (London: Academic Press), pp. 129–153.

Grasso, P. and Hinton, R. H., 1991, Evidence for and possible mechanisms of non-genotoxic carcinogenesis in rodent liver. *Mutation Research*, **248**, 271–290.

Gray, T. J. B., Lake, B. G., Beamand, J. A., Foster, J. R. and Gangolli, S. D., 1983, Peroxisome proliferation in primary cultures of rat hepatocytes. *Toxicology and Pharmacology*, **67**, 15–25.

Herrero, M. E. and Castell, J. V., 1994, Quantification of CYP1A1 and 2B1/2 in rat hepatocytes cultured in microwells by immunological methods. *Toxicology in Vitro*, **8**, 1167–1175.

Lake, B. G., 1987, Preparation and characterization of microsomal fractions for studies of xenobiotic metabolism. In K. Snell and B. Mullock (eds), *Biochemical Toxicology: A Practical Approach* (Oxford: IRL), pp. 183–215.

Lake, B. G., 1995, Mechanisms of hepatocarcinogenicity of peroxisome-proliferating drugs and chemicals. *Annual Review of Pharmacology and Toxicology*, **35**, 483–507.

Lake, B. G., 1997, *In vitro* methods. In R. S. McCuskey and D. L. Earnest (eds), *Comprehensive Toxicology*, vol. 9: *Hepatic and Gastrointestinal Toxicology* (Oxford: Pergamon), pp. 233–249.

Lake, B. G., Lewis, D. F. V., Gray, T. J. B. and Beamand, J. A., 1993, Structure-activity relationships for induction of peroxisomal enzyme activities in primary rat hepatocyte cultures. *Toxicology in Vitro*, **7**, 605–614.

Lake, B. G., Renwick, A. B., Cunninghame, M. E., Price, R. J., Surry, D. and Evans, D. C., 1998, Comparison of the effects of some CYP3A and other enzyme inducers on replicative DNA synthesis and cytochrome P450 isoforms in rat liver. *Toxicology*, **131**, 9–20.

LeCluyse, E. L., Bullock, P. L. and Parkinson, A., 1996, Strategies for restoration and maintenance of normal hepatic structure and function in long-term cultures of rat hepatocytes. *Advanced Drug Delivery Reviews*, **22**, 133–186.

Lowry, O. H., Rosebrough, N. J., Farr, A. L. and Randall, R. J. 1951, Protein measurement with the Folin phenol reagent. *Journal of Biological Chemistry*, **193**, 265–275.

Mayer, R. T., Netter, K. J., Heubel, F., Hahnemann, B., Buchheister, A., Mayer, G. K. and Burke, M. D., 1990, 7-Alkoxyquinolines: new fluorescent substrates for cytochrome P450 monooxygenases. *Biochemical Pharmacology*, **40**, 1645–1655.

Nelson, D. R., Koymans, L., Kamataki, T., Stegeman, J. J., Feyereizen, R., Waxman, D. J., Waterman, M. R., Gotoh, O., Coon, M. J., Estabrook, R. W., Gunsalus, I. C. and Nebert, D. W., 1996, P450 superfamily: update on new sequences, gene mapping, accession numbers and nomenclature. *Pharmacogenetics*, **6**, 1–42.

Nerurkar, P. V., Park, S. S., Thomas, P. E., Nims, R. W. and Lubet, R. A., 1993, Methoxyresorufin and benzyloxyresorufin: substrates preferentially metabolized by cytochromes P4501A2 and 2B respectively, in the rat and mouse. *Biochemical Pharmacology*, **46**, 933–943.

Nims, R. W., Devor, D. E., Henneman, J. R. and Lubet, R. A., 1987, Induction of alkoxyresorufin *O*-dealkylases, epoxide hydrolase, and liver weight gain: correlation with tumor-promoting potential in a series of barbiturates. *Carcinogenesis*, **8**, 67–71.

Okey, A. B., 1990, Enzyme induction in the cytochrome P-450 system. *Pharmacology and Therapeutics*, **45**, 241–298.

Paine, A. J., 1990, The maintenance of cytochrome P-450 in rat hepatocyte culture: some applications of liver cell culture to the study of drug metabolism, toxicity and the induction of the P-450 system. *Chemico-Biological Interactions*, **74**, 1–31.

Parkinson, A., 1996, Biotransformation of xenobiotics. In C. D. Klaassen (ed.), *Casarett and Doull's Toxicology: The Basic Science of Poisons* 5th edn (New York: McGraw Hill), pp. 113–186.

Pelkonen, O., Mäenpää, J., Taavitsainen, P., Rautio, A. and Raunio, H., 1998, Inhibition and induction of human cytochrome P450 (CYP) enzymes. *Xenobiotica*, **28**, 1203–1253.

Rubinstein, L. V., Shoemaker, R. H., Paull, K. D., Simon, R. M., Tosini, S., Skehan, P., Scudiero, D. A., Monks, A. and Boyd, M. R., 1990, Comparison of *in vitro* anticancer-drug-screening data generated with a tetrazolium assay versus a protein assay against a diverse panel of human tumor cell lines. *Journal of the National Cancer Institute*, **82**, 1113–1118.

Sidhu, J. S., Farin, F. M. and Omiecinski, C. J., 1993, Influence of extracellular overlay on phenobarbital-mediated induction of CYP2B1, 2B2, and 3A1 genes in primary adult rat hepatocyte culture. *Archives of Biochemistry and Biophysics*, **301**, 103–113.

Sidhu, J. S. and Omiecinski, C. J., 1995, Modulation of xenobiotic-inducible cytochrome P450 gene expression by dexamethasone in primary rat hepatocytes. *Pharmacogenetics*, **5**, 24–36.

Silva, J. M., Morin, P. E., Day, S. H., Kennedy, B. P., Payette, P., Rusmore, T., Yergey, J. A. and Nicoll-Griffith, D. A., 1998, Refinement of an *in vitro* cell model for cytochrome P450 induction. *Drug Metabolism and Disposition*, **26**, 490–496.

Skehan, P., Storeng, R., Scudiero, D., Monks, A., McMahon, J., Vistica, D., Warren, J. T., Bokesch, H., Kenney, S. and Boyd, M. R., 1990, New colorimetric assay for anticancer-drug-screening. *Journal of the National Cancer Institute*, **82**, 1107–1112.

Surry, D., McAllister, G., Meneses-Lorente, G. and Evans, D. C., 1999, High throughput ribonuclease protection assay for the determination of CYP3A mRNA induction in cultured rat hepatocytes. *Xenobiotica*, **29**, 827–838.

White, I. N. H., 1988, A continuous fluorimetric assay for P-450-dependent mixed function oxidases using 3-cyano-7-ethoxycoumarin. *Analytical Biochemistry*, **172**, 304–310.

Whysner, J., Ross, P. M. and Williams, G. M., 1996, Phenobarbital mechanistic data and risk assessment: enzyme induction, enhanced cell proliferation and tumour proliferation. *Pharmacology and Therapeutics*, **71**, 153–191.

Wortelboer, H. M., de Kruif, C. A., van Iersel, A. A. J., Falke, H. E., Noordhoek, J. and Blaauboer, B. J., 1991, Comparison of cytochrome P450 isoenzyme profiles in rat liver and hepatocyte cultures. The effects of model inducers on apoproteins and biotransformation activities. *Biochemical Pharmacology*, **42**, 381–390.

XENOBIOTICA, 2000, VOL. 30, NO. 8, 797–813

Pharmacokinetics of the M1-agonist talsaclidine in mouse, rat, rabbit and monkey, and extrapolation to man

A. LEUSCH*, W. TRÖGER, A. GREISCHEL and W. ROTH

Department of Pharmacokinetics and Drug Metabolism, Boehringer Ingelheim Pharma KG, 88397 Biberach, Germany

Received 6 January 2000

1. Talsaclidine is an M1-agonist under development for the treatment of Alzheimer's disease. The aim of the study was to investigate the absorption, distribution, metabolism and excretion (ADME) of single intravenous and oral doses of [^{14}C]-talsaclidine in mouse, rat, rabbit and monkey. Previous data in humans showed that the drug was mainly excreted into the urine as the unchanged parent drug. The hypothesis was tested if animal data of drugs, which are mainly excreted renally, could be extrapolated to human.

2. The apparent volume of distribution at steady-state (V_{ss}) was comparable in all animal species (2–5 l.kg^{-1}) indicating an extensive distribution of the drug into tissues. The plasma protein binding was low and comparable in all species including man ($\leqslant 7\%$). Elimination in terms of clearance was rapid-to-moderate depending on the species. The total plasma clearance (Cl) decreased in the order: mouse (128 ml.min^{-1}.kg^{-1}) > rat (73.9) > monkey (10.6). Urinary excretion is the dominant route of excretion ($\geqslant 86\%$).

3. A good correlation was achieved with human and animal data in allometric scaling of Cl and V_{ss}. This confirms the hypothesis that renal filtration is scalable over the species and, given a comparable protein binding, animal data is predictive for man.

Introduction

Alzheimer's disease (AD) is a progressive degenerative illness characterized by continuing loss of memory, impaired cognition and a change in personality. Drug development in recent years has aimed at boosting the cholinergic system, either by sustaining the level of the natural transmitter or by substituting acetylcholine itself (Lawrence *et al*. 1998). Initial attempts based on acetylcholine precursors such as lecithin or choline were unsuccessful, whereas compounds which prevented acetylcholine degradation in the synaptic cleft by inhibiting acetylcholinesterase (AChE) proved a promising approach. Tacrine (Davies *et al*. 1989, Giacobini 1998) was introduced in 1993 into the US market. Furthermore, another AChE-inhibitor, Donepezil (Barner *et al*. 1998, Rogers *et al*. 1998) was subsequently put on the market.

A different approach, based on the cholinergic hypothesis, is the direct stimulation of post-synaptic muscarinic receptors. These receptors appear to be unaffected in AD and, therefore, the post-synaptic neurone excitation would still occur despite the low levels of the endogenous neurotransmitter. Early attempts (e.g. arecoline, pilocarpine) faced serious drawbacks, as most of these early compounds were quaternary derivatives that penetrated the blood–brain barrier poorly and which had undesired peripheral side-effects (Arnt *et al*. 1992). The next generation of compounds took advantage of the observation that different muscarinic

* Author for correspondence; e-mail: andreas.leusch@bc.boehringer-ingelheim.com

Xenobiotica ISSN 0049-8254 print/ISSN 1366-5928 online © 2000 Taylor & Francis Ltd
http://www.tandf.co.uk/journals

receptor subtypes existed in tissues (Hulme *et al*. 1990). Compounds such as xanomeline (Bymaster *et al*. 1998, Delapp *et al*. 1998), SB202026 (Bromidge *et al*. 1997) and LU 25–109 (Sramek *et al*. 1998) have been developed with a more or less functional selectivity.

The ideal cholinomimetic in AD would be a centrally acting M1 agonist, as the post-synaptic muscarinic receptors in the cortex and hippocampus are predominantly of the M1 subtype (Messer *et al*. 1989) and serious side-effects could be avoided due to the limited stimulation of peripheral M2 and M3 subtypes. Talsaclidine exhibits functional selectivity with regard to stimulation of the neuronal muscarine M1 receptor subtype *in vitro* (Ensinger *et al*. 1993, 1997) and *in vivo* in animals.

Previous results in the rat (Ensinger *et al*. 1997) indicated a high proportion of renally excreted drug and/or metabolites. In man (Adamus *et al*. 1995), the parent drug was mainly excreted in urine. The aim of the present study was to determine the basic pharmacokinetics of talsaclidine in animal species to test the hypothesis if animal data of mainly renally excreted drugs are predictive for man.

Materials and methods

Radiolabeled compound

Talsaclidine was radiolabelled by introducing a ^{14}C-atom in the position 3 of the 1-aza-bicyclo[2,2,2]octane ring system, at a position considered least likely to be affected by metabolic transformation (figure 1). In all studies, the specific radioactivity was ~ 13 MBq.mg^{-1} (active entity), which was diluted with the unlabelled drug to the appropriate activity for the experimental set-up. Radiochemical purity was $> 99\%$ in all experiments.

Radiometry

The concentrations of [^{14}C]talsaclidine and its metabolites in blood, plasma, urine and faeces were measured using a liquid scintillation counter (Packard TriCarb 1500 or TriCarb 460 CD, Packard, Frankfurt, Germany) or model LS 3801 (Beckman Instruments GmbH, Munich, Germany), and Quickszint (Zinsser Analytik, Frankfurt, Germany) was used as a scintillation cocktail unless otherwise specified. Other LSC cocktails used were Optifluor (Canberra-Packard, Frankfurt, Germany) or Oxysolve C-400 (Zinsser Analytik, Frankfurt, Germany) for samples combusted in a sample oxidizer (Biological Oxidizer OX 500, J. Harvey Instrument Corp., Zinsser Analytik GmbH, Frankfurt, Germany). Quench correction was made using the transformed spectral index of the internal standard spectrum (tSIE), which was calculated from the Compton spectrum, induced in the sample by the external standard source (^{133}Ba). The radioactivity measured in dpm.ml^{-1} or g blood or plasma was converted into the concentration of drug and metabolites by division by the specific radioactivity of [^{14}C]talsaclidine. Because the method measures both talsaclidine and radioactive metabolites of talsaclidine, concentrations were expressed as equivalents of [^{14}C]talsaclidine. The radioactivity in urine and faeces was expressed as a percentage of the radioactivity administered. All reported data refer to the active entity talsaclidine (free base).

GC/MS assay for talsaclidine

A sensitive and specific internally standardized gas chromatographic assay with mass selective detection in electron-impact mode (GC/MS-EI) for quantitative determination determined talsaclidine in plasma samples of different species, in rat brain tissue and cerebrospinal fluid (CSF). Before extraction, brain tissue samples were homogenized with 2 ml saline (0.9% NaCl) with an Ultra-Turrax. 0.5 ml homogenate or 0.5 ml plasma/CSF were spiked with the internal standard (pentadeuterated talsaclidine-d_5). Buffer (1 ml, pH 11; H_3BO_3, KCl, NaOH, Merck, Darmstadt, Germany) and 50 μl NaOH 4 M (Merck) were added and the samples extracted with 4 ml of a mixture of toluene/dichloromethane/ethyl acetate (TDE, 5:3:2 v/v/v). After vortexing, the extracts were separated by centrifugation or freezing and further purified by re-extraction with 200 μl sulphuric acid 0.4 N (Baker, Griesheim, Germany) and re-extracted with 250 μl organic solvent mixture (TDE) containing additionally 100 μl buffer, pH 11, and 50 μl NaOH 4 M. Of the organic supernatant, 200 μl was transferred into an autosampler vial, mixed with 10 μl acetic acid and dried (vacuum centrifuge). The residues were reconstituted in 20 μl TDE containing

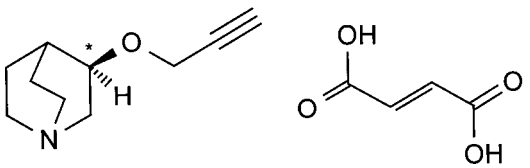


Figure 1. Chemical structure of [^{14}C]-radiolabelled talsaclidine fumarate, the salt of the active entity talsaclidine (1-azabicyclo[2.2.2]octan,3-(2-propynyloxy)-,(*R*)-,(E)-2-butenedioate). *Position of radioactive label.

12.5% triethylamine (Fluka, Buchs, Switzerland). An aliquot was employed to chromatographic separation on a 100% cross-linked methyl-silicone capillary column (Hewlett Packard Ultra 1, 12 m × 0.2 mm, film thickness 0.33 μm) in a Hewlett Packard 5890 A gas chromatograph was equipped with a mass selective detector (HP 5970A) running at an EI mode at 70 eV (Hewlett Packard, Waldbronn, Germany). The temperature gradient programme started with 60 °C for 1 min and increased at 30 °C.min^{-1} to a final 280 °C held for 5 min. The masses of 126 *m/z* for talsaclidine and 131 *m/z* for the internal standard were used for identification and quantification of the analytes. The GC-MS method was validated according to current international guidelines (Shaw *et al*. 1992) and exhibited a calibration range of 1–118 ng.ml^{-1}. The imprecision and inaccuracy of the method were < 15%. All reported data refer to the active entity talsaclidine (free base).

Sampling of biological materials

Blood samples from mouse and rat were obtained under halothane, ether or chloroform anaesthesia by puncture of the orbital venous sinus or by cardiac puncture. Additionally, a new procedure of obtaining multiple blood samples from mouse by puncturing the tail vein with a butterfly (Abbott, Wiesbaden, Germany) connected with a 1 ml syringe (Primo, Rødby, Denmark) was developed and used to obtain concentration–time profiles from single animals. Blood samples from rabbit and rhesus monkey were taken from the ear vein and from the leg or arm vein (contralaterally to the intravenous (i.v.) administration) respectively.

CSF was collected by puncturing the cisterna magna through the foramen occipitale using a disposable syringe and a cannula no. 18 (0.45 × 23 mm; Neolus Terumo, Leuven, Belgium). Samples were only accepted if they were colourless or with a minor contamination of blood. Brain tissue was collected by decapitation of the rat. The skull was then opened by dissection of a skull calotte along the lateral sutures starting from the foramen occipitale. The brain was removed with a micro spatula, wiped with absorbent tissues and the medulla oblongata dissected.

Urine and faeces were collected up to 192 h and the radioactivity of the samples was determined.

Preparation of samples for liquid scintillation counting

In general, each of three blood aliquots was weighed in plastic vials, haemolyzed by 0.5 ml digestin (1 M N-ethyl-N-dodecyl-N,N-dimethylammonium-hydroxid in methanol; Merck): ethanol (1:2) at 50 °C in a shaking water bath and decolourized with 0.2 ml 30% H_2O_2 (Sigma, Deisenhofen, Germany) under the same conditions. The samples were left overnight after the addition of 0.2 ml HCl (1 M; Merck) and measured by liquid scintillation counting (LSC). Plasma was prepared by centrifugation of blood at 3000*g*. Radioactivity was determined in duplicate or triplicate 50–200-μl fractions.

The total volume of urine was determined, and three 0.1–0.5 ml portions of urine were measured in the LSC after addition of 20 ml Quickszint. Faecal samples were diluted with ~ 5–10 vols water and homogenized with an Ultra-Turrax (Jahnke and Kunkel, Stauffen, Germany). Three aliquots of 0.1–0.4 g were treated with 1 ml Digestin for 2 h at 50 °C in a shaking water bath and decolourized with 0.15 ml H_2O_2 under the same conditions. After the addition of 20 ml scintillation cocktail, and a decay of > 24 h, the radioactivity was measured. However, in one experiment, weighed blood and faeces samples were dried and combusted in an automatic combustion chamber absorbing the $^{14}CO_2$ in 15 ml Oxysolve C-400.

Protein binding of talsaclidine

Plasma protein binding was investigated by means of equilibrium dialysis in mouse, rat, rabbit, monkey and human. Stored human plasma and freshly obtained animal plasma were used for the species comparison. The concentration dependence of the plasma protein binding was tested with triplicate human plasma samples containing 0.2, 1.0 or 20 μg.ml^{-1} [^{14}C]talsaclidine. All samples were dialysed in triplicate against a phosphate buffer according to Sörensen (67 mmol.l^{-1}, pH 7.4) in a Dianorm-4Drive dialysis apparatus (Diachema, Munich, Germany) containing 1.3 μg.ml^{-1} [^{14}C]talsaclidine. The chamber

Table 1. Doses and administration routes in the animal experiments.

Species	Route of administration	Dose of talsaclidine ($mg.kg^{-1}$)	Number of animals per dose	Experiment
Mouse	i.v.	1·2	2 m/2 f*	parent compound
	i.v.	1·2	5 m/4 f*	radioactivity
	i.v.	5·9	5 m/5 f*	excretion
	p.o.	5·9	2 m/2 f*	parent compound
	p.o.	5·9	4 m/4 f*	radioactivity
	p.o.	5·9	5 m/5 f*	excretion
Rat	i.v.	1·2	4 m/4 f	parent compound
	i.v.	6·5	5 m	radioactivity
	i.v.	5·9	5 m	excretion
	p.o.	5·9	4 m/5 f	parent compound
	p.o.	6·5	5 m	radioactivity
	p.o.	8·8, 17·6, 35·2, 52·9	2 m/2 f	excretion
	p.o.	5·9	6 m*	blood brain barrier
Rabbit	p.o.	5·9	3 f	parent compound
	p.o.	5·9	2 m/2 f	radioactivity
	p.o.	5·9	2 m/2 f	excretion
Monkey	i.v.	2·9	2 m/2 f	parent compound
	i.v.	2·9	2 m/2 f	radioactivity
	i.v.	2·9	2 m/1 f	excretion
	p.o.	5·9	2 m/2 f	parent compound
	p.o.	5·9	2 m/2 f	radioactivity
	p.o.	5·9	2 m/2 f	excretion

* Per timepoint.
m, Male; f, female.

volume was 1 ml (macrocell: Macro1) and the membrane was a visking dialysis tube (type 20/32, wall thickness 0.02 mm, pore size 22A; Serva, Heidelberg, Germany). The chambers were rotated for 3 h at 37 °C (water bath) and radioactivity was measured in 0.5-ml aliquots by LSC.

Pharmacokinetic analysis

Pharmacokinetic parameters were determined using non-compartmental methods in the TopFit program package (Heinzel *et al*. 1993). C_{max} and t_{max} for talsaclidine and drug-related radioactivity were determined by direct observation of the data. λ_z was calculated by logarithmic–linear regression of the plasma concentration–time curve. The elimination $t_{1/2}$ was calculated as $\ln 2/\lambda_z$. AUC_{0-t} to the final measurable sample was calculated using the logarithmic trapezoidal rule for concave concentration–time profiles and extrapolated to infinity ($AUC_{0-\infty}$) with the final plasma concentration being divided by λ_z. MRT_{tot} ($MRT_{abs}+MRT_{disp}$) was calculated according to the method of Gibaldi and Perrier (1982). Total plasma clearance, Cl, was calculated by dividing the dose by $AUC_{0-\infty}$, and volume of distribution at steady-state (V_{ss}) was calculated as $V_{ss} = Cl \cdot_{disp}$ (i.v. bolus). Mean pharmacokinetic parameters in mouse, rabbit (radioactivity) and monkey were calculated from male and female animals due to no sex difference in the plasma concentration data. In rat, means were calculated for males and females separately. SD was given where appropriate. Further statistical analysis of the data was not performed due to the limited number of animals.

Animals

Rationale. Pharmacokinetic information was required for mouse, rat, rabbit and rhesus monkey because the species were used in drug safety studies. The rat was of primary interest because it was also used extensively in pharmacological studies. The studies in rhesus monkey were undertaken to obtain data from primates. For safety reasons, doses in man (highest dose 94 mg; Adamus *et al*. 1995) were several times lower than doses in the animal species (1–10 $mg.kg^{-1}$). Maximum drug plasma concentrations (C_{max}) in animals turned out to be two-to-three-fold higher than in humans at the highest dose level. C_{max} in humans increased proportionally to the dose in the range 0.3–94 mg and therefore linear kinetics was assumed. All doses (table 1) refer to the active entity talsaclidine (free base). The drug was generally dissolved in physiological saline for i.v. administration or in distilled water for oral gavage. Animals were housed individually in metabolism cages and excreta were collected in the excretion balance experiments. All animals were fasted overnight before administration.

Table 2. Pharmacokinetic parameters of talsaclidine in plasma after the intravenous administration of talsaclidine to the male and female mouse, rat and rhesus monkey.

Parameter		Mouse m+f	Rat# m	Rat# f	Monkey m+f
Dose	($mg.kg^{-1}$)	1·2	1·2	1·2	2·9
C_{max}	($ng.ml^{-1}$)	442·5±69·9	371·9±6·2	451·6±90·9	2645±2221
t_{max}	(h)	0·083*	0·083*	0·083*	0·25*
$AUC_{0-\infty}$	($ng.h.ml^{-1}$)	154·2±14·6	212·4	352·8	5400±2698
$MRT_{0-\infty}$	(h)	0·4±0·1	1·0	1·2	3·9±1·4
$t_{1/2}$	(h)	1·0±1·3	1·6	1·4	4·8±1·4
Cl	($ml.min^{-1}.kg^{-1}$)	128±11·7	92·2	55·5	10·6±4·4
V_{ss}	($l.kg^{-1}$)	3·2±0·6	5·7	4·0	2·3±0·7

* Median.

\# Owing to a staggered design, the mean concentration–time profile of four males or four females was evaluated and a SD is not available.

m, Male; f, female.

Mouse. Experiments to characterize talsaclidine pharmacokinetics were carried out with the male and female Crl:CD-1 (ICR) BR mouse (Charles River Wiga GmbH, Sulzfeld, Germany) and drug-related radioactivity in blood was determined in the male and female Chbb:NMRI animal (Experimental Animal Breeding Station, Dr Karl Thomae GmbH, Biberach/Riß, Germany). Blood samples were taken by puncturing the tail vein. The body weight of all animals used varied between 15.9 and 31.4 g.

Rat. All animal studies were conducted with the male and female albino rat (Chbb:THOM; Dr Karl Thomae GmbH; body weight 200–250 g).

Rabbit. Pharmacokinetic properties were assessed in the male and female rabbit (Chbb:HM; Dr Karl Thomae GmbH; body weight 2.5–3.1 kg).

Rhesus monkey. Experiments were carried out in the male and female rhesus monkey (*Macaca mulatta*; Animal Centre, Boehringer Ingelheim KG, Ingelheim am Rhein, Germany; body weight 5.6–10.4 kg).

Allometric scaling

Pharmacokinetic parameters in man, mouse, rat and monkey were correlated using the allometric scaling approach according to the relation: $x = a \cdot BW^b$, where x is the test parameter (total plasma clearance, Cl_{tot} and V_{ss}), BW is body weight and a, b are constants calculated by non-linear regression. Data on Cl_{tot} and V_{ss} in man are from Adamus *et al*. (1995). Mean Cl_{tot} and V_{ss} data in mouse, rat and monkey (male and female), obtained after i.v. administration (table 2), were used for the regression. Intravenous data in rabbit were not available and the species was excluded from the regression.

Results

Mouse

The concentration–time profile of talsaclidine and drug-related radioactivity in the male and female mouse is given in figure 2. Corresponding pharmacokinetic parameters are listed in tables 2–5.

After i.v. administration of 1.2 $mg.kg^{-1}$, no differences between the male and female were observed. Maximum talsaclidine plasma concentrations of 442.5 $ng.ml^{-1}$ (C_{max}) were detected 5 min (t_{max}) after administration (figure 2, A). Plasma concentrations declined rapidly in a polyphasic manner with a terminal half-life of 1.0 h. Mean residence was 0.4 h. The elimination was fast with a Cl of 128 $ml.min^{-1}.kg^{-1}$. V_{ss} was 3.2 $l.kg^{-1}$. Following oral administration of 5.9 $mg.kg^{-1}$, maximum talsaclidine plasma levels of 1041 $ng.ml^{-1}$ were observed 0.25 h after

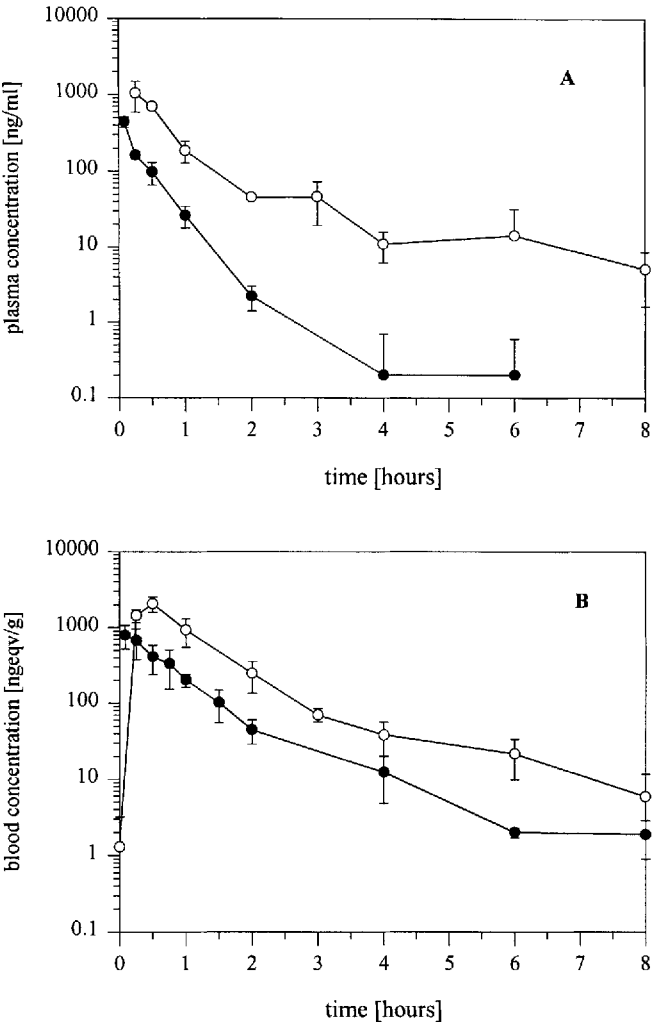


Figure 2. Plasma concentration–time curve for talsaclidine (A) and drug-related radioactivity in blood (B) in the male and female mouse after the i.v. administration of 1.2 mg.kg^{-1} and oral administration of 5.9 mg.kg^{-1}. ●, 1.2 mg.kg^{-1} i.v.; ○, 5.9 mg.kg^{-1} oral. Data are the mean ± SD of four-to-nine animals.

administration (figure 2, A). The terminal half-life (1.7 h) was almost comparable with the i.v. route, although the terminal phase was different between the two routes due to assay sensitivity. When comparing the $AUC_{0-\infty}$ after i.v. administration (154.2 ng·h.ml^{-1}) with that after oral administration (749.4 ng·h.ml^{-1}), an oral bioavailability of 99% was calculated.

The concentration–time profile of drug-related radioactivity in blood after the i.v. administration of 1.2 mg.kg^{-1} (figure 2, B) was characterized by a higher C_{max} (795.9 ng eq.ml^{-1}; table 4) and a longer elimination phase ($t_{1/2}$ = 7.6 h) compared with the profile of the parent compound. After oral administration of 5.9 mg.kg^{-1}, maximum plasma concentration in blood was 2065 ng eq.ml^{-1} at 0.5 h (table 5). Terminal half-life (8.0 h) and mean residence time (2.0 h) were comparable with the i.v. route.

Table 3. Pharmacokinetic parameters of talsaclidine in plasma after the oral administration of talsaclidine to the male and female mouse, rat, rabbit and rhesus monkey.

Parameter		Mouse m+f	Rat# m	Rat# f	Rabbit f	Monkey m+f
Dose	($mg.kg^{-1}$)	5.9	5.9	5.9	5.9	5.9
C_{max}	($ng.ml^{-1}$)	1041±451.4	846.8±2006	1488±258	9.5±8.6	963.6±518.1
t_{max}	(h)	0.25*	0.25*	0.25*	1.0*	2.8*
$AUC_{0-\infty}$	($ng*h.ml^{-1}$)	749.4±96.7	963.7	1623	27.7±4.2	4152±1295
$MRT_{0-\infty}$	(h)	1.3±0.1	2.0	1.5	5.0±1.1	6.4±3.8
$t_{1/2}$	(h)	1.7±0.4	3.2	4.4	4.7±0.9	3.7±0.5

* Median.

\# Owing to a staggered design, the mean concentration–time profile of four males or five females was evaluated and a SD is not available.

m, Male; f, female.

Table 4. Pharmacokinetic parameters for drug-related radioactivity in blood after the intravenous administration of [^{14}C]talsaclidine to the male and female mouse, rat and rhesus monkey.

Parameter		Mouse# m+f	Rat m	Monkey m+f
Dose	($mg.kg^{-1}$)	1.2	6.5	2.9
C_{max}	($ng.eq.ml^{-1}$)	795.9±278.2	5222±687.2	3299±2519
t_{max}	(h)	0.083*	0.083*	0.25*
$AUC_{0-\infty}$	($ng.eq \cdot h.ml^{-1}$)	672.8	6160±267	10870±4540
$MRT_{0-\infty}$	(h)	1.4	9.5±1.1	5.4±2.1
$t_{1/2}$	(h)	7.6	15.6±1.2	5.9±1.2

* Median.

\# Owing to a staggered design, the mean concentration–time profile of five males and four females was evaluated and a SD is not available.

m, Male; f, female.

Table 5. Pharmacokinetic parameters for drug-related radioactivity in blood after the oral administration of [^{14}C]talsaclidine to the male and female mouse, rat, rabbit and rhesus monkey.

Parameter		Mouse# m+f	Rat m	Rabbits m+f	Monkey m+f
Dose	($mg.kg^{-1}$)	5.9	6.5	5.9	5.9
C_{max}	($ng.eq.ml^{-1}$)	2065±476.6	1966±295	5960±1071	2138±884
t_{max}	(h)	0.5*	0.5*	0.5*	2.5*
$AUC_{0-\infty}$	($ng.eq \cdot h.ml^{-1}$)	2221	2975±146	20240±10540	10840±3474
$MRT_{0-\infty}$	(h)	2.0	2.7±0.7	3.9±1.4	7.1±3.4
$t_{1/2}$	(h)	8.0	6.7±3.2	2.9±1.1	4.8±0.9

* Median.

\# Owing to a staggered design, the mean concentration–time profile of four males and four females was evaluated and a SD is not available.

m, Male; f, female.

Drug-related radioactivity was mainly excreted in urine after both routes of administration (table 6). After i.v. administration, 92.7% of the administered dose was renally excreted within the collection period and 88.8% after oral administration. Comparing the urine data, an absorption of 96% was calculated, which is in accordance with the high bioavailability of the drug. Accordingly, only 5.1 (i.v.) and 6.3% (p.o.) of the administered dose were found in the faeces, and the mass

Table 6. Excretion of drug-related radioactivity (in % of administered dose, mean ± SD) in urine, faeces and bile after the administration of [^{14}C]talsaclidine to mouse, rat, rabbit and rhesus monkey.

Matrix	Mouse		Rat		Rabbit	Monkey	
	5.9 mg.kg^{-1} i.v.	5.9 mg.kg^{-1} oral	5.9 mg.kg^{-1} i.v.	8.8, 17.6, 35.2, 52.9 mg.kg^{-1} oral #	5.9 mg.kg^{-1} oral	2.9 mg.kg^{-1} i.v.	5.9 mg.kg^{-1} oral
Urine							
0–24 h	85.6 ± 1.7	83.1 ± 7.8	–	84.7–96.9	85.2 ± 2.8	81.0 ± 6.4	76.7 ± 6.9
0 h–end	92.7 ± 2.4	88.8 ± 2.5	86.8 ± 9.4	92.1–102.2	90.9 ± 3.1	88.7 ± 3.9	85.9 ± 4.5
Faeces							
0–24 h	3.6 ± 2.2	5.3 ± 0.1	–	1.2–3.6	0.7 ± 0.6	1.7 ± 0.7	1.2 ± 0.6
0 h–end	5.1 ± 2.1	6.3 ± 0.4	8.3 ± 6.3	2.1–5.5	2.2 ± 0.5	5.9 ± 4.1	2.1 ± 0.5
Mass balance	97.8 ± 0.3	95.1 ± 2.1	95.1 ± 3.6	95.2–104.6	93.1 ± 3.0	94.6 ± 1.0	88.1 ± 4.9
Collection period (h)	0–96	0–96	0–72	0–96	0–192	0–192	0–192

Range.

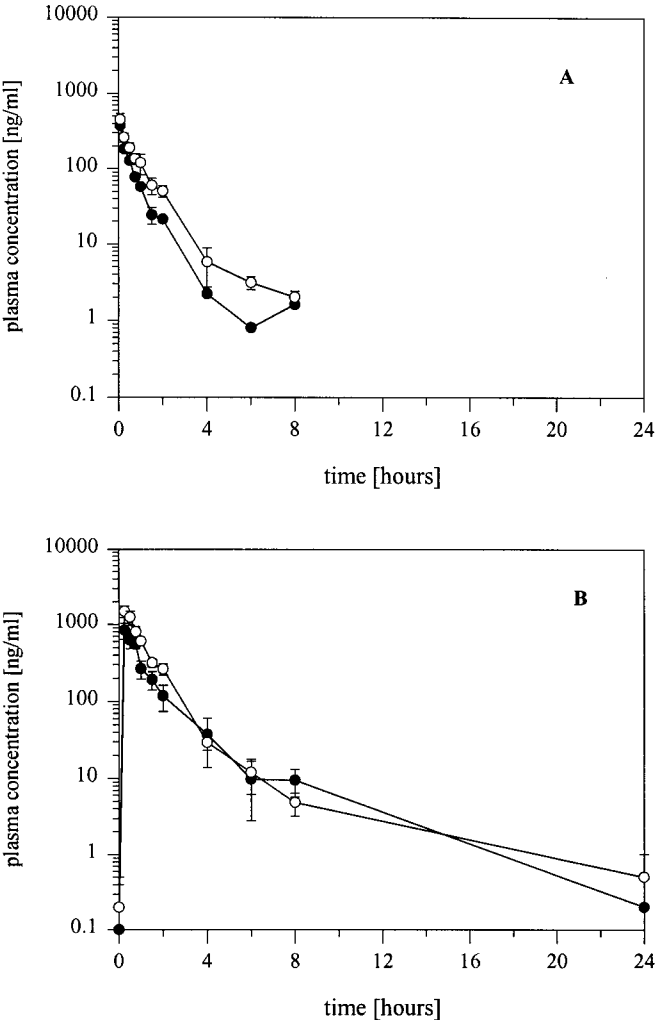


Figure 3. Plasma concentration–time curve for talsaclidine in the male and female rat after i.v. administration of 1.2 mg.kg^{-1} (A) and oral administration of 5.9 mg.kg^{-1} (B). ●, Male; ○, female. Data are mean ± SD from four-to-five animals.

balance was complete. Drug-related radioactivity was excreted rapidly as indicated by the 0–24-h fractions. The protein binding of talsaclidine to mouse plasma proteins was low. At 0.6 μg.ml^{-1} [^{14}C]talsaclidine, only 7.3% was bound to plasma proteins.

Rat

After i.v. administration of 1.2 mg.kg^{-1} talsaclidine to the male and female rat, plasma concentrations in the female were higher when compared with the male (figure 3). Maximum plasma concentrations were 371.9 ng.ml^{-1} (male) and 451.6 ng.ml^{-1} (female), which were observed shortly after administration (t_{max} = 0.083 h; table 2). The elimination was high indicated by a total clearance of 92.2 (male) and 55.5 ml.min^{-1}.kg^{-1} (female). The rapid elimination of the drug was

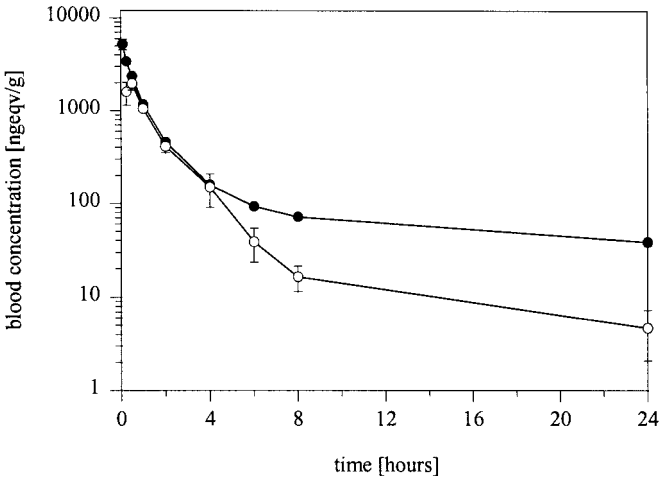


Figure 4. Drug-related radioactivity in blood after the i.v. administration of 6.5 mg.kg^{-1} and the oral administration of 6.5 mg.kg^{-1} to rat. ●, 6.5 mg.kg^{-1} i.v.; ○, 6.5 mg.kg^{-1} oral. Data are the mean ± SD from five animals.

confirmed by the short terminal half-life and mean residence time, which were between 1.0 and 1.6 h. The volume of distribution was determined as 5.7 (male) and 4.0 l.kg^{-1} (female) indicating an extensive distribution into tissues. After oral administration of 5.9 mg.kg^{-1}, talsaclidine plasma concentrations quickly (t_{max} = 0.25 h) reached a maximum of 846.8 for males and 1488 ng.ml^{-1} for females and the peak ratio ($C_{max,m}/C_{max,f}$) was 1.8 (table 3). Terminal half-life and mean residence time were prolonged (between 1.5 and 4.4 h; figure 3, B) compared with the i.v. route, but this could be explained by the different definition of the terminal phase (2–8 for i.v. versus 6–24 h for oral). Comparing $AUC_{0-\infty}$ data, an oral bioavailability of 92% for males and 94% for females was estimated.

The concentration–time profile of drug-related radioactivity in blood after i.v. administration of 6.5 mg.kg^{-1} [^{14}C]talsaclidine is depicted in figure 4. Maximum blood concentrations of 5222 ng eq.ml^{-1} were reached at 0.083 h (table 4). The terminal half-life was 15.6 h and the mean residence time of 9.5 h indicated a prolonged persistence of radioactivity in the body compared with the parent compound. After oral administration of 6.5 mg.kg^{-1} [^{14}C]talsaclidine, maximum plasma concentrations of 1966 ng eq.ml^{-1} were observed at 0.5 h (table 5). The terminal half-life of 6.7 h is shorter compared with the i.v. route.

Drug-related radioactivity was mainly excreted in urine and almost independent of the dose. Radioactivity (92.1–102.2%) was excreted renally at oral dose levels of 8.8, 17.6, 35.2 and 52.9 mg.kg^{-1} (table 6). The faecal excretion was low with 2.1–5.5%. The drug-related radioactivity was completely recovered (95.2–104.6%). The mass balance after i.v. administration of 5.9 mg.kg^{-1} [^{14}C]talsaclidine was also complete (table 6), with a similar fraction recovered in urine. Based on the urine data, an absorption of $\geqslant$ 92% was estimated. As indicated by 0–24-h fractions, excretion was as rapid as in the mouse.

Protein binding was low. At a plasma concentration of 0.6 μg.ml^{-1}, only 2.4% was bound to plasma proteins.

Talsaclidine concentrations in rat brain, CSF and plasma were determined after oral administration of 5.9 mg.kg^{-1} (figure 5). The drug penetrates the blood–brain

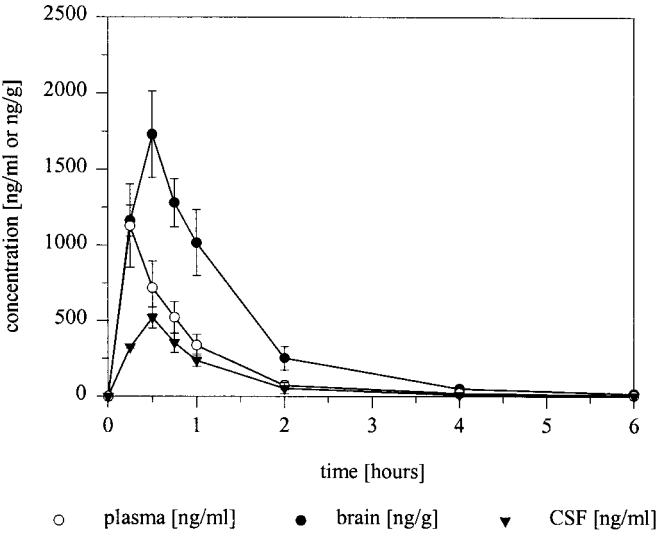


Figure 5. Concentration–time profile of talsaclidine in the plasma, brain tissue and CSF after oral administration of 5.9 mg.kg^{-1} to the male rat. Data are the mean ± SD of three-to-six animals per time-point.

barrier well, which is illustrated by the drug concentrations in the CSF and brain tissue. $AUC_{0-\infty}$ ratios (brain/plasma, CSF/plasma) were 2.2 and 0.6 respectively. The brain tissue was not sectioned in this study and no conclusion was possible about whether the drug concentrates in certain brain regions. The data, therefore, reflect the average of different brain regions.

Rabbit

After oral administration of 5.9 mg.kg^{-1} talsaclidine to the female rabbit, plasma concentrations of the parent drug were very low (table 3, figure 6). The maximum plasma concentration (C_{max} = 9.5 ng.ml^{-1}) was reached 1 h after administration. Plasma concentrations declined thereafter with a half-life of 4.7 h and the mean residence time was 5.0 h and $AUC_{0-\infty}$ was 27.7 ng·h.ml^{-1}.

The concentration–time curve of drug-related radioactivity after oral administration of 5.9 mg.kg^{-1} [^{14}C]talsaclidine was much higher than the corresponding parent drug profile (table 5, figure 6). Maximum plasma concentrations of 5960 ng eq.ml^{-1} were detected at 0.5 h (t_{max}). This observation points to extensive metabolism in the rabbit. Less than 1% of the circulating drug-related radioactivity corresponded to the parent compound. The terminal half-life for radioactivity (2.9 h) was slightly shorter than the $t_{1/2}$ of the parent drug (4.7 h), which might be due to difficulties in estimating the terminal phase of the parent drug with concentrations near or below the detection limit. The mean residence time was 3.9 h and $AUC_{0-\infty}$ was 20240 ng eq·h.ml^{-1}.

Drug-related radioactivity was mainly excreted in urine (table 6). Of it, 90.9% was in urine at the end of the collection period and, therefore, absorption was as high as in the other animal species. Accordingly, faecal excretion was low (2.2%). Of dosed radioactivity, 93.1% was recovered during the collection period. As observed in mouse and rat, radioactivity was excreted rapidly, i.e. within the first 24 h.

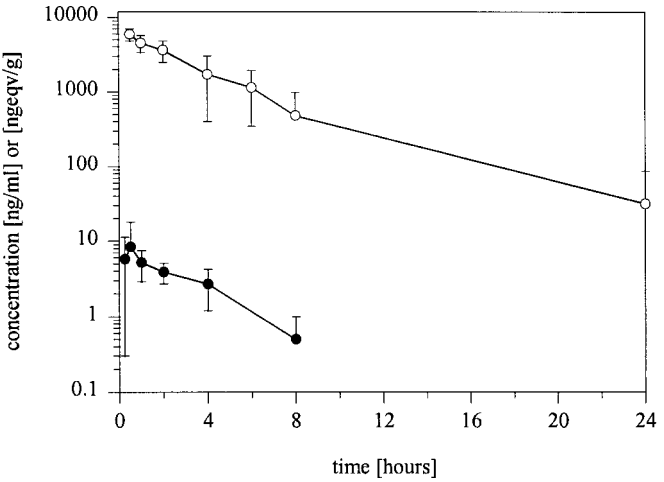


Figure 6. Plasma concentration–time curve for talsaclidine (●) and the drug-related radioactivity in blood (○) in rabbit after the oral administration of 5.9 mg.kg^{-1}. Data are the mean ± SD of three-to-four animals.

The protein binding of talsaclidine to rabbit plasma proteins was low. At 0.6 μg.ml^{-1} [^{14}C]talsaclidine, only 0.3% was bound to plasma proteins.

Monkey

The concentration–time profile of the parent drug was comparable in the male and female rhesus monkey after the i.v. administration of 2.9 mg.kg^{-1} [^{14}C]talsaclidine (figure 7, A). Maximum plasma concentrations (C_{max}) of 2645 ng.ml^{-1} were reached at 0.25 h (t_{max}; table 2) and plasma levels declined rapidly with a terminal half-life of 4.8 h. The mean residence time was 3.9 h. Elimination in terms of clearance was rapid (Cl = 10.6 ml.min^{-1}.kg^{-1}) and an extensive distribution of the drug into tissues was observed (V_{ss} = 2.3 l.kg^{-1}). After oral administration of 5.9 mg.kg^{-1} [^{14}C]talsaclidine, maximum plasma levels of the parent compound (C_{max}) of 963.6 ng.ml^{-1} were observed 2.5 h (t_{max}) after administration (table 3). Terminal half-life and mean residence time were 3.7 and 6.4 h respectively, which were close to the corresponding values observed after i.v. administration. Based on $AUC_{0-\infty}$, an oral bioavailability of 38% was calculated.

Figure 7 (B) shows the concentration–time profile of drug-related radioactivity in blood after i.v. administration. Maximum blood concentrations of 3299 ng eq.g^{-1} were reached 0.25 h after i.v. administration (table 4). In terms of $t_{1/2}$ and MRT, there was no significant indication of a longer persistence of drug-related radioactivity compared with the parent drug. After oral administration of 5.9 mg.kg^{-1} [^{14}C]talsaclidine, maximum blood concentrations of drug-related radioactivity of 2138 ng eq.g^{-1} were reached 2.5 h (table 5) after administration and declined afterwards with a terminal half-life of 4.8 h.

After i.v. administration, drug-related radioactivity was mainly excreted renally as observed with the other species (table 6). Of radioactivity, 88.7% was excreted in urine, whereas only 5.9% was excreted in faeces during the collection period of 192 h. After oral administration, the values were 85.9% and 2.1%. The mass balance was almost complete for the i.v. route but was incomplete for the oral route.

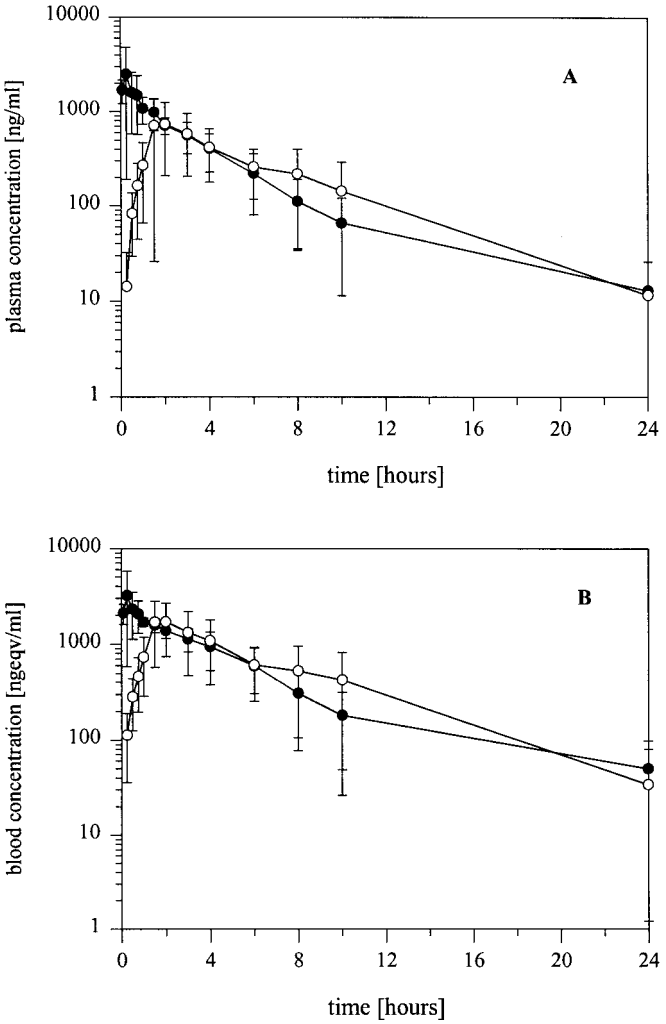


Figure 7. Plasma concentration–time curve for talsaclidine (A) and the drug-related radioactivity in blood (B) in the male and female rhesus monkey after the i.v. administration of 2.9 mg.kg^{-1} and oral administration of 5.9 mg.kg^{-1}. ●, 2.9 mg.kg^{-1} i.v.; ○, 5.9 mg.kg^{-1} oral. Data are the mean ± SD of four animals.

It was not assumed that the lower recovery reflected a metabolically labile radiolabelled position. From the urine data, an absorption of 97% could be estimated.

The protein binding of [^{14}C]talsaclidine to plasma proteins in rhesus monkey was low. At a concentration of 0.6 μg.ml^{-1}, only 2.6% of drug-related radioactivity was bound to plasma proteins.

Allometric scaling

Whether animal parameters are predictive for human pharmacokinetics of talsaclidine was examined. The allometric scaling approach used data of both human and animal species and showed that Cl_{tot} and V_{ss} correlated well to body weight

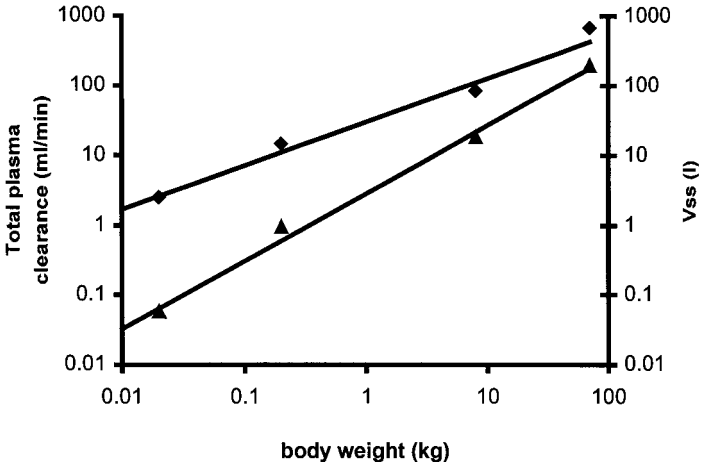


Figure 8. Allometric scaling of total plasma clearance (◆, Cl_{tot}) and volume of distribution at steady-state (▲, V_{ss}) in mouse, rat, monkey and human.

(figure 8). Differences between experimental and predicted values (from the regression) were < 40%. Calculated values for the proportionality factor 'a' were 30.2 (Cl) and 3.0 (V_{ss}) and values for the exponent b were 0.62 (Cl) and 0.96 (V_{ss}).

Protein binding in human

The plasma protein binding in human plasma was low (< 1%) and independent of the concentration used (0.1, 0.6 and 12 $\mu g.ml^{-1}$ [^{14}C]talsaclidine).

Discussion

Comparing i.v. data generated in mouse, rat and monkey, the animal pharmacokinetics of talsaclidine was governed by a rapid elimination (Cl) from the circulation and a high distribution into tissues (V_{ss}). Cl_{tot} was higher than the hepatic blood flow in all tested species (Davies *et al.* 1993) characterizing the drug as having a high extraction ratio. V_{ss} was between 2 and 5 $l.kg^{-1}$ in the animal species, which was clearly higher than total body water (~ 0.6 $l.kg^{-1}$) suggesting an additional binding of talsaclidine in tissues. In addition, rapid diffusion of talsaclidine into tissues due to its small size might be assumed and an extensive distribution seems to be reasonable. The plasma protein binding was low (< 7%) and therefore did not restrict distribution and elimination as most of the drug circulates as unbound, free drug in the body. The variability of drug plasma levels was moderate. High deviations between the animals were only observed at the first or last sampling point, which was related to experimental difficulties in sampling or the measurement near the limit of quantitation (LOQ). The terminal half-life and the mean residence time did not deviate appreciably in the animal species. The above parameters for the i.v. route are similar to those reported by Ensinger *et al.* (1997).

Following oral administration of talsaclidine, concentration–time profiles in mouse, rat, rabbit and monkey confirmed a good absorption. This observation was consistent with the physicochemical parameters of the drug. The drug is highly soluble in water and at physiological pH it is almost completely protonated (pK_a =

10.5). Other drugs with a comparable pK_a and log P such as ephedrine and propanolol showed also an *in vivo* absorption of $>90\%$ in man (Pade *et al*. 1998). Absorption was also fast as maximum plasma levels were reached after 0.25 h in mouse and rat and after 1 h in rabbit. Only in monkey was the t_{max} prolonged (2.5 h). The absolute bioavailability in the rat (92% for males, 94% for females) was in accordance with previous data (96%; Ensinger *et al*. 1997). Mouse had an equally high bioavailability (99%), whereas in monkey only 38% bioavailability was observed. In the latter species, this was possibly due to first-pass metabolism (e.g. CYP P450). Surprisingly low plasma concentrations of parent drug were observed in rabbit after oral dosing in contrast to much higher concentrations of drug-related radioactivity. This pointed to a high degree of first-pass metabolism in rabbit because the absorption was as good as in the other three animal species ($\geqslant 91\%$ of the dosed [^{14}C]talsaclidine was in urine). The relatively low bioavailability in monkey and rabbit might also be caused by contributing efflux pumps (e.g. *p*-glycoprotein). In all species examined, terminal half-lives and mean residence times were comparable with the values measured after i.v. dosing. The variability of drug plasma levels was moderate as described for i.v. dosing.

Drug-related radioactivity persisted longer in the animal species compared with the parent compound, confirmed by a longer terminal half-life and mean residence time. Circulating metabolites seemed to be eliminated more slowly than the parent compound. A comparison of blood C_{max} data of drug-related radioactivity with plasma C_{max} data of parent compound after i.v. administration is only possible when the blood–plasma ratio (C_b/C_p) was taken into account. C_b/C_p was ~ 1.0 for the rhesus monkey (data not shown). Therefore, the ratio (radioactivity/unchanged drug) was 1.2 in monkey suggesting no relevant contribution of metabolites at early time-points. However, after oral administration, the ratio was 2.2, which indicated again a higher contribution of metabolites by first-pass metabolism. Even more striking was the calculated ratio in the rabbit (630, $C_b/C_p = 1.0$ assumed), indicating relevant amounts of circulating metabolites.

A gender effect was only observed in rat but not in mouse or monkey, and a conclusion was not possible on rabbit due to the limited data. The gender-related differences in the pharmacokinetics of drugs, particularly in rat, have been well known and can be a result of the differences in hormone levels, plasma protein binding and/or the extent of metabolism (Tanaka *et al*. 1991, Gleiter *et al*. 1996, Lin *et al*. 1996, Prakash *et al*. 1997). The female rat had a 21% higher C_{max} and a 66% higher $AUC_{0-\infty}$ compared with the male (parent compound data) after i.v. administration. This translated into a lower clearance in the female. Minor differences were observed with V_{ss}, terminal half-life and mean residence time. Elimination processes rather than distribution processes therefore drive the observed differences between the male and female rat. The observed differences were also apparent after oral administration of talsaclidine. Only the male rat was examined in the radioactivity experiments and a conclusion on drug-related radioactivity was therefore not possible.

Talsaclidine penetrated the blood–brain barrier well. The ratios of brain tissue/plasma and CSF/plasma were 2.2 and 0.6 for $AUC_{0-\infty}$ respectively. CSF is a more accurate indicator of blood–brain barrier permeability as free drug concentration is more relevant for efficacy. Both brain tissue and CSF had a delayed t_{max} (0.5 h), which indicated that the drug needed time to cross the barriers. In Ensinger *et al*. (1997), only two time points (0.5 and 2 h) were measured by radioreceptor

assay with respect to drug concentration in plasma and brain tissue after oral dosing. Ratios of 2.5–3.0 in favour of brain tissue were reported, which were comparable with data of the present study. The high uptake in the brain correlates also with the $\log P = 0.3$, which illustrates sufficient lipophilicity of the drug. This property is no contradiction to the high renal clearance of Talsaclidine as the drug circulated almost completely unbound in blood (low protein binding) and therefore the drug is easily filtered in the glomeruli of the kidney.

Talsaclidine was mainly excreted renally. More than 86% of the administered radioactivity was excreted in urine in all four investigated animal species. In addition, renal excretion was rapid, which means that a high degree was excreted during the first 24 h. Taking into account the high amount of unbound Talsaclidine in blood as a protonated quaternary ammonium ion, one might speculate that specific cation transporters (Ullrich 1994) in the tubuli of the kidney are involved in excretion. The urine data was used to calculate the extent of absorption (96% mouse $>$ 92% rat, 97% monkey), which was in accordance with the high bioavailability in mouse and rat. However, the monkey exhibited a high extent of absorption but a much lower bioavailability which could be related to first-pass metabolism. Owing to the high amount of renal excretion, the amount of total radioactivity in faeces was low and $<$ 9% was found in all animal species. The drug-related radioactivity was almost entirely recovered except in the orally dosed monkey study (88.1%). The dose dependence of renal and faecal excretion was investigated in rat at oral dose levels of 8.8–52.9 $mg.kg^{-1}$. No relevant change was observed with respect to renal and faecal excretion suggesting dose linearity and no saturation effects.

Most of the animal data corresponded well to the human pharmacokinetic data (Adamus *et al.* 1995). For instance, pharmacokinetic data in man indicated a rapid and extensive absorption and an oral bioavailability of $>$ 70%. Mean maximum concentrations of 1.6–429 $ng.ml^{-1}$ (recalculated to talsaclidine base) were reached at dose levels of 0.3–94 mg (t_{max} between 1 and 2 h) and a dose linearity was established for C_{max} and $AUC_{0-2/1\,h}$ data (Ensinger *et al.* 1997). Renal excretion of parent drug also predominated in man. All these features suggested that animal data of talsaclidine is predictive to human. An allometric scaling approach with human and animal data was therefore chosen in order to test this hypothesis. Only two pharmacokinetic parameters, namely Cl and V_{ss}, were investigated, because they govern the disposition of talsaclidine. A good correlation between the clearance data of mouse, rat, monkey, human and the corresponding body weight was achieved. This was attributed to the fact that talsaclidine was mainly excreted in urine as parent compound. The renal function (filtration) has been shown to follow the allometric approach (Lin 1998). Furthermore, V_{ss} showed a good correlation across the animal species and in man as well. This might be attributed to the fact that the protein binding is low and comparable over the species. Talsaclidine is a compound with a low molecular weight which could freely diffuse into tissues lacking a specific binding in a given species. However, high V_{ss}'s showed that tissue binding contributes mainly to the distribution of talsaclidine. The calculated exponent b (0.62 for Cl, 0.97 for V_{ss}) indicated an almost linear relationship between V_{ss} and body weight. Clearance seemed to correlate better with body surface area (body surface area = $A \cdot B^{0.67}$) than in a linear fashion. For other drugs data has been reported with respect to clearance (Chiou *et al.* 1998) and volume of distribution (Ings 1990), which were comparable with the calculated b in the present study. Despite the fact that these exponents have been confirmed with many drugs, further

interpretation of results obtained by allometric scaling should be exercised with caution as this method is empirical. In conclusion, talsaclidine is an example that emphasizes that animal data is predictive for man.

Acknowledgement

The excellent technical assistance of G. Müller, B. Eichhorn, H. Weil, S. Goldner, E. M. Ecker and M. Müller is gratefully acknowledged.

References

Adamus, W. S., Leonard, J. P. and Tröger, W., 1995, Phase I clinical trials with WAL 2014, a new muscarinic agonist for the treatment of Alzheimer's disease. *Life Science*, **56**, 883–890.

Arnt, J., Lembol, H. L., Meier, E. and Pedersen, H., 1992, Discriminative stimulus properties of the muscarinic receptor agonists Lu 26–046 and O-Me-THPO in rats: evidence for involvement of different muscarinic receptor subtypes. *European Journal of Pharmacology*, **218**, 159–169.

Barner, E. L. and Gray, S. L., 1998, Donepezil use in Alzheimer disease. *Annals of Pharmacotherapy*, **32**, 70–77.

Bromidge, S. M., Brown, F., Cassidy, F., Clark, M. S., Dabbs, S., Hadley, M. S., Hawkins, J., Loudon, J. M., Naylor, C. B., Orlek, B. S. and Riley, G. J., 1997, Design of [*R*-(Z)]-(+)-alpha-(methoxyimino)-1-azabicyclo[2.2.2]octane-3-acetonitrile (SB 202026), a functionally selective azabicyclic muscarinic M1 agonist incorporating the N-methoxy imidoyl nitrile group as a novel ester bioisostere. *Journal of Medical Chemistry*, **40**, 4265–4280.

Bymaster, F. P., Carter, P. A., Peters, S. C., Zhang, W., Ward, J. S., Mitch, C. H., Calligaro, D. O., Whitesitt, C. A., DeLapp, N., Shannon, H. E., Rimvall, K., Jeppesen, L., Sheardown, M. J., Fink-Jensen, A. and Sauerberg, P., 1998, Xanomeline compared with other muscarinic agents on stimulation of phosphoinositide hydrolysis *in vivo* and other cholinomimetic effects. *Brain Research*, **795**, 179–190.

Chiou, W. L., Robbie, G., Chung, S. M., Wu, T. C. and Ma, C., 1998, Correlation of plasma clearance of 54 extensively metabolized drugs between humans and rats: mean allometric coefficient of 0.66. *Pharmaceutical Research*, **15**, 1474–1479.

Davies, B., Andrewes, D., Stargatt, R., Ames, D., Tuckwell, V. and Davis, S., 1989, Tacrine in Alzheimer's disease. *Lancet*, **II**, 163–164.

Davis, B. and Morris, T., 1993, Physiological parameters in laboratory animals and humans. *Pharmaceutical Research*, **10**, 1093–1095.

DeLapp, N., Wu, S., Belagaje, R., Johnstone, E., Little, S., Shannon, H., Bymaster, F., Calligaro, D., Mitch, C., Whitesitt, C., Ward, J., Sheardown, M., Fink-Jensen, A., Jeppesen, L., Thomsen, C. and Sauerberg, P., 1998, Effects of the M1 agonist xanomeline on processing of human beta-amyloid precursor protein (FAD, Swedish mutant) transfected into Chinese hamster ovary-m1 cells. *Biochemical and Biophysical Research Communications*, **244**, 156–160.

Ensinger, H. A., Bechtel, W. D., Birke, F. W., Mendla, K. D., Mierau, J., Speck, G. and Tröger, W., 1997, WAL 2014 FU (talsaclidine): a preferentially neuron activating muscarinic agonist for the treatment of Alzheimer's disease. *Drug Development and Research*, **40**, 144–157.

Ensinger, H. A., Doods, H. N., Immel-Sehr, A. R., Kuhn, F. J., Lambrecht, G., Mendla, K. D., Mueller, R. E., Mutschler, E., Sagrada, A., Walther, G. and Hammer, R., 1993, WAL 2014—a muscarinic agonist with preferential neuron-stimulating properties. *Life Sciences*, **52**, 473–480.

Giacobini, E., 1998, Invited Review: Cholinesterase inhibitors for Alzheimer's disease therapy: from tacrine to future applications. *Neurochemistry International*, **32**, 413–419.

Gibaldi, M. and Perrier, D., 1982, *Pharmacokinetics*, 2nd edn (New York: Marcel Dekker), pp. 409–417.

Gleiter, C. H. and Gundert-Remy, 1996, Gender differences in pharmacokinetics *European Journal of Drug Metabolism*, **21**, 123–128.

Heinzel, G., Woloszczak, R. and Thomann, P., 1993 Non-compartmental analyses: methods. In *TOPFIT version* 2.0: *Pharmacokinetic and Pharmacodynamic Analysis System for the PC* (New York: Gustav Fisher), pp. 2.6–29.

Hulme, E. C., Birdsall N. J. and Buckley N. J., 1990, Muscarinic receptor subtypes. [Review]. *Annual Reviews of Pharmacology and Toxicology*, **30**, 633–673.

Ings, R. M. J., 1990, Interspecies scaling and comparison in drug development and toxicokinetics. *Xenobiotica*, **20**, 1201–1231.

Lawrence A. D. and Sahakian B. J., 1998, The cognitive psychopharmacology of Alzheimer's disease: focus on cholinergic systems [Review]. *Neurochemistry Research*, **23**, 787–794.

Lin, J. H., 1998, Applications and limitations of interspecies scaling and *in vitro* extrapolation in pharmacokinetics. *Drug Metabolism and Disposition*, **26**, 1202–1212.

Lin, J. H., Chiba, M., Chen, I. W., Nishime, J. A. and Vastag, K. J., 1996, Sex-dependent pharmacokinetics of indinavir: *in vivo* and *in vitro* evidence. *Drug Metabolism and Disposition*, **24**, 1298–1306.

Messer, W. S. Jr, Ellerbrock, B., Price, M. and Hoss, W., 1989, Autoradiographic analyses of agonist binding to muscarinic receptor subtypes. *Biochemical Pharmacology*, **38**, 837–850.

Pade, V. and Stavchansky, S., 1998, Link between drug absorption and permeability measurements in CaCo-2 cells. *Journal of Pharmaceutical Science*, **87**, 1604–1607.

Prakash, C. and Soliman, V., 1997, Metabolism and excretion of a novel antianxiety drug candidate, CP-93,393, in Long–Evans rats. *Drug Metabolism and Disposition*, **25**, 1288–1297.

Rogers, S. L., Doody, R. S., Mohs, R. C. and Friedhoff, L. T., 1998, Donepezil improves cognition and global function in Alzheimer disease: a 15-week, double-blind, placebo-controlled study. *Archives of Internal Medicine*, **158**, 1021–1031.

Shaw, V. P., Midha, K. K., Dighe, S., McGilveray, I. J., Skelly, J. P., Yacobi, A., Layloff, T., Viswanathan, C. T., Cook, C. E., McDowall, R. D., Pittmann, K. A. and Spector, S., 1992 Analytical methods validation: bioavailability, bioequivalence and pharmacokinetic studies. *Pharmaceutical Research*, **9**, 588–592.

Sramek, J. J., Forrest, M., Mengel, H., Jhee, S. S., Hourani, J. and Cutler, N. R., 1998, A bridging study of LU 25–109 in patients with probable Alzheimer's disease. *Life Sciences*, **62**, 195–202.

Tanaka, Y., Deguchi, Y., Ishii, I. and Terai, T., 1991, Sex differences in excretion of zenarestat in rat. *Xenobiotica*, **21**, 1119–1125.

Ullrich, K. J., 1994, Specificity of transporters for organic anions and organic cations in the kidney. *Biochimica et Biophysica Acta*, **1197**, 45–62.

XENOBIOTICA, 2000, VOL. 30, NO. 8, 815–830

Pharmacokinetics and metabolism of a vitamin D analogue (Seocalcitol) in rat and minipig

A.-M. KISSMEYER†* and J. T. MORTENSEN‡

Departments of † Pharmacokinetics and Metabolism, and ‡ Toxicology, Leo Pharmaceutical Products, DK-2750 Ballerup, Denmark

Received 25 February 2000

1. Seocalcitol (EB 1089), a vitamin D analogue with strong antiproliferative effects *in vitro* and *in vivo*, is presently under clinical evaluation for the systemic treatment of various solid tumours.

2. The aim was to investigate the pharmacokinetics of Seocalcitol after single and multiple oral administration to rat and minipig. Furthermore, the hepatic metabolism of Seocalcitol was studied both *in vitro* and *in vivo*. *In vitro* metabolism was also investigated in human.

3. In rat, the pharmacokinetic profile of Seocalcitol (C_{max}, AUC, T_{max}, $T_{\frac{1}{2}}$) was the same after single and oral administration. Pharmacokinetics were also demonstrated as dose-independent. The same was more difficult to evaluate in the minipig due to a great variation among individual animals.

4. In the male rat, the serum $T_{\frac{1}{2}}$ was 3 h, but in the female rat and minipig (both genders) $T_{\frac{1}{2}}$ = 8 h.

5. At T_{max} the concentration of Seocalcitol in the liver (both species) was 10-fold higher than the concentration in serum. The major metabolites in the liver were various isomers of 26-hydroxy Seocalcitol, although the concentration of the individual isomers in rat and minipig were not the same.

6. The same metabolites were formed *in vitro* following incubations with rat, minipig and human S9 fractions.

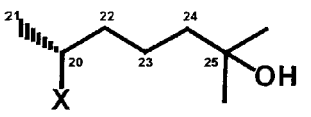
Introduction

Seocalcitol [1(*S*),3(*R*)-dihydroxy-20(*R*)-(5′ethyl-5′-hydroxy-hepta-1′(E), 3′(E)-dien-1′-yl)-9,10-secopregna-5(Z),7(E),10(19)-triene] (EB 1089) is an analogue of 1α,25-dihydroxyvitamin D_3 [1α,25$(OH)_2D_3$], the physiologically active form of vitamin D_3 (figure 1). 1α,25$(OH)_2D_3$ plays a crucial role in the regulation of calcium homeostasis (Deluca *et al*. 1990) and in cell growth regulation (Reichel *et al*. 1989). The effects of 1α,25$(OH)_2D_3$ are believed to be mediated via a specific intracellular receptor found in many cells and tissues, and are not restricted to those involved in the regulation of calcium metabolism (Haussler *et al*. 1995). The clinical usefulness of 1α,25$(OH)_2D_3$ is primarily limited by its effect on calcium homeostasis, with the risk of inducing hypercalcaemia and soft tissue calcifications. However, a synthetic analogue has been developed, namely Seocalcitol, with pronounced antiproliferative effects both *in vitro* and *in vivo*, but with reduced effects on calcium metabolism (Binderup *et al*. 1991, Colston *et al*. 1992, Haq *et al*. 1993, Mathiasen *et al*. 1993). Seocalcitol is presently under clinical evaluation for the systemic treatment of various solid tumours including hepatocellular carcinoma (Dalhoff *et al*. 1998).

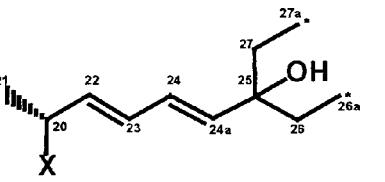
Very little data on the pharmacokinetics of Seocalcitol in animals and humans have been published (Kissmeyer *et al*. 1995, 1997). One of the major reasons is a lack of sensitive analytical methods to quantify the concentration of Seocalcitol in serum

* Author for correspondence; e-mail: Anne-Marie.Kissmeyer@leo-pharma.com

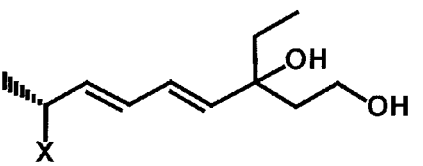
Xenobiotica ISSN 0049-8254 print/ISSN 1366-5928 online © 2000 Taylor & Francis Ltd
http://www.tandf.co.uk/journals



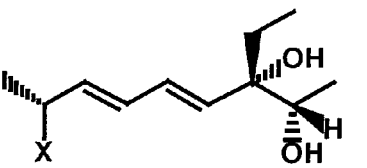
$1\alpha,25(OH)_2D_3$



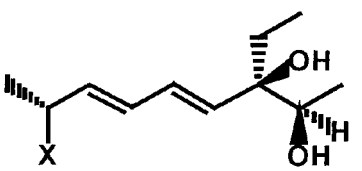
EB 1089



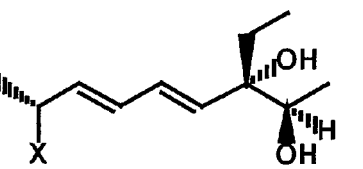
26a-OH EB 1089
(Leo Code EB 1435)



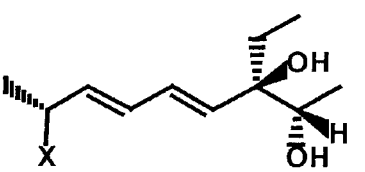
(25S),26S-OH EB 1089
(Leo Code EB 1436)



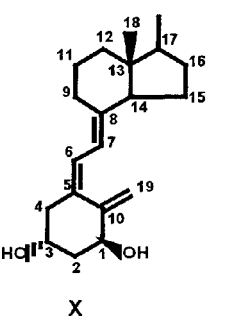
(25R),26R-OH EB 1089
(Leo Code EB 1445)



(25S),26R-OH EB 1089
(Leo Code EB 1446)



(25R),26S-OH EB 1089
(Leo Code EB 1470)



X

Figure 1. Chemical structures of $1\alpha,25(OH)_2D_3$, Seocalcitol (EB 1089) and Seocalcitol derivatives. X, vitamin D ring system.

after administration of doses in the pharmacological range. However, the present authors recently developed a sensitive liquid chromatography tandem mass spectrometry assay (Kissmeyer *et al*. 2000), which made possible the investigation of the pharmacokinetic profile of Seocalcitol in animals and human at pharmacological doses. The objective of the present investigations was to study the pharmacokinetics of Seocalcitol after single and multiple oral dosing to rat and minipig to support both toxicological and pharmacological observations. It has previously been shown that the major metabolites of Seocalcitol formed *in vitro* in liver homogenate from rat, minipig and human were 26- and 26a-hydroxy derivatives of Seocalcitol (figure 1), although these six isomers were not completely separated (Kissmeyer *et al*. 1997). As it is now possible to separate all six isomers of the 26-hydroxy and 26a-hydroxy Seocalcitol, the metabolic profiles observed in the liver and kidney from rat and minipig dosed with Seocalctiol were compared with the profiles obtained after incubation of Seocalcitol in the post-mitochondrial liver fraction from the male and female rat, minipig and human. Since, it has been demonstrated that 3-epi-1α,25(OH)$_2$D$_3$ is a minor metabolite of 1α,25(OH)$_2$D$_3$ (Sekimoto *et al*. 1999), it was also investigated whether a similar 3-epi-Seocalcitol metabolite could be found in liver and kidney from both the Seocalctiol-dosed rat and minipig.

Materials and methods

Chemicals

Seocalctiol, [d_6]-Seocalcitol (internal standard), 3-epi-Seocalcitol, the four diastereoisomeric forms of 26-hydroxy Seocalcitol, the two 26a-hydroxy epimers of Seocalcitol (not separated) and [d_6]-1α,25(OH)$_2$D$_3$ (internal standard) (figure 1) were synthesized at Leo Pharmaceutical Products (Ballerup, Denmark) (Binderup *et al*. 1991, Kissmeyer *et al*. 1997). Stock solutions in 2-propanol were prepared taking purity into account. All other chemicals and reagents were commercially available. All solvents were HPLC grade, ammonium acetate was Analytical Reagent Grade, and nitrogen gas was 99.999% pure.

Dosing formulation

Rat. Seocalcitol was formulated in a propylene glycol buffer solution (1.8 mg Na_2HPO_4, $2H_2O$, 200 mg water, and 830 mg propylene glycol per ml) (= formulation used in the toxicity studies).

Minipig. Seocalcitol was formulated in soft entero-coated capsules containing 1 or 5 μg Seocalcitol (= formulation used in the toxicity studies).

Pharmacokinetic studies

Rat. One hundred and thirty-two males weighing 260$\pm$23 g and 132 females weighing 189$\pm$10 g Sprague–Dawley rats (M&B, Lille Skensved, Denmark) with free access to water and feed (pelleted Altromin 1324®, Brogaarden, Gentofte, Denmark) were included in the study. Rats were divided evenly into four groups. Groups 1 and 2 were given a single oral dose of 0.6 and 2.4 μg/kg respectively. The doses are close to those used in the toxicological studies. Groups 3 and 4 were given one dose of 0.6 and 2.4 μg/kg respectively per day for 7 days. Using heart puncture under CO_2 anaesthesia, blood samples were collected 0, 0.5, 1, 2, 4, 6, 8, 16 and 24 h after dosing from three animals per sampling time per group per gender.

Minipig

Experiment 1. Three male and three female Ellegaard–Göttingen minipigs weighing 10$\pm$0.4 kg (Ellegaard, Dalmose, Denmark) were treated once a day for 8 days with 3 μg (0.3 μg/kg) Seocalcitol per animal administered as capsules containing 1 μg per capsule. The dose corresponds to the highest dose in long-term toxicological studies. Blood samples were collected 0, 2, 4, 6, 8 and 24 h after the first and eighth dose. The number of blood samples was restricted due to animal welfare.

Experiment 2. Four female Ellegaard–Göttingen minipigs weighing 7$\pm$1.3 kg were given a single oral dose of 20 μg per animal (2.9 μg/kg) as four capsules containing 5 μg per capsule. The dose was chosen as a compromise between a tolerable dose and one that would give higher and more reliable serum concentrations of Seocalcitol. Blood samples were collected 0, 0.5, 1, 2, 3, 4, 5, 6, 8, 9, 10, 12 and 24 h after

dosing. In both experiments, the animals had access to water *ad libitum* and were fed twice daily with a commercially available pelleted minipig diet (Type SMP MOD (E) POLY SQC from Special Diet Services Ltd, Witham, UK). Half of the daily ration was given immediately following dosing and the remaining half ration 5–6 h later.

Serum was prepared and kept at −80 °C until analysis.

Metabolic studies

Rat. Twelve male and 12 female rats from the highest single and multiple dosing groups in the pharmacokinetic experiment were selected for examination of the metabolic profile in the liver and kidney. Blood was collected and, after exsanguination, the liver and kidney were removed from the animals 0 (before treatment) and 2 h (about C_{max}) after last dosing. The tissues were immediately placed in one part of an ice-cold phosphate buffer followed by homogenization using a Potter–Elvehjem type Teflon–glass, motor-driven homogenizer.

Minipig. After a washout period, the three male and three female minipigs remaining from the multiple dosing pharmacokinetic experiment were used to study the metabolic profile of Seocalcitol in the liver and kidney. The animals were given a single oral dose of 20 μg per animal. A blood sample was collected 6 h (about C_{max}) after dosing, and the animals were killed immediately thereafter. After exsanguination, samples of the liver and kidneys were collected and homogenized in one part of an ice-cold phosphate buffer.

All homogenates were kept at −80 °C until analysis.

Incubation with liver homogenates

Seocalcitol was incubated with a liver-metabolizing system containing the post-mitochondrial liver fraction (S9) from the male and female pools from rat, minipig (S9: in-house production) and human (Human Biologics International, Scottsdale, AZ, USA) corresponding to 5 mg protein per ml in 8 mM $MgCl_2$, 33 mM KCl, 5 mM glucose 6-phosphate and 4 mM $NADP^+$ in 0.1 M phosphate buffer, pH 7.4. The final concentration of Seocalcitol was 4 μM. Incubations were performed at 37 °C, and samples collected 0, 2 and 4 h after addition of the test compound. Metabolism was stopped by addition of 2 vols acetonitrile.

Quantitation of Seocalcitol in serum and tissues

The concentration of Seocalcitol in rat and minipig serum was determined by a LC/MS/MS method (Kissmeyer *et al*. 2000). Briefly, 1 ml serum was precipitated with 2 ml acetonitrile after addition of internal standard, before the supernatant was diluted with water. The mixture was loaded to a Isolute™ MF C18 SPE column (100 mg; 1 ml) (IST, Mid-Glamorgan, UK) using an ASPEC™ XL4 sample processor with a 404 Syringe Pump and 724 Software package (Gilson, Middleton, WI, USA). The analytes were eluated with heptane-2-propanol (93:7 v/v). The organic solvent was then evaporated and the residue was reconstituted in mobile phase before injection to the LC/MS/MS system. The reversed-phase HPLC system consisted of a Waters Alliance 2690 Separation Module with cooling on the autosampler, online vacuum degassing and column oven (Waters, Milford, MA, USA). The analytical column was a Symmetri C8 50 × 2.1 mm 3.5 μm (Waters) and kept at 30 °C. The mobile phase was a linear gradient from 75 to 99% methanol with a constant concentration of 2 mM ammonium acetate with a flow rate of 0.3 ml/min. The injection volume was 150 μl. The mass detector was a PE/Sciex API 3000 Mass Spectrometer using a PE/Sciex TurboIonSpray ion source (Concord, Ontario, Canada). The ion source was operated in the positive electrospray ionization (ESI) mode at 250 °C, and the mass spectrometer was operated in the selected reaction monitoring (SRM) mode. The lower limit of quantitation of Seocalcitol in serum was 10 pg/ml. Similarly, liver and kidney samples were analysed, but the injection volume was only 100 μl.

Profiles of 26- and 26a-hydroxy metabolites in liver and kidney

A modification of the above assay was used to investigate the profile of the 26- and 26a-hydroxy metabolites of Seocalcitol from tissue homogenates from the Seocalcitol-dosed rat and minipig, and from incubations of Seocalcitol with liver homogenates from rat, minipig and human. No deuterated metabolites were available. Instead d_6-1α,25$(OH)_2D_3$ was the internal standard as its polarity is close to the one of the metabolites (EB 1446). The analytical column was a Symmetri C18 150 × 2.1 mm 3.5 μm (Waters) and kept at 25 °C. The ternary gradient system used was solvent A: water; solvent B: methanol–1 M ammonium acetate–water (990:2:8 v/v/v); solvent C: acetonitrile–1 M ammonium acetate–water (900:2:98 v/v/v). Flow rate was 0.3 ml/min; injection volume was 100 μl. Only EB 1446 was quantified, as the standard curves from the other metabolites were difficult to interpret.

Determination of 3-epi-Seocalcitol in liver and kidney

The samples were cleaned using the same procedure as above, but the samples were reconstituted in hexane–methanol–isopropanol (92:1:7 v/v/v) and injected into a straight-phase HPLC system consisting of a Merck Hitachi pump L-7100 and UV detector L-7400 (E. Merck, Darmstadt, Germany), a Spark Holland Basic Marathon autosampler (Spark Holland, Emmen, The Netherlands) and a Millennium 32 Chromatography Manager (Waters). The analytical column was a Merck Superspher Si 60, 4 μm, 250 × 4 mm column. The eluent was hexane–isopropanol–methanol (92:1:7 v/v/v) with a flow-rate of 2.5 ml/min. The wavelength for the detection of the standards was 264 nm. The fractions corresponding to the retentions of 3-epi-Seocalcitol (~ 15 min) and Seocalcitol (~ 18 min) were collected separately. The organic phase was evaporated and the samples were finally reconstituted in the mobile phase and further analysed as described above.

Quantitation of serum calcium

The total serum calcium was determined by complex formation with *o*-cresolphtalein (Sarkar and Chanhan 1967) in samples collected before dosing, and 24 h after the seventh and eighth dose of Seocalcitol to rat and minipig respectively.

Pharmacokinetic calculations

Maximum serum concentration (C_{max}) and time (T_{max}) at which C_{max} occurred were found by inspection of the Seocalcitol serum concentration–time data from individual animals. Serum half-life ($T_{\frac{1}{2}}$) and the area under the curve (AUC) were calculated by non-compartmental analysis using the WinNonlin Standard v.2.1 (Pharsight Corp., Mountain View, CA, USA). AUC was calculated using the linear–log trapezoidal method. The linear trapezoidal rule was used up to C_{max}, and the logarithmic trapezoidal rule was used after C_{max}. The logarithmic trapezoidal rule is used as the serum concentration after C_{max} falls exponentially.

Results

Serum concentrations after oral administration of Seocalcitol to rat

Figure 2 shows the concentration of Seocalcitol in serum after one and seven oral doses of 0.6 and 2.4 μg/kg to rat. Its concentration was above the limit of quantitation in all animals 0.5–8 h after last dose. In female animals given 2.4 μg/kg, Seocalcitol was still detectable at the last sampling time, i.e. 24 h after dosing. $T_{\frac{1}{2}}$ was ~ 3 h in males and 8 h in females. The mean maximum serum concentrations (calculated from the three highest concentrations found in each group) were reached at ~ 2 h (T_{max}) in all groups except from females given 0.6 μg/kg, where the maximum did not peak until 4–5 h after dosing (table 1). The maximum concentrations of Seocalcitol in serum (C_{max}) were very similar after a single dose and after seven doses without any gender difference. AUCs were also the same after single and multiple dosing in male animals, but were higher in females and with a tendency of being higher after multiple dosing. C_{max} is almost directly proportional to the dose with an increase in C_{max} being 88–120% of theoretical values. On the other hand, AUCs increased less than the suggested rise in the dose, but AUCs in the lower dosing groups were calculated with some inaccuracy as up to 39% of the area was extrapolated.

Serum concentrations after oral administration of Seocalcitol to minipig

The concentrations of Seocalcitol in serum after a single and eight oral administrations of 0.3 μg/kg/day to minipig are shown in figure 3. The concentration of Seocalcitol in serum was below the limit of quantitation in 20% of the samples collected between 2 and 8 h. The mean C_{max} and AUCs were higher in females compared with males, but with a great variation within each gender (table 2). T_{max} was observed almost 5 h after the last dosing in both genders. Owing to the low serum concentrations, it was impossible to calculate the serum half-life. Therefore,

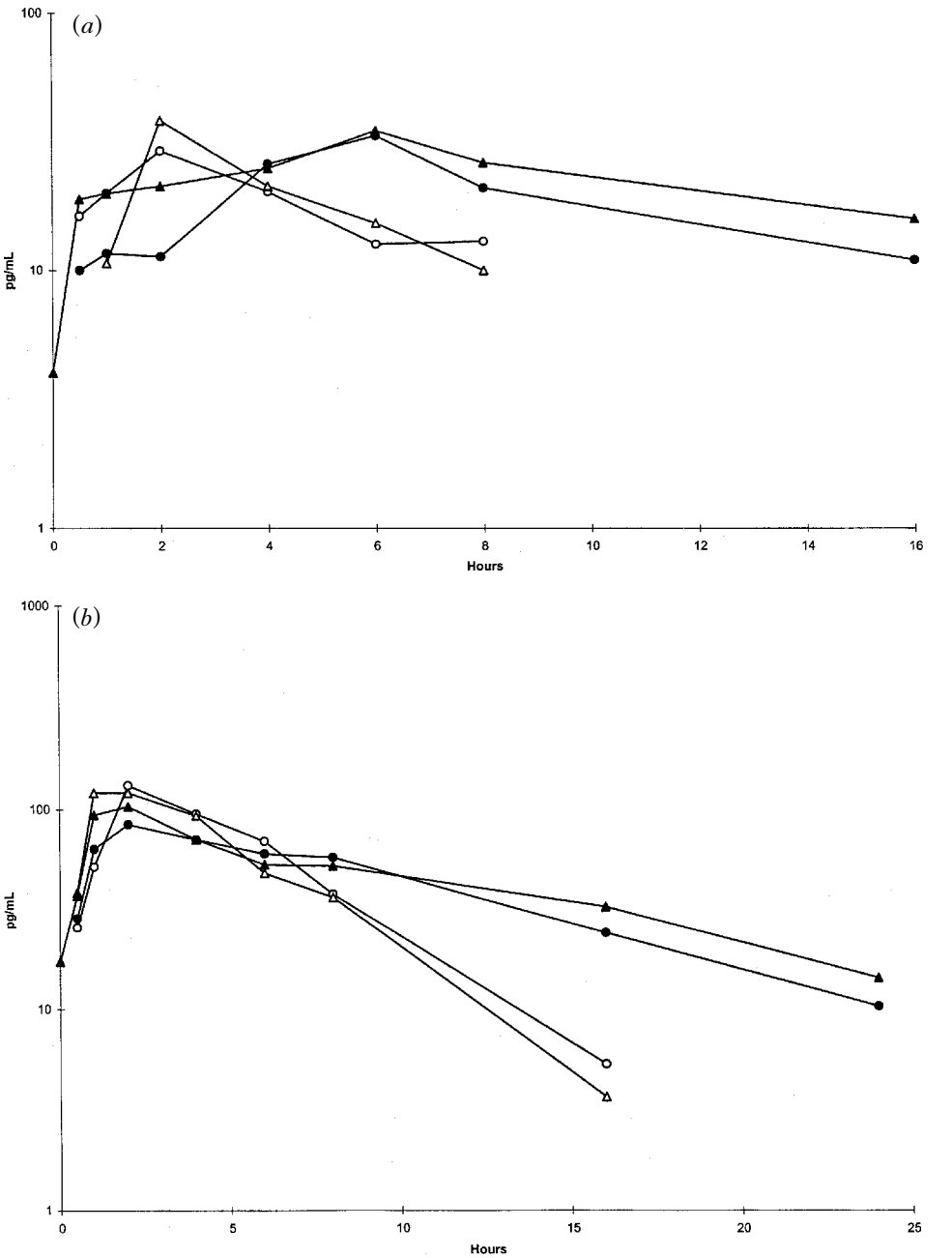


Figure 2. Concentrations of Seocalcitol in serum from rat after oral administrations of 0.6 (a) and 2.4 μg/kg (b) Seocalcitol. Male single dose (○), male seven doses (△), female single dose (●) and female seven doses (▲). Mean of three animals per sampling time.

to obtain higher serum concentrations and, thus, more reliable pharmacokinetic parameters, four female minipigs were given a single dose of 20 μg per animal. This high dose could not be administered repeatedly to the minipigs as it would cause severe clinical symptoms in the animals. Figure 4 shows the individual concen-

Table 1. Pharmacokinetics of Seocalcitol after single and multiple oral administration to rats.

Gender	Dose (μg/kg/day)	No. of doses	C_{max} (pg/ml) mean ± SD	T_{max} (h) mean ± SD	AUC_{∞} (pg/ml × h)	$T_{\frac{1}{2}}$ (h)
Male	0·6	1	30 ± 8	1·7 ± 0·6	236	3·5 (r = 0·99)*
	0·6	7	38 ± 14	2·0 ± 0	223	3·2 (r = 0·99)
	2·4	1	137 ± 40	2·7 ± 1·2	763	2·9 (r = 0·99)
	2·4	7	146 ± 34	1·7 ± 0·6	738	2·8 (r = 0·99)
Female	0·6	1	32 ± 4	5·3 ± 1·2	400	6·7 (r = 0·94)
	0·6	7	34 ± 1	3·7 ± 2·5	585	9·5 (r = 0·96)
	2·4	1	107 ± 26	2·3 ± 1·5	1047	7·1 (r = 0·99)
	2·4	7	146 ± 35	1·7 ± 0·6	1234	8·5 (r = 0·96)

Data are derived from three animals each sampling time.

C_{max} and T_{max}: no significant difference between single and repeated dosing (Student's t-test, p = 0·05); $T_{\frac{1}{2}}$ was calculated from C_{max} and onwards. * The 8-h sampling result was not included in $T_{\frac{1}{2}}$.

AUC_{∞}: 12–39% was extrapolated in the low-dose group and 2–14% was extrapolated in the high-dose group.

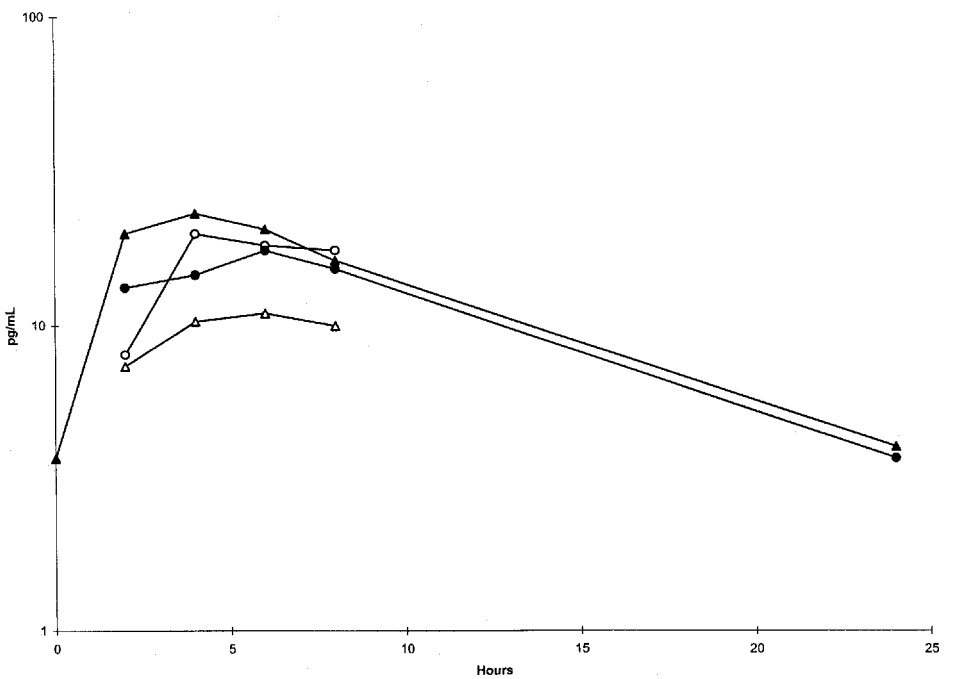


Figure 3. Concentrations of Seocalcitol in serum from minipig after oral administration of 3 μg/animal (0·3 μg/kg) Seocalcitol. Male single dose (○), male eight doses (△), female single dose (●) and female eight doses (▲). Mean of three animals per sampling time.

trations of Seocalcitol in serum. Taking the dose into consideration, the mean C_{max} and AUC were lower than expected from the result in the low-dose animals. These results are based on concentrations near the limit of quantitation and therefore are not completely reliable. However, in the high dose experiment, T_{max} was also 5 h; $T_{\frac{1}{2}}$ was 8.3 h.

Table 2. Pharmacokinetics of Seocalcitol after single and multiple oral administration to minipig.

Gender	Dose (μg/animal)	No. of doses	C_{max} (pg/ml) mean ± SD	T_{max} (h) mean ± SD	AUC (pg/ml × h) mean ± SD	$T_{\frac{1}{2}}$ (h) mean ± SD
Male	3	1	22 ± 11	5.0 ± 1.2	110 ± 69	—
(n = 3)	3	8	14 ± 4	4.7 ± 2.3	64 ± 50	—
Female	3	1	24 ± 14	5.5 ± 2.5	175 ± 89	—
(n = 3)	3	8	33 ± 8	3.3 ± 1.2	236 ± 199	—
Female	20	1	144* ± 60	5.0 ± 2.9	1842* ± 668	8.3 ± 1.6
(n = 4)						

3 μg/animal = 0.30 ± 0.01 μg/kg: AUC_{0-8}.
20 μg/animal = 2.9 ± 0.5 μg/kg: AUC_{∞}.
* Values were dose corrected before calculation of means.

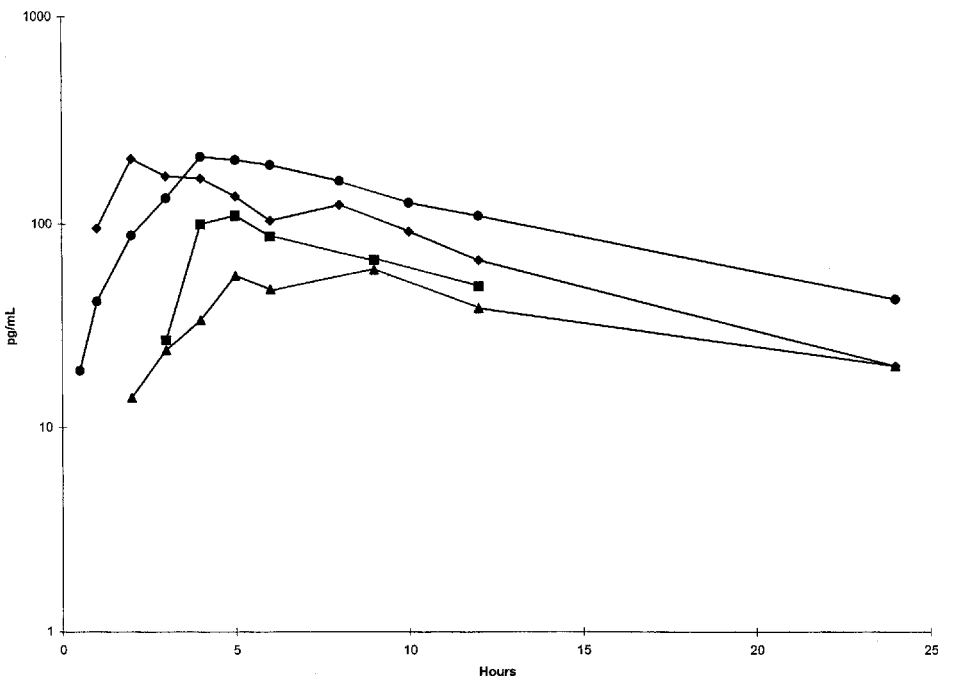


Figure 4. Concentrations of Seocalcitol in serum from minipig given a single oral dose of 20 μg/animal (2.9 μg/kg).

Distribution of Seocalcitol in serum, liver and kidney

The levels of Seocalcitol in serum and liver about T_{max} are given in table 3. In both rat (single and repeated dosing) and minipig (single dosing), the concentration of Seocalcitol in liver was ~10-fold higher than that in serum. The exact concentrations of Seocalcitol in the kidney were more difficult to determine because the kidney was more difficult to homogenize than the liver. Furthermore, there was a greater variation in individual animals. However, the concentration of Seocalcitol in rat kidneys was estimated as ~2-fold higher than in serum, and in the minipig kidneys the concentration was slightly higher than 2-fold (compared with serum).

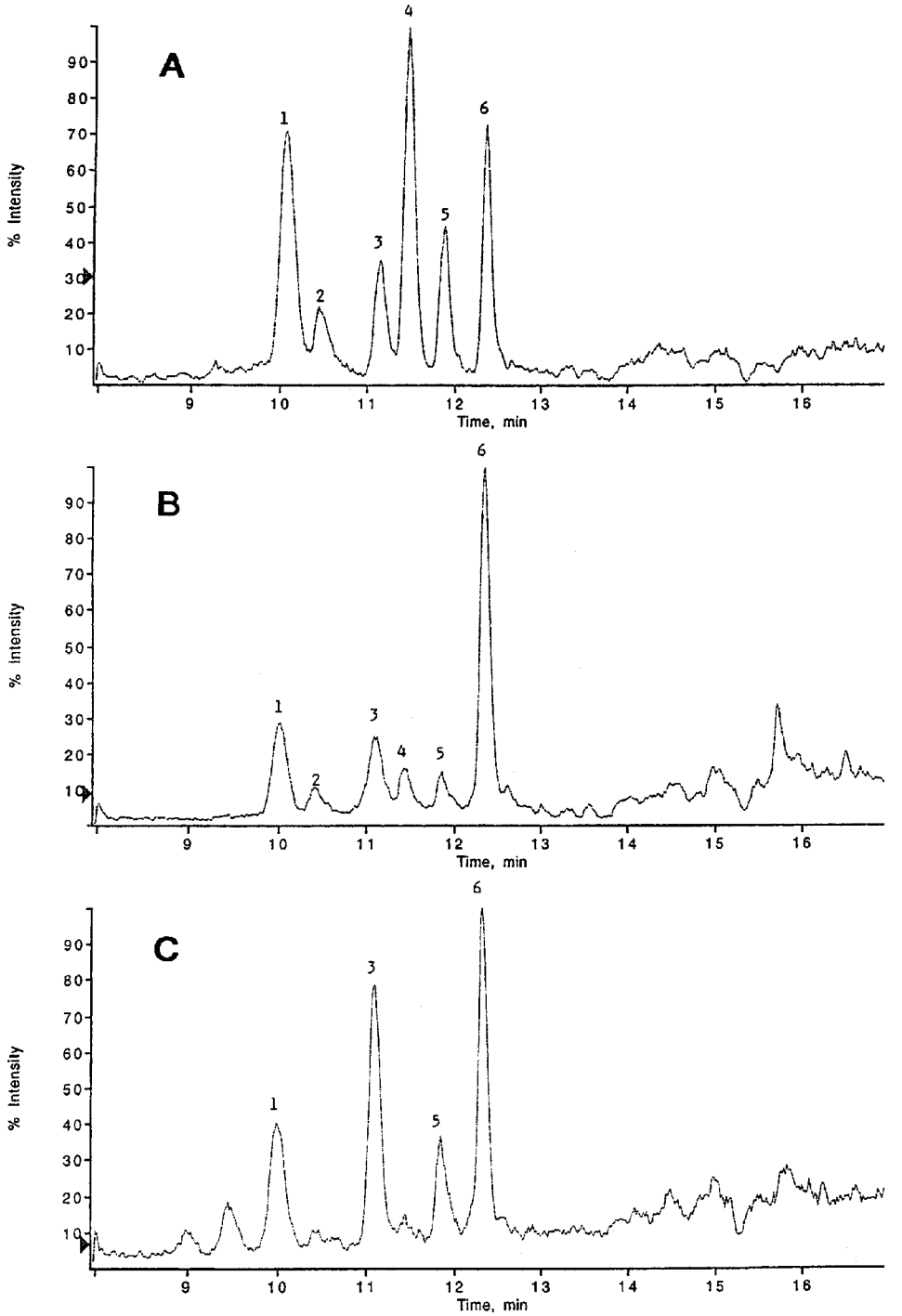


Figure 5. Selected reaction monitoring (SRM) ion chromatograms (transition: m/z 488.4 → 453.4): authentic standards of EB 1435a (1), EB 1445 (2), EB 1470 (3), EB 1435b (4), EB 1436 (5) and EB 1446 (6) in the relative concentrations 0.5:1:1:0.4:1:1 (A). Livers (pooled) from three male rats taken 2 h after a single oral dose of 2.4 μg/kg Seocalcitol (B). Livers (pooled) from three male minipigs taken 6 h after a single oral dose of 20 μg Seocalcitol per animal (C). No interferences were observed in similar blank livers.

Table 3. Concentrations of Seocalcitol in serum and liver from rat and minipig after oral administration.

Species	Gender	Dose (μg/kg/day)	No. of doses	Concentration of Seocalcitol		Concentration of EB1446 in liver
				Serum (pg/ml)	Liver (pg/g)	
Rat	M	2·5	1	151	1548	1422
	M	2·5	7	131	1776	—
	F	2·5	1	93	1014	542
	F	2·5	7	123	790	—
Minipig	M	1·8	1	117	1134	432
	F	1·8	1	106	1018	688

Concentrations were determined from a pool of three animals. Samples were collected close to the T_{max} for serum (at 2 and 6 h after dosing in rat and minipig respectively).

Metabolism of Seocalcitol in liver and kidney from rat and minipig

The metabolic profile of Seocalcitol was also investigated in the liver and kidney collected from the Seocalcitol-dosed rat and minipig. The very different MS/MS ionization efficiency of the 26- and 26a-hydroxy Seocalcitol derivatives as shown in figure 5A must be taken into account when estimating the relative concentrations of the metabolites in liver. Thus, from figure 5, it can be seen that the major metabolite of Seocalcitol in liver from the male rat was EB 1446 and its concentration is similar to Seocalcitol (table 3). In the same tissue, the level of the second major metabolite (EB 1470) was estimated as about half the concentration of Seocalcitol. A similar picture was observed in the female rat, but with lower concentrations of metabolites. Moreover, no change in the profiles was observed after single and multiple dosing. In the male and female minipig, the major hepatic metabolite was EB 1470 being present in about twice the concentration of EB 1446 and thus in a similar concentration as Seocalcitol (table 3). EB 1446 was the second major metabolite, but the concentration of EB 1436 was estimated as being almost as high as EB 1446. The metabolic profiles in the kidney from both species appeared similar to the profiles seen in the liver.

The same liver and kidney samples were also examined for the presence of 3-epi-Seocalcitol. Under reversed-phase LC conditions, it was difficult to separate Seocalcitol and 3-epi-Seocalcitol. Therefore, the two compounds were separated and isolated in a straight-phase HPLC system before their analysis in the LC/MS/MS system. It was not possible to detect any 3-epi-Seocalcitol, so it is questionable if it ever was present, but if so, its concentration corresponded to $< 5\%$ of the concentration of Seocalcitol in the liver and kidney samples from rat and minipig.

In vitro *metabolism in liver homogenates from rat, minipig and humans*

As for the *in vivo* samples, the different MS/MS responses of the metabolites must be taken into account when estimating the relative concentrations of the metabolites formed *in vitro*. The profiles of the 26- and 26a-hydroxy metabolites obtained after incubation of Seocalcitol in the post-mitochondrial liver fraction from rat, minipig and humans are shown in figure 6. In rat, very similar profiles were observed *in vitro* and *in vivo* with EB 1446 being the major metabolite. As seen *in vivo*, the concentration of metabolites was higher in the male animals compared with

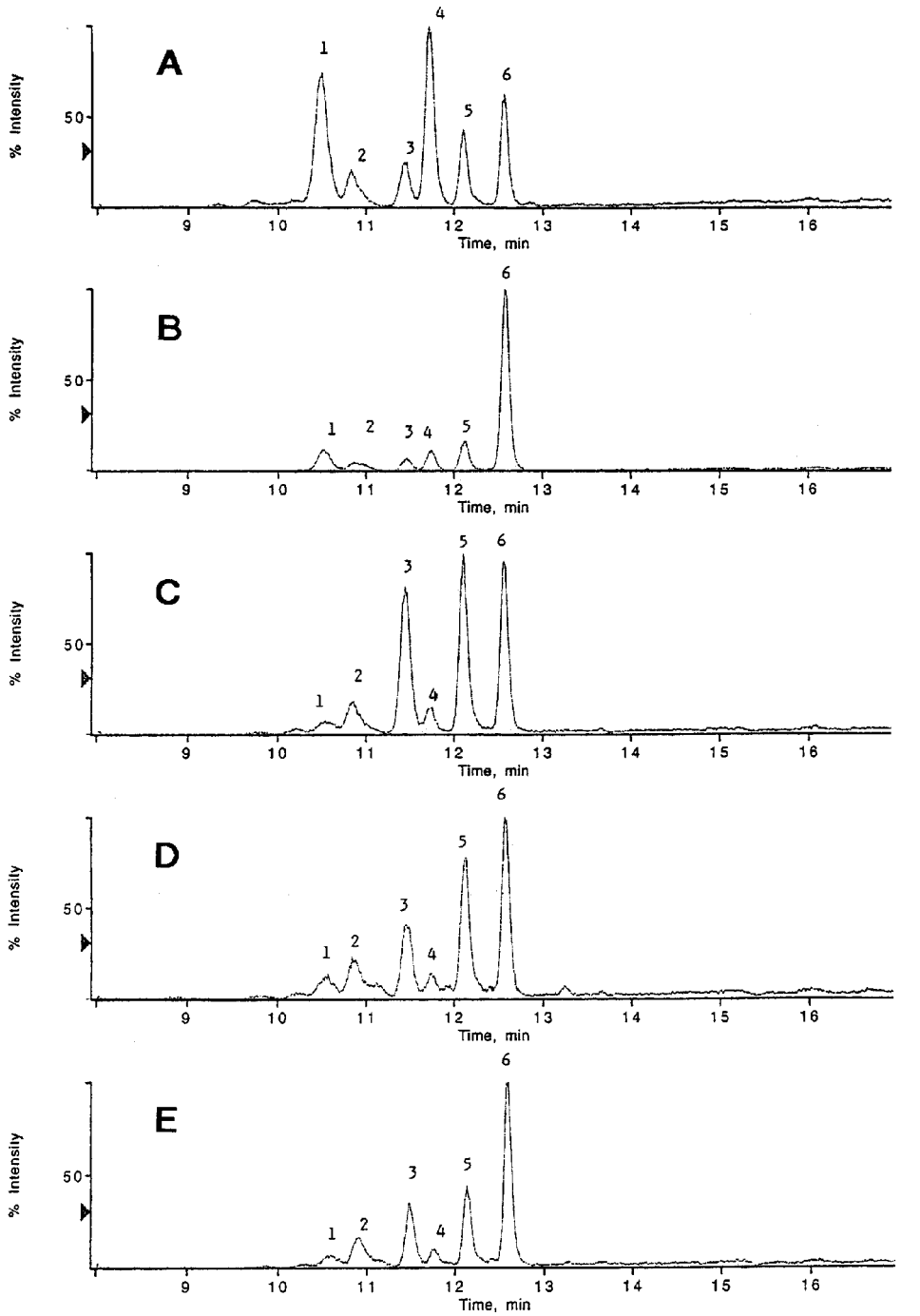


Figure 6. Selected reaction monitoring (SRM) ion chromatograms (transition: m/z 488.4 → 453.4): authentic standards of EB 1435a (1), EB 1445 (2), EB 1470 (3), EB 1435b (4), EB 1436 (5) and EB 1446 (6) in the relative concentrations 0.5 : 1 : 1 : 0.4 : 1 : 1 (A). Two-hour incubation of Seocalcitol with post-mitochondrial liver fraction from the male rat (B), male minipig (C), male human (D) and female human (E). No interferences were observed in similar blank incubations.

Table 4. Serum calcium in rat and minipig after multiple oral administration of Seocalcitol.

Species	Gender	Dose (μg/kg/day)	Days (no. of doses)*	Serum calcium (mmol/l) mean ± SD
Rat	M	0	0	2·97 ± 0·06 (n = 9)
	M	0·6	7	3·07 ± 0·19 (n = 3)
	M	2·4	7	3·67 ± 0·08 (n = 3)
	F	0	0	2·92 ± 0·08 (n = 9)
	F	0·6	7	3·50 ± 0·05 (n = 3)
	F	2·4	7	3·77 ± 0·48 (n = 3)
Minipig	M	0	0	2·74 ± 0·03 (n = 3)
	M	0·3	8	3·13 ± 0·10 (n = 3)
	F	0	0	2·87 ± 0·09 (n = 3)
	F	0·3	8	3·33 ± 0·40 (n = 3)

* Serum was collected 24 h after dosing from the Seocalcitol-treated animal.

the females (data not shown). In both genders, the quantitative and qualitative profiles were almost the same after 2 and 4 h incubation (data from 4 h not shown). In minipig, the major *in vitro* metabolite was EB 1470, followed by EB 1436 and EB 1446 found in the relative concentrations similar to the *in vivo* findings. No major differences were observed between males and females nor between 2- and 4-h incubation. In the homogenates from the male human, EB 1446, EB 1470, and EB 1436 were almost present in equal amounts after a 2-h incubation, and in the female human the concentration of EB 1446 was estimated as slightly higher than EB 1470 and EB 1436. In contrast to the two other species, the total concentration of metabolites is reduced to be about one-third after 4- compared with 2-h incubation, indicating a higher capacity for further metabolism in the human system.

Effects on calcium metabolism

The dose-limiting factor of most vitamin D analogues is related to their effect on the calcium metabolism. As seen in table 4, all the doses used in the multiple-dosing studies gave rise to increases in the concentration of calcium in serum. The effect on serum calcium is genetically regulated and appears at ~24 h after treatment. Therefore, animals given a single dose were probably not hypercalcaemic during the period, where the single dose pharmacokinetics was investigated.

Discussion

The objective of the present investigations was to study the pharmacokinetics of Seocalcitol after single and multiple oral administration to rat and minipig to support both toxicological and pharmacological observations, as well as the studies are useful for the design of later studies in humans (e.g. blood sampling times). Based on previous results (Kissmeyer *et al.* 1997) demonstrating that the hepatic metabolism *in vitro* of Seocalcitol led to the formation of 26- and 26a-hydroxy derivatives, the present authors have further investigated the presence of each of these metabolites in liver and kidney from rat and minipig. These findings were correlated with the profiles observed *in vitro* after incubation of Seocalcitol in liver homogenates from rat, minipig and human.

The pharmacokinetic data have revealed that almost the same C_{max} and AUC were found in rat after one and seven doses indicating no induction/inhibition of the

enzymes involved in the biotransformation of Seocalcitol. However, the higher AUC observed in the female compared with the male are explained by a slower clearance in the female. Consequently, a higher $T_{\frac{1}{2}}$ was also observed and a slightly higher AUC at steady-state was observed after multiple dosing to the female. In contrast to the male with the short $T_{\frac{1}{2}}$ combined with the once-a-day dose regimen, the steady-state level was obtained after the first daily dose. A difference in $T_{\frac{1}{2}}$ is also known from other drugs (Maurizis *et al*. 1997, Pargal *et al*. 1998) and is generally due to higher levels of metabolizing enzymes in the male rat (Kato and Yamazoe 1993, Imamura *et al*. 1999). Furthermore, the pharmacokinetic data were calculated using non-compartmental analysis, although a one-compartment model with a first order elimination is suggested from the log–linear relationship observed from the data (figure 2). Moreover, both the dose-corrected C_{max} and $T_{\frac{1}{2}}$ were constant at the two dose levels, which indicates dose-independent pharmacokinetics. This is further supported by the fact that the $T_{\frac{1}{2}}$ in the male is in the same range as that found previously after a single intravenous administration of 200 μg/kg Seocalcitol to the male rat ($T_{\frac{1}{2}}$ = 2.1 h) (Kissmeyer *et al*. 1997). This observation indicates that the pharmacokinetics of Seocalcitol, at least in the male rat, is independent of the dose in a wide range. This observation is reassuring because classification of the metabolic stability of numbers of vitamin D analogues was previously determined after administration of such a high dose before the sensitive LC/MS/MS assay became available and a less sensitive HPLC assay with UV detection was used (Kissmeyer *et al*. 1995). In contrast to the above, dose independence was not so pronounced for AUC_{∞}, but in this context it must be stressed that up to 39% of AUC_{∞} in the low-dosing groups was extrapolated and therefore not fully reliable.

In minipig after single and multiple dosing of 0.3 μg/kg Seocalcitol, the pharmacokinetic data demonstrated an apparent variation between individual animals. Therefore, no hypothetic differences in C_{max} and AUC after single and multiple dosing as well as between the male and female were revealed. The variation in the pharmacokinetics data cannot solely be explained by the fact that many of the calculations were based on concentrations found near the limit of quantitation, as a somewhat great variation was also observed in the female giving a 10-fold higher dose producing much higher and therefore more reliable serum concentrations. Therefore, taking these variations into account, it was similarly impossible to evaluate the pharmacokinetic dose dependency in minipig.

Comparison of the pharmacokinetic data in minipig and rat revealed that the maximal concentration of Seocalcitol peaked $\sim$ 2 h later in minipig than in rat. This can be explained by the difference in the gastrointestinal tract between the two species because administration of Seocalcitol to minipig as a propylene glycol buffer solution has demonstrated the same late T_{max} (data not shown). Otherwise, the pharmacokinetic data from the two species are comparable with the best correlations between the minipig (both genders) and the female rat.

In spite of having used the current sensitive assay to quantify the concentration of Seocalcitol in serum, it is reasonable to note that one can still only describe the pharmacokinetics of Seocalcitol after administration of doses that are close or have given rise to increases in serum calcium after multiple administration. Thus, 0.6 μg/kg Seocalcitol to rat is comparable with the highest doses that have been included in the long-term toxicity studies. Similarly, in minipig the highest dose used in long-term toxicity studies was 0.2–0.3 μg/kg. As it is solely the effect of Seocalcitol on calcium metabolism that limits the dose levels, it is reassuring that the

pharmacokinetic data of Seocalcitol have not been affected by the rise in serum calcium observed after multiple administration of Seocalcitol. Therefore, there is no reason to believe that the pharmacokinetic profile of Seocalcitol would be different at lower, non-calcaemic doses.

In addition to the investigation of the pharmacokinetic profile of Seocalcitol in serum, it is important to understand the major catabolic pathway of Seocalcitol. From studies in rat using radiolabelled Seocalcitol, high concentrations of radioactivity were primarily measured in the liver (Kissmeyer *et al*. 1997). Also demonstrated were that the major metabolites found in liver samples collected from rat dosed with ^{14}C-Seocalcitol and from incubation of Seocalcitol in the post-mitochondrial liver fraction from rat, minipig and human were the 26- and 26a-hydroxy metabolites of Seocalcitol. A complete separation of all six isomers was not performed. However, this work has continued and now all six isomers can be separated and the metabolic profiles regarding these metabolites were investigated further. In rat and minipig, an excellent *in vitro*/*in vivo* correlation was found comparing the profiles generated from Seocalcitol dosed animals and from incubations of Seocalcitol in the post-mitochondrial liver fractions from the same species, although much higher concentrations were used *in vitro* in comparison with the concentrations obtained in the livers *in vivo*. This finding is important, especially because a very limited amount of information regarding the metabolism of Seocalcitol in humans can be generated from *in vivo* studies. On the other hand, the relative concentrations of the metabolites are different between the three species. In rat, the major metabolite was EB 1446, and in minipig the major metabolite was EB 1470. However, in humans, the *in vitro* system generated EB 1446, EB 1470 and EB 1436 in almost the same concentrations, which then also is expected to be the case *in vivo*. It has been reported that the relative calcaemic activities of EB 1470 and EB 1436 were comparable with Seocalcitol, whereas the calcaemic activity of EB 1446 was $\sim$10-fold less (Kissmeyer *et al*. 1997). The formation of more calcaemic metabolites in minipig than in the rat combined with a longer $T_{\frac{1}{2}}$ (at least compared with male rat) would suggest a lower tolerance of Seocalcitol in minipig, which also was the case when comparing the maximal tolerated doses from long-term toxicity studies (unpublished data). In contrast, the dose corresponding to the 'no observable effect level' of Seocalcitol was slightly higher in minipig than in rat. Therefore, the two species might have a slightly different susceptibility towards modulation of calcium homeostasis. Thus, rat seems to be more sensitive to renal mineralization although it can tolerate a higher dose.

It has been demonstrated that 3-epi-1α,25(OH)$_2$D$_3$ is a minor metabolite of 1α,25(OH)$_2$D$_3$ (Sekimoto *et al*. 1999). Therefore, it was interesting to examine whether a similar metabolite of Seocalcitol could be found in liver and kidney from rat and minipig. However, 3-epi-Seocalcitol was not detectable in any of the tissues (i.e. $<$ 5% of the concentration of Seocalcitol), but it cannot be ruled out that 3-epi-Seocalcitol was present in a small concentration or it might be formed in other tissues.

The enzyme(s) involved in the metabolism of Seocalcitol have not yet been identified. However, it has been demonstrated that the cytochrome P450 inhibitor ketoconazole blocks the metabolism of Seocalcitol suggesting that cytochrome P450 enzymes are involved in the metabolism of Seocalcitol (Shankar *et al*. 1997). On the other hand, it has also been shown that neither the cytochrome P450 enzyme CYP24 (24-hydroxylase involved in, for example, the metabolism of 1α,25(OH)$_2$D$_3$) nor

CYP27 (mitochondrial 25-hydroxylase involved in, for example, formation of 25OH D_3) plays an important role in the metabolism of Seocalcitol, as both CYP24- and CYP27-transfected monkey kidney COS-1 cells failed to generate 26- and 26a-hydroxy Seocalcitol. This agrees with the fact that Seocalcitol was readily metabolized in the post-mitochondrial fraction (cytosol and microsomal fractions), as CYP27 is an enzyme primarily found in the liver mitochondria catalysing the C-25 hydroxylation of vitamin D_3 and 1αOHD_3 (Okuda 1994). However, in the hepatic microsomal fraction, another enzyme is known to hydroxylate a broad spectrum of substrate also including vitamin D_3 and 1αOHD_3 (Hayashi *et al*. 1986). This enzyme must have been present during the time where the 26- and 26a-hydroxy metabolites were generated, and therefore it is a possibility that the microsomal 25-hydroxylase is involved in the metabolism of Seocalcitol. Moreover, the microsomal 25-hydroxylase has been described to be much more active in the male rat compared with the female (Kato *et al*. 1993). So if the microsomal 25-hydroxylase is involved in the metabolism of Seocalcitol, it may explain the faster metabolism of Seocalcitol observed in male rat ($T_{\frac{1}{2}}$ = 3 h) compared with the female and the minipig ($T_{\frac{1}{2}}$ = 8 h). However, further studies are needed to clarify this theory and also to understand the mechanism behind the generation of the various isomers of 26-and 26a-hydroxy Seocalcitol. In that context it is important to note that the relative formation of each isomer in the various systems is very consistent.

In conclusion, the present data have revealed that the pharmacokinetic profile of Seocalcitol is the same after single and repeated oral dosing as well as the $T_{\frac{1}{2}}$ is constant over a wide dose range. In addition, the pharmacokinetic parameters did not change, although the animals became hypercalcaemic. These findings are important because of analytical limitations, as many studies on the metabolism and pharmacokinetics of Seocalcitol are still forced to be conducted at slightly hypercalcaemic doses to detect the parent compound or its metabolites. Moreover, a 10-fold higher concentration of Seocalcitol in liver compared with serum was observed at T_{max} in rat and minipig. The same presumable accumulation of Seocalcitol in human livers may thus be anticipated, as Seocalcitol is under clinical evaluation for the treatment of liver cancer (Dalhoff *et al*. 1998). In the liver, the major metabolites were identified as the 26-hydroxy Seocalcitol derivatives, although the concentration of the various isomers was different in rat and minipig. On the other hand, a good correlation between the metabolic profile obtained *in vitro* and *in vivo* was found, which is important, as most knowledge of the hepatic metabolism of Seocalcitol in human must be based on the present *in vitro* findings. Further studies are required to explore the further metabolism of Seocalcitol, for example, the major metabolites in the faeces. Moreover, studies of the pharmacokinetics in human are in the planning stage and it will be interesting to compare the preclinical and clinical data to evaluate the usefulness of rat and minipig as models for this class of compound.

Acknowledgements

The authors thank Drs H. Aaes, A.-M. Paarup, J. Schützsack and Mr O. Larsen for handling the minipigs. The technicians in the Department of Pharmacokinetics and Metabolism are thanked for technical support.

References

Binderup, E., Calverley, M. and Binderup, L., 1991, Synthesis and biological activity of 1α-hydroxylated vitamin D analogues with poly-unsaturated side chains. In *Proceedings of the Eighth Workshop on Vitamin D*, 5–10 July, Paris, pp. 192–193.

Colston, K., Mackay, A. G., James, S. Y., Binderup, L., Chander, S. and Coombes, R. C., 1992, EB 1089: A new vitamin D analogue that inhibits the growth of breast cancer cells *in vivo* and *in vitro*. *Biochemical Pharmacology*, **44**, 2273–2280.

Dalhoff, K., Astrup, L., Bach-Hansen, J., Burcharth, F., Haahr, H. L. O., Hamberg, K. J., Evans, T. R. J., Lofts, F., Møller, S., Ranek, L., Skovsgaard, T. and Steward, W. P., 1998, Seocalcitol (EB 1089), a vitamin D analogue, in hepatocellular carcinoma. *Hepatology*, **28**, 2–12.

DeLuca, H. F., Krisinger, J. and Darwish, H., 1990, The vitamin D system: 1990. *Kidney International*, **38 (suppl. 29)**, S-2–8.

Haq, M., Kremer, R., Golzman, D. and Rabbani, S. A., 1993, A vitamin D analogue (EB1089) inhibits parathyroid hormone-related peptide production and prevents the development of malignancy-associated hypercalcemia *in vivo*. *Journal of Clinical Investigation*, **91**, 2416–2422.

Haussler, M. R., Jurutka, P. W., Hsieh, J. C., Thompson, P. D., Selznick, S. H., Haussler, C. A. and Whitfield, G. K., 1995, New understanding of the molecular mechanism of receptor-mediated genomic actions of the vitamin D hormone. *Bone*, **17**, 33S–38S.

Hayashi, S.-I., Noshiro, M. and Okuda, K., 1986, Isolation of a cytochrome P-450 that catalyzes the 25-hydroxylation of vitamin D3 from rat liver microsomes. *Journal of Biochemistry*, **99**, 1753–1763.

Imamura, Y., Kaneko, M., Mori, Y. and Otagiri, M., 1999, Sex-dependent pharmacokinetics and *in vitro* reductive metabolism of acetohexamide in Wistar–Imamichi rats. *Biological Pharmaceutical Bulletin*, **22**, 435–438.

Kato, R. and Yamazoe, Y., 1993, Hormonal regulation of cytochrome P450 in rat liver. In J. B. Shenkman and H. Greim (eds), *Handbook of Experimental Pharmacology Volume* 105 (Berlin: Springer), pp. 445–459.

Kissmeyer, A.-M., Binderup, E., Binderup, L., Hansen, C. M., Andersen, N. R., Makin, H. L. J., Schroeder, N. J., Shankar, V. N. and Jones, G., 1997, Metabolism of the vitamin D analog EB 1089: identification of *in vivo* and *in vitro* liver metabolites and their biological activities. *Biochemical Pharmacology*, **53**, 1087–1097.

Kissmeyer, A.-M., Mathiasen, I. S., Latini, S. and Binderup, L., 1995, Pharmacokinetics studies of vitamin D analogues: relationship to vitamin D binding protein (DBP). *Endocrine*, **3**, 263–266.

Kissmeyer, A.-M., Sonne, K. and Binderup, E., 2000, Determination of the vitamin D analog EB 1089 (Seocalcitol) in human and pig serum by liquid chromatography tandem mass spectrometry. *Journal of Chromatography B*, **740**, 117–128.

Mathiasen, I. S., Colston, K. and Binderup, L., 1993, EB 1089, a novel vitamin D analogue, has strong antiproliferative and differentiation inducing effects on cancer cells. *Journal of Steroid Biochemical Molecular Biology*, **46**, 365–371.

Maurizis, J. C., Madelmont, J. C., Rapp, M., Marijnen, C., Cerf, M. C., Gillardin, J. M., Lepage, F. and Veyre, A., 1997, Disposition and metabolism of 2,6-dimethylbenzamide N-(5-methyl-3-isoxazolyl) (D2916) in male and female rats. *Drug Metabolism and Disposition*, **25**, 33–39.

Okuda, K. I., 1994, Liver mitochondrial P450 involved in cholesterol catabolism and vitamin D activation. *Journal of Lipid Research*, **35**, 361–372.

Pargal, A., Cherian, B., Rant, S. and Joshi, D., 1998, Flurbiprofen pharmacokinetics: interstrain and sex differences in rats. *Pharmaceutical and Pharmacological Communication*, **4**, 407–410.

Reichel, H., Koeffler, H. P. and Norman, A. W., 1989, The role of the vitamin D endocrine system in health and disease. *New England Journal of Medicine*, **320**, 980–991.

Sarkar, R. B. C. and Chanhan, U. P. S., 1967, A new method for determining microquantities of calcium in biological materials. *Analytical Biochemistry*, **20**, 155–166.

Sekimoto, H., Siu-Caldera, M.-L., Weiskopf, A., Vouros, P., Muralidharan, K. R., Okamura, W. H., Uskokovic, M. R. and Reddy, G. P., 1999, 1α,25-Dihydroxy-3-epi-vitamin D3: *in vivo* metabolite of 1α,25-dihydroxyvitamin D3 in rats. *FEBS Letters*, **448**, 278–282.

Shankar, V. N., Dilworth, F. J., Makin, H. L. J., Schroeder, N. J., Trafford, D. J. H., Kissmeyer, A.-M., Calverley, M. J., Binderup, E. and Jones, G., 1997, Metabolism of the vitamin D analog EB1089 by cultured human cells: redirection of hydroxylation site to distal carbons of the side-chain. *Biochemical Pharmacology*, **53**, 783–793.

XENOBIOTICA, 2000, VOL. 30, NO. 8, 831–841

Diltiazem blood pharmacokinetics in the pregnant and non-pregnant rabbit: maternal and foetal tissue levels

M. A. BREGANTE†, J. J. ARAMAYONA†*, L. J. FRAILE†, M. A. GARCIA‡ and C. SOLANS†

Departments of †Pharmacology and Physiology and ‡Analytical Chemistry, Faculty of Veterinary Science, Miguel Servet 177, E-50013 Zaragoza, Spain

Received 25 February 2000

1. The aim was to investigate the pharmacokinetics of diltiazem (DTZ) and its metabolites, deacetyldiltiazem (M1) and N-demethyldiltiazem (MA), in the pregnant rabbit following DTZ intravenous administration. In addition, DTZ tissue distribution in both the non-pregnant and pregnant rabbit and foetuses was also studied.

2. The slope of the α- and β-phases increased slightly in six of the eight pregnant rabbits as compared with the non-pregnant animal, but the other pharmacokinetic parameters that largely determine drug disposition (AUC, V_D, CL) showed no significant differences.

3. MA blood disposition was unaltered by pregnancy. However, all the pharmacokinetic parameters calculated for the deacetylated metabolite of DTZ were significantly modified in the pregnant as compared with the non-pregnant rabbit.

4. DTZ tended to concentrate in most of the tissues examined. Significant differences were observed in the DTZ concentration in the uterus and kidney from the pregnant as compared with the non-pregnant rabbit.

5. The findings suggest that DTZ diffuses easily through the placenta, reaching DTZ blood concentrations equivalent to that observed in maternal blood. However, the concentration of DTZ and its metabolites in the selected foetal tissues was either higher (in brain and muscle) or lower than that observed in maternal tissues, suggesting a different tissue affinity and/or a different metabolic activity in the foetuses as compared with the mothers.

Introduction

Diltiazem (DTZ) is one of the several effective therapies for the management of hypertension (Weir 1995). As a consequence, its use for the treatment of hypertension occurring in pregnancy has been postulated (Holbrook *et al*. 1988), especially in those clinical cases refractory to traditional therapy. The pharmacokinetics of DTZ have been widely described in adult animals and in man (Yeung *et al*. 1990, 1993). The drug is extensively metabolized by at least five distinct pathways including deacetylation, N-demethylation, O-demethylation, ring hydroxylation and acid formation (Sugawara *et al*. 1988). The deacetylation and N-demethylation of DTZ seem to be the most important pathways leading to the production of basic metabolites in the rabbit (Yeung *et al*. 1991). These basic metabolites retain a certain degree of pharmacological activity and may contribute to the overall pharmacological action of the drug (Yabana *et al*. 1985).

Despite the extensive information available on DTZ pharmacokinetics, there are no reports on DTZ disposition in the pregnant animal. This represents a gap in the knowledge of DTZ during this particularly critical period. In fact, the physiologic changes occurring in gestation may alter the pharmacokinetics of a drug (Jeffries *et*

* Author for correspondence; e-mail: aramayon@posta.unizar.es

Xenobiotica ISSN 0049-8254 print/ISSN 1366-5928 online © 2000 Taylor & Francis Ltd
http://www.tandf.co.uk/journals

al. 1988, Loebstein *et al*. 1997), making the extrapolation of findings obtained in other physiologic or pathologic situations inappropriate. Because of the lack of basic information on DTZ pharmacokinetics in the pregnant animal, the aim of the present study was to investigate the pharmacokinetics of DTZ in the pregnant rabbit following intravenous (i.v.) administration, and to compare its disposition with that observed in the non-pregnant rabbit. Rabbit was chosen as the animal model because its DTZ pharmacokinetics (including metabolism) are very similar to those in man (Yeung *et al*. 1990). In addition, the DTZ tissue distribution in both the non-pregnant and pregnant rabbit and their foetuses has also been studied, given the high tissue affinity reported for the drug (Renton *et al*. 1985, Nakamura *et al*. 1987).

Materials and methods

Animals

Twenty-three New Zealand White rabbits (body weight 4.5–5.0 kg, age 1.5–2.0 years) were acclimatized in our laboratory for 7 days before their enrolment in the experiment. During this period, the does were housed in rooms with a controlled temperature (20 °C) and a 12-h light/dark cycle, and rabbits were maintained on water and standard laboratory chow *ad libitum*. Each animal was judged to be normal by way of physical examination before the experiment. During this procedure, both the heart and respiratory rates and the rectal temperature had to be considered normal before including the animals in the experiments.

Reagents

Diltiazem (DTZ) and imipramine were from Sigma Chemical Co. (St Louis, MO, USA). Deacetyldiltiazem (M1) and demethyldiltiazem (MA) were gifts from the Mario Negri Institute (Milan, Italy) via Dr R. Latini. All other chemicals were of reagent or HPLC grade.

Intravenous bolus administration

The effect of pregnancy on DTZ pharmacokinetics was studied in eight rabbits in a crossover design (washout period of 6 weeks). The female rabbits were cohabited with male breeders and pregnancy were determined 11 days later by abdominal palpation. When necessary, the mating protocol was repeated. When pregnancy was confirmed, the weight of the animals was recorded every 4 days to verify a normal course of gestation. In the pregnant rabbit, the experiment was performed on day 28 of gestation. The does were whelped from days 30 to 32 of gestation. The litter sizes, perinatal mortality and offspring growth were recorded. The rabbits were administered DTZ i.v. as a bolus dose of 5 $mg.kg^{-1}$ body weight in the marginal ear vein. Serial blood samples (1 ml) were drawn from a catheter inserted in the contralateral central ear artery at 0, 5, 15, 30, 45, 60, 90, 120, 180, 240, 300, 360 and 480 min. Blood samples were immediately haemolysed by the addition of an equal volume of water. Thereafter, samples were placed in 20 ml of cold (−20 °C) extraction medium (hexane–isobutanol, 98:2 v/v) and assayed for DTZ, M1 and MA concentrations.

Maternal and foetal tissue distribution of DTZ and its metabolites following an i.v. infusion of DTZ

Nine female rabbits, four on day 28 of gestation, were used. To obtain the steady-state concentration of DTZ, an infusion programme was set up using the average of the estimated pharmacokinetic parameters obtained from the i.v. bolus experiment. Infusion rate (Q) was calculated as:

$$Q = C_{ss}{*}\mathrm{CL},$$

where C_{ss} is the desired maternal blood concentration at steady-state (300 $ng.ml^{-1}$) and CL is blood clearance (43 $ml.min^{-1}.kg^{-1}$). DTZ solutions were prepared by dilution to an appropriate concentration that permitted infusion rates in every animal of < 0.2 $ml.min^{-1}$. The time at which the equilibrium between maternal and foetal DTZ concentration was achieved was determined in a pilot experiment. Briefly, a pregnant rabbit was maintained under i.v. pentobarbital anaesthesia for 3 h after DTZ infusion was started. The uterus was exposed to allow foetal blood sampling. Maternal and foetal blood samples were simultaneously drawn at 60, 120 and 180 min and assayed for DTZ, M1 and MA concentrations.

In the main experiment ($n = 3$), maternal blood samples were drawn through a catheter inserted in the ear artery at 0, 5, 15, 30, 45, 60, 90, 120 and 180 min after the start of the DTZ infusion. After reaching steady-state (180 min after the start of the infusion), does were anaesthetized by an i.v. administration of sodium pentobarbital (30 $mg.kg^{-1}$) and a midline incision was carried out in the ventral abdominal wall passing through the skin and linea alba. In the pregnant animal, the horns of the uterus were exteriorized and an incision was made in the dorsal surface of the uterine body such that the placental sacs were intact ($n = 4$ in each dam). A syringe drew amniotic fluid (0.5 ml) from each implantation site. The foetuses

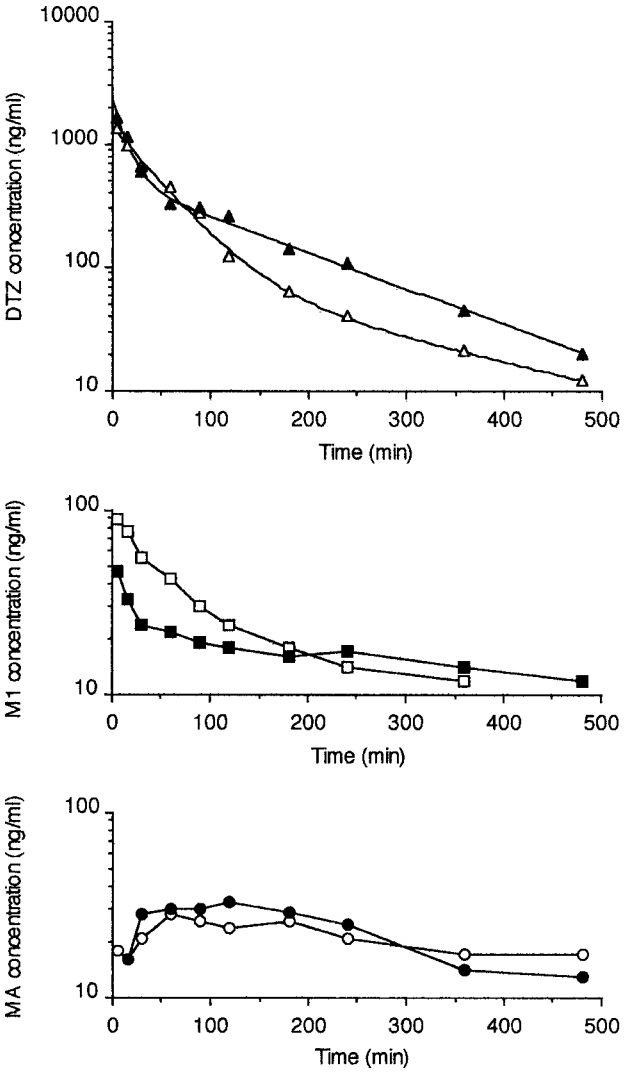


Figure 1. DTZ (top), deacetyl diltiazem (central) and N-demethyl diltiazem (bottom) blood concentrations following an intravenous bolus dose of 5 $mg.kg^{-1}$ DTZ in a representative rabbit. Non-pregnant (open symbols); pregnant (filled symbols). ▲, △, DTZ; ■, □, M1; ●, ○, MA.

were then freed from membranes and placenta. Blood samples (0.5 ml) were obtained from the foetuses by cardiac puncture under light ether anaesthesia. Maternal and foetal tissues were quickly excised in the following order: perirenal fat, spleen, kidney, uterus, liver, heart, lung, brain, muscle. Thereafter, tissues were rinsed with cold saline, blotted and weighed. All specimens were rapidly frozen at −20 °C until assayed for DTZ, M1 and MA concentrations. The same protocol was performed in the non-pregnant rabbit (n = 6) but, obviously, without foetal sampling.

Tissue samples (~ 2 g) were homogenized at 13500 rpm for 2 min in 10 ml cold 0.01 M phosphate buffer, pH 7.4, using a tissue homogenizer (Ultra-Turrax T25, Janke and Kunkel, GmbH and Co. Germany). Thereafter, homogenates were centrifuged for 5 min at 1000 g (Beckman Model J2–21; Palo Alto, CA, USA) and the supernatant fraction was collected. An aliquot of 5 ml homogenate was separated for analysis.

Hplc assay of DTZ and its metabolites

DTZ and its metabolites were assayed in blood and tissue homogenates following hexane–isobutanol (98:2 v/v) extraction according to the HPLC method of Yeung *et al.* (1989). The HPLC system consisted of an isocratic pump (Model 145), a 5-μm reversed-phase column (Novapack C18, 150 × 3.9 mm i.d.) and

Table 1. Mean (±SD) pharmacokinetic variables of diltiazem and its M1 and MA metabolites determined following endovenous administration of 5 mg diltiazem kg^{-1} of body weight to the non-pregnant (n = 8) and pregnant rabbit (n = 8) (concentration data fit to equation 1).

Parameters	Non-pregnant rabbit	Pregnant rabbit
Diltiazem		
C_1 ($ng.ml^{-1}$)	1·674±611	1·757±268
λ_1 (min^{-1})	0·0300±0·0098	0·0665±0·0199#
C_z ($ng.ml^{-1}$)	479±248	575±122
λ_z (min^{-1})	0·0054±0·0008	0·0073±0·0013#
$t_{1/2^i1}$ (min)	23*	11*
$t_{1/2^iz}$ (min)	128*	95*
AUC_{DTZ} ($ng.min.ml^{-1}$)	127·592±41·006	113·600±20·507
V_1 ($ml.kg^{-1}$)	2·567±745	2·078±185
V_{1D} ($ml.kg^{-1}$)	8·218±3·496	6·346±1·044
CL ($ml.min^{-1}.kg^{-1}$)	42·7±13·1	45·8±8·1
Deacetyl diltiazem		
C_{max} ($ng.ml^{-1}$)	88±26	46±16#
λ_z (min^{-1})	0·0061±0·0032	0·0022±0·0014#
AUC_{M1} ($ng.min.ml^{-1}$)	8·803±4·134	5·571±2·585#
AUC_{M1}/AUC_{DTZ}	0·0670±0·0292	0·0478±0·0186#
N-demethyl diltiazem		
C_{max} ($ng.ml^{-1}$)	36±15	34±7
λ_z (min^{-1})	0·0043±0·0031	0·0031±0·0012
AUC_{MA} ($ng.min.ml^{-1}$)	7·841±4·306	8·979±3·006
AUC_{MA}/AUC_{DTZ}	0·0602±0·0308	0·0796±0·0269

Each value is the mean±SD of eight animals.

C_1 and C_z are the coefficients, and λ_1 and λ_z are the exponents derived by non-linear least-squares regression fit of concentration data to equation (1). The terms are related to rate constants for the specific two-compartment pharmacokinetic model and were used to derive the following pharmacokinetic values: $t_{1/2^i1}$, distribution half-life; $t_{1/2^iz}$, elimination half-life; V_1, volume of the central compartment; V_{1D}, apparent volume of distribution calculated by area method; AUC, area under the blood concentration-time curve; CL, body clearance. C_{max} is the maximum concentration observed in the M1 or MA blood concentration–time curve.

* Harmonic mean.

\# Significantly different from the non-pregnant rabbit.

an UV-VIS detector set at 237 nm (Model 484; all Waters Associates, Milford, MA, USA). Quantitation was performed using a calibration curve of spiked blank blood or tissue homogenates over the range of concentrations assayed. The method was linear for concentrations of 10–5000, 10–1000 and 10–500 $ng.ml^{-1}$ DTZ, M1 and MA respectively. The detection limit was 6, 12 and 9 $ng.ml^{-1}$ for DTZ, M1 and MA respectively. Recovery was determined as >85% for each analyte. Inter- and intra-assay precisions, determined by injection of control standards, were 7 and 3% for DTZ, 9 and 4% for M1 and 9 and 5% for MA respectively.

Data analysis

The following equation was used, describing the time course of DTZ in non-pregnant or pregnant rabbit, namely

$$C = \sum_{i=1}^{n} A_i^* e^{-\lambda_i t}, \quad (1)$$

where A_i and λ_i are the compartmental kinetic variables obtained by non-linear least-squares regression analysis, using a weighting factor of $1/c^2$. The number of exponents (n) to fit the experimental data to the mathematical model (1) was calculated using Akaike's information criterion (Yamaoka *et al*. 1978). The half-lives in the α- and β-phases were calculated as:

$$t_{1/2}\lambda_i = \ln 2/\lambda_i,$$

where λ_i is the slope of the α- and β-phases. Total body clearance was calculated as:

$$CL = dose/AUC_{DTZ},$$

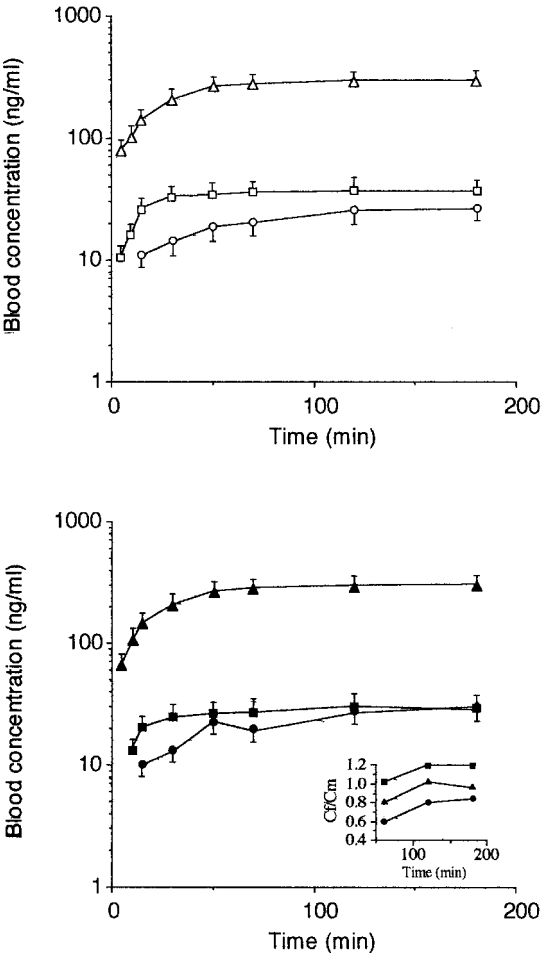


Figure 2. Blood concentration (mean ± SD) of DTZ, M1 and MA during the DTZ infusion program in the non-pregnant (n = 6) (open symbols) and pregnant rabbit (n = 3) (filled symbols). ▲, △, DTZ; ■, □, M1; ●,○, MA. The insert in the bottom panel is the foetal–maternal blood concentration ratio (C_m/C_f) of DTZ, M1 and MA determined in an additional pregnant rabbit (pilot study).

where AUC_{DTZ} is the area under the DTZ blood concentration–time curve calculated by the trapezoidal rule to the last datum point and extrapolated to infinity by dividing C_{last} for the slope of the elimination phase. Finally, the volume of distribution under the area was calculated as:

$$V_{Darea} = \text{dose}/(AUC_{DTZ} \cdot \lambda_n).$$

M1 and MA blood concentrations versus times were analyzed using a non-compartmental model. The slope of the terminal phase (λ_n) was calculated using non-linear least-squares regression analysis of the concentration–time data points forming a straight line, and AUC (AUC_{M1} and AUC_{MA}) was calculated as described for the parent drug.

Statistics

The pharmacokinetic values obtained in the non-pregnant and pregnant rabbits are given as mean ± SD, except for half-life, where the harmonic mean was calculated. Comparisons between i.v. pharmacokinetic parameters from the non-pregnant and pregnant rabbit were carried out by using a Student's paired t-test. The differences between the DTZ, M1 or MA tissue concentrations observed in the non-pregnant and pregnant rabbit, as well as in foetuses, were determined by one-way analysis of variance (ANOVA). In all instances, $p < 0.05$ was considered as statistically significant.

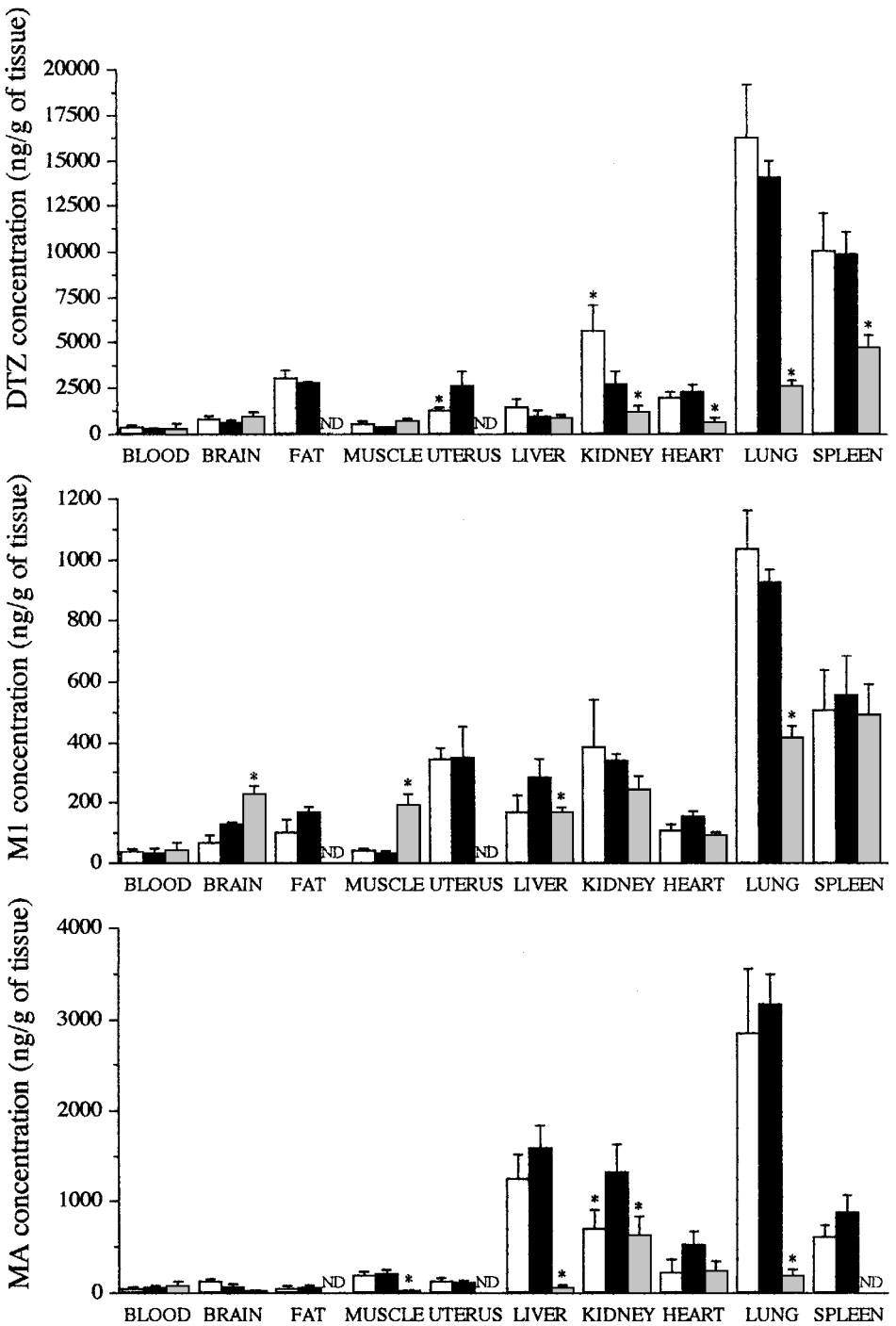


Figure 3. Concentrations (mean ± SD) of DTZ (top), M1 (central) and MA (bottom) in several tissues and in whole blood determined in the non-pregnant ($n = 6$) and pregnant rabbit ($n = 3$), and foetuses ($n = 12$) after reaching steady-state following DTZ infusion. □, Non-pregnant; ■, pregnant; ▤, foetuses. ND, not determined. *Significantly different from the pregnant rabbit ($p < 0.05$).

Results

Intravenous bolus administration

The rabbits used in the present study were similar in age, weight at delivery and weight at 6 weeks postpartum. Deliveries occurred at term (30–32 days of gestation) with a mean litter size of seven individuals. Perinatal mortality was maintained at a minimum (2% stillbirth, 3% dead postpartum) and showed no differences when compared with routine controls carried out in our laboratory. Throughout the study, the pups grew according to a logarithmic pattern, indicating that sucking was adequate.

A non-linear least-squares regression analysis of individual DTZ blood concentration versus time obtained in the pregnant and non-pregnant rabbit was performed. In all instances, the best fit was obtained for $n = 2$, as determined by using Akaike's information criterion (Yamaoka *et al.* 1978). Diltiazem had a slow distributive phase in the non-pregnant rabbit (figure 1), which extended for ~ 200 min after i.v. bolus administration. Thereafter, a linear elimination decrease began and extended until the last time point examined. A comparison of blood DTZ concentrations between the pregnant and non-pregnant rabbit is shown in figure 1, while the pharmacokinetic parameters are compared between the two groups in table 1. The slopes of the α- and β-phases increased slightly in the pregnant rabbit ($p < 0.05$). However, this general trend was reversed in the case of two of the eight rabbits. The other parameters that largely determine drug disposition (AUC, V_D, CL) showed no significant differences between the two groups.

After i.v. bolus administration of the parent compound, the M1 and MA metabolites were detected in the blood (figure 1) in both the pregnant and non-pregnant rabbit. All the pharmacokinetic parameters calculated for M1 (C_{max}, λ_z, AUC_{M1}, AUC_{M1}/AUC_{DTZ}) showed significant differences between the pregnant and non-pregnant rabbit (table 1), suggesting that pregnancy may alter the blood disposition of the deacetylated metabolite of DTZ. However, the pharmacokinetic parameters calculated for MA in the pregnant and non-pregnant rabbit did not show significant differences between both groups of animals (table 1).

Tissue distribution

The mean blood levels of DTZ and of its metabolites, M1 and MA, during the i.v. infusion of DTZ in the pregnant and non-pregnant rabbit are shown in figure 2. The i.v. infusion of DTZ resulted in blood levels in the range of 300 $ng.ml^{-1}$, indicating that there was no difference between the two groups with respect to body clearance. A steady-state plateau was reached ~ 100 min after the beginning of the infusion. Throughout the infusion period, the presence of M1 and MA could be observed. Nevertheless, by contrast with that observed following the i.v. bolus administration, no statistical differences were detected in the blood concentration of DTZ metabolites in the pregnant and non-pregnant animal. DTZ, M1 and MA foetal–maternal ratios were observed to be constant 180 min after the start of DTZ infusion, indicating that the steady-state had been reached.

In all the tissues examined from the pregnant and non-pregnant rabbit, the DTZ concentration was higher than that measured in whole blood. Nevertheless, tissue affinity may be specific for each tissue. For example, the DTZ concentration observed in lung homogenates was ~ 50 times higher than that observed in blood, but the muscle–blood ratio was ~ 1.5, suggesting that some tissues selectively

Table 2. Foetal–maternal ratios (±SD) of DTZ and its metabolites (M1 and MA) in the blood and selected tissues after reaching steady-state following an i.v. infusion of DTZ in three pregnant rabbits.

Organ	DTZ	M1	MA
Blood	0·96±0·43	1·21±0·19	1·17±0·22
Brain	1·48±0·19	1·82±0·28	1·40±0·21
Muscle	2·27±0·59	6·06±0·70	0·10±0·08
Heart	0·27±0·13	0·58±0·10	0·46±0·13
Spleen	0·48±0·15	0·88±0·30	–
Kidney	0·44±0·07	0·71±0·08	0·47±0·11
Liver	0·93±0·15	0·59±0·06	0·03±0·01
Lung	0·18±0·06	0·45±0·10	0·06±0·03

Each value is the mean±SD of 12 animals (four foetuses from each dam).

accumulate DTZ. A similar phenomenon was observed for both M1 and MA. M1 mainly accumulated in the lung, spleen, kidney and uterus, whereas MA mainly accumulated in the lung, liver, kidney, heart and spleen. In most of the tissues examined, there were no statistical differences when comparing the tissue levels of DTZ and its metabolites in the pregnant and non-pregnant rabbit. Nevertheless, some interesting differences could be observed (figure 3). The DTZ concentration in the uterus was about twice as high in the pregnant as compared with the non-pregnant rabbit. In addition, the DTZ and MA concentrations in the kidney of the pregnant rabbit were statistically different from that observed in the non-pregnant animal.

The concentration of DTZ and its metabolites observed in the foetal blood did not show significant differences with the levels of these substances found in the does blood, suggesting that DTZ readily diffuses through the placenta. The DTZ and M1 concentrations in the amniotic fluid were 74±40 and 20±7 $ng.ml^{-1}$ respectively, but the concentration of MA was below the detection limit of the assay. The foetal tissues showed higher DTZ and M1 concentrations than those found in foetal blood. However, MA concentration in the foetal tissues was lower than that observed in the foetal blood, except in the kidney, heart and lung. The ratio between the DTZ, M1 or MA concentration in the foetal and maternal tissues is shown in table 2. As mentioned above, the maternal–foetal ratio was close to 1 in the blood for all three substances. However, the ratio was < 1 for DTZ, M1 and MA in the heart, spleen, kidney, liver and lung, indicating a lower accumulation in the foetal tissues than that observed in the pregnant animal. On the other hand, both the brain and muscle showed ratios >1 for all substances, with the exception of the ratio determined for MA in muscle.

Discussion

The pharmacokinetics of DTZ have been widely described in several animal species. Reports indicate that DTZ is eliminated by multiple and simultaneous mechanisms, including hepatic and extrahepatic metabolism (Fraile *et al*. 1996) and renal excretion. Many of the processes related with drug elimination have been shown to be modified during gestation, as a consequence of the physiologic adaptation taking place in the pregnant female (Loebstein *et al*. 1997). The first objective of the present study, therefore, was to determine if pregnancy modifies the disposition of DTZ. To that end, the non-pregnant and pregnant rabbit were administered i.v. DTZ (5 $mg.kg^{-1}$ body weight) to determine the blood disposition

of the drug and its metabolites in both physiological states. The results indicate that the slopes of both the α- and β-phases were significantly modified by pregnancy. In fact, λ_1 and λ_z tended to be higher in the pregnant than in the non-pregnant animal. This finding can be explained by the increase in cardiac output, the alteration in regional blood flow to the organs and/or the modification in body composition occurring during pregnancy (Mitani *et al*. 1987). However, two rabbits showed the reverse trend, indicating an inconsistent effect of pregnancy on DTZ disposition after i.v. administration. Therefore, the observed interindividual variability may determine the lack of differences observed in other important parameters which describe DTZ disposition (AUC, CL, apparent volume of distribution). DTZ has a high hepatic extraction ratio and, as a result, its hepatic clearance is largely dependent on blood flow to the liver. Failure to demonstrate a change in body clearance between the pregnant and non-pregnant state may simply reflect the absence of any significant alteration in hepatic blood flow in pregnancy. Confirming this approach, Witter (1993) pointed out that highly extracted drugs do not usually show an altered disposition as a consequence of pregnancy. Furthermore, others have observed that propranolol (O'Hare *et al*. 1984) and fenoterol (Hildebrandt *et al*. 1993) dispositions (drugs which are mainly dependent on metabolism for elimination) showed hardly any modification during pregnancy. All these reports may question the validity of the differences observed in the present work after DTZ i.v. administration, and they illustrate the fact that such differences probably have no practical implications. In fact, in the second set of experiments in which DTZ was administered by i.v. infusion, DTZ blood concentrations were essentially the same in the pregnant and non-pregnant rabbit.

Following a single i.v. dose of DTZ to the pregnant and non-pregnant rabbit, the presence of M1 and MA in the blood was observed. Blood MA disposition was unaltered by pregnancy. However, the pharmacokinetic parameters associated with M1 disposition after DTZ i.v. bolus administration were significantly altered in the pregnant as compared with the non-pregnant rabbit. The formation of M1 by a specific esterase has been reported in dog, rat, rabbit and human (Yeung *et al*. 1991). In rabbit, this enzyme is present in several organs such as the brain, lung, liver, small intestine and blood (Fraile *et al*. 1996). Los *et al*. (1996) suggested that esterase-metabolized drugs might have an altered disposition in the pregnant animal. Nevertheless, alternative interpretations must be considered. For example, a higher formation of M1 may be accompanied by an altered renal elimination of both DTZ and M1 in this period. In addition, variations in body composition (e.g. the increment in body water or the creation of new compartments, which occur in pregnancy) may largely account for differences in the distribution pattern of a drug.

Most of the tissues examined in both the non-pregnant and pregnant rabbit showed higher levels of DTZ and its metabolites than those present in the blood, indicating that DTZ was extensively accumulated in tissues. For example, in the lung the concentrations of DTZ, M1 and MA were 60, 22 and 140 times higher than those observed in the blood at the same time. It has been widely reported that several tissues have a high affinity (mainly saturable and reversible) for DTZ and its metabolites (Hussain *et al*. 1994). This is true not only for DTZ, but also for most drugs with basic amine characteristics that tend to accumulate in specific tissues (Wilson *et al*. 1979). This particular characteristic may be relevant from a pharmacodynamic point of view because some of these tissues are considered as target organs for DTZ and its metabolites. In some of the tissues examined in the

present research, significant differences were detected when the DTZ, M1 and MA tissue levels were compared in the pregnant and non-pregnant rabbit. For example, DTZ concentration was four times higher in the uterus of the pregnant as compared with the non-pregnant rabbit. However, the DTZ concentration observed in other tissues was either lower or unchanged in the pregnant animal. These differences may be caused by a different tissue affinity of DTZ and/or differences in the blood flow that reaches particular organs. It is known that cardiac output and regional blood flow change depending on physiological state (non-pregnant versus pregnant) (Knott 1991). As mentioned above, no significant differences were found between the pregnant and non-pregnant rabbit in the main pharmacokinetic parameters calculated after i.v. administration, but this fact does not directly imply that drug concentration in a particular tissue must remain constant. The present results indicate that, in general, the tissue distribution of DTZ and its metabolites after i.v. infusion is only marginally affected by pregnancy. However, the variation in DTZ concentration described in some tissues in the pregnant as compared with the non-pregnant rabbit may have important clinical consequences in target tissues and in tissues directly related with the gestation process (e.g. uterus and placenta).

The present results further indicate that DTZ passes through the placenta in a measurable quantity and that DTZ concentrations observed in the foetal blood were not significantly different from those detected in maternal blood. This fact could be interpreted as a similar foetal exposure to DTZ with respect to their mothers. However, the concentration of DTZ and its metabolites in the selected tissues was either higher (in brain and muscle) or lower than that observed in maternal tissues, indicating a different tissue affinity and/or metabolic activity in the foetus as compared with its mother. It has been reported that the foetus and newborn rabbit are essentially unable to metabolize most drugs via the microsomal mixed-function oxidase system (Nouws 1992). However, recent reports have demonstrated that the rabbit foetus has a higher DTZ deacetylase activity to that observed in the adult (Fraile *et al*. 1997). The role of the placenta in determining the transfer of a particular drug (or metabolite) selectively from the maternal to the foetal side should also be borne in mind when differences have been described between the tissue concentrations of DTZ and its metabolites of foetal and maternal origin.

In conclusion, the differences observed in DTZ disposition in the pregnant rabbit following DTZ i.v. administration are not thought to have any practical clinical significance. The different tissue levels of DTZ and its metabolites in the foetus, pregnant and non-pregnant rabbit illustrate that the modifications in the tissue level of a drug may not necessarily be accompanied by significant modifications in the blood disposition of the drug.

Acknowledgements

This work was supported by the Spanish DGICYT (PB92-0350), L. J. F. was supported by the Diputacion General de Aragón (BCB-17/93). The authors thank Dr R. Latini and the Istituto di Ricerche Farmacologiche 'Mario Negri' for providing the diltiazem metabolites, and also Ms M. Gascón for excellent technical assistance.

References

Fraile, L. J., Aramayona, J. J., Bregante, M. A., Garcia, M. A. and Abadia, A. R., 1996, Deacetylation of diltiazem by several rabbit tissues. *Pharmaceutical Research*, **13**, 1875–1880.

Fraile, L. J., Aramayona, J. J., Bregante, M. A., Garcia, M. A. and Solans, C., 1997, Enhanced diltiazem deacetylase activity in pre-term and full-term rabbits compared with adult rabbits. *Biology of the Neonate*, **72**, 51–61.

Hildebrandt, R., Weitzel, H., Warnke, K. and Gundert-Remy, U., 1993, Pharmacokinetics of fenoterol in pregnant and nonpregnant women. *European Journal of Clinical Pharmacology*, **45**, 275–277.

Holbrook, R. H., Gibson, R. N. and Voss, E. M., 1988, Tocolytic and cardiovascular effects of the calcium antagonist diltiazem in the near-term pregnant rabbit. *American Journal of Obstetrics and Gynecology*, **159**, 591–595.

Hussain, M. D., Tam, Y. K., Gray, M. R. and Coutts, R. T., 1994, Mechanisms of time-dependent kinetics of diltiazem in the isolated perfused rat liver. *Drug Metabolism and Disposition*, **22**, 36–42.

Jeffries, W. S. and Bochner, F., 1988, The effect of pregnancy on drug pharmacokinetics. *Medical Journal of Australia*, **149**, 675–677.

Knott, C., 1991, The treatment of hypertension in pregnancy: clinical pharmacokinetic considerations. *Clinical Pharmacokinetics*, **21**, 233–241.

Loebstein, R., Lalkin, A. and Koren, G., 1997, Pharmacokinetics changes during pregnancy and their clinical relevance. *Clinical Pharmacokinetics*, **33**, 328–343.

Los, L. E., Welsh, D. A., Herold, E. G., Bagdon, W. J. and Zacchei, A. G., 1996, Gender differences in toxicokinetics, liver metabolism, and plasma esterase activity: observations from a chronic (27-week) toxicity study of enalapril/diltiazem combinations in rats. *Drug Metabolism and Disposition*, **24**, 28–33.

Mitani, G. M., Steinberg, I., Lien, E., Harrison, C. and Elkayan, U., 1987, The pharmacokinetics of antiarrythmic agents in pregnancy and lactation. *Clinical Pharmacokinetics*, **12**, 253–291.

Nakamura, S., Suzuki, T., Sugawara, Y., Usuki, S., Ito, Y., Kume, T., Yoshikawa, M., Endo, H., Ohashi, M. and Harigaya, S., 1987, Metabolic fate of diltiazem. Distribution, excretion and protein binding in rat and dog. *Arzneim.-Forsch/Drug Research*, **37**, 1244–1252.

Nouws, J. F. M., 1992, Pharmacokinetics in immature animals: a review. *Journal of Animal Science*, **70**, 3627–3634.

O'Hare, M. F., Kinney, C. D., Murnaghan, G. A. and McDevitt, D. G., 1984, Pharmacokinetics of propranolol during pregnancy. *European Journal of Clinical Pharmacology*, **27**, 583–587.

Renton, K. W., 1985, Inhibition of hepatic microsomal drug metabolism by the calcium channel blockers diltiazem and verapamil. *Biochemical Pharmacology*, **34**, 2549–2553.

Sugawara, Y., Nakamura, S., Usuki, S., Ito, Y., Suzuki, T., Oshashi, M. and Harigaya, S., 1988, Metabolism of diltiazem. II. Metabolic profile in rat, dog, and man. *Journal of Pharmacobiodynamics*, **11**, 224–233.

Weir, M. R., 1995, Diltiazem: Ten years of clinical experience in the treatment of hypertension. *Journal of Clinical Pharmacology*, **35**, 220–232.

Wilson, A. G. E., Pickett, R. D., Eling, T. E. and Anderson, M. W., 1979, Studies on the persistence of basic amines in the rabbit lung. *Drug Metabolism and Disposition*, **76**, 420–424.

Witter, F. R., 1993, Clinical pharmacokinetics in the treatment of rheumatoid arthritis in pregnancy. *Clinical Pharmacokinetics*, **25**, 444–449.

Yabana, H., Nagao, T. and Sato, M., 1985, Cardiovascular effects of the metabolites of diltiazem in dogs. *Journal of Cardiovascular Pharmacology*, **7**, 152–157.

Yamaoka, K., Nakagawa, T. and Uno, T., 1978, Application of the Akaike's information criterion (AIC) in the evaluation of linear pharmacokinetics. *Journal of Pharmacokinetics and Biopharmaceutics*, **6**, 165–175.

Yeung, P. K. F., Montague, T. J., Tsui, B. and McGregor, C., 1989, High-performance liquid chromatographic assay of diltiazem and six of its metabolites in plasma: application to a pharmacokinetic study in healthy volunteers. *Journal of Pharmaceutical Sciences*, **78**, 592–597.

Yeung, P. K. F., Mosher, S. J., Quilliam, M. A. and Montague, T. J., 1990, Species comparison of pharmacokinetics and metabolism of diltiazem in humans, dogs, rabbits and rats. *Drug Metabolism and Disposition*, **18**, 1055–1059.

Yeung, P. K. F., Mosher, S. J. and Pollak, P. T., 1991, Pharmacokinetics and metabolism of diltiazem in rabbits after a single intravenous or single oral administration. *European Journal of Drug Metabolism and Pharmacokinetics*, **16**, 69–74.

Yeung, P. K. F., Prescott, C., Haddad, C., Montague, T. J., McGregor, C., Quilliam, M. A., Xei, M., Farmer, P., Li, R. and Klassen, G. A., 1993, Pharmacokinetics and metabolism of diltiazem in healthy males and females following a single oral dose. *European Journal of Drug Metabolism and Pharmacokinetics*, **18**, 199–206.

XENOBIOTICA, 2000, VOL. 30, NO. 9, 843–856

Human hepatic metabolism of a novel 2-carboxyindole glycine antagonist for stroke: *in vitro–in vivo* correlations

R. A. H. J. GILISSEN, L. FERRARI, R. J. BARNABY and M. KAJBAF*

GlaxoWellcome S.p.A, Department of Bioanalysis and Drug Metabolism, Medicines Research Centre, Via A. Fleming 4, 37135, Verona, Italy

Received 6 January 2000

1. The hepatic metabolism of 3-[-2(phenylcarbamoyl) ethenyl]-4,6-dichloroindole-2-carboxylic acid (GV150526), a novel glycine antagonist for stroke, was investigated.

2. After a single intravenous administration of 800 mg GV150526 to healthy volunteers, six metabolites were observed. The major metabolites detected in human plasma have been shown by mass spectrometry to be glucoronides and one sulphate conjugate.

3. After incubation of GV150526 for 6 and 24 h with human liver slices, three glucuronide metabolites were observed. After incubation of GV150526 with pooled human liver microsomes, only one metabolite was observed, with the same molecular weight and HPLC retention time as the synthetic standard GV217053 (GV150526 hydroxylated on the *para*-position of the phenyl ring).

4. GV150526 hydroxylase enzyme kinetics—a step before sulphation—was determined using pooled human microsomes and was shown to be catalysed by cytochrome P4502C9. Glucuronidation kinetics towards GV150526 using microsomal preparations were also determined. Glucuronidation of GV150526 was observed with UGT1A1 cDNA-expressed protein, but not with UGT1A6.

5. The above enzyme kinetic data were used to calculate intrinsic clearance after scaling-up and hepatic clearance were calculated. Since GV150526 has a high plasma protein binding capacity, the effect of GV150526 binding to microsomal protein was determined. Thus, enzyme kinetic data were corrected, plotting the free (unbound) concentration of GV150526 versus enzymatic velocities: apparent V_{max} did not alter significantly but apparent K_m was ~10-fold lower. Correlation of these corrected enzyme kinetic data to predict clearance with *in vivo* clearance of GV150526 was good when both fu_{plasma} and $fu_{\text{microsomes}}$ were included in the clearance calculations.

Introduction

It is widely accepted that in ischaemic or hypoxic conditions such as stroke (abrupt onset of a neurological condition caused by insufficient cerebral circulation), the N-methyl-D-aspartate (NMDA) receptor is overstimulated by an increased amount of endogenous glutamate (Collinridge and Watkins 1994). This results in a massive Ca^{2+} influx into the post-synaptic neurones, activating several destructive cascades and ultimately leading to excitotoxic cell death (Collinridge and Bliss 1987). Among the different modulatory sites associated with the NMDA receptor, the strychnine-insensitive glycine binding site has attracted particular interest mainly due to the expected greater therapeutic index as compared with the first glycine antagonists identified (Chiamulera *et al*. 1990). Indeed, in the past few years, a number of potent and selective glycine antagonist have been identified (Rogawski 1992). Some are currently undergoing clinical trials to evaluate their efficacy in the acute treatment of stroke in man (Sacchetti *et al*. 1997).

* Author for correspondence; e-mail: Mk30297@glaxowellcome.co.uk

Xenobiotica ISSN 0049–8254 print/ISSN 1366–5928 online © 2000 Taylor & Francis Ltd
http://www.tandf.co.uk/journals

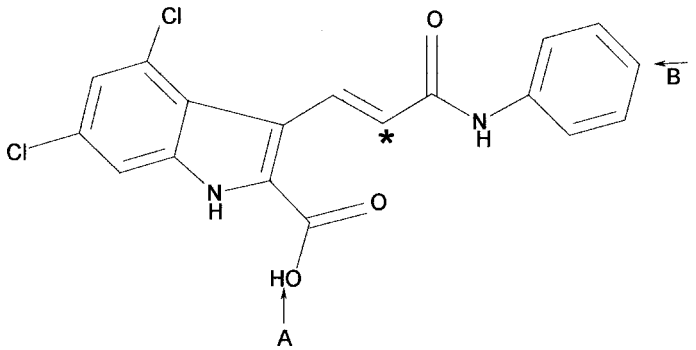


Figure 1. Chemical structure of GV150526 (GV150526-sodium salt MW = 396.3). *Position of ^{14}C label. The sites of glucuronidation (A) and 4′-hydroxylation (B) are indicated.

The 2-carboxyindole derivative, GV150526 (3-[-2(phenylcarbamoyl) ethenyl]-4,6-dichloroindole-2-carboxylic acid; figure 1), is a highly potent antagonist of NMDA-induced convulsions (Gaviraghi *et al.* 1996). Its effect is reversed by D-serine (glycine agonist) confirming that GV150526's mechanism of action is through the glycine site associated with the NMDA receptor. GV150526 has a clear neuroprotective action both after pre- and post-ischaemic administration as tested in the permanent MCA occlusion model in rat (Gaviraghi *et al.* 1996, Bordi *et al.* 1997). Moreover, no side-effects at doses significantly higher than the neuroprotective ones are observed in rat and mouse (Gaviraghi *et al.* 1996). The latter observation suggests that glycinergic modulation of abnormal overactivation of the NMDA receptor following stroke, might be a safe approach to block the ischaemic-induced neurodegeneration.

Since the liver is the main organ involved in the biotransformation of drugs and endogenous compounds, the *in vitro* human hepatic metabolism of GV150526 was investigated utilizing liver slices, microsomal preparations and cDNA expressed enzymes. Metabolite profiles obtained *in vitro* were compared with *in vivo* human plasma and urine metabolite profiles, and the enzyme kinetics for 4′-hydroxylase activity and carboxylic acid glucuronidation of GV150526 were also determined. These enzyme kinetic data allowed the prediction of the hepatic clearance of GV150526 using both the well-stirred and parallel tube models (Wilkinson 1987), and the effect of microsomal binding of GV150526 in both models was assessed. Clearances obtained were compared with the *in vivo* clearance of GV150526 in healthy human volunteers administered with a single dose of 800 mg. The present data suggest that, for both models, a good correlation between the *in vitro* and *in vivo* data was observed when both plasma protein (fu_{plasma}) and microsomal binding ($fu_{microsomes}$) are included in the analysis.

Materials and methods

Chemicals and materials

The 2-carboxyindole derivatives, GV150526 (as the sodium salt, purity > 99%), ^{14}C-GV150526 (4.14 $mBq \cdot mg^{-1}$, 112 $\mu Ci \cdot mg^{-1}$, purity > 99%) and GV217053 (4′-hydroxy-GV150526, purity > 97%; figure 1) were synthesized by the Department of Medicinal Chemistry and Chemical Development, GlaxoWellcome S.p.A. (Verona, Italy). Bovine serum albumin (BSA), magnesium chloride, saccharo 1,4-lactone, β-nicotinamide-adenosine dinucleotide phosphate, reduced form (NADPH), William's E medium and UDP-glucuronic acid were from Sigma Chemical Co. (Milan, Italy). Cell line microsomes containing human cDNA-expressed proteins: CYP2C9*1 (Arg_{144}), CYP2C9*2 (Cys_{144}), CYP2C19,

CYP2D6 and CYP3A4 (all expressed with human NADPH-cytochrome P450-reductase), and the glucuronosyl transferase UGT1A6 were from GenTest (Woburn, MA, USA). These cDNAs were expressed in a human B lymphoblast cell line AHH-1; the vector (plasmid) used for cDNA protein expression was a pHEBo-derivative. Cell-line microsomes of UGT1A1 cDNA-expressed protein were from Panvera (Cambridge, UK). All other materials were of analytical or HPLC grade and used without further purification.

Administration of GV150526 to human volunteers

A single dose of 800 mg GV150526 (free acid) in a 5% dextrose solution was administered intravenously to healthy human volunteers (four males, four females, age range 23–94 years). The administration protocol was: the first 400 mg was given over 30 min (time = 0) and the remaining dose over 210 min. Blood was collected 3 and 12 h after the first GV150526 administration, and urine was collected from 0 to 24 and 24 to 48 h. To 50 μl blood plasma or urine samples, 150 μl methanol was added as was 100 μl water. Thereafter, samples were centrifuged at 3000 *g* for 10 min at 4 °C. Of the resulting supernatant, 50 μl was injected onto the HPLC column for metabolite identification.

Human liver preparations

Human liver tissues (5–100 g, histologically normal) were from patients undergoing liver resection surgery at Borgo Roma Hospital (Verona, Italy), with the consent of the donors and the Hospital. Human liver microsomes were prepared according to the method described by Gorrod *et al*. (1975). Briefly, 50% (w/v) homogenates was made with a Potter S homogenizer (Braun, Milan, Italy) fitted with a Teflon pestle in ice-cold 0.1 M phosphate buffer (pH 7.4). Homogenates were centrifuged for 20 min at 9000 *g* (4 °C), and the resulting supernatant for 60 min at 100000 *g* (4 °C). The pellet was resuspended in 1 ml 0.1 M phosphate buffer (pH 7.4) per 1 g wet liver tissue, and designated as microsomes. Total cytochrome P450 and cytochrome-b_5 levels were determined according to Omura and Sato (1962). Protein concentrations were determined with the Bio-Rad (Milan, Italy) protein solution based on Bradford (1976), using BSA (fraction V) as standard. Microsomes were aliquoted and stored at −80 °C until use.

Pooled human liver microsomes (six males, three females, all Caucasian) were prepared to minimize the effect of the known interindividual variability in human cytochrome P450 activities (Iyer and Sinz 1999). Total cytochrome P450 and cytochrome-b_5 levels and protein concentration were determined as mentioned above. The three female organ donors were 54, 59 and 62 years old; the six males, 32, 57, 60, 65, 66 and 67 years old.

Preparation of human liver slices and incubation with GV150526

Human liver samples were placed in ice-cold Earle's balanced salt buffer (Krumdieck *et al*. 1980). Cores of liver were prepared from liver samples using a sharpened cylindrical stainless steel tube (i.d. 8 mm) attached to a tissue-coring press and a clean glass plate as support. Thin tissue slices (200–300 μm) were prepared from this core of tissue using a Krumdieck tissue slicer (Alabama Research & Development Co., AL, USA).

Human tissue slices (four pieces, ~ 50 mg total weight) were placed in 3.0 ml William's E′ medium buffer. Incubation was started by addition of GV150526 (45 μM in 6.5 μl DMSO; DMSO content was < 1% v/v) and incubated for 6 and 24 h at 37 °C under constant oxygenation (at an O_2/CO_2 ratio of 95/5%). Thereafter, slices were removed and then homogenized in 50% (v/v) methanol–water using an Ultra-Turrax Drive T25 (Janke & Kunkel, GmbH & Co. KG, Germany) homogenizer. Homogenates and supernatant were combined and centrifuged for 10 min at 900 *g* (4 °C). Of the resulting supernatant, 100 μl was analysed by HPLC-UV (see below).

Hydroxylation of GV150526

Enzyme kinetics for the hydroxylation of GV150526 was performed using pooled human microsomes (n = 9) and cytochrome P450 cDNA expressed microsomes. The assay mixtures (final incubation volume of 0.2 ml) in 0.1 M phosphate buffer, pH 7.4, contained: GV150526 (8 to 1000 μM), 2 mM NADPH and 0.5 mg·ml^{-1} pooled microsomes or 0.2 mg·ml^{-1} cDNA expressed protein. The enzymatic reaction was initiated by addition of protein and incubated for 30 min (it was decided to use an incubation time of 30 min to obtain adequate quantities of hydroxy metabolite) at 37 °C. The reaction was terminated by adding 1 volume of ice cold methanol (250 μl), and samples were subsequently centrifuged at 900 g for 10 min (4 °C). Of the resulting supernant, 100 μl was analysed by HPLC (see below).

Glucuronidation of GV150526

Enzyme kinetics for the glucuronidation of GV150526 was performed using pooled human microsomes (*n* = 9) and cDNA expressed UGT. The assay mixtures in 0.1 M phosphate buffer (pH 7.4) contained ^{14}C-GV150526 (0.5–250 μM, at various specific activities), 4 mM UDPGA, 4 mM saccharo

1,4-lactone, 10 mM magnesium chloride and 0.4 mg·ml^{-1} protein, in a total volume of 500 μl. The enzymatic reaction was initiated by addition of protein and incubated for 30 min at 37 °C. The reaction was terminated by adding 200 μl acetonitrile and samples were subsequently centrifuged at 900 *g* for 10 min at 4 °C. Aliquots of 100 μl were analysed by HPLC.

Binding of GV 150526 to human liver microsomes

GV150526 (0.5–1000 μM) was mixed with 0.4 mg pooled human (n = 9) microsomes in 0.146 M phosphate-buffered saline, pH 7.4. The mixture (0.8 ml) was transferred to one side of a dialysis cell (Dianorm, Munich, Germany) containing a preconditioned dialysis membrane (Spectra/Por, Laguna Hills, CA, USA; molecular weight cut off 6000–8000 Daltons). To the other side of the membrane was placed 0.8 ml of 0.146 M phosphate-buffered saline, pH 7.4. The cells were sealed and the apparatus incubated, with the cells rotating in a water bath for 210 min. After incubation, the dialysates were removed. Analysis of free GV150526 concentration was performed by isocratic HPLC-UV. GV150526 was separated on a Hypersil ODS column (100 × 2.1 mm, 5 μm, 35 °C) prefitted with a RP8 (20 × 2 mm, 30–40 μm) guard column. The HPLC instrumentation comprised of a Gilson 305/306 (Milan, Italy) delivery system equipped with a Jasco 975 UV-detector (λ = 343 nm). Data integration was achieved with Access*Chrom (Perkin-Elmer, Milan, Italy). Elution was with 60% (v/v) methanol–40% (v/v) 0.146 M phosphate-buffered saline, pH 7.4, at 0.3 ml·min^{-1}. A calibration curve of GV150526 was prepared and linearity was observed over the investigated concentration range of 1.3–6300 pmol (R = ~ 0.995).

Sample preparation for mass spectrometry

Human plasma samples (200 μl) were extracted in the presence of sodium chloride (0.1 g) with 3 × 3 ml acetonitrile by continuous mixing using a rocking device for 30 min. The tubes were centrifuged at 1000 *g* for 10 min using a bench centrifuge, and the organic phase was transferred to a new test tube. The organic extracts were combined and evaporated to dryness using vacuum centrifugation (final recovery of GV150526 and its metabolites was ~ 98%). The residues were redissolved in 200 μl methanol–water (50:50). Aliquots of 50 μl were injected into the HPLC-TS-MS.

HPLC identification and quantification of metabolites

GV150526 and its metabolites were separated on a Hypersil ODS column (250 × 4.6 mm, 5 μm, 35 °C) prefitted with a RP8 (20 × 2 mm, 30–40 μm) guard column. The HPLC instrumentation comprised of a Gilson 305/306 delivery system equipped with a Jasco 975 UV-detector (λ = 343 nm). Data integration was achieved with Access*Chrom. Elution was with buffer A (25 mM ammonium acetate, pH 8.0) and B (100% methanol) at 1.0 ml·min^{-1}. The gradient employed was: methanol concentration increased linear from 40 to 50% over 5 min, thereafter to 60% over 15 min, followed by an increase to 85% over 15 min. A calibration curve of GV217053 (4′-hydroxy-GV150526) was prepared and was linear over the investigated range (15.6–2000 pmol, R ~ 0.998). Radiochemical detection was used for the determination of GV150526 glucuronide and metabolites were detected in the HPLC effluent by using an on-line radioactive monitor (Flo-one-β, Canberra Packard, Milan, Italy). The scintillator flow was 3 ml·min^{-1}; cell size was 0.5 ml.

High-performance liquid chromatography/mass spectrometry (HPLC/TS-MS)

The chromatographic system for HPLC-TS-MS analysis was a binary solvent delivery system 1090A (Hewlett Packard). The HPLC eluent was transferred into a single quadrupole mass spectrometer 5988 A (Hewlett Packard) via a HP thermospray interface.

The analysis of metabolites from extracted mixtures using HPLC/TS-MS was carried out using a reverse-phase column Hypersil ODS (25 H 0.46 cm, 5 μm) with a mobile phase of ammonium acetate 14 mM, pH 8.0 (pump A) and methanol (B), flow rate 1 ml·min^{-1}. Elution was achieved by starting with 60% A, and after 4 min changing to 40% A over 20 min and after 16 min changed to 60% A over 1 min and held for a further 10 min for re-equilibration of the column. The thermospray interface temperatures were set to achieve 90% of vaporization of the mobile phase.

The thermospray source was maintained at 300 °C with the filament off and the measurements were performed under positive-ion conditions. The analyser manifold pressure was 3.5 H 10^{-6} Torr, and the following ions were selected for identification of metabolites, m/z 331, 333, 391, 393, 375, 377, 498, 500, 551, 553, 567 and 569.

Data analysis

Initial estimates of apparent K_m and V_{max} were obtained by linear regression of Lineweaver–Burke plots. Values were than used as the first estimates for a Michaelis–Menten model (Microsoft Graphit, v.3.0), an extended least-squares modelling program.

Results

Metabolites of GV150526 in human plasma and urine

Each metabolite was given the prefix 'MET' and an arabic number depending on its retention time. In human plasma, GV150526 was the main peak observed (figure 2a). Metabolites of GV150526 were: 1, 3ab, 4, 5ab and 6. In human urine (0–24, 24–48 h) GV150526, MET3ab, MET4 and MET5ab were observed (figure 2b), but no hydroxy-GV150526 (MET2) or its sulphated derivative (MET1) were detected. The HPLC/TS-MS analysis of the human plasma sample confirmed the presence of glucoronides and sulphate derivatives (table 1). MET1, with molecular ion m/z 471, corresponded to the protonated GV150526 sulphate conjugate. The fragment ion a m/z 391[471-SO_3]$^+$, corresponded to GV150526 with one hydroxy group. MET3ab, MET4 and MET5ab all contain a strong signal at m/z 551 corresponding to GV150526 plus a 176 mass unit. This ion was tentatively attributed to a glucuronide conjugated compound. When these metabolites were exposed to alkaline conditions (pH >12.0), only parent compound was observed (data not shown). Also, when MET4 was stored for prolonged period under neutral conditions, formation of MET3ab and MET5ab was observed (data not shown). The latter suggests that acyl-migration occurs, a common feature of acyl glucuronides (Spahn-Lagguth and Benet 1992). Taken together, these data indicate that MET3ab, MET4 and MET5ab are glucuronic acid metabolites, and MET1 is the sulphoconjugate of hydroxy GV150526. A further, longer retention time component (MET6) was observed in some plasma and urine samples, and is thought to be an artefact. The occurrence of MET6 may be due to the presence of methanol in the samples for deproteinization, which at neutral pH may esterify parent compound and/or its glucuronide metabolites (Smith *et al*. 1985).

Metabolism of GV150526 in human liver slices

When GV150526 was incubated with human liver slices for 6 or 24 h, the three glucuronide metabolites were observed, namely MET3ab, 4 and 5ab (figure 3). These metabolites were enzymatically formed since no traces of them were detected in any control incubations (inactivated tissue slices or without tissue slices; data not shown). No MET2 or MET1 were detected under these conditions.

Determination of non-specific binding of GV150526 to human liver microsomes

GV150526 exhibits high plasma protein binding: $fu_{\text{plasma}} = 0.00002$ (Hoke *et al*. 1998) and drugs known to have a high protein plasma binding may non-specifically bind to microsomal proteins (Obach 1997). The latter phenomenon may therefore influence enzyme kinetic data and hence clearance calculations. Therefore, the effect of non-specific microsomal binding of GV150526 was determined. GV150526 demonstrated reversible binding to pooled human liver microsomes when subjected to equilibrium dialysis. The binding experiments were performed at 37 °C using 0.4 and 0.5 mg·ml^{-1} protein concentrations to mimic *in vitro* enzyme kinetic studies. However, no cofactors (NADPH or UDPGA) were included so that metabolism could not occur. Equilibrium was reached after 180 min (data not shown) and routine equilibrium dialysis experiments were therefore performed for 210 min at 37 °C. No corrections for volume shifts occurring during dialysis had to be made for free and unbound GV150526 concentrations. The reversible binding of GV150526

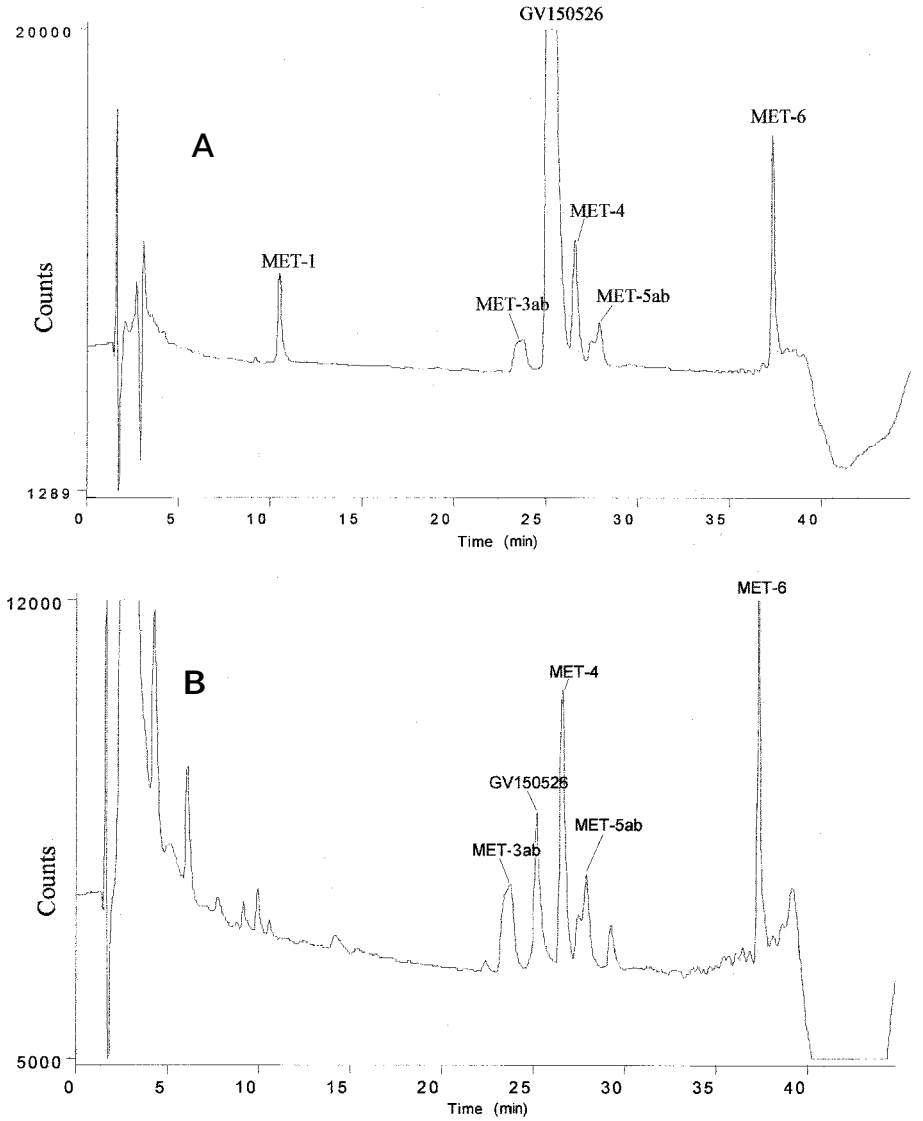


Figure 2. Typical HPLC profiles of human plasma samples 3 h (A) and urine sample 0–24 h (B) after intravenous administration of 800 mg (free acid) of GV150526 to human volunteers.

Table 1. Pseudomolecular and fragment ions were observed in the selected ion spectra of the human plasma mixture by HPLC/TM-MS.

Metabolite	Ion (*m/z*)	Possible structure of ion detected	Fragment ion (*m/z*)	Possible structure of ion detected
MET1	471, 473	$MH^+ + SO_4$	391, 393	$MH^+ + O$
MET3ab	551, 553	$MM + C_6H_9O_6$	377, 375	MH^+
MET4	551, 554	$MM + C_6H_9O_6$	377, 375	MH^+
MET5ab	551, 553	$MM + C_6H_9O_6$	377, 375	MH^+
GV150526A	375, 377	MH^+		

MH^+ = protonated GV150526A.
$C_6H_9O_6$ represents the glucuronide moiety.

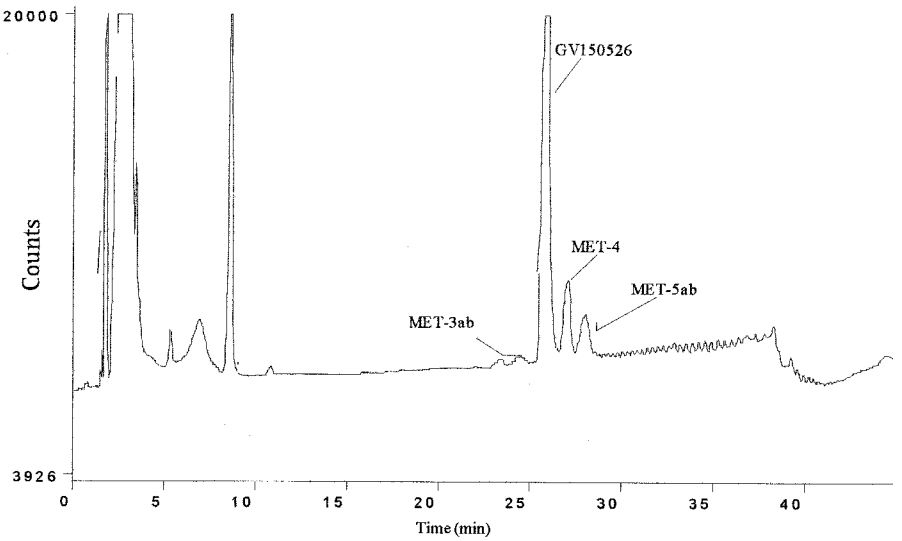


Figure 3. Typical HPLC profile of metabolites formed after 6-h incubation of GV150526 with human liver slices.

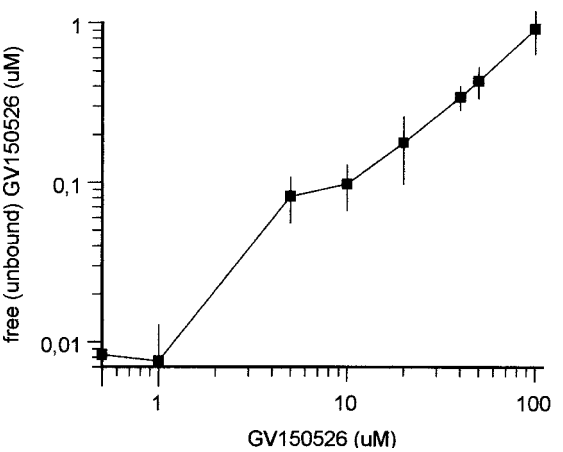


Figure 4. Determination of free (unbound) concentration of GV150526 after binding to microsomal protein (0.4 mg·ml^{-1}) using an equilibrium dialysis model. Each point represents the mean of three independent measurements.

was independent of microsomal protein concentration (0.1–1.0 mg·ml^{-1}), species (rat, dog, human) or protein source (liver microsomes, cDNA expressed protein microsomes). However, with increasing GV150526 concentrations (0.5–100 μM, 0.5 mg·ml^{-1}; figure 4), the free concentration increased from 0.007 to 1 μM. Based on these results, $fu_{\text{microsomes}}$ of GV150526 was calculated as 0.01 (figure 4).

Enzyme kinetics of hydroxylase and glucuronidation activity towards GV150526

The rate of GV150526 hydroxylase activity was linear with an incubation up to 180 min at 37 °C (figure 5a). Linearity between GV150526 hydroxylase activity and protein amount was also observed up to 0.5 mg (1.0 mg·ml^{-1}; figure 5b). Therefore,

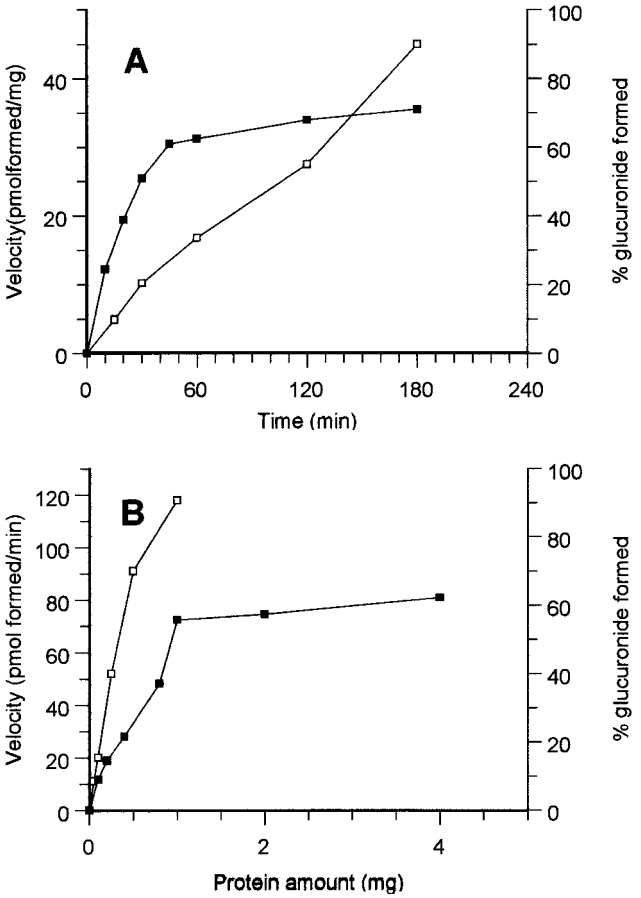


Figure 5. 4′-Hydroxylation (□) and glucuronidation (■) enzyme activities with respect to incubation time (A) and protein concentration (B). 4′-Hydroxylase activity towards GV150526 is expressed as pmol product formed·mg protein^{-1} (A, left axis) and pmol product formed·min^{-1} (B, left axis), and glucuronosyl transferase activity is expressed as % GV150526 glucuronide formed (right axis). GV150526 concentration used was 50 μM. All points are the mean of three determinations.

Table 2. Enzyme kinetics for the hydroxylation and glucuronidation of GV150526 in human liver microsomes.

	K_m (μM)	V_{max} (nmol/min/mg)	V_{max}/K_m (μl/min/mg)
Hydroxylation			
uncorrected[a]	30±5	0·26±0·01[b]	8·7
Corrected	2·2±0·02	0·24±0·01	109·0
Glucuronidation			
uncorrected[a]	7·6±3·2	0·13±0·01	16·5
Corrected	0·53±0·02	0·11±0·02	213

[a] Uncorrected refers to the total concentration of GV150526 added to incubation assays, whereas corrected is defined as the free (unbound) concentration.

[b] Data are mean±SD (n = 3).

Table 3. Hydroxylation and glucuronidation of GV150526 by human liver cDNA-expressed protein preparations.

	Rate of conversion (pmol product formed·min^{-1}·mg^{-1})[a]	
cDNA-expressed enzymes	$N = 1$[c]	$N = 2$
CYP2C9-Arginine$_{144}$	96	109
CYP2C9-Cysteine$_{144}$	18·2	21·1
CYP2C19	0	0
CYP2D6	0	0
CYP3A4	16·9	18·8
Control	0	0
UGT1A1	240	255
UGT1A6	0	0
Control	0	0

[a] Rate of conversion was measured using 0·4 mg·ml^{-1} expressed protein and an incubation of 60 min for the cytochrome P450 cDNA-expressed proteins. Rate of conversion using UGT cDNA expressed proteins was determined with 0·4 mg ml^{-1} protein and an incubation of 30 min.

[b] Control is a microsomal preparation of host cells transfected with plasmid only.

[c] Determinations were performed using two different batches of cDNA expressed protein (n = 1 and 2).

hydroxylase enzyme kinetics of GV150526 were performed for 30 min at 37 °C using a final protein concentration of 0.5 mg·ml^{-1}.

Enzyme kinetics over the concentration range 8–1000 μM GV150526 were determined (table 2). The corrected apparent K_m calculated after plotting unbound GV150526 concentrations versus velocity was 14-fold lower, whereas apparent V_{max} was not affected. A pronounced substrate inhibition of hydroxy-GV150526 formation occurred at concentrations >250 μM (data not shown), and is probably due to the non-specific binding of GV150526.

Glucuronidation activity towards GV150526 was linear with incubations up to 45 min at 37 °C (figure 5a) and linearity between GV150526 glucuronide formation and protein amount was observed up to 0.5 mg (1.0 mg·ml^{-1}; figure 5b). Therefore, glucuronidation enzyme kinetics of GV150526 were performed for 30 min at 37 °C using a final protein concentration of 0.4 mg·ml^{-1}. Enzyme kinetics for the glucuronidation of GV150526 (0.5–100 μM GV150526) using pooled liver microsomal preparations are given in table 2. After correction for microsomal binding, the apparent K_m was $\sim$ 15-fold lower, whereas apparent V_{max} was not affected (table 2).

Identification of CYP and UGT isoforms involved in the biotransformation of GV150526

Cytochrome P450 enzymes involved in the formation of hydroxyl-GV150526 were identified using cell line microsomes of cDNA-expressed enzymes. The cytochrome P450s 2C9-Arginine$_{144}$, 2C9-Cysteine$_{144}$ and 3A4 hydroxylated GV150526 (table 3). In addition, only sulphaphenazole (20 μM) inhibited the hydroxylation of GV150526 in human liver microsomes, whereas α-naphthoflavone (10 μM), tranylcypromine (20 μM), quinidine (20 μM), disulphiram (20 μM) and ketoconazole (5 μM) had no effect (data not shown).

Of the two cDNA-expressed UGT isoforms examined, only UGT1A1 glucuronidated GV150526 (table 3).

Table 4. Human clearances (CL) of GV150526 by scaling of *in vitro* intrinsic clearance (CL_{int}) data using equations describing the well-stirred and parallel tube models of hepatic clearance and including or excluding plasma protein and microsome binding.

		Well-stirred model: CL hepatic calculations[b]			Parallel tube model: CL hepatic calculations[c]		
Glucuronidation	CL_{int}[a] ($\mu l \cdot min^{-1} \cdot kg^{-1}$)	No protein binding included ($ml \cdot min^{-1} \cdot kg^{-1}$)	fu_{plasma} included[d] ($\mu l \cdot min^{-1} \cdot kg^{-1}$)	fu_{plasma} and $fu_{microsomes}$ included[e] ($\mu l \cdot min^{-1} \cdot kg^{-1}$)	No protein binding included ($ml \cdot min^{-1} \cdot kg^{-1}$)	fu_{plasma} included[d] ($\mu l \cdot min^{-1} \cdot kg^{-1}$)	fu_{plasma} and $fu_{microsomes}$ included[e] ($\mu l \cdot min^{-1} \cdot kg^{-1}$)
Pooled microsomes							
Uncorrected	5.6	4.4	0.09	0.8	4.0	0.09	0.9
Corrected[f]	72.5	16.1	0.32	32	11.2	0.32	32
Hydroxylation							
Uncorrected	2.95	2.6	0.006	0.5	2.4	0.005	0.5
Corrected	37.1	13.3	0.27	26	9.8	0.27	27

[a] CL_{int} was scaled up from V_{max}/K_m data assuming 45 mg protein g^{-1} wet liver (Wilkinson 1987).

[b] The following equations calculated hepatic clearance in a well-stirred model:
no protein binding: $CL = Q \times CL_{int}/Q + CL_{int}$.
including fu_{plasma}: $CL = Q \times fu_{plasma} \times CL_{int}/Q + fu_{plasma} \times CL_{int}$.
including fu_{plasma} and $fu_{microsomes}$: $CL = Q \times fu_{plasma} \times (CL_{int}/fu_{microsomes})/(Q + fu_{plasma} \times (CL_{int}/fu_{microsomes}))$.
A value of 20.7 $ml \cdot min^{-1} \cdot kg^{-1}$ as Q (hepatic blood flow) was used.

[c] The following equations were used to calculate hepatic clearance in a parallel-tube model:
no protein binding: $CL = Q \times (1 - e^{-CLint/Q})$
including fu_{plasma}: $CL = Q \times (1 - e^{-CLint \times fu_{plasma})/Q})$
including fu_{plasma} and $fu_{microsomes}$: $CL = Q \times (1 - e^{-CLint \times fu_{plasma}/fu_{microsomes} \times Q})$
A value of 20.7 $ml \cdot min^{-1} \cdot kg^{-1}$ as Q (hepatic blood flow) was used.
A value of 20.7 $ml \cdot min \cdot kg^{-1}$ as Q (hepatic blood flow) was used.

[d] fu_{plasma} is 0.00002 (Hoke *et al.* 1998).

[e] $fu_{microsomes}$ is 0.01.

[f] Free concentration of GV150526 was determined 210 min after equilibrium dialysis. The free concentration of GV150526 was plotted versus enzyme velocity to calculated apparent K_m and V_{max}, which were used to calculate V_{max}/K_m.

Table 5. Total hepatic clearance calculated from *in vitro* data.[a]

	Predicted total clearance from *in vitro* data		*In vivo* determined clearance[b] ($80\ \mu l \cdot min^{-1} \cdot kg^{-1}$)
	Uncorrected	Corrected	
Well-stirred model			
−protein binding ($ml \cdot min^{-1} \cdot kg^{-1}$)	7·0	29·4	
+fu_{plasma} ($ml \cdot min^{-1} \cdot kg^{-1}$)	0·14	0·59	
+fu_{plasma} and $fu_{microsomes}$ ($\mu l \cdot min^{-1} \cdot kg^{-1}$)	14·0	59·0	
Parallel-tube model			
−protein binding ($ml \cdot min^{-1} \cdot kg^{-1}$)	6·4	21·0	
+fu_{plasma} ($\mu l \cdot min^{-1} \cdot kg^{-1}$)	0·15	0·59	
+fu_{plasma} and $fu_{microsomes}$ ($\mu l \cdot min^{-1} \cdot kg^{-1}$)	15·0	59·0	

[a] Total hepatic clearance was calculated as the sum of the individual metabolic pathways contributing to the elimination of a given drug (Wilkinson 1987). Thus, glucuronidation and hydroxylation CL_{int} were summed.

[b] *In vivo* determined clearance of GV150526 (Hoke *et al*. 1997).

In vitro *hepatic clearance calculations*

Scaling-up of V_{max}/K_m data was performed assuming 45 mg protein g^{-1} wet liver and a liver weight of 1.8 kg for an individual of 70 kg (Wilkinson 1987), and these scaling factors were used in the well-stirred and parallel tube model (Wilkinson 1987) to calculate total clearance. These calculations were performed including and excluding plasma protein and microsomal binding of GV150526. In general, no difference in the clearance values were noted using either the well-stirred or parallel tube model (tables 4 and 5).

The previously determined *in vivo* plasma clearance of GV150526 is $80\ \mu l \cdot min^{-1} \cdot kg^{-1}$ (range 50–100 $\mu l \cdot min^{-1} \cdot kg^{-1}$; Hoke *et al*. 1998). Comparison of the *in vivo* determined with the *in vitro* predicted clearances showed that correction for microsomal binding in the determination of V_{max} and apparent K_m and inclusion of fu_{plasma} and $fu_{microsomes}$ would predict *in vivo* clearance (1.3-fold underestimation). Under all other circumstances, major deviations occur, namely: (1) an 80-fold overestimation when protein and microsomal binding is ignored and no correction for substrate concentration is made; (2) a 370-fold overestimation when protein and microsomal binding is ignored but correction for substrate concentration has been taken into account; (3) a 570-fold underestimation when only fu_{plasma} is included, but no correction for free substrate concentration; and (4) a 140-fold underestimation when only fu_{plasma} is included and correction for free substrate concentration is made (table 5).

Discussion

The human hepatic metabolism of GV150526 was investigated *in vitro* compared with the metabolite profile and clearance *in vivo*. HPLC and LC-TS/MS data of the plasma and urine confirm MET1 as a sulpho-conjugate of MET2, the latter being the 4′-hydroxylase product of GV150526 and MET3a,b, MET4 and MET5 as glucuronic acid conjugates of GV150526.

Based on HPLC retention times, formation of the same GV150526 glucuronic acid conjugates was observed *in vitro* utilizing liver slices as had been observed *in vivo*. The sulpho-conjugate or its hydroxy-GV150526 precursor were not detected *in vitro*. This may be due to limitation of detection or because no or low hydroxylase activity was present in the samples used.

It appears that three superfamilies of the drug-metabolizing enzymes are involved in the biotransformation of GV150526, namely the cytochrome P450s, sulphotransferases and glucuronosyl transferases. One biotransformation pathway involves hydroxylation of GV150526 at the *para*-position of the phenyl moiety, followed by conjugation with sulphate. This latter metabolite has been observed in plasma of some humans, whereas the former has never been observed in man. This suggests that once hydroxy-GV150526 is formed at the endoplasmic reticulum, it is rapidly sulphated by cytosolic sulphotransferases. Therefore, sulphation of GV150526 is not a rate-limiting factor. Sulphation and glucuronidation may compete for the same compound (Mulder *et al.* 1990). However, glucuronidation of the hydroxyl group (rendering an O-ether glucuronide, which is readily cleaved by β-glucuronidases) has not been observed in man *in vivo* or *in vitro*. This reinforces the hypothesis that sulphation is a high-affinity and low-capacity metabolic pathway, whereas glucuronidation has a low affinity but a high capacity (Mulder *et al.* 1990). The identification of human liver sulphotransferases (P-PST, M-PST, EST, HST) involved in the sulpho-conjugation of hydroxy-GV150526 is currently being conducted.

As mentioned, the sulphate conjugate of hydroxy-GV150526 was observed in the plasma of some individuals, whereas its precursor was never observed. These results suggest that hydroxylation of GV150526 is hindered, but not sulpho-conjugation. The present results show that CYP2C9 actively supports the hydroxylation of GV150526. Some allelic variants of CYP2C9 have been reported and the nature of the allelic variants of CYP2C9 may influence catalytic activity towards various substrates (Goldstein and de Morais 1994). For instance, the single amino acid change $Cys_{144} \rightarrow Arg$ appears to increase tolbutamide hydroxylase activity (Veronese *et al.* 1991). In addition, Cys_{144} had a 10-fold lower V_{max} for warfarin 7-hydroxylation than the Arg_{144} variant (Retti *et al.* 1994). Preliminary results obtained in our laboratory also indicate that the CYP2C9 allelic variant used determines hydroxylase activity towards GV150526: the Cys_{144} variant (allele CYP2C9*2) had a 5-fold lower hydroxylation rate than the Arg_{144} variant (CYP2C9*1 allele or wild-type).

The other biotransformation pathway for GV150526 elimination occurs by direct glucuronidation of the carboxylic acid moiety and glucuronidation of GV150526 is thought to be the major elimination pathway. The 4-fold higher affinity of GV150526 for glucuronosyl transferases as compared with cytochrome P450s might account for this. Identification of glucuronosyl transferases involved in the glucuronidation of GV150526 is hampered by the fact that, as yet, only two cDNA-expressed proteins are commercially available. Our data indicate that UGT1A1 is involved in the glucuronidation of GV150526. This finding is of interest since UGT1A1 is expressed in extrahepatic tissues, including in the small intestine (Radominska-Pandya *et al.* 1999). Consequently, extrahepatic metabolism may occur and contribute to the clearance of GV150526. It may be that other glucuronosyl transferases are also involved. The most likely candidates are UGT1A8 and/or UGT2B7, since drugs containing a carboxylic acid group are glucuronidated by these isoenzymes (Ritter *et al.* 1992, Ebner and Burchell 1993, Jin *et al.* 1993). Inhibition studies using UGT isoenzyme-specific substrates are currently being conducted to address this issue.

The use of *in vitro*-generated enzyme kinetic data permits the prediction of the *in vivo* clearance of a drug at an early stage of drug development. Comprehensive

reviews of the process of scaling-up of *in vitro* metabolism data to *in vivo* clearance have described both theoretical and practical aspects (Houston and Carlile 1997, Iwatsubo *et al*. 1997). Non-specific binding of drugs to *in vitro* protein matrices was suggested to be of minor importance for the scaling-up process because the protein concentration used for *in vitro* experiments was low when compared with plasma protein concentrations. However, the importance of possible binding of drugs to protein sources used in *in vitro* studies has recently been addressed. Improved prediction of *in vivo* clearance from *in vitro* metabolic data for phenytoin was observed when albumin was added to the assay mixtures (Ludden *et al*. 1997). In addition, the non-specific binding of warfarin, propanolol and imipramine to *in vitro* incubation matrices was assessed (Obach 1997). Obach concluded that the unbound fraction of drug should be determined and included in the process of scaling-up to predict the *in vivo* clearance. Our data for the prediction of *in vivo* clearance of GV150526 based on *in vitro* metabolism data are in agreement with this. Thus, if no correction was made for microsomal binding in the determination of K_m and V_{max}, *in vivo* clearance prediction was always poor. This is a direct result of the calculated K_m for the separate biotransformation pathways. Furthermore, the importance of inclusion of fu_{plasma} and $fu_{microsomes}$ for predicting *in vivo* clearances from *in vitro* data has also been outlined (Obach 1997). Again, our results are in good agreement with this conclusion. Ignoring $fu_{microsomes}$ from the equations to predict *in vivo* clearance always resulted in an underestimation, while ignoring both fu_{plasma} and $fu_{microsomes}$ resulted always in an overestimation.

In conclusion, a good prediction of the *in vivo* GV150526 clearance results when the free (unbound) *in vitro* concentration was used to determine hepatic enzyme kinetics and when the plasma protein and microsomal binding *fu* of GV150526 were taken into account.

Acknowledgement

The authors thank Dr M. Almi for synthesis of ^{14}C-GV150526, Dr F. Hoke for helpful discussions and Mr A. Ruffo for excellent technical assistance.

References

Bordi, F., Pietra, C., Ziviani, L. and Reggiani, A., 1997, The glycine antagonist GV150526 protects somatosensory evoked potentials and reduces the infarct area in the MCAo model of focal ischemia in the rat. *Experimental Neurology*, **145**, 425–433.

Bradford, M., 1976, A rapid and sensitive method for the quantitation of microgram of quantity of protein utilizing the principle of dye binding. *Analytical Biochemistry*, **72**, 248–254.

Chiamulera, C., Costa, S. and Reggiani, A., 1990, Effect of NMDA- and strychnine-insensitive glycine site antagonists on NMDA-mediated convulsions and learning. *Psychopharmacology*, **102**, 551.

Collinridge, G. L. and Bliss, T. V. P., 1987, NMDA receptors – their role in long term potentiation. *Trends Neurosciences*, **10**, 288–293.

Collinridge, G. L. and Watkins, J. C., 1994, *The NMDA Receptor*, 2nd edn (Oxford: Oxford University Press).

Ebner, T. and Burchell, B., 1993, Substrate specificities of two stably expressed human liver UDP-glucuronosyl transferases of the UGT1 gene family. *Drug Metabolism and Disposition*, **21**, 50–55.

Gaviraghi, G., Di Fabio, R., Cugola, A., Donati, D., Feriani, E., Trist, D. G. and Reggiani, A., 1996, Novel glycine antagonists as potent neuroprotective agents. *Pharmacochemistry Library*, **28**, 81–95.

Goldstein, J. A. and De Morais, S. M. F., 1994, Biochemistry and molecular biology of the human CYP2C subfamily. *Pharmacokinetics*, **4**, 285–299.

Gorrod, J. W., Temple, D. J. and Beckett, A., 1975, The metabolism of *N*-ethyl-*N*-methylaniline by rabbit liver microsomes: the measurement of metabolites by gas–liquid chromatography. *Xenobiotica*, **5**, 453–462.

Hoke, J. F., Dyker, A. G., McAllister, A. M. and Lees, K. R., 1998, Pharmacokinetics of GV150526 following multiple intravenous doses in acute stroke patients. Abstract, 6th European Stroke Conference, Amsterdam, The Netherlands.

Houston, J. B. and Carlile, D. J., 1997, Prediction of hepatic clearance from microsomes, hepatocytes, and liver slices. *Drug Metabolism Reviews*, **29**, 891–922.

Iwatsubo, T., Hirota, T., Ooie, T., Suzuki, H., Shimada, H., Chiba, K., Ishizaki, T., Green, C. E., Tyson, C. A. and Sugiyama, Y., 1997, Prediction of *in vivo* drug metabolism in the human liver from *in vitro* metabolism data. *Pharmacology and Therapeutics*, **73**, 147–171.

Iyer, K. R. and Sinz, M. W., 1999, Characterisation of Phase I and Phase II hepatic drug metabolism activities in a panel of human liver preparations. *Chemico-Biological Interactions*, **118**, 151–169.

Jin, C. J., Miners, J. O., Lillywhite, K. J. and Mackenzie, P. I., 1993, Complementary deoxyribonucleic acid cloning and expression of a human liver uridine disphosphate-glucuronosyltransferase glucuronidating carboxylic acid-containing drugs. *Journal of Pharmacology and Experimental Therapeutics*, **264**, 475–479.

Krumdieck, C. L., Dos Santos, J. E. and Ho, K. J., 1980, A new instrument for the rapid preparation of tissue slices. *Analytical Biochemistry*, **104**, 118–123.

Ludden, L. K., Ludden, T. M., Collins, J. M., Pentikis, H. S. and Strong, J. M., 1997, Effect of albumin on the estimation, *in vitro*, of phenytoin V_{max} and K_m values: implications for clinical correlations. *Journal of Pharmacology and Experimental Therapeutics*, **282**, 391–396.

Mulder, G. J., Coughtrie, M. H. W. and Burchell, B., 1990, Glucuronidation. In G. J. Mulder (ed.), *Conjugation Reactions in Drug Metabolism* (London: Taylor & Francis), pp. 51–107.

Obach, R. S., 1997, Nonspecific binding to microsomes: impact on scale-up of *in vitro* intrinsic clearance to hepatic clearance as assessed through examination of warfarin, imipramine, and propranolol. *Drug Metabolism and Disposition*, **42**, 1359–1369.

Omura, T. and Sato, R., 1962, A new cytochrome in liver microsomes. *Journal of Biological Chemistry*, **237**, 1375–1376.

Radominska-Pandya, A., Czernik, P. J. and Little, J. A. 1999, Structural and functional studies of UDP-glucuronosyltransferases. *Drug Metabolism Reviews*, **31**, 817–899.

Retti, A. E., Wienkers, L. C., Gonzalez, F. J., Trager, W. F. and Korzekwa, R., 1994, Impaired (*S*)-warfarin metabolism catalyzed by the R144C allelic variant of CYP2C9. *Pharmacokinetics*, **4**, 39–42.

Ritter, J. K., Chen, F., Yheun, Y. S., Lubet, R. A. and Owens, I. S., 1992, Two human liver cDNAs encode UDP-glucuronosyl transferases with 2 log differences in activity towards parallel substrates including hyodeoxycholic acid and certain estrogen derivatives. *Biochemistry*, **212**, 3409–3414.

Rogawski, M. A., 1992, The NMDA receptor, NMDA antagonists and epilepsy therapy. *Drugs*, **44**, 279–292.

Sacchetti, M. L., Toni, M., Fiorelli, M., Argentino, C. and Fieschi, C., 1997, The concept of combination therapy in acute ischemic stroke. *Neurology*, **49**, S70–74.

Smith, P. C., Hasegawa, J., Langendijk, P. N. and Benet, L. Z., 1985, Stability of acyl glucuronides in blood, plasma, and urine: studies with zomepirac. *Drug Metabolism and Disposition*, **13**, 110–112.

Spahn-Lagguth, M. and Benet, L. Z., 1992, Acyl-glucuronides revisited: Is the glucuronidation process a toxification as well as a detoxification mechanism? *Drug Metabolism Reviews*, **24**, 5–48.

Veronese, M. E., Mackenzie, P. I., Doecke, C. J., McManus, M. E., Miners, J. O. and Birkett, D. J., 1991, Tolbutamide and phenytoin hydroxylations by cDNA-expressed human liver cytochrome P4502C9. *Biochemical and Biophysical Research Communications*, **175**, 1112–1118.

Wilkinson, G. R., 1987, Clearance approaches in pharmacology. *Pharmacological Reviews*, **39**, 1–47.

XENOBIOTICA, 2000, VOL. 30, NO. 9, 867–879

Biotransformation of the xenoestrogen 4-*tert*-octylphenol in hepatocytes of rainbow trout (*Oncorhynchus mykiss*)

R. T. PEDERSEN and E. M. HILL*

School of Chemistry, Physics and Environmental Science, University of Sussex, Falmer, Brighton BN1 9QJ, UK

Received 25 February 2000

1. The biotransformation of a 4-*tert*-alkylphenol in rainbow trout (*Oncorhynchus mykiss*) liver was studied to determine the possible fate and activity of these xenoestrogens in fish.

2. Primary trout hepatocytes were incubated with 30 μM 4-(1′,1′,3′,3′-tetramethylbutyl)[U-^{14}C]phenol (4-*tert*-octylphenol; 4-*t*-OP) for up to 3 h. Radiolabelled metabolites were detected by radio-HPLC and the structures were determined by GC-MS analysis of the conjugated or aglycone products.

3. During the first 15 min, 4-*t*-OP was metabolized at 1.06 pmol·min^{-1}·10^{-6} cells. The amount of parent compound metabolized was maximum after a 1-h incubation, when 86% of 4-*t*-OP was transformed to five other products.

4. The major metabolite comprised 61% of the total recovered radioactivity and was identified as 4-*t*-OP-β-glucuronide.

5. The remaining metabolites were formed from the hydroxylation of 4-*t*-OP on either the C2 (w-3) or C4 (ω) positions of the alkyl chain, or *ortho* on the aromatic ring to form a catechol. These oxidized products were also metabolized to glucuronide derivatives conjugated on the phenol ring.

6. The results suggest that oestrogenic alkylphenols could be rapidly transformed in fish liver by both phase I and II metabolic pathways to a number of conjugated products which are unlikely to be active at the oestrogen receptor.

Introduction

Alkylphenols are present in the aquatic environment through the degradation of alkylphenol polyethoxylate detergents in sewage treatment works. These long-chain surfactants are transformed to persistent short-chain alkylphenol ethoxylates, alkylphenol ethoxycarboxylic acids and alkylphenols, which are subsequently released in the wastewater effluent into the receiving waters (Brunner *et al*. 1988, Ahel *et al*. 1994a, b). Both *in vitro* and *in vivo* studies have reported that these alkylphenol polyethoxylate derivatives are weak oestrogen mimics and that the alkylphenols are the most oestrogenic of the degradation products (Jobling and Sumpter 1993, Jobling *et al*. 1996, Routledge and Sumpter 1996). The alkylphenol moiety of these surfactants consists of a mixture of *para*-substituted secondary and tertiary nonylphenols although smaller amounts of octyl or dodecylphenols are also present (Bhatt *et al*. 1992, Wheeler *et al*. 1997). In oestrogen receptor-binding studies, 4-*tert*-alkylphenols exhibited greater activity than 4-*sec*-alkylphenols and activity was greatest with compounds possessing an alkyl chain of six-to-eight carbon atoms (Routledge and Sumpter 1997). In *in vivo* studies, 4-*tert*-octylphenol

* Author for correspondence; e-mail: e.m.hill@sussex.ac.uk

Xenobiotica ISSN 0049–8254 print/ISSN 1366–5928 online © 2000 Taylor & Francis Ltd
http://www.tandf.co.uk/journals

(4-*t*-OP) was reported to stimulate oestrogen-dependent vitellogenin production and to inhibit testicular growth in male rainbow trout (*Oncorhynchus mykiss*) at 5–30 $\mu g \cdot l^{-1}$ (Jobling *et al*. 1996). Technical grade 4-nonylphenol (4-NP), a mixture of branched-chain alkyl isomers, caused the development of testis–ova (intersex) in male medaka (*Oryzias latipes*) at 50 $\mu g \cdot l^{-1}$ (Gray and Metcalfe 1997) whereas exposure to 4-*tert*-pentylphenol (100 $\mu g \cdot l^{-1}$) resulted in the development of an oviduct in male carp (*Cyprinus carpio*) (Gimeno *et al*. 1996). The concentrations of 4-NP in British rivers have been reported to range from < 0.1 to 180 $\mu g \cdot l^{-1}$ and in sediments to vary from 0.1 to 15 $\mu g \cdot g^{-1}$ depending on the levels of industrial pollution (Blackburn and Waldock 1995, Blackburn *et al*. 1999). The high concentrations of alkylphenolic compounds present in the water and sediments of certain rivers receiving industrial effluents could be responsible for the hormonal disruption of fish in these waters (Harries *et al*. 1997).

In oestrogen receptor-binding studies, the potency of 4-*tert*-alkylphenols is between 1/1000th to 10,000th that of 17β-oestradiol. However, *in vivo*, the potency for the induction of vitellogenin is only 1/100th and 1/1000th that of 17β-oestradiol (Jobling *et al*. 1996). This raises the question as to whether the higher activity *in vivo* is a result of bioconcentration of these compounds and/or is due to metabolism of alkylphenols to more active structures. Studies have shown that these lipophilic compounds can bioaccumulate in organisms with reported bioconcentration factors for 4-NP in whole fish ranging from 280 to 1300 (McLeese *et al*. 1981, Ekelund *et al*. 1990). Straight chain and secondary 4-alkylphenols have been reported to be rapidly metabolized by phase I and II enzyme systems in fish (Meldahl *et al*. 1996, Thibaut *et al*. 1998). However, there is limited information on the metabolism of 4-*tert*-alkylphenols in fish or other vertebrates. 4-*tert*-Octylphenol, a degradation product of octylphenol polyethoxylates, is the most oestrogenic of the alkylphenolic compounds (Jobling *et al*. 1996, Routledge and Sumpter 1997). This study reports the detailed structural analysis of 4-*tert*-octylphenol metabolites formed by primary rainbow trout hepatocytes in order to determine the likely oestrogenic activity of these compounds in fish.

Materials and methods

Materials

Radiolabelled 4-(1′,1′,3′,3′-tetramethylbutyl)[U-^{14}C]phenol (4-*t*-OP, 666 Mbq $\cdot$ mmol^{-1}, radiochemical purity $> 98\%$) was synthesized by Amersham International (Amersham, UK) and was a kind gift from Professor J. Sumpter, Brunel University, UK. Collagenase grade H from *Clostridium histolyticum* was from Boehringer Mannheim (Germany). Methylbenzothonium hydroxide tissue solubilizer, CytoScint and EcoLume liquid scintillation cocktails were from ICN Radiochemicals (Irvine, CA, USA). All solvents were of HPLC grade from Rathburn Chemicals (Walkerburn, UK). Heparin, β-glucuronidase type VII-A (sulphatase-free) from *Escherichia coli* and all other chemicals were from Sigma-Aldrich Co. (Poole, UK).

Hepatocyte preparation

Female rainbow trout (*O. mykiss*), 600 g, were from Chalk Spring Fish Farm (Arundel, UK). Fish were held on a 12-h light/dark cycle in a constantly aerated flow through tank supplied with municipal water passed through an activated carbon filter. Water temperature remained constant at 12 °C. Fish were fed a commercial feed (Trout Rapid, BOCM Paul's Fish Feed Group, Renfrew, UK) *ad libitum*. After 1 week, fish were killed by a blow to the head followed by destruction of the brain. Hepatocytes were prepared by a two-step perfusion of the liver using a procedure modified from Maitre *et al*. (1986). Heparin (300 USP units) was injected into the heart and the hepatic portal vein was cannulated. The liver was perfused for 20 min at 10 ml $\cdot$ min^{-1} with oxygenated calcium-free buffer consisting of 160 mM NaCl,

10 mM HEPES, 3 mM KCl, 0.3 mM Na_2HPO_4 adjusted to pH 7.65 with 1 M NaOH. The liver was perfused for a further 20–30 min at 10 ml·min^{-1} on a recirculating system with 100 ml oxygenated buffer (pH 7.8) containing 260 mg·l^{-1} collagenase (equivalent to 148 U·l^{-1} collagenase activity), 140 mM NaCl, 30 mM HEPES, 3 mM KCl and 2 mM $CaCl_2$. Liver cells were dispersed by gentle teasing in 200 ml incubation buffer at 10 °C containing 130 mM NaCl, 10 mM HEPES, 3 mM KCl, 2 mM $CaCl_2$, 1 mM $MgCl_2$, 0.3 mM $MgSO_4$ and 5.6 mM D-(+)-glucose adjusted to pH 7.65 with 1 M NaOH. Hepatocytes were purified by centrifuging at 50*g* for 4 min, decanting the supernatant and resuspending the pellet in 50-ml incubation buffer. After two further purification steps, hepatocytes were resuspended in incubation buffer to a final concentration of 10^7 cells·ml^{-1}. Cell viability was determined by trypan blue exclusion and in the final suspension was > 95%.

Incubations

Hepatocytes (1 ml) were incubated with 30 μM radiolabelled 4-*t*-OP at 15 °C with constant agitation for up to 3 h. The concentration of ethanol carrier was 0.1% (v/v). Control incubations were heat inactivated at 100 °C for 5 min, then cooled to 15 °C before dosing. At the end of incubations, an aliquot of the suspension was taken to determine final cell viability. Incubations were terminated by addition of an equal volume of ice cold methanol and stored at −20 °C before analysis.

Isolation of metabolites

The methanolic cell suspensions were centrifuged (3000*g*, 10 min, 4 °C), the supernatant drawn off and the pellet extracted three times in 0.5 ml methanol. Supernatants were combined and an aliquot assayed for recovery of radioactivity. Residual radioactivity in the hepatocyte pellets was determined after solubilization with 1 M (1 ml) methylbenzothonium hydroxide in methanol.

A 60 mg polymer solid-phase extraction cartridge (Oasis, Waters Corp., Milford, MA, USA) was preconditioned with 1 ml methanol followed by 1 ml 5% (v/v) methanol in 17.5 mM ammonium acetate buffer (pH 4.0). The supernatant liquor, diluted with 10 parts buffer (pH 4.0), was drawn through the extraction cartridge on a vacuum manifold at 2 ml·min^{-1}. The cartridge was washed with 2 ml 5% (v/v) methanol in buffer (pH 4.0) and metabolites were eluted with 2 ml methanol. The methanol was removed under reduced pressure and the sample dissolved in 50% (v/v) methanol in buffer (pH 4.0) before HPLC analysis. Total recovery of the radioactive sample by solid phase extraction was typically 83%.

High-performance liquid chromatography

Metabolites were analysed by reverse-phase-high performance liquid chromatography (RP-HPLC) using a C_{18} column (Nova-Pak, 5 μM, 4.6 × 150 mm; Waters). A step gradient program was employed using methanol:water:acetic acid (30:70:0.1 v/v, adjusted to pH 4.0 with ammonium hydroxide) for 10 min, increasing to 40% (v/v) methanol (20 min), 50% (v/v) methanol (35 min), then to 100% methanol in a linear gradient over 15 min at 1 ml·min^{-1}. Metabolites were detected by a photodiode array UV absorbance spectrophotometer (Waters 996) followed in series by an on-line radioactivity monitor (LB 506 C-1, Berthold, Wildbad, Germany).

To separate metabolites for structural analysis, some hepatocyte incubations were pooled, concentrated under reduced pressure and subject to RP-HPLC analysis. Separated metabolites were collected and evaporated under reduced pressure to dryness before derivitization for GC-MS analysis.

β-Glucuronidase hydrolysis

Aliquots of some metabolites fractionated by HPLC were incubated with β-glucuronidase. Samples were evaporated to dryness under reduced pressure and re-dissolved in 1 ml sodium phosphate buffer (4 mM, pH 6.8) containing 100 Fishman units β-glucuronidase solution and incubated for 12 h at 37 °C. Enzyme incubations were acidified to pH 4 with 1 M HCl and extracted three times with 1 ml ethyl acetate. The ethyl acetate extractions were pooled and evaporated to dryness under a stream of nitrogen before derivitization for GC-MS analysis.

Derivatization

Trimethylsilylation. Some samples were solubilized in 25 μl dry pyridine and 25 μl bis(trimethylsilyl)-trifluoroacetamide (BSTFA) containing 1% trimethylchlorosilane (TMCS). The solution was incubated for 30 min at 65 °C. Before analysis by GC-MS, incubations were evaporated to dryness under a stream of nitrogen and dissolved in 10 μl hexane.

Table 1. Levels of radiolabelled metabolites formed from incubation of trout hepatocytes with [^{14}C]4-*t*-OP (30 μM).

	% Radioactivity[a]	
Metabolite	15-min incubation	60-min incubation
4-*t*-OP (parent compound)	47.2±3.3	13.5±4.6
1	42.9±3.6	60.6±3.9
2	2.0±0.2	5.1±0.3
3	4.2±0.5	8.6±0.3
4	0.6±0.2	4.1±0.6
5	2.9±0.5	8.0±0.9
Total metabolites	52.8±3.3	86.5±4.6

[a] Values are expressed as the average percentage of total radioactivity±SE (three experiments) from radio-HPLC analysis of the metabolite profiles.

Methylation. Ethereal diazomethane was prepared from 1-methyl-3-nitro-1-nitrosoguanidine (MNNG). Samples were methylated in a two-step procedure. To methylate phenolic hydroxyl groups, methanol and ethereal diazomethane were added to the sample to give a final concentration of 20% (v/v) methanol. The sample was left to stand in darkness for 48 h and evaporated to dryness under nitrogen. To esterify carboxylic acids, methanol and ethereal diazomethane were added to a final composition of 1% (v/v) methanol and left to stand in the dark for 24 h. Reactions were evaporated to dryness under nitrogen and silylated before GC-MS analysis.

Butylboronate esterification. Samples were spiked with 4-*tert*-butylcatechol (500 ng) and 4-*n*-hexylrescorcinol (500 ng) as positive and negative controls respectively and evaporated to dryness under a stream of nitrogen. *tert*-Butylboronic acid (2 μg) in pyridine (20 μl) was added and the reaction left to stand for 4 h. Vial contents were evaporated to dryness under nitrogen, dissolved in 10 μl hexane, concentrated by evaporation to a volume of $\sim$0.5 μl and analysed by GCMS.

Gas chromatography mass spectrometry

Electron ionization mass spectrometry was performed on a Kratos MS890 instrument coupled to a Carlo Erba MFC500 gas chromatograph. Samples were injected in splitless mode onto a capillary column (DB-5, 0.25 μm film thickness, 15 m × 0.25 mm i.d., J&W Scientific, Folsom, CA, USA). The injector temperature was held at 320 °C and the column temperature was programmed at 100 °C (4 min) increasing to 320 °C at 10 °C·min^{-1}. Helium carrier gas flow rate was 7 m·s^{-1}. Ion source temperature was 250 °C, electron energy 70 eV, accelerating potential 4 kV and the magnetic sector cycled from 1000 to 50 amu during 0.8 s.

Results

RP-HPLC analysis of 4-t-OP metabolites

During incubations with 4-*t*-OP, >90% of hepatocytes remained viable for up to 3 h. Over 97% of the radioactivity was recovered by methanol extraction of the hepatocytes. The remaining radioactivity was covalently bound within the pellet and only extracted by incubation with tissue solubilizer.

RP-HPLC analysis of the methanolic extracts of hepatocyte incubations with 30 μM 4-*t*-OP showed five major metabolites (figure 1). The incubation concentration of 4-*t*-OP was chosen to reflect an exposure of fish to low levels of alkylphenols (5 μg·l^{-1}) combined with a high bioconcentration factor (1000). In addition, there were no qualitative differences in the RP-HPLC profile of metabolites formed after incubations with either 10 or 50 μM 4-*t*-OP (data not shown). After a 15-min incubation, >53% 4-*t*-OP was metabolized, and after 60 min 86% 4-*t*-OP was transformed to other products (table 1). Incubations of

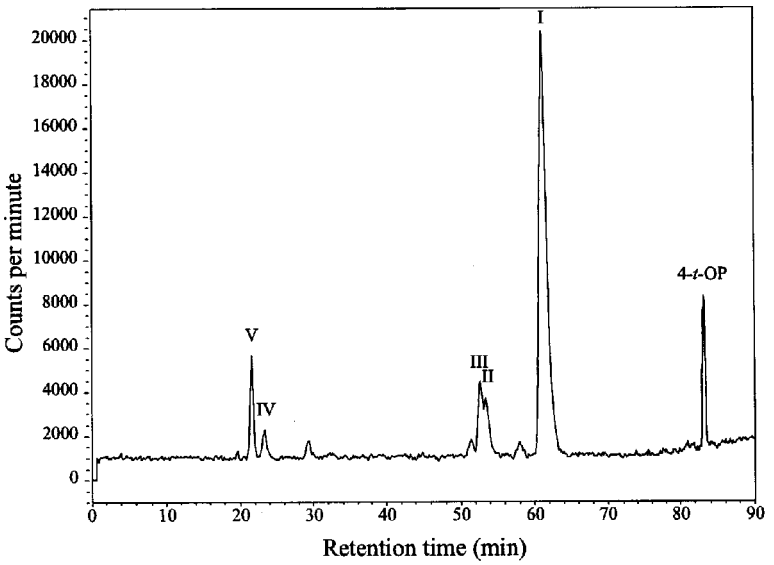


Figure 1. Typical radio-HPLC profile of metabolites formed from the incubation of [^{14}C]4-*t*-OP (30 μM) with primary trout hepatocytes for 1 h.

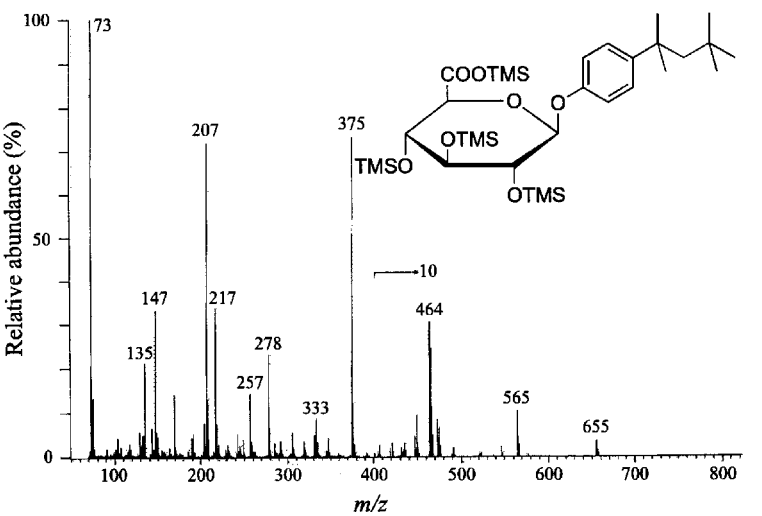


Figure 2. GC-MS spectrum of the trimethylsilylated derivative of M1. TMS, trimethylsilyl.

hepatocytes with 4-*t*-OP for >1 h resulted in no further metabolism. After 1 h, the major metabolic peak (M1) accounted for 61% of the total recovered radioactivity and the remaining metabolites were present at levels of between 4 and 8% of the total radioactivity. Transformation of 4-*t*-OP was not detected in control incubations with heat-inactivated hepatocytes (data not shown).

Identification of metabolites

Metabolite 1. The UV spectra of M1 (λ_{max} = 221.5 and 272.1 nm) was typical of a phenolic structure and the same as 4-*t*-OP (data not shown). GC-MS analysis of the

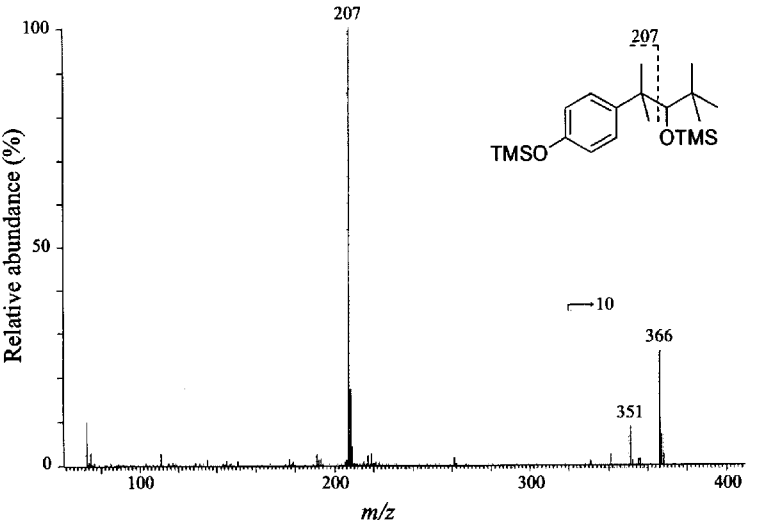


Figure 3. GC-MS spectrum of the trimethylsilylated derivative of M2. TMS, trimethylsilyl.

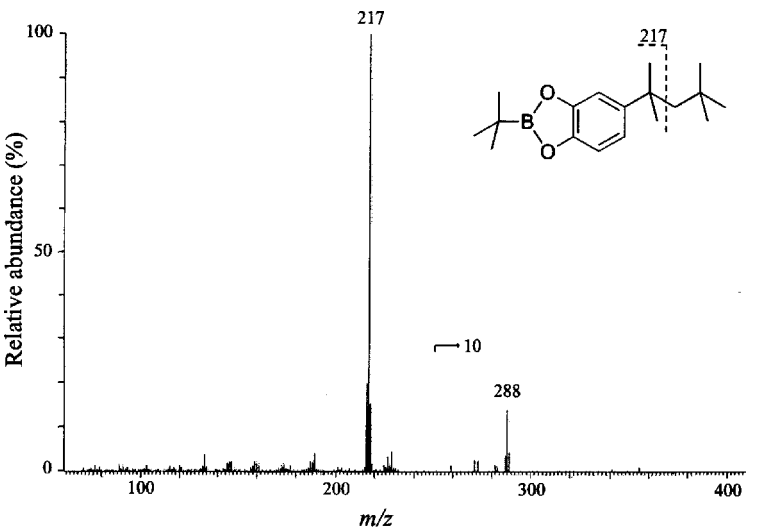


Figure 4. GC-MS spectrum of the butylboronate ester of M3 aglycone.

trimethylsilyl (TMS) ether/ester derivative revealed ions at m/z 655 $[M\text{-}CH_3]^+$ and 565 $[M\text{-}CH_3\text{-}TMSOH]^+$, which indicated a molecular mass of 670 amu (figure 2). Elimination of the 4-*t*-OP aglycone from the molecular ion via hydrogen rearrangement yielded the ion at m/z 464. The fragment ion present at m/z 465 arose by loss of the aglycone radical from the molecular ion and further stepwise elimination of TMSOH yielded m/z 375. The fragment ion at m/z 278 originated from the aglycone moiety via a rearrangement of TMS; subsequent cleavage of the alkyl chain yielded a fragment ion at m/z 207. The fragment ions at m/z 135 arose from the aglycone moiety via a hydrogen rearrangement and cleavage of the alkyl

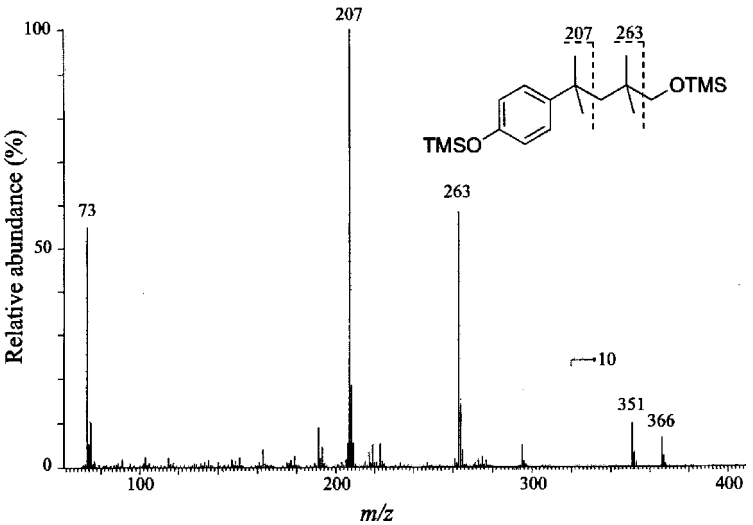


Figure 5. GC-MS spectrum of the trimethylsilylated derivative of M4 aglycone. TMS, trimethylsilyl.

chain. These ions indicated there was no hydroxylation of the aglycone moiety. The mass spectrum also contained a series of ions characteristic of fragmentation of glucuronides (*m/z* 147, 169, 217, 257; DeJongh *et al.* 1969).

After incubation with *β*-glucuronidase, the retention time on RP-HPLC increased from 60.5 to 82.6 min, suggesting the loss of a glucuronic acid group (data not shown). GC-MS of the silyated derivative of the aglycone revealed ions at *m/z* 278 $[M]^+$, 263 $[M\text{-}CH_3]^+$ and 207 $[M\text{-}C_5H_{11}]^+$ consistent with the structure of 4-*t*-OP (data not shown). From these data, M1 was identified as 4-(1′,1′,3′,3′-tetramethylbutyl)phenoxy-*β*-glucuronide.

Metabolite 2. The UV spectra of M2 (λ_{max} = 222.7 and 276.8 nm) was typical of a phenolic structure (data not shown). The retention time of the metabolite on RP-HPLC was not altered after incubation with *β*-glucuronidase. GC-MS analysis of the TMS derivative showed ions at *m/z* 366 $[M]^+$, *m/z* 351 $[M\text{-}CH_3]^+$, *m/z* 261 $[M\text{-}TMSOH\text{-}CH_3]^+$, *m/z* 207 $[M\text{-}C_5H_{10}OTMS]^+$ (figure 3). M2 was identified as 4-(2′-hydroxy-1′,1′,3′,3′-tetramethylbutyl)phenol.

Metabolite 3. The UV spectra of M3 (λ_{max} = 218.0 and 278.0 nm) suggested substitution on the aromatic ring (data not shown). GC-MS analysis of the silylated derivative gave fragments *m/z* 653 $[M\text{-}CH_3\text{-}TMSOH]^+$, *m/z* 563 $[M\text{-}CH_3\text{-}TMSOH\text{-}TMSOH]^+$, *m/z* 366 (rearrangement of TMS to the aglycone), *m/z* 295 (loss of C_5H_{11} from *m/z* 366) and ions at *m/z* 147, 169, 217, 375 and 464 characteristic of fragmentation of a glucuronic acid moiety (data not shown). Hydrolysis with *β*-glucuronidase increased the retention time of M3 from 52.0 to 80.0 min. GC-MS analysis of the silylated hydrolysis product revealed ions at *m/z* 366 $[M^+]$ and *m/z* 295 $[M\text{-}C_5H_{11}]^+$ (data not shown). These data suggested hydroxylation of 4-*t*-OP on the aromatic ring. To determine whether the structure was a catechol or resorcinol, an aliquot of the hydrolysed metabolite was treated with *tert*-butylboronic acid. GC-MS analysis of this derivative revealed ions at *m/z* 288 $[M]^+$ and *m/z* 217 $[M\text{-}C_5H_{11}]^+$ consistent with the formation of the butylboronate

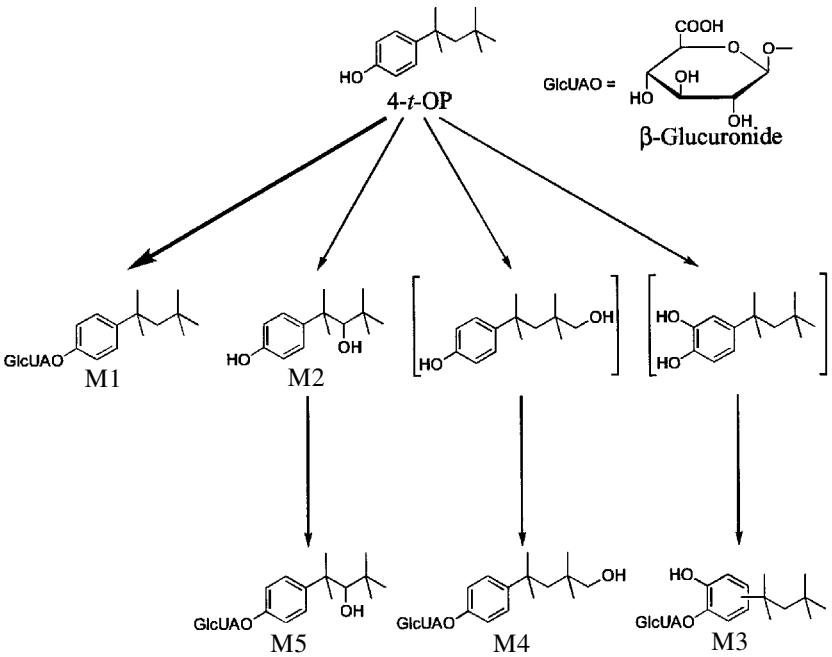


Figure 6. Proposed pathway for the metabolism of 4-*tert*-octylphenol in trout hepatocytes. The bold arrow indicates the major biotransformation product.

ester of a catechol (figure 4). M3 was therefore identified as 2-β-glucuronoxy-4[5]-(1′,1′,3′,3′-tetramethylbutyl)phenol.

Metabolite 4. The UV spectra of M4 (λ_{max} = 221.5 and 270.9 nm) was typical of a phenolic structure. GC-MS analysis of a silyated aliquot revealed ions at m/z 743 $[M\text{-}CH_3]^+$, 653 $[M\text{-}CH_3\text{-}TMSOH]^+$ and 563 $[M\text{-}CH_3\text{-}TMSOH\text{-}TMSOH]^+$, which indicated that the molecular mass was 758 amu (data not shown). Ions at m/z 147, 217, 375, 464 and 465 were characteristic of fragmentation of a glucuronic acid moiety. The fragment ions at m/z 263, 207 and 135 arose from the aglycone portion of the molecule and suggested hydroxylation at the C4 position of the alkyl chain.

Hydrolysis of an aliquot of M4 with β-glucuronidase increased the retention time on RP-HPLC from 22.8 to 55.7 min. GC-MS analysis of the silyated derivative of the hydrolysis product revealed ions at m/z 366 $[M]^+$, m/z 351 $[M\text{-}CH_3]^+$, m/z 263 $[M\text{-}CH_2OTMS]^+$ and m/z 207 $[M\text{-}C_5H_{10}OTMS]^+$ (figure 5). These data were consistent with the addition of an extra hydroxyl group on the C4 position of the alkyl chain.

To investigate whether glucuronide conjugation was on the alkoxy or phenoxy group of the metabolite, an aliquot of the original conjugate was methylated by diazomethane followed by silylation. GC-MS analysis of this derivative yielded ions at m/z 685 $[M\text{-}CH_3]^+$, 595 $[M\text{-}CH_3\text{-}TMSOH]^+$ and 505 $[M\text{-}CH_3\text{-}TMSOH\text{-}TMSOH]^+$, which indicated that the molecular weight was 700 amu and it suggested mono-methylation of the metabolite (data not shown). Fragment ions at m/z 406, 317 and 275 indicated methylation was on the carboxyl group of the glucuronide

moiety. The fragment ions at m/z 263, 207 and 135 arose from the aglycone portion of the molecule and indicated that the phenoxy group was not methylated. This mass spectrum was consistent with glucuronide conjugation on the phenoxy group. From these data, M4 was identified as 4-(4′-hydroxy-1′,1′,3′,3′-tetramethylbutyl)-phenoxy-β-glucuronide.

Metabolite 5. The UV absorbance spectrum of M5 (λ_{max} = 220.3 and 262.7 nm) indicated a phenolic structure. GC-MS analysis of the TMS derivative revealed ions at m/z 743 [M-CH_3]$^+$, 653 [M-CH_3-TMSOH]$^+$ and 563 [M-CH_3-TMSOH-TMSOH]$^+$, which indicated that the molecular mass was 758 amu (data not shown). Other ions at m/z 147, 217, 375 and 464 were characteristic of a glucuronic acid conjugate. The fragment ions at m/z 366, 207 and 135 derived from the aglycone portion of the molecule and indicated hydroxylation on the alkyl chain.

An aliquot of M5 was hydrolysed by β-glucuronidase, which increased the retention time on HPLC from 21.0 to 51.8 min. The TMS derivative of the aglycone yielded a mass spectrum identical to that of M2, which suggested that M5 was the glucuronic acid conjugate of 4-(2′-hydroxy-1′,1′,3′,3′-tetramethylbutyl)-phenol (data not shown).

To investigate the position of the glucuronide group the methyl-ester TMS-ether derivative was analysed by GC-MS. The mass spectrum revealed ions at m/z 685 [M-CH_3]$^+$ and 595 [M-CH_3-TMSOH]$^+$, which indicated that the molecular mass was 700 amu (data not shown). Fragment ions at m/z 406, 317 and 275 indicated methylation was on the carboxyl group of the glucuronide moiety. The fragment ions derived from the aglycone at m/z 366, 207 and 135 indicated the phenolic group was not methylated. This mass spectrum was consistent with glucuronide conjugation on the phenoxy group. From this data M5 was identified as 4-(2′-hydroxy-1′,1′,3′,3′-tetramethylbutyl)phenoxy-β-glucuronide.

Discussion

This study showed that 4-*t*-OP was rapidly metabolized in trout hepatocytes to five compounds. The major metabolite was the glucuronide conjugate of 4-*t*-OP (M1; figure 6). Minor products arose from the oxidative metabolism of 4-*t*-OP to form hydroxylated derivatives which were also metabolized to glucuronide conjugates (M3–5). Thibaut *et al*. (1998) also reported that when 4-*n*-NP was administered orally to immature rainbow trout, the major biliary metabolite was 4-*n*-NP-glucuronide. Together, these studies suggest that glucuronidation of the phenol ring is not affected by the structure of the alkyl chain.

In many vertebrates, sulphation and glucuronidation are competing pathways in the liver for the conjugation of phenolic substrates. Generally, although sulphotransferases have a higher affinity for phenolic substrates, they become saturated with increased substrate loading so that at high substrate concentrations the end products are mainly glucuronide conjugates (Pang 1990). Both sulphate and glucuronide metabolites were excreted by zebra fish (*Brachydanio rerio*) exposed to phenol or substituted phenols (Kasokat *et al*. 1987). However, in many species of fish, glucuronidation is the major pathway for the conjugation and excretion of

phenolic xenobiotics (Clarke *et al*. 1991). It is possible that in these *in vitro* studies, exposure to a lower substrate concentration would result in the formation of sulphate conjugates. However, in the current study, the only conjugates detected were glucuronides, even with incubations at a lower concentration of 10 μM 4-*t*-OP. In addition, only a minor amount of a sulphate metabolite was identified in rainbow trout hepatocytes incubated with 10 μM 4-NP (Coldham *et al*. 1998), which suggests that in this species mainly glucuronide conjugates of alkylphenols are formed in the liver.

After a 1-h incubation, 26% of 4-*t*-OP was oxidized to form metabolites, which were hydroxylated on either the C2 (ω-3), the C4 (ω) positions of the alkyl chain or *ortho* on the aromatic ring to form a catechol. These pathways were typical of cytochrome P450 monooxygenase metabolism. In other studies, phase I metabolism has also been shown to be important in the metabolism of 4-alkylphenols. Incubation of a mixture of three alkyl isomers of 4-*sec*-NP with microsomal preparations of rainbow trout hepatocytes formed glucuronide conjugates that were hydroxylated on the ω-1 position of the alkyl chain, but ω- or ring-hydroxylated metabolites were not detected (Meldahl *et al*. 1996). Thibaut *et al*. (1998) administered rainbow trout orally with a single dose of 4-*n*-NP and they detected biliary glucuronide conjugates of metabolites hydroxylated at both the ω-and ω-1 positions of the alkyl chain. The ω-metabolites were further oxidized to the corresponding carboxylic acids, which were then subject to β-oxidation and chain-shortening to form C_7, C_5 and C_3 carboxylic acids. Chain-shortening by β-oxidation is hindered in terminally branched chain alkanes and the present study shows that highly branched 4-*tert*-alkylphenols are unlikely to be chain-shortened and, in trout, will be hydroxylated on the terminal regions of the alkyl chain. Coldham *et al*. (1998) reported that a technical mixture of 4-NP was metabolized by trout *in vivo* to products hydroxylated on the ring or the alkyl chain. Although the position of hydroxylation on the alkyl chain was not determined, no further oxidation to carboxylic acids nor products of β-oxidation were detected.

In the present studies, 4-*t*-OP was hydroxylated at both the ω-and ω-2 positions of the alkyl chain (M4, 2 and 5). Hydroxylation of alkanes such as lauric acid has been reported in hepatic microsomes isolated from a number of fish species (Buhler *et al*. 1997, Haasch *et al*. 1998, Sabourault *et al*. 1998). Juvenile trout liver microsomes incubated with lauric acid formed products hydroxylated at the ω, ω-1, ω-2, ω-3, ω-4, ω-5 and ω-6 positions (Buhler *et al*. 1997). The regiospecific hydroxylation is thought to be dependent on the cytochrome P450 isoform. Some cytochrome P450 isoforms have been isolated from rainbow trout liver (Buhler and Wang-Buhler 1998). Purified trout hepatic CYP2K1 catalyzed the production of lauric acid hydroxylated at the ω-1 and ω-2 positions, whereas CYP2M1 formed the ω-6 hydroxylation product (Buhler *et al*. 1997). In mammals, ω-and ω-1 hydroxylations of alkanes are associated with isoforms of the CYP4A family (Lewis 1996). To date, only the CYP4T1 and CYP4T2 isoforms have been reported in fish and there is no information on their catalytic activity (Falckh *et al*. 1997, Sabourault *et al*. 1998). It is not clear which cytochrome P450 isoforms catalyze the hydroxylation of branched alkyl chains in fish.

The present studies showed that 4-*t*-OP was also hydroxylated on the phenol ring and GC-MS analysis of the butylboronate ester of the aglycone of M3 revealed that hydroxylation was at the *ortho* position to form a catechol structure. A ring-hydroxylated metabolite was also detected in bile of trout dosed with a technical

mixture of 4-NP (Coldham *et al.* 1998). It is not clear which isoform in fish is responsible for ring hydroxylation of the alkylphenol, but in mammals, cytochrome P450 isoforms that hydroxylate phenolics, such as steroids or biphenols, to catechols tend to be either in the CYP1A, 2B and 3A gene subfamilies (Martucci and Fishman 1993, Stresser and Kupfer 1997). Lee *et al.* (1996a, b) reported that 4-NP inhibited the catalytic activity of CYP1A and CYP3A enzymes in rat liver and down-regulated CYP1A but up-regulated CYP3A hepatic protein, suggesting that NP maybe a substrate of these enzymes. CYP2B2 was also shown to metabolize 4-*sec*-NP. However, the identity of the products was not determined (Lee *et al.* 1998).

These studies indicate that in female trout, 4-*t*-OP is metabolized by some pathways that are similar to the catabolism of oestrogens in fish and other vertebrates, namely by glucuronidation of the phenol ring and catechol formation (Clarke *et al.* 1991, Zhu and Conney 1998). It is not known whether the cytochrome P450 and the uridine diphosphate glucuronosyltransferase enzymes involved in alkylphenol metabolism are sex-specific and whether they are the same isoforms responsible for catabolism of endogenous steroids. Further investigation is needed to determine whether alkylphenols can competitively inhibit the catalytic activity and/or alter gene expression of steroid-metabolizing enzymes and thereby alter circulating steroid profiles.

It is not clear whether the higher oestrogenic activity of 4-alkylphenols *in vivo* in fish compared with *in vitro* activity is due to bioconcentration of the parent compound and/or due to bioactivation to more active structures (Jobling *et al.* 1996). The present study shows that 4-*t*-OP is rapidly metabolized by trout liver to a variety of glucuronide conjugates. Detailed GC-MS analysis of the methylated derivatives of all the conjugated 4-*t*-OP metabolites showed that conjugation was on the phenol ring and not on the hydroxylated alkyl chain. Steroid glucuronides conjugated on the A ring show little or no receptor activity (Anstead *et al.* 1997), which suggests that the 4-*t*-OP conjugates are unlikely to possess oestrogen receptor activity. Conjugated steroids can undergo enterohepatic circulation and circulate as the active aglycone. It is possible that 4-*t*-OP glucuronides could be deconjugated in the large intestine and re-enter the bloodstream as the parent compound and its hydroxylated metabolites. It remains to be investigated whether M2 and the aglycone products of M3 and 4 retain oestrogen receptor activity.

In fish, although the liver is recognized as an important site of xenobiotic-metabolizing enzymes, extrahepatic tissues such as the gill, kidney and intestine can also contribute to xenobiotic metabolism in some species. However, in trout, unlike some fish species, the liver appears to be the main organ for activity of phase I and II metabolizing enzymes (Lindström-Seppä *et al.* 1981, Clarke *et al.* 1991). Cravedi *et al.* (1999) also reported that the *in vitro* biotransformation of simple phenols in primary trout hepatocytes correlated well with the products obtained *in vivo*. In summary, the present study shows that highly branched oestrogenic 4-*tert*-alkylphenols are likely to be rapidly metabolized in fish by both phase I and phase II pathways to a number of conjugated metabolites. These glucuronide conjugates are unlikely to be oestrogen receptor active, but *in vivo* studies are necessary to determine if deconjugated active metabolites are produced from enterohepatic circulation.

Acknowledgements

The authors thank Dr S. Jobling of Brunel University and Dr M. Titherage of the University of Sussex for advice on hepatocyte preparation.

References

Ahel, M., Giger, W. and Koch, M., 1994a, Behaviour of alkylphenol polyethoxylate surfactants in the aquatic environment—I. Occurrence and transformation in sewage treatment. *Water Research*, **28**, 1131–1142.

Ahel, M., Giger, W. and Schaffner, C., 1994b, Behaviour of alkylphenol polyethoxylate surfactants in the aquatic environment—II. Occurrence and transformation in rivers. *Water Research*, **28**, 1143–1152.

Anstead, G. M., Carlson, K. E. and Katzenellenbogen, J. A., 1997, The estradiol pharmacophore: ligand structure–estrogen receptor binding affinity relationships and a model for the receptor binding site. *Steroids*, **62**, 268–303.

Bhatt, B. D., Prasad, J. V., Kalpana, G. and Ali, S., 1992, Separation and characterization of isomers of *p*-nonylphenols by capillary GC/GC-MS/GC-FTIR techniques. *Journal of Chromatographic Science*, **30**, 203–210.

Blackburn, M. A., Kirby, S. J. and Waldock, M. J., 1999, Concentrations of alkylphenol polyethoxylates entering UK estuaries. *Marine Pollution Bulletin*, **38**, 109–118.

Blackburn, M. A. and Waldock, M. J., 1995, Concentrations of alkylphenols in rivers and estuaries in England and Wales. *Water Research*, **7**, 1623–1629.

Brunner, P. H., Capri, S., Marcomini, A. and Giger, W., 1988, Occurrence and behaviour of linear alkylbenzenesulfonates, nonylphenol, nonylphenol monophenol and nonylphenol diethoxylates in sewage and sewage-sludge treatment. *Water Research*, **22**, 1465–1472.

Buhler, D. R., Miranda, C. L., Deinzer, M. L., Griffin, D. A. and Henderson, M. C., 1997, The regiospecific hydroxylation of lauric acid by rainbow trout (*Oncorhynchus mykiss*) cytochrome P450s. *Drug Metabolism and Disposition*, **25**, 1176–1183.

Buhler, D. R. and Wang-Buhler, J. L., 1998, Rainbow trout cytochrome P450s: purification, molecular aspects, metabolic activity, induction and role in environmental monitoring. *Comparative Biochemistry and Physiology C—Pharmacology Toxicology and Endocrinology*, **121**, 107–137.

Clarke, D. J., George, S. J. and Burchell, B., 1991, Glucuronidation in fish. *Aquatic Toxicology*, **20**, 35–56.

Coldham, N. G., Sivapathasundaram, S., Dave, M., Ashfield, L. A., Pottinger, T. G., Goodall, C. and Sauer, M. J., 1998, Biotransformation, tissue distribution, and persistence of 4-nonylphenol residues in juvenile rainbow trout (*Oncorhynchus mykiss*). *Drug Metabolism and Disposition*, **26**, 347–354.

Cravedi, J. P., Lafuente, A., Baradat, M., Hillenweck, A. and Perdu-Durand, E., 1999, Biotransformation of pentachlorophenol, aniline and biphenyl in isolated rainbow trout (*Oncorhynchus mykiss*) hepatocytes: comparison with *in vivo* metabolism. *Xenobiotica*, **29**, 499–509.

DeJongh, D. C., Radford, T., Hribar, J. D., Hanessian, S., Bieber, M., Dawson, G. and Sweeley, C. C., 1969, Analysis of trimethylsilyl derivatives of carbohydrates by gas chromatography and mass spectrometry. *Journal of the American Chemical Society*, **91**, 1728–1740.

Ekelund, R. Bergman, Å., Granmo, Å. and Berggren, M., 1990, Bioaccumulation of 4-nonylphenol in marine animals—a re-evaluation. *Environmental Pollution*, **64**, 107–120.

Falckh, P. H. J., Wu, Q. K. and Ahokas, J. P., 1997, CYP4T1—a cytochrome P450 expressed in rainbow trout (*Oncorhynchus mykiss*) liver. *Biochemical and Biophysical Research Communications*, **236**, 302–305.

Gimeno, S., Gerritsen, A., Bowmer, T. and Komen, H., 1996, Feminization of the male carp. *Nature*, **384**, 221–222.

Gray, M. A. and Metcalfe, C. D., 1997, Induction of testis–ova in Japanese medaka (*Oryzias latipes*) exposed to *p*-nonylphenol. *Environmental Toxicology and Chemistry*, **16**, 1082–1086.

Haasch, M. L., Henderson, M. C. and Buhler, D. R., 1998, Induction of lauric acid hydroxylase activity in catfish and bluegill by peroxisome proliferating agents. *Comparative Biochemistry and Physiology C—Pharmacology Toxicology and Endocrinology*, **121**, 297–303.

Harries, J. E., Sheahan, D. A., Jobling, S., Matthiessen, P., Neall, M., Sumpter, J. P., Taylor, T. and Zaman, N., 1997, Estrogenic activity in five United Kingdom rivers detected by measurement of vitellogenesis in caged male trout. *Environmental Toxicology and Chemistry*, **16**, 534–542.

Jobling, S., Sheahan, D., Osborne, J. A., Matthiessen, P. and Sumpter, J. P., 1996, Inhibition of testicular growth in rainbow trout (*Oncorhynchus mykiss*) exposed to estrogenic alkylphenolic chemicals. *Environmental Toxicology and Chemistry*, **15**, 194–202.

Jobling, S. and Sumpter, J., 1993, Detergent components in sewage effluent are weakly oestrogenic to fish: an *in vitro* study using rainbow trout (*Oncorhynchus mykiss*) hepatocytes. *Aquatic Toxicology*, **27**, 361–372.

Kasokat, T., Nagel, R. and Urich, K., 1987, The metabolism of phenol and substituted phenols in zebra fish. *Xenobiotica*, **17**, 1215–1221.

Lee, P. C., Chakraborty Patra, S. and Struve, M., 1996a, Modulation of rat hepatic CYP3A by nonylphenol. *Xenobiotica*, **26**, 831–838.

Lee, P. C., Chakraborty Patra, S., Stelloh, C. T., Lee, W. and Struve, M., 1996b, Interaction of nonylphenol and hepatic CYP1A in rats. *Biochemical Pharmacology*, **52**, 885–889.

Lee, P. C., Marquardt, M. and Lech, J. J., 1998, Metabolism of nonylphenol by rat and human microsomes. *Toxicology Letters*, **99**, 117–126.

Lewis, D. F. V., 1996, *Cytochromes P450* (London: Taylor & Francis).

Lindström-Seppä, P., Koivusaari, U. and Hänninen, O., 1981, Extrahepatic xenobiotic metabolism in North-European freshwater fish. *Comparative Biochemistry and Physiology C—Pharmacology Toxicology and Endocrinology*, **69**, 259–263.

Maitre, J. L., Valotaire, Y. and Guguen-Guillouzo, C., 1986, Estradiol-17β stimulation of vitellogenin synthesis in primary culture of male rainbow trout hepatocytes. *In Vitro Cellular and Developmental Biology*, **22**, 337–343.

Martucci, C. P. and Fishman, J., 1993, P450 enzymes of estrogen metabolism. *Pharmacology and Therapeutics*, **57**, 237–257.

McLeese, D. W., Zitko, V., Sergeant, D. B., Burridge, L. and Metcalfe, C. D., 1981, Lethality and accumulation of alkylphenols in aquatic fauna. *Chemosphere*, **10**, 723–730.

Meldahl, A. C., Nithipatikom, K. and Lech, J. J., 1996, Metabolism of several ^{14}C-nonylphenol isomers by rainbow trout (*Oncorhynchus mykiss*): *in vivo* and *in vitro* microsomal metabolites. *Xenobiotica*, **26**, 1167–1180.

Pang, K. S., 1990, Kinetics of conjugation reactions in eliminating organs. In G. J. Mulder (ed.), *Conjugation Reactions in Drug Metabolism: An Integrated Approach* (London: Taylor & Francis), pp. 5–39.

Routledge, E. J. and Sumpter, J. P., 1996, Estrogenic activity of surfactants and some of their degradation products assessed using a recombinant yeast screen. *Environmental Toxicology and Chemistry*, **15**, 241–248.

Routledge, E. J. and Sumpter, J. P., 1997, Structural features of alkylphenolic chemicals associated with estrogenic activity. *Journal of Biological Chemistry*, **272**, 3280–3288.

Sabourault, C., Berge, J. B., Lafaurie, M., Girard, J. P. and Amichot, N., 1998, Molecular cloning of a phthalate-inducible CYP4 gene (CYP4T2) in kidney from the sea bass, *Dicentrarchus labrax*. *Biochemical and Biophysical Research Communications*, **251**, 213–219.

Stresser, D. M. and Kupfer, D., 1997, Catalytic characteristics of CYP3A4: requirement for a phenolic function in *ortho* hydroxylation of estradiol and mono-*O*-demethylated methoxychlor. *Biochemistry*, **36**, 2203–2210.

Thibaut, R., Debrauwer, L., Rao, D. and Cravedi, J. P., 1998, Characterization of bilary metabolites of 4-*n*-nonylphenol in rainbow trout (*Oncorhynchus mykiss*). *Xenobiotica*, **28**, 745–757.

Wheeler, T. F., Heim, J. R., La Torre, M. R. and Janes, A. B., 1997, Mass spectral characterization of *p*-nonylphenol isomers using high-resolution capillary GC-MS. *Journal of Chromatographic Science*, **35**, 19–30.

Zhu, B. T. and Conney, A. H., 1998, Functional role of estrogen metabolism in target cells: review and perspectives. *Carcinogenesis*, **19**, 1–27.

XENOBIOTICA, 2000, VOL. 30, NO. 9, 881–890

Metabolism, excretion and distribution of the flame retardant tetrabromobisphenol-A in conventional and bile-duct cannulated rats

H. HAKK†*, G. LARSEN†, Å. BERGMAN‡ and U. ÖRN†

† US Department of Agriculture, Agricultural Research Service, Biosciences Research Laboratory, PO Box 5674-University Station, Fargo, ND 58105, USA
‡ Department of Environmental Chemistry, Stockholm University, SE-106 91 Stockholm, Sweden

Received 25 February 2000

1. ^{14}C-TBBP-A (2,2-bis(4-hydroxy-3,5-dibromophenyl)propane) was administered orally to the conventional and bile-duct cannulated male Sprague–Dawley rat (2.0 mg/kg body weight). Urine, bile and faeces were collected daily for 72 h, and selected tissues were removed for distribution studies.

2. Faeces was the major route of elimination of TBBP-A in the conventional rat (91.7% of dose), and urine was a minor elimination route (0.3%). Enterohepatic circulation was suggested by biliary excretion of 71.3% and faecal excretion of 26.7% of the administered radioactivity in the bile-duct cannulated rat.

3. ^{14}C-labelled residues in tissues were 2% in the conventional rat, and $< 1\%$ in the bile-duct cannulated rat. The large and small intestines contained the majority of the tissue ^{14}C activity for both groups of rat. Levels of TBBP-A in liver were $< 0.1\%$, and in fat were below the level of quantification.

4. Three metabolites were characterized in 0–24 h bile samples. Glucuronic acid and sulphate ester conjugates were characterized by mass spectrometry. More than 95% of the extractable faecal ^{14}C was identified as parent TBBP-A.

5. Negligible amounts of TBBP-A-derived ^{14}C were associated with carrier proteins in the urine and bile.

Introduction

Flame retardants are used in a variety of commercial products including electronic equipment and textiles, and all contain bromine atoms responsible for the flame retardance in the gas phase. Tetrabromobisphenol-A (2,2-bis(4-hydroxy-3,5-dibromophenyl)propane; TBBP-A) is the most common flame retardant currently in use, and is principally found covalently bound to epoxy resin circuit boards. The worldwide demand for TBBP-A and its polymeric derivatives reaches upwards of 60000 tons (van Esch 1995). This compares with the 150000 tons worldwide for all brominated flame retardants.

Owing to its high usage and limited water solubility (octanol:water partition coefficient 4.5–5.3), TBBP-A may be expected to persist in the environment and thereby to accumulate in biological systems. It has been found in river sediment samples in Osaka, Japan, although not in marine sediment (Watanabe and Kashimoto 1983). TBBP-A has also been found at the ppb level in river sediments near an industrial area of Sweden (Sellström and Jansson 1995). Absorption and elimination studies have been previously performed with TBBP-A in mammals and fish (Brady 1979, Nye 1978), but to the authors' knowledge, no metabolism studies

* Author for correspondence; e-mail: hakkh@fargo.ars.usda.gov

Xenobiotica ISSN 0049-8254 print/ISSN 1366-5928 online © 2000 Taylor & Francis Ltd
http://www.tandf.co.uk/journals

have been performed. Therefore, the goal of the study was to administer a single oral dose of TBBP-A to both conventional and bile-duct cannulated rat, and to investigate the tissue distribution, excretion and metabolism of the abundant flame retardant in a mammalian system.

Materials and methods

Chemicals

Bis-[^{14}C]phenol-A was prepared from [UL-^{14}C]phenol (2·0 mCi, 25 mCi·mmol^{-1}) and acetone according to Susan *et al*. (1979). [^{14}C]2,2-bis(4-hydroxy-3,5-dibromophenyl)propane (TBBP-A) was synthesized by brominating bis-[^{14}C]phenol-A with 4·2 equiv. bromine in 1:1 methanol:water. The resulting specific activity of TBBP-A was 48·4 mCi·mmol^{-1} as determined by gas chromatography and radioactivity measurements. The purity of TBBP-A (>98%) was determined by silica TLC (50:50 hexane:methylene chloride) and HPLC (C18; H_2O:CH_3CN gradient). Radiolabelled TBBP-A was diluted with unlabelled material until the desired specific activity was achieved (3265 dpm·μg^{-1}).

Instruments

Negative-ion fast-atom bombardment mass spectrometry (FAB/MS) was obtained with a VG Autospec mass spectrometer equipped with a cesium gun. GC/MS was performed on a VG Autospec mass spectrometer operating at 70 eV, using a Model 5890 GC (Hewlett-Packard, Palo Alto, CA, USA) with a 15-m DB-5 ms column (J&W Scientific, Folsom, CA, USA) run from 70 to 310 °C·min^{-1}.

High-performance liquid chromatography (HPLC) analyses were performed with a Gilson System 45NC Gradient Analytical HPLC (Gilson Medical Electronics, Middleton, WI, USA) equipped with a variable wavelength UV detector set to 254 nm, and a liquid scintillation flow-through detector linked in series. Injections were made with a Model 7125 Rheodyne injector. HPLC fractionations were accomplished in reversed-phase mode using a C-18 DeltaPak column (8× 100 mm; Waters Associates, Milford, MA, USA).

Animal dosing and sample collection

Ten male Sprague–Dawley rats (310–354 g) received a single oral dose of ^{14}C-tetrabromobisphenol-A (2·0 mg·kg^{-1} body weight; 1·0 μCi per rat) dissolved in 0·5 ml peanut oil. The doses were administered via a stomach tube device constructed of a 1·0 ml glass syringe fitted with 15 cm Teflon tubing (1/32 inch). These rats were referred to as 'conventional'. Eight bile-duct cannulated male Sprague–Dawley rats (311–349 g) received the identical dose, and were referred to as 'cannulated'. Both groups of rats were housed in a controlled environment of 20 °C, 12 h light/dark cycle, and a relative humidity of 25±5%. The cannulated rats were anaesthetized with halothane prior to surgery. A ventral midline incision was made, and the bile duct was cannulated with medical polyethylene tubing 1·5 cm from the base of the liver. The cannula was fastened with 4-0 silk ligature, and exited near the base of the tail. Rats were housed in stainless steel metabolism cages (Bollman 1948) that allowed for the separate collection of urine, bile and faeces, and were allowed free access to water and feed (Lab Diet 5012, PMI Nutritional International, Brentwood, MO, USA).

At 72 h the rats were killed by CO_2 asphyxiation (conventional), or halothane anaesthesia followed by exsanguination (cannulated). Blood samples were collected into heparinized vials to prevent clotting. The tissues listed in table 2 were removed and stored at −40 °C until combustion could be performed. Small and large intestines included contents.

Quantification of radioactivity

Aliquots of urine, bile or faeces extracts (500 μl) were pipetted into 5 ml LCS cocktail (Ecolite, ICN Biomedicals, Inc., Costa Mesa, CA, USA) and radioactivity was measured in a Packard Model 1900 CA liquid scintillation counter (LSC). Tissues and carcass were homogenized, and aliquots were removed in triplicate, weighed and combusted on a Packard Model 307 tissue oxidizer (0·5 g for most tissues, 0·1 g for fat). ^{14}C-CO_2 was trapped in CARBO-SORB® E (Packard, Meriden, CT, USA). Samples were then measured in Permafluor scintillator (Packard) for ^{14}C content on an LSC.

Fractionation and characterization of biliary metabolites

Bile from each time point was pooled, applied onto a Porapak Q column (PQ; Waters Associates), and eluted with water, then methanol (figure 1). The methanol PQ fraction was applied to a Sephadex LH-20 column (Pharmacia; Piscataway, NJ, USA) and eluted with water. Three major fractions from the

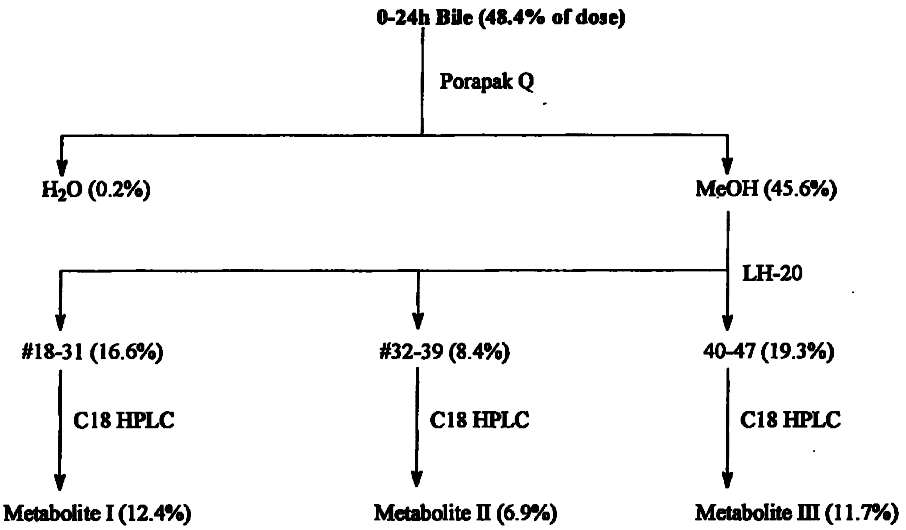


Figure 1. Fractionation of ^{14}C in 0–24 h bile from the male rat orally administered ^{14}C-TBBP-A in peanut oil. Values in parentheses are the percentage of administered dose present in the bile fractions. The structures of the metabolites are shown in table 3.

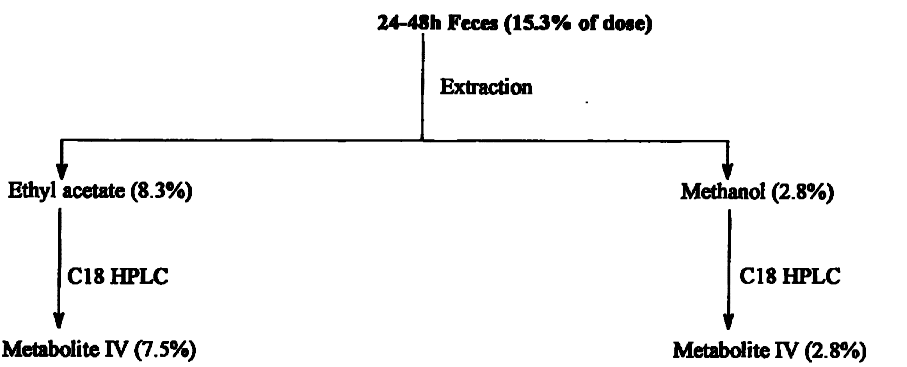


Figure 2. Fractionation of ^{14}C in 24–48 h faeces from the male rat orally administered ^{14}C-TBBP-A in peanut oil. Values in parentheses are the percentage of administered dose in the faeces fractions. The structure of M4 is that of parent TBBP-A (see table 3).

LH-20 column were further chromatographed by reversed-phase HPLC as described above, and identified by FAB/MS analysis.

Fractionation and characterization of faecal metabolites

Faeces were pooled according to time of collection and lyophilized. The dried faeces was extracted three times each with 500 ml ethyl acetate, then with 500 ml methanol (figure 2). The pooled extracts were purified by HPLC in reversed-phase mode using a step gradient beginning at 5% acetonitrile in water to 100% acetonitrile during 60 min. Isolated fractions were submitted for GC/MS analysis after derivatization to the methoxy derivative with diazomethane, or to the trimethylsilyl (TMS) ether with Regisil® (Regis Technologies, Morton Grove, IL, USA).

Binding study with carrier proteins in aqueous excreta

Pooled 0–48 h urine samples and 0–24 h, 24–48 h and 48–72 h bile collections were separately chromatographed by size exclusion on a Sephadex G-75 column (4·5 × 90 cm) as described by Larsen *et al.* (1990). Briefly, the column was eluted with 0·05 M potassium phosphate (pH 7·2). The protein-bound

fractions were combined and re-chromatographed by size exclusion on a Sephacryl S-200 column (2·2 × 85cm) with 0·05 M potassium phosphate buffer (pH 7·2). The method used for SDS-PAGE (sodium dodecyl sulphate-polyacrylamide gel electrophoresis) was that of Mazel (1971), and was performed under reducing conditions. SDS-PAGE gels were stained with Coomassie blue.

Results

The data presented in table 1 indicate that TBBP-A is readily excreted in the male Sprague–Dawley rat, and > 91% of the administered dose was excreted in the faeces of the conventional rat. Faecal excretion was only 7% at 0–24 h, peaked at 24–48 h (65%) and declined to 20% by 72 h (table 1).

In the bile-duct cannulated rat, > 71% of the administered dose was excreted via the bile in 72 h. Nearly 50% of the dose was excreted in the bile by 24 h, but it dropped steadily at subsequent time points. More than 26% of the dose was excreted in the faeces of the cannulated rat by 72 h. Faecal excretion peaked at the 24–48 h time point. Urine was a minor route for excretion of TBBP-A in both the conventional and cannulated rat. The cumulative urine excretion was considerably < 1% of the dose, i.e. 0·3 and 0·7% respectively (table 1).

Owing to the extensive elimination of TBBP-A, total tissue retention at 72 h was limited. In the conventional rat, 2% of the dose was retained in the tissues, but < 1% in the cannulated rat (table 2). The tissues in the conventional and cannulated rat with the highest retention of TBBP-A at 72 h were the large and small intestine and lung. Essentially, no deposition of TBBP-A could be detected in adipose tissue, heart, spleen, testis or thymus in the conventional or cannulated rat (limit of quantification was 0·0005% of the dose; table 2).

The 0–24 h bile sample was fractionated as described in figure 1 to characterize metabolites. Three metabolites were indicated by the LH-20 column results, i.e. fractions #18–31, 32–39 and 40–47. LH-20 fractions were further purified by HPLC, then characterized by FAB/MS. The mass spectrum of LH-20 #18–31 was consistent with a diglucuronide ether conjugate of TBBP-A (M1; table 3). Ions at 891, 715 and 539 corresponded to losses of a hydrogen atom, a glucuronic acid moiety, and two glucuronic acids respectively. Hydrolysis of M1 with β-glucuronidase (*E. coli* recombinant, pH 6·8, 37 °C, 16 h; Sigma, St Louis, MO, USA), derivatization with diazomethane, and GC/MS analysis were used to confirm the assignment. The resulting mass spectrum was consistent with the dimethoxy derivative of TBBP-A [M^+. 568 (4 Br); M-15 (553); M-109 (459)].

The FAB mass spectrum of LH-20 #32–39 was consistent with that of a glucuronic acid/sulphate ester diconjugate of TBBP-A (M2; table 3). Ions at 795 and 537 corresponded to losses of a hydrogen atom, and sulphate plus glucuronic acid moieties respectively. LH-20 #40–47 was identified as the monoglucuronic acid conjugate of TBBP-A (M3; table 3). The FAB/MS showed losses of a hydrogen atom at m/z 715, and a glucuronic acid loss at 539. Hydrolysis of M3 with β-glucuronidase and derivatization with diazomethane resulted in a mass spectrum identical with that of the dimethoxy derivative of TBBP-A (table 3).

The 24–48 h faeces sample was fractionated as described in figure 2 to obtain purified metabolites that could be characterized by GC/MS. Nearly 28% of the radiolabel was non-extractable. The non-extractable levels were even higher at the 0–24 h and 48–72 h time points, i.e. 54·0 and 39·3% respectively. The overwhelming majority of the extractable TBBP-A derived radioactivity at all time points was the parent compound by GC/MS analysis following derivatization with

Table 1. Recovery of ^{14}C from the conventional and bile-duct cannulated male Sprague–Dawley rat administered a single oral dose of TBBP-A (2.0 mg/kg body weight) in 0.5 ml peanut oil (mean ± SD).

	Percent of dose	
Excreta	Conventional (n = 10)	Cannulated (n = 8)
Urine		
0–24 h	0.1 ± 0.07	0.4 ± 0.4
24–48 h	0.2 ± 0.07	0.3 ± 0.4
48–72 h	0.02 ± 0.02	0.03 ± 0.04
Subtotal	0.3 ± 0.07	0.7 ± 0.84
Bile		
0–24 h	—	48.4 ± 15.6
24–48 h	—	21.0 ± 13.1
48–72 h	—	1.9 ± 1.9
Subtotal		71.3 ± 7.2
Faeces		
0–24 h	6.6 ± 7.1	6.0 ± 6.0
24–48 h	65.6 ± 22.7	15.3 ± 5.6
48–72 h	19.5 ± 8.8	5.0 ± 5.3
Subtotal	91.7 ± 17.4	26.3 ± 6.3
Total Excreted	92.0	98.5

Table 2. Tissue recovery of ^{14}C from the conventional and bile-duct cannulated male Sprague–Dawley rat administered a single oral dose of TBBP-A (2.0 mg/kg body weight) in 0.5 ml peanut oil (mean ± SD).

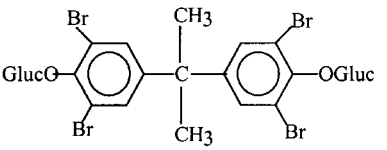
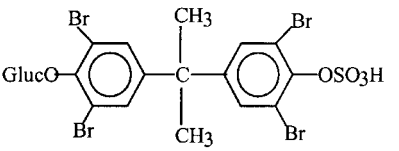
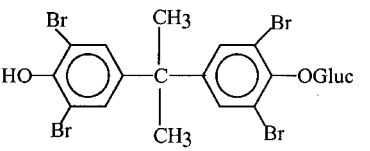
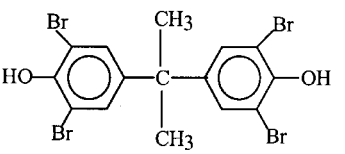
	Percent of dose	
Tissue	Conventional (n = 10)	Cannulated (n = 8)
Adipose (epididymal)	< 0.0005[a]	< 0.0005[a]
Blood	< 0.0005[a]	< 0.0005[a]
Carcass	0.2 ± 0.1	0.3 ± 0.5
Intestine:		
Large	1.0 ± 0.7	0.4 ± 0.3
Small	0.7 ± 0.6	0.2 ± 0.2
Heart	< 0.0005[a]	< 0.0005[a]
Kidney	0.003 ± 0.001	0.001 ± 0.001
Liver	0.06 ± 0.04	0.05 ± 0.05
Lung	0.2 ± 0.3	0.07 ± 0.1
Spleen	< 0.0005[a]	< 0.0005[a]
Testis	< 0.0005[a]	< 0.0005[a]
Thymus	< 0.0005[a]	< 0.0005[a]
Total for tissues	2.1	1.0

[a] Limit of quantification was 0.0005% of dose.

diazomethane. The resulting mass spectra were identical to standard dimethoxy TBBP-A (compound M4; table 3). In addition, the extracted faecal sample was also silylated with Regisil®. The GC retention time and mass spectrum of this silylated derivative were the same as the diTMS ether of authentic TBBP-A (data not shown). No metabolites of TBBP-A could be detected by HPLC.

Almost 18% of TBBP-A and/or its metabolites associated with carrier proteins in the pooled 0–48 h urine sample (500–1300 ml; figure 3). However, the amount of protein-bound ^{14}C was insufficient to allow for protein characterization by the methods utilized. The majority of TBBP-A derived ^{14}C in the urine (> 82%) was

Table 3. Negative-ion fast atom bombardment (−FAB) and electron-impact (EI) mass spectral evidence for the structure of ^{14}C-labelled metabolites present in 0–24 h bile and 24–48 h faeces from the male rat dosed orally with ^{14}C-TBBP-A.

 M1	[M - H^+] 891; [M + Na^+ - H^+] 913; [M - Gluc - H^+] 715; [M - 2(Gluc) - H^+] 539 (FAB/MS)
 M2	[M + Na^+ - 2H^+] 817; [M - H^+] 795; [M - SO_3^- + Na^+ - H^+] 737; [M - SO_3^- - Gluc - 2H^+] 537; [M - Gluc + Na^+ - H^+] 639 (FAB/MS)
 M3	[M - H^+] 715; [M + Na^+ - 2H^+] 737; [M - Gluc] 539 (FAB/MS)
 M4	[$M^{+\cdot}$] 568 (4Br); [M-CH_3] 553 (4Br); [M-CH_2OBr] 459 (3Br): [M-$C_6H_2Br_2OCH_3$] 305 (2Br) (EI/MS as the dimethoxy derivative)

unbound as indicated by the radioactivity eluting between 1800 and 2500 ml on G-75 (figure 3). In addition, total protein excreted remained relatively constant in the urine following the TBBP-A dose when compared with levels obtained before TBBP-A administration (data not shown).

In 0–24 h bile samples, essentially no measurable level of protein binding of TBBP-A could be demonstrated. However, in 24–48 h bile samples, 2·0% of the TBBP-A derived ^{14}C associated with protein (500–700 ml; figure 4), which increased to 6·6% at 48–72 h. The protein was characterized as a 79 kDa protein by SDS-PAGE (data not shown). The majority of the TBBP-A in bile at each time point was unbound, and eluted from the G-75 size exclusion column as two radioactive peaks, i.e. 1700–2200 and 2300–2800 ml (figure 4).

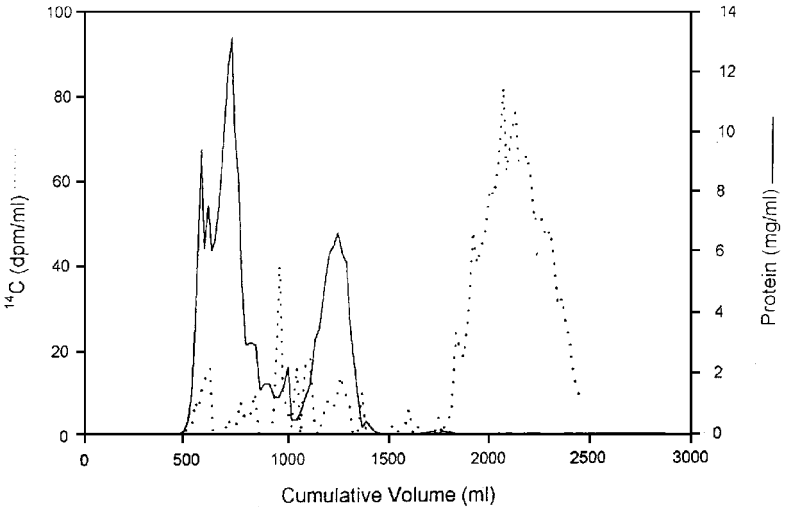


Figure 3. Sephadex G-75 size exclusion fractionation of pooled 0–48 h urine samples from the male rat orally dosed with ^{14}C-TBBP-A. The protein-bound region extends from 500 to 1300 ml, and the unbound region is from 1750 to 2500 ml. Fractions were assayed for protein and ^{14}C as described in the Materials and methods. —, Protein concentration; · · · · ·, quantity of radioactivity.

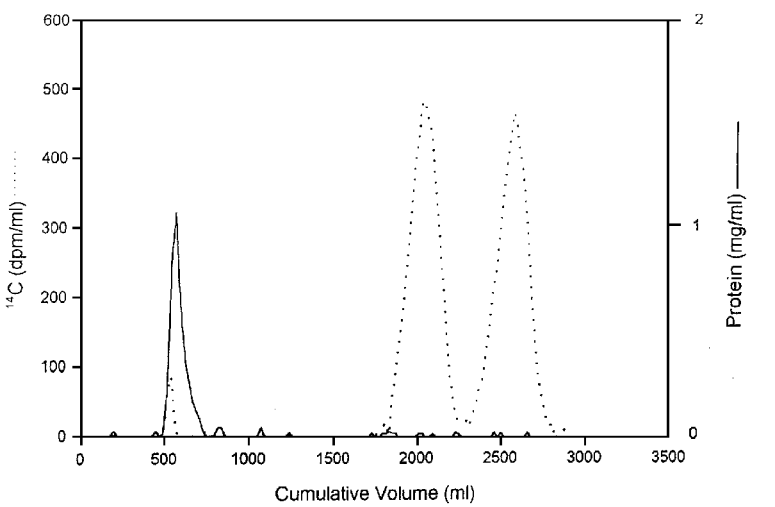


Figure 4. Sephadex G-75 size exclusion fractionation of 24–48 h bile samples from the male rats orally dosed with ^{14}C-TBBP-A. The protein-bound region extends from 500 to 700 ml, and the unbound region is from 1700 to 2800 ml. Fractions were assayed for protein and ^{14}C as described in the Materials and methods. —, Protein concentration; · · · · ·, quantity of radioactivity.

Discussion

TBBP-A was largely eliminated from the conventional male rat via the faeces. Nearly 92% of the dose appeared in the faeces by 72 h, while only 0·3% was eliminated in the urine (table 1). It was expected that TBBP-A, with a relatively high molecular weight of 540, would exhibit preferential biliary excretion when compared with renal excretion into the urine, due to the molecular weight cutoffs in the proximal tubule of the kidney (Timbrell 1991). These excretion results compare favourably with previous data (Brady 1979), which reported that 95% of a 6·5–7·5

$mg \cdot kg^{-1}$ body weight dose of [^{14}C]TBBP-A was excreted in the faeces of the male Sprague–Dawley rat within 72 h, while $< 1{\cdot}1\%$ of the TBBP-A dose could be measured in the urine. The conclusion from previous research with the conventional male rat (Brady 1979) was that TBBP-A was poorly absorbed from the intestinal tract of the male rat. However, the present data demonstrated a delay in faecal excretion, i.e. 66% faecal excretion in the 24–48 h time period versus only $6{\cdot}6\%$ by 24 h (table 1), which provided circumstantial evidence that intestinal absorption was followed by enterohepatic circulation. The time-dependent process of enterohepatic circulation would involve the hepatic conjugation of absorbed TBBP-A, excretion via the bile, deconjugation by bacterial microflora, and reabsorption in the lower gut. Results from the bile-duct cannulated rat also confirmed that absorption of the TBBP-A dose had occurred (table 1). Greater than 71% of the dose administered to the bile-duct cannulated rat was excreted in the bile by 72 h. Only 26% of the dose could be identified in the faeces of the bile-duct cannulated male rat. Therefore, the excretion data with the conventional and cannulated rat indicated that TBBP-A was readily absorbed from the gut, metabolized and excreted within 72 h.

The chromatographic and mass spectrometry results demonstrated that the net result of mammalian metabolism was the excretion of TBBP-A largely as the unchanged compound via the faeces, and may have significant environmental and toxicological ramifications. TBBP-A may persist in the environment for years despite the fact that it can be absorbed and undergo metabolic conversion in mammalian systems. As a result, the environmental inventories of TBBP-A, the most abundant flame retardant currently in use, could increase in the future to levels where toxicological effects may be observed in susceptible species. Previous studies have demonstrated that TBBP-A is not mineralized to a significant extent by sewage sludge in 28 days (CITI 1992), although other research has reported that TBBP-A is subject to biodegradation in soil, sediment and a sediment/water microbial test system under aerobic and anaerobic conditions (Fackler 1989a–c).

The facile absorption and elimination of TBBP-A by the male rat indicates a low potential for bioaccumulation in the male. Based on criteria proposed by the International Council of Chemical Associations, a primary indicator for bioaccumulation potential for a xenobiotic is a fish bioconcentration factor of > 5000. Bioaccumulation studies with bluegill sunfish (Nye 1978), fathead minnows (Fackler 1989d), and carp (CITI 1992) have failed to establish bioaccumulation factors of > 1200 for TBBP-A. Although actual bioconcentration factors were not determined in the present rat study, the ^{14}C combustion data in table 2 demonstrated that all tissues contained considerably $< 1\%$ of the administered dose at 72 h. The tissues with the highest residues in the conventional rat were the large intestine ($1{\cdot}0\%$), small intestine ($0{\cdot}7\%$), lung ($0{\cdot}2\%$) and carcass ($0{\cdot}2\%$). The higher intestinal levels may be partially explained by the fact that the intestines were not purged of contents. Despite the lipophilic character of TBBP-A, it was not detected in lipophilic tissues, i.e. the adipose tissue or testis. In addition, TBBP-A was not deposited in heart, spleen or thymus, and $< 0{\cdot}1\%$ of the dose was detected in the livers of the conventional and cannulated rat. Earlier results (Brady 1979) have previously shown that the highest tissue levels of TBBP-A in the male rat were found in the liver and testis. Therefore, the collective data would indicate that TBBP-A does not appear to present a potential to bioaccumulate in terrestrial or aquatic species.

The two hydroxyl groups in TBBP-A provide functional groups for conjugation. The FAB/MS results indicated hepatic β-glucuronosyl transferase and arylsulpho-

transferase activity toward the TBBP-A substrate. β-Glucuronosyl transferase enzymes are microsomal, whereas arylsulphotransferase enzymes are cytosolic (Eadsforth and Hutson 1984). Based on the quantified levels of the three identified metabolites in 0–24 h bile samples (figure 1), it would appear that TBBP-A served as a better substrate for β-glucuronosyl transferase than for arylsulphotransferase by perhaps partitioning preferentially in the hepatocyte microsomes rather than the cytosol. The monoglucuronic and diglucuronic acid conjugates of TBBP-A (M1 and 3) accounted for 78·8% of the 24–48 h biliary activity. Furthermore M2 was conjugated to glucuronic acid as well as being sulphated. Refractoryness to phenol sulphation has been reported when methyl or methoxy groups are in an *ortho* position (Mulder 1984), and a tertiary butyl substitution in the *ortho* position of phenols abolished sulphation completely. TBBP-A contains two relatively bulky bromine atoms on each ring, both situated *ortho* to the phenolic hydroxyl groups. The steric hindrance introduced by the *ortho* bromines may serve to make TBBP-A a poor substrate for the arylsulphotransferase enzyme, and favour the β-glucuronosyl transferase system.

An endogenous dimethoxy TBBP-A metabolite was not detected in the bile or faeces of the male rat. This suggested that the rat and perhaps other mammalian species are not capable of methylating TBBP-A. Results obtained from river sediment samples from Japan (Watanabe and Tatsukawa 1990) and downstream from a plastics production facility in Sweden (Sellstrom and Jansson 1995) demonstrated the dimethoxy TBBP-A was present at levels ranging from 0·6 to 1500 ppb on a dry weight basis. Dimethoxy TBBP-A is not used commercially as a flame retardant, nor is it thought to be a contaminant of commercial preparations of TBBP-A. Therefore, the presence of dimethoxy TBBP-A in environmental samples is thought to occur by microbial methylation of TBBP-A.

Mammalian carrier proteins have been identified in urine and bile which associate with various halogenated xenobiotics and/or their metabolites. In male rat urine, albumin and α2u-globulin are associated with non-toxic (Larsen *et al*. 1995) and toxin dioxins (Hakk *et al*. 1999), and brominated diphenyl ethers (Larsen *et al*. 1999). In the bile, an uncharacterized, monomeric 79 kDa protein with a isoelectric point of 5·7 is associated with many halogenated aromatic hydrocarbons (Wiener and Larsen 1997). In the present study, the authors attempted to identify and quantify the level of carrier protein mediation in the excreta following an oral dose of TBBP-A. In the urine, 82·3% of TBBP-A and/or its metabolites were not associated with carrier proteins (figure 3). The greater hydrophilicity of TBBP-A when compared with dioxins and brominated diphenyl ethers would probably make elimination in the aqueous media via a carrier system unnecessary. Similarly in the bile, very little association of the parent and/or the conjugated TBBP-A metabolites to carrier proteins was observed (figure 4). Therefore, the risk of disrupting the native function of urinary albumin and α2u-globulin, or the 79 kDa protein in the bile via association with TBBP-A and/or its metabolites would appear to be insignificant.

Acknowledgements

The authors thank Barbara Magelky and Colleen Pfaff for technical expertise in handling the rats, tissues and fractionated excreta. Additional thanks to Margaret Lorentzsen for obtaining the mass spectral data.

References

Bollman, J. L., 1948, A cage which limits the activity of rats. *Journal of Laboratory and Clinical Medicine*, **33**, 1348.

Brady, U. E., 1979, Pharmacokinetic Study of Tetrabromobisphenol A (BP-4A) in Rats. Report from Athens, GA, University of Georgia. Report to Velsicol Chemical Corporation, Chicago, submitted to WHO by the Brominated Flame Retardant Industry Panel.

Chemicals Inspection and Testing Institute, 1992, *Biodegradation and Bioaccumulation Data of Existing Chemicals Based on the CSCL* (Tokyo: Japan Chemical Industry Ecology, Toxicology and Information Center), pp. 4–14.

Eadsforth, C. V. and Hutson, D. H., 1984, Formation of carbohydrate, sulfate and other xenobiotic compounds. In J. Caldwell and G. D. Paulson (eds), *Foreign Compound Metabolism* (London: Taylor & Francis), pp. 171–184.

Fackler, P. H., 1989a, Determination of the Biodegradability of Tetrabromobisphenol A in Soil under Aerobic Conditions (Final Report). Wareham, Massachusetts, Springborn Life Sciences, Inc. Report no. 88-11-2848 submitted to WHO by the Brominated Flame Retardant Industry panel.

Fackler, P. H., 1989b, Determination of the Biodegradability of Tetrabromobisphenol A in Soil under Anaerobic Conditions. Wareham, Massachusetts, Springborn Life Sciences, Inc. Report no. 88-11-2849 submitted to WHO by the Brominated Flame Retardant Industry panel.

Fackler, P. H., 1989c, Tetrabromobisphenol A-Determination of the Biodegradability in a Sediment/Soil Microbial System. Wareham, Massachusetts, Springborn Life Sciences, Inc. Report no. SLI 89-8-3070 submitted to WHO by the Brominated Flame Retardant Industry panel.

Fackler, P. H., 1989d, Bioconcentration and Elimination of ^{14}C-Residues by Fathead Minnows (*Pimiphales promelas*) exposed to Tetrabromobisphenol A. Wareham, Massachusetts, Springborn Life Sciences, Inc. Report no. 89-8-2952 submitted to WHO by the Brominated Flame Retardant Industry panel.

Hakk, H., Larsen, G. and Feil, V. J., 1999, The binding of 1,2,3,7,8-pentachlorodibenzo-*p*-dioxin metabolites with rat urinary and biliary carrier proteins. *Organohalogen Compounds*, **40**, 125–128.

Larsen, G. L., Bergman, Å. and Klasson-Wehler, E., 1990, A methylsulphonyl metabolite of a chlorinated biphenyl can serve as a ligand for α_{2u}-globulin in rat and major urinary protein in mice. *Xenobiotica*, **20**, 1343–1352.

Larsen, G., Hakk, H., Klasson-Wehler, E., Örn, U. and Bergman, Å., 1999, Binding of 2,2′4,′,5-pentabromodiphenyl ether (BDE-99) and/or its metabolites to mammalian urinary and biliary carrier proteins. *Organohalogen Compounds*, **40**, 371–374.

Larsen, G. L., Wiener, C., Hakk, H. and Feil, V. J., 1995, Interaction of 1,2,7,8-tetrachlorodibenzo-*p*-dioxin metabolites with mammalian carrier proteins. *Organohalogen Compounds*, **25**, 249–251.

Mazel, J. V., Jr, 1971, Polyacrylamide gel electrophoresis of viral proteins. *Methods in Virology*, **5**, 179–246.

Mulder, G. J., 1984, Sulfation-metabolic aspects. In J. W. Bridges and L. F. Chasseaud (eds) *Progress in Drug Metabolism*, **8** (London: Taylor & Francis), pp. 35–99.

Nye, D. E., 1978, The Bioaccumulation of Tetrabromobisphenol A in the Bluegill Sunfish. Santa Clara, CA, Stoner Laboratories, Inc. Report to Velsicol Chemical Corporation, Chicago, IL, submitted to WHO by the Brominated Flame Retardant Industry Panel.

Sellström, U. and Jansson, B., 1995, Analysis of tetrabromobisphenol A in a product and environmental samples. *Chemosphere*, **31**, 3085–3092.

Susan, A. B., Ebert, D. A. and Duncan, W. P., 1979, Synthesis of carbon-14-labeled flame retardants. Carbon-14-labeled-tetrabromophthalic anhydride and tetrabromobisphenol-A. *Journal of Labelled Compounds and Radiopharmacology*, **16**, 579–589.

Timbrell, J. A., 1991, *Principles of Biochemical Toxicology*, 2nd edn (London: Taylor & Francis).

van Esch, G. J. (eds), 1995, *Tetrabromobisphenol A and Derivatives.* International Programme on Chemical Safety, Environmental Health Criteria, **172** (Geneva: WHO), pp. 25–31.

Watanabe, I. and Kashimoto, T., 1983, The flame retardant tetrabromobisphenol-A and its metabolite found in river and marine sediments in Japan. *Chemosphere*, **12**, 1533–1539.

Watanabe, I. and Tatsukawa, R., 1990, Anthropogenic brominated aromatics in the Japanese environment. In L. Freih (ed.), *Proceedings of Workshop on Brominated Aromatic Flame Retardants*, Skokloster, 24–26 October, 1989 (Solna: National Chemicals Inspectorate), pp. 63–71.

Wiener, C. and Larsen, G. L., 1997, Covalent binding of dioxin metabolites to a 79 kDa protein isolated from bile of rats dosed with either 1,2,7,8-; 1, 3, 7, 8-; or 1, 4, 7, 8-tetrachlorodibenzo-*p*-dioxin. *Organohalogen Compounds*, **34**, 195–198.

XENOBIOTICA, 2000, VOL. 30, NO. 9, 891–903

High conservation of both phase I and II drug-metabolizing activities in cryopreserved rat liver slices

A.-K. SOHLENIUS-STERNBECK*, E. FLOBY, M. SVEDLING and A. ORZECHOWSKI

Preclinical Development, AstraZeneca R&D Södertälje, S-151 85 Södertälje, Sweden

Received 6 April 2000

1. Xenobiotic-metabolizing enzymes, including both cytochrome P450 and phase II-conjugating systems, have been characterized in rat liver slices cryopreserved in 12 or 18% dimethylsulphoxide (DMSO).

2. Several cytochrome P450 isoforms in rat liver slices metabolized testosterone to a variety of hydroxylated products. The rates of formation of these same products were well maintained during cryopreservation of the slices in both 12 or 18% DMSO.

3. After cryopreservation of rat liver slices in 18% DMSO, the rates of metabolism of ropivacaine to 3-hydroxyropivacaine, 4-hydroxyropivacaine and PPX (all catalysed by different cytochrome P450 isoforms) were ~94, 79 and 82% respectively of the corresponding rates observed with fresh slices.

4. The rates of conjugation of 7-hydroxycoumarin and 1-naphthol by rat liver slices were significantly decreased after cryopreservation in 12% DMSO, but they were maintained when the concentration of this cryopreservant was increased to 18%.

5. After cryopreservation in 12% DMSO, the mitochondrial reduction of the tetrazolium salt MTT by rat liver slices was significantly lowered. In contrast, slices cryopreserved in 18% DMSO demonstrated no significant decrease in their capacity to reduce MTT.

6. Thus, in agreement with previous studies, it was found that cytochrome P450-dependent activities are retained after cryopreservation of liver slices. Although phase II-conjugating enzyme activities are more sensitive to cryopreservation, it was shown that increasing the concentration of DMSO present during cryopreservation could circumvent the problem. This modification improves the usefulness of cryopreserved rat liver slices as a tool in drug metabolism studies.

Introduction

To date, the use of precision-cut liver slices for *in vitro* studies of drug metabolism has been rather limited. This is somewhat surprising, since liver slices are unique as an *in vitro* system, which retains *in vivo*-like properties (for general reviews, see Ekins, 1996; Olinga *et al*. 1997) and contains physiological concentrations of cofactors and intact cell–cell interactions. Moreover, liver slices are easy to prepare and handle, requiring, in contrast to the preparation of isolated hepatocytes, no use of digestive enzymes. Cytochrome P450-dependent activities have been extensively characterized in cultured liver slices from rat, mouse and man (Lake *et al*. 1996, Gokhale *et al*. 1997).

During the past few years, several groups of investigators have reported that liver slices can be stored without undue damage by cryopreservation (Ekins *et al*. 1996, Fisher *et al*. 1996, de Kanter *et al*. 1997, 1998, Glockner *et al*. 1998). For example, liver slices from different species, including man, can be cryopreserved with efficient

* Author for correspondence.

Xenobiotica ISSN 0049–8254 print/ISSN 1366–5928 online © 2000 Taylor & Francis Ltd
http://www.tandf.co.uk/journals

maintenance of cytochrome P450-catalysed activities (de Kanter *et al*. 1997, 1998; Glockner *et al*. 1998). Such a system could provide a valuable method for drug metabolism studies, allowing optimal use of biological material, which is difficult to obtain, e.g. human liver.

At present, information concerning activities of phase II-conjugating enzymes in cryopreserved liver slices is scarce. This may well reflect difficulties involved in obtaining maintenance of these enzyme activities in liver slices after cryopreservation. De Kanter *et al*. (1998) demonstrated that cryopreserved human slices could conjugate 7-hydroxycoumarin. However, the rate of formation of conjugates appeared to be much lower than in fresh slices. In addition, Ekins *et al*. (1996) demonstrated that the rate of conjugation of 7-hydroxycoumarin by cryopreserved dog liver slices is only ~ 20% of the corresponding value for fresh slices.

The protectant most often employed for cryopreservation of liver slices is dimethylsulphoxide (DMSO), usually at a concentration of 10 or 12% (v/v) (de Kanter *et al*. 1997, 1998; Glockner *et al*. 1998). After incubation of the slices with the cryopreserving medium at low temperature for at least 15 min, the slices are rapidly frozen in the medium by immersion into liquid nitrogen. A recent study revealed that liver slices cryopreserved in 18% DMSO are more viable (with respect to histomorphology and K^+ content) than are slices frozen in 12% DMSO (de Graaf *et al*. 1999). The present authors decided, therefore, to compare xenobiotic-metabolizing enzyme activities, including phase II-conjugating systems, in fresh liver slices and in slices cryopreserved in 12 or 18% DMSO.

The pattern of hydroxylation of testosterone by isoforms of cytochrome P450 is commonly employed to characterize phase I xenobiotic metabolism (Arlotto *et al*. 1991, Gokhale *et al*. 1997). Accordingly, the metabolism of testosterone by fresh and cryopreserved rat liver slices was examined. Ropivacaine, an amide-type local anaesthetic agent, is also metabolized by cytochrome P450 (Ekstrom and Gunnarsson 1996) and the present authors studied its metabolism by fresh and cryopreserved slices of rat liver.

The phase II-conjugating enzymes UDP-glucuronosyltransferase and sulphotransferase are often assayed using 1-naphthol or 7-hydroxycoumarin as diagnostic substrates (Schwenk *et al*. 1991, Walsh *et al*. 1995, Boström *et al*. 2000). In the present study, conjugation of these substrates by fresh and cryopreserved rat liver slices was also characterized.

The tetrazolium salt MTT is reduced by mitochondria, and this reduction is often employed as an indicator of viability, i.e. capacity for cell growth and survival (Mosmann 1983). MTT reduction by cryopreserved rat liver slices was compared with the same process in fresh slices.

Materials and methods

Materials

Williams' medium E was from Life Technologies AB (Täby, Sweden); testosterone from Janssen, Chimica (Geel, Belgium); testosterone metabolites were kindly provided by AstraZeneca R&D Lund (Sweden); 6β-hydroxytestosterone for quantitative determination was from Ultrafine Chemicals (Manchester, UK); agarose, Dulbecco's phosphate-buffered saline (without calcium chloride), 7-hydroxycoumarin, Krebs–Hanseleit buffer (without calcium chloride), MTT, naphthol, 1-[^{14}C]-naphthol and trizma-base were from Sigma Chemical Co. (St Louis, MO, USA). Dimethylsulphoxide, *n*-butanol and propionic acid were from Merck (Darmstadt, Germany). Ropivacaine, 3-hydroxy-ropivacaine, 4-hydroxyropivacaine and PPX were synthesized at AstraZeneca R&D Södertälje. All other chemicals were of analytical grade and from common commercial sources.

Animals

Male Sprague–Dawley rats (B&K Universal AB, Sollentuna, Sweden), weighing 225–250 g, were maintained under a 12-h light/dark cycle in steel cages with free access to commercial food pellets (Lactamin, Stockholm, Sweden).

Preparation of rat liver slices

After anaesthetizing the rats with isofluran® (Abbott Scandinavia AB, Kista, Sweden), the liver was perfused *in situ* with ice-cold Krebs–Hanseleit buffer. A drill press (diameter 8 mm) was used to produce cores of the liver. Liver slices were prepared in an ice-cold phosphate-buffered saline with 0.1% agarose (wt/v) using a Krumdieck tissue slicer (Krumdieck *et al*. 1980) set at a thickness of 250 μm. This same preparation buffer was employed previously for slicing of liver and kidney tissue (Obatomi *et al*. 1998). It was then suggested that the presence of agarose in the buffer could help to prevent mechanical stress during slicing. In initial experiments in our laboratory, Krebs–Hanseleit buffer was present during the slicing procedure. It was observed, however, that the use of the buffer resulted in a higher degree of damaged slices. After slicing in ice-cold phosphate-buffered saline with 0.1% agarose, ~ 80% of the total number of slices could be used for incubation, whereas only ~ 50% of the total number of slices could be used after preparation in Krebs–Hanseleit buffer.

The slices obtained were subsequently stored in ice-cold Krebs–Hanseleit buffer until use (within 1 h after preparation).

Cryopreservation of rat liver slices

The procedure employed for cryopreservation was a modification of that described by de Kanter *et al*. (1998). The cryopreservation medium consisted of Williams' medium E containing 12 or 18% DMSO (v/v) as cryoprotectant. Five slices were incubated in an Erlenmeyer flask in 10 ml of this medium. The flask was shaken horizontally 54 times.min^{-1} for 30 min at 2 °C under an atmosphere of 5% CO_2/95% O_2. In initial experiments, the shaking speed during exposure to DMSO was 110 times.min^{-1}. This higher speed was reported by de Kanter *et al*. (1998) to provide good results with human liver slices. After incubation in the presence of DMSO, the five slices were transferred directly into a freezing vial containing 1 ml fresh ice-cold cryopreservation medium and this vial immediately immersed into liquid nitrogen (−196 °C).

Thawing and pre-incubation of rat liver slices

The rat liver slices were stored in liquid nitrogen for as long as 3 days before thawing and use. To achieve thawing, the vial was moved directly from liquid nitrogen into a water bath at 37 °C. After washing in 150 ml Williams' medium E, each slice was pre-incubated for 1 h in 3.2 ml Williams' medium E or Krebs–Hanseleit buffer at 37 °C under an atmosphere of 5% CO_2/95% O_2. Fresh slices were preincubated under these same conditions.

Incubations

All incubations were performed in Falcon tissue culture plates with six wells (Labora AB, Johanneshov, Sweden). All enzyme assays were performed with saturating substrate concentration and conditions of linearity with time for at least 90 min.

Testosterone metabolism by rat liver slices. Fresh and cryopreserved rat liver slices were incubated individually with 250 μM testosterone in 3.2 ml Williams' medium E at 37 °C for 30–90 min. Metabolism was terminated by hand homogenizing the slice (using 15 up-and-down strokes of a glass homogenizer) at 2 °C and subsequently freezing this homogenate on ethanol/dry ice. After thawing, the homogenate was extracted with dichloromethane and the resulting organic phase removed and evaporated to dryness under a stream of nitrogen. The dried residues were re-dissolved in ethanol:water (30:70 v/v) and analysed by reverse-phase HPLC.

The samples were injected at room temperature onto a LiChroCART column (250 × 4 mm, LiChropher 100, RP-18, 5 μm) with a LiChroCART (4 × 4 mm) guard column (Merck, Darmstadt, Germany). The mobile phases employed were (A) 30% (v/v) ethanol in water and (B) 60% (v/v) ethanol in water. During the 60-min run, the proportion of B in the mobile phase was increased from 0 to 67%. Flow rate was maintained at 0.8 ml.min^{-1}. The absorption of the eluant at 254 nm was monitored continuously using a UV/VIS detector (Spectra-Physics, Stockholm, Sweden). Finally, the formation of 6β-hydroxytestosterone was quantitated using a standard curve obtained with synthetic 6β-hydroxytestosterone.

Ropivacaine metabolism by rat liver slices. Fresh and cryopreserved rat liver slices were incubated individually with 1 mM ropivacaine in 3.2 ml Williams' medium E at 37 °C for 30–90 min. Metabolism was terminated by hand homogenizing the slice (using 15 up-and-down strokes of a glass homogenizer)

at 2 °C and subsequently freezing this homogenate on ethanol/dry ice. After thawing, the homogenate was extracted with diethyl ether: hexane (4:1 v/v) and the organic phase removed and evaporated to dryness under a stream of nitrogen. The dried residues were re-dissolved in the mobile phase (without acetonitril) used for reverse-phase HPLC separation (see below).

The samples were injected at room temperature onto a LiChroCART column (125 × 4 mm, Superspher 60 RP-select B®, 4 μm) with a LiChroCHART (4 × 4 mm, LiChrospher 60) guard column (Merck). The mobile phase consisted of sodium phosphate buffer (pH 2, I = 0.05) containing 5 mM 1-octane sulphonic acid and 20% acetonitrile. The flow rate was maintained at 1 ml.min^{-1}. Detection was achieved by monitoring the absorption of the eluant at 210 nm with a Spectra-Physics UV/VIS detector.

Conjugation of 7-hydroxycoumarin by rat liver slices. Fresh and cryopreserved rat liver slices were incubated individually with 25 μM 7-hydroxycoumarin in 2.0 ml Krebs–Hanseleit buffer at 37 °C for 30–120 min. At the end of this incubation period, the medium was removed, filtered through a filter with 0.22-μm pores and subsequently analysed by HPLC (Walsh *et al.* 1995). Each slice was hand homogenized (using 15 up-and-down strokes of a glass homogenizer) in Krebs–Hanseleit buffer and its protein content was determined.

1-Naphthol conjugation by rat liver slices. The conjugation of 1-naphthol was determined according to Schwenk *et al.* (1991) and Boström *et al.* (2000) with certain modifications. Fresh and cryopreserved rat liver slices were incubated individually with 100 μM [^{14}C]-1-naphthol (0.256 μCi) in 2.0 ml Williams' medium E at 37 °C for up to 90 min. Conjugation was terminated by hand homogenizing the slice (using 15 up-and-down strokes of a glass homogenizer) at 2 °C and subsequently freezing this homogenate on ethanol/dry ice. After thawing, the homogenate was extracted with chloroform and the radioactivity present in the aqueous upper phase (containing conjugates) and the organic lower phase (containing remaining substrate and unconjugated metabolites) determined using a liquid scintillation counter.

Of the aqueous upper phase, 500 μl was evaporated under a stream of nitrogen, redissolved in 25 μl water and subsequently applied to a thin-layer silica gel plate (LKD silica gel 60 Å, Whatman, Inc., Clifton, NJ, USA). 1-Naphthyl sulphate was separated from 1-naphthyl glucuronide using *n*-butanol:0.01 M Tris:propionic acid (75:14:1.1) as the solvent system. A radioactivity scanner (System 200 Imaging scanner, Bioscan, Washington, DC, USA) was employed for the quantification of radioactive compounds.

Reduction of MTT

MTT reduction was determined essentially as described previously (Mosmann 1983). In short, fresh and cryopreserved rat liver slices were incubated individually with 1.2 mM MTT in 2 ml Williams' medium E at 37 °C for 3 h and subsequently transferred to 1 ml acidified isopropanol. After extraction overnight at 4 °C, the absorbance of the organic phase at 595 nm was determined using a microtiter plate reader (EmaxTM, Molecular Devices, Sunnyvale, CA, USA).

Protein determination

The protein concentrations in liver slice homogenates were determined according to Bradford (1976) using a protein assay kit (Bio-Rad Laboratories, Richmond, CA, USA) with bovine serum albumin as standard.

Statistical analysis

The data are means ± SD of the number of experiments indicated. The results of statistical analysis using a Student's t-test are given where appropriate.

Results

Rate of shaking during cryopreservation

During incubation in the cryopreservation medium containing DMSO for 30 min at 1–2 °C, the slices were shaken in a water bath. All the results presented here were obtained using slices shaken horizontally 54 times.min^{-1} during this period. In earlier experiments, 110 shakes.min^{-1} were used, but it was found that this higher speed resulted in a dramatic decrease in the rate of metabolism of testosterone by rat liver slices. For example, after shaking at 110 shakes.min^{-1} during incubation of rat liver slices in 12% DMSO, the rate of formation of 6β-hydroxytestosterone from testosterone was only ~ 33% of the corresponding formation in fresh slices (average of two independent experiments).

Table 1. Reduction of MTT by fresh and cryopreserved rat liver slices. Slices were incubated individually with 1.2 mM MTT. They were extracted in acidified isopropanol and the absorbance of the organic phase at 595 nm was determined. For further details, see the Materials and methods. The level of absorbance reflects the degree of MTT reduction.

	MTT reduction by rat liver slices (OD_{595}/slice)	
Fresh	Cryopreserved in 12% DMSO (% of fresh)	Cryopreserved in 18% DMSO (% of fresh)
0.882±0.244	0.369±0.099 (42%)*	0.762±0.136 (86%)

*$p < 0.05$ compared with fresh slices and with slices cryopreserved in 18% DMSO.

Data are means±SD of three-to-six independent experiments.

Table 2. Formation of metabolites of testosterone by fresh and cryopreserved rat liver slices. Slices were incubated individually with 250 μM testosterone. Samples were analyzed by reverse-phase HPLC and metabolites were detected on the basis of their UV absorbance. For further details, see the Materials and methods.

	Testosterone metabolism by rat liver slices		
Metabolite	Fresh (pmol.min^{-1}.mg protein^{-1})	Cryopreserved in 12% DMSO (% of formation by fresh slices)	Cryopreserved in 18% DMSO
6α-OH[b]	3.22±0.94	85.8±14.5	74.7
7α-OH[b]	12.5±2.99	96.8±24.2	63.3
6β-OH[a]	22.6±3.80	142±56.6	95.4±24.1
16α-OH	49.1±19.0	240±139	106±15.7
2α-OH[b]	31.2±9.0	185±88.1	110±12.3
Androstenedione[b]	300±132	91.7±33.7	73.9±5.6

Data are means±SD of three independent experiments, except in the case of 6α- and 7α-hydroxytestosterone formation by slices cryopreserved in 18% DMSO, where the average of two independent experiments is given.

[a] Specific rate of formation of 6β-hydroxytestosterone was determined from a standard curve prepared with synthetic 6β-hydroxytestosterone.

[b] This same standard curve as in (a) was also used to estimate the specific rates of formation of all other metabolites of testosterone.

Reduction of MTT

As shown in table 1, the reduction of MTT by rat liver slices cryopreserved in 12% DMSO was 42% of the corresponding reduction in fresh slices. In contrast, slices cryopreserved in 18% DMSO demonstrated no significant decrease in their capacity to reduce MTT (table 1). The presence of testosterone, ropivacaine, 7-hydroxycoumarin or 1-naphthol in the incubation medium was without effect on the reduction of MTT by fresh or cryopreserved rat liver slices (data not shown).

Testosterone metabolism by rat liver slices

Incubation of rat liver slices with testosterone resulted in the formation of a variety of hydroxylated products. This formation of testosterone metabolites was linear with time for at least 90 min under our incubation conditions (data not shown).

As shown in table 2, the formation of 6β-hydroxytestosterone by liver slices cryopreserved in 18% DMSO was ~95% of the corresponding formation in fresh slices. Rat liver slices cryopreserved in 18% DMSO, produced 16α-hydroxy-

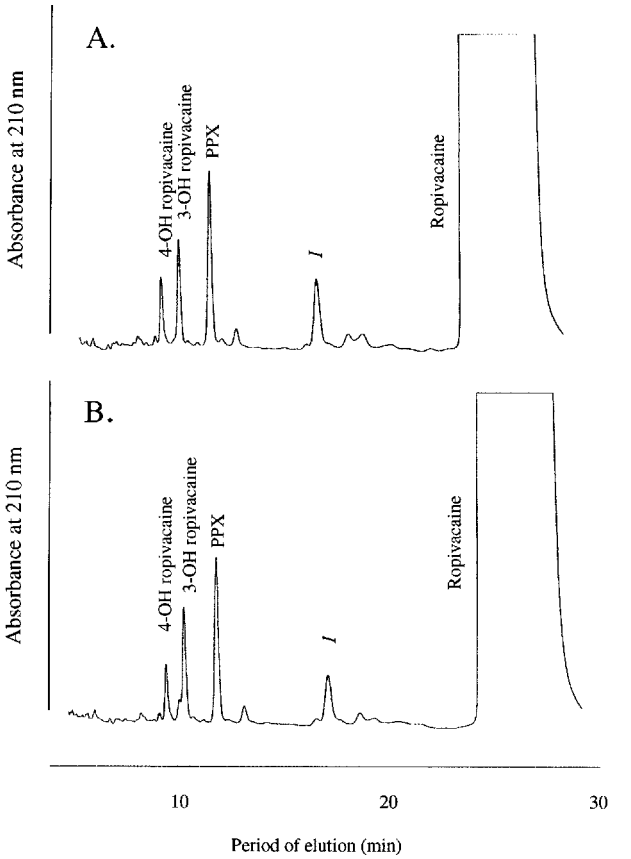


Figure 1. Reverse-phase HPLC analysis of metabolites of ropivacaine produced by (A) fresh liver slices and (B) rat liver slices cryopreserved in 18% DMSO. Fresh and cryopreserved rat liver slices were incubated individually with 1 mM ropivacaine for 60 min. The metabolites formed were subsequently analysed by reverse-phase HPLC and were detected on the basis of their UV absorbance. For further details, see the Materials and methods. I, impurity. The chromatograms are representative of three independent experiments.

testosterone and 2α-hydroxytestosterone at levels which were ~110% of the corresponding formation in fresh slices. Conversion of testosterone to androstenedione by these same cryopreserved slices was 74% of the corresponding metabolism in fresh slices. There were no statistically significant differences between the rates of formation of testosterone metabolites by fresh rat liver slices and rat liver slices cryopreserved in 18% DMSO.

In rat liver slices cryopreserved in 12% DMSO, the rates of formation of 6α-, 7α-, 6β-, 16α- and 2α-hydroxytestosterone were 86, 97, 142, 240 and 185% respectively of the corresponding rates in fresh slices (table 2). The formation of androstenedione was 92% of the corresponding value in fresh slices (table 2). There were, however, no statistically significant differences between the rates of formation of testosterone metabolites by fresh rat liver slices and rat liver slices cryopreserved in 12% DMSO, nor between the rates of metabolite formation by slices cryopreserved in 12 and 18% DMSO.

Table 3. Metabolism of ropivacaine by cryopreserved rat liver slices. Fresh and cryopreserved slices were incubated individually with 1 mM ropivacaine. The samples were subsequently analysed by reverse-phase HPLC and metabolites were detected on the basis of their UV absorbance. For further details, see the Materials and methods. The levels of metabolites were calculated on the basis of the areas under the absorption peaks in the HPLC chromatogram and are expressed as percentages of the corresponding values for fresh slices.

	Ropivacaine metabolism by rat liver slices (% of formation by fresh slices)	
Metabolite	Cryopreserved in 12% DMSO	Cryopreserved in 18% DMSO
3-OH-Ropivacaine	104±23.1	94.0±11.1
4-OH-Ropivacaine	93.5±14.5	79.4±6.50
PPX	105±27.0	82.4±8.7

Data are means±SD of three independent experiments.

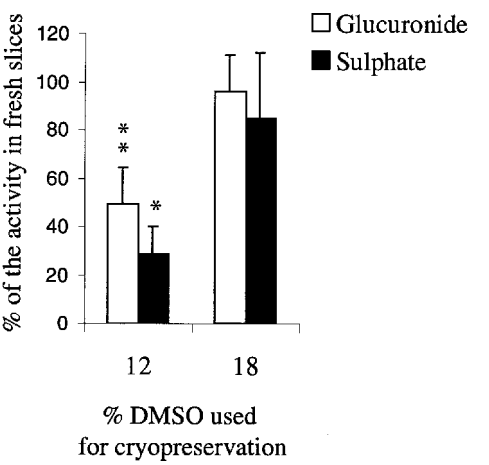


Figure 2. Glucuronidation and sulphation of 7-hydroxycoumarin by rat liver slices cryopreserved in 12 and 18% DMSO. Fresh and cryopreserved rat liver slices were incubated individually with 25 μM 7-hydroxycoumarin. The conjugates formed were subsequently analysed by reverse-phase HPLC and were detected on the basis of their UV absorbance. For further details, see the Materials and methods. The rates of glucuronidation and sulphation (estimated from the ratio between the area under the absorption peak for each conjugate and the sum of the areas of all absorption peaks) in fresh slices (i.e. 100%) were 79±17 and 52±13 pmol.min^{-1} and mg.protein^{-1} respectively. These data are means±SD of three-to-four independent experiments. *$p < 0.05$, **$p < 0.01$ compared with slices cryopreserved in 18% DMSO.

Ropivacaine metabolism by rat liver slices

Incubation of rat liver slices with ropivacaine resulted in the formation of 3-hydroxyropivacaine, 4-hydroxyropivacaine and PPX (the *N*-depropylated product of ropivacaine). The formation of ropivacaine metabolites was linear with time for at least 90 min under the present incubation conditions (data not shown).

Figure 1 depicts two representative HPLC chromatograms obtained after incubation with fresh rat liver slices (A) and rat liver slices cryopreserved in 18% DMSO (B) with 1 mM ropivacaine for 60 min. The absolute rate of formation of ropivacaine metabolites varied somewhat between different rat livers. However, when the rate of metabolite formation in cryopreserved slices was expressed as the percentage of formation by fresh slices from the same liver, the result between the

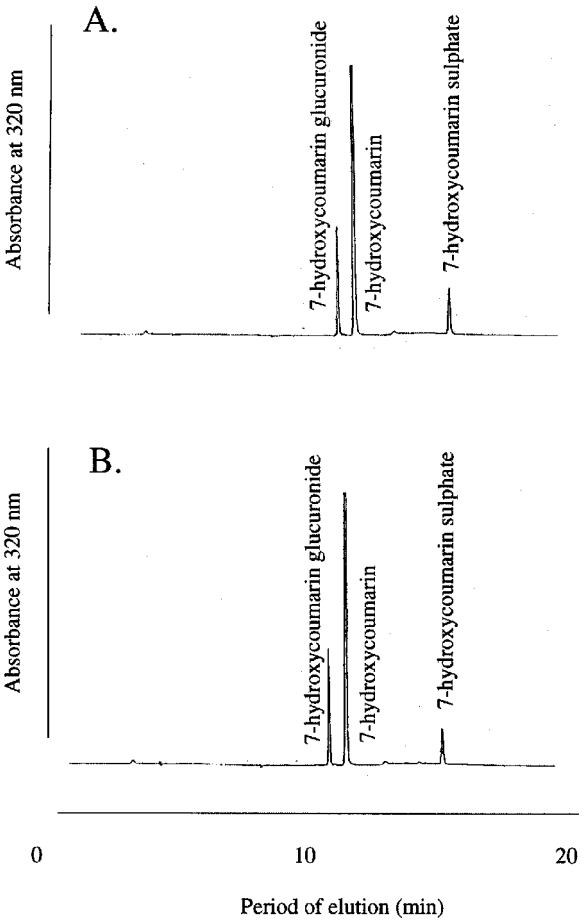


Figure 3. Reverse-phase HPLC analysis of conjugates of 7-hydroxycoumarin produced by (A) fresh liver slices and (B) liver slices cryopreserved in 18% DMSO. Fresh and cryopreserved rat liver slices were incubated individually with 25 μM 7-hydroxycoumarin for 60 min. The conjugates formed were subsequently analysed by reverse-phase HPLC and detected on the basis of their UV absorbance. For further details, see the Materials and methods. The chromatograms are representative of three independent experiments.

different rat livers was more constant (table 3). In rat liver slices cryopreserved in 18% DMSO, the rates of formation of 3-hydroxyropivacaine, 4-hydroxyropivacaine and PPX were 94, 79 and 82% respectively of the corresponding values for fresh slices (table 3). There were no statistically significant differences between the rates of formation of ropivacaine metabolites by slices cryopreserved in 12 and 18% DMSO.

With fresh slices from three independent experiments, the estimated mean specific rates of formation (based on the ratio between the area under the absorption peak for each metabolite and the sum of the areas for all peaks, including remaining substrate) were 41 ± 23, 24 ± 16 and 72 ± 42 pmol.min^{-1} and mg.protein^{-1} for 3-hydroxyropivacaine, 4-hydroxyropivacaine and PPX respectively.

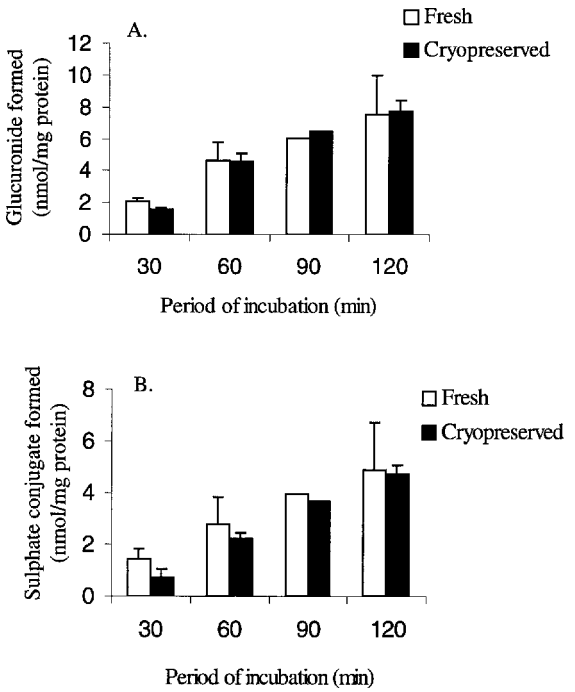


Figure 4. Time-course for the glucuronidation (A) and sulphation (B) of 7-hydroxycoumarin by fresh rat liver slices and rat liver slices cryopreserved in 18% DMSO. Fresh and cryopreserved rat liver slices were incubated individually with 25 μM 7-hydroxycoumarin for 30–120 min. The conjugates formed were subsequently analysed by reverse-phase HPLC and detected on the basis of their UV absorbance. For further details, see the Material and methods. These data are means ± SD of three independent experiments, except in the case of incubation for 90 min, where the average of two independent experiments is given. The specific rates of formation of 7-hydroxycoumarin sulphate and 7-hydroxycoumarin glucuronide were estimated from the ratio between the area under the absorption peak for each conjugate and the sum of the areas under all absorption peaks.

Conjugation of 7-hydroxycoumarin by rat liver slices

Incubation of rat liver slices with 25 μM 7-hydroxycoumarin gave rise to both sulphate and glucuronic acid conjugates. The formation of conjugates was linear with time for at least 120 min under the incubation conditions.

Figure 2 illustrates that the rates of 7-hydroxycoumarin glucuronidation and sulphation by rat liver slices cryopreserved in 12% DMSO were 49±15% and 28±11% respectively of the corresponding rates with fresh slices.

Figure 3 depicts two representative HPLC chromatograms obtained after incubation of fresh rat liver slices (A) or rat liver slices cryopreserved in 18% DMSO (B) with 25 μM 7-hydroxycoumarin for 60 min. The time-course for the glucuronidation and sulphation of 7-hydroxycoumarin by rat liver slices cryopreserved in 18% DMSO is shown in figure 4. There were no significant differences in the rates of formation of 7-hydroxycoumarin conjugates by fresh slices and slices cryopreserved in 18% DMSO.

1-Naphthol conjugation by rat liver slices

Incubation of rat liver slices with 100 μM 1-naphthol resulted in the formation of both sulphate and glucuronic acid conjugates. However, the level of sulphate conjugates was very low (< 5% of the total conjugate formation) in both fresh and

Table 4. Rate of conjugation of 1-naphthol by fresh and cryopreserved rat liver slices. Slices were incubated individually with 100 μ_M 1-[^{14}C]-naphthol. Conjugates were subsequently extracted and the overall rate of formation calculated on the basis of their radioactivity. For further details, see the Materials and methods.

Rate of formation by liver slices (pmol.min^{-1}.mg protein^{-1})		
Fresh	Cryopreserved in 12% DMSO (% of fresh)	Cryopreserved in 18% DMSO (% of fresh)
721±136	371±113 (51%)**	532±193 (74%)

**$p < 0.01$ compared with fresh slices.
Data are mean±SD of three-to-six independent experiments.

cryopreserved rat liver slices. The formation of conjugates of naphthol by rat liver slices was linear with time for at least 90 min under our incubation conditions (data not shown).

The total formation of conjugates by rat liver slices cryopreserved in 12% DMSO was significantly decreased to 51% of the corresponding value for fresh slices (table 4). In contrast, there was no statistically significant difference between 1-naphthol conjugation by fresh slices and by slices cryopreserved with 18% DMSO, although there was a trend slightly to decreased conjugation activity (74% of the corresponding value for fresh slices).

Discussion

In the present study, the usefulness of cryopreserved rat liver slices was examined as an *in vitro* system for characterizing drug metabolism. Various enzyme activities, including both cytochrome P450 and phase II-conjugating systems, in these slices were compared with the corresponding activities in fresh rat liver slices.

The liver slices were incubated with the cryoprotectant (i.e. DMSO) at low temperature and thereafter quickly transferred to freeze vials containing the cryopreservation medium, after which these vials were immersed in liquid nitrogen. It is important that the slices are shaken gently (54 times.min^{-1}) during incubation with DMSO. When 110 shakes.min^{-1} is employed, the rat liver slices loose much of their capacity to metabolize testosterone. However, this higher speed was reported by de Kanter *et al*. (1998) as providing good results with human liver slices. Since human liver is denser than rat liver, human liver slices may require a more vigorous shaking to obtain efficient distribution of DMSO within the slices.

Incubation of rat liver slices with testosterone resulted in the formation of a variety of hydroxylated products. Formation of these same hydroxylated products was efficiently maintained after cryopreservation of the slices in both 12 and 18% DMSO (table 2). Some values for testosterone metabolism by rat liver slices cryopreserved in 12% DMSO were apparently high (185 and 240% of the corresponding values with fresh slices). It is however difficult to draw any conclusions concerning these discrepancies, since the differences were not statistically significant.

The metabolism of testosterone has been well characterized in rat liver (Arlotto *et al*. 1991). Conversion of testosterone to 6α-hydroxytestosterone and 2α-hydroxytestosterone is catalysed by rat liver CYP2A1 and CYP2C11 respectively.

Both CYP2B1 and CYP2C11 are involved in the formation of 16α-hydroxytestosterone. The 7α-hydroxytestosterone metabolite is formed by CYP2A isoforms, while CYP2C11 and CYP2B1/2B2 form androstenedione. Several rat liver cytochrome P450 isoforms are involved in the conversion of testosterone to 6β-hydroxytestestosterone.

It has been reported that human CYP3A catalyses the metabolism of ropivacaine to 4-hydroxyropivacaine and PPX (the *N*-depropylated product of ropivacaine), whereas the formation of 3-hydroxyropivacaine is catalysed by human CYP1A (Ekstrom and Gunnarsson 1996). After cryopreservation of rat liver slices in 12 or 18% DMSO, the rate of metabolism of ropivacaine to 3-hydroxyropivacaine, 4-hydroxyropivacaine and PPX (also presumably catalysed by CYP1A and CYP3A) was efficiently maintained (table 3).

After cryopreservation of rat liver slices in 12% DMSO, the rates of conjugation of 7-hydroxycoumarin and 1-naphthol were significantly lowered. On the other hand, the use of 18% DMSO for cryopreservation efficiently preserved the rates of 7-hydroxycoumarin glucuronidation and sulphation (figure 2). Moreover, there were no significant differences in 1-naphthol conjugation by fresh slices and slices cryopreserved with 18% DMSO (table 4).

The decreased conjugating capacity of rat liver slices cryopreserved in 12% DMSO may reflect impaired synthesis of the cofactors UDP-glucuronic acid and PAPS. Earlier studies have indeed shown that a decrease in the cellular level of ATP results in decreased production of these cofactors, and, consequently, in decreased UDP-glucuronosyltransferase and sulphotransferase activities (Reinke *et al*. 1994, Klaassen and Boles 1997). The present authors observed a decrease in the capacity of mitochondrial reduction of MTT in slices cryopreserved in 12% DMSO compared with fresh slices (table 1). In addition, a histomorphology study showed that liver slices cryopreserved in 12% DMSO have a higher degree of cell integrity damage than do slices cryopreserved in 18% DMSO (de Graaf *et al*. 1999). Thus, it appears likely that our slices cryopreserved in 12% DMSO have a defective respiratory chain and reduced production of ATP, which may explain the observed decreases in UDP-glucuronosyltransferase and sulphotransferase activities.

In the present experiments, rat liver slices were stored in liquid nitrogen for as long as 3 days before thawing and use. De Kanter *et al*. (1998) demonstrated that cytochrome P450-dependent activities are maintained in human liver slices stored in this manner for 3–129 days. Thus, a successful outcome would appear to be more dependent on the conditions employed during cryopreservation and thawing of the liver slices, than on the period of storage in liquid nitrogen. To establish definitely whether the length of storage of rat liver slices cryopreserved in 18% DMSO affects the hepatocytes, characterization should be performed after various periods of storage.

The results here confirm previous findings that cytochrome P450-catalysed activities in liver slices are unaffected by cryopreservation (de Kanter *et al*. 1998, Glockner *et al*. 1998). The present authors also demonstrate that phase II enzyme activities were more susceptible to cryopreservation than were cytochrome P450-dependent activities. However, using a higher concentration of DMSO during cryopreservation can circumvent this problem.

Thus, cryopreserved rat liver slices may be a useful *in vitro* system for characterizing both phase I and II drug metabolism. Cryopreservation of tissue slices allows more efficient use of biological material of limited availability, including

human liver. Consequently, a more thorough characterization of various drug-metabolizing systems in cryopreserved liver slices from different species, including man, is highly desirable. In connection with such studies, the metabolism of a variety of phase I and II diagnostic substrates should be examined.

Acknowledgements

The authors thank Professor Joseph W. DePierre at the Unit for Biochemical Toxicology, Stockholm University for correcting the text. They are also grateful to Annica Rask and Lotta Halvarsson at AstraZeneca R&D Södertälje for excellent help with the animals.

References

Arlotto, M. P., Trant, J. M. and Estabrook, R. W., 1991, Measurement of steroid hydroxylation reactions by high-performance liquid chromatography as indicator of P450 identity and function. *Methods in Enzymology*, **206**, 454–462.

Boström, M., Becedas, L. and DePierre, J. W., 2000, Conjugation of 1-naphthol in primary cell cultures of rat ovarian cells. *Chemico-Biological Interactions*, **124**, 103–118.

Bradford, M. M., 1976, A rapid and sensitive method for the quantitation of microgram quantities of protein utilizing the principle of protein–dye binding. *Analytical Biochemistry*, **72**, 248–254.

De Graaf, I. A. M., van der Voort, D., Brits, J. H. F. G. and Koster, H. J., 1999, Critical factors in cryopreservation of precision-cut liver slices. Poster presented at the 7th European ISSX Meeting, 22–26 August, Budapest.

De Kanter, R., Olinga, P., Hof, I., de Jager, M., Verwillegen, W. A., Slooff, M. J., Koster, H. J., Meijer, D. K. and Groothuis, G. M., 1998, A rapid and simple method for cryopreservation of human liver slices. *Xenobiotica*, **28**, 225–234.

De Kanter, R., Olinga, P., Koster, H. J., de Jager, M., Slooff, M. J. H., Meijer, D. K. F. and Groothuis, G. M. M., 1997, A simple method for the cryopreservation of liver slices from man and other species. In L. F. M. van Zutphen and M. Balls (eds), *Animal Alternatives, Welfare and Ethics* (Elsevier: Amsterdam), pp. 851–856.

Ekins, S., 1996, Past, present, and future applications of precision-cut liver slices for *in vitro* xenobiotic metabolism. *Drug Metabolism Reviews*, **28**, 591–623.

Ekins, S., Williams, J. A., Murray, G. I., Burke, M. D., Marchant, N. C., Engeset, J. and Hawksworth, G. M., 1996, Xenobiotic metabolism in rat, dog, and human precision-cut liver slices, freshly isolated hepatocytes, and vitrified precision-cut liver slices. *Drug Metabolism and Disposition*, **24**, 990–995.

Ekstrom, G. and Gunnarsson, U. B., 1996, Ropivacaine, a new amide-type local anesthetic agent, is metabolized by cytochromes P450 1A and 3A in human liver microsomes. *Drug Metabolism and Disposition*, **24**, 955–961.

Fisher, R. L., Hasal, S. J., Sanuik, J. T., Hasal, K. S., Gandolfi, A. J. and Brendel, K., 1996, Cold- and cryopreservation of dog liver and kidney slices. *Cryobiology*, **33**, 163–171.

Glockner, R., Steinmetzer, P., Drobner, C. and Muller, D., 1998, Application of cryopreserved precision-cut liver slices in pharmacotoxicology - principles, literature data and own investigations with special reference to CYP1A1-mRNA induction. *Experimental and Toxicologic Pathology*, **50**, 440–449.

Gokhale, M. S., Bunton, T. E., Zurlo, J. and Yager, J. D., 1997, Cytochrome P450 isoenzyme activities in cultured rat and mouse liver slices. *Xenobiotica*, **27**, 341–355.

Klaassen, C. D. and Boles, J. W., 1997, Sulfation and sulfotransferases 5: the importance of 3′-phosphoadenosine 5′-phosphosulfate (PAPS) in the regulation of sulfation. *FASEB Journal*, **11**, 404–418.

Krumdieck, C. L., dos Santos, J. E. and Ho, K. J., 1980, A new instrument for the rapid preparation of tissue slices. *Analytical Biochemistry*, **104**, 118–123.

Lake, B. G., Charzat, C., Tredger, J. M., Renwick, A. B., Beamand, J. A. and Price, R. J., 1996, Induction of cytochrome P450 isoenzymes in cultured precision-cut rat and human liver slices. *Xenobiotica*, **26**, 297–306.

Mosmann, T., 1983, Rapid colorimetric assay for cellular growth and survival: application to proliferation and cytotoxicity assays. *Journal of Immunological Methods*, **65**, 55–63.

Obatomi, D. K., Brant, S., Anthonypillai, V., Early, D. A. and Bach, P. H., 1998, Optimizing pre-incubation conditions for precision-cut rat kidney and liver tissue slices: effect of culture media and antioxidants. *Toxicology in Vitro*, **12**, 725–737.

Olinga, P., Meijer, D. K. F., Slooff, M. J. H. and Groothuis, G. M. M., 1997, Liver slices in *in vitro* pharmacotoxicology with special reference to the use of human liver tissue. *Toxicology in Vitro*, **12**, 77–100.

Reinke, L. A., Kauffman, F. C. and Thurman, R. G., 1994, Cofactor supply as a rate-limiting determinant of hepatic conjugation reactions. In F. C. Kauffman (ed.), *Conjugation–Deconjugation Reactions in Drug Metabolism and Toxicity* (*Handbook of Experimental Pharmacology*) (Berlin: Springer), pp. 219–244.

Schwenk, M., Linz, C. and Kobusch, A. B., 1991, Conjugation of 1-naphthol in the gastric mucosa of guinea pigs. *Biochemical Pharmacology*, **42**, 469–473.

Walsh, J. S., Patanella, J. E., Halm, K. A. and Facchine, K. L., 1995, An improved HPLC assay for the assessment of liver slice metabolic viability using 7-ethoxycoumarin. *Drug Metabolism and Disposition*, **23**, 869–874.

XENOBIOTICA, 2000, VOL. 30, NO. 9, 905–914

Identification of cytochrome P4503A as the major subfamily responsible for the metabolism of roquinimex in man

H. TUVESSON†‡*, L. C. WIENKERS§, P. O. GUNNARSSON†, J. SEIDEGÅRD‡ and R. PERSSON†

† Pharmacokinetics and Metabolism, Active Biotech Research AB, PO Box 724, Lund, Sweden
‡ Department of Cell and Molecular Biology, Lund University, Sölvegatan 21, SE-223 62 Lund, Sweden
§ Drug Metabolism Research, Pharmacia & Upjohn, Kalamazoo, MI, USA

Received 25 February 2000

1. Roquinimex, a novel immunomodulator, is metabolized in liver microsomes from mouse and rat via cytochrome P450s to four hydroxylated and two demethylated metabolites (R1–6). The study investigated which cytochrome P450 enzyme(s) is responsible for the metabolism of roquinimex in man.

2. Enzyme kinetic analysis demonstrated an apparent K_m = 1.28–7.00 mM and V_{max} = 50–159 pmol·mg^{-1} microsomal protein·min^{-1} for the primary metabolites in human liver microsomes. The sum of Cl_{int} for the primary pathways was 0.167 μl·mg^{-1} microsomal protein·min^{-1}.

3. A correlation between the formation rate of R1–6 and 6β-hydroxylation of testosterone was obtained within a panel of liver microsomes from 11 individuals (r^2 = 0.72–0.97). Furthermore, significant inhibition (> 90%) of roquinimex primary metabolism was demonstrated by ketoconazole and troleandomycin, specific inhibitors of CYP3A4 as well as with anti-CYP3A4 antibodies. Moreover, a similar metabolite pattern was produced from roquinimex by incubation with cDNA-expressed CYP3A4 as by human liver microsomes.

4. In conclusion, these data indicate a major role for CYP3A4 in the formation of roquinimex primary metabolites in human liver microsomes.

Introduction

Roquinimex (Linomide®, *N*-methyl-*N*-phenyl-1,2-dihydro-4-hydroxy-1-methyl-2-oxoquinoline-3-carboxamide) is a compound in a series of quinoline 3-carboxamide derivatives with immunomodulating capacity. The immunomodulating effects of roquinimex are incompletely defined. However, roquinimex manifests an inhibitory effect on disease progression in a variety of animal models of autoimmune diseases such as insulin-dependent diabetes mellitus in the non-obese diabetic (NOD) mouse and experimental autoimmune encephalomyelitis (EAE) (Tarkowski *et al*. 1986a, b, Karussis *et al*. 1993, Gross *et al*. 1994). The main effect of roquinimex in EAE, the animal model of human multiple sclerosis (MS), was suggested to be on antigen-presenting cells (Lehman *et al*. 1997). In two double-blind placebo-controlled phase II studies, Linomide was demonstrated to suppress the progression of MS as measured by magnetic resonance imaging (MRI) as well as with the expanded disability status scale (EDSS) (Karussis *et al*. 1995, Andersen *et al*. 1996).

The pharmacokinetics of roquinimex in human is characterized by complete

* Author for correspondence at Active Biotech Research; e-mail: helen.tuvesson@activebiotech.com

Xenobiotica ISSN 0049–8254 print/ISSN 1366–5928 online © 2000 Taylor & Francis Ltd
http://www.tandf.co.uk/journals

bioavailability, a small volume of distribution and a low plasma clearance, 5 $ml \cdot h^{-1} \cdot kg^{-1}$ (Nived *et al.* 1994, Strandgården *et al.* 2000). Furthermore, roquinimex is eliminated mainly via metabolism and < 2% of a dose given to patients was excreted unchanged in urine. Hydroxylated, demethylated, as well as conjugated metabolites have been identified in urine samples. Hydroxylation and demethylation are reactions known to be catalysed by the cytochrome P450 (CYP) enzyme system (Nelson *et al.* 1996), which suggests a role for these enzymes in the metabolism of roquinimex. Previous experiments with liver microsomes from mouse and rat demonstrated that roquinimex was metabolized by microsomes from both species and four hydroxylated and two demethylated primary metabolites were formed (the same as those identified *in vivo* in urine from various species) (Tuvesson *et al.* 2000). Furthermore, the formation of these metabolites was potently induced in liver microsomes from mouse and rat pretreated with pregnenolone 16α-carbonitrile, a typical inducer of CYP enzymes of subfamily 3A in both mouse and rat (Simmons *et al.* 1985, Gonzalez *et al.* 1986).

In the present study, the phase I metabolism of roquinimex in man was investigated using human liver microsomes, with and without specific chemical or immunological inhibitors, as well as using microsomes from recombinant CYP enzymes expressed in insect cells.

Materials and methods

Chemicals

^{3}H-PNU-212616 (roquinimex), with the specific activity of 10.4 $Ci \cdot mmol^{-1}$ and with a radiochemical purity > 95% was synthesized at Amersham International plc (Amersham, UK) and ^{14}C-PNU-212616 with the specific activity of 12.2 $mCi \cdot mmol^{-1}$ was synthesized at Pharmacia & Upjohn AB (Helsingborg, Sweden) with a radiochemical purity > 95%. The non-radioactive reference substances, PNU-212616, PNU-212684 (R1), PNU-213708(R2), PNU-214608 (R3), PNU-213831 (R4), PNU-212679 (R5) and PNU-211944 (R6) were also synthesized at Pharmacia & Upjohn with a chemical purity > 95%. NADPH, troleandomycin (TAO), sulphaphenazole and coumarin were from Sigma Chemical Co. (St Louis, MO, USA). Furafylline and ketoconazole were from Research Biochemicals International (Natick, MA, USA). All other chemicals were of analytical grade and commercially available.

Human liver microsomes

Pooled human liver microsomes (from both sexes) were from Human Biologics, Inc. (Phoenix, AZ, USA), Xenotech (Cambridge, KS, USA) and Pharmacia & Upjohn (Kalamazoo, MI, USA). Human liver microsomes from individual subjects were from Pharmacia & Upjohn (Kalamazoo). Specific activities of individual cytochrome CYP enzymes were determined from their catalytic activity for the biotransformation of the following substrates: CYP1A2 (7-ethoxyresorufin *O*-dealkylation), CYP2A6 (coumarin 7-hydroxylation), CYP2C9 (tolbutamide hydroxylation), CYP2C19 (*S*-mephenytoin 4-hydroxylation), CYP2E1 (*p*-nitrophenol hydroxylation), CYP2D6 (dextromethorphan *O*-demethylation) CYP3A4 (testosterone 6β-hydroxylation). Microsomes containing human-expressed CYP enzymes (1A2, 2C9, 2C19, 2D6, 3A4) from insect cells and non-transfected as well as anti-CYP1A2 (polyclonal antibody, rabbit anti-human CYP1A2), CYP2C9 (polyclonal antibody, goat anti-human CYP2C13) and 3A4 (polyclonal antibody, rabbit anti-human CYP3A4) antibodies were from Gentest (Woburn, MA, USA).

Assay conditions

Incubations were performed with roquinimex (5–3010 μ_M), 4 $mg \cdot ml^{-1}$ microsomal protein (pooled microsomes) in 50 mM sodium phosphate buffer, pH 7.4, at 37 °C for 60 min. Preliminary experiments established conditions for reasonable substrate consumption, and time- and protein-linearity of all metabolite formation. The incubation mixture was pre-incubated for 5 min before addition of NADPH (10 mM, final concentration). The reaction was terminated by addition of an equal volume of ice-cold acetone and centrifuged at 10000*g* for 10 min. The supernatant was transferred to autosample vials and analysed by HPLC.

In the correlation studies, the metabolism of roquinimex was determined across a panel of 11 different

human liver microsomal preparations, which had been characterized for specific CYP substrate activities. To give an appropriate evaluation of the metabolism for this correlation study, 500 μM roquinimex was incubated with 4 mg·ml^{-1} microsomal protein.

In the inhibition studies, incubations were performed with human liver microsomes and specific inhibitors of CYP enzymes. Roquinimex (1000 μM) was incubated in 4 mg·ml^{-1} microsomal protein and one of the following enzyme inhibitors: furafylline (5, 10, 20 μM), sulphaphenazole (50 μM), ketoconazole (25 μM), troleandomycin (1 mM), or serum anti-CYP1A1, 2C9 or 3A4 antibodies at pH 7.4 for 60 min at 37 °C. Each inhibitor was added in ethanol to a final concentration of 2% ethanol. A pre-incubation equilibrium and inactivation period was performed, in the case of the mechanism-based inhibitors troleandomycin and furafylline for 10 min at 37 °C and in the case of serum anti-CYP antibodies, for 30 min at room temperature. The metabolic reactions were initiated by the addition of NADPH (10 mM, final concentration). Incubation reactions were terminated by addition of an equal volume of ice-cold acetone and centrifuged at 10000*g* for 10 min. The obtained supernatants were transferred to autosample vials and analysed by HPLC.

The metabolism of roquinimex by cDNA-expressed CYP enzymes was performed by incubating roquinimex (500 μM) with microsomes containing one of the following expressed CYP isoforms from insect cells: CYP1A2, 2C9, 2C19, 2D6 or 3A4 (2 mg microsomal protein·ml^{-1}). Microsomes from non-transfected cells were used as controls.

HPLC analyses

Quantification of roquinimex and metabolites was obtained with an HPLC system. The samples were injected (10–100 μl) into the chromatographic system and separated on a radial packed Nova-Pak C18 column, 4 μm (3.9 × 150 mm) with Nova-Pak C18 guard column (Waters Associates, Milford, MA, USA) and with a linear gradient system from 15:65:20 to 80:0:20 (methanol with 20% tetrahydrofuran:deionized water:25% formic acid). Analyses were performed at room temperature at 1.0 ml.min^{-1}. Radioactivity was detected by a flow detector (Flo-One β, Radiomatic Instruments, Meriden CT, USA), with a 0.5 ml flow cell. The mobile phase was mixed post-column with Ultima Flo AP (Packard Instrument Co., Meriden CT, USA) at 3 ml·min^{-1}. The retention times of formed metabolites were compared with the retention times of synthesized reference standards and their identity was further confirmed by electrospray ionization mass spectrometry.

Calculations and kinetic analysis

The metabolite peak areas from the HPLC analysis were converted into pmol and expressed as in relation to mg protein·min^{-1}.

The nature of roquinimex microsomal metabolism was characterized graphically by Eadie–Hofstee plots for the different metabolites and the kinetic parameters K_m, V_{max} and microsomal clearance (Cl_{int}) were estimated by the non-linear procedure PROC NLIN in the SAS statistical software (*SAS/STAT User's Guide*). The model

$$\log(V) = \log[V_{max}{*}S^n/(K_m{}^n + S^n)] = \log[K_m{*}Cl_{int}{*}S^n/(K_m{}^n + S^n)],$$

where n was derived from the Hill equation, were fitted to data. The weight after log-transformation was 1, which corresponds to a multiplicative error on untransformed data. Intrinsic clearance (Cl_{int}) was estimated as V_{max}/K_m. The parameters were estimated in two steps, where the parameter n was fixed as 1 in the main analysis and was estimated in a second step. The initial K_m, V_{max} and Cl_{int} were varied until both functions gave the same results.

The correlation coefficients (r^2) were calculated using linear regression analysis.

Results

Kinetics of roquinimex metabolism

Roquinimex was metabolized by human liver microsomes and six primary metabolites, R1–6, were detected (figure 1). Identification of R1–6 by mass spectrometry (data not shown) demonstrated hydroxylation of roquinimex in the phenyl ring (R1, *p*-OH) and at different sites in the quinoline moiety (R2, 6-OH, R3, 7-OH and R4, 8-OH). Furthermore, roquinimex was *N*-demethylated in the quinoline part of the molecule (R5) and at the aniline nitrogen (R6). The formation of metabolites was NADPH-dependent, linear with time and protein concentration (data not shown). To determine the Michaelis–Menten parameters for the formation of the primary metabolites, roquinimex at concentrations 5–3010 μM was incubated for 60 min with a microsomal protein concentration of 4 mg·ml^{-1}.

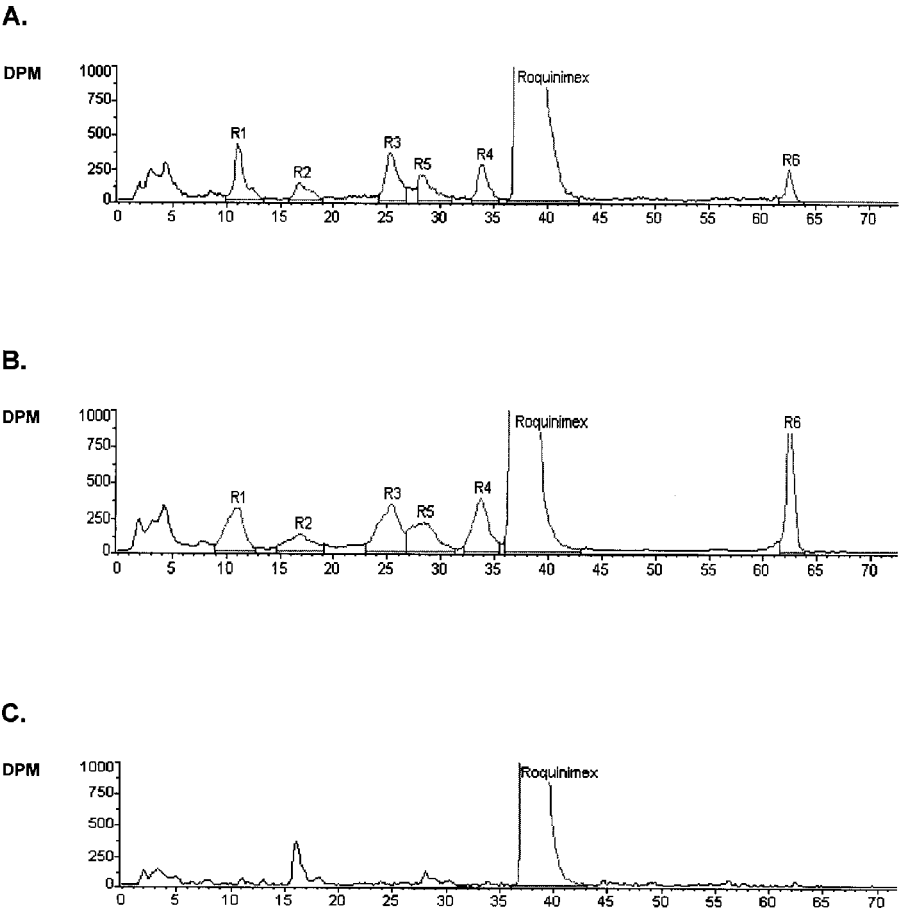


Figure 1. HPLC-radiochromatograms of metabolites formed in incubations of roquinimex with pooled human liver microsomes (A), cDNA expressed CYP3A4 (B) and control microsomes (insect control).

Table 1. Kinetic parameters for the formation of roquinimex metabolites in human liver microsomes.

	R1	R2	R3	R4	R5	R6
V_{max} (pmol·mg^{-1} protein·min^{-1})	50 (6)	104 (53)	59 (6)	63 (8)	159 (81)	71 (28)
K_m(mM)	1.86 (0.26)	7.00 (3.81)	1.28 (0.16)	1.70 (0.24)	6.67 (3.60)	3.93 (1.70)
Cl_{int} (nl·mg^{-1} protein·min^{-1})	27 (1)	15 (1)	46 (2)	37[a] (1)	24[b] (1)	18[c] (1)

Incubation of ^{3}H-roquinimex at eight different concentrations within the range 5–3010 μM was conducted for 60 min at 37 °C with human liver microsomes (4 mg protein·ml^{-1}). All experiments were performed in duplicate. Results are presented as obtained values (SE) from non-linear regression analysis.

[a] n from Hill equation = 1.04 and Cl_{int} 44 (4).
[b] n from Hill equation = 1.07 and Cl_{int} 32 (5).
[c] n from Hill equation = 1.09 and Cl_{int} 26 (4).

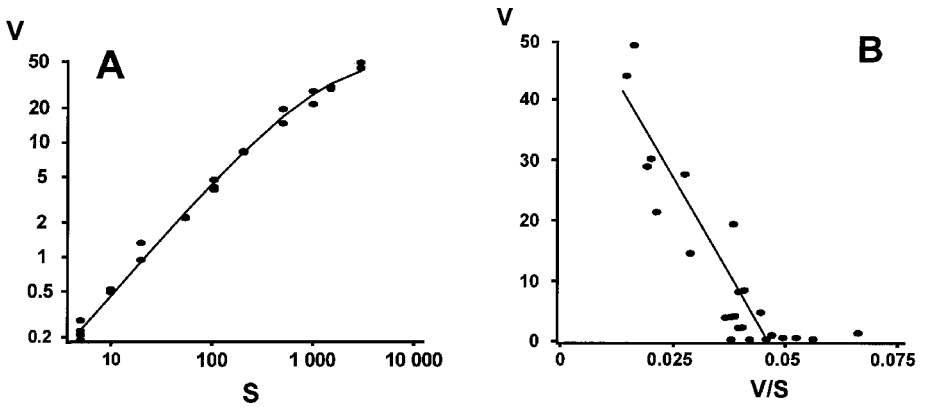


Figure 2. Saturation curve (A) and Eadie–Hofstee plot (B) for the formation of R3 in human liver microsomes.

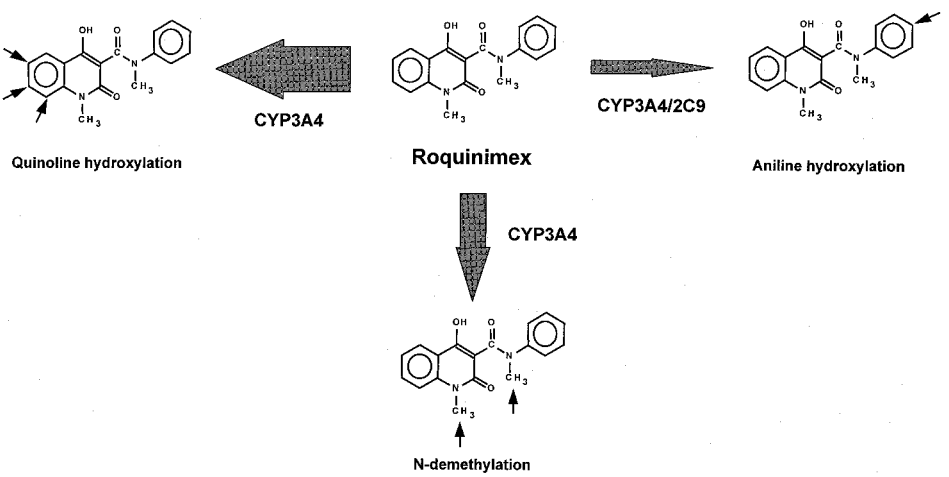


Figure 3. Metabolic pathways of roquinimex in human liver microsomes. →, Site of metabolism.

Apparent $K_{m,}$ V_{max}, and Cl_{int} are shown in table 1. The saturation curve and Eadie–Hofstee plot for the formation of R3 are shown in figure 2. For R4–6, a weak deviation from linearity was indicated ($n < 1.1$). Hydroxylation in the quinoline moiety was the major pathway, representing ~ 59% of total metabolism, whereas the *N*-demethylation and the hydroxylation in the phenyl ring constituted 25 and 16% each (figure 3).

Correlation of roquinimex metabolism and CYP marker activities across a panel of human livers

Roquinimex metabolism was determined in microsomal preparations from 11 human livers, which have been characterized for different CYP marker activities. The rate of metabolite formation varied ~ 35-fold among the samples (data not shown). Correlations between the rate of formation of R1–6 and different CYP marker activities are shown in table 2. For the formation of R3–6, the strongest

Table 2. Correlation of roquinimex metabolites R1–6 formation with total CYP content and with specific CYP activities across a panel of different human liver microsomes (n = 11).

		Correlation (r^2)					
Marker activity	CYP	R1	R2	R3	R4	R5	R6
Total CYP content		0.79[a]	0.24	0.84[a]	0.85[a]	0.74[a]	0.81[a]
7-Ethoxyresorufin *O*-dealkylation	1A2	0.28	–[b]	0.24	0.29	0.27	0.14
Coumarin 7-hydroxylation	2A6	0.42	–[b]	0.62[b]	0.57[a]	0.49	0.66[a]
Tolbutamide methyl-hydroxylation	2C9	0.93[a]	–[b]	0.38	0.44	0.39	0.35
S-mephenytoin 4-hydroxylation	2C19	0.01	–[b]	0.02	0.01	0.04	0.04
Dextromethorphan *O*-demethylation	2D6	0.36	–[b]	0.65[a]	0.65[a]	0.75[a]	0.62[a]
p-Nitrophenol hydroxylation	2E1	0.23[a]	–[b]	0.02	0.02	0.03	0.02
Testosterone 6β-hydroxylation	3A4	0.72[a]	–[b]	0.96[a]	0.97[a]	0.90[a]	0.93[a]

[a] $p < 0.0001$.
[b] Not detectable.

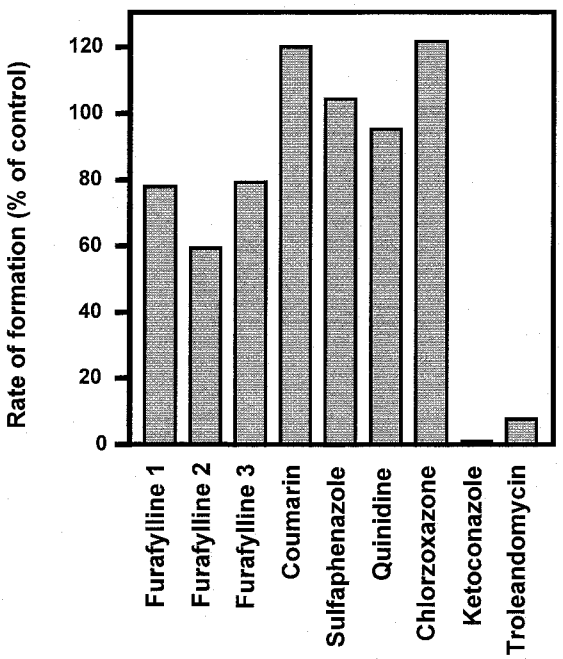


Figure 4. Effect of the CYP inhibitors furafylline 5 μM (1), 10 μM (2), 20 μM (3), coumarin 25 μM, sulphaphenazole 50 μM, quinidine 25 μM, chlorzoxazone 50 μM, ketoconazole 25 μM and troleandomycin 300 μM on the formation rate (% of control) of roquinimex metabolites R1–6, expressed as a sum, at 1 mM roquinimex in human liver microsomes. Data are the average of two determinations.

correlation was found towards testosterone 6β-hydroxylation (CYP3A4) (r^2 = 0.90–0.97). A relatively high correlation was also found for these metabolites and coumarin 7-hydroxylation (CYP2A6) and dextromethorphan *O*-demethylation (CYP2D6). However, both CYP2A6 and CYP2D6 activities correlated with CYP3A4 activity when the activities for the specific CYP enzymes were compared with each other (r^2 = 0.62 and 0.58 for CYP2A6 and CYP2D6 respectively). The formation of R1 was correlated to testosterone 6β-hydroxylation (r^2 = 0.72) but a stronger correlation was found for R1 and tolbutamide methyl hydroxylation

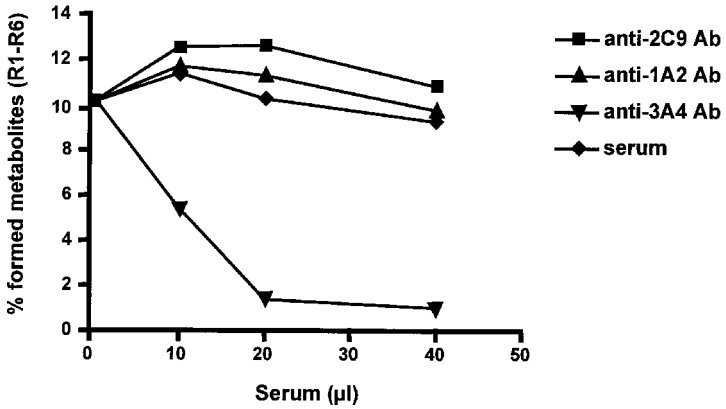


Figure 5. Effect of serum anti-CYP antibodies on the formation rate of roquinimex metabolites R1–6, expressed as sum, at 1 mM roquinimex in human liver microsomes. Data are the average of two determinations.

(CYP2C9, $r^2 = 0.93$). The formation rate of R2 was too low to detect a significant correlation towards any of the marker activities. However, the formation of R3 was only quantitatively detectable in six of the 11 liver samples, all of which had relatively high CYP3A4 activity. A good correlation was also obtained toward total CYP content and the formation of roquinimex metabolites ($r^2 = 0.74$–0.85).

Inhibition of roquinimex metabolism

Competitive substrates, irreversible inhibitors and serum anti-CYP1A2, 2C9 and 3A4 antibodies were used to evaluate the CYP enzymes involved in roquinimex metabolism. Incubations were performed with a concentration of 1 mM roquinimex and pooled human liver microsomes. Metabolite formation was quantified compared with control incubations (without inhibitor) performed in parallel.

Chemical inhibition

As shown in figure 4, furafylline, a mechanism-based inhibitor of CYP1A2 (Kunze and Trager 1993), demonstrated a weak inhibition ($< 30\%$) of roquinimex metabolism at concentrations used in this study. Sulphaphenazole, a competitive inhibitor of CYP2C9 (Relling *et al*. 1990), as well as quinidine, a specific inhibitor of CYP2D6 (Inaba *et al*. 1985), did not have any effect on the metabolism of roquinimex. An extensive inhibition ($> 90\%$) of roquinimex metabolism (including formation of R1–6) was observed with ketoconazole, a competitive inhibitor of CYP3A4 and troleandomycin a mechanism-based inhibitor of CYP3A enzymes (Guengerich 1990). Sulphaphenazole competitive inhibitor of CYP2C9, did not significantly affect the formation of R1.

Serum anti-CYP antibodies

Anti-CYP1A2 and anti-CYP2C9 antibodies did not affect the metabolism of roquinimex, whereas the formation of all metabolites (including R1–6) was significantly inhibited by co-incubation of anti-CYP3A4 antibodies (figure 5).

Roquinimex metabolism in cDNA-expressed CYP enzymes

Roquinimex metabolism carried out in the presence of different human cDNA-expressed cytochrome CYP enzymes revealed a similar metabolic pattern with expressed CYP3A4 as with human liver microsomes (figure 1). Neither of the other enzymes tested (CYP1A2, 2C9, 2C19, 2D6) displayed any catalytic activity towards roquinimex (data not shown).

Discussion

In the present study, liver microsomal preparations from humans were used to establish the enzymatic basis for the phase I metabolism of roquinimex in man. Roquinimex was metabolized to the primary hydroxylated metabolites, R1–4 and demethylated metabolites, R5–6. The metabolite formation exhibited single enzyme Michaelis–Menten kinetics with K_m in the range 1.28–7.0 mM for R1–6, and V_{max} from 50 to 159 pmol·mg^{-1} protein·min^{-1}. Examination of the Eadie–Hofstee plots indicated a minor deviation from linearity ($n \cong < 1.1$) for some of the metabolites, e.g. R4, R5 and R6, which could be indicative of positive cooperativity. The allosteric phenomenon has been described for CYP3A4 and compounds such as α-naphthoflavone have been shown to activate as well as to inhibit CYP3A4 reactions (Lasker *et al*. 1984, Baldwin *et al*. 1995, Lewis *et al*. 1998).

Hydroxylation at different sites in the quinoline moiety (R2–4) was the major pathway (59%) followed by *N*-demethylation (25%) and hydroxylation in the *para*-position of the phenyl ring (16%). It remains to be clarified if any of the roquinimex metabolites display pharmacologic or toxicologic activity.

The strong correlation observed between the formation rate of R1–6 and 6β-hydroxylation of testosterone (CYP3A4) in the panel of human liver microsomes, implies that both the hydroxylation and the demethylation of roquinimex at different sites are mediated mainly through enzymes of the CYP3A subfamily. The notable correlation also obtained toward total CYP content is in accordance with immunochemical studies indicating that ~30% of the total CYP content in the human liver is CYP 3A isoenzymes (Shimada *et al*. 1994). The 35-fold variability for the metabolism of roquinimex across the panel is also in good agreement with the large variability reported for CYP3A activity within the general population (Wilkinson 1996).

A strong correlation for R1 was also found towards tolbutamide methyl-hydroxylation (CYP2C9). However, the formation of R1 was not inhibited by sulphaphenazole, an inhibitor of CYP2C9 (Relling *et al*. 1990) at concentrations used in this investigation. On the other hand, the role of CYP3A4 was further supported by the significant inhibition exerted by the specific inhibitors of CYP3A4, troleandomycin, ketoconazole and anti-CYP3A4 antibodies on the formation of roquinimex primary metabolites (including R1). Moreover, a similar metabolite pattern was produced by incubation with cDNA-expressed CYP3A4 as by incubation with human liver microsomes, whereas no metabolism was detectable in incubations with the other cDNA-expressed enzymes. Taken together, the presented data strongly support the CYP3A subfamily as the major CYPs catalysing hydroxylation as well as demethylation of roquinimex in human liver microsomes. However, participation of other CYP enzymes in the metabolism of roquinimex can not be excluded, especially in patients expressing low amounts of CYP3A4.

The identification of CYP3A4 as a major enzyme in the oxidative metabolism of

a compound could be of clinical importance with regard to drug–drug interactions, since it has been estimated that > 50% of drugs used in humans are metabolized by this enzyme. This includes drugs such as calcium channel antagonists, immunosuppressant agents, cholesterol-lowering agents, non-sedating antihistamines, benzodiazepines and macrolide antibiotics (Shou *et al*. 1994). The low affinity (high K_m) between roquinimex and enzyme, demonstrated in the present study, might reduce the risk for competitive inhibition of the metabolism of other CYP3A4 substrates. On the other hand, a possible influence of other drugs on the metabolism of roquinimex in man, which might affect the clearance of the compound, cannot be excluded. Thus, the role of CYP3A4 as a major catalyst in the primary metabolism of roquinimex should be considered for drug–drug interactions.

It has been previously reported that roquinimex is metabolized by CYP enzymes in liver microsomes from mouse and rat (Tuvesson *et al*. 2000). Furthermore, these enzymes have been demonstrated to play a major role in determining the clearance of roquinimex *in vivo* in these species. The sum of the Cl_{int} for the primary metabolites provides a comparison with the clearance of roquinimex *in vivo* in man. Prediction of *in vivo* clearance, using a microsomal protein scaling factor of 35.4 $mg.g^{-1}$ liver, determined in our own laboratory, according to Carlile *et al*. (1997) resulted in a clearance of roquinimex of ~ 7 $ml \cdot h^{-1} \cdot kg^{-1}$, which is in good agreement with the reported clearance of the compound in man, namely 5 $ml \cdot h^{-1} \cdot kg^{-1}$ (Nived *et al*. 1994).

In conclusion, it has been demonstrated that roquinimex is metabolized through a low-affinity process primarily by CYP3A4 in man. Despite the low intrinsic clearance, the data obtained showed high predictability of the situation *in vivo*.

Acknowledgements

The authors thank Lillemor Halvarsson for excellent technical assistance and Örjan Nordle for statistical analysis of the enzyme kinetics.

References

Andersen, O., Lycke, J., Tollesson, P. O., Svenningsson, A., Runmarker, B., Linde, A. S., Åström, M., Gjörstrup, P. and Ekholm, S., 1996, Linomide reduces the rate of active lesions in relapsing-remitting multiple sclerosis. *Neurology*, **47**, 895–900.

Baldwin, S. J., Bloomer, J. C., Smith, G. J., Ayrton, A. D., Clarke, S. E. and Chenery, R. J., 1995, Ketoconazole and sulphaphenazole as the respective inhibitors of P4503A and 2C9. *Xenobiotica*, **25**, 261–270.

Carlile, D. J., Zomorodi, K. and Houston, B., 1997, Scaling factors to relate drug metabolic clearance in hepatic microsomes, isolated hepatocytes and the intact liver. *Drug Metabolism and Disposition*, **25**, 903–911.

Gonzalez, F. J., Song, B.-J. and Hardwick, J. P., 1986, Pregnenolone 16-α carbonitrile-inducible P450 gene family: gene conversion and differential regulation. *Molecular Cell Biology*, **6**, 2969–2976.

Gross, D. J., Sidi, H., Weiss, L., Kalland, T., Rosenmann, E. and Slavin, S., 1994, Prevention of diabetes mellitus in non-obese diabetic mice by Linomide, a novel immunomodulating drug. *Diabetologia*, **37**, 1195–1201.

Guengerich, F. P., 1990, Mechanism-based inactivation of human microsomal cytochrome P450 IIIA4 by gestodene. *Chemical Research in Toxicology*, **3**, 363–371.

Inaba, T., Jurima, M., Mahon, W. A. and Kalow, W., 1985, *In vitro* inhibition studies of two isozymes of human liver cytochrome p-450: mephenytoin *p*-hydroxylase and sparteine monooxygenase. *Drug Metabolism and Disposition*, **13**, 443–448.

Karussis, D. M., Lehmann, D., Slavin, S., Kalland, T., Vourka-Karussis, U., Mizrachi-Koll, R., Ovadia, H. and Abramsky, O., 1995, Immunomodulation of autoimmunity by Linomide. *Israel Journal of Medical Sciences*, **31**, 38–41.

Karussis, D. M., Lehmann, D., Slavin, S., Vourka-Karussis, U., Mizrachi-Koll, R., Ovadia H., Kalland, T. and Abramsky, O., 1993, Treatment of chronic-relapsing experimental autoimmune encephalomyelitis with the synthetic immunomodulator Linomide (quinoline-3-carboxamide). *Proceedings of the National Academy of Sciences, USA*, **90**, 6400–6404.

Kunze, K. L. and Trager, W. F., 1993, Isoform selective mechanism-based inhibition of human CYP1A2 by furafylline. *Chemical Research in Toxicology*, **6**, 649–656.

Lasker, J. M., Huang, M. T. and Conney, A., 1984, *In vitro* and *in vivo* activation of oxidative drug metabolism by flavonoids. *Journal of Pharmacology and Experimental Therapeutics*, **229**, 162–170.

Lehmann, D., Karussis, D. M., Fluresco, D., Mizrachi-Koll, R., Ovadia, H., Shezen, E., Kalland, T. and Abramsky, O., 1997, Immunomodulation of autoimmunity by linomide: inhibition of antigen presentation through down regulation of macrophage activity in the model of experimental autoimmune encephalomyelitis. *Journal of Neuroimmunology*, **74**, 102–110.

Lewis, D. F. V., Dickins, M., Weavers, R. J., Eddershaw, P. J., Goldfarb, P. S. and Tarbit, M. H., 1998, Molecular modelling of human CYP2C subfamily enzymes CYP2C9 and CYP2C19: rationalization of substrate specificity and site-directed mutagenesis experiments in the CYP2C subfamily. *Xenobiotica*, **28**, 235–268.

Nelson, D. R., Koymans, L., Kamataki, T., Stegeman, J. J., Feyereisen, R., Waxman, D. J., Waterman, M. R., Gotoh, O., Coon, M. J., Estabrook, R. W., Gunsalus, I. C. and Nebert, D. W., 1996, P450 superfamily: update on new sequences, gene mapping, accession numbers and nomenclature. *Pharmacogenetics*, **6**, 1–42.

Nived, O., Sturfelt, G., Nilsson, B., Termander, B., Gunnarsson, P. O., Strandgården, K. and Wollheim, F., 1994, Clinical pilot study of roquinimex (Linomide) in patients with autoimmune disease. *International Journal of Immunotherapy*, **10**, 49–59.

Relling, M. V., Aoyama, T., Gonzalez, F. J. and Meier, U. R., 1990, Tolbutamide and mephenytoin hydroxylation by cytochrome P450s in the 2C subfamily. *Journal of Pharmacology and Experimental Therapeutics*, **252**, 442–427.

SAS/STAT, 1989, *SAS/STAT User's Guide, Version* 6, 4th edn, vol. 1 (Cary: SAS Institute, Inc.).

Shimada, T., Yamazaki, H., Mimura, M., Inui, Y. and Guengerich, F. P., 1994, Interindividual variations in human liver cytochrome P-450 enzymes involved in the oxidation of drugs, carcinogenes and toxical chemicals: studies with liver microsomes of 30 Japanese and 30 Caucasians. *Journal of Pharmacology and Experimental Therapeutics*, **270**, 414–423.

Shou, M., Grogan, J., Mancewicz, J.-A., Krausz, K. W., Gonzalez, F. J., Gelboin, H. V. and Korzekwa, K. R., 1994, Activation of CYP3A4: evidence for simultaneous binding of two substrates in a cytochrome P450 active site. *Biochemistry*, **33**, 6450–6455.

Simmons, D. L., Lalley, P. A. and Kasper, C. B., 1985, Chromosomal assignment of genes coding for component of the mixed-function oxidase system in mouse *Journal of Biology and Chemistry*, **260**, 515–521.

Strandgården, K., Höglund, P., Grönquist, L., Svensson, L. and Gunnarsson, P. O., 2000, Absorption and disposition including circulation of ^{14}C-roquinimex after oral administration to healthy volunteers. *Biopharmaceutics and Drug Disposition* (submitted).

Tarkowski, A., Gunnarsson, K., Nilsson, L., Lindholm, L. and Stålhandske, T., 1986b, Successful treatment of autoimmunity in MRL/I mice with LS 2616, a new immunomodulator. *Arthritis and Rheumatics*, **29**, 1405–1409.

Tarkowski, A., Gunnarsson, K. and Stålhandske, T., 1986a, Effects of LS 2616 administration upon the autoimmune disease of (NZB NZW) F_1 hybrid mice. *Immunology*, **59**, 589–594.

Tuvesson, H., Strandgården, K., Nordle, Ö., Gunnarsson, P. O., Seidegård, J. and Persson, R., 1999, Microsomal metabolism of roquinimex in mouse and rat. *Xenobiotica* 2000, **30**, 371–380.

Wilkinson, G. R., 1996, Cytochrome P4503A (CYP3A) metabolism: prediction of *in vivo* activity in humans. *Journal of Pharmacokinetics and Biopharmaceutics*, **24**, 475–490.

XENOBIOTICA, 2000, VOL. 30, NO. 9, 915–932

Biotransformation of 1,8-cineole in the brushtail possum (*Trichosurus vulpecula*)

R. BOYLE†*, S. McLEAN† and N. W. DAVIES‡

† Tasmanian School of Pharmacy, University of Tasmania, GPO Box 252-26, Hobart 7001, Tasmania, Australia.
‡ Central Science Laboratory, University of Tasmania, GPO Box 252-74, Hobart 7001, Tasmania, Australia.

Received 14 March 2000

1. The metabolic fate of 1,8-cineole was investigated in the brushtail possum. Six possums were fed an artificial diet to which 0.5% 1,8-cineole (wet weight) was added for 2 days. Urine and faeces were collected after the second day. A sample of each was extracted into ethyl acetate and analysed for metabolites. Both free and total levels of metabolites were identified by GC-MS and LC-MS and quantified by GC-MS.

2. The pattern of metabolite excretion was very complex in the brushtail possum. Nineteen metabolites were found in total. Metabolites were categorized into four groups according to the oxidation they had undergone: hydroxycineoles ($n = 3$), cineolic acids ($n = 2$), dihydroxycineoles ($n = 3$) and hydroxycineolic acids ($n = 11$). No hydroxycineolic acid metabolites have been previously reported as metabolites of 1,8-cineole.

3. Fractional recovery of the ingested dose (2.4 ± 0.5 g; mean ± SD) was 0.44 ± 0.14 (mean ± SD) in 24 h. Sixty percent of excreted metabolites were hydroxycineolic acids, the most extensively oxidized metabolites. Conjugation with glucuronic acid was inversely related to metabolite polarity, being greatest for hydroxycineoles (41–82%) and minimal for hydroxycineolic acids.

4. Traces of most metabolites were also found in the faeces.

Introduction

Marsupial eucalypt folivores inevitably encounter monoterpenes such as 1,8-cineole (figure 1) in their diet and often consume many grams per day. These significant quantities would be toxic to many animal species, including humans (Jenner *et al*. 1964, Patel and Wiggins 1980, Webb and Pitt 1993, Barnes 1996). Therefore, marsupial eucalypt folivores, such as the brushtail possum (*Trichosurus vulpecula*), have developed the ability to detoxify and eliminate large quantities of such compounds. 1,8-Cineole is the most abundant terpene found in *Eucalyptus* spp. In many species, it is the dominant monoterpene, often accounting for $> 90\%$ of the terpene content (Guenther 1950, Boland and Brophy 1991, Li *et al*. 1994).

Metabolites of 1,8-cineole have been studied in various animals. Flynn and Southwell (1979) reported the first structural elucidations of 1,8-cineole metabolites in possums, including 9-hydroxy-1,8-cineole and 9-cineolic acid. Since then other new metabolites have been reported in the possum, namely 7-hydroxy-1,8-cineole and 7-cineolic acid (Bull *et al*. 1993), 2α,4-dihydroxy-1,8-cineole (Carman and Rayner 1994), 7,9-dihydroxy-1,8-cineole and 2α,7-dihydroxy-1,8-cineole (Carman and Garner 1996) and 2,9-dihydroxy-1,8-cineole and 2,10-dihydroxy-1,8-cineole

* Author for correspondence.

Xenobiotica ISSN 0049-8254 print/ISSN 1366-5928 online © 2000 Taylor & Francis Ltd
http://www.tandf.co.uk/journals

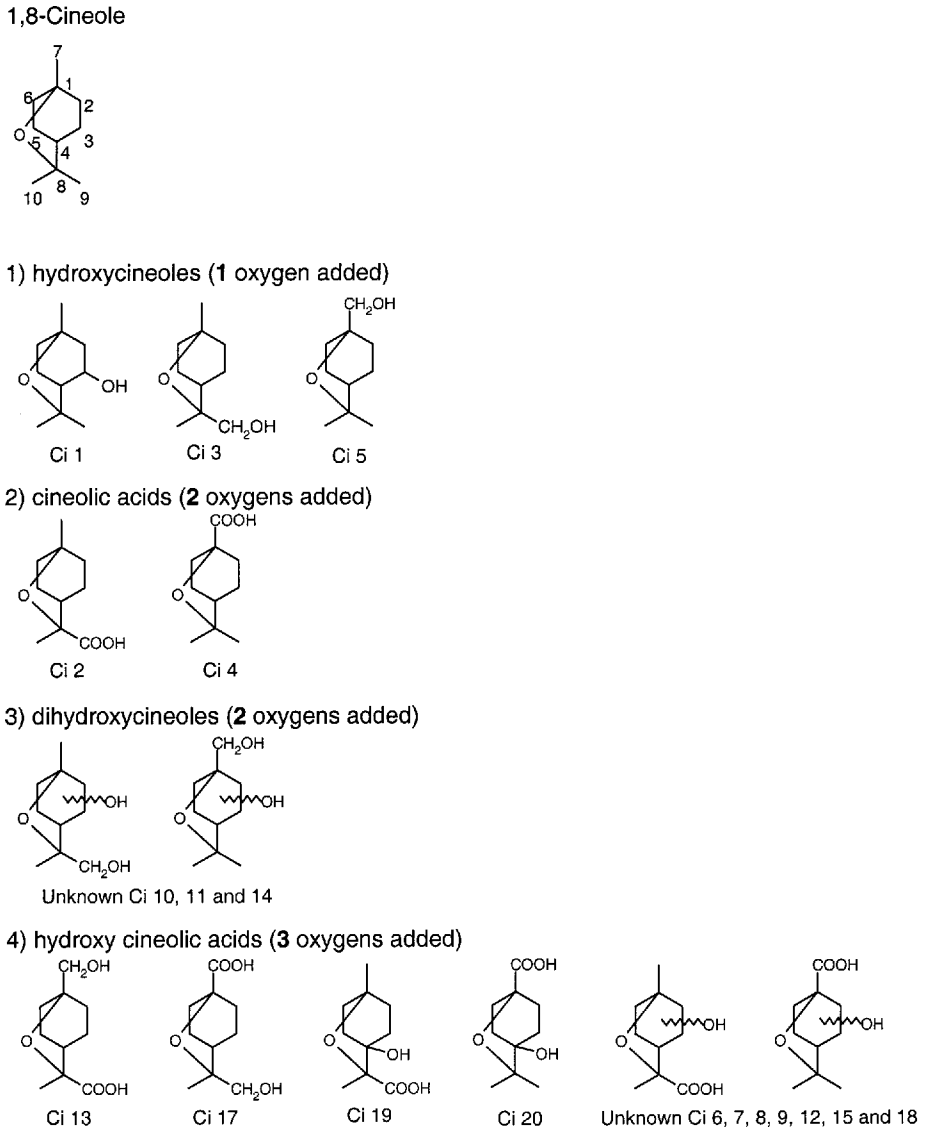


Figure 1. Chemical structure of 1,8-cineole and its metabolites. Metabolites are grouped according to the number of oxygen atoms acquired and type of oxidation. Metabolites are shown in their underivatized states. See table 1 for metabolite names where known.

(Carman *et al*. 1994). The fate of 1,8-cineole in insects and microbes has also been studied, resulting in the elucidation of other novel metabolites (MacRae *et al*. 1979, Carman *et al*. 1986, Liu and Rosazza 1990, Southwell *et al*. 1995).

As part of an investigation into the mechanisms that allow *Eucalyptus* leaf-eating marsupials to avoid terpene intoxication, the current study sought to characterize and quantitate the major urinary metabolites of 1,8-cineole in the brushtail possum. This is the first comprehensive study of the metabolism of 1,8-cineole in any mammalian species.

Methods and materials

Materials

All reagents used were obtained from commercial suppliers and were of analytical grade. 1,8-Cineole (purity 99%) was from Aldrich Chemical Co., Inc. (Castle Hill, Australia).

Animal experiments

Six brushtail possums (two females, four males) were trapped around the Hobart area. Possums were individually housed in covered, outdoor enclosures and were provided with a nest box and aerial branches. They were maintained on a diet of chopped apples, carrots, lettuce leaf and occasionally bread, dog biscuits and bananas for variety. They were weighed regularly and their weights remained constant (3.73 ± 0.82 kg, mean $\pm$ SD) throughout captivity.

Dosing and urine collection

During experiments, possums were transferred to stainless steel metabolism cages ($60 \times 60 \times 45$ cm), housed in a room controlled for temperature (20 °C) and light (12-h light/dark). Food and water were supplied *ad libitum* and the daily intake of each was measured (control samples for both food and water allowed adjustment of intake due to evaporative losses).

Possums were offered a basal diet (lucerne; ground to 1 mm mesh, carrot, apple, silver beet, brown sugar and water) for the duration of the feeding experiments. A food processor grated the apple, carrot and silver beet and then all ingredients were thoroughly mixed by hand. This diet was highly acceptable to the animals.

Possums spent 2 days (days 1 and 2) adjusting to the metabolism cages and were fed a 1,8-cineole free diet. On the third and fourth day 0.5% wet weight 1,8-cineole was mixed into the diet. The diet was divided into seven individual trays (six possums and one control) and weighed before being offered to the possums and again on removal the following day.

Urine was collected over ice and pH and volume were measured daily. Cage floors and collecting funnels were washed with distilled water, which was combined with the urine for analyses. A sample of each collection was stored at -18 °C for later analysis. Urine collected at the end of day 4 was analysed for 1,8-cineole metabolites.

Urinary analysis

Instruments. Gas chromatography-mass spectrometry (GC-MS) was used for identification and quantitation of 1,8-cineole metabolites in urine and faecal extracts. The GC-MS was carried out with a Hewlett-Packard (HP) 5890 gas chromatograph and HP 5970B mass-selective detector with HP 59970A Chemstation software (Hewlett-Packard Australia Ltd, Melbourne, Australia). The Chemstation software was modified to enable exporting of mass spectra to the NIST MS Search Program (NIST 1998). GC-MS chromatography was carried out on a 25 m HP-1 capillary column (0.32 mm i.d., coated with 0.52 μm cross-linked methyl silicone). GC-MS operating conditions were: split injector (1:10) at 250 °C, injection volume 2 μl, He carrier gas (12 psi), oven 50 °C for 1 min then 10 °C $\cdot$ min^{-1} to 290 °C and held for 2 min, detector 290 °C, solvent delay of 2 min for methylated only extracts and 6 min for methylated plus trimethylsilyl (TMS) derivatized extracts, electron multipler voltage +600 V relative to the Autotune value and the range m/z 40–600 was scanned on a 1-s cycle.

Chemical ionization (CI) GC-MS and high resolution MS analyses were carried out on a Hewlett-Packard model 5890 Series II GC directly coupled to a Kratos Concept ISQ high-resolution mass spectrometer. For chemical ionization, ammonia was the reagent gas, with an accelerating voltage of 5.3 kV, a scan rate of 0.9 s/scan, m/z range 100–550 and resolution of 1000 (3000 for accurate mass determinations). Perfluorokerosene (PFK) was used as an internal calibrant for accurate mass measurements.

Liquid chromatography-mass spectrometry (LC-MS) of possum urine confirmed molecular weights for each group of metabolites and their respective glucuronides. Mass spectrometry-mass spectrometry (MS-MS) of 1,8-cineole derived metabolites, obtained by automatic data-dependent selection and collisional activation of the most intense ion in the spectrum, provided further evidence for metabolite identification. The LC-MS used was a Waters Alliance 2690 HPLC coupled to a Finnigan LCQ using atmospheric pressure chemical ionization (APCI). Chromatography was carried out on a 3.9×150 mm Waters NovaPak C18 analytical column. The mobile phase was 10% methanol/90% water (with 2% acetic acid) and graded to methanol 100% at 40 min, with a flow-rate of 0.8 ml $\cdot$ min^{-1} and injection volume 15 μl. Urine samples were filtered (0.45 μm) after dilution (1:10) with distilled water. Positive-ion APCI was used to identify most 1,8-cineole metabolites in the brushtail possums.

Extraction, derivatization and analysis of urine samples. Urine samples were analysed for both free and total metabolites. Free metabolites were analysed by measuring 0.5 ml thawed urine and diluting with 0.5 ml distilled water. To each sample, internal standard was added (0.5 mg 2,5-dimethylbenzoic acid in

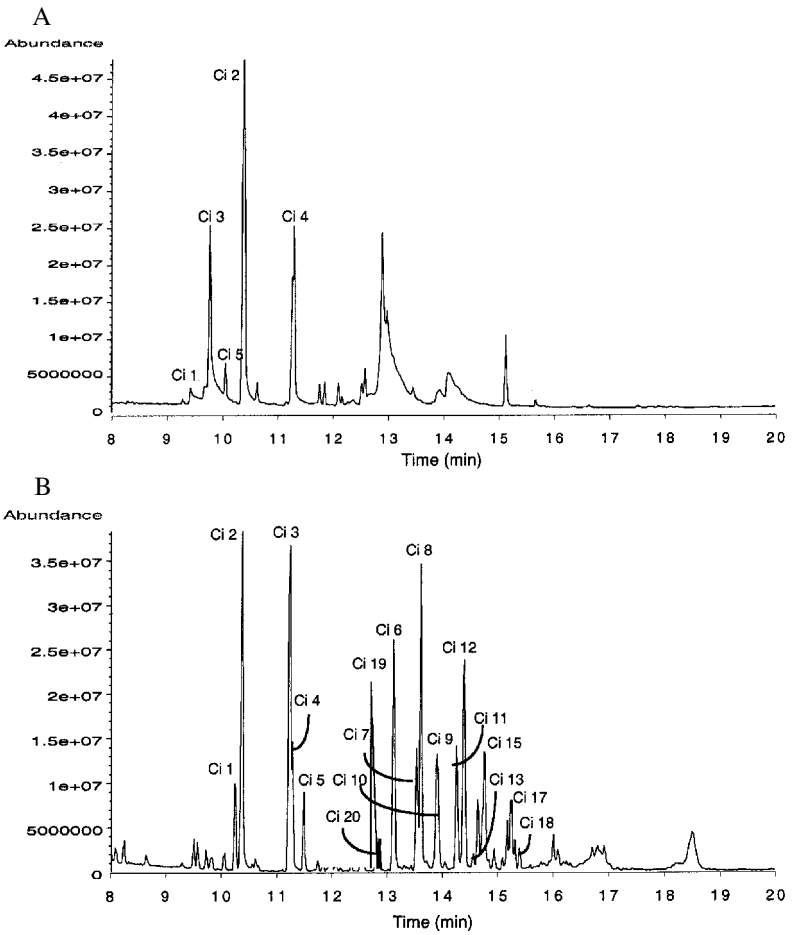


Figure 2. TIC chromatograms from GC-MS of brushtail possum urine extracts comparing derivatization methods. (A) Chromatography of extract after derivatisation of carboxylic acids to their methyl esters resulted in poor resolution of many metabolites. (B) Double derivatization of carboxylic acid and hydroxy moieties of metabolites to their methyl ester and TMS forms, respectively, improved their chromatography markedly. Metabolites are labelled with assigned names. See table 1 for identification of individual metabolites.

50 μl methanol). The urine was acidified to pH 1 with 20 μl 5 M HCl and then extracted with three sequential volumes of ethyl acetate (1×1 ml and 2×0.5 ml). Vortexing for 30 s and subsequent centrifuging at 2000 rpm for 5 min ensured thorough mixing and separation of ethyl acetate and urine. Carboxylic acid metabolites were then derivatized to their methyl esters. About 100 μl of the ethyl acetate extract was transferred to a 5-ml screw-capped glass vial and 200 μl diazomethane in diethyl ether (0.2 mmol·ml^{-1}; Schwartz and Bright 1974, Aldrich 1983) added. The vial was capped and allowed to sit for 30 min in an ice bath. Excess diazomethane was evaporated under a stream of N_2 at 40 °C and the final volume readjusted to $\sim$ 100 μl with ethyl acetate.

GC-MS of methylated-only urine resulted in chromatograms with many poorly resolved 1,8-cineole derived peaks (figure 2A). Development of a double derivatization method resulted in both methyl esters and trimethylsilyl ether (TMS) derivatives being formed. This method greatly improved the separation of metabolites by GC (figure 2B). Aliquots (20 μl) of the methylated ethyl acetate extract were transferred into 100-μl glass inserts in septum sealed crimp cap autosampler vials and 20 μl *N,O*-bis(trimethyl) trifluoroacetamide (BSTFA; Alltech Associates, Inc., Deerfield, IL, USA) added. Vials were sealed and heated at 70 °C for 20 min before GC analysis.

Total metabolites were measured by hydrolysing the urine before extracting. The same urine dilutions and internal standard were used as for the free metabolite assays. To diluted urine samples, 100 μl 1.1 M acetate buffer and 25 μl extract of *Helix pomatia* (β-glucuronidase 141 000 units·ml^{-1} plus

aryl sulphatase 3950 units·ml^{-1}; Boehringer Mannheim, Germany) were added. Samples were heated at 37.5 °C overnight in a water bath. After incubation, samples were treated identically to other urine samples except that 40 μl 5 M HCl was required to acidify the acetate buffer.

Identification of 1,8-cineole metabolites

Reference standards for a number of metabolites were kindly donated by Dr Ray Carman, University of Queensland. These metabolites had been either synthesized or isolated from brushtail possum urine and were: 9-hydroxycineole, 9-cineolic acid, 2,4-dihydroxycineole, 2-hydroxycineole and 7-cineolic acid. Purities of standards were variable, but all were $>80\%$ pure. GC retention times and mass spectra of these metabolites were determined.

For the many metabolites that did not correspond to the above available standards, the primary aim was to identify the degree and type of oxidation (i.e. hydroxy, carboxy), and where possible the position(s) of substitution. This was done by a series of derivatizations, mass spectrometric experiments to determine molecular weights and empirical formulae, and where possible position-specific daughter ions. Allowing for the formation of enantiomers, there are three theoretically possible carboxycineoles (cineolic acids), 12 possible hydroxycineoles, 58 possible dihydroxycineoles (assuming substitution on different carbons) and 33 possible hydroxycarboxycineoles (hydroxycineolic acids). Given that the latter turned out to be a dominant class in the possum urine, formal assignment of structure of the numerous isomers detected was not feasible in this study. For those compounds where the position of substitution was apparent from the MS evidence, no further attempt was made to determine their absolute stereochemistry.

Most metabolites did not produce molecular ions (M^+) after electron ionization (EI)-MS, therefore CI/GC-MS was used to determine protonated molecular ions ($[M+H]^+$), and empirical formulae were derived from subsequent accurate mass measurements of these. Reference EI mass spectra and GC retention times were obtained for all metabolites.

Where possible, these characteristics were obtained from isolated metabolites. Otherwise, they were obtained directly from urine extracts. Once metabolites had been identified and their mass spectra characterized, all metabolites could be separated in the chromatogram by extracting mass chromatograms of diagnostic ions. This procedure also enhanced the detection of minor metabolites that were otherwise difficult to detect from the background noise of the total ion current (TIC) chromatogram.

It was necessary to relate the abundance of the diagnostic ions to the actual amount of metabolite to allow quantitation of metabolites from calibration curves prepared for structurally similar metabolites. The abundance of the diagnostic ion as a fraction of the TIC was calculated from a good quality TIC chromatogram produced for each metabolite. The inverse of each fraction could then be multiplied by future diagnostic ion abundances to calculate the TIC (table 1).

Isolation of metabolites

Two metabolite mixtures were isolated from brushtail possum urine for use as metabolite standards for quantitation. The first was a mixture of 9- and 7-cineolic acids (Ci 2 and Ci 4), and the other a mixture of 9- and 7-hydroxycineole (Ci 3 and Ci 5). 7-Hydroxy-9-cineolic acid (Ci 13) was used to quantify all hydroxycineolic acids. This metabolite was obtained from koala urine as part of a separate study.

Excess possum urine from the dosing experiments was combined for the purpose of isolating metabolites. About 1000 ml urine was thawed and hydrolysed by adding 100 ml 1.1 M acetate buffer, 3 ml of extract of *Helix pomatia* and 100 mg sodium fluoride (as an antibacterial agent) in a large conical flask and heating at 37.5 °C for 5 days.

Sufficient hydrolysis had occurred after 5 days, determined by substantial increases in the amounts of 9-hydroxycineole and 7-hydroxycineole when a small volume of the urine was extracted and analysed by GC.

The urine was then fractionated into strong acid, weak acid and neutral fractions. About 500 ml hydrolysed urine was placed in a separating funnel, acidified to pH 1 with 100 ml 5M HCl and extracted with ethyl acetate (3×150 ml). The resultant extract was washed sequentially with chilled 5% aqueous $NaHCO_3$ (4×50 ml) to re-extract strong acids and 5% aqueous NaOH (4×50 ml) solutions to re-extract weak acids, leaving a neutral extract. The basic solutions were acidified with 20 and 25 ml concentrated HCl respectively. The acidified aqueous fractions were then back extracted into ethyl acetate using 3×100-ml washes for each fraction. A small portion of each fraction was methylated for analysis by GC-MS. The strong acid fraction contained predominantly 9-cineolic acid and 7-cineolic acid plus several other minor peaks.

Surprisingly, the hydroxycineolic acids remained in the acidified $NaHCO_3$ after back extraction with ethyl acetate. This result was presumably due to the influence of salts in the solution and their polarity. The hydroxycineolic acids were finally extracted using a more polar solvent (dichloromethane and *n*-propanol, 50:50). The dichloromethane/*n*-propanol solvent was removed by evaporation and the residue weighed (358 mg). The mixture was complex and contained all the hydroxycineolic acids. It was

Table 1. Assigned metabolite names and derivatisations for each 1,8-cineole metabolite found. Diagnostic ions (DI) used to extract mass chromatograms, the conversion factor used to calculate the TIC from the diagnostic ion abundance, protonated molecular ions $[M+H]^+$, accurate mass data, empirical formulae and molecular weights (MW) for 1,8-cineole metabolites derived from CI and high resolution GC/MS are also shown.

	Metabolites	Derivative[1]	Diagnostic ion (DI)	DI–TIC[2] factor	CI-MS $[M+H]^+$	CI-MS Accurate mass[3]	Calc. mass[4] $[M+H]^+$	Empirical formulae	Underivatized MW[5]
IS	2,5-dimethylbenzoic acid		164	9.05					
Group 1—hydroxycineoles									
Ci 1	3-hydroxycineole	TMS	159	10.47	243	243.1779	243.178	$C_{13}H_{26}SiO_2$	170
Ci 3	9-hydroxycineole	TMS	139	2.97	243	243.1749		$C_{13}H_{26}SiO_2$	170
Ci 5	7-hydroxycineole	TMS	183	14.91	243			$C_{13}H_{26}SiO_2$	170
Group 2—cineolic acids									
Ci 2	9-cineolic acid	M	139	2.83	199	199.1336	199.1334	$C_{11}H_{18}O_3$	184
Ci 4	7-cineolic acid	M	183	7.08	199	199.1328		$C_{11}H_{18}O_3$	184
Group 3—dihydroxycineoles									
Ci 10	dihydroxycineole A	TMS	243	11.10	331	331.2145	331.2125	$C_{16}H_{34}Si_2O_3$	186
Ci 11	dihydroxycineole B	TMS	227	5.01	331			$C_{16}H_{34}Si_2O_3$	186
Ci 14	dihydroxycineole C	TMS	227	6.90	331			$C_{16}H_{34}Si_2O_3$	186
Group 4—hydroxycineolic acids									
Ci 6	hydroxycineolic acid A	M+TMS	227	13.36	287	287.1682	287.1679	$C_{14}H_{26}SiO_4$	200
Ci 7	hydroxycineolic acid B	M+TMS	227	12.31	287			$C_{14}H_{26}SiO_4$	200
Ci 8	hydroxycineolic acid C	M+TMS	227	9.81	287			$C_{14}H_{26}SiO_4$	200
Ci 9	hydroxycineolic acid D	M+TMS	227	13.46	287			$C_{14}H_{26}SiO_4$	200
Ci 12	hydroxycineolic acid E	M+TMS	227	12.36	287			$C_{14}H_{26}SiO_4$	200
Ci 13	7-hydroxy-9-cineolic acid	M+TMS	227	13.91	287	287.17092		$C_{14}H_{26}SiO_4$	200
Ci 13	7-hydroxy-9-cineolic acid	M	155	10.58					
Ci 15	hydroxycineolic acid I	M+TMS	227	22.89	287			$C_{14}H_{26}SiO_4$	200
Ci 17	9-hydroxy-7-cineolic acid	M+TMS	183	3.50	287			$C_{14}H_{26}SiO_4$	200
Ci 18	hydroxycineolic acid H	M+TMS	227	12.01	287			$C_{14}H_{26}SiO_4$	200
Ci 19[6]	4-hydroxy-9-cineolic acid	M	155	7.00	215			$C_{11}H_{18}O_4$	200
Ci 20[6]	4-hydroxy-7-cineolic acid	M	155	11.22	215			$C_{11}H_{18}O_4$	200

[1] Methyl ester (M) and/or TMS ether (TMS).
[2] The conversion of diagnostic ion abundances to TIC abundances is described in the text.
[3] Accurate mass data were obtained from at least one metabolite in each group.
[4] Calc. mass = calculated mass (to four decimal points).
[5] Underivatised metabolites are inferred from CI-MS $[M+H]^+$.
[6] Ci 19 and 20 did not form the TMS derivative due to steric hinderance at the OH group.

considered too difficult to separate individual hydroxycineolic acids from this mixture. Instead, it was decided to use 7-hydroxy-9-cineolic acid, isolated from koala urine, as the standard for all hydroxycineolic acid metabolites.

The neutral fraction contained predominantly 9-hydroxycineole and small amounts of 7-hydroxycineole. The weak acid fraction contained no peaks at all and was discarded.

Further separation and purification of each fraction by HPLC and silica gel thin layer chromatography (TLC) was based on non-1,8-cineole compounds (see Discussion) and is described as follows. The strong acids, 9- and 7-cineolic acid, were further purified using TLC. Preliminary tests with small analytical TLC plates determined that the best separation of UV fluorescence quenching and vanillin sensitive compounds (i.e. non-1,8-cineole derived compounds such as hippuric acid and phenyl acetyl glycine) was achieved using unmethylated extracts in a mobile phase of ethyl acetate/hexane, 50:50. It was assumed that this method would also result in the best separation of the non-visible cineolic acids.

Preparative (pTLC) plates were prepared with powdered silica gel (60 GF 254, Keiselgel, Merck, Germany) and the concentrated strong acid fraction was applied to two pTLC plates. Zones (0–5) were removed according to bands detected by UV fluorescence quenching and vanillin spray. Each zone was re-dissolved in sequential methanol washes (3 × 15 ml). Methanol extracts were evaporated to dryness and the residue re-dissolved in ethyl acetate, methylated and analysed by GC. Both 9- and 7-cineolic acid were in the same zone (R_f = 0.71).

Further attempts using TLC to separate 9- and 7-cineolic acid as either their acid or methyl ester forms, using various mobile phases, were unsuccessful so a mixture of the two metabolites was used for quantitation. The purity, by GC, of the combined acids in the final standard used for quantitation was 98.4% and the proportions of 9-cineolic acid to 7-cineolic acid were 91.7 and 8.3% respectively.

TLC was also used for separating and purifying 9- and 7-hydroxycineole, respectively. The same TLC system as used for the separation of the acids was used for the hyroxycineoles. Both 9- and 7-hydroxycineole were present across three zones (R_f = 0.44–0.59) and the purest (97.4%) was used for the purpose of standards. The relative proportions of 9-hydroxycineole and 7-hydroxycineole were 85.6 and 14.4% respectively.

Quantitation of 1,8-cineole metabolites

Calibration curves for five metabolites were prepared. These metabolites were 9- and 7-hydroxycineole, 9- and 7-cineolic acid and 7-hydroxy-9-cineolic acid. As it was not practical to isolate all metabolites, these calibration curves were used to quantify structurally similar metabolites for which no standard was available. For example, the calibration curve prepared for Ci 13 was used to quantify all hydroxycineolic acids.

One group of metabolites, the dihydroxycineoles, did not have a representative standard isolated and quantitation of these metabolites used the calibration curve for the structurally similar 9-hydroxycineole. The hydroxycineolic acids Ci 19 and 20 did not accept a TMS group during derivatization with BSTFA. Therefore, these two metabolites were quantified separately using a calibration curve of Ci 13 that had been methylated only.

A stock solution of metabolites was prepared. Each metabolite standard, or metabolite mix, was accurately weighed into an autosampler vial, made to 400 μl with methanol and sealed with a Teflon/rubber septum and screw cap. Five aliquots of the stock solution were made to 50 μl with methanol, covering appropriate concentration ranges (Ci 2, 0–11.23 μmol/0.5 ml; Ci 3, 0–12.34 μmol/0.5 ml; Ci 4, 0–1.02 μmol/0.5 ml; Ci 5, 0–2.08 μmol/0.5 ml and Ci 13, 0–20.98 μmol/0.5 ml). It was necessary to hydrolyse methylated standard metabolites, by saponification, to return them to their excreted state. The standard metabolites could then be subject to the same assay procedure as genuine urine samples. NaOH (250 μl 0.2 M) was added to each dilution and the tubes heated at 40 °C. Aliquots were taken from the control tube at intervals and analysed by GC to monitor hydrolysis progress. The absence of the derivatized peaks from the chromatogram after 24 h confirmed complete hydrolysis. Finally, 250 μl of control brushtail possum urine and internal standard (0.5 mg 2,5-dimethylbenzoic acid in 50 μl methanol) was added to each dilution. The dilutions were then acidified, extracted, derivatized and analysed by GC-MS as described previously.

Faecal metabolite analyses

Faecal pellets were also analysed quantitatively for 1,8-cineole metabolites. Pellets were ground separately in a mortar and pestle and weighed. About 1 g (accurately weighed) of grindings was measured into a large centrifuge tube and 10 ml distilled water added. Tubes were placed on a rotary mixer for 5 h and then left standing overnight to ensure complete breakdown and dissolution of ground faeces.

About 500-mg aliquots of faecal slurry were accurately weighed into clean centrifuge tubes with internal standard (0.5 mg 2,5-dimethylbenzoic acid in 50 μl methanol). The slurry was hydrolysed by adding 200 μl 1.1 M acetate buffer and 50 μl of extract of *Helix pomatia* and heating at 37.5 °C overnight. Samples of faecal slurry were also analysed for free metabolite. These were analysed in the same manner as the hydrolysed samples, but omitting the enzyme incubation step. Faecal samples were acidified to pH 1 with three drops of 5 M HCl. Metabolites were extracted into three washes (1 × 2 and 2 × 1 ml) of

dichloromethane/*n*-propanol 80:20. A sample of the dichloromethane/*n*-propanol extract was evaporated to dryness and re-dissolved in 500 μl ethyl acetate and methylated with 1 ml diazomethane and finally 20 μl methylated extract was trimethylsilylated with 20 μl BSTFA.

Faecal extracts were analysed by GC-MS using the same instrument and conditions as those described for urine. Calibration curves for quantitation of faecal metabolites were the same as those prepared for urine quantitation.

Results

Food and 1,8-cineole intake

Possums ingested 2.4 ± 0.5 g (mean ± SD; 4.5 ± 1.0 mmol·kg^{-1}) 1,8-cineole on the last day of the diet.

Identification of 1,8-cineole metabolites

The structure of 1,8-cineole and its metabolites are shown in figure 1. Table 1 reports the assigned names for all metabolites identified plus the type of derivative, the diagnostic ion used for extracting mass chromatograms and the conversion factor for calculating the TIC from diagnostic ion abundances for each metabolite.

Identification of both known and novel 1,8-cineole metabolites was by a number of methods. Direct comparison of urine extracts from pre- and post-ingestion of 1,8-cineole by GC and LC-MS identified 1,8-cineole-related peaks. CI/GC-MS and high resolution GC-MS analysis of urine extracts provided molecular weights and empirical formulae for each metabolite (table 1). The EI mass spectrum of each metabolite is reported in table 2. For simplicity, mass spectra are only reported for metabolites in the fully derivatized state. Comparison of mass spectra with published data and donated reference metabolites was possible for 9- and 7-hydroxycineole and 9- and 7-cineolic acid. Other metabolites required additional derivatization before GC could resolve them. Finally LC-MS analysis of a diluted urine sample provided strong supportive evidence of metabolite structure, as well as providing direct evidence of glucuronidated 1,8-cineole metabolites (figure 3 and table 3).

Of the 19 metabolites identified, detailed structures of only five (Ci 2–5 and 13) are known and the structures of four others (Ci 1, 17, 19 and 20) were tentatively assigned. Eleven novel hydroxycineolic acid metabolites were found in the urine and structures have been tentatively assigned to four of these metabolites (Ci 13, 17, 19 and 20). The justification for the assignment of structures is as follows.

Mass spectrometry determined Ci 1 to be a hydroxycineole that formed a TMS derivative. Since hydroxylation on carbons 2, 7 and 9 resulted in known metabolites and we know that the 4 position does not accept a TMS group (see below), Ci 1 was deduced by the process of elimination to be a 3-hydroxycineole. Ci 13 was identified as 7-hydroxy-9-cineolic acid in a separate study by NMR and mass spectrometry. Ci 17 was tentatively assigned as 9-hydroxy-7-cineolic acid based on its EI-MS fragmentation pattern, which was very similar to that of 7-cineolic acid (Ci 4). The MS of the methyl ester/TMS ether of the latter is dominated by an ion at m/z 183, resulting from the loss of one of the methyl groups at C9 or C10 to form a very stable oxonium ion. Substitution on carbons 9 or 10, with subsequent loss of the substituent and any added derivative, would readily yield the same ion. The position of hydroxylation for Ci 19 and 20 were deduced from the fact that they failed to produce a TMS derivative, with the sterically hindered 4 position the only likely position for hydroxylation in these cases. Ci 19 and 20 were therefore tentatively assigned as 4-hydroxy-9-cineolic acid and 4-hydroxy-7-cineolic acid respectively,

Table 2. EI mass spectra for all 1,8-cineole metabolites in the brushtail possum.

Metabolite[1]	R_t GC/MS	Significant EI ions (m/z)[2] *Relative abundance* (%)																													
Ci 1	10.38	242	227	199	169	160	159	157	152	143	137	130	129	117	111	109	108	101	93	83	77	75	73	71	69	67	59	55	47	45	43
		21	*34*	*11*	*13*	*13*	*100*	*32*	*20*	*37*	*28*	*13*	*1 6*	*25*	*17*	*24*	*45*	*10*	*45*	*13*	*12*	*44*	*53*	*13*	*15*	*10*	*11*	*12*	*11*	*23*	*70*
Ci 2	10.49	198	140	139	95	71	67	59	53	43	41																				
		tr	*10*	*100*	*32*	*9*	*7*	*3*	*4*	*52*	*6*																				
Ci 3	11.37	140	139	121	95	93	81	75	73	71	67	45	43	41																	
		11	*100*	*4*	*24*	*7*	*5*	*10*	*14*	*7*	*5*	*7*	*63*	*5*																	
Ci 4	11.42	184	183	155	152	151	140	139	123	111	108	95	83	81	80	79	69	67	59	55	53	45	43	41							
		11	*100*	*2*	*5*	*37*	*23*	*33*	*21*	*18*	*11*	*12*	*17*	*27*	*19*	*25*	*30*	*12*	*16*	*26*	*12*	*34*	*54*	*35*							
Ci 5	11.64	242	227	199	183	169	159	143	139	137	135	111	109	107	103	95	94	93	91	84	81	79	75	73	69	67	59	55	45	43	41
		65	*81*	*21*	*100*	*20*	*20*	*44*	*38*	*45*	*33*	*45*	*15*	*25*	*23*	*14*	*16*	*52*	*14*	*24*	*11*	*37*	*60*	*60*	*16*	*16*	*10*	*25*	*20*	*44*	*36*
Ci 6	13.28	228	227	183	143	138	137	111	109	95	93	75	73	59	45	43															
		12	*65*	*39*	*12*	*11*	*93*	*12*	*11*	*19*	*97*	*29*	*46*	*13*	*31*	*100*															
Ci 7	13.71	228	227	183	143	138	137	111	109	95	93	75	73	59	45	43															
		11	*57*	*8*	*13*	*11*	*100*	*11*	*12*	*15*	*94*	*25*	*35*	*10*	*27*	*89*															
Ci 8	13.77	286	254	244	243	228	227	211	153	138	137	117	116	111	109	101	95	93	75	73	59	45	43								
		2	*16*	*12*	*65*	*24*	*100*	*11*	*13*	*11*	*14*	*11*	*55*	*21*	*22*	*61*	*24*	*21*	*42*	*62*	*15*	*25*	*79*								
Ci 9	14.06	227	138	137	131	109	95	94	93	75	73	45	43																		
		50	*12*	*100*	*13*	*16*	*10*	*10*	*99*	*29*	*56*	*28*	*66*																		
Ci 10	14.12	228	227	138	137	117	116	111	109	101	95	93	75	73	59	45	43														
		22	*100*	*11*	*24*	*11*	*47*	*18*	*17*	*48*	*14*	*21*	*26*	*40*	*11*	*17*	*40*														
Ci 11	14.43	227	225	183	157	156	143	137	95	93	75	73	45	43																	
		100	*13*	*12*	*11*	*19*	*10*	*12*	*11*	*16*	*22*	*46*	*10*	*21*																	
Ci 12	14.55	286	271	227	197	181	169	149	143	138	137	137	129	117	111	109	107	101	95	93	83	79	75	73	67	59	55	45	43	39	
		1	*98*	*100*	*34*	*11*	*10*	*10*	*20*	*12*	*44*	*55*	*20*	*10*	*24*	*10*	*10*	*13*	*13*	*41*	*14*	*19*	*42*	*71*	*12*	*22*	*12*	*28*	*53*	*22*	
Ci 13	14.73	271	227	211	137	119	109	94	93	91	79	75	73	59	45	43															
		11	*23*	*7*	*68*	*12*	*11*	*10*	*100*	*15*	*13*	*44*	*49*	*20*	*33*	*54*															
Ci 14[3]	14.78	271	227	209	195	157	156	145	137	105	95	93	75	73	45	43															
		tr	*100*	*16*	*6*	*11*	*26*	*21*	*14*	*15*	*15*	*18*	*33*	*60*	*17*	*36*															
Ci 15	14.84	227	210	196	195	156	145	120	105	93	91	79	77	75	73	45	43														
		34	*45*	*21*	*100*	*11*	*54*	*26*	*38*	*15*	*13*	*9*	*10*	*36*	*69*	*20*	*36*														
Ci 17	15.35	183	151	123	79	75	73	45	43																						
		100	*50*	*23*	*11*	*8*	*14*	*35*	*23*																						
Ci 18	15.42	227	138	137	133	109	93	75	73	45	43																				
		46	*11*	*84*	*10*	*10*	*100*	*27*	*57*	*26*	*21*																				
Ci 19	12.95	156	155	139	138	127	111	110	109	96	95	93	71	67	55	43															
		12	*91*	*17*	*16*	*14*	*30*	*19*	*22*	*13*	*50*	*27*	*10*	*14*	*15*	*100*															
Ci 20	13.03	155	137	95	93	55	45	43																							
		42	*49*	*15*	*68*	*10*	*15*																								

[1] Mass spectra are reported for metabolites in their fully derivatized state. Metabolites and their derivatizations are reported in table 1 and chemical structures for underivatized metabolites are shown in figure 1. tr, trace.

[2] Significant ions were those with >10 % relative abundance, and those with high mass which provide good structural data. In addition, for compounds with little fragmentation, most ions were reported.

[3] Ci 14 was not quantified as it was detectable in only very small amounts in some possums.

Table 3. Positive ion APCI LC-MS and MS-MS data for 1,8-cineole metabolites in brushtail possum urine (diluted 1:10).

		MS (m/z)[3]							
R_t[1] LC/MS	Metabolite group[2]	$[M+H]^+$	$[M+H_2O]^+$	$[M+H+CH_3OH]^+$	MS/MS (m/z) of major MS ion[4] explanation of fragmentation				
Glucuronides									
3.95	3*	**363**	380		345 $[M+H-H_20]^+$	187 $[M+H\text{-gluc}]^+$	169 $[M+H\text{-gluc-}H_2O]^+$	151 $[M+H\text{-gluc-}2H_2O]^+$	
4.75	3*	**363**	380		345 $[M+H-H_20]^+$	327 $[M+H-2H_20]^+$	309 $[M+H-3H_20]^+$	187 $[M+H\text{-gluc}]^+$	151 $[M+H\text{-gluc-}2H_2O]^+$
6.58	3*	**363**	380		345 $[M+H-H_20]^+$	327 $[M+H-2H_20]^+$	309 $[M+H-3H_20]^+$	187 $[M+H\text{-gluc}]^+$	151 $[M+H\text{-gluc-}2H_2O]^+$
5.32	4*		**394**		No MS/MS data as metabolite co-elutes with a stronger peak				
13.14	2*		**378**		202 $[M+H_2O\text{-gluc}]^+$	185 $[M+H_2O\text{-gluc-}H_2O]^+$	139 cineole ion		
15.84	1*	**347**			329 $[M+H-H_20]^+$	311 $[M+H-2H_20]^+$	293 $[M+H-3H_20]^+$	171 $[M+H\text{-gluc}]^+$	
16.63	1*	**347**			329 $[M+H-H_20]^+$	311 $[M+H-2H_20]^+$	293 $[M+H-3H_20]^+$	171 $[M+H\text{-gluc}]^+$	
17.44	1*	**347**			329 $[M+H-H_20]^+$	311 $[M+H-2H_20]^+$	293 $[M+H-3H_20]^+$	171 $[M+H\text{-gluc}]^+$	

[1] Retention times (R^t) from HPLC conditions described in text. Diluted neat urine was used—therefore metabolites were underivatized.

[2] 1* = hydroxycineole glucuronide, 2* = cineolic acid glucuronide, 3* = dihydroxycineole glucuronide, 4* = hydroxycineolic acid glucuronide, 1 = hydroxycineole, 2 = cineolic acid and 4 = hydroxycineolic, gluc = glucuronic acid-H_2O (loss of 176).

[3] Mass spectra of water or methanol adducts or metabolite dimers were common. In some cases these were the major ions and MS/MS data was acquired for these ions. The ion from which MS/MS data originated is highlighted in bold.

[4] Daughter ion fragmentation patterns are explained where possible. Similar patterns of fragmentation recurred, especially for the glucuronides where multiple water ions were lost.

Table 3. (*cont.*) Positive ion APCI LC-MS and MS-MS data for 1,8-cineole metabolites in brushtail possum urine (diluted 1:10).

R_t[1] LC/MS	Metabolite group[2]	MS (m/z)[3] $[M+H]^+$	$[M+H_2O]^+$	$[M+H+CH_3OH]^+$	MS/MS (m/z) of major MS ion[4] explanation of fragmentation		
Free metabolites							
6.05	4	**201**	218	233	183 $[M+H-H_20]^+$	165 $[M+H-2H_20]^+$	155 cineole ion
8.00	4	**201**	218		No MS/MS data as metabolite co-elutes with a stronger peak		
9.78	4	**201**			183 $[M+H-H_20]^+$	165 $[M+H-2H_20]^+$	155 cineole ion
11.09	4	201	**218**	233	201 $[M+H_2O-OH]^+$	165 $[M+H_2O-2H_2O-OH]^+$	155 cineole ion
12.40	4	**201**	218	233	183 $[M+H-H_20]^+$	165 $[M+H-2H_20]^+$	155 cineole ion
18.93	2	**185**	202		139 cineole ion		
19.24	2	**185**	202		167 $[M+H-H_20]^+$	139 cineole ion	
18.23	1	**171**	188		153 $[M+H-H_20]^+$	135	
19.86	1	**171**			153 $[M+H-H_20]^+$	135	

[1] Retention times (R^t) from HPLC conditions described in text. Diluted neat urine was used—therefore metabolites were underivatized.

[2] 1* = hydroxycineole glucuronide, 2* = cineolic acid glucuronide, 3* = dihydroxycineole glucuronide, 4* = hydroxycineolic acid glucuronide, 1 = hydroxycineole, 2 = cineolic acid and 4 = hydroxycineolic, gluc = glucuronic acid-H_2O (loss of 176).

[3] Mass spectra of water or methanol adducts or metabolite dimers were common. In some cases these were the major ions and MS/MS data was acquired for these ions. The ion from which MS/MS data originated is highlighted in bold.

[4] Daughter ion fragmentation patterns are explained where possible. Similar patterns of fragmentation recurred, especially for the glucuronides where multiple water ions were lost.

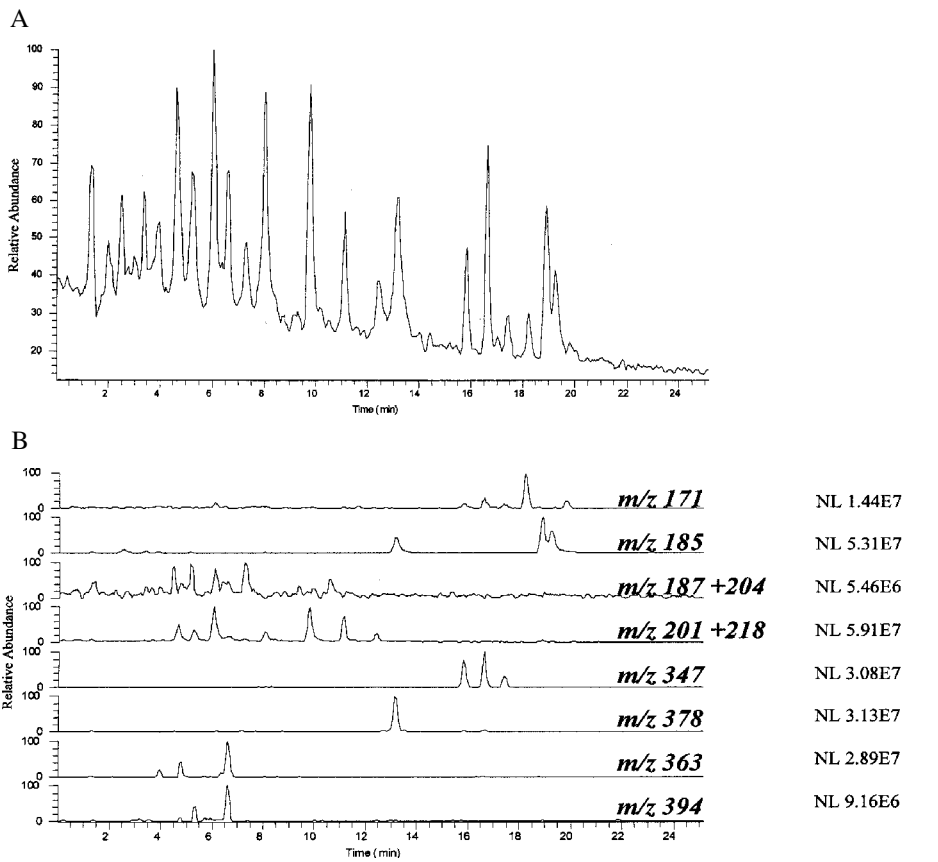


Figure 3. (A) Total ion current chromatogram from APCI LC-MS of diluted possum urine. (B) Selected mass chromatograms from APCI LC-MS of possum urine. Most but not all peaks represent molecular species, e.g. the peak just after 13 min in the m/z 185 chromatogram is derived from the glucuronide ion observed in the m/z 378 chromatogram. NL represents the normalization level for each trace. Selected ions represent the following metabolite groups: m/z 171 hydroxycineoles $[M+H]^+$, m/z 185 carboxycineoles $[M+H]^+$, m/z 187+204 dihydroxycineoles $[M+H]^+$ and $[M+H_2O]^+$, m/z 201+218 hydroxycarboxycineoles $[M+H]^+$ and $[M+H_2O]^+$, m/z 347 hydroxycineole glucuronides $[M+H]^+$, m/z 378 carboxycineole glucuronides $[M+H_2O]^+$, m/z 363 dihydroxycineole glucuronides $[M+H]^+$ and m/z 394 hydroxycarboxycineole glucuronides $[M+H_2O]^+$.

based on their relative abundance compared to that of 9-cineolic acid to 7-cineolic acid and 9-hydroxycineole to 7-hydroxycineole.

Three dihydroxycineole metabolites were found but the double derivatization meant that they could not be correlated with the five dihydroxycineole metabolites reported by Carman *et al.* (1994), Carman and Rayner (1994) and Carman and Garner (1996).

Although formal structures of the many metabolites were not elucidated, the functional groups for each compound were determined from their empirical formulas, mass spectra and types of derivatives formed (methyl ester, TMS ether).

The chromatogram resulting from positive ion APCI LC-MS of brushtail possum urine is shown in figure 3 and MS/MS data of metabolite peaks are reported in table 3. Metabolites frequently formed adducts with the mobile phase components

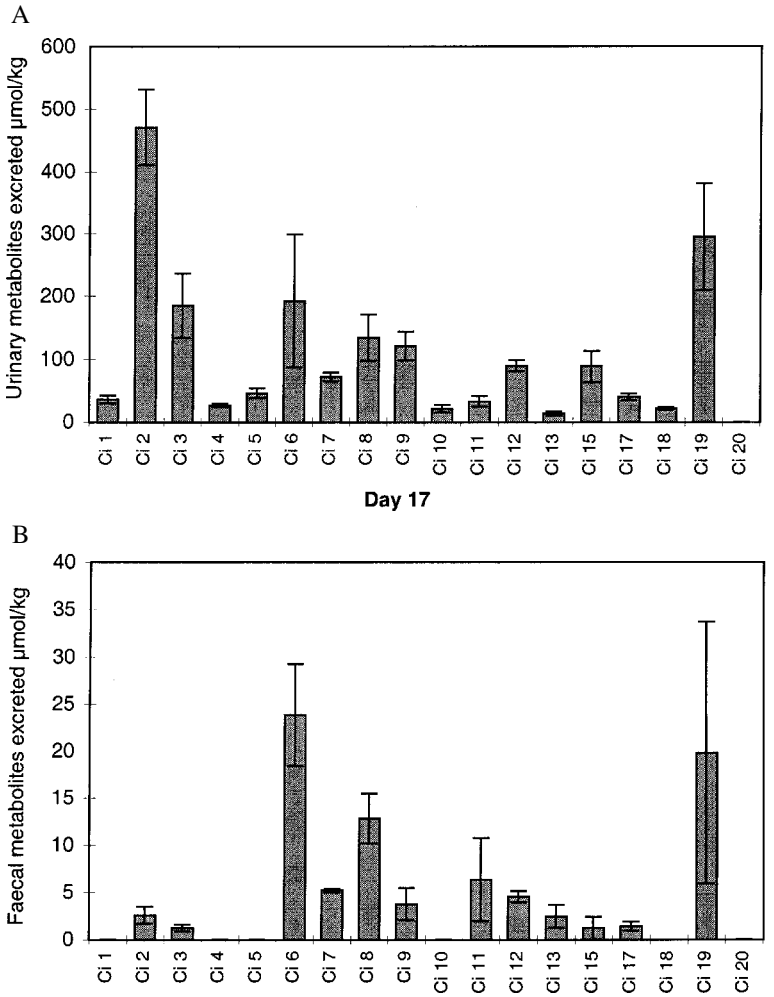


Figure 4. Individual 1,8-cineole metabolite recoveries (μmol/kg^{-1}) for (A) urine after hydrolysis (mean $\pm$ SE) and (B) faecal extracts after hydrolysis (mean $\pm$ SE). Metabolites are identified in table 1. Data are derived from six possums on the final day of collection.

(water and methanol) and these are also reported. For some metabolites the adduct produced the major ion and MS/MS data are therefore reported for the adduct.

MS/MS of the MH^+ of 1,8-cineole metabolites resulted in similar fragmentation patterns and free metabolites frequently lost water and produced a characteristic 1,8-cineole ion (e.g. m/z 139 or 155). Sequential losses of water were characteristic for glucuronides, as was a loss of 176 amu.

Since a reverse phase HPLC column was used for the chromatography, the retention times could be used as a measure of metabolite polarity, with the earlier eluting metabolites being the most polar. This sequence indicates that some glucuronide metabolites are less polar than the dihydroxycineole and the hydroxycineolic acid metabolites (at least in the acid mobile phase used).

Quantitation of 1,8-cineole metabolites

The fraction of the calculated ingested dose recovered in the urine on the final

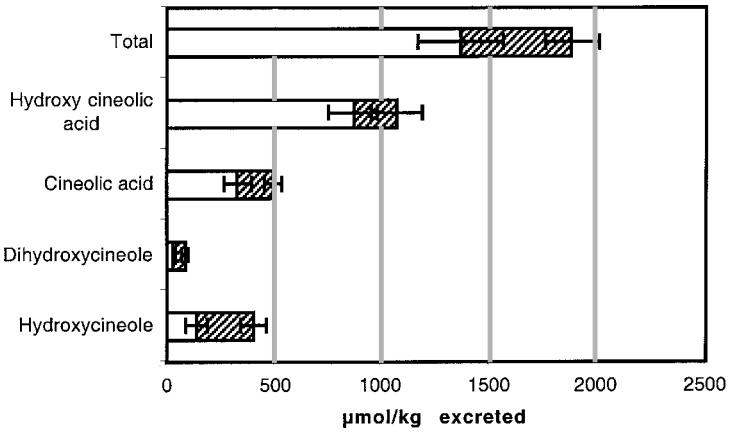


Figure 5. Comparison of free (blank) and conjugated (hatched) metabolites (μmol/kg^{-1}) for each group of 1,8-cineole metabolites (mean$\pm$SE). Data are derived from six possums on the final day of urine collection.

day was 0.44 ± 0.14 (mean$\pm$SD) and the pattern of metabolite excretion in urine is shown in figure 4A. To facilitate the interpretation of the pattern of metabolite excretion, metabolites were assigned to groups according to the extent of oxidation they had undergone and the functional groups they acquired during oxidation. A summary of the four groups follows:

- Hydroxycineoles—Ci 1 (3-hydroxycineole), Ci 3 (9-hydroxycineole) and Ci 5 (7-hydroxycineole). These metabolites acquired a single oxygen to form alcohol metabolites.
- Cineolic acids—Ci 2 (9-cineolic acid) and Ci 4 (7-cineolic acid) result from further oxidation of 9- and 7-hydroxycineoles respectively.
- Dihydroxycineoles—Ci 10 and Ci 11 were excreted as minor metabolites in the possum and traces of Ci 14 were found in some urine extracts. The positions of the hydroxy groups were not elucidated.
- Hydroxycineolic acids—these were the most extensively oxidized metabolites found in the possum and eleven hydroxycineolic acids were present in quantifiable amounts (Ci 6–9, 12, 13, 15, 17–20). Additional hydroxycineolic acids were present in trace amounts in some urine samples.

Figure 5 shows the recovery of free and conjugated metabolites in each group, excreted by the possum. The hydroxycineolic acid group accounted for the greatest proportion of recovered metabolites ($56\pm9\%$; mean$\pm$SD). Cineolic acids accounted for $27\pm5\%$, hydroxycineoles accounted for $14\pm6\%$ and dihydroxycineoles accounted for $3\pm2\%$ of recovered metabolites. A significant proportion of the dose was excreted as glucuronides. Conjugation with glucuronic acid was inversely related to metabolite polarity, being greatest for hydroxycineoles (41–82%) and minimal for hydroxycineolic acids.

Faecal analysis of 1,8-cineole metabolites

Most of the urinary 1,8-cineole metabolites were also found in the faeces. The pattern of faecal metabolite excretion is shown in figure 4B. The overall extractable content of faeces was much more extensive than urine and the 1,8-cineole metabolites were minor in the total faecal extract. The mass chromatograms of

diagnostic ions used to extract 1,8-cineole metabolites revealed a similar metabolite profile in the faecal and urine extracts of possums, although the least oxidized metabolites were under-represented in the faeces. Hydrolysis of the faecal extracts did not increase the recovery of any metabolite.

Discussion

It has been shown that a complicated array of 1,8-cineole metabolites is excreted by the brushtail possum and in this study 19 metabolites were identified in their free and/or glucuronidated forms.

Figure 1 shows the complexity of the metabolic products of 1,8-cineole in the brushtail possum. The complexity arises from a number of influences. First, oxidation can occur on most carbon atoms in the molecule. Second, serial oxidations, firstly to alcohols and then secondly to carboxylic acids occurs. Third, multiple stereoisomers are possible from a single oxidation, further increasing the range of products formed. As the number of oxidations increases, the number of possible isomers escalates, resulting in more than 100 possible structures when considering only hydroxy, carboxy, dihydroxy and hydroxy-carboxy metabolites. The pattern of metabolite excretion by brushtail possums could therefore be even more complex than appears to be the case. Presumably the cytochrome P450s and the other oxidation enzymes exhibit some specific regioselectivity in the oxidation reactions responsible for the production of metabolites, but this remains to be clarified. The complexity of possible isomers was somewhat simplified in our study as the GC capillary column used did not separate enantiomers. A chiral capillary column would be required to separate these metabolites, but was beyond the scope of this study. Interestingly, Carman and Klika (1992) reported some preliminary evidence that enantiomeric ratios of 9-hydroxycineole and 9-cineolic acid differ between male and female possums and suggested they may have a role in chemical communication.

Of the 19 metabolites, eleven hydroxycineolic acids have not previously been reported as 1,8-cineole metabolites. Taken collectively, these metabolites accounted for the major part of the urinary metabolites excreted ($\sim 60\%$). That this group of metabolites has yet to be detailed in the literature is testament to the complexity of 1,8-cineole metabolism. In the decade of detailed research into 1,8-cineole metabolism, only the non-acidic urinary metabolites and the previously known simple monoacids have been studied to date (R. Carman, personal communication, 1999). Others may have missed these compounds in the past due to their polarity requiring the double derivatization of acid and alcohol moieties before adequate resolution is achieved by gas chromatography, and the relative difficulty in extracting them from the urine

The structures of five dihydroxycineoles excreted by brushtail possums have been reported in the literature (Carman *et al.* 1994, Carman and Rayner 1994, Carman and Garner 1996). Only three were detected and they could not be correlated with the dihydroxycineoles reported in the literature since it was necessary doubly to derivatize urine extracts, altering their mass spectra from published data.

There were insufficient quantities of the donated standards to use for quantitation. Furthermore, the supply of 2,4-dihydroxycineole had been exhausted before the double derivatization technique had been developed. Therefore, only 9-hydroxycineole, 2-α-hydroxycineole, 9-cineolic acid and 7-cineolic acid were

available to be derivatized in the same manner as the urine extracts. The present authors, therefore, could not specifically match any of the diyhdroxy cineole metabolites found in the urine samples with the 2,4-dihydroxycineole supplied.

The derivatives of individual metabolites had to be carefully considered when mass spectra were used for identification since metabolites were susceptible to either one or both derivatizations. For example, the hydroxycineolic acids generally formed both methyl ester and TMS derivatives. However, two metabolites in this group (Ci 19 and Ci 20) did not accept the TMS group due to steric hindrance, and this in itself provides evidence for the position of hydroxylation being on carbon 4.

Glucuronidation was significant for 1,8-cineole metabolites excreted by the brushtail possum. Each group of metabolites underwent a degree of conjugation with the less oxidized metabolites undergoing a greater degree of glucuronidation. The pattern of conjugation is being further investigated as part of another study that examines the pattern of metabolite excretion during chronic ingestion of 1,8-cineole.

LC-MS results supported the mass spectral findings from GC-MS. It was particularly useful as MS and MS/MS data for underivatized metabolites confirmed the presence and identity of metabolites and their glucuronides. Further identification of metabolites was not possible by this method without reference standards. Nor was it possible to directly reconcile metabolites identified by GC-MS to those detected by LC-MS as the different modes of mass spectrometry produce incomparable mass spectra due to their respective characteristic sensitivities.

It may not be surprising that 1,8-cineole metabolites were detected in faecal extracts from possums. A study examining the fate of L-menthol in rats reported extensive enterohepatic circulation of menthol glucuronide and as much as half of the dose was recovered from the faeces (Yamaguchi *et al*. 1994). Another study also reported on the conjugated biliary metabolites of the terpene pulegone (Thomassen *et al*. 1991). However, it is interesting to note that in previous studies the present authors failed to find faecal metabolites of terpenes in folivorous marsupials (McLean *et al*. 1993, Boyle *et al*. 1999, 2000). Before these reports, examination of faeces has generally been limited to searching for unchanged oil (Southwell *et al*. 1980, Foley *et al*. 1987).

Biliary excretion of metabolites would require metabolites to be conjugated, as only larger molecular weight compounds (>300–500) are considered to be excreted by this route (Pratt and Taylor 1990). This indicates that hydrolysis of 1,8-cineole metabolites occurred *in vivo*, as metabolites were excreted in their free form. Presumably reabsorption and reuse of glucuronic acid occurs and enterohepatic circulation of 1,8-cineole metabolites may also occur.

The lower molecular weight metabolites were under-represented in the faecal metabolite profile compared to urine. Hydroxycineole glucuronides and cineolic acid glucuronides have molecular weights of 346 and 360 respectively. That these metabolites do not undergo biliary excretion suggests that molecular weights of 1,8-cineole glucuronides are borderline for biliary excretion in the brushtail possum (molecular weights of hydroxycineolic acid glucuronides are 376).

Isolation of 1,8-cineole metabolites from possum urine was difficult as it was not possible to detect them by UV-dependent methods since these metabolites did not absorb UV strongly (UV absorbance maxima were ~ 194 nm for hydroxycineole metabolites), nor were they susceptible to other trialled indicators (e.g. 1% vanillin in conc. sulphuric acid, or iodine) that would allow their detection on TLC. For this

reason separation and purification of metabolite standards by HPLC and TLC used unrelated urinary compounds such as hippuric acid and phenylacetylglycine as chromatographic markers.

Because of the number and complexity of 1,8-cineole metabolites excreted by the brushtail possum, it was not feasible to have standards for the purpose of quantitation for individual metabolites. Where possible metabolites were isolated, otherwise quantitation relied on calibration curves prepared for structurally similar metabolites. Justification for using this approach was based on the fact that response factors for compounds with serial positional isomers have been shown to be essentially constant (Dibeler 1979). In most cases, the standards used for quantitation in each group of metabolites had undergone the same functionalization. However no representative metabolite standard for dihydroxycineoles was isolated and these were quantified using the calibration curve for 9-hydroxycineole. These were minor metabolites and this estimation was considered satisfactory for the purpose of studying the metabolite pattern.

The elucidation of all 1,8-cineole metabolite structures and their absolute stereochemistry represents a major chemical research project and was beyond the scope of this study. The purpose of investigating the metabolic fate of 1,8-cineole in the brushtail possum was to examine the detoxification strategies employed by the brushtail when challenged by a chronic toxic diet. For this purpose, grouping metabolites according to their degree of oxidation satisfied this requirement and permitted an insight into the metabolic processes in this species.

Acknowledgements

The authors thank Dr R. Carman, University of Queensland, for supplying 1,8-cineole metabolite standards. The koala urine samples were obtained as part of a collaborative study with Dr W. J. Foley and B. Moore, Australian National University, Canberra.

References

Aldrich, 1983, Diazald™, MNNG and diazomethane generators. *Aldrichchimica Acta*, **16**, 1.

Barnes, W., 1996, *Eucalyptus* oil poisoning in children. *Australian Journal of Emergency Care*, **3**, 15–20.

Boland, D. J. and Brophy, J. J., 1991, *Eucalyptus Leaf Oils: Use, Chemistry, Distillation and Marketing* (Melbourne: Inkata).

Boyle, R., McLean, S., Foley, W. J. and Davies, N. W., 1999, Comparative metabolism of dietary terpene, *p*-cymene, in generalist and specialist folivorous marsupials. *Journal of Chemical Ecology*, **25**, 2109–2126.

Boyle, R., McLean, S., Foley, W. J., Moore, B. D., Davies, N. W. and Brandon, S., 2000c, Fate of the dietary terpene, *p*-cymene, in the koala. *Journal of Chemical Ecology* **26**, 1095–1111.

Bull, S. D., Carman, R. M., Carrick, F. N. and Klika, K. D., 1993, 7-Hydroxy-1,8-cineole and 7-cineolic acid. Two new possum urinary metabolites. *Australian Journal of Chemistry*, **46**, 441–447.

Carman, R. M. and Garner, A. C., 1996, 7,9-Dihydroxy-1,8-cineole and 2α,7-dihydroxy-1,8-cineole: two new possum urinary metabolites. *Australian Journal of Chemistry*, **49**, 741–749.

Carman, R. M., Garner, A. C. and Klika, K. D., 1994, 2,9-Dihydroxy-1,8-cineole and 2,10-dihydroxy-1,8-cineole—2 new possum urinary metabolites. *Australian Journal of Chemistry*, **47**, 1509–1521.

Carman, R. M. and Klika, K. D., 1992, Partially racemic compounds as brushtail possum urinary metabolites. *Australian Journal of Chemistry*, **45**, 651–657.

Carman, R. M., MacRae, I. C. and Perkins, M. V., 1986, The oxidation of 1,8-cineole by *Pseudomonas flava*. *Australian Journal of Chemistry*, **39**, 1739–1746.

Carman, R. M. and Rayner, A. C., 1994, 2-Alpha,4-dihydroxy-1,8-cineole—a new possum urinary metabolite. *Australian Journal of Chemistry*, **47**, 2087–2097.

Dibeler, V. H., 1979, Chemical analysis by mass spectrometry. In C. A. McDowell (ed.), *Mass Spectrometry* (New York: McGraw-Hill).

Flynn, T. M. and Southwell, I. A., 1979, 1,3-Dimethyl-2-oxabicyclo[2,2,2]-octane-3-methanol and 1,3-dimethyl-2-oxabicyclo[2,2,2] octane-3-carboxylic acid, urinary metabolite of 1,8-cineole. *Australian Journal of Chemistry*, **32**, 2093–2095.

Foley, W. J., Lassak, E. V. and Brophy, J., 1987, Digestion and absorption of *Eucalyptus* essential oils in greater glider (*Petauroides volans*) and brushtail possum (*Trichosurus vulpecula*). *Journal of Chemical Ecology*, **13**, 2115–2130.

Guenther, E., 1950, The *Eucalyptus* oils. In *The Essential Oils* (New York: D. van Nostrand), pp. 437–525.

Jenner, P. M., Hagan, E. C., Taylor, J. M., Cook, E. L. and Fitzhugh, O. G., 1964, Food flavourings and compounds of related structure i. acute oral toxicity. *Food and Cosmetic Toxicology*, **2**, 327–343.

Jorgensen, A. D., Picel, K. C. and Stamoudis, V. C., 1990, Prediction of gas chromatography flame ionization detector response factors from molecular structures. *Analytical Chemistry*, **62**, 683–689.

Li, H., Madden, J. L. and Davies, N. W., 1994, Variation in leaf oils of *Eucalyptus nitens* and *E. denticulata*. *Biochemical Systematics and Ecology*, **22**, 631–640.

Liu, W. G. and Rosazza, J. P. N., 1990, Stereospecific hydroxylation of 1,8-cineole using a microbial catalyst. *Tetrahedron Letters*, **31**, 2833–2836.

MacRae, I. C., Alberts, V., Carman, R. M. and Shaw, I. M., 1979, Products of 1,8-cineole oxidation by a *Pseudomonad*. *Australian Journal of Chemistry*, **32**, 917–922.

McLean, S., Foley, W. J., Davies, N. W., Brandon, S., Duo, L. and Blackman, A. J., 1993, Metabolic fate of dietary terpenes from *Eucalyptus radiata* in common ringtail possum (*Pseudocheirus peregrinus*). *Journal of Chemical Ecology*, **19**, 1625–1643.

NIST, 1998, NIST Mass Spectral Library (US Department of Commerce).

Patel, S. and Wiggins, J., 1980, Eucalyptus oil poisoning. *Archives of Disease in Childhood*, **55**, 405–406.

Pratt, W. B. and Taylor, P., 1990, *Principles of Drug Action: The Basis of Pharmacology* (New York: Churchill Livingston).

Schwartz, D. P. and Bright, R. S. 1974, A column procedure for esterification of organic acids with diazomethane at the microgram level. *Analytical Biochemistry*, **61**, 271–274.

Southwell, I. A., Flynn, T. M. and Degabriele, R., 1980, Metabolism of α- and β-pinene, *p*-cymene and 1,8-cineole in the brushtail possum, *Trichosurus vulpecula*. *Xenobiotica*, **10**, 17–23.

Southwell, I. A., Maddox, G. D. A. and Zalucki, M. P., 1995, Metabolism of 1,8-cineole in tea tree (*Melaleuca alternifolia* and *M. linariifolia*) by pyrgo beetle (*Paropsisterna tigrina*). *Journal of Chemical Ecology*, **21**, 439–453.

Thomassen, D., Pearson, P. G., Slattery, J. T. and Nelson, S. D., 1991, Partial characterization of biliary metabolites of pulegone by tandem mass spectrometry—detection of glucuronide, glutathione, and glutathionyl glucuronide conjugates. *Drug Metabolism and Disposition*, **19**, 997–1003.

Webb, N. J. A. and Pitt, W. R., 1993, Eucalyptus oil poisoning in childhood: 41 cases in south-east Queensland. *Journal of Paediatric Child Health*, **29**, 368–371.

Yamaguchi, T., Caldwell, J. and Farmer, P. B., 1994, Metabolic fate of [H-3]-l-menthol in the rat. *Drug Metabolism and Disposition*, **22**, 616–624.

XENOBIOTICA, 2000, VOL. 30, NO. 9, 933–941

Hepatotoxicity of acetaminophen and *N*-acetyl-*p*-benzoquinone imine and enhancement by fructose

M. HOJO, K. HANIOKA†, M. MIYATA* and Y. YAMAZOE
Division of Drug Metabolism and Molecular Toxicology, Graduate School of Pharmaceutical Sciences, Tohoku University, Aoba-ku, Sendai, 980-8578, Japan

Received 25 February 2000

1. Although oral administration of 400 mg/kg acetaminophen (APAP) or 1·8–3·4 g/kg sucrose had no effect on serum levels of alanine aminotransferase (ALT) and sorbitol dehydrogenase (SDH), their co-administration resulted in 20-fold increases in ALT/SDH activities. APAP alone (1250 mg/kg, p.o.) caused the elevation hepatotoxicity parameters, but the levels were lower than observed with co-administration of APAP (400 mg/kg) and sucrose (2·6 or 3·4 g/kg).

2. Sucrose-associated increase in serum ALT/SDH activities was selective with APAP and not detected with carbon tetrachloride (160 mg/kg, i.p.), D-galactosamine (400 mg/kg, i.p.) or α-naphthyl isothiocyanate (100 mg/kg, p.o.).

3. To verify the synergistic mechanism of sucrose, a major reactive intermediate of APAP, *N*-acetyl-*p*-benzoquinone imine (NAPQI), was given via the portal vein to rat pretreated with sucrose. Clear elevation of ALT/SDH activities was detected in the co-treated group. These results, together with an allopurinol-inhibition experiment, suggest the involvement of high-dose sucrose at a step(s) occurring after the metabolic activation of APAP.

4. Co-administration of glucose or fructose as well as sucrose elevated APAP-induced hepatotoxicity parameters in rat. Fructose but not glucose elevated APAP- or NAPQI-induced LDH leakage in a primary hepatocyte system. The results suggest the primary role of fructose is on the sucrose enhancement of APAP toxicity in rat.

Introduction

Acetaminophen (APAP) is commonly used for the treatment of pain or fever. High doses of the drug, however, sometimes result in serious liver necrosis in man (Davidson and Eastham 1966, Prescott *et al*. 1971) as well as experimental animals (Mitchell *et al*. 1973). It is believed that the hepatotoxicity of APAP is triggered by cytochrome P450- or peroxidase-mediated bioactivation of APAP to *N*-acetyl-*p*-benzoquinoneimine (NAPQI) (Dahlin *et al*. 1984, Ji *et al*. 1986, Esterline *et al*. 1989). Experiments using the knockout mouse showed that CYP2E1 and CYP1A2 are mainly involved in NAPQI formation (Zaher *et al*. 1998). Excessive production of NAPQI results in the depletion of the cellular GSH levels and allows NAPQI to bind covalently to cellular macromolecules (Potter *et al*. 1974). The critical mechanism of APAP- and NAPQI-induced hepatotoxicity, however, remains unclear in spite of extensive research (Nelson *et al*. 1995, Cohen and Khairallah 1997, Pumford *et al*. 1997).

To improve the efficacy and safety of drugs, drug interactions are a major issue in drug metabolism studies. Drug interactions are either pharmacodynamic or pharmacokinetic in nature. APAP is sometimes prescribed in the form of syrup and

* Author for correspondence; e-mail: miyata@mail.pharm.tohoku.ac.jp
† Present address: Toxicological Research Laboratory, Fujisawa Pharmaceutical Co. Ltd, Japan.

Xenobiotica ISSN 0049-8254 print/ISSN 1366-5928 online © 2000 Taylor & Francis Ltd
http://www.tandf.co.uk/journals

it has been reported that sugar co-administration influences the potency of APAP-induced hepatotoxicity in rodents (Hassing *et al*. 1979, Martinelli *et al*. 1989, Price and Jollow 1989, Chanda and Mehendale 1995, Ishida *et al*. 1997). In the present preliminary experiments, enhanced APAP-induced hepatotoxicity was observed in rat co-administered with sucrose.

In the present study, the effects of glucose and fructose on APAP- and NAPQI-induced hepatotoxicity have been examined in rat *in vivo* and primary hepatocytes to understand the mechanism underlying the enhanced APAP-induced hepatotoxicity by sucrose co-administration.

Materials and methods

Chemicals

α-Naphthyl isothiocyanate, D-galactosamine, allopurinol were from Sigma Chemical Co. (St Louis, MO, USA). APAP, assay kits for ALT and LDH, collagenase type I were from Wako Pure Chemical Co. (Osaka, Japan). NAPQI (purity 99%) was prepared by the oxidation of APAP according to the method of Dahlin and Nelson (1982).

Animals and treatments

Male Sprague–Dawley rats (6 weeks old, 180–230 g body weight) were allowed free access to water and were used in all experiments after a 1-week acclimation. APAP, D-galactosamine or allopurinol was dissolved in saline (10, 10 or 0·625% w/v respectively). α-Naphthyl isothiocyanate and carbon tetrachloride were dissolved in corn oil (2 and 20% w/v respectively). Sucrose, glucose and fructose were dissolved in saline (85% w/v). NAPQI was dissolved in DMSO (500 mM). α-Naphthyl isothiocyanate, APAP, sucrose, glucose or fructose were given p.o., whereas D-galactosamine, allopurinol or carbon tetrachloride were given i.p. to animals following an 18-h fasting. Animals were euthanized at 24 h after APAP or NAPQI treatment. In the NAPQI experiment, rats were treated with sucrose following an 18-h fasting. Rats were then anaesthetized with ether and received NAPQI solution via the hepatic portal vein 1 h after sucrose administration.

Isolation of primary hepatocytes

Hepatocytes were prepared by a collagenase perfusion of liver (Murayama *et al*. 1991). Cell number and viability were estimated by a Trypan blue exclusion method. Aliquots (1.0×10^7 cells) were plated in 10-cm tissue-culture plates and incubated in serum-free Dulbecco's modified Eagle medium (glucose free) at 37 °C in an atmosphere of 5% CO_2. APAP and NAPQI were added 4 h after plating. LDH leakage was measured 20 and 1 h after APAP and NAPQI treatment respectively.

Assessment of toxicity

Blood was collected from the lower vena cava under ether anaesthesia, stored at room temperature for 30 min and centrifuged for 10 min at 1000*g*. Serum was collected and frozen at −80 °C for subsequent analysis. Wako kits (GPT-UV Test Wako and LDH-Cytotoxic Test Wako) from Wako Pure Chemical Co. (Osaka,

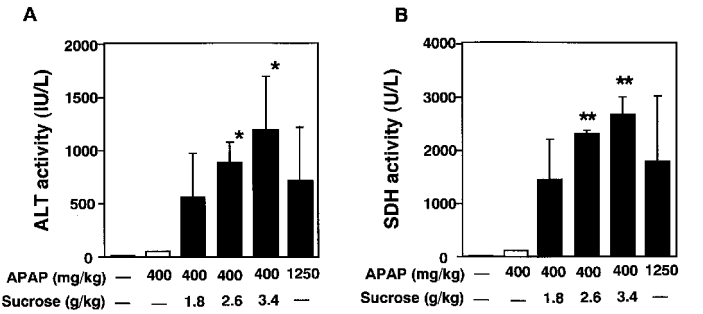


Figure 1. Effects of sucrose co-administration on APAP-induced hepatotoxicity. (A) ALT activity and (B) SDH activity were measured 24 h after APAP and sucrose administration. Data are the mean ± SD (n = 3). *$p < 0.05$, **$p < 0.01$ (compared with APAP, 400 mg/kg).

Japan) measured ALT and LDH activities. SDH activity was measured by the method of Gerlach and Hiby (1974). LDH leakage is defined as the ratio of LDH activity in medium to total LDH activity.

Results

Effect of sucrose co-administration on chemical-induced hepatotoxicity in rat

APAP is known to induce hepatotoxicity in human and rat. To understand the influence of co-administered chemicals, sucrose was co-administrated together with APAP in rat. No increase in serum levels of ALT and SDH activities was detected in rat treated with 400 mg/kg APAP, although a clear increase was detected in rat given 1250 mg/kg APAP (figure 1). Administration of sucrose alone did not affect ALT and SDH activities (data not shown). Sucrose co-administration to rat receiving 400 mg/kg APAP, however, significantly enhanced serum ALT and SDH activities in a dose-dependent manner (figure 1). Serum levels of ALT and SDH activities in rat co-treated with 400 mg/kg APAP and 2.6 or 3.4 g/kg sucrose were higher than those in rat treated with 1250 mg/kg APAP alone.

Carbon tetrachloride, D-galactosamine and α-naphthyl isothiocyanate are known to induce hepatotoxicity through distinct mechanisms (Gregus and Klaassen 1996, Moslen 1996). To verify whether the effect of sucrose co-administration is APAP-specific, sucrose was co-administrated with these hepatotoxins. Sucrose administration at 3.4 g/kg had no significant enhancement on ALT and SDH activities in rat treated with carbon tetrachloride, D-galactosamine or α-naphthyl isothiocyanate (figure 2).

Effect of sucrose on total P450 content

To verify the association of APAP-metabolizing capacity to the sucrose enhancement effect, microsomal cytochrome P450 levels were determined after the treatment of rat with APAP, sucrose, or APAP and sucrose. As shown in figure 3, no clear change was detected in total liver P450 content between control and sucrose- or APAP-treated groups. However, a decrease in total P450 and also the content of CYP1A2 and CYP2E1 responsible for the activation of APAP was observed in the sucrose and APAP co-administrated group. These results suggest the dissociation

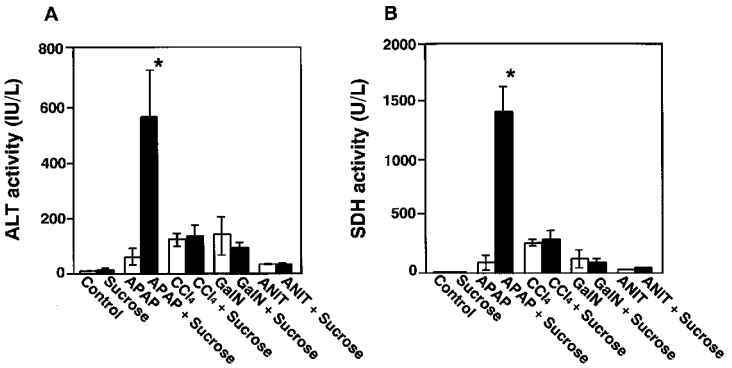


Figure 2. Effects of sucros co-administration on hepatotoxicity induced by various chemicals. (A) ALT activity and (B) SDH activity were measured 24 h after the chemical and sucrose administration. APAP, 400 mg/kg (p.o.); sucrose, 3·4 g/kg (p.o.); CCl_4, carbon tetrachloride, 160 mg/kg (i.p.); GalN, D-galactosamine, 400 mg/kg (i.p.); ANIT, α-naphthyl isothiocyanate, 100 mg/kg (p.o.). Data are the mean ± SD (n = 3). $*p < 0.05$ (compared with APAP).

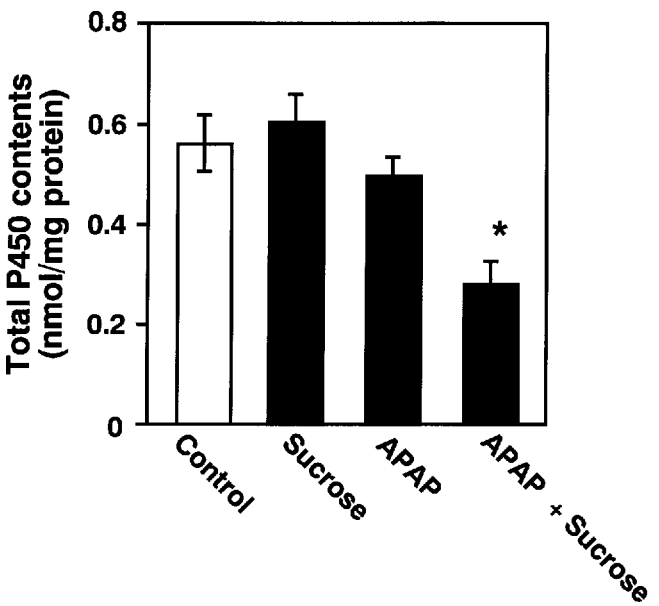


Figure 3. Total microsomal cytochrome P450 content in liver. Rats were treated with APAP and/or sucrose. Total microsomal P450 contents in liver were measured 24 h after administration. Sucrose, 3.4 g/kg (p.o); APAP, 400 mg/kg (p.o.). Data are the mean ± SD (n = 3). $*p < 0.05$ (compared with control).

between APAP-induced hepatotoxicity and the increase of reactive intermediate production such as NAPQI.

Effect of a xanthine oxidase inhibitor on hepatotoxicity induced by co-administration of APAP and sucrose

APAP is known to produce activated oxygen species through activation of xanthine oxidase. The activation of xanthine oxidase is considered a major process in APAP-induced hepatotoxicity (Jaeschke 1990, Tirmenstein and Nelson 1990).

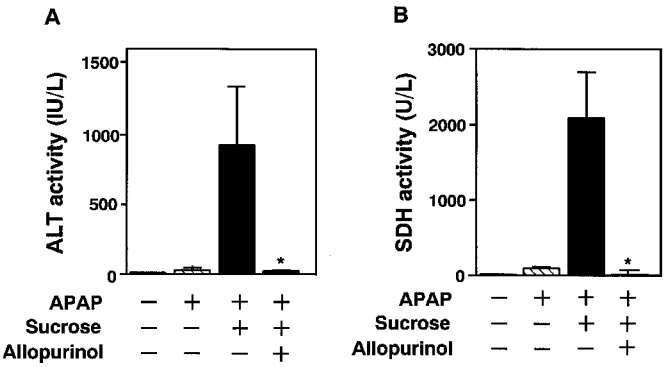


Figure 4. Effect of allopurinol on hepatotoxicity induced by co-administration of acetaminophen and sucrose. Rats were treated with acetaminophen (400 mg/kg) and/or sucrose (3·4 g/kg) after the administration of allopurinol (125 mg/kg). Data are the mean ± SD (n = 3 or 4). $*p < 0.05$ (compared with APAP + sucrose).

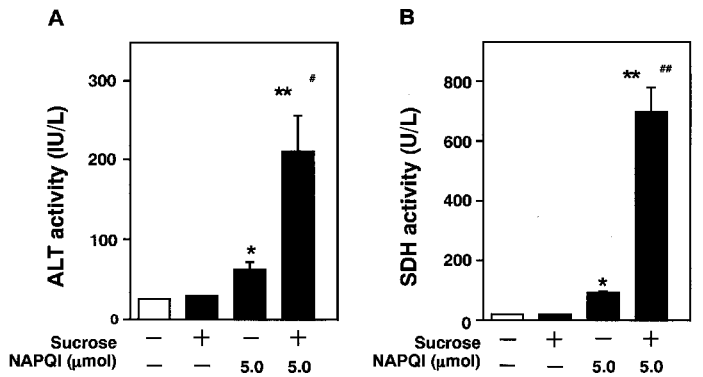


Figure 5. Effects of sucrose on NAPQI-induced hepatotoxicity. NAPQI-DMSO or DMSO were injected into the hepatic portal vein 1 h after the administration of sucrose or saline. (A) ALT activity and (B) SDH activity were measured 23 h after injection. Sucrose, 3·4 g/kg (p.o.). Data are the mean ± SD (n = 3 or 4). $*p < 0.05$, $**p < 0.01$ (compared with sucrose(−)/NAPQI(−)), $\#p < 0.05$, $\#\#p < 0.01$ (compared with sucrose(−)/NAPQI(5·0)).

To examine whether the xanthine oxidase inhibitor, allopurinol, affects the enhancement of APAP-induced hepatotoxicity by sucrose, rat was pretreated with allopurinol before APAP and sucrose co-administration. As shown in figure 4, allopurinol treatment completely blocked increases in ALT and SDH activities induced by APAP and sucrose co-administration.

Effect of sucrose co-administration on NAPQI-induced hepatotoxicity in rat

The experiment suggests the independence of the sucrose effect from NAPQI formation. To assess more directly the influence on APAP-induced hepatotoxicity, the effect of chemically synthesized NAPQI was examined *in vivo* in rat. Injection of NAPQI (5 μmol) to rat via the portal vein significantly enhanced the serum levels of ALT and SDH activities (figure 5). Although pretreatment with sucrose (3·4 g/kg) had no effect on ALT and SDH activities in vehicle-treated controls, clearly enhanced ALT and SDH activities were detected in the NAPQI plus sucrose-treated rat.

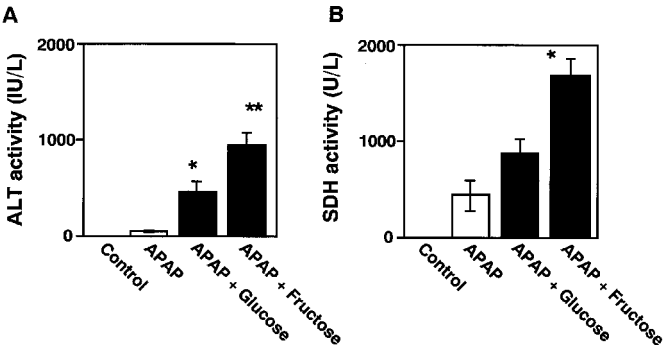


Figure 6. Effects of glucose and fructose co-administration on APAP-induced hepatotoxicity. Rats were treated with APAP and glucose or fructose. (A) ALT activity and (B) SDH activity were measured 24 h after the administration. APAP, 400 mg/kg (p.o.); glucose, 3.6 g/kg (p.o.); fructose, 3.6 g/kg. Data are the mean ± SD (n = 3). $*p < 0.05$, $**p < 0.01$ (compared with APAP).

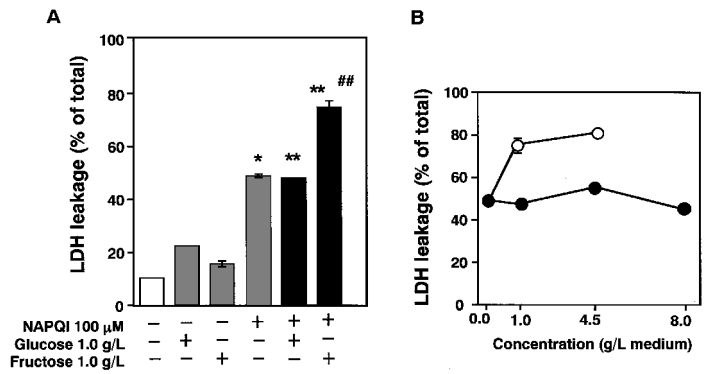


Figure 7. Effects of glucose and fructose on NAPQI-induced cytotoxicity. Hepatocytes prepared from rat livers were incubated for 1 h in medium (DMEM) with NAPQI (100 μM) or DMSO (0.1% as control) plus concomitantly added (A) glucose (0, 1.0 g/l) or fructose (0, 1.0 g/l) and added (B) glucose (0, 1.0, 4.5, 8.0 g/l) (closed circle) or fructose (0, 1.0, 4.5 g/l) (open circle). LDH leakage was measured in conditioned medium and cell lysate. Data are the mean ± SEM (n = 3) $*p < 0.05$, $**p < 0.01$ (compared with NAPQI(−)/sucrose(−)/fructose(−)), $\#\#p < 0.01$ (compared with NAPQI (100 μM)/sucrose(−)/fructose(−)).

Effect of glucose and fructose on APAP-induced hepatotoxicity

Sucrose is hydrolyzed to glucose and fructose and then absorbed from the gut *in vivo*. To examine further the sucrose effect on APAP-induced hepatotoxicity, rat was pretreated with glucose or fructose instead of with sucrose. As shown in figure 6, both glucose and fructose enhanced serum ALT and SDH levels in the APAP-treated rat. These serum levels were, however, higher in the fructose-treated rat than those in the glucose-treated animal. In rat primary hepatocytes, lactate dehydrogenase (LDH) leakage was observed in the presence of > 4 mM APAP (data not shown) and attained a maximum at 20 h after APAP treatment. In this condition, the addition of fructose (1.0 g/l), but not glucose increased LDH leakage in rat hepatocytes, as compared with the group treated only with APAP (data not shown). Furthermore, the addition of 100 μM NAPQI, but not that of glucose (1.0 g/l) or fructose (1.0 g/l) significantly induced LDH leakage from rat hepatocyte (figure 7A). An increase in fructose concentration from 0 to 4.5 g/l

medium enhanced the amounts of NAPQI-induced LDH leakage (figure 7B). In contrast, glucose did not exhibit a synergistic effect on NAPQI-induced LDH leakage, even at 8 mM concentration.

Discussion

In the present study, NAPQI was shown to induce directly hepatotoxicity *in vivo*. In addition, high levels of sucrose and fructose enhanced APAP- and NAPQI-induced hepatotoxicity. Chanda *et al*. (1995) reported that rat pretreated with glucose increased the lethality of APAP, whereas fructose was shown to suppress the hepatotoxicity of APAP (Mourelle *et al*. 1991, Strubelt and Younes 1992, Ishida *et al*. 1997). Although the reason for this latter conflict is unclear, the effect of sucrose and fructose on APAP-induced hepatotoxicity might depend on the method of fructose treatment. Simultaneous treatment with fructose and APAP was done in the present experiment, which is different from that of other groups.

Sucrose co-administration resulted in the enhancement of APAP-induced hepatotoxicity in rat. Similar experiments with other typical hepatotoxins such as carbon tetrachloride, D-galactosamine, α-naphthyl isothiocyanate had no clear effect, suggesting sucrose selectivity on the hepatotoxicity of APAP. These phenomena prompted the investigation of the mechanism of APAP-induced hepatotoxicity from the point of food and drug interactions. Administration of glucose or fructose (hydrolysis products of sucrose) enhanced APAP-induced hepatotoxicity in rat, although the effect of fructose was more pronounced than that of glucose. Fructose but not glucose enhanced APAP-induced cytotoxicity in rat primary hepatocytes. These results are partially inconsistent with the *in vivo* data but suggest that fructose is directly associated with enhanced APAP-induced hepatotoxicity. Reciprocal changes of fructose and glucose *in vivo* may explain at least partially the discrepancy observed.

Zaher *et al*. (1998) showed that liver CYP2E1 and CYP1A2 activate APAP to NAPQI. In the present study, sucrose administration did not increase, but it decreased total liver P450 and also the content of CYP2E1 and CYP1A2 (data not shown). These results support the hypothesis that sucrose primarily affects toxicity after NAPQI production rather than the level of NAPQI production. This idea is further strengthened by the data of the NAPQI injection experiment in rat (figure 5).

Several mechanisms have been proposed for APAP-induced hepatotoxicity (Nelson *et al*. 1995, Cohen and Khairallah 1997, Pumford *et al*. 1997). Xanthine oxidase has been implicated in APAP-induced hepatotoxicity in mouse (Tirmenstein and Nelson 1990). Allopurinol, a xanthine oxidase inhibitor, completely suppressed the sucrose-enhancing effect on APAP-induced hepatotoxicity (figure 4). This result suggests the association of sucrose-enhancement of toxicity with a xanthine oxidase-mediated process. Although NAPQI is known to be a reactive intermediate causing hepatotoxicity, the subsequent process leading to hepatotoxicity remains undefined. When rat is administered large amount of sucrose, fructose moves to the liver through the portal vein. In spite of the structural similarity, the role of fructose on the production of ATP is different from that of glucose *in vivo*. Glucose produces ATP by the glycolytic pathway, whereas fructose causes ATP depletion in the liver (Berghe *et al*. 1977). This difference may be related to a difference in APAP-induced hepatotoxicity between fructose and

glucose, because cellular ATP level is known as a key regulator of intracellular Ca^{2+} concentration and purine levels involved in APAP-induced hepatotoxicity (Tirmenstein and Nelson 1989, Weis *et al*. 1992).

Based on the present studies, fructose may play an important role in sucrose-mediated enhancement of APAP-induced hepatotoxicity.

Acknowledgements

This work is supported by Grants-in-Aids from Ministry of Education, Science, and Culture and Ministry of Health and Welfare, and by the Japan Health Sciences Foundation.

References

Berghe, G., Bronfman, M., Vanneste, R. and Hers, H.-G., 1977, The mechanism of adenosine triphosphate depletion in the liver after a load of fructose. *Biochemical Journal*, **162**, 601–609.

Chanda, S. and Mehendale, H. M., 1995, Nutritional impact on the final outcome of liver injury inflicted by model hepatotoxicants: effect of glucose loading. *FASEB Journal*, **9**, 240–245.

Cohen, S. and Khairallah, E., 1997, Selective protein arylation and acetaminophen-induced hepatotoxicity. *Drug Metabolism Reviews*, **29**, 59–77.

Dahlin, D., Miwa, G., Lu, A. and Nelson, S. D., 1984, *N*-acetyl-*p*-benzoquinoneimine: a cytochrome P-450 mediated oxidation product of acetaminophen. *Proceedings of the National Academy of Sciences, USA*, **81**, 1327–1331.

Dahlin, D. C. and Nelson, S. D., 1982, Synthesis, decomposition kinetics, and preliminary toxicological studies of pure *N*-acetyl-*p*-benzoquinone imine, a proposed toxic metabolite of acetaminophen. *Journal of Medicinal Chemistry*, **25**, 885–886.

Davidson, D. G. D. and Eastham, W. N., 1966, Acute liver necrosis following overdose of paracetamol. *British Medical Journal*, **2**, 497–499.

Esterline, R., Ray, S. and Ji, S., 1989, Reversible and irreversible inhibition of hepatic mitochondrial respiration by acetaminophen and its toxic metabolite, *N*-acetyl-*p*-benzoquinoneimine (NAPQI). *Biochemical Pharmacology*, **38**, 2387–2390.

Gerlach, U. and Hiby, W., 1974, *Methods of Enzymatic Analysis* (New York: Academic Press), pp. 569–573.

Gregus, Z. and Klaassen, C. D., 1996, Mechanisms of toxicity. In C. D. Klaassen (ed.), *Casarett & Doull's Toxicology: The Basic Science of Poisons* (New York: McGraw-Hill), pp. 35–74.

Hassing, J. M., Rosenberg, H. and Stohs, S. J., 1979, Acetaminophen-induced glutathione depletion in diabetic rats. *Research Communications in Chemical Pathology and Pharmacology*, **25**, 3–11.

Ishida, K., Sakazume, M., Hirai, N., Ikegami, H., Sakai, T. and Doi, K., 1997, Effects of fructose-induced hypertriglyceridemia on hepatorenal toxicity of acetaminophen in rats. *Experimental and Toxicologic Pathology*, **49**, 39–46.

Jaeschke, H., 1990, Glutathione disulfide formation and oxidant stress during acetaminophen-induced hepatotoxicity in mice *in vivo*: the protective effect of allopurinol. *Journal of Pharmacology and Experimental Therapeutics*, **255**, 935–941.

Ji, S., Ray, S. and Esterline, R., 1986, Intracellular dissipative structures as the ultimate targets of cytotoxicity. *Advances in Experimental Medicine and Biology*, **197**, 871–889.

Martinelli, A., Meneghelli, U., Zucoloto, S. and Lima, S., 1989, Effect of the intake of an exclusive sucrose diet on acetaminophen hepatotoxicity in rats. *Brazilian Journal of Medical and Biological Research*, **22**, 1381–1387.

Mitchell, J., Jollow, D., Potter, W., Davis, D., Gillette, J. and Brodie, B., 1973, Acetaminophen-induced hepatic necrosis. I. Role of drug metabolism. *Journal of Pharmacology and Experimental Therapeutics*, **187**, 185–197.

Moslen, M. T., 1996, Toxic responses of the liver. In C. D. Klaassen (ed.), *Casarett & Doull's Toxicology: The Basic Science of Poisons* (New York: McGraw-Hill), pp. 403–416.

Mourelle, M., Beales, D. and McLean, A. E., 1991, Prevention of paracetamol-induced liver injury by fructose. *Biochemical Pharmacology*, **41**, 1831–1837.

Murayama, N., Shimada, M., Yamazoe, Y. and Kato, R. 1991, Difference in the susceptibility of two phenobarbital-inducible forms, P450IIB1 and P450IIB2, to thyroid hormone- and growth hormone-induced suppression in rat liver: phenobarbital-inducible P450IIB2 suppression by thyroid hormone acting directly, but not through the pituitary system *Molecular Pharmacology*, **39**, 811–817.

Nelson, S. D., 1995, Mechanisms of the formation and disposition of reactive metabolites that can cause acute liver injury. *Drug Metabolism Reviews*, **27**, 147–177.

Potter, W., Thorgeirson, S., Jollow, D. and Mitchell, J., 1974, Acetaminophen-induced hepatic necrosis. V. Correlation of hepatic necrosis, covalent binding and glutathione depletion in hamsters. *Pharmacology*, **12**, 129–143.

Prescott, L. F., Roscoe, P., Wright, N. and Brown, S. S., 1971, Plasma-paracetamol half-life and hepatic necrosis in patients with paracetamol overdosage. *Lancet*, **1**, 519–522.

Price, V. and Jollow, D., 1989, Effect of glucose and gluconeogenic substrates on fasting-induced suppression of acetaminophen glucuronidation in the rat. *Biochemical Pharmacology*, **38**, 289–297.

Pumford, N., Halmes, N. and Hinson, J., 1997, Covalent binding of xenobiotics to specific proteins in the liver. *Drug Metabolism Reviews*, **29**, 39–57.

Strubelt, O. and Younes, M., 1992, The toxicological relevance of paracetamol-induced inhibition of hepatic respiration and ATP depletion. *Biochemical Pharmacology*, **44**, 163–170.

Tirmenstein, M. and Nelson, S. D., 1989, Subcellular binding and effects on calcium homeostasis produced by acetaminophen and a nonhepatotoxic regioisomer, 3′-hydroxyacetanilide, in mouse liver. *Journal of Biological Chemistry*, **264**, 9814–9819.

Tirmenstein, M. and Nelson, S. D., 1990, Acetaminophen-induced oxidation of protein thiols Contribution of impaired thiol-metabolizing enzymes and the breakdown of adenine nucleotides. *Journal of Biological Chemistry*, **265**, 3059–3065.

Weis, M., Kass, G., Orrenius, S. and Moldeus, P., 1992, *N*-acetyl-*p*-benzoquinone imine induces Ca^{2+} release. *Journal of Biological Chemistry*, **267**, 804–809.

Zaher, H., Buters, J. T. M., Ward, J. M., Bruno, M. K., Lucas, A. M., Stern, S. T., Cohen, S. D. and Gonzalez, F. J., 1998, Protection against acetaminophen toxicity in CYP1A2 and CYP2E1 double-null mice. *Toxicology and Applied Pharmacology*, **126**, 267–275.

XENOBIOTICA, 2000, VOL. 30, NO. 10, 943–953

Characterization of cytochrome P450 enzymes involved in drug oxidations in mouse intestinal microsomes

C. EMOTO†, H. YAMAZAKI†, S. YAMASAKI†,
N. SHIMADA‡, M. NAKAJIMA† and T. YOKOI†*

† Faculty of Pharmaceutical Sciences, Kanazawa University, Kanazawa 920-0934, Japan
‡ Daiichi Pure Chemicals, Ibaraki 319-1182, Japan

Received 4 April 2000

1. Cytochrome P450 (P450, CYP) enzymes involved in drug oxidations in mouse intestines were characterized for their role in the first-pass metabolism of xenobiotics.

2. Preparation of mouse intestinal microsomes using a buffer containing glycerol and protease inhibitors including (*p*-amidinophenyl) methanesulphonyl fluoride, EDTA, soybean trypsin inhibitor, aprotinin, bestatin and leupeptine gave the highest testosterone 6*β*-hydroxylase activity among several preparation buffers tested in this study. Testosterone 6*β*-hydroxylase activity catalysed by mouse intestinal microsomes subjected to freezing and thawing was lower than that catalysed by unfrozen intestinal microsomes.

3. Low but significant catalytic activities of nifedipine oxidation, midazolam 1′- and 4-hydroxylation, chlorzoxazone 6-hydroxylation, bufuralol 1′- and 6-hydroxylations and tolbutamide methylhydroxylation were observed in mouse intestinal microsomes. Testosterone 6*β*-hydroxylation, chlorzoxazone 6-hydroxylation, and bufuralol 1′- and 6-hydroxylations were inhibited by ketoconazole, diethyldithiocarbamate and quinine respectively.

4. Immunoblot analysis using anti-rat CYP3A antibodies demonstrated two immunoreactive bands showing similar migration in mouse intestinal and hepatic microsomes, although studies using anti-CYP1A, anti-CYP2C, anti-CYP2D and anti-CYP2E1 antibodies did not detect any band in mouse intestinal microsomes.

5. The results suggest that mouse intestinal microsomes should be prepared with glycerol and several protease inhibitors and that Cyp3a enzymes probably play an important role in drug oxidations catalysed by mouse intestine.

Introduction

Cytochrome P450 (P450, CYP) consists of a superfamily of haem-containing monooxygenases associated with the metabolism of substrates, such as drugs, environmental pollutants and endogenous substrates with broad overlapping specificities (Guengerich 1991). P450s are microsomal enzymes that exist mainly in liver as well as in extrahepatic tissues such as intestines, lungs and kidneys (Krishna and Klotz 1994). Recently, the intestine has been recognized as a potential site for drug oxidations because of early exposure to orally administered xenobiotics. The upper part of the small intestine serves as the major site for intestinal CYP3A-mediated first-pass metabolism in man (Paine *et al*. 1997). There have been reports on the metabolism of midazolam by CYP3A4 in human intestine (Paine *et al*. 1996, 1997). The CYP3A subfamily accounts for 30% of the total P450 content in the adult human liver and for the majority of P450 in the human intestine (Watkins *et al*.

* Author for correspondence: e-mail: TYOKOI@kenroku.kanazawa-u.ac.jp.

Xenobiotica ISSN 0049-8254 print/ISSN 1366-5928 online © 2000 Taylor & Francis Ltd
http://www.tandf.co.uk/journals

1987, Shimada *et al*. 1994). CYP3A enzymes are known to have a broad substrate specificity and about half the drugs on the market are substrates for CYP3A4 (Guengerich 1995).

Recently, considerable progress has been made in the identification and characterization of intestinal P450 enzymes. Several species of experimental animals have been used in early toxicology and metabolism studies by the pharmaceutical industry. Intestinal microsomes from experimental animals and humans have been prepared by various methods in different laboratories. In rat and non-rodent species including dog and monkey, characterization of small intestinal P450s has been reported (Prueksaritanont *et al*. 1996, Zhang *et al*. 1996). However, few studies have been conducted so far in mouse. Furthermore, little attention has been paid to the use of protease inhibitors and glycerol in the preparation of intestinal microsomes. It should also be mentioned that little is known about changes in the stability of intestinal microsomes by freezing and thawing, in contrast to a large number of studies on human liver microsomes (Pearce *et al*. 1996, Yamazaki *et al*. 1997). Therefore, it was planned to investigate the methods for preparation of mouse intestinal microsomes and to characterize the intestinal drug-metabolizing enzymes.

In this study, methods for preparing intestinal microsomes from the upper part of the mouse small intestine, particularly the effects of protease inhibitors and glycerol, were investigated. The oxidation of testosterone, nifedipine, midazolam, chlorzoxazone, bufuralol and tolbutamide were measured in mouse intestinal microsomes and the inhibitory effects of P450 inhibitors were examined. Immunochemical detection of Cyp3a enzymes in mouse intestinal microsomes was also performed.

Materials and methods

Chemicals

Testosterone and 6β-hydroxytestosterone were from Steraloids (Wilton, NH, USA). Midazolam and 1′- and 4-hydroxymidazolam were kindly provided by Yamanouchi Pharmaceuticals (Tokyo, Japan). Chlorzoxazone, aprotinin, bestatin, leupeptin and trypsin inhibitor (Type II-S: soybean) were from Sigma (St Louis, MO, USA). (±)-Bufuralol, tolbutamide and their metabolites and 6-hydroxychlorzoxazone were from Ultrafine Chemicals (Manchester, UK). (*p*-Amidinophenyl) methanesulphonyl fluoride (APMSF) was from Wako Pure Chemicals (Osaka, Japan). Other reagents were of the highest grade commercially available.

Preparation of intestinal and hepatic microsomes

Male C57BL/6CrSlc mice (8 weeks old, ~ 30 g) were from Japan SLC, Inc. (Hamamatsu, Japan). Microsomes from mouse small intestines were prepared according to Iatsimirskaia *et al*. (1997) with slight modifications. Immediately after excision of the small intestine, a 10-cm segment of the upper part of the small intestine was placed on an ice-cold stainless dish and cut longitudinally, then washed with ice-cold washing solution (0.9% NaCl, 1 mM APMSF, 1 mM EDTA) by gentle swirling for 1 min. The mucosal cells were gently scraped off with a micro-cover glass. The scraped sample was dipped in 3 vols ice-cold buffer A (50 mM Tris-HCl buffer, pH 7.4) containing 150 mM KCl, 1 mM APMSF, 1 mM EDTA, 1 mg/ml trypsin inhibitor, 10 μM leupeptin, 0.04 unit/ml aprotinin, 1 μM bestatin, and 20% (v/v) glycerol, and was homogenized using a motor-driven Teflon-tipped pestle (three strokes). The homogenates were centrifuged at 9000 *g* for 20 min at 4 °C and the resultant supernatant centrifuged at 105000 *g* for 60 min at 4 °C. The fatty layer on the surface was removed carefully and the microsomal pellets were resuspended in ice-cold buffer A.

To investigate the effects of protease inhibitors and glycerol, the following buffers were used instead of buffer A: B, Tris-HCl buffer (pH 7.4) containing KCl, APMSF, EDTA, trypsin inhibitor, aprotinin, bestatin and leupeptin; C, Tris-HCl buffer (pH 7.4) containing KCl, glycerol, APMSF, EDTA and trypsin inhibitor; D, Tris-HCl buffer (pH 7.4) containing KCl, glycerol, APMSF and EDTA at the above concentrations.

Hepatic microsomes were prepared by the same method above except for the use of 0.9% NaCl instead of the washing solution described above.

The effects of freezing and thawing on testosterone 6β-hydroxylase activities in mouse intestinal and hepatic microsomes were examined with microsomes frozen in liquid nitrogen and thawed in water at room temperature within 1 day.

Protein concentrations were determined according to Lowry *et al*. (1951) using bovine serum albumin as the standard.

Enzyme assays

Testosterone 6β-hydroxylation, nifedipine oxidation, midazolam 1′- and 4-hydroxylation, bufuralol 1′- and 6-hydroxylation, tolbutamide methylhydroxylation, and chlorzoxazone 6-hydroxylation were determined as described (Kronbach *et al*. 1987, 1989, Brian *et al*. 1989, Peter *et al*. 1990, Yamazaki *et al*. 1994, Yamazaki and Shimada 1997). The standard incubation mixture (final volume 0.25 ml) contained 0.3 mg protein mouse intestinal microsomes, 100 mM potassium phosphate buffer (pH 7.4), an NADPH-generating system consisting of 0.5 mM $NADP^+$, 5 mM glucose 6-phosphate, 0.5 unit/ml glucose 6-phosphate dehydrogenase and 100 μM substrates except for tolbutamide methylhydroxylation. The incubation mixture for tolbutamide methylhydroxylation contained 0.3 mg protein mouse intestinal microsomes, 50 mM potassium phosphate buffer (pH 7.4), the NADPH-generating system and 250 μM tolbutamide. In the case of hepatic microsomes, 0.1 mg mouse hepatic microsomes was used. The reaction mixtures were incubated at 37 °C for 10 min for testosterone 6β-hydroxylation, nifedipine oxidation, midazolam 1′- and 4-hydroxylation, and chlorzoxazone 6-hydroxylation and for 15 min for bufuralol hydroxylation and tolbutamide methylhydroxylation. The reactions with testosterone, nifedipine, chlorzoxazone and tolbutamide were terminated by the addition of 1.5 ml dichloromethane and 0.3 M NaCl for testosterone 6β-hydroxylation, 0.2 M NaCl–0.1 M sodium carbonate for nifedipine oxidation, 4.3% phosphoric acid for chlorzoxazone hydroxylation, and 0.1 N HCl for tolbutamide methylhydroxylation. After mixing vigorously and centrifugation at 900 *g* for 10 min, the organic phase was evaporated at 40 °C under a gentle nitrogen stream. The residue was dissolved in 200 μl HPLC mobile phase, and a 100-μl portion was subjected to HPLC. The reactions of midazolam and bufuralol were terminated by the addition of 0.25 ml methanol and 10 μl 60% percloric acid respectively. After mixing vigorously, the mixtures were centrifuged at 900 *g* for 10 min. The supernatants (100 μl) were subjected to HPLC analysis.

The substrates and P450 inhibitors (dissolved in methanol) were added simultaneously to the microsomal preparations. The final concentration of solvent in the incubation mixture was $< 1\%$.

HPLC analyses

HPLC analyses were performed using an LC-6A pump, SIL-6B autosampler, SPD-6A UV detector (all Shimadzu, Kyoto, Japan), FP-920 II fluorescence detector (Jasco, Tokyo, Japan) and C-R4A integrator (Shimadzu) equipped with a C_{18} 5-μm analytical column (Mightysil, 150 × 4.6 mm i.d.; Kanto Chemicals, Tokyo, Japan) except for the case of chlorzoxazone hydroxylation (C_8 5-μm analytical column, Mightysil, 150 × 4.6 mm i.d.; Kanto). The column temperature was set at 35 °C in a CTO-6A column oven (Shimadzu). The elution of both testosterone and nifedipine metabolites was conducted with a 64% CH_3OH (v/v) at 1 (testosterone) or 1.5 ml/min (nifedipine). The eluate was monitored at 240 and 254 nm respectively. The elution of midazolam metabolites was conducted with 24% methanol/33% acetonitrile/43% 10 mM potassium phosphate buffer (pH 7.4) (v/v) at 1 ml/min. The eluate was monitored at 220 nm. The elution of bufuralol metabolites was conducted with 33% acetonitrile/67% 20 mM sodium perchloric acid (pH 2.5) (v/v) at 1.5 ml/min. The eluate was monitored fluorometrically (excitation 252 nm, emission 302 nm). The elution of tolbutamide metabolites was conducted with 30% acetonitrile containing 0.04% phosphoric acid (v/v) at 1.5 ml/min. The eluate was monitored at 230 nm. The elution of chlorzoxazone metabolites was conducted with a mixture of 27% acetonitrile containing 0.5% phosphoric acid (v/v) at 1.5 ml/min. The eluate was monitored at 287 nm.

Immunoblot analyses

Polyclonal goat anti-rat CYP1A1, CYP2C6, CYP2E1 and CYP3A2 antisera were from Daiichi Pure Chemicals (Tokyo, Japan). Polyclonal rabbit anti-rat CYP2D1 antiserum was from Funakoshi (Tokyo, Japan). Immunoblot analysis was performed according to Laemmli (1970) with slight modifications. The microsomal proteins were separated on 7.5% polyacrylamide gel electrophoresis and transferred electrophoretically to a nitrocellulose membrane. The secondary antibodies used were anti-goat IgG (anti-rabbit IgG for CYP2D1) and detection was carried out with diaminobenzidine staining.

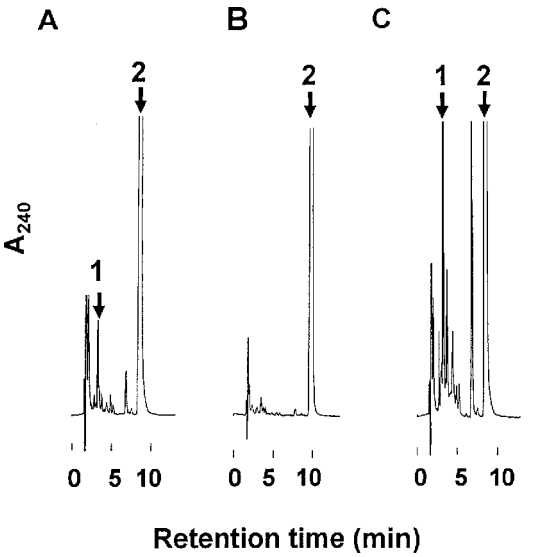


Figure 1. Representative HPLC chromatograms of testosterone metabolites in mouse intestinal and hepatic microsomes. (A) Mouse intestinal microsomes prepared with buffer A; (B) mouse intestinal microsomes prepared with buffer A excluding protease inhibitors and glycerol; (C) mouse hepatic microsomes prepared with buffer A. Peak: 1, 6β-hydroxytestosterone; 2, testosterone. Precision was $< 10\%$ and inaccuracy was $< 10\%$ with control samples containing 50 and 250 pmol 6β-hydroxytestosterone ($n = 5$). Detection limit was < 1 pmol/min/mg intestinal microsomal protein.

Statistical analysis

Statistical analysis was performed by a Student's *t*-test using an InStat computer program (Graphpad Software, San Diego, CA, USA).

Results

Effects of protease inhibitors and glycerol in the preparation buffers and of freezing and thawing on testosterone 6β-hydroxylase activity in intestinal and hepatic microsomes from the mouse

Testosterone 6β-hydroxylase activity was determined in mouse intestinal and hepatic microsomes (figure 1). 6β-Hydroxytestosterone was observed when intestinal microsomes prepared in buffer A were used as an enzyme source (figure 1A). However, when glycerol and these protease inhibitors were omitted from buffer A, testosterone 6β-hydroxylase activity could not be detected (figure 1B). On the other hand, the formation of 6β-hydroxytestosterone catalysed by mouse hepatic microsomes was similar in these two preparation buffers.

The effects of combinations of protease inhibitors and of glycerol in buffer A on testosterone 6β-hydroxylase activity of mouse intestinal and hepatic microsomes were investigated (figure 2). Intestinal microsomes from mouse prepared with buffer A gave the highest activities among those prepared with the buffer systems used in this study (figure 2(1A)). Therefore, intestinal microsomes from mouse were prepared using buffer A thereafter and used as an enzyme source. The effects of freezing and thawing of mouse intestinal microsomes on testosterone 6β-hydroxylase activities were investigated. Testosterone 6β-hydroxylase activities of mouse

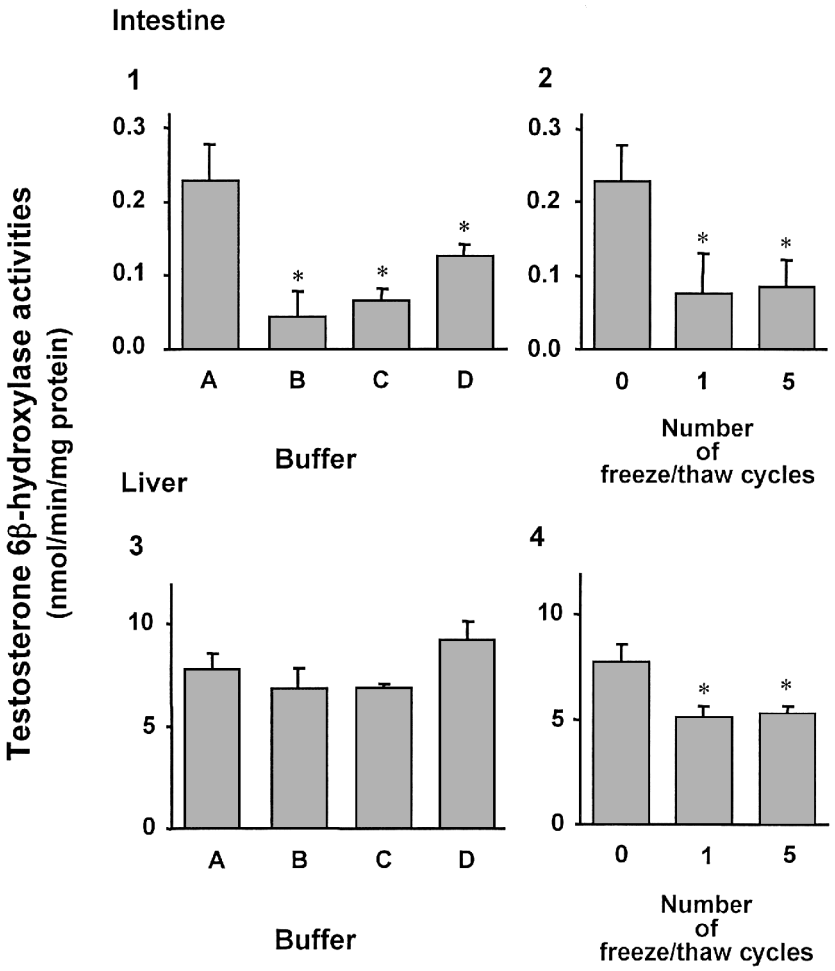


Figure 2. Effects of protease inhibitors and glycerol in preparations of microsomes and of freezing and thawing of microsomes on the testosterone 6β-hydroxylase activity. Intestinal (1) and hepatic (3) microsomes from mice were prepared using buffers A–D and catalytic activities determined in an unfrozen condition according to the method described in the Materials and methods. Both intestinal (2) and hepatic (4) microsomes prepared with buffer A were subjected to one or five cycles of freezing and thawing. * Significantly different from activities of unfrozen intestinal (1 and 2) and hepatic microsomes (3 and 4) prepared with buffer A from mice ($p < 0.05$). Each column represents the mean $\pm$ SD from three mice.

intestinal microsomes were decreased to 30% by only one cycle of freezing and thawing (figure 2(2)). Five cycles of freezing and thawing did not further affect the activities decreased by one cycle.

In contrast, the effects of combinations of protease inhibitors and of glycerol on the testosterone 6β-hydroxylase activities of hepatic microsomes were not significant (figure 2(3)). One cycle of freezing and thawing resulted in a 40% decrease of the catalytic activities in mouse hepatic microsomes (figure 2(4)). The degree of decrease of testosterone 6β-hydroxylase activities in mouse hepatic microsomes by freezing and thawing was smaller than that of mouse intestinal microsomes.

Table 1. Drug oxidation activities in intestinal and hepatic microsomes from mouse.

Drug oxidation	Microsomes	
	Intestine (pmol/min/mg protein)	Liver (pmol/min/mg protein)
Testosterone 6β-hydroxylation	230±50	7800±51
Nifedipine oxidation	88±51	1400±140
Midazolam 1′-hydroxylation	24±5	260±28
Midazolam 4-hydroxylation	21±5	240±23
Chlorzoxazone 6-hydroxylation	67±54	4100±910
Bufuralol 1′-hydroxylation	55±11	3200±220
Bufuralol 6-hydroxylation	0·3±0·1	8·5±0·7
Tolbutamide methylhydroxylation	8±3	670±240

Microsomes were prepared with buffer A and were used for assays without freezing.
Data are the mean±SD from three mice.

Comparison of drug oxidation activities in intestinal and hepatic microsomes from the mouse

Drug oxidation activities of intestinal and hepatic microsomes from mouse are summarized in table 1. Low but significant activities of nifedipine oxidation, midazolam 1′- and 4-hydroxylation, chlorzoxazone 6-hydroxylation, bufuralol 1′- and 6-hydroxylation, and tolbutamide methylhydroxylation were observed in mouse intestinal microsomes. The maximal turnover number was observed for testosterone 6β-hydroxylation in both intestinal and hepatic microsomes. The ratios of midazolam 1′- and 4-hydroxylation activities in intestinal and hepatic microsomes from mouse were similar.

Effects of P450 inhibitors on oxidation activities in mouse intestinal and hepatic microsomes

The effects of P450 inhibitors on testosterone 6β-hydroxylase, chlorzoxazone 6-hydroxylase, and bufuralol 1′- and 6-hydroxylase activities in intestinal and hepatic microsomes from mouse were investigated (figure 3). Testosterone 6β-hydroxylase activities in both intestinal and hepatic microsomes were extensively inhibited by ketoconazole (figure 3A) and were similar in intestinal microsomes freshly prepared and subjected once to freezing (data not shown). Chlorzoxazone 6-hydroxylase activities in intestinal and hepatic microsomes were inhibited to 68 and 58% respectively by diethyldithiocarbamate (figure 3B). Bufuralol 1′-hydroxylase activities in both intestinal and hepatic microsomes were extensively inhibited by quinine rather than by quinidine (figure 3C). Quinine, quinidine and α-naphthoflavone inhibited bufuralol 6-hydroxylase activities in intestinal microsomes in a similar manner (figure 3D). Bufuralol 6-hydroxylase activity in hepatic microsomes was inhibited to 16% by α-naphthoflavone.

Immunoblot analyses of mouse P450s in intestinal microsomes

Two immunoreactive bands could be observed in intestinal and hepatic microsomes from mouse, showing similar migration detected by anti-rat CYP3A2

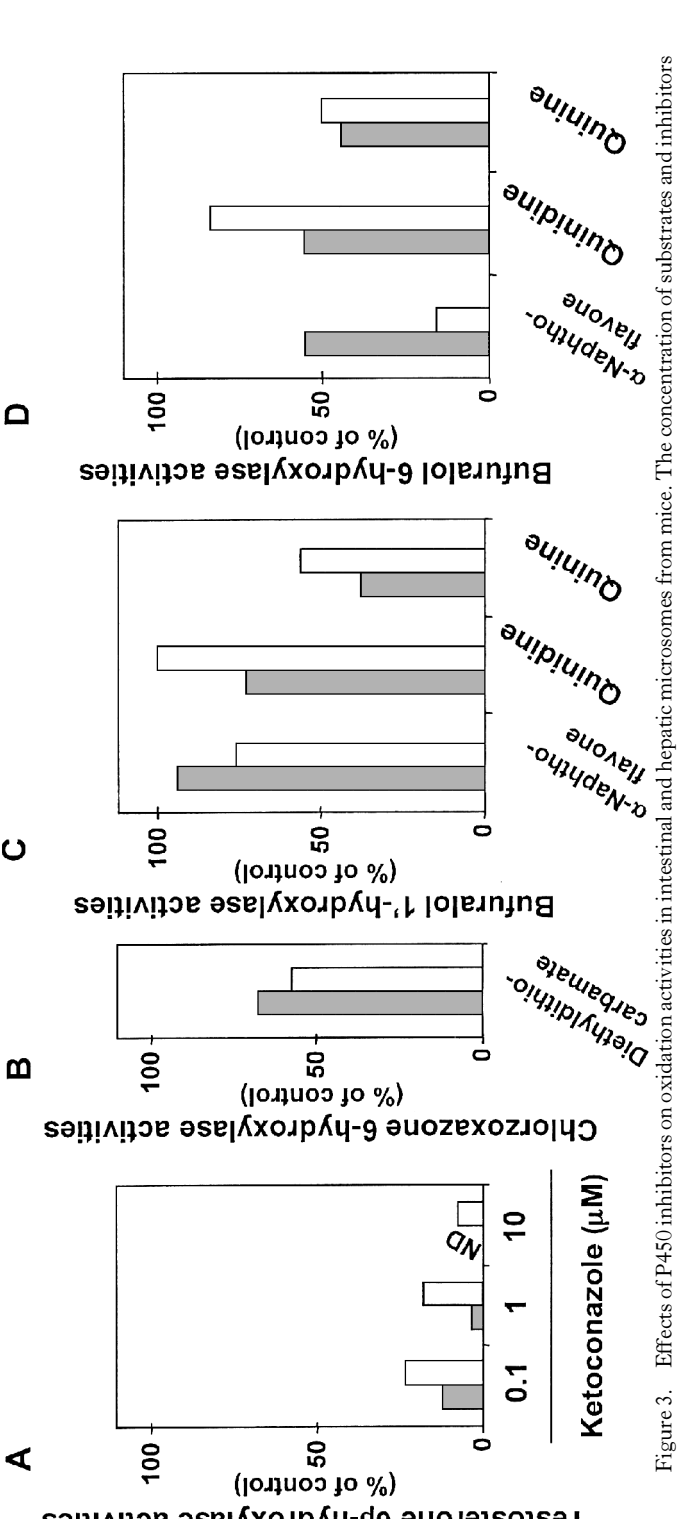


Figure 3. Effects of P450 inhibitors on oxidation activities in intestinal and hepatic microsomes from mice. The concentration of substrates and inhibitors was 0.1 mM except that of ketoconazole (as indicated). Drug oxidation activities in intestinal (close column) and hepatic (open column) microsomes subjected once to freezing were measured. (A) Control activity (without inhibitors) of testosterone 6β-hydroxylation by intestinal and hepatic microsomes was 131 and 7040 pmol/min/mg protein respectively. (B) Control activity of chlorzoxazone 6-hydroxylation by intestinal and hepatic microsomes was 48 and 3080 pmol/min/mg protein respectively. (C) Control activity of bufuralol 1′-hydroxylation by intestinal and hepatic microsomes was 43 and 2950 pmol/min/mg protein respectively. (D), Control activity of bufuralol 6-hydroxylation by intestinal and hepatic microsomes was 0.19 and 7.8 pmol/min/mg protein respectively. Each column represents the average of duplicate determinations. ND, not detected.

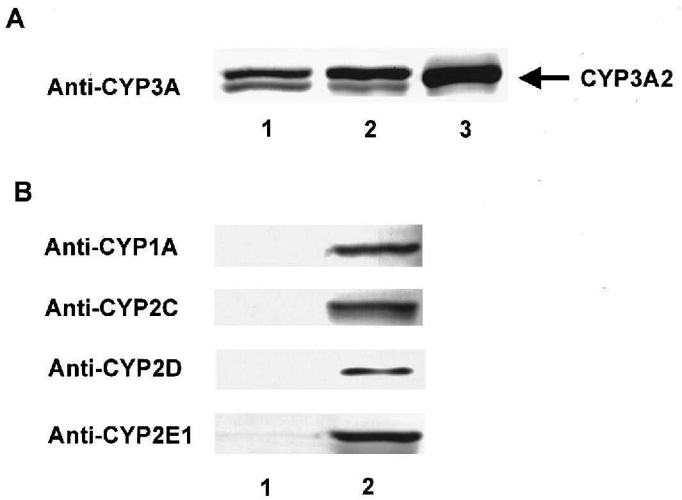


Figure 4. Immunoblot analyses of mouse intestinal and hepatic microsomes. (A) Immunoblot analyses of mouse intestinal and hepatic microsomes were performed using anti-rat CYP3A2 antibodies. Lanes 1, intestinal microsomes (30 μg) from upper part of mouse small intestine; 2, mouse hepatic microsomes (10 μg); 3, rat hepatic microsomes for standard (corresponding to 0.23 pmol CYP3A2). (B) Immunoblot analyses of mouse intestinal and hepatic microsomes were performed using anti-rat CYP1A1, anti-rat CYP2C6, anti-rat CYP2D1 and anti-rat CYP2E1 antibodies. Lanes 1 and 2 were the same as those in (A).

antibodies (Figure 4A). Rat hepatic microsomes showed a single band. Compared with intestinal samples of mouse, the density of the upper band in hepatic microsomes was higher than the lower band. On the other hand, anti-rat CYP1A1, anti-rat CYP2C6, anti-rat CYP2D1 and anti-rat CYP2E1 recognized mouse hepatic P450 enzymes; however, no immunoreactive bands in mouse intestinal microsomes could be detected (figure 4B).

Discussion

In general, the preparation of intestinal microsomes is relatively difficult compared with hepatic microsomes because intestinal microsomes are exposed to an abundance of proteases during preparation. In the preparation of intestinal microsomes from human, monkey and rodent, different laboratories have used different combinations of protease inhibitors. One popular combination of protease inhibitors is phenyl methanesulphonyl fluoride (PMSF) and EDTA, and they have been occasionally used in combination with a trypsin inhibitor or leupeptine (Rosenberg and Mankowski 1994, Kashfi *et al.* 1995). Shimizu *et al.* (1998) reported that PMSF was effective in the preparation of intestinal microsomes from human, although PMSF was not effective in those from monkey. Komura *et al.* (1998) employed a combination of a trypsin inhibitor and EDTA without PMSF in the preparation of intestinal microsomes from dog. In the preparation of recombinant human P450 enzymes from bacterial membranes, protease inhibitors such as PMSF, leupeptine, bestatin, aprotinin and EDTA have been used (Guengerich *et al.* 1998). Therefore, the methods for the preparation of intestinal microsomes from each type of animal should be considered carefully.

In the present study, combinations of protease inhibitors as well as glycerol (buffer A) were necessary to obtain good testosterone 6β-hydroxylase activities in mouse intestinal microsomes (figure 2(1)). In our preliminary experiments, testosterone 6β-hydroxylase activities in intestinal microsomes based on total protein were 4.1-fold higher than those of 9000 *g* supernatant of intestine, although the catalytic activities of 9000 *g* supernatant from mouse intestines were not dependent on the constituents of the preparation buffer (data not shown). These results suggested that P450 enzymes in intestinal microsomes would lose the activities during the ultracentrifugation of 9000 *g* supernatant and/or resuspension process in the absence of protease inhibitors and glycerol. The preparation of intestinal microsomes without glycerol caused a significant loss of catalytic activities in an unfrozen condition compared with those prepared with glycerol in spite of the addition of protease inhibitors (figure 2(1)). Therefore, glycerol could play an important role in the preparation of catalytically active intestinal microsomes (figure 2(1)) in a similar manner as reported in liver microsomes (Guengerich 1994). Intestinal microsomes from rat prepared with buffer A showed lower testosterone 6β-hydroxylase activities (41 ± 9 pmol/min/mg protein, mean $\pm$ SD, $n = 3$) than those from mice in unfrozen condition (data not shown). These results also suggested that there would be species differences in the effects of protease inhibitors for the maintenance of catalytic activities in microsomal preparations.

Several drug oxidation activities were demonstrated in the upper part of small intestine from mouse (table 1). The inhibitory effects of typical P450 inhibitors on testosterone 6β-hydroxylase, chlorzoxazone 6-hydroxylase, and bufuralol 1′- and 6-hydroxylase activities in intestinal and hepatic microsomes from mouse were observed (figure 3). These drug oxidation activities in mouse intestine should be catalysed by P450 enzymes. However, immunoreactive bands of Cyp1a, Cyp2c, Cyp2d and Cyp2e1 enzymes were not detected in mouse intestine, and only Cyp3a proteins were clearly detected using anti-rat CYP3A2 antibodies (figure 4). These results suggested that catalytic analysis might have higher sensitivity than immunoblot analysis to characterize microsomal P450 enzymes in mouse intestine.

The density of two immunoreactive bands detected using anti-rat CYP3A2 antibodies was different in intestinal and hepatic microsomes (figure 4A). Sakuma *et al*. (2000) reported that both Cyp3a11 and Cyp3a13 were the major Cyp3a enzymes in mouse small intestine and liver. In livers of the male mouse, Cyp3a11 predominated over Cyp3a13 (Yanagimoto *et al*. 1997). The molecular weights of mouse Cyp3a11 (SwissProt accession no. Q64459), Cyp3a13 (Q64464) and rat CYP3A2 (P05183) have been reported to be 57.9, 57.5 and 57.7 kDa respectively (SWISS-PROT protein database). Although there was an organ difference with respect to the expression of Cyp3a enzymes, the upper and lower bands observed immunochemically are very likely Cyp3a11 and Cyp3a13 respectively.

In conclusion, proposed here is an appropriate method for the preparation of intestinal microsomes from mouse using glycerol and a combination of protease inhibitors. Freezing of mouse intestinal microsomes should be avoided as much as possible for the analysis of catalytic activities. The present authors are currently examining the metabolic profiles of drugs in the intestine using intestinal microsomes from other animals and humans.

Acknowledgements

The work was supported in part by a Pharmaceutical and Medical Safety Research Grant from the Ministry of Health and Welfare of Japan. The authors thank Ms Ayaka Shibata for skilful technical assistance and Brent Bell for reviewing the manuscript.

References

Brian, W. R., Srivastava, P. K., Umbenhauer, D. R., Lloyd, R. S. and Guengerich, F. P., 1989, Expression of a human liver cytochrome P450 protein with tolbutamide hydroxylase activity in *Saccharomyces cerevisiae*. *Biochemistry*, **28**, 4993–4999.

Guengerich, F. P., 1991, Reaction and significance of cytochrome P-450 enzymes. *Journal of Biological Chemistry*, **266**, 10019–10022.

Guengerich, F. P., 1994, Analysis and characterization of enzymes. In A. W. Hayes (ed.), *Principles and Methods of Toxicology* (New York: Raven), pp. 1259–1313.

Guengerich, F. P., 1995, Human cytochrome P450 enzymes. In P. R. Oritiz de Montellano (ed.), *Cytochrome P450* (New York: Plenum), pp. 473–535.

Guengerich, F. P., Hosea, N. A. and Martin, M. V., 1998, Purification of cytochromes P450: products of bacterial recombinant expression systems. In I. R. Phillips and E. A. Shephard (eds), *Cytochrome P450 Protocols* (Totowa: Humana), pp. 77–83.

Iatsimirskaia, E., Tulebaev, S., Storozhuk, E., Utkin, I., Smith, D., Gerber, N. and Koudriakova, T., 1997, Metabolism of rifabutin in human enterocyte and liver microsomes: kinetic parameters, identification of enzyme systems, and drug interactions with macrolides and antifungal agents. *Clinical Pharmacology and Therapeutics*, **61**, 554–562.

Kashfi, K., McDougall, C. J. and Dannenberg, A. J., 1995, Comparative effects of omeprazole on xenobiotic metabolizing enzymes in the rat and human. *Clinical Pharmacology and Therapeutics*, **58**, 625–630.

Komura, H., Sagami, M. and Yoshida, N. H., 1998, Establishment for evaluation system of small intestinal metabolism. Abstract for the 5th annual meeting of the HAB Discussion Group, **5**, 1.

Krishna, D. R. and Klotz, U., 1994, Extrahepatic metabolism of drugs in humans. *Clinical Pharmacokinetics*, **26**, 144–160.

Kronbach, T., Mathys, D., Gut, J., Catin, T. and Meyer, U. A., 1987, High-performance liquid chromatographic assays for bufuralol 1′-hydroxylase, debrisoquine 4-hydroxylase, and dextromethorphan *O*-demethylase in microsomes and purified cytochrome P450 isozymes of human liver. *Analytical Biochemistry*, **162**, 24–32.

Kronbach, T., Mathys, D., Umeno, M., Gonzalez, F. J. and Meyer, U. A., 1989, Oxidation of midazolam and triazolam by human liver cytochrome P450IIIA4. *Molecular Pharmacology*, **36**, 89–96.

Laemmli, U. K., 1970, Cleavage of structural proteins during the assembly of the head of bacteriophage T4. *Nature*, **227**, 680–685.

Lowry, O. H., Rosebrough, N. J., Farr, A. L. and Randall, R. J., 1951, Protein measurement with the Folin phenol reagent. *Journal of Biological Chemistry*, **193**, 265–275.

Paine, M. F., Khalighi, M., Fisher, J. M., Shen, D. D., Kunze, K. L., Marsh, C. L., Perkins, J. D. and Thummel, K. E., 1997, Characterization of interintestinal and intraintestinal variations in human CYP3A-dependent metabolism. *Journal of Pharmacology and Experimental Therapeutics*, **283**, 1552–1562.

Paine, M. F., Shen, D. D., Kunze, K. L., Perkins, J. D., Marsh, C. L., McVicar, J. P., Barr, D. M., Gillies, B. S. and Thummel, K. E., 1996, First-pass metabolism of midazolam by the human intestine. *Clinical Pharmacology and Therapeutics*, **60**, 14–24.

Pearce, R. E., McIntyre, C. J., Madan, A., Sanzgiri, U., Draper, A. J., Bullock, P. L., Cook, D. C., Burton, L. A., Latham, J., Nevins, C. and Parkinson, A., 1996, Effects of freezing, thawing, and storing human liver microsomes on cytochrome P450 activity. *Archives of Biochemistry and Biophysics*, **331**, 145–169.

Peter, R., Böcker, R., Beaune, P. H., Iwasaki, M., Guengerich, F. P. and Yang, C. S., 1990, Hydroxylation of chlorzoxazone as a specific probe for human liver cytochrome P450IIE1. *Chemical Research in Toxicology*, **3**, 566–573.

Prueksaritanont, T., Gorham, L. M., Hochman, J. H., Tran, L. O. and Vyas, K. P., 1996, Comparative studies of drug-metabolizing enzymes in dog, monkey, and human small intestines, and in Caco-2 cells. *Drug Metabolism and Disposition*, **24**, 634–642.

Rosenberg, D. W. and Mankowski, D. C., 1994, Induction of cyp2e-1 protein in mouse colon. *Carcinogenesis*, **15**, 73–78.

Sakuma, T., Takai, M., Endo, Y., Kuroiwa, M., Ôhara, A., Jarukamjorn, K., Honma, R. and

Nemoto, N., 2000, A novel female-specific member of the CYP3A gene subfamily in the mouse liver. *Archives of Biochemistry and Biophysics*, **377**, 153–162.

Shimada, T., Yamazaki, H., Mimura, M., Inui, Y. and Guengerich, F. P., 1994, Interindividual variations in human liver cytochrome P450 enzymes involved in the oxidation of drugs, carcinogens and toxic chemicals: studies with liver microsomes of 30 Japanese and 30 Caucasians. *Journal of Pharmacology and Experimental Therapeutics*, **270**, 414–423.

Shimizu, R., Hanano, M. and Sato, T., 1998, Preparation and storage of human intestinal microsomes. *Xenobiotic Metabolism and Disposition*, **13**, S254.

Watkins, P. B., Wrighton, S. A., Schuetz, E. G., Molowa, D. T. and Guzelian, P. S., 1987, Identification of glucocorticoid-inducible cytochromes P450 in the intestinal mucosa of rats and man. *Journal of Clinical Investigation*, **80**, 1029–1036.

Yamazaki, H., Guo, Z., Persmark, M., Mimura, M., Inoue, K., Guengerich, F. P. and Shimada, T., 1994, Bufuralol hydroxylation by cytochrome P450 2D6 and 1A2 enzymes in human liver microsomes. *Molecular Pharmacology*, **46**, 568–577.

Yamazaki, H., Inoue, K., Turvy, C. G., Guengerich, F. P. and Shimada, T., 1997, Effects of freezing, thawing, and storage of human liver samples on the microsomal contents and activities of cytochrome P450 enzymes. *Drug Metabolism and Disposition*, **25**, 168–174.

Yamazaki, H. and Shimada, T., 1997, Progesterone and testosterone hydroxylation by cytochromes P450 2C19, 2C9, and 3A4 in human liver microsomes. *Archives of Biochemistry and Biophysics*, **346**, 161–169.

Yanagimoto, T., Itoh, S., Sawada, M. and Kamataki, T., 1997, Mouse cytochrome P450 (Cyp3a11): predominant expression in liver and capacity to activate aflatoxin B_1. *Archives of Biochemistry and Biophysics*, **340**, 215–218.

Zhang, Q. Y., Wikoff, J., Dunbar, D. and Kaminsky, L., 1996, Characterization of rat small intestinal cytochrome P450 composition and inducibility. *Drug Metabolism and Disposition*, **24**, 322–328.

XENOBIOTICA, 2000, VOL. 30, NO. 10, 955–969

Metabolism of 7-benzyloxy-4-trifluoromethyl-coumarin by human hepatic cytochrome P450 isoforms

A. B. RENWICK†, D. SURRY‡, R. J. PRICE†,
B. G. LAKE†* and D. C. EVANS§

† TNO BIBRA International Ltd, Carshalton SM5 4DS, UK
‡ Merck Sharp and Dohme Ltd, Neuroscience Research Centre, Terlings Park, Harlow CM20 2QR, UK
§ Merck and Co., Inc., 126 East Lincoln Avenue, Rahway, NJ 08535, USA

Received 14 April 2000

1. The metabolism of 7-benzyloxy-4-trifluoromethylcoumarin (BFC) to 7-hydroxy-4-trifluoromethylcoumarin (HFC) was studied in human liver microsomal preparations and in cDNA-expressed human cytochrome P450 (CYP) isoforms.

2. Kinetic analysis of the NADPH-dependent metabolism of BFC to HFC in four preparations of pooled human liver microsomes revealed mean (±SEM) K_m and V_{max} of 8.3±1.3 μM and 454±98 pmol/min/mg protein respectively.

3. The metabolism of BFC to HFC was determined in a characterized bank of 24 individual human liver microsomal preparations employing BFC substrate concentrations of 20 and 50 μM (i.e. about two and six times K_m respectively). With 20 μM BFC the highest correlations were observed between BFC metabolism and markers of CYP1A2 (r^2 = 0.784–0.797) and then with CYP3A (r^2 = 0.434–0.547) isoforms, whereas with 50 μM BFC the highest correlations were observed between BFC metabolism and markers of CYP3A (r^2 = 0.679–0.837) and then with CYP1A2 (r^2 = 0.421–0.427) isoforms. At both BFC substrate concentrations, lower correlations were observed between BFC metabolism and enzymatic markers for CYP2A6, CYP2B6, CYP2C9, CYP2C19, CYP2D6, CYP2E1 and CYP4A9/11.

4. Using human β-lymphoblastoid cell microsomes containing cDNA-expressed CYP isoforms, 20 μM BFC was metabolized by CYP1A2 and CYP3A4, with lower rates of metabolism being observed with CYP2C9 and CYP2C19. Kinetic studies with the CYP1A2 and CYP3A4 preparations demonstrated a lower K_m with the CYP1A2 preparation, but a higher V_{max} with the CYP3A4 preparation.

5. The metabolism of 20 μM BFC in human liver microsomes was inhibited to 37–48% of control by 5–100 μM of the mechanism-based CYP1A2 inhibitor furafylline and to 64–69% of control by 5–100 μM of the mechanism-based CYP3A4 inhibitor troleandomycin. While some inhibition of BFC metabolism was observed in the presence of 100 and 200 μM diethyldithiocarbamate, the addition of 2–50 μM sulphaphenazole, 50–500 μM *S*-mephenytoin and 2–50 μM quinidine had little effect.

6. The metabolism of 20 μM BFC to HFC in human liver microsomes was also inhibited by an antibody to CYP3A4, whereas antibodies to CYP2C8/9 and CYP2D6 had no effect.

7. In summary, by correlation analysis, use of cDNA-expressed CYP isoforms, chemical inhibition and inhibitory antibodies, BFC appears metabolized by a number of CYP isoforms in human liver. BFC metabolism appears to be primarily catalysed by CYP1A2 and CYP3A4, with possibly some contribution by CYP2C9, CYP2C19 and perhaps other CYP isoforms.

8. The results also demonstrate the importance of the selection of an appropriate substrate concentration when conducting reaction phenotyping studies with human hepatic CYP isoforms.

* Author for correspondence; e-mail: blake@bibra.co.uk

Xenobiotica ISSN 0049-8254 print/ISSN 1366-5928 online © 2000 Taylor & Francis Ltd
http://www.tandf.co.uk/journals

Introduction

The cytochrome P450 (CYP) superfamily of isoforms is known to have a major role in the oxidative metabolism of xenobiotics and certain endogenous compounds including fatty acids, steroids and vitamins (Parkinson 1996a, b). In human liver microsomes members of the CYP1A, CYP2A, CYP2B, CYP2C, CYP2D, CYP2E and CYP3A subfamilies have been shown to metabolize a wide variety of drugs (Wrighton *et al*. 1993a, 1995, Nelson *et al*. 1996, Parkinson 1996a, b, Pelkonen *et al*. 1998). Knowledge of the CYP isoforms responsible for the metabolism of a new therapeutic agent is required for a number of reasons. For example, such information can help predict likely drug interactions and identify whether some individuals will be poor metabolizers of the drug as a consequence of known genetic polymorphisms (Parkinson 1996a, b, Pelkonen *et al*. 1998).

In recent years extensive use has been made of *in vitro* techniques employing human liver microsomes and cDNA-expressed human liver CYP isoforms (Wrighton *et al*. 1993a, 1995, Crespi *et al*. 1997, 1998, Clarke 1998, Pelkonen *et al*. 1998, Rodrigues 1999). Using these systems, it is possible to identify which CYP isoforms will be involved in the metabolism of a new chemical entity and from CYP isoform inhibition studies to obtain information on the potential for *in vivo* drug interactions. One requirement for conducting such studies is the availability of suitable probe substrates for the CYP isoforms of interest. For example, rapid screening for CYP isoform inhibition may be performed in a 96-well plate format using either liver microsomes or cDNA-expressed CYP isoforms and substrates that are metabolized to highly fluorescent products (Crespi *et al*. 1997, 1998, 1999).

Recently, the present authors have been developing some more rapid procedures for the determination of CYP1A2, CYP2C9, CYP2C19, CYP2D6, CYP2E1 and CYP3A4 isoform enzyme activities in human liver microsomes. As part of this work, the metabolism of 7-benzyloxy-4-trifluoromethylcoumarin (BFC) has been examined using a 96-well plate format coupled to fluorimetric quantitation of the 7-hydroxy-4-trifluoromethylcoumarin (HFC) product. Using a bank of characterized human liver microsomes, good correlations (r^2 = 0.77–0.84) were observed between BFC metabolism and the metabolism of the CYP3A isoform substrates testosterone and midazolam (Surry and Evans, unpublished data). Others have reported that BFC is a selective substrate for cDNA-expressed CYP3A4 (Crespi *et al*. 1999). The availability of selective fluorescent CYP3A4 substrates would be very useful for rapid CYP isoform metabolism and inhibition screening studies. Currently, many substrates used as CYP3A4 probes are not readily amenable for use in rapid screens as the assays often involve chromatographic separation of the metabolites before quantitation by spectroscopic, radiometric or mass spectrometry techniques. One exception appears to be 3-(3,4-difluorobenzyloxy)-5,5-dimethyl-4-(4-methylsulphonylphenyl)-5*H*-furan-2-one (DFB), which has been reported to be a specific fluorescent probe for CYP3A4/5 in human liver microsomes (Chauret *et al*. 1999).

The objective of this study was to identify which CYP isoforms are responsible for BFC metabolism in human liver in order to ascertain if BFC is a specific substrate for CYP3A isoforms. CYP isoform 'reaction phenotyping' (Parkinson 1996a, b, Rodrigues 1999) was performed by correlation analysis, the use of cDNA-expressed human CYP isoforms, chemical inhibition and inhibitory antibodies.

Materials and methods

Materials

NADPH, Tris, diethyldithiocarbamate, quinidine, sulphaphenazole and troleandomycin were obtained from Sigma-Aldrich Co. Ltd (Poole, Dorset, UK) and BFC, HFC, furafylline and *S*(+)-mephenytoin from Salford Ultrafine Chemicals and Research Ltd. (Manchester, UK). Microsomes from human β-lymphoblastoid cells containing cDNA-expressed human CYP isoforms (Gentest Corp., Woburn, MA, USA) were obtained from Cambridge Bioscience (Cambridge, UK) and stored at –80 °C. The samples of human β-lymphoblastoid cell microsomes comprised control cell microsomes (i.e. no transfected human CYP isoform cDNA but contains native CYP1A1 activity) and cell microsomes containing CYP1A2, CYP2A6+OR (i.e. CYP2A6 cDNA plus human NADPH-cytochrome P450 reductase (OR) cDNA), CYP2B6, CYP2C8+OR, CYP2C9+OR, CYP2C19, CYP2D6+OR, CYP2E1+OR and CYP3A4+OR. Inhibitory antibodies against CYP2C8/9, CYP2D6 and CYP3A4 were provided by MSD Research Laboratories (Harlow, Essex, UK) and stored at −80 °C. The specificity and use of the CYP3A4 antibody has been recently described (Mei *et al*. 1999).

Human liver microsomes

Samples of human liver (surplus to transplant requirements) were transported on ice to TNO BIBRA from other institutions and were stored at –80 °C. Washed microsomal fractions were prepared in 0.154 M KCl containing 50 mM Tris-HCl pH 7.4 as described previously (Lake, 1987). Liver microsomal fractions were assayed for protein (Lowry *et al*. 1951) employing bovine serum albumin as standard. The washed microsomal fractions were diluted to 10 mg protein/ml and aliquots stored at –80 °C. Four separate batches, designated pools A, B, C and D, of pooled human liver microsomes were prepared. Each batch was prepared by pooling liver samples from five subjects. Pool A comprised liver samples from males aged 15, 29 and 44 years and females aged 12 and 42 years; pool B comprised liver samples from males aged 26, 29 and 41 years and females aged 14 and 42 years; pool C comprised liver samples from male subjects aged 15, 17 and 29 years and female subjects aged 31 and 42 years and pool D comprised liver samples from male subjects aged 2.5 and 58 years and female subjects aged 14, 59 and 74 years. Studies were also conducted with a bank of 24 individual human liver microsomal preparations that had been previously characterized for total CYP content and CYP isoform enzyme activities (Renwick *et al*. 1998).

Metabolism of BFC by human liver microsomes

Incubations were performed in Nunc MicroWell™ (Life Technologies Ltd., Paisley, Scotland, UK) polystyrene 96-well plates with conical wells. The NADPH-dependent metabolism of BFC was studied in incubation mixtures containing 2–100 μM BFC, 2–50 μg of microsomal protein and 70 mM phosphate buffer pH 7.4 in a final volume of 100 μl. Stock solutions of BFC were prepared in methanol and diluted 1 in 300 with 100 mM phosphate buffer pH 7.4 so that the final methanol concentration in the incubations was 0.2% (v/v). For each BFC substrate concentration, microsomal protein concentration and incubation time, 6 wells were incubated with NADPH (tests) and 2 wells without NADPH (blanks). After mixing, the plates were pre-incubated for 10 min in a 37 °C incubator and the reaction then initiated by the addition of 1 mM (final concentration) NADPH. Incubations were performed for 5–30 min at 37 °C and were terminated by the addition of 100 μl of Tris base in 60% (v/v) acetonitrile. The plates were centrifuged at 260 *g* for 10 min at 4 °C and a 120 μl aliquot removed from each well into a white Porvair 96-well plate (Perkin Elmer Ltd., Beaconsfield, Bucks, UK). All fluorescence measurements were performed with a Perkin Elmer model LS-50B luminescence spectrophotometer equipped with a Perkin-Elmer model LS50 plate reader. Fluorescence measurements were made at excitation and emission wavelengths of 410 and 510 nm respectively, employing 3 nm slit widths. Standard curves were constructed with 0–50 pmol HFC/well.

BFC metabolism correlation analysis

Incubations were conducted as described above with either 20 or 50 μM BFC and 10 μg microsomal protein for 15 min. For each of the 24 preparations of human liver microsomes 6 wells were incubated with NADPH and 2 wells (blanks) without NADPH.

BFC metabolism by cDNA-expressed CYP isoforms

For each of the β-lymphoblastoid cell cDNA-expressed CYP isoform preparations and each incubation time, 4 wells were incubated with NADPH and 1 well (blank) without NADPH. Incubation mixtures contained 20 μM BFC (added in 0.2% (v/v) methanol), 1 mM NADPH and 100 mM phosphate buffer pH 7.4 in a final volume of 100 μl. After a 10 min pre-incubation at 37 °C, the reaction was initiated with 100 μg of β-lymphoblastoid cell microsomal protein (equivalent to 2.3–25.5 pmol of each CYP isoform) and incubations terminated after 10 and 40 min. A direct fluorescence monitoring procedure was used for the kinetic studies with the cDNA-expressed CYP1A2 and CYP3A4 preparations. The

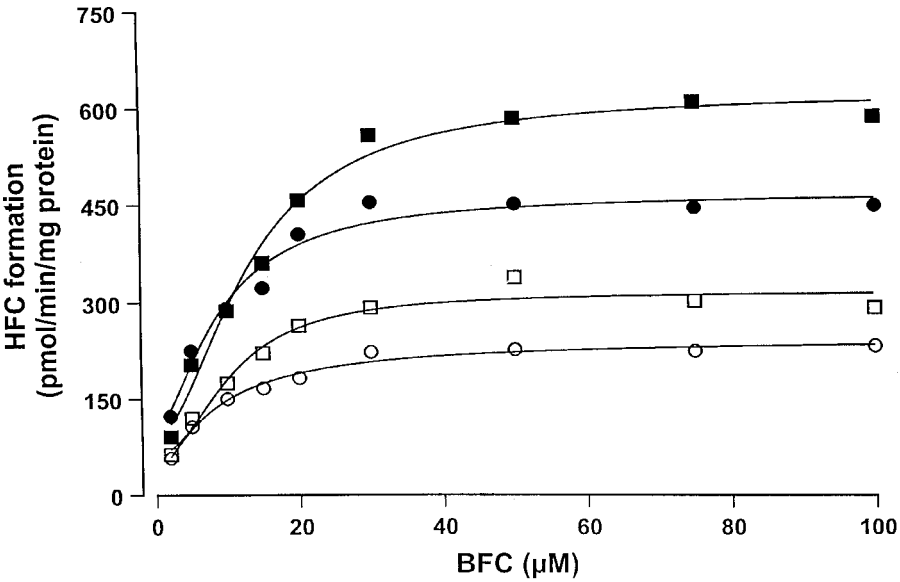


Figure 1. Michaelis–Menten plots of BFC metabolism to HFC in four pooled human liver microsomal preparations. Incubations (n = 6 wells for each BFC substrate concentration) were performed with 10 μg protein/well of the pool A (○), B (●), C (□) and D (■) microsomal preparations with 2–100 μM BFC for 15 min.

incubations were performed in a Molecular-Devices (Wokingham, UK) Gemini Fluorescence Plate Reader with readings being made every 45 seconds at excitation and emission wavelengths of 430 and 538 nm respectively. Following each fluorescence reading the plates were agitated for 3 seconds. Incubation mixtures contained 0.24–250 μM BFC (added in 5 μl of acetonitrile), 8.9–9.9 pmol CYP isoform in Dulbecco's phosphate buffered saline pH 7.4 in a final volume of 250 μl. For each of the CYP isoform preparations and BFC substrate concentration 2 wells were incubated with NADPH and 2 wells (blanks) without NADPH. After a 10 min pre-incubation at 37 °C the reaction was initiated by the addition of 2 mM (final concentration) NADPH. Incubations were performed at 37 °C for 15 min and the rate determined over the linear portion of the reaction curve. Standard curves were constructed with 0–100 pmol HFC/well.

BFC metabolism inhibition studies

Incubations were conducted as described above with 20 μM BFC, 10 μg human liver microsomal protein and 70 mM phosphate buffer pH 7.4 for 15 min. For each inhibitor concentration 6 wells were incubated with NADPH and 2 wells (blanks) without NADPH. To study the effect of the mechanism-based inhibitors furafylline (CYP1A2), diethyldithiocarbamate (CYP2E1) and troleandomycin (CYP3A4), the compounds were pre-incubated for 30 min at 37 °C with 1 mM NADPH and liver microsomes before the addition of BFC and a further aliquot of 1 mM NADPH. In the studies with the inhibitors sulphaphenazole (CYP2C9) and quinidine (CYP2D6) and the substrate *S*-mephenytoin (CYP2C19), the compounds were pre-incubated with liver microsomes for 10 min at 37 °C before the joint addition of BFC and 1 mM NADPH. Stock solutions of the inhibitors and *S*-mephenytoin were prepared in dimethyl sulphoxide and added to give a final solvent concentration in the incubation mixtures of 0.25% (v/v). The effects of antibodies to CYP2C8/9, CYP2D6 and CYP3A4 were studied in incubation mixtures containing 20 μM BFC, 1 mM NADPH, 10 μg human liver microsomal protein, 0.005, 0.05 or 0.5 μl of each antibody and 70 mM phosphate buffer pH 7.4 for 15 min. For each concentration of each inhibitor 6 wells were incubated with NADPH and 2 wells (blanks) without NADPH. The antibodies were pre-incubated with the liver microsomes and buffer for 10 min at 37 °C before the joint addition of BFC and NADPH.

Results

Kinetics of BFC metabolism

Initial BFC metabolism studies were conducted with a substrate concentration of 20 μM. The pool D human liver microsomal preparation was used as this

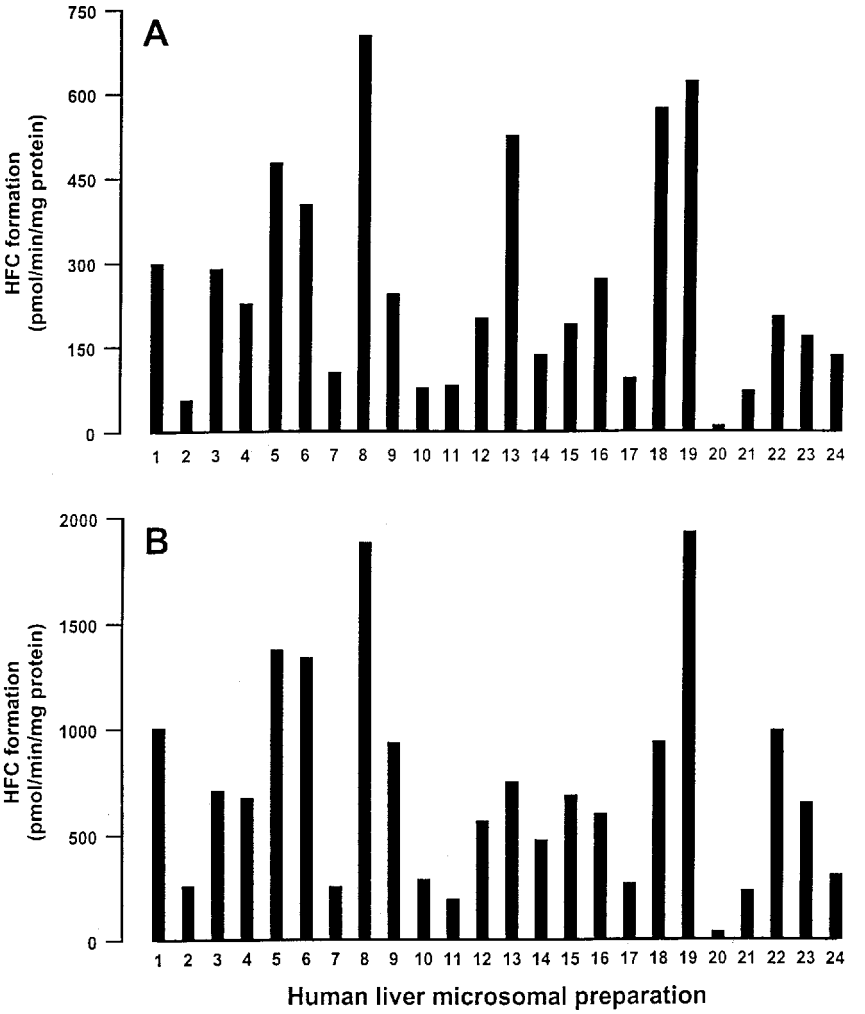


Figure 2. Variability in the metabolism of 20 (A) and 50 (B) μM BFC to HFC in a panel of 24 individual human liver microsomal preparations. Incubations (n = 6 wells for each microsomal preparation) were performed with 10 μg protein/well for 15 min.

preparation was found to have the highest rate of BFC metabolism. BFC was metabolized by human liver microsomes in the presence of NADPH to HFC. The formation of HFC was linear with respect to incubation time for at least 15 min and microsomal protein concentration up to at least 15 μg/well (data not shown).

Using all four pooled human liver microsomal preparations, the metabolism of BFC was investigated over a substrate concentration range of 2–100 μM (figure 1). Kinetic analysis of Michaelis–Menten plots revealed K_m of 6.7, 6.0, 8.7 and 11.8 μM for the pool A, B, C and D human liver microsomal preparations respectively (figure 1). Corresponding V_{max} were 253, 498, 359 and 705 pmol/min/mg protein respectively. For the four pooled human liver microsomal preparations mean ($\pm$SEM) K_m and V_{max} were 8.3 ± 1.3 μM and 454 ± 98 pmol/min/mg protein respectively.

Table 1. Correlation analysis for BFC metabolism to HFC with various CYP isoform-dependent enzyme activities in human liver microsomes.

CYP isoform	Enzyme activity[a]	r^2 20 μM BFC	r^2 50 μM BFC
–	Total CYP	0.460	0.632
1A2	7-ethoxyresorufin *O*-deethylase	0.797	0.421
	caffeine *N*3-demethylase	0.784	0.427
2A6	coumarin 7-hydroxylase	0.012	0.033
2B6	*S*-mephenytoin *N*-demethylase	0.085	0.207
2C9	tolbutamide methylhydroxylase	0.336	0.401
2C19	*S*-mephenytoin 4′-hydroxylase	0.330	0.267
2D6	dextromethorphan *O*-demethylase	0.078	0.092
2E1	chlorzoxazone 6-hydroxylase	0.036	0.114
3A4/5	testosterone 6β-hydroxylase	0.510	0.814
	testosterone 2β-hydroxylase	0.497	0.786
	testosterone 15β-hydroxylase	0.484	0.760
	diazepam 3-hydroxylase	0.547	0.837
	caffeine 8-hydroxylase	0.434	0.679
4A9/11	lauric acid 12-hydroxylase	0.272	0.208

[a] Total CYP content and the CYP isoform enzyme activities shown were correlated with data obtained from the metabolism of either 20 or 50 μM BFC (figure 2) in a panel of 24 individual human liver microsomal preparations.

BFC metabolism correlation analysis

The metabolism of BFC was examined with a characterized bank of 24 human liver microsomal preparations employing substrate concentrations of 20 and 50 μM (i.e. approximately two and six times K_m respectively). BFC was metabolized to HFC by all 24 liver microsomal preparations examined (figure 2). Microsomal BFC metabolism varied from 9 to 702 and from 35 to 1924 pmol/min/mg protein at substrate concentrations of 20 and 50 μM respectively.

The rates of BFC metabolism were correlated with obtained for total CYP content and a range of CYP isoform enzyme activities (table 1). With 20 μM substrate the highest correlations (r^2 = 0.797 and 0.784) were observed between BFC metabolism and 7-ethoxyresorufin *O*-deethylase (figure 3A) and caffeine *N*3-demethylase activities. Lower correlations were observed between BFC metabolism and testosterone 6β-hydroxylase (figure 3B) and other CYP3A isoform enzyme activities (r^2 = 0.434–0.547). In contrast, with 50 μM BFC substrate the highest correlations were with testosterone 6β-hydroxylase (figure 3D) and other CYP3A isoform enzyme activities (r^2 = 0.679–0.837). Lower correlations were observed between BFC metabolism and 7-ethoxyresorufin *O*-deethylase (figure 3C; r^2 = 0.421) and caffeine *N*3-demethylase (r^2 = 0.427) activities.

Metabolism of BFC by cDNA-expressed CYP isoforms

In initial studies the metabolism of 20 μM BFC was examined in Gentest β-lymphoblastoid cell microsomes containing human cDNA-expressed CYP1A2, CYP2A6, CYP2B6, CYP2C8, CYP2C9, CYP2C19, CYP2D6, CYP2E1 and CYP3A4, together with microsomes from control (wild type) cells. High rates of BFC metabolism to HFC were observed with the cDNA-expressed CYP1A2 and CYP3A4 preparations (figure 4). BFC was also metabolized to HFC by the cDNA-expressed CYP2C9 and CYP2C19 preparations, whereas a low rate of BFC

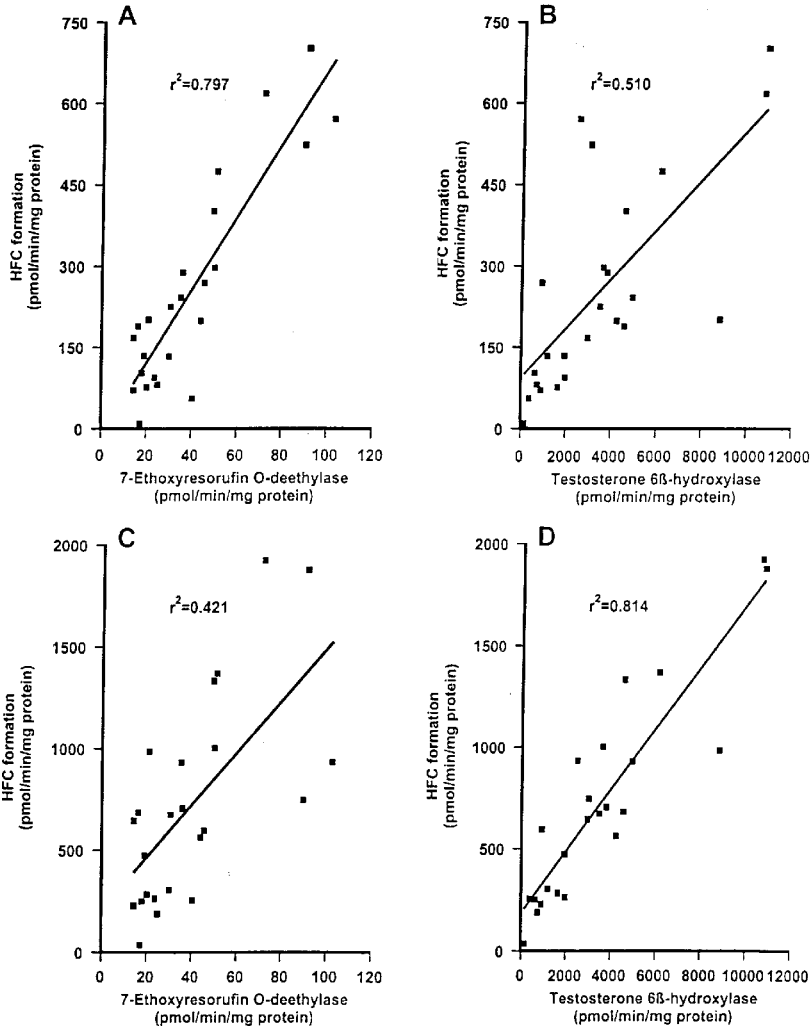


Figure 3. Correlation between BFC metabolism to HFC and 7-ethoxyresorufin *O*-deethylase (A, C) and testosterone 6β-hydroxylase (B, D) enzyme activities in a characterized panel of 24 human liver microsomal preparations. Incubations (n = 6 wells for each microsomal preparation) were performed with both 20 (A, B) and 50 (C, D) μM BFC substrate concentrations.

metabolism was observed with the CYP2B6 preparation. Only trace amounts of BFC metabolism was observed with the CYP2A6, CYP2C8, CYP2D6 and CYP2E1 preparations (figure 4) and with the control β-lymphoblastoid cell preparation (data not shown).

The kinetics of BFC metabolism were investigated over a substrate concentration range of 0.24–250 μM using β-lymphoblastoid cell microsomes containing cDNA-expressed CYP1A2 and CYP3A4 (figure 5). For the cDNA-expressed CYP1A2 and CYP3A4 preparations, K_m were 4.1 and 26.0 μM respectively, with corresponding V_{max} of 11.1 and 61.2 pmol/min/pmol CYP isoform respectively.

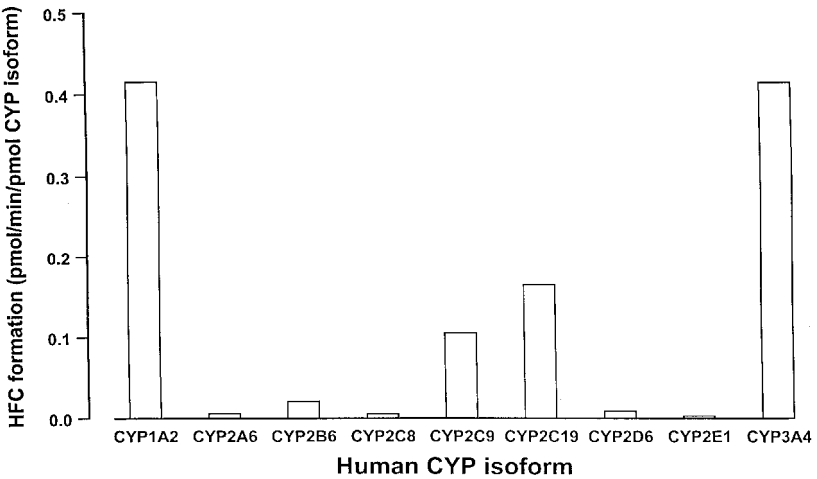


Figure 4. Metabolism of 20 μM BFC by β-lymphoblastoid cell microsomes containing cDNA-expressed human CYP isoforms. Incubations (n = 4 wells for each microsomal preparation) were performed with 100 μg protein/well for 10 and 40 min.

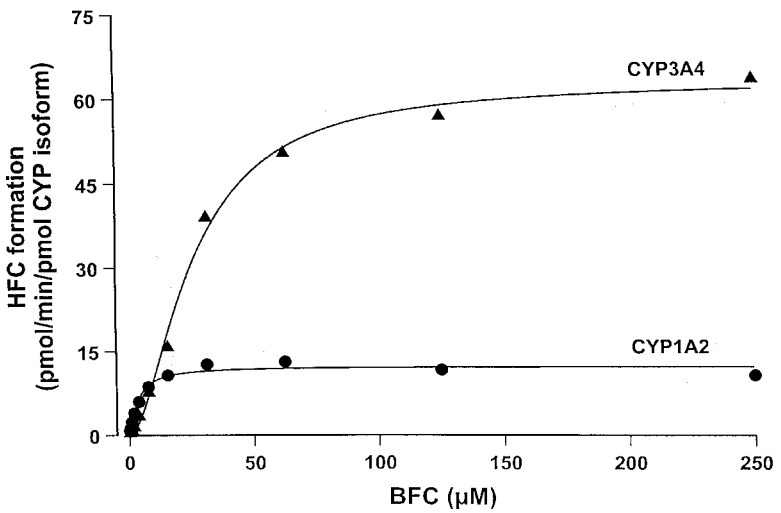


Figure 5. Kinetics of metabolism of 0.24–250 μM BFC by β-lymphoblastoid cell microsomes containing cDNA-expressed CYP1A2 (●) and CYP3A4 (▲). Incubations (n = 2 wells for each BFC substrate concentration) were performed with 9.9 and 8.9 pmol CYP/well respectively for 15 min.

Inhibition of BFC metabolism

The effect of some known CYP inhibitors and one substrate on the metabolism of 20 μM BFC in human liver microsomes (pool D) was studied. For the mechanism-based inhibitors (Newton *et al.* 1995) furafylline, diethyldithiocarbamate and troleandomycin, the compounds were pre-incubated with NADPH and the liver microsomes before addition of BFC. Treatment with 5–100 μM furafylline and 5–100 μM troleandomycin inhibited BFC metabolism to 37–48 and 64–69% of control respectively (figure 6A). While 10–50 μM diethyldithiocarbamate had little effect on BFC metabolism, the addition of 100 and 200 μM diethyldithiocarbamate

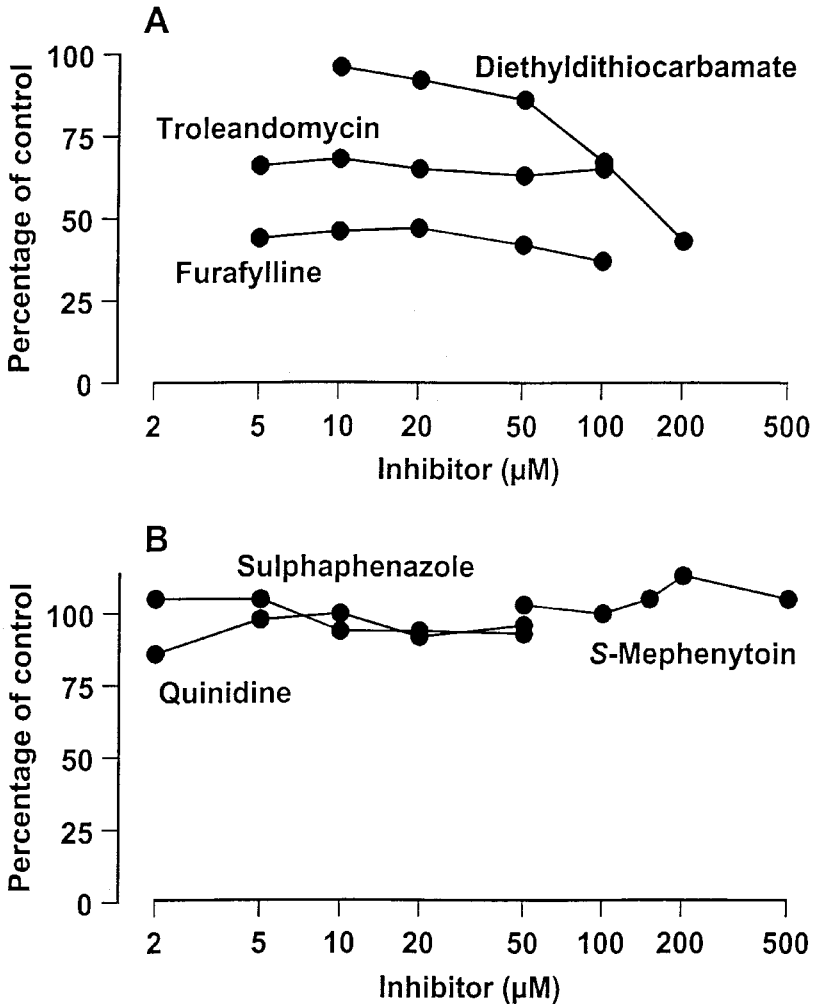


Figure 6. Inhibition of 20 μM BFC metabolism to HFC in human liver microsomes. To study the effects of 5–100 μM furafylline, 10–200 μM diethyldithiocarbamate and 5–100 μM troleandomycin (A), but not 2–50 μM sulphaphenazole, 50–500 μM *S*-mephenytoin and 2–50 μM quinidine (B), the compounds were pre-incubated with liver microsomes and NADPH at 37 °C before addition of BFC. Incubations (n = 6 wells for each inhibitor concentration) were performed with 10 μg protein/well of the pool D human liver microsomal preparation for 15 min and the results expressed as percentage of control (no inhibitor added) incubations. Control rates of metabolism of BFC to HFC were 345 and 424 pmol/min/mg protein for the mechanism-based inhibitors (A) and the other compounds (B) respectively.

inhibited enzyme activity to 67 and 43% of control respectively (figure 6A). In contrast, treatment with 2–50 μM sulphaphenazole, 50–500 μM *S*-mephenytoin and 2–50 μM quinidine had little effect on the metabolism of BFC in human liver microsomes (figure 6B).

Also examined were the effects of three available inhibitory antibodies on BFC metabolism in human liver microsomes. Using two pooled human liver microsomal preparations (pools C and D) treatment with either 0.005, 0.05 or 0.5 μl/well of inhibitory antibodies to CYP2C8/9 and CYP2D6 had no effect on BFC metabolism (figure 7A and B). In contrast, the addition of 0.005, 0.05 or 0.5 μl/well (i.e. 0.005,

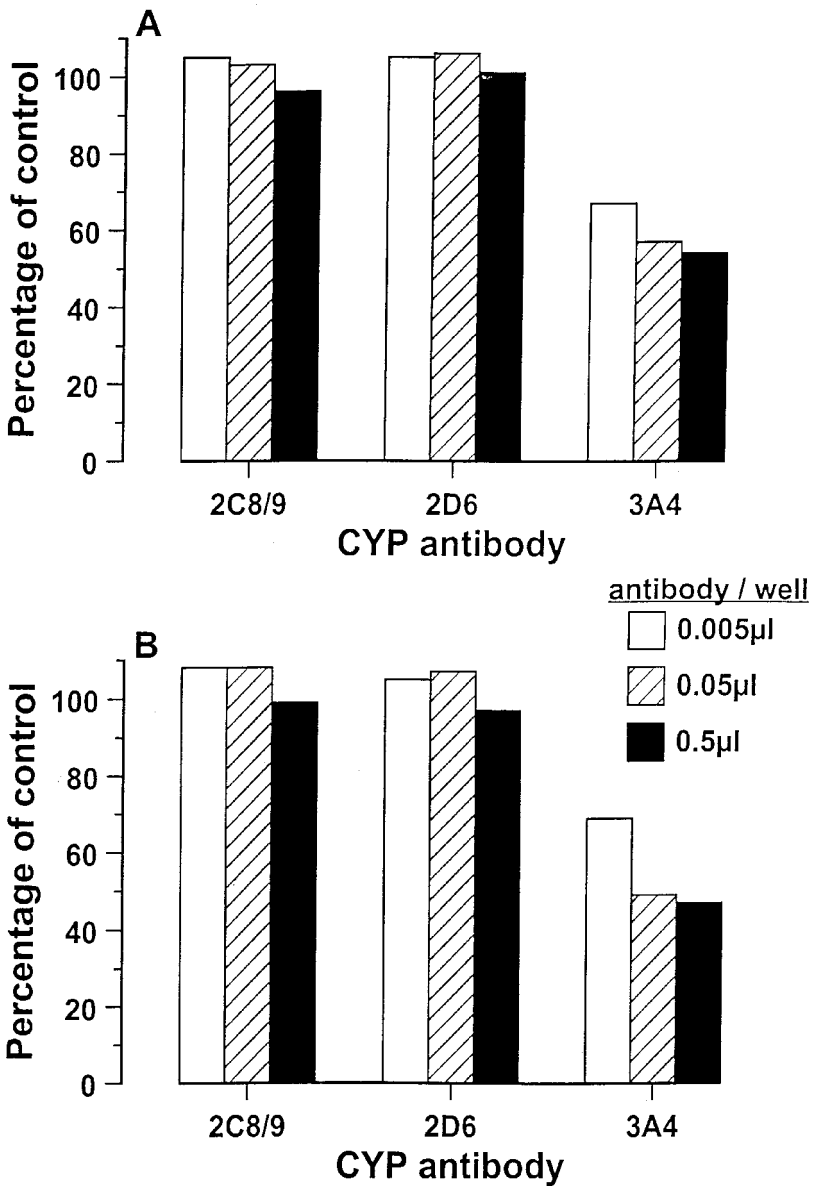


Figure 7. Inhibition of 20 μM BFC metabolism to HFC in human liver microsomes by antibodies to CYP2C8/9, CYP2D6 and CYP3A4. The antibodies (0.005, 0.05, 0.5 μl/well) were pre-incubated with the pool C (A) and pool D (B) human liver microsomal preparations at 37 °C before addition of NADPH and BFC. Incubations (n = 6 wells for each inhibitory antibody concentration) were performed with 10 μg microsomal protein/well for 15 min and the results are expressed as percentage of control (no antibody added) incubations. Control rates of BFC metabolism to HFC by the pool C (A) and pool D (B) human liver microsomal preparations were 341 and 677 pmol/min/mg protein respectively.

0.05 and 0.5 μl/100 μl incubation mixture) of an inhibitory antibody to CYP3A4 reduced BFC metabolism to 68, 53 and 50% of control (mean of both human liver microsomal preparations) respectively (figure 7A and B). Additional studies with the pool D microsomal preparation demonstrated that tolbutamide methyl-

hydroxylase activity was inhibited to 66 and 25% of control by the addition of 0.05 and 0.5 μl/100 μl incubation mixture respectively of the CYP2C8/9 antibody (data not shown). In contrast, no inhibition of tolbutamide methylhydroxylase activity was observed by the addition of 0.01–1.0 μl/100 μl incubation mixture of the CYP3A4 antibody (data not shown).

Discussion

In this study the metabolism of BFC to HFC by human liver microsomal preparations and cDNA-expressed CYP isoforms has been investigated. BFC metabolism was observed in all 24 individual and the four pooled human liver microsomal preparations examined. Previous studies have demonstrated that other HFC derivatives are also substrates for human hepatic CYP isoforms. For example, 7-methoxy-4-trifluoromethylcoumarin has been reported as a good substrate for cDNA-expressed CYP2C9 (Crespi *et al*. 1999) and 7-ethoxy-4-trifluoromethylcoumarin is metabolized by a number of CYP isoforms including CYP1A2, CYP2B6, CYP2C9 and CYP2E1 (Buters *et al*. 1993, Code *et al*. 1997).

Investigations into the kinetics of BFC metabolism in human liver microsomes revealed a mean ($\pm$SEM, $n = 4$) $K_m = 8.3 \pm 1.3$ μM. This is similar to the 14.2 ± 3.4 μM ($n = 3$) observed in the present authors' previous investigations (Surry and Evans, unpublished data). Higher rates of BFC metabolism (and hence V_{max} values) were observed when the 96-well plates were agitated during the incubations (Surry and Evans, unpublished data). In the present investigations, with the exception of the kinetic studies with cDNA-expressed CYP1A2 and CYP3A4, a static incubation system was employed.

In this study 'reaction phenotyping' for BFC metabolism was performed by correlation analysis, the use of cDNA-expressed CYP isoforms, chemical inhibition and three available inhibitory antibodies. BFC metabolism correlation analysis was conducted with substrate concentrations of 20 and 50 μM (i.e. about two and six times K_m respectively). At a substrate concentration of 20 μM, high correlations ($r^2 = 0.797$ and 0.784) were observed between BFC metabolism and the activities of 7-ethoxyresorufin *O*-deethylase and caffeine *N*3-demethylase (table 1). These two enzyme activities are considered to be catalysed by CYP1A2 in human liver (Fuhr *et al*. 1992, Wrighton *et al*. 1993a, Tassaneeyakul *et al*. 1994, Parkinson 1996a, b, Pelkonen *et al*. 1998). Some correlations ($r^2 = 0.434$–0.547) were also observed between BFC metabolism and testosterone 2β-, 6β- and 15β-hydroxylases, diazepam 3-hydroxylase and caffeine 8-hydroxylase activities. These enzyme activities are considered to be catalysed by CYP3A isoforms in human liver (Tassaneeyakul *et al*. 1994, Parkinson 1996a, b, Yang *et al*. 1999). Lower correlations were observed between BFC metabolism and tolbutamide methylhydroxylase ($r^2 = 0.336$) and *S*-mephenytoin 4′-hydroxylase ($r^2 = 0.330$) activities, which are known to be catalysed by CYP2C9 and CYP2C19 respectively (Wrighton *et al*. 1993b, Parkinson 1996a, b, Miners and Birkett 1998). No correlations ($r^2 = 0.012$–0.085) were observed between BFC metabolism and coumarin 7-hydroxylase, *S*-mephenytoin *N*-demethylase, dextromethorphan *O*-demethylase and chlorzoxazone 6-hydroxylase activities, which are catalysed by CYP2A6, CYP2B6, CYP2D6 and CYP2E1 respectively in the human liver (Wrighton *et al*. 1993a, Heyn *et al*. 1996, Pelkonen *et al*. 1998).

However, with 50 μM BFC substrate a different pattern of correlations was apparent (table 1). The highest correlations (r^2 = 0.679–0.837) were obtained between BFC metabolism and the CYP3A isoform markers and some correlation (r^2 = 0.632) was also observed with total CYP content. This latter observation may be attributable to CYP3A isoforms being relatively abundant in the human liver (Wrighton *et al*. 1993, Lecoeur *et al*. 1994, Shimada *et al*. 1994, Rodrigues 1999). The good correlations with CYP3A isoform enzyme activities are in agreement with previous investigations (Surry and Evans, unpublished data) where a BFC substrate concentration of 50 μM was also used. Weaker correlations were obtained with the enzymatic markers of CYP1A2 (r^2 = 0.421–0.427) and CYP2C9 (r^2 = 0.401). The higher affinity of BFC for CYP1A2 and CYP3A4 at low and high substrate concentrations respectively is contrasted in figure 3 with data for 7-ethoxyresorufin *O*-deethylase and testosterone 6β-hydroxylase activities.

The effect of chemical inhibitors and inhibitory antibodies on BFC metabolism in human liver microsomes was also investigated. Previous work has demonstrated that furafylline, sulphaphenazole, *S*-mephenytoin, quinidine, diethyldithiocarbamate and troleandomycin may be considered as either inhibitors or substrates of human hepatic CYP1A2, CYP2C9, CYP2C19, CYP2D6, CYP2E1 and CYP3A4 respectively (Wrighton *et al*. 1993a, Chang *et al*. 1994, Clarke *et al*. 1994, Baldwin *et al*. 1995, Newton *et al*. 1995, Bourrié *et al*. 1996, Ono *et al*. 1996, Parkinson 1996a, b, Rodrigues 1999). BFC metabolism (20 μM substrate) to HFC was inhibited to 37–48% of control by 5–100 μM furafylline and to 64–69% of control by 5–100 μM troleandomycin. Other work has demonstrated that at the concentrations examined furafylline and troleandomycin may be considered relatively specific mechanism-based inhibitors of CYP1A2 and CYP3A4 respectively (Newton *et al*. 1995). However, both furafylline and troleandomycin only inhibited a fraction of the total metabolism of BFC (figure 6A), suggesting that CYP1A2, CYP3A4 and possibly other CYP isoforms can metabolize BFC in human liver microsomes. The inhibition of BFC metabolism by high concentrations of diethyldithiocarbamate (figure 6A) is unlikely to reflect metabolism by CYP2E1, but rather that this compound also inhibits other CYP isoforms (Chang *et al*. 1994, Ono *et al*. 1996). The involvement of CYP3A4 in BFC metabolism was also demonstrated by the studies with the three available inhibitory antibodies. At the concentrations examined the CYP3A4 antibody inhibited a fraction of total BFC metabolism in human liver microsomes, whereas the CYP2C8/9 and CYP2D6 antibodies were without any effect (figure 5).

The metabolism of BFC by cDNA-expressed CYP isoforms was also examined. At a substrate concentration of 20 μM, the highest rates of BFC metabolism were observed with cDNA-expressed CYP1A2 and CYP3A4, then with CYP2C9 and CYP2C19, with a low level of BFC metabolism being catalysed by CYP2B6. Only trace amounts of BFC metabolism were observed with the other cDNA-expressed CYP isoforms examined and with the control β-lymphoblastoid cell microsomes. Kinetic studies with cDNA-expressed CYP1A2 and CYP3A4 revealed a lower K_m for CYP1A2, but a higher V_{max} for CYP3A4.

Overall, the results of the reaction phenotyping studies demonstrate that BFC can be metabolized by a number of CYP isoforms in human liver. At low substrate concentrations BFC is a more specific substrate for CYP1A2 than for CYP3A4, whereas the reverse is true at high substrate concentrations. BFC may also be a substrate for CYP2C9 and CYP2C19, as indicated by the studies with the cDNA-expressed CYP isoforms and to some extent by correlation analysis. However,

CYP2C9 would only appear to have a minor role in the metabolism of BFC in human liver microsomes, as neither sulphaphenazole nor the CYP2C8/9 inhibitory antibody had any marked effect on the metabolism of 20 μM BFC. The studies with the cDNA-expressed isoforms indicated that BFC could be metabolized by CYP2C19 and possibly also by CYP2B6. However, compared with the levels of CYP3A4 and even CYP1A2, these two CYP isoforms are present at only low levels in human liver microsomes (Wrighton *et al*. 1993, Lecoeur *et al*. 1994, Shimada *et al*. 1994, Rodrigues 1999). Thus, overall BFC metabolism in human liver is likely to be primarily catalysed by CYP1A2 and CYP3A4.

These studies also demonstrate the importance of the selection of appropriate substrate concentrations for reaction phenotyping studies with human hepatic CYP isoforms. For therapeutic agents, ideally such studies should be performed with pharmacologically relevant substrate concentrations. For example, lansoprazole 5-hydroxylation is predominantly catalysed by CYP2C19 *in vivo*, yet in studies with human liver microsomes at high substrate concentrations lansoprazole 5-hydroxylation is dominated by CYP3A4/5, a low-affinity high-capacity enzyme (Pearce *et al*. 1996). Other studies have demonstrated that diazepam *N*-demethylation can be catalysed by CYP2C19 and CYP3A isoforms, with CYP2C19 predominating at low substrate concentrations (Yasumori *et al*. 1993, Andersson *et al*. 1994, Yang *et al*. 1999).

In summary, BFC appears to be a useful substrate for CYP isoform metabolism studies employing either human liver microsomes or cDNA-expressed CYP isoforms (Crespi *et al*. 1999). Like 7-ethoxyresorufin (Kennedy and Jones 1994), BFC is metabolized to a highly fluorescent product that permits the assay of enzyme activity in a 96-well plate format using only small amounts of tissue (e.g. 10 μg human liver microsomal protein). However, unlike 7-ethoxyresorufin, which is considered a relatively specific marker for CYP1A2 in human liver microsomes (Wrighton *et al*. 1993a, Parkinson 1996a, b, Pelkonen *et al*. 1998), BFC appears to be a substrate for a number of CYP isoforms. BFC metabolism in human liver appears to be primarily catalysed by CYP1A2 and CYP3A4, with possibly some contribution by CYP2C9, CYP2C19 and perhaps other CYP isoforms.

Acknowledgements

The authors are grateful to MSD Research Laboratories, Harlow, Essex, for the provision of a research grant. They thank Drs T. A. Baillie and T. H. Rushmore, Merck Research Laboratories, West Point, PA, for the generous gifts of the CYP2C8/9, CYP2D6 and CYP3A4 inhibitory antibodies.

References

Andersson, T., Miners, J. O., Veronese, M. E. and Birkett, D. J., 1994, Diazepam metabolism by human liver microsomes is mediated both by *S*-mephenytoin hydroxylase and CYP3A isoforms. *British Journal of Clinical Pharmacology*, **38**, 131–137.

Baldwin, S. J., Bloomer, J. C., Smith, G. J., Ayrton, A. D., Clarke, S. E. and Chenery, R. J., 1995, Ketoconazole and sulphaphenazole as the respective selective inhibitors of P4503A and 2C9. *Xenobiotica*, **25**, 261–270.

Bourrié, M., Meunier, V., Berger, Y. and Fabre, G., 1996, Cytochrome P450 isoform inhibitors as a tool for the investigation of metabolic reactions catalysed by human liver microsomes. *Journal of Pharmacology and Experimental Therapeutics*, **277**, 321–332.

Buters, J. T. M., Schiller, C. D. and Chou, R. C., 1993, A highly sensitive tool for the assay of cytochrome P450 enzyme activity in rat, dog and man. Direct fluorescence monitoring of the deethylation of 7-ethoxy-4-trifluoromethylcoumarin. *Biochemical Pharmacology*, **46**, 1577–1584.

Chang, T. K. H., Gonzalez, F. J. and Waxman, D. J., 1994, Evaluation of triacetyloleandomycin, α-naphthoflavone and diethyldithiocarbamate as selective chemical probes for inhibition of human cytochromes P450. *Archives of Biochemistry and Biophysics*, **311**, 437–442.

Chauret, N., Tremblay, N., Lackman, R. L., Gauthier, J.-Y., Silva, J. M., Marois, J., Yergey, J. A. and Nicoll-Griffith, D. A., 1999, Description of a 96-well plate assay to measure cytochrome P4503A inhibition in human liver microsomes using a selective fluorescent probe. *Analytical Biochemistry*, **276**, 215–226.

Clarke, S. E., 1998, *In vitro* assessment of human cytochrome P450. *Xenobiotica*, **28**, 1167–1202.

Clarke, S. E., Ayrton, A. D. and Chenery, R. J., 1994, Characterization of the inhibition of P4501A2 by furafylline. *Xenobiotica*, **24**, 517–526.

Code, E. L., Crespi, C. L., Penman, B. W., Gonzalez, F. J., Chang, T. K. H. and Waxman, D. J., 1997, Human cytochrome P4502B6. Interindividual hepatic expression, substrate specificity, and role in precarcinogen activation. *Drug Metabolism and Disposition*, **25**, 985–993.

Crespi, C. L., Miller, V. P., Ackermann, J. M., Stresser, D. M. and Busby, W. F., Jr, 1999, Novel high throughput fluorescent cytochrome P450 assays. *Toxicological Sciences*, **48(1-S)**, 69.

Crespi, C. L., Miller, V. P. and Penman, B. W., 1997, Microtiter plate assays for inhibition of human, drug-metabolizing cytochromes P450. *Analytical Biochemistry*, **248**, 188–190.

Crespi, C. L., Miller, V. P. and Penman, B. W., 1998, High throughput screening for inhibition of cytochrome P450 metabolism. *Medical Chemistry Research*, **8**, 457–471.

Fuhr, U., Doehmer, J., Battula, N., Wölfel, C., Kudla, C., Keita, Y. and Staib, A. H., 1992, Biotransformation of caffeine and theophylline in mammalian cell lines genetically engineered for expression of single cytochrome P450 isoforms. *Biochemical Pharmacology*, **43**, 225–235.

Heyn, H., White, R. B. and Stevens, J. C., 1996, Catalytic role of P4502B6 in the *N*-demethylation of *S*-mephenytoin. *Drug Metabolism and Disposition*, **24**, 948–954.

Kennedy, S. W. and Jones, S. P., 1994, Simultaneous measurement of cytochrome P4501A catalytic activity and total protein concentration with a fluorescent plate reader. *Analytical Biochemistry*, **222**, 217–223.

Lake, B. G., 1987, Preparation and characterisation of microsomal fractions for studies of xenobiotic metabolism. In K. Snell and B. Mullock (eds), *Biochemical Toxicology*: *A Practical Approach* (Oxford: IRL Press), pp. 183–215.

Lecoeur, S., Bonierbale, E., Challine, D., Gauter, J.-C., Valadon, P., Dansette, P. M., Catinot, R., Ballet, F., Mansuy, D. and Beaune, P. H., 1994, Specificity of *in vitro* covalent binding of tienilic acid metabolites to human liver microsomes in relationship to the type of hepatotoxicity: comparison with two directly hepatotoxic drugs. *Chemical Research in Toxicology*, **7**, 434–442.

Lowry, O. H., Rosebrough, N. J., Farr, A. L. and Randall, R. J. 1951, Protein measurement with the Folin phenol reagent. *Journal of Biological Chemistry*, **193**, 265–275.

Mei, Q., Tang, C., Assang, C., Lin, Y., Slaughter, D., Rodrigues, A. D., Baillie, T. A., Rushmore, T. H. and Shou, M., 1999, Role of a potent inhibitory monoclonal antibody to cytochrome P-450 3A4 in assessment of human drug metabolism. *Journal of Pharmacology and Experimental Therapeutics*, **291**, 749–759.

Miners, J. O. and Birkett, D. J., 1998, Cytochrome P4502C9: an enzyme of major importance in human drug metabolism. *British Journal of Clinical Pharmacology*, **45**, 525–538.

Nelson, D. R., Koymans, L., Kamataki, T., Stegeman, J. J., Feyereisen, R., Waxman, D. J., Waterman, M. R., Gotoh, O., Coon, M. J., Estabrook, R. W., Gunsalus, I. C. and Nebert, D. W., 1996, P450 superfamily: update on new sequences, gene mapping, accession numbers and nomenclature. *Pharmacogenetics*, **6**, 1–42.

Newton, D. J., Wang, R. W. and Lu, A. Y. H., 1995, Cytochrome P450 inhibitors. Evaluation of specificities in the *in vitro* metabolism of therapeutic agents by human liver microsomes. *Drug Metabolism and Disposition*, **23**, 154–158.

Ono, S., Hatanaka, T., Hotta, H., Satoh, T., Gonzalez, F. J. and Tsutsui, M., 1996, Specificity of substrate and inhibitor probes for cytochrome P450s: evaluation of *in vitro* metabolism using cDNA-expressed human P450s and human liver microsomes. *Xenobioticia*, **26**, 681–693.

Parkinson, A., 1996a, An overview of current cytochrome P450 technology for assessing the safety and efficacy of new materials. *Toxicologic Pathology*, **24**, 45–57.

Parkinson, A., 1996b, Biotransformation of xenobiotics. In C. D. Klaassen (ed.), *Casarett and Doull's Toxicology*: *The Basic Science of Poisons*, 5th edn (New York: McGraw Hill), pp. 113–186.

Pearce, R. E., Rodrigues, A. D., Goldstein, J. A. and Parkinson, A., 1996, Identification of the human P450 enzymes involved in lansoprazole metabolism. *Journal of Pharmacology and Experimental Therapeutics*, **277**, 805–816.

Pelkonen, O., Mäenpää, J., Taavitsainen, P., Rautio, A. and Raunio, H., 1998, Inhibition and induction of human cytochrome P450 (CYP) enzymes. *Xenobiotica*, **28**, 1203–1253.

Renwick, A. B., Mistry, H., Ball, S. E., Walters, D. G., Kao, J. and Lake, B. G., 1998, Metabolism of zaleplon by human hepatic cytochrome P450 isoforms. *Xenobiotica*, **28**, 337–348.

Rodrigues, A. D., 1999, Integrated cytochrome P450 reaction phenotyping. Attempting to bridge the gap between cDNA-expressed cytochromes P450 and native human liver microsomes. *Biochemical Pharmacology*, **57**, 465–480.

Shimada, T., Yamazaki, H., Mimura, M., Inui, Y. and Guengerich, F. P., 1994, Interindividual variations in human liver cytochrome P-450 enzymes involved in the oxidation of drugs, carcinogens and toxic chemicals: studies with liver microsomes of 30 Japanese and 30 Caucasians. *Journal of Pharmacology and Experimental Therapeutics*, **270**, 414–423.

Tassaneeyakul, W., Birkett, D. J., McManus, M. E., Tassaneeyakul, W., Veronese, M. E., Andersson, T., Tukey, R. H. and Miners, J. O., 1994, Caffeine metabolism by human hepatic cytochromes P450: contributions of 1A2, 2E1 and 3A isoforms. *Biochemical Pharmacology*, **47**, 1767–1776.

Wrighton, S. A., Ring, B. J. and Vandenbranden, M., 1995, The use of *in vitro* metabolism techniques in the planning and interpretation of drug safety studies. *Toxicologic Pathology*, **23**, 199–208.

Wrighton, S. A., Stevens, J. C., Becker, G. W. and Vandenbranden, M., 1993b, Isolation and characterization of human liver cytochrome P450 2C19: correlation between 2C19 and *S*-mephenytoin 4′-hydroxylation. *Archives of Biochemistry and Biophysics*, **306**, 240–245.

Wrighton, S. A., Vandenbranden, M., Stevens, J. C., Shipley, La., Ring, B. J., Rettie, A. E. and Cashman, J. R., 1993a, *In vitro* methods for assessing human hepatic drug metabolism: their use in drug development. *Drug Metabolism Reviews*, **25**, 453–484.

Yang, T. J., Krausz, K. W., Sai, Y., Gonzalez, F. J. and Gelboin, H. V., 1999, Eight inhibitory monoclonal antibodies define the role of individual P-450s in human liver microsomal diazepam, 7-ethoxycoumarin and imipramine metabolism. *Drug Metabolism and Disposition*, **27**, 102–109.

Yasumori, T., Nagata, K., Yang, S. K., Chen, L.-S., Murayama, N., Yamazoe, Y. and Kato, R., 1993, Cytochrome P450 mediated metabolism of diazepam in human and rat: involvement of human CYP2C in *N*-demethylation in the substrate concentration-dependent manner. *Pharmacogenetics*, **3**, 291–301.

XENOBIOTICA, 2000, VOL. 30, NO. 10, 971–982

Use of everted sacs of mouse small intestine as enzyme sources for the study of drug oxidation activities *in vitro*

C. EMOTO†, H. YAMAZAKI†, S. YAMASAKI†,
N. SHIMADA‡, M. NAKAJIMA† and T. YOKOI†*

†Faculty of Pharmaceutical Sciences, Kanazawa University, Kanazawa 920–0934, Japan
‡Daiichi Pure Chemicals, Ibaraki 319–1182, Japan

Received 4 April 2000

1. The use of everted sacs of the small intestine as an enzyme source for the study of the first-pass metabolism of xenobiotics by cytochrome P450s (P450, CYP) is described. Several drug oxidation activities for testosterone, chlorzoxazone, tolbutamide, bufuralol and warfarin were observed when everted sacs (1-cm segment) from different parts of mouse small intestine were incubated with an NADPH-generating system and each substrate.

2. Most of the drug hydroxylase activities resided in the upper part of mouse small intestine and these activities were much higher than those of intestinal microsomes. Drug oxidation activities decreased along the distance from the upper part of the small intestine except for warfarin hydroxylation.

3. Testosterone 6β-hydroxylation in the everted sacs exhibited the highest catalytic activities among the drug oxidations tested here. In the upper part of the small intestine, the testosterone 6β-hydroxylase activities of everted sacs subjected once to freezing and thawing were substantially decreased compared with the untreated everted sacs.

4. Testosterone 6β-hydroxylase activities in the everted sacs of the small intestine were significantly inhibited by ketoconazole. Immunoreactive proteins using anti-CYP3A antibodies were detected in the upper and middle parts of the small intestine.

5. The results demonstrated that the upper part of the mouse small intestine serves as the major site for intestinal P450 mediated first-pass metabolism. Everted sacs of the small intestine are therefore useful for the study of drug metabolism as well as of transport and absorption.

Introduction

Cytochrome P450 (P450, CYP) consists of a superfamily of haem-containing monooxygenases, and multiple forms of P450 enzymes exist in mammals. These P450 enzymes are responsible for the oxidation of many drugs, environmental chemicals and endogenous substances (Nelson *et al*. 1996). P450s are microsomal enzymes existing mainly in the liver as well as in the extrahepatic tissues such as intestine, lung and kidney (Krishna and Klotz 1994). The metabolism of xenobiotics has been studied most extensively in the liver because of its high drug-metabolizing enzyme activities. Recently, the intestine has been recognized as a potential site for drug metabolism because the intestine is a major absorption route of orally dosed xenobiotics and contributes substantially to the first-pass metabolism effect (Paine *et al*. 1996).

Concerning the CYP3A family in man, CYP3A enzymes are the most abundant P450 enzymes in liver and small intestine (Watkins *et al*. 1987, Shimada *et al*. 1994).

* Author for correspondence: e-mail: TYOKOI@kenroku.kanazawa-u.ac.jp

Xenobiotica ISSN 0049-8254 print/ISSN 1366-5928 online © 2000 Taylor & Francis Ltd
http://www.tandf.co.uk/journals

CYP3A enzymes have a broad substrate specificity (Guengerich 1995), and about half the drugs currently on the market are substrates of CYP3A enzymes (Bertz and Granneman 1997). Intestinal slices have been used for metabolic studies similar to liver slices (Vickers *et al*. 1992, 1995), and recently intestinal microsomes have been frequently used for metabolic studies (Jacobsen *et al*. 1999). However, the preparation of intestinal microsomes is considered to be difficult compared with hepatic microsomes, because intestinal microsomes would be exposed to abundant intestinal proteases during their isolation. Typical marker activities of intestinal microsomes from experimental animals and humans prepared by various methods in different research laboratories and commercial enzyme manufacturers are not always similar. Therefore, it is very difficult to validate the drug oxidation activities of intestinal microsomes.

Everted sacs of the small intestine were originally used for studies of the transfer of substances from the mucosal to the serosal surfaces (Wilson and Wiseman 1954). Recently, Hashimoto *et al*. (1998) reported that tacrolimus was metabolized in everted sacs of rat small intestine under a 95% O_2/5% CO_2 atmosphere. However, there are no reports in which metabolites are measured directly using everted sacs of small intestine.

In the current study, everted sacs were incubated with an NADPH-generating system and several substrates, and the oxidative metabolites were determined by HPLC analysis. The relationship between the localization of the segment and the drug oxidation activities was investigated in mouse small intestine and the stability of catalytic activities during freezing and thawing of the small intestine. Immunoblot analyses of mouse intestinal microsomes from different organs were also examined.

Materials and methods

Chemicals

Testosterone and its metabolite were from Steraloids (Wilton, NH, USA). Chlorzoxazone, aprotinin, bestatin, leupeptin and trypsin inhibitor (type II, soybean) were from Sigma (St Louis, MO, USA). (±)-Bufuralol, *R*- and *S*-warfarin, tolbutamide, their metabolites, and 6-hydroxychlorzoxazone were from Ultrafine Chemicals (Manchester, UK). (*p*-Amidinophenyl)methanesulphonyl fluoride hydrochloride (APMSF) was from Wako Pure Chemicals (Osaka, Japan). Other reagents used were of the highest grade commercially available.

Preparation of everted sacs of small intestine

Male C57BL/6CrSlc mice, 8 weeks old (~ 30 g), were from Japan SLC, Inc. (Hamamatsu, Japan). Everted sacs were prepared according to Wilson and Wiseman (1954) with slight modifications. The mice were killed by exsanguination from the carotid artery. The abdominal cavity was opened via a midline incision, and the small intestine was removed by cutting from the upper end of the duodenum to the lower end of the ileum. To evert the intestine quickly, a vinyl-covered wire was pushed into the intestinal lumen until it appeared and rolling the proximal portion of the intestine completed the eversion. The everted sac (~ 30 cm long) was then slipped off the wire and washed in 30 ml ice-cold washing buffer (0.9% NaCl, 1 mM APMSF, 1 mM EDTA) for 1 min by gentle swirling. The everted sac was cut into 1-cm segments from the duodenum to the ileum. To study the effects of freezing and thawing of this tissue, everted sacs were frozen in liquid nitrogen, stored at −80 °C for overnight, and then thawed on ice.

Preparation of intestinal and hepatic microsomes

Microsomes from mouse small intestines were prepared according to Iatsimirskaia *et al*. (1997) with slight modifications. Immediately after excision, the small intestine (from duodenum to ileum) was divided into three 10-cm segments (upper, middle, lower part) to prepare intestinal microsomes. Each 10-cm segment of the small intestine was placed on a stainless dish kept on ice and was cut longitudinally,

then washed in ice-cold washing buffer for 1 min by gentle swirling. The mucosal cells were gently scraped off with a microcover glass and then processed into microsomes. The scraped off sample was dipped in 3 vols ice-cold buffer A (50 mM Tris-HCl buffer, pH 7.4, containing 150 mM KCl, 20% (v/v) glycerol, 1 mM EDTA, 1 mM APMSF, 1 mg/ml trypsin inhibitor, 10 μM leupeptin, 0.04 U/ml aprotinin, 1 μM bestatin) and homogenized using a motor-driven Teflon-tipped pestle (three strokes). The homogenate was centrifuged at 9000*g* at 4 °C for 20 min and then the supernatant was centrifuged at 105 000*g* at 4 °C for 60 min. The fatty layer on the surface was removed carefully, and the microsomal pellets were resuspended in ice-cold buffer A. Aliquots of the final microsomal suspension were stored at –80 °C until use.

Hepatic microsomes were prepared according to the method described above except for the use of 0.9% NaCl instead of the washing buffer.

Protein concentrations were determined according to Lowry *et al*. (1951).

Enzyme assays

Testosterone 6β-hydroxylation, bufuralol 1′- and 6-hydroxylation, tolbutamide methylhydroxylation, chlorzoxazone 6-hydroxylation, and *S*- and *R*-warfarin 6- and 7-hydroxylation were determined as described (Kronbach *et al*. 1987, Brian *et al*. 1989, Peter *et al*. 1990, Yamazaki *et al*. 1994, Lang and Böcker 1995, Yamazaki and Shimada 1997). The standard incubation mixture (final volume of 1 ml for everted sacs or 0.25 ml for microsomes) contained 1-cm segments of the everted sac or 0.3 mg protein of intestinal microsomes prepared from mouse, 100 mM potassium phosphate buffer (pH 7.4), an NADPH-generating system (0.5 mM $NADP^+$, 5 mM glucose 6-phosphate, 0.5 U/ml of glucose 6-phosphate dehydrogenase), and 100 μM substrates except for tolbutamide hydroxylation. The incubation mixture for tolbutamide methylhydroxylation contained 50 mM potassium phosphate buffer (pH 7.4), the NADPH-generating system and 250 μM tolbutamide. The choices of substrate concentrations were based on ~2-fold K_m in human liver microsomes. In the case of hepatic microsomes, 0.1 mg mouse hepatic microsomes was used. The mixtures including everted sacs were incubated at 37 °C for 30 min with shaking for all tested drug oxidations. The mixtures including intestinal or hepatic microsomes were incubated for 10 min for testosterone 6β-hydroxylation, chlorzoxazone 6-hydroxylation, and *S*- and *R*-warfarin 6- and 7-hydroxylation and for 15 min for bufuralol 1′- and 6-hydroxylation and tolbutamide methylhydroxylation. The reactions with testosterone, tolbutamide and chlorzoxazone were terminated by the addition of dichloromethane (5 ml for everted sacs or 1.5 ml for microsomes) and 0.3 M NaCl for testosterone 6β-hydroxylation, 0.1 N HCl for tolbutamide methylhydroxylation, and 4.3% phosphoric acid for chlorzoxazone 6-hydroxylation. After mixing vigorously, the mixtures were centrifuged at 900*g* for 10 min. Organic phases were evaporated at 40 °C under a gentle nitrogen stream. The residue was dissolved in 200 μl mobile phase, and a 50-μl portion was subjected to HPLC analysis. The reactions of bufuralol and warfarin were terminated by the addition of 60% perchloric acid (50 μl for everted sacs and 10 μl for microsomes). These reaction mixtures were centrifuged at 900*g* for 10 min. These supernatants (50 μl) were subjected to HPLC analysis.

The specific enzymatic activities of the everted sacs were calculated with a knowledge of the corresponding intestinal microsomal protein content (mean of three mice).

HPLC analysis

HPLC analyses were performed using an LC-6A pump, SIL-6B autosampler, SPD-6A UV detector (all Shimadzu, Kyoto, Japan), FP-920II fluorescence detector (Jasco, Tokyo, Japan) and C-R4A integrator (Shimadzu) equipped with a C_{18} 5-μm analytical column (Mightysil, 150 × 4.6 mm i.d., Kanto Chemicals, Tokyo, Japan) except for chlorzoxazone 6-hydroxylation (C_8 5-μm analytical column, Mightysil, 150 × 4.6 mm i.d.; Kanto). The column temperature was 35 °C. The elution of testosterone metabolites was conducted with a 64% methanol (v/v) at a flow rate of 1 ml/min. The eluate was monitored at 240 nm. Retentions of 6β-hydroxytestosterone and testosterone were 3.4 min and 9.6 min respectively. The elution of bufuralol metabolites was conducted with acetonitrile/20 mM sodium perchloric acid, pH 2.5 (33/67 v/v) at a flow rate of 1.5 ml/min. The eluate was monitored at 254 nm and by fluorescence (excitation 252 nm, emission 302 nm). Retentions of 1′- and 6-hydroxybufuralol and bufuralol were 2.5, 3.2 and 10.7 min respectively. The elution of tolbutamide metabolites was conducted with acetonitrile/0.04% phosphoric acid (30/70 v/v) at a flow rate of 1.5 ml/min. The eluate was monitored at 230 nm. Retentions of methylhydroxylated tolbutamide and tolbutamide were 2.8 and 12.5 min respectively. The elution of warfarin metabolites was conducted with acetonitrile/0.04% phosphoric acid (36/64 v/v) at 2 ml/min. The eluate was monitored by fluorescence (excitation 320 nm, emission 415 nm). Retentions of 6- and 7-hydroxywarfarin and warfarin were 4.8, 5.8 and 12.8 min respectively. Under the fluorescence conditions used, the molecular coefficient of 7-hydroxywarfarin was ~10-fold higher than that of 6-hydroxywarfarin (Lang and Böcker 1995, Yamazaki *et al*. 1998). The elution of chlorzoxazone metabolites was conducted with acetonitrile/0.5% phosphoric acid (27/43 v/v) at 1.5 ml/min. The eluate was monitored at 287 nm. Retentions of 6-hydroxychlorzoxazone and chlorzoxazone were 3.0 and 5.9 min respectively.

Immunoblot analysis

Polyclonal goat anti-rat CYP1A1, CYP2C6, CYP2E1 and CYP3A2 antisera were from Daiichi Pure Chemicals (Tokyo, Japan), which also provided rat liver microsomes with known contents of respective P450 isoforms for positive control in the immunoblot analysis. Polyclonal rabbit anti-rat CYP2D1 antiserum was from Funakoshi (Tokyo, Japan). Immunoblot analysis was performed according to the method of Laemmli (1970) with slight modifications. The microsomal proteins were separated on 7·5% polyacrylamide gel electrophoresis and transferred electrophoretically to a nitrocellulose membrane. The secondary antibodies used were anti-goat IgG (anti-rabbit IgG for CYP2D1) and detection was carried out using diaminobenzidine as a substrate for peroxidase.

Statistical analysis

Statistical analysis was performed by Student's *t*-test and by two-way ANOVA using computer programs of InStat and of Prism (Graphpad Software, San Diego, CA, USA) respectively.

Results

Testosterone 6β-hydroxylase activities catalysed by everted sacs of mouse small intestine and effects of freezing and thawing on catalytic activities

Testosterone 6β-hydroxylase activities of the everted sacs of mouse small intestine were measured by HPLC. Everted sacs (1-cm segment) from different parts of the small intestine were incubated with an NADPH-generating system and substrate with shaking. Representative HPLC chromatograms are shown in figure 1. The 6β-hydroxytestosterone formation was decreased markedly from the upper to the lower part of the intestine. A time-dependent formation of 6β-hydroxy-testosterone by everted sacs of the upper and middle parts of the mouse small intestine was observed until 180 min (figure 2). The mean of testosterone 6β-hydroxylase activities catalysed by everted sacs of the upper part of the small intestine were 3·6 times significantly higher than those of the middle part (table 1).

To examine the effect of freezing and thawing of the everted sacs on testosterone 6β-hydroxylase activities, everted sacs from different parts of the small intestine were frozen and thawed once. Everted sacs prepared from one mouse were divided alternately to fresh ones and frozen and thawed ones. A marked decrease of testosterone 6β-hydroxylase activities was observed in the upper parts of the small intestine (figure. 3). Table 1 summarizes the mean activities of three segments of testosterone 6β-hydroxylase activities in fresh and frozen and thawed everted sacs from the upper, middle and lower parts of the mouse small intestine. The mean of catalytic activities by everted sacs of upper part of small intestine were significantly decreased by 44% by freezing and thawing ($p < 0.05$). In contrast, relatively low catalytic activities by everted sacs of the middle and lower parts of the small intestine were not affected by freezing and thawing.

In addition, the effects of ketoconazole (a potent inhibitor of CYP3A) on testosterone hydroxylase activities of everted sacs were investigated. Figure 4 shows that ketoconazole significantly inhibited these activities throughout the intestinal tract ($p < 0.01$; figure 4).

Other drug oxidation activities of everted sacs

Chlorzoxazone 6-hydroxylation, tolbutamide methylhydroxylation, and bufuralol 1′- and 6-hydroxylations catalysed by the segments of everted sacs of mouse small intestine are shown in figure 5. These activities decreased from the upper to

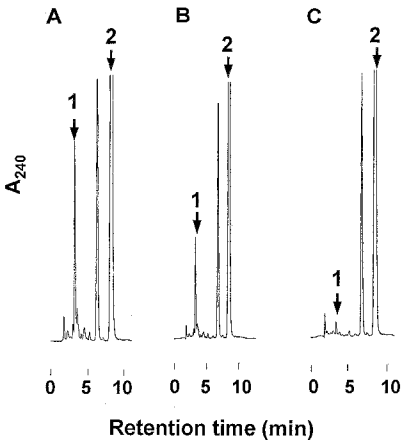


Figure 1. Representative HPLC chromatograms of testosterone 6β-hydroxylation catalysed by everted sacs. Everted sacs of mouse small intestine from upper (A), middle (B) and lower (C) part (1-cm segment) were used. Peak: 1, 6β-hydroxytestosterone; 2, testosterone.

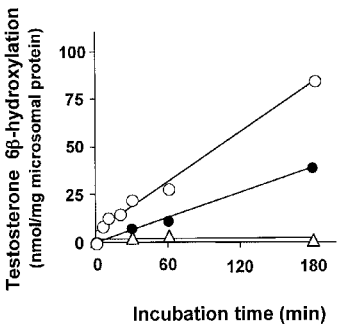


Figure 2. Testosterone 6β-hydroxylase activity catalysed by everted sacs. Everted sacs prepared from upper (○), medium (●) and lower (△) part of small intestine were incubated with testosterone and an NADPH-generating system up to 180 min at 37 °C. Data are derived from a single determination and several points were confirmed by independent experiments.

the lower parts of the small intestine. Low but significant *S*- and *R*-warfarin 6- and 7-hydroxylase activities were observed in mouse everted sacs (figure 6). The metabolites of bufuralol 6-hydroxylase (figure 5D) and *S*-warfarin 6-hydroxylase (figure 6A) activities were detected only in the upper part of the small intestine.

Comparison of drug oxidation activities catalysed by everted sacs of small intestine and intestinal or hepatic microsomes from mice

Drug oxidation activities catalysed by the everted sacs were compared with those catalysed by intestinal and hepatic microsomes (table 2). Testosterone 6β-hydroxylase activity was higher than other catalytic activities. The drug oxidation activities catalysed by everted sacs were significantly higher than those catalysed by intestinal microsomes except for chlorzoxazone 6-hydroxylase activity.

Bufuralol 1′-hydroxylase activity was higher than its 6-hydroxylase activity in all enzyme sources and the ratios of bufuralol 1′- to 6-hydroxylase activities catalysed by everted sacs were twice as large as those catalysed by intestinal microsomes, but similar to those by hepatic microsomes.

Table 1. Effects of freezing and thawing of everted sacs of mouse small intestine on testosterone 6β–hydroxylase activities.

	Testosterone 6β–hydroxylation	
Segment	Fresh (nmol/min/mg microsomal protein)	Frozen/thawed†
Upper	0.32 ± 0.07[a]	0.14 ± 0.01[c]
Middle	0.09 ± 0.01[b]	0.12 ± 0.03[d]
Lower	0.04 ± 0.02	0.02 ± 0.01

† Everted sacs were frozen in liquid nitrogen and thawed once.

Data are expressed as mean ± SE from each 1-cm segment of everted sacs (n = 10).

[a] Significantly different from the middle and lower parts of fresh everted sacs ($p < 0.05$).

[b] Significantly different from the lower part of fresh everted sacs ($p < 0.05$).

[c] Significantly different from the upper part in fresh everted sacs ($p < 0.05$) and from the lower part of frozen/thawed everted sacs ($p < 0.05$).

[d] Significantly different from the lower part of frozen/thawed everted sacs ($p < 0.01$).

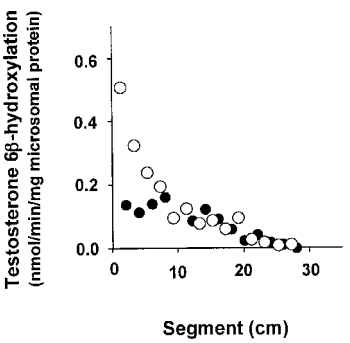


Figure 3. Effects of freezing and thawing on the testosterone 6β-hydroxylase activity catalysed by mouse everted sacs. Everted sacs, untreated (○) and frozen and thawed once (●), were incubated with testosterone and an NADPH-generating system. Data are derived from a single determination and several points were confirmed by independent experiments.

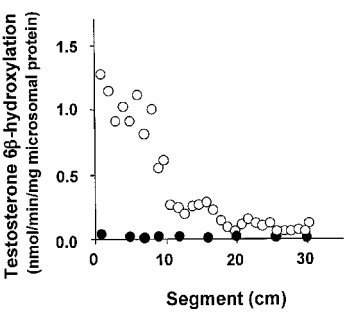


Figure 4. Effects of ketoconazole on testosterone 6β-hydroxylase activities catalysed by everted sacs. Everted sacs were incubated with testosterone and an NADPH-generating system in the absence (○) or presence (●) of ketoconazole (1 μM). Testosterone 6β-hydroxylation activities in the presence of ketoconazole were significantly lower than those in the absence of ketoconazole ($p < 0.01$, two-way ANOVA). Data are derived from a single determination and several points were confirmed by independent experiments. The limits of quantitation of testosterone 6β-hydroxylase activities were 1 pmol/min/mg protein.

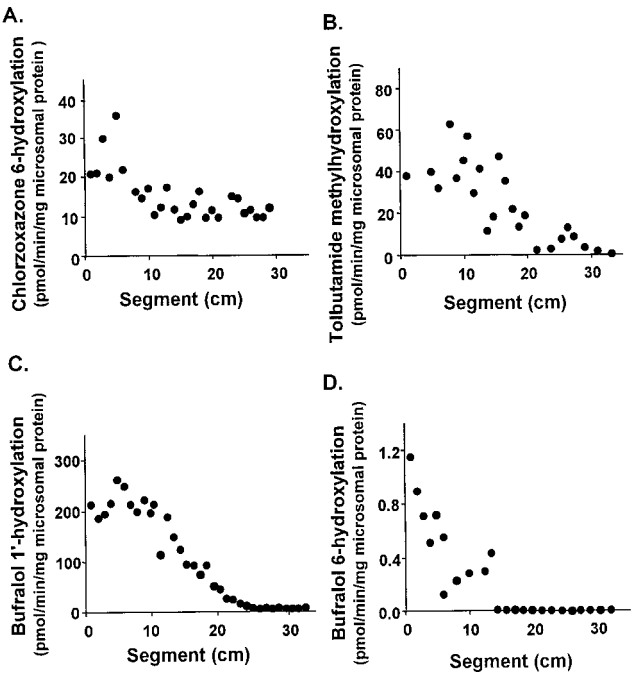


Figure 5. Drug oxidation activities catalysed by mouse everted sacs. Chlorzoxazone 6-hydroxylase (A), tolbutamide methylhydroxylase (B) bufuralol 1′- and 6-hydroxylase (C and D respectively) activities catalysed by everted sacs were determined according to the Materials and methods. Data are derived from a single determination and several points were confirmed by independent experiments. The limits of quantitation of activities of chlorzoxazone 6-hydroxylase, tolbutamide methylhydroxylase, and bufuralol 1′- and 6-hydroxylase were 1, 1, 0·1, and 0·1 pmol/min/mg protein respectively.

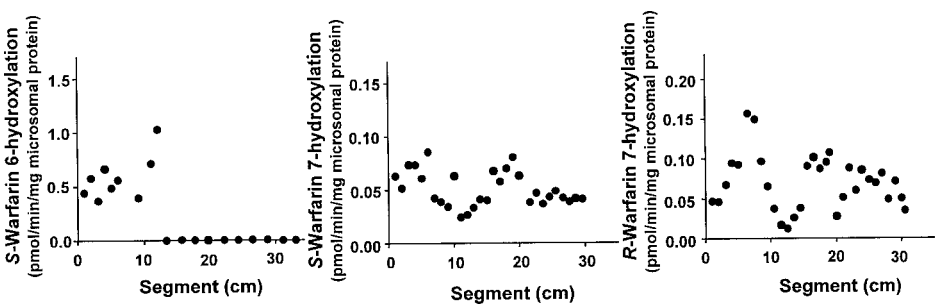


Figure 6. Warfarin hydroxylase activities catalysed by everted sacs. *S*-warfarin 6-hydroxylase (A), *S*-warfarin 7-hydroxylase (B) and *R*-warfarin 7-hydroxylase (C) activities catalysed by everted sacs were determined according to the Materials and methods. The limits of quantitation of warfarin 6- and 7-hydroxylase activities were 0·10 and 0·01 pmol/min/mg protein respectively. Data are derived from a single determination and several points were confirmed by independent experiments.

The 6- and 7-hydroxylation activities of *S*- and *R*-warfarin catalysed by everted sacs were compared with those catalysed by microsomal fractions (table 3). There was a different regioselectivity in *S*-warfarin hydroxylation between everted sacs and hepatic microsomes from mice. Mouse everted sacs had 11-fold higher *S*-

Table 2. Drug oxidation activities in everted sacs of mouse small intestine and in intestinal and hepatic microsomal fractions from mice

	Testosterone 6β-hydroxylation	Chlorzoxazone 6-hydroxylation	Tolbutamide methyl hydroxylation	Bufuralol 1′-hydroxylation	Bufuralol 6-hydroxylation
	(pmol/min/mg microsomal protein)				
Everted sacs (upper part)	930±73**	21±2.3	38±4.4**	210±7.7**	0.58±0.09
Intestinal microsomes (upper part)	170±29	67±31*	7.6±1.8	55±6.7	0.29±0.07
Hepatic microsomes	7750±480	4100±520	670±140	3200±130	8.5±0.39

Data for everted sacs are expressed as mean±SE from 1-cm segment of upper part of small intestine (n = 10).
Data for microsomes are expressed as mean±SE from three mice.
Significantly different between everted sacs and intestinal microsomes (*$p < 0.05$, **$p < 0.01$).

Table 3. Warfarin 6- and 7-hydroxylation activities catalyzed by everted sacs and by intestinal and hepatic microsomal fractions from mice.

Enzyme	Substrate	6-Hydroxylation	7-Hydroxylation	6/7 ratio[a]	S/R ratio of 7-Hydroxylation
		(pmol/min/mg protein)			
Everted sacs (upper part)	*S*-Warfarin	0.67	0.06	11.2	0.60
	R-Warfarin	< 0.10	0.10	–	
Intestinal microsomes (upper part)	*S*-Warfarin	< 0.10	0.01	–	0.50
	R-Warfarin	< 0.10	0.02	–	
Hepatic microsomes	*S*-Warfarin	< 0.10	1.89	–	0.16
	R-Warfarin	6.33	11.6	0.55	

[a] 6/7 ratio; ratio of 6- and 7-hydroxylase activities.
Data for everted sacs are expressed as mean from each 1 cm-segment of the upper part of the small intestine (n = 10).
The limit of the quantitation of warfarin 6- and 7-hydroxylation activities was the same as in the legend of figure 6.

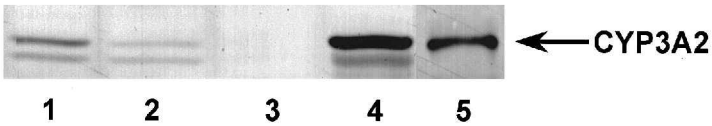


Figure 7. Immunoblot analysis of intestinal and hepatic microsomes from mice using anti-rat CYP3A2 antibodies. Intestinal microsomes (30 μg) from upper (1), middle (2) and lower (3) part, mouse hepatic microsomes (4) (10 μg), and rat hepatic microsomes provided by the manufacturer for standard (5) (corresponding to 0.23 pmol CYP3A2) were fractionated by electrophoresis described in the Materials and methods.

warfarin 6-hydroxylase activities than 7-hydroxylase activities. In contrast, mouse hepatic microsomes had higher *S*-warfarin 7-hydroxylase activities than 6-hydroxylase activities. On the other hand, both mouse everted sacs and intestinal microsomes showed higher 7-hydroxylase activities for *R*-warfarin than those for *S*-warfarin.

Immunoblot analysis of mouse P450s in intestinal microsomes

Two immunoreactive bands were observed in intestinal microsomes showing similar migration to that in hepatic microsomes using anti-rat CYP3A2 antibodies (figure 7). Rat liver microsomes gave a single band. The density of immunoreactive bands decreased from the upper to the lower part of the mouse intestine. On the other hand, anti-rat CYP1A1, anti-rat CYP2C6, anti-rat CYP2D1 and anti-rat CYP2E1 antibodies did not detect any immunoreactive band (data not shown).

Discussion

Several published studies that address the issue of enzyme distribution and biotransformation in the gut are summarized in Waldron *et al.* (1994). In general, preparation of intestinal microsomes is thought to be difficult compared with that of hepatic microsomes because intestinal microsomes are exposed to several intestinal proteases during their preparation. Many laboratories have reported different combinations of protease inhibitors in the preparations of intestinal microsomes of human and experimental animals (Stralka and Strobel 1989, Rosenberg and Mankowski 1994, Kashfi *et al.* 1995). The typical marker activities of intestinal microsomes in different research laboratories are not always similar. In our preliminary experiments, various combinations of protease inhibitors were necessary for preparing mouse intestinal microsomes with high catalytic activities (data not shown). However, it is unknown whether these catalytic activities would reflect the original activities. A simple and reliable method of preparation of the enzyme source which can maintain the original catalytic activities is required for studying intestinal drug metabolism. Hansen *et al.* (2000) reported the capacity of isolated and cultivated pig enterocyte to carry out intestinal drug oxidations. Everted sacs have been used for the study of transport and/or absorption (Hughes *et al.* 1995, Kitagawa *et al.* 1996). Hashimoto *et al.* (1998) reported that everted sacs of rat small intestine metabolize tacrolims in Krebs–Hensleit bicarbonate buffer under continuous bubbling with 95% O_2/5% CO_2. In the present study, a simple method is

proposed for metabolism using everted sacs with shaking incubation under air. Intestinal enzymes in the everted sacs functioned effectively in testosterone 6β-hydroxylation for at least 3 h in phosphate buffer (pH 7.4) (figure 2).

In the present study, the testosterone 6β-hydroxylase activities decreased along the distance from the upper to the lower parts of the small intestine (figure 3). The upper part of the everted sacs was more sensitive to enzyme inactivation by freezing and thawing than the middle or lower parts (table 1). Testosterone 6β-hydroxylase activities would be predominantly catalysed by CYP3A enzymes in the everted sac, because testosterone 6β-hydroxylase activities, a typical CYP3A-mediated reaction, were significantly inhibited by ketoconazole ($p < 0.01$; figure 4), which is a potent inhibitor of CYP3A. In addition, the density of immunoreactive bands detected using anti-CYP3A antibodies decreased from the upper to the lower parts of the mouse intestine (figure 7). These results were coincident with the decrease of testosterone 6β-hydroxylase activities from the upper to the lower part of the small intestine. Therefore, the majority of CYP3A enzymes would reside in the proximal region of the small intestine.

The density of two immunoreactive bands detected using anti-CYP3A antibodies was different between intestinal and hepatic microsomes. Both mouse Cyp3a11 and Cyp3a13 are the major CYP3A enzymes in small intestine, but in livers of male mice, Cyp3a11 mainly existed rather than CYP3A13 (Yanagimoto *et al*. 1997, Sakuma *et al*. 2000). The molecular weights of mouse Cyp3a11, Cyp3a13 and rat CYP3A2 were reported as 57.9, 57.5 and 57.7 kDa respectively (SWISS-PLOT). Although there was an organ difference with respect to the existence of CYP3A enzymes, the upper and lower bands observed by immunoblot analysis would be Cyp3a11 and Cyp3a13 respectively.

Several drug oxidation activities in the everted sacs were observed. These drug oxidations might be catalysed by P450s in the everted sacs, which could not be detected immunochemically. The localization of activities of chlorzoxazone 6-hydroxylation, tolbutamide methylhydroxylation, and bufuralol 1′- and 6-hydroxylations were in agreement with testosterone 6β-hydroxylase activity (figure 5). In contrast, those of *S*- and *R*-warfain 6- and 7-hydroxylation were not (figure 6). These differences might have been caused by the hydrophobicity of the substrate. Experiments of everted sacs take no account of the absorption of substrates by mucosal cells. The concentrations of the substrate might be different in the reaction mixture and mucosal cells. Therefore, each drug oxidation experiment using everted sacs could not be treated in the same way.

Several drug oxidation activities catalysed by the everted sacs were higher than those by intestinal microsomes under our experimental conditions (table 2). Differences in catalytic activities between everted sacs and intestinal microsomes might be partly attributed to the local conditions of several enzymes. P450 systems that exist in everted sacs would be in a better condition than intestinal microsomes in *in vitro* experiments, because the everted sacs are whole tissues that closely resemble the *in vivo* situation. In general, drug oxidation is carried out in the P450 cycle consisting of P450 enzymes, P450 reductase, NADPH, a substrate, and oxygen. It has been reported that CYP3A activities, P450 contents, and P450 reductase activities increased slightly from the duodenum to middle jejunum and then declined markedly in the distal jejunum and ileum in humans, although cytochrome b_5 contents and cytochrome b_5 reductase activities are reported to vary throughout the intestinal tract (Paine *et al*. 1997, Zhang *et al*. 1999). These findings

of catalytic activities were almost coincident with our drug oxidation activities using mouse everted sacs, except for the slight increase in the middle jejunum in humans. The characteristic localization of catalytic activities may be caused by differences in the localization of enzymes involved in drug oxidation. The concentrations of substrate and/or oxygen in mucosal cells of intestine may be also indispensable for intestinal drug metabolisms *in vivo*. In comparison with liver, extrapolation of intestinal drug oxidation from *in vitro* to *in vivo* should be difficult from the viewpoint of the localization of P450 systems and of the absorbed substrates in drug oxidation.

In conclusion, a simple method of using everted sacs for drug metabolism studies in intestine is proposed. The present study has demonstrated that the upper part of the small intestine serves as the major site of CYP3A-mediated first-pass metabolism. The everted sacs are useful for the study of drug metabolism as well as transport and absorption.

Acknowledgements

This work was supported by a Pharmaceutical and Medical Safety Research Grant from the Ministry of Health and Welfare of Japan. The authors thank Mr Brent Bell for reviewing the manuscript.

References

Brian, W. R., Srivastava, P. K., Umbenhauer, D. R., Lloyd, R. S. and Guengerich, F. P., 1989, Expression of a human liver cytochrome P450 protein with tolbutamide hydroxylase activity in *Saccharomyces cerevisiae*. *Biochemistry*, **28**, 4993–4999.

Bertz, R. J. and Granneman, G. R., 1997, Use of *in vitro* and *in vivo* data to estimate the likelihood of metabolic pharmacokinetic interactions. *Clinical Pharmacokinetics*, **32**, 210–258.

Guengerich, F. P., 1995, Human cytochrome P450 enzymes. In P. R. Oritiz de Montellano (ed.), *Cytochrome P*450 (New York: Plenum), pp. 473–535.

Guengerich, F. P., 1999, Cytochrome P-450 3A4: regulation and role in drug metabolism. *Annual Reviews in Pharmacology and Toxicology*, **39**, 1–17.

Hansen, T., Borlak, J. and Bader, A., 2000, Cytochrome P450 enzyme activity and protein expression in primary porcine enterocyte and hepatocyte cultures. *Xenobiotica*, **30**, 27–46.

Hashimoto, Y., Sasa, H., Shimomura, M. and Inui, K., 1998, Effects of intestinal and hepatic metabolism on the bioavailability of tacrolimus in rats. *Pharmaceutical Research*, **15**, 1609–1613.

Hughes, J. A., Avrutskaya, A. V., Brouwer, K. L., Wickstrom, E. and Juliano, R. L., 1995, Radiolabeling of methylphosphonate and phosphorothioate oligonucleotides and evaluation of their transport in everted rat jejunum sacs. *Pharmaceutical Research*, **126**, 817–824.

Iatsimirskaia, E., Tulebaev, S., Storozhuk, E., Utkin, I., Smith, D., Gerber, N. and Koudriakova, T., 1997, Metabolism of rifabutin in human enterocyte and liver microsomes: kinetic parameters, identification of enzyme systems, and drug interactions with macrolides and antifungal agents. *Clinical Pharmacology and Therapeutics*, **61**, 554–562.

Jacobsen, W., Kirchner, G., Hallensleben, K., Mancinelli, L., Deters, M., Hackbarth, I., Baner, K., Benet, L. Z., Sewing, K. F. and Christians, U., 1999, Small intestinal metabolism of the 3-hydroxy-3-methylglutaryl-coenzyme A reductase inhibitor lovastatin and comparison with pravastatin. *Journal of Pharmacology and Experimental Therapeutics*, **291**, 131–139.

Kashfi, K., McDougall, C. J. and Dannenberg, A. J., 1995, Comparative effects of omeprazole on xenobiotic metabolizing enzymes in the rat and human. *Clinical Pharmacology and Therapeutics*, **58**, 625–630.

Kitagawa, S., Sato, K., Sato, S. and Sasaki, M., 1996, Absorption of methochlorpromazine in rat small intestinal everted sac. *Biological and Pharmaceutical Bulletin*, **19**, 998–1000.

Krishna, D. R. and Klotz, U., 1994, Extrahepatic metabolism of drugs in humans. *Clinical Pharmacokinetics*, **26**, 144–160.

Kronbach, T., Mathys, D., Gut, J., Catin, T. and Meyer, U. A., 1987, High-performance liquid chromatographic assays for bufuralol 1′-hydroxylase, debrisoquine 4-hydroxylase, and dextromethorphan *O*-demethylase in microsomes and purified cytochrome P450 isozymes of human liver. *Analytical Biochemistry*, **162**, 24–32.

Laemmli, U. K., 1970, Cleavage of structural proteins during the assembly of the head of bacteriophage T4. *Nature*, **227**, 680–685.

Lang, D. and Böcker, R., 1995, Highly sensitive and specific high-performance liquid chromatographic analysis of 7-hydroxywarfarin, a marker for human cytochrome P450 2C9 activity. *Journal of Chromatography B: Biomedical Applications*, **672**, 305–309.

Lowry, O. H., Rosebrough, N. J., Farr, A. L. and Randall, R. J., 1951, Protein measurement with the Folin phenol reagent. *Journal of Biological Chemistry*, **193**, 265–275.

Nelson, D. R., Koymans, L., Kamataki, T., Stegeman, J. J., Feyereisen, R., Waxman, D. J., Waterman, M. R., Gotoh, O., Coon, M. J., Estabrook, R. W., Gunsalus, I. C. and Nebert, D. W., 1996, P450 superfamily: update on new sequences, gene mapping, accession numbers and nomenclature. *Pharmacogenetics*, **6**, 1–42.

Paine, M. F., Khalighi, M., Fisher, J. M., Shen, D. D., Kunze, K. L., Marsh, C. L., Perkins, J. D. and Thummel, K. E., 1997, Characterization of interintestinal and intraintestinal variations in human CYP3A-dependent metabolism. *Journal of Pharmacology and Experimental Therapeutics*, **283**, 1552–1562.

Paine, M. F., Shen, D. D., Kunze, K. L., Perkins, J. D., Marsh, C. L., McVicar, J. P., Barr, D. M., Gillies, B. S. and Thummel, K. E., 1996, First-pass metabolism of midazolam by the human intestine. *Clinical Pharmacology and Therapeutics*, **60**, 14–24.

Peter, R., Bocker, R., Beaune, P. H., Iwasaki, M., Guengerich, F. P. and Yang, C. S., 1990, Hydroxylation of chlorzoxazone as a specific probe for human liver cytochrome P450IIE1. *Chemical Research in Toxicology*, **3**, 566–573.

Rosenberg, D. W. and Mankowski, D. C., 1994, Induction of cyp2e-1 protein in mouse colon. *Carcinogenesis*, **15**, 73–78.

Sakuma, T., Takai, M., Endo, Y., Kuoiwa, M., Ôhara, A., Jarukamjorn, K., Honma, R. and Nemoto, N., 2000, A novel female-specific member of the CYP3A gene subfamily in the mouse liver. *Archives of Biochemistry and Biophysics*, **377**, 153–162.

Shimada, T., Yamazaki, H., Mimura, M., Inui, Y. and Guengerich, F. P., 1994, Interindividual variations in human liver cytochrome P450 enzymes involved in the oxidation of drugs, carcinogens and toxic chemicals: studies with liver microsomes of 30 Japanese and 30 Caucasians. *Journal of Pharmacology and Experimental Therapeutics*, **270**, 414–423.

Stralka, D. J. and Strobel, H. W., 1989, Cytochrome P450 activity and distribution in the human colon mucosa. *Cancer*, **64**, 2111–2116.

Vickers, A. E., Fisher, R. L., Brendel, K., Guertler, J., Dannecker, R., Keller, B. and Fischer, V., 1995, Sites of biotransformation for the cyclosporin derivative SDZ IMM 125 using human liver and kidney slices and intestine. Comparison with rat liver slices and cyclosporin A metabolism. *Drug Metabolism and Disposition*, **23**, 327–333.

Vickers, A. E., Fischer, V., Connors, S., Fisher, R. L., Baldeck, J. P., Maurer, G. and Brendel, K., 1992, Cyclosporin A metabolism in human liver, kidney, and intestine slices. Comparison to rat and dog slices and human cell lines. *Drug Metabolism and Disposition*, **20**, 802–809.

Waldron, K. W., Johnson, I. T. and Fenwick, G. R. (eds), 1994, Food and Cancer Prevention: Chemical and Biological Aspects. Special publication 123 (London: Springer).

Watkins, P. B., Wrighton, S. A., Schuetz, E. G., Molowa, D. T. and Guzelian, P. S., 1987, Identification of glucocorticoid-inducible cytochromes P450 in the intestinal mucosa of rats and man. *Journal of Clinical Investigation*, **80**, 1029–1036.

Wilson, T. H. and Wiseman, G., 1954, The use of sacs of everted small intestine for the study of the transference of substances from the mucosal to the serosal surface. *Journal of Physiology*, **123**, 116–125.

Yamazaki, H., Guo, Z., Persmark, M., Mimura, M., Inoue, K., Guengerich, F. P. and Shimada, T., 1994, Bufuralol hydroxylation by cytochrome P450 2D6 and 1A2 enzymes in human liver microsomes. *Molecular Pharmacology*, **46**, 568–577.

Yamazaki, H., Inoue, K. and Shimada, T., 1998, Roles of two allelic variants (Arg144Cys and Ile359Leu) of cytochrome P450 2C9 in the oxidation of tolbutamide and warfarin by human liver microsomes. *Xenobiotica*, **28**, 103–115.

Yamazaki, H. and Shimada, T., 1997, Progesterone and testosterone hydroxylation by cytochromes P450 2C19, 2C9, and 3A4 in human liver microsomes. *Archives of Biochemistry and Biophysics*, **346**, 161–169.

Yanagimoto, T., Itoh, S., Sawada, M. and Kamataki, T., 1997, Mouse cytochrome P450 (CYP3A11): predominant expression in liver and capacity to activate aflatoxin B_1. *Archives of Biochemistry and Biophysics*, **340**, 215–218.

Zhang, Q. Y., Dunbar, D., Ostrowska, A., Zeisloft, S., Yang, J. and Kaminsky, L. S., 1999, Characterization of human small intestinal cytochromes P450. *Drug Metabolism and Disposition*, **27**, 804–809.

XENOBIOTICA, 2000, VOL. 30, NO. 10, 983–991

Pharmacokinetics and disposition of the novel dopamine agonist Z-7760 in rat after intravenous and oral administration

M. BOLLARD†, J. CALDWELL†*, G. W. TAYLOR‡, M. STROLIN-BENEDETTI§ and C. SEMERARO§

† Division of Biomedical Sciences, Imperial College School of Medicine, Sir Alexander Fleming Building, South Kensington, London SW7 2AZ, UK
‡ Division of Medicine, Imperial College School of Medicine, Ducane Road, London W12 0HS, UK
§ Zambon Group Spa, PO Box 091 Bresso, Milan, Italy

Received 8 March 2000

1. Z-7760 (S(–)-N-[N-2-phenylethyl)-6-hexylamino]-N-propyl-5,6-dihydroxy-1,2,3,4-tetrahydro-2-naphthylamine dihydrobromide) is a potent dopamine D-1 and D-2 agonist synthesized during a search for agents to treat heart failure. Reported is the fate of the drug in rat.

2. ^{3}H-Z-7760 was administered p.o. and i.v. to male Sprague–Dawley rats (0.4 mg and 400 μCi/kg in 0.1% ascorbic acid) and venous blood samples collected at intervals up to 48 h. Comparison of the AUC for total ^{3}H showed that 37% of an oral dose of Z-7760 was absorbed. The percentage plasma ^{3}H present as the parent compound fell from 82% 30 min after i.v. dosing to 12% after 24 h. After oral dosing, the fraction of plasma ^{3}H present as unchanged Z-7760 was $< 5\%$ and this was essentially unaltered throughout the study. The long terminal elimination phase evident from 6 h was notable after both routes of administration.

3. The bile duct-cannulated rat was given ^{3}H-Z-7760 p.o. (0.4 mg and 40 μCi/kg) and bile was collected for up to 22 h. Biliary excretion accounted for 30% of the dose. No parent compound was detected in the bile.

4. In further studies, other rats were dosed p.o. or i.v. with ^{3}H-Z-7760 (0.4 mg and 400 μCi/kg) and urine and faeces were collected daily for 3 days. The major route of excretion was the faeces with 94–97% ^{3}H recovered after oral and 70–73% after i.v. dosing. A further 4–7% was recovered in the urine after oral and 12–13% after i.v. dosing.

5. After oral administration of Z-7760 (100 mg/kg, 40 μCi/kg) to rats, the major metabolites in the urine were identified as the 5-O-methyl and glucuronic acid conjugates of Z-7760 by LC and MS. The glucuronide was only seen in urine after oral administration but 5-O-methyl-Z-7760 was present in urine and faeces after both routes of administration.

6. The low bioavailability of Z-7760 is the consequence of its poor absorption from the gastrointestinal tract as well as extensive first-pass metabolism that further reduces systemic blood concentrations after oral administration.

Introduction

Z-7760 (S(–)-N-[N-2-phenylethyl)-6-hexylamino]-N-propyl-5,6-dihydroxy-1,2,3,4-tetrahydro-2-naphthylamine dihydrobromide) (figure 1) is a representative of a series of novel dopamine D-2 receptor agonists developed in a search for new agents for the treatment of heart failure (Santangelo *et al*. 1995, Semeraro *et al*. 1997). The best-studied congener is Z-1046 (S-6-[[6[[2-(2-methoxyphenoxy)-ethyl]amino]propyl]amino]-5,6,7,8-tetrahydro-1,2-naphthalenediol dihydro-

* Author for correspondence; e-mail: j.caldwell@ic.ac.uk

Xenobiotica ISSN 0049-8254 print/ISSN 1366-5928 online © 2000 Taylor & Francis Ltd
http://www.tandf.co.uk/journals

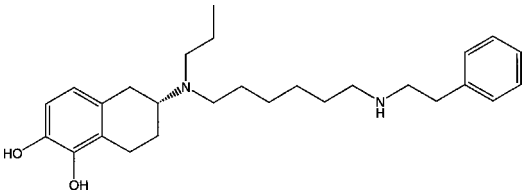


Figure 1. Structure of Z-7760 ((–)S-N-[N-2-phenylethyl)-6-hexylamino]-N-propyl-5,6-dihydroxy-1,2,3,4-tetrahydro-2-naphthylamine dihydrobromide).

chloride) that has excellent activity by intravenous (i.v.) infusion but not when given orally (p.o.) (Montanari *et al*. 1993). This prompted the search for congeners with good oral activity, which led to interest in Z-7760.

The poor activity of orally administered drugs is arguably the greatest problem facing drug development today. It is important that the two major causes of this, namely poor absorption across the gastrointestinal tract and presystemic metabolism, be evaluated to inform the design and selection of molecules with desirable pharmacodynamic and pharmacokinetic properties (Lipinski *et al*. 1996). Although empirical approaches to the problem of poor bioavailability, such as chemical modification at sites likely to influence metabolism e.g. bio-isosteric substitution, have both been claimed to lead to improvements in some cases, there remains a need for a systematic understanding of the origins of the problem within individual drug classes. Reported are the results of a series of *in vivo* investigations into the fate of Z-7760 in rat, following administration of ^{3}H-Z-7760 by different routes. Some data have been communicated to the International Society for the Study of Xenobiotics (Bollard *et al*. 1997).

Materials and methods

Compounds

[U-^{3}H]-Z-7760 (>98% radiochemical purity), Z-7760 (>95% chemical purity) ((–)-S-N-[N-2-phenylethyl)-6-hexylamino]-N-propyl-5,6-dihydroxy-1,2,3,4-tetrahydro-2-naphthylamine dihydrobromide) and Z-12962 (5-O-methyl-Z-7760) were synthesized at Zambon SpA (Bresso, Italy). HPLC-grade solvents were from BDH Merck Ltd (Lutterworth, UK). Sagatal (pentobarbitone, 60 mg/ml) was from Veterinary Services (York, UK). PBA and C_{18} BondElut columns were from Waters (Watford, UK) and Phenomenex UK Ltd (Macclesfield, UK) respectively. Ecoscint scintillation cocktail was from National Diagnostics (Atlanta, GA, USA). All other chemicals were of analytical grade and from Aldrich Chemical Co. Ltd (Gillingham, UK) or Sigma Chemical Co. Ltd (Poole, UK).

Plasma pharmacokinetics

Male Sprague–Dawley rats (250 g, $n = 6$) were from Charles River (Margate, UK). They received ^{3}H-Z-7760 (0.4 mg and 400 μCi/kg) dissolved in 0.1% ascorbic acid (2.5 ml/kg) by i.v. injection via a tail vein ($n = 3$) or by oral gavage ($n = 3$). Blood samples were collected from a tail vein into heparinized vials at regular intervals up to 48 h post-dose and were centrifuged for 10 min at 8500*g*. Plasma was stored at −20 °C before determination of ^{3}H activity. The percentage of the total radioactivity present in the plasma as parent compound was determined by radio-HPLC using system 2 (see below). The peak eluting from the column at the retention time corresponding to that of Z-7760 was collected and analysed for ^{3}H activity.

Balance study

Rats ($n = 8$) received ^{3}H-Z-7760 (0.4 mg and 400 μCi/kg) dissolved in 0.1% ascorbic acid by i.v. injection ($n = 4$) or oral gavage ($n = 4$) as above, and were housed individually in all-glass metabolism cages. They were given pelleted food (Special Diet Services, Witham, UK) and water *ad libitum*. Urine

and faeces were collected for 24 h predose, 0–24, 24–48 and 48–72 h after administration and stored at −20 °C. Urine was collected into flasks containing 2% ascorbic acid (1 ml) over solid CO_2. After 72 h, the rats were killed and the carcasses digested for analysis of ^{3}H activity. In further studies, rats were given 100 mg/kg ^{3}H-Z-7760 (40 μCi/kg) by oral gavage and their 0–24-h urine collected for the characterization of metabolites.

Bile duct cannulation

Rats (n = 3) received ^{3}H-Z-7760 (0.4 mg and 40 μCi/kg) by oral gavage before cannulation of the common bile duct using the surgical procedure of Mulder *et al*. (1981). Rats were anaesthetized with pentobarbitone (60 mg/kg i.p.) and a tail vein was cannulated. A 3-cm incision was made along the midline, and the bile duct was located and cannulated with polythene tubing (i.d. 0.40 mm, o.d. 0.80 mm). Rats were placed in restraining cages with free access to 4.3% dextrose/0.18% saline. Body temperature was maintained by placing the animal under a lamp; fluid loss was replaced by i.v. infusion of 0.9% saline at regular intervals. Bile was collected hourly for up to 22 h and stored at –20 °C before analysis for ^{3}H.

High-performance liquid chromatography (HPLC)

HPLC used Shimadzu (Düsseldorf, Germany) LC10AS pumps, a Pye (Cambridge, UK) LC3 UV detector set at 220 or 270 nm or a Shimadzu RF-535 fluorescence detector (λ_{ex} = 235 nm, λ_{em} = 305 nm) and a Waters 715 UltraWISP autoinjector under the control of Raytest (Sheffield, UK) Gina software. A Nucleosil 5 C_{18} 100 A column (25 cm × 3.2 mm i.d., 5 μm particle size) was employed for analysis using one of the gradient elution programmes given below.

System 1. This gradient system employed acetonitrile and sodium perchlorate (0.02 M, pH 3.0), with a flow rate of 0.6 ml/min and an acetonitrile gradient of 0–5 min at 10%, 5–25 min at 10–35%, 25–35 min at 35–50%, 35–60 min at 50–60%, 60–65 min at 60–80% and 65–75 min at 80–100%.

System 2. This gradient system employed acetonitrile and sodium perchlorate (0.02 M, pH 3.0) with a flow rate of 0.6 ml/min and an acetonitrile gradient of 0–5 min at 10%, 5–15 min at 10–35%, 15–20 min at 35–50%, 20–30 min at 50–60% and 30–35 min at 60–80%.

System 3. The final gradient system employed solvent A, aqueous acetonitrile (acetonitrile, 0.04% v/v aq. trifluoroacetic acid, 70:30) and solvent B, trifluoroacetic acid (0.04% v/v aq.) with a flow rate of 0.6 ml/min. The gradient used was 0–10 min at 0–60% solvent A, 10–15 min at 60%, 15–30 min at 60–80% and 30–35 min at 80–100% solvent A.

Electrospray mass spectrometry

A VG Biotech (Altrincham, UK) Quattro II tandem quadrupole instrument equipped with a pneumatically assisted electrospray probe was used. Samples were dissolved in acetonitrile/H_2O (1:1 v/v) and analysed by flow injection analysis (FIA) at 20–30 μl/min and a source temperature of 70 °C. A capillary voltage of 3 kV was used in conjunction with a cone voltage of 30 V and 10% valley resolution. CID experiments were performed at a collision energy of 50–70 eV with argon as the collision gas at 10^{-3} mBar. Positive-ion spectra were collected over a mass range of 130–500 or 130–700 amu with a scan cycle time of 1 s.

Radiochemical techniques

Aliquots of urine (0.1 ml), bile (50 μl) or plasma (20 μl) and other solutions (0.1–1.0 ml) were mixed with 1 ml methanol and 15 ml Ecoscint scintillation cocktail, and their ^{3}H activity was determined with a Packard (Pangbourne, UK) TriCarb Minaxi 4000 liquid scintillation spectrometer, using the external standard method to correct for quenching.

Faeces were lyophilized, ground in a mortar and pestle, and 50-mg samples were oxidized to ^3H_2O using a Packard 306 Oxidizer and assayed for radioactivity as above.

Carcasses were dissolved in 1 ml per body weight of 40% sodium hydroxide (w/v) and were left in the dark for 5–7 days at room temperature until no solid matter remained. The digests were homogenized and 0.2-ml aliquots were mixed with 0.4 ml water and 0.4 ml Triton X-405:methanol (1:3 v/v) in glass scintillation vials and left to stand overnight. Solutions were then neutralized with 10 M nitric acid before addition of 1 ml methanol and 15 ml Ecoscint and were analysed for radioactivity by liquid scintillation spectrometry.

Urinary ^3H_2O content

Duplicate 0.1-ml aliquots of urine of known ^3H activity were lyophilized and reconstituted with the same volume of distilled water. The ^3H activity of the reconstituted residue was determined by liquid scintillation spectrometry and the loss of ^3H_2O on lyophilization was calculated as a percentage of the ^3H activity of the urine.

Determination of ^3H metabolite profiles for urine, bile and faeces

Whole urine and bile samples were subjected to solid-phase extraction (SPE) before HPLC analysis. Urine samples (1 ml) were adjusted to pH 2 using 0.1 M hydrochloric acid and loaded on to a C_{18} BondElut cartridge preconditioned with methanol. More than 80% of the ^3H activity in the urine was recovered from the cartridge by elution with 3 ml methanol. The solvent was evaporated under a stream of nitrogen and the residue taken up in 200 μl 10% acetonitrile:sodium perchlorate (0.2 M, pH 3.0) for HPLC using system 2. Metabolite profiles were established by measuring the ^3H activity of serial 12-s fractions of the HPLC column eluent.

Bile samples (300 μl) were loaded on PBA BondElut cartridges, preconditioned with 30% aqueous isopropanol. Up to 80% of the ^3H activity of bile was eluted with 3 ml propanol:5% w/v aqueous acetic acid (30:70 v/v). The extracts were dried under a stream of nitrogen and reconstituted in 200 μl 10% acetonitrile:sodium perchlorate (0.2 M, pH 3.0) for HPLC analysis using system 2. Metabolite profiles were established as above.

Faeces (0.5 g) were lyophilized and the residues extracted with 5-ml aliquots of methanol. More than 90% ^3H was recovered after five extractions. The extracts were combined, evaporated to dryness under N_2 and reconstituted in acidified H_2O (1 ml). This was then applied to a preconditioned C_{18} BondElut cartridge. More than 80% of the applied ^3H was recovered with 3 ml methanol. The solvent was evaporated under nitrogen and the residue taken up in 200 μl 10% acetonitrile:sodium perchlorate (0.2 M, pH 3.0). ^3H metabolite profiles were established as above using HPLC system 2.

Urinary metabolite identification

Urine (5 ml) from rats given 100 mg/kg (40 μCi/kg) Z-7760 was subjected to SPE as above and the extracts freeze dried and reconstituted in 200 μl 10% acetonitrile and sodium perchlorate (0.2 M, pH 3.0) to concentrate the metabolites. Aliquots (100 μl) were analysed using HPLC system 2. Metabolite peaks were collected, the acetonitrile evaporated under nitrogen and then lyophilized. Dried samples were reconstituted in 200 μl 0.04% v/v trifluoroacetic acid and rechromatographed using HPLC system 3. Radioactive peaks were again collected, lyophilized and reconstituted in 50% aqueous acetonitrile for analysis by electrospray mass spectrometry.

Pharmacokinetic analysis

Plasma concentration–time data for total ^3H and Z-7760 were analysed with PK Summit (Summit Research Services, USA). Bioavailability and the percentage absorption of Z-7760 were calculated from the dose-corrected mean AUCs (obtained by the trapezoidal rule) thus:

$$AUC_{0-\infty} \text{ p.o.}/AUC_{0-\infty} \text{ i.v.} \times 100$$

for total plasma ^3H after i.v. and oral administration.

Results

Plasma pharmacokinetics

The plasma level time curves for total ^3H and parent drug after i.v. and oral administration of Z-7760 are shown in figure 2 and a selection of the pharmacokinetic parameters describing these are presented in table 1. After i.v. administration, the percentage plasma ^3H as parent compound fell from 82% at 30 min to 12% after 24 h. After oral administration, the fraction of plasma ^3H as Z-7760 was essentially unaltered throughout the study ($< 5\%$), the levels being close to the limit of detection (0.1 pmol) in most samples. After oral administration, the maximum ^3H concentration in plasma was reached after 1.5 h followed by a sustained plateau established from 6 to 48 h (not shown in figure 2).

The extent of absorption of ^3H after oral administration, calculated from the ratio of the AUCs for ^3H after i.v. and oral administration, was 37%. The oral

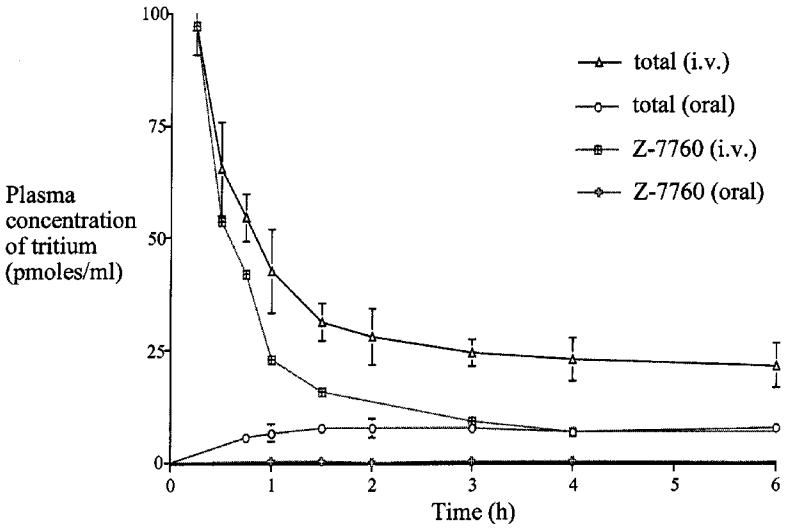


Figure 2. Plasma concentration–time curves for total ^{3}H and unchanged Z-7760 after i.v. (n = 3) and oral (n = 3) administration of Z-7760 (0.4 mg and 400 μCi/kg) to the male rat.

Table 1. Pharmacokinetic parameters describing the plasma concentration–time curves of total ^{3}H in rat given ^{3}H-Z-7760 (0.4 mg and 400 μCi/kg^{-1}) by i.v. infusion (n = 3) or orally (n = 3).

Parameter	Intravenous Mean ± SD	Oral Mean ± SD
Distribution/absorption rate (h^{-1})	2.41 ± 1.00	1.31 ± 1.14
Elimination rate (h^{-1})	0.08 ± 0.04	0.06 ± 0.03
Distribution/absorption half-life (h^{-1})	0.33 ± 0.17	1.41 ± 1.22
Elimination half-life (h^{-1})	9.95 ± 5.02	19.10 ± 17.62
$AUC_{0-6\,h}$ (observed area) (ng h ml^{-1})	939.30 ± 16.90	334.70 ± 13.60

Table 2. Excretion balance of ^{3}H by rat given ^{3}H-Z-7760 (0.4 mg and 400 μCi/kg^{-1}) by i.v. infusion (n = 4) or orally (n = 4).

	Intravenous	Oral
Urine	12.7 (12.0–13.5)	5.1 (4.0–7.2)
Faeces	71.6 (69.9–73.3)	95.3 (93.8–96.7)
Carcass	9.8 (4.9–14.8)	2.4 (2.2–2.8)
Total	94.1 (91.1–96.8)	102.8 (102.7–102.9)

Figures are % ^{3}H dose recovered in that sample in 72 h, with ranges in parentheses.

bioavailability of unchanged Z-7760 was estimated as $< 0.1\%$, a value which cannot be calculated more accurately due to the low levels of drug present in the great majority of plasma samples after oral administration.

Balance study

The excretion balance of ^{3}H from rat given ^{3}H-Z-7760 is presented in table 2, which shows the essentially quantitative recovery achieved after i.v. and oral administration. The principal route of excretion of ^{3}H was the faeces after both i.v.

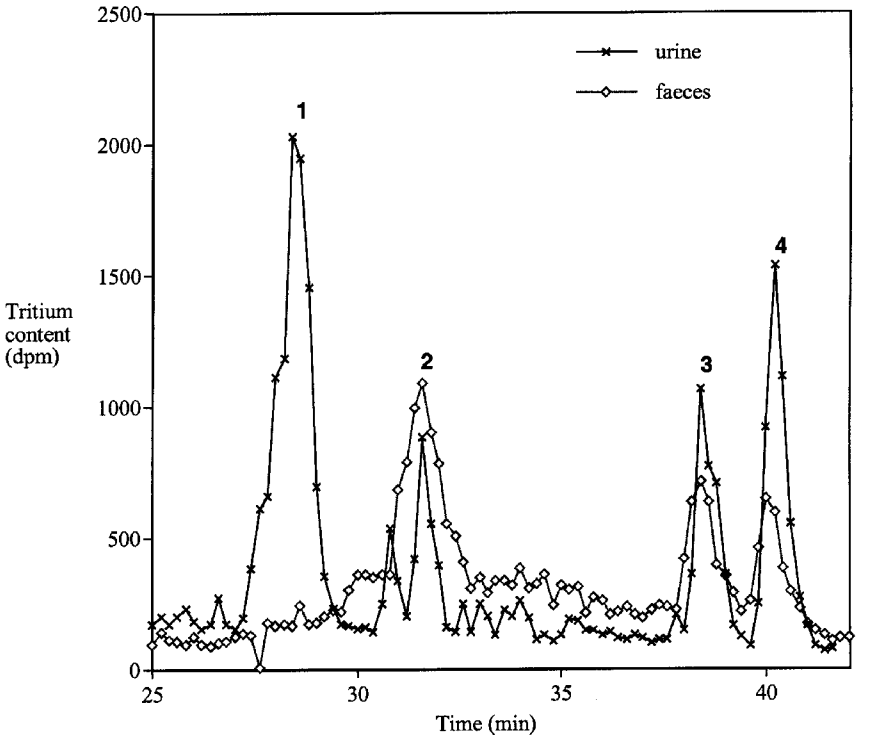


Figure 3. ^{3}H profiles of extracts of 0–24-h urine and faeces from rat given Z-7760 (100 mg/kg^{-1}, 40 μCi/kg^{-1}) p.o., using HPLC system 2. 1, Glucuronide of Z7760; 2, unknown.

(>69%) and oral (>93%) administration, with the remainder excreted in the urine (i.v. 12%, oral 5%). The balance of the dose was retained in the carcass after 72 h (i.v. 10%, oral 2%).

Biliary excretion

The biliary excretion of ^{3}H from rat given ^{3}H-Z-7760 p.o. totalled 30% in 22 h. Excretion was sustained at ~1% of dose/h throughout the collection period.

Urinary, biliary and faecal metabolites

Of the total urinary ^{3}H, 98% was recovered after freeze-drying of all samples, indicating the biological stability of the ^{3}H label and that the excretion of $^{3}H_2O$ was negligible.

Up to 20 tritiated compounds were present in the ^{3}H HPLC profiles (using system 2) of SPE extracts of the 0–24-h urine after oral administration of Z-7760. After i.v. administration, 13 tritium-containing peaks were observed. The HPLC profile of extracts of urine of the orally dosed rat was dominated by six compounds, with retentions of 13.8 (6% of urinary ^{3}H), 28.4 (15%), 30.6 (6%), 31.6 (9%), 38.4 (9%) and 40.2 (14%) min in system 2, which together accounted for 59% of urinary ^{3}H. In the HPLC profiles of urinary extracts from the i.v. dosed rat, six tritiated peaks dominated at retentions of 13.8 (13% of urinary ^{3}H), 25.5 (14%), 30.6 (7%), 31.6 (6%), 38.4 (10%) and 40.2 (14%) min. The peak with a retention time of 28.4 min seen after oral administration was absent from urine after i.v. dosage.

The peak at 38.4 min seen in the urine of both oral (9% of urinary tritium) and i.v. (10%) dosed rat co-eluted with an authentic sample of Z-7760. The peak at 40.2 min, also seen in the urinary extracts from the oral (14%) and i.v. (14%) treated rat, co-eluted with an authentic sample of 5-O-methyl-Z-7760. These assignments were confirmed by electrospray mass spectrometry, the peaks having $[M+H]^+$ ions of m/z 425 and m/z 439 respectively. The third peak, with a retention of 28.4 min, was present after oral (15% of urinary ^3H) but not i.v. administration. This peak had an $[M+H^+]$ ion of m/z 601 and was identified by electrospray mass spectrometry as a glucuronide of Z-7760. The peaks at 13.8, 25.5, 30.6 and 31.6 min (totalling 21 and 40% of urinary ^3H after oral and i.v. administration respectively, or 2.7 and 2.0% of the dose of 0.4 mg/kg) remain uncharacterized due to the very small quantities present.

Three major ^3H peaks were present in the HPLC profiles (using system 2) of faecal extracts after SPE from rat dosed orally with Z-7760 and five in rat dosed i.v. ^3H peaks at 38.4 (13% oral, 13% i.v.) and 40.2 min (12% oral, 5% i.v.) co-eluted with Z-7760 and 5-O-methyl-Z-7760 respectively. The peak at 31.6 min was not identified. In addition, ^3H peaks at 30.6 and 33.9 min (9 and 35% of faecal ^3H) after i.v. administration remained uncharacterized. The glucuronide of Z-7760 was not detected in the faeces after oral or i.v. administration.

The ^3H HPLC profiles in HPLC system 2 of 0–24-h urine and faeces extracts from rat given 100 mg/kg Z-7760 (40 μCi/kg) are shown in figure 3.

Two metabolite peaks, with retentions of 21.0 and 24.0 min, were observed in the ^3H profiles (using system 1) of SPE extracts of bile obtained after oral administration of ^3H-Z-7760. However, the parent compound (retention of 28.0 min) was not detected. The proportion of each tritiated component varied between bile samples collected at different time points.

Discussion

At present, a failure to achieve therapeutically effective blood levels of drugs intended for oral administration is one of the greatest pharmacokinetic problems in the development of New Chemical Entities (Lipinski *et al*. 1996). There are two major reasons underlying such findings, namely poor absorption from the gastrointestinal tract and intestinal and/or hepatic first-pass metabolism of absorbed drug (Caldwell and Marsh 1982, Lin *et al*. 1999). Z-7760 is a member of a series of novel dopamine agonists, many of which are much less effective when given orally than by i.v. infusion (Montanari *et al*. 1993). By analogy with related compounds, it was assumed that this was due to their presystemic metabolism by O-methylation and/or sulphation in the gut wall. This is exemplified by catechol-containing drugs such as isoprenaline (George *et al*. 1974) and L-DOPA (Hashizume *et al*. 1987) and related phenolic amines such as 8-hydroxy-DPAT (Mason *et al*. 1995). These compounds are well absorbed ($>80\%$) across the gastrointestinal wall. The present work uses a relatively straightforward approach to show that the poor oral pharmacodynamic effect of Z-7760 is due to poor absorption and hepatic first-pass metabolism of absorbed drug. The plasma level-time curves for ^3H after the i.v. and p.o. administration of Z-7760 are indicative of the relatively poor absorption of ^3H after oral administration and comparison of the AUCs of ^3H show that only 37% of an oral dose of ^3H-Z-7760 is absorbed from the gastrointestinal tract. That fraction of the oral dose absorbed is then subject to extensive first-pass metabolism,

so that $< 0.1\%$ of the dose reaches the systemic circulation unchanged. As mentioned above, it is not surprising that this catechol drug shows low oral bioavailability due to its propensity for extensive first-pass metabolism. In the present case, this is associated with glucuronidation and O-methylation. However, it is important to appreciate that Z-7760 is also relatively poorly absorbed, a feature which may be associated with the bulky lipophilic side chain that this series of compounds possesses.

Absorbed Z-7760 is completely eliminated from the animal body within 3 days, with the bulk of the compound being excreted in the faeces. This is largely due to unabsorbed drug after oral administration, but there is also a contribution from biliary excretion. Studies after oral gavage have shown that there occurs a slow and sustained biliary excretion of up to 30% of the dose within 22 h. It thus appears that biliary elimination contributes to faecal excretion after oral administration and accounts for the majority of faecal ^{3}H after i.v. administration (72% of dose in 72 h). There was no evidence of parent drug in the bile while $< 1\%$ of the dose (9% of the total ^{3}H activity) was present in the 24-h urine as parent drug from the orally dosed rat.

Extensive metabolism of Z-7760 occurs in rat with six major HPLC peaks found in the urine after oral administration and three major peaks in the faeces. The two most dominant ^{3}H peaks in the urine from the orally dosed rat were the 5-O-methyl and glucuronic acid conjugates of Z-7760, which together with unchanged Z-7760 and three unknown metabolites accounted for 59% of the total ^{3}H content. It is interesting to note that this glucuronide was resistant to hydrolysis when urine was incubated with a beef liver β-glucuronidase preparation (Glusulase; Sigma).

The major metabolic routes of Z-7760 are conjugation by glucuronidation and 5-O-methylation, with no evidence for sulphation. Conjugation of the phenolic hydroxyl with glucuronic acid rather than sulphate is consistent with the structural complexity and high molecular weight (424.7) of Z-7760. Relatively unhindered monocyclic phenols undergo principally sulphate in rodents but the pattern of conjugation moves towards one dominated by glucuronidation with increasing molecular weight and steric hindrance around the hydroxyl group (Caldwell 1980, Mulder 1982, 1990). It is likely that the conjugate is an ether glucuronide, since the phenolic 5- and 6-hydroxy groups of the catechol moiety are the most likely sites for the transfer of glucuronic acid. It appears that phase I metabolic pathways are only relatively minor for Z-7760 and are unlikely to make a major contribution to its extensive first-pass metabolism. The 5-O-methyl conjugate is found in the urine after both oral and i.v. administration, suggesting that it is formed systemically, most likely in the liver. In contrast, the glucuronide is excreted in the urine only after oral dosing, consistent with its presystemic formation in the intestinal mucosa and/or the liver. The 5-O-methyl conjugate is found in the faeces after both oral and i.v. dosing, suggesting that it is formed systemically and then undergoes biliary excretion. The failure to detect the glucuronide of Z-7760 in faeces after either route of administration is consistent with excretion in the bile after bacterial hydrolysis in the lumen of the intestine.

Acknowledgements

The assistance of Dr N. J. Swales with the bile duct cannulation is gratefully acknowledged.

References

Bollard, M. E., Strolin-Benedetti, M., Semeraro, C. and Caldwell, J., 1997, The metabolic fate of the dopamine agonist Z7760 in the rat. *ISSX Proceedings*, **11**, 133.

Caldwell, J., 1980, Comparative aspects of detoxication in mammals. In W. B. Jakoby (ed.), *Enzymatic Basis of Detoxication*, vol. 1 (New York: Academic Press), pp. 85–114.

Caldwell, J. and Marsh, M. V., 1982, Metabolism of drugs by the gastrointestinal tract. In C. F. George, D. Shand and A. G. Renwick (eds), *Presystemic Drug Elimination* (London: Butterworths), pp. 29–42.

George, C. F., Blackwell, E. W. and Davies, D. S., 1974, Metabolism of isoprenaline in the intestine. *Journal of Pharmacy and Pharmacology*, **26**, 265–267.

Hashizume, K., Yamatodani, A., Yamamoto, T., Ogihara, T., Kumahara, Y. and Wada, H., 1987, Effects of oral and intravenous administration of dopamine and L-dopa on plasma levels of two isomers of dopamine sulphate in man. *Life Sciences*, **41**, 2697–2704.

Lin, J. H., Chiba, M. and Baillie, T. A., 1999, Is the role of the small intestine in first-pass metabolism over-emphasised? *Pharmacological Reviews*, **51**, 135–157.

Lipinski, C. A., Lombardo, F., Dominy, B. W. and Feeney, P. J., 1996, Experimental and computational approaches to estimate solubility and permeability in drug discovery. *Advances in Drug Delivery Research*, **23**, 3–25.

Mason, J. P., Caldwell, J. and Dring, L. G., 1995, The pharmacokinetics of the 5-hydroxytryptamine1A agonist 8-hydroxy-2-(N,N-di-*n*-propylamino)tetralin (8-OHDPAT) in the rat after intravenous and oral administration. *Xenobiotica*, **25**, 1371–1380.

Montanari, S., Bertolini, G., Casagrande, C., Cavelleri, P., Ferlenga, P., Marchini, F., Pradella, L., Pocchiari, F., Santangelo, F. and Semeraro, C., 1993, Z1046, a novel peripheral dopaminergic agent. *Bioorganic and Medicinal Chemistry Letters*, **6**, 2795–2800.

Mulder, G. J.,1982, Conjugation of phenols. In W. B. Jakoby, J. R. Bend and J. Caldwell (eds), *Metabolic Basis of Detoxication* (New York: Academic Press), pp. 247–269.

Mulder, G. J., 1990, Competition between conjugations for the same substrate. In G. J. Mulder (ed.), *Conjugation Reactions in Drug Metabolism* (London: Taylor & Francis), pp. 41–50.

Mulder, G. J., Scholtens, E. and Meijer, O. K., 1981, Collection of metabolites in bile and urine in the rat. *Methods in Enzymology*, **77**, 21–30.

Santangelo, F., Montanan, S., Bertolini, G., Cavalleri, P., Marchini, F., Pocchian, F., Pradella, L., Semeraro, C. and Zanzottera, D., 1995, Synthesis and biological evaluation of Z1046 and analogues as novel and potent peripheral dopaminergic agonists. *Abstracts of Papers of the American Chemical Society*, **209**, 67-Medi.

Semeraro, C., Marchini, F., Ferlenga, P., Masotto, C., Morazzoni, G., Pradella, L. and Pocchiari, F., 1997, The role of dopaminergic agonists in congestive heart failure. *Clinical and Experimental Hypertension*, **19**, 201–215.

XENOBIOTICA, 2000, VOL. 30, NO. 10, 993–1003

Determination, pharmacokinetics and protein binding of a novel tissue-type plasminogen activator, pamiteplase in human plasma

K. OIKAWA†*, T. WATANABE†, I. MIYAMOTO‡ and S. HIGUCHI†

†Drug Metabolism Laboratories and ‡Clinical Development Department, Yamanouchi Pharmaceutical Co. Ltd, 1–8 Azusawa 1-chome Itabashi-ku, Tokyo 174–8511, Japan

Received 14 April 2000

1. An enzyme-linked immunosorbent assay (ELISA) and functional bioassay to determine immunoreactive and bioactive concentrations of pamiteplase, a novel thrombolytic agent, in human plasma were developed. The ELISA and functional bioassay showed satisfactory accuracy and precision within a concentration range of 0·5–25 ng.ml^{-1} and of 0·127–16·2 ng.ml^{-1} respectively.

2. The pharmacokinetics of pamiteplase in healthy human subjects were evaluated using the ELISA and functional bioassay. Irrespective of the method used, plasma concentrations declined bi-exponentially. Half-lives in the β phase were 1·25 and 0·78 h, and AUCs were 507·9 and 286·4 ng.h.ml^{-1} respectively. Total clearances of pamiteplase decreased to 19 and 31% of those of the wild-type tissue-type plasminogen activator.

3. The protein binding of pamiteplase in human plasma was investigated by gel filtration chromatography. Pamiteplase formed three high molecular weight complexes with α_2-macroglobulin, C_1-esterase inhibitor and α_2-plasmin inhibitor in human plasma. This complex formation was relatively slow, and was thought to be irreversible and covalently bounded. Furthermore, this protein binding in humans resulted in the termination of biological action.

Introduction

Pamiteplase is a novel tissue-type plasminogen activator (t-PA) bearing a deletion in the Kringle-1 domain and a point mutation ($Arg_{275} \rightarrow Glu$) in the Kringle-2 domain (Kawauchi *et al*. 1991). These structural modifications have lengthened the plasma half-life compared with that of wild-type t-PA (wt-PA), which is rather short (Katoh *et al*. 1991). Plasma concentrations after intravenous administration of pamiteplase to rat or dog are greater than those of wt-PA because of the decrease in total clearance (Cl_{total}) compared with that of wt-PA (Oikawa *et al*. 1996a). Despite these structural modifications, pamiteplase possesses almost the same affinity for fibrinous thrombi as dose wt-PA, and it degrades fibrin by converting plasminogen to plasmin (Katoh *et al*. 1991). These properties of pamiteplase have been supported by results showing that pamiteplase has almost the same thrombolytic activity as wt-PA at one-third the dose of wt-PA in rat and dog with induced thrombi (Kawasaki *et al*. 1993a–c). In a thrombolytic therapy, wt-PAs have to be administered using bolus and 60-min infusion regimes. However, these findings have suggested that pamiteplase may achieve clinically sufficient efficacy by bolus administration alone.

The pharmacokinetics of a high molecular-weight compound (HWMC) such as pamiteplase have usually been examined by quantifying plasma concentrations using two kinds of method. One is the enzyme-linked immunosorbent assay

* Author for correspondence; e-mail: oikawa@yamanouchi.co.jp

Xenobiotica ISSN 0049–8254 print/ISSN 1366–5928 online © 2000 Taylor & Francis Ltd
http://www.tandf.co.uk/journals

(ELISA), which can be simple and highly sensitive. The other is a functional bioassay based on biological activity. However, such assays usually have poorer sensitivity than ELISAs and they show relatively less accuracy and precision compared with ELISAs in the presence of matrices such as plasma and urine. It is extremely important and better necessary to measure plasma concentrations by both methods to understand the pharmacokinetics of HWMCs. On the other hand, endogenous proteins existing in plasma are usually regulated by a physiological homeostasis, in which endogenous inhibitors bind them to control their biological activities. Therefore, the specificity of determination methods for HWMCs should be carefully examined to interpret their pharmacokinetics correctly.

In this study, techniques to determine plasma concentrations of pamiteplase were considered in preparation for human pharmacokinetic studies. ELISA (Holvoet *et al*. 1985, Buessecker *et al*. 1993, Schrauwen *et al*. 1994), the fibrin plate method (Walton *et al*. 1966) and the synthetic substrate method (Verheijen *et al*. 1982) have been reported as quantification methods for wt-PAs. An ELISA and functional bioassay were investigated and used to determine the pharmacokinetics of pamiteplase in healthy human subjects. There are differences in measured pamiteplase concentrations between these two assays, suggesting that human plasma components on the assays. Consequently, the protein binding of pamiteplase in human plasma was examined *in vitro*.

Materials and methods

Subjects

The study protocol was approved by the Institutional Review Board of Yamanouchi Pharmaceutical Co. Ltd. The normal health of adult male subjects was confirmed from their medical history and by physical and laboratory examinations including electrocardiography, haematology, blood chemistry, urinalysis, titre, coagulation-fibrinolysis parameters (PT, APTT, ELT, ELA, fibrinogen, FDP, D-dimmer, plasminogen, α_2-macroglobulin, α_2-plasmin inhibitor, α_2-PIC, PAI-1), and bleeding time measured by the Ivy method. Five people judged suitable for the study were admitted. The mean + SE of their ages was 29.1 and 1.2 years (range 25–30 years), and those of their body weights were 62.5 and 3.7 kg (54.0–76.0 kg). The subjects were informed of the objectives and procedures of the study, of the anticipated effects and potential adverse reactions of pamiteplase, and of the right to withdraw at any time. All subjects gave written informed consent before study registration. All subjects were controlled under the supervision of the study doctor from the evening before drug administration until the 24-h test after administration, and also had to abstain from alcohol, caffeine-containing beverages and tobacco during the study. Furthermore, all subjects were examined for possible allergic reactions using the prick test just before drug administration, and none of the subjects showed any indication of allergic reactions.

Materials

Pamiteplase contained a finger domain, an epidermal growth factor domain, a Kringle-2 domain, a serine protease domain and a site mutation at the Kringle-2 ($Arg_{275} \rightarrow Glu$) (Kawauchi *et al*. 1991). A lyophilized pharmaceutical preparation of pamiteplase was used in this study. Monoclonal antibody SP-322 (Ab-SP-322) was prepared from BALB/C mouse hybridoma SP-322 (Watanabe *et al*. 1989). Horseradish peroxidase labelled goat anti-human t-PA IgG (HRP-anti t-PA Ab) was from Biopool (Umea, Sweden), and a t-PA activity kit and human t-PA-deficient plasma were from Technoclone (Vienna, Austria). Carrier free $Na^{125}I$ was from DuPont NEN (Boston, MA, USA). Blank plasma was isolated by adding 3.8% sodium citrate (final concentration 10%; Kokusai Shiyaku, Koube, Japan) to blood obtained from healthy subjects and by centrifugation (1800*g* for 15 min at 4 °C). Gel filtration standard was from BIO-RAD (Hercules, CA, USA). Rabbit antibody anti-human α_2-macroglobulin, rabbit antibody anti-human C_1-esterase inhibitor, rabbit antibody anti-human α_2-plasmin inhibitor, and goat anti-rabbit immunoglobulin for immunoprecipitation were from DAKO (Glostrup, Denmark).

Evaluation of the ELISA

Sample preparation for the ELISA. Pamiteplase stock solution (1 $mg.ml^{-1}$) was prepared by dissolving a pamiteplase lyophilized formulation in physiologic saline. Pamiteplase standard solutions for ELISA were prepared by diluting the pamiteplase stock solution with 10 mM Tris-buffered saline containing

0·2% BSA and 0·05% Tween 20 (pH 7·5, BSA-TBS-Tw). Calibration curve samples were prepared by adding the pamiteplase standard solution to a t-PA-deficient plasma at final concentrations of 0·5–25 ng.ml^{-1}. To establish a precision and an accuracy of ELISA, three quality control samples (0·5, 2·5, 12·5 ng.ml^{-1}) were prepared by adding the pamiteplase standard solution to a t-PA-deficient plasma.

ELISA procedure. ELISA samples were incubated with 1·0 M acetic acid solution (pH 3·9) for 15 min at 37 °C, and then neutralized with 0·1 M NaH_2PO_4/0·4 M NaOH solution.

Ab-SP-322 dissolved in 0·05 M Na_2CO_3 solution (pH 9·6) was added to each well of 96-well microplate (Nunc, Roskilde, Denmark), and the plate was incubated at 4 °C overnight. After the coating of the capture antibody, the plate was incubated with 10 mM Tris-buffered saline containing 1% BSA and 0·05% Tween 20 (pH 7·5) at room temperature (RT) for 2 h. After washing the plate with BSA-TBS-Tw, plasma samples were added to each well of the coated plate, and the plate was incubated at RT for 3 h. After washing with BSA-TBS-Tw, 1:700 HRP-anti t-PA Ab solution was added to each well and the plate was incubated for 3 h at RT. After washing with BSA-TBS-Tw, a enzyme substrate comprising 0·1 M acetic acid/sodium citrate buffer (pH 5·8) containing 0·02% H_2O_2 and 3,3′,5,5′-tetramethylbenzidine (0·1 mg.ml^{-1}) was added to each well, and the plate was incubated for 5 min at RT. The colour development was stopped with 3 M H_2SO_4, and an absorbance was read at 450 nm on a microplate reader (Titertek Multiscan MCC/340, Dainihon Pharmaceutical, Suita, Japan).

Evaluation of the functional bioassay

Sample preparation for the functional bioassay. Pamiteplase standard solutions for the functional bioassay were prepared by diluting the pamiteplase stock solution with dilution buffer A (0·15 M Tris/Cl buffer containing 0·1% BSA and 0·1% Tween 80, pH 9·0). The calibration curve was prepared in a dilution buffer A because no effect of plasma on the assay was observed, and the calibration curve samples were prepared by adding the pamiteplase standard solution to a dilution buffer A at final concentrations ranging from 0·127 to 16·2 ng.ml^{-1}. To establish the precision and accuracy of the functional bioassay, four quality control samples (0·127, 0·33, 1·62, 13 ng.ml^{-1}) were prepared by adding the pamiteplase standard solution to a dilution buffer A.

Bioassay procedure. Acetic acid solution (0·05%) was added to the functional bioassay samples, and the mixture was incubated for 10 min and centrifuged at 1800*g* for 10 min at 4 °C. After discarding the supernatant, the precipitates (euglobulin fraction) were dissolved in dilution buffer A, and then the solutions were added to a 96-well microplate (Nunc). A synthetic plasmin substrate solution (0·1 M Tris/Cl buffer containing H-D-norleucyl-hexahydrotyrosyl-lysine-*p*-nitroanilide diacetate, Glu-plasminogen, CNBr-fragments of fibrin and 0·1% Tween 80) was added to each well, and the mixture was incubated at 37 °C for 2·5 h. An absorbance was read at 405 nm on a microplate reader (SJeia autoreader ER-8000, Sakou Pure Pharmaceutical, Tokyo, Japan).

Study design

Dosing solution (10 ml) prepared by dissolving the lyophilized pamiteplase formulation in sterile physiologic saline at 400 μg.ml^{-1} was administered intravenously to each of four of five healthy subjects within 2 min. One received placebo. Blood samples were drawn predosing and at 2, 5, 10, 15, 30 min, 1, 2, 4, 6 and 24 h post-dosing. The samples were mixed gently, followed by centrifugation (1800*g* for 15 min at 4 °C) to separate the plasma. The plasma was stored at –80 °C until analysis.

Pharmacokinetic analysis

Endogenous t-PA exists in human plasma with individual differences and intraday variation in concentration (Holvoet *et al*. 1985, Huber *et al*. 1989, Tahara *et al*. 1989). The ELISA and functional bioassay quantification methods for plasma pamiteplase concentrations also detected endogenous t-PA. Because concentrations measured by both methods are the sum of pamiteplase and endogenous t-PA, the values subtracting the concentrations predosing from values measured at each time point were taken as exogenous pamiteplase concentrations to evaluate the pharmacokinetics of pamiteplase.

Plasma immunoreactive and bioactive concentrations for each of the subjects were analysed using WinNonlin software (v.1·5, Pharsight, Inc., CA, USA) to calculate the half-life in the α phase ($t_{1/2}\alpha$), half-life in the β phase ($t_{1/2}\beta$), area under the plasma concentration–time curve from zero to infinity ($AUC_{0\rightarrow\infty}$), total body clearance (Cl_{total}), distribution volume at the steady state (Vd_{ss}), and mean residence time (MRT).

Preparation of ^{125}I-labelled pamiteplase (^{125}I-pamiteplase)

^{125}I-pamiteplase was synthesized by the chloramine T method using carrier-free Na^{125}I (Oikawa *et al*. 1996b). The specific activity, concentration and purity of radioactivity of ^{125}I-pamiteplase were 214·3 MBq.mg^{-1}, 11·4 MBq.ml^{-1} and > 95% respectively.

Incubation of ^{125}I-pamiteplase with human citrated plasma

Incubation solutions were prepared using pamiteplase stock solution, ^{125}I-pamiteplase solution and vehicle A (0·127 M phosphoric acid containing 0·2 M arginine and 0·01% Tween 80). After adding the incubation solution to human plasma (final concentration 1 $\mu g.ml^{-1}$), the mixture was incubated at 37 °C, and samples were collected at 10, 30, 60 and 120 min after incubation. The samples were analysed using gel filtration chromatography.

Gel filtration chromatography (GFC)

GFC conditions were: precolumn: TSK guardcolumn SW_{XL} (6·0 mm × 4 cm, TOSOH, Tokyo, Japan,); column: TSK-GEL G-3000 SW_{XL} (7·5 mm × 30 cm, TOSOH, Tokyo, Japan); column temperature: room temperature; eluent: 0·1 M Na_2HPO_4-NaH_2PO_4 buffer (pH 6·0) containing 0·01% Tween 80 and 0·2 M L-arginine; flow: 0·5 $ml.min^{-1}$; detection: UV 280 nm; 200 ml of incubation mixtures was injected into the column. Eluate (400 μl) was collected using fraction collector (SF-2120, ADVANTEC, Tokyo, Japan). The radioactivity of each fraction was measured in a γ-counter (Autogamma 5530, Packard, Tokyo, Japan).

The immunoreactive and bioactive concentrations of each fraction were measured by the ELISA and functional bioassay methods as described above.

Immunoprecipitation of various fractions using rabbit anti-human plasma protein

An antibody solution (anti-human α_2-macroglobulin rabbit IgG, anti-human C_1-esterase inhibitor rabbit IgG or anti-human α_2-plasmin inhibitor rabbit IgG) was added to fractions after adjusting pH with 0·1 M Tris buffer (pH 8·8). The mixture was incubated at 4 °C overnight. After adding goat anti-rabbit immunoglobulin to the mixture, the mixture was incubated at 4 °C overnight. After measuring the total radioactivity of the mixture, the radioactivity of the precipitable fraction obtained by centrifugation (1800 × *g* for 15 min at 4 °C) was measured.

Results

Evaluation of ELISA and functional bioassay

A calibration curve for the ELISA was prepared using t-PA-deficient plasma because of the existence of endogenous t-PA in human plasma (Holvoet *et al.* 1985, Huber *et al.* 1989, Tahara *et al.* 1989). A typical calibration curve over the concentration range 0·5–25 $ng.ml^{-1}$ concentration is shown in figure 1. Table 1 shows the within-day accuracy (expressed as CV) and precision (expressed as RE) of the ELISA. CV and RE at each concentration ranged from 2·78 to 12·53% and from −10·60 to 5·28% respectively. The results of between-day precision and accuracy test were equal to those of the within-day test (data not shown). To measure higher concentration samples, the sample was diluted with a t-PA-deficient plasma, and the linearity of the dilution was confirmed in the range 1–10 000 $ng.ml^{-1}$. The specificity of the ELISA assay was confirmed using six individual samples with and without pamiteplase.

A typical calibration curve for the functional bioassay obtained by fitting each bioactive concentration to a four-parameter logistic curve (Aloka RIA program, Aloka, Japan) is shown in figure 1. Table 1 shows the within-day accuracy and precision of this functional bioassay. CV and RE at each concentration ranged from 2·5 to 4·3% and from 2·0 to 25·8% respectively. The results of the between-day precision and accuracy test were equal to those of the within-day test (data not shown). To measure higher concentration samples over calibration curve, the sample dilution was conducted with dilution buffer A, and the linearity of the dilution was confirmed in the range 1–10 000 $ng.ml^{-1}$. The specificity of bioassay was confirmed using six individual samples with and without pamiteplase, resulting that no interfered matrix was observed. The bioactive concentration of endogenous materials in blank human plasma ranged from 7·6 to 25·2 $ng.ml^{-1}$, and CV of the endogenous t-PA measurement ranged from 0·6 to 2·7%.

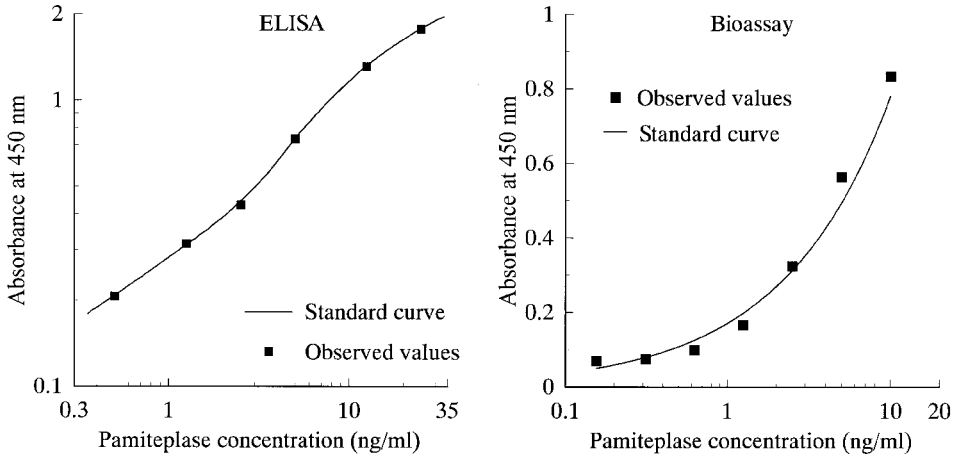


Figure 1. ELISA and functional bioassay standard curves. Each datum point represents the average of three determinations.

Table 1. Accuracy and precision of the ELISA and functional bioassay methods.

Method	Prepared concentration ($ng.ml^{-1}$)	Observed concentration[a] ($ng.ml^{-1}$)	Coefficient of variation (%)	Relative error (%)
ELISA	0.5	0.450±0.03	12.53	−10.60
	2.5	2.63±0.12	10.22	5.28
	12.5	12.7±0.16	2.78	1.62
Bioassay	0.127	0.129±0.001	3.8	2.0
	0.33	0.41±0.004	3.3	25.8
	1.62	1.81±0.023	4.3	11.7
	13.0	13.3±0.094	2.5	2.3

[a] Data are the mean ± SE of five determinations.

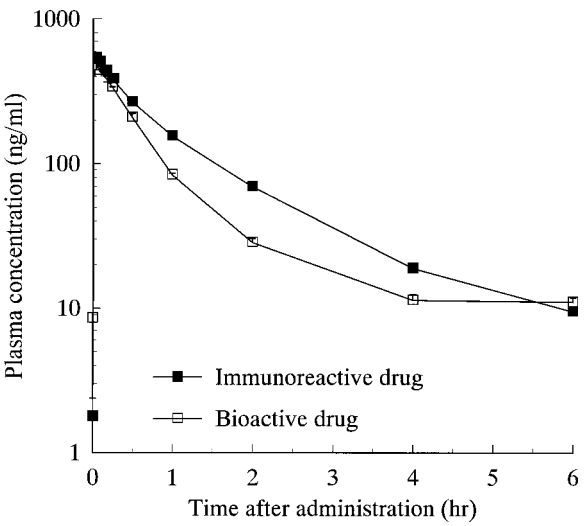


Figure 2. Concentration–time profile of immunoreactive and bioactive plasma concentrations after intravenous administration of 4.0 mg pamiteplase to healthy subjects. Data represent the mean + SE of four subjects.

Table 2. Pharmacokinetic parameters of immunoreactive and bioactive concentration after intravenous administration of 4.0 mg pamiteplase to healthy subjects.

Method	$t_{1/2}\alpha$ (h)	$t_{1/2}\beta$ (h)	$AUC_{0\to\infty}$ ($ng.h.ml^{-1}$)	Cl_{total} ($l.h^{-1}.kg^{-1}$)	Vd_{ss} ($l.kg^{-1}$)	MRT (h)
Immunoreactive	0.33±0.04	1.25±0.06	507.9±25.3	0.13±0.01	0.17±0.01	1.31±0.03
Bioactive	0.32±0.01	0.78±0.10	286.4±11.0	0.23±0.01	0.14±0.01	0.65±0.02

Data are mean±SE of four subjects.
Values were calculated from the subtracted values for endogenous t-PA concentration.

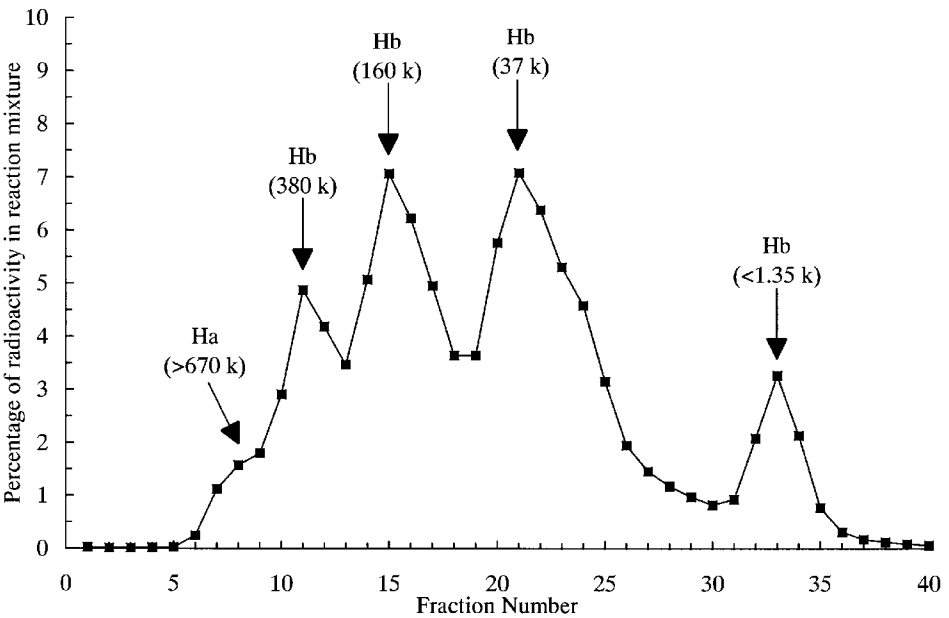


Figure 3. Typical gel filtration radiochromatogram of human plasma at 60 min after incubation with ^{125}I-pamiteplase. Data represent the results from one experiment.

Pharmacokinetics

Figure 2 shows the time-profile for the immunoreactive and bioactive concentration in plasma after intravenous administration of 4.0 mg pamiteplase to healthy subjects, and table 2 shows the pharmacokinetic parameters.

Immunoreactive and bioactive concentrations in healthy subjects declined in a bi-exponential manner, thus pharmacokinetic parameters were calculated using a two-compartment model. $t_{1/2}\alpha$ of the immunoreactive and bioactive pamiteplase were 0.33 and 0.32 h, and $t_{1/2}\beta$ were 1.25 and 0.78 h, MRT were 1.31 and 0.65 h respectively. The $AUC_{0\to\infty}$ of bioactive concentrations was about half that of immunoreactivity. Vd_{ss} were similar to each other.

Plasma protein binding

Figure 3 shows a typical gel filtration chromatogram examining the molecular weight distribution of radioactivity at 60 min after incubation of ^{125}I-pamiteplase in human plasma. Table 3 shows a immunoprecipitation of each peak observed in figure 3. Five radioactive peaks, designated Ha, Hb, Hc, Hd and He, were observed

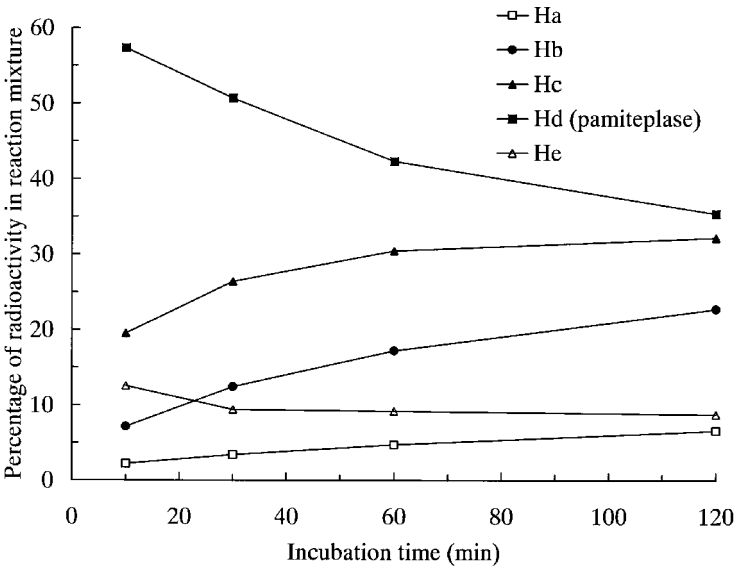


Figure4. Concentration–timeprofileofradioactivepeaksinhumanplasmaafterincubationwith^{125}I-pamiteplase. Data represent the mean of three experiments.

Table 3. Immunoprecipitation of GFC fractions of human plasma to various rabgit IgCs at 60 min after incubation with ^{125}I-pamiteplase.

	Percentage of precipitable radioactivity			
Rabbit IgG	Ha[a]	Hb[a]	Hc[a]	Hd[a]
Anti-human α_2-macroglobulin rabbit IgG	42.3	10.4	5.3	3.7
Anti-human C_1-esterase rabbit IgG	8.9	40.2	8.9	13.2
Anti-human α_2-plasmin inhibitor rabbit IgG	5.7	5.0	59.8	11.0

[a] GFC peak.
Data are the mean of three experiments.

in the chromatogram. Molecular weights of these peaks were calculated as >670, 380, 160 and 37 k and low molecular weight (<1350 k) in order of increasing elution time. As shown in table 3, Ha, Hb and Hc showed a distinct immunoprecipitability with anti-α_2-macroglubulion IgG, anti-C_1-esterase inhibitor IgG and anti-α_2-plasmin inhibitor IgG respectively. Consequently, Ha, Hb and Hc were identified as the probable complexes of pamiteplase with α_2-macroglubulion, C_1-esterase inhibitor and α_2-plasmin inhibitor respectively. Hd was identified as the unchanged form of pamiteplase by retention time. Furthermore, the He fraction was thought to be either a complex of ^{125}I with low molecular material (oligopeptides, amino acids) or a free ^{125}I.

Figure 4 shows the time-profile of five radioactive peaks after incubation of ^{125}I-pamiteplase in human plasma. After incubation for 10 min, the radioactivity in Hd (pamiteplase) was the highest of all peaks. As the length of incubation increased, the radioactivity in Hd decreased and that in Ha, Hb and Hc increased. No time-dependent variation in He was observed.

Figure 5 shows the comparison between radioactive, immunoreactive and bioactive concentrations of GFC fractions. Of five peaks, Hb, Hc and Hd

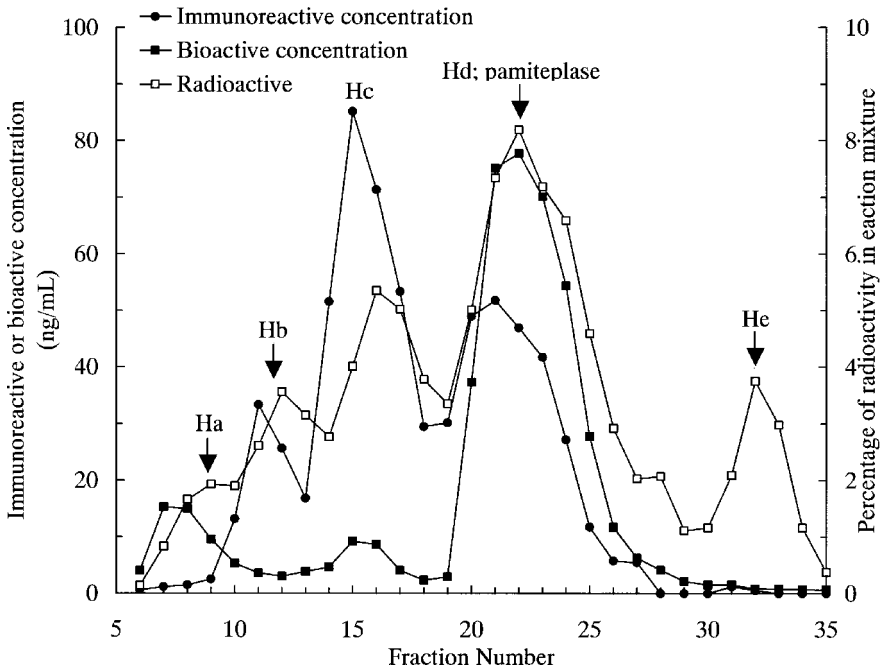


Figure 5. Relationship between radioactive, immunoreactive and bioactive concentrations in GFC fractions of human plasma at 60 min after incubation with ^{125}I-pamiteplase. Data represent the results from one experiment.

(pamiteplase) were detectable by the ELISA, while Hd (pamiteplase) was only reactive in the functional bioassay. In the case of the Hd fraction, the immunoreactive concentrations were almost equal to those of the bioactive.

Discussion

This study developed and tested quantification methods for human pharmacokinetic studies of pamiteplase. ELISA for immunoreactive concentrations of pamiteplase was examined using the monoclonal antibody SP-322, which recognizes the Kringle-2 domain of wt-PA (Watanabe *et al.* 1989). Therefore, the relative cross-reactivity between the wt-PA and pamiteplase in the assay was 100%. In the ELISA steps, the treatment with acetic acid was necessary to inactivate the enzyme. The CV and RE in the ELISA were within 15% of all concentrations determined, so this new ELISA has a satisfactory accuracy and precision to be an appropriate assay method to evaluate the human pharmacokinetics of pamiteplase.

ELISAs may detect pharmacologically inactive drug forms because antibodies used in ELISAs recognizes a part of HWMCs. Therefore, it is important for the evaluation of pharmacokinetics to measure concentrations by functional bioassay in relation to a pharmacological efficacy as well. The fibrin plate method (Walton *et al.* 1966) and synthetic substrate method (Verheijen *et al.* 1982) have already been reported as a functional bioassay of wt-PA. A synthetic substrate method was examined using a t-PA activity kit because it is more precise than a fibrin plate method. Therefore, the relative cross-reactivity between the wt-PA and pamiteplase in the functional bioassay was 100%. In the first step of this process, test compounds

activate Glu-plasminogen with CNBr-fragments (stimulator) of fibrin, producing Glu-plasmin. In the second step, Glu-plasmin cleaves H-D-norleucyl-hexahydrotyrosyl-lysine-*p*-nitroanilide diacetate salt (synthetic substrate), producing *p*-nitroaniline (*p*-NA). The amount of *p*-NA produced is measured by absorbance at 405 nm. The calibration curve for the functional bioassay was prepared using the dilution buffer A because human plasma components have no effect on the functional bioassay (data not shown). The CV and RE for the functional bioassay were within 25% at all concentrations determined, showing sufficient accuracy and precision to test human pharmacokinetics. Furthermore, CV at a measurement of endogenous t-PA in humans was satisfactory.

Endogenous wt-PA is well known to exhibit the circadian fluctuation and individual variability (Holvoet *et al*. 1985, Huber *et al*. 1989, Tahara *et al*. 1989). The maximum level of endogenous wt-PA is ~ 20 ng.ml^{-1} (Holvoet *et al*. 1985, Huber *et al*. 1989, Tahara *et al*. 1989), which is relatively low compared with the plasma concentration after administration of pamiteplase. Both endogenous wt-PA and pamiteplase have the same pharmacological activity. Furthermore, the increase in the level of pamiteplase results in the homeostatic suppression of production of endogenous wt-PA.

Examinations of pamiteplase pharmacokinetics in healthy subjects revealed that both immunoreactive and bioactive concentrations declined bi-exponentially. $t_{1/2}\beta$ of pamiteplase showed marked prolongation compared with wt-PA, whose half-life in humans is 3 min (Seifried *et al*. 1988, Tanswell *et al*. 1989, Kerins *et al*. 1992). Cl_{total} of pamiteplase was smaller than hepatic blood flow, indicating that pamiteplase was a capacity-limited drug. Furthermore, Vd_{ss} is roughly proportional to the sum of volume of plasma and extracellular fluid, indicating that tissue distribution of pamiteplase was relatively low.

Pharmacokinetics of wt-PA in humans have reported that Cl_{total} of immunoreactive and bioactive concentrations ranges from 35.3 to 41.2 l.h^{-1} and from 54.4 to 74.1 l.h^{-1} respectively (Seifried *et al*. 1988, Tanswell *et al*. 1989, Kerins *et al*. 1992). Cl_{total} of immunoreactive and bioactive concentrations of pamiteplase decreased to $\sim 20\%$ those of wt-PA. These results suggested that wt-PAs require bolus and infusion methods to provide a sufficient thrombolytic therapy, whereas pamiteplase shows the same thrombolytic efficacy by bolus administration only. The elimination of both compounds is due to metabolic clearance (Iida *et al*. 1988, Komuro *et al*. 1989, Okumura *et al*. 1989, Oikawa *et al*. 1996b). Since no urinary excretion of either compound is observed in humans, elimination in humans is thought to be due to a similar metabolic clearance process as found in rat. The results of tissue distribution in rat have shown that both compounds are eliminated mainly by the hepatic uptake (Iida *et al*. 1988, Komuro *et al*. 1989, Okumura *et al*. 1989, Oikawa *et al*. 1996b), so higher plasma concentrations of pamiteplase compared with wt-PAs are thought to be due to a lower hepatic uptake of pamiteplase (Oikawa *et al*. 1996b).

The elimination of wt-PAs has been achieved by complex formation with plasma proteins, in addition to a hepatic uptake (Korninger and Collen 1981, Haggroth *et al*. 1984, Iida *et al*. 1988, Komuro *et al*. 1989, Okumura *et al*. 1989). wt-PAs form complexes with α_2-macroglobulin and α_2-plasmin inhibitor in rat and rabbit plasma, and with α_2-macroglobulin, C_1-esterase inhibitor and α_2-plasmin inhibitor in human and dog plasma. Species differences of wt-PA in complex formation have been observed (Korninger and Collen 1981).

The metabolism of plasma protein bindings of pamiteplase in human was

examined by GFC analysis. Pamiteplase in human plasma exists as complexes with α_2-macroglobulin, C_1-esterase inhibitor and α_2-plasmin inhibitor similar to wt-PAs. Free pamiteplase was the major form just after addition to human plasma, but decreased time-dependently, suggesting that complex formation was a relatively slow reaction. As no time-dependent variation in the low molecular weight fraction (< 1350) was observed, pamiteplase was not thought to be degraded into low molecular weight components in human plasma. The glycoproteins α_2-macroglobulin, C_1-esterase inhibitor and α_2-plasmin inhibitor inhibit serine protease activity by binding covalently to a serine residue at an active site (Barret and Starkey 1973, Moroi and Aoki 1976). These inhibitors were thought to bind irreversibly and covalently to serine residues in the active site of pamiteplase supported by the fact that the structure of active site of pamiteplase (His_{322}, Asp_{371}, Ser_{478}) shows high structural homology with other serine proteases (Kawauchi *et al*. 1991). Therefore, pamiteplase bound to these proteins could not return the free form and was thought to be taken up by the liver.

As there was a difference in the time-profile between immunoreactive and bioactive concentration of pamiteplase in humans, the specificity of ELISA and functional bioassay was examined by investigating the reactivity of complexes with both assays. The complex with α_2-macroglobulin was not detected by the ELISA but slightly detected by the functional bioassay, showing lower detectability than the unchanged form. The complexes with C_1-esterase inhibitor and α_2-plasmin inhibitor were detected by the ELISA but not detected by the functional bioassay. Furthermore, the low molecular weight fraction (< 1350) was not detected by either assays. Consequently, immunoreactive concentrations included values for the two complexes of pamiteplase with C_1-esterase inhibitor and α_2-plasmin inhibitor as well as those of the unchanged form, whereas bioactive concentrations consisted almost entirely of the unchanged form. In the case of wt-PAs, ELISAs detect not only the unchanged form but also the complexes, whereas bioassays only detect wt-PAs (Colucci *et al*. 1985, Iida *et al*. 1988). Therefore, the protein binding of pamiteplase in humans resulted in the termination of biological action.

The previously described observations lead to the following conclusions. An ELISA and functional bioassay to determine pamiteplase immunoreactive and bioactive concentrations in human plasma showed satisfactory accuracy and precision. The pharmacokinetic properties of pamiteplase in healthy subjects were examined with these two assays. Cl_{total} of pamiteplase was markedly lower than that of wt-PA, suggesting that pamiteplase may show clinically sufficient thrombolytic activity by bolus administration only. In human plasma, ^{125}I-pamiteplase existed in complexes with α_2-macroglobulin, C_1-esterase inhibitor and α_2-plasmin inhibitor. The complexes with C_1-esterase inhibitor and α_2-plasmin inhibitor were detected by the ELISA but not by the functional bioassay.

References

Barret, A. J. and Starkey, P. M., 1973, The interaction of α_2-macroglobulin with proteinases. Characteristics and specificity of the reaction, and a hypothesis concerning its molecular mechanism. *Biochemical Journal*, **133**, 709–724.

Buessecker, F., Reinartz, J., Schirmer, U. and Kramer, M. D., 1993, Enzyme-linked immunosorbent assays for plasminogen activator. *Journal of Immunological Methods*, **162**, 193–200.

Colucci, M., Parama, J. A. and Collen, D., 1985, Generation in plasma of a fast-acting inhibitor of plasminogen activator in response to endotoxin stimulation. *Journal of Clinical Investigation*, **75**, 818–824.

Haggroth, L., Mattsson, C. and Friberg, J., 1984, Inhibition of the human tissue plasminogen activator in plasma from different species. *Thrombosis Research*, **33**, 583–594.

Holvoet, P., Cleemput, H. and Collen, D., 1985, Assay of human tissue-type plasminogen activator (t-PA) with an enzyme-linked immunosorbent assay (ELISA) based on three murine monoclonal antibodies to t-PA. *Thrombosis and Haemostasis*, **54**, 684–687.

Huber, K., Beckmann, R., Lang, I., Schuster, E. and Binder, B. R., 1989, Circadian fluctuations in plasma levels of tissue plasminogen activator antigen and plasminogen activator inhibitor activity. *Fibrinolysis*, **3**, 41–43.

Iida, S., Iwamoto, M., Suzuki, M. and Komatsu, T., 1988, Metabolic fate of recombinant human tissue plasminogen activator (rt-PA) (1). *Xenobiotic Metabolism and Disposition*, **3**, 309–329.

Katoh, M., Suzuki, Y., Miyamoto, I. and Watanabe, T., 1991, Biochemical and pharmacokinetics properties of pamiteplase, a novel fibrinolytic agent. *Thrombosis and Haemostasis*, **65**, 1193.

Kawasaki, T., Kawamura, S., Katoh, S. and Takenaka, T., 1993a, Experimental model of carotid artery thrombosis in rats and the thrombolytic activity of YM866, a novel modified tissue-type plasminogen activator. *Japanese Journal Pharmacology*, **63**, 135–142.

Kawasaki, T., Katoh, M., Kaku, S., Gushima, H., Takenaka, T., Yui, Y. and Kawai C., 1993b, Thrombolytic activity of a novel modified tissue-type plasminogen activator, YM866, in a canine model of coronary artery thrombosis. *Japanese Journal Pharmacology*, **63**, 9–16.

Kawasaki, T., Katoh, M., Kaku, S., Gushima, H., Takenaka, T., Yui, Y. and Kawai C., 1993c, Thrombolysis with intracoronary administration of YM866, a novel modified tissue-type plasminogen activator, in a canine model of coronary artery thrombosis. *Japanese Journal Pharmacology*, **63**, 319–325.

Kawauchi, Y., Morinaga, T., Yokota, M., Kinoshita, A., Kawamura, K., Suzuki, Y., Takayama, M., Furuichi, K. and Gushima, H., 1991, Gene construction and large scale production of a novel fibrinolytic agent (pamiteplase) in CHO cells. *Thrombosis and Haemostasis*, **65**, 1193.

Kerins, D. M., Roy, L., Kunitada, S., Adedoyin, A., Fitzgerald, G. A. and Fitzgerald, D. J., 1992, Pharmacokinetics of tissue-type plasminogen activator during acute myocardial infarction in men. *Circulation*, **85**, 526–532.

Komuro, S., Yamamoto, R., Itou, M., Iba, I., Yoshitake, A., Sakurama, T. and Kaneko, M., 1989, Metabolic fate of SM-9527 in rats. *Clinical report*, **23**, 115–132.

Korninger, C. and Collen, D., 1981, Neutralization of human extrinsic (tissue-type) plasminogen activator in human plasma: No evidence for a specific inhibitor. *Thrombosis and Haemostasis*, **46**, 662–665.

Moroi, M. and Aoki, N., 1976, Isolation and characterization of α_2-plasmin inhibitor from human plasma. *Journal of Biochemical Chemistry*, **251**, 5956–5965.

Oikawa, K., Kamimura, H., Watanabe, T., Higuchi, S. and Miyamoto I., 1996a, Pharmacokinetics of YM866 and t-PA after intravenous administration to rats and dogs. *Clinical Pharmacology and Therapy*, **6**, 2391–2396.

Oikawa, K., Kamimura, H., Watanabe, T., Miyamoto, I. and Higuchi, S., 1996b, Metabolic fate of YM866, a novel fibrinolytic agent. *Xenobiotic Metabolism and Disposition*, **11**, 1–10.

Okumura, I., Aoki, S., Ohno, T., Iba, Y., Nishimoto, K. and Baba, S., 1989, Metabolic fate of TD-2061(I). *Progress Medicine*, **9**, 483–503.

Schrauwen, Y., Emeis, J. J. and Kooistra, T., 1994, A sensitive ELISA for human tissue-type plasminogen activator applicable to the study of acute release from cultured human endothelial cells. *Thrombosis and Haemostasis*, **71**, 225.

Seifried, E., Tanswell, P., Rijken, D. C., Barrett-Bergshoeff, M. M., Su, C. A. P. F. and Kluft, C., 1988, Pharmacokinetics of antigen and activity of recombinant tissue-type plasminogen activator after infusion in healthy volunteers. *Arzneimittel-Forschung/Drug Research*, **38**, 418–422.

Tahara, C., Kazama, M., Miyajima, Y. and Abe, T., 1989, Circadian fluctuation of plasmatic plasminogen activator and its inhibitor PAI-1 of Japanese adults. *Blood and Vessel*, **20**, 67–69.

Tanswell, P., Seifried, E., Su, P. C. A. F., Feuerer, W. and Rijken, D. C., 1989, Pharmacokinetics and systemic effects of tissue-type plasminogen activator in normal subjects. *Clinical Pharmacology and Therapeutics*, **46**, 155–162.

Verheijen, J. H., Mullaart, E., Chang, G. T. G., Kluft, C. and Wijngaards, G., 1982, A simple, sensitive spectrophotometric assay for extrinsic (tissue-type) plasminogen activator applicable to measurements in plasma. *Thrombosis and Haemostasis*, **48**, 266–269.

Walton, P. L., 1966, An improved fibrin plate method for the assay of plasminogen. *Clinica et Chimica Acta*, **13**, 680–684.

Watanabe, S., Sasamata, M. and Katoh, M., 1989, t-PA activity assay method in blood sample using dipstick coated with a monoclonal antibody SP-322. *Thrombosis and Haemostasis*, **62**, 95.

XENOBIOTICA, 2000, VOL. 30, NO. 10, 1005–1017

Metabolic activation of *o*-phenylphenol to a major cytotoxic metabolite, phenylhydroquinone: role of human CYP1A2 and rat CYP2C11/CYP2E1

S. OZAWA†*, K. OHTA†‡, A. MIYAJIMA†, H. KUREBAYASHI†, M. SUNOUCHI†, M. SHIMIZU†‡, N. MURAYAMA*, Y. MATSUMOTO‡, M. FUKUOKA‡ and Y. OHNO†

†Division of Pharmacology, National Institute of Health Sciences, 1–18–1 Kamiyoga, Setagaya-ku, Tokyo 158–8501, Japan
‡Department of Clinical Pharmacology and Toxicology, Showa Pharmaceutical University, 3–3165 Higashitamagawagakuen, Machida, Tokyo 194–8543, Japan

Received 31 March 2000

1. The *in vitro* metabolic activation of *o*-phenylphenol has been evaluated as yielding a toxic metabolite, 2,5-dihydroxybiphenyl (phenylhydroquinone), by *p*-hydroxylation in liver microsomes of rat and human. The involvement of rat CYP2C11, CYP2E1 and human CYP1A2 in the *p*-hydroxylation of *o*-phenylphenol is suggested.

2. 2,3- and phenylhydroquinone, which induced DNA single-strand scission in the presence of 1 μM $CuCl_2$, were the most cytotoxic chemicals examined to cultured mammalian cell lines among *o*-phenylphenol, *m*-phenylphenol, *p*-phenylphenol, 2,2′-, 4,4′-, 2,3- and phenylhydroquinone.

3. Rat and human liver microsomes catalysed the formation of phenylhydroquinone, but not 2,3-dihydroxybiphenyl, using *o*-phenylphenol as a substrate. A higher rate of metabolic activation of *o*-phenylphenol was observed with livers of the male than the female rats by 5.6- and 2.6-fold respectively.

4. Inhibitory antibodies against the male-specific CYP2C11 inhibited hepatic *o*-phenylphenol *p*-hydroxylation in the male F344 and Sprague–Dawley rat by >70%. Liver microsomes from the isoniazid-treated rats produced 1.8- and 3-fold induction of *o*-phenylphenol *p*-hydroxylation and chlorzoxazone 6-hydroxylation (a CYP2E1-dependent activity) respectively.

5. Human CYP1A2, expressed by baculovirus-mediated cDNA expression systems, exhibited a remarkably higher capacity for *o*-phenylphenol *p*-hydroxylation at concentrations of 5 (>5-fold), 50 (>2-fold) and 500 μM (>2-fold) than CYP2A, CYP2B, CYP2Cs, CYP2D6, CYP2E1 and CYP3A4 on the basis of pmol P450.

6. Among various CYP inhibitors tested here, 7,8-benzoflavone and furafylline, typical human CYP1A2 inhibitors, inhibited the microsomal *p*-hydroxylation of *o*-phenylphenol in human livers most potently by 70 and 50% respectively.

7. The results thus indicate the involvement of rat CYP2C11/CYP2E1 and human CYP1A2 in the hepatic *p*-hydroxylation of *o*-phenylphenol.

Introduction

o-Phenylphenol (OPP) is used as a fungicide for harvested citrus fruits and its toxicity has been extensively studied, including acute toxicity, mutagenicity and teratogenic effects (Luster *et al*. 1981). Long-term carcinogenicity testing (Hodge *et al*. 1952) did not give clear evidence on any carcinogenic effects by OPP. From these early results, no significant hazardous effect was anticipated with the exposure of

*Author for correspondence; e-mail: sozawa@nihs.go.jp

Xenobiotica ISSN 0049-8254 print/ISSN 1366-5928 online © 2000 Taylor & Francis Ltd
http://www.tandf.co.uk/journals

man to low doses of OPP. However, in 1981 (Hiraga and Fujii 1981), OPP was first shown to induce urinary bladder tumours by administration of an OPP-containing diet to the male F344 rat. Subsequently, a clear sex-related difference was observed in the susceptibility to bladder carcinogenicity by OPP (Hasegawa *et al*. 1991), with males being more sensitive than females.

OPP was shown to undergo oxidative metabolism in livers of mouse and rat to produce a toxic metabolite, 2,5-dihydroxybiphenyl or phenylhydroquinone (PHQ) (Ushiyama *et al*. 1992). PHQ is thought to be readily auto-oxidized to phenylbenzoquinone (PBQ) via a semiquinone radical (Tayama *et al*. 1994). A significant correlation was reported between the incidence of bladder cancer and the level of reactive intermediates including PBQ in urine after administration of OPP to the male F344 rat (Morimoto *et al*. 1987, 1989). Several lines of evidence have accumulated to support the concept that the OPP metabolite, PHQ, causes oxidative damage to exposed cells by the induction of DNA damage, to produce 8-hydroxy deoxyguanosine, adduct formation and DNA strand breakage (Nagai *et al*. 1990, 1995, Sasaki *et al*. 1997, Murata *et al*. 1999). Among the several forms of xenobiotic-metabolizing enzymes in rat and mouse, neither phenobarbital- nor 3-methylcholanthrene-induced cytochrome P450 (CYPs) were likely to be the major forms catalysing the oxidative metabolism of OPP to yield PHQ (Halpaap-Wood *et al*. 1981). Furthermore, in spite of use of OPP as a food additive, little is known about human CYP forms involved in the metabolic activation of OPP. An attempted, therefore, is made to elucidate which CYPs play major roles in the oxidative metabolism of OPP to produce the reactive metabolite, PHQ.

In the present study, microsomal oxidation of OPP was quantitated by HPLC using hepatic microsomes from the male and female rat and human. Inhibition of PHQ formation catalysed by male rat liver microsomes was examined by the aid of inhibitory antibodies against various rat CYPs. Also compared was the oxidation of OPP to produce PHQ catalysed by human CYPs expressed by baculovirus-mediated systems. Typical inhibitors of human CYPs were used to confirm the results obtained from the cDNA-mediated human CYP expression systems. Thus, rat CYP2C11 and possibly CYP2E1, and human CYP1A2 were shown to be the major CYPs involved in the metabolic activation of OPP to PHQ in the present *in vitro* systems.

Materials and methods

Reagents and hepatic microsomes

All reagents used were of the highest grade available. OPP, *p*-phenylphenol (PPP), 2,2′-dihydroxybiphenyl, 2,3-dihydroxybiphenyl and 4,4′-dihydroxybiphenyl, 7,8-benzoflavone, coumarin and diethyldithiocarbamate were from Wako Pure Chemical Industries Ltd (Tokyo, Japan). *m*-Phenylphenol (MPP) and PHQ were from Tokyo Kasei Organic Chemicals (Tokyo, Japan). The purity of OPP, PPP, 2,2′-dihydroxybiphenyl, 2,3-dihydroxybiphenyl, 4,4′-dihydroxybiphenyl, MPP and PHQ was $>99\%$, since no other hydroxybiphenyl was detected on HPLC with any of the hydroxylated biphenyls used in the present study. The chemical structures of the hydroxybiphenyls studied and PBQ are shown in figure 1. Diclofenac, troleandomycin, cyclophosphamide and β-naphthol were from Sigma Chemical Co. Ltd (St. Louis, MO, USA). Furafylline was from Ultrafine Chemical Co. (Manchester, UK) through Daiichi Chemicals (Tokyo, Japan), omeprazole was from Astra Japan Ltd (Osaka, Japan), and quinidine was from Kanto Chemicals (Tokyo, Japan). SKF-525A was from Smith Kline & French Labs. $NADP^+$ and NADPH were from Oriental Yeast (Tokyo, Japan) and glucose 6-phosphate and glucose 6-phosphate dehydrogenase were from Boehringer Mannheim. Mixed liver microsomes of human individuals (six males, six females) and inhibitory antibodies against rat CYP forms were from GENTEST Corp. (Woborn, MA, USA) through Daiichi Chemicals (Tokyo, Japan). Male and female rat liver microsomes were prepared from 10 male and 10 female F344 rats (8 weeks old; Japan SLC, Inc., Hamamatsu, Japan) respectively, and those from 20 male and 42 female Sprague–Dawley rats were from

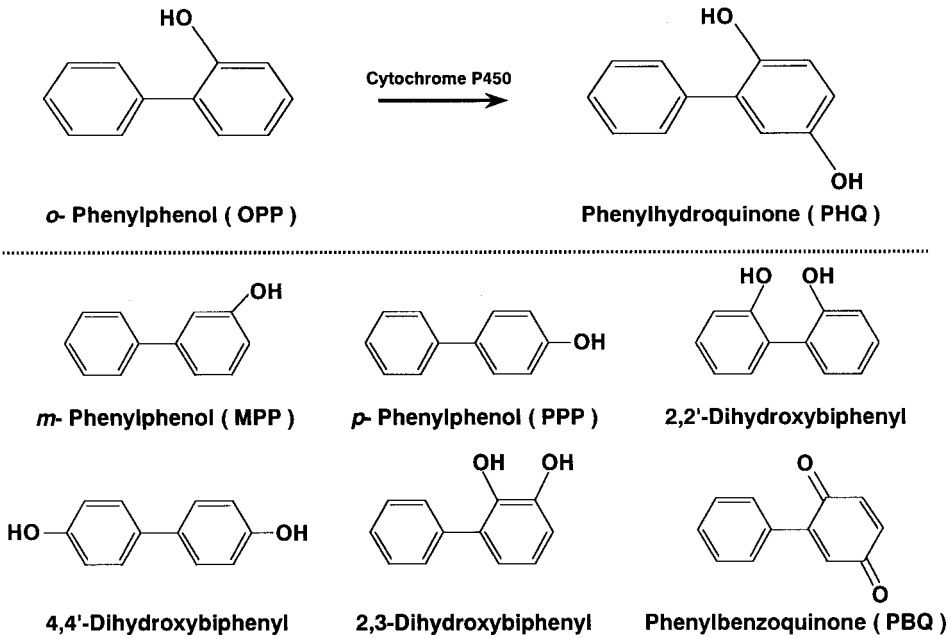


Figure 1. Enzymatic reaction of *o*-phenylphenol *p*-hydroxylation and the chemical structures of other related hydroxybiphenyls and phenylbenzoquinone. Metabolic activation of *o*-phenylphenol catalysed by cytochrome P450 is depicted as well as the chemical structures of other related hydroxybiphenyls and phenylbenzoquinone.

Xenotech LLC (Kansas City, KS, USA) to examine sex-related differences in hepatic PHQ formation. Male rat liver microsomes from corn oil- or saline-administered Sprague–Dawley rats (20 each) and various CYP inducer-treated 15 (phenobarbital-treated), 16 (5,6-benzoflavone-treated) or 18 (isoniazid-treated) male Sprague–Dawley rats (8 weeks old) were from Xenotech LLC (Yokohama, Japan). 5,6-Benzoflavone (a CYP1A inducer; Sigma) dissolved in corn-oil was administered to 16 male Sprague–Dawley rats at 100 mg.kg^{-1} body weight once per day on days 1–4, and liver microsomes were prepared on day 5. Hepatic 7-ethoxyresorufin *O*-dealkylation (the CYP1A-dependent activity) was 3940 pmol.mg^{-1} protein.min^{-1} in mixed microsomes of the inducer-treated 16 animals and 280 pmol.mg^{-1} protein.min^{-1} in corn oil-administered 20 animals. Phenobarbital (a CYP2B inducer; Spectrum Chemical Mfg. Co.) dissolved in saline was administered to 15 male Sprague–Dawley rats at 80 mg.kg^{-1} body weight once per day on days 1–4, and liver microsomes were prepared on day 5. Hepatic 7-penthoxyresorufin *O*-dealkylation (the CYP2B-dependent activity) was 1490 pmol.mg^{-1} protein.min^{-1} in mixed microsomes of the inducer-treated 15 animals and 18 pmol.mg^{-1} protein.min^{-1} in saline-administered 20 animals. Isoniazid (a CYP2E1 inducer; Sigma) dissolved in saline was administered to 18 male Sprague–Dawley rats at 200 mg.kg^{-1} body weight once per day on days 1–4, and liver microsomes were prepared on day 5. Hepatic chlorzoxazone 6-hydroxylation (the CYP2E1-dependent activity) was 13.3 nmol.mg^{-1} protein.min^{-1} in mixed microsomes of the inducer-treated 18 animals and 4.4 nmol.mg^{-1} protein.min^{-1} in saline-administered 20 animals.

Cell kill and growth inhibitory assays in cultured mammalian cells

HepG2 cells were cultured in Dulbecco's MEM supplemented with 10% foetal calf serum (FCS). Culture media for MIAPaCa-2, V79 and rabbit cornea derived SIRC cells were Eagle's MEM supplemented with 10% FCS and that for Morris5123DTC was RPMI1640 with 10% FCS. Cell kill assays were done according to the inhibition of colony formation induced by OPP and related compounds using human cancer cell lines, HepG2 (liver) and MIAPaCa-2 (pancreas), rat cancer cell line, Morris5123DTC (liver) and Chinese hamster fibroblast cell line, V79 (lung). Concentrations of *o*-, *m*-, *p*-phenylphenol and 2,2′-dihydroxybiphenyl used were 1000, 500, 250, 125, 62.5, 31.3 and 15.6 μM; those of 4,4′-dihydroxybiphenyl were 1000, 500, 250, 125, 62.5, 31.3 and 15.6 μM; and those of 2,3-dihydroxybiphenyl and PHQ were 125, 62.5, 31.3, 15.6, 7.8, 3.9, 1.9 and 1.0 μM. Hydroxybiphenyls were dissolved in H_2O. Cells (100–4000) were inoculated in 60-mm (diameter) dishes and cultured overnight at 37 °C in a humidified atmosphere of 95% air and 5% CO_2. Either OPP or related compounds were added at various concentrations and further cultured for 48 h. Culture media were changed, and cultured for 1–2 weeks depending on the growth rates of each cell line. Colonies were counted after 0.4% crystal

violet staining. A growth inhibition assay was performed according to Itagaki *et al*. (1995) and Ohno *et al*. (1998). Briefly, SIRC cells were inoculated at a cell density of 20 000 cells per well of 96-well plates. The cells were further cultured with various concentrations of hydroxybiphenyls for 72 h at 37 °C. Inhibition of cell growth was determined after the cells were stained with 0·4% crystal violet.

In vitro DNA strand scission induced by OPP and related compounds

Covalently closed circular (ccc) DNA (pTrcHisB, Invitrogen, Carlsbad, CA, USA) was treated with various concentration of OPP and related compounds. The reaction mixture (10 μl) consisted of 50 mM Tris-HCl (pH 8·0), 1 μM $CuCl_2$, 0·4 μg cccDNA and various concentrations of OPP and related compounds. DNA strand breakage was analysed on 1% agarose gel electrophoresis according to mobility differences between cccDNA, open circular DNA and linearized DNA, after incubation performed at room temperature for 30 min.

Assays of microsomal OPP-hydroxylating activities by rat and human hepatic microsomes

The microsomal oxidation of OPP to PHQ was examined using rat and human liver microsomes. A typical incubation mixture (250 μl) contained 100 mM potassium phosphate buffer (pH 7·4), 0·5 mM OPP, 0·33 mM NADPH and 50 μg hepatic microsomes from rat or 100 μg mixed human microsomes. The reaction was initiated by the addition of NADPH, incubated for 20–40 min and terminated by the addition of 250 μl ethyl ether. The reaction was linear with time up to 40 min. OPP and hydroxylated metabolites were extracted twice with ethyl ether. Amounts of OPP metabolites formed were analysed together with β-naphthol as an internal standard by reverse-phase HPLC system (Shimadzu LC-VP series) equipped with a L-column ODS (4·6 × 250 mm). The initial mobile phase was acetonitrile: 0·5% acetic acid (3:7), and was kept for 2 min with a flow rate of 0·8 $ml.min^{-1}$. The acetonitrile concentration was then raised as a linear gradient up to acetonitrile: 0·5% acetic acid (8:2) over 22 min. Metabolites were detected at 312 nm by a UV-VIS detector (SPD-10Avp). The elution times of PHQ, β-naphthol and OPP were 14·7, 20·3 and 28·6 min respectively.

Inhibitory antisera against rat CYP1A1/2, CYP2B1, CYP2C11, CYP2E1 and CYP3A1 (0, 10, 20 or 50 μl) were incubated with rat hepatic microsomes at room temperature for 30 min as suggested by the manufacturer. Normal goat antisera were added so that total volume of antisera was 50 μl. The mixture was added to 100 mM potassium phosphate buffer (pH 7·4), 0·5 mM OPP, 0·33 mM NADPH, in a total volume of 250 μl. The reaction was started by the addition of 0·33 mM NADPH, incubated for 20 min, and was terminated by the addition of 250 μl ethyl ether. The aqueous layer was extracted twice with ethyl ether and the PHQ extracted into the organic layer was quantitated by HPLC.

Also measured was OPP hydroxylation in microsomes from rat treated with CYP inducers.

Hydroxylation of OPP by human CYP forms, which had been expressed together with cytochrome P450 reductase in baculovirus-mediated cDNA-expression systems (SUPERSOMES™, GENTEST Corp., Woburn, MA, USA), was examined. The CYP forms used were: CYP1A2, CYP2A6, CYP2B6, CYP2C8, CYP2C9, CYP2C19, CYP2D6, CYP2E1 and CYP3A4. Insect cell microsomes expressing cytochrome b_5 and cytochrome P450 reductase were also used. The reaction mixture for OPP hydroxylation (250 μl) consisted of 100 mM potassium phosphate buffer (pH 7·4), either 500 or 5 μM OPP, 0·33 mM $NADP^+$, 3·3 mM glucose 6-phosphate, 0·4 U/ml glucose 6-phosphate dehydrogenase, 3·3 mM $MgCl_2$ and insect cell microsomes expressing each human CYP form. Reactions were performed for 20 min and metabolites analysed by HPLC.

Effects of typical CYP inhibitors or substrates on OPP hydroxylation catalysed by human liver microsomes were examined (5 μM OPP). The following substances were used for inhibition of CYP-dependent enzymatic activities: 7,8-benzoflavone and furafylline for CYP1A2, coumarin for CYP2A6, cyclophosphamide for CYP2B6, diclofenac for CYP2C9, omeprazole for CYP2C19, quinidine for CYP2D6, diethyldithiocarbamate for CYP2E1, troleandomycin for CYP3A4 (Ono *et al*. 1996, Teramura *et al*. 1997). Human microsomes (100 μg) were pre-incubated with various concentrations of CYP inhibitors or substrates at 37 °C for 15 min. OPP was then added at a concentration of 5 μM. The reaction was performed at 37 °C for 20 min and terminated by the addition of 250 μl ethyl ether. The aqueous layer was extracted twice with ethyl ether, and then metabolites formed were quantified by HPLC.

Results

Cell kill and growth inhibitory effects of OPP and biphenyl-related compounds with hydroxyl moieties

The potency of cytotoxicity and growth inhibition of OPP and other hydroxylated biphenyls were compared using established cell lines derived from various animals. Based on the IC_{50}, 2,3-dihydroxybiphenyl and PHQ were the most cytotoxic of the hydroxy biphenyls studied (table 1). 2,3-Dihydroxybiphenyl, PHQ

Table 1. Inhibition of colony formation or cell growth of various mammalian cells treated with OPP and related compounds.

	IC_{50} (μM)				
	Human		Rat	Chinese hamster	Rabbit
	HepG2	MIAPaCa-2	Morris5123DTC	V79	SIRC
o-Phenylphenol	270	100	420	130	290
m-Phenylphenol	210	70	250	160	250
p-Phenylphenol	230	110	170	200	170
2,2′Dihydroxybiphenyl	400	310	560	340	420
4,4′Dihydroxybiphenyl	42	90	16	90	40
2,3′Dihydroxybiphenyl	50	5	19	9	70
2,5′Dihydroxybiphenyl	30	3	21	9	40

Inhibition of colony formation of HepG2, MIAPaCa-2, Morris5123DTC and V79 cells was examined; and growth inhibition of SIRC cells was determined as described by Ohno *et al*. (1998) respectively. IC_{50} shown are the average of three determinations.

and 4,4′-dihydroxy biphenyl showed a tendency to be the most potent inhibitors of colony formation (cell lines listed in table 1 except for SIRC cells) or cell growth (SIRC cells) among the hydroxylated biphenyl derivatives studied.

Induction of DNA strand breakage by OPP and hydroxylated derivatives of biphenyl

Induction of DNA strand breakage by OPP and other mono- and di-hydroxylated biphenyl derivatives was examined in the presence of 1 μM $CuCl_2$. Both PHQ and 2,3-dihydroxybiphenyl (at 10–20 μM) caused nicks on the plasmid DNA molecules used, and DNA strand breakage was much weaker with OPP, MPP, PPP, 2,2′-dihydroxybiphenyl and 4,4′-dihydroxybiphenyl at even 500 μM (figure 2).

Microsomal PHQ formation catalysed by rat liver microsomes

Microsomal PHQ formation was compared between livers of the male and female F344 and Sprague–Dawley rat and a clear male dominance was observed (table 2), namely 5·64-fold higher in the male F344 rat than in the female, and 2·60-fold in the male Sprague–Dawley rat than in the female.

Effects of inhibitory antibodies of rat CYPs on PHQ formation

Inhibitory antibodies against rat CYP forms were used to elucidate the specific rat CYPs involved in PHQ formation by the male F344 and Sprague–Dawley rat liver microsomes. In both the male F344 and Sprague–Dawley rat, antisera against the male-specific CYP2C11 showed the most effective and concentration-dependent inhibition of microsomal PHQ formation from OPP by 88 and 70% respectively (figure 3A and B).

Hydroxylation of OPP in liver microsomes from rat treated with various CYP-inducers

It was examined whether hepatic microsomes from rat treated with CYP inducers exhibit induction of OPP hydroxylation. 5,6-Benzoflavone (a CYP1A inducer) failed to induce microsomal OPP *p*-hydroxylation in the Sprague–Dawley

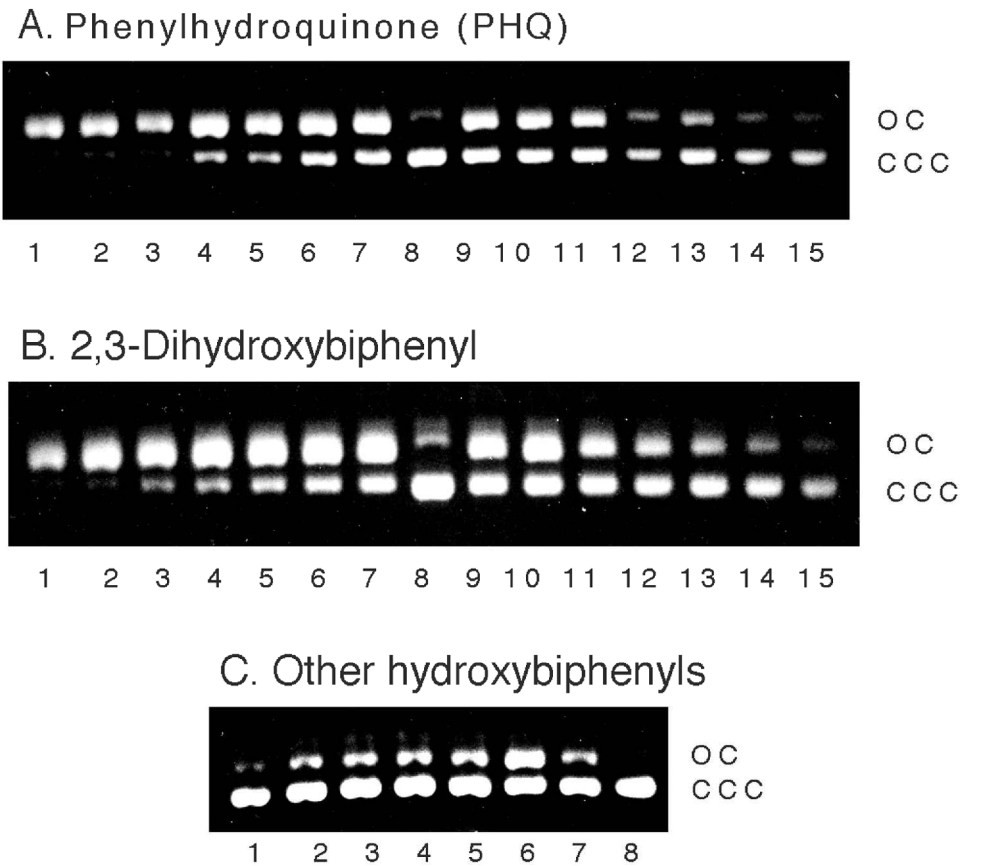


Figure 2. DNA single-strand breaks induced by OPP and other hydroxylated biphenyl derivatives. Covalently closed circular DNA (cccDNA) was treated with various concentration of OPP and related compounds in the presence of 1 μM $CuCl_2$. DNA strand breakage was analysed according to the reduction in the amount of cccDNA and the increase in the amount of nicked open circular (OC) DNA. (A) Concentrations (μM) of PHQ used were: 12.5 (lane 1); 10 (2); 8 (3); 6.4 (4); 5.1 (5); 4.1 (6); 3.3 (7); 0 (control, 8); 2.6 (9); 2.1 (10); 1.7 (11); 1.3 (12); 1.1 (13); 0.9 (14); 0.7 (15). (B) Concentrations (μM) of 2,3-dihydroxy-biphenyl used were: 25 (lane 1); 20 (2); 16 (3); 12.8 (4); 10.2 (5); 8.2 (6); 6.5 (7); 0 (control, 8); 5.2 (9); 4.2 (10); 3.4 (11); 2.6 (12); 2.1 (13); 1.7 (14); 1.3 (15). (C) Biphenyl and other hydroxylated biphenyl (500 μM): biphenyl (lane 1); 2-hydroxy (*o*-phenylphenol; 2); 3-hydroxy (*m*-phenylphenol; 3); 4-hydroxy (*p*-phenylphenol; 4); 2,2′-dihydroxybiphenyl (5); 4,4′-dihydroxybiphenyl (6); 3-hydroxy (*m*-phenylphenol; 7); none (control; 8).

Table 2. Male-dominant *p*-hydroxylation of OPP in liver microsomes of the F344 and Sprague–Dawley rat.

Strain	Male	Female	p[a]
F344	3.67 ± 0.40	0.65 ± 0.10	< 0.001
Sprague–Dawley	2.06 ± 0.05	0.79 ± 0.02	< 0.001

Hepatic *p*-hydroxylation of OPP (500 μM, nmol·min^{-1}·mg microsomal protein) was determined using mixed liver microsomes from 10 male and 10 female F344 rats and those from 20 male and 42 female Sprague–Dawley rats as described in the Materials and methods.

Data are the mean ± SD of four determinations.

[a] Degree of statistical significance.

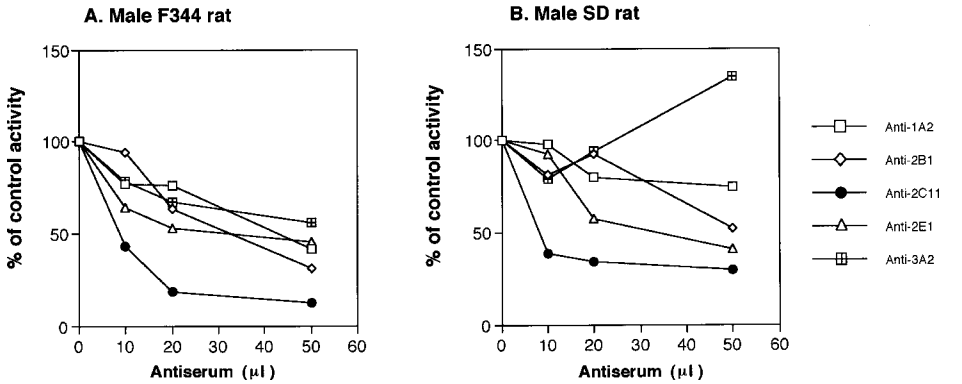


Figure 3. Effects of antisera against rat CYP forms on OPP *p*-hydroxylation in rat liver microsomes. Effects of inhibitory antibodies on microsomal OPP *p*-hydroxylation in rat livers were examined as described in the Materials and methods. The concentration of OPP was 500 μM and OPP was incubated for 40 min with rat liver microsomes (50 μg protein). Control activities (mean ± SD, nmol.min^{-1}.mg^{-1} microsomal protein) in the male F344 rat and male Sprague–Dawley (SD) rat were 1·17 ± 0·10 and 1·61 ± 0·05 respectively. Data points are the average of four determinations.

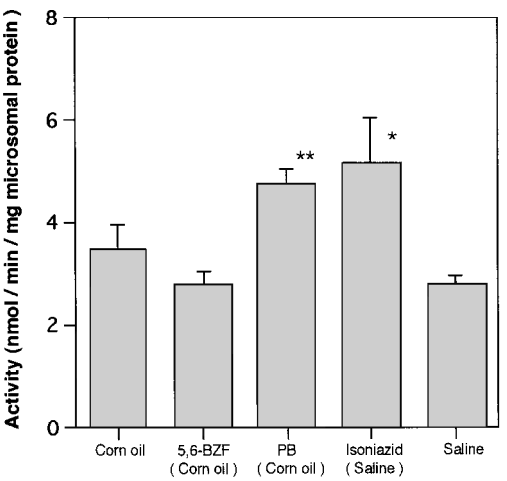


Figure 4. OPP *p*-hydroxylation in microsomes from the male Sprague–Dawley rat pretreated with CYP inducers. The concentration of OPP was 500 μM and OPP was incubated for 40 min with microsomes (50 μg protein). Data from 5,6-benzoflavone-treated (5,6-BZF) and phenobarbital-treated (PB) rats were compared with those from the corn oil-treated rat as controls. Data from the isoniazid-treated rat were compared with those from the saline-treated rat as controls. Each column represents the mean ± SD of triplicate determinations. Control activities (nmol.min^{-1}.mg^{-1} microsomal protein) in the presence of corn oil and saline were 3·48 ± 0·46 in quadruplicate determinations and 2·81 ± 0·15 in triplicate determinations respectively. The degree of statistical significance is expressed as $*p < 0.02$ or $**p < 0.01$.

rat liver, although 7-ethoxyresorufin *O*-deethylation, a typical CYP1A-dependent activity, was induced by 14-fold. Microsomal OPP *p*-hydroxylation was minimally induced (1·36-fold) by the administration of phenobarbital (a CYP2B inducer), whereas 7-pentoxyresorufin *O*-dependentylation, a typical CYP2B-dependent activity, was induced by 85-fold. These results indicated that both CYP1A and CYP2B were not the major isoforms involved in the microsomal of *p*-hydroxylation OPP (figure 4). On the other hand, the largest induction (1·8-fold) of OPP *p*-hydroxylation was observed by isoniazid-administration.

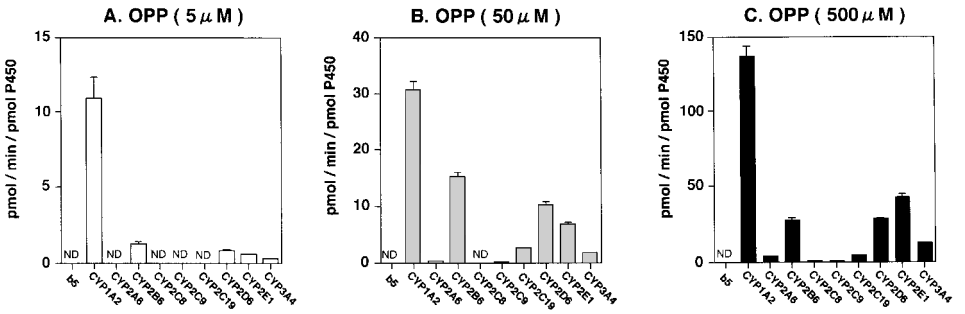


Figure 5. OPP *p*-hydroxylation in microsomes from baculovirus-infected insect cells expressing individual human CYPs. OPP was incubated for 20 min with CYP-expressing microsomes (10 pmol CYP) and the concentration of OPP was 5 μM (A), 50 μM (B) and 500 μM (C). Each column represents the mean ± SD of three separate experiments. ND (not detectable) indicates that metabolic activity was < 0·18 pmol.min^{-1}/pmol CYP.

Human CYPs responsible for PHQ formation

Mixed liver microsomes derived from human individuals (n = 12) also catalysed the *p*-hydroxylation of OPP (500 μM) at 2·54 ± 0·48 nmol.min^{-1}.mg^{-1} protein in triplicate determinations, which was as high as the rate of formation in male rat liver microsomes. Forms of human CYP expressed in baculovirus-mediated cDNA expression systems were used to examine the specific CYPs catalysing OPP hydroxylation. In the reaction mixtures using 10 pmol of each expressed CYP, CYP1A2 catalysed PHQ formation the most efficiently of the CYP forms tested in the present study (figure 5A-C). The PHQ formation was tested at the OPP concentration of 5 μM (figure 5A), 50 μM (B) and 500 μM (C). At 5 μM substrate concentration, CYP1A2 predominantly exhibited OPP *p*-hydroxylation at 11·94 pmol.min^{-1}/pmol CYP. The next highest was observed with CYP2B6 (1·26 pmol.min^{-1}/pmol CYP). CYP2D6, CYP2E1 and CYP3A4 showed lower activities at rates of 0·76, 0·58 and 0·23 pmol.min^{-1}/pmol CYP respectively. At 50 μM substrate concentration, catalytic activities by CYP1A2, CYP2B6, CYP2D6, CYP2E1 and CYP3A4 were 30·6, 15·2, 10·1, 6·7 and 1·7 pmol.min^{-1}/pmol CYP respectively. At 500 μM, CYP1A2, CYP2E1, CYP2D6, CYP2B6 and CYP3A4 converted OPP to PHQ at 136·8, 42·4, 27·9, 27·2 and 12·5 pmol.min^{-1}/pmol CYP respectively. In addition, CYP2C19, CYP2C9, CYP2C8 and CYP2A6, which did not exhibited catalytic activity at 5 μM, showed lower activities at 50 and 500 μM.

Hence, the overall conclusion is that CYP1A2 was the most efficient isoform for OPP *p*-hydroxylation.

Inhibition of OPP hydroxylation catalysed by human liver microsomes

Effects of typical CYP substrates or inhibitors on human hepatic OPP hydroxylation were examined to support results obtained using the microsomes of insect cells expressing different forms of human CYP. 7,8-Benzoflavone and furafylline, typical CYP1A inhibitors, exhibited the most potent inhibition of OPP *p*-hydroxylation (figure 6). By contrast, inhibitors of other forms of CYP showed lesser extent of inhibition of OPP *p*-hydroxylation. These results supported the results obtained by the recombinant CYP experiments in that CYP1A2 most efficiently catalysed OPP *p*-hydroxylation.

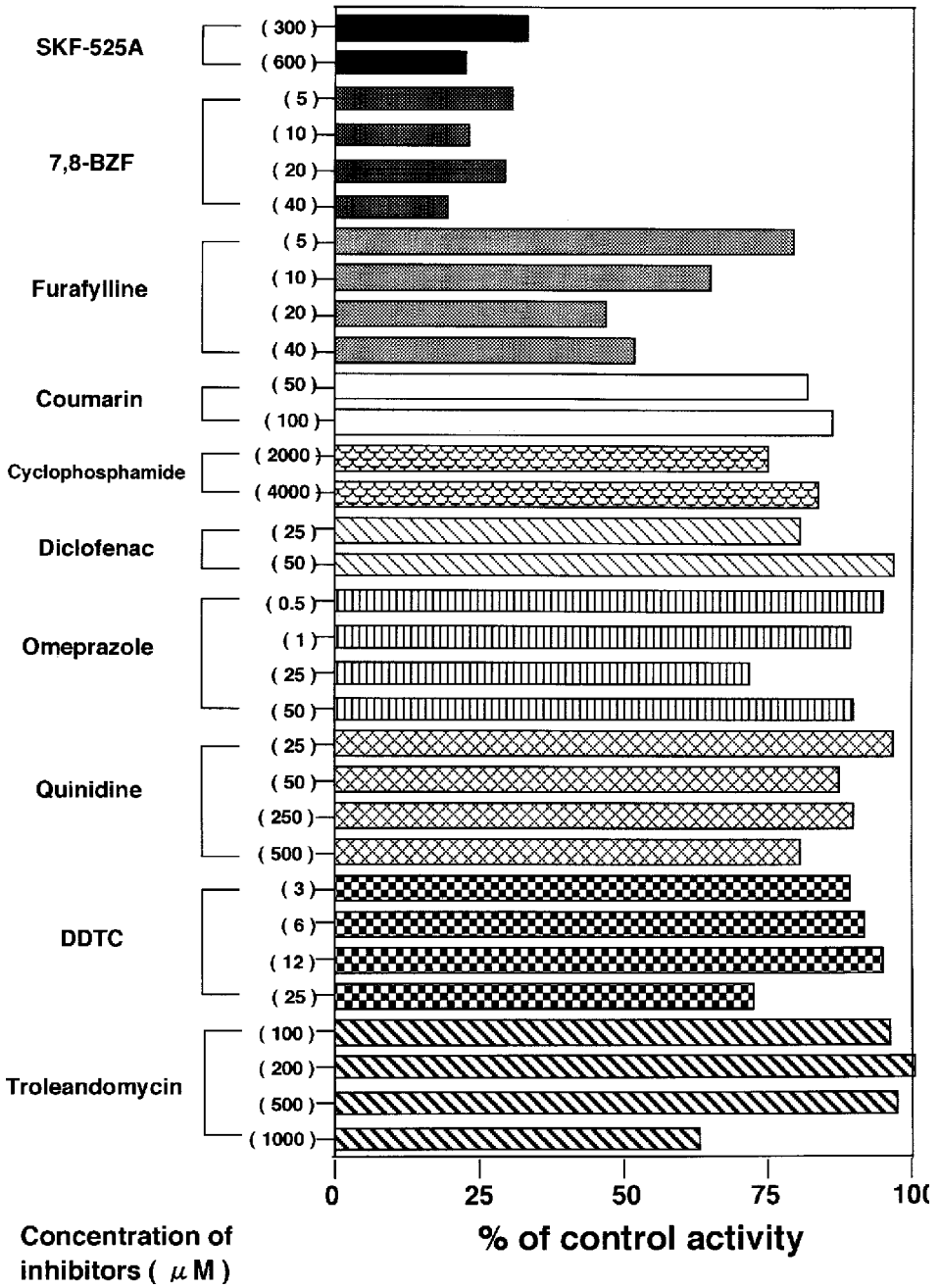


Figure 6. Effect of CYP inhibitors on OPP *p*-hydroxylation in human liver microsomes. The concentration of OPP was 5 μM and each column represents the average of duplicate experiments. OPP was incubated for 20 min with pooled human microsomes (100 μg protein). SKF-525A, furafylline, coumarin, cyclophosphamide, diclofenac, omeprazole, quinidine, diethyldithiocarbamate (DDTC) and troleandomycin were dissolved in distilled water. 7,8-Benzoflavone (7,8-BZF) was dissolved in methanol. Control activities (mean $\pm$ SD, nmol.min^{-1}.mg^{-1} protein) in the presence of distilled water and methanol were 0.32 ± 0.06 in six determinations and 0.31 ± 0.04 in triplicate determinations respectively.

Discussion

The involvement of rat CYP2C11 (a male-specific form), rat CYP2E1 and human CYP1A2 has been demonstrated *in vitro* for the metabolic activation of OPP to the toxic metabolite, PHQ by hepatic microsomes of the male rat and human.

2,3-Dihydroxybiphenyl and PHQ were cytotoxic in cell lines derived from several animal species and also for DNA strand break at the lowest concentration of the hydroxylated biphenyl derivatives used in this study. 4,4′-Dihydroxybiphenyl failed to induce efficient DNA strand break but was relatively cytotoxic, suggesting different mechanisms of cytotoxicity from those of 2,3-dihydroxybiphenyl and PHQ (table 1 and figure 2).

2,3-Dihydroxybiphenyl was not detected in the microsomal systems from either rat or human. Male dominance in the liver microsome-mediated conversion of OPP into PHQ was observed (table 2), consistent with the fact that a higher incidence in OPP-induced bladder cancer was also observed in the male F344 rat as compared with the female (Hasegawa *et al*. 1991). It was also observed that hepatic OPP *p*-hydroxylation catalysed by the male F344 and Sprague–Dawley rat was best inhibited by inhibitory antibodies against the male-specific rat CYP2C11 (figure 3). Antibodies against CYP3A seemed to enhance hepatic OPP *p*-hydroxylation. These results might suggest a possible interaction of OPP with CYP3A, although the exact mechanisms are unknown at present (figure 3). Recently, OPP was reported to induce cell injury in hepatocytes, associated with a substantial decrease in intracellular glutathione (Sugihara *et al*. 1997). Potencies of damage in cultured cells and induction of DNA strand breaks seemed to correlate among the hydroxybiphenyls, including PHQ used in the present study. Renal expression of the male-specific CYP2C11 has been documented (Ryan *et al*. 1993). Thus, male-specific rat CYP2C11, which has been proposed to be involved in the metabolic activation of OPP in this study, might play an important role in mediating cell damage in OPP-exposed rat. Whether the observed male-dominance in hepatic OPP *p*-hydroxylation could also be attributed to the bladder cancer incidence in the male rat clearly depends on the stability of the resultant toxic metabolite (PHQ) in the circulating blood and uro-epithelial tracts.

PHQ is further oxidized to yield PBQ (figure 1; Lambert and Eastmond 1994). CYP-catalysed one-electron reductive bioactivation has been reported as an important metabolic activation of compounds with a quinone moiety (Goeptar *et al*. 1995). The resultant PBQ is likely to undergo reductive bioactivation by CYP form(s). Elucidation of forms of CYP involved in the PBQ formation and the reductive bioactivation is required for clarification of the complete metabolic activation pathway of OPP.

Neither phenobarbital- nor 5,6-benzoflavone-administered rat liver microsomes exhibited substantially higher OPP *p*-hydroxylation than those from the corn oil-administered rat (figure 4). Failure of 5,6-benzoflavone to induce OPP *p*-hydroxylation is consistent with the results reported by Halpaap-Wood *et al*. (1981).

Among various human CYPs expressed in the baculovirus-mediated systems, CYP1A2 catalysed the OPP *p*-hydroxylation most efficiently among the CYP forms which are known to be expressed in human livers, over the OPP concentration examined (i.e. 5, 50 and 500 μM; figure 5). At higher OPP concentrations, CYP2D6 catalysed the OPP *p*-hydroxylation. Apparently, the K_m of CYP2D6 for the reaction was higher than that of CYP1A2 (figure 5). CYP2D6 is known to catalyse

C-hydroxylation of debrisoquin. It has been shown that ring-hydroxylation of debrisoquin was catalysed by CYP2D6 (Lightfoot *et al*. 2000). These results may support our results on OPP being a substrate of CYP2D6 to form PHQ, though further investigation is required.

It was decided to examine the major hepatic CYP forms catalysing the reaction at an OPP concentration of 5 μM, since this lowest concentration adopted in the present study might be of the highest toxicological significance. The results on the potent inhibition by 7,8-benzoflavone and furafylline, typical CYP1A inhibitors, on OPP hydroxylation catalysed by mixed human liver microsomes were quite consistent with the efficient catalytic activities by cDNA-expressed CYP1A2. K_m for microsomal OPP hydroxylation was $\sim$ 110 μM in human liver systems (data not shown). The approximate hepatic levels (pmol.mg^{-1} protein) of CYP forms in human livers are (Shimada *et al*. 1996): 55 $\pm$ 28 for CYP1A; 83 $\pm$ 29 for CYP2C; 10 $\pm$ 5 for CYP2D6; 33 $\pm$ 17 for CYP2E1; and 147 $\pm$ 57 for CYP3A. Thus, taking the substantially high rate of OPP *p*-hydroxylation by the recombinant CYP1A2 and the hepatic CYP levels into consideration, CYP1A2 likely plays a major role in PHQ formation in human livers. It was reported that 7,8-benzoflavone stimulated human CYP3A4-mediated phenacetin *O*-deethylation (Nakajima *et al*. 1999). 7,8-Benzoflavone inhibited OPP *p*-hydroxylation by human liver microsomes at concentrations of 5–40 μM (figure 6), which also enhanced CYP3A4-mediated phenacetin *O*-deethylation (data not shown). These results suggested the important role of CYP1A2 in hepatic OPP-hydroxylation, although CYP3A4 was also shown to catalyse the reaction (figure 5A).

CYP1A2-dependent activity is known to show remarkable individual difference and to be polymorphically distributed in the human population (Minchin *et al*. 1985, Butler *et al*. 1992, Nakajima *et al*. 1994). Thus, the present results on the role of CYP1A2 in the metabolic activation of OPP raise the possibility of potential toxic effects by this food additive in human individuals with high CYP1A2 expression.

Acknowledgements

This work was supported in part by a Grant-in-Aid from the Ministry of Health and Welfare of Japan and a grant for the research project 'Humanised Testing Systems' from the Organisation for Pharmaceutical Safety and Research (97-14). The authors express their deep thanks to Noriaki Shimada of Daiichi Chemical Co. for all his supports and helpful discussions.

References

Butler, M. A., Lang, N. P., Young, J. F., Caporaso, N. E., Vineis, P., Hayes, R. B., Teitel, C. H., Massengill, J. P., Lawsen, M. F. and Kadlubar, F. F., 1992, Determination of CYP1A2 and NAT2 phenotypes in human populations by analysis of caffeine urinary metabolites. *Pharmacogenetics*, **2**, 116–127.

Goeptar, A. R., Scheerens, H. and Vermeulen, N. P. E., 1995, Oxygen and xenobiotic reductase activities of cytochrome P450. *Critical Reviews in Toxicology*, **25**, 25–65.

Halpaap-Wood, K., Horning, E. C. and Horning, M. G., 1981, The effect of phenobarbital and β-naphthoflavone induction on the metabolism of biphenyl in the rat and mouse. *Drug Metabolism and Disposition*, **9**, 97–102.

Hasegawa, R., Fukuoka, M., Takahashi, T., Yamamoto, A., Yamaguchi, S., Shibata, M.-A., Tanaka, A. and Fukushima, S., 1991, Sex difference in *o*-phenylphenate rat urinary bladder

carcinogenesis: urinary metabolites and electrolytes under conditions of aciduria and alkaliuria. *Japanese Journal of Cancer Research*, **82**, 657–664.

Hiraga, K. and Fujii, T., 1981, Induction of tumours of the urinary system in F344 rats by dietary administration of sodium *o*-phenylphenate. *Food and Cosmetic Toxicology*, **19**, 303–310.

Hodge, H. C., Maynard, E. A., Blanchet, H. J., Jr, Spencer, H. C. and Rowe, V. K., 1952, Toxicological studies of orthophenylphenol (Dowcide 1). *Journal of Pharmacology and Experimental Therapeutics*, **104**, 202–210.

Itagaki, H., Shibata, M., Tani, N., Kinoshita, S., Kakishima, H., Seyama, Y., Ohuchi, J., Kasai, Y., Okada, J., Kojima, H., Okamoto, Y., Kotani, M., Ohno, Y., Miyajima, A., Takanaka, A., 1995, First-phase inter-laboratory validation of the *in vitro* eye irritation tests for cosmetic ingredients. X-Evaluation of cytotoxicity tests on SIRC cells. *AATEX*, **3**, 201–209.

Lambert, A. C. and Eastmond, D. A., 1994, Genotoxic effects of the *o*-phenylphenol metabolites phenylhydroquinone and phenylbenzoquinone in V79 cells. *Mutation Research*, **322**, 243–256.

Lightfoot, T., Ellis, S. W., Mahling, J., Ackland, M. J., Blaney, F. E., Bijioo, G. J., De Groot, M. J., Vermeulen, N. P., Blackburn, G. M., Lennard, M. S. and Tucker, G. T., 2000, Regioselective hydroxylation of debrisoquine by cytochrome P4502D6: implications for active site modelling. *Xenobiotica*, **30**, 219–233.

Luster, M. I., Dean, J. H., Boorman, G. A., Archer, D. L., Lauer, L., Lawson, L. D., Moore, J. A. and Wilson, R. E., 1981, The effect of orthophenylphenol, tris(2,3-dichloroporpyl)phosphate, and cyclophosphamide on the immune system and host susceptibility of mice following subchronic exposure. *Toxicology and Applied Pharmacology*, **58**, 252–261.

Minchin, R. F., McManus, M. E., Boobis, A. R., Davies, D. S. and Thorgeirsson, S. S., 1985, Polymorphic metabolism of the carcinogen 2-acetylaminofluorene in human liver microsomes. *Carcinogenesis*, **6**, 1721–1724.

Morimoto, K., Fukuoka, M., Hasegawa, R., Tanaka, A., Takahashi, A. and Hayashi, Y., 1987, DNA damage in urinary bladder epithelium of male F344 rats treated with 2-phenyl-1,4-benzoquinone, one of the non-conjugated urinary metabolites of sodium *o*-phenylphenate. *Japanese Journal of Cancer Research (Gann)*, **78**, 1027–1030.

Morimoto, K., Sato, M., Fukuoka, M., Hasegawa, R., Takahashi, T., Tsuchiya, T., Tanaka, A., Takahashi, A. and Hayashi, Y., 1989, Correlation between the DNA damage in urinary bladder epithelium and the urinary 2-phenyl-1,4-benzoquinone levels from F344 rats fed sodium *o*-phenylphenate in the diet. *Carcinogenesis*, **10**, 1823–1827.

Murata, M., Moriya, K., Inoue, S. and Kawanishi, S., 1999, Oxidative damage to cellular and isolated DNA by metabolites of a fungecide *ortho*-phenylphenol. *Carcinogenesis*, 20, 851–857.

Nagai, F., Ushiyama, K., Satoh, K. and Kano, I., 1990, DNA cleavage by phenylhydroquinone: the major metabolite of a fungicide *o*-phenylphenol. *Chemico-Biological Interactions*, **76**, 163–179.

Nagai, F., Ushiyama, K., Satoh, K., Kasai, H. and Kano, I., 1995, Formation of 8-hydroxydeoxyguanosine in calf thymus DNA treated *in vitro* with phenylhydroquinone, the major metabolite of *o*-phenylphenol. *Carcinogenesis*, 16, 837–840.

Nakajima, M., Kobayashi, K., Oshima, K., Shimada, N., Tokudome, S., Chiba, K. and Yokoi, T., 1999, Activation of phenacetin *o*-deethylase activity by α-naphthoflavone in human liver microsomes. *Xenobiotica*, **29**, 885–898.

Nakajima, M., Yokoi, T., Mizutani, M., Shin, S., Kadlubar, F. F. and Kamataki, T., 1994, Phenotyping of CYP1A2 in Japanese population by analysis of caffeine urinary metabolites: absence of mutation prescribing the phenotype in the *CYP1A2* gene. *Cancer Epidemiology Biomarkers Prevention*, **3**, 413–421.

Ohno, Y., Miyajima, A. and Sunouchi, M., 1998, Alternative methods for mechanistic studies in toxicology. Screening of hepatotoxicity of pesticides using freshly isolated and primary cultured hepatocytes and non-liver-derived cells, SIRC cells. *Toxicology Letters*, **102–3**, 569–573.

Ono, S., Hatanaka, T., Hotta, H., Satoh, T., Gonzalez, F. J. and Tsutsui, M., 1996, Specificity of substrate and inhibitor probes for cytochrome P450s: evaluation of *in vitro* metabolism using cDNA-expressed human P450s and human liver microsomes. *Xenobiotica*, **26**, 681–693.

Ryan, D. E., Thoma, P. E., Levin, W., Maines, S. L., Bandiera, S. and Reik, L. M., 1993, Monoclonal antibodies of differentiating specificities as probes of cytochrome P450h (2C11). *Archives in Biochemistry and Biophysics*, **301**, 282–293.

Sasaki, Y. F., Saga, A., Akasaka, M., Yoshida, K., Nishidate, E., Su, Y. Q., Matsusaka, N. and Tsuda, S., 1997, *In vivo* genotoxicity of *ortho*- phenylphenol, biphenyl, and thiabendazole detected in multiple mouse organs by the alkaline single cell gel electrophoresis assay. *Mutation Research*, 395, 189–198.

Shimada, T., Yamazaki, H., Mimura, M., Wakamiya, N., Ueng, Y.-F., Guengerich, F. P. and Inui, Y., 1996, Characterization of microsomal cytochrome P450 enzymes involved in the oxidation of xenobiotic chemicals in human fetal livers and adult lungs. *Drug Metabolism and Disposition*, **24**, 515–522.

Sugihara, N., Shimomichi, K. and Furuno, K., 1997, Cytotoxicity of food preservatives in cultured rat hepatocytes loaded with linolenic acid. *Toxicology*, **120**, 29–36.

Tayama, S. and Nakagawa, Y., 1994, Effect of scavengers of active oxygen species on cell damage caused in CHO-K1 cells by phenylhydroquinone, an *o*-phenylphenol metabolite. *Mutation Research*, 324, 121–131.

Teramura, T., Fukunaga, Y., van Hoogdalem, E. J., Watanabe, T. and Higuchi, T., 1997, Examination of metabolic pathways and identification of human liver cytochrome P450 isozymes responsible for the metabolism of barnidipine, a calcium channel blocker. *Xenobiotica*, **27**, 885–900.

Ushiyama, K., Nagai, F., Nakagawa, A. and Kano, I., 1992, DNA adduct formation by *o*-phenylphenol metabolite *in vivo* and *in vitro*. *Carcinogenesis*, **13**, 1469–1473.

xenobiotica, 2000, vol. 30, no. 11, 1019–1032

Effects of clofibrate and indocyanine green on the hepatobiliary disposition of acetaminophen and its metabolites in male CD-1 mice

CHUAN CHEN†, GAYLE E. HENNIG‡, DENIS J. MCCANN§¶ and JOSÉ E. MANAUTOU†*

Toxicology Program, Departments of † Pharmaceutical Sciences and ‡ Pathobiology, University of Connecticut, Storrs, CT 06269, USA
§ Drug Disposition and Metabolism Department, AstraZeneca Pharmaceuticals, Wilmington, DE 19850, USA

Received 4 May 2000

1. The effects of clofibrate (CFB) and indocyanine green (ICG) on the biliary excretion of acetaminophen (APAP) and its metabolites were investigated.

2. Male CD-1 mice were pretreated with 500 mg CFB/kg, i.p. for 10 days. Controls received corn oil vehicle only. After overnight fasting, common bile duct-cannulated mice were challenged with a non-toxic dose of APAP (1 mmol/kg, i.v.).

3. CFB pretreatment did not affect bile flow rate, nor did it affect the cumulative biliary excretion of APAP and its conjugated metabolites.

4. Additional CFB or corn oil pretreated mice were given 30 μmol indocyanine green (ICG)/kg, i.v., immediately before APAP dosing. ICG is a non-metabolizable organic anion that is completely excreted into the bile through a canalicular transport process for organic anions.

5. ICG significantly decreased the bile flow rate and biliary concentration of APAP-glutathione, APAP-glucuronide and APAP-mercapturate within the first hour after dosing without affecting the biliary concentration of APAP.

6. The results indicate that CFB pretreatment does not affect the total amount of APAP and its metabolites excreted in bile. They also suggest that the biliary excretion of several conjugated metabolites of APAP share the same excretory pathway with the organic anion ICG.

Introduction

The widely used analgesic and antipyretic drug acetaminophen (N-acetyl-*p*-aminophenol, paracetamol, APAP) can produce severe centrilobular liver necrosis in both humans and laboratory animals following overdosing (Davidson and Eastham 1966, Boyer and Rouff 1971, Placke *et al*. 1987). APAP hepatotoxicity depends on a balance between detoxification pathways, such as sulphation and glucuronidation, and bioactivation through cytochrome P450 to the reactive intermediate N-acetyl-*p*-benzo-quinonimine (NAPQI) (Mitchell *et al*. 1973b, Hazelton *et al*. 1986). Hepatic glutathione (GSH) status is also an important determinant in APAP toxicity (Mitchell *et al*. 1973a, Strubelt *et al*. 1974, Harman and Self 1986). Factors that can shift the balance between detoxification and bioactivation pathways for APAP and/or alter the hepatic GSH status have been demonstrated to modulate the severity of APAP hepatotoxicity (Mitchell *et al*. 1973a, McClain *et al*. 1980, Hazelton *et al*. 1986).

* Author for correspondence; e-mail: manautou@uconnvm.uconn.edu
¶ Present address: Lilly Research Laboratories, Lilly Corporate Center, Indianapolis, IN 46285, USA.

Xenobiotica ISSN 0049-8254 print/ISSN 1366-5928 online © 2000 Taylor & Francis Ltd
http://www.tandf.co.uk/journals DOI: 10.1080/00498250010002252

Clofibrate [2-(*p*-chlorophenoxy)-2-methyl-propionic acid ethyl ester] (CFB) is a hypolipidemic drug that also belongs to a group of structurally diverse chemicals known as peroxisome proliferators. Peroxisome proliferators can induce multiple responses ranging from hepatomegaly, induction of peroxisomal and microsomal enzymes associated with fatty acid oxidation, and increased incidence of liver tumours in rodents (Reddy and Lalwani 1983). Studies have reported that treatment with CFB and other peroxisome proliferators protects mice from acute APAP hepatotoxicity (Nicholls-Grzemski *et al*. 1992, Manautou *et al*. 1994, Nguyen *et al*. 1999). In this model of hepatoprotection, APAP covalent binding to microsomal and cytosolic protein targets, as well as hepatic GSH depletion are substantially reduced, suggesting that this treatment regimen decreases net availability of NAPQI (Manautou *et al*. 1994). Interestingly, *in vivo* and *in vitro* studies have demonstrated that CFB pretreatment does not alter bioactivation of APAP to the toxic metabolite NAPQI, nor the activity of detoxification pathways for APAP (Manautou *et al*. 1994, Manautou *et al*. 1996, Nicholls-Grzemski *et al*. 1996). Despite the lack of changes in APAP biotransformation, its elimination from both liver and plasma was determined to be much more rapid in the CFB-pretreated mice (Manautou *et al*. 1996). Additionally, no differences in 24-h urinary output of APAP and its metabolites were detected in our previous studies. A possible explanation could be that CFB pretreatment enhances the biliary disposition of APAP.

Many endogenous compounds, xenobiotics and their conjugated metabolites are eliminated from the body through biliary excretion. In recent years, several canalicular transport systems belonging to the ATP-binding cassette (ABC) transporter superfamily have been cloned and characterized (Croop *et al*. 1989, Buchler *et al*. 1996, Paulusma *et al*. 1996). For example, the functionally characterized canalicular multispecific organic anion transporter (cMOAT), which is responsible for the biliary secretion of a wide variety of amphiphilic organic anions such as bilirubin glucuronides, glutathione *S*-conjugates, reduced and oxidized glutathione, has been cloned and identified as an isoform of the multidrug resistance-associated protein, MRP (Keppler *et al*. 1998). This transport protein is referred interchangeably as MRP2 or cMOAT. Other well-characterized ATP-dependent transport proteins involved in hepatobiliary secretion include the P-glycoproteins MDR1 and MDR3 (Muller and Jansen 1997). Although the enhanced expression of certain transport proteins such as MRP1 and P-glycoprotein, MDR1 have been strongly associated with acquired resistance to chemotherapeutic agents in certain types of tumours (Gottesman and Pastan 1993, Keppler *et al*. 1998), it remains unclear whether xenobiotic-induced changes in liver transport protein expression could lead to changes in hepatic disposition and susceptibility to model hepatotoxicants. Fibrate-type peroxisome proliferators have been shown to induce *mdr*2 gene expression in the mouse liver, leading to an increased biliary phospholipid secretion (Chianale et al. 1996). The same group recently showed that the herbicide 2,4,5-trichlorophenoxyacetic acid increases cMoat/mrp2 protein expression, whereas CFB treatment does not (Wielandt *et al*. 1999). These data do not preclude the possibility that CFB treatment may enhance the expression of a related, yet unidentified transporter for organic anions.

The current study was conducted to determine if CFB pretreatment could enhance the biliary excretion of APAP and its metabolites. Also, to understand better the mechanisms for the biliary excretion of APAP and its conjugated metabolites, additional groups of mice received the non-metabolizable organic anion

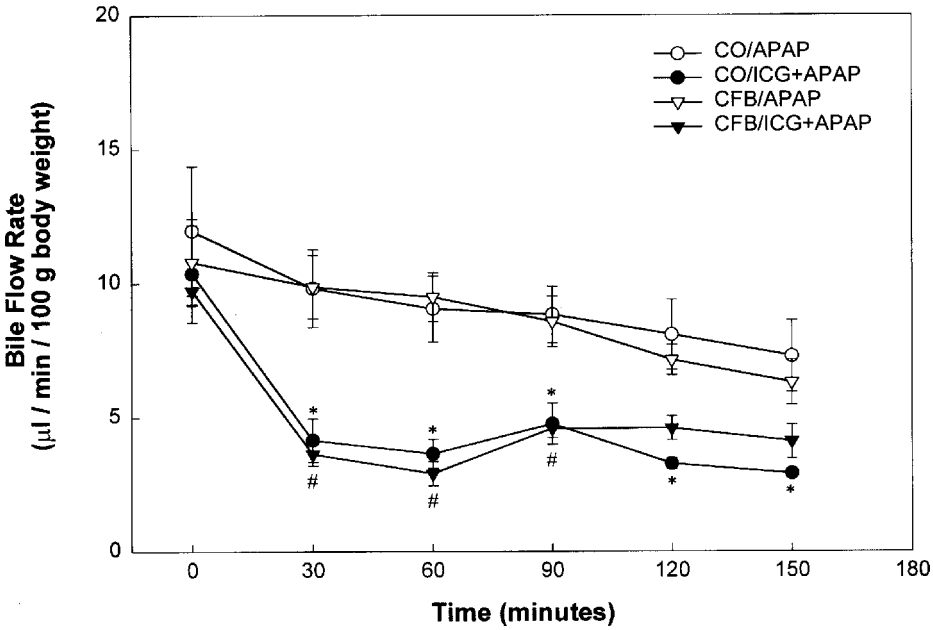


Figure 1. Effects of CFB pretreatment and the organic anion ICG on bile flow. Male CD-1 mice received either corn oil (CO) (5 ml/kg) or CFB (500 mg/kg), i.p. daily for 10 days. Following overnight fasting, mice were anaesthetized and the common bile duct was cannulated. Fifteen minutes later, APAP (1 mmol/kg) was given i.v. Additional groups of the corn oil- or CFB-pretreated mice received 30 μmol ICG/kg immediately before APAP dosing. Bile was collected for 150 min at 30-min intervals. Results are the means ± SEM for three-to-six mice per treatment group. * Significantly different ($p < 0.05$) from corn oil-pretreated mice receiving APAP only; # significantly different ($p < 0.05$) from CFB-pretreated mice receiving APAP only.

indocyanine green (ICG) before APAP dosing. Interference by ICG with the biliary excretion of APAP and its metabolites would be suggestive of a common biliary excretory pathway.

Materials and methods

Reagents

Clofibrate, 4-acetamidophenol (APAP), indocyanine green, propylene glycol, and corn oil were from Sigma Chemical Co. (St Louis, MO, USA). High-performance liquid chromatography (HPLC)-grade methanol and acetic acid were from Fisher Scientific (Springfield, NJ, USA). APAP metabolite standards (e.g. APAP-glutathione, -glucuronide, -sulphate, -mercapturate, -cysteine) were a generous gift from Dr Sidney Nelson (University of Washington, Seattle, WA). All other chemicals used were reagent grade or better.

Animals

Three-to-four-month-old male Crl:CD-1 (ICR)BR mice (Charles Rivers Laboratories, Wilmington, MA, USA) were housed in community stainless steel cages (five per cage) on hardwood shavings (Sani-Chip Dry, P. J. Murphy Forest Products, Montville, NJ, USA). They had free access to tap water and Laboratory Rodent Diet No. 5001 (PMI Feeds, Inc., St Louis, MO, USA). Lights were maintained on a 12/12-h light/dark cycle, and room temperature was maintained at 22 °C.

Treatment regimen and biliary excretion studies

Mice received 500 mg CFB/kg or corn oil vehicle (5 ml/kg), i.p., daily for 10 days (Nicholls-Grzemski *et al.* 1992, Manautou *et al.* 1994). Following overnight fasting (18 h), mice were anaesthetized with a combination of 100 mg ketamine/kg and 10 mg xylazine/kg i.p. (Fort Dodge Animal Health, Fort Dodge, IA, USA) and the common bile duct was cannulated using 1.2-Fr polyurethane catheter tubing (Access Technologies, Skokie, IL, USA). Rectal temperature was monitored with a thermistor thermometer unit (Harvard Apparatus, Holliston, MA, USA) and maintained between 35 and 37 °C

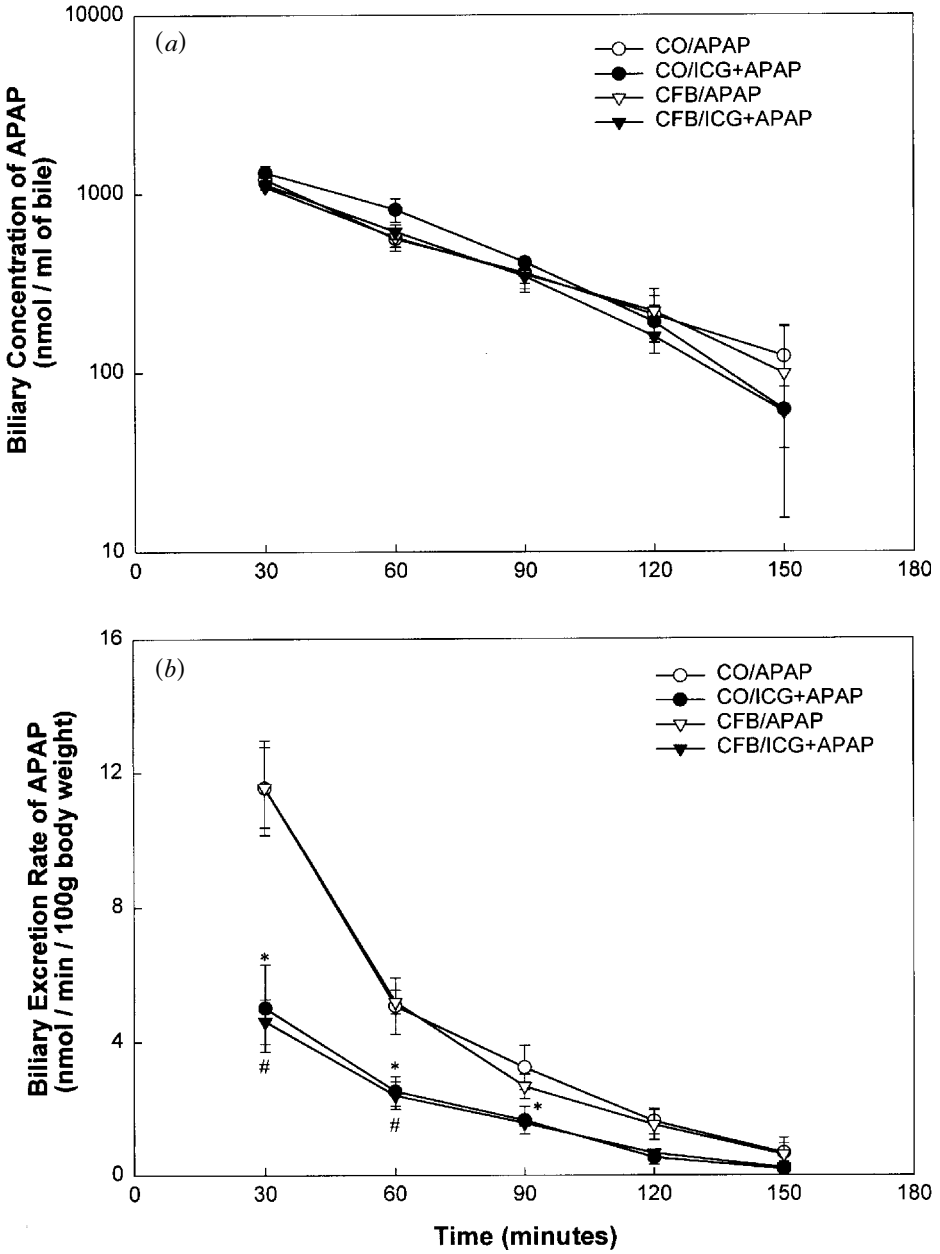


Figure 2. Effects of CFB pretreatment and the organic anion ICG on biliary excretion of APAP. For details on treatment regimens and experimental procedures, see figure 1. (a) Biliary concentration of APAP; (b) biliary excretion rate of APAP. Results are the means ± SEM for three-to-six mice per treatment group. * Significantly different ($p < 0.05$) from corn oil-pretreated mice receiving APAP only; # significantly different ($p < 0.05$) from CFB-pretreated mice receiving APAP only.

using a heat lamp. ICG and APAP were dissolved in physiological saline and 20% propylene glycol, respectively. Fifteen minutes after bile duct cannulation, a non-toxic dose of APAP (1 mmol/kg) (Gregus *et al.* 1988) was injected with or without prior administration of 30 μmol ICG/kg, both via the tail vein. This dose of ICG has been reported to produce a maximal rate of biliary excretion for this organic anion in both rats and mice when given i.v. (Gregus and Klaassen 1982). Bile was collected into preweighed

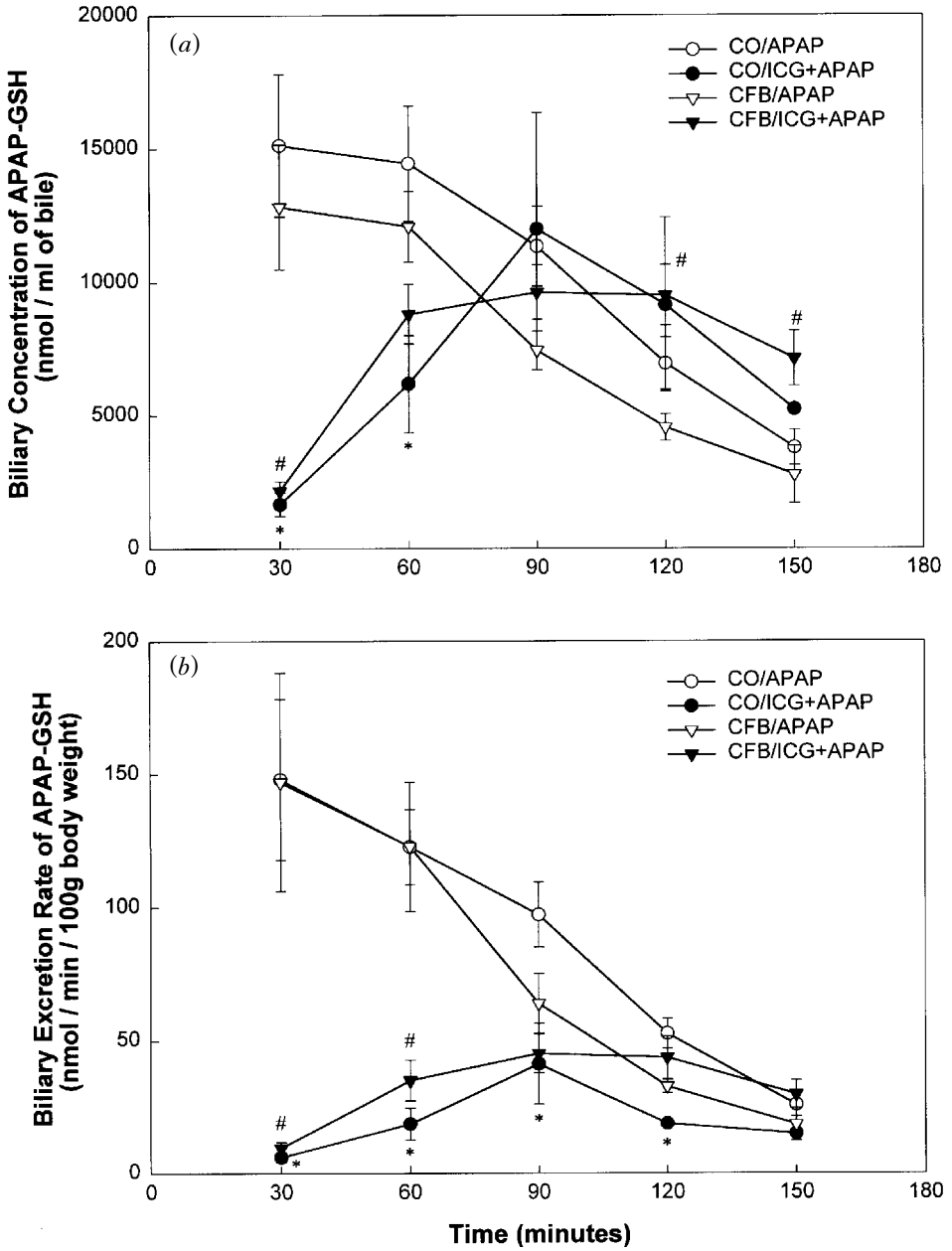


Figure 3. Effects of CFB pretreatment and the organic anion ICG on biliary excretion of APAP-GSH. For details on treatment regimens and experimental procedures, see figure 1. (a) Biliary concentration of APAP-GSH; (b) biliary excretion rate of APAP-GSH. Results are the means ± SEM for three-to-six mice per treatment group. * Significantly different ($p < 0.05$) from corn oil-pretreated mice receiving APAP only; # significantly different ($p < 0.05$) from CFB-pretreated mice receiving APAP only.

microcentrifuge tubes kept on ice at 30-min intervals for up to 150 min. Anaesthesia was maintained by i.m. injection with 1/10 to 2/10 of the initial dosage of ketamine/xylazine every 30 min. Bile volume was determined gravimetrically assuming a specific gravity of one. Samples were stored at −70 °C until assayed. The University of Connecticut Institutional Animal Care and Use Committee (IACUC) approved all animal protocols.

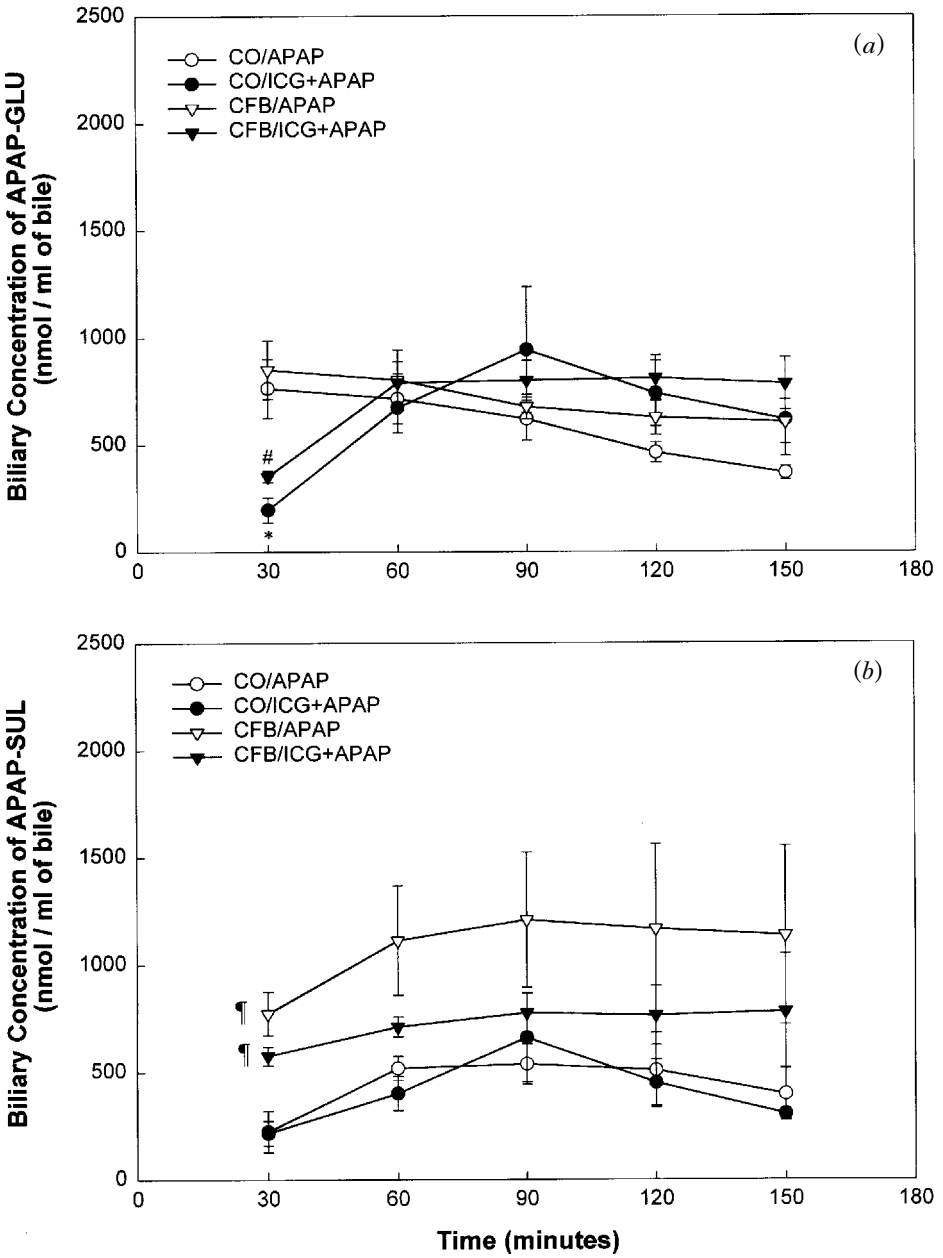


Figure 4. For legend see opposite.

HPLC analysis of bile samples

APAP and its metabolites in bile were analysed using an HPLC method modified from that of Howie *et al.* (1977) as previously described (Manautou *et al.* 1996). Bile samples were diluted with 2 vols ice-cold HPLC-grade methanol and centrifuged at 1200*g* for 30 min (Sorvall RMC 14 refrigerated micro-centrifuge, Dupont Co., Wilmington, DE, USA). Then two-thirds of the resulting supernatant was added to 3–5 vols double de-ionized water, depending on the time of bile collection. Diluted bile samples were filtered through a 0.20-μm nylon filter, and analysed using a Beckman System Gold HPLC system equipped with a 128 NM solvent module and a 166 NM detector (Beckman Instruments, Inc., Fullerton, CA, USA). Aliquots (20 μl) of the processed bile samples were injected onto a Zorbax SB 5 μm C_{18}reserve-phase column (4.6 × 250 mm, MAC-MOD Analytical, Inc., Chadds Ford, PA, USA). APAP

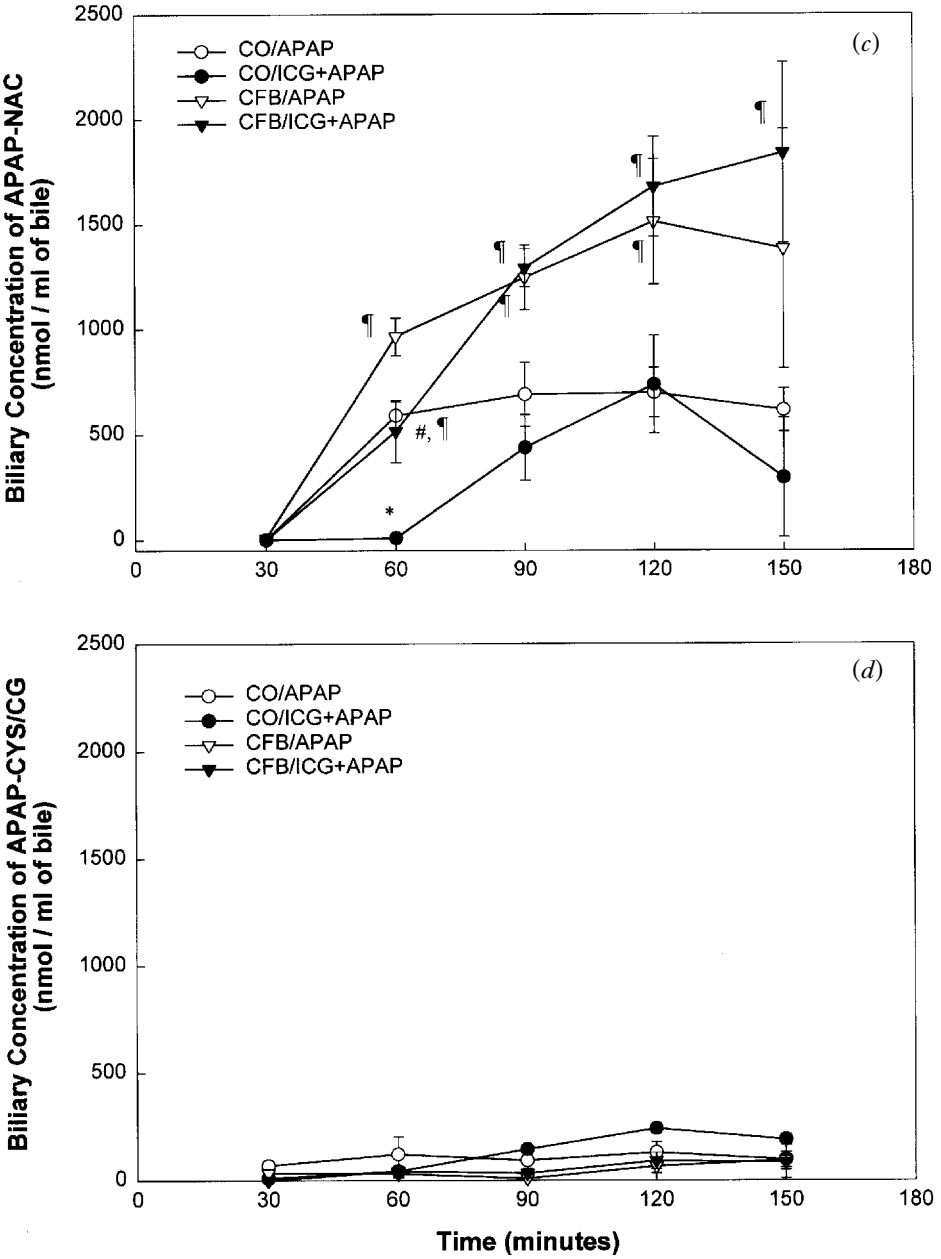


Figure 4. Effects of CFB pretreatment and the organic anion ICG on the biliary concentration of other APAP conjugates. For details on treatment regimens and experimental procedures, see figure 1. (a) APAP-GLU, (b) APAP-SUL, (c) APAP-NAC, (d) APAP-CYS/CG. Results are the means ± SEM for three-to-six mice per treatment group. *Significantly different ($p < 0.05$) from corn oil-pretreated mice receiving APAP only; # significantly different ($p < 0.05$) from CFB-pretreated mice receiving APAP only; ¶ significantly different ($p < 0.05$) from its respective corn oil vehicle control.

and its metabolites were eluted using a mobile phase composed of 12.5% HPLC-grade methanol, 1% glacial acetic acid and 86.5% water, run isocratically at a flow rate of 1.2 ml/min. The elution of metabolites was monitored at a wavelength of 254 nm. Retention times for APAP and its metabolites were determined by comparison with those of authentic standards. Since this HPLC method did not separate

the cysteinylglycine and cysteine conjugates of APAP, they were quantitated together as APAP-CYS/CG. Preliminary chromatographic analysis of control bile samples from mice treated with CFB and ICG showed no interfering peaks. Quantitation was based on integrated peak areas. The concentration of APAP and its metabolites was calculated using an APAP standard curve since the molar extinction coefficients of APAP and its conjugated metabolites are the same (Howie *et al*. 1977). The amount of APAP and its metabolites excreted into the bile was expressed as nmol/min/100 g body weight, and biliary concentrations were expressed as nmol/ml bile.

Statistical analysis

Results are expressed as mean ± SEM of at least three mice per treatment group. One-way analysis of variance (ANOVA) followed by the post-hoc Duncan's multiple range test was used to compare means from different treatment groups at individual time points, and $p < 0.05$ were considered statistically significant.

Results

Bile flow rate

The effect of CFB pretreatment and dosing with the organic anion ICG on bile flow rate is depicted in figure 1. Mice receiving CFB for 10 days and challenged with APAP only had no change in bile flow rate when compared with corn oil controls. However, administration of ICG before APAP challenge resulted in a significant decrease in bile flow rate in both groups of CFB and corn oil pretreated mice. A cholestatic effect for ICG has been previously reported (Gregus and Klaassen 1982).

Effects of CFB and ICG on biliary concentration and excretion rate of APAP and its metabolites

The time-course for biliary concentration and excretion rate of APAP, APAP-glutathione (APAP-GSH), APAP-glucuronide (APAP-GLU), APAP-mercapturate (APAP-NAC), APAP-sulphate (APAP-SUL) and APAP-cysteine/cysteinylglycine (APAP-CYS/CG) are shown in figures 2–4.

Biliary concentration of APAP was not affected by either CFB pretreatment or ICG dosing. APAP concentration in bile declined with time in a logarithmic fashion (figure 2a). Similarly, CFB pretreatment had no effect on the biliary excretion rate of APAP (figure 2b). However, all groups of mice receiving ICG had significantly lower excretion rates of APAP. This reduction is most likely due to the effect of ICG on the bile flow rate.

In CFB pretreated mice receiving APAP only, the biliary concentration of APAP-GSH was consistently lower than, but not significantly different from corn oil-pretreated mice at all time points measured (figure 3a). This was the major APAP metabolite secreted in bile, which is consistent with previous reports (Wong *et al*. 1981, Gregus *et al*. 1988). The highest concentration of APAP-GSH was detected at 30 min after APAP dosing in these two groups of mice. In CFB- and corn oil-pretreated mice receiving ICG before APAP, the biliary concentration of APAP-GSH at 30 min was significantly lower than that in mice dosed with APAP only. Then, APAP-GSH concentration gradually increased after 30 min to values similar to or even higher than those seen in mice that did not receive ICG. Since dosing with ICG produced a marked decrease on the initial concentration of APAP-GSH in bile, but not on that of the parent compound (figure 2a), these results suggest that ICG and this prominent metabolite of APAP are competing for the same biliary transport process. The time-course for the biliary excretion rate of APAP-GSH is presented in figure 3b. Again, CFB pretreatment

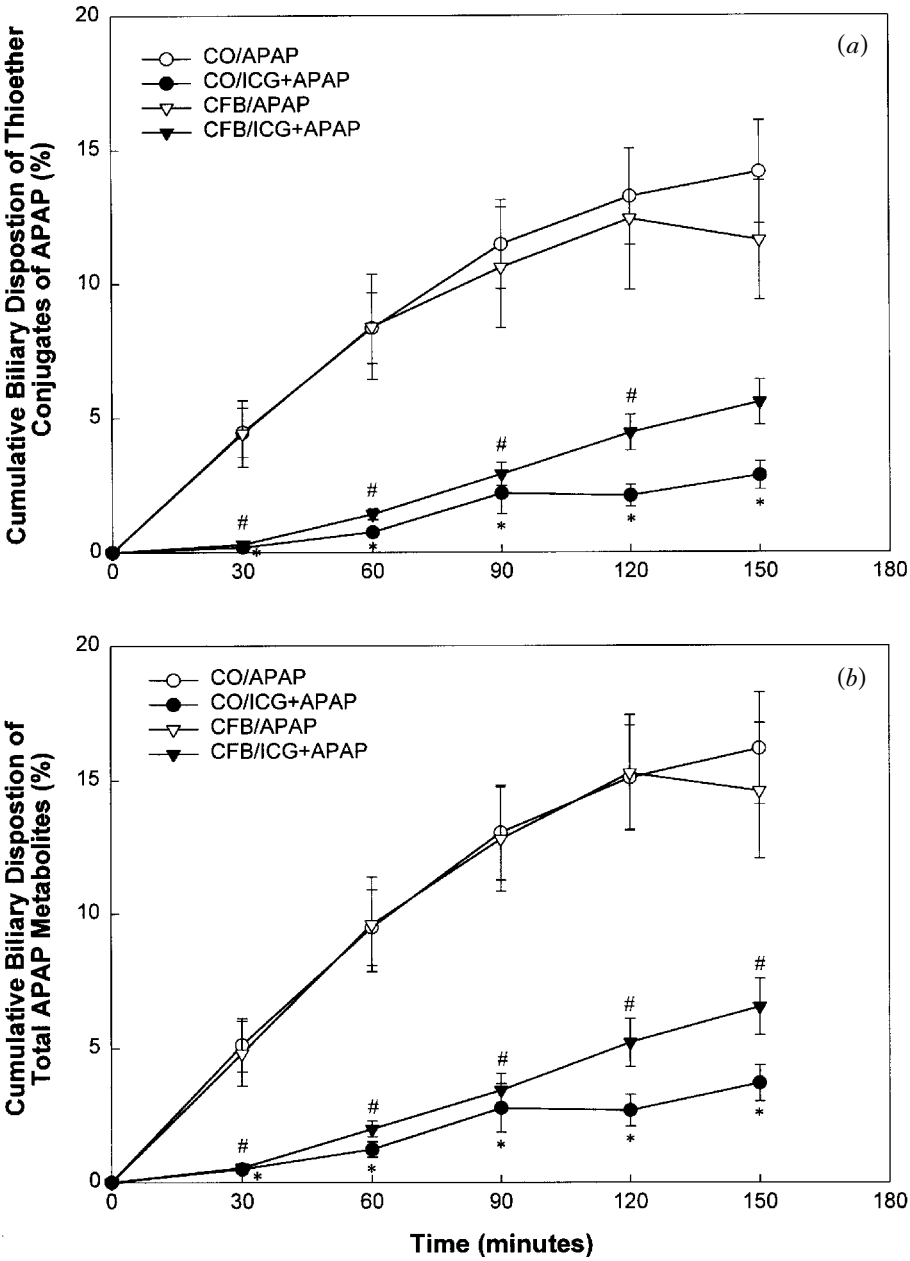


Figure 5. Effects of CFB pretreatment and the organic anion ICG on the cumulative biliary disposition of APAP thioether conjugates and total APAP metabolites. For details on treatment regimens and experimental procedures, see figure 1. The cumulative biliary disposition of APAP is expressed as the percentage of the given dose. (a) Cumulative biliary disposition of APAP thioether conjugates; (b) cumulative biliary disposition of total APAP metabolites. Results are the means ± SEM for three-to-six mice per treatment group. *Significantly different ($p < 0.05$) from corn oil-pretreated mice receiving APAP only; # significantly different ($p < 0.05$) from CFB-pretreated mice receiving APAP only.

did not change the biliary excretion rate of APAP-GSH. However, the excretion rate for this metabolite was significantly reduced by ICG in both corn oil- and CFB-pretreated mice at many time points examined.

Figure 4 shows the effects of CFB and ICG on the biliary concentration of other APAP conjugates detected in bile including APAP-GLU, APAP-SUL, APAP-NAC and APAP-CYS/CG. Similarly, CFB pretreatment did not affect the biliary concentration of APAP-GLU when compared with corn oil pretreated controls (figure 4a). In contrast, administration of ICG resulted in a significant decrease ($>50\%$) in APAP-GLU concentration at 30 min after APAP dosing in both groups of corn oil and CFB pretreated mice. At later time points, these values were similar to those seen in mice that did not receive ICG. This is consistent with the effects of ICG on biliary APAP-GSH excretion (figure 3a).

The biliary concentration of APAP-SUL in mice pretreated with CFB was apparently consistently higher than that seen in corn oil controls at all time points measured. However, this difference was only significant at 30 min after APAP dosing (figure 4b). In CFB pretreated mice receiving ICG before APAP, the biliary concentration of APAP-SUL was apparently lower, but not significantly different from mice receiving APAP only. In corn oil pretreated mice, ICG had no effect on the biliary concentration of APAP-SUL.

APAP-NAC concentration was undetectable in most 30 min bile samples from all treatment groups, but started to increase thereafter (figure 4c). Mice pretreated with CFB showed significantly higher biliary APAP-NAC concentrations at 60 min and later, whereas ICG produced a significant decrease in APAP-NAC concentrations only at 60 min after APAP.

APAP-CYS/CG was the least abundant set of APAP metabolites present in bile as indicated in figure 4d. The highest concentration of APAP-CYS/CG detected in bile was only 300 nmol/ml. Neither CFB pretreatment nor ICG produced any significant effect on the biliary concentration of APAP-CYS/CG.

Effect of CFB and ICG on cumulative biliary disposition of APAP thioether conjugates and total APAP metabolites

APAP-thioether conjugates include APAP-GSH, and its hydrolysis products: APAP-CYS/CG and APAP-NAC. As shown in figure 5, APAP-thioether conjugates accounted for approximately 90% of total APAP metabolites excreted in bile in all treatment groups. No significant differences in the cumulative biliary disposition of APAP thioether conjugates (figure 5a) nor total APAP metabolites (including the parent compound) (figure 5b), were detected between CFB and corn oil pretreated groups at any of the time points examined. However, administration of ICG before APAP considerably decreased the cumulative biliary disposition of APAP thioether conjugates (figure 5a) and total APAP metabolites (figure 5b). In mice dosed with APAP only, the cumulative biliary disposition of APAP and its metabolites within 150 min was 15–16% of the dose; whereas only 3–5% of the same dose was recovered in bile from all groups of mice receiving ICG before APAP.

Discussion

In addition to the large number of biochemical and morphological changes commonly associated with peroxisome proliferation, peroxisome proliferators are also known to reduce dramatically the toxicity that ensues following administration

of high doses of APAP (Nicholls-Grzemski *et al*. 1992, Manautou *et al*. 1994). Previous studies from our laboratory support the hypothesis that hepatoprotection by CFB involves an enhanced capacity to detoxify the reactive electrophile NAPQI by conjugation with GSH (Manautou *et al*. 1994). In agreement with this, we also reported that the concentration of APAP-GSH in bile collected by aspiration of gall bladder contents at 2 h after a hepatotoxic dose of APAP (700 mg/kg, p.o.) was significantly higher in CFB pretreated mice (Manautou *et al*. 1996). However, it should be noted that gallbladder concentrations of metabolites might not accurately reflect the rate at which APAP and its metabolites are excreted into bile. To investigate further the effect of CFB on the hepatobiliary output of APAP and its conjugated metabolites, mice were pretreated with corn oil or CFB for 10 days (Manautou *et al*. 1994). Following pretreatment, the common bile duct was cannulated, and bile was collected for 150 min after APAP challenge. Additional groups of corn oil or CFB pretreated, bile duct cannulated mice received the model organic anion ICG immediately before APAP dosing. Studies with ICG provide valuable information regarding the mechanism(s) by which APAP and its metabolites are secreted into bile.

Theoretically, any variation in APAP's bioactivation, detoxification or hepatobiliary transport capacity could contribute to potential differences in biliary excretion of APAP and its metabolites. However, it is unlikely that CFB pretreatment has any major effect on APAP bioactivation, since no differences in CYP450-mediated bioactivation of APAP were observed in previous *in vivo* and *in vitro* studies (Manautou *et al*. 1994, Manautou *et al*. 1996, Nguyen *et al*. 1999). Also, the rates of APAP-GSH formation in primary culture of hepatocytes prepared from the control and CFB pretreated mice were similar (Nicholls-Grzemski *et al*. 1996). In agreement with these findings, the present studies now demonstrate that dosing with CFB does not enhance the cumulative hepatobiliary disposition of APAP thioether conjugates, which are derived from the conjugation of the toxic electrophilic metabolite with GSH. Similarly, we have also reported that CFB does not affect the capacity of the liver to conjugate APAP with glucuronic acid or sulphate, which are the main detoxification pathways for APAP (Manautou *et al*. 1996). In the past, hepatoprotective treatment regimens that enhance hepatic glucuronide conjugation prevent the toxic effects of APAP by increasing substantially the formation and disposition of APAP-glucuronide conjugate (Madhu and Klaassen 1991, Davies and Schnell 1991, Liu *et al*. 1993). The lack of changes in biliary output of APAP-GLU due to CFB pretreatment in the current studies, along with previous observations from urinary metabolites studies (Manautou *et al*. 1996), further supports the absence of changes in hepatic APAP glucuronidation. Collectively, measuring the hepatobiliary disposition of APAP and its metabolites in bile duct cannulated mice provides additional information about the effects of CFB pretreatment on this route of disposition of APAP.

In contrast to previous observations (Manautou *et al*. 1996), the present work demonstrates that CFB does not affect the biliary excretion of APAP-GSH and the amount of total APAP metabolites excreted in bile. Additionally, our current results cannot explain the previous findings that CFB pretreatment enhances the elimination of APAP from plasma and liver at 2 and 6 h after challenge (Manautou *et al*. 1996). In the earlier studies, a higher dose of APAP was used. Therefore, it is possible that the observed effects of CFB pretreatment may be simply due to differences in pharmacokinetics associated with APAP toxicity.

Although CFB pretreatment does not change significantly the total amount of APAP and its metabolites excreted in bile, the concentrations of APAP-SUL and APAP-NAC in bile were significantly higher in mice receiving CFB. The reason for this change is unclear. It could be that CFB pretreatment induces the expression of canalicular transport proteins other than cMOAT with specificity towards the two conjugated metabolites of APAP, or that CFB enhances their formation. However, the contribution of these changes to the protective effect of CFB against APAP hepatotoxicity may be limited, since sulphation of APAP is a high affinity, low capacity detoxification pathway compared with glucuronidation (Hjelle and Klaassen 1984). Also, a less than one fold increase in APAP-SUL concentration in bile is unlikely to account for the dramatic reduction in toxicity seen with this CFB dosing regimen. Moreover, since CFB pretreatment does not increase the biliary output of APAP thioether conjugates, the increased excretion of APAP-NAC by itself does not indicate that CFB affects APAP bioactivation either. While the precise mechanism(s) for the hepatoprotection induced by CFB is not fully understood, the current bile duct cannulation studies now indicate that changes in biliary disposition of APAP are not involved, and that the mechanism for such resiliency resides elsewhere.

APAP-GLU, APAP-SUL, and APAP thioether conjugates are all organic compounds with negative charges. A prominent difference in terms of routes of elimination for those APAP metabolites is well documented (Wong *et al*. 1981, Gregus *et al*. 1988). In mice, ~ 50–80% of the initial APAP dose (1 mmol/kg, i.v.) appears in the urine and bile within 2–3 h after challenge, 50% of which is composed of metabolites generated from CYP450-mediated bioactivation pathway. APAP-GSH and its derived adducts make up to > 90% of the total APAP excreted into the bile, whereas APAP-GLU makes up ~ 75% of the total urinary excretion of APAP (Gregus *et al*. 1988). Little is known about the mechanisms underlying this difference except the observation that compounds with molecular weights less than 350 Dalton are predominantly excreted into urine, whereas those with larger molecular weights are preferentially transported into bile (Klaassen and Watkins 1984). One may speculate that the transport systems on the basolateral and canalicular sites responsible for the efflux of these organic anions might have quite different but overlapping substrate specificity.

To understand better the canalicular transport processes for APAP and its metabolites, additional groups of corn oil or CFB pretreated mice were given the model organic anion ICG immediately before APAP dosing. ICG is not biotransformed and is almost completely excreted into bile (Ott 1998). The biliary excretion of ICG is reduced to 75% of normal in the mutant TR^- rat lacking the ATP dependent transporter for organic anions cMoat/mrp2 (Jansen *et al*. 1993). Sathirakul *et al*. (1994) reported that the primary transport system for ICG is distinct from that for leukotriene C4, the highest affinity substrate for cMOAT. Taken together, these observations indicate that in addition to cMOAT, other organic anion transport processes are responsible for the biliary excretion of ICG. In the present study, the biliary concentrations of APAP-GSH and APAP-GLU were substantially decreased at 30 min following ICG injection, whereas those of APAP itself and APAP-SUL were not affected by ICG. In addition, the biliary concentration of APAP-NAC was significantly decreased at 60 min after ICG treatment.

The concentration of APAP itself in bile has been postulated to reflect APAP

concentration in the liver (Gregus and Klaassen 1982). If this assumption is true, the present results support the notion that APAP diffuses passively across the canalicular membrane instead of through a transport mechanism. Therefore, the fact that ICG also significantly decreased the biliary excretion rate of APAP itself without any effect on the biliary concentration can only be attributed to the reduction in bile flow produced by ICG. In summary, these results suggest that APAP conjugates, such as APAP-GSH, APAP-GLU and APAP-NAC may compete with ICG for biliary excretion. Additional studies employing other model organic anions that do not produce cholestasis, and the use of mutant rats lacking cMoat/mrp2 should further clarify the role of biliary transport processes involved in the excretion of APAP and its metabolites.

In conclusion, the present work demonstrated that CFB pretreatment does not enhance the biliary disposition of APAP, and that ICG significantly decreases the biliary excretion of APAP-GSH, as well as APAP-GLU and APAP-NAC, suggesting that these APAP metabolites share the same canalicular transport process for ICG.

Acknowledgements

The paper was presented in part at the 38th annual meeting of the Society of Toxicology in March 1999, New Orleans, LA, and was supported by a grant from AstraZeneca Pharmaceuticals and Boehringer Ingelheim Pharmaceutical, Inc. Predoctoral Fellowship in Toxicology to Chuan Chen.

References

Boyer, T. D. and Rouff, S. L., 1971, Acetaminophen-induced hepatic necrosis and renal failure. *Journal of the American Medical Association*, **218**, 440–441.

Buchler, M., Konig, J., Brom, M., Kartenbeck, J., Spring, H., Horie, T. and Keppler, D., 1996, cDNA cloning of the hepatocyte canalicular isoform of the multidrug resistance protein, cMRP, reveals a novel conjugate export pump deficient in hyperbilirubinemic mutant rats. *Journal of Biological Chemistry*, **271**, 15091–15098.

Chianale, J., Vollrath, V., Wielandt, A. M., Amigo, L., Rigotti, A., Nervi, F., Gonzalez, S., Andrade, L., Pizarro, M. and Accatino, L., 1996, Fibrates induce mdr2 gene expression and biliary phospholipid secretion in the mouse. *Biochemical Journal*, **314**, 781–786.

Croop, J. M., Raymond, M., Harber, D., Devault, A., Areci, R. J., Gros, P. and Housman, D. E., 1989, The three mouse multidrug resistance (mdr) genes are expressed in a tissue-specific manner in normal mouse tissue. *Molecular and Cellular Biology*, **9**, 1346–1350.

Davidson, D. G. and Eastham, W. N., 1966, Acute liver necrosis following overdose of paracetamol. *British Medical Journal*, **2**, 497–499.

Davies, M. H. and Schnell, R. C., 1991, Oltipraz-induced amelioration of acetaminophen hepatotoxicity in hamsters. II. Competitive shunt in metabolism via glucuronidation. *Toxicology and Applied Pharmacology*, **109**, 29–40.

Gottesman, M. M. and Pastan, I., 1993, Biochemistry of multidrug resistance mediated by the multidrug transporter. *Annual Review of Biochemistry*, **63**, 385–427.

Gregus, Z. and Klaassen, C. D., 1982, Comparison of biliary excretion of organic anions in mice and rats. *Toxicology and Applied Pharmacology*, **63**, 13–20.

Gregus, Z., Madhu, C. and Klaassen, C. D., 1988, Species variation in toxification and detoxification of acetaminophen *in vivo*: a comparative study of biliary and urinary excretion of acetaminophen metabolites. *Journal of Pharmacology and Experimental Therapeutics*, **244**, 91–99.

Harman, A. W. and Self, G., 1986, Comparison of the protective effects of N-acetylcysteine, 2-mercaptopropionylglycine and dithiothreitol against acetaminophen toxicity in mouse hepatocytes. *Toxicology*, **41**, 83-93.

Hazelton, G. A., Hjelle, J. J. and Klaassen, C. D., 1986, Effects of butylated hydroxyanisole on acetaminophen hepatotoxicity and glucuronidation *in vivo*. *Toxicology and Applied Pharmacology*, **83**, 474–485.

Hjelle, J. J. and Klaassen, C. D., 1984, Glucuronidation and biliary excretion of acetaminophen in rats. *Journal of Pharmacology and Experimental Therapeutics*, **228**, 407–413.

Howie, D., Adriaenssens, P. I. and Prescott, L. F., 1977, Paracetamol metabolism following overdosage: application of high performance liquid chromatography. *Journal of Pharmacy and Pharmacology*, **29**, 235–237.

Jansen, P. L. M., van Klinken, J., van Gekder, M., Ottenhoff, R. and Oude Elferink, R. P. J., 1993, Preserved organic anion transport in mutant TR$^-$ rats with a hepatobiliary secretion defect. *American Journal of Physiology*, **265**, G445–G452.

Keppler, D., Leier, I., Jedlitschky, G. and Konig, J., 1998, ATP-dependent transport of glutathione *S*-conjugates by the multidrug resistance protein MRP1 and its apical isoform MRP2. *Chemico-Biological Interactions*, **111**, 153–161.

Klaassen, C. D. and Watkins, J. B., 1984, Mechanisms of bile formation, hepatic uptake and biliary excretion. *Pharmacological Reviews*, **36**, 1–67.

Liu, J., Liu, Y. P., Madhu, C. and Klaassen, C. D., 1993, Protective effects of oleanolic acid on acetaminophen-induced hepatotoxicity in mice. *Journal of Pharmacology and Experimental Therapeutics*, **266**, 1607–1613.

Madhu, C. and Klaassen, C. D., 1991, Protective effect of pregnenolone-16-alpha-carbonitrile on acetaminophen-induced hepatotoxicity in hamsters. *Toxicology and Applied Pharmacology*, **109**, 305–313.

Manautou, J. E., Hoivik, D. J., Tveit, A., Hart, S. G., Khairallah, E. A. and Cohen, S. D., 1994, Clofibrate pretreatment diminishes acetaminophen's selective covalent binding and hepatotoxicity. *Toxicology and Applied Pharmacology*, **129**, 252–263.

Manautou, J. E., Tveit, A., Hoivik, D. J., Khairallah, E. and Cohen, S. D., 1996, Protection by clofibrate against acetaminophen hepatotoxicity in male CD-1 mice is associated with an early increase in biliary concentration of acetaminophen-glutathione adducts. *Toxicology and Applied Pharmacology*, **140**, 30–38.

McClain, C. J., Kromhout, J. P., Peterson, F. J. and Holtzman, J. L., 1980, Potentiation of acetaminophen hepatotoxicity by alcohol. *Journal of the American Medical Association*, **244**, 251–253.

Mitchell, J. R., Jollow, D. J., Potter, W. Z., Davis, D. C., Gillette, J. R. and Brodie, B. B., 1973b, Acetaminophen-induced hepatic necrosis. I. Role of drug metabolism. *Journal of Pharmacology and Experimental Therapeutics*, **187**, 185–194.

Mitchell, J. R., Jollow, D. J., Potter, W. Z., Gillette, J. R. and Brodie, B. B., 1973a, Acetaminophen-induced hepatic necrosis. IV. Protective role of glutathione. *Journal of Pharmacology and Experimental Therapeutics*, **187**, 211–217.

Muller, M. and Jansen, P., 1997, Molecular aspects of hepatobiliary transport. *American Journal of Physiology*, **272**, G1285-G130.

Nguyen, K. A., Carbone, J. M., Silva, V. M., Chen, C., Hennig, G. E., Whiteley, H. E. and Manautou, J. E., 1999, The PPAR activator docosahexaenoic acid prevents acetaminophen hepatotoxicity in male CD-1 mice. *Journal of Toxicology and Environmental Health*, **58**, 171–186.

Nicholls-Grzemski, F. A., Burcham, P. C., Calder, I. C. and Priestly, B. G., 1996, Pretreatment with peroxisome proliferators protects mice against some but not all hepatotoxins. *Annals of the New York Academy of Sciences*, **804**, 742–744.

Nicholls-Grzemski, F. A., Calder, I. C. and Priestly, B. G., 1992, Peroxisome proliferators protect against paracetamol hepatotoxicity in mice. *Biochemical Pharmacology*, **43**, 1395–1396.

Ott, P., 1998, Hepatic elimination of indocyanine green with special reference to distribution kinetics and the influence of plasma protein binding. *Pharmacology and Toxicology*, **82**, 1–48.

Paulusma, C. C., Bosma, P. J., Zaman, G. J. R., Bakker, C. T. M., Otter, M., Scheffer, G. L., Scheper, R. J., Borst, P. and Oude Elferink, R. P. J., 1996, Congenital jaundice in rats with a mutation in a multidrug resistance-associated protein gene. *Science*, **271**, 1126–1128.

Placke, M. E., Ginsberg, G. L., Wyand, D. S. and Cohen, S. D., 1987, Ultrastructural changes during acute acetaminophen-induced hepatotoxicity in the mouse: a time and dose study. *Toxicologic Pathology*, **15**, 431–438.

Reddy, J. K. and Lalwani, N. D., 1983, Carcinogenesis by hepatic peroxisome proliferators: evaluation of the risk of hypolipidemic drugs and industrial plasticizers to humans. *Critical Review in Toxicology*, **12**, 1–58.

Sathirakul, K., Suzuki, H., Yamada, T., Hanano, M. and Sugiyama, Y., 1994, Multiple transport systems for organic anions across the bile canalicular membrane. *Journal of Pharmacology and Experimental Therapeutics*, **268**, 65–73.

Strubelt, O., Siegers, C. P. and Schutt, A., 1974, The curative effects of cysteamine, cysteine, and dithiocarb in experimental paracetamol poisoning. *Archives of Toxicology*, **33**, 55–64.

Wielandt, A. M., Vollrath, V., Manzano, M., Miranda, S., Accatino, L. and Chianale, J., 1999, Induction of the multispecific organic anion transporter (cMOAT/mrp2) gene and biliary glutathione secretion by the herbicide 2,4,5-trichlorophenoxyacetic acid in the mouse liver. *Biochemical Journal*, **341**, 105–111.

Wong, L. T., Whitehouse, L. W., Solomonraj, G. and Paul, C. J., 1981, Pathways of disposition of acetaminophen conjugates in the mouse. *Toxicology Letters*, **9**, 145–151.

XENOBIOTICA, 2000, VOL. 30, NO. 11, 1033–1045

In vitro identification of the cytochrome P450 isoform responsible for the metabolism of α-dihydroergocryptine

M. ALTHAUS†*, A. RETZOW†, J. V. CASTELL‡, M.-J. GÓMEZ-LECHÓN‡, Z. AMALOU§, T. ROSE§ and K. APPEL§

† Desitin Arzneimittel GmbH, Weg beim Jäger 214, D-22335 Hamburg, Germany
‡ Unidad de Hepatologia Experimental, Centro de Investigacion, Hospital Universitario La Fe, E-46009 Valencia, Spain
§ Pharmbiodyn GmbH, Ferdinand-Porsche-Straße 5, D-79211 Denzlingen, Germany

Received 2 June 2000

1. The *in vitro* metabolism of α-dihydroergocryptine (DHEC, Almirid®), an ergot-derived dopamine agonist for the treatment of Parkinson's disease, has been studied in cultured cell lines following incubation with DHEC. Human hepatocytes as well as two sets of metabolically competent cell lines expressing one single human cytochrome P450 (1A1, 1A2, 1B1, 2A6, 2C8, 2C9, 2C18, 2C19, 2D6, 2E1, 3A4) were used.

2. Mono- and dihydroxy metabolites of DHEC could only be detected in the culture media of the cell line expressing human cytochrome CYP3A4. The same metabolites were found in the media of cultured human hepatocytes derived from three different donors. After 24-h incubation with 1 μM DHEC, ~ 60% mono- and ~ 20% dihydroxy metabolites were detected, i.e. ~ 80% of DHEC was metabolized. Further, DHEC demonstrated an inhibitory effect on CYP3A4-mediated testosterone metabolism and additionally could induce CYP3A4 and CYP2E1 mRNA when added at 10 μM to cultured human hepatocytes.

3. The data suggest that DHEC metabolism in humans is primarily mediated by the CYP3A4 isoform. The results are in accordance with findings derived from other ergot alkaloids.

Introduction

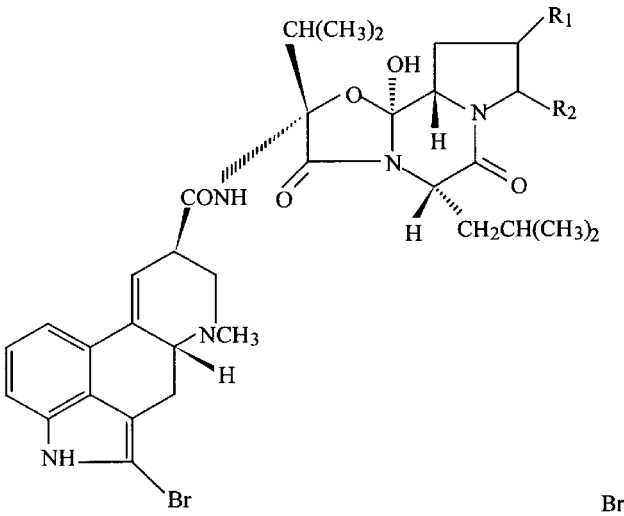
α-Dihydroergocryptine (DHEC), a dopamine agonist, is a hydrogenated derivative of the ergoline compound ergocryptine. It has agonistic effects at the D_2-receptor and partially at the D_1-receptor (Markstein 1983). The methansulphonate salt of α-dihydroergocryptine has been approved for the treatment of Parkinson's disease (Battistin *et al*. 1999, Bergamasco *et al*. 2000) in several European countries.

As for other ergot alkaloids, DHEC undergoes extensive first-pass metabolism in the liver where two of the metabolites amount to 80–90% of the total dose administered (Ronca *et al*. 1996, Mas-Chamberlin *et al*. 1997). The molecule differs from bromocriptine, another dopamine agonist, by the saturation of the Δ^{9-10} double bond (Peyronneau *et al*. 1994). Although the metabolism of DHEC has not been investigated in detail so far, the structural similarity with bromocriptine (figure 1) suggests that major biotransformation occurs by oxidation of the pyrrolidine moiety (Maurer *et al*. 1982). This also represents the principal pathway for β-dihydroergocryptine (Maurer 1977) and dihydroergotamine (Maurer and Frick 1984).

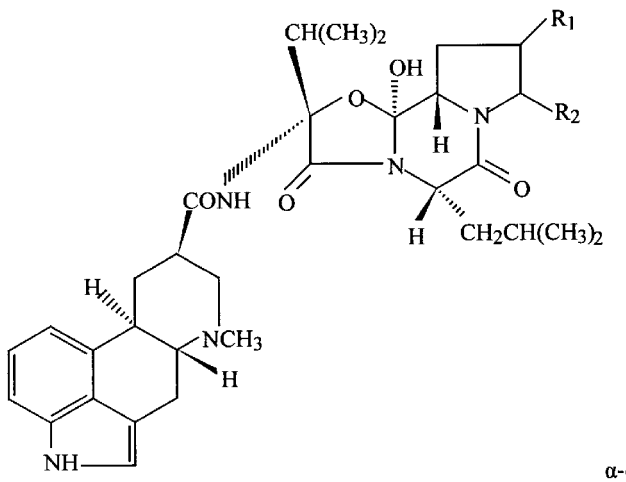
Published data from related compounds suggest that the cytochrome P450 system is responsible for the oxidation of DHEC in the liver (Delaforge *et al*. 1989).

* Author for correspondence; e-mail: althaus@desitin.de

Xenobiotica ISSN 0049-8254 print/ISSN 1366-5928 online © 2000 Taylor & Francis Ltd
http://www.tandf.co.uk/journals DOI: 10.1080/00498250010002261



Bromocriptine



α-dihydroergocryptine

Figure 1. Chemical structure of bromocriptine, α-dihydroergocryptine and their metabolites: monohydroxy metabolites: R_1 = OH, R_2 = H; dihydroxy metabolites: R_1 = OH, R_2 = OH.

This enzyme family comprises isoforms with different substrate specificities (Lewis *et al.* 1999). Accordingly, it is not surprising that they catalyse the metabolism of a vast number of drugs (Correia 1998, Murray 1999). The assignment of a drug's metabolic pathway to one or more cytochrome P450 isoforms is thus one prerequisite for the prediction of possible drug interactions.

CYP3A4 has been demonstrated to metabolize bromocriptine and other structurally similar ergot derivatives (Ball *et al.* 1992, Peyronneau *et al.* 1994, Rauschenbach *et al.* 1995). In addition, bromocriptine is a potent inhibitor of CYP3A4 (Winalda and Wienkers 1997). Studies with [^{3}H]dihydroergocryptine in human and rat liver cells have shown that the metabolites are excreted without further glucuroconjugation or sulphoconjugation (Mas-Chamberlin 1997).

Therefore, the present investigation focuses on the possible role of CYP3A4 in the metabolism of DHEC, but the contribution of other isoforms was also examined.

The study in hand specifically addresses the quantification of DHEC and its mono- and dihydroxy metabolites in the culture medium of different cell lines. A liquid chromatography/mass spectrometry (LC-MS) method was developed for this purpose and the metabolites were further characterized by LC-MS/MS. A battery of cell lines each expressing one specific human cytochrome P450 isoform (Doehmer 1993, Pfeifer 1995) as well as cultured human hepatocytes was investigated. In addition, the inhibitory effect of DHEC at CYP3A4 was examined. Furthermore, a possible induction of CYP isoforms by DHEC was assessed in cultured human hepatocytes using a quantitative reverse transcription polymerase chain reaction (RT-PCR) assay (Rodriguez-Antona 2000).

Materials and methods

Materials

α-Dihydroergocryptine mesylate (purity 99%) was from Desitin Arzneimittel GmbH (Hamburg, Germany). Testosterone, 6β-hydroxytestosterone and corticosterone were from Sigma, Deisenhofen, Germany. Further supply sources were DMEM (Cell Concepts, Umkirch, Germany), Ham's F-12 and Lebovitz F-15 (Gibco, Karlsruhe, Germany), foetal bovine serum (Eurobio, Schwerte, Germany), Rneasy Total RNA Kit (Quiagen, Hilden, Germany), High pure PCR purification kit (Roche Diagnostics, Mannheim, Germany), Picogreen and Ribogreen (Molecular Probes, Göttingen, Germany), and Oligonucleotide primers and Dnase I (Gibco, Karlsruhe, Germany). All chemicals used for HPLC were from Merck, Darmstadt, Germany, HPLC grade.

CYP-engineered cell lines

Chinese hamster V79 cell lines were genetically manipulated to express specific CYP genes (Doehmer 1993). Cell lines expressing CYP1A1, CYP1A2, CYP1B1, CYP2A6, CYP2D6 and CYP3A4 were cultured in six-well dishes containing Dulbecco's modified Eagle medium (DMEM) supplemented with 10% FBS, penicillin (100 $U.ml^{-1}$), streptomycin (100 $\mu g.ml^{-1}$) and 1 mM L-glutamine. The cultures were incubated at 37 °C, 5% CO_2 and 90% saturated atmospheric humidity.

Immortalized human liver epithelial cells (THLE) were genetically manipulated to express specific CYP genes. Cell lines expressing CYP2C8, CYP2C9, CYP2C18, CYP2C19 and CYP2E1 were cultured on fibronectin/collagen coated flasks in serum free medium, as described (Pfeifer 1993, 1995, Macé 1997, Bort 1999). Cells were incubated with DHEC (10 μM) and samples of the culture media were withdrawn at 4 and 24 h. All cell lines, V79 as well as THLE, also expressed NADPH-reductase activity.

Preparation and culture of human hepatocytes

Human hepatocytes were obtained from surgical liver biopsies (2–4 g) of patients undergoing cholecystectomy, after having taken informed consent. Donors were: HB-386, male, 77 years; HB-387, female, 78 years; and HB-388, female, 59 years. Cells were isolated by microperfusion of the tissue sample with collagenase, as described by Gómez-Lechón (1990). Cellular viability was assessed by the trypan blue dye exclusion test and was usually 85–90%. Hepatocytes were seeded on fibronectin-coated (3.5 $\mu g.cm^{-2}$) plastic dishes (60 mm diameter) at 8×10^4 viable cells cm^{-2} and cultured in Ham's F-12/Lebovitz L-15 (1:1) medium supplemented with 2% new-born calf serum, 50 $U.ml^{-1}$ penicillin, 50 $\mu g.ml^{-1}$ streptomycin, 0.2% BSA and 10^{-8} M insulin. The medium was changed after 1 h, and after 24 h the cells were shifted to serum-free hormone-supplemented medium (10^{-8} M dexamethasone, 10^{-8} M insulin). Four hours after the culture medium change, human hepatocytes were exposed to DHEC (10, 50, 100 μM) for 8 and 24 h (metabolic study) or 48 h (induction study) respectively.

LC-MS/MS

A LC-MS/MS assay was developed to detect DHEC and its mono- and dihydroxy metabolites. The samples were injected with an autosampler, which was coupled to an extra pump for the extraction mobile phase (50 mM ammonium bicarbonate/2-propanol (v/v 96/4), flow: 0.5 $ml.min^{-1}$). After extraction, extraction column valve switches and the sample, extracted on a Bio Trap 500, were flushed back onto the analytical column by the analytical mobile phase (A: 50 mM formic acid, 1 mM ammonium acetate/acetonitrile (v/v 90/10); B: acetonitrile, flow: 0.5 $ml.min^{-1}$). The analytes were identified by a

chromatographic run employing the automated MS/MS data acquisition technique of the mass spectrometer (LCQ Finnigan MAT). The LCQ was set-up to perform data on the unmetabolized DHEC (m/z = 577.7–578.7, used as reference for the tuning of the LCQ MS detector in the ESI/MS mode) and the mono- (m/z = 593.7–594.7) or dihydroxy metabolites (m/z = 609.7–610.7).

Inhibition studies

The V79h3A4/hOR cell line expressing human cytochrome P4503A4 and human NADPH cytochrome P450 reductase were incubated with testosterone (250 μM) and the indicated concentration of ketoconazole (positive control) and DHEC. Samples of the culture media were withdrawn at 6 and 24 h. After incubation, the supernatants were collected and kept at −20 °C until analysis. Samples were analysed by HPLC as described below.

HPLC analysis of 6β-hydroxytestosterone

Incubation medium (2 ml) was taken with 10 μl corticosterone (1 mg.ml^{-1}) as internal standard and loaded on Isolute C18 (ICT). After solid-phase extraction the samples were concentrated using the TurboVap LV Evaporator (Zymark). Samples were analysed by HPLC using a reverse-phase, 250 mm/4 μM column. The mobile phase (A: methanol 20% (v/v), tetrahydrofuran 7% (v/v), water 73%; B: methanol 93% (v/v), tetrahydrofuran 7% (v/v)) was delivered at 0.5 ml.min^{-1}. The column effluent was monitored at 254 nm (Platt *et al*. 1989).

Induction studies

Total RNA of human hepatocytes was extracted from 6-cm diameter culture plates using 'Rneasy Total RNA Kits'. The amount of purified RNA was estimated by ribogreen fluorescence and its purity by the absorbance ratio 260/280 nm (> 2.5). RNA was incubated for 15 min at 23 °C with DNase I (1 unit μg^{-1}), followed by thermal inactivation of the enzyme (65 °C for 10 min). A quantitative RT-PCR assay was performed to measure the mRNA content of the major human CYPs (1A1, 1A2, 2A6, 2B6, 2C9, 2C19, 2D6, 2E1, 3A4, 3A5). The PCR primers (for oligonucleotide sequences, see Rodriguez-Antona 2000) were selected specifically to match each CYP mRNA, to have a very close annealing temperature and to render PCR products of similar sizes. The PCR conditions were designed to allow the simultaneous measurement of the various human liver CYPs in a single run (Rodriguez-Antona 2000). Measurements were done in triplicate. Assays were normalized versus β-actin mRNA content and expressed as fold increase over control, i.e. non-treated cells. As positive controls, methylcholantrene (1 μM), phenobarbital (1 mM) and rifampicin (50 μM) were added.

Results

Incubation of cell lines with stable expression of single human CYP isoforms with DHEC

After 4 and 24 h of incubation with 10 μM DHEC, significant amounts of mono- and dihydroxy metabolites were detectable in the culture medium of the V79 cell line expressing human CYP3A4 (V79h3A4) (tables 1 and 2). Incubation of this cell line with 1 μM DHEC showed comparable results (table 3). After 24 h, > 50% of DHEC was metabolized, mainly into monohydroxy metabolites. The average ratio between mono- and dihydroxy metabolites was 6:1. At concentrations of 100 μM, however, no significant metabolism was detectable (table 3), reflecting a toxic concentration to this cell line, as assessed by the trypan blue test. The mono- and dihydroxy metabolites of DHEC were determined using LC-MS analysis (figure 2) and the metabolites were further characterized by means of the LC-MS/MS method. In all other cell lines, unchanged DHEC accounted for > 97% of the total dose after 4 and 24 h of incubation, indicating the absence of any relevant metabolism. The same is true for the experiments with the V79 and THLE control cell lines not expressing any human CYP. The existence of the low amounts of metabolites found in controls (media only) could not be confirmed by an additional LC-MS/MS.

Table 1. DHEC and metabolite content in the culture media of different V79 cell strains after incubation with DHEC.

V79 cell line CYP expressed	Incubation time (h)	DHEC (% of total)	Monohydroxy metabolites (% of total)	Dihydroxy metabolites (% of total)
1A1	4	99.8	0.0	0.2
1A1	24	99.8	0.1	0.2
1A2	4	100.0	0.0	0.0
1A2	24	99.2	0.2	0.6
1B1	4	99.8	0.0	0.1
1B1	24	99.3	0.1	0.7
2A6	4	99.4	0.4	0.2
2A6	24	99.5	0.4	0.1
2D6	4	99.7	0.2	0.1
2D6	24	99.4	0.4	0.2
3A4	4	93.1	5.9	1.1
3A4	24	42.9	48.6	8.5
V79 control	4	99.8	0.1	0.1
V79 control	24	99.4	0.3	0.3

CYP-expressing V79 cells were incubated with 10 μM DHEC for 4 and 24 h respectively. The samples were stored at −20 °C until analysis by LC-MS. The percentage of DHEC and metabolites was calculated from the peak areas. Data are means of two independent incubations.

Table 2. DHEC and metabolite content in the culture media of different THLE cell strains after incubation with DHEC.

THLE Cell line CYP expressed	Incubation time (h)	DHEC (% of total)	Monohydroxy metabolites (% of total)	Dihydroxy metabolites (% of total)
2C8	4	99.5	0.4	0.1
2C8	24	98.4	1.2	0.5
2C9	4	97.7	1.6	0.7
2C9	24	97.7	1.5	0.8
2C18	4	99.3	0.7	0.0
2C18	24	98.4	1.6	0.0
2C19	4	98.2	1.3	0.5
2C19	24	97.4	2.3	0.4
2E1	4	98.5	1.0	0.5
2E1	24	97.4	2.1	0.6
Control	4	98.0	0.8	0.4
Control	24	98.5	1.4	0.3

CYP-expressing THLE cells were incubated with 10 μM DHEC for 4 and 24 h, respectively. The samples were stored at −20 °C until analysis by LC-MS. The existence of the low amounts of metabolites found in controls (media only) could not be confirmed by an additional LC-MS/MS. Data are means of two independent incubations.

Effect of DHEC on the CYP3A4 enzyme activity

Ketoconazole is a well-known inhibitor of the CYP3A4 (Eagling *et al*. 1998) isoform and CYP3A4 activity was quantified by the determination of testosterone 6β-hydroxylase activity. In V79h3A4/hOR cells, ketoconazole at concentrations of 1 μM or more significantly decreased the 6β-hydroxy testosterone concentration in the culture medium (49% inhibition at 1 μM; 90% inhibition at 10 μM after 6-h incubation). Results of 24-h incubation were comparable (data not shown).

Incubation of V79h3A4/hOR cells with DHEC showed a concentration-dependent inhibition of testosterone 6β-hydroxylase activity (figure 3). Inhibition was initially observed at a concentration of 1 μM and increased dose-dependently:

Table 3. DHEC and metabolite content in the culture media of the cell V79h3A4 strain after incubation with different concentrations of DHEC.

DHEC concentration (μM)	Incubation time (h)	DHEC (% of total)	Monohydroxy metabolites (% of total)	Dihydroxy metabolites (% of total)
1	4	76.8	21.1	2.1
1	24	52.2	41.7	6.1
10	4	93.1	5.9	1.0
10	24	42.9	48.6	8.5
100	4	98.5	0.7	0.8
100	24	98.3	1.1	0.6

CYP3A4-expressing V79 cells were incubated with increasing concentrations of DHEC for 4 and 24 hours, respectively. The samples were stored at −20 °C until analysis by LC-MS. The identity of the metabolites was confined by an additional LC-MS/MS. Data are means of two independent incubations.

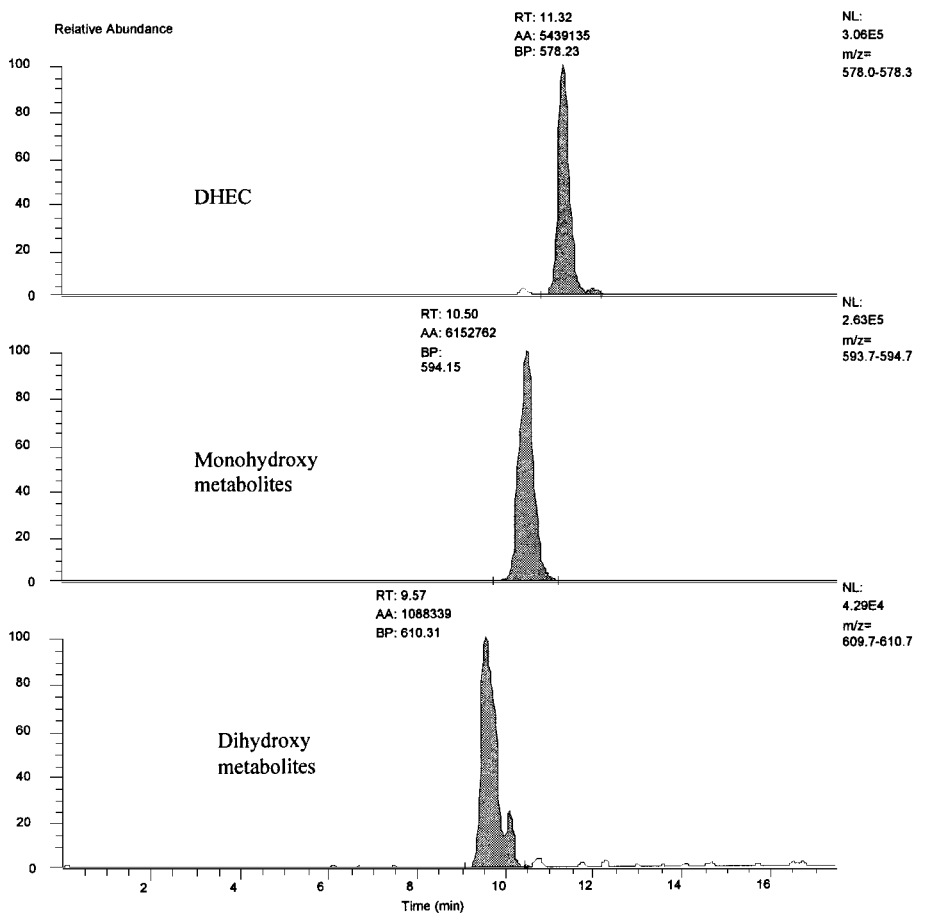


Figure 2. LC-MS detection of DHEC and its metabolites in the media of V79h3A4 cells. V79h3A4 cells were incubated with 10 μM DHEC for 24 h. Samples were stored at −20 °C until analysis. Further characterization of the metabolites was obtained by additional LC-MS/MS.

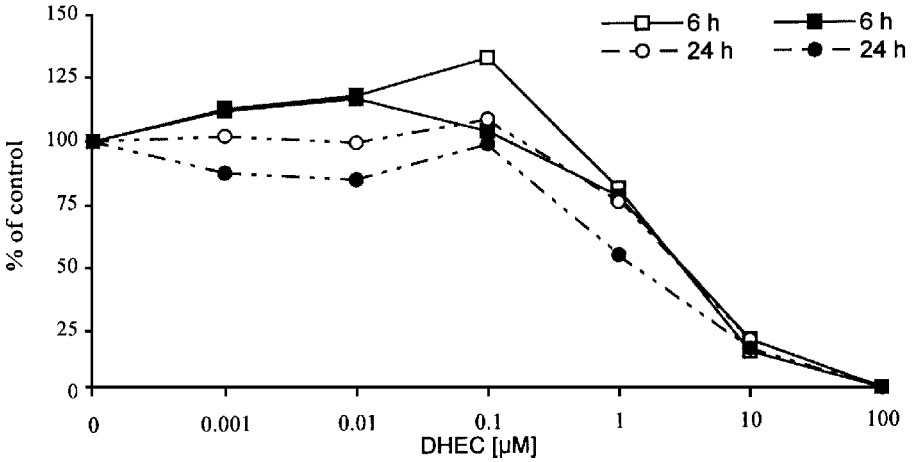


Figure 3. Inhibition of testosterone-6β-hydroxylation in the V793A4/hOR cell line by increasing concentrations of DHEC. V79h3A4/hOR cells were incubated in presence of the substrate, testosterone (250 μM), and in absence (control) or presence of α-dihydroergocryptine (0.001–100 μM) for 6 and 24 h respectively. Control activities were 5.34 and 5.75 pmol.min^{-1} 10^6 cells (6 h) and 3.00 and 3.55 pmol.min^{-1} 10^6 cells (24 h). Semilogarithmic plot. Four independent incubations are shown.

Table 4. Relative amount of DHEC and metabolites in the culture media of hepatocytes derived from different donors.

Cell preparation	DHEC concentration (μM)	DHEC (% of total)	Monohydroxy metabolites (% of total)	Dihydroxy metabolites (% of total)
BH388	1	22.7	49.4	27.9
Control	1	100	0	0
BH387	1	25.8	66.5	7.7
Control	1	100	0	0
BH388	10	30.5	62.4	7.2
Control	10	98.9	1.0	0.1
BH387	10	73.8	24.8	1.5
Control	10	98.7	1.3	0
BH388	50	69.7	27.5	2.8
Control	50	99.5	0.6	0
BH387	50	93.9	5.7	0.4
Control	50	99.5	0.5	0
BH386	50	45.4	49.1	5.5
Control	50	99.3	0.6	0.1

Human hepatocytes were obtained from three different donors and incubated with different concentrations of DHEC for 24 h. The samples were stored at −20 °C until analysis with LC-MS. The identity of the metabolites was confirmed by additional LC-MS/MS. Control is incubation with medium only. Data are means of two independent incubations.

~30% inhibition after incubation with 1 μM DHEC, ~80% inhibition at a concentration of 10 μM and complete inhibition at 100 μM. No differences were found between 6 and 24 h of incubation.

Incubation of human hepatocytes with DHEC

Hepatocytes were obtained from three different human donors and incubated with various concentrations of DHEC. In the presence of 1 μM DHEC, 80% of the substrate was metabolized after 24 h and ~60% monohydroxy and ~20%

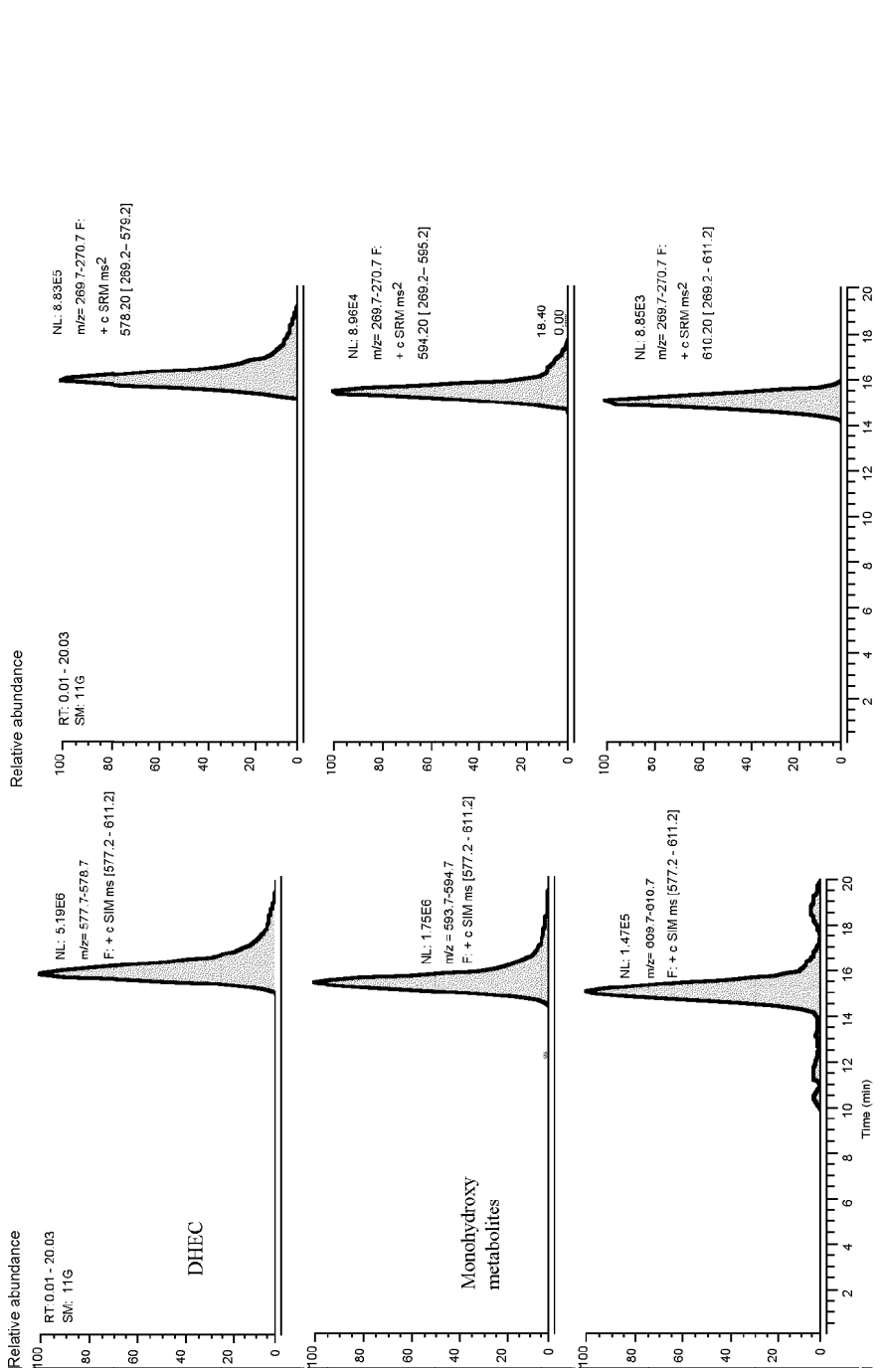


Figure 4. Detection of DHEC and its metabolites in the media of cultured human hepatocytes by LC-MS and LC-MS/MS. Human hepatocytes were incubated with 50 μM DHEC for 8 h. DHEC, monohydroxy and dihydroxy metabolites were detected (left). The identity of the peaks was confirmed by LC-MS/MS (right). A relative collision energy of 20% was applied on the molecules, which resulted in the fragment at m/z = 270.2 (α-dihydrolysergic acid).

Table 5. Relative increase in CYP mRNA in cultured human hepatocytes after incubation with DHEC and three standard enzyme inducers.

Hepatocytes	Substrate	Concentration (μM)	Incubation (h)	CYP mRNA (times induction compared with control) 1A1	1A2	2A6	2B6	2C9	2C19	2D6	2E1	3A4	3A5
HB386	DHEC	50	24	2.3 ±1.4	2.0 ±0.5	0.2 ±0.2	3.6 ±0.7	3.3 ±0.5	2.7 ±0.2	1.5 ±0.3	3.5 ±0.4	4.3 ±1.2	2.4 ±1.1
HB388	DHEC	10	48	2.4 ±0.1	2.1 ±0.0	1.6 ±0.2	1.5 ±0.1	0.7 ±0.5	2.5 ±0.8	2.2 ±0.2	3.5 ±1.0	3.5 ±0.5	1.8 ±0.3

Human hepatocytes derived from two different donors were incubated with DHEC for 24 h (50 μM) or 48 h (10 μM). Total RNA was extracted and purified. cDNA was prepared by reverse transcription. Selective amplification of each CYP cDNA was achieved by PCR and its content was finally determined by fluorescence. For positive control, cells were incubated with methylcholantrene (MC), phenobarbital (PB) and rifampicin (RIF). Means of triplicate determination ± SD are shown.

dihydroxy metabolites were detected (table 4). Metabolites were characterized by an additional LC-MS/MS analysis (figure 4). Incubation for 8 h led to similar results (data not shown). Further increases in DHEC concentration in the culture medium considerably enhanced the variability between the different cell preparations. Cells derived from donor BH388 gave comparable results with incubation of either 1 or 10 μM, irrespective of the incubation time. Only at 50 μM did the relative amount of metabolites detected in the medium markedly decline.

In contrast, cells derived from donor BH387 already showed lower relative amounts of metabolites at 10 μM DHEC concentration (table 4). A concentration of 100 μM was toxic to all cell preparations. Viability of hepatocytes as measured by the trypan blue and MTT tests were 100% of control after 24-h incubation with 1 and 10 μM DHEC respectively, but declined to 5% when incubated with 100 μM DHEC.

Quantitative RT-PCR measurement of human cytochrome P450 mRNA

Incubation with three well-described CYP inducers, i.e. methylcholanthrene, rifampicin and phenobarbital produced, as expected, an increase in mRNA for the specific CYP isoforms and demonstrates the metabolic integrity of the hepatocyte preparations. The cells were further incubated with 10, 50 and 100 μM DHEC for 48 h (HB388) and in an additional experiment with 50 μM DHEC for 24 h (HB386). After 48-h incubation, RNA could only be extracted from the plates incubated with the lowest concentration (10 μM) due to the decline in cell viability, thus preventing the investigation of long-term induction effects and higher concentrations. CYP3A4 and CYP2E1 showed measurable induction (by about a factor of 3.5–4) at both concentrations, whereas CYP2B6 and CYP2C9 mRNA was only increased at concentrations of 50 μM (table 5).

Discussion

The metabolism of DHEC has not been entirely elucidated to date, but it is likely that major biotransformation occurs by the oxidation of the pyrrolidine moiety. Therefore, the present investigation was focused on the detection of the mono- and dihydroxy metabolites of DHEC. Although the LC-MS/MS did not provide information on the steric structure of the metabolites, it was assumed that with the known metabolites of β-dihydroergocryptine, bromocriptine and dihydroergotamine, that the peaks detected with LC-MS/MS (m/z = 593.7–594.7 and 609.7–610.7 respectively) corresponded to the mono- and dihydroxy metabolites of DHEC.

The results derived from the *in vitro* metabolizing systems, i.e. different cell lines expressing specific CYPs, demonstrate that CYP3A4 is the primarily responsible isoform for DHEC metabolism. These data are in accordance with the findings for other ergot alkaloids, e.g. bromocriptine (Peyronneau 1994). The results were further substantiated by the ability of DHEC to inhibit the 6β-hydroxylation of testosterone, a marker substrate for CYP3A4. The estimated IC_{50} for DHEC in the present experiments was 2–5 μM. This is comparable with the data reported for bromocriptine with an IC_{50} of 1.69 μM (Wynalda and Wienkers 1997).

The metabolites detected in the culture media were monohydroxy and, to a smaller extent, dihydroxy metabolites. Since the V79 and THLE cell lines represent

only test systems for a single CYP, experiments with human hepatocytes were necessary to corroborate the results. We decided for fresh hepatocytes derived from biopsies. Compared with microsomal fractions, the use of hepatocytes allows for additional induction experiments. Fresh hepatocytes are superior to frozen cells in terms of viability but suffer from the disadvantage of limited availability and the time consuming isolation procedures. Therefore, the number of experiments in our investigation was restricted and unfortunately hindered by toxic effects of DHEC to the cultured cells in concentration exceeding 50 μM. In particular, the mRNA induction experiment should be confirmed by further studies.

Incubation of human hepatocytes with DHEC resulted in the detection of significant amounts of mono- and dihydroxy metabolites in the culture medium and ~ 80% of DHEC was metabolized. In agreement with the above, estimates of unchanged drug in human urine samples collected after the administration of ^{3}H-α-dihydroergocryptine was 12% of the total urine radioactivity (Ronca *et al*. 1996). The differences between the three hepatocyte preparations, which became evident in the induction experiment, may be related to differences in gender and age of the donors (Beierle *et al*. 1999, Tanaka, 1999). Hepatic CYP3A4 content has been shown to vary at least 20-fold among individuals (Dresser *et al*. 2000) and is in accordance with the results of Mas-Chamberlin *et al*. (1997) who detected different patterns of ^{3}H-DHEC metabolites in human hepatocytes derived from different donors.

The relevance of CYP3A4 in DHEC metabolism is confirmed by the fact that the drug could induce CYP3A4 and CYP2E1 mRNA in human hepatocytes at concentrations of 10 μM. Whether DHEC can induce other isoforms at higher concentrations is less clear. Further experiments are needed and the present preliminary results should be strictly interpreted in an exploratory sense.

What is the clinical relevance of the findings? Human cytochrome P4503A4 is the most abundant P450 enzyme in the liver and is involved in the metabolism of a broad range of drugs (Flockhart 2000), including steroids, antiretroviral agents (Barry *et al*. 1999) and anti-arrhythmics. Considerable amounts of the enzyme are also found in the gut wall (Kolars *et al*. 1994). Finally, hepatic and enteric CYP3A4 content appear to be regulated independently from each other (Dresser *et al*. 2000), which further complicates the prediction of *in vivo* interactions in an individual patient.

Wynalda and Wienkers (1997) concluded for bromocriptine that as long as the co-administration of bromocriptine did not dramatically alter the dispositional characteristics of a drug primarily mediated by CYP3A4, the data suggested that bromocriptine should not significantly modify the metabolism of a second drug metabolized by CYP3A4. Since the IC_{50} determined here for DHEC is comparable with that of bromocriptine, the same may apply to DHEC. Inasmuch as DHEC could induce CYP3A4, only the results of *in vivo* studies may provide an answer to the above.

Nelson *et al*. (1990) demonstrated a significantly enhanced bioavailability of bromocriptine in healthy volunteers after the pretreatment and co-administration of erythromycin, a potent inhibitor of CYP3A4. In the same study population, the co-administration of caffeine, a CYP1A2 substrate, only slightly altered the C_{max} of bromocriptine without reaching statistical significance. Whether the same is true for DHEC should be addressed by appropriate drug interaction studies. Clinical trials with DHEC are under way to investigate further the pharmacokinetics of DHEC in

patients with impaired hepatic function and to assess possible drug interactions with erythromycin and other substances.

References

Ball, S. E., Maurer, G., Zollinger, M., Ladona, M. and Vickers, A. E. M., 1992, Characterization of the cytochrome P-450 gene family responsible for the *N*-dealkylation of the ergot alkaloid CQA 206–291 in humans. *Drug Metabolism and Disposition*, **20**, 56–63.

Barry, M., Mulcahy, F., Merr, C., Gibbons, S. and Back, D., 1999, Pharmacokinetics and potential interactions amongst antiretroviral agents used to treat patients with HIV infection. *Clinical Pharmacokinetics*, **36**, 289–304.

Battistin, L., Bardin, P., G., Ferro-Milone, F., Ravenna, C., Toso, V. and Reboldi, G., 1999, Alpha-dihydroergocryptine in Parkinson's disease: a multicentre randomized double blind parallel group study. *Acta Neurologica Scandinavica*, **99**, 36–42.

Beierle, I., Meibohm, B. and Derendorf, H., 1999, Gender differences in pharmacokinetics and pharmacodynamics. *International Journal of Clinical Pharmacology and Therapeutics*, **37**, 529–547.

Bergamasco, B., Frattola, L., Muratorio, A., Piccoli, F. and Parnetti, L., 2000, Alpha-dihydroergocryptine in the treatment of *de novo* Parkinsonian patients: results of a multicentre, randomized, double blind, placebo-controlled study. *Acta Neurologica Scandinavica*, **101**, 372–380.

Bort, R., Macé, K., Boobis, A., Gómez-Lechón, M.-J., Pfeifer, A. and Castell, J., 1999, Hepatic metabolism of diclofenac: role of human CYP in the minor oxidative pathways. *Biochemical Pharmacology*, **58**, 787–796.

Correia, A. M., 1998, Drug biotransformation. In B. G. Katzung (ed.), *Basic & Clinical Pharmacology*, 7th edn (Stamford: Appleton & Lange), pp. 50–61.

Delaforge, M., Rivière, R., Sartori, E., Doignon, J. L. and Grognet, J. M., 1989, Metabolism of dihydroergotamine by a cytochrome P-450 similar to that involved in the metabolism of macrolide antibiotics. *Xenobiotica*, **19**, 1285–1295.

Doehmer, J., 1993, V79 Chinese hamster cells genetically engineered for cytochrome P450 and their use in mutagenicity and metabolism studies. *Toxicology*, **82**, 105–118.

Dresser, G. K., Spence, J. D. and Bailey, D. G., 2000, Pharmacokinetic-pharmacodynamic consequences and clinical relevance of cytochrome P450 3A4 inhibition. *Drug Interactions*, **38**, 41–57.

Eagling, V. A., Tjia, J. F. and Back, D. J., 1998, Differential selectivity of cytochrome P450 inhibitors against probe substrates in human and rat liver microsomes. *British Journal of Clinical Pharmacology*, **45**, 107–114.

Flockhart, D. A., 2000, Cytochrome P450 drug interaction table, Georgetown University Medical Center, Division of Clinical Pharmacology [http://www.dml.georgetown.edu/depts/pharmacology/davetab.html].

Gómez-Lechón, M.-J., Lopez, P., Donato, T., Montoya, A., Larrauri, A., Gimen Trullenque, R., Fabra, R. and Castell, J. V., 1990, Culture of human hepatocytes from small surgical biopsies. Biochemical characterization and comparison with *in vivo*. *In Vitro Cellular and Developmental Biology*, **26**, 67–74.

Kolars, J. C., Lown, K. S., Schmiedlin-Ren, P., Ghosh, M., Fang, C., Wrighton, S., Merion, R. M. and Watkins, P. B., 1994, CYP3A gene expression in human gut epithelium. *Pharmacogenetics*, **4**, 247–259.

Lewis, D. F., Dickins, M., Eddershaw,P. J., Tarbit, M. H. and Goldfarb, P. S., 1999, Cytochrome P450 substrate specificities, substrate structural templates and enzyme active site geometries. *Drug Metabolism and Drug Interaction*, **15**, 1–49.

Macé, K., Aguilar F., Wang, J. S., Vautravers, P., Gómez-Lechón, M., Gonzalez, F. J., Groopman, J., Harris, C. C. and Pfeifer, A. M., 1997, Aflatoxin B1-induced DNA adduct formation and p53 mutations in CYP450-expressing human liver cell lines. *Carcinogenesis*, **18**, 1291–1297.

Markstein, R., 1983, Dopamine receptor profile of co-dergocrine (Hydergine-) and its components. *European Journal of Pharmacology*, **86**, 145–155.

Mas-Chamberlin, C., Bromet, N., Olgiati, V., Giradello, R, and Lowenthal, D. T., 1997, Metabolism study of dihydro-α-ergocryptine,9,10-[9,10^{-3}H(N)] in rat and human hepatocyte cultures and rat, monkey, and human microsomes. *American Journal of Therapeutics*, **4**, 291–299.

Maurer, G., 1977, Isolement et Structure de Metabolites Biliaires de la Dihydro-*β*-ergokryptine chez le Rat. Doctoral thesis, University Claude Bernard, Lyon I, pp. 1–184.

Maurer, G. and Frick, W., 1984, Elucidation of the structure and receptor binding studies of the major primary metabolite of dihydroergotamine in man. *European Journal of Clinical Pharmacology*, **26**, 463–470.

Maurer, G., Schreier, E., Delaborde, S., Loosli, H. R., Nufer, R. and Shukla, A. P., 1982, Fate and disposition of bromocriptine in animals and man. I: Structure and elucidation of the metabolites. *European Journal of Drug Metabolism and Pharmacokinetics*, **7**, 281–292.

Murray, M., 1999, Mechanisms and significance of inhibitory drug interactions involving cytochrome P450 enzymes [Review]. *International Journal of Molecular Medicine*, **3**, 227–238.

Nelson, M. V., Berchou, R. C., Karetti, D. and LeWitt, P. A., 1990, Pharmacokinetic evaluation of erythromycin and caffeine administered with bromocriptine. *Clinical Pharmacology and Therapeutics*, **47**, 694–697.

Peyronneau, M.-A., Delaforge, M., Riviere, R., Renaud, J.-P. and Mansuy, D., 1994, High affinity of ergopeptides for cytochrome P450 3A. *European Journal of Biochemistry*, **223**, 947–956.

Pfeifer, A. M., Cole, K. E., Smoot, D. T., Weston, A., Groopman, J. D., Shields, P. G., Vignaud, J. M., Juillerat, M., Lipsky, M. M., Trump, B. F., Lechner, J. F. and Harris, C. C., 1993, Simian virus 40 large tumor antigen-immortalized normal human liver epithelial cells express hepatocyte characteristics and metabolize chemical carcinogens. *Proceedings of the National Academy of Sciences, USA*, **90**, 5123–5127.

Pfeifer, A. M., Macé, K., Tromvoukis, Y. and Lipsky, M. M., 1995, Highly efficient establishment of immortalized cells from adult human liver. *Methods of Cellular Science*, **17**, 83–89.

Platt, K. L., Molitor, E., Döhmer. J., Dogra, S. and Oesch, F., 1989, Genetically engineered V79 Chinese hamster cell expression of purified cytochrome P-450IIBI monooxygenase activity. *Journal of Biochemical Toxicology*, **4**, 1–6.

Rauschenbach, R., Gieschen, H., Husemann, M., Salomon, B. and Hildebrand, M., 1995, Stable expression of human P450 3A4 in V79 cells and its application for metabolic profiling of ergot derivatives. *European Journal of Pharmacology Environmental Toxicology and Pharmacology Section*, **293**, 183–190.

Rodriguez-Antona, C., Gomez-Lechon, M. J. and Castell, J. V., 2000, Quantitative RT-PCR measurement of human cytochrome P-450 application to drug induction studies. *Archives of Biochemistry and Biophysics*, **376**, 109–116.

Ronca, F., Guazzelli, M., Salvadori, O., Palumbo, R., Neuteboom, B., Ambrosoli, L., Poli, A., Giradello, R. and Lowenthal, D. T., 1996, Pharmacokinetic and metabolism study in healthy volunteers after administration of single oral dose of ^{3}H-α-dihydroergocryptine mesylate. *American Journal of Therapeutics*, **3**, 553–562.

Tanaka, E., 1999, Gender-related differences in pharmacokinetics and their clinical significance. *Journal of Clinical Pharmacy and Therapeutics*, **24,** 339–346.

Wynalda, M. A. and Wienkers, L. C., 1997, Assessment of potential interactions between dopamine receptor agonists and various human cytochrome P450 enzymes using a simple *in vitro* inhibition screen. *Drug Metabolism and Disposition*, **25**, 1211–1214.

XENOBIOTICA, 2000, VOL. 30, NO. 11, 1047–1054

Glucuronidation of resveratrol, a natural product present in grape and wine, in the human liver

C. DE SANTI†, A. PIETRABISSA‡, F. MOSCA‡ and G. M. PACIFICI†*

† Department of Neurosciences, Section of Pharmacology, Medical School, Via Roma 55, I-56126 Pisa, Italy

‡Department of Oncology, Section of Surgery, Cisanello Hospital, at University of Pisa, I-56124 Cisanello, Pisa, Italy

Received 15 June 2000

1. Resveratrol, a polyphenolic compound present in grape and wine, has beneficial effects against cancer and protective effects on the cardiovascular system. It has been shown that the compound is sulphated in human liver and the aims of the present investigation were to study resveratrol glucuronidation in human liver microsomes and to determine whether flavonoids inhibit resveratrol glucuronidation.

2. A simple and reproducible radiometric assay for resveratrol glucuronidation was developed. The assay employed uridine-5′-diphosphoglucuronic acid-[^{14}C] and unlabelled resveratrol. Resveratrol-glucuronide was isolated by TLC. The intra- and interassays variabilities were 1 and 1.5%, respectively.

3. The rate of resveratrol glucuronidation was measured in 10 liver samples. The mean ± SD and median of resveratrol glucuronidation rate were 0.69 ± 0.34 and 0.80 nmol/min/mg, respectively. Resveratrol glucuronosyl transferase followed Michaelis–Menten kinetics and the K_m and V_{max} (mean ± SD; n = 5) were 0.15 ± 0.09 mM and 1.3 ± 0.3 nmol/min/mg, respectively. The intrinsic clearance was $11 \pm 4 \times 10^{-3}$ ml/min.mg.

4. The flavonoid quercetin inhibited resveratrol glucuronidation and its IC_{50} (mean ± SD; n = 3) was 10 ± 1 μM. Myricetin, catechin, kaempferol, fisetin and apigenin (all at 20 μM) inhibited resveratrol glucuronidation and the percent of control ranged between 46% (catechin) to 72% (apigenin).

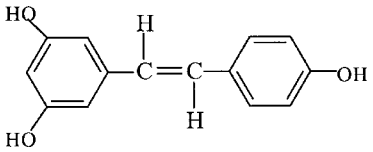
5. The present results show that resveratrol is glucuronated in the human liver. Glucuronidation may reduce the bioavailability of this compound however, flavonoids inhibit resveratrol glucuronidation and such an inhibition might improve the bioavailability of resveratrol.

Introduction

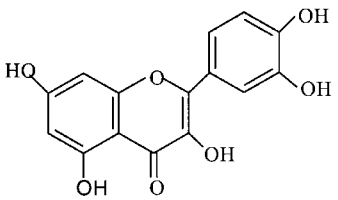
Trans-resveratrol (3,5,4′-trihydroxy-*trans*-stilbene; figure 1) (hereafter resveratrol) is a polyphenolic compound present in grapes and wine (Jeandet *et al*. 1991, 1993, Goldberg *et al*. 1995) and has recently gained increasing interest for its beneficial effects against cancer and protection of the cardiovascular system. In the past 5 years, over 180 articles have been published on the effects of resveratrol and selected information includes the following. Resveratrol causes dose-dependent inhibition of human oral squamous cell carcinoma (Elattar and Virji 1999), has anticancer effects in LNCaP prostate cancer cells (Mitchell *et al*. 1999), prevents apoptosis in K562 cells by inhibiting lipocyclooxygenase (MacCarrone *et al*. 1999), inhibits the growth of human breast cancer cells (Lu and Serrero, 1999) and decreases tumour growth in a rat model (Carbo *et al*. 1999). Resveratrol has a protective effect on myocardial function (Sato *et al*. 2000), protects the isolated heart rat from ischaemia (Ray *et al*. 1999), increases nitric oxide synthesis (Hsieh *et al*.

* Author for correspondence; e-mail: pacifici@biomed.unipi.it

Xenobiotica ISSN 0049-8254 print/ISSN 1366-5928 online © 2000 Taylor & Francis Ltd
http://www.tandf.co.uk/journals DOI: 10.1080/00498250010002487



Resveratrol



Quercetin

Figure 1. Molecular structures of resveratrol and quercetin.

1999), has relaxant effect on isolated porcine coronary arteries (Jager and Nguyen-Duong 1999) and inhibits factor expression in vascular cells (Pendurthi *et al.* 1999).

It has been shown that resveratrol is sulphated in human liver (De Santi *et al.* 2000a) and the rate of sulphation is inhibited by flavonoids (De Santi *et al.* 2000b), quercetin (figure 1) being the most potent as an inhibitor. Sulphotransferase and glucuronosyl transferase often share the same substrate, and the first aim of the current study was to see whether resveratrol was glucuronated and if so, to develop an assay for measuring the rate of resveratrol glucuronidation in human liver. The second aim of this investigation was to study resveratrol glucuronidation in human liver. Finally, the third aim was to see whether flavonoids inhibit resveratrol glucuronidation.

Materials and methods

Chemicals

Uridine 5′-diphosphoglucuronic acid-[^{14}C] (UDPGA, specific activity 295 mCi/mmol; chemical purity >97%) was from NEN Life Science Products, Inc. (Brussels, Belgium). Unlabelled uridine 5′-diphosphoglucuronid acid, polyoxyethylene 20 cetyl ether (Brij 58), *p*-nitrophenyl-*β*-D-glucuronide, quercetin, myricetin, catechin, kaempferol, fisetin, apigenin and bovine serum albumin (BSA) were from Sigma Chemical Co. (Milan, Italy). Glacial acetic acid, 30% ammonia, *n*-butanol, acetone, tris-[hydroxymethyl]aminomethane (Tris) and magnesium chloride were from Carlo Erba (Milan, Italy). *Trans*-resveratrol (chemical purity >99%) was a generous gift from Professor Luca Giovannini, Department of Neurosciences, University of Pisa. TLC plates were 19-channel LK5DF silica gel glass (0.25 μM in thickness) with loading zone from Whatman (Milan, Italy).

Biological material

The Ethical Committee of the Medical School of the University of Pisa approved this project. Liver specimens were obtained after clinically indicated partial hepatectomy, from seven men and three women aged between 41 and 71 years (mean ± SD = 60 ± 11 years). Table 1 summarizes the liver function tests of the patients from whom the liver samples were derived. Liver function tests were mainly within the normal values.

Isolation of the microsomal fraction

After the tissue specimens were obtained, they were immediately chilled in ice and transported to our laboratory within a few minutes where they were frozen and stored at −80 °C. Liver samples (~1 g) were homogenized in 5 vols 0.25 M sucrose dissolved in 5 mM potassium orthophosphate buffer (pH 7.4)

Table 1. Clinical data for the patients undergoing clinically indicated partial hepatectomy from which liver samples were derived.

	Minimum	Maximum	Mean ± SD	Median	Normal values
Age (year)	41	71	60 ± 11	63	–
Albumin (d/dl)†	3·4	4·3	3·8 ± 0·3	3·8	3·5–5·5 g/dl
Bilirubin (mg/dl)‡	0·3	0·7	0·5 ± 0·2	0·6	⩽ 1·1 mg/dl
GOT (U/L)	17	83	39 ± 26	31	< 45 U/l
GPT (U/L)	12	96	30 ± 29	24	< 45 U/l
PT (s)	11·6	12·3	11·8 ± 6·1	11·7	10·9–12·8 s

† Plasma albumin concentration; ‡ total bilirubin plasma concentration; GOT, glutamic-oxalacetic transaminase activity; GPT, glutamic-pyruvic transaminase activity; PT, prothrombin time.

using a Polytron homogenizer (power 4, 3 × 5 s). The homogenates were homogenized again in a glass–Teflon homogenizer and were transferred into centrifuge tubes. The homogenates were centrifuged at 12000 *g* for 15 min and the supernatants centrifuged again at 105000 *g* for 1 h. The high-speed pellets were suspended in 2 ml 100 mM Tris-HCl (pH 7.4) containing 30% glycerol (v/v). The membrane suspensions, designated microsomal fraction, were divided into aliquots and stored at −80 °C.

Assays

Protein concentration was measured as described by Lowry *et al*. (1951) using BSA as a standard.

The assay for resveratrol glucuronidation was essentially as that described by Bansal and Gessner (1980) with minor modifications. The volume of the incubation mixture was 50 μl. The final concentration of resveratrol and UDPGA was 1 mM. To each tube was added 50 nmoles unlabeled UDPGA containing 0.025 μCi UDPGA-[^{14}C] (~ 55000 dpm). The nmol of UDPGA contained in 0.025 μCi UDPGA-[^{14}C] were 0.08 and were considered negligible. The incubation mixture also contained the following compounds at the stated final concentrations: Brij 58 (0.05% w/v), 0.1 M Tris-HCl (pH 7.4), 5 mM $MgCl_2$, and 1 mM resveratrol. Resveratrol was dissolved in acetone and was added in 2 μl to the incubation mixture. This volume of acetone did not affect the rate of glucuronosyl transferase. Finally, 20 μl of the microsomal suspension was added to the incubation mixture to give a final protein concentration ranging between 1.2 and 5.0 mg/ml. Each sample was assayed in duplicate and had two blank samples that had the same composition of the test samples with the exception that resveratrol was replaced by 2 μl acetone. The incubations were started by the addition of UDPGA, carried out at 37 °C for 30 min and stopped by the addition of 100 μl absolute ethanol. The tubes were vortexed and immediately chilled in ice. Of the samples, 50 μl were applied to the loading zone of TLC plates. Chromatography was developed using the following mixture: *n*-butanol:acetone:glacial acetic acid:30% ammonia:water (70:50:18:1.5:60 by vol.) (Bansal and Gessner 1980). *p*-Nitrophenyl-β-D-glucuronide was used as a reference standard, as the glucuronides of the various aglycones have similar R_f (Bansal and Gessner 1980). Of 5 mM p-nitrophenyl-β-D-glucuronide, 50 μl were applied at the first and last channels of the plate. After chromatography was developed, the plates were gently dried in an air stream and then placed under UV light. The spots that had the same R_f of *p*-nitrophenyl-β-D-glucuronide were scraped out and transferred into scintillation vials. Absolute ethanol (1 ml) was added, the vials shaken and 10 ml scintillation cocktail (Emulsifier Scintillator Plus, Packard, Milan, Italy) added. Radioactivity was measured in a liquid-phase scintillator Beckman LS1701. Enzyme activity was measured, after correction of the test samples for the blank samples, on the specific radioactivity of UDPGA-[^{14}C]. The sample to blank ratios ranged between 4 and 7. The intra-assay variability was determined in six replicates and the interassays variability was determined by measuring the rate of resveratrol glucuronidation in six assays performed on different days.

Kinetics of resveratrol glucuronosyl transferase

The kinetics of resveratrol glucuronosyl transferase were studied in five liver samples from three men and two women aged between 47 and 71 years. The concentrations or resveratrol were 0.0625, 0.125, 0.25, 0.5 and 1 mM and the concentration of UDPGA was kept constant at 1 mM.

Inhibition of resveratrol glucuronidation

The inhibition of resveratrol glucuronidation by quercetin was studied in three liver samples from two men and one woman aged between 47 and 71 years. The inhibition curves were constructed using the following concentrations 1.25, 2.5, 5, 10, 20 and 40 μM quercetin and the concentrations of UDPGA and resveratrol were kept constant at 1 mM. The type of inhibition of resveratrol glucuronidation by quercetin was studied in three liver samples. Each assay consisted of three saturation curves for

resveratrol whose concentration were 0.0625, 0.125, 0.25, 0.5 and 1 mM. One set did not contain the inhibitor (control) and the other two sets contained quercetin at final concentrations of 5 and 10 μM. The concentration of UDPGA was kept constant at 1 mM. The inhibition by the flavonoids: myricetin, catechin, kaempferol, fisetin and apigenin was studied in three livers and the flavonoid final concentration was 20 μM. At higher concentrations, these flavonoids underwent glucuronidation and could not be used as inhibitors of glucuronosyl transferase. A bottle of red Chianti wine, produced in 1998, was opened just before the inhibition study. The content of alcohol was 12% (v/v), pH was 3 and was increased to 6 by addition of 1 N NaOH drop by drop. Wine (4 μl) was added to the incubation mixture.

Calculations

The kinetic parameters V_{max} and K_m were determined using the non-linear correlation option of the software package Prism 3 (GraphPad Software, San Diego, CA, USA). The intrinsic clearance was measured by dividing V_{max} by K_m. IC_{50} was calculated using the software package Dose–Effect Analysis (Biosoft, Cambridge, UK). K_i and K_{ies} were calculated by using the computer program 'Enzpack 3' (Biosoft, Cambridge, UK). The effectiveness of inhibitor binding to free enzyme was measured by the dissociation constant K_i of the reaction, defined as:

$$K_i = ([E] \times [I])/[EI]$$

and the effectiveness of its binding to the enzyme substrate complex is measured by K_{ies} defined as:

$$K_{ies} = ([ES] \times [I])/EIS],$$

where [E] is the concentration of the enzyme, [I] is the concentration of the inhibitor, [ES] is the concentration of the enzyme–substrate complex and [EIS] is the concentration of the enzyme–substrate inhibitor complex. In a mixed, non-competitive inhibition type, when $K_i = K_{ies}$, the binding of the substrate to the enzyme does not modify the affinity of the enzyme for the inhibitor.

ANOVA analysis, followed by the Tukey–Kramer multiple comparisons test, assessed the difference of K_m and V_{max} estimates measured in the absence and in the presence of two concentrations of the inhibitor. The software package used for statistical analysis was Instat for Windows (GraphPad). The activities and the kinetic parameters of resveratrol glucuronidation were measured in the same samples used to study resveratrol sulphation (De Santi *et al.* 2000a). The levels of difference between the activities and the kinetic parameters of glucuronosyl transferase and sulphotransferase were tested by paired *t*-test. The levels of significance of correlations were tested by the Spearman-rank test. Descriptive analysis was performed by the software package Statistica (StatSoft Inc., Tulsa, OK, USA). The intra- and interassays coefficients of variation were calculated by dividing the SD by the mean.

Results and discussion

The optimal conditions for resveratrol glucuronidation were first determined. The highest rate of resveratrol glucuronidation was found at pH 7, but it had little variation between pH 6.5 and 7.5 (figure 2a). The results described hereafter were obtained at pH 7.4. The amounts of resveratrol-glucuronide formed increased linearly with time up to at least 40 min of incubation (figure 2b) and up to at least 0.2 mg microsomal protein per ml incubation mixture (figure 2c). The coefficients of intra- and interassays variabilities were 1.0 and 1.5% respectively.

The rate of resveratrol glucuronidation (nmol/min/mg) was measured in 10 liver samples (figure 2d) and ranged between 0.23 and 1.2 with the mean ± SD and the median being 0.69 ± 0.34 and 0.80, respectively. The fold variation between the 5th and 95th percentiles was 5. The rate of resveratrol glucuronidation were not correlated with the age of the patients from whom the liver samples were obtained ($r = 0.282$, $p = 0.430$) and was not gender-dependent being 0.58 ± 0.33 in men and 0.96 ± 0.23 in women ($p = 0.108$). The hepatic rate of resveratrol sulphation reported by De Santi *et al.* (2000a) was measured in the same samples used to asses the rate of resveratrol glucuronidation. The mean ± SD and the median of resveratrol sulphation rate were 90 ± 21 and 80 pmol/min/mg. The rate of sulphation was lower ($p < 0.001$) than that of glucuronidation and the rates of resveratrol sulphation and glucuronidation were not correlated ($r = 0.244$, $p = 0.492$).

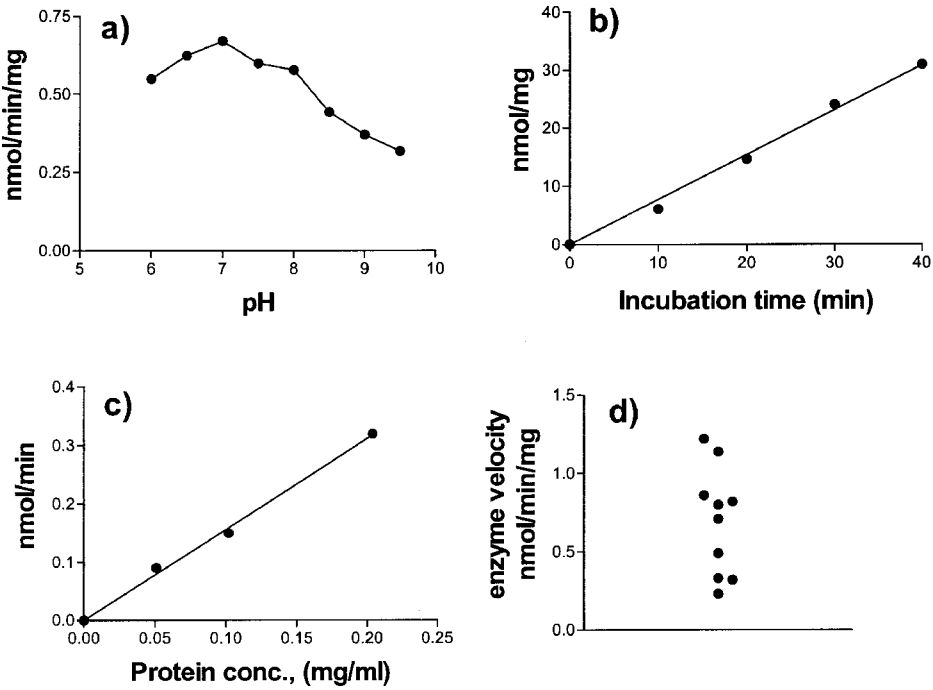


Figure 2. Glucuronidation of resveratrol in human liver. Effects of pH (a), incubation time (b) and protein concentration (c) on the formation rate of resveratrol glucuronide. Data are from a 64-year-old woman. Activity of glucuronosyl transferase towards resveratrol in 10 human liver samples and the median estimate was 0.80 nmol/min/mg (d).

The kinetics of glucuronosyl transferase toward resveratrol were studied in five liver samples and the enzyme followed Michaelis–Menten kinetics. Representative results from one liver (both the saturation curve and the transformation of the enzyme activity into the Lineweaver–Burk plot) are shown in figure 3 (a, b, curve 'control'). The kinetic parameters (mean ± SD) were $K_m = 0.15 \pm 0.09$ mM and $V_{max} = 1.3 \pm 0.3$ nmol/min/mg and the goodness of fit (r^2) ranged between 0.9928 and 0.9994. The intrinsic clearance of resveratrol glucuronidation was $11 \pm 4 \times 10^{-3}$ ml/min.mg. The kinetic parameters of resveratrol sulphotransferase have been determined in the same samples used to assess the kinetics of resveratrol glucuronosyl transferase (De Santi *et al.* 2000a). The intrinsic clearance for resveratrol sulphation was 0.22 ± 0.07 ml/min.mg, one order of magnitude greater than that for resveratrol glucuronidation. The intrinsic clearances for resveratrol sulphation and glucuronidation were significantly different ($p < 0.0001$).

Quercetin was a potent inhibitor of resveratrol glucuronidation, with an IC_{50} value (mean ± SD; $n = 3$) of 10 ± 1 μM and the inhibition curve is shown in figure 3 (c). K_i and K_{ies} values (mean ± SD; μM) were 10 ± 4 and 9 ± 2, respectively ($p = 0.662$). K_m values (mean ± SD; mM) were 0.15 ± 0.09 (control), 0.06 ± 0.04 (5 μM quercetin) and 0.13 ± 0.06 (10 μM quercetin), and the control value was not different from those of 5 and 10 μM quercetin. V_{max} values (mean ± SD; nmol/min/mg) were 1.3 ± 0.3 (control), 0.73 ± 0.07 (5 μM quercetin) and 0.46 ± 0.23 (10 μM quercetin), and the of control value was greater than that for 10 μM quercetin ($p < 0.05$). The type of inhibition was mixed, non-competitive and the representative results from a liver are shown in figure 3 (a, b).

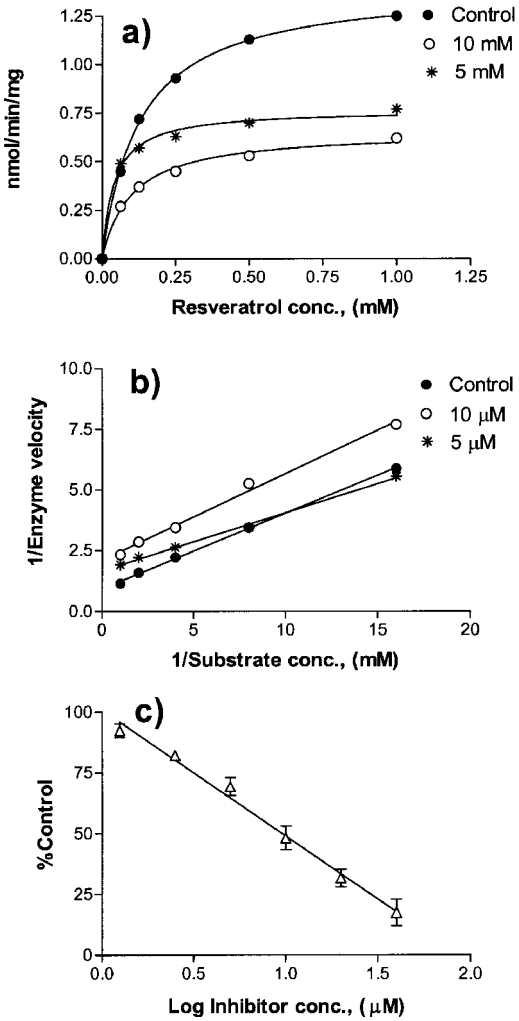


Figure 3. Inhibition of resveratrol glucuronidation by quercetin. (a) Saturation curves for resveratrol and (b) transformation of the enzyme activity into Lineweaver–Burk plots. Control (no quercetin; filled circles), 5 μM quercetin (stars) and 10 μM quercetin (unfilled circles). Data are from a 71-year-old woman. (c) Inhibition curve of resveratrol glucuronidation by quercetin. Data points are the mean $\pm$ SD of three livers. Vertical bars are 2 $\times$ SD.

The effect of 20 μM myricetin, catechin, kaempferol, fisetin and apigenin on the rate of resveratrol glucuronidation was also determined and the percent of control value were 50 ± 3, 46 ± 2, 55 ± 13, 72 ± 14, 66 ± 8, respectively. Flavonoids therefore inhibit resveratrol glucuronidation but the extent of inhibition is less than that for resveratrol sulphation (De Santi *et al.* 2000b).

IC_{50} of quercetin for inhibition of resveratrol sulphation is 12 pM (De Santi *et al.* 2000b) and that for resveratrol glucuronidation is three orders of magnitude greater indicating that quercetin is a more potent inhibitor of resveratrol sulphation than glucuronidation. Chianti red wine (4 μl), corresponding to 7% of the incubation mixture volume, decreased the rate of resveratrol glucuronidation to 65 ± 3% of the control value. The addition of 8 μl wine to the incubation mixture (final volume 150 μl) for the assay of resveratrol sulphation, corresponding to 5% of

the incubation mixture volume, decreased the rate of resveratrol sulphation to $9 \pm 0.4\%$ of control value (De Santi *et al*. 2000b). Glucuronidation is therefore less susceptible inhibition by wine than sulphation.

Resveratrol concentration in Chianti wine produced in 1990 and 1991 was 5.1 and 5.6 μM, respectively (Goldberg *et al*. 1996). Assuming a resveratrol concentration of 5.6 μM in the wine used in the study, the amounts of resveratrol in 4 μl were 22.4 pmoles, which is $\sim 0.4\%$ of the total amount of resveratrol in the incubation mixture. Thus, the inhibition of resveratrol glucuronidation by wine is not due to an excess of substrate and is likely caused by the cumulative effects of many compounds.

In conclusion, a simple and reproducible assay has been described to measure the rate of resveratrol glucuronidation in human liver, which is one order of magnitude greater than that of resveratrol sulphation (De Santi *et al*. 2000a). The comparison of the present results with those previously described on the inhibition of resveratrol sulphation by flavonoids (De Santi *et al*. 2000b) indicates that glucuronidation of resveratrol is less susceptible than sulphation to the inhibition by flavonoids and this result accords with that obtained with wine. The present results are consistent with the view that glucuronidation of resveratrol has a greater capacity and a lower affinity than that of sulphation.

Acknowledgements

The authors thank Professor Luca Giovannini for the generous gift of resveratrol. The work was supported by contract BMH1-CT94–1622 of the European Commission (Brussels, Belgium), by the Italian Ministry of the University (Rome, Italy) and the Italian Association for Cancer Research (Milan, Italy).

References

Bansal, S. K. and Gessner, T., 1980, A unified method for the assay of uridine diphosphoglucuronosyltransferase activities toward various aglycones using uridine diphospho[U-^{14}C]glucuronic acid. *Analytical Biochemistry*, **109**, 321–329.

Carbo, N., Costelli, P., Baccino, F. M., Lopez-Soriano, F. J. and Argiles, J. M., 1999, Resveratrol, a natural product present in wine, decreases tumour growth in a rat tumour model. *Biochemical and Biophysical Research Communications*, **254**, 739–743.

De Santi, C., Pietrabissa, A., Spisni, R., Mosca, F. and Pacifici, G. M., 2000a, Sulphation of resveratrol, a natural product present in grapes and wine, in the liver and duodenum. *Xenobiotica* **30**, 609–617.

De Santi, C., Pietrabissa, A., Spisni, R., Mosca, F. and Pacifici, G. M., 2000b, The sulphation of resveratrol, a natural compound present in wine, and its inhibition by natural flavonoids. *Xenobiotica* **30**, 857–866.

Elattar, T. M. and Virij, A. S., 1999, Modulating effect of resveratrol and quercetin on oral cancer cell growth and proliferation. *Anticancer Drugs*, **10**, 187–193.

Goldberg, D. M., Tsang, E., Karumanchiri, A., Diamandis, E. P., Soleas, G. and Ng, E., 1996, Method to assay the concentrations of phenolic constituents of biological interest in wines. *Analytical Chemistry*, **68**, 1688–1694.

Goldberg, D. M., Yan, J., Ng, E., Diamandis, E. P., Karumanchiri, A., Soleas, G. and Waterhouse, A. L., 1995, A global survey of *trans*-resveratrol concentrations in commercial wines. *American Journal of Enology and Viticulture*, **46**, 159–165.

Hertog, M. G. L., Hollman, P. C. H., Katan, M. B. and Kromhout, D., 1993, Intake of potentially anticarcinogenic flavonoids and their determinants in adults in the Netherlands. *Nutrition and Cancer*, **20**, 21–29.

Hsieh, T. C., Juan, G. and Wu, J. M., 1999, Resveratrol increases nitric oxide synthase, induces accumulation of p53 and p21 (WAF1/CIP1), and suppresses cultured bovine pulmonary artery endothelial cell proliferation by perturbing progression through S and G2. *Cancer Research*, **59**, 2596–2601.

Jager, U. and Nguyen-Duong, H., 1999, Relaxant effect of *trans*-resveratrol on isolated porcine coronary arteries. *Arzneimittelforschung/Drug Research*, **49**, 207–211.

Jeandet, P., Bessis, R. and Gautheron, B., 1991, The production of resveratrol (3,5,4′-trihydroxystilbene) by grape berries in different developmental stages. *American Journal of Enology and Viticulture*, **42**, 41–46.

Jeandet, P., Bessis, R., Maume, B. F. and Mohamed Sbaghi, 1993, Analysis of resveratrol in Burgundy wines. *Journal of Wine Research*, **4**, 79–85.

Lowry, O. H., Rosebrough, N. J., Farr, A. and Randall, R. J., 1951, Protein measurement with Folin phenol reagent. *Journal of Biological Chemistry*, **193**, 265–275.

Lu, R. and Serrero, G., 1999, Resveratrol, a natural product derived from grape, exhibits antiestrogenic activity and inhibits the growth of human breast cancer cells. *Journal of Cellular Physiology*, **179**, 297–304.

MacCarrone, M., Lorenzon, T., Guerrieri, P. and Agro, A. F., 1999, Resveratrol prevents apoptosis in K562 cells by inhibiting lipoxygenase and ciclooxygenase activity. *European Journal of Biochemistry*, **265**, 27–34.

Mitchell, S. H., Zhu, W. and Young, C. Y., 1999, Resverarol inhibits the expression and function of the androgen LNCaP prostate cancer cells. *Annals of the New York Academy of Sciences*, **889**, 214–223.

Pendurthi, U. R., Williams, J. T. and Rao, L. V., 1999, Resveratrol, a polyphenolic compound found in wine, inhibits tissue factor expression in vascular cells: a possible mechanism for the cardiovascular benefits associated with moderate consumption of wine. *Arteriosclerosis and Thrombosis Vascular Biology*, **19**, 419–426.

Ray, P. S., Maulik, G., Bertelli, A. A., Bertelli, A. and Das, D. K., 1999, The red wine antioxidant resveratrol protects isolated rat hearts from ischemia reperfusion injury. *Free Radical Research Communications*, **27**, 160–169.

Sato, M., Maulik, G., Bagchi, D. and Das, D. K., 2000, Myocardial protection by protykin, a novel extract of *trans*-resveratrol and emodin. *Free Radical Research Communications*, **32**, 135–144.

XENOBIOTICA, 2000, VOL. 30, NO. 11, 1055–1062

Metabolism of 26,27-hexafluoro-1α,25-dihydroxyvitamin D_3 and 26,27-hexafluoro-1α,23(*S*)25-trihydroxyvitamin D_3 in ROS17/2.8 cells transfected with a plasmid expressing CYP24

T. MIYAHARA†*, S. GOMYO†, Y. UEDA†, Y. OHYAMA‡, C. SIGENO§, A. KOZAKAI¶, T. TAKAMURA¶, R. YAMAZAKI¶, S. HIGUCHI¶, M. YAMAMOTO†, T. SAKUMA† and N. NEMOTO†

† Department of Toxicology, Faculty of Pharmaceutical Sciences, Toyama Medical & Pharmaceutical University, 2630 Sugitani, Toyama-shi, Toyama, 930-0194, Japan
‡ Graduate Department of Gene Science, Faculty of Science, Hiroshima University, 1-3-1 Kagamiyama, Higashi-hiroshima-shi, Hiroshima, 739-8526, Japan
§ Department of Radiology and Nuclear Medicine, Faculty of Medicine, Kyoto University, Shogoin, Sakyo-ku, Kyoto 606-8397, Japan
¶ Research Center, Taisho Pharmaceutical Company, Ltd, Yoshinohara, Ohmiya-shi, Saitama, 330-0031, Japan

Received 2 June 2000

1. To clarify the possibility that the metabolism of 26,27-hexafluoro-1α,25-dihydroxyvitamin D_3 [F_6-1,25$(OH)_2D_3$] to 26,27-hexafluoro-1α,23(*S*),25-trihydroxyvitamin D_3 [F_6-1,23,25$(OH)_3D_3$ and that of F_6-1,23,25$(OH)_3D_3$ to 26,27-hexafluoro-23-oxo-1α,25-dihydroxyvitamin D_3 [F_6-23-oxo-1,25$(OH)_2D_3$] are catalysed by 25-hydroxyvitamin D_3 24-hydroxylase (CYP24), ROS17/2.8 cells transfected with a plasmid expressing CYP24 [pSVL-CYP24(+)] and a corresponding blank plasmid [pSLV-CYP24R(−)] were used.

2. Incubation of [1β-^{3}H]-F_6-1,25$(OH)_2D_3$ for 2 and 5 days with ROS17/2.8 cells transfected with pSVL-CYP24(+) generated a metabolite that co-migrated with authentic F_6-1,23,25$(OH)_3D_3$ in both normal phase and reversed-phase HPLC systems.

3. Incubation of [1β-^{3}H]-F_6-1,23,25$(OH)_3D_3$ for 5 days with pSVL-CYP24(+)-transfected ROS 17/2.8 cells generated a metabolite that co-migrated with authentic F_6-23-oxo-1,25$(OH)_2D_3$. In contrast, the metabolites F_6-1,23,25$(OH)_3D_3$ or F_6-23-oxo-1,25$(OH)_2D_3$ were not generated in the cells transfected with pSVL-CYP24R(-).

4. The results indicate that CYP24 catalyses the conversion of F_6-1,25$(OH)_2D_3$ to F_6-1,23,25$(OH)_3D_3$ and that of F_6-1,23,25$(OH)_3D_3$ to F_6-23-oxo-1,25$(OH)_2D_3$.

Introduction

26,27-Hexafluoro-1α,25-dihydroxyvitamin D_3 [F_6-1,25$(OH)_2D_3$] is a hexafluorinated analogue of the active form vitamin D_3, 1α,25-dihydroxyvitamin D_3 [1,25$(OH)_2D_3$]. The potency of F_6-1,25$(OH)_2D_3$ to enhance bone mobilization *in vivo* was 5–10 times higher than that of 1,25$(OH)_2D_3$ (Tanaka *et al*. 1984). In a 48-h organ culture system using foetal rat limb bones, however, the effect of F_6-1,25$(OH)_2D_3$ on bone resorption was reported as being similar to that of 1,25$(OH)_2D_3$ (Stern *et al*. 1984). To clarify this discrepancy between the *in vivo* and *in vitro* systems, we subsequently used neonatal mouse parietal bones and extended the culture period from 48 to 144 h (Harada *et al*. 1992). In cultures of 0–48 h, the

* Author for correspondence.

Xenobiotica ISSN 0049-8254 print/ISSN 1366-5928 online © 2000 Taylor & Francis Ltd
http://www.tandf.co.uk/journals DOI: 10.1080/00498250010002496

activity of F_6-1,25$(OH)_2D_3$ was similar to that of 1,25$(OH)_2D_3$. In cultures of 48–144 h, however, F_6-1,25$(OH)_2D_3$ was much more effective than 1,25$(OH)_2D_3$. The results suggest that there is a difference between the metabolism of two compounds. In fact, it was recognized in the present organ culture that the conversion of F_6-1,25$(OH)_2D_3$ to a bioactive metabolite, 26,27-hexafluoro-1α,23(*S*),25-trihydroxyvitamin D_3 [F_6-1,23,25$(OH)_3D_3$] increased and was retained in the bones with an increase in the culture period (Harada *et al*. 1994), but 1,25$(OH)_2D_3$ was converted to inactive forms. The bone-resorbing activity of F_6-1,23,25$(OH)_3D_3$ was similar to that of 1,25$(OH)_2D_3$ in organ culture (Harada *et al*. 1992). A higher activity of F_6-1,25$(OH)_2D_3$ in cultures of 48–144 h was suggested to be due to the formation of F_6-1,23,25$(OH)_3D_3$ from F_6-1,25$(OH)_2D_3$.

Conversion of F_6-1,25$(OH)_2D_3$ to F_6-1,23,25$(OH)_3D_3$ has been reported *in vitro* (HL-60 cells, Honda *et al*. 1993, Inaba *et al*. 1993; MG-63 cells, Ishibashi *et al*. 1996), *ex vivo* (Miyahara *et al*. 1999) and *in vivo* (Komuro *et al*. 1996).

25-Hydroxyvitamin D_3[25$(OH)D_3$]-24-hydroxylase (CYP24) hydroxylates at the C-24 position of 25$(OH)D_3$ and 1,25$(OH)_2D_3$ (Akiyoshi-Shibata *et al*. 1994). As CYP24 also has the ability to hydroxylate at the C-23 position of 25$(OH)D_3$ (Beckman *et al*. 1996), it was proposed that CYP24 hydroxylated at the C-23 position of F_6-1,25$(OH)_2D_3$. To clarify this point, ROS17/2.8 cells transfected with a plasmid expressing CYP24 [pSVL-CYP24(+)] were used. In addition, 26,27-hexafluoro-23-oxo-1α,25-dihydroxyvitamin D_3 [F_6-23-oxo-1,25$(OH)_2D_3$], a metabolite of F_6-1,23,25$(OH)_3D_3$ was identified *in vivo* (Komuro *et al*. 1996) but was not found *in vitro*. Also investigated was the possibility that F_6-1,23,25$(OH)_3D_3$ was converted to F_6-23-oxo-1,25$(OH)_2D_3$ by CYP24.

Materials and methods

Materials

F_6-1,25$(OH)_2D_3$, F_6-1,23,25$(OH)_3D_3$, F_6-23-oxo-1,25$(OH)_2D_3$ and [1β-^{3}H]-F_6-1,25$(OH)_2D_3$ (450 MBq/mmol, as radiochemical purity ~ 90%, it was purified by HPLC before use) were generous gifts from Sumitomo Pharmaceuticals (Osaka, Japan). 25$(OH)D_3$ and 24,25$(OH)_2D_3$ were from Funakoshi Co. Ltd. (Tokyo, Japan) [26,27-3H(N)]-25$(OH)D_3$ (6327 GBq/mmol, radiochemical purity ~ 100%) was from NEN Life Science Products, Inc. The plasmid expressing CYP24 [pSVL-CYP24(+)] and a corresponding blank plasmid [pSVL-CYP24R(−)] were prepared in our laboratory (Ohyama *et al*. 1991).

Transfection of ROS17/2.8 cells with pSVL-CYP24(+) or pSVL-CYP24(−)

ROS17/2.8 cells were seeded in 100-mm plates at a density of 1.5×10^6 cells/dish and cultured in Ham F12 containing 5% foetal calf serum (FCS) for 24 h. Eighty percent of confluent cells was transfected with pSVL-CYP24(+) or pSVL-CYP24R(−) using Transfast transfection reagent (Promega, Inc.) as described in the manufacture's manual. Forty-eight hours after transfection, the medium was replaced and the cells incubated with 3H-labelled substrate for 2 or 5 days.

Metabolism of [^{3}H]-25(OH)D_3 in pSVL-CYP(+)-transfected cells

Transfected cells were suspended in 180 μl 2% FCS-Ham F12 medium. Ten microliters of [^{3}H]-25$(OH)D_3$ (37 kBq) and 10 μl unlabeled 25$(OH)D_3$ (0.1 nmol) were added to the cell suspension, which was shaken vigorously at 37 °C for 2 h and then sonicated with Astrason XL (Heatsystem, Inc.). Sterols were extracted by the method of Bligh and Dyer (1957) with a slight modification. Sonicated solution was mixed with 0.64 ml methyl alcohol/chloroform (2:1) and vortexed for 3 min, and centrifuged at 10000 rpm for 5 min at 4 °C. The lower layer was added to a new microtube (1.5 ml). Aqueous layer was mixed with 500 μl chloroform, vortexed for 2 min, and centrifuged at 10000 rpm for 15 s at 4 °C. The second chloroform layer was added to the first. The combined chloroform layers were dried under

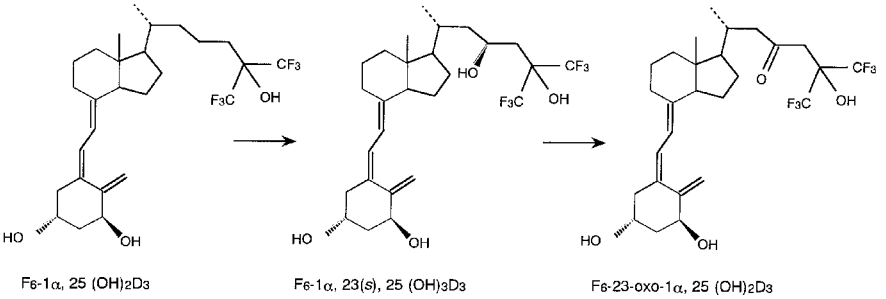


Figure 1. Metabolism of F_6-1,25$(OH)_2D_3$.

nitrogen and dissolved in 200 μl toluene:ethanol (1:1) for storage. 25$(OH)D_3$ and 24,25$(OH)_2D_3$ were separated by normal phase HPLC (Hitachi, Japan; column, Zorbax-Sil 4.6 × 250 mm; mobile phase, dichloromethane/methanol, 96:4; flow rate 1 ml/min). The effluent was collected in 1-min fractions. The radioactivity of each fraction was measured with a liquid scintillation spectrophotometer.

Metabolism of [^{3}H]-F_6-1,25$(OH)_2D_3$ and [^{3}H]-F_6-1,23,25$(OH)_3D_3$ in pSVL-CYP24(+)-transfected cells

Transfected cells were incubated with [^{3}H]-F_6-1,25$(OH)_2D_3$ or [^{3}H]-F_6-1,23,25$(OH)_3D_3$ (1.5 KBq, 150 pmol) in 15 ml of 2% FCS-Ham F12 medium for 2 and 5 days, respectively. After the cells were washed with Ca^{2+}- and Mg^{2+}-free phosphate-buffered saline [PBS(−)], 2 ml PBS(−) was added to the cell pellets. Cell suspension was sonicated for 2 min at 0 °C with Astrason XL. Sterols were extracted by the method of Harada *et al.* (1994). The sonicated solution was mixed with 1 ml tetrahydrofuran and 4 ml ethyl acetate, vortexed and centrifuged at 2200 rpm for 5 min at 4 °C. The aqueous layer was extracted with 4 ml ethyl acetate four times. The organic layer was dried with anhydrous sodium sulphate and evaporated. Dried extracts were dissolved in *n*-hexane containing 4% isopropanol and the solution was passed through a Sep-Pak cartridge (Waters Associates, Milford, MA, USA) equilibrated with *n*-hexane containing 20% isopropanol. The eluate was dried under nitrogen and dissolved in 200 μl toluene:ethanol (1:1) for storage. The sample was subjected to HPLC on normal phase Zorbax Sil (4.6 × 250 mm) at 1.5 ml/min and eluted with *n*-hexane/isopropanol/dichloromethane (49:3:48). The effluent was collected in 1-min fractions. In addition, when [^{3}H]-F_6-1,25$(OH)_2D_3$ and [^{3}H]-F_6-1,23,25$(OH)_3D_3$ were separated, we also used reversed-phase HPLC (column, Sumipax ODS A212, 6 × 150 mm; mobile phase, acetonitrile/water/tetrahydrofuran, 45:50:5; flow rate 1.5 ml/min). [1β-^{3}H]-F_6-1,23,25$(OH)_3D_3$ was prepared by incubation of [1β-^{3}H]-F_6-1,25$(OH)_2D_3$ with the osteogenic cell line, MC3T3-E1. [1β-^{3}H]-F_6-1,25$(OH)_2D_3$ and its metabolite were extracted with ethyl acetate from the cells, and [1β-^{3}H]-F_6-1,23,25$(OH)_3D_3$ was isolated from the mixture by HPLC.

Results

Metabolism of 25$(OH)D_3$ in pSVL-CYP24(+)-transfected ROS17/2.8 cells

To confirm that pSVL-CYP24(+)-transfected cells have CYP24 activity, [^{3}H]-25$(OH)D_3$ was incubated with ROS17/2.8 cells which were transfected at transfection reagent:plasmid DNA ratio of 1:1 (figure 2A), 2:1 (figure 2B) and 3:1 (figure 2C). [^{3}H]-24,25$(OH)_2D_3$ was detected by HPLC. When the reagent:DNA ratio was 2:1, the peak height of 24,25$(OH)_2D_3$ was maximum (figure 2B). As shown in figure 2D, [^{3}H]-24,25$(OH)_2D_3$ was not detected in pSVL-CYP24R(−)-transfected cells which were incubated with [^{3}H]-25$(OH)D_3$.

Metabolism of F_6-1,25$(OH)_2D_3$ in pSVL-CYP24(+)-transfected ROS17/2.8 cells

In figure 3, HPLC pattern of F_6-1,25$(OH)_2D_3$, F_6-1,23,25$(OH)_3D_3$ and F_6-23-oxo-1,25$(OH)_2D_3$ was shown. Incubation of [1β-^{3}H]-1,25$(OH)_2D_3$ with pSVL-CYP24(+)-transfected ROS17/2.8 cells for 2 and 5 days generated a metabolite that

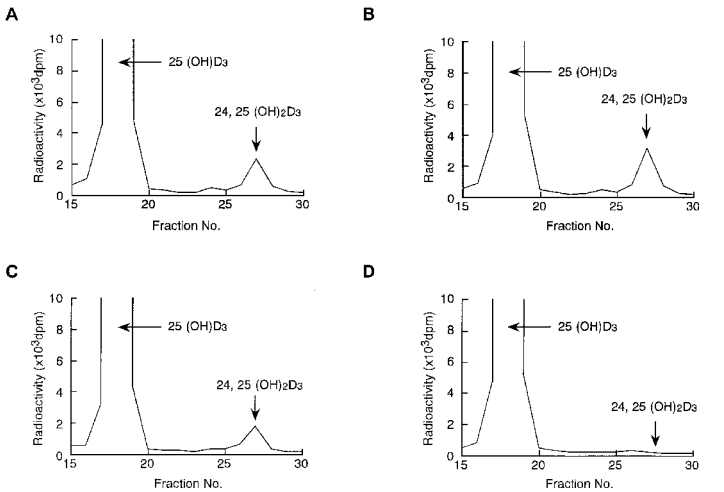


Figure 2. Conversion of $25(OH)D_3$ to $24,25(OH)_2D_3$ in ROS17/2.8 cells transfected with pSVL-CYP24(+). Eighty percent of confluent ROS17/2.8 cells were transfected with pSVL-CYP24(+) at 1:1 (A), 2:1 (B), 3:1 (C) reagent:plasmid DNA ratio or pSVL-CYP24R(−) at 2:1(D) reagent:DNA ratio. One hour after transfection, 5% FCS-Ham F12 medium was added to the plate. After 48-h incubation, the cells were shaken vigorously with 10 nM [^{3}H]-$25(OH)D_3$ for 2 h at 37 °C. The chloroform layer from the extract of the reaction mixture was subjected on normal phase HPLC (Zorbax-Sil) to detect [^{3}H]-$24,25(OH)_2D_3$.

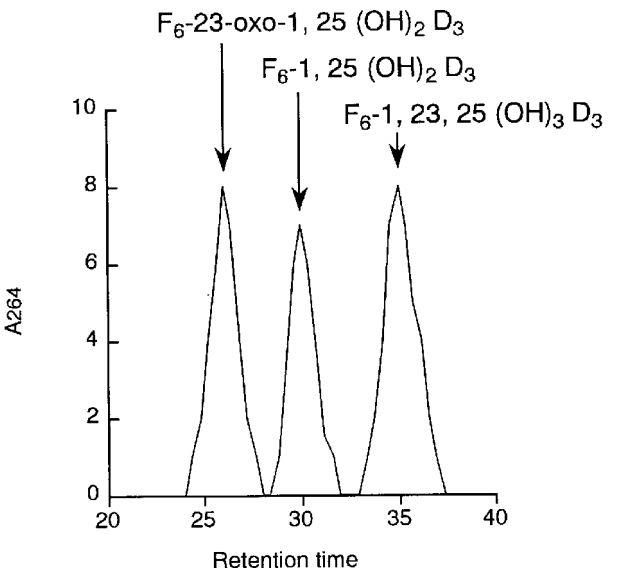


Figure 3. HPLC pattern of authentic F_6-$1,25(OH)_2D_3$ metabolites. Authentic F_6-$1,25(OH)_2D_3$ metabolites were subjected to HPLC on a Zorbax Sil (4.6× 250 mm) column using *n*-hexane/isopropanol/dichloromethane (49:3:48 by vol.) at 1.5 ml/min by monitoring UV absorption at 264 nm.

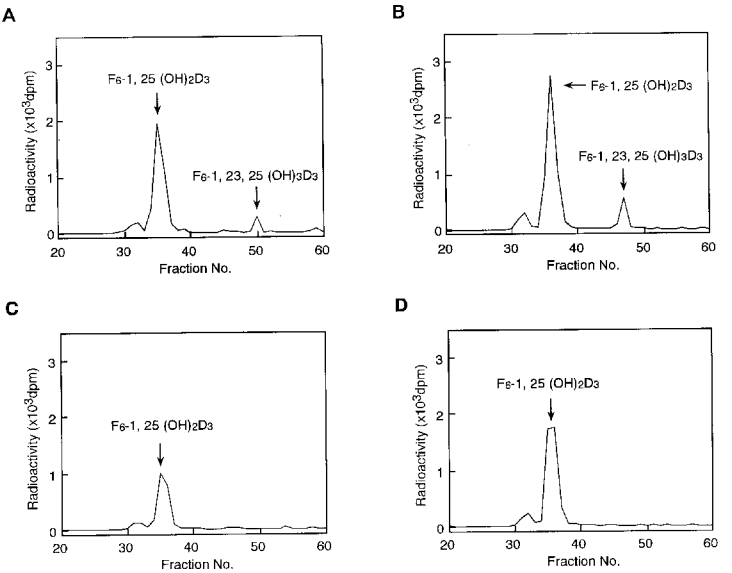


Figure 4. Conversion of F_6-1,25$(OH)_2D_3$ to F_6-1,23,25$(OH)_3D_3$ in ROS17/2.8 cells transfected with pSVL-CYP24(+). Eighty percent of confluent ROS17/2.8 cells were transfected with pSVL-CYP24(+) (A, B) or pSVL-CYP24R(−) (C, D) at 2:1 transfection reagent:plasmid DNA ratio. One hour after the transfection, 5% FCS-Ham F12 medium was added to the culture dish. After 48 h, cells were cultured with 10 nM [1β-^{3}H]-F_6-1,25$(OH)_2D_3$ for 2 days (A, C) or 5 days (B, D). The ethyl acetate layer from the cell extract was analysed by normal phase HPLC to detect F_6-1,23,25$(OH)_3D_3$.

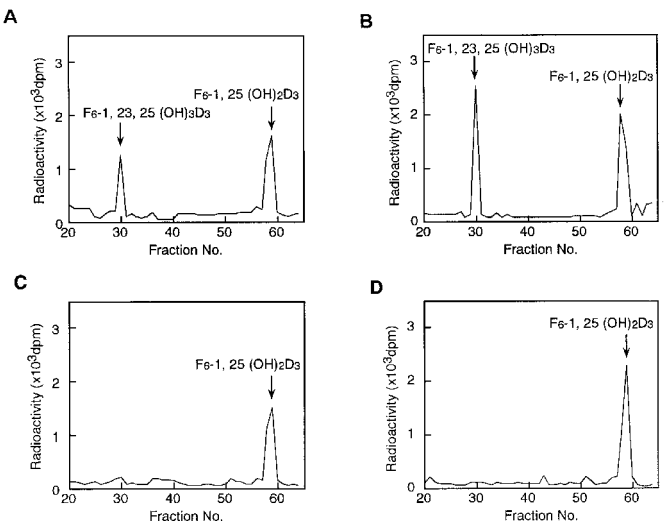


Figure 5. Conversion of F_6-1,25$(OH)_2D_3$ to F_6-1,23,25$(OH)_3D_3$ in pSVL-CYP(+)-transfected ROS17/2.8 cells. Eighty percent of confluent cells was transfected with pSVL-CYP24(+) (A, B) or pSVL-CYP24R(−) (C, D) at 2:1 transfection reagent:plasmid DNA ratio. Transfected cells were incubated with 10 nM [1β-^{3}H]-F_6-1,25$(OH)_2D_3$ for 2 days (A, C) or 5 days (B, D). The ethyl acetate layer from the cells was analyzed by reversed-phase HPLC (Sumipax ODS A-212).

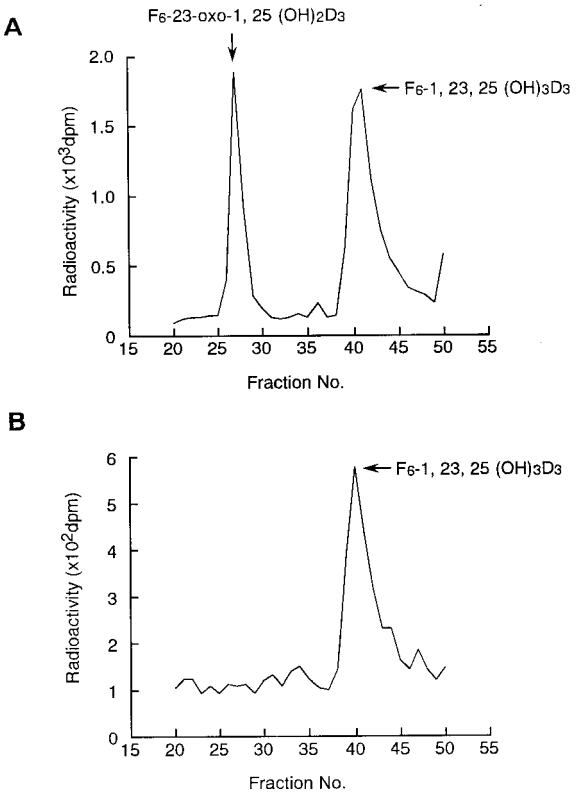


Figure 6. Conversion of F_6-1,23,25$(OH)_3D_3$ to F_6-23-oxo-1,25$(OH)_2D_3$ in pSVL-CYP24(+)-transfected ROS17/2.8 cells. Eighty percent of confluent cells was transfected with pSVL-CYP(+)24 (A) or pSVL-CYP24R(−) (B) at 2 : 1 reagent plasmid DNA ratio. Transfected cells were incubated with 10 nM [1β-^{3}H]-F_6-1,23,25$(OH)_3D_3$ for 3 days. The ethyl acetate layer from the cells was analysed by normal phase HPLC (Zorbax-Sil).

co-migrated with authentic F_6-1,23,25$(OH)_3D_3$ on normal phase HPLC (figure 4) and on reversed-phase HPLC (figure 5). As shown in figures 4 and 5, ROS 17/2.8 cells transfected with pSVL-CYP24R(−) did not generate F_6-1,23,25$(OH)_3D_3$.

Metabolism of F_6-1,23,25$(OH)_3D_3$ in pSVL-CYP24(+)-transfected ROS17/2.8

When [1β-^{3}H]-1,23,25$(OH)_3D_3$ was incubated with pSVL-CYP24(+)-transfected cells for 3 days, we detected a metabolite that co-migrated with authentic F_6-23-oxo-1,25$(OH)_2D_3$. In ROS17/2.8 transfected with pSVL-CYP24R(−), a metabolite was not recognized (figure 6).

Discussion

CYP24 was identified as the enzyme responsible for the hydroxylation at the C-24 position of 1,25$(OH)_2D_3$ and 25$(OH)D_3$ (Ohyama and Okuda 1991) and human recombinant CYP24 additionally catalyses the hydroxylation at the C-23 position of 25$(OH)D_3$ (Beckman *et al.* 1996). Miyamoto *et al.* (1997) reported that 24,24-difluoro-1α,25-dihydroxyvitamin D_3 is metabolized to 24,24-difluoro-1α,25,26$(OH)_3D_3$ by pSVL-CYP(+)-transfected ROS17/2.8 cells. These results

indicate that CYP24 has multicatalytic functions. Therefore, it is generally accepted that CYP24 also hydroxylates the C-23 position of F_6-1,25$(OH)_2D_3$. Recently, Hayashi *et al*. (1998) demonstrated that F_6-1,25$(OH)_2D_3$ was metabolized to F_6-1,23,25$(OH)_3D_3$ by rat kidney mitochondrial 24-hydroxylase expressed in *E. coli*. This report supports our result that F_6-1,25$(OH)_2D_3$ is metabolized to F_6-1,23,25$(OH)_3D_3$ in pSVL-CYP24(+)-transfected ROS17/2.8.

On the other hand, it is established that the osteoblastic cell line, UMR106, in addition to kidney and intestine, catalyses the conversion of 1,24,25-trihydroxy-vitamin D_3 to 1,25-dihydroxy-24-oxo-vitamin D_3 (Reddy and Makin 1989). This step is speculated to consist of the following reaction mechanism. CYP24 first hydroxylates 1,25$(OH)_2D_3$ at position 24, then introduces another hydroxy group at the same position to form a *gem*-diol intermediate, which spontaneously rearranges with loss of water to form the corresponding ketone (Akiyoshi-Shibata *et al*. 1994). Conversion of F_6-1,23,25$(OH)_3D_3$ to F_6-23-oxo-1,25$(OH)_2D_3$ also is suggested to be catalysed by CYP24 in a similar fashion. A similar multiple reaction mechanism has been reported in the formation of oestrogen by P450arom (Watanabe and Ishimura 1989).

In conclusion, metabolism of F_6-1,25$(OH)_2D_3$ to F_6-1,23,25$(OH)_3D_3$ and that of F_6-1,23,25-$(OH)_3D_3$ to F_6-23-oxo-1,25$(OH)_2D_3$ was confirmed to be catalysed by CYP24.

References

Akiyoshi-Shibata, M., Sakaki, T., Ohyama, Y., Noshiro, M., Okuda, K. and Yabusaki, Y., 1994, Further oxidation of hydroxycalcidiol by calcidiol 24-hydroxylase: a study with the mature enzyme expressed in *Escherichia coli*. *European Journal of Biochemistry*, **224**, 335–343.

Beckman, M. J., Tadikonda, P., Werner, E., Prahl, J., Yamada, S. and DeLuca, H. F., 1996, Human 25-hydroxyvitamin D_3-24-hydroxylase, a multicatalytic enzyme. *Biochemistry*, **35**, 8465–8472.

Harada, M., Miyahara, T., Miyata, M., Tomita, I., Okayachi, H., Ikemoto, Y., Higuchi, S., Otomo, S., Kozuka, H. and Ikekawa, N., 1992, Effect on cultured neonatal mouse calvariae of 1α, 25-dihydroxyvitamin D_3, 26,26,26,27,27,27-hexafluoro-1α,25-dihydroxyvitamin D_3 and 26,26,26,27,27,27-hexafluoro-1α,23,25-trihydroxyvitamin D_3. *Bone and Mineral*, **18**, 41–49.

Harada, M., Miyahara, T., Kajita-Kondo, S., Kozakai, A., Higuchi, S., Otomo, S. and Kozuka, H., 1994, Differences in metabolism between 26,26,26,27,27,27-hexafluoro-1α,25-dihydroxyvitamin D_3 and 1α,25-dihydroxyvitamin D_3 in cultured neonatal mouse calvaria. *Research Communications in Molecular Pathology and Pharmacology*, **86**, 183–193.

Hayashi, K., Akiyoshi-Shibata, T., Sakaki T. and Yabusaki, Y., 1998, Rat CYP24 catalyses 23S-hydroxylation of 26,26,26,27,27,27-hexafluorocalcitriol *in vitro*. *Xenobiotica*, **28**, 457–463.

Honda, A., Nakashima, N., Shida, Y., Mori, Y., Nagata, A. and Ishizuka, S., 1993, Modification of 1α,25-dihydroxyvitamin D_3 metabolism by introduction of 26,26,26, 27,27,27-hexafluoro atoms in human promyelocytic leukemia (HL-60) cells: isolation and identification of a novel bio-active metabolite, 26,26,26,27,27,27-hexafluoro-1α,23(*S*)25-trihydroxyvitamin D_3. *Biochemical Journal*, **295**, 509–516.

Inaba, M., Okuno, S., Nisizawa, Y., Imanishi, Y., Katsumata, T., Sugata, I. and Morii, H., 1993, Effect of substituting fluoride for hydrogen at C-26 and C-27 on the side chain of 1,25-dihydroxyvitamin D_3. *Biochemical Pharmacology*, **45**, 2331–2336.

Ishibashi, E., Seki, H. and Katsumata, M., 1996, Effects of Falecalcitriol on osteocalcin secretion and its metabolism in human osteosarcoma cell line, MG-63. *Clinical Report*, **30**, 2983–2990.

Komuro, S., Kanamaru, H., Nakatsuka, I. and Yoshitake, A., 1996, Disposition and metabolism of ST-630(2): metabolism after single administration of ^{3}H-ST-630 in rats. *Xenobiotic Metabolism and Disposition*, **11**, 518–529.

Makin, G., Lohnes, D., Byford, V., Ray, R. and Jones, G., 1989, Target cell metabolism of 1,25-dihydroxyvitamin D_3 to calcitroic acid. *Biochemical Journal*, **262**, 173–180.

Miyahara, T., Harada, M., Kozakai, A., Matsumoto, M., Hashimoto, K., Inoue, H., Yoda, K., Nakatsu, T., Kajita, S., Yamazaki, R., Higuchi, S., Kozuka, H. and Nemoto, N., 1999, Comparison of 26,27-hexafluoro-1α,25-dihydroxyvitamin D_3 and 1α,25-dihydroxyvitamin D_3 on the resorption of bone explants *ex vivo*. *Journal of Nutritional Science and Vitaminology*, **45**, 239–249.

Miyamoto, Y., Shinki, T., Yamamoto, K., Ohyama, Y., Iwasaki, H., Hosotani, R., Kasawa, T., Takayama, H., Yamada, S. and Suda, T., 1997, 1α-25-dihydroxyvitamin D_3-24-hydroxylase (CYP24) hydroxylates the carbon at the end of the side chain (C-26) of the C-24-fluorinated analog of 1α, 25-dihydroxyvitamin D_3. *Journal of Biological Chemistry*, **272**, 14115–14119.

Ohyama, Y., Noshiro, M. and Okuda, K., 1991, Cloning and expressing of cDNA encoding 25-hydroxyvitamin D_3 24-hydroxylase. *FEBS Letters*, **278**, 195–198.

Stern, P. H., Marreas, T., Tanaka, Y., DeLuca, H. F., Ikekawa. N. and Kobayashi Y., 1984, Fluoride substitution of vitamin D analogs at C-26 and C-27: enhancement of activity of 25-hydroxyvitamin D but not of 1,25-dihydroxyvitamin D on bone and intestine *in vitro*. *Journal of Pharmacology and Experimental Therapeutics*, **229**, 9–13.

Tanaka, Y., DeLuca, H. F., Kobayashi, Y. and Ikekawa, N., 1984, A highly potent, long-lasting analog of 1,25-dihydroxyvitamin D_3. *Archives of Biochemistry and Biophysics*, **229**, 348–354.

Watanabe, Y. and Ishimura, Y., 1989, Aromatization of tetralone derivatives by FeIIIPFR(Cl)/ PHIO and cytochrome P-450cam: a model study on aromatase P-450 reaction. *Journal of the American Chemical Society*, **111**, 410–411.

XENOBIOTICA, 2000, VOL. 30, NO. 11, 1063–1077

Isolation and cultivation of Ca^{2+} tolerant cardiomyocytes from the adult rat: improvements and applications

T. THUM and J. BORLAK*

Fraunhofer Institute of Toxicology and Aerosol Research, Center of Drug Research and Medical Biotechnology, Hannover, Germany

Received 31 March 2000

1. Primary cultures of cardiomyocytes provide a valuable tool for the study of the pharmacological and toxicological properties of drugs and chemicals, but for several technical reasons cardiomyocytes from adult animals are not routinely used in long-term culture. Because of significant advances in cardiovascular research, tissue engineering and cell transplantation, the need to isolate primary cells from adult animal and/or human tissue is likely to increase in the future.

2. The most common protocols for the isolation and cultivation of cardiomyocytes have been reviewed and the various approaches have been compared. The recent advances in cell culture techniques and the use of the cytoprotective agent, e.g. 2,3-butanedione monoxime greatly increases cell yield and cell viability of isolated and cultured cardiomyocytes. New concepts emerge that enabled an assessment of cellular differentiation in cultured cardiomyocytes and certain specific nuclear transcription factors may play a pivotal role in this process.

Introduction

Shortly after birth, cardiomyocytes lose their ability to proliferate *in vivo* (Rumyantsev 1963) and growth of heart tissue is governed by cellular growth rather then by cell proliferation. Although the majority of investigators prefer the isolation of cardiomyocytes from foetal and/or neonatal tissue to establish a confluent cell layer, these initial proliferative cells dedifferentiate rather quickly, e.g. development of pseudopodial extensions and changes in the expression of subtypes of myosin (Nag *et al*. 1985, Ghanbari and McCarl 1980). Cardiomyocytes have been isolated since the early 1950s, and one of the first protocols for the isolation of embryonic cardiomyocytes of the rat was by Cavanaugh (1955). Thereafter, a number of isolation protocols for neonatal laboratory animals have been reported (Harary and Farley 1960, Nag *et al*. 1985, Marino *et al*. 1989). All of these isolation protocols depend heavily on the use of new-born animals, but Vahouny *et al*. (1970) were one of the first to report the isolation of cardiomyocytes from the adult rat. The highlights of the most important isolation protocols and a summary of various experimental parameters are given in table 1.

Despite the above-named achievements, there are still major problems that need to be overcome when cardiomyocytes are isolated from adult animals and these include yield and viability and maintenance of cardiomyocytes in culture for prolonged periods. Furthermore, as adult cardiomyocytes are evaluated for their use in clinical cell transplantation, the need for a robust and well-characterized culture model is greater than ever, which justifies the renewed attempts in developing an

* Author for correspondence at: Fraunhofer Institute of Toxicology and Aerosol Research, Department of Molecular Toxicology and Pharmacokinetics, Nicolai-Fuchs-Str. 1, D-30659 Hannover, Germany; e-mail: Borlak@ita.fhg.de

Xenobiotica ISSN 0049-8254 print/ISSN 1366-5928 online © 2000 Taylor & Francis Ltd
http://www.tandf.co.uk/journals DOI: 10.1080/00498250010005196

Table 1. Compilation of isolation protocols to obtain cardiomyocytes from the adult rat.

Reference	Washing solution	Enzyme solution+treatment	Cultivation media	Cell count (% of rod-shaped cells)	Calcium tolerance
Vahouny (1970)	—	incubation of sliced heart with collagenase and trypsin	none	55 (after 100 min; 30)	no
Fabiato and Fabiato (1972)	—	incubation of sliced heart with collagenase and trypsin or hyaluronidase	none	10	no
Grosso *et al.* (1977)	—	Ca-free PBS, collagenase, hyaluronidase, BSA, then slices of heart incubated with enzyme solution	none	90	no
Nag and Zak (1979)	KRP with 2 mM EDTA	collagenase, hyaluronidase, BSA, then cells shaken in KRP	Eagles' minimum essential medium, epidermal growth factor, insulin–transferrin–selenium mixture, norepinephrine, triiodothyronine, ascorbic acid	65	yes
Nag *et al.* (1983),	Ca-free KRP	collagenase, hyaluronidase, BSA	see above	60 (varied)	yes
Bkaily *et al.* (1984)		collagenase, trypsin Sr or Ba ions instead of Ca ions	not known	63	yes
Van der Heide (1990)	Ca-free buffer	collagenase	Dulbecco's modified Eagle medium	74 (after 120 min 63%)	yes
Weisensee (1995),	Ca-free tyrode	collagenase, hyaluronidase	Dulbecco's modified Eagle medium	?(not reported)	yes
Kivisto (1995)	tyrode solution 2 mM Ca for 3 min, then Ca-free tyrode solution for 6 min	tyrode solution with collagenase A, BDM heart sliced and filtrated	tyrode solution	?(not reported)	yes
Thum and Borlak (2000a)	Joklik solution with 15 mM BDM, 500 μM EDTA	Joklik solution with 15 mM BDM, 1 mg/ml collagenase II, 1% BSA, heart sliced and filtrated	Joklik medium, foetal calf serum	92	yes

improved protocol for the isolation and cultivation of cardiomyocytes. These systems, although experimental at this stage, may be the therapies of the future, e.g. cardiomyocytes for local drug delivery and for cell transplantation into infarcted tissue (Soonpaa *et al*. 1994). From a clinical point of view, transplantation of foetal cardiomyocytes is unlikely, which necessitates the development of a cell culture model based on adult cardiomyocytes.

Improvements and applications

Various isolation and cultivation protocols for rodent cardiomyocytes

The isolation of cardiomyocytes from adult animals was initially carried out by slicing heart tissue and transferring the slices into an enzyme digestive solution. Alternatively, the retrograde perfusion of the heart was carried out by inserting a cannula into the aorta ascendens and perfusion of the heart with an enzymatic solution to digest the tissue. In early studies, cell isolation could only be achieved for calcium-intolerant cells with survival rates of a few hours only (Vahouny *et al*. 1970) and additions of physiological calcium concentration to the culture media produced metabolically deregulated cardiomyocytes, leading to hypercontractility, ischaemia and membrane damage, e.g. actin aggregates leading to bleb formation of the cytoskeleton (Brierley *et al*. 1985). In addition, aggressive enzyme digestion results in low yield and viability of cardiomyocytes during isolation and therefore a fine balance between good digestion of connective tissue but non-aggressive preparation of cells is needed. Thus, a number of enzyme preparations have been tested, including collagenase of various types (I-IV), hyaluronidase and trypsin (Fabiato *et al*. 1971, Nag and Zak 1979, Nag *et al*. 1985). Cells that have been aggressively isolated appear to be more vulnerable towards cell ischaemia and other cytotoxic effects in response to the isolation procedure, but unfortunately, membrane damage can not be easily determined in culture. Typical changes in response to membrane damage include the formation of spherical (figure 1a) as opposed to rod shaped cells (figure 1b) and high levels of lactate dehydrogenase and creatine kinase activity (figure 2).

The process of cellular dedifferentiation in culture appears to be gradual starting with the loss of rod-shape morphology and changes in the cytoskeleton leading to the formation of pseudopodium like structures (figure 1c). Of note, these cells are not ischaemic (spherical shape) *per se* before their change in morphology. For comparison, typical ischaemic cardiomyocytes are round and are shown in figure 1a.

Cellular dedifferentiation of cardiomyocytes in culture is presumably irreversible and is accompanied with a change in electrical conductivity, as shown by the lack of syncytial contractility and the very significant increase in beats per minute (60–100 beats/min[1]).

Well-cultured and healthy cardiomyocytes should not contract, as a large number of contracting cells in culture may be viewed as membrane damaged and metabolically deregulated (Brierley *et al*. 1985).

From the studies of several investigators, evidence has been obtained that ischaemic cells suffer from a disorganization of myofilaments leading to the formation of blebs of the sarcolemma (Sage and Jennings 1988, Vanwinkle *et al*. 1994, Jans *et al*. 1997) and, indeed, a major step forward was the method of Powell and Twist (1976), who reported the isolation of calcium-tolerant cardiomyocytes. A

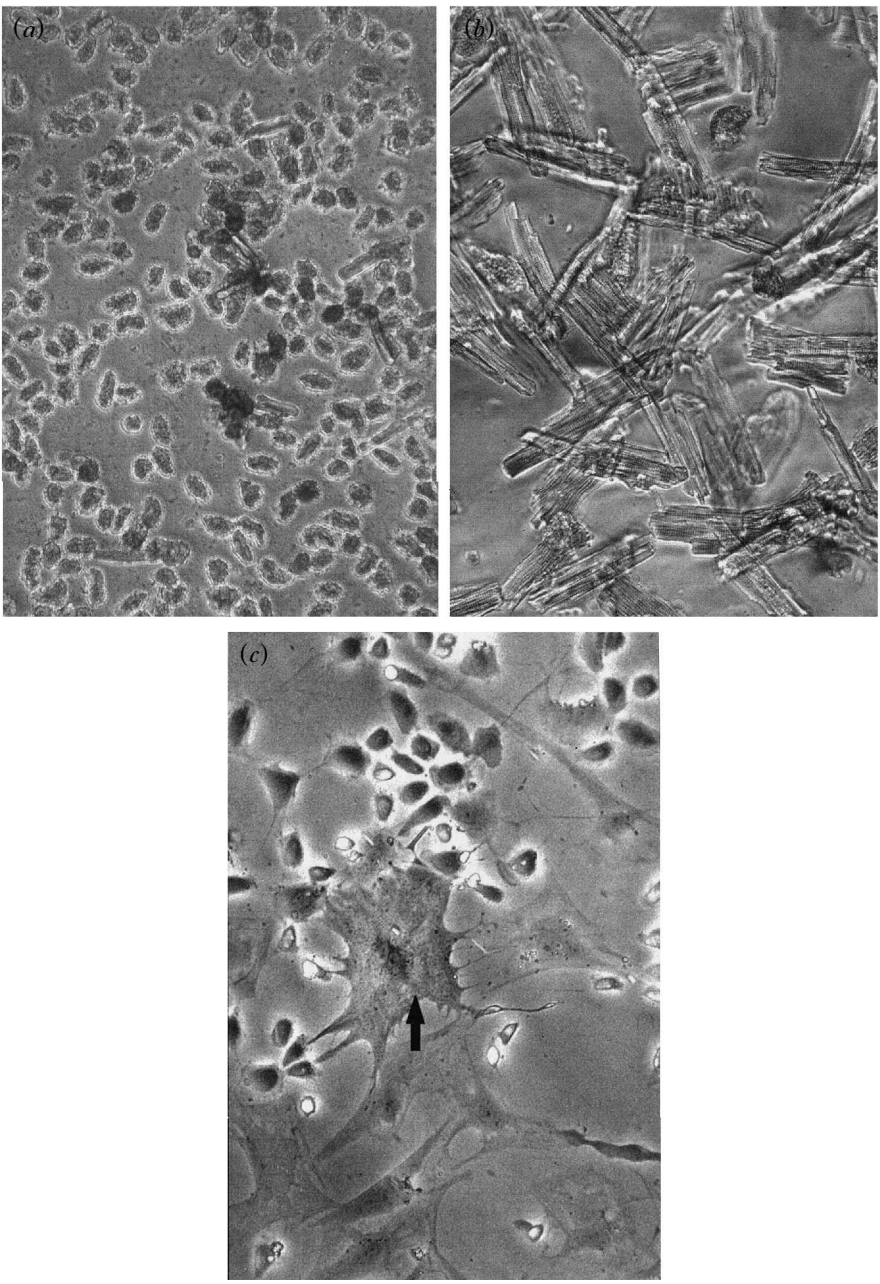


Figure 1. (a) Ischaemic (spherical) cardiomyocytes in culture. (b) Freshly isolated rod-shaped cardiomyocytes. (c) Dedifferentiated cardiomyocytes cultured for 4 weeks. Dark arrows show the cardiac myocyte with multiple pseudopodial extensions.

variety of different culture media and perfusion conditions were then investigated to improve the yield of calcium-tolerant cardiomyocytes, of which a summary is given in table 1. With the method of Powell and Twist (1976), cells that maintained calcium homeostasis and calcium overload could be prevented by avoiding metabolic deregulation of sodium calcium exchange pumps (Altschuld *et al*. 1980).

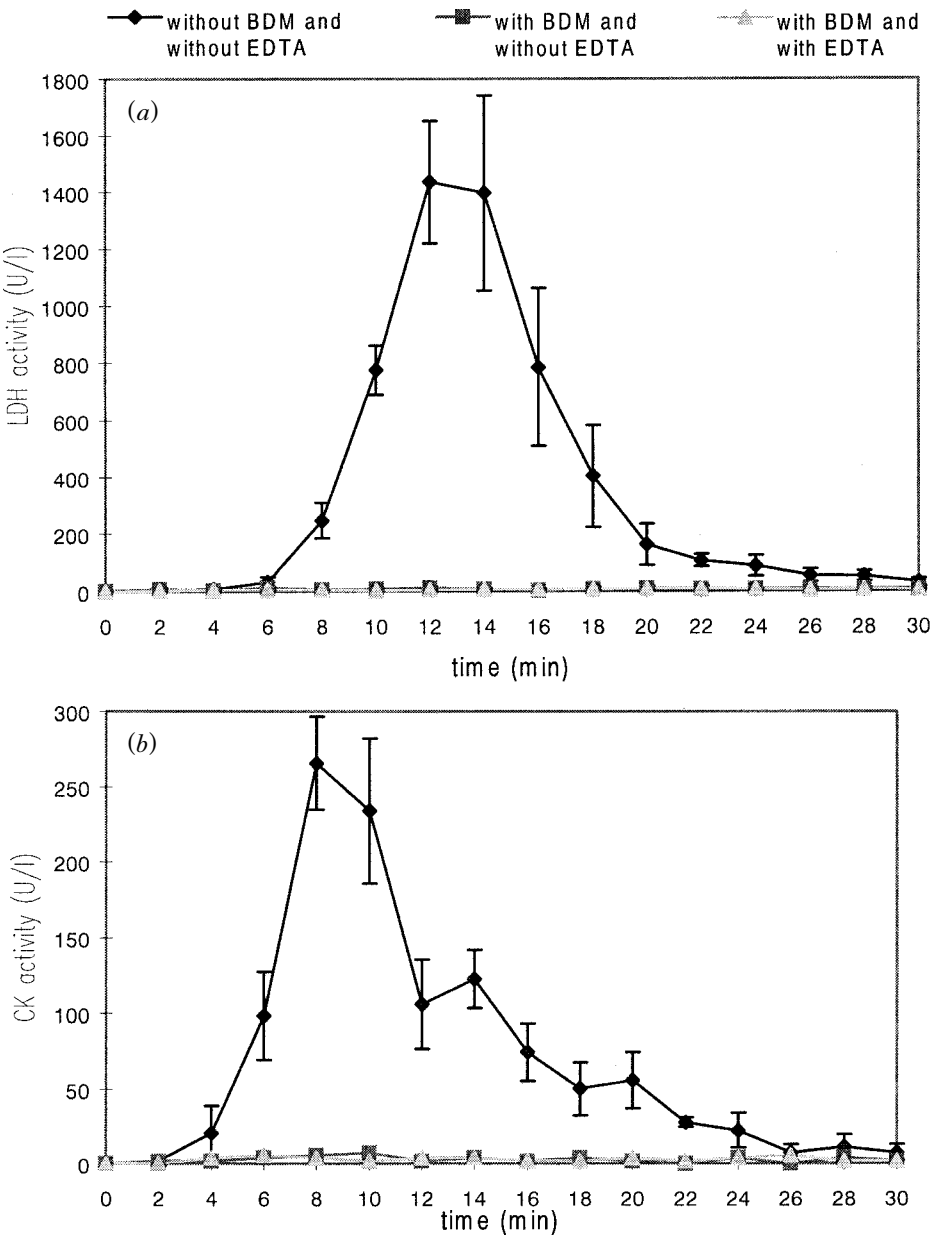


Figure 2. (a) Lactate dehydrogenase (LDH) activity during isolation of cardiomyocytes. (b) Creatine kinase (CK) activities during isolation of cardiomyocytes.

Van der Heide *et al*. (1990) isolated ~ 70% of intact cells, but cardiomyocytes lost their rod-shaped morphology within a few hours. The isolation procedure itself and the use of various proteases, e.g. collagenase, trypsin or hyaluronidase, are also given in table 1 and there is a very significant increase in the markers LDH and CK during isolation (figure 2). Both enzymes are important for membrane integrity and membrane damage with CK being a specific marker for muscle cells. Although, LDH and CK activities did increase during retrograde perfusion the addition of the

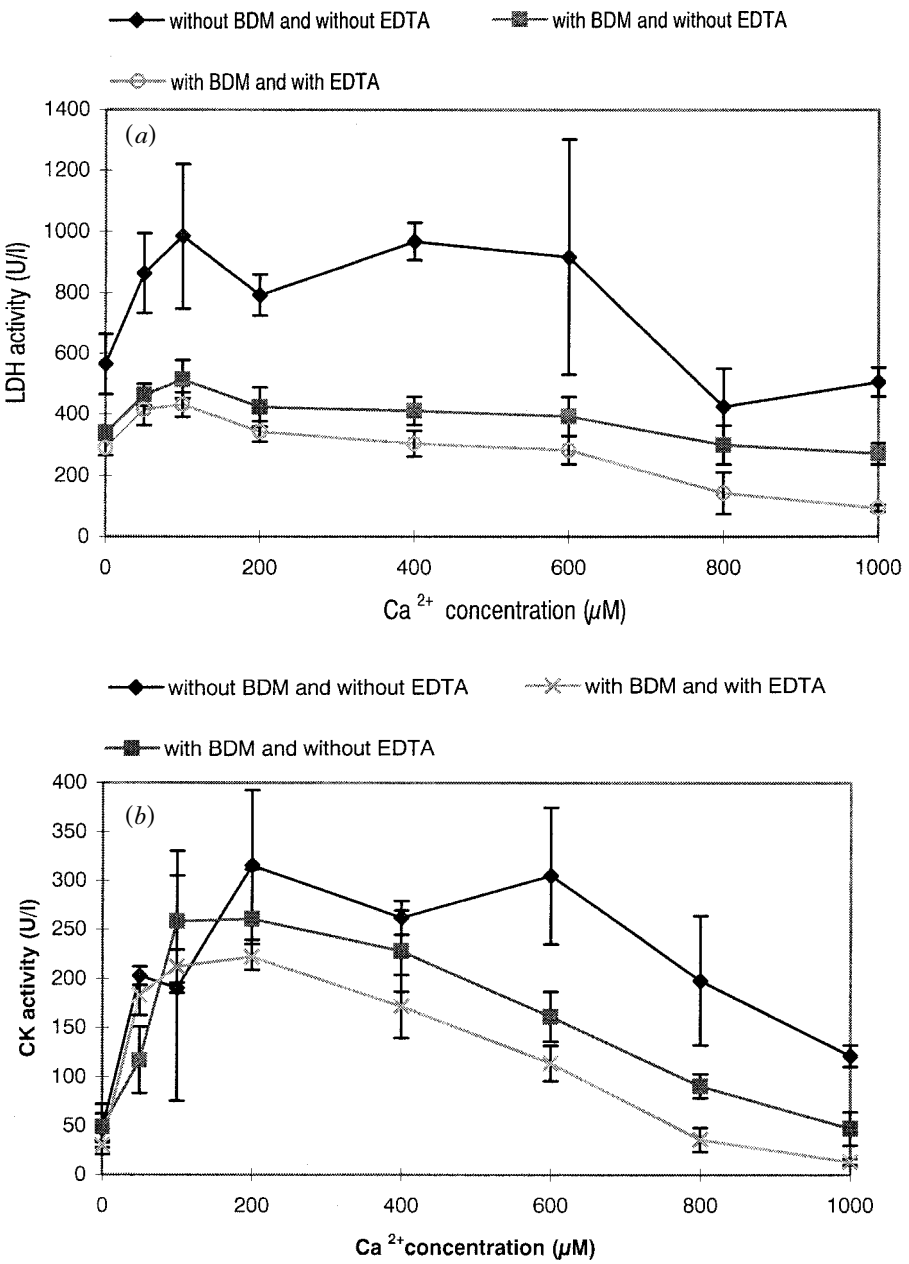


Figure 3. (a) Lactate dehydrogenase (LDH) activity during the calcium replacement phase. (b) Creatine kinase (CK) activity during the calcium replacement phase.

cytoprotective agent butanedione monoxime (BDM) alleviated this rise in enzyme activity very significantly (figure 2), thus producing favourable results.

It is interesting that these increase in enzyme activities are somewhat similar to these reported for myocardial infarction as observed during post myocardial infarction (Herlitz *et al*. 1988). Based on the latter endpoints, *in vitro* experiments may simulate cell damage as observed during myocardial infarction.

The majority of investigators isolate and cultivate cardiomyocytes from foetal, perinatal or neonatal animals due to the difficulties in working with heart tissue from adult animals and there are several advantages when foetal/new-born animals are used including formation of confluent cardiomyocyte cell layers and maintenance of cell cultures for prolonged periods of time (Nag *et al*. 1985). On the other hand, foetal cardiomyocytes differ morphologically and biochemically and thus may be of limited value (Pin and Merrifield 1993, Kato *et al*. 1996). This includes developmental changes in action potential and membrane currents (Kato *et al*. 1996) or the expression of different myosin heavy chain phenotypes (Pin and Merrifield 1993). Therefore, foetal cells do not necessarily provide the appropriate test system for predicting *in vivo* organ toxicity when compared with adult cardiomyocytes.

Previously, calcium-tolerant cardiomyocytes could not be isolated and on addition of calcium to the culture media, cardiomyocytes changed their rod-shape morphology immediately to become spherical (Haworth *et al*. 1989). A swift and irreversible calcium-intoxication of cells is then observed leading to cell death. Kao *et al*. (1980) were one of the first to isolate calcium-tolerant cells with a modified culture media, e.g. containing insulin. Warming of the culture media to 37 °C during the calcium-depletion phase improved additionally cell yield and viability. BDM is shown to be cytoprotective during the calcium repletion phase (figure 3).

Utility of BDM in the isolation and cultivation of adult cardiomyocytes

As stated above, BDM caused a dramatic decline in the release of LDH and CK during isolation and in culture (figure 2). The cytoprotective properties of BDM have been attributed to the negative inotropic property of BDM (Takasago *et al*. 1997). A further property of BDM shows it to produce a reversible blockade of the gap junctions in cardiomyocytes (Verrecchia *et al*. 1997). BDM is already used in solutions to preserve hearts for transplantation (Stringham *et al*. 1992), because of its favourable properties and its known usefulness as an organ-protective agent.

A further improvement in the isolation procedure of Thum and Borlak, 2000a was the use of EDTA at the beginning of the isolation, as EDTA produced improved viability and yield of cardiomyocytes. Various protocols were compared by Thum and Borlak in the isolation of cardiomyocytes from the adult rat. Briefly, in the presence of EDTA $11.0 \pm 0.3 \times 10^6$ cardiomyocytes could be isolated the viability being $92.7 \pm 1.8\%$. In contrast, omission of EDTA resulted in similar yields ($11.3 \pm 2 \times 10^6$ cells) but reduced cell viability ($34 \pm 9.5\%$) (figure 4).

Others have also used calcium-chelating agents but primarily for the isolation of hepatocytes (Rivas *et al*. 1993). Most likely, EDTA modulates tight junctions of cardiomyocytes, thereby improving yield and vitality of cells. Presumably, this modulation of tight junctions between cells leads to a less dramatic damage of membranes, as less time is needed for dissolving the connective tissue (Artursson and Magnusson 1989).

BDM also stabilizes membrane function and prevents the formation of blebs (cytoskeleton damage) (Habazettl *et al*. 1998), and therefore these findings with BDM warrant further investigations into its cytoprotective properties. Recently, the favourable effects of BDM on the gene expression of the stress marker ANP (atrial natriuretic peptide) was investigated in cardiomyocyte cultures (Thum and Borlak, 2000b; figure 5).

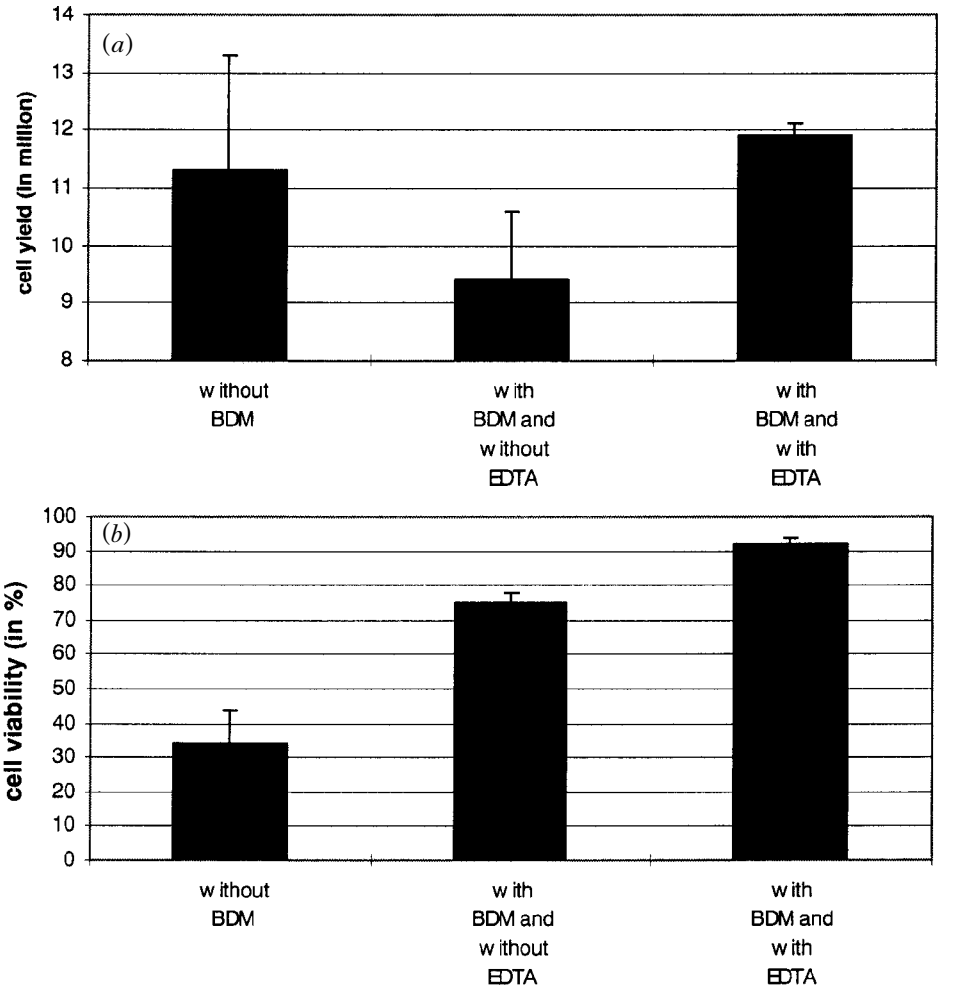


Figure 4. (a) Cell yield of adult cardiomyocytes using different isolation protocols. (b) Cell viability of adult cardiomyocytes after isolation using different isolation protocols.

Cytochrome P450 (P450) system in cardiomyocytes

Previous studies have reported that high levels of P450 occur in cardiac microsomes of *Stenotomus chrysops* (Stegeman *et al.* 1982). In addition, P4501A1 induction and localization in endothelium of vertebrate heart tissue (teleost) has been reported by the same group (Stegeman *et al.* 1989). The authors reported that treatment of *S. chrysops* (scup) with β-naphthaflavone produced an extensive ($\sim$ 10-fold) induction of spectrally measured P450 in cardiac microsome with the specific P450 content reaching levels similar to those induced in scup liver. Using a monoclonal antibody, Stegeman *et al.* (1989) also reported the immunohistochemical localization of environmentally induced P4501A1 in multiple organs of the marine scup and P4501A1 was specifically detected in vascular tissue and particularly in endothelial cells but not in other cell types.

In the scup hearts staining was detected in the endocardium of atrium and ventricle and endothelium of the coronary vasculature and in the great vessels (Stegeman *et al.* 1989).

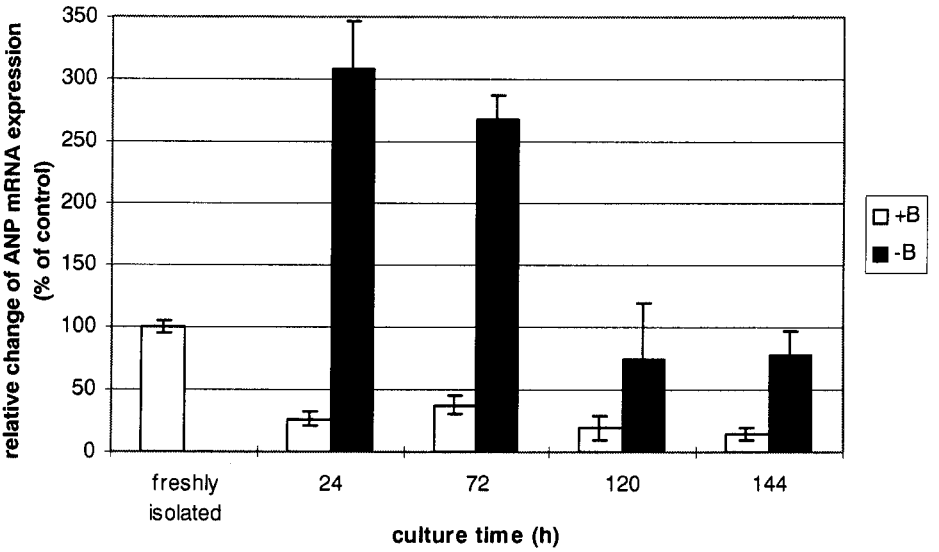


Figure 5. Semiquantitative RT-PCR of ANP mRNA expression in cardiomyocytes isolated from the adult male rat ($p < 0.05$).

Geetha *et al.* (1991) studied the effects of α-tocopherol on doxorubicin-induced changes in the rat heart. When rats were treated with doxorubicin for a total of 8 weeks, P450, NADH-b_5 reductase and glucose 6-phosphatase activities were highly significantly decreased on treatment with this cytotoxic drug. Interestingly, co-administration of α-tocopherol reduced significantly the alteration observed in microsomes of rat heart tissue. The tissue-specific expression, induction and inhibition through metabolic intermediate complex formation of guinea pig P450 was studied by Yamada *et al.* (1992). They reported that treatment with dexamethasone or *p,p'*-dichlorodiphenyltrichloroethane and/or isoafrole produced very significant induction in the expression of P450 isozymes in guinea pig heart tissue.

The microsomal P4501A1-dependent monooxygenase activity in guinea pig heart was also studied by McCallum *et al.* (1993). They reported the induction, inhibition and increased activity of P4501A1 in guinea pig heart microsomes. Interestingly, treatment of guinea pig with β-napthaflavone resulted in a marked increase in activity (20-fold induction of EROD). The authors reported that the low rates of EROD activity in cardiac microsomes were due, at last in part, to a deficiency of the flavoprotein NADPH-P450 reductase activity and the addition of exogenous NADPH-P450 reductase dramatically increased EROD activity in cardiac microsomes of the guinea pig. Both EROD and 7-methoxyresorufin *O*-demethylase activities were ~ 4-fold higher in microsomes prepared from the ventricle than the atrium of the β-napthaflavone-induced guinea pig, thus suggesting that the regulation of P450 monooxygenases differed when atria and ventricular tissue were compared.

Stegeman *et al.* (1995) also reported the induction of P4501A1 by aryl hydrocarbon receptor agonists in porcine aorta endothelial cells in culture and P4501A1 activity in intact cells. They used a number of different chemicals to produce induction of P4501A1, including not only 2,3,7,8-tetrachlorodibenzo-*p*-

dioxin (TCDD) and BNF in addition to benzo(α)pyrene, but also the congeneric 3,3′,4,4′-tetrachlorobiphenyl. P4501A1, but not P4501A2, is induced in porcine endothelial cells in culture and P4501A1 activity is measurable, but the rates are low. Xiao *et al*. (1998) suggested a role of P450 in modulating calcium channel expression and contraction in mammalian heart cells. Indeed, the modulatory effects of P450 on the L-type calcium current intracellular-free Ca^{2+} signal and cell shortening were assessed in the single ventricular myocytes of the adult rat. Clear evidence was presented to suggest that P450 modulated cardiac L-type Ca^{2+} currents and cell contraction, and the modulation might result from changes in intercellular levels of cAMP by P450-mediated metabolites of arachidonic acid.

Recently, it was reported that P4501A1, 2B6/7, 2C8–19, 2D6 and 4B1 were predominantly expressed in the right ventricle of the human heart, but mRNA transcripts for epoxide hydrolase, P450 2E1 and flavin-containing monooxygenases 2 and 5 were detected in all regions of the heart and the great vessels (Thum and Borlak 2000c). Also investigated was the metabolic capacity in cultures of adult cardiomyocytes (Thum and Borlak 2000a) and diligence was shown in which heart muscle cells produce biotransformation products of testosterone. This finding is of considerable interest as androgen receptors are present in cardiomyocytes and may signal hypertrophy in cardiac tissue (Marsh *et al*. 1998).

Drug testing with cultured cardiomyocytes of adult animals

The long-term culture of primary cardiomyocytes provides a valuable tool for studying the pharmacological and toxicological properties of drugs and chemicals. The pro-arrhythmogenic potential of new chemical entities can also be studied in cultures of primary cardiomyocytes of the adult rat. Investigations into drug/drug interactions or metabolic processes leading to adverse drug effects may additionally be studied with cultured cardiomyocytes. To the best of our knowledge, only limited information is available on the metabolic competence of cardiomyocytes and includes metabolism studies with antidiabetic drugs (troglitazone) (Bahr *et al*. 1996), anti-anginal and anti-arrhythmic drugs (trimetazidine) (Fantini *et al*. 1994, Kessler-Icekson *et al*. 1996, Nuss *et al*. 1999), linoleic acid (Lopez Jimenez *et al*. 1997), sympathomimetic agents (methamphetamine) (He 1995) and hormones (insulin, trijodthyronine) (Orfali *et al*. 1995).

Cell transplantation, future studies and clinical applications

A new and exciting area of research is the application of adult cardiomyocytes in tissue engineering and cell transplantation. These systems, although being experimental at this stage, may be the therapies of the future, e.g. cardiomyocytes for local drug delivery or for cell transplantation (Soonpaa *et al*. 1994). Studies with genetically engineered cardiomyocytes are a further area of intense research. Indeed, cardiomyocytes can be modified leading to an enhanced expression of proteins of interest, including skeletal troponine 1 (Westfall *et al*. 1997) or cell cycle proteins such as c-myc and c-fos (Green *et al*. 1997) and angiogenic factors, e.g. endothelial growth factor (Maruyama *et al*. 1999). The expression of the latter protooncogenes also play an important role in myocardial growth and differentiation and a precise knowledge of the regulation of these factors is of importance, if cardiomyocytes are to be used in cell transplantation or in local drug delivery.

Koh *et al*. (1993), Li *et al*. (1998) and Leor *et al*. (1997) demonstrated improved therapeutic outcome when cardiomyocytes were transplanted into ischaemic heart tissue. These authors also demonstrated that transplanted cardiomyocytes become adherent and developed gap junctions with the native heart tissue (Soonpaa *et al*. 1994). The same group also showed that transplanted cardiomyocytes undergo structural and architectural organization, which are termed 'intracordal disks' in the region of transplantation. It is therefore possible that transplanted cardiomyocytes may provide a better outcome for animals with myocardial infarction as judged by infarct size and myocardial functions. Therefore, transplantation of cardiomyocytes may be a therapeutic approach of the future with transplantation of cells into dead or damaged tissue.

In addition to studies with small laboratory animals, experiments with the pig have also demonstrated the therapeutic benefit of cell transplantation (Watanabe *et al*. 1998). Isolated cardiomyocytes may be used for local drug delivery, which includes the release of angiogenic factors into areas of ischaemia. For instance, Arras *et al*. (1998) described the injection of microspheres coupled with angiogenic factors into smaller coronary arteries via a catheter and although it is possible to inject angiogenetic factors and other growth factors directly into ischaemic heart tissue, cardiomyocytes may prove to be more valuable for therapy when transplanted into the deceased tissue and could release cytoprotective agents and other medication into the area of cell damage, acting as a depot for the slow release of these chemicals. In contrast, direct injection of therapeutic agents into heart is often rapidly removed (Darsinos *et al*. 1993).

Molecular markers for cellular differentiation of cardiomyocytes

It is now established that pathological changes in heart tissue are linked to changes in the gene expression pattern of a number of genes and during hypertrophy, foetal isoforms of the β-myosin heavy chain (β-MHC) and α-skeletal actin are upregulated, whereas the corresponding adult isoforms, α-myosin heavy chain (α-MHC) and α-cardiac actin are down-regulated (Schwartz *et al*. 1993, Nakao *et al*. 1997). Cellular stress and metabolic deregulation in cardiomyocytes fosters the expression of the 28 amino acid polypeptide atrial natriuretic peptide (ANP) and the b-type natriuretic peptide (BNP), which are mainly secreted in atrial and ventricular tissue, respectively to cause decreased blood pressure by vasodilatation and natriuresis, all of which are upregulated in the heart in response to hypertrophic signals (Yoshimura *et al*. 1993, Lowes *et al*. 1997). Whether β-MHC and α-skeletal actin, as well as ANP and BNP, are coordinately regulated in pathological processes remains uncertain, but common binding sites for several transcription factors of the above-named marker genes are suggestive of a coordinated response during cardiac remodelling and disease.

There is also growing evidence for transcription factors (e.g. GATA4, MEF-2c, Nkx2.5, Oct-1) to be of critical importance in the onset of human heart failure as well as congenital heart disease (Durand *et al*. 1995, Molkentin *et al*. 1998, Schott *et al*. 1998, Pehlivan *et al*. 1999).

The transcription factors GATA-4, MEF-2c, Nkx2.5 and Oct-1 were examined for their specific role in the gene regulation of ANP, BNP, α-MHC, β-MHC and cardiac α-actin as reported (Lee *et al*. 1997, Sepulveda *et al*. 1998, Charron *et al*. 1999). The latter target genes are also considered to be good diagnostic markers in

the onset of human heart failure as well as congenital heart disease (Schwartz *et al*. 1993, Yoshimura *et al*. 1993, Lowes *et al*. 1997, Nakao *et al*. 1997). It is intriguing that the gene expression pattern in cardiomyocyte cultures (Thum and Borlak, 2000b) resembles to such an extent that of diseased patients in various clinical settings and could therefore be of considerable importance for the development of new pharmacotherapeutic approaches, e.g. targeting transcription factor gene expression.

Conclusions

Because of significant improvements in isolation and cultivation procedures, primary cardiomyocytes may be used more frequently in preclinical pharmacology and toxicology testing and in cell therapy approaches for the purpose of local drug delivery or replacement of damaged cells. In addition, it is now possible to assess simultaneously the gene expression of transcription factors and target genes, as a means of evaluation of the level of cellular differentiation of cultured cardiomyocytes.

References

Altschuld, R. A., Gibb, L., Ansel, A., Hohl, C., Kruger, F. A. and Brierley, G. P., 1980, Calcium tolerance of isolated rat heart cells. *Journal of Molecular and Cellular Cardiology*, **12**, 1383–1395.

Arras, M., Mollnau, H., Strasser, R., Wenz, R., Ito, W. D., Schaper, J. and Schaper, W., 1998, The delivery of angiogenic factors to the heart by microsphere therapy. *Nature Biotechnology*, **16**, 159–162.

Artursson, P. and Magnusson, C., 1989, Epithelial transport of drugs in cell culture. II: Effect of extracellular calcium concentration on the paracellular transport of drugs of different lipophilicities across monolayers of intestinal epithelial (CaCo-2) cells. *Journal of Pharmaceutical Science*, **7**, 595–600.

Bahr, M., Spelleken, M., Bock, M., Von Holtey, M., Kiehn, R. and Eckel, J., 1996, Acute and chronic effects of troglitazone (CS-045) on isolated rat ventricular cardiomyocytes. *Diabetologia*, **39**, 766–774.

Bkaily, G., Sperelakis, N. and Doane, J., 1984, A new method for preparation of isolated single adult myocytes. *American Journal of Physiology*, **247**, 1018–1028.

Brierley, G. P., Wenger, W. C. and Altschuld, R. A., 1985, Heart myocytes as models of the cellular response to ischaemia. *Advances in Experimental Medicine and Biology*, **194**, 303–314.

Cavanaugh, N. W., 1955, Pulsation, migration and division in dissociated chick embryo heart cells *in vitro*. *Journal of Experimental Zoology*, **128**, 573–585.

Charron, F., Paradis, P., Bronchain, O., Nemer, G. and Nemer, M., 1999, Cooperative interaction between GATA-4 and GATA-6 regulates myocardial gene expression. *Molecular Cell Biology*, **19**, 4355–4365.

Darsinos, J. T., Samouilidou, E. C., Krumholz, B., Kontoyanni, M., Pestevos, A. K., Karli, J. N., Theodorakis, M. G., Levis, G. M. and Moulopoulos, S. D., 1993, Distribution of lidocaine and digoxin in heart tissues and aorta following intrapericardial administration. *International Journal of Clinical Pharmacology and Therapeutic Toxicology*, **31**, 611–615.

Durand, J. B., Bachinski, L. L., Bieling, L. C., Czernuszewicz, G. Z., Abchee, A. B., Yu, Q. T., Tapscott, T., Hill, R., Ifegwu, J. and Marian, A. J., 1995, Localization of a gene responsible for familial dilated cardiomyopathy to chromosome 1q32. *Circulation*, **92**, 3387–3389.

Fabiato, F., Fabiato, A. and Sonnenblick, E. H., 1971, Isolated myocardial cells of adult mammals. Analytical study of contractility and excitation-contraction coupling. *Journal of Physiology* (*Paris*), **63**, 210A.

Fabiato, A. and Fabiato, F., 1972, Excitation-contraction coupling of isolated cardiac fibers with disrupted or closed sarcolemmas. Calcium-dependent cyclic and tonic contractions. *Circulation Research*, **31**, 293–307.

Fantini, E., Demaison, L., Sentex, E., Grynberg, A. and Athias, P., 1994, Some biochemical aspects of the protective effect of trimetazidine on rat cardiomyocytes during hypoxia and reoxygenation. *Journal of Molecular and Cellular Cardiology*, **26**, 949–958.

Geetha, A., Marar, T. and Devi, C. S., 1991, Effect of alpha-tocopherol on doxrubicin-induced changes in rat liver and heart microsomes. *Indian Journal of Experimental Biology*, **2**, 782–785.

Ghanbari, H. A. and McCarl, R. L., 1980, A comparative study of myosin and its subunits in adult and neonatal-rat hearts and in rat heart cells from young and old cultures. *Biochemical Journal*, **191**, 627–635.

Green, N. K., Franklyn, J. A., Ohanian, V., Heagerty, A. M. and Gammage, M. D., 1997, Transfection of cardiac muscle: effects of overexpression of c-myc and c-fos protooncogene proteins in primary cultures of neonatal rat cardiac myocytes. *Clinical Science* (*Colch*), **92**, 181–188.

Grosso, D. S., Frangakis, C. J., Carlson, E. C. and Bressler, R., 1977, Isolation and characterisation of myocytes from the adult rat heart. *Preparations in Biochemistry*, **7**, 383–401.

Habazettl, H., Voigtlander, J., Leiderer, R. and Messmer, K., 1998, Efficacy of myocardial initial reperfusion with 2,3 butanedione monoxime after cardioplegic arrest is time-dependent. *Cardiovascular Research*, **37**, 684–690.

Harary, I. and Farley, B., 1960, *In vitro* studies of single isolated beating heart cells. *Science*, **131**, 1674–1675.

Haworth, R. A., Goknur, A. B., Warner, T. F. and Berkoff, H. A., 1989, Some determinants of quality and yield in the isolation of adult heart cells from rat. *Cellular Calcium*, **10**, 57–62.

He, S. Y., 1995, Methamphetamine-induced toxicity in cultured adult rat cardiomyocytes. *Nippon Hoigaku Zasshi*, **49**, 175–186.

Herlitz, J., Waldenstrom, J. and Hjalmarson, A., 1988, Infarct size limitation after early intervention with metoprolol in the MIAMI trial. *Cardiology*, **75**, 117–122.

Jans, S. W., Willems, J., van Bilsen, M., Reutelingsperger, C. P. and van der Vusse, G. J., 1997, Phospholipid degradation in energy-deprived cardiac myocytes: does annexin V play a role? *Journal of Molecular and Cellular Cardiology*, **29**, 1401–1410.

Kao, R. L., Christman, E. W., Luh, S. L., Krauhs, J. M., Tyers, G. F. and Williams, E. H., 1980, The effects of insulin and anoxia on the metabolism of isolated mature rat cardiac myocytes. *Archives in Biochemistry and Biophysics*, **203**, 587–599.

Kato, Y., Masumiya, H., Agata, N., Tanaka, H. and Shigenobu, K. J., 1996, Developmental changes in action potential and membrane currents in foetal, neonatal and adult guinea-pig ventricular myocytes. *Journal of Molecular and Cellular Cardiology*, **28**, 1515–1522.

Kessler-Icekson, G., Schlesinger, H., Djaldetti, M., Brodie, C., Sampson, S. R. and Bergmann, M., 1996, Cardiomyocytes in culture – a model to study the cellular actions of amiodarone. *Israeli Journal of Medical Science*, **32**, 1212–1216.

Kivisto, T., Makiranta, M., Oikarinen, E. L., Karhu, S., Weckstrom, M. and Sellin, L. C., 1995, 2,3-Butanedione monoxime (BDM) increases initial yields and improves long-term survival of isolated cardiac myocytes. *Japanese Journal of Physiology*, **45**, 203–210.

Koh, G. Y., Soonpaa, M. H., Klug, M. G. and Field, L. J., 1993, Long-term survival of AT-1 cardiomyocyte grafts in syngeneic myocardium. *American Journal of Physiology*, **264**, 1727–1733.

Lakich, M. M., Diagana, T. T., North, D. L. and Whalen, R. G., 1998, MEF-2 and Oct-1 bind to two homologous promoter sequence elements and participate in the expression of a skeletal muscle-specific gene. *Journal of Biological Chemistry*, **273**, 15217–15226.

Lee, Y., Nadal-Ginard, B., Mahdavi, V. and Izumo, S., 1997, Myocyte-specific enhancer factor 2 and thyroid hormone receptor associate and synergistically activate the alpha-cardiac myosin heavy-chain gene. *Molecular Cell Biology*, **17**, 2745–2755.

Leor, J., Prentice, H., Sartorelli, V., Quinones, M. J., Patterson, M., Kedes, L. K. and Kloner, R. A., 1997, Gene transfer and cell transplant: an experimental approach to repair a 'broken heart'. *Cardiovascular Research*, **35**, 431–441.

Li, R. K., Yau, T. M., Sakai, T., Mickle, D. A. and Weisel, R. D., 1998, Cell therapy to repair broken hearts. *Canadian Journal of Cardiology*, **14**, 735–744.

Lopez Jimenez, J. A., Bordoni, A., Lorenzini, A., Rossi, C. A., Biagi, P. L. and Hrelia, S., 1997, Linoleic acid metabolism in primary cultures of adult rat cardiomyocytes is impaired by aging. *Biochemical and Biophysical Research Communications*, **237**, 142–145.

Lowes, B. D., Minobe, W., Abraham, W. T., Rizeq, M. N., Bohlmeyer, T. J., Quaife, R. A., Roden, R. L., Dutcher, D. L., Robertson, A. D., Voelkel, N. F., Badesch, D. B., Groves, B. M., Gilbert, E. M. and Bristow, M. R., 1997, Changes in gene expression in the intact human heart. Downregulation of alpha-myosin heavy chain in hypertrophied, failing ventricular myocardium. *Journal of Clinical Investigation*, **100**, 2315–2324.

Marino, T. A., Walter, R. A., Dámbra, K. and Mercer, W. E., 1989, Effects of catecholamines on foetal rat cardiocytes *in vitro*. *American Journal of Anatomy*, **186**, 127–132.

Marsh, J. D., Lehmann, M. H., Ritchie, R. H., Gwathmey, J. K., Green, G. E. and Schiebinger, R. J., 1998, Androgen receptors mediate hypertrophy in cardiac myocytes. *Circulation*, **98**, 256–261.

Maruyama, K., Mori, Y., Murasawa, S., Masaki, H., Takahashi, N., Tsutusumi, Y., Moriguchi, Y., Shibazaki, Y., Tanaka, Y., Shibuya, M., Inada, M., Matsubara, H. and Iwasaka, T., 1999, Interleukin-1 beta upregulates cardiac expression of vascular endothelin growth factor and its receptor KDR/flk-1 via activation of protein tyrosine kinases. *Journal of Molecular and Cellular Cardiology*, **31**, 607–617.

McCallum, G. P., Horton, J. E., Falkner, K. C. and Bend, J. R., 1993, Microsomal cytochrome P4501A1 dependent monooxygenase activity in guinea pig heart: induction, inhibition, and increased activity by addition of exogenous NADPH-cytochrome P450 reductase. *Canadian Journal of Physiology Pharmacology*, **71**, 151–156.

Molkentin, J. D., Lu, J. R., Antos, C. L., Markham, B., Richardson, J., Robbins, J., Grant, R. R. and Olson, E. N., 1998, A calcineurin-dependent transcriptional pathway for cardiac hypertrophy. *Cell*, **93**, 215–228.

Nag, A. C., Cheng, M., Fischman, D. A. and Zak, R., 1983, Long-term cell culture of adult mammalian cardiac myocytes: electron microscopic and immunofluorescent analyses of myofibrillar structure. *Journal of Molecular and Cellular Cardiology*, **15**, 301–317.

Nag, A. C., Ingland M. and Cheng, M., 1985, Factors controlling embryonic heart cell proliferation in serum-free synthetic media. *In Vitro Cellular and Developmental Biology*, **21**, 553–562.

Nag, A. C. and Zak, R., 1979, Dissociation of adult mammalian heart into single cell suspension: an ultrastructural study. *Journal of Anatomy*, **129**, 541–559.

Nakao, K., Minobe, W., Roden, R., Bristow, M. R. and Leinwand, L. A., 1997, Myosin heavy chain gene expression in human heart failure. *Journal of Clinical Investigation*, **100**, 2362–2370.

Nuss, H. B., Marban, E. and Johns, D. C., 1999, Overexpression of a human potassium channel suppresses cardiac hyperexcitability in rabbit ventricular myocytes. *Journal of Clinical Investigation*, **103**, 889–896.

Orfali, K. A., Fryer, L. G., Holness, M. J. and Sugden, M. C., 1995, Interactive effects of insulin and triiodothyronine on pyruvate dehydrogenase kinase activity in cardiac myocytes. *Journal of Molecular and Cellular Cardiology*, **27**, 901–908.

Pehlivan, T., Pober, B. R., Brueckner, M., Garrett, S., Slaugh, R., Van Rheeden, R., Wilson, D. B., Watson, M. S., Hing, A. V., 1999, GATA4 haploinsufficiency in patients with interstitial deletion of chromosome region 8p23.1 and congenital heart disease. *American Journal of Medical Genetics*, **83**, 201–206.

Pin, C. L. and Merrifield, P. A., 1993, Embryonic and foetal rat myoblasts express different phenotypes following differentiation *in vitro*. *Developmental Genetics*, **14**, 356–368.

Powell, T. and Twist, V. W., 1976, A rapid technique for the isolation and purification of adult cardiac muscle cells having respiratory control and a tolerance to calcium. *Biochemical and Biophysical Research Communications*, **72**, 327–333.

Rivas, P. A., Fabrega, A. J., Schwartz, D. and Pollak, R., 1993, The morphology and function of rabbit hepatocytes isolated using ethylendiaminetetraacetate. *Transplantation*, **55**, 335–339.

Rumyantsev, P. P., 1963, A morphological and autoradiographical study of the peculiarities of differentiation rate, DNA synthesis and nuclear division in the embryonal and postnatal histogenesis of cardiac muscles of white rats. *Histochemica et Cytochemica*, **1**, 463–471.

Sage, M. D. and Jennings, R. B., 1988, Cytoskeletal injury and subsarcolemmal bleb formation in dog heart during *in vitro* total ischaemia. *American Journal of Pathology*, **133**, 327–337.

Schott, J. J., Benson, D. W., Basson, C. T., Pease, W., Silberbach, G. M., Moak, J. P., Maron, B. J., Seidmann, C. E., Seidmann, J. G., 1998, Congenital heart disease caused by mutations in the transcription factor Nkx2–5. *Science*, **281**, 108–111.

Schwartz, K., Chassagne, C. and Boheler, K. R., 1993, The molecular biology of heart failure. *Journal of the American College of Cardiology*, **22**, 30A–33A.

Sepulveda, J. L., Belaguli, N., Nigam, V., Chen, C. Y., Nemer, M. and Schwartz, R. J., 1998, GATA-4 and Nkx2. 5 coactivate Nkx-2 DNA binding targets: role for regulating early cardiac gene expression. *Molecular Cell Biology*, **18**, 3405–3415.

Soonpaa, M. H., Koh, G. Y., Klug, M. G. and Field, L. J., 1994, Formation of nascent intercalated disks between foetal cardiomyocytes and host myocardium. *Science*, **264**, 98–101.

Stegeman, J. J., Hahn, M. E., Weisbrod, R., Woodin, B. R., Joy, J. S., Najibi, S. and Cohen, R. A., 1995, Induction of cytochrome P4501A1 by aryl hydrocarbon receptor agonists in porcine aorta endothelial cells in culture and cytochrome P4501A1 activity in intact cells. *Molecular Pharmacology*, **47**, 296–306.

Stegeman, J. J., Miller, M. R. and Hinton, D. E., 1989, Cytochrome P4501A1 induction and localization in endothelium of vertebrate (teleost) heart. *Molecular Pharmacology*, **36**, 723–729.

Stegeman, J. J., Woodin, B. R., Klotz, A. V., Wolke, R. E. and Orme-Johnson, N. R., 1982, Cytochrome P-450 and monooxygenase activity in cardiac microsomes from the fish *Stenotomus chrysops*. *Molecular Pharmacology*, **21**, 517–526.

Stringham, J. C., Paulsen, K. L., Southard, J. H., Fields, B. L. and Belzer, F. O., 1992, Improved myocardial ischaemic tolerance by contractile inhibition with 2,3-butanedione monoxime. *Annals of Thoracic Surgery*, **54**, 859–860.

Takasago, T., Goto, Y., Kawaguchi, O., Hata, K., Saeki, A., Taylor, T. W., Nishioka, T. and Suga, H., 1997, 2,3-Butanedione monoxime suppresses excitation-contraction coupling in the canine blood-perfused left ventricle. *Japanese Journal of Physiology*, **47**, 205–215.

Thum, T. and Borlak, J., 2000a, Cytochrome P450 monooxygenase gene expression and protein activity in cultures of adult cardiomyocytes of the rat. *British Journal of Pharmacology*, **130**, 1745–1752.

Thum, T. and Borlak, J., 2000b, Reprogramming of gene expression in cultures of cardiomyocytes and in explanted hearts by the myosin ATPase inhibitor butanedione monoxime. *Transplantation* (in press).

Thum, T. and Borlak, J., 2000c, Gene expression in distinct regions of the heart. *Lancet*, **355**, 979–983.

Vahouny, G. V., Wie, R., Starkweather, R. and Davis, C. M., 1970, Preparation of beating heart cells from adult rats. *Science*, **167**, 1616–1618.

Van der Heide, R. S., Rim, D., Hohl, C. M. and Ganote, C. E., 1990, An *in vitro* model of myocardial ischaemia utilising isolated adult rat myocytes. *Journal of Molecular and Cellular Cardiology*, **22**, 165–181.

Vanwinkle, W. B., Snuggs, M., Miller, J. C. and Buja, L. M., 1994, Cytoskeletal alterations in cultured cardiomyocytes following exposure to the lipid peroxidation product, 4-hydroxynonenal. *Cellular Motility and the Cytoskeleton*, **28**, 119–134.

Verrecchia, F. and Herve, J. C., 1997, Reversible blockade of gap junctional communication by 2,3-butanedione monoxime in rat cardiac myocytes. *American Journal of Physiology*, **272**, 875–885.

Watanabe, E., Smith, D. M. Jr., Delcarpio, J. B., Sun, J., Smart, F. W., Van Meter, C. H. Jr and Claycomb, W. C., 1998, Cardiomyocyte transplantation in a porcine myocardial infarction model. *Cell Transplantation*, **7**, 239–246.

Weisensee, D., Seeger, T., Bittner, A., Bereiter-Hahn, J., Schoeppe, W. and Low-Friedrich, I., 1995, Cocultures of foetal and adult cardiomyocytes yield rhythmically beating rod shaped heart cells from adult hearts. *In Vitro Cellular and Developmental Biology*, **31**, 190–195.

Westfall, M. V., Rust, E. M. and Metzger, J. M., 1997, Slow skeletal troponin I gene transfer, expression, and myofilament incorporation enhances adult cardiac myocyte contractile function. *Proceeding of the National Academy of Sciences, USA*, **94**, 5444–5449.

Xiao, Y. F., Huang, L. and Morgan, J. P., 1998, Cytochrome P450: a novel system modulating Ca^{2+} channels and concentration in mammalian heart cells. *Journal of Physiology*, **508**, 377–392.

Yamada, H., Kaneko, H., Takeuchi, K., Oguri, K. and Yoshimura, H., 1992, Tissue-specific expression, induction, and inhibition through metabolic intermediate-complex formation of guinea pig cytochrome P450 belonging to the CYP2B subfamily. *Archives in Biochemistry and Biophysics*, **299**, 248–254.

Yoshimura, M., Yasue, H., Okumura, K., Ogawa, H., Jougasaki, M., Mukoyama, M., Nakao, K. and Imura, H., 1993, Different secretion patterns of atrial natriuretic peptide and brain natriuretic peptide in patients with congestive heart failure. *Circulation*, **87**, 464–469.

XENOBIOTICA, 2000, VOL. 30, NO. 11, 1079–1090

Skeletal muscle kinetics of propofol in anaesthetized sheep: effect of altered muscle blood flow

D. ZHENG, R. N. UPTON and A. MARTINEZ

Anaesthesia and Intensive Care, University of Adelaide/Royal Adelaide Hospital, North Terrace, Adelaide, SA 5005, Australia

Received 3 July 2000

1. The kinetics of propofol were studied *in vivo* in a skeletal muscle bed of the hindlimb of the anaesthetized sheep at normal and low rates of blood flow.

2. Propofol kinetics in muscle were determined during and after a 20-min i.v. infusion of propofol (10 mg min^{-1}) via paired arteriofemoral venous blood sampling. One-and-a-half hours later, the study was repeated but with a concurrent left femoral artery infusion of adrenaline (0.004 mg min^{-1}) to lower the muscle blood flow by vasoconstriction.

3. Muscle blood flow in the low flow state was 28% of that in the normal state. The kinetics were poorly described by a single flow-limited compartment model, but were better described by a model with a flow-limited component and a deeper distribution component. There were no significant differences in muscle retention of propofol between normal and low flow states.

4. There was an apparent arteriovenous shunt of ~ 24% of total muscle blood flow for the low flow state, but not for the normal blood flow state.

Introduction

Critically ill patients may respond in an unpredictable manner to intravenous anaesthetic drugs such as propofol, and a lack of knowledge of the determinants of propofol disposition could contribute to adverse outcomes following its administration in these patients (Warden and Lunn 1993). The pioneering work of Benowitz *et al*. (1974a) showed that physiological pharmacokinetic models could be used to describe and predict the effect of critical illness (as represented by haemorrhage and sympathomimetic administration) on drug disposition. A physiologically based pharmacokinetic-pharmacodynamic model of the induction of anaesthesia with propofol in sheep has been previously reported (Ludbrook and Upton 1997, Upton and Ludbrook 1997). Although the representation of propofol kinetics in the lungs and brain was detailed, the systemic kinetics of propofol in the remainder of the body was represented only as two pooled compartments with a clearance term. It was felt that further knowledge about the disposition of propofol in other organs of the body would allow the refinement of this model with respect to describing and predicting propofol disposition in critical illness.

Of the remaining organs of the body, it was considered that skeletal muscle would be important as it comprises ~ 40% of the body mass in man. Furthermore, blood flow in skeletal muscle changes dramatically in various disease states, and was shown to be an important determinant of the uptake of lignocaine into muscle by Benowitz *et al*. (1974b). In many physiological pharmacokinetic models, particularly those of lipophilic drugs, the kinetics of the drug in skeletal muscle is inferred from muscle mass, blood flow and the steady-state muscle:blood partition coefficient (Benowitz *et al*. 1974a, b, Parham *et al*. 1997). Muscle kinetics were therefore

* Author for correspondence; e-mail: da.zheng@adelaide.edu.au

Xenobiotica ISSN 0049-8254 print/ISSN 1366-5928 online © 2000 Taylor & Francis Ltd
http://www.tandf.co.uk/journals DOI: 10.1080/00498250010006582

represented as single-flow limited compartments in these models. It has been reported that tissue kinetics of some lipophilic drugs can not be described using such flow-limited models (Bjorkman *et al*. 1993). Furthermore, there have been reports of disparities in kinetics extrapolated from steady-state partition coefficients and kinetics inferred from other methods (Dutta *et al*. 1998). It is unclear whether the kinetics of propofol in skeletal muscle are compatible with this flow-limited model, and in particular whether the model can account for kinetics when muscle blood flow is altered.

The present authors published an *in vivo* method for the manipulation and continuous measurement of muscle blood flow in sheep hindlimb, with the potential for afferent and efferent blood sampling for pharmacokinetic studies across muscle (Zheng *et al*. 2000). The method was used to examine the kinetics of propofol in muscle at both normal and low blood flows. The aims of the study were (1) to define the kinetics of propofol in skeletal muscle using this method at a normal muscle blood flow; (2) to define how propofol kinetics in muscle differ when muscle blood flow is reduced; and (3) to examine the ability of various regional kinetic models (including a single flow-limited compartment) to describe the kinetics of propofol in skeletal muscle over a range of blood flows. The hypothesis to be examined is that the kinetics of propofol in muscle can be described using a single compartment flow-limited kinetic model.

Materials and methods

General experimental preparation

The Animal Ethics Committee of the University of Adelaide approved the study. For a detailed description of the experimental preparation, see Zheng *et al*. (2000). In brief, five healthy sheep of 2–3 years of age and of similar body mass (~ 50 kg) were prepared under halothane anaesthesia. Intravascular catheters were placed, via the right femoral artery or vein, with their tips in the abdominal aorta (for measurement of blood pressure and arterial blood sampling), in the right atrium (for drug administration), and in the pulmonary artery (for measurement of body temperature). After the sheep recovered from anaesthesia, they were housed in metabolic crates with free access to food (lucerne chaff) and water.

On the experimental day, the sheep were again anaesthetized (thiopentone 1.5 g induction, halothane 2% maintenance). The inspired oxygen was 40% (balance nitrogen) and the sheep were mechanically ventilated to an end-expired carbon dioxide tension of 40 mmHg. The left femoral artery and vein (i.e. on the opposite side to the previously placed catheters) were dissected free of surrounding tissue. Silicone cuffed Doppler probes (Titronics Medical Instruments, Iowa City, IA, USA) of size 4 or 3.7 mm (i.d.) were placed on each vessel to measure an index of femoral arterial and venous blood flow respectively as described (Zheng *et al*. 2000). A 4-French catheter was placed into the left femoral vein (for sampling of muscle effluent blood).

The following haemodynamic measurements were made using methods reported by Zheng *et al*. (2000). Indices of femoral arterial and venous blood flow were derived from the output of the cuffed Doppler flow probes. Mean arterial blood pressure (MAP) was measured using a pressure transducer on an arterial catheter. The haemodynamic parameters were recorded using an analogue-to-digital card and a personal computer.

Experimental protocol

Once the instrumentation had been placed, propofol kinetic studies were conducted in normal and low muscle blood flow states achieved as described below. Heparin (25 000 i.u.) was given i.v. immediately before each propofol study to prevent clots forming in the left femoral vein that hindered blood sampling. The studies were not conducted in random order because pilot studies showed long recovery times from some low flow states.

Propofol infusion in normal muscle blood flow state

This study was not commenced until at least 120 min after the induction of anaesthesia, and when the haemodynamic measurements had been stable for at least 10 min. After 5 min of baseline haemodynamic measurements, 200 mg propofol was infused i.v. via the right atrial catheter over 20 min (10 mg min^{-1}).

The start of the infusion was designated as time zero. Arterial and femoral venous blood samples (1 ml) were taken at 0, 1, 3, 5, 10, 15, 18, 20, 21, 23, 25, 30, 35, 40, 45, 50 and 60 min. Blood samples were frozen and propofol concentrations in whole blood were later assayed using a high-pressure liquid chromatography and fluorescence detection technique (Ludbrook *et al*. 1996).

Propofol infusion in low muscle blood flow state

At the end of the normal blood flow study, muscle blood flow was decreased by infusing adrenaline (0.004 mg min^{-1}) directly into the left femoral artery via an acutely placed 26-gauge needle. Flow was monitored using the Doppler flow probes. Once flow had reached a stable level about one-quarter of baseline and at least 90 min after the last propofol infusion, the propofol infusion and blood sampling protocol described above was repeated.

Model independent data analysis

The extraction ratio (ER) of propofol at a given time across the skeletal muscle was calculated using:

$$\mathrm{ER} = 1 - \frac{C_{\mathrm{ven}}}{C_{\mathrm{art}}}, \tag{1}$$

where C_{art} is the femoral arterial propofol concentration and C_{ven} is the femoral venous propofol concentration.

The retention ($R\%$) of propofol in muscle at the end of each study was calculated using:

$$R\% = \left(1 - \frac{\mathrm{AUC}_{\mathrm{ven}}}{\mathrm{AUC}_{\mathrm{art}}}\right) \cdot 100. \tag{2}$$

where $\mathrm{AUC}_{\mathrm{art}}$ is the area under the curve of the femoral arterial propofol concentrations and $\mathrm{AUC}_{\mathrm{ven}}$ is the area under the curve of the femoral venous propofol concentrations, both determined using the trapezoidal rule.

The flux of propofol into or out of skeletal muscle at the times of the blood samples was calculated as follows:

$$\mathrm{Flux} = (C_{\mathrm{art}} - C_{\mathrm{ven}}) \cdot Q_{\mathrm{s}}, \tag{3}$$

where Q_{s} is skeletal muscle blood flow.

The time-course of the apparent amount of propofol in skeletal muscle (A_{ske}) was calculated using balance principles (Upton 1994). The amount at a given time (t) is given by the time integral of the difference in the flux of propofol entering the skeletal muscle and the flux leaving the skeletal muscle.

$$A_{\mathrm{ske}} = \int_0^t Q_{\mathrm{s}} \cdot (C_{\mathrm{art}} - C_{\mathrm{ven}})\, \mathrm{d}t. \tag{4}$$

Muscle oxygen consumption and blood gases

Additional blood samples were taken during the baseline period and at 20 min immediately before stopping the propofol infusion for both the low and normal flow states. These were analysed using a blood gas analyser (ABL Radiometer Medical A/S, Copenhagen, Denmark) to determine blood oxygen tension ($P\mathrm{o}_2$), pH, blood carbon dioxide tension ($P\mathrm{co}_2$) and oxygen saturation ($S\mathrm{o}_2$). Skeletal muscle oxygen consumption ($SV\mathrm{o}_2$) was calculated as the product of skeletal muscle blood flow and the arteriovenous (a-v) oxygen content gradient, assuming that baseline muscle blood flow in the normal flow state was 65 ml min^{-1} as reported (Zheng *et al*. 2000).

Statistical analysis

To compare the effect of blood flow state on propofol retention and flux in skeletal muscle, MAP, arterial, venous concentrations, amount of propofol in muscle, blood gases, $SV\mathrm{o}_2$ and skeletal muscle blood flow between the normal and low blood flow studies, the differences between the normal and low blood flow values at each time point were calculated, and their mean and 95% confidence limits plotted. If both the expected value and 95% confidence limits lay above or below 0, the value was recorded as being statistically difference at that time. To compare the effect of propofol on skeletal muscle blood flow and $SV\mathrm{o}_2$, the baseline and 95% confidence limits were plotted. If both the expected value and 95% confidence limits lay outside of 95% confidence limits of baseline, the value was recorded as being statistically changed from baseline. Data are presented as mean (95% confidence limits).

Kinetic modelling

Hybrid modelling (Upton 1996) was used to examine the ability of various kinetic models to describe the observed propofol concentrations in femoral venous blood. Models were constructed as a series of differential equations using the Scientist for Windows software package (v.2.01; Micromath Scientific

Software, Salt Lake City, UT, USA), and were fitted to mean data for the five sheep. The measured arterial propofol concentrations (C_{art}) and blood flow entering the muscle were fitted to forcing functions (exponential and polynomial functions respectively) and these were used as the input functions for the muscle kinetic models. The measured femoral venous concentrations (C_{ven}) were used to estimate the parameters of the models by curve fitting. Curve fitting was by a least-squares method based on the maximization of Model Selection Criteria (MSC) of the Scientist program. MSC is essentially the Akaike Information Criterion scaled to compensate for data sets of different magnitudes (Scientist for Windows manual), and is calculated from the following formula, where p is the number of parameters and n the number of data points.

$$\mathrm{MSC} = \ln\left(\frac{\sum_{i=1}^{n}(Y_{\mathrm{obs}_i} - \bar{Y}_{\mathrm{obs}})^2}{\sum_{i=1}^{n}(Y_{\mathrm{obs}_i} - Y_{\mathrm{cal}_i})^2}\right) - \frac{2p}{n}. \tag{5}$$

The coefficient of variation of a parameter estimate was calculated from the estimated value and its SD in the normal manner. Three models were examined as outlined below, where Q_s is skeletal muscle blood flow and V_s is the apparent volume of propofol in the compartment including venous blood.

A single flow-limited compartment model:

$$V_s \cdot \frac{dC_{ven}}{dt} = Q_s \cdot (C_{art} - C_{ven}). \tag{6}$$

A single flow-limited compartment with an apparent first-order loss:

$$V_s \cdot \frac{dC_{ven}}{dt} = Q_s \cdot (C_{art} - C_{ven}) - k \cdot C_{ven}, \tag{7}$$

where k is apparent clearance term describing the loss. This could represent a loss due to metabolism, or loss into a second compartment sufficiently deep to make the distribution essentially irreversible in the time-scale of the study.

A membrane-limited compartment model: here, 'PS' is used to represent membrane permeability in keeping with standard principles of capillary exchange, C_{deep} is the propofol concentration in the deep compartment of the skeletal muscle in the hindlimb with a volume given by V_{deep}:

$$V_s \cdot \frac{dC_{ven}}{dt} = Q_s(C_{art} - C_{ven}) + \mathrm{PS} \cdot (C_{deep} - C_{ven})$$

$$V_{deep} \cdot \frac{dC_{deep}}{dt} = \mathrm{PS} \cdot (C_{ven} - C_{deep}) \tag{8}$$

These models were fitted to the data for the normal and low flow studies separately. All three models were also fitted to the data with and without a concurrent a-v shunt. For this, the ratio of blood flow bypassing the muscle was represented by the term 'a-v shunt' and was constrained during fitting to be between 0 and 1. The venous muscle concentration (C_{ven}) was calculated as the weighted mean of the concentration in blood by-passing the muscle (where $C_{ven} = C_{art}$) and that passing through the structural model as given by equations (6–8).

Results

Haemodynamic changes

There were no significant differences in the time-course of MAP between the studies at normal and low blood flows. There were also no significant differences in baseline arterial pH, $P\mathrm{co}_2$, $P\mathrm{o}_2$ (table 1) and $SV\mathrm{o}_2$ between the two studies, suggesting no progressive change in the general physiological state of the sheep between the studies.

As expected, the time-courses of skeletal muscle blood flow were significantly different between the normal and low blood flow studies (figure 1). This reduction in blood flow was presumably due to vasoconstriction caused by the adrenaline, but was not associated with changes in acid or carbon dioxide production by the

Table 1. Physiological data at baseline (0 min) and at the end of the propofol infusion (20 min) for normal and low blood flow states. Data are mean and 95% confidence intervals.

		pH		$Paco_2$ (mmHg)		Pao_2 (mmHg)	
Min	Site	Normal	Low	Normal	Low	Normal	Low
0	art	7·52 (7·49–7·56)	7·47 (7·39–7·55)	32 (30–34)	37 (33–40)	236 (16–311)	211 (162–260)
	ven	7·48 (7·45–7·50)	7·39 (7·32–7·47)	37 (33–43)	41 (33–50)	49 (32–67)	39 (31–47)
20	art	7·47 (7·39–7·54)	7·45 (7·39–7·51)	38 (33–43)	37 (34–40)	177 (78–275)	206 (150–262)
	ven	7·44 (7·39–7·50)	7·33 (7·25–7·41)	40 (36–44)	49 (41–56)	44 (28–60)	43 (31–55)

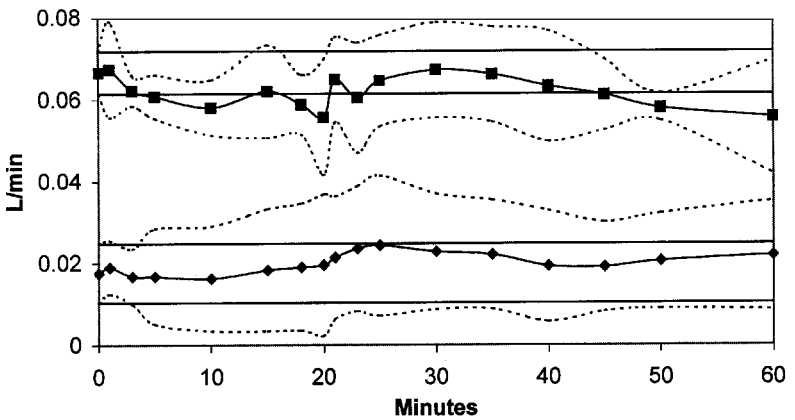


Figure 1. Time-courses of skeletal muscle blood flow for the normal (squares) and low (diamonds) flow studies. Propofol administrated at $t = 0$ for 20 min. Data are the mean (symbols) and 95% confidence limits (dashed line). The 95% confidence limits of the baseline data are shown as the solid lines. At any particular time, a statistically significant difference occurs if the observed value and 95% confidence intervals lay outside of 95% confidence intervals of the baseline period.

muscle (table 1). Furthermore, SVo_2, although a relatively noisy calculated parameter, was unchanged with the reduction in flow. The baseline values for the normal and low blood flow states were 11.8 (−1.8 to 24.9) and 14.2 (4.7–23.6) ml min^{-1}/100 g respectively. These data taken together suggest that the low flow state was not associated with muscle acidosis, hypoxia or decreased metabolism.

The data also provide some insight into the effect of propofol on muscle blood flow and oxygen consumption. During and after infusion of propofol, the time-courses of skeletal muscle blood flow were not greatly changed from baseline for both the normal and low flow states (figure 1). Comparison of the 0 and 20 min measurements show that propofol did not effect SVo_2 for either flow states.

Effect of blood flow on propofol concentrations

The arterial concentrations for both the normal and low flow studies rose progressively to ~2 mg l^{-1} during the infusions, but did not reach steady state (figure 2). There were no statistically significant differences between the arterial propofol concentrations between the studies (except at 35 min). This is not

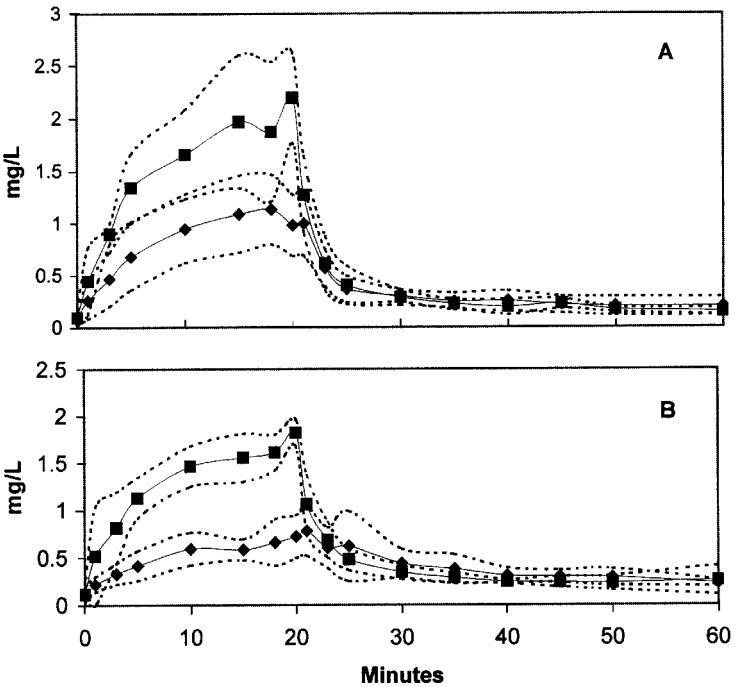


Figure 2. Observed arterial (squares) and femoral venous (diamonds) propofol concentrations for the normal (A) and low (B) flow states. Propofol administrated at $t = 0$ for 20 min. Data are the mean (symbols) and 95% confidence limits (dotted lines).

surprising given the relatively small size (657 g) of the skeletal muscle bed in which flow was altered (Zheng *et al.* 2000), which constitutes ~ 1.3% of the total body mass. The influence of altered flow in such a small region on the systemic kinetics would be expected to be minimal.

The femoral venous propofol concentrations in low skeletal muscle flow state were significantly lower than those in normal skeletal muscle flow state at 10, 15, 18 min, but significantly higher at 35 and 40 min (figure 2). This was not manifested as a significant difference in the time-course of the extraction ratio of propofol across the muscle between the two flow states, which was a relatively noisy measurement (figure 3a). However, differences in the rate of uptake between the two flow states were more apparent when expressed as a flux, which was higher for normal state from 3 to 20 min but significantly lower at 40 min (figure 3b). There were large differences in the calculated amount of propofol in skeletal muscle from 1 to 60 min (figure 3c). Importantly, not all the propofol that entered the skeletal muscle had left by the end of the study period – the retention of propofol is shown in table 2. There were no significant differences in the retention between the flow states.

Modelling

During initial data analysis, both individual and mean data sets were used for modelling. The fit of the models to each individual set was consistent with the fit of models to the mean data set for both the normal and low flow states. Therefore, for reasons of brevity only the modelling of the mean data set is reported. The goodness

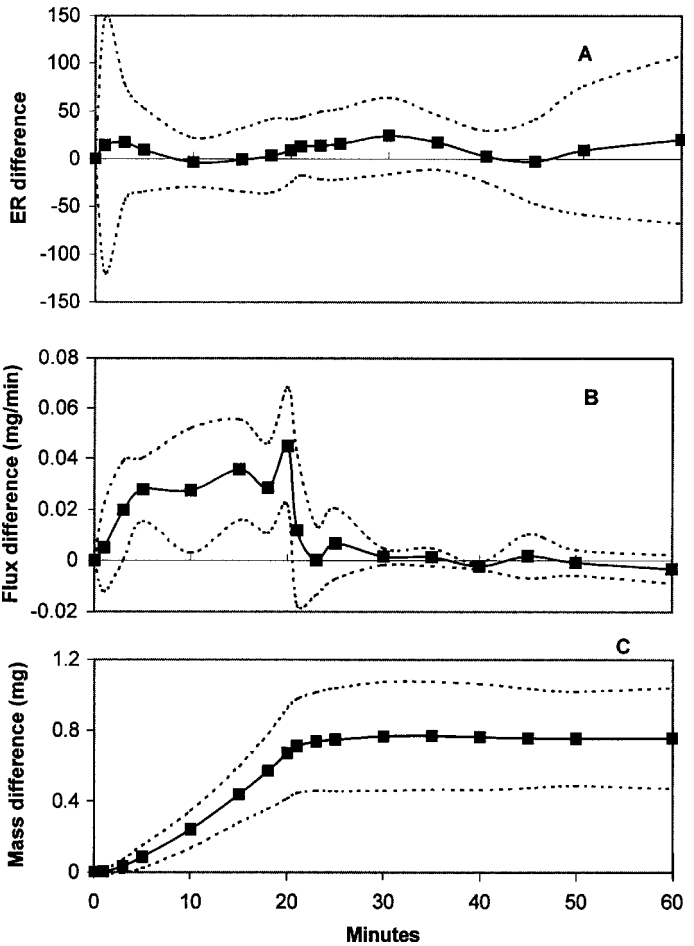


Figure 3. Time-course of the difference between the normal and low flow studies (high minus low) for (A) apparent extraction ratio, (B) propofol flux and (C) amount of propofol in the muscle. Propofol administrated at $t = 0$ for 20 min. Data are the mean (symbols) and 95% confidence limits (dashed line). At any particular time, a statistically significant difference occurs if the expected value and 95% confidences lay above or below 0.

Table 2. Parameters of the best-fit models of skeletal muscle kinetics of propofol for both low and normal flow data sets. Parameters are the apparent distribution volume (V_s), membrane permeability (PS) for the membrane limited model or apparent loss term (k) for the flow-limited with loss model (as appropriate), and the apparent distribution volume of the deep compartment (V_{deep}). A-v shunt is the ratio of blood shunted through arterio-venous shunt. Parameter estimates are the mean and upper and lower 95% confidence intervals returned by the curve-fitting program. The calculated retention of propofol (R%) in muscle for the duration of the study is also shown.

Date set	Best model	V_s (litres)	PS or k (1/min)	V_{deep} (litre)	A-v shunt (%)	R%
Low	flow-limited with loss	0.457 (0.284–0.631)	0.007 (0.0002–0.014)		24.2 (15.1–33.4)	28.9 (10.8–47.1)
Normal	membrane-limited	0.058 (0.011–0.105)	0.053 (0.044–0.062)	3.24 (1.73–4.74)	no shunt	37.9 (27.6–48.3)

Table 3. Goodness of fits of the models of the muscle kinetics of propofol for the data collected at normal and low blood flow states. Data are for models with and without a concurrent a-v shunt. MSC is the model selection criteria—the higher the number, the better the fit. The coefficient of variation of the noisiest parameter of the model (CV_{max}) is also shown.

		No shunt		A-V shunt	
Model	Data	MSC	CV_{max} (%)	MSC	CV_{max} (%)
Flow-limited	low	−0.00	15.1	1.40	12.6
	normal	−0.12	23.4	2.49	25.7
Flow-limited with loss	low	0.65	23.1	1.54[a]	42.8
	normal	2.52	30.7	2.40	>1000
Membrane-limited	low	1.27	140.9	1.42	>1000
	normal	3.24[b]	37.9	3.20	>1000

[a] Best model of low flow data.
[b] Best model of normal flow data.

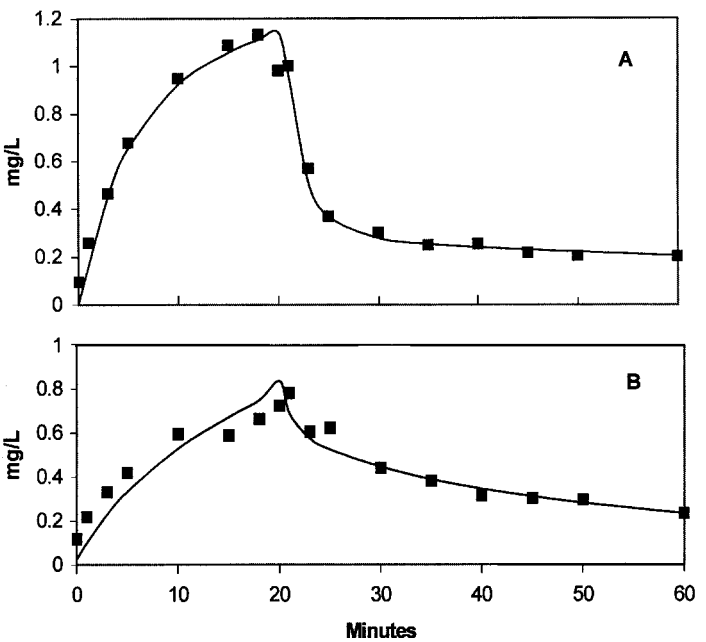


Figure 4. Measured propofol concentrations in venous blood from muscle (symbol), and the predicted concentrations for the best-fit model (line) to the normal (A) and low (B) flow data sets. Propofol administrated at $t = 0$ for 20 min.

of fit of the various models is shown in table 3. The flow-limited model alone was a poor fit of the data, but was improved by the addition of an a-v shunt. The poor fit was presumably due to the retention of propofol in muscle, which is uncharacteristic of a flow-limited system. The best fit of the low flow data was a flow-limited model with an a-v shunt and an apparent first-order loss. For the normal flow data, a better fit was achieved by sequestering this 'lost drug' in a relatively large deep distribution compartment in the membrane-limited model. There was no evidence of an a-v shunt for this data set.

The parameter estimates of the best fit models are shown in table 2, and the lines of best fit to the venous concentration data are shown in figure 4. By comparing the

values for the fits of the low and normal data sets, it can be seen that the apparent distribution volume of the vascular compartment (V_s) and the loss from this compartment (PS or k) were greatly affected by blood flow.

Discussion

This study has revealed two key aspects of the kinetics of propofol in skeletal muscle. The first was the existence of an apparent a-v shunt of $\sim 24\%$ of total muscle blood flow in the low flow state produced by localized adrenaline infusion. The second was the existence of two distinct kinetic components to the kinetics – a flow-limited component (as represented by 'vascular' compartment of the membrane-limited model) and a deeper distribution component (as represented by the retention of propofol in muscle) that was not affected by changes in blood flow. These will be discussed in turn.

With respect to the first aspect, a-v shunts have been described in both muscle and skin of the hindlimb. In sheep, a-v shunts in the skin have an important role in thermoregulation and shunts of up to 24% have been reported (Hales 1984). However, as other tissues including skin contribute $< 6\%$ to the tissue mass studied in the present preparation (Zheng *et al*. 2000), this is unlikely to contribute to the observed shunts. In muscle, the role of a-v shunt is less clear, with some reports showing a reduction in shunt and hind-limb capillary flow with electrical stimulation of sympathetic nerve chain (Cronenwett *et al*. 1983) whereas others report decreased capillary blood flow but increased shunt with adrenaline infusion (Berk *et al*. 1967). The latter mechanism would be consistent with the present data.

With respect to the second aspect, there have been a number of earlier models of drug and solute kinetics in skeletal muscle that must be placed in context of the present work. A large body of work has used solutes of different properties to study the micro-vascular structure of muscle (Renkin 1959, Renkin and Rosell 1962, Oliver *et al*. 1997). A feature of this work is the use of an 'impulse-response' experimental design. The solute (or solutes) is injected as an instantaneous bolus (impulse) into the afferent blood supply of the muscle, and rapid or continuous blood sampling is used to define the concentration profile of the emerging solute (response). Owing to the distribution of intravascular transit times of blood through the muscle (i.e. some capillary paths are longer than others) and other factors, this concentration profile is analogous to a statistical distribution curve, and is usually skewed to the right. Models to describe these types of data are relatively complex, and incorporate some element to account for this transit time distribution (Cross *et al*. 1993, Weiss and Roberts 1996). However, the transit of intravascular markers through rat hindlimb muscle is rapid, with mean intravascular transit times of ~ 9 s (Weiss and Roberts 1996). Work has shown that models of this type are less applicable to some *in vivo* situations where drug concentrations change sufficiently slowly that kinetic process slower than intravascular transit dominate regional kinetics (Doolette *et al*. 1998, Upton and Doolette 1999, Upton *et al*. 2000). It was felt that intravascular transit time would make a minimal contribution to the kinetics of propofol in skeletal muscle over the course of a 20-min infusion, and these types of models were therefore not applied to the data.

A key finding of this earlier work has been that lipophobic molecules (i.e. those that cannot pass through cell membranes) enter the interstitial space of the muscle via pores in the capillaries. Their rate of uptake is relatively slow, and distribution

volume in muscle is small. Their kinetics can be described using models that account for the molecular size of the solute and the size of the pores (McNamee and Wolf 1998).

In marked contrast are models of the kinetics of lipophilic drugs such as propofol. These drugs are thought to cross cell membranes more rapidly than can be supplied to the muscle via the blood flow. Their kinetics are often represented in physiological pharmacokinetic models as a single well-stirred compartment. Muscle kinetics are therefore defined by only two parameters – muscle blood flow and the steady-state muscle : blood partition coefficient. In general, physiological pharmacokinetic models based on these relatively simple regional kinetic models and steady-state partition coefficient data have been successful in describing the measured concentration data. Most notable was the observation that haemorrhage reduced skeletal muscle blood flow and that this slowed the uptake of lignocaine into muscle (Benowitz *et al*. 1974a, b).

With respect to the present experimental design, it is useful to consider what form the a-v concentration data would take if the muscle behaved in a well-stirred (single compartment flow-limited) manner. The rates of uptake and elution in muscle would be similar, as blood flow and apparent distribution volume govern them both. Therefore, the a-v difference observed during the infusion (arterial > venous) will be of a similar magnitude but 'reversed' (venous > arterial) during the post-infusion period. Altered blood flow would not be expected to change the steady-state partition coefficient of propofol in muscle, but the slower flow would produce larger a-v differences as uptake was slowed.

It is clear from considering these issues that the propofol kinetics in skeletal muscle did not behave in a manner consistent with single compartment flow-limited kinetics. This was confirmed by the poor fit of the flow-limited model to the data. However, the fit of the data at both flow states could be improved if a flow-limited distribution volume was combined with an apparent first order loss or a deeper distribution compartment. For the former, the loss term could be due to distribution or metabolism, but the better fit of the membrane-limited model to the normal flow data sets suggests that distribution was the most likely mechanism. The observation that the volume of the vascular compartment of the models was affected by blood flow is curious. This may indicate that this volume is to some extent affected by capillary blood volume and the extent of intravascular mixing. The fact that kinetics in the deep distribution compartment (as given by retention in muscle) were less dependent of blood flow is consistent with the general concept that the permeability barrier is extra-vascular. However, the value of the permeability term ($\sim 0.05\ l\ min^{-1}$) is comparable with that of muscle blood flow ($\sim 0.06\ l\ min^{-1}$ for the normal flow state), suggesting the membrane limitation is only partial.

Some recent evidence supports membrane limitation in the organ kinetics as diverse as nitrous oxide in the brain (Doolette *et al*. 1998) and fentanyl in various organs (Bjorkman *et al*. 1993). Propofol and thiopentone both exhibit partial membrane limitation in their cerebral kinetics (Upton and Ludbrook 1999). At a macroscopic level, the membrane barrier may be diffusion of the drug into adjacent high capacity tissues such as fat – this would explain why the effect is more pronounced for muscle than the brain of sheep, as muscle is generally adjacent to fat. An alternative explanation is that the barrier is at the microscopic level due to accumulation of propofol in specific intracellular structures – the mitochondria (Miniati *et al*. 1996) and liposomes (MacIntyre and Cutler 1988) have been

implicated. However, these mechanisms are based on ion trapping within the organelles, and it should be noted that propofol is unionized at most physiological pH. The most likely mechanism for the deep distribution may therefore be uptake into lipid pools within or around the muscle.

Acknowledgements

The National Health and Medical Research Council of Australia supported the work.

References

Benowitz, N., Forsyth, R. P., Melmon, K. L. and Rowland, M., 1974a, Lidocaine disposition kinetics in monkey and man. II. Effects of hemorrhage and sympathomimetic drug administration. *Clinical Pharmacology and Therapeutics*, **16**, 99–109.

Benowitz, N., Forsyth, R. P., Melmon, K. L. and Rowland, M., 1974b, Lidocaine disposition kinetics in monkey and man. I. Prediction by a perfusion model. *Clinical Pharmacology and Therapeutics*, **16**, 87–98.

Berk, J. L., Hagen J. F., Beyer, W. H. and Niazmand, R., 1967, The effect of epinephrine on arteriovenous shunts in the pathogenesis of shock. *Surgery, Gynecology and Obstetrics*, **124**, 347–355.

Bjorkman, S., Stanski, D. R., Harashima, H., Dowrie, R., Harapat, S. R., Wada, D. R. and Ebling, W. F., 1993, Tissue distribution of fentanyl and alfentanil in the rat cannot be described by a blood flow limited model. *Journal of Pharmacokinetics and Biopharmaceutics*, **21**, 255–279.

Cronenwett, J. L., Zelenock, G. B., Whitehouse, W. M., Jr, Stanley, J. C. and Lindenauer, S. M., 1983, The effect of sympathetic innervation on canine muscle and skin blood flow. *Archives of Surgery*, **118**, 420–424.

Cross, S. E., Wu, Z. and Roberts, M. S., 1994, Effect of perfusion flow rate on the tissue uptake of solutes after dermal application using the rat isolated perfused hindlimb preparation. *Journal of Pharmacokinetics and Biopharmaceutics*, **46**, 844–850.

Doolette, D. J., Upton, R. N. and Grant, C., 1998, Diffusion limited, but not perfusion limited, compartmental models describe cerebral nitrous oxide kinetics at both high and low flows. *Journal of Pharmacokinetics and Biopharmaceutics*, **26**, 649–672.

Dutta, S., Matsumoto, Y., Muramatsu, A., Matsumoto, M., Fukuoka, M. and Ebling, W. F., 1998, Steady-state propofol brain:plasma and brain:blood partition coefficients and the effect-site equilibration paradox. *British Journal of Anaesthesia*, **81**, 422–424.

Hales, J. R., 1984, Skin arteriovenous anastomoses, their control and role in thermoregulation. In K. Johansen and W. Burggren (eds), *Cardiovascular Shunts* (Copenhagen: Munksgaard), pp. 433–485.

Ludbrook, G. L. and Upton, R. N., 1997, A physiological model of the induction of anaesthesia with propofol in sheep. 2. Model analysis. *British Journal of Anaesthesia*, **79**, 505–513.

Ludbrook, G. L., Upton, R. N., Grant, C. and Gray, E. C., 1996, Brain and blood concentrations of propofol after rapid intravenous injection in sheep, and their relationships to cerebral effects. *Anaesthesia and Intensive Care*, **24**, 445–452.

MacIntyre, A. C. and Cutler, D. J., 1988, The potential role of lysosomes in tissue distribution of weak bases. *Biopharmaceutics and Drug Disposition*, **9**, 513–526.

McNamee, J. E. and Wolf, M. B., 1998, Prediction of permeability-surface area product data by continuous-distribution pore models. *Microcirculation*, **5**, 275–280.

Miniati, M., Paci, A., Cocci, F., Ciarimboli, G., Monti, S. and Pistolesi, M., 1996, Mitochondria act as a reservoir for the basic amine HIPDM in the lung. *European Journal of Respiratory Disease*, **9**, 2306–2312.

Oliver, R. E., Heatherington, A. C., Jones, A. F. and Rowland, M., 1997, A physiologically based pharmacokinetic model incorporating dispersion principles to describe solute distribution in the perfused rat hindlimb preparation. *Journal of Pharmacokinetics and Biopharmaceutics*, **25**, 389–412.

Parham, F. M., Kohn, M. C., Matthews, H. B., DeRosa, C. and Portier, C. J., 1997, Using structural information to create physiologically based pharmacokinetic models for all polychlorinated biphenyls. *Toxicology and Applied Pharmacology*, **144**, 340–347.

Renkin, E M., 1959, Transport of potassium-42 from blood to tissue in isolated mammalian skeletal muscles. *American Journal of Physiology*, **197**, 1205–1210.

Renkin, E. M. and Rosell, S., 1962, The influence of sympathetic adrenergic vasoconstrictor nerves on transport of diffusible solutes from blood to tissues in skeletal muscle. *Acta Physiologica Scandinavica*, **54**, 223–240.

Upton, R. N., 1994, An analysis of errors arising from the direct use of mass balance principles to describe regional drug uptake and elution. *Journal of Pharmacokinetics and Biopharmaceutics*, **22**, 309–321.

Upton, R. N., 1996, A model of the first pass passage of drugs from i.v. injection site to the heart-parameter estimates for lignocaine in the sheep. *British Journal of Anaesthesia*, **77**, 764–772.

Upton, R. N. and Doolette, D. J., 1999, Kinetic aspects of drug disposition in the lungs. *Clinical and Experimental Pharmacology and Physiology*, **26**, 381–391.

Upton, R. N. and Ludbrook, G. L., 1997, A physiological model of the induction of anaesthesia with propofol in sheep. 1. Structure and estimation of parameters. *British Journal of Anaesthesia*, **79**, 497–504.

Upton, R. N. and Ludbrook, G. L., 1999, A model of the kinetics and dynamics of the induction of anesthesia in sheep. Parameter estimation for thiopentone and comparison with propofol. *British Journal of Anaesthesia*, **82**, 890–899.

Upton, R. N., Ludbrook, G. L., Grant, C. and Doolette, D. J., 2000, The effect of altered cerebral blood flow on the cerebral kinetics of thiopental and propofol in sheep. *Anesthesiology*, **93**, 1085–1094.

Warden, J. C. and Lunn, J. N., 1993, The role of anaesthesia in death. In M. Fisher (ed.), *Bailliere's Clinical Anaesthesiology* (London: Bailliere Tindall), pp. 199–214.

Weiss, M. and Roberts, M. S., 1996, Tissue distribution kinetics as determinant of transit time dispersion of drugs in organs: application of a stochastic model to the rat hindlimb. *Journal of Pharmacokinetics and Biopharmaceutics*, **24**, 173–196.

Zheng, D., Doolette, D. J. and Upton, R. N., 2000, *In vivo* manipulation and continuous measurement of muscle blood flow with venous effluent sampling. *Clinical and Experimental Pharmacology and Physiology*, **27**, 625–629.

XENOBIOTICA, 2000, VOL. 30, NO. 11, 1091–1110

Mass spectrometric and NMR characterization of metabolites of roxifiban, a potent and selective antagonist of the platelet glycoprotein IIb/IIIa receptor

A. E. MUTLIB†*, S. DIAMOND†, J. SHOCKCOR†, R. WAY†, G. NEMETH‡, L. GAN† and D. D. CHRIST†

† Drug Metabolism and Pharmacokinetics Section and ‡ Department of Chemical and Physical Sciences, DuPont Pharmaceuticals Company, Stine-Haskell Research Center, PO Box 30, Elkton Road, Newark, DE 19714, USA

Received 8 March 2000

1. The methyl ester prodrug roxifiban is an orally active, potent and selective antagonist of the platelet glycoprotein GPIIb/IIIa receptor and is being developed for the prevention and treatment of arterial thrombosis.

2. Roxifiban was rapidly hydrolyzed to the zwitterion XV459 *in vivo* and by liver slices from the rat, mouse and human and by intestinal cores from dog. XV459 was metabolized to only a small extent *in vitro* and *in vivo*.

3. Studies with rat and dog given radiolabelled roxifiban showed limited oral absorption with the majority of the radiolabel being excreted in faeces. After i.v. doses of ^{14}C-roxifiban, most of the radioactivity was recovered in the urine of rat whereas the dog excreted significant amounts of radioactivity in bile and urine.

4. XV459 could be metabolized extrahepatically by dog gut flora to produce an isoxazoline ring-opened metabolite. *In vitro* hepatic metabolism of XV459 was mainly by hydroxylation at the prochiral and chiral centres of the isoxazoline ring. These hydroxylated metabolites were not detected in the urine and plasma of human volunteers administered roxifiban.

5. Initial LC/MS identification of metabolites was achieved by dosing the rat with an equimolar mixture of d_0:d_4 roxifiban and detecting isotopic clusters of pseudomolecular ions. Unequivocal characterization of these metabolites was achieved by LC/MS, LC/NMR and high-field NMR techniques using synthetic standards of the metabolites.

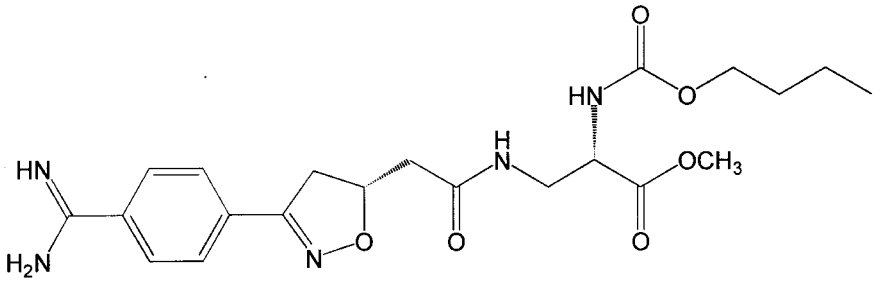
6. The synthesis of one hydroxylated metabolite enabled the assignment of the correct stereochemistry of the substituted hydroxyl group on the isoxazoline ring.

Introduction

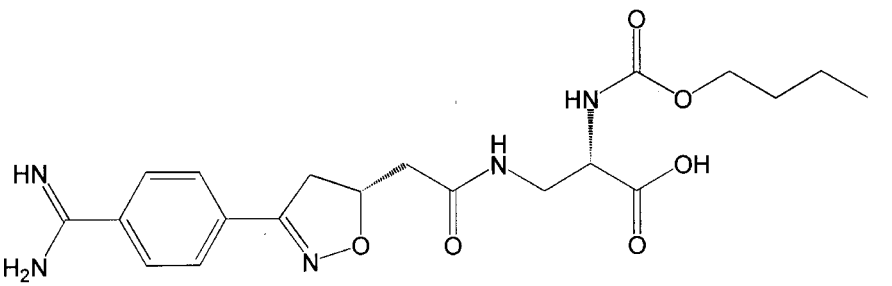
Roxifiban (methyl N^3-[2-{3-(4-formamidino-phenyl)-isoxazolin-5(*R*)-yl}-acetyl]-N^2-(1-butyloxycarbonyl)-2,3-(*S*)-diaminopropionate;acetate salt) is an ester prodrug that requires *in vivo* hydrolysis to the zwitterion XV459 (figure 1), producing a potent and selective antagonist of the platelet glycoprotein (GP) IIb/IIIa receptor (Xue *et al*. 1996, Wityak *et al*. 1997). XV459 inhibits agonist-induced platelet aggregation by blocking fibrinogen binding to the GP IIb/IIIa receptor. This novel antagonist binds to the GP IIb/IIIa receptor complex of activated and resting platelets with the same affinity (Xue *et al*. 1996, Wityak *et al*. 1997) and is active in dog and human but not in rat. Roxifiban is being developed as an antiplatelet agent for the prevention and treatment of arterial thrombosis. To

* Author for correspondence; e-mail: abdul.mutlib@dupontpharma.com

Xenobiotica ISSN 0049-8254 print/ISSN 1366-5928 online © 2000 Taylor & Francis Ltd
http://www.tandf.co.uk/journals DOI: 10.1080/00498250010006591



Roxifiban



XV459

Figure 1. Structures of roxifiban and XV459.

facilitate the clinical development of the compound, the metabolism and excretion of roxifiban was studied in rat and dog. Additionally, the *in vitro* metabolism was studied using human, rat and mouse liver slices as well as dog intestinal cores.

Large doses of roxifiban were administered to rat so that sufficient quantities of metabolites could be isolated for characterization purposes. Preliminary metabolism studies showed that XV459 was formed rapidly from roxifiban in the presence of liver microsomes, liver slices or intestinal segments. Because of the rapid hydrolysis of roxifiban, only the metabolites of the zwitterion were isolated and characterized. Using radioactivity, deuterium-labelled roxifiban and synthetic standards of metabolites facilitated the identification of these metabolites in biological fluids. Because isomeric metabolites could be formed it was imperative that appropriate synthetic standards were available to make spectroscopic and spectral comparisons with isolated metabolites. The metabolites were characterized by electrospray ionization-liquid chromatography/mass spectrometry (ESI-LC/MS), high-field NMR and liquid chromatography/nuclear magnetic resonance (LC/NMR) experiments. The techniques have been used previously to characterize unambiguously the metabolites of other polar drugs (Spraul *et al.* 1993, Mutlib *et al.* 1995, Shockcor *et al.* 1996, Lindon *et al.* 1997).

Materials and methods

Chemicals and supplies

Roxifiban (methyl N^3-[2-{3-(4-formamidino-phenyl)-isoxazolin-5(*R*)-yl}-acetyl]-N^2-(1-butyloxy-carbonyl)-2,3-(*S*)-diaminopropionate; acetate salt); XV459 ((*R*)-3-[[[3-[4-(aminoiminomethyl)phenyl]-4,5-dihydro-5-isoxazoly]acetyl]amino]-*N*-(butoxycarbonyl)-L-alanine); 3-[[[3-[4-aminoiminomethyl-

phenyl]-4-(*S*,*R*)-hydroxy-4,5-dihydro-5-(*R*,*S*)-isoxazolyl]acetyl]amino]-*N*-(butoxycarbonyl)-(*S*)-alanine trifluoroacetate (*trans*-4-hydroxy isomer of M2); 3-[[[3-[4-aminoiminomethylphenyl]-4-(*R*,*S*)-hydroxy-4,5-dihydro-5-(*R*,*S*)-isoxazolyl]acetyl]amino]-*N*-(butoxycarbonyl)-(*S*)-alanine trifluoroacetate (*cis*-4-hydroxy isomer of M2) and 3-[[[3-[4-aminoiminomethylphenyl]-5-(*R*,*S*)-hydroxy-4,5-dihydro-5-isoxazolyl]acetyl]amino]-*N*-(butoxycarbonyl)-(*S*)-alanine trifluoroacetate (5-hydroxy metabolite, M3) were synthesized and characterized by DuPont Pharmaceuticals Company (Batt *et al*. 1999). The purity of all synthetic standards was $>99.5\%$ as determined by HPLC. ^{14}C-roxifiban and ^{14}C-XV459 were synthesized and characterized by New England Nuclear (Boston, MA, USA) with specific activities of 99 and 91 μCi mg^{-1} respectively. The radiochemical purity of ^{14}C-roxifiban and ^{14}C-XV459 were 99.7 and 99.9% respectively. Flo-Scint II® was from Packard Instrument Company (Downers Grove, MO, USA). Mega Bond-Elut C_{18} cartridges (10 g/60 cc, 500 mg/10 ml and 500 mg/3 ml) were from Varian Sample Preparation Products (Harbor City, CA, USA). A C_{18} semipreparative column (10 × 300 mm, 5 μm) and a C_{18} analytical column (4.6 × 250 mm, 5 μm, both Ultrasphere®) were from Beckman Instruments, Inc. (Fullerton, CA, USA). All general solvents and reagents were the highest grade available commercially.

Liquid chromatography/mass spectrometry

LC/MS was carried out by coupling a Waters HPLC system to a Sciex API 300 mass spectrometer. The HPLC eluent was introduced into the source using a Turbo ionspray® interface held at 450–480 °C. The electrospray needle was maintained at 4500 V with the orifice potential set at 50–60 V. The nebulizer gas was ultrapure nitrogen set at 40 psi. The Turbo ionspray® gas flow rate was 6–8 l min^{-1}. The mass spectrometer was operated in the positive-ion mode. Mass spectrometry/mass spectrometry (MS/MS) was carried out using nitrogen as the collision gas. The collision energy was kept at 25–35 eV.

For the analyses of urine samples, HPLC was carried out using Waters quaternary pump coupled in sequence to a Waters WISP (Model 717 plus) and to a Beckman C_{18} column (250 × 4.6 mm, 5 μm). Unless otherwise stated, the metabolites were separated by a gradient solvent system consisting of acetonitrile/10 mM ammonium formate, pH 3.3 (15:85 v/v) delivered at 0.8–1.0 ml min^{-1}. Aliquots of urine samples were injected directly onto the column. A post-column split (1:1) introduced ~ 0.4–0.5 ml min^{-1} eluent to the mass spectrometer.

To obtain the ESI-LC/MS of the isolated metabolites, aliquots of dissolved metabolites (in methanol or water) were introduced to the mass spectrometer by flow injection. The mobile phase consisted of acetonitrile/10 mM ammonium formate, pH 3.3 (1:1 v/v) delivered at 0.3 ml min^{-1}.

Liquid chromatography/NMR

LC/NMR data for M1 was obtained using a Bruker LC22 pump to deliver the mobile phase. The eluent from the Waters Symmetry C_{18} column (3.9 × 150 mm, 5 μm) was monitored at 254 nm using a Bischoff Lambda 1010 UV detector. A gradient solvent system consisting of acetonitrile and D_2O (each containing 0.05% trifluoroacetic acid) separated the metabolite from endogenous components. The percentage of acetonitrile was increased linearly from 10 to 50% over 30 min. ^{1}H-NMR spectra were obtained in stop-flow mode using a Bruker Avance 500 MHz NMR spectrometer equipped with a ^{1}H/^{13}C LC/NMR flow-probe, with a cell volume of 120 μl. Suppression of the residual water and acetonitrile signals was carried out using the WET solvent suppression method (Smallcombe *et al*. 1995). Data were acquired with 256 transients into 32 K data points with a pulse repetition time of 2.8 s. Chemical shifts were referenced to acetonitrile at δ2.0 ppm.

The NMR data for M2–6 were obtained in DMSO-d_6 on a Bruker Avance 500 MHz spectrometer. The NMR data for M7 was obtained using a Varian VXR-Unity 400 MHz instrument. The structures of these metabolites were determined from ^{1}H-NMR as well as proton-proton total correlated spectroscopy (TOCSY), proton-carbon heteronuclear single quantum coherence (HSQC) and long-range proton-carbon heteronuclear multiple-bond correlation (HMBC) two-dimensional NMR using standard parameter sets.

Metabolite profiling with HPLC/radiochemical detection

Analysis of rat and dog plasma, urine, bile and faeces was conducted by HPLC using a Radiomatic FLO-ONE/Beta Model A500 radiocativity detector (Packard Instruments, Meriden, CT, USA). Plasma (pooled from each time point) was extracted using a BondElut C8 SPE cartridge and eluted with methanol. Lyophilized faeces (200 mg) from each time point was extracted overnight with 6 ml methanol/0.1% formic acid (90:10 v/v) and the extracts were evaporated to dryness. The dried residues were reconstituted with water/acetonitrile (90:10 v/v) and injected onto a YMC-Pack C8 column (250 × 4.6 mm) and the components resolved using a gradient HPLC system. Urine (50–100 μl) and bile (20 μl) samples were injected directly onto the HPLC column. The mobile phase consisted of two solvents: A (50 mM phosphoric acid/acetonitrile, 90:10 v/v) and B (50 mM phosphoric acid/acetonitrile,

75:25 v/v). The proportion of B was increased from 0 to 100% over 8 min with a solvent flow rate of 1.0 ml min^{-1}. After washing the column with 100% B for an additional 10 min, the column was re-equilibrated with the mobile phase A.

In vivo *studies*

Excretion of ^{14}C by bile duct-cannulated rat after i.v. and oral dosing of either roxifiban or XV459. The bile duct-cannulated male Sprague-Dawley rat (~400 g each) obtained commercially (Charles River, Raleigh, NC, USA) received a single 0.5 mg kg^{-1} dose by i.v. bolus into the jugular vein ($n = 4$) or a single 2.5 mg kg^{-1} oral gavage ($n = 4$) of ^{14}C-roxifiban or ^{14}C-XV459. Bile salts were replenished during the course of this and subsequent experiments involving the bile duct-cannulated rat. Each rat received ~20 or 75 μCi ^{14}C-labelled compound for the i.v. and oral studies respectively. Rats were placed in individual metabolic cages and urine, bile and faeces were collected separately from 0–24, 24–48, 48–72 and 72–96 h. Urine and bile were collected on dry and wet ice respectively. All collection vessels contained 1 mM phenylmethylsuphonyl fluoride to inhibit the *ex vivo* hydrolysis of roxifiban. Aliquots of urine (1 ml) and bile (250 μl) were added in triplicate to 15 ml scintillant (Ultima Gold®, Packard) and the radioactivity present was determined by LSC. The radioactivity (dpm) was calculated using a quench curve after the subtraction of background. Faeces from each rat were lyophilized, ground, weighed and 100 mg placed in Combusto-Cones®. Samples were burned in a Packard Oximate 80® sample oxidizer, the liberated CO_2 trapped in a solution of Carbo-sorb and Permafluor E+, and the radioactivity counted by LSC. Control samples containing a known amount of radioactivity were routinely oxidized to determine the percent recovery from the combustion process and used to correct the results of faeces samples.

In a separate experiment, platelet poor plasma was prepared from whole blood collected at 0, 15, 30 and 90 min after an oral dose of ^{14}C-XV459 (2.5 mg kg^{-1}, 60 μCi). The plasma was pooled at each time point and extracted using a C8 SPE cartridge, as described above.

Excretion of ^{14}C by dog after i.v. and oral dosing of either roxifiban or XV459. In separate experiments, the male beagle dog ($n = 3$) weighing ~8 kg received single oral doses of either ^{14}C-roxifiban (2.5 mg kg^{-1}, 333 μCi) or ^{14}C-XV459 (2.5 mg kg^{-1}, 333 μCi). The animals were placed in individual cages and urine and faeces were collected from 0–24, 24–48, 48–72 and 72–96 h. Blood was collected at 0, 0.5, 1.5, 2.5 and 3.5 h post-dose, and platelet poor plasma prepared immediately. The samples were kept frozen at −20 °C until analysed. In another study, three male beagle dogs were administered ^{14}C-XV459 i.v. (40 μg/kg, 36 μCi) and urine, plasma and faeces collected. An i.v. dose of ^{14}C-roxifiban (40 μg/kg, 36 μCi) was administered to a single bile duct-cannulated male beagle dog, and urine, bile and faeces were collected. The excretion profiles of radioactivity in urine, bile and faeces were obtained by treating the samples in the same manner as described above in the rat study.

To obtain the metabolite profiles in urine, bile, plasma and faeces of dog given either oral or i.v. doses of XV459 or roxifiban, samples were treated, as described above. Aliquots of bile and urine were injected directly onto the HPLC column without any sample treatment.

LC/MS profiling of metabolites present in urine and bile of rat given d_0:d_4 roxifiban. A single male bile duct-cannulated Sprague–Dawley rat was dosed with 100 mg kg^{-1} equimolar mixture of d_0:d_4-roxifiban (four unsubstituted positions on the aromatic ring labelled with deuterium) and bile and urine were collected at 0–8 and 8–24 h intervals. Urine and bile samples were extracted by C_{18} SPE cartridges before analysis by LC/MS. About 2 ml of each sample was loaded onto a preconditioned BondElut C_{18} SPE cartridge (500 mg, 10 cc) and allowed to elute under gravity. The cartridges were washed with 2 ml water followed by a rinse with 10% methanol in water. The metabolites were eluted with 30% methanol in water. The extracts were dried, reconstituted in the HPLC mobile phase and injected onto the LC/MS.

LC/MS profiling of metabolites present in urine and plasma of human subjects given roxifiban. Roxifiban (1–2 mg) was administered orally once daily for 7–10 days to healthy male Caucasian volunteers (aged 40–65 years, weighing 54–75 kg) enrolled in the first phase of clinical trials. Eleven volunteers provided written informed consent and the protocol was approved by the local ethics committee. The drug was administered as a tablet with 180 ml water to subjects who had fasted for at least 8 h overnight before each dose. Urine samples were collected at 0–6, 6–12, 12–24 and 24–48 h after the dose and stored at −20 °C. Plasma and urine samples were analysed. After extraction on C_{18} cartridges as described above, the cartridges were eluted with 80% methanol in water. The eluent was dried under nitrogen and reconstituted in the HPLC mobile phase. Aliquots (30 μl) were injected onto the LC/MS and full scan and selected ion monitoring (SIM) profiles obtained in separate experiments.

Infusion of rat with XV459 and roxifiban for spectroscopic characterization of metabolites. Preliminary studies in rat suggested that the metabolites produced at high doses (100 mg kg^{-1}) were the same as those produced at low doses (2.5 mg kg^{-1}). To generate large quantities of metabolites, eight male bile duct-cannulated Sprague–Dawley rats were infused with roxifiban at 100 mg kg^{-1} h^{-1} for 6 h. Urine and bile

samples were collected at 0–7 and 7–24 h intervals, and blood was collected 1 h after the end of the infusion and the plasma was then stored at −20 °C until analysed. In another study, a single male bile duct-cannulated Sprague-Dawley rat was infused with XV459 at 100 mg kg^{-1} h^{-1} for 60 min. Plasma (at t = 2 h), urine and bile samples were collected over 24 h and stored frozen until analysed.

In vitro *studies*

Metabolism of ^{14}C-roxifiban by liver slices. ^{14}C-roxifiban (5 μM, 2×10^6 dpm ml^{-1}) was incubated for 4 h with liver slices from rat and mouse, two species suitable for carcinogenicity studies, and a male 46-year-old human transplant donor. After the incubation, aliquots of the supernatants were analysed by HPLC with radiochemical detection to determine the metabolite profiles.

Metabolism of ^{14}C-roxifiban by dog intestinal cores. One male beagle dog was killed by ensanguination, and 5-inch segments of the duodenum, ileum, ascending colon and descending colon were isolated immediately. Longitudinal sections were cut through the mucosa, rinsed with saline and immediately placed in Krebs-Henseleit buffer (pH 7.4) on ice. From each intestinal section, 8-mm cores were cut from the tissue using a skin biopsy punch, placed in fresh Krebs buffer and pre-incubated separately at 37 °C for 10 min. Cores (n = 10) were then placed in fresh Krebs buffer containing ^{14}C-roxifiban (5 μM, 2×10^6 dpm ml^{-1}), and gassed with O_2/CO_2 (95/5%). Samples were incubated at 37 °C in a shaking water bath and aliquots of buffer (0.75 ml) were collected at 0, 5, 10, 20, 60 and 120 min and snap frozen. A sample containing only ^{14}C-roxifiban and buffer and incubated for 120 min was included as a control to monitor ester hydrolysis in the absence of tissue. Samples were analysed by HPLC using a Radiomatic FLO-ONE/Beta Model A500 radioactivity detector, as described above.

Metabolism of ^{14}C-roxifiban by dog faeces under anaerobic incubation conditions. Dog faeces were freshly collected and 1 g was immediately suspended in 2 ml reduced trypticase soy broth and capped immediately. A portion of this faecal suspension was boiled for 5 min to be used as control. The complete incubation contained 0.4 ml active faeces suspension, 2 ml trypticase soy broth and ^{14}C-roxifiban (5×10^6 dpm, 5 μM). After inoculation, samples were transferred to an Atmosbag™ purged of room atmosphere and the bag was sealed. Nitrogen was introduced into the bag through a sealed port at 2 psi with a constant vacuum applied at the second sealed port. The bag was subsequently placed in a 37 °C incubator for 48 h. After incubation, methanol (4 ml) was added and samples extracted overnight. The homogenate was centrifuged, and supernatant removed and dried. Samples were analysed by HPLC with a Radiomatic FLO-ONE/Beta Model A500 radioactivity detector, as described above.

Isolation of roxifiban metabolites. M1–6 were obtained from rat urine samples and M7 was isolated from dog faeces. Because only a small percentage of the dose was eliminated in bile (table 1), the metabolites were isolated only from urine. Urine (200 ml) from rat dosed with roxifiban were extracted with solid-phase extraction (SPE) MegaBond Elut C_{18} cartridges (10 g/60 ml, Varian Sample Preparation Products) conditioned with 20 ml methanol followed by 20 ml water. Urine was loaded onto the cartridges and sequentially washed with 20 ml aliquots of varying percentages of methanol in water (0, 5, 15, 20, 25, 30, 35, 40, 50, 60, 70, 80, 100% methanol). Each fraction was analysed by LC/MS for the presence of metabolites and the fractions containing the appropriate metabolite(s) were pooled and dried under vacuum. Further purification of individual metabolites was carried out on HPLC and C_{18} cartridges, as described below.

- M1: the 30% methanol fraction was dried and repurified on a 500 mg/10 ml C_{18} cartridge after reconstituting in water. Elutions were carried out with 2 ml 0, 10, 15, 20, 25, 30, 35, 40 and 45% methanol in water. The fractions containing M1 were pooled, dried and repurified on a semipreparative C_{18} column (Beckman, 250 × 10 mm) using an isocratic mobile phase consisting of 12% acetonitrile in 10 mM ammonium formate (pH 3.3) delivered at 3.3 ml min^{-1}. The HPLC eluent was monitored at 254 nm by a variable wavelength UV detector. M1, eluting at 5.2 min, was collected from several injections, pooled, dried, weighed (11.1 mg) and submitted for NMR and LC/NMR analyses.
- M2 and M3: M2 and M3 co-eluted in the 35 and 40% methanolic fractions of the initial clean up of the urine samples. The samples were dried and re-extracted on a 500 mg/10 ml C_{18} cartridge, as described above. The fractions containing M2 and M3 were pooled, dried and repurified on a semipreparative C_{18} column (250 × 10 mm) using the same conditions as for M1 except the percent organic was increased to 17% acetonitrile. The two metabolites were collected as separate peaks, pooled and dried under vacuum. Each metabolite sample was subsequently reconstituted in 0.01 M HCl and extracted on a 500 mg/10 ml cartridge to remove any salts. M2 and M3 were eluted from the cartridge with 50% methanol in water (2 ml). The samples were dried and the yield determined (4.1 mg for M2; 3.9 mg for M3) before submitting them for NMR analyses.
- M4: this was a less polar metabolite than XV459, eluting at a longer retention time than other metabolites. M4 co-eluted with XV459 during the initial purification of the urine samples. The extract

Table 1. Excretion of total radioactivity in 96 h by the bile duct-cannulated rat following an i.v. (A) or oral (B) dose (0.5 or 2.5 mg kg^{-1} respectively) of either ^{14}C-roxifiban or ^{14}C-XV459.

	Percent of the dose excreted			
	Urine	Bile	Faeces	Total
I.v. (0.5 mg kg^{-1})				
Roxifiban	76.5±32.3	8.6±2.2	2.0±0.6	81.8±23.7
XV459	66.6±10.9	11.1±1.8	7.1±10.6	84.8±19.1
Oral				
Roxifiban	11.8±12.5	0.8±0.4	78.7±28.1	91.2±19.6
XV459	14.1±7.4	0.5±0.2	85.6±21.1	91.4±19.5

Data are the mean±SD (n = 4).

containing M4 was purified further using the same HPLC conditions as those used for M2 and M3. The isolated metabolite fraction was dried and submitted for NMR analyses. The structure of M4 was subsequently confirmed by comparing the retention time and mass spectral fragmentation of the methylated analogue with a synthetic standard. A portion of partially purified M4 was dissolved in 1:1 v/v mixture of ether:methanol and excess of diazomethane, generated *in-situ* from Diazald®, added.

- M5: one of the minor metabolites isolated during the purification of M2 and M3 had the same MH^+ (at m/z 448) as roxifiban. Sufficient quantities of this metabolite were isolated during the semipreparative purification of M2 and M3 for NMR analyses.
- M6: M6 co-eluted with M1 in the 30% methanol fraction of the SPE extract. However, M6 was retained on the C_{18} HPLC column much longer than M1. Hence, M6 was purified on the Beckman C_{18} column (250×10 mm) using an isocratic HPLC mobile phase consisting of acetonitrile and 10 mM ammonium formate, pH 3.3 (25:75 v/v) delivered at 3.3 ml min^{-1}. The peak corresponding to M6 was collected, dried and submitted for NMR analyses.
- M7: radiochromatographic analysis of dog faeces following an oral dose of ^{14}C-roxifiban showed one major metabolite with MH^+ at m/z 437. To isolate sufficient quantities of M7, two male beagle dog were given 2.5 mg kg^{-1} roxifiban by oral gavage. Faeces were collected from 0 to 24 h, lyophilized and homogenized. Samples (200 mg) were shaken overnight with 6 ml methanol/0.1% formic acid (90:10 v/v), centrifuged and the supernatant evaporated to dryness. The dried extracts were reconstituted in water and extracted using a BondElut C8 SPE cartridge. The metabolite was selectively extracted by water/acetonitrile (70:30 v/v). All samples were dried, reconstituted in water/methanol (90:10 v/v) and injected onto a YMC-Pack C8 column and resolved using the same HPLC system as described above. The 50 mM phosphoric acid was replaced by 0.1% formic acid in the mobile phases. The appropriate HPLC fractions were collected, evaporated to dryness and reconstituted in methanol/water (50/50 v/v) and repurified by a second gradient HPLC system developed by pumping 100% mobile phase A (water:methanol, 90/10 v/v) to 100% mobile phase B (water:methanol, 60/40 v/v) over 15 min. The HPLC fractions containing the metabolite were collected, pooled and evaporated to dryness using the Savant Speed Vac® (model SC110). The sample was submitted for NMR analyses and the structure confirmed with the synthetic metabolite.

Results

Excretion of total radioactivity by rat

The recovery of total radioactivity after 96 h in rat dosed with ^{14}C-roxifiban was 81.8±23.7 and 91.2±19.6% of the administered i.v. and oral doses respectively (table 1). The majority of the radioactivity after i.v. administration was excreted in the urine (76.5±32.3%) and small amounts were excreted in bile and faeces. However, after oral administration of ^{14}C-roxifiban, 78.7±28.1% of the radioactivity was excreted in the faeces. Similarly, the recovery of total radioactivity after 96 h in rat dosed with ^{14}C-XV459 was 84.8±19.1% and 91.4±19.5% of the administered i.v. and oral doses respectively (table 1). The majority of the radioactivity after i.v. administration was excreted in the urine, whereas after an oral administration most of the radioactivity was found in faeces. The percent of dose

Table 2. Excretion of total radioactivity in 96 h by dog following an i.v. r oral dose (40 or 2·5 mg kg^{-1} respectively) of either ^{14}C-roxifiban or ^{14}C-XV459.

	Percent of the dose excreted			
	Urine	Bile	Faeces	Total[a]
I.v. (40 μg/kg)				
Roxifiban	34[b]	55[b]	5[b]	94[b]
XV459	25·8±4·4	ns[c]	71·2±17·7	96·8±19·5
	28·6[b]	54·7[b]	ns[c]	83·3[b]
Oral				
Roxifiban	6·0±2·1	ns[c]	87·8±21·2	94·0±22·1
XV459	3·4±0·7	ns[c]	63·2±14·7	66·6±14·6

[a] Data are the mean ± SD (n = 3), except for the single bile duct-cannulated dog.
[b] which was dosed i.v. with XV459 or roxifiban.
[c] ns, No sample.

excreted in the bile and urine of rat dosed i.v. (with either roxifiban or with XV459) when compared with animals dosed orally suggest a very low oral bioavailability of the two compounds. In addition, the high percentage of radioactivity recovered in faeces of bile duct-cannulated rats after oral doses of either roxifiban or XV459 also suggests low oral absorption of the compounds.

The radiochemical profiles of urine, bile and faeces after oral administration of ^{14}C-XV459 showed that only a small percentage of the dose was eliminated in urine and bile as the unchanged XV459 (2.4 and 0.4% respectively; data not shown). The excretion of metabolites in urine and bile was minimal, accounting for 4.7 and $< 0.5\%$ of total dose respectively. In rat faeces, 5.2% of the excreted radioactivity was present as XV459, and 83.8% was identified as the ring-opened M7.

Excretion of total radioactivity by dog

Following an i.v. dose of ^{14}C-roxifiban to a single bile duct-cannulated dog, 55 and 34% of the dose was eliminated in bile and urine respectively. Faecal excretion was the primary route of elimination following an oral dose of ^{14}C-roxifiban, with 87.8% ± 21.2 of the dose excreted in the faeces. A small percentage of the dose (6.0 ± 2.1) was eliminated in the urine (table 2). Faecal excretion was the primary route of elimination for dog given either i.v. or oral doses of ^{14}C-XV459. After the i.v. dose, 25.8 and 71.2% of the dose was eliminated in the urine and faeces respectively within 96 h. These data suggested that biliary excretion of XV459 was important, and studies in a bile duct-cannulated dog given an i.v. dose of either ^{14}C-roxifiban or ^{14}C-XV459 confirmed this observation (table 2). After an oral dose of ^{14}C-XV459, 63.2% ± 14.7 and 3.4% ± 0.7 of the administered radioactivity was recovered in dog faeces and urine respectively (table 2). The low total recovery of radioactivity after 96 h in dog given ^{14}C-XV459 orally could not be explained.

Radiochromatographic analysis of bile and urine from the bile duct-cannulated dog given ^{14}C-roxifiban (i.v.), showed that only XV459 was present. In dog dosed orally with roxifiban, the majority of the radioactivity is eliminated in faeces principally as M7, after microbial degradation of unabsorbed XV459. After a single i.v. dose of ^{14}C-XV459, the unchanged compound and M7 were major components in dog urine and faeces respectively. Metabolite profiles of excreta collected after an oral dose of ^{14}C-XV459 showed that 86% of the radioactivity in faeces chromato-

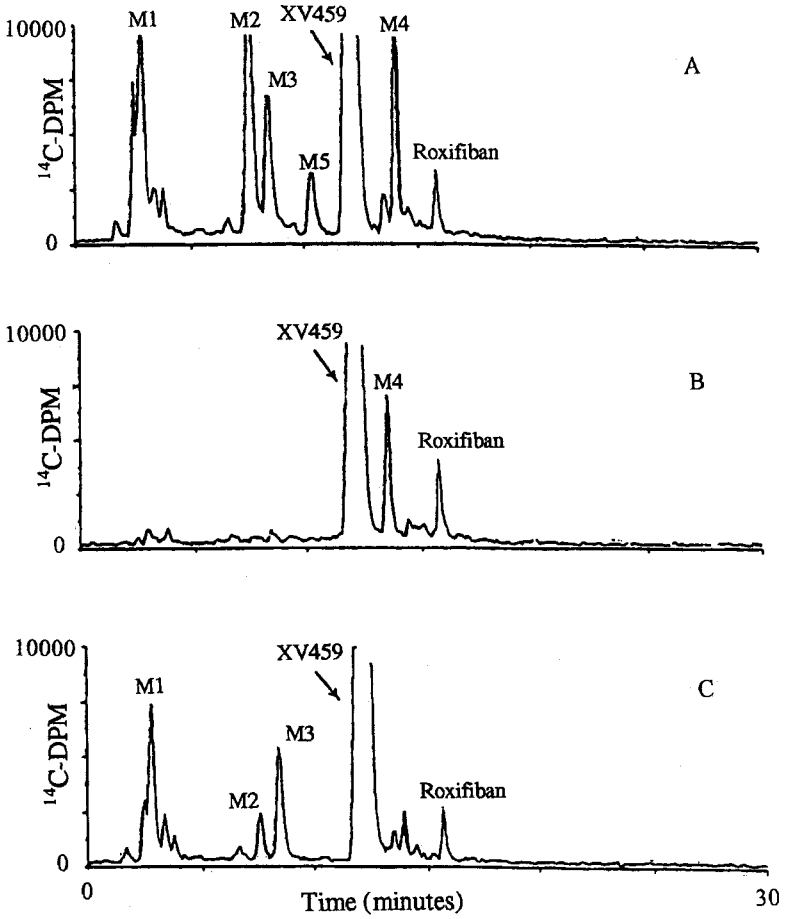


Figure 2. Metabolite profiles of ^{14}C-roxifiban incubated with rat (A), mouse (B) and human (C) liver slices.

graphed as M7 and 5% as unchanged XV459. Whereas XV459 accounted for most of the radioactivity in urine collected after an oral dose of ^{14}C-XV459, at least five minor unidentified peaks were also present. However, XV459 and its metabolites accounted for $< 5\%$ of the dose in urine after oral administration of XV459.

In dog biliary excretion is a significant route of elimination for these compounds. Dog given an i.v. dose of ^{14}C-XV459 excreted most of the dose in the faeces (table 2) after extensive biliary excretion.

Rat and dog plasma profiles

After oral or i.v. doses of ^{14}C-XV459, only the parent compound was present in dog and rat plasma. XV459 was the major component in urine and plasma from rat and dog dosed either orally or i.v. with ^{14}C-roxifiban.

Metabolite profiles of ^{14}C-roxifiban incubated with rat, mouse and human liver slices

The major metabolite XV459 produced by rat, mouse and human liver slices after a 4-h incubation with ^{14}C-roxifiban represented 79, 97 and 96% of the chromatographed radioactivity respectively (figure 2). Several metabolites were

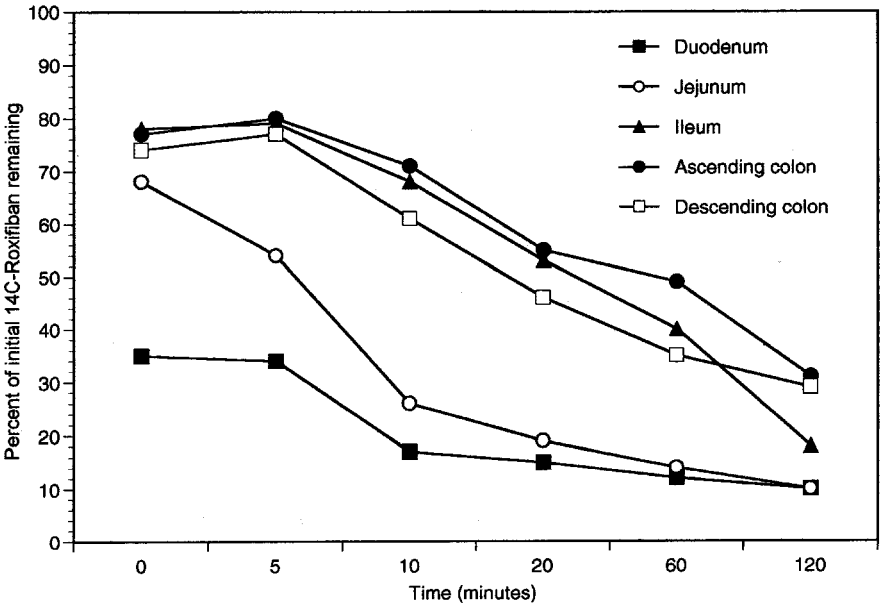


Figure 3. Metabolism of ^{14}C-roxifiban by dog intestinal cores over 2 h. Data are from 10 cores.

detected in rat, mouse and human liver slice supernatants representing 21, 3 and 4% of the chromatographed radioactivity respectively. These data confirmed that hydrolysis of ^{14}C-roxifiban in rat, mouse and human liver slices to XV459 was the major pathway and that the rodent and human produce similar metabolite profiles. Furthermore, this experiment demonstrated that the active compound, XV459, was further metabolized by the liver but only to a small extent. M1–5 were identified as minor metabolites and their structures were tentatively established by comparing the HPLC retention times with standards isolated from rat urine (figure 2).

Metabolism of ^{14}C-roxifiban by dog intestinal cores

The duodenum and jejunum segments hydrolyzed roxifiban to XV459 to the greatest extent, and after 5 min only 34 and 54% ^{14}C-roxifiban remained respectively. Other intestinal sections also metabolized ^{14}C-roxifiban rapidly, with $< 50\%$ of the parent drug remaining after 1 h in all samples. In the absence of tissue, $< 10\%$ ^{14}C-roxifiban was hydrolyzed to XV459 (figure 3).

Roxifiban is hydrolyzed rapidly to XV459 by both intestinal and liver tissues, contributing to the rapid and total conversion of the prodrug. The small intestine hydrolyses roxifiban to XV459 faster than the large bowel.

Metabolism of ^{14}C-roxifiban by dog faeces

Under anaerobic conditions, dog faeces converted roxifiban to M7 (major) and to the zwitterion, XV459. In the presence of inactivated gut contents, most of the radioactivity was recovered as unchanged roxifiban with small quantities of XV459 being detected.

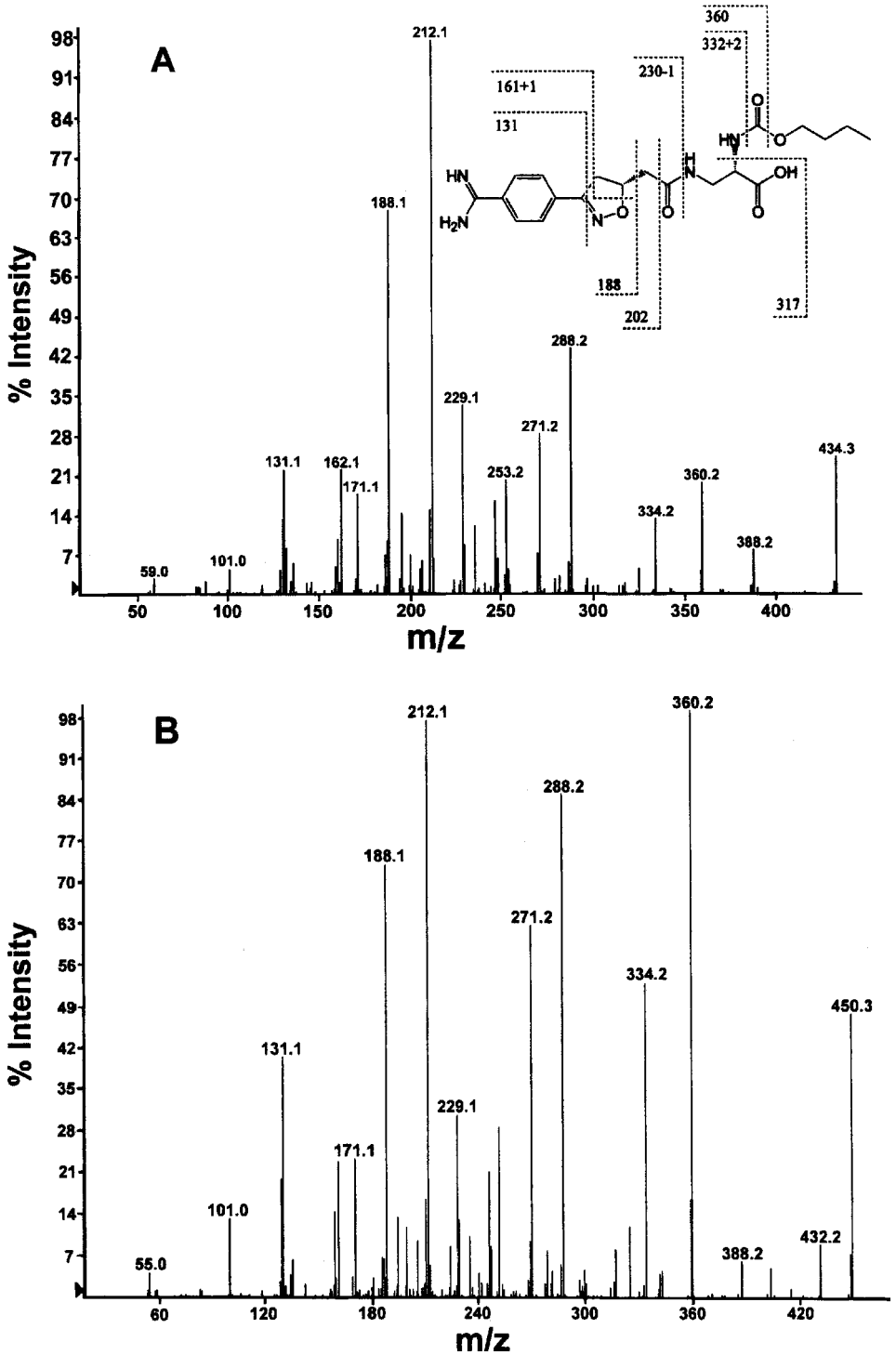


Figure 4. MS/MS spectra of XV459 (A) and of M1 (B). Fragmentation patterns were similar for both the compounds.

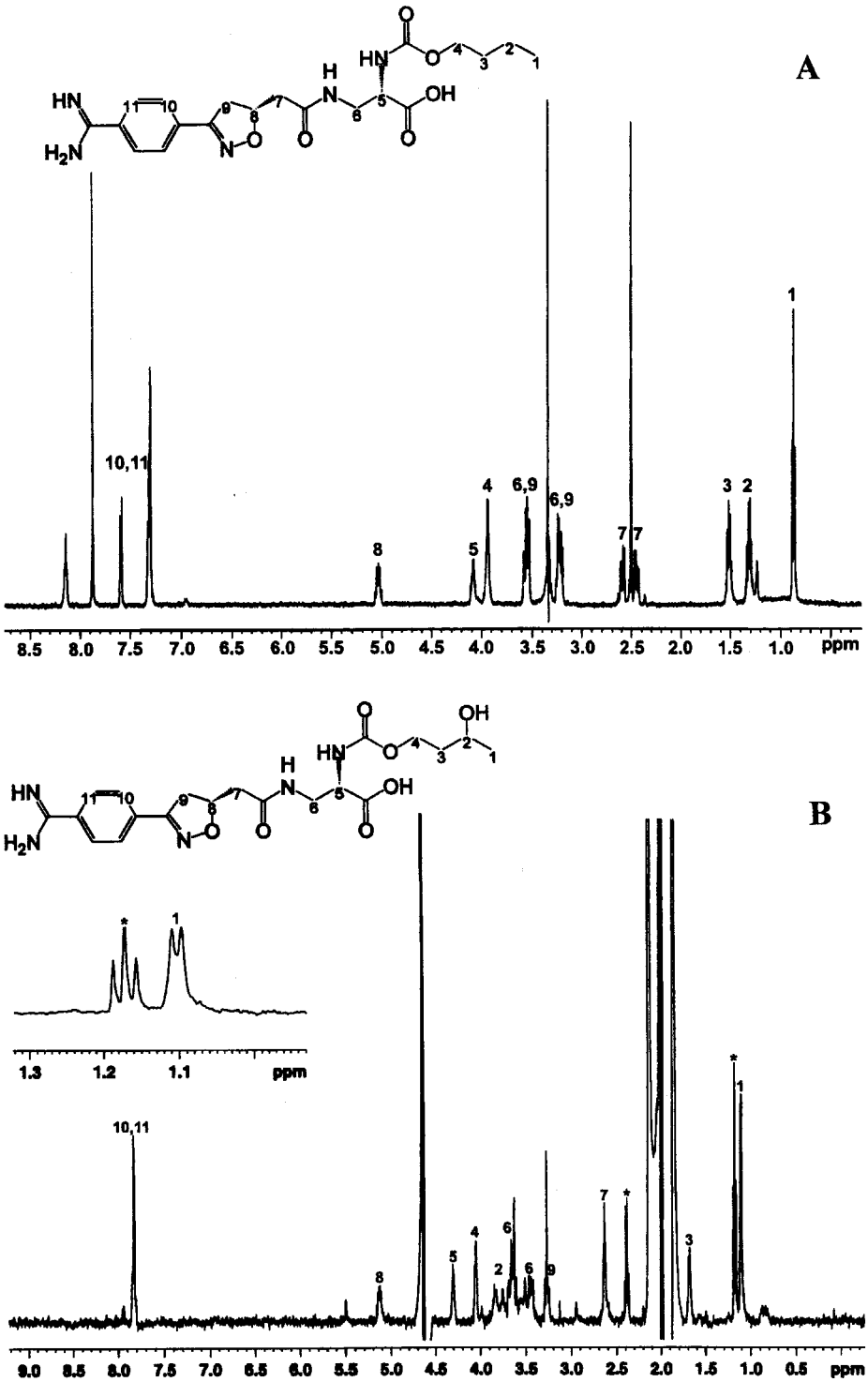


Figure 5. ^{1}H-NMR of the zwitterion, XV459 (top) and ^{1}H-LC/NMR of M1 isolated from rat urine (bottom).

Excretion of metabolites in d_0:d_4 *roxifiban dosed rat*

The initial identification of metabolites in rat bile and urine was facilitated by dosing the rat with a 1:1 mixture of d_0:d_4 roxifiban. The mass spectra of metabolites showed pairs of twin ions separated by 4 amu, thus enabling the detection of roxifiban metabolites in the presence of endogenous components. The major metabolite found in the bile and urine of rat was XV459. Some hydroxylated metabolites of XV459 with MH^+ at m/z 450/454 were also found as minor metabolites. Interestingly, no metabolites were found as glucuronide conjugates either in bile or urine of rat.

Metabolism of roxifibanby human

Analyses of plasma and urine samples from subjects dosed with 1–2 mg roxifiban showed that XV459 was the major component in both matrices. LC/MS profiling of plasma and urine in both full scan and SIM modes revealed that none of the previously identified metabolites from animal studies were detectable in human plasma or urine.

Characterization of M1–7

M1–6 were isolated from urine of rat infused with roxifiban, while M7 was isolated from dog faeces.

- M1: the MS/MS spectra for M1 (MH^+ at m/z 450) and XV459 (MH^+ at m/z 434) are shown in figure 4. The MS/MS fragmentation pattern suggested that hydroxylation had taken place on the *n*-butyl side chain because the fragment ions formed by M1 and XV459 were similar. The position of hydroxylation on M1 was assigned unambiguously by LC/NMR experiments. The ^{1}H-LC/NMR analyses of M1 showed characteristic changes in the ^{1}H-NMR consistent with a ω-1 hydroxylated product. The characteristic triplet and quartet patterns seen for an intact $-CH_2CH_3$ spin system (see figure 5(A) for the ^{1}H-NMR of XV459) was replaced by a doublet at δ1·10 ppm ($-CH_3$) and a multiplet at 3.8 ppm ($-CH(OH)CH_3$). The other methylene multiplets appeared at δ1·68 and 4.05 and are consistent with the addition of an OH in the position labelled 2 (figure 5(B)). The rest of the proton signals remained unchanged as compared with the parent compound.
- M2: M2 also produced MH^+ at m/z 450, with the mass spectral fragmentation pattern different from M1. The MS/MS of ion at m/z 450 suggested hydroxylation on the isoxazoline ring. The fragment ion at m/z 131 indicated an intact benzamidine, while the ions at m/z 204 (188+16), 228 (212+16) and 246 (230+16) were consistent with a hydroxylated isoxazoline ring (see figure 4 for ion fragments from XV459 for comparison). The structure and the stereochemistry of M2 were confirmed by comparing the LC/MS/MS and NMR data with synthetic standards (both *trans*- and *cis*-4-hydroxy metabolite standards). The mass spectral fragmentation pattern and the HPLC retention time of M2 matched those of the synthetic standard bearing the hydroxyl group in the trans configuration. The LC/MS fragmentation pattern and the retention time of the *cis*-4-hydroxy isomer were different and clearly distinguishable from M2 and the *trans*-isomer. The ^{1}H-NMR results confirmed the structure with the hydroxyl group on C9 (figure 6). Comparison of this spectrum with that of the parent

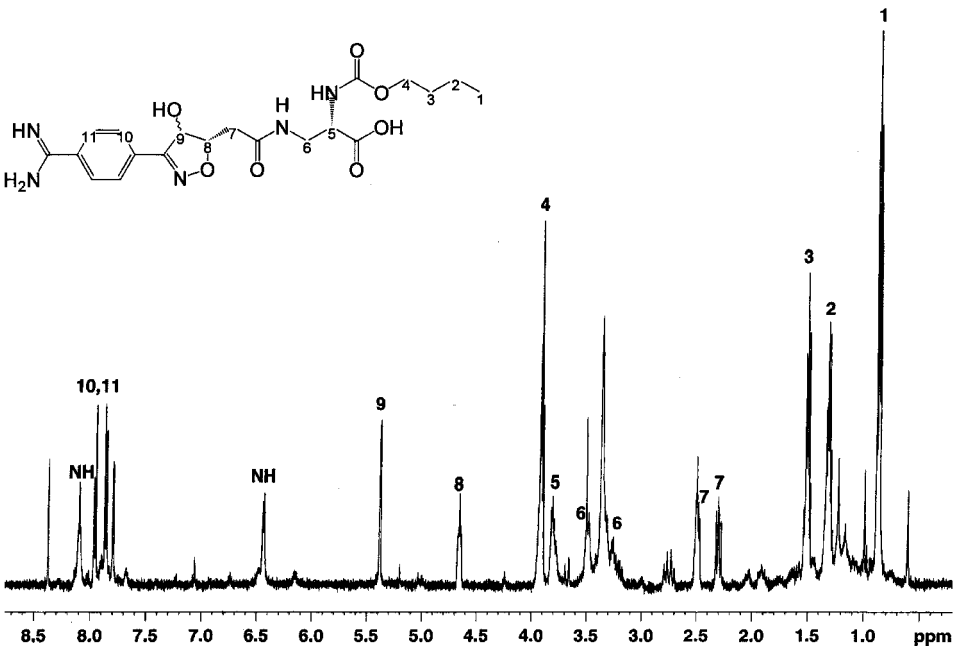


Figure 6. ^{1}H-NMR of M2 isolated from rat urine.

compound XV459 (figure 5 (A)) showed the spin system of protons in the 5- and 6-positions and the two NH resonances are present whereas the spin-system of the protons in the 7–9-positions was altered. The methylene in the 9-position of the parent has been shifted down-field and was now a methine doublet at 5.38 ppm with a 3.35 Hz coupling to the methine in the 8-position which was also shifted down-field. The resonances arising from the methylene in the 7-position were essentially unchanged. These data are consistent with hydroxylation in the 9-position. Nuclear Overhauser effect spectroscopy (NOESY) data obtained on this sample were inconclusive as to the absolute stereochemistry of the metabolite. The ^{1}H-NMR data obtained for the synthetic *trans*-4-hydroxy isomer was similar to the isolated metabolite.

- M3: the formation of the hydroxylated M3 from XV459 produced a compound with a fixed stereochemistry (figure 7). The ESI-LC/MS of M3 produced MH^+ at m/z 450 with the major fragment ion at m/z 432 (base peak) formed by neutral loss of water. Other characteristic fragments included ions at m/z 358, 332, 286, 269, 246, 228 and 204. The assigned ^{1}H-NMR spectrum of M3 is shown in figure 8. The structure of M3 was confirmed by NMR experiments and by comparing the LC/MS retention time and mass spectral fragmentation pattern with the 5-hydroxy synthetic standard. Comparison of this spectrum with that of the parent compound XV459 (figure 5(A)) shows loss of the resonance of the methine in the 8-position and is consistent with hydroxylation at that position. Although M2 and M3 were regio-isomers formed by hydroxylation of the isoxazoline ring, the mass spectral fragmentation patterns were very different from each other.
- M4: the metabolite with MH^+ at m/z 432 was apparently formed by the dehydration of either M2 or M3. The similarity in mass spectral fragmentation pattern between M3 and M4 suggested that M4 was likely to be formed from M3

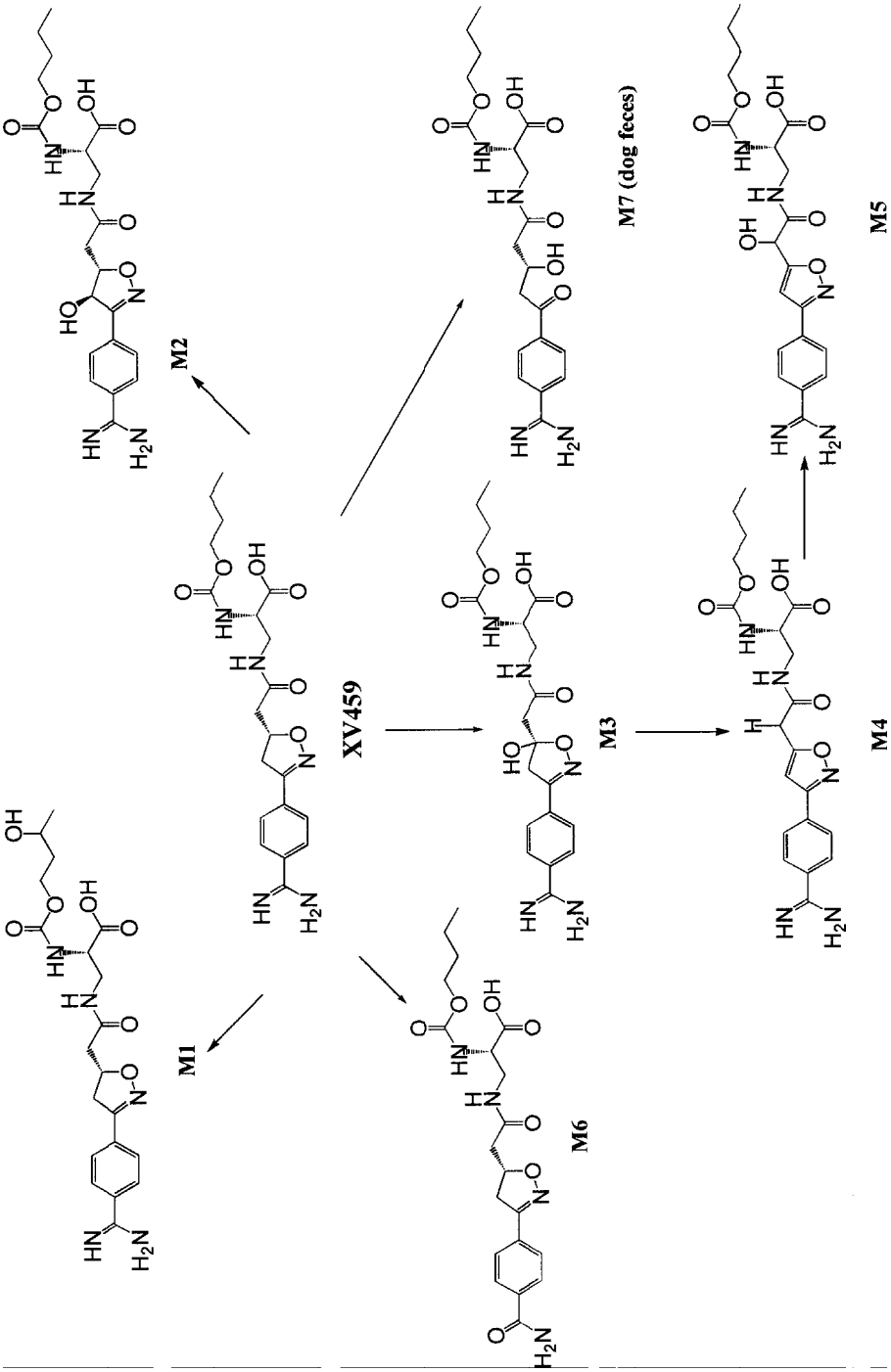


Figure 7. Proposed metabolic pathways of XV459, the zwitterion derived from the prodrug roxifiban.

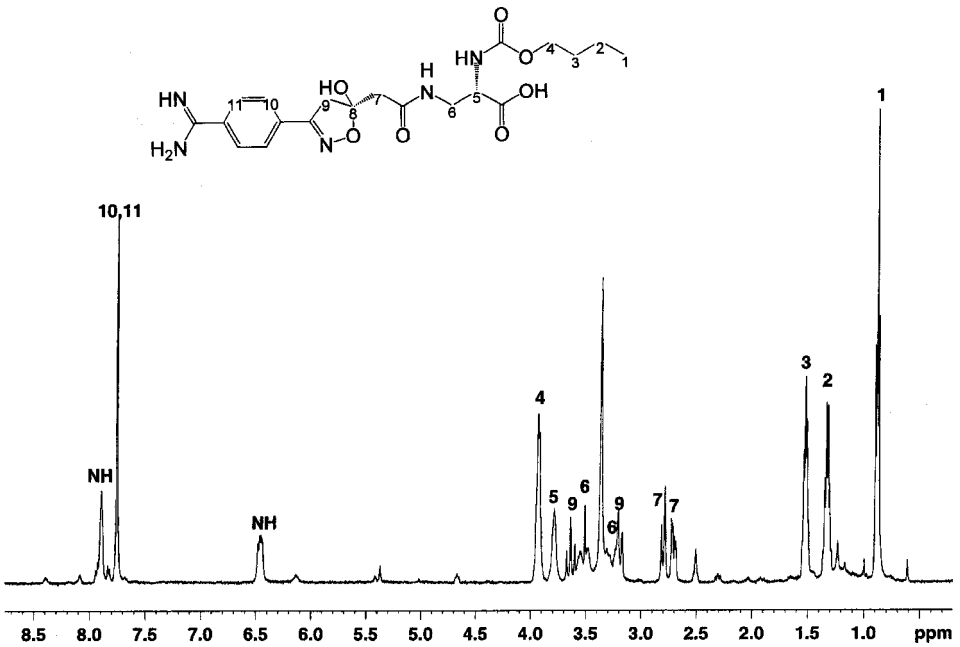


Figure 8. ^{1}H-NMR of M3 isolated from rat urine.

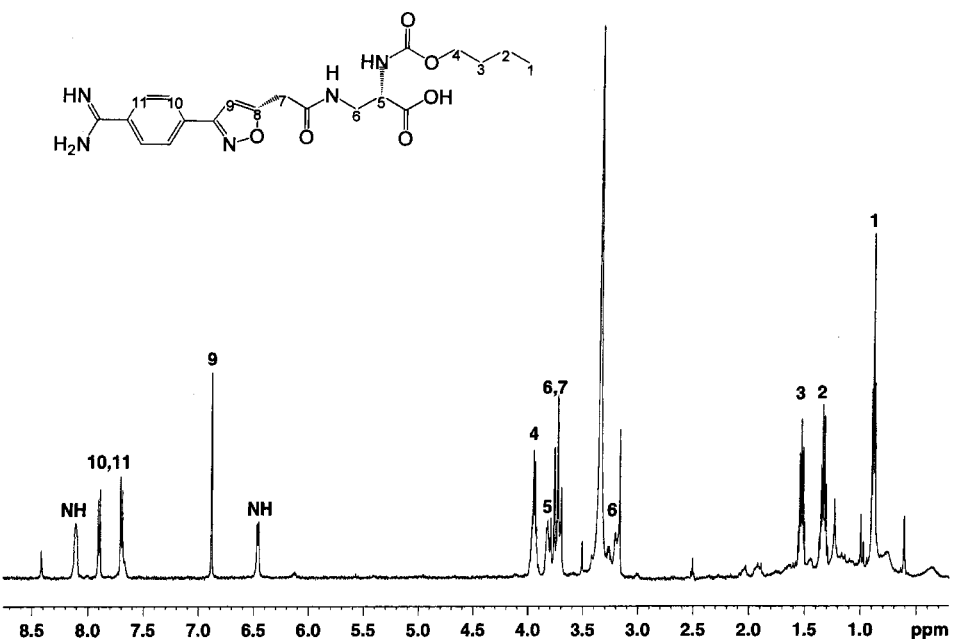


Figure 9. ^{1}H-NMR of M4 isolated from rat urine.

rather than from M2. M3 under acidic conditions overnight produced M4. This was confirmed by LC/MS experiments whereby the retention times and mass spectral fragmentation patterns were matched with those of M3 and M4. The structure of M4 was confirmed by comparing the LC/MS data of the methylated

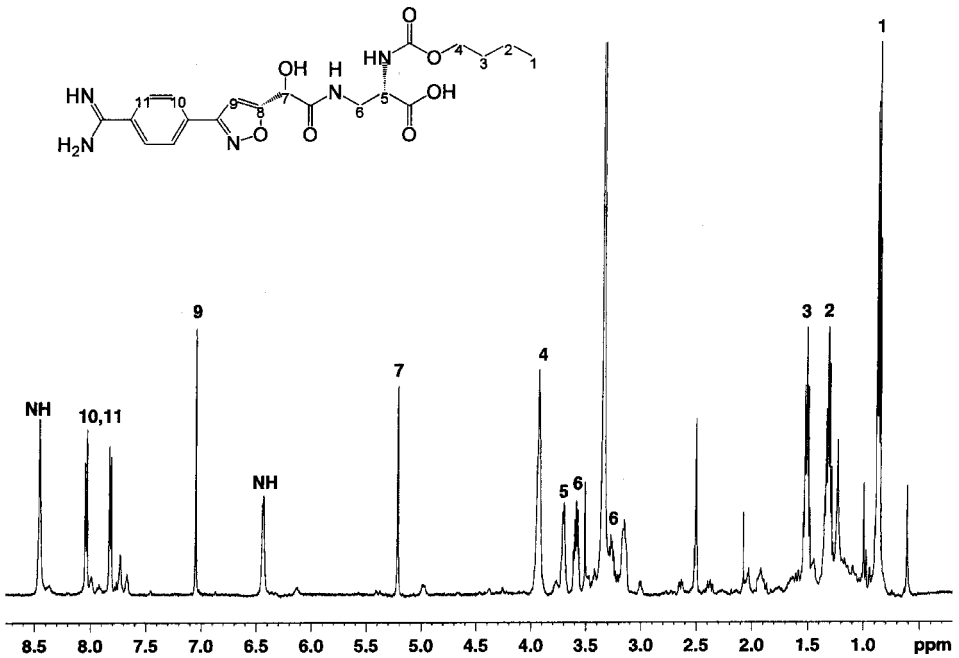


Figure 10. ^{1}H-NMR of M5 isolated from rat urine.

M4 with an authentic standard. Furthermore, the structure of M4 was confirmed unambiguously by NMR. The ^{1}H-NMR spectrum showed the presence of all the proton signals as in the parent compound except for the C8 and C9 protons. The structure of M4, based on comparison with the synthetic standard, is shown in figures 7 and 9. Introduction of the double bond in the isoxazoline ring produced a characteristic signal for the vinylic proton at δ6·8 ppm (=CH, singlet). The proton attached to C8 (δ4·5–5.0 ppm) was distinctly absent in the spectrum, indicating that the double bond was within the isoxazoline ring. The loss of the chirality at C8, with the formation of a double bond, led to the observation of allylic C7 protons ($-CH_2-$, δ3·8 ppm) as a singlet for this metabolite (figure 9).

- M5: this was a minor metabolite isolated from rat urine. The ESI-LC/MS gave MH^+ at m/z 448. The assigned ^{1}H-NMR spectrum of M5 is shown in figure 10. The singlets at 7.05 and 5.21 ppm and the loss of the resonance for the methine in the 8-position are consistent with hydroxylation in the 7-position and the formation of a double bond between the 8- and 9-positions and intact *n*-butyl side chain and benzamidine ring.
- M6: M6 gave MH^+ at m/z 435. The change in the MH^+ from even to odd number suggested a change in the number of nitrogens present in the molecule. The assigned ^{1}H-NMR spectrum of M6 is shown in figure 11. The spectrum is similar to that of the parent compound, XV459 (figure 5(A)) and is consistent with the proposed structure.
- M7: M7 isolated from dog faeces gave MH^+ at m/z 437. The addition of 3 amu to the pseudomolecular ion suggested that the isoxazoline ring was opened (Mutlib *et al*. 1995) with a concurrent loss of a nitrogen atom. The mass spectrum of M7 showed a characteristic fragment ion at m/z 419, formed by the neutral loss of a molecule of water. The shift of one mass unit from m/z 162 (for roxifiban) to m/z

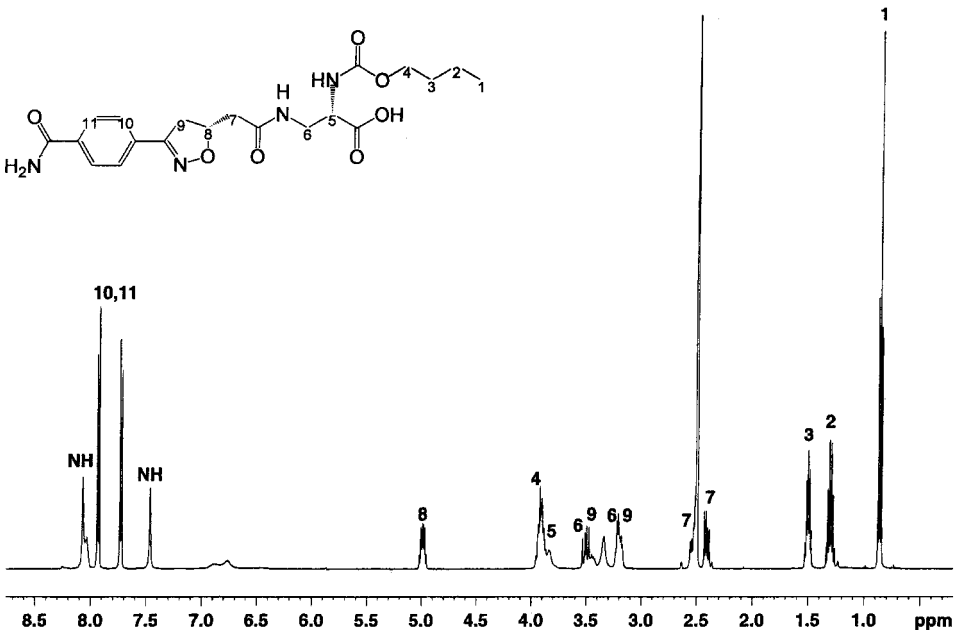


Figure 11. ^{1}H-NMR of M6 isolated from rat urine.

163 further indicated the replacement of a nitrogen atom with the oxygen atom in this fragment. The NMR spectra of the isolated metabolite and the synthetic standard were identical (figure 12). The hydroxyl and carboxylate resonances were not observed in the collected metabolite due to exchangeable protons.

Discussion

Roxifiban possesses an isoxazoline ring that is required for pharmacological activity. Compounds possessing such a moiety are metabolically unstable, yielding the ring-opened products on incubation with liver subcellular fractions or on exposure to gastrointestinal microbes. One objective of these studies was to demonstrate the stability of isoxazoline ring of roxifiban to liver enzymes or to intestinal microbial flora. XV459 is metabolized easily to an isoxazoline ring-opened metabolite, M7, by dog faecal homogenates. Isoxazole rings are reductively cleaved to ring-opened metabolites (Stiff and Zemaitis 1990, Stiff *et al.* 1992, Mannens *et al.* 1993, Meuldermans *et al.* 1994, Mutlib *et al.* 1995). The opening of the benzisoxazole ring of risperidone was attributed to reduction by gut microflora (Meuldermans *et al.* 1994); however, studies of zonisamide, a compound possessing the same benzisoxazole ring, showed that ring cleavage was mediated by liver enzymes instead of gut flora (Stiff *et al.* 1992). An initial reductive cleavage of the 1,2-benzisoxazole ring system to an intermediate with a phenol and imine was postulated, with the imine being further hydrolyzed non-enzymatically to a carbonyl function. Similarly, iloperidone was metabolized by rat hepatic enzymes to the benzisozaxole ring-opened metabolite (Mutlib *et al.* 1995). XV459 also undergoes reductive metabolism by dog gut microflora in the same manner as risperidone, producing the intermediate with an imine and a hydroxyl functional group. The imine is apparently hydrolyzed non-enzymatically to a carbonyl functional as been

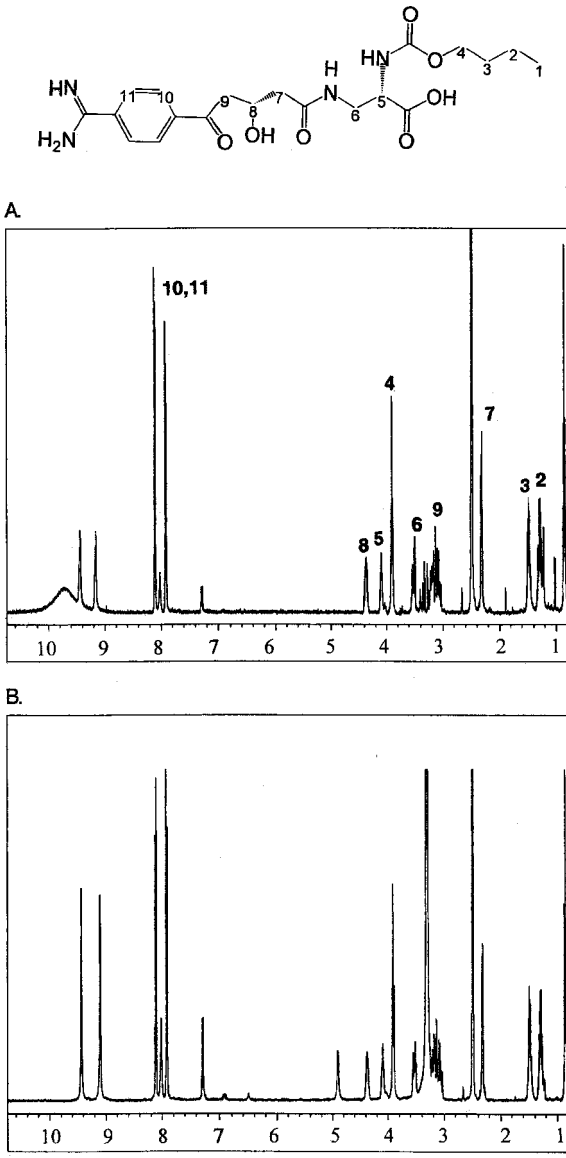


Figure 12. ^{1}H-NMR of isolated faecal M7 (A) and of the synthetic standard (B).

documented for zonisamide (Stiff *et al.* 1992). Incubations of XV459 or roxifiban with liver slices from rat, mouse and human did not produce this metabolite, hence the formation of the isoxazoline ring-opened M7 appears to be mediated solely by gut flora and not by hepatic enzymes.

Intravenous administration of either XV459 or roxifiban in rat produced metabolites that were isolated, characterized and used as reference standards to monitor the formation of metabolites by human. XV459 is the only detectable metabolite found in the plasma and urine of human subjects given oral doses of roxifiban. No other metabolites are detected by LC/MS operated in the SIM mode. LC/MS and NMR techniques accomplished characterization of the metabolites of roxifiban. Some hydroxylated metabolites were isolated after repeated chromato-

graphies on a semipreparative column. The structures of M1–6 were readily determined from NMR data. The structure of M1, the ω-1 hydroxylated metabolite, was determined by stopped flow LC/NMR experiments. The use of LC/NMR in recent years (Spraul *et al*. 1993, Mutlib *et al*. 1995, Shockcor *et al*. 1996, Lindon *et al*. 1997) has made it easier to characterize trace metabolites present in complex biological matrices. Nonetheless, to obtain full NMR characterization of some metabolites, isolation of compounds from endogenous components may still be required. In this study LC/NMR was used to obtain initial information on the nature of M1. The ^{1}H-LC/NMR analysis was adequate for complete structural characterization of M1. This technique was useful because M1 is fairly polar in comparison with other hydroxylated metabolites and hence was difficult to isolate from the endogenous components. Initial characterization of metabolites was also facilitated by dosing rat with a 1:1 w/w mixture of d_4:d_0 roxifiban. This enabled the present authors to detect and identify, by LC/MS, the metabolites of roxifiban in a complex biological matrix like bile. The use of stable isotopes in characterizing the metabolites of compounds has been described (Mutlib *et al*. 1995, *passim*).

Because the formation of M2 produces a chiral centre, it is impossible to determine the absolute configuration of the hydroxyl group by NMR experiments. Both the *cis*- and *trans*-isomers were synthesized for comparison with the isolated metabolite because the relative stereochemistry of the 4-hydroxy group with respect to the 5-substituent of M2 was unclear. Availability of the *cis*- and *trans*-isomer synthetic standards of M2 enabled us to assign the correct structure for M2. A synthetic standard of M3 was also made and compared with the isolated metabolite. Since the stereochemistry at the C8-position was fixed, hydroxylation at this position led to the formation of only one product whose structure was confirmed by comparison with the standard.

In summary, the metabolism studies with roxifiban show that this compound is rapidly hydrolyzed to its zwitterionic form, XV459, *in vivo* and in the presence of liver slices and intestinal segments. Further hepatic metabolism of XV459 is minimal, with the major metabolites being formed by modification of the isoxazoline ring. These studies also show that XV459 undergoes extrahepatic reductive cleavage of the isoxazoline to produce the ring-opened metabolite, M7 in the presence of gut flora. The identification of the metabolites, formed in small quantities from XV459, was achieved by application of LC/MS, LC/NMR and high-field NMR techniques along with the availability of deuterated analogues and appropriate synthetic standards. Analyses of plasma and urine samples from human subjects dosed with roxifiban show the presence of only XV459 in these matrices. The minor hydroxylated metabolites found in rat are not detected in the biological samples from these subjects.

Acknowledgements

The authors thank Dr William Ebling, Drug Metabolism and Pharmacokinetics Section, DuPont Pharmaceuticals, for providing the urine and plasma samples from human subjects given roxifiban.

References

Batt, D. G., Houghton, G. C., Danekar, W. F. and Jadhav, P. K., 1999, Synthesis of *cis*- and *trans*-isomers of an isoxazoline ring-hydroxylated metabolite of roxifiban, a platelet glycoprotein IIb/IIIa receptor antagonist. *Journal of Organic Chemistry* (in press).

Lindon, J. C., Nicholson, J. K., Sidelmann U. G. and Wilson I. D., 1997, Directly coupled HPLC-NMR and its application to drug metabolism. *Drug Metabolism Reviews*, **29**, 705–747.

Mutlib, A. E., Strupczewski, J. T. and Chesson, S. M., 1995, Application of hyphenated LC/NMR and LC/MS techniques in rapid identification of *in vitro* and *in vivo* metabolites of iloperidone. *Drug Metabolism and Disposition*, **23**, 951–964.

Meuldermans, W., Hendrickx, J., Mannens, G., Lavrijseri, K., Janssen, C., Bracke, J. and Jeune, L. L., 1994, The metabolism and excretion of risperidone after oral administration in rats and dogs. *Drug Metabolism and Disposition*, **21**, 129–136.

Mannens, G., Huang, M., Meuldermans, W., Hendrickx, J., Woestenborghs, R. and Heykants, J., 1993, Absorption, metabolism and excretion of risperidone in humans. *Drug Metabolism and Disposition*, **21**, 1134–1141.

Shockcor, J. P., Wurm, R. M., Frick, L. W., Sanderson, P. N., Farrant, R. D., Sweatman, B. C. and Lindon, J. C., 1996, HPLC-NMR identification of the human urinary metabolites of (−)-*cis*-5-fluoro-1-[2-(hydroxymethyl)-1,3-oxathiolan-5-yl]cytosine, a nucleoside analogue active against human immunodeficiency virus (HIV). *Xenobiotica*, **26**,189–199.

Spraul, M., Hofmann, M., Wilson, I. D., Lenz, E., Nicholson, J. K. and Lindon, J. C. 1993, Coupling of HPLC with ^{19}F- and ^{1}H-NMR spectroscopy to investigate the human urinary excretion of flurbiprofen metabolites. *Journal of Pharmaceutical and Biomedical Applications*, **11**,1009–1015.

Smallcombe, S. H., Patt, S. L. and Keifer, P. 1995, WET solvent suppression and its applications to LC NMR and high-resolution NMR spectroscopy. *Journal of Magnetic Resonance A*, **117**, 295–303.

Stiff, D. D., Robicheau, J. T. and Zemaitis, M. A., 1992, Reductive metabolism of the anticonvulsant agent zonisamide, a 1,2-benzisoxazole derivative. *Xenobiotica*, **22**, 1–11.

Stiff, D. D. and Zemaitis, M. A., 1990, Metabolism of the anticonvulsant agent zonisamide in the rat. *Drug Metabolism and Disposition*, **18**, 888–894.

Still, W. C., Kahn, M. and Mitra, A., 1978, Rapid chromatographic technique for preparative separations with moderate resolution. *Journal of Organic Chemistry*, **43**, 2923–2925.

Tucker, C. E., Davidson, J. and Knochel, P., 1992, Mild and stereoselective hydroborations of functionalized alkynes and alkenes using pinacolborane. *Journal of Organic Chemistry*, **57**, 3482–3485.

Wityak, J., Sielecki, T. M., Pinto, D. J., Emmett, G., Sze, J. Y., Liu, J., Tobin, A. E., Wang, S. and Jiang, B., 1997, Discovery of potent isoxazoline glycoprotein IIb-IIIa receptor antagonists. *Journal of Medicinal Chemistry*, **40**, 50–60.

Xue, C. B., Rafalski, M., Roderick, J., Eyermann, C. J., Mousa, S., Olson, R. E. and De Grado, W. F., 1996, Design, synthesis and *in vitro* activities of a series of benzimidazole/benzoxazole glycoprotein IIb/IIIa inhibitors. *Bioorganic Medicinal Chemistry Letters*, **6**, 339–344.

XENOBIOTICA, 2000, VOL. 30, NO. 12, 1111–1121

NADH-dependent reduction of sulphamethoxazole hydroxylamine in dog and human liver microsomes

L. A. TREPANIER* and J. L. MILLER

Department of Medical Sciences, School of Veterinary Medicine, University of Wisconsin-Madison, Madison, WI 53706–1102, USA

Received 3 July 2000

1. Reduction of hydroxylamine drug metabolites by NADH-dependent hydroxylamine reductase (NDHR) has been suggested to be involved in the pathogenesis of idiosyncratic sulphonamide toxicity in humans. The dog represents a naturally occurring clinical model for sulphonamide toxicity in humans. The purpose of these studies, therefore, was to characterize the presence of hepatic NADH-dependent hydroxylamine reductase activity in the dog and to compare this activity with that found in humans.

2. NDHR activity was characterized by the presence of two enzymes in both dog and human liver microsomes, with comparable estimates of K_m (K_{m1} = 75 μM, K_{m2} = 404 μM in dog; K_{m1} = 69 μM, K_{m2} = 503 μM in human). Estimates of maximal velocity were significantly, but not dramatically, higher for dog NDHR (V_{max1} = 2.09 nmole mg^{-1} min^{-1}, V_{max2} = 4.58 nmole mg^{-1} min^{-1}) compared with human NDHR (V_{max1} = 0.42 nmole mg^{-1} min^{-1}, V_{max2} = 1.56 nmole mg^{-1} min^{-1}). NDHR in dog, as in humans, preferred NADH to NADPH, was more active at pH 6.3 than at 7.4 and was not inhibited by carbon monoxide, azide, anaerobic conditions, the CYP substrate inhibitors tolbutamide, dextromethorphan, or erythromycin, or antibodies directed against CYP2C, CYP2D or CYP3A.

3. It is concluded that two forms of NDHR are present in dog and humans with similar biochemical characteristics. Although NDHR activity has been attributed to a CYP2D isoform in pig, there is no evidence for involvement of CYP450 in the reduction of sulphamethoxazole hydroxylamine in either dogs or humans.

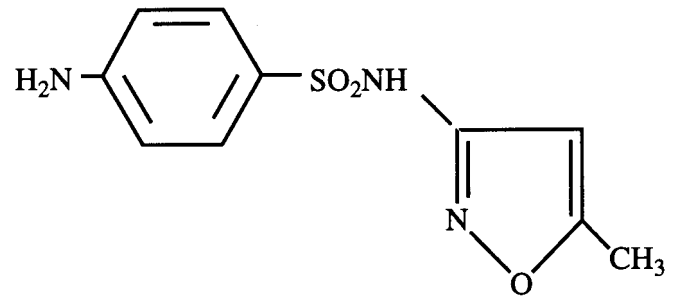
Introduction

Sulphamethoxazole (SMX) is a sulphonamide antimicrobial prescribed for the treatment of a number of gastrointestinal, urinary and respiratory pathogens, including *Pneumocystis carinii* pneumonia in patients with AIDS (Mandell and Petri 1996). However, the use of sulphamethoxazole and other sulphonamides is limited by the occurrence of delayed, idiosyncratic, multisystemic drug toxicity in humans, including fever, rash, skin eruptions, blood dyscrasias and hepatotoxicity (Cribb *et al*. 1996). Similar reactions also occur in dog, the only other species in which these reactions have been well documented (Cribb 1989, Trepanier 1999).

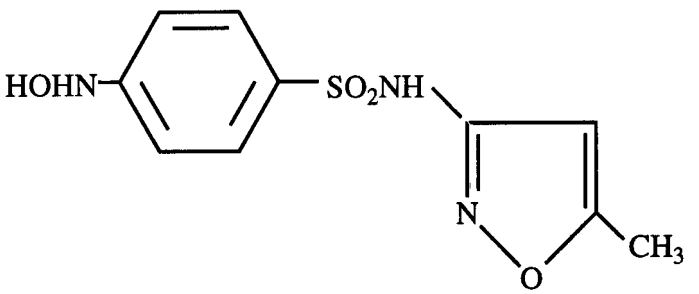
It has been hypothesized that delayed, idiosyncratic sulphonamide toxicity reactions are mediated by oxidized metabolites of the parent sulphonamide (Cribb *et al*. 1996). In humans and dog, sulphamethoxazole is oxidized by cytochrome P450 to its hydroxylamine metabolite (figure 1), (Cribb and Spielberg 1990a,b). Sulphamethoxazole hydroxylamine (SMX-HA) is cytotoxic (Rieder *et al*. 1989) and is oxidized spontaneously to the even more toxic nitroso metabolite (Rieder *et al*. 1995). Using leukocytes incubated with SMX-HA, *in vitro* cytotoxicity assays have demonstrated that patients with delayed sulphonamide toxicity reactions have a decreased ability to detoxify SMX-HA, and that this defect is shared by family members (Shear *et al*. 1986, Wolkenstein *et al*. 1995). Individual dogs may also

* Author for correspondence; e-mail: LATrepanier@facstaff.wisc.edu

Xenobiotica ISSN 0049–8254 print/ISSN 1366–5928 online © 2000 Taylor & Francis Ltd
http://www.tandf.co.uk/journals
DOI:10.1080/00498250010013908



Sulphamethoxazole



Sulphamethoxazole hydroxylamine

Figure 1. Structures of sulphamethoxazole and its metabolite, sulphamethoxazole hydroxylamine.

express a similar defect (Cribb and Spielberg 1990b). These findings have lead to the hypothesis that a genetic defect in hydroxylamine detoxification predisposes patients to idiosyncratic sulphonamide toxicity (Shear *et al.* 1986, Wolkenstein *et al.* 1995).

Sulphamethoxazole hydroxylamine is detoxified by microsomal NADH-dependent hydroxylamine reductase (NDHR) (Cribb *et al.* 1995), also termed microsomal O_2-insensitive benzamidoxime reductase (Clement *et al.* 1997) or NADH-dependent *N*-hydroxy amine reductase (Kadlubar and Ziegler 1974). Hydroxylamine reductase has several unique characteristics: it is a reductase active under aerobic conditions, it prefers NADH (over NADPH) as a cofactor and, although active at physiologic pH, it has a pH optimum of ~ 6.3 (Kadlubar *et al.* 1973, Clement and Jung 1994). The identity of NDHR is not clear. In one species (pig), NDHR activity has been purified and has been attributed to a CYP2D isoform, along with NADH cytochrome-b_5 reductase and cytochrome-b_5 (Clement *et al.* 1997). This would represent an unusual role for a cytochrome P450, and it is not known whether CYP2D or other CYP isoforms are involved in hydroxylamine reduction in humans or dog. The purpose of these studies, therefore, was to characterize the presence of hepatic NADH-dependent hydroxylamine reductase activity in the dog to compare the activity with that found in humans, and to determine whether cytochrome P450 is likely to be involved in this pathway in either species.

Materials and methods

Chemicals

All chemicals were from Sigma Chemical Co. (St Louis, MO, USA), except for sulphamethoxazole hydroxylamine, which was from Dalton Chemical Co. (Toronto, Ontario, Canada).

Microsome preparation

Liver samples were from healthy dogs (beagle, greyhound, Labrador retriever, mixed breed hound; two males, nine females, ranging from 9 months to 2 years of age) that were being euthanized or were recipient dogs in an unrelated experimental liver transplant protocol. Livers were harvested immediately after euthanasia or within 5 min of surgical ligation of the blood supply respectively. Livers were handled on ice, perfused with cold PBS and snap-frozen in liquid nitrogen within 30 min of harvest. Microsomes were prepared from whole liver homogenized in HEPES pH 7.4, using standard differential ultracentrifugation. Protein was quantitated using the method of Lowry *et al*. (1951), using a commercially available kit (BioRad, Hercules CA, USA). Microsomes were stored at −80 °C until use. Pooled human liver microsomes (derived from five male and five female donors, ranging from 21 to 61 years of age; eight Caucasian, one Hispanic, one African-American) were from Gentest Corp. (Woburn, MA, USA).

Kinetic characterization of SMX-HA reduction

Canine hepatic microsomes (1 mg protein ml^{-1}) or pooled human liver microsomes (0.5 mg protein ml^{-1}) were incubated with 1 mM NADH in HEPES buffer, pH 7.4, for 15 min at 37 °C, with varying concentrations of SMX-HA. Under these conditions, reaction velocities approximated linear kinetics. Preliminary studies indicated that 1 mM glutathione and ascorbic acid markedly increased the stability of the hydroxylamine, so both reagents were included in all reactions. Sulphamethoxazole hydroxylamine (20 mM stock in 50% DMSO/3 mM ascorbic acid) was made fresh daily, and was added to each reaction to a final concentration ranging from 1.1 μM to 1 mM. Some reactions were also performed with 1 mM NADPH substituted for, or in addition to, NADH. To evaluate the pH dependence of the reaction, microsomes were diluted in HEPES buffer pH 6.3 for some experiments. The effect of inhibitors in both humans and dog was determined by co-incubating reactions with final concentrations of either 1 mM azide, 1 mM N-methylhydroxylamine or 1 mM of *p*-hydroxymercuribenzoate. The final incubation volume was 1 ml.

Reactions were stopped with the addition of a half volume of methanol on ice, and samples were filtered through a centrifugal filtration device (Centrifree, 30000 M.W. cut-off; Millipore Corp, Bedford, MA, USA) at 750*g* to remove protein. Samples of the ultrafiltrate (100 μl) were loaded onto a C18 Ultrasphere ODS column (4.6 mm × 25 cm) with an isocratic mobile phase consisting of 20% acetonitrile, 0.05% triethylamine and 1.0% glacial acetic acid in water, run at 2 mls min^{-1}. Reactions were analysed for SMX and SMX-HA following HPLC using UV detection at 270 nm (Beckman Instruments, Inc., Schaumburg, IL, USA). Retention times for SMX and SMX-HA HA were 8.5 and 6.5 min respectively. The identity of SMX in the reactions was determined by co-chromatography with the authentic SMX standard. Confirmation of the specificity of this assay for SMX and SMX-HA using mass spectroscopy has been previously reported (Rieder *et al*. 1988). SMX was quantitated by comparison to SMX external standards ranging from 1 mM to 0.12 μM. SMX standards were handled in a manner identical to experimental reactions except for substitution of 1 mg ml^{-1} BSA for microsomal protein, and omission of the incubation step. The interassay coefficient of variation for the SMX concentrations tested ranged from 6.4 to 21.2%, while the intra-assay coefficient of variation ranged from 2.9 to 10.5%.

Role of P450 in SMX-HA reduction

To determine the role, if any, of cytochrome P450 enzymes in hydroxylamine reduction, reactions were performed under carbon monoxide or nitrogen atmospheres, in the presence of 1 mM azide, in the presence of substrate inhibitors of CYP2C, CYP3A or CYP2D, or following pre-incubation with anti-CYP antibodies. For oxygen tension experiments, reaction mixtures containing human or canine microsomes (minus cofactor) were injected into sealed vials held on ice. Either carbon monoxide or nitrogen gas, bubbled through a solution containing 0.05% 2-anthraquinone sodium sulphonate, 0.5% sodium dithionite and 0.1 N NaOH (Cribb *et al*. 1995) was introduced through a 22-gauge needle inserted into the vial septum. A second 22-gauge needle acted as a vent. Following a 5-min purge of the reaction mixtures on ice, the vent needles were removed and gas flow was stopped. The sealed containers were then injected with NADH (final concentration 1 mM) to start the reaction, which was carried out at 37 °C. For substrate inhibitor studies, dextromethorphan (a CYP2D substrate in humans and dogs; Roussel *et al*. 1998); erythromycin (a CYP3A substrate in humans and dogs; Born *et al*. 1996), and tolbutamide (a CYP2C9 substrate in humans; CYP2C substrates have yet to be well characterized in dogs; Blaisdell *et al*. 1998) were co-incubated with reactions as described for kinetic characterization experiments, using substrate concentrations of either 25 or 250 μM SMX-HA. Substrate inhibitors were

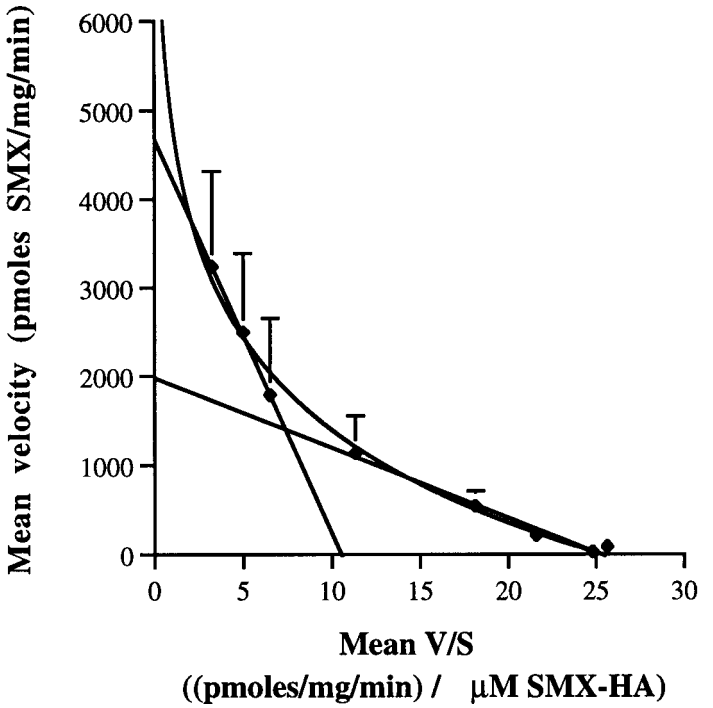


Figure 2. Eadie-Hofstee transformation of kinetic data for the NADH-dependent reduction of sulphamethoxazole hydroxylamine in liver microsomes from six dogs. All reactions contained 1 mM NADH, 1 mM glutathione, 1 mM ascorbic acid, and 1 mg ml^{-1} microsomal protein at pH 7.4. For this transformation, the slope is equal to $-K_m$ and the *y*-intercept provides an estimate of V_{max}. The results suggest the involvement of two enzymes in hydroxylamine reduction in the dog.

diluted in DMSO (final reaction concentration 5%) to a final inhibitor concentration of 1 mM. DMSO vehicle (final concentration 5%) was used in control reactions. For antibody inhibition experiments, polyclonal goat anti-rat CYP2C, polyclonal rabbit anti-human CYP2D6, and polyclonal rabbit anti-rat CYP3A (Daiichi Pure Chemicals Co. Ltd, Tokyo, Japan) were pre-incubated for 30 min at room temperature with canine pooled liver microsomes (100–250 μg ml^{-1}) or human pooled liver microsomes (100 μg ml^{-1}). Antiserum (10–50 μl; equivalent to 100–500 μg IgG) was used for each reaction. Negative controls contained the appropriate volumes of pre-immune sera as provided with each antibody.

Statistical analysis

Data for kinetic analyses for individual dogs were from two to three separate kinetic determinations for each animal. All other results were from duplicate determinations in three separate experiments. Estimates of K_m and V_{max} were made from Eadie-Hofstee transformations of the data (Cornish-Bowden 1995). Data are mean $\pm$SD. For comparison of different experimental conditions, a Student's *t*-test (both paired and unpaired as appropriate) or an ANOVA followed by a Fisher's least significant difference *post-hoc* test was used, with $p < 0.05$ considered significant.

Results

Kinetic characterization of SMX reduction in dog and humans

Reduction of SMX-HA to SMX was readily detected in 11 dog livers tested; kinetics of SMX-HA reduction were further characterized in six dogs. For all dogs, Eadie-Hofstee transformations of the data were biphasic in the substrate range of 1.1 μM to 1 mM (figure 2), consistent with the involvement of two enzymes. Similar

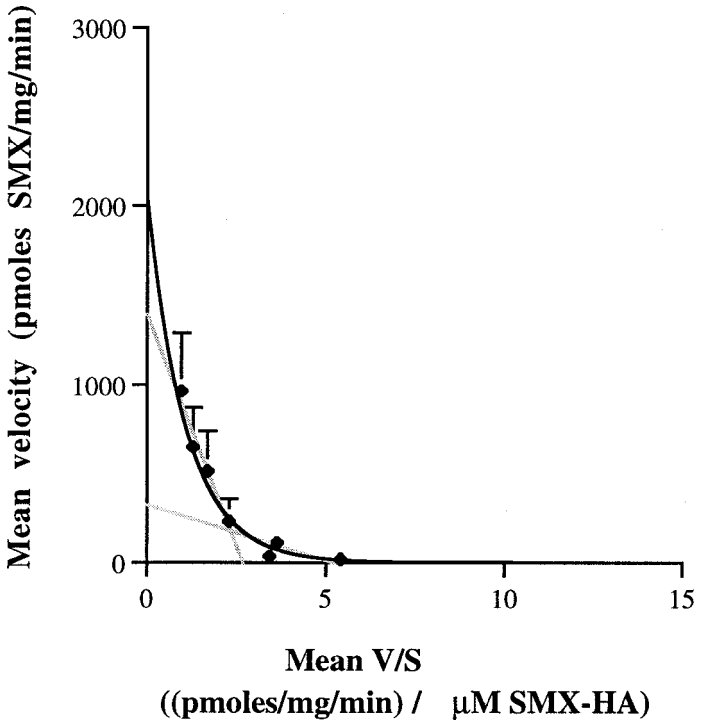


Figure 3. Eadie-Hofstee transformation of kinetic data for the NADH-dependent reduction of sulphamethoxazole hydroxylamine in pooled human hepatic microsomes. All reactions were performed as described in figure 2 except for the use of 0.5 mg ml^{-1} microsomal protein. Data are the mean of three experiments, each run in duplicate. The results suggest the involvement of two enzymes in hydroxylamine reduction in humans, although overall activities are lower in humans compared with dogs (figure 2).

Table 1. Kinetics of sulphamethoxazole hydroxylamine reduction in dog and human liver microsomes. All reactions were performed in HEPES pH 7.4 with 1 mM NADH and 1 mg ml^{-1} microsomal protein (dog) or 0.5 mg ml^{-1} microsomal protein (human), with 1 mM glutathione and 1 mM ascorbic acid included to stabilize the hydroxylamine. Parameters listed were derived from Eadie–Hofstee transformations of the data, and represent the mean of two to three individual kinetic determinations for each dog, or three separate experiments in pooled human microsomes, each run in duplicate.

Dog	K_{m1} (μM)	V_{max1} (nmole mg^{-1} min^{-1})	K_{m2} (μM)	V_{max2} (nmole mg^{-1} min^{-1})
1	91	2.12	366	4.91
2	65	2.79	279	6.27
3	101	2.41	557	4.86
4	73	1.71	372	3.41
5	77	2.90	303	5.61
6	41	0.58	544	2.42
Canine microsomes	75±21	2.09±0.86	404±119	4.58±1.42
Human microsomes	69±40	0.42±0.04*	503±197	1.56±0.16**

Significantly different from canine V_{max}; * $p = 0.04$; ** $p = 0.008$.

results were found in human liver microsomes (figure 3). The estimates of K_m for the dog (K_{m1} = 75±21 μM, K_{m2} = 404±119 μM) were very similar to those found in pooled human liver microsomes (K_{m1} = 69±40 μM, K_{m2} = 503±197 μM) (table 1). The estimates for V_{max} in dog (V_{max1} = 2.09±0.86 nmole mg^{-1} min^{-1}; V_{max2} =

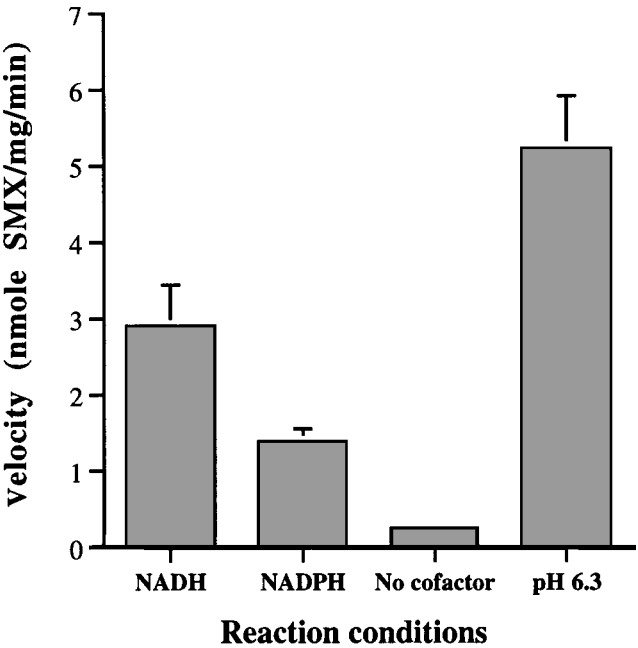


Figure 4. Effect of cofactor and pH on sulphamethoxazole hydroxylamine reduction in canine liver microsomes. Reactions were performed as described in figure 2, using 500 μM SMX-HA. Significantly more activity was observed in the presence of 1 mM NADH compared with 1 mM NADPH, and at pH 6.3 compared with pH 7.4 (both $p < 0.001$). No additional activity was observed when both NADPH and NADH were added compared with NADH alone (data not shown). Similar results were observed over a wide range of SMX-HA concentrations (10 μM to 6 mM; data not shown). Data are the mean ($\pm$SD) of three individual dogs, each run in duplicate.

4.58$\pm$1.42 nmole mg^{-1} min^{-1}) were significantly, but not dramatically, higher than those found in human liver (V_{max1} = 0.42$\pm$0.04 nmole mg^{-1} min^{-1}; V_{max2} = 1.56$\pm$0.16 nmole mg^{-1} min^{-1}) (table 1). No reduction of SMX hydroxylamine was evident in the presence of boiled microsomes or buffer instead of microsomes (data not shown).

Biochemical characterization of hydroxylamine reduction in dog

NADH was the preferred cofactor for SMX-HA reduction in dog, with nearly 2.5-fold greater activity with NADH compared with NADPH (figure 4). This preference for NADH over NADPH was seen over a wide range of substrate concentrations (10 μM to 6 mM), and no further increase in activity was seen when both NADPH and NADH were included in the reactions (data not shown). Similar results were found in human liver microsomes (data not shown). Like NDHR in other species, NDHR activity in dogs was more than twofold greater at pH 6.3 compared with pH 7.4 (figure 4).

Rates of SMX-HA reduction in canine and human liver microsomes were unaffected by azide or carbon monoxide (table 2). As reported in humans (Cribb *et al.* 1995), canine NDHR was similarly not inhibited by a nitrogen atmosphere (data not shown).

Table 2. Lack of effect of carbon monoxide or azide on sulphamethoxazole hydroxylamine reduction in canine and human liver microsomes. All reactions were performed as described in figure 2 with either 25 or 250 μM concentrations of SMX-HA. Reactions were coincubated with 1 mM azide, or were pre-incubated with carbon monoxide, bubbled through 0.05% 2-anthraquinone sodium sulphonate, 0.5% sodium dithionite and 0.1 N NaOH for 5 min on ice before addition of NADH. Velocities are the mean of three experiments, each run in duplicate.

Condition [SMX-HA]	Velocity (nmole SMX mg^{-1} min^{-1}) Dog microsomes 25 μM	Dog microsomes 250 μM	Human microsomes 25 μM	Human microsomes 250 μM
Room air	0.93±0.02	2.58±1.08	0.15±0.00	0.69±0.00
Carbon monoxide	0.89±0.00	2.57±0.96	0.14±0.00	0.77±0.03
No azide	0.42±0.04	3.16±1.29	0.08±0.01	0.52±0.10
Azide	0.41±0.08	3.51±0.80	0.11±0.02	0.68±0.07

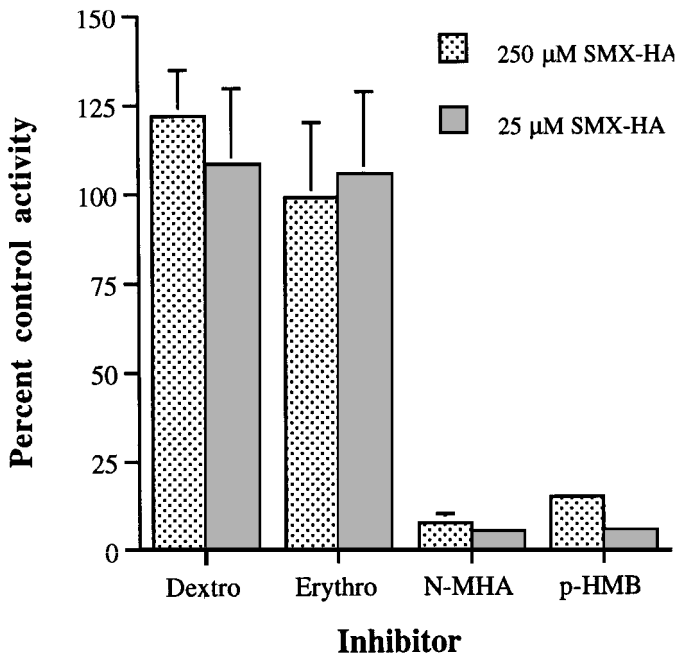


Figure 5. Effect of CYP substrates and inhibitors on sulphamethoxazole hydroxylamine reduction in dog liver microsomes. Reactions, performed as described for figure 2, were co-incubated with 250 or 25 μM SMXHA and 1 mM dextromethorphan (Dextro), erythromycin (Erythro), *N*-methylhydroxylamine (NMHA) or *p*-hydroxymercuribenzoate (*p*-HMB) in DMSO (final reaction concentration, 5% DMSO). Control reactions contained DMSO vehicle. Data are the mean of three individual dogs, each run in duplicate. P450 substrate inhibitors had no significant effect on SMX-HA reduction. However, *N*-methylhydroxylamine (an inhibitor of NDHR in other species), and *p*-hydroxymercuribenzoate (an inhibitor of NADH cytochrome-b_5 reductase) each inhibited SMX-HA reduction by $>80\%$.

Effect of inhibitors and inhibitory antibodies

Reduction of SMX-HA reduction was not significantly inhibited in either dog or human liver microsomes by 1 mM dextromethorphan or erythromycin (dog and human experiments), or 1 mM tolbutamide (human experiments only) (figures 5 and 6). Tolbutamide was not used in canine experiments because it is a very poor CYP substrate in the dog (Prueksaritanont *et al.* 1996, Chauret *et al.* 1997), and

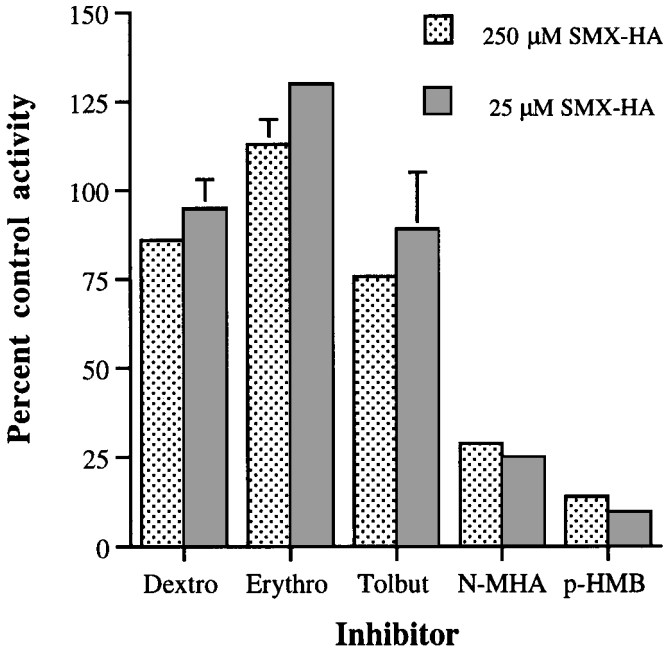


Figure 6. Effect of CYP substrates and inhibitors on sulphamethoxazole hydroxylamine reduction in human liver microsomes. Reactions, performed as described in figures 2 and 3, were co-incubated with 250 or 25 μM SMXHA and 1 mM dextromethorphan (Dextro), erythromycin (Erythro), tolbutamide (Tolbut), *N*-methylhydroxylamine (NMHA) or *p*-hydroxymercuribenzoate (*p*-HMB) in DMSO (final reaction concentration, 5% DMSO). Control reactions contained DMSO vehicle. Data are the mean (±SD) of three experiments in pooled human microsomes, each run in duplicate. As in dog, P450 substrate inhibitors had no effect on SMX-HA reduction, but *N*-methylhydroxylamine and *p*-hydroxymercuribenzoate each inhibited hydroxylamine reduction by >70%.

alternative canine CYP2C substrates have not yet been well characterized (Blaisdell *et al.* 1998). However *N*-methylhydroxylamine (an inhibitor of NDHR in other species (Clement *et al.* 1993)) and *p*-hydroxymercuribenzoate (an inhibitor of NADH cytochrome-b_5 reductase activity (Shimada *et al.* 1998)) inhibited hydroxylamine reduction by >70% in both species (figures 5 and 6). Antibodies directed against CYP2C, CYP2D6 and CYP3A (100–500 μg IgG per 250 μg microsomal protein) did not significantly inhibit reduction of SMX-HA in pooled canine or human liver microsomes when compared with pre-immune sera controls (figure 7).

Discussion

Sulphamethoxazole hydroxylamine reduction was readily detected in the dog. In both dog and humans, Eadie-Hofstee transformation of kinetic data suggested the involvement of two enzymes in hydroxylamine reduction. Over a broad range of substrate concentrations, hydroxylamine reduction in both species was active under aerobic conditions, preferred NADH to NADPH, and had greater activity at pH 6.3 than at physiological pH (Cribb *et al.* 1995). This is similar to that reported for NDHR in pig, rabbit and rat (Kadlubar *et al.* 1973, Clement *et al.* 1993, 1996).

Both dog and human liver had similar estimates of K_m for both forms of NDHR

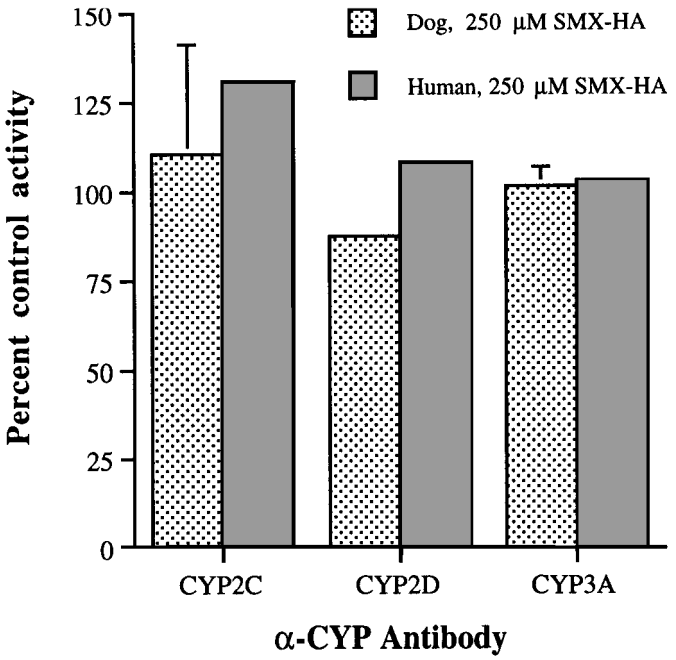


Figure 7. Lack of inhibition of sulphamethoxazole hydroxylamine reduction by CYP antibody inhibitors in dog and human liver microsomes. Reactions were performed as described in figures 2 and 3, except that 100–250 μg microsomal protein was used per reaction. Antibodies directed against CYP2C9/19, CYP2D6, and CYP3A4 (500 μg IgG antisera per 250 μg microsomal protein) were pre-incubated with pooled canine or human microsomes for 30 min before initiation of the reactions. Pre-immune sera, provided by the manufacturer, were used for negative controls. Data shown are for 250 μM SMX-HA; similar results were obtained using 25 μM SMX-HA (not shown). Experiments were performed in duplicate for each antibody in each species, at both 250 μM SMX-HA (data shown) and 25 μM SMX-HA (data not shown). Similar results were found under all conditions.

(69–75, 400–500 μM), which are comparable with those reported for rat and rabbit microsomal hydroxylamine reductases (23–27, 200–300 μM) (Clement *et al*. 1993, 1996). Neither of these enzymes would be predicted to be very active at therapeutically attainable plasma concentrations of SMX-HA in humans. For example, after an 800 mg oral dose of SMX, peak plasma concentrations of SMX-HA reach only 1–2 μM (Van der Ven *et al*. 1994). However, local tissue concentrations of hydroxylamine may be much higher in organs such as the liver and leukocytes that generate hydroxylamines. The NDHR pathway may be particularly important in dogs, which are unique as a species in that an alternative detoxification pathway, arylamine *N*-acetylation, is completely absent (Bridges and Williams 1963, Caldwell 1980, Trepanier *et al*. 1997).The consistently higher velocities for SMX-HA reduction in dog compared with humans, if borne out by a larger sample population, may represent an adaptation to the lack of arylamine *N*-acetylation in the dog.

Despite its initial description more than 25 years ago, the identity of NDHR is still not clear. NADH cytochrome-b_5 reductase and cytochrome-b_5 are important components of this activity in the pig (Clement *et al*. 1997). This is consistent with inhibition of NDHR in both humans and dogs by *p*-hydroxymercuribenzoate, a sulphydryl blocking reagent that inhibits NADH cytochrome-b_5 reductase

activity (Shimada *et al*. 1998). Protein purification studies in pig have suggested that a CYP2D isoform is also required for hydroxylamine reduction (Clement *et al*. 1997), which would represent an unusual role for cytochrome P450. However, in humans and dog, hydroxylamine reduction was not inhibited by either substrate or antibody inhibitors of CYP2C, CYP2D and CYP3A. Negative results of antibody inhibition in dog do not rule out the involvement of cytochrome P450, since species differences in antibody binding may exist. However, the lack of inhibition by azide, nitrogen and carbon monoxide strongly suggests that a cytochrome P450 is not involved in sulphamethoxazole hydroxylamine reduction in dog or humans. This is consistent with the lack of correlation between hydroxylamine reduction in human liver microsomes and the activities of either CYP1A2, 2A6, 2C8, 2C9, 2C19, 2D6, 2E1, 3A4, 3A5 or flavin monoxygenase form 3 (FMO3), reported by others (Lin et al. 1996).

It is as yet unclear whether NADH-dependent hydroxylamine reduction is catalysed by one protein with two active sites or by two distinct proteins (likely isozymes) with similar chemical characteristics but different kinetic behaviour. Enzymes known to be involved in nitrogen reduction include alcohol dehydrogenases, aldo-keto reductases, NADPH cytochrome P450 reductase, NADH cytochrome-b_5 reductase, xanthine and aldehyde oxidoreductases, and others (Testa 1995). Of these, only NADH cytochrome-b_5 reductase has the characteristics, like NDHR, of microsomal localization and preference for NADH. Studies are ongoing in our laboratory to characterize the identity of NDHR in humans and dogs, and to determine whether individual variability in this pathway is associated with the outcome of idiosyncratic sulphonamide toxicity in either species.

Acknowledgements

The study was supported in part by a Basic Science Grant Award from the University of Wisconsin-Madison, School of Veterinary Medicine.

References

Blaisdell, J., Goldstein, J. A. and Bai, S. A., 1998, Isolation of a new canine cytochrome P450 cDNA from the cytochrome P450 2C subfamily (CYP2C41) and evidence for polymorphic differences in its expression. *Drug Metabolism and Disposition*, **26**, 278–283.

Born, S. L., Fraser, D. J., Harlow, G. R. and Halpert, J. R., 1996, *Escherichia coli* expression and substrate specificities of canine cytochrome P450 3A12 and rabbit cytochrome P450 3A6. *Journal of Pharmacology and Experimental Therapeutics*, **278**, 957–963.

Bridges, J. and Williams, R., 1963, Species differences in the acetylation of sulphanilamide. *Biochemical Journal*, **87**, 19P.

Caldwell, J., 1980, Comparative aspects of detoxication in mammals. In W. Jakoby (ed.), *Enzymatic Basis of Detoxication* (New York: Academic Press), pp. 85–114.

Chauret, N., Gauthier, A., Martin, J. and Nicoll-Griffin, D. A., 1997, *In vitro* comparison of cytochrome P450-mediated metabolic activities in human, dog, cat, and horse. *Drug Metabolism and Disposition*, **25**, 1130–1136.

Clement, B., Demesmaeker, M. and Linne, S., 1996, Microsomal catalysed *N*-hydroxylation of guanabenz and reduction of the *N*-hydroxylated metabolite: characterization of the two reactions and genotoxic potential of guanoxabenz. *Chemical Research in Toxicology*, **9**, 682–688.

Clement, B. and Jung, F., 1994, *N*-hydroxylation of the antiprotozoal drug pentamidine catalysed by rabbit liver cytochrome P-450 2C3 or human liver microsomes, microsomal retroreduction, and further oxidative transformation of the formed amidoximes. *Drug Metabolism and Disposition*, **22**, 486–497.

Clement, B., Lomb, R. and Moller, W., 1997, Isolation and characterization of the protein components of the liver microsomal O_2-insensitive NADH-benzamidoxime reductase. *Journal of Biological Chemistry*, **272**, 19615–19620.

Clement, B., Schultze-Mosgau, M.-H. and Wohlers, H., 1993, Cytochrome P450 dependent *N*-hydroxylation of a guanidine (debrisoquine), microsomal catalysed reduction and further oxidation of the *N*-hydroxy-guanidine metabolite to the urea derivative. *Biochemical Pharmacology*, **46**, 2249–2267.

Cornish-Bowden, A., 1995, *Fundamentals of Enzyme Kinetics* (London: Portland).

Cribb, A. E., 1989, Idiosyncratic reactions to sulphonamides in dogs. *JAVMA*, **195**, 1612–1614.

Cribb, A. E., Lee, B. L., Trepanier, L. A. and Spielberg, S. P., 1996, Adverse reactions to sulphonamide and sulphonamide-trimethoprim antimicrobials: clinical syndromes and pathogenesis. *Advances in Drug Reactions and Toxicological Reviews*, **15**, 9–50.

Cribb, A. E. and Spielberg, S. P., 1990a, Hepatic microsomal metabolism of sulphamethoxazole to the hydroxylamine. *Drug Metabolism and Disposition*, **18**, 784–787.

Cribb, A. E. and Spielberg, S. P., 1990b, An in vitro investigation of predisposition to sulphonamide idiosyncratic toxicity in dogs. *Veterinary Research Communications*, **14**, 241–252.

Cribb, A. E., Spielberg, S. P. and Griffin, G. P., 1995, N4-hydroxylation of sulphamethoxazole by cytochrome P450 of the cytochrome P4502C subfamily and reduction of sulphamethoxazole hydroxylamine in human and rat hepatic microsomes. *Drug Metabolism and Disposition*, **23**, 406–414.

Kadlubar, F. F., McKee, E. M. and Ziegler, D. M., 1973, Reduced pyridine nucleotide-dependent *N*-hydroxy amine oxidase and reductase activities of hepatic microsomes. *Archives of Biochemistry and Biophysics*, **156**, 46–57.

Kadlubar, F. F. and Ziegler, D. M., 1974, Properties of a NADH-dependent *N*-hydroxy amine reductase isolated from pig liver microsomes. *Archives of Biochemistry and Biophysics*, **162**, 83–92.

Lin, J., Beerkman, C. E. and Cashman, J. R., 1996, *N*-oxygenation of primary amines and hydroxylamines and retroreduction of hydroxylamines by adult human liver microsomes and adult flavin-containing monooxygenase 3. *Chemical Research in Toxicology*, **9**, 1183–1193.

Lowry, O. H., Rosebrough, N. J., Farr, A. L. and Randall, R. J., 1951, Protein measurement with the Folin phenol reagent. *Journal of Biological Chemistry*, **193**, 265–275.

Mandell, G. L. and Petri, W. A., 1996, Antimicrobial agents: sulfonamides, trimethoprim-sulphamethoxazole, quinolones, and agents for urinary tract infections. In J. G. Hardman, L. E. Limbard, P. B. Molinoff, R. W. Ruddon and A. G. Gilman (eds), *Goodman and Gilman's The Pharmacological Basis of Therapeutics* (New York: McGraw-Hill), pp. 1057–1072.

Prueksaritanont, T., Gorham, L. M., Hochman, J. H., Tran, L. O. and Vyas, K. P., 1996, Comparative studies of drug-metabolizing enzymes in dog, monkey, and human small intestines, and in Caco-2 cells. *Drug Metabolism and Disposition*, **24**, 634–642.

Rieder, M. J., Krause, R. and Bird, I. A., 1995, Time-course of toxicity of reactive sulphonamide metabolites. *Toxicology*, **95**, 141–146.

Rieder, M. J., Uetrecht, J., Shear, N. H., Cannon, M., Miller, M. and Spielberg, S. P., 1989, Diagnosis of sulphonamide hypersensitivity reactions by *in-vitro* 'rechallenge' with hydroxylamine metabolites. *Annals of Internal Medicine*, **110**, 286–289.

Rieder, M. J., Uetrecht, J., Shear, N. H. and Spielberg, S. P., 1988, Synthesis and in vitro toxicity of hydroxylamine metabolites of sulphonamides. *Journal of Pharmacology and Experimental Therapeutics*, **244**, 724–728.

Roussel, F., Duignan, D. B., Lawton, M. P., Orbach, R. S., Strick, C. A. and Tweedie, D. J., 1998, Expression and characterization of canine cytochrome P450 2D15. *Archives of Biochemistry and Biophysics*, **357**, 27–36.

Shear, N. H., Spielberg, S. P., Grant, D. M., Tang, B. K. and Kalow, W., 1986, Differences in metabolism of sulphonamides predisposes to idiosyncratic toxicity. *Annals of Internal Medicine*, **105**, 179–184.

Shimada, H., Hirai, K.-I., Simamura, E. and Pan, J., 1998, Mitochondrial NADH-quinone oxidoreductase of the outer membrane is responsible for paraquat cytotoxicity in rat livers. *Archives of Biochemistry and Biophysics*, **351**, 75–81.

Testa, B., 1995, *Biochemistry of Redox Reactions* (San Diego: Academic Press).

Trepanier, L. A., 1999, Delayed hypersensitivity reactions to sulphonamides: syndromes, pathogenesis, and management. *Veterinary Dermatology*, **10**, 241–248.

Trepanier, L. A., Ray, K., Winand, N., Spielberg, S. P. and Cribb, A. E., 1997, Cytosolic arylamine N-acetyltransferase deficiency in the dog and other canids due to an absence of *NAT* genes. *Biochemical Pharmacology*, **54**, 73–80.

Wolkenstein, P., Charue, D., Laurent, P., Revuz, J., Roujeau, J.-C. and Bagot, M., 1995, Metabolic predisposition to cutaneous adverse drug reactions: role in toxic epidermal necrolysis caused by sulphonamides and anticonvulsants. *Archives in Dermatology*, **131**, 544–551.

XENOBIOTICA, 2000, VOL. 30, NO. 12, 1123–1130

Effects of flupyrazofos on liver microsomal cytochrome P450 in the male Fischer 344 rat

HYE SUK LEE†, HEE YONG LEE†, HEE KYOUNG GU‡, SANG SEOP HAN‡, CHUL-HO YUN§, JEONG HAN KIM‖, JUNG-AE KIM¶, EUNG-SEOK LEE¶, DOO-HYUN NAM¶ and TAE CHEON JEONG¶*

† College of Pharmacy, Wonkwang University, Iksan, 570–749, Korea
‡ Toxicology Research Center, KRICT, Taejon, 305-606, Korea
§ Department of Biochemistry, Pai-Chai University, Taejon, 302–735, Korea
‖ College of Agriculture, Seoul National University, Suwon, 441-744, Korea
¶ College of Pharmacy, Yeungnam University, Kyungsan, 712-749, Korea

Received 31 July 2000

1. The effects of flupyrazofos on liver microsomal cytochrome P450 were investigated in the male Fischer 344 rat. When rats were treated intraperitoneally with flupyrazofos for 3 consecutive days, the activities of ethoxyresorufin *O*-deethylase and testosterone 2 β-hydroxylase were significantly reduced, whereas the activities of pentoxyresorufin *O*-depentylase and testosterone 6 β- and 7 α-hydroxylases were induced in liver microsomes.

2. Within 24 h after treatment with 50 m kg^{-1} flupyrazofos, most enzyme activities were decreased, indicating the interaction of flupyrazofos with cytochrome P450.

3. In Western immunoblotting, cytochrome P4502B1/2 proteins were clearly induced by treatment with flupyrazofos, whereas P4501A1/2 and 2C6 proteins were reduced in liver microsomes.

4. The present results indicate that flupyrazofos modulates the expression of cytochrome P450 in rat.

Introduction

Flupyrazofos [*O*,*O*-diethyl *O*-(1-phenyl-3-trifluoromethyl-5-pyrazoyl) thiophosphoric acid ester] is a new insecticide developed in 1987 against the diamondback moth (*Plutella xylostella*). Flupyrazofos acts as a contact and stomach poison by inhibiting acetylcholinesterase (Lee *et al*. 1997b). The oral LD_{50} of flupyrazofos in rat was reported to be 372–605 mg kg^{-1} (Song *et al*. 1998). In addition, flupyrazofos may be neither phototoxic, mutagenic, teratogenic nor neurotoxic (Park *et al*. 1997). Good thermostability and photostability were reported with small amounts of degradation products, including unstable flupyrazofos oxon [*O*,*O*-diethyl *O*-(1-phenyl-3-trifluoromethyl-5-pyrazoyl) phosphoric acid ester], *O*,*S*-diethyl *O*-(1-phenyl-3-trifluoromethyl-5-pyrazoyl) phosphorothiolate and relatively stable 1-phenyl-3-trifluoromethyl-5-hydroxypyrazole (PTMHP) (Cho and Han 1992, Cho *et al*. 1993). The structures of parent compound and metabolites are illustrated in figure 1. Moreover, in rat liver microsomes, cytochrome P450 enzymes produced flupyrazofos oxon and PTMHP. The desulphuration of flupyrazofos to its oxon form was selectively enhanced in the microsomes induced by pretreatment of rat with phenobarbital, indicating that P4502B1/2 isozymes may be responsible for the metabolism of flupyrazofos (Lee *et al*. 1997a).

* Author for correspondence; e-mail: taecheon@yu.ac.kr

Xenobiotica ISSN 0049–8254 print/ISSN 1366–5928 online © 2000 Taylor & Francis Ltd
http://www.tandf.co.uk/journals
DOI:10.1080/00498250010013917

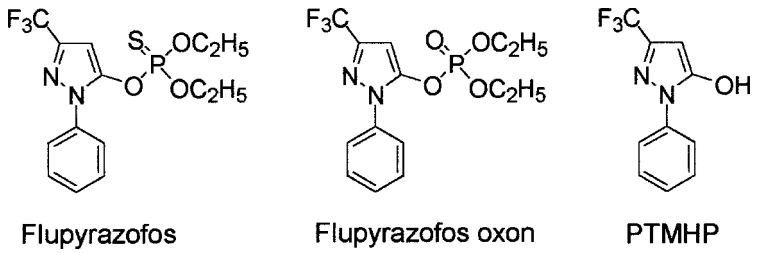


Figure 1. Structures of flupyrazofos and its metabolites.

In the present studies, the effects of flupyrazofos on liver microsomal activities of P450 were investigated in the male Fischer 344 rat. Because information on the effects of flupyrazofos on P450 was absent, the dose-response and time-course studies were performed. Liver microsomes isolated from the flupyrazofos-treated rat were used to determine P450-associated monooxygenase activities and protein levels as measured by Western immunoblotting analyses.

Materials and methods

Animals

Specific pathogen-free male Fischer 344 rats were obtained from the animal-breeding laboratory at this institute. The animals received at 4–5 weeks of age (100–150 g) were acclimated for at least 3 weeks. On arrival, rats were randomized and housed four or five per cage. All animals were maintained on γ-irradiated Jeil Lab Chow (Taejon, Korea) and UV-irradiated tap water *ad libitum*. When animals were 8–10 weeks old (200–300 g), they were used in the studies. The animal quarters were strictly maintained at 23 ± 3 °C and 40–60% relative humidity. A 12-h light/dark cycle was used with an intensity of 150–300 lux.

Materials

Sung Bo Chemical Co. (Ansan, Korea) kindly provided flupyrazofos (99%) and PTMHP (99%). Reagents for assaying P450-associated enzymes and nitrocellulose filters were from Sigma Chemical Co. (St Louis, MO, USA). Alkaline phosphatase-conjugated goat anti-rabbit IgG antibody, alkaline phosphatase substrate kit and a kit for protein determination were from Bio-Rad Laboratory (Richmond, CA, USA). All other chemicals used were of reagent grade commercially available.

Animal treatment and microsome preparation

Animals were treated intraperitoneally with flupyrazofos in corn oil at 25, 50 and 100 mg kg^{-1}/10 ml for 3 consecutive days in the dose-response studies. Corn oil at 10 ml kg^{-1} was given for vehicle control. Livers were isolated 24 h after the last dosing. For the time-course studies, 50 mg kg^{-1}/10 ml flupyrazofos in corn oil was administered intraperitoneally for 2, 4, 6, 8 or 24 h. Microsomes were prepared from livers by the differential centrifugation method, as described (Jeong *et al.* 1995) and were resuspended in 0.1 M potassium phosphate buffer, pH 7.4, containing 20% glycerol and 0.1 mM EDTA. Aliquots of liver microsomes were stored at -80 °C until use. The content of microsomal protein was determined according to Bradford (1976) using bovine serum albumin as a standard.

Monooxygenase assays

Ethoxyresorufin *O*-deethylase (EROD) activity was determined spectrofluorometrically as described by Blank *et al.* (1987) with a slight modification. The reaction mixture (2 ml) consisted of 0.1 M potassium phosphate buffer, pH 7.4, containing 2 mg ml^{-1} bovine serum albumin, 10 μM dicumarol, 5 mM glucose 6-phosphate, 1 unit glucose 6-phosphate dehydrogenase, 5 μM NADPH and 2.5 μM 7-ethoxyresorufin. The formation of resorufin was monitored fluorometrically at an excitation maximum of 550 nm and an

emission maximum of 585 nm. Pentoxyresorufin *O*-dependentylase (PROD) activity was determined spectrofluorometrically by measuring the amount of resorufin produced from 7-pentoxyresorufin (Lubet *et al*. 1985). The assay procedure was exactly the same as the assay of EROD, except that the substrate concentration was 2.0 μM. The activities of chlorzoxazone hydroxylase and testosterone hydroxylases were determined by measuring the amounts of hydroxychlorzoxazone and hydroxytestosterones formed, respectively, in an hplc system. For the chlorzoxazone hydroxylase assay, the method of Guengerich and Kim (1991) was slightly modified. The reaction mixture (1 ml) contained 100 μM chlorzoxazone, 5 mM glucose 6-phosphate, 1.0 mM $NADP^+$ and 1 unit glucose 6-phosphate dehydrogenase in 50 mM potassium phosphate buffer, pH 7.4. After the reaction termination by phosphoric acid, the product was extracted with dichloromethane and methanol. The activities of microsomal testosterone hydroxylases were determined as described previously (Brian *et al*. 1990, Yamazaki *et al*. 1994). The assay procedure was exactly the same as the assay of chlorzoxazone hydroxylase, except that the substrate was 100 μM testosterone.

Western immunoblotting

Microsomal proteins (10 μg/well) were resolved by a 10% SDS-PAGE and were transferred to nitrocellulose filters. The filters were incubated with 2.5% non-fat dry milk for 30 min to block non-specific binding, and then were incubated with rabbit polyclonal antibodies against rat individual P450, followed by an alkaline phosphatase-conjugated goat anti-rabbit IgG antibody. The primary antibodies against individual P450 were prepared as described using purified individual isozymes (Kaminsky *et al*. 1981). The specificity of each antibody raised has been described elsewhere (Jeong *et al*. 1995, 1998, Jeong and Yun 1995). For immunostaining, the nitrocellulose filters were developed with a mixture of 5-bromo-4-chloro 3-indolyl phosphate, nitroblue tetrazolium and 0.1 M Tris buffer (1:1:10) under an instruction by the manufacturer.

Statistics

Dunnett's *t*-test compared the significance of data obtained. Significant values were taken as $*p < 0.05$.

Results

The effects of flupyrazofos on liver microsomal activities of P450-associated monooxygenases were investigated in the male Fischer 344 rat (figure 2). Rats were treated intraperitoneally with 25, 50 and 100 mg kg^{-1} flupyrazofos for 3 consecutive days. The EROD activity was significantly reduced by the treatment with 100 mg kg^{-1} flupyrazofos. In addition, testosterone 2 β-hydroxylase activity was dose-dependently suppressed from 25 mg kg^{-1} flupyrazofos. Conversely, the activities of PROD, testosterone 6 β-hydroxylase and testosterone 7 α-hydroxylase were induced dose-dependently by treatment with flupyrazofos. Chlorzoxazone 4-hydroxylase activity was not changed significantly by flupyrazofos.

The time-course effects of flupyrazofos on liver microsomal activities of P450-associated monooxygenases were investigated within 24 h (figure 3). EROD activity was reduced from 2 h after the flupyrazofos treatment and reached a maximum inhibition at 6 h after the treatment. PROD activity was also inhibited from 2 h after the flupyrazofos treatment, but was induced at 24 h after the treatment. Testosterone 2 β-hydroxylase activity was significantly inhibited from 8 h after the treatment. The effects of flupyrazofos on other enzyme activities were not significant.

The results of Western immunoblotting analyses are shown in figure 4. Liver microsomes isolated from the flupyrazofos-treated rat were subjected to the SDS-PAGE, followed by the incubation of blotted filters with polyclonal antibodies raised against rat P4501A1/2, 2B1/2, 2C6, 2E1 and 3A1/2 respectively. The levels of P4501A1/2 and 2C6 proteins were clearly reduced by treatment with

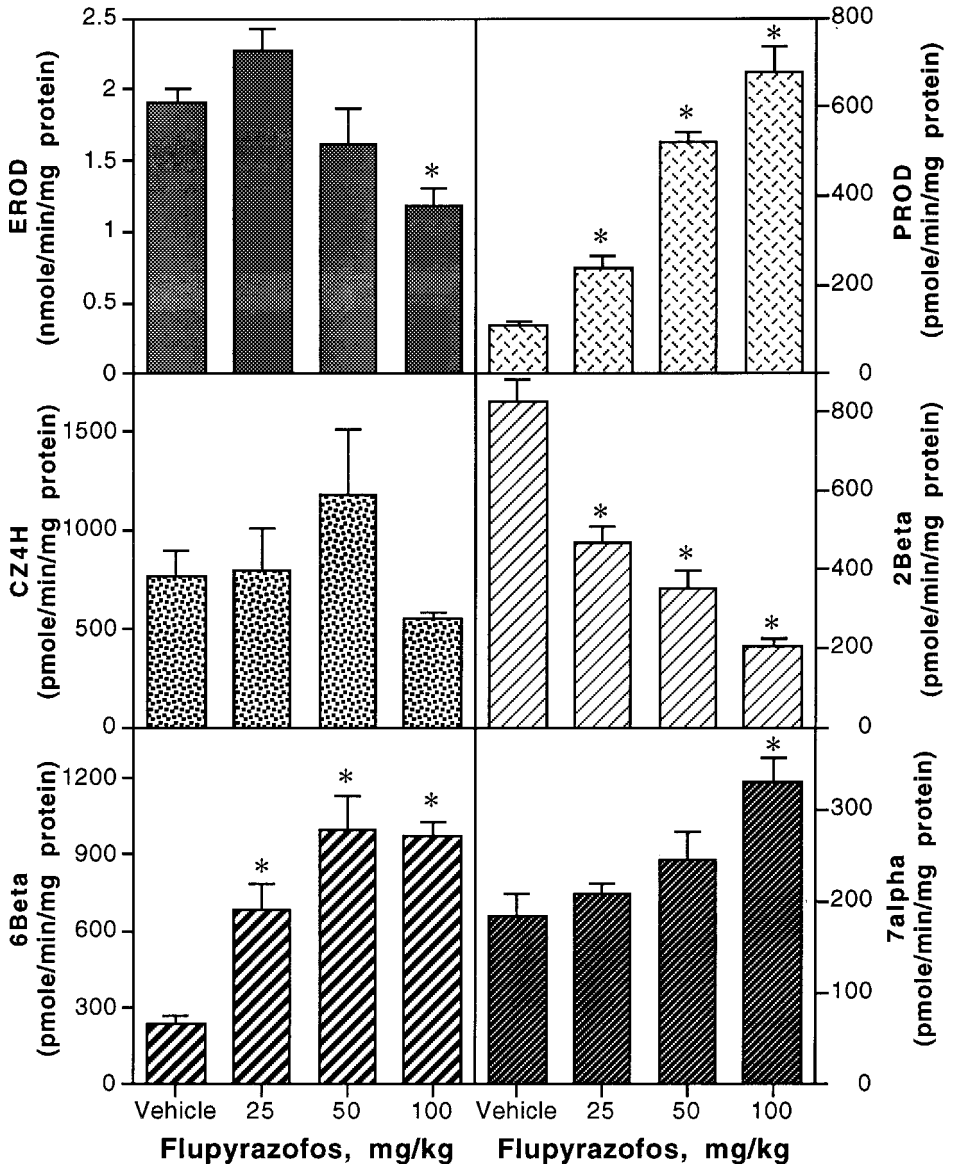


Figure 2. Effects of flupyrazofos on P450-associated monooxygenase activities in liver microsomes of the male Fischer 344 rat. A dose-response study. Rats were treated intraperitoneally with 25, 50 and 100 mg kg^{-1} flupyrazofos for 3 consecutive days. Twenty-four hours after the last treatment, the livers were removed to prepare the microsomes. Each bar represents the mean activity + SE of four animals. *Significantly different from the vehicle control at $p < 0.05$. EROD, ethoxyresorufin *O*-deethylase; PROD, pentoxyresorufin *O*-dependentylase; CZ4H, chlorzoxazone 4-hydroxylase; 2beta, testosterone 2 β-hydroxylase; 6beta, testosterone 6 β-hydroxylase; 7alpha, testosterone 7 α-hydroxylase.

flupyrazofos. The level of P4502E1 was slightly induced at 50 and 100 mg kg^{-1} flupyrazofos. P4503A1/2 was not clearly changed by flupyrazofos. And P4502B1/2 proteins were substantially induced in rat liver microsomes prepared from rat treated with flupyrazofos for 3 consecutive days.

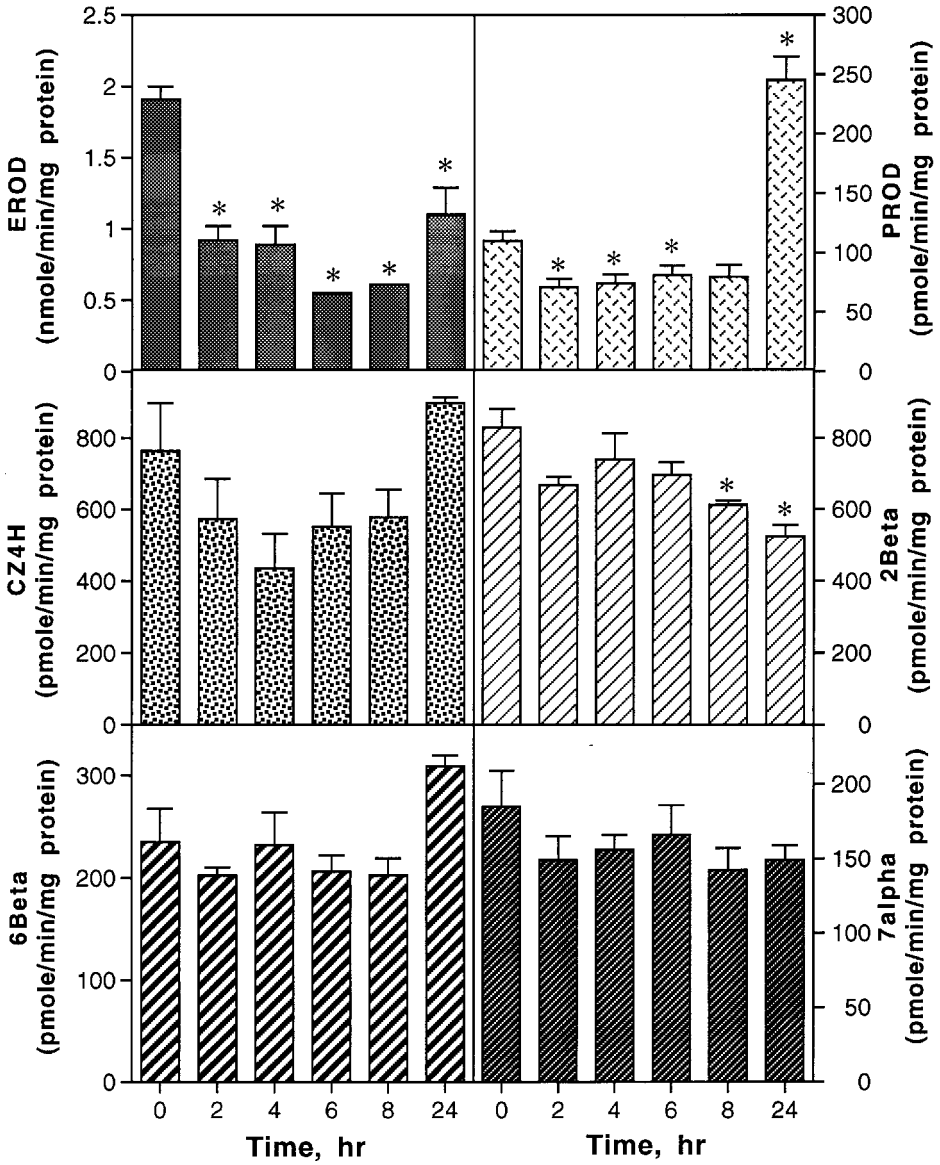


Figure 3. Effects of 50 mg kg^{-1} flupyrazofos on P450-associated monooxygenase activities in liver microsomes of the male Fischer 344 rat. A time-course study. Rats were treated intraperitoneally with 50 mg kg^{-1} flupyrazofos for 2, 4, 6, 8 or 24 h. At the designated time, livers were removed to prepare the microsomes. Each bar represents the mean activity + SE of four animals. *Significantly different from the 0-h control at $p < 0.05$. EROD, ethoxyresorufin *O*-deethylase; PROD, pentoxyresorufin *O*-dependentylase; CZ4H, chlorzoxazone 4-hydroxylase; 2beta, testosterone 2 β-hydroxylase; 6beta, testosterone 6 β-hydroxylase; 7alpha, testosterone 7 α-hydroxylase.

Discussion

Interaction of P450 enzymes with certain chemicals may cause either toxicant activation or detoxication, and severe drug–drug interactions in body (Wrighton and Stevens 1992). For these reasons, studies on the expression of P450 enzymes by new

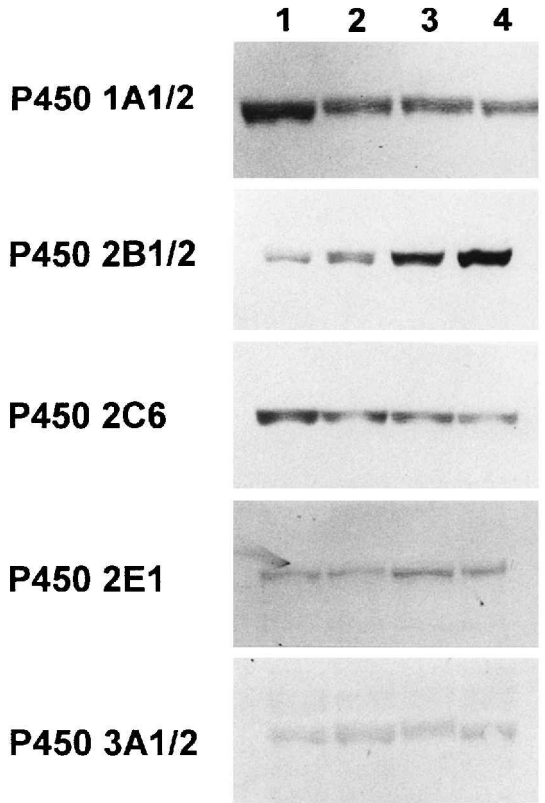


Figure 4. Effects of flupyrazofos on liver microsomal P450 in the male Fischer 344 rat. Western immunoblotting analyses. Rats were treated intraperitoneally with 25, 50 and 100 mg kg^{-1} flupyrazofos for 3 consecutive days. Twenty-four hours after the last treatment, the livers were removed to prepare the microsomes. The pooled liver microsomal proteins (10 μg/well) isolated from the flupyrazofos-treated rat were subjected to 10% SDS-PAGE and transferred to the nitrocellulose filters. Lanes 1, corn oil-treated control; 2, flupyrazofos at 25 mg kg^{-1}; 3, flupyrazofos at 50 mg kg^{-1}; 4, flupyrazofos at 100 mg kg^{-1}.

chemical entities are essentially required in development processes not only just for new drugs, but also for new pesticides. In the present studies, the effects of flupyrazofos, a new insecticide for the diamond-back moth, on P450 expression were investigated because many organophosphate insecticide are known to inhibit P450 enzymes non-specifically.

It was found that PROD activity was significantly induced by the treatment of the male Fischer 344 rat with flupyrazofos treatment for 3 consecutive days, and that these enzyme activities were reduced shortly after the treatment (figures 2 and 3). In the Western immunoblotting analyses, the levels of P4502B1/2 proteins were increased, showing a consistency with the induction of enzyme activity (figure 4). Therefore, flupyrazofos may be a strong inducer of P4502B1/2. In addition to P4502B1/2, testosterone 6 β-hydroxylase activity was also induced by the treatment with flupyrazofos. According to the literature, testosterone 6 β-hydroxylation can be catalysed by several isozymes, including P4501A1, 2A2, 3A1/2 and 2C13 (Arlotto *et al*. 1991). Because testosterone 2 β-hydroxylase is also a marker for P4503A1/2 (Arlotto *et al*. 1991) and was dose-dependently decreased by flupyrazofos in the

present studies (figure 2), the induction was definitely not due to P4503A1/2. In addition, the present results demonstrated that P4501A1 and 2C6 were decreased by flupyrazofos treatment (figures 2 and 4). Therefore, the induction of testosterone 6 β-hydroxylase activity by flupyrazofos might result from the induction of P4502A proteins. In this regard, testosterone 7 α-hydroxylase activity, which is one of the markers for P4502A1/2 (Arlotto *et al*. 1991, Yamazaki *et al*. 1994), was induced in the current studies (figure 2). However, the degree of induction of testosterone 6 β-hydroxylase and 7 α-hydroxylase was not comparable and a possible role of other isozymes should be investigated further. This possibility is currently under study.

The effects of flupyrazofos on P450 expression might be due to flupyrazofos or its oxon metabolite, but not by the stable metabolite PTMHP. From the studies on the effects of PTMHP on P450-associated enzymes activities, it was found that the inductive and inhibitory effects of PTMHP were moderate when compared with the effects of flupyrazofos (data not shown). These results indicate that flupyrazofos or its unstable oxon metabolite may cause either the induction or inhibition. From studies on the *in vitro* metabolism of flupyrazofos by rat liver microsomes, the biotransformation of flupyrazofos or flupyrazofos oxon was particularly enhanced by the pretreatment with phenobarbital, indicating that P4502B1/2 isozymes might be responsible for the desulphuration of flupyrazofos (Lee *et al*. 1997a). In addition, the present results indicated that P4502B1/2 isozymes were mostly induced by flupyrazofos treatment among others after a rapid reduction of enzyme activities (figures 2–4). Although the mechanism of induction was not studied in these particular studies, many P450 inhibitors can induce P450 enzymes after repeated doses. SKF 525-A can induce P4502B1/2 enzymes when treated for >1 day at doses capable of inhibiting P450 enzyme activities in the mouse (manuscript in preparation). In addition, flupyrazofos inhibited several P450 enzyme activities *in vitro* (manuscript in preparation).

Flupyrazofos had inhibitory effects on the activities of EROD and testosterone 2 β-hydroxylase in liver microsomes of the Fischer 344 male rat when treated for 3 consecutive days (figure 2). In particular, the activity of testosterone 2 β-hydroxylase was substantially inhibited by flupyrazofos treatment. In the Western immunoblotting analyses, P4503A1/2 proteins were not greatly influenced by flupyrazofos treatment (figure 4). These results indicate that the decreased activity of P4503A1/2 might be regulated at the level of enzyme activity, not at the level of either transcription or translation. Other possible mechanism for the discrepancy between protein levels and enzyme activity would be that flupyrazofos and/or its metabolites ligand to P450 proteins, preventing the activity to be fully expressed. In fact, flupyrazofos and flupyrazofos oxon, but not PTMHP, inhibited testosterone hydroxylation and chlorzoxazone hydroxylation *in vitro* (manuscript in preparation). This may account for the discrepancy in the results that treatment with flupyrazofos elevated the levels of P4502E1 protein, but not the enzyme activity of chlorzoxazone hydroxylases (figures 2 and 4). Further studies are needed to understand the exact mechanism of discrepancy between activity and protein level of certain isozymes caused by flupyrazofos.

Acknowledgement

The work was supported by the grants from the Ministry of Science and Technology, Korea.

References

Arlotto, M. P., Trant, J. M. and Estabrook, R. W., 1991, Measurement of steroid hydroxylation reactions by high-performance liquid chromatography as indicator of P450 identity and function. *Methods in Enzymology*, **206**, 454–462.

Blank, J. A., Tucker, A. N., Sweatlock, J., Gasiewicz, T. A. and Luster, M. I., 1987, α-Naphthoflavone antagonism of 2,3,7,8-tetrachlorodibenzo-*p*-dioxin induced murine ethoxyresorufin *O*-deethylase activity and immunosuppression. *Molecular Pharmacology*, **32**, 168–172.

Bradford, M. M., 1976, A rapid and sensitive method for the quantitation of microgram quantities of protein utilizing the principles of protein-dye binding. *Analytical Biochemistry*, **72**, 248–254.

Brian, W. R., Sari, M. A., Iwasaki, M., Shimada, T., Kaminsky, L. S. and Guengerich, F. P., 1990, Catalytic activities of human liver cytochrome P450IIIA4 expressed in *Saccharomyces cerevisiae*. *Biochemistry*, **29**, 11280–11292.

Cho, B. Y. and Han, D. S., 1992, Thermal decomposition of a new insecticide KH-502 [*O*,*O*-diethyl *O*-(1-phenyl-3-trifluoromethyl-5-pyrazoyl)thiophosphoric acid ester]. *Korean Journal of Environmental Agriculture*, **11**, 225–234.

Cho, B. Y., Han, D. S. and Yang, J. E., 1993, Photolysis of a new insecticide KH-502 [*O*,*O*-diethyl *O*-(1-phenyl-3-trifluoromethyl-5-pyrazoyl)thiophosphoric acid ester]. *Korean Journal of Environmental Agriculture*, **12**, 176–183.

Guengerich, F. P. and Kim, D. H., 1991, Enzymatic oxidation of ethyl carbamate to vinyl carbamate and its role as an intermediate in the formation of 1,N^6-ethenoadenosine. *Chemical Research in Toxicology*, **4**, 413–421.

Jeong, H. G. and Yun, C.-H., 1995, Induction of rat hepatic cytochrome P450 enzymes by myristicin. *Biochemical and Biophysical Research Communications*, **217**, 966–971.

Jeong, T. C., Gu, H. K., Chun, Y. J., Yun, C.-H., Han, S. S. and Roh, J. K., 1998, Effects of β-ionone on the expression of cytochrome P450 and NADPH-cytochrome P450 reductase in Sprague-Dawley rats. *Chemico-Biological Interactions*, **114**, 97–107.

Jeong, T. C., Kim, H. J., Yun, C.-H., Lee, S. S., Yang, K. H., Han, S. S. and Roh, J. K., 1995, Induction of liver cytochrome P450 2B1 by β-ionone in Sprague-Dawley rats. *Biochemical and Biophysical Research Communications*, **216**, 198–202.

Kaminsky, L. S., Fasco, M. J. and Guengerich, F. P., 1981, Production and application of antibodies to rat liver cytochrome P-450. *Methods in Enzymology*, **74**, 262–272.

Lee, H. S., Jeong, S., Kim, K., Kim, J. H., Lee. S. K., Kang, B. H. and Roh, J. K., 1997a, *In vitro* metabolism of the new insecticide flupyrazofos by rat liver microsomes. *Xenobiotica*, **27**, 423–429.

Lee, S. G., Hwang, C. Y., Yoo, J. K., Lee, S. W., Cho, B. R. and Lee, J. O., 1997b, Insecticidal activity of flupyrazofos against *Plutella xylostella* (Lepidoptera: Yuponomontidae) and *Spodoptera exigua* (Lepidoptera: Noctuidae). *Korean Journal of Pesticide Science*, **1**, 48–51.

Lubet, R. A., Meyer, R. T., Cameron, J. W., Nims, R. W., Burke, M. D., Wolff, J. and Guengerich, F. P., 1985, Dealkylation of pentoxyresorufin: a rapid and sensitive assay for measuring induction of cytochrome(s) P-450 by phenobarbital and other xenobiotics in the rat. *Archives of Biochemistry and Biophysics*, **238**, 43–48.

Park, J. H., Seo, K. W., Nam, K. H., Han, S. S. and Lee, Y. S., 1997, A study on acute delayed neurotoxicity of KH-502, a new synthesized insecticide. *Korean Journal of Toxicology*, **13**, 317–322.

Song, S. W., Kim, H. C., Shin, C. C., Lim, K. H., Ha, C. S. and Han, S. S., 1998, Acute toxicity test of KH-502 (flupyrazofos) in rats and mice. *Journal of Toxicology and Public Health*, **14**, 227–235.

Wrighton, S. A. and Stevens, J. C., 1992, The human cytochrome P450 involved in drug metabolism. *Critical Review in Toxicology*, **22**, 1–21.

Yamazaki, H., Mimura, M., Sugahara, C. and Shimada, T., 1994, Catalytic roles of rat and human cytochrome P450 2A enzymes in testosterone 7 α- and coumarin 7-hydroxylations. *Biochemical Pharmacology*, **48**, 1524–1527.

XENOBIOTICA, 2000, VOL. 30, NO. 12, 1131–1152

Determining the best animal model for human cytochrome P450 activities: a comparison of mouse, rat, rabbit, dog, micropig, monkey and man

J. J. P. BOGAARDS†*, M. BERTRAND‡, P. JACKSON‡, M. J. OUDSHOORN†, R. J. WEAVER§, P. J. VAN BLADEREN† and B. WALTHER‡

† TNO Pharma, Department of Kinetics and Metabolism, PO Box 360, 3700 AJ Zeist, The Netherlands
‡ Technologie Servier, Rue du Eugène Vignat, Orléans, France
§ Servier Research and Development, Fulmer Hall, Fulmer, Slough SL3 6HH, UK

Received 4 May 2000

1. In the present study, nine cytochrome P450 enzyme activities in seven species were characterized to allow a practical means of comparing this important metabolic step between various test animals and man.

2. Enzyme activities and kinetic parameters were first determined towards marker substrates for human cytochrome P450 enzymes. Inhibition profiles were then determined with both antibodies directed against various cytochrome P450 enzymes and with chemical inhibitors.

3. Both the enzyme kinetic parameters/enzyme activities, and the inhibition profiles obtained for the animal species were compared with those obtained for human liver microsomes in order to postulate the animal species most similar to man with regard to each individual cytochrome P450 enzyme activity.

4. It was found that, as expected, none of the tested species was similar to man for all the measured P450 enzyme activities, but that in each species only some of the P450 enzyme activities could be considered as similar to man.

5. When it is known which human cytochrome P450 enzymes are involved in the metabolism of a compound, the comparative data presented here can be used for selecting the most suitable species for *in vitro* and *in vivo* experiments.

Introduction

The cytochrome P450 superfamily is involved in numerous oxidative reactions and as such often plays a decisive role in the metabolism and kinetics of xenobiotics (Guengerich and Shimada 1991, Guengerich *et al*. 1991, Wrighton and Stevens 1992, Daly *et al*. 1993, Gonzalez and Gelboin 1994, Gonzalez and Idle 1994). Animal models are used to predict kinetics and toxicity in humans. The interspecies comparison that has to be made suffers from two difficulties. First, in human organs large interindividual variations exist between individual cytochrome P450 enzymes (Guengerich and Turvey 1991, Forrester *et al*. 1992, Lucas *et al*. 1993, Shimida *et al*. 1994, Bogaards *et al*. 1995), as a consequence of phenotypic differences of genetic polymorphisms (Cholerton *et al*. 1992, Daly *et al*. 1993, Nakachi *et al*. 1993, Furuya *et al*. 1995, Daniel and Edeki 1996). Second, although cytochrome P450 enzymes are classified into distinct subfamilies based on amino acid sequence identity (Nelson *et al*. 1993), a high degree of sequence identity does not automatically mean similar catalytic specificity (Guengerich 1997). A single amino acid substitution may even give a change in substrate specificity (Lindberg and

* Author for correspondence; e-mail: Bogaards@voeding.tno.nl

Xenobiotica ISSN 0049–8254 print/ISSN 1366–5928 online © 2000 Taylor & Francis Ltd
http://www.tandf.co.uk/journals
DOI:10.1080/00498250010021684

Negishi 1989). Therefore, orthologous genes/enzymes do not automatically allow comparison of catalytic specificities between species (Nelson *et al.* 1993). In addition, very different cytochrome P450 enzymes can catalyze the same activity (Guengerich 1997).

With respect to species–species extrapolation, it is important to know which similarities and/or differences exist between the cytochrome P450 enzymes/subfamilies, as well as their levels of expression. In humans, the most important P450 enzymes/subfamilies involved in the metabolism of xenobiotics and endogenous compounds in man are cytochromes P4501A2, 2A6, 2B6, 2C, 2D6, 2E1 and 3A4, accounting on average for 13, 4 < 1, 18, 1.5, 6.6 and 30% of the total amount of hepatic P450 respectively (Shimada *et al.* 1994). In animal species, the levels of related enzymes/subfamilies may be very different. For example, coumarin 7-hydroxylase activities in humans have been reported which were up to 200-fold higher than in rat (Pearce *et al.* 1992, Yamazaki *et al.* 1994). With respect to hepatic CYP3A activity, a sex-related difference in rat has been described (Kato and Yamazoe 1992, Werner *et al.* 1995, Tomlinson *et al.* 1997), with the male rat having 5–10-fold higher activities than the female rat, while similar CYP3A activities were observed in the male rat and in human (Tomlinson *et al.* 1997). Therefore, to predict kinetics and toxicity in humans, species differences between cytochrome P450 enzymes should be taken into account when animal species are selected for *in vitro* and *in vivo* experiments.

Some studies have been reported in which species differences with respect to cytochrome P450 enzyme activities were investigated (e.g. Boobis *et al.* 1990, Pearce *et al.* 1992, Ohmori *et al.* 1993, Stevens *et al.* 1993, Yasumori *et al.* 1993, Weaver *et al.* 1994, 1999, Yamazaki *et al.* 1994, Sharer *et al.* 1995, Ghosal *et al.* 1996, Tomlinson *et al.* 1997, Anzenbacher *et al.* 1998, Eagling *et al.* 1998). However, in some of these studies only two or three species were studied (Ohmori *et al.* 1993, Stevens *et al.* 1993, Yamazaki *et al.* 1994, Sharer *et al.* 1995, Ghosal *et al.* 1996, Anzenbacher *et al.* 1998, Eagling *et al.* 1998, Weaver *et al.* 1999), while in others only one or two substrates were investigated (Pearce *et al.* 1992, Ohmori *et al.* 1993, Yasumori *et al.* 1993, Yamazaki *et al.* 1994, Ghosal *et al.* 1996, Tomlinson *et al.* 1997). In addition, not always the more common cytochrome P450 probe substrates were used (Stevens *et al.* 1993, Weaver *et al.* 1994, Ghosal *et al.* 1996, Tomlinson *et al.* 1997). Therefore, the species differences reported with respect to cytochrome P450 enzyme activities seem to be rather fragmental.

It was therefore the aim of the present study to characterize within one study nine cytochrome P450 enzyme activities in seven species to allow a practical means of comparing this important metabolic step between various test animals and man. First, enzyme activities and kinetic parameters were determined towards 7-ethoxyresorufin, coumarin, 7-ethoxy-4-trifluoro-methylcoumarin, diclofenac, *S*-mephenytoin, bufuralol, chlorzoxazone, testosterone and lauric acid, using liver microsomes of mouse (B6C3F1), rat (Wistar), rabbit (New Zealand White), dog (Beagle), micropig (Yucatan), monkey (Macaca fascicularis) and man. These substrates are well-known marker substrates for human cytochrome P450 enzymes. Subsequently, inhibition profiles were determined both with antibodies directed against various cytochrome P450 enzymes, and with the chemical inhibitors α-naphthoflavone, furafylline, pilocarpine, sulphaphenazole, quinidine, quinine, diethyldithiocarbamate and ketoconazole. In this way, the present study hoped to provide additional important information about interspecies comparative metab-

olism. Both the enzyme kinetic parameters/enzyme activities and the inhibition profiles obtained for the animal species were compared with those obtained for human liver microsomes to postulate the animal species most similar to man with regard to the various cytochrome P450 activities.

Materials and methods

Materials

7-Ethoxyresorufin, coumarin, diclofenac and pilocarpine were from Sigma Chemical Co. (St Louis, MO, USA). Resorufin, 7-hydroxycoumarin, chlorzoxazone, quinidine, quinine and diethyldithiocarbamate from Aldrich (Bornem, Belgium). 7-Ethoxy-4-trifluoromethyl-coumarin and 7-hydroxy-4-trifluoromethyl-coumarin were from Enzyme Systems Products (Dublin, CA, USA). *S*-mephenytoin, 4′-hydroxymephenytoin, bufuralol, 1′-hydroxybufuralol, 6-hydroxy-chlorzoxazone, furafylline and sulphaphenazole were from Ultrafine Chemicals (Manchester, UK). Testosterone, 6β-hydroxytestosterone and 11β-hydroxytestosterone were from Steraloids, Inc. (Wilton, NH, USA). *S*-[4-^{14}C]mephenytoin, [2-^{14}C]chlorzoxazone, [4-^{14}C]testosterone and [4-^{14}C]lauric acid were from Amersham Life Science Ltd (Amersham, UK).

4′-Hydroxydiclofenac was a kind gift from Ciba-Geigy (Basel, Switzerland). Ketoconazole was a kind gift from Janssen (Beerse, Belgium). Antiserum for human CYP1A (raised against rat CYP1A2), anti-rat CYP2B1, anti-rat CYP2C11, anti-human CYP2D6, anti-rat CYP2E1, anti-rat CYP3A2 and anti-rat CYP4A1 (all polyclonal antibodies) were kind gifts from Daiichi Pure Chemicals Company (Tokyo, Japan). Anti-human CYP2A6 (MAB-2A6, monoclonal) was kindly provided by GENTEST Corp. (Woburn, MA, USA).

According to the manufacturers, anti-human CYP2A6 shows minor cross-reactivity towards human CYP2E1, anti-rat CYP2B1 shows cross-reactivity with rat CYP2B2, and anti-rat CYP2C11 shows minor cross-reactivity with rat CYP2B1/CYP2B2. For the other antibodies, no detectable cross-reactivities were found towards rat or human cytochrome P450 enzymes. All other chemicals were of the highest available quality.

Animals and preparation of liver microsomes

Liver homogenates of B6C3F1 mouse (Charles River, Germany; aged 8–10 weeks), Wistar rat (Charles River, Germany; aged 12 weeks), New Zealand White rabbit (Broekman, The Netherlands; aged 16 weeks), and beagle dog (Harlan, The Netherlands; aged 12–13 months) were prepared from fresh livers. Liver homogenates of Yucatan micropig (Charles River, France; aged 9–10 months) and *Macaca fascicularis* monkey (Servier, UK; aged 26–27 months (males) and 18–24 months (females) were from frozen livers. Microsomes were prepared both from male and female animals. Three animals were used for each species and gender, with the exception of mouse (six animals) and monkey (two). Livers were homogenized in 0.01 M Tris-HCl/0.14 M KCl, pH 7.4 buffer (1:3 w/w) at 0–4 °C. Microsomes were prepared by ultracentrifugation (100000 ***g*** for 75 min) of the post-mitochondrial supernatant (10000 ***g*** for 20 min). The microsomal pellet was resuspended in homogenization buffer and centrifuged for 60 min at 100000 ***g***. The washed microsomes were suspended in homogenization buffer (weight equal to the amount of liver homogenized) and stored at approximately −80 °C. Pooled microsomes contained equal amounts of the individual microsomal preparations. Liver microsomes prepared from mouse, rat, dog, micropig and monkey were from untreated animals. Rabbit liver microsomes were from animals used for acute dermal irritation studies, in which no significant dermal effects were found.

Human liver microsomes

Human liver microsomes were from Human Biologics, Inc. (Phoenix, AZ, USA) and Gentest Corp. In the experiments performed for the estimation of K_m and V_{max}, male human liver microsomes comprised a pool of four samples (HBI03, HBI05, HBI07 and HBI11) and female liver microsomes comprising a pool of six samples (HBI02, HBI06, HBI09, HBI10, HBI12 and HBI13; all Human Biologics). In the inhibition experiments, male human liver microsomes comprised a pool of three samples (HBI05, HBI07 and HBI20; Human Biologics) and female liver microsomes a pool of three samples (HG30, HG56 and HG93; Gentest).

Enzyme assays for cytochrome P450 probe substrates

7-Ethoxyresorufin *O*-dealkylase, coumarin 7-hydroxylase, 7-ethoxy-4-trifluoromethyl-coumarin *O*-dealkylase, diclofenac 4′-hydroxylase, bufuralol 1′-hydroxylase, chlorzoxazone 6-hydroxylase and testosterone 6β-hydroxylase activities were determined as described by Bogaards *et al.* (1995, 1996). In

Table 1. Cytochrome P450 marker substrates and concentrations used for the estimation of enzyme kinetic parameters and the inhibition experiments.

Cytochrome P450 marker substrate	Selective for human	Marker substrate concentrations (μM)	
		Estimation of K_m/V_{max}	Inhibition experiment
7-Ethoxyresorufin	CYP1A2	0.01–2	2
Coumarin	CYP2A6	0.5–500	100
7-Ethoxy-4-trifluoromethylcoumarin	CYP2B6	1–100	100
Diclofenac	CYP2C9	1–100	100
S-mephenytoin	CYP2C19	–	100
Bufuralol	CYP2D6	0.5–150	100
Chlorzoxazone	CYP2E1	5–500	200
Testosterone	CYP3A	5–400	400
Lauric acid	CYP4A	–	100

–, Enzyme kinetic parameters not determined.

the inhibition experiments, chlorzoxazone 6-hydroxylase and testosterone 6β-hydroxylase activities were determined with radiolabeled substrates. Incubations with [2-^{14}C]chlorzoxazone were terminated with perchloric acid, and incubations with [4-^{14}C]testosterone with ice-cold acetonitrile. After centrifugation, HPLC analysis was performed as described by Bogaards *et al*. (1995) using on-line radiochemical detection (Canberra Packard A500).

S-mephenytoin 4-hydroxylase activity was determined by incubation with *S*-[4-^{14}C]mephenytoin and reversed-phase HPLC. Incubations were performed at 37 °C in 100 μl incubation mixtures containing 0.1 M potassium phosphate buffer, pH 7.4, 3 mM NADPH and 100 μM ^{14}C-*S*-mephenytoin. The reaction was terminated by the addition of 25 μl ice-cold acetonitrile. After centrifugation, the supernatant was subjected to HPLC analysis. HPLC analysis of 4′-hydroxymephenytoin was performed using a 250×4.6 mm Zorbax ODS C18 column, and a gradient of 20 mM sodium perchlorate pH 2.5/methanol/acetonitrile (60:35:5 v/v) (solvent A) and methanol (solvent B). Elution was performed at 0% B for 12 min, followed by a linear gradient from 0 to 95% B in 4 min and isocratic elution at 95% B for 9 min. The flow-rate was 0.8 ml min^{-1}. Radioactivity in the effluent was measured by on-line radiochemical detection (Canberra Packard A500).

Lauric acid 12-hydroxylase activity was determined by incubation with [1-^{14}C]lauric acid and reversed-phase HPLC. Incubations were performed at 37 °C in 200 μl incubation mixtures containing 0.05 M Tris-HCl buffer, pH 7.4, 3 mM NADPH and 100 μM ^{14}C-lauric acid. The reaction was terminated by the addition of 100 μl ice-cold acetonitrile/acetic acid = 94:6 (v/v). After centrifugation, the supernatant was subjected to HPLC analysis. HPLC analysis was performed at 50 °C using a 250×4.6 mm Zorbax ODS C18 column, and a gradient of methanol/acetonitrile/water = 23:23:54 (v/v), containing 5 mM perchloric acid (solvent A) and methanol (solvent B). Elution was performed using a linear gradient from 0 to 28% B in 20 min, followed by elution with methanol for 10 min. The flow-rate was 1.0 ml min^{-1}. Radioactivity in the effluent was measured by on-line radiochemical detection (Canberra Packard A500).

Concentrations of P450 marker substrates and chemical inhibitors

For the estimation of enzyme kinetic parameters K_m and V_{max}, seven concentrations of P450 marker substrates were used. The selected marker substrate concentrations for the inhibition experiments were based on the obtained K_m for the various species and are, in general, V_{max} conditions for all species. To compare the inhibition profiles of the various species, standard (V_{max}) conditions were chosen with respect to the P450 marker substrate concentrations (same concentration for all species). Therefore, these conditions do not have to be the most optimal conditions with respect to complete inhibition of cytochrome P450 enzyme activities. The selected concentrations of *S*-mephenytoin and lauric acid were based on literature values reported elsewhere and are at least two-times the K_m (Powell *et al*. 1996, Schmider *et al*. 1996). The range of marker substrate concentrations used are summarized in table 1. Enzyme kinetic parameters K_m and V_{max} were calculated with the curve-fitting program for the analysis of enzyme kinetic data EZ-FIT® (Perella 1988).

Antiserum for human CYP1A, anti-human CYP2A6, anti-rat CYP2B1, anti-rat CYP2C11, anti-human CYP2D6, anti-rat CYP2E1, anti-rat CYP3A2 and anti-rat CYP4A1 were used at the following concentrations: 10, 2.5, 50, 25, 15, 50, 35 and 50 μl per 100 μg microsomal protein respectively. These concentrations were based on the results of preliminary experiments, in which three different concentrations of antibodies were used (data not shown). The selected chemical inhibitors and inhibitor

concentrations were based on literature data (Kunze and Trager 1993, Chang *et al*. 1994, Wrighton and Ring 1994, Kimonen *et al*. 1995, Newton *et al*. 1995, Ono *et al*. 1996, Eagling *et al*. 1998): α-naphthoflavone (1 μM), furafylline (25 μM), pilocarpine (20 μM), sulphaphenazole (10 μM), quinidine (5 μM), quinine (5 μM), diethyldithiocarbamate (100 μM) and ketoconazole (1 μM). For furafylline, a concentration of 5 μM was used at first. However, at this concentration, only 50% inhibition was found in human liver microsomes while no inhibition was found in the other species (data not shown). Therefore, the furafylline concentration was increased to 25 μM. At this concentration, furafylline was still selective with respect to the inhibition of CYP1A2 activity in human liver microsomes (inhibition of CYP1A2 activity: 88% CYP2D6 activity: 19%, no inhibition of other activities). Inhibition experiments were performed in duplicate. Inhibition experiments with male and female liver microsomes were performed in two separate experiments, both for antibodies and chemical inhibitors. Controls in the immuno-inhibition experiments were incubated without antibody, but with the same amount of pre-immune rabbit or goat serum (Daiichi antibodies), or with Tris buffer (anti-human CYP2A6). Chemical inhibitors were added to the incubation mixtures as solutions in methanol. For the controls, only methanol was added. The amount of organic solvent in the incubation mixtures was $< 2.5\%$ (v/v). Since organic solvents inhibit CYP2E1, incubations with chlorzoxazone in the presence of chemical inhibitors were performed by evaporation of the chemical inhibitor solutions prior to the addition of the incubation mixture components. Blanks were incubated without pre-immune serum/buffer/chemical inhibitor and without NADPH. Before starting the enzymatic reactions, the samples were pre-incubated for 5 min at 37 °C in the presence of antibody/chemical inhibitor.

Results

The enzyme kinetic parameters/enzyme activities and the inhibition results are presented in tables 2A–H. The enzyme kinetic parameters/enzyme activities are presented both for males and females. Because the extent of inhibition in males and females was rather similar, the inhibition results are presented as the means of males and females with the exception of rat testosterone 6β-hydroxylase activity. For this enzyme activity, anti-rat CYP3A2 and ketoconazole were very potent inhibitors in the male rat, while almost no inhibition was found in females (table 2G). This sex-related CYP3A difference has been reported before (Kato and Yamazoe 1992, Werner *et al*. 1995, Tomlinson *et al*. 1997). With respect to the classification of the inhibition results, an antibody or chemical inhibitor was considered a weak inhibitor if the percentage of inhibition ranged from 15 to 30%, a moderate inhibitor if the inhibition ranged from 30 to 60%, a strong inhibitor from 60 to 80%, and a very strong inhibitor if $>80\%$ of the enzyme activity was inhibited. The antibody or chemical inhibitor was considered not to be an inhibitor of cytochrome P450, under the conditions used, if the amount of inhibition was $< 15\%$: small amounts of inhibition could also be due to intra-assay variations, etc. In addition to the inhibition of the enzyme activity the antibody or chemical inhibitor was directed against, cross-reactivities with other enzyme activities are also presented in table 2, if moderate or stronger inhibition of this enzyme activity was found for at least in one of the species.

Inhibition experiments with *S*-mephenytoin were only performed with monkey and human liver microsomes, because *S*-mephenytoin 4′-hydroxylase activity in the other species was near or below the limit of detection (table 2D).

7-Ethoxyresorufin O-dealkylase activity (table 2A)

Cytochrome P4501A2 has been purified from mouse, rat, rabbit and human. All these enzymes showed characteristically 7-ethoxyresorufin and phenacetin *O*-dealkylation activities (Guengerich 1997). In addition, CYP1A2 genes or gene products have been found in dog and monkey (Nelson *et al*. 1993, 1996; http://drnelson.utmem.edu/Nomenclature.html).

Table 2A. Enzyme kinetic parameters for and inhibition of 7-ethoxyresorufin *O*-dealkylase activity.

	Male		Female		Amount of inhibition[1]							
	K_m	V_{max}	K_m	V_{max}	Antiserum for human CYP1A			α-Naphthoflavone			Furafylline	
Species	Enzyme activity: EROD				EROD	7-ETC	CHLZ	EROD	DICLO	CHLZ	EROD	CHLZ
Mouse	0.055	66	0.052	63	++++	–	–	++++	–	–	++	–
Rat	0.220	78	0.045	67	++	–	–	++	–	–	+	–
Rabbit	0.145	123	0.186	142	++++	–	–	++++	+	+	+	+
Dog	0.070	409	0.063	411	++++	++	++	++++	–	++	++	++
Micropig	0.059	57	0.098	116	++	–	–	+++	–	–	–	–
Monkey	0.187	129	0.296	118	++	–	–	+++	++	–	–	–
Man	0.265	95	0.179	25	++++	++	–	++++	–	–	++++	–

Apparent K_m is expressed as μM; V_{max} as pmol min^{-1} mg^{-1} microsomal protein.

[1] –, No inhibition (0–15%); +, weak inhibition (15–30%); ++, moderate inhibition (30–60%); +++, strong inhibition (60–80%); ++++, very strong inhibition (80–100%); EROD, 7-ethoxyresorufin *O*-dealkylation; 7-ETC, 7-ethoxy-4-trifluoromethyl-coumarin *O*-dealkylation; DICLO, diclofenac 4′-hydroxylation; CHLZ, chlorzoxazone 6-hydroxylation. Data are derived from duplicate determinations.

In the present study, the inhibition profiles obtained for antiserum for human CYP1A and α-naphthoflavone were rather similar. The only obvious difference was that diclofenac 4′-hydroxylase activity in monkey was inhibited by α-naphthoflavone, but not by anti-human CYP1A. A possible explanation could be that α-naphthoflavone acts directly towards the active site while the antibody binds to a larger region of the enzyme molecule.

In rat (anti-CYP1A and α-naphthoflavone) and monkey (anti-CYP1A) 7-ethoxy-resorufin *O*-dealkylase activity was inhibited to a lesser extent than in the other species. In rat, this can be explained by the fact that several P450 isoforms are involved in the metabolism of 7-ethoxyresorufin in untreated animals (Burke *et al*. 1994).

Both dog and human liver microsomes showed moderate inhibition of 7-ethoxy-4-trifluoromethyl-coumarin *O*-dealkylase activity by antiserum for human CYP1A. For α-naphthoflavone, only a weak inhibition (17–19%) of this enzyme activity was found in dog and human liver microsomes (data not presented in table 2A). In human liver microsomes, 7-ethoxy-4-trifluoromethyl-coumarin is metabolized not only by CYP2B6, but also by other P450 enzymes, mainly CYP1A2 (Bogaards *et al*. 1996, Lewis *et al*. 1999). Therefore, the inhibition of this activity in human liver microsomes is most likely due to the role of CYP1A2 in the metabolism of this probe substrate. In dog liver microsomes, this could also be the case due to the involvement of a functionally related CYP1A protein. In dog, both antiserum for human CYP1A and α-naphthoflavone inhibited chlorzoxazone 6-hydroxylase activity, which indicates a structural relationship between dog CYP1A and CYP2E. Maybe that is why a higher 7-ethoxyresorufin activity was found in the dog as compared with the other species. In addition, chlorzoxazone could possibly not be specific for CYP2E1 in dog. Differences between the inhibition profiles obtained for α-naphthoflavone and furafylline could be due to the fact that α-naphthoflavone inhibits both CYP1A1 and CYP1A2 (related proteins), while furafylline only inhibits CYP1A2 (related protein) (Kunze and Trager 1993, Chang *et al*. 1994, Eagling *et al*. 1998). However, immuno-inhibition experiments with anti-rat CYP1A1 and antiserum for human CYP1A1 showed no inhibition of 7-ethoxyresorufin *O*-dealkylase activities in any of the species (data not shown), indicating that CYP1A1 (related protein) is not constitutively expressed in the various species, which has already been described by Guengerich (1997). Therefore, the obtained differences between α-naphthoflavone and furafylline can be explained by differences between the active site amongst species (Boobis *et al*. 1990).

Taking into account the role of human CYP1A2 in the metabolism of 7-ethoxy-4-trifluoromethyl-coumarin, mouse, rabbit, micropig and human liver microsomes showed the most similar inhibition profiles obtained for antiserum for human CYP1A and α-naphthoflavone. Because this inhibition is selective in these species (no or weak inhibition of other enzyme activities), the role of other P450 isoforms in the metabolism of 7-ethoxyresorufin seems to be limited. From these species, the mouse showed the most similar furafylline inhibition profile compared to human liver microsomes. Because K_m and V_{max} of the various species were rather similar, maybe with exception of the V_{max} of dog, mouse, followed by rabbit seem to be the most similar species as compared with man with respect to CYP1A2 (related protein).

In human liver microsomes, a four-fold difference was found between males and females with regard to V_{max}. However, this is not due to a sex-related difference

because in the pooled human liver microsomes used for the inhibition experiments, the control incubations showed similar activities for males and females (103 and 140 pmol min^{-1} mg^{-1} protein) under V_{max} conditions.

Coumarin 7-hydroxylase activity (table 2B)

Cytochrome P4502A enzymes have been studied in mouse, rat, rabbit, hamster, monkey and human. These CYP2A proteins differ markedly in catalytic specificity, which is strongly determined by four single amino acid residues (Guengerich 1997). Honkakoshi and Negishi (1997) have proposed a classification based on these specificities and relates the activities to these four amino acid residues. All these CYP2A enzymes showed coumarin 7-hydroxylase activity (Guengerich 1997). However, it was also demonstrated that coumarin 7-hydroxylase activity in rat liver microsomes was very low (Pearce *et al*. 1992, Yamazaki *et al*. 1994, present study).

In the present study, the obtained K_m for the 7-hydroxylation of coumarin were rather similar, although the K_m for human female liver microsomes was 3–17-fold lower than in the other species. Furthermore, a large range of V_{max} was found. Rabbit, micropig and monkey seem to be the most similar species to man. The male micropig showed a relatively low V_{max} compared with the female micropig. Because only three animals were used in the present study, and because of the limited information available in the literature, it is not known whether this has to do with a sex-related difference in micropig. Female human liver microsomes also showed a rather low V_{max}. However, in the inhibition experiments a different pool of female human liver microsomes was used, which showed an activity of 779 pmol min^{-1} mg^{-1} protein under V_{max} conditions. Furthermore, the monkey livers used in the present study appeared to have rather high coumarin 7-hydroxylase activities, because in other studies cynomolgus monkey and human liver microsomes appeared to have rather similar coumarin 7-hydroxylase activities (Pearce *et al*. 1992, Sharer *et al*. 1995). The anti-human CYP2A6 inhibition profiles obtained for micropig and monkey were most similar to man regarding the 7-hydroxylation of coumarin. All three species showed moderate to strong inhibition of coumarin 7-hydroxylase activities, with only weak inhibition of 7-ethoxy-4-trifluoromethyl-coumarin metabolism in micropig and human liver microsomes. Therefore, micropig and monkey seem to be the most similar species as compared to man with respect to CYP2A (related protein).

The inhibition profiles obtained for pilocarpine in the various species were very different. In mouse, rat and human liver microsomes, chlorzoxazone 6-hydroxylase activity was inhibited to the largest extent (28–40%). In dog and monkey, diclofenac 4′-hydroxylase activity was inhibited most efficiently (44–89%), while in rabbit almost complete inhibition of coumarin 7-hydroxylase activity was observed. Kimonen *et al*. (1995) have reported pilocarpine to be a very potent inhibitor of coumarin 7-hydroxylase activity in mouse and man (IC_{50} = 6 μM for both species). Therefore, pilocarpine was selected as chemical inhibitor in the present study. However, inhibition of coumarin 7-hydroxylase activity could not be confirmed in the present study. Only in rabbit, a strong inhibition of coumarin 7-hydroxylase activity was found (90%), while in the other species no inhibition or weak inhibition was found (5–15%). Because Kimonen *et al*. (1995) used a coumarin concentration of 2 μM while in the present study a concentration of 100 μM was used, differences

Table 2B. Enzyme kinetic parameters for and inhibition of coumarin 7-hydroxylase activity.

	Male		Female		Amount of inhibition[1]					
	K_m	V_{max}	K_m	V_{max}	Anti-human CYP2A6			Pilocarpine		
Species	Enzyme activity: coumarin 7-hydroxylase				COUMA	7-ETC	CHLZ	COUMA	DICLO	CHLZ
Mouse	6.1	51	11.8	48	++	–	++	–	+	++
Rat	–	< 5	–	< 5	n.d.	–	–	n.d.	–	+
Rabbit	7.7	654	10.0	890	++	++	++	++++	–	++
Dog	2.0	68	4.3	180	+++	+	++	–	++++	–
Micropig	4.4	180	22.1	966	+++	+	–	–	+	+
Monkey	5.2	2398	11.0	7175	+++	–	–	–	++	–
Man	4.4	1275	1.3	357	++++	+	–	–	–	++

Apparent K_m is expressed as μM; V_{max} as pmol min^{-1} mg^{-1} microsomal protein.

[1]–, No inhibition (0–15%); +, weak inhibition (15–30%); ++, moderate inhibition (30–60%); +++, strong inhibition (60–80%); ++++, very strong inhibition (80–100%); n.d., not determined; COUMA, coumarin 7-hydroxylation; 7-ETC, 7-ethoxy-4-trifluoromethyl-coumarin *O*-dealkylation; DICLO, diclofenac 4′-hydroxylation; CHLZ, chlorzoxazone 6-hydroxylation. Data are derived from duplicate determinations.

Table 2C. Enzyme kinetic parameters for and inhibition of 7-ethoxy-4-trifluoromethylcoumarin *O*-dealkylase activity.

Species	Male		Female		Amount of inhibition[1]		
	K_m	V_{max}	K_m	V_{max}	Anti-rat CYP2B1		
	Enzyme activity: 7-ETC				7-ETC	COUMA	DICLO
Mouse	3.7	572	4.8	604	++	+	–
Rat	6.6	1509	5.0	1550	+	n.d.	++
Rabbit	6.7	2136	4.1	1620	++	–	–
Dog	2.7	2124	3.5	2578	++	++	–
Micropig	2.3	286	1.8	353	++	–	–
	29	875	37	979			
Monkey	3.4	3225	3.1	2996	–	–	–
Man	2.4	271	2.8	178	++	++	–

Apparent K_m is expressed as μM; V_{max} as pmol min^{-1} mg^{-1} microsomal protein.

[1] –, No inhibition (0–15%); +, weak inhibition (15–30%); ++, moderate inhibition (30–60%); +++, strong inhibition (60–80%); ++++, very strong inhibition (80–100%); n.d., not determined; COUMA, coumarin 7-hydroxylation; 7-ETC, 7-ethoxy-4-trifluoromethyl-coumarin *O*-dealkylation; DICLO, diclofenac 4′-hydroxylation. Data are derived from duplicate determinations.

between both studies are probably due to differences in coumarin concentrations. Therefore, the results obtained with pilocarpine were not used for the prediction of the animal species most comparable with man.

7-Ethoxy-4-trifluoromethyl-coumarin O*-dealkylase activity* (table 2C)

Cytochrome P4502B enzymes have been studied in rat, rabbit, dog, monkey and human (Guengerich 1997). In addition, CYP2B genes or gene products have been found in mouse (Nelson *et al*. 1993, 1996; http://drnelson.utmem.edu/Nomenclature.html). The rabbit P4502B enzymes seem to have the same catalytic specificities as the rat 2B enzymes. Dog P4502B11 seems to be somewhat different because of its ability to oxidize polychlorinated biphenyls (Guengerich 1997). Species differences between rat and dog with regard to the 16-hydroxylation of testosterone, which is considered to be a CYP2B-catalyzed reaction, have been reported (Ohmori *et al*. 1993) with rat liver microsomes showing a 3–4-fold higher testosterone 16α-hydroxylase activity than dog liver microsomes.

In the present study, rat and dog showed rather similar enzyme kinetics towards 7-ethoxy-4-trifluoromethylcoumarin. The anti-rat CYP2B1 antibody used in the present study was not selective with respect to the inhibition of 7-ethoxy-4-trifluoromethyl-coumarin *O*-dealkylation. Indeed, antibodies raised against rat P4502B1 have been reported to give unreliable results (Guengerich 1997). Furthermore, the probe substrate used is not metabolized primarily by CYP2B6 in human liver microsomes (Bogaards *et al*. 1996, Lewis *et al*. 1999), which will most likely also be the case in the animal species. Therefore, the inhibition profiles obtained do not allow a prediction with respect to the species most similar to man. Rather large differences were observed between the V_{max} of the various species. Microsomes of micropig appeared to have two affinity components, one component having an apparent K_m similar to the other species, and one component with a >10-fold higher K_m. Mouse and human liver microsomes showed the most similar V_{max}. Therefore, taking everything into account, the mouse seems to be the most similar species to man with respect to cytochrome P4502B.

Diclofenac and S-*mephenytoin 4′-hydroxylase activities* (table 2D)

CYP2C genes or gene products have been detected in mouse, rat, rabbit, dog, monkey and man (Nelson *et al*. 1993, 1996; http://drnelson.utmem.edu/Nomenclature.html). The human and rabbit CYP2C enzymes have been studied most extensively (Guengerich 1997). In humans, four CYP2C enzymes have been found (Guengerich 1997): 2C8, 2C9, 2C18 and 2C19. In rabbits, seven CYP2C enzymes have been found that differ markedly in substrate specificity. P4502C3 is the predominant steroid 6β-hydroxylase enzyme in rabbit, while in rat and human the CYP3A subfamily is involved is this activity (Guengerich 1997). In human, *S*-mephenytoin is a probe substrate for CYP2C19 (Schmider *et al*. 1996, Guengerich 1997). Rat CYP2C11 also shows *S*-mephenytoin 4′-hydroxylase activity (Yasumori *et al*. 1993).

In the present study, anti-rat CYP2C11 appeared not to be a selective antibody. Therefore, the results are not presented in table 2D. Anti-rat CYP2C11 inhibited diclofenac 4′-hydroxylase activity moderately in rat, rabbit, dog and micropig (30–54%) and strongly in mouse, monkey and human (68–78%). In monkey and man, *S*-mephenytoin 4′-hydroxylase activity was inhibited very strongly (91–7%). However, in addition to these CYP2C activities, anti-rat CYP2C11 inhibited the metabolism of 7-ethoxyresorufin (rat), coumarin (mouse, rabbit, dog, micropig, monkey, human), 7-ethoxy-4-trifluoromethylcoumarin (mouse, rat, rabbit, micropig, monkey), bufuralol (rat, rabbit, monkey, human) and testosterone (rabbit) moderately (30–60%) to (very) strongly (60–100%).

Dog, followed by micropig and monkey, showed the most similar sulphaphenazole inhibition profiles as compared with human. With respect to the obtained enzyme kinetic parameters towards diclofenac, rat, rabbit and monkey were the most similar species with regard to V_{max} as compared with human, although only rat showed a K_m in the same order of magnitude as found in human liver microsomes. However, in rat liver microsomes, no inhibition of diclofenac metabolism by sulphaphenazole was found, as it was also the case for tolbutamide metabolism (Eagling *et al*. 1998), thus indicating a difference between the active sites of human CYP2C9 and rat CYP2C9 related protein. Therefore, based on the *in vitro* enzyme kinetics and the results obtained with anti-rat CYP2C11 and sulphaphenazole, a reliable prediction with respect to the species most similar to man cannot be achieved.

With respect to the 4′-hydroxylation of *S*-mephenytoin, monkey and human liver microsomes showed the most similar enzyme activities, with the dog having a 4–5-fold lower activity. In addition, Sharer *et al*. (1995) found similar K_m for the 4′-hydroxylation of *S*-mephenytoin in liver microsomes of monkey and man. Although rat CYP2C11 is involved in the metabolism of *S*-mephenytoin (Yasumori *et al*. 1993), this activity was about 14-fold lower than in human liver microsomes (present study). Both for monkey and human liver microsomes, *S*-mephenytoin metabolism was inhibited almost completely by anti-rat CYP2C11, while no inhibition was found for sulphaphenazole in both species. These results, consistent with those described for the inhibition in monkey (anti-CYP2C) and human (sulphaphenazole) liver microsomes (Yasumori *et al*. 1993, Ono *et al*. 1996), do not indicate a difference between both species. Therefore, monkey seems to be the most similar species to man with respect to CYP2C19 (related protein).

Table 2D. Enzyme kinetic parameters for and inhibition of diclofenac 4′-hydroxylase and *S*-mephenytoin 4-hydroxylase activities.

	Male		Female				Amount of inhibition[1]
	K_m	V_{max}	K_m	V_{max}	Male	Female	Sulphaphenazole
Species	Enzyme activity: diclofenac 4′-hydroxylase				Enzyme activity: S-MEPH		Diclofenac 4′-hydroxylase
Mouse	9.8	90	18	197	0.5	0.6	–
Rat	11	538	16	715	1.6	0.6	–
Rabbit	64	358	58	246	1.2	1	–
Dog	89	71	65	98	3.2	5	++
Micropig	40	64	30	22	< 0.4	< 0.3	+
Monkey	160	1035	291	669	23.0	19.7	+
Man	6.7	1513	8.2	1915	19.8	9.6	+++

Apparent K_m is expressed as μM; V_{max} as pmol min^{-1} mg^{-1} microsomal protein.

[1] –, No inhibition (0–15%); +, weak inhibition (15–30%); ++, moderate inhibition (30–60%); +++, strong inhibition (60–80%); ++++, very strong inhibition (80–100%); S-MEPH, *S*-mephenytoin 4′-hydroxylation (activities measured at a concentration 100 μM). Data are derived from duplicate determinations.

Table 2E. Enzyme kinetic parameters for and inhibition of bufuralol 1′-hydroxyse activity.

	Male		Female		Amount of inhibition		
	K_m	V_{max}	K_m	V_{max}	Anti-human CYP2D6	Quinidine	Quinine
Species	Enzyme activity: bufuralol 1′-hydroxylase				BUFUR	BUFUR	BUFUR
Mouse	1.2	936	1.4	1084	–	–	–
Rat	1.3	1021	1.6	596	++	–	+
Rabbit	1.8	581	1.1	509	–	–	–
Dog	14.3	191	14.2	260	–	++	++
Micropig	1.9	653	1.7	638	–	–	–
Monkey	2.9	1167	2.5	955	++	+	+
Man	15.5	151	9.7	87	++	+++	–

Apparent K_m is expressed as μM; V_{max} as pmol min^{-1} mg^{-1} microsomal protein.

[1] –, No inhibition (0–15%); +, weak inhibition (15–30%); ++, moderate inhibition (30–60%); +++, strong inhibition (60–80%); ++++, very strong inhibition (80–100%); BUFUR, bufuralol 1′-hydroxylation. Data are derived from duplicate determinations.

Bufuralol 1′-hydroxylase activity (table 2E)

CYP2D genes or gene products have been detected in mouse, rat, rabbit, dog, minipig, monkey and human (Nelson *et al*. 1993, 1996; http://drnelson.utmem.edu/Nomenclature.html). The human CYP2D6 enzyme is particularly of interest because of its genetically defined polymorphism in man (Guengerich and Shimada 1991, Daly *et al*. 1993, Gonzalez and Idle 1994).

In the present study, dog and human liver microsomes showed similar enzyme kinetics with respect to the 1′-hydroxylation of bufuralol. In addition, the quinidine inhibition profiles obtained for dog and human liver microsomes were also the most similar: moderate to strong inhibition of bufuralol 1′-hydroxylase activity was found in dog and human liver microsomes, while none of the other enzyme activities were inhibited. In contrast to human liver microsomes, the quinine isomer also showed moderate inhibition in dog.

Anti-human CYP2D6 showed moderate inhibition of bufuralol 1′-hydroxylase in rat, monkey and human liver microsomes. However, in contrast to the inhibition found with quinidine/quinine, no inhibition was observed in dog liver microsomes. The weak inhibition observed in rat and monkey by quinine and quinidine respectively as compared with the moderate inhibition observed in dog and human liver microsomes could be due to (1) the lower K_m observed in rat and monkey with respect to bufuralol 1′-hydroxylation and/or (2) lower K_i for quinidine towards bufuralol 1′-hydroxylation in dog and man, as compared with rat and monkey. At least the latter seems to be the case for rat and man, since IC_{50} = 240 and 0.2 μM respectively have been reported (Boobis *et al*. 1990) for the inhibition of bufuralol 1′-hydroxylase activity by quinidine.

Both the 1′-hydroxylation of bufuralol and the competitive inhibition of this substrate by quinidine/quinine occur directly at the active site of the P450 molecule, while inhibition by anti-human CYP2D6 is more directed against a certain region of the molecule. Therefore, because of the similar enzyme kinetics and quinidine inhibition profiles, dog seems to be the most similar species to man with respect to CYP2D, followed by rat and monkey.

Table 2F. Enzyme kinetic parameters for and inhibition of chlorzoxazone 6-hydroxylase activity.

	Male		Female		Amount of inhibition[1]				
	K_m	V_{max}	K_m	V_{max}	Anti-rat CYP2E1				
Species	Enzyme activity: chlorzoxazone 6-hydroxylase				CHLZ	EROD	7-ETC	DICLO	MEPH
Mouse	78	1933	68	2194	+++	+++	++	+	n.d.
Rat	306	3184	220	2233	+++	++	–	++	n.d.
Rabbit	153	2470	98	1833	+	+	–	–	n.d.
Dog	42	573	82	1129	+	+	–	–	n.d.
Micropig	25	285	37	714	–	+	–	–	n.d.
Monkey	202	1761	116	989	+	+	–	–	–
Man	87	1326	152	2764	++	+	–	–	++

Apparent K_m is expressed as μM; V_{max} as pmol min^{-1} mg^{-1} microsomal protein.

[1] –, No inhibition (0–15%); +, weak inhibition (15–30%); ++, moderate inhibition (30–60%); +++, strong inhibition (60–80%); ++++, very strong inhibition (80–100%); EROD, 7-ethoxyresorufin *O*-dealkylation; 7-ETC, 7-ethoxy-4-trifluoromethyl-coumarin *O*-dealkylation; DICLO, diclofenac 4′-hydroxylation; MEPH, *S*-mephenytoin 4′-hydroxylation; CHLZ, chlorzoxazone 6-hydroxylation. Data are derived from duplicate determinations.

Chlorzoxazone 6-hydroxylase activity (table 2F)

Cytochrome P4502E1 has been purified from rat, rabbit and human (Guengerich 1997). CYP2E1 genes or gene products have also been detected in mouse, dog, and monkey (Nelson *et al*. 1993, 1996; http://drnelson.utmem.edu/Nomenclature.html). CYP2E1 enzymes in the various species seem to have similar catalytic specificities (Guengerich 1997). Besides the metabolism of small molecules (Guengerich 1991, Gonzalez and Gelboin 1994), P4502E1 enzymes are also involved in the metabolism of fatty acids (Guengerich 1997). Most animal species appear to have only a single P4502E gene, CYP2E1 (Guengerich 1997).

In the present study, anti-rat CYP2E1 inhibited chlorzoxazone 6-hydroxylase activity in all species, with exception of micropig. However, in all species, the extent of inhibition of chlorzoxazone 6-hydroxylase activity was not much higher than the inhibition observed for some of the other 450 enzyme activities. Therefore, anti-rat CYP2E1 is considered not to be selective with regard to the inhibition of the cytochrome P450 enzyme activities. Diethyldithiocarbamate showed a very low specificity. The results obtained are, therefore, not presented in table 2F. Chlorzoxazone 6-hydroxylase activity was inhibited moderately in micropig and monkey, and (very) strongly in the other species. However, moderate to very strong inhibition was also observed for the metabolism of coumarin (mouse, rabbit, dog, micropig, monkey, human), diclofenac (all species), bufuralol (dog, micropig, monkey, human) and testosterone (all species with exception of the female rat). Therefore, diethyldithiocarbamate cannot be used as a selective inhibitor of CYP2E activity (Chang *et al*. 1994, Ono *et al*. 1996, Eagling *et al*. 1998), although this suggestion has been made previously (Newton *et al*. 1995).

Because the inhibition of chlorzoxazone 6-hydroxylase activity by anti-rat CYP2E1 and diethyldithiocarbamate was non-specific, the inhibition profiles obtained could not be used to rank the species most comparable with human. The obtained enzyme kinetic parameters showed a narrow range of K_m and V_{max} for the various species, maybe with exception of micropig, which showed the lowest K_m and V_{max}. Based on the enzyme kinetic parameters, very few differences seem to exist amongst species with respect to chlorzoxazone 6-hydroxylase activity.

Testosterone 6β-hydroxylase activity (table 2G)

CYP3A genes or gene products have been detected in mouse, rat, rabbit, dog, minipig, monkey and human (Nelson *et al*. 1993, 1996; http://drnelson.utmem.edu/Nomenclature.html). In humans, CYP3A is the most important subfamily, with cytochrome P4503A4 as its major representative (Guengerich 1990). Relatively little is known about catalytic specificities between species, although all P4503A enzymes show testosterone 6β-hydroxylase activity (Nagata *et al*. 1990). In rat, a sex-related difference in hepatic CYP3A activity has been described (Kato and Yamazoe 1992, Werner *et al*. 1995, Tomlinson *et al*. 1997). Table 2G shows that this sex-related difference was also detected in the present study.

The anti-rat CYP3A2 inhibition profiles obtained for mouse and the male rat showed the greatest similarities with the inhibition profile of human liver microsomes. The inhibition profiles of ketoconazole confirmed these similarities, although the profiles of micropig and monkey could possibly be included. Anti-rat CYP3A2 and/or ketoconazole showed inhibition of diclofenac 4′-hydroxylase

Table 2G. Enzyme kinetic parameters for and inhibition of testosterone 6β-hydroxylase activity.

Species	Male		Female		Amount of inhibition[1]						
	K_m	V_{max}	K_m	V_{max}	Anti-rat CYP3A2		Ketoconazole				
	Enzyme activity: testosterone 6β-hydroxylase				TESTOS	DICLO	TESTOS	EROD	DICLO	BUFUR	CHLZ
Mouse	99	2732	76	3321	+++	++	+++	–	+	–	–
Rat	84	3396	582	378	+++[2]/+[3]	+	++[2]–[3]	+	+	–	–
Rabbit	101	4111	121	5160	–	+	++	++	+	+	–
Dog	192	1488	194	1656	+	++	++	–	–	++	–
Micropig	79	4852	49	4116	–	+	+++	–	+	–	++
Monkey	141	11941	132	10764	++	++	++++	++	++	+	–
Man	72	5307	87	8997	++	–	+++	–	–	–	–

Apparent K_m is expressed as μM; V_{max} as pmol min^{-1} mg^{-1} microsomal protein.

[1] –, No inhibition (0–15%); +, weak inhibition (15–30%); ++, moderate inhibition (30–60%); +++, strong inhibition (60–80%); ++++, very strong inhibition (80–100%).

[2], Males.

[3], Females.

EROD, 7 ethoxyresorufin *O*-dealkylation; DICLO, diclofenac 4′-hydroxylation; BUFUR, bufuralol 1′-hydroxylation; CHLZ, chlorzoxazone 6-hydroxylation; TESTOS, testosterone 6β-hydroxylation. Data are derived from duplicate determinations.

Table 2H. Enzymatic activities for and inhibition of lauric acid 12-hydroxylase activity (pmol min^{-1} mg^{-1} microsomal protein). Lauric acid concentration was 100 μM.

	Male	Female	Amount of inhibition[1] anti-rat CYP4A1
Species	Enzyme activity: LAURIC		LAURIC
Mouse	396	361	++++
Rat	492	373	++++
Rabbit	1501	1362	++++
Dog	860	926	++++
Micropig	717	808	++++
Monkey	1736	1661	+++
Man	1230	1674	++++

[1] −, No inhibition (0–15%); +, weak inhibition (15–30%); ++, moderate inhibition (30–60%); +++, strong inhibition (60–80%); ++++, very strong inhibition (80–100%); LAURIC, lauric acid 12-hydroxylation. Data are derived from duplicate determinations.

activity in all the animal species, which was not found in humans. This could indicate that the CYP2C and CYP3A enzymes in the animal species are more related to each other than in man.

In rabbit liver microsomes, no immuno-inhibition of testosterone 6β-hydroxylase activity was observed. This could be due to the fact that in rabbit, P4502C3 is the predominant steroid 6β-hydroxylase enzyme (Guengerich 1997). However, ketoconazole showed moderate (55%) inhibition of testosterone 6β-hydroxylase in rabbit. Therefore, the predominant role of rabbit P4502C in the metabolism of testosterone could not be confirmed unless ketoconazole is an inhibitor of rabbit P4502C.

With respect to the obtained enzyme kinetic parameters, no large differences were found between the various species, with exception of the female rat (higher K_m and lower V_{max}) and maybe the dog (lower V_{max}). Therefore, mouse and the male rat, followed by micropig and monkey, seem to be the most similar species to man regarding cytochrome P4503A.

Lauric acid 12-hydroxylase activity (table 2H)

Cytochrome P4504A enzymes have been identified in mouse, rat, rabbit, guinea pig and human (Nelson *et al*. 1993, 1996; http://drnelson.utmem.edu/Nomenclature.html). Cytochromes P4504A are involved in the $\tilde{\omega}$-hydroxylation of fatty acids, and the induction of lauric acid 12-hydroxylation, a P4504A-catalyzed reaction, is associated with peroxisome proliferation in rodents (Sharma *et al*. 1988, Dirven *et al*. 1991, Makowska and Gibson 1992, Amet *et al*. 1998).

In the present study, the immuno-inhibition profiles of the various species all showed a strong and selective inhibition of lauric acid 12-hydroxylase activity. In addition, no large differences were found between species with respect to the 12-hydroxylation of lauric acid. Therefore, CYP4A (related protein) catalyzed lauric acid 12-hydroxylase activity seems to be well conserved between species.

Discussion

The aim of the present study was to characterize nine cytochrome P450 enzyme activities in seven species to compare this important metabolic step between various test animals and man. Enzyme activities and kinetic parameters were determined

Table 3. Prediction of species most comparable with man with respect to cytochromes P450.

P450 activity towards	Antibody/chemical inhibitor	Inhibition pattern most similar to man	K_m/V_{max} or enzymatic activity most similar to man	Species most similar to man
7-Ethoxy-resorufin	antiserum for human CYP1A	mouse, rabbit micropig	mouse, rat, rabbit, micropig, monkey	(1) mouse, (2) rabbit, micropig
	furafylline	mouse		
	α-naphthoflavone	mouse, rabbit, micropig		
Coumarin	anti-human 2A6	micropig, monkey	rabbit, micropig, monkey	micropig, monkey
7-ETC	anti-rat 2B1	–	mouse	mouse
Diclofenac	anti-rat 2C11	–	rat	?
	sulphaphenazole	dog, micropig, monkey		
Mephenytoin	anti-rat 2C11	–	monkey[1]	monkey
	sulphaphenazole	no inhibition		
Bufuralol	anti-human 2D6	rat, monkey	dog	(1) dog, (2) rat, monkey
	quinidine	dog		
	quinine	moderate inhibition in dog, weak in rat/monkey		
Chlorzoxazone	anti-rat 2E1	–	no large differences between species	no large differences between species
	DDC	–		
Testosterone	anti-rat 3A2	mouse, male rat	mouse, male rat, rabbit, micropig, monkey	(1) mouse, male rat, (2) micropig, monkey
	ketoconazole	(1) mouse, male rat, (2) micropig, monkey		
Lauric acid	anti-rat 4A1	no large differences between species	no large differences between species[1]	no large differences between species

7-ETC, 7-ethoxy-4-trifluoromethylcoumarin; DDC, diethyldithiocarbamate; –, prediction not reliable due to the large extent of cross-reactivity of the antibody/chemical inhibitor.

[1] Similarities not based on K_m and V_{max}, but on enzymatic activity.

towards well-known marker substrates for human cytochrome P450 enzymes. Because different cytochrome P450 enzymes can catalyze the same activity (Guengerich 1997), additional information is required to postulate the animal species most similar to man with regard to the various cytochrome P450 activities. Therefore, inhibition profiles were determined for a broad selection of antibodies and chemical inhibitors. The more similar the inhibition profile of a species to that of man, the more similar the cytochrome P450 catalytic specificities of this species will be. Both the enzyme kinetic parameters/enzyme activities (expression levels) and the inhibition profiles (catalytic specificities) were used to make a prediction with regard to the animal species most similar to man. These results are summarized in table 3. However, it must be considered that in humans the various cytochrome P450 levels show a (wide) range of activities due to interindividual variation and/or genetic polymorphism (Guengerich and Turvey 1991, Forrester *et al.* 1992, Shimada *et al.* 1994). In the present study, pools of human liver microsomes were used, having about mean enzymatic activities towards the various P450 probe substrates. Therefore, when V_{max} of human liver microsomes were compared with those of the animal species, V_{max} of 'mean individuals' were compared.

A number of studies have been reported in which species differences with respect to cytochrome P450 enzyme activities were investigated (e.g. Boobis *et al*. 1990, Pearce *et al*. 1992, Ohmori *et al*. 1993, Stevens *et al*. 1993, Yasumori *et al*. 1993, Weaver *et al*. 1994, 1999, Yamazaki *et al*. 1994, Sharer *et al*. 1995, Ghosal *et al*. 1996, Tomlinson *et al*. 1997, Anzenbacher *et al*. 1998, Eagling *et al*. 1998). In general, the results described in these studies are consistent with the results described here. However, some differences were observed with respect to the metabolism and inhibition of tolbutamide, compared to that of diclofenac. Eagling *et al*. (1998) investigated the inhibition of tolbutamide 4-hydroxylase activity, a CYP2C9/10-catalyzed reaction, in human and rat liver microsomes, by a number of inhibitors. Furafylline, a human CYP1A2 inhibitor, showed no inhibition of tolbutamide 4-hydroxylase activity in human liver microsomes, but rat liver microsomes showed an IC_{50} = 24 μM. In the present study, diclofenac was used as probe substrate for CYP2C9 (related protein). Using this substrate, no inhibition by furafylline was found in rat liver microsomes. Therefore, diclofenac could be a better substrate for CYP2C9-related protein in rat than tolbutamide. Sharer *et al*. (1995) compared the tolbutamide 4-hydroxylase activity in human, cynomolgus monkey and beagle dog liver microsomes. In dog, no detectable tolbutamide 4-hydroxylase activity was found. However, in contrast with tolbutamide metabolism, diclofenac 4′-hydroxylase activity was detectable in this species (table 2D). Although Sharer *et al*. (1995) found rather similar V_{max} in monkey and human, which is consistent with the results of the present study, a K_m for tolbutamide metabolism in monkey was found which was 4-fold higher than in human liver microsomes. For diclofenac metabolism (present study), a 25–35-fold higher K_m was found, indicating a much higher affinity of human CYP2C9 towards diclofenac than monkey CYP2C9-related protein, as compared with tolbutamide.

Guengerich (1997) has proposed a tentative group of 'catalytic preservation' with respect to species extrapolation:

(1) P450 subfamilies in which species extrapolation appears to hold well: 2E1.
(2) P450 subfamilies in which some caution is required in extrapolation: 1A1, 1A2 and 4A.
(3) P450 subfamilies in which more caution is advised in extrapolation: 2D and 3A.
(4) Major problems in extrapolations: 2A, 2B and 2C.

This classification is not strict. In the present study a different approach was used. It was not the aim to rank the cytochrome P450 subfamilies with respect to species extrapolation, but to predict the species most similar to man with respect to the various cytochrome P450 subfamilies. Based on enzyme kinetic parameters, activities and inhibition profiles, no large differences were found between species regarding chlorzoxazone 6-hydroxylase and lauric acid 12-hydroxylase. For 7-ethoxyresorufin *O*-dealkylase, bufuralol 1′-hydroxylase and testosterone 6β-hydroxylase three or four species were selected as species most similar to man, while for coumarin 7-hydroxylase, 7-ethoxy-4-trifluoromethylcoumarin *O*-dealkylase and *S*-mephenytoin 4′-hydroxylase only one or two species were similar enough to man. For diclofenac metabolism, no reliable prediction could be achieved. If the results summarized in table 3 would be used for classification into these groups, CYP2E and CYP4A would be classified in group 1, CYP2A, CYP2B and CYP2C in group 4,

while CYP1A, CYP2D and CYP3A would be classified in groups 2 or 3. Thus, overall, the results presented in table 3 are consistent with the classification proposed by Guengerich.

Finally, the present study was designed to characterize nine cytochrome P450 enzymes/enzyme activities in seven different species to provide additional important information regarding interspecies comparative metabolism. The results were used to select the species most similar to man for each individual P450 enzyme (activity). When it is known which human cytochrome P450 enzyme is involved in the metabolism of a compound, the data in table 3 should be considered as a tool for selecting the most suitable species for *in vitro* and *in vivo* experiments. In this way, the present study hopes to provide additional important information regarding interspecies comparative metabolism.

Acknowledgements

The authors thank Dr Noriaki Shimada of Daiichi Pure Chemicals Co., Ltd, Tokyo and Dr Charles L. Crespi of the GENTEST Corp., Woburn, MA for sponsoring the present study by kindly providing the antibodies.

References

Amet, Y., Adas, F. and Nanji, A. A., 1998, Fatty acid omega- and (omega-1)-hydroxylation in experimental alcoholic liver disease: relationship to different dietary fatty acids. *Alcoholism: Clinical and Experimental Therapeutics*, **22**, 1493–1500.

Anzenbacher, P., Soucek, P., Anzenbacherova, E., Gut, I., Hruby, K., Svoboda, Z. and Kvetina, J., 1998, Presence and activity of cytochrome P450 isoforms in minipig liver. Comparison with human liver samples. *Drug Metabolism and Disposition*, **26**, 56–59.

Bogaards, J. J. P., van Ommen, B. and van Bladeren, P. J., 1995, Human cytochrome P450 enzyme selectivities in the oxidation of chlorinated benzenes. *Toxicology and Applied Pharmacology*, **132**, 44–52.

Bogaards, J. J. P., Venekamp, J. C. and van Bladeren, P. J., 1996, The biotransformation of isoprene and the two isoprene monoepoxides by human cytochrome P450 enzymes, compared to mouse and rat liver microsomes. *Chemico-Biological Interactions*, **102**, 169–182.

Boobis, A. R., Sesardic, D., Murray, B. P., Edwards, R. J., Singleton, A. M., Rich, K. J., Murray, S., De la Torre, R., Segura, J., Pelkonen, O., Pasanen, M., Kobayashi, S., Zhi-Guang, T. and Davies, D. S., 1990, Species variation in the response of the cytochrome P-450-dependent monooxygenase system to inducers and inhibitors. *Xenobiotica*, **20**, 1139–1161.

Burke, M. D., Thompson, S., Weaver, R. J., Wolf, C. R. and Mayer, R. T., 1994, Cytochrome P450 specifities of alkoxyresorufin *O*-dealkylation in human and rat liver. *Biochemical Pharmacology*, **48**, 923–936.

Chang, T. K. H., Gonzalez, F. J. and Waxman, D. J., 1994, Evaluation of triacetyloleandomycin, α-naphthoflavone and diethyldithiocarbamate as selective chemical probes for inhibition of human cytochrome P450. *Archives of Biochemistry and Biophysics*, **311**, 437–442.

Cholerton, S., Daly, A. K. and Idle, J. R., 1992, The role of individual human cytochromes P450 in drug metabolism and clinical response. *TiPS Reviews*, **13**, 434–439.

Daly, A. K., Cholerton, S., Gregory, W. and Idle, J. R., 1993, Metabolic Polymorphisms. *Pharmacology and Therapeutics*, **57**, 129–160.

Daniel, H. I. and Edeki, T. I., 1996, Genetic polymorphism of *S*-mephenytoin 4′-hydroxylation. *Psychopharmacology Bulletin*, **32**, 219–230.

Dirven, H. A. A. M., Bruijn, A. A. G. M. de, Sessink, P. J. M. and Jongeneelen, F. J., 1991, Determination of the cytochrome P450 4 marker, ω-hydroxylauric acid by high performance liquid chromatography and fluorometric detection. *Journal of Chromatography*, **564**, 266–271.

Eagling, V. A., Tjia, J. F. and Back, D., 1998, Differential selectivity of cytochrome P450 inhibitors against probe substrates in human and rat liver microsomes. *British Journal of Clinical Pharmacology*, **45**, 107–114.

Forrester, L. M., Henderson, C. J., Glancey, M. J., Back, D. J., Park, B. K., Ball, S. E., Kitteringham, N. R., McLaren, A. W., Miles, J. S., Skett, P. and Wolf, C. R., 1992, Relative expression of cytochrome P450 isoenzymes in human liver and association with the metabolism of drugs and xenobiotics. *Biochemical Journal*, **281**, 359–368.

Furuya, H., Fernandez-Salguero, P., Gregory, W., Taber, H., Steward, A., Gonzaleze, F. J. and Idle, J. R., 1995, Genetic polymorphism of CYP2C9 and its effect on warfarin maintenance dose requirement in patients undergoing anticoagulation therapy. *Pharmacogenetics*, **5**, 389–392.

Ghosal, A., Satoh, H., Thomas, P. E., Bush, E. and Moore, D., 1996, Inhibition and kinetics of cytochrome P4503A activity in microsomes from rat, human, and cDNA-expressed human cytochrome P450. *Drug Metabolism and Disposition*, **24**, 940–947.

Gonzalez, F. J. and Idle, J. R., 1994, Pharmacogenetic phenotyping and genotyping. *Clinical Pharmacokinetics*, **26**, 59–70.

Gonzalez, F. J. and Gelboin, H. V., 1994, Role of human cytochromes P450 in the metabolic activation of chemical carcinogens and toxins. *Drug Metabolism Reviews*, **26**, 165–183.

Guengerich, F. P., 1990, Mechanism-based inactivation of human liver microsomal cytochrome P450 IIIA4 by gestodine. *Chemical Research in Toxicology*, **3**, 363–371.

Guengerich, F. P., 1991, Oxidation of toxic and carcinogenic chemicals by human cytochrome P-450 enzymes. *Chemical Research in Toxicology*, **4**, 391–407.

Guengerich, F. P., 1997, Comparisons of catalytic selectivity of cytochrome P450 subfamily enzymes from different species. *Chemico-Biological Interactions*, **106**, 161–182.

Guengerich, F. P., Kim, D. and Iwasaki, M., 1991, Role of human cytochrome P-450 IIE1 in the oxidation of many low molecular weight cancer suspects. *Chemical Research in Toxicology*, **4**, 168–179.

Guengerich, F. P. and Shimada, T., 1991, Oxidation of toxic and carcinogenic chemicals by human cytochrome P-450 enzymes. *Chemical Research in Toxicology*, **4**, 391–407.

Guengerich, F. P. and Turvey, C. G., 1991, Comparison of levels of several human microsomal cytochrome P-450 enzymes and epoxide hydrolase in normal and disease states using immunochemical analysis of surgical liver samples. *Journal of Pharmacology and Experimental Therapeutics*, **256**, 1189–1194.

Honkakoshi, P. and Negishi, M., 1997, The structure, function and regulation of cytochrome P450 2A enzymes. *Drug Metabolism Reviews*, **29**, 977–996.

Kato, R. and Yamazoe, Y., 1992, Sex-specific cytochrome P450 as a cause of sex- and species-related differences in drug toxicity. *Toxicology Letters*, **64/65**, 661–667.

Kimonen, T., Juvonen, R. O., Alhava, E. and Pasanen, M., 1995, The inhibition of CYP enzymes in mouse and human liver by pilocarpine. *British Journal of Pharmacology*, **114**, 832–836.

Kunze, K. L. and Trager, W. F., 1993, Isoform-selective mechanism-based inhibition of human cytochrome P450 1A2 by furafylline. *Chemical Research in Toxicology*, **6**, 649–656.

Lewis, D. F. V., Laje, B. G., Dickins, M., Eddershaw, P. J., Tarbit, M. H. and Goldfarb, P. S., 1999, Molecular modelling of CYP2B6, the human CYP2B isoform, by homology with the substrate-bound CYP102 crystal structure: evaluation of CYP2B6 substrate characteristics, the cytochrome b_5 binding site and comparisons with CYP2B1 and CYP2B4. *Xenobiotica*, **29**, 361–393.

Lindberg, R. L. and Negishi, M., 1989, Alteration of mouse cytochrome $P450_{coh}$ substrate specificity by mutation of a single amino-acid residue. *Nature*, **339**, 632–634.

Lucas, D., Berthou, F., Dréano, Y., Lozac'h, P., Volant, A. and Ménez, J., 1993, Comparison of levels of cytochromes P-450, CYP1A2, CYP2E1, and their related monooxygenase activities in human surgical samples. *Alcoholism: Clinical and Experimental Research*, **17**, 900–905

Makowska, J. M. and Gibson, G. G., 1992, Species differences in cipofibrate induction of hepatic cytochrome P450 4A1 and peroxisome proliferation. *Journal of Biochemical Toxicology*, **7**, 183–191.

Nagata, K., Gonzalez, F. J., Yamazoe, Y. and Kato, R., 1990, Purification and characterization of four catalytically active testosterone 6β-hydroxylase P-450s from rat liver microsomes: comparison of a novel form with three structurally and functionally related forms. *Journal of Biochemistry*, **107**, 718–725.

Nakachi, K., Imai, K., Hayashi, S. and Kawajiri, K., 1993, Polymorphisms of the CYP1A1 and glutathione *S*-transferase genes associated with susceptibility to lung cancer in relation to cigarette dose in a Japanese population. *Cancer Research*, **53**, 2994–2999.

Nelson, D. R., Kamataki, T., Waxman, D. J., Guengerich, F. P., Estabrook, R. W., Feyereisen, R., Gonzalez, F. J., Coon, M. J., Gunsalus, I. C., Gotoh, O., Okuda, K. and Nebert, D. W., 1993, The P450 superfamily: update on new sequences, gene mapping, accession numbers, early trivial names of enzymes, and nomenclature. *DNA and Cell Biology*, **12**, 1–51.

Nelson, D. R., Koymans, L., Kamataki, T., Stegeman, J. J., Feyereisen, R., Waxman, D. J., Waterman, M. R., Gotoh, O., Coon, M. J., Estabrook, R. W., Gunsalus, I. C. and Nebert, D. W., 1996, P450 superfamily: update on new sequences, gene mapping, accession numbers and nomenclature. *Pharmacogenetics*, **6**, 1–42.

Newton, D. J., Wang, R. W. and Lu, A. Y. H., 1995, Evaluation of specificities in the *in vitro* metabolism of therapeutic agents by human liver microsomes. *Drug Metabolism and Disposition*, **23**, 154–158.

Ohmori, S., Taniguchi, T., Rikihisa, T., Kanakubo, Y. and Kitada, M., 1993, Species differences of testosterone 16-hydroxylase in liver microsomes of guinea pig, rat and dog. *Xenobiotica*, **23**, 419–426.

Ono, S., Hatanaka, T., Hotta, H., Satoh, T., Gonzalez, F. J. and Tsutsui, M., 1996, Specificity of substrate and inhibitor probes for cytochrome P450s: evaluation of *in vitro* metabolism using cDNA-expressed human P450s and human liver microsomes. *Xenobiotica*, **26**, 681–693.

Pearce, R., Greenway, D. and Parkinson, A., 1992, Species differences and interindividual variation in liver microsomal cytochrome P450 2A enzymes: effects on coumarin, dicumarol, and testosterone oxidation. *Archives of Biochemistry and Biophysics*, **298**, 211–225.

Perella, F. W., 1988, EZ-FIT: a practical curve-fitting microcomputer program for the analysis of enzyme kinetic data on IBM-PC compatible computers. *Analytical Biochemistry*, **174**, 437–447.

Powell, P. K., Wolf, I. and Lasker, J. M., 1996, Identification of CYP4A11 as the major lauric acid omega-hydroxylase in human liver microsomes. *Archives of Biochemistry and Biophysics*, **335**, 219–226.

Schmider, J., Greenblatt, D. J., Moltke, L. L. von, Harmatz, J. S., Duan, S. X., Karsov, D. and Shader, R. I., 1996, Characterization of six *in vitro* reactions mediated by human cytochrome P450: application to the testing of cytochrome P450-directed antibodies. *Pharmacology*, **52**, 125–134.

Sharer, J. E., Shipley, L. A., Vanderbranden, M. R., Binkley, S. N. and Wrighton, S. A., 1995, Comparisons of phase I and phase II *in vitro* enzyme activities of human, dog, rhesus monkey, and cynomolgus monkey. *Drug Metabolism and Disposition*, **23**, 1231–1241.

Sharma, R., Lake, B. G., Foster, J. and Gibson, G. G., 1988, Microsomal cytochrome P452 induction and peroxisome proliferation by hypolipidaemic agents in liver. A mechanistic inter-relationship. *Biochemical Pharmacology*, **37**, 1193–1201.

Shimada, T., Yamazaki, H., Mimura, M., Inui, Y. and Guengerich, F. P., 1994, Interindividual variations in human liver cytochrome P-450 enzymes involved in the oxidation of drugs, carcinogens and toxic chemicals: studies with human liver microsomes of 30 Japanese and 30 Caucasians. *Journal of Pharmacology and Experimental Therapeutics*, **270**, 414–423.

Stevens, J. C., Shipley, L. A., Cashman, J. R., Vandenbranden, M. and Wrigthon, S. A., 1993, Comparison of human and rhesus monkey in vitro phase I and phase II hepatic drug metabolism activities. *Drug Metabolism and Disposition*, **21**, 753–760.

Tomlinson, E. S., Maggs, J. J., Park, B. K., and Back, D. J., 1997, Dexamethasone metabolism *in vitro*: species differences. *Journal of Steroid Biochemistry and Molecular Biology*, **62**, 345–352.

Weaver, R. J., Dickins, M. and Burke, M. D., 1999, A comparison of basal and induced hepatic microsomal cytochrome P450 monooxygenase activities in cynomolgus monkey (*Macaca fascicularis*) and man. *Xenobiotica*, **29**, 467–482.

Weaver, R. J., Thompson, S., Smith, G., Dickins, M., Elcombe, C. R., Mayer, R. T. Burke, M. D., 1994, A comparative study of constitutive and induced alkoxyresorufin O-dealkylation and individual cytochrome P450 forms in cynomolgus monkey (*Macaca fascicularis*), human, mouse, rat and hamster liver microsomes. *Biochemical Pharmacology*, **47**, 763–773.

Werner, M., Birner, G. and Dekant, W., 1995, The role of cytochrome P4503A1/2 in the sex-specific sulfoxidation of the hexachlorobutadiene metabolite, *N*-acetyl-*S*-(pentachlorobutadienyl)-L-cysteine in rats. *Drug Metabolism and Disposition*, **23**, 861–868.

Wrighton, S. A. and Ring, B. J., 1994, Inhibition of human CYP3A catalyzed by 1′-hydroxy midazolam formation by ketoconazole, nifedipine, erythromycin, cimetidine, and nizatidine. *Pharmaceutical Research*, **6**, 921–924.

Wrighton, S. A. and Stevens, J. C., 1992, The human hepatic cytochromes P450 involved in drug metabolism. *Critical Reviews in Toxicology*, **22**, 1–21.

Yamazaki, H., Mimura, M., Sugahara, C. and Shimada, T., 1994, Catalytic roles of rat and human cytochrome P450 2A enzymes in testosterone 7α- and coumarin 7-hydroxylations. *Biochemical Pharmacology*, **48**, 1524–1527.

Yasumori, T., Chen, L., Nagat, K., Yamazoe, Y. and Kato, R., 1993, Species differences in stereoselective metabolism of mephenytoin by cytochrome P450 (CYP2C and CYP3A). *Journal of Pharmacology and Experimental Therapeutics*, **264**, 89–94.

XENOBIOTICA, 2000, VOL. 30, NO. 12, 1153–1157

Metabolism of *N*-isopropylacetanilide in rat

G. L. LARSEN*, V. J. FEIL† and J. E. BAKKE†

USDA ARS Biosciences Research Laboratory, PO Box 5674-University Station, Fargo, ND 58105, USA

Received 11 September 2000

1. Radioactivity from oral doses of *N*-isopropyl[1-^{14}C]acetanilide was excreted in urine (53.5%), faeces (8.1%) and expired air (17.0%) of rat.

2. Enterohepatic circulation occurred during formation of ~ 34% of the metabolites. *N*-isopropylacetanilide was metabolized by oxidation in all moieties of the molecule with subsequent conjugation with glucuronic and sulphuric acids.

3. The sulphate ester of 4′-hydroxyacetanilide (acetaminophen) was the major metabolite (28% of the dose).

Introduction

Hutson *et al*. (1984) reported that an acetanilide intermediate (4′-cyanoacetanilide) formed during rat metabolism of *p*-*N*,*N*-dimethylaminobenzonitrile was excreted, in part, as 4′-cyano-2-methylsulphonylacetanilide (figure 1). The 2-methylsulphonyl acetanilides formed during propachlor (2-chloro-*N*-isopropylacetanilide) metabolism were catabolites of the glutathione (GSH) conjugate (Bakke *et al*. 1981a, b). This catabolism involved cysteine conjugate-β-lyase cleavage of the cysteine conjugate of a xenobiotic to a xenobiotic thiol, methylation of the thiol, and oxidation of the sulphur to the sulphone (figure 1).

Propachlor is also metabolized by reductive dehalogenation to *N*-isopropylacetanilide in plants (Lamoureux *et al*. 1971), soil (Lee *et al*. 1982), and animals (rat, Bakke and Price 1979; chicken, Bakke and Larsen 1985). The *N*-isopropylacetanilide detected in these studies was probably formed in the pathway described by Hutson *et al*. (1976). This pathway involves glutathionolysis of the GSH conjugate to yield oxidized glutathione (GSSG) and the reduced xenobiotic moiety (figure 2). The glutathionolysis probably occurs with conjugates resulting from proteolytic degradation of the GSH conjugate in addition to the GSH conjugate because labelled *N*-isopropylacetanilide was excreted when the cysteine conjugate of [1-^{14}C]propachlor was dosed to chicken (Bakke and Larsen 1985) (figure 2).

The purpose of the present study was to determine if the *N*-isopropylacetanilide formed by reductive dehalogenation in propachlor metabolism served as a precursor for any of the 2-methylsulphonyl-containing metabolites formed in rat dosed with propachlor.

Materials and methods

Radiolabelled compound

N-isopropyl[1-^{14}C]acetanilide (**I**; table 2) was synthesized as follows: a solution of 350 μl silicon tetrachloride in 1 ml methylene chloride was slowly added to a solution of 1 mCi acetic[1-^{14}C] acid (sp. act. 7.49 mCi mM^{-1}, Pathfinder Laboratories, Inc., St Louis, MO, USA), 72 mg acetic acid, 270 mg *N*-isopropylaniline, and 2 ml pyridine in 4 ml methylene chloride. The reaction mixture was stirred at

* Author for correspondence; e-mail: larseng@fargo.ars.usda.gov † Retired.

Xenobiotica ISSN 0049–8254 print/ISSN 1366–5928 online © 2000 US Government
http://www.tandf.co.uk/journals
DOI: 10.1080/00498250010021693

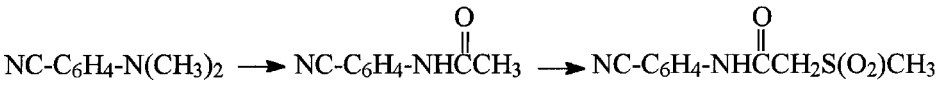


Figure 1. Reaction 1.

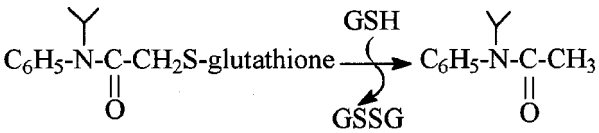


Figure 2. Reaction 2.

room temperature for 16 h, 75 ml methylene chloride was added and the solution washed twice with 10-ml portions of 2.5 N sodium hydroxide and finally with two 10-ml portions of water. The methylene chloride solution was dried over magnesium sulphate and passed through a small column of silica to yield 293 μCi *N*-isopropyl[1-^{14}C]acetanilide (**I**). No radioactive impurities could be detected by TLC on silica with the following solvent systems: methylene chloride, ethyl acetate or methylene chloride-ethyl acetate 1:1.

Animal treatments

Ten control and six bile-duct-cannulated, male Sprague–Dawley rats (250–290 g) were each given a single oral dose of *N*-isopropyl[1-^{14}C]acetanilide (**I**; 5.2 mg containing 0.99 μCi ^{14}C per rat) in 0.3 ml ethyl acetate. Seven control rats were kept in stainless steel metabolism cages. Three control rats and three rats with cannulated bile ducts were housed in metabolism cages equipped for the collection of CO_2. Rats with cannulated bile ducts were kept in restraining cages (Bollman 1948) and were dosed 20–24 h after surgery. All rats were given food (Purina Rodent Chow, Ralston Purina Co., St Louis, MO, USA) and water *ad libitum* (cannulated rats were given physiological saline in place of water). Urine and faeces were collected daily for 2 days. Rats were killed with CO_2.

Instrumentation and quantitation of radioactivity

Liquid scintillation counting quantitated radioactivity in urine, bile and various extracts. $^{14}CO_2$ in expired air was trapped in ethanolamine solution and quantitated as according to Robbins and Bakke (1967). Tissue and faecal samples were homogenized in water, freeze-dried and combusted in a Packard Tri-Carb sample oxidizer (model 305; Packard Instrument Co., Meriden, CT, USA). $^{14}CO_2$ was quantitated by liquid scintillation counting.

Electron impact mass spectra were obtained using the solid sample inlet probe of a Varian-MAT CH5 DF mass spectrometer (Varian Inst. Co., Bremen, Germany). Fast-atom bombardment (FAB) mass spectra (negative-ion mode) were obtained on the same equipment fitted with an Ion-Tech argon gun (Teddington, UK). For FAB mass spectrometry, samples were run in a glycerol matrix. Capillary gas chromatography coupled with mass spectrometry (GLC/MS) was done on a Hewlett-Packard 5988 instrument (Agilent Technologies, Inc., Wilmington, DE, USA). The column was 25 m long with an inside diameter of 0.32 mm coated with methylsilicone (0.52 μm). The sample was directly injected onto the column and the following GLC parameters were used: gas flow 1 ml min^{-1}; initial injector temperature was 85 °C; and the initial column temperature was held at 80 °C for 2 min then programmed at 10 °C min^{-1} to 240 °C. The MS was operated at 240 °C at 300 mA and 70 Ev.

Isolation of metabolites

A column containing Porapak Q (Waters Assoc., Milford, MA, USA; 1×10 cm) was used for extraction of labelled metabolites from the urine and bile. The column was packed as a slurry in methanol, then washed with water before sample application. Urine was adjusted to pH 4 with HCl before application to the column; bile was applied as collected. Unbound materials were washed off the column with water and absorbed materials were eluted from the column with methanol.

The radioactivity that eluted from the Porapak Q column was next applied to a column (2×150 cm) of water-equilibrated Sephadex LH-20 (Pharmacia, Biotech AB, Uppsala, Sweden). The radioactivity was eluted from the column with water pumped at 1 ml min^{-1}. Two radioactive fractions were separated. These fractions were then further purified by HPLC on a μ-Bondapak-C_{18} column (Waters Assoc.). The samples were applied to the column in water, and the ^{14}C was eluted from the column with a linear gradient of water to 100% acetonitrile. Radioactivity in the effluent was detected with a flow monitor (Tri-Carb RAM 7500).

Table 1. Recovery of ^{14}C from rat 48 h after a single oral dose of *N*-isopropyl[1-^{14}C]acetanilide.

	% of dose	
	Control (n = 10)	Cannulated bile duct (n = 6)
Bile	—	42.7±3.7
Urine	53.5±4.9	32.2±3.2
Faeces	8.1±2.5	0.5±0.4
CO_2	17.0±0.7 (n = 3)	9.8±1.2 (n = 3)
Carcass	10.8±2.7	2.7±1.3
Total recovery	89.4	87.9

—, Not applicable.
Values are mean±SD.

A Hewlett Packard gas chromatograph (5790A) equipped with an effluent splitter was used for packed-column GLC. About 10% of the column effluent went to a flame ionization detector and 90% was trapped in glass tubes for ^{14}C detection or instrumental analysis. The column was a 1 m×0.32 cm i.d. glass column packed with 3% SE-30 on 60/80 mesh Chromasorb W. The carrier gas was helium at 30 ml min^{-1}. Oven temperature was programmed at 10 °C min^{-1} from 100 to 300 °C. The injector and detector were maintained at 250 °C. When necessary, samples were derivatized for GLC by reaction with *bis*-trimethylsilyl-trifluoroacetamide containing 1% trimethylchlorosilane at 100 °C overnight.

Results

Recovery of radioactivity

The recoveries of radioactivity from rats dosed orally with *N*-isopropyl[1-^{14}C]acetanilide (**I**) are given in table 1. Urine was the major route for excretion of ^{14}C; however, metabolism of the carbonyl group to $^{14}CO_2$ and tissue residues was also important. Biliary excretion was also a major route of excretion and indicated that enterohepatic circulation was involved in formation of urinary and faecal metabolites, expired $^{14}CO_2$ and contributed to ^{14}C-residues in tissue.

Characterization of metabolites

Glucuronides (**II–IV**) were characterized using electron-impact and both positive- and negative-ion fast-atom bombardment mass spectrometry. For electron-impact mass spectrometry, the per-trimethylsilyl derivatives of the intact glucuronides were formed and purified as a group by GLC on the packed column. The fraction containing ^{14}C was trapped and separated on the capillary GLC/MS. Three components were separated that gave fragmentation patterns characteristic for per-trimethylsilyl-glucuronides (Bakke 1976). The aglycones were recovered from the glucuronidase hydrolysate of the mixture of glucuronides, the trimethylsilyl derivatives were formed, and three isomers were separated and characterized using capillary GLC/MS. *p*-Hydroxy-*N*-isopropylacetanilide (aglycone of **II**) was characterized by the absence of the m/z 120 ($C_6H_5NHCO^+$) fragment ion, which is characteristic of the acetanilide moiety. 2-Hydroxy-*N*-isopropylacetanilide (aglycone of **III**) was identified by NMR spectroscopy and the third isomer (aglycone of **IV**) was assumed to have a primary hydroxyl on the isopropyl moiety because of the $[M\text{-}(CH_3)_3SiOCH_2]^+$ ion at m/z 162, and the m/z 120 ion in the mass spectrum. *N*-Isopropyl-*N*-phenyloxamic acid (**V**; Bakke and Price 1979), acetanilide (**VII**) and *p*-hydroxyacetanilide (aglycone of **VI**) were identified by comparison with authentic standards. The sulphate ester of *p*-hydroxyacetanilide (**VI**)

Table 2. Labelled metabolites from urine and bile of rat dosed with *N*-isopropyl[1-^{14}C]-acetanilide (**I**).

		Percent of dose		
		Control urine	Cannulated bile duct	
			Urine	Bile
C_6H_5-N($CH(CH_3)_2$)-C(O)CH_3	parent, **I**	1	1	10
Gl-O-C_6H_4-N($CH(CH_3)_2$)-C(O)CH_3	**II**	3	1	20
C_6H_5-N($CH(CH_3)_2$)-C(O)CH_2-O-Gl	**III**	3	2	10
C_6H_5-N(CH_3CHCH_2OGl)-C(O)CH_3	**IV**	6	—	1
C_6H_5-N($CH(CH_3)_2$)-C(O)C(O)OH	**V**	3	< 1	—
$^{-}O_3S$-O-C_6H_4-HN-C(O)CH_3	**VI**	28	12	3
C_6H_5-HN-C(O)CH_3	**VII**	7	—	—

Gl, glucuronic acid.

was detected using negative-ion fast-atom bombardment mass spectrometry. The yields of the urinary metabolites formed in the control and in the bile duct-cannulated rat are shown in table 2.

Discussion

There was no evidence for either GSH conjugation or the formation of 2-methylsulphonyl acetanilides as metabolites of *N*-isopropylacetanilide (**I**) in the control rat or in rat with a cannulated bile duct. The proposed precursors for GSH conjugation in *N*-isopropylacetanilide metabolism would be the sulphate esters of either 2-hydroxy-*N*-isopropylacetanilide (aglycone of **III**) or 2-hydroxyacetanilide (**VII**). Although the glucuronide of 2-hydroxy-*N*-isopropylacetanilide (**III**) was a biliary metabolite (10% of dose), the aglycone formed before glucuronidation or after intestinal hydrolysis of the biliary glucuronide probably never became a substrate for sulphotransferase in a tissue where reaction with and displacement of GSH could occur.

All moieties of the *N*-isopropylacetanilide (**I**) molecule were metabolized; the major excreted products in control rat urine were acetanilide (**VII**) and *p*-hydroxyacetanilide (acetaminophen) as the sulphate ester (**VI**). Comparison of the metabolite profiles in bile and urine from the cannulated rat with that in urine from the controls (table 2) shows extensive metabolism associated with enterohepatic circulation. This metabolism during enterohepatic circulation included all moieties of the molecule and included a near doubling of the formation of respiratory $^{14}CO_2$ and a tripling of tissue residues of ^{14}C from the acetyl moiety (table 1). The fate of the de-acetylated aromatic portion was not determined.

Note

The use of trade, firm or corporation names in this publication is for the information and convenience of the reader. Such use does not constitute an official endorsement or approval by the US Department of Agriculture or the Agricultural Research Service of any product or service to the exclusion of others that may be suitable.

References

Bakke, J. E., 1976, Recent advances in the isolation and identification of glucuronide conjugates. In D. D. Kaufman, G. G. Still, G. D. Paulson and S. K. Bandal (eds), *Bound and Conjugated Pesticide Residues*. Symposium Series no. 29 (Washington, DC: American Chemical Society), pp. 55–67.

Bakke, J. E. and Larsen, G. L., 1985, Metabolism of 2-chloro-*N*-isopropylacetanilide in chickens. *Chemosphere*, **14**, 1749–1754.

Bakke, J. E., Larsen, G. L., Aschbacher, P. W., Rafter, J. J., Gustaffson, J.-Å. and Gustaffson, B. E., 1981a, Role of gut microflora in metabolism of glutathione conjugates of xenobiotics. In *Sulfur in Pesticide Action and Metabolism*. ACS Symposium Series no. 158 (Washington, DC: American Chemical Society), pp. 165–178.

Bakke, J. E. and Price, C. E., 1979, Metabolism of 2-chloro-*N*-isopropylacetanilide (propachlor) in the rat. *Journal of Environmental Science and Health*, **B14**, 427–441.

Bakke, J. E., Rafter, J., Larsen, G. L., Gustaffson, J.-Å. and Gustaffson, B. E., 1981b, Enterohepatic circulation of the mercapturic acid and cysteine conjugates of propachlor. *Drug Metabolism and Disposition*, **9**, 525–528.

Bollman, J. L., 1948, A cage which limits the activity of rats. *Journal of Laboratory and Clinical Medicine*, **33**, 1348.

Hutson, D. H., Holmes, D. S. and Crawford, M. J., 1976, The involvement of glutathione in the reductive dechlorination of a phenacyl halide. *Chemosphere*, **5**, 79.

Hutson, D. H., Lakeman, S. K. and Logan, C. J., 1984, The fate of 4-cyano-N,N-dimethylaniline in rats; a novel involvement of glutathione in the metabolism of anilines. *Xenobiotica*, **14**, 925–934.

Lamoureux, G. L., Stafford, L. E. and Tanaka, F. S., 1971, Metabolism of 2-chloro-*N*-isopropylacetanilide (propachlor) in the leaves of corn, sorgum, sugarcane and barley. *Journal of Agricultural and Food Chemistry*, **19**, 346–350.

Lee, J. K., Minard, R. D. and Bollag, J. M., 1982, Microbial metabolism of propachlor (2-chloro-*N*-isopropylacetanilide) in soil suspension. *Journal of the Korean Agricultural Chemical Society*, **25**, 44–54.

Robbins, J. D. and Bakke, J. E., 1967, Sheep and goat metabolism unit for the collection of excreta and expired $^{14}CO_2$. *Journal of Animal Science*, **26**, 424–429.